

Table of Contents

Award Winners, Thursday 17:00-18:00

AWARD_1--Simulating The Effects Of Crouch Gait Surgeries On Knee Mechanics--(Lenhart)	1
AWARD_2--Achilles Tendon Deformations And The Age-Related Reduction In Plantarflexor Performance During Walking--(Franz)	3
AWARD_3--MRI Assessments Of Cartilage Mechanics, Morphology And Composition Following ACL-Reconstructive Surgery--(Kaiser)	5
AWARD_4--Assessment Of The Contributions Of Elastic Energy In The Human Plantar Aponeurosis--(Wager)	7

Concurrent Session 1, Thursday 8:00-9:30

TP1A_1--The Influence Of Solid Ankle-Foot-Orthoses On Forward Propulsion And Dynamic Balance In Healthy Adults During Walking--(Vistamehr)	9
TP1A_2--The Influence Of Passive-Dynamic Ankle-Foot Orthosis Bending Axis On Gait Performance In Individuals With Lower-Limb Impairments--(Ranz)	11
TP1A_3--Effects Of Ankle Bending Stiffness Of Ankle-Foot Orthosis On Gait Patterns With Cerebral Palsy- A Pilot Study With Single-Subject Design--(Sanchez Posada)	13
TP1A_4--Adaptive Gain For Proportional Myoelectric Control Of A Robotic Ankle Exoskeleton During Human Walking--(Koller)	15
TP1A_5--Implementing A Virtual Gait Assistance Device Within A Musculoskeletal Simulation Framework--(Akbas)	17
TP1B_1--Surveying The Interest Of Individuals With Upper Limb Loss In Novel Prosthetic Control Techniques--(Engdahl)	19
TP1B_2--Quick, Low-Cost, Sensitive Motor Assessment Using Markerless Motion Capture--(Charles)	21
TP1B_3--Portable Myoelectric Brace Use In Chronic, Post Stroke Hemiparesis--(Willigenburg)	23
TP1B_4--Improving Finger Movement Repertoire In Stroke--(Ranganathan)	25
TP1B_5--Scapular Kinematic Is Altered After Electromyography Biofeedback Training--(San Juan)	27
SM1C_1--Using Sensors To Improve Sport Safety--(Duma)	29
SM1C_2--Quantifying Field-Based Warfighter Performance Via A Body-Worn Array Of Wireless Inertial Sensors--(McLean)	31
SM1C_3--Clinical Interventions For Gait Abnormalities- Mode Of Feedback And Lower Extremity Mechanical Effects--(Williams III)	33
SM1C_4--Assessing Load And Load Symmetry Outside The Lab--(Queen)	35
PD1D_1--Open Knee(S) Comprehensive Patellofemoral Joint Testing For Specimen Specific Next Generation Knee Models--(Colbrunn)	37
PD1D_2--An ACL Denervation Model For Determination Of The Effects Of Sensory Afferents On Joint Function--(Nagelli)	39
PD1D_3--Pediatric Obesity And Walking Duration Affect Medial And Lateral Tibiofemoral Compartment Contact Forces--(Lerner)	41
PD1D_4--Effect Of Knee Bracing And Wedged Insoles Upon Knee Joint Contact Forces--(Tse)	43
PD1D_5--Can Osteoarthritis Radiographic Severity And Pain Be Explained By Joint Mechanics--(Hassan)	45
PD1D_6--Active And Passive Knee Stability In Patients With Severe OA--(Freisinger)	47
PD1E_1--Influence Of Tendon Stiffness On Muscle-Tendon Interaction Dynamics During Cyclic Contractions--(Doering)	49
PD1E_2--3D Finite-Element Modeling Of The Soft Palate Reveals Synergic Actions Of Speech Muscles--(Inouye)	51
PD1E_3--Agent-Based Model Of Inflammation And Regeneration Following Contraction-Induced Muscle Injury--(Martin)	53
PD1E_4--Effects Of Q-Angle And Tibial Slope On Anterior Cruciate Ligament Force- A Finite Element Study--(Amerinatanzi)	55
PD1E_5--Effect Of Deep Medial Collateral Ligaments On Meniscus Motion--(Guess)	57
PD1E_6--Muscle Architecture Analysis Using Computational Fluid Dynamics--(Inouye)	59

Concurrent Session 2, Thursday 10:00-11:30

TP2A_1--Individual Differences In Required Coefficient Of Friction Affect Slip Risk During Level Walking--(Beschoner)	61
TP2A_2--Falls Resulting From A Laboratory-Induced Slip Occur At A Higher Rate Among Young And Older Adults Who Are Obese--(Allin)	63
TP2A_3--Obesity Increases Fall Rate Following A Laboratory-Induced Trip--(Garman)	65
TP2A_4--Vibration Training Could Reduce Risk Of Falls Among Young Adults With Obesity--(Munoz)	67
TP2A_5--An Evaluation Of Fall Biomechanics That May Underlie The Incidence Of Wrist And Hip Fractures In Older Adult Women--(Crenshaw)	69
TP2B_1--Automation Of Stride-Specific Belt Velocities On Instrumented Treadmills For Gait Rehabilitation And Training--(Hinkel-Lipsker)	71
TP2B_2--Gait Retraining To Improve Stance Time Asymmetry Reduces Knee External Adduction Moments- A Case Study Of A Unilateral Transtibial Amputee--(Rice)	73
TP2B_3--Development Of A Visual Biofeedback System For Center Of Pressure Modification During Gait--(Browne)	75
TP2B_4--Modifying Ankle Joint Neuromechanics Using An Ankle Foot Orthosis With Vibrotactile Feedback During Human Walking--(Westbrook)	77
TP2B_5--Individuals With Incomplete Spinal Cord Injury Change Locomotor Stability After Exposure To A Viscous Force Field--(Gordon)	79
SM2C_1--Grand Challenges In Upper-Limb Biomechanics--(Charles)	81
PD2D_1--Methods For Full Body Inverse Dynamics Analysis Of Standing Jump--(Ashby)	84
PD2D_2--Synthesis Of Subject-Specific Task-Level Motions For Predictive Simulations Of Balance Recovery--(Mansouri)	86

PD2D_3--Simulation-Based Design Of Devices To Augment Human Movement--(Rogers)	88
PD2D_4--Simulated Soft-Tissue Oscillation Increases Stability In Passive-Dynamic Walkers--(Masters)	90
PD2D_5--Generating Predictive Simulations Of Musculoskeletal Movement Using Optimal Control, Matlab And OpenSim--(Lee)	92
PD2D_6--Influence Of Stiffness Of An Ankle-Foot Orthosis On Gait - A Predictive Simulation Study--(Koelewijn)	94
PD2E_1--Biomechanical, Clinical, And Functional Changes With Achilles Tendon Pathology--(Zellers)	96
PD2E_2--Variation In The Human Achilles Tendon Moment Arm During Walking--(Rasske)	98
PD2E_3--Lumbar Intervertebral Disc Deformation In Vivo During Lifting Motion--(Byrne)	100
PD2E_4--Quantifying Microstructural Damage Accumulation In The Annulus Fibrosus During Induced Intervertebral Disc Herniation--(Noguchi)	102
PD2E_5--Relative Strain In Anterior Cruciate Ligament And Medial Collateral Ligament During Simulated Athletic Tasks- Implications For Injury Risk--(Bates)	104
PD2E_6--The Effect Of Isolated And Combined Tibial Rotations On ACL And MCL Biomechanics During Simulated Deceleration Tasks--(Bates)	106

Concurrent Session 3, Friday 15:00-16:30

TP3A_1--1/f Characteristics Of Step Width During Treadmill Walking--(Grabner)	108
TP3A_2--Gait Speed Is Influenced By Secondary Tasks In Persons With Unilateral Transtibial Amputation--(Hendershot)	110
TP3A_3--Lower Prosthetic Stiffness Minimizes The Metabolic Cost Of Running For Individuals With Bilateral Leg Amputations--(Beck)	112
TP3A_4--The Effects Of Prosthetic Foot Stiffness On Amputee Turning Mechanics--(Shell)	114
TP3A_5--When Should We Biomechanically Examine A Lower-Limb Amputee A Systematic Review Of Accommodation Times--(Wanamaker)	116
TP3B_1--Sarcomere Length Organization As A Design For Cooperative Function Amongst All Lumbar Spine Muscles--(Zwambag)	118
TP3B_2--Functional Importance Of Fascia In The Preservation Of Muscle Tension--(Ruttiman)	120
TP3B_3--Multiscale Muscle Models Predict How Accumulated Microtears Lead To Acute Muscle Injury--(Virgilio)	122
TP3B_4--Effects Of Strength Training On Muscle Force Production And Muscle Function In Children With Cerebral Palsy--(Hegarty)	124
TP3B_5--Extensor Muscle Sequencing During Return To Stand In A Subgroup Of Individuals With Low Back Pain- Response To Exercise--(Nelson-Wong)	126
SM3C_1--Bringing Mechanics To Life--(Zaferiou)	128
SM3C_2--Experiential, Low Cost Neuroscience Outreach For All Ages - Muscles Alive!--(Tracy)	130
SM3C_3--The Rebel Stem Academy- Bringing Students To The Science--(Dufek)	131
SM3C_4--Bridging Engineering, Science And Technology In Medicine (Best Medicine)--(Davis)	132
PD3D_1--Subchondral Strains And Initiation Of Osteoarthritis In The Radiocarpal Joint--(Johnson)	133
PD3D_2--A Simulation Study Of The Wrist And Thumb- Why Do Wrist Surgeries Decrease Lateral Pinch Strength--(Nichols)	135
PD3D_3--Effects Of Carpal Tunnel Syndrome On Force Coordination And Muscle Coherence During Precision Pinch--(Lu)	137
PD3D_4--A Mathematical Model For Measuring Scapular Motion--(Nicholson)	139
PD3D_5--Quantifying Kinematic And Muscular Adaptations To Rotator Cuff Fatigue--(McDonald)	141
PD3D_6--Identification Of Multidimensional Shoulder Impedance With Passive And Active Muscles--(Lipps)	143

Concurrent Session 4, Friday 16:45-18:15

TP4A_1--Loading Patterns Vary By Direction, Footwear, And Foot-Strike In Running--(Nordin)	145
TP4A_2--The Immediate Effects Of Footstrike Loudness Feedback In Reducing Impact Loading In Runners--(Tate)	147
TP4A_3--The Effect Of Highly Cushioned Shoes On Tibial Acceleration In Runners--(Ruder)	149
TP4A_4--Subject-Specific Tibial Stresses During Shod And Barefoot Running--(Boyer)	151
TP4A_5--Frequency Content Of The Vertical Impact Peak During Rearfoot And Forefoot Running--(Gruber)	153
TP4B_1--Effort-O-Meter- The Relationship Between Effort Of Walking And Amount Of Walking Performed--(Wu)	155
TP4B_2--Biomechanical Determinants Of Muscle Metabolic Energy Consumption In Locomotion--(Johnson)	157
TP4B_3--Is The Foot Working With Or Against The Ankle During Human Walking--(Zelik)	159
TP4B_4--A Kinematic And Energetics Model Of Shank Progression During Stance--(Pollen)	161
TP4B_5--Asymmetric Forces Increase The Metabolic Cost Of Running For Individuals With A Unilateral Leg Amputation--(Beck)	163
PD4D_1--Kinematic Strategies For Asymmetric Bilateral Landing After Anterior Cruciate Ligament Injury--(Wordeman)	165
PD4D_2--Sagittal Plane Knee Excursion Is Key Predictor Of Lower Extremity Performance During Single Leg Hop--(Hoffman)	167
PD4D_3--Kinematic_Kinetic Differences Between Subjects With_Without Knee Osteoarthritis After Unilateral Anterior Cruciate Ligament Reconstruction	169
PD4D_4--Single-Limb Drop Landing Biomechanics Following Anterior Cruciate Ligament Reconstruction--(Pozzi)	171
PD4D_5--The Impact Of Various Measures Of Quadriceps Strength On Landing Mechanics In Young Athletes After Anterior Cruciate Ligament Reconstruction- Implications For Second ACL	173
PD4D_6--Single-Leg Hop Distance As A Functional Surrogate For Lower Extremity Joint Power In Healthy Adults--(Tatarski)	175

PD4E_1--Trial-Trial Temporal Variability In Upper Limb Functional Task Performance Differentiates Amputees From Controls And Decreases With Practice--(Major)	177
PD4E_2--Joint Power Adaptations To Running Speed In Individuals With Amputation Using Running-Specific Prostheses--(Baum)	179
PD4E_3--Body-In-The-Loop Optimization For The Selection Of Prosthetic Control Parameters - A Pilot Study--(Felt)	181
PD4E_4--Emulating Candidate Ankle-Foot Prostheses To Inform Prescription--(Caputo)	183
PD4E_5--The Effect Of Multi-Axial Prosthetic Stiffness On Angular Momentum In People With Transtibial Amputation Walking Over Uneven Terrain--(Childers)	185
PD4E_6--Whole-Body Angular Momentum During Sloped Walking With Powered And Passive Ankle-Foot Prostheses--(Pickle)	187

Concurrent Session 5, Saturday 9:00-10:30

TP5A_1--Effects Of Intentional Effort Manipulation On Balance Tested Under A Dual-Task Paradigm--(Neville)	189
TP5A_2--Single And Dual-Task Turning In Recently Concussed Athletes And Matched Controls- Preliminary Results--(Fino)	191
TP5A_3--Effect Of Sex On Recovery Of Gait Balance Control Following Concussion--(Peterson)	193
TP5A_4--Balance Measurements Using A Smartphone At The Upper Arm Compared To The Balance Error Scoring System--(Fino)	195
TP5A_5--The Relationship Between Head Acceleration And Heart Rate Variability- A Possible Diagnostic Tool For Head Injury Severity--(Dufek)	197
TP5B_1--A Comparison Of Measures To Assess Balance In Post-Stroke Subjects--(Vistamehr)	199
TP5B_2--Body Weight Support Effects Lateral Stability During Treadmill Walking--(Dragunas)	201
TP5B_3--Dynamic Gait Stability- The Reciprocal Relationship Between Lower Limb And Trunk Control In Response To Segmental Loading--(Beaudette)	203
TP5B_4--Does Dynamic Balance Of Transtibial Amputees Change After A Three Week Adaptation Period On A New Prosthetic Foot--(Kent)	205
TP5B_5--Relationship Between Postural Balance Parameters And Gait Asymmetries In Unilateral Transtibial Amputees--(Akins)	207
SM5C_1--Follow This Fellow Fine, But Give It Your Own Twist--(DeVita)	209
SM5C_2--A Career Path- From Get Smart... To Getting Smarter--(Davis)	210
SM5C_3--Using Biomechanics To Try To Understand The Mechanisms Of Unintentional Injuries So They Can Better Be Prevented--(Ashton-Miller)	212
PD5D_1--How Obesity Affects Hip Joint Contact Forces During Walking In Children--(Browning)	216
PD5D_2--Frontal Hip Power Absorption During Weight Acceptance Among Individuals With Incomplete Spinal Cord Injury--(Worthen-Chaudhari)	218
PD5D_3--Knee Moments Increase More Than Ground Reaction Forces Increase With Added Loads--(Fellin)	220
PD5D_4--Prospective Gait Analysis Of Ankle Arthrodesis And Arthroplasty--(Pomeroy)	222
PD5D_5--Analysis Of The Tripod Theory Using Plantar Shear Forces--(Crow)	224
PD5D_6--Adaptations In Lower Extremity Work Due To Changes In Walking Speed--(Ebrahimi)	226
PD5E_1--Systems Engineering Approach To Identifying Core Control Strategies In Individuals With And Without Low Back Pain During A Novel Unstable Sitting Task--(Davidson)	228
PD5E_2--Influence Of Input Device, Work Surface Angle, And Task On Spine Kinematics During Simulated Office Work--(Riddell)	230
PD5E_3--Physical Ergonomics Of Tablet Interaction While Sitting--(Bachynskyi)	232
PD5E_4--Sitting And Standing Alter Upper Extremity Joint Loading And Localised Discomfort During Manual Materials Handling Tasks--(Cudlip)	234
PD5E_5--Influence Of Jackhammer Weight On Hand-Arm Vibration Transmission--(Johnson)	236
PD5E_6--A Novel Multiple Comparison Procedure For Functional Data- The Effect Of Fitness- And Movement-Centric Exercise On Trunk Posture Among Firefighters--(Noguchi)	238

Concurrent Session 6, Saturday 11:00-12:30

TP6A_1--A Bootstrapping Method To Access The Influence Of Gender On Probability Of Tripping As A Function Of Obstacle Height--(Garman)	240
TP6A_2--Sex-Specific Differences In Lower Extremity Joint Power During A Single-Leg Hop Test In Healthy Adults--(Tatarski)	242
TP6A_3--Sex Based Differences In Anterior Cruciate And Medial Collateral Ligament Biomechanics In Robotically Simulated Deceleration Tasks--(Bates)	244
TP6A_4--Climbing Direction, Number Of Contact Points And Gender Influence Recovery From Ladder Falls But Not Glove Use--(Pliner)	246
TP6A_5--The Lumbopelvic Ratio During Trunk Flexion- The Effects Of Age, Gender And Motion Pace--(Vazirian)	248
TP6B_1--The Effect Of Exercise Training On Shoulder Joint Position Sense--(Lin)	250
TP6B_2--How Humans Use Visual Optic Flow To Regulate Stepping Movements--(Salinas)	252
TP6B_3--Proximal-Distal Differences In Movement Smoothness Reflect Differences In Biomechanics, Not Neural Control--(Charles)	254
TP6B_4--Beta Frequency Sensorimotor Cortical Oscillations During Ankle Plantarflexion Are Related To Spatiotemporal Gait Kinematics--(Arpin)	256

TP6B_5--Outcome Measures For Hand And Leg Function Naturally Reveal Latent Domains Of Strength, Limb Coordination, And Sensorimotor Processing--(Lawrence)	258
SM6C_1--Pregnancy Induced Adaptations In Intramuscular Extracellular Matrix Of Rat Pelvic Floor Muscles--(Alperin)	260
SM6C_2--Biomechanical Modeling Of Anterior Vagina Wall Prolapse--(Chen)	262
SM6C_3--Resolving The Surface Detection Challenge In Nanoindentation Of Soft Materials For Applications In Reproductive Tissue Mechanics--(Wagoner Johnson)	264
SM6C_4--Sheep As An Animal Model For Pelvic Organ Prolapse And Urogynecological Research--(Patnaik)	266
SM6C_5--Biomechanical Evaluation Of The Effectiveness Of Prosthetic Meshes--(Maurer)	268
SM6C_6--The Effect Of Fetal Membrane Prestretch On Cervical Loading During Pregnancy--(Fernandez)	270
PD6D_1--Redistribution Of Lower-Limb Joint Power During Uphill And Downhill Walking And Running--(Nuckols)	272
PD6D_2--Muscle Function During Sloped Walking--(Pickle)	274
PD6D_3--Uphill Walking Enhances The Retention Of A New Stepping Pattern Learned On A Split-Belt Treadmill--(Calvert)	276
PD6D_4--Muscle Function And Coordination During Stair Ascent--(Harper)	278
PD6D_5--Biomechanical Changes During Stair Climbing At The Knee, Hip, And Trunk After Total Knee Arthroplasty--(Lewis)	280
PD6D_6--Simulated Hip Abductor Strengthening Reduces Peak Joint Contact Forces During Stair Descent In Patients With Total Hip Arthroplasty--(Myers)	282
PD6E_1--Longitudinal Evaluation Of Postural Stability In Breast Cancer Patients Treated With Taxane-Based Chemotherapy--(Monfort)	284
PD6E_2--Balance Control During Reactive Stepping- The Effect Of Increased Passive Trunk And Hip Stiffness--(Weaver)	286
PD6E_3--Improving Neuropathic Gait And Balance Via Sensory Substitution--(Bauman)	288
PD6E_4--Postural Control Changes Associated With Ankle-Foot Orthoses In Individuals With Peripheral Neuropathy--(Bigelow)	290
PD6E_5--Effect Of Sensory Augmentation Via Skin Stretch Feedback On Quiet Standing Balance--(Pan)	292
PD6E_6--Recovery From Hip Abductor Fatigue Is Influenced By The Presence Of Low Back Pain--(Viggiani)	294

Concurrent Session 7, Saturday 14:45-16:15

TP7A_1--Stride-To-Stride Control Of Treadmill Walking In Healthy Elderly--(Dingwell)	296
TP7A_2--Age-Associated Redistribution Of Relative Joint Moment Angular Impulses Is Robust To Stride Length Manipulations--(Buddhadev)	298
TP7A_3--The Effect Of Fatigue On Knee Mechanics In Older Adults- Does Physical Activity Matter--(Hafer)	300
TP7A_4--Increased Lateral Forefoot Pressure Regularity In Older Adults Is Independent Of Gait Velocity--(Pisciotta)	302
TP7A_5--Visual Perturbations, But Not A Cognitive Challenge, Induce An Increase In Muscle Co-Activation During Gait In Healthy Old Adults--(Francis)	304
TP7B_1--Quantifying Performance And Effects Of Load Carriage During Completion Of A Window Obstacle Using An Array Of Wireless Inertial Sensors--(Cain)	306
TP7B_2--Duration Of Exertion And SCBA Design Affect Firefighter Balance--(Deetjen)	308
TP7B_3--Contributions Of An Integrated Bolster System To Dynamic Load Stability While Wearing A Backpack Over Body Armor--(Higginson)	310
TP7B_4--Physiological And Biomechanical Changes During Execution Of Three Load Carriage Paradigms--(Hasselquist)	312
TP7B_5--Effects Of Load Carriage And Surface Inclination On Slip And Trip Risks--(Rashedi)	314
SM7C_1--A Clinical Perspective On Prosthetics--(Van Der Watt)	316
SM7C_2--Ankle-Foot Prostheses For Improved Balance And Stability During Standing And Sloped Walking--(Hansen)	318
SM7C_3--A Rugged Microprocessor Controlled Ankle-Foot Prosthesis For Running--(Ward)	320
SM7C_4--Prosthetic Limbs That Reduce The Energy Cost Of Walking To Below Non-Amputee Levels Are Possible But Hard To Discover--(Collins)	322
SM7C_5--Optimizing Leg Prostheses For Walking And Running- Can We Augment Performance--(Jeffers)	324
PD7D_1--Characterizing Fluoroscopy Based Kinematic Accuracy Based On Pulse Width And Velocity--(Ellingson)	326
PD7D_2--Dynamic Tracking Influenced By Anatomy In Patellar Instability--(Elias)	328
PD7D_3--Intra-Operative Fragment Tracking For Articular Fracture Reduction--(Kern)	330
PD7D_4--Comparing The Effective Quadriceps And Patellar Tendon Moment Arms In Asymptomatic Controls And Subjects With Patellofemoral Pain--(Thomeer)	332
PD7D_5--Method For Three-Dimensional Analysis Of Skeletal Muscle Strain--(Jensen)	334
PD7D_6--Stiffening Of The Transverse Carpal Ligament In Pianists Detected By Acoustic Radiation Force Impulse Imaging--(Mhanna)	336
PD7E_1--Validation Of An Instrumented Figure Skating Blade To Measure Force--(King)	338
PD7E_2--Using Sample Entropy On Continuous And Discontinuous Data To Assess Jumping And Landing--(Queen)	340
PD7E_3--Using An Accelerometer To Monitor Recovery Of Gait Balance Control Following Concussion--(Chou)	342
PD7E_4--Energy Flow Analysis Of High And Low Velocity Baseball Pitchers--(McNally)	344
PD7E_5--Kinetics Of Youth Baseball Pitchers And Catchers--(Washington)	346

Posters 1-40

1AE--The Effects Of Military Body Armor On Knee Mechanics During Box Drop And Prone To Standing Tasks--(Phillips)	350
2AF--Lower Extremity Joint Kinematics In Alternative Footwear During Slip Events--(Chander)	352
3BF--Effects Of Proximal And Distal Muscle Fatigue On Repetitive Movements--(Cowley)	354
4BD--Larger Horizontal Affordances For Perceived Safe Handling Are Associated With Injury-Risk Lifting Kinematics--(Doan)	356
5CD--Validity Of Accelerometers In Predicting Occupationally Related Lower Extremity Exposures--(Dutt)	358
6CE--Low Back Pain Status And Prolonged Standing Alter Center Of Pressure Profiles During Constrained Standing--(Gallagher)	360
7AE--Standing In Ankle Plantarflexion Reduces Low Back Pain Reports During Prolonged Standing--(Gallagher)	362
8AF--The Influence Of Interactions Between External Task Demands In Lifting On Estimates Of In Vivo Low Back Joint Loads--(Gooyers)	364
9BF--Perceived Risk Of Biomechanical Factors Related To Low Back Injury In The Workplace--(Snow)	366
10BD--Ergonomic Evaluation Of A Prototype Quick-Release Body Armor System--(Higginson)	368
11CD--Low Back Physical Demands During A Simulated Dental Hygiene Task--(Howarth)	370
12CE--Effects Of Fatigue And Asymmetric Load Carriage On Firefighter Obstacle Crossing Performance--(Angelini)	372
13AE--Contributory Factors To Muscular Demand In Cashiers--(Maciukiewicz)	374
14AF--Effect Of Unilateral And Bilateral Load Carriage On Gait And Trunk Orientation In Healthy Young Adult Females--(McGinnis)	376
15BF--The Effect Of Early And Frequent Seated Breaks On Low Back Pain Development During Prolonged Standing Work--(McKinnon)	378
16BD--Novel Assessment Of Trunk Regional Peak Torque And Range Of Motion In Healthcare Workers--(Nyman)	380
17CD--External Force And Deltoid Surface EMG Relationship During Relative And Absolute Isometric Ramp Contractions At Three Angles--(Phillips)	382
18CE--Biomechanical Effects Of Cranio-Cervical Positions On Cervical Musculoskeletal Disorders--(REN)	384
19AE--The Effect Of Submaximal Hand Force Exertion On Shoulder Muscle Activation--(Vidt)	386
20AF--Effects Of Ergonomic Factors On Stair Navigation In Older Adult Multifocal Lens Glasses Wearers--(Weston)	388
21BF--Three-Dimensional Finite Element Model Of The Brain Responses To The Top Impacts Of A Construction Helmet--(Wu)	390
22BD--Effects Of Working Environment Factors On Upper Extremity Mechanical Properties During Powered Hand Tool Use0--(Xu)	392
23CD--Lower Extremity Joint Strategy Varies With Step When Transitioning Onto Different Stair Risers With And Without Ankle Load--(Ajisafe)	394
24CE--Average Minimum Toe Clearance May Not Contribute To Increased Fall Risk In Patients With Chronic Obstructive Pulmonary Disease--(Arnold)	396
25AE--Factors Influencing Frontal Plane Kinematics And Kinetics Before And After Total Knee Arthroplasty--(Baker)	398
26AF--The Effects Of Varus And Valgus Midfoot Orthotic Posting On Ankle And Midtarsal Joint Angles During Walking- A Multi-Segment Foot Analysis--(Barrios)	400
27BF--Muscular And Metabolic Changes Identified During Prolonged Load Carriage On Variable Grades--(Batty)	402
28BD--Effect Of Plantar Fascia Stiffness On Foot Energy Absorption During Overground Walking--(Bell)	404
29CD--Plantar Regional Peak Pressure And Minimal Shear Stress Profiles In Diabetic And Non-Diabetic Patients--(Berki)	406
30CE--Gait Affects Both Kinesthetic And Visual Perception Of Distance Traversed--(Bischoff)	408
31AE--Knee Joint Impulse While Running With Varied Step Lengths--(Bowersock)	410
32AF--Tibial Characteristics Of Habitual Mid_Forefoot And Rearfoot Strikers--(Boyer)	412
33BF--Identification Of Compensatory Movement Patterns In Patients With Amputation Using Separation Of Angular Momentum--(Brecca)	414
34BD--A Simulated Inverted Pendulum Applied To Hemiplegic Cerebral Palsy Gait--(Buczek)	416
35CD--A Telescoping Inverted Pendulum Applied To Hemiplegic Cerebral Palsy Gait--(Buczek)	418
36CE--The Effect Of Hip Abductor Fatigue On Frontal Plane Kinematics During Walking And Running--(Capehart)	420
37AE--Does The Addition Of Perturbation Training Improve Gait Asymmetries In Athletes After ACLR With Different Mechanisms Of Injury--(Capin)	422
38AF--Association Of Spinal Deformity And Pelvic Tilt With Gait Asymmetry In Adolescent Idiopathic Scoliosis Patients- Ground Reaction Force Investigation--(Chu)	424
39BF--A Principal Component Analysis-Based Correction Method For Anatomical Frame Variation In Gait Analyses--(Clouthier)	426
40BD--Prediction Of Medial Knee Contact Force Using External Measures Is Population Dependent--(Clouthier)	428

Posters 41-80

41CD--Dynamic Thickness Change Of Rectus Femoris Muscle During Gait Measured Using Ultrasound Is Related To Hip And Knee Joint Moments And Muscle Electrical Activation--(Eddo)	430
42CE--Differences In Stance Phase Kinematics And Muscle Activity After Eight Weeks Of Insole Use--(Cotter)	432
43AE--Approximate Entropy Of Trunk And Foot Accelerations During Walking--(Craig)	434

44AF--Barefoot Versus Shod- Effects Of Backpack Loads On Walking Mechanics--(Dames)	436
45BF--Averaging Trials Versus Averaging Trial Peaks- Impact On Statistical Tests--(Dames)	438
46BD--The Effect Of Step Height Perturbation On Human Gait--(Darici)	440
47CD--Development Of An Elastic Force-Field To Influence Mediolateral Foot Placement During Walking--(Broadway)	442
48CE--Dynamic Reliability And Validity Of Pressure-Measuring Insoles--(DeBerardinis)	444
49AE--Femoral Neck Loads In Young And Older Adults During Stair Ascent And Descent--(Deng)	446
50AF--Gender Differences In The Association Between Acute Articular Cartilage Metabolism And Ambulatory Kinetics--(Denning)	448
51BF--Sample Entropy Outperforms Approximate Entropy For Hour-Long Overground And Treadmill Walking--(Denton)	450
52BD--The Effect Of Leg Retraction On Stability During Running--(Dhawale)	452
53CD--Studying The Progression Of Compensation Changes During Simulated Recovery From Injury--(DiBerardino)	454
54CE--Changes In Walking Kinematics Following Bilateral Isolated Lower Extremity Joint Fatigue--(Hovey)	456
55AE--Complexity Of Gait Post Stroke--(Dugan)	458
56AF--Energy Substrate Use During Walking As A Function Of Step Rate--(Ehtemam)	460
57BF--Ground Reaction Force Comparison Of Prediction-Based And Direct Force Measurement Systems--(Flowers)	462
58BD--Kinematic Comparison Of Marker-Based And Markerless Motion Capture Systems--(Flowers)	464
59CD--Foot And Ankle Kinematics During Descent From Varying Step Heights--(Gerstle)	466
60CE--Foot Placement Optimization During Lateral Maneuvers--(Acasio)	468
61AE--The Relationship Between Variability And Asymmetry During Gait--(Gregory)	470
62AF--Partial Least Squares For Discriminant Analysis Of Kinematic And Kinetic Data--(Hassan)	472
63BF--Foot Dissipation During Ankle Push-Off- Human Walking Insights From A Multiarticular EMG-Driven Musculoskeletal Model--(Honert)	474
64BD--Accuracy Of Running Data From The Garmin Forerunner--(Hunter)	476
65CD--Validation Of Determining Stance Time Using Accelerometer Data--(Jamison)	478
66CE--Quantitative Assessment Of Movement Smoothness During Emotional Gait--(Kang)	480
67AE--Obesity Is Associated With Increased Joint Torques And Relative Effort During Gait- Preliminary Findings--(Koushyar)	482
68AF--Knee Joint Moments During Single-Leg Forward Hopping--(Krupenevich)	484
69BF--Mechanical Work Performed By The Legs Of Children With Hemiplegic Cerebral Palsy--(Gehringer)	486
70BD--The Effect Of Shoe Heel Elevation Angle On Strike Pattern--(Kwon)	488
71CD--The Relationship Between Clinical Measures And Stair Climbing Biomechanics In Patients With Total Knee Arthroplasty--(Lewis)	490
72CE--Effects Of Prolonged Walking At Preferred Speed In Individuals With Multiple Sclerosis--(Liddy)	492
73AE--Heel Rocker Mechanics In Gait Are Different Between Limbs And Compared To Controls Following ACL Reconstruction--(Lin)	494
74AF--A Planar Dual-Slip Model Of Incline And Decline Walking--(Liu)	496
75BF--Individual Limb Transition Work During Walking In Service Members With Transfemoral Amputation--(Mahon)	498
76BD--Audio And Visual Biofeedback As Methods Of Gait Retraining To Reduce Tibial Acceleration Upon Foot Strike--(Morgan)	500
77CD--Gait Biomechanics In Patients With Peripheral Arterial Disease Can Be Predicted By Functional Measures Using Stepwise Regression.--(Bowman)	502
78CE--The Relationship Between Perceived Health Status And Gait Improvement Following Surgical Intervention In Peripheral Arterial Disease.--(Holscher)	504
79AE--Peak EMG Characteristics Of Lower-Extremity Musculature Indicate Upcoming Locomotor Transition--(Nakamura)	506
80AF--Variability Of Shear Stresses On The Plantar Surface Of The Foot During Gait--(Papp)	508

Posters 81-120

81BF--Control Strategies During A Step Up And Over Task In Patients Six Months After Total Knee Arthroplasty And Healthy Controls--(Pozzi)	510
82BD--Comparison Of Three Plug-In-Gait Protocol Variations In Gait Analysis--(Razu)	512
83CD--Bilateral Vertical Stiffness Asymmetry During A Low-Intensity Run In Youth Male Athletes--(Ryu)	514
84CE--Gait Alterations In Peripheral Arterial Disease Are Not Worsened By The Presence Of Diabetes--(Schieber)	516
85AE--Muscle Function Differences Between Young And Older Adults During Gait--(Schloemer)	518
86AF--A New Method For Identifying Toe-Off Event Running On A Treadmill Using Kinematic Data--(Seneli)	520
87BF--Comparison Of Overground, Outdoor Running Between Limb Salvage Individuals And Patients With Transtibial Amputations- Initial Findings--(Sharp)	522
88BD--Lower Limb Trauma Impairs Lateral Walking Transitions In A Virtual Obstacle Course--(Sheehan)	524
89CD--Attention Allocation Ability In Dual Task Among Different Ages--(Liu)	526
90CE--Influence Of Heel Type On Stride Length--(Smallwood)	528
91AE--Modeling The Lean Release, Lean Release With Waist Pulls And Waist Pull While Walking Perturbations With An Inverted Pendulum--(Pierre)	530

92AF--The Sensitivity Of Predicted Knee Contact Mechanics During Gait To Variations In Ligament Properties--(Smith)	532
93BF--Joint Moment Patterns During A Fatiguing Run--(Smith)	536
94BD--Effects Of Transcutaneous Electrical Nerve Stimulation On Gait Kinetics In Individuals With Experimentally Induced Knee Joint Pain--(Son)	538
95CD--Dance Alters Subjective And Objective Biomechanical Gait And Balance Measures In Parkinson's Disease- A Case Study--(Sowalsky)	540
96CE--Low Strength Increases Functional Demand During Walking In Older Women--(Spinoso)	542
97AE--Walk-To-Run Transitions On A Split-Belt Treadmill--(Stenum)	544
98AF--Fractal Scaling Exponent Of Spatio-Temporal Variables Due To Three Types Of Belt Speed Control Modes During Treadmill Walking--(Choi)	546
99BF--Anterior Laxity In Healthy Young Women With Knee Hyperextension--(Teran-Yengle)	548
100BD--Differences In Synergistic Control Of Muscles During Treadmill Walking In Anterior Cruciate Ligament Reconstructed Legs--(Churchwell)	550
101CD--Co-Contraction Index During Gait And Relationship To Quadriceps Strength In Individuals With Focal Cartilage Defects In The Knee--(Thoma)	552
102CE--Cognitive Influence On Obstacle Avoidance- Auditory And Structural Interference--(Vallis)	554
103AE--Foot Pressure Masking Differences With And Without Kinematic Data For Unilateral Clubfoot--(Wallace)	556
104AF--Effects Of Customized Knee Replacement Surgeries On Walking Mechanics--(Wang)	558
105BF--Effects Of Walking Speed On The Stump-Socket Interface In Transtibial Amputees--(Wedge)	560
106BD--Individuals Using An Ankle-Foot Orthosis Have Minimal Gait Deviations When Accommodating To Walking On A Cross Slope--(Whitehead)	562
107CD--COPD Patients Exhibit Similar Joint Angle Variability Compared To Older, Healthy Control Subjects--(Wiens)	564
108CE--Kinematic Predictors Of Tibiofemoral And Patellofemoral Joint Impulse During Running--(Willson)	566
109AE--Ankle Kinematics Of Service Members With And Without Transtibial Amputation While Walking On A Split Belt Treadmill--(Wolf)	568
110AF--The Effects Of Longitudinal Training On Walking Navigation Through A Complex Environment--(Worden)	570
111BF--Walking Pattern In Children With And Without Down Syndrome Via An Force-Driven Harmonic Oscillator Model--(Wu)	572
112BD--Children Display Adult-Like Kinetic Pattern In The Time Domain But Not In The Frequency Domain While Walking With Ankle Load--(Wu)	574
113CD--2DOF External Fixator And Surgical System For Clubfoot Correction--(Wu)	576
114CE--Shod Vs. Barefoot Walking- Why Do Humans Change Their Step Frequency--(Yandell)	578
115AE--Body Mass And Height Are Not Good Predictors Of Plantar Shear Stress--(Master)	580
116AF--More Ulcers Develop At Peak Shear Locations Than At Peak Pressure Locations. A Call To Revisit Ulceration Pathomechanics--(Yavuz)	582
117BF--Association Between High Temperatures And Triaxial Plantar Loading In Diabetic Patients--(Yavuz)	584
118BD--Gait Patterns Following Anterior Cruciate Ligament Reconstruction Differ With Graft Type--(Zarzycki)	586
119CD--Knee Joint Loads And Surrounding Muscle Forces During Stair Ascent In Total Knee Replacement Patients And Healthy Controls--(Zhang)	588
120CE--Validity Of The Two-Dimensional Sagittal Plane Assumption In Modeling The Standing Long Jump--(Hickox)	590

Posters 121-160

121AE--Using A Dynamic Musculoskeletal Model To Explore Human Pinch--(Barry)	592
122AF--Investigation Of The Stresses Induced In Bone During Walking And Stair Climbing Pre And Post THR--(Bendjaballah)	594
123BF--Effect Of Jump Impact Load On Menisci,Femoral,Tibial And Patellar Cartilages During Full Joint Knee Flexion--(ELSAGHEIR)	596
124BD--Modeling The Aging Achilles Tendon- Inter-Fascicle Adhesions And Tendon Compliance Affect Plantarflexor Behavior During Walking--(Franz)	598
125CD--Performance Of A Versatile In Vitro Joint Simulator With Kinetic Chain Testing Capabilities--(Green)	600
126CE--Multi-Segment Foot Modeling To Maximize Reliability And Clinical Relevance--(Gutekunst)	602
127AE--Effect Of Morphology, Cross-Section Type, And Apparent Density On The Elastic Properties Of Open-Cell Structures--(Hedayati)	604
128AF--Kinetic Validation Of A Link-Segment Trunk Model--(Hutchinson)	605
129BF--Design And Validation Of A TDNN Human Walking Model--(Iqbal)	607
130BD--Effect Of Age On Body Segment Parameters In Normal Weight Females--(Knewton)	609
131CD--Estimation Of Impact Forces On Human Hip And Wrist Joints Based On Rear-Side Falling Simulation Using A Musculoskeletal Model--(BAE)	611
132CE--Dynamic Stability Of Structures For An Electric Handbike By Motion Analysis During Durability Test--(BAE)	613
133AE--Comparison Of Bone Strength Between Osteoporosis And Normal Mouse Femora Using Fe Analysis--(HAN)	615

134AF--Effect Of Increased Body Mass Index On Body Segment Parameters In Males--(Merrill)	617
135BF--Impact Of Mass Redistribution On Lower Extremity Biomechanics During Slipping--(Merrill)	619
136BD--Multiscale Computational Modeling Of Shoe-Floor Friction--(Moghaddam)	621
137CD--Validating A Computational Model Of Reverse Shoulder Arthroplasty--(Permeswaran)	623
138CE--Simulation Of Reduced Ankle Torque During The Anticipatory Postural Adjustments For Gait Initiation--(Petrucchi)	625
139AE--Evaluation Of The Transverse Metatarsal Arch Of The Foot--(Rezvanifar)	627
140AF--Glenohumeral Abduction And Flexion Muscle Moment Arms- A Verification Study Of A New Musculoskeletal Model Of The Shoulder--(Richardson)	629
141BF--Development Of An Open-Source, Discrete Element Knee Model--(Schmitz)	631
142BD--Improving Patient Simulator Upper Arm Biomechanics--(Singh)	633
143CD--The Effects Of Added Foot Stiffness On Soleus Muscle Fascicle Behavior During Human Walking--(Takahashi)	635
144CE--Assessing Wire Navigation Performance In Treating Hip Fractures--(Taylor)	637
145AE--Tracking The Trunk Segment- Backpack Vs. Elastic Strap--(Willigenburg)	639
146AF--Specifics Of A Lower Extremity Biomechanical Model That Yields Reliable Kinematics And Kinetics During Landing In Athletes--(Willigenburg)	641
147BF--Predictive Simulation Of Rowing Exercise Using GPOPS II--(Zarei)	643
148BD--Isometric And Dynamic Activation Characteristics Of The Human Latissimus Dorsi Muscle--(Beaudette)	645
149CD--Relationships Between Clinical And Biomechanical Measures Of Core Stability--(Butowicz)	647
150CE--The Effect Of Structured Rhythmic Auditory Stimuli On The Performance Of A Repetitive Hammering Task--(Catlett)	649
151AE--Visualizing The Structure Of High Dimensional Feasible Activation Sets For Static Force Production--(Cohn)	651
152AF--Lumbar Angle And Muscle Activation Time Series Are Strongly Related In Individuals Asymptomatic For Low Back Pain--(Nairn)	653
153BF--Decreased Dynamical Complexity During Quiet Sitting In Children With Autism Spectrum Disorders--(Fournier)	655
154BD--Muscle Activation Strategies Of Stepping Onto A Compliant Surface In Healthy Adults--(Johnson)	657
155CD--Movement Quality During Unimanual And Bimanual Functional Reaching Movements--(Sriram)	659
156CE--Motor Cortex Activation And Landing Neuromuscular Control After Anterior Cruciate Ligament Reconstruction--(Grooms)	661
157AE--Dual-Task Effects On Motor Performance In Healthy Younger Adults--(Wehry)	663
158AF--Synchronization Of Gait With Fractal Musical Stimuli Occurs Differently At Short And Long Time Scales--(Hough)	665
159BF--Simultaneous Turn And Step Task For Investigating Control Strategies In Healthy Young And Community Dwelling Older Adults--(Huntley)	667
160BD--Shared And Task-Specific Muscle Synergies During Normal Walking And Slipping--(Nazifi)	669

Posters 161-200

161CD--High Knee Flexion And Lower Limb Muscle Activation- Does Movement Pattern Matter--(Kingston)	671
162CE--Distinctive Control Strategy Of Dynamic Fingertip Force In Individuals With Mild To Moderate Parkinson's Disease And Its Clinical Implications--(Ko)	673
163AE--Intra-Auditory Integration In A Constant Force Production Task--(Koh)	675
164AF--Representation Of Wrist Motion Characteristics Using The Axis Of Rotation--(Lahroodi)	677
165BF--Modulation Of Tremor During Isometric Force Tracking--(Laine)	679
166BD--Carpal Tunnel Syndrome Impairs Finger Responses To Unpredictable Perturbation--(Xiu)	681
167CD--Postural Stability, Motor Skills, And Repetitive Behaviors In Children With Autism Spectrum Disorder--(Mache)	683
168CE--Patients With Symptomatic Femoroacetabular Impingement (FAI) Demonstrate Different Lower Extremity Joint Coordination Compared To Healthy Controls During A Double Leg Squat Task--(Malloy)	685
169AE--Reductions In Structural And Frequency Coupling Between Posture And Surface Motion Are Facilitated By Plantar Tactile Stimulation--(Lueders)	687
170AF--The Ability To Dynamically Regulate Instabilities With The Leg Is Susceptible To Repetitive Eccentric Contractions.--(Nagamori)	689
171BF--Can Paravertebral Facet Injection Improve Motor Performance In Patients With Degenerative Facet Osteoarthopathy--(Toosizadeh)	691
172BD--Subject-Specific Landing Strategies Identify Changes In Movement Control--(Nordin)	693
173CD--The Effects Of Vibratory Stimuli On Cortical And Spinal Neuron Excitability- Implications For Osteoarthritis Treatment And Prevention--(Pamukoff)	695
174CE--Information About How Another Person Is Moving Through The Environment Is Conveyed In The Movements Of Their Limbs--(Reynolds)	697
175AE--Adaptation Strategies Of Individuals With Anterior Cruciate Ligament Reconstruction--(Roper)	699
176AF--Hamstring Strength Deficits Three Years After Anterior Cruciate Ligament Reconstruction In Individuals With Hamstring Autografts Alter Knee Mechanics During Gait And Jogging--(Abourezk)	701
177BF--Effects Of Simulated Surgical Repositioning Of The Tibial Tubercle On Patellofemoral Kinematics In Knees With Patellofemoral	

Malalignment--(Amerinatanzi)	703
178BD--Effects Of Follower Load And Rib Cage On Intervertebral Disc Pressures In Static Tests Of Cadaveric Thoracic Spines--(Anderson)	705
179CD--Determinants Of Aponeuroses Shape Change During Muscle Contraction--(Arellano)	707
180CE--Removable Anchoring Pedicle Screw Restores Pull Out Strength In An Osteoporotic Vertebra To Normal Bone Value- A Finite Element Analysis--(Asadollahi)	709
181AE--Improved Rod Fixation Reduction In Loosening Of The Pedicle Screws Due To Peek_Titanium Screw Concept- A Finite Element Analysis--(Asadollahi)	711
182AF--Robotic Simulation Of In Vivo Kinematics On Cadaveric Limbs Exhibit Minimal Mechanical Differences Between Contralateral Pairs--(Bates)	713
183BF--Tibial Slope Correlations With Peak Knee Joint Loads And Anterior Cruciate Ligament Strain During Simulations Of Controlled Athletic Tasks--(Bates)	715
184BD--The Influence Of Internal And External Tibial Rotation Offsets On Knee Joint And Ligament Biomechanics During Simulated Athletic Tasks--(Bates)	717
185CD--Screw Pull Out Under Cyclic Fatigue Loading In Synthetic And Cadaveric Bone--(Baumann)	719
186CE--Comparisons Of Three Hip Joint Center Estimation Methods In Estimating Knee Mechanical Axis Using Motion Capture--(Bennett)	721
187AE--Effect Of Rotation Angle On Disc Torsional Mechanics--(Bezci)	723
188AF--Optimization Of The Digitized Grood And Suntay Knee Joint Coordinate System--(Bonner)	725
189BF--Inter-Segmental Spine Joint Reaction Forces During Activities Of Daily Living--(Brelhoff)	727
190BD--Frontal Plane Trunk And Knee Angles During Unilateral Landing Tasks One Year After Anterior Cruciate Ligament Reconstruction--(Briggs)	729
191CD--Knee Adduction Moment Impulse At Baseline Predicts Change In Medial Tibial Cartilage Volume Over 2.5 Years In Knee Osteoarthritis--(Brisson)	731
192CE--The Effect Of Different Ranges Of Motion On Local Dynamic Stability Of The Elbow During Unloaded Repetitive Flexion-Extension Movements--(Gsell)	733
193AE--Investigating The Relationship Between Hip Position And Lumbar Spine Range Of Motion--(Glofcheskie)	735
194AF--A Biomechanical Mechanism To Explain High Incidence Of Thoracolumbar Vertebral Fractures--(Bruno)	737
195BF--Biomechanical Evaluation Of Patellar Fracture Risk After Tendon Graft Harvest For Cruciate Ligament Reconstruction- A Finite Element Study--(Carey)	739
196BD--Evaluation Of A Simple Method For Determining Muscle Volume In Vivo--(Challis)	741
197CD--Comparing Failure Rates Of Autografts And Allografts In Anterior Cruciate Ligament Reconstruction- A Systematic Review--(Chen)	743
198CE--Comparisons Of Coordination Patterns Between Lumbar Spine Versus Leading And Trailing Hips In Golf Downswing--(Choi)	745
199AE--Evaluation Of Rotational Quasi-Stiffness In The Hip Joints During Golf Downswing Of Experienced Golfers--(Choi)	747
200AF--Effects Of Pelvis Impact Angle And Hip Muscle Forces On Hip Fracture Risk During A Fall Using An Advanced Hip Impact Simulator--(Choi)	749

Posters 201-240

201BF--Influence Of Pelvis Impact Angle During A Fall On The Protective Benefit Of Hip Protectors--(Choi)	751
202BD--Effect Of Muscle Contraction On Impact Velocities Of The Head During Backward Falls In Young Adults--(Choi)	753
203CD--Comparison Of Rectus Femoris Force Output And Activation In Seated Vs. Prone Extension--(Colucci)	755
204CE--Age And Sex Effects On Force Asymmetry During Jump And Push-Up Tasks In Youth Soccer Players--(Cosgrove)	757
205AE--Automated Calculation Of Long Bone Bending Stiffness From Ct Scans And One-Dimensional Finite Element Analysis--(Arnold)	759
206AF--The Effects Of Medial And Lateral Wedges On Iliotibial Band Strain During Overground Running--(Day)	761
207BF--Tibial Stress During Landings From Two Heights--(Dado)	763
208BD--Self-Reported Hip Function Is Related To Ankle Joint Moment Asymmetry During Landing In Individuals With Femoroacetabular Impingement--(Di Stasi)	765
209CD--Comparison Of Objective Fracture Severity Measures In Tibial Plateau And Pilon Fractures--(Dibbern)	767
210CE--Dynamic Simulation Of Patellar Tracking For Knees With Instability--(Kelly)	769
211AE--The Biomechanical Advantage Of Locked Versus Non-Locked Symphyseal Plating Of Unstable Pelvic Ring Injuries--(Godinsky)	771
212AF--Agreement Between 3D Reconstructions From Fluoroscopic Cone Beam And Conventional High Resolution CT For Tracking Native Knee Kinematics--(Ellingson)	773
213BF--Effect Of Long-Term Use Of High-Heeled Shoes And Knee Position On Calf Muscle Isokinetic Strength--(Elsayed)	775
214BD--A Novel Planning Paradigm For Augmentation Of Osteoporotic Femur--(Farvardin)	777
215CD--Exploring The Regional Response Of The Intervertebral Disc Under Postural Varying Loads--(Fewster)	779

216CE--Preliminary Finite Element Analysis Of Subchondral Bone Cysts In The Stifle Of The Horse--(Frazer)	781
217AE--Validation Of A Finite Element Model Of The Humerus For Fracture Risk Assessment During Assisted Ambulation--(Fritz)	783
218AF--Finite Element Assessment Of Pediatric Femoral Response To Loading During Ambulation- Normal Vs. Osteogenesis Imperfecta (OI) Bone--(Fritz)	785
219BF--PTH Signaling Mediates Perilacunar Remodeling During Exercise--(Gardinier)	787
220BD--Lumbar Spine Kinematics For End-Range Trunk Positions In Healthy Individuals Using Upright MRI--(Rubin)	789
221CD--The Effect Of Age On The Mechanical Properties Of Porcine Intervertebral Discs Following A Cyclic Loading Protocol--(Gruevski)	791
222CE--The Effects Of A Five-Week Exercise Intervention Using EMG Biofeedback On Scapular Kinematics And Scapular Stabilizer Muscle Activation--(Gundersen)	793
223AE--Using Digital Image Correlation To Investigate The Effect Of Impact Velocity On The Response Of A Vertebra--(Gustafson)	795
224AF--Finite Element-Based Adjacent Level Intersegmental Rotation And Intradiscal Pressure Analysis After Lumbar Fusion For Scoliosis--(Haddas)	797
225BF--Lifting Risk After Lumbar Fusion In Scoliosis--(Haddas)	799
226BD--Peak Knee Joint Contact Force Increases With Body Borne Load During Run-To-Stop Task--(Hancock)	801
227CD--Measuring Capulohumeral Rhythm With Supraspinatus Impairment--(Hannon)	803
228CE--Changes In Muscle Work With Disease Progression During Gait In Duchenne Muscular Dystrophy--(Heberer)	805
229AE--Effects Of A Long Term Stretching Intervention On The Material Properties Of Muscle- Preliminary Results--(Hibbert)	807
230AF--Matrix Stiffness Affects Human Mesenchymal Stem Cell Differentiation Uniquely In 2D And 3D Culture--(Hogrebe)	809
231BF--A Probabilistic Model Of The Subacromial Space- Implications For Subacromial Impingement Syndrome--(Hurley)	811
232BD--Predicting Patellofemoral Contact Mechanics- A Computational Study--(Jahandar)	813
233CD--Lower Extremity Kinetics During Stop-Jump Of Individuals With Adolescent Idiopathic Scoliosis After Surgical Fusion Of Spine--(Kakar)	815
234CE--Comparison Of Medial-Lateral Contact Force Balance In Knee Joint Before And After High Tibial Osteotomy For Osteoarthritis--(Purevsuren)	817
235AE--Comparative Analysis Of Stress And Strain Of Spinal Cord In Various Posterior Decompression Extents For Cervical Ossification Of The Posterior--(Khuyagbaatar)	819
236AF--Dynamical Finite Element Analysis To Reproduce The Typical Patterns Of Pelvic Insufficiency Fractures--(Kiriama)	821
237BF--High-Dimensional Analysis Reveals Patterns Of Lower Limb Muscle Volume Dissimilarities Across Clinical And Athlete Populations--(Knaus)	823
238BD--Analysis Of 3D Strain In Medial Meniscal Allograft Transplants Following Two Surgical Techniques--(Kolaczek)	825
239CD--Comparative Evaluation Of Morphometric And Biomechanical Properties Of The Cervine Femur--(Libruk)	827
240CE--Adjusting Thinking About IM Nails- Mechanical Evaluation Of An Adjustable Intramedullary Nail Prototype--(Hedgeland)	829

Posters 241-280

241AE--Activities Of Daily Living Induce Vertebral Fractures Despite Healthy BMD--(Corbiere)	831
242AF--Monitoring Acoustic Events In Bone During Screw Insertion--(Langdale)	833
243BF--Validation Of The Subject-Specific Finite Element Analysis Under Quasi-Static And Dynamic Gait Conditions--(Isvilanonda)	835
244BD--Patient-Specific Mechanical Properties Of Diabetic And Healthy Plantar Soft Tissue From Gated MRI--(Williams)	837
245CD--Quantifying Muscle Material Properties Of Passive And Active Stroke-Impaired Biceps Brachii--(Lee)	839
246CE--Principal Component Analysis Of The 3D Structural Stiffness Of The Wrist--(Gabra)	841
247AE--Carpal Tunnel Creep During External Compressive Force Application--(Galey)	843
248AF--Carpal Arch Compression Decreases Median Nerve Flattening In Carpal Tunnel Syndrome Patients--(Marquardt)	845
249BF--Predictors Of Patellofemoral Joint Stress- An Examination Of Patellofemoral Joint Morphology--(Liao)	847
250BD--The Effect Of Exercise Training On Shoulder Kinematics And Muscle Electromyography During Arm Elevation--(Lin)	849
251CD--The Effects Of Entheseal Shape On Strain Fields In A Planar Model Of The Anterior Cruciate Ligament--(Luetkemeyer)	851
252CE--A Comprehensive Meta-Analysis Of Skeletal Muscle Architecture In Humans--(Luu)	853
253AE--Kinetics And Kinematics Of The Ankle During Foot External Rotation--(Mait)	855
254AF--Biaxial Quantification Of Transverse Carpal Ligament Elastic Properties By Sex And Region--(Mathers)	857
255BF--Axial Rotation Causes Bilateral Differences In The Size Ratio Of Intervertebral Foramen To Nerve Root--(Mayberry)	859
256BD--Maximal Biceps Contraction During Supination Causes Proximal Radial Head Translation--(Bergman)	861
257CD--Associations Between Quadriceps Muscle Strength, Power, And Knee Joint Mechanics In Knee Osteoarthritis- A Cross-Sectional Study--(Murray)	863
258CE--Sensitivity Of Cartilage Pressure To Ligament Stiffness During Shoulder Abduction--(Rahman)	865
259AE--Arthrokineatic Effects Of Joint Mobilization Of The Talocrural Joint- An In Vitro Study--(McNally)	867
260AF--Comparison Of Two Functional Shoulder Joint Center Protocols--(Levasseur)	869

261BF--Vibration Of Quadriceps Muscle Afferents Affects Both Ipsilateral And Contralateral Quadriceps And Hamstrings Ratio Of Torque, Power, And Acceleration Time--(Schilaty)	871
262BD--Hierarchical Control Improves Joint Motion Simulator Performance--(Schimoler)	873
263CD--Changes In Tibiofemoral Contact Forces Following Alterations In Joint Capsule Stiffness--(Schmitz)	875
264CE--Experimental Anterior Knee Pain Affects Activation Of Certain Muscles Differently During Landing And Jumping--(Seeley)	877
265AE--Reduced Rate Of Proximal Junctional Fractures Above Long-Segment Instrumented Constructs Utilizing A Tapered Dose Of Bone Cement For Prophylactic Vertebroplasty--(Anoli)	879
266AF--Three-Dimensional Humeral Shape Morphology Throughout The Pediatric Age Spectrum In Children With Unilateral OBPP--(Jackson)	881
267BF--Influence Of Age And Gender On Lumbar Shear Tolerance--(Shimada)	883
268BD--Age-Related Differences In Mechanical Response Of Lower Back Tissues And The Resultant Spinal Loads During Lifting--(Shojaei)	885
269CD--Advances In Hyperelastic Finite Element Modeling Of Biological Tissues- Explicit Strain Energy Function Specification--(Inouye)	887
270CE--Isometric Squat Peak Force In Range Of Knee Flexion Angles Strongly Related To Countermovement Jump Peak Force--(Stephenson)	889
271AE--The Effects Of Stimulus Timing On The Kinetics Of A Directed Jump Landing--(Stephenson)	891
272AF--Altered Trabecular Microarchitecture In Brachial Plexus Birth Palsy- A Rat Model Study--(Stolfi)	893
273BF--Influence Of Fatigue On Lower Extremity Biomechanical Variability During Forward Lunge--(Stone)	895
274BD--Comparison Of Standalone PLIF Expandable Cage And TLIF Standard Cage- An In Vitro And Finite Element Study--(Sudershan)	897
275CD--Modeling Of Human Intent For Classification Of A Weight Lifting Task--(Totah)	899
276CE--Assessment Of Bone Quality By Novel Spectroscopic Biomarkers--(UNAL)	901
277AE--Spectral Evidence For Association Between Collagen Denaturation And Bone Toughness--(UNAL)	903
278AF--Shorter Heels Are Associated With Stiffer Plantarflexor Tendons--(van Werkhoven)	905
279BF--Relationship Between ACL Graft Geometry And Tibiofemoral Kinematics--(Vignos)	907
280BD--Biceps Brachii And Brachialis Cross-Sectional Areas Are Major Determinants Of Muscle Moment Arms--(Vigotsky)	909

Posters 281-320

281CD--Effect Of Scapular Misalignment During Setup On Stability Of The Shoulder--(Walia)	911
282CE--Minimal Effect Of Compressive Loading On The Glenohumeral Joint Stability Ratio--(Walia)	913
283AE--Effect Of Musculoskeletal Model Choice On Muscle Activations During Landing, Running, And Lateral Cutting--(Fontenot)	915
284AF--The Effects Of Squat Depth On Right Leg Kinematics And Kinetics--(Sievert)	917
285BF--Patient-Based Predictors Of High-Risk Biomechanics In Anterior Cruciate Ligament-Reconstructed Subjects--(Wordeman)	919
286BD--Protective Hip And Knee Kinematics During Unilateral And Bilateral Landings After Neuromuscular Training In ACL-Reconstructed Subjects--(Wordeman)	921
287CD--Lack Of Association Between Subjective And Objective Assessment Of Spinal Stiffness--(Xia)	923
288CE--A Comparison Of Two Superficial MCL Reconstruction Including Single-Bundle Anterior Cruciate Ligament (ACL) Reconstruction--(Zhu)	925
289AE--The Relationship Between Arch Height And Arch Flexibility--(Zifchock)	927
290AF--Long-Range Correlations Of Center Of Pressure Are Stronger For AP Perturbations Than ML Perturbations In Healthy Young Adults--(Ambati)	929
291BF--Virtual Time To Contact Is More Strongly Related To Disease Severity Than Sway Excursion In People With Diabetes And Diabetic Neuropathy--(Becker)	931
292BD--Leg Stiffness And Postural Control In Children During Single-Leg Hopping--(Beerse)	933
293CD--Assessment Of Knee Mechanics And Muscle Activity During Balance Exercises--(Benson)	935
294CE--Hand And Foot Responses That Improve Ladder Fall Recovery--(Pliner)	937
295AE--Changes In Dynamic Balance Control And Postural Stability Between Level And Sloped Walking--(Brelloff)	939
296AF--Comparing Trunk Proprioceptive Ability And Muscle Responses To Sudden Trunk Perturbations Between Athletes And Non-Athletes--(Glofcheskie)	941
297BF--Compliant Flooring And Its Effect On Posture- Differences Between Young And Older Populations--(Buschman)	943
298BD--Lower Extremity Net Joint Moments During Lateral Load Transferring- Differences Between High And Low Surface Friction--(Catena)	945
299CD--Effects Of Blurry Vision On Standing Balance--(Clough)	947
300CE--Principal Component Analysis Of Human Balance On A Tunable Balance Board--(Cruise)	949
301AE--Postural Changes In Young Adults When Wearing A Traditional Backpack Versus The Backpack--(Dahl)	951

302AF--Effects Of White Noise Achilles Tendon Vibration On Standing Posture--(Gaffney)	953
303BF--Electromyographic Analysis Of Core Muscle Activation During Lumbar Stabilization Exercises- Implications For Rehabilitation And Training--(Deoghare)	955
304BD--Using Mutual Information To Capture Major Concerns Of Postural Control In A Tossing Activity--(Gazula)	957
305CD--Relationship Between Thoracic And Lumbar Spinal Curvature During Unsupported Sitting--(Givens)	959
306CE--The Relationship Between Knee Proprioception And Balance In Anterior Cruciate Ligament Reconstructed Individuals--(Seidel)	961
307AE--Development Of A Novel Proprioceptive Perturbation During Standing Balance--(Guyer)	963
308AF--Relationships Between Hip Abductor Strength And Measures Of Single-Leg Stability In Fit, Young Adults--(Heise)	965
309BF--The Relationship Between Foot Contact Area And Single-Legged Postural Stability--(Richmond)	
310BD--Impact Of Visual Guidance On Diabetes' Toe Elevation During Virtual Obstacle Crossing Tasks--(Huang)	969
311CD--Perception Of Self-Motion Impacts The Variability Of Plantar Propulsion Force In Diabetes--(Huang)	971
312CE--Assessment Of Slip-Risk Using A Portable Slip Simulator--(Iraqi)	973
313AE--Intrinsic And Extrinsic Foot Muscles Have Unique Roles In Functional Standing Postures--(Kurihara)	975
314AF--The Effect Of Static Stimulus On The Nonlinear Dynamics Of Posture In Children With ASD--(Motz)	977
315BF--Changes To Force Control Stability After Anterior Cruciate Ligament Rupture And Reconstruction--(Lanier)	979
316BD--Redistribution Of Joint Moments And Dynamic Balance Control Of Persons With Parkinson's Disease--(Lee)	981
317CD--Effect Of Whole Body Vibration On Center Of Mass Movement In Healthy Young Adults--(Liang)	983
318CE--Postural Stability In Adolescents With Ehlers-Danlos Syndrome (Hypermobility Type) Following An Exercise Intervention--(Long)	985
319AE--Head Accelerations After Slipping And Tripping Exceed Those During Walking--(Arena)	987
320AF--Obesity Does Not Increase Likelihood Of Slipping While Descending Ramps--(Scanlon)	989

Posters 321-360

321BF--Lumbar Spine Movement Patterns During A Clinical Test And A Functional Activity In People With Low Back Pain And People Without Low Back Pain--(Marich)	991
322BD--Stance Time Variability Is The Best Physical And Gait Biomechanical Parameter To Discriminate Older Fallers And Non-Fallers--(Marques)	993
323CD--Role Of The Paretic And Nonparetic Limbs To Arrest Forward Momentum Following A Perturbation--(Reimold)	995
324CE--A Comparison Of Tandem Walk Performance Between Bed Rest Subjects And Astronauts--(Miller)	997
325AE--Using The Feasible Balance Region To Estimate The Strength Requirements Of One Leg Balance: Effects Of Age And Diabetic Peripheral Neuropathy--(Shahshahani)	999
326AF--Stride Time Variability And Fall Risk In Persons With Multiple Sclerosis--(Moon)	1001
327BF--Biomechanics Of The Functional Reach Test--(Nandi)	1003
328BD--Error Augmentation Feedback For Dynamic Lateral Weight Shifting--(O'Brien)	1005
329CD--Role Of Multi-Sensory Integration Relevant For Balance In Slip Recovery--(O'Connell)	1007
330CE--Low Back Fatigue Influences Postural Variability--(Olson)	1009
331AE--Gait Adaptations To Unexpected Drop-Away Flooring Perturbations--(Peterson)	1011
332AF--Dynamic Stability During Single Stance In Multiple Sclerosis Patients--(Reinholdt)	1013
333BF--Cop Parameters For ACL Repaired Individuals During Stair Negotiation--(Rullestad)	1015
334BD--Balance Control During Common Rehabilitation Exercises In Obese Females--(Singh)	1017
335CD--Locomotor Control During Planned And Unplanned Gait Termination In Essential Tremor--(Skinner)	1019
336CE--Validation Of A Clinical Test To Assess Hip Abductor Muscle Control In Patients With Hip Arthroplasty--(Thompson)	1021
337AE--Effects Of A Combined Inversion And Plantarflexion Surface On Knee And Hip Kinematics During Landing--(Valenzuela)	1023
338AF--Effects Of Different Perturbation Levels During Fall Risk Assessment For Older Adults At Higher Fall Risk--(Vallabhajosula)	1025
339BF--The Influence Of Locomotor Training On Dynamic Balance And Its Relation To Increased Walking Speed In Post-Stroke Hemiparetic Subjects--(Vistamehr)	1027
340BD--Postural Stability During Stair Negotiation While Carrying Asymmetric Loads--(Wang)	1029
341CD--The Effect Of Load Magnitude And Distribution On Lumbar Spine Posture In Active-Duty Marines--(Rodriguez-Soto)	1031
342CE--The Effect Of Posterior Foot Placements On Sit-To-Stand Kinetics, Energetics And Muscle Activity--(Pitman)	1033
343AE--Alternative Footwear's Influence On Muscle Activation Patterns Of The Lower Leg Following A One Mile Walk--(Wilson)	1035
344AF--A Biomechanical Model To Personalize AFO Footplates To Promote Natural Shank Kinematics With Limited Dorsiflexion--(Arch)	
345BF--Biomechanical Analysis Of Two Novel Tapered Hip Screw Systems--(Ashworth)	1039
346BD--Techniques Used To Optimize Wheelchair Propulsion Startup--(Bass)	1041
347CD--Running-Specific Prosthesis Modeling Effects On Joint Moments During Overground Running--(Baum)	1043
348CE--Spatiotemporal And Metabolic Impacts On Gait Of A Powered Ankle Exoskeleton In Persons With Multiple Sclerosis--(Boes)	1045
349AE--A Strengthening Program Designed To Minimize Knee Loads In Women With Knee Osteoarthritis- A Proof-Of-Principle Study--(Brenneman)	1047

350AF--A Pilot Program To Determine Intramuscular Fat Percentage In The Quadriceps And Hamstrings Muscles In Women With Knee Osteoarthritis--(Brenneman)	1049
351BF--Effect Of Ankle Foot Orthosis Alignment On Muscle Activity--(Brown)	1051
352BD--Clinical Measurements With A Device To Enable Weightbearing Ct In A Horizontal Gantry--(Campbell)	1053
353CD--Using Hybrid Neuroprostheses To Improve Stand-To-Sit Maneuver For Individuals With Paraplegia--(Chang)	1055
354CE--Spinal Curvature And Shoulder Kinematics During Wheelchair Propulsion- Evaluating The Impact Of Spinal Cord Injury Level--(Cloud)	1057
355AE--Identification Of Finger Forces Over Ranges Of Motions: A Comparison Between Healthy And Reduced Hand Functionality Participants--(Drost)	1059
356AF--Comparison Of Tibia Strain Between Simulated Exoskeleton-Assisted Gait And Normal Gait--(Fang)	1061
357BF--Predicting Inertial Properties For Individuals With Transtibial Amputation--(Ferris)	1063
358BD--Use Of Medical Imaging And Mechanics To Quantify The Stiffness Connecting Lower-Limb Prostheses And Transfemoral Amputees--(Fey)	1065
359CD--Assistive Ankle Power Prompts Muscular Compensations During Gait--(Gardinier)	1067
360CE--Metabolic Cost Changes With The Amount Of Prosthetic Ankle Power Provided--(Davidson)	1069

Posters 361-400

361AE--Developing A Robotic Elbow Joint Controlled By EMG Stimulus--(Christensen)	1071
362AF--Mechanical Energy Differences In Arm-Constrained Human Rolling--(Hassan)	1073
363BF--Variability In Torso Kinematics In Arm-Constrained Human Rolling--(Vu)	1075
364BD--Human-Exoskeleton Hybrid Model To Produce Stable Gait Through Inter-Limb Coordination--(Wei)	1077
365CD--Wrist Compressive Forces Affect The Median Nerve Response To Wheelchair Propulsion And Other Markers For Carpal Tunnel Syndrome In People With Paraplegia--(Hogaboom)	1079
366CE--Weekly Changes In Vastus Lateralis Volume After ACL Injury--(Yoh)	1081
367AE--Upper Extremity Joint Dynamics And Electromyography (EMG) During Standard And Geared Manual Wheelchair Propulsion--(Jahanian)	1083
368AF--Effect Of Prosthetic Foot Damping On Ankle Push-Off Work In Late Stance--(Jin)	1085
369BF--Design Of Sensory Augmentation System For Postural Control Rehabilitation--(Kim)	1087
370BD--Improving The Mobility And Postural Balance Of Individuals With Multiple Sclerosis--(Davies)	1089
371CD--Comparing Effects Of Body Weight Supported Treadmill Training On Bone And Muscle Following Complete And Incomplete Spinal Cord Injury--(Loftus)	1091
372CE--Determining The Sagittal Plane Function For A Model Prosthetic Foot--(Martin)	1093
373AE--Hand Kinematics Before And After Tendon Transfer Surgery In Hansen's Disease Patient With Ulnar Nerve Palsy--(Abreu)	1095
374AF--Knee Kinetics And Contact Forces Of The Intact Limb In Amputee Walking--(Miller)	1097
375BF--Does Unilateral Transtibial Amputation Affect 90° Turning Strategies--(Nottingham)	1099
376BD--Design And 3D Printing Of A Dynamic Wrist Splint In The Dart Throw Motion Plane--(Portnoy)	1101
377CD--Optimal Method For Estimating Scapular Kinematics During Upper Extremity Cycling--(Rapp)	1103
378CE--The Effect Of Ankle-Foot Orthosis Alignment On Roll-Over Shape In Patients With Lower Limb Reconstruction--(Ruble)	1105
379AE--Biomechanical Adaptations To Ankle-Foot Orthosis Stiffness During Running--(Russell Esposito)	1107
380AF--Frontal Plane Stepping Control In Persons With Transtibial Amputation--(Rylander)	1109
381BF--Pediatric Joint Dynamics During Manual Wheelchair Mobility--(Schnorenberg)	1111
382BD--The Influence Of Speed And Grade On Wheelchair Propulsion Hand Pattern--(Slowik)	1113
383CD--Evaluating The Assumption Of Symmetry In Manual Wheelchair Propulsion--(Soltau)	1115
384CE--Predicting Isolated Lumbar Multifidus Activation During Neuromuscular Electrical Stimulation With Near Infrared Spectroscopy--(Sung)	1117
385AE--Optimal Running Prostheses For Sprinters With Bilateral Leg Amputations--(Taboga)	1119
386AF--Optimal Running Prostheses For Sprinters With Unilateral Leg Amputations--(Taboga)	1121
387BF--Motor Learning Effects On Variability In Goal-Directed Upper Limb Movements Using Time Warping Analysis--(Thies)	1123
388BD--Mechanical Properties Of Dynamic Elastic Response Prosthetic Feet--(Webber)	1125
389CD--Elevated Vacuum Pressure To Quantify Prosthetic Socket Mechanics--(Wernke)	1127
390CE--Design Of Two Lightweight High Bandwidth, Torque-Controlled Ankle Exoskeletons--(Witte)	1129
391AE--Severity Of Functional Impairment Influences Reach Kinematics In People Post Stroke--(Wutzke)	1131
392AF--Effect Of Customized Haptic Feedback On Navigation Characteristics And Performance--(Yoon)	1133
393BF--Proportional Myoelectric Control Of A Robotic Hip Exoskeleton--(Young)	1135
394BD--Comparison Of Torque Controllers For An Ankle Exoskeleton With A Series Elastic Actuator Driven By A Uni-Directional Bowden Cable During Walking--(Zhang)	1137

395CD--Lower Body Joint Kinetics In Standing Broad, Vertical, And Squat Jumps--(Bean)	1139
396CE--Biomechanical Factors Associated With Medial Tibial Stress Syndrome- A Prospective Study--(Becker)	1141
397AE--Joint Moment Differences In Dancers Landing In Turned-out Verse Parallel Positions--(Spitzley)	1143
398AF--Turnout Generation Strategies And Resulting Joint Moments In Dancers--(Jackson)	1145
399BF--Kinematic Differences Between Drop Jump, Cutting, And Rebound Landings--(Moreno)	1147
400BD--The Relationship Between Center Of Mass Excursion And ACL Injury Risk Variables In The Stationary Single Leg Hop (Stash)--(Cerne)	1149

Posters 401-440

401CD--Kinematic And Temporal Parameters Of High School Baseball Pitchers In Different Velocity Groups--(Kumar)	1151
402CE--Prediction Of Functional Movement Screen Performance From Lower Extremity Range Of Motion And Core Tests--(Chimera)	1153
403AE--Gluteal Activity During Pitching- Comparing The Traditional Leg Kick And Slide Step Deliveries--(Concha)	1155
404AF--Quantifying Warfighter Performance During A Prone-Running-Prone Movement Task Using Wireless Inertial Sensors--(Davidson)	1157
405BF--Validation Of Center Of Pressure Measurements With Artificial Turf--(Du Bois)	1159
406BD--The Countermovement Jump Is More Functional Than The Squat Jump In Measuring Elite Basketball Player Performance--(Epp-Stobbe)	1161
407CD--The Effects Of Two Different Pulling Strategies On Barbell Kinematics During The Clean Pull Exercise.--(Ficklin)	1163
408CE--The Effect Of Different Start Styles On Base Stealing Kinematics In Division I Softball Players.--(Parrott)	1165
409AE--WITHDRAWN	1167
410AF--Influence Of A Self-Induced Drop On Vertical Jump Performance--(Fox)	1169
411BF--No Angular Swing Kinematic Differences In Female Softball Players With Differently Weighted Warm-Up Bats--(Fu)	1171
412BD--Detrended Fluctuation Analysis Of Running Gait Tracks Changes In Performance When Athletes Are Overtrained--(Fuller)	1173
413CD--Jump Performance Variables Are Not Different In Female D1 Lacrosse Athletes With Generalized Joint Hypermobility.--(Geiser)	1175
414CE--Estimating Joint Contributions In Functional Motions To Create A Metric For Injury Prevention Using Motion Capture And Opens- A Preliminary Study--(Kozlowski)	1177
415AE--Impact Of Error Sonification Auditory Feedback For Neuromuscular Training Across Two Degrees Of Freedom--(Hale)	1179
416AF--Plie Flexibility In Dancers- Difference Between Positions, Measurement Methods, And Limbs--(Harmon-Matthews)	1181
417BF--Turnout In Dance- Examination Of Measurement Method And Limb Asymmetry Across Training Levels--(Harmon-Matthews)	1183
418BD--Relationships Between Quadriceps Strength Symmetry, Internal Knee And Hip Extension Moment Impulse Symmetry Is Stronger In Women Than Men--(Hartigan)	1185
419CD--Performance Biomechanics Of Running And Cutting Tasks--(Havens)	1187
420CE--WITHDRAWN	1189
421AE--ACL Injury Trends By Position And Team Activity In The National Football League Between 2009-2014--(Hoffman)	1191
422AF--Fatigue Effects On Lower Extremity Coordination And Coordination Variability During Multi-Joint Ballistic Movement--(Jagodinsky)	1193
423BF--Unloading Reactions During Sudden Ankle Inversion In Individuals With Functional Ankle Instability--(Jain)	1195
424BD--The Effects Of An Exhaustive Run On Multi-Muscle Patterns In Forefoot Running--(Jewell)	1197
425CD--Effects Of Foot Strike Pattern And Step Frequency On Achilles Tendon Stress During Running--(Lyght)	1199
426CE--Vertical Ground Reaction Force Magnitudes And Rates Not Positively Correlated With Prospective Running Injury--(Kiernan)	1201
427AE--Energy Absorption In Subjects With Ankle Instability During A Forward-Side Jump--(Kim)	1203
428AF--Standing Vertical Jumps With Countermovement Accommodate Biomechanical Constraints--(Kim)	1205
429BF--Muscle Architectural Parameters Predict Force-Velocity Parameters Derived From Loaded Countermovement Jumps--(Kipp)	1207
430BD--Difference In Force Generation While Deadlifting With Chains--(Lawrence)	1209
431CD--Differences In Lower Extremity, Pelvic And Trunk Kinematics Between Single Leg Squat And Step Down Tasks--(Lewis)	1211
432CE--Does Medial Knee Displacement Represent Knee Abduction Angle During Single-Leg Squats In Females--(Linde)	1213
433AE--Abdominal Muscle Activation Techniques Reduce Peak Knee Abduction And Peak Hip Adduction During Single-Leg Squats In Females.--(Linde)	1215
434AF--Muscle Activation During Single Leg Squat Is Affected By Position Of The Non-Stance Limb--(Loverro)	1217
435BF--Kinetic And Kinematic Based Algorithm For Processing Lateral Cut Maneuver--(Marmon)	1219
436BD--Eyes-Closed Single Limb Balance Is Not Related To Hypermobility Status In Dancers--(Marulli)	1221
437CD--Influence Of Forefoot Anthropometry On Pain In Minimalist Runners--(Casto)	1223
438CE--Effects Of Load On The Hip-To-Knee Torque Ratio In A Squat Exercise--(Meyer)	1225
439AE--A GRF Comparison Between Landing From A Countermovement Jump And Landing From Hanging And Dropping- A Pilot Study--(Miranda)	1227

440AF--A Biomechanical Profile Of Fear In ACL Reconstructed Athletes--(Nagelli)	1229
--	------

Posters 441-480

441BF--Wearing A Wetsuit Alters Arm Motion During Simulated Surfboard Paddling--(Nessler)	1231
442BD--Multivariate Models Utilize Accelerometers To Estimate Peak Vertical Ground Reaction Force--(Nicolozakes)	1233
443CD--Soft Tissue Movement Of The Shank During Landings--(Furlong)	1235
444CE--Absolute And Relative CMJ Performance Across Different Age Groups And Sports In Young Male Athletes--(Palazzi)	1237
445AE--Are Variables Associated With Knee Injuries Different Before And After A 40Min Run--(Paquette)	1239
446AF--The Effects Of MSM Supplementation On Knee Kinetics During Running, Muscle Strength, And Muscle Soreness Following Eccentric Exercise-Induced Quadriceps Damage--(Peel)	1241
447BF--A Prospective Comparison Of Biomechanical Variables Associated With Running-Related Injuries In Collegiate Cross Country Runners--(Kuhman)	1243
448BD--Effects Of Imposed Foot Strike Pattern Before And After A Long Run On Joint Stiffness In Rearfoot Strike Runners--(Melcher)	1245
449CD--Does Fatigue And Imposed Forefoot Strike Alter Strike Pattern Variability And Loading Rate In Rear Foot Strike Runners--(Paquette)	1247
450CE--Hip Loading During Forward And Side Lunges--(Zorn)	1249
451AE--Facilitation Of Short-Latency Rate Of Force Development Of Neck Muscles--(Pelland)	1251
452AF--Development Of A Novel Protocol To Temporarily Reduce Core Stability--(Raabe)	1253
453BF--Biomechanical Consequences Of Running With Deep Core Muscle Weakness--(Raabe)	1255
454BD--Estimating Vertical And Long Jump Power In Female Collegiate Soccer Athletes--(Razu)	1257
455CD--Comparative Evaluation Of The Microsoft Kinect With The Vicon Motion Capture System To Obtain 3D Knee Angles--(Razu)	1259
456CE--Bilateral Symmetry During A Power Clean In Recreational Vs. Competitive Weightlifters--(Rider)	1261
457AE--The Effects Of A Foot Strengthening Programs On Intrinsic Foot Muscles Size And Strength - A Pilot Study--(Ridge)	1263
458AF--Re-Examination Of The Relationship Between Bi-Articular Muscle Coactivation And Running Economy--(Schornstein)	1265
459BF--Relationship Between Landing, Taking-Off Kinematic Variables And Maximum Running Velocity Performance--(sha)	1267
460BD--Effects Of Wearing Toe Cage On Knee Biomechanics During Stationary Cycling--(Shen)	1269
461CD--Predictors Of Loading Rate In Heel-Strike Runners--(Shih)	1271
462CE--Knee Joint Loads And Surrounding Muscle Forces Of Selected Knee Unfriendly Movement Elements In 42-Form Tai Ji--(Wen)	1273
463AE--Whole Body Mechanics During Japanese Elite And Non-Elite Male Wrestlers During A Tackle--(Yamashita)	1275
464AF--Thromboelastographic Clot Parameters Of Autologous Blood Products--(Ghassab)	1277
465BF--Walking-Mediated Upregulation Of Follistatin-Like 3 Expression Is Insufficient To Increase Muscle Contractile Force--(Blazek)	1278
466BD--Temporal Gene Expression Patterns Reveal That Walking-Generated Biomechanical Signals Maintain Cartilage Health And Regulate Genes Associated With Osteoarthritis--(Blazek)	1280
467CD--Full Field In Vivo Characterization Of Skin Deformation Under Pressure Loading--(Bong)	1282
468CE--Stopped Teaching Physics, Started Teaching Biomechanics And Flipped The Classroom--(Brelloff)	1284
469AE--Modeling Reperfusion Responses In Patients With Leg Wounds--(Pan)	1286
470AF--Blood Perfusion Responses Of Lower Legs- Study Of Venous Stasis Ulcers--(Pan)	1288
471BF--Mechanical Work Of Massage After Eccentric Exercise In A Rabbit Model--(Crawford)	1290
472BD--Investigation Of Neck And Head Injury Potential During Inertial Of The Pediatric Head- Implications To Shaken Baby Syndrome Characterization--(Davison)	1292
473CD--Using A Hybrid Course Format To Teach Biomechanics Research Methods--(Feser)	1294
474CE--A Joint Coordinate System To Describe Relative 3D Motion Between The Rear And Front Body Segments Of Rodents- Application In The Study Of Neurodegenerative Diseases	1296
475AE--Characteristics Of Peri-Implant Bone Quality With Guided Bone Regeneration--(Johnson)	1298
476AF--Measurement Of Contact Pressure Of Femoral Fracture Fixation Plate Made Of Shape Memory Alloy--(BYUN)	1300
477BF--Activities To Promote Reflective Learning In The Biomechanics Classroom--(Kuxhaus)	1302
478BD--Validation Of Inertial Sensors For Use In Shooting Event Detection--(Lindecker)	1304
479CD--The Effect Of Skin Motion On Dynamic Ultrasound Of The Vastus Lateralis--(Lipps)	1306
480CE--A Vision Based, Hybrid Reality, Wire Navigation Simulator--(Long)	1308

Posters 481-491

481AE--Reliability Of A MRI-Based Technique For Quantification Of Dynamic Motion Of Solid Bodies--(Mahato)	1310
482AF--Methodology, Validation And Testing Of An Inexpensive Optical Planar-Motion Capture System--(Mahoney)	1312
483BF--Between Day Reliability Of Markerless Versus Traditional Marker Based Motion Capture During A Stepdown Task--(Morgan)	1314
484BD--Post Processing Technique For Approximating Projectile Trajectory In 3D Space--(Pfeifer)	1316
485CD--The Effect Of Forceplate Data Error On Joint Torques During Running--(Schmitz)	1318
486CE--Automatic Classification Of Mouse Motor Function From Markerless Measurements--(Sheets)	1320

487AE--PyCellAnalyst- A Robust, Open-Source Tool For 3D Image Segmentation And Deformation Analysis--(Sibole)	1322
488AF--Upper Extremity Injuries In Low-Speed Motor Vehicle Accidents Without Air Bag Deployment--(Toosi)	1324
489BF--Pre-Shot Jitter During Self-Paced Firing Using Small Arms Weapon Systems--(Webster)	1326
490BD--Automatic Segmentation And Reconstruction Of Extraocular Muscles From MRI Using Superpixel And Normalized Cut--(Xing)	1328
491CD--Investigating The Mechanism Of Neonatal Brachial Plexus Palsy Using Biomechanical Testing--(Zamorski)	1330

SIMULATING THE EFFECTS OF CROUCH GAIT SURGERIES ON KNEE MECHANICS

¹Rachel L. Lenhart, ¹Colin R. Smith, ²Michael H. Schwartz, ²Tom F. Novacheck, ¹Darryl G. Thelen

¹University of Wisconsin-Madison, Madison, WI, USA

²Gillette Children's Specialty Healthcare (St. Paul) and University of Minnesota (Minneapolis), MN, USA
email: rlenhart@wisc.edu, web: uwnmb1.engr.wisc.edu

INTRODUCTION

Crouch is a common gait abnormality in cerebral palsy that is characterized by excessive knee flexion during stance. Distal femoral extension osteotomy (DFEO) and patellar tendon advancement (PTA) procedures [1] are promising approaches to treat impairments underlying crouch. DFEO compensates for knee flexion contractures by creating an extension deformity of the distal femur. PTA corrects knee extensor insufficiency and tightens the quadriceps by advancing the patellar tendon (PT) insertion distally on the tibia. The combined procedures improve knee kinematics during gait more than traditional techniques or either procedure in isolation [2]. However, the degree of improvement remains variable and the procedures have not been standardized across institutions. Further, it is uncertain if additional procedures (e.g. hamstring lengthening) should be performed simultaneously. To address these issues, we are using dynamic musculoskeletal models to assess how surgical decisions made in DFEO and PTA procedures influence knee mechanics, muscle lengths, and articular cartilage loading in gait.

METHODS

Knee Model: We constructed a multi-body knee model with 6 DOF tibiofemoral and patellofemoral joints [3] (Fig. 1). This model was created using bony and cartilage geometries and ligament attachment sites obtained from MR images of a healthy adult female (61 kg, 1.65 m). The knee was incorporated into a lower extremity musculoskeletal model with 43 muscle-tendons acting about the hip, knee, and ankle [4]. This new construct was shown to accurately reproduce passive and active *in vivo* knee kinematics, as measured by dynamic MRI [3].

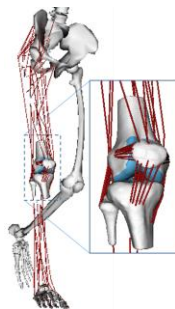


Figure 1: Model with 12 DOF knee joint.

DFEO Surgical Simulation: The knee model was modified to include a 30° knee flexion contracture. The reference strain of the posterior capsule ligaments was set to restrict knee extension to 30° when a 5 Nm extension torque was applied. A DFEO was then virtually performed by removing an anterior wedge of the distal femur geometry. The distal fragment was rotated to close the gap (Fig. 2), and translated to maintain the knee axis in the same anterior-posterior (AP) location [1]. A passive forward simulation was then run to determine the new resting knee posture. This process was repeated for a series of wedge apex locations. For each apex, we characterized the change in femur length, and medial hamstrings and vastii lengths.

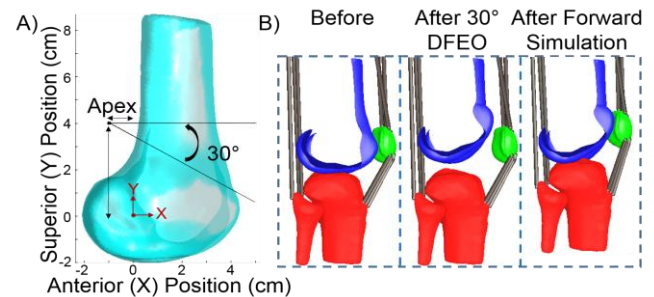


Figure 2: A) Creation of the DFEO wedge. Sensitivity analyses were conducted by moving the wedge apex in the AP and superior-inferior directions. B) Altered orientation of distal femur after removal of 30° anterior wedge from A, and after forward simulation.

PTA Surgical Simulation: PTA was simulated by varying the patellar tendon length such that the reference patellar position varied between 3 cm superior (alta) and 2 cm inferior (baja) to nominal. For each patellar position, we simulated the knee mechanics through a normal gait cycle. To do this, an enhanced static optimization method was used to simultaneously predict muscle and ligament forces, secondary knee kinematics, and cartilage contact pressure necessary to generate normal gait kinematics. Maximum quadriceps and PT forces during stance and mean patellar contact pressures in stance were compared between conditions.

RESULTS

DFEO Surgical Simulation: Varying the AP location of the apex of the DFEO wedge had a larger effect on femur and muscle lengths than varying the superior-inferior position (Fig. 3). Varying the apex AP location by 1 cm led to a 0.45 cm change in femur length. The osteotomy tended to increase semimembranosus (SM) lengths compared to their state in a contracted posture, though they were shorter than lengths that would occur in a fully extended knee. Vastus medialis (VM) lengths were substantially reduced compared to that seen in both contracted and extended postures pre-surgically.

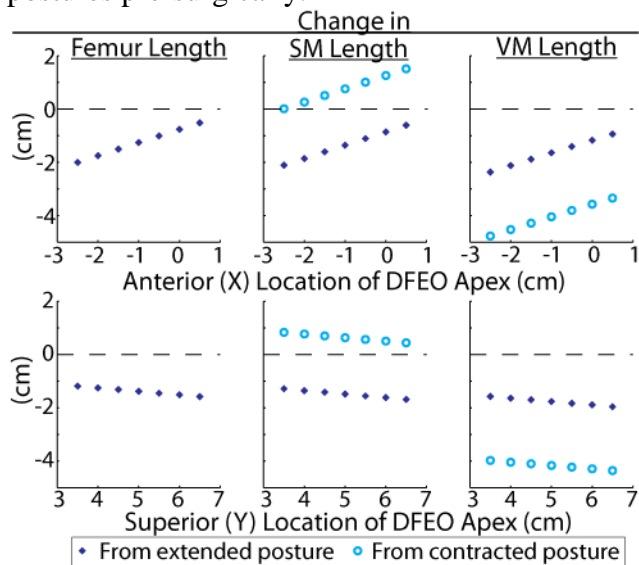


Figure 3: Change in femur, SM, and VM lengths between the original model and the model with DFEO performed. Muscle lengths are referenced to the model in an extended posture and with a 30° knee flexion contracture. Nominal Y location for the DFEO wedge was 4 cm, and X location was -1 cm (Fig 2).

PTA Surgical Simulation: Varying the patellar position substantially altered the quadriceps and PT forces and patellar pressures during walking (Fig. 4). A small amount of alta required the lowest quadriceps forces needed during gait, but induced larger PT forces and mean patellar contact pressures. Alta also migrated the patella contact to the inferior edge of the patella. The patella baja positions had a tendency to increase quadriceps force needed during walking, and drive contact to the superior edge of the patellar facets.

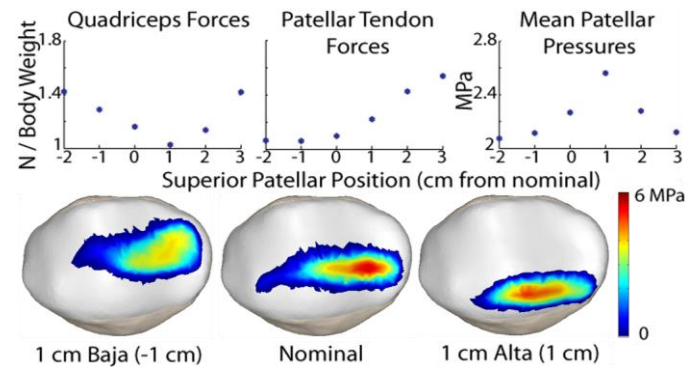


Figure 4: Maximum quadriceps (sum of all components) and PT forces during stance and mean patellar pressure at the maximum stance phase knee flexion angle. Negative numbers on the x-axes represent baja, whereas positive numbers represent alta. Patellar pressure distributions are shown below.

CONCLUSIONS

Our DFEO simulations suggest that the procedure has the potential to induce substantial shortening of the femur and quadriceps, with the greatest effect occurring when a cuneiform wedge of bone is removed (i.e. -X apex locations). In contrast, the hamstrings are most lengthened when the apex is near the posterior edge of the bone (X=0.05 cm), and a triangular wedge is removed. The latter observation is a concern surgically where there is a concern of introducing increased tension in the posterior compartment structures. The PTA simulations demonstrate that advancing the patella alters both the knee extensor mechanism, and cartilage loading. PTA procedures are often performed in a way that induces patella baja, which the model suggests may induce higher quadriceps load and superior patellar pressure if upright gait is achieved post-surgically. The greater quadriceps loading seems to result from a diminished effective moment arm of the extensor mechanism with baja. We conclude that the insights gained through this type of study can enhance the understanding and planning of complex surgeries used to treat crouch.

REFERENCES

1. Novacheck TF et al *J Bone Joint Surg Am* **91**, 271-86, 2009.
2. Stout JL, et al. *J Bone Joint Surg Am* **90**, 2470-84, 2008.
3. Lenhart RL, et al. *Ann Biomed Eng*, in review.
4. Arnold EM, et al. *Ann Biomed Eng* **38**, 269-79, 2010.

ACKNOWLEDGEMENTS: NIH F30AR065838, NIH T32GM008692, NIH UL1TR000427, NIH EB015410

ACHILLES TENDON DEFORMATIONS AND THE AGE-RELATED REDUCTION IN PLANTARFLEXOR PERFORMANCE DURING WALKING

Jason R. Franz^{1,2} and Darryl G. Thelen¹

¹University of Wisconsin, Madison, WI, USA

²University of North Carolina and North Carolina State University, Chapel Hill, NC, USA
email: jrfranz2@wisc.edu, web: <http://uwnmb1.engr.wisc.edu>

INTRODUCTION

Plantarflexor performance (i.e., net ankle joint kinetics) during the push-off phase of walking decreases precipitously in old age [1-2]. Although potentially important, few studies of walking have investigated the role of age-related changes in the behavior of the Achilles tendon (AT) [3]. The free AT governs the transmission of gastrocnemius and soleus muscle forces, and consists of distinct bundles of tendon fascicles arising from each of these muscles: superficial fascicles arise from the medial gastrocnemius and deep fascicles arise from the soleus [4]. We recently proposed that sliding between AT fascicle bundles may facilitate relatively independent gastrocnemius and soleus muscle fiber behavior, and thus muscle-tendon coordination tuned for effective force or power generation in walking [5]. Aging may reduce the capacity for sliding between tendon fascicle bundles [6], thereby potentially contributing to diminished plantarflexor performance commonly observed in old adults.

We coupled dynamic ultrasound imaging, quantitative motion capture, and inverse dynamic analyses to investigate age-related changes in free AT deformations *in vivo* during walking and their

relation to plantarflexor mechanical performance. We first hypothesized that superficial-deep variations in free AT deformations would be smaller in old than young adults. Second, we hypothesized that these more uniform AT deformations in old adults would be accompanied by proportional reductions in net ankle joint kinetics compared to young adults.

METHODS

9 healthy young (mean age, 23.9 years) and 8 healthy old (69.9 years) adults walked at three speeds (0.75, 1.00, and 1.25 m/s) on a force-sensing treadmill. Subjects completed one 2 min walking trial at each speed in random order. A linear array transducer secured via a custom orthotic recorded ultrasound radiofrequency data from the free AT approximately 6 cm superior to the calcaneal insertion (Fig. 1A). A custom 2D speckle tracking algorithm [5] tracked superficial and deep tissue displacements within the free AT. We used motion capture to record lower extremity kinematics and the position and orientation of the ultrasound transducer. We estimated superficial and deep AT elongation (i.e., change in length) relative to the calcaneal insertion by transforming the orthotic, transducer, and calcaneus

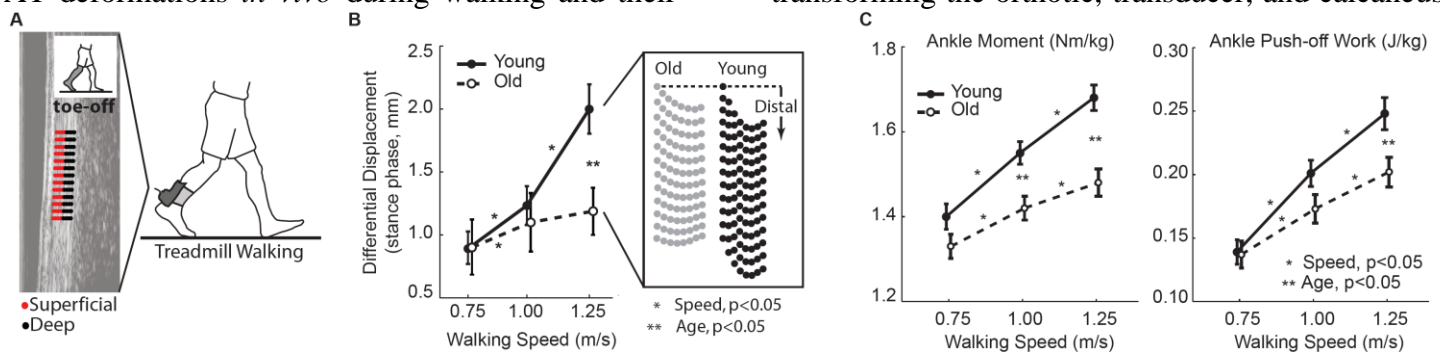


Figure 1. (A) We tracked superficial and deep tissue displacements within the free AT using a 2D speckle tracking algorithm. (B) Group mean (SE) differential (i.e., deep-superficial) free AT displacements and representative deformations. (C) Group mean (SE) peak ankle moment and positive ankle work during push-off.

kinematics into a common reference frame. Finally, we calculated peak ankle moment and power, and positive ankle work performed during push-off via inverse dynamics. A repeated measures ANOVA tested for significant main effects of and interactions between age and speed on each outcome measure. We also computed bivariate correlations between tendon deformations and net ankle joint kinetics.

RESULTS AND DISCUSSION

We observed significant depth-dependent variations in free AT deformations, wherein the superficial tendon displaced significantly less and elongated significantly more during stance than the deep tendon at all speeds for both old and young adults. The difference in displacements and elongations between superficial and deep AT regions did not differ between old and young adults at the slower two walking speeds (p 's > 0.63) (Fig. 2). However, a significant age \times speed interaction revealed that only young adults exhibited a progressive increase in relative motion between the superficial and deep AT with faster walking speed (p < 0.01). Consequently, depth-dependent variations in free AT deformations were 41% smaller in old vs. young adults at 1.25 m/s (p = 0.01) (Fig. 1B). Compared to young adults, old adults averaged 8% and 12% smaller peak ankle moments at 1.00 m/s (p < 0.01) and 1.25 m/s (p < 0.01), and performed 19% less positive ankle push-off work at 1.25 m/s (p = 0.02) (age \times speed, p < 0.01) (Fig. 1C). More uniform tendon deformations in old adults most strongly predicted reduced peak ankle moment (R^2 = 0.40), but also significant correlated with reduced peak power generation (R^2 = 0.15) and positive ankle work during push-off (R^2 = 0.19) (p 's < 0.01) (Fig. 2).

One interpretation of our findings is that a reduced capacity for sliding in old tendons [6] may act to couple gastrocnemius and soleus muscle-tendon behavior, thereby reducing net plantarflexor performance. This coupling would be undesirable for at least two reasons. First, the triceps surae muscles perform different biomechanical functions during walking, with the prevailing opinion that the gastrocnemius contributes more to forward propulsion and the soleus to vertical support. Thus, a loss of independent actuation of the gastrocnemius

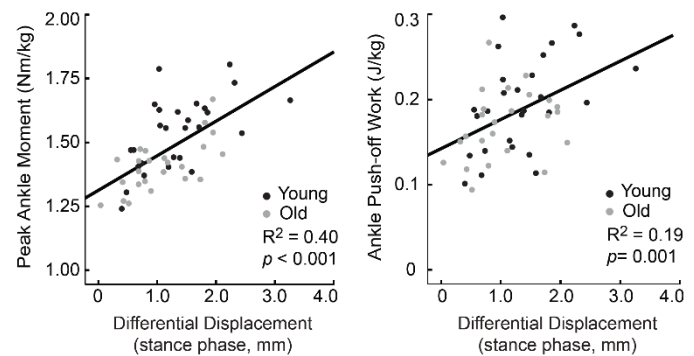


Figure 2. Bivariate correlations between free AT differential (i.e., deep-superficial) displacements and peak ankle moment and positive work during push-off for all subjects and walking speeds.

and soleus muscles may reduce old adults' ability to optimally modulate relative levels of propulsion and support during push-off. Second, the gastrocnemius and soleus muscles exhibit markedly different muscle fiber kinematics during walking [7] which may be facilitated by differences in tendon elasticity. A reduced capacity for sliding in old tendons may alter series elasticity and thus muscle fiber operating lengths and muscle-tendon mechanical output.

CONCLUSIONS

Advanced age brings more uniform free AT deformations that predict reduced plantarflexor performance in old adults during the push-off phase of walking. Together, our findings: 1) demonstrate a potential role for non-uniform AT deformations in governing gastrocnemius and soleus muscle-tendon function, and 2) allude to altered tendon behavior that may contribute to the age-related reduction in plantarflexor performance during walking.

REFERENCES

1. DeVita and Hortobagyi, J Appl Physiol 2000.
2. Winter et al., Phys Ther 1990.
3. Mian et al., Acta Physiol 2007.
4. Szaro et al., Ann Anat 2009.
5. Franz et al., Gait Posture 2015.
6. Thorpe et al., Eur Cell Mater 2013.
7. Ishikawa et al., J Appl Physiol 2005.

ACKNOWLEDGEMENTS

We gratefully acknowledge Dr. Laura Slane and Kristen Rasske. Funded by NIH (F32AG044904).

MRI ASSESSMENTS OF CARTILAGE MECHANICS, MORPHOLOGY AND COMPOSITION FOLLOWING ACL-RECONSTRUCTIVE SURGERY

¹ Jarred Kaiser, ¹ Michael F. Vignos, ¹ Fang Liu, ¹ Richard Kijowski, and ¹ Darryl G. Thelen

¹ University of Wisconsin - Madison, Madison, WI, USA
email: jmkaiser2@wisc.edu, web: <http://uwnmbl.engr.wisc.edu/>

INTRODUCTION

Despite regaining joint stability, patients who undergo ACL-reconstructive (ACL-r) surgery often exhibit radiographic signs of osteoarthritis (OA) within 10 years [1]. It is theorized that abnormal knee mechanics may persist after ACL-r, leading to altered tissue loading that initiates cartilage degeneration [2]. However, it remains challenging to test this theory as morphological changes with OA are often not detectable for many years.

In the early stages of OA, there are changes in the cartilage composition, such as the degradation of collagen and proteoglycan and an increase of water content. Quantitative MR imaging of T2 relaxation time has been used to indirectly assess these compositional changes, though the traditional T2 relaxation parameter is nonspecific and influenced by multiple factors [3]. More recently, multi-component driven equilibrium single shot observation of T1 and T2, termed mcDESPOT, has been introduced to distinguish the contributions of the fast relaxing T2 signal, which is correlated with water tightly bound to proteoglycan, and the slow relaxing T2 signal assigned to the bulk water [4]. Thus, quantitative MR imaging is an attractive modality to identify early signs of cartilage degeneration following ACL-r before the onset of cartilage volume loss and radiographic OA.

In this abstract, we describe our use of static, dynamic and quantitative MR imaging to investigate links between altered mechanics and early cartilage degeneration in reconstructed knees. We hypothesize that ACL-r knees exhibit normal morphology but abnormal cartilage contact patterns after surgery. We also show initial evidence that links spatial locations of abnormal contact and quantitative MR measures of cartilage degeneration.

METHODS

Eight subjects with a primary unilateral, isolated ACL-reconstruction (4 F, 25.8 ± 4.9 yrs, 86.3 ± 18.2 kg, 2.3 ± 0.6 yrs since surgery, 5 patellar tendon grafts, 3 hamstrings grafts, 1 partial lateral meniscectomy) and nine healthy controls (2F, 22.7 ± 3.1 yrs, 79.3 ± 8.9 kg) were tested after obtaining informed consent according to an IRB-approved protocol. Control subjects had no history of knee pain, injury or surgery and no history of inflammatory or crystalline induced arthritis.

Subjects underwent a bilateral static MR protocol consisting of a fat-suppressed 3D SPGR sequence ($0.37 \times 0.37 \times 0.90$ mm resolution) and a 3D FSE Cube sequence (0.31 mm isotropic resolution). Distal femur, and proximal tibia bone geometries were segmented from the SPGR images. Articular cartilage surfaces were segmented from the FSE Cube images. Cartilage thickness maps of the tibia plateau were generated by determining the distance from the articular cartilage surface to bone surface.

Dynamic MR imaging was used to measure knee kinematics and cartilage contact during an active flexion-extension task. Subjects were positioned supine with their lower leg secured on a MR-compatible loading device. Cyclic knee flexion and extension was performed at 0.5 Hz for 5 min while SPGR-VIPR images were continuously collected [5]. Model-based tracking was used to determine femoral and tibial bone position and orientation at each frame of the motion cycle. Regions of cartilage contact were assessed by computing the proximity between tibia and femoral cartilage surfaces, with negative proximity indicative of contact. Contact maps were generated by determining the closest proximity of each tibial cartilage mesh face through the motion cycle.

A mcDESPOT sequence (0.6x0.6x3.0 mm resolution) was performed unilaterally on the reconstructed knee of the subjects and a healthy knee of the controls. Fraction maps for the fast relaxing water component (F_{pg}) were calculated as the ratio of water bound to proteoglycan to the total amount of water in a voxel.

Bounding boxes surrounding the medial and lateral plateaus were subdivided into 20 regions of interest (ROIs). Average contact and cartilage thickness were computed for each ROI. A one-way ANOVA tested the effect of surgery on thickness and contact between the ACL-r knees and the control subject knees. A repeated measures ANOVA was used to compare the ACL-r knees and their contralateral knees. If a significant difference was found ($p < 0.05$), a post-hoc Tukey test was performed to identify the location of group differences ($p < 0.05$). A correction was made for an uneven N between ACL-r and control subjects.

RESULTS AND DISCUSSION

As hypothesized, there were no significant differences in ACL-r tibial cartilage thickness when compared to the contralateral knee or control knees. However, cartilage contact patterns in the reconstructed knees were significantly different (Fig. 1). In particular, ACL-r knees exhibited greater contact in the posteromedial aspect of the medial plateau and the posterior aspect of the lateral plateau. Initial evaluations of the F_{pg} maps also

reveals potential evidence of reduced proteoglycan content in similar regions of the ACL-r tibia plateaus (Fig. 1).

To our knowledge, this is the first study to show that abnormal tibiofemoral cartilage contact patterns can be detected in reconstructed knees with dynamic MRI. Prior studies using biplanar fluoroscopy have identified altered contact during gait [6], suggesting that the changes seen in the simpler flexion-extension task may be representative of functional tasks. The absence of changes in cartilage thickness in this population is consistent with prior studies suggesting that long time periods are needed to detect changes in cartilage morphology following ACL-r [7]. However, it is notable that quantitative MR does detect potential evidence of altered cartilage composition within 1-2 years of reconstruction [3]. Further study is needed to see if the decline in fraction of rapidly relaxing water component is consistently evident in reconstructed knees and is associated with cartilage loss over time.

REFERENCES

- [1] Linden, M et al. *Arthroscopy* **24**: 10, 2008.
- [2] Andriacchi, TP et al. *Ann Biomed Eng* **32**:11, 2004
- [3] Li, X et al. *Radiology* **258**: 10, 2011.
- [4] Liu, F et al. *JMRI* **39**: 8, 2014.
- [5] Kaiser, J et al. *MRM* **7**, 2013.
- [6] Hoshino, Y et al. *Clin Ortho* **471**: 8, 2013.
- [7] Andreisek, G et al. *OA Cart* **17**: 8, 2009.

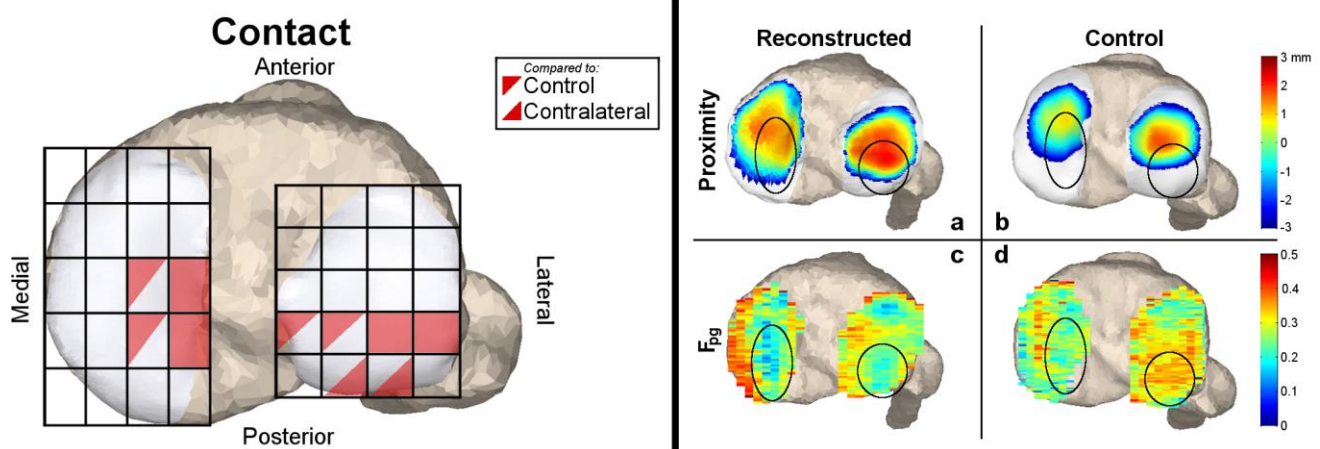


Figure 1. *Left.* Significantly increased contact, denoted by red, is present in the posteromedial portion of the medial plateau and the posterior aspect of the lateral plateau. *Right.* Example maps of cartilage contact (a,b) and F_{pg} (c,d) for an ACL-r subject (a,c) and a control subject (b,d). Note that regions of abnormal contact, denoted by the ovals, display a decrease in F_{pg} .

ASSESSMENT OF THE CONTRIBUTIONS OF ELASTIC ENERGY IN THE HUMAN PLANTAR APONEUROSIS

Justin C. Wager and John H. Challis

Biomechanics Lab, The Pennsylvania State University, University Park, PA, USA
email: jcw296@psu.edu

INTRODUCTION

The arch of the human foot has received considerable attention for its potential to store and release elastic energy (EE) and possibly influence the metabolic cost of running [1]. While *in situ* testing has demonstrated that the spring-like function of the arch exists under simple loading conditions, it remains unclear whether this function exists during the more complex task of human locomotion. The aim of this study was to investigate one of the main elastic tissues in the arch (the plantar aponeurosis; PA) to examine its ability to store EE and contribute to the movement of the foot. A second aim was to investigate the influence of the initial foot contact pattern (IFCP) on the function of the PA during the stance phase of running.

METHODS

A 10 degree of freedom rigid body model of the human lower leg and foot was created that consisted of five segments (tibia, calcaneus, talus, midfoot, combined toes). A non-linear spring (tuned to match *in situ* data [2]) connecting the calcaneus to the great toe was added to represent the PA. This model was then scaled to match the anthropometry of eight men and women and driven using kinematics of running barefoot at 3.1 m/s under two IFCP conditions: rearfoot initial contact (RF; foot strike angle, mean \pm SD: $12.3 \pm 2.7^\circ$) and non-rearfoot initial contact (NRF; foot strike angle: $-1.4 \pm 4.0^\circ$). PA strain was computed using the length of the PA during stance. Initial and peak strains were used to determine the average strain rate from foot contact to peak PA strain. The joint moments were determined using inverse dynamics. To investigate the contribution of the PA to the movement of the foot, the joint moments arising from the PA force were calculated using the PA moment arms over the course of the stance phase. PA joint power (P_{PA}) at the

talonavicular (TN) joint and metatarsophalangeal (MTP) joint was determined from the PA moments and the joint angular velocities; positive PA joint work (W_{PA}) was computed as the time integral of P_{PA} . EE_{PA} stored was calculated as the integral of the spring's non-linear force-strain relation. PA strain rate as well as peak measures of strain, force, P_{PA} and EE_{PA} were compared between the conditions using paired t-tests ($\alpha = 0.05$).

RESULTS AND DISCUSSION

Average strain rate of the PA from foot contact to peak strain was significantly higher in the NRF condition compared with the RF condition. This is due to both a lower initial strain ($p < 0.001$) as well as less time to peak strain ($p < 0.001$) in the NRF condition. Peak values of PA strain, force, EE_{PA} , P_{PA} , and W_{PA} were not significantly different between conditions (Table 1). The temporal profiles of PA strain for the two conditions illustrate both the increased strain rate in early stance as well as the lack of differences at peak strain and beyond (Figure 1).

Table 1: Means (\pm standard deviation) of peak values for the IFCP conditions. Subscript PA-TN denotes PA joint power or work at the TN joint.

	RF	NRF	<i>p</i>
PA strain	0.062 ± 0.013	0.063 ± 0.014	0.09
PA strain rate (s^{-1})	0.18 ± 0.05	0.31 ± 0.06	<0.001
PA force (BW)	1.22 ± 0.44	1.20 ± 0.41	0.07
EE_{PA} (J)	3.0 ± 1.5	3.1 ± 1.7	0.07
P_{PA-TN} ($W \cdot kg^{-1}$)	1.56 ± 0.87	1.54 ± 0.88	0.70
W_{PA-TN} ($J \cdot kg^{-1}$)	0.10 ± 0.05	0.09 ± 0.05	0.31

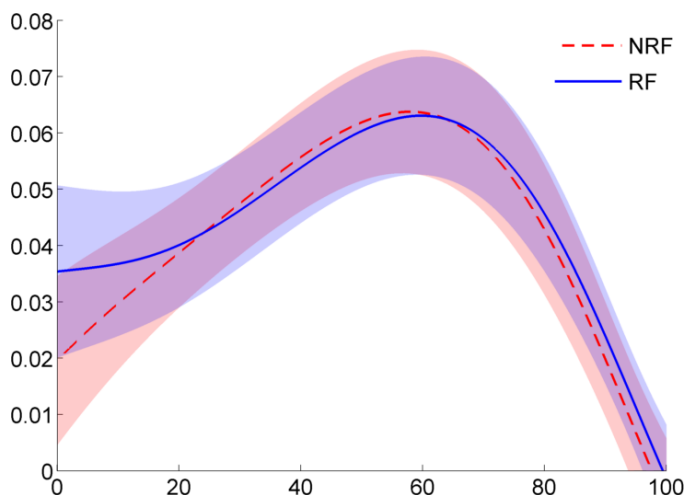


Figure 2: Group means for PA strain for the NRF (dashed red) and RF (solid blue) conditions. Shaded regions are ± 1 S.D.

As no significant differences were found from peak strain to toe-off, the two conditions were collapsed into one data set to examine the function of the PA during pushoff. Peak PA strain (0.063 ± 0.013 at $58.8 \pm 3.7\%$ of stance) was slightly higher than and occurred slightly earlier than peak PA strain during walking [3]. Peak PA force (1.21 ± 0.43 BW) was also slightly higher than that found during *in situ* simulations of walking [2]. Peak EE stored in the PA (3.1 ± 1.6 J) was similar to the decrease in EE storage obtained upon sectioning of the PA during simple loading of cadaveric specimens [1].

The contributions of the PA to foot dynamics were the largest at the talonavicular (TN) joint. Of the peak TN joint moment, the PA accounted for $19.4 \pm 11.0\%$ (23.1 ± 5.1 N·m). In addition, the PA produced power at the TN joint (peak: 1.54 ± 0.88 W·kg⁻¹ at 77% of stance) and performed positive work at the TN joint from 55% of stance to toe-off (Figure 2). However, the magnitudes of the joint power and joint work are small compared to power and work at other joints during running [4].

At the MTP joint, the PA accounted for $18.8 \pm 14.8\%$ (1.3 ± 0.7 N·m) of the peak joint moment. PA joint power at the MTP joint followed a pattern of power generation early in stance before power absorption from 37% of stance to toe-off, which is consistent with the pattern of MTP joint power previously found during running [5].

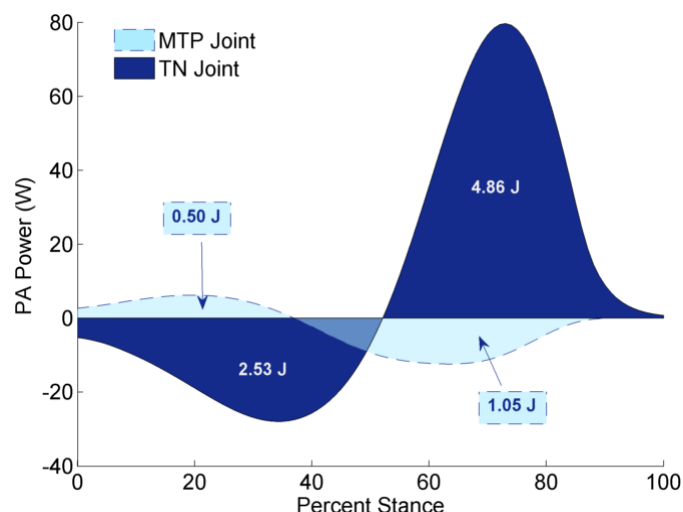


Figure 1: Mean PA joint power & joint work at the TN and MTP joints for one representative subject.

CONCLUSIONS

It has been speculated that the spring-like function of the arch of the foot stores and releases EE, reducing the energetic cost of running [1]. The present study examined this speculation within the scope of the PA, using a multi-segment rigid body foot model driven by experimental running data. The results support the storage and release of EE in the PA, with magnitudes of energy storage that agree with the results of *in situ* testing. This storage and release of EE was not different between IFCP conditions (RF and NRF). During pushoff, the PA produced power at the TN joint of the foot, which suggests that the PA can contribute to the shortening of the arch during late stance. However, the magnitude of the TN joint power generated by the PA is small compared to the power generated at more proximal joints during running [4]. This study demonstrates that the PA does store EE during running gait, but that the return of this energy does not make a large contribution to the energetics of running gait.

REFERENCES

1. Ker RF, et al. *Nature* **325**, 147-149, 1987.
2. Erdemir A, et al. *J Bone Joint Surg Am* **86**, 546-552, 2004.
3. Caravaggi P, et al. *J Anat* **217**, 254-261, 2010.
4. Winter, DA. *J Biomech* **16**, 91-97, 1983.
5. Stefanyshyn, DJ & Nigg, BM. *J Biomech* **30**, 1081-1085, 1997

THE INFLUENCE OF SOLID ANKLE-FOOT-ORTHOSES ON FORWARD PROPULSION AND DYNAMIC BALANCE IN HEALTHY ADULTS DURING WALKING

Arian Vistamehr¹, Steven A. Kautz^{2,3} and Richard R. Neptune¹

¹ Department of Mechanical Engineering, The University of Texas, Austin, TX

² Department of Health Sciences and Research, Medical University of South Carolina, Charleston, SC

³ Ralph H Johnson VA Medical Center, Charleston, SC

email: arian.vistamehr@utexas.edu web: <http://www.me.utexas.edu/~neptune>

INTRODUCTION

Solid polypropylene ankle-foot-orthoses (AFOs) are frequently prescribed to assist with gait impairments in post-stroke hemiparetic subjects (e.g., [1]). These AFOs hold the ankle in a near neutral position to assist in foot clearance during swing while bracing the ankle during stance. While most studies have reported increased walking speed and improved toe clearance when walking with an AFO (e.g., [1]), the effects of solid AFOs on other aspects of walking are unclear.

Improving mobility is a common rehabilitation goal. Mobility demands, such as changing walking speed and direction, are accomplished by accelerating or decelerating the body while maintaining dynamic balance. Previous studies have shown that the ankle plantarflexors are primary contributors to regulating forward propulsion (e.g., [2]) and dynamic balance [3]. However, with AFOs limiting ankle motion and plantarflexor output during stance, execution of these walking subtasks may be compromised.

The purpose of this study was to assess the influence of a commonly prescribed solid polypropylene AFO on forward propulsion and dynamic balance in healthy subjects across a range of walking conditions including steady-state, accelerated and decelerated walking. Assessing the influence of AFOs on healthy subjects' walking mechanics will provide a baseline for comparison with hemiparetic subjects, which collectively can provide clinicians with quantitative rationale as to whether solid AFOs improve paretic leg impairments and overall walking mobility.

METHODS

Ten healthy young subjects (age = 27.3 ± 2.7) walked on an instrumented treadmill in randomized trials of steady-state (0.6 m/s and 1.2 m/s), accelerated (0-1.8 m/s at 0.06 m/s^2) and decelerated (1.8-0 m/s at -0.06 m/s^2) walking. Subjects walked with and without wearing a unilateral solid AFO (Fig. 1) on a randomly assigned leg. Kinematic and ground reaction force (GRF) data were collected at 120Hz and 2000Hz, respectively. An inverse dynamics model was used to calculate the center-of-mass position and velocity for all body segments.

Dynamic balance was assessed using the range of whole-body angular momentum (H) in each plane, which was calculated as the difference between the maximum and minimum value of H over the entire gait cycle as described in [4]. Propulsion was assessed using the propulsive and braking GRF impulses, which were calculated using the time integral of the positive and negative anterior-posterior GRFs, respectively.

The range of H was compared between the AFO and no AFO (NAFO) conditions at each walking speed using a paired t-test. Braking and propulsive impulses were compared using a one-factor (AFO condition) repeated measures ANOVA ($\alpha = 0.05$) with three levels (AFO leg, contralateral leg, and average of both legs during the NAFO condition).

RESULTS AND DISCUSSION

The propulsive impulses decreased in the AFO leg compared to the contralateral leg and no AFO condition at steady-state moderate, accelerated and decelerated walking conditions (Fig. 2). With no change in the propulsive impulse at the slow steady-

state walking speed, the present results suggest that a solid AFO may hinder forward propulsion to a greater extent during non-steady-state walking.

Walking with an AFO resulted in a greater range of H in the frontal plane for all the walking conditions and in the sagittal plane during the steady-state moderate (Fig. 3), accelerated and decelerated walking conditions [4]. Whole-body angular momentum has previously been found to be highly regulated during walking and that successful regulation of H is needed in older adults to prevent a fall following a trip [5]. Thus, poor regulation of H during walking results in higher magnitudes of H , which may indicate a decreased ability to control dynamic balance.

In summary, common clinically prescribed solid polypropylene AFOs adversely influenced the generation of forward propulsion and dynamic balance in healthy adults during steady-state and non-steady-state walking. These results suggest that AFOs limit the successful execution of these important mobility tasks, especially when changing walking speed is important, and that the prescription of AFOs should be carefully considered. In cases where an AFO is needed to compensate for gait impairments such as foot drop, perhaps more advanced AFO designs that promote ankle plantarflexion or functional electrical stimulation systems (e.g., The WalkAide System, Austin, TX, USA) that promote dorsiflexion can improve rehabilitation outcomes.



Figure 1: Solid polypropylene ankle-foot-orthosis (AFO) used in this study.

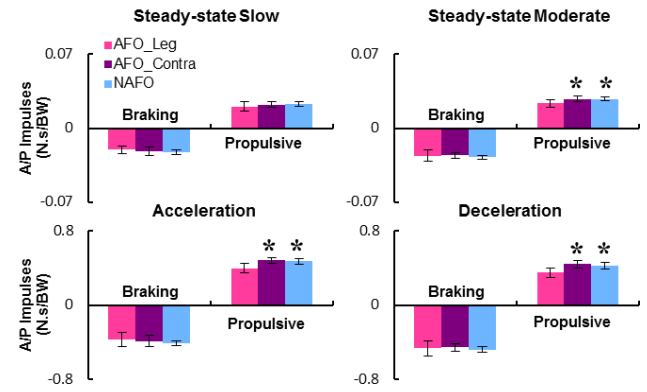


Figure 2: Mean braking and propulsive impulses (normalized by body weight) for the AFO leg (AFO_Leg), contralateral leg (AFO_Contra) and average of both legs in the no AFO condition (NAFO). A significant difference between the AFO leg and other conditions (contralateral leg and NAFO) is indicated with ‘*’ ($p < \frac{\alpha}{3}$, $\alpha = 0.05$).

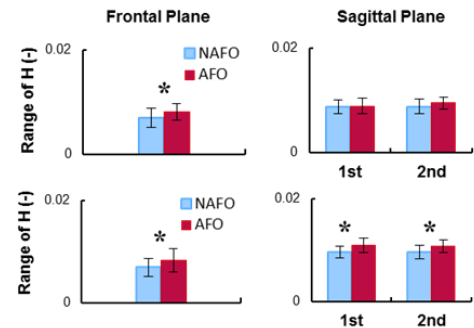


Figure 3: Mean (\pm SD) range of H during the steady-state slow (top row) and moderate (bottom row) walking conditions with (AFO) and without (NAFO) an AFO. ‘1st’ and ‘2nd’ indicate the first and second halves of the gait cycle. A significant difference between the AFO and no AFO conditions is indicated with ‘*’ ($p < 0.05$).

ACKNOWLEDGEMENTS

This work was supported by AHA SouthWest Affiliate pre-doctoral fellowship (12PRE12030414) and the Rehabilitation Research and Development Service of the Department of Veteran’s Affairs.

REFERENCES

1. Carse B, et al. *Prosthet Orthot Int*, 2014 (in press).
2. Peterson CL, et al. *Gait & Posture* **33**, 562-567, 2011.
3. Neptune RR. and McGowan CP. *J Biomech* **44**, 6-12, 2011.
4. Vistamehr A, et al. *Clin Biomech* **29**, 583-589, 2014.
5. Pijnappels M, et al. *Gait & Posture* **21**, 388-394, 2005.

THE INFLUENCE OF PASSIVE-DYNAMIC ANKLE-FOOT ORTHOSIS BENDING AXIS ON GAIT PERFORMANCE IN INDIVIDUALS WITH LOWER-LIMB IMPAIRMENTS

¹Ellyn C. Ranz, ^{2,3}Elizabeth Russell Esposito, ^{2,3}Jason M. Wilken, ¹Richard R. Neptune

¹Department of Mechanical Engineering, The University of Texas at Austin, Austin, TX, USA

²Center for the Intrepid, Department of Orthopaedics and Rehabilitation, Brooke Army Medical Center, JBSA Ft Sam Houston, TX, USA, ³DoD-VA Extremity Trauma and Amputation Center of Excellence

email: ellynrantz@gmail.com, web: <http://www.me.utexas.edu/~neptune>

INTRODUCTION

Passive-dynamic ankle-foot orthoses (PD-AFOs) are commonly prescribed to augment impaired ankle muscle function by providing elastic energy storage and return and improve gait performance. Previous studies have examined the benefits of PD-AFOs over traditional designs [e.g., 1] and the influence of PD-AFO mechanical properties, such as stiffness, on pathological gait [e.g., 2]. However, the design and prescription process remain largely qualitative and modifications to other PD-AFO design characteristics may be advantageous.

One PD-AFO design includes a molded footplate, a cuff worn below the knee and a strut rigidly connecting the two (Fig. 1a). During gait, deflection occurs along the length of the strut, with the greatest deflection occurring at a central bending axis. A previous study indicated that a correlation may exist between AFO instantaneous center of rotation (representing the axis of a hingeless AFO as determined by AFO deformation) and ankle joint mechanics [3]. Thus, PD-AFO bending axis is a design characteristic that may influence gait performance, yet it has been largely uninvestigated. However, previous work has demonstrated that misalignment of articulated AFOs with the natural ankle joint may increase resistance torque [4] and cuff movement [5] which may cause discomfort.

The overall goal of this study was to investigate the influence of altering the bending axis location on gait performance. We hypothesize that subjects will prefer a bending axis closer to the natural ankle joint, and this preference will correspond to improvements in biomechanical gait measures.

METHODS

Thirteen subjects who had experienced unilateral

lower extremity trauma and were clinically prescribed a PD-AFO by their orthopedic surgeon were enrolled in this study. A previously developed framework [6] was used to fabricate selective laser sintered (SLS) PD-AFO struts with bending stiffnesses matching each subject's prescribed PD-AFO. A second SLS strut incorporated a 2.5cm radius circular extrusion located at 30% of the inner bolthole-to-bolthole distance from the strut center. Strut orientation was used to manipulate the device bending axis (Fig. 1 b or d).

In the experimental data collection protocol, subjects completed overground walking trials at self-selected speed while electromyographic (EMG), kinetic and kinematic data were collected. Subjects completed testing in three different PD-AFO bending axis conditions (Fig. 1): proximal (high), central (nominal) and distal (low), and indicated the order of their bending axis preference once testing was completed.



Figure 1: PD-AFO with the a) prescribed strut, b) proximal (high) bending axis, c) central (nominal) bending axis, and d) distal (low) bending axis.

Integrated EMG (iEMG), joint work and ground reaction force (GRF) impulses were calculated as the time integrals of EMG, joint powers and GRFs, respectively. Biomechanical measures were computed in six gait regions: 1) first double-leg support, 2) early single-leg support, 3) late single-leg support, 4) second double-leg support, 5) early

swing, and 6) late swing. Three way (limb, bending axis, subject preference) repeated measures ANOVAs were conducted to test for significant differences. Significant main and interaction effects were adjusted using a Huynh-Feldt correction and examined using post-hoc pairwise comparisons with a Bonferonni correction (unadjusted $p < 0.05$).

RESULTS AND DISCUSSION

Contrary to what was hypothesized, the majority of subjects (seven) preferred the nominal bending axis, with two subjects preferring the high and four preferring the low condition. Altering PD-AFO bending axis had few effects on peak joint kinematics and kinetics. In region 1, peak ankle plantarflexion was greater in the low compared to nominal condition ($p=0.018$) in both limbs.

Some differences were observed in joint work, primarily at the hip (Fig. 2). In region 1, positive hip work was greater in the nominal compared to high condition in both limbs ($p=0.027$). In region 2, positive ankle work was greater in the low compared to nominal condition in both limbs ($p=0.003$). Negative hip work was also altered by bending axis in region 4 (limb*bending axis*preference; $p=0.004$).

Bending axis had little effect on GRF impulses. In region 3, the vertical GRF impulse was greater in the nominal compared to both low ($p=0.043$) and high ($p=0.002$) conditions in both limbs.

Bending axis altered vastus medialis (VAS), medial gastrocnemius (GAS) and rectus femoris (RF) activity (iEMG). In region 1 and region 4, bending axis altered VAS activity (limb*bending axis*preference; region 1: $p=0.015$, 4: $p=0.002$). Bending axis also altered GAS activity in regions 1, 4 and 5 (bending axis*preference; region 1: $p=0.046$, 4: $p=0.028$, 5: $p=0.034$) and RF activity in region 5 (bending axis*preference: $p=0.028$).

Although several changes were observed, they were generally small and not likely of functional relevance. This suggests that one bending axis does not significantly improve gait and factors such as preference and comfort may play a more important role in prescription. As differences found were often based on preference, future work should examine the relationship between etiology and preference.

Understanding this relationship and the influence of bending axis on gait performance may allow for improved PD-AFO prescription guidelines and rehabilitation outcomes.

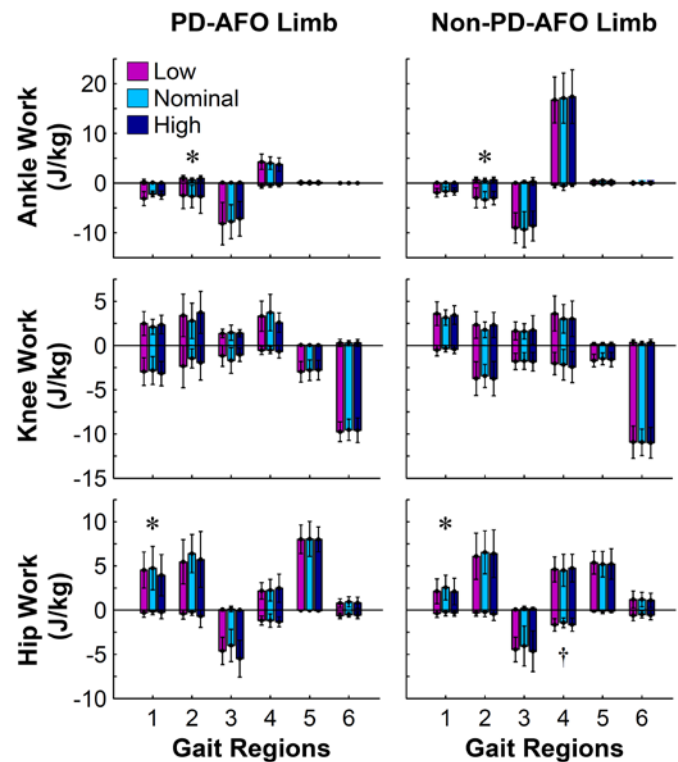


Figure 2: Joint work across gait regions. Significant main (*) and interaction (†) effects are indicated.

REFERENCES

1. Patzkowski JC, et al. *J Bone Joint Surg Am*, **94**, 507-515, 2012.
2. Russell Esposito E, et al. *Clin Orthop Relat Res*, **472**, 3026-3035, 2014.
3. Sumiya T, et al. *J Rehabil Res Dev*, **34**, 279-285, 1997.
4. Gao F, et al. *Prosthet Orthot Int*, **35**, 181-189, 2011.
5. Fatone S and Hansen AH. *Prosthet Orthot Int*, **31**, 76-87, 2007.
6. Harper NG, et al. *J Biomech Eng*, **136**, 091001-1-091001-7, 2014.

ACKNOWLEDGEMENTS

This study was supported in part by a research grant from the Center for Rehabilitation Sciences Research, Department of Physical Medicine and Rehabilitation, Uniformed Services University of Health Sciences, Bethesda, MD. The views expressed herein are those of the authors and do not reflect the official policy or position of Brooke Army Medical Center, the U.S. Army Medical Department, the U.S. Army Office of the Surgeon General, the Department of the Army, Department of Defense or the U.S. Government.

EFFECTS OF ANKLE BENDING STIFFNESS OF ANKLE-FOOT ORTHOSIS ON GAIT PATTERNS WITH CEREBRAL PALSY: A PILOT STUDY WITH SINGLE-SUBJECT DESIGN

¹Juliana Sánchez P, ¹Jaebum Son, ¹Juan Carlos Briceño, ²Jose Luis Duplat; ²Fernando Ortiz; ²Luis Eduardo Rueda.

¹Department of Biomedical Engineering, Universidad de los Andes, Bogotá, Colombia

² Instituto de Ortopedia Infantil Roosevelt, Bogotá, Colombia

e-mail: j.sanchez679@uniandes.edu.co, web: <http://www.uniandes.edu.co>

INTRODUCTION

The selection of the correct orthosis to improve the gait pattern of children with cerebral palsy (CP) is a complex task for orthopaedic physicians, since it should match the condition of spasticity and weakness of the muscles of each patient [1, 2]. The prescription of an orthosis for a patient is currently based on the physician's experience and is not specific in terms of the mechanical and/or geometrical properties the orthosis should have [1]. Therefore, we aim to assess the effect of ankle bending stiffness of a posterior leaf spring ankle-foot orthosis (AFO), on the gait pattern of one hemiplegic child with spastic CP, which could provide some suggestions about how this characteristic feature of orthosis affects a child's gait pattern.

METHODS

Subject

One child (11.6 years, 29.8kg), diagnosed with spastic unilateral CP on the left side, and evaluated in the clinical gait analysis laboratory from the Instituto de Ortopedia Infantil Roosevelt (IOIR) in Bogotá, Colombia, participated in this study. The following inclusion criteria were used: independent gait without assistive devices, GMFCS I and II; cognitive ability to understand and follow instructions taking part of the experimentation protocol. The exclusion criteria were: orthopaedic lower limbs surgery in the past year; applied Botulinum toxin in the last six months; rigid equinus; symptoms of dystonia and other conditions that may affect balance and/or gait pattern.

Subject assent and parental consent was approved by the Institutional Review Board of the IOIR.

AFOs with different stiffness

An orthopaedic technician of IOIR fabricated three different posterior leaf spring AFOs for the child. Orthoses were fabricated from 3.0 mm thick polypropylene, extending distally under the toes and proximally on the posterior surface of the leg to about 3-5cm below the knee. All were fabricated with a fixed 90° plantar flexion. Different bending stiffness were achieved in their fabrication by increasing the width of the back part and the width of the reinforcement placed in the back (Fig. 1a).



Figure 1a: Posterior view of the posterior leaf spring AFOs fabricated for the subject, from left to right in order of bending stiffness (low to high).

Figure 1b. BRUCE design suggested by Bregman *et al* [3].

Characterization of the ankle bending stiffness

A device was constructed based on the BRUCE design [3] (Fig. 1b) to determine the ankle bending stiffness of the AFO over a functional range of deflections in the sagittal plane. Inverse dynamics were used to obtain the moment exerted by the AFO for different angles, based on the geometry of the device, the vertical displacement velocity (1mm/s) and the vertical force registered by the Instron machine (5586). **Error! Reference source not found.** describes stiffness obtained for the three different orthoses manufactured for the subject.

Table 1. Ankle bending stiffness [N·m/°] (n=5)

Orthosis	Mean	St. Deviation
Low stiffness	0.0318	0.0082
Medium stiffness	0.0931	0.0209
High stiffness	0.1311	0.0082

Experimental design

A single-subject A-B-C-D experimental design was used, in which a baseline phase (A) was followed by three different intervention conditions (B, C and D). In each intervention phase, the child tested one of the three different fabricated AFOs (with high, medium and low stiffness) in randomized order.

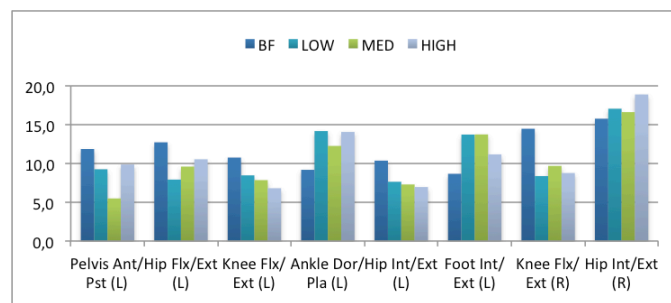
Three-dimensional kinematic data were collected using the BTS Motion System. Markers were placed over the skeletal landmarks according to Davis *et al* standard clinical protocol. Kinetic data were collected using two force plates (AMTI). For each test, the subject was instructed to walk along a 10 m laboratory walkway at his/her self-selected comfortable walking speed. Two trials per phase were finally selected and averaged, for the analysis. All the kinematic information was processed and normalized in biomechanical indexes (MAP).

RESULTS AND DISCUSSION

Kinematic results showed that the principal effect of the ankle bending stiffness is the resulting amount of ankle mobility during the stance phase. Fig. 2 shows the change in MAP of the reviewed subject of some gait characteristics of both sides (L: Left, R: Right), when walking barefoot (BF) and with low (LOW), medium (MED) and high (HIGH) ankle bending stiffness AFO.

Not all the MAP indexes show an improvement when increasing the ankle bending stiffness of the orthosis. Although, some such as the Knee Flx/Ext (L) and the Hip Int/Ext (L) show an improvement, some others such the Ankle Dor/Pla (L) show a deterioration of the gait pattern when increasing this characteristic. This happened during the analysis of both sides. In addition, none of the indexes of gait pathology include in their calculation process the subject's kinetic information obtained during the

gait analysis; hence there is no evidence of those results in the values obtained by this indexes.

**Figure 2:** MAP indexes for each condition.

CONCLUSIONS

Ankle bending stiffness of posterior leaf spring AFOs is a feature that produces an immediate effect over the gait pattern of hemiplegic child, creating changes in the kinematic and kinetic data of the patient. The results obtained with the MAP indexes, showed that an overall evaluation of changes in the gait pattern cannot be made just using the indexes of gait pathology, since they do not include in their definition the kinetic data from which physicians gather important information about the physiological characteristics of the patient's muscles.

In clinical practice it is convenient to find the optimal AFO for a specific patient, by testing different AFOs with different stiffness. In this process physicians should study not only the kinematic but also the kinetic data obtained from the patient testing all the orthosis, and determine which orthosis addresses best the particular patient's gait pathology. The final selection should be consistent with the results the physician is expecting, taking into account that there is a trade-off in the correction.

REFERENCES

1. Bregman DJJ, van der Krogt MM, de Groot V, Harlaar J, Wisse M, Collins SH. *Clin. Biomech*, **26**(9). 2011.
2. Ries AJ, Novacheck TF, Schwartz MH. *Gait Posture*, **40**, 2014.
3. Bregman DJJ, Rozumalski A, Koops D, de Groot V, Schwartz M, Harlaar J. *Gait Posture*, **30**, 2009.

ADAPTIVE GAIN FOR PROPORTIONAL MYOELECTRIC CONTROL OF A ROBOTIC ANKLE EXOSKELETON DURING HUMAN WALKING

Jeffrey R. Koller, Daniel A. Jacobs, Daniel P. Ferris, C. David Remy

University of Michigan, Ann Arbor, USA

jrkoller@umich.edu, jacobsda@umich.edu, ferrisdp@umich.edu, cdremy@umich.edu

INTRODUCTION

There exists a large disconnect between the natural fluid motion of unconstrained human walking and the unnatural, rigid motion of human walking with a robotic exoskeleton. This unnatural movement of walking in a robotic exoskeleton is largely due to poor controller design and can make the motion energetically inefficient for the user [1]. Our research group has been developing techniques to use neural signals from the wearer to directly control exoskeleton actuation timing and amplitude. By using neural signals to control the device we are attempting to alleviate the issues that come with relying on intrinsic mechanical measurements for exoskeleton control.

In our work, we use electromyography (EMG) to directly control walking robotic exoskeletons. In the past, these controllers created a control signal for actuation by using a *constant* mapping gain to map the EMG linear envelope to an actuation voltage. This constant mapping gain was hand tuned by the researcher. The researcher would tune the gain such that it mapped the peak EMG linear envelope during walking to the saturation voltage of the actuators. We call this max-to-max mapping the calibration mapping gain. The researcher would then scale the calibration mapping gain by 2.0 to encourage a reduction in the user's own muscle recruitment [2]. Because of this scaling, subjects were forced to adapt to walking with a peak muscle recruitment 50% lower than their normal walking muscle recruitment in order to achieve an unsaturated control signal. This technique has resulted in large reductions in metabolic cost; however, the constant mapping gain could be a limiting factor of the controller.

The constant gain constrained the way the user walked in previous ankle exoskeleton studies from

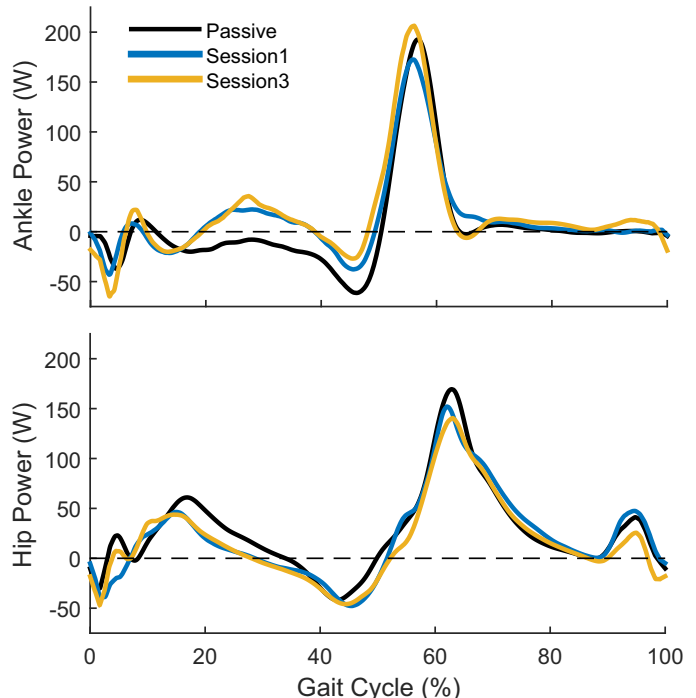


Figure 1: Subjects chose to use more ankle power at the ankle in order to reduce their effort at the hip. Data representing Session 1 and Session 3 were collections that occurred at the end of the powered walking portion of the corresponding testing days.

our lab. The 2.0 scaling of the calibration gain led to a muscle recruitment of the user that may not reflect their preferred manner to walk with the exoskeleton. To overcome this limitation, we developed an EMG based control scheme that frees this mapping gain to *dynamically* adapt to the user as the user adapts to the device. This allows the wearer to use whatever muscle recruitment level they see fit while still receiving maximum unsaturated actuation from the device. By doing so, our adaptive controller refrains from constraining the user to specific dynamics at the ankle. This controller allows us to study what amount of ankle power is preferred by subjects during walking with a robotic exoskeleton. We hypothesized that

subjects would learn to co-adapt with the device in order to achieve a metabolic reduction.

METHODS

For this study, we designed and built a simple one degree of freedom robotic ankle exoskeleton (2.09 kg). The exoskeleton used artificial pneumatic muscles to assist with plantar flexion and was controlled by an off board real-time processor. We used EMG from the user’s soleus to control actuation.

Our controller processed the raw EMG to get the signal’s linear envelope and then conducted a real-time max search of the linear envelope on a stride by stride basis. The detected maximum of each stride was added to a moving average of the previous fifty strides. Our controller then calculated the mapping gain necessary for this moving average to map to a desired maximum actuator voltage. The controller then updated the mapping gain after every stride. In other words, the exoskeleton always operated at its maximal power output while subjects were able to alter the amount of their own soleus recruitment; thereby adjusting the amount of total ankle power.

We tested three subjects (male, $19.3 \pm .7$ years, 70.8 ± 3.7 kg, 182.0 ± 6.6 cm; means \pm s.e.m.) during treadmill walking at 1.2 m s^{-1} . All subjects walked in the device continuously for 50 minutes on three separate training days. Each training day was identical and consisted of 10 minutes of unpowered (passive) walking, 30 minutes of powered (active) walking, followed by 10 minutes of unpowered walking. We collected electromyography, metabolic, kinematic, and kinetic data across all sessions. All joint kinematics and dynamics were processed in OpenSim.

RESULTS AND DISCUSSION

We found that by the end of the third session, our adaptive controller had chosen gains that were a 1.76 ± 0.24 (mean \pm s.e.m.) scaling of the would be calibration mapping gain. Previous studies used a constant scaling factor of 2.0. The scaling results show that subjects opted to

Table 1: Results percent change relative to passive conditions (mean \pm s.e.m.)

Measurement	Session 1	Session 3
Peak Ankle Power	$-15.8 \pm 8.0\%$	$4.9 \pm 8.9\%$
Peak Hip Power	$-8.5 \pm 9.3\%$	$-12.2 \pm 1.0\%$
Metabolic Cost	$-19.0 \pm 6.7\%$	$-24.6 \pm 1.8\%$

use higher peak soleus activity than what was enforced in previous studies with a static mapping gain.

Additionally, subjects chose to increase their peak ankle power across training days when using the adaptive controller. This increase in ankle power was coupled with a decrease in hip power (Figure 1 & Table 1). Because our adaptive controller did not constrain subjects to walk in any specified manner, this trade off between ankle and hip dynamics was discovered by subjects voluntarily. This trade off seen between ankle and hip dynamics is supported by the work of Lewis et al. [3]. We believe subjects adapted to these joint dynamics for their energetic benefits due to the metabolic reduction seen across training days. The energetic benefits from actuating the ankle as opposed to the hip has been shown in simulation by Kuo [4] and supports our findings.

Our results suggest that subjects voluntarily increased effort at the ankle in order to reduce effort at the hip. This finding opens an interesting discussion as to what is the best way of providing assistance to the human gait. Should we be employing similar strategies to intrinsically controlled exoskeletons or prosthesis as opposed to replicating ‘normal’ joint dynamics?

REFERENCES

- [1] DP Ferris et al. *International Journal of Humanoid Robotics*, 4(3):507–528, 2007.
- [2] GS Sawicki et al. *Journal of Experimental Biology*, 211(9):1402–1413, 2008.
- [3] CL Lewis et al. *Journal of Biomechanics*, 41(10):2082–2089, 2008.
- [4] AD Kuo. *Journal of Biomechanical Engineering*, 124(1):113–120, 2002.

IMPLEMENTING A VIRTUAL GAIT ASSISTANCE DEVICE WITHIN A MUSCULOSKELETAL SIMULATION FRAMEWORK

Tunc Akbas and James Sulzer, Ph.D

The University of Texas at Austin, Austin, TX, USA

email: tuncakbas@utexas.edu

INTRODUCTION

Exoskeletons are promising tools for gait assistance in those with neurological impairments [1]. Our goal is to develop exoskeletal assistance for post-stroke Stiff-Knee gait (SKG). We have developed a lightweight, transparent knee flexion actuator intended to assist knee flexion torque during pre-swing in those with SKG after stroke [2]. We initially hypothesized that knee flexion torque assistance would reduce the need for compensatory kinematics such as hip circumduction. However, our results showed that circumduction increased during assistance in people with SKG compared to healthy controls [3]. We concluded that abnormal coordination patterns following stroke, independent from biomechanics, were responsible for this finding.

The suspected abnormal coordination patterns could be involved in any number of superficial or deep musculature, some of which were not detectable using surface electromyography (sEMG). Musculoskeletal simulation packages such as OpenSim have become a powerful complement to experimental approaches, with the ability to estimate muscle activations that may be difficult to directly measure. As such, our goal is to simulate the activation dynamics resulting from exoskeletal assistance in those with SKG to uncover these abnormal coordination patterns. Here we introduce the challenges involved in this novel neuromuscular simulation of exoskeletal gait assistance.

METHODS

The active knee brace (Figure 1a) was used by nine stroke patients with SKG and five healthy controls on an instrumented treadmill using a motion capture system to monitor lower body kinematics. The hip and knee flexion torque assistance was provided during the preswing phase. We encountered a number of challenges while integrating this data

into OpenSim, including adjustment of motion capture data, application of the external device, and accounting for unmeasured handrail forces and torques. We used the reduced residual algorithm (RRA) [4], and inverse dynamics approaches to assure dynamic consistency and obtain the joint moments, respectively.

OpenSim assumes a full-body marker set where all markers are fixed to the human model. However, our experimental data only constituted a lower body marker set, with left thigh and knee markers on the actuator. Patients also wore ankle-foot orthoses (AFOs) that reduced ankle mobility. To account for these factors, we condensed the weight of the torso to the pelvis and reduced the marker weightings on the orthosis to account for the non-rigid connection to the body. For patients with SKG, we fixed the ankle joint of the impaired side perpendicular to the shank to accurately model the aforementioned kinematic constraint.

The assistive device, which provides a torque couple for hip and knee flexion, is modeled as external force couples at the femur (thigh) and tibia (shank). These couples are applied in opposite directions to provide hip flexion and knee flexion torques (Fig. 1) and set with equal distance from the center of mass of the corresponding bodies (Fig. 1c). The simulated torque assistance is calculated using Eq. 1 and added as an external force to the RRA algorithm (Eq. 2).

$$\tau_{device} = \sum_{i=1}^4 F_i \times d \quad (1)$$

$$\sum_{i=1}^{11} m a = F_{GRF} + \tau_{device} + F_{residual} \quad (2)$$

Where τ_{device} is the experimental torque measure from the device, F_{GRF} is the ground reaction force vector, $F_{residual}$ is residual forces and moments, F_i is the decomposed force couples of the device and d is the distance of these force couples from the center of mass of the corresponding bodies.

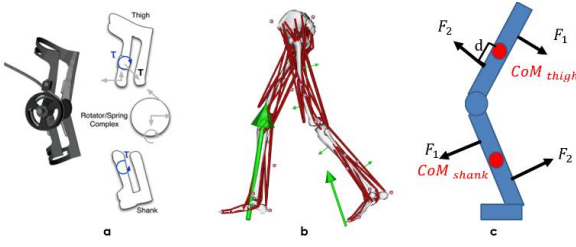


Figure 1: **a.** Free body diagram of the device **b.** Implementation of the device in OpenSim **c.** Free body diagram of the modeled external forces

We validated the model by comparing the simulated torque at the knee with and without modeled assistance to the measured torque at the brace (Fig. 2). The maximum average RMS error was below 0.002 Nm.

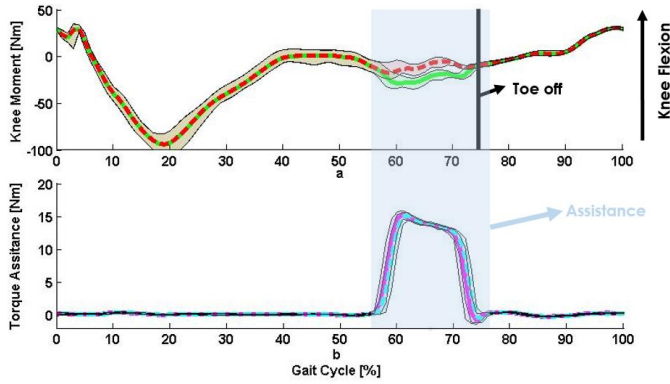


Figure 2: **a.** Averaged knee joint moments obtained from RRA analysis with (dashed line) and without (solid line) the introduction of the device **b.** Modeled assistance (dashed line) and the assistive torque measured by the experiments (solid line)

Another challenge was accounting for unmeasured unilateral handrail use of stroke patients that would reduce the accuracy of the model. In recent studies it has been shown that handrail forces in the vertical direction can be successfully estimated using residual forces [5]. But the residuals may have originated from various sources such as inaccessible movement artifacts in the upper body or inconsistencies between marker data and force plate readings. Therefore, we subtracted the difference between the forces and torques generated by the body kinematics and ground reaction forces to account for handrail support. We then applied these forces and torques on the pelvis segment to model the handrail support. The following equations were

used to obtain the differences between forces and torques:

$$F_{total} = \sum_{i=1}^{11} ma, \quad F_{diff} = F_{total} - F_{GRF} \quad (3)$$

$$\tau_{diff} = \sum_{i=1}^{11} \frac{d\bar{H}}{dt} - \hat{r} \times F_{GRF} \quad (4)$$

$$\sum_{i=1}^{11} ma = F_{GRF} + \tau_{device} + F_{residual} + \tau_{diff} + F_{diff} \quad (5)$$

Where i is the index of the corresponding body in the OpenSim model, F_{diff} and τ_{diff} are force and torque differences between the body kinematics driven equations and ground reaction forces, \bar{H} is the angular momentum and \hat{r} is the position vector from the contact point to center of mass (CoM) location.

RESULTS AND DISCUSSION

To verify the dynamic consistency of our simulations we compared the average residuals of the initial model (absence of modeled device and handrail force feedback) and modified model of a stroke patient. All of the residuals were decreased by considerable amount (Table 1) except the residual moment around x -axis (M_x), which is negligible (0.85 Nm). Using these methods on a larger data set, we intend on delineating the neuromuscular mechanisms of abnormal muscle coordination in people with SKG. We believe neuromuscular simulation could be a valuable tool in development of exoskeletons for those with post-stroke SKG and similar neuromuscular impairments.

REFERENCES

1. Mertz L., *Pulse*, IEEE 3.4, 56-61, 2012.
2. Sulzer JS, et al. *Robotics*, IEEE Transactions on 25.3, 539-548, 2009.
3. Sulzer JS, et al. *Stroke* 41.8, 1709-1714, 2010.
4. Delp SL, et al. *Biomedical Engineering*, IEEE Transactions on 54.1, 1940-1950, 2007.
5. Knarr BA, et al. *ASME 2012 Summer Bioengineering Conference*. Fajardo, Puerto Rico, 2012.

Table 1: Average residuals from initial and modified model and average residual threshold values provided by OpenSim.

	F_x	F_y	F_z	M_x	M_y	M_z
Initial Model	10.34 N	40.80 N	1.72 N	1.03 Nm	1.21 Nm	4.39 Nm
Modified Model	3.48 N	0.16 N	0.69 N	1.88 Nm	0.22 Nm	0.20 Nm
Residual Thresholds	5-10 N	5-10 N	5-10 N	0-30 Nm	0-30 Nm	0-30 Nm

SURVEYING THE INTEREST OF INDIVIDUALS WITH UPPER LIMB LOSS IN NOVEL PROSTHETIC CONTROL TECHNIQUES

Susannah M. Engdahl, Breanne P. Christie, Brian Kelly, Alicia Davis, Cynthia A. Chestek, Deanna H. Gates

University of Michigan, Ann Arbor, MI, USA

email: sengdahl@umich.edu web: <http://rehab-biomech-lab.kines.umich.edu/>

INTRODUCTION

Acquiring reliable control signals for upper limb prostheses is a challenge that obstructs further development of advanced devices. Recent research has focused on ways to collect control data by interfacing directly with the nervous system. These efforts fall into three categories: targeted muscle reinnervation (surgically moving nerves to residual muscles in the missing limb to create additional control sites) [1], peripheral nerve interfaces (electrodes implanted in the residual limb to record signals directly from the peripheral nervous system) [2], and cortical interfaces (electrode arrays implanted in the brain to record action potentials directly from motor neurons) [3]. Given the surgically invasive nature of these techniques, it is important to understand whether individuals with upper limb loss are willing to try them. The goal of this work was to evaluate the general interest in surgically invasive and noninvasive prosthetic control techniques.

METHODS

An anonymous online survey was made available to individuals over age 18 with a major upper limb amputation. The survey contained closed and open-ended questions regarding interest in four prosthetic control techniques: myoelectric control, targeted muscle reinnervation, peripheral nerve interfaces, and cortical interfaces. Participants viewed a simple drawing and a brief explanation of each technique, along with a description of any associated medical procedures and potential risks. Participants were then asked to rate their likelihood of using the technique at each of six theoretical performance levels, which were roughly ordered from basic to advanced (Fig. 1). Participants were also asked to rate the overall importance of each feature, in order

to gauge their general interest in the features. All responses were collected on a 5-point Likert scale.

A two-way repeated measures analysis of variance with Greenhouse-Geisser corrections was used to examine the effect of technique type and performance level on participants' interest in each technique. Pairwise comparisons were performed using Fisher's Least Significant Difference method.

RESULTS AND DISCUSSION

A total of 104 responses were collected. The mean age was 47 ± 15 years and 67% were male. Most participants (92%) had unilateral limb loss, which primarily occurred at the transradial and transhumeral levels. Trauma was the most common reason for limb loss.

When the responses were collapsed across all six performance levels, participants expressed the most interest in myoelectric control and the least interest in cortical interfaces. Out of all 104 participants, 83% responded positively to the myoelectric control. Only 39% responded positively to the cortical interfaces, while targeted muscle reinnervation and peripheral nerve interfaces were roughly equivalent (63% and 68%, respectively).

We anticipated that participants would be more likely to try each prosthetic control technique if it offered higher levels of functionality. However, the initial responses did not follow this expected trend – participants generally responded less positively to more advanced performance levels (Fig. 1). A similar trend was present in participants' theoretical interest in each performance level (Fig. 1). To address this concern, we altered the wording to be explicitly cumulative. Thirty-five participants used the original “discrete” wording of the performance levels (Fig. 1A) and 69 used the subsequent

“cumulative” wording (Fig. 1B). Changes in the wording did not substantially affect our findings: there were significant differences in participants’ interest in different performance levels for both the discrete ($p = 0.008$) and cumulative ($p = 0.031$) wording. This fact strengthens our findings, suggesting that participants truly viewed the advanced features as less important.

Written comments from the participants revealed that common concerns regarding myoelectric control included weight, difficulty of use, cost and

durability. The inherent risk of surgery with the other interfaces was difficult for many participants to accept. However, some respondents reported that the potential benefits would justify the surgical risks and recovery time.

The results of this work will be instrumental in the development of advanced devices that are appealing to individuals with upper limb loss. Larger studies investigating the relationship between demographic factors and interest in novel prosthetic control techniques are still needed to fully inform the design of future devices.

REFERENCES

1. Kuiken TA, et al. *J Am Med Assoc* **301**, 619-628, 2009.
2. Urbanek MG, et al. *Plast Reconst Surg* **130**, 55-56, 2012.
3. Chestek CA, et al. *J Neural Eng* **8**, 2011.

ACKNOWLEDGMENTS

Support was provided by a University of Michigan Office of Research Grant. D. Gates is supported by the NIH under K12HD073945. S. Engdahl is supported by the NSF Graduate Research Fellowship Program under DGE 1256260.



Figure 1: Percentage of positive (“likely” or “very likely”) responses for each technique, shown separately for the discrete (A) and cumulative (B) wording. The rightmost column shows the percentage of participants who indicated a feature was “important” or “very important”. (MYO = myoelectric control, TMR = targeted muscle reinnervation, PI = peripheral nerve interface, CI = cortical interface)

QUICK, LOW-COST, SENSITIVE MOTOR ASSESSMENT USING MARKERLESS MOTION CAPTURE

^{1,2}Steven K. Charles, ²Paula Johnson, and ¹Clay Kincaid

¹ Mechanical Engineering and ²Neuroscience, Brigham Young University, Provo, UT
email: skcharles@byu.edu, web: neuromechanics.byu.edu

INTRODUCTION

There is a nationally recognized need for more sensitive motor assessments to evaluate and diagnose motor impairments following traumatic brain injury (TBI). Conventional motor assessments rely on subjective observations and often fail to detect subtle impairments common in TBI. The purpose of our research is to 1) develop a quantitative motor assessment (QMA) that is quick, low-cost, and highly sensitive, and 2) establish a normative database to allow comparison of a patient's motor assessment relative to a healthy norm.

To this end, we developed a system to administer traditional motor tests using low-cost markerless motion capture. Our system consists of an \$80 Leap Motion sensor and custom software (Figure 1). This system automates traditional motor tests and measures the position of finger tips with a resolution of 0.01mm and a sampling frequency of 100Hz. We have seeded a normative database by administering this QMA to 50 control subjects.



Figure 1: Test setup. For most tests (A), subjects pointed to objects on a screen while a Leap Motion sensor (C) captured their movements. In the balance test (B), subjects' head sway was extracted from the motion of dowels attached to a helmet.

METHODS

Fifty healthy, right-handed subjects (age range 18-30 years; 23 females, 27 males) completed five QMA tests (described below). To allow for comparison with traditional assessments, we included 3 traditional tests as well: Halstead-Reitan Finger Tapping Test, grip strength, and the Beery Visual Motor Integration Test. Tests were performed in random order. Positions and velocities of the finger tips and palm were recorded at 100 Hz. Movements were performed by both hands. The entire assessment required 1 hour 45 minutes.

Each subject performed the following QMA tests:

Finger Oscillation Test

- Participants were instructed to make oscillatory finger movements as fast as possible for 10s
- Subjects received visual feedback of their finger location on a graphical user interface (GUI) (Figure 2A) and needed to oscillate their finger above and below a band to achieve a tap
- Subjects needed 5 trials within 5 oscillations of each other (10 trials max)
- 30-90s rests between trials

Visually Guided Movement

- Subjects moved the tip of their index finger, represented as a red dot, as quickly as possible to targets appearing in random order (Figure 2B)
- The next target appeared after the finger had rested on the target for 500ms.

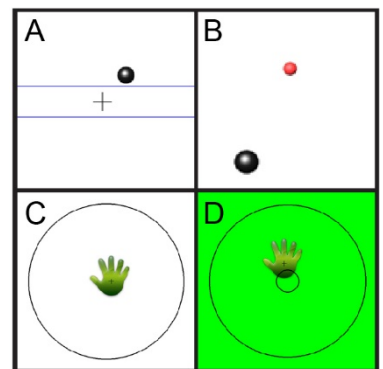


Figure 2: Graphical User Interface for QMA tests: finger oscillation (A), visually guided movements (B), postural tremor (C), and reaction time (C-D).

- Two trials, each with 12 paths executed 5 times in random order were completed

Postural Tremor

- Participants were instructed to hold their hand over the motion capture sensor with palm down and fingers spread (Figure 2C)
- Two trials of 30s each for each hand

Reaction Time

- Participants held their hand over the sensor (Figure 2C)
- Subjects were instructed to remove their hand as quickly as possible as soon as the background color changed from white to green (Figure 2D)

Balance

- Participants stood with feet together and hands across the chest for 30s (Figure 1B)
- Five different trials were completed, each in a different pose
 - Hard surface eyes open
 - Hard surface eyes closed
 - Soft surface eyes open
 - Soft surface eyes closed
 - Tandem stance, preferred foot in front

The data from each test were analyzed to extract test-specific measures (Table 1). Together these measures form a normative database against which patients' QMA results can be compared to evaluate the degree of their impairment.

RESULTS AND DISCUSSION

Being normative data from young, healthy subjects, the QMA results were generally stereotyped, with few differences between men and women or dominant and non-dominant hands (Figure 3).

Novel markerless motion capture technology allows for collection of an abundance of quantitative movement information. Using this technology and the associated normative databases will allow for

quick, low-cost, and highly sensitive motor assessment in clinical settings, which we expect will result in improved diagnosis, prognosis, and rehabilitation following TBI. Because of the gaming industry, markerless technology is bound to continue to improve, creating more sensitive instruments. This QMA and its normative database will be available. We invite others to take advantage of it and contribute to the database.

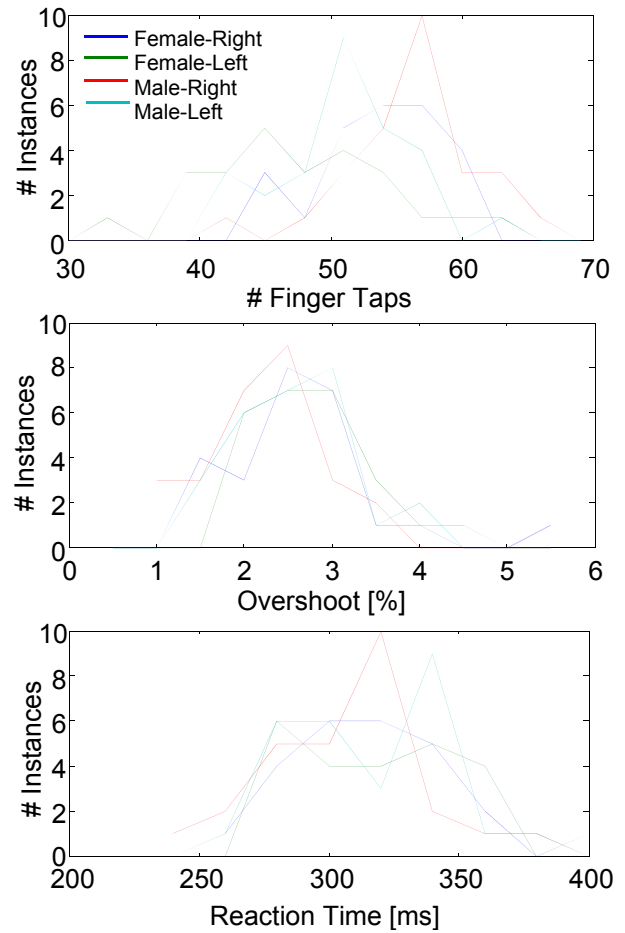


Figure 3: Histograms of QMA measures for the finger oscillation (top), visually guided movement (middle), and reaction time (bottom) tests.

ACKNOWLEDGEMENTS

Utah NASA Space Grant Consortium and EPSCoR

QMA Test	Behavioral Attributes	Measures
Finger Oscillation	Strength, movement efficiency	Number and regularity (approximate entropy) of taps
Visually Guided Movements	Visuomotor control, kinetic tremor	Dysmetria, duration, smoothness, power spectrum area
Postural Tremor	Tremor, chorea, strength, impersistence	Area under power spectrum between 4 and 12 Hz
Reaction Time	Processing time	Reaction time
Balance	Postural stability	Mean path, max. excursion of the crown of the head

Table 1: Each QMA test was designed to assess particular behavioral attributes that were defined and quantified as measures.

PORTABLE MYOELECTRIC BRACE USE IN CHRONIC, POST STROKE HEMIPARESIS

Nienke W. Willigenburg, Michael P. McNally, Nathan D. Schilaty, Timothy E. Hewett, Stephen J. Page
Sports Health and Performance Institute & Health and Rehabilitation Sciences
The Ohio State University, Columbus (OH), United States
email: nienkewilligenburg@gmail.com

INTRODUCTION

Stroke frequently causes debilitating upper extremity (UE) motor impairments that are retained well beyond rehabilitation discharge. Several UE motor rehabilitative approaches have been developed, with most adhering to the P.R.A.C.T.I.C.E. principles¹. Yet, many promising UE rehabilitative strategies²⁻⁴ are only efficacious in individuals already exhibiting high levels of active, paretic UE movement; only a small portion of the growing stroke survivor population.

Reduced UE impairment and increased function were reported among survivors with moderate UE impairment participating in repetitive task-specific practice (RTP) that integrated a portable, electromyography (EMG) triggered, brace ("Myomo")⁵⁻⁷. We wished to compare the efficacy of this regimen with the use of RTP only (the standard of care in most outpatient environments) while concurrently characterizing the motor behavior of stroke survivors exhibiting moderate UE impairment.

METHODS

Subjects: Twelve subjects gave written consent to participate (4 males; age=53.5±5.35 years; mean time post-stroke=61.7 months; 11 Caucasians, 1 African-American; 6 left-sided strokes; 10 ischemic strokes; 1 basal ganglia stroke; 3 strokes in the left-middle cerebral artery; 1 in the frontal lobe; 2 in the parietal lobe; 5 in unspecified locations). They were randomized into two groups: 7 subjects were administered RTP+Myomo, and 5 RTP-only.

Apparatus: The Myomo e100 (Fig. 1) is an FDA approved, lightweight (~2lbs), myoelectric brace that uses surface EMG signals from the biceps and triceps brachii from active paretic UE movement attempts to assist the active muscle with movement

of the paretic UE⁷. A treating therapist can adjust the system parameters to alter the amount of mechanical assistance provided.



Figure 1. Myoelectric brace used in the study.

Intervention: Both groups (RTP+Myomo and RTP-only) participated in individualized, 45-minute therapy sessions occurring 3 days/week over an 8-week period. As described previously⁷, the intervention's design and therapy session content involved progressive difficulty in tasks. In all cases, the latter tasks were selected collaboratively with the patient, caregiver, and therapist. With or without the Myomo, chosen tasks were functional/goal directed, integrating the paretic UE into whole-arm tasks that were salient to the subject. Therapy included both bilateral and unilateral UE tasks, and included components of muscle control, coordination, strength, endurance, and proprioception.

Behavioral data: We administered the Stroke Impact Scale (SIS); a 64-item self-report measure. For this study, we focused on changes in the paretic UE (SIS arm and hand scales), ability to perform activities of daily living, and recovery scales.

Kinematic data: An 11-camera motion capture system (Motion Analysis Corporation Raptor-12 system, Santa Rosa, CA, USA) tracked 3D-motion of subjects' paretic and less affected UEs during the experimental tasks. Twenty-six reflective markers were placed on the upper body (Fig. 2). Each subject performed 5 repetitions of two reaching

tasks with the paretic and non-paretic UE. For the ‘reach-out’ task, a cylinder-shaped object was placed in front of the subject on the table, aligned with the subject’s sternum at 2/3 of paretic UE length. For the ‘reach-up’ task, the same object was elevated by 24 cm. Subjects were instructed to reach for the object as if they were reaching for a glass of water, without specific instructions on movement speed. Joint angles were calculated based on a standard UE model and conventions for the shoulder joint.⁸ Main outcome measures were shoulder flexion (range), elbow extension (range) and hand velocity (peak).

Statistics: Mann Whitney U tests compared all behavioral and kinematic changes between intervention groups.

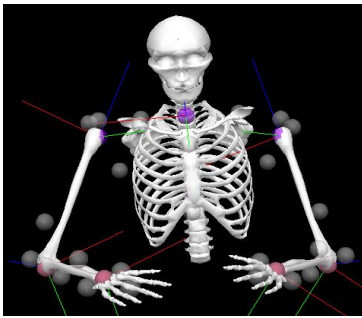


Figure 2. Kinematic model of subject in the starting position

RESULTS AND DISCUSSION

Subjects administered RTP+Myomo tended to exhibit larger improvements on all scales than subjects administered RTP-only. This difference between groups reached significance for SIS recovery ($U=4$, $p=0.032$, point probability=0.015), and came close to significance for SIS ADL ($U=6$, $p=0.061$, point probability=0.001).

None of the subjects were able to grasp and lift the object with their paretic limb. Therefore, kinematic analyses focused on the reaching part of the movement, which ended when the hand touched the object. When subjects were unable to touch the object, we analyzed the full attempt. Most patients demonstrated improved capability to move the object after completing the intervention. The change in hand velocity from pre-test to post-test in the ‘reach-up’ task was significantly larger in the RTP-only group compared to the RTP+Myomo group ($U=3$, $p=0.018$, point probability=0.04). None of the other changes in kinematic variables from pre-test

to post-test were significantly different between groups (all $p>0.53$).

A trend towards a significant correlation was observed between the change in the SIS arm subscale and the change in range of elbow extension during the reach up task. However, Spearman’s correlation coefficient was negative ($\rho=-0.57$, $p=0.054$), which indicates that subjects with larger elbow range of motion while reaching up tended to report lower arm function SIS scores. None of the changes in other kinematic variables significantly correlated with any of the changes in SIS subscales (all $p\geq 0.12$).

CONCLUSIONS

RTP integrating myoelectric bracing might be more beneficial than RTP only in improving subjects’ perceptions of their overall recovery. This approach does not convey superior benefits to RTP only in terms of UE kinematics, and no significant correlations were observed between changes in self-reported outcomes and reaching kinematics. Our findings suggest that clinicians may be able to reduce the debilitating impact of moderate UE impairment using RTP+Myomo.

REFERENCES

- [1] S. Page and H. Peters, “Mental practice: applying motor PRACTICE and neuroplasticity principles to increase upper extremity function,” *Stroke*, vol. 45, no. 11, pp. 3454–60, Nov. 2014.
- [2] S. J. Page, P. Levine, and A. Leonard, “Mental practice in chronic stroke: results of a randomized, placebo-controlled trial,” 2007.
- [3] S. J. Page, P. Levine, A. Leonard, J. P. Szaflarski, and B. M. Kissela, “Modified constraint-induced therapy in chronic stroke: results of a single-blinded randomized controlled trial,” *Phys. Ther.*, vol. 88, pp. 333–340, 2008.
- [4] T. J. Kimberley, S. M. Lewis, E. J. Auerbach, L. L. Dorsey, J. M. Lojovich, and J. R. Carey, “Electrical stimulation driving functional improvements and cortical changes in subjects with stroke,” *Exp. Brain Res.*, vol. 154, pp. 450–460, 2004.
- [5] J. Stein, K. Narendran, J. McBean, K. Krebs, and R. Hughes, “Electromyography-controlled exoskeletal upper-limb-powered orthosis for exercise training after stroke,” 2007.
- [6] S. J. Page, V. Hill, and S. White, “Portable upper extremity robotics is as efficacious as upper extremity rehabilitative therapy: a randomized controlled pilot trial,” *Clin. Rehabil.*, vol. 27, no. 6, pp. 494–503, Jun. 2013.
- [7] S. J. Page, V. H. Hermann, P. G. Levine, E. Lewis, J. Stein, and J. DePeel, *Portable neurorobotics for the severely affected arm in chronic stroke: a case study*, vol. 35, 2011, pp. 41–46.
- [8] G. Wu, F.C.T. van der Helm, H.E.J. Veeger, et al., “ISB recommendation on definitions of joint coordinate systems of various joints for the reporting of human joint motion-Part II: shoulder, elbow, wrist and hand,” 2005. *J Biomech.*, vol. 38, pp. 981–9

IMPROVING FINGER MOVEMENT REPERTOIRE IN STROKE

Rajiv Ranganathan

Michigan State University, East Lansing, MI, USA

email: rrangana@msu.edu, web: <https://sites.google.com/site/motrelab/>

INTRODUCTION

Stroke often results in an impairment of hand function, which severely impairs activities of daily living [1]. One common deficit that is observed after stroke is a loss of finger independence [2], which is associated with reduced hand dexterity. The purpose of the current study was to examine if we could use a body-machine interface to increase the repertoire of finger movements in stroke survivors. Specifically, we examined if we could elicit different patterns of finger movements by manipulating which finger motions contributed to task performance.

METHODS

Participants were 8 chronic stroke survivors (mean 7 years after stroke) who had mild to moderate deficits in hand function as quantified by the Chedoke-McMaster test of hand function. Participants wore an instrumented glove (Cyberglove, Cyberglove Systems, San Jose, CA) which measured finger kinematics of the affected hand. The motions at the MCP joint of the index, middle, ring and little fingers were mapped to the horizontal motion of a cursor on a screen [3]. The task of the participants was to move the cursor between two targets shown on the screen (Fig. 1).

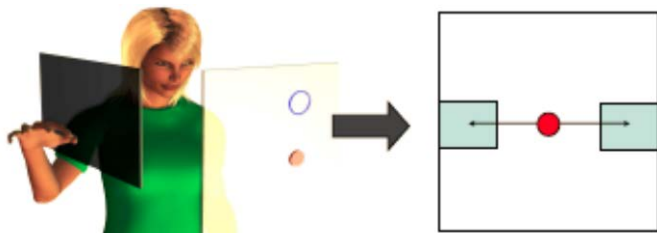


Figure 1: Finger kinematics were mapped on to the horizontal position of a cursor (shown in red). The task was to move the cursor between two targets.

The critical manipulation in the experiment was to alter the mapping between the finger motions and the motion of the cursor. Initially, all fingers were given uniform weights so that the typical power grasp motion (where all fingers jointly perform flexion and extension with no finger individuation) could be used to perform the task. However, after the first 25 trials, the weights were gradually altered over the next 25 trials so that this motion was shifted to the null space (i.e. performing the same power grasp motion now resulted in little to no motion of the cursor). At this point, participants had to reorganize their finger coordination, and find an alternative coordination pattern to continue moving the cursor to the remaining 50 targets. Each session took about 1 hour and participants performed the task for 5 sessions spread over 2.5 weeks. Here, we focus only on the first (Pre) and last session of practice (Post).

We used the path length (i.e. the distance traveled by the cursor in going from one target to another) as a measure of task performance. In order to examine the reorganization in the coordination pattern, we used principal component analysis (PCA) on the finger kinematics. Specifically, we examined the change in the first principal component (which accounts for the most variance) using a dot product.

RESULTS AND DISCUSSION

Task performance (as measured by the path length) showed significant increases as the weights changed, indicating that participants were engaged in exploration of different coordination patterns while attempting to move the cursor between the two targets. The amount of this exploration was significantly reduced at the last session of practice, indicating that participants were now able to switch to a different coordination pattern more quickly (Fig. 2).

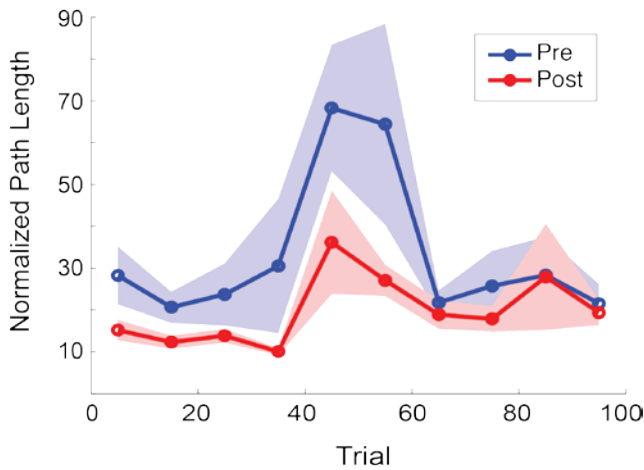


Figure 2: Path length of the cursor (summed over 10 trials) during the experiment. Trials 1-25 indicate the uniform weights for each finger, 26-50 indicate the gradual transition to the new weights, and 51-100 indicate the performance with the new weights. A lower value indicates fewer reversals in cursor direction when moving between targets.

In terms of the coordination patterns (as measured by the PCA), we found significant changes in the dominant coordination mode (i.e. PC1) as participants transitioned from the old weights to the new weights. The average change was about 20 degrees, both initially in practice as well as the final session of practice (Fig. 3).

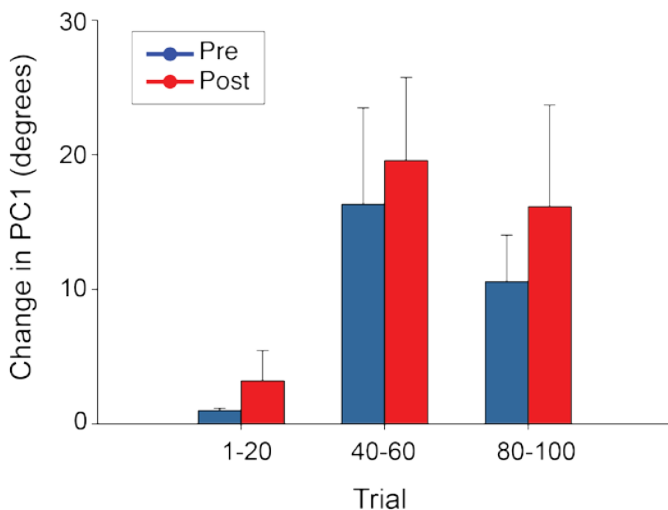


Figure 3: Change in the first principal component during the experiment both in the first and last session of practice. There was a significant increase in the angle when the weights were changed indicating reorganization of coordination patterns.

These results show that stroke participants are able to reorganize their finger coordination patterns when provided with appropriate feedback in a game-like environment. Specifically, participants were able to move out of the dominant non-individuated pattern that is normally seen in stroke, and were able to not only learn but also retain these new coordination patterns to solve the task.

CONCLUSIONS

The results here suggest that the paradigm described here has potential for the rehabilitation of hand function in participants with mild to moderate deficits. Given that the changes here are implicit (i.e. no explicit instruction was given regarding the finger coordination pattern), this paradigm could be combined with game-like environments and virtual reality [4] to improve hand movement repertoire and facilitate rehabilitation in stroke.

REFERENCES

1. Hunter SM, et al. *Reviews in Clinical Gerontology* **12**, 68-81, 2002.
2. Lang CE, et al. *J Neurophysiol* **90**, 1160-1170, 2003.
3. Mosier KM, et al. *J Neurophysiol* **94**, 4362-4372, 2005.
4. Adamovich SV, et al. *Neurorehabilitation* **25**, 29-44, 2009.

ACKNOWLEDGMENTS

This work was supported by a grant from the National Institutes of Health (NIH R03HD 069806). We also thank Meghan Buell, OT for her assistance.

SCAPULAR KINEMATIC IS ALTERED AFTER ELECTROMYOGRAPHY BIOFEEDBACK TRAINING

¹ Jun G. San Juan, ¹ Samantha R. Gunderson, ¹ Kai Kane-Ronning and ¹ David N. Suprak

¹ Western Washington University, Bellingham, WA, USA
email: jun.sanjuan@wwu.edu

INTRODUCTION

Electromyography (EMG) biofeedback training has become a more useful tool with rehabilitation of subacromial impingement syndrome. Biofeedback affords patients a better sense of different muscle activations involved in the movement of the shoulder girdle [1]. It is important to address scapular kinematics in the healthy population, because those who have daily routines involving large amounts of lifting at shoulder level or higher are at a heightened risk of developing subacromial impingement syndrome (SAIS) [2]. Understanding the effects of scapular stabilization exercises in order to prevent subacromial impingement syndrome to these population is beneficial. As a result, the aim of this study was to investigate the effects of scapular stabilization exercises with EMG biofeedback training in scapular kinematics.

METHODS

Nineteen healthy subjects (14 males, 5 females) volunteered for the study. The mean age was 22.9 ± 3.1 y/o, mean height of 1.76 ± 0.1 m and mean mass of 75.1 ± 11.0 kg. To measure muscle activation, a Noraxon Telemetry DTS (Gain 500, CMRR > 100dB, input impedance > 100Mohm) was utilized and sampled at 1500 Hz. The EMG data were normalized using maximum voluntary isometric contraction (MVIC) for all the muscles tested. Bipolar surface electrodes were placed parallel to the muscle fibers of the upper and lower trapezius, serratus anterior, and lumbar paraspinals of the dominant arm with an inter-electrode distance of 2.0 cm (Figure 1). The EMG data were displayed on a stationary overhead projector connected to a PC-type of computer using MR3.4 MyoMuscle software (Figure 1). A Polhemus Fastrak magnetic tracking device was used to measure 3-dimensional scapular kinematics. The receivers were attached to

the spine of the scapula using a customized scapular jig, sternum (inferior to the jugular notch), and distal humerus (Figure 1). A Polhemus sensor pen was utilized to digitize the spinous process of C7, T1, T7, and T8, the sternal notch, the sternoclavicular joint, and lateral and medial epicondyles of the humerus to set-up the coordinate system following the standard set by the International Society of Biomechanics [3].

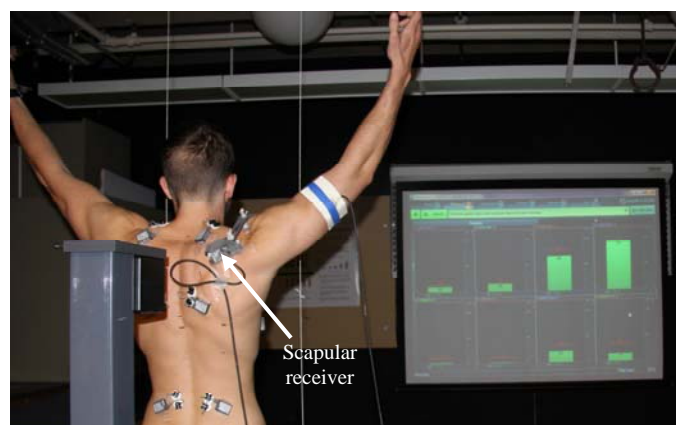


Figure 1: EMG and Magnetic tracking device set-up.

A customized LabVIEW program was utilized to collect and analyze scapular kinematics. The kinematics data were sampled at 40 Hz. After a standardized warm-up protocol, subjects underwent scapular kinematic testing before and after biofeedback training that consisted of three humeral elevation trials in the scapular plane. Subjects were afforded to practice humeral elevation trial before the data collection commenced. Then EMG biofeedback began with scapular stabilization exercises (I, W, T, Y) performed at 1 set of 10 repetitions (Figure 2). Subjects were told to actively try and reduce the muscle activation shown on the screen for the upper trapezius during the exercises. A two-way repeated measures ANOVA was utilized to compare scapular kinematics before and after the EMG biofeedback scapular stabilization exercises.

The independent variables were humeral elevation (30°, 60°, 90° & 110°) and time (Pre and Post biofeedback training). The dependent variable was scapular kinematics. Alpha level was set to 0.05.



Figure 2: Scapular stabilization exercises (I, W, T, Y)

RESULTS AND DISCUSSION

There was a statistically significant difference at all humeral elevation angles during scapular external rotation ($p < 0.004$) between times (Figure 3). After the exercises, the scapula was in a more externally rotated orientation with a mean difference of 6.8 degrees. There were no significant differences found for scapular upward rotation and posterior tilt at all humeral elevation angles between times.

We hypothesize a significant change in scapular kinematics after EMG biofeedback training. The current study's result was able to observed changes in scapular kinematics after the scapular stabilization exercises. Scapular kinematics is altered by EMG biofeedback training. However, only external rotation was significantly affected by the exercises. We did not see any significant differences in upward/downward rotation and anterior/posterior tilt of the scapula. According to the literature, increase in subacromial space can be attained by an increase in upward rotation, external rotation and posterior tilt of the scapula during humeral elevation. It can decrease the chance of

SAIS. The change in external rotation observed in the current study can be attributed to the exercises implemented, which targeted the serratus anterior. The action of the serratus anterior muscle is to prevent scapular “winging” or excessive internal rotation of the scapula. The exercises used in this current study combined with EMG biofeedback has a valuable effect in preventing shoulder pain.

CONCLUSIONS

Scapular stabilization exercises together with EMG biofeedback can help change scapular kinematics in healthy individuals. A more externally rotated scapula might result in an increase in subacromial space that can be beneficial in decreasing the development of subacromial impingement syndrome. Workers that necessitate large amount of lifting above their shoulder and overhead athletes (e.g. pitchers, tennis players) will benefit from these type of exercises for shoulder injury prevention.

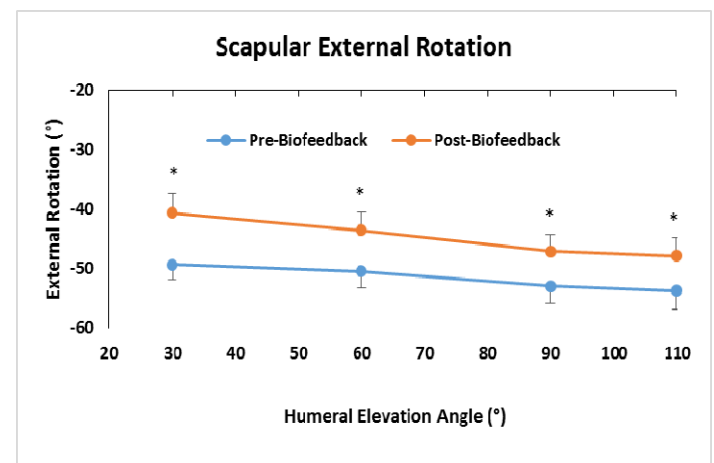


Figure 3: Scapular external rotation before and after EMG biofeedback training.

REFERENCES

1. Holtermann BE, et al. *J of Electromyogr Kines* **20(2)**, 359-365, 2010.
2. Lewis JS, et al. *J Orthop Sports Phys Ther* **35(2)**, 72-87, 2005.
3. Wu G, et al. *J Biomech*, **38(5)**, 9881-992, 2005.

ACKNOWLEDGEMENTS

We would like to thank Jennifer Estep and Zoe Geiger for assistance with data collection.

USING SENSORS TO IMPROVE SPORT SAFETY

¹ Stefan M. Duma and ¹ Steven Rowson

¹ Virginia Tech, Department of Biomedical Engineering and Mechanics
Blacksburg, VA, USA

email: Headbiomed@vt.edu, web: www.vt.edu/helmet

INTRODUCTION

In the fall of 2003, Virginia Tech became the first collegiate football team to utilize wireless helmet mounted accelerometer systems [1]. Throughout the next decade, over 2,000,000 head impact data points were collected on football teams across the country using the same Head Impact Telemetry (HIT) technology (Simbex) [2]. This abstract provides a very brief discussion of this research area and introduces the future Sensor STAR system that will help guide the widespread implementation of sensors in all sports.

FOOTBALL HELEMET SENSORS

The original HIT system consists of six accelerometers that are mounted in the crown of the football helmet. The individual sensors are used to calculate linear and rotational head acceleration values for each head impact. These data are relayed in real time to a sideline controller that can then alert the medical staff if there is a high impact. These alerts are not diagnostic, but simply a page to a beeper to alert the physicians of a high impact. Over the past decade, multiple systems have been developed by Simbex and used throughout all ages of football (Figure 1) [3].

The sensor data has proven dramatically valuable and has resulted in two specific sport safety improvements. First, the data on youth football was used to provide guidelines for safer practice structures that were adopted nationally by Pop Warner [4,5]. Second, these data were used to develop advanced concussion risk functions and subsequently the Virginia Tech helmet rating program that has resulted in improved helmet design [6,7,8,9]

SENSOR STAR

Over the past several years, there has been an explosion of new head impact measuring systems. Many of these will allow for data collection in non-helmeted sports and in particular will allow for data collection in female sports (Figure 2). In order to evaluate the effectiveness of these new sensors, we have introduced the Sensor STAR program. This program will utilized a three step process to access the accuracy of the sensor systems.

The first step of the process will be to mount the sensors onto a dummy head form and subject the system to a range of impact severities and impact directions. The new sensor data will be compared to the reference data measured at the center of gravity of the head form. It is important to note that we are looking for reasonably accurate systems and not perfect systems, as those may never exist for wide-spread volunteer use. For example, a sensor with a 10% error would measure 45g or 55g for an impact with a 50g reference value. There is no meaningful difference between these three impact values.

Once a sensor has passed the first step, the second level includes evaluation on volunteers during low level impact events, such as heading soccer balls. This evaluation will evaluate the sensors ability to trigger and count impacts correctly. This is particularly important as the head impact counts are being used to modify league rules, and the need to be reasonably accurate prior to rule changes. The last level of evaluation will utilize high impacts on human surrogates to evaluate the sensor's ability to accommodate surface interaction conditions. The Sensor STAR information will be provided on-live via our ratings web page: www.vt.edu/helmet



Figure 2: New sensor technologies will allow for widespread data collection on female and youth athletes in non-helmeted sports. A female subject is shown with Triax Technologies headband sensor.

REFERENCES

1. Duma, S. M., *et al*, *Clin J Sport Med.* **15**(1):3-8, 2005.

2. Duma, S. M. and S. Rowson. *Exerc Sport Sci Rev.* **39**(1):2-3, 2011.
3. Daniel, R. W., S. Rowson and S. M. Duma. *Ann Biomed Eng.* **40**(4):976-81, 2012.
4. Cobb, B., *et al*, *Ann Biomed Eng.* **41**(12):2463-73, 2013.
5. Daniel, R. W., S. Rowson and S. M. Duma. *J Biomech Eng.* **136**(9):094501, 2014.
6. Rowson, B., S. Rowson and S. M. Duma. *Ann Biomed Eng.* 2015. DOI: 10.1007/s10439-015-1278-7
7. Rowson, S. and S. M. Duma. *Ann Biomed Eng.* **41**(5):873-82, 2013.
8. Rowson, S. and S. M. Duma. *Ann Biomed Eng.* **39**(8):2130-40, 2011.
9. Rowson, S., *et al*, *J Neurosurg.* **120**(4):919-22, 2014.

ACKNOWLEDGEMENTS

The authors appreciate the support and assistance from the Virginia Tech Department of Biomedical Engineering and Mechanics, the Virginia Tech Institute of Critical Technologies and Applied Sciences, and the Lewis Family Foundation.



Figure 1: Simbex, sold through Riddell, produces a range of helmet mounted technologies that have been used since 2003 to quantify head impact exposure at youth, middle school, high school, and collegiate levels. The original HIT system, the 6DOF system, and the InSite system are shown overlaying youth data collection.

QUANTIFYING FIELD-BASED WARFIGHTER PERFORMANCE VIA A BODY-WORN ARRAY OF WIRELESS INERTIAL SENSORS

¹ Scott G. McLean, ¹ Stephen M. Cain, ² Ryan S. McGinnis, ¹ Steven P. Davidson, ¹ Rachel V. Vitali and ¹ Noel C. Perkins

¹ The University of Michigan, Ann Arbor, MI, USA, ² MC10 Inc., Cambridge, MA, USA
email: smcain@umich.edu

INTRODUCTION

Warfighter performance is inherently challenging to monitor, quantify and ultimately interpret. These challenges originate from the varied and complex tasks that warfighters perform, the underlying variability in human task performance, the environments in which they operate, and a limited knowledge of the measures that truly characterize task performance success/failure. Adding to these challenges are the confounding effects on physical performance due to equipment (e.g., load, bulk and stiffness), task training, and explicit performance degradation. Our ongoing research in this rapidly growing area aims to address these challenges by engineering and evaluating a complete performance approach to quantify and report warfighter performance in naturalistic outdoor environments.

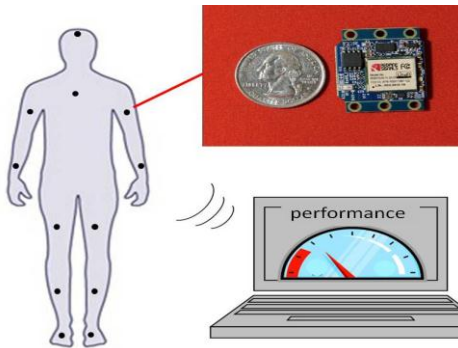


Figure 1: Body-won sensor array for the warfighter

Continued efforts rest on advancing our ongoing research utilizing body-worn arrays of miniature inertial measurement units (IMUs) that synchronously measure and transmit data defining the spatial mechanics of major body segments and their interactions with external equipment. Our current array utilizes up to ten IMU nodes attached to the task-relevant segments/equipment of interest. The IMU data encode the thumbprint of task

performance. For example, during walking or running gait, performance metrics include timing events (e.g., ground contact), gait speed, and explicit segmental dynamics. To date, we have developed an integrated functional IMU array and companion (Matlab™ based) computational algorithms for analysis of select warfighter tasks. Currently the end user is required to have significant expertise in human biomechanics, experimental methods, and software development/manipulation to implement the integrated system in a functional setting. Current efforts aim to mitigate these limitations and extend system capabilities by engineering and evaluating a fully automated measurement system. Our ultimate goal is to deliver an integrated hardware/software system that enables easy and reliable assessment and comparison of warfighter performance. Specifically, we will generate a complete measurement system that discriminates warfighter performance using IMU data within naturalistic (and often random) movement environments encountered by the warfighter.

METHODS

We have collected data on a large number of young healthy subjects, both for the purposes of the IMU-based system validation and to subsequently assess the effects of load-carriage within a simulated warfighter environment [1, 2]. For the purposes of validation, we compared a number of IMU-derived body and segmental kinematical measures during a variety of (e.g., walking, running, jumping, rifle aiming) movement tasks to those obtained via “gold-standard” motion capture techniques. Mocap derived data were generated using or well established methods [3]. Load-carriage effects were evaluated with the validated IMU-system for subjects moving within an outdoor obstacle course. The course was consistent with those adopted

within the military, containing a series of running, jumping, crawling, climbing and rifle aiming tasks. Specifically, subjects completed the course with and without additional (20.5kg) load.

Throughout the testing protocol, subjects had eight wireless IMUs (Opal, APDM, Inc.) secured to specific body segments (feet, shanks, thighs, sacrum, and torso). Each IMU contains a 3-axis accelerometer, angular rate gyro, and magnetometer; a proprietary Kalman filter estimates the directions of gravity and magnetic north relative to sensor-fixed axes. Subjects initial perform calibration movements to determine segment-to-sensor alignments for post-processing purposes.

RESULTS AND DISCUSSION

Results from our extensive efforts to date have yielded four major findings; namely: 1) IMU-derived kinematical measures of human movement accurately replicate those determined from standard motion capture; 2) these kinematical measures distinguish performance in a spectrum of highly relevant warfighter tasks; 3) our chosen performance measures are sensitive to extreme load carriage (e.g., loaded versus unloaded), warfighter fitness and/or task induced performance degradation (e.g., fatigued versus non-fatigued); and 4) IMU technology and the embedded algorithms readily translate to and be largely immune to the inherently random nature of outdoor environments. More specifically, our validation experiments have revealed excellent agreement between IMU and mocap measurements of linear acceleration and angular velocity as well as quantities derived therefrom, including linear velocity and angular orientation. Less accurate, in general, are position estimates, particularly for unconstrained tasks, which is consistent with the raw data being measured by a sensor, as position would be an integrated parameter from the raw velocity and acceleration signals. A key outcome of our obstacle course work, which is particularly relevant to the already encumbered warfighter, is that a rich and highly applicable dataset can be generated with a minimum number of sensors. For example, walking and running performance can be successfully

quantified and compared across (e.g., load and or performance degradation) conditions using relatively straightforward IMU-derived gait parameters (e.g., stride period, length, and speed; duration of single/double support phases and swing phases). Similarly, jumping, climbing and landing performance can be successfully quantified and compared using sacral IMU-derived measures of vertical acceleration and velocity as well as jump height.

CONCLUSIONS

Our research provides an innovative and critical vertical step in field-based warfighter performance assessment techniques. Specifically, we have shown that meaningful and readily comparable and translatable performance outcomes can be obtained from a small number of body-worn miniature IMU sensors. By extending beyond the confines of the traditional laboratory setting, this approach will ultimately enable warfighter performance to be successfully monitored and optimized within a variety of complex and often random environments. Moving forward, we will extend our approach to more effectively characterize critical movement metrics that can consistently distinguish levels of performance success. Additionally, we will automate the assessment approach so that it can be used by the non-expert evaluator. Through these steps, we expect this integrated technology will readily translate to a variety of clinical settings.

REFERENCES

1. Pandorf CE, et al. *Can J Appl Physiol* **28**, 27-37, 2003.
2. O'Neal EK, et al. *Military Medicine* **179**, 950-954, 2014.
3. McLean SG, et al., *Clin Biomech* **25**, 781-788, 2010

ACKNOWLEDGEMENTS

Supported by NSRDEC W911QY-13-C-0011.

CLINICAL INTERVENTIONS FOR GAIT ABNORMALITIES: MODE OF FEEDBACK AND LOWER EXTREMITY MECHANICAL EFFECTS

¹ D. S. Blaise Williams III

¹ VCU RUN LAB, Virginia Commonwealth University, Richmond, VA USA
email: dswilliams@vcu.edu, web: <https://khs.vcu.edu/about/vcu-run-lab/>

INTRODUCTION

The yearly incidence of injuries across all runners varies between 24% to 71% (Fields, 2011). Of these injuries, the majority involves the lower extremity with 70-80% occurring from the knee distally (van Gent, 2007). These high injury rates for runners result from multiple reported causes including, poor training, abnormal structure, weakness, inflexibility and poor motor control. It is likely that these differences in running-related injuries are due to a combination of these factors. While the comprehensive understanding of the etiology of running-related injuries is incomplete, it is generally accepted that running injuries are related to three main factors: overexposure, lower extremity structure, and lower extremity biomechanics. Exposure or training can be easily monitored or changed while structure is much more difficult to change or account for. Biomechanical changes are attainable but often difficult to learn or slow to change.

Gait training has been an integral part of physical therapy practice since the beginning of the profession. However, interventions related to gait are often subjective or based on predetermined norms. Because there are likely multiple biomechanical factors involved in lower extremity injury, there are consequently multiple approaches available to address these factors. Recently, evidence has emerged investigating the mechanical effects of modification of gait. Specifically, gait can be modified with 3 main types of feedback: auditory, visual and motor feedback. The purpose of this presentation is to demonstrate the acute biomechanical effects (particularly on ground reaction forces, stride frequency, strike position and strike pattern) of various types of feedback. Further

discussion will be added regarding clinical application.

METHODS

All subjects will undergo running assessment via 3D motion analysis. Data will be presented based on various feedback interventions. During the gait assessment, retroreflective markers (at least three per segment) will be placed bilaterally on the segments of the rearfoot, shank, thigh and pelvis. A standing calibration trial will be collected. The subject will then be asked to run on a specialized treadmill instrumented with a force platform and surrounded by an 8-camera, motion analysis system. The subjects will run at a constant speed (3.35 m/s). Kinematic data will be sampled at 240 Hz, and force data will be collected at 1200 Hz. Thirty seconds of data will be collected for pre- and post-conditions. Kinematic and kinetic data will be time-synchronized. The three-dimensional coordinates of each marker are reconstructed using a direct linear transformation method. The reconstruction errors in a volume of approximately 1m X 1m X 2m are typically on the order of 0.5 mm. The 3-dimensional coordinates will be filtered using a 2nd order recursive Butterworth filter with a 12 Hz cutoff frequency.

The following modes of feedback will be employed for pre- and post- comparison: step rate via metronome and cuing, hip drop via video and cuing, strike position via video and cuing, strike pattern via video and cuing, trunk lean via video and cuing, soft landing via cuing. Additionally, mechanical outcomes following acute bouts of stretching, strengthening and repetitive motion will be examined. Mechanical variables of loading rate, peak vertical GRF, strike position, strike pattern and vertical stiffness will be evaluated. Lower extremity

stiffness will be determined during running by dividing vertical ground reaction force by vertical displacement of the body's center of mass (Farley & Gonzalez, 1996). Based on the results of these laboratory tests, similar clinical interventions will be used and outcomes evaluated in runners with injuries or performance deficits.

RESULTS AND DISCUSSION

There were distinct differences in outcomes post intervention across most variables. Feedback with metronome was successful for immediate change in stride frequency, strike position and strike pattern. With cuing, there were immediate changes but the changes were not as distinct and were not consistent after 1 minute. These will be demonstrated in clinical settings utilizing free apps and basic clinical feedback methods.

Differences were realized in hip drop with visual cuing and verbal cuing. Visual cuing resulted in slower changes that deteriorated when feedback was removed. Cuing resulted in immediate changes that were longer lasting but deviated further from baseline. Strike position and strike pattern were less consistent in their response to both video and cuing. Clinical examples that result in short term and long term changes in pain will be demonstrated.

Trunk lean feedback, whether through video or cuing resulted in varying mechanical outcomes and subjects were less able to successfully change trunk lean. Soft landing via cuing was successful but not symmetrical. Lower extremity stiffness was greater pre cuing for soft landing 14.15Nm/kg compared to post 10.11Nm/kg which represents a 27% decrease in stiffness. Clinical examples of trunk lean and soft landing will be presented.

Mechanical outcomes following acute bouts of stretching resulted in reductions in lower extremity stiffness and loading rates. After acute bouts of strengthening exercises, there were no differences in mechanics. With repetitive motion, there were changes in stiffness and stride rate.

CONCLUSIONS

In general, runners are able to quickly and easily respond to most feedback methods in the clinic. Based on mechanical outcomes, stride rate and soft landing cues appear to be the most effective and easily realized. The fact that runners are able to change running mechanics does not indicate they have adapted to a particular running style. The current study was not designed to develop permanent adaptations and therefore does not suggest that these or other runners are able to maintain these gait patterns. In fact, depending on the type of feedback, it may not be maintained over a single training session. This suggests that caution should be exercised when training runners with new or different mechanics as the intended changes may not be realized (4).

It appears that runners are able to quickly alter their gait patterns based on a number of different feedback modes. While auditory feedback for stride frequency seems to be most successful, verbal cuing has reasonable success for many variables. Visual feedback, particularly for trunk lean is least effective in achieving changes. More practice may be necessary to further train runners in specific gait parameters. Future studies are still needed to determine if runners permanently adapt to changes in their running mechanics and whether these changes alter any risk for running-related injuries.

REFERENCES

1. Fields KB. Curr Sports Med Rep. **10**:299-303, 2011.
2. van Gent RN, et al. Br J Sports Med. **41**:469-80, 2007.
3. Farley CT & Gonzalez O. J Biomech. **29**:181-186, 1996
4. Williams DS et al. J Appl Biomech. **16**: 210-8, 2000.

ASSESSING LOAD AND LOAD SYMMETRY OUTSIDE THE LAB

¹Robin M Queen, PhD, FACSM

¹ Duke University Medical Center, Michael W. Krzyzewski Human Performance Lab, Durham, NC, USA
email: robin.queen@duke.edu, web: <http://klab.surgery.duke.edu/>

INTRODUCTION

Biomechanical assessment has been traditionally completed in a controlled laboratory setting. With advances in technology it is now possible to assess movement in athletes and patients outside of the lab and therefore to more closely recreate normal movement during a variety of activities in both athletic as well as patient populations. Previous work has demonstrated that both movement and loading asymmetry is present in a variety of populations from orthopaedic patients following surgical intervention to athletes as they return to completion following an injury. While previous studies have demonstrated that these movement and loading deficits are present in a variety of populations all of this work has been completed in a controlled laboratory environment.

Following both total hip replacement (Queen, Clin Biomech 2015), and total ankle replacement surgery (Queen, JBJS 2014), Queen Clin Biomech, 2014) both movement and loading asymmetry have been reported to persist for up to 24 months. These asymmetries have been associated with incomplete recovery and it has been proposed that additional post-operative interventions might be needed in order to improve long-term outcomes and restore both loading and movement symmetry. In addition, Paterno, et al as well as other have reported a similar asymmetrical movement pattern that persists following anterior cruciate ligament (ACL) reconstruction (Paterno, CJSJ 2007, Dai, AJSM 2012, Butler, Sports Health, 2014). This asymmetrical pattern in post-operative ACL patients has been associated with an increased risk for a secondary injury and therefore an area of focus for rehabilitation as well as injury prevention programs (Paterno, CJSJ 2007).

Previous studies have examined changes in loading patterns outside of the lab setting on a variety of athletic surfaces (Queen, BJSM 2008, Orendurff, AJSM 2008). However the collection of this information was not without limitations and at times

the set-up and collection of this data can be difficult due to the need for data logging and or a close proximity to the computer. Based on these and other limitations a method of collecting data that can provide real-time feedback without needing to be in the laboratory setting will be essential as we begin to explore how various injuries and pathologic conditions impact activities of daily living in a variety of settings.

METHODS

The purpose of the symposium and this presentation are to stimulate discussion within the biomechanics community and raise awareness about the variety of techniques that can be used for the collection of biomechanical data in a variety of non-laboratory based settings. The collection of plantar loading data has been possible for years using in-shoe pressure systems such as Pedar-X (Novel Electronics, St. Paul, MN) as well as the F-Scan (Tekscan, South Boston, MA). However, the collection and interpretations of this data can be time consuming and have limited applications for immediate feedback to the subject. The current options for the collection of in-shoe pressure data will allow the researcher to collect the data either through data logging, which does not provide immediate feedback to the researcher or the subject or the researcher is required to have the subject move in close proximity to a computer in order to use Bluetooth to obtain the plantar loading data. While these collection methods have provided invaluable information about how the foot is being loaded during a variety of conditions and in a variety of settings, this method does not allow for the flexibility that is needed for the assessment of movement in a “real-life” setting.

The PodoPed (Novel Electronics, St. Paul, MN) is a new device that is designed to deliver on many of the current needs for the assessment of loading in a variety of environments. The PodoPed is a single sensor insole (up to 300Hz) that fits within most

shoes (US Women's 5.5 – Men's 15). The PodoPed does not require a separate transmitter or battery to be worn by the subject. The PodoPed uses Bluetooth technology to link to an iPhone app for data collection. The application allows for the real-time visualization of the vertical force for each foot in two graphical forms. Data collected from the PodoPed can be stored on the iPhone and then downloaded through iTunes for additional analysis.



Figure 2: Real-time biofeedback during a squat in a patient with an asymmetric loading pattern.

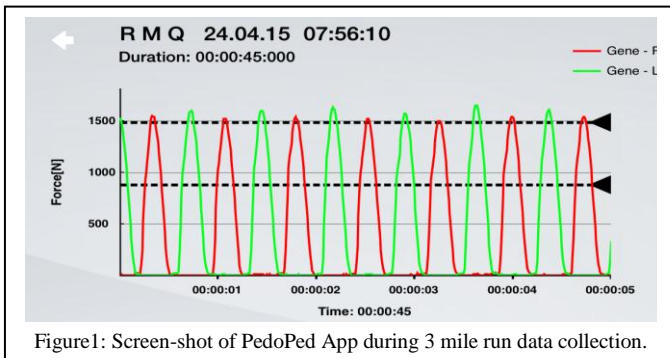


Figure 1: Screen-shot of PodoPed App during 3 mile run data collection.

The preparation and subject set-up take no more than 5 minutes from the time the insole is placed in the shoe until the first trial is collected. All that is required to begin is an accurate body weight (converted to newtons). Once the load information is entered into the iPhone app the subject is asked to stand on one foot and then the other (fingertip touch for stability) in a sequence in order to calibrate the system. Once this is completed and then the insoles are zeroed, data collection can begin.

Throughout the presentation a variety of scenarios for the use of the PodoPed device in a variety of settings from a controlled laboratory environment to running and walking on a nature trail will be described. These examples, including running (Figure 1), biofeedback (Figure 2), and orthopedic rehabilitation (Figure 3), will demonstrate the versatility of the PodoPed as well as its uses for both the collection of research data as well as the ability to set thresholds and provide immediate biofeedback (Figure 2) to the patient independent of the testing location.

RESULTS AND DISCUSSION

A 67 year old female, 5 years post-op from a right TKA was asked to complete a 1 mile walk in a location of her choosing while wearing the PodoPed

insoles. The total set-up time was 7 minutes and the subject chose to walk on the sidewalks around town. The calibration was completed with a single fingertip touch to improve balance and stability prior to data collection. Data was collected for 30 second every 2 minutes throughout the walk.

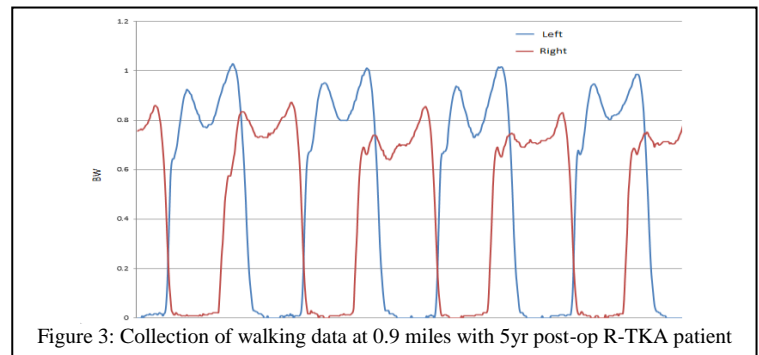


Figure 3: Collection of walking data at 0.9 miles with 5yr post-op R-TKA patient

This data (Figure 3) would indicate that this subject has a significant asymmetry with an overload of her non-operative limb.

Through the use of technology like PodoPed and other, researchers and clinicians will be able to monitor movement in any environment in order to replicate specific activities and conditions. The ability to collect in any environment will allow for the design and implementation of interventions to improve long-term health, decrease injury risk factors and hopefully allow individuals to maintain an active and healthy lifestyle.

REFERENCES

1. Queen, et al. JBJS. 96(12):987-993, 2014
2. Queen, et al. Clinical Biomechanics.29: 418-422, 2014
3. Queen, et al. Clinical Biomechanics. 30(1): 53-58, 2015
4. Paterno et al. CJSM. 2007;17:258-262
5. Butler, et al. Sports Health. 6(3):203-209, 2014
6. Dai, et al. AJSM. 40(12): 2756-2763, 2012.
7. De Biasio, Journal of Athletic Training 48(5):601-609, 2013
8. Queen, et al. BJSM, 42 (4): 278-284, 2008.
9. Orendurff, et al AJSM, 36(3): 566-571, 2008

OPEN KNEE(S): COMPREHENSIVE PATELLOFEMORAL JOINT TESTING FOR SPECIMEN SPECIFIC NEXT GENERATION KNEE MODELS

Robb W. Colbrunn¹, Tara F. Bonner¹, Snehal K. Chokhandre², Craig J. Bennetts², Jason Halloran³ and Ahmet Erdemir²

¹BioRobotics and Mechanical Testing Core

²Computational Biomodeling (CoBi) Core
Department of Biomedical Engineering
Lerner Research Institute, Cleveland Clinic
Cleveland, Ohio, 44195, USA

³Mechanics and Control of Living Systems

Department of Mechanical Engineering
Cleveland State University
Cleveland, Ohio, 44115, USA

email: colbrur@ccf.org web: <http://simtk.org/home/openknee>

INTRODUCTION

Developing virtual knee models for clinical and scientific simulations of the patellofemoral joint requires evaluating their predictive capacity, to represent physiological joint kinematics-kinetics and contact mechanics, in order to establish model credibility [1]. With comprehensive testing, specimen-specific models can be developed to represent not only individualized anatomy, but also tissue mechanical properties. In addition, with joint level mechanical testing data, the accuracy of the model can be confirmed.

Recently, the Open Knee(s) project has been launched to mitigate various uncertainties in modeling and simulation of the knee joints with the aim to build completely specimen-specific (geometry and material) three-dimensional finite element representations from different populations with varying gender, age and grades of osteoarthritis [1]. Within this project's framework, specimen-specific patellofemoral joint mechanics have been measured such that specimen-specific evaluation of model performance can be conducted in an elaborate manner. The goal of this document is to provide the specific details of the patellofemoral testing within the framework of the Open Knee(s) project.

METHODS

Six knee specimens were obtained (Table 1). All specimens were absent of knee injury, surgeries or inflammatory arthritis. A specimen preparation protocol allowed placement of optoelectronic measurement sensors (Optotrak, Northern Digital Inc., Waterloo, Ontario, Canada) and registration

markers (to relate mechanics data to imaging) on the tibia, femur, and patella.

Table 1: Specimen Characteristics

Specimen #	Gender	Age	Height	Weight	BMI
oks001	Male	71	1.83 m	77.1 kg	23.1 kg/m ²
oks002	Female	67	1.55 m	45.3 kg	18.9 kg/m ²
oks003	Female	25	1.73 m	68.0 kg	22.8 kg/m ²
oks004	Female	46	1.58 m	54.4 kg	21.9 kg/m ²
oks006	Female	71	1.52 m	49.4 kg	21.3 kg/m ²
oks007	Male	71	1.7 m	65.8 kg	22.7 kg/m ²

Anatomical landmarks and MRI-opaque registration spheres were digitized relative to the optoelectronic sensors, respectively, on the tibia, femur and patella and standardized joint coordinate systems (JCS) were created and defined for the tibiofemoral and patellofemoral joints [2]. The specimen was then secured to the robotic Universal Musculoskeletal Simulator [3], capable of six degrees-of-freedom and real-time force feedback using simVITROTM software (Cleveland Clinic, Cleveland OH). The tibia was secured to two 6 DOF force-torque sensors (SI-1900-80, ATI Industrial Automation, Apex, NC) embedded in a custom stage rigidly attached to the robot. These sensors were used to measure force vectors applied to the tibia by the femur and provide feedback needed to drive the robot. A quadriceps loading system was developed utilizing a Baldor (Fort Smith, AR) model BSM80N-275AE servomotor and a harmonic drive system (CSG-40-50, Hauppauge, NY). The quadriceps tendon was held by a custom wire mesh grip (DCD Design and Manufacturing Ltd., Richmond BC, Canada) and frozen with liquid nitrogen. Quadriceps loading was applied under force feedback control synchronized with the robot to achieve a desired joint loading state.

A Tekscan (Boston, MA) sensor (5051, 1,200 psi range) was inserted in the patellofemoral joint to measure contact mechanics.

Patellofemoral mechanics were characterized under quadriceps loading at tibiofemoral flexion angles of 0°, 15°, 30°, 45°, and 60°. At each flexion angle the tibiofemoral joint was set to a position approximating passive flexion (20 N quadriceps, 20 N tibiofemoral compression, and all other off-axis loads minimized). Then, quadriceps loads were applied at 20, 100, 200, 300, 400, 500, and 600 N. At each loading state, the patellofemoral contact mechanics, patellofemoral kinematics, tibiofemoral kinematics, and tibial loads were measured.

RESULTS AND DISCUSSION

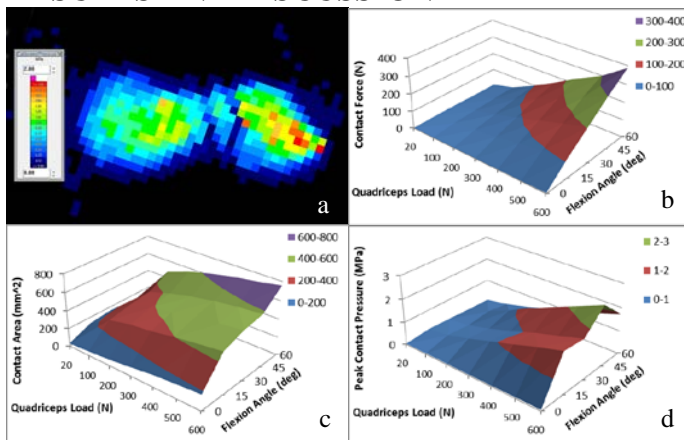


Figure 1: Patellofemoral contact mechanics for oks007 specimen. a) pressure distribution at 60° flexion and at 600 N quadriceps force, b-d) contact force, area, and peak pressure at all flexion angles and loading conditions, respectively.

For the purpose of this abstract, one specimen's results were highlighted. Patellofemoral contact mechanics for a single specimen (oks007) are shown in Figure 1. The pressure distribution at 60° flexion with a 600 N of quadriceps load a dual contact area is shown in Figure 1a. The contact force and area increased with both flexion and quadriceps loading and the peak contact pressure monotonically increased with quadriceps loading (Figures 1b-d), but not with flexion. The highest contact pressure recorded for this specimen was at 45 degrees of flexion. Table 2 illustrates the variability of peak contact pressure across specimens at this same loading condition.

Table 2: Peak contact pressure for each specimen at 45 degrees of flexion and 600 N of quadriceps load.

Peak Contact Pressure (MPa)					
oks001	oks002	oks003	oks004	oks006	oks007
1.76	2.90	2.90	2.22	3.37	2.61

In order to build virtual knee models with accurate specimen-specific joint mechanics, the model predicted joint kinematics-kinetics and contact mechanics should be similar to the experimental measurements for the corresponding specimen. This document outlined the specific details on how patellofemoral testing was completed within the framework of the Open Knee(s) project to provide the opportunity for specimen-specific evaluation. Anatomical images and tissue properties were also collected for the same specimens as part of the Open Knee(s) initiative, aiming to build geometric and mechanically consistent specimen-specific models.

When specimen-specific patellofemoral joint mechanics data are not available, data from the literature can be utilized. However, it is evident that contact mechanics vary largely amongst specimens and such comparisons may suffer from uncertainties associated with anatomical and mechanical variations between specimens (Table 2).

Open Knee(s) project targets to complement the reported data by testing four additional specimens, to further diversify the population of patellofemoral joint data. The next steps involve development of specimen-specific knee models to evaluate against the contact mechanics data collected in this study, for each respective specimen. These models can then be used by any and all interested investigators to further elucidate patellofemoral pathologies and potential treatment options for patients.

ACKNOWLEDGMENTS

This study was funded by NIGMS, NIH (R01GM104139, PI: Erdemir). Assistance from Katie Stemmer, Dylan Beckler, Sam Doerle and Erin Merico is appreciated. Open Knee(s) is an open development modeling project; specifications, models, and data can be accessed at <http://wiki.simtk.org/openknee>.

REFERENCES

- [1] Erdemir, A. *J Med Device*, 7:0409101, 2013.
- [2] Grood, E.S. et al. *J Biomech Eng.*, 105:136–144, 1983.
- [3] Noble, L.D. et al, *J Biomech Eng*, 132(2), 2010.

AN ACL DENERVATION MODEL FOR DETERMINATION OF THE EFFECTS OF SENSORY AFFERENTS ON JOINT FUNCTION

¹Christopher Nagelli, ²James L. Cook, ²Keiichi Kuroki, ²Chantelle Bozynski, ¹Timothy Hewett

¹Sports Health and Performance Institute, OSU Sports Medicine, The Ohio State University, Columbus, OH
²Comparative Orthopaedic Laboratory, University of Missouri, Columbia, MO
email: christopher.nagelli@osumc.edu

INTRODUCTION

Anterior cruciate ligament (ACL) injuries are extremely common. Patients sustaining ACL injury also incur damage to other joint tissues with resultant dysfunction. Surgical ACL reconstruction (ACLR) is performed to regain knee stability and allow return to function in a timely manner. Autografts and allografts used for ACLR must undergo cellular repopulation, revascularization, and re-innervation for joint function to return to normal. The most common complications after ACL injury and ACLR include continued dysfunction, re-tear, and secondary osteoarthritis (OA).¹ These complications may be inter-related and may stem from the inability to fully restore ACL, and whole-joint, integrity and function. Importantly, 50-100% of ACLR patients experience early onset OA with radiographic evidence seen as early as 5 years after ACL injury.² These sequelae indicate that current management strategies for ACL injuries are suboptimal and have profound clinical implications regarding long-term prognosis and related healthcare costs.

Several mechanisms for development of OA secondary to ACL injury have been reported, including altered tibiofemoral biomechanics after injury, chondrocyte death due to initial trauma, and neuromuscular control deficits.^{3,4} Recent evidence indicates that an absence of sensory information may play a critical role in the development of OA.⁵ To investigate this potential mechanism, we developed a novel large animal model to assess the relative contributions of sensory afferents in the ACL and the joint to knee function and early development of OA. We hypothesized that ACL sensory denervation would manifest in knee joint dysfunction and development of early OA.

METHODS

With IACUC approval, purpose-bred, adult research dogs (n=9 dogs, 18 knees) underwent aseptic arthroscopic surgery to create 6 treatment cohorts (**Table 1**). An immunotoxin was used to induce sensory denervation. OX7-saporin has been reported to successfully denervate 80% of the sensory nerve fibers projecting to the knee.⁵ Once injected, this immunotoxin was taken up by a nerve through endocytosis and transported back to the cell body where it deactivated the ribosomes, killing the nerve. For this study, OX7-saporin (50ug) was injected into the ACL for the ACL insufficient (denervated) group and into the knee joint for the Joint insufficient (whole-joint denervation) group. Partial transection of the ACL was performed to provide a positive control of known mechanical dysfunction (ACL deficient group) and sham procedures were performed in the contralateral knees (**Table 1**).

Table 1: Project Cohort Description

<i>Study Group</i>	<i>Control</i>	<i>Representative</i>
ACL denervation (n=3)	ACL saline (n=3)	ACL Insufficient
ACL transection (n=3)	ACL sham transection (n=3)	ACL Deficient
Joint denervation (n=3)	Joint Saline (n=3)	Joint Insufficient

After intervention, dogs were enrolled in a regimented exercise program in which they were leash-walked for 20 minutes/day 5 days/week. Gait analysis was performed at weeks 1, 4, 8, and 12 using a pressure-sensitive walkway. Clinically relevant functional assessments of the knees were performed by a board-certified veterinary surgeon,

blinded to treatment, at weeks 4, 8, and 12. At week 12, the animals were humanely euthanatized for arthroscopic, gross, and histologic assessments. Two different raters assessed the histological results in blinded fashion.

RESULTS AND DISCUSSION

The ACL insufficient group demonstrated joint dysfunction as evidenced by reduced limb loading and comfortable range of motion compared to the contralateral control limb. Interestingly, knee dysfunction and ACL pathology scores associated with ACL denervation were relatively more severe than that associated with whole-joint denervation, but less severe than ACL deficiency. These results indicate that sensory dysfunction of the ACL has effects on knee joint health and function, which has profound implications for management of ACL injuries.

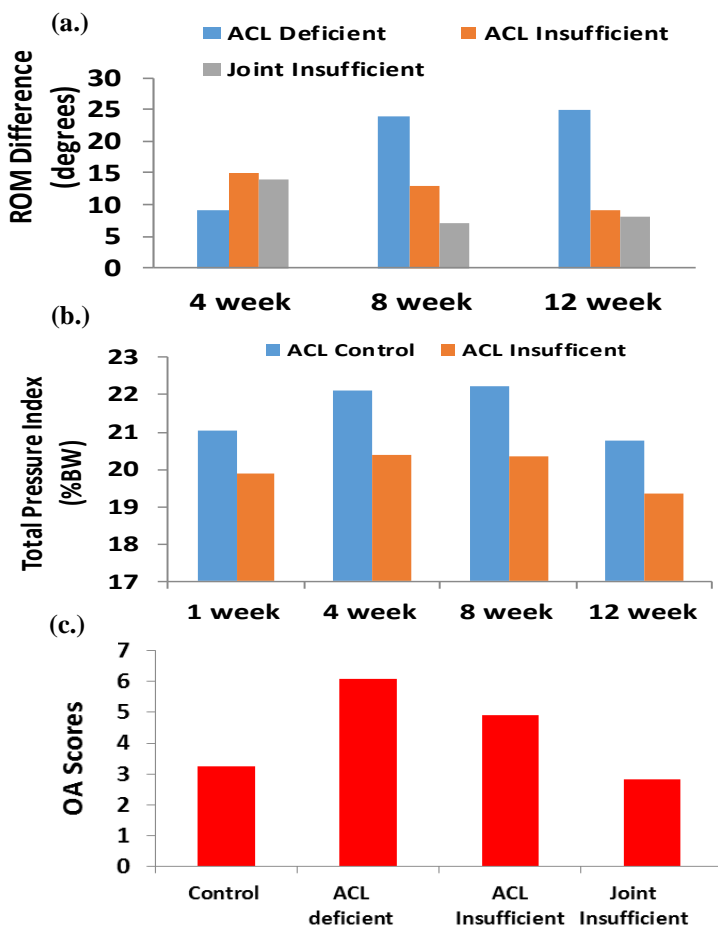


Figure 1: A change in overall joint function (1a and 1b) and tissue health (1c) was observed between the study groups.

Early onset OA secondary to ACL injury is likely a multi-factorial process. Aberrant biomechanics, arthrogenic muscle inhibition, and trauma to the subchondral bone have been strongly associated with the degradation of articular cartilage seen in OA. The present findings indicate that it is necessary to elucidate the effects of ACL afferents on osteoarthritic changes in the knee after ACL injury as the neurologic function of the ligament appears to play important roles in this disease process. This novel model may provide a platform to: (1) investigate the neural mechanisms of osteoarthritis and (2) understand the consequences of selective sensory ablation on joint function. The current study has limitations. In addition to the small number of dogs included in each cohort, the relatively short duration of the study limits the conclusions that can be made from these observations. The effects of the toxin OX7-saporin on sensory afferents in the dog have not been validated, but are part of our ongoing analyses.

CONCLUSION

To the investigators' knowledge, this is the first study to investigate the effects of local sensory denervation of the ACL on knee joint function and health. Further development and use of this novel model holds importance as the ACL is a major sensory structure for knee joint function. After ACL injury, there is disruption in the sensory-motor connection to the knee, which ACL reconstruction does not immediately re-establish. The results of our study indicate denervation of the ACL may lead to joint dysfunction and subsequent osteoarthritic changes. These findings have implications for management of patients with ACL injuries, including rehabilitation programs that focus on re-establishment of sensory-motor function, which may ameliorate rapid development of OA knee.

REFERENCES

1. Helmick et al. *Arthritis Rheum.* 58.1.15-25. 2008.
2. Kessler et al. *Knee Surg Sports Traumatol Arthrosc.* 93.11.994-1000. 2008
3. Quatman et al. *J Knee Surg.* 25.3.197-206. 2012.
4. Palmieri-Smith et al. *Exerc sport Sci Rev.* 37.3.147-153.2009
5. Salo et al. *Orthop Res.* 20.6.1256-1264.2002.

ACKNOWLEDGEMENTS

The authors acknowledge funding support from the National Institutes of Health / National Institute of Arthritis and Musculoskeletal and Skin Diseases grants R01-AR049735 and R01-AR056259.

PEDIATRIC OBESITY AND WALKING DURATION AFFECT MEDIAL & LATERAL TIBIOFEMORAL COMPARTMENT CONTACT FORCES

Zachary F. Lerner, Wayne J. Board, and Raymond C. Browning

Colorado State University, Fort Collins, CO, USA

email: Zach.Lerner@ColoState.edu web: <http://pal.colostate.edu>

INTRODUCTION

Obese children can improve their health outcomes by engaging in sufficient walking and running physical activity. However, since obese children have greater muscle force requirements relative to lean-mass during locomotion [1], continuous bouts of walking or running may elicit fatigue, which may alter joint loading and increase injury risk. Altered tibiofemoral loading during daily physical activity in obese children is theorized to contribute to their well-documented increased risk of orthopedic disorders of the knee (e.g. growth plate suppression and joint malalignment); conditions thought to lead to a cycle of weight gain [2,3]. However, it is unknown how tibiofemoral loading is altered by pediatric obesity during walking and this limits our ability to evaluate the risk-benefit ratio of physical activity on the musculoskeletal system. *This study sought to determine the effects of pediatric obesity and walking duration on the magnitudes, distribution, and loading rates of medial and lateral tibiofemoral contact forces.*

METHODS

We collected experimental biomechanics data during treadmill walking at $1 \text{ m}\cdot\text{s}^{-1}$ for 20 minutes in 10 obese ($\text{BMI}_Z > 95\%$) and 10 healthy-weight ($5\% < \text{BMI}_Z < 85\%$) 8-12 year-olds. Age, sex, and leg length were similar between groups.

We used dual x-ray absorptiometry to capture whole body and higher-resolution knee radiographs for each child (Fig. 1A, B). We defined a medial tibial epiphysis region of interest (ROI) and measured the areal bone mineral density (BMD) (Fig. 2A). In a prior model development and methodology validation study, we introduced a knee

mechanism into a full-body OpenSim gait model that was capable of incorporating subject-specific tibiofemoral alignment and centers-of-pressure, and accurately resolving medial & lateral compartment contact forces [4] (Fig. 1C). In the present study, we created subject-specific musculoskeletal models by specifying leg alignment and compartment centers-of-pressure by analyzing the radiographs for each child using established methods [5]. In OpenSim, we used weighted static optimization to estimate the muscle forces that reproduced the measured walking motions, and calculated the contact force in each compartment using Joint Reaction [4].

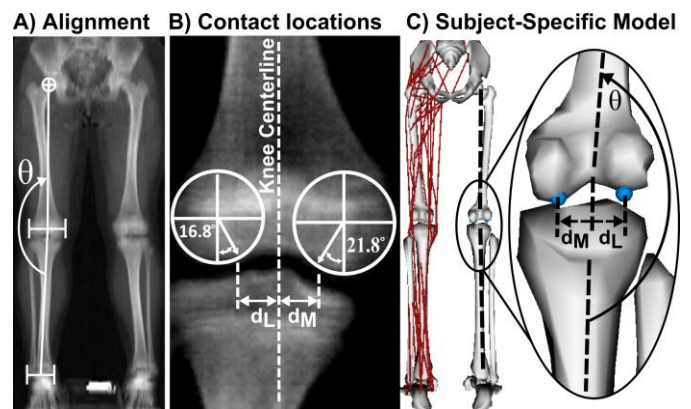


Figure 1: Measurement (A,B) and specification (C) of alignment (θ) & medial and lateral compartment contact locations (d_M/d_L) [5] for each subject-specific model.

RESULTS AND DISCUSSION

Obesity and walking duration affected tibiofemoral loading (Fig. 2-4). In the obese vs. healthy-weight children, peak contact forces (N) during stance were 2.1 times greater in the medial compartment ($p < 0.001$) (Fig. 2B), but similar in the lateral compartment ($p = 0.406$). Normalized to the BMD in the medial tibial epiphysis ROI, peak medial forces ($\text{N}\cdot\text{kg}^{-1}\cdot\text{cm}^2$) were 1.77 times larger in the obese vs. healthy-weight individuals (Fig. 2C).

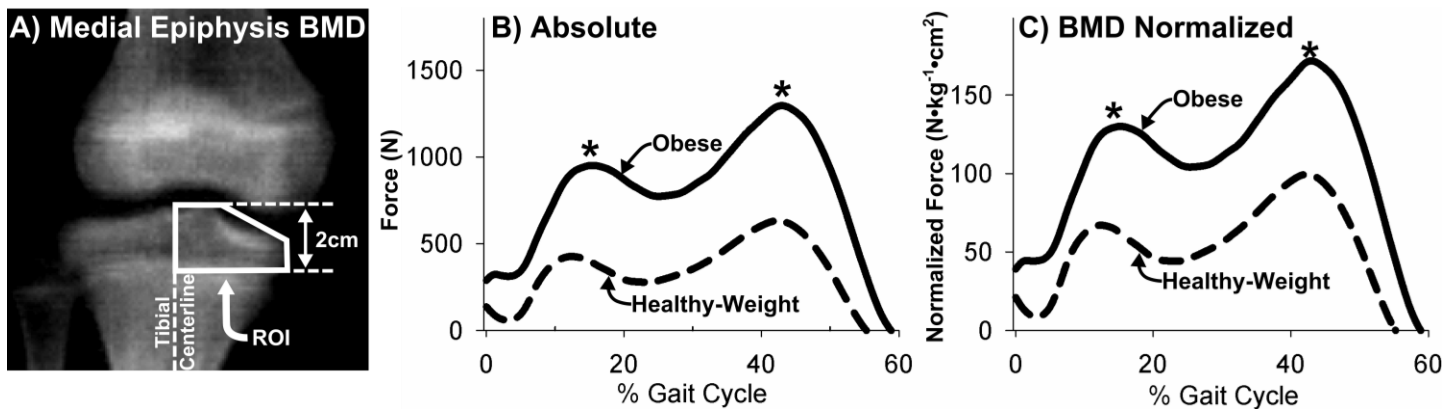


Figure 2: Medial tibial epiphysis ROI (A), and absolute (B) and BMD normalized (C) medial compartment contact forces in the obese (solid) and healthy-weight (dashed) children. * denotes a significant difference.

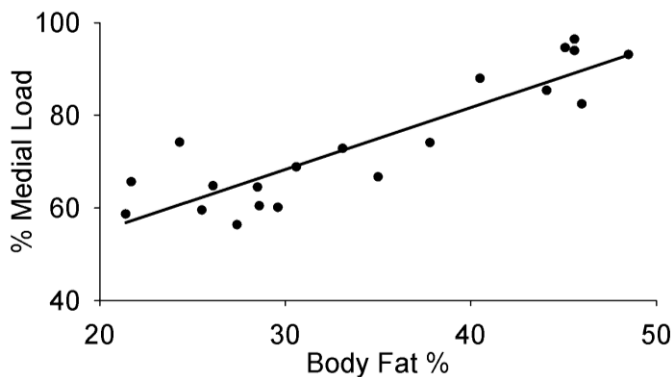


Figure 3: The linear relationship ($r^2=0.79$) between % medial load (%ML) and body fat % (BF%); $\%ML = 1.3 \cdot BF\% + 28.3$.

At the start time-point (1st minute after 5 minute acclimation period), the average medial load share during stance was 85% in the obese children vs. 63% in the healthy-weight children. At the end time-point (20th minute), the average medial load share was 90% in the obese children vs. 72% in the healthy-weight children (Fig. 4).

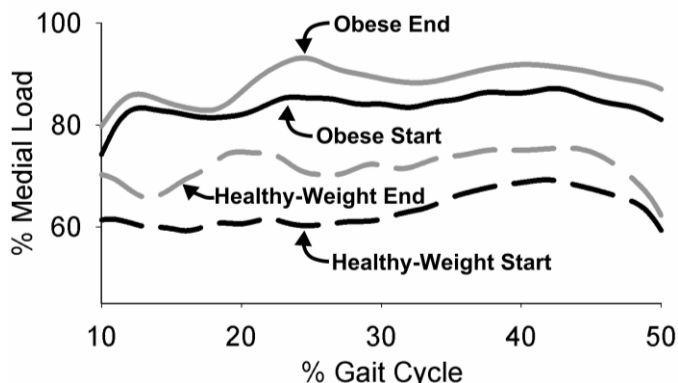


Figure 4: Media load share in obese and healthy-weight children at the start and end time-points.

Medial compartment loading rates were 1.78 times greater in the obese vs. healthy-weight participants

and increased 17% in both groups at the end vs. the beginning time-point ($p=0.001$).

CONCLUSIONS

During adolescence there is a disassociation between longitudinal bone growth and mineral accrual, affecting bone microarchitecture. Our finding of elevated medial compartment force relative to the underlying BMD supports the theory that altered loads in obese children during walking may contribute to their increased risk of developing orthopedic disorders of the knee. The strong relationship between medial load share and body fat % (Fig. 3) also supports the previously reported positive association between pediatric obesity and knee pain/pathology. Walking duration affected loading in both groups, yet the baseline values were greater in the obese children. Thus, longer activity durations may increase the risk of musculoskeletal injury more in obese vs. healthy-weight children, so shorter durations may be advisable.

REFERENCES

1. Lerner ZF, et al. *J Biomech* **47**, 2975-2982, 2014.
2. Wearing SC, et al. *Obes Rev* **7**, 209-218, 2006.
3. Davids JR, et al. *J Ped Ortho* **16**, 461-468, 1996.
4. Lerner ZF, et al. *J Biomech*, In Press, doi:10.1016/j.jbiomech.2014.12.049, 2015
5. Li G, et al. *Am J Sport Med* **33**, 102-107, 2005.

ACKNOWLEDGEMENTS

Funding from NIH/NICHD F31 HD080261 and ACSM Foundation doctoral student research grants.

EFFECT OF KNEE BRACING AND WEDGED INSOLES UPON KNEE JOINT CONTACT FORCES

¹Jim Tse, ¹Walter Bohne, MD, ¹Lilly Tran, MS, ²Darryl D. D'Lima, MD, PhD, ²Shantanu Patil, MD, ³Benjamin J. Fregly, PhD, ¹Sherry I. Backus, PT, DPT, MA, ¹Andrew P. Kraszewski, MS, ¹Glenn Garrison, CPO, ¹Andreas Kontaxis, PhD, ¹Mark Lenhoff, BS, ¹Howard J. Hillstrom, PhD

¹Hospital for Special Surgery, New York, NY, USA

²Scripps Clinic, La Jolla, CA, USA,

³University of Florida, Gainesville, FL, USA

E-mail: HillstromH@hss.edu

INTRODUCTION

Malalignment, high body mass index, and soft tissue injuries have all been associated with knee osteoarthritis (OA). Patients with knee OA most typically suffer from varus malalignment, which overloads the medial compartment. Medial knee compartment contact forces can be reduced by the use of valgus bracing^{1,2} and lateral knee compartment forces can be reduced by the use of varus bracing¹. The effect of lateral and medial foot wedges with and without valgus knee bracing upon compressive joint loading is unknown. Total knee contact force was measured on an individual wearing medial and lateral foot wedged insoles with and without a knee brace. The test subject has been fitted with an instrumented knee replacement (e-tibia) that measures total knee contact force *in vivo*. We hypothesize: **(H1)** lateral wedged foot insoles will decrease medial compartment forces, while medial wedged foot insoles will decrease lateral compartment forces, and **(H2)** that wedged foot orthoses will further decrease total knee contact forces compared with knee bracing alone.

METHODS

A pilot study was conducted on a single-subject (female, 69 years old, 81 kg) who had an e-tibia total knee replacement (TKR). Composed of a polyethylene insert, tibial tray, and telemetry system, the e-tibia measured three forces (F_x , F_y , F_z) and three moments (M_x , M_y , M_z) through 12 load cell strain gages integrated within the TKR³. The subject walked at her self-selected speed on a level walkway while simultaneously measuring e-tibia contact loading and 3D inverse dynamics (12 Eagle

cameras, Motion Analysis Corp, Santa Rosa, CA; 2 Bertec, Columbus, Ohio; and 2 AMTI, Bilarica, MA force plates). The test subject walked with a knee brace (Unloader Select, Ossur Americas, Foothill Ranch, CA) adjusted to 4° valgus and in the unbraced condition representing baseline (control). In addition, the test subject was fitted with 5° medial and lateral wedged full length foot insoles which were assessed with and without the knee brace. Inverse dynamics and e-tibia data were simultaneously collected from the subject with four trials per condition. Total contact forces from the e-tibia were stratified into medial and lateral compartment forces using subject-specific regression equations.

RESULTS AND DISCUSSION

Medial (solid) and lateral (dashed) compartment contact forces were measured by the e-tibia (Fig. 1). The unbraced condition (control) shown in purple demonstrated the largest peak forces in both the medial and lateral compartments of the knee. The Unloader Select knee brace (4° valgus correction) shown in green significantly reduced peak contact forces in the medial compartment (~20%). Medial wedges alone shown in dark blue significantly reduced the 1st peak contact force in the medial compartment but not the 2nd. The lateral wedges alone shown in yellow significantly reduced the 2nd peak contact force but not the 1st. Neither wedge alone had a substantial impact on lateral compartment forces. The medial and lateral wedges in conjunction with knee bracing are shown in light blue and red and were both effective at reducing medial compartment contact forces.

A valgus knee brace alone or with wedged foot insoles was able to significantly reduce peak contact forces within the medial compartment of the knee (Fig. 1). Wedged foot orthoses alone were able to reduce medial peak contact forces preferentially. Neither wedged insole was effective at reducing lateral compartment forces supporting partial acceptance of hypothesis 1. The addition of either medial or lateral wedged foot insoles to knee bracing did not further reduce peak contact forces. This suggests the mechanism for reducing contact forces is through load sharing via the brace hinge.⁴ Wedge insoles employ a different strategy, which is to shift the load through altering foot alignment. Given that the addition of wedged insoles did not further reduce contact forces compared knee bracing alone hypothesis 2 is rejected.

CONCLUSIONS

Wedged foot orthoses were able to preferentially reduce the 1st or 2nd peak of the medial compartment

knee contact force. Knee braces alone were capable of reducing both the 1st and 2nd peak of the contact force and the addition of medial or laterally wedged foot insoles did not provide additional benefit to braces alone.

REFERENCES

1. Tse et al. Proceedings of GCMAS, 2015, Portland Orgeon, USA, 2015.
2. Kutzner at al. J Biomech. 2011; Apr 29;44(7):1354-60.
3. D'Lima, D. D. et al. *Journal of Biomechanics* 38; 2 (2005): 299-304.
4. Pollo, F. E. et al. *Am J Sports Med.* 30; 3 (2002): 414-21.

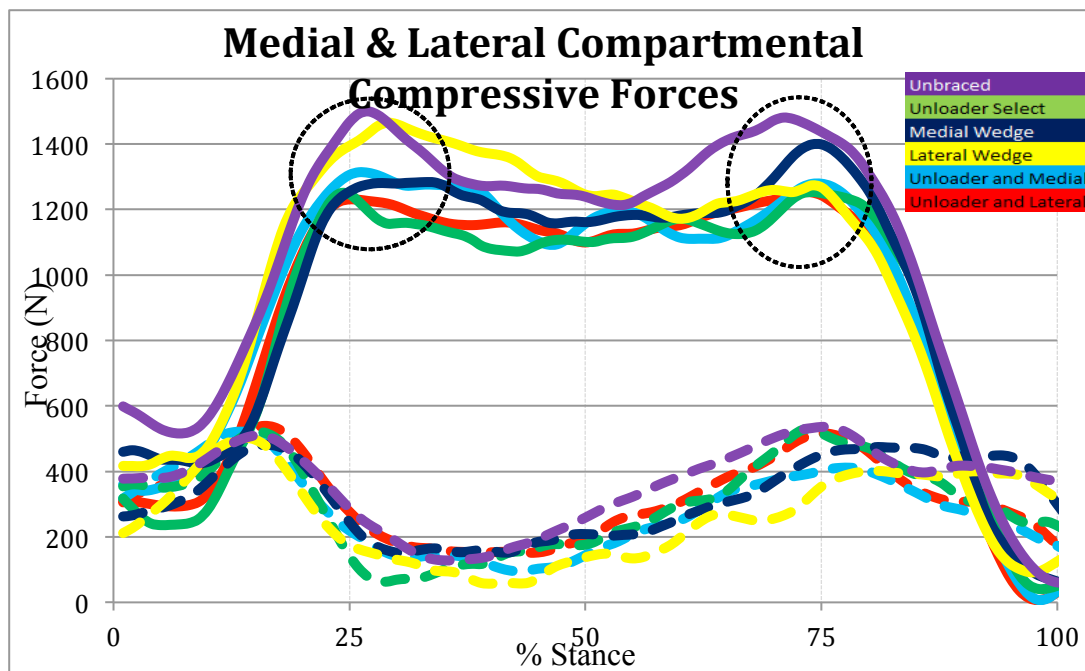


Figure 1: Medial Compartmental forces are depicted in solid lines while the lateral compartmental forces are depicted in dashed lines. The Unbraced condition (reference) is shown in purple, the Unloader Select knee brace is in green, medial and lateral wedges alone are in dark blue and yellow, and the medial and lateral wedges in conjunction with knee bracing are shown in light blue and red.

CAN OSTEOARTHRITIS RADIOGRAPHIC SEVERITY AND PAIN BE EXPLAINED BY JOINT MECHANICS?

¹ Elizabeth A Hassan and ¹ Kevin J Deluzio

¹ Dept. of Mechanical Engineering, Queen's University, Kingston, ON, Canada
email: elizabeth.hassan@queensu.ca

INTRODUCTION

Intuitively, it would make sense for radiographic signs of osteoarthritis severity to be closely related to pain and joint mechanics during gait. However, quantifying this relationship has proven to be analytically challenging, particularly in patients with mild or moderate severe osteoarthritis. The previous literature is not conclusive on the topic, Astephen *et al* [1] linked pain to stride characteristics, but not to mechanics, but was able to link knee adduction moment to radiographic severity, and Zifchock *et al* [2] found that pain did not correlate with knee adduction moment, but did correlate with radiographic indicators of severity. In contrast, Henriksen *et al* [3] linked increased pain to decreased peak knee adduction moment. This abstract proposes that links between pain, radiographic severity and mechanics can be quantified using Partial Least Squares, and that this technique offers some interpretation advantages over more traditional tools such as multiple linear regression.

Partial Least Squares (PLS) [4] is a generalized form of principal component analysis (PCA). An advantage of PLS over PCA and multiple linear regression is that it is possible to analyze multiple, continuous response (Y) variables simultaneously. This advantage is particularly useful in cases with multiple correlated predictors and responses.

METHODS

To evaluate the performance of PLS as an analysis and interpretation tool for biomechanical data, it was tested on an already published data set. The data set includes hip, knee and ankle kinematic and kinetic data from 37 subjects with mild to moderate osteoarthritis; the details of the data collection are

summarized in Astephen *et al* [1]. The analysis procedure was as follows:

Preprocessing:

Calculate PC scores for 3 components on each variable

$$[PC_1^{Knee\ Ax} \ PC_2^{Knee\ Ax} \ PC_3^{Knee\ Ax}] = PCA(Knee\ Flexion\ Angle\ Ax_{37 \times 101})$$

$$[PC_1^{Knee\ Ay} \ PC_2^{Knee\ Ay} \ PC_3^{Knee\ Ay}] = PCA(Knee\ Adduction\ Angle\ Ay_{37 \times 101}) \text{ etc...}$$

X is composed of all PC Scores for all variables

$$X = [PC_1^{Knee\ Ax} \ PC_2^{Knee\ Ax} \ PC_3^{Knee\ Ax} \ PC_1^{Knee\ Ay} \ \dots]_{37 \times 45}$$

Y is composed of outcome measures, VAS and pain

$$Y = [VAS \ Pain]$$

Variable Selection:

Calculate the PLS model, reject least important variable, repeat until 5 variables remain in X

PLS:

Calculate scores for 2 Latent Variables

$$[T_1 \ T_2] = PLS(X, Y)$$

MLR:

Predict Y based on T_1 and T_2

$$Y_{VAS} = a_0 + a_1 T_1 + a_2 T_2$$

$$Y_{pain} = b_0 + b_1 T_1 + b_2 T_2$$

The PCA analysis was conducted using MATLAB code written by our lab group. Three principal components were extracted for the flexion and abduction-adduction angles, and all moments at the hip, knee and ankle. The PLS analysis was conducted using MATLAB code written by the author, based on the algorithm outlined in Abdi [5]. The number of columns in X was reduced to a more parsimonious set of 5 variables using the criteria described in Andersen and Bro [6]. Multiple linear regression (MLR) on the PLS latent vector scores was conducted with built in MATLAB functions.

RESULTS AND DISCUSSION

The response (Y) variables were radiographic VAS (Visual Analog Scale, average of grade from two surgeons, mean 4.4, range 1.1 to 8.3) and the pain

subscale from the WOMAC Score (mean 7.2, range 0 to 18). The Kellgren-Lawrence (KL) Score for these patients ranged from 1 to 4.

The predictor variables selection process extracted kinematic and kinetic variables as shown in Figure 1, along with the regression weights calculated as part of the PLS process. The knee moment variables were of similar importance to the prediction of VAS and pain, but in the opposite direction. Hip adduction moment PC2 score (corresponding to the first peak) was an important predictor for pain, but was not an important factor in predicting radiographic severity. The ankle toe in-toe out moment PC1 (corresponding to magnitude) was important for predicting radiographic severity, but not pain. However, severity and pain are not associated with each other, and the relationship between mechanics and pain and the relationship between mechanics and radiographic severity are different. Multiple linear regression revealed that mechanics better explained radiographic severity than pain, with R^2 values of 0.3 for VAS, 0.2 for pain.

The importance of knee adduction moment is consistent with the previous literature relating radiographic severity and this feature. Henriksen *et al* [2] noted the relationship between this variable and pain, but Henriksen analyzed the peak knee adduction moment, and the PC2 extracted by this analysis appears to also related to the curve shape, as shown in Figure 2.

CONCLUSIONS

The results of the PLS analysis suggests that mechanics can be linked to both radiographic severity and pain in moderate OA patients. The Astephen *et al* 2011 paper was not able to link pain to joint mechanics, but the current analysis was able to using the same data, which indicates that multivariate methods may be required to quantify the pain-radiographic severity-mechanics relationship.

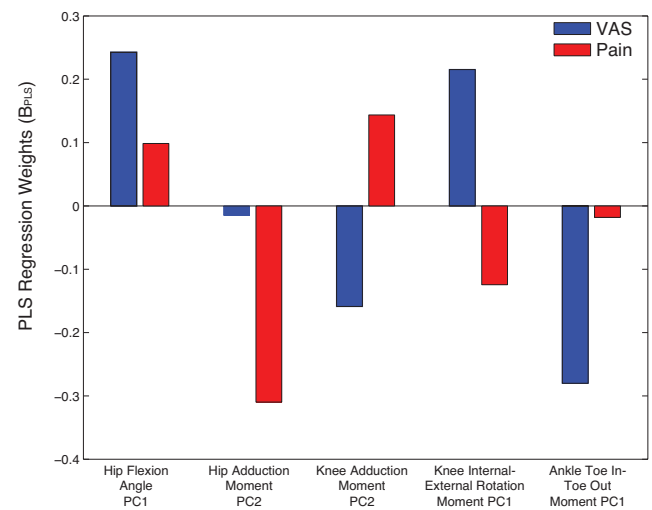


Figure 1: Regression weights for retained variables to explain radiographic severity (VAS) and pain

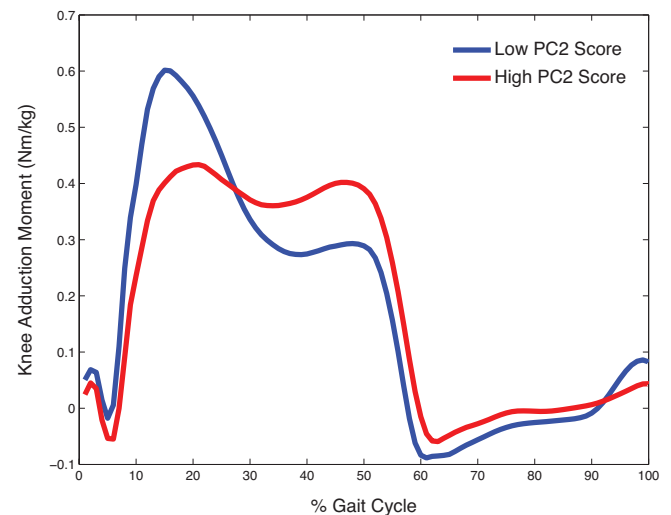


Figure 2: Waveforms corresponding to high and low PC scores (+/- 1 SD)

REFERENCES

1. Astephen Wilson JL et al. *Osteoarthritis Cartilage* **19**, 186-93, 2011.
2. Zifchock RA et al. *Clin Orthop Relat Res* **469**: 10, 2866-2873, 2011.
3. Henriksen M et al. *The Knee* **19**:4, 392-398, 2012.
4. Wold S & Sjöström M. *Chemometrics and Intelligent Laboratory Systems* **58** 109-130 2001
5. Abdi, H. *WIREs Comp Stat.* 2010.
6. Andersen, CM & Bro, R. *J. Chemom.* **24**, 728-737. 2010.

ACTIVE AND PASSIVE KNEE STABILITY IN PATIENTS WITH SEVERE OA

¹ Gregory Freisinger, ¹ Erin Hutter, ¹ Jackie Lewis, ¹ Rachel Baker, ¹ Jeffrey Granger, ² Matthew Beal,
¹ Xueliang Pan, ¹ Laura Schmitt, ¹ Robert Siston and ¹ Ajit Chaudhari

¹ The Ohio State University, Columbus, OH, USA

² Northwestern University, Evanston, IL, USA

email: gregory.freisinger@gmail.com, web: <http://u.osu.edu/osusportsbiomechanics/>

INTRODUCTION

Osteoarthritis (OA) is the largest single cause of disability in the United States, and the knee joint is most frequently affected [1]. Increased knee laxity has been reported in knee OA patients compared to controls [2], and additional active knee stability, by increased muscle activation or co-contraction of antagonist muscles, has been hypothesized to assist in knee stabilization [3]. Muscle guarding may reduce the magnitude of measured laxity, and it is currently unknown how large of an effect this plays in identifying a relationship to active stability.

The primary purpose of this study was to identify the association between passive knee laxity, measured when each participant is under general anesthesia, and contributors to active knee stability in participants with severe OA. We hypothesized that increased passive knee laxity would be associated with increased quadriceps muscle activity and co-contraction indices during gait.

METHODS

Twenty individuals (22 total knees: 7 male / 15 female, age=59.0 ± 7.3 y, ht=1.68 ± 0.11 m, mass=93.5 ± 15.3 kg, BMI=33.3 ± 4.5 kg/m²) completed this study after providing IRB approved consent. Participants had predominantly medial compartment tibiofemoral OA and were awaiting total knee arthroplasty (TKA). Prior to surgery, each participant completed gait analysis in Ohio State's Movement Analysis and Performance Lab. Participants walked along a 10 m path at a self-selected speed (0.98 ± 0.26 m/s). Marker data were collected at 150 Hz utilizing 10 motion-capture cameras (MX-F40; Vicon; Oxford, UK). A modified point-cluster technique marker set was

used in conjunction with a functional hip joint center to calculate lower extremity kinematics.

Wireless surface electromyography (EMG) (Telemetry DTS; Noraxon USA, Inc; Scottsdale, AZ) was recorded at 1500 Hz for specific lower extremity muscles that cross the knee joint on the involved limb. Three separate, unweighted tasks were used as submaximal reference activities to normalize EMG signals. Seated uni-lateral knee extension was used to normalize the rectus femoris (RF), vastus medialis (VM), and vastus lateralis (VL). Standing uni-lateral knee flexion was used to normalize semimembranosus (SM) and biceps femoris (BF). Standing bi-lateral ankle plantarflexion was used to normalize medial and lateral gastrocnemius (MG & LG). The highest 500ms running average of EMG for each muscle was used for normalization.

The average quadriceps activation (avgQUAD) and average co-contraction indices (avgCCI) were used as active stability measures for their potential to stabilize the knee joint during gait. avgQUAD was found by calculating the mean of RF, VM, and VL muscle activity and avgCCIs were calculated using Equation 1 [4] for the following antagonist muscle pairs: quadriceps and hamstring (QH); quadriceps and gastrocnemii (QG); VM and SM (MQH); VL and BF (LQH); VM and MG (MQG); and LV and LG (LQG).

$$avgCCI = \frac{1}{n} \sum_{i=1}^n \left(\frac{lower\ EMG_i}{higher\ EMG_i} \times (lower\ EMG_i + higher\ EMG_i) \right)$$

Equation 1. Average co-contraction index (avgCCI) was calculated using the relatively lower and higher EMG signals for antagonistic muscles.

avgQUAD and avgCCIs were calculated over the weight acceptance phase of gait (WA), which was defined as the time period from initial heel contact to peak knee flexion. Four trials of gait were used to calculate ensemble averages for the muscle activations during WA. Selected muscle activation values from specific participants were dropped from further analysis due to poor signal quality, so the number of participants used are shown in Table 1.

Passive varus-valgus knee laxity was measured intra-operatively using a custom navigation system and knee stability device [5] in the osteoarthritic knee before TKA. Laxity was calculated as the difference in varus-valgus knee angle when the knee was loaded with 10 Nm of varus and valgus moment, respectively. Each participant's overall varus-valgus laxity was the average value found during three trials in the operating room.

Non-parametric statistics were chosen after an initial inspection of the data revealed 4 of the 7 EMG variables were not normally distributed (Anderson-Darling test; $p < 0.05$). Spearman's rank order correlations were calculated for varus-valgus laxity and EMG variables of interest. A p -value < 0.05 was used to indicate statistical significance.

RESULTS AND DISCUSSION

No association was observed between passive varus-valgus laxity and any active stability measure during the WA phase of gait. The distribution of passive varus-valgus laxity, avgQUAD activation and avgCCIs are reported in Table 1.

Quadriceps force can create a moment to counteract varus-valgus rotation, as a result of the bicondylar nature of the knee joint and attachment point of the quadriceps on the tibia; however this was not related to varus-valgus laxity in this cohort. While no CCI was related to laxity, LQH was significantly larger than MQH (Mann-Whitney U test, $p = 0.005$). This may be a neuromuscular strategy to stabilize the adduction moment during weight acceptance, and prevent the lateral side of the femur from lifting off the tibia [3].

Table 1. Variables of interest and Spearman's rank order correlation to varus-valgus laxity

	n	Mean \pm SD / Median [IQR]	rho	P-value
VV Laxity, $^{\circ}$	22	4.7 \pm 2.4	1	n/a
avgQUAD, %	22	90.4 [46.3]	-0.171	0.446
QH avgCCI	19	1.15 [0.65]	0.070	0.775
QG avgCCI	21	0.26 [0.28]	-0.136	0.556
MQH avgCCI	22	0.57 [0.61]	0.067	0.786
LQH avgCCI	19	1.51 [0.74]	0.103	0.647
MQG avgCCI	22	0.24 [0.22]	-0.094	0.687
LQG avgCCI	21	0.30 [0.36]	-0.132	0.559
Footnotes: Interquartile range (IQR); varus-valgus (VV); average (avg); co-contraction index (CCI); quadriceps/hamstrings (QH); quadriceps/gastrocnemii (QG); medial (M); lateral (L).				

CONCLUSIONS

The primary purpose of this study was to identify the relationship between passive knee laxity and contributors to active knee stability in participants with severe OA. Contrary to our hypothesis, we found no associations between passive varus-valgus laxity and average quadriceps activity or any of the co-contraction indices during gait. Stability of the knee joint necessitates a complex control strategy; further study is needed to understand the contributions of passive and active structures in osteoarthritic populations.

REFERENCES

1. CDC. *MMWR: Morbidity and Mortality Weekly Report* **58**, 421-426, 2009.
2. Sharma L. *Arthritis Rheum* **42**, 861-870, 1999.
3. Schipplein OD and Andriacchi TP. *JOR* **9**, 113-119, 1991.
4. Rudolph KS, et al. *KSSTA* **8**, 262-269, 2000.
5. Siston RA, et al. *J Biomech Eng* **134**, 115001, 2012

ACKNOWLEDGEMENTS

Funding for this study came from award number R01AR056700 from the National Institute of Arthritis and Musculoskeletal and Skin Diseases.

INFLUENCE OF TENDON STIFFNESS ON MUSCLE-TENDON INTERACTION DYNAMICS DURING CYCLIC CONTRACTIONS

¹ Jonathan A. Doering and ¹ Gregory S. Sawicki

¹UNC-NC State Joint Department of Biomedical Engineering, Raleigh, NC, USA
email: jadoerin@ncsu.edu

INTRODUCTION

Series elastic elements (SEE) (e.g., tendon and aponeurosis) are critical for efficient contractions during cyclic, steady locomotion tasks (e.g., walking, hopping, running), as they can store and return significant mechanical energy, reducing mechanical work required by muscle (CE) [1]. In many clinical conditions, the SEE stiffness is altered, becoming either more or less stiff [2]. In addition, the SEE of muscle-tendon units (MTU) tend to get relatively longer when moving from proximal to distal lower-limb joints. The goal of this study was to examine how changes in MTU architecture via altered SEE stiffness impact the ‘tuned’ interaction between CE and SEE during cyclic locomotion. We hypothesized that there would be an optimal, intermediate SEE stiffness that generated high MTU forces, isometric strut-like CE behavior, and facilitated large amounts of elastic energy storage and return in the SEE (i.e., ‘tuned’ MTU dynamics).

METHODS

We employed a MTU model containing a muscle contractile element (CE) with a parallel elastic element (PEE) and a series elastic element (SEE) that acted in opposition to a point mass experiencing constant gravitational forces, simulating MTU dynamics of the lumped ankle plantarflexors during cyclic contractions [3] (Fig. 1). Force was generated in the modeled CE by a Hill-type muscle with classic force-length and – velocity relationships, with stimulation modeled as a square wave pulse with a duty of 10% relative to the cycle period. The PEE and SEE followed non-linear force-displacement relationships taken from recent literature, and the SEE compliance was parametrized by specifying the stiffness, k_{SEE} , in the linear region. To address the role of SEE stiffness on MTU interaction dynamics we compared MTUs with k_{SEE} in a compliant ($=60\text{kN/m}$), baseline ($=180\text{kN/m}$) and stiff ($=540\text{kN/m}$) setting. Then we performed two simulation protocols on each case: (1) a ‘passive pluck’ of the modeled MTU where the passive components oscillated against the load (i.e. no stimulation, to establish the natural frequency) and (2) a dynamic contraction, where the MTU was actively driven with neural stimulus at the passive natural frequency from baseline condition ($\approx 2.2\text{Hz}$) and 10% duty factor. Finally, to address the hypothesis, we extracted and compared force, length change and mechanical power dynamics of the MTU, CE and SEE from each simulation case.

RESULTS

The passive resonant frequencies, ω_0 , computed based on a period of oscillation from ‘passive plucks’ for $k_{SEE}/3$, k_{SEE} , and $k_{SEE} \cdot 3$ were 1.64, 2.20, and 2.36 Hz, respectively. Results from the dynamic contractions driven at $\omega_{DRIVE} = 2.2\text{Hz}$ and 10% duty (i.e., stimulation period = 450ms; duration=45ms)

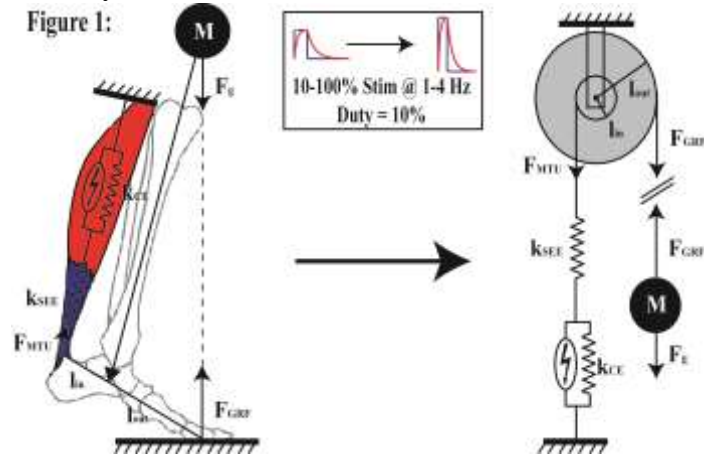


Figure 1. Lumped ankle plantarflexor MTU model of vertical hopping. A bodymass in gravity with fixed mechanical advantage (L_{in}/L_{out}) simulates ankle MTU dynamics during cyclic contractions. Simulations were performed with series elastic stiffness, k_{SEE} at baseline (180kN/m), $k_{SEE}/3$ (54kN/m) and $k_{SEE} \cdot 3$ (540kN/m).

demonstrated that in the compliant $k_{SEE}/3$ condition (i.e., $\omega_{DRIVE} > \omega_0$) (Fig. 2, left), the MTU produced less force, underwent more excursion at lower velocity, and produced less mechanical power than the baseline k_{SEE} condition (Fig. 2, middle). With a compliant SEE, the CE underwent significant length changes, shortening in the first half of the contraction and performed more mechanical work than baseline. In the stiff $k_{SEE} \cdot 3$ condition (i.e., $\omega_{DRIVE} < \omega_0$) (Fig. 2, right) the MTU produced similar force but at higher rate and with more passive contribution, underwent less excursion at lower velocity and produced less mechanical power than baseline. With a stiff SEE, the CE underwent significant length changes, lengthening in the first half of the contraction and performed more mechanical work than baseline.

CONCLUSIONS

These results strongly support our hypothesis that there is a ‘sweet spot’ in SEE stiffness that leads to ‘tuned’ MTU interaction with high forces and the

majority of the MTU mechanical power cycled in elastic tissues. If the SEE is too compliant, the CE undergoes internal shortening, performs significant mechanical work suffers reduced force production force output suffers due to force-length relationship of muscle. If the SEE is too stiff, the CE is passively stretched, and can produces high forces at high rate, but at dangerously long lengths. These results suggest an underlying fundamental principle; that for optimal function, neural drive of an MTU should match its architecture such that it is driven near its passive natural frequency.

REFERENCES

1. Roberts, T.J., et al., *Science*, 1997. **275**(5303): p. 1113-5.
2. Roy, A., et al., *Journal of Rehabilitation Research and Development*, 2013. **50**(4): p. 555-571.
3. Robertson, B.D. and G.S. Sawicki, *J Theor Biol*, 2014. **353**: p. 121-32.

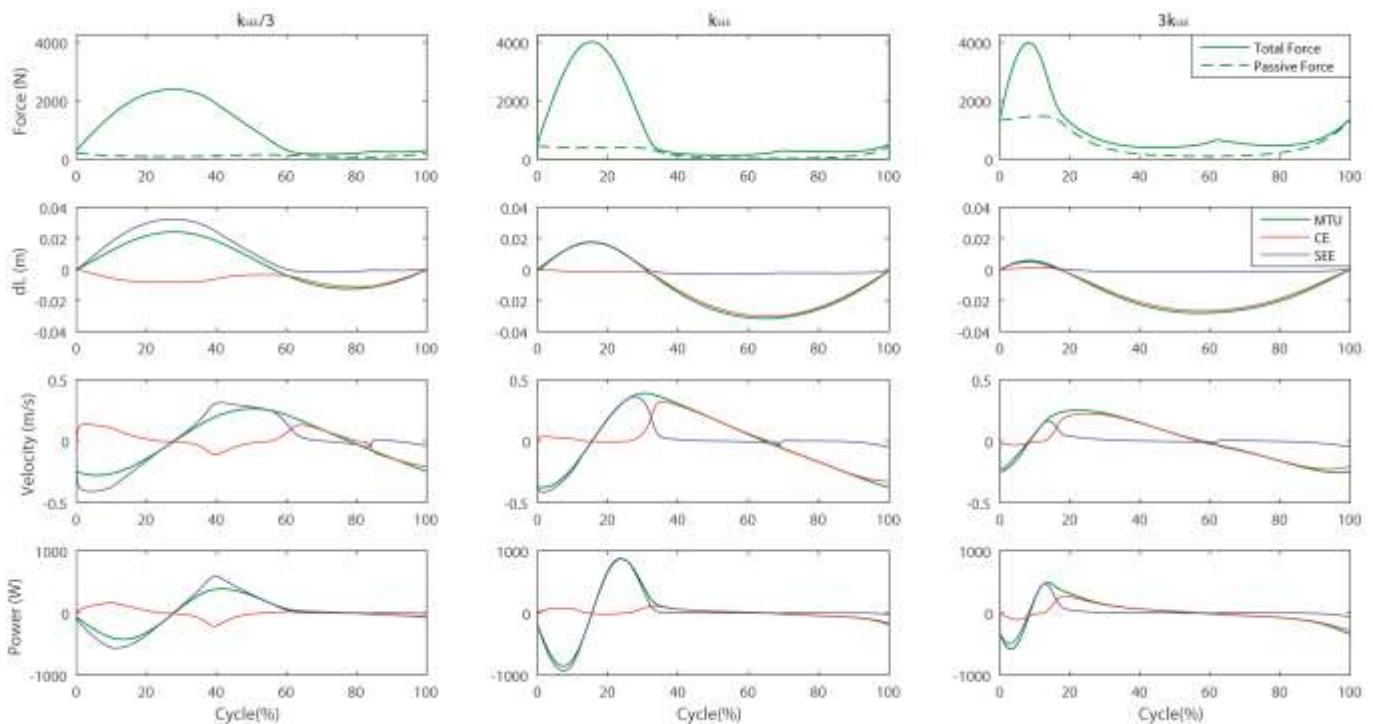


Figure 2. Simulated ankle plantarflexor contraction dynamics for MTUs of varying compliance in steady locomotion cycles. Force, length change, velocity and mechanical power (top to bottom) for MTU (green), CE (red) and SEE (blue) during contraction cycles with k_{SEE} going from compliant ($k_{SEE}/3=60\text{kN/m}$) to baseline ($k_{SEE}=180\text{kN/m}$) to stiff ($k_{SEE}=540\text{kN/m}$) (left to right). Baseline shows optimal ‘tuning’ for efficient contractions dominated by elastic energy storage and return in SEE.

3D FINITE-ELEMENT MODELING OF THE SOFT PALATE REVEALS SYNERGIC ACTIONS OF SPEECH MUSCLES

¹ Joshua M. Inouye, ² Jamie L. Perry, ¹ Kant L. Lin, and ¹ Silvia S. Blemker

¹ University of Virginia, Charlottesville, VA, USA

² East Carolina University, Greenville, NC, USA

email: ssblemker@virginia.edu

INTRODUCTION

The velopharyngeal (VP) mechanism is a complex deformable system consisting of several muscles and complicated soft tissue geometry within the soft palate. Understanding the mechanics of this system is essential for developing effective treatments for speech disorders and improving surgeries for cleft palate patients. However, the mechanics of the soft palate are complex. Several muscles interact with one another to move the soft palate during speech, and the physics of the interactions between these muscles are poorly understood. The goal of this work is to develop a multi-muscle model of the soft palate and use model to examine how the various muscles of the soft palate contribute to the movement of the soft palate during speech.

METHODS

We created a 3D finite element model of the VP mechanism based on MRI scans of a 20-year-old Japanese male subject with normal VP anatomy. The model components included the soft palate, the posterior pharyngeal wall (PPW), the levator veli palatini muscle (L), the musculus uvulae (U), and the palatopharyngeus muscle (P) (Figure 1).

Simulations were based on the muscle and soft tissue mechanical properties from the literature [1,2]. The soft tissue was modeled as an isotropic, hyperelastic Mooney-Rivlin material with elastic modulus of 25kPa and muscle was modeled as a transversely isotropic material. Muscle fiber trajectories for the muscle material were determined using computational fluid dynamics [3]. We used SefeaTM (Strain-Enriched FEA, AMPS Technologies) finite element solver with explicit strain energy function specification and automatic meshing of 4-node enhanced tetrahedral elements to

run the simulations [4]. In these half-symmetry simulations, we activated all combinations of the three simulated palate muscles. We measured soft palate elevation, closure force, and contact length (Figure 2a) for each combination at muscle activation levels ranging from inactive to fully active, smoothing the variables to remove numerical noise.

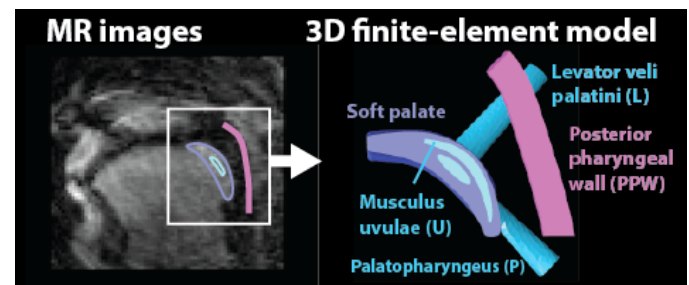


Figure 1: We used MR images to create a 3D finite-element model of the velopharyngeal mechanism with three muscles (cyan).

RESULTS

The different combinations of muscle activations show markedly different deformations (Figure 2b). Deformations in dynamic speech MRI data [5] compared favorably with model deformations for L activation (Figure 2c). L and LU activation reached similar soft palate elevations as the MRI data (Figure 2d). Experimental speech data for closure force [6] compared most favorably with L and LU activation (Figure 2d). L, LU, LP, and LUP activation combinations were able to produce contact length ranges measured in a previous MRI study [7] (Figure 2d).

DISCUSSION

The different deformations created by muscle activations show both synergistic and antagonistic actions. For example, L and P synergize to retract

the velum towards the PPW. However, their effects on soft palate elevation are antagonistic. Proper action of L (the largest palate muscle) is necessary but not sufficient to reproduce data comparing favorably with experimental data in normal speech (Figure 2d). These deformation patterns and future modeling studies will help in surgical planning for cleft palate patients (where the musculature must be surgically reconstructed) and aid in clinical assessment of dysfunctional motor control during speech. More broadly, these simulations demonstrate the applicability of muscle biomechanical analysis to studies of speech function.

REFERENCES

1. Inouye JM, et al. *J Craniofac Surg*, In press, 2014.
2. Blemker SS, et al. *J Biomech* **38**, 657-665, 2005.
3. Inouye JM, Handsfield GG, et al. *Submitted to Proc. Am. Soc. Biomech*, Columbus, OH, USA, 2015.
4. Inouye JM, Perry JL, et al. *Submitted to Proc. Am. Soc. Biomech*, Columbus, OH, USA, 2015.
5. Perry JL, et al. *Cleft Palate-Cran J* **51**(4), 476-85, 2014.
6. Kuehn DP, Moon JB. *J Speech Lang Hear R.* **41**(1), 51-62, 1998.
7. Inouye JM, et al. *Proc. Am. Cleft Palate Assoc.*, Orlando, FL, USA, 2013.

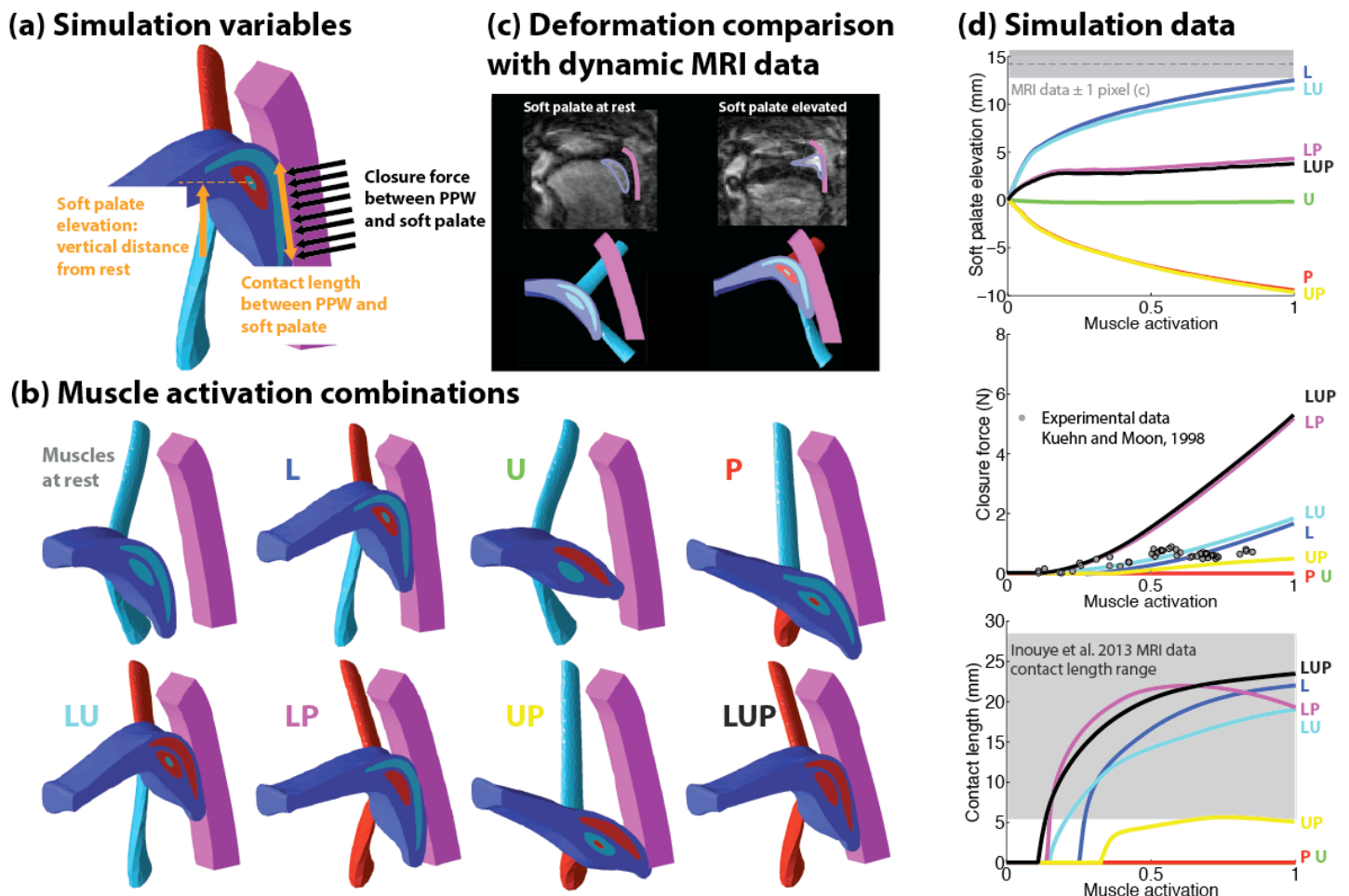


Figure 2: (a) Measured simulation variables. (b) Different muscle activations produced markedly different deformations. Red muscles are active; cyan muscle are inactive. (c) Deformations in dynamic MRI data [1] compared favorably with model deformations for L activation (d) Activation of L is necessary for the model data to compare favorably with experimental values, highlighting the importance of its proper reconstruction in cleft palate repair.

AGENT-BASED MODEL OF INFLAMMATION AND REGENERATION FOLLOWING CONTRACTION-INDUCED MUSCLE INJURY

Kyle S Martin, Kelley M Virgilio, Shayn M Peirce and Silvia S Blemker
The University of Virginia, Charlottesville, VA, USA
email: ksm5ha@virginia.edu

INTRODUCTION

Skeletal muscle has an extraordinary ability to regenerate and recover from injury. After the initial insult (such as a contusion, toxin, laceration, contraction-induced injury, etc.), muscle tissue regenerates through a sterile inflammatory response [1]. This response involves the spatially dynamic recruitment and activation of numerous cells, including neutrophils, macrophages, satellite stem cells, muscle fibers, and fibroblasts [1]. The timing and magnitude of response is dependent on the type and severity of injury. For instance, muscle regeneration and speed of recovery is different between a single lengthening contraction with large strain vs. multiple contractions with a small strain [2]. Additionally, the timing of recruitment of inflammatory cells have been shown to be dependent the number of muscle contractions.

In this study, we wish to probe the differences in the inflammation and muscle regeneration responses across varying levels of strain-induced injury. We have developed a novel multi-scale modeling platform that couples micromechanical finite element modeling with cellular level agent-based modeling in order to explore injury-related inflammation and muscle regeneration.

METHODS

The flow of our modeling framework can be summarized in six steps. Step 1: we utilized an agent-based model to create a cross-section of a muscle fascicle (muscle fibers and ECM) [3]. Step 2: we created a micromechanical model reflecting the same cross-sectional geometry [4, 5]. Step 3: we applied boundary conditions to the micromechanical model based on a macro-scale simulation of an eccentric contraction (similar to [5]). Step 4: the predicted strains were mapped onto our agent based model. Areas of strain above a threshold of 15% were considered damaged and

simulated as necrotic tissue. Step 5: we simulated inflammation and regeneration at the cellular level using our agent based model. In agent based modeling (ABM), agents are given rules or behaviors to follow. In our model, each cell was considered an agent. Over 50 rules were defined in the ABM, many of which are stochastic in nature. A subsample of these rules is provided in Table 1. We tracked the interactions between and among satellite stem cells, neutrophils, pro- and anti-inflammatory macrophages (labeled M1 and M2 in Table 1 and Fig 1), muscle fibers, and fibroblasts. Our primary output focused on inflammatory cell populations through 10 days of regeneration.

RESULTS

The simulations were able to generate inflammation responses similar to published literature [1,6]. In particular, the timing and peak populations of the simulated neutrophils and M1 macrophages were generally consistent with muscle injury studies [1,6]. However, muscle injuries often result in a M2 macrophage population peak around day 4-7, and ours peaked around day 3. However, the predicted M2 population remained elevated for the entire 10-day simulation period, which has been seen in the literature [1,6].

DISCUSSION

The presented results illustrate the potential of predicting the inflammatory and regenerative response from injury. While our current data includes one strain profile and threshold of damage, which resulted in ~20% damage, future work will include predicting the response from low, medium, and high levels of strain. We wish to explore changes in inflammation and recovery from different damage profiles, something that has been seen previously [2]. Furthermore, the model has application to prediction of the behavior of many cell types and muscle fiber metrics that are also

highly applicable to the regenerative response of muscle, including fibroblast and satellite stem cell populations, necrotic/damaged area, and average fiber cross sectional area (CSA).

REFERENCES

1. Tidball, JG. *Am J Physiol Regul Integr Comp Physiol* **298**, R1173 – 87, 2010.

2. Lovering, RM. *Arch Phys Med Rehabil* **88**, 617 – 25, 2007.

3. Martin, KS. *J Appl Physiol* 2015

4. Virgilio, KM. *Interface Focus* 2015

5. Virgilio, KM. *ASB annual meeting* 2015 (submitted abstract)

6. Paulsen, G. *Med Sci Sports Exerc* **42**, 75 – 85, 2010.

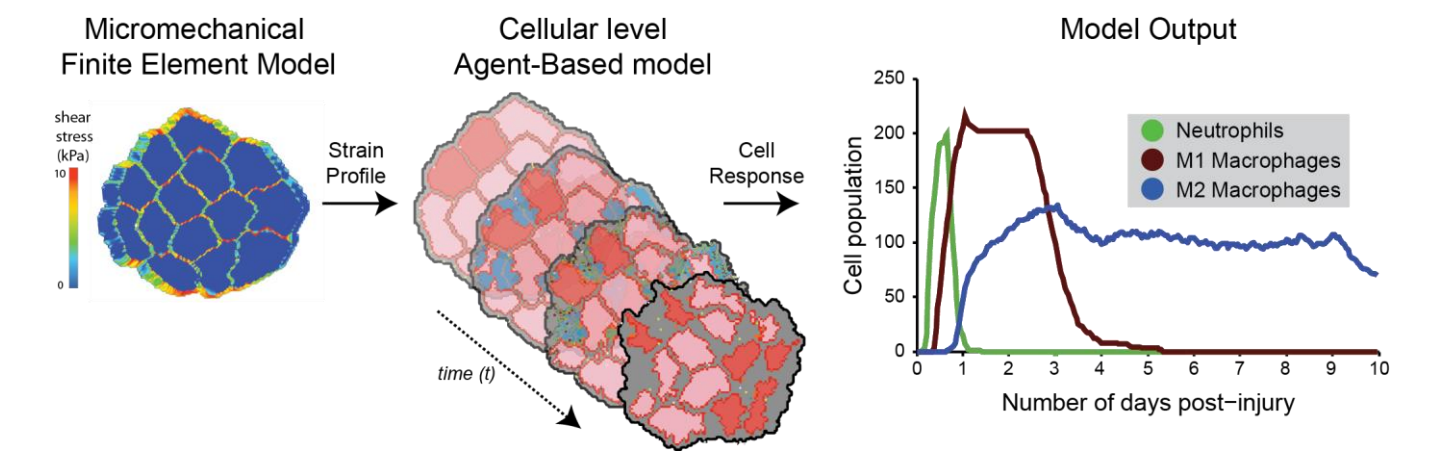


Figure 1: Multiscale computational model simulates how changes in strain affect dynamic muscle remodeling and inflammation. (From left) Screen shot of a simulated muscle fascicle cross-section showing how the micromechanical finite element model predicts shear stress throughout the muscle cross-section. A strain profile was outputted to the agent-based model (middle); where strain levels exceeding a threshold proscribed the locations of muscle fiber damage. Muscle fibers that are damaged become necrotic and produce damage-related proteins that invoke inflammation in the model. Populations of different inflammatory cells are tracked over the course of 10 days (right).

Table 1. Example rules implemented in the ABM	
Behavior	Rule
Fibroblast secretion of IGF-1 as function of strain	8.8×10^{-5} pg/cell/hr
Fibroblast apoptosis in response to TNF-alpha, where baseline apoptosis rate equals one cell every 15 days	If $0.2 < \text{TNF} < 20$ ng/ml: apoptosis rate = baseline apoptosis rate + $(2.5 * (\log \text{TNF-alpha}) + 2.75) * 100 - 100$
Change in muscle fiber cross-sectional area as a function of protein synthesis and degradation.	$d\text{CSA}/dt = \beta S - \beta D * \text{CSA}$ βS : protein synthesis coefficient ($\mu\text{m}^2/\text{hr}$) βD protein degradation coefficient (1/hr). CSA: Cross sectional area
Neutrophils apoptose after phagocytosis of necrotic tissue, and each phagocytosis event makes it more likely to apoptose	Neutrophil: If $\text{random}(3) + 3 \leq \# \text{ of phagocytosis events}$ then become apoptotic
Macrophages switch phenotype when they engulf apoptotic neutrophils: if a macrophage engulfs 2 apoptotic neutrophils it has a chance of polarizing from M1 to M2.	M1 Macrophage: If $\text{random}(6 - \# \text{ of neutrophils engulfed}) < 1$ then become M2 Macrophage
Activated satellite cells sense growth factor and secrete chemokines that attract macrophages.	If Hepatic Growth Factor > 10 ng/ml then satellite cells produce MCP-1 at a rate of 0.15 ng/hr/cell

EFFECTS OF Q-ANGLE AND TIBIAL SLOPE ON ANTERIOR CRUCIATE LIGAMENT FORCE: A FINITE ELEMENT STUDY

¹A. Amerinatanzi, M. Ingels, J. Kinn, R. Summers, E. Nyman, A. Kiapour, ²A.M. Kiapour, ³T.E. Hewett, ¹V. Goel

¹Engineering Center for Orthopaedic Research Excellence (E-CORE), The University of Toledo, Toledo, OH, USA

²Sports Medicine Research Laboratory, Department of Orthopaedic Surgery, Boston Children's Hospital, Harvard Medical School, Boston, MA

³Sports Health and Performance Institute, The Ohio State University, Columbus, OH

Email: Vijay.Goel@utoledo.edu

INTRODUCTION

Many factors contribute to the resultant forces in the anterior cruciate ligament (ACL). Rapid generation of ACL force has the capability to induce ruptures that can lead to significant osteoarthritis and reduction in sport activity. Substantial research has contributed to understanding the effects of subject-specific geometry and its relation to force propagation in the ACL. Important geometric parameters of the knee joint include the Q-angle, and coronal, lateral, and medial tibial slopes. The goal of this study was to evaluate the effect of patient-specific Q-angles and coronal/lateral/medial tibial slopes on ACL force during flexion through the use of subject specific validated finite element models of the knee joint.

METHODS

MRI and CT images were obtained from three subjects with no history of knee injury. The Q-angle, and coronal, lateral, and medial tibial slopes were calculated using ImageJ (NIH, Bethesda, Maryland) and Mimics v15.0 (Materialise, Leuven, Belgium). Q-angle was calculated by the angle formed by the intersection of the center of the patella, the center of the femoral shaft, and the center of the tibial tuberosity [1]. The tibial slope was determined by identifying the outer-most points of the lateral and medial sides of the tibial plateau, and bisecting that line with a line generated from multiple points along the center of the tibial shaft [2]. Subject-specific finite element models were developed from three sets of MRI and CT images. 3D geometries of hard and soft tissues were digitized using Mimics v15.0 (Materialise, Leuven, Belgium). Geometries were converted into solid 8-node hexahedral elements for the patella, ligaments (ACL, MCL, LCL, and PCL), and menisci. The geometries of the femur, fibula, and tibia were constructed with an outer layer of wedge C3D6

elements for cortical bone and tetrahedral C3D4 elements for cancellous bone. Cartilage utilized tetrahedral C3D4 elements. Meshes were imported into ABAQUS 6.11-2 (SIMULIA, Providence, RI, USA). Capsules, muscles, tendons, and remaining ligaments were simulated using uniaxial truss elements.

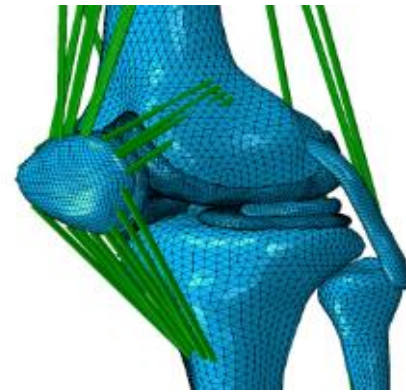


Figure 1 – ABAQUS Knee Joint Model

The material properties of the ACL, PCL, and MCL were modeled with hyper-elastic properties. Material properties of all other tissues were modeled as linear elastic with different moduli assigned to the corresponding tissue. The femur, fibula, and tibia were defined as non-deformable rigid bodies. All uniaxial truss elements were defined as incompressible. The resultant models were validated against cadaveric testing on 18 fresh frozen legs undertaken at our lab [3]. Model validation was achieved by subjecting cadaveric specimens to loading conditions to simulate tibial rotation, anterior shear, and valgus/varus moments during knee flexion. Simulations consisted of a 100N anterior shear force in static loading conditions at 0, 10, 20, and 30 degrees of flexion.

RESULTS

Geometric Angle (Deg)	MODEL 1	MODEL 2	MODEL 3
Coronal Tibial Slope	1.41	5.03	4.76
Lateral Tibial Slope	5.18	5.62	4.10
Medial Tibial Slope	0.85	1.22	1.60
Q-Angle	18.99	14.27	18.00

Table 1 – Q-Angle and tibial slope comparison between models

The Q-Angle ranged from14.3 to 19.0 degrees and the range of the slopes for the three models are listed in Table 1.

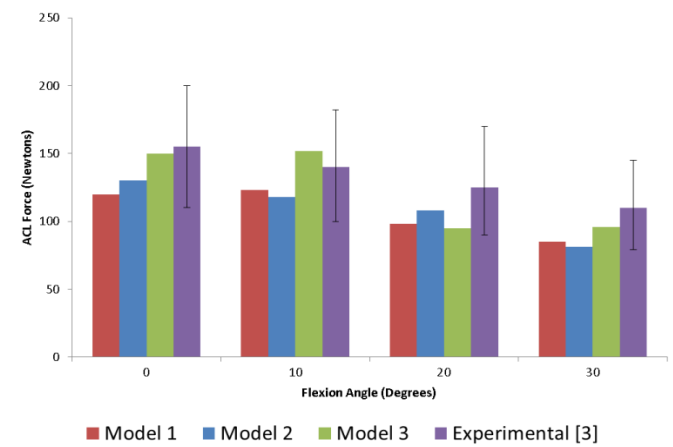


Figure 2 – ACL force prediction as a function of flexion angle as compared with ex-vivo data [3].

ACL force varied amongst the three models, as shown in Figure 2. Model 3 demonstrated a 25% increase in force at lower flexion angles (i.e., 10 degrees of flexion).

DISCUSSION

As supported by these preliminary results, variability in model-specific geometric factors and relative positioning (knee joint flexion angle) contribute to ACL force. Tibial geometry (coronal, lateral, and medial tibial slope) and Q-angle contributed to up to a 25% change in ACL force in the 0-10 degree flexion range. Variability in geometry has been previously implicated in changes of joint kinematics and kinetics. This study provides a solid framework upon which to build future studies with sensitivity analysis, greater sample sizes, and more comprehensive geometric and kinematic variability.

REFERENCES

1. Smith T, Knee Surg Sports Traumatol Arthrosc. 2008: 16:1068-79
2. Hashemi J, J Bone Joint Surg Am. 2008: 90:2724-34
3. Kiapour A, ASME 2014: 136:011002
4. Markolf K, JORS 1995: 13.6:930-935

ACKNOWLEDGEMENTS

Work supported by National Institutes of Health (Grants 5- R01 AR056259-06-TEH).

EFFECT OF DEEP MEDIAL COLLATERAL LIGAMENTS ON MENISCUS MOTION

¹Trent M. Guess, ¹Swithin Razu and ¹Hamidreza Jahandar

¹The University of Missouri, Columbia, MO, USA

email: guesstr@health.missouri.edu, web: www.mizzoumotioncenter.com

INTRODUCTION

The extent of meniscus motion on the tibia plateau and the role of peripheral attachments in limiting this motion are not completely understood. Anatomical studies of the deep medial collateral ligament (dMCL) have separated it into two functional units, the menisiofemoral and menisiotibial divisions, with stout attachments to the meniscus described [1]. But, based on their cadaver study, Stein et. al. concluded that the medial collateral ligament did not affect the stability of the medial meniscus [2]. In the current study, subject specific computational models coupled with subject specific leg motion are used to predict meniscus excursion on the tibial plateau. The effect of the dMCL meniscal attachments on medial meniscus motion is also explored.

METHODS

Two adult females (Subject 1: age 20 years, height 159.5 cm, mass 59.0 kg, Subject 2: age 29 years, height 170 cm, mass 70.3 kg) free of any lower extremity problems participated in this study after providing written informed consent approved by the institution's human subjects review board. Magnetic resonance images (MRI) were acquired of each subject's right leg and the images converted to geometries of bone, cartilage and menisci. Ligament insertions and origins were also determined. Leg motion during passive movement of the knee (laxity test) was recorded using a VICON motion capture system. During these laxity tests, an orthopaedic surgeon manipulated the knee of each subject through its complete range of flexion-extension, abduction-adduction and internal-external rotations while taking care to minimize any applied forces.

Computational models were developed in the multibody dynamic analysis program ADAMS (MSC Software Corporation, Santa Ana, CA).

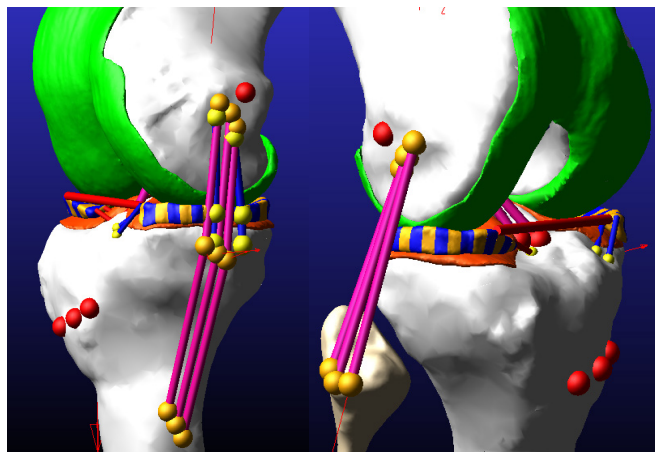


Figure 1: Medial and lateral view of subject 2 multibody knee model.

Deformable contacts were defined between tibial and femoral cartilages. The ligaments were attached to the bones according to the identified origin and insertion sites. The anterior cruciate ligament and posterior cruciate ligament were both separated into two bundles. The lateral collateral ligament was separated into three bundles and the medial collateral ligament was separated into five bundles, three superficial (sMCL) and two deep bundles (dMCL). The three bundles of the sMCL wrapped around the tibia. Each ligament bundle was modeled as a tension only nonlinear spring using a piecewise function that described its force-length relationship [3]. The menisci were modeled as previously described [4]. Briefly, the menisci geometries were sectioned into multiple wedge shaped rigid bodies connected by 6 x 6 stiffness matrices. The medial and lateral menisci were sectioned at 10° intervals radiating from the geometric center of each meniscus. For the two subjects, the medial meniscus was divided into 20 rigid bodies and the lateral meniscus was divided into 25 rigid bodies. Mass properties were assigned to each meniscus element based on its volume and a density of 1,100 kg/m³. Deformable contacts were defined between each meniscus element and tibial cartilage and femoral cartilage geometries. The menisci were connected

to the tibia via four horn attachments and the anterior intermeniscal ligament was also included. The two bundles of the dMCL were connected to the medial menisci via three-axis springs.

Localizers that appeared in both the MRI and motion capture system were worn by each subject and used to place the knee model relative to the motion capture markers. Motion constraints that followed motion capture marker trajectories were used in the initial simulation. The motion constraints were connected to the femur and tibia via three-axis springs. These initial laxity simulations were used for fine adjustment of the femur and tibia position and to determine the zero-load lengths of each ligament bundle. After adjustments, relative motion between the tibia and femur using Grood and Suntay [5] local coordinates was recorded during simulation. For the final laxity simulations, the femur was held fixed and the recorded tibia motion was applied to the bone through a 6-axis spring. The laxity simulations included multiple flexion-extension cycles ranging from 0 to 140°. Additional simulations included internal-external knee rotation (range of 40°) added to the laxity motion and simulations with the dMCL attachments to the menisci removed.

RESULTS AND DISCUSSION

During the laxity simulation both knees exhibited the screw home mechanism, rotating externally from 25° flexion to full extension. In addition, the max force required to move the tibia through the laxity motion was less than 30 N for both knees and maximum torque less than 0.7 N-m. Anterior-posterior menisci excursion on the tibia plateau during laxity simulations are provided in Table 1. The medial and lateral menisci translated posteriorly with flexion. Lateral excursion is greater than medial excursion for both knees and the excursion distance is within that measured by Yao et. al. during passive extension and flexion (lateral meniscus 8.2 ± 3.2 mm, medial meniscus 3.3 ± 1.5 mm, $n=10$) [6]. For the laxity simulations with added internal-external rotation, the excursion distance increased for both the lateral and medial menisci (Table 2). Removing the dMCL meniscal attachments increased anterior-posterior excursion

of the medial meniscus. Additionally, the increase in motion occurred during internal rotation (Fig. 1).

Table 1: Anterior-posterior excursion of the middle meniscus element during laxity simulation.

Laxity		
	Lateral	Medial
Sub 1	6.9 mm	4.2 mm
Sub 2	9.8 mm	3.5 mm

Table 2: Anterior-posterior excursion of the middle meniscus element during the laxity with internal-external rotation simulation.

Laxity with Internal External Knee Rotation			
	Lateral	Medial dMCL intact	Medial dMCL transected
Sub 1	11.2 mm	8.5 mm	14.4 mm
Sub2	16.4 mm	7.5 mm	14.1 mm

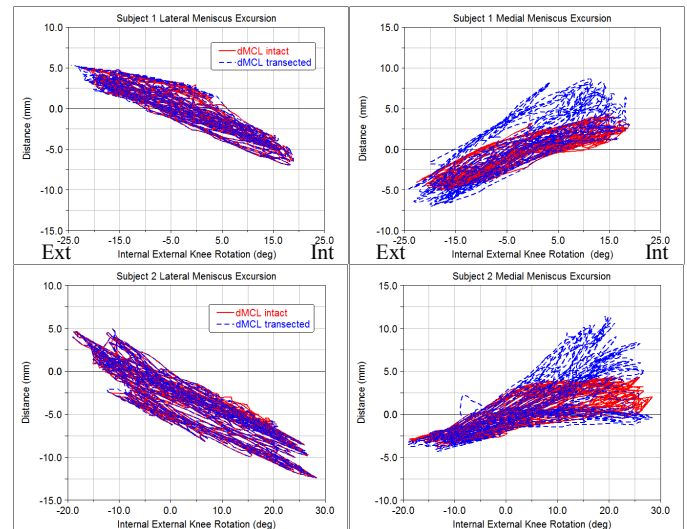


Figure 2: Anterior-posterior excursion versus internal-external knee rotation for dMCL intact and dMCL transected models.

REFERENCES

1. Laprade RF, et al., J Orthop Sports Phys Ther, 2012. **42**(3): p. 221-33.
2. Stein G., et al., Surg Radiol Anat, 2011. **33**(9): p. 763-6.
3. Guess TM, et al., J Biomech Eng, 2014. **136**(2): p. 021032-021032-9.
4. Guess TM, et al., Med Eng Phys, 2010. **32**(5): p. 505-15.
5. Grood ES, et al., J Biomech Eng, 1983. **105**(2): p. 136-44.
6. Yao, J., et al., J Orthop Res, 2008. **26**(5): p. 673-84.

MUSCLE ARCHITECTURE ANALYSIS USING COMPUTATIONAL FLUID DYNAMICS

¹ Joshua M. Inouye, ¹ Geoffrey G. Handsfield, and ¹ Silvia S. Blemker

¹ University of Virginia, Charlottesville, VA, USA
email: ssblemker@virginia.edu

INTRODUCTION

The trajectories of skeletal muscle fascicles are critical to their function, and many skeletal muscles across the body have fascicles with highly complex trajectories. Architectural descriptions of muscles account for fascicle trajectories by reporting parameters such as fascicle length, physiological cross-sectional area, and pennation angle. These parameters are typically reported as constants [1], yet it has been shown that some muscles have large distributions of these parameters [2]. Cadaveric studies of muscle architecture can be time-consuming and do not represent young healthy or patient-specific populations, and MRI diffusion tensor imaging (DTI) studies of muscle architecture can suffer from noisy data acquisition [3]. We present a method to calculate architecture parameters from arbitrarily complex muscles automatically using computational fluid dynamics (CFD). This method can be used to map and examine the three-dimensional architecture of a given muscle, and it can also be used as input to 3D finite-element models of muscle [4].

METHODS

Our method of generating fascicle trajectories using CFD analysis consists of three key steps. Step 1 is to create an image-based solid model of the muscle in Autodesk Inventor® (Autodesk Inc.). Step 2 is to export the solid model to Autodesk Simulation CFD® (Autodesk Inc.) and set up the simulation. We set the inlet pressure to 1Pa and the outlet pressure to 0Pa at the regions of fascicle origin and termination. The other surfaces are set to slip boundary conditions (Figure 1a). The fluid is set to be incompressible with a viscosity of 1Pa-s and density of 1g/cm³. This resulted in very low Reynolds numbers (<1) and good convergence.

Incompressible, laminar, viscous, and steady-state flow are prescribed. These conditions along with the boundary conditions help satisfy the observations about fascicle trajectories in muscle [3]: i) they are coaxially aligned and do not cross each other (viscous flow) ii) they do not branch (incompressible flow) iii) they will not reverse their directions abruptly (laminar flow) and iv) they must connect between attachment points (boundary conditions).

Step 3 is to export the flow direction vectors from the CFD mesh into Matlab (Mathworks Inc.) to perform fascicle and pennation angle analysis. The fascicles are traced and their length distributions are computed (Figure 1b). In addition, pennation angle distributions are calculated using a tendon vector specification from the distal tendon, as in [1] (Figure 1c).

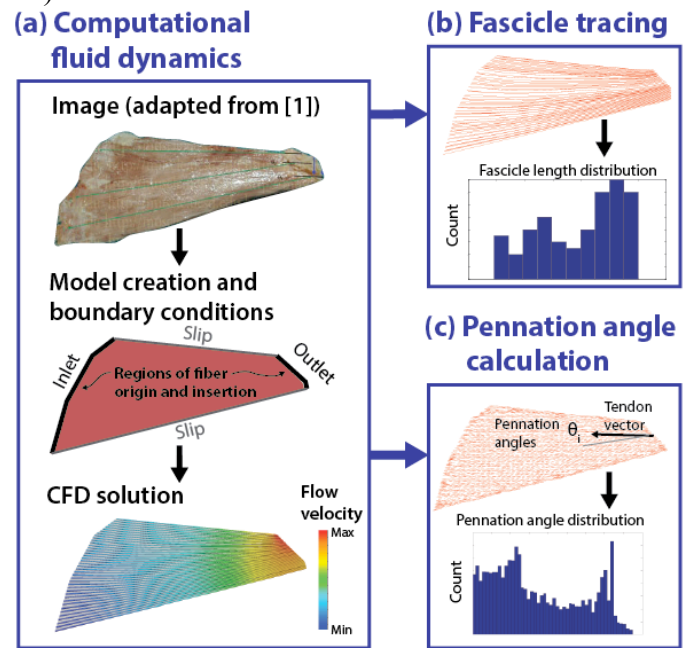


Figure 1: (a) We create image-based models and use CFD to determine muscle architecture parameter distributions for (b) fascicle lengths and (c) pennation angles.

We performed the process on a 2-D image of the adductor brevis [1] and a 3-D MRI-based model of the biceps femoris longhead [5]. We compared the adductor brevis calculations with a previous cadaver study [1].

RESULTS

The mean fascicle length for the 2D adductor brevis model (raw, unadjusted for sarcomere length) was 12.9cm (Figure 2a). This can be compared to the published raw fascicle length average measurements of 11.1cm with standard deviation of 1.53cm across 21 cadavers (10.3 ± 1.42 cm optimal fascicle length and 2.91 micron average sarcomere length). The pennation angle distribution ranged from 0 to 17 degrees, with an average of 6.9 degrees (Figure 2a). The cadaver study measured 6.1 degrees mean and 3.1 degrees standard deviation averaged across cadavers.

The CFD solution for the 3D biceps femoris longhead model computed realistic fascicle trajectories and enabled automatic calculations of the fascicle length and 3D pennation angle distributions (Figure 2b).

DISCUSSION

We have proposed a method using computational fluid dynamics to automatically compute muscle architecture parameters and their distributions

within the muscle. The method leverages the power of CFD solvers and also enables efficient fascicle mapping for finite-element studies of muscle. The advantages of this method over other methods include ease of implementation and objective, efficient calculation of 3D muscle architecture parameters. Flow guiding surfaces can be incorporated so that complex observed features such as twisting or MRI-DTI data can be incorporated. One limitation of this method is that the fascicles are measured implicitly from the geometry of the muscle and not directly measured. However, the close correlation of the direct cadaver measurements with our computational measurements for the adductor brevis provides preliminary validation of the method. This method has great potential to enhance and empower *in vivo* architecture studies (e.g., using MRI) on arbitrarily complex muscle geometries.

REFERENCES

1. Ward SR, et al. *Clin Orthop Relat Res.* **467**(4), 1074-1082, 2009.
2. Blemker SS, et al. *Ann Biomed Eng* **33**(5), 661-673, 2005.
3. Choi HF and Blemker SS. *PLoS One.* **8**(10), e77576, 2013.
4. Inouye JM, et al. *J Craniofac Surg*, In press, 2014.
5. Rehorn MR and Blemker SS. *J Biomech* **43**(13), 2574-2581, 2010.

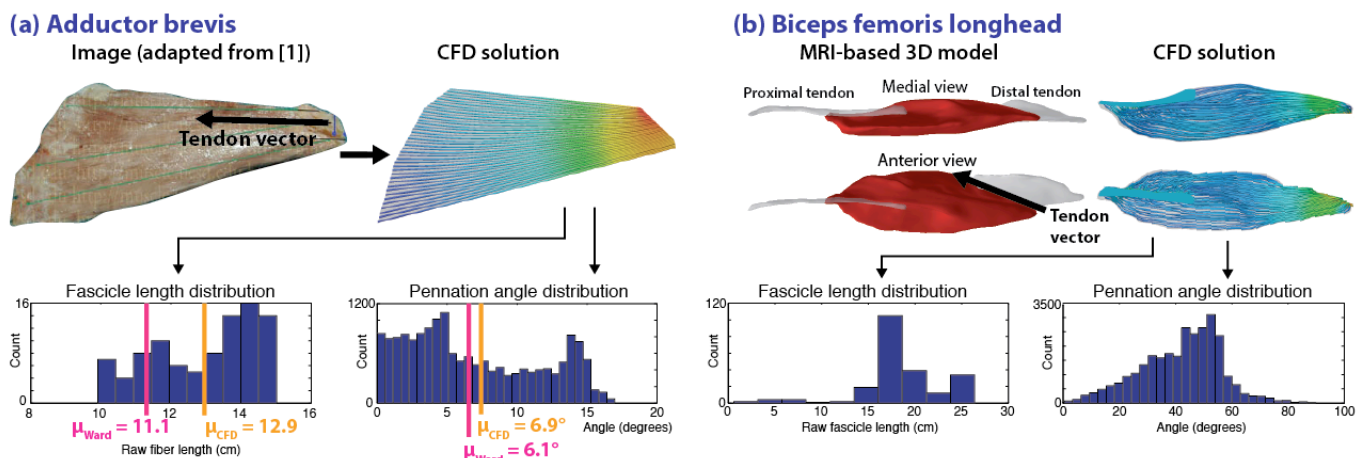


Figure 2: (a) Mean muscle architecture parameters calculated with CFD compare favorably with those in a previous cadaver study [1]. (b) CFD computes realistic fascicle trajectories and fascicle length and pennation angle distributions in 3D.

INDIVIDUAL DIFFERENCES IN REQUIRED COEFFICIENT OF FRICTION AFFECT SLIP RISK DURING LEVEL WALKING

¹ Kurt Beschorn, ¹ Devon Albert, ¹ Mark S. Redfern

¹ The University of Pittsburgh, Pittsburgh, PA, USA

email: beschorn@pitt.edu, web: <http://www.engineering.pitt.edu/KurtBeschorn/>

INTRODUCTION

Slip and fall accidents are a major source of occupational and public health injuries. Previous studies have demonstrated that slipping risk can be predicted from the difference between the available coefficient of friction (ACOF) and the required coefficient of friction (RCOF) using a logistic regression equation [1]. This logistic regression equation predicts that slipping risk is most sensitive to RCOF when the RCOF and ACOF are approximately equal and that increased RCOF is associated with a higher risk of slipping. Several studies have used RCOF as a measure of individual slip risk [2, 3] under the assumption that subtle changes in RCOF alter slipping risk. Surprisingly, however, the link between individual RCOF and slip risk has not been confirmed experimentally.

The purpose of this study is to determine if individual differences in RCOF are predictive of slip risk. The shoe-floor-contaminant conditions were selected such that the shoe-floor ACOF was approximately equal to RCOF for gait.

METHODS

Thirty healthy and young subjects (13 female, 17 male) between the ages of 20 and 35 years were recruited to participate. Participants signed informed consent and the study was approved by the University of Pittsburgh Internal Review Board.

Each participant performed a series of baseline walking trials to characterize their RCOF and two unexpected slipping trials. Boots with three different outsole materials were used in this study. Subjects wore tight-fitting clothing, a safety harness and reflective markers including one placed on the heel of the boot to track slip distance. After being

randomly assigned to an initial pair of boots, subjects completed between five and eight baseline walking trials, were unexpectedly slipped, changed into a different pair of boots with a different outsole material, completed 10-23 additional baseline walking trials and then were unexpectedly slipped again. A 50% glycerol/50% water solution was applied to a vinyl floor during the unexpected slips. The three boots had an identical upper region, identical tread pattern but different materials. The three materials included a hard material (Shore A: 85), a moderate hardness material (Shore A: 76) and a soft material (Shore A: 64). ACOF values were measured as the ratio of shear forces to normal forces recorded by a force plate while a slip tester applied a normal force of 250 N, a sliding speed of 0.3 m/s and a shoe-floor angle of 7°. ACOF values for the three shoes were: 0.149 (hard), 0.168 (moderate hardness) and 0.179 (soft).

RCOF was calculated and averaged for the five baseline walking trials preceding each slip. The RCOF was defined as the peak ratio of resultant shear to normal force for the intervals when the normal force exceeded 100 N, the ratio was increasing with time, and the anterior/posterior force was in the anterior direction [4]. The resultant sliding distance of the heel marker between heel contact and slip stop (defined by the first minimum in slip velocity after the maximum velocity or when the foot sliding off of the force plate) was used to characterize a slip. A slip distance exceeding 10 mm was considered a slip, while smaller slip distance were considered a non-slip.

ANOVA methods were used to determine if the boot outsole material, the slip order or their interaction (independent variables) affected the RCOF (dependent variable). The effect of RCOF on slipping risk was examined using a logistic

regression model with slip outcome as the dependent variable and RCOF as the prediction variable.

RESULTS AND DISCUSSION

RCOF did not vary significantly across the different boot materials or between the first and second slip. The interaction between outsole material and slip order was also not significant. The minimum RCOF was 0.135, the maximum RCOF was 0.272 and the mean RCOF was 0.201 (standard deviation: 0.026). The lack of difference in RCOF across the boots suggests that the modest change in available COF across the boots did not have an impact on the amount of RCOF required for gait. The average RCOF values reported in this study (0.201) was similar to what has been reported in other studies for level walking (0.18) [1].

Twenty-nine percent of the trials resulted in a slip. Increased RCOF led to an increase in slipping risk ($p < 0.05$) (Figure 1). This model suggests that the risk of slipping for the subject with the highest RCOF value (0.272) was 79% whereas the risk of slipping was just 7% for the subject with the lowest RCOF value (0.135). The slip risk for mean RCOF value (0.201) was 34%. These findings suggest that RCOF is a valid measure of an individual's slip risk and that persons with a high individual RCOF have an increased risk of slipping whereas individuals with a low RCOF have a reduced risk of slipping.

The findings of this study confirm the relevance of previous research that utilized RCOF as an individual measure of slip risk [2,3]. This supports the conclusions from previous research that quadriceps fatigue increases slip risk [2] and that anticipating a slippery surface reduces slipping risk [3]. Furthermore, the results of this study can be used as justification for future research studies that may use RCOF as a measure of slip risk when it is impractical to unexpectedly slip subjects.

This study is limited in its ability to generalize the developed slip risk model. The slip risk model that was developed in this study is specific to just the shoe-floor-contaminant conditions that were considered. A different relationship between RCOF

and slip risk is expected for other shoe-floor-contaminant combinations, particularly when the ACOF is much larger or smaller than the RCOF. The trend observed in this study (i.e., that slip risk increases with RCOF) is expected to be similar in other studies where ACOF was approximately equal to RCOF.

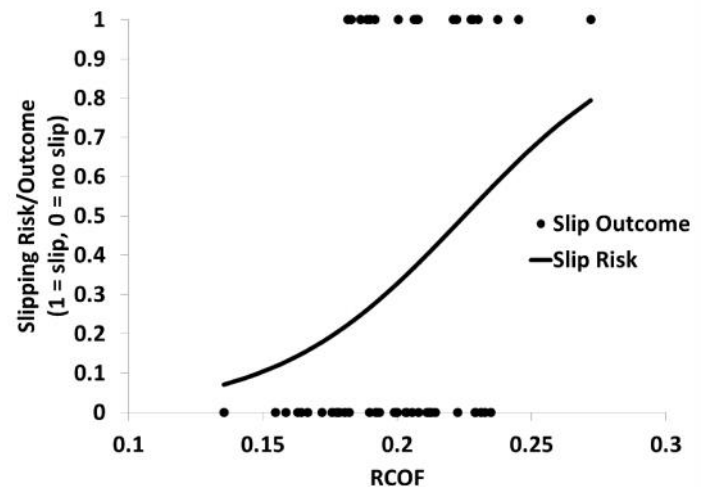


Figure 1: Effect of RCOF on slip outcomes and the predicted slip risk. Each data point represents the outcome of an individual slip. The solid line represents the logistic regression prediction model.

CONCLUSIONS

This study confirmed that RCOF values have a significant impact on slipping risk when the available COF is similar to the RCOF. The RCOF magnitudes that were observed in this study ranged from 0.135 to 0.272, which corresponded to a predicted slipping risk ranging from 7% to 79%. Thus, individual differences in RCOF can have a dramatic impact on their slipping risk.

REFERENCES

1. Hanson et al. *Ergonomics* **42**, 1619-33, 1999.
2. Parijat and Lockhart, *Gait Post* **28**, 568-73, 2008.
3. Cham and Redfern, *Gait Post* **15**, 159-71, 2002.
4. Chang et al., *App Ergo* **39**, 766-71, 2008.

ACKNOWLEDGEMENTS

This study was funded by the National Institute of Occupational Safety and Health (R01OH008986).

FALLS RESULTING FROM A LABORATORY-INDUCED SLIP OCCUR AT A HIGHER RATE AMONG YOUNG AND OLDER ADULTS WHO ARE OBESE

¹Leigh J. Allin, ²Xuefang Wu, ²Maury A. Nussbaum, and ³Michael L. Madigan

¹University of Virginia, Charlottesville, VA, USA

²Virginia Polytechnic Institute and State University, Blacksburg, VA, USA

³Texas A&M University, College Station, TX, USA

Email: leigh.allin@virginia.edu

INTRODUCTION

Falls due to slipping are a serious occupational concern. Slipping is estimated to cause 40-50% of all fall-related injuries [1]. Epidemiological data suggest that individuals who are older or obese fall more frequently than younger, non-obese adults [2]. The problem of slip-related falls may be exacerbated by a high prevalence of obesity and an aging workforce in the United States. The purpose of this study was to investigate the effects of obesity and age on slip severity and fall frequency following a laboratory-induced slip. Results from this study can help to identify obesity and/or age as risk factors for falling from slipping, and may aid in the development of fall-prevention strategies

METHODS

Seventy-two adults completed the study including: 26 young (18-29 years) non-obese (BMI 17.7-24.9 kg/m²); 25 young obese (BMI 29.1-40.4 kg/m²); 10 older (50-66 years) non-obese (BMI 19.5-26.3 kg/m²); and 11 older obese (BMI 30.1-45.1 kg/m²) individuals. During each experimental session, participants wore a harness and walked at a comfortable, but purposeful, pace along a 10m walkway. After 10-20 walking trials, a thin layer of vegetable oil was applied to the surface of a force platform to induce a slip of the dominant foot.

Positions of selected anatomical landmarks were sampled at 100 Hz using a six-camera motion analysis system (Vicon Motion Systems, Centennial, CO) and low-pass filtered at 7 Hz (second-order, zero-phase-lag Butterworth filter). Ground reaction forces under the slipping foot and force applied to the harness were sampled at 1000

Hz using a force platform (Bertec Corporation, Columbus, OH) and a uniaxial load cell (Cooper Instruments and Systems, Warrenton, VA), respectively. Both were low-pass filtered at 20 Hz.

Slip outcomes were classified as falls, recoveries, or harness-assisted based on methods similar to Brady et al. [3] and Yang and Pai [5]. Gait speed, step length, and four measures of slip severity (slip duration, slip distance, peak slip velocity, and mean slip velocity) were calculated for each slip classified as either a fall or recovery. Slip severity thresholds, separating most falls from most recoveries, were iteratively determined. The effects of obesity and age group on gait speed and step length were analyzed using two-way analyses of variance. Slip severity measures were analyzed using three-way analyses of covariance, with independent variables of obesity group, age group, and gender, and with gait speed as a covariate. Slip outcome was analyzed using a logistic regression model with independent variables of obesity group, age group, gender, and gait speed. Statistical analyses were performed using JMP 10 (SAS Institute Inc., Cary, NC) with a significance level of $p \leq 0.05$.

RESULTS AND DISCUSSION

Slip outcome differed between obesity groups ($p=0.005$; Table 1) in that 33.3% of obese participants fell after slipping, while only 8.3% of non-obese participants fell. The odds ratio for obesity group indicated that obese participants were 8.24 [95% C.I.: 1.81, 57.10] times more likely to fall than non-obese participants when adjusting for age group, gender, and gait speed. Slip outcome did not differ between age groups ($p=0.937$) or genders ($p=0.399$; Table 1).

Table 1: Slip outcomes among groups

	Fall	Recovery	Harness-Assisted	Total
Total	15	48	9	72
Obese	12	21	3	36
Non-obese	3	27	6	36
Older	5	12	4	21
Young	10	36	5	51
Male	5	24	4	33
Female	10	24	5	39

Mean slip velocity was 8.3% higher ($p=0.022$) among obese participants, but slip duration ($p=0.974$), slip distance ($p=0.121$), and peak slip velocity ($p=0.065$) did not differ between obesity groups (Table 2). Age group did not affect any slip severity measures. Slip distance ($p=0.005$), peak slip velocity ($p<0.001$), and mean slip velocity ($p<0.001$) increased with gait speed, but gait speed did not affect slip duration ($p=0.148$). Gait speed and step length did not differ between obesity (speed $p=0.486$, step length $p=0.886$) or age groups (speed $p=0.245$, step length $p=0.593$; Table 2).

In general, participants who fell experienced more severe slips. The majority of falls occurred at slip distances beyond 50 cm, slip durations longer than 0.3 s, peak slip velocities above 2.5 m/s, and mean slip velocities above 1.0 m/s. More specifically, a slip distance of 56.5 cm separated 85.4% of recoveries from 86.7% of falls, a slip duration of

0.35 s separated 54.2% of recoveries from 86.7% of falls, a peak slip velocity of 2.57 m/s separated 91.7% of recoveries from 80.0% of falls, and a mean slip velocity of 1.19 m/s separated 79.2% of recoveries from 86.7% of falls.

CONCLUSIONS

Laboratory-induced slips resulted in more severe slips and a higher fall rate among individuals who are obese. However, no obesity \times age interaction effects were found for slip outcome or slip severity. These results suggest that the higher fall rates reported among obese individuals may be due, at least in part, to a greater rate of falling after slipping while walking. Slip severity thresholds that separated the majority of falls from recoveries were also reported, and may have practical value in the design of fall-resistant flooring.

ACKNOWLEDGEMENTS

This work was supported by award R01OH009880 from the CDC-NIOSH.

REFERENCES

1. Courtney et al. *Ergonomics* **44**, 1118-1137, 2001.
2. Fjeldstad et al. *Dynamic Medicine* 7:4, 2008.
3. Brady et al. *J Biomech* **33**, 803-808, 2000.
4. Cham and Redfern, *J Biomech* **34**, 1439-1445, 2001.
5. Yang and Pai, *J Biomech* **44**, 2243-2249, 2011

Table 2: Gait and slip severity measures (mean \pm standard deviation)

	Gait Measures		Slip Severity Measures			
	Gait Speed (m/s)	Step Length (m)	Slip Duration (s)	Slip Distance (cm)	Peak Slip Velocity (m/s)	Mean Slip Velocity (m/s)
Obese	1.25 \pm 0.14	0.70 \pm 0.07	0.42 \pm 0.27	42.1 \pm 27.2	1.89 \pm 0.98	1.05 \pm 0.59*
Non-obese	1.31 \pm 0.17	0.69 \pm 0.13	0.38 \pm 0.24	38.4 \pm 23.9	1.70 \pm 0.89	0.97 \pm 0.61*
Older	1.32 \pm 0.19	0.70 \pm 0.08	0.32 \pm 0.10	42.2 \pm 25.5	1.84 \pm 0.90	1.16 \pm 0.66
Young	1.27 \pm 0.14	0.71 \pm 0.06	0.36 \pm 0.12	40.2 \pm 25.3	1.81 \pm 0.93	0.97 \pm 0.56
Male	1.29 \pm 0.16	0.73 \pm 0.06	0.31 \pm 0.09	34.2 \pm 23.4	1.67 \pm 0.90	0.96 \pm 0.60
Female	1.27 \pm 0.16	0.69 \pm 0.07	0.38 \pm 0.12	46.5 \pm 25.6	1.95 \pm 0.91	1.08 \pm 0.58

* Significantly different between BMI groups

OBESITY INCREASES FALL RATE FOLLOWING A LABORATORY-INDUCED TRIP

¹Christina R. Garman, ¹Maury A. Nussbaum, ²Michael L. Madigan

¹Virginia Tech, Blacksburg, VA, USA

²Texas A&M University, College Station, Texas, USA

email: rossic@vt.edu

INTRODUCTION

Tripping accounts for an estimated 53% of falls among adults aged 65 and older [1]. A common strategy to prevent a fall after tripping is to step to extend the base of support anteriorly, and thereby provide vertical and posterior ground reaction forces that can help arrest the forward momentum of the trunk [2]. As such, stepping characteristics and trunk kinematics are critically important during trip recovery.

Obese adults exhibit a higher rate of falls than those who are normal-weight [3], but the reason for this higher rate is unclear. The purpose of this study was to investigate: 1) obesity- and age-related differences in trip recovery, and 2) differences between successful and failed recoveries. Dependent variables included measures of fall rate, stepping characteristics, and trunk kinematics.

METHODS

Participants included 10 young (age 18-30 years) normal-weight (body mass index, BMI, of 18-24.9 kg/m²) adults, 10 young obese adults (BMI over 30 kg/m²), 10 older (age 60-70 years) normal-weight adults, and 10 older obese adults. Participants were tripped near mid-swing using a 7-cm-high obstacle while walking at a speed of 1.4-1.6 m/s. Forces applied to a safety harness were sampled from a load cell (Cooper Instruments and Systems, Warrenton, VA) at 1000 Hz and low-pass filtered at 20 Hz (eighth-order, zero-phase-shift Butterworth filter). Kinematic data using a modified Helen Hayes marker set were collected at 100 Hz with a 6-camera motion analysis system (MX-T10, Vicon Motion Systems Inc., L.A, CA) and low-pass filtered at 5 Hz (8th-order, zero-phase-shift Butterworth filter).

Harness load was used to classify trip recovery outcome as either a recovery (peak load less than 30% body weight), a harness-assisted recovery (peak load 30-50% body weight), or a fall (peak load exceeded 50% of body weight). Trials classified as harness assisted were removed from further analysis.

Logistic regression analyses were used to investigate the effects of obesity and age on fall rate and stepping strategy (elevating or lowering). A three-way analysis of variance was used to investigate the effects of obesity, age, and trip recovery outcome on recovery step time and length, and peak trunk angle and angular velocity. All statistical analyses were performed using JMP 10 (SAS Institute Inc., Cary, NC) with a significance level of $p \leq 0.05$.

RESULTS AND DISCUSSION

Obesity affected several aspects of trip recovery. Fall rate was 52% among obese adults and 22% among normal-weight adults, with an odds ratio indicating obese adults were 8.79 (C.I.: 4.62, 394.8; $p=0.026$) times more likely to fall when adjusting for age and gender. Stepping strategy ($p=0.151$), recovery step time ($p=0.499$), and recovery step length ($p=0.854$) did not differ between obesity groups. Peak trunk angle was 13 degrees higher among obese adults ($p=0.046$) (Figure 1). Peak trunk angular velocity was affected by an obesity level x age interaction ($p=0.038$; Figure 1). Peak trunk angular velocity was 216 degrees/s higher among obese older adults compared to normal-weight older adults ($p=0.012$), and 245 degree/s higher among obese older adults compared to obese young adults ($p=0.005$).

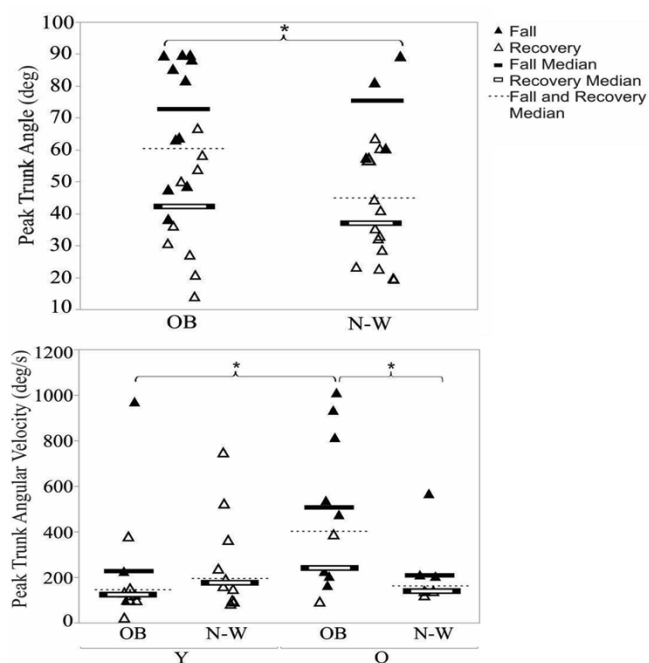


Figure 1: Peak trunk angle (top) and peak trunk angular velocity (bottom) separated by obesity group, and obesity and age group. Brackets indicate significant differences between groups. Note: OB=obese, N-W=normal-weight, Y=young, O=older.

Comparing dependent variables between falls and recoveries also revealed several differences. A lowering strategy was used during 73% of falls and 25% of recoveries with odds ratios indicating users of a lowering strategy were 8.25 (C.I.: 2.03; 40.18; $p=0.003$) times more likely to fall. Recovery step time and length did not differ between falls and recoveries ($p=0.541$ and $p=0.758$). Peak trunk angle was 32 degrees higher during falls ($p<0.001$), and peak trunk angular velocity was 287 degrees/second higher during falls ($p=0.027$).

The higher rate of falls among obese adults may have resulted from differing trunk kinematics, and three intrinsic factors associated with obesity could be responsible for these differences. First, an anterior shift of the trunk COM among obese adults [4] could increase the gravitational moment that rotates the body forward after tripping. Second, greater trunk mass would increase trunk momentum that needs to be decelerated through trunk and lower extremity muscle exertions [5]. Third, reduced relative strength

among obese adults could reduce the ability to decelerate trunk momentum.

Although recovery step time and length were not affected by obesity or trip recovery outcome, the success of trip recovery was dependent upon the choice of stepping strategy. Other studies have reported a higher prevalence of a lowering strategy among obese adult fallers [6]. For older adults it has been shown that practicing balance recovery from a simulated trip improves recovery kinematics following an actual trip [7]. This training may be effective in promoting more frequent use of the elevating strategy during mid-swing trips, and may help improve the success of trip recovery.

In conclusion, obese adults exhibited a higher fall rate after tripping. This higher fall rate was not due to altered stepping characteristics, but appeared to be related to trunk kinematics. These results suggest the higher rate of falls among obese adults reported elsewhere may be due to impaired trip recovery, and support the use of interventions to improve trip recovery capability to help prevent falls among obese adults.

REFERENCES

1. Blake, A.J., et al. Age Ageing, 1998. 17(6): p. 365-372.
2. Grabiner, M.D., et al., J. Gerontol. 1996. 48(3): p. M97-M102.
3. Fjeldstad, C., et al. Dyn Med. 2008. 7(4).
4. Corbeil, P., et al., IEEE Trans Neural Syst Rehabil Eng. 2001. 9(2): p. 126-136.
5. Pijnappels, M., et al. JOB. 2004. 37(12): p. 1811-1818.
6. Rosenblatt, N.J., et al. Arch. Phys. Med. 2012. 93(4): p. 718-722.
7. Bieryla, K.A., et al. Gait & posture, 2007. 26(2): p. 208-213

ACKNOWLEDGEMENTS

This work was supported by award R01OH009880 from the CDC-NIOSH and National Science Foundation Graduate Research Fellowship under grant DGE 0822220

VIBRATION TRAINING COULD REDUCE RISK OF FALLS AMONG YOUNG ADULTS WITH OBESITY

Jose Munoz, JaeEun Kim, Maria Sanchez and Feng Yang

The University of Texas at El Paso, TX, USA

E-mail: fyang@utep.edu

INTRODUCTION

Obesity is a major health concern all over the world. One of the major concerns related to obesity is that it leads to increased risk of falls. It has been reported that individuals with obesity have a higher likelihood of falls in comparison to their non-obese counterparts. High risk of falls among individuals with obesity has been associated with several factors, such as muscle weakness, postural instability, and abnormal body mass distribution [1]. As falls are considered the most common cause of injuries in obese community, it is pressing needed to develop an effective training paradigm which can reduce those aforementioned risk factors of falls.

Though training programs based on weight loss and strength training have been applied to reduce the risk of falls among individuals with obesity [2], they may not be suitable for the entire obese community. For example, a significant portion of individuals with obesity is unable or unwilling to comply with or manage conventional training regimens requiring high intensity and long duration. Therefore, alternative training approaches requiring less intensive physical activities involved to prevent falls targeting persons with obesity are highly demanded.

Controlled whole-body vibration training (CWBV) has recently emerged as a relatively novel modality to train older adults to reduce their fall risk [3]. It has been proven that a short-term (6-10 weeks) CWBV training course enhances neuromuscular performance and reduces risk of falls among older adults [4]. The transmission of mechanical vibrations and oscillations to the human body can lead to physiological and neuromuscular changes on numerous levels [5]. Some common risk factors of falls shared by older adults and individuals with

obesity suggest that CWBV could be a promising approach to prevent falls in the stroke community. However, no study has investigated the potential effect of CWBV training on reducing falls among populations with obesity. Therefore, the primary purpose of this study was to systematically examine the overall effectiveness and feasibility of CWBV training in reducing risk of falls among individuals with obesity. We were particularly interested in studying the impact of a 6-week CWBV training on reducing body fat percentage, improving muscle strength, and enhancing dynamic gait stability.

METHODS

Five young adults (age: 26.2 ± 9.04 years; body height: 172.16 ± 4.43 cm; body mass: 100.18 ± 6.28 kg; 2 females) with obesity were recruited to participate in this preliminary study. Obesity level was determined based on both the body mass index ($\text{BMI} \geq 30 \text{ kg/m}^2$) and the body fat percentage ($\geq 30\%$). All subjects gave informed consent for participating in this study.

This study adopted a pretest-posttest design. All subjects received CWBV training 3 days a week for 6 weeks. The training was delivered by a vibration platform (Orthometrix, NY) in an intermittent way: each 1-min vibration was followed by a 1-min rest for 10 minutes when they stood on the platform. The vibration frequency was 25 Hz and the amplitude 7.8 mm. Immediately prior to (or pre-training) and following (or post-training) the 6-week CWBV training, each subject was evaluated for their risk of falls quantified in terms of the muscle strength, body fat percentage, and dynamic stability during walking.

Subjects' knee joint extensor strength capacity was assessed under isometric condition on the right side

via an isokinetic dynamometer (Biodex, NY). The body fat percentage was measured by a bioelectric impedance analysis (BIA) machine (RJL-101, MI). To evaluate the dynamic gait stability, each subject was required to walk on a 12-m walkway at their preferred gait speed. Their full body kinematics was collected from 28 retro-reflective markers placed on the subjects' body and floors by using an 8-camera motion capture system (Vicon, UK).

The body center of mass (COM) kinematics was computed using gender-dependent segmental inertial parameters [6] from the filtered markers paths. The two components of the COM motion state, i.e. its position and velocity were calculated relative to the rear of base of support (i.e. the leading heel) and normalized by foot length and $\sqrt{g \times bh}$, respectively, where g is the gravitational acceleration and bh the body height. The timing for two events in the gait cycle: touchdown (TD) of the leading foot and liftoff (LO) of the trailing foot, was identified from feet kinematics. The stability was calculated at both time instants as the shortest distance from the COM motion state to the limits of stability against backward balance loss [7].

Paired t -tests were used to compare all risk factors between the two evaluation sessions (i.e. pre-training vs. post-training) in order to determine the possible effect of the CWBV training. All statistics were performed using SPSS 19.0 (IBM, NY), and a significance level of 0.05 was used.

RESULTS AND DISCUSSION

The 6-week CWBV training significantly improved the maximum isometric knee extensor strength among the obese adults in this study. Specifically, the maximum knee extensor strength increased to 1.83 ± 0.23 Nm/kg in the post-training evaluation from 1.66 ± 0.28 Nm/kg in the pre-training evaluation ($p < 0.05$). Similarly, the dynamic gait stability was improved as the result of the vibration training. In detail, the stability values were 0.61 ± 0.02 and 0.32 ± 0.06 respectively for TD and LO before the training. The stability at TD and LO became 0.70 ± 0.05 ($p < 0.01$) and 0.40 ± 0.03 ($p < 0.05$), respectively post the training.

Interestingly, the body fat percentage did not show difference between two evaluations (37.45 ± 7.40 vs 37.45 ± 7.65 , $p > 0.05$). One explanation for this could be that the 6-week CWBV training actually does not affect body composition. Alternatively, the small sample size or the accuracy level of the BIA machine employed in this study could also contribute to the similar body fat percentage between tests. The stability examined in this study was the one against backward falling. Therefore, it remains unknown how CWBV training affect the stability against balance loss in other directions. These warrant our further investigation.

CONCLUSIONS

A 6-week CWBV training course can increase muscle strength and improve dynamic gait stability control among young obese adults. As these two factors closely relate to falls, CWBV training could serve as a promising training method to reduce fall risk among individuals with obesity. However, it may not change the body composition at least in the sample studied in this experiment. Still, the finding from this study sheds light on the feasibility of applying CWBV training to reduce falls among individuals with obesity.

REFERENCES

- 1 Madigan M, et al. Cur Obes Rep 3, 348-354, 2014.
- 2 Matrangola SL, et al. Med. Sci. Sports Exerc 41, 1488-1493, 2009.
- 3 Lam FMH, et al. Maturats 72, 206-213, 2012.
- 4 Furness TP, et al. J Streng Condit Research 23, 1508-1513, 2009.
- 5 Madou KH, et al. Hong Kong Physiotherapy Journal 26, 24-38, 2008.
- 6 de Leva P, et al. J. Biomech 29, 1223-1230, 1996.
- 7 Yang F, et al. J. Biomech 41, 1818-1822, 2008.

ACKNOWLEDGEMENTS

Funding from the Retirement Research Foundation and University Research Institute (UTEP) supported this study.

AN EVALUATION OF FALL BIOMECHANICS THAT MAY UNDERLIE THE INCIDENCE OF WRIST AND HIP FRACTURES IN OLDER ADULT WOMEN

^{1,2} Jeremy R. Crenshaw, ¹ Kathie A. Bernhardt, ¹ Shreyasee Amin, and ¹ Kenton R. Kaufman

¹ Mayo Clinic, Rochester, MN, USA

² University of Delaware, Newark, DE, USA

email: kaufman.kenton@mayo.edu, web: <http://www.mayo.edu/research/labs/motion-analysis>

INTRODUCTION

After the age of 75 years (yrs), the incidence of wrist fractures in women declines [1], while the incidence of hip fracture begins to rise [2]. Differences in fall biomechanics with aging have been hypothesized to account for these concurrent trends. Possible fall biomechanics proposed include:

- M1. An age-related inhibition of protective arm movements during a fall that results in less impact to the hand/wrist, in turn reducing the risk of wrist fracture, but increasing the risk of hip fracture.
- M2. An interaction between age and direction-specific fall risk that predisposes the oldest women to more posterior and lateral falls, but fewer anterior falls. This interaction likely reduces the incidence of wrist fracture and increases the risk of hip fracture [3].

The purpose of this study was to evaluate fall biomechanics in women age ≥ 65 yrs through i) laboratory assessments of fall recovery and ii) the prospective tracking of falls over 1 yr in the free-living environment. We compared women age 65-75 yrs to women age >75 yrs given the dramatically altered incidences in fractures at the wrist and hip between these age groups [1,2]. We hypothesized that, based on laboratory assessments, women age >75 yrs would have diminished protective arm movements (M1) and would demonstrate recovery responses that reflect greater risk of falling posteriorly and laterally (M2). We also hypothesized that, over 1-yr follow-up, women age >75 yrs would demonstrate fewer fall impacts to the hands (M1) and would exhibit a higher incidence of posterior and lateral falls (M2).

METHODS

We recruited an age-stratified sample of 125 ambulatory, community-dwelling women. There were 58 women age 65-75 yrs (mean \pm s.d.

age=69.7 \pm 3.3 yrs, BMI=28.5 \pm 5.3 kg/m²), and 67 women age >75 yrs (age=82.6 \pm 4.2 yrs, BMI=26.2 \pm 4.5 kg/m²).

Laboratory Assessments of Fall Recovery

A subset of participants (65-75 yrs: n=49; >75 yrs: n=50) completed assessments to determine anterior (AMST) and posterior (PMST) multiple-stepping thresholds. These thresholds were determined using a progressive series of treadmill-induced postural disturbances that induced anterior or posterior falls [4]. Participants were asked to recover balance with a single step, and thresholds represent the disturbance magnitudes that elicited more than one step or a fall into a safety harness over the course of four attempts. AMST, PMST, and the ratio of the two thresholds (AMST/PMST) were evaluated to determine direction-specific fall risk (M2).

The stepping-threshold assessment of 67 participants (65-75 yrs: n=32; >75 yrs: n=35) were recorded with motion capture technology. For failed attempts to recover in a single step, the following variables were calculated:

- The largest anterior (AMST) or posterior (PMST) distance ($d_{wrist-pelvis}$) between a wrist marker and the pelvic center 500 ms after the disturbance onset (M1). Positive values indicate a wrist positioned in the direction of the fall relative to the pelvis.
- The lateral distance between the whole-body center of mass (COM) and the stepping-foot toe (AMST) or heel (PMST) marker at foot contact [5,6]. (M2)

Free-Living Environment Assessments of Fall Risk

Falls were recorded by all participants using semimonthly questionnaires. The questionnaires included fall orientation and anatomical figures in order to ascertain, respectively, the direction of the fall (M2) and impact locations (M1).

RESULTS AND DISCUSSION

Laboratory Assessments of Fall Recovery

The older group demonstrated smaller protective arm movements compared to the younger group when falling anteriorly ($p=0.003$), but not posteriorly (Table 1). We did note that 25% of younger participants demonstrated negative $d_{wrist-pelvis}$ during a posterior fall, which may reflect a strategy aimed at fall recovery, not impact preparation [7]. In contrast, only 6% of older participants demonstrated negative $d_{wrist-pelvis}$. Negative $d_{wrist-pelvis}$ values were not observed in either group for anterior falls.

The ability to recover from anterior and posterior falls, as quantified by multiple-stepping thresholds, was impaired with older age (Table 1). Group differences in AMST/PMST ratio approached significance ($p = 0.058$, effect size = 0.52). A post-hoc linear regression analysis determined a significant relationship between age and this ratio ($AMST/PMST = 0.849 + 0.013 \cdot \text{age}$, $p=0.01$). Such results suggest that older age impairs posterior fall-recovery more than anterior fall-recovery.

In response to an anterior fall, the lateral distance between the COM and stepping-foot toe was wider for the >75 yr group ($p=0.03$) (Table 1). This finding suggests that, with advanced age, anterior fall-recovery mechanics are altered in a way that may increase lateral fall risk. This effect of age was not observed during posterior falls.

Free-Living Environment Assessments of Fall Risk

There was a trend for women age >75 yrs to be more likely to fall posteriorly (37% vs. 28%,

$p=0.25$) (Table 1). For those individuals who experienced a fall, older age did not decrease the odds of having an impact to the hand (OR [95% CI] = 0.83 [0.36-1.93]). Furthermore, older age did not increase the odds of having a hip impact with no impact to the hand (OR = 1.13 [0.47-2.73]).

CONCLUSIONS

These results suggest that, in response to an anterior fall, a reduction in protective arm movements in older women may explain a late-age decline in wrist fractures (M1). Furthermore, late age may involve a change in anterior fall recovery that predisposes women to a lateral fall, in turn increasing the risk of hip fracture (M2). An apparent age-related impairment of posterior fall-recovery and an increase in posterior fall incidence may also increase the risk of hip fracture with older age (M2).

REFERENCES

1. Falch JA. *Acta Orthop Scand* **54**, 291-5, 1983.
2. Samelson EJ, et al. *Am J Public Health* **92**, 858-62, 2002.
3. Nevitt MC, et al. *J Am Geriatr Soc* **41**, 1226-34, 1993.
4. Crenshaw JR, et al. *Gait Posture* **39**, 810-5, 2014.
5. Troy KL et al., *Gait Posture* **28**, 461-5, 2008.
6. Rogers MW and Mille ML, *Exerc Sport Sci Rev* **31**, 182-7, 2003.
7. Troy KL, et al. *J Biomech* **42**, 1339-44, 2009.

ACKNOWLEDGEMENTS

We thank L. McCready and D. Hansen for study coordination, data collection, and data processing. Funding provided by NIH R01AR027065, NIH T32HD07447, and NIH UL1TR000135.

Table 1: Fall recovery and mechanics.

	Variable	Age 65-75 yrs	Age > 75 yrs	Significance
Laboratory	Anterior fall $d_{wrist-pelvis}$ (cm)	51 \pm 14	41 \pm 13	$p = 0.003$
	Posterior fall $d_{wrist-pelvis}$ (cm)	14 \pm 20	19 \pm 13	$p = 0.256$
	AMST (N·m)	627 \pm 163	425 \pm 91	$p < 0.001$
	PMST (N·m)	360 \pm 105	234 \pm 67	$p < 0.001$
	AMST/PMST	1.75 \pm 0.29	1.90 \pm 0.45	$p = 0.058$
	PMST lateral heel-COM distance (cm)	18 \pm 6	17 \pm 6	$p = 0.571$
	AMST lateral toe-COM distance (cm)	11 \pm 4	13 \pm 3	$p = 0.030$
Free-Living Environment	Fell anteriorly (%)	29%	33%	$p = 0.671$
	Fell posteriorly (%)	28%	37%	$p = 0.248$
	Fell laterally (%)	28%	24%	$p = 0.636$

AUTOMATION OF STRIDE-SPECIFIC BELT VELOCITIES ON INSTRUMENTED TREADMILLS FOR GAIT REHABILITATION AND TRAINING

Jacob W. Hinkel-Lipsker and Michael E. Hahn

University of Oregon, Eugene, OR, USA
email: jhinkell@uoregon.edu, web: <http://bssc.uoregon.edu>

INTRODUCTION

Split-belt treadmill training has been shown to be effective in normalizing gait symmetry by inducing a motor adaptation to an asymmetry in belt velocity [1]. This method of training has shown positive outcomes in clinical populations such as those who suffer from stroke [2], and has been used to investigate the effects of introducing a novel gait to healthy populations [3]. Gait training methods that have utilized changes in belt velocity from step-to-step between training blocks require the treadmill operator to quickly adjust belt velocities through the controlling device [3]. This form of manual control can become a source of error and even impossible if the belt velocity changes are frequent (eg. stride-by-stride). Further, timing of velocity changes is of crucial importance to insure that the adjustment happens during the desired phase of gait.

As research into treadmill gait rehabilitation progresses, the need has arisen for automated treadmill operation. While some virtual reality interfaces have utilized kinematic data for user-driven control schemes [4], there is currently a lack of operator-driven schemes that can be pre-set to change speeds given a specified gait event. Therefore, a scheme was implemented to automate an operator-driven control system for split-belt treadmill walking. The purpose of this study was to detail the process of automated treadmill control and test its performance during a trial of random asymmetrical split-belt training.

METHODS

A random training protocol, which represents the most challenging practice difficulty according to contextual interference theory [5], was implemented. This practice method involved the

non-dominant limb being driven at the user's self-selected walking speed (SSWS) while the dominant limb was randomly changed within an upper and lower velocity limit of ± 0.5 m/s of SSWS for every step. These velocities were randomized prior to the trial in order to decrease computation time. One subject (185 cm, 84 kg, SSWS = 1.57 m/s) walked for 100 strides on the treadmill. Ground reaction force (GRF) data were collected by the force plate embedded under the dominant leg treadmill belt at 1200 Hz and were used to calculate swing phase time (ms) for each step of the dominant leg.

A Bertec split-belt instrumented treadmill (Bertec, Columbus, OH) was used for this study due to its ability to be remotely controlled through TCP/IP protocol. The control scheme was as follows: analog force plate data (volts) were streamed (T1) to an Arduino Mega 2560 at 25 Hz (T2), which then interfaced with a Windows 7 machine (2.7 GHz, 8 GB RAM) using a USB serial connection (T3). These data were streamed into MATLAB (Mathworks Inc.) using the Data Acquisition Toolbox (T4). As the analog data is streamed, this custom-written program detects swing phase for the dominant foot and issues a command at the first sample where $GRF > 0$ volts to change speeds (T5) from the pre-set speed randomization file to a TCP/IP controller via USB (T6), which interfaces with the treadmill motor to drive the belt. The acceleration of the belt (T7) during each velocity was set at 20 m/s^2 (Figure 1).

For this control scheme to function as intended, the treadmill belt needed to be fully accelerated during swing phase, prior to the next foot contact. To assess performance, the total time (TT) for the scheme to process and perform its commands was calculated as the sum of the seven time points previously specified. Assuming T1, T3, T5, and T6

were nearly instantaneous, only T2, T4, and T7 were used to calculate TT. T2 was calculated to be 40 ms, which would represent the longest possible time for the Arduino board to capture a GRF > 0 signal while sampling at 25 Hz. T4 was calculated using a MATLAB function to compute the time between signal input and output. T7 was calculated as the change in velocity for each step divided by the 20 m/s² acceleration of the treadmill belt. A factor of safety (FOS) was calculated by dividing TT for each step by the minimum swing phase time over the 100 strides.

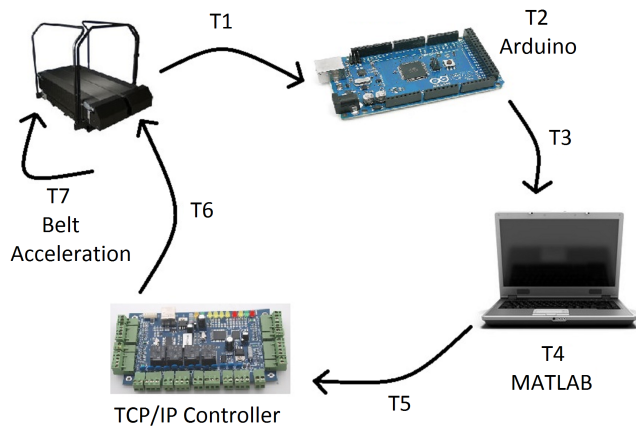


Figure 1: Treadmill control scheme with time points for calculation of total time. Analog force plate data are sampled by an Arduino A/D board, then streamed in real-time into custom written MATLAB software. Once swing phase is detected, a command for a pre-set velocity change is sent to a TCP/IP controller, which controls the motor to drive the treadmill belts.

RESULTS AND DISCUSSION

Minimum swing phase time was calculated to be 300 ms. At a maximum belt velocity change of 0.43 m/s, TT was calculated to be 66 ms, resulting in a FOS of 5. A polynomial fit of the relationship between velocity change and TT ($R^2 = 0.93$), indicates that sampling rate and device processing time were not large factors in calculating TT (Figure 2).

These results indicate that, with a maximum TT of 66 ms, this control scheme is sufficient to accommodate treadmill belt velocity changes within

the ± 0.5 m/s limit imposed on this study. This approach would function well for given patient populations with much shorter swing phases, such as hemiplegic stroke patients [6]. Further, given the polynomial equation calculated, this control scheme can accommodate a treadmill velocity change ranging from -1.77 m/s to + 1.47 m/s.

This control scheme can be implemented for future split-belt treadmill studies that require automated belt velocity changes. It can also be combined with user-driven kinematic parameters in virtual reality interfaces to detect gait events and implement operator-controlled gait rehabilitation or training programs.

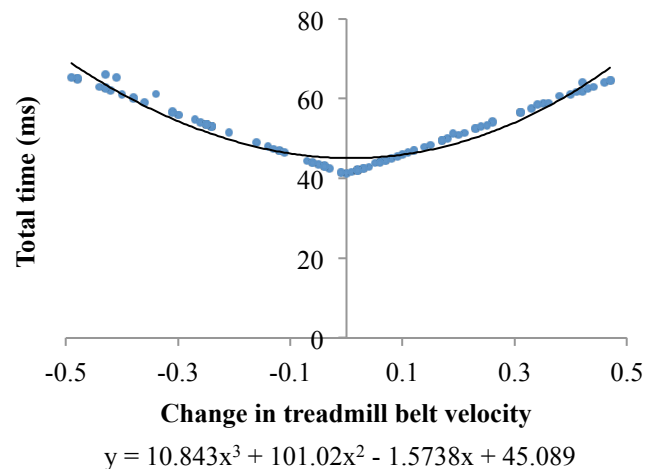


Figure 2: Total time as a function of belt velocity change. Total time increased as treadmill velocities reached their upper and lower limits ($R^2 = 0.93$).

REFERENCES

1. Stubbs PW, Gervasio S. *J Neurophysiol* **108**: 1225-27, 2012.
2. Reisman DS, et al. *Brain* **130**, 1861-72, 2007.
3. Sawers A, et al. *J Mot Behav* **45**, 405-14, 2013.
4. Yoon J, et al. *J Neuroeng Rehabil* **9**, 2012.
5. Shea, JB, Morgan, RL. *J Exp Psychol Learn Mem Cogn* **5**, 179-87, 1979.
6. Kramers de Quiervain IA, et al. *J Bone Joint Surg Arm* **78**, 1506-14, 1996.

ACKNOWLEDGEMENTS

Thanks to Sabin Kafle for assistance in programming TCP/IP control.

GAIT RETRAINING TO IMPROVE STANCE TIME ASYMMETRY REDUCES KNEE EXTERNAL ADDUCTION MOMENTS: A CASE STUDY OF A UNILATERAL TRANSTIBIAL AMPUTEE

¹ Hannah M. Rice, ^{1,2} Steve T. Jamison, ^{3,4} Alison L. Pruziner, ¹ Irene S. Davis

¹ Spaulding National Running Center, Harvard Medical School, Cambridge, MA, USA.

² The University of Delaware, Newark, DE, USA

³ Department of Rehabilitation, Walter Reed National Military Medical Center, Bethesda, MD, USA.

⁴ DoD-VA Extremity Trauma and Amputation Center of Excellence
email: ricehm204@gmail.com

INTRODUCTION

Individuals with a unilateral transtibial amputation (TTA) are at increased risk of developing osteoarthritis (OA) in their intact limb knee [1]. During walking, these individuals load their intact limb for longer than their amputated limb and this asymmetric loading may result in joint pain [2]. Furthermore, greater knee external adduction moments (KEAM) have been reported in the intact versus amputated limb of these individuals [3].

Real-time feedback has previously been used to decrease asymmetry during a single treadmill walking session in individuals with a unilateral TTA [4]. It remains unclear whether a treadmill-based gait retraining program with a faded feedback design can improve symmetry in individuals with a unilateral TTA, and whether such changes translate to a reduced KEAM in the intact limb during overground walking.

The objective of this case study was to evaluate the effect of gait retraining using real-time feedback on stance time asymmetry and intact limb KEAM during overground walking in an individual with a unilateral TTA. It was hypothesized that following retraining, stance time asymmetry would decrease, resulting in reduced intact limb KEAM.

METHODS

This case study involved a 40 year old female (67.9kg; 1.67m) with a left traumatic TTA. The participant had high functional capability, and reported no discomfort during walking. Following screening to ensure the participant met the inclusion criterion of $\geq 5\%$ stance time asymmetry, a pre-training gait assessment was completed, followed by gait retraining, and finally a post-training assessment. During assessments, 7 trials were collected in which the participant walked along a

30-m runway at $1.1\text{m}\cdot\text{s}^{-1} \pm 5\%$, contacting a force plate (AMTI, Watertown, MA) at its center, with the intact limb. Kinematic data were obtained using a 10-camera Vicon (Oxford, UK) system and full-body markers.

Twelve gait retraining sessions were conducted on an instrumented treadmill (AMTI, Watertown, MA) over a 7 week period. A harness was worn throughout retraining sessions to prevent injury if a fall occurred. A custom program (C-motion, Germantown, MD) calculated and displayed real-time stance time asymmetries for each gait cycle. This was displayed on a large screen positioned in front of the treadmill (Fig. 1).

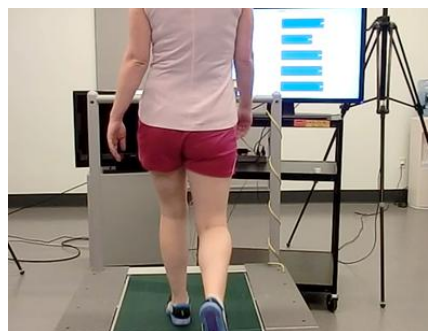


Figure 1: Demonstration of real-time stance time asymmetry feedback. Colored bars indicate the magnitude and side of the stance time asymmetry.

Duration of retraining sessions increased from 10 to 30 minutes over 12 sessions. Feedback was provided for the entirety of the first 6 sessions. The amount of feedback was reduced in each of the final 6 sessions in a faded feedback design, to encourage internalization of the new walking pattern [5].

RESULTS

Following gait retraining, stance time asymmetry was reduced by 32% (Fig. 2), and this corresponded with a 14% decrease in KEAM (Fig. 3). Post retraining there was a 2% increase in peak vertical

GRF, an 8% reduction in peak medial GRF, and a 3° increase in peak knee adduction angle (Table 1).

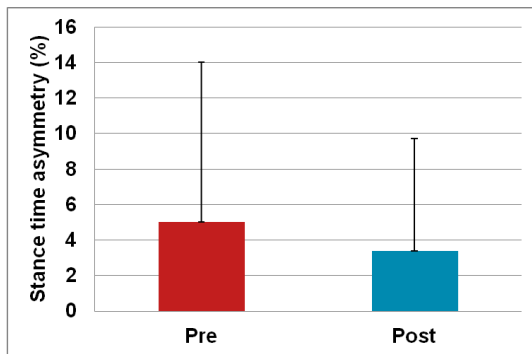


Figure 2: Mean (SD) stance time asymmetry during walking pre and post gait retraining.

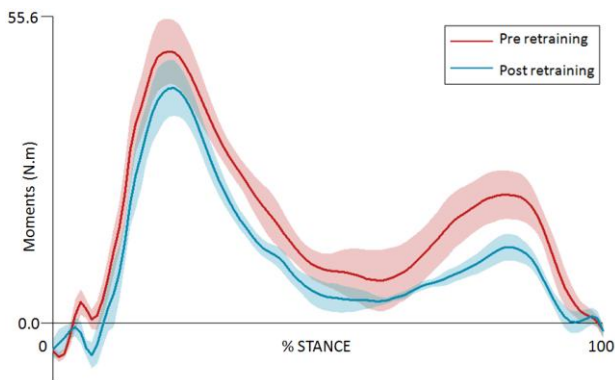


Figure 3: Mean (SD) KEAM in the intact limb during walking pre and post gait retraining.

DISCUSSION

The gait retraining program reduced stance time asymmetry in a participant with unilateral TTA. Intact limb KEAM was also reduced, likely as a result of the reduced peak medial GRF, despite the fact that the real-time feedback exclusively provided stance time asymmetry information. It is important to highlight that the changes in stance time asymmetry and intact limb KEAM observed in this case study occurred in a participant with a high

baseline level of symmetry. It is plausible that the magnitude of change from pre to post training would be greater in a more asymmetric participant.

Additional research is required to determine the success of this program in a larger population, and the ability of the participant to maintain changes without exposure to real-time feedback. As such, a follow-up assessment is planned after a period in which the participant undertakes focused walk training without feedback. If a more symmetric gait pattern can be maintained, the long-term risk of knee OA in the intact limb of individuals with a unilateral TTA may be reduced.

CONCLUSIONS

Based on this case study, gait retraining using visual real-time feedback is promising for improving stance time symmetry and reducing KEAM in individuals with a unilateral transtibial amputation.

REFERENCES

1. Lloyd CH, et al. *Gait Posture* **32**, 296-300, 2010.
2. Nolan L, et al. *Gait Posture* **17**, 142-51, 2003.
3. Royer TD, et al. *Gait Posture* **23**, 303-6, 2006.
4. Dingwell JB, et al. *POI* **20**, 101-10, 1996.
5. Crowell HP, et al. *Clin Biomech*, **26**, 78-83, 2011.

ACKNOWLEDGEMENTS

This work was supported by the BADER Consortium (DoD OR100017), a Department of Defense, Congressionally Directed Medical Research Programs cooperative agreement (W81XH-11-2-0222) and the DoD-VA Extremity Trauma & Amputation Center of Excellence (Public Law 110-417, National Defense Authorization Act 2009, Section 723). The views expressed in this abstract are those of the authors and do not necessarily reflect the official policy of the Departments of the Army, Navy, Defense, nor Veteran's Affairs.

Table 1: Temporal, kinetic and kinematic parameters, pre and post gait retraining in the intact limb.

Variable	Mean (SD) pre	Mean (SD) post	% change
Stance time asymmetry (%)	5.0 (9.0)	3.4 (6.3)	-32
Peak KEAM (N.m)	49.7 (5.9)	42.9 (5.0)	-14
Peak vertical GRF (N)	832.5 (41.0)	851.5 (25.4)	+2
Peak medial GRF (N)	63.3 (4.0)	58.1 (13.9)	-8
Peak knee adduction angle (°)	1.3 (0.5)	4.6 (0.5)	change (°) + 3.3

DEVELOPMENT OF A VISUAL BIOFEEDBACK SYSTEM FOR CENTER OF PRESSURE MODIFICATION DURING GAIT

^{1,2}Michael G. Browne and ^{1,2}Gregory S. Sawicki

¹North Carolina State University, Raleigh, NC, USA

²University of North Carolina, Chapel Hill, NC, USA
email: mgbrown2@ncsu.edu

INTRODUCTION

Visual biofeedback has been utilized for mobility modification in various impaired populations for a considerable amount of time [1-4]. With the advent of new technologies capable of both collecting and portraying physiological information in real time, new techniques for mobility modification are now available. Center of pressure (COP), defined as the centroid of all external forces acting on the plantar surface of the foot, it is a direct combination of kinetic and kinematic variables making it an intriguing function to investigate within mobility modification [5]. In order to evaluate this claim, we have developed a system to visually show COP trajectory in the transverse plane of the foot along with target locations for heel strike and toe off location. **The overall goal of this project is to modify COP during gait as a method to alter functional mobility in healthy adults in order to further understand and develop rehabilitation techniques and strategies.**

We hypothesize that:

- 1.) All healthy walkers will be able to volitionally modify and maintain an altered COP trajectory when provided visual biofeedback and
- 2.) Shifting the COP trajectory medially and laterally will decrease/ increase frontal plane ankle moments, respectively, while anterior and posterior shifts will increase and decrease sagittal plane ankle moments, respectively.

METHODS

In this feasibility study, one adult subject walked at 1.25 m/s on a split belt instrumented treadmill (Bertec, Columbus, OH) while motion capture

(Vicon Nexus, Denver, CO) data of the lower extremities was collected.

Utilizing a software development kit capable of connecting motion capture and ground reaction force data with computation software (MathWorks, Natick, MA) we provided a visual/graphical representation of the COP trajectory in real-time to the walking subject through the use of a custom Matlab code. Using the subject's normal/neutral COP trajectory as the basis, we graphically provided a target toe off location which was shifted medially, laterally, posteriorly and anteriorly along the length of the foot.

In the extended study with no fewer than 12 healthy subjects, we will also use electromyography (EMG) to understand specific ankle muscle compensations (tibialis anterior, gastrocnemius and soleus) caused by the modified COP. Finally, using indirect calorimetry, the metabolic energy expenditure required to maintain each modified COP trajectory will be collected.

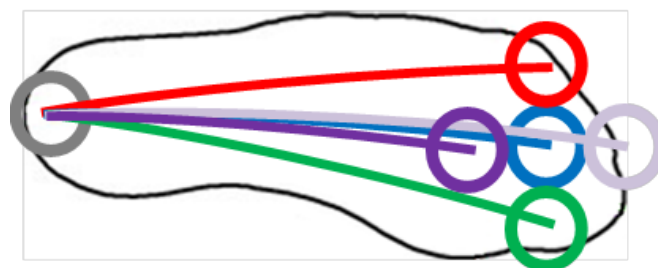


Figure 1: Graphical depiction of output from custom Matlab code. Purple represents neutral toe off location alongside four potential shifted targets (red, green, purple, and light grey target locations for shifts laterally, medially, posteriorly and anteriorly, respectively).

RESULTS AND DISCUSSION

This proof of concept study demonstrated the general ability of an individual to modify their toe off location along the foot's x-axis (medial/lateral) shown in **Figure 2**. These results represent the average COP trajectory over 20 consecutive steps for one healthy adult male walking at 1.25 m/s.

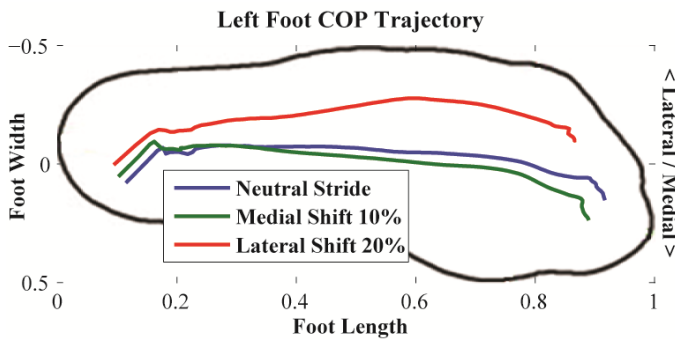


Figure 2: Transverse plane view of COP trajectory while provided no biofeedback/neutral walking (Blue), toe off shifted 10% of foot width medially (Green) and toe off shifted 20% of foot width laterally (Red). Axes normalized to foot width and foot length, respectively.

Mechanics data shown below in **Figure 3** provided some key insight into the underlying effects caused by modifying the COP trajectory. The most prominent alterations occurred with the 20% lateral shift of the toe off while the 10% medial shift generated largely similar mechanical outcomes in both the sagittal and frontal planes.

The lateral shift had implications in the sagittal plane (decreased dorsiflexion angle contributing to a reduction in moment magnitude during stance phase and, thus, reduced peak power during push-off). Frontal plane kinematics showed an approximately 10 degree offset throughout the entire gait cycle towards ankle inversion that had substantial effects on the frontal plane moment (~150% increase). Power generation, while visibly affected, had peak magnitudes of only ~3% of those seen in the sagittal plane.

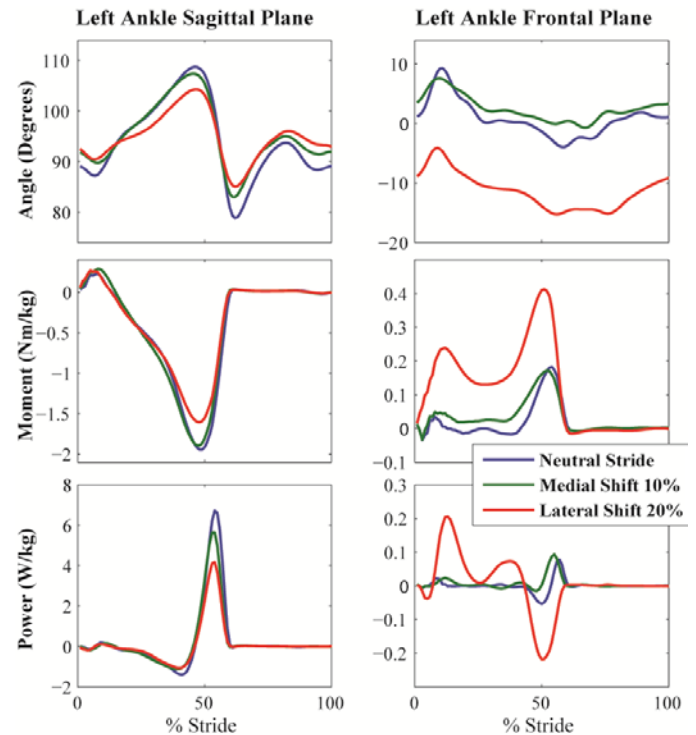


Figure 3: Sagittal and frontal plane mechanics for the left ankle joint while provided no biofeedback/neutral walking (Blue), toe off shifted 10% of foot width medially (Green) and toe off shifted 20% of foot width laterally (Red).

Ultimately, this pilot study and data has demonstrated the capacity of healthy walkers to modify their COP trajectory via our biofeedback application. We will continue validating the approach through further data collection including evaluation of compensations at more proximal joints (i.e. knee and hip) and also new parameters including EMG and metabolic expenditure.

REFERENCES

1. E. Aiello, et al. *Journal/Conf Proc IEEE Eng Med Biol Soc* **7**, 2005.
2. M. E. Khallaf, et al. *Journal/Neurol Res Int*, 2014.
3. D. S. Nichols. *Journal/Phys Ther* **77**, 1997.
4. J. R. Franz, et al. *Journal/Clin Biomech (Bristol, Avon)* **29**, 2014.
5. V. Lugade, et al. *Journal/Gait Posture* **40**, 2014.

MODIFYING ANKLE JOINT NEUROMECHANICS USING AN ANKLE FOOT ORTHOSIS WITH VIBROTACTILE FEEDBACK DURING HUMAN WALKING

Audrey E. Westbrook and Gregory S. Sawicki

North Carolina State University, Raleigh, NC, USA

email: aewestbr@ncsu.edu, greg_sawicki@ncsu.edu

INTRODUCTION

Two common walking-related problems in impaired populations are the inability to propel the body forward during push-off at end of stance and/or clear the foot during forward leg swing (foot drop). A key factor contributing to these symptoms may be inadequate ankle joint control in the weakened limb. A potential solution to improve ankle joint control is through the use of biofeedback. For example, studies have investigated the capability of biofeedback in older adults with propulsive deficits, finding that this population has “considerable and underutilized propulsive reserve available” [1], making real-time biofeedback a promising method of rehabilitation. We have developed an ankle foot orthosis (AFO) with built-in vibrotactile biofeedback to provide dynamic feedback and encourage activation of ankle muscles during walking. The goal of this project was to test the effectiveness of this device in healthy subjects by asking the user to modify ankle kinematics by altering control of their own muscles based on biofeedback cues.

METHODS

A custom fabricated, unilateral carbon fiber/fiber glass composite AFO was created for eight healthy participants (age = 23.63 ± 3.29 years; mass = 74.72 ± 10.82 kg; height = $1.75 \pm .08$ m). The device uses a microcontroller with inputs from an encoder and pressure sensors to control biofeedback through the use of a buzzer and a vibration motor (Fig. 2a). Time series data between each step is shown in Figs. 2b,c. Each participant was asked to walk in four 7 minute conditions: (1) No AFO, (2) AFO – No Feedback, (3) AFO encouraging increased plantarflexion (i.e. improve push-off), and (4) AFO encouraging increased dorsiflexion (i.e. prevent foot-drop). An instrumented treadmill was used to record ground reaction forces (Bertec,

Columbus, OH) while a motion capture system (Vicon, Oxford, UK) was used to determine joint kinematics. A combination of the two was used in an inverse dynamic analysis to compute joint powers using Visual 3D software (C-Motion Inc., Germantown, MD). EMG was collected through surface electrodes (SX230 Biometrics Ltd.) processed and integrated while a portable indirect calorimetry system (Oxycon Mobile, Yorba Lina, CA) was used to measure inspired O₂ and expired CO₂ and compute metabolic power. Data was averaged over 10 steps and ANOVA with a Bonferroni adjustment was used to compare differences between No AFO and AFO with the different forms of biofeedback.

RESULTS AND DISCUSSION

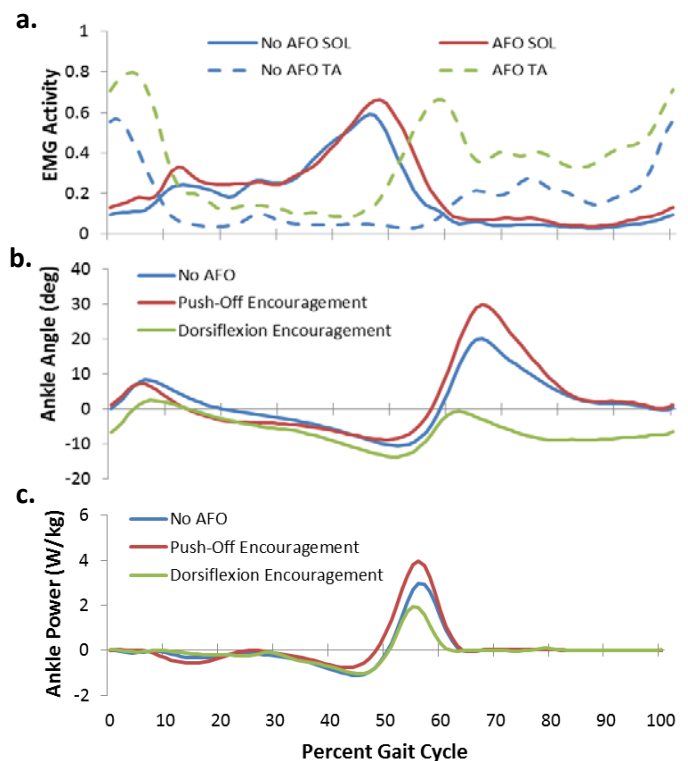


Figure 1: (a) Soleus (solid) and Tibialis Anterior (dotted) EMG ; (b) ankle angle ; (c) ankle power. Data are group means.

For the increase dorsiflexion/prevent foot drop biofeedback framework, users exhibited increased tibialis anterior muscle activity (Fig. 1a) and dorsiflexion of the ankle (Fig. 1b) during the swing phase of gait. However compensations such as decreased ankle power (Fig. 1c) and increased hip power were observed during swing, contributing to increases in metabolic cost while walking with the AFO turned on (Table 1). These results lead us to believe that this type of rehabilitation will be best for users with foot drop not accompanied by other neuromuscular impairments by strengthening their tibialis anterior muscle and increasing ankle dorsiflexion. However, for those who suffer from foot-drop and propulsion deficits (e.g., post-stroke), intensely focusing on using ankle dorsiflexors to keep a lifted toe would negatively impact propulsion performance. In these cases, strategies that focus more on knee flexion to achieve toe clearance, might be better.

In the second framework, increase plantarflexion/improve ankle propulsion deficiencies, increases in propulsive ankle power (Fig. 1c) and soleus muscle activity (Fig. 1a) were observed, as well as decreases in peak hip power (Table 1), indicating that users could recruit unused reserves of ankle ‘push-off’ power for limb

advancement by trading off with power at the hip. Slight increases in metabolic cost were observed, however this was expected as enforced gait patterns can elicit higher metabolic energy cost [2]. If an impaired population, such as those with hemiparesis following stroke can attempt to replicate these results, we are hopeful that gait symmetry and walking economy could be restored, leading to improved quality of life.

CONCLUSIONS

This study lays the groundwork for future testing on a vibrotactile biofeedback AFO to prevent foot drop and assist push-off in impaired populations. This targeted, on-line biofeedback approach, could positively impact rehabilitation practices if impaired populations can recruit muscle activity that they are not using on a daily basis.

REFERENCES

1. Franz JR., et al., Real-time feedback enhances forward propulsion during walking in old adults. *Clinical Biomechanics*. 2014; **29**: 68-74.
2. Wezenberg D., et al. Mind your step: Metabolic energy cost while walking an enforced gait pattern. *Gait & Posture*. 2011; **33**: 544-549.

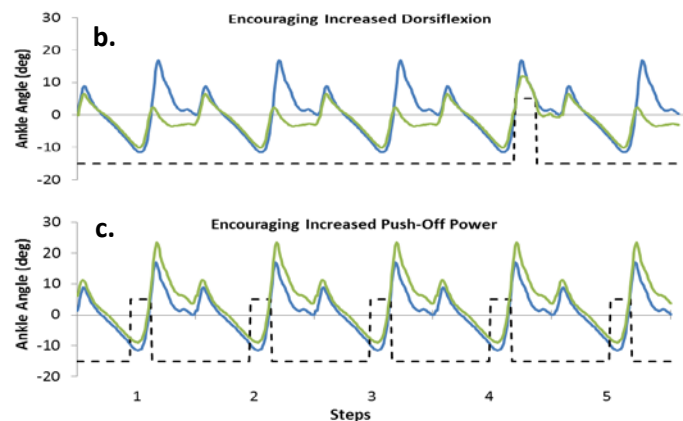
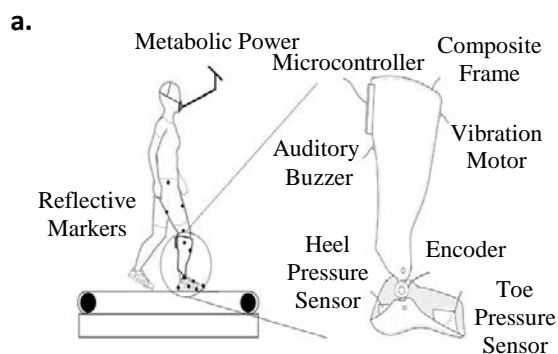


Figure 2: (a) Vibrotactile AFO; and time series demonstrating (b) dorsiflexion encouragement (i.e., decrease foot drop) and (c) plantarflexion encouragement (i.e., increase push-off power)

Table 1: Comparison of peak values for foot drop and push-off paradigms to no AFO condition

Foot Drop	No AFO	AFO	Push Off	No AFO	AFO
Peak TA Activity	0.19	0.26	Peak SOL Activity	0.21	0.23
Peak Ankle Dorsiflexion*	20.66 deg	-0.244 deg	Peak Ankle Plantarflexion*	20.66 deg	30.45 deg
Peak Positive Ankle Power*	3.15 W/kg	2.04 W/kg	Peak Positive Ankle Power*	3.15 W/kg	4.07 W/kg
Peak Positive Hip Power	0.76 W/kg	0.96 W/kg	Peak Positive Hip Power	0.26 W/kg	0.17 W/kg
Metabolic Cost	2.71 W/kg	3.45 W/kg	Metabolic Cost	2.71 W/kg	3.13 W/kg

Individuals with Incomplete Spinal Cord Injury Change Locomotor Stability After Exposure to a Viscous Force Field

^{1,2} Keith Gordon, ¹ Geoffrey Brown, ¹ Kristen Jakubowski, and ¹ Mary Wu

¹ Northwestern University, Chicago, USA

² Edward Hines Jr. VA Hospital, Hines, USA

Email: keith-gordon@northwestern.edu

INTRODUCTION

All strategies for stabilizing gait are not equal. Individuals with neurologic impairments rely heavily on general stabilization strategies that are present every step to resist and respond to any potential perturbation. General stabilization strategies (e.g. taking wide steps and increasing percent time in double support) decrease the necessity of sensing and responding to specific perturbations but inherently limit maximum walking speed, increase the metabolic cost of transport, and decrease maneuverability. Training individuals to utilize specific stabilization strategies (e.g. corrective steps, anticipatory postural adjustments) that are present only when needed could improve gait stability, speed, efficiency and adaptability. However, inducing individuals to practice task-specific stabilization strategies is very difficult, because general stabilization strategies can act as a physiological “crutch” that reduce the requirement to perform specific corrective actions when practicing walking in a balance-challenging environment.

The purpose of this study was to induce a temporary after-effect of reduced reliance on general stabilization strategies during gait in ambulatory individuals with incomplete spinal cord injury by exposing them to a brief period of walking with external lateral stability.

METHODS

Two ambulatory subjects with chronic, AIS (American Spinal Injury Association Impairment Scale) D, incomplete spinal cord injury, completed 600 steps of treadmill walking at their preferred speed. The first 200 steps established a **Baseline**

measure of how subjects walked with no external assistance. The next 200 steps occurred in the presence of an added **Viscous lateral force field**. After these 200 steps, the force field was turned off and the subject continued to walk for another 200 steps to measure any **After Effects**. The forces were applied via a cable/pulley system attached to the subjects' hips and driven by two brushless AC linear motors (Baldor, USA). Force control was maintained using feedback from load cells placed in series between the subject and the motors. The Viscous lateral force field consisted of a 66 N baseline force, applied bilaterally to the subject, and an additional variable force proportional to the subject's lateral center of mass velocity. The effect of the viscous field was to resist subjects' lateral motion. Motion capture cameras were used to measure mediolateral pelvis kinematics and foot placement variability.

RESULTS AND DISCUSSION

As shown in Figures 1 and 2, during the **After-Effects** period, subjects demonstrated an increase in mediolateral center of mass excursion variability (~70-220%), step width variability (~100% - 350% increase), and minimum lateral margin of stability variability (~40% - 350% increase) when compared with **Baseline** walking. Step width mean and margin of stability mean both tended to decrease (~10% - 50%), double-support time decreased (~4-30%), and no consistent trend was found for center of mass excursion mean. These results suggest decreased reliance on general stabilization strategies during the **After-Effects** period as compared to **Baseline**.

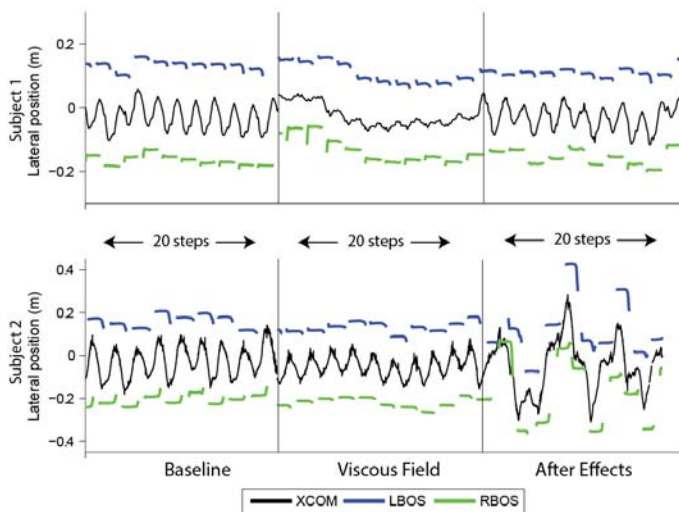


Figure 1: Extrapolated center of mass (XCOM), left base of support (LBOS), and right base of support (RBOS) data for two subjects walking during baseline, exposure to a viscous lateral force field, and after-effects immediately after removing the force field. Data shown is for the last 20 steps of the baseline and viscous field trials, and the first 20 steps during the after-effects period.

CONCLUSIONS

A temporary period of reduced reliance on general stabilization strategies during gait can be induced in individuals with incomplete spinal cord injury by exposing them to a brief period of walking with external lateral stabilization. We believe that external stabilization can be used to prime the motor system for acquiring specific stabilization strategies during targeted gait rehabilitation interventions, by temporarily decreasing an individual's reliance on the physiological “crutch” of general stabilization strategies

ACKNOWLEDGEMENTS

This work was supported in part by Career Development Award #1 IK2 RX000717-01 from the United States Department of Veterans Affairs, Rehabilitation Research and Development Service.

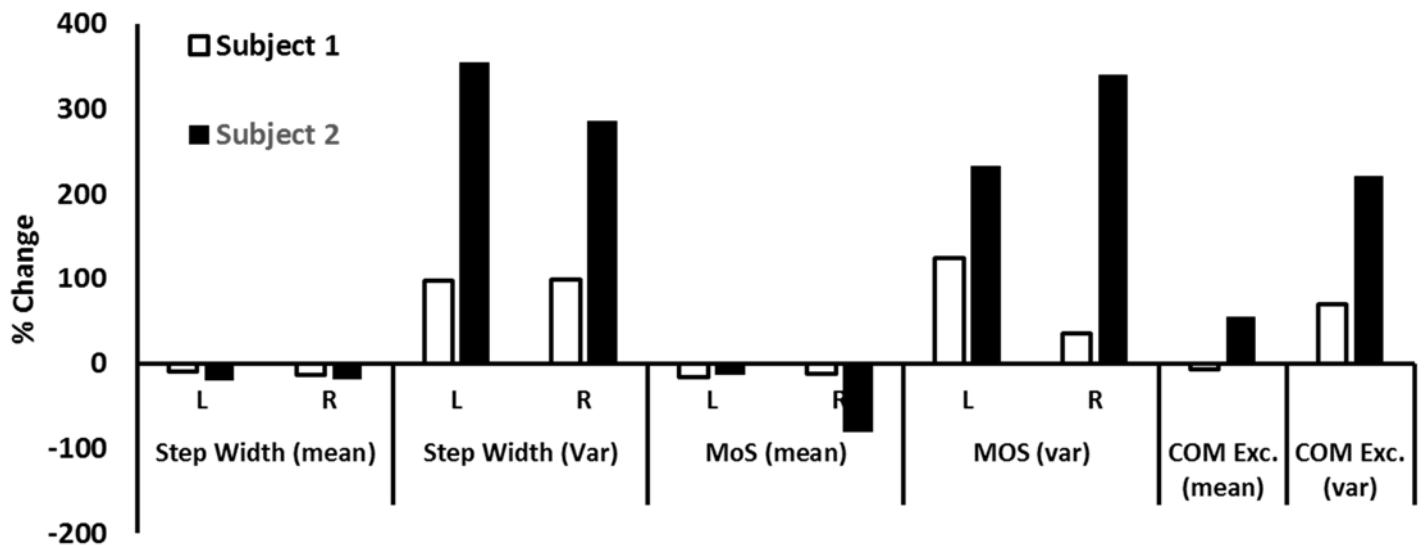


Figure 2: Percent change of kinematic measures from baseline walking to the after-effects period created from exposure to the force field. Mean and variability of step width, margin of stability (MoS), and center of mass excursion (COM Exc.) are shown for both limbs (L = left, R = right) of each subject.

GRAND CHALLENGES IN UPPER-LIMB BIOMECHANICS

¹ Steven K. Charles, ² Zong-Ming Li, ³ Wendy Murray, ³ Eric Perreault, ⁴ Francisco Valero-Cuevas, and ⁵ Meghan E. Vidt

¹ Mechanical Engineering and Neuroscience, Brigham Young University, Provo, UT, USA

² Biomedical Engineering, Cleveland Clinic, Cleveland, OH, USA

³ Biomedical Engineering and Physical Medicine and Rehab., Northwestern University, Chicago, IL, USA

⁴ Biomedical Engineering and Biokin. and Physical Ther., Univ. of Southern California, Los Angeles, CA, USA

⁵ Kinesiology, University of Waterloo, Waterloo, ON, Canada

email: skcharles@byu.edu

INTRODUCTION

Identifying priority research areas has a variety of positive effects. In addition to focusing individual researchers' attention on issues that are important and urgent, it requires an honest assessment of the state and direction of one's field of research, creates community-wide communication around a common theme, and invites collaboration and cross-fertilization.

The Grand Challenge to Predict In Vivo Knee Loads was announced in 2009 and has had a positive impact on the biomechanics community. The associated competitions have benchmarked current methods, encouraged innovation, raised awareness, and increased conversation in the lower-limb biomechanics community [1, 2].

However, upper limb biomechanists face a different set of important and urgent issues. There are fundamental differences between lower- and upper-biomechanics on a variety of levels, including function, loading, control, and pathology. In addition, methods employed in upper-limb biomechanics research are generally less standardized than lower-limb methods, making comparisons and community-wide communication more difficult. The upper-limb biomechanics community would greatly benefit from efforts to identify its own set of priority areas and grand challenges. Although identifying such priority areas and grand challenges is beyond the scope of a single symposium (let alone coming to agreement), this symposium can serve to start a community-wide discussion of priority areas and potential grand challenges (for the purposes of this symposium, a

priority area is defined as a research area of exceptional importance, whereas a grand challenge is defined as a specific, tightly defined problem that addresses an aspect of a priority area and draws attention to it, often through an organized competition).

SYMPOSIUM FORMAT

The symposium will begin with a short presentation by each author in which he/she presents his/her opinion of priority areas in upper-limb biomechanics, and suggestions for potential grand challenges. After these presentations, the audience will be divided into groups and encouraged to discuss the presentations and develop their own priority areas and grand challenges, which each group will briefly present to the entire audience. The symposium will end with a moderated debate involving the authors and the audience.

PRESENTATIONS

Charles: The gap between researchers and clinicians is a significant obstacle to the progress of upper-limb biomechanics research. This gap is arguably larger for upper limb movements than for lower-limb movements, perhaps in part because standardization is more pervasive for the lower limb (gait is more easily standardized than upper limb function) and because the lower-limb research community has more researchers who bridge that gap (e.g. researchers in exercise science, who often pursue applied research, make up a large part of the lower-limb biomechanics research community but rarely

research upper limb biomechanics). There appears to be relatively little discussion (or even common ground) between researchers in upper-limb biomechanics and motor control and clinicians such as occupational therapists and surgeons. Greater communication between researchers and clinicians would greatly benefit patients with movement disorders by informing researchers of clinically relevant problems and by assisting clinicians in adopting more quantitative tools for evaluation and diagnosis. One potential first step may be to take advantage of recently developed motion capture systems that are low-cost, quick-and-easy (markerless), *and* high-resolution (e.g. Leap Motion sensor). Gathering and sharing upper-limb movement data from large numbers of subjects would allow us to establish quantitative norms of upper limb movements (intra- and inter-subject variability as well as means). Although such an endeavor is difficult because upper limb function is highly variable, it could enable identification of subtle movement abnormalities believed to cause the movement impairment syndromes so common in clinical practice (60% of patients seen by physical therapists, for example [3]).

Li: Biomechanics is an applied science that bridges basic research and clinical applications, effectively translating research findings to benefit patients. Research in musculoskeletal biomechanics has led to significant advances in clinical practice in orthopedic surgery and rehabilitation, including implant design, joint replacements, medical devices, surgical techniques, orthotics and prosthetics, and performance evaluation. However, biomechanics for the hand is somewhat underdeveloped in comparison to other musculoskeletal areas. Yet, the hand offers a unique research opportunity for biomechanics research because of its anatomical complexity, functional versatility, and pathological vulnerability. My research for over 15 years has focused on hand biomechanics and motor control with a clinical application to carpal tunnel syndrome. I will share my experiences of disease-centered research development and discuss the challenges and opportunities of biomechanics research related to several main hand disorders.

Murray: In biomechanics, the upper limb is often considered somewhat of a niche area. In addition to the complexity of the system and the difficulty in stereotyping the most common way humans use their arms and hand (compared to gait, for example), this viewpoint is a challenge to progress and momentum in the field of upper-limb biomechanics. Researchers interested in the upper limb need to continue to demonstrate how advances in this area add and advance a common knowledge base that should be of interest to a wide community, not to just those who focus their efforts in this area.

Similarly, upper limb researchers often face difficulties in translating their research to the clinic. Without a specialized journal or society that brings researchers and clinicians together (such as the Gait and Clinical Movement Analysis Society), researchers interested in the upper limb often have difficulty finding clinicians who are familiar with upper-limb biomechanics research. This can limit the clinical collaborations and can make distribution of research findings challenging; sometimes findings are considered too clinical for a scientific journal and too research-oriented for a journal with clinical interests.

Finally, in the lower limb, joint replacements are considered to be one of the most successful medical devices of our time. In contrast, joint replacements in the upper limb have had relatively limited success; degenerative pain in the wrist and thumb is most commonly treated by simply removing the bones associated with the degeneration, without any replacement.

Perreault: Understanding the proximal-distal differences in the neural control of upper limb biomechanics is a priority area. Different levels of the nervous system are engaged in different proportions as we consider proximal and distal joints in the human arm. We do not presently have a good understanding of how these differences contribute to our ability to complete various motor tasks, or how these abilities are altered by injury. This is arguably a much greater issue for the upper limb than it is for the lower limb.

Also, efforts to identify neural control strategies need to incorporate task and biomechanical constraints. Many studies attempt to infer neural control strategies from recorded muscle activations but fail

to consider how those activations are constrained by the biomechanics of the limb and the task being performed. This issue is relevant to both upper and lower limbs, though solutions may be more feasible for the upper limb.

Valero-Cuevas: We should re-evaluate the current cortico-centric view of the neural control of the upper extremity and hand. For over a century, researchers have agreed that our anatomy and brains exhibit dramatic, specific, and useful adaptations for control of the upper extremity and hand. But if we roll back evolutionary time, it is not at all clear what were the evolutionary pressures that drove such drastic neural adaptations. For example, the advantages of monosynaptic corticospinal projections are often taken to be self-evident for biomechanical function—but it is equally evident that the larger proportion of oligosynaptic corticospinal and rubrospinal projections serve humans and other dexterous vertebrates well. Similarly, time delays argue against cortical circuits being the dominant drivers of time-critical biomechanical dexterity. Roger Lemon has argued that these adaptations cannot be the sine qua non of dexterity [4], yet this caveat has largely gone unheeded. Therefore, let us explore a hierarchical and distributed neuromechanical architecture that leverages, yet does not supersede, phylogenetically older structures shared by humans and other dexterous vertebrates.

Vidt: There is a movement toward developing models for individualized medicine, but more work is needed before this can become a plausible solution for the upper-limb. There are several aspects of shoulder biomechanics notably absent or simplified in current models [5]. These exclusions necessitate further model development and should be considered as priority areas for the upper limb research community. For example, muscle scaling and humeral head translation are needed to more accurately represent different individuals, and these

parameters become increasingly important in the context of orthopaedic injury (e.g. rotator cuff tears, subacromial impingement). Muscle force and the relative positions of the bony structures are essential determinants of the magnitude and direction of joint contact forces. To bridge the gap between biomechanics and the clinic, it is important to quantify how these measures change following injury and the extent to which they affect joint loading and contribute to subsequent joint damage during typical upper limb movements.

A potential grand challenge would include model prediction of glenohumeral joint contact forces measured using instrumented shoulder implants. Being able to accurately predict *in vivo* loads would require a model that effectively captures the muscular changes associated with injury, as well as the intrinsic bony kinematics. The challenge would be in the same spirit as that of the lower limb, but due to the anatomical and functional differences of the shoulder, it would require a markedly different approach.

REFERENCES

1. Fregly BJ, Besier TF, Lloyd DG, Delp SL, Banks SA, Pandy MG, and D'Lima DD. *Journal of Orthopaedic Research* **30**, 503-513, 2012.
2. Kinney AL, Besier TF, D'Lima DD, and Fregly BJ. *Journal of Biomechanical Engineering-Transactions of the ASME* **135**, Article #021012, 2013.
3. Sahrmann SA. *Diagnosis and Treatment of Movement Impairment Syndromes*, Mosby, Inc., 2002.
4. Lemon RN. The G. L. Brown Prize Lecture. Cortical control of the primate hand. *Experimental Physiology* **78**, 263-301, 1993.
5. Prinold JA, Masjedi M, Johnson GR, Bull AMJ. *Proceedings of the Institution of Mechanical Engineers, Part H: Journal of Engineering in Medicine* **227**, 1041-1057, 2013.

METHODS FOR FULL BODY INVERSE DYNAMICS ANALYSIS OF STANDING LONG JUMP

¹ Blake M. Ashby, ^{1,2} Nathaniel Vlietstra, ¹ Lauren J. Hickox, ¹ Gordon J. Alderink

¹ Grand Valley State University, Grand Rapids, MI, USA

² Disher Design & Development, Zeeland, MI, USA

email: ashbybl@gvsu.edu, web: <http://www.gvsu.edu/engineering>

INTRODUCTION

The standing long jump is an athletic event that has been frequently studied to analyze and improve athletic mechanics and performance. Analysis of the biomechanics of the standing long jump can be complex due to requisite coordination of the upper and lower body movements. The net muscle torques at anatomic joints can be calculated using inverse dynamics on kinematic and kinetic data obtained from a motion capture system. The conventional calculation of joint torques involves modeling the body as a series of rigid segments connected by joints and iteratively solving the Newton-Euler equations of motion for each segment in the model. Measurement and modeling errors compound as the solution to one segment is used to solve for the solution to the next. For systems involving more than a few segments, the errors can become larger than physiologically possible [1]. Including the ground reaction forces measured by force plates can be used to increase accuracy but results in an over-determined set of equations. This over-determinacy is often resolved by arbitrarily ignoring the equations from or applying residual forces and a torque to the top-most segment.

The objective of the present study was to investigate various strategies for performing inverse dynamics for the standing long jump including neglecting the equations of motion for different segments to yield determinate conventional solutions and by simultaneously solving all of the equations using a least squares static optimization solution method [2].

METHODS

Six adult males (mean \pm standard deviation, mass: 90.3 ± 12.0 kg and height: 182.0 ± 6.3 cm) each completed a series of eight standing long jumps.

The positions of reflective markers placed on their bodies were recorded by an eight-camera motion capture system (Vicon Motion Systems Ltd., Los Angeles, CA) and the ground reaction forces and center of pressure locations were recorded by two in-ground force plates (Advanced Mechanical Technology Inc., Watertown, MA). The locations of the reflective markers were selected to allow for the creation of a two-dimensional, seven segment (foot, shank, thigh, pelvis, trunk/head, upper arm, and forearm/hand) link model. The volunteers were given the opportunity to warm up and familiarize themselves with the standing long jump motion through practice jumps. For the recorded trials, the participants were instructed to stand with one foot on each force plate and perform standing long jumps for best distance.

The planar Newton-Euler equations of motion were derived for all seven segments. The joint torques at the ankle, knee, hip, lower back, shoulder, and elbow were calculated using a conventional “bottom-up” inverse dynamics procedure by applying the measured ground reaction force data and neglecting the equations of motion for the forearm/hand segment. The same joint torques were calculated using a conventional “top-down” inverse dynamics procedure by applying the known zero external loading at the hand and neglecting the equations of motion for the foot. Conventional solutions neglecting the equations for each of the other segments were obtained by simultaneously completing the “bottom-up” and “top-down” procedures until the eliminated segment was reached. In addition, a static optimization procedure was used to obtain the joint torques by including the measured ground reaction force data and simultaneously solving the equations of motion for all seven segments in a least squares sense similar to the procedure proposed by Kuo [2].

A one-way single variable ANOVA blocking on the six participants was created in SAS JMP 10.0 (SAS Institute, Cary, NC, USA) and used to calculate the mean joint torque with 95% confidence intervals at each frame for each inverse dynamics method.

RESULTS AND DISCUSSION

The joint torques for the conventional “bottom-up” and “top-down” inverse dynamics and the least-squares static optimization procedures for the last 1.2 s before take-off are shown in Figure 1.

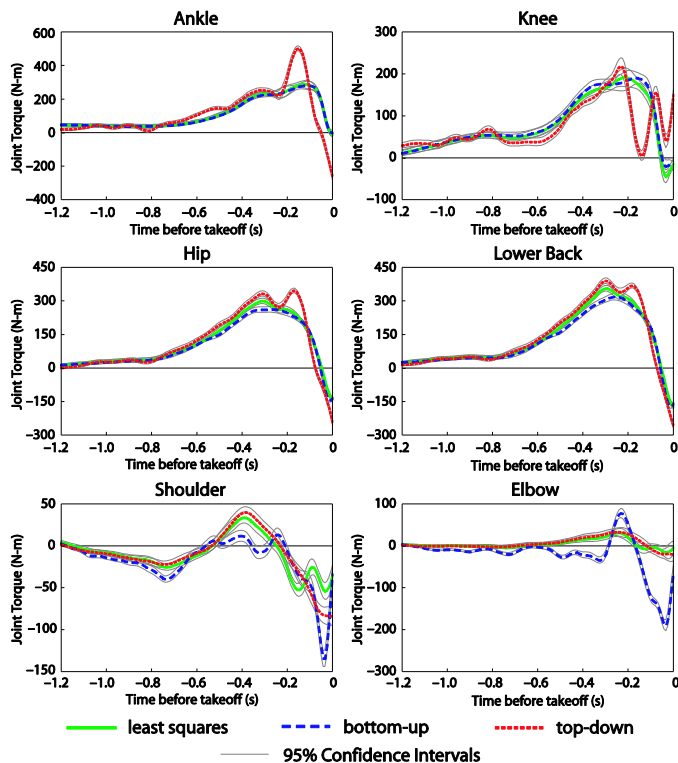


Figure 1: Comparison of joint torques for “bottom-up” and “top-down” conventional solutions and least squares solution (+ extension/plantarflexion).

The hip and lower back torques demonstrated the greatest agreement for the three methods, with overlapping confidence intervals through the jump. The least squares solution almost entirely coincided with the “bottom-up” solution at the ankle and with the “top-down” solution at the elbow. The conventional joint torques calculated for the two joints furthest from the known applied force (shoulder and elbow for the “bottom-up” solution, knee and ankle for the “top-down” solution) substantially differed from the least squares

solution. The propagation of error for the inverse dynamics solutions crossing more than three or four segments was considerable.

The effects of discarding equations for segments other than the forearm/hand and foot segments were explored by using the “bottom-up” solution “up” to the segment of interest and the “top-down” solution “down” to the segment. Neglecting the equations for the trunk yielded joint torques over the full-body model that were most similar to the least squares analysis, which suggests that greater accuracy in conventional full body inverse dynamics may be obtained by ignoring the equations of motion for the trunk segment.

CONCLUSION

Conventional methods of inverse dynamics result in well-established errors in the calculated joint torques that increase considerably as the number of segments increases. Including known or measured external forces at the ground and/or at the hand can increase accuracy but results in an over-determined system of equations. The present study explored various strategies for resolving this over-determinacy including leaving out the equations of motion for various segments and solving all of the equations simultaneously using a least squares static optimization procedure. The calculated torques for joints more than three or four segments away from a known external force demonstrated questionable reliability as they substantially diverged from the other two solution methods. The results from this study suggest that the reliability in the calculated torques for a full body model can be enhanced considerably by discarding the equations of motion for the trunk segment through a combined “bottom-up” and “top-down” conventional inverse dynamics solution or by solving all of the equations simultaneously using a least squares static optimization procedure.

REFERENCES

1. Hatze H. *J Biomech* **35**, 109-115, 2002.
2. Kuo, AD. *J Biomech Eng-T ASME* **120**, 148-159, 1998

SYNTHESIS OF SUBJECT-SPECIFIC TASK-LEVEL MOTIONS FOR PREDICTIVE SIMULATIONS OF BALANCE RECOVERY

¹ Misagh B. Mansouri, ² Cyril J. Donnelly, ³ Mark Robinson, ³ Jos Vanrenterghem, and ¹ Jeffrey A. Reinbolt

¹ University of Tennessee, Knoxville, TN, USA, ² University of Western Australia, Perth, AUS,

³ Liverpool John Moores University, Liverpool, UK

email: misagh@utk.edu, web: http://rrg.utk.edu

INTRODUCTION

Among older adults in the U.S., falls are the leading cause of nonfatal injuries, with 2.5 million treated in 2013 alone [1], at a direct healthcare cost of 30-billion dollars annually [2]. The number of fall events continues to rise each year, providing a rationale to study balance control and how it relates to a fall event. Through this approach prophylactic exercise prescriptions can be developed, to reduce the number of preventable falls. Experiments have identified many aspects of falls; however, simulations can complement experiments to help uncover mechanisms of coordinated and uncoordinated movements for predicting balance recovery. Synthesis of subject-specific movements requires accurate musculoskeletal modeling, complex dynamic simulation, and robust control system design. Human movement involves closed-loop control and a combination of biomechanics and robotics approaches offers great potential for improving fall-related interventions; in addition, it will accelerate the study of human movement control and subject-specific outcome prediction.

METHODS

Motion capture and electromyography (EMG) data (Gluteus Maximus, Gluteus Medius, Rectus Femoris, Vastus Medialis & Lateralis, Biceps

Femoris, Semitendinosus, and Medial Gastrocnemius) of balance recovery were collected from a healthy female (height 1.72 m; mass 68 kg) and male (height 1.79 m; mass 84.5 kg) using a Computer Assisted Rehabilitation Environment (CAREN) system (Fig. 1). The CAREN base was randomly (1 to 3 sec into trial) translated (6 cm) anterior or posterior at maximum viable speed (40 cm/s), while each subject stood on one foot lifting the contralateral foot (>10 cm) above the surface.

Subject-specific dynamic simulations with supporting contacts were created from a three-dimensional, full-body musculoskeletal model with 17 degrees of freedom and 92 muscle-tendon actuators using OpenSim [3] and a custom MATLAB S-function [4]. The simulated motion was combined with surrogate models of experimental motion capture data to begin forming the closed-loop control (Fig. 1; Fig. 2 top right). Separate quadratic response surfaces were developed for each desired subtask (e.g., swing foot position) as a function of a primary task (e.g., center of mass position) to approximate subject-specific task-level movement coordination allowing synthesis of a range of motions (e.g., prediction of post-treatment outcome from pre-treatment motion).

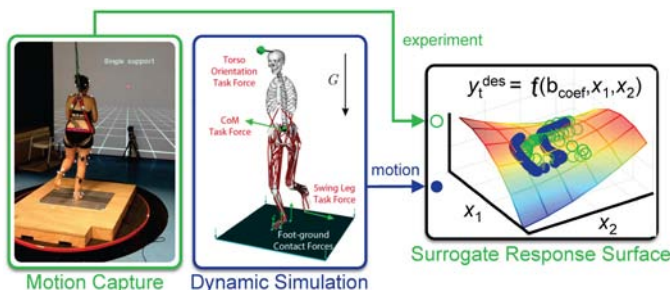


Figure 1: Subject-specific surrogate models created from experimental motion capture data and used for desired task-level coordination during simulations.

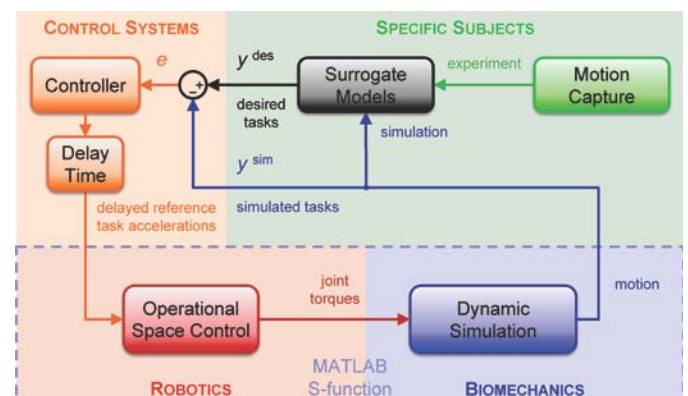


Figure 2: Overview of task-level simulation using OpenSim and MATLAB.

Differences between simulated and desired tasks were used to compute task errors (Fig. 2 top left). Differences between simulated and experimental tasks were minimized by tuning proportional-integral-derivative (PID) controller gains in the feedback loop to a specific subject. Desired task accelerations were delayed (60 ms) to represent time lags for neuromechanical processes.

Task accelerations were used to synthesize whole-body motions using prioritized, multi-task approaches for a support-consistent formulation maintaining the foot-ground contact [5, 6] (Fig. 2 bottom left). Each task force is comprised of the task acceleration multiplied with its task space inertia matrix, plus velocity and gravity compensation terms. Composite joint torques to simultaneously control all tasks are found by multiplying task forces by their respective reduced Jacobians and dynamically-consistent, priority-level-determined, null space matrices for each task.

Joint torques from the prioritized operational space motion control were used for a musculoskeletal dynamic simulation with supporting contacts (Fig. bottom right). Static optimization minimized the sum of muscle activations squared subject to bounds (0 to 1) and constraints on net muscle moments, the product of muscles forces and their moment arms, equaling the total joint torques for the tasks.

The synthesized motions were compared with the experimental ones from each subject. In addition, the model's muscle activations were compared with processed experimental EMG from each subject.

RESULTS AND DISCUSSION

The synthesized motions and muscle activations reproduced the balance recovery experiments. The

simulated whole-body center of mass displacements were, on average, within 0.7 cm (female) and 1.3 cm (male) of experimental ones (Fig. 3a male subject). Model muscle activations (Fig. 3b bottom row) matched experimental EMG (Fig. 3b top row) in timing of peak muscle excitations. Differences between simulated and experimental balance recovery were similar in both anterior and posterior translation directions of the CAREN base.

The combination of biomechanics and robotics approaches for closed-loop control simulations allowed synthesis of subject-specific task-level motions. The surrogate response surfaces allowed synthesis of new, coordinated motions without additional experimental motion capture data. The optimal PID gains allowed control over simulated tasks for each subject. The operational space control allowed multiple prioritized tasks to balance on a single supporting limb in contact with the ground. The four areas of the closed loop (Fig. 2: specific subjects, control systems, robotics, and biomechanics) offer numerous directions for future work to advance the study of human balance control and subject-specific outcome predictions.

REFERENCES

1. CDC, *WISQARS*, accessed online, August 2013.
2. Stevens JA, et al. *Injury Preven* **12**, 290–5, 2006.
3. Delp, et al. *IEEE Trans BME* **55**, 1940–50, 2007.
4. Mansouri, et al. *J Biomech* **45**, 1517–21, 2012.
5. De Sapiro, et al. *Multi Sys Dyn* **16**, 73–102, 2006.
6. Sentis, et al. *IEEE Trans Rob* **26**, 483–501, 2010.

ACKNOWLEDGEMENTS

We are grateful to Vince De Sapiro for helpful discussions and the National Science Foundation (CAREER #1253317) for support.

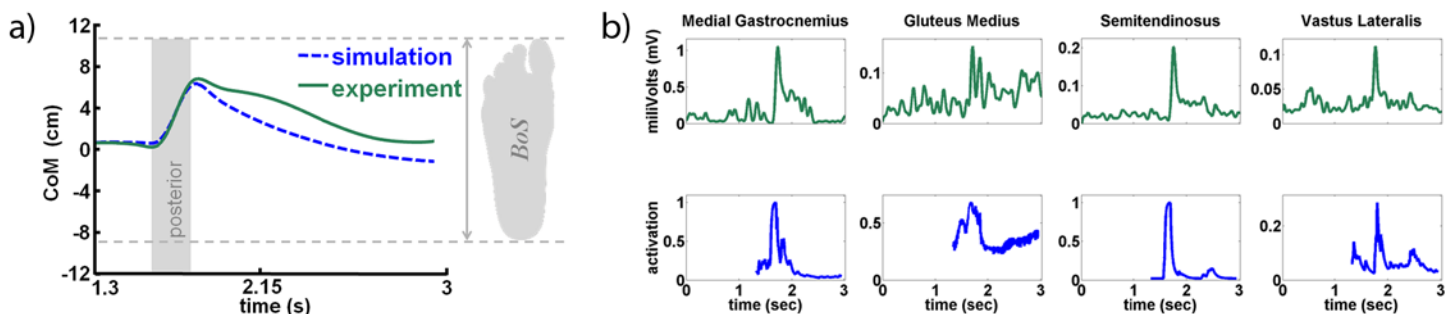


Figure 3: Center of mass displacement for one male subject in the anterior-posterior direction (a) and muscle activities for four selected muscles (b) from the balance recovery experiment (green) and simulation (blue).

SIMULATION-BASED DESIGN OF DEVICES TO AUGMENT HUMAN MOVEMENT

John R Rogers

United States Military Academy, West Point, NY, USA

email: john.rogers@usma.edu

INTRODUCTION

Musculoskeletal dynamic simulation can aid the design of devices that augment human movement. These devices can be used for rehabilitation or for enhancing athletic performance; in the latter role the device relieves some of the metabolic work done by muscles acting over a joint. The design of powered devices requires knowledge of the speed and torque at the joint over time. In-vivo measurement of these quantities is inherently difficult, but they can be predicted by simulation. The objective of this study is to intelligently design wearable robotic devices, including selection of motors, springs, etc.

Exoskeleton systems that transmit force to the human body have been developed for rehabilitation [1], for load carrying [2], and for enhancing strength and endurance [3]. The simulation-based design method described in this paper is applied to a prototype hip actuator, the purpose of which is to help a person run fast. The device is light, of few parts, and is capable of delivering a significant fraction of hip power. Hamner et al. [4, 5] and Dorn [6] describe simulations of human running. The author has not found any physics-based musculoskeletal simulations of humans with exoskeletons in the literature.

This study demonstrates simulation-based selection of springs and electric motors for a hip actuator to assist running. The author's vision is to utilize external power to enable an average runner to maintain his or her sprint pace for a mile.

METHODS

Simulation is based on a human body model that accounts for the sizes and masses of body segments, muscle-to-bone attachment points, and muscle dynamics. OpenSim is software for simulating musculoskeletal dynamics of human and animal

movement. OpenSim executes inverse kinematics, inverse dynamics, residual reduction, and computed muscle control algorithms. Simulation results include joint moments, joint angular velocities, and joint power, and metabolic rate [7]. The human body model used in this work contains 92 musculotendon actuators of the lower extremities and torso [4, 5]. The hip actuator is also included in the model.

The action of the hip actuator prototype is reciprocating: a flexion moment applied by the device to the right leg is accompanied by an equal and opposite moment (extension moment) applied to the left leg. The mechanism does not restrict hip abduction and adduction, thus it minimizes interference with the natural motion of running. The controls and battery are in a backpack.

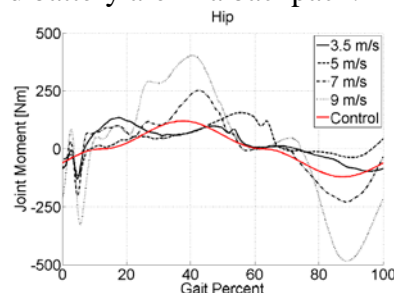


Figure 1: Hip actuator torque (red) is timed to maximize the contribution to hip flexion moment.

Extension and flexion moments exerted by the hip actuator are synchronized to the runner's gait. The torque profile is shown in Fig. 1 on the same plot with hip joint moments from an OpenSim analysis of over-ground running at four speeds up to 9 m/s [6]. A four minute mile is run at 6.7 m/s for comparison. The torque profile must accommodate the reciprocating action: force on the right leg must be equal and opposite to the reaction force on the left leg. The peak magnitude of the torque profile shown is 120 Nm; such a torque would require a peak force of 300 N (68lb) applied to the leg proximal to the knee. Gain control is used to reduce

the magnitude of the torque applied. The phase of the control signal is aligned with the positive and negative peaks of the hip muscle moment to maximize the contribution of the system.

The angular position of the system is equal to the angular position of one leg relative to the other, Fig. 2A, and the motor speed is the system speed multiplied by the motor gear ratio, Fig. 2B.

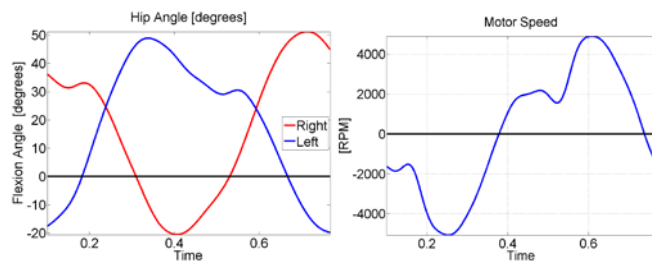


Figure 2a: Hip flexion angles for right and left legs over one gait cycle. **Figure 2b:** Motor speed.

A motor is selected to satisfy the speed and torque profiles, iteratively analyzing the current-, voltage- and power-versus-time profiles with candidate motors.

RESULTS AND DISCUSSION

The motor input power profile for one gait cycle is shown in Fig.3. This figure is for running at 4 m/s. The RMS power is 170 W; the peak is 320 W.

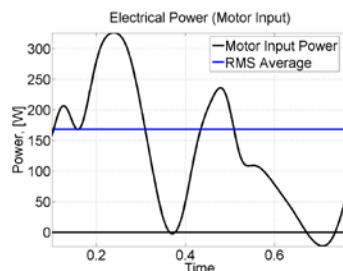


Figure 3: Motor input power over one gait cycle.

CONCLUSIONS

This paper presents a method of incorporating mechanical devices in OpenSim for the purpose of design.

An important limitation of this analysis is the assumption that gait kinematics are the same with the device as they are without the device. This

approach can answer the question “if a runner runs the same way with the device as he runs without it, will there be a metabolic savings?” If the runner adapts his or her gait to accommodate wearing the system, this analysis does not account for the change.

The next step in this project is to run the OpenSim metabolic analysis with and without the hip actuator, the hypothesis being that metabolic rate will be less with the device. OpenSim will be also used to identify potential negative effects on non-hip muscles, and bone-bone contact forces. Once the prototype is assembled and subjected to pilot testing, the author will seek approval for a trial from the Institutional Review Board for human subject testing.

Simulation-based prediction of the effects of machines on human metabolics and muscle force is helpful to understand the impact of such devices on the user. An OpenSim analysis can output joint angular velocities and joint torques, the principle quantities necessary for the design of wearable robotic systems.

REFERENCES

1. Veneman, J et al. *Int J Robot Res* **25.3**, 261-281, 2006
2. Zoss, A et al. *Mechatronics*, IEEE/ASME Trans **11.2**, 128-138, 2006
3. Pratt, J et al., *Robot and Autom ICRA2004*
4. Hamner, S et al. *J Biomech*, **43.14** 2709-2716, 2010
5. Hamner, S et al. *J Biomech*, **46.44** 780-787, 2013
6. Dorn, T et al. *J Exp Biol*, **215** 1944-1956
7. Delp, S et al. *Biomed Engr*, IEEE Trans, **54.11** 1940-1950, 2007

ACKNOWLEDGEMENTS

The views expressed herein are those of the author and do not purport to reflect the position of the United States Military Academy, the Department of the Army, or the Department of Defense. The author wishes to acknowledge the ARL-USMA Mathematical Sciences Center which funded this research in part.

SIMULATED SOFT-TISSUE OSCILLATION INCREASES STABILITY IN PASSIVE-DYNAMIC WALKERS

Samuel E. Masters and John H. Challis

Biomechanics Lab, The Pennsylvania State University, University Park, PA, USA
email: sem361@psu.edu

INTRODUCTION

The majority of human body mass is comprised of soft tissue that oscillates during human locomotion. As a result, models of human locomotion that ignore soft tissue vibration may affect the measurement accuracy of gait kinematics and kinetics. Models of human locomotion that contain a soft-tissue component can be used to study the potential role of soft-tissue oscillation. Passive-dynamic walkers (PDWs) are simple human ambulation models that can be used to study the underlying dynamics of walking gait. A bipedal, point-mass walker with masses located at the hip and both feet can ambulate on an incline solely due to gravity [1]. A PDW model can be modified to study the dynamics of biologically-inspired systems (e.g., energy storage and release in a muscle-tendon unit, or arm swing). A simple PDW with a soft-tissue component was modeled to study the effects of soft-tissue oscillation on human gait dynamics.

The objectives of the study were: (1) quantify the effects of soft-tissue oscillation on the stability of human walking gait; and (2) to measure the kinematic differences between a bipedal walker with and without a soft-tissue component.

METHODS

A two-dimensional PDW was modeled to study the effects of soft-tissue oscillation on gait dynamics. The control passive-dynamic walker (CPDW) contained a point mass at the hip and each foot. The legs were massless and rigid. The oscillating passive-dynamic walker (OPDW) was identical to the CPDW except for the addition of spring-mass-damper system attached to the hip mass to simulate soft-tissue oscillation (Fig. 1).

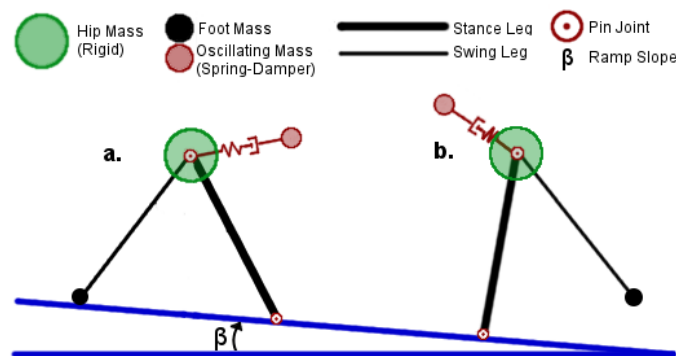


Figure 1: Diagram of a passive oscillating mass walker. (a) The initial position of a step cycle. (b) An intermediate position of a step cycle.

Stable gait cycles were found by systematically incrementing the spring-damper (S-D) parameters until the walker failed to ambulate. The damping values analyzed were between 0 and 12 N.s.m⁻¹ in increments of 0.25 N.s.m⁻¹, and the spring stiffness value was incremented by 0.1 N.m⁻¹. The conditions for foot-ground contact were such that each step was mathematically dependent upon the angular position of the stance leg exclusively [1]. Therefore, the stance leg state trajectory was analyzed in order to assess stability.

The gait stability of the control and oscillating PDWs were measured by Floquet multipliers (FMs), basin of attraction (BOA), and step-time variability (STV). The S-D parameters that resulted in period-1 gait were analyzed for stability. A period-1 gait cycle is such that each cycle is kinematically identical, therefore, the PDW could ambulate indefinitely if unperturbed. The FMs and BOA were analyzed by perturbing the initial state of the stance leg and analyzing the subsequent gait cycles.

To test PDW robustness to an isolated perturbation in the terrain, the slope was perturbed and the subsequent steps were recorded. The perturbation was systematically increased and

decreased until the PDW failed to ambulate. The slope perturbation range (SPR) was the range of slope perturbation values that the walker could ambulate without failing in the subsequent steps. To further test robustness, the CPDW and the OPDW for varying S-D parameters were simulated for 200 steps on uneven terrain. The slope was randomly varied and the standard deviation of the step time was calculated for the CPDW and an OPDW with varying S-D parameters.

RESULTS AND DISCUSSION

The OPDW gait dynamics were sensitive to the S-D parameters. The S-D parameters could be tuned such that the OPDW exhibited stable period-1, period-n ($n>1$), or chaotic gait cycles.

A FM with a magnitude less than one constitutes a system that is stable step-to-step. The S-D parameters could be tuned such that the step-to-step stability of the OPDW was greater than that of the CPDW (Tab. 1). The range of slope values for which an OPDW with S-D parameters of 62.4 N.m^{-1} and 3.5 N.s.m^{-1} could ambulate was 112.9% greater than that of the CPDW. The most stable FM value for this OPDW occurred at a mid-range slope value, which corresponded to a relatively moderate walking speed.

Table 1: Floquet multiplier values for the CPDW and varying spring-damper parameters for the OPDW.

	Control	-----Oscillating-----		
c (N.s.m^{-1})	0	3.5	10.0	12.0
k (N.m^{-1})	0	25.8	32.3	39.1
Floquet Multiplier	0.5883	0.3545	0.3644	0.3651

The phase space of the BOA plane was the Poincare section of the initial state for each step. The S-D parameters for the OPDW with the largest BOA were 1.1 N.m^{-1} - 2.5 N.s.m^{-1} . The area was 111.6% larger than that for the CPDW.

The S-D parameters that resulted in the largest SPR were 53.7 N.m^{-1} and 3.5 N.s.m^{-1} . The SPR for this OPDW was 0.0167 radians, which was 131.9% larger than the SPR of the CPDW. The standard

deviation of the step time for the CPDW on varying terrain was 0.12810 seconds. The standard deviation of the step time for the OPDW on the same randomly varied terrain was 0.07017 seconds, which is 45.2% less than the CPDW.

The S-D parameters for the oscillating mass could be tuned such that PDW exhibited an increase in step-to-step stability, global stability, and robustness to changes in the terrain. In fully rigid body models of human ambulation, stability is largely attained by muscle actuation. The extent to which the neuromuscular system controls stability may be overestimated. Soft-tissue vibration passively increases stability, which would decrease the necessity of the neuromuscular system to aid stability.

It has been illustrated that varying the S-D parameters will drastically change the gait dynamics of a bipedal walker. Stability in human walking gait has been shown to be different amongst different age groups and body types. Differing levels of stability amongst humans may be attributed, in part, to inter-human soft tissue composition variability. Adipose tissue, which is less stiff than other soft tissues, will passively affect the walking kinetics and kinematics of human gait differently than other types of soft tissue (e.g., muscle tissue, skin tissue, and tendon tissue).

CONCLUSIONS

Passive-dynamic walkers can be utilized to obtain insights into human locomotion. These simple PDW models were extended to study the effects of soft-tissue oscillation on walking gait dynamics. Importantly the walking gait of the PDW model with an oscillating component was much more stable than the fully rigid model. This suggests damped soft-tissue oscillations may, in addition to their other roles, make gait more stable.

REFERENCES

1. Garcia M, et al. *J Biomech Eng* **120**, 281-288, 1998.

GENERATING PREDICTIVE SIMULATIONS OF MUSCULOSKELETAL MOVEMENT USING OPTIMAL CONTROL, MATLAB AND OPENSIM

¹ Leng-Feng Lee and ² Brian R. Umberger

¹ Stony Brook University, New York, USA

² University of Massachusetts Amherst, Amherst, MA, USA
email: lengfenglee@gmail.com, umberger@kin.umass.edu

INTRODUCTION

Computer simulation and optimization are powerful tools for studying the biomechanics of movement. Dynamic optimizations can be categorized as either data-tracking or predictive problems. The open-source software OpenSim [3] provides tools for generating tracking simulations but not predictive simulations. However, OpenSim includes a robust application programming interface (API) that permits extending its capabilities with scripting languages such as MATLAB [e.g., 2]. In the work presented here, we combine the computational tools provided by MATLAB with the musculoskeletal modeling capabilities of OpenSim to create a framework for generating predictive simulations of musculoskeletal movement based on direct collocation (DC) optimal control techniques [1,4].

METHODS

The optimal control problem can be stated as: find the state and control trajectories that minimize an objective function, subject to constraints represented by the system dynamical equations, bound constraints on the controls, and arbitrary task constraints [4]. With DC, both the states and controls are discretized in time and treated as unknowns, and the original optimal control problem is transformed into a large-scale, nonlinear programming problem [1]. In our approach (Fig. 1), we use MATLAB to set-up and solve the optimization problem using the fmincon solver (interior-point algorithm) and to communicate with OpenSim via the API. OpenSim is used to calculate the derivatives of the state variables, given a set of discretized states and controls, as well as to return any other quantities of interest (e.g., muscle or contact forces). In evaluating the system dynamical

equation constraints, we used a backward Euler discretization.

For demonstration purposes, we used a simple 1 degree of freedom (DOF) model consisting of a block acted upon by two muscles (6 states, 2 controls), that was modified from the “Tug of War” example provided with OpenSim. Task constraints were defined such that the block should move from a starting position of -0.08 m to a position of 0.08 m and back to the original position in 1.0 s. The objective function to be minimized was the sum of squared muscle activation integrals.

We evaluated the solutions by comparing them at different mesh densities between 25-201 nodes, and by comparing them with forward simulations based on the resulting initial conditions and controls from DC. To evaluate the scalability of the Matlab-OpenSim DC approach, we also present preliminary result for a predictive human walking simulation using a two-dimensional (2-D) model with 12 DOF and 18 muscles (60 states, 18 controls).

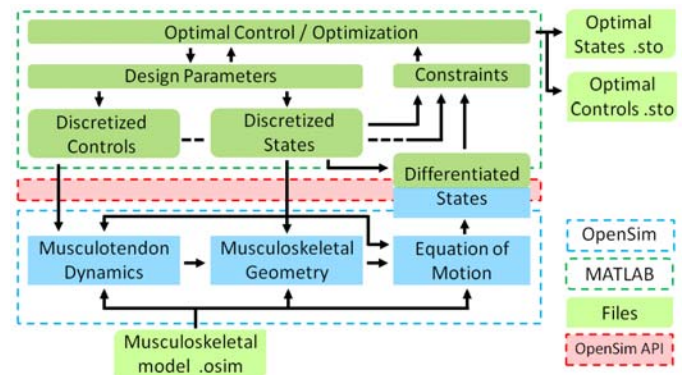


Figure 1: MATLAB-OpenSim interface for solving optimal control problems using DC.

RESULTS AND DISCUSSION

For the 1-DOF model, all node densities resulted in approximately sinusoidal motions that satisfied the constraints (tolerance = $1e-6$) even when the initial guess (blue lines in Fig. 2) was far from the final result (black and green lines in Fig. 2).

With increasing node density, the minimum objective function value (related to the activation integrals in Fig. 2b) decreased considerably until 101 nodes, with little further reduction at 201 nodes.

The forward simulation based on the 201 node solution (red lines in Fig. 2) was nearly identical to the DC result, with a maximum discrepancy of 2.8 mm in the block position at the end of the 1.0 s simulation.

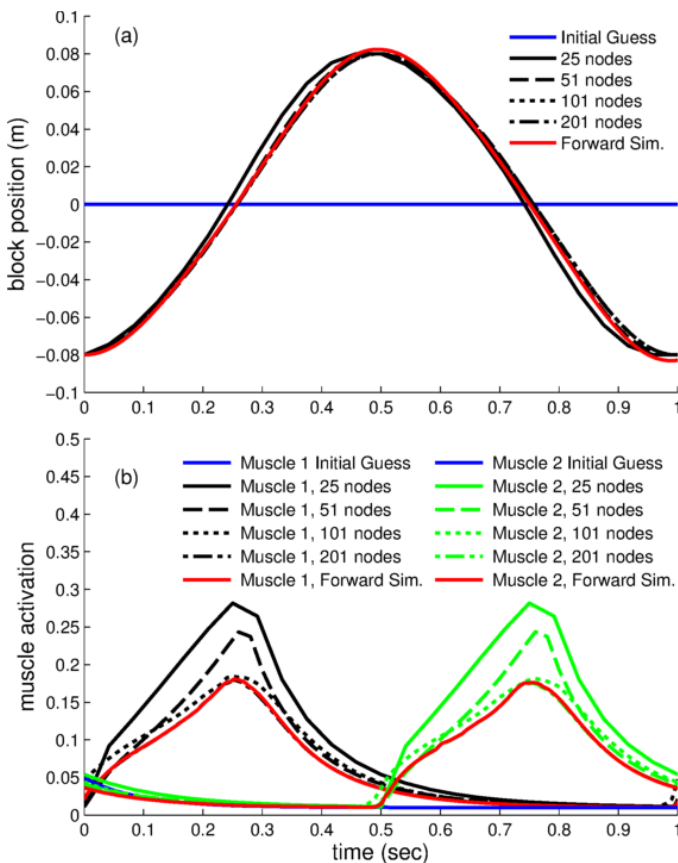


Figure 2: (a) Optimized block position and (b) optimized muscle activations for different numbers of nodes, and for the forward solution. The 201 node activations (dash-dot lines) are hidden behind the forward simulation results (red lines).

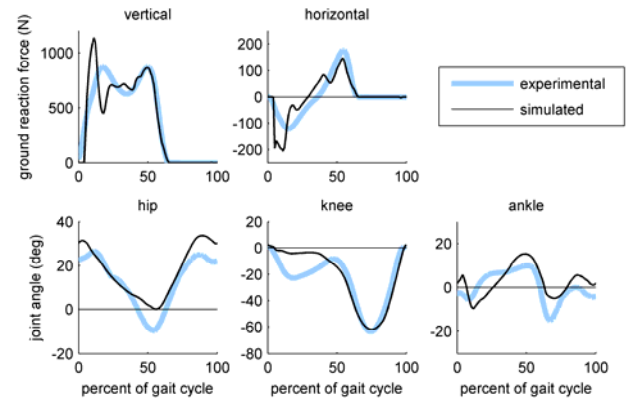


Figure 3: Results for the predictive 2-D walking simulation. Experimental data were not tracked.

The results for the 2-D walking simulation (Fig. 3), while still preliminary, were also encouraging, with ground reaction forces and joint angles that were in reasonable agreement with experimental data. However, convergence to an acceptable tolerance was slow (>100 hr) using the fmincon solver.

CONCLUSIONS

The MATLAB-OpenSim interface provides a powerful and flexible approach for generating predictive musculoskeletal movement simulations using the DC optimal control approach. We are currently investigating replacing fmincon with the IPOPT and/or SNOPT solvers [4], which should substantially reduce the computational time needed to generate the simulations.

REFERENCES

1. Betts JT. *Practical Methods for Optimal Control Using Nonlinear Programming*. SIAM, 2001.
2. Mansouri M, Reinbolt JA. *J Biomech* **45**, 1517-1521, 2012.
3. Seth A, et al. *Procedia IUTAM* **2**, 212-232, 2011.
4. Van Den Bogert AJ, et al. *Procedia IUTAM* **2**, 297-316, 2011.

ACKNOWLEDGEMENTS

We thank Dr. Ross Miller for assistance with the DC approach. This project was supported by grants from NSF (BCS 0935327) and the National Center for Simulation in Rehabilitation Research.

INFLUENCE OF STIFFNESS OF AN ANKLE-FOOT ORTHOSIS ON GAIT A PREDICTIVE SIMULATION STUDY

Anne Koelewijn and Antonie J. van den Bogert

Cleveland State University, Cleveland, OH

email: a.koelewijn@csuohio.edu, web: <http://hmc.csuohio.edu>

INTRODUCTION

An ankle-foot orthosis (AFO) is often prescribed to patients with instability or weakness in the lower leg to assist plantarflexion or dorsiflexion [1]. A limited number of studies focuses on the optimal stiffness of the AFO. It is known that excessive AFO stiffness introduces buckling in the knee [1]. It would be desirable to have the ability to predict the effect of an AFO on the gait of a specific patient. This would make customized prescriptions possible and reduce the need for trial and error. Bregman et al. used a simplified gait model and found that patient energy cost might be reduced by choosing the correct stiffness [2]. However, this model did not have muscles.

In the present study, a dynamic musculoskeletal model will be used to predict the effect of the stiffness of the AFO on gait parameters. We hypothesize that less muscular effort is required in the lower leg with an increased stiffness in the AFO due to the higher moment generated in the AFO.

METHODS

Predictive simulations of gait were performed with a sagittal plane model having nine degrees of freedom and 16 muscles. An open loop optimal control problem was formulated to find a gait cycle that minimizes a weighted sum of muscular effort and deviation from normal gait kinematics. The model and solution method were identical to [3], but a full gait cycle was simulated. Also, tracking was not performed on the ankle where the AFO was applied, since this could make the muscles “fight” the orthosis.

The optimal control problem was solved for an able-bodied system with and without an AFO. The AFO was modelled as a rotational spring that was

applied to one of the ankle joints. The stiffness of the AFO ranges from 50 to 400 Nm/rad, similar to the range of stiffnesses that were tested in [2].

RESULTS AND DISCUSSION

Figure 1 shows the ankle moment and muscle forces in the lower leg of the predictive simulations. The color of the line gets lighter with an increased stiffness. The black line shows the result without an AFO.

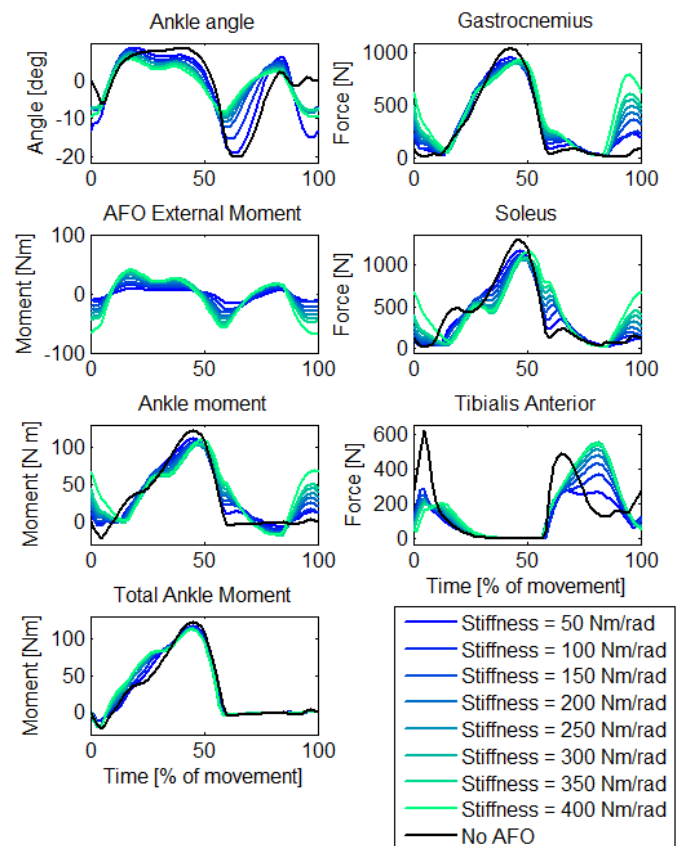


Figure 1: Results of the predictive simulations of gait with and without an AFO.

Figure 1 shows that the AFO decreases the force required in the Tibialis Anterior during initial stance significantly. However, there is little benefit of having a higher stiffness, since the decrease is much

higher between the no-AFO simulation and any simulation with AFO. Also, the stiffness does not have an effect on the size of the peak Gastrocnemius and Soleus force during stance. Both are lower than in gait without AFO, but there is no significant effect of the stiffness.

It was found that this is due to the timing of the moments that are generated by the AFO. During push-off, the ankle angle is almost zero, so the AFO is not able to provide much assistance during this phase. However, during the stance phase, when the ankle angle is larger, the total ankle moment increases with AFO stiffness.

The AFO stiffness has a significant effect on the Tibialis Anterior force during the swing phase. The muscle is counteracting the AFO to provide sufficient toe-clearance, for which a dorsiflexion angle is required. This suggests that a too large stiffness is not beneficial, since it increases the necessary force in the Tibialis Anterior.

There is also a significant effect of the stiffness of the AFO on the Gastrocnemius and Soleus during the initial and final phase of the swing phase. It was found that this was due to the tracking of the vertical ground reaction force, which requires a nonzero ankle angle during the swing phase, yielding a moment in the AFO. The Soleus and Gastrocnemius were activated to reduce the total ankle moment to 0. Further research is necessary to find if this behavior is also present in reality, or if it is an artifact of the cost function that was used in the optimal control problem.

Studies on impaired patients walking with and without an AFO confirm our finding that there is no decrease in peak muscle force in the Gastrocnemius and Soleus muscle [4]. Balmaseda et al., in a study on healthy subjects, reported a reduction of the mean stance phase duration of 4.83% with an AFO compared to without an AFO [5]. This reduction is confirmed by this study, which also yielded a reduction in the stance phase of approximately 5%.

CONCLUSIONS

The hypothesis that an increase in AFO stiffness yields a decrease in muscular effort was not confirmed. It was found that there was only little effect of the stiffness of the AFO on the peak force in the Gastrocnemius and Soleus.

Future studies should include a verification of these results using a subject study, for example to see if humans also increase their force in the Gastrocnemius and Soleus during the swing phase. If it is found that this is an artifact of the optimal control problem, such results can be used to further improve the formulation of suitable cost functions.

REFERENCES

- [1] Yokoyama, O., et al. "Kinematic effects on gait of a newly designed ankle-foot orthosis with oil damper resistance: A case series of 2 patients with hemiplegia." *Arch. Phys. Med. Rehabil.* 86.1 (2005): 162-166.
- [2] Bregman, D. J. J., et al. "The effect of ankle foot orthosis stiffness on the energy cost of walking: A simulation study." *Clin. Biomech.* 26.9 (2011): 955-961.
- [3] Van den Bogert, A. J., et al. "Predictive musculoskeletal simulation using optimal control: effects of added limb mass on energy cost and kinematics of walking and running." *Proc Inst Mech Eng, P: J of Sports Eng Technol* 226.2 (2012): 123-133.
- [4] Ohata, Koji, et al. "Effects of an ankle-foot orthosis with oil damper on muscle activity in adults after stroke." *Gait & posture* 33.1 (2011): 102-107.
- [5] Balmaseda Jr, M. T., et al. "Ground reaction forces, center of pressure, and duration of stance with and without an ankle-foot orthosis." *Arch. Phys. Med. Rehabil.* 69.12 (1988): 1009-1012.

ACKNOWLEDGEMENTS

This research was supported by the National Science Foundation under Grant No. 1344954.

Biomechanical, Clinical, and Functional Changes with Achilles Tendon Pathology

¹ Jennifer A. Zellers, ¹ Daniel H. Cortes, and ¹ Karin Gravare Silbernagel

¹ The University of Delaware, Newark, DE, USA
email: jzellers@udel.edu

INTRODUCTION

Achilles tendon injury is associated with pain, functional impairment and an inability to return to prior level of function in activities of daily living as well as sport activity. Early viscoelastic recovery of the tendon has been suggested to correlate with functional gains following Achilles tendon rupture [1]. Prior studies have been limited by an inability to adequately measure tendon viscoelastic properties non-invasively. A novel, non-invasive ultrasound elastography technique using continuous shear wave elastography (cSWE) has been developed to measure viscoelastic properties of the tendon [2,3]. This technique has been validated and applied to a healthy population, however, application of this technique to Achilles tendon dysfunction has only been described in one subject [2,3]. This study evaluated tendon viscoelastic properties via cSWE and functional capacity of three subjects with Achilles tendon dysfunction.

METHODS

Three subjects with varying tendon pathologies were included in this case series. This study was approved by the University of Delaware Institutional Review Board.

Subjects were examined by a licensed physical therapist to confirm Achilles tendon injury. Tendon geometry was obtained via B-mode ultrasound imaging to measure tendon length from the calcaneal notch to the soleus insertion and gastrocnemius myotendinous junction. Viscoelastic properties of the tendons were measured using cSWE. Data was collected at eleven frequencies (323, 340, 358, 379, 403, 430, 461, 496, 538, 586, 645 Hz) due to the variation in wave propagation of healing tissue. Six frequencies which produced a

complete sine wave in the visualized region were used in the calculation of shear and viscous moduli.

Subjects completed functional testing including the heel-rise test for ankle plantar flexor muscular endurance. This test has been found to correlate with tendon length and functional outcomes [4]. Subjects completed questionnaires regarding self-reported symptoms and function including the Victorian Institute of Sport – Achilles Questionnaire (VISA-A), the Achilles Tendon Total Rupture Score (ATRS), and the Foot and Ankle Outcome Score (FAOS).

RESULTS AND DISCUSSION

Case 1 is a 72 year-old male, presenting with chronic, tendinopathic changes. Case 2 is a 56 year-old male, presenting with Achilles tendinopathy. Case 3 is a 25 year-old female, presenting seven weeks status-post acute Achilles tendon rupture currently undergoing conservative treatment.

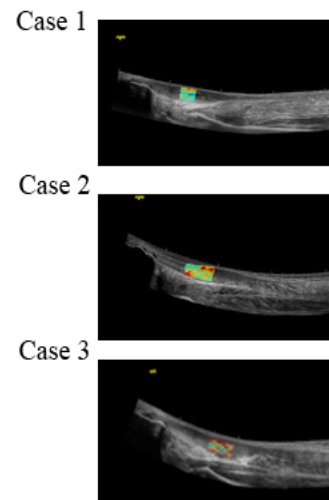


Figure 1: Viscoelastic map of shear modulus superimposed on B-mode ultrasound image for the symptomatic tendon in each of the three cases.

Achilles tendon length, viscoelastic properties, heel-rise test total work and maximum heel-rise height, VISA-A and ATRS scores are included in Table 1. Viscoelastic maps were constructed for each of the subjects (Fig. 1). None of the subjects were able to complete a unilateral heel-rise on their affected side. FAOS scores are shown in Figure 2.

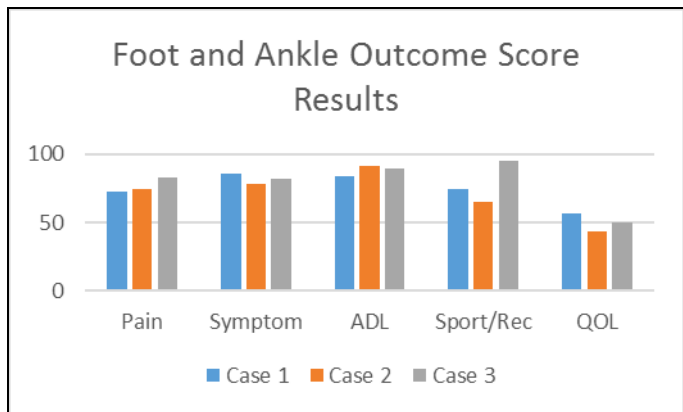


Figure 2: Results of the FAOS for each case in pain, symptom, activity of daily living (ADL), sport and recreation, and quality of life (QOL) subscales.

CONCLUSIONS

Each of the three subjects included in this case series were diagnosed with Achilles tendon injury. Two demonstrated varying severity of Achilles tendinopathy and one was status-post acute Achilles tendon rupture. All subjects demonstrated differences in shear and viscous moduli compared to their asymptomatic side. All subjects also demonstrated decreased functional performance as evidenced by the inability to perform a single heel

rise and by subject self-report using the VISA-A, ATRS and FAOS.

This is the first study to identify differences in Achilles tendon viscoelastic properties using the cSWE technique and associate them with clinical outcomes in an unhealthy population. Additional studies with larger subject numbers are required to identify whether there are correlations between viscoelastic properties and functional outcomes and whether these properties change over time with healing.

REFERENCES

1. Schepull T et al. *Scand J of Med and Sci in Sports* **22**, 18-23, 2012.
2. Cortes DH et al. *Ultra. Med & Biol*, In press.
3. Suydam et al. *J Orthopaedic Research*, Accepted.
4. Silbernagel KG et al. *Am J Sports Med* **40**, 1564-1571, 2012.

ACKNOWLEDGEMENTS

Research reported in this publication was supported by the National Institute of Arthritis and Musculoskeletal and Skin Diseases of the National Institutes of Health under Award Numbers R01AR050052, R21AR067390, P30-GM103333. The content is solely the responsibility of the authors and does not necessarily represent the official views of the National Institutes of Health.

Table 1: Tendon geometry, viscoelastic properties, and total work performed with the heel-rise test in three case subjects (symptomatic/asymptomatic sides).

Case	Length to Soleus	Length to Gastroc.	Shear Modulus	Viscosity	Heel-Rise – Total Work	Heel-Rise – Max Height	VISA-A or ATRS Score
1	9.9 cm / 10.6 cm	24.4 cm / 22.6 cm	73.55 kPa / 141.42 kPa	16.6 Pa-s / 51.3 Pa-s	0 J / 1234.9 J	0 cm / 9.9 cm	VISA-A: 25/100
2	8.6 cm / 9.9 cm	21.4 cm / 21.0 cm	88.68 kPa / 122.62 kPa	25.2 Pa-s / 48.8 Pa-s	0 J / 1185.53 J	0 cm / 10.7 cm	VISA-A: 52/100
3	8.6 cm / 4.2 cm	21.4 cm / 19.0 cm	101.22 kPa / 92.69 kPa	28.3 Pa-s / 68.4 Pa-s	0 J / Not tested	0 cm / Not tested	ATRS: 43/100

VARIATION IN THE HUMAN ACHILLES TENDON MOMENT ARM DURING WALKING

Kristen Rasske¹, Darryl G. Thelen¹, and Jason R. Franz^{1,2}

¹University of Wisconsin-Madison, Madison, WI, USA

²University of North Carolina and North Carolina State University, Chapel Hill, NC, USA

email: krasske@wisc.edu web: <http://uwnmbl.engr.wisc.edu/>

INTRODUCTION

The Achilles tendon (AT) moment arm is an important biomechanical measure that converts gastrocnemius and soleus muscle forces into a joint moment at the ankle, ultimately contributing to the generation of mechanical power during walking. However, existing measurements of the AT moment arm are limited to isolated ankle exercises, which are then assumed to apply during walking [1-4]. For example, current modeling approaches presume a kinematic AT moment arm that increases with plantarflexion over the range of motion observed in walking. Yet, recent evidence suggests that the relation between AT moment arm and ankle joint rotation is load dependent and varies significantly from rest with increasing muscle activity [2]. Thus, the AT moment arm may vary in a complex manner during gait, reflecting considerable and compound changes in joint angle and muscle forces.

Our purpose was to couple ultrasound imaging and quantitative motion capture to dynamically estimate the AT moment arm *in vivo* during walking. We hypothesized that the AT moment arm varies considerably during walking, but not as a strict kinematic function of ankle joint angle.

METHODS

Ten healthy, young adults (age: 23.9 ± 4.0 years; 6 males and 4 females) walked barefoot at 1.25 m/s on a dual-belt, force measuring treadmill. A custom orthotic positioned a 38 mm linear array transducer over the free AT of subjects' right leg, on average ~6 cm superior to the calcaneal insertion (Fig. 1). For each subject, we recorded ultrasound radiofrequency (RF) data at 155 frames/s over five strides. In synchrony, an 8-camera motion capture system (Motion Analysis, Corp., Santa Rosa, CA) recorded

the 3D trajectories of retroreflective markers placed on subjects' pelvis, right and left legs, and the ultrasound orthotic. We also collected electromyographic (EMG) activities of the lateral gastrocnemius and soleus.

We manually tracked the superficial and deep edges of the AT at three locations (proximal, middle, and distal) using down-sampled (2x) B-mode images created from the RF data. We defined the AT midline as the best fit line through the average of the superficial and deep tendon edges. We defined the right ankle joint center as the midpoint of the lateral and medial malleoli markers. Finally, by transforming the ultrasound, orthotic, and motion capture kinematics into a common reference frame, we estimated the AT moment arm over the gait cycle as the perpendicular distance from AT midline to the ankle joint center (Fig. 1). A repeated measures ANOVA tested for significant ($p < 0.05$) main effects of gait cycle phase (20% bins) on estimates of the AT moment arm.

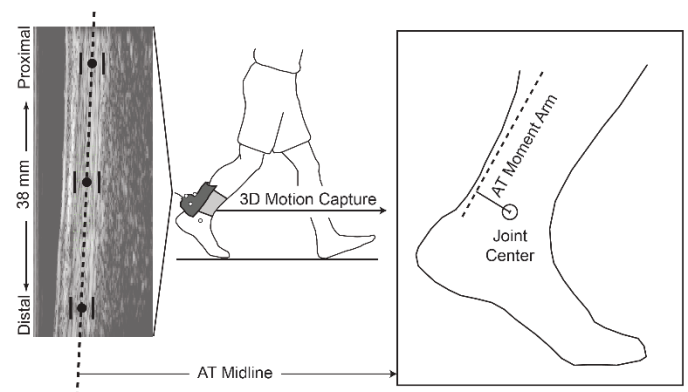


Figure 1: We used ultrasound imaging and quantitative motion capture to estimate the AT moment arm during treadmill walking at 1.25 m/s.

RESULTS AND DISCUSSION

We found that the AT moment arm varied considerably during walking, increasing significantly and progressively from initial contact until after toe-off (Fig. 2B) ($p < 0.001$). The progressive increase in AT moment arm during stance corresponded with increasing plantarflexor muscle activity (Fig. 2A). In addition, the AT moment arm reached its maximum near the instant of peak plantarflexion. However, as hypothesized, and in contrast to current musculoskeletal modeling approaches, the AT moment arm during walking could not be expressed as a strict function of ankle joint angle (Fig. 2C). Our results imply that the AT moment arm varies with load during gait, presumably arising from a co-interaction between gastrocnemius and soleus forces and ankle angle.

Interestingly, we do observe some similarities between the AT moment arm measured during walking and that during isolated ankle exercises. For example, the AT moment arm immediately after initial contact, an instant of negligible muscle force [5], coincides with that previously reported at rest for the same joint angle (Fig. 2C) [1]. Additionally, the AT moment arm during late stance, when the AT is maximally loaded [5], corresponds to that reported during MVC at the same joint angle [1].

By measuring the AT moment arm *in vivo* during gait, we might better elucidate the relation between muscle-tendon architecture and performance. For example, the AT moment arm is modestly correlated

with walking speed in slower old adults [6], a change that may contribute to diminished ankle power output seen in this population. This potential link between musculoskeletal geometry and performance can be directly tested using the proposed *in vivo* measurements during gait.

CONCLUSIONS

We provide evidence that the AT moment arm during walking is load dependent, likely reflecting compound changes in joint angle and muscle forces. Our results have important implications for the development of musculoskeletal models, suggesting that the AT moment arm measured during isolated ankle exercises may not accurately predict that during walking. Moreover, measuring the AT moment arm *in vivo* during walking has the potential to provide new and mechanistic insight into triceps surae muscle-tendon performance.

REFERENCES

1. Maganaris CN. *Eur J Appl Physiol* **91**, 130-139, 2004.
2. Olszewski K, et al. *J Biomech*, In press.
3. Fath F, et al. *J Appl Physiol* **109**, 1644-1652, 2010.
4. Manal K, et al. *Physiol Rep* **1** (6), e00139, 2013.
5. Finni T, et al. *Eur J Appl Physiol Occup Physiol* **77**(3), 289-91, 1998.
6. Lee S, et al. *J Biomech* **45**, 1601-1606, 2012.

ACKNOWLEDGEMENTS

Funded in part by a grant from NIH (F32AG044904).

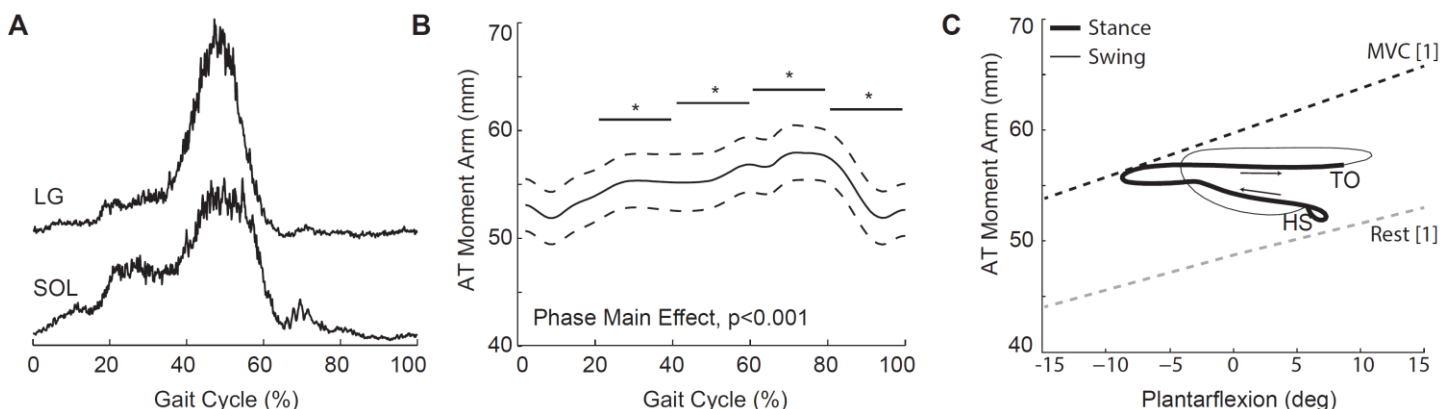


Figure 2: (A) Group mean EMG profiles of the lateral gastrocnemius (LG) and soleus (SOL) muscles and (B) group mean (standard error) AT moment arm over an average gait cycle. Asterisks (*) indicate significantly different from preceding 20% gait cycle ($p < 0.05$). (C) Group mean AT moment arm versus ankle joint angle compared to previous values during maximum voluntary contraction (MVC) and at rest from isolated ankle exercises [1].

LUMBAR INTERVERTEBRAL DISC DEFORMATION IN VIVO DURING LIFTING MOTION

¹ Ryan Byrne, ² William Anderst, ^{1,2} Xudong Zhang

¹ Department of Mechanical Engineering & Materials Science

² Department of Orthopaedic Surgery, University of Pittsburgh, Pittsburgh, PA, USA

email: xuz9@pitt.edu

INTRODUCTION

Low back disorders (LBD) remain one of the most prevalent, debilitating, and costly public health problems. Excessive mechanical loading on the lumbar intervertebral discs is a major risk factor for causing LBD. Assessment of the disc loading or deformation in vivo during functional activities is challenging. Most prior studies have either used models to predict the disc forces without taking into account the disc deformation [1] or have examined the force-deformation relationship in vitro by cadaveric tests and used the data to verify finite element model (FEM) predictions [2]. One study quantified the lumbar disc deformation in vivo but only for static positions [3]. We have recently succeeded in measuring 3D continuous lumbar vertebral kinematics in vivo during lifting activities, using a dynamic stereo-radiography system [4]. The purpose of the current study was to characterize the lumbar intervertebral disc deformation based on the skeletal kinematics data acquired.

METHODS

We used data of 8 asymptomatic subjects (5 male, 3 female; age: 24 ± 2 years) who performed a straight-legged lifting motion and static standing trials while a dynamic stereo-radiography system captured their lumbar vertebral kinematics at 30 Hz. Data of two trials of lifting a 10-lbs load and one trial of static upright standing with no load were included. The recorded dynamic radiographic images were then processed using a volumetric model-based tracking procedure, resulting in 3D motion data of the vertebral bones (from L2 to S1). Details of the experimental setup, data acquisition, and data processing were described in a prior publication [4].

The intervertebral disc deformation was defined based on the relative motion between adjacent vertebral endplates, with the static position in upright standing as the reference state (Fig. 1). The disc was modeled by line segments (grey lines) perpendicular to the average (blue line) of planes fit to the adjacent endplates (red lines) in the static upright position [5]. The disc height was calculated at over 100 discrete line segments that were evenly distributed in the anterior-posterior direction throughout the mid 1/3rd of the disc. Line segments representing the disc remained connected to the endplates as the vertebrae moved relative to each other. The deformation at each time frame was decomposed into two orthogonal components: compression and shear component; the percent change in length in the compression direction with respect to the static position was then determined (Fig. 2).

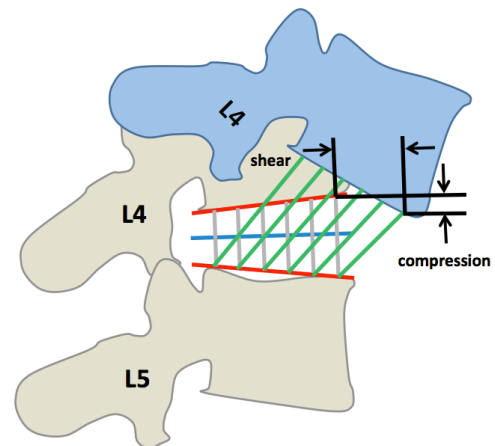


Figure 1: Definitions of the compression and shear components of disc deformation as a result of intervertebral motion. Deformation is exaggerated for visualization purpose.

Disc deformation was analyzed for three 2mm radius circular areas (most anterior, central, and most posterior) consistently defined within each disc. The line segment within each circle

experiencing the median compression-distraction at the beginning of dynamic motion was selected and tracked throughout the rest of lifting. The correlation between disc deformation and extension was determined for each motion segment for each participant.

RESULTS AND DISCUSSION

The anterior compression and posterior distraction, computed as disc height percent changes from the upright standing posture, were greatest at the beginning of a lift where the lumbar spine was most flexed (Fig. 2). The average maximum disc compression and distraction were comparable across L2-L5, but were distinctively less at L5-S1 (Table 1). The anterior compression and posterior distraction reduced, in a relatively linear fashion, with the progression of lifting (see ranges of R² values in Table 2).

Table 1: Maximum lumbar disc deformation.

Disc	Max Compression	Max Distraction
	Mean±SD	Mean±SD
L2-L3	-34% (±25%)	+65% (±34%)
L3-L4	-36% (±22%)	+70% (±44%)
L4-L5	-38% (±11%)	+59% (±18%)
L5-S1	-17% (±12%)	+30% (±12%)

Table 2: Ranges of R² values quantifying the correlation between deformation and extension.

Disc	Anterior Compression	Posterior Distraction
L2-L3	.90 - .98	.79 - .99
L3-L4	.82 - .98	.90 - .98
L4-L5	.75 - .99	.88 - .99
L5-S1	.44 - .99	.61 - .99

Minimal deformation changes were incurred in the central areas of the discs, which on average varied from -4% to +6%, during the lifting motions.

The results that the L5-S1 disc experiences much less deformation change during a lifting motion may point to one or both of the following interpretations: (1) it is under significantly more pre-stress and deformation at the static positions, therefore reducing the appearance of compression-distraction change throughout the flexion; (2) the L5-S1 disc has distinctively different structural or material properties (e.g., is stiffer) than the other discs.

CONCLUSION

This study quantified the lumbar intervertebral disc deformation in vivo during lifting motions, showing that the discs underwent substantial deformation in the anterior and posterior regions while the L5-S1 disc exhibited unique deformation characteristics in comparison to the L2 to L5 lumbar discs.

REFERENCES

- Granata KP & Marras WS. *J Biomech* **28**, 1309-1317, 1995.
- Goel VK, et al. *Spine*, **20**, 1719-1727, 1995.
- Wang S, et al. *J Biomech* **42**, 705-711, 2009.
- Aiyanger AK, et al. *J Biomech Eng* **136**, 011004, 2014.
- Anderst WJ, et al. *J Orthop Res* **31**, 1881-1889, 2013.

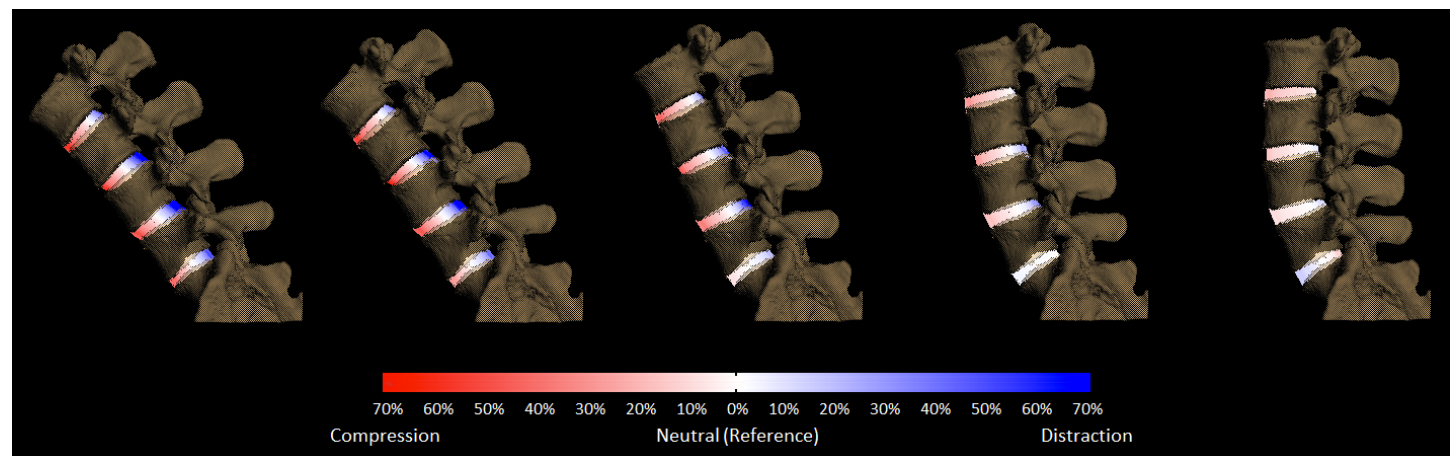


Figure 2: L2-S1 lumbar disc compression-distraction deformation during a representative lifting trial.

QUANTIFYING MICROSTRUCTURAL DAMAGE ACCUMULATION IN THE ANNULUS FIBROSUS DURING INDUCED INTERVERTEBRAL DISC HERNIATION

Mamiko Noguchi*, Alexander Wong, Ibrahim Ben Daya, Troy L. Campbell, Joe Quadrilatero and Jack P. Callaghan

University of Waterloo, Waterloo, ON, Canada

*email: mnoguchi@uwaterloo.ca

INTRODUCTION

Structural damage to the annulus fibrosus is commonly observed in degenerated intervertebral discs (IVD) [1]. Approximately 40% of low back pain cases are attributed to internal disc disruption [2], which is characterized by damage to the internal structure of the IVD and is the precursor of herniation. Previous studies have proposed damage progression mechanisms by examining the magnitude of microstructural damage [3,4]. Results from these studies suggest that herniation initiates from a formation of clefts within the intralamellar matrix [3] and the most severe damage occurs in the inner annulus fibrosus [4]. However, both these studies only examined herniated discs, and only qualitatively. Therefore, it is unknown how this microstructural damage accumulates over a protocol known to induce herniation and whether the magnitude of damage can be quantified. The purpose of this study was to quantify microstructural damages to the annulus fibrosus at various time points during a herniation protocol in order to characterize accumulation of clefts (number, area, length, and major to minor axis ratio) leading up to IVD herniation.

METHODS

Ten porcine cervical functional spine units (mean age = 6 months; C3-C4 and C5-C6), each consisting of two adjacent vertebrae and the intervening IVD were used in this study. There were five loading conditions: 4000, 3000, 2000, and 1000 cycles of a herniation inducing protocol (1500 N load control; 1 Hz flexion-extension cycle), and pre-conditioning only as a control (preload at 300 N for 15 minutes followed by four cycles of passive flexion-extension test). Previous studies have shown that approximately 80% of porcine specimens partially herniate between 3000 and 7000 cycles of this protocol, suggesting that development of macrostructural damage would be captured within the design of the study [5,6].

Following the loading protocol, three tissue samples were excised from the posterior regions of the discs. These tissue samples were embedded in Optimum Cutting Temperature compound (Tissue-Tek OCT; Sakura Finetek, Torrance, CA, USA) and frozen in liquid nitrogen. Each frozen specimen was serially sectioned into 10 μm thick slices in the frontal (superficial and deep layers) and sagittal planes and stained with hematoxylin and eosin (H&E). Each section was examined using a digital camera (PixeLink, Ottawa, ON, Canada) linked to a brightfield microscope (Nikon Instruments Inc., Melville, NY, USA) and captured using Image ProPlus analysis software (Media Cybernetics, Rockville, MD, USA) (Fig.1). Three representative images were taken from each section and processed using a custom Matlab program. A Gaussian Mixture Model was used to identify the cluster for the clefts, and four cleft properties were calculated: i) number of clefts, ii) major axis length, iii) cleft area, and iv) major to minor axis ratio. The average and standard deviation of each dependent variable was calculated to demonstrate the trend across different time points during the herniation protocol.

RESULTS AND DISCUSSION

From 1000 to 3000 cycles, the number of clefts increased (over 300% increase or appearance of more than 55 clefts), while there were minimal increases in major axis length ($< 9 \mu\text{m}$) and cleft area ($< 33 \mu\text{m}^2$), suggesting that number of clefts may be an indicator of the magnitude of microstructural damage (Fig.2).

Despite the lack of any mechanical loading, the number of clefts and cleft length were higher in control (zero cycle; pre-condition only) compared to the 1000 and 2000 cycle conditions. In addition, the average cleft area was similar between control and 3000 cycles ($< 10\%$ difference). However, when comparing the total area (sum of each cleft area), it increased from control to 3000 cycles by approximately 40% in both superficial and deep

layers. By examining the images qualitatively, this trend can be explained: gaps (inherent imperfections) between collagen fibers were visible when the fibers were still crimped in the control condition (Fig.1), whereas after 1000 and 2000 cycles, the collagen fibers stretched to the point where these gaps disappeared. By 3000 cycles, the fibers began to pull apart, forming ellipse-shaped clefts, which resulted in larger total cleft area (Fig.1).

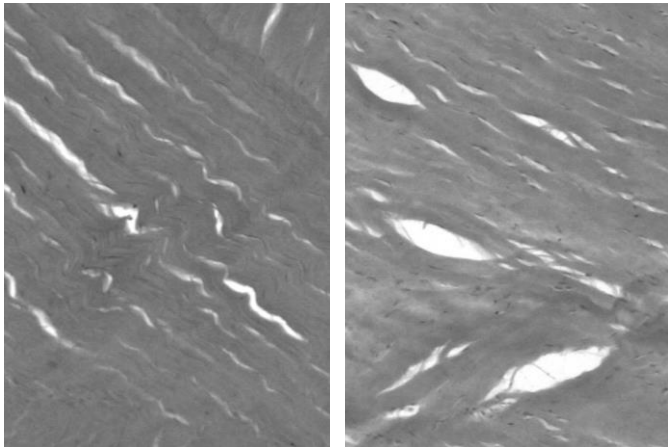


Figure 1: Images from the superficial layers in control (left) and 3000 cycle (right) conditions, highlighting the difference between inherent and mechanical loading-induced clefts, respectively.

From 3000 to 4000 cycles, a prominent decrease in the number of clefts and increases in major axis length and cleft area were observed (Fig.2), suggesting a shift from accumulation of small clefts to formation of larger clefts by the joining of minor clefts. The number of clefts decreased to approximately half while the length and area increased by almost two- and seven-fold, respectively. The ratio between major and minor axes demonstrated less than 10% change on average, indicating that the shapes of clefts remained similar.

These results, taken together suggest that microstructural damage progresses predominantly due to the increases in number of clefts, as opposed to major axis length or cleft area increases, similar to the mechanisms reported for bone crack initiation and propagation [7]. Overall, changes seen between the conditions were similar between superficial and deep layers; however, the damage in the superficial layers appears to be larger. A study examining the amount of radial bulge using MRI demonstrated that the superficial layers bulge out more than the deep layers by approximately 80% (0.2 mm) in flexion

[8], suggesting that the superficial layers may be more susceptible to accumulation of microstructural damages during the cyclic flexion-extension protocol as used in this study. Although some trends have emerged from this study, only a limited number of specimens have been collected. Further investigation is necessary to provide insight into why a number of degenerated discs exhibit inward collapse of the inner annulus fibrosus (inter-lamellar damage) as well as damage to the anterior annulus fibrosus.

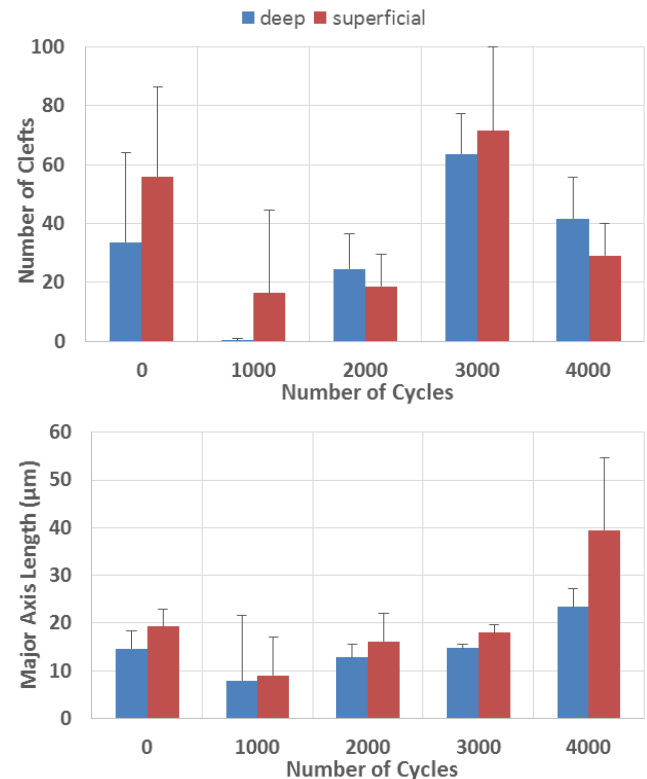


Figure 2: The average number of clefts (top) and major axis length (bottom) across different loading cycles for the deep (blue) and superficial (red) layers.

CONCLUSION

A pathway leading up to IVD herniation may be explained by accumulation of small clefts that bridge to form major clefts - not an expansion of a single cleft.

REFERENCES

- [1] Tanaka M, et al. *Spine* **18**, 1456-62, 1993.
- [2] Schwarzer AC, et al. *Spine* **20**, 1878-83, 1995.
- [3] Tampier C, et al. *Spine* **32**, 2869-74, 2007.
- [4] Pezowicz CA, et al. *Spine* **31**, 2891-903, 2006.
- [5] Drake JDM, et al., *Clin Biomech* **20**, 1038-45, 2005.
- [6] Yates JP, et al. *Spine* **35**, 734-9, 2010.
- [7] O'Brien FJ, et al. *J Biomech* **36**, 973-80, 2003.
- [8] O'Connell GD, et al. *J Orthop Res* **29**, 547-55, 2010.

RELATIVE STRAIN IN ANTERIOR CRUCIATE LIGAMENT AND MEDIAL COLLATERAL LIGAMENT DURING SIMULATED ATHLETIC TASKS: IMPLICATIONS FOR INJURY RISK

Nathaniel A. Bates^{a,b,c}, Rebecca J. Nesbitt^b, Jason T. Shearn^b,
Gregory D. Myer^{a,c}, Timothy E. Hewett^{a,b,c}

^aOSU Sports Medicine Sports Health & Performance Institute, Ohio State University, Columbus, OH, USA

^bUniversity of Cincinnati, Cincinnati, OH, USA

^cCincinnati Children's Hospital Medical Center, Cincinnati, OH, USA

email: batesna@gmail.com website: <http://sportsmedicine.osu.edu/>

INTRODUCTION

The medial collateral (MCL) and anterior cruciate ligaments (ACL) are primary and secondary ligamentous restraints against knee abduction during gait, respectively.[1] Knee abduction is an ACL injury risk predictor and component of valgus collapse, which is often observed during ACL rupture.[2] The MCL is a primary ligamentous restraint to knee abduction at knee flexion angles under 30°. Despite this, MCL ruptures only occur concomitantly in 20-40% of ACL injuries.[3] The purpose of this investigation was to understand how athletic tasks load the knee joint in a manner that leads to ACL failure without concomitant MCL failure. The hypothesis tested was that the ACL would provide a greater overall contribution to intact knee forces than the MCL during simulated motion tasks. A second tested hypothesis was that the ACL would demonstrate greater relative peak strain than the MCL during simulated motion tasks.

METHODS

A 6-degree-of-freedom robotic manipulator articulated 18 cadaveric knees from 11 unique donors (age = 47.6 ± 7.3 years; mass = 829 ± 199 N) through simulations of kinematics recorded from *in vivo* athletic tasks.[4] Four athletic tasks were simulated (male drop vertical jump (DVJ), female DVJ, male sidestep cutting, and female sidestep cutting) while recording forces, torques, and changes in ligament strain simultaneously. Specimens were tested in both intact-knee and isolated-ligament conditions. The isolated ligament condition was also used to identify each ligament's neutral strain position, allowing the absolute ligament strain throughout each motion to be

determined. Following simulation, a uniaxial servohydraulic system tensioned each ACL and MCL to failure along their fiber orientations at a strain rate of 20% per second. Univariate ANOVA was used to evaluate statistical significance ($\alpha < 0.05$) between the ACL & MCL within each robotically simulated task.

RESULTS AND DISCUSSION

During a DVJ in the intact-knee, the ACL showed greater peak strain than the MCL (6.1% vs. 0.4%; $P < 0.01$). Greater peak ACL strains were also observed during sidestep cutting tasks (5.4% vs. 0.5%; $P = 0.02$). In all simulated tasks for the intact-knee, the ACL was continuously under greater strain than the MCL throughout the duration of landing phase (Figure 1). The isolated-ACL condition also showed greater peak anterior force (4.8% bodyweight vs. 0.3% bodyweight; $P < 0.01$), medial force (1.6% bodyweight vs. 0.4% bodyweight; $P < 0.01$), flexion torque (8.4 N*m vs. 0.4 N*m; $P < 0.01$), abduction torque (2.6 N*m vs. 0.3 N*m; $P < 0.01$), and adduction torque (0.5 N*m vs. 0.0 N*m; $P = 0.03$) than the isolated-MCL condition. During uniaxial tensioning, ACL specimens preferentially loaded in the AM-bundle exhibited plastic strain of 28.0% and failure strength of 637 N, while MCLs exhibited plastic strain of 15.0% and failure strength of 776 N.

The data confirmed the hypothesis that the ACL would make larger mechanical contributions to knee joint restraint during athletic tasks than the MCL. Irrespective of gender, DVJ and sidestep cutting tasks generated significantly greater peak loads in the ACL than in the MCL. This confirms previously reported bias in ligament loading ratios.[5]

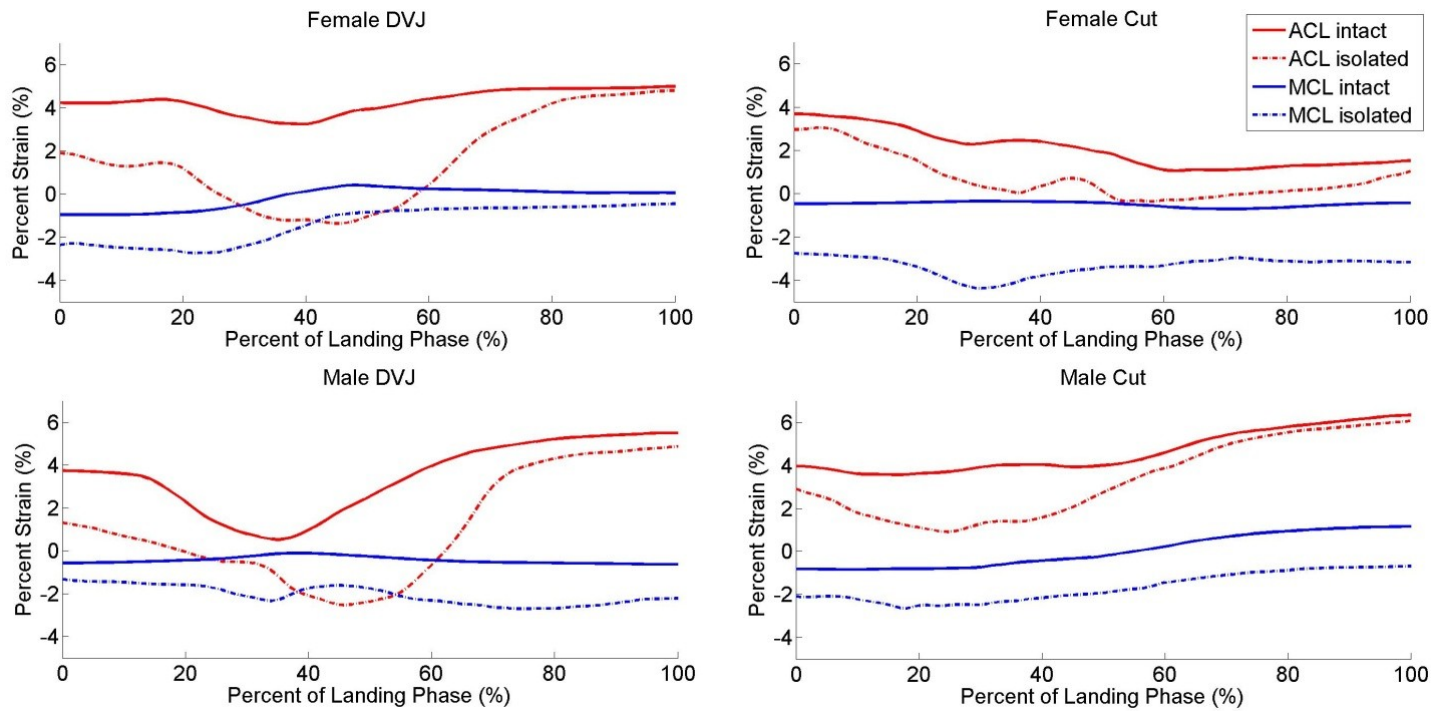


Figure 1: Population average absolute strains for the ACL (red) and MCL (blue) in the intact-knee (solid) and isolated-ligament (dashed) condition throughout each simulated motion task. Throughout the majority of simulated tasks, the MCL was unstrained, while the ACL expressed up to 6.3% strain.

ACL:MCL loading ratios were exacerbated as the level of rigor for the simulated task increased. During the DVJ the mean ACL:MCL strain ratio was 15.3 while the sidestep cut ratio was 10.8. The increased ratios in the present study were the result of minimal strain being observed on the MCL throughout each simulation.

The ACL contributed significant torque (> 1.0 N*m) to the flexion and abduction DOFs, but not to internal torque resistance. Significant evidence, has supported valgus collapse as a primary mechanism of noncontact ACL injury.[2] In the present simulation model, the ACL made significant contributions (force $> 1.0\%$ bodyweight) to the anterior and medial forces. This corresponds with previous literature that identifies the ACL as a primary resistor to anterior tibial translation and a secondary resistor to medial tibial translation.[1]

CONCLUSIONS

Data from this investigation demonstrated the relative contributions of the ACL and MCL to knee joint restraint during simulated *in vivo* athletic tasks. In these controlled physiologic athletic tasks, where

no ligament damage was inflicted on the specimen, the ACL provided greater contributions to knee restraint than the MCL, which was generally unstrained and minimally loaded. The current findings support that multi-planar loading during athletic tasks preferentially loads the ACL over the MCL, leaving it more susceptible to injury. A greater understanding of joint loading during *in vivo* tasks may provide insight that improves the efficacy of injury prevention protocols.

REFERENCES

1. Nesbitt RJ, et al. *J Biomech.* **47**, 2022-7. 2013.
2. Hewett TE, et al. *Am J Sports Med.* **33**, 492-501. 2005.
3. Yoon KH, et al. *J Bone Joint Surg.* **93**, 240-6. 2011.
4. Bates NA, et al. *Submitted for Publication.* 2015.
5. Quatman CE, et al. *Am J Sports Med.* **42**, 177-86. 2014.

ACKNOWLEDGEMENTS

Funding from NIH Grants R01-AR049735, R01-AR05563, R01-AR056660, and R01-AR056259.

THE EFFECT OF ISOLATED AND COMBINED TIBIAL ROTATIONS ON ACL AND MCL BIOMECHANICS DURING SIMULATED DECELERATION TASKS

Nathaniel A. Bates^{a,b,c}, Rebecca J. Nesbitt^b, Jason T. Shearn^b,
Gregory D. Myer^{a,c}, Timothy E. Hewett^{a,b,c}

^aOSU Sports Medicine Sports Health & Performance Institute, Ohio State University, Columbus, OH, USA

^bUniversity of Cincinnati, Cincinnati, OH, USA

^cCincinnati Children's Hospital Medical Center, Cincinnati, OH, USA

email: batesna@gmail.com website: <http://sportsmedicine.osu.edu/>

INTRODUCTION

The anterior cruciate ligament (ACL) serves as the primary soft tissue restraint to anterior tibial translation and as a secondary restraint to motion in additional degrees of freedom in the knee, while the medial collateral ligament (MCL) is aligned to primarily resist knee abduction.[1] Unfortunately, data extracted from various methods of mechanical knee simulations is not consistent.[2] However, novel methods of *in vitro* simulation driven by *in vivo* recorded kinematics have recently been developed to directly investigate knee mechanics during athletic tasks that may relate to ACL injury.[3] The purpose of this study was to apply robotically-controlled kinematic stimuli to joint orientations derived from *in vivo* recorded athletic activities of landing and pivoting in order to determine the effects of abduction, internal, and combined rotations on knee ligament biomechanics.

METHODS

In vivo kinematics were recorded for male and female athletic tasks using 3D motion capture. Kinematics were filtered and processed to be usable in robotic simulation.[3] 17 cadaveric lower extremities from 11 unique donors were obtained from an anatomical donations program and accepted for use in this study (age = 47.6 ± 7.3 years; mass = 829 ± 199 N). A six-degree-of-freedom robotic arm and custom mechanical fixtures were used to drive each specimen to the male- and female-specific initial contact orientations recorded for drop vertical jump (DVJ) and sidestep cutting tasks. The robotic manipulator then sequentially applied isolated $\pm 4^\circ$ rotational perturbations to the tibia in the frontal and transverse planes. Combined abduction/internal and

adduction/external perturbations were also applied to each joint. Throughout each perturbation, joint forces and torques were recorded by a six-axis load cell aligned with the tibial axis and ligament strains were recorded by differential variable force transducers implanted on the ACL and MCL. A 2 x 3 ANOVA with a least significant difference post-hoc analysis evaluated significant differences ($\alpha < 0.05$) in ligament strain and joint loading between motion task and type of rotational perturbation.

RESULTS AND DISCUSSION

Perturbations ordered from greatest to least strain induced on the ACL were abduction/internal, abduction, adduction, internal, adduction/external, and external rotation (Figure 1). However, strain differences between each incremental perturbation were not statistically significant and only abduction/internal perturbation strains were significantly different than neutral alignment. Mean change induced by internal rotation was 1.01% less than abduction rotation, which was 0.26% less than combined abduction/internal rotation.

MCL strain significantly increased relative to the neutral orientation only when abduction and abduction/internal perturbations were applied. Adduction and combined adduction/external rotations completely unstrained the MCL. The MCL exhibited less change in strain than the ACL during external, internal, adduction, and adduction/internal perturbations. Similarly, the MCL exhibited smaller strain magnitudes than the ACL in all conditions apart from isolated abduction perturbation.

The ACL was most susceptible to combined abduction/internal perturbations as their magnitude

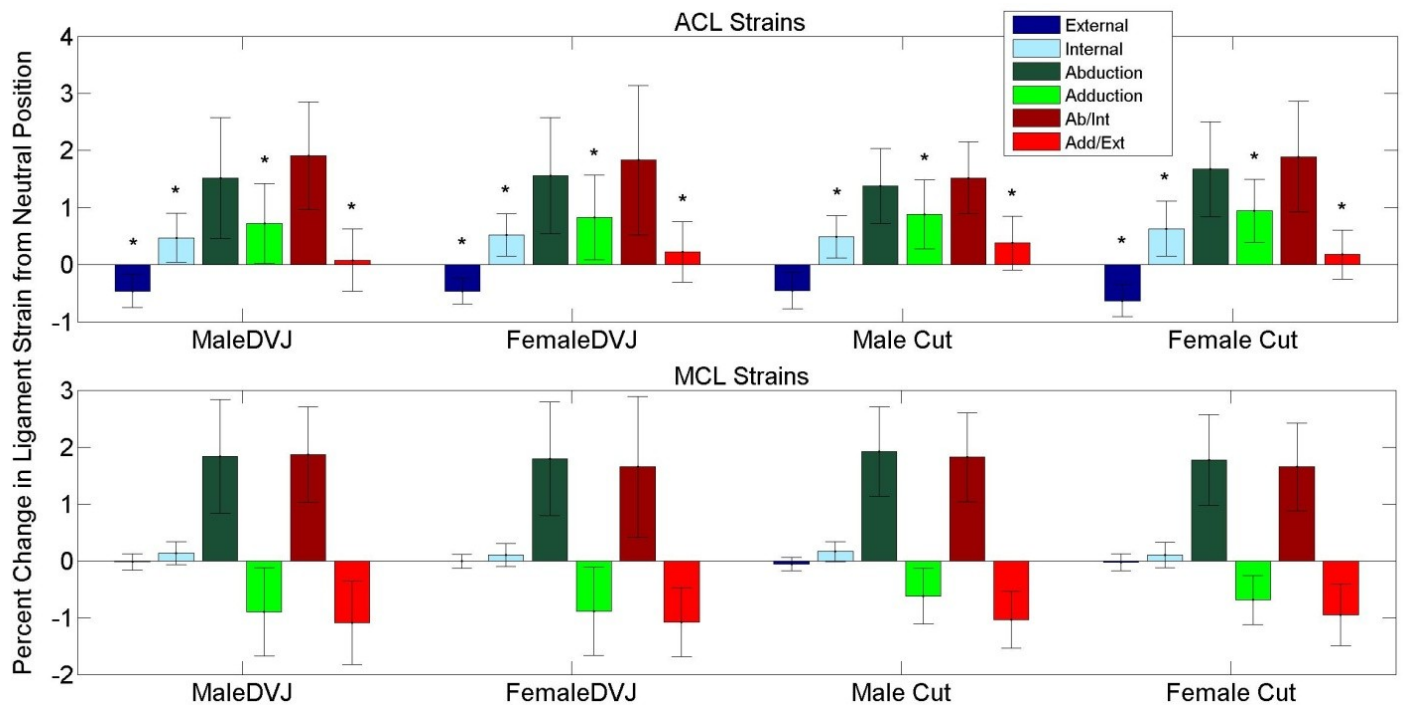


Figure 1: Displays the mean change (relative to the neutral position) in ACL (top) and MCL (bottom) ligament strain generated in the intact knee by each rotational stimuli. For the ACL, the mean strain changes were -0.5% external, 0.5% internal, 1.5% abduction, 0.8% adduction, 1.8% combined abduction/internal, and 0.2% combined adduction/external. For the MCL, the mean strain changes were -0.0% external, 0.1% internal, 1.8% abduction, -0.8% adduction, 1.8% combined abduction/internal, and -1.0% combined adduction/external. * indicated significant differences between ligaments.

of effected strain change was respectively 239% and 116% larger than isolated internal or abduction perturbations. This trend is supported by previous literature.[2] Transverse plane stimuli produced a linear range of strain change in the ACL, but this was not true of frontal plane rotations as both abduction and adduction perturbations increased ACL strain. Therefore, any frontal plane deviation from a neutral path throughout motion is likely to increase load on the ACL.

The present study corroborated that the MCL serves as the primary resistor to pure knee abduction rotation as this was the only perturbation that produced significant strain differences in the MCL. The generally reduced response of MCL strain to rotational stimuli may help explain why MCL failure is only observed in 20-40% of ACL failures despite a shared abduction loading mechanism.[4]

CONCLUSIONS

Combined abduction and internal rotations had the greatest influence on ACL strain. Isolated abduction

produced larger magnitudes of change than isolated internal rotation, though the differences were not statistically significant. Therefore, reduction of knee valgus through a neutral knee alignment during athletic tasks should be a focus of ACL injury prevention programs. Also, knee abduction had the greatest influence on MCL strain; however, the MCL generally expressed less absolute strain than the ACL, which may be indicative of how and why ACL failure often occurs without MCL injury.

REFERENCES

1. Nesbitt RJ, et al. *J Biomech.* **47**, 2022-27. 2013.
2. Bates NA, et al. *Clin Biomech.* **30**, 1-13. 2015.
3. Bates NA, et al. *Submitted for Publication.* 2015.
4. Yoon KH, et al. *J Bone Joint Surg.* **93**. 1510-18. 2011.

ACKNOWLEDGEMENTS

Funding from NIH Grants R01-AR049735, R01-AR05563, R01-AR056660, and R01-AR056259.

1/f characteristics of step width during treadmill walking

¹Mark D. Grabiner, ²Marilynn P. Wyatt, ³Pinata H. Sessoms, ⁴Kenton R. Kaufman

¹University of Illinois at Chicago, Chicago, Illinois USA

²Naval Medical Center San Diego, San Diego, California

³Naval Health Research Center, San Diego, California USA

⁴Mayo Clinic, Rochester, Minnesota, USA

email: grabiner@uic.edu, web: <http://www.uic.edu/ahs/biomechanics/>

INTRODUCTION

During treadmill walking, step width variability is a “robust indicator of step-to-step balance” [1]. This is underscored by the significant relationship ($R^2=0.54$) between step width and mediolateral kinematics of the trunk, a segment representing more than 50% of body mass [2]. Step width variability, generally calculated as a standard deviation, ignores the possibility of important information related to gait dynamics that may be imbedded in the step-to-step variations. Such variations in step time have been characterized by a shift from long-range correlations reflective of “healthy performance variability”, i.e., pink noise, toward less complex, uncorrelated white noise. These shifts have been widely reported and linked to aging and fall-risk [3]. We have observed decreased fractal-like, 1/f properties of step width during treadmill walking associated with both age and with simultaneous performance of a cognitively demanding task (unpublished).

The gait of lower extremity amputees, who have a higher risk of falls than non-amputees, is generally characterized by larger step width [4,5] and larger step width variability [5] than that of non-amputees. In the present work we conducted a secondary analysis to establish if the fractal-like 1/f properties of step width during treadmill walking by transtibial amputees varies from that of non-amputee control subjects.

METHODS

Fourteen male military service members with traumatic unilateral transtibial amputations (TTA) and a control group of 12 male non-amputee military service members, walked for 10 minutes in

a Computer-Assisted Rehabilitation Environment (CAREN; Motek Medical BV, Amsterdam, the Netherlands). CAREN is a fully immersive virtual environment that includes a 6 DOF motion platform and dual-belt instrumented treadmill. A visual input, synchronized to the subject's treadmill walking velocity (Froude number = 0.2) was projected onto a 180 degree visual surround (Figure 1)



Figure 1: Subject walking in the CAREN at the Naval Health Research Center in San Diego [6].

The step width time series for the 10 minute walking trial was calculated from the trajectories of and markers located on the heels collected using a 14 camera motion capture system operating at 120 Hz (Motion Analysis Corp, Santa Rosa, CA USA).

Three dependent variables were extracted from the step width time series, the average step width and its standard deviation (step width variability), and a variable, β , representative of the randomness of the time series (Fig.1). β was computed by first converting the step width time-amplitude series to a frequency-amplitude power spectrum, which was then log transformed. The resulting data were fit using linear regression. The regression coefficient

from the regression, β , was used as an index of the extent of signal randomness where as β approaches zero the signal approaches the characteristics of white noise. In contrast, as β approaches 1.0, the signal approaches the characteristics of pink noise, reflective of activity of multiple interacting control systems acting over different temporal and/or spatial scales [7].

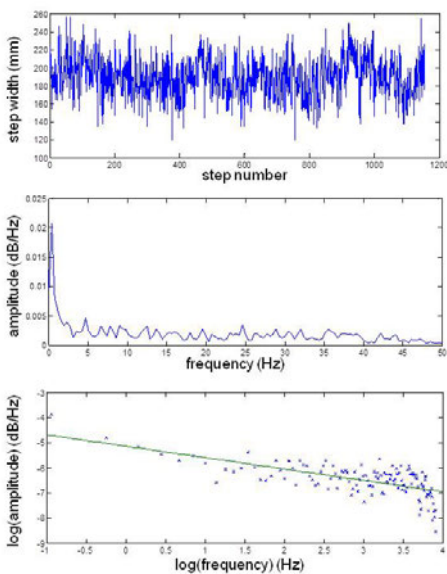


Figure 1: (Top panel) Time series of step width ($n=1124$) of a non-amputee subject. (Middle panel) Power spectrum of step width time series. (Bottom panel) Log-transform of power spectrum data with the linear regression line, the slope of which, β , is interpreted to reflect the presence of randomness in the original time series.

The presence of between-group differences for the dependent variables were examined using three independent t-tests. Pearson correlation coefficients were computed to characterize the co-dependency of the dependent variables.

RESULTS AND DISCUSSION

Contrary to expectations, the step width of the TKA subjects (135 ± 36 cm) was not significantly different than that of the control subjects (147 ± 31 cm). However, the step width variability of the TKA subjects was significantly larger (34 ± 7 cm) than that of the control subjects (28 ± 7 cm).

β revealed an unexpectedly large presence of randomness for both the TKA and control group subjects, the between-group difference (TKA

subjects: -0.52 ± 0.14 ; control subjects: -0.51 ± 0.16) of which was not significant. This was not expected because, in our preliminary work, β ranged between -0.85 and 1.0 for young subjects during conditions that included normal treadmill walking, narrow base of support treadmill walking and treadmill walking while performing an attention-demanding task.

The largest contributor to this outcome may be the between-site differences in the testing environment, which includes the design and dimensions of the treadmill. The width of the CAREN treadmill is almost 2X than that of the previously used treadmill. Although the larger presence of randomness may reflect more entrainment of gait dynamics on the CAREN treadmill, it is not clear why, or even if, treadmill dimensions would modify this effect in a frontal plane gait variable.

Ultimately, the potential clinical utility of this measure will be defined by the extent to which it is affected by the variations specific to environment in which the primary data are collected as well as the relationship between β collected in these environments and that which occurs during community-based ambulation.

REFERENCES

1. Collins, Kuo. *PLOS*, 8:e73597, 2013.
2. Hurt et al., *Gait Posture*, 31:461-464, 2010.
3. Hausdorff, *Hum Mov Sci*, 26:555-589, 2007.
4. Hak et al., *Arch Phys Med Rehab*, 94:2186-2193, 2013
5. Beurskens, et al., *J Biomech*, 47:1675-1681, 2014.
6. Kaufman et al., *CORR*, 472:3076-3084, 2014.
7. Sejdić and Lipsitz, *Comput Methods Programs Biomed*, 111:459-470, 2013.

ACKNOWLEDGEMENTS

This work was supported by DOD Grant Number W81X-WH-11-2-0058 (Log No. DM090896) and the Navy Bureau of Medicine and Surgery, Wounded, Ill, and Injured Program. The views expressed in this article are those of the authors and do not necessarily reflect the official policy or position of the Department of the Navy, Department of Defense, or the U.S. Government. Approved for public release; distribution is unlimited.

GAIT SPEED IS INFLUENCED BY SECONDARY TASKS IN PERSONS WITH UNILATERAL TRANSTIBIAL AMPUTATION

^{1,2}Brad D. Hendershot, ^{1,3}Jennifer L. Cooper, ^{1,4}Erik J. Wolf, and ^{1,4}Alison L. Pruziner

¹ Department of Rehabilitation, Walter Reed National Military Medical Center, Bethesda, MD, USA

² Center for Rehabilitation Sciences Research, Uniformed Services University of the Health Sciences, Bethesda, MD, USA

³ Department of Exercise and Nutrition Sciences, George Washington University, Washington, DC, USA

⁴DOD/VA Extremity Trauma and Amputation Center of Excellence

email: bradford.d.hendershot2.ctr@mail.mil

INTRODUCTION

Cognitive and motor functions are not independent processes. For example, the attentional demands of dual-tasking can influence the control and quality of gait [1, 2]. Among healthy individuals, common effects of dual-tasking on gait include reduced walking speed and increased gait variability; such deviations in gait with secondary tasks are often more pronounced in populations with cognitive or motor impairments [2].

Learning to walk with a prosthetic device following lower limb amputation likely imposes distinct challenges on cognitive and motor functions; however, the effects of dual-tasking on gait in this population are not well understood. Our preliminary data suggest limited biomechanical adaptations to dual-tasking in persons with amputation, though we hypothesized factors associated with forcing a consistent gait (treadmill) speed throughout the tasks confounded the results. Therefore, the objective of this study was to investigate the effects of dual-tasking on gait speed in persons with unilateral transtibial amputation (TTA) and able-bodied controls using a self-paced treadmill application. We posited that allowing participants to modulate walking speed, rather than forcing to a set pace, would better capture influences of dual-tasking during gait, and that variations in gait speed would be larger among persons with vs. without TTA across tasks.

METHODS

Five persons with traumatic, unilateral TTA, and nine able-bodied controls, completed a repeated measures design in which each participant completed three 2-minute walking trials while performing secondary tasks (“easy” and “hard”) – each involving distinct attentional demands – and a

no task (“baseline”) trial. For the easy task, a single object was displayed on a screen within direct line-of-sight with changing shapes and participants were asked to press a button whenever a square appeared. For the hard task, two objects were displayed simultaneously, with individually changing shapes and colors, and participants were asked to press a button when both objects were either the same shape or same color. The no task condition consisted of a constant blue target, requiring no active response.

A self-paced treadmill speed algorithm was used within the Computer Assisted Rehabilitation Environment (CAREN; Motek Medical BV, Netherlands), which controls belt speed by tracking anterior-posterior pelvic position, velocity, and acceleration [e.g., 3]. Following a 4-minute acclimation period, participants walked for 2 minutes in each condition (in a random order). Treadmill belt speed was collected (300 Hz) continuously throughout each trial, and used as a proxy for gait speed [4]. Mean and standard deviation of belt speed – and their ratio (coefficient of variation; CV) – were computed in 20s windows throughout each trial, to compare among tasks and between groups. All participants provided written informed consent, and all study procedures were approved by the local IRB.

RESULTS AND DISCUSSION

Decreases in walking speed, and increases in gait variability, are common gait changes with dual-tasking [1, 2]; however, the current results did not fully support this finding. While walking speed was initially slower in the hard condition among controls (Fig. 1), they generally approached, over time, a similar speed regardless of task. In contrast, persons with TTA tended to walk faster in the easy/hard conditions relative to no task (Fig. 1), and never

approached a similar speed over time. Overall, walking speed variability, as evidenced by the CV, was also larger among persons with TTA vs. controls (Fig. 1); in both groups, these tended to decrease with time and secondary task difficulty. Faster gait speeds with secondary tasks among persons with TTA suggest these individuals may differentially prioritize cognitive and motor functions. Additionally, the attentional demands of the secondary tasks appear to influence the variability in gait speed, whereby both groups (but especially those with TTA) walked with more variability in the no vs. easy/hard tasks.

Several other factors should be considered when interpreting the results. Changes in mean gait speed and its variability, over time, may be more related to treadmill habituation than dual-tasking [5]; although participants completed a 4-min acclimation period, additional habituation time may be required. The secondary tasks used here were also visually dependent; objects were displayed on a blank screen, and did not incorporate optical flow within the virtual environment [6]. Finally, the presence of a harness (though not weight supporting) can influence gait variability and confidence in walking ability [7], perhaps “encouraging” participants to walk faster than they otherwise would unrestrained (e.g., psychologically minimizing the consequence or fear of falls). Additional biomechanical analyses are needed to better understand how these

individuals modulate walking speed while dual-tasking, as well as to determine the specific influences of these additional factors.

REFERENCES

1. Montero-Odasso M, et al. *Arch Phys Med Rehabil* **93**, 293-99, 2012.
2. Yogev G, et al. *Mov Disord* **23**, 329-42, 2008.
3. Sloop LH, et al. *Gait Posture* **39**, 478-84, 2014.
4. Fusco N, et al. *Gait Posture* **28**, 663-67, 2008.
5. Wall, C. *Ergonomics* **24**, 531-42, 1981.
6. Hollman et al. *Gait Posture* **23**, 441-44, 2006.
7. Decker LM, et al. *J Neuroeng Rehab* **9**, 8, 2012.

ACKNOWLEDGEMENTS

This work was supported, in part, by: the Center for Rehabilitation Sciences Research, of the Uniformed Services University of the Health Sciences (DOD Defense Health Program – NF90UG), and the DoD-VA Extremity Trauma & Amputation Center of Excellence (Public Law 110-417, National Defense Authorization Act 2009, Section 723). The authors also wish to thank Vanessa Q. Gatmaitan, MS (CAREN Operator) for her assistance with data collection. The views expressed in this abstract are those of the authors and do not necessarily reflect the official policy or position of the Departments of the Army, Navy, Defense, nor the United States Government.

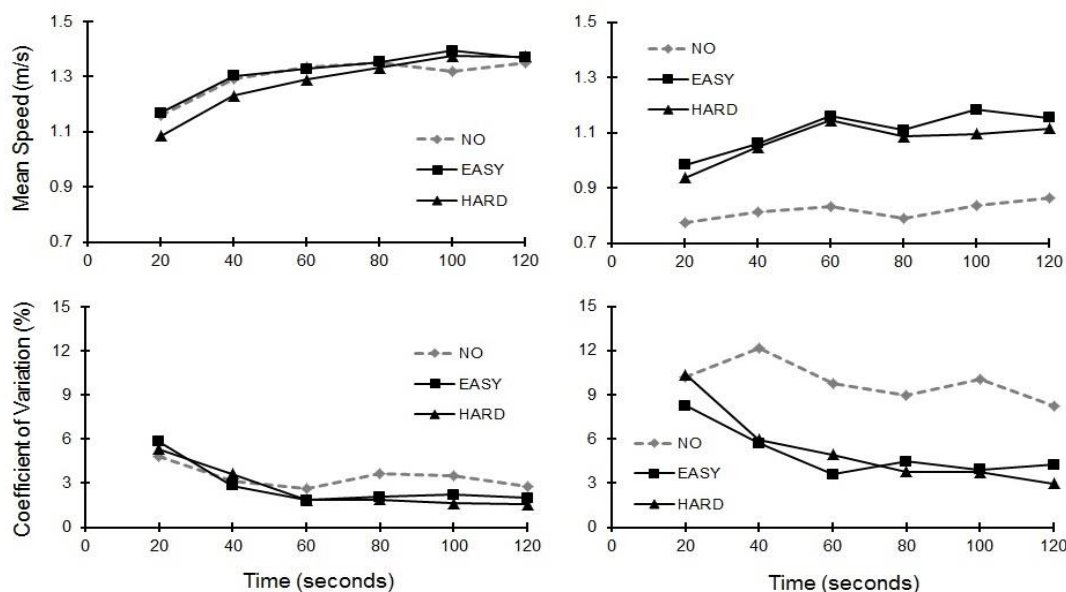


Fig. 1. Mean walking speed (top) and variability (bottom) by task condition, over time, for controls (left) and persons with TTA (right).

Lower Prosthetic Stiffness Minimizes the Metabolic Cost of Running for Individuals with Bilateral Leg Amputations

¹Owen N. Beck, ¹Paolo Taboga, and ^{1,2}Alena M. Grabowski

¹University of Colorado, Boulder, CO, USA; ²VA Eastern Colorado Healthcare System, Denver, CO, USA
email: owen.beck@colorado.edu

INTRODUCTION

Non-amputee runners increase leg stiffness (k_{leg}) and decrease contact time (t_c) to achieve faster running speeds [1, 2]. Kram and Taylor [3] suggest that longer t_c reduces the rate of muscular force production, thereby facilitating the recruitment of slower more economical muscle fibers which decreases the energetic cost of running. Thus, it is likely that a lower k_{leg} (and longer t_c) reduces the metabolic cost of running.

While running with passive-elastic running-specific prostheses (RSPs), bilateral transtibial amputees have a lower k_{leg} with faster running speeds [2]. Due to the singular stiffness of a given RSP, it is suggested that RSPs dominate k_{leg} , thus runners with bilateral leg amputations may be able to alter their metabolic cost of running by changing the stiffness of their RSPs. We hypothesize that using RSPs with lower stiffness will reduce the metabolic cost of transport (CoT) during running in runners with bilateral leg amputations. Also, we were curious how RSP model or height affect CoT, and due to insufficient evidence, we hypothesize that neither RSP model nor RSP height will influence CoT. To test our hypotheses we measured metabolic demand, ground reaction forces (GRFs), stride kinematics, and k_{leg} from runners with bilateral leg amputations using RSPs that varied by model, stiffness category, and height.

METHODS

Three male runners with bilateral transtibial amputations participated. We obtained informed written consent, and then a certified prosthetist fit each subject with three RSP models (RSP1, RSP2, RSP3) at the recommended and ± 1 stiffness categories. The height of each RSP was set to match the tallest allowed standing height as determined by

the International Paralympic Committee [4] and ± 2 cm. If the shortest attainable height for a RSP model was taller than recommend, the shortest height was used for that subject/model; then we altered RSP height by +2 cm, and +4 cm.

On days following the fitting session, subjects performed 5 min running trials on a force-instrumented treadmill at either 2.5 m/s ($n=2$) or 3.0 m/s ($n=1$). Each trial was completed using a different RSP model, stiffness category, and height combination. First, subjects ran using the recommended height while RSP model and/or stiffness categories were changed. Then, RSP height was altered ± 2 cm (or +2 cm, +4 cm) at the optimal stiffness category; the stiffness category that elicited the lowest CoT. All trials were randomized.

We used indirect calorimetry to determine net metabolic power from the average metabolic rates during the final 2 min of each trial [5]. We converted average net metabolic power to work and divided by the product of mass and running speed, yielding CoT in J/kg/m.

We measured GRFs from 10 consecutive strides during the last 2 min of each trial. We combined the average GRFs from both legs, sampled at 1000 Hz, and processed them using a custom MATLAB script. We calculated k_{leg} according to [6]. A statistical linear mixed model was used to determine the associations of RSP model, stiffness category, and height on CoT. We also compared the effect of RSP stiffness category on peak k_{leg} , peak vertical GRF ($vGRF$), and peak displacement of the leg-spring (ΔL).

RESULTS AND DISCUSSION

For every one reduction in RSP stiffness category, CoT decreased by 5.1% ($p<0.01$) (Fig. 1).

Moreover, with our limited number of subjects ($n=3$), we were unable to detect significant effects from either RSP model ($p=0.14$) or height ($p=0.59$) on CoT. Based on our current sample size, our data support our hypotheses that RSP stiffness, but not model or height, influence CoT.

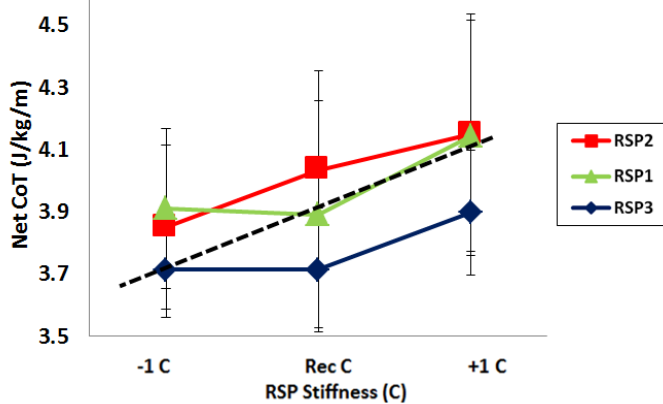


Figure 1. Mean (\pm SEM) net metabolic cost of transport (CoT) as a function of RSP stiffness category (C) for three RSP models. Dashed line is the regression line ($\text{CoT} = 3.90 + 0.20 \times \Delta \text{Rec C}$).

k_{leg} increased linearly with RSP stiffness ($p<0.01$) (Fig. 2). Across all conditions, k_{leg} increased by 6% with a one category increase in RSP stiffness. Interestingly, peak vGRF was independent of changes in RSP stiffness category ($p=0.60$). Therefore, the decrease in k_{leg} was primarily due to a 7.5% increase in ΔL with each RSP stiffness category ($p<0.01$). Additionally, t_c increased with decreases in RSP stiffness (and k_{leg}) ($p<0.01$).

Therefore our data support the idea that RSP stiffness dominates k_{leg} . Because peak vGRF was invariant across RSP stiffness categories, softer RSPs (lower stiffness categories) resulted in greater leg-spring compression. The more compliant k_{leg} elicited by our subjects increased the elastic energy storage (and return) of their leg-spring.

$$EE = \frac{1}{2} k(x)^2$$

Elastic energy storage (EE) is equal to half the spring stiffness (k) multiplied by the displacement of the spring (x) squared. This increased elastic energy storage and return of the leg, coupled with

longer t_c , contribute to the decreased CoT elicited by softer RSPs.

CONCLUSIONS

Runners with bilateral transtibial amputations had lower CoT, k_{leg} , and t_c when using RSPs with lower stiffness categories. However, neither RSP model nor height significantly affected CoT.

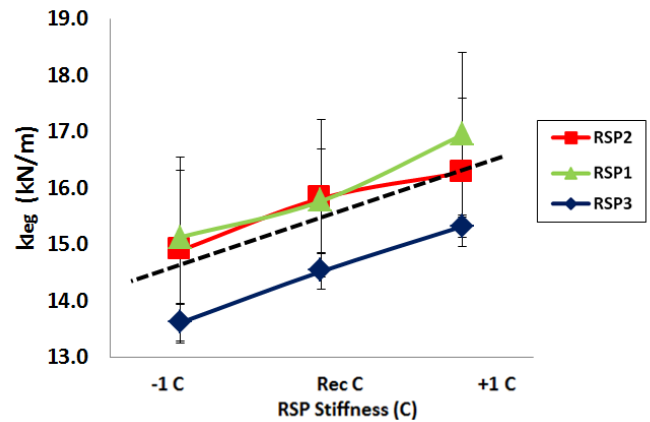


Figure 2. Mean (\pm SEM) leg stiffness (k_{leg}) as a function of RSP stiffness category (C). Dashed line is the regression line ($k_{\text{leg}} = 15.32 + 0.92 \times \Delta \text{Rec C}$).

REFERENCES

1. Grabowski AM, et al. *Biol. Lett* **6**, 201-204, 2010.
2. McGowan CP, et al. *J R Soc Interface* **9**, 1975-1982, 2012.
3. Kram R & Taylor CR. *Nature* **346**, 265-267, 1990.
4. IPC Athletics Rules and Regulations 2014-2015. www.Paralympic.org/athletics
5. Brockway JM. *Hum nutr. Clin nutr* **41**, 463-471, 1987.
6. Farley CT et al. *J Exp Biol* **185**, 71-86, 1993.

ACKNOWLEDGEMENTS

We thank Freedom Innovations, Ossur, and Ottobock for the donation of RSPs. This project was supported by the BADER Consortium, Department of Defense, CDMRP cooperative agreement (W81XWH-11-2-0222).

THE EFFECTS OF PROSTHETIC FOOT STIFFNESS ON AMPUTEE TURNING MECHANICS

¹Courtney E. Shell, ²Glenn K. Klute and ¹Richard R. Neptune

¹ The University of Texas at Austin, Austin, TX, USA

² VA Center for Limb Loss Prevention and Prosthetic Engineering, Seattle, WA, USA
email: c.shell@utexas.edu, web: <http://www.me.utexas.edu/~neptune/>

INTRODUCTION

Compared to non-amputees, amputees experience increased difficulty with maneuvering tasks such as turning, which are common in daily living activities [1, 2]. While changes in sagittal-plane prosthetic foot stiffness have been shown to influence amputee walking mechanics and can be tuned to provide desired levels of body support and forward propulsion [e.g., 3], the influence of prosthetic foot stiffness on amputee turning is unknown. Turning requires the generation of appropriate mediolateral ground reaction forces (GRFs) and ankle kinematics [1, 4], which are both influenced by prosthetic foot stiffness. The purpose of this study was to assess the influence of prosthetic foot stiffness on amputee turning mechanics, which has important implications for the design and prescription of prosthetic devices.

METHODS

Three prosthetic ankles (compliant, nominal and stiff) were manufactured using an additive manufacturing process (Vanguard HiQ/HS Sinterstation, 3D Systems Corp.). The ankles were combined in series with a low-profile version of a commonly-prescribed carbon fiber prosthetic foot (Category 9, LP Vari-Flex® with EVO™, Össur) to create a set of ankle-foot combinations that spanned a range of stiffness values.

Unilateral transtibial amputees (n=7) free of musculoskeletal disorders and pain completed an IRB-approved protocol of turning maneuvers with each of the three ankle-foot combinations. Subjects walked overground at their self-selected speed clockwise and counterclockwise around a 1-meter radius circle with six embedded force plates (Advanced Mechanical Technology, Inc.; Kistler

Instrument Corp.). Repeated trials were collected for each ankle-foot combination to obtain at least five force plate strikes per foot.

GRF and kinematic data were collected at 1200 Hz and 120 Hz, respectively, using a 12-camera motion capture system (Vicon Nexus, Vicon Motion Systems). In addition to the Plug-In Gait marker set, reflective markers were placed bilaterally on the greater trochanter and fifth metatarsal heads and four-marker clusters were placed bilaterally on the thigh and shank. Residual limb markers were placed symmetrically with intact limb markers. Hip functional joint centers were found using trials with at least five hip circumduction movements while knee functional joint axes were found using trials with at least five knee flexion-extension movements (Visual 3D, C-Motion, Inc.).

GRF and marker data were filtered using a 4th-order, low-pass Butterworth filter with cutoff frequencies of 20 and 6 Hz, respectively. Joint angles and powers were calculated using Visual 3D. Peak joint angles were averaged across trials. Positive and negative joint work were calculated as the time-integral of the positive and negative joint power, respectively, then averaged across trials. Joint work was examined in each of the six phases of the gait cycle.

RESULTS AND DISCUSSION

As in previous studies [e.g., 3], decreasing stiffness increased ankle dorsiflexion and knee flexion as well as decreased hip extension (Table 1). In addition, when the residual limb was inside the turn, prosthetic ankle energy storage and return increased with decreasing stiffness (Fig. 1). In the coronal plane, decreased ankle stiffness caused a decrease in hip adduction and, when the limb was inside the

turn, an increase in hip abduction (Table 1). Compared to the compliant and stiff combinations, the nominal ankle-foot caused greater ankle eversion when the limb was inside the turn and less ankle inversion when the limb was outside the turn (Table 1). Late stance ankle coronal-plane positive and negative work were also greater when the limb was inside the turn and lower when the limb was outside the turn for the nominal ankle-foot (Fig. 1).

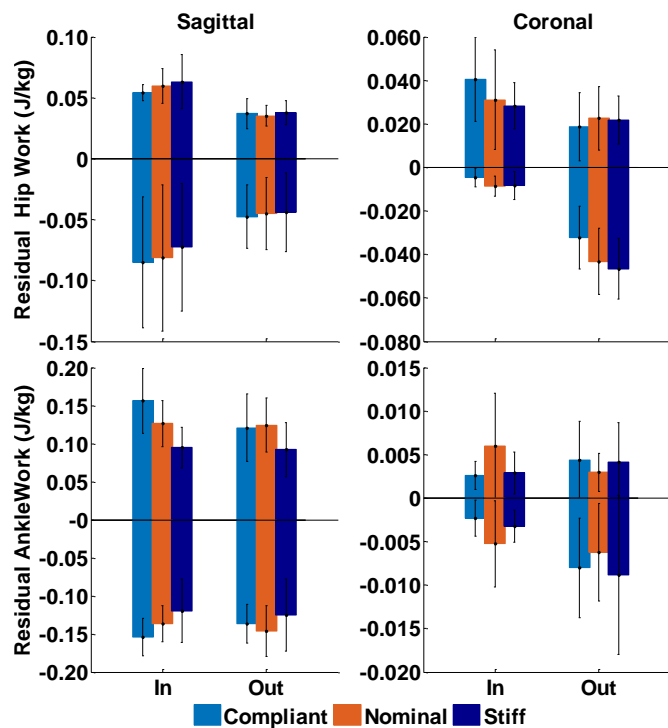


Figure 1: Coronal and sagittal plane positive and negative work at the residual limb ankle and hip when the limb was inside (In) and outside (Out) of the turn with the compliant, nominal and stiff ankle-foot combinations during late stance.

Since the prosthetic foot acts like an elastic spring, deforming the ankle more in the coronal plane allowed it to store greater energy during the second

half of stance and subsequently return more coronal-plane energy at push-off (Fig. 1). A decrease in ankle stiffness caused a decrease in late-stance negative coronal-plane hip work when the limb was outside the turn and an increase in late-stance positive coronal-plane hip work when the limb was inside the turn (Fig. 1). The increased positive hip work may be a response to decreased ankle stiffness and necessary to rotate the pelvis and complete the turning task.

CONCLUSIONS

Changes in stiffness influenced sagittal-plane kinematics during turning, which were similar to those previously observed during straight-line walking [e.g., 3]. Stiffness changes also caused coronal-plane adaptations at the ankle and hip. Thus, when tuning stiffness to balance body support and forward propulsion, the effects on turning mechanics should also be considered.

REFERENCES

1. Segal AD, et al. *Gait Posture*. 2011; **33**(1):41-47.
2. Ventura JD, et al. *Gait Posture*. 2011; **34**(3):307-312.
3. Fey NP, et al. *Clin Biomech*. 2011; **26**(10):1025-1032.
4. Orendurff MS, et al. *Gait Posture*. 2006; **23**(1):106-111.

ACKNOWLEDGEMENTS

This work was supported by the National Science Foundation Graduate Research Fellowship Program (Grant DGE-1110007) and the Dept. of Veterans Affairs (Grant I01 RX000311).

Table 1: Select residual limb peak joint angles with trends caused by changes in ankle stiffness when the limb was inside (In) and outside (Out) of the turn with the compliant, nominal and stiff ankle-foot combinations.

Peak Sagittal Joint Angle (°)		Ankle-Foot Combination			Peak Coronal Joint Angle (°)	Ankle-Foot Combination		
		Compliant	Nominal	Stiff		Compliant	Nominal	Stiff
Ankle Dorsiflexion (+)	In	20.4±4.2	11.6±2.2	8.8±2.5	Ankle Inversion (+)	-3.1±1.3	-3.9±1.9	-3.2±1.6
	Out	19.1±3.6	12.0±2.3	8.6±2.6		5.3±1.6	4.8±1.3	5.2±0.8
Knee Flexion (-)	In	-67.3±4.7	-65.0±6.3	-63.2±7.9	Hip Adduction (+)	5.7±4.6	7.0±3.7	7.5±4.4
	Out	-68.9±6.2	-66.1±5.8	-64.9±7.4		-0.5±4.3	1.1±3.1	2.1±3.1
Hip Extension (-)	In	-15.2±5.5	-17.8±6.8	-17.7±6.6	Hip Abduction (-)	-2.4±5.3	-1.9±5.6	-0.6±5.3
	Out	-14.4±5.2	-17.1±6.0	-16.9±7.3		-6.8±4.4	-7.0±4.3	-5.8±4.0

WHEN SHOULD WE BIOMECHANICALLY EXAMINE A LOWER-LIMB AMPUTEE? A SYSTEMATIC REVIEW OF ACCOMMODATION TIMES

Andrea B. Wanamaker and Ajit M.W. Chaudhari

The Ohio State University, Columbus, OH, USA
email: Wanamaker.178@osu.edu

INTRODUCTION

Over two million Americans are currently living with limb loss, with 185,000 new amputations occurring annually. Of these, approximately 65% involve loss of a lower-extremity. Fifty-four percent of amputations are due to diabetic complications and 45% are due to trauma [1].

Technological advances, particularly over the past 30 years, have completely transformed the care of musculoskeletal disorders, including more advanced prosthetic devices that use a combination of sensing, actuation, and microprocessors to enhance function on even surfaces, hills and stairs, and in other high-demand applications. However, our understanding of how and when patients adapt to a new conventional or advanced prosthesis is unclear. Only one study to our knowledge specifically examined stabilization of data over time but the study was limited to one male above-knee amputee over only three weeks [2]. Other previous studies on above-knee amputees appear to have a wide range of testing timepoints, ranging from testing immediately after receiving a new prosthesis to testing after two years, making it unclear when testing should be performed to ensure accurate and relevant results.

The goal of this systematic review was to identify evidence-based consensus of when biomechanical analysis on amputees should occur after a patient receives a new prosthetic limb.

METHODS

A systematic literature search was conducted in January 2015 using PUBMED (1964-January 2015) and Scopus (1948-January 2015). The databases were searched using generic terms related to lower-limb amputation and prosthetic devices. The

following lines were used: (lower limb OR lower-limb OR leg OR thigh OR shank) AND (amput* OR transtibial OR transfemoral) AND (prosth* OR (C-Leg) OR (Intelligent Prosth*) OR (BiOM)).

As the goal of this systematic review was to gather any articles related to an investigation of a prosthesis the inclusion and exclusion criteria were kept simple. The search was limited to peer-reviewed journal articles, human subjects, and the English language. Titles, abstracts, and full texts were then screened as necessary to further exclude articles: conference proceedings; theses; dissertations; reviews; case reports; studies examining bilateral amputees or subjects under the age of 18; studies examining new prosthetic components, such as prosthetic sockets and pylons, or alignment changes; and studies that did not include biomechanical analyses were all excluded from the review.

Once the search was complete, relevant data were pulled from each article. We were most interested in the amputee participant populations and if an accommodation time was given. Data extracted included sex, height, weight, age, type of amputation and cause, time since amputation, experience with a prosthetic, prosthetic device worn prior to testing, prosthetic device(s) tested, and time given to accommodate prior to testing a new prosthetic limb.

RESULTS AND DISCUSSION

A total of 7901 unique hits were found between PUBMED and Scopus. After reviewing titles and abstracts, a total of 283 articles remained. Of these, 116 matched our criteria and were included in this review. For completeness, the references of these articles were examined which resulted in an additional 28 articles for a final total of 144 articles.

A total of 2026 amputees were investigated from all 144 studies. Of these, 1113 (55%) had amputations due to trauma, 286 (14%) were due to vascular causes, 172 (8%) were due to cancer or tumor, 150 (7.4%) due to other causes, and 305 (15%) were not specified.

Of the 144 articles, there were a total of four investigations involving hip or pelvis amputation, 65 involving an above-knee amputation or knee disarticulation, and 85 involving a below-knee amputation. The median number of days given for accommodation for all investigations was 8.5 days with in interquartile range (IQR) of 30 days (Figure 1,2).

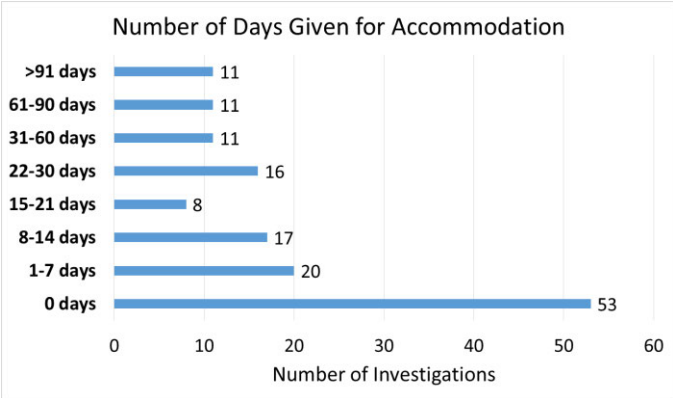


Figure 1: Number of accommodation days for the 144 investigations. Range 0-154 days.

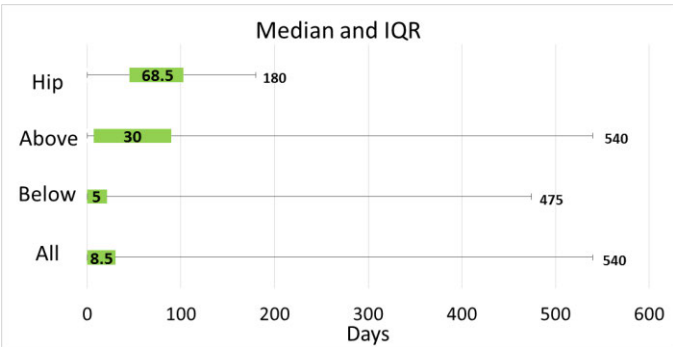


Figure 2: For hip, above-knee, below-knee, and total population the IQR for accommodation was 57.8, 83, 21, and 30 days, respectively. Median reported in IQR range.

While many investigations clearly stated how much time was given for accommodation, many did not. A total of 53 investigations tested the day of receiving a new limb or did not specifically mention

an accommodation time (Figure 3). Phrases such as “given as long as necessary”, “intensive practice phase”, and “break in period” were frequently used. These investigations were placed into the not reported (NR) category and it was assumed testing was done the day of receiving a new prosthetic limb.

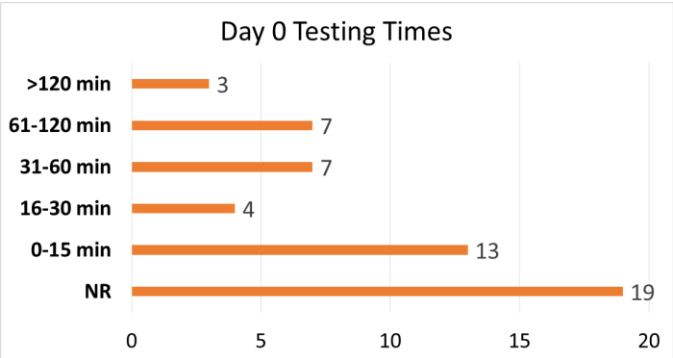


Figure 3: Detailed results for testing on the day of receiving a new limb. Not reported (NR).

From these results, we can see that there is no clear consensus on when a biomechanical investigation should be performed on an amputee subject. Testing time points range from within minutes or hours of receiving a new limb to 5+ months after fitting.

CONCLUSIONS

Our systematic literature search resulted in 144 unique biomechanical investigations involving the amputee population. The median number of days to accommodate to a new prosthetic limb was 8.5 days with an IQR of 30 days. Above-knee and hip amputees were given more time to accommodate than below-knee amputees.

REFERENCES

1. Ziegler-Graham K, et al. *Arch Phys Med Rehab* **89**, 422-429, 2008.
2. English RD, et al. *J Rehabil Res Dev* **32**, 32-35, 1995.

ACKNOWLEDGMENTS

The authors gratefully acknowledge Fern Cheek of OSU Libraries for her assistance in developing the search strategy.

SARCOMERE LENGTH ORGANIZATION AS A DESIGN FOR COOPERATIVE FUNCTION AMONGST ALL LUMBAR SPINE MUSCLES

Derek P. Zwambag, T. Alexander Ricketts, and Stephen H.M. Brown
Human Health and Nutritional Sciences, University of Guelph, Guelph, ON, Canada
email: shmbrown@uoguelph.ca

INTRODUCTION

The functional design of spine muscles in part dictates their role in moving, loading, and stabilizing the lumbar spine. There have been numerous studies that have examined the isolated properties of these individual muscles, and some have highlighted an interesting characteristic of the multifidus muscle; it has short sarcomeres in the neutral spine posture and reaches optimal length for force production when the spine is flexed [1]. Contrarily, longer than optimal sarcomere lengths have been measured from psoas major when the spine is in a neutral position and the hip is mildly flexed [2]. Understanding of how all the lumbar muscles interact and work together is lacking. The objective of this study was to measure sarcomere lengths of all lumbar muscles in a neutral cadaveric position and predict the operating ranges of these muscles throughout full ranges of spine movements.

METHODS

Small muscle samples (0.5 cm^2) were removed from iliocostalis, longissimus, multifidus, quadratus lumborum, intertransversarii, psoas major, and psoas minor of seven cadaveric donors embalmed in an approximate neutral spine position. Single fascicles were excised from each sample and sarcomere lengths were measured using laser diffraction. Muscle length changes through full lumbar range of motion (flexion, extension, lateral bend and axial twist) were predicted using an anatomically detailed computational model of the spine [3]. Sarcomere length operating ranges were predicted from the changes in muscle fibre length to determine force-length characteristics of each muscle in a neutral position and at end ranges of motion (Fig 1).

RESULTS AND DISCUSSION

Each of the lumbar extensors (multifidus, longissimus, and iliocostalis) was measured to have short sarcomere lengths (2.36 ± 0.05 , 2.43 ± 0.05 , and $2.41 \pm 0.06 \mu\text{m}$, respectively) in the neutral cadaveric spines (Fig 2A). The intermediate and anterior muscles had longer sarcomeres than the posterior extensors with quadratus lumborum close to optimal ($2.66 \pm 0.09 \mu\text{m}$), intertransversarii slightly below optimal ($2.53 \pm 0.05 \mu\text{m}$), and psoas major and minor longer than optimal (3.41 ± 0.07 , $3.17 \pm 0.12 \mu\text{m}$, respectively).

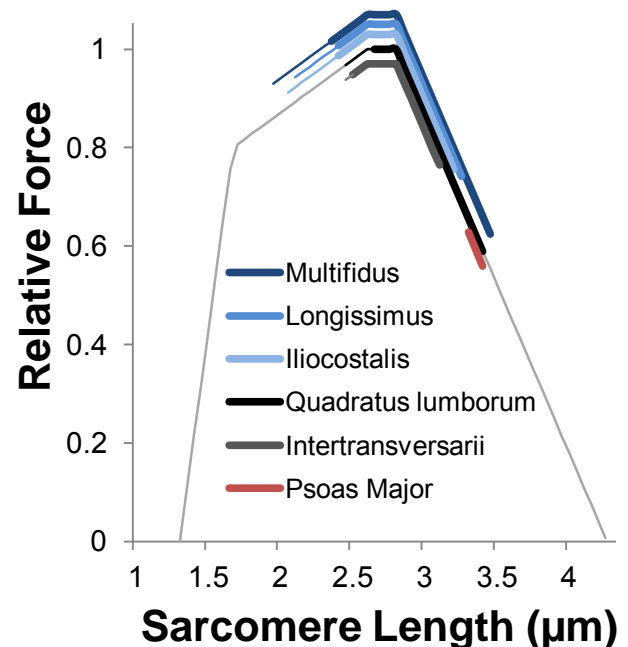


Figure 1: Sarcomere length operating range of lumbar spine muscles. Thick lines are from a neutral posture to full flexion and thin lines are from neutral to full extension. Muscles are offset from force length curve for clarity.

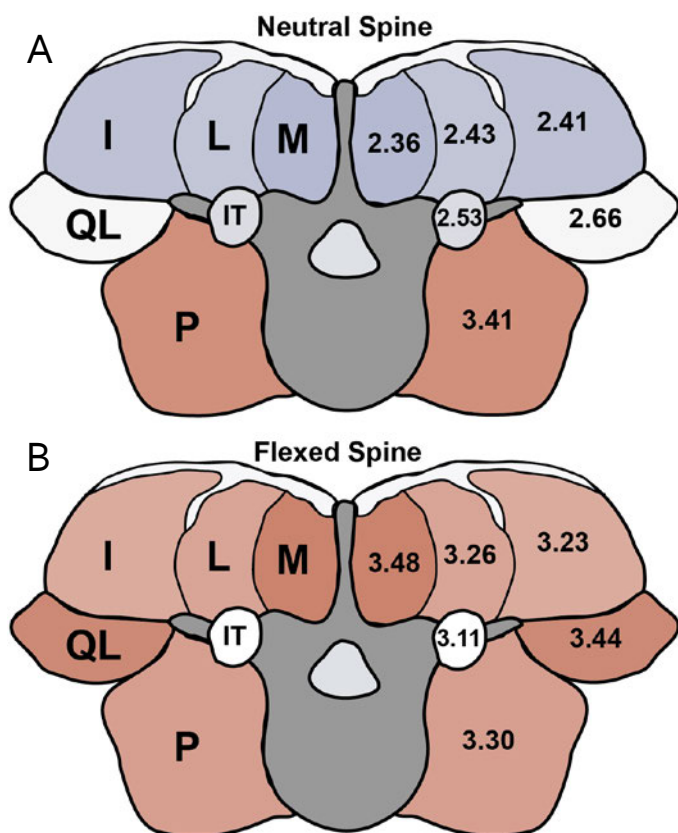


Figure 2: (A) Sarcomere lengths (μm) measured from lumbar spine muscles in a neutral cadaveric position and (B) modelled sarcomere lengths at full spine flexion. Blue, white, and red corresponds to sarcomeres on the ascending limb, plateau, and descending limb of the sarcomere force length curve, respectively. M, multifidus; L, longissimus; I, iliocostalis; QL, quadratus lumborum; IT, intertransversarii; and P, psoas major.

During modelled flexion the extensor and intermediate muscles lengthened so that all muscles operated in the approximate same location on the descending limb (range 3.11-3.48 μm ; Table 1) of the force-length relationship (Fig 2B). Flexion caused multifidus fibres to lengthen by 50.0%, while iliocostalis and longissimus fibres

lengthened by 38.1%. Quadratus lumborum and intertransversarii were less affected by spine flexion lengthening 29.2% and 23.3%, respectively. The anterior muscles were largely unaffected by spine flexion.

During lateral bend, quadratus lumborum had the largest operating range due its location furthest from the axis of rotation. Axial twist had minimal effect on sarcomere lengths of all lumbar muscles.

CONCLUSIONS

The sarcomere lengths of multifidus and psoas major in a neutral spine posture were consistent with those in the literature [1,2]. However, multifidus is not unique in comparison to sarcomere lengths of the other low back muscles. In a neutral position, there appears to be a pattern for muscles anterior to the spine to have long sarcomere lengths and those posterior to have short sarcomeres. Spine posture significantly altered the maximum isometric active force generating capability of lumbar muscles. The extensor muscles are all designed to produce maximum force in a mid-flexed posture, and all lumbar muscles operate at similar locations of the force-length relationship at full spine flexion. The intrinsic design of sarcomere organization appears to provide an inherent mechanism for balancing force production throughout spine motion.

REFERENCES

1. Ward S, et al. *J Bone Jt Surg* **9**, 176-185, 2009.
2. Regev G, et al. *Spine* **36**, E1666-E1674, 2011.
3. Cholewicki J, McGill SM. *Clin Biomech* **11**, 1-15, 1996

Table 1: Modeled sarcomere lengths (μm) of lumbar muscles at end ranges of motion

	Ilio	Long	Mult	QL	IT	P.Maj	P.Min
Flexion	3.23	3.26	3.48	3.44	3.11	3.30	3.12
Extension	2.09	2.11	1.97	2.46	2.45	3.30	3.12
Contralateral bend	2.65	2.67	2.46	3.29	2.85	3.52	3.33
Ipsilateral bend	2.03	2.05	2.16	2.00	2.22	3.15	2.98
Contralateral axial rotation	2.32	2.34	2.26	2.59	2.54	3.36	3.19
Ipsilateral axial rotation	2.40	2.42	2.41	2.76	2.53	3.37	3.18

Modeled ranges of motion were flexion 52°, extension 16°, lateral bend 29°, and axial rotation 13°

FUNCTIONAL IMPORTANCE OF FASCIA IN THE PRESERVATION OF MUSCLE TENSION

Roy J. Ruttiman, David Sleboda, Thomas J. Roberts

Brown University, Providence, RI, USA

roy_ruttiman@brown.edu, <http://brown.edu/research/labs/robertslab/>

INTRODUCTION

Fibrous extra-muscular connective tissue, also known as fascia, delineates and encloses functional muscle groups, thus forming discrete fascial compartments. These fascial compartments have clinical significance, as increased pressure within a compartment can compromise the blood supply and function of the tissues enclosed. However, it is unclear how fascial compartments influence normal muscle performance. We explored the relationship between fascial compartments and muscle tension in the ventral interosseous of the wild turkey (*Meleagris gallopavo*), a bipennate distal wing muscle bordered by bone and enclosed within a fascial compartment.

METHODS

Birds were anesthetized with inhaled isoflurane. The *Ramus superficialis*, a distal branch of the ulnar nerve, was isolated immediately distal to the carpometacarpal junction and connected to a bipolar stimulating electrode. The wing was fixed to a rigid custom-made aluminum frame, and the distal tendon of the muscle was isolated and attached to the lever of a servomotor via Kevlar thread (Figure 1).

Muscles were stimulated supramaximally under isometric conditions. Each muscle was subjected to approximately 5-7 contractions at different muscle lengths. The muscle was allowed a minimum of 5 minutes between contractions to prevent fatigue. After length-tension (LT) relationship of the muscle was established, a repeat isometric contraction was performed at optimum length (L_o) to assess muscle fatigue.

Fascial release treatment was achieved via skin incision on the ventrum of the distal wing; followed by careful surgical removal of the ventral fascia

overlying the ventral interosseous. The muscle was once again subjected to approximately 5-7 contractions at different muscle lengths, constructing a post-fascial release LT relationship. Repeat isometric contraction assessed muscle fatigue.

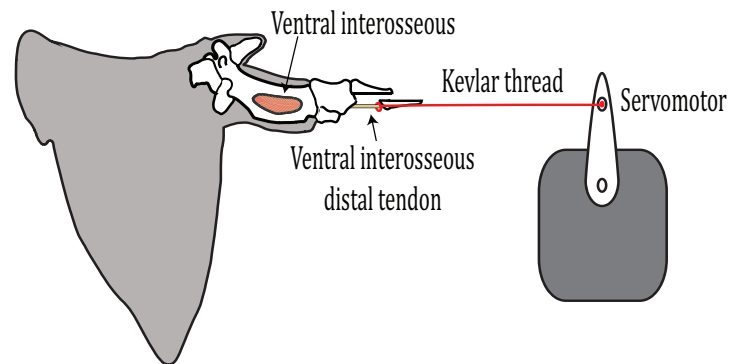


Figure 1: *In situ* preparation. Distal tendon of ventral interosseous attached to the servomotor lever via Kevlar thread. The distal tendon was maneuvered until a direct line of pull between the muscle and the servomotor was established.

RESULTS AND DISCUSSION

In trials performed on the plateau region of the LT curve, peak isometric force decreased by 22.3% following fascial release (Figure 2). Aside from peak magnitude, there was no noticeable difference in the contraction waveform between the intact compartment condition and the post-fascial release condition. Within each segment of the ventral interosseous's length tension curve, fascial release was associated with a reduction in isometric force production.

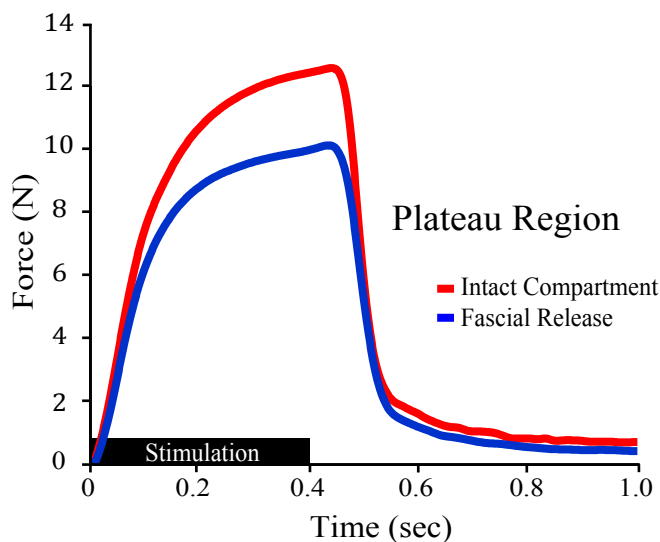


Figure 2: Pre and post-fascial release contraction patterns from the plateau region of the muscle in the same individual. Muscle was stimulated for a 400ms train duration.

In five individuals, fascial release resulted in an average decrease in muscle force output of approximately 19% along the ascending, plateau and descending regions of the length-tension curve. The force deficit associated with fascial release increased as muscle length increased, ranging from 13% along the ascending limb to 24% on the descending limb.

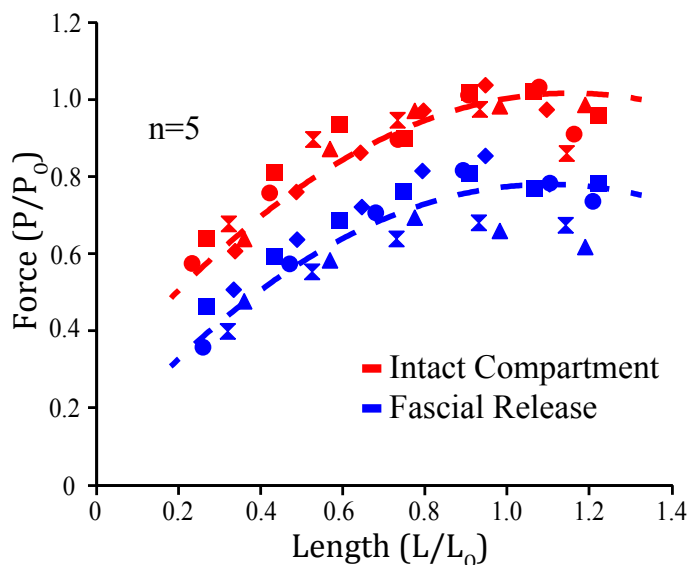


Figure 3: The effect of fascial release on maximal force generation along the length-tension curve of ventral interosseous muscle. Normalized isometric contractions from five experiments demonstrate

ventral interosseous muscle force generating capacity within an intact fascial compartment (red) and after fascial release (blue). Each marker represents an individual experiment.

CONCLUSIONS

Gross partitioning of synergistic muscles into fascial compartments is a widespread feature of mammalian limb anatomy. Yet few studies have explored the functional importance of having such a muscle and connective tissue arrangement. In this study, we accounted for muscle length and supramaximally simulated the ventral interosseous to achieve maximal force production along different muscle lengths both before and after fascial release treatment. Fascial release repeatedly and reliably reduced peak force production in the ventral interosseous muscle. These results, along with previous work on dog hindlimb muscles [1], suggest that releasing fascial constraints reduces muscle force output; and by extension suggests that fascia may play a critical role in preservation of muscle tension.

A mechanistic explanation for the observed reduction in muscle tension after fascial release remains elusive. Our findings question whether fascial release treatment is an entirely benign procedure, particularly in cases of chronic exertional compartment syndrome [2].

The National Institutes of Health research grant [AR055295] awarded to TJR supported this research.

REFERENCES

1. Garfin SR. *Journal of Applied Physiology*, San Diego, CA, USA, 1981.
2. Roberts AJ. *J R Army Med Corps*, Epsom, Surrey, UK, 2015.

MULTISCALE MUSCLE MODELS PREDICT HOW ACCUMULATED MICROTURNS LEAD TO ACUTE MUSCLE INJURY

¹Kelley M. Virgilio, ¹Kyle M. Martin, ¹Shayn M. Peirce, and ¹Silvia S. Blemker

¹The University of Virginia, Charlottesville, VA, USA
Email: kam8kc@virginia.edu

INTRODUCTION

Eccentric contractions have been linked to muscle injuries [1]; however, the mechanisms leading to acute strain injury are poorly understood. At the macro-level, a gait analysis study which captured an acute sprinting-related muscle strain injury indicated that the injury was not caused by a dramatic change in gait or misstep, suggesting that accumulated damage (microtears) may escalate to a major injury [1]. At the tissue level, previous work has demonstrated that the inherent architecture of the muscle influences its injury susceptibility by generating regions of high-localized strains [2]. At the fiber level, studies have shown a loss of force-transmitting proteins (dystrophin) immediately after eccentric contractions [3], which would compromise the mechanical integrity of the fibers since dystrophin is known to protect the muscle membrane from damage [4]. Together, these important factors all influence the resulting extent of muscle injury; however, since they cross multiple scale lengths, it is challenging to integrate them into one holistic understanding. The goal of this study was to address this critical gap in the field by creating multiscale models of skeletal muscle that represent the macro-scale loading, the tissue-level strains, and the micro-level damage during sprinting. Once developed, we used the models to explore the mechanisms underlying accumulated muscle damage and resulting injury.

METHODS

The modeling framework included seven key steps. Step 1 was to use a finite element (FE) model of the biceps femoris long head (BFLH) to determine the along fiber shear strain distribution throughout the muscle [2]. Step 2 was to utilize an agent-based model (ABM) to create a cross-section of a muscle fascicle for the micromechanical FE model, with

fibers, ECM, and nonlinear elastic springs to represent dystrophin. The ABM allowed for the rapid generation of muscle cross-sections that account for physiological variability [5]. Step 3 was to apply boundary conditions based on the shear strains in two regions (high and low strain) of the macroscale BFLH model (Fig 1). Step 4 was to simulate contraction by applying the representative shear displacements to the micromechanical model. Step 5 was to calculate the strain between the muscle fiber and the ECM (membrane strain). Step 6 was to update the model so that proteins with a membrane strain greater than the prescribed threshold, based on the estimated extensibility of dystrophin [6], were deleted. Step 7 was to create a new “damaged” micromechanical model with the remaining proteins. Step 4-7 were repeated until no additional damage was generated in the membrane.

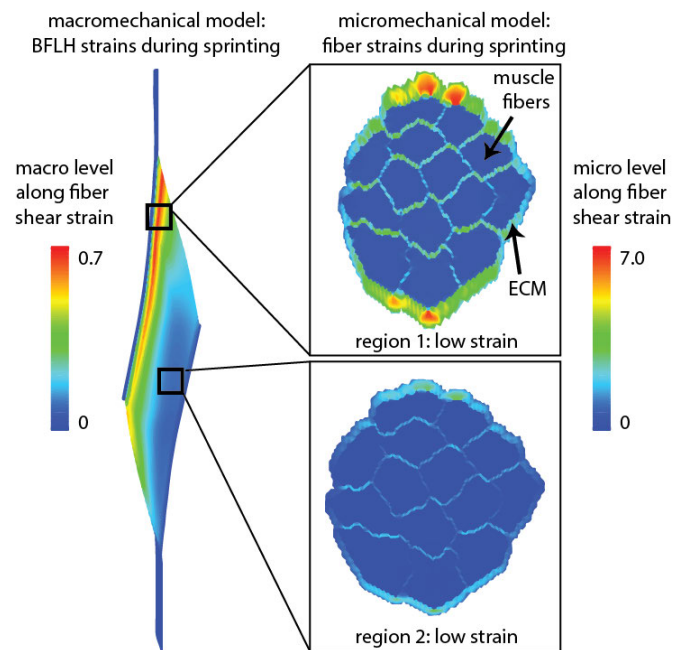


Figure 1: A BFLH model indicates non-uniform along fiber shear strain during sprinting. Two micromechanical models of muscle fascicles were developed with boundary conditions to simulate the local mechanics at high and low strain regions

RESULTS AND DISCUSSION

The whole-muscle model of the BFLH illustrated how local peak strains during eccentric contractions could lead to damage in specific regions of the muscle (Fig 1). At a smaller scale, the micromechanical model demonstrated this same phenomenon of non-uniform shear strain profiles within the fibers, based on the geometry and material properties of the ECM and the fiber. We found that micro-damage at the force-transmitting proteins (dystrophin) escalated from a single small tear (after a single eccentric contraction), into a substantial tear in the muscle membrane (after multiple contractions), which could ultimately result in an acute injury (Fig 2). In comparison, the region of the muscle with low local strains did not exhibit this same behavior and did not lead to acute muscle injury, consistent with the observation that injuries only occur in certain regions of a muscle.

This modeling framework illustrated a potential mechanism for the initial mechanical injury that could lead to an acute muscle injury, and suggested a number of important avenues for future exploration. First, we found that the prescribed thresholds for the damage to the dystrophin proteins and the onset of an acute muscle injury are

important determinants of the outcome, and thus need to be better characterized from experimental studies of membrane damage and dystrophin structure. Additionally, although the micro-scale model was informed by deformation patterns from the whole muscle, our future work aims to expand the simulations to include multiple deformation patterns, and verification with animal models of eccentric contraction injury.

CONCLUSIONS

This study proposed a novel multi-scale modeling framework to describe how high localized strains in the muscle during eccentric contraction could introduce small microtears that rapidly develop into an acute muscle injury.

REFERENCES

1. Schache A. *Gait and Posture* **32**, 136-140, 2010.
2. Fiorentino NM. *J Biomech* **47**, 3325-3333, 2014.
3. Lovering RM. *AM J Physiol Cell Physiol* **6**, C230-C238, 2004.
4. Bloch R. *Exerc. Sport Sci. Rev.* **31**, 73-78, 2003.
5. Virgilio KM. *Interface Focus* **5**, 2015.
6. Bhasin N. *J Mol Bio*, **352**, 795-806.

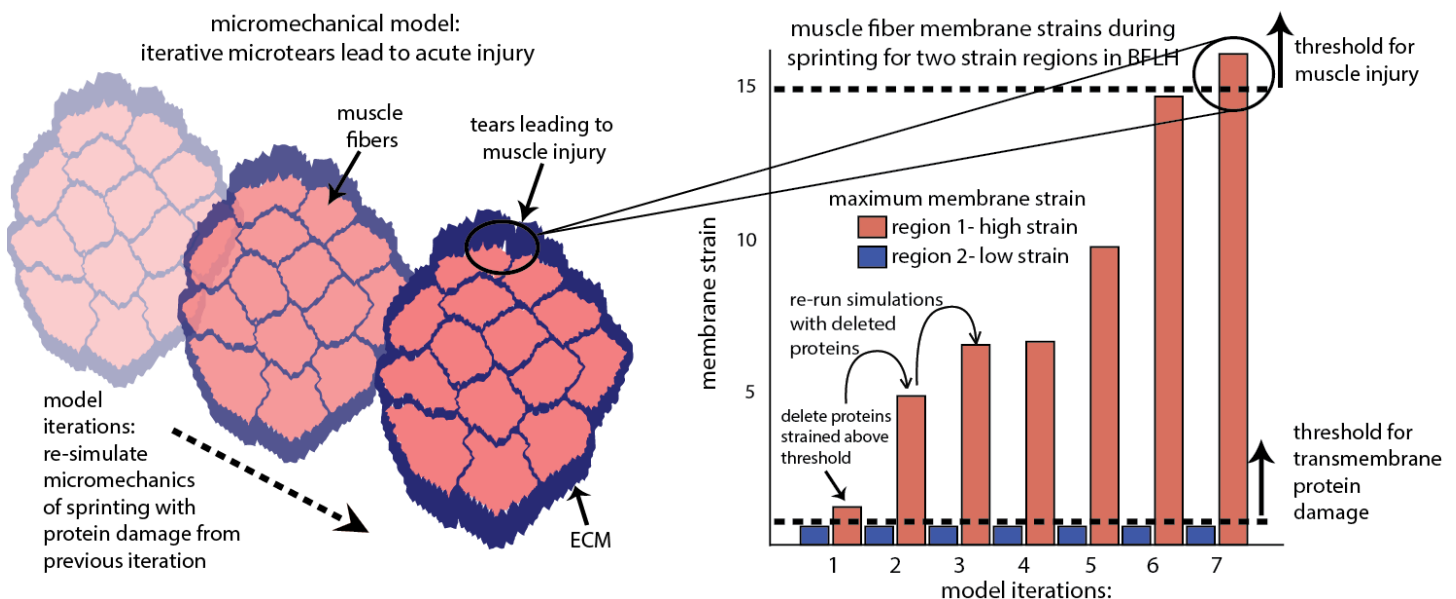


Figure 2: Iterations of the model analyses illustrate how small losses in membrane proteins could instantaneously lead to an acute muscle injury during eccentric contraction. After each simulation, proteins above the threshold for protein damage were deleted and a simulation with the remaining proteins was re-run. Model iterations represent the progressive increase in maximum membrane strain as proteins are deleted.

EFFECTS OF STRENGTH TRAINING ON MUSCLE FORCE PRODUCTION AND MUSCLE FUNCTION IN CHILDREN WITH CEREBRAL PALSY

Amy K. Hegarty¹, Max J. Kurz², Wayne Stuber² and Anne K. Silverman¹

¹Department of Mechanical Engineering, Colorado School of Mines, Golden, CO, USA

²Physical Therapy Dept., Munroe-Meyer Institute, University of Nebraska Medical Center, Omaha, NE, USA
email: ahegarty@mymail.mines.edu, web: <http://fbl.mines.edu>

INTRODUCTION

Cerebral palsy (CP) is a neurological disorder caused by an insult to the brain, which often leads to neuromuscular impairments. Strength training for children with CP increases isometric muscle strength and walking speed [1, 2], as well as affects muscle force and lower limb extension capacity during walking [3]; however, changes in muscle contributions to body center of mass (COM) accelerations after training have not been evaluated. The purpose of this study was to expand on previous work by evaluating changes in dynamic muscle force production and function in a group of children who participated in strength training.

METHODS

Four children with spastic CP participated in a six-week strength training protocol. Lower body kinematics and ground reaction forces were collected at 120 Hz during overground walking. Isometric muscle strength was measured with a handheld dynamometer for lower-limb joints before and after training. A generic musculoskeletal model with 14 segments, 21 degrees of freedom, and 92 Hill-type musculotendon actuators was scaled for each child. Three walking trials for each child before and after strength training were simulated in OpenSim 3.2 (www.simtk.org). A computed muscle control algorithm was used to estimate muscle excitations required to reproduce the experimentally measured kinematics. The contributions to body COM acceleration were analyzed using an induced acceleration analysis. Changes in mean dynamic muscle force production and contributions to COM acceleration before and after strength training were quantified over three stance phases of the gait cycle (GC) including: Double Support 1 (DS1, ~0-10% GC), Single Limb Stance (SS, ~10-50% GC), and

Double Support 2 (DS2, ~50-60% GC). A two-way repeated-measures ANOVA was used to assess differences ($\alpha=0.05$) in muscle forces, joint isometric strength, and muscle contributions to COM acceleration between legs, and as a result of training.

RESULTS and DISCUSSION

Few significant training main effects were found (Fig. 1). Several significant leg main effects indicated bilateral asymmetry not affected by training. Significant leg \times training effects indicated different left and right leg muscle responses to training. Soleus (SOL) contributions to the body COM vertical acceleration (support) were significantly increased after training in DS2. Also in DS2, significantly increased unilateral dynamic force in the gastrocnemius (GAS) was found.

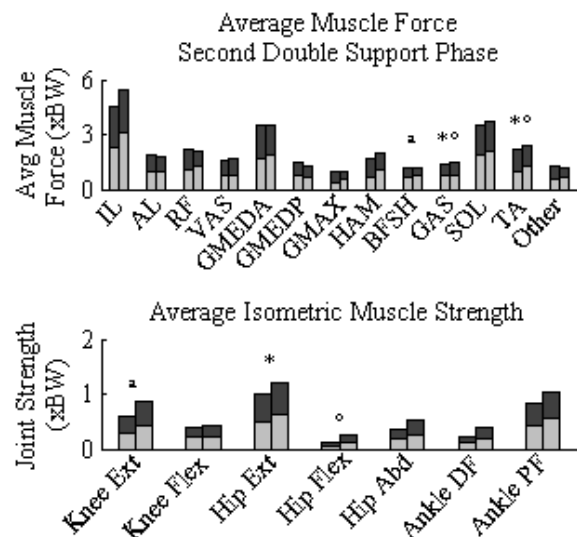


Figure 1: Mean dynamic muscle forces during DS2 (top) and average isometric joint strength (bottom). Left leg (light gray) and right leg (dark gray) were compared before (left bar) and after (right bar) training. Significant ANOVA leg (^a), training ([°]), and leg \times training interaction (^{*}) effects are shown.

However, muscles that had significant increases in dynamic force production after training did not correspond with muscle groups that had significantly greater isometric strength. Isometric strength of the hip extensors and hip flexors significantly increased after training (Fig. 1), but this was not found in the walking simulation results. Bilateral asymmetry in isometric knee extensor strength, not affected by training, was not found in the dynamic knee extensor muscle force estimates during walking.

Increased dynamic force production in the GAS and increased SOL contributions to body support in DS2 suggest a shift toward able-bodied mechanics after training [4-6]. However, high variability was found across children in muscle contributions to the COM acceleration. Thus, evaluating muscle results on an individual child basis may be a better approach for evaluating the effects of strength training on muscle function. For example, one child in the study had substantial changes in muscle contributions to support in the gluteus medius, vasti and soleus, all shifting towards able-bodied muscle function (Fig. 2) [6,7]. However, these results were not consistent for all children, and were not apparent in the group average results.

Increases in isometric strength measurements did not correspond to increases in dynamic muscle force production during walking. These results suggest that increases in static strength do not always translate to how a muscle is used dynamically during a movement. Similar changes in dynamic and static joint ranges of motion were found after strength training [8]. This may help explain why highly variable mobility improvements are associated with strength training [2]. In addition, these results

highlight how modeling and simulation analyses can assess dynamic muscle behavior during movement tasks that are not reflected in joint-level static testing.

CONCLUSIONS

These results suggest that strength training results in increased dynamic force and improved function in the ankle plantarflexors during gait. Strength training may also improve muscle function to provide body support and propulsion in other muscles groups, as in Child 1 (Fig. 2), although the responses of individual children are highly variable. Modeling and simulation analyses have the potential to guide therapy protocols that address muscle functional deficits on an individual child basis, and provide additional information regarding muscle mechanics not revealed by isometric strength testing.

REFERENCES

1. Dodd KJ, et al. *Arch. Phys. Med.* **38**, 1157–64, 2002.
2. Steele KM. et al. *Pediatr. Rehabil. Med.* **5**, 99–106, 2012.
3. Damiano DL. et al. *Phys. Ther.* **90**, 1-11, 2010.
4. Steele KM. et al. *J. Biomech.*, **43**, 2099–2105, 2010.
5. Neptune RR. et al. *J. Biomech.* **34**, 1387–98, 2001.
6. Liu MQ. et al. *J. Biomech.* **39**, 2623–30, 2006.
7. Steele KM. et al. *Gait Posture*. **38**, 86–91, 2013.
8. McMulkin M. et al. *J. Ped. Ortho.* **20**, 366-9, 2000.

ACKNOWLEDGEMENTS

This work was partially supported by the NSF GRFP (DGE-1057607) and a research grant from the Pediatrics Section of the APTA.

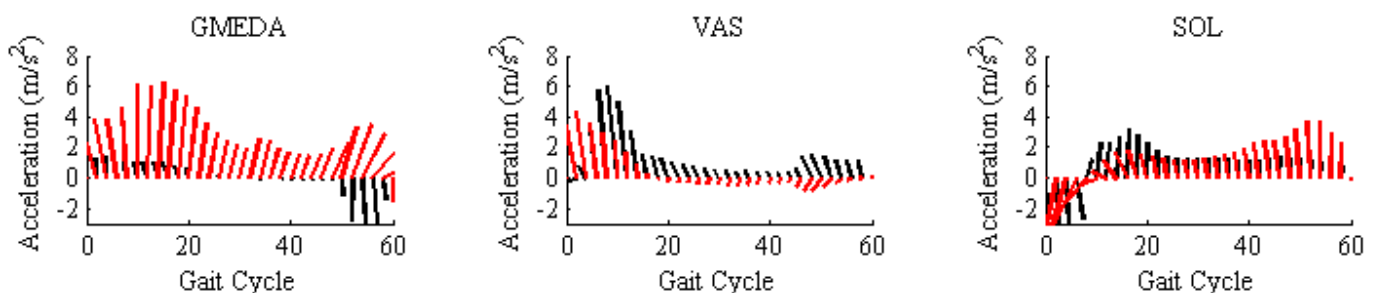


Figure 2: Child 1 anterior gluteus medius (GMEDA), vasti (VAS) and soleus (SOL) contributions to support (vertical component) and propulsion (horizontal component) before (black) and after (red) strength training.

EXTENSOR MUSCLE SEQUENCING DURING RETURN TO STAND IN A SUBGROUP OF INDIVIDUALS WITH LOW BACK PAIN: RESPONSE TO EXERCISE

Erika Nelson-Wong

Regis University School of Physical Therapy, Denver, CO, USA

email: enelsonw@regis.edu

INTRODUCTION

It has been recognized that LBP cannot be treated as a singular disorder and outcomes improve when individuals are subgrouped according to etiology and clinical presentation. Several sub-classification paradigms are used clinically, with Treatment Based Classification (TBC) being one of the more common approaches used by physical therapists. This approach categorizes individuals with LBP into 1 of 4 subgroups, Manipulation, Direction Specific Exercise, Traction, and Motor Control/Stabilization according to their clinical presentation [1], and is meant to direct appropriately matched interventions. Observation of aberrant motions during forward flexion in standing (FS) is one of the criteria for classification into the Motor Control/Stabilization (Stab) subgroup, with reversal of lumbopelvic rhythm being one of the aberrant motions described. Observation of lumbopelvic reversal during FS has poor inter- and intra-rater reliability [2], which makes its inclusion in the sub-classification algorithm questionable. However, there is evidence that sequencing of extensor muscle activity during FS differs between individuals with and without LBP. A 'bottom up' (gluteus maximus followed by erector spinae) muscle activation sequence is considered to be typical in healthy individuals during the return to stand (RTS) phase of FS. A reversal of this pattern during RTS has been observed in individuals predisposed to LBP during a prolonged standing protocol [3]. Extensor muscle activation sequencing during FS, and response to appropriately matched intervention, has not been investigated in individuals meeting TBC criteria for Stab. Therefore the purpose of this study was to investigate differences in extensor muscle sequencing during the RTS phase of FS between healthy controls and individuals with LBP classified into the Stab subgroup, and to determine response to a stabilization-based exercise intervention.

METHODS

Fourteen individuals with LBP (36% male, age 36.9 ± 13.8 years) meeting TBC criteria for Stab and 13 healthy control participants (36% male, age 30.6 ± 9.5 years) enrolled in this study. Following baseline data collection, participants completed a standard stabilization-based, progressive exercise program for 6 weeks, then returned for a post-intervention assessment. The protocol for baseline and post-intervention data collections was identical. Surface electromyography (EMG) data were collected from left lumbar erector spinae (ES) and gluteus maximus (GMx) muscles. Kinematic data were collected to construct a 4-segment (trunk, pelvis, bilateral thighs) model. Participants performed a single trial of self-paced FS. EMG data were filtered for noise removal, linear enveloped and normalized to reference contractions. Kinematic data were used to extract windows isolating the RTS phase of motion. Cross correlation analyses were used to quantify relative timing between the ES and GMx muscles, with phase lag at maximal spatial correlation extracted from a physiological window of ± 250 msec [3]. Phase lags were dichotomized as Bottom Up (BU) where GMx activated first, or Top Down (TD) where ES activated first, strategies. Chi-square analyses were used to determine associations between LBP status and baseline strategy and changes in strategy following intervention for the LBP group with $\alpha = .05$.

RESULTS AND DISCUSSION

The individuals with LBP in this study reported relatively low disability with mean baseline pain (100 mm visual analog scale, VAS) of 12.1 mm (range: 0 - 52 mm) and Oswestry Disability Questionnaire (ODQ) scores of 15.1% (range: 2 - 42 %). Reversal of lumbopelvic rhythm (visual observation) was noted in 57% of the LBP sample

at baseline. There was a significant association between LBP status and extensor muscle sequencing strategy at baseline ($\chi^2=6.0$, $p<.05$) with most control participants utilizing a typical BU strategy (76.9%) and most LBP cases demonstrating a TD strategy (71.4%) (Figure 1).

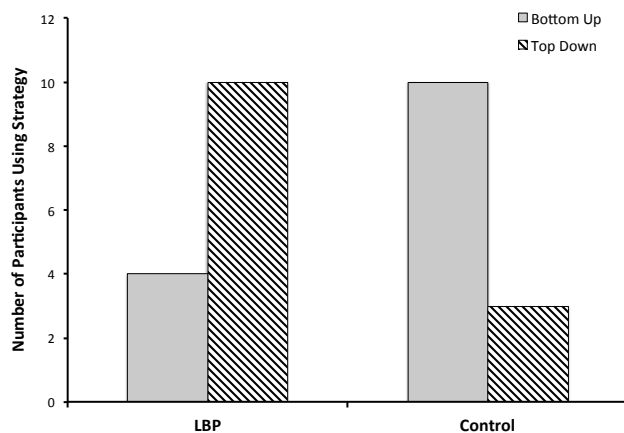


Figure 1: Individuals with LBP primarily used a top down strategy while healthy controls used a bottom up strategy.

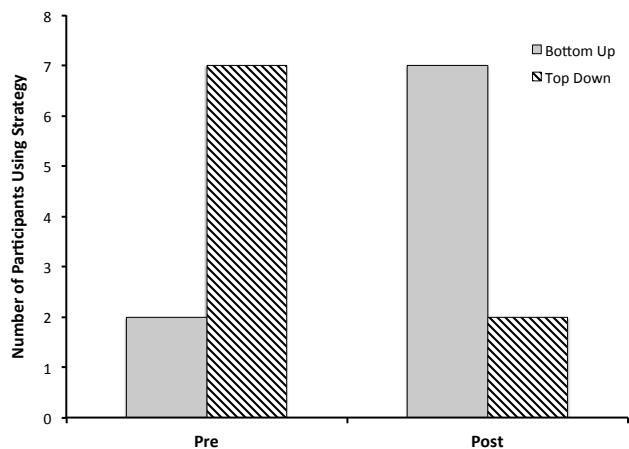


Figure 2: There was a favorable change in muscle activation strategy for individuals with LBP following exercise intervention.

Of the 14 individuals with LBP, 10 completed the exercise intervention and post-intervention assessment (2 withdrew for medical reasons, 2 were completing the intervention at time of abstract submission). EMG data were not available for 1 participant due to technical issues. Therefore, pre-post intervention analysis includes data from 9 participants with LBP. Following exercise intervention there was a decrease in average pain on

VAS (4.9 mm, range: 0 – 15 mm) and disability on ODQ (9.9%, range: 2 – 24%). Observed reversal of lumbopelvic rhythm was noted in 11% of the sample. There was a significant change in extensor muscle sequencing strategy following exercise intervention ($\chi^2=5.6$, $p<.05$) with 77.8% of LBP cases demonstrating a BU strategy (compared with 22.2% baseline) and 22.2% using TD strategy (versus 77.8% at baseline) (Figure 2). Of the LBP cases using TD strategy at baseline, 71.4% converted to a BU strategy following exercise intervention.

CONCLUSIONS

These findings showed clear differences in extensor muscle strategy during RTS phase of FS between healthy controls and individuals with LBP meeting the TBC criteria for Stab. Although reliability of observed lumbopelvic rhythm reversal has been questioned, individuals in the TBC Stab subgroup demonstrated altered movement strategies in FS. It is encouraging that these atypical strategies appear to be modifiable through a standard exercise program targeted towards the Stab subgroup. It should be noted that the intervention did not include any exercises involving standing flexion. It may be that improvements in trunk and hip strength and control gained through the intervention allowed participants to use a more typical BU strategy during the RTS phase of FS. These findings provide further support for stabilization based exercise intervention in patients with LBP meeting the TBC criteria for Motor Control/Stabilization sub-classification.

REFERENCES

1. Stanton TR, et al. *Phys Ther* **91**, 496-509, 2011.
2. Hicks G, et al. *Arch Phys Med Rehabil* **84**, 1858-1864, 2003.
3. Nelson-Wong E, et al. *Clin Biomech* **27**, 994-998, 2012.

ACKNOWLEDGEMENTS

Regis University Research and Scholarship Council for funding. Regis DPT students for assisting with data collection.

BRINGING MECHANICS TO LIFE

Antonia Zaferiou¹, Edward V. Wagner², Travis Peterson¹, Jani Macari Pallis⁴, and Jill L. McNitt-Gray^{1,3}
Departments of Biomedical Engineering¹, Aerospace and Mechanical Engineering², Biological Sciences³
University of Southern California, Los Angeles, CA, USA 90089
Department of Mechanical Engineering⁴, University of Bridgeport, USA
email: mcnitt@usc.edu

INTRODUCTION

Biomechanics provides an engaging vehicle for exploring fundamental questions at the interface of engineering, physiology, and health. Through guided-experiential learning, students can gain exposure, experience, and expertise as they begin to embed the use of fundamental principles in their self-discovery¹ of mechanisms governing movement. Since 1988, members of the USC Biomechanics Research Lab have been actively involved in a wide range of Science, Technology Engineering, Art, and Mathematics (STEAM) outreach activities. The focus of this paper is to share what we have found to be “Best Practices” for engaging young audiences and embedding the use of scientific processes and engineering design in the study of human biomechanics.

METHODS

Two outreach initiatives will be discussed: Body Engineering-Los Angeles (BELA) and Get SSET Academy (Sport Science, Engineering and Technology). BELA is a year-long program that partners doctoral students in engineering with teachers in urban middle schools. STEM standards are met by investigating the human body as a machine. Lessons are generated and led by both the teacher and doctoral student on a weekly basis throughout the year. This project has been funded in part by National Science Foundation Grant DGE 1045595) and the USC Viterbi School of Engineering.

The *Get SSET* (Sport Science, Engineering, and Technology) Academy is an informal educational experience aimed at first-generation college-bound 9-10 grade female students interested in sports and science. Our aim in this 3.5 day residency program is to provide students with an experience of college life and exposure to engineering, prior to making decisions regarding high school coursework.

Participants are recommended by both their science or mathematics teacher and their coach to confirm that the student-athlete has the desire to improve. Advancement in sport often involves hours of practice, failures, observation of performance related issues, and resolution of these issues through creative solutions and persistence. These same processes are key in becoming an effective engineer or scientist. While academy activities have varied, all have included a sport aerodynamics activity, a design methodology activity, a biomechanics motion capture and analysis activity, a visit to a local sport, science or other engineering facility, and final presentations from the students to the sponsors, faculty, staff and their families.

RESULTS AND DISCUSSION

“Best Practices” in both of these initiatives has involved an intriguing hook that engages and is relevant to the participants. This hook must be supported with fundamental science and engineering principles through interactive discussion and exploration of concepts. By balancing lecture (<7 minutes) with video and structured participation, students develop active interest. This allows the educators to transition into inquiry-based experiments or engineering design challenges. To facilitate implementation, low-cost readily available materials are typically used with open-source software. To measure learning outcomes, student presentations, electronic journals, and peer review sessions can be used.

REFERENCES

1. Farkas, RD et al., J Edu Res 97(1), 42-51, 2003

ACKNOWLEDGEMENTS

National Science Foundation, USC Center for Excellence in Teaching, Center for Scholarly Technology, Undergraduate Research Program in Biomechanics.

EXPERIENTIAL, LOW COST NEUROSCIENCE OUTREACH FOR ALL AGES – *MUSCLES ALIVE!*

Brian L. Tracy, Ph.D.

Neuromuscular Function Laboratory
Department of Health and Exercise Science
Colorado State University, Fort Collins, CO, USA
Email: brian.tracy@colostate.edu

INTRODUCTION

Interactive, immersive, and engaging science lessons can have lasting effects in students. For diverse student populations, optimal learning occurs via different modes (experiential, tactile, auditory, visual). Our lab conducts human neuromuscular EMG studies with expensive lab-based equipment not suitable for use in the outreach setting. We have leveraged our scientific expertise to create novel, effective community-based neuroscience outreach.

METHODS

In 2012, our CSU group helped Backyard Brains, Inc. produce the new EMG Spikerbox, a small, inexpensive bioamplifier that for the first time allowed students to experience, hear, see, and record their own muscle electrical activity outside of the research lab. The EMG signal is detected with 10-cent disposable electrodes made from popsicle sticks and brass brads, displayed visually in real time on iPods with the Spike Recorder App, and the audio is played through hobby speakers.

We also use commonly available vibrating massagers to elicit the tonic vibration reflex and attention-getting, fun, experiential proprioceptive illusions.

The novel EMG kits and proprioception demos are the centerpiece of our 2.5 yr-old program *Muscles Alive!*, named as an homage to the classic EMG text. Offering vivid visual and audio feedback, our participatory demonstrations usually involve small groups of students and include:

- 1) Live visual/auditory display of raw EMG signals from muscles of the hand, arm, leg, and face during different tasks.
- 2) Jaw muscle activity - chewing experiments with foods of different consistencies.
- 3) Weight lifting and arm wrestling.
- 4) Motor Unit Hunt – perhaps surprisingly, we can commonly record single motor unit discharge

with these 10-cent electrodes, allowing direct observation of motor neuron discharge behavior.

- 5) Tendon vibration demos with 60Hz massagers that target afferent muscle sensors: *The Phantom Limb* (biceps brachii tonic vibration reflex) and *The Neurophysiology Trust Fall* (a robust proprioceptive illusion).
- 6) Live recording of the EMG of the patellar tendon tap reflex (stretch reflex).
- 7) Stretch reflex circuit timing (25-40ms) with a \$15 instrumented reflex hammer.
- 8) Human-to-Human interface: control your friend's arm with your own EMG.

RESULTS AND DISCUSSION

Our demonstrations are accompanied by age-appropriate displays designed to teach students about 1) biological electricity and excitable cells, 2) the relation between brain command and muscle activation, 3) how action potentials are transmitted efferently to muscle and converted to force, 4) the role and extreme sensitivity of muscle sensors (spindles) in reflexes and proprioception, 5) the speed and necessity of reflexes, 6) neuromuscular anatomy, and 7) the critical role of voluntary muscle control in making us human.

We maintain an undergrad/grad team who lead the demonstrations and benefit from the teaching and community involvement. They must use their classroom knowledge in an applied context.

Impact - We have interacted with ~3,200 9-18 year-olds during > 45 events in public schools, science fairs, expos, science museums, community events, university events, and after school programs. The same equipment and concepts have been used successfully in public science settings with adults. Recently we have used these kits and techniques in university courses in neuromuscular physiology and anatomical kinesiology.

THE REBEL “STEM” ACADEMY: BRINGING STUDENTS TO THE SCIENCE

¹Janet S. Dufek and ²Christopher L. Heavey

¹Department of Kinesiology and Nutrition Sciences

²Assistant Vice Provost for Undergraduate Education

University of Nevada, Las Vegas, Las Vegas, NV, USA

email: janet.dufek@unlv.edu; website: <http://www.unlv.edu/kns/kinesiology>

INTRODUCTION

The Rebel Science, Technology, Engineering, and Mathematics (STEM) Academy, developed jointly by the Office of the Provost and the Office of Admissions, brings high-achieving local high school students and their teachers to the University of Nevada, Las Vegas (UNLV) campus to spend a Saturday participating in hands-on experiences in STEM laboratories. The REBEL (Rehabilitation, Engineering, Biomechanics, Exercise Science, Life Sciences) Human Performance Group, formerly, the “Biomechanics Laboratory” is a participant in this event.

METHODS

Invitations are sent out the local school district’s STEM teachers to gather students and participate in the event. Note that the “local” school district (Clark County School District) is the fifth largest in the country, thus a wide net is cast. Participating teachers and their students visit the UNLV campus on what is affectionately referred to as “STEM Saturday”. Up to 10 high-profile laboratories on the UNLV campus participate in the event. The students visit laboratories that are conducting research in solar energy, water quality, renewable energy research, genomics, and *biomechanics*.

RESULTS AND DISCUSSION

The inaugural REBEL STEM Academy was held during the spring of 2013. It was attended by five teachers and 23 of their students. Each student participated in two different laboratory experiences spread across five different laboratories offered by faculty and graduate students from the College of Engineering, Sciences, School of Allied Health Sciences, and School of Community Health

Sciences. Subsequent STEM Academies have averaged 10 teachers and 42 students. Our next Rebel STEM Academy is scheduled for April 2015. We already have 10 teachers and over 100 students signed up to participate. In addition to participating in the hands-on laboratory experiences, students and teachers join us for lunch, receive some UNLV swag, and learn about degrees and opportunities available at UNLV. Those who have attended have described it as a wonderful and eye-opening day.

When the students arrive at the site of the REBEL Human Performance Group, they are introduced to a variety of biomechanics tools. We demonstrate motion capture techniques by instrumenting one of the students and capturing locomotion data. Three-dimensional images are reconstructed and discussed. Other student participants will run or jump on the force platforms. Not only do students see force-time curves illustrated, but we explain salient characteristics, which typically leads to eagerness to repeat the experiment by running faster or jumping higher (adding a second “experimental condition”). One of the annual highlights is placing someone in our positive pressure treadmill and allowing them to run at reduced body weight. Here, we demonstrate that biomechanics can lead to a sense of weightlessness!

CONCLUSION

The Rebel STEM Academy is a fun day and a great way to showcase the impressive scientific research being done on our campus, including the lesser known science of biomechanics. We expect this event to continue to grow in the future as more teachers and students learn about it and as we continue to increase the number of participating STEM laboratories. We encourage others adopt this model to encourage biomechanics to “get younger”.

BRIDGING ENGINEERING, SCIENCE AND TECHNOLOGY IN MEDICINE (BEST MEDICINE)

¹ Brian L. Davis, and ¹Carin A. Helfer

¹ Department of Biomedical Engineering
The University of Akron, Akron, OH, USA

email: bdavis3@uakron.edu; website: <http://www.uakron.edu/bestmedicine>

INTRODUCTION

“Bridging Engineering, Science and Technology in Medicine,” (aka BEST Medicine) is an engineering fair in which 6th-12th graders create solutions to medical problems. BEST Medicine inspires students to seek solutions to health issues (often musculoskeletal) that they encounter in their home or social environment – while reinforcing math and science concepts they learn at school (Table 1).

Table 1. Goals and relationships to standards.

Goal	Relevant Standards
Grow vocabularies in science, engineering, and medicine	Common Core State Standards Connections (CCSSC) ELA/Literacy RST.6-8.8
Become proficient at testing a concept and improving ideas	Next Generation Science Standard (NGSS) MS-ETS1-4
Present logical arguments based on substantive claims, sound reasoning, and evidence	CCSSC ELA/Literacy SL8.5
Develop familiarity with 21st century media and technology	CCSSC ELA/Literacy SL8.5
Apply mathematical thinking to real world challenges	CCSSC Mathematics 7.EE.3
Become familiar with the engineering design process	NGSS MS-ETS1

Incorporating the engineering design process into the curriculum at the middle school level may seem a challenge at first glance. However, including engineering is a necessity since the Next Generation Science Standards (NGSS Lead States 2013) include engineering design process at the middle school level. At this grade level, the students are to “learn to sharpen the focus of problems by precisely specifying criteria and constraints of successful solutions” (NGSS Lead States 2013). Also, students should understand that engineering is critical to addressing future challenges in society (NRC 2012). Within the broad field of engineering, our experience shows that biomechanics is particularly suited to this endeavor. Each year, students showcase novel ideas for prosthetic and other rehabilitation devices, footwear, robotic approaches in medicine and human movement projects.

METHODS

BEST Medicine has been hosted for the past 5 years at the National Inventors Hall of Fame Middle School in Akron, Ohio. Typically 120 students (who have been preselected through other school or regional science fairs) participate. Holding a fair that highlights biomechanics is an excellent approach for teaching students about interdisciplinary science and/or the engineering design process. Local medical professionals (biomechanics faculty, physical therapists, clinicians etc.) attend the fair and this allows students to explore potential career opportunities. Concurrent teacher workshops are offered while the student projects are being judged.

RESULTS AND DISCUSSION

Each year approximately 30 to 40% of all projects submitted to BEST Medicine are related to biomechanics. Examples include (i) reducing the risk of concussion in sports, (ii) developing improved prosthetic sockets, (iii) decreasing the risk of bathroom falls, (iv) predicting knee stress through a computer model and (v) an ergonomic power-assisted wheelchair transfer system.

CONCLUSION

By middle school, students are aware of many medical problems, often through personal experiences of friends and family members. Therefore, projects that involve engineering solutions to biomechanical issues allow students to solve real human problems for which they have a personal interest.

REFERENCES

National Research Council (NRC). 2012. A framework for K-12 science education: Practices, crosscutting concepts, and core ideas. Washington, DC: National Academies Press.

NGSS Lead States. 2013. Next Generation Science Standards: For states, by states. Washington, DC: National Academies Press. www.nextgenscience.org/next-generation-science-standards.

SUBCHONDRAL STRAINS AND INITIATION OF OSTEOARTHRITIS IN THE RADIOCARPAL JOINT

¹ Joshua E. Johnson and ¹ Karen L. Troy
¹ Worcester Polytechnic Institute, Worcester, MA, USA
email: jejohnson@wpi.edu

INTRODUCTION

Prevalence of radiographic osteoarthritis (OA) is highest in the hand, and secondary OA due to injury is a significant problem. Peak contact pressure (CP) on the radius articular surface is an important mechanical factor in OA initiation, and is affected by joint injury and subsequent abnormal load transfer [1]. However, distal radius strains due to abnormal joint loads may also influence the degenerative response from the subchondral level. The goal of this study was to investigate whether changes in distal radius subchondral strains are related to changes in peak CP, to better understand the mechanism of OA initiation. Our hypothesis was that increases in peak CP would result in a similar (or greater) increase in peak strains.

METHODS

Radiocarpal joint finite element (FE) models were created using computed tomography (CT) data acquired from two female subjects (mean age 27.5 years), after IRB approval. Proximal wrist and forearm images were acquired at 234×234×625 μm voxel size (Fig. 1A).

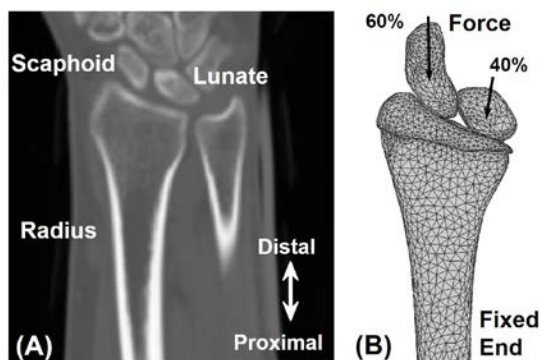


Figure 1: (A) CT data used to construct FE models of the radiocarpal joint (B).

The methods used have been previously validated for evaluation of distal radius mechanics [2]. The

radius and carpal bones (lunate, scaphoid) were segmented from the images in Mimics (Materialise, Leuven, Belgium). Cartilage was created by expanding the distal radius surface to achieve an average thickness of 1.4 mm, similar to values reported in literature. Bone and cartilage geometries were converted to quadratic tetrahedral meshes (Fig. 1B). Cartilage was assigned a Neo-Hookean hyperelastic material property. Based on an established density-elasticity relationship, the radius was assigned a linear elastic, inhomogeneous property. Normal behavior between the contacting surfaces was modeled using a finite sliding formulation, while a penalty method was used to model tangential behavior. To simulate physiologic loading (leaning onto the palm), proximal radius nodes were fixed, while an axial force was applied through the scaphoid and lunate centroids based on percentage of load transfer through the joint.

Loads were applied ranging from 50-500 N (50 N increments) to represent abnormal changes due to joint injury, resulting in 10 simulations per subject. All simulations were performed in Abaqus (Simulia, Providence, RI). Energy equivalent strain $\bar{\epsilon}$ ($\sqrt{2 \times U/E}$, U =strain energy density; E =modulus) was chosen as the strain outcome because of its association with bone adaptation. For both the radioscapoid (RS) and radiolunate (RL) articulations, percent changes versus baseline (50 N) in peak CP were compared to percent changes in peak $\bar{\epsilon}$, determined from subchondral radius elements (3 mm average length) in regions underlying contact pressure distribution.

RESULTS AND DISCUSSION

Average results of the two subjects were analyzed. With increasing load, percent changes in peak $\bar{\epsilon}$ versus baseline for the RS articulation trended higher than peak CP (Fig. 2). On the other hand, changes in peak $\bar{\epsilon}$ trended lower than peak CP for

the RL articulation (Fig. 3). Figure 4 shows example CP distributions (top row) from 100 N and 300 N joint load simulations for the RS and RL articulations, and corresponding $\bar{\epsilon}$ distributions on the distal radius surface (bottom row).

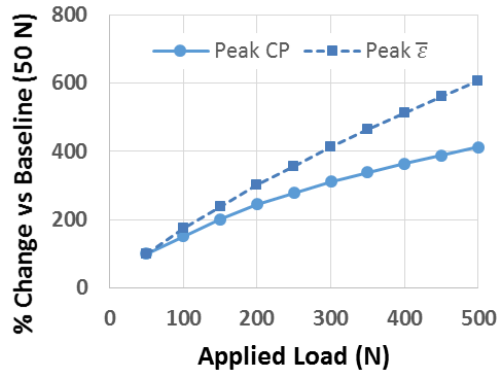


Figure 2: Percent changes in RS peak CP and $\bar{\epsilon}$.

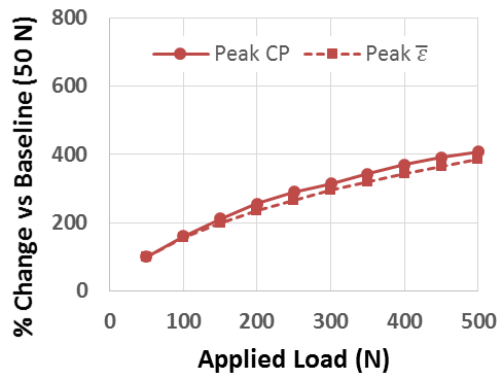


Figure 3: Percent changes in RL peak CP and $\bar{\epsilon}$.

The mechanism leading to the onset of post-traumatic OA is not well understood. Only a portion of the radius cartilage is loaded during normal functional wrist motion (average 21%) [3]. It is possible that the tissue preconditions to physiologic loading over time, and may be sensitive to changes in magnitude or location of peak contact pressure. Also, $\bar{\epsilon}$ values above a threshold are associated with bone apposition and vice versa. Higher changes in peak $\bar{\epsilon}$ were observed only on the scaphoid side. These higher strains could result in local bone formation and consequently local increases in stiffness. This could lead to local stress concentrations at the cartilage-bone interface, resulting in a degenerative response also at the subchondral level. Also, the increased stiffness of the subchondral bed would lead to subsequent increases in peak contact pressure - essentially a

positive feedback loop. This combination of peak contact pressure and $\bar{\epsilon}$ could predispose the scaphoid fossa to higher OA risk, which interestingly, is clinically observed to initiate on the scaphoid side [4]. Further, shift in location of peak contact pressure due to injury may result in even higher increases in peak strain. Due to its shape, the lunate articulation may be protected from increases in subchondral strains as a result of even load distribution. However, the progression of joint instability and degeneration eventually result in the lunate fossa also succumbing to OA (scapholunate advance collapse pattern of wrist OA).

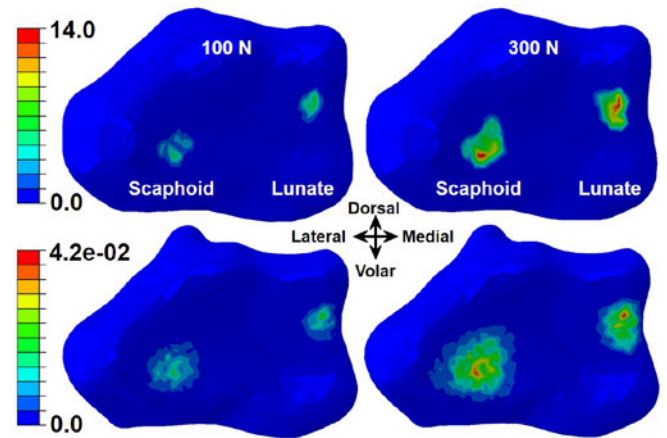


Figure 4: CP (top; MPa) and $\bar{\epsilon}$ (bot) distributions.

One limitation of the study was using a “projected” cartilage surface, which is less accurate to estimate contact pressure than actual cartilage surface. However, using the radius surface instead of an idealized surface, improved the geometric accuracy of the scaphoid and lunate articular fossae.

CONCLUSIONS

We observed higher changes in peak $\bar{\epsilon}$ in relation to peak CP, which suggests a mechanism of OA initiation also at the subchondral level.

REFERENCES

1. Johnson J, et al. *J Orthop Res* **31**, 1455-60, 2013.
2. Bhatia V, et al. *J Biomech* **47**, 2759-65, 2014.
3. Patterson R, et al. *J Hand Ther* **8**, 97-105, 1995.
4. Watson H, et al. *J Hand Surg* **9**, 358-65, 1984.

ACKNOWLEDGEMENTS

NIH R01AR063691 grant funding.

A SIMULATION STUDY OF THE WRIST AND THUMB: WHY DO WRIST SURGERIES DECREASE LATERAL PINCH STRENGTH?

¹Jennifer A. Nichols, ^{2,3}Michael S. Bednar, ^{4,5}Sarah J. Wohlman, and ^{2,4,5}Wendy M. Murray

¹University of Utah, Salt Lake City, UT; ²Edward Hines Jr. VA Hospital, Hines, IL;

³Loyola University Medical Center, Maywood, IL

⁴Northwestern University, Chicago, IL; ⁵SMPP, Rehabilitation Institute of Chicago, Chicago, IL

email: jen.nichols@utah.edu, web: <http://smpp.northwestern.edu/research/arms/>

INTRODUCTION

A healthy wrist is essential for hand function. Yet, the complexity of these two, highly integrated, multi-body, multi-joint systems often necessitates studying their biomechanical features in isolation. Experimental studies, for example, have separately studied the kinematics of carpal, metacarpal, and phalangeal joints [1-3]. Even simulation studies rarely integrate the wrist and hand, due to the computational challenges associated with building robust musculoskeletal models of these intricate, low mass, low inertia systems. For example, the wrist has previously been excluded from models implemented to analyze force production by the thumb, index finger, and in multi-finger grip [4-6].

This study leverages the available experimental data and the computational advances of previous models to develop simulations of lateral pinch force that integrate the wrist and thumb. We specifically study scaphoid-excision four-corner fusion (SE4CF) and proximal row carpectomy (PRC), common surgeries to treat wrist osteoarthritis. These procedures provide an ideal context to examine biomechanical coordination between the wrist and thumb. Notably, even though SE4CF and PRC surgically alter only the wrist, they are known to result in decreased lateral pinch strength [7]. Also, these surgeries dramatically, but distinctly, alter the wrist's bone geometry (Fig. 1A) and kinematic function.

METHODS

To examine how surgically altering the wrist affects lateral pinch force production, biomechanical models of the nonimpaired wrist [8] and thumb [5] were adapted to develop dynamic simulations for three wrist conditions (nonimpaired, SE4CF, and

PRC; Fig. 1). The three models included fourteen muscles (5 primary wrist, 4 extrinsic thumb, and 5 intrinsic thumb muscles). Condition-specific joint kinematics and moment arms for each model were based on experimental data [8, 9, 10].

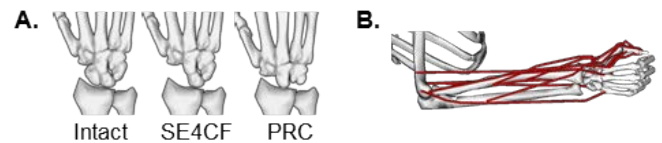


Fig. 1. (A) Wrist bone geometry. (B) Pinch posture.

Seven lateral pinch tasks (magnitude 0-60 N in 10 N increments; direction pure palmar) were simulated with each of the three biomechanical models using two simulation approaches (Fig. 2). All simulations were performed in OpenSim v. 3.1 [11].

To compare the joint torques necessary to produce a given level of lateral pinch force across wrist conditions, we implemented a computed torque control algorithm (Fig. 2A). Each simulation involved maintaining a static wrist posture while producing the target endpoint force. These simulations did not include muscle-tendon units. Differences in the resulting torques isolate the effects of wrist kinematics on the transformation from joint torques to thumb-tip endpoint force.

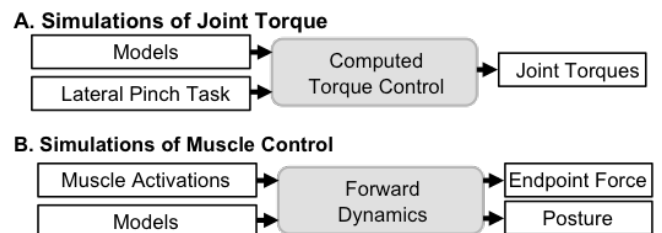


Fig. 2. Summary of the simulation approaches.

To compare how effectively muscles produce lateral pinch force across wrist conditions, forward dynamic simulations were performed (Fig. 2B). In each forward simulation, the inputs were the muscle activations required to reproduce the lateral pinch tasks in the nonimpaired model, calculated using computed muscle control. Because muscle activations were held constant across wrist models, any differences in the simulated pinch force vectors arise from the changes to wrist joint kinematics and musculoskeletal geometry imposed by the surgeries. Results of the forward simulations were compared when the simulations reached equilibrium.

RESULTS AND DISCUSSION

Regardless of the magnitude of endpoint force simulated, the SE4CF and PRC models required wrist torques larger than those required by the nonimpaired model (Fig. 3). The PRC model consistently required the largest wrist torques (more than 3.5 times larger than the nonimpaired model). Torques across the three thumb joints were similar across all models (results not shown).

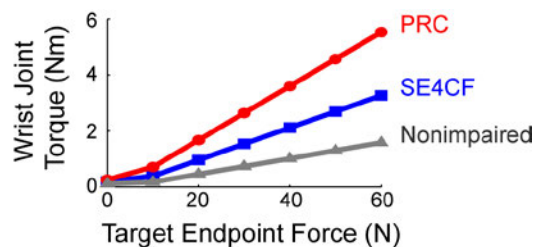


Fig. 3 Magnitudes of wrist joint torque versus thumb-tip endpoint force for the nonimpaired (gray), SE4CF (blue), and PRC (red) models. Torques were decomposed into a common anatomical frame for direct comparison.

Given the same muscle activations, the SE4CF and PRC models produced thumb-tip endpoint forces that were smaller in magnitude and misdirected compared to the nonimpaired model (Fig. 4). The misdirection of the force depended on the surgery; SE4CF produced force in palmar and medial directions, PRC produced force in palmar and proximal directions (Fig. 4). The posture at equilibrium was also different across the three models. In addition to changes in thumb joint posture (Fig. 4), the wrist moved by nearly 10° in both surgical models. The equilibrium wrist posture was neutral for the nonimpaired model, combined radial-extension for SE4CF, and ulnar deviation for

PRC. These postures reflect post-operative changes in muscle moment arms [10].

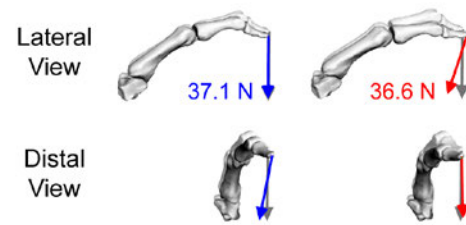


Fig. 4 Representative endpoint forces from forward simulations to produce 40 N target endpoint force. The SE4CF (blue) and PRC (red) results are superimposed on the nonimpaired (gray) results. Arrows represent force (magnitude and direction); thumb illustrates the final, equilibrium posture.

CONCLUSIONS

Changes in joint kinematics and musculoskeletal geometry following wrist surgery likely contribute to impairments in lateral pinch strength. Our simulations indicate that muscles must generate larger torques about the wrist following surgery to produce a given magnitude of lateral pinch force (Fig. 3). Many muscles actuating the wrist also actuate the hand. Thus, impairments in lateral pinch may reflect an inability to effectively coordinate muscle activation patterns across the wrist and hand to meet this additional task requirement. In addition, we demonstrate that altered wrist musculoskeletal geometry changes the transformation between muscle activations and lateral pinch force (Fig. 4). Both simulation studies suggest new muscle control strategies must be learned following surgery. As a whole, our work highlights the complex, integrated biomechanics of the wrist and thumb.

REFERENCES

1. Crisco et al. *J Bone Joint Surg Am* 87(12): 2005.
2. Buffi et al. *J Biomech* 46(12): 2013.
3. Hollister et al. *Clin Orthop Relat Res* 320: 1995.
4. Valero-Cuevas et al. *J Biomech* 31(8): 1998.
5. Wohlman and Murray *J Biomech.* 46(5): 2013.
6. Sancho-Bru et al. *J Biomech Eng.* 125(1): 2003.
7. Mulford et al. *J Hand Surg. Eur.* 34(2): 2009.
8. Saul et al. *CMBBE*, 18(13): 2015.
9. Blankenhorn et al. *J Hand Surg. Am.* 32(1): 2007.
10. Nichols *PhD Thesis*, Northwestern University: 2014.
11. Delp et al. *IEEE Trans Biomed Eng* 54(11): 2007.

ACKNOWLEDGEMENTS

This work was funded by NIH F31 AG041627.

EFFECTS OF CARPAL TUNNEL SYNDROME ON FORCE COORDINATION AND MUSCLE COHERENCE DURING PRECISION PINCH

¹Szu-Ching Lu, ¹Kaihua Xiu, ¹Tamara L. Marquardt, ²Peter J. Evans, ²William H. Seitz Jr., ^{1,2,3}Zong-Ming Li

Hand Research Laboratory, Departments of ¹Biomedical Engineering, ²Orthopaedic Surgery, and ³Physical Medicine and Rehabilitation, Cleveland Clinic, Cleveland, OH, USA
email: liz4@ccf.org, web: <http://www.handlab.org>

INTRODUCTION

Carpal tunnel syndrome (CTS) is a common compression neuropathy of the upper extremity, caused by entrapment of the median nerve in the carpal tunnel. Deficient sensorimotor function associated with CTS may cause dyscoordination of digit forces and muscle activities in dexterous tasks. There has been report about unstable pinch forces in CTS patients [1], however, there is limited understanding of CTS effects on muscle activities during precision pinch. Coherence between two electromyography (EMG) signals can be used to quantify the coordination of muscle pairs. Specifically, muscle coherence in the 15-30 Hz range (β -band) has been shown to be associated with maintaining steady force output [2]. The purpose of this study was to investigate the effects of CTS on force coordination between digits and β -band coherence between intrinsic muscles during sustained precision pinch. In addition, wrist flexion (i.e. Phalen's maneuver) is commonly used to provoke CTS symptoms for diagnosis purpose. Therefore, a precision pinch task with varied wrist postures was implemented for investigation of force and muscle dyscoordination.

METHODS

Eight CTS patients (50.9 ± 10.8 years old) and eight asymptomatic controls (47.6 ± 14.9 years old) participated in this study. An apparatus consisting of two six-component force/torque transducers was developed to measure the digit forces. A surface EMG system was used to monitor the activities of the abductor pollicis brevis (APB) and first dorsal interosseous (FDI) muscles. Customized splints were used to stabilize the wrist in 30° extension, anatomical neutral, and 30° flexion (Fig. 1). First,

participants were instructed to maximally pinch the apparatus with the thumb and index finger, reaching their maximum force within 5 sec. Three maximum pinch trials were performed for each wrist posture. Then, the maximal pinch forces at each posture were averaged and 10% of the averaged maximal force was set as the target for the subsequent submaximal task. For the submaximal task, participants were asked to pinch the apparatus and match the target force for 15 sec according to graphical feedback. Ten submaximal trials were performed for each wrist posture. The three wrist postures were randomized and a 1-minute rest was given between trials. Force and EMG data were collected at a sampling rate of 1000 Hz. To avoid the non-stationary effects at the beginning of each submaximal trial, the data in the first 5-sec were excluded from analyses. A force difference index was determined as the magnitude difference between the resultant forces of the index finger and thumb normalized by target force. In addition, a force angle was calculated between the 3D force vectors of the two digits to quantify the directional opposition. Muscle coherence was computed as the cross-spectrum normalized with respect to the square root of the auto-spectra of the associated EMG signals, followed by a Fisher's Z-transformation. The average coherence in the β -band between the APB and FDI muscles was calculated.

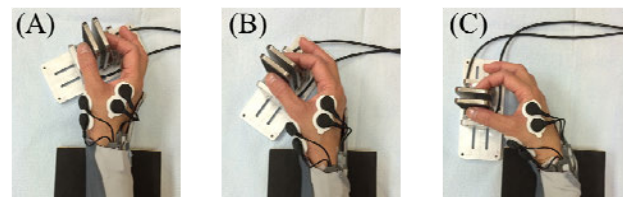


Figure 1: Experimental setup with the wrist in 30° extension (A), anatomical neutral (B), and 30° flexion (C).

Two-way repeated measures ANOVAs (one factor repeated) were performed to test the effects of group (CTS and control) and wrist posture (extension, neutral, and flexion) on force difference index, force angle, and muscle coherence. Post hoc Tukey's tests were performed for pairwise comparisons. The α level was set at 0.05.

RESULTS AND DISCUSSION

An interaction effect of group and posture was found on the force difference index ($p = 0.01$), although the main effect of group or posture was insignificant. Within the control group, there was a significantly higher value of force difference index in flexion than in extension (Fig. 2A). On average, the greatest group difference in the force difference index was found in wrist flexion (0.34 ± 0.23 for controls and 0.17 ± 0.29 for CTS patients). For the force angle, the difference between groups was on average greatest in wrist flexion (Fig. 2B), although the difference was not significant. In wrist flexion the control group had a force angle of $158.3 \pm 4.5^\circ$, whereas the CTS group had an angle of $164.8 \pm 6.2^\circ$. For the β -band coherence, the largest difference between groups was also found in wrist flexion (Fig. 2C). The control group had a coherence value of 0.14 ± 0.03 in wrist flexion while the CTS group had a value of 0.16 ± 0.03 ; however, the difference was not statistically different.

The wrist flexion posture at 30° employed in this study was relatively moderate in comparison to the clinically used wrist flexion for Phalen's test. We expect that a more flexed wrist flexion would allow us to observe a greater difference between groups. Furthermore, this preliminary study has a small sample size. Statistical power is expected to increase when more subject data are collected. Consistent with previous findings [1], the index finger generated more force than the thumb during submaximal pinch. In the control group, the force contribution of the index finger significantly increased in wrist flexion relative to extension, which may be due to more diminished thumb flexor function with flexed wrist [3]; however, the trend was not observed in the CTS group. Additionally, on average, the CTS group had a greater force angle (i.e. better opposition) than the control group. This

counterintuitive result may be attributable to thenar muscle weakness in CTS patients [4]. Weak thenar muscles decrease thumb abduction, making the thumb force vector orient more towards opposition. Furthermore, better opposition of the thumb and index finger may lead to less force difference between digits for the torque balance. Although thenar muscle weakness may result in greater digit force opposition during pinching on a stabilized object, this mechanism may not be practical for daily activities requiring high-level sensorimotor control. In the results of muscle coherence, on average, a higher value of β -band coherence was observed in CTS patients with their wrists in flexion. The modulation of muscle coherence has been associated with sensorimotor processing, which could be sensitive to changes in peripheral inputs [2]. It could be postulated that the increase in β -band coherence in CTS patients is a compensatory mechanism for flexion-induced exacerbation of symptoms.

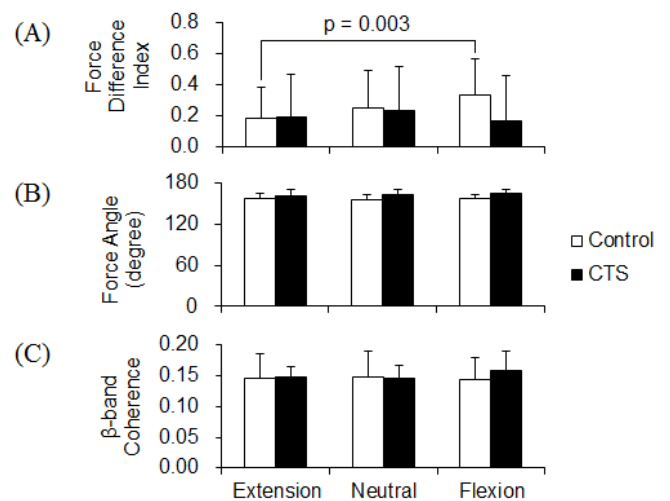


Figure 2: Force coordination (A and B) and muscle coherence (C) during submaximal precision pinch.

REFERENCES

1. Li K, et al. *Clin Neurophysiol* **126**, 194-201, 2015.
2. Kilner JM, et al. *J Neurophysiol* **92**, 790-796, 2004.
3. Harvey L, et al. *Clin Biomech* **25**, 194-198, 2010.
4. Pease WS, et al. *Am J Phys Med Rehabil* **67**, 117-119, 1988.

ACKNOWLEDGEMENTS

NIH/NIAMS R01AR056964

A MATHEMATICAL MODEL FOR MEASURING SCAPULAR MOTION

¹ Kristen Nicholson, ¹ Tyler Richardson, ¹ Elizabeth Rapp, ¹ Garry Quinton, ² Kert Anzilotti, and ¹ James Richards

¹ The University of Delaware, Newark, DE, USA

² Christiana Care Health Systems, Newark, DE, USA

email: kristent@udel.edu

INTRODUCTION

The goal of this study was to develop and validate a new clinically applicable approach to measuring scapulothoracic (ST) kinematics among typically developed individuals. Accurate assessment of ST kinematics is important for understanding functional limitations of the shoulder and upper extremity [1]. Current efforts to measure shoulder function often provide no differentiation between scapulothoracic and glenohumeral joint contributions to shoulder motion [2]. Techniques that attempt to quantify these measures are often inaccurate, invasive, time consuming, induce large amounts of radiation exposure, and/or require the subject to lie horizontally in an enclosed space. Traditional 3D motion capture has been used effectively to measure kinematics of bones that move with the skin, such as the humerus, but has failed to provide accurate estimates of scapular kinematics. We believe, however, that 3D motion capture data can be used in an innovative way to estimate scapular kinematics. Individualized mathematical algorithms that estimate dynamic scapular orientation based on measured humeral orientations and/or acromion process (AP) displacements were developed using motion capture data collected in multiple static poses. The mathematical algorithms were validated using a technique recently established by our lab that utilizes bone models and biplane fluoroscopy to perform a 2D to 3D matching process [3]. The algorithms provide a clinically useful tool for measuring ST kinematics that can be extended to patient populations.

METHODS

Individualized mathematical algorithms were developed for two subjects. Algorithm development is based on the principle that scapular orientation is

a function of humeral orientation and AP displacement. For any given humeral orientation and AP displacement, the scapular orientation is expected to be consistent, regardless of the path of motion used to reach that position. This approach also assumes that the scapula moves in a consistent manner throughout an individual's entire range of motion. Mathematical algorithms were created for each subject using motion capture data (Motion Analysis Corp, Santa Rosa, CA) from eleven static positions: neutral, abduction, hand to mouth, hand to neck, elevation, forward reach, extension, hand to spine, external rotation, internal rotation, and flexion. Equations to estimate scapular orientation from AP displacement data and humeral orientation were developed using two different approaches: multiple linear regression (LR) and artificial neural networks (NN). Humeral orientation was calculated as humerothoracic (HT) helical angles, i.e. the helical angle between the trunk and the humerus, and AP displacement was calculated as the displacement of the AP marker along the Y axis (inferior/superior) and the X axis (anterior/posterior) of the trunk. The predicted values were scapula orientation, calculated as ST helical angles, i.e. the helical angle between the trunk and the scapula. Helical angles are calculated as a theta angle and an XYZ vector. The theta and vector are then resolved into the X, Y, and Z components. Each individual has an equation to estimate the ST X component, an equation to estimate the ST Y component, and an equation to estimate the ST Z component. The LR algorithms and the NNs were applied to dynamic trials in which the individual moved continuously through the eleven positions listed above. The accuracy of the algorithms was determined by the correlations and average differences between the algorithms predicated ST angles and the validation ST angles.

RESULTS AND DISCUSSION

The ST X and ST Z angles estimated from the linear regression algorithms for subject 1 were highly correlated with the validation ST X and ST Z angles, while the ST Y angles were mildly correlated (Table 1). All three ST angles estimated from the linear regression algorithms for subject 2 were highly correlated with the validation ST angles. Subject 2's neural network estimated ST angles were all highly or mildly correlated with the validation ST angles (Table 1). Subject 1's ST Y neural network angles were poorly correlated with the validation angles, but the ST X and ST Z neural network angles were very highly correlated with the validation ST angles.

Table 1: Correlations

	LR X	LR Y	LR Z	NN X	NN Y	NN Z
Subj 1	0.93	0.54	0.90	0.90	*0.43	0.91
Subj 2	0.90	0.75	0.96	0.89	0.51	0.67

* $r < 0.5$ signifies a poor correlation

Clinical accuracy was determined with average differences presented in Table 2. All average differences were less than 10° for both subjects and both mathematical approaches. Figure 1 shows the actual ST motion about all three axes as compared to the ST motion estimated with LR and NN during the dynamic trials.

Although both mathematical approaches were able to estimate ST angles throughout the entire motion, the LR technique estimated ST angles that resulted in higher correlations and smaller average differences when compared to the validation angles. The LR technique is also easier to implement, making this method extremely clinically applicable.

Regional clinicians have expressed that errors less than 10° provide the accuracy needed to aid in reconstructive surgery decisions, outcome

assessments, and rehabilitation strategies. While the LR equations were not as highly correlated for the ST Y angles, the average differences for all axes were well below 10° . It takes less than thirty seconds of computing time to generate the three LR equations for one subject, and less than thirty minutes to collocate the necessary motion capture data, making the algorithm development a fast, non-invasive, and clinically accurate tool for determining dynamic scapular orientation. This new technique is expected to drive future work in musculoskeletal modeling, clinical trials, and basic research that will add further insight into impaired shoulder function.

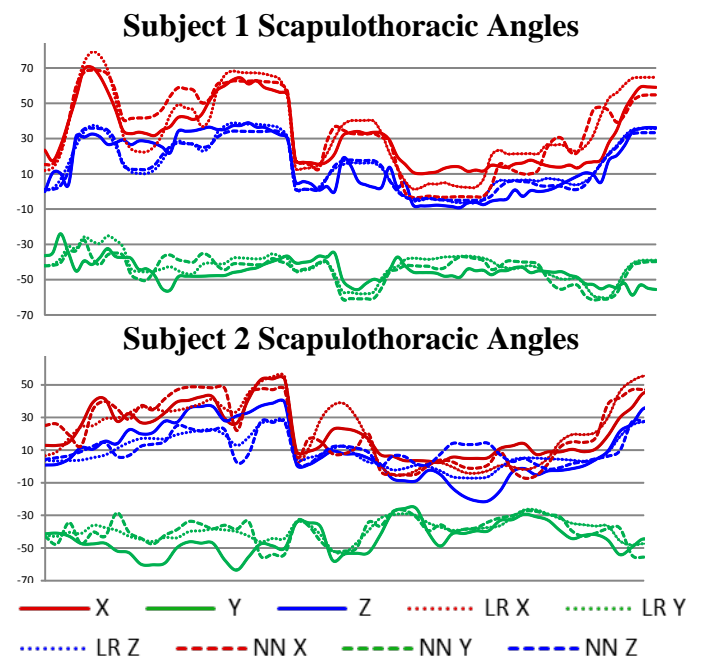


Figure 1: ST angles during dynamic trials compared to the validation standard ST angles.

REFERENCES

1. Bourne DA, et al. *Ann Biomed Eng* **39**, 777-85, 2004.
2. Lin J, et al. *Phys Ther* **86**, 1065-74, 2006.
3. Nicholson KF, et al. *GCMAS Annual Conference Proceedings*, 2013.

Table 2: Average difference (mean \pm standard deviation)

	LR X	LR Y	LR Z	NN X	NN Y	NN Z
Subject 1	$7.6^\circ \pm 4.6^\circ$	$6.1^\circ \pm 4.2^\circ$	$5.6^\circ \pm 4.5^\circ$	$7.9^\circ \pm 6.8^\circ$	$6.4^\circ \pm 4.4^\circ$	$5.4^\circ \pm 4.1^\circ$
Subject 2	$7.2^\circ \pm 4.8^\circ$	$6.5^\circ \pm 5.1^\circ$	$6.9^\circ \pm 4.7^\circ$	$7.7^\circ \pm 4.7^\circ$	$7.5^\circ \pm 6.5^\circ$	$9.3^\circ \pm 9.2^\circ$

QUANTIFYING KINEMATIC AND MUSCULAR ADAPTATIONS TO ROTATOR CUFF FATIGUE

Alison C. McDonald, Daanish M. Mulla and Peter J. Keir

Department of Kinesiology, McMaster University, Hamilton, ON, Canada, L8S 4K1
email: pjkeir@mcmaster.ca

INTRODUCTION

Work-related musculoskeletal disorders (MSDs) of the upper extremity are one of the most frequently reported workplace injuries in Ontario Canada [1]. The rotator cuff muscles of the shoulder are frequently injured in the workplace. These muscles are important in maintaining glenohumeral stability and function. These roles make it valuable to understand the implications of fatigue in this muscle group. Muscle fatigue during repetitive work can cause people to adopt kinematic and muscular strategies to continue working and maintain task performance [2]. These compensations can be adaptive to maintain task performance or maladaptive and increasing risk of injury. To understand these complex compensations during work tasks we must first understand how simple movements are impacted by muscle fatigue. The purpose of this study was to quantify kinematic and muscular compensations to rotator cuff muscle fatigue during simple glenohumeral motions.

METHODS

Male participants ($n=10$) completed 5 glenohumeral motions before (pre-fatigue) and after (post-fatigue) a fatigue protocol designed to target the internal and external rotators of the shoulder complex. The 5 glenohumeral motions were: (i) 120° sagittal plane elevation, (ii) 120° scapular plane elevation, (iii) 120° frontal plane elevation, (iv) cross-flexion/extension, (v) internal/external rotation. All exertions were performed while holding a 2 kg weight. Participants were given 10 seconds to complete each exertion and instructed to move at their own pace. The fatigue protocol consisted of a series of dynamic and isometric efforts completed in a cyclic manner using a dynamometer (Biodex System 4, Biodex Medical Systems, NY, USA). The dynamic efforts consisted of 10 concentric-concentric isokinetic exertions (60°/s, 15% MVC)

and the static efforts were 30 seconds of external rotation followed by 30 seconds of internal rotation (both at 45° external rotation, 25% MVC). The dynamometer constrained movement speed and torque level was maintained using visual feedback (Labview 8.2, National Instruments, Texas, USA). This cycle was continued until participants were unable to maintain the required 25% force output for 2 consecutive cycles or voluntarily ended the protocol. The 5 glenohumeral motions were repeated immediately following the fatigue protocol. To minimize order effects, the pre- and post-fatigue exertion orders were randomized.

Kinematic data were collected using an electromagnetic tracking system (Polhemus 3Space, Fastrak, Colchester, VT, USA). Scapular kinematics were measured using an electromagnetic sensor placed on the base of a custom scapular tracker [3]. A digitizing stylus was used to digitize bony landmarks. Muscle activity from 14 upper extremity, back and chest muscles were recorded using surface electromyography (Trigno™, Delsys, MA, USA). To quantify fatigue, submaximal static reference efforts and maximal internal-external rotation efforts (Series 5 Mark-10 force gauge) were performed before and immediately after the fatigue protocol.

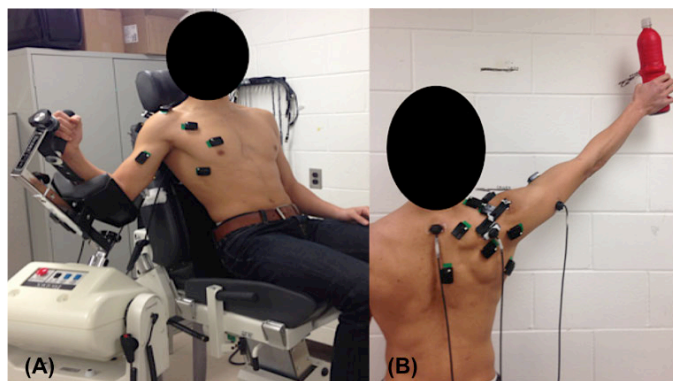


Figure 1. (A) Internal/external rotation fatigue protocol in Biodex dynamometer (B) Participant performing 120° of elevation in the frontal plane.

Joint angles for the humerus, thorax and scapula were calculated in accordance with ISB standards. EMG data were linear enveloped ($F_c=3$ Hz) and normalized to each muscle's maximum activation. Using the resultant humeral angular displacement, the EMG and kinematic data were cut to include the motion portion of each trial. Summary variables (mean, peak) were calculated for 3D joint angles and muscle activity. Time to peak angular displacement, velocity and acceleration were also included in the analysis. Multiple repeated measures ANOVA were used for the statistical analyses (SPSS 20.0, SPSS Inc., Chicago, IL, USA).

RESULTS AND DISCUSSION

Following the fatigue protocol, participants displayed signs of muscle fatigue ($>8\%$ decline in median power frequency between pre and post fatigue submaximal reference exertions) in 5/14 of the monitored muscles: infraspinatus, clavicular head of pectoralis major, triceps brachii, latissimus dorsi, and serratus anterior.

Specific muscle activity compensations following fatigue were dependent on the glenohumeral motion examined. After the fatigue protocol, participants used a combination of increased mean deltoid (anterior, middle and posterior), trapezius (middle, upper) and latissimus dorsi activity (all $p < 0.05$) to elevate the arm in the scapular plane.

Most participants displayed noticeable kinematic differences during the post-fatigue movements. Variability in the response between participants (Figure 2), make it challenging to fully capture these compensations using descriptive statistics. No significant kinematic changes were seen during elevation in the scapular plane. However, there was a slight reduction in trunk flexion in the frontal plane. During cross flexion, humeral, scapular and trunk joint angles were all affected by rotator cuff muscle fatigue ($p < 0.05$). Preliminary analyses suggest scapular adaptations may serve to increase the width of the subacromial space. These impingement sparing adaptations have also been observed during more complex work tasks [2].

Participants were able to utilize the kinematic and muscular flexibility afforded by the shoulder to perform glenohumeral motions following rotator cuff fatigue. Applying these compensations to more complex workplace tasks will give insight into expected strategies to repetitively perform these tasks.

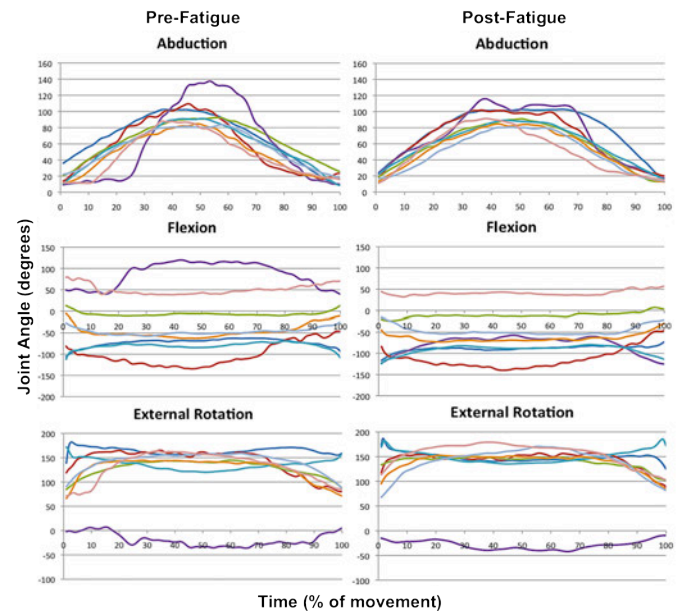


Figure 2: Humeral angles with respect to the thorax during a glenohumeral abduction-adduction movement (frontal plane) pre- and post-fatigue. Each line colour represents a different participant ($n=8$). The length of each trial is normalized to 100% of the motion.

REFERENCES

1. Workplace Safety & Insurance Board. (2013) Ontario, Canada.
2. McDonald A.C., Tse C.T.F., & Keir P.J. (2014) International Shoulder Group Conference
3. Karduna A.R., McClure P.W., Michener L.A. & Sennett, B. (2001). *J Biomech Eng* 123: 184-190

ACKNOWLEDGEMENTS

This study was supported by funding from the Natural Sciences and Engineering Research Council Discovery Grant # 217382-09 and Automotive Partnership Canada (APC).

IDENTIFICATION OF MULTIDIMENSIONAL SHOULDER IMPEDANCE WITH PASSIVE AND ACTIVE MUSCLES

^{1,2}David B. Lipps, ^{1,2}Emma M. Baillargeon, ^{1,2}Daniel Ludvig, and ^{1,2}Eric J. Perreault

¹Northwestern University, Evanston, IL, USA

²Rehabilitation Institute of Chicago, Chicago, IL USA

email: dlipps@ricres.org

INTRODUCTION

The shoulder is stabilized by passive structures and active muscle forces. The interaction between these factors is critical for normal joint function and the evaluation of shoulder pathologies. The objective of this study was to investigate how passive structures and active muscle forces regulate three-dimensional (3D) joint mechanics during volitional contractions. We quantified impedance of the shoulder in three clinically relevant planes of motion to reliably assess multidimensional joint function. We hypothesized that the coupling of joint impedance between different planes of motion of the shoulder would be significant and enhanced with muscle activation. This work may provide a novel approach for quantifying the 3D mechanics of the human shoulder, and ultimately for tracking altered mechanics following injury or rehabilitation.

METHODS

The right shoulder of four male subjects (mean age: 35 yrs, weight: 71 kg, height: 176 cm) with no history of shoulder injury was placed in a removable cast and attached to a high-precision rotary motor with an encoder and six-degree of freedom load cell. Subjects were perturbed in one of three planes of motion in a random order, while the resultant torques were measured in all three degrees of freedom (Fig. 1). Our measurement coordinate system was aligned with established biomechanical guidelines [1]. Subjects were asked to maintain a constant shoulder torque during 60-second experimental trials. In each perturbation direction, measurements were acquired as subjects maintained a net torque level scaled to $\pm 10\%$ of their maximum voluntary contraction (MVC) in each of the three torque directions. Measurements were also made in the passive condition. Two trials were performed in each of the seven testing conditions and three perturbation directions, yielding 42 trials.

Joint impedance, the dynamic relationship describing the torque response to an imposed change in joint angle, was estimated using small, stochastic perturbations. Model structure was determined with nonparametric identification; these estimates were then approximated by a 2nd order linear system with inertial, viscous and elastic parameters [2]. The current study focused on the elastic parameter, otherwise known as stiffness. For each perturbation and torque direction, stiffness was represented as 3 x 3 matrix, where the diagonal terms are the direct response and the off-diagonal terms are the coupled response to a perturbation of posture. A bootstrapping procedure was used to estimate the mean and confidence intervals for the stiffness matrices for the different experimental conditions for each subject. These matrices were represented as 3D stiffness ellipsoids. Descriptions of these ellipsoids (size, shape, and orientation) were adapted from prior work [3].

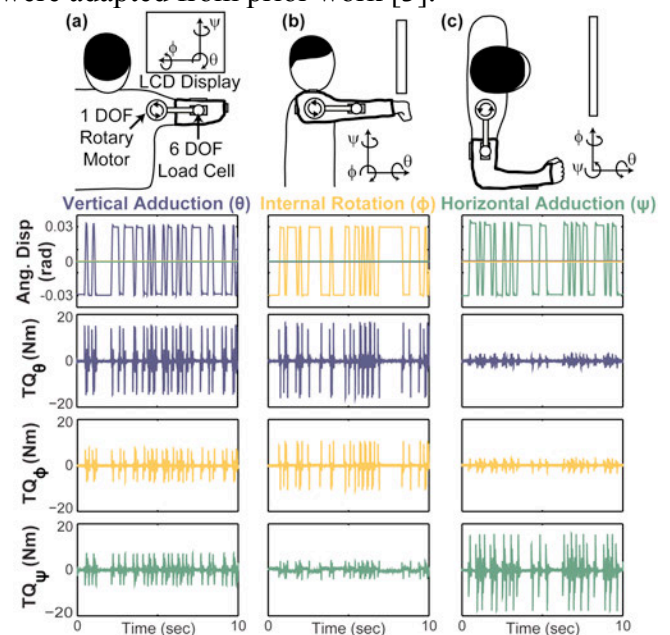


Figure 1. A single-axis rotary motor perturbed the shoulder in one of three orthogonal directions (a)–(c). Visual feedback assisted subjects in matching the desired target. The coordinate system is also shown. Exemplar passive trials show the resultant 3D torque response to the imposed perturbation is shown below each illustration.

RESULTS AND DISCUSSION

Stiffness ellipsoids for a typical subject are shown in Figure 2, which graphically depict the directions where the shoulder is most resistant to external perturbations of posture. Muscle activation increased stiffness, as demonstrated by the larger size of the active ellipsoids when compared to the passive ellipsoid. The norm of the stiffness matrix eigenvalues is indicative of the greater shoulder stiffness across subjects with volitional activation (Table 1). Shoulder stiffness was highly anisotropic, or stiffer in certain direction than others. Shape, or the ratio of the matrix eigenvalues, is indicative of this anisotropy. Ratios equal to one are indicative of isotropic stiffness, but these ratios were less than one across subjects (Table 1).

The stiffness ellipsoids provide insights into the coupling between different degrees of freedom of the shoulder. The production of a net torque in a given direction should orient the stiffness ellipsoid along the orthogonal axis of torque generation if no stiffness coupling was present. The ellipsoids in Figure 2 indicate stiffness coupling is present. Passive shoulder stiffness was orientated away from the orthogonal shoulder axes, as the relative angle

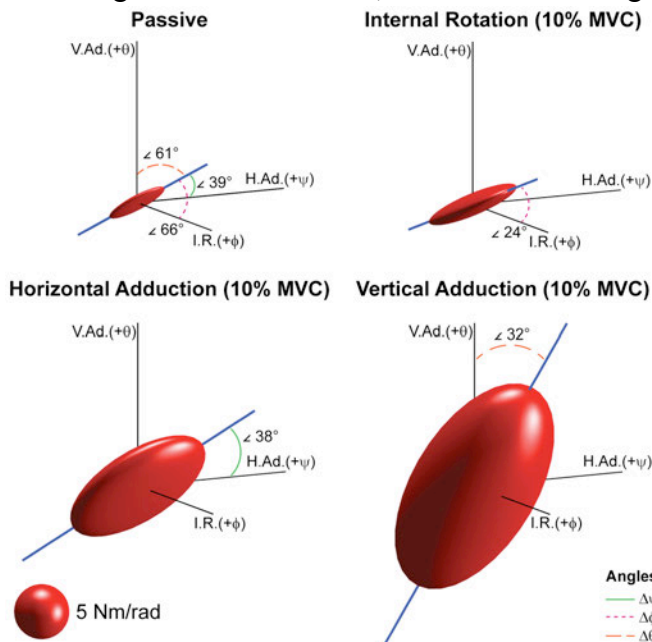


Figure 2. 3-D stiffness ellipsoids under passive and active conditions for a representative subject. Stiffness ellipsoids representing passive and net torques of 10% MVC in internal rotation, horizontal adduction, and vertical adduction are shown. The principal axis of each ellipsoid is shown as a blue line projecting out of the ellipsoid. The relative angle between the principal axis and the orthogonal shoulder axes are labeled. To highlight the anisotropy of these ellipsoids, a scale drawing of a 5 Nm/rad isotropic ellipsoid is depicted on the bottom.

between the principal axis of the passive stiffness ellipsoid and the closest orthogonal shoulder axis was $30.5 \pm 8.1^\circ$. The direction of torque production altered the degree of coupling as well, as the stiffness ellipsoids were aligned closest to the axis of torque generation (Table 1).

There is a pertinent clinical need to better prevent, diagnose and treat shoulder injuries. The current study shows the utility of quantitative impedance methods in estimating the 3D mechanics of the healthy shoulder. The anisotropy of shoulder stiffness indicates certain directions are less resistant to external perturbations, and therefore may be more prone to injury. The observed stiffness coupling within the shoulder is indicative of underlying neuromuscular mechanisms. These methods will enable future work to compare how coupling differs for different shoulder pathologies.

CONCLUSIONS

The shoulder muscles provide significant mechanical coupling between different degrees of freedom, and may offer a more complete description of healthy joint mechanics.

REFERENCES

- [1] Wu G, et al. *J Biomech* **38**, 981-992, 2005.
- [2] Perreault EJ, et al. *Exp Brain Res* **141**, 312-323, 2001.
- [3] Krutky MA, et al. *J Neurophysiol* **109**, 1045-1054, 2013.

ACKNOWLEDGEMENTS

Funding: NIH T32-HD07418 and R01-NS053813.

Table 1: Mean (± 1 S.D.) size, orientation and shape of shoulder stiffness ellipsoid across subjects.

Condition	Norm ($\lambda_1 \lambda_2 \lambda_3$)	Rel. Angle (deg)	Int/Maj	Min/Maj
0%	56 \pm 25		0.76 \pm 0.13	0.33 \pm 0.14
10% V.Ad	752 \pm 310	29 \pm 3	0.60 \pm 0.18	0.43 \pm 0.07
-10% V.Ad	1132 \pm 208	34 \pm 23	0.53 \pm 0.14	0.24 \pm 0.06
10% I.R.	240 \pm 97	44 \pm 17	0.69 \pm 0.19	0.38 \pm 0.15
-10% I.R.	358 \pm 158	34 \pm 17	0.65 \pm 0.10	0.33 \pm 0.08
10% H.Ad	368 \pm 99	27 \pm 19	0.69 \pm 0.07	0.31 \pm 0.04
-10% H.Ad	553 \pm 322	40 \pm 20	0.64 \pm 0.08	0.28 \pm 0.07

Abbreviations: Torques were scaled to MVCs generated in vertical adduction (V.Ad), internal rotation (I.R.), and horizontal adduction (H.Ad). The size of the ellipsoids is the norm of the eigenvalues. Orientation is the relative angle between the principal axis and the axis of torque generation. Shape is the ratio of the intermediate (Int) or minor (Min) eigenvalues relative to the major (Maj) eigenvalue.

LOADING PATTERNS VARY BY DIRECTION, FOOTWEAR, AND FOOT-STRIKE IN RUNNING

Andrew D. Nordin and Janet S. Dufek

University of Nevada, Las Vegas, Las Vegas, NV, USA
email: nordina@unlv.nevada.edu

INTRODUCTION

Foot-strike pattern manipulations in running have previously identified alterations in three-dimensional (3D) loading rates, with potential implications for understanding injury mechanisms [1,2]. The use of minimalist footwear has also been promoted as a means of reducing running injuries, ostensibly mimicking barefoot running and facilitating foot-strike changes [3]. Comprehensive analysis of 3D loading patterns across footwear and foot-strike manipulations may therefore provide insight into interactions among these factors.

The purpose of this investigation was to examine 3D loading patterns following footwear and foot-strike manipulations in over-ground running. Inter-axis loading pattern changes were hypothesized in contrasting footwear and foot-strike conditions.

METHODS

Twenty volunteers free of lower extremity injuries (9M, 11F, age: 25.3 ± 3.6 y, mass: 73.2 ± 13.7 kg, height: 1.68 ± 0.09 m) provided institutionally approved informed consent prior to participation. Subjects completed 15 over-ground running trials (14 analyzed) in each of 6 experimental conditions, including 3 foot-strike (forefoot, mid-foot, rear-foot strike; FFS, MFS, RFS, respectively) and 2 footwear conditions (neutral cushioned [New Balance ® 680V2] & minimalist [New Balance ® Minimus Hi-Rez]).

Prior to over-ground running trials, a treadmill warm-up was completed using each subject's natural foot-strike pattern (self reported and visually identified: 50% RFS & 50% MFS/FFS among subjects). Approximately 5-minute accommodation periods were provided in each footwear type, simultaneously obtaining preferred running speed.

Over-ground running trials were carried out on a 20m runway, controlling running speed via timing gaits ($\pm 5\%$ preferred speed; Lafayette Model 63501IR). Instructional videos and practice trials were provided before blocked foot-strike and footwear conditions. Condition order was counterbalanced.

Kinetic data were collected during the stance phase of the right limb using a force platform (Kister Type 9281CA; 2000Hz; GRFz > 20N), with synchronized kinematic data collected via 10-camera motion capture system (Vicon Plugin-Gait; MX-T40S; 200Hz) and sagittal reference video of the foot at ground contact (Basler piA640-210gc; 50Hz). Kinematic analyses were limited to foot segment angle at ground contact and point of foot contact from sagittal video as means of corroborating foot-strike patterns. Kinematic and kinetic data were low-pass filtered (15 & 50Hz cutoffs, respectively). GRFz data were normalized to bodyweight (BW), with loading rate-time profiles computed independently for X, Y, & Z axes using first central difference differentiation (BW/s).

Loading patterns were assessed using principal component analysis (PCA) on the 3D loading rate-time series in each axis, footwear and foot-strike condition. Prior to performing PCA, each time series was temporally normalized to 101 data points using cubic spline interpolation. Loading rate time series variables were converted to z-scores in each axis (X, Y, Z), subtracting the mean and normalizing to the standard deviation of each subject's condition. PCA was then performed on a 5040x101 dimension matrix (20 subjects x 14 trials x 3 axes x 3 foot-strike x 2 footwear). PCs exceeding 10% explained variance were interpreted. Inferential testing was carried out on PC scores after computing the mean from each participant.

Separate 3-way repeated measures factorial ANOVAs (3x3x2; axis x foot-strike x footwear) were conducted for each PC, testing differences among loading patterns observed in each axis, foot-strike, and footwear condition. Follow-up factorial and one-way repeated measures ANOVAs, along with pairwise comparisons, were carried out as necessary. Degrees of freedom were adjusted with Huynh-Feldt corrections, with Bonferroni adjusted pairwise comparisons ($\alpha=0.05$). Differences among foot segment angle at ground contact in each desired foot-strike pattern were tested via one-way repeated measures ANOVA.

RESULTS AND DISCUSSION

Foot segment angle at contact differed among desired foot-strike patterns (FFS: $-12.0 \pm 7.1^\circ$, MFS: $2.5 \pm 10.8^\circ$, RFS: $20.3 \pm 5.3^\circ$; $F[2,38]=122.0$, $p<.001$, $\eta^2=.87$; pairwise comparisons: $p<.001$), verifying the distinction among foot-strike conditions.

Two PCs were extracted (PC1: 42.5% & PC2: 22.8% explained variance). From visual inspection, PC1 captured a source of variation characteristic of loading rate-time curves lacking an observable GRF impact peak during braking [1,2]. In contrast, PC2 captured a source of variation characteristic of loading rate-time curves demonstrating a GRF impact peak during braking [1,2]. The interaction among axis, footwear and foot-strike was significant in each PC (PC1: $F[2.1,40.1]=5.6$, $p=.007$, $\eta^2=.23$; PC2: $F[2.0,38.4]=62.3$, $p<.001$, $\eta^2=.77$).

PC1 scores were interpreted in the context of impact attenuation, differing by axis, footwear, and foot-strike pattern. In each footwear condition, vertical PC1 scores during FFS exceeded MFS and RFS ($p \leq .016$), indicating FFS impact attenuation. Vertical impact attenuation in cushioned RFS exceeded minimalist RFS ($p<.001$). In each footwear condition, anterior-posterior PC1 scores differed by foot-strike (RFS>MFS>FFS, $p<.001$), highlighting anterior-posterior impact attenuation in RFS. Anterior-posterior impact attenuation in minimalist FFS exceeded cushioned FFS ($p<.001$), while cushioned RFS impact attenuation exceeded minimalist RFS ($p=.013$). In each case, vertical PC1 scores exceeded anterior-posterior and medial-

lateral ($p<.001$), demonstrating lesser sensitivity to vertical impact features [2].

PC2 scores were interpreted relative to impact characteristics typically observed during braking in 3D loading rate-time series [1,2]. Greater vertical PC2 scores were observed in minimalist RFS, relative to minimalist FFS and MFS ($p<.001$), indicating greater impact characteristics in minimalist RFS. Cushioned FFS demonstrated greater impact characteristics relative to minimalist FFS ($p<.001$). In each footwear condition, anterior-posterior PC2 scores differed by foot-strike (FFS>MFS>RFS, $p \leq .003$), indicating greater anterior-posterior impact characteristics in FFS and MFS. Anterior-posterior impact characteristics in cushioned FFS exceeded minimalist FFS ($p<.001$). Medial-lateral impact characteristics were lesser in RFS, relative to FFS and MFS in both cushioned and minimalist shoes ($p<.001$). Medial-lateral impact characteristics for cushioned shoes exceeded minimalist for both FFS and RFS ($p \leq .002$).

CONCLUSIONS

Assessment of the loading rate-time series via PCA allowed distinct impact features to be identified, highlighting inter-axis changes among footwear and foot-strike conditions. Cushioned footwear provided vertical impact attenuation in RFS running, though minimalist footwear demonstrated anterior-posterior and medial-lateral impact attenuation relative to cushioned FFS running. The selection of appropriate footwear is therefore likely dependent on foot-strike pattern. Changes in foot-strike, however, alter impact-loading direction, which likely requires time for adaptation following interactive footwear and foot-strike adjustments.

REFERENCES

1. Boyer ER, et al. *MSSE*, **46**(7), 1384-1391, 2014.
2. Nordin AD, et al. *ICRS*, Aug. 2014, Calgary, CA.
3. Trudeau MB et al., *MSSE*, ePub ahead of print.

ACKNOWLEDGEMENTS

Footwear was provided from a New Balance ® Production Footwear Research Award.

THE IMMEDIATE EFFECTS OF FOOTSTRIKE LOUDNESS FEEDBACK IN REDUCING IMPACT LOADING IN RUNNERS

¹ Jeremiah J. Tate, ² Clare E. Milner

¹ The University of Tennessee at Chattanooga, Chattanooga, TN, USA

² Drexel University, Philadelphia, PA, USA

email: Jeremiah-Tate@utc.edu

INTRODUCTION

Past studies have investigated the use of gait retraining programs aimed at reducing impact loading in runner at risk of tibial stress fractures. In one study, Crowell and Davis [1] attached a hardwired accelerometer to runner's legs to provide them with visual feedback of the tibia shock associated with impact. Runners were also instructed to "run softer" and "make their footfalls quieter". Runners successfully demonstrated a significant reduction in impact forces and tibial shock after 2 weeks of training and 1 month later. One limitation to this method of gait retraining is the cost of the equipment and technical training required to provide the accelerometer feedback.

Verbal instructions related to the sound of impact have been implemented successfully in the retraining of other motor activities, such as jump landings [2]. Recent advances in technology have provided researchers with mobile devices (eg, smart phones and tablets) that are capable of providing objective feedback (eg, decibel levels) via built in microphones. It remains unknown if a simple verbal instruction and external feedback of the loudness of a runner's impact could result in meaningful reductions in impact forces during running. Therefore, the aim of this study was to assess the immediate effects of verbal instructions with and without decibel meter feedback during running on key variables associated with tibial stress fractures [3].

METHODS

A total of 19 recreational runners participated in this study. Participants either received verbal instructions only (VO) or verbal instruction plus decibel meter feedback (V+DM) (Table 1). Each

participant met the following criteria: 1) currently running at least 6 miles/week; 2) rearfoot striker; 3) familiar with treadmill running; 4) no known hearing problems; and 5) free of any current lower extremity injuries. The study was approved by the university's IRB and informed consent was obtained from each participant.

Table 1: Mean (SD) for group demographics.

	VO group n=8; 2F/6M	V+DM group n=11; 9F/2M
Age, yr	20.4 (2.1)	24.0 (2.0)
Height, m	1.67 (0.8)	1.74 (0.07)
Weight, kg	59.2 (7.5)	66.9 (9.6)
Running speed, m*s ⁻¹	2.98 (0.32)	2.93 (0.25)

Participants first performed a 5-minute run on a treadmill to serve as a warm-up and establish their self-selected running speed. Baseline data collection was then performed for over-ground running. Participants ran along a 10m runway landing with the right foot on a 40 X 60cm force plate (sampled at 1200Hz) centered along the runway. Each participant performed 5 good trials at their self-selected running speed. After baseline data collection, participants underwent gait retraining on the treadmill. Participants in the VO group were instructed to "run as quietly as possible". Participants in the V+DM group received continuous decibel meter feedback provided visually via an iPad application (SPLnFFT Sound Meter, version 5.2) and were instructed "to decrease the decibel level as much as possible while trying to run as quietly as possible". Each participant performed the gait retraining for 15 minutes at his or her self-selected speed. After gait retraining, participants performed 5 more acceptable trials of over-ground running at their previously determined speed. Participants were reminded to use the same

running strategy he or she used during gait retraining.

Kinetic variables of interest were identified using a custom LabVIEW program. An independent t-test determined whether there were group differences in running speed. Mixed-model ANOVAs were used to analyze differences in the following variables at baseline and after gait retraining: vertical impact peak (VIP), vertical instantaneous loading rate (VILR), vertical average loading rate (VALR), and vertical propulsion peak (VPP).

RESULTS AND DISCUSSION

No group difference was demonstrated in self-selected running speed. Each mixed-model ANOVA revealed a significant main effect for time for VIP, VILR, and VALR indicating a decrease in magnitude as a result of gait retraining (Table 2). The main effect for group was not statistically significant for VIP, VILR, or VALR. A trend ($P=0.07$) for VIP interaction effect indicated a greater decrease in the V+DM group compared to the VO group. Percent changes in VIP, VILR, and VALR for the VO group ranged from 10-22%, while percent changes in the same variables for the V+DM ranged from 30-38%. There were no significant main effects or interactions for VPP.

Gait retraining consisting of verbal instructions with and without decibel meter feedback resulted in clinically meaningful changes in variables associated with tibia stress fractures. Based on the percent changes, it appears that the addition of the decibel meter feedback resulted in a greater reduction in vertical impact peaks and vertical loading rates.

Verbal instructions with decibel meter feedback provided via portable devices that many people own may provide clinicians with a simple way to provide gait retraining to runners at risk of tibial stress fracture. It remains unknown if the immediate reductions demonstrated in this study would become permanent. Further research is needed to demonstrate if permanent change (ie, motor learning) would occur with additional training. Further research is also warranted to compare the magnitude of reductions in loading achieved with this method of gait retraining to comparable methods (eg, cadence modification).

REFERENCES

1. Crowell HP and Davis IS. *Clin Biomech* **26**, 78-83, 2011.
2. Prapavessis H, et al. *J Orthop Sports Phys Ther* **38**, 204-207, 2003.
3. Milner CE, et al. *Med Sci Sports Exerc*, **38**, 223-328, 2006.

Table 2: Means (SD) for variables of interest in both groups at baseline and after gait retraining.

Variable	Baseline	After Gait Retraining
Vertical impact peak (BW)		
VO group	1.51 (0.25)	1.36 (0.15)*
V+DM group	1.58 (0.30)	1.11 (0.37)*
Vertical instantaneous loading rate (BW*s⁻¹)		
VO group	100.54 (24.90)	64.65 (22.89)*
V+DM group	85.68 (26.60)	67.49 (16.94)*
Vertical average loading rate (BW*s⁻¹)		
VO group	86.35 (22.57)	53.80 (18.87)*
V+DM group	74.36 (22.78)	58.80 (16.27)*
Vertical propulsion peak (BW)		
VO group	2.43 (0.15)	2.37 (0.23)
V+DM group	2.30 (0.11)	2.30 (0.20)

Abbreviations: BW, % body weight; VO, verbal instruction only; V+DM, verbal instruction plus decibel meter feedback.

*significant main effect for time ($p<0.05$)

THE EFFECT OF HIGHLY CUSHIONED SHOES ON TIBIAL ACCELERATION IN RUNNERS

¹ Matthew C Ruder, ¹ Phattarapon Atimetin, ^{1,2} Steve T Jamison, and ¹ Irene Davis

¹ Spaulding National Running Center, PM & R, Harvard Medical School, Cambridge, MA, USA.

² University of Delaware, Newark, DE, USA

INTRODUCTION

In stark contrast to the recent trend of minimalist running shoes, highly cushioned shoes have begun to emerge on the running shoe market. These types of shoes have noticeably thicker midsoles, with up to 2.5 times more cushioning than standard running shoes. Manufacturers claim their designs offer more shock attenuation upon impact, thereby reducing injury risk as (Fig. 1a). [1] It has been documented that vertical impact loading and loading rates have been linked to injuries in runners. [2,3] We have previously reported higher vertical ground reaction force loading rates in runners while wearing highly cushioned shoes compared to standard neutral shoes. [4] Ground reaction forces are measured at the shoe-ground interface and may not directly reflect what the leg is experiencing. Therefore, we sought to examine the effect of the additional cushioning on distal tibial accelerations. Based on our previous findings [4], we expected that tibial accelerations would be higher when running in the highly cushioned shoes.



Figure 1: Medial right foot in A) high-cushioned and B) standard shoes. C) Accelerometer coordinate system.

METHODS

7 healthy male runners (age = 32.9 ± 12.3 years, height = 1.767 ± 0.040 m, weight = 72.58 ± 12.75 kg) have been recruited, to date, in this ongoing study. All participants had to run at least 10 miles per week in standard running shoes. Prior to data collection, tri-axial accelerometers (IMeasureU, Auckland, NZ) were strapped around the ankles bilaterally. The accelerometer was affixed tightly to the distal medial tibia such that the vertical axis was aligned with the long axis of the tibia (Fig. 1c). A single marker was placed on the lateral aspect of the

right foot in order to match the foot to the correct ground reaction force data. Following a 3-minute warm-up period, subjects ran on an instrumented treadmill (AMTI, Watertown, MA) in a standard neutral shoe (SNS; Nike Air Pegasus) at a self-selected speed (mean: 2.61 m/s) and 20 consecutive footstrikes were collected. The process was then repeated in the highly cushioned shoes. (HCS; Hoka One One, Stinson). An 8-camera motion capture system (Vicon, Oxford, UK) recorded both the force (1500 Hz) and marker (250 Hz) data. Acceleration data was collected at 1000 Hz using a trigger from Vicon to start and stop collection.

To ensure accelerometers were on the tibia, they were placed slightly anterior (Fig 1c). This results in the accelerometer's AP and ML axes only being in the vicinity of tibial anatomical AP and ML axes, respectively. Because the accelerometer and anatomical axes are not aligned, results will be reported in the coordinate system of the accelerometer (Acc). The longitudinal axis of the tibia and the vertical axis of the accelerometer (VAcc) were better aligned.

Variables of interest were the peak tibial accelerations in the vertical (VAcc), medial (MAcc), lateral (LAcc) and posterior (PAcc) directions, as well as the resultant acceleration (RAcc). The vertical average loading rates (VALR) was also assessed.

Due to the preliminary nature of these data, only descriptive statistics are being presented. This includes the comparison of means (sd) and percent differences across groups as well as a scatterplot relating VAcc with VALR. A more robust analysis will be performed once the study is complete.

RESULTS AND DISCUSSION

The acceleration data for two of the subjects exceeded the maximum range of the accelerometer (16G) thereby clipping the signal. One subject exceeded this in both their neutral and highly

cushioned shoe conditions, the other in just their highly cushioned shoe condition. Therefore, these two subjects were excluded, leaving 5 subjects for analysis. The three components of the tibial acceleration from a representative participant are seen in Figure 2. The vertical component is the largest, followed by the anterior, then medial.

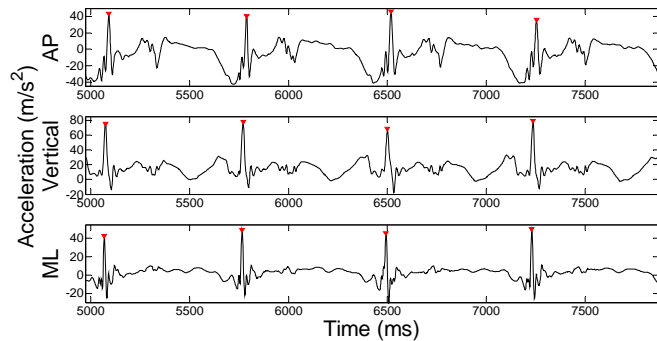


Figure 2: Representative acceleration signals in the vertical, mediolateral and anteroposterior directions.

All acceleration variables were greater in the HCS on average (Fig. 3). Variables ranged between 8.1 and 24.3% higher in the HCS.

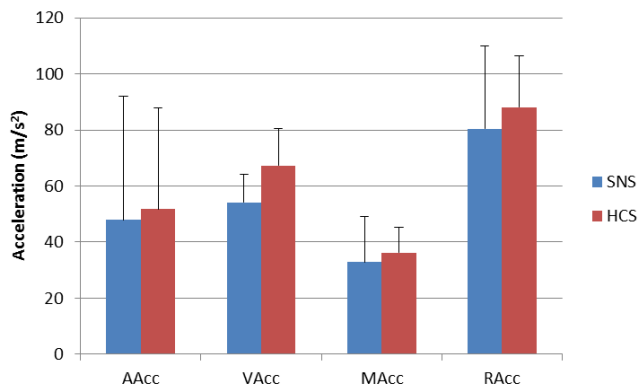


Figure 3: Comparison of peak tibial accelerations in the SNS and HCS.

It might be argued that the additional cushioning in the highly cushioned shoes should reduce the shock experienced by the lower extremity. However, it has been shown that individuals tend to stiffen their leg when landing on soft surfaces [5]. A stiffer leg during landing is not likely to attenuate shock as well as a compliant one. This will result in greater shock experienced by the leg.

The association between the VAcc and the VALR can be seen in Figure 4. While these data are preliminary, this plot suggests there may be a moderate relationship between these variables. If this is confirmed with additional data, measurement

of VAcc may be a good surrogate for VALR. This can be extremely useful in the clinic when a force plate is not available or when monitoring of vertical loading during running in the community is desired.

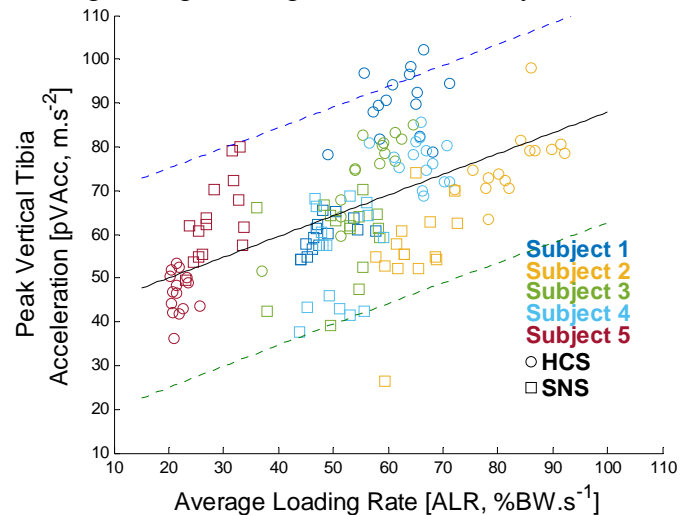


Figure 4: Correlation between peak VAcc and Vertical Average Loading rate with confidence intervals.

Because kinematics were not yet available for this investigation, it is not known how gait patterns differ between the two conditions. It is also important to note that the subjects in this study were not habituated to running in highly cushioned shoes. Therefore, these results may not represent those of runners who are habituated to this footwear. We are currently collecting data on these runners as well.

CONCLUSIONS

These preliminary results suggest that running in highly cushioned running shoes results in increased tibial shock compared with a standard neutral shoe.

REFERENCES

1. "Technology." HOKA ONE ONE Running. Accessed March 10, 2015. <http://www.hokaoneone.com/technology.html>.
2. Milner CE, et al. *MSSE* **38**, 323-328, 2006.
3. Butler RJ, et al. *Clin Biomech* **18**, 511-517, 2003.
4. Ruder MR. *ACSM '15*, San Diego, CA, 2015.
5. Ferris, DP et al. *Proceedings of the Royal Society of London: Biological Sciences*, 265:989-9

SUBJECT-SPECIFIC TIBIAL STRESSES DURING SHOD AND BAREFOOT RUNNING

¹ Elizabeth R. Boyer and ¹ Tim R. Derrick

¹ Iowa State University, Ames, IA, USA

email: ehageman@iastate.edu, web: <http://www.kin.hs.iastate.edu/>

INTRODUCTION

Our purpose was to compare distal tibia bone stresses in habitual rearfoot strikers (hRF) and habitual mid/forefoot strikers (hFF) during 1) shod rearfoot striking (RF), 2) shod mid/forefoot striking (M/FF), and 3) barefoot M/FF (BF). The secondary purpose was to see if these stresses decrease with an 8% shorter stride length.

METHODS

Recreational/competitive runners age 18-35 were recruited (Table 1). Participants ran overground at 3.5 m/s ($\pm 3\%$). Preferred stride length (PSL) was determined while participants ran on the treadmill at 3.5 m/s. They then performed 6 overground conditions: 1) shod RF at PSL, 2) shod M/FF at PSL, 3) BF at PSL, 4) shod RF at -8% PSL, 5) shod M/FF at -8% PSL, 6) BF at -8% PSL. Force platform data were collected at 1000 Hz and marker positions at 200 Hz.

A 2-mm thickness CT scan was obtained for each participant's right leg 1/3 of the way from the ankle to the knee. This location was chosen because it is a common site for stress fractures [1]. Based on the relationship between the Hounsfield scale and apparent bone density, the elastic modulus of all elements was determined from the CT image. Joint reaction forces and moments were combined with muscle forces (estimated using static optimization) to calculate joint contact forces. Forces and moments acting at the level of the CT scan were estimated and used as inputs to a finite element mesh to estimate bone stresses [2]. Peak compressive (C), tensile (T), and shear (S) stresses during stance phase were the dependent variables.

Data were analyzed with a repeated measures MANOVA ($2 \times 3 \times 2$) (group \times run style \times SL). Significance was assessed at $\alpha < 0.05$.

RESULTS AND DISCUSSION

Five hRF and 6 hFF have completed the study. Groups did not significantly differ based on age, height, mass, BMI, or weekly mileage (all $p > 0.37$).

The three-way interaction was not significant ($p = 0.252$), nor was group \times SL ($p = 0.225$), SL \times run style (0.419), or group \times run style ($p = 0.389$). There was not a main effect for group ($p = 0.295$), and SL bordered on significance ($p = 0.089$). Run style was significant ($p = 0.002$). Data are shown in Figure 1 and Table 2.

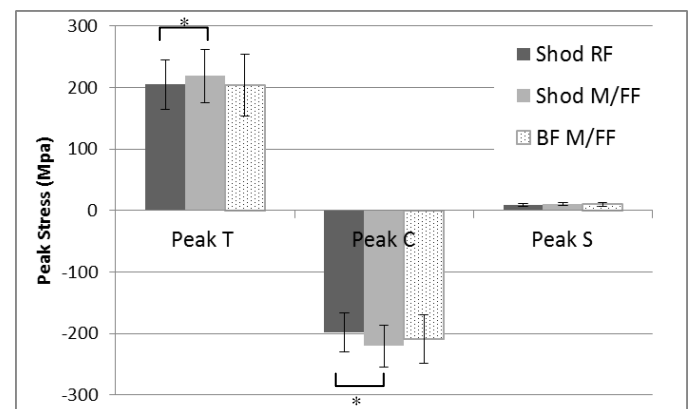


Figure 1. Peak stresses for the PSL condition. Significant differences are indicated by the *.

Both peak C and T stresses were larger for the shod M/FF condition relative to RF, but not different for the other pairwise comparisons. Our data agree with the trends previously observed [3].

The highest C stress consistently occurred in the posteromedial quadrant, which agrees with the location stress fractures most commonly occur in

runners [1]. Tensile stresses were highest in the anterolateral quadrant.

The greater work performed by the plantarflexors during M/FF and BF likely resulted in the greater tibial stresses at the cross-section of interest. Like Altman and Davis [3] hypothesized, perhaps shod M/FF compressive stress was larger than BF because a larger plantarflexion angle is needed to accommodate the shoe midsole. Interestingly, peak plantarflexion moment was greatest for BF (RF: -0.271 ± 0.25 , M/FF: -0.322 ± 0.28 , BF: -0.333 ± 0.32 BW*m), but that did not equate to the largest stresses. Perhaps the larger vertical knee reaction forces for M/FF v. BF (2.09 ± 0.17 v. 2.04 ± 0.14 BW, $p=0.034$) partially explains the differences.

It has been suggested that decreased loads during BF running are primarily due to a shorter SL [4]. Since we controlled for SL, the differences observed in tibial stresses seem to be due to foot strike/footwear. An 8% shorter SL did not significantly decrease peak compressive stress (1.4%, $p=0.305$) but decreased peak tensile stress $\sim 2.1\%$ ($p=0.062$) and peak shear stress $\sim 7.0\%$ ($p=0.015$) across the 3 running styles. While these decreases seem small, because of the exponential association between stress magnitude and cycles to failure in bone [5], use of a shorter SL may significantly decrease bony injury risk.

Our peak tibial stresses are relatively high compared to the literature. As such, the relative differences are more important than the absolute stress values.

CONCLUSIONS

Peak T and C tibial stresses are greatest during shod M/FF. Runners choosing to switch to this M/FF running should do so gradually to allow adequate time for bones to adapt to the higher stresses to help avoid injury. An 8% shorter stride length only minimally decreases peak stresses.

REFERENCES

1. Crossley et al. *Med Sci Sports Exerc*, **31**, 1088- 93, 1999.
2. Kourtis LC et al. *Computer Meth Biomech Biomed Eng*, **11**, 463-476. 2008.
3. Altman A & Davis I. *Proceedings of the 36th Annual Meeting of ASB*, Gainesville, FL, USA, 2012.
4. Thompson et al. *J Biomech*, **47**, 2745-50. 2014.
5. Edwards & Derrick. *Track Cross Country Journal*, **1**, 17-22. 2011.

ACKNOWLEDGEMENTS

Thank you to ASB for the Grant-In-Aid 2014 Award to fund this research.

Table 1: Subject characteristics (mean \pm SD).

	<i>hRF</i>	<i>hFF</i>
Gender (M, F)	3, 2	3,3
Age (yr)	24 \pm 5	26 \pm 6
Height (m)	1.75 \pm 0.14	1.73 \pm 0.09
Mass (kg)	63.9 \pm 12.9	65.4 \pm 12.7
BMI	20.6 \pm 1.3	21.8 \pm 2.6
Weekly Mileage (mi/wk)	29 \pm 30	29 \pm 20

Table 2: Mean \pm SD peak tensile (T), compressive (C), and shear (S) stresses for the 6 conditions, averaged across groups. Only shear stresses significantly decreased with an 8% shorter stride length.

	<i>Peak T</i>	<i>Peak C</i>	<i>Peak S*</i>
RF	197 \pm 44	-190 \pm 40	9 \pm 2
RF -8%	195 \pm 42	-188 \pm 35	9 \pm 3
M/FF	211 \pm 50	-210 \pm 45	11 \pm 2
M/FF -8%	208 \pm 49	-210 \pm 44	10 \pm 2
BF	198 \pm 52	-201 \pm 46	10 \pm 3
BF -8%	191 \pm 51	-197 \pm 42	9 \pm 3

FREQUENCY CONTENT OF THE VERTICAL IMPACT PEAK DURING REARFOOT AND FOREFOOT RUNNING

¹Allison H. Gruber, ²W. Brent Edwards, ³Joseph Hamill

¹Biomechanics Laboratory, Indiana University Bloomington, Bloomington, IN, USA

²Human Performance Laboratory, University of Calgary, Calgary, AB, CAN

³Biomechanics Laboratory, University of Massachusetts Amherst, Amherst, MA, USA
email: ahgruber@indiana.edu

INTRODUCTION

The wavelet transform has been used to evaluate the frequency content of various biological signals such as heart rate [e.g. 1] and vertical ground reaction forces [e.g. 2]. One benefit of the wavelet transform over other frequency analyses is that both time- and frequency-domain information of the signal is maintained. Therefore, wavelet transforms permit examination of specific events within a time series that may lead to improved understanding of the biological significance of such events.

The impact peak within the vertical component of the ground reaction force (GRF) has been suggested to be a major factor in the development of running related overuse injuries. This impact peak is observed in the time-domain during running with the rearfoot (RF) pattern but is blunted or absent when running with a forefoot (FF) pattern. However, a previous study using the continuous wavelet transform identified that the vertical impact peak was present in FF running but was visually obscured in the time-domain by the active peak [3]. Although there are many benefits of the continuous wavelet transform, the frequency component of a time-series event cannot be assigned exactly from the scaling parameter and decisions as to what frequency ranges to examine must be made *a priori*. The discrete wavelet transform, however, does not require *a priori* decisions of the frequency ranges to analyze and may be more accurate at reconstructing finite, non-periodic, and non-stationary signals compared with the Fourier and continuous wavelet transforms. The purpose of the present study was to compare the frequency components within the vertical GRF impact peak between RF and FF running using the discrete wavelet transform. This analysis may

provide greater insight to the potential biological significance of this event between footfall patterns.

METHODS

Twenty habitual RF runners (males/females 13/7; age 26 ± 6 yrs; height 1.8 ± 0.1 m; mass 69.9 ± 9.8 kg) and twenty habitual FF runners (males/females 15/5; age 25 ± 6 yrs; height 1.8 ± 0.1 m; mass 70.3 ± 10.6 kg) participated after given written informed consent. Participants ran over a force platform (1200 Hz) that was located in the center of a 20 m runway. Participants ran with their habitual footfall pattern at a standardized speed ($3.5 \text{ m} \cdot \text{s}^{-1} \pm 5\%$). Raw vertical GRFs during the stance phase were processed with the discrete wavelet transform (DWT) for levels 1–6 using the discrete Meyer mother wavelet. Each level acted similarly to a band-pass filter with different cut-off frequencies. The ‘approximates’ comprised the filtered reconstruction of the original signal in the time-domain. The ‘details’ comprised the frequency components of the original signal that were filtered out then reconstructed in the time-domain. The Hilbert transform was performed on the details to determine signal amplitude [1]. The impulse of the signal amplitude of the details (ImpA) was calculated by numeric integration with respect to time. Differences in signal impulse at each level between groups was assessed with a student’s t-test ($\alpha=0.01$).

The range of frequencies contained within the details of each level were determined by performing the DWT analysis on a chirp function which linearly increased in frequency from 0–80 Hz in 0.23 s. This frequency range and time equated to the range of frequencies that contain 98% of the power in the vertical GRF and the average stance time of all trials performed by the participants (0.23 ± 0.02 s).

RESULTS AND DISCUSSION

Levels 4–6 caused some attenuation of the impact peak compared with the original signal (Fig. 1, column 1). The signal details of these levels show a prominent impact peak in both footfall patterns (Fig. 1, column 2). Compared with the other levels, RF running resulted in a greater impact peak magnitude at level 5 (Fig. 1, column 2) but greater ImpA at level 6 (Table 1). FF running resulted in a greater impact peak and ImpA at level 6 compared with the other levels (Fig. 1, Table 1).

ImpA was not different between RF and FF running at levels 1–2 (Table 1). RF running resulted in significantly greater ImpA than FF running for levels 4 and 5, indicating greater vertical GRF signal power of frequencies between 20–80 Hz ($P>0.000$). FF running resulted in greater ImpA than RF running for levels 3 and 6 ($P>0.000$). ImpA at level 3 was less than 1 Ns for both footfall patterns and thus the statistical difference at this level may not be biologically meaningful. The largest difference in ImpA between patterns was observed at level 5 representing frequencies 20–37 Hz.

CONCLUSIONS

The DWT identified that the RF and FF patterns contain a vertical impact peak that may have a primary frequency content of 9–20 Hz for both patterns. Due to the limitations of the DWT, some of the power in this frequency band may be attributed to the active peak. Future studies should separate the impact peak from the active peak before calculating time domain variables such as vertical loading rate.

REFERENCES

1. Tanaka K, et al. *Med Eng Phys*, **26**, 313-319, 2004.
2. Verdini F, et al. *Clin Biomech*, **12**, 607-610, 2000.
3. Gruber AH, et al. *Proceedings of ACSM'15*, San Diego, CA, USA, 2015.

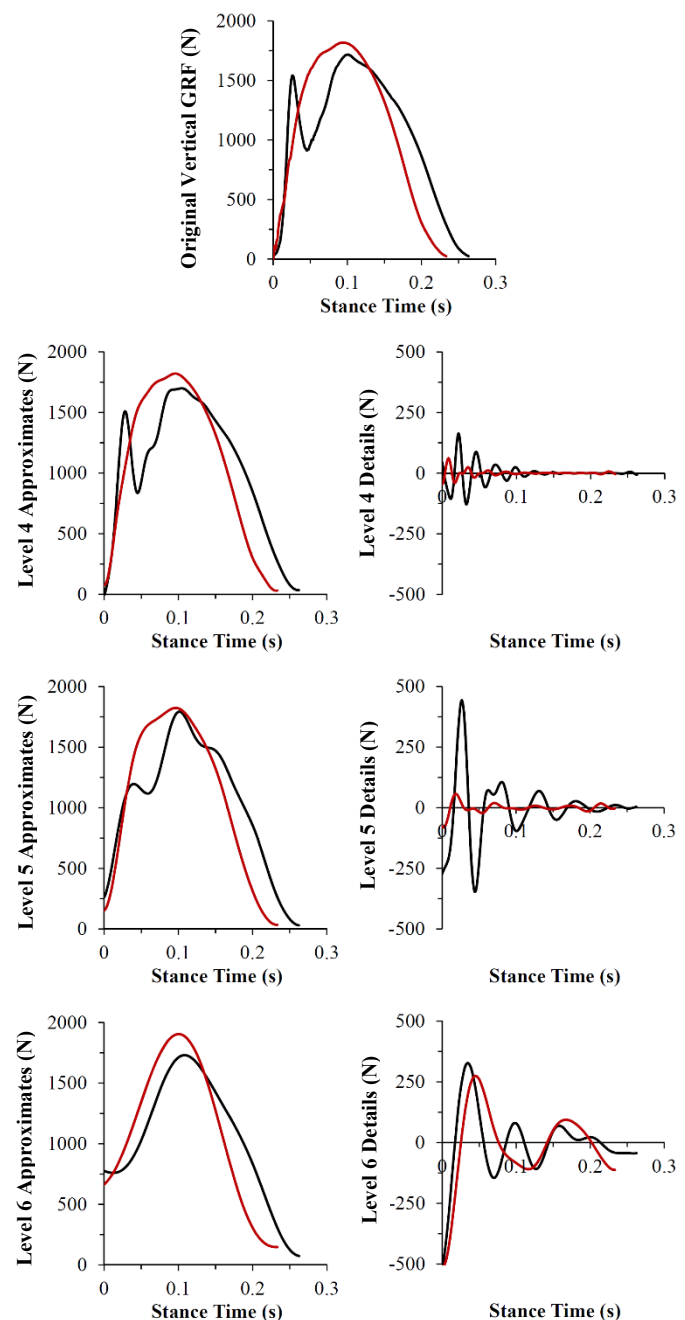


Figure 1: Row 1: Original vertical GRF generated from a representative RF (black) and FF (blue) runner. Row 2–4: Signal approximates (column 1) and details (column 2) of discrete wavelet transform levels 4–6.

Table 1: Impulse of signal amplitude at each level. *indicates $P<0.01$.

Level	1	2	3*	4*	5*	6*
Frequency (Hz)	>80	>80	>80	37 – 80	20 – 37	9 – 20
RF group (Ns)	0.3 ± 0.1	0.4 ± 0.1	0.6 ± 0.2	3.9 ± 1.8	20.1 ± 5.4	28.3 ± 8.4
FF group (Ns)	0.3 ± 0.1	0.4 ± 0.1	0.7 ± 0.3	2.7 ± 0.8	5.7 ± 2.1	34.6 ± 6.7

EFFORT-O-METER: THE RELATIONSHIP BETWEEN EFFORT OF WALKING AND AMOUNT OF WALKING PERFORMED

¹ Mailing Wu, ² Peter Adamczyk, and ¹ Steve Collins

¹ Carnegie Mellon University, Pittsburgh, PA, USA

² Intelligent Prosthesis Systems, LLC, Ann Arbor, MI, USA

email: mailingwu@cmu.edu

INTRODUCTION

Walking is an effective method for promoting activity among sedentary groups, and people adhere to walking routines more than other, more vigorous exercise regimens [1, 2]. Slightly increasing the metabolic cost of walking could be a simple method of increasing overall physical activity in the overweight or obese. However, while increasing the energy cost per step would increase net metabolic cost if all conditions (distances, velocities, etc.) were kept constant, this benefit could be reduced or eliminated if the subject reduces overall activity due to the higher cost.

We explored whether a modest increase in energy cost per step affected overall energy consumption from walking over a one week period compared to normal walking energy expenditure. We hypothesized that even a small increase in energy cost per step would cause the amount of walking performed to be reduced so dramatically that the overall energy cost would be decreased. The results of this study not only have implications for prescribing exercise regimens to improve public health and promote weight loss, but also help understand the expected impact of energy-saving prostheses and orthoses on exercise obtained during walking.

METHODS

Two pairs of sneakers were constructed: one pair weighted and one pair unweighted. A platform was attached to the sole to house an inertial monitoring unit (Sapphire Inertial Monitor, APDM, Inc.) and weight, if applicable. A steel bar was used to generate the appropriate mass, which was calibrated to equal approximately 2.5% of the user's body weight. The total load was expected to correspond

to roughly a 25% energy increase per step in the user [3].

24 able-bodied participants with no major health concerns were recruited at Carnegie Mellon University. Five voluntarily withdrew before completion of the protocol due to discomfort while wearing the shoes, especially the weighted shoes. An additional nine had unusable data for a variety of reasons, including not wearing the shoes for more than 12 hours per day, large periods of unexplained time (> 4 hours) spent with the shoes off, and changing environmental conditions between the two weeks.

The remaining subjects (n=10, 7 male, 3 female, 23.60 ± 2.88 years, 22.86 ± 2.52 kg/m² body mass index) were asked to wear both shoes all day except when sleeping or bathing for one week each. Additional activities that required the use of other shoes or no shoes (running, swimming, etc.) were logged and kept consistent between the two weeks to minimize misrepresentations in total energy costs. Subjects were not informed of the exact nature of the data being collected and motivation behind the study to minimize data biases due to conscious decisions to alter walking behavior. Study protocol was approved by the Carnegie Mellon University Institutional Review Board, and written informed consent was obtained from all subjects after the nature and possible consequences of the study were explained.

At the completion of the community-based collection, the participant answered a survey regarding the shoes (Fig. 1). Subjects then walked on a treadmill wearing each pair of shoes at various speeds and grades while oxygen consumption was measured using an indirect respirometry system (Jaeger Oxycon Mobile).

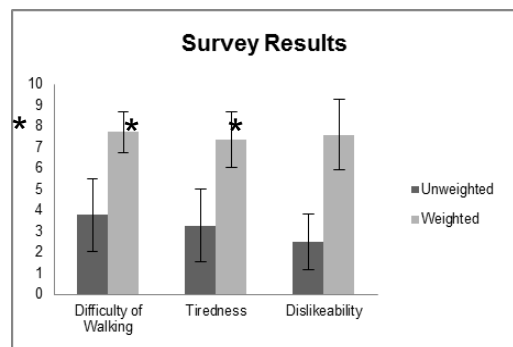


Figure 1: Survey results from all participants showing strong dislike of the heavy shoes. Asterisks denote a significant difference.

Data from the inertial monitor was numerically integrated [4] using IMUWalk software (Intelligent Prosthetic Systems, LLC) to estimate foot placement and timestamps for each step. Subjects' metabolic power data was used in conjunction with the processed monitor data to determine total metabolic cost while wearing the shoes. A paired t-test was used to determine statistical significance at 95% CI.

RESULTS AND DISCUSSION

The shoes were worn for at least 12 hours per day (14.25 ± 1.32 hours unweighted, 13.95 ± 0.97 hours weighted) and no significant difference in times ($p = 0.22$). The weighted shoes created a $27.1 \pm 16.4\%$ increase in metabolic rate while walking at 1.25 m/s on level ground.

Increasing metabolic cost of walking caused acute discomfort in users. Survey results (Fig. 1) revealed participants strongly disliked wearing the weighted shoes ($p < 0.001$), and found them much more tiring ($p < 0.01$).

Despite their dislike of the shoes, participants maintained the same distance walked per day ($p = 0.91$) and number of strides per day ($p = 0.87$), with no change in average velocity ($p = 0.98$), resulting in a significant increase in total energy cost when wearing the weighted shoes compared to the unweighted shoes ($6,739 \pm 5,576$ J/kg/day in unweighted, $8,058 \pm 6,152$ J/kg/day in weighted, $p = 0.002$) (Fig. 2). Indeed, all but one subject had increased energy expenditure in the weighted shoes despite large differences in baseline energy use.

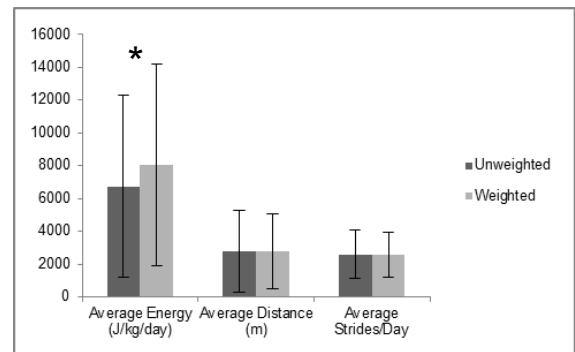


Figure 2: Average values for energy cost, distance traveled, and strides/day. Asterisks denote a significant difference.

Ultimately, our hypothesis was incorrect; subjects did not significantly change their behavior when presented with high-effort shoes. However, more extreme behavioral changes may appear over longer periods of time. Poor protocol adherence was major problem among our subjects, largely due to the discomfort of the weighted shoes, an effect which may be compounded in the long term. More study is needed among clinically overweight and obese individuals who lead sedentary lifestyles.

REFERENCES

1. Perri, MG., et al. (2002) Adherence to exercise prescriptions: effects of prescribing moderate versus higher levels of intensity and frequency. *Health Psychology* **21**(5): 452.
2. Siegel, PZ., Brackbill RM, Heath GW. (1995) The epidemiology of walking for exercise: implications for promoting activity among sedentary groups. *American journal of public health* **85**(5): 706-710.
3. Browning, RC., et al. (2007) The effects of adding mass to the legs on the energetics and biomechanics of walking. *Medicine and science in sports and exercise* **39**(3): 515.
4. Rebula JR, Ojeda LV, Adamczyk PG, Kuo AD. (2013) Measurement of Foot Placement and Its Variability with Inertial Sensors. *Gait & Posture* **38**(4): 974–980.

ACKNOWLEDGEMENTS

This material is based upon work supported by the National Science Foundation under Grant No. IIS-1355716

BIOMECHANICAL DETERMINANTS OF MUSCLE METABOLIC ENERGY CONSUMPTION IN LOCOMOTION

Russell T. Johnson and Brian R. Umberger

University of Massachusetts Amherst, Amherst, MA, USA
email: russellj@kin.umass.edu, web: <http://www.umass.edu/locomotion>

INTRODUCTION

Individuals tend to walk at a speed that minimizes the metabolic energy consumption per unit distance. Within a speed, individuals self-select a stride frequency (SF) that minimizes the energy cost for that particular speed [1]. It remains unclear exactly why metabolic energy is minimized at the preferred SF. A better understanding of the factors that determine the cost of locomotion would shed light on this issue. Two different hypotheses have been proposed regarding the biomechanical determinants of the metabolic cost of locomotion. One hypothesis states that the mechanical work done by the muscles is the primary determinant of the metabolic cost [1]. The other hypothesis states that the metabolic cost of locomotion is determined by the magnitude and rate of muscle force generation [2]. Since force and work are not completely independent, another possibility is that both are important determinants of locomotor costs.

A U-shaped relationship between metabolic energy and SF has been well established in whole body studies [1]. However, the nature of the relationships for individual muscle groups is unknown. Energy consumption cannot easily be measured in individual muscles while human subjects are walking. However, using a computer modeling approach [3] it is possible to estimate the metabolic energy consumed by individual muscles during walking. We focused on the triceps surae muscles for this study due to the relative simplicity of the ankle plantar flexors and the important role they play in locomotion. The specific purpose of this study was to examine the relationships among metabolic energy consumption, mechanical work and rate of force generation during walking in the triceps surae muscle group.

METHODS

Data were collected for five able-bodied male ($n=3$) and female subjects [age = 25 ± 1.8 years, height = 1.74 ± 0.08 m, mass = 77.1 ± 12.7 kg]. The subjects provided written informed consent before participating in the study. Three dimensional kinematic and kinetic data were collected using a motion capture system as subjects walked overground at their preferred SF (PSF), and at frequencies 20% greater (+20% SF) and 20% less (-20% SF) than preferred. Subjects matched their SF to the beat of a metronome. Five trials were collected for each subject at each SF.

Lower limb joint angles and joint moments were calculated in OpenSim [4]. Static optimization was performed for each trial using a musculoskeletal model with 23 degrees of freedom and 92 muscle actuators to obtain estimates of the individual muscle forces. OpenSim was also used to obtain estimates of the instantaneous muscle-tendon lengths over the stride. The muscle-tendon length and muscle force data were averaged across trials and subjects for each SF, and then analyzed using a custom MATLAB program to calculate muscle mechanic and metabolic variables [3].

Muscle metabolic power was plotted versus average positive mechanical power and versus the rate of force generation for the triceps surae muscles. We predicted that if either mechanical power or rate of force generation was a strong determinant of the cost, then there would be a linear trend with metabolic cost. However, given the nature of the data, correlation coefficients were not calculated.

RESULTS AND DISCUSSION

The triceps surae metabolic power was lowest at the PSF and highest at the -20% SF (Fig. 1A), consistent with whole-body results [1]. Mechanical power followed a similar trend (Fig. 1B), resulting in a linear dependence of metabolic power on mechanical power (Fig. 2A). The rate of force generation was greater at higher SFs (Fig. 1C). The average triceps surae force was similar across SFs, so the trend was due almost entirely to the smaller ground contact times at higher SFs. There was no clear relationship between muscle metabolic power and rate of force generation (Fig. 2B).

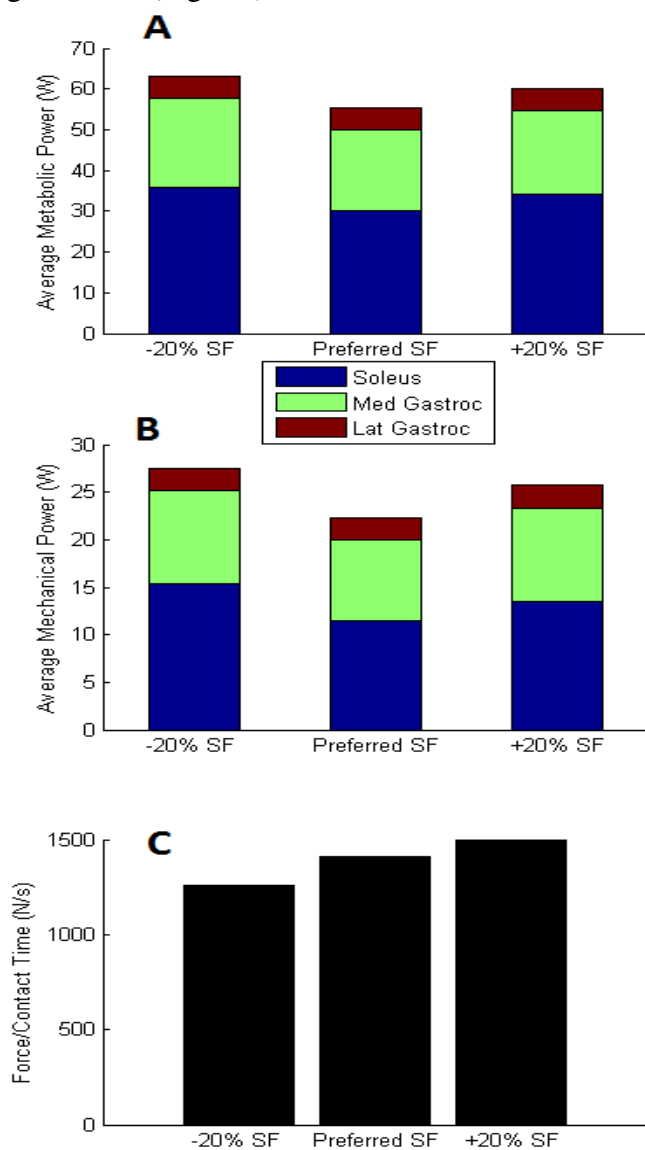


Figure 1: A: metabolic power vs. stride frequency, B: positive mechanical power vs. stride frequency, C: rate of force vs. stride frequency.

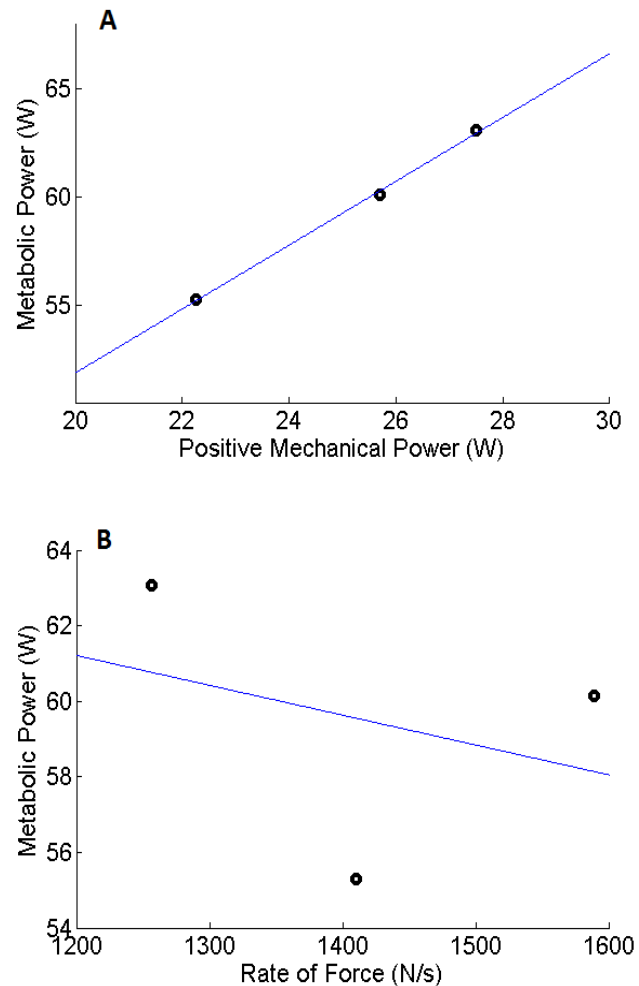


Figure 2: A: metabolic power vs. mechanical power. B: metabolic power vs. rate of force generation.

CONCLUSIONS

The demand to generate mechanical power appears to be the primary biomechanical determinant of the metabolic cost incurred by the triceps surae in human walking. In future research, we will extend the present analyses to include other major muscle groups of the lower limb.

REFERENCES

1. Minetti AE, et al. *Med Sci Sports Exerc*, **27**, 1194-1202, 1995.
2. Kram R, et al. *Nature*, **346**, 265-267, 1990.
3. Umberger BR, et al. *Comput Methods Biomech Biomed Engin*, **6**, 99-111, 2003.
4. Delp SL, et al. *IEEE Trans Biomed. Eng*, **54**, 1940-1950, 2007.

IS THE FOOT WORKING WITH OR AGAINST THE ANKLE DURING HUMAN WALKING?

¹ Karl E. Zelik

¹ Vanderbilt University, Nashville, TN, USA

email: karl.zelik@vanderbilt.edu, web: my.vanderbilt.edu/batlab/

INTRODUCTION

The muscles and tendons acting about the ankle joint perform a critical Push-off function that facilitates economical human gait. This ankle Push-off, due in part to elastic recoil of the Achilles tendon, is primarily transmitted upward along the leg to the rest of the body, and helps to redirect the body's center-of-mass during step-to-step transitions in walking. However, biomechanical estimates indicate that the foot dissipates substantial energy during this Push-off phase of gait. This foot energy absorption detracts from the positive ankle Push-off work, and may therefore undermine the power transferred to the rest of the body and the energetic benefits of the Achilles tendon, potentially degrading gait economy. From a basic science perspective the foot's behavior is perplexing. From a translational science perspective, it is unclear if prosthetic feet should be designed to mimic this dissipative foot behavior, or if non-biomimetic prostheses might instead improve gait beyond natural capabilities. These unresolved questions motivated our recent studies of foot function. The purpose of this research abstract is threefold:

1. To summarize our recent work on the coordination of foot muscles during gait
2. To review our recent findings on foot kinetics within the context of prior experimental and theoretical research
3. To discuss various plausible explanations for the seemingly wasteful foot behavior, and its interplay with the ankle during walking

METHODS

We performed two studies of healthy human walking. The first investigated the coordination of intrinsic and extrinsic foot muscles [1], and the second quantified foot and lower-limb joint kinetics during gait [2]. Experiment 1: We analyzed surface

electromyographic (EMG) recordings of 11 foot muscles in healthy individuals during level treadmill walking at 1.1 m/s (3 males, 4 females, 25.9 ± 2.7 , years old, 1.76 ± 0.11 m, 74 ± 16 kg). Experiment 2: We analyzed 6 degree-of-freedom (6DOF) foot kinetics, in conjunction with 6DOF ankle, knee and hip kinetics during human gait (7 males, 3 females, 24 ± 2.5 years old, 1.76 ± 0.11 m, 73.5 ± 15 kg). We computed power due to compression and rotation of the foot (and shoe), using a deformable body model [3] to account for the foot's many internal degrees of freedom (e.g., metatarsophalangeal (MTP) joints, heel pad, arch).

RESULTS AND DISCUSSION

We found that groups of intrinsic and extrinsic foot muscles exhibited peak activations in a consistent progression during forward walking. The period around Push-off could be roughly characterized by sequential peak muscle activity from the ankle plantarflexors, MTP flexors, then MTP extensors and finally ankle dorsiflexors (Fig. 1). Functionally, this muscle activation sequence represents torque contributions to ankle plantarflexion Push-off, followed by an MTP flexion moment near terminal stance phase. MTP flexor activity has been suggested to support/stabilize the foot arch, but these muscle-tendon units may also perform negative work against the extending toe joint, contributing to energy absorption in the foot.

We estimated ankle Push-off work to be approximately 23 J at 1.4 m/s (Fig. 2). However, we also found about -6 J of simultaneous work done by the foot, similar to previous studies (e.g., [4]). The magnitude of foot work during Push-off was comparable to the simultaneous work performed about the knee joint, indicating that foot contributions should not be neglected in understanding whole-body gait dynamics.

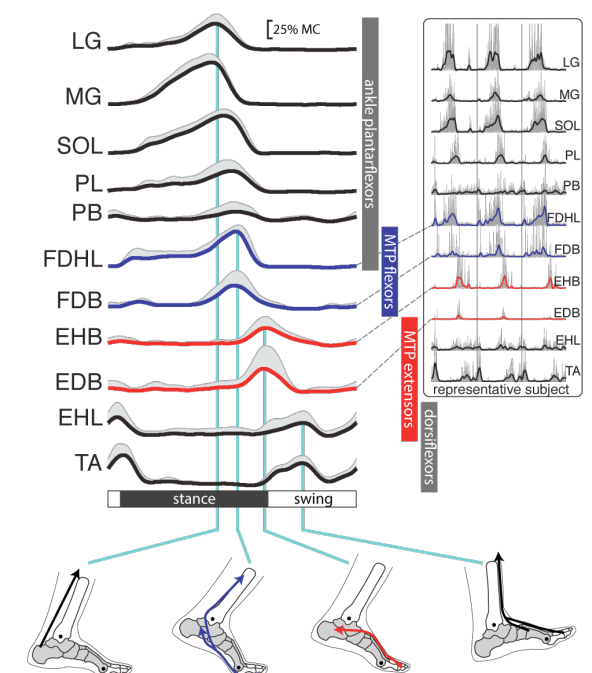


Figure 1: Foot muscle EMGs during walking [1]. Lateral (LG) & medial (MG) gastroc., soleus (SOL), peroneus longus (PL) & brevis (PB), flexor dig./hal. longus (FDHL), flexor dig. brevis (FDB), extensor hal. (EHB) & dig. brevis (EDB), extensor hal. longus (EHL), tibialis anterior (TA). EMG is depicted as percent of maximum contraction (MC).

We observed evidence that substantial energy is absorbed during the Push-off phase of walking, which may be due in part to negative muscle-tendon work as the toes extend in late stance. This foot behavior may subvert the energy-saving benefits of Achilles tendon recoil and ankle Push-off during walking. Several plausible explanations exist for this observed phenomenon:

I. The foot is working *against* the ankle... One possibility is that the foot absorbs substantial energy through deformation and rotation of structures within the foot/shoe, and that this dissipation is indeed detrimental to level-ground walking economy [5]. However, perhaps this foot behavior is useful for other reasons (e.g., balance, adaptability, non-level terrains), and it would be valuable to further explore functional trade-offs.

II. The foot is working *with* the ankle, indirectly... Another possibility is that the foot absorption is beneficial to gait economy, albeit indirectly; for example, by facilitating economical

force production of the calf muscles [6], or contributing to arch support during gait.

III. The foot is working *with* the ankle, but our conventional biomechanical estimates fail to capture it... Yet another possibility, and one that has received little attention, is that the foot may not absorb as much energy as it presently appears. Methodological limitations might result in over-estimating the magnitude of negative foot work, and failing to capture positive work performed by structures within the foot and shoe. For instance, apparent foot dissipation may be due to limitations in conventional biomechanical estimates, which fail to account for multiarticular muscle contributions.

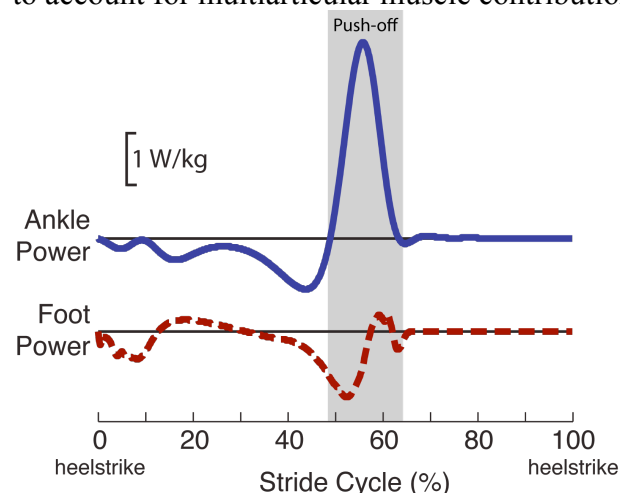


Figure 2: Ankle Push-off may be undermined by energy dissipation in the foot during walking [2].

In summary, we present recent findings on foot muscle coordination and kinetics, and propose several potential explanations for the peculiar foot behavior observed during the Push-off phase of walking. Additional studies are needed to discern these various explanations of foot function during gait, which have implications for prosthetic foot design, walking simulations and our fundamental understanding of bipedal locomotion.

REFERENCES

1. Zelik KE, et al. *Eur. J. Appl. Physiol.*, 2014.
2. Zelik KE, et al. *J Exp. Biol.*, 2015.
3. Takahashi KZ, et al. *J Biomech.*, 45(15), 2012.
4. Takahashi KZ, et al. *Gait & Posture.*, 2013.
5. Song S. and Geyer H. *IEEE ROBOTICS*, 2011.
6. Carrier DR, et al. *Science*, 1994.

A KINEMATIC AND ENERGETICS MODEL OF SHANK PROGRESSION DURING STANCE

Travis R. Pollen, Elisa S. Arch, Steven J. Stanhope

University of Delaware, Newark, DE, USA
email: trpollen@udel.edu, web: http://www.udel.edu/bioms

INTRODUCTION

Individuals with transtibial amputations depend on prosthetic ankle-feet to ambulate. However, due to the design of modern devices, analyzing prosthetic systems using traditional methods like inverse dynamics proves challenging [1]. As a result, appropriate characterization of prosthetic ankle-foot function and, subsequently, objective guidelines for the prescription and customization of these systems are lacking. Component selection depends on the prosthetist's training and intuition. Roll-over shape, the geometry the ankle-foot conforms to during the stance phase of gait, has been proposed as an improved characterization method [2]. While useful, roll-over shape fails to account for the period of late stance during which propulsion occurs.

The kinematics (rotation and translation) and energetics (flow of segmental power) of shank progression may provide a more complete description of ankle-foot function. The purpose of this study was to quantify and model the kinematics and energetics of shank progression over the stance phase of typical gait.

METHODS

Analyses were performed on ten typical adult participants (age 20-29, height 1.63-1.84 m, body mass 59.5-86.5 kg) who completed barefoot overground instrumented gait analysis at a scaled normal walking velocity (0.8 statures/second). Kinematic data were tracked using a 6 degrees-of-freedom marker set and sampled at 240 Hz using a six-camera motion capture system (Motion Analysis Corp. Santa Rosa, CA). Kinetic data were sampled at 1200 Hz using a strain gauge force platform (AMTI, Watertown, MA). Kinematic and kinetic data were filtered at 6 Hz and 25 Hz, respectively, using Visual3D software (C-Motion, Inc.,

Germantown, MD). From these data, kinematic and energetics models of shank progression were developed. The models were evaluated by comparing model predictions to shank progression quantified from the ten participants.

RESULTS AND DISCUSSION

A kinematic model (Fig. 1) was developed to predict stance phase ankle and knee joint center anterior-posterior (y) and superior-inferior (z) positions in the laboratory coordinate system:

$$y_{ankle} = y_{MH2} - \sin(\theta) * L_{foot} \quad (1)$$

$$z_{ankle} = z_{MH2} + \cos(\theta) * L_{foot} \quad (2)$$

$$y_{knee} = y_{ankle} - \sin(\theta_0 - \varphi) * L_{shank} \quad (3)$$

$$z_{knee} = z_{ankle} + \cos(\theta_0 - \varphi) * L_{shank} \quad (4)$$

where L_{foot} and L_{shank} are the lengths of the foot and shank; $MH2$ is the position of the second metatarsal head; θ is the foot-to-floor angle; θ_0 is the foot-to-floor angle normalized to 0° in the static pose; φ is the ankle (shank-to-foot) angle; and $\theta_0 - \varphi$ is the shank angle relative to the z-axis of the lab. Model-based and motion-capture derived positions were all strongly correlated ($R^2 > .98$).

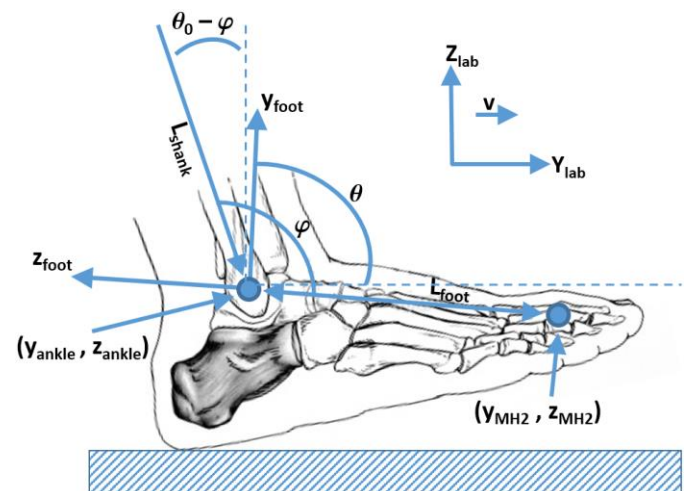


Figure 1: Kinematic model of shank progression in the laboratory sagittal plane.

Model-based and motion capture derived shank angles were also strongly correlated ($R^2 = 0.999$), and the contributions of the ankle and foot-to-floor angles to shank angle were determined (Table 1). Using the model, it was determined that foot-to-floor motion produces the forward rotation of the shank during late stance, while ankle plantar flexion produces the trajectory of the knee joint center necessary for forward propulsion.

A sagittal plane energetics model of shank progression during stance was also developed as per Robertson & Winter [3]. Net segmental power of the shank (P_{shank}) was calculated as the sum of the proximal muscle power (P_{pm}), proximal joint force power (P_{pj}), distal muscle power (P_{dm}), and distal joint force power (P_{dj}) of the shank:

$$\begin{aligned} P_{shank} &= P_{pm} + P_{pj} + P_{dm} + P_{dj} \\ &= M_{proximal} \bullet \omega_{shank} + F_{proximal} \bullet v_{proximal} \\ &\quad + M_{distal} \bullet \omega_{shank} + F_{distal} \bullet v_{distal} \end{aligned} \quad (5)$$

$M_{proximal}$ and M_{distal} correspond to the moments applied to the shank about the medio-lateral x-axis at the proximal and distance ends; $F_{proximal}$ and F_{distal} to the joint reaction forces applied to the proximal and distal ends of the shank; $v_{proximal}$ and v_{distal} to the translational velocities of the proximal and distal ends of the shank; and ω_{shank} to the angular velocity of the shank about the x-axis. Analogous calculations were made for the foot.

Mean scaled peak ankle power for the 10 participants occurred at 89% of stance. At this point in stance, the ankle plantar flexors were generating power through the active muscle terms, and the shank received 6.12 W/kg of power via the distal joint force segmental power term (Fig. 2). A small amount of energy (1.62 W/kg) left the foot distally via the joint force power term.

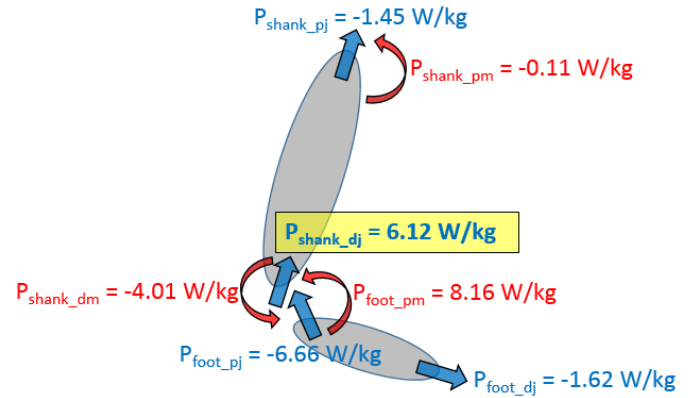


Figure 2: Dynamics of energy flow at peak ankle power (89% of stance). The shank received 6.12 W/kg of power via joint force power.

CONCLUSIONS

The kinematic and energetics shank progression models capture ankle-foot function during the entire stance phase of gait more completely than other methods, like roll-over shape. This study reveals the interrelationships between the ankle, foot-to-floor, and shank angles, as well as the dynamics of energy flow into the shank via the distal joint force segmental power term. These results can be used in the future to design novel prosthetic ankle-foot systems that better mimic natural shank progression, which may lead to improved functional outcomes for individuals with transtibial amputation.

REFERENCES

1. Geil MD, et al. *J Biomech* **33**, 1745–1750, 2000.
2. Hansen AH and Childress DS, *Disabil Rehabil* **32**, 2201–2209, 2010.
3. Robertson DG and Winter DA, *J Biomech* **13**, 845–854, 1980.

Table 1: Ankle, foot-to-floor, shank, and model-based shank angles during stance

Gait Event (% Stance)	Ankle Angle	Foot-to-Floor Angle	Shank Angle	Model Shank Angle
Heel strike (0%)	0° (neutral)	+16°	+16° (reclined)	+16° (reclined)
Foot flat (21%)	0° (neutral)	0° (flat)	0° (vertical)	0° (vertical)
Heel off (52%)	+10° (dorsiflexion)	0°	-11° (inclined)	-11° (inclined)
Max. DF (73%)	+15° (dorsiflexion)	-6°	-21° (inclined)	-21° (inclined)
Toe off (101%)	-14° (plantar flexion)	-65°	-50° (inclined)	-51° (inclined)

Asymmetric Forces Increase the Metabolic Cost of Running for Individuals with a Unilateral Leg Amputation

¹Owen N. Beck, ¹Paolo Taboga, and ^{1,2}Alena M. Grabowski

¹University of Colorado, Boulder, CO, USA; ²VA Eastern Colorado Healthcare System, Denver, CO, USA
email: owen.beck@colorado.edu

INTRODUCTION

Asymmetrical step lengths and step frequencies are associated with an elevated metabolic cost of locomotion [1]. Runners with a unilateral transtibial amputation using running-specific prostheses (RSPs) exhibit asymmetric ground reaction forces (GRFs), contact times (t_c), step lengths, step frequencies, and leg stiffness (k_{leg}) over a range of running speeds [2, 3]. Furthermore, a study of two runners with unilateral transtibial amputations using RSPs showed that changes in RSP stiffness (± 0.5 category) and height (± 1.27 cm) resulted in altered GRF and kinematic asymmetry between the affected leg (AL) and unaffected leg (UL) [4]. However, it is uncertain how asymmetric GRFs and stride kinematics affect the metabolic cost of runners with leg amputations. Therefore, we compared amputee runners using RSPs that varied by model, stiffness category, and height while measuring metabolic cost, GRFs, stride kinematics, and k_{leg} . We hypothesized that more symmetric vertical GRFs and stride kinematics would lower the metabolic cost of running for individuals with a unilateral leg amputation.

METHODS

Nine runners with unilateral transtibial amputations (7 M; 2 F) gave written informed consent to participate. Subjects were fit with three different RSP models (RSP1, RSP2, and RSP3) at the manufacturer recommended and ± 1 stiffness categories by a certified prosthetist. Next, the prosthetist aligned each RSP at the manufacturer recommended height and ± 2 cm.

On subsequent days, subjects performed 5 min running trials on a force-instrumented treadmill. Subjects ran $3 \text{ m}\cdot\text{s}^{-1}$ unless they were unable to maintain primarily oxidative metabolism, denoted by a $\text{RER} \geq 1.0$, in which case they ran $2.5 \text{ m}\cdot\text{s}^{-1}$. Each subject ran using 15 different combinations of

RSP model, stiffness category, and height. Initially, subjects ran using each RSP model at the 3 different stiffness categories with the recommended height. The stiffness category for each RSP model that required the lowest metabolic cost of transport (CoT) was deemed optimal. Subsequently, subjects ran with the optimal stiffness category of each model at heights of ± 2 cm. All trials were randomized.

We measured metabolic energy expenditure using indirect calorimetry to calculate the average net metabolic power during the last 2 min of each trial using a standard equation [4]. Then, we converted average net metabolic power to work and divided by the product of mass and running speed to yield CoT in J/kg/m.

We measured GRFs from 10 consecutive strides during each trial (1000 Hz) and processed the data using a custom MATLAB script. We defined asymmetry as:

$$\frac{UL - AL}{0.5(UL + AL)}$$

and reported it as a percentage [5]. We used a statistical linear mixed model to test the associations between RSP model, stiffness category, and height on CoT. Next, we determined the associations between peak vertical GRF, step length, step frequency, t_c , and k_{leg} asymmetries on the CoT using the same statistical method.

RESULTS AND DISCUSSION

While controlling for other variables, across all conditions, RSP3 elicited a 5.2 and 4.2% lower CoT than RSP1 and RSP2, respectively ($p < 0.01$) (Fig. 1). The CoT elicited from using RSP1 and RSP2 were similar ($p = 0.27$). Across RSP models, stiffness category had no effect on CoT ($p = 0.54$) (Fig. 1), whereas decreased RSP height was associated with a lower CoT ($p = 0.02$). For every 2 cm reduction in RSP height, CoT decreased by 1.3% (Fig. 2).

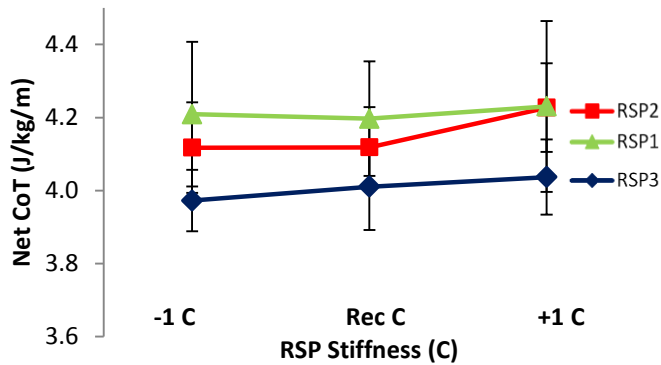


Figure 1. Average (\pm SEM) net metabolic cost of transport (CoT) while using three RSP models with the recommended stiffness category (Rec C) and $\pm 1C$ at the recommended height.

Consistent with previous research, subjects exhibited lower peak vertical GRFs, longer t_c , and lower k_{leg} with their AL compared to their UL ($p < 0.01$) (Table 1). Yet, CoT was independent of step length, step frequency, t_c , and k_{leg} asymmetries ($p \geq 0.30$). Peak vertical GRF asymmetries were associated with higher (worse) CoT ($p < 0.01$). For example, across all conditions our subjects generated 14% lower peak vertical GRFs with their AL compared to their UL ($p < 0.01$). If their legs had produced symmetric peak vertical GRFs, CoT would have decreased by 2.7%. Interestingly, when legs were compared separately, CoT was independent of the AL peak vertical GRF ($p = 0.18$), yet was higher with increases in UL peak vertical GRF ($p < 0.01$).

Practical implications from our study are that shortening RSP height and reducing peak vertical GRF asymmetries by lowering UL peak GRFs may

reduce the metabolic cost of running for individuals with a unilateral transtibial amputation.

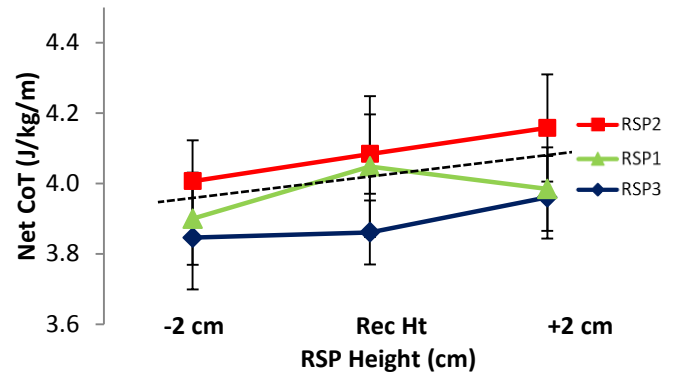


Figure 2. Average (\pm SEM) net metabolic cost of transport (CoT) using three RSP models with the optimal stiffness categories at the recommended height (Rec Ht) and ± 2 cm. The dashed line is the regression line ($\text{CoT} = 4.00 + 0.03 \times \Delta \text{RSP Ht}$).

REFERENCES

1. Ellis RG, et al. *Proc R Soc B* **280**, 1-7, 2013.
2. Grabowski AM, et al. *Biol. Lett* **6**, 201-204, 2010.
3. McGowan CP, et al. *J R Soc Interface* **9**, 1975-1982, 2012.
4. Wilson JR, et al. *Prosthet Orthot Int* **33**, 218-229, 2009.
5. Brockway JM. *Hum nutr. Clin nutr* **41**, 463-471, 1987.

ACKNOWLEDGEMENTS

We thank Freedom Innovations, Ossur, and Ottobock for the donation of RSPs. This project was supported by the BADER Consortium, Department of Defense, CDMRP cooperative agreement (W81XWH-11-2-0222)

Table 1. Mean peak vertical ground reaction forces (vGRF) & contact time (t_c) asymmetries (%). Positive numbers indicate higher values for the unaffected leg (UL) vs. affected leg (AL). *Italics* indicate the lowest asymmetry. Rec is recommended, C is category, and Ht is height. $n=9$ at Rec Ht, & <9 at each ± 2 cm condition.

		RSP1			RSP2			RSP3		
Peak vGRF Asymmetry		-1 C	RecC	+1 C	-1 C	RecC	+1 C	-1 C	RecC	+1 C
	+2 cm	27.9	26.3	31.5	33.5	22.4	-	20.9	1.2	7.2
	Rec Ht	14.2	19.0	19.6	14.7	17.4	18.7	2.3	7.2	10.1
	-2 cm	5.1	15.7	2.1	6.5	13.4	-	0.4	-1.2	7.2
t_c Asymmetry		-1 C	RecC	+1 C	-1 C	RecC	+1 C	-1 C	RecC	+1 C
	+2 cm	-15.7	-10.8	-14.4	-12.6	-5.8	-	-12.6	2.0	8.5
	Rec Ht	-11.1	-8.1	-5.6	-5.6	-2.6	-2.2	-2.4	-0.9	2.1
	-2 cm	-4.0	-4.8	-6.1	1.9	-3.5	-	-2.5	-2.1	7.8

KINEMATIC STRATEGIES FOR ASYMMETRIC BILATERAL LANDING AFTER ANTERIOR CRUCIATE LIGAMENT INJURY

¹Samuel C. Wordeman PhD, ^{1,2}Stephanie Di Stasi PT, PhD, and ¹⁻³Timothy E. Hewett PhD

¹ Sports Health and Performance Institute, The Ohio State University, Columbus, OH, USA

² Department of Orthopaedics, The Ohio State University, Columbus, OH, USA

³ Departments of Physiology and Cell Biology, Family Medicine, and Biomedical Engineering, The Ohio State University, Columbus, OH, USA

Email: Samuel.Wordeman@osumc.edu, **Web:** sportsmedicine.osu.edu

INTRODUCTION

Strength and performance symmetry are common benchmarks for rehabilitation and readiness for return to sport after anterior cruciate ligament (ACL) reconstruction. However, movement symmetry is less frequently used in clinical decision-making. Asymmetries in movement patterns and decreases in external moments on the involved limb are frequently reported in ACL-reconstructed subjects. [1] Identification of such asymmetries usually requires complex, costly motion analysis equipment that may not be available clinically. Avoidance strategies should be mitigated to reduce the likelihood of developing strong limb preferences, and to create the optimal scenario for safe return to sport after ACL reconstruction. [2] The goals of this study were to: 1) Identify ACL-reconstructed patients who exhibit under-loading [lower peak vertical ground reaction force (vGRF)] of the injured limb during the drop vertical jump (DVJ) test, and 2) identify the kinematic strategies that characterize under-loading to guide clinical evaluations of biomechanical symmetry. The hypothesis tested was that patients who demonstrated decreased peak vGRF on the involved limb would also demonstrate significant kinematic asymmetries.

METHODS

Twenty-five ACL-reconstructed patients (12 males and 13 females, 19.6 ± 7.2 years old) were evaluated upon discharge from supervised rehabilitation. Patients performed three successful trials of a drop vertical jump (DVJ) in the capture volume following several practice repetitions to ensure consistency in performance. The DVJ task involves a bilateral drop from a 31 cm high box, followed

directly by a maximum effort vertical jump. Patients were specifically instructed to leave the box with both feet simultaneously, to avoid any asymmetry in landing due to stepping off with one leg first. The contact phase of the DVJ task was normalized so that initial contact occurred at 0% of the contact phase, and takeoff occurred at 100%. Hip, ankle, and knee joint angles in all three anatomical planes were calculated in Visual3D. Discrete variables for statistical analysis included joint angles at initial contact, maximum and minimum joint angles, and joint excursions during the landing. Two-by-two (group-by-limb) analysis of variance (ANOVA) models were used for statistical comparisons. *Post-hoc*, two-tailed t-tests were used to compare values between the involved and uninvolved limbs (paired tests) or between groups (unpaired tests).

RESULTS AND DISCUSSION

Eighteen (18/25, 72%) patients were classified as under-loaders (UL), and demonstrated $25 \pm 14\%$ lower peak vGRF on the involved limb compared to the uninvolved limb. Under-loaders demonstrated significantly increased hip flexion (UL_Involvement: 34.2 ± 7.7 degrees, UL_Uninvolved: 29.8 ± 7.7 degrees; $p=0.0001$) and knee flexion (UL_Involvement: -21.6 ± 8.5 degrees, UL_Uninvolved: -16.2 ± 5.5 degrees; $p=0.002$) on the involved limb, and a trend toward greater ankle plantar flexion at initial contact compared to subjects who did not under-load (Others, 7/25, 38%) (UL: -46.3 ± 7.0 degrees, Others: -40.7 ± 8.5 degrees; $p=0.07$). Conversely, in patients who did not under-load the involved extremity, hip and knee flexion at initial contact were greater on the uninvolved limb.

The purpose of this investigation was to assess hip, knee, and ankle kinematic asymmetries during a drop vertical jump task in individuals

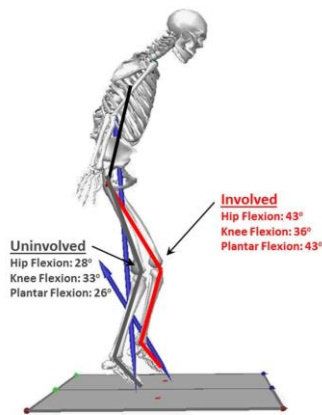


Figure 1: Representative sagittal view of a subject at initial contact that exhibited under-loading strategies on the involved limb. Joint flexion values indicated in the figure are actual values from this frame.

following ACL reconstruction and supervised physical therapy. Nearly three quarters (18/25) of our patients demonstrated a lower peak vGRF on the involved limb, with an average 25% reduction in this subgroup of “under-loaders”. The primary findings of this study are that under-loaders appear to land with greater ankle plantar flexion compared to patients who do not under-load, and demonstrate significant asymmetries in hip and knee flexion at initial contact. Specifically, at initial contact patients classified as under-loaders demonstrate greater hip and knee flexion at initial contact on the involved limb (**Figure 1**). The magnitude of asymmetries in sagittal plane knee kinematics in subjects that did not under-load was comparable to the asymmetries observed in under-loaders; however, the off-loading tendencies were observed in the uninvolved limb. While neither of these asymmetries was observed in the “other” (non-

under-loader) group, this may be attributable to the relatively small group sample size.

CONCLUSIONS

We focused on the identification of kinematic strategies that could potentially be observed in a clinical setting, without complex biomechanical analyses. This paper demonstrates residual avoidance patterns in a vast majority of ACL-reconstructed subjects during a common screening task, and identifies movement patterns associated with under-loading the involved limb. Future studies may benefit from identifying patients as ‘under-loaders’ or ‘over-loaders’ to identify limbs at increased risk for second injury, or quantify existing deficiencies in movement patterns. Despite discharge from physical therapy, the majority of ACL-reconstructed patients demonstrated under-loading of the surgical limb. Kinematic strategies consistent with under-loading may be identifiable through techniques such as sagittal plane video analysis, particularly during bilateral tasks where the patient may rely on the uninvolved limb.

REFERENCES

1. Paterno MV, et al. *Clin J Sports Med* **17**, 258-262, 2007.
2. Di Stasi SL, et al. *J Orthop Sports Phys Ther* **43**, 777-792, 2013.

ACKNOWLEDGEMENTS

The authors would like to acknowledge Joshua Hoffmann and the entire staff of the Sports Biodynamics Lab at The Ohio State University for their assistance, as well as NIH 2R01-AR056259

Table 1: Subject and group demographics from a cohort of 25 subjects in this analysis

Under-loaders	Males	Females	Group
n=18	8	10	18
Age (years)	20.3 ± 5.4	19.0 ± 6.1	19.3 ± 5.7
Height (m)	1.75 ± 0.07	1.64 ± 0.04	1.69 ± 0.08
Mass (kg)	82.2 ± 13.7	67.2 ± 7.5	73.9 ± 12.9
Post-Op (weeks)	38.8 ± 11.4	39.0 ± 21.7	38.9 ± 17.7
Others	Males	Females	Group
n=7	4	3	7
Age (years)	24.5 ± 13.5	15.7 ± 0.6	20.7 ± 10.7
Height (m)	1.76 ± 0.09	1.62 ± 0.07	1.69 ± 0.11
Mass (kg)	80.6 ± 16.9	56.4 ± 7.9	70.2 ± 18.2
Post-Op (weeks)	31.1 ± 5.1	41.7 ± 15.1	37.2 ± 12.4

SAGITTAL PLANE KNEE EXCURSION IS KEY PREDICTOR OF LOWER EXREMITY PERFORMANCE DURING SINGLE LEG HOP

¹Joshua T. Hoffman MS, ¹Samuel C. Wordeman PhD, and ¹⁻⁵Timothy E. Hewett PhD

¹Sports Health and Performance Institute (SHPI) OSU Sports Medicine, ²Department of Biodomedical Engineering, ³School of Health and Rehabilitative Sciences, ⁴Department of Orthopaedics, ⁵Department of Physiology and Cellular Biology and Family Medicine, Ohio State University, Columbus, OH

INTRODUCTION

Each year, approximately 125,000 people in the United States require surgical reconstruction of the anterior cruciate ligament (ACL) [1]. Following surgery, most athletes exhibit significant biomechanical and performance-based asymmetries between the injured and uninjured limbs [2]. Clinicians frequently utilize the single leg hop (SLH) for distance and isokinetic quadriceps strength tests to identify residual functional deficits in the ACL-injured population. While biomechanical imbalances are observed between involved and uninvolved limbs during both tasks, the relationship(s) of these deficits to power generation and joint work are unclear [2]. The purpose of this study was to analyze power generation and total joint work in the lower extremities of ACL-reconstructed subjects. We aimed to establish key biomechanical asymmetries during the propulsion phase of a SLH task. In addition, we used clinically-based measures to develop predictive models for total power and work output at the joints.

METHODS

Nineteen (n=19, males n=5, females n=14) ACL-injured subjects cleared for discharge from supervised rehabilitation were included in this study. Peak isokinetic quadriceps strength normalized by body mass was recorded at 60°/s. Three-dimensional (3-D) motion capture data from the propulsion phases of two bilateral SLH trials, and the total distance hopped were analyzed for each subject. The distance hopped was averaged for each limb over the two trials. Kinematics and kinetics at the hip, knee, and ankle were averaged for each limb over the propulsion phase of the two trials. The propulsion phase was operationally defined as the period between peak knee flexion and toe off. The sum of peak sagittal plane hip, knee, and ankle power and peak sagittal plane total joint power were examined. In addition, joint work was determined by Trapezoidal Riemann Summation of hip, knee, and

ankle power time series curves. Individual joint work curves were summed to calculate total joint work. Paired *t*-tests were used to determine limb asymmetries. In addition, multivariate linear regression models were developed to predict power and work output.

RESULTS AND DISCUSSION

Normalized peak isokinetic strength (p-value, uninvolved limb mean \pm standard deviation, involved limb mean \pm standard deviation; $p < 0.001$, 2.46 ± 0.47 Nm/kg, 2.14 ± 0.51 Nm/kg) and SLH distance ($p = 0.019$, 127.0 ± 28.4 cm, 119.0 ± 32.0 cm) were significantly greater for the uninvolved limb compared to the involved limb. In addition, the uninvolved limb generated statistically greater sum of peak hip, knee, and ankle joint powers ($p = 0.007$, 23.7 ± 6.1 Watt/kg, 21.5 ± 6.8 Watt/kg) and peak total joint power ($p = 0.012$, 17.6 ± 4.1 Watt/kg, 15.7 ± 5.2 Watt/kg). Finally, more total joint work was produced by the uninvolved limb ($p = 0.008$, 1106.1 ± 312.3 J/kg, 985.9 ± 332.3 J/kg).

Sagittal plane knee excursion (KE_{SAG}), defined as the range between peak knee flexion and peak knee extension during SLH propulsion, was significantly greater ($p < 0.001$, $37.8 \pm 8.8^\circ$, $30.6 \pm 9.9^\circ$) for the uninvolved limb. KE_{SAG} symmetry ratio (involved/uninvolved) was 0.81 ± 0.14 , and 18 of the 19 subjects displayed less knee excursion in the sagittal plane on the involved limb.

Three multivariate linear regression models were constructed with summed peak joint power, peak total joint power, and total joint work as dependent outcome variables. For each model, KE_{SAG} and SLH distance hopped were the independent predictor variables. The adjusted R^2 value for the summed peak joint powers regression model was 0.757 (Figure 1a), and the p-values for KE_{SAG} and SLH distance were < 0.001 and 0.002, respectively (Table 1). The model for TJP demonstrated an adjusted R^2 of 0.695 (Figure 1b). The p-values for this model were < 0.001 for KE_{SUM}

and 0.042 for SLH distance hopped (Table 1). Finally, the adjusted R^2 value for the total joint work regression model was 0.621, and the p-values for KE_{SAG} and SLH distance were <0.001 and 0.032, respectively (Table 1). Separate models that included peak isokinetic quadriceps strength were performed, but this measure was not statistically significant.

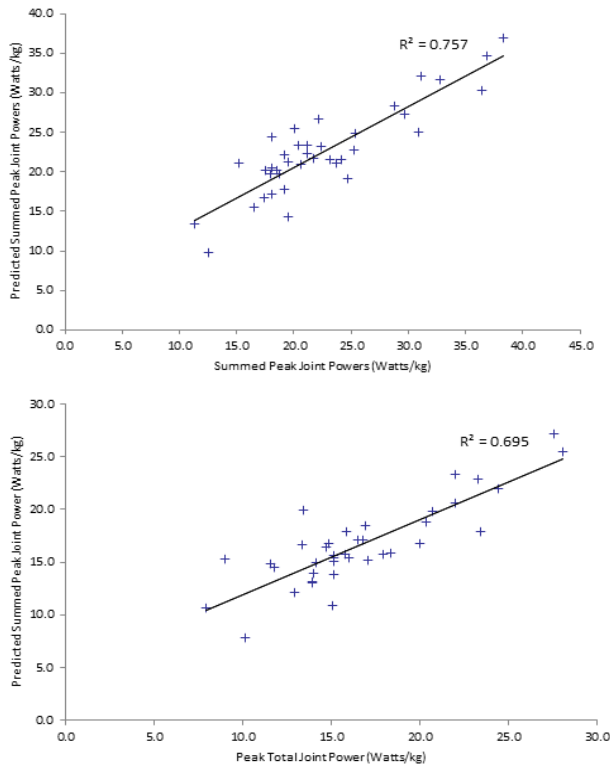


Figure 1. Fit of Power Generation Regression Models: This figure illustrates the fit for the summed peak joints powers [top (a)] and the peak total joint power [bottom (b)] regression models.

This study demonstrates significant performance imbalances between the involved and uninvolved limb. Furthermore, the regression models exhibit good-to-excellent correlation with actual total power and work produced at the joints. Although the kinematic and kinetic imbalances are consistent with outcomes previously reported by Orishimo et al, our models must be validated in an

independent data set prior to clinical implementation [2].

While this study shows significant differences between limbs in an injured population, comparison of performance and biomechanical measures to a healthy population has not been performed. In addition, the small sample size and predominantly female cohort may limit the impact of these findings. Therefore, future research should compare power generation and work done between injured and healthy populations. Furthermore, the injured population should be expanded to include more male subjects.

CONCLUSION

The multivariate linear regression models developed for summed peak joint power, peak total joint power, and total joint work indicate that both KE_{SAG} and SLH distance are significant predictors of total power and work output at the joints. Currently, clinicians utilize SLH distance and peak isokinetic quadriceps strength to assess power generation imbalances. However, these models illustrate that differences in KE_{SAG} between limbs during the SLH task should be considered. KE_{SAG} can be measured by sagittal plane reference video recording of SLH tasks. Most clinics are equipped with the hardware and software to calculate KE_{SAG} , so application of this model in a clinical setting is feasible. Therefore, measurement of these predictors for total power and work outputs at the joint following ACL reconstruction may provide clinicians an improved understanding of performance during rehabilitation.

REFERENCES

1. Kim S, et al. *J Bone Joint Surg, Am.* 93, 994-1000. 2011.
2. Orishimo, et al. *Knee Surg, Sports Traumatol, Arthroscopy.* 18, 1587-593. 2010

ACKNOWLEDGEMENTS

The authors would like to acknowledge the OSU Sports Medicine research staff, internal funds, and the NIH (R01-AR056259)

	Summed Peak Joint Powers	Peak Total Joint Power	Total Joint Work
Adjusted R^2	0.757	0.695	0.621
KE_{SUM} p-value	<0.001	<0.001	<0.001
SLH p-value	0.002	0.042	0.032

Table 1. Multivariate Linear Regression Models

KINEMATIC/KINETIC DIFFERENCES BETWEEN SUBJECTS WITH/WITHOUT KNEE OSTEOARTHRITIS AFTER UNILATERAL ANTERIOR CRUCIATE LIGAMENT RECONSTRUCTION, AND THE INFLUENCE ON STRESS DISTRIBUTION

Ashutosh Khandha, Kurt Manal, Lynn Snyder-Mackler and Thomas S. Buchanan

The University of Delaware, Newark, DE, USA
email: ashutosh@udel.edu, web: <http://bme.udel.edu/>

INTRODUCTION

In subjects with unilateral anterior cruciate ligament reconstruction (ACLR), changes in knee joint mechanics post-surgery are thought to contribute to altered cartilage stresses, which in turn is believed to cause premature knee osteoarthritis (OA) [1]. We have reported that unilateral ACLR subjects who get medial compartment OA in the involved knee demonstrate lower joint forces compared to non-OA subjects, as early as six months post-surgery [2]. In subjects that get OA five years after unilateral ACLR, we have observed that radiographic osteophytes are most commonly seen near the medial margin of the medial knee compartment, i.e. the joint region closer to the midline of the body. While it has been shown that the knee cartilage is thinner in that region (compared to the central region of the joint) [3], the spatial variation that occurs in knee cartilage stress distribution after ACLR is not clearly understood [4]. Specifically, it is not clear whether cartilage stresses near the medial margin of the medial knee compartment can be higher (and hence detrimental) even though the joint force is lower, in OA vs. non-OA subjects.

With that background, the purpose of this study is to evaluate kinematic/kinetic differences in the involved knee between subjects with/without knee OA five years after unilateral ACLR. The comparisons are made at the first peak of vertical ground reaction force (vGRF) during gait. We further evaluate the effect of typical kinematics/kinetics on medial tibial cartilage stress distribution, for a non-OA vs. OA subject.

METHODS

The subject population includes 37 unilateral ACLR subjects (14 females, 23 males, Age Range: 14 to 46

years) at the five year post-surgery time point. Weight-bearing anterior-posterior radiographs were graded using the Kellgren-Lawrence (K-L) scale. A K-L grade ≥ 2 was defined to be indicative of OA. 8 out of 37 subjects showed signs of OA in the medial compartment. The testing protocol included gait analysis using an 8-camera video system (Vicon, Oxford Metrics Limited, London, UK) and a force platform (Bertec Corporation, Worthington, OH). Electromyography (EMG) analysis was conducted using surface-EMG recordings (Motion Lab Systems, Baton Rouge, LA) collected from seven muscles crossing the knee joint. A validated Hill-type EMG-informed musculoskeletal model [5] was used to estimate joint force. Student's t-test ($\alpha = 0.05$) was used to evaluate differences in kinematics/kinetics between the non-OA vs. OA group, at the first peak of vGRF.

Quasi-static finite element analysis at the first peak of vGRF was conducted using Open Knee [6] in FEBio (Musculoskeletal Research Laboratories, Salt Lake City, UT), with material properties derived from literature [6-9]. The Open Knee model (Figure 1) was scaled based on subject-specific knee epicondylar width measurements of one non-OA and one OA subject, each of whom demonstrated kinematics/kinetics similar to mean values demonstrated by their respective groups. The tibia was held fixed while the knee flexion angle was prescribed to the femur. Subject-specific joint force, frontal plane moment and transverse plane moment were applied to the femur. The resultant medial tibial cartilage stress distributions for the non-OA vs. OA subject were compared.

RESULTS AND DISCUSSION

The OA group demonstrated significantly lower flexion angle, sagittal plane moment and transverse

plane moment, compared to the non-OA group (Table 1. Mean \pm 1 standard deviation). The OA group also demonstrated a lower joint force and a higher frontal plane moment, but these differences were not significant.

Differences in medial tibial cartilage stress distribution were observed for typical kinematics/kinetics representing the non-OA vs. OA subject (Figure 1). While the maximum medial tibial cartilage stress for the OA subject was lower (non-OA: 6.2 MPa, OA: 4.9 MPa), the maximum stress near the medial margin of the medial tibial cartilage (region circled in red in Figure 1) was higher for the OA subject (non-OA: 3.3 MPa, OA: 4.9 MPa). This is the region where cartilage tends to be thinner (compared to the central region of the joint) and also the region where we have observed radiographic osteophytes in unilateral ACLR subjects.

In summary, these results provide insight pertaining to altered cartilage stress distribution as a result of altered joint mechanics, and can help solidify the

link between altered joint mechanics and premature knee OA in unilateral ACLR subjects.

REFERENCES

1. Zabala ME, et al. *J Biomech* **46**, 515-520, 2013.
2. Wellsandt E, et al. *Proceedings of ORS*, New Orleans, LA, USA, 2014.
3. Andriacchi T, et al. *Ann Biomed Eng* **32:3**, 447-457, 2004.
4. Imhauser C, et al. *Am J Sports Med* **41**, 815-825, 2013.
5. Manal K, et al. *J Biomech Eng* **135:2**, 2013.
6. Erdemir A, et al. *Proceedings of ISB*, Brussels, Belgium, 2011
7. Kiapour A, et al. *J Biomech Eng* **136**, 2014
8. Pena E, et al. *J Biomech* **39:9**, 1686-1701, 2006
9. Sibole S, et al. *PLoS ONE* **7**, e37538, 2012

ACKNOWLEDGEMENTS

Work supported by National Institutes of Health (P30-GM103333, R01-AR046386, and R01-AR048212)

Table 1: Mean (\pm 1 SD) @ 1st peak of vGRF.

(SD = standard deviation, vGRF = vertical ground reaction force, OA = osteoarthritis, BW = body weight, HT = height)

Kinematic and Kinetic Parameters	non-OA (n=29)	OA (n=8)	p-value
Knee Flexion Angle (Degrees)	25.1 \pm 4.3	17.7 \pm 2.2	0.01
Joint Force (BW)	3.8 \pm 0.9	3.4 \pm 0.8	0.29
Flexion Moment (%BW*HT)	4.9 \pm 1.0	3.4 \pm 1.1	0.01
Adduction Moment (%BW*HT)	3.0 \pm 0.7	3.2 \pm 0.5	0.36
External Rotation Moment (%BW*HT)	1.4 \pm 0.3	1.0 \pm 0.2	0.01

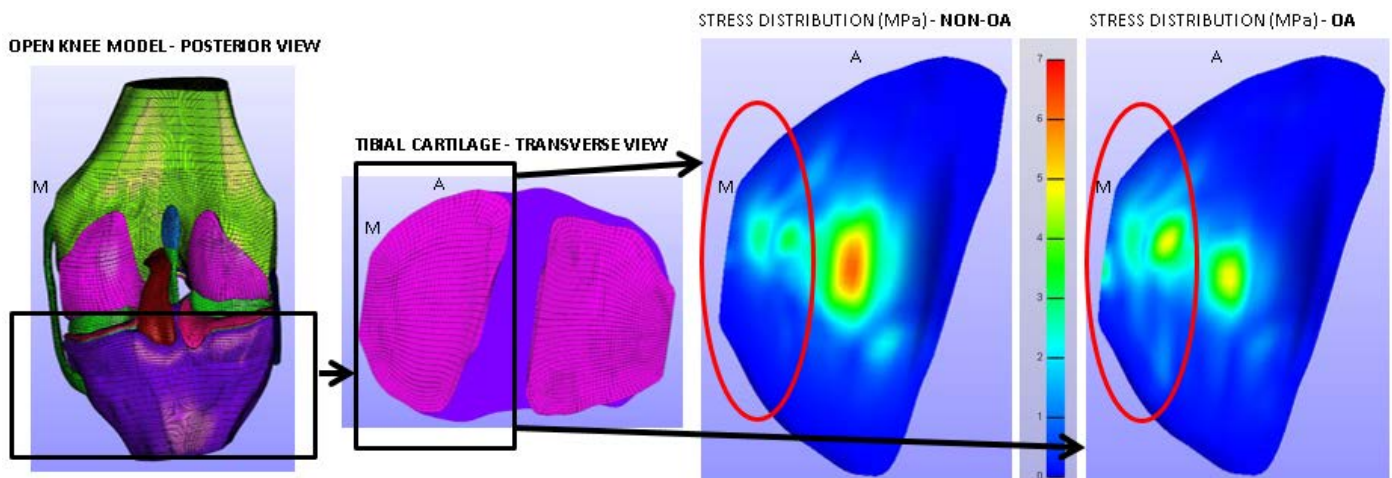


Figure 1: Stress distribution (MPa): Medial tibial cartilage of the involved knee: non-OA vs. OA.

(A = anterior, M = medial, OA = osteoarthritis)

SINGLE-LIMB DROP LANDING BIOMECHANICS FOLLOWING ANTERIOR CRUCIATE LIGAMENT RECONSTRUCTION

¹Federico Pozzi, ¹Andrew Rombach, ¹Joseph Zeni, ²Stephanie Di Stasi, ³Joaquin Barrios

¹University of Delaware, Newark, DE, USA

²The Ohio State University, Columbus, OH, USA

³University of Dayton, Dayton, OH, USA

email: jbarrios1@udayton.edu

INTRODUCTION

Biomechanical maladaptations during double-limb drop vertical jumping increase the risk for primary anterior cruciate ligament (ACL) injury.¹ Following ACL surgery, the contralateral limb may be used to compensate for unilateral deficits.² As such, unilateral landing tasks may be better able to elicit and identify deficits in individuals at risk for ACL injury or following surgery.³ Therefore, the purpose of this case-control study was to evaluate single-limb drop landing biomechanics in individuals after successful ACL surgery and rehabilitation.

METHODS

Twenty patients at least one year following ACL surgery and 20 healthy individuals matched by gender, age, body mass index, limb dominance and activity level, participated in this study (Table 1).

Table 1. Demographic characteristics of the participants.

	ACL (n=20)	Control (n=20)
Gender	17 F, 3 M	17 F, 3 M
Age (yr)	22 ± 2.5	21 ± 3.2
Height (m)	1.7 ± .07	1.7 ± .09
Weight (kg)	65 ± 10.7	62 ± 10.4
BMI, (kg/m ²)	22.8 ± 2.2	22.2 ± 1.8
Tegner Activity Level	6.8 ± .89	6.9 ± .93
Time since surgery (mo)	58.4 ± 33.2	

Retro-reflective markers were placed on the trunk, pelvis, thigh, shank, and foot of either the involved leg of the ACL patients or the dominance-matched leg of the control group. After the calibration trials, subjects stood on a 30cm tall box with all their body weight on the test leg. They were told to drop down onto the force plate in front of them, to land on the test leg only, and to briefly hold the landing position. Landings that involved any temporary loss of balance or involved double-striking were

excluded. Subjects were allowed to practice the drop landing task as needed. Five landing trials were captured.

Marker trajectories and kinetic data were acquired at 150Hz and 1500Hz, respectively, and smoothed using low-pass filtering (8Hz and 50Hz). Data were analyzed during the interval between initial contact (IC) and lowest vertical position of the L5S1 marker (LOW). IC was determined when the ground reaction force exceeded a 25N threshold. Data were then time normalized according to the interval between IC and LOW. Five trials were collected and averaged for the analysis. Time series curves were visually inspected for quality control considerations. Discrete variables were calculated at 25, 50, 75, and 100% of the landing time-series interval (IC – LOW).

The vertical displacement of the L5S1 marker between IC and LOW was calculated and reported as percentage of the subject's height. Kinematic and kinetic variables at the ankle, knee and hip joint were calculated in the sagittal plane. Kinematic variables included joint angles and angular velocities. Kinetic variables included normalized (body mass, kg) vertical ground reaction force (vGRF), external joint moment, and joint power; these were calculated using an inverse dynamic approach and normalized to body mass*height (kg*m). Total support moment (TSM) represents the magnitude of the lower limb extensor synergy, and was calculated by summing the internal extensor moments at the ankle, knee, and hip joints. Percentage contributions of each joint to the TSM were calculated by separately dividing the internal moment of the ankle, knee and hip by the TSM at the 25, 50, 75, and 100% indexed timepoints. Data were compared between groups using independent samples t-tests.

RESULTS AND DISCUSSION

There were no group differences at any indexed interval for L5S1 marker displacement, vGRF, or TSM, suggesting that overall whole-body COM descent and external demands of the drop landing were similar between groups (Figure 1A and 1D).

At 25% of the landing, no group differences were observed. Visual analysis of the time-series curves revealed that vGRF and TSM were increasing throughout the 0-25% time interval and this pattern was consistent between groups.

At 50% of the landing, the joint power data showed that greater energy was absorbed by the control group at the knee (+40%, $p = 0.02$), but no other differences were seen. By 50% of the interval, the vGRF and TSM curves had already peaked (Figures 1A and 1D).

At 75% of landing, a number of group differences emerged. The ACL group had a larger moment at the hip (+86%, $p = 0.02$) and a smaller moment at the knee (-23%, $p < 0.01$, Figure 1E). Also, the relative contributions of the hip and knee joints to the TSM were 13% greater ($p < 0.01$) at the hip and 10% lower ($p < 0.01$) at the knee in the ACL group. The ACL group also had less angular velocity (-25 and -33°/sec, Figure 1F) and less power absorption (-40 and -43%, Figure 1C) at the ankle and knee joints, respectively (all $p < 0.05$), suggesting a stiffer landing strategy.

The differences in the joint moments and the percent TSM contributions were still present at the

end of landing (100%). The knee joint moment was 21% smaller ($p < 0.01$, Figure 1E), and the contribution of the hip and knee joints to the TSM were 7% greater at the hip ($p = 0.02$) and 6% lower at the knee ($p < 0.01$) in the ACL group compared to the control group.

CONCLUSIONS

The demands of the external loads during the earlier phases of landing did not elicit altered joint mechanics. Further exploration of this kinematic-kinetic relationship during early loading is warranted. Conversely, later in the task, the ACL group did demonstrate an altered neuromuscular strategy that largely affected the proximal joints. Greater reliance on the hip joint and decreased reliance on the knee to meet the extensor demands of the task were observed. Overall, these data suggest that movement abnormalities persist years after successful ACL reconstruction and conventional rehabilitation. Understanding both the inability to compensate during the initial portions of the task and the different adaptations during the latter portion of the task will inform evidence-based care of these individuals.

REFERENCES

1. Paterno MV et al., *Am J Sports Med*, **38**, 1968-78, 2010.
2. Schmitt LC et al., *Med Sci Sports Exerc*, Epub 2014.
3. Myer GD et al., *J Orthop Sports Phys Ther*, **41**, 377-87, 2011.

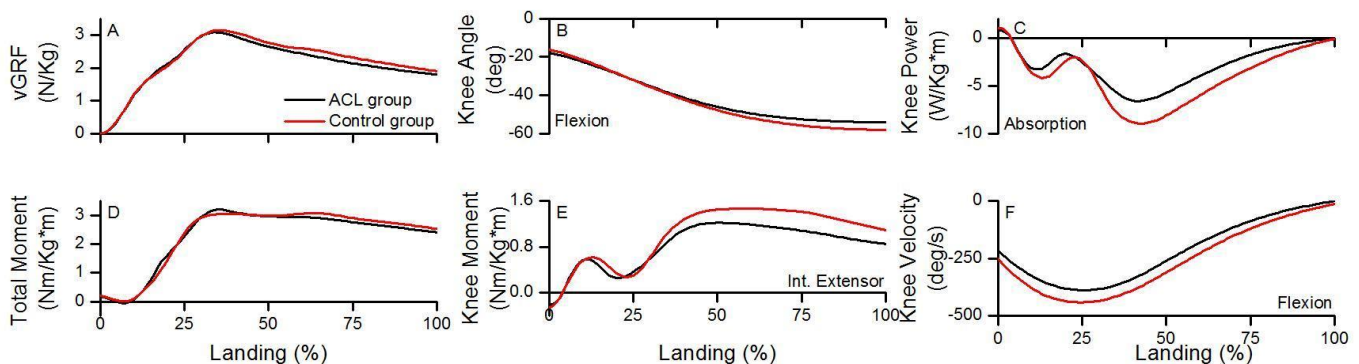


Figure 1. Time series curves of the vertical ground reaction force (A), knee angle (B), knee power (C), total support moment (D), knee moment (E), and knee velocity (F) during landing. 0 represent initial contact, 100 represent the lowest point of the L5S1 marker.

THE IMPACT OF VARIOUS MEASURES OF QUADRICEPS STRENGTH ON LANDING MECHANICS IN YOUNG ATHLETES AFTER ANTERIOR CRUCIATE LIGAMENT RECONSTRUCTION: IMPLICATIONS FOR SECOND ACL INJURY RISK

Matthew P. Ithurburn¹, Mark V. Paterno², Kevin R. Ford³, Timothy E. Hewett^{1,2}, Laura C. Schmitt^{1,2}

¹The Ohio State University, Columbus, OH; ²Cincinnati Children's Hospital Medical Center, Cincinnati, OH;

³High Point University, High Point, NC

Email: Matthew.Ithurburn@osumc.edu

INTRODUCTION

Alterations in landing mechanics are common after anterior cruciate ligament (ACL) reconstruction (ACLR) and contribute to second ACL injury risk in young, active individuals. Specifically, frontal plane knee motion, transverse plane hip kinetics, and side-to-side asymmetries in sagittal plane knee moment were risk factors for a second ACL injury after ACLR and return-to-sport [1]. While decreased quadriceps strength, a persistent impairment after ACLR, contributes to altered mechanics [2, 3], it remains unknown which measures of quadriceps strength impact landing mechanics that contribute to second ACL injury risk after ACLR. The hypothesis tested was that in young athletes after ACLR, kinematic and kinetic variables of interest during a double-leg landing task would be predicted by isometric and isokinetic quadriceps strength at 180°/s, but not by isokinetic quadriceps strength at 300°/s.

METHODS

Participants included 84 young athletes (age=17.4 yrs; 59 females, 25 males) after primary, unilateral ACLR cleared and planning to return to cutting/pivoting sports. All participants and/or parents provided written informed consent prior to participation. An isokinetic dynamometer (Biodex) was used to quantify peak isometric quadriceps torque (Nm) and peak isokinetic quadriceps torque at 180°/s and 300°/s (Nm). Kinematic and kinetic data were collected by tracking 37 retroreflective markers with a 10-camera motion analysis system (Motion Analysis Corp.; 240 Hz) during the initial landing phase of a drop vertical jump task (Figure 1). Participants landed with each foot onto a separate force plate (AMTI; 1200 Hz). Kinematic and kinetic variables of interest were calculated with Visual3D and MATLAB. Variables of interest

were based upon biomechanical risk factors for second ACL injury and common asymmetries in landing after ACLR. These included involved and uninvolved knee flexion motion (initial contact through peak flexion); involved and uninvolved frontal plane knee motion (initial contact through peak valgus); involved, uninvolved, and side-to-side differences in peak internal knee extension moment; involved, uninvolved, and side-to-side differences in peak vertical ground reaction force (VGRF); and involved and uninvolved transverse plane hip kinetics. Low-pass Butterworth filters were used to filter trajectories and force plate data used in calculating joint moments (12 Hz) and to filter force plate data (100 Hz). Joint moments were not normalized. Linear regressions were used to identify the impact of each quadriceps strength measure on variables of interest, after controlling for weight and height ($\alpha < .05$).



Figure 1. Example of the drop vertical jump task (From Paterno 2010 [1], with permission).

RESULTS AND DISCUSSION

Isometric and isokinetic quadriceps strength at 180°/s and 300°/s predicted involved peak internal knee extension moment (Table 1). Both isometric and isokinetic quadriceps strength at 180°/s predicted side-to-side differences in peak internal knee extension moment, uninvolved peak VGRF,

side-to-side differences in peak VGRF, and involved hip rotation moment impulse (all $p < .05$) (Table 1). Quadriceps strength measures were not predictive of involved or uninvolved knee flexion motion or frontal plane knee motion, uninvolved peak internal knee extension moment, involved peak VGRF, or uninvolved hip rotation moment impulse (all $p > .05$).

The cohort in this study consisted of young, active individuals that at the time of return-to-sport were planning on returning to cutting and pivoting sports. Previous work has demonstrated second ACL injury rates as high as 29.5% within 2 years of ACLR and return-to-sport in this population [4]. Thus, given that quadriceps strength deficits are nearly ubiquitous after ACLR, understanding the impact of common measures of quadriceps strength testing on known contributors to the risk of second injury is critical. All measures of quadriceps strength in this study predicted side-to-side differences in knee extension moment, which has been linked with second ACL injury risk during a drop vertical jump [1]. Across all variables of interest for which isometric and isokinetic quadriceps strength at 180°/s were significant predictors, isometric quadriceps strength predicted more of the variance in each variable, excluding involved peak internal knee extension moment (Table 1). While previous work has shown that individuals with decreased isometric quadriceps strength symmetry

demonstrate altered landing mechanics during a drop vertical jump task after ACLR [3], this appears to be the first study to identify the impact of several commonly used measures of quadriceps strength on altered landing mechanics that contribute to increased second ACL injury risk. Interestingly, in addition to not contributing to most kinetic variables of interest in this study, isokinetic quadriceps strength testing at 300°/s has also previously not been correlated with functional performance tests after ACLR [5].

CONCLUSIONS

Both isometric and isokinetic quadriceps strength at 180°/s predict important biomechanical variables during landing that are known contributors to second ACL injury risk after ACLR and return-to-sport. Measuring isokinetic quadriceps strength at 300°/s may not be important in predicting double-leg landing mechanics after ACLR.

REFERENCES

1. Paterno MV, et al. *Am J Sports Med.* 2010; **38**: 1968-1978.
2. Schmitt LC, et al. *Med Sci Sports Exerc.* Nov 4 2014; [Epub ahead of print]
3. Lewek M, et al. *Clin Biomech.* 2002; **17**: 56-63.
4. Paterno MV, et al. *Am J Sports Med.* 2014; **42**: 1567-1573.
5. Noyes FR, et al. *Am J Sports Med.* 1991; **19**: 513-518.

Table 1. Regression Models for Quadriceps Strength Measures on Kinematic and Kinetic Variables of Interest

	Model 1: Including Height/Weight (R² adj.)	QF-Iso (R² change from Model 1, P- value)	QF-180 (R² change from Model 1, P- value)	QF-300 (R² change from Model 1, P- value)
Involved Peak IKEM	21.4%	4.5%, .028	14.3%, <.001	5.4%, .016
Side-to-Side Differences in Peak IKEM	7.4%	18.1%, <.001	13.5%, <.001	2.8%, .111
Uninvolved Peak VGRF	47.6%	11.7%, <.001	6.7%, .001	1.9%, .083
Side-to-Side Differences in Peak VGRF	2.1%	16.4%, <.001	14.8%, <.001	3.0%, .108
Involved Hip Rotation Moment Impulse	2.1%	19.1%, <.001	4.8%, .048	3.1%, .110

Each model with strength measure (columns 3-5) demonstrates R² change after accounting for height and weight; QF-Iso = peak isometric quadriceps torque; QF-180 = peak isokinetic quadriceps torque at 180°/s; QF-300 = peak isokinetic quadriceps torque at 300°/s; IKEM = internal knee extension moment; VGRF = vertical ground reaction force; Hip rotation moment impulse over first 10% of landing

SINGLE-LEG HOP DISTANCE AS A FUNCTIONAL SURROGATE FOR LOWER EXTREMITY JOINT POWER IN HEALTHY ADULTS

^{2,6}Rachel L. Tatarski, ^{2,6}Joshua Hoffman, and ¹⁻⁶Timothy E. Hewett

¹Department of Biomedical Engineering, ²Sports Health and Performance Institute (SHPI) OSU Sports Medicine, ³ Mayo Clinic, Rochester, MN, ⁴Department of Orthopaedics, ⁵Department of Physiology and Cellular Biology and Family Medicine, ⁶The Ohio State University, Columbus, OH, USA

email: rachel.tatarski@osumc.edu, web: http://sportsmedicine.osu.edu/ourteam/research_staff/index.cfm

INTRODUCTION

Joint power is a good indicator of muscle function in many populations. However, joint power cannot be easily measured in a clinical setting without access to biomechanical tools such as 3D motion capture and force plates. For this reason, it is important to find a comparable measurement for function that can be easily implemented and used in a clinical or athletic performance setting. A forward single-leg hop for distance is a common test for overall function in physically active populations. However, function is usually determined by limb symmetry rather than hop distance [1].

Therefore, the purpose of this study was to determine the relationship between lower extremity joint power and function (single-leg hop distance). The hypothesis tested was that there would be a positive relationship between total lower extremity joint power and hop distance.

METHODS

Sixteen healthy adults volunteered to participate in this study and gave written informed consent (n = 8 females; n = 8 males). To measure whole body kinematics, each subject was fitted with 55 retro-reflective markers to define joints and segments. Markers were tracked in 3-dimensional space using 12 Motion Analysis cameras. To measure kinetics, ground reaction forces were measured using 4 imbedded Bertec force plates. Data were analyzed using Motion Analysis Cortex, Visual3D, and MatLab.

All measurements were taken for the dominant limb. Limb dominance was determined by asking the subject which leg he or she would choose to kick as soccer ball. To measure the take-off phase of a single-leg hop for distance, subjects began the

movement on the force plate with their foot lined up with the edge of a standard measuring tape. Subjects were instructed to hop as far as they could forward on one leg and maintain balance on or 'stick' the landing. The distance of the hop was measured at the location of the heel in the nearest centimeter. Subjects were allowed to practice the hop twice and then performed two successful trials. A trial was considered successful if the subject only used one leg to push off and land.

Total peak lower extremity power was determined from the sum of the peak hip, peak knee, and peak ankle powers for each subject. Pearson's product-moment correlation was used to determine the relationship between total lower extremity joint power and hop distance.

RESULTS

A strong positive correlation was observed between single-leg hop distance and peak total lower extremity joint power (Figure 1). In addition, hip range of motion accounted for ~56% of the variance in hop distance, knee range of motion for ~32%, and ankle range of motion accounted for ~4% of the variance in hop distance (Table 1). Peak hip power accounted for ~60% of the variance in hop distance, peak knee power for ~13%, and peak ankle power accounted for ~11% of the variance in single-leg hop distance (Table 1).

DISCUSSION

The results from this study confirm the postulate of a strong positive relationship between total lower extremity joint power and single-leg hop distance. Furthermore, these results offer promising evidence for the use of a single-leg hop test as a measure of function. Previous research has demonstrated very good reliability of functional tests such as the

single-leg hop [1] and their usefulness at discriminating between injury recovery status [2]. Therefore, clinicians should consider the use of hop distance as a measure of function as well as distance asymmetry between limbs due to the strong positive correlation between hop distance and total lower extremity joint power.

Moreover, the strong positive relationships between lower extremity joint ranges of motion and lower extremity joint power offer another simple and straightforward measure of function. Two-dimensional video analysis is a cheap and readily available too for clinical use and can quickly assess joint ranges of motion during functional tasks such as the single-leg hop.

CONCLUSIONS

Utilization of a combination of outcome measures such as total hop distance, distance symmetry between limbs, and lower extremity joint ranges of motion, clinicians and athletic performance specialists can quickly and effectively screen patients for muscle function as it relates to risk of injury and recovery of injury. Further research will investigate the role of limb dominance on functional test performance.

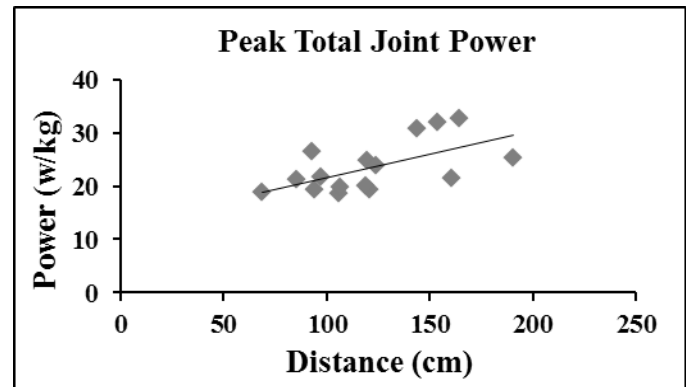


Figure 1: Single-leg hop distance versus peak total lower extremity joint power ($R^2 = 0.36$).

REFERENCES

1. Reid A, et al. *Phys Ther*, **87**(3), 337-349, 2007.
2. Nyland J, et al. *The Knee*, **21**(6), 1191-1197, 2014.

ACKNOWLEDGEMENTS

The authors acknowledge funding support from the National Institutes of Health / National Institute of Arthritis and Musculoskeletal and Skin Diseases grants R01-AR049735 and R01-AR056259 (TEH) and the OSU Sports Medicine Sports Health and Performance Institute.

Table 1: Correlations between single-leg hop distance and joint excursions, single-leg hop distance and peak joint powers, and joint excursions and peak joint powers.

	Single-Leg Hop Distance	Hip Excursion	Knee Excursion	Ankle Excursion
Hip Excursion	$R^2 = 0.56$			
Knee Excursion	$R^2 = 0.32$			
Ankle Excursion	$R^2 = 0.04$			
Peak Hip Power	$R^2 = 0.60$	$R^2 = 0.75$		
Peak Knee Power	$R^2 = 0.13$		$R^2 = 0.26$	
Peak Ankle Power	$R^2 = 0.11$			$R^2 = 0.003$

TRIAL-TRIAL TEMPORAL VARIABILITY IN UPPER LIMB FUNCTIONAL TASK PERFORMANCE DIFFERENTIATES AMPUTEES FROM CONTROLS AND DECREASES WITH PRACTICE

^{1,2}Matthew J Major, ^{1,2}Rebecca Stine, ³Sibylle Thies, ^{3,4}Mohammad Sobuh, ³Adam Galpin, ⁵Peter Kyberd and ³Laurence Kenney

¹Northwestern Univ., Chicago, IL, USA; ²Jesse Brown VA Medical Center, Chicago, IL, USA

³Univ. of Salford, Salford, UK; ⁴Univ. of Jordan, Amman, Jordan; ⁵Univ. of New Brunswick, Canada
email: matthew-major@northwestern.edu

INTRODUCTION

Many of the clinical tests to assess skill in using an upper limb prosthesis measure speed of performance of a pre-defined set of tasks [1]. However, speed of task completion is only one of several factors which characterize skilled prosthetic use [2]. Recently, Major et al. [3] showed that joint angle variability is higher in amputees than controls, and in amputees it is correlated with years of experience of prosthetic use. In common with almost all studies of upper limb functional task performance, in [3] joint angle trajectories were first linearly normalized with respect to time. However, the relative duration of different phases of the task can vary from trial to trial, linear time normalization of the entire task cannot take this into account [4]. In this paper we report on the characterization of functional task performance using an upper limb myoelectric prosthesis using a time warping method which allows for differentiation between temporal and trajectory variability. In Study 1 we validated the approach with a comparison of amputees and anatomically intact (AI) controls. In Study 2 we report on the changes in temporal and trajectory variability with practice using a myoelectric prosthesis simulator in AI subjects.

METHODS

Study 1 (carried out at Northwestern University, USA): Full details of the protocol are provided in [3]. Following ethical approval, six AI individuals (3 male, 35±11 years of age) and seven myoelectric transradial prosthesis users (5 male, 49±18 years of age, 20±18 years of prosthesis experience) were recruited to the study. Subjects visited the lab on one occasion to perform five trials of three seated

tasks (selected from the Southampton Hand Assessment Procedure (SHAP) [1]): 1) lifting a carton and emptying liquid contents into a jar using their non-dominant or prosthetic limb, 2) lifting and transferring a weighted container across a low-level barrier using their non-dominant or prosthetic limb, and 3) lifting and transferring a tray across a low-level barrier using both hands. Subjects also completed the entire SHAP protocol. During each task, marker position approximating location of the radial and ulnar styloid processes were collected and used to track the virtual wrist joint center. Estimation of wrist joint three-axis accelerations were used to calculate inter-trial temporal (warp cost) and trajectory (RMS error) variability [4,5].

Study 2 (carried out at University of Salford, UK): Full details of the protocol are provided in [6]. Following ethical approval, seven AI individuals (4 male, 6 right handed, 36±10 years of age) were recruited to the study. Subjects visited the lab on four occasions, spaced over approximately 2 weeks. On visit one, subjects were asked to perform a seated task which involved reaching with their anatomic hand for a juice carton, picking it up and pouring the liquid into a cup, before returning it to its original location, then moving their hand back to the original resting point. The location of the carton, cup and starting point for the hand were fixed for each subject across all trials. Subjects repeated the task 12 times on each visit. For visits 2-4 subjects performed the task with a custom-made myoelectric prosthesis simulator [6]. In between visits subjects carried out the SHAP with the prosthesis simulator on four occasions between visits 2 and 4 for practice. During task performance, position data of a cluster of 4 reflective markers located on the forearm were collected. These data were then used

to calculate the simulated output of a three-axis accelerometer [5]. Subsequently, temporal and trajectory variability within session were calculated.

RESULTS AND DISCUSSION

Table 1 displays results of Study 1 comparing AI control and prosthesis user task performance. Tables 2 and 3 display results of Study 2 observing changes in variability due to practice.

Table 1: Inter-trial variability and SHAP outcomes (mean \pm 1SD) of AI and prosthesis users.

		AI Controls	Prosthesis Users
Carton Pouring	Warp Cost	52.08 \pm 10.19	138.84 \pm 86.64
	RMSE (m/s ²)	0.48 \pm 0.05	0.57 \pm 0.30
Container Transfer	Warp Cost	6.84 \pm 2.26	69.76 \pm 47.35
	RMSE (m/s ²)	0.78 \pm 0.28	0.74 \pm 0.21
Tray Transfer	Warp Cost	12.99 \pm 8.19	43.32 \pm 21.52
	RMSE (m/s ²)	1.02 \pm 0.31	1.02 \pm 0.31
SHAP Index of Function		96 \pm 3	53 \pm 12

Table 2: Inter-trial temporal variability (warp cost) across practice sessions.

	Visit 1 (Anatomic hand)	Visit 2 (Prosthesis simulator)	Visit 4 (Prosthesis simulator)
AI 1	43.16 \pm 17.60	81.84 \pm 27.00	76.53 \pm 27.80
AI 2	91.61 \pm 90.82	101.15 \pm 37.20	108.68 \pm 56.04
AI 3	61.61 \pm 29.83	158.57 \pm 74.85	79.35 \pm 30.84
AI 4	42.55 \pm 23.93	159.48 \pm 73.31	57.50 \pm 18.60
AI 5	68.40 \pm 35.11	116.44 \pm 68.66	54.53 \pm 15.07
AI 6	63.86 \pm 26.51	133.44 \pm 58.51	58.00 \pm 16.17
AI 7	51.99 \pm 23.48	213.44 \pm 80.91	83.05 \pm 43.66
mean\pm1SD	60.45 \pm 17.02	137.77 \pm 43.92	73.95 \pm 19.27

Table 3: Inter-trial trajectory variability (RMS error [m/s²]) across practice sessions.

	Visit 1 (Anatomic hand)	Visit 2 (Prosthesis simulator)	Visit 4 (Prosthesis simulator)
AI 1	0.58 \pm 0.26	0.36 \pm 0.09	0.31 \pm 0.06
AI 2	0.39 \pm 0.13	0.46 \pm 0.19	0.35 \pm 0.13
AI 3	0.48 \pm 0.15	0.42 \pm 0.13	0.31 \pm 0.11
AI 4	0.39 \pm 0.16	0.49 \pm 0.14	0.39 \pm 0.08
AI 5	0.50 \pm 0.21	0.36 \pm 0.10	0.28 \pm 0.08
AI 6	0.36 \pm 0.07	0.52 \pm 0.26	0.31 \pm 0.06
AI 7	0.56 \pm 0.16	0.54 \pm 0.27	0.39 \pm 0.13
mean\pm1SD	0.47 \pm 0.09	0.45 \pm 0.07	0.33 \pm 0.04

Study 1 found differences in temporal inter-trial variability between amputees and controls, but less clear differences in trajectory variability. The finding demonstrates for the first time the nature of

differences in trial-to-trial variability between experienced users of myoelectric prostheses and controls. These results reflect those previously observed in [3] regarding greater joint-level kinematic variability and reduced SHAP scores of prosthesis users compared to controls, thereby validating this method and demonstrating the contribution of temporal variability to prostheses user movement quality during task execution.

In Study 2 we demonstrated that trial-to-trial temporal variability in a carton pouring task increases dramatically on first use of a prosthesis simulator, then declines with practice. Consistent with the findings in Study 1 trajectory variability showed less clear changes both on first introduction of the prosthesis simulator and with practice.

The reasons for these findings requires further work, but it is possible to speculate that in this case when using a prosthesis the limb trajectory variability is relatively constrained by the limited degrees of freedom and fixed task characteristics. However, all of the tasks studied involved acquiring and releasing objects using the prosthetic hand; if opening the hand to acquire the object, or release the object was difficult, then this may be one of the sources of higher timing variability seen in prosthesis results. The study reported here used camera based techniques to derive overall task completion time and simulated accelerometer trajectories. However, both of these parameters could be derived from a real accelerometer located on the wrist and hence the approach offers the potential for clinicians to characterise both overall task completion time and trial-trial temporal and trajectory variability using low cost instrumentation.

REFERENCES

1. Light CM, et al. *Arch Phys Med Rehabil* **83**, 776-83, 2002.
2. Bongers RM, et al. *J Pros Orthot* **24**, 67-76, 2012
3. Major MJ, et al. *J Neuroeng Rehabil* **11**, 132, 2014.
4. Thies S, et al. *J Neuroeng Rehabil* **6**, 2, 2009.
5. Thies S, et al. *Med Eng Phys* **29**:967-72, 2007
6. Sobuh M, et al. *J Neuroeng Rehabil* **11**, 72, 2014.

JOINT POWER ADAPTATIONS TO RUNNING SPEED IN INDIVIDUALS WITH AMPUTATION USING RUNNING-SPECIFIC PROSTHESES

^{1,2} Brian S. Baum, ³ Hiroaki Hobara, and ^{2,4} Jae Kun Shim

¹ Regis University, Denver, CO, USA

² The University of Maryland, College Park, MD, USA

³ The National Institute of Advanced Industrial Science and Technology, Tokyo, Japan

⁴ Kyung Hee University, Seoul, Korea

email: bbaum@regis.edu

INTRODUCTION

Running after lower limb amputation leads to altered joint powers. The ankle joint is the primary power generator during able-bodied running [1, 2], and prostheses may not effectively replace this joint's function. Existing literature is conflicting with limited sample sizes reporting joint powers. Two athletes with unilateral transtibial amputations generated lower peak ankle power with their running-specific prostheses (RSPs) than their intact ankle joint while sprinting [3]; however, a sprinter with bilateral transtibial amputations has exhibited greater peak ankle powers than a control group [4]. To account for altered ankle powers, knee powers may be reduced [3, 4] or increased [3] relative to control limbs, while longer positive hip power periods have been observed in prosthetic limbs [3].

Further study of joint powers in running after amputation will provide insights into muscular adaptations, which can lead to advances in training and rehabilitation. Joint powers when using RSPs at submaximal speeds and across a range of speeds are poorly understood since prior literature focuses on sprinting. Hence, the purpose of this study was to investigate lower limb joint powers when running with RSPs at different speeds. We hypothesized that (1) the prosthetic limb would exhibit lower peak joint powers than the intact and control limbs at each speed, and (2) increased speed would result in increased peak joint powers in the limbs.

METHODS

8 males with unilateral transtibial amputation wearing RSPs and 8 male controls ran overground at three speeds (2.5, 3.0, and 3.5 m/s). 10 motion

capture cameras captured kinematic data (200 Hz) while 10 force platforms collected ground reaction forces (1000 Hz). Tracking markers were placed bilaterally on the lower extremities and on the prostheses. The prosthetic limb "ankle" joint was defined as the RSP's most acute point of curvature. Ankle, knee, and hip joint powers were calculated via inverse dynamics using Visual3D (C-Motion). A 3-way (Group x Leg x Speed) ANOVA was used to test for peak joint power differences with $\alpha=0.05$.

RESULTS

Table 1 presents the peak power data. Peak ankle powers showed significant speed effects ($p<0.001$) where generation and absorption increased with speed. Significant leg effects ($p=0.018$) and leg x group interactions ($p=0.009$) existed where the prosthetic limb generated less power than the intact limb. The prosthetic limb generated lower ankle power than the control limbs at 3.5 m/s ($p=0.036$).

Stance phase knee power absorption and generation exhibited significant speed effects ($p<0.001$) where peak magnitudes increased with speed. These variables had significant leg x group interactions ($p<0.007$) where the prosthetic limb knee absorbed and generated less power than the intact and control limb knees. Knee swing power absorption showed significant speed ($p<0.001$), leg ($p=0.014$), leg x group interaction ($p=0.005$), speed x leg interaction ($p=0.001$), and speed x leg x group interaction ($p=0.005$). All limbs increased peak knee absorption with speed during swing phase, and the prosthetic limb knee absorbed less power than the intact and control limbs. During swing phase, the intact and control limbs both increased peak power absorption with speed at a greater rate than the prosthetic limb.

Peak hip powers had significant speed effects ($p \leq 0.004$) where power absorption and generation increased with speed during both stance and swing phases. The prosthetic limb generated greater peak power during stance than the control group ($p = 0.035$). Significant leg \times group interactions for peak hip stance absorption ($p = 0.029$) and swing generation ($p = 0.034$) indicated that the amputation group limbs had greater differences than the control group limbs. The prosthetic limb hip absorbed and generated less power than the intact limb hip.

DISCUSSION AND CONCLUSIONS

Our first hypothesis that ILEA would exhibit lower peak joint powers in the prosthetic limb than the intact and control limbs at each speed was supported for most parameters, but notably not for hip power generation. The prosthetic ankle had lower power absorption and generation than the intact limb, supporting the idea that running prostheses are much more limited in their ability to contribute to energy used during running [3]. However, since prosthetic ankle power was only lower than controls at 3.5 m/s, this limitation may only be exacerbated at faster running speeds. Lower prosthetic limb knee powers suggest either greater muscular co-contractions that reduce the net joint moments, or that ILEA adapt their running style to use the knee joint more passively [5]. The prosthetic limb also generated greater hip power compared to the control limbs. This correlates to the prolonged hip extension moments observed in ILEA running

with RSPs [3]. The prosthetic limb further produced lower swing phase knee power absorption and hip power generation that can be attributed to smaller inertial properties of the lower limb with the RSP.

Our second hypothesis that increased running speed would be associated with similar increases in peak powers of the intact and prosthetic limbs was accepted. As the demands of running faster increase, the peak joint powers responded accordingly. However, in several cases, the intact limb joints increased power generation and absorption at a greater rate than the prosthetic limb. This suggests that in stance phase, the potential limitations of the prosthesis resulted in greater power output requirements by the intact limb to achieve faster running speeds. In swing phase, the speed demands had a greater impact on the intact limb due to its greater inertial properties. As peak joint powers offer a limited view into mechanical energy requirements of ILEA running, additional study of joint work profiles are needed to further elucidate compensatory mechanisms.

REFERENCES

1. Winter DA. *J Biomech* **16**, 91-97, 1983.
2. Novacheck TF. *Gait Posture* **7**, 77-95, 1998.
3. Buckley JG. *Clin Biomech* **15**, 352-358, 2000.
4. Brüggemann GP et al. *Sports Technol* **1**, 220-227, 2009.
5. Czerniecki JM et al. *Am J Phys Med Rehabil* **71**, 209-218, 1992.

Table 1: Average \pm SD peak power values, in watts/kg, for the prosthetic (P), intact (I), and control (C) limbs across each of the tested speeds. White areas indicate stance phase and grey areas indicate swing phase.

	2.5 m/s			3.0 m/s			3.5 m/s		
	P	I	C	P	I	C	P	I	C
Ankle Abs ^v	-5.3 \pm 2.3	-5.7 \pm 1.4	-5.6 \pm 1.2	-6.4 \pm 3.0	-7.0 \pm 1.3	-7.0 \pm 1.4	-6.8 \pm 2.6 ⁱ	-8.4 \pm 2.9	-8.5 \pm 1.4
Ankle Gen ^v	5.0 \pm 2.0 ⁱ	7.9 \pm 1.8	6.2 \pm 1.2	6.0 \pm 2.0 ⁱ	9.7 \pm 1.3	7.7 \pm 1.4	6.7 \pm 2.4*	11.4 \pm 2.0	9.1 \pm 1.5
Knee Abs ^v	-3.2 \pm 1.8*	-9.3 \pm 2.8	-8.6 \pm 1.7	-3.8 \pm 2.1*	-11.0 \pm 4.0	-9.7 \pm 1.9	-4.4 \pm 2.6*	-10.6 \pm 4.7	-10.4 \pm 1.7
Knee Gen ^v	3.2 \pm 1.9*	6.5 \pm 2.5	5.7 \pm 1.5	3.8 \pm 2.0*	7.5 \pm 3.2	6.5 \pm 1.8	4.8 \pm 2.8*	7.8 \pm 3.1	7.3 \pm 1.7
Knee Abs ^v	-2.5 \pm 0.7*	-3.6 \pm 1.3	-3.5 \pm 0.7	-3.0 \pm 0.9*	-4.7 \pm 1.4	-4.5 \pm 0.8	-3.6 \pm 1.1*	-5.9 \pm 1.8	-5.5 \pm 0.8
Hip Abs ^v	-1.3 \pm 0.9 ⁱ	-2.6 \pm 0.9 ^c	-1.9 \pm 0.4	-1.8 \pm 0.9 ⁱ	-2.6 \pm 1.3	-2.5 \pm 0.7	-2.3 \pm 1.8	-3.1 \pm 1.4	-3.0 \pm 0.8
Hip Gen ^v	2.2 \pm 1.2	1.5 \pm 0.9	1.0 \pm 0.5	2.6 \pm 1.3	1.6 \pm 1.3	1.4 \pm 0.5	2.8 \pm 1.4	2.4 \pm 2.0	1.9 \pm 0.6
Hip Abs ^v	-0.4 \pm 0.3	-0.4 \pm 0.5	-0.6 \pm 0.3	-0.5 \pm 0.3	-0.5 \pm 0.5	-0.5 \pm 0.3	-0.6 \pm 0.3	-0.6 \pm 0.3	-0.7 \pm 0.2
Hip Gen ^v	2.0 \pm 0.7	2.4 \pm 0.6 ^c	2.0 \pm 0.2	2.2 \pm 0.7 ⁱ	3.1 \pm 0.5	2.7 \pm 0.4	3.1 \pm 0.9 ⁱ	3.9 \pm 0.7	3.5 \pm 0.3

Abs=power absorption; Gen = power generation; v=significant speed effect; *=prosthetic limb significantly differs from intact and control limbs; i=significant difference between prosthetic and intact limb; c=significant difference between intact and control limb.

BODY-IN-THE-LOOP OPTIMIZATION FOR THE SELECTION OF PROSTHETIC CONTROL PARAMETERS – A PILOT STUDY

Wyatt Felt, Emily S. Gardinier, Jeffrey Wensman, Deanna H. Gates, C. David Remy

The University of Michigan, Ann Arbor, MI, USA
email: cdremy@umich.edu, web: <http://ram-lab.engin.umich.edu/>

INTRODUCTION

Like many assistive devices, the BiOM T2 powered ankle-prosthesis (BiOM, Inc., Bedford, MA) has numerous software settings that need to be tuned. Four basic parameters control stiffness and ankle power, while seven advanced parameters control the timing of push-off and other functionalities [1]. Selecting appropriate values for these parameters or those of similar devices can be a challenge. Evaluating many different device settings can be a slow and fatiguing process for the user and the resulting settings might suffer from a subjective bias of the clinician. Therefore, a faster and more objective method for identifying proper device settings would be a valuable tool. “*Body-in-the-Loop*” optimization refers to a process of parameter selection that utilizes physiological measures to drive an algorithmic parameter selection process [2]. The purpose of this study was to determine if such a process could be used to accelerate the identification of metabolically optimal device settings for a powered prosthesis.

METHODS

The proposed process relies on real-time measures of metabolic cost acquired while parameters are continuously varied. We estimate the instantaneous metabolic cost, x , using transient metabolic measurements (rather than using “steady-state” measurements [3]). To this end, we represent the relationship between the parameter setting \mathbf{p} , and the instantaneous metabolic cost, x , with a fifth-order polynomial of \mathbf{p} with a vector of coefficients, $\boldsymbol{\lambda}$. Modeling the dynamics of the measured metabolic response, y , as a first-order, linear system with inputs, x , and a time constant, τ , yields an estimated series of breath measurements, \bar{y}^i . The dynamics of the breath-to-breath oxygen

consumption measures can be written in terms of the breath-number, i , and the time between breaths, h_i :

$$\bar{y}^i = \left(1 - \frac{h_i}{\tau}\right) \bar{y}^{(i-1)} + \frac{h_i}{\tau} x^i(\mathbf{p}^i, \boldsymbol{\lambda})$$

The vector of coefficients, $\boldsymbol{\lambda}$, is optimized to minimize the error between a set of predicted breath measurements, \bar{y}^i , and actual measurements, \hat{y}^i .

$$\min_{\boldsymbol{\lambda}, \bar{y}^1} e = (\hat{y}^1 - \bar{y}^1)^2 + \sum_{i=2}^n (\hat{y}^i - \bar{y}^i(x(\boldsymbol{\lambda}, \mathbf{p}^i), \bar{y}^{i-1}))^2$$

In this equation, we recursively propagate an initial measurement, \bar{y}^1 , that is also being estimated.

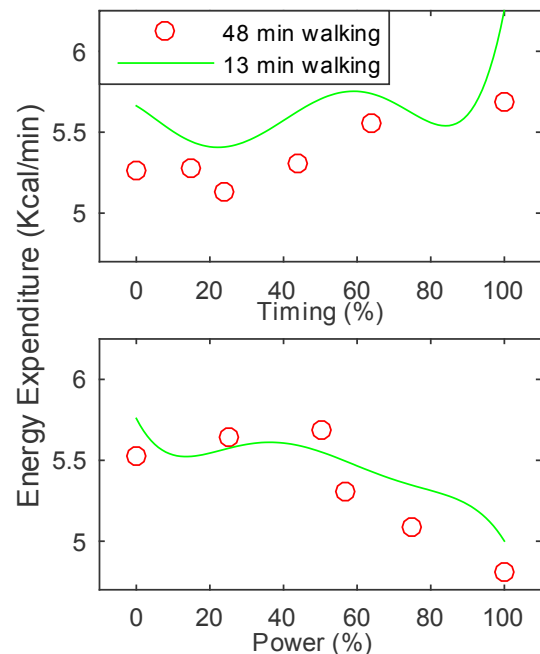


Figure 1: Using continuous measures of metabolic cost, we identified metabolically optimal parameter settings in a fraction of time needed by traditional methods. The red dots are means energy expenditure from steady-state tests. The green line is the fifth-order polynomial, $x(\mathbf{p}, \boldsymbol{\lambda})$, that was fit to breath measures taken while the parameters were varied continuously.

We applied this process to approximate the metabolically optimal parameters of the BiOM T2 Ankle System for a 59-year-old male with unilateral transtibial amputation. The device was fit and the settings were adjusted by a manufacturer-certified prosthetist. The subject's BMI and walking speed were 28.9 kg/m² and 1.16 m/s respectively. Energy use was measured with a portable respirometer (K4b2, COSMED, Rome, Italy).

The BiOM manufacturer allows the power and timing parameters to be varied between 0% and 100%. We tested each parameter independently. While varying the timing parameter, the power was fixed at the prosthetist-selected 57%. Similarly, in the power trials, the timing was fixed at 44%. All other device parameters were fixed at prosthetist-selected settings.

We ran two tests to identify the relationship between the energy expenditure and the parameters. The first test evaluated energy expenditure by averaging several minutes of data at steady-state conditions. The total walking time for each parameter was approximately 48 minutes.

The second test applied the methods of “body-in-the-loop” optimization. The walking time required for these trials was approximately 13 minutes per parameter. In these trials, the dynamics of the metabolic response were first identified by asking the subject to stand at rest for three minutes and then walk for three minutes. The parameters were then varied between 0% and 100% (or vice-versa) over the course of ten-and-a-half minutes. A fifth-order polynomial was used as a surrogate function.

RESULTS AND DISCUSSION

For the power setting, both methods indicated the 100% power setting as the metabolically optimal choice. For timing, the results of the two methods differed slightly. In the “Body-in-the-Loop” optimization, the best-fit 5th-order polynomial predicted the optimal timing parameter to be 22%. A 5th-order polynomial fit to the means of the steady-state measures had a minimum at 28%.

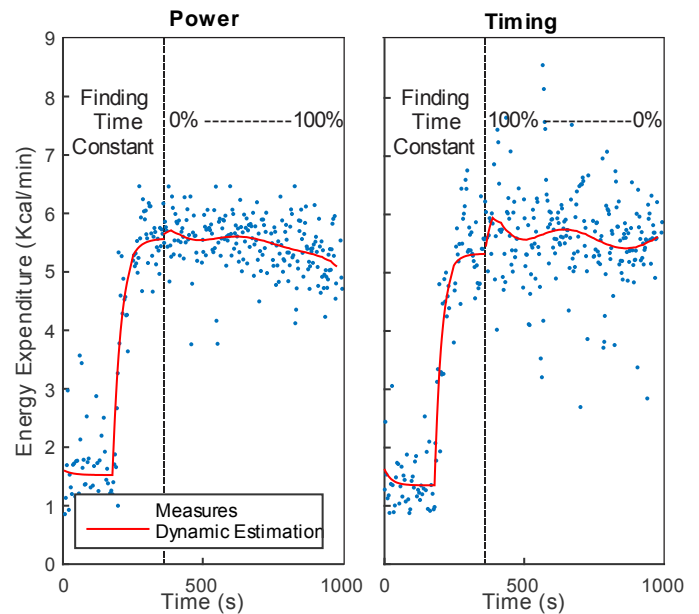


Figure 2: Our method enables us to estimate relationships between device parameters and metabolic cost in real-time, using noisy and dynamically changing measures of energetic cost (\hat{y}^i , blue dots). The first part of the experimental trial was used to identify the time constant of the metabolic response. The red line is the best-fit, predicted metabolic response, \bar{y}^i .

Though these methods were only tested on a single subject, “Body-in-the-loop” optimization techniques hold promise for improving the selection of parameter settings. They allow for the rapid and objective evaluation of parameter settings without an excessive amount of subject fatigue.

REFERENCES

1. BiOM Personal Bionics. T2 Product Brochure.
2. Felt W, Selinger J, Donelan JM, and Remy CD. Dynamic Walking 2014.
3. Selinger JC and Donelan JM. *J Appl Physiol* **117.11** (2014): 1406-1415

ACKNOWLEDGEMENTS

Funding for this work was provided by the MCubed program at the University of Michigan.

EMULATING CANDIDATE ANKLE-FOOT PROSTHESES TO INFORM PRESCRIPTION

^{1,2} Joshua M. Caputo, ² Peter G. Adamczyk, and ¹ Steven H. Collins

¹ Carnegie Mellon University, Pittsburgh, PA, USA

² Intelligent Prosthetic Systems, Ann Arbor, MI, USA

email: joshua.m.caputo@gmail.com, web: <http://biomechatronics.cit.cmu.edu/>

INTRODUCTION

Robotic ankle-foot prostheses can improve walking performance for amputees compared to conventional designs [1], but prescription has been hindered by their high cost and uncertainty about the degree to which individuals will benefit. The typical prescription process cannot well predict how an individual will respond to a device they have never used, as it bases decisions on subjective assessment of an individual's current activity level [2]. We propose a new approach to prescription in which individuals 'test drive' candidate devices using a prosthesis emulator while their walking performance is quantitatively assessed and results are distilled to inform prescription decisions [3].

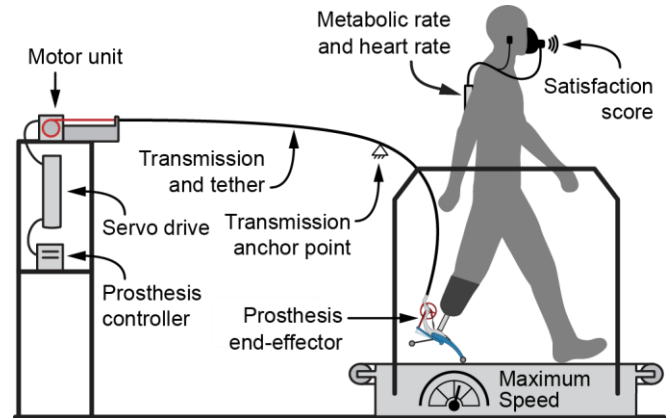


Figure 1: The emulator consists of a lightweight prosthesis actuated through a tether by a powerful motor and controller. Metabolic and heart rate, maximum walking speed, and user satisfaction are measured to assess the emulated behaviors.

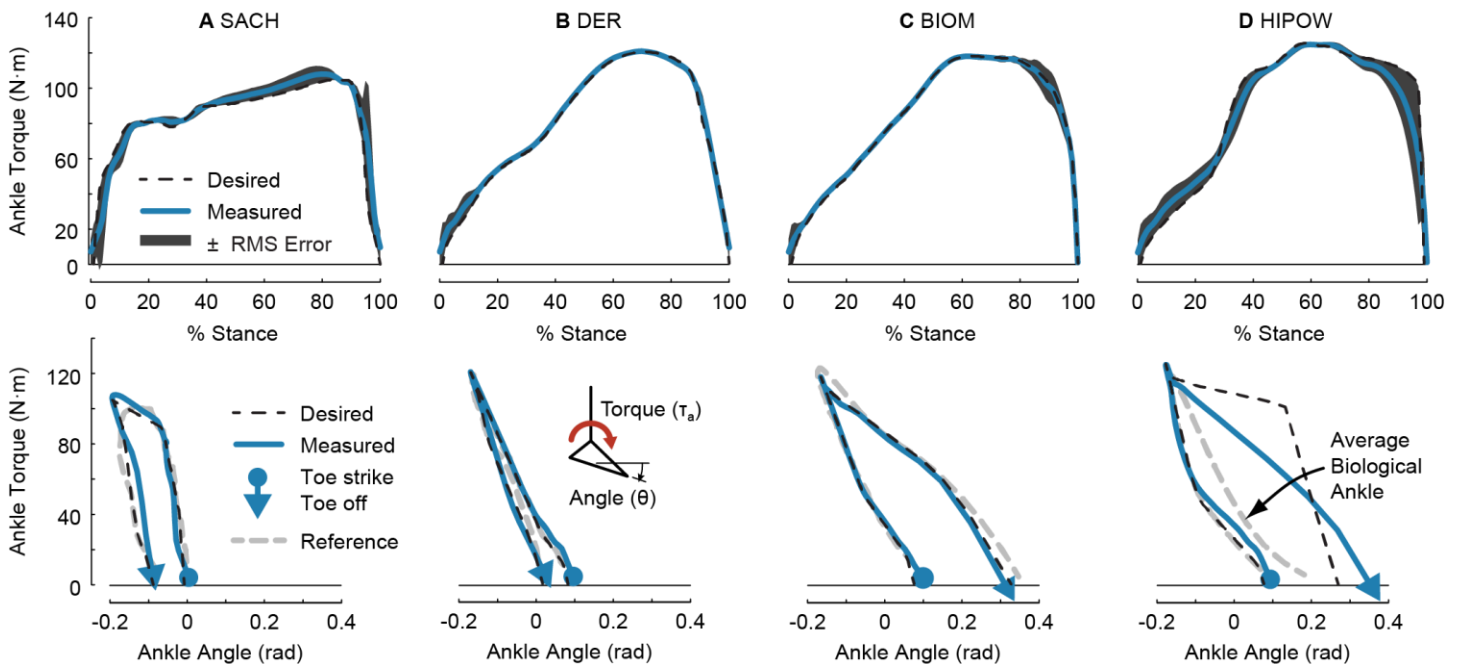


Figure 2: We programmed the behavior of **A** a solid ankle cushioned heel (SACH), **B** a dynamic-elastic response (DER), **C** the BiOM® T2 powered robotic, and **D** a conceptual high-powered robotic (HIPOW) prosthesis. Emulation was performed by joint torque control with the ankle torque vs. angle relationships of commercially-available prostheses as the reference torque. Data presented are from a single representative subject walking at 1.25 m/s on level ground over approximately 150 strides.

We propose a new approach to prescription in which individuals ‘test drive’ candidate devices using a prosthesis emulator while their walking performance is quantitatively assessed and results are distilled to inform prescription decisions [3]. By emulating, rather than purchasing and fitting candidate devices, behavior can be changed quickly through a software interface rather than by swapping mechanical components, so users can experience a broader range of devices than is possible using traditional approaches.

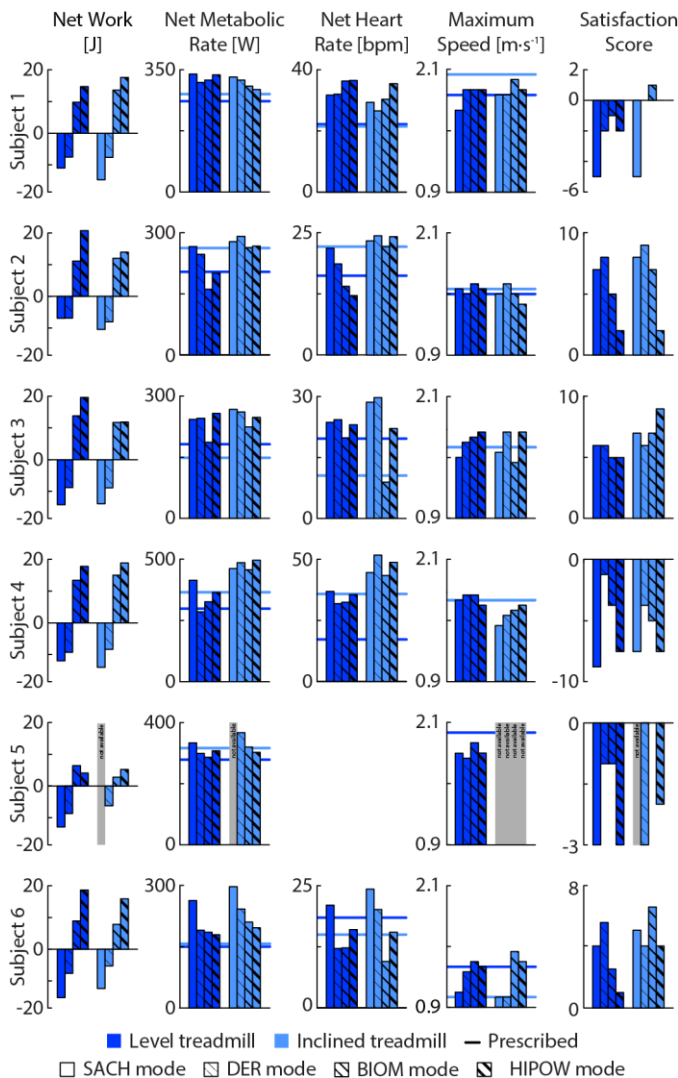


Figure 3: Walking performance outcome metrics listed for each subject across different emulator modes and two treadmill incline conditions.

METHODS

To test the viability of the approach, we developed a prototype ankle-foot prosthesis emulator (Fig. 1)

and assessment protocol, leveraging hardware and methods we previously developed [4] for basic science experiments (eg. [5]), and conducted a treadmill walking experiment with 6 unilateral transtibial amputees (δ , K3, aged 49 ± 5 yrs, 15 ± 16 yrs as amputee, 184 ± 15 lbs).

RESULTS AND DISCUSSION

We demonstrated an emulator that closely tracked the ankle torque vs. angle relationships of an array of commercially-available ankle-foot prostheses (Fig. 2). Average RMS torque tracking errors were between 2 and 4% of the maximum ankle torque. Users indicated that emulations were subjectively convincing representations of each device class. We demonstrated a protocol for measuring users' walking performance across emulator modes that discerned individuals' needs using simple quantitative measures (Fig. 3). All unilateral transtibial amputees we tested appeared to benefit from robotic assistance strategies to some degree but with individual subject differences. The five DER users demonstrated potential for improved walking performance and satisfaction with a robotic prosthesis, but were never able to explore this option within the conventional prescription process. The BiOM® T2 user showed benefits from robotic assistance, but only when walking uphill, and always preferred walking in the passive modes. By exploring candidate device behaviors through haptic emulation, prosthesis prescriptions could be objectively justified prior to device purchase and fitting to ensure that users reach an appropriate balance of cost and benefit.

REFERENCES

1. Herr HM. *P. Roy. Soc. Lond. B. Bio.*, 2012.
2. Hofstad C. *Cochran Db. Syst. Rev.*, 2004.
3. Caputo JM. *ICRA 2015*.
4. Caputo JM. *J. Biomech. Eng.*, 2014.
5. Caputo JM *Sci. Rep.*, 2014.

ACKNOWLEDGEMENTS

This work was supported by the National Institutes of Health under Award No. R43HD076518.

THE EFFECT OF MULTI-AXIAL PROSTHETIC STIFFNESS ON ANGULAR MOMENTUM IN PEOPLE WITH TRANSTIBIAL AMPUTATION WALKING OVER UNEVEN TERRAIN

W. Lee Childers, Ryan D. Funderburk, Adam T. Smith, C. Jake Davidson

Alabama State University, Montgomery, AL, USA
email: lchilders@alasu.edu, web: <http://www.alasu.edu/biomechanics>

INTRODUCTION

Individuals with transtibial amputation face serious challenges when negotiating uneven terrain. Prosthetic foot manufacturers have attempted to minimize these challenges by designing prosthetic feet that can deform and adapt to uneven terrain. Feet incorporating “multi-axial” features have been traditionally prescribed to individuals expected to negotiate uneven environments. However, there is limited information on the effect of multi-axial prosthetic ankle stiffness on measures of gait stability.

The purpose of this study was to define the effect of prosthetic multi-axial stiffness on gait stability in people with uni-lateral transtibial amputation. Study results should strengthen the evidence-base of prosthetic/rehabilitation interventions.

METHODS

Eight participants (of twelve recruited) with uni-lateral transtibial amputation secondary to trauma (101 ± 20.5 kg, 1.84 ± 0.14 m, 42.5 ± 13.4 yrs) have completed this IRB approved study.

Participants walked ten times over even and uneven terrain to a metronome (108 bpm). The uneven terrain (Figure 1) consisted of a 7.3 x 0.8m walkway with 80 x 25 x 20 cm blocks specifically placed in a rotating pattern (0°, 45°, 90°, and 135°). The center of each block was spaced 200 cm apart from each other. A 1 cm thick rubber mat was placed over the uneven walkway reducing visual feedback while making the floor appear even. A track mounted harness system (Solo-step Inc. North Sioux City, SD, USA) was used to safe ambulation over the uneven walkway. A full-body marker (Vicon PlugInGait) in conjunction with an eight camera

motion capture system (Vicon Motion Systems, Oxford, UK) recorded limb kinematics. The participant's normal prosthesis and an Endolite Multi-flex foot with four different ankle unit stiffnesses (soft, medium, firm, and locked out) were tested in random order. The ankle design of the Endolite multi-flex foot was used because it consists of a ball and socket joint and stiffness can be controlled by interchanging rubber isolators between the joint's shank and foot sections.



Figure 1: The uneven walkway with part of the mat removed to show the blocks underneath.

Matlab 2013b was used to calculate whole body center of mass based on a 14 limb-segment model [1] and the range of angular momentum about the coronal and sagittal planes when the amputated limb was in stance [2]. Angular momentum was normalized to the participant's mass, velocity, and height [1]. Minimum toe clearance during swing for the amputated limb and stance width variability were also quantified to provide indirect measures of gait stability [3]. A two factor Repeated Measures ANOVA (terrain x ankle) with Bonferroni post-hoc tested statistical significance ($p < .05$).

RESULTS AND DISCUSSION

There were significant effects from terrain and prosthetic ankle for toe clearance, angular

momentum in the coronal and sagittal planes. Stance width variability only demonstrated significant effect between terrains. There were no significant effects related to gait speed (1.06 ± 0.02 m/s), cadence (106 ± 2.4 strides/min), or Froude number (0.14 ± 0.004) indicating these effects were minimized. The locked ankle condition significantly increased the range of angular momentum in both planes when compared with the participant's normal prosthesis and the soft ankle condition (Figure 2). Toe clearance was significantly smaller comparing the normal, soft, and medium ankle stiffnesses to the locked condition (Figure 3). Stance width variability only demonstrated significant effects between terrain but showed a trend toward minimization at the medium stiffness (Figure 3).

The uneven terrain destabilized gait across all measures of gait stability (range of angular momentum, toe clearance, and stance width variability). The locked prosthetic ankle also tended to destabilize gait. There were general trends in the data suggesting that prosthetic ankle stiffness had a greater effect on the uneven terrain. Generally, the softer ankle stiffnesses was related to increasing gait stability over uneven terrain, likely because the softer ankles better allowed the prosthetic foot to alter its orientation and conform to the terrain.

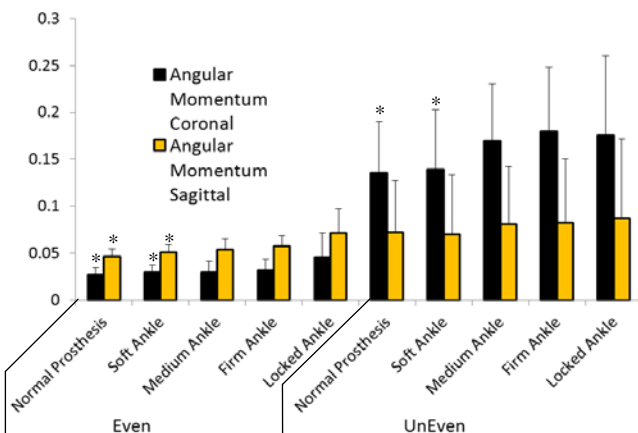


Figure 2: The participants' normal prosthesis and the soft ankle minimized the range of angular momentum. Decreasing the range of angular momentum indicate an increase in gait stability [1]. * indicates statistical significant difference from the locked ankle condition.

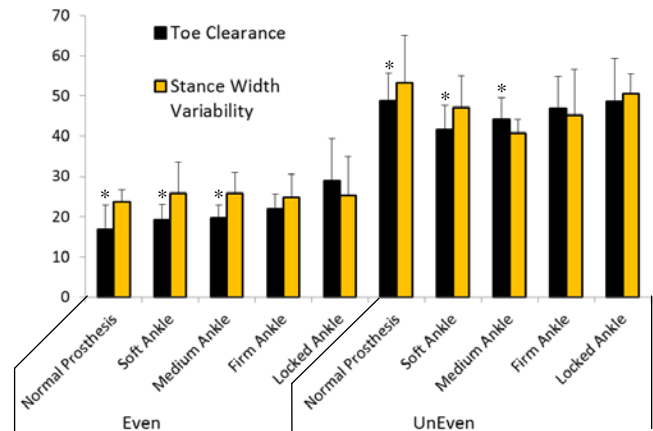


Figure 3: The locked ankle condition significantly increased prosthetic toe clearance compared to the soft and medium ankle stiffnesses. Decreasing the toe clearance or stance width variability indicate an increase in gait stability [3]. * indicates statistical significant difference from the locked ankle condition.

CONCLUSIONS

These data indicate prosthetic feet with multi-axial features will increase gait stability over even and uneven terrain. Therefore, prosthetic users will benefit from the use of prosthetic foot/ankle systems that allow for multi-axial movement. Optimal prosthetic ankle stiffness will be more apparent when ambulating over uneven terrain and softer ankles demonstrate a trend toward more stability; however, more participants need to complete the study before a definitive conclusion can be drawn.

REFERENCES

1. De Leva P. *J Biomech* **29**, 1223-1230, 1996
2. Herr H. & Popovic M. *J Exp Biol* **211**, 467-481, 2008.
3. Bruijn SM., et al. *J R Soc Interface* 10, 20120999, 2013.

ACKNOWLEDGEMENTS

Funding for this study provided by the American Orthotics and Prosthetics Association, Center for Orthotics and Prosthetic Learning and Outcomes/ Evidence-Based Practice Grant #EBP-043014.

WHOLE-BODY ANGULAR MOMENTUM DURING SLOPED WALKING WITH POWERED AND PASSIVE ANKLE-FOOT PROSTHESES

¹Nathaniel T. Pickle, ²Jason M. Wilken, ²Jennifer M. Aldridge Whitehead and ¹Anne K. Silverman

¹Department of Mechanical Engineering, Colorado School of Mines, Golden, CO, USA

²Center for the Intrepid, Department of Orthopaedics and Rehabilitation, Brooke Army Medical Center, Ft. Sam Houston, TX, USA

email: npickle@mines.edu website: fbl.mines.edu

INTRODUCTION

Sloped walking places increased demand on the ankle joint [1], and results in a greater risk of slipping than level walking due to an increased shear force between the foot and ground [2]. Sloped walking may thus be especially challenging for individuals with transtibial amputation (TTA), who have a greater risk of falling compared to able-bodied individuals (AB) [3]. This increased fall risk is partially attributed to the functional loss of the ankle muscles, which are critical for controlling dynamic balance during walking [4].

Whole-body angular momentum (H) has been previously used to investigate dynamic balance [5, 6], but has not been quantified for individuals with TTA during sloped walking. In addition, powered prostheses (PWR) actively generate torque at the ankle joint, which may affect dynamic balance differently than passive energy storage and return prostheses (ESR). The influence of PWR on dynamic balance during sloped walking is unclear, and thus the purpose of this study was to analyze H during sloped walking while using both powered and passive prostheses.

METHODS

Six adult males with ($n=3$) and without ($n=3$) TTA walked on slopes of $\pm 10^\circ$, $\pm 5^\circ$, and 0° . Individuals with TTA were assessed using their clinically prescribed ESR prosthesis and also with the BiOM (BiOM, Bedford, MA) powered prosthesis. Whole-body kinematics were collected at 120 Hz while participants walked at a fixed walking speed based on leg length.

Kinematic data were filtered at 6 Hz using a 4th order low pass Butterworth filter. A 13-segment inverse dynamics model was used to compute H as:

$$\vec{H} = \sum_{i=1}^n [(\vec{r}_i^{COM} - \vec{r}_{body}^{COM}) \times m_i (\vec{v}_i^{COM} - \vec{v}_{body}^{COM}) + I_i \vec{\omega}_i]$$

where n is the number of segments, \vec{r}_i^{COM} , \vec{v}_i^{COM} , and $\vec{\omega}_i$ are, respectively, the position, velocity, and angular velocity of the i^{th} segment, \vec{r}_{body}^{COM} and \vec{v}_{body}^{COM} are, respectively, the position and velocity of the body center of mass (COM), and m_i and I_i are the mass and inertia matrix of the i^{th} segment. For each of the three anatomical planes as well as the overall vector magnitude, H was normalized by body height and weight and expressed from 0 to 100% of the left or prosthetic limb gait cycle. Characteristic features (range, mean) of H during the first (0-50%) and second (50-100%) halves of the gait cycle were compared across groups and slopes using a linear mixed effects ANOVA with slope angle and group (AB, ESR, PWR) as fixed effects and subject as a random effect nested within type (AB, TTA). Post-hoc pairwise comparisons were performed when significant main or interaction effects were found, and p -values were adjusted using Tukey's method. All tests used a significance level $\alpha=0.05$.

RESULTS AND DISCUSSION

Although H was analyzed in each of the three anatomical planes, the primary findings were in the sagittal plane and in the vector magnitude of H during the first half (0-50%) of the prosthetic (left) limb gait cycle (Fig. 2). For all slope conditions, both ESR and PWR resulted in increased range of sagittal-plane H relative to AB (Figs. 1 & 2). In addition, the mean magnitude of H was increased in ESR relative to AB on declines, and was increased in both ESR and PWR relative to AB on inclines. The increased range and magnitude of H in individuals with TTA suggest that it may be more difficult for them to maintain their balance on slopes, since the affected limb lacks ankle muscles

that are important for regulating H [7]. This potential increase in fall risk for individuals with TTA is in addition to the already increased risk of falls on slopes relative to level ground [2].

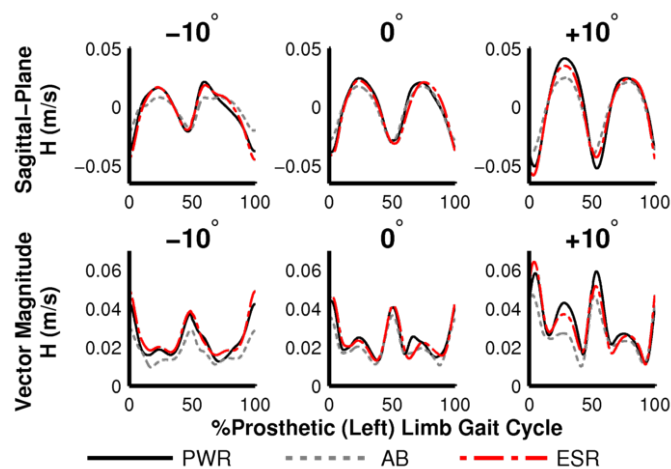


Figure 1: Normalized whole-body angular momentum (H) trajectories in the sagittal plane (top row) and total vector magnitude (bottom row) for 3 sloped walking conditions.

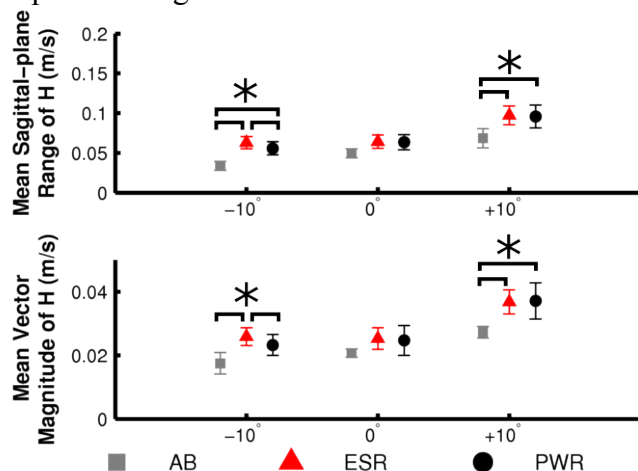


Figure 2: Mean (\pm SD) of the range (peak-to-peak value) of sagittal H (top) and magnitude of the H vector over the first 50% of the gait cycle. Significant differences between groups are indicated by ‘*’.

Few differences were observed in H when using ESR relative to PWR, similar to previous results on stairs [6]. However, one notable difference was that individuals with TTA had increased sagittal-plane range and mean magnitude of H with ESR compared to PWR when walking on a 10° decline. This result suggests that PWR performs more similarly to AB than ESR, potentially because of controlled plantarflexion in early stance and active

plantarflexion in late stance [8]. These functions may help in regulating H during decline walking for individuals with TTA.

All groups had increased sagittal-plane range and mean vector magnitude of H at +10° relative to 0° in the first half of the gait cycle. However, only AB had a decreased mean magnitude of H at -10° relative to 0°, suggesting that individuals with TTA do not regulate H as tightly as AB during decline walking. The risk of falling during decline walking is greater than during incline walking because of differences in the timing of the peak shear GRF [2]. AB may be more tightly controlling H in response to this greater risk of falling [5], which may be difficult for individuals with TTA.

CONCLUSIONS

Differences in H suggest altered control of dynamic balance across different sloped walking conditions, between individuals with TTA and AB, and when using different prostheses. Future work will incorporate additional subjects and investigate the external moment to further understand dynamic balance control.

REFERENCES

1. McIntosh AS, et al. *J Biomech* **39**, 2491-2502, 2006.
2. Redfern MS, et al. *Ergonomics* **44**, 1138-1166, 2001.
3. Miller WC, et al. *Arch Phys Med Rehabil* **82**, 1031-1037, 2001.
4. Neptune RR and McGowan CP. *J Biomech* **44**, 6-12, 2011.
5. Silverman AK, et al. *J Biomech* **45**, 965-971, 2012.
6. Pickle NT, et al. *J Biomech* **47**, 3380-3389, 2014.
7. Pijnappels M, et al. *J Biomech* **38**, 627-634, 2005.
8. Eilenberg MF, et al. *IEEE Trans Neur Sys Rehab* **18**, 164-173, 2010.

ACKNOWLEDGEMENTS

Research supported by NIH NICHD Award No. R03HD075946 and the Center for Rehabilitation Sciences Research, Department of Physical Medicine and Rehabilitation, Uniformed Services University of Health Sciences, Bethesda, MD.

EFFECTS OF INTENTIONAL EFFORT MANIPULATION ON BALANCE TESTED UNDER A DUAL-TASK PARADIGM

¹ Christopher Neville and ¹ Ryan Charboneau

¹ Upstate Medical University, Syracuse, NY, USA
email: nevillec@upstate.edu

INTRODUCTION

Balance is routinely tested in athletes at high risk for mild traumatic brain injury (mTBI, also known as concussion) before the start of an athletic season (baseline testing). Poor performance on baseline tests due to intentional acts or reduced effort may lead to failed injury identification. More precise measurement of balance using inertial sensors may allow improved ability to identify effort related manipulation as well as change due to injury.[1] Additionally, measuring balance while subjects concurrently complete a balance and cognitive test (dual-task) may further uncover effort related changes.[2] Therefore, the purpose of this study was to compare 3 consecutive data sessions collected from a healthy study cohort. The first two data sessions included test-retest data collected as reliability data to represent baseline performance. The third data session was collected after subjects were instructed to simulate being injured following a published “malingering” protocol. It was hypothesized that the third session would be different than the two baseline sessions. Further, it was hypothesized that dual-task tests would identify that injury symptoms were simulated.

METHODS

Twenty healthy college students volunteered to participate in a study where they would be asked to complete a balance assessment on two separate occasions to establish reliability. In addition, 10 of the subjects completed a third session where they acted impaired following a protocol to elicit malingering type symptoms and responses.[3] The balance tests were instrumented with an inertial sensor (Motion Intelligence, Ithaca NY) and tri-axial acceleration data was output at 250Hz for each of the 30-second tests. The balance assessment consisted of 11 common balance test but two tests

were chosen for comparison in the current analysis to address the stated hypotheses. These tests included a balance test in isolation; tandem stance eyes open (TSEO) standing on the floor, and a similar test where the subject stood in the same position but also held a tablet-computer and completed a cognitive test (trail-making Part B: TMB). The first two testing sessions were completed 2 days apart (baseline reliability) while the third data set was collected one week later. Data was output graphically (Figure 1) to identify patterns across the 3 sessions of data. A noted change in the variance of the accelerations between the third (malingering) session and the first two (baseline) sessions prompted calculation of a variance metric. The variance metric was calculated to represent 95% of the variance in the acceleration signal (P95), similar to 2 standard deviations but not assuming a normal distribution. The data was compared between sessions using a repeated-measures ANOVA with an alpha level of 0.05 followed by individual subject comparisons to aid in the interpretation of the ANOVA model in the cohort of 10 subjects. Finally, a ratio was calculated as balance alone (TSEO) divided by dual-task balance (TMB). This ratio was tested between sessions using a t-test.

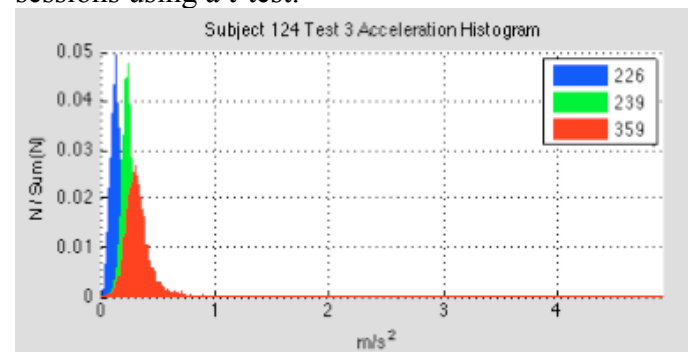


Figure 1: Histogram of the frequency (number) of Acceleration values observed across the 30-second balance test (TSEO) for 1 subject completing 3 separate sessions (2 baseline-reliability (blue and green), 1 malingering (red))

RESULTS AND DISCUSSION

As expected, for the isolated balance test, TSEO, session 3 was significantly ($p<0.01$) greater than session 1 or 2 but there were no differences between session 1 and 2 ($p=0.73$)(Table 1, Figure 1). For the dual-task balance test, TMB, there was again a significant ($p<0.01$) difference between session 3 and 1 or 2, and no difference between session 1 and 2 ($p=0.54$)(Figure 2). For the ratio of balance alone (TSEO) to dual-task (TMB) there was a significant ($p<0.01$) difference between baseline reliability sessions, and session 3 (simulated injury).

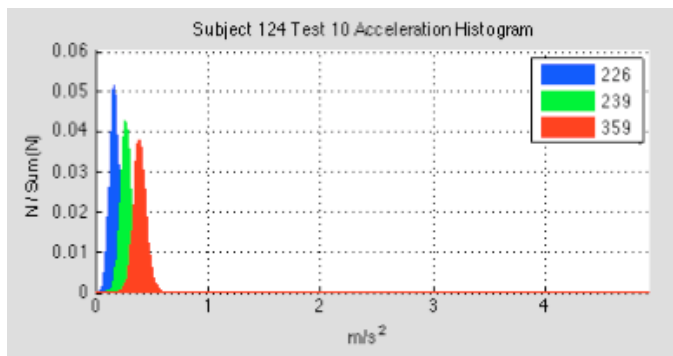


Figure 2: Histogram of the frequency (number) of Acceleration values observed across the TMB dual-task test for 1 subject completing 3 separate sessions (2 baseline-reliability (blue and green), 1 malingering (red))

CONCLUSIONS

The purpose of this study was to identify potential effects of simulated injury compared to typical baseline performance. The group comparisons for sessions 1 and 2 suggest good overall consistency allowing good comparisons to simulated injury in session 3. Session 3 results demonstrate that

subjects increased the variance of their acceleration by increasing their sway in attempts to simulate injury. The variance was observed to increase in the dual-task balance test compared to the isolated balance test during the baseline session. This may be due to the added cognitive load distracting participants from the balance task or the effect of simply adding upper extremity movement to complete the cognitive test. Interestingly, this was not observed during session 3 while subject simulated injury. It is hypothesized that the added cognitive task makes efforts to act injured more difficult resulting in atypical decreases in sway compared to the isolated balance test. Only 2 of the 10 subjects were able to maintain their efforts to simulate injury by increasing sway during the dual-task test. Additional studies to identify effort related effects are needed but metrics that target acceleration variance show promise over common metrics such as root-mean-square (RMS) which capture average acceleration.[1]

REFERENCES

1. King L, et al. *Arch Physical Med and Rehab* **95**, 353-359, 2014.
2. Catena RD, et al. *J Neuroeng Rehabil* **8**, 1-8, 2011.
3. Mittenburg W. *Professional Psychology* **26** 491-498, 2010.

ACKNOWLEDGEMENTS

Motion Intelligence, LLC, Ithaca, NY for use of the inertial sensor for testing.

Table 1: Mean and standard deviations for the P95 metric for balance and dual-task measures completed across 3 sessions.

Balance Alone (TSEO)	S1 TSEO	S2 TSEO	S3 TSEO	S2-S1	sig	S3-S1	sig
Mean (m/s^2)	0.214	0.211	0.803	0.019	$p=0.73$	0.607	$p<0.01$
Stdev (m/s^2)	0.070	0.048	0.540				
Dual-Task Balance (TMB)	S1 TMB	S2 TMB	S3 TMB	S2-S1	sig	S3-S1	sig
Mean (m/s^2)	0.320	0.332	0.788	0.040	$p=0.54$	0.499	$p<0.01$
Stdev (m/s^2)	0.149	0.145	0.579				

SINGLE AND DUAL-TASK TURNING IN RECENTLY CONCUSSED ATHLETES AND MATCHED CONTROLS: PRELIMINARY RESULTS

¹ Peter C. Fino, ² P. Gunnar Brolinson, ³ Thurmon E. Lockhart, ¹ Maury A. Nussbaum

¹ Virginia Tech, Blacksburg, VA, USA

² Edward Via College of Osteopathic Medicine, Blacksburg, VA, USA

³ Arizona State University, Tempe, AZ, USA

email: fino@vt.edu

INTRODUCTION

Typical sports-related concussion symptoms resolve within 7-10 days post-concussion [1]. However, use of challenging motor control tasks indicate that deficits can persist beyond this typical timeframe. For example, concussed athletes have increased medio-lateral (ML) sway during dual-task gait up to two months post-concussion [2]. After being cleared for competition, recently concussed athletes demonstrate greater reorientation variability [3] and greater clearance when circumventing obstacles [4] compared to controls in turning tasks. Other changes to turning mechanics due to concussions and their potential impact on performance and/or injury remain unknown. This study examined turning in recently concussed collegiate athletes and matched controls, after the athletes were cleared to return to play, to examine differences in path curvature and ML inclinations.

METHODS

Four recently concussed athletes (C) and four healthy matched controls (H) were tested a mean (SD) of 23 (2) days after each concussion. The C athletes were cleared 12 (4) days post-concussion. Concussions were clinically diagnosed by Virginia Tech sports medicine physicians. Controls were selected from the same team as each concussed athlete and matched based on position, age, stature and weight. Participants gave written consent and protocols were approved by the Virginia Tech IRB.

Participants walked continuously around a course marked with 1.5 m tall pylons and consisting of straight and non-straight segments with $\sim 90^\circ$ turns (Figure 1). Participants walked at their normal pace (single task = ST) around the course 14 times, seven

laps in each direction. Participants then repeated the procedure while serially subtracting by sevens (dual task = DT).

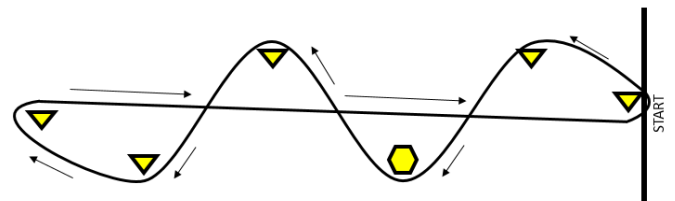


Figure 1: Depiction of the 18 m long course. Triangles indicate pylons, and the hexagon indicates the pylon location where motions were tracked.

Kinematic data was sampled at 120 Hz for each lap using four ProReflex (Qualysis, Sweden) cameras located around the middle pylon. Reflective markers were placed over the xiphoid process, approximate T9 vertebra, and on each calcaneus (heel). The upper body center-of-mass (COM_{UB}) location was estimated as the mean of the xiphoid process and T9 vertebral markers. Kinematic data was filtered using a 6 Hz 4th order phaseless Butterworth filter.

The maximum instantaneous curvature of the horizontal COM_{UB} trajectory identified the apex of the turn. Heel contact was identified using the local minima of the heel marker vertical location. The turning stance limb was identified as the heel contact closest to the apex, with the turning stride encompassing one step forward and backward (Figure 2). The ML inclination angle (θ) was calculated as the angle from vertical in the frontal plane from the heel to the COM_{UB} at each heel contact in the turning stride (Pre-Apex, θ_{Pre} , Apex, θ_{Apex} , Post-Apex, θ_{Post}).

Mean curvature and ML inclination angles were compared between groups (C vs. H) using GEE

models with compound symmetry covariance structures across laps. Turning strategy (inside vs. outside stance limb), task (ST vs. DT), velocity of the COM_{UB}, and all group-paired interactions were included in the model as covariates, with significant interactions retained in the final models. A 0.05 significance level was used throughout and analyses were performed using MATLABTM.

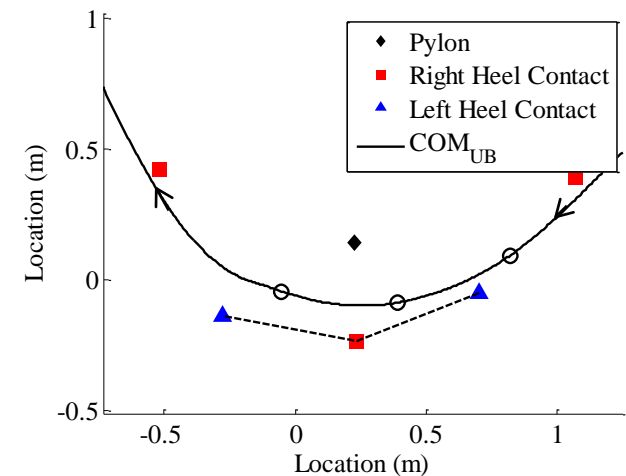


Figure 2: Example overhead view of a turning stride (dotted line) connecting the left-right-left heel contacts around the apex. Black circles show the location of the COM_{UB} at each heel contact.

RESULTS AND DISCUSSION

Summary statistics for each outcome measure are given in Table 1. Significant differences in mean curvature were found between groups ($p = 0.012$), COM_{UB} velocities ($p < 0.001$), and turning strategy ($p < 0.001$). Significant group ($p = 0.002$) and turning strategy ($p < 0.001$) differences were found for θ_{Pre} . The angle θ_{Apex} was significantly different between turning strategy ($p < 0.001$) and task ($p = 0.019$), and the θ_{Post} differed by COM_{UB} velocity ($p = 0.02$), strategy ($p < 0.001$), and task ($p = 0.03$).

Overall, the group differences in curvature and θ_{Pre} support other studies that suggested concussions can affect dynamic task performance, even after athletes return to play [2-4]. Although measured during walking and not competition speed (i.e. running), the lower curvatures found here suggest a potential effect on performance, with recently concussed athletes taking wider, less abrupt turns that may inhibit their ability to respond to competitive demands. Furthermore, the decreased θ_{Pre} suggests delayed anticipation of the turn that may manifest in declined performance and/or increased injury risk. However, it is unclear whether these differences are caused by the neurophysiology of the concussion or are a result of potential detraining during recovery. The increased curvature and θ_{Apex} for outside stance limb compared to inside stance limb agree with a previous report [5].

In summary, these results encourage further research examining the effects of concussions on turning behaviors and on the competitive readiness of athletes returning/recovering from concussions.

REFERENCES

1. McCrory P, et al. *Br J Sports Med* **45.5**, 250-258, 2013.
2. Howell DR, et al. *Arch Phys Med Rehabil* **94**, 1513-1520, 2013.
3. Powers KC, et al. *Gait Posture* **39**, 728-732, 2014.
4. Fait P, et al. *J Head Trauma Rehab* **28.4**, 293-301, 2013.
5. Fino PC, et al. *J Biomech* **48.1**, 104-112, 2015.

ACKNOWLEDGEMENTS

The first author was supported by an NSF Graduate Research Fellowship (Grant No. DGE 0822220).

Table 1: Means (SD) of curvature and ML inclination angles for each combination of group, strategy, and task.

	Concussed				Healthy Controls			
	Inside Leg		Outside Leg		Inside Leg		Outside Leg	
	ST	DT	ST	DT	ST	DT	ST	DT
Curvature (m ⁻¹)	1.7 (0.4)	1.9 (0.8)	2.6 (1.1)	2.6 (1.2)	2.4 (1.3)	2.5 (1.3)	3.1 (1.0)	2.9 (1.3)
θ_{Pre} (deg.)	4.7 (1.7)	4.7 (2.7)	1.8 (2.4)	1.5 (2.1)	6.8 (1.4)	5.1 (3.4)	2.5 (2.4)	2.4 (2.5)
θ_{Apex} (deg.)	5.3 (1.7)	4.7 (2.2)	7.6 (2.3)	7.5 (1.6)	6.4 (2.3)	5.7 (2.4)	9.0 (1.4)	8.3 (1.5)
θ_{Post} (deg.)	6.8 (1.7)	6.3 (2.5)	1.4 (3.5)	0.2 (3.4)	7.5 (3.1)	5.9 (1.6)	2.7 (2.4)	0.8 (3.4)

EFFECT OF SEX ON RECOVERY OF GAIT BALANCE CONTROL FOLLOWING CONCUSSION

Quinn Peterson, Rachel Klas, David Howell, and Li-Shan Chou

Department of Human Physiology, University of Oregon, Eugene, OR, USA
email: chou@uoregon.edu, web: <http://biomechanics.uoregon.edu/MAL>

INTRODUCTION

Concussion is an acutely evolving injury that can result in a wide array of functional and neuropsychological deficits, including, but not limited to, clinical signs, physical symptoms, cognitive impairment, and gait balance impairments [1]. The role of sex as an indicator of concussion severity is not well understood but has been hypothesized as a potential risk factor and/or predictor of injury severity [2]. However, a study investigating sex differences in concussion recovery reported no differences in neuropsychological test measures following injury, and no differences in long-term recovery outcomes [3].

Due to anatomical and physiological differences between sexes that may result in differences in sustaining and recovering from concussion, differences in gait balance between female and male concussion subjects can potentially be measured [4]. Therefore, the purpose of this study was to longitudinally examine differences in gait balance impairment between female and male subjects following concussion.

METHODS

38 subjects (14F/24M; mean age: 18.6 ± 3.2 and 17.3 ± 3.2) diagnosed with concussion by healthcare professionals were referred to the lab for the first testing session within 72 hours of injury and returned at approximate time points of: 1wk, 2wk, 1mo, and 2mo post-injury. 38 control subjects matched for age, sex, height, weight, and sport participation were tested in a similar timeline following their initial visit. Concussion symptoms were assessed based on a 22-symptom inventory using a Likert-like scale (ranking each symptom from 0-6) [1].

Subjects walked barefoot along a walkway at a self-selected speed while performing a continuous auditory Stroop test for 8-10 trials. The Stroop test consisted of a recorded voice saying the word “high” or “low” in a high- or low-pitch voice four consecutive times. Subjects were instructed to identify the pitch, regardless if the pitch was congruent with the meaning of the word.

29 retro-reflective markers were placed on bony landmarks and whole body movement was recorded using a ten camera motion analysis system (Motion Analysis Corp., Santa Rosa, CA) at a sampling rate of 60 Hz. Whole body COM position was calculated with a 13-link model [4]. Three dependent variables were identified from each gait cycle: the peak anterior COM velocity (A_v), total COM medial/lateral displacement (MLdisp), and average walking speed. A_v and MLdisp have previously been reported to provide sensitive detection of gait imbalance in concussion subjects [4].

Three-way mixed-effects ANOVA were used to analyze each of the walking dependent variables and symptom scores in order to determine the effect of sex (female/male), group (concussion/control), and time (72hr, 1wk, 2wk, 1mo, 2mo), and interactions between these independent variables. For all omnibus tests, significance was set at $p < .05$. Follow up pairwise comparisons were examined using the Bonferroni procedure to control Family Wise Type I Error.

RESULTS AND DISCUSSION

For the average walking speed, no significant effect of sex was detected ($P = .218$), while main effect of group on average walking speed was nearly significant ($p = .059$). Both concussion and control groups increased average walking speed across the 2-month testing period (time x group interaction, $P = .001$).

On average, concussion subjects were observed to have significantly greater MLdisp compared to control subjects across the 2-month testing period (main effect of group, $P < .01$; main effect of time, $P = .001$). However, there was no significant interaction or effect of sex found for MLdisp during dual-task walking ($P = .66$) (Figure 1); indicating gait balance impairment for concussion subjects up to 2-months post-injury with no difference between male and female subjects.

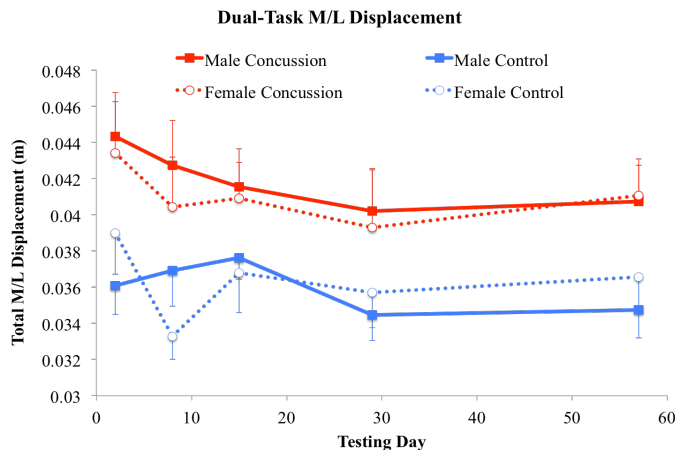


Figure 1: Average total medial/lateral displacement in female/male concussion and control subjects across testing time points.

Additionally, no significant differences were observed between male and female subjects for peak anterior velocity ($P = .295$). The peak anterior velocity increased for concussion subjects at each time point across the 2-month testing period, while control subjects showed no significant difference across time (time x group interaction $P < .01$).

On average, all female subjects reported significantly greater total symptom scores than male subjects, regardless of concussion (main effect of sex, $P < .05$) (Figure 2). Symptom scores of male concussion subjects were found to be resolved to the control level between the 1mo and 2mo time points, whereas female concussion subjects did not reach symptom resolution throughout the 2-months of testing. Concussion subjects reported greater symptom scores than matched controls (main effect of group, $P < .001$) and demonstrated significant

decreases in total symptom scores at each visit across the 2-month testing period, while control subject symptom scores did not significantly change during the testing period (group x time interaction, $P < .001$).

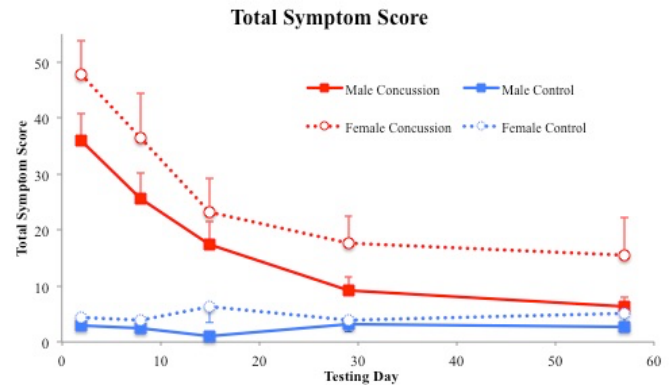


Figure 2: Average total symptom score in female/male concussion and control subjects across testing time points.

DISCUSSION AND CONCLUSIONS

The present data suggest similar recovery patterns over time between female and male concussion subjects in terms of balance control during dual-task walking. However, self-report symptom scores were resolved to control levels for male concussion subjects between the 1mo and 2mo time points, whereas female concussion subjects did not reach symptom resolution throughout the 2-months of testing. Females also reported greater total symptom scores throughout the entire testing period. It is likely that females perceive and/or self-report the effects of concussion differently than males.

REFERENCES

1. McCrory, P. et al. (2013) British Journal of Sports Medicine, 47(5):250-8.
2. Marar, M. et al. (2012) American Journal of Sports Medicine, 40(4):747-55.
3. Tsushima, WT. et al. (2009) Brain Injury, 23(10):809-14.
4. Howell, D.R. et al. (2013) Archives of Physical Medicine and Rehab., 94(8):1513-20

BALANCE MEASUREMENTS USING A SMARTPHONE AT THE UPPER ARM COMPARED TO THE BALANCE ERROR SCORING SYSTEM

¹ Peter C. Fino, ² Matthew D. Weirath, ³ Rahul Soangra, ³ Thurmon E. Lockhart, ⁴ P. Gunnar Brolinson

¹ Virginia Tech, Blacksburg, VA, USA

² Belleville Family Medicine Residency, 375th Medical Group, Scott AFB, IL, USA

³ Arizona State University, Tempe, AZ, USA

⁴ Edward Via College of Osteopathic Medicine, Blacksburg, VA, USA
email: fino@vt.edu

INTRODUCTION

Concussions can affect balance and stability, making balance assessments an important component of concussion test batteries [1]. The balance error scoring system (BESS) has become the standard field test to identify balance deficits following concussions using a trained clinician to count errors [2]. Instrumenting the BESS with inertial measurement units can produce better diagnostic classification than the traditional “error count” which can be challenging for the clinician [3]. Removing the clinician’s error count reduces the challenge of administering the BESS. Furthermore, using publicly familiar IMUs will allow more widespread use when a clinician is not readily available (e.g., youth sports, at-home monitoring). This study compared the traditional BESS error count with the sway measurements of a common smartphone attached with a standard sport armband in healthy young adults.

METHODS

Twenty healthy young males (ages 18-22) previously unfamiliar with the BESS gave written consent and were tested two separate times with one week in between sessions. All protocols were approved by the Virginia Tech IRB. A smartphone (iPhone 5, Apple Inc.) was placed laterally on the upper arm, midway between the elbow and shoulder using a standard smartphone sport armband (Belkin Sport-Fit Armband, Belkin). Participants performed three stances (double, single leg, tandem) on firm ground and on a foam Airex balance pad. Participants were instructed to keep their hands on their iliac crests and maintain each stance for 20 seconds with their eyes closed, returning to that

position as soon as possible if they moved their hands, feet, opened their eyes, or lost balance.

A trained sports medicine physician counted BESS errors for each stance [2]. The smartphone calculated sway using tri-axial accelerometers, sampled at 31.5 Hz, and computed the angles between the sensitive axes and the direction of gravity using α , β , and γ , the angles of the resultant acceleration with respect to the local reference frame (Figure 1) [4]. The projection’s coordinates (d_x , d_y) were calculated using these angles and the height of the smartphone dz . The circular sway area was calculated using the mean radius of sway and sway velocity was the sway length over time.

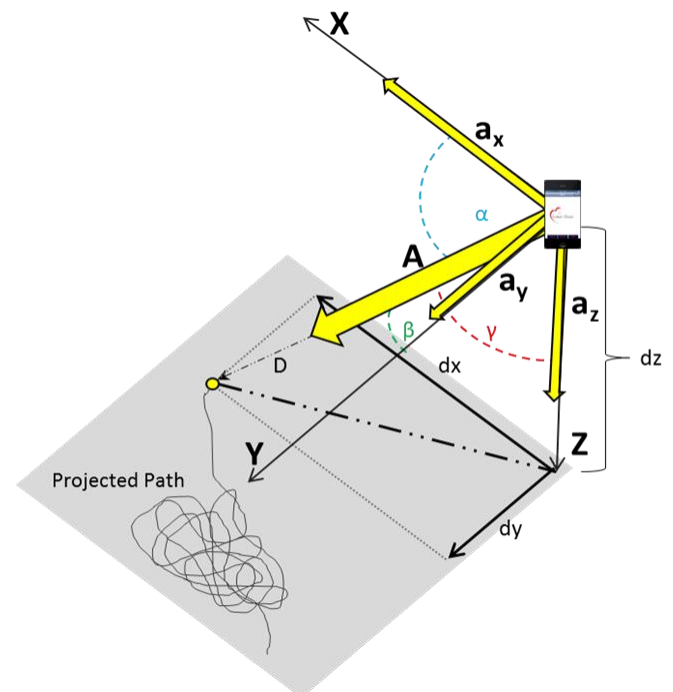


Figure 1: Schematic diagram of projected sway using the iPhone accelerometers. Adapted from [4].

Spearman's rank correlation coefficient (ρ) was used to compare all measurements of sway area and sway velocity to the BESS errors overall and separated by ground (firm vs. foam). Interclass correlation coefficients (ICC (2,1)) compared the repeatability of the BESS and sway measurements on each individual from the first to second weeks.

RESULTS AND DISCUSSION

Spearman's ρ between all BESS scores and sway area was 0.86, and 0.85 between BESS scores and sway velocity. On the firm surface, $\rho = 0.76$ for sway area and 0.77 for sway velocity. On the foam surface, $\rho = 0.83$ for sway area and 0.79 for sway velocity. ICC values are given in Table 1. Medians and inter-quartile ranges (IQRs) for each measure are given in Table 2.

Table 1: ICC's comparing between weeks.

ICC	All	Firm	Foam
BESS errors	0.01	0.45	-0.27
Sway area	-0.04	0.40	-0.10
Sway velocity	-0.01	0.08	-0.02

Overall, the smartphone based measures showed good (> 0.80) clinical reliability to the BESS scores, especially for a system located on an upper extremity. While the repeatability was poor, the sway area's repeatability was similar to the BESS, and both showed the highest repeatability on firm ground, the most likely surface for BESS tests without a clinician. Because the BESS errors do not take into account movements of the upper body unless an error is committed, it is possible the smartphone based measures of sway area and sway velocity may more accurately represent the postural control of individuals, with differences between methods attributed to discrepancies in the BESS reliability and repeatability [5]. This discrepancy between methods is evident when examining the

single leg stance measurements, where large upper body movements resulted in very large sway amplitudes and velocities, but may have only counted as one error. However, this study is limited because the smartphone based measures were not compared to a ground truth (i.e. force plate) and no concussed individuals were tested, limiting conclusions about the clinical classification ability of the sway area and velocity. By placing the smartphone on the upper arm, the measurements were also biased against arm movements, which resulted in large sway amplitudes and velocities, compared to foot movements or opening eyes, which the BESS treats equal to arm movements but produced small sway amplitudes.

CONCLUSIONS

Overall, a common smartphone and sport armband achieved good reliability and comparable repeatability with the BESS, encouraging further studies in clinical and concussed populations to extend the use of smartphone-based balance testing.

REFERENCES

1. McCrory P, et al. *Br J Sports Med* **45.5**, 250-258, 2013.
2. Guskiewicz KM. *Clin Sports Med* **30.1**, 89-102, 2011
3. King LA, et al. *Arch Phys Med Rehab* **95**, 353-359, 2014.
4. Seimetz C, et al. *Biomed Sci Instrum* **48**, 386-392, 2012.
5. Hunt TN, et al. *Clin J Sport Med* **19.6**, 471-475, 2009

ACKNOWLEDGEMENTS

The first author was supported by an NSF Graduate Research Fellowship (Grant No. DGE 0822220).

Table 2: Medians (IQR) for BESS errors, sway areas, and sway velocities for each stance.

	Firm Ground			Foam Ground		
	Double	Single Leg	Tandem	Double	Single Leg	Tandem
BESS errors	0 (0)	2.5 (3.5)	1 (2)	0 (0)	8 (3.5)	5 (5)
Sway area (cm²)	3.0 (1.1)	14.1 (8.8)	8.8 (4.2)	5.5 (1.9)	26.8 (106.8)	22.3 (11.7)
Sway velocity (cm*s⁻¹)	1.2 (1.0)	28.0 (47.9)	7.4 (11.1)	4.2 (1.9)	171.8 (1469.3)	70.0 (147.6)

THE RELATIONSHIP BETWEEN HEAD ACCELERATION AND HEART RATE VARIABILITY: A POSSIBLE DIAGNOSTIC TOOL FOR HEAD INJURY SEVERITY

¹ Janet S. Dufek, ² Nancy A. Ryan-Wenger, ¹ Aaron Prado and ¹ Austin Coupé

¹ University of Nevada, Las Vegas, Las Vegas, NV, USA

² Nationwide Children's Hospital, Columbus, OH, USA

email: janet.dufek@unlv.edu; website: <http://www.unlv.edu/kns/kinesiology>

INTRODUCTION

Traumatic brain injury (TBI) is one of the leading causes of death in the United States with over 1.7 million people affected annually.¹ Four typical events contribute to the occurrence of TBI including: 1) contact with objects and equipment, 2) falls, 3) motor vehicle accidents, and 4) assault or violent acts.² These events suggest vulnerability to TBI for a large segment of the population, including the elderly, due to the high rate of falls they experience. Along with children (0-4 years) and adolescents (15-19 years), adults 65 years of age and older are the most likely group to experience TBI resulting from a fall.¹

Several neuroimaging techniques are currently used to assess injury severity following a jolt or blow to the head. These include magnetic resonance imaging (MRI) and computerized tomography (CT). Additionally, new techniques are being developed including diffusor tensor imaging and magnetic resonance spectroscopy. The latter are not without shortcomings including both cost and the inability to detect incidence of lesser severe TBI cases.³

Heart rhythm is controlled by the sinoatrial node, which is modulated by the parasympathetic and sympathetic branches of the autonomic nervous system. Slight changes in these nervous system inputs result in variations in heart rate. Spectral analysis of heart rate variability (HRV) has been shown to be related to Glasgow coma scale results as well as brain damage severity.⁴ Thus, our research team sought to explore the use of a direct biological measurement (HRV) to determine fall injury severity. The purpose of the study was to examine the relationship between HRV and linear head acceleration. Head acceleration was used as a simulation of the magnitude of head impact.

METHODS

Nine apparently healthy male volunteers (175.9±2.4 cm, 75.1±7.3 kg, 25.3±2.4 yrs), with no history of lower extremity injury in the last six months granted institutionally approved written consent to participate. A heart rate monitor (Polar RS800cx; Polar Electro, Kempele, Finland), set to R-R interval mode, was secured to the chest with data transmitted to a wireless receiver secured to the wrist. Sampling frequency was set to 1,000 Hz providing temporal resolution of 1 ms for each R-R period. A plastic helmet with an attached uniaxial accelerometer (PCB Piezotronics Inc. 52456; Depaw, NY) was donned. Bioware software (Kistler 4.0; Amherst, NY; 1000 Hz) was used to measure head vertical acceleration (HA) values.

The experimental protocol consisted of quiet sitting followed by continuous landing. An initial resting heart rate measurement was recorded over 5min. Participants were then instructed to continuously step onto a 45cm platform, step off the platform, and come to rest on the floor "softly". Participants repeated this process over a 5min period as both heart rate and head acceleration were measured. Next, a second 5min resting heart rate measurement was recorded followed by 5min of continuous 45cm step-off landings, this time minimizing the amount of knee flexion upon landing (stiff landing). A final 5min resting heart rate measurement was obtained. Data were extracted over the 5min sample using Polar Pro Trainer 5 software (Polar Electro, Kempele, Finland) and each R-R interval file was analyzed using Kubios HRV Analysis Software 2.0 (Biomedical Signal and Medical Imaging Analysis Group, Kuopio, Finland).

Dependent variables in the time domain included maximum head acceleration (HA), the standard

deviation of R-R intervals (RRsd) and the root mean square (RMSsd) of R-R intervals. Frequency domain measures of power in the low frequency (LF; 0.04-0.15 Hz) and high frequency (HF; >0.15-0.40 Hz) ranges were also extracted. All dependent variables were evaluated using repeated measures ANOVAs ($\alpha = 0.05$) with Huynh-Feldt corrections as necessary. Correlations between HA and the indices of HRV were also computed. All statistical comparisons were conducted using SPSS v22 Statistics software (IBM; Armonk, NY).

RESULTS AND DISCUSSION

There was a significant difference ($p=0.001$) observed between HA_{soft} ($3.05 \pm 1.11 \text{ g's}$) and HA_{stiff} ($7.61 \pm 2.73 \text{ g's}$), which confirmed that participants did distinguish performance between landing conditions, as instructed. There were no significant differences among resting conditions for RRsd (70.9 ± 15.3 , 74.8 ± 10.0 , $72.6 \pm 13.3 \text{ ms}$, for pre-, mid- and final rest, respectively) or similarly for RMSsd (44.2 ± 16.1 , 37.2 ± 17.5 , $31.4 \pm 10.4 \text{ ms}$, respectively). A significant RRsd ANOVA result ($F_{(1,8)}=2.056$, $p=0.001$, $\eta^2=.836$) was followed up with *post hoc* contrasts using Sidak adjustments. RRsd for both the soft ($37.6 \pm 9.2 \text{ ms}$) and stiff ($32.4 \pm 8.1 \text{ ms}$) landing conditions were significantly less ($p=0.007$ and $p=0.001$, respectively) than any of the resting conditions. RRsd between landing conditions was not significantly different. A similar trend was observed for RMSsd with the source of the significant ANOVA ($F_{(1,8)}=25.24$; $p<0.001$; $\eta^2=.759$) between both the soft ($10.5 \pm 5.6 \text{ ms}$) and stiff ($9.5 \pm 5.0 \text{ ms}$) landings compared to the three resting conditions (44.2 ± 16.1 , 37.2 ± 17.5 , and $31.4 \pm 10.5 \text{ ms}$, respectively).

In the frequency domain, no significant differences were observed among LF or HF measures (Figure 1). Correlations between HA and HRV measures ranged from ± 0.162 - 0.664 with a significant relationship demonstrated between HA_{stiff} and RMSsd ($r=-0.664$, $p = 0.026$).

HRV is posited to mirror the control of the cardiovascular system. In the time domain, the measures of HRV (RRsd, RMSsd) significantly decreased with increased HA, with no differences

observed in HRV among the rest conditions. Surprisingly, a similar outcome was not observed at the group level between the soft and stiff landing conditions. There were no observed differences in the frequency domain, perhaps due to lesser agreement between LF and HF measures from the Polar monitor versus a 12-lead ECG.⁵ Increased variability in HF for the stiff landing condition (Figure 1), might also have influenced this outcome.

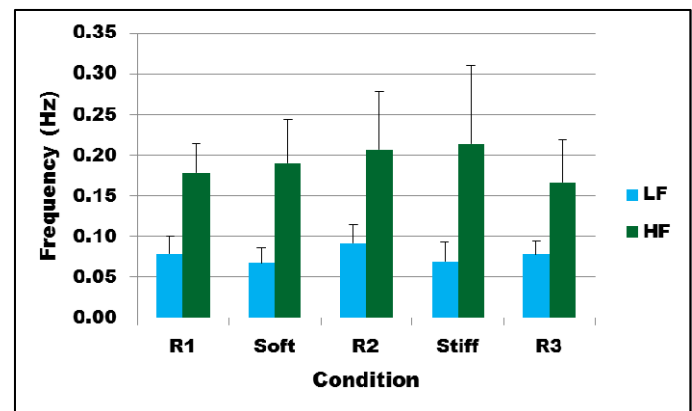


Figure 1. Mean and standard deviation values for frequency domain analysis.

CONCLUSIONS

Results suggest the potential application of HRV as a quantifiable, non-invasive diagnostic measure of head impact severity. Future research should consider head and neck rotational components relative to HRV across a wider range of impact activities, as well as examining LF/HF ratio.

REFERENCES

1. Faul, M., et al. CDC Blue Book. 2010.
2. Tiesman H.M., et al. *Am J Prev Med.* 41:61-67, 2011.
3. Flanagan S.R., et al. *Neuro Disease Trtmt.* 4:877-892, 2008.
4. Su C.F. et al. *Clin Neuro.* 116:1273-1279, 2005.
5. Nunan D., et al. *Eur J Appl Physiol.* 103: 529-537, 2008.

ACKNOWLEDGEMENT

Partially support by a Faculty Opportunity Award, #2221-272-76MH, University of Nevada, Las Vegas.

A COMPARISON OF MEASURES TO ASSESS BALANCE IN POST-STROKE SUBJECTS

Arian Vistamehr¹, Leah M. Carter¹, Steven A. Kautz^{2,3}, Mark G. Bowden^{2,3} and Richard R. Neptune¹

¹ Department of Mechanical Engineering, The University of Texas, Austin, TX

² Department of Health Sciences and Research, Medical University of South Carolina, Charleston, SC

³ Ralph H Johnson VA Medical Center, Charleston, SC

email: arian.vistamehr@utexas.edu web: <http://www.me.utexas.edu/~neptune>

INTRODUCTION

Balance control is a challenging task in many patient populations such as in post-stroke hemiparetic subjects. More than 50% of stroke survivors experience falls within one year post stroke (e.g., [1]). Lack of balance control can lead to physical injuries and long-term disabilities. Thus, it is important to assess dynamic balance using reliable methods in order to detect and treat balance disorders.

Various methods have been used to evaluate balance performance. These methods range from simple clinical scores such as Berg Balance Scale (BBS) (e.g., [2]) and Dynamic Gait Index (DGI) (e.g., [3]) to more comprehensive laboratory-based measures such as margin of stability (MoS) (e.g., [4]) and peak-to-peak range of whole-body angular momentum (H) (e.g., [5]). Further, clinical balance scores are based on discrete score assignments while completing a series of movement tasks, whereas the laboratory-based measures are obtained using whole-body kinematic and kinetic data during walking, often on a treadmill.

A recent study investigated the relationship between clinical balance scores and the rate of change of H in post-stroke subjects and found that a higher rate of change of H during the paretic leg stance was associated with poorer BBS and DGI scores [6]. However, no study has investigated whether the other methods report consistent findings in assessing balance in post-stroke subjects. This information can assist clinicians in selecting the appropriate method to evaluate balance. Thus, the purpose of this study was to assess frontal-plane balance using BBS, DGI, MoS and peak-to-peak range of H in post-stroke hemiparetic subjects and determine if these measures are correlated.

METHODS

Previously collected [7] three-dimensional kinematics and ground reaction force (GRF) data were collected at 100 Hz and 2000 Hz, respectively, while 19 post-stroke hemiparetic subjects (14 left hemiparesis; age: 62 ± 11 years; 6 female) walked on a split-belt instrumented treadmill at their self-selected walking speeds. In addition, BBS and DGI data were collected for each subject.

A 13-segment inverse dynamics model was used to calculate the center-of-mass (CoM) position and velocity for all the body segments. Margin of stability (MoS), which is the minimum distance between the extrapolated CoM and the base of support, was calculated in the mediolateral direction as described in [4]. MoS values were calculated at each step for the paretic foot placement, the nonparetic foot placement and the sum of both legs. Whole-body angular momentum (H) in the frontal plane was calculated as the sum of individual segments angular momenta about the body CoM and was normalized as described in [5]. The peak-to-peak range of H was calculated as the difference between the minimum and maximum values of H over the entire gait cycle.

To determine whether these four measures assess balance performance consistently, correlation analyses were performed. Pearson's correlation analyses were performed between MoS and the range of H using both the mean values across all subjects and the individual step data. Also, non-parametric Spearman's correlation analyses were performed between the clinical balance scores (BBS and DGI) and the laboratory-based measures (MoS and range of H).

RESULTS AND DISCUSSION

Significant correlations were found among all the balance measures (Table 1). BBS was positively correlated with DGI. That is, subjects with a lower BBS also had a lower DGI, indicating poor balance control. Also, MoS (sum from both legs) and the range of H were positively correlated. This was true both for the mean values across all the subjects (Table 1) as well as the individual step data ($r = 0.52$, $P < 0.001$). However, both of the laboratory-based measures (MoS and the range of H) were inversely correlated with the clinical scores (BBS and DGI) (Table 1). In other words, subjects with a higher range of H had a higher MoS (sum from both legs) and lower BBS and DGI scores, indicating poor balance control. These results are consistent with previous studies [5-6]. Further, examining MoS for each foot revealed that only the MoS corresponding to the paretic foot placement was correlated with other balance measures (Fig. 1). Thus, the use of MoS to assess balance performance in stroke subjects should be carefully implemented.

In summary, all measures led to similar conclusions in assessing balance in post-stroke hemiparetic subjects. However, balance being multidimensional, each measure may provide insight about different aspects of balance. The advantage of clinical balance scores is that they provide a simple and quick global assessment which does not require collection and processing of kinematic and kinetic data. However, contrary to the laboratory-based measures, the clinical balance scores cannot provide insight into the mechanisms for maintaining dynamic balance. MoS can provide some insight into foot placement mechanisms, but not the GRFs. Further, it does not account for the segmental moment of inertia and rotational motion that influence dynamic balance. Although a more complex in calculation, whole-body angular momentum can provide insight into how the sum of linear and angular momenta of all the body segments (about the body CoM) can be controlled

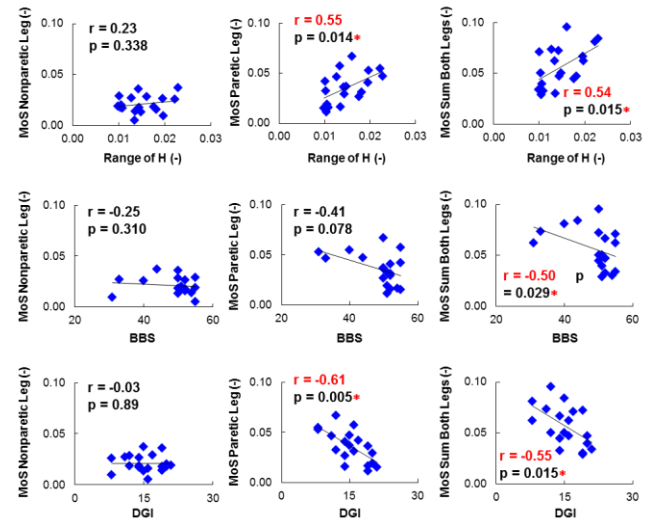


Figure 1: Top row shows the Pearson's correlations between normalized margin of stability (MoS) and the range of whole-body angular momentum (H). Middle and bottom rows show the Spearman's correlations between MoS & Berg Balance Scale (BBS) and MoS & Dynamic Gait Index (DGI), respectively. The left, middle and right columns respectively correspond to the MoS for the nonparetic leg, the paretic leg, and the sum of both legs. Significant correlations ($p < 0.05$) are shown in red with '*'.

by adjustments in foot placement and generation of the appropriate GRFs. The results of this study can assist clinicians with selecting the most suitable method for assessing balance performance.

ACKNOWLEDGEMENTS

This work was supported by AHA SouthWest Affiliate pre-doctoral fellowship (12PRE12030414) and the Rehabilitation Research and Development Service of the Department of Veteran's Affairs.

REFERENCES

1. Ashburn A, et al. *Age Ageing* **37**, 270-276, 2008.
2. Blum L and Korner-Bitensky N. *Phys Ther* **88**, 559-566, 2008.
3. Dye DC, et al. *Phys Ther* **93**, 809-818, 2013.
4. Hof AL, et al. *J Biomech* **25**, 250-258, 2007.
5. Vistamehr A, et al. *Clin Biomech* **29**, 583-589, 2014.
6. Nott CR, et al. *Gait & Posture* **39**, 129-134, 2014.
7. Bowden MG, et al. *Arch Phys Med Rehabil* **94**, 856-62, 2013.

Table 1: Correlations between various balance measures in post-stroke hemiparetic subjects ($n = 19$). Significant correlations ($p < 0.05$) are shown with '*'. The acronyms are as follows: (H): range of whole-body angular momentum, (MoS): margin of stability sum from both legs, (BBS): Berg Balance Scale, (DGI): Dynamic Gait Index.

	H & MoS	H & BBS	H & DGI	MoS & BBS	MoS & DGI	BBS & DGI
r	0.54	-0.55	-0.48	-0.50	-0.55	0.64
p	0.015*	0.014*	0.036*	0.029*	0.015*	0.003*

Body Weight Support Effects Lateral Stability during Treadmill Walking

^{1,2} Andrew Dragunas and ^{1,3} Keith Gordon

¹ Department of Physical Therapy & Human Movement Sciences, Northwestern University, Chicago, IL, USA

² Department of Biomedical Engineering, Northwestern University, Chicago, IL, USA

³ Edward Hines Jr. VA Hospital, Hines, IL, USA

Email: AndrewDragunas@u.northwestern.edu

INTRODUCTION

Dynamic, overhead body weight support (BWS) systems are often used during gait rehabilitation. By applying an upward force through an overhead lift at a fixed medio-lateral location, some external lateral stabilization will be provided to a subject during walking. Our purpose was to quantify this interaction between BWS and lateral stability during treadmill walking.

Previous research suggests that smaller step widths, and less step width variability are typically observed when walking in a stable environment [1]. We hypothesized that increasing BWS would reduce the requirements for active lateral stabilization when gait speed was held constant. With BWS, we expected to find decreases in step width, step width variability, and minimum lateral margin of stability (MoS). In dynamically similar environments, we did not expect to see significant differences in lateral stability.

To create dynamically similar environments, in which the ratio of inertial forces to gravitational forces experienced during walking were similar across varying levels of BWS, walking speed was varied. Specifically, walking velocity was calculated using a set Froude number (Fr), a factor used to compare motions of different body size, velocity, and gravity. Walking velocities were calculated as:

$$V = \sqrt{\frac{Fr}{gl}}$$

where g is the gravitational constant, and l is the leg length. $Fr=0.25$ was used for all subjects as it represented the optimal walking speed [3].

METHODS

Eight able-bodied subjects walked on a treadmill with BWS provided by a motorized overhead support

system (ZeroG, Aretech, Ashburn, VA). Subjects walked with BWS of 0%, 20%, 40%, and 60% body weight. At each BWS level, a walking velocity, where $Fr=0.25$, was calculated. These calculated speeds and BWS levels were paired to form a set of *Dynamically Similar* conditions. Each BWS level was also repeated with the absolute speed calculated for 0% BWS, to form a set of *Speed Matched* conditions. The order of the conditions was randomized. Subjects accommodated to each condition for five minutes, after which data was collected for two minutes.

For each condition, we calculated step width, step width variability, and minimum lateral MoS. Calculation for MoS was adapted from [2], and taken as the minimum difference between the extrapolated center of mass, a measure accounting for both center of mass position and velocity, and the lateral base of support for each step. Statistical comparisons were made in MATLAB (Mathworks, Natick, MA) with a one-way repeated measures ANOVA. Bonferroni post-hoc comparisons were made when the ANOVA indicated there were significant differences between conditions. A p value of ≤ 0.05 was considered statistically significant for all tests.

RESULTS AND DISCUSSION

We found significant differences in step width, step width variability and MoS between conditions (ANOVA, $p < 0.05$; all variables). Step width tended to increase as BWS was increased. Step width was 13% larger during the 60% BWS than the 0% BWS for both the Dynamically Similar (post-hoc, $p < 0.001$) and Speed Matched (post-hoc, $p < 0.001$) conditions (Figure 1). Step width variability tended to decrease as BWS increased. For both the Dynamically Similar and Speed Match conditions, step width variability was significantly smaller during all levels of BWS when compared to the 0%

BWS condition (post hoc, $p<0.001$) (Figure 2). For minimum lateral MoS, there was only a significant difference between 60% and 0% BWS for the Speed Matched condition ($p<0.001$). During the Speed Matched 60% condition, MoS was 12% larger than during 0% BWS.

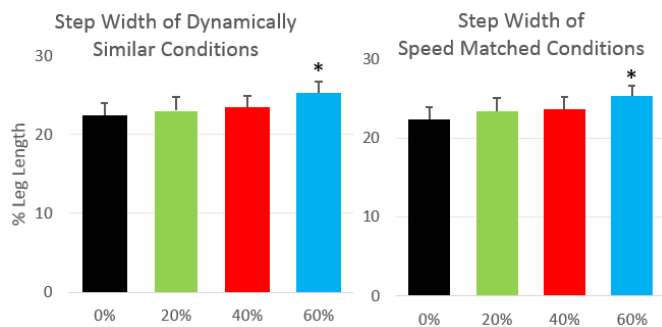


Figure 1: Normalized step width changes for dynamically similar conditions (left) and speed matched (right) conditions. Asterisks indicate significance from 0% BWS ($p<0.001$).

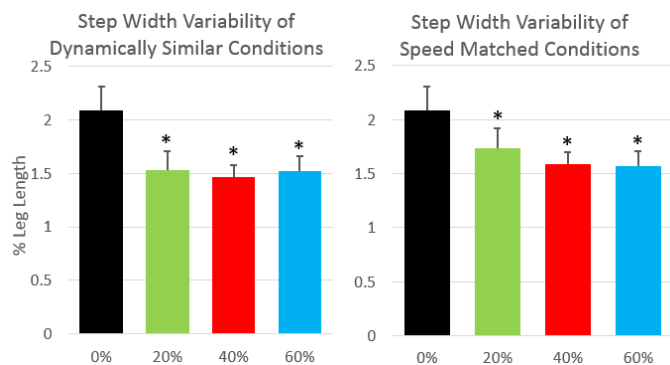


Figure 2: Normalized step width variability changes for dynamically similar conditions (left) and speed matched (right). Asterisks indicate significance from 0% BWS ($p<0.001$).

CONCLUSIONS

In both the Dynamically Similar and Speed Matched conditions, subject step width became less variable when subjects were provided with BWS. This reduction in variability suggests that, as we

hypothesized, the BWS system may provide lateral stability during gait. However, subjects also adapted wider steps and demonstrated an increased lateral MoS as BWS increased. Both these adaptations are typically observed in destabilizing environments. Subjects' choice to increase step width with BWS was contrary to our hypothesis. It is possible that subjects increased step width with BWS for reasons other than to increase lateral stability. Wider steps may have given subjects greater ability to control their yaw moments that may have been affected by increasing BWS forces. Future research investigating how BWS affects ground reaction forces and joint moments will provide further insight.

Overall our results indicate that overhead BWS effects frontal plane gait kinematics. Reductions in step width variability suggest that the BWS system may provide an external lateral stabilization and decrease the requirements for subjects to actively stabilize. However, increases in step width with BWS suggest that changes in frontal plane kinematics may occur for reasons other than controlling lateral stability. BWS creates a unique environment that needs to be considered before designing therapeutic interventions.

REFERENCES

1. Donelan JM, et al. *J Biomech* **37**, 827-835 (2004).
2. Hof AL, et al. *J Biomech* **38**, 1-8.
3. Leurs F, et al. *J Exp Biol* **214**, 2276-2282.

ACKNOWLEDGEMENTS

This work was supported in part by Career Development Award #1 IK2 RX000717-01 from the United States Department of Veterans Affairs, Rehabilitation Research and Development Service. The authors would also like to thank Mary Wu and members of the Human Agility Lab for their assistance in the preparation of this work.

DYNAMIC GAIT STABILITY: THE RECIPROCAL RELATIONSHIP BETWEEN LOWER LIMB AND TRUNK CONTROL IN RESPONSE TO SEGMENTAL LOADING

¹ Shawn M. Beaudette, ¹ Timothy A. Worden, ¹ Lori Ann Vallis and ¹ Stephen H.M. Brown

¹ University of Guelph, Guelph, ON, Canada
email: sbeaudet@uoguelph.ca, tworden@uoguelph.ca

INTRODUCTION

For successful walking to occur, the central nervous system (CNS) requires implicit information about the mechanical properties of body segments, including segment masses and moments of inertia [1]. Alterations in segment mechanical properties, such as those induced by an asymmetrically applied mass to a leg segment during walking, have been shown to alter stepping kinematics [2], however, the effect of limb mass reweighting on both upper body and joint (hip, knee, ankle and lumbar spine) dynamic stability remains unknown.

The purpose of this study was to examine the effect of an asymmetrically applied mass to individual leg segments on upper body (combined Head, Trunk and Pelvis segments, termed 'HTP') and lower limb dynamic stability. Furthermore, temporal changes in dynamic stability induced by the segment weighting were examined over the duration of cyclical treadmill walking trials. We hypothesized that distal loading would produce larger instabilities in HTP dynamic stability, while it would stabilize individual joints of the lower limb and lumbar spine due to increased muscular activation. Conversely, we hypothesized that proximal loading would stabilize HTP, while destabilizing joints distal to the applied load. Temporally, we expected both HTP and individual joints to become more stable over time as the CNS adapted to any altered segment properties.

METHODS

Fourteen healthy young adults walked on a treadmill (1.5 m/s; 5 min) while completing three different asymmetrical segment loading conditions (THIGH, SHANK and FOOT) as well as an UNLOADED control trial. The applied masses were 50 % of each estimated individual segment mass

[3], and were securely applied to the non-dominant leg for the entire walking trial. Each trial was divided into five, non-overlapping stride epochs (E1, E2, E3, E4 and E5; 50 strides per epoch) to examine the temporal effects of segmental reweighting.

Margins of Stability (MOS) and Local Dynamic Stability (Lyapunov Analysis) estimates were computed from anteroposterior (AP) and mediolateral (ML) HTP velocities to approximate neuromuscular control of the center of mass [4]. Three-dimensional angular joint kinematics were collected, and Lyapunov analyses were performed to obtain estimates of LDS for the lumbar spine, hip, knee and ankle. A two-way repeated measures statistical design was conducted, with the loading conditions and temporal epochs as independent variables. Post-hoc analyses were performed with a Tukey's adjustment, $p < 0.05$.

RESULTS AND DISCUSSION

When examining HTP dynamic stability across the different weighting conditions in the ML direction, MOS demonstrated that FOOT weighting was more destabilizing as compared to the THIGH, SHANK and UNLOADED conditions (Figure 1). Both MOS and LDS detected similar trends, although MOS detected more significant differences between conditions, with proximally applied loads (THIGH and SHANK) being more stable than the UNLOADED condition (Figure 1). Similar trends for both dynamic stability measures were also apparent in the AP direction, with distal weighting being more destabilizing as compared to proximal weighting. This was likely due to the larger accelerations the foot segment experiences; with distal loading being a more challenging perturbation to the control system. Temporally, the only effect on HTP dynamic stability was detected by LDS in

the AP direction, with the first time epoch being less stable than all other epochs.

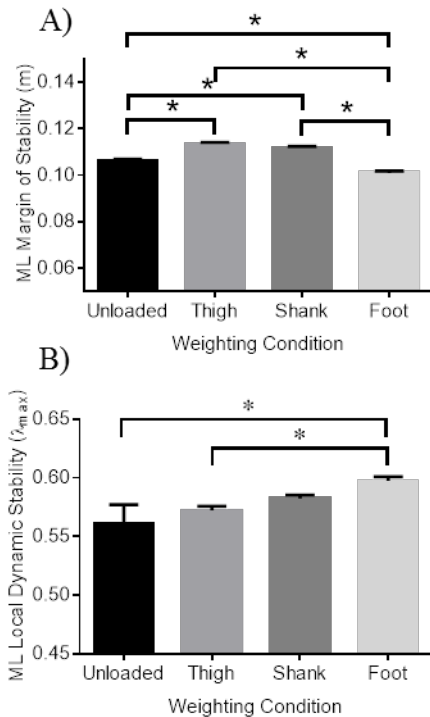


Figure 1: The effects of segment reweighting on HTP A) MOS and, B) LDS (* $p < 0.05$). Note that a higher LDS (λ_{max}) indicates lower stability.

For individual joint stability, it was found that a mass applied proximal to a joint had a destabilizing effect as determined by increased LDS. Conversely, masses applied distal to a joint had a stabilizing effect at the joint. As illustrated in Figure 2, the ankle joint was destabilized when the mass was more proximally applied (THIGH and SHANK), and conversely was as stable as the UNLOADED condition when the mass was applied to the foot. Similar spatial weighting effects were also observed at the knee and hip. This may be due to the increased muscular activation about the proximal joints required to stabilize the distally applied load, thereby stiffening each joint and increasing stability.

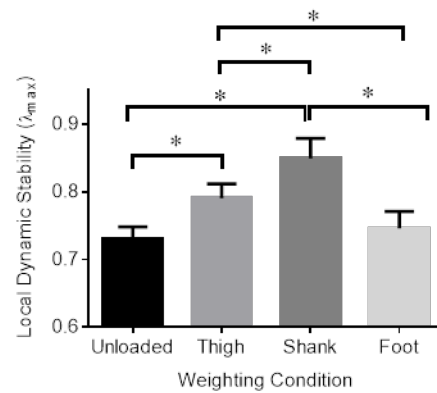


Figure 2: LDS of the ankle joint for the four weighting conditions (* $p < 0.05$). Note that a higher LDS (λ_{max}) indicates lower stability.

Temporally, the hip and ankle LDS stabilized over the duration of the trial (independent of which loading condition was applied, including Unloaded). This indicates that the hip and ankle joints may be responsible for the control of adaptation to walking on a treadmill.

CONCLUSIONS

Our results indicate that adding a mass distal to a joint increases the dynamic stability of that joint. Interestingly, the increased stability at the joint level appears at the cost of reduced stability of the HTP segment. We propose that the increased joint stability is the result of increased muscular activation about the joint, which in turn stiffens the leg segments. This stiffness in leg segments presumably changes foot strike patterns, thereby destabilizing HTP MOS measures. Temporally, the ankle and hip joints stabilized over time while walking on the treadmill, indicating that overall HTP stability is achieved via alterations occurring at the joint level.

REFERENCES

1. Gribble PL & Scott SH. *Nature* **417**, 938-941, 2002.
2. Noble JW & Prentice SD. *Exp Brain Res* **169**, 482-495, 2006.
3. Winter DA. *Biomechanics and Motor Control of Human Movement*, John Wiley & Sons, 2005.
4. Hak L et al. *PLoS One* **8**(12), e82842, 2013.

DOES DYNAMIC BALANCE OF TRANSTIBIAL AMPUTEES CHANGE AFTER A THREE WEEK ADAPTATION PERIOD ON A NEW PROSTHETIC FOOT?

¹Jenny A. Kent, ^{1,2}Nicholas Stergiou, and ^{1,3}Shane R. Wurdeman

¹University of Nebraska at Omaha, Omaha, NE, USA

²University of Nebraska Medical Center, Omaha, NE, USA; ³Hanger Clinics, Omaha, NE, USA

email: swurdeman@unomaha.edu, web: <http://www.unomaha.edu/college-of-education/cobre/index.php>

INTRODUCTION

Assessment of the suitability of a prosthetic device immediately following delivery to a patient with lower limb amputation is complicated by the ability of an individual to adapt to the device. Forming a judgment on device efficacy before this adaptation has occurred could lead to inappropriate prescription decisions. It is therefore important to understand the changes that may be expected to take place as the individual adapts. Measures that show consistency at baseline with later assessment, regardless of adaptation are valuable for the decision process, providing objective support to currently subjective decision methods.

Balance during walking is of high importance to transtibial amputees [1] and its assessment a fundamental consideration in limb prescription. The margin of stability (MOS) is a measure of dynamic balance that has been adapted from traditional static base-of-support measures to account for the inertial factors associated with center of mass (COM) motion during movement [2]. The velocity of the COM is multiplied by a factor $\sqrt{\text{leg length/acceleration due to gravity}}$ to obtain the Extrapolated Center of Mass (XcoM). This vector is then added to the vertical projection of the COM onto the ground in the anterior-posterior (AP) and medial-lateral (ML) directions to generate MOS. MOS in the ML direction (MOS_{ML}) is defined as the minimum distance between the XcoM and the lateral margin of the base of support during movement. We defined MOS in the AP direction (MOS_{AP}) as the maximum distance past the base of support that the XcoM is allowed to progress in swing prior to contra-lateral heel strike.

We hypothesized that changes in balance, evident in MOS_{ML} and MOS_{AP} values, over a three week adaptation period with a new prosthesis would differ depending on the individual's prescribed Medicare functional classification level [3]. Specifically, improvements in balance would be exaggerated when adapting to a foot of a lower activity level than the person's functional level, compared to a foot of the correct functional level.

METHODS

21 unilateral transtibial amputees (age 27-76 yrs; height 1.78 (0.81) m; mass 100.6 (18.8) kg; etiology traumatic (n=13), vascular (n=5), other (n=3)) participated in a randomized crossover trial. Participants were tested on two foot components rated 'higher activity' (HA) (i.e. energy-storage-and-return type feet) and 'lower activity' (LA) (e.g. SACH) with order of provision randomized. All subjects were previously categorized as K3 or K4 and appropriately wore high activity feet with their personal prostheses. Prosthesis provision and alignment was conducted by a certified prosthetist.

A new foot component was provided at the initial session (V1) after which participants immediately undertook baseline gait assessment. Movement of the lower limbs was recorded with 27 retroreflective markers (60 Hz; 12 camera Motion Analysis Corp., Santa Rosa, CA, USA) [2]. Each participant completed ten traverses of the laboratory at a self-selected walking speed, with 10-15 steps per leg extracted for analysis. Following a three-week adaptation period, participants returned for a repeat assessment (V2). The foot component was then swapped for an alternative component of a higher or lower activity rating and the process (V1, V2) was repeated with the second foot. The vertical

projection of the midpoint of the pelvis markers onto the floor was used to represent COM [4]. For MOS_{ML} the lateral malleolus marker was used to approximate the lateral base of support. MOS_{AP} was defined as the maximum anterior deviation of the XcoM beyond the base of support defined by the ipsilateral toe marker in terminal swing (i.e. at the point of contralateral foot contact). MOS_{ML} and MOS_{AP} were examined using a three way repeated measures ANOVA (leg x prosthesis x visit) with Fisher's LSD post hoc tests.

RESULTS AND DISCUSSION

With HA, from V1 to V2 the MOS_{ML} on the prosthetic side decreased while sound limb MOS_{ML} increased. Although these changes were not significant, in V2 this resulted in the elimination of the significant inter-limb difference that was apparent at V1. No such change was seen with LA (Figure 1). MOS_{AP} was greater on the sound limb compared to the prosthetic limb on both HA and LA during both visits, although the difference was only significant for LA. Significant increases in MOS_{AP} on both the sound and prosthetic limbs were seen from V1 to V2 on HA but not on LA (Figure 2).

Our hypothesis was refuted given the significant changes in both MOS_{AP} and MOS_{ML} across visits that were greater on average for HA. The changes seen however resulted in a more symmetrical

MOS_{ML} , which may suggest reduced favoring of the sound limb, and an increased MOS_{AP} , indicative of a greater balance confidence.

CONCLUSIONS

Changes in dynamic balance indicated by MOS_{ML} and MOS_{AP} occurred over a three week adaptation period on a new prosthetic limb of the individual's prescribed Medicare functional classification level. Our results oppose the use of MOS at initial fitting to assess function on a given device, regardless of the appropriateness of its activity level for the individual.

REFERENCES

1. Legro MW, et al. *JRRD* **36**(3), 155, 1999.
2. Hof AL, et al. *J Biomech* **38**(1), 1-8, 2004.
3. NHIC, 2015. Accessed Mar 18, 2015 from URL https://www.noridianmedicare.com/dme/coverage/docs/lcds/current/lower_limb_prostheses.htm
4. Hak L, et al. *Gait Posture* **36**, 260-264, 2012.

ACKNOWLEDGEMENTS

This work was supported by the Center for Research in Human Movement Variability of the University of Nebraska Omaha, NIH (P20GM109090).

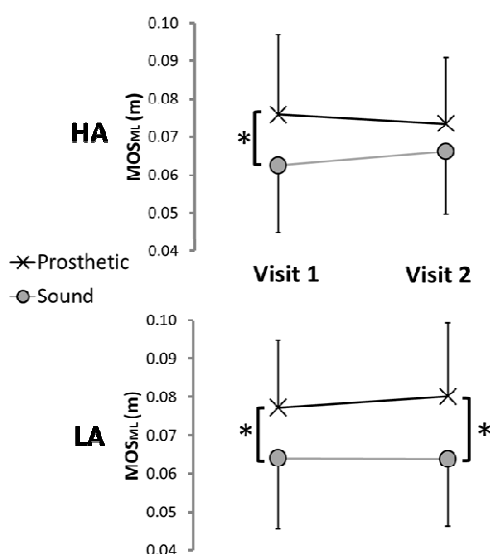


Figure 1: ML Margin of stability across visits. HA – higher activity foot, LA – lower activity foot.

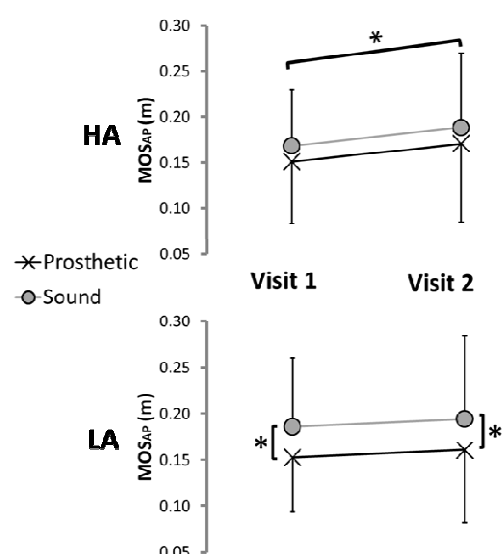


Figure 2: AP Margin of stability across visits. HA – higher activity foot, LA – lower activity foot.

RELATIONSHIP BETWEEN POSTURAL BALANCE PARAMETERS AND GAIT ASYMMETRIES IN UNILATERAL TRANSTIBIAL AMPUTEES

^{1,2} Jonathan S. Akins, ^{1,2} Rory A. Cooper, and ¹ David M. Brienza

¹ University of Pittsburgh, Pittsburgh, PA, USA

² VA Pittsburgh Healthcare System, Pittsburgh, PA, USA
email: jsa14@pitt.edu

INTRODUCTION

Greater than half of community dwelling amputees are at risk of falling and this rate is more than twice the fall rate among the general community dwelling population (24.7%) [1]. Among amputees that fall, up to 50% sustain a physical injury [1]. Physical injuries are compounded by psychological consequences that include fear of falling and lack of confidence. The causes of falls are complex and numerous fall mechanisms are not readily modifiable (e.g., environment, prosthetic entanglements, and terrain). However, mechanisms such as postural balance and gait are modifiable via rehabilitation and exercise. Previous research has examined inter-limb asymmetries of amputees during postural balance [2] and gait [3], but no known research has determined if correlations exist. The purpose of this study was to explore relationships between medial-lateral (ML) balance parameters and gait asymmetries. We hypothesized that reduced ML balance parameters were correlated with greater gait asymmetries.

METHODS

Unilateral transtibial amputees were recruited and written informed consent was obtained prior to the initiation of study procedures. Lower extremity kinematics and kinetics were measured in a computer assisted rehabilitation environment (CAREN, Motek Medical, Amsterdam, Netherlands) using a conventional gait model.

Quiet Stance Participants stood on separate force platforms with their hands on their hips and attention focused straight forward at a target placed at eye level. Three, 30-second trials were conducted with the mean values of the three trials used for

analysis. Parameters were ML center of pressure (COP) excursion, mean ML distance from geometric mean, root mean square (RMS) ML distance from geometric mean, and ML range of COP. ML parameters were selected because they have been associated with future falls [4].

Perturbed Balance Participants stood in the same posture and four linear support surface translations were applied in the horizontal plane – anterior, posterior, towards the prosthetic limb, towards the sound limb. Perturbation magnitude was 2% of the participant's height and was applied with the CAREN's 6 degree-of-freedom motion platform. Three trials were conducted for each direction; perturbation direction and time were randomized. Peak joint moments were calculated within the active force production range (160-400 ms). Response latencies were calculated as the time from onset of platform perturbation (0 ms) to peak ankle and hip moments. The symmetry index was calculated for the ankle and hip: $SI(\%) = (X_S - X_P) / (0.5(X_S + X_P)) * 100$, where X_S is the sound limb and X_P is the prosthetic limb. The mean of three trials was used for analysis and only ML perturbations were analyzed.

Gait Participants walked at a preferred walking velocity in a virtual environment. The scene was a straight trail in the woods with flat terrain; optic flow was matched to walking velocity. After participants performed a 3-minute accommodation task and took a rest break, a 3-minute trial was conducted. Twenty strides were used for analysis. Symmetry of the full normalized gait cycle waveforms were calculated using the method proposed by Kaufman et al., 2012 [2], which uses singular value decomposition. Values of + 1 indicated perfect symmetry between waveforms, 0

indicated no relationship between waveforms, and -1 indicated perfect asymmetry.

Statistics Spearman's rank correlation coefficients were calculated between ML quiet stance parameters and gait asymmetries, and between ML perturbed balance parameters and gait asymmetries. Statistical significance was set as $P \leq .05$ *a priori*.

RESULTS AND DISCUSSION

Ten unilateral transtibial amputees participated: 9 men and 1 woman; 56.3 ± 13.1 years of age; 174.7 ± 11.4 cm; 89.4 ± 14.2 kg; 9.0 ± 5.84 years since amputation; and 6 traumatic and 4 dysvascular amputations.

Decreased mean ML distance, RMS ML distance, and ML range were significantly correlated with increased ankle kinematic and kinetic gait symmetry parameters (Table 1). Decreased quiet stance parameters correspond with better balance and increased symmetry parameters are generally accepted to correspond with better gait, although a debate exists. The correlation between ML quiet stance parameters and ankle gait symmetries support the importance of gait symmetry in unilateral transtibial amputees because previous studies have demonstrated that ML quiet stance parameters are associated with future falls [4]. While Piirtola and Era [4] was a review of prospective follow-up studies with elderly participants, no such study has been performed with the unilateral transtibial amputee population.

Quiet stance parameters were not correlated with knee ($r = -.527 - .285$) or hip ($r = -.515 - -.127$) symmetry parameters. Few perturbed balance parameters were correlated with ankle, knee, or hip symmetry parameters and no clear relationships were identified. Gait symmetry index parameters

Table 1: Spearman's rank correlation coefficients between medial-lateral center of pressure parameters during quiet stance and gait symmetries

Joint	Symmetry Parameter	COP Excursion	Mean Distance	RMS Distance	Range
Ankle	Angle ($^{\circ}$)	-.127	-.697*	-.758*	-.697*
	Moment (Nm/kg)	-.042	-.685*	-.673*	-.612
	Power (W/kg)	-.515	-.855**	-.879**	-.939**

* $P \leq .05$ ** $P \leq .01$

were generally symmetric ($+1$) with a few outliers for ankle angle, knee moment, and ankle and hip powers (Figure 1).

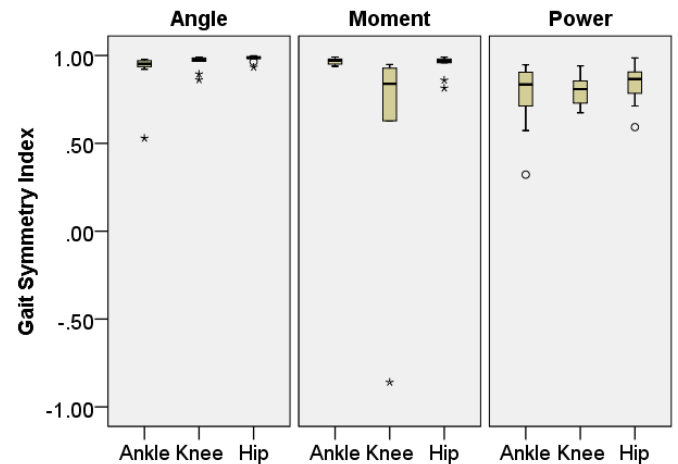


Figure 1: Boxplots of gait symmetry index parameters for sagittal plane kinematics and kinetics.

Limitations of this study include a cohort of traumatic and dysvascular amputees and no control group. Matched-control participants are currently being recruiting and tested.

CONCLUSIONS

The importance of gait symmetry in unilateral transtibial amputees is supported by the correlations between ML quiet stance parameters and ankle gait symmetries shown in this study.

REFERENCES

1. Miller et al. *Arch Phys Med Rehabil* **82**, 1031-1037, 2001.
2. Vanicek, et al. *Arch Phys Med Rehabil* **90**, 1018-1025, 2009.
3. Kaufman KR, et al. *Clin Biomech* **27**, 460-465, 2012.
4. Piirtola M and Era P. *Gerontology* **52**, 1-16, 2006.

FOLLOW THIS FELLOW? FINE, BUT GIVE IT YOUR OWN TWIST.

Paul DeVita, Ph.D.

Department of Kinesiology, East Carolina University, Greenville, NC 27858

[Biomechanics Lab on Facebook](#) (more fun than Lab website)

CAREER OVERVIEW

Believe it or not, I was educated: Maplewood Elementary, Memorial Junior High, [Walt Whitman High](#), SUNY at Binghamton and U. of Oregon. All that yet I still can't spel champaign. Since then I have progressed through the ranks at Southern Illinois and [East Carolina Universities](#). I have also been highly active in ASB, of course, and ACSM.

SCIENTIFIC QUESTIONS ADDRESSED

I have worked as a locomotion biomechanist investigating ACL injury, aging, obesity, osteoarthritis, and healthy gait. The common theme throughout is the [biomechanical plasticity in locomotion](#) (1) induced by various health issues. Through this work, I learned that while the mechanics of biomechanics provide our methods, the bio of biomechanics provides the mystery. Animals are adaptable, flexible, malleable, compliant, transformable, and ever-so-changeable. Thus we find the not-always-easily-predictable responses humans make to a change in our state, i.e. the mystery of biomechanics.

REFLECTIONS ON CAREER

When starting a career, we think about ourselves and the work we can and will do. Later however, we start to think about other people and how we can assist them in performing the work they can do. We migrate from first to last authors on our papers. I like this because while we should all like our work, we should like our colleagues and students more, especially our students. As we get better at our jobs we contribute more to the professional and personal growth of young people and we must do that with passion and sincerity.

WHAT DIRECTIONS WOULD I GET INTO NOW?

Vertical? Oh, not that kind of direction. Personally, I wanted to be the NY Yankees Biomechanist but this job didn't exist in 1986. Probably still doesn't but it soon will. Biomechanics will not always be dominated by researchers but will one day have practitioners, to use this term. Of course, many biomechanists today work in commercial settings using biomechanics to, "improve performance," of people or things. [As I look into the future](#), I foresee more commercial biomechanics opportunities. Name the industry... sports, film-making, medicine, construction, manufacturing... biomechanists will be employed to explain, exploit, and expand the human movement element. Of course, I love doing biomechanics science and always have. I think however future biomechanists will be employed as both science-creators and science-users and some of the users will have PhDs. Brave new world.

ADVICE FOR YOUNGER SCIENTISTS

- Create hypotheses that are comprehensive, fundamental ideas, not statements of expected results. Write introductions that lead to hypotheses not purpose statements.
- Avoid university service as much as you can. Do not serve on the Library Committee, the Should-Students-Wear-Blue-On-Tuesdays Committee, and most other committees. Do not be exploited by the university to do service tasks unrelated to your science. Provide biomechanics service for your university and for biomechanics (e.g. contribute to ASB). Of course, service is part of the tenure triumvirate and you must perform some activities defined as service but keep them to a minimum and fly under the university service radar.
- **Get some advice from people who have been working for ~8 years. They have been around the block yet are still part of the modern world.**
- Work hard when you are young and energetic.

(1) [This phrase developed by my long-time colleague, Tibor Hortobagyi](#)

A Career Path: From Get Smart ... to Getting Smarter

Irene S. Davis

Department of Physical Medicine and Rehabilitation, Harvard Medical School, Cambridge, MA 02138

www.runsnrc.org

CAREER OVERVIEW

I graduated from Sandwich High School, Sandwich, MA with 60 kids that I had spent the majority of my schooling with. I had originally wanted to be an FBI agent, but was denied a summer internship by J. Edgar Hoover because of my sex (no females allowed!). Thus, I took a year off, bought a motorcycle and travelled the US. With a secondary interest in the human body, I then went on to complete a BS in Exercise Science from the University of Massachusetts, a BS in physical therapy from the University of Florida, an MEd in Biomechanics from the University of Virginia and a PhD in Biomechanics from Penn State University. I subsequently accepted a faculty position in the Dept. of Physical Therapy at the University of Delaware. I remained there for 21 years until accepting a position in the Dept. of Physical Medicine and Rehabilitation at Harvard Medical School to develop and direct the Spaulding National Running Center where I now work.

SCIENTIFIC QUESTIONS ADDRESSED

My research has been aimed at understanding the relationship between lower extremity mechanics and overuse musculoskeletal injuries associated with gait. This has included injuries such as stress fractures, patellofemoral pain, iliotibial band syndrome, plantar fasciitis and Achilles tendinitis. A second focus has been on the development and assessment of gait retraining interventions to address abnormal mechanics leading to these particular injuries. While my emphasis has been on injured runners, I have also studied retraining interventions for other populations such as those with knee osteoarthritis and amputations. Two areas of much interest to me are patellofemoral mechanics and foot mechanics, neither of which are very amenable to standard motion analysis techniques. Therefore, I have very recently become involved in studying these mechanics using biplanar videoradiography techniques. Another recent area

of exploration is the mobile monitoring of gait. I hope to better understand how mechanics might change out in the natural environment. I am also working to provide realtime biomechanic feedback to alter walking and running mechanics out in the community to improve the reinforcement of new motor patterns.

REFLECTIONS ON CAREER

What I have learned about a career is that it is a professional path that has a beginning, and an initial direction. However, it is dynamic and can be significantly altered by the people you come in contact with and/or who join you along its course. I started out wanting to be an FBI agent – and that course was altered forever with a rejection letter from J. Edgar Hoover.

Thus, I started my undergraduate program without any real direction...and a bit worried. An exercise science course sparked my interest and an advisor who was a physical therapist further influenced my path towards physical therapy. As a rehab physical therapist working with patients with spinal cord injuries, I became intrigued about the biomechanics of patients being able to move their bodies with only 25% of their muscle power. This propelled me to pursue graduate work in biomechanics – another alteration of my professional path. Through my Masters' work, I developed an interest in lower extremity mechanics and sought out a PhD program focusing on this. Being accepted into Penn State University to work with Peter Cavanagh on running mechanics set the primary course for the rest of my career. Wanting to merge my clinical and scientific focuses, my path was set in the direction of understanding the relationship between lower extremity mechanics and injury.

During the first half of my career at the University of Delaware, my goal was to understand the mechanics associated with specific injuries. This provided the justification to then develop

interventions to alter these mechanics to reduce injury risk. This is the work I pursued during the second half of my tenure at UD. However, after over 20 years, I was ready for a new challenge. I wanted to apply our research findings into a clinical environment. I also wanted that clinical environment to be continually shaped by evidence derived from ongoing research. Thus the idea of a clinical and research center focused on running injuries began to develop. Boston was my home and I felt it was the ideal location for such a center, so I began to network in this area. One day, I found myself sitting across from the Chair of Physical Medicine and Rehabilitation at Harvard Medical School, describing my idea for this new center.....and my career path diverged once again to where I am now.

What I have learned is that it is nearly impossible to predict where your career will take you. But, whatever path you take, you should keep it open to new directions.

WHAT DIRECTIONS WOULD I GET INTO NOW?

Dynamic imaging techniques such as ultrasound and biplanar videoradiography are two of the new frontiers in biomechanics. These techniques provide a way to assess muscle action as well as bony motions not possible with current techniques using external markers. This relatively new line of research can provide important new information about musculoskeletal mechanics not possible without these techniques. I also think the time and mobile technology has come to promote the study of mechanics outside the laboratory environment and especially when individuals are not conscious of their gait being observed. These are the types of data that will be the most ecologically valid, and likely the most valuable.

Another area I find fascinating is tissue engineering. While we have progressed in our surgical techniques and implant technologies, nothing takes the place of nature. I believe the closer we come to restoring our natural state, the better our outcomes will be. It is entirely possible that we will soon be growing new joints using biological scaffolds and stem cell technology. This will be an incredibly

impactful and exciting area of future biomechanical research that I believe will be quite fundable.

Finally, I believe strongly in preventative medicine. Unfortunately, this is not currently an area with strong funding support. However, if this funding environment changes, I believe this is a critical area of research that biomechanists could contribute significantly to, whether it be in the area of occupational, sports, or clinical biomechanics. Promoting preventative medicine in this way could significantly improve the quality of lives and reduce the remarkably high costs of healthcare.

ADVICE FOR YOUNGER SCIENTISTS

Choose your work carefully and live by the four Ps. Have a noble Purpose, doing something that you are Passionate about. Be Persistent with your approach and Patient with results. Plan a line of research that logically builds progressively. A scattered research history is heavily scrutinized during promotion reviews. Collaborate early and often. Collaborations with those more experienced will help you in your funding efforts. Your research will become so much more dimensional and interesting through collaborations with scientists with skills outside your own area of expertise. Pick your collaborators wisely – you will be working closely with them and there truly needs to be a mutual trust and respect between you. Keep a steady influx of young scientists with new ideas into your lab to keep your research ideas fresh and relevant. Keep an open mind to shifts in paradigms that might shake the core of your current beliefs. Remember that the truth of 10 years ago may not be the truth of today, and the truth of today may not be the truth 10 years from now.

It is a privilege to live an academic life, but it is very easy for it to consume you. In terms of balance, you wear three hats: your professional hat, your family hat and your personal hat. It is difficult to be at your best in all three areas at the same time. Sometimes one or two areas have to take priority. My advice is just not to let any one area go too long without attention. Also, if you feel your plate is full, do not add another responsibility until you eliminate one first. Finally, I have found that it is so important to be able to completely disconnect from your work at times – so work hard, but play hard.

USING BIOMECHANICS TO TRY TO UNDERSTAND THE MECHANISMS OF UNINTENTIONAL INJURIES SO THEY CAN BETTER BE PREVENTED

James A. Ashton-Miller, Ph.D.

Department of Mechanical Engineering,
University of Michigan, Ann Arbor
jaam@umich.edu; webpage: <http://me.engin.umich.edu/brl/>

EARLY YEARS

I grew up in England with four sisters and a brother in Flax Bourton, a village of 250 near the southwest coast of England. When I was five my mother died unexpectedly after childbirth. It was iatrogenic - a needless death caused by a blood clot due to a doctor ordering too much bed rest. Thankfully, medical practice changed soon after. My father, a surgeon, remarried a Norwegian. At 7 years I was sent to her mother on a small farm in Norway for 6 months to learn Norwegian and attend school. With 6 feet of snow, it was heaven. The local boys introduced me to the joys of gliding down hills on my skis. They dared me to try their ski jumps, so they could enjoy the inevitable head plant with glee. But the Telemark bindings prevented serious injuries, and I slowly became a passable skier. Back in England I also became an inveterate tinkerer. By age 10 my friend and I had bought two 1929 cars for £1 each. We stripped them to their engine and chassis and had two full-size go carts to race around the neighbor's farm after the crops were in. In school I played soccer and cricket, ran track and cross-country and took up squash. My first real injury was a lumbar intervertebral disc herniation; now a known risk factor for cricket fast bowlers. By 15 I had acquired and rebuilt a 1936 MG PB sports car that would later carry me the 300 miles to college, along with a toolbox that could be needed at any time. After high school a stipend allowed me to study physical education for a year at Romerike Folkehøgskole in Norway, where I got certificates as a children's gymnastics, swimming and ski instructor. That was where I learned my first anatomy and physiology, and first heard about biomechanics. Back in England I attended Newcastle University to study mechanical engineering. A senior design class provided my first

introduction to biomechanics, and I found the experience of the collaborating with physicians to help patients very gratifying. That was what I wanted to do – apply my engineering to humans. But in 1972 there were only a couple of openings to study biomechanics in the U.K –at Strathclyde University. Surmising that I had a very small chance of being accepted there I never applied and moved to the U.S. to study for a masters degree at M.I.T. in mechanical engineering. I did research on spinal cord injuries. Every winter weekend I raced the Vermont and New Hampshire X-C ski circuit. In 1975 my bride, Kathy, and I moved to Norway so I could improve my X-C racing and she could find her roots. I volunteered as a biomechanical engineer at a University of Oslo orthopedic hospital while Kathy supported us by teaching. Luckily, I was granted a fellowship by the Norwegian government to study the biomechanics of idiopathic scoliosis for a doctorate. In 1980 I happened to see an IBM computer advertisement in a U.S. national newspaper showing how Albert Schultz (a later ASB Borelli winner) had used a computer to model spine scoliosis. By chance he was on sabbatical in Gothenberg, Sweden, so I invited him to Oslo to give a seminar. We found common interests and he offered me a job at the University of Illinois at Chicago. In 1983 we were both recruited to the University of Michigan (U-M) in Ann Arbor, where I have worked ever since. It is interesting how job opportunities seemed to materialize at fortuitous times.

REFLECTIONS ON SCIENTIFIC QUESTIONS ADDRESSED

Spine Biomechanics: My doctoral work involved demonstrating that higher vertebral growth rates in children with idiopathic scoliosis than normal.,

measuring the 3-D biomechanical properties of two child spines, and building a 17-vertebra 3-D mathematical model of the child spine stabilized by 144 muscle slips controlled by an optimization algorithm. I used the model to study how different neuromuscular recruitment strategies might affect curve progression risk under gravitational loading. I learned the hard way that complex theoretical models can be almost impossible to validate. I am forever grateful to Al Schultz for teaching me the power of using simple biomechanical models to capture the essence of the behavior of interest, and to Gunnar Andersson for modeling how orthopedic surgeons can effectively collaborate with engineers.

Falls in the Elderly: In the early 1990s Al and I were encouraged by a U-M gerontologist to examine how aging affected balance and gait. We performed some of the first studies of stepping over obstacles. Working with geriatrician Neil Alexander and neuropsychologist Bruno Giordani we studied obstacle avoidance with and without divided attention. With Darrel Thelen as a post-doc, we studied the biomechanics of forward falls and how much age and sex adversely affected rate of ankle torque development. Later doctoral students Kurt DeGoede and Josh Lo helped me analyze optimal fall strategies, both theoretically and experimentally. More recently physiatrist James Richardson and I have studied gait on uneven surfaces, especially in diabetic neuropathy.

Anterior Cruciate Ligament Injuries: About 10 years ago I suggested to a U-M orthopedist, Ed Wojtys, that we figure out which 3-D impulsive loading causes the highest ACL strain during a simulated jump landing. It took three doctoral dissertations (Tom Withrow, Youken Oh and David Lipps) to find the answer. Since then doctoral students David Lipps and Melanie Beaulieu have helped us use that experimental model to demonstrate that, while a single overload can cause an ACL rupture, repeated sub-maximal loading can also cause failure - due to low-cycle ACL tissue fatigue. This is especially true in the presence of femoroacetabular impingement.

Maternal Injuries during Vaginal Birth and Pelvic Floor Function and Dysfunction. A serendipitous meeting with John DeLancey (Obgyn) about 25 years ago over a cadaver led us to meet every Friday morning to try to understand how, why and when women are injured during birth, and why those injuries lead to pelvic organ prolapse and incontinence later in life. Aided by our Pelvic Floor Research Group we have made steady progress. Our data challenge the prevailing dogma that prolapse is caused by a problem with the vaginal wall connective tissue, and hopefully they will lead to improved treatments.

REFLECTIONS ON CAREER

Whether it was orthopedics, geriatrics, physical medicine, gynecology, urology, or neuropsychology it seemed to take about two years to learn enough about the new field to get a good feel for what is and is not possible. I have been privileged to find physicians who are open minded and respectful of what other disciplines can bring to the table to help their patients. Part of the reason I survived on soft money for 40 years, through good and bad funding cycles, is that I purposely diversified my portfolio to spread the risk of failure. I have found that competing for funding to put bread on the table means only submitting one's very best work. Anything else is a waste of time.

ADVICE FOR YOUNGER SCIENTISTS

- 1) Work on important socioeconomic problems - they are easier to get funded and they will open doors for you. If one's research is not going to make a difference, then move on to a topic that will.
- 2) Life is too short to work with people you don't respect or who don't respect you, your time, or your efforts.
- 3) Be considerate of your collaborator's time and give credit where credit is due.
- 4) The best way to get a collaboration going is to meet every week, come rain or shine, and preferably with an interested student.

REGRETS, I'VE HAD A FEW; BUT THEN AGAIN, TOO FEW TO MENTION – Frank Sinatra

Rodger Kram

University of Colorado Boulder

rodger.kram@colorado.edu; www.colorado.edu/intphys/people/kram.html

CAREER OVERVIEW

- High School (1975-1979): Realized in ~1977 that I could combine my 2 obsessions (running and science) via exercise physiology. Collected my first VO₂max data. Biomechanics not yet on radar; ASB only formed 1977.
- Northwestern University (1979-1982) Biology major: Abysmal classroom student (GPA 2.74) but worked in a lab and never lost confidence or fascination with science.
- Penn State University (1982-1985): Lab tech, then M.S. student under Peter Cavanagh. Lived the dream, ran ~80 miles/week while studying biomechanics and energetics of human running.
- Harvard University (1985-1991): Lab tech, then Ph.D. student under Dick Taylor & Tom McMahon. Studied biomechanics and energetics of locomotion in humans, kangaroos, horses and antelope +.
- University of California Berkeley (1992-2000): Post-doc under Bob Full, then Assistant Professor. Studied biomechanics and energetics of locomotion in insects, humans, penguins and elephants.
- University of Colorado Boulder (2000-present): Associate Professor, research evolved towards health related topics (obesity, amputations, aging) and sports related topics (xc skiing, cycling, and as always, running)

SCIENTIFIC QUESTIONS ADDRESSED

What is the biomechanical basis for the metabolic energy cost of legged locomotion in humans and other animals? It's been a tough question; I'm still working on it after 30+ years.

REFLECTIONS ON CAREER

I figured out what I wanted to be when I was just a kid and at key junctures, I audaciously pursued opportunities. I am amazed that I get paid to read, think and tinker/invent things. I am gratified to see young scientists extend (and/or disprove) my ideas. Mentoring grad students and seeing them succeed

on their own is my greatest career satisfaction. Good ideas will get you through times of no money better than money will get you through times of no ideas.

WHAT DIRECTIONS WOULD I GET INTO NOW?

Understanding how the brain controls movement is a daunting challenge, one that was quite primitive when I was a student. Merging the new tools of neuroscience (fMRI etc.) and imaging (PET) with biomechanics and energetics seems promising. PET scanning or something better will help us to understand energetics at the muscle level and even more locally. It is impossible to be an expert in every technology. I would pursue collaborations with experts in these techniques who are looking for questions to answer.

NIH etc. funding opportunities can be very frustrating and inefficient. Industry funding can be infinitely faster and the odds are much better. In my mind, grants are means to an end, but some departments view grants as ends in themselves.

WHAT WOULD I DO DIFFERENTLY IF I WERE STARTING AGAIN?

Mistake #1. I was really good at math in high school but I got in over my head in my first college math course. I squeaked by with a C and never took another math class.

Mistake #2. I had been OK at programming in grad school and as a post-doc. But when I was an Assistant Professor, I felt that I was too busy to learn Matlab when it came on the scene. As a result, I've had to depend on my students and post-docs for any serious data processing. Both of these mistakes restricted later options. Learn as much math and computer science as you can, in a formal class or on-line, DIY etc. You'll have a bigger toolbox.

Mistake #3. I am not very patient and I became frustrated by the time involved in writing grants, the delays and low odds of getting NIH funding. I have not applied for NIH grants as PI in many years. That resulted in my grad students doing more TA-ing than their peers (not always a bad thing) and it is why I have not advanced to the rank of Full Professor. Lack of funding has forced me to be more creative, but it also has limited my research to some extent. By writing papers, I have made good use of the time that I could have spent writing grants. But in hindsight, I should not have given up on grants without more fight.

Mistake #4. Also after tenure, I tried to develop a parallel career track developing research tools into clinical devices and growing my own business. That was a disaster. I do not belong in a world where the goal is making money and truth is not valued. It is better to patent and license your practical ideas. A scientist trying to be a businessperson can be as pathetic as a businessperson trying to do science or a fish riding a bicycle.

ADVICE FOR YOUNGER SCIENTISTS

My strengths have always been as an experimentalist and inventor. Although modeling and simulation are now a huge part of biomechanics, there is still plenty of room for clever experiments and equipment design. The best scientific papers develop a model and test it with experiments. Few people are both excellent modelers and experimentalists. Find a collaborator who complements your strengths/weaknesses.

Science can be like being on a whale-watching boat trip. When a whale is spotted off the starboard side, everyone runs to that side, the boat lurches to that direction and only a few people get to see the whale. Government initiatives (RFPs) and new hot areas

are like whale sightings. Aging research was a hot area at one point and I avoided it in part because the crowd was all running in that direction. Later in my career, when I had some original ideas percolate up about aging and locomotion, I was able to make significant contributions. In short, pursue your own ideas, don't try to study what someone else says is important.

- Undergrads: If majoring in engineering, take some biology classes and vice versa. Learn to write!
- Grad students: ABR = Always Be Reading high quality scientific papers. Learn to ask important scientific questions and design experiments. Best Dissertation = series of papers published 1 or 2 per year, not a single *magnum opus* published after graduation. You don't get a Ph.D. for surfing the Internet; write your damn paper.
- Post-docs: Become a Reese's Peanut Butter Cup (chocolate + peanut butter) i.e. combine Ph.D. expertise with that of post-doc advisor to become a unique and powerful combination.

Don't take work so seriously. Be intense but make sure to have fun in and outside of the lab. Cultivate a lifetime form of exercise/sport and do it regularly. Many faculty are quite macho/proud about how many hours they work per week and how little vacation time they take. I find that planned vacations result in very productive pre-vacation frenzies of work and vacations result in greater energy and enthusiasm when I return. I get perspective on my work when I am away from it and the creative ideas flow.

REFERENCES

Two of my favorite books:

Zinzer, W. *On writing well*. Available free on-line.

Tufte, E. *The Visual Display of Quantitative Information*. www.edwardtufte.com

HOW OBESITY AFFECTS HIP JOINT CONTACT FORCES DURING WALKING IN CHILDREN

Raymond C. Browning and Zachary F. Lerner

Colorado State University, Fort Collins, CO, USA

email: Zach.Lerner@ColoState.edu web: <http://pal.colostate.edu>

INTRODUCTION

Obese children are at an increased risk of developing orthopedic disorders of the lower-extremity. At the hip, a strong, positive association exists between pediatric obesity and a reduction in femoral neck anteversion angle and slipped capital femoral epiphysis (SCFE), the most common hip disorder in children [1, 2]. SCFE is a debilitating condition that results in an inferior-posterior slip of the femoral head relative to the femoral neck along the physis. It has been theorized that altered hip joint loading during daily physical activity (e.g. walking) in obese children may contribute to their increased risk of developing these orthopaedic disorders of the hip [1, 2]. However, it remains unknown how pediatric obesity affects hip joint loads during walking. This gap in the literature limits our ability to evaluate the risk-benefit ratio of walking physical activity on the musculoskeletal system of obese children. *This study sought to determine the effects of pediatric obesity on compressive and shear hip joint contact forces and loading rates during walking.*

METHODS

Kinematic and kinetic data was collected during treadmill walking at $1 \text{ m} \cdot \text{s}^{-1}$ in 10 obese ($\text{BMI}_Z > 95\%$) and 10 healthy-weight ($5\% < \text{BMI}_Z < 85\%$) 8-12 year-olds. Age, sex, and leg length were similar between groups. We used dual x-ray absorptiometry (DXA) to determine body composition, segment masses, lower-extremity alignment, and femoral neck angle (Fig. 1) and width for each child.

To validate our musculoskeletal model and optimization scheme used to predict muscle forces, we compared measured to predicted axial, mediolateral, and anteroposterior hip joint contact

forces for an individual with an instrumented hip prosthesis walking at $1.08 \text{ m} \cdot \text{s}^{-1}$ [3]. Predicted loads had similar magnitudes and waveforms. At peak loading, which occurred during early-mid stance, peak axial, anteroposterior, and mediolateral contact force predictions had accuracies of 98.6%, 90.3%, and 85.7%, respectively.

We scaled a generic OpenSim musculoskeletal model to the size of each participant and subsequently specified lower-extremity alignment and segment masses to create a subject-specific model for each child. We used a weighted static optimization approach to estimate the muscle forces that reproduced the measured walking mechanics determined from inverse dynamics, and calculated hip joint contact forces using the joint reaction analysis [4]. To compute compressive and shear forces, we transformed the contact forces from the reference frame of the hip to that of each child's femoral neck (Fig. 1).

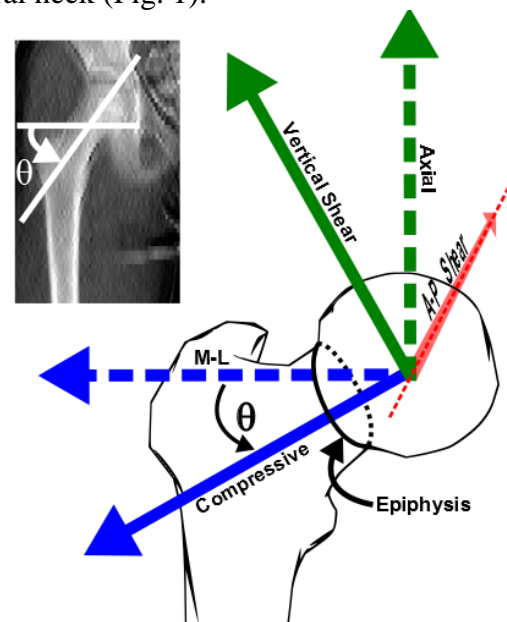


Figure 1: Measurement of femoral neck angle (θ) from a representative participant's DXA radiograph (inset) and transformation of the hip joint contact forces.

RESULTS AND DISCUSSION

Obesity affected compressive and shear hip joint loading (Fig. 2). First peak compressive contact forces (N) during stance were 1.8 times greater in the obese vs. healthy-weight participants ($p<0.001$). Similarly, first peak distal and posterior shear forces were 1.8 and 1.5 times greater ($p<0.001$), respectively, in the obese vs. healthy-weight children.

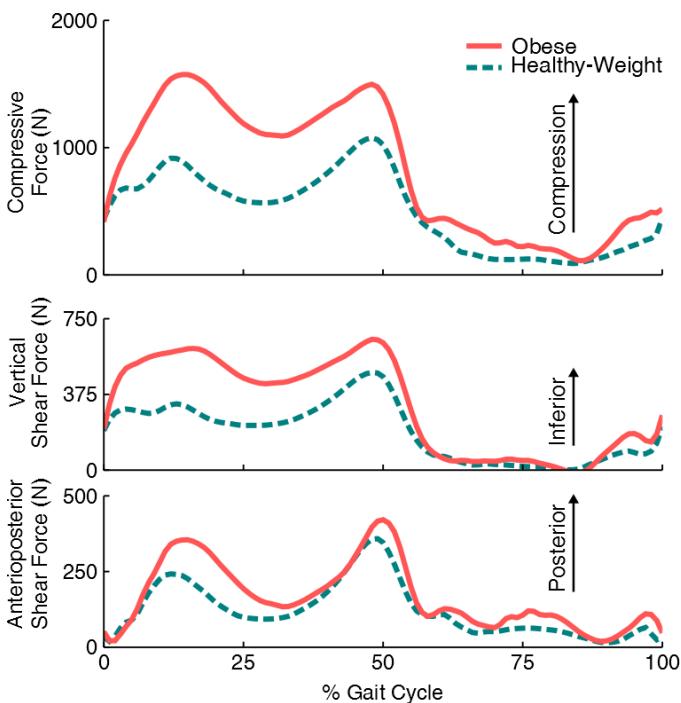


Figure 2: Compressive (top), vertical shear (middle), and anteroposterior shear (bottom) hip joint contact forces in obese (red, solid) and healthy-weight (blue, dashed) children.

Peak compressive and resultant shear loading rates, which occurred during early stance, were 1.47 times (10.15 vs. 6.89 $\text{kN}\cdot\text{s}^{-1}$, $p<0.001$) and 1.43 times (4.35 vs. 3.03 $\text{kN}\cdot\text{s}^{-1}$, $p=0.002$) greater in the obese vs. healthy-weight participants, respectively.

The hip joint contact force load vectors had similar directions but greater magnitudes in both the sagittal and transverse planes for the obese vs. healthy-weight children (Fig. 3). The directions of the applied shear forces (inferior and posterior) are consistent with the direction of femoral head slippage in the SCFE condition (inferior-posterior).

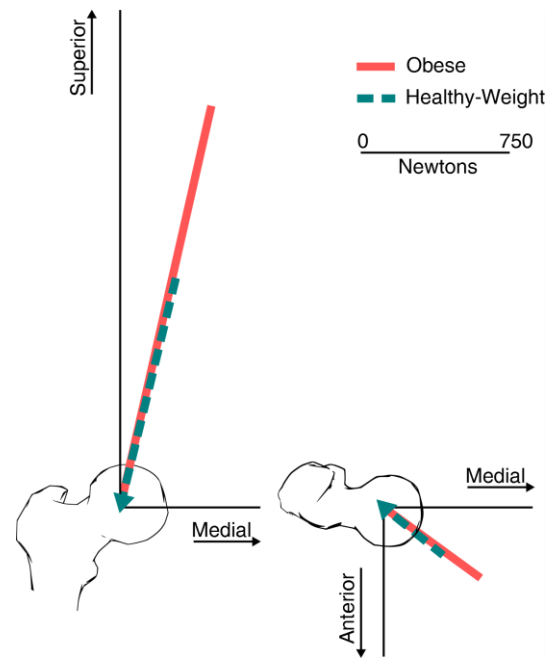


Figure 3: First peak hip contact force load vectors in the sagittal (left) and transverse (right) planes for the obese (red, solid) and healthy-weight (blue, dashed) children.

CONCLUSIONS

Our results of greater compressive and shear forces at the hip during walking in obese children provides biomechanical evidence that altered loading during daily walking physical activity may contribute to their increased risk of developing orthopaedic disorders at the hip. Femoral neck diameter was similar between groups. This suggests that our findings of greater contact forces in the obese children likely represent similarly elevated compressive and shear stresses at the growth-plate. The results of this study may help clinicians weigh the risk-benefit ratio of increased physical activity on the musculoskeletal system in obese children.

REFERENCES

1. Wills M, *Ped Phys Thera* **47**, 230-235, 2004.
2. Wearing SC, et al. *Obes Rev* **7**, 209-218, 2006.
3. Bergmann, et al. *J Biomech* **34**, 859-871, 2001.
4. Lerner ZF, et al. *J Biomech*, In Press, doi:10.1016/j.jbiomech.2014.12.049, 2015

ACKNOWLEDGEMENTS

Funding from NIH/NICHD F31HD080261 and ACSM Foundation doctoral student research grants.

FRONTAL HIP POWER ABSORPTION DURING WEIGHT ACCEPTANCE AMONG INDIVIDUALS WITH INCOMPLETE SPINAL CORD INJURY

¹ Lise Worthen-Chaudhari, ² James Schmiedeler, and ¹ D. Michele Basso

¹ The Ohio State University, Columbus, OH, USA

² University of Notre Dame, Notre Dame, IN, USA

email: lise.worthen-chaudhari@osumc.edu

INTRODUCTION

During locomotion, power absorption in the lower extremity joints serves to decelerate the center of mass of the body (i.e., brake), prevent joint collapse [1], maintain forward propulsion and provide vertical support [2]. Within the frontal plane of the hip joint, power absorption is prevalent during the weight acceptance (WA) phase of locomotion [3]. Despite the importance of power absorption for functional success, the WA phase of locomotion has received little attention in neurorehabilitation research of locomotor recovery. In addition, frontal plane hip dynamics may play a more important role in WA than previously realized [3,4]. We hypothesized that individuals with incomplete spinal cord injury (iSCI) who had shown substantial gains during prior locomotor training (LT) would evidence persistent deficits in power absorption about the frontal hip during the WA phase of walking.

METHODS

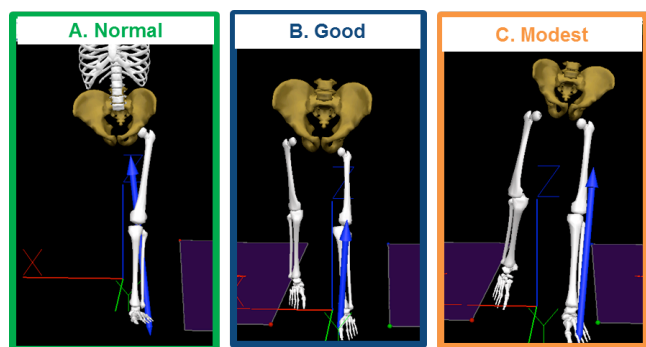
This research was approved by The Ohio State University Institutional Review Board. Two participants with iSCI, who had undergone more than 50 LT sessions by the day of testing, and eight control participants consented to participate. The 2 participants with iSCI had recovered full (blue; Fig. 1) or limited (gold; Fig. 1) community ambulation during LT participation prior to participating in this study, as measured by standard clinical measures such as the 10 meter walk test and the Spinal Cord Injury Functional Ambulation Inventory. Their treadmill walking speeds (0.6 m/s, 0.54 m/s) were similar to the mean speed of the controls (0.64 m/s; representative data at 0.57 m/s shown in green; Fig. 1), although BWS was applied at 30% vs 0% for control. At low speeds, power production about the

frontal hip in controls is not significantly different at 30% and 0% BWS [5].

Kinematic data were collected using a 7-camera system (Vicon, 200Hz), and force data were collected using a split belt instrumented force platform treadmill (Bertec, 1000Hz). Body weight support (BWS) was provided by a hydraulic BWS system and harness. Subjects were asked to walk normally per condition, to look at a target positioned at the head of the treadmill at eye level, and to walk at steady-state speed for approximately 25 seconds per trial. Low-pass filters were applied to kinematic (Butterworth, 1st order, bi-directional, 6Hz) and force (critically damped, 1st order, bi-direction, 10Hz) data. Joint power calculations were performed in Visual 3D (C-Motion, Inc). WA phase was isolated [4], and peak power with corresponding hip ab/duction angle was detected using custom MATLAB software.

RESULTS AND DISCUSSION

Participants with iSCI demonstrated delayed onset of hip adduction (Fig. 1E) and prolonged, exaggerated weight acceptance activity about the frontal hip (Fig. 1F). The end of weight acceptance in controls occurred at $22.8 \pm 4.8\%$ of stride (mean \pm STD), consistent with the representative case in Fig. 1F. At the time of peak power absorption about the frontal hip, participants with iSCI exhibited less hip adduction than did controls (Fig. 1D), with the modestly recovered iSCI participant even exhibiting abduction at this instant in some cases. These aberrant hip motions tend to be distinctly different from those caused by gluteus medius weakness, such as in a Trendelenburg gait, in that the pelvis and hip of the swing leg are elevated rather than dropped (Fig. 1B,C).



CONCLUSIONS

Individuals with iSCI who have undergone LT show persistent deficits in hip abductor function during the WA phase of gait, as evidenced by prolonged, exaggerated power absorption about the frontal hip in WA. Specific training to address persistent deficits may provide a way to tap into additional potential for neurologic recovery.

REFERENCES

- [1] Winter DA. Overall principle of lower limb support during stance phase of gait. *J Biomech.* 1980; **13**(11): 923-927.
- [2] Liu MQ, Anderson FC, Pandy MG, Delp SL. Muscles that support the body also modulate forward progression during walking. *J Biomech.* 2006; **39**(14): 2623-2630.
- [3] Worthen-Chaudhari L, Bing J, Schmiedeler JP, Basso DM. A new look at an old problem: Defining weight acceptance in human walking. *Gait Posture.* 2014; **39**(1): 588-592.
- [4] Kim CM, Eng JJ. Magnitude and pattern of 3D kinematic and kinetic gait profiles in persons with stroke: relationship to walking speed. *Gait Posture.* 2004; **20**(2): 140-146.
- [5] Worthen-Chaudhari L, Schmiedeler JP, Basso DM. Training conditions that best reproduce the joint powers of unsupported walking. *Gait Posture.* 2015, doi: 10.1016/j.gaitpost.2015.01.003.
- [6] Andriacchi TP, Alexander EJ, Toney MK, Dyrby C, Sum J. A point cluster method for in vivo motion analysis: applied to a study of knee kinematics. *J Biomed Eng.* 1998; **120**(6): 743-749.

ACKNOWLEDGEMENTS

Partial funding for this research was provided by the Ohio Chapter of the Fraternal Order of Eagles.

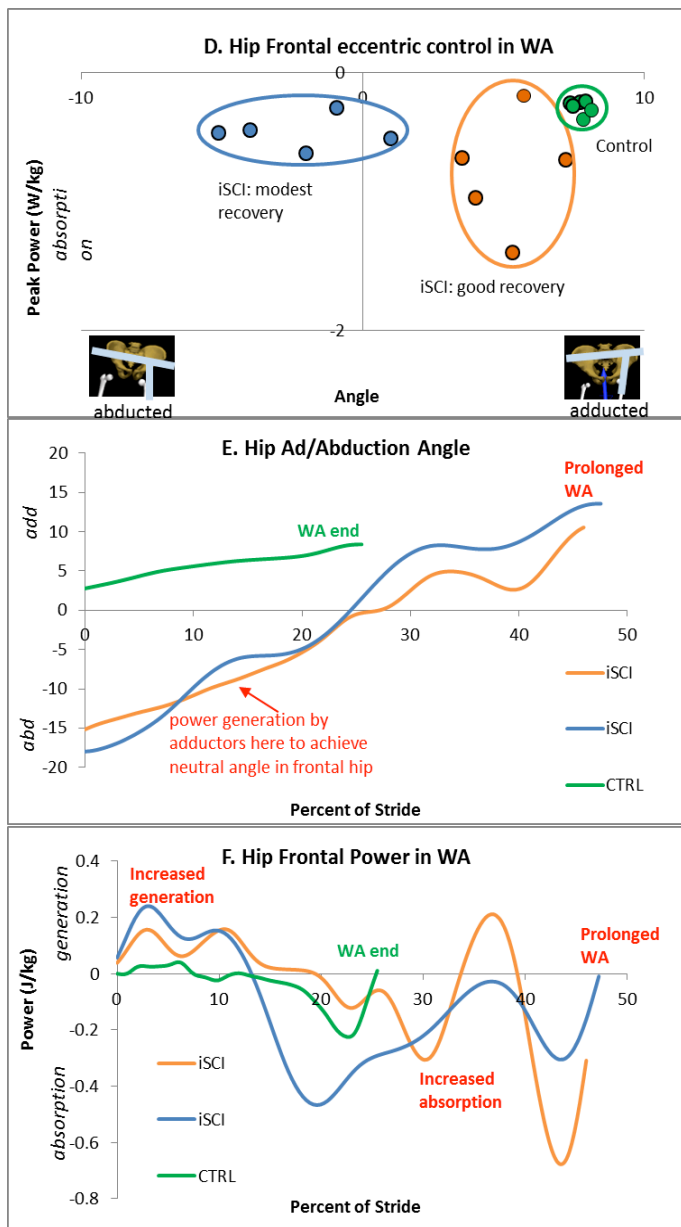


Figure 1: Depictions of left side frontal hip function for three functional levels: Normal, Good locomotor recovery, and Modest locomotor recovery following iSCI and LT. (A,B,C) depicts lower extremity position and ground reaction force, (D) plots peak power by corresponding angle for five trials, (E) shows time to WA end, and (F) depicts hip frontal power.

KNEE MOMENTS INCREASE MORE THAN GROUND REACTION FORCES INCREASE WITH ADDED LOADS

Rebecca E. Fellin, Shane G. Sauer, Peter N. Frykman and Joseph F. Seay

U.S. Army Research Institute of Environmental Medicine, Natick, MA, USA
email: rebecca.e.fellin.civ@mail.mil, web: <http://www.usariem.army.mil/>

INTRODUCTION

Soldiers often carry heavy loads (up to 55-kg) while on missions. Soldiers who frequently carry heavy loads are more likely to sustain knee injuries than soldiers who do not often carry heavy loads [1] although the precise mechanisms of injury are unclear. For example, increases in vertical ground reaction force (vGRF) were 5-6 percent bodyweight (%BW) for every 10% increase in relative load, load normalized to %BW [3]. Recent research found that joint moments increased as added load increased [2,3]. However, researchers have not explored the relationship between increases in joint moments compared to increases in relative load. In order to better understand the possible relationship between knee loads and knee injury, a comprehensive analysis of joint moments in the lower extremity and relative load is necessary.

Therefore, the purpose of this study was to compare increases in ground reaction forces and joint moments to increases in relative load. We hypothesized that the ground reaction forces would increase at the same rate as increases in relative load. We further hypothesized that the joint moments would increase at a lower rate than relative load.

METHODS

Thirty male soldiers (20.6 ± 3.1 yrs; ht: 1.77 ± 0.08 m; wt: 84.7 ± 14.4 kg; mean \pm SD) volunteered to participate in this study. Only males were included as infantry roles in the Army are limited to males, currently. During an orientation session, subjects walked on an instrumented treadmill at the speed and maximum weight they would experience in the data collection. During the data collection session, subjects were instrumented with retro-reflective markers to track pelvis and bilateral lower extremity motion. Subjects then walked in their combat boots

at 3 MPH on the treadmill for 5 minutes following which 30 seconds of data were recorded during 6 load conditions: bodyweight (BW) only, 15-kg, 25-kg, 35-kg, 38-kg and 55-kg. The BW only condition was presented first followed by the 5 loads presented in random order. The 15-kg load was an armored vest, and subsequent loads were weighted vests. Subjects rested for a minimum of 3 minutes between loads.

Kinematic and kinetic data were filtered at 10 and 20 Hz, respectively. Five strides from the right side were selected for analysis. Spatiotemporal parameters, including step rate, stride length and double support time, as well as vGRF, 3D joint angles and moments at the hip, knee and ankle were computed. Knee range of motion (ROM) was calculated as knee flexion angle between footstrike and mid-stance. vGRF was normalized to BW. Joint moments were normalized to body mass. Peak moments in early (0-50%) and late (51-100%) stance were extracted. Variables were averaged across the 5 strides for each condition. Relative load, load normalized to percent bodyweight (%BW), was calculated for each subject. Percent increases compared to BW only values for all variables were computed. To minimize regression bias, BW percentages $>70\%$ (11 data points) and outliers ($3 \times$ interquartile range) were removed from the analyses. Outliers removed were hip extension (1) and knee flexion (1) moments and knee flexion peak angle (2). To identify the sensitivity of variables to load increases, regression analyses for each individual variable (spatiotemporal, knee ROM, and kinetics) with %BW load as a predictor variable were conducted.

RESULTS AND DISCUSSION

As hypothesized, vGRF peaks for loading and push-off increased at a similar rate to %BW increases in relative load, 0.93% and 0.81%, respectively

(Figure 1). Additionally, our hypotheses for hip and ankle moments were supported with increases of 0.65-0.67% in early stance and 0.65-0.77% in late stance for each %BW increase in relative load. Interestingly, knee moments were the most sensitive to increases in relative load. Knee extension moment increased 1.3% for every 1% increase in relative load. A scatterplot of the knee extension moment revealed most data points were above a 1:1 relationship, indicated by the dotted line (Figure 2). Knee flexion moment in late stance increased 0.86% for every 1% increase in relative load.

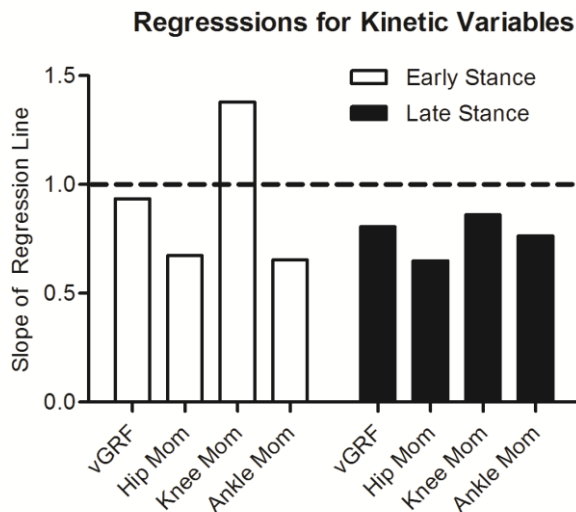


Figure 1: Slopes of regression lines, which compared effects of increases in relative load to percent increases in peak values of kinetic variables over baseline values. All slopes significantly different from zero. Dashed line at 1.0 indicates a 1:1 relationship between increases in relative load and kinetic variables. vGRF=vertical ground reaction force peak, mom=moment peak.

These increases in knee extension moment occurred despite potential mechanisms to decrease the effects of the relative load. For each added %BW of relative load, there was a significant increase in double support time (0.33%). Smaller, yet statistically significant, protective changes occurred in step rate, 0.09%, peak angle for knee flexion, 0.08% and stride length, -0.05%, for each %BW increase in relative load. However, knee ROM did not increase with relative load (slope 0.02%). The lack of change in knee ROM, indicated that the knee musculature appear to share a higher burden of

the increased load, which was previously found between 15-kg and 55-kg loads in this dataset [2].

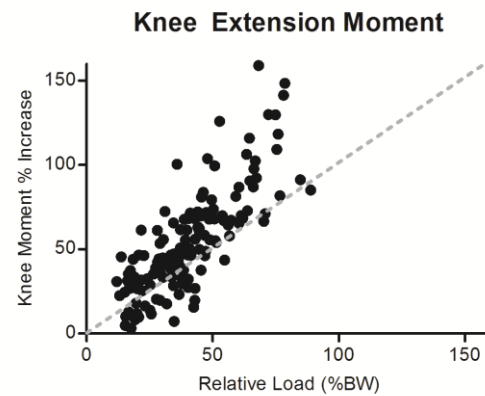


Figure 2: Knee extension moment increases for added loads. Dotted line is 1:1 relationship. Values >70% relative load removed prior to analyses to minimize bias and no outliers remained.

These findings of similar increases in vGRF peaks to increases in relative load are in contrast to findings of vGRF increases of only half the relative load increase [3]. These differences may be due to load carriage experience of soldiers in our cohort versus civilians and/or due to wearing combat boots compared to what was likely other footwear.

CONCLUSIONS

Despite adaptive strategies to decrease joint loads in the lower extremity, some joint loads still increased at rates similar to increases in relative load. These data suggest a potential mechanism of why the knee joint is more commonly injured in soldiers who frequently carry heavy loads.

REFERENCES

1. Hill OT, et al. *Mil Med* **178**, 676-682, 2013
2. Seay JF, et al. *Mil Med* **179**, 85-91, 2014.
3. Silder A, et al. *J Biomech* **46**, 2522-2528, 2014.

ACKNOWLEDGEMENTS

The views expressed in this abstract are those of the authors and do not reflect the official policy of the Department of Army, Department of Defense, or the U.S. Government. The investigators have adhered to the policies for protection of human subjects as prescribed in DOD Instruction 3216.02 and the research was conducted in adherence with the provisions of 32 CFR Part 219.

PROSPECTIVE GAIT ANALYSIS OF ANKLE ARTHRODESIS AND ARTHROPLASTY

¹Shannon M. Pomeroy, ¹Michael E. Hahn, ²Ava D. Segal, ²Eric C. Whittaker, ²Marisa Benich, ^{2,4}William R. Ledoux and ^{2,4}Bruce J. Sangeorzan

¹ Department of Human Physiology, University of Oregon, Eugene, OR, USA

² Department of Veterans Affairs, VA Puget Sound, Seattle, WA, USA

³ Departments of Mechanical Engineering and ⁴ Orthopaedic and Sports Medicine, University of Washington, Seattle, WA
email: mhahn@uoregon.edu | web: www.bssc.uoregon.edu

INTRODUCTION

Historically, the treatment for ankle arthritis has been arthrodesis, which provides a relatively painless and stable joint. However, the diminished joint ROM has been reported to increase the risk for developing distal foot pain [1]. In recent years arthroplasty has become available. With this replacement technique, closer to normal kinematics have been achieved [2]. Both operations have displayed improved gait function, with one retrospective study concluding that patients with arthrodesis were able to walk faster, however, their gait was more asymmetrical than patients with arthroplasty [3].

Although studies have separately examined the effects of each operation on functional outcomes, limited studies have made direct comparisons, with a lack of long-term prospective studies. Thus, in this prospective work, it was hypothesized that post-surgery, there would be improved temporospatial parameters, altered ankle ROM, increased internal plantarflexor moment and increased power in both surgeries. It was further hypothesized that improvements pre- to post-surgery would be greater in the arthroplasty group than in the arthrodesis group, with an increasing disparity over time.

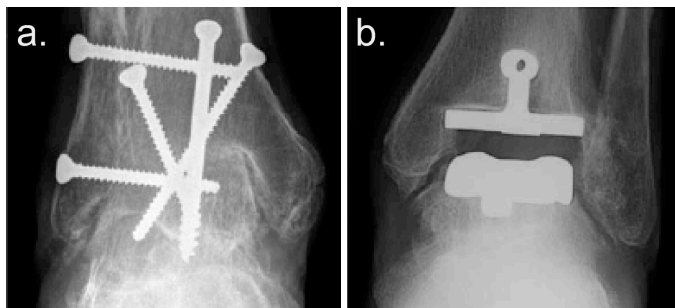


Figure 1. Radiographs of the ankle following (a) arthrodesis and (b) arthroplasty.

METHODS

Twenty-three patients scheduled for surgical treatment of end-stage ankle arthritis were recruited for participation in the study following a surgical decision. Exclusion criteria included having

neurologic, metabolic, or orthopaedic lower limb impairment of ambulatory ability, a recent surgical intervention, or systemic inflammatory arthritis. Subjects were stratified based on chosen surgical procedure, either tibiotalar arthrodesis using a screw fixation or standard arthroplasty technique (Figure 1; Table 1). Patients were evaluated prior to surgery (t_0) and at 1, 2, and 3 years post-surgery (t_1 , t_2 , and t_3). Due to time commitment and relocation, some patients opted out of return visits (Table 2). Each patient engaged in standard rehabilitation protocols [4]. Subject informed consent and Institutional Review Board approval was obtained prior to study initiation.

Table 1. Demographics of patients enrolled; Mean (SD).

	Arthrodesis	Arthroplasty
N	8	15
Sex	2 female; 6 male	8 female; 7 male
Age (years)	55.3 (3.7)	59.4 (7.1)
Side	6 right; 2 left	4 right; 11 left
BMI (kg/m ²)	28.2 (2.1)	31.3 (4.6)

Kinematic and Kinetic Analysis

Three-dimensional marker coordinate data of the affected limb and ground reaction forces were collected for 5 successful barefoot gait trials along a 10-m walkway at self-selected walking speed using previously reported motion capture techniques [4]. Net internal joint forces, moments, and power for the hip, knee, and ankle were subsequently calculated using inverse dynamics. Peak stance phase kinetic values and sagittal plane ankle ROM were extracted and averaged for each subject across trials. Gait velocity (m/s), stride length (m), and cadence (steps/min) were also calculated (Table 2).

A mixed effects linear model was used to compare temporospatial variables, peak kinetics, and ankle ROM between visits for both groups ($\alpha=0.05$). Kinematic and kinetic comparisons included gait velocity as a covariate and changes across time were tested for group effects.

RESULTS AND DISCUSSION

Sagittal plane ankle ROM was significantly affected by surgery type, with a decrease of 4.8° following fusion and increase of 1.9° following arthroplasty at 3-years follow-up (Figure 2; $p < 0.01$). Significant pair-wise differences were found for peak internal plantar flexor ankle moment between t_1 , t_2 and t_3 .

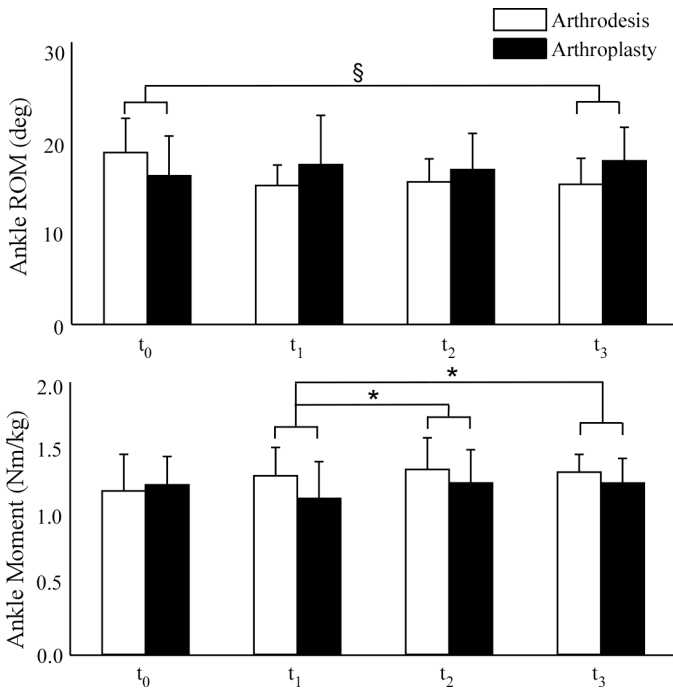


Figure 2: Ankle joint kinematics and kinetics (mean \pm standard deviation) pre- (t_0) and post-surgery (*, pair-wise difference between time points, $p < .05$; §, significant change by surgery type, $p < .01$).

Though not statistically significant, many observations were noted which can aid in the interpretation of primary findings (Table 2). Gait velocity stabilized following surgery in arthroplasty patients, however a decreasing trend was found in arthrodesis patients across the 3-year follow-up. Arthroplasty patients displayed decreased peak internal plantar flexor moment and increased ankle ROM with an increasing trend in ankle joint power across the 3-year follow-up. At the same time point, the arthrodesis group produced increased peak

ankle, knee, and hip moments along with decreased joint power. It is possible in a fusion patient that the proximal joints become involved due to the complex coupling between knee and ankle with a fixed tibiotalar joint. These observations should be examined further in future studies.

CONCLUSIONS

Outcomes demonstrated that regardless of operation, surgery to address end-stage ankle arthritis is able to improve gait function. However, gait function seems to decline at 3 years post-surgery in arthrodesis patients, with gait velocity reduced close to pre-surgical values. It is plausible that at this time compensations such as increased ankle joint moments with significantly reduced ankle ROM are beginning to compromise surrounding joints [1]. To better explain how gait function is maintained in both groups following surgery a more robust multi-segment foot model is necessary. Future consideration of the current data coincident with recorded physical function in daily activities as well as center of mass movement will afford extrapolation of the mechanisms utilized and resulting quality of life. Presently, the findings provide insight to the ongoing debate regarding surgical outcomes in treating end-stage ankle arthritis, providing data highlighting the beginning stages of altered kinematics and associated risk.

REFERENCES

- Coester L, et al., *JBone Joint Surg.* **83-A**:219-28, 2001.
- Valderrabano V, et al., *Foot Ank Int.* **24**:881-96, 2003.
- Piriou P, et al., *Foot Ankle Int.* **29**:3-9, 2008.
- Hahn ME, et al., *Foot Ankle Int.* **33**:282-289, 2012.

ACKNOWLEDGMENTS

Thanks to Jane Shofer for statistical analysis. This study was funded by grants from the VA RR&D (A4513R, F7968R).

Table 2. Patient inclusion numbers, temporospatial parameters, and kinetics over time; Sample Mean (SD).

	Arthrodesis				Arthroplasty			
	t_0	t_1	t_2	t_3	t_0	t_1	t_2	t_3
Number of patients	8	8	7	6	15	15	12	9
Gait velocity (m/s)	1.06 (0.20)	1.16 (0.20)	1.14 (0.16)	1.09 (0.13)	1.02 (0.19)	1.12 (0.19)	1.13 (0.16)	1.13 (0.16)
Stride length (m)	1.14 (0.17)	1.25 (0.15)	1.19 (0.14)	1.22 (0.14)	1.05 (0.22)	1.14 (0.19)	1.18 (0.14)	1.19 (0.13)
Cadence (steps/min)	108 (14)	109 (11)	109 (7)	106 (6)	106 (10)	111 (9)	111 (10)	111 (7)
Ankle Power (W/kg)	1.72 (0.66)	1.78 (0.58)	1.84 (0.63)	1.74 (0.65)	1.75 (0.57)	1.79 (0.92)	1.88 (0.85)	1.84 (0.67)
Ankle Moment (Nm/kg)	1.19 (0.27)	1.30 (0.21)	1.35 (0.23)	1.33 (0.13)	1.23 (0.21)	1.14 (0.27)	1.25 (0.24)	1.25 (0.18)
Knee Moment (Nm/kg)	0.29 (0.26)	0.35 (0.24)	0.39 (0.18)	0.39 (0.09)	0.41 (0.16)	0.46 (0.25)	0.42 (0.25)	0.39 (0.17)
Hip Moment (Nm/kg)	0.47 (0.17)	0.48 (0.15)	0.43 (0.19)	0.48 (0.13)	0.30 (0.15)	0.41 (0.13)	0.38 (0.15)	0.35 (0.15)

ANALYSIS OF THE TRIPOD THEORY USING PLANTAR SHEAR FORCES

¹Mariam J. Crow, ¹Visar Berki and ¹Brian L. Davis, Ph.D.

¹ The University of Akron, Akron, OH, USA

email: mjc73@zips.uakron.edu <http://bme.uakron.edu>

INTRODUCTION

In 1970, Kapandji proposed the notion that “Viewed as a whole, the plantar vault [of the foot] can be compared with an architectural vault supported by three arches”. The three ground supports to which Kapandji was referring occur at the first and fifth metatarsal heads (MTHs), as well as the calcaneus¹. The present study focused on (i) the existence of a tripod under the foot, and (ii) the ability of neuropathic, diabetic patients to support the arches.

METHODS

Pressure and shear stress data were collected on 29 human subjects: 16 control patients (9M, 7F; Age: 47.6 ± 5.8 years; Weight: 824 N) and 13 neuropathic, diabetic patients (8M, 5F, Age: 61.6 ± 14 years, Weight: 944 N). Each subject walked barefoot across a custom built shear and pressure collection system that is aligned in the center of a 3 m. x 0.6 m. platform². Four steps were analyzed for each subject and all plantar surfaces were divided into ten regions (Figure 1) using custom-written Matlab code. The present study focuses on four of the ten regions: regions 4, 6, 9 and 10 (Figure 1).

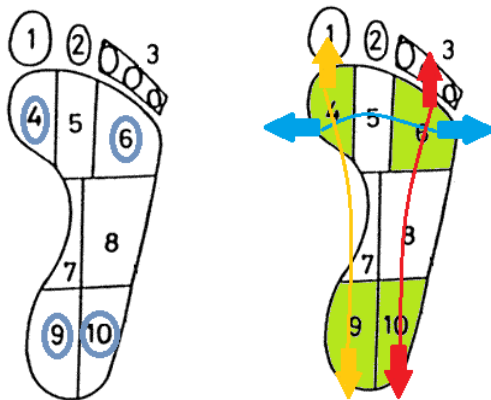


Figure 1: Display of shear force directions for regions of primary interest in present study. The green areas correspond to the base of a tripod.

It was hypothesized that evidence of a collapse of a plantar tripod could be demonstrated using the mean shear values in the regions previously listed. In support of the medial longitudinal arch, the differences were determined between mean anterior shear under the first MTH and mean posterior shear under the medial heel. For the lateral longitudinal arch, the differences were calculated between mean anterior shear under the fourth and fifth MTHs and mean posterior shear under the lateral heel. Lastly, for the transverse arch, shear differences were examined between the mean medial shear under the first MTH and the mean lateral shear under the fourth and fifth MTHs. These values were determined for all 116 steps then steps compared between control and diabetic, neuropathic groups.

RESULTS AND DISCUSSION

The presence of peripheral neuropathy correlates with loss of nerve, as well as intrinsic muscle control. Therefore, it was hypothesized that the existence of three arches could be demonstrated using differences in shear values, and moreover that diabetic patients would exhibit greater shear differences due to splaying of their foot (i.e., the tripod) during gait.

The differences in shear forces for each element of the tripod were significant for all three elements of the tripod. The medial longitudinal arch had mean values of 11.5 ± 3.7 kPa and 15.1 ± 5.4 kPa for control and diabetic, neuropathic participants, respectively ($p < 0.01$). The mean values of force differences for the lateral longitudinal arch were 9.3 ± 2.8 kPa and 13.1 ± 4.0 kPa for control and experimental subjects, respectively ($p < 0.01$). Lastly, the mean differences across the metatarsal heads were 17.7 ± 4.6 kPa for the control group and 22.5 ± 9.0 kPa for the diabetic, neuropathic subjects ($p < 0.01$) (Figure 2 and Table 1.)

CONCLUSIONS

This is the first study to examine the relationship between shearing forces on the plantar surface of the foot and each element of “Kapandji’s tripod”. In our opinion, any diminished ability to maintain these arches would be manifested through slippage of the skin relative to the support surface, and concomitant changes in shearing stresses on the plantar surface of the foot.

Due to the presence of peripheral neuropathy in the diabetic subjects, it was hypothesized that intrinsic muscles would have diminished capabilities to oppose the collapsing of the three arches during gait. The differences were determined between mean anterior shearing forces under the first MTH and fourth and fifth MTHs and the mean posterior shears under the medial and lateral calcaneus, respectively. The same methods were utilized for medial shear under the first MTH and lateral shear under the fourth and fifth MTHs to demonstrate the collapse of the transverse arch. Significantly higher differences were found for the diabetic, neuropathic

subjects along all three arches in comparison to the control subjects. These data not only support the existence of three arches and in turn the tripod theory; but also support the claim that the feet of diabetic subjects with peripheral neuropathy are less capable of opposing the outward shear forces that lead to the collapse of these three arches.

REFERENCES

1. Kapandji IA. (1970). The Physiology of the Joints. 2nd ed. Edinburgh: Churchill Livingstone, 196-219.
2. Stucke, S. et al. (2012). "Spatial relationships between shearing stresses and pressure on the plantar skin surface during gait." Journal of biomechanics 45(3), 619-622.

ACKNOWLEDGEMENTS

This research was possible due to support from National Institutes of Health (Grant # 4R44DK084844-02) & the collaborations of Akron General Medical Center.

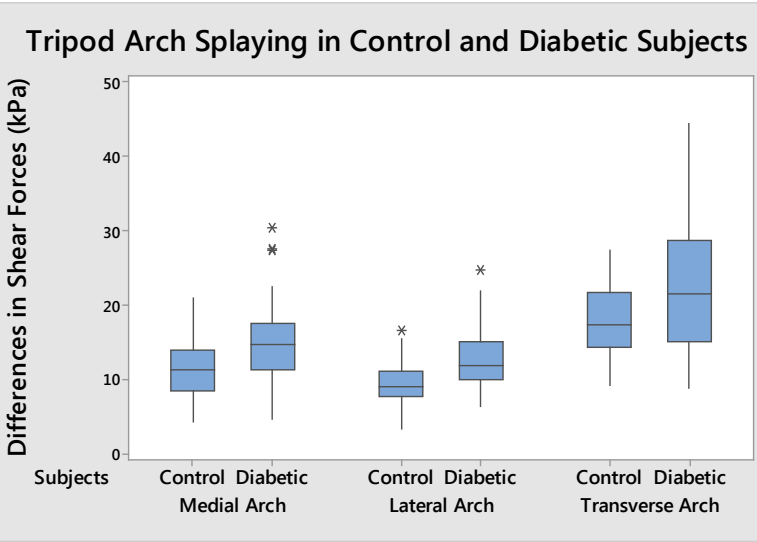


Figure 2: Boxplot displaying mean shear differences across three plantar arches

Table 1: Numerical differences in shearing forces for each element of the tripod.

	Shear Force Splaying (kPa)		
	Medial Arch	Lateral Arch	Transverse Arch
Control Subjects	11.5 ± 3.7	9.3 ± 2.8	17.7 ± 4.6
Diabetic Subjects	15.1 ± 5.4	13.1 ± 4.0	22.5 ± 9.0
P - Value	< 0.01	< 0.01	< 0.01

ADAPTATIONS IN LOWER EXTREMITY WORK DUE TO CHANGES IN WALKING SPEED

¹Anahid Ebrahimi, ²Saryn R. Goldberg, ¹Steven J. Stanhope

¹University of Delaware, Newark, DE, USA, ²Hofstra University, Hempstead, NY

e-mail: anahide@udel.edu web: <http://me.udel.edu>

INTRODUCTION

The ability to modulate walking speed is often an important goal for individuals with gait impairments. To aid in developing proper treatments and corrective devices for individuals with impairments, it is important to first understand the gait adaptations of unimpaired individuals ambulating from slow to typical walking speeds. Studying the energetics of the lower extremity allows for causal analysis of movement. While energetics studies have historically been limited to 3 degree-of-freedom (DOF) work calculations of the joints (ankle, knee, and hip), recent literature has supported the use of 6 DOF inverse dynamics work calculations of these joints and the inclusion of a distal foot work term [1].

The objective of this study was to understand the work adaptations of all the lower extremity limb constituents (ankle, knee, hip, and distal foot) that occur in order to increase walking speed. We investigated changes in the 6 DOF work of the limb constituents over slow to typical walking speeds during the stance and swing phases of gait. Furthermore, we quantified the proportional change of the constituents' contributions to the absolute work produced by the limb with increased speed.

METHODS

A subset of the data collected by Goldberg and Stanhope (2013) was used for data analysis [2]. Eight unimpaired adult subjects (height 177 ± 7.5 cm, mass 74 ± 13.1 kg) walked on a calibrated [3] instrumented split-belt treadmill (Bertec, Columbus, OH) at three height-normalized velocities (0.4, 0.6, and 0.8 statures/s). Three-dimensional movement analysis data were collected via a six-camera system (Vicon, Los Angeles, CA). Using Visual3D software (C-Motion, Inc. Germantown, MD), 6 DOF powers of each constituent (ankle, knee, hip, and distal foot) were calculated using methods described elsewhere [4,5]. Stride length was calculated by multiplying the treadmill velocity in meters per second by the

subject's average stride time (heel-strike to ipsilateral heel-strike) in seconds. Positive (negative) constituent work values were calculated for each subject by integrating the positive (negative) portion of the respective constituent power curves over stance and swing phases. Net constituent work was the sum of the positive and negative constituent work for each constituent. Positive, negative, or net limb work was the sum of the positive, negative, or net constituent work values, respectively (e.g., net limb work in Eq. 1). Absolute limb work (W_{limb}^{abs}) was the sum of the positive limb work and absolute value of the negative limb work. Relative work (RW) was the absolute value of each constituent's work divided by the absolute limb work (e.g., relative negative ankle work in Eq. 2). All work values were normalized by body mass and stride length.

$$W_{limb}^{net} = W_{ankle}^{net} + W_{knee}^{net} + W_{hip}^{net} + W_{distal\ foot}^{net} \quad (1)$$

$$RW_{ankle}^{-} = |W_{ankle}^{-}| \div W_{limb}^{abs} \quad (2)$$

Differences in net work and relative work were compared separately across the three walking speeds using several repeated measures ANOVAs with Bonferroni corrections ($p < 0.05$) using SPSS software (IBM Corp., Armonk, NY).

RESULTS AND DISCUSSION

Average stride length increased with faster walking speed (mean \pm SD): 0.877 ± 0.153 m, 1.165 ± 0.110 m, and 1.306 ± 0.253 m for 0.4, 0.6, and 0.8 statures/s, respectively. In stance, net ankle work and net distal foot work significantly increased, while net hip work significantly decreased with speed ($p < 0.05$) (Table 1). In swing, net hip work during swing significantly increased with speed ($p < 0.05$). Net limb work did not differ significantly with speed in stance or swing. Absolute limb work did not significantly differ with faster walking speed: 1.056 ± 0.189 J/kg/m, 1.092 ± 0.170 J/kg/m, and 1.376 ± 0.703 J/kg/m for 0.4, 0.6, and 0.8 statures/s, respectively. The sizes of the pie charts in Figure 1 are relative to the amount of absolute limb work performed at that speed.

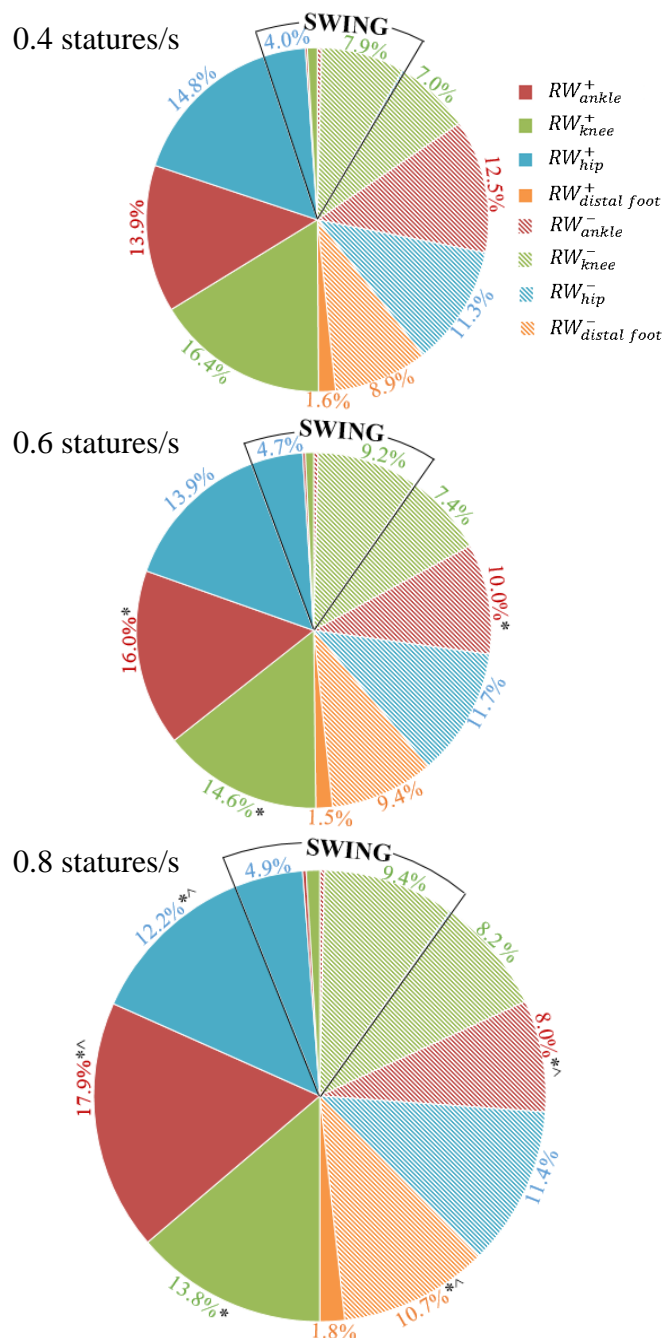


Figure 1: Relative constituent work (J/kg/m) as % of absolute limb work across speeds. Slices not labeled are $\leq 1\%$. * and ^ indicate a significant difference from 0.4 statures/s and 0.6 statures/s, respectively.

Our findings indicate that while net limb work per distance does not change significantly with increased walking speed, the net constituent work does change. All constituent net work values showed some change with walking speed except for the net knee work. Using the same data set presented here, it was previously shown that peak knee extension moments do not significantly differ with speed [2]. In addition, Figure 1 provides a unique analysis of the proportional change in constituent work relative to absolute limb work with speed, separated by the phase of the gait cycle in which the relative constituent adaptations occur. In stance, the positive ankle and negative distal foot work contributions increased while the negative ankle contribution decreased with faster speeds, supporting trends seen in previous literature [5]. Interestingly, as speed increased, the knee and hip generated less relative positive work in stance. Conclusions must be limited to unimpaired individuals walking at slow to typical walking speeds. Future studies will characterize work across a broader range of gait intensities, including faster walking conditions.

CONCLUSION

The net limb work did not change significantly with speed, while net constituent work did change (except at the knee). Relative constituent work helps identify the extent of individual joint adaptations and where in the gait cycle they occur to enable unimpaired persons to walk at faster speeds.

REFERENCES

1. Zelik KE, et al. *J Exp Biol* in print, 2015.
2. Goldberg SR, et al. *J Biomech* **46**, 1176-83, 2013.
3. Goldberg SR, et al. *J Appl Bio* **25**, 401-6, 2009.
4. Buczec FL, et al. *J Biomech* **12**, 1447-57, 1994.
5. Takahashi K, et al. *Gait & Pos* **38**, 818-23, 2013.

Table 1: Net constituent and limb work normalized by body mass and stride length (mean \pm SD). * and ^ indicate a significant difference from 0.4 statures/s and 0.6 statures/s, respectively.

Net Work J/kg/m $\times 10^{-2}$	0.4 statures/s		0.6 statures/s		0.8 statures/s	
	Stance	Swing	Stance	Swing	Stance	Swing
Ankle	1.681 \pm 2.564	-0.225 \pm 0.087	6.666 \pm 3.482*	-0.168 \pm 0.157	14.023 \pm 9.650*^	-0.122 \pm 0.174
Knee	9.792 \pm 3.317	-7.258 \pm 1.740	7.915 \pm 3.229	-9.036 \pm 2.042	7.862 \pm 5.439	-10.712 \pm 2.500
Hip	3.361 \pm 3.264	3.908 \pm 1.083	2.190 \pm 3.110	4.901 \pm 1.585	0.203 \pm 4.129*	5.877 \pm 2.113*^
Distal Foot	-7.553 \pm 1.360	N/A	-8.699 \pm 1.145	N/A	-12.004 \pm 4.558*	N/A
Limb	7.280 \pm 2.449	-3.575 \pm 1.014	8.071 \pm 3.146	-4.303 \pm 0.751	10.084 \pm 6.229	-4.956 \pm 1.510

SYSTEMS ENGINEERING APPROACH TO IDENTIFYING CORE CONTROL STRATEGIES IN INDIVIDUALS WITH AND WITHOUT LOW BACK PAIN DURING A NOVEL UNSTABLE SITTING TASK

¹Bradley S. Davidson and ²Sheri P. Silfies

¹University of Denver, Denver, CO, USA

²Drexel University, Philadelphia, PA, USA

email: bradley.davidson@du.edu, web: www.du.edu/biomechanics

INTRODUCTION

Individuals with recurrent and chronic low back pain (LBP) have impaired core neuromuscular control [1,2], which may influence recurrence of symptoms [3,4]. Understanding differences in core neuromuscular control between healthy individuals and those with LBP will help advance clinical assessment and in planning rehabilitation interventions. We propose that insight into neuromuscular control within LBP is gained within a multi-joint task that requires coordination and stabilization of all musculoskeletal elements by the central nervous system. Prior characterization of neuromuscular control in patients with LBP has produced inconsistent findings. Most analyses have focused on a single parameter within neuromuscular control (e.g. proprioception, muscle timing) or neglected the dynamic interdependence between key musculoskeletal elements (e.g. trunk, pelvis).

The objective of this investigation was to implement an assessment of overall system function by applying a well-established system identification paradigm to a novel seated dynamic stabilization task. We used this approach to characterize differences in performance and motor control strategies of the trunk and pelvis system between patients with LBP and healthy controls.

METHODS

Six patients with current low back pain (average: pain 4.8 ± 2.2 [NPRS, 0-10]; disability $27.3 \pm 8.6\%$, [Oswestry, 0-100%]) and six age and gender matched healthy controls participated in the investigation (8/12 female, average age 36.8 ± 15.1 years). Each participant performed four trials of a dual control task on an unstable seat that required them to simultaneously: 1) maintain upright sitting

and 2) tilt the seat to match a target. The seat was attached to a sphere that rolled without slipping on a force platform. Weight of the lower extremities was counterbalanced so that the participant was in a neutral configuration (vertical trunk and horizontal thighs). Targets were based on center of pressure (COP) repositioning, which were achieved by reconfiguration of the trunk and pelvis from neutral (Fig. 1). Each participant received real-time visual feedback of the COP on a computer monitor during all portions of the task.

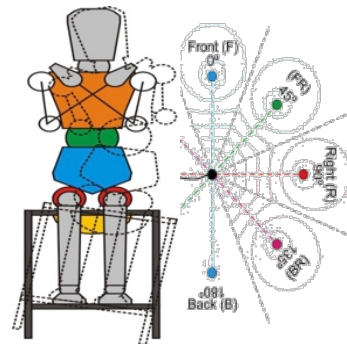


Figure 1: Neutral configuration and reconfiguration (dotted lines) of trunk and pelvis (left) required to reposition COP on targets (right).

Within a single trial, eight targets 35mm away from the neutral COP in eight directions (0°, 45°, 90°, 135°, 180°, 225°, 270°, 315°) were sequentially displayed on the monitor (Fig. 1). For each target, the participant started in the neutral position, and was instructed to “move directly toward the target as quickly and accurately as possible, pausing on the target.” Force platform data were collected at 2400 Hz during the entire trial, filtered (piecewise-linear), and used for subsequent analyses.

To characterize neuromuscular control for each

participant, we performed 2nd-order nonparametric system identification on time series data to identify three system coefficients (Fig. 2). The input, $U(s)$, was a series of eight step functions equivalent to the eight targets at 35mm from neutral, and the output $Y(s)$ was the series of recorded COP trajectories within a trial (Fig 2a).

Validity of the model structure was assessed for each participant with a leave-one-out cross validation (% accuracy) for the four trials. Representative coefficients were averaged across the four trials, and mean coefficients were compared across groups using two-tailed t -tests.

RESULTS AND DISCUSSION

The 2nd-order model structure provided high accuracy for both groups (Control Group: 94.2(1.0)%, LBP group 93.4(1.2)%). The participant-specific models demonstrated clear differences in performance between the groups (Fig. 2b), which were reflected by differences in two of the three identified coefficients (Table 1).

Table 1: Mean (SD) coefficients identified for each group. Asterisk indicates group difference ($P < 0.05$).

Coefficient	Control Group	LBP Group
a_0	1.09 (0.38)*	0.68 (0.17)
b_0	1.53 (0.28)	1.56 (0.35)
b_1	1.10 (0.38)*	0.69 (0.17)

Interpreting these changes within the context of classical second order systems analysis provides coarse insight into strategy and performance of the LBP group. Lower a_0 in the LBP group compared to control group indicates an overall lower system gain and corresponds with the slower rise time to the target observed in the COP traces. Higher b_1 in the control group compared to the LBP group indicates more damping, which may be necessary to limit the overshoot during a faster target acquisition strategy.

Our approach represents a unique paradigm compared to past systems approaches because the trunk and pelvic reconfiguration for each target is initiated by executive command (internal perturbation). Previously applications in the low back used externally applied perturbations with a

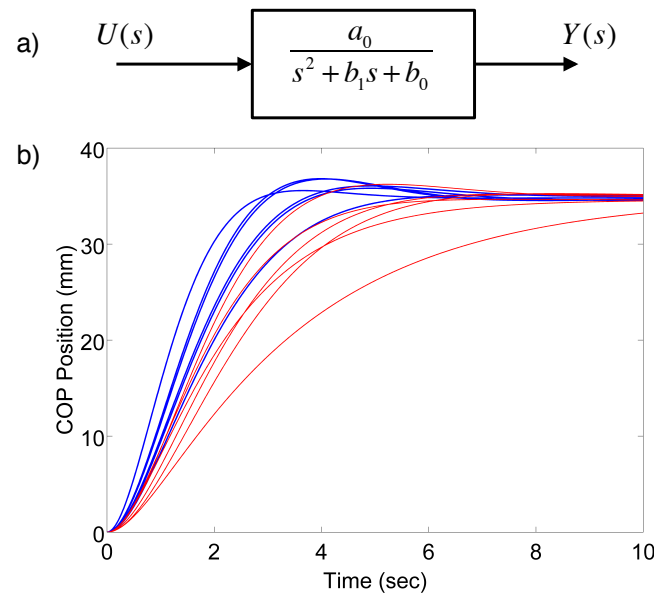


Figure 2: a) 2nd-order system with coefficients. b) Simulated responses to the target task using participant-specific models (blue: healthy; red: low back pain)

fixed pelvis [5,6] and identified mechanical properties of the trunk segment alone.

Nonparametric analysis is an appropriate first step, but cannot identify performance of individual system components and limits our interpretation to general differences between groups. In future work, we will develop a parametric analysis that considers parameters needed in neuromuscular control to complete the target task.

CONCLUSIONS

Nonparametric system identification was used to establish differences in neuromuscular control between LBP and control groups. This foundation will allow us to develop analyses that lead toward a more comprehensive understanding of neuromuscular control in the context of assessment of and rehabilitation for LBP.

REFERENCES

1. Silfies et al. *Clin Biomech* **20**,465-73,2005
2. Silfies et al. *Arch Phys Med Rehabil*, **90**, 1159-69, 2009
3. MacDonald et al. *Pain* **142**, 183-8, 2009
4. Lomond et al. *Man Ther* **5**, 425-32, 2014
5. Moorhouse & Granata *J Biomech* **40**, 1058-65, 2007
6. Bazrgari et al. *Comp Meth Biomech* **15**, 1000-9, 2012

ACKNOWLEDGEMENTS

Supported in part by NIH K01HD053632 (Silfies).

INFLUENCE OF INPUT DEVICE, WORK SURFACE ANGLE, AND TASK ON SPINE KINEMATICS DURING SIMULATED OFFICE WORK

¹ Maureen F. Riddell, ² Kaitlin M. Gallagher, ¹ Colin D. McKinnon, and ¹ Jack P. Callaghan

¹ University of Waterloo, Waterloo, ON, CAN

² University of Arkansas, Fayetteville, AR, USA
email: m2riddell@uwaterloo.ca

INTRODUCTION

Modern software and touch technology have enabled tablets to perform nearly all the advanced functions of desktop computers. Their mobility allows tablets to be versatile across industries and favoured in off-site and non-traditional office settings. Being a stand-alone device, tablets provide users with location mobility and the ability to perform tasks in standing or sitting postures with ease. Contemporary equipment, such as an adjustable work surface slope, is often used in conjunction with tablets and other input devices, adding to an increasingly complex workstation environment. The type of work task heavily influences trunk posture [1] as well as the location of the device due to viewing angle [2]. Changing these elements of a work surface slope may facilitate a closer interaction and proper viewing angle between the device and the user resulting in the maintenance of neutral spine postures. The purpose of this study was to analyze the kinematics of the cervical and lumbar spine segments during simulated computer tasks using a desktop computer and a tablet, on both a sloped and horizontal work surface.

METHODS

Fourteen participants (6 male and 8 female) volunteered for this study. Three-dimensional kinematics of the cervical and lumbar spine were sampled at 32 Hz using a motion capture system (Optotrak Certus, NDI, Waterloo, Canada). Participants sat for 1-hour at a hybrid sit-stand workstation with a work surface that could vary slope from 15° to horizontal (Focal Upright Furniture, New York, USA). The adjustable foot platform and height of the seat-pan was modified to match the participant's height, and to position the

participant's thigh-to-trunk angle at 135°. The session was separated into four randomized 15-min conditions: horizontal-computer, horizontal-tablet, sloped-computer, and sloped-tablet. A 2nd generation iPad was used (Apple, Cupertino, CA, USA). Within each condition, participants completed three 5-min tasks: reading (READ), emailing (MAIL) and filling out a form on a device from a paper copy (FORM). Cervical and lumbar median angles and range of motion (ROM) (10th to 90th percentile angles) were extracted from amplitude probability distribution functions (APDF) calculated from the angle data. All outcome measures were entered into a three-way general linear model with three repeated factors of device (TABLET/ PC), desk (HORIZONTAL/ SLOPED), and task (READ/ MAIL/ FORM).

RESULTS AND DISCUSSION

There was a significant main effect of task on cervical spine posture ($p=0.0008$). The FORM task produced the greatest median neck flexion angle ($20.3 \pm 2.5^\circ$) compared to the MAIL ($14.2 \pm 2.5^\circ$) and READ ($11.8 \pm 2.7^\circ$) tasks. A table-by-device interaction effect ($p=0.0228$) showed higher cervical flexion angles in TABLET conditions that were more influenced by the change from HORIZONTAL to a SLOPED work surface than the same tasks performed on a PC ($p=0.0228$) (Table 1). A three-way interaction was seen for cervical spine ROM between table, device, and task ($p=0.0212$). There was a device-by-table interaction effect for all tasks (MAIL: $p<0.0001$; FORM: $p=0.0005$; READ: $p=0.0332$). Participants experienced more neck flexion when using a tablet on a horizontal versus a sloped work surface, which has been found in previous studies and was consistent for both devices [2,3]. Extreme neck flexion angles have been associated with the flexion

relaxation phenomenon (FRP). Even though participants were free to either hold or place the tablet on the table, participants assumed a posture resulting in more neck flexion when interacting with a HORIZONTAL work surface, demonstrating participants do not choose a neutral posture under these conditions. The FRP may have similar implications for pain development in the cervical spine as it does in the lumbar spine. The degree of neck flexion is highly influenced by task and the degree of tablet tilt by means of viewing/gaze angle (0° or 15°). To mitigate this viewing issue, external devices should be used if interacting with tablet on a non-sloping surface to prevent high cervical flexion angles.

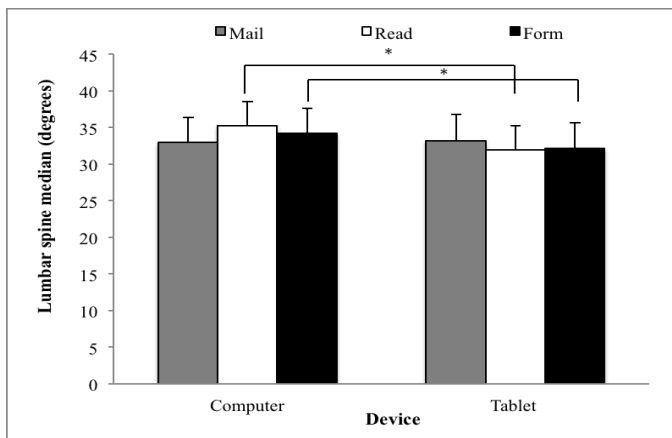


Figure 1: Relative lumbar median spine angle with respect to a neutral posture between tasks while using a desktop computer and tablet. Note: (*) signifies a significant difference.

A device-by-task interaction ($p=0.0061$) was observed for relative lumbar spine angles (Fig. 1). FORM ($p=0.0106$, $35.3 \pm 3.4^\circ$) and READ ($p<0.0001$, $34.2 \pm 3.5^\circ$) resulted in greater lumbar spine flexion while using a PC compared to a TABLET (READ: $31.9 \pm 3.4^\circ$; FORM: $32.1 \pm 3.5^\circ$). A main effect of task ($p=0.0242$) was found for lumbar spine ROM. This finding was accompanied by a trend towards significance in the

lumbar spine ROM for the main effect of device ($p=0.0592$). This increase in lumbar flexion while using a PC was likely due to the lack of mobility compared to the TABLET, which can be moved closer to the participant while they were using it. The influence of task on posture cannot be ignored as the physical properties of the task, (layout and tools) heavily determines the postures users adopt [4]. Differences are hypothesized to be due to the requirement of either direct finger contact or mousing to complete the tasks.

CONCLUSIONS

Based on the task specific responses of spine postures, when selecting a device one should consider the physical nature of the task and the work surface adjustability. Working with a TABLET on a HORIZONTAL work surface slope resulted in high amounts of cervical flexion. Therefore, when possible, external aids such as a monitor arm and keyboard should be used to reduce flexion and facilitate a neutral posture if a tablet is the primary device used to complete tasks.

REFERENCES

1. Gregory DE, et al. *Hum Factors* **48**, 142-153, 2006
2. Young JG, et al. *Work* **41**, 81-91, 2012
3. Asundi K, et al. *Ergonomics* **53** 74-82, 2010
4. Dennerlein JT, et al. *Ergonomics* **49**, 45-61, 2006

ACKNOWLEDGEMENTS

The authors would like to thank the Natural Sciences and Engineering Research (NSERC) of Canada for funding this project. Dr. Jack P. Callaghan is supported by the Canada Research Chair in Spine Biomechanics and Injury Prevention.

Table 1: Neck median and range of motion angles from the APDF when reading in sloped or horizontal desk positions (in degrees – mean (standard error)). An * denotes a significant difference in angles.

	Horizontal		Sloped	
	Median	Range	Median	Range
Computer	6.9 (2.9)	10.3 (1.9)	5.5 (2.7)	13.8 (2.7)
Tablet	26.6 (2.5)*	16.9 (4.9)	22.7 (2.4)*	10.4 (1.6)

PHYSICAL ERGONOMICS OF TABLET INTERACTION WHILE SITTING

Myroslav Bachynskyi

Max Planck Institute for Informatics and Saarland University, Saarbrücken, Germany
email: mbachyns@mpi-inf.mpg.de, web: <http://resources.mpi-inf.mpg.de/biomechanics/>

INTRODUCTION

We present physical ergonomics assessment of typical tablet device usage. Tablet devices are becoming widespread and often even displace personal computers and laptops. However, while physical ergonomics of PCs and laptops was extensively studied in the past, there is only little knowledge of ergonomics of tablet devices. In particular the user assessment is complex due to portability of tablets, which allows a variety of tablet locations, orientations and holds which can be adopted by users. The purpose of this work was to identify typical postures, set of recruited muscles and health risks related to the tablet interaction.

Few previous works [1, 2] have measured head and neck posture, or wrist and shoulder posture of tablet usage, however they used predefined set of tablet hold configurations. They extracted joint angles directly from locations of markers attached to anatomical landmarks, which ignores such sources of error as marker drift during movement, joint displacement, or absence of skeletal anatomy. In contrast to this in our work we do not assume a particular posture for interaction and ask participants to take a pose and hold the tablet as comfortable for them. We record motion of the whole human body and analyze biomechanical indices simulated using an anatomically-correct musculoskeletal model.

METHODS

For the analyses we have used the dataset created by Bachynskyi et al. [3]. The data comes from 40 participants (26 males and 14 females) recruited on the local university campus. Mean age is 24.9, height 171.4 cm, and weight 67.4kg. The participants were asked to perform a repetitive target selection task on an iPad-sized and shaped surface. Targets were of 12 types depending on the

size and approach angle, and participants performed 50 target selections in each condition. During the tasks the participants used sitting postures which they have considered comfortable, without constraints from the experimenter. 12 cameras of PhaseSpace Impulse motion capture system have tracked 38 active markers attached to all body segments of a participant at 480 Hz. To record main external forces acting on a user, the chair and platform under the feet were equipped with 8 force sensors collecting data at 125 Hz.

The data was pre-processed by custom Matlab scripts. Biomechanical simulation was performed in an open source software OpenSim [4] with a commercial musculoskeletal model of the Full-Body¹. The outputs generated by Inverse Kinematics, Inverse Dynamics and Static Optimization are further consolidated into the single dataset. This allows fast and simple analysis of frame-level and aggregated data. The dataset contains posture and moment values for 109 joints, forces and activations for 236 muscles covering the whole human body.

We use Matlab and an interactive visualization tool [5] to perform analyses on the data. We compute average postures of each joint and compare it to movement ranges and neutral postures. Postures close to extreme are considered as health risk after prolonged use. Further, we consider average and peak joint moments. High values of average joint moments pose health risk after prolonged use; high peak moments can lead to an injury even in short interaction. We consider peak muscle forces, as a factor that can lead to a muscle or tendon injury. High average muscle forces lead to muscle stress and fatigue. In our analyses we focus on the body segments the most affected by the tablet usage: upper back and neck, shoulder and arm supporting the tablet, and shoulder and arm interacting on the

¹ <http://www.musculographics.com>

device. The most extreme value at each segment defines health risk for the whole segment.

RESULTS AND DISCUSSION

The results show that the typical posture selected for interaction with a tablet is incorrect and has high risk for users' health. In particular, the posture of upper back and neck is stressful and impose serious risk: average neck flexion differs by 42.6° from the neutral pose. Average and peak joint moments are also high for the neck which can lead to both RSI after prolonged use, or to an acute injury in neck joint. Average muscle forces are moderate which means that muscles are not actively recruited to support head and will not suffer from fatigue, however the peak muscle force is high, and can lead to injuries in neck extensor muscles.

Average elevation angle of the supporting shoulder is slightly larger than neutral zone, so the joint angle is not extreme, but muscles can fatigue after relatively short period. Average joint moment at shoulder is high which can lead to RSI after prolonged use, however peak joint moment is moderate, as result an acute injury is less probable. Average muscle force is high, as a result muscles will fatigue relatively fast. Peak muscle force is also high which can lead to a muscle strain. The elbow joint is in the neutral zone. Average joint moment is low and peak moment is also low. Average muscle force and peak muscle force are high for some muscles, however, there are redundant muscles with similar action which can be recruited if necessary, for example biceps can generate force if brachialis

is fatigued. There is no such reserve for shoulder muscles to recruit in the case of fatigue.

Average shoulder elevation of the interacting arm is in the neutral zone. Average and peak joint moments are moderate, average moment is 35% lower than the moment of the supporting shoulder. Average muscle forces and peak muscle forces are only slightly lower than in the supporting shoulder, however the set of recruited muscles is different and there is more variability in recruitment. As a result the muscles of the interacting shoulder can be fatigued, but much slower than in the supporting shoulder. Average elbow flexion is 110.4° , which is at the border of neutral zone. Average and peak joint moments are moderate. Average muscle forces are low, but peak muscle forces are still high for some muscles. There is more variability in muscle groups of the interacting arm. This adds to more balanced usage of the musculature without exhaustion of a particular muscle.

The largest risks of tablet interaction in the typical postures are related with bad neck posture and fatigue of the supporting shoulder muscles.

REFERENCES

1. Young JG, et al., *J Work* **41.1**, 81-91, 2012.
2. Young JG, et al., *J Work* **45.1**, 59-71, 2013.
3. Bachynskyi M, et al., *Proceedings of CHI'15*, Seoul, Korea, 2015.
4. Delp SL, et al., *IEEE Trans. Biomed. Eng.* **54.11**, 1940-1950, 2007.
5. Palmas G, et al., *IEEE Trans. Vis. Comput. Graphics* **20.12**, 2359-2368, 2014.

Table 1: Biomechanical indices for tablet interaction.

Body part	Biomechanical indices					
	Av. j. angle	Av. j. moment	Peak j. moment	Peak m. force	Av. m. force	Stress level
Neck	-31.5°	2.9 N·m	411.9 N·m	260.4 N	20.2 N	High
Supporting Shoulder	38°	2.3 N·m	184.8 N·m	2588.8 N	83 N	Moderate
Supporting Arm	59.8°	1.2 N·m	46.1 N·m	2006.9 N	73.8 N	Low
Interacting Shoulder	19.2°	1.5 N·m	208.8 N·m	2351.7 N	77.5 N	Low
Interacting Arm	110.4°	1.8 N·m	137 N·m	2010.2 N	53.2 N	Low

SITTING AND STANDING ALTER UPPER EXTREMITY JOINT LOADING AND LOCALISED DISCOMFORT DURING MANUAL MATERIALS HANDLING TASKS

¹Alan C. Cudlip, ¹Jack P. Callaghan, and ¹Clark R. Dickerson

¹Department of Kinesiology, University of Waterloo, Waterloo, ON, Canada
email: accudlip@uwaterloo.ca, web: <http://ahs.uwaterloo.ca/kin/research/diesel/index.html>

INTRODUCTION

Musculoskeletal injuries in the workplace delimit corporate productivity and individual worker performance health. Work-related claims involving the low back and shoulder are designated as a “high impact” claim group, representing over one third of all lost time claims and almost half of all lost time benefits [1]. Upper extremity use during manual materials handling (MMH) tasks is quite variable and can be affected by whole body postures; previous research has not quantified the biomechanical exposures associated with sitting and standing during MMH tasks. Understanding the physical demands associated with task performance in seated and standing positions will facilitate the development of schedules to rotate between these configurations. The purpose of this research was to determine if differences in workplace configurations between seated and standing postures creates changes in joint moments or local body discomfort levels during MMH tasks.

METHODS

Twenty right-handed males (22.5±2.2y, 1.79±0.07m, 79.5±9.06kg) and twenty right-handed females (22.3±1.9y, 1.64±0.07m, 61.2±8.78kg) performed 4 MMH tasks: a 40N static push, a 40N static pull, a weighted bottle transfer set at 15% of the participant’s maximal arm elevation strength, and a light assembly task. All tasks were completed once each while both seated and standing. Seat height was set so that sagittal hip, knee and ankle joint angles were all 90°. Three-dimensional motion was tracked using reflective markers placed over bony landmarks and recorded at 50 Hz using eight VICON MX20 optoelectric cameras with VICON Nexus software (VICON Motion Systems, Oxford, UK). During the push and pull tasks, force outputs were measured using an AMTI 6-DOF force

transducer (MC3A, AMTI MA, USA) rigidly fixed between a D-shaped handle and a MOTOMAN HP-50 robotic arm (Motoman Robotics Division, Yaskawa America, USA), and sampled at 1500 Hz. Ratings of local body discomfort were measured on a 100mm visual-analog scale, with participants indicating local body discomfort in 18 body sections before collection and after each MMH task. Local joint moments at each time sampled were calculated for the wrist, elbow, shoulder, and low back joints. Amplitude probability distribution functions (APDFs) of the X, Y and Z components of each joint were then calculated and a joint trade-off index was used to examine potential inter-joint loading differences (Eq. 1):

$$TOI = \frac{NM_{standing_i}}{NM_{sitting_i}} \quad (1)$$

where TOI = trade-off index, $NM_{standing}$ = resultant joint moment at the 0.9 APDF level for joint i in standing, $NM_{sitting}$ = resultant joint moment at the 0.9 APDF level for joint i in sitting. Joints with trade-off values greater than 1.0 within a task represented significant increases in joint loading in standing compared to sitting. A mixed model ANOVA was used to assess differences in joint loading and body discomfort ratings. Two within subject factors (MMH task, workspace configuration) and one interaction factor (task*configuration) with a between subject factor of gender were used in the analysis with post-hoc testing to confirm significant differences at $p < 0.05$. All statistical analyses were performed using JMP 10.0 software (SAS Institute, Cary, NC, USA).

RESULTS AND DISCUSSION

Joint trade-offs between sitting and standing occurred at the wrist, elbow, and shoulder for most MMH tasks. These differences appeared in both wrists in the push and pull tasks, the left wrist in the transfer task, and the right shoulder during the push task (Table 1). Low back trade-offs were below

1.00 in the push, pull and transfer tasks, indicating decreased moments in sitting compared to standing. No joint experienced a significant sit-stand trade-off in the assembly task.



Figure 1. Local body discomfort changes between sitting and standing in the assembly task. Blue regions indicate decreased discomfort when moving from sitting to standing, while red regions indicate an increase.

Differences in local body discomfort were primarily discriminated by task, but also by the task*configuration interaction. Interaction effects were observed in the shoulders, mid back, right lower back, and shank/foot sections ($p<0.0244$), with most areas decreasing when moving to standing. Post-hoc testing indicated decreased discomfort in the left shoulder (60%), right shoulder (21%), left mid back (88%), right mid back (76%) and right low back (58%) in standing. Shank/foot discomfort increased by 273% and 609% for left and right sides, respectively (Figure 1).

Trade-off effects were primarily observed in the wrists and low back across the MMH tasks. When

Table 1: Joint trade-off indices across tasks. Significant sit/stand trade-offs ($p\leq0.05$) are indicated by shading.

	Left Wrist	Left Elbow	Left Shoulder	Right Wrist	Right Elbow	Right Shoulder	L5/S1
Push	1.19	1.11	1.11	1.22	0.95	1.05	0.71
Pull	1.26	1.13	1.23	1.34	1.07	1.05	0.73
Transfer	8.21	1.30	1.74	1.11	1.03	0.82	0.94
Assembly	1.05	0.94	0.98	1.08	1.06	0.84	0.95

standing, wrist load increased and low back load decreased. Within the same MMH task, wrist flexion was often increased while standing, resulting in greater net moments [2]. This trade-off resulted in net moments 8.2 times greater in standing, however this large change was likely due to the small absolute values of the wrist joint moments. Despite the small hand loads, resultant wrist moments in sitting and standing postures had differences of up to 4.17Nm. This magnitude represents over 30% of mean population wrist strength, and warrants consideration in industrial design [3]. Low back trade-offs appeared in the push, pull, and transfer tasks, with decreased moments in standing compared to sitting. Greater low back flexion in sitting increased joint moments, which agrees with previous work [4].

Most body regions experienced increased discomfort in sitting, however seated postures were not universally worse. Foot/shank discomfort increased in standing, and is likely attributable to the rest provided to the lower limbs in sitting.

CONCLUSIONS

Future recommendations regarding upper extremity and low back mechanical exposures during MMH tasks should consider placing workers in standing postures to minimize musculoskeletal loading. The task*configuration interactions identified in this study should be considered in the development of workspaces and tasks, in which musculoskeletal risks are generally reduced while standing.

REFERENCES

1. WSIB, *2011 Statistical Report*, 2011.
2. Hedge et al, *Ergonomics* 2005.
3. Stobbe, U. Michigan PhD thesis, 1982
4. Callaghan & McGill, *Ergonomics* 2001.

INFLUENCE OF JACKHAMMER WEIGHT ON HAND-ARM VIBRATION TRANSMISSION

Blake Johnson, MS, Naira Campbell-Kyureghyan, PhD, Wilkistar Otieno, PhD, Kristian O'Connor, PhD
University of Wisconsin-Milwaukee, Milwaukee, WI, USA
email: john2742@uwm.edu

INTRODUCTION

To better understand the onset of Hand Arm Vibration Syndrome, the biodynamic responses of the hand-arm system (HAS) to vibration have been extensively studied. The transmissibility of vibration has often been investigated as a way to quantify the biomechanical response to a vibration stimulus (1). Previous laboratory research has identified that vibration attenuates in the structures as it moves up the HAS (2). Resonance frequencies have also been identified for the hand to be in the range of 16-40 Hz and for the upper arm in the range of 8-12 Hz (3, 4). The previous research has helped identify important characteristics of hand-arm vibration (HAV) from a frequency perspective. However, no study attempted to investigate the affect of the weight of the vibrating tool on the vibration transmission.

The goal of this research is to quantify the vibration transmission in the HAS while operating two different weights of jackhammers (JH). It was hypothesized that the reduction in weight of the lightweight jackhammer will increase the amplitude of the vibration transmission to the hand-arm. The findings of this research will help to better understand how the weight of a vibrating tool contributes to the transmitted HAV.

METHODS

Eight JH operators (7 males and 1 female) with experience ranging between 3-20 years participated in this study. The average weight and height of the operators were 85(\pm 24) kg and 167(\pm 10) cm, respectively. All operators signed an IRB approved consent form before participating in the study.

Two pneumatically powered JHs were selected for this study: 40.8 kg conventional (CJH) and 27.2 kg lightweight (LJH). Each subject broke a 91cm x 91cm section of 15cm thick reinforced concrete twice in a random order, once with the CJH and

once with the LJH. The operators were required to break along specific diagonal lines to control for task variation. No other instructions were given to the operators to allow for normal use of the JHs.

Jackhammer accelerations were recorded on the handle using a Biometrics W4X system and S2-G10-MF accelerometers (Nexgen Ergonomics, USA). The same system was used to collect accelerations on the hand. Accelerations on the forearm and upper arm were measured using Delsys Trigno wireless sensors (Delsys, USA). The placement of the accelerometers on the hand-arm was done in accordance with the ISO standard 5349 part one (Figure 1). All accelerometer data was collected at 500 Hz and processed using Vibration Analysis Toolset software (Nexgen Ergonomics, USA), high pass filtered at 4 Hz and root mean squared. Dominant frequencies were found through a power spectral density analysis of each trial. Transmission was calculated as the difference in acceleration between source and hand-arm segment.

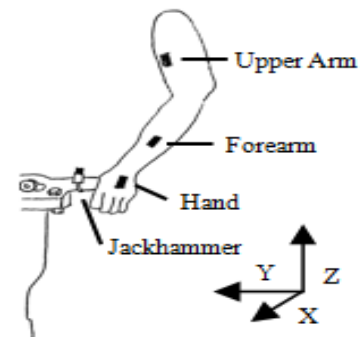


Figure 1: Sensor locations and directions of the axes

Grip pressure was measured with an FSA 24 sensor pressure glove (Vista Medical, CA). The overall sum of all grip pressure sensors was calculated at each step. The average grip pressure during JH operation was then calculated for each trial.

A paired t-test was performed on the results to compare the different weighted JHs. The alpha value for significance was set at 0.05.

RESULTS AND DISCUSSION

There were no differences in average acceleration magnitude measured on the handle between the JHs ($p=0.422$). In both weight cases an increase in the vector summed acceleration magnitude from the source to the hands was measured (19% for CJH and 28% for LJH), while a reduction at the forearm (36% for CJH and 43% for LJH) and upper arm (72% for CJH and 71% for LJH) was observed (Figure 2). The overall increase in hand acceleration is due to the increases in acceleration amplitude in the X and Y axes (Figure 3). It has been previously found that vibration transmissibility increases in these axes as frequency increases, up to 2.5 times the input acceleration from 16–50 Hz (5). The reductions found at the forearm and upper arm could be due to the attenuation of vibration at the joints and tissues. Similar reductions were found by Adewusi et al (6).

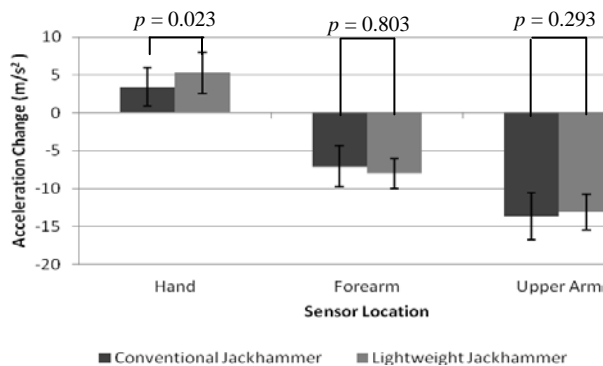


Figure 2: Overall change in acceleration from source

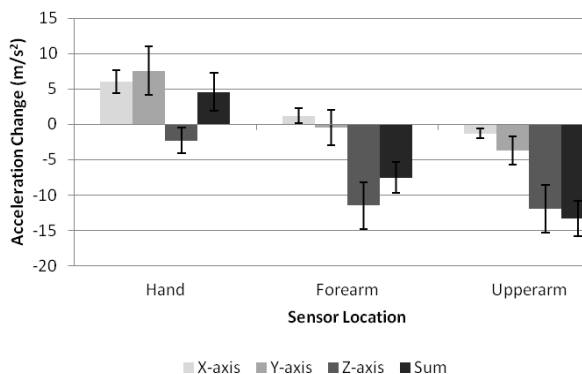


Figure 3: Change in acceleration from source per by axis

On average the increase in hand acceleration in the case of the LJH was 1.67 times greater than the CJH (Figure 2) ($p=0.023$). This difference between JH weight acceleration transmission could be attributed to the operating frequency. The LJH has a dominant

frequency of 22 Hz versus 19 Hz for the CJH. It has been previously found that as the vibration frequency at the hand increases, the transmissibility increases as well, peaking at 35 Hz (5). No differences in acceleration of the forearm and upper arm were found due to the two weights of JHs ($p=0.803$ and 0.293).

Another explanation for the differences in acceleration transmission to the hand could be the differences in grip pressure between the JH weights. Although grip pressure differences were observed (0.46 MPa CJH and 0.40 MPa LJH) the differences were not statistically significant ($p=0.126$). Note that higher relative grip pressures were measured for the LJH, indicating that more control was exerted. It is therefore possible that more motion was allowed for the CJH, leading to some of the vibrational energy being directed into inertial effects of the JH instead of transmitting to the hand.

CONCLUSIONS

JH weight was found to affect acceleration transmission to the hand, with the LJH exhibiting greater transmission than the CJH. Differences in dominant frequency and relative grip pressure may explain the observed differences in JH-hand acceleration transmission. The current study further supports previous findings of increasing vibration transmission at the hand above the ISO standard considered frequency range of 16-20 Hz, and therefore the current weighting used in the standard might not accurately reflect the risk for the hand (5).

REFERENCES

1. Dong RG, et al. *J Sound Vib* **332**, 6193-6202, 2013.
2. Pyykkö I, et. al. *Scan. J. Work Environ and Health* **2**, 87-95, 1976.
3. Dong RG, et al. *J Sound Vib* **331**, 1191-1206, 2012.
4. Adewusi SA, et al. *J Ind Ergon* **42**, 249-260, 2012.
5. Welcome DE, et al. *Int J of Ind Ergo* **45**, 21-23, 2015
6. Adewusi SA, et al. *J Sound Vib* **329**, 2953-2971, 2010.

ACKNOWLEDGEMENTS

This study was funded by the Gas Technology Institute, Chicago, IL. The authors would like to thank Alexa Hernandez, Dennis Jarnecke, John Bubaris, Nikolas Daniels, and Patrick Dix for their assistance in data collection.

A NOVEL MULTIPLE COMPARISON PROCEDURE FOR FUNCTIONAL DATA: THE EFFECT OF FITNESS- AND MOVEMENT-CENTRIC EXERCISE ON TRUNK POSTURE AMONG FIREFIGHTERS

¹ Mamiko Noguchi*, ² Kimihiro Noguchi, ³ Tyson A. C. Beach, ³ David M. Frost, ⁴ Bert Ji, and ¹ Jack P. Callaghan

¹ University of Waterloo, Waterloo, ON, Canada, ² Western Washington University, Bellingham, WA, USA,

³ University of Toronto, Toronto, ON, Canada, ⁴ Independent Scholar, Kitchener, ON, Canada

*email: mnoguchi@uwaterloo.ca

INTRODUCTION

Among firefighters, overexertion accounts for over one third of all injuries, with 40% of those injuries affecting the low back region [1]. Approximately 50% of overexertion injuries have a specific cause of 'lifting', typically resulting from inadequate help or procedure during heavy lifting [1]. In addition to this high occurrence rate, overexertion-related injuries are associated with high compensation costs: in medical cost alone, the average overall per-claim mean was \$1,973 whereas the overexertion injury mean was \$3,458 [1]. Since the job demands of fire-ground operations cannot be modified or predicted easily, increasing firefighters' capacity via exercise may be the key to reducing low back injuries. Two approaches can be used to train firefighters [2]: i) primarily emphasizing movement outcomes (fitness-centric) and ii) emphasizing both the way the movement was completed and its outcomes (movement-centric). It is hypothesized that movement-centric exercise would provide additional benefit since an individual's injury risk is determined by their capacity and how this capacity is utilized. For instance, risk of injury may not change if an individual adopts postures that increase the tissue load.

There have been several methods used to examine time-varying (functional) data, including principal component analysis (PCA) and fractal analysis [3]; however, the difficulty of these methods lies in interpretation of the results and examination of local differences in curves, respectively. Herein, a novel statistical method – namely, the parametric bootstrap-based minP procedure with Welch's t-test, was used to investigate whether each group's average response differs from another and where in time the difference becomes significant [4]. This multiple comparison procedure also provides simultaneous overall and pairwise comparison adjusted p-values without any discrepancy in the conclusion between the two. Therefore, the objective

of this study was to use this statistical method to analyze the phases of symmetrical lifting or lowering tasks where statistically significant differences may occur among different exercise interventions with professional firefighters.

METHODS

Fifty-three career firefighters (males) from the Pensacola Fire Department (Pensacola, FL, US) were included in the analyses. All participants were free of any activity-limiting health conditions and were randomly separated into three groups: fitness-centric exercise group (FIT; N = 16), movement-centric exercise group (MOV; N = 22), and control group (CON; N = 15). Each intervention group participated one of two 12-week exercise programs and were coached by accredited strength and conditioning coaches. Coaches provided different instructions and feedback according to the objectives of each group: FIT group was given extrinsic feedback to maximize the performance outcomes (i.e. improving the physical fitness scores) and MOV group was given intrinsic feedback to improve physical fitness while maintaining quality of coordination and control of movement. There were no restrictions on activities outside of this program for all groups.

To examine the effect of the two exercise programs, a symmetrical lifting and lowering task, simulating manual material handling was performed before and after the 12-week interventions. Four task conditions were performed in order of increasing demand: low load, low velocity (LLLV); low load, high velocity (LLHV); high load, low velocity (HLLV); and high load, high velocity (HLHV). In low and high load conditions, 6.8 and 22.7 kg weights were used, respectively. In high velocity conditions, participants were instructed to complete each trial as fast as they were comfortable with. In each condition, three repetitions of lift and lower trials (bending down to lift a crate from the floor to

the upright posture and back to the floor) were performed with rest in between. Three-dimensional kinematics of the trunk, pelvis, and upper and lower extremities were captured using a 10-camera Vicon motion capture system (Vicon, Oxford, UK) at 160 Hz using Vicon Nexus Motion Capture software (Version 1.5, Vicon, Oxford, UK). Post-processing was performed using Visual3D software (Version 4, C-Motion, Inc., Germantown, MD, United States). The kinematic data were low-pass filtered (Butterworth, 4th order, zero-lag, 6Hz cutoff) and the trunk angle was calculated with an Euler rotation sequence of flexion/extension, abduction/adduction, and axial rotation. Each phase (lift and lower) was normalized by time, and a curve produced by taking the difference between the pre- and post-intervention measure was used in the statistical analysis. Parametric bootstrap based minP procedure with Welch's t-test was performed for statistical analysis [5]. Welch's t-test was used since the group variances were unequal in this study. Parametric bootstrap with 1000 resamples was used to better control the familywise error rate [6].

RESULTS AND DISCUSSION

Significant or trending towards significant sagittal motion (flexion/extension) differences between CON and FIT/MOV groups were observed mainly in the lowering phase (Table 1). CON and FIT groups were significantly different in the LLLV condition in the middle (40-60%) of lowering phase ($p = 0.041$) (Figure 1). Trending towards significant ($p < 0.10$) differences were seen in the lowering phase (HLHV, LLHV, LLLV) and the lifting phase (HLHV) between CON and MOV groups, in which the largest difference occurred at the beginning through mid-phase (30-60%) of the trial. In all conditions and phases, the MOV group adopted more favorable (less flexed) trunk posture following the exercise program. In a study examining the kinematics of lifting and lowering, horizontal displacement during lowering has been shown to be larger (further away from the trunk) than during lifting due to the anterior momentum of the load [7],

indicating increased risk of injury. Therefore, a reduction in trunk flexion in the middle of the lowering phase, where horizontal displacement is reaching its peak [7], can be considered a favorable adaptation to minimize tissue load on the low back. Although there was no significant difference between FIT and MOV groups ($p > 0.10$), the difference between MOV and CON was trending towards significantly different in half of the conditions, indicating that MOV may yield better "transfer" of training. There were no significant differences between the groups in transverse (axial rotation) and frontal plane motion (abduction/adduction). Future studies will include examining variability between groups using a similar statistical method.

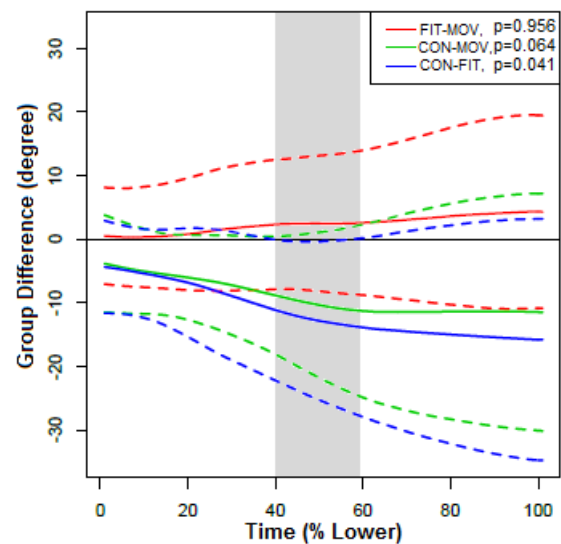


Figure 1: Mean (solid) and 95% simultaneous confidence band (dotted) of each group difference in the LLLV lowering phase. Shaded area indicates where the significant difference occurred between CON and FIT ($p < 0.05$).

REFERENCES

- [1] Walton S, et al. *Am J Ind Med* **43**, 454-458, 2003. [2] Beach TA, et al. *Ergonomics* **57**, 744-63, 2014. [3] Chau T. *Gait Posture* **13**, 49-66, 2001. [4] Noguchi K, et al. working paper, 2015. [5] Westfall, PH. *J Biopharm Stat* **21**, 1187-1205, 2011. [6] Konietzschke F, et al. *Centre de Recherches Mathematiques Proceedings*, Montreal, ON, CA, 2012. [7] McKean C & Potvin, J. *Int J Ind Ergonom* **28**, 1-15, 2001.

Table 1: Pairwise comparison adjusted p-values in each condition for sagittal plane motion. Note: * indicates trending towards significant ($p = 0.05 - 0.10$) and ** indicates significant results ($p < 0.05$).

Pairwise comparison adjusted p-value	Lift				Lower			
	HLHV	HLLV	LLHV	LLLHV	HLHV	HLLV	LLHV	LLLHV
Fitness – Movement	0.460	0.752	0.137	0.961	0.781	0.998	0.536	0.956
Control – Movement	0.094*	0.384	0.172	0.412	0.070*	0.143	0.058*	0.064*
Control – Fitness	0.658	0.900	0.719	0.294	0.239	0.173	0.197	0.041**

A BOOTSTRAPPING METHOD TO ACCESS THE INFLUENCE OF GENDER ON PROBABILITY OF TRIPPING AS A FUNCTION OF OBSTACLE HEIGHT

¹Christina R. Garman, ¹Christopher T. Franck ¹Maury A. Nussbaum, ²Michael L. Madigan

¹ Virginia Tech, Blacksburg, VA, USA

² Texas A&M University, College Station, Texas, USA

email: rossic@vt.edu

INTRODUCTION

Tripping accounts for an estimated 53% of falls among older adults [1]. The most common measure for characterizing the probability of tripping is the minimum foot clearance (MFC) during swing. A decrease in the central tendency (i.e. mean/median) of MFC, or an increase in MFC variability, are both associated with an increased probability of tripping [2-4]. These indirect measures of probability of tripping can lead to ambiguous results, though, when both increase or decrease simultaneously. Moreover, median MFC and MFC IQR are positively correlated [3], indicating concurrent increases or decreases in both are to be expected.

The purpose of this study was to determine the probability of tripping using a method that avoids this ambiguous situation, and to demonstrate how this method can be used to compare this probability between groups of interest. This method was used to investigate differences in the probability of tripping between females and males, based upon reports of elevated risks of falling and sustaining a fall-related injury among females [5].

METHODS

Forty males and forty females completed 16 trials walking along a 10 m walkway at a self-selected speed. All participants wore the same brand of athletic shoes, to which were attached three reflective markers. A Vicon MX T10 motion analysis system (Vicon Motion Systems Inc., LA, CA) was used to sample marker positions at 100 Hz. MFC was determined using a method adopted from Startzell et al [6].

MFC values from all trials were used to create trip probability curves that indicated how the probability of tripping varied as a function of the height of a

potential tripping obstacle (Figure 1). For potential tripping obstacle heights ranging from 0 - 7 cm, in increments of 2 mm, each MFC value was dichotomized as either a trip (if the potential obstacle height was greater than MFC) or a non-trip (if the potential obstacle height was equal to or less than MFC). The percentages of trips at each obstacle height were then computed, serving as an estimate of the probability of tripping versus obstacle height.

A statistical bootstrapping technique was used at each potential obstacle height to determine whether the probability of tripping differed between females and males. The first step was to randomly reassign participant group labels (i.e., male or female) to each participant's 16 MFC values. A probability curve was then created for each group, and the difference in trip probability between groups was calculated at each potential obstacle height. This process was repeated a large number of times (100,000 in our analysis) to obtain a distribution of differences at each potential obstacle height that would occur if group assignment was random. The second step was to examine the position, within the distribution of differences, of the actual observed difference in probability of tripping between groups. This was done to determine if this difference was statistically significant at a level of $\alpha=0.05$. A multiplicity correction was used to avoid inflation of type I errors. As such, if the difference was positioned in the outer 0.14% of the distribution, then the difference in trip probability between groups was considered statistically significant ($\alpha=0.0014$). The percentage of the distribution of differences outside of the actual observed difference yielded a bootstrap p -value. This second step was performed at each potential obstacle height to determine the specific heights at which the probability of tripping differed between females and males.

Group differences identified from this statistical bootstrapping technique were compared with group differences identified using the traditional measures of median MFC and MFC IQR and mixed-factor analyses of covariance (ANCOVA). Analyses were performed using JMP v7 (Cary, North Carolina, USA).

RESULTS AND DISCUSSION

The probability of tripping was higher among females across a range of obstacle heights (1.2-4.4 cm), while both median MFC and MFC IQR were lower among females (Figure 1).

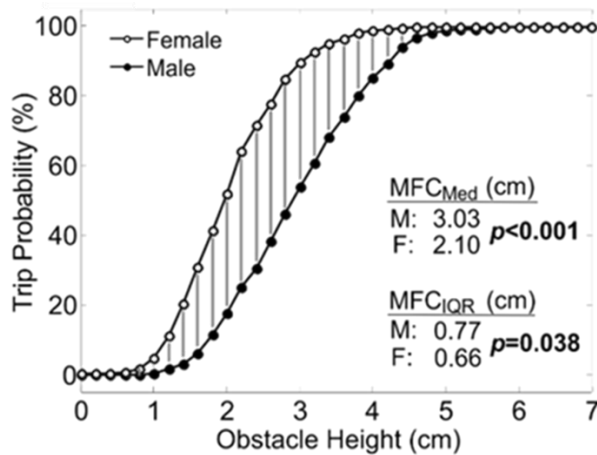


Figure 1: Trip probability curve and median/IQR MFC. Differences in trip probability between groups are indicated by a solid vertical line, and differences in median/IQR are indicated by bold. Note: m=male, and f=female

This technique identified clear gender differences in the probability of tripping versus obstacle height despite ambiguous results from the ANCOVA analysis in that both median MFC and MFC IQR were both lower among females. Furthermore, characterizing the probability of tripping as a function of obstacle height provides additional information on how individual factors may affect the probability of tripping. For example, results

suggest that trip probability does not differ between males and females unless obstacle heights are greater than 1.2 cm (Figure 1). Such information may be helpful in establishing safety guidelines.

Two limitations to the method presented here warrant mentioning. First, this method focuses on foot clearance at the instant that MFC occurs even though a trip could occur at other instances during the swing phase. Second, unlike an ANOVA based upon median/mean MFC and/or MFC IQR, the current method cannot incorporate measures of covariance, or statistically control for the effects of other variables, when evaluating an independent variable of interest.

In conclusion, a pragmatic method is reported to characterize the probability of tripping as a function of obstacle height, and which can identify effects of factors not identifiable by the commonly used ANOVA analysis using MFC central tendency and variability

REFERENCES

1. Blake, A.J., et al., Age Ageing, 1998. 17(6): p. 365-372.
2. Winter, D.A., Physical Therapy, 1992. 72(1): p. 45-53.
3. Begg, R., et al., Gait & Posture, 2007. 25(2): p. 191-198.
4. Mills, P.M., et al., Gait & Posture, 2008. 28(1): p. 101-107.
5. Fjeldstad, C., et al., Dynamic Medicine, 2008. 7(4).
6. Startzell, J.K. et al. Hum. Movement Sci. 1999. 18(5): p. 603-611.

ACKNOWLEDGEMENTS

This work was supported by award R01OH009880 from the CDC-NIOSH and National Science Foundation Graduate Research Fellowship under grant DGE 0822220

SEX-SPECIFIC DIFFERENCES IN LOWER EXTREMITY JOINT POWER DURING A SINGLE-LEG HOP TEST IN HEALTHY ADULTS

^{2,6}Rachel L. Tatarski, ^{2,6}Joshua Hoffman, and ¹⁻⁶Timothy E. Hewett

¹Department of Biomedical Engineering, ²Sports Health and Performance Institute (SHPI) OSU Sports Medicine, ³ Mayo Clinic, Rochester, MN, ⁴Department of Orthopaedics, ⁵Department of Physiology and Cellular Biology and Family Medicine, ⁶The Ohio State University, Columbus, OH, USA

email: rachel.tatarski@osumc.edu, web: http://sportsmedicine.osu.edu/ourteam/research_staff/index.cfm

INTRODUCTION

Females are typically at greater risk for musculoskeletal injury compared to their male counterparts. Often, this increased risk is attributed to modifiable risk factors such as strength and neuromuscular movement patterns. Females use quadriceps-dominant movement strategies, whereas males use hip extensor dominant movement strategies [1,2]. This quadriceps-dominant movement strategy puts females at greater risk for knee injury. Thus, determination of which females are a greater risk of knee injury is an important goal for health care professionals such as athletic trainers, physical therapists, and physicians.

Functional tests such as the single-leg hop are often used in physically active populations to test for risk of injury or deficits due to injury. Asymmetry between limbs in hop distance is usually the outcome of interest, but this measure does not take into account sex-specific movement strategies. Moreover, the distance hopped is likely related to the power generation strategy during the take-off phase of the hop and could serve as another measure of function. Therefore, the purpose of this study was to compare the power generation strategies between healthy males and females. We hypothesized that females would display a quadriceps-dominant strategy, while males will display a hip-extensor-dominant strategy.

METHODS

Sixteen subjects volunteered to participate and provided written informed consent (n = 8 females; n = 8 males). To measure whole body kinematics, each subject was fitted with 55 retro-reflective markers to define joints and segments. Markers were tracked in 3-dimensional space using 12 Motion Analysis cameras. Ground reaction forces were measured

using 4 imbedded Bertec force plates. Data were analyzed using Motion Analysis Cortex, Visual3D, and MatLab. To measure the take-off phase of a single-leg hop for distance, subjects were instructed to begin the movement on the force plate with their foot lined up with a tape measure. Subjects were instructed to hop as far as they could forward on one leg and stick the landing. The distance of the hop was measured at the location of the heel. Subjects were allowed to practice the hop twice on each leg and then performed two successful trials per leg. A trial was considered successful if the subject only used one leg to push off and land. Pearson's product-moment correlation was used to assess the relationship between power generation and hop distance. *Student's t*-test was used to test for significant differences between sexes. The alpha level was set to 0.05, *a priori* to determine significant results.

RESULTS

Overall, there was a strong, positive correlation between peak total lower extremity joint power and hop distance ($r = 0.60$). Males demonstrated a stronger relationship between peak total joint power and hop distance ($r = 0.58$) than females ($r = 0.24$). In addition, males hopped significantly farther than females (Table 1). For either hip or ankle excursion, there were no significant differences between sexes; however, males had significantly more knee excursion than females (Table 1). Peak hip power accounted for ~60% of the variance in hop distance in males, but only ~13% of the variance in hop distance for females (Figure 1A). Peak knee power accounted for ~4% of the variance in hop distance in males and ~11% variance in hop distance for females (Figure 1B). Peak ankle power accounted for ~29% of the variance in hop distance for males and ~1% in females (Figure 1C).

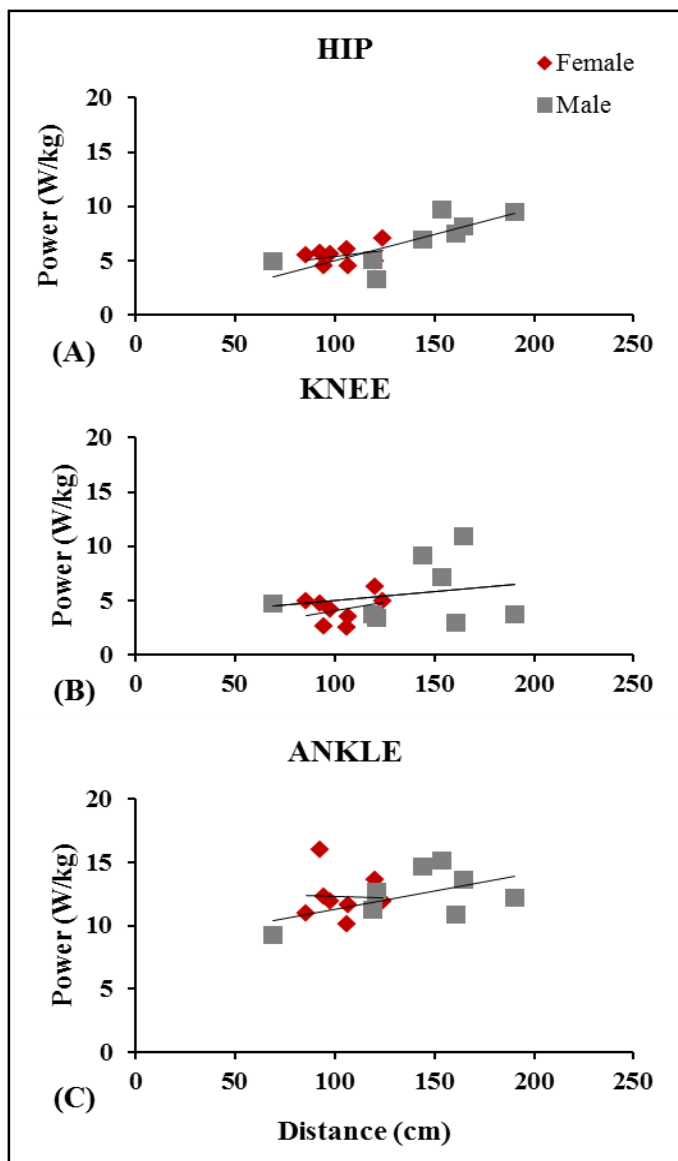


Figure 1: Relationships between single-leg hop distance and peak joint powers between males and females (A = hip, B = knee, C = ankle).

DISCUSSION

The findings from this study confirm our hypothesis that males would use a hip-extensor strategy for power generation during a single-leg hop, while females would rely on a quadriceps-dominant

strategy. These sex-specific differences in performance are similar to previous findings in functional tests such as the drop vertical jump [3]. However, it is interesting to note that the data from our female subjects showed a clustering trend, while the data from our male subjects were more varied. The lower R-squared values for the female subjects is likely due in part to the clustered nature of this data. However, exponential transformation did not affect this pattern. Individual variation between female subjects may also account for this low association.

CONCLUSIONS

Overall, females tended to use less total lower extremity excursion, instead females utilized a more upright posture and thereby limited the power-generating function of their muscles. Furthermore, females tended to use a quadriceps-dominant strategy, whereas males used a hip-extensor strategy to perform the task. Since a quadriceps-dominant strategy is a known risk factor for knee injury, an easy, simple and straightforward test such as the single-leg hop may be a useful tool to assess injury risk in this population.

REFERENCES

1. Mendiguchia J, et al. *Sports Med*, **41**(7), 541-557, 2011.
2. Ford KR, et al. *AM J Sports Med*, **38**(9), 1829-1837, 2010.
3. Ford KR, et al. *J Strength Cond Res*, **19**(2), 394-399, 2005.

ACKNOWLEDGEMENTS

The authors acknowledge funding support from the National Institutes of Health / National Institute of Arthritis and Musculoskeletal and Skin Diseases grants R01-AR049735 and R01-AR056259 (TEH) and OSU Sports Health and Performance Institute.

Table 1: Kinematics during single-leg hop (* difference between males and females $p < 0.05$).

	Males	Females
Distance (cm)*	140.3 \pm 37.1	103.4 \pm 13.4
Hip Excursion (degrees)	63.3 \pm 18.0	47.6 \pm 12.6
Knee Excursion (degrees)*	49.9 \pm 6.4	40.6 \pm 8.6
Ankle Excursion (degrees)	50.5 \pm 4.8	48.5 \pm 5.9

SEX BASED DIFFERENCES IN ANTERIOR CRUCIATE AND MEDIAL COLLATERAL LIGAMENT BIOMECHANICS IN ROBOTICALLY SIMULATED DECELERATION TASKS

Nathaniel A. Bates^{a,b,c}, Rebecca J. Nesbitt^b, Jason T. Shearn^b,
Gregory D. Myer^{a,c}, Timothy E. Hewett^{a,b,c}

^aOSU Sports Medicine Sports Health & Performance Institute, Ohio State University, Columbus, OH, USA

^bUniversity of Cincinnati, Cincinnati, OH, USA

^cCincinnati Children's Hospital Medical Center, Cincinnati, OH, USA

email: batesna@gmail.com website: <http://sportsmedicine.osu.edu/>

INTRODUCTION

Anterior cruciate ligament (ACL) injury rates are 4-8 times greater in female athletes than their male counterparts.[1] As female athletes are at increased risk of ACL injury compared to males, it is important to understand the underlying mechanics that contribute to this sex bias. The purposes of this investigation were to employ a robotic manipulator to simulate male and female kinematics from athletic tasks on cadaveric specimens and to identify sex-based mechanical differences relative to the ACL. The primary hypothesis tested was that simulations of female motion would generate higher ACL loads associated with greater ACL injury risk than simulations of male motion when executed on the same cohort of cadaveric specimens. A second hypothesis tested was that female motion simulations would exhibit greater ACL strains than male motion simulations.

METHODS

A 6-degree-of-freedom robotic manipulator articulated 19 cadaveric lower extremity specimens from 12 unique cadaveric donors of mixed sex (9 males; 3 females, age = 47.9 ± 7.0 years; mass = 832 ± 190 N) through simulations of *in vivo* knee kinematics that were recorded from male and female sidestep cutting and drop vertical jump tasks (DVJ).[2] A six-axis load cell aligned with the mechanical axis of the tibia recorded joint forces and torques at the joint center point, while differential variable resistance transducers implanted on the anteromedial bundle of the ACL recorded ligament strain. Univariate ANOVA was used to evaluate statistical significance of mechanical simulations between genders ($\alpha < 0.05$).

RESULTS AND DISCUSSION

Peak ACL strain during a simulated DVJ was 6.27% and 6.61% for the female and male models, respectively ($P = 0.86$; Table 1). For the sidestep cut peak ACL strain was 4.33% and 7.57% for the female and male models, respectively ($P = 0.21$). Female simulations exhibited lower peak lateral joint force during the DVJ and lower peak anterior joint force, lateral joint force, and external joint torque during the sidestep cut compared with male simulations ($P < 0.05$; Figure 1).

ACL strain was only different between sexes at peak knee flexion during sidestep cutting. The sidestep cut simulations exhibit peak flexion angles of approximately 62° and 50° for the male and female, respectively. This indicated that the only significant gender differences in ACL strain occurred at a position where the ligament is likely unloaded or minimally loaded.[3] Further, the female motion did not generate higher joint loads compared to the male motion. The simulations performed were relative to controlled athletic tasks

Table 1: Peak ACL strains observed at various stages of landing phase during sex-specific simulations of DVJs and sidestep cutting.

	Landing Phase	First 50 msec	Initial Contact	Peak Flexion
DVJ				
Male	6.6	3.7	3.7	6.0
Female	6.3	4.5	4.2	5.0
Sidestep Cut				
Male	7.6	4.8	4.8	6.4*
Female	4.3	4.1	4.1	2.4*

* statistically significant difference between sexes ($P < 0.05$)

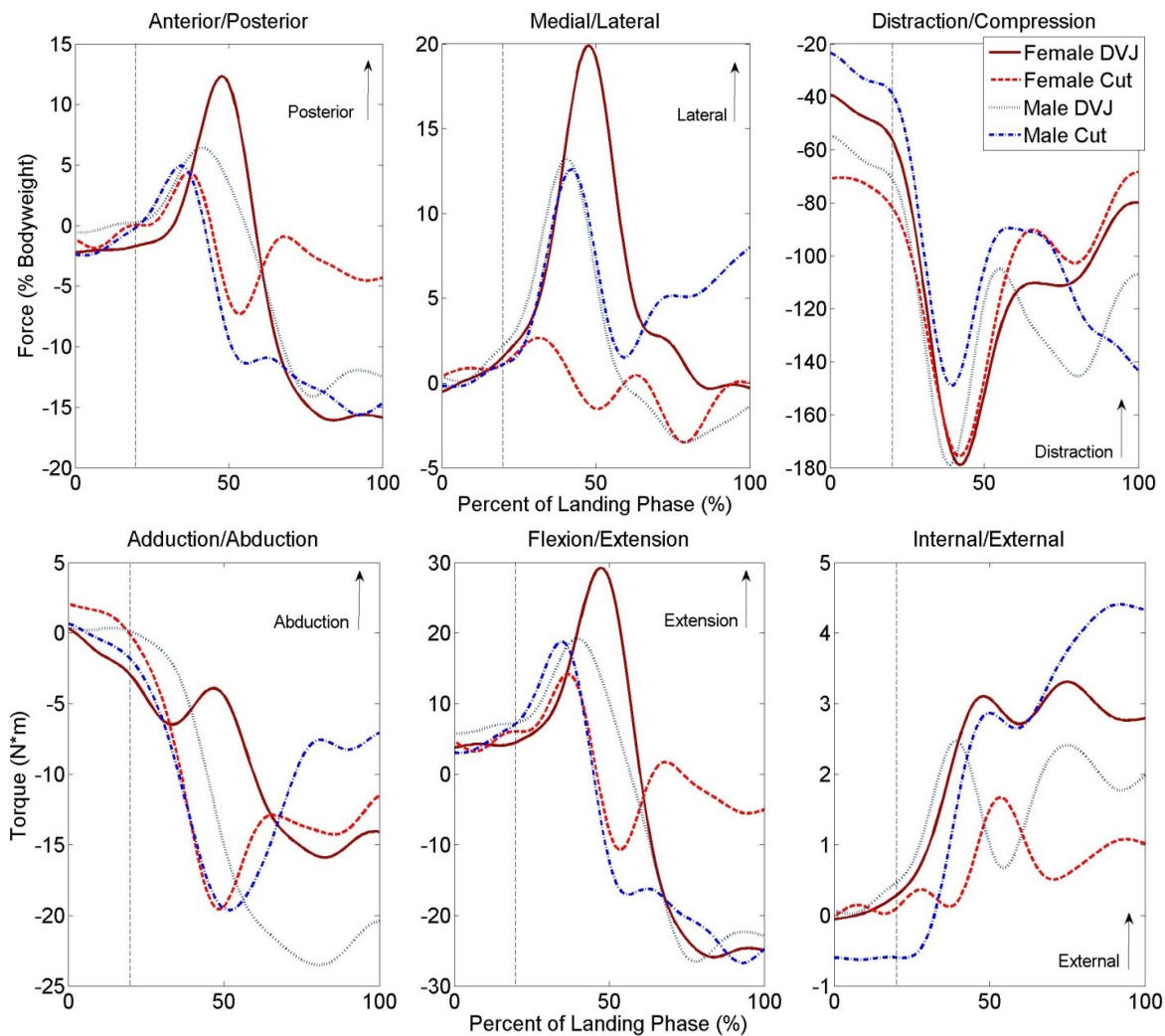


Figure 1: Displays the population average force (top row) and torque (bottom row) measured at the tibiofemoral joint in response to simulated male and female DVJ and sidestep cut articulations. The vertical, dashed line represents the approximate cutoff for the first 50 msec after initial contact, where ACL injuries are most likely to occur.

with minimal perturbation to the athlete and no injuries. In this setting, the male and female simulations exhibited minimal mechanical differences; however, more rigorous activities that offer greater perturbation and exhibit additional sex-based loading differences.

CONCLUSIONS

The sex-based loading and strain differences noted do not appear to explain the increased rate of ACL injuries observed in female athletes for the athletic tasks simulated, assuming parity of ligament properties between sexes. Therefore, additional perturbation is likely necessary to invoke the mechanical differences that lead to higher rates of ACL injury in female populations. In the current

Investigation, data indicated that, during the performance of regulated athletic tasks, sex-specific movement patterns exhibit similar levels of ACL strain. As such, the rehabilitation and prevention of ACL injuries should be similarly focused on known risk factors across sexes.

REFERENCES

1. Boden BP, et al. *Orthop.* **23**, 573-8. 2000.
2. Bates NA, et al. *Submitted for Publication.* 2015.
3. Renstrom P, et al. *Am J Sports Med.* **14**, 83-7. 1986.

ACKNOWLEDGEMENTS

Funding from NIH Grants R01-AR049735, R01-AR05563, R01-AR056660, and R01-AR056259.

Climbing Direction, Number of Contact Points and Gender Influence Recovery from Ladder Falls but not Glove Use

¹ Erika M. Pliner, ² Na Jin Seo and ³ Kurt E. Beschorn

¹ The University of Wisconsin-Milwaukee, Milwaukee, WI, USA

² Medical University of South Carolina, Charleston, SC, USA

³ The University of Pittsburgh, Pittsburgh, PA, USA

email: beschorn@pitt.edu

INTRODUCTION

Ladder falls account for 16% of fatal falls and 8% of non-fatal falls [1]. Injuries from ladder falls are severe, but can be prevented from safer ladder climbing practices and proper ladder climbing training [2]. Previous research has investigated the effects of gloves on grasping ladder rungs in hopes to improve ladder climbing practices [3, 4]. High friction gloves were found to increase the maximum gripping force when the rung is forcibly pulled from their hand [3]. Also, more muscle activity is needed to stabilize the rung with low-friction gloves [4]. However, these studies only considered the interaction between the hand and the rung, which may be an over-simplification of ladder recovery.

Other risk factors for ladder falls may include gender, utilizing 3 points of contact and climbing direction. For example, differences in strength across genders [5] may alter recovery risk. Three points of contact is a common safety suggestion and requirement of OSHA. Lastly, falls have been observed more frequently during egress of mining equipment than ingress suggesting that ladder descent may be more difficult than ascent [6]. A paucity of objective data exists regarding how each of these factors impacts recovery from a ladder fall event.

The purpose of this study was to quantify the impact of gloves, 3-point contact, gender and climbing direction on recovery after a ladder perturbation.

METHODS

Thirty-five (10 female, 25 male) healthy participants between the ages of 18 and 29 were recruited for this study. IRB approval and written informed consent were obtained prior to testing. All participants were equipped with standardized attire, footwear and a safety harness that was equipped with a load cell to measure the support force (1000 Hz). Forty-seven reflective markers were placed on

participant's anatomical landmarks to record their kinematic data (100 Hz), including the hands, feet, and the anterior/posterior superior iliac spines.

Participants climbed a vertical 12-foot custom-designed ladder. The ladder was equipped with strain gauges and load cells to estimate forces placed on several of the ladder rungs. The fourth rung on the ladder was designed such that the rung could be released under the participants' foot electronically. The armed rung was programmed to release when the contralateral leg stepped off of the previous rung. This timing corresponds approximately to when subjects typically slip [7], leaving the hands as the primary means of recovery. Each participant experienced six simulated ladder missteps corresponding to three glove conditions (bare hands, high friction gloves and low friction gloves) and two climbing directions (ascent and descent). Participants performed between five and eight baseline trials before each perturbation to minimize anticipation. The order of gloves and climbing direction were randomized.

A participant's ability to recover was based on the force supported by the safety harness. The harness force was normalized to the participant's body weight and calculated as the peak harness force between the start of fall and end of fall time points. The start of fall was the point in time the fourth rung was triggered to release. The end of fall was the point in time of the first minimum of the mid-hip joint center's vertical displacement after the start of fall. Hip joint centers were calculated based on the pelvic markers [8]. The number of body to ladder contact points at the start of fall was visually determined from kinematic data. Point of contact varied between two point contact (2 Pt, 1 hand and 1 foot) and three point contact (3 Pt, 2 hands and 1 foot). An ANOVA was performed with gender, climbing direction, point of contact and glove

condition as independent variables and harness force as the dependent variable.

RESULTS AND DISCUSSION

Females had higher harness forces than males ($p < 0.001$). Descending perturbations resulted in higher harness forces ($p < 0.001$). Participants who had three point contact with the ladder at the start of fall had lower harness forces ($p < 0.05$). Glove condition did not affect harness force (Figure 1).

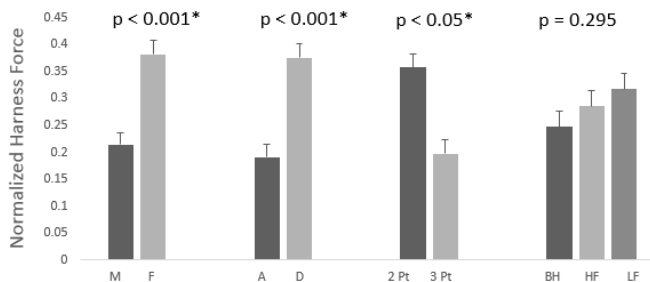


Figure 1: Average harness force normalized to body weight for males (M) vs. females (F), ascend (A) vs. descend (D), 2-point contact (2 Pt) vs. 3-point contact (3 Pt) and bare hand (BH), high-friction (HF) vs. low-friction (LF).

The discrepancy between males' and females' ability to recover may be due to physiological factors. Young male adults typically have higher upper body strength [5] than female adults, which may have assisted their ability to recover from a fall.

The difference in harness forces of ascending and descending perturbations may be due to the momentum of the body at the time of perturbation. Ascending the ladder may provide climbers with more time to respond since downward falling will be delayed and downward fall velocity is reduced. Thus, descending a ladder may be a more hazardous task than ascending a ladder, which may explain the higher injury rates reported during the egress process over the ingress process on mining equipment [6].

The finding that 3 points of contact enhances recovery is largely consistent with safety practices that promote utilizing three points of contact at all times on ladders. Less supporting points of contact will increase the required reaction load at each contact point, which may be too much for a single

hand after losing the support foot. It should be noted that few subjects maintained 3 points of contact during the whole climbing process (40%) and that the number of points of contact was just assessed at the moment of perturbation onset. Thus, the results of this study indicate that utilizing 3 points of contact when the body is most vulnerable to a slip (i.e., just after foot off [7]) may be sufficient to reduce fall risk.

Surprisingly, no effects were found between gloves and harness forces. Increased force capability from high friction gloves may not necessarily translate to better recovery during full body recovery. One potential reason for this finding may be that other factors (positioning of the hands, personal strength) may be more important than the maximum pull strength when an actual fall event is occurring.

CONCLUSIONS

This study found that fall risk was higher for female participants than male participants, for descent than ascent and when only 2 extremities are contacting the ladder compared with 3 extremities. Gloves did not affect recovery. This study suggests that ladder safety should prioritize maintaining three points of contact over glove use. Also, this study suggests that additional protection may be needed during ladder descent and for female ladder climbers.

REFERENCES

1. Webster T, *Compensation and working conditions* **2000**, 28-38, 2000.
2. Socias C, et al. *Morbidity and Mortality Weekly Report* **63**, 341-368, 2014.
3. Hur P, et al. *J Biomech* **45**, 958-964, 2012.
4. Hur P, et al. *J Electromyography and Kinesiology* **24**, 159-164, 2014.
5. Miller A, et al. *Europ. J Applied Physiology & Occupational Physiology* **66**, 254-262, 1993.
6. Moore S, et al. *J Safety Research* **40**, 455-460, 2009.
7. Paul A, et al. *Proceedings of ASB'13*, Omaha, NE, USA, 2013
8. Bell A, et al. *J Biomech* **23**, 617-621, 1990.

ACKNOWLEDGEMENTS

This work was funded by NIOSH/CDC (R21OH010038).

THE LUMBOPELVIC RATIO DURING TRUNK FLEXION: THE EFFECTS OF AGE, GENDER AND MOTION PACE

¹Milad Vazirian, ¹Iman Shojaei, ¹Anuj Agarwal and ¹Babak Bazrgari

¹ University of Kentucky, Lexington, KY, USA
email: milad.vazirian@uky.edu

INTRODUCTION

The prevalence of low back pain (LBP) increases with aging. Given the projected increase in the number of older individuals at workplace, management of occupational LBP will require an understanding of the reason(s) behind such increase in risk of LBP with aging [1]. A recent study by Tafazzol et al. [2] has shown that a reduction of lumbar contribution to a given angle of trunk flexion, as reflected in a reduction of lumbopelvic ratio (LPR), was associated with an increase in spinal loads. The objective of this study was to quantify age-related changes in LPR under fast and slow trunk flexion motions. On the basis of the suggested relationship between the LPR and spinal loads, it was hypothesized that, for a given task, the LPR of older versus younger individuals and faster versus slower motion paces will be smaller.

METHODS

Sixty individuals participated in the study after completing a consenting procedure approved by the University of Kentucky IRB. Participants were grouped in five age ranges of 22-28 (11 male and 7 female), 32-38 (7 male and 7 female), 42-48 (3 male and 6 female), 52-58 (4 male and 6 female) and 62+ (4 male 5 and female) years old with respective mean (SD) stature (cm) of 172 (1.9), 171 (1.8), 170 (2.3), 173 (4.2) and 171 (2.7) , and respective mean (SD) body mass (kg) of 69 (2.5), 72 (3.4), 77 (5.2), 81 (3.7) and 71 (4.2). Each participant attended two data collection sessions during which they completed three repetitions of slow and three repetitions of fast trunk flexion-extension tasks. Participants started each task from the standing posture and bent forward to reach their maximum comfortable trunk flexion, and then returned to the upright posture. The paces of trunk flexion for fast and slow motions were self-selected and

participants were instructed to remain in full flexion posture for 5 s during the slow tasks. The thoracic and pelvic relative rotations from the upright standing posture were measured using two inertial-magnetic sensors (Xsens Technologies, Enschede, Netherlands) attached to the subject's back at the levels of T12 and S1. Lumbar flexion during each task was estimated as the difference between the measured thoracic and pelvic rotations. Finally, the LPR, was calculated as the ratio of lumbar flexion to pelvic rotation at the instant of full trunk flexion. Kinematics data were collected by a sampling rate of 50 Hz and were low-pass filtered using a fourth-order, bidirectional, Butterworth filter with cutoff frequency of 6 Hz. Repeated measures analysis of variance (ANOVA) was conducted to determine the effects of age and gender (i.e., between-subject factors) as well as flexion pace (i.e., within subject factor) on the maximum values of thoracic and pelvic rotations along with corresponding lumbar flexion and the LPR.

RESULTS AND DISCUSSION

The maximum thoracic rotation did not change with age ($p=0.433$) or gender ($p=0.395$), but was larger ($p<0.001$) during the fast vs. slow flexion tasks (Table 1).

Table 1: Mean maximum thoracic rotations along with 95% confidence interval for the slow and fast tasks (all values are in degrees)

Pace	Mean	95% Confidence Interval	
		Lower Bound	Upper Bound
Slow	82.9	79.4	86.4
Fast	95.8	92.4	99.1

The pelvic rotations increased with age ($p<0.001$), pace of task ($p<0.001$) and was larger ($p<0.001$) in females vs. males. (Table 2).

In contrast to the pelvic rotation, the lumbar flexion decreased generally with age ($p=0.003$). However, it was larger in the males than females ($p=0.017$), and similar to the thoracic and pelvic rotations, was found to increase with pace of task motion ($p<0.001$). (Table 3).

Table 2: Mean maximum pelvic rotation along with 95% confidence interval for each age group, gender and pace (all values are in degrees)

Age	Mean	95% Confidence Interval	
		Lower Bound	Upper Bound
22-28	24.0	20.0	28.1
32-38	26.4	21.9	30.9
42-48	29.3	23.4	35.3
52-58	35.3	29.9	40.7
62+	40.4	34.3	46.6
Male	26.7	23.1	30.9
Female	35.5	32.5	38.6
Slow	26.5	24.3	28.7
Fast	35.6	33.1	38.0

Table 3: Mean lumbar flexion along with 95% confidence interval for each age group, gender and pace (all values are in degrees)

Age	Mean	95% Confidence Interval	
		Lower Bound	Upper Bound
22-28	60.4	56.0	64.9
32-38	65.2	60.4	70.1
42-48	59.5	53.1	66.0
52-58	51.9	46.0	57.8
62+	52.0	45.9	58.1
Male	60.9	57.1	64.6
Female	54.7	51.4	58.0
Slow	55.9	53.3	58.5
Fast	59.7	57.1	62.2

The main effects of age, gender and pace on the LPR were all significant ($P<0.001$). Specifically, the LPR was smaller under fast versus slow trunk motions, older (>40 years old) versus younger (<40 years old), and female versus male participants. There was an interaction between the pace and age, however, the slow motion was associated with a higher LPR in all age groups, although with highly different values.

Our results concur with earlier findings of reduction in lumbar range of flexion with aging [4].

Furthermore, on the basis of the suggested relationship between the LPR and spinal loads [2], our results suggest that older versus younger individuals and females versus males may experience larger spinal loads when doing the same flexion-extension task. Given the important role of mechanical loading in development of LBP, it is likely that the adopted lumbopelvic motion by older individuals to perform physical activity put them at higher risk of lower back injury as compared to younger individuals. It is also important to mention that LBP patients demonstrate a smaller LPR during trunk flexion as compared to asymptomatic individuals [4]. Future investigation of whether such differences in LPR, and potentially in the lower back biomechanics, between people with and without LBP is a cause or consequence of LBP can further enhance our understanding related to etiology of LBP among older individuals.

Table 4: Mean LPR along with 95% confidence interval for each age group, gender and pace

Age	Mean	95% Confidence Interval	
		Lower Bound	Upper Bound
22-28	2.998	2.538	3.458
32-38	3.038	2.529	3.546
42-48	2.273	1.600	2.946
52-58	1.733	1.118	2.347
62+	1.368	.729	2.006
Male	2.754	2.361	3.147
Female	1.809	1.465	2.154
Slow	2.620	2.280	2.959
Fast	1.944	1.740	2.148

REFERENCES

1. Johannes CB, et al. *J Pain*, **11**, 1230-1239.
2. Tafazzol A, et al. *Clin Biomech*, **29**, 7-13, 2014.
3. Intolo P, et al. *Man Ther*, **14**, 596-604, 2009.
4. Porter JL and Wilkinson A. *Spine (Phila Pa 1976)*, **22**, 1508-1513, 1997.

ACKNOWLEDGEMENTS

This work was supported by CDC-NIOSH grant number R21OH010

THE EFFECT OF EXERCISE TRAINING ON SHOULDER JOINT POSITION SENSE

Yin-Liang Lin and Andrew Karduna

University of Oregon, Eugene, OR, USA

email: yinliang@uoregon.edu, web: <http://karduna.uoregon.edu/>

INTRODUCTION

The central nerve system uses proprioception to help coordinate muscle activity around the shoulder to provide dynamic stability during movement. Impaired proprioception has been found to be associated with shoulder injuries [1].

Exercise is an important part of shoulder rehabilitation, but the effect of exercise on proprioception is still controversial [2, 3]. To our knowledge, no study has focused on training rotator cuff and scapular muscles, which are the dynamic stabilizers of the shoulder. The purpose of this study is to investigate the effect of rotator cuff and scapular muscle strengthening exercise on the shoulder joint position sense.

METHODS

Twelve healthy subjects were recruited (4 males and 7 females, 18 – 26 years old). They received exercise training three times per week for four weeks, with an average duration of 30 minutes per session. All training sessions were supervised to ensure compliance with the training protocol. The exercise protocol contained six exercises, including full can, prone full can, external rotation in sidelying, diagonal exercise, push up with plus, and push up on exercise ball. The training consisted of three sets of 10 repetitions using variable resistance: one set at 50% of the 10-repetition maximum (RM), one at 75% of the 10 RM, and one at 100% of the 10 RM.

JPS was tested with an active position reproduction test before and after the exercise training. A magnetic tracking device (Polhemus Liberty, Colchester, VT) was used to measure scapular, humeral and thoracic kinematics. Subjects wore a head mounted display, which provided visual cues for the target position and blocked the visual

feedback on the arm position. A custom written LabVIEW program (National Instruments, Austin, TX) guided subjects to move their arm to a specific target elevation of the humerus with respect to the thorax in scapular plane (Figure 1).

After the subject had maintained the arm in the target position for one second, the display turned completely black, thus removing all visual feedback. Subjects held their arms for two seconds, memorizing the target position. Then subjects were instructed to return to the rest position. After three seconds, subjects were prompted with another verbal cue to return to the target position. The subjects indicated when they believed they had reached the target by pushing a button on a wireless presenter remote with their contralateral hand [4].

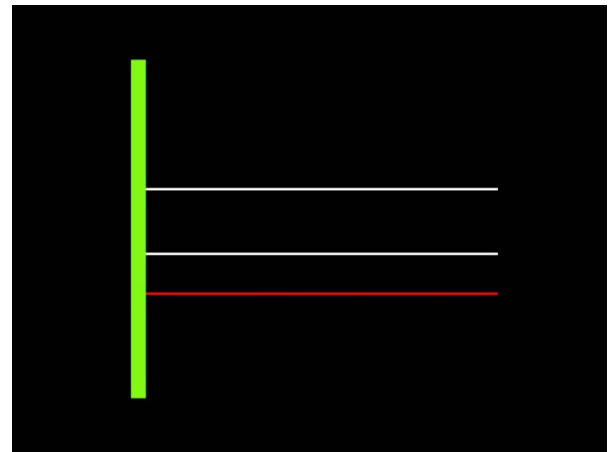


Figure 1. The white bars indicate the target. The red bar represents the humerothoracic elevation angle. The green bars indicate if the arm deviates from the scapular plane

Three target positions were presented: humerothoracic elevation angles of 50°, 70°, and 90°. This study focused on humerothoracic elevation, glenohumeral elevation, and scapular helical angles. Percentage errors were calculated by dividing the errors between the reposition angle and target angle by the reposition range of motion. The

error of the scapular helical angles was calculated from the rotational matrix at the reposition with respect to the target position. The scapular range of motion is calculated from the rotational matrix at the reposition with respect to rest position. Constant errors (CE) and variable errors (VE), which were calculated from percentage errors, were used to represent joint position sense. A two-way repeated measures ANOVA was used to examine the changes after the training.

RESULTS AND DISCUSSION

Figure 2 and figure 3 show the CE and VE of humerothoracic elevation, glenohumeral elevation and scapular helical angles before and after exercise training. No significant interaction was found in CE and VE in three joints. There was a significant main effect in angle found in both CE and VE in three joints, indicating that when the target angles increased, the CE and VE decreased.

There was no significance difference after the exercise training in humerothoracic and

glenohumeral elevation angles. The errors of humerothoracic and glenohumeral elevation demonstrate similar patterns. Significant difference in CE before and after exercise training was found in scapular helical angles, with CEs decrease after the training.

CONCLUSIONS

Although the overall shoulder and glenohumeral joint position sense did not change, scapular joint position sense improved after the exercise training of rotator cuff and scapular muscle. The exercise may be important for the control of scapula.

REFERENCES

1. Machner A, et al. *Acta Orthop Scan* **74**, 85-88, 2003.
2. Rogol IM, et al. *J Athl Train* **33**, 315-318, 1998.
3. Padua DA, et al. *J Sport Rehabil* **13**, 75-95.
4. King J. et al. *J Mot Behav* **45**, 479-486, 2011.

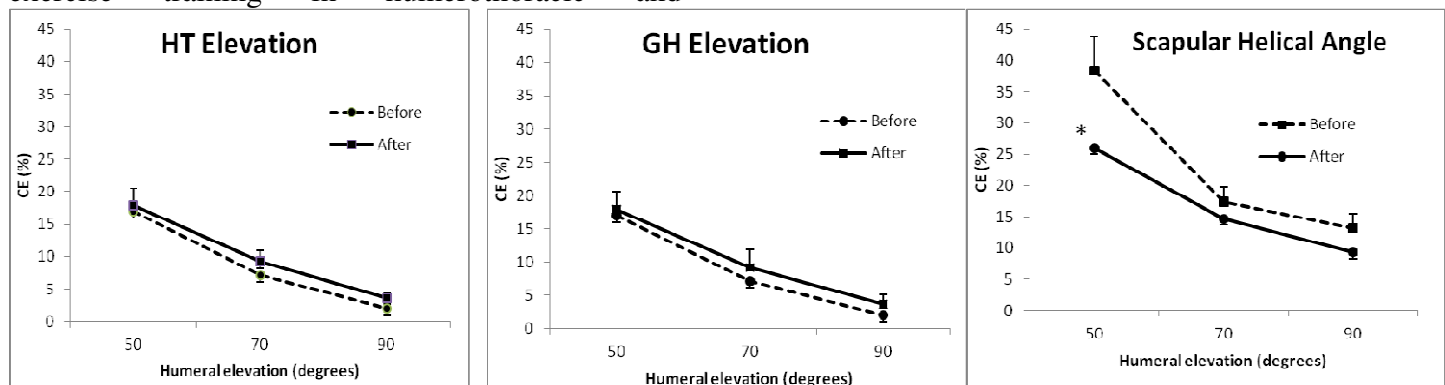


Figure 2. The constant errors (CE) in the percentage of reposition range of motion of humerothoracic (HT) elevation, glenohumeral (GH) elevation and scapular helical angles

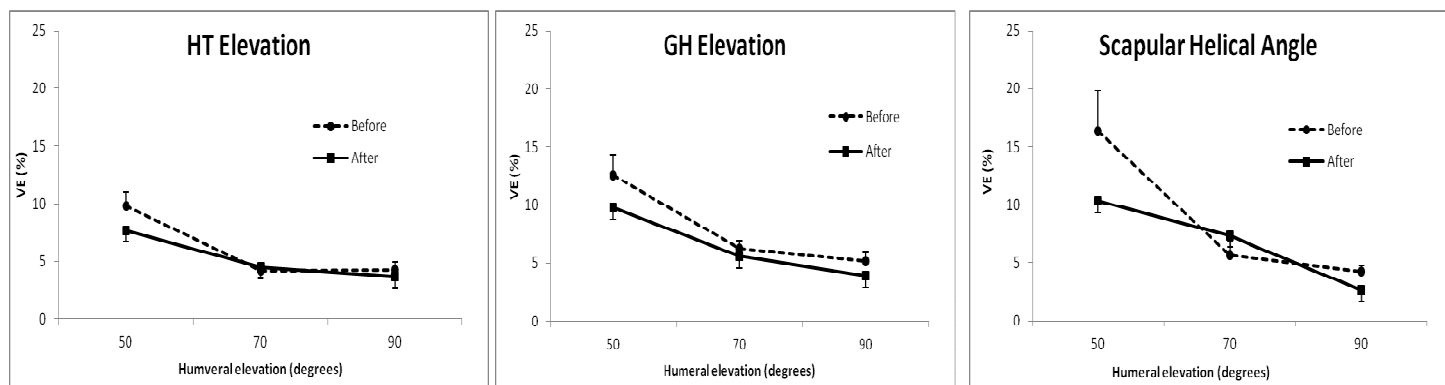


Figure 3. The variable errors (VE) in the percentage of reposition range of motion of humerothoracic (HT) elevation, glenohumeral (GH) elevation and scapular helical angles

HOW HUMANS USE VISUAL OPTIC FLOW TO REGULATE STEPPING MOVEMENTS

¹ Mandy M. Salinas, ² Jason M. Wilken, and ¹ Jonathan B. Dingwell

¹ The University of Texas at Austin, Austin, TX, USA

² Center for the Intrepid, Brooke Army Medical Center, Ft. Sam Houston, TX, USA
email: flyingcape@austin.utexas.edu, web: <http://www.edb.utexas.edu/khe/nbl/>

INTRODUCTION

Visual optic flow is critical for regulating walking [1]. Healthy humans walking on a motorized treadmill (no optic flow) maintain approximately constant stride speeds (S_n) at each stride, n [2]. Subjects allowed deviations in stride length (L_n) and time (T_n) to persist across strides, but rapidly corrected deviations in S_n . In contrast, during overground walking, fluctuations in L_n , T_n , and S_n all exhibit strong persistence [3]. Optic flow provides information about *motion* (i.e. speed) [4]. Differences in optic flow may explain these different experimental results. Here, we determined how humans alter stride-to-stride stepping control by systematically removing or altering optic flow in a virtual (VR) walking environment.

METHODS

Twenty healthy adults (10M/10F; age 19-34) walked on a motorized treadmill at fixed speed (v_w). They were presented 5 optic flow conditions: static VR scene (STA), blank screen (BLK), and VR scene with optic flow speed either matched to (MAT), slower (SLO), or faster (FAS) than v_w . Whole-body kinematic data were recorded to compute time series of L_n , T_n , S_n , and absolute treadmill position, P_n .

During treadmill walking, all $[T_n, L_n]$ combinations that equally achieve the same speed (i.e., $L_n/T_n = v_w$) define a Goal Equivalent Manifold [2] (Fig. 1). Deviations tangent to the GEM (δ_T) do not affect speed (v_w), while deviations perpendicular to the GEM (δ_P) do affect speed (v_w) (Fig.1). Time series of δ_T and δ_P fluctuations relative to the GEM were also computed.

Means and standard deviations were computed for each time series. Detrended Fluctuation Analysis (DFA) was used to compute exponents, α , that quantified the degree of statistical persistence / anti-persistence in each time series. Smaller α indicate

greater likelihood of correcting stride-to-stride deviations on the next stride (i.e. greater *control*) [2].

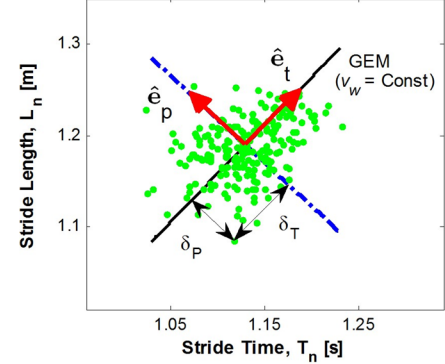


Figure 1: Goal Equivalent Manifold (GEM, $L_n/T_n = v_w$) for walking, showing example $[T_n, L_n]$ data (each dot represents one individual stride n) [2].

RESULTS

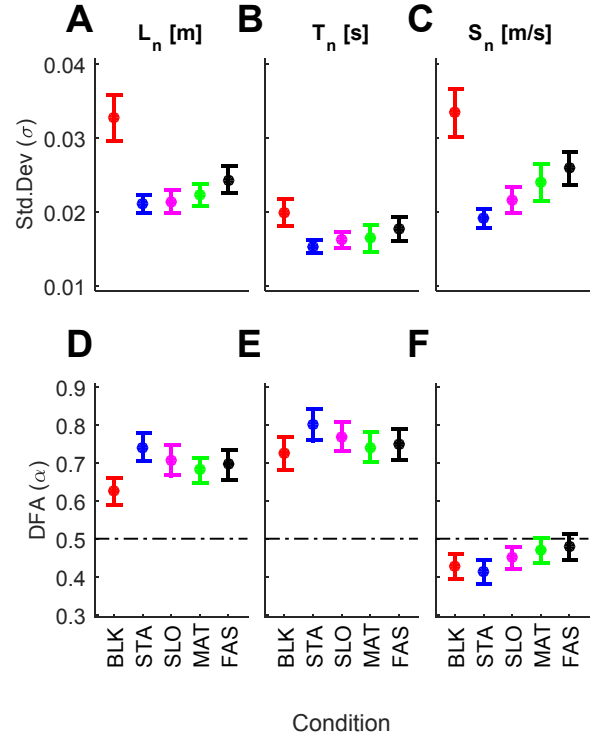


Figure 2: Variability (σ) and Statistical Persistence (α) of Stride Parameters (L_n , T_n , S_n).

Across conditions, participants exhibited stride-to-stride statistical persistence (i.e. $\alpha \gg \frac{1}{2}$) in both L_n (Fig. 2A) and T_n (Fig. 2B), suggesting weaker control of these deviations. Anti-persistence (i.e. $\alpha < \frac{1}{2}$) was observed in S_n across all conditions (Fig. 2C). During BLK, participants exhibited significantly increased variability for all three stride parameters (Fig. 2A-C), and L_n was less persistent compared to the other conditions (Fig. 2D), indicating greater control [2].

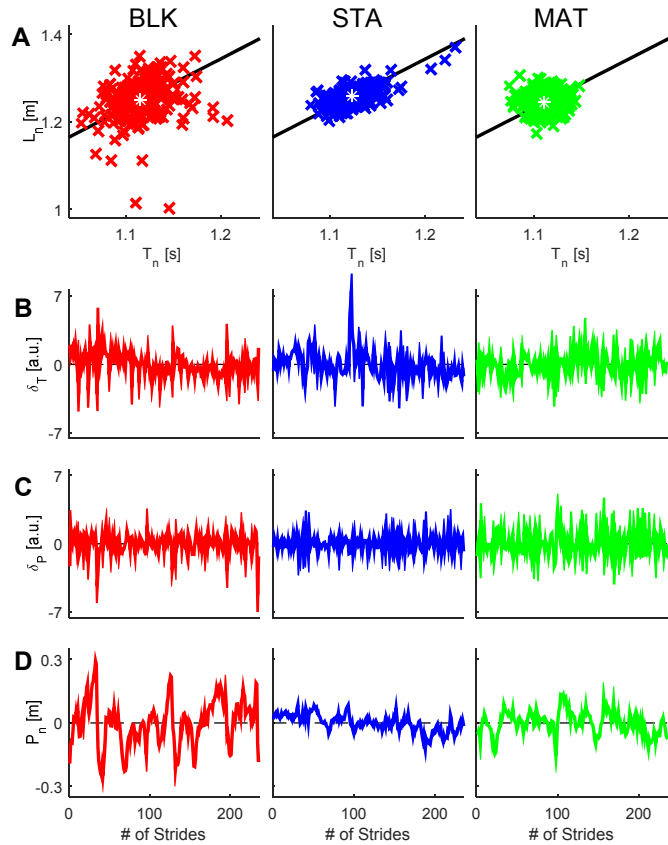


Figure 3: Example $[T_n, L_n]$ and time series data for typical subject for BLK, STA, and MAT conditions.

In the BLK condition, participants exhibited qualitatively more variance in all directions (Fig. 3A). In the STA condition compared to the MAT condition, participants exhibited more variance along and less variance perpendicular to the GEM (Fig. 3A).

Participants exhibited greater variability for δ_T than for δ_P deviations across all conditions (Fig. 4A-B). For the STA condition, variance ratios ($\sigma(\delta_T)/\sigma(\delta_P)$) were highest and ($\sigma(P_n)$) was lowest. Participants exhibited greater statistical persistence for δ_T than for δ_P and strong persistence of P_n across all conditions

(Fig. 4D-F). No significant differences were found for statistical persistence of δ_T , δ_P , or P_n (Fig. 4D-F).

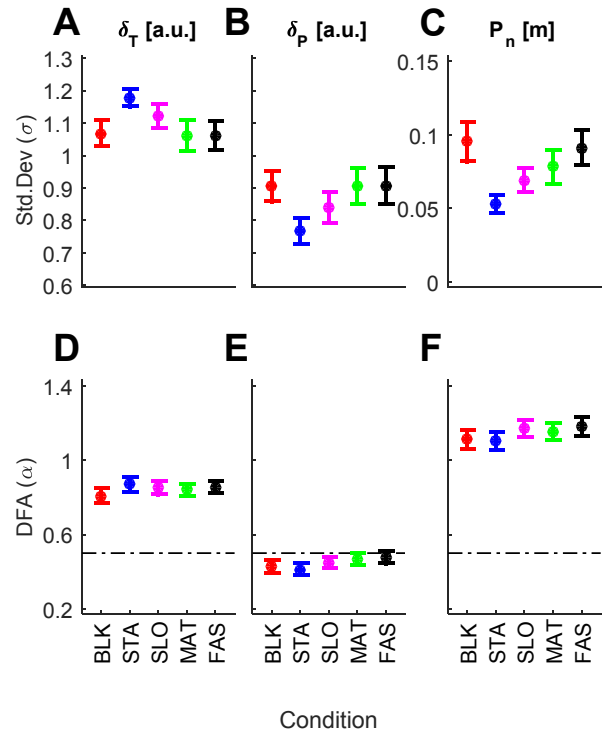


Figure 4: Variability (σ) and Statistical Persistence (α) of both δ_T and δ_P deviations and absolute position (P_n).

DISCUSSION AND CONCLUSIONS

Participants did not adopt stepping control strategies observed during overground walking [3]. However, manipulating optic flow did significantly alter walking variability and how that variability was regulated. Lack of a visual reference (BLK) lead to significantly greater movement variability. However, the level of stride-to-stride control remained similar for these healthy young adult subjects.

REFERENCES

1. Warren WH et al. (2001) *Nat. Neurosci.* **4**(2): 213-6.
2. Dingwell, JB et al. (2010) *PLoS Comput. Biol.* **6**(7): e1000856.
3. Terrier, P et al. (2005) *Hum. Mov. Sci.* **24**(1): 97-115.
4. Gibson JJ (1954) *Psychol. Rev.*, **61**(5): 304-14.

ACKNOWLEDGEMENTS

Partial support provided by: DoD / CDMRP / BADER Consortium, #W81XWH-11-2-0222 (to JBD & JWM).

PROXIMAL-DISTAL DIFFERENCES IN MOVEMENT SMOOTHNESS REFLECT DIFFERENCES IN BIOMECHANICS, NOT NEURAL CONTROL

^{1,2}Steven K. Charles, ¹Layne H. Salmond, and ¹Andrew D. Davidson

¹Mechanical Engineering and ²Neuroscience, Brigham Young University, Provo, UT, USA
email: skcharles@byu.edu, web: neuromechanics.byu.edu

INTRODUCTION

Smoothness is a hallmark of healthy movement and has the potential to be used as a marker of recovery in rehabilitation settings. However, while much past research has focused on how the neuromuscular system plans and controls shoulder and elbow movements (reaching), which are remarkably smooth, little is known about the smoothness of wrist rotations despite the importance of wrist rotations in everyday life. Because the smoothness of wrist rotations has not been characterized, it cannot be used as a marker for diagnosis and evaluation. This study examined the smoothness of wrist rotations in comparison to the known baseline of reaching movements. We found that wrist rotations are significantly less smooth than reaching movements, and that this difference reflects differences in the low-pass filtering properties of the shoulder/elbow vs. the wrist joint.

METHODS

Ten young, healthy subjects were asked to perform 15-degree wrist rotations and 14cm reaching movements in eight different directions at fast, medium, and slow speeds (300, 550, and 900ms durations, respectively). Position data were recorded using trakSTAR (Ascension Technologies, Milton, VT), low-pass filtered and differentiated to get velocity, acceleration, and jerk, and individual movements were extracted as the portion of each movement continuously above 10% of the maximum speed. The smoothness of each individual movement was quantified using two measures: the ratio of the integrated square jerk of the movement to that of the corresponding minimum-jerk trajectory, and the number of maxima in the speed profile. To compare the smoothness between factors (joint, speed, target, and direction), we performed on both measures mixed-model ANOVA with subject as a random factor.

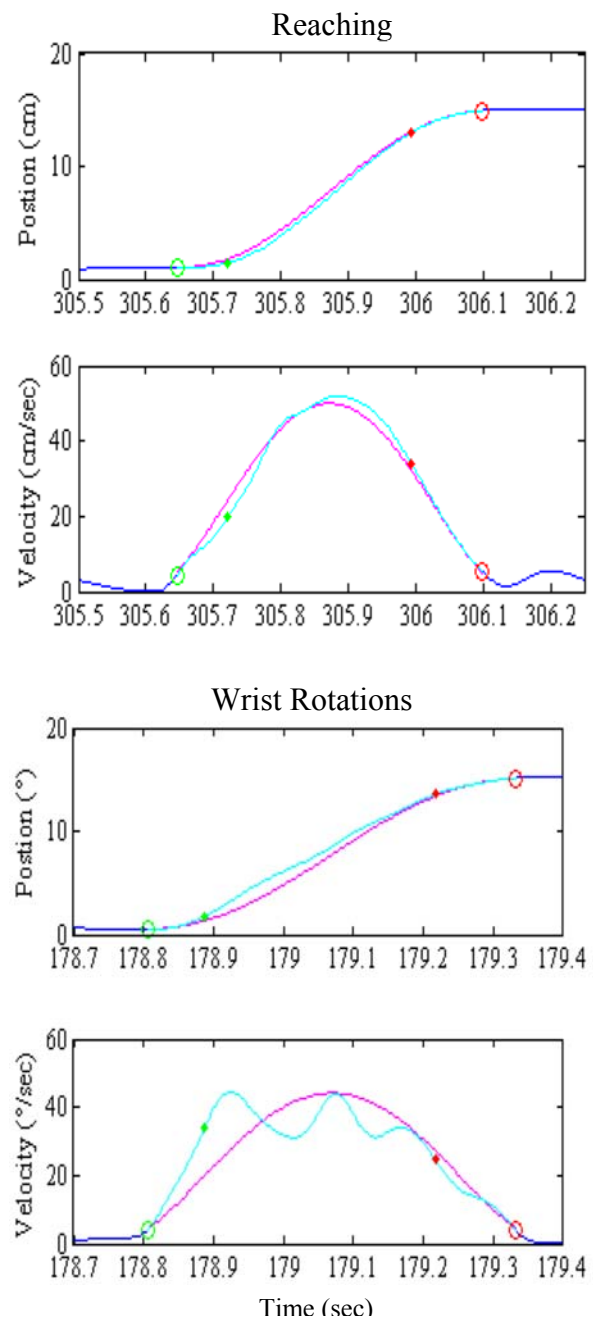


Figure 1: Position and velocity of typical reaching movements (top) and wrist rotations (bottom). Actual movements (blue and cyan) are compared to corresponding minimum-jerk trajectories (pink). Green and red open circles indicate the start and stop of movements (based on 10% of maximum speed).

RESULTS AND DISCUSSION

Position and velocity data of representative fast reaching movements and wrist rotations are shown in Figure 1. Comparing the velocity plots in Figure 1 suggests that wrist rotations were less smooth than reaching movements. Indeed, our analysis showed that 1) wrist rotations were significantly less smooth than reaching movements ($p \leq 0.005$; Figure 2), 2) smoothness decreased significantly as speed decreased ($p < 0.0001$; Figure 2), and 3) wrist rotations exhibited a pattern of smoothness that varied significantly between targets and outbound/inbound movement directions ($p < 0.0001$; not shown).

We further investigated potential causes for these findings. The cause behind the first finding was explored by testing whether the observed difference in smoothness between wrist rotations and reaching movements was due to differences in mechanical, muscular, neural, or protocol-related properties. To investigate the cause behind the third finding, we tested whether differences in wrist smoothness between directions was due to anisotropy in the musculoskeletal dynamics of the wrist or anisotropy in movement duration. Prior studies revealed for reaching and finger movements that faster movements are smoother, so we relied on these studies for an explanation of the second finding.

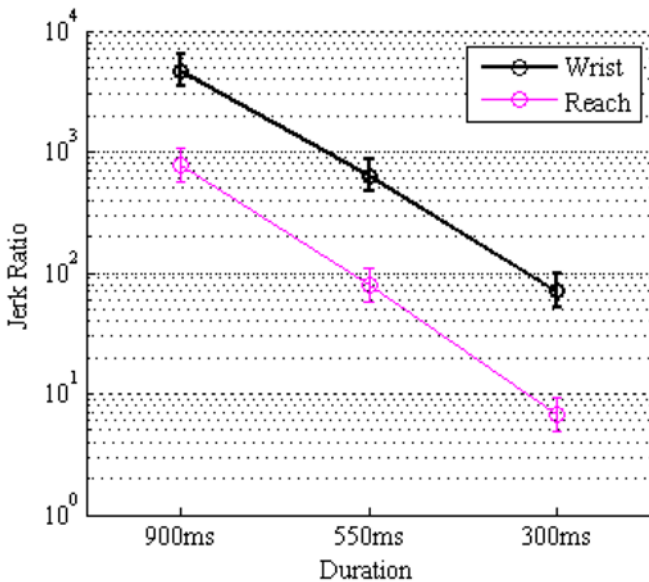


Figure 2: Wrist rotations were found to be significantly less smooth (higher jerk ratio) than reaching movements. For wrist rotations and reaching movements, slower movements were significantly less smooth than faster movements.

Modeling the power spectra of the shoulder/elbow and wrist revealed that the bandwidth of the wrist is significantly larger than that of the shoulder and elbow, and that there is considerable power in the bandwidth of the wrist that would be low-pass filtered in reaching movements, indicating that at least some of the difference in smoothness between wrist and reaching movements is due to differences in mechanical properties (Figure 3). Differences in muscular, neural, or protocol-related properties (signal-dependent noise, proprioceptive acuity, and the speed requirements of the task, respectively) do not appear to be capable of causing the observed difference in smoothness between wrist and reaching movements. Differences in wrist smoothness between movement directions reflects differences in movement duration between directions.

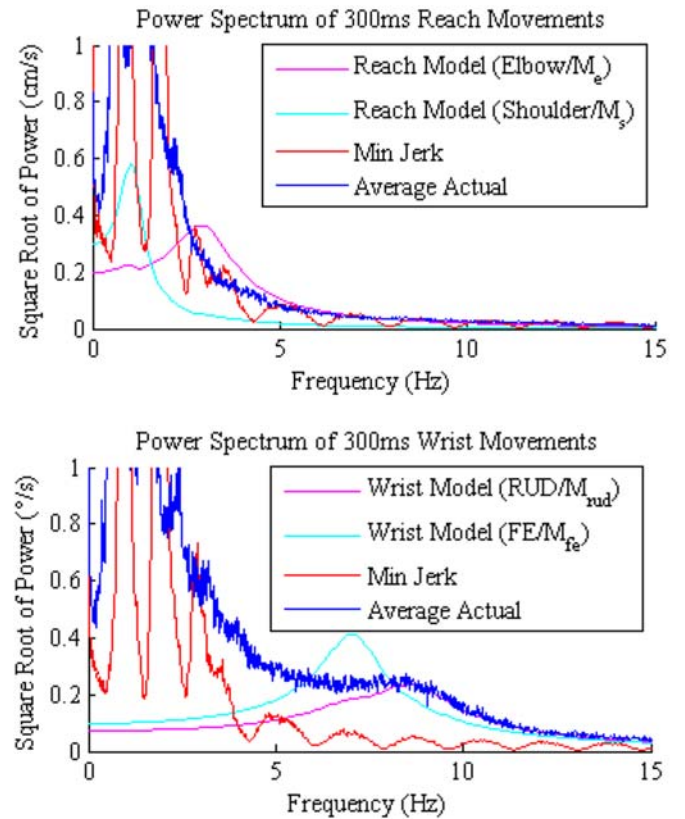


Figure 3: Power spectrum of reaching movements (top) and wrist rotations (bottom). The spectra of actual movements are shown in blue, while the spectra of corresponding minimum-jerk trajectories are shown in red. Superimposed on the power spectrum plots are scaled versions of the magnitude responses (cyan and pink). The power spectrum of the wrist shows considerable power above 4Hz that is not required by the task (hinted by the fact that the minimum-jerk spectrum drops off). Assuming that the input to reaching movements has a similar bandwidth, the power in the 4-10Hz band could not pass through the shoulder/elbow, resulting in smoother movements.

BETA FREQUENCY SENSORIMOTOR CORTICAL OSCILLATIONS DURING ANKLE PLANTARFLEXION ARE RELATED TO SPATIOTEMPORAL GAIT KINEMATICS

¹David J. Arpin, ²Elizabeth Heinrichs-Graham, ²Tony W. Wilson & ^{1,2}Max J. Kurz

¹Munroe-Meyer Institute, University of Nebraska Medical Center, Omaha, Nebraska

²Center for Magnetoencephalography, University of Nebraska Medical Center, Omaha, Nebraska

Email: mkurz@unmc.edu Web: <http://www.unmc.edu/mmi/>

INTRODUCTION

Numerous investigations have examined the kinematics and kinetics of human locomotion; however, few have attempted to explore how the brain is involved in the control of the gait biomechanics [1,2]. A prior study that used electroencephalography (EEG) has shown that there are changes in the sensorimotor cortical oscillations in the beta-frequency (15-30 Hz) range during gait [2]. While identifying that beta oscillatory activity is likely involved in the control of gait is insightful, we still have a substantial knowledge gap in our understanding of how they are linked with control of the lower extremity muscular force production during gait. This information is imperative as we strive to develop brain computer interfaces (BCI) that can be used to control robotic exoskeletons for gait.

The ankle plantarflexors are responsible for producing approximately 80% of the total power during gait [3]. As such, the ankle plantarflexors are largely responsible for the forward progression of the center of mass, and have a direct impact on the sustainment and change of the walking speed. Therefore, understanding how the sensorimotor cortex is involved in controlling the ankle joint musculature may provide further insight on the cortical processes involved in controlling gait. The purpose of this investigation was 1) to assess sensorimotor cortical activity at the beta frequency range during performance of an ankle plantarflexion motor task, and 2) to determine if there is a relationship between sensorimotor cortical activity in the beta frequency range during the ankle plantarflexion task and the spatiotemporal kinematics of gait.

METHODS

Nine adults (Age = 25 ± 3 yrs.) performed an isometric ankle plantarflexion target matching task. Custom Labview software was used to collect and display the isometric forces measured from an isokinetic dynamometer at 1 kHz (Biodex Inc., Shirley, NY). The amount of torque generated was graphically displayed on a large monitor as a single box that moved vertically depending on the amount of torque the subject applied to the foot pedal. The experimental paradigm involved the subjects matching and holding their isometric force at a target torque that was at 20% of their maximum. 60 target matching trials were performed, with each trial consisting of 5 s of isometric torque generation followed by a 10 s rest period where the subject's gaze was fixed on a cross. A 64 channel EEG system was used to concurrently measure the somatosensory cortical activity during the ankle plantarflexion task at 1 kHz (Advanced Neuro Technology, Enschede, Netherlands). Artifact-free epochs for each electrode were transformed into the time-frequency domain and averaged over the respective trials to generate plots of the mean spectral density. The data were then normalized by dividing the power value of each predetermined time-frequency bin by the respective bin's baseline power, which was calculated as the mean power during the baseline period. This normalization procedure allowed power changes to be visually discerned in the individual electrodes. A linearly-constrained minimum variance vector beamformer algorithm was used to reconstruct the electrical neural signals that generated the observed power changes. The images were derived from the cross spectral densities of all combinations of EEG electrodes within the beta frequency, and the solution of the forward problem for each location on

a grid specified by input voxel space. The source power in these images was normalized per subject using a separately averaged pre-stimulus noise period of equal duration and bandwidth. Task effects were analyzed using one-sample t-tests to identify brain areas with significant beta activity. The participants additionally walked across a digital mat at their preferred and fast-as-possible walking speeds in order to assess their gait spatiotemporal kinematics (GAITRite, CIR Systems Inc., Sparta, NJ). Each walking condition was repeated twice and an average was used for the final analysis. For the correlation analysis, the amplitude of the peak voxel for the task effect was extracted from each participant's beamformer output image. Spearman rho rank order correlations were subsequently performed between the peak amplitude and the respective spatiotemporal kinematics.

RESULTS AND DISCUSSION

A representative plot of the time frequency components for the electrode located over the leg motor region (e.g., Cz) is shown in Figure 1A. Inspection of this plot reveals substantial beta frequency activity was present during the ankle plantarflexion task. The beamformer results indicated that the source of this beta activity resided within the leg area of the precentral and postcentral gyri ($p < 0.000005$; cluster-corrected; Fig. 1B).

There were strong correlations between the strength of activity within the peak sensorimotor voxel and the spatiotemporal gait kinematics. For the preferred walking speed, a strong negative correlation was found between the strength of beta neural activity and the cadence ($r = -0.67$, $p = 0.05$). During the fast-as-possible walking speed, we found strong negative correlations between the strength of beta sensorimotor cortical activity and the walking speed ($r = -0.78$, $p = 0.01$) and cadence ($r = -0.87$, $p = 0.01$). This indicated that stronger cortical activity at the beta frequency was related to faster walking speed and quicker cadence. We additionally found a strong positive correlation between the strength of the beta somatosensory cortical activity and step width ($r = 0.67$, $p = 0.05$), suggesting that stronger beta activity was related to a narrower step width.

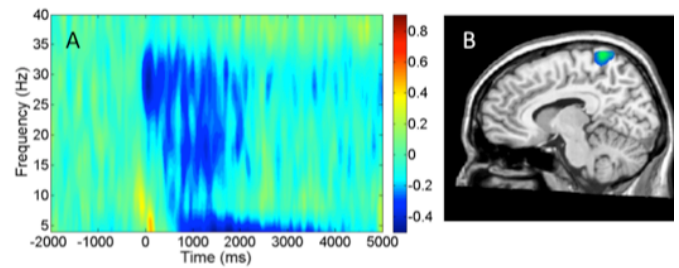


Figure 1. A) Group average time-frequency plot for the electrode located over the leg motor region (Cz) B) Beamformer image of the task effect for the 16-22 Hz response from 750-950 ms. The movement related beta-frequency changes are in blue (pre- and postcentral gyri).

Our results show that there is an increased amount of sensorimotor cortical activity at the beta frequency while performing an ankle plantarflexion force task. These results are aligned with prior investigations that have noted that the beta oscillations may be linked with the control of the lower extremity musculature [4]. More importantly, our results show that there are strong correlations between the amount of beta activity within the somatosensory cortices that are involved in the control of ankle plantarflexion musculature and the gait spatiotemporal kinematics. This implies that the beta frequency oscillations previously noted from the EEG collected during gait may reflect the control of the ankle musculature [2]. Based on our strong correlations, we suspect that monitoring the beta frequency oscillations within the leg region of the somatosensory cortices may provide an innovative index for BCI that use robotic exoskeletons to control the ankle plantarflexion force production during gait.

ACKNOWLEDGEMENT

Partial funding for this study was provided by an ASB Student Research Award.

REFERENCES

1. Kurz et al. *NeuroImage* **59**, 1602-7, 2012.
2. Gwin JT, et al. *NeuroImage* **54**, 1289-1296, 2011.
3. Winter DA. *The biomechanics and motor control of human gait: Normal, elderly and pathological*, 1991.
4. Gwin JT, Ferris DP. *J Neuroeng Rehabil* **9** 35.

OUTCOME MEASURES FOR HAND AND LEG FUNCTION NATURALLY REVEAL LATENT DOMAINS OF STRENGTH, LIMB COORDINATION, AND SENSORIMOTOR PROCESSING

¹Emily L. Lawrence, ¹Sudarshan Dayanidhi, ¹Guilherme Ceasar,
¹Susan M. Sigward, ¹Francisco J. Valero-Cuevas

¹University of Southern California, Los Angeles, CA, USA
email: ellawren@usc.edu

INTRODUCTION

The International Classification of Functioning, Disability and Health (ICF) construct by the World Health Organization emphasizes clinical assessments related to body structure and function, activity, and participation [1]. But the question remains whether and how individual outcome measure relate to—and reveal—these latent functional domains. We developed a multidimensional approach to examine the interactions among available outcomes measures to reveal latent functional domains in both hand and leg function.

METHODS

Sixty-six healthy older adult participants (38F, 28M, 66.1±11.6yrs, range: 45-88yrs) consented to perform upper extremity outcome measures with their dominant hand. Thirty-seven healthy young adults (18F, 19M, 24.7±2.7yrs, range: 18-30yrs) completed the lower extremity outcome measures with their self-reported dominant leg.

The upper extremity measures included six outcome measures: Grip, Key and Precision Pinch strengths, Box and Block test (BBT), Nine Hole Pegboard test (NHPT) and the Strength-Dexterity test compression force (SD_F). The lower extremity measures included ten outcome measures from five assessment tools: Vertical Jump (VJ), Y-balance (YBT), center of pressure variability (COP) during Single Limb Hop and Balance (SLHB) and Single Limb Balance (SLB) tests, and the Lower Extremity Dexterity (LED) test). In [2] we describe how the compression forces in the SD and LED tests quantify the maximal instability that can be controlled.

We used principal components analyses (PCA) to examine whether and how the associations among outcomes measures reveal latent functional domains. We limited our analyses to the PCs that sufficed to capture $\geq 75\%$ of the total variance for both datasets.

RESULTS AND DISCUSSION

In the upper extremity, the 1st PC shows that measures of hand strength are the leading factors. The 2nd PC is dominated by measures of upper limb coordination (BBT and NHPT with inverted scales, hence the negative correlations). The 3rd PC has sensorimotor processing (SD_F) as the sole contributor (Fig. 1).

In the lower extremity, the 1st PC contains outcome measures requiring more strength for successful performance (VJ and YBT), with moderate, positive correlations with SLB COP_{AP} and COP_{ML}. The 2nd and 3rd PCs featured measures of coordinated lower limb ability (SLHB and SLB). Interestingly, while the associations between SLHB and SLB COP variables were positive in the 2nd PC, they were negatively associated in the 3rd PC. Moreover, in the 3rd PC, LED compression force (LED_F; a measure of maximal instability that can be controlled) was positively correlated with dynamic balance variables (SLHB), but LED force variability (LED_{RMS}) was more closely associated with static balance variables (SLB). The 4th PC revealed that outcome measures of sensorimotor processing (LED_{RMS} and LED_F) were highly, positively correlated with each other and no other measure (Fig. 2).

Hand and leg functions are inherently multidimensional [1]. The ICF construct offers a language and a framework for quantifying health

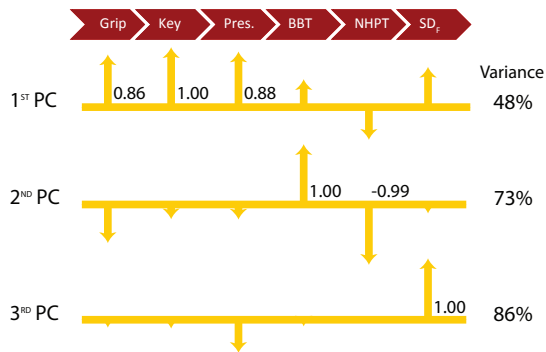


Figure 1: Latent domains of hand function. The scaled loadings for the first three PCs are shown. For ease of comparison, the outcome measures were ordered on a continuum of decreasing strength requirement. Strength-related measures are on the left, sensorimotor measures are on the right, and measures of limb coordination are between them.

and disability. But the link to real-world tasks (e.g., clinically practical outcome measures) is less developed, reducing its utility. The strong and distinct associations and dissociations that emerged naturally among outcome measures reveal—to our knowledge for the first time—three distinct latent functional domains: strength, limb coordination, and sensorimotor processing.

By mapping commonly used functional assessment tools to latent functional domains of hand and leg function, this work critically extends the meaning and utility of the ICF. Strength and sensorimotor processing fit within the structure and function category; and limb coordination fits within activity (reach to grasp, mobility, and balance) and participation (necessary for work, play, and everyday activities) categories.

Importantly, these distinct domains emerged naturally from the data, for both hand *and* leg function despite the obvious evolutionary, anatomical, and functional differences. Despite, also, of the fact that strength is often required in combination with limb coordination for activity and participation, and sensorimotor processing and limb coordination are needed to perform everyday tasks such as in-hand manipulation and maintaining balance.

We present an integrative approach to quantifying hand and leg function that draws from multiple

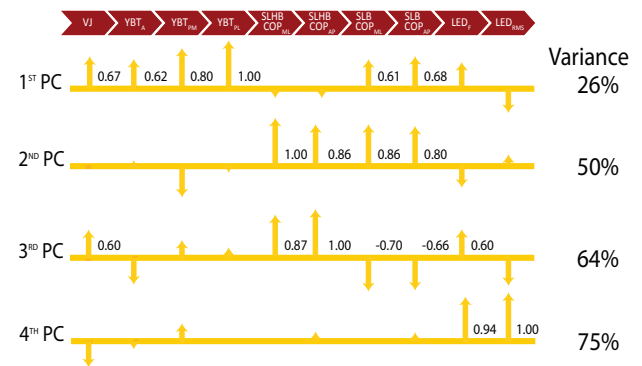


Figure 2: Latent domains of leg function. The scaled loadings for the first four lower extremity PCs are shown.

areas including biomechanics, neuroscience, and general well being. Our novel approach of mapping outcome measures to latent domains of hand and leg function provides a critical new perspective for basic science and clinical research: It enables the design of research studies and treatment modalities to target each of the latent domains of function using available outcome measures.

CONCLUSIONS

When assessing one's the level of hand or leg function, it is particularly important to acknowledge their multidimensional nature—and explicitly consider each outcome measure as it relates to these three latent domains of function. Our novel approach enables a clearer view into the underlying physiological mechanisms that enable, impair, or restore ability in everyday life.

REFERENCES

1. *International classification of functioning, disability and health*: World Health Organization, Geneva, 2001.
2. Lawrence EL, et al. *Frontiers in Neurology*, 5(53), 2014.

ACKNOWLEDGEMENTS

We thank Martha Bromfield, Richard Peterson, Philip Requejo, Carolee Winstein, Isabella Fassola, and Caroline Leclercq. This work was supported by NIH grants AR050520 and AR052345 to FVC and K12 HD0055929 to SMS.

PREGNANCY INDUCED ADAPTATIONS IN INTRAMUSCULAR EXTRACELLULAR MATRIX OF RAT PELVIC FLOOR MUSCLES

Marianna Alperin¹ and Richard L. Lieber^{2,3}

¹Reproductive Medicine, Division of FPMRS, University of California, San Diego, La Jolla, CA, United States.

²Orthopaedic Surgery, University of California, San Diego, La Jolla, CA, United States.

³Rehabilitation Institute of Chicago, Chicago, IL, United States.

email: malperin@ucsd.edu

INTRODUCTION

Birth trauma to pelvic floor muscles (PFMs) is a major risk factor for pelvic floor disorders. Modeling and imaging studies suggest that demands placed on PFMs during childbirth exceed their physiologic limits; however many parous women do not sustain PFM injury [1]. Skeletal muscle extracellular matrix (ECM) supports muscle fibers and determines muscle stiffness. Adaptation during pregnancy of most pelvic tissues results in substantial stiffness decrease in preparation for delivery. However, the effects of pregnancy on structural and mechanical properties of intramuscular ECM in PFMs have not been investigated. This may have significant implications for understanding the pathogenesis of PFMs birth injury caused by mechanical strain. In this study, we sought to determine if pregnancy induces adaptations in the PFM ECM in a rat model.

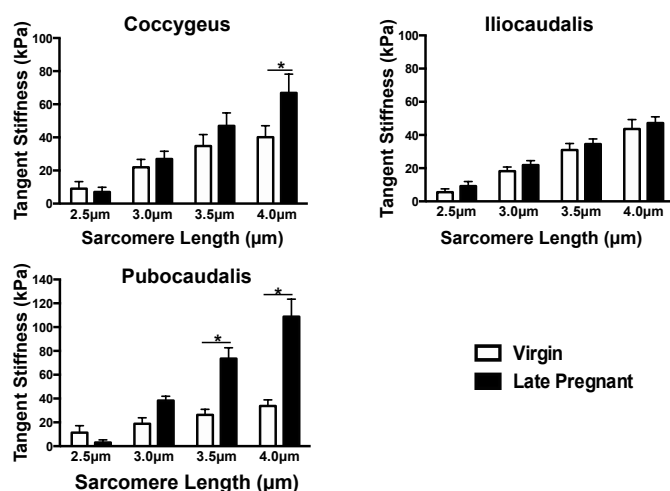
METHODS

Coccygeus (C), Iliocaudalis (IC), and Pubocaudalis (PC) were harvested from 20 3-months old Sprague-Dawley virgin and late-pregnant rats. Stiffness was determined at a bundle level, which reflects mechanical behavior predominantly due to ECM. To establish if parallel changes occur in muscles outside of the PFM, we also examined a hind limb muscle, tibialis anterior (TA). Custom apparatus was used to test 3 bundles from each muscle [2]. Baseline parameters, including cross-sectional area, were measured. A stress-relaxation protocol consisted of increasing sarcomere length (L_s) by 0.25 μm /stretch and relaxing for 3 min, after which force and L_s were recorded. Bundles were stretched until failure or to L_s of 4.0 μm . Force was converted to stress and

tangent stiffness was calculated as the slope of the stress- L_s curve between 2.5 and 4.0 μm . Tissue was processed for quantification of total collagen content using spectrophotometric hydroxyproline assay and elastin content using enzyme-linked immunosorbent assay. Collagen crosslinks (Hydroxylysyl Pyridinoline (HP), Lysyl Pyridinoline (LP), Pentosidine (PE)) were determined by HPLC system, as previously described [3]. Data were compared between groups using two-way ANOVA with Tukey's *post-hoc* testing. Linear regressions were performed to determine correlations between measured parameters. Significance was set at $p < 0.05$, all values are reported as mean \pm SEM.

RESULTS

Pregnant rats demonstrated significantly greater stiffness in C and PC when compared to virgin controls, with 66.86 ± 11.33 kPa vs. 40.09 ± 6.95 kPa ($P < 0.05$) in C and 108.74 ± 14.77 kPa vs. 33.78 ± 5.13 kPa ($P < 0.0001$) in PC at L_s of 4 μm (*see Figure*). IC stiffness was unchanged ($P > 0.05$). Total collagen content was significantly increased in the ECM of all PFMs in pregnant rats relative to virgin controls. Elastin content, on the other hand, remained unchanged (*see Table*). Analyses of enzymatic collagen crosslinks revealed a differential response of individual PFMs, with significant decrease in HP in PC and LP in C in pregnant rats. On the contrary, PE levels were significantly elevated in all three PFMs in pregnancy (*see Table*). When muscle stiffness was plotted against biochemical parameters examined, there were no consistent significant correlations. Importantly, biomechanical and biochemical changes observed in the PFMs, were not present in the TA.



CONCLUSIONS

In contrast to other pelvic tissues, the total collagen content of intramuscular ECM and PFM stiffness does not decrease in pregnancy. Instead, pregnancy induces a significant rise in the ECM collagen and stiffness in PFMs. The above adaptation has the potential to shield PFM fibers from excessive mechanical strain during parturition. Pregnancy results in decrease in enzymatic collagen crosslinks in C and PC, while significantly escalating non-enzymatic crosslinks in all PFMs. It remains unclear which biochemical components of PFMs ECM dictate tissue stiffness.

REFERENCES

1. Hoyte L, et al. *AJOG* 2008. **199**(2):198
2. Lieber RL, et al. *Muscle Nerve* 2003. **28**: 464-71
3. Bank RA, et al. *J Chromatogr*, 1997. **703**: 37-44

Figure: Tangent stiffness of pelvic floor muscles in virgin and late-pregnant groups, measured as mean \pm standard error of the mean.

Table: Content of elastin, total collagen, and collagen crosslinks in intramuscular extracellular matrix in pelvic floor muscles of virgin and late-pregnant rats, measured as mean \pm standard error of the mean.

Total Collagen ($\mu\text{g}/\text{mg}$ tissue)	Virgin	Late-Pregnant	P-value
C	3.1 ± 0.47	7.5 ± 0.65	0.0005
IC	2.9 ± 0.21	4.3 ± 0.12	0.04
PC	3.5 ± 0.52	6.1 ± 0.62	0.001
Elastin (pg/mg tissue)			
C	52.34 ± 10.56	48.48 ± 6.28	0.96
IC	23.25 ± 2.61	17.78 ± 1.99	0.88
PC	18.67 ± 0.96	17.48 ± 1.96	0.99
Hydroxylysyl Pyridinoline (HP) (pmole/mg tissue)			
C	0.080 ± 0.004	0.111 ± 0.011	0.24
IC	0.150 ± 0.012	0.116 ± 0.013	0.17
PC	0.182 ± 0.011	0.127 ± 0.014	0.01
Lysyl Pyridinoline (LP) (pmole/mg tissue)			
C	0.091 ± 0.009	0.036 ± 0.002	<0.0001
IC	0.057 ± 0.013	0.050 ± 0.004	0.88
PC	0.053 ± 0.005	0.045 ± 0.004	0.84
Pentosidine (PE) (pmole/mg tissue)			
C	0.083 ± 0.007	0.122 ± 0.007	0.0002
IC	0.057 ± 0.002	0.081 ± 0.003	0.02
PC	0.037 ± 0.002	0.081 ± 0.010	<0.0001

BIOMECHANICAL MODELING OF ANTERIOR VAGINA WALL PROLAPSE

¹Luyun Chen, ¹James Asthon-Miller, and ²John DeLancey

¹Biomedical Engineering Department

²Obstetrics and Gynecology Department

The University of Michigan, Ann Arbor, MI, USA

email: luyunc@umich.edu

INTRODUCTION

In the US, approximately 200,000 women have surgery to repair prolapse annually with a cost to society that exceeds 1 billion dollars per year. Anterior vaginal wall prolapse, clinically known as cystocele, is the most common form of pelvic organ prolapse and has the highest rate of recurrence.

Dynamic magnetic resonance imaging (MRI) studies have revealed that anterior compartment prolapse is highly correlated with loss of apical support provided by cardinal and uterosacral ligament (1). There are also connective tissues attaching the mid-portion of the vagina laterally to the pelvic floor sidewalls providing "paravaginal support" (2). In addition to the connective tissue attachments, studies have also revealed levator ani muscle damage in women with prolapse. Women with prolapse are 4 times more likely to have the visible damage to the levator ani muscle than women with normal support (3). Sometimes there is a loss of muscle substance but the overall shape of the muscle remains intact. In other instances, gross distortion of the muscle origin occurs (4) presumably due to avulsion of muscle from the pubic bone.

Each of these observations concerns a particular aspect of anterior vaginal wall support and failure. To integrate these observations into a single disease model, we developed a series of biomechanical models from 2D lumped parameter model to 3D finite element models seeking to understand the interactions between different support elements.

METHODS

We first developed a simple 2D lumped parameter model of anterior vaginal wall support (5) (Figure 1). This model simulated anterior vaginal

wall deformation in the mid-sagittal plane and provided an important insight on the interaction between muscular support to the anterior vaginal wall provided by the levator ani and apical connective tissue support provided by the cardinal and uterosacral ligaments. Then we developed a 3D finite element model with paravaginal support and deformable posterior compartment to study the interaction between connective tissue impairment and levator ani muscle impairment based on intact nulliparous anatomy (6). Most recently, a series of three finite element models (unilateral model, bilateral model and normal model) have been developed to investigate the effect of the structure distortion caused by the avulsion of pubococcygeus muscle on pelvic floor support. Then the sensitivity analysis were performed using a using a $2^3 \times 3$ factorial design in Abaqus 6.8 TM to assess all possible combinations of site impairments as shown in Figure 2. Anterior vaginal wall descent was been evaluated at point Aa and apex relative to a hymenal reference plane. The relative theoretical contributions of those four types of impairment to the descent of anterior vaginal wall have been quantified as their effect on Aa and apex decent, which were determined by calculating the their main effect, an aggregate measure that estimates the overall impact on the dependent variable by comparing all of the models.

RESULTS

In all generations of biomechanical models, we were able to generate the cystocele similar to what observed clinically. Cystocele size was sensitive to abdominal pressure and impairment of connective tissue and muscle. Figure 3 shows the example simulation results from the most recent models and the sensitivity analysis of how the cystocele size is sensitive to four different types of the impairments.

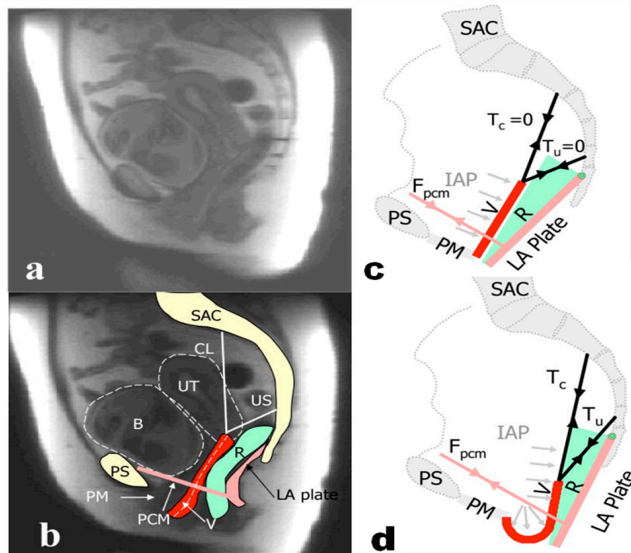


Figure 1. 2D lumped parameter model of anterior vaginal wall support. **A:** mid-sagittal MR image. **B:** modeled elements. **C:** loading lumped parameter model with normal muscular support; **D:** loaded biomechanical model with defective muscular support. Pubovisceral muscle: PCM; PS: pubic symphysis; SAC: sacrum; PM: perineal membrane; LA plate: levator plate; R: rectum; V: vagina; CL: cardinal ligament spring; US: uterosacral ligament spring; B: bladder; UT: uterus. IAP: intra-abdominal pressure.

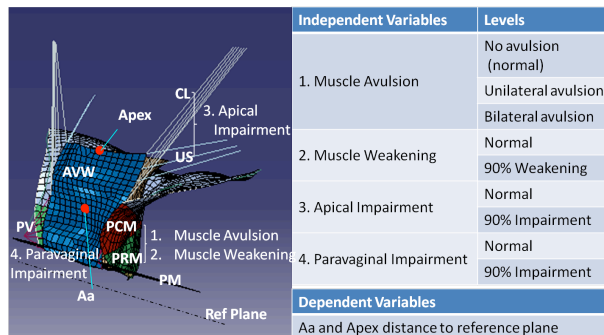


Figure 2. Left panel shows the unilateral defect finite element model resting geometry in oblique view where the right pubococcygeal muscle is missing including: AVW: anterior vaginal wall; PCM: pubococcygeus muscle; PRM: puborectalis muscle; ICM: iliococcygeus muscle; PV: Paravaginal support; PM: perineal membrane. Four different impairments were selected as independent variables and the levels of impairment used in sensitivity analysis showed in the table. Aa and apex locations (the red dots) and their distance from reference plane used as dependent variables.

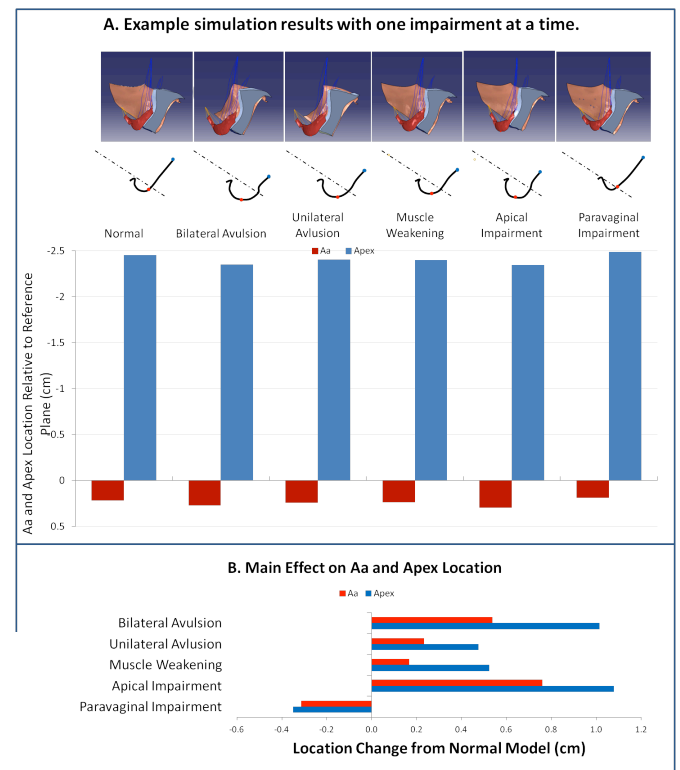


Figure 3. Panel A. Example simulation results with one impairment at a time. Panel B. Result of sensitivity analysis shows the main effect of four impairments on Aa, and Apex of anterior vaginal wall location deviated from normal model.

CONCLUSIONS

Apical support and the bilateral levator ani muscle avulsion are most influential parameters in the anterior vaginal wall descent.

REFERENCES

- Summers A et al. Am J Obstet Gynecol. 2006 May; 194(5):1438-43.
- DeLancey JOL. Am J Obstet Gynecol.1992;166:1717-1728.
- DeLancey JOL et al, Obstet Gynecol. 2007;109:295-302
- Huebner M, Margulies R, DeLancey J. Int Urogynecol 2008 19:863-867
- Chen L et al Obstet Gynecol. 2006 Aug ;108(2):324-32
- Chen L et al. J Biomechanics 2009; 42:1371-1377

RESOLVING THE SURFACE DETECTION CHALLENGE IN NANOINDENTATION OF SOFT MATERIALS FOR APPLICATIONS IN REPRODUCTIVE TISSUE MECHANICS

Amy J. Wagoner Johnson and Jie Wei

Department of Mechanical Science and Engineering,
University of Illinois at Urbana-Champaign, Urbana, IL USA
email: ajwj@illinois.edu

INTRODUCTION

Instrumented nanoindentation (NI) is increasingly used to characterize the mechanical properties of soft materials, including tissues. IN is attractive because testing is done on small samples, for example a tissue biopsy. Further, the testing process itself is non-destructive, leaving tested samples available for other analyses such as by histology. NI also has the potential to measure local properties of heterogeneous soft tissues. This capability is valuable both from a basic science and a clinical perspective. Accurate characterization of local properties, as compared to bulk measurements, allows for the development of more accurate computational models, which can help to understand and diagnose a range of clinical pathologies as well as to monitor treatment. We are particularly interested in characterizing the local properties of pregnant and non-pregnant cervix tissue, especially in the context of assessing risk for preterm birth and for developing better computational models of the pregnant cervix and surrounding tissue structures.

While NI has potential for measuring soft tissue properties, there are major challenges that must be addressed before it can be widely used. The most significant challenge is surface detection. Without accurate surface detection, the indentation test often begins with the probe already at some unknown depth, h_i , below the sample surface (Fig. 1). If this is not taken into account, the value used for the contact depth, h_c , is incorrect and therefore the calculation of the sample Young's modulus, E_s , can be grossly inaccurate (Eqn. 1 and 2).

Here, we present and validate a new approach to overcome the surface detection limitation for soft

materials during NI. Use of this approach will make it possible to use NI to characterize the local mechanical properties for cervix and other reproductive tissues, as well as for a range of other soft materials.

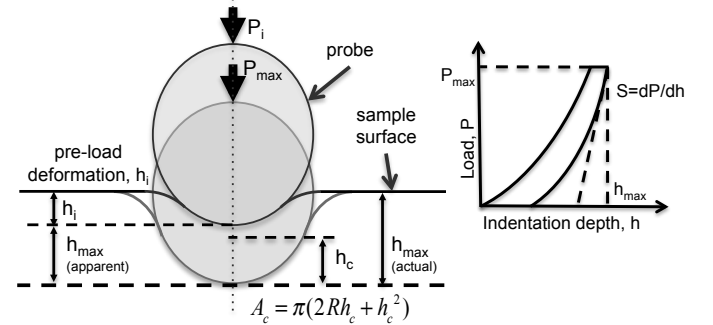


Figure 1: Schematic of the indentation at the initial unknown depth, h_i , and the final depth, h_{max} . The apparent h_{max} is measured, and h_i is calculated using the MIM approach. A schematic of the load-indentation response is shown (right).

METHODS

Polyacrylamide gels with nominal Young's modulus of 19kPa and 49kPa were prepared for uniaxial compression tests and for NI. The moduli obtained from the bulk compression tests were used as the standard for comparison to those obtained by NI. Compression tests were carried out on a Bose Biodynamic Test system and the modulus was

$$S = \beta \frac{2}{\sqrt{\pi}} \frac{E_s}{(1-\nu_s^2)} \sqrt{\pi(2Rh_c + h_c^2)} \quad (1)$$

$$h_c = h_{max(actual)} - \epsilon \frac{P_{max}}{S} \quad (2)$$

$$h_{max(actual)} = h_i + h_{max(apparent)} \quad (3)$$

$$h_i = \frac{S_m^2(h_{max(apparent)-n} - \epsilon \frac{P_{max-n}}{S_n}) - S_n^2(h_{max(apparent)-m} - \epsilon \frac{P_{max-m}}{S_m})}{S_n^2 - S_m^2} \quad (4)$$

calculated from the linear portion of the stress-strain curve ($N=3$). Samples for NI were cast with a flat surface using a custom mold, and affixed to a glass dish petridish. Two samples of each stiffness were tested via NI, and indents were performed on five different spots for each sample. The method described below requires at least two indents to different maximum depths for each spot. The modulus determined using both test methods was compared using an unpaired t-test with significance of $p<0.05$. These were also compared to the modulus determined using the standard Oliver-Pharr approach (Eqn. 1 and 2)[1].

Our approach uses a multi-indent method (MIM), to determine h_i , which allows us then to accurately calculate the modulus. The important parameters used in MIM are shown in Fig. 1.

According to the Oliver-Pharr model[1] E_s , is determined from the stiffness, S , obtained from the linear portion of the load-indentation curve on unloading (Fig. 1), the radius of the probe, R , the sample poissons ratio, ν_s , a geometric constant, β , and the depth of contact, h_c . Depth of contact depends on the maximum load, P_{max} , and corresponding maximum indentation depth, h_{max} (Eqn. 2). ϵ is a constant that depends on the tip geometry and is 0.75 for a spherical tip[2], used here. The actual maximum indentation depth (Eqn. 3), $h_{max(actual)}$, is the sum of the initial unknown indentation depth, h_i , and the apparent maximum depth, $h_{max(apparent)}$, obtained from the load-indentation data (Fig.1). Using the MIM approach two indents of different depths, indent m and n , are made on the same spot. S_m and S_n are the stiffnesses determined for each indent, m and n . By squaring each and taking the ratio, we can solve for h_i , the result of which is shown in Eqn. 4, which relates to h_c through Eqn. 2 and 3. From this we can then determine the sample modulus (Eqn. 1).

RESULTS AND DISCUSSION

Results show that the modulus measured by uniaxial compression tests and the modulus obtained using the MIM approach are in excellent agreement. In contrast, if the initial indentation depth, h_i , is not

taken into account and the standard Oliver-Pharr method is used, the modulus is as much as twice the value obtained by MIM and compression tests. The modulus obtained in this way is significantly different ($p<0.0001$) from those obtained by compression tests and using MIM (Fig.2).

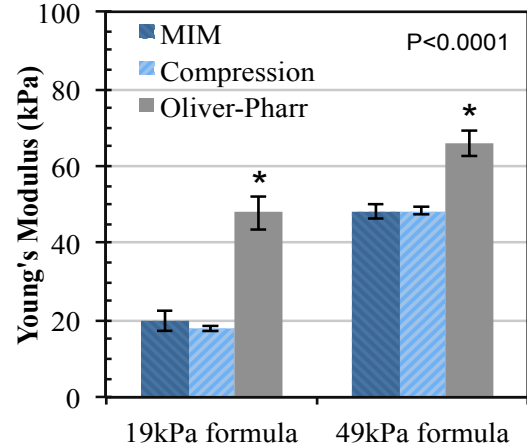


Figure 2: Results show excellent agreement between the Young's modulus determined by compression tests and the MIM approach, while results from the standard Oliver-Pharr model give inaccurate results.

CONCLUSIONS

We developed a multi-indent method (MIM) based on the Oliver-Pharr model that solves the major limitation of NI: the challenge in detecting the sample surface for soft materials. The excellent agreement between the Young's modulus obtained from compression tests and that obtained by MIM validates the approach and demonstrates the error associated with the standard Oliver-Pharr approach for soft materials. Thus, MIM provides a much more accurate way of assessing the modulus of soft materials. We are currently adapting MIM to test pregnant and non-pregnant rat cervix for applications in preterm birth.

REFERENCES

1. Z. Ilke, Kalcioğlu, R. M. Soft Matter , 8, 3393-3398, 2012
2. W.C. Oliver, G.M. Pharr, J Materials Research, 2003.

SHEEP AS AN ANIMAL MODEL FOR PELVIC ORGAN PROLAPSE AND UROGYNECOLOGICAL RESEARCH

¹ Sourav S. Patnaik, ¹ Bryn Brazile, ² Vani Dandolu, ³ Margot Damaser, ⁴ C.H. van der Vaart, and ^{1,*} Jun Liao

¹ Mississippi State University, Mississippi State, MS, USA; ² University of Nevada Medical School, Las Vegas, NV, USA; ³ Cleveland Clinic Foundation, Cleveland, OH, USA; ⁴ Utrecht Medical Center, Utrecht, Netherlands

*Email: jliao@abe.msstate.edu, web: <http://tbl.abe.msstate.edu/>

INTRODUCTION

Animal models can be best utilized to study for POP, immunological responses of mesh implants, biomechanical characteristics of these meshes over time, and the time-dependent tissue-mesh interaction [1]. A variety of animal models, including non-human primates, rodents, murine, rabbit, etc., has been used in the past decade for studying POP and surgical implantation of meshes/grafts. Recently, scientists have projected sheep as an ideal large animal model for biomedical research due to their similar fetal size, comparative anatomy, being best suited for surgical procedures, ease of handling, and economical advantage. Therefore, in order to establish sheep a rigorous animal model, it is important to understand and evaluate the biomechanical characteristics (*in vitro* and *in vivo*) of sheep pelvic floor tissues.

METHODS

Samples for *in vitro* biomechanical testing (biaxial mechanical testing and ball burst testing) were obtained from a local abattoir. Nulliparous Rambouillet-Suffolk breed female lambs of 9-11 months old (weighing 110-135 lbs) were chosen. For this study, we compared the biomechanical characteristics of sheep pelvic floor tissues namely vagina, bladder, broad ligament, and rectum (n = 8 per group). Biaxial mechanical testing was carried out as per previously established protocols [2]. For biaxial testing, the excised sheep tissue (vagina, bladder, rectum, or broad ligament) was dissected into ~20 mm x 20 mm square samples, with one edge of the sample aligned along the longitudinal direction and the other edge aligned along the circumferential (or transverse) direction. Four black markers were placed on the tissue specimens for

tracking local deformation (using CCD camera). Tissue specimens were securely connected to each actuator arms of the biaxial device using custom designed hooks, which were attached to 000 size polyester sutures (4 hooks per edge). Specimens were then preloaded up to 1 gram, preconditioned ten times, and subjected to an equibiaxial stress of 15 kPa. Maximum stretches of the specimen, in both directions, were analyzed to reveal the tissue extensibility. Ball burst testing (Fig. 3) was carried out by a scaled American Society of Testing and Materials (ASTM) standard ball-burst apparatus. The testing apparatus used a stainless steel ball of 12.7 mm diameter, and the sample surface area was set at ~1013.41 mm² (ASTM Test Method D3787). Specimens for ball burst testing (~28 x 28 mm) were mounted between two metal plates with a 19.05 mm diameter hole and ruptured at a rate of 10 mm per minute. Data from ball burst tests were processed to obtain max load (g) and max displacement (mm) for the respective tissues.

In vivo biomechanical testing was carried out on live nulliparous lambs (n=3; Katahdin-Dorpers breed; about 9 months old and 120 lbs.) using a novel balloon based insertable probe (Patent US 20140275841 A1) [3]. All animal experiments were performed by a Diplomate of American College of Veterinary Surgeons (ACVS), as per IACUC protocol number 12-088. Once inserted into the vaginal tract, the probe was inflated to 100 cm H₂O (~1.5 psi), and the corresponding vaginal wall displacement in both axes (anterior to posterior, and left to right) was measured in millimeters.

RESULTS AND DISCUSSION

Biaxial testing of these sheep pelvic tissues was performed to reveal the anisotropic behavior of these materials. Anisotropic behavior at 15 kPa was

found to be highest in vagina, followed by rectum, broad ligament, and finally bladder (Fig.1 A-D). For all four pelvic tissues, the longitudinal direction was found to be more extensible than the circumferential (or transverse) direction. For vaginal tissues, the average stretch was 1.18 ± 0.08 mm/mm (longitudinal) vs. 1.02 ± 0.01 mm/mm (circumferential); whereas, for bladder tissues the longitudinal direction was found to be slightly more extensible than the circumferential direction (1.35 ± 0.09 mm/mm vs. 1.31 ± 0.13 mm/mm). Similarly, for ball burst tests, max load was highest for vaginal tissue, whereas max displacement was highest for rectum tissue (Fig.1 E-F).

With biaxial testing under physiological range, we observed a marked difference in the mechanical behavior of the sheep vaginal wall tissues in their respective loading directions (Fig.1 A). This observation, however, is in contrast to a previously published study, which reports sheep vaginal tissue as isotropic material and less extensible beyond physiological range [4]. The *in vivo* data further indicates that, under physiological loading conditions, sheep vaginal tract can accommodate stretching in either direction by virtue of its microstructural organization. Similarly, *in vivo* human biomechanical measurements of female patients with vaginal wall prolapse have shown a greater degree of structural compliance and a reduced elastic behavior [1]. Under the influence of hormone and other biochemical factors, we expect to observe an altered compliance (or dilation) from the *in vivo* biomechanical measurements in the vaginal tract of prolapsed sheep, and perhaps an altered elastic behavior as well.

CONCLUSIONS

We have developed a baseline protocol for *in vitro* and *in vivo* biomechanical characterizations of sheep pelvic tissues/vaginal tract. Sheep have similar supporting structures for the pelvic organs and their structural and mechanical properties share similarities with humans [1]. Furthermore, sheep are advantageous for surgical research owing to their size, anatomy, and relatively quick prolapse timeline. These commonalities make sheep the ideal vehicle for advancing our knowledge of pelvic prolapse.

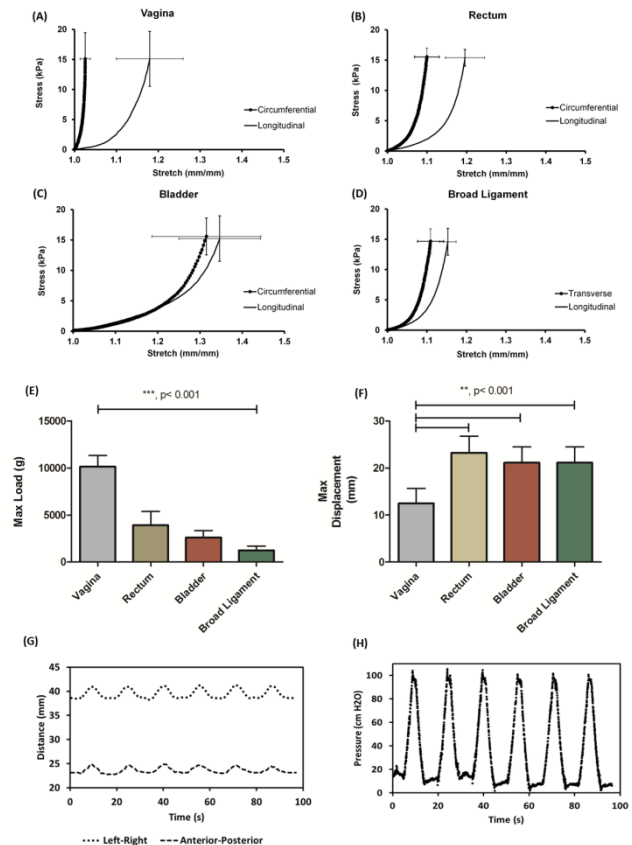


Figure 1: *In vitro* and *in vivo* biomechanical testing results of sheep pelvic floor tissues. Biaxial mechanical testing results of vagina (A), rectum (B), bladder (C), and broad ligament (D) shows the anisotropic characteristics of each tissue. Ball burst test results of these pelvic floor tissues are shown as Max load (E) and Max displacement (F) parameters. Displacement (G) and Pressure profiles (H) of *in vivo* biomechanical testing of sheep pelvic floor, obtained by the insertable probe is shown here.

REFERENCES

1. Abramowitch SD, et al. *Eur J Obstet Gynecol Reprod Biol.* **May; 144 Suppl 1**:S146-58, 2009.
2. Patnaik SS, et al. ASME Proceedings: Summer Bioengineering Conference. SBC2012-80886: 1193-1194, 2012.
3. Borazjani A, et al., *Insertable probe*. Google Patents, 2014.
4. Rubod C, et al. *J Urol* **Jul; 178(1)**:320-5, 2007.

ACKNOWLEDGEMENTS

- ICS Emerging Research Team Grant 2015-16
- NSF EPS-0903787
- Ag. & Bio. Engg. Dept. and I²AT at Mississippi State University

BIOMECHANICAL EVALUATION OF THE EFFECTIVENESS OF PROSTHETIC MESHES

¹ Manfred M. Maurer, ¹ J. Menze, ¹ B. Röhrnbauer, ² A. Feola, ² J. Deprest and ^{1,3} E. Mazza

¹ Institute of Mechanical Systems, ETH Zurich, Leonhardstrasse 21, 8092 Zurich, Switzerland

² Center for Surgical Technologies, Faculty of Medicine, Universitair Ziekenhuis “Gasthuisberg” Leuven, Katholieke Universiteit Leuven, Leuven, Belgium

³ EMPA Materials Science and Technology, Überlandstrasse 129, 8600 Dübendorf, Switzerland

email: maurer@imes.mavt.ethz.ch

INTRODUCTION

This study addresses the open question on which factors influence clinical complications related to insertion of prosthetic meshes for hernia and pelvic organ prolapse (POP) repair. The material itself (usually a polymer such as polypropylene) has been proven to be “biocompatible”, e.g. [1]. However, *mechanical biocompatibility*, related to the ability of implants to display a mechanical behavior compatible with its function and favoring its integration in the surrounding native tissue [2], is an important factor which is not determined only by the chemical composition of the implant material. It recently became clear that the deformation behavior of meshes in a physiological range, also called “comfort zone” [3], is of major importance and it is suggested that implants designed to mimic biomechanical properties of the area of application are advantageous.

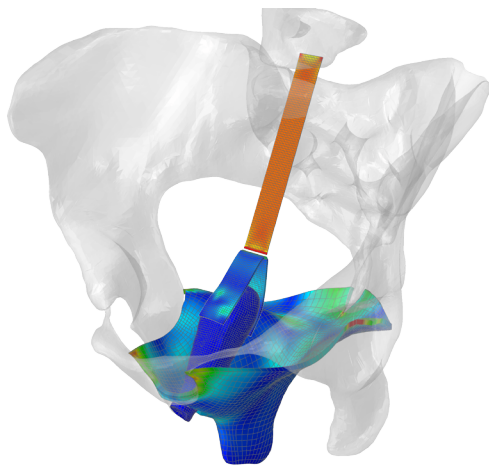


Figure 1: Finite element model simulation of stresses during Valsalva after the sacrocolpopexy procedure.

However, the definition of a reasonable physiological range of loads in-vivo, thus serving as a basis to evaluate experimental results and providing a design target for future meshes, still remains an open challenge, since corresponding in-vivo measurements are currently not feasible. Additionally, the surgical technique and implant handling strongly influence the mechanical behavior of the implant in-vivo.

We use extensive experimental testing and data analysis to evaluate the mechanical biocompatibility of mesh implants [4]. Finite element modeling is employed in order to qualitatively analyze the influence of mesh properties and surgical technique based on an exemplary case of the Valsalva maneuver after a sacrocolpopexy procedure (Fig. 1).

METHODS

Experimental protocol: Nine different mesh types were investigated. Each mesh type was tested in eight different configurations:

2 (uniaxial tension OR biaxial tension) x 2 (dry OR embedded) x 2 (0° OR 90° direction)

Experiments with uniaxial tension and biaxial tension (realized as uniaxial strain test) were performed on the same tensile test machine. Test piece dimensions were selected to generate a free area of 30mm x 15mm (uniaxial) and 50mm x 15mm (biaxial). Each specimen was loaded to a maximum of 30% nominal strain (loading rate of $\sim 10^{-3} \text{s}^{-1}$) and unloaded back to a pre-force threshold of 0.01 N for 10 cycles. Local strains were extracted optically in the center of the specimen with the aid of an image analysis algorithm.

Finite Element Modeling: The FE model was originally developed in the group of M. Brieu [5] and has been modified for the present application. It

is based on MR images and consists of the homogenized pelvic floor muscle structure, the vaginal stump after hysterectomy and a Y-shaped mesh system attached to anterior and posterior vaginal wall as well as the sacrum. Material laws of muscle and vaginal canal are taken from the literature [5,6]. Two meshes were simulated, one stiffer (DynaMesh® PRS) and one softer (DynaMesh® Endolap) with material laws (2nd order reduced polynomial hyperelastic) fitted to our experimental data. Valsalva pressure is applied to the pelvic muscle sheet. In order to investigate the influence of surgical technique, a pre-stretch of 10% is applied to the upper mesh arm, simulating the surgeon pulling the mesh before fixing it to the sacrum.

RESULTS AND DISCUSSION

The mechanical properties of mesh implants show large variation, depending on their knitting pattern, weight, area density and state of loading. In fact, one cannot simply infer properties of the knitted mesh from the source material or pore size and weight. Rather, implants need to be analyzed as a structure. The specific stress and/or strain, at which experimental data is interpreted in terms of mechanical biocompatibility plays another major role. This poses the question of meaningful corresponding physiological reference values (Fig. 2).

Our simulations of the specific exemplary case of Valsalva after the sacrocolpopexy procedure show however, that surgical technique strongly influence the in-vivo structural behavior. By simply pulling the upper mesh arm before attaching it to the sacrum, the mechanical response of the mesh can be altered. An initially soft mesh can become much stiffer and the stresses and strains experienced by the mesh and underlying vaginal tissue strongly increased. Furthermore, the techniques used to attach the mesh to the vaginal wall determines the local interaction of mesh and tissue.

These results indicate the relevance of quantitative biomechanical studies in order to define guidelines for mesh manufacturing and surgical techniques, improving the performance of implants.

REFERENCES

1. Shtilman MI, *Polymeric Biomaterials*, Brill Academic Pub., 2003
2. Mazza E, et al. *J Mech Behav Biomed Mater* **48**, 100-124, 2015
3. Ozog Y, et al. *Int Urogynecol J* **22**, 1099-1108, 2011
4. Maurer MM, et al. *J Mech Behav Biomed Mater* **40**, 42-58, 2014
5. Lecomte-Grosbras P, et al. *Proceedings of MICCAI 2013*, Nagoya, Japan, 2013
6. Chantreau P et al. *Int Urogynecol J* **25**, 1547-1553, 2014

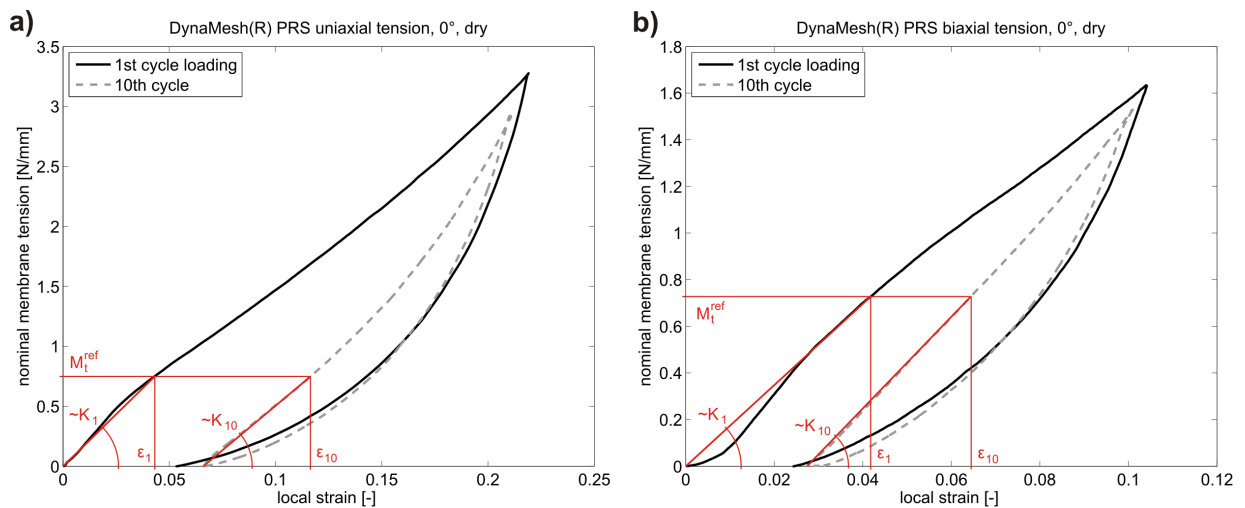


Figure 2: Exemplary tension-strain curves for DynaMesh® PRS for illustration of secant stiffness determination. a) uniaxial tension in 0° direction, dry mesh, loading and unloading in 1st and 10th cycle. b) biaxial tension in 0° direction, dry mesh, loading and unloading in 1st and 10th cycle. Secant stiffness in 1st and 10th cycle are shown in both.

THE EFFECT OF FETAL MEMBRANE PRESTRETCH ON CERVICAL LOADING DURING PREGNANCY

¹Michael J. Fernandez, ²Alexander E. Ehret, ²Edoardo Mazza, ³Michael House, ⁴Joy S. Vink, ⁴Ronald Wapner,

¹Kristin M. Myers

¹Columbia University, New York, NY, USA

²Swiss Federal Institute of Technology, ETH Zurich, Switzerland

³Tufts Medical Center, Boston, MA, USA

⁴Columbia University Medical Center, New York, NY, USA

INTRODUCTION

Preterm birth (PTB), defined as birth before 37 weeks of gestation, is a major healthcare problem around the world [1]. The dominant structural and material factors that lead to premature rupture of membranes and/or early cervical shortening, major risk factors for PTB [2], are unknown. This study analyzes what role the fetal membrane (FM) may play in the progression of cervical dilation by simulating intrauterine pressure (IUP), membrane-uterus-cervix interactions, and varying levels of membrane *in vivo* prestretch in a finite element (FE) analysis. We constructed an FE model based on an idealized anatomical geometry at term and utilized experimentally-supported material models [3-5] to calculate the loads and stretches in the fetal membrane, uterus, and cervix. We demonstrate that the fetal membrane's *in vivo* stretch level affects its contribution to load sharing, which in turn dictates the loading experienced by the cervix and lower uterine segment.

It is hypothesized that the mechanical failure of tissues supporting the fetus plays a role in PTB. The soft tissues surrounding the fetus are equipped to grow, remodel, stretch and remain intact during the course of gestation. Then at term, in a reversal of their previous role, these tissues allow for delivery of the baby. The uterus contracts, the FM ruptures, and the cervix shortens and dilates. If the remodeling events of these tissues are mistimed, the load-bearing capability could be compromised, leading to PTB.

The contribution of each organ to load sharing is dependent on the material characteristics of the particular tissue and the amount of prestretch in an

organ after its growth and remodeling process. Evidence suggests that the FM grows until the 2nd trimester [6], then stretches over the rest of pregnancy to accommodate the enlarging amniotic cavity. Additionally, the area stretch of the FM at term has been measured to be 1.7 by comparing ultrasonic intrauterine area and post-delivery membrane area [7], and IUP has been reported to be 2.66kPa at baseline uterine tone at term (between contractions) [8]. Lastly, we know that the material response of the FM is nonlinear [3]. Given these lines of evidence, we provide a preliminary FE framework to explore the consequences of FM prestretch. We demonstrate that the load-sharing between the LUS, cervix, and FM at term is largely influenced by the amount of FM prestretch.

METHODS

We created an idealized 3D model (Fig. 1) of the uterus, cervix, and fetal membrane using Trelis Pro 15 (csimsoft, LLC, 2015). The uterus was represented by 1/8 of a spherical shell section with an inner diameter of 10cm and a wall thickness of 1cm. We defined the cervix to be a cylindrical tube with an outer diameter of 3cm, an inner diameter of 1cm, and a length of 3.5cm. Since the amnion is the primary load-bearing component of the fetal membrane, we modeled it as a spherical shell section with a thickness of 0.1mm. Its outer diameter in the reference configuration was parameterized in this study in order to investigate two different levels of *in vivo* stretch. The final mesh contained 6688 hexahedral elements with a mean volume of 7.6mm³. We used a fiber composite material with neo-Hookean ground substance for the uterus and cervix. The cervical model was fitted to mechanical tension and

compression tests of full-term pregnant cervical tissue specimens [4,5]. The uterine material properties were chosen as in [4]. An Ogden material model based on equibiaxial tensile loading of human amnion was employed for the fetal membrane layer. A frictionless sliding interface was defined between the exterior surface of the membrane and the interior of the uterus and cervix. The model was assembled and solved using FEBio 2.2.6 (<http://febio.org/>).

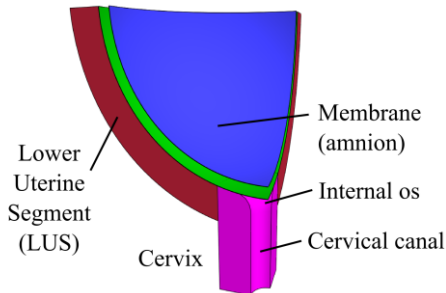


Figure 1: Quarter model of the idealized LUS (red), cervix (magenta) and two different membrane reference states (blue and green).

We analyzed two states of prestretch: no prestretch and the prestretch corresponding to a baseline *in vivo* IUP. To achieve the latter, we scaled the membrane in its reference state such that it would come into contact with the un-deformed uterus and cervix when subjected to the *in vivo* IUP of 2.66kPa reported by Buhimschi [8]. For comparison purposes we consider also the IUP of 8.60kPa, which represents the peak value during contractions in the second stage of labor.

RESULTS AND DISCUSSION

An increased membrane prestretch resulted in a stiffer membrane response and reduced mechanical loading of the cervix. Increasing the membrane prestretch from 1 (no prestretch) to 1.08 (corresponding to an area stretch of 1.17) decreased the stretch at the cervical internal os from 1.25 to 1.1 at an IUP of 8.60kPa (Fig. 2).

This preliminary investigation suggests that FM prestretch is an important contributing factor to the mechanical loading that occurs in pregnancy. Future work will seek to reconcile these simulations with literature studies on FM area change and *in vivo*

stretch state. We will also refine the amnion material model to include fiber dispersion and the ability to parameterize fiber orientation, and work toward improved uterine muscle modeling.

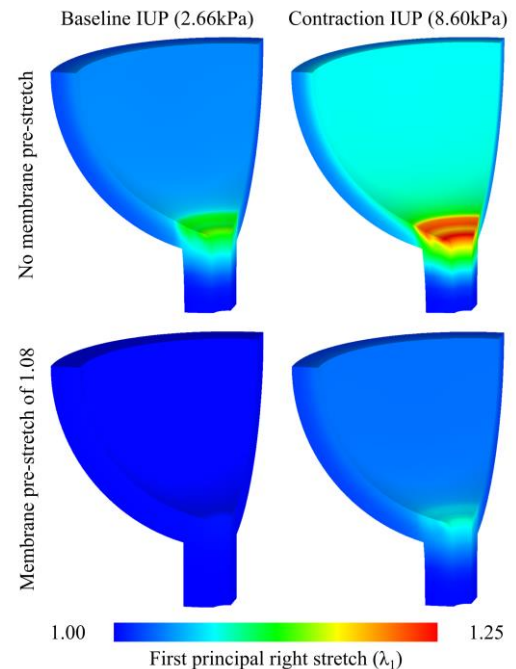


Figure 2: Cervical stretch levels for IUP at baseline and contraction level under two assumptions for membrane prestretch state. Membranes hidden for stretch state visibility.

CONCLUSIONS

Our model demonstrates that the fetal membrane's *in vivo* stretch level affects its contribution to load sharing, which in turn dictates the loading experienced by the cervix and lower uterine segment. The membrane and its *in vivo* loading state should not be ignored in future studies of pregnancy biomechanics.

REFERENCES

1. World Health Organization. Preterm birth: fact sheet no. 363. 2014.
2. To, et al. *Ultrasound Obstet Gynecol* **18**, 200–203, 2001.
3. B r zle W, et al. *J Biomech* **46(11)**, 1777–1783, 2013.
4. Fernandez, M., et al. *Comput Methods Biomech Biomed Engin*, 2015. In press.
5. Myers KM, et al. *J Biomech*, 2015. In press.
6. Alger LS, et al. *Clin Obstet Gynecol* **29(4)**, 758–770, 1986.
7. Millar LK, et al. *Am J Obstet Gynecol* **182(1.1)**, 128–134, 2000.
8. Buhimschi CS, et al. *Obstet Gynecol* **103**, 225–230, 2004.

REDISTRIBUTION OF LOWER-LIMB JOINT POWER DURING UPHILL AND DOWNHILL WALKING AND RUNNING

Richard W. Nuckols¹, Dominic Farris², Raziel Riemer³, Gregory S. Sawicki¹

¹Joint Dept. of Biomedical Engineering, NCSU and UNC-Chapel Hill

²University of Queensland, Australia; ³Ben-Gurion University of the Negev, Israel
email: rwnuckol@ncsu.edu

INTRODUCTION:

Mechanical output of the lower-limbs during gait is modulated in response to changing environmental demands. For example, at steady speed on level ground, the majority of positive work is performed by the ankle and hip over a range of walking and running speeds (1). On an incline during walking (2) and running (3), joint power contributions are re-distributed, with the hip becoming the predominant source of net work to raise the center of mass against gravity. Our aim was to characterize the distribution of positive and negative mechanical power output across the lower-limb joints in walking and running up and downhill in order to guide design of assistive devices (i.e., exoskeletons and prostheses). We hypothesized that the hip would dominate mechanical energy generation needed to go uphill and the knee would dominate mechanical energy absorption needed to go downhill at steady speed.

METHODS:

3D lower-limb kinematics and kinetics were collected on eight subjects across 5 walking (1.25 m/s; -15%, -10%, 0%, 10%, 15% grade) and running (2.25 m/s; -10%, -5%, 0%, 5%, 10% grade) during 7 minute trials. Using inverse dynamics analysis we computed joint moments and powers for the ankle, knee, and hip in each condition and computed average positive and negative power pie charts including both limbs following (1).

RESULTS AND DISCUSSION:

The distribution of joint power and work output among the ankle, knee, and hip depended on both surface gradient and gait. During walking, positive work shifted from the ankle to hip with increasing grade while the knee was the dominant source of negative work across all grades (Fig. 1a). Net work followed similar trends. On inclines, the majority of net work was performed at the hip, while on

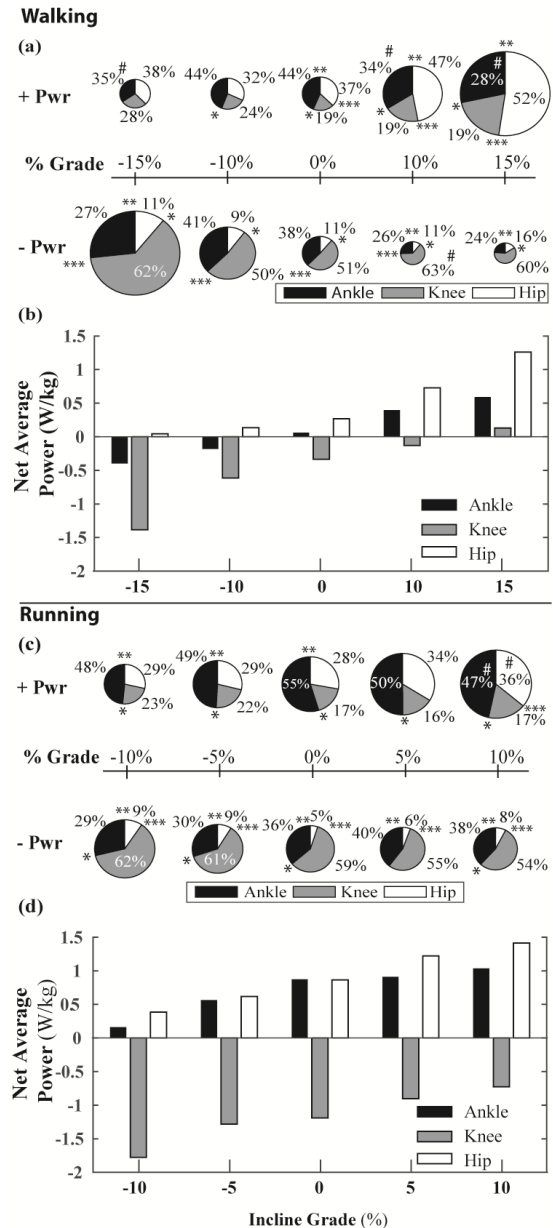


Figure 1: (a) Percent distribution of average positive and negative lower-limb joint power for (a) walking (1.25 m/s) and (c) running (2.25 m/s) over a range of grades. The area of each pie is normalized to the average positive power at level grade for walking (1.02 W/kg) and running (3.66 W/kg). A significant change ($p < 0.05$) in the individual joint's percent work distribution compared to level walking or running is marked by a hash sign (#). A significant difference ($p < 0.05$) in pairwise comparisons between percent joint work at a given grade is marked by a * (Hip to Knee), ** (Knee to Ankle), and *** (Ankle to Hip). Net average power of each joint across grade conditions for (b) walking and (d) running.

declines the largest source of net work was the knee (Fig. 1b).

During running, the ankle was the dominant source of positive work and the knee was the dominant source of negative work across all grades (Fig. 1c). The hip did very little negative work during running, and was therefore the dominant source of net work during incline running (Fig. 1d).

Time series plots show the redistribution of joint moment and power over the stride cycle for walking (Fig. 2) and running (Fig. 3). Again, the general trend was a shift in positive power to the hip with increasing incline, while the knee was the primary site of negative work (i.e. absorption). Changes in ankle positive power were predominately seen at push-off (~60% stride), with changes in the knee negative power and hip positive power coming in initial stance.

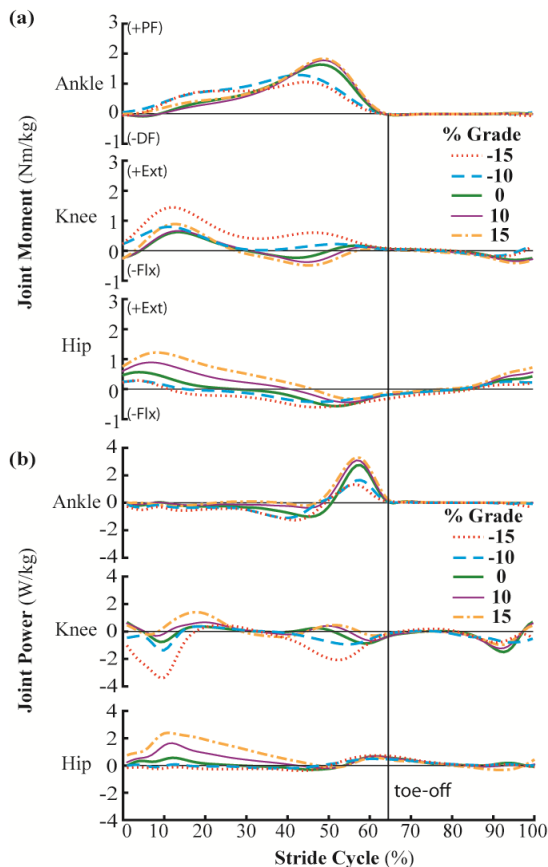


Figure 2: Normalized time series plots of the joint moments (a) and powers (b) during walking across grades. Data shown are a group mean over one complete stride defined with 0% and 100% = heel-strike of same limb.

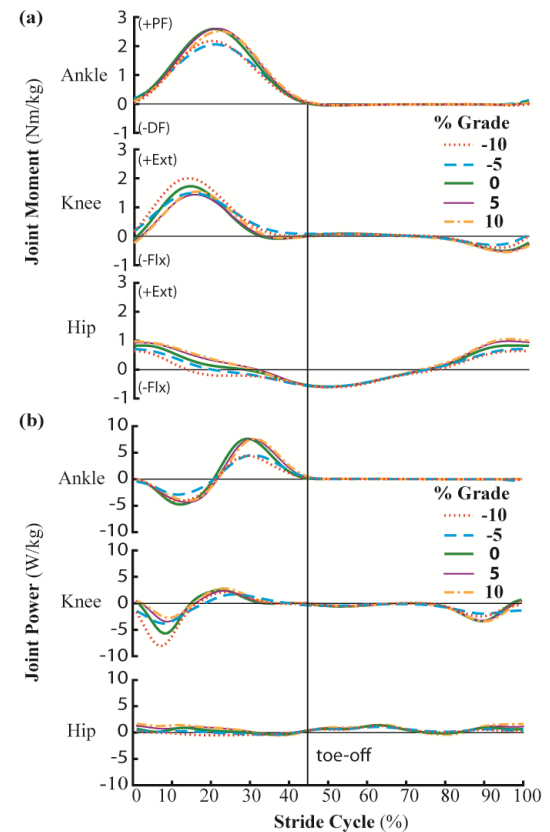


Figure 3: Normalized time series plots of the joint moments (a) and powers (b) during running across grades. Data shown are a group mean over one complete stride defined with 0% and 100% = heel-strike of same limb.

These results support our hypothesis and the previous work of others (1,2,3) that for uphill locomotion, the hip is an important source of net mechanical energy generation. In addition, we have demonstrated that the knee is the predominant source of absorption during both walking and running downhill-highlighting a strong opportunity for energy harvesting during downhill gait. Interestingly, during uphill running, the ankle joint remains an important contributor to overall positive work, making it an ideal site for assistance with simple exoskeletal devices. Future work will be directed at assessing the mechanical and metabolic effects of assistive devices in similar conditions of increased mechanical demand.

REFERENCES

1. Farris DJ, *J R Soc Interface*. 2012 Jan 7;9(66):110-8.
2. Franz JR, *Gait Posture*. 2014 Jan;39(1):135-40.
3. Roberts TJ, *J Exp Biol*. 2005 May;208(Pt 10):1963-70

MUSCLE FUNCTION DURING SLOPED WALKING

Nathaniel T. Pickle¹, Alena M. Grabowski^{2,3}, Arick G. Auyang⁴ & Anne K. Silverman¹

¹Department of Mechanical Engineering, Colorado School of Mines, Golden, CO USA

²Department of Integrative Physiology, University of Colorado, Boulder, CO USA

³VA Eastern Colorado Healthcare System, Denver, CO USA

⁴Nike Explore Team Sports Research Lab, Beaverton, OR USA

email: npickle@mymail.mines.edu, web: fbl.mines.edu

INTRODUCTION

Uphill and downhill walking are fundamentally different biomechanical tasks than level-ground walking, as evidenced by altered electromyography (EMG) signals [1] and kinematics and kinetics [2]. However, it is unknown how muscles work in synergy to achieve altered biomechanics on slopes. Musculoskeletal modeling and simulation can be used to estimate the forces and function of individual muscles during movement, and have provided important insight into muscle functional roles during level-ground walking [3, 4]. However, these tools have not been applied to sloped walking. Thus, we sought to use musculoskeletal modeling and simulation to characterize muscle function during walking on uphill and downhill slopes.

METHODS

Thirteen healthy adult subjects (9 male, 4 female) walked on an instrumented treadmill at 1.25m/s and $0^\circ \pm 3^\circ$, $\pm 6^\circ$, and $\pm 9^\circ$. Ground reaction forces (GRFs) (1500 Hz, Bertec Corp.), whole-body kinematics (100 Hz, Vicon Inc.), and EMG signals (1500 Hz, Noraxon) from eight muscles on each leg were collected. Joint angles were computed using an inverse kinematics algorithm and low-pass filtered at 6 Hz in Visual3D (C-Motion, Inc.). GRFs were also low-pass filtered at 6 Hz to maintain consistency between signals [5].

Subject-specific musculoskeletal models were created in OpenSim 3.1 [6] by scaling the segment lengths and total mass of a generic model with 23 degrees of freedom and 92 Hill-type musculotendon actuators. Passive torques were added to each joint to represent forces from ligaments and soft tissues [7]. A residual reduction algorithm was used to improve dynamic consistency in the simulations between the measured kinematics and GRFs. A computed muscle control algorithm was used to

solve the muscle redundancy problem and determine muscle excitations that produced the experimental walking kinematics while minimizing the sum of squared muscle excitations at each time step. Muscle excitations were constrained based on EMG signals from the lower limbs. For each subject, three gait cycles per slope were simulated, resulting in a total of 273 simulations.

After the simulations were generated, left leg muscle contributions to the acceleration of the body center of mass (COM) were determined with an induced acceleration analysis using a rolling without slipping kinematic constraint between the foot and the ground [8]. The induced accelerations in the treadmill reference frame were analyzed by calculating the mean parallel (braking/propulsion), normal (perpendicular to the treadmill), and mediolateral accelerations induced by each muscle group during early (0-30% gait cycle) and late (30-60% gait cycle) stance. A linear mixed effects ANOVA was performed ($\alpha=0.05$) with slope as a fixed effect and subject as a random effect. When a significant slope main effect was found, post-hoc pairwise comparisons ($\alpha=0.05$) were performed using Dunnett's test to compare sloped to level-ground walking.

RESULTS AND DISCUSSION

Nearly all ANOVAs indicated a significant slope main effect, demonstrating that muscle function is greatly affected by both uphill and downhill slopes. The major contributors to acceleration in the parallel and normal directions were the rectus femoris (RF), vasti (VAS), hamstrings (HAMS), gluteus maximus (GMAX), and biarticular plantarflexors (BPF) (Fig. 1). The hip abductors were the primary contributors to mediolateral accelerations, but the accelerations in this direction were small and had fewer significant results.

In the parallel direction, RF and VAS were major contributors to braking on downhill slopes. RF provided braking throughout stance, while VAS contributed during early stance. The greater braking from RF and VAS compared to level-ground walking was consistent with greater knee extensor moments previously observed on downhill slopes [2]. On uphill slopes, HAMS and GMAX had an increased contribution to propulsion during early stance compared to level-ground walking. BPF, which primarily delivers energy to the leg to initiate swing in level-ground walking [3], provided increased body propulsion during late stance on uphill slopes. The greater propulsion from HAMS, GMAX, and BPF on uphill slopes was also consistent with greater hip extensor and ankle plantarflexor moments [2].

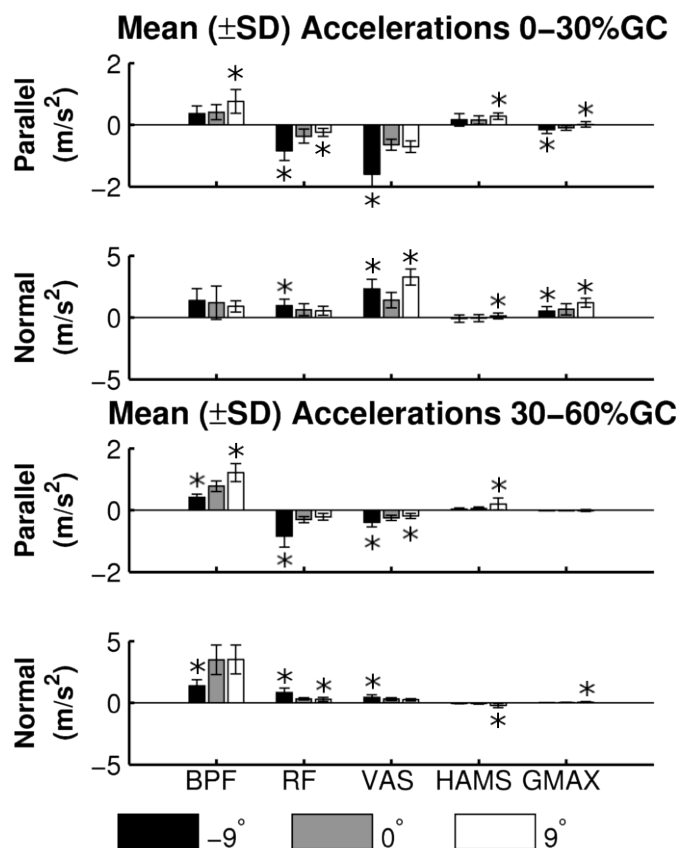


Figure 1: Mean (\pm SD) contributions of left leg muscles to body center of mass acceleration during 0-30% (top two plots, early stance) and 30-60% (bottom two plots, late stance) of the left leg gait cycle (GC), in the directions parallel and normal to the treadmill. * indicates a significant difference compared to 0° .

In the normal direction, VAS provided greater upward acceleration (away from the treadmill) of the COM during early stance on uphill and downhill slopes compared to level ground, which was consistent with previous observations of increased knee extensor activity on uphill and downhill slopes [1]. HAMS provided greater upward acceleration in early stance, but only on uphill slopes. During late stance on downhill slopes, BPF provided less upward acceleration, suggesting a reduced need for energy delivered to the leg for swing initiation compared to level-ground walking [3]. RF provided greater upward acceleration in late stance, which was consistent with greater muscle activity [1].

CONCLUSIONS

This study described the specific functions of major muscle groups during uphill and downhill walking. In particular, the ankle plantarflexors and knee extensors provided the largest accelerations to the body COM during all walking conditions, and provided even greater accelerations during uphill and downhill walking. These results can serve as a baseline for identifying functional deficits in impaired populations and aid in the analysis of devices that are intended to replicate muscle function, such as prosthetic feet.

REFERENCES

1. Lay AN, et al. *J Biomech* **40**, 1276-1285, 2007.
2. Lay AN, et al. *J Biomech* **39**, 1621-1628, 2006.
3. Neptune RR, et al. *J Biomech* **34**, 1387-1398, 2001.
4. Silverman AK and Neptune RR. *J Biomech* **45**, 2271-2278, 2012.
5. Kristianslund E, et al. *J Biomech* **45**, 666-671, 2012.
6. Delp SL, et al. *IEEE Trans BME* **54**, 1940-1950, 2007.
7. Anderson FC. *Unpublished Dissertation*, University of Texas at Austin, TX, 1999.
8. Hamner SR, et al. *J Biomech* **43**, 2709-2716, 2010.

ACKNOWLEDGEMENTS

This work is partially supported by a VA Career Development Award (VA RR&D A7972-W) to A.M.G.

UPHILL WALKING ENHANCES THE RETENTION OF A NEW STEPPING PATTERN LEARNED ON A SPLIT-BELT TREADMILL

¹ Jonathan S. Calvert, Carly J. Sombric, and Gelsy Torres-Oviedo

¹ University of Pittsburgh, Pittsburgh, PA, USA

email: jsc53@pitt.edu, web: <http://www.engineering.pitt.edu/MARGroup/Home/>

INTRODUCTION

Stroke patients often possess an asymmetric walking pattern that affects their mobility and quality of life. Promising studies have shown that patients can correct their gait asymmetries after walking on a split-belt treadmill, which forces their legs to move at different speeds [1]. Thus, there is an interest for enhancing the duration of these positive effects after split-belt walking. We hypothesize that the duration of the walking pattern learned on the split-belt treadmill is modulated by the forces experienced at the subjects' feet (i.e., ground reaction forces) during split-belt walking. To test this, we assessed the retention of adaptation effects after split-belt walking when healthy subjects walked uphill or downhill, which are conditions that naturally modulate ground reaction forces during walking.

METHODS

Twenty healthy volunteers (12 men, mean age 25.2 ± 5.4) participated in the study. The subjects were divided among three groups: flat, uphill, and downhill walking. The three groups walked on a split-belt treadmill (Bertec), in which one leg moved at 0.5 m/s and the other leg moved at 1.5 m/s (3:1 belt speed ratio) for 600 strides. Subjects also walked on the treadmill when the two belts moved at the same speed (1 m/s) before and after the split-belt condition. Kinematic data were recorded in all groups with a motion tracking system (Vicon) via reflective markers placed bilaterally on the trunk and legs. In the uphill and downhill groups, the treadmill was inclined to a 15% grade before, during, and after split-belt walking.

We used the kinematic data to compare the walking pattern of the three groups when the two belts were moving at the same speed before and after split-belt walking. To accomplish this, we computed in each group their asymmetry in 1) step length, 2) step position, and 3) step time, which are measures known to adapt independently during split-belt walking [2]. We evaluated the extent of adaptation effects (i.e. after-effects) on these outcome measures by comparing their average values before split-belt walking and the initial steps (i.e., average of the first 5 steps) after split-belt walking. We also compared the decay of adaptation effects across the three groups. To this end we computed the number of steps that subjects took before their walking pattern returned to baseline behavior after the split-belt perturbation was removed.

The raw kinematic data was extracted from Vicon and processed in MATLAB. Step length asymmetry, step position asymmetry, and step time asymmetry were calculated as defined in previous split-belt adaptation studies [2]. Values from pre-split-belt walking were subtracted from the post-split-belt walking values to assess how well the subjects retained the new walking pattern. Divergence from baseline walking was defined as the points at which the asymmetry was greater than two times the standard deviation of the baseline walking data. A one-way ANOVA with Tukey post hoc analysis was used to determine if there were differences between the walking conditions ($\alpha=0.05$).

RESULTS AND DISCUSSION

Figure 1 shows the step length, step position, and step time asymmetries after split-belt walking. The uphill group had step length and step position

asymmetries that were significantly different to those of the other two groups. However, the step time asymmetry was not significantly different across groups. Additionally, the flat and downhill groups were not significantly different among any of the asymmetry values.

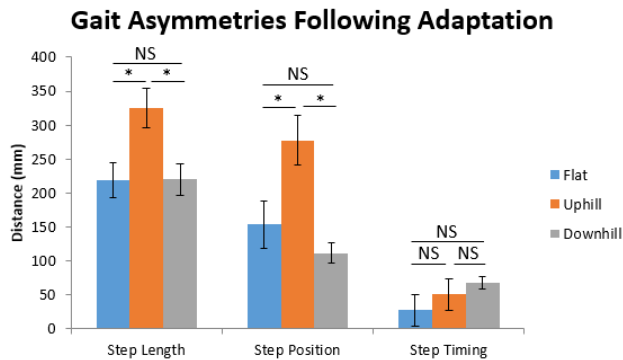


Figure 1: The average step length, step position, and step timing asymmetries immediately following the adaptation period. The uphill group is significantly different for step length and step position, but not step timing. Asterisks indicate statistical significance.

Additionally, subjects in the uphill group took longer to return to baseline values in the spatial parameters than the temporal parameters. Specifically, subjects in the uphill group took an average of 60 steps to return to baseline values for step position asymmetry vs. 49 and 21 steps in the flat and downhill groups, respectively. Conversely, all groups took an average of 15 steps to return to step time asymmetry baseline values.

Uphill walking significantly increased the retention of the new walking pattern in the spatial domain, but not the temporal domain. Previous studies have shown that slope walking in humans may require specialized neural control strategies [3]. Therefore,

the increased retention of spatial parameters after split-belt walking may be due to a different motor control strategy than what is used during flat split-belt walking.

This increase in after-effects in step position and step length, but not step time, in the uphill condition suggests that split-belt walking on an incline could enhance the correction of spatial asymmetries via split-belt walking. An increase in the retention of spatial adaptation effects is important because stroke patients often have larger deficits in one domain than the other [4]. Therefore, it is pertinent to identify ways to adapt spatial and temporal asymmetries independently.

CONCLUSIONS

Overall, this study shows that we able to increase the effects in the spatial domain during and after split-belt walking in healthy controls by inclining the treadmill. This increase in spatial parameters may be useful in creating individualized rehabilitation for stroke patients who have a large spatial asymmetry. In future studies, stroke patients will be tested with this paradigm to see if these results transfer across populations

REFERENCES

1. Reisman et al. *Brain* **130.7**, 1861-1872, 2007.
2. Finley et al. *Neural*. Submitted. 2014.
3. Lay et al. *J Biomechanics*, **39.9**, 1621-1628, 2006.
4. Malone and Bastian, *Neurorehabilitation and Neural Repair*. **28.3** 230-240. 2014.

MUSCLE FUNCTION AND COORDINATION DURING STAIR ASCENT

¹ Nicole G. Harper, ² Jason M. Wilken and ¹ Richard R. Neptune

¹ Department of Mechanical Engineering, The University of Texas at Austin, Austin, TX, USA

² Center for the Intrepid, Department of Orthopaedics and Rehabilitation, Brooke Army Medical Center,
JBSA Ft. Sam Houston, TX, USA

email: nicole.harper@utexas.edu, web: <http://www.me.utexas.edu/~neptune>

INTRODUCTION

Stair ascent is a critical task for mobility independence in daily living. However, stair ascent can be biomechanically challenging, requiring an individual to simultaneously propel the center-of-mass horizontally and vertically [e.g., 1] while also controlling mediolateral motion and modulating leg swing to avoid contact with the intermediate step [e.g., 1]. While the plantarflexors, knee extensors and hip abductors have been identified as important contributors to stair ascent, it remains unclear how the individual muscles function in synergy to accomplish this task. The purpose of this study was to develop a three-dimensional muscle-actuated forward dynamics simulation of unimpaired stair ascent to determine the contributions of individual lower-extremity muscles to the biomechanical subtasks of vertical propulsion, horizontal propulsion, mediolateral control and leg swing. Such an analysis will provide additional insight into muscle function and coordination in stair ascent and help guide the development of effective, targeted rehabilitation programs aimed at improving an individual's ability to ascend stairs.

METHODS

A three-dimensional muscle-actuated forward dynamics simulation of stair ascent was generated to emulate group-averaged experimental kinematics and ground reaction forces (GRFs) for 27 unimpaired subjects. To develop the simulation, the musculoskeletal system, foot-ground contact and muscle force generation were modeled based on previous work [e.g., 2] and dynamic optimization was used to identify the muscle excitation patterns for 38 Hill-type musculotendon actuators that minimized the difference between the simulated and experimental kinematics and GRFs. To identify the contributions of individual muscles to the

biomechanical subtasks of stair ascent, previously-described GRF decomposition, induced acceleration and segment power analyses were performed [e.g., 3]. The 38 individual muscles were combined into 15 muscle groups for analysis based on similar functional and anatomical classification [4].

RESULTS AND DISCUSSION

The optimization framework identified a set of muscle excitations that successfully emulated the experimental kinematics and GRFs. In addition, the timing profiles for the optimized muscle excitations compared well with published EMG data [1] and the primary contributors to the subtasks of stair ascent were identified (Table 1).

The vasti (VAS) and plantarflexors (SOL and GAS), which were the primary contributors to vertical propulsion in the first and second halves of stance, respectively, generated vertical power to the trunk and ipsilateral leg (Fig. 1: Vertical Power). The hamstrings (HAM) opposed vertical propulsion in the second half of stance by absorbing vertical power from the legs, although they did redistribute some of that power to the trunk to propel it upward.

Gluteus maximus (GMAX) and HAM, the primary contributors to forward propulsion in the first and second halves of stance, respectively, generated horizontal power to both legs while simultaneously transferring power from the trunk to the legs (Fig. 1: Horizontal Power). SOL contributed to braking in the first half of stance by absorbing horizontal power from the ipsilateral leg while rectus femoris (RF) contributed to braking in the second half of stance by absorbing horizontal power from both legs, although some of this power was transferred to the trunk to propel it forward.

VAS, the primary contributor to lateral control in the first half of stance, absorbed power from the

trunk and transferred some power from the trunk to the contralateral leg (Fig. 1: Mediolateral Power). While this decelerated the trunk's lateral motion, it accelerated the contralateral leg's medial motion which accelerated the overall body laterally. The anterior compartments of gluteus medius and minimus (GMEDA), the primary contributor to medial control in the first half of stance, generated power to the trunk and initially transferred some power from the ipsilateral leg to the trunk prior to generating power to the ipsilateral leg. While this accelerated the trunk laterally, it also decelerated and then accelerated the ipsilateral leg's lateral and medial motion, respectively. During the second half of stance, most of the power distributed by the muscles was very small (not shown).

During pre- and early swing, iliacus (IL) generated power to the ipsilateral leg and transferred power from the trunk to the ipsilateral leg (Fig. 1: Net Power). In contrast, VAS absorbed power from the ipsilateral leg and transferred power from the ipsilateral leg to the trunk. During late swing, tibialis anterior (TA) generated power to the ipsilateral leg while SOL absorbed power from the ipsilateral leg in preparation for contact with the ground.

The plantarflexors, knee extensors, hip extensors and hip abductors were found to work in synergy to accomplish the biomechanical subtasks of stair ascent, with additional contributions from the dorsiflexors and hip flexors to leg swing. By understanding the function and coordination of these muscle groups, targeted rehabilitation programs can be designed to improve an individual's ability to ascend stairs.

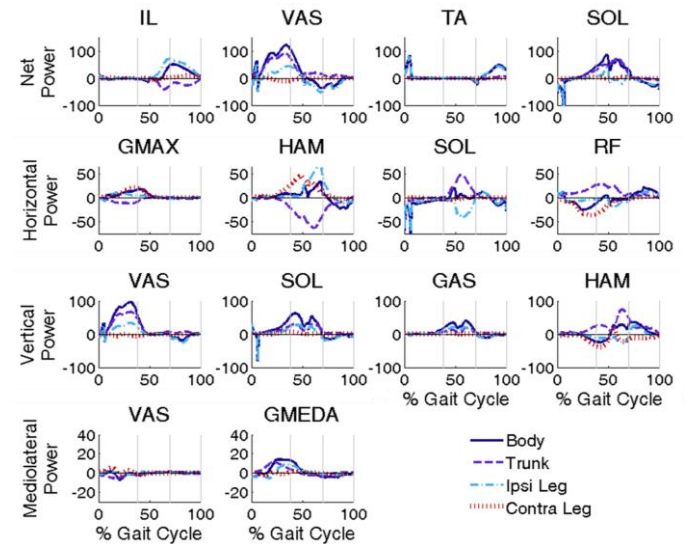


Figure 1: Net, Horizontal, Vertical and Mediolateral mechanical power distributed to the body, trunk, ipsilateral leg and contralateral leg by the primary muscle contributors to the biomechanical subtasks of stair ascent.

REFERENCES

1. McFadyen, BJ and Winter, DA. *J Biomech* **21**, 733-744, 1988.
2. Peterson, CL, et al. *J Biomech* **43**, 2348-2355, 2010.
3. Neptune, RR, et al. *Gait Posture* **19**, 194-205, 2004.
4. Silverman AK and Neptune RR. *J Biomech* **45**, 2271-2278, 2012.

ACKNOWLEDGEMENTS

This study was supported by an NSF Graduate Research Fellowship (DGE-1110007). The views expressed herein are those of the authors and do not reflect the official policy or position of the Brooke Army Medical Center, the U.S. Army Medical Department, the U.S. Army Office of the Surgeon General, the Department of the Army, Department of Defense or the U.S. Government.

Table 1: The primary positive and negative contributors (listed in order) to vertical propulsion, horizontal propulsion (+ forward propulsion; - braking), mediolateral (ML) control (+ lateral; - medial), and leg swing.

Subtask	First half of stance		Second half of stance			
	(+) Contributor	(-) Contributor	(+) Contributor	(-) Contributor		
Vertical Propulsion	VAS, GMAX, SOL GMEDP, GMEDA		SOL, GAS	HAM		
Horizontal Propulsion	GMAX, TA, VAS, GMEDP, GMEDA	SOL, RF, GAS, TFL	HAM	RF, VAS		
ML Control	VAS	GMEDA, GMEDP	HAM, AL	GMEDP, GMEDA		
	Pre-swing		Early Swing		Late Swing	
	(+) Contr.	(-) Contr.	(+) Contr.	(-) Contr.	(+) Contr.	(-) Contr.
Leg Swing	IL, GAS, HAM, AL	VAS, GMEDA	IL, HAM	VAS, GMEDP	TA, IL, RF	SOL, GMEDP, HAM, GAS

BIOMECHANICAL CHANGES DURING STAIR CLIMBING AT THE KNEE, HIP, AND TRUNK AFTER TOTAL KNEE ARTHROPLASTY

Jacqueline Lewis, Gregory Freisinger, Laura Schmitt, Robert Siston, and Ajit Chaudhari

The Ohio State University, Columbus, OH, USA
email: lewis.1127@osu.edu

INTRODUCTION

Osteoarthritis (OA) is the most common cause of disability in the United States and its prevalence continues to increase [1]. Total knee arthroplasty (TKA) is used to treat end-stage knee OA and is generally considered successful; however, patients with OA and TKA tend to have decreased stair climbing performance compared to healthy adults [2].

Peak knee adduction moment (pKAM) provides an estimate of the balance between the medial and lateral compartments of the knee. Higher pKAM is associated with medial compartment knee OA but is typically reduced to match those of healthy controls after TKA [3]. Peak knee flexion angle (pKFA) and peak knee flexion moment (pKFM) are typically less in knee pathology populations compared to healthy controls [4]. Increased trunk lean is seen in OA and TKA populations and is thought to decrease demand at the quadriceps, but may also increase demand on the hip extensors [5, 6].

Although these abnormal kinematic and kinetic patterns are well defined in knee OA and TKA populations, it remains unknown whether TKA alters the biomechanics from the preoperative status, or if a patient's pre-TKA biomechanical adaptations persist after TKA. We hypothesized that the biomechanical variables would change after TKA to more closely match those of healthy controls. Specifically, pKFA and pKFM would increase, while pKAM, trunk lean, peak hip flexion angle (pHFA) and peak hip flexion moment (pHFM) would decrease after TKA.

METHODS

20 patients (7M / 13F, age: 59.4 ± 6.1 y, mass: 92.0 ± 14.3 kg, ht: 1.7 ± 0.1 m) with predominantly

medial compartment osteoarthritis were recruited by three orthopedic surgeons at The Ohio State University Wexner Medical Center and provided IRB-approved informed consent. All participants underwent a primary TKA, using a posterior stabilized (PS) prosthesis. (Zimmer, NexGen LPS Flex; Warsaw, IN). Biomechanical assessments were completed approximately 1 month before and approximately 6 months following surgery.

During the biomechanical assessment, each patient performed stair ascent and descent trials foot over foot on a custom made 3-step staircase (tread depth: 25.5 cm, tread height: 20 cm). The first two steps of the staircase were attached to force plates (Bertec 4060-10; Columbus, OH) embedded in the floor to capture stair climbing ground reaction forces at 1500 Hz. A modified point-cluster marker set in conjunction with a functional hip joint center was used to calculate lower extremity kinematics for the involved limb (10 Vicon MX-F40; Oxford, UK). Marker and force data were filtered with fourth order low-pass Butterworth filters at a cutoff frequency of 6 Hz. All moments were expressed as externally applied to the joint of interest and were normalized by body weight times height. Forward trunk lean angle was calculated using the vector created by the markers placed on the 10th thoracic and 7th cervical vertebrae relative to global vertical axis in the sagittal plane.

Only 17 of the 20 study patients (6M / 11F, age: 59.5 ± 6.5 y, mass: 91.8 ± 14.2 kg, ht: 1.7 ± 0.1 m) were able to descend the staircase foot over foot. Paired t-tests were used to test for a difference between each variable of the involved limb during stair ascent and descent, before and after TKA.

RESULTS AND DISCUSSION

During both stair ascent and descent, pKAM significantly decreased after TKA (Table 1), suggesting that TKA results in a more equally distributed load between the medial and lateral compartments. Although there was a significant change in pKFA and pKFM during stair ascent, the change was a decrease, which contradicted our hypothesis (Table 1). Hip biomechanics and trunk lean during both stair ascent and descent, and sagittal plane knee biomechanics during stair descent did not change after TKA (Table 1).

The results of this study suggest that many biomechanical adaptations utilized by patients with knee OA persist after TKA. It is possible that these biomechanical adaptations persist due to neuromuscular adaptations learned during the progression of OA that are not easily changed. Quadriceps strength deficits are still visible six months after TKA, and therefore, the trunk lean and hip extensors may still be used to compensate for quadriceps weakness. Clinicians should be aware of these potential adaptations when a patient increases stair climbing speed, and may want to focus on decreasing trunk lean during stair climbing, thereby decreasing the role of the hip extensors, and increasing the role of the knee extensors. This could promote more normal knee biomechanics and ultimately improve stair climbing ability after TKA.

In addition to the measurement and estimation limitations associated with optical motion capture, force platforms and inverse dynamics, a potential limitation of this study is the fact that all participants received a PS prosthesis. Changes in femoral rollback have previously been observed

with PS designs [5], but the *in vivo* functional consequences of altered femoral rollback remain an avenue for future investigation.

CONCLUSIONS

TKA using a PS prosthesis yielded sagittal plane stair climbing biomechanics that were not different from the biomechanics observed before surgery. The only result that supported our hypothesis was in the frontal plane where pKAM did decrease after TKA, indicating that intraoperative realignment and soft-tissue balancing corrected the varus deformity associated with medial compartment OA. Clinicians may want to focus decreasing the amount of trunk lean in patients with TKA to promote more normal kinematic and kinetic patterns. Further analysis is needed to differentiate between biomechanical adaptations used by patients with OA that persist after surgery and those that form due to the surgery itself.

REFERENCES

1. MMWR Morb Mort Wkly Rep, **59**, 1261-5, 2005.
2. Bade MJ, et al. *J Orthop Sports Phys Ther* **40**(9), 559-67, 2010.
3. Mandeville D., et al. *Clin Biomech*, **23**(8), 1053-8, 2008.
4. Andriacchi TP, et al. *J Bone & Joint* **62-A**, 749-757, 1980.
5. Asay JL, et al. *J Orthop Res* **27**(3), 325-9, 2009.
6. Andriacchi TP, et al. *J Arthro*, **1**(3), 211-9, 1986.

ACKNOWLEDGEMENTS

Funding from NIAMS, award number R01AR056700 supported this study.

Table 1: Mean±StDev for OA and TKA variables with p-value of the paired t-test

Variable	Ascent (n=20)			Descent (n=17)		
	OA	TKA	p-value	OA	TKA	p-value
pKFA (°)	72.7±5.8	68.4±5.8	0.009*	89.3±4.4	87.4±7.8	0.422
pKFM (%bw*ht)	4.0±1.1	3.1±1.3	0.039*	5.2±1.3	4.6±1.2	0.098
pKAM (%bw*ht)	2.5±1.2	1.9±1.1	0.005*	3.0±1.5	1.8±1.1	<0.001*
pHFA (°)	73.0±5.8	70.8±4.9	0.213	33.3±7.5	32.4±7.4	0.677
pHFM (%bw*ht)	5.9±1.0	6.4±1.3	0.122	1.8±1.3	2.0±1.1	0.357
Trunk Lean (°)	26.6±7.6	23.5±5.9	0.211	14.8±5.7	13.4±5.5	0.312

SIMULATED HIP ABDUCTOR STRENGTHENING REDUCES PEAK JOINT CONTACT FORCES DURING STAIR DESCENT IN PATIENTS WITH TOTAL HIP ARTHROPLASTY

¹Casey A. Myers, ¹Peter J. Laz ¹Kevin B. Shelburne, ²Dana L. Judd, ²Cory L. Christiansen,
²Jennifer E. Stevens-Lapsley, ¹Bradley S. Davidson

¹Center for Orthopaedic Biomechanics, University of Denver, Denver, CO, USA

²Physical Therapy Program, University of Colorado, Aurora, CO, USA

email: casey.myers@du.edu

INTRODUCTION

Rehabilitation following total hip arthroplasty (THA) is designed to reduce the impairments associated with the surgery and to optimize overall functional recovery. It is common for lower extremity muscle strength training to be a focus of rehabilitation as strength deficits can decrease overall function. Through the use of rehabilitation, investigators have reported improvement in muscle strength in the first six months of recovery compared to preoperative values. Typical strength gains ranged from 0-30%, with more common gains of 15-20% [1]. While strength deficits relative to the uninvolved side may persist, early stage strength gains may be beneficial to long-term function and in reducing the loading experienced by the implant.

The strength of the hip abductor muscle group is an important predictor of overall function following THA. This may be due to its influence on the internal joint contact force (JCF), where excessive forces associated with muscle weakness [2] can lead to loosening of the implanted components and overall functional deficits [3]. Targeting deficits in this muscle group may improve functional recovery following surgery. However, the relationship between hip abductor strength and JCF has not been fully investigated, particularly during tasks with high muscle demand. Additionally, identifying which abductor muscles have the most impact on JCF can direct rehabilitation strategy and inform surgical approach. The purpose of this study was to investigate the effects of simulated increases in hip abductor strength following rehabilitation on JCFs during stair descent.

METHODS

Five patients who had undergone THA (2 M, 3F; age: 63±7.5 yrs; BMI: 27.5±2.0) participated in a laboratory testing session that consisted of lower

extremity maximum isometric strength tests and a stair descent task from a height of 20 cm as part of a larger study. Subject-specific musculoskeletal models were created by scaling a model that included detailed hip musculature [4] to segment dimensions and mass. Additionally, the subject-specific muscle maximum isometric strength values of each model were scaled to minimize differences between model-predicted and measured preoperative maximum isometric joint torques in hip flexion, extension, and abduction as well as knee flexion and extension.

A baseline forward dynamic simulation of each subject performing the stair descent was constructed using their corresponding subject-specific model to predict JCFs at the ankle, knee, hip, and low back. The hip abductor muscle strength for gluteus medius (glut med), gluteus minimus (glut min), anterior section of the gluteus maximum (glut max), tensor fasciae latae (tfl), piriformis (piri) and gemellus (gem) were then increased relative to baseline in a probabilistic framework using the advanced mean value method [5]. A range of possible strength increases was simulated with a mean of 15% and a standard deviation of 5% to result in a $\pm 3\sigma$ range of 0-30% of possible increase in abductor muscle strength.

The output range of peak JCF at each joint was generated by calculating the values with 0.5% (lower) and 99.5% (upper) probability. Muscle strengths were individually varied to calculate sensitivity factors from the advanced mean value method, which quantify the relative impact of increased strength of each muscle on the peak JCF.

RESULTS AND DISCUSSION

Simulated hip abductor strengthening resulted in peak JCFs at lower and upper probabilities that

were reduced relative to baseline for all five patients at the hip (18.9-23.8±16.5%) and knee (20.5-23.8±11.2%). Four of the five patients had reductions at the ankle (7.1-8.5±11.3%) and low back (3.5-7.0±5.3%) with one patient demonstrating no change. Reductions at the ankle and low back were smaller than the hip and knee, but demonstrate the ability of the hip abductor group to influence loading at these joints in some patients (Table 1). The large variability in percent reduction in JCF was associated with preoperative strength. In general, patients with weaker preoperative strength resulted in the greatest reductions in JCF in response to simulated strengthening.

Simulated strengthening resulted in a redirection of JFCs at the lower extremity joints as demonstrated by changes to the force components. The largest differences occurred in the vertical component at each joint and accounted for 82.5±13.1% of the JCF reductions, on average (Table 1).

The two posterior sections of the gluteus medius had a 20.3% greater effect on low back JCF than any other joint, while the anterior section had 46.3% greater effect on knee JCF than any other joint.

The smaller muscles (tfl, gem) had the greatest influence overall for the relative increase in hip strength. Knee JCFs demonstrated sensitivity factors of 0.24±0.8 and 0.26±0.8 for the tfl and gem, respectively, and were the highest of any muscle-joint relationship. However, sensitivity factors varied between subjects, likely due to differences in anthropometry and stair descent kinematics that can influence moment arm and muscle mechanics.

CONCLUSION

Simulated strengthening of the hip abductor muscle

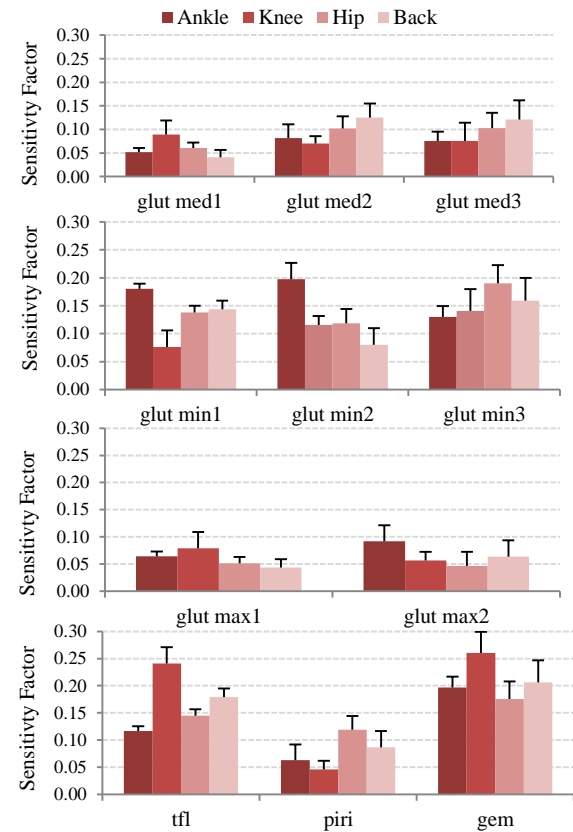


Figure 1: Sensitivity factors for hip abductor muscles with respect to ankle, knee, hip and low back joint contact forces.

group produced reductions in JCF when muscle demand was high, which indicates that targeting this muscle group in early THA rehabilitation may lead to higher overall patient function with reduced JCF on the implant. In addition, JFC was most sensitive to simulated strengthening in what may be considered minor muscles of the hip, and may play an important role in surgical approach and rehabilitation planning.

REFERENCES

1. Judd, DL. *Clin Orthop Relat Res*, **472**, 654-664, 2014.
2. Valente, G. *J Biomech*, **46**, 2186-2193, 2013.
3. Di Monaco, M. *Eur J Phy Rehab Med*, **45**, 303-317, 2009.
4. Shelburne, K. *Trans Annu Meet Orthop Res Soc*, 0149-6433, 2010.
5. Laz, P. *J Eng Med*, **224**, 927-943, 2010.

Table 1: Mean (SD) joint contact forces in body weight for ankle (A), knee (K), hip, (H) and low back (B) in anterior-posterior (x), vertical (y), and medial-lateral (z) components across 5 subjects. Included is the difference between the lower and upper (L/U) probability levels.

	Ax	Ay	Az	A	Kx	Ky	Kz	K	Hx	Hy	Hx	H	Bx	By	Bz	B
Baseline (pre-op)	-0.31 (.31)	-3.36 (.68)	-0.34 (.38)	3.64 (1.05)	0.21 (.77)	-3.42 (1.35)	-0.31 (.26)	3.51 (1.36)	0.03 (.50)	-3.30 (.34)	0.81 (.31)	3.43 (.38)	0.08 (.08)	1.56 (.60)	0.04 (.06)	1.56 (.60)
Lower (0.5%)	-0.33 (.31)	-3.25 (.67)	-0.30 (.33)	3.53 (.93)	0.22 (.71)	-2.65 (.92)	-0.22 (.19)	2.84 (.86)	0.19 (.35)	-2.61 (.37)	0.65 (.16)	2.80 (.45)	0.07 (.07)	1.51 (.65)	0.06 (.06)	1.51 (.65)
Upper (99.5%)	-0.35 (.31)	-3.28 (.67)	-0.31 (.33)	3.50 (.93)	0.19 (.69)	-2.76 (.82)	-0.24 (.19)	2.73 (.96)	0.16 (.35)	-2.71 (.44)	0.59 (.15)	2.70 (.40)	0.06 (.07)	1.46 (.66)	0.05 (.06)	1.46 (.66)
L/U Diff	0.02	0.03	0.01	0.04	0.03	0.10	0.02	0.11	0.04	0.10	0.05	0.10	0.01	0.05	0.01	0.05

LONGITUDINAL EVALUATION OF POSTURAL STABILITY IN BREAST CANCER PATIENTS TREATED WITH TAXANE-BASED CHEMOTHERAPY

¹ Scott M. Monfort, ² Maryam B. Lustberg, ² Robyn Patrick, ¹ Xueliang Pan, and ¹ Ajit M.W. Chaudhari

¹ The Ohio State University, Columbus, OH, USA

² The Ohio State University Comprehensive Cancer Center, Columbus, Ohio, USA

email: monfort.30@osu.edu **web:** <http://u.osu.edu/osusportsbiomechanics/>

INTRODUCTION

Chemotherapy-induced peripheral neuropathy (CIPN) is a neurotoxic side effect of several classes of common chemotherapy agents including taxanes. CIPN is associated with a decreased quality of life due to symptoms including pain and impaired function [1]. Similar to peripheral neuropathies in other populations, an increased risk of falling has been observed in patients with CIPN that suggests underlying balance deficits are likely present [2,3]. However, it is unknown how these balance deficits progress as patients proceed through chemotherapy. Establishing the natural history of postural instability in this population may elucidate balance parameters that are able to identify patients early in treatment who are likely to subsequently develop severe symptoms. Improved ability to quantify the effects of CIPN may also better enable researchers to evaluate and develop effective interventions that have remained elusive to date.

The purpose of this pilot study was to establish the feasibility of implementing quantitative, objective balance measures into the clinical setting. We proposed to gain insight into the natural history of postural instability in breast cancer patients being treated with taxane-based chemotherapy.

METHODS

At the time of analysis, 29 breast cancer patients (f/m = 28/1; age = 47.1 ± 11.2 years; mass = 75.1 ± 20.3 kg; height = 1.64 ± 0.08 m) being treated with taxane-based chemotherapy for the first time had been accrued for this study after providing IRB-approved informed consent.

Patients were assessed at 5 timepoints: within 1 month of starting chemotherapy (timepoint 1), at the

beginning of subsequent chemotherapy cycles (timepoints 2-4), and 1-3 months after completing their chemotherapy regimen (timepoint 5). At each visit, patients filled out patient-reported outcomes and performed balance and gait tasks. All data was collected by trained clinical research coordinators in the clinic where the patients were receiving treatment. Balance tasks consisted of quiet standing with eyes open (1 trial for 30 sec), quiet standing with eyes closed (1 trial for 30 sec), limits of stability (1 trial), functional reach with foot (5 trials for maximum distance), and functional reach with hand (3 trials for maximum distance), as shown in Figure 1.

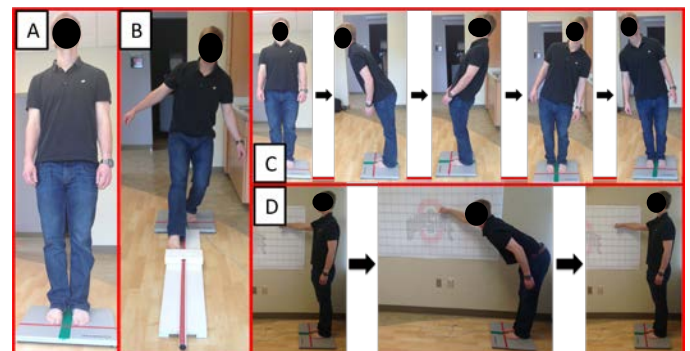


Figure 1. Standing balance tasks collected in the clinic. A. Quiet standing; B. Functional reach with foot; C. Limits of stability; D. Functional reach with hand.

Quiet standing consisted of patients standing as still as possible with their arms relaxed at their sides. The limits of stability task involved patients leaning forward, backward, left, and right as far as possible without losing their balance or picking their feet off of the balance plate. For the functional reach with foot task, patients were asked to balance on their left foot and push a slider as far as possible with their right foot in a single controlled motion. For the hand reaching task, patients reached with a locked elbow and closed fist along a graduated poster with

both feet flat on the balance plate. Foot measurements and standardized positioning enabled estimation of each patient's boundaries of support.

Center of pressure (CoP) data was collected during all balance tasks through a Bertec BP5046 balance plate. A custom LabVIEW interface was developed to guide clinical personnel through the protocol and collect CoP data. Processing of balance data was performed through custom Matlab scripts with all CoP data low-pass filtered at 20 Hz using a 4th order Butterworth filter. Preliminary analysis of the data was performed using linear mixed model least squares means for repeated measures to estimate changes in balance parameters over time.

RESULTS AND DISCUSSION

The results of this pilot study support the feasibility of implementing balance measures into a clinical setting to quantify postural instability in breast cancer patients. Testing in the clinic was performed without interfering with normal operations. At the time of analysis, patients were at varying stages of the study with more than half of the patients having completed timepoint 4. Five of the 29 patients dropped out of the study (n=4 after timepoint 1, n=1 after timepoint 2). The preliminary results presented here are for the quiet standing with eyes closed task at timepoints 1-4 using 95% confidence ellipse area of CoP trajectory. Progressive increases in ellipse area were observed, as shown in Figure 2.

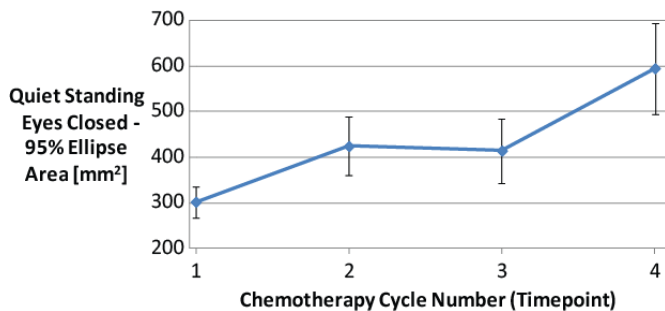


Figure 2. Least squares means \pm standard error of 95% ellipse area during eyes closed task.

An increase in ellipse area was observed as early as timepoint 2. Changes between timepoints are presented in Table 1.

Table 1. Change in 95% confidence ellipse area from timepoint 1 during quiet stance with eyes closed.

Timepoint Comparison	% Change from Timepoint 1	p-value
1→2	40%	0.046
1→3	37%	0.058
1→4	97%	0.004

Higher 95% confidence ellipse areas have been associated with balance deficits [4]. The changes observed in this pilot study suggest that patients become progressively less stable as they continue through chemotherapy treatment. This result is consistent with a loss of proprioception and/or vestibular acuity. Further analysis will be conducted after completing testing of the breast cancer cohort including comparing changes in balance measures with changes in patient-reported CIPN symptoms. Future research will evaluate this approach in other cancer populations as well as in a larger sample of breast cancer patients to further assess the scope of these findings.

CONCLUSIONS

Balance testing in the clinical setting with trained clinical personnel was conducted in this pilot study, which supports the feasibility of this approach. Preliminary analysis showed a progressive increase in 95% confidence ellipse area during quiet stance with eyes closed.

REFERENCES

1. Ocean AJ, Vahdat LT. *Support Care Cancer* 12(9):619-625, 2004.
2. Toftagen C, et al. *Support Care Cancer* 20:583-589, 2012.
3. Richardson, JK, Hurvitz EA. *J of Gerontol A Biol Sci Med Sci*. 50A(4) M211-M215, 1995.
4. Prieto TE, et al. *IEEE Trans Biomed Eng*. 43(9):956-966, 1996.

ACKNOWLEDGEMENTS

We would like to thank our funding sources:

- NCI R03 CA182165-01
- NSF GRF DGE-13430

BALANCE CONTROL DURING REACTIVE STEPPING: THE EFFECT OF INCREASED PASSIVE TRUNK AND HIP STIFFNESS

Tyler B. Weaver and Andrew C. Laing

Department of Kinesiology, University of Waterloo, Waterloo, Ontario, Canada
Injury Biomechanics and Aging Laboratory, University of Waterloo, Waterloo, Ontario, Canada
E-mail: tweaver@uwaterloo.ca

INTRODUCTION

Age-related changes in the control of the trunk and hips may be one factor influencing fall-risk in older adults. Previous research suggests that older adults exhibit greater trunk stiffness compared to young adults [1], with abnormal trunk movement after a perturbation [2]. Increased trunk stiffness could help to resist gravitational effects, but it could also inhibit compensatory movements after a balance perturbation. Therefore, it is of interest to determine how increased passive stiffness of the trunk and hips influences balance control during a reactive forward step. It was hypothesized that increased passive stiffness would result in detriments during a reactive step, inferred through changes in the centre of mass (COM) displacement and ground reaction forces.

METHODS

Sixteen young adults participated in the study (mean (SD) age: 22.5 (2.5) y; height: 1.70 (0.10) m; mass: 68.4 (9.7) kg). Balance perturbations were applied using a tether-release paradigm, which required participants to react with a forward step and hold their final position for ten seconds. Separate tethers attached to each hip allowed for three perturbation directions to be applied: 1) forward; 2) forward-left rotation; 3) forward-right rotation. Starting foot-position for all participants was standardized to 50% of hip-width. All participants assumed an initial lean position equivalent to 15% of body weight, monitored in real-time. Instructions were provided to

participants to lean forward as one rigid segment above the ankles with their arms crossed over their chest, and to let the tethers and harness support their body weight.

Three-dimensional kinematics were collected using a four-bank Optotrak Certus system (NDI, Waterloo, ON) at 100 Hz, and used to calculate the whole body COM position via an 11-segment model in the anterior-posterior (AP) and medio-lateral (ML) directions. Forces from each reactive step were measured using a floor-mounted force platform (AMTI, Watertown, MA) at 2000 Hz. Passive stiffness was increased using a rigid, plastic “corset” which crossed the hips and extended upwards to the xiphoid process. Movement was restricted in both the sagittal and frontal planes.

First, a point of equilibrium, referred to as the ‘restabilisation’ point, was calculated as the point when the COM velocity waveform entered and remained inside an amplitude bandwidth bordered by two standard deviations of the mean velocity during the last two seconds of the trial [3]. In order to calculate the maximum COM displacement after a step, the ‘restabilisation’ point established after foot-contact was subtracted from both the maximum global AP and ML COM values observed after foot-contact. To compare the size of ‘restabilisation’ displacement between the corset and no corset conditions, the starting COM position (prior to the onset of a tether-release) was also subtracted from ‘restabilisation’ point for each condition to

determine if differences existed between conditions regarding where participants established their new equilibrium after foot-contact (referenced to their COM position at the start of the trial).

Accordingly, the following dependent variables were calculated: 1) maximum AP and ML COM displacement after foot-contact (as defined above) ($COM_{MaxDisp}$); 2) the size of AP and ML COM 'restabilisation' displacement, referenced to the COM start ($COM_{RestabSize}$); 3) AP and ML ground reaction forces at the maximum COM position after foot-contact (GRF). For all metrics means and standard deviations (representing within-subject trial-to-trial variability) were computed and compared. Standard deviation was included as a measure of variability as existing research has reported that variability is larger in older adults [4].

RESULTS AND DISCUSSION

AP COM Movement: AP $COM_{MaxDisp}$ was 36% larger (i.e., forward) with the corset (7.3 cm) vs. without (5.3 cm) ($p=0.002$). The corset also caused AP $COM_{MaxDisp}$ to be 28% more variable compared to the no corset condition ($p=0.015$).

In the AP direction, $COM_{RestabSize}$ was influenced by a corset x perturbation direction interaction ($p<0.001$). Post-hoc analysis revealed that for both the forward-left and forward-right perturbations the $COM_{RestabSize}$ was smaller with the corset vs. without (left: $p=0.003$, 26% smaller; right: $p=0.007$, 25% smaller). AP $COM_{RestabSize}$ was also 22% more variable with vs. without the corset ($p=0.049$).

ML COM Movement: ML $COM_{MaxDisp}$ was not different ($p=0.689$) or more variable ($p=0.918$) between corset and no corset conditions. Further, in the ML direction, $COM_{RestabSize}$ was not statistically different ($p=0.126$), although the corset mean (3.6 cm) was 65% smaller than the no corset mean (10.2 cm) (i.e., smaller = closer to the step leg). ML $COM_{RestabSize}$ was not more variable with vs. without the corset ($p=0.767$).

AP Ground Reaction Forces: AP GRFs were 31% smaller with the corset, compared to without ($p=0.004$). However, AP GRF variability was not different between corset conditions ($p=0.657$).

ML Ground Reaction Forces: ML GRFs were influenced by a corset x perturbation direction interaction ($p=0.031$), where for a forward-right perturbation, the corset condition resulted in a 16% larger ML GRF, with no difference for the other two perturbation directions. The ML GRFs were not more variable with or without the corset ($p=0.315$).

Overall, balance control after foot-contact is influenced by increased passive trunk/hip stiffness. With the corset, participants adopted an AP 'restabilisation' point which was closer to the pre-perturbation AP COM position. Perhaps the stiffness resulted in less trunk flexion during this period with the end result of COM being located more posterior. This may also explain the reduced AP GRFs which were used by participants after foot-contact. In the ML direction, the almost 7 cm mean difference in COM_{Restab} suggests that while wearing the corset, participants adopted a 'restabilisation' point closer to their step leg. Interestingly, when maximum ML COM values were referenced to the starting ML COM position, the corset resulted in 35% greater ML COM movement towards the step leg ($p=0.036$) compared to the no corset condition.

To conclude, increased passive trunk/hip stiffness influences balance recovery after foot-contact. However, researchers should be cognisant of how different methods of reporting COM movement can influence their results. Moving forward, research is needed to determine how increased stiffness influences balance after foot-contact in older adults.

REFERENCES

1. Allum JHJ, et al. *J Physiol* **542**, 643-663, 2002.
2. Troy KL, et al. *Gait & Posture* **28**, 461-465, 2008.
3. Singer JC, et al. *Gait & Posture* **35**, 106-110, 2012.
4. Singer JC, et al. *Gait & Posture* **38**, 679-683, 2013.

IMPROVING NEUROPATHIC GAIT AND BALANCE VIA SENSORY SUBSTITUTION

¹ Jay Bauman, ¹ Marc LeVangie, ¹ Sandro Nigg, ^{2,3} Breanne Everett, and ¹ Benno Nigg

¹ The University of Calgary, Calgary, AB, Canada

² Orpyx Medical Technologies Inc., Calgary, AB, Canada

³ The University of Calgary, Department of Surgery, Section of Plastic Surgery, Calgary, AB, Canada

email: jmbauman@ucalgary.ca

INTRODUCTION

Peripheral neuropathy (PN) is a condition characterized by nerve impairment in the distal extremities. PN can result in debilitating problems with balance and walking, putting these patients at an increased risk of falls [1]. A class of medical technologies termed “sensory substitution systems” (SSS) aims to utilize neuroplasticity — the capacity of the central nervous system to rewire neural pathways — to restore lost sensory function. The goal of a SSS is to collect information on behalf of a deficient sensory modality and convert it into a form that can be perceived by the patient [2].

Orpyx Medical Technologies Inc. has developed a SSS to replace lost sensory function in the feet. As the user walks, plantar pressures are measured in real time by insoles worn in the shoes. The magnitude and spatial position of the plantar pressures are wirelessly transmitted to a belt worn around the subject’s lower back. Motors within the belt vibrate in correspondence with each pressure sensor to create a mapping of the feet on the back.

We hypothesized that after four weeks of training with this novel SSS device, subjects would exhibit improvements in gait and balance parameters, and further, that any changes in gait and balance would then disappear after a four-week washout period without the device.

METHODS

Eight individuals diagnosed with PN were recruited (6 male, 2 female; 69.3 ± 9.6 years). All participants provided written informed consent in accordance with the University of Calgary’s Conjoint Health

Research Ethics Board. Each subject made six visits to the Human Performance Lab for periodic gait and balance assessment (Table 1).

Table 1: Timeline of assessments

Stage	Time (Weeks)
1. Familiarization	-1
2. Baseline	0
3. Mid-Training	2
4. Post-Training	4
5. Mid-Washout	6
6. Post-Washout	8

Each subject was initially fitted for the device and familiarized with the measurement protocols before actual testing. After baseline measurements at the subsequent visit, subjects were given the SSS device to take home for a four-week training period. They were requested to use it actively (ambulating) at least one hour per day with no upper limit to its use. Subjects returned the device after the post-training session, and were not exposed to it for the ensuing four-week “washout” period.

Balance was assessed through distance travelled by the center of pressure (CoP) during quiet standing. Ground reaction forces were recorded on a force plate sampling at 2400 Hz (Kistler Instruments AG). Subjects executed three different postural conditions (eyes open, narrow stance, eyes closed) for each of two device conditions (power on, power off). Gait was assessed through stride frequency and its variability in the form of coefficient of variation (CV). Subjects walked a 44m path twice for each device condition (on, off) while wearing a set of instrumented insoles that recorded plantar pressures at 100 Hz (Pedar-X, Novel). A training effect was

defined as a significant interaction between time and device condition in a two-way ANOVA.

RESULTS AND DISCUSSION

For the eyes closed balance task, the CoP path length was significantly shorter while standing with the device in the on condition compared to the off condition across all time points ($F=11.9$, $p<0.03$). There was no significant training effect (improvement over time) for balance (Fig. 1).

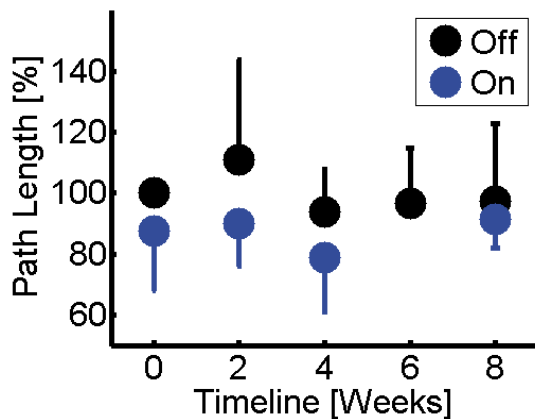


Figure 1: Normalized changes in CoP path length over time while standing with eyes closed.

Across all time points, the CV of stride frequency was significantly smaller while walking in the on condition compared to off ($F=21.7$, $p<0.01$). In addition, the mean stride frequency was significantly higher while walking in the on condition compared to off ($F=12.1$, $p<0.02$). There was no significant training effect of the device for stride variability during walking (Fig. 2).

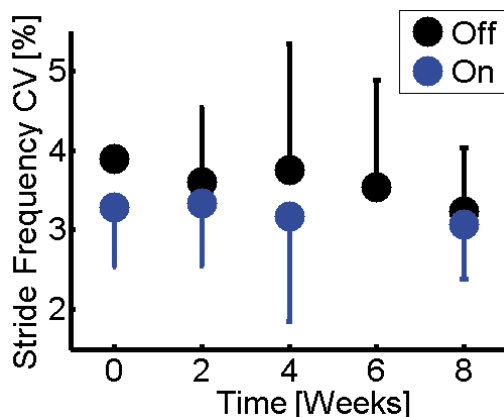


Figure 2: Changes in coefficient of variation of stride frequency over time while walking.

There were significant differences between on and off conditions independent of time, which suggests this device can elicit instantaneous improvements in balance and gait. More stable balance was observed in shorter CoP path lengths while standing with eyes closed. Without visual feedback and with their own feedback from the feet compromised, subjects may have been primed to consciously detect the vibration response to large shifts in balance and perform appropriate postural corrections. Improved gait was evidenced by reduced variability in stride parameters as well as increased cadence, which are both associated with healthier walking in PN [3]. Changes in stride frequency during walking could be explained by locomotor rhythm entrainment to the oscillating left-right vibration signal.

It was anticipated that improvement in balance and gait would be the product of training, i.e. differences between the on and off conditions would change over time. Variability in training factors could explain why the instantaneous effects of the device were not enhanced through training. Subjects wore the device for 1-8 hours per day across a variety of activities. Moreover, the spatial position of the device may have been inconsistent due to potential mediolateral and craniocaudal movement relative to the subjects' bodies. The subject pool also featured a wide degree of PN severity (from 1-8 on the MNSI-B and 0-10 on the NDS inventories) and a range of PN etiologies, including diabetic, idiopathic, and chemotherapy-induced PN [4].

Users of this sensory substitution device exhibited instantaneous improvements in gait and balance. More regimented protocols are required to better assess its training effects over time. Manipulating locomotion and posture through augmented sensory feedback has broad potential applications in gait rehabilitation and skill acquisition.

REFERENCES

1. Lafond D, et al. *Diabetes Care* **27**, 173-178, 2004.
2. Bach-y-Rita P & Kercel SW. *Trends in Cognitive Sciences* **7**, 541-546, 2003.
3. Richardson J, et al. *Journal of the American Geriatric Society* **52**, 1532-1537, 2004.
4. Meijer J, et al. *Diabetes Care* **23**, 750-753, 2000.

POSTURAL CONTROL CHANGES ASSOCIATED WITH ANKLE-FOOT ORTHOSES IN INDIVIDUALS WITH PERIPHERAL NEUROPATHY

Kimberly E. Bigelow and Kurt Jackson

University of Dayton, Dayton, OH, USA
email: Kimberly.bigelow@udayton.edu

INTRODUCTION

Peripheral Neuropathy (PN) affects an estimated 8% of individuals aged sixty-five and older living in the community and up to 26.4% of those with Type II diabetes [1,2]. Individuals with PN often experience problems with balance and mobility and are more likely to fall [3]. Recently there has been some evidence that the use of ankle-foot orthoses (AFOs) may provide augmented feedback to individuals with sensory loss due to PN [4,5]. Developments in the design and manufacture of AFOs further this potential. Newer anterior shell carbon composite AFOs are lightweight and provide a large surface area of tactile contact over much of the shank. The limited work done to date in individuals with PN has largely concentrated on the effect of AFOs on static balance, with limited research focusing on dynamic aspects of balance and mobility. This seems especially important to consider because of the potential tradeoffs with regard to mechanical restrictions of the AFOs. Because of this, the aim of this study was to examine the effect of AFOs on individuals with PN on measures of posturography and clinical assessments of balance and mobility. It was hypothesized that AFOs would result in improved quiet-standing balance but would negatively impact tasks requiring leaning, rapid stepping, and other quick and dynamic movements.

METHODS

Twelve subjects with PN, who had not previously used AFOs, participated in this study (mean age: 75.1 ± 7.4 , mean body mass index: 28.7 ± 5.1). These subjects were screened to ensure significant sensory loss in the feet/lower legs (mean sensory threshold: 5.59 ± 1.03 , mean vibration values: 0.98 ± 1.41 on a scale of 0 to 8). For the aim of the study, individuals

were excluded if sensory loss was accompanied by notable deficits in range of motion or strength.

Participants were assessed in two conditions: while wearing non-articulated, rigid anterior shell carbon composite AFOs bilaterally (ToeOFF, Allard USA, Rockaway, NJ, USA) and while not wearing the AFOs (typical function). The order of these conditions was counterbalanced to reduce potential ordering effects. For the AFO condition, participants were guided in a series of brief exercises to become familiar with the AFOs.

In each condition, individuals underwent the same set of assessments. First, participants completed a quiet-standing posturography protocol. Participants stood on the force plate for 20 seconds at a time in four test conditions: eyes open and closed on the firm plate, and eyes open and closed on a foam pad placed on the plate. Each test condition was repeated three times, and anterior-posterior (A/P) and medial-lateral (M/L) center of pressure (COP) was collected. Participants then completed a Limits of Stability task on the flat plate, leaning as far forward, backward, left, and right as possible using an ankle strategy. A/P sway range, M/L sway range, and mean velocity were calculated for quiet-standing trials and averaged across the three trials of the same condition. A/P sway range and M/L sway range were calculated for Limits of Stability.

Clinical balance and gait assessments that required more dynamic movement were then conducted. Participants completed the Mini Balance Evaluation Systems Test (Mini-BESTest), walking speed assessment, and the Timed Up and Go (TUG). These assessments include tasks that an individual would regularly do in everyday life such as: standing up from a chair, rising on toes, compensatory stepping, and dynamic gait.

Paired t-tests were done to compare the with and without AFO conditions for the posturography measures, the gait speed assessment, and the TUG. Wilcoxon signed rank test was used to compare results of the Mini-BESTest. A significance of 0.05 was used for all testing.

RESULTS AND DISCUSSION

For the quiet-standing posturography assessments, statistical differences were found in the eyes closed, flat plate condition for both A/P sway range ($p=0.012$) and M/L sway range ($p=0.047$). In both cases, participants exhibited reduced sway ranges, indicating improved postural control in the AFO condition. Additionally, all parameters associated with eyes open on the firm plate, eyes closed on the firm plate, and eyes open on the foam pad revealed a similar, albeit non-statistically significant trend of reduced and slower sway while wearing the AFOs. The eyes closed, foam pad condition proved to be quite difficult for both AFO conditions. 8 of 12 subjects lost balance on at least one eyes closed, foam trial, limiting the ability to draw conclusions.

The findings of the quiet-standing assessment seemed to support that AFOs were helpful for individuals with sensory impairment. The Limits of Stability results, however, showed a significant reduction in anterior-posterior sway range when the AFOs were worn (146.78 ± 29.6 mm without to 128.03 ± 27.2 mm, $p=0.000$). This suggested that the AFOs provided mechanical rigidity that restricted how far an individual was able to lean. This has potential implications for tasks such as reaching into a high cabinet safely without losing balance.

The clinical and gait assessments results indicated no statistically significant differences in the mean values for the AFO versus non-AFO condition for any of the outcome measures. Individual performance, though, was quiet variable with the AFOs providing meaningful improvements to some and being detrimental to others. For example, on the Mini-BESTest, two individuals had scores that exceeded the minimal clinically important difference score of 4 points when they wore the AFOs (+4 points and +8 points), but the performance of another two was reduced by more

than the minimally important change value (-6 pts. And -5pts.). This suggests that these individuals experienced changes that would likely have functional implications and that for some individuals these changes associated with wearing the AFOs were positive, whereas for others they could be quite detrimental.

This work suggests that while AFOs may provide additional tactile feedback that improves standing balance, the mechanical restrictions associated with the brace may introduce additional trade-offs. The results of the clinical assessments, in particular, seem to suggest that different individuals may respond differently to AFOs. Future work should seek to determine the characteristics of those who benefit more from the AFOs than others and evaluate whether these differences lessen with time, use, and/or familiarization. Future work should also explore whether the sensory benefits seemingly observed in quiet-standing transfer to a reduction in fall incidence in individuals with PN.

CONCLUSIONS

Anterior-shell carbon fiber AFOs were found to significantly improve quiet-standing balance in individuals with peripheral neuropathy, especially when vision was compromised. Performance on tasks that required more dynamic movement was more variable with no group significant differences.

REFERENCES

1. Martyn CN, Hughes RA. *J Neurol Neurosurg Psychiatry* **62**, 310-318, 1997.
2. Davies M, et al. *Diabetes Care* **29**, 1518-1522, 2006.
3. DeMott TK, et al. *Am J Phys Med Rehabil* **86**, 125-132, 2007.
4. Rao N, Aruin AS. *Diabetes Res Clin Pract* **74**, 48-56, 2006.
5. Rao N, Aruin AS. *Neurorehabil Neural Repair* **25**, 110-117, 2011.

ACKNOWLEDGEMENTS

The authors thank Allard USA for providing the AFOs used in this study and Mark Horowitz, CPO

EFFECT OF SENSORY AUGMENTATION VIA SKIN STRETCH FEEDBACK ON QUIET STANDING BALANCE

Yi-Tsen Pan, Yoo-Seok Kim and Pilwon Hur

Mechanical Engineering, Texas A&M University, College Station, TX, USA
Email: {yitsenpan, yooseokteam, pilwonhur}@tamu.edu web: <http://hurgroup.net>

INTRODUCTION

Postural control and balance are two important factors to humans in performing activities of daily living (ADL). In the past two decades, studies [1] have shown that light touch (contact force less than 1N) of fingers on fixed surfaces can reduce postural sway during quiet standing and walking for people with or without dysfunction of sensory systems. With the help of additional sensory information from biofeedback, individuals with neurological impairments may improve their balance in ADL, which eventually can lead to enhanced quality of life. Recently, a portable sensory augmentation device was developed [2]. However, the efficacy of the device is not studied yet.

In this study, we examined whether augmented sensation at the fingertip via a newly developed portable sensory augmentation device (SAD) can modulate quiet standing postural sway. A closed-loop control strategy was implemented in this system for postural control. Furthermore, it is not known if the effect of sensory augmentation in balance enhancement depends on the availability of sensory modality. The objective of this study is to examine the effect of augmented sensation at the fingertip due to SAD on quiet standing balance of healthy young adults for various sensory modalities. It is hypothesized that augmented sensation enhances quiet standing balance more effectively when more sensory modalities are removed.

METHODS

Fifteen healthy young adults (four females and eleven males; mean age \pm s.d.: 26.4 ± 5.6 years) with neither neurological nor musculoskeletal impairments participated in this study. Subjects were asked to stand quietly on a force plate (OR6, AMTI, Watertown, MA) under three conditions of availability of sensation: i) eyes-open (EO), ii) eyes-closed (EC) and iii) tilting head backwards with eyes closed (ECHU). Subjects put SAD on their

right index finger (Fig. 1a). A belt enclosing an inertia measurement unit (IMU) (MPU-9150, InvenSense Inc., San Jose, CA) and an embedded control unit (myRIO, National Instruments, Austin, TX) was wrapped around waist of subjects (Fig. 1b). The details of SAD and control unit can be found at [2].

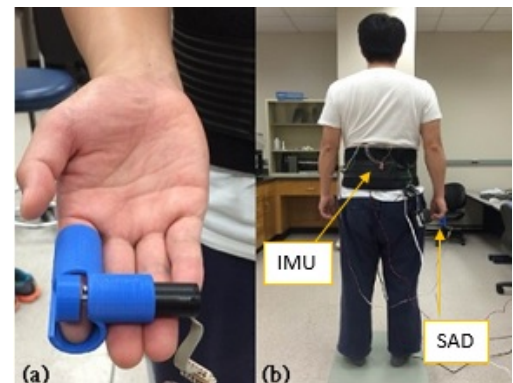


Figure 1: a) SAD, b) experiment setup

The experiments consisted of two parts: 1) practice session, and 2) main session. In the practice session, subjects were instructed to stand quietly on a force plate under three conditions of availability of sensation (EO, EC, and ECHU). The purpose of the session was to calibrate IMU by computing subject's reference angle while quietly standing, and to familiarize the subject with the testing environment. In the main session, subjects were asked to stand quietly on a force plate for 30s, with 10 repetitions for each sensory modality condition (EO, EC, ECHU) and SAD condition (on vs. off). Subjects were unaware of the function of SAD. Force plate data and pitch angle were sampled at 1kHz and 500Hz, respectively. Two-minute rests were given every five trials to avoid muscle fatigue.

SAD contactor was controlled by a position control where angular velocity of contactor was proportional to the angular deviation of pitch angle from the reference angle [2]. For example, when subject leaned forward (or backward) during quiet standing, the contactor rotated clockwise (or

counterclockwise) so that the fingertip pad was stretched backward (or forward). This way, the subject was provided augmented sensory feedback of his/her postural sway.

From the force plate data, center of pressure (COP) was computed. From COP data, several traditional parameters such as maximum distance (*MaxDist*), range (*Range*), and mean frequency (*MeanFreq*) in anterior-posterior (AP), medial-lateral (ML) directions were computed [3].

To study the effect of availability of sensation and SAD on quiet standing balance, a two-way repeated measures ANOVA was performed. Level of significance was set to $\alpha=0.05$ (SPSS, v21, Chicago, IL).

RESULTS AND DISCUSSION

Availability of sensory information significantly affected balance. *MaxDistAP*, *MaxDistML*, *RangeAP*, and *RangeML* indicated that postural sway was the smallest when all sensory information was available (EO), followed by when vision was lacking (EC), and followed by when both vision and vestibular information was deprived (ECHU) in both AP and ML direction (Table 1). These results agreed with previous studies that removing sensory information or challenging balance significantly increased postural sway [4].

Sensory augmentation due to SAD significantly affected balance. *MeanFreqAP* and *MeanFreqML* significantly decreased when sensory augmentation was provided (Table 1). *MeanFreq* is proportional to ratio of *Total Excursion* to *Mean Distance* or equivalently to ratio of *Mean Velocity* to *Mean Distance* [3]. This result suggests that sensory augmentation from SAD can reduce effective postural sway that cannot be captured by the mean values of postural sway.

Our hypothesis that the effect of sensory augmentation due to SAD will be more prominent

when less sensory modality was available was also supported. *MaxDistAP* and *RangeAP* had significant interaction effects between sensory availability and SAD. This interaction came from the fact that for EO/EC condition, SAD increased the mean values of *MaxDistAP* and *RangeAP* whereas for ECHU condition, SAD decreased the mean values of *MaxDistAP* and *RangeAP*.

One possible explanation is that sensory information during EO/EC conditions was enough to make stable balance whereas sensory information during ECHU condition was not enough to make stable balance so that additionally provided sensory augmentation could help improve balance.

Limitation of this study was as follows. Since SAD used position control and subject's reference angle kept changing over time during experiment, the quality of sensory feedback could be suboptimal. One possible solution would be applying velocity-based control where the reference angle does not affect the performance of SAD.

CONCLUSIONS AND FUTURE WORK

The efficacy of the developed sensory augmentation system via skin stretch feedback is evaluated. Our results indicate that the presence of additional sensory input helped maintaining balance when both visual and vestibular inputs were removed, substantiating our hypothesis. Future works include to 1) develop velocity-based controller (derivative control) and change the approach of obtaining the subject's reference angle, and 2) recruit groups of patients with impaired sensory systems to compare the quiet standing performance with normal subjects.

REFERENCES

1. Jeka JJ et al. *Physical Therapy* 77(5): 476-487, 1997
2. Kim YS et al. *ASB*, Columbus, OH. August, 2015 (Submitted)
3. Prieto TE et al. *IEEE Trans Biomed Eng* 43, 1996
4. Nashner et al. *J Neuroscience* 2(5): 536-544, 1982

Table 1: Measures of postural sway. Value represents mean (standard deviation). Superscript denotes significant differences from indicated main effect condition ($p < .05$).

Parameters	Available Sensory Modality			Sensory Augmentation		Interaction <i>p</i> -value
	EO (A)	EC (B)	ECHU (C)	With SAD (D)	No SAD (E)	
<i>MaxDistAP</i> (m)	.012 (.001) ^{BC}	.014 (.001) ^{AC}	.017 (.001) ^{AB}	.015 (.001)	.014 (.001)	.013
<i>MaxDistML</i> (m)	.006 (.0005) ^C	.006 (.001)	.007 (.001) ^A	.007 (.001)	.006 (.001)	.184
<i>RangeAP</i> (m)	.021 (.001) ^{BC}	.024 (.001) ^{AC}	.029 (.002) ^{AB}	.026 (.002)	.024 (.001)	.019
<i>RangeML</i> (m)	.010 (.001) ^C	.011 (.001)	.012 (.001) ^A	.011 (.001)	.011 (.001)	.181
<i>MeanFreqAP</i> (Hz)	.360 (.024) ^B	.395 (.022) ^A	.391 (.024)	.370 (.025) ^E	.395 (.021) ^D	.421
<i>MeanFreqML</i> (Hz)	.461 (.027)	.441 (.028)	.430 (.028)	.421 (.029) ^E	.466 (.025) ^D	.029

RECOVERY FROM HIP ABDUCTOR FATIGUE DURING STANDING IS INFLUENCED BY THE PRESENCE OF LOW BACK PAIN

Daniel Viggiani and Jack P. Callaghan

Department of Kinesiology, University of Waterloo, Waterloo, ON, Canada

INTRODUCTION

Muscle fatigue and pain are two factors often associated with musculoskeletal injury. Both muscle fatigue and pain are task-dependent^[1], therefore the specific interactions between muscle fatigue and pain will differ based on how fatigue and pain are generated. However, previous research approaches examining the fatigue-pain interaction have used methods that are rarely encountered outside of laboratory settings. This study's purpose is to determine how the pain developed during prolonged standing, interacts with a type of fatigue that is also frequently encountered in workplace settings – repetitive low-level muscular activity. The hip abductor muscle group was chosen as it is both relevant to postural control^[2] and the pain pathway^[3] reported during prolonged standing.

METHODS

Thirty participants (15 female) completed two, 2-hour standing sessions. During one of the sessions, participants performed a side-lying repetitive leg-raising exercise using their dominant leg just prior to the start of standing; the other session was used as a control session with participants completing 2 hours of prolonged standing work. The order of the sessions was randomized.

Surface electromyography (EMG) of bilateral gluteus medius was measured continuously while participants were standing. Raw EMG data was linear enveloped and expressed as a percentage of maximal isometric voluntary contraction. The normalized EMG data was used to compute cocontraction indices between the left and right gluteus medii^[3]. Self-reported levels of pain for the low back were recorded using 100 mm visual analog scales (VAS) prior to the start of and every 15 minutes during standing. VAS scores were used to classify participants as pain (PD) or non-pain (NPD) developers using a 10 mm minimum threshold based on control data^[3,4]. Participants were asked to

maximally abduct their dominant leg against isometric resistance provided by a tethered cuff positioned just above their femoral condyles. These abduction contractions (ABCs) occurred at time points 0, 1, 2, 3, 5, 10, 15, 30 minutes and every 15 minutes thereafter during the standing work. Force measures from the ABCs were normalized to a baseline ABC completed at least 5 minutes prior to the start of each standing session. The difference of normalized strengths between the control and fatigue sessions was then computed.

Paired t-tests were performed on cocontraction indices and ABCs with pain group as the independent variable. A mixed-model ANOVA with a within factor of session and between factor of pain group was performed on VAS scores.

RESULTS AND DISCUSSION

Twelve of 30 participants were classified as PDs (8 female) based on VAS scores. PDs had a trend of smaller cocontraction indices during the first 15 minutes of standing in the fatigue session (591.9 ± 777.9 %MVC) compared to the control session (854.4 ± 1216.9 %MVC; $p = 0.0736$). PDs also reported lower peak low back pain during the fatigue session (Figure 1), having a peak pain reduction of 8.6 mm (SD = 5.0 mm; $p < 0.0001$). Only 3 out of 12 PDs reported pain below the 10 mm threshold and as a whole, the PD group was still experiencing clinically significant levels of pain while standing^[4]. There was no difference in NPD pain reporting between control and fatigue sessions (mean difference: -0.7 mm; SD = 3.3 mm; $p = 0.3096$).

PDs had greater strength differences between control and fatigue sessions than NPDs at time points 30 minutes ($p = 0.0313$), 105 minutes ($p = 0.0264$) and 120 minutes ($p = 0.0111$; Figure 2). In the last 30 minutes of standing, PDs had a trend of

greater strength losses while standing while NPDs were able to recover strength losses (Figure 2).

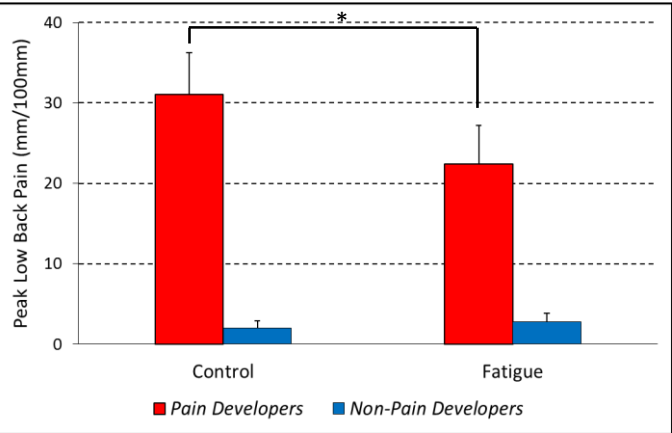


Figure 1: Peak low back pain reported by participants during the control and fatigue dates.

CONCLUSIONS

Using fatigue to alter the PD hip abductor activity patterns reduced their low back pain during standing, but NPDs responses were unaffected. This implies that the hip abductor muscle group is one of multiple potential causes of the low back pain in prolonged standing. It appears as though PDs did not recover force as well as NPDs after a fatiguing exercise, however PDs reported less low back pain during the two hours in which they were recovering from fatigue. Prolonged standing in itself may introduce

muscle fatigue in PDs but not NPDs based on differences in muscle activation patterns^[3], and may place this group at a higher risk for incurring low back injuries while standing^[1].

REFERENCES

1. Enoka, R. et al. (2008). Muscle fatigue: what, why and how it influences muscle function. *J Physiol*, **586** (1); p. 11-23.
2. Winter, D.A. et al. (1996). Unified theory regarding A/P and M/L balance in quiet stance. *J Neurophysiol*, **75** (6); 2334-43.
3. Nelson-Wong, E. et al., (2010). Is muscle co-activation a predisposing factor for low back pain development during standing? *JEK*, **20** (2); p. 256-63.
4. Kelly, A.M., (1998). Does the clinically significant difference in visual analog scale pain score vary with gender, age or cause of pain? *Acad Emerg Med*, **5** (11); p. 1086-90.

ACKNOWLEDGEMENTS

Financial support for this project was provided by the Natural Science and Engineering Research Council. Jack P. Callaghan is supported by the Canada Research Chair in Spine Biomechanics and Injury Prevention.

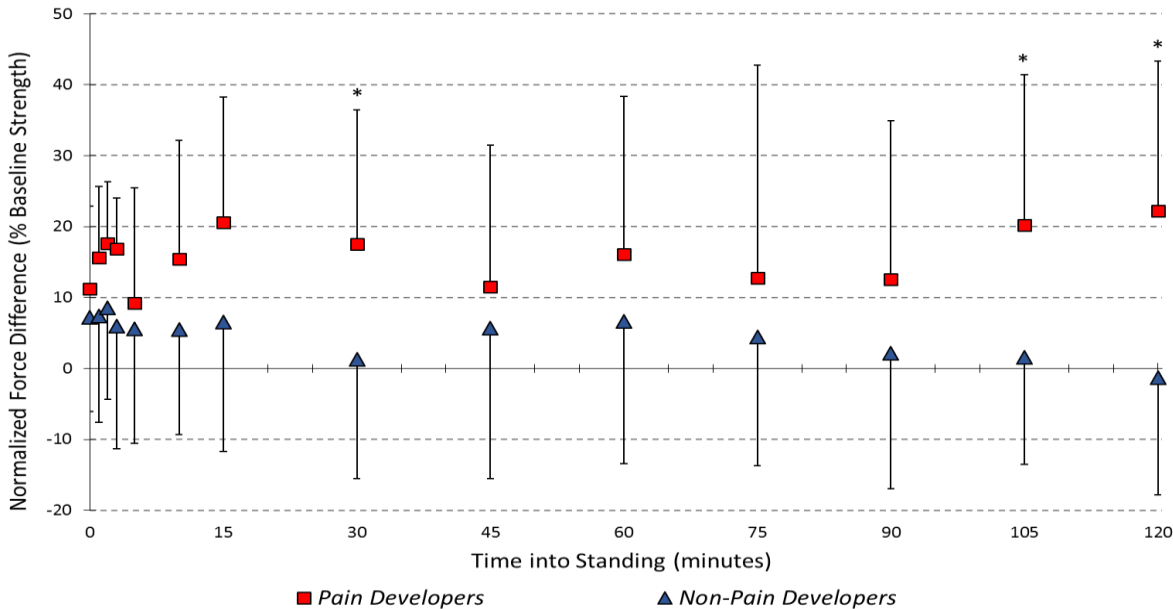


Figure 2: Differences in % Baseline Strength between control and fatigue dates. A larger positive number indicates greater levels of fatigue. Differences between PDs and NPDs are indicated by an asterisk (p < 0.05).

STRIDE-TO-STRIDE CONTROL OF TREADMILL WALKING IN HEALTHY ELDERLY

¹ Jonathan B. Dingwell, ¹ Mandy M. Salinas, and ² Joseph P. Cusumano

¹ The University of Texas at Austin, Austin, TX, USA

² The Pennsylvania State University, University Park, PA, USA

email: jdingwell@austin.utexas.edu, web: <http://www.edb.utexas.edu/khe/nbl/>

INTRODUCTION

Intrinsic noise is ubiquitous to all biological systems and [1] and increases with age [2]. This contributes to increased gait variability as we age [3]. Increased gait variability also prospectively predicts increased fall risk in the elderly [4]. However, it is not known if such correlations are *causal*: i.e., if variability predicts fall risk *because* it indicates deleterious changes in locomotor *control*, or if it reflects “just noise”.

Young healthy humans exploit redundancy to regulate variability [5,6] in walking [7] (Fig. 1). Here we determined whether healthy elderly exploit redundancy in the same way, in spite of the increased biological noise [1,2] that naturally accompanies aging.

METHODS

Young adults walking on a treadmill do *not* tightly regulate fluctuations in stride length (L_n), time (T_n), or position, but instead try to maintain speed, v , at each stride, n [7]. All $[T_n, L_n]$ combinations that equally achieve this goal (i.e., $L_n/T_n = v$) define a “Goal Equivalent Manifold” [6,7] (Fig. 1). *Goal equivalent* tangential deviations (δ_T) do not affect v . Only *goal relevant* perpendicular deviations (δ_P) do.

17 young (YH) and 17 older (OH) healthy adults each walked on a treadmill for 2 trials of 5 min each at each of 5 speeds [3]. 3D movements of their feet were recorded (Vicon, Oxford Metrics, Oxford, UK) to compute time series of L_n , T_n and stride speeds (i.e., $S_n = L_n/T_n$), as well as time series of δ_T and δ_P fluctuations relative to each GEM ([7]; Fig. 1).

Means and standard deviations were computed for each variable. We used Detrended Fluctuation Analysis (DFA) [6-8] to compute exponents, α , that quantified the degree of statistical persistence / anti-persistence in each time series. Smaller α are predicted

by controllers that rapidly *correct* stride-to-stride deviations and thus reflect greater *control* [6-8].

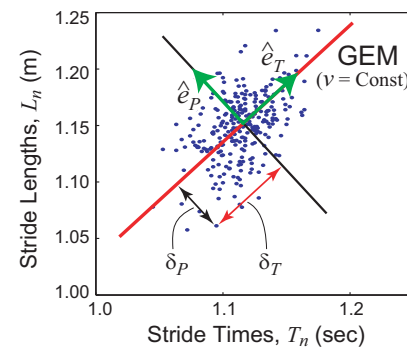


Figure 1: Stride lengths (L_n) vs. times (T_n) for a typical subject, showing the GEM ($L_n/T_n = v$) and scalar deviations δ_T and δ_P relative to the GEM [6,7].

We also extended our computational model of these stepping control strategies [7] to quantify how *independently* varying the noise and degree of control effort in our model would reflect observed behavior.

RESULTS

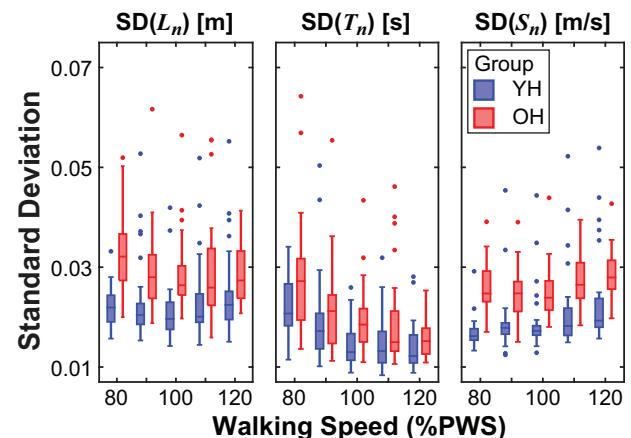


Figure 2: Variability of stride parameters (L_n , T_n , & S_n) for Young (YH) and Older (OH) healthy adults.

Elderly subjects took shorter ($p = 0.02$) and faster ($p < 0.001$) steps than young, but maintained the same

speeds ($p = 0.57$) [3]. Our elderly also exhibited significantly greater variability ($p < 0.04$) than young subjects for all stride variables quantified (Fig. 2).

However, despite their greater variability (Fig. 2), OH subjects exhibited no differences ($p = 0.52$) in the relative *shapes* of their variability distributions within the $[T, L]$ plane (not shown). These OH subjects likewise exhibited no differences in statistical persistence (α) for fluctuations in any of the stride parameters (all $p > 0.56$; Fig. 3A) or for fluctuations with respect to the GEM ($p = 0.86$; Fig. 3B).

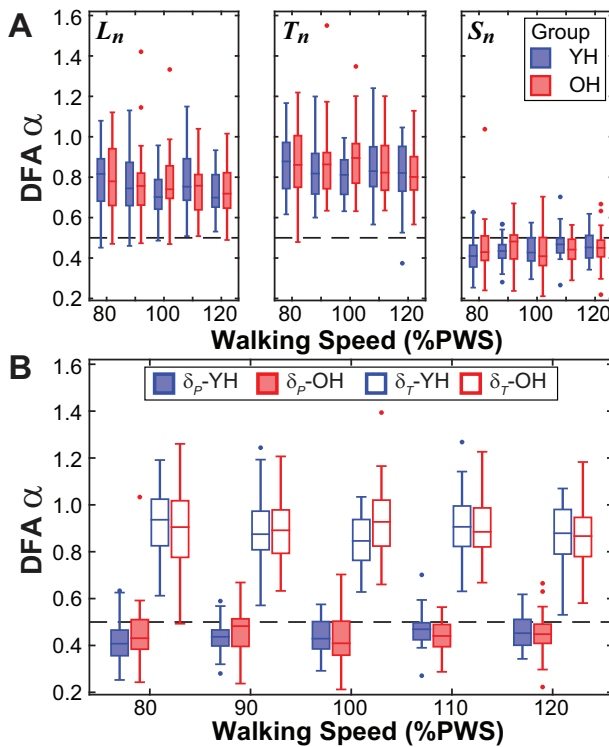


Figure 3: DFA exponents (α) for stride parameters (A) and GEM variables (B) for YH and OH adults.

In our model (Fig. 4) increasing only intrinsic noise [1,2] produced greater variability, but no changes in statistical persistence (Fig. 4A), consistent with our experiments (Figs. 2-3). Conversely, manipulating only the degree of *control* led to minimal changes in variability, but substantial shifts in DFA α (Fig. 4B). This was contrary to our experiments, but fully consistent with theoretical expectations [6-8].

DISCUSSION AND CONCLUSIONS

These healthy elderly exploited the available $[T_n, L_n]$ redundancy to maintain \sim constant walking speed at

each stride in the same way as young subjects (Fig. 3) [7]. They exhibited the same degree of stride-to-stride control [5,6] despite increased variability (Fig. 2; [3]). We emphasize these were very *healthy* elderly who had not yet fallen and did not yet walk slower than our healthy controls. Thus, age-related increase in neuronal variability [2] alone may not indicate degraded neuromuscular *control*.

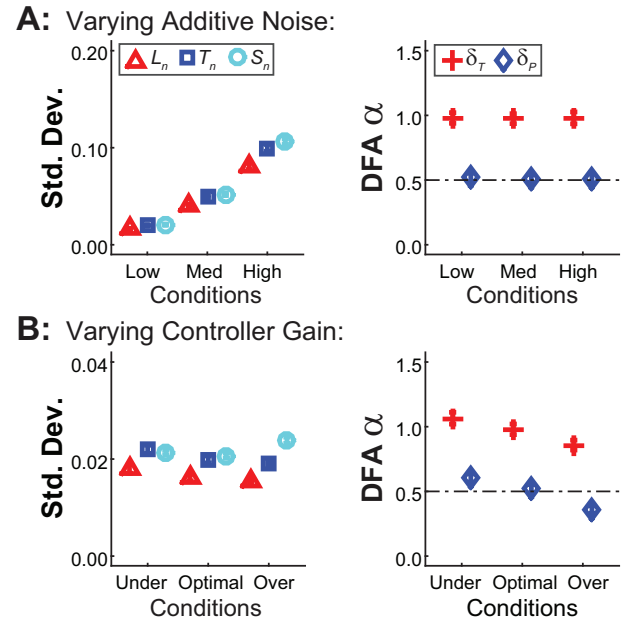


Figure 4: Computational model results.

REFERENCES

1. Faisal AA, Selen LPJ, & Wolpert DM. *Nat Rev Neurosci* **9**(4): 292-303, 2008.
2. Shaffer SW & Harrison AL. *Phys Ther* **87**(2): 193-207, 2007.
3. Kang HG & Dingwell JB. *J Biomech* **41**(14): 2899-2905, 2008; *J Biomech* **42**(14): 2231-2237, 2009.
4. Brach JS et al. *Gait & Post* **31**(2): 175-179, 2010.
5. Todorov E. *Nat Neurosci* **7**(9): 907-915, 2004.
6. Cusumano JP & Dingwell JB. *Hum Mov Sci* **32**(5): 899-923, 2013.
7. Dingwell JB, John J, & Cusumano JP. *PLoS Comput Biol* **6**(7): e1000856, 2010.
8. Dingwell JB & Cusumano JP. *Gait & Posture* **32**(3): 348-353, 2010.

ACKNOWLEDGEMENTS

Whitaker Foundation #RG-02-0354 (JBD), NIH EB007638 (JBD), NSF #0625764 (JPC).

AGE-ASSOCIATED REDISTRIBUTION OF RELATIVE JOINT MOMENT ANGULAR IMPULSES IS ROBUST TO STRIDE LENGTH MANIPULATIONS

Harsh Buddhadev, Ann L. Smiley-Oyen and Philip E. Martin
Iowa State University, Ames, IA, USA
email: harshb@iastate.edu

INTRODUCTION

Compared to young adults, older adults display higher relative joint moment and power contributions at the hip and lower contributions at the ankle joint at any given speed of walking [1]. DeVita and Hortobagyi [1] speculated age-related decline in plantarflexor muscle strength is one cause for redistribution of joint moments observed in the elderly. Two recent studies [2,3] demonstrated that systematically increasing stride length (SL) at a fixed walking speed resulted in higher peak and average net joint moments and powers at the ankle and lower values at the hip in young adults. Allet et al. [3] suggested differences between young and older adults in joint moment contributions may originate in SL and cadence differences between the two age groups. However, both studies [2,3] used only young adults as participants.

There is a need for further assessment of the relationship between SL and distribution of effort across the ankle, knee, and hip during walking in young and older adults. The purpose of the study was to determine if age-associated differences in distribution of joint moment impulses are robust to SL manipulation. Hypotheses: 1) Older adults demonstrate a proximal redistribution (i.e., lower ankle and higher hip and knee contributions) compared to young adults, and; 2) longer strides are associated with higher ankle and lower hip relative contributions in both older and young adults.

METHODS

Participants were 16 healthy young (8 males and 8 females; age, 25.3 ± 4.3 yrs; height, 172.0 ± 6.6 cm; mass, 66.1 ± 8.9 kg) and 18 older adults (8 males and 10 females; 71.8 ± 5.8 yrs, 170.7 ± 9.4 cm, 74.4 ± 16.3 kg), who were free from conditions that can affect normal walking. Reflective markers (n=21) were placed on anatomical landmarks of the

participant's pelvis and right lower extremity. Participants completed three successful overground walking trials at $1.5 \text{ m} \cdot \text{s}^{-1}$ ($\pm 3\%$) under three SL conditions (preferred SL, preferred SL -10% of leg length (LL), preferred SL +10% LL) conditions. Three dimensional marker positions and ground reaction forces were sampled synchronously at 100 Hz and 500 Hz, respectively.

A three-segment sagittal plane inverse dynamics model was used to estimate net joint forces and moments at the ankle, knee and hip. Segment inertial properties were predicted using methods outlined by Vaughan [4]. Average extensor joint impulses normalized to body mass were calculated over the stance phase of a gait cycle for ankle, knee, and hip as described previously [2]. Based on total average extensor impulse (computed as a sum of all three average joint extensor impulses), relative impulse at the three joints were computed as a percentage of the total. A 2 x 3 repeated measures ANOVA examined the effects of age and SL on ankle, knee, and hip average and relative extensor impulses. Significant differences were considered at $p < 0.05$.

RESULTS AND DISCUSSION

For average joint impulses, a main effect was observed for knee impulse, which was greater for older compared to young adults. The total average joint moment impulses and average ankle, knee, and hip moment impulses increased as SL increased (Table 1). These results were in partial agreement with Allet and colleagues [3], who reported higher average ankle and knee impulses, but not hip impulses, for longer SL's. In partial agreement with our first hypothesis, older adults generated lower ankle and higher knee relative angular impulses compared to young adults. However, relative hip impulse was not different for young and older adults (Figure 1). In contrast to our second hypothesis,

relative ankle impulse decreased and knee impulse increased as SL increased. Relative hip impulse was unaffected by changes in SL.

These data suggest that average and relative joint impulses could change as a function of SL in both young and older adults. However, the age-associated distal-to-proximal redistribution of relative joint impulses is yet apparent as stride length was manipulated at a fixed walking speed. These findings imply that age-associated distal-to-proximal redistribution may not originate from differences in SL's chosen by young and older adults as suggested by Allet et al. [2]. Dynapenia, reduction in torque and power generating ability of the lower limb muscles, especially in the plantarflexor muscles may one of the factors underlying to the age-associated redistribution of relative joint moment impulses as suggested by previous studies. Strengthening exercises aimed at improving power in the lower limb muscles, especially the plantarflexors, may help to improve and sustain walking abilities in older adults.

CONCLUSIONS

Relative joint moment impulses displayed an age-associated distal-to-proximal redistribution (i.e., lower ankle and higher knee contributions) when SL's was manipulated at fixed walking speed. With increase in SL, relative ankle moment impulses reduced and knee moment impulses increased. Dynapenia of lower limb muscles may the mechanism contributing to the distal-to-proximal shift. Thus, strengthening exercises aimed at improving power in the lower limb muscles may help to improve and sustain walking abilities in older adults.

REFERENCES

- 1.DeVita P et al. *J Applied Physiology* **88**, 1804-1811, 2000.
- 2.Allet L et al. *Gait & Posture* **33**, 300-306, 2011.
- 3.Umberger BR et al. *J Exp Biology* **210**, 3255-3265, 2007.
- 4.Vaughan CE et al. *Dynamics of Gait*, Kiboho Publishers,1992.

Table 1: Average joint extensor impulses ($\text{Nm}\cdot\text{kg}^{-1}$) as a function of age and stride length (SL). Total extensor impulse and ankle, knee, and hip impulses increased systematically as a function of SL ($p=0.000$) for both older and young adults. Older adults exerted higher ($p=0.005$) knee extensor angular impulses than young adults.

	Preferred SL - 10%LL		Preferred SL		Preferred + 10%LL	
	Older	Young	Older	Young	Older	Young
Ankle	0.36 ± 0.07	0.38 ± 0.05	0.40 ± 0.09	0.44 ± 0.06	0.45 ± 0.08	0.48 ± 0.06
Knee	0.09 ± 0.03	0.06 ± 0.03	0.11 ± 0.03	0.07 ± 0.04	0.15 ± 0.05	0.10 ± 0.05
Hip	0.12 ± 0.05	0.11 ± 0.04	0.14 ± 0.05	0.12 ± 0.05	0.17 ± 0.06	0.14 ± 0.05
Total	0.57 ± 0.10	0.55 ± 0.08	0.64 ± 0.13	0.63 ± 0.10	0.77 ± 0.13	0.73 ± 0.11

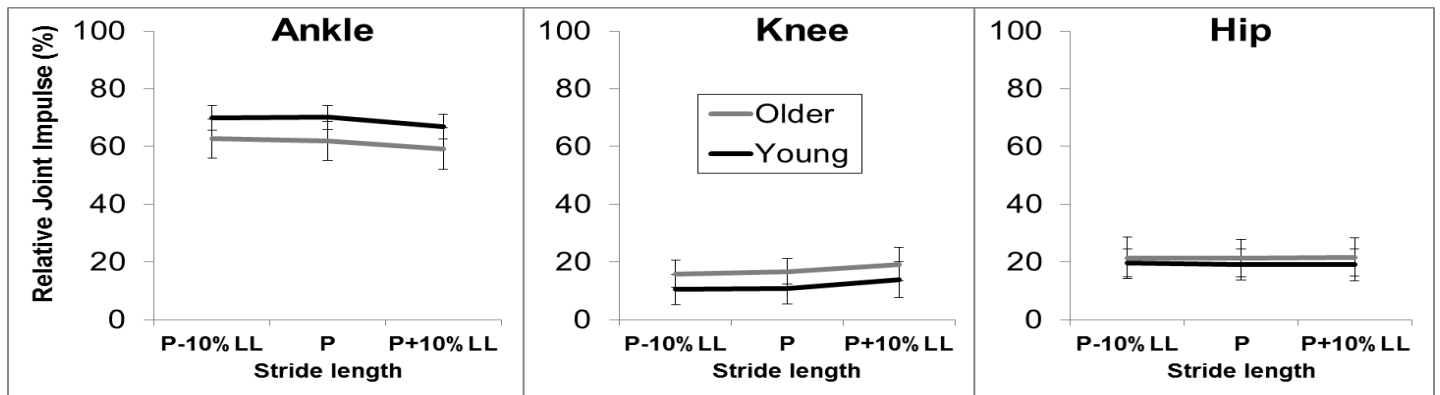


Figure 1: Relative joint extensor impulses (%) as a function of age and SL during the stance phase of walking at $1.5 \text{ m}\cdot\text{s}^{-1}$. Older adults exerted lower relative ankle ($p=0.000$) and higher relative knee ($p=0.003$) impulses compared to young adults. Relative ankle impulses decreased ($p=0.000$), knee impulses increased ($p=0.000$), and hip impulses were unchanged ($p=0.632$) as SL was increased. These relative extensor impulse data were computed over the stance phase at a walking speed of $1.5 \text{ m}\cdot\text{s}^{-1}$.

THE EFFECT OF FATIGUE ON KNEE MECHANICS IN OLDER ADULTS: DOES PHYSICAL ACTIVITY MATTER?

Jocelyn F. Hafer, Jane A. Kent, and Katherine A. Boyer
University of Massachusetts Amherst
email: jhafer@kin.umass.edu

INTRODUCTION

Aging is often associated with a change in gait mechanics and it is possible that these changes contribute to the incidence of knee osteoarthritis (OA), a mechanically mediated, age-related disease. Differences in gait mechanics between healthy young and older adults appear to follow a similar trend as differences between healthy older adults and older adults with knee OA [1]. Given the potential importance of gait mechanics for maintenance of joint health, there exists an urgent need to understand the factors that contribute to age-related changes in gait mechanics.

Compared with young adults, older adults have lower baseline knee extensor strength and greater muscle fatigue during rapid, high-velocity dynamic contractions. As the knee extensors are prime movers in gait, fatigue accumulated throughout the day in these muscles could result in changes in gait mechanics. The purpose of this study was to determine whether a bout of treadmill walking induces knee extensor fatigue and changes in knee mechanics in healthy older adults. Because habitual physical activity (PA) is a potential mediator of knee extensor strength in aging, we also examined the effect of usual PA level by comparing the responses to treadmill walking in sedentary and highly active older adults. We hypothesized that the treadmill protocol would induce a larger drop in knee extensor power as well as larger changes in knee mechanics in older sedentary adults compared with older runners.

METHODS

Healthy adults aged 55-75 with BMI <25 were recruited in two groups: those who ran ≥ 15 miles/wk, and those who were sedentary (<150 min of moderate to vigorous PA per week). Participants completed baseline gait and strength testing, a 30 minute bout of treadmill walking (30MTW), and post-30MTW gait and strength testing.

Gait testing consisted of motion capture of 5 strides of right-sided overground walking data at each participant's preferred walking speed. Joint kinematics were calculated using the point cluster technique, which allows for calculation of joint rotations as well as translations at the knee [2]. Externally referenced moments were calculated using inverse dynamics and normalized to body mass and height. Knee extensor (KE) concentric and eccentric power were assessed at 90, 180, and 270°/s using an isokinetic dynamometer (Humac Norm, Cybex). KE isometric strength was assessed at 60° of knee flexion.

After baseline gait and strength testing, all participants completed the 30MTW at their preferred overground speed. This protocol, which includes 3 1-minute "challenge" periods during which the grade is increased to 3%, has been shown to induce knee extensor fatigue in older women [3]. Pre- to post- 30MTW changes in KE power and strength (%), as well as changes in knee mechanics relevant to knee OA (knee flexion at heel strike, peak knee flexion during loading response, peak knee adduction angle, anterior femoral displacement at heel strike, anterior femoral displacement during loading response, peak knee flexion moment, and peak knee adduction moment) were calculated. Paired t-tests were used to compare changes within groups in KE power pre- to post-30MTW. Unpaired t-tests were used to compare changes in power and knee mechanics between groups post-30MTW. T-tests were one-tailed as we hypothesized a larger drop in KE power and a larger increase in knee mechanics variables in sedentary older adults. Due to the preliminary nature of the current results, significance was set at $p \leq 0.10$. Effect sizes were calculated for unpaired tests at a 95% confidence level.

RESULTS

Currently, participants include 6 runners (2 female), 62.8 ± 4.3 years, BMI 22.6 ± 1.6 kg/m² and 3

sedentary older adults (1 female), 64.7 ± 3.1 years, BMI 23.13 ± 2.1 kg/m². KE power data were excluded for one runner due to a strong learning effect from pre- to post- strength testing. Average preferred walking speed and stride length normalized to height for the runners and sedentary adults were 1.4 ± 0.1 m/s, 0.9 ± 0.1 ; and 1.4 ± 0.1 m/s, 0.8 ± 0.1 , respectively.

In response to the 30MTW, sedentary older adults displayed a significant drop in eccentric muscle power at $270^\circ/\text{s}$ while older runners had decreases in eccentric KE power at 270 and $180^\circ/\text{s}$ and in concentric KE power at $270^\circ/\text{s}$. For eccentric power at $270^\circ/\text{s}$ and for isometric strength, the drop was larger in sedentary older adults compared to runners, with effect sizes of 1.14 and 0.87, respectively (Figure 1).

For knee mechanics outcomes in response to the 30MTW, the sedentary group showed an increase in peak knee adduction angle and peak knee adduction moment, while these variables decreased in the runners. Effect size calculations indicated larger increases in sedentary older adults than runners in peak knee flexion and femoral anterior displacement during loading response, as well as in peak knee flexion moment (Table 1).

CONCLUSIONS

In response to the 30MTW, older sedentary adults displayed a larger decrease in eccentric KE power at $270^\circ/\text{s}$ as well as in isometric strength compared with older runners. In addition, runners displayed a significant decrease in KE power at high eccentric

and concentric contraction velocities (Figure 1). These findings demonstrate that both inactive and active older adults experience measurable muscle fatigue in response to a bout of walking comparable to daily activity.

Sedentary older adults had larger increases in most of the knee mechanics variables in response to the 30MTW as compared to older runners. The finding of larger increases in peak frontal plane variables are particularly relevant to knee joint health, as frontal knee malalignment and increased knee adduction moment have been tied to higher risk of knee OA [4]. This shift in knee mechanics in sedentary older adults follows the direction of differences observed between older asymptomatic adults and older adults with knee OA [1] and may indicate that these individuals are at risk of accumulating cartilage damage as they fatigue through daily activity. Our results suggest that maintenance of vigorous habitual PA may protect older adults from changes in gait mechanics induced by muscle fatigue.

REFERENCES

1. Favre J et al., *Osteoarthritis Cartilage*, 22(3), 464-71, 2014
2. Andriacchi TP et al., *J Biomech Eng*, 120(6), 743-9, 1998
3. Foulis S, *Open Access Dissertations*, 792, 2013
4. Lynn SK et al., *Knee*, 14(1), 22-28, 2007

ACKNOWLEDGEMENTS

Funding for this study was provided by an ACSM Foundation Doctoral Student Research Grant

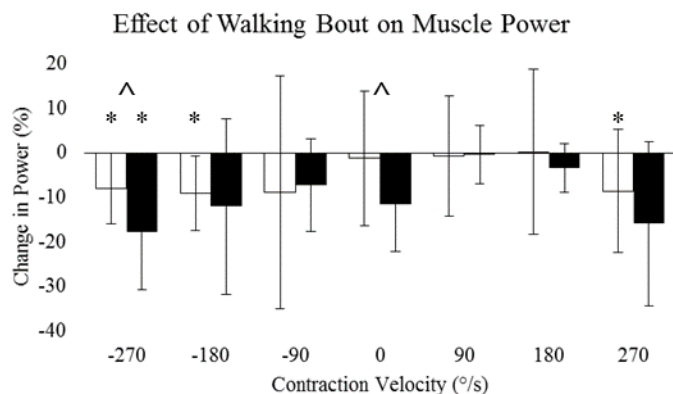


Figure 1: Group mean (SD) changes in knee extensor power in response to the 30MTW. White bars: runners, black bars: sedentary. *: $p \leq 0.1$ for paired comparison; ^: effect size > 0.6 for unpaired comparison.

Table 1: Changes in knee mechanics pre- to post- 30MTW in runners and sedentary older adults. KF: knee flexion, KA: knee adduction, HS: heel strike, LR: loading response, FAD: femoral anterior displacement.

	Runners		Sedentary		p-value	Effect size
	Mean	SD	Mean	SD		
KF HS (°)	0.75	1.47	1.40	0.37	0.24	0.59
KF LR (°)	0.23	2.28	1.89	1.49	0.15	0.90
KA Peak (°)	-0.38	0.84	0.49	0.90	0.10	1.15
FAD HS (mm)	0.88	3.56	1.88	2.84	0.34	0.34
FAD LR (mm)	1.94	2.08	4.28	7.45	0.24	0.61
KFM (%BW*Ht)	-0.16	0.56	0.24	0.47	0.16	0.85
KAM (%BW*Ht)	-0.01	0.40	0.42	0.36	0.08	1.25

INCREASED LATERAL FOREFOOT PRESSURE REGULARITY IN OLDER ADULTS IS INDEPENDENT OF GAIT VELOCITY

¹ Eric J. Pisciotto and ¹ Jennifer M. Yentes

¹ University of Nebraska at Omaha, Omaha, NE, USA
email: episciotto@unomaha.edu, web: cobre.unomaha.edu

INTRODUCTION

Aging is a non-homogenous degeneration of biological processes ultimately leading to a loss of physiologic complexity [1]. As we age, the foot bone and ligament structural properties are altered leading to changes in plantar pressure distributions [2]. In addition, plantar soft tissue in older adults displays increased stiffness and an altered response to changing impact velocity [3]. Older adults walk with a conservative gait pattern [4] and one out of three present with a foot deformity [5]. Moreover, studies investigating the effects of aging on plantar pressure distributions have found decreased peak pressures in the heel and medial foot masks in older adults [6]. The regularity of peak pressures, within a spectrum of walking velocities, can provide insight into the preferred loading behavior and potential gait differences due to aging.

If a movement is too regular, it lacks the flexibility to adapt to an external perturbation whereas, a highly irregular movement is uncoordinated. Either of these extreme conditions are a potential mechanism for gait abnormalities among older adults. The theory of optimal variability proposes that there exists an ideal range of variation in the inherent fluctuations during movement that is advantageous to human performance and describes healthy movement patterns [7]. Optimal variability models the complexity and predictability (i.e., regularity) of a time series; moderate levels of predictability and high complexity are key components of a healthy physiologic process.

The primary goal of this research was to identify alterations in peak plantar pressure variability due to aging and walking velocity. Specifically, we aimed to quantify the amount and temporal structure of peak pressure variability under distinct anatomical regions of the foot during consecutive stance cycles.

It was hypothesized that older adults would present with a decreased amount of variability (as measured by standard deviation (SD) and coefficient of variation (CV)) and increased regularity (as measured by sample entropy (SampEn) of peak pressures in the lateral forefoot due to changes in foot structure and a reduction in medial pressures but not lateral in older adults [3, 6]. Secondly, it was hypothesized that, for both groups, the amount of variability would decrease and the temporal structure would become increasingly regular at faster walking velocities due to increased effects of inertia on foot roll over dynamics.

METHODS

Ten healthy young adults ($25.8y \pm 2.7$) and 10 healthy older adults ($75.1y \pm 6.7$) participated in this study. A clinical foot evaluation was conducted in order to document foot deformities and anthropometric measurements were obtained. Subjects were then fitted to a control shoe (Dart VI, Nike) with a pair of pressure sensitive insoles (PedarX, Novel Electronics) inside. Subjects were given a 5-10 minute period to adapt to the footwear and treadmill. During this time self-selected walking speed (SSWS) was determined. Subjects then walked on the treadmill for 10 minutes for three different speed conditions (3 minutes rest between trials) while plantar pressure data was collected. The first trial was always the SSWS condition. The following two speed conditions were randomized to either $\pm 20\%$ of the SSWS.

The pressure insole was masked into 7 anatomic regions (Figure 1). The amount and temporal structure of peak pressure variability in the right foot was used for comparisons. Regional peak pressure SD, CV, and SampEn ($r=0.25$, $m=2$) was calculated from 400 consecutive steps (N). SSWS was compared between groups using an

independent t-test. The SD, CV, and SampEn of the regional peak pressures were compared using a 2x3 repeated measures ANOVA (2 groups x 3 speeds). If a dependent variable violated assumptions of sphericity, a Greenhouse-Geisser correction was reported.

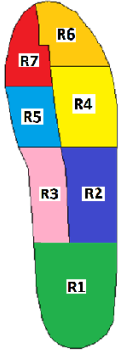


Figure 1: Plantar pressures were masked into the following regions for analysis: R1) Heel, R2) Lateral mid-foot, R3) Medial mid-foot, R4) Lateral metatarsals, R5) First metatarsal, R6) Lateral toes, and R7) Hallux.

RESULTS AND DISCUSSION

The SSWS of older adults was significantly reduced as compared to the younger group ($p=0.02$). A main effect for group was found in the SampEn of the lateral metatarsal region, R4, ($F_{2,36}=17.79$, $p=0.001$) indicating a significant increase in the lateral forefoot regularity in older adults. This result partially supports the first hypothesis. It was also hypothesized that there would be decreases in the SD and CV in the lateral forefoot, however, no changes were identified. This is not unexpected, as temporal structure of variability measures have been shown to discriminate between groups when amount of variability cannot [7]. Despite insignificant findings, other lateral regions trended towards regularity in older adults. A group effect was nearly detected in the SampEn of the lateral mid-foot, R2, ($F_{2,36}=3.95$, $p=0.06$) and lateral toes, R6, ($F_{2,36}=3.2$, $p=0.09$). Increased sample size may improve significance in these regions.

A main effect for speed was found for the SD of the lateral mid-foot, R2, ($F_{1,39,25.05}=14.1$, $p<0.001$) and the medial mid-foot, R3, ($F_{1,29,23.29}=3.98$, $p=0.049$). In addition, a main effect for speed was found in the CV of the heel, R1, ($F_{2,36}=14.1$, $p<0.001$), lateral mid-foot, R2, ($F_{1,43,25.7}=8.79$, $p=0.003$), lateral metatarsals, R4, ($F_{2,36}=6.48$, $p=0.004$), lateral toes, R6, ($F_{2,36}=9.32$, $p=0.001$). These variables were all decreased in the fast velocity compared to both of the other conditions. The slow speed was

significantly increased from both other conditions in the lateral mid-foot, R2, SD and for CV in the heel and lateral mid-foot, R1 and R2. These results support part of the second hypothesis, however, no main effects for speed were found in SampEn. Mean pressure increased with higher velocity resulting in the amount of variability, SD and CV, to decrease. However, SampEn is independent of the mean and depends on the fluctuations in the behavior from step to step. It is possible that the $\pm 20\%$ SSWS was an insufficient perturbation to one or both of these populations.

A significant interaction was found in the CV of the hallux, R7, ($F_{2,36}=4.33$, $p=0.021$). Both groups demonstrated a decrease in CV from slow to the fastest speed; however, in young adults reduction in CV from SSWS to $+20\%$ was significantly greater. This is likely attributed to similar variation but reduced pressure in older adults.

CONCLUSIONS

These results suggest increasingly repetitive peak pressures under the lateral metatarsals in older adults. Increasing regularity indicates an adaptive process to gait that allows older adults to gain consistent sensory information from the environment. These findings indicate that amount of variability is more sensitive to changing gait velocity. These results support findings from other studies that the amount and temporal structure of variability provide different information [7]. This may have further implications for elderly persons with foot pain, diabetic ulcers, or at risk for falls.

REFERENCES

1. Lipsitz LA, et al. *JAMA* **267**, 1806-1809, 1992.
2. Rodgers MM, *J Orthop Sport Phys Ther* **21**, 306-316, 1992.
3. Hsu CC, et al. *Ultrasound Med Bio* **31**, 1423-9, 2005.
4. Winter DA, et al. *Phys Ther* **70**, 340-347, 1990.
5. Dunn JE, et al. *Am J Epidemiol* **159**, 491-8, 2004.
6. Hessert MJ, et al. *BMC Geriatrics* **5**, 2004.
7. Stergiou S, *J Neuro Phys Ther* **30**, 120-29, 2006.

ACKNOWLEDGEMENTS

Funding provided by the UNO GRACA and UCRCA

Visual Perturbations, but not a Cognitive Challenge, Induce an Increase in Muscle Co-Activation during Gait in Healthy Old Adults

Carrie A. Francis, Jason R. Franz and Darryl G. Thelen

University of Wisconsin-Madison, Madison, WI, USA
email: carrie.francis@wisc.edu, web: <http://uwnmbi.engr.wisc.edu/>

INTRODUCTION

Old adults are often at greater risk of falling during locomotion. Age-related declines in integration and quality of sensory feedback likely contribute to fall risk. Our recent studies show that old adults rely more on vision to inform balance control during gait [1-2]. This visual reliance may compensate for age-related declines in quality of somatosensory and vestibular feedback [3-4]. Alternatively, changes in executive function may alter the integration of sensory information and planning motor actions [5]. Fear of falling may also contribute to greater fall risk by leading old adults to limit physical activity, compounding losses in strength and coordination [6]. Moreover, increases in antagonist muscle co-activation – a presumably protective mechanism to stiffen the joints, often seen in old adults – may be an indicator of fear of falling or a sign of disrupted balance [7]. Better understanding of the way that sensorimotor changes with age affect balance during gait may allow earlier detection of fall risk and improved intervention strategies.

To this end, a number of studies have investigated biomechanical differences in gait between healthy old and young adults, often focusing on gait variability. In these studies, age-related differences in gait variability are enhanced by making walking more challenging. However, there is little consensus on the challenge to use with approaches including physical and cognitive (dual-task) challenges and sensory manipulation. In this study, we investigated changes in leg muscle activation patterns in old and young adults walking normally, with a visual perturbation, and while performing a dual task (serial 7 subtractions).

Based on kinematic findings with these tasks [2], we hypothesized that when healthy old and young adults

walked normally or with a dual task, the two groups would exhibit similar muscle activation patterns. We further hypothesized that old adults would perceive visual perturbations as a greater threat to balance than young adults, which would be reflected in an increase in muscle co-activation.

METHODS

Twelve healthy young (23.6 ± 3.9 years) and ten healthy old adults (71.0 ± 4.4 years) walked on a treadmill facing a semi-circular screen showing a speed-matched virtual hallway (Fig. 1a). Subjects walked at their preferred overground speed on a treadmill and completed a 3-minute trial for each of three conditions: normal walking, visual perturbations, and a dual task.

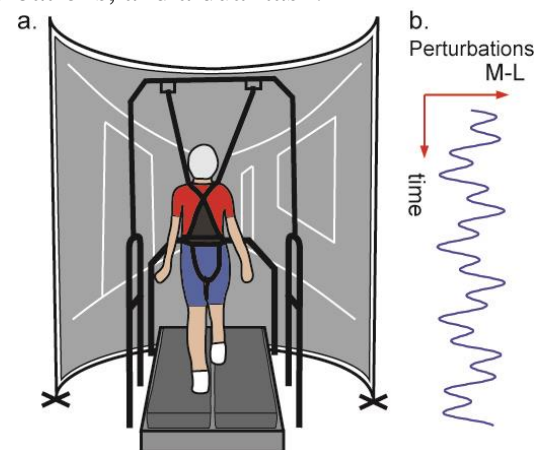


Figure 1. a) A subject walks on an instrumented treadmill while watching a virtual hallway. b) The sum of sinusoids used to produce mediolateral perturbation of the virtual hallway.

During the visual perturbation, the virtual hallway rotated continuously in the mediolateral direction according to the sum of two sinusoids (0.135 and 0.0442 Hz) with 0.175 m amplitudes (Fig. 1b). For the dual task, subjects performed serial 7 subtractions starting at a given three-digit number.

We collected lower limb kinematics and bilateral EMG from five muscles - medial hamstrings (MH), vastus lateralis (VL), medial gastrocnemius (MG), soleus (SL), and tibialis anterior (TA). EMG data were band-pass filtered (1 – 350 Hz), rectified, and then low-pass filtered with a 10 Hz cut-off to obtain activation envelopes. EMG data were partitioned into gait cycles identified from the kinematic data. Subjects' EMG data were averaged over each trial and normalized to the root-mean-square for the normal trial. Left and right EMG were then combined and group averages computed. Using a repeated measures ANOVA, we compared EMG signals from five periods of the gait cycle: loading response (0-10%), mid-stance (10-30%), terminal stance and pre-swing (30-60%), initial swing (60-73%), and terminal swing (87-100%) [7].

RESULTS AND DISCUSSION

Muscle activation patterns did not differ between healthy old and young adults during normal walking, and only exhibited minor differences in the dual task condition. Young adults increased TA activity during the loading response of the dual task. Young adults' TA activity was also greater than that of old adults during loading response and terminal swing. Previously observed gait changes in healthy adults under dual task conditions is mixed, but some studies suggest that young adults are more likely than old to prioritize gait in an attention-dividing condition [5].

Substantial aging effects were observed in visually perturbed gait, with old adults increasing activation of the quadriceps, hamstrings and plantarflexors. Specifically, compared to normal walking, old adults increased MH and VL activity during terminal swing and increased MH, VL, and SL activity during mid-stance. Compared to young adults, old adults had higher MH and VL activation during terminal swing, loading response, and mid-stance, and higher MH activation in terminal stance and pre-swing. Changes in old adults' upper leg muscle activations during visually perturbed walking were consistent with greater antagonist muscle co-activation, presumably to stabilize the leg during contact. Since the physical demands of walking during the visual trial were not altered, the increases in old adults' muscle activation would seem to be an attempt to compensate for a

perceived threat to their balance from a decline in the quality of the visual information provided.

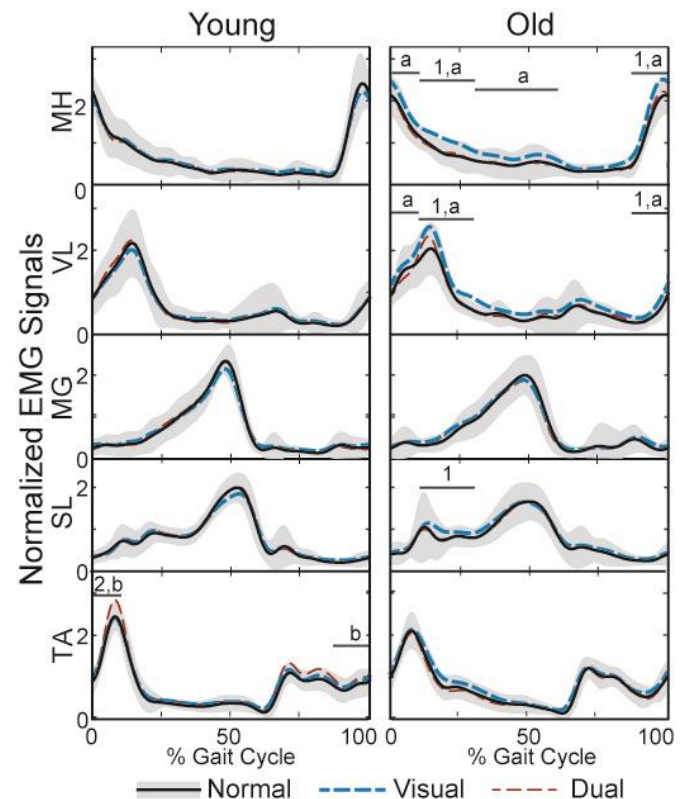


Figure 2: Mean \pm standard deviation EMG activity for normal walking in each group plotted with mean activity for challenge trials. Significant differences are denoted: Visual vs. Normal (1), Dual Task vs. Normal (2), Age Effect-Visual (a), Age Effect-Dual Task (b).

REFERENCES

1. Franz, et al. *Hum Movement Sci* **40**, 2015
2. Franics, et al. *Gait Posture*, In Review
3. Skinner, et al. *Clin Orthop Relat Res* **184**, 1984
4. Sloane, et al. *Am J Otolaryngol* **10**, 1980
5. Yogev-Seligmann, et al. *Mov Disord* **23**, 2008
6. Li, et al. *J Gerontol B* **58B**, 2003
7. Schmitz et al. *J Electromyogr Kinesiol* **19**, 2009

ACKNOWLEDGEMENTS

We would like to acknowledge Dr. Shawn O'Connor, Mike Schmidt, and Holly Schoenberg. Funded by NIH F31AG046945 and NIH F32AG044904

QUANTIFYING PERFORMANCE AND EFFECTS OF LOAD CARRIAGE DURING COMPLETION OF A WINDOW OBSTACLE USING AN ARRAY OF WIRELESS INERTIAL SENSORS

¹ Stephen M. Cain, ² Ryan S. McGinnis, ¹ Steven P. Davidson, ¹ Rachel V. Vitali,
¹ Noel C. Perkins and ¹ Scott G. McLean

¹ The University of Michigan, Ann Arbor, MI, USA, ² MC10 Inc., Cambridge, MA, USA
email: smcain@umich.edu

INTRODUCTION

Warfighter performance is inherently challenging to quantify due to the complex tasks that warfighters perform, variations in technique, the environments in which warfighters operate, and limited knowledge of measures that truly characterize task performance beyond simple success or failure. Occupational physical performance tests, or obstacle courses, are one approach to assess the effects of fatigue and/or load on warfighter performance [1, 2]. Unfortunately, measures of the total time to complete an obstacle course or time required to complete each obstacle are typically the only quantitative metrics obtained from such tests.

Advancements in inertial measurement unit (IMU) technology make it possible for researchers to unobtrusively measure body segment kinematics in real-world environments. In this study, we utilized an array of wireless IMUs to measure the movements of subjects completing a window obstacle as quickly as possible, both with and without external load. Our objectives were: 1) to quantify changes in performance due to load, 2) to quantify changes in subject movement and 3) to identify performance metrics. We hypothesized that carrying external load would: increase the time required for subjects to complete the obstacle, decrease the ranges of motion of the pelvis and torso (due to effects of armor [3]), and decrease the angular velocities of the torso and pelvis (due to increased inertia).

METHODS

We tested 30 subjects (11 females, 19 males; age = 20.8 ± 2.6 years; body mass = 75.4 ± 11.1 kg; height = 1.75 ± 0.08 m; mean \pm standard deviation). The University of Michigan IRB approved the study,

and all subjects gave informed consent. Subjects completed an outdoor obstacle course both with and without a 20.5 kg load (body armor and tactical assault panel); the order of trials (load or no load) was random. Subjects carried a mock-rifle (3.4 kg) in both load conditions. The window obstacle is a freestanding wooden wall with a 0.91 m \times 0.91 m opening 1.22 m off of the ground. Subjects approached the window and used any technique they chose to pass through the window as quickly as possible. The subjects then repeated the process, going through the window in the opposite direction.

We secured eight wireless IMUs (Opal, APDM, Inc.) to each subject's feet, shanks, thighs, sacrum, and torso. Each IMU contains a 3-axis accelerometer, angular rate gyro, and magnetometer; a proprietary Kalman filter estimates the directions of gravity and magnetic north relative to sensor-fixed axes. Subjects performed calibration movements prior to testing, allowing us to deduce body segment-to-sensor alignments in post-processing. Sacrum accelerations were resolved in an inertial frame and integrated to obtain vertical velocity of the sacrum. Peaks in the vertical velocity signal revealed the jump up onto and down from the window, which identified the time required for a subject to complete the window obstacle (Fig. 1) without a stopwatch or timing gates. Orientations of the torso and sacrum-mounted IMUs relative to gravity and magnetic north were used to calculate medial-lateral (ML), anterior-posterior (AP), and heading (rotation about vertical) ranges of motion for both the torso and pelvis.

We focused our analysis on 12 candidate performance metrics: total time through window (performance), 3-D ranges of motion for the torso and pelvis, and mean angular velocity magnitudes of the feet, shanks, thighs, pelvis and torso. We used

paired t-tests with a Bonferroni correction ($\alpha = 0.05/12 = 0.004$) to test for significant differences between loaded and unloaded conditions.

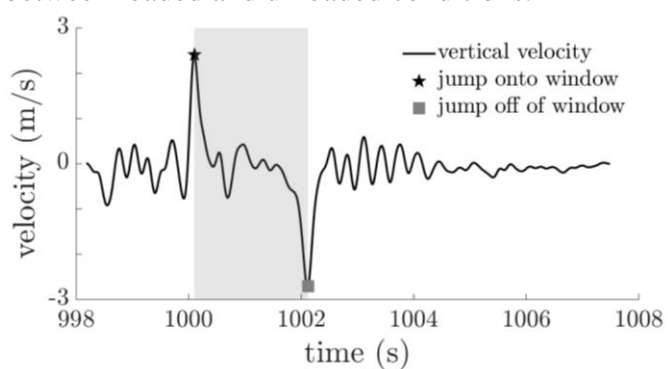


Figure 1: Representative plot of vertical velocity of the sacrum versus time. The shaded region highlights the time interval that the subject is completing the obstacle.

RESULTS AND DISCUSSION

Load carriage resulted in a significant increase in the total time through the window (mean diff = 1.81s, $t=3.67$, $p=0.001$), consistent with other studies that demonstrate that external load decreases obstacle course performance [2]. Subjects reduced their pelvis heading angle range of motion when carrying load (mean diff = -12.35deg, $t=-4.06$, $p<0.001$) but did not significantly alter ML and AP ranges of motion of the pelvis or torso ranges of motion. The largest changes in torso and pelvis orientation typically occurred when subjects passed through the window opening. The decrease in pelvis heading angle range of motion with load indicates that subjects chose to keep their pelvises more in line with the direction of travel through the window while keeping other movements relatively unchanged from the unloaded condition. All segment mean angular velocity magnitudes decreased significantly with load carriage ($t<-8.77$, $p<0.001$ for all segments). While we expected torso and pelvis mean angular velocities to decrease due to increased inertia when carrying load, we were surprised to find that lower limb segment angular velocities also decreased, as no mass or inertia was added to the lower limbs.

Larger values of mean segment angular velocity magnitudes were correlated to higher performance (faster times); Fig. 2 illustrates this relationship for

the torso. A power-law provides a good fit to the data ($R^2=0.74$); other segments exhibit a similar relationship. This result indicates that faster moving subjects (larger mean segment angular velocities) are able to complete the obstacle more quickly. Performance in other obstacles is likely also correlated to measures of segment angular velocity.

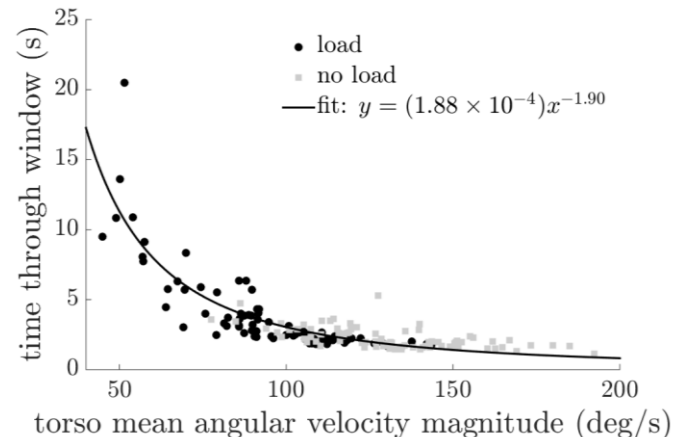


Figure 2: Total time to complete the window obstacle versus torso mean angular velocity magnitude.

CONCLUSIONS

Load carriage significantly reduces performance on a window obstacle, reducing the speed at which subjects move (segment angular velocities) and altering pelvis range of motion. Subject technique varies widely, and therefore it is possible that additional load effects may be revealed by considering subject technique. We also plan to continue to work with this data set to reveal common strategies that our subjects used to negotiate the window obstacle through the use of a cluster analysis or principal components analysis.

REFERENCES

1. Pandorf CE, et al. *Can J Appl Physiol* **28**, 27-37, 2003.
2. O'Neal EK, et al. *Military Medicine* **179**, 950-954, 2014.
3. Benseck CK, et al. NSRDEC, Natick, MA, 1980.

ACKNOWLEDGEMENTS

Supported by NSRDEC W911QY-13-C-0011.

DURATION OF EXERTION AND SCBA DESIGN AFFECT FIREFIGHTER BALANCE

¹Grace S. Deetjen, ¹Michael J. Angelini, ²Richard M. Kesler, ¹Matthew N. Petrucci, ³Karl S. Rosengren,
^{1,2}Gavin P. Horn, ¹Elizabeth T. Hsiao-Wecksler

¹The University of Illinois at Urbana-Champaign, Urbana, IL, USA

²Illinois Fire Service Institute, University of Illinois at Urbana-Champaign, Champaign, IL, USA

³The University of Wisconsin-Madison, Madison, WI, USA

email: deetjen2@illinois.edu, web: hdcl.mechanical.illinois.edu

INTRODUCTION

Slips, trips and falls are among the leading causes of fireground firefighter injury [1]. With several sizes of compressed air tanks available and fire departments tending towards larger, extended duration tanks, changes in body kinematics are anticipated. This study investigated the effects of self-contained breathing apparatus size and design as well as fatigue from simulated firefighting activities on balance during a functional balance test [2].

METHODS

Thirty firefighters (29 male) used each of four self-contained breathing apparatuses (SCBA): standard cylinders providing 30, 45, and 60 minutes of air when breathing at 40 L/min (S30, S45, S60); and a low-profile prototype (P45, 45-minute) (MSA, Inc.; Murrysville, PA, USA). The functional balance test (FBT) used a ground-level balance beam with a raised platform on each end. A trial consisted of walking across the balance beam to the opposite raised platform and then returning to the starting position. Subjects performed two trials each with and without a light-weight bar across the middle of the balance beam at 75% of the subject's height. Subjects were instructed to move at fireground pace, which is common fire service terminology for moving quickly but safely.

FBT performance was quantified by completion time (sec) and error count – minor (MI) and major (MA). MI included not turning within a 24" × 24" marked space on either platform or contacting the overhead bar. MA included walking off the beam or knocking the bar off its supports. To quantify

overall performance, a unit-less performance index was calculated for each trial: $PI = completion\ time + MI + 2*MA$. Thus, a lower PI is considered to be a better performance.

FBT trials were performed before (pre) and after (post) subjects completed an exercise protocol in a heated environmental chamber (47°C, 20% humidity) consisting of two minutes each of four simulated firefighting tasks, with two-minute rests between tasks, such that the total time for one bout was 16 minutes. The firefighting tasks were stair ascent and descent, hose advance, floor search, and ceiling pull [3]. During separate visits, subjects completed one bout (1B), two bouts with a five-minute break (2B), or back-to-back bouts in the chamber (BB). Repeated-measures ANOVAs assessed time, MI, MA, and PI for three comparison groups based on SCBA characteristics or fatigue ($\alpha = 0.05$):

CG1) SCBA size (S30_1B, S45_1B, S60_1B)

CG2) SCBA design (S60_1B, P45_1B)

CG3) Bouts of exertion (S60_1B, S60_2B, S60_BB)

Subjects were binned into groups based on years of firefighting experience for additional analysis.

RESULTS AND DISCUSSION

Analysis of time, error counts, and PI indicated that there are variations in FBT-crossing ability as a result of SCBA size/design and extended duration of firefighting activities.

The CG1 analysis investigated increasing size of SCBA with one bout of activity. A significant increase in minor errors ($p=0.001$) was observed with the addition of an overhead bar, as well as an

increase in time ($p<0.001$). There was a significant increase in PI as SCBA size increased, especially for the condition with a bar overhead (Fig. 1, $p<0.001$). These results suggest that firefighters may have difficulty moving quickly and carefully with larger capacity tanks, increasing fall risk [4]. Binning subjects into experience groups revealed a main effect of experience for minor error counts ($p=0.04$). Post-hoc analysis showed that inexperienced firefighters made fewer MI than subjects with intermediate firefighting experience (Table 1, $p=0.03$). This trend indicates that novice firefighters may be more careful in FBT performance than intermediate ones.

Table 1: Average minor error counts for all 1B test conditions with a standard SCBA (S30, S45, S60).

Subjects binned based on years of experience.

Experience Group	Years of Experience	Average MI Count (\pm SE)
Novice (n=9)	0.5 – 2	0.08 ± 0.07
Intermediate (n=12)	4 – 10	0.32 ± 0.06
Advanced (n=9)	16 – 25	0.21 ± 0.07

The CG2 analysis sought to determine whether the low-profile prototype P45 would be helpful for avoidance of an overhead obstacle. The P45 was comparable in weight to the S60. No significant difference was found in MA because the counts were so low. PI dramatically decreased from S60 to P45 with the bar overhead, showing improved balance (Fig. 1, $p=0.008$).

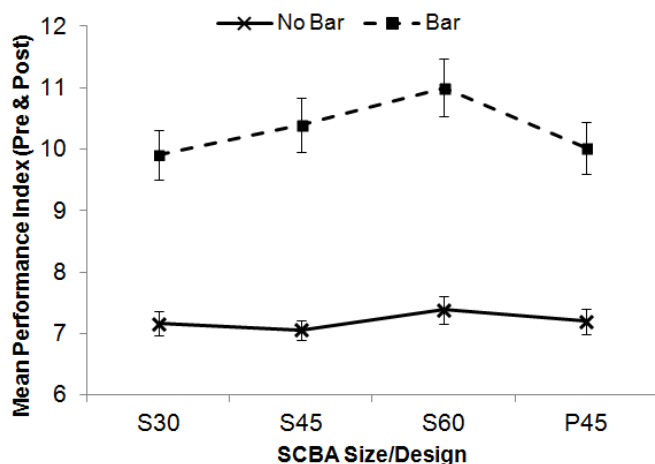


Figure 1: Performance index relative to SCBA size and obstacle presence (used in CG1 and CG2). Standard error bars are shown.

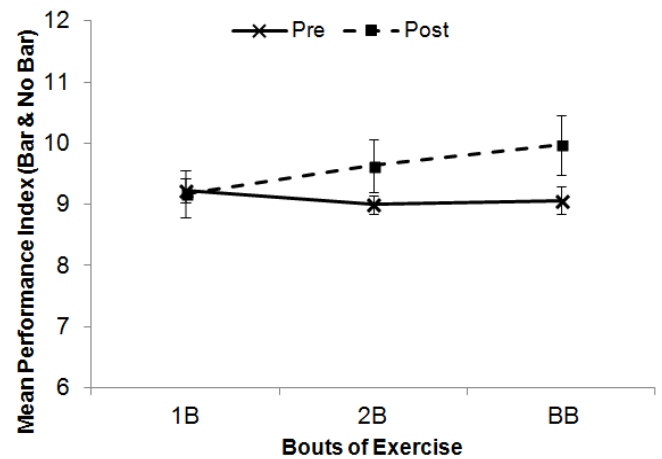


Figure 2: Comparison of varied exercise duration with the S60 SCBA. Standard error bars are shown.

The CG3 analysis varied bouts of exercise using the S60 SCBA. An interaction effect between period and bouts was observed for PI (Fig. 2, $p=0.002$), showing an increased PI after longer duration of exercise. This suggests that being fatigued following BB exercise may lead to a decrease in obstacle-crossing performance.

CONCLUSIONS

These data demonstrate that changes in SCBA size/design and exercise duration can significantly affect functional balance in firefighters. Larger SCBAs may result in a loss of balance and increased mistakes when crossing obstacles, resulting in an increased risk of injury. These findings should be considered by fire departments using larger SCBA with extended duration of firefighting.

REFERENCES

1. Karter MJ. *Patterns of Firefighter Fireground Injuries*, Quincy, MA, USA, 2012.
2. Hur P, et al. *J Ergonomics* **48**, 49-55, 2015.
3. Horn GP, et al. *Ergonomics*, Published online: 19 Jan, 2015.
4. Punakallio A, et al. *Safety Science*, **43** 455-468, 2005.

ACKNOWLEDGEMENTS

This study was funded by DHS grant #EMW-2010-FP-0160.

CONTRIBUTIONS OF AN INTEGRATED BOLSTER SYSTEM TO DYNAMIC LOAD STABILITY WHILE WEARING A BACKPACK OVER BODY ARMOR

¹ Brian K. Higginson and ² Jennifer L. Wheeler

¹ Gonzaga University, Spokane, WA, USA

² Montana State University, Bozeman, MT, USA
email: higginson@gonzaga.edu

INTRODUCTION

Load carriage systems (such as backpacks) are typically designed to interface with the user directly. In many military applications, duty requirements often dictate that load carriage systems be worn over body armor. This change in load-user interface often results in a decrease in load stability. In many military career fields, such as special forces/special ops, load stability can directly affect performance and survivability, particularly during tactical engagements. The two most viable solutions to maximize load stability when an external load is worn over body armor is to develop an integrated armor/load carriage system, or modify the existing load carriage systems to provide a more stable load-user interface. While development of an integrated armor/load carriage system is ongoing, there remains many load carriage and armor systems already in use that may benefit from a redesigned user interface to maximize load stability when being worn over armor.

The purpose of this study was to quantify backpack motion relative to the user/armor system at two treadmill walking speeds, and determine the magnitude of load stabilization offered by an integrated 'bolster' system under these conditions.

METHODS

Backpack-experienced subjects (14 men, Mean \pm SD: 32 \pm 7 yrs, 177.6 \pm 4.4 cm, 78.3 \pm 10.1 kg) were fitted with body armor and a pack frame onto which was mounted a 60 lb military backpack. Subjects then performed a 3-5 minute walking warm-up session in order get accustomed to the treadmill and ensure they were able to comfortably perform at the

two required walking speeds (3 and 4 mph) while carrying the required load used in the study.

At each of the two walking speeds, the subjects carried the load with and without an integrated bolster system attached to the pack, for a total of four test conditions. The integrated bolster system was attached to the pack frame and served to increase contact area laterally between the load and armor system. The load remained unchanged across all testing conditions. In addition to the armor system and pack load, subjects were required to carry an M-16A2 'Rubber Ducky' rifle (i.e., simulating carrying a rifle on patrol), which weighed another 4.1 kg. The four test conditions (two walking speeds and two bolster conditions) were counterbalanced across subjects. Each trial lasted three minutes in duration, with data sampled and averaged over five strides 30 second prior to the end of each trial. A three minute rest period was provided between trials.

Linear and angular measures of motion were quantified for both the armor system and the load (backpack). Angular measures of motion included lateral (side-to-side) and anterior/posterior (front-to-back) changes in angular orientation measured directly using two 2-D inclinometers, one attached to the front plate of the armor system, and the second attached to the back of the pack. Linear measures of motion consisted of vertical, lateral, and forward linear acceleration measured using two 3-D accelerometers attached directly to each of the inclinometers on the armor system and pack. Each measure of motion was averaged over five strides and evaluated for significant differences across conditions using a multivariate 2-factor repeated measures analysis of variance ($\alpha=0.05$).

RESULTS AND DISCUSSION

All measures of linear and angular motion increased for both the pack and armor system as walking speed increased from 3 to 4 mph. With the exception of vertical acceleration, pack motion was always greater than motion of the armor system. Pack angular motion in the lateral direction was twice as much as that associated with the armor (14.1 vs 6.7 degrees respectively, $p<0.001$), and 25% greater (14.7 vs 11.9 degrees respectively, $p<0.001$) in the forward direction. Linear measures of pack motion were 81% ($p<0.001$) greater than armor motion in the lateral direction, and three times greater in the forward direction ($p<0.001$). This difference between pack and armor motion was more pronounced as walking speed increased from 3 to 4 mph. The greatest increases in pack motion as speed increased were seen in the side-to-side angular motion (56% increase, $p<0.001$), and lateral (89% increase, $p<0.001$) and forward (87% increase, $p<0.001$) acceleration. Motion (acceleration) of the pack and armor system in the vertical direction were very similar at the lowest walking speed, and increased by the same magnitude (~60%) as speed increased to the highest walking speeds. This was the only measure tested that was similar for both the pack and armor system across conditions ($p=0.577$).

Use of the integrated bolster system was most effective at reducing pack motion at the higher walking speeds, particularly in the forward and side-to-side directions (both linear and angular measures). Pack motion was reduced by 11% ($p=0.010$) for side-to-side angular motion, 20% for lateral acceleration ($p=0.027$), and 7% for forward acceleration ($p=0.024$) at the fastest walking speed (4 mph). Little difference was seen in pack motion when the bolster system was used at the slowest walking speed. The integrated bolster system had little influence on vertical acceleration ($p=0.805$) or angular pack motion in the front-to-back direction ($p=0.555$). This result is not surprising as the bolster system is located on the lateral aspects of the pack/load system and, as such, has very little potential to affect motion in the vertical or forward direction.

CONCLUSIONS

The results of the current study show that both pack and armor system measures of motion increase as walking speed increases, with pack motion increasing to a greater extent than armor motion for almost all measures. The use of an integrated bolster system was found to decrease the amount of pack motion, particularly at faster walking speeds. The highest walking speed tested in the current study was just under the walk/run transition speed for most subjects. Given the observed increase in pack motion associated with increased walking speeds, it is logical to assume that these increases in pack motion would be exaggerated once walk/run transition speed is exceeded and that the integrated bolster system may be even more effective at reducing pack motion with speeds exceeding the walk/run transition.

PHYSIOLOGICAL AND BIOMECHANICAL CHANGES DURING EXECUTION OF THREE LOAD CARRIAGE PARADIGMS

Leif Hasselquist, Meghan O'Donovan, Kari Loverro, and Carolyn K. Bense

Natick Soldier Research, Development and Engineering Center, Natick MA.

E-mail: Leif.hasselquist.civ@mail.mil

INTRODUCTION

The effects of prolonged load carriage on military populations are not well characterized. Research evaluating the effects of prolonged marching by soldiers carrying an external load has focused on energy cost and not alterations to gait mechanics. Epstein et al. [1] hypothesized that fatigue of skeletal muscles alters gait biomechanics and that this change is the proximal cause of increased energy cost over time when carrying heavy loads. Patton et al. [2] maintained that several mechanisms are probably responsible for the rise in energy cost with prolonged load carrying and proposed, as Epstein et al. [1] did, that a factor of particular importance is a reduction over time in mechanical efficiency due to altered biomechanics. Changes in energy cost and in gait biomechanics that might be associated with long-duration load carriage have critical implications for successful execution of military operations by dismounted soldiers. The purpose of this study was to measure kinematic changes over time associated with three increasingly difficult prolonged load carriage paradigms, while concurrently measuring oxygen consumption ($\dot{V}O_2$).

METHODS

Eleven U.S. Army soldiers (Age, 23 ± 3 years; Ht, 178.6 ± 6.5 cm; Wt, 83.1 ± 9.0 kg; $\dot{V}O_{2peak}$, 49.1 ± 4.3 ml·kg⁻¹·min⁻¹) walked on a treadmill at 1.35 m·s⁻¹ for 2 h on three nonconsecutive days. On each occasion, the soldiers were tested on a different one

of 3 march paradigms: I — 6-kg load, 0% grade; II — 40-kg load, 0% grade; III — 40-kg load, 4% grade (Table 1). $\dot{V}O_2$ data (CPET, COSMED, Chicago, IL) were collected for 2 min at the beginning of the march and then every 30 min (5, 30, 60, 90, and 120 min). A mean was obtained over each 2-min recording period and the data were normalized to the individual's body mass (ml·kg⁻¹·min⁻¹). Kinematic data were also collected at the beginning of the march and then every 30 min via a 12 camera motion capture system (Oqus, Qualisys AB, Gothenburg, Sweden). Joint angles were calculated [minimum, maximum, range of motion (ROM), in degrees] for the ankle, knee, hip and trunk and averaged over 5 consecutive strides (Visual3D™, C-Motion, Inc., Germantown, MD). Single two-way, repeated-measures analyses of variance (ANOVAs) were performed to assess the effects of the 3 march paradigms and elapsed march time. In those instances in which an ANOVA yielded a significant effect ($p < .05$), post hoc analyses were performed with a Bonferroni correction applied.

RESULTS

The $\dot{V}O_2$ analysis yielded a significant interaction ($p < .001$) between march paradigm and time on the march. $\dot{V}O_2$ increased significantly from paradigm I through III, revealing increasing levels of exertion. Steady state energy expenditure was achieved early in the march with paradigm I, whereas $\dot{V}O_2$ increased as time progressed for paradigms II and III (Table 1).

Table 1: Mean (SD) $\dot{V}O_2$ (ml·kg⁻¹·min⁻¹) normalized to body mass for each paradigm and time on the march.

Paradigm (Load, Grade)	2-h March	Time (min)				
		5	30	60	90	120
I: 6 kg, 0%	13.07 (1.27) _A	13.03 (1.09) _A	13.13 (0.98) _A	13.05 (1.11) _A	13.06 (1.42) _A	13.07 (1.20) _A
II: 40 kg, 0%	17.37 (1.73) _B	16.71 (1.46) _A	16.82 (1.94) _{AB}	17.46 (1.71) _{AB}	17.56 (1.51) _B	18.3 (1.81) _C
III: 40 kg, 4%	23.86 (1.68) _C	22.84 (1.45) _A	23.42 (1.50) _A	23.86 (1.41) _B	24.40 (1.51) _B	24.76 (1.99) _B

In each row, means for Time that do not share the same subscript differed significantly in post hoc tests ($p < .05$).

There was a significant main effect of paradigm on ankle ($p < .001$), knee ($p < .02$), and hip ($p < .001$) ROMs. Paradigm III differed significantly from paradigms I and II in post hoc tests, with higher ankle and hip and lower knee ROM (Table 2). There were significant paradigm by march time interactions for maximum trunk ($p < .001$) and hip angles ($p < .05$). As the march progressed, there was little change in these maximum angles for paradigm I, whereas paradigms II and III revealed increased flexion (Figure 1).

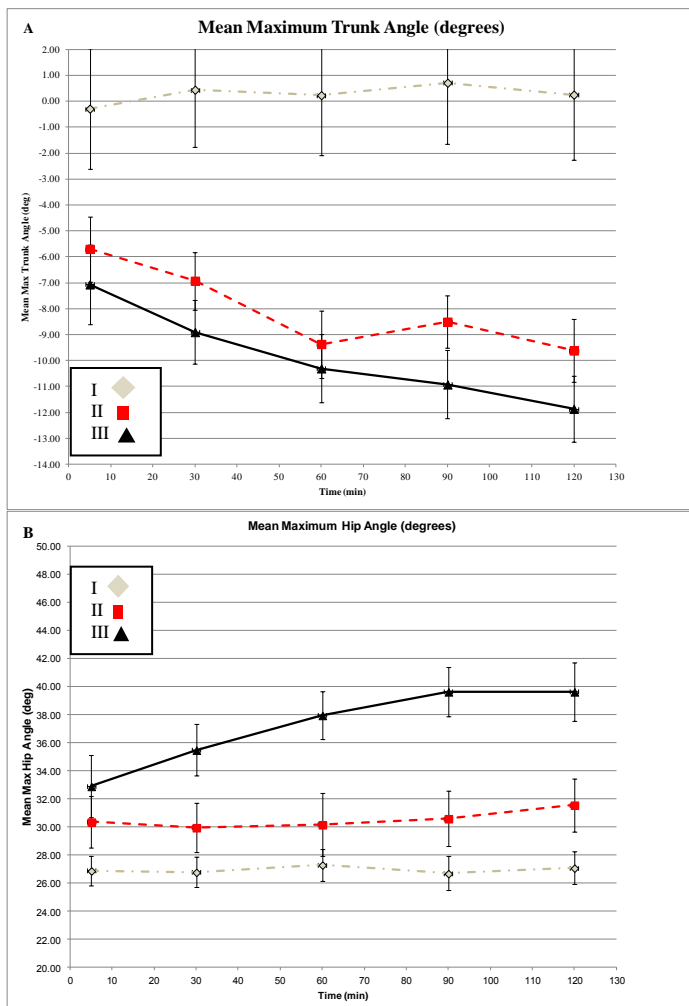


Figure 1: Means (SE) for paradigm by march time interactions on the (A) maximum trunk angle and (B) maximum hip angle measures.

Table 2: Mean (SD) joint ROM (degrees) for each march paradigm (I-III).

Joint	I	II	III
Ankle	29.59 (0.90) _A	31.27 (1.26) _A	32.68 (0.27) _B
Knee	73.07 (0.23) _A	73.07 (1.17) _A	69.67 (0.15) _B
Hip	42.61 (0.33) _A	47.57 (1.41) _A	51.22 (0.81) _B

In each row, means that do not share the same subscript differed significantly in post-hoc tests ($p < .05$).

DISCUSSION

A particular focus of this investigation was the alteration in gait biomechanics that previous researchers [1, 2] hypothesized was the proximal cause of the increases in the energy cost of load carrying. In consonance with the earlier findings, the results of this study showed increases in $\dot{V}O_2$ as march time increased when the heavier (40 kg) load was carried (paradigms II and III). In addition, analysis of kinematic data in the current study supported the hypotheses of Epstein et al. [1] and Patton et al. [2] insofar as changes in gait kinematics were obtained for the more strenuous march paradigms. As time on the march progressed, maximum trunk and hip angles reflected an increased flexed posture with the heavier load (paradigms II and III) compared to the lighter load (paradigm I). Joint angles for paradigm III, when compared to I and II, also differed significantly, with higher ankle and hip and lower knee ROM.

CONCLUSIONS

These study results demonstrate an association between the increases in energy cost and changes in biomechanics. Changes in energy cost and in gait biomechanics that are associated with long-duration load carriage have critical implications for successful execution of military operations by dismounted soldiers. The higher metabolic costs are likely to have a negative effect on efficient completion of a march and success in undertaking subsequent tactical operations. In addition, alterations in gait biomechanics over time may increase the probability of musculoskeletal injury.

REFERENCES

1. Epstein Y, et al. *Eur J Appl Phys* **57**, 243-247, 1988.
2. Patton JF, et al. *Eur J Appl Phys* **63**, 89-93, 1991.

Effects of Load Carriage and Surface Inclination on Slip and Trip Risks

Ehsan Rashedi, Hema Bhatt, and Maury A. Nussbaum

Virginia Tech, Blacksburg, VA, USA
email: nussbaum@vt.edu

INTRODUCTION

Slips, trips, and falls continue to be significant occupational safety concerns, and causes of occupational injuries and fatalities in the workplace and daily activities. While extensive gait research has focused mainly on level walking, less evidence is available for inclined surfaces. The latter is particularly important since walking on inclined surfaces increases the risk of instability and slips, due to the generation of higher shear forces.

Diverse work environments (e.g., construction and agriculture) require load carriage during walking on inclined surfaces. However, few studies have assessed the risks of slips or trips in such conditions. To our knowledge, this is the first study that specifically investigated different methods of load carriage without the use of packs or other assistive devices and the influence of walking on inclined surfaces. We hypothesized that surface inclination, load carriage method, and load magnitude would significantly affect biomechanical parameters related to the risks of slipping or tripping.

METHODS

Twenty participants (gender balanced), with no self-reported musculoskeletal disorders, completed the experiment after giving informed consent (procedures approved by the VT IRB). Respective means (SD) for age, stature, and body mass were 26.1 (3.3) yrs, 167.9 (7.4) cm, and 72.3 (9.0) kg. Each participant walked in 12 different loaded conditions (e.g., Fig. 1). The 12 conditions involved all combinations of: 1) three *surface inclinations* (SIs): level, up and down a 20° incline, 2) two types of *Load Carriage* (LC): on head and posterior load carriage (on upper back), and 3) two *Load Magnitudes* (LM): medium (7.5 kg) and heavy (15 kg) loads. Dependent variables were step length (SL), walking velocity (WV), required coefficient

of friction (RCOF), heel contact velocity (HCV), and minimum toe clearance (MTC), each of which were normalized to values from additional no-load conditions.

Consistent shoes were provided to the participants, and 18 passive retro-reflective markers were placed over bony landmarks to track segmental kinematics using a 9-camera system (Vicon Motion System Inc., Los Angeles, CA, USA). Kinematic data were recorded at 120 Hz, and low-pass filtered with a cutoff frequency of 5 Hz. Ground reaction forces were sampled (960 Hz) from two force platforms (AMTI OR6-7-1000, Watertown, MA, USA), and low-pass filtered at 12 Hz.

Separate repeated-measures analyses of variance were performed to assess the effects of SI, LC, and LM on each normalized dependent measure, with *post hoc* comparisons done using Tukey's HSD. Student *t* tests were used to compare conditions to the relevant no-load conditions. All statistical analyses were conducted using JMP Pro 11 (SAS Institute Inc., Cary, NC), and statistical significance was determined when $p < 0.05$.

RESULTS AND DISCUSSION

All dependent measures were significantly affected by SI (Table 1), with substantial effects in some cases (Fig. 2). Compared to the level walking, SL decreased by 5.3% going uphill, while WV and HCV respectively decreased by 2.4 and 10.4% going downhill. There were 7.4 and 6.4% decreases in RCOF during downhill and uphill walking, respectively. MTC during downhill walking was 8.9% larger than in level walking. Main effects of LC and LM were only significant on WV. Normalized WV was 1% lower when carrying the heavier loads, while it was 2% higher carrying the load on the back. During level walking, RCOF was

larger for on head versus posterior load carriage (~5%).

RCOF and HCV are the main parameters associated with friction demand during human gait [1]. A slip event can be initiated when the required friction demand exceeds the available friction. In all surface conditions, RCOF increased relative to the no-load condition, especially during level walking (~9.3%), indicating a higher risk of slip initiation. An increase in HCV has been considered to increase the likelihood of slip-induced falls [2]. Similar to previous work [1], HCV decreased with load carriage, and is likely related to adoption of slower gait (~3.8%). However, the decrease in WV was not as large as the decline of HCV, which was more pronounced in downhill walking. Specifically, WV decreased by 5.3%, while HCV decreased by 13.6%, and which might indicate adoption of safer gait to decrease slip risk during the most risky condition (walking downhill). Decreased MTC increases trip risk, and which may increase the risk of fall-related injuries [3]. While carrying a load, MTC decreased during uphill (~0.9%) and flat (~3.3%) walking, and suggests a higher trip risk.

Overall, SI was the most influential factor in this study. Except for WV, use of different LMs did not significantly affect any of the dependent variables. Similarly, the main effect of LC method (i.e., on head versus posterior load carriage) was only significant on WV. Considering RCOF, LC method was mainly influential while walking over the flat surface. In summary, interventions to decrease the risk of slips, trips, and falls while carrying a load on different surfaces may focus more on *Surface Inclination*, rather than the *Load Magnitude* or the *Load Carriage* method.

Table 1: Summary of ANOVA results (*p* values) for main and interactive effects of SI, LC, and LM.

	SI	LC	LM	SI×LC	SI×LM	LC×LM
SL	<0.0001	0.19	0.48	0.39	0.65	0.82
WV	0.0013	0.0132	0.0170	0.08	0.21	0.94
HCV	0.0033	0.31	0.15	0.06	0.70	0.94
RCOF	<0.0001	0.28	0.40	0.0053	0.61	0.50
MTC	<0.0001	0.15	0.52	0.41	0.63	0.88



Figure 1: Experimental setup, walking uphill while participant carried the heavy load on the head.

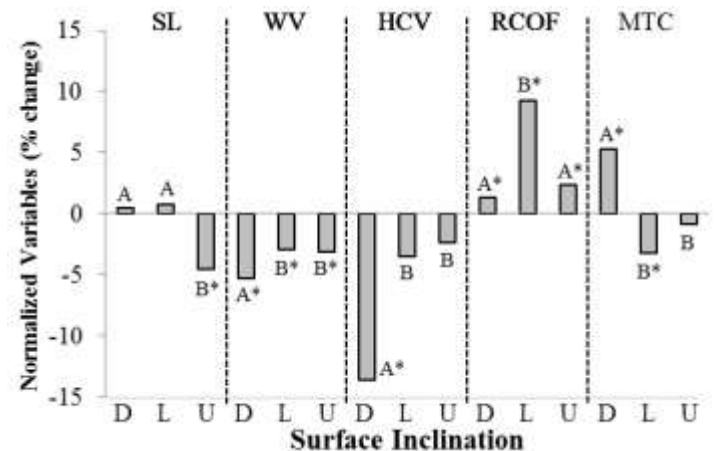


Figure 2: Effects of *Surface Inclination* (D: downhill, L: level, U: uphill) on SL, WV, HCV, RCOF, and MTC. Letters indicate significant pairwise differences between SI conditions, and * a significant difference from the no-load condition.

REFERENCES

1. Redfern M. et al., *Ergonomics*, 44(13), 1138-1166, 2001.
2. Mills PM et al., *Human Movement Science*, 20(4-5), 427-446, 2001.
3. Winter DA, *Physical Therapy*, 72(1), 45-53, 1992.

A CLINICAL PERSPECTIVE ON PROSTHETICS

¹ Francois. J. Van Der Watt

¹ LIM Innovations, San Francisco, CA, USA

email: fvanderwatt@liminnovations.com, web: www.liminnovations.com

INTRODUCTION

To better understand the capabilities of wearable active and passive leg prostheses, it is important to gain a perspective of the history of these devices. Thus, I will provide a general overview of lower limb prosthetic devices that will cover prosthetic device development since World War II [1] as well as the functional and clinical limitations of these devices for people with lower limb amputations. I will also present an introduction to present day micro-processor controlled devices and powered prosthetic devices for different levels of amputation. Sport or activity specific devices will also be discussed as many people with lower limb amputation require prosthetic devices that can improve their sport performance as well as allow them to lead an active lifestyle that would not be possible with conventional prosthetic devices.

TECHNOLOGY

Following WWII, the need for prosthetic devices grew substantially due to injuries sustained in the war. This dramatic increase in service members with amputations facilitated rapid development of lower limb prostheses. To understand the potential functional benefits or drawbacks of these devices, I will establish a timeline of the advancements made in prosthetic devices and the technological development of prostheses up to today (Fig. 1). Further, I will discuss the role and contribution of the Department of Veterans Affairs (VA) in the development and research of prosthetic devices.

CURRENT PROSTHETIC DEVICES

Current day commercially available prosthetic devices and components have the potential to improve locomotion and function for people with a leg amputation. Examples of these prostheses and components include microprocessor controlled (MPC) and powered controlled (PC) prosthetic devices, the C-Leg by Otto Bock (Germany), the

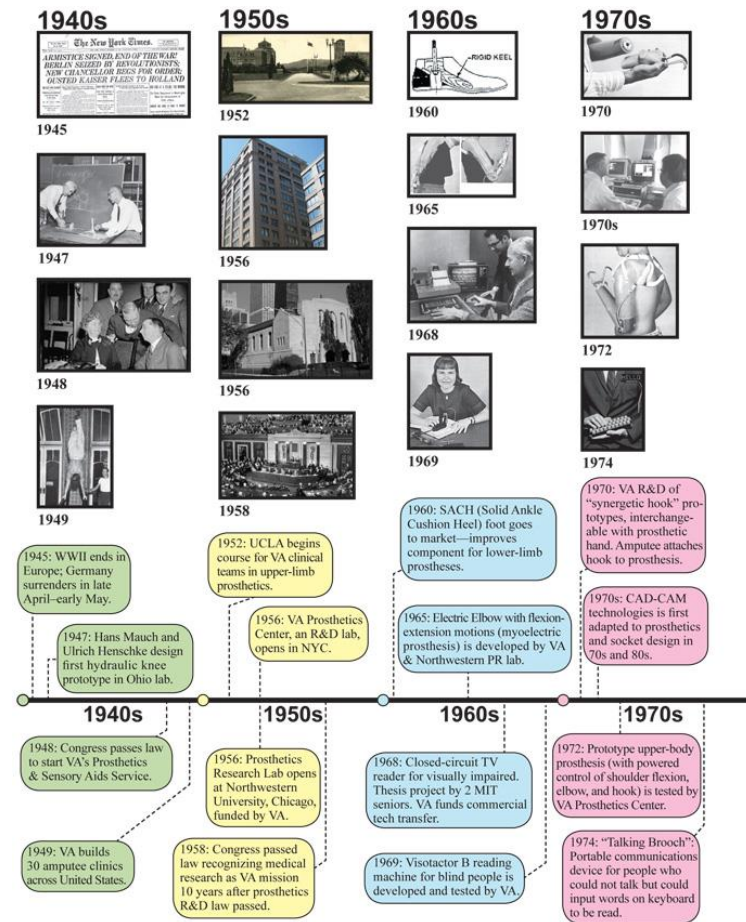


Figure 1. Chronology of Department of Veterans Affairs (VA) Optimization Study.



Figure 2. Power Knee (Össur)

Rheo Knee and Power Knee (Fig. 2) by Össur (Iceland), the BiOM T2 System Foot (Fig. 3) by BiOM (USA) and the Proprio Foot by Össur

(Iceland) [2-5]. Sport specific prosthetic devices like the Cheetah foot (Fig. 4) by Össur can improve activity specific sport performance and I will discuss the implications for future development of these activity specific devices.



Figure 3. BiOM T2 Foot (BiOM)



Figure 4. Cheetah Foot (Össur)

FUTURE DEVELOPMENTS

Clinical indications for future developments are needed in the functioning of prosthetic devices. The future functional and outcome requirements of the amputee population should be considered in developing the next generation of prosthetic devices that include a powered driven or a passive prosthetic device. Considerations for integrated prosthetic devices to include the socket system will also be discussed. Integrated systems can include various levels of micro processing function and communication of control mechanisms in the complete prosthetic device. A brief discussion will follow of the future development and research of

neuro-integrated and osseointegrated (Fig. 5) prosthetic devices.



Figure 5. Osseointegration

CONCLUSIONS

The history of prosthetic device development post WWII up to present day provides an important context for current devices. The advancement of technology and the role in prosthetic device development to improve function and outcomes for the lower limb amputee will be presented. The clinical considerations will be discussed in the development of the next generation of advanced prosthetic devices for the lower limb amputee population. The continued need for sport performance for amputee athletes and the role of prosthetic devices used in human performance will demonstrate the need for improved future prosthetic device design and development.

REFERENCES

1. McAleer N. *J Rehabil Res Dev.* **48(2)** vii-xvi, 2011
2. Ossur.com <http://www.ossur.com/prosthetic-solutions/products/knees-and-legs/bionic-knees/power-knee>
3. BiOM.com <http://www.biom.com/prosthetists/bionic-benefits/>
4. ProMotion.com <http://pmp prosthetics.com.au/teaching/>
5. Ossur.com <http://www.ossur.com/prosthetic-solutions/products/feet/feet/cheetah-xtreme>

ANKLE-FOOT PROSTHESES FOR IMPROVED BALANCE AND STABILITY DURING STANDING AND SLOPED WALKING

¹⁻² Andrew Hansen, ¹ Eric Nickel, ³ Jonathan Sensinger, ¹⁻² Stuart Fairhurst,
¹ Steve Morin, ¹ Sara Koehler-McNicholas, ¹⁻² John Ferguson

¹ Minneapolis VA Health Care System, Minneapolis, MN, USA

² University of Minnesota, Minneapolis, MN, USA

³ University of New Brunswick, Fredericton, New Brunswick, Canada

e-mail: Andrew.Hansen2@va.gov

INTRODUCTION

Many persons with lower-limb amputations have low balance confidence, which is associated with reduced mobility and social activities [1]. Persons with amputations also fall at a high rate [2, 3]. The circumstances that lead to falling and reduced balance confidence are not well understood. However, differences in biomechanics between physiologic and prosthetic ankle-foot systems for different functional tasks (e.g. standing) and walking conditions (e.g. sloped terrain) suggest advancements that may improve future outcomes.

The physiologic ankle-foot system conforms to a curved effective rocker shape for level walking and to a flat effective rocker shape for standing and fore-aft swaying [4]. Our measurements of over forty prosthetic feet commercially available in the 2000s suggest that designs were focused on providing good function for level walking, with less focus on standing function. Roll-over shapes of prosthetic feet tested had radii much closer to that of the able-bodied ankle-foot system during walking than during standing and fore-aft swaying.

The physiologic lower-limb system adapts for uphill and downhill walking, with a net “dorsiflexion” of the leg’s effective rocker shape for uphill slopes and a net “plantarflexion” of the effective rocker shape for downhill slopes [5]. Many prosthetic feet provide good function for level walking. However, most do not alter their characteristics for walking on sloped surfaces. The systems that do adapt their function for sloped walking often have delays associated with the use of sensors to estimate the surface slope, or they utilize damping that removes energy from the system.

Our group’s development efforts in ankle-foot prostheses have been focused on improving balance and stability during standing and sloped walking. Improving balance and stability of lower-limb prosthesis users during standing and sloped walking may lead to increased balance confidence, reductions in falling, and increased participation in life activities (e.g. family, work, and community).

METHODS

Our group has recently developed a bimodal ankle foot-system [6] that provides a curved effective rocker shape for walking and a flat effective rocker shape for standing (Fig. 1). The bimodal ankle-foot system has an automatic switching circuit that utilizes a gyroscope to determine whether the user is walking or standing. A smartphone application can be used to manually control the ankle when the automatic mode is not desired.

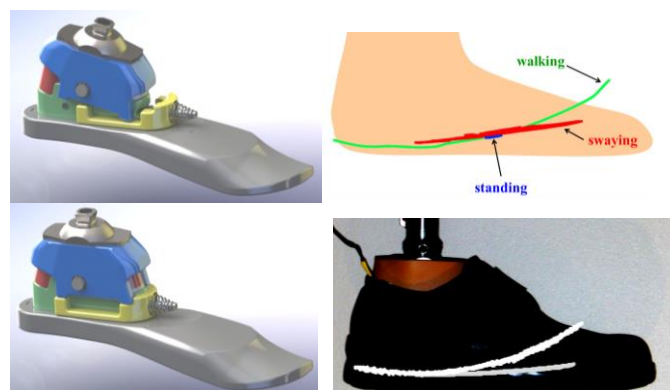


Figure 1: (Left) Bimodal ankle in walking mode (top) and standing mode (bottom). (Right) Effective shapes for walking, standing, and swaying for able-bodied persons (top) and for the bimodal ankle (bottom).

Our group has also been working on ankle-foot prostheses that adapt their equilibrium-point by allowing the foot to “find” the walking surface under a low stiffness, and then engaging a higher stiffness element at foot flat [7]. This “EquiFoot” approach provides adaptation to walking slopes on every step of walking and has been demonstrated with mechanically passive prototypes (Fig. 2).



Figure 2: (Left) Photograph of the EquiFoot adaptable ankle-foot prosthesis. (Right) The EquiFoot at “foot flat” on different slopes (i.e., the time used to set the equilibrium-point of the ankle).

RESULTS AND DISCUSSION

Our group has built working prototypes of both the bimodal and EquiFoot ankle-foot prostheses and has conducted limited pilot testing in the laboratory. Results from mechanical testing of the bimodal ankle demonstrate that the standing mode provides a rocker radius that is above the center of mass of the body, creating a mechanically stable system [6].

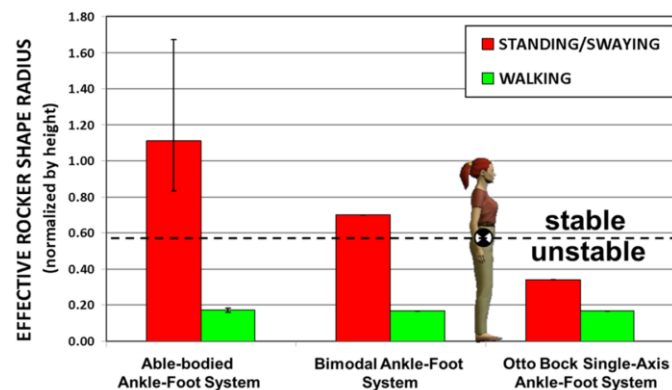


Figure 3: Effective rocker radii for able-bodied, bimodal, and single-axis prosthetic feet. The bimodal ankle provides a stable base for standing.

Testing of the bimodal ankle-foot system with one person with transtibial amputation demonstrated improvements in balance when using the system in standing mode compared with walking mode. The subject also commented that it was the most stable he had felt during standing since his amputation.

Three persons with transtibial amputations have provided feedback on the EquiFoot prototype shown in Fig. 2. For all subjects, the ankle torque versus ankle angle curves were shifted toward dorsiflexion for uphill walking and toward plantarflexion for downhill walking. Subjects commented that it was more comfortable and took less exertion to walk on sloped surfaces with the EquiFoot compared to their usual non-adaptable prosthetic feet.

Current work on these projects includes further development toward commercially-viable ankle-foot prostheses as well as human subjects testing in the laboratory. Future work will include technology transfer and long-term clinical testing to determine if use of these systems will lead to increased participation in life activities.

REFERENCES

1. Miller et al. *Arch Phys Med Rehabil*, **82**(9): 1238-1244, 2001.
2. Miller et al. *Arch Phys Med Rehabil*, **82**(8): 1031-7, 2001.
3. Gauthier-Gagnon F et al. *Arch Phys Med Rehabil*, **80**(6): 706-13, 1999.
4. Hansen and Wang, *Gait and Posture*, **32**: 181-184, 2010.
5. Hansen et al. *Human Movement Science*, **23**(6): 807-821, 2004.
6. Hansen and Nickel, *ASME Journal of Medical Devices*, **7**(3):035001, 2013.
7. Nickel et al, *J Rehabil Res Dev*, **51**(5): 903-814, 2014.

ACKNOWLEDGEMENTS

The research reported here was supported by the Department of Veterans Affairs, Veterans Health Administration, Rehabilitation Research and Development Service under awards A1531-R and A1514-R.

A RUGGED MICROPROCESSOR CONTROLLED ANKLE-FOOT PROSTHESIS FOR RUNNING

Jeffrey Ward¹, PhD, Kyle Schroeder¹, PhD, Dustin Vehon¹, Robert Holgate¹, Alexander Boehler¹, Martin Grimmer², PhD

¹SpringActive, Inc., Tempe Arizona

² Technische Universität, Darmstadt Germany

E-mail: Jeff.Ward@springactive.com, Web: www.springactive.com

INTRODUCTION

Lower limb amputees typically expend 10-30% additional metabolic cost to walk depending on gait speed and amputation level as compared with able-bodied individuals. Many also experience significant gait asymmetry, lower back pain, slower walking speeds, reduced activity levels, and overuse injuries on their unaffected limb.

An intelligent, powered ankle prosthesis has been developed that provides the user with a fully powered and properly timed push-off, picks the toe up in the swing phase, and provides a more natural and energy efficient gait to below the knee amputees. The Ruggedized Odyssey Ankle (ROA), Fig. 1, utilizes a compliant actuator to store the natural braking energy just after heel strike, while a small lightweight motor adds additional energy to the step[1].

Table 1 lists important properties of the ROA device. These performance specifications are made possible by the uniquely tuned ankle spring, the energy store and release actuation scheme, and our continuous (non-state based) gait controllers [2]. Our control scheme examines the phase plane of the tibia's angular velocity and elevation angle to determine a proper actuator position. An actuator position surface was previously developed in terms of walking gait percent and stride length [2]. This surface was recently adapted to include running gait, Fig. 2.

Table 1: ROA Specifications

Mass of Device (kg)	2.5
Maximum Dorsiflexion (deg)	26
Maximum Plantarflexion (deg)	38
Peak Ankle Torque Output (Nm)	190
Max Output Power @ Ankle (W)	1,100
Motor Portion (W)	250
Spring Portion (W)	850
Motor Power Amplification	4.4

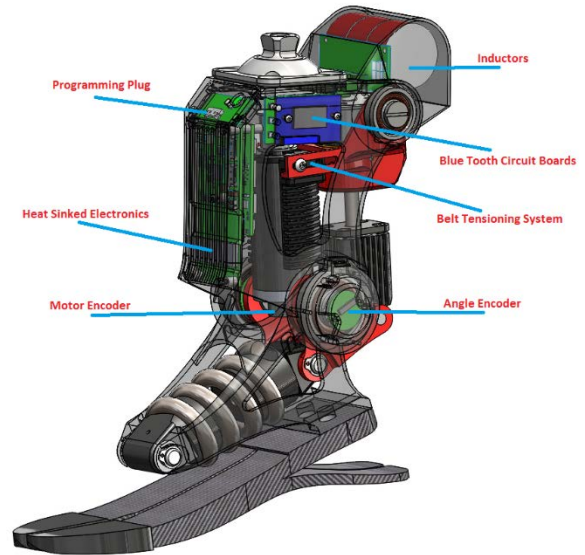


Figure 1: 3D Model; Ruggedized Odyssey Ankle

Able-bodied input data for the running controller was provided by the Lauflabor Locomotion Lab (TU Darmstadt, Germany, www.lauflabor.de) [3].

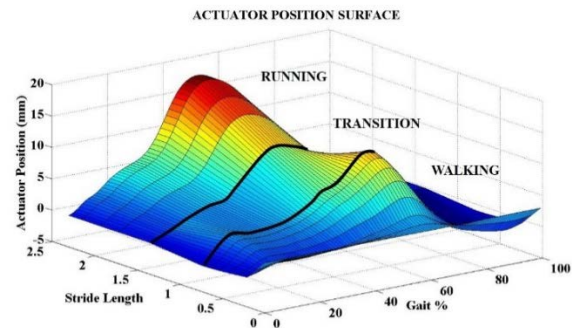


Figure 2: Actuator Position Surface; Illustrates the Walking, Transition, and Running Regions.

METHODS

Pilot data have been collected from two otherwise healthy and high functioning unilateral transtibial amputees, Table 2. Ankle angle, moment and power information were derived from embedded sensors on ROA. Video recordings were made from several of the sessions. Prior to data collection, each participant

wore ROA and walked or ran on the treadmill at various speeds while the device's timing and power were tuned. After completion of the tuning procedure adequate time was allowed for the participant to gain familiarity with the device. This included walking and running over ground.

Table 2: Specification for the two male participants of the pilot study.

Sub #	Weight	Age	K-Level	Affliction
001	72 (kg)	58	K4	Transtibial
002	84 (kg)	36	K4	Transtibial

RESULTS & DISCUSSION

Fig. 3 (left) compares ROA treadmill running (Subject# 001) from 1.6 to 2.5 m/s (3.6 to 6 mph) to able-bodied treadmill running data³ at 2.0 m/s (4.5 mph). This figure demonstrates that the kinematics and kinetics supported by ROA have similar characteristics as able-bodied gait. The ROA walking data, Fig. 3 (right), were collected on the treadmill at 1.2 m/s (2.7 mph), while the able-bodied comparison data is for treadmill gait at 1.04 m/s (2.3 mph) and 1.55 m/s (3.5 mph). Measured ankle

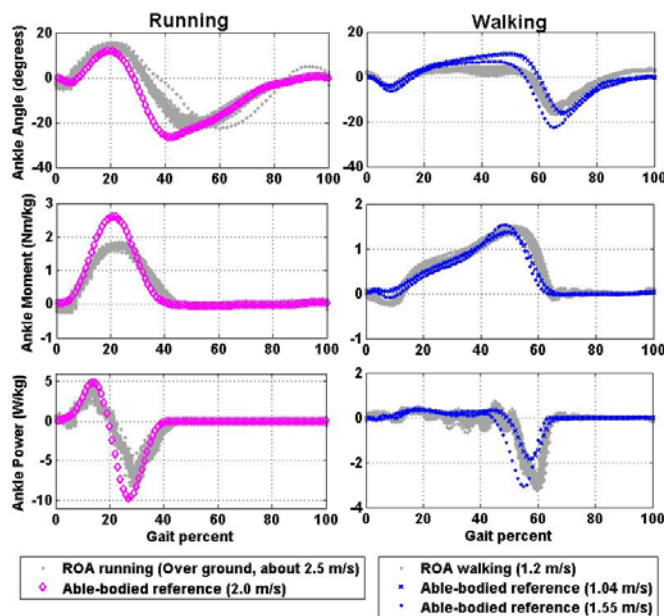


Figure 3: Ankle Angle, Normalized Moment and Power of ROA during Running and Walking for Subject# 001 Compared to Able-Bodied Data

angles, moments and powers are comparable to the able-bodied data.

Fig. 4, illustrates the average kinematics and kinetics over 18 treadmill walking steps for subject 002 at 3.3 mph. Ankle range of motion, moment and power

have shape, timing and amplitude characteristics of able-bodied norms.

CONCLUSION

Initial testing of ROA shows a strong correlation with able-bodied kinematics and kinetics for both walking and running gaits. Future work will focus on clinical trials to fully understand how powered ankle systems affect amputees from a whole-body perspective and to identify the amputee groups that will benefit the most from the technology.

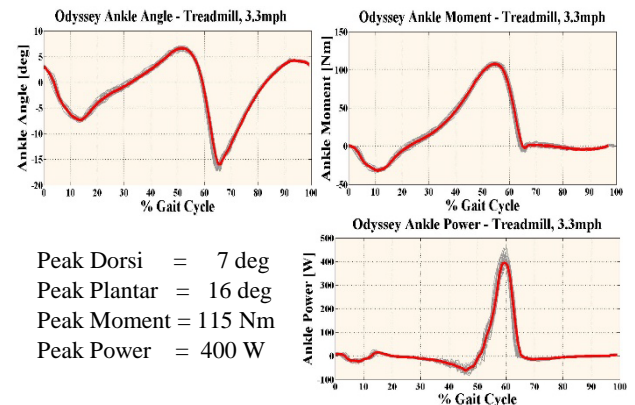


Figure 4: Average of 18 treadmill walking steps for Sub 002, 3.3 mph gait.

REFERENCE

1. Sugar, T. G., Hollander, K. W., Boehler, A. & Ward, J. Comparison and Analysis of a Robotic Tendon and Jackspring™ Actuator for Wearable Robotic Systems. *J. Med. Devices* **7**, 041003–041003 (2013).
2. Holgate, M. A., Sugar, T. G. & Bohler, A. W. A novel control algorithm for wearable robotics using phase plane invariants. *In Robotics and Automation, ICRA, IEEE International Conference on* 3845–3850 (2009).
3. Grimmer, M., Eslamy, M. & Seyfarth, A. Energetic and Peak Power Advantages of Series Elastic Actuators in an Actuated Prosthetic Leg for Walking and Running. *Actuators* **3**, 1–19 (2014).

ACKNOWLEDGEMENTS

This work is supported by the US Army Medical Research and Materiel Command under Contract No.W81XWH-12-C-0266.

The views, opinions and/or findings contained in this report are those of the author(s) and should not be construed as an official Department of the Army position, policy or decision unless so designated by other documentation.

PROSTHETIC LIMBS THAT REDUCE THE ENERGY COST OF WALKING TO BELOW NON-AMPUTEE LEVELS ARE POSSIBLE BUT HARD TO DISCOVER

Steven H. Collins

Carnegie Mellon University, Pittsburgh, PA, USA
stevecollins@cmu.edu, <http://biomechatronics.cit.cmu.edu>

INTRODUCTION

This symposium addresses the question: Can active or passive prosthetic legs augment performance in people with amputation? In terms of reducing the energy cost of locomotion, all signs point to 'yes'. In principle, walking at constant speed on level ground requires no energy input. In practice, both powered [1] and unpowered [2] ankle exoskeletons can reduce the energy cost of unimpaired human walking to below normal levels. Powered prostheses can reduce the energy cost of walking compared to passive devices [3, 4] and passive prostheses can allow the same cost of transport as for unimpaired controls [5]. Ankle-foot prosthesis controllers can even reduce the energy used for active balance [6]. It is likely that powered, semi-active and unpowered prostheses will eventually lead to more economical gait than possible with biological legs.

Despite these positive signs, we cannot predict now the formula for success. Many devices expected to augment gait, powered or passive, have failed. The benefits of powered prostheses, and their effects on gait mechanics, have not been consistent [4], and many studies have found performance deficits with passive prostheses. Some amputees experience lower metabolic rate or increased satisfaction with emulations of robotic prostheses, while others respond better to emulations of passive devices [7]. Net work performed during ankle push-off might be responsible for the benefits of active prostheses, where present, but has not been studied in isolation from other prosthesis features. In non-amputee subjects wearing amputation-simulating boots, increasing prosthetic ankle push-off work in isolation leads to decreased metabolic rate [8], but only if push-off occurs late in stance [9] and without hypothesized reductions in center of mass work.

In this presentation, we will review recent studies that address the theme of augmenting locomotor performance and present the results of a new study intended to isolate the effects of ankle push-off work on the energetics of amputee walking [10].

METHODS

Participants with unilateral, trans-tibial amputation ($N = 6$, 47 ± 6 yrs, 1.79 ± 0.04 m, 88 ± 8 kg) with congenital ($N = 1$) or traumatic ($N = 5$) causes, at least one year post amputation (1-45 yrs) provided written informed consent to a protocol approved by the Carnegie Mellon Institutional Review Board.

Subjects wore an ankle-foot prosthesis emulator [11] in place of their prescribed foot. This tethered, robotic device can apply higher mechanical power than mobile prostheses or the biological ankle joint, without varying other prosthesis features such as mass, stiffness or contact geometry. We applied seven push-off conditions in which net ankle work ranged from -2 to 8 times of the value observed during normal walking at $1.25 \text{ m}\cdot\text{s}^{-1}$. Mechanics during the lead-up to push-off were held constant. Subjects underwent three acclimation days, three training days, and one collection day.

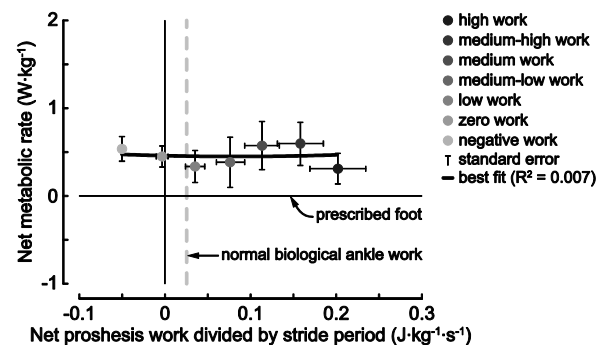


Figure 1: Metabolic rate was not significantly affected by net ankle-foot prosthesis push-off work on average.

We measured lower-limb joint mechanics, muscle activity, center of mass mechanics, and metabolic rate, and performed ANOVA to test for an effect of push-off work on each outcome. We fit quadratic relationships between net ankle work and metabolic rate on average and for each subject.

RESULTS AND DISCUSSION

On average, work input from the prosthesis did not affect metabolic rate (Fig. 1; $P = 0.2$; $R^2 = 0.03$). Effects were inconsistent between subjects (Fig. 2). Negative, low, or moderate net ankle work seemed to minimize metabolic cost in most cases, and no subjects trended towards lower metabolic rate with higher push-off work. Only one subject had lower metabolic rate than with their prescribed foot, achieved at about zero net work. Subjects also preferred medium-low net work ($P = 3 \cdot 10^{-4}$).

Push-off work affected some mechanics and muscle activity outcomes during the period of active push-off, but with inconsistent implications for metabolic rate. With increasing push-off work, prosthesis-side hip work decreased ($H3$; $P = 8 \cdot 10^{-5}$), prosthesis-side negative knee work increased ($K3$; $P = 6 \cdot 10^{-4}$), and intact biceps femoris activity decreased ($P = 3 \cdot 10^{-4}$). Contrary to predictions based on simple dynamic models of walking, increased trailing-limb push-off work did not reduce leading-limb collision work.

CONCLUSIONS

Augmenting gait is not simple. Net work input is thought to be responsible for reduced metabolic rate with powered prostheses, but humans are complex and it is very doubtful that this is the only factor. Subtle mechanical details may have unexpected

effects on, e.g., muscle-tendon dynamics. Details of prosthesis control may also be important, and can reduce or increase energy cost without changing average work input [6]. These and other aspects of prosthesis function are most efficiently studied in experiments with versatile emulator systems [11], which allow single factors to be isolated, rather than comparisons of multi-featured devices.

It is certain that individual differences play an important role in selecting user-optimal device characteristics, illustrated here by the range of responses to increased push-off work. Optimization on an individual basis is challenging for many reasons, but is possible [12] and will be critical to augmentation of amputee locomotion.

REFERENCES

1. Malcolm P, et al. *PLoS ONE* **8**, e56137, 2013.
2. Collins SH, et al. *Nature* **in press**, 2015.
3. Herr HM & Grabowski AM. *Proc Royal Society London B* **279**, 457-464, 2012.
4. Esposito ER, et al. *Prosth Orth Int*, 2015.
5. Esposito ER, et al. *JRRD* **51**, 1287-1296, 2014.
6. Kim M & Collins SH, *JNER*, **12**, 43, 2015.
7. Caputo JM, et al. *Proc. ICRA*, Seattle, WA, 2015.
8. Caputo JM & Collins SH. *Sci Rep* **4**, 7213, 2014.
9. Malcolm P, et al. *JNER*, **12**, 21, 2015.
10. Quesada RE, et al. in preparation.
11. Caputo JM & Collins SH. *J Biomech Eng* **136**, 035002, 2014.
12. Caputo JM & Collins SH, in preparation.

ACKNOWLEDGEMENTS

Based upon work supported by the National Science Foundation under Grant No. CMMI-1300804.

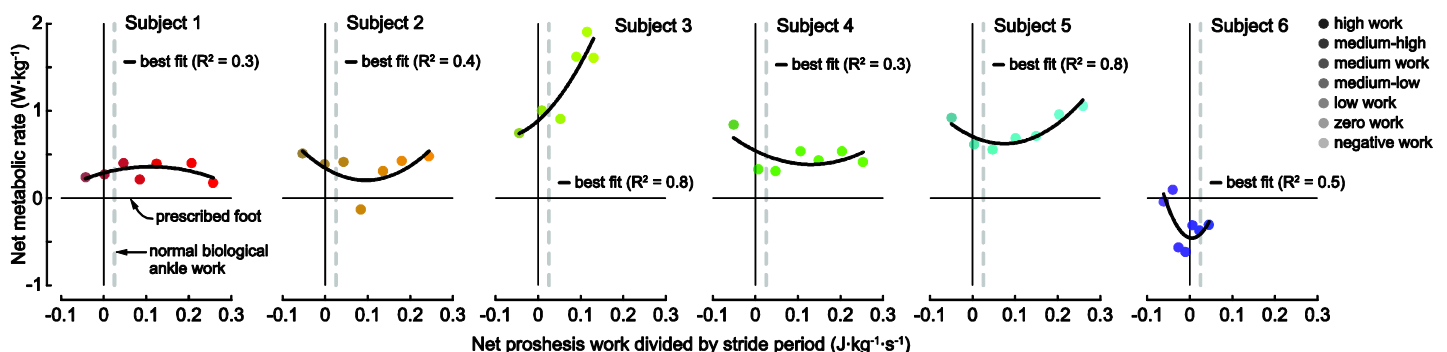


Figure 2: Subjects exhibited widely varying trends in metabolic rate as net work from the ankle-foot prosthesis was increased.

OPTIMIZING LEG PROSTHESES FOR WALKING AND RUNNING: CAN WE AUGMENT PERFORMANCE?

¹Jana R. Jeffers, ¹Owen N. Beck, ¹Paolo Taboga & ^{1,2}Alena M. Grabowski

¹University of Colorado Boulder, CO, USA, ²VA Eastern Colorado Healthcare System, Denver, CO, USA
email: alena.grabowski@colorado.edu, web: <http://spot.colorado.edu/~grabowsa>

INTRODUCTION:

Recent technology incorporates stance-phase power into prosthetic ankles for walking. These powered prostheses generate net positive work by utilizing a motor and battery, could restore full function to people with an amputation [1], and thus may inhibit the sedentary lifestyle adopted by many people with leg amputation using passive prostheses [2]. However, previous studies suggest powered prostheses cannot replicate biological ankle joint function on uneven terrain [3]. Accordingly, we hypothesize that powered ankle-foot prostheses will require robust control to restore biomechanics and metabolic demands during up- and down-hill walking.

Specialized carbon-fiber running-specific prostheses (RSPs) emulate the spring-like function of tendons during level-ground steady-speed running and allow considerable elastic energy return [4]. However, passive-elastic RSPs cannot generate mechanical power, vary stiffness, or dorsiflex to allow foot-ground clearance during leg swing. Because RSPs cannot adapt, the biomechanics of people with a leg amputation are asymmetrical [5], yet metabolic costs may be comparable to those of non-amputees [6]. Optimizing RSP mechanical properties, such as stiffness and height, could improve symmetry, metabolic demands, and performance. We hypothesize that RSPs that elicit symmetrical biomechanics will decrease metabolic costs during running and increase top sprinting speeds in athletes with unilateral leg amputation, and that less stiff RSPs will decrease metabolic costs during running and taller RSPs will increase top sprinting speed for athletes with bilateral leg amputations.

METHODS:

Walk: 3 males with unilateral transtibial amputation were fit with the BiOM and walked 1.25 m/s on a dual-belt force treadmill (Bertec Corp., USA) at 7 slopes (0°, ±3°, ±6°, ±9°) while we measured

kinetics and kinematics (Vicon, USA). We optimized the BiOM tuning for level ground (LVL) and at each slope (ADJ) by iteratively changing tuning parameters until prosthetic ankle joint biomechanics matched those of non-amputees within 1 SD. We measured metabolic rates (Parvo Medics, USA) for 5 min during standing and walking at each slope for LVL and ADJ. We calculated net cost of transport (CoT) with a standard equation and by subtracting standing from walking CoT from the last two minutes of each trial.

Run/Sprint: A certified prosthetist fit 9 runners with unilateral (7 M; 2 F), 3 runners with bilateral (3M), 3 sprinters (2M, 1F) with unilateral, and 3 sprinters with bilateral (3M) transtibial amputations with three different RSP models (RSP1, RSP2, and RSP3) at the manufacturer recommended and ±1 stiffness categories, and at the manufacturer recommended height and ±2 cm; 15 combinations of RSP model, stiffness category, and height.

Runners performed 5 min trials on a force treadmill (Treadmetrix, Park City, UT) at 2.5-3.0 m/s while we measured ground reaction forces (GRFs) and metabolic rates. Sprinters performed sets of trials on the force treadmill while we measured GRFs. Sprinters started each set of trials at 3 m/s, speed was incremented 1 m/s until they approached top speed, then smaller speed increments were employed until subjects reached top speed, which occurred when sprinters could not maintain their position for ten consecutive strides.

RESULTS AND DISCUSSION:

Walk: BiOM ankle net work values for ADJ were within one S.D. of non-amputee values at ±3° and +6°. Net CoT was not different at ±3°, ±6°, or ±9° (p=0.39-0.96) in ADJ versus LVL (Fig. 1). Net CoT was higher for subjects with an amputation compared to non-amputees at -6° and -9° (p<0.05).

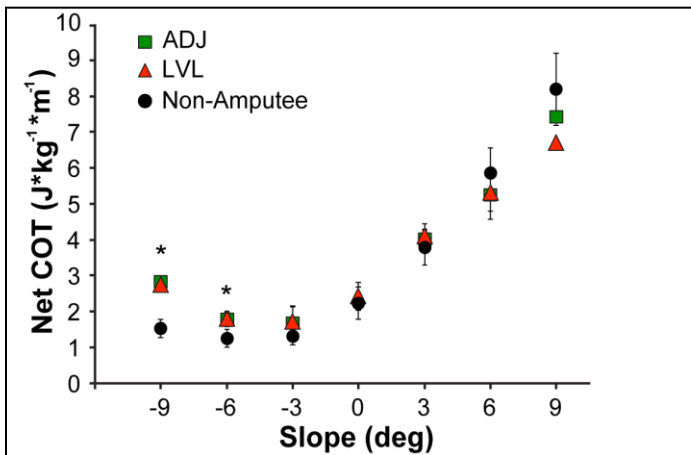


Figure 1: Average (\pm SD) net CoT at 1.25 m/s on up- and downhill slopes with the BiOM tuned for each slope (ADJ) and level ground (LVL), compared to non-amputees.

Run: Runners with unilateral amputations had 4.2-5.2% lower CoT using one RSP model compared to the other two ($p<0.01$), 1.3% lower CoT with -2 cm ($p=0.02$) (Fig. 2), and asymmetrical peak vertical GRFs correlated with higher CoT ($p<0.01$). Runners with bilateral amputations had 5.1% lower CoT with -1 RSP stiffness category ($p<0.01$).

Sprint: Sprinters with unilateral amputations had 8-11% faster top speeds using two RSP models compared to one model ($p<0.005$). For one model, -1 stiffness category increased top speed 5% ($p=0.02$), while -1 cm increased top speed 7% ($p<0.001$). Sprinters with bilateral amputations increased top speed 0.06 m/s with -1 cm RSP height ($p<0.001$) (Fig. 3).

CONCLUSIONS:

Walk: Tuning the BiOM for each slope resulted in normative ankle biomechanics, but no differences in metabolic cost compared to level-ground tuning. The BiOM did not augment performance. Thus, future research is needed to better understand ankle biomechanics and metabolic costs on slopes.

Run/Sprint: Reducing RSP height and peak vertical GRF asymmetry reduced metabolic costs for runners with unilateral leg amputations. Reducing RSP stiffness category reduced metabolic costs for runners with bilateral leg amputations. Faster top speeds were achieved by shortening contact time, and increasing peak vertical GRF in sprinters with unilateral leg

amputations. Surprisingly, shorter RSPs improved top speed in sprinters with bilateral leg amputations. Thus, optimizing RSP mechanical properties improved performance in athletes with leg amputations.

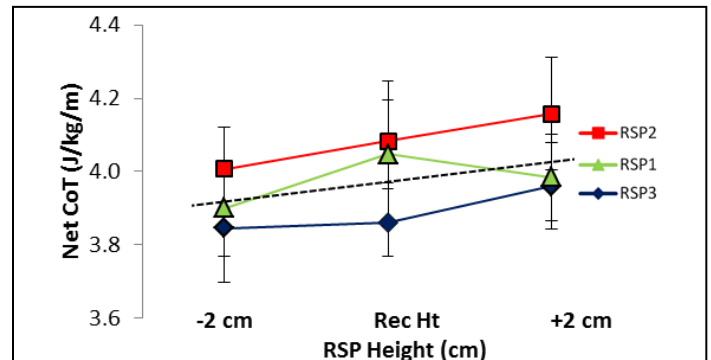


Figure 2: Average (\pm SEM) net CoT for unilateral runners using 3 RSP models at recommended height (Rec Ht) and ± 2 cm. Dashed line is regression line.

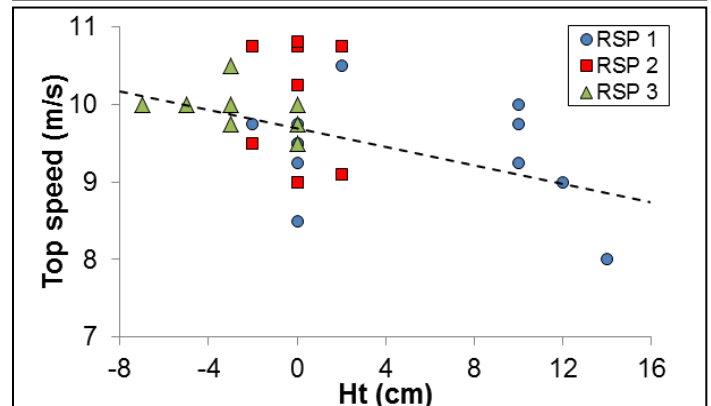


Figure 3: Top speed for each bilateral sprinter and condition relative to RSP height (Ht). Dashed line is regression line.

REFERENCES:

- Herr HM & Grabowski AM. *Proc R Soc B-Biol Sci* **279**, 457-464, 2012
- Hsu MJ, et al. *Arch Phys Med Rehabil* **87**, 123-129, 2006.
- Gates DS, et al. *Clin Biomech* **28**, 467-472, 2013.
- Bruggemann G-P, et al. *Sports Tech* **1**, 220-227, 2008.
- Grabowski AM, et al. *Biol Lett* **6**, 201-204, 2010.
- Brown MB, et al. *Med Sci Sport Exerc* **41**, 1080-1087, 2009.

ACKNOWLEDGEMENTS:

Research supported by a VA CDA-2 (VA RR&D A7972-W) and by the BADER Consortium, DoD, CDMRP cooperative agreement (W81XWH-11-2-0222). We thank Freedom Innovations, Ossur, and Ottobock for donation of prostheses.

CHARACTERIZING FLUOROSCOPY BASED KINEMATIC ACCURACY BASED ON PULSE WIDTH AND VELOCITY

Arin M. Ellingson, Joseph D. Mozingo, Dixon J. Magnuson, Mark W. Pagnano, and Kristin D. Zhao

Mayo Clinic, Rochester, MN, USA

email: zhao.kristin@mayo.edu

INTRODUCTION

Fluoroscopic imaging has become an increasingly popular method to investigate total knee arthroplasty (TKA) kinematics non-invasively. Briefly, 3D implant models are aligned with 2D image projections, and optimized via an edge-detection algorithm (Fig. 1). Prior studies aimed to assess the accuracy of this shape-matching technique, though largely ignore the importance of fluoroscopic imaging parameters [1, 2]. A particularly sensitive parameter in dynamic applications is the pulse width, or exposure time per frame, which if too long may lead to blur (Fig. 1F) and subsequent degradation in image edge quality. This phenomenon has been anecdotally described previously [3]. However, to our knowledge, no studies have quantified the errors associated with increased pulse widths and movement velocity. *Therefore, the purpose of this study was to assess the accuracy of 6 degree-of-freedom TKA kinematics as pulse width and flexion velocity were systematically varied.*

METHODS

One intact, fresh-frozen cadaver right leg was acquired from the Mayo Clinic Bequest Program. Femoral and tibial total knee replacement components (Triathlon® Knee System, Stryker Orthopaedics, Mahwah, NJ, USA) were implanted by an orthopedic surgeon. A portion of the knee was left partially exposed to facilitate digitization of landmarks to establish local anatomical coordinate systems.

The femur and tibia were secured in a custom apparatus that allowed for unconstrained knee flexion at a manually guided rate. The knee was centered in the imaging volume created by the 48 cm flat-panel Multi-Diagnost Eleva C-arm single-plane x-ray system (Philips Medical Systems, Best, Netherlands) perpendicular to the primary plane of bending. X-ray images were acquired at 30 Hz (63 kV, 160 mA). Infrared marker sets were

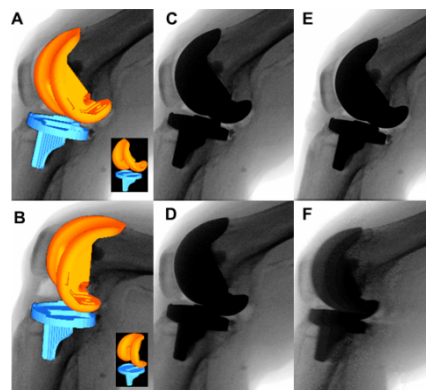


Figure 1- Workflow of 2D/3D Shape Matching. Left: 3D TKA models aligned with silhouette when initially fully extended (A) and fully flexed (B). Middle: Silhouette of 1ms pulse width at initial position (C) and position of maximal flexion velocity (D). Right: Silhouette of 16ms pulse width at initial position (E) and at maximal flexion velocity (F).

attached to bone pins that were embedded in the femur and tibia. 3D kinematics were simultaneously acquired using an Optotrak Certus (Northern Digital Inc., Waterloo, Ontario, Canada) and subsequently downsampled to 30 Hz. The rotation rate was varied between 50°/s, 100°/s, 225°/s for pulse widths of 1ms, 8ms, and 16ms.

An open source model-based tracking program was used to manipulate the position and orientation of 3D CAD models of the femoral and tibial components, such that model edges were coincident with edges of the projected silhouettes on the radiograph (JointTrack, University of Florida, Gainesville, FL, USA). Following manual placement, poses were optimized with a built-in simulated annealing algorithm [4]. Relative orientation was defined using Euler angles (Z-X-Y sequence; flexion/extension, abduction/adduction, external/internal rotation) [5]. The 3D position and orientation of the tibia relative to the femur were determined for all frames of each trial and the limits of agreement were defined using a Bland-Altman technique.

RESULTS AND DISCUSSION

The average kinematic differences between the optoelectric and fluoroscopic methods for the

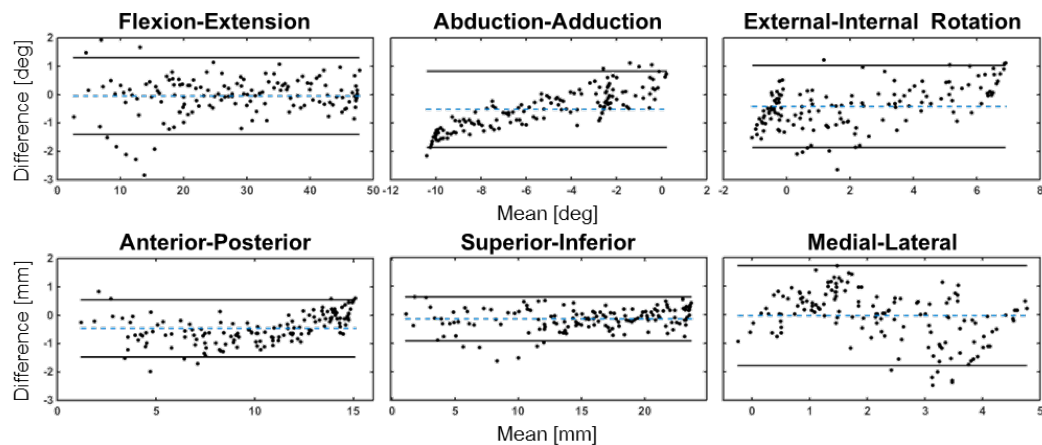


Figure 2: Bland-Altman plots. Demonstrate agreement in kinematic measures between fluoroscopic and optoelectronic methods for 1ms pulse width, 50/s rotation rate trial. Each point represents the mean and difference of relative joint angles (top row) and translations (bottom row) between each method, at a given frame. The dashed and solid lines are the mean difference between methods, and the 95% confidence intervals respectively.

optimal 1ms pulse width was 1.2° and 0.6 mm or less for all trials (Table 1). Figure 2 depicts a Bland-Altman plot demonstrating the agreement between the two kinematic collection techniques. A linear trend was only detected in the abduction rotation ($R^2=0.73$). The overall largest mean differences were in abduction-adduction across trials, but varied in translation.

Comparable mean differences and agreement were observed for the 8ms pulse width – less than 1.2° and 0.8mm (Table 1).

The 16 ms pulse width yielded the greatest mean differences, which were intensified during the most dynamic flexion activity. The mean rotational and translational differences were nearly double (2.0°) and triple (1.6mm) those from 1ms, respectively. Furthermore, the agreement between the systems, represented by the confidence interval, also increased dramatically for the 16ms pulse width.

CONCLUSIONS

In conclusion, this work defines the accuracy of our fluoroscopy system in conjunction with a 2D/3D shape-matching protocol for TKA models, which

was well below previously acceptable levels [2]. This provides a basis for future trials investigating TKA kinematics *in vivo*.

Additionally, the importance of pulse width and velocity should not be overlooked for future studies – greater than 1ms pulse widths should be used cautiously and pulse widths of 16ms and greater avoided. This parameter has proven to be a sensitive metric in the quantification of joint motion via fluoroscopy and must be identified and reported in future studies.

REFERENCES

1. Banks SA. *IEEE Trans Biomed Eng*, **43**(6), 638-649, 1996.
2. Acker S. *J Biomech*, **44**(4), 784-787, 2011.
3. Tashman, S. *J Biomech*, **41**(15), 3290-3291, 2008.
4. Mahfouz MR. *IEEE Trans Med Imaging*, **22**(12), 1561-1574, 2003.
5. Grood ES. *J Biomech Eng*, **105**(2), 136-144, 1983.

ACKNOWLEDGEMENTS

Funding was provided through NIH/NIAMS T32AR56950 and Minnesota Partnership for Biotechnology and Medical Genomics.

Table 1 Mean differences between methods (bold). The limits of agreement in parentheses (95% confidence interval)

Difference	1ms Pulse Width			8ms Pulse Width			16ms Pulse Width		
	50 °/s	100 °/s	225 °/s	50 °/s	100 °/s	225 °/s	50 °/s	100 °/s	225 °/s
Flexion (deg)	-0.1 (-1.4 to 1.3)	1.0 (-0.4 to 2.5)	-0.4 (-2.7 to 1.9)	0.5 (-0.9 to 1.9)	0.5 (-1.1 to 2.1)	0.5 (-1.8 to 2.8)	-0.2 (-1.7 to 1.3)	0.7 (-1.7 to 3.1)	0.8 (-3.1 to 4.6)
Abduction (deg)	-0.5 (-1.9 to 0.8)	-0.4 (-1.7 to 1.0)	-1.2 (-3.9 to 1.5)	-1.0 (-2.3 to 0.3)	-1.2 (-2.8 to 0.5)	-1.2 (-3.2 to 0.8)	-0.9 (-2.2 to 0.5)	-1.5 (-3.1 to 0.1)	-2.0 (-4.2 to 0.3)
Internal (deg)	-0.4 (-1.9 to 1.0)	-0.1 (-1.7 to 1.4)	-0.4 (-2.5 to 1.8)	-0.1 (-0.9 to 0.7)	0.2 (-1.1 to 1.4)	0.7 (-0.7 to 2.0)	0.3 (-1.1 to 1.7)	0.2 (-1.1 to 1.5)	1.0 (-1.0 to 3.0)
Ant / Post. (mm)	-0.5 (-1.5 to 0.6)	-0.4 (-1.6 to 0.8)	-0.3 (-1.6 to 1.0)	0.3 (-0.8 to 1.3)	0.1 (-0.9 to 1.0)	0.1 (-1.7 to 1.9)	0.1 (-1.3 to 1.5)	1.5 (0.2 to 2.8)	1.6 (-0.9 to 4.0)
Sup / Inf (mm)	-0.2 (-0.9 to 0.6)	0.2 (-0.9 to 1.4)	-0.2 (-1.7 to 1.2)	-0.4 (-1.7 to 0.8)	-0.1 (-1.4 to 1.2)	-0.3 (-1.9 to 1.4)	-0.3 (-1.5 to 0.8)	0.8 (-0.5 to 2.2)	-0.9 (-2.8 to 1.1)
Med / Lat (mm)	-0.0 (-1.8 to 1.7)	-0.2 (-2.6 to 2.2)	-0.6 (-2.0 to 0.8)	-0.6 (-2.7 to 1.4)	0.6 (-1.3 to 2.5)	0.8 (-2.2 to 3.9)	0.1 (-2.1 to 2.2)	-0.6 (-3.1 to 1.9)	-0.3 (-2.4 to 1.8)

DYNAMIC TRACKING INFLUENCED BY ANATOMY IN PATELLAR INSTABILITY

¹ John J. Elias, ² Neil T. Soehrlen, ¹ Loredana M. Guseila, and ³ Andrew J. Cosgarea

¹ Akron General Medical Center, Akron, OH, USA

² Northeast Ohio Medical University, Rootstown, OH, USA

³ Johns Hopkins University, Baltimore, MD, USA

email: john.elias@akrongeneral.org

INTRODUCTION

Excessive lateral patellar tracking leading to instability is most common with the knee near full extension. Anatomical factors that are considered contributors to instability include a lateralized tibial tuberosity, trochlear dysplasia, and patella alta. The current study evaluates the influence of these anatomical factors on dynamic in vivo patellar tracking as a function of flexion angle in knees experiencing patellar instability.

METHODS

Eight patients with recurrent instability who had not undergone a previous patellar stabilizing osteotomy were included in the IRB-approved study. Each patient participated in a dynamic CT scan (Aquilion ONE, Toshiba Medical Systems) as part of clinical evaluation. The scans were performed during extension against gravity from a flexed position to full extension over 10 seconds [1]. Computational models of the femur, tibia and patella were reconstructed from 5 to 7 volumes of images spanning the extension range. Shape matching techniques were used to represent each position of knee extension with a single model of each of the three bones. [1, 2].

Patellar tracking was correlated with anatomical parameters. Patellar lateral shift was measured in terms of the bisect offset index as the portion of the patellar width lateral to the deepest point of the trochlear groove (Fig. 1). The measurement was made within a plane perpendicular to the long axis of the patella with the lateral direction defined by the femoral posterior condylar axis. Patellar lateral tilt was measured as the angle between a line along the medial-lateral axis of the patella and the

posterior condylar axis. Trochlear dysplasia was measured in terms of lateral trochlear inclination as the angle between the lateral trochlear ridge and the posterior condylar axis. The tibial tuberosity to trochlear groove (TT-TG) distance was measured as the lateral distance from the deepest point of the trochlear groove to the patellar tendon attachment on the tibial tuberosity. Patella alta was characterized by the Caton-Deschamps index as the ratio of the distance from the superior-anterior aspect of the tibia to the distal point of cartilage on the patella and the length of the cartilage surface along the patella. All measures of patellar tracking and anatomy were quantified using an automated algorithm. Based on previous studies, errors for measures of tilt and lateral trochlear inclination are on the order of 1°, errors for TT-TG distance are on the order of 1 mm, and errors for bisect offset index and Caton-Deschamps index are on the order of 0.05 [1, 2].

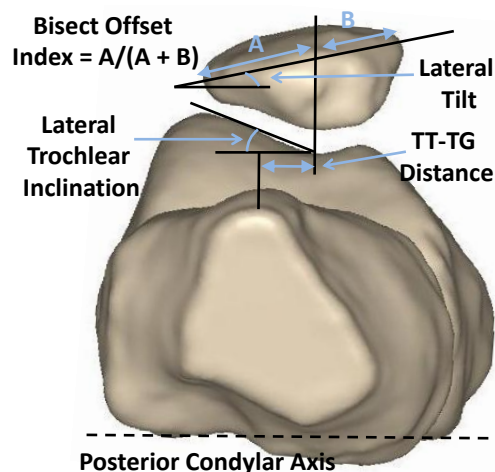


Figure 1: Measures of anatomy and patellar tracking.

Patellar tracking was related to the anatomical parameters using stepwise multivariable linear regression analyses, with $p < 0.15$ required to enter.

The data was separated into flexion angles less than and greater than 20°, based on the approximate angle at which the patella starts to engage the trochlear groove.

RESULTS AND DISCUSSION

At flexion angles less than 20°, bisect offset index was primarily correlated with lateral trochlear inclination, with the relationship with TT-TG distance also significant (Table 1). Lateral tilt was significantly correlated with lateral trochlear inclination. At flexion angles greater than 20°, bisect offset index was significantly correlated with only TT-TG distance. Lateral tilt was significantly correlated with only lateral trochlear inclination. Caton-Deschamps index was not significantly correlated with tracking. The relationships between tracking and anatomy were stronger at flexion angles < 20°. Additional assessment of the relationship between patellar tracking and anatomy with loading conditions more representative of those that produce instability is warranted.

CONCLUSIONS

The results indicate that the relationship between dynamic patellar tracking and knee anatomy in patients with patellar instability varies with the flexion angle. Near full extension, where the patella is most likely to dislocate, patellar tracking is strongly correlated with trochlear dysplasia. Lateral position of the tibial tuberosity has a weaker correlation with patellar lateral shift over all flexion angles. Understanding the relationship between anatomy and tracking helps clinicians assess the risk of recurrent instability and plan effective surgical treatment options.

REFERENCES

1. Elias JJ, et al. *Knee Surg Sports Traumatol Arthrosc*, 22, 2350-6, 2014.
2. Biyani R, et al. *Knee Surg Sports Traumatol Arthrosc*, 22, 2334-41, 2014.

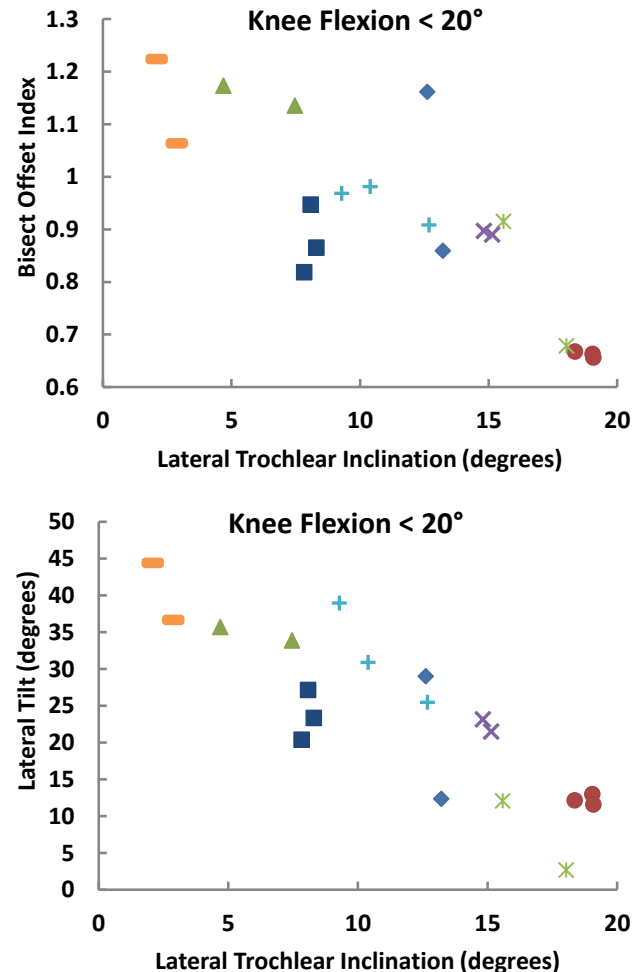


Figure 2: Bisect offset index and patellar lateral tilt vs. lateral trochlear inclination for flexion angles < 20°, with 8 knees distinguished by different symbols.

Table 1: Results of linear regression analyses relating anatomy to patellar tracking

	Bisect Offset Index				Lateral Tilt			
	< 20°		> 20°		< 20°		> 20°	
	p-value	r ²	p-value	r ²	p-value	r ²	p-value	r ²
LTI	< 0.001	0.62	> 0.15	0.00	< 0.001	0.71	0.04	0.11
TT-TG	0.02	0.21	0.02	0.21	> 0.15	0.03	0.08	0.05
CD index	> 0.15	0.00	> 0.15	0.00	> 0.15	0.05	> 0.15	0.00
multivariate	< 0.001	0.72	0.02	0.23	< 0.001	0.71	0.002	0.20

LTI: Lateral trochlear inclination, CD: Caton-Deschamps

INTRA-OPERATIVE FRAGMENT TRACKING FOR ARTICULAR FRACTURE REDUCTION

Andrew M. Kern, Steven A. Long, Geb W. Thomas and Donald D. Anderson

The University of Iowa, Iowa City, IA, USA

email: andrew-kern@uiowa.edu, web: <http://tinyurl.com/UIOBL>

INTRODUCTION

Restoring a joint surface to its original state is the primary goal in the surgical treatment of articular fractures. This is done to minimize articular contact stress and to restore the joint contact mechanics. Despite surgeons' best efforts, the articular reduction is often less than perfect.

Visualizing fracture reduction intra-operatively is a challenging task. It requires constructing a mental 3D model working from 2D images. 3D-to-2D computational registration algorithms have been used to deduce the 3D pose of objects from 2D images^{1,2}. Computer hardware has recently become sufficiently powerful to provide near-real-time performance with these algorithms. Foundational work for an intra-operative, markerless, fragment tracking system is presented here. The system allows for the position and orientation of individual bone fragments to be derived, in near-real time, using intra-operative 2D fluoroscopy images.

METHODS

The basis of the markerless fragment tracking system is iterative comparison of digitally reconstructed radiographs (DRRs) computed from pre-op CT scan data to intra-operative fluoroscopic images. The poses of individual bone fragments are varied *in silico* to maximize the agreement between the real and synthetic images. The system has three separate components: image segmentation, DRR generation, and pose optimization (Fig 1).

The pre-op CT image is pre-processed for DRR generation by converting the Hounsfield Units (HU) to linear attenuation coefficients ($\mu \text{ cm}^{-1}$). A semi-

automated, watershed-based, image segmentation is performed to uniquely identify individual fragments in a label map. A sub-volume is created for each bone fragment by using the label map to tightly crop a bounding box around each region (Fig 2).

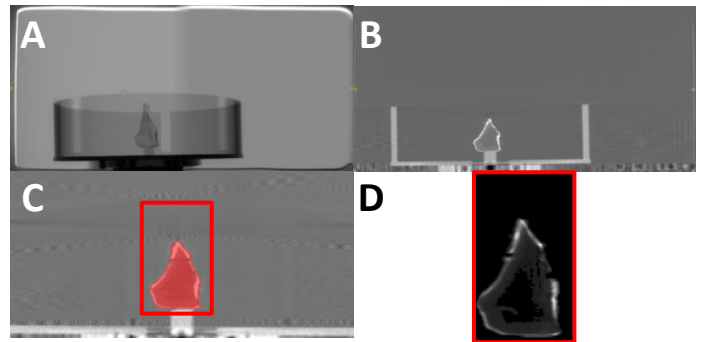


Figure 2. 2D radiograph of calibration frame taken from WBCT (A). CT image reconstructed by the WBCT (B). Segmentation of the surrogate bone fragment along with bounding box defining its subvolume (C). Subvolume containing bone fragment after removal of background (D).

In order to obtain real-time feedback for intra-operative use, a DRR algorithm was written in CUDA C++ for use on a graphics processing unit (GPU). After initialization, DRRs are computed by approximating the integral of X-ray attenuation along the path between the source and each pixel on a detector³. Within this framework, the pose of the virtual detector unit, soft-tissue, and bone fragments (sub-volumes) can be varied independently to change each subsequent DRR.

Similarity between the DRR and an intra-op fluoro image is computed using normalized cross correlation (NCC). When multiple images from different views are involved, the NCC from each view is combined into a single similarity metric².

$$Similarity = \log \prod_{i=0}^n (1 - NCC_i)$$

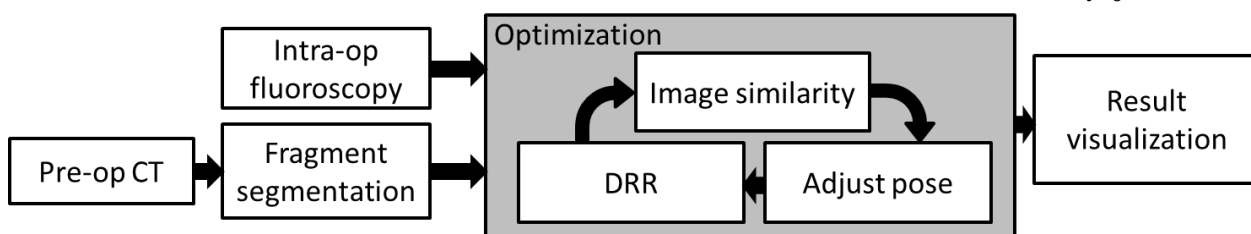


Figure 1. Intra-operative fragment tracking begins with a pre-operative CT, which is segmented and preprocessed. Each individual fragment pose is identified in an optimization loop. Final result is visualized.

The position and orientation of each bone fragment is then varied to minimize the similarity metric and thereby deduce the 3D pose of each fragment.

The DRR algorithm and pose estimation were tested using a prototype weight bearing CT (WBCT) scanner (Curvebeam), where a series of 2D cone beam images (0.38x0.38 mm pixels) are used to reconstruct a 3D CT volume (0.37x0.37x0.37 mm voxels). A surrogate bone fragment (Sawbones, Vashon Island, WA) was placed within a device that allowed the precise spatial manipulation (within 3 μ m and 5 arc minutes) in all 6 degrees of freedom. One neutral pose, 3 translated poses, and 2 rotated poses were imaged. The bone fragment, segmented from the neutral pose CT data, was aligned to orthogonal 2D images from the poses using an optimizer to minimize the similarity metric.

The performance of two different optimizers was characterized in terms of the speed and accuracy in reproducing the known bone pose. Covariance matrix adaptation evolution strategy (CMA-ES) was tested, as it is a well known gradient free optimizer used frequently in this application^{1,4}. A Simplex algorithm was also tested, as it is a gradient free optimization method that requires relatively few function evaluations to converge^{1,5}.

RESULTS AND DISCUSSION

Upon visual comparison, the DRRs reproduced the experimental data accurately, albeit with less sharp edge information, likely due to discretization errors and artifact within the CT volume (Fig 3). A single DRR is computed within ~2 ms, and the average optimization times for CMA-ES and the Simplex algorithms were 167.9 and 10.7 seconds, respectively.

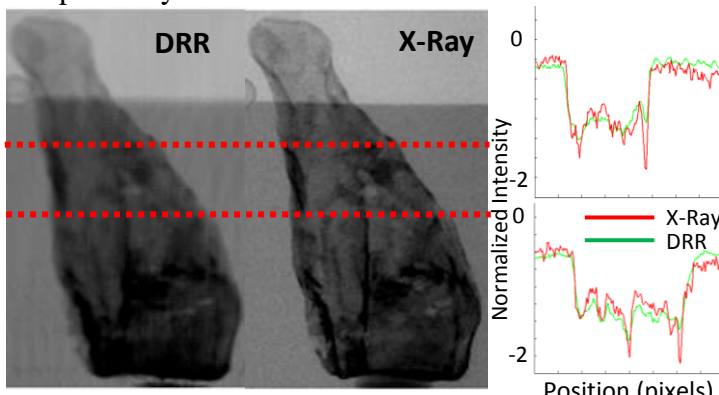


Figure 3. Comparison of DRR of bone fragment (following *in silico* translation) compared to experimentally gathered 2D X-Ray. Line profiles were sampled from the resulting images to show that DRR resulted in similar image but with higher frequency information lost.

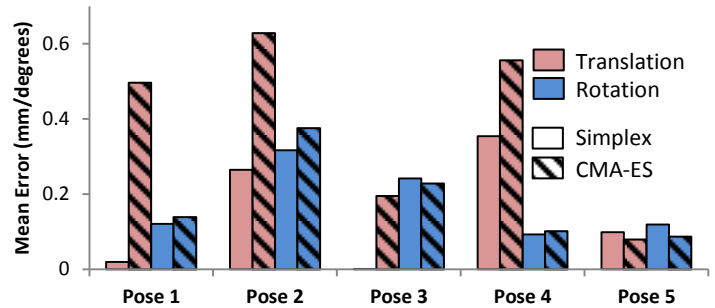


Figure 4. Mean error in translation and rotation following alignment of bone fragment to known rigid transformations. Poses 1-3 were translations in an arbitrarily selected direction of 5 mm. Poses 4 and 5 were an arbitrary rotation of up to 45 degrees.

The methods presented show promise for the real-time measurement intra-operative fragment pose. The accuracy of the fragment pose identification was sub-mm/degree for both optimization techniques (Fig. 4), but the Simplex algorithm was ~15 times faster. Even the fastest optimizations required ~10 seconds to converge to the correct solution, which is still too slow for real-time application. The DRR computation is currently performed within C++ CUDA, and the optimization within MATLAB, where ~80% of computation time is spent within MATLAB. It is expected that implementing optimization features within the C++ CUDA software and reducing the image resolution of early optimization steps will dramatically improve time performance¹.

This work was limited by the use of a non-clinical setting (single surrogate bone fragment with no soft tissue or surgical instrumentation present), and by the use of relatively small movements of the bone fragment. Future work will involve improving both temporal and spatial performance of the optimization, developing optimization strategies for multiple simultaneous bone fragments, and developing methods for translation into the OR.

REFERENCES

1. Otake et. al. **IEEE Trans on Med Img.** 2012
2. Haque et. al. **Med Eng Phys.** 2013
3. Siddon R.L, **Med Phys.** 1986.
4. Hansen, N. et al. **8th International Conf. on Parallel Problem Solv.** 2004
5. Lagarias J.C et al, **SIAM J. Optimization**, 1998.

ACKNOWLEDGEMENTS

This work was supported by a grant from NIH/NIAMS (P50 AR055533).

COMPARING THE EFFECTIVE QUADRICEPS AND PATELLAR TENDON MOMENT ARMS IN ASYMPTOMATIC CONTROLS AND SUBJECTS WITH PATELLOFEMORAL PAIN

¹Lucas T. Thomeer, ¹Frances T. Sheehan, PhD, ¹Jennifer N. Jackson, PhD

¹Rehabilitation Medicine Department, National Institutes of Health, Bethesda, MD, USA
email: gavellif@cc.nih.gov

INTRODUCTION

Knowledge of a tendon's moment arm (ma) is crucial to understanding joint kinetics, as it defines the relationship between a muscle's linear force and the moment it creates. However, because the patella acts as a dynamic fulcrum, the quadriceps' moment on the tibia cannot be directly calculated. Instead, the term effective quadriceps moment arm (EQma) was coined to define this relationship [1]. The EQma has not been quantified during dynamic *in vivo* movements. In addition, there is disagreement on how pathology influences EQma. Patella alta in patients with cerebral palsy is assumed to weaken knee extension capacity by reducing the EQma [2]. Conversely, a larger EQma has been reported for subjects with patella alta, relative to controls [3]. However, patellofemoral (PF) pain was reported by some subjects in both cohorts [3]. Characterizing the relationship between the EQma and patella alta in cohorts affected by pathologies associated with patella alta will provide crucial data for surgical interventions aimed at altering PF kinematics in these cohorts. Thus, the purpose of this study was to compare the *in vivo* EQma, captured during dynamic knee extension, of asymptomatic controls to subjects with PF pain using dynamic magnetic resonance (MR) imaging. A sub-analysis compared subjects with both PF pain and patella alta to controls. A secondary goal was to correlate the EQma to the PF superior position.

METHODS

The data were collected as part of an ongoing IRB approved study. All volunteers gave informed consent. The control cohort consisted of 38 healthy knees (29F/9M, 26.7 ± 5.7 years, 62.2 ± 10.8 kg, 167.5 ± 10.4 cm). All subjects in the cohort with PF pain had a diagnosis of PF pain with a minimum six

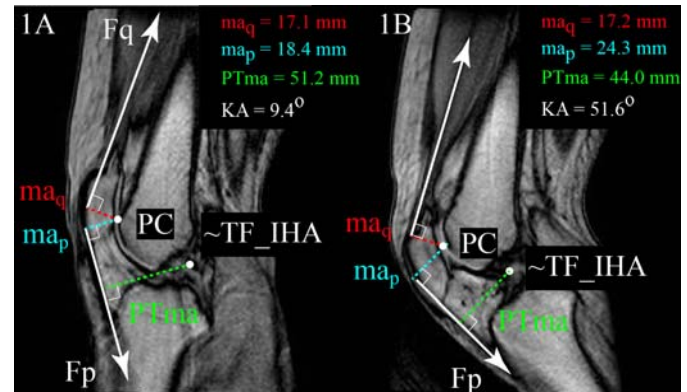


Figure 1: Analysis of two time frames for a single control subject. **A.** PTma, relative to the TF_IHA (shown approximately), was quantified by tracking the patellar tendon insertions through integration of the CPC data. **B.** maq and map were defined through direct image-based measures.

month history of PF pain (30F/3M, 22.3 ± 11.8 years, 57.8 ± 12.3 kg, 162.3 ± 7.4 cm).

A dynamic cine-phase contrast (CPC) MR acquisition and a multi-plane cine (MPC) MR acquisition were captured (3T, Philips Medical Systems) as each subject extended and flexed their knee through a range of motion of 10° to at least 40° . To rule out any underlying pathology, high-resolution static 3D MR images were acquired and read by a radiologist.

The CPC data was integrated to quantify the PF and tibiofemoral kinematics, allowing the patellar tendon moment arm (PTma) about the tibiofemoral instantaneous helical axis (TF_IHA) to be quantified. The EQma was quantified using a visual analysis of the ratio of the patellar tendon to quadriceps force (F_p/F_q , Fig 1) and the moment balance equation for the patella relative to the PF point of contact (PC, assumed to be the center of PF line of contact in the image containing the largest patellar section):

$$EQma = PTma * (F_p/F_q) = PTma * (ma_q/ma_p)$$

map: ma of the patellar tendon, relative to PC
 ma_q: ma of the quadriceps tendon, relative to PC

Since the dynamic data were acquired in even temporal increments, all kinematic data were interpolated to 10° knee angle (KA) increments from 10° to 50°. All distance measures were scaled by the ratio of the average control epicondylar width to the subject's epicondylar width.

A cohort with patella alta (10F, 23.2 ± 13.2 years, 61.0 ± 16.0 kg, 162.3 ± 8.9 cm) was taken as a subset of the cohort with PF pain. All knees in the cohort with PF pain that had a superior displacement of more than one standard deviation above the control mean were included.

A two-way analysis of variance (2x4 ANOVA, SPSS 22.0) was used to assess main and interaction effects of cohort (control vs. PF pain and control vs. PF pain with patella alta) and knee angle comparisons. Pearson's correlation coefficients were found between the superior displacement of the patella and the three moment arm variables (F_p/F_q ratio, PTma, and EQma) for the control cohort and the full cohort with PF pain.

RESULTS AND DISCUSSION

The cohort with PF pain was younger ($p = 0.046$) and shorter ($p = 0.017$) than the control cohort. Age was likely not a confounding factor, as all subjects were screened for arthritis. Height was removed as a confounding factor through scaling.

Cohort (control vs. PF pain) was not a main effect for F_p/F_q , PTma, or EQma. As in other studies [3, 4], the ratio of F_p/F_q was greater than 1.0 for knee angles less than ~20° in the control cohort. For the cohort with PF pain, the ratio of F_p/F_q was greater than 1.0 for knee angles less than ~15° (Fig 2).

Cohort (control vs. PF pain with patella alta) was a main effect for F_p/F_q (significant at 40° KA), but not for PTma or EQma. This lack of difference in EQma disagrees with previous work that found an increase in EQma [1, 3]. These differences were most likely due to differing methodologies. The current study was dynamic, not static. The EQma

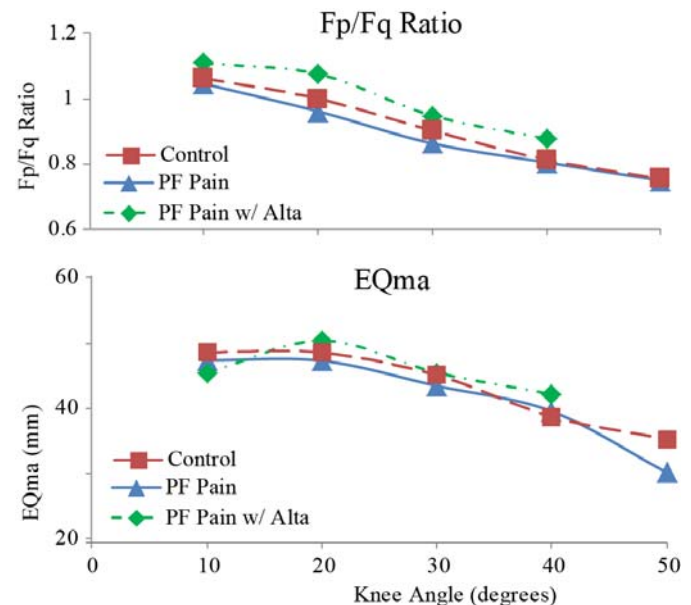


Figure 2: Comparisons of the cohorts (control, PF pain, PF pain with patella alta) across knee angles for F_p/F_q (top) and EQma (bottom).

was based on the PTma referenced to the TF_IHA, not the crossing point of the cruciate ligaments [3] or the tibiofemoral point of contact [1].

For two main cohorts, the F_p/F_q ratio showed a positive ($r = 0.35$ to 0.72 , $p < 0.05$) and the PTma an inverse correlation ($r = -0.38$ to -0.55) with PF superior position. This resulted in EQma not showing a correlation to the PF superior position, except at 40° KA in the cohort with PF pain. This stands in opposition to past work that indicated the EQma is associated with patella alta [3].

CONCLUSIONS

These novel *in vivo* data acquired across a large asymptomatic control population and a population of individuals with PF pain during a dynamic extension activity requiring active quadriceps contraction fills a critical gap in our understanding of musculoskeletal dynamics. As patella alta does not result in an increased EQma, surgically altering the height of the patella in the femoral groove would not reduce the quadriceps' efficiency.

REFERENCES

1. Yamaguchi GT, et al. *J Biomech* **22**, 1-10, 1989
2. Topoleski TA, et al. *J Pediatr Orthop* **20**, 636-9, 2000
3. Ward SR, et al. *J Biomech* **38**, 2415-22, 2005
4. van Eijden TM, et al. *J Biomech* **19**, 219-29, 1986

METHOD FOR THREE-DIMENSIONAL ANALYSIS OF SKELETAL MUSCLE STRAIN

^{1,2} Elisabeth R. Jensen, ¹ Duane A. Morrow, ³ Joel P. Felmlee, and ¹ Kenton R. Kaufman

¹ Division of Orthopedic Research, ² Mayo Graduate School, ³ Department of Radiology
Mayo Clinic, Rochester, MN, USA

email: Kaufman.Kenton@mayo.edu, web: <http://mayoresearch.mayo.edu/mayo/research/biomechanics/>

INTRODUCTION

Skeletal muscle weakness is frequently associated with stiffness changes [1,2], which may alter functional contraction and passive elongation dynamics. Cine Phase Contrast (CPC) MRI has been successfully used to quantify skeletal muscle strain distribution in a single plane [3,4]. The strain distribution was found to be non-uniform, indicating complex internal dynamics of skeletal muscle. The objective of this study was to advance CPC MRI-based analysis of muscle strain to three dimensions and to establish the output validity.

METHODS

A healthy female subject (24 y.o., 61 kg) was recruited and informed consent was obtained prior to her participation. The subject was positioned in a 1.5T MRI scanner (Signa HDX 16.0, GE Medical Systems, Waukesha, WI) and her right ankle was passively rotated between neutral and 26 degrees of plantar-flexion at 30 deg/sec for ~1300 cycles using a custom MRI-compatible apparatus. Data were collected using a commercial Fast 2D Phase Contrast sequence (50 mm/s venc, 12 time segments, 4 vps). The sequence and the apparatus were gaited to a two second cycle using a function generator. Nine adjacent sagittal image slices were acquired (5x0 mm thick, 24 cm FOV, 192x192 in-plane resolution) to cover the width of the tibialis anterior (TA). Velocity was encoded in each of the three spatial dimensions independently. Axial T2-weighted image stacks were collected with the ankle stationary at neutral and in plantarflexion (5x0 mm thick, 20 cm FOV, 320x320 in-plane resolution).

The TA muscle was manually segmented from the neutral-ankle T2-weighted images (Mimics, Materialise NV, Leuven, Belgium), then exported as

a surface mesh. A 3D hexahedral mesh with 10824 elements was generated by projecting a “butterfly” volume mesh to the TA surface mesh (TrueGrid, XYZ Scientific, Livermore, CA) and was exported as an Abaqus input file (SIMULIA, Waltham, MA). Local element axis 1 was defined as parallel to the TA’s long axis. Local element axis 2 was defined to be parallel to the internal aponeurosis, identified from the T2-weighted images, which varied across the TA length. The CPC-generated velocity maps (smoothed and corrected according to [5]) were used to track the 3D trajectory of each mesh node with custom software (MATLAB, The MathWorks, Natick, MA) that incorporated forward-backward integration and linear interpolation between voxels [4]. By applying these trajectories as nodal boundary conditions in Abaqus, the deformed 3D mesh of the lengthened TA was obtained.

The validity of the final deformed 3D mesh of the TA was tested in two ways: 1) The surface of the deformed mesh (exported from Abaqus) was overlaid on the T2-weighted images (plantarflexed ankle) to validate the final position. 2) The positive-to-negative transition of E13 shear strain was compared to the internal aponeurosis seen on the T2-weighted images. These lines were expected to coincide due to opposite fascicle rotation on either side of the aponeurosis (Figure 1).

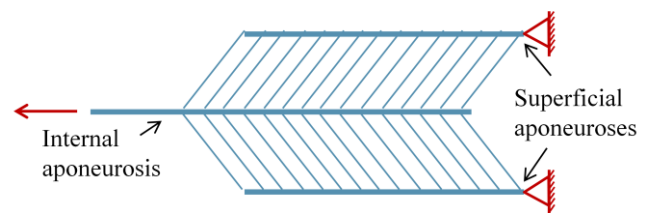


Figure 1: Muscle fibers on opposing sides of an internal aponeurosis in a bi-pennate muscle (such as the TA) experience opposite shear strains with passive muscle lengthening.

RESULTS AND DISCUSSION

The validity of the deformed mesh was supported by the data. The three-dimensional surface boundary of the deformed mesh matched the position of the TA in the strained condition, as confirmed by the T2-weighted images (example cross-section shown in Figure 2). Specifically, the anterior, posterior, and lateral boundaries of the deformed mesh coincided with anatomical landmarks such as skin, tendon, and fat near which the original mesh was defined (Figure 2b,c). This means that the trajectories of the most superficial nodes behaved as expected, indicating that motions of the internal nodes were appropriate in both magnitude and direction. The medial boundary of the mesh did not follow the anatomical landmarks as closely due to partial volume effects: the sagittal slices which included both muscle and bone volume were noisy due to a lack of signal in cortical bone.

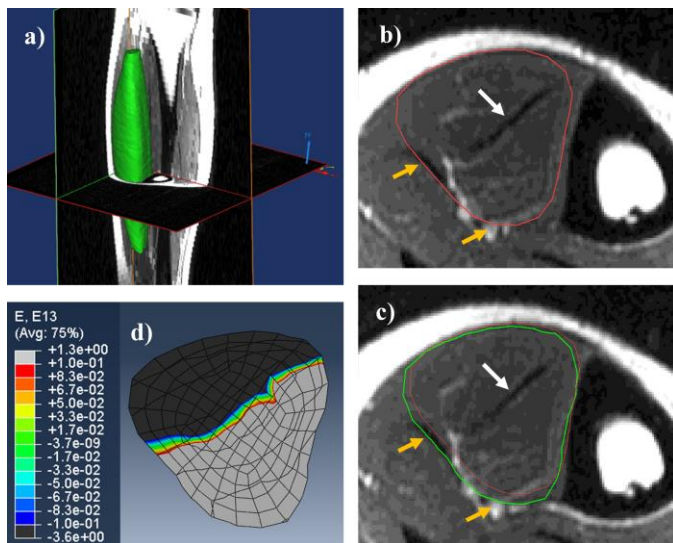


Figure 2: a) Deformed mesh (green) superimposed on axial T2-weighted MRI image stack (plantar-flexed ankle). b) Axial T2-weighted image (neutral ankle) with TA segmentation outlined in red. Slice corresponds to cross-section identified in (a). White arrow points to aponeurosis; yellow arrows point to identifiable anatomical landmarks of TA. c) Axial image (plantarflexed ankle) corresponding to (a) and (b) identifying segmented TA position (red) and deformed mesh outline (green). d) Corresponding cross section of deformed mesh, displaying positive-to-negative E13 shear strain transition.

More significantly, the positive-to-negative transition of the E13 shear strain matched the image-identified internal aponeurosis throughout its length (Figure 2c,d). This supports model validity of the internal mesh elements. Mechanical analysis of bi-pennate muscle under passive elongation predicts opposite direction fascicle rotation on either side of the aponeurosis, generating opposite shear strains. The ability of the model to identify the proper transition line demonstrates strong validity.

CONCLUSIONS

Quantification of three-dimensional skeletal muscle strain may provide important insights into the internal dynamics of weak and injured muscle. Previous studies on this topic have, out of necessity, attempted to represent complex 3D dynamics in two dimensions. This study demonstrates a novel approach to quantify 3D muscle strain using CPC MRI. The current study is limited to analysis of passive elongation due to the long duration of the data collection, but future application of accelerated CPC sequences will enable analysis of active muscle contraction due to significantly reduced data collection time [6].

REFERENCES

- [1] Gajdosik, RL et al. *Journal of Orthopaedic & Sports Physical Therapy*, 29:181-190, 1999.
- [2] Lampe, AK and Bushby, K. *Journal of Medical Genetics*, 42(9):673-685, 2005.
- [3] Sinha, S et al. *Journal of Magnetic Resonance Imaging*, 20(6):1008-19, 2004.
- [4] Zhou, H et al. *Journal of Magnetic Resonance Imaging*, 25(1):175-184, 2007.
- [5] Jensen, ER et al. *Journal of Biomechanics*, 48(1):95-103, 2015.
- [6] Johnson, KM et al. *Magnetic Resonance in Medicine*, 60(6): 1329-1336, 2008.

ACKNOWLEDGEMENTS

Funding for this study provided by Mayo Graduate School and the National Institutes of Health (T32AR56950 and R01HD31476). Special thanks to Dr. John Novotny for sharing data analysis code.

STIFFENING OF THE TRANSVERSE CARPAL LIGAMENT IN PIANISTS DETECTED BY ACOUSTIC RADIATION FORCE IMPULSE IMAGING

¹Christiane Mhanna, ¹Tamara L. Marquardt, ^{1,2,3}Zong-Ming Li

Hand Research Laboratory, Departments of ¹Biomedical Engineering, ²Orthopaedic Surgery, and ³Physical Medicine and Rehabilitation, Cleveland Clinic, Cleveland, OH, USA
email: liz4@ccf.org, web: <http://www.handlab.org>

INTRODUCTION

The transverse carpal ligament (TCL) anchors the thenar muscles that are critical to thumb function. Contractions of the thenar muscles biomechanically stimulate the TCL and such repetitive stimulations may cause pathomechanical tissue changes such as TCL thickening and stiffening [1]. While practicing and performing, pianists forcefully and repetitively exercise their thumbs and may be at risk for TCL modifications [2]. By examining TCL stiffness *in vivo* using acoustic radiation force impulse (ARFI) ultrasound imaging, there is potential for identifying etiological factors of carpal tunnel syndrome (CTS) such as TCL pathomechanics. Thus, the purpose of this study was to investigate stiffness changes in the TCL among pianists using ARFI. We hypothesized that pianists would exhibit a stiffer TCL in comparison to non-pianist controls.

METHODS

A total of twenty healthy, right handed female volunteers participated in the study. Ten of the participants were pianists (20.4 ± 1.6 years) who practice at least ten hours per week and have at least ten years of piano experience (18.6 hours/week of practice, 12.8 years of piano experience). The remaining ten participants served as a control group (23.8 ± 3.4 years) and were non-pianists that reported fewer than five hours per day typing, texting, or performing repetitive hand movements.

Each participant sat next to a testing table with the right arm submerged in a tank of room temperature water. The hand and wrist of each subject was stabilized in a supine, anatomically neutral position within a thermoplastic splint secured with Velcro® straps (Fig. 1). ARFI images were obtained with a

Siemens Acuson S2000 ultrasound system using a 9L4 linear array transducer that was stabilized using a positioning arm. The ultrasound system was equipped with Virtual Touch™ Tissue IQ software that permitted quantitative assessment of tissue stiffness by measuring the shear wave velocity (SWV) of tissues using ARFI technology. For each trial, a B-mode ultrasound image of the TCL and surrounding tissues was captured along with its corresponding ARFI grayscale map. Four images of the TCL were collected at the distal level of the carpal tunnel for each subject and then the experiment was repeated on the left hand.

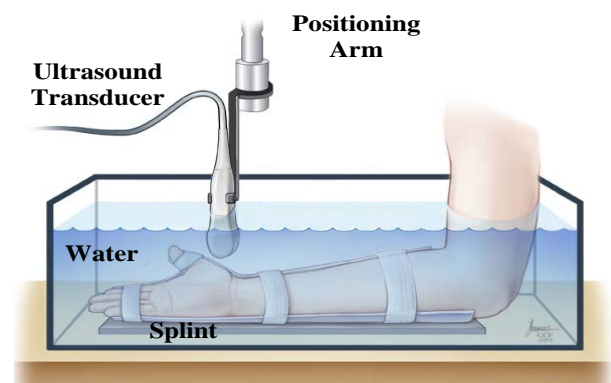


Figure 1: Illustration of the experimental setup to obtain ARFI images of the TCL.

A customized MATLAB script calculated the SWV by manually tracing the TCL on the B-mode side and translating the selection to the ARFI image side (Fig. 2). The SWV value of each pixel within the selection was calculated and the median SWV was determined. Additionally, the thenar muscles' ulnar point (TUP), the most ulnar insertion point of the thenar muscles on the TCL, was identified. For further analysis, the TCL was divided into ulnar and radial sides, i.e. uTCL and rTCL. The uTCL was defined as the region from the TUP towards the hook of hamate, while the rTCL was defined as the

region from the TUP towards the trapezium. The median values from the four trials were averaged for each participant and then the data from the right and left hands were averaged. A one-way ANOVA was used to compare the TCL SWV of pianists and controls. Additionally, a two-way ANOVA was performed with factors of group (pianist and control) and TCL side (uTCL and rTCL). The significance level was $\alpha = 0.05$.

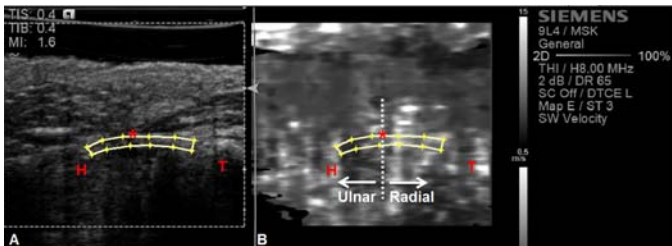


Figure 2: A representative ultrasound image with the TCL selection outlined on both the B-mode side (A) and ARFI side (B). The hamate (H), trapezium (T), and TUP (★) are identified. The vertical line indicates the division location for uTCL and rTCL.

RESULTS AND DISCUSSION

The SWV of the TCL, uTCL, and rTCL for the control group were 5.01 ± 0.58 , 4.52 ± 0.59 , and 4.99 ± 0.82 m/s, respectively. The SWV of the TCL, uTCL, and rTCL for the pianist group were 5.52 ± 0.46 , 4.84 ± 0.38 , and 6.09 ± 0.63 m/s, respectively. One-way ANOVA revealed that the SWV of the TCL was significantly greater in pianists as compared to the control group ($p < 0.05$) (Fig. 3). Two-way ANOVA showed that the SWV was significantly affected by group ($p < 0.001$) and side ($p < 0.001$) factors. Further comparisons showed that the SWV of the rTCL was not significantly different from that of the uTCL for the control group ($p = 0.109$). For the pianist group, however, the SWV of the rTCL was significantly greater than that of the uTCL ($p < 0.001$). The ratios of rTCL to uTCL SWV were 1.10 ± 0.10 and 1.26 ± 0.14 for the controls and pianists, respectively. Comparisons across the groups showed that the controls and pianists did not significantly differ for the SWV of the uTCL ($p = 0.172$), but the SWV of the rTCL for the pianists was 18.2% greater than that for the controls ($p < 0.005$).

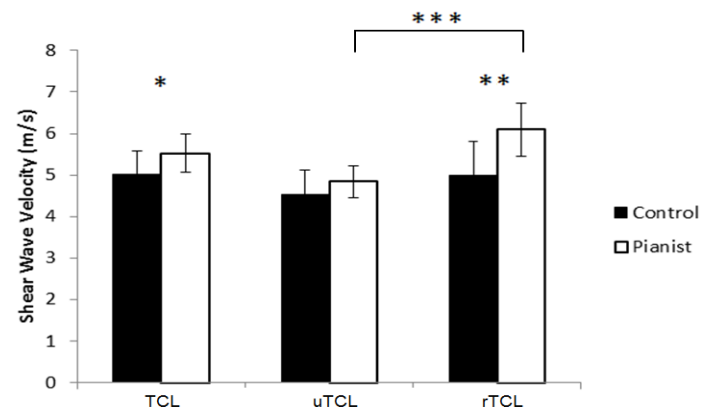


Figure 3: SWV of TCL, uTCL, and rTCL in pianists and controls. * $p < 0.05$, ** $p < 0.01$, and *** $p < 0.001$

ARFI imaging permitted *in vivo* examination of TCL SWV. SWV values of the control group agree well with findings of a previous study [3]. This study additionally revealed that pianists exhibit a higher TCL SWV than non-pianists. An increase in SWV is correlated with an increase in tissue stiffness [4]. While it was indicated that the TCL was generally stiffer among pianists, detailed analysis revealed that the adaptation was location dependent. The rTCL may be stiffer in pianists because that region of the TCL is physically attached to the thenar muscles and is under biomechanical stimulation when pianists play octaves and scales [5]. Previous research has shown that the thenar muscles are commonly overused in pianists and that this overuse may contribute to pain or stiffness [6]. Our study explores early signs of TCL stiffening among pianists, which could ultimately lead to CTS. Future studies are needed to determine if TCL stiffness is correlated with years of piano playing and with CTS.

REFERENCES

1. Shen ZL, et al. *Ultrasound Med Biol* **38**, 982-988, 2012.
2. Hochberg FH, et al. *JAMA* **249**, 1869-1872, 1983.
3. Shen ZL, et al. *PLoS ONE* 8(7): e68569, doi:10.1371/journal.pone.0068569, 2013.
4. Nightingale KR, et al. *Ultrasound in Med. & Biol* **28**(2), 227-235, 2002.
5. Parry CB. *Hand Clin* **19**(2), 317-324, 2003.
6. Sakai N, et al. *J Hand Surg* **31A**, 830-835, 2006.

ACKNOWLEDGEMENTS

NIH/NIAMS R21AR064957

VALIDATION OF AN INSTRUMENTED FIGURE SKATING BLADE TO MEASURE FORCE

¹Deborah L. King, ²J. Brandon Adamo, ²Blake R. Harper, ¹Timothy Snyder, ²Nicholas J. Whipple, ¹Stephanie R. Zybert, ²Steven K. Charles, ²Sarah T. Ridge

¹ Ithaca College, Ithaca, NY, USA

² Brigham Young University, Provo, UT, USA

email: dking@ithaca.edu, web: <http://www.ithaca.edu/hshp/depts/ess/>

INTRODUCTION

Competitive figure skating involves an intricate combination of artistry and athleticism. To perfect the difficult jumps, spins, and throws, skaters often train 3-6 hours per day, 4-6 days per week performing over 50 jumps each day [1,2]. With this intense training, injuries are all too frequent; over 70% of elite singles skaters have reported overuse injuries [3]. Understanding the forces that act on skaters will provide information related to a better understanding of injury mechanisms in figure skating.

However, measuring impact force in skating is not trivial. Previous studies have measured on-ice forces using pressure sensitive insoles or off-ice forces on a force plate, but neither method captures all of the forces experienced on ice [2,4,5]. Recently [6], a figure skating blade (Jackson Ultima Matrix) instrumented with strain gauges was developed to measure on-ice forces (Fig. 1). Data from one landing onto a force-plate was compared between the instrumented blade and a force-plate. An r-value of 0.88 between the two force curves was reported with errors in peak force magnitude of 780N (Fz1) and 20 N (Fz2) [6]. The purpose of the current study was to validate the instrumented blade using multiple landings onto a force-plate from different heights.

METHODS

A total of 16 simulated figure skating landings were performed onto a .01 m thick rubber mat (density $1.3 \times 10^3 \text{ kg/m}^3$) covering an AMTI (OR6, Watertown, MA) force-plate with the instrumented figure skating blade. Eight landings were performed from a height of 0.18 m and eight from a height of

0.27 m. Data were collected at 1000 Hz from both the blade and force-plate. Reflective markers were placed on the heel and toe of the boot parallel to the blade for sagittal plane recording with a SVSI StreamVision camera (Southern Vision Systems, Huntsville, AL) operating at 150 Hz.



Figure 1. Instrumented blade: Wheatstone bridge boards and strain gauges (a) - front two wrapped for data collection), signal processing board (b), compact flash card slot (c), and battery (d) wrapped for data collection. Details are in [6].

Four landings, 2 from each height, were randomly selected to perform a calibration. Blade angles were measured (MaxTraQ 2D, Innovision, Columbiaville, MI) 10 frames prior to contact to a minimum of 100 frames after contact, filtered at 20 Hz and re-sampled at 1000 Hz using linear interpolation (LabView 2013, National Instruments, Austin, TX). Blade strain gauge data in volts (perpendicular to and parallel to blade) were transformed to the global (force-plate) coordinate system (vertical and horizontal), cropped from contact to 500 ms, and entered into a linear least squares regression with the corresponding force-plate data in N synchronized at contact. In total, 2000 data points were used to create the calibration matrix.

Blade angles were measured for the remaining 12 landings and force was calculated in the global coordinate system using angles and the calibration matrix. The blade and force-plate data were cropped from contact to 500 ms and low-pass filtered at 150 Hz. A zero-lag cross correlation was computed between the blade and force-plate data for each landing. Paired t-tests were used to compare peak vertical impact forces with $\alpha = 0.05$.

RESULTS AND DISCUSSION

A representative force curve comparing blade data to force-plate data is shown in Fig. 2. Zero-lag cross-correlations (r-values) ranged from 0.78 to 0.97 with a median r-value of 0.90 and mode of 0.93.

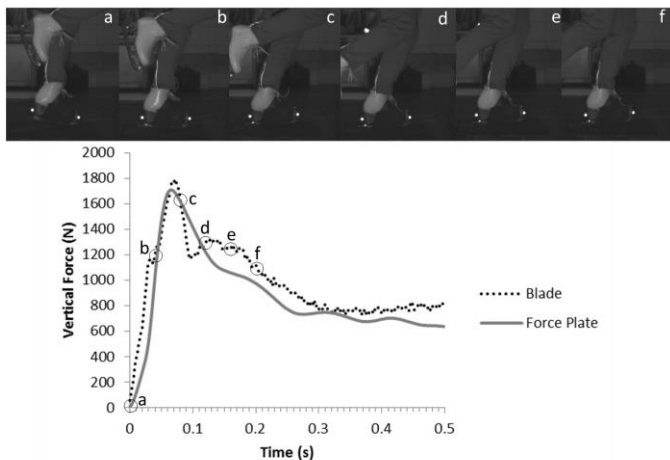


Figure 2: Instrumented blade and force-plate forces for landing 10 with corresponding video frames. For this landing $r = 0.93$.

The difference in peak force between the blade and force-plate was not significant ($p = 0.528$). The difference ranged from the blade underestimating by 152 N to overestimating by 145 N with a mean difference of -17 ± 89 N (Fig. 3).

The data suggest good to excellent agreement between the forces measured from the instrumented blade to those from the force-plate. The large standard deviations in peak force differences could be due to quantization of strain from the instrumented blade designed with a resolution of 30 N compared to a 1.5 N resolution of the force-plate.

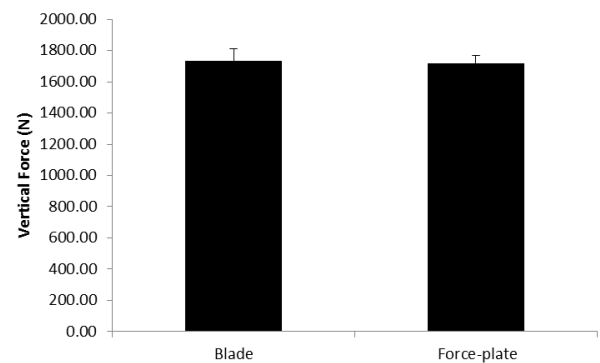


Figure 3: Average (+SD) peak force from the blade and force-plate for the 12 landings.

Non-quantified differences were observed in the shape of the two force curves. The blade often measured a small Fz1 peak (passive peak from the toe-impact seen near symbol b in Fig. 2) that was not registered on the force-plate. This could be due to the rubber mat, used to allow the skater to safely land on the force-plate, or differences in dynamics of the blade and force-plate. Further validation is recommended on an artificial ice-type surface to better mimic on-ice landings. It is also recommended that the blade be validated across different skaters to ensure that landing technique does not affect the validity of the calibration matrix and that reliability of the instrumented blade be established across days.

CONCLUSIONS

An instrumented figure skating blade self-contained underneath the boot of a skate was found to accurately measure vertical force in simulated figure skating landings performed in a laboratory setting.

REFERENCES

1. Smith, AD. *Clin Sport Med*, **19**, 741, 2000.
2. Breuning, DA & Richards, JG. *J Appl Biomech*, **22**, 285-295, 2006.
3. Pecina, Bojanic, & Dubrvicic, *Am J Sports Med*, **18**, 277-279, 1990
4. Kho, M. *M.S. Thesis*, University of Waterloo, CA, 1996.
5. Lockwood, K & Gervais, P. *Clin Biomech*, **12**, S11, 1997.
6. Acuna, SA et al. *Meas Sci & Tech*, **25**, pp6, 2014.

Using Sample Entropy on Continuous and Discontinuous Data to Assess Jumping and Landing

¹Robin M Queen, ¹Edward Merenda, ²Douglas Powell, and ³DS Blaise Williams

¹ Duke University Medical Center, Michael W. Krzyzewski Human Performance Lab, Durham, NC, USA

² Campbell University AIMS Laboratory, Buies Creek, NC, USA

³ Virginia Commonwealth University VCU RUN LAB, Richmond, VA, USA

email: robin.queen@duke.edu, web: <http://klab.surgery.duke.edu/>

INTRODUCTION

Musculoskeletal injuries are common in athletes and often result in loss of time from training and competition. Often, the injuries experienced by athletes are the result of overuse and repetitive wear on the musculoskeletal system. It has been suggested that healthy neuro-musculoskeletal systems exhibit an appropriate amount of variability interpreted as either the exploration of alternate movement strategies or a measure of adaptability within the system (Preatoni et al, 2013). Previous literature has associated limited variability, within a biological system, with unhealthy systems (Stergiou & Decker, 2011). While this theory is most commonly applied within cardiovascular or neuromuscular signals, this theory may also be applied to musculoskeletal injury. Specifically, a musculoskeletal system that exhibits limited variability would result in repeated loading and stress on the same tissues. This repeated stress to the musculoskeletal system could result in overuse injuries.

Emerging literature has suggested that nonlinear measures of variability may be more sensitive to subtle differences or changes within a movement pattern compared to traditional measures of centrality (Stergiou & Decker, 2011). A limitation of using nonlinear measures of variability is the reported need to have a continuous, deterministic time-series. This is a key limitation in certain movement patterns associated with injury including jumping and landing. However, the effect of using a continuous versus discontinuous time-series on values of nonlinear calculations such as sample entropy has not been previously evaluated.

Therefore, the purpose of this study was to determine if sample entropy (SampEn) calculated

using a continuous series of jumping and landing data is statistically different from assessing a merged series of continuous landing phase data. The hypothesis was that there will be no difference in SampEn between the two sets of data.

METHODS

16 recreational athletes (Table 1) with experience in jumping and landing sports were recruited for this study. Prior to participation in the experimental protocol, each participant signed an approved informed consent form.

	Male (n=8)	Female (n=8)
Age (years)	19.0 ± 1.1	24.6 ± 5.4
Height (m)	1.81 ± 0.08	1.72 ± 0.04
Mass (kg)	66.6 ± 9.2	59.9 ± 8.7

The subjects performed three trials of 10 repeated bilateral vertical jumps for maximum height during each trial. Subjects were allowed a 30 second rest between each of the repeated jumping trials. During each of the jumping trials, subjects were instructed to land with both feet, but ensure that one foot landed on each force plate (AMTI, Watertown, MA). Three-dimensional kinematic and kinetic data were collected during each of the jumping trials using an eight camera motion capture system (Motion Analysis Corporation, Santa Rosa, CA). Lower extremity joint angles and joint resultant moments were calculated for the right limb using Visual 3D (Germantown, MD). Joint moments were calculated using standard inverse dynamic techniques and the moment was normalized to body mass multiplied by height. The variables of interest for this study were sagittal plane knee joint angles and moments as well as frontal plane knee joint angles. Two datasets were used for analysis including continuous (CONT) and discontinuous data sets. The discontinuous (DISC) dataset was characterized by removing the flight phase from

each participant's data set and splicing together the data associated with load absorption and vertical jump prior to take off to create a continuous dataset.

Sample entropy (SampEn) was used to quantify the regularity of each variable of interest for both CONT and DISC datasets (Richman & Moorman, 2000). SampEn calculations yield a value between zero and infinity which reflects the predictability of future values within a time-series based on the preceding values of that time-series. Low SampEn values (i.e. 0) represent a predictable time-series such as a sine waveform while high SampEn values (i.e. > 2-3) represent an unpredictable time-series such as white noise. SampEn values each of the variables of interest were calculated using the following algorithm:

$$SampEn(m, r, N) = \ln \frac{\sum_{i=1}^{N-m} n_i^m}{\sum_{i=1}^{N-m} n_i^{m+1}}$$

where m was the length of the compared runs (m=2), r was the similarity criterion between points in a time-series ($r = 0.2 * SD$), N was the number of measurements in the time-series (i.e. number of points). The SampEn values were calculated for each variable of interest for each trial for each subject. A subject mean was then calculated as the average SampEn of all trials within a given calculation method for a given subject. Subject means were used in statistical analysis of the data. A series of paired t-tests were completed to determine if any differences existed between the two datasets (CONT and DISC) with the level of significance set at $\alpha = 0.05$.

RESULTS AND DISCUSSION

When comparing the two different datasets (CONT and DISC), no difference existed for the sagittal plane knee angle ($p=0.451$) or moment ($P=0.798$). However, the frontal plane knee angle was different between the two groups ($p=0.001$). In the frontal plane, the DISC data demonstrated a greater SampEn when compared to the CONT data set (Table 2).

The results of this study demonstrate that SampEn

can be used to assess movement variability during dynamic tasks such as jumping and landing as a relative measure between two movements or two groups. For sagittal plane angle and moments no difference was found between the DISC and CONT data indicating that using non-continuous data and mathematically merging it into a continuous series might be a possibility when trying to assess dynamic movements that can't easily be done in sequence.

	CONT	DISC	p-value
Sagittal Knee Angle	0.283 ± 0.071	0.298 ± 0.077	0.451
Sagittal Knee Moment	0.421 ± 0.140	0.432 ± 0.153	0.798
Frontal Knee Angle	0.690 ± 0.264	1.097 ± 0.356	0.001

The only measure that was different between the two data sets was the frontal plane joint angle. The differences in frontal plane motion could have resulted from greater variability inconsistencies in movement during the flight phase which would be present only in the CONT data, which is similar to what has previously been reported in walking and running (Kadaba et al, 1989). Therefore, future work needs to examine the differences in frontal plane linear variability to better understand the basic movement differences in order to provide information on the utility of this type of measure outside of the sagittal plane. Based on the results from this work, future studies should begin to examine the differences in both linear and non-linear variability during jumping and landing in both healthy as well as patient populations, such as those with ACL reconstruction.

REFERENCES

1. Sawicki GS. *Proceedings of NACOB'08*, Ann Arbor, MI, USA, 2008.
2. Gardner JG, et al. *J Biomech* **38**, 1861-1868, 2004.
3. Holzapfel GA. *Nonlinear Solid Mechanics*, John Wiley & Sons, Ltd., 2000.
4. Richman JS, Moorman JR. *Am J Physiol: Heart & Circulat Physiol* **278** (6): 2039-49, 2000.
5. Stergiou & Decker. *Hum Mov Sci* **30**(5): 869-888. 2011.
6. Preatoni E et al, *Sports Biomech*, 12, 69-92, 2013.
7. Kadaba et al, 1989, *J Orthop Res*. 7(6):849-60, 1989

USING AN ACCELEROMETER TO MONITOR RECOVERY OF GAIT BALANCE CONTROL FOLLOWING CONCUSSION

¹Li-Shan Chou, ^{1,2}David Howell, and ¹Louis Osternig

¹Department of Human Physiology, University of Oregon, Eugene, OR, USA

²Division of Sports Medicine, Department of Orthopedics, Children's Hospital Boston, Boston, MA, USA

E-mail: chou@uoregon.edu; Web: biomechanics.uoregon.edu/MAL

INTRODUCTION

An increased risk of a second concussion following the first has been reported (Guskiewicz et al., 2000; Zemper, 2003). This indicates that a sensitive examination of post-injury recovery may be a critical component in concussion management. Gait balance disturbances have been identified in individuals following concussion. Individuals with concussion exhibit greater displacement and velocity of whole body center-of-mass (COM) in the frontal plane and smaller peak COM velocity in the sagittal plane during dual-task walking than individually matched and uninjured controls (Howell et al., 2013, 2014, 2015; Parker et al., 2006).

Laboratory-based measurements require substantial equipment not often available in clinical settings where post-concussion assessments are conducted. Hence, a need exists to develop protocols utilizing inexpensive, easily implemented alternatives that provide detection comparable to camera-based systems for measuring gait stability. Accelerometry offers such a cost-effective, readily available alternative for the objective measurement of gait following concussion.

The objective of this study was to examine sagittal and frontal plane accelerations, measured with an accelerometer during dual-task walking, in a cohort of participants with concussion regularly over a 2-month post-injury period and similarly in uninjured controls. It was hypothesized that differences in sagittal and frontal plane accelerations at critical gait events would be observed between concussion and control groups.

METHODS

Seventeen subjects were identified and recruited for testing. Ten subjects (7M/3F; mean age: 19.0±5.5 years) were diagnosed with a concussion by a healthcare professional (physician/athletic trainer) and were assessed in the laboratory within 72 hours of injury and approximately one week, two weeks, one month, and two months post-injury. Seven control subjects (3M/4F; mean age: 20.0±4.5 years) were also tested according to the same timeline. Prior to data collection, all subjects and parents/guardians (if under the age of 18) provided written consent to participate in the study.

All study participants walked barefoot at a self-selected speed along a walkway while simultaneously completing an auditory Stroop test. The Stroop test consisted of the subject listening to four auditory stimuli: the recorded words “high” or “low” spoken in either a high or low pitch. Subjects were instructed to identify the pitch of the word, regardless of whether the pitch was congruent with the word. While walking, participants wore an accelerometer (APDM Opal Sensor, Portland, OR) attached with an elastic belt at L5, so that the reference coordinate system x-axis was oriented vertically downward, the y-axis was oriented to the right, and the z-axis was oriented orthogonal to the x- and y-axes toward the front. Accelerometer data were used to identify linear accelerations in the anterior-posterior and medial-lateral directions, obtained at a sampling frequency of 128Hz and saved via data-logger for offline post-processing.

The peak forward acceleration was identified at approximately 50% of the gait cycle (Figure 1A). Three distinct peak medial-lateral accelerations were identified: 1) during 25–45% of the gait cycle, 2) during 45–55% of the gait cycle, and 3) during

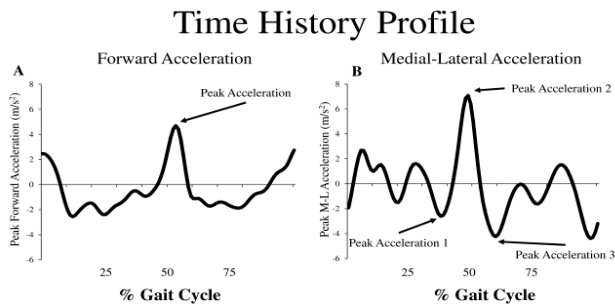


Figure 1: Exemplary COM acceleration profiles in the (A) forward and (B) medial-lateral directions for a gait cycle.

55–75% of the gait cycle (Figure 1B). Absolute values were used in further analysis to normalize between right and left directions. Peak accelerations were analyzed by two-way mixed effects analyses of covariance, with average gait velocity as a covariate, in order to determine the effect of group (concussion and control), time (72 hours, 1 week, 2 weeks, 1 month, and 2 months post-injury) and the interaction between these two independent variables.

RESULTS

Results indicated no significant interactions, or main effects of group or time for mean peak forward acceleration (Figure 2A, $p > .05$). Peak medial-lateral accelerations 1 and 2 analyses also revealed no significant interaction effects, or main effects of group or time (Figures 2B and 2C, $p > .05$). Peak acceleration 3 results indicated that subjects with concussion displayed less peak frontal plane acceleration during 55%-75% of the gait cycle during dual-task walking than control participants throughout the two months of testing (main effect of group $p = .04$, Figure 2D).

DISCUSSION AND CONCLUSIONS

Data from this study indicate that during dual-task walking, participants with concussion displayed less peak medial-lateral acceleration than control participants during 55%-75% gait cycle, representing the transition from double-support to single-support phases and suggest that concussion

may affect the ability to regulate whole-body side-to-side balance control during dual-task gait, possibly due to poor COM acceleration generation and regulation. The examination of acceleration may provide a feasible way to detect dynamic balance deficits in the clinical setting using readily available technology.

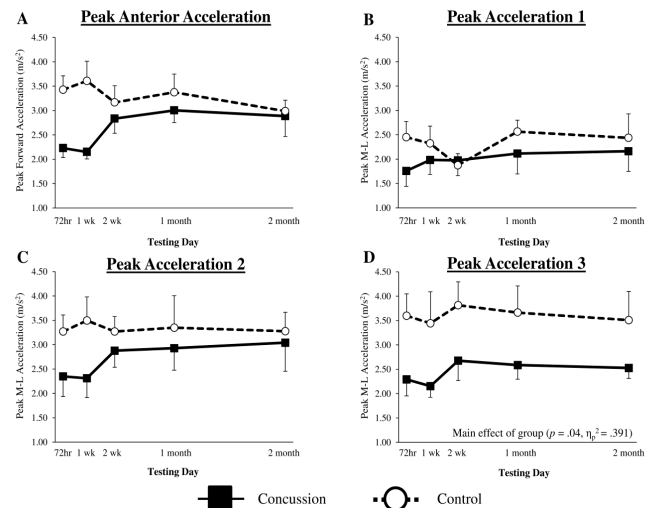


Figure 2: Mean \pm SE peak acceleration data for concussion and control groups across the two months of testing peak forward (A) and peak medial-lateral (B/C/D) directions. Including average gait velocity as a covariate, results indicated a significant difference between groups across the two months of testing for peak acceleration 3 (D).

REFERENCES

1. Guskiewicz et al., Am. J. Sports Med. 28, 643–650, 2000.
2. Zemper, Am. J. Phys. Med. Rehabil. Assoc. Acad. Physiatr. 82, 653–659 2003.
3. Howell, et al., Arch. Phys. Med. Rehabil. 94, 1513–20. 2013.
4. Howell et al., Exp. Brain Res. 232, 1773–1782, 2014.
5. Howell et al., Med. Sci. Sports Exerc. (doi: 10.1249/MSS.0000000000000462), 2015.
6. Parker et al., Med. Sci. Sports Exerc. 38, 1032–1040, 2006.

ENERGY FLOW ANALYSIS OF HIGH AND LOW VELOCITY BASEBALL PITCHERS

Michael P. McNally, John D. Borstad, James A. Oñate, and Ajit M.W. Chaudhari

The Ohio State University, Columbus, OH, USA

email: Michael.mcnally@osumc.edu, web: <http://u.osu.edu/osusportsbiomechanics/>

INTRODUCTION

The throwing motion is characterized by the sequential motion of distal to proximal segments, which is assumed to be indicative of the transfer of energy through the kinetic chain [3]. This kinetic chain is a common focus both clinically and in research for improving performance, as well as for preventing or rehabilitating throwing injuries to the elbow [1]. While most studies investigating the kinetic chain tend to utilize correlational analysis, energy flow analysis enables us to estimate energy flowing into and out of segments, providing an estimate of the role muscles play in generating, dissipating, and transferring energy between segments [4]. This approach has been used to investigate differences between injured and uninjured elite tennis players during the overhead serve [2], but there has been little to no research investigating the role of energy flow in performance and injury risk during an overhead baseball throw. Therefore, it was the purpose of this study to explore differences in upper extremity energy transfer between high and low performing baseball pitchers.

METHODS

Thirty-two male high school baseball pitchers (height = 1.83 ± 0.07 m, mass = 75.6 ± 10.9 kg, hand velocity = 21.1 ± 2.0 m/s) were recorded at 300 Hz using a 10-camera passive optical motion capture system (Vicon, Oxford, UK) while throwing 15 fastballs towards a target. An upper extremity marker set consistent with the ISB recommendations was used to define shoulder joint angles, and joint torques were calculated using standard inverse dynamics equations in Visual3D (C-Motion, Inc., Germantown, MD). The last three pitches with complete data were chosen for analysis.

The 10 pitchers with the highest and lowest average peak hand velocity were separated into high and low velocity groups for comparison. Segment power (SP) was calculated as the sum of joint force power (JFP) and segment torque power (STP) at the distal and proximal ends of each segment for the trunk, upper arm, forearm, and hand of the throwing extremity throughout the pitch cycle (Equations 1-3; Winter, 1978).

$$\text{Eq. 1) } JFP = \text{Joint reaction force} \cdot \text{linear joint velocity}$$

$$\text{Eq. 2) } STP = \text{Segment torque} \cdot \text{joint angular velocity}$$

$$\text{Eq. 3) } SP_{\text{segment}} = JFP_{\text{prox}} + JFP_{\text{dist}} + STP_{\text{prox}} + STP_{\text{dist}}$$

Net energy transfer was calculated as the integral of power for each segment of the arm during the arm cocking phase (stride foot contact to maximum shoulder external rotation) and arm acceleration phase (maximum shoulder external rotation to ball release), when energy is being applied to accelerate the ball.

One way ANOVA's were performed to compare net energy flow between high and low velocity groups using height and mass as covariates. A Bonferroni-adjusted alpha level of $p < 0.00625$ was set *a priori* to account for multiple comparisons.

RESULTS AND DISCUSSION

Figure 1 shows energy flow through the trunk and throwing arm during the arm cocking and arm acceleration phases for high and low velocity pitchers. Pitchers with high velocity demonstrated greater net energy flow out of the trunk (-165.9 vs. -90.9 J; $p < 0.001$), and into the forearm (105.7 vs. 63.0 J; $p < 0.001$) and hand (93.3 vs. 56.2 J; $p < 0.001$) during the arm cocking phase.

Greater flow of energy out of the trunk and into the arm early in the pitch cycle increases the energy of the arm, which may aid in accelerating the ball. This finding supports the importance of the trunk musculature to generate and transfer energy into the arm to improve performance. While it may seem counter-intuitive that the upper arm, forearm and hand receive more energy during the arm cocking phase than the arm acceleration phase, this result occurs because these segments actually move forward relative to the ground during the arm cocking phase, even though they are moving backward relative to the shoulder.

This analysis gives unique insights into how energy flows through the kinetic chain, and may be an alternative method to previous kinematic analyses for assessing the kinetic chain. This analysis can also be extended further down the kinetic chain to determine the role of core and lower extremity muscles in generating and transferring energy from the ground up. Energy flow may also be a useful analysis when investigating interventions aimed at core and shoulder stability, or other interventions with a purpose of improving energy transfer between segments. Due to the exploratory nature of

this study, further research is needed to corroborate these findings and determine how energy transfer relates to actual injury occurrences.

CONCLUSIONS

Performance may be improved through a greater transfer of energy out of the trunk and into the arm early in the pitch cycle. The power flow analysis used may be an effective measurement technique for better understanding the effectiveness of interventions aimed at improving the kinetic chain. Further research is needed though to understand the validity and utility of this analysis in kinetic chain tasks.

REFERENCES

1. Kibler WB, et al. *Clin Sports Med* **32**, 637-651, 2013.
2. Martin C, et al. *Am J Sports Med* **42**, 2751-2760, 2014.
3. Putnam CA. *J. Biomechanics* **26s1**, 125-135, 1993.
4. Winter DA, et al. *Biol. Cybernetics* **29**, 137-142, 1978.

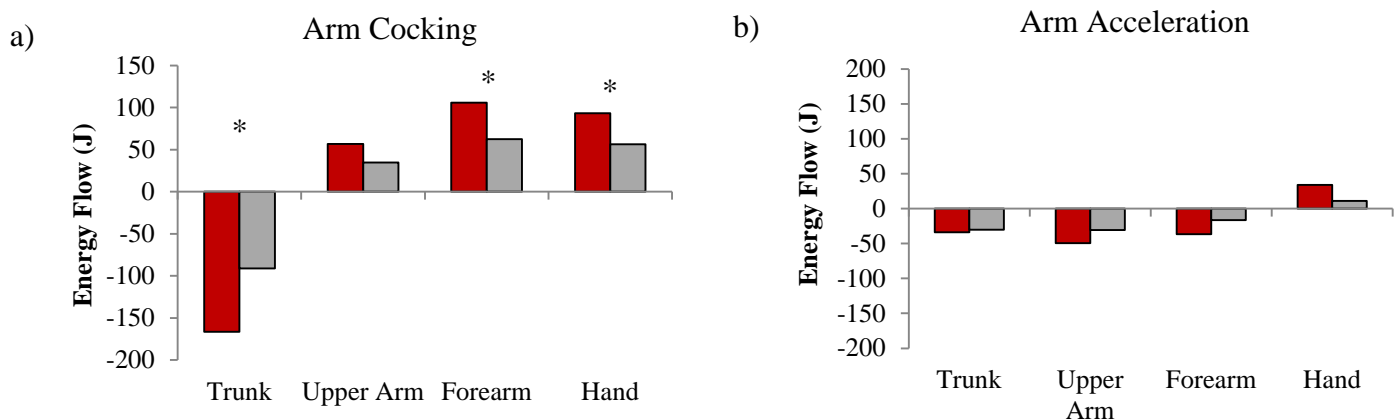


Figure 1. Net segment energy flow during the a) arm cocking phase and b) arm acceleration phases. Positive values indicate net energy input to the segment, negative values indicate net energy output from the segment.

* indicates $p < 0.00625$

KINETICS OF YOUTH BASEBALL PITCHERS AND CATCHERS

Jessica Washington, Hillary A. Plummer and Gretchen D. Oliver

Auburn University, Auburn, AL, USA

email: goliver@auburn.edu

INTRODUCTION

Sports medicine professionals have reported elbow and shoulder injuries in youth baseball pitchers for decades [1,2], where to date these injuries have been considered an epidemic [3]. Rules and guidelines have been implemented for youth pitcher safety. Additionally in 2009 Little League added rules to prohibit pitchers from playing catcher in the same game. As it has been a coaching trend in baseball for youth pitchers to concomitantly play catcher. Furthermore, it has been reported that pitchers also playing catcher appeared to double or even triple their risk of injury [3]. With the increased injury risk of pitchers playing catcher, it was our purpose to examine the upper extremity kinetics in youth baseball pitchers and catchers.

METHODS

Baseball pitchers ($n = 25$; 11.5 ± 1.2 years; 153.5 ± 7.9 cm; 47.0 ± 7.3 kg) and catchers ($n = 25$; 11.2 ± 2.3 years; 150.6 ± 13.2 cm; 46.6 ± 10.6 kg) reported for testing prior to engaging in resistance training or any vigorous activity that day. The University's Institutional Review Board approved testing protocols.

Kinematic and kinetic data were collected using The MotionMonitorTM motion capture system (Innovative Sports Training, Chicago IL) at a rate of 144Hz. Prior to testing participants had 11 electromagnetic sensors attached at the following locations: (1) the posterior/medial aspect of the torso at C7, (2) posterior/medial aspect of the pelvis at S1, (3-4) bilateral distal/posterior aspect of the upper arm, (5) the flat, broad portion of the acromion of the scapula, (6-7) bilateral distal/posterior aspect of the forearm, (8-9) bilateral distal/posterior aspect of the lower leg, and (10-11) bilateral distal/posterior aspect of the upper leg [4].

A twelfth sensor was attached to a stylus that was used for digitization of the bony landmarks described by the International Shoulder Group of the International Society of Biomechanics. Two points described the longitudinal axis of the segment, and a third point described the plane. A second axis was defined perpendicular to the plane, and the third axis was defined as perpendicular to both the first and second axis. Participants stood in anatomical position during digitization to guarantee accurate bony landmark identification.

Participants were given an unlimited time to warm-up. Following warm-up, pitchers were instructed to throw maximal effort fastballs for strikes over a regulation distance (46 feet; 14.0 meters) to a catcher, while catchers were instructed to receive a pitch from a pitcher and then throw the ball to a position player on second base (90 feet; 27.4 meters).

To calculate kinetics, inertial properties of the hand, forearm, and upper arm were calculated from previously published data [5] and scaled to each participant's body size. Biomechanical parameters investigated were based on previous throwing comparisons. Peak values of four kinetic parameters were analyzed: elbow varus torque, shoulder internal rotation torque, shoulder horizontal adduction torque, and shoulder proximal force. The kinetic parameters were examined during three phases of the throwing motion: arm cocking, arm acceleration and arm deceleration.

RESULTS AND DISCUSSION

For statistical analysis, (2) x (3) between-subjects repeated measures analysis of variance (ANOVAs) were performed to evaluate each upper extremity kinetic variable among youth pitchers and catchers. A significance level of 0.05 was adopted and all

statistical analyses were performed with IMB SPSS 22 software. Shoulder proximal torque was the only variable that produced significant differences between pitchers and catchers ($F_{1,48} = 4.71$; $p = 0.035$; partial eta squared = 0.089; power = 0.566). A follow-up t-test was then performed to determine where the difference occurred in the throwing motion and the results revealed that shoulder proximal torque was significantly different in pitchers and catchers during the deceleration phase ($p = 0.027$). Kinetic results are shown in Table 1.

It is known that most shoulder and elbow injuries in youth baseball are the result of the repetitive forces created during the throwing motion. During the arm-cocking phase of the throwing motion the shoulder must externally rotate and the elbow is flexed. Then to initiate the acceleration phase, the shoulder must rapidly internally rotate while the elbow extends. Shoulder internal rotation torque is produced to decelerate the external rotation and initiate internal rotation. The current study revealed no differences in shoulder internal rotation torque between pitchers and catchers. These results are similar to those found when comparing flat ground throwing to pitching from a mound [6]. However, the current study revealed greater shoulder proximal force during the deceleration phase of catchers throwing to second versus pitchers pitching from a mound. One explanation for this difference may be what has previously been reported when throwing from a mound that throwing from a mound has a mechanical advantage that may also serve as a

protective mechanism versus throwing from flat ground [6].

CONCLUSIONS

To the author's knowledge this is the first study to examine a sample of youth pitchers and catchers who were similar in age, height and weight. As the trend in youth baseball is for pitchers to also train as catchers, it is important to understand the kinetics involved with the two positions. Large kinetics about the upper extremity may predispose these players to an increased incidence of shoulder and elbow injury. Additionally, further investigation should focus on the kinematic differences that may be present in youth pitchers and catchers in attempt to gain a better understanding of the kinetics about the upper extremity.

REFERENCES

1. Gugenheim JJ, et al. *Am J Sports Med* **4**, 189-200, 1976.
2. Dun S, et al. *Am J Sports Med* **36**, 686-188, 2008.
3. Fleisig GS, et al. *Am J Sports Med* **39**, 253-257, 2011.
4. Oliver GD, et al. *J Sports Sciences* **29**, 1071-1077, 2011.
5. Dempster WT. *Proceedings of WADC Technical Report 55-159*, Patterson Air Force Base, Ohio, USA, 1955.
6. Slenker NR, et al. *Am J Sports Med* **42**, 1226-1242.

Table 1: Kinetic means and standard error of the mean for youth pitchers and catchers

Phases of Throwing	Shoulder IR Torque N/m	Shoulder Horizontal Add Torque N/m	Shoulder Proximal Force N/m	Elbow Varus Torque N/m
Arm Cocking				
Pitchers	-13.39 ± 1.15	-12.32 ± 1.68	-12.32 ± 1.68	3.33 ± 0.93
Catchers	-13.16 ± 2.25	-13.79 ± 2.25	-13.79 ± 2.25	0.18 ± 1.15
Acceleration				
Pitchers	-2.52 ± 3.15	-22.75 ± 5.67	-22.61 ± 4.56	11.69 ± 2.60
Catchers	-2.28 ± 1.96	-28.07 ± 4.20	-21.20 ± 4.42	15.25 ± 3.07
Deceleration				
Pitchers	-2.77 ± 2.67	-17.55 ± 5.93	8.91 ± 5.18	12.44 ± 2.71
Catchers	-11.06 ± 3.42	-11.49 ± 7.35	25.17 ± 4.89*	16.56 ± 3.33

Varus Angle Differences and Band Lengthening During the Moving Valgus Stress Test

¹Thomas Maher, ²Patrick J Schimoler, ¹Ahkila Veerubhotla, ¹Michael Wigton, ¹Alexander Kharlamov,
¹Patrick J. DeMeo, ^{1,2}Mark Carl Miller

¹Orthopaedic Surgery, Allegheny General Hospital, Pittsburgh, PA, USA

²University of Pittsburgh, Pittsburgh, PA, USA

INTRODUCTION

Athletes who participate in sports that require overhand throwing motions have an increased risk of developing injuries to the medial Ulnar Collateral Ligament (mUCL). While advanced imaging is useful for diagnosing complete tears of the ligament; physical examinations are effectively used to diagnose partial tears or ligament damage. The Moving Valgus Stress Test (MVST) is used to diagnose injuries, which are not readily apparent on imaging.¹ A valgus torque is applied to the elbow of a patient with the shoulder abducted and the arm is then extended from full flexion (135°) to complete extension (at least 30°) or until pain is too severe. If the MVST reproduces the pain experienced by the patient during physical activity, the mUCL is likely damaged. The current work using cadaveric elbows, sought to quantify the dynamic movement inherent to the MVST, in order to compare dynamic and static anterior bundle band lengths and varus/valgus angles. Loaded elbows were compared using three different cases (flexion, extension and static loadings), which were then compared against an unloaded static case. The null hypothesis was that there would be no significant difference between band lengths and varus/valgus angulation in the three loaded cases.

METHODS

Seven cadaveric elbows, without histories of elbow injuries, were obtained and dissected by the chief orthopedic surgery resident. There were 5 male elbows (age 49.8±13) and 2 female elbows (age 39±24). The brachialis and triceps muscles were identified and sutured with fishing line. The mUCL was then carefully exposed and the three bands of the anterior bundle were identified. Three rows of small black spherical markers (0.8 mm diameter)

were placed longitudinally along fibers of the three parallel bands (anterior, central, posterior).

Each elbow was mounted in a custom-built physiologic elbow simulator so that flexion and extension were in a horizontal plane. A follower arm was used to measure the flexion and extension angles of the free-swinging elbow using a precision encoder (US Digital HB5M). The varus/valgus angles were measured with an inclinometer (US Digital X3Q-V) attached to the forearm. Two conditions for each elbow were used: 1) no valgus load while 89 N of tension was applied to the brachialis and triceps and 2) loaded with only 4.5 N of tension applied to the brachialis and triceps but with an additional 6 N weight hanging from the wrist. This load was added to where the humeral trochlear groove meets the trochlear notch in order to provide consistent reference angles and lengths.

After calibration, cameras mounted above the elbow simulator captured the movement of the markers. The markers' locations in space were determined using a Spicatek Motion Capture Suite. The lengths of the mUCL bands were calculated from these locations. For a given angle in the loaded dynamic and static trials, differences of length and varus angle were determined by a comparison with a static unloaded trial. Two-way repeated measures ANOVAs (MiniTab, State College, PA) were used with Tukey's least significant difference for post-hoc testing if an ANOVA found significance.

RESULTS AND DISCUSSION

The statistical analysis found that the loading variable was significant, indicating that the static, dynamic flexion and dynamic extension were different ($p < 0.001$). All three bands of the anterior bundle of the mUCL consistently increased in

length with a load applied to the wrist. This increase in ligament band length was determined by comparing the three loaded trials, all of which were conducted with a reference to a static unloaded trial at each angular position. The differences that existed between the loaded and unloaded trials were expected because it was reasonable to assume that any weight applied to the wrist would necessarily translate the arm in a downward direction, lengthening the three bands of the ligament.

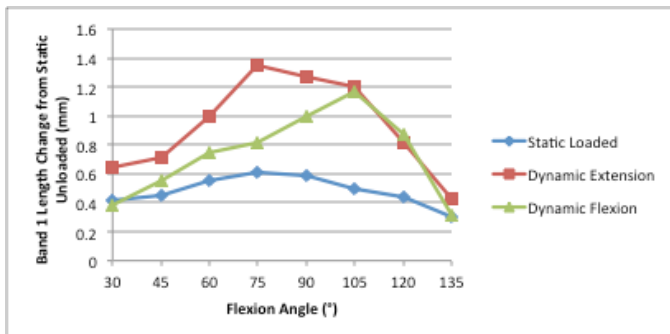


Figure 1: A comparison of anterior band lengths for the three loaded trials using Flexion angle and Static Unloaded Band length.

The data, however, indicated that the amount of lengthening associated with the loading was not consistent among the three loaded trials. (Figure 1) The dynamic movements, both flexion and extension, both lengthen noticeably more than the static loaded trial. The increased lengthening of the ligament associated with dynamic movement was also associated with a greater change in varus angle for dynamic loaded trials than the static loaded trial. (Figure 2)

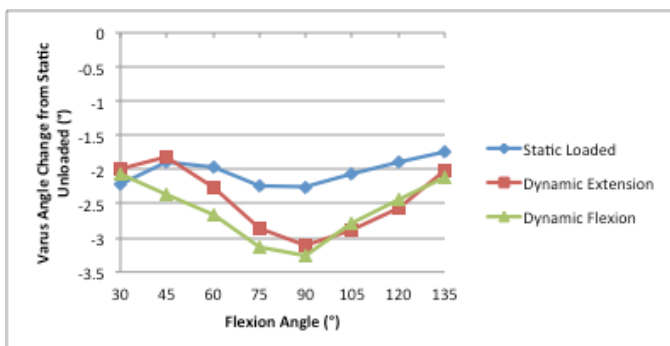


Figure 2: A comparison of changes in Varus Angle for loaded trials as a function of Flexion Angle.

While it is possible that the movement associated with the test caused the ligament to lengthen more because more fibers may be loaded at different

flexion angles, the explanation for the difference may also be simpler. For instance, do to the nature of the experiment the elbow is loaded for a longer period of time during the dynamic movement. One may have to consider the viscoelastic nature of the ligament as it hangs during dynamic movement as opposed to a static loaded trial.

The quantification of the lengths of the fibrous bands of the anterior bundle furthers the understanding of the morphology of the mUCL. The data from this study combined with the work by Jackson² can be seen as a continuation of the work of Dugas³. Dugas was able to provide data about the overall anatomical structure of the anterior bundle of the mUCL.³ Jackson was able to determine that the posterior and anterior fibrous bands of the anterior bundle were indistinguishable structurally. The difference in strain between the bands was a consequence of movement and insertion. The anterior band remained under relatively constant strain but the strain on the posterior band increased with flexion angle.²

The knowledge that movement and angle are contributing factors to the amount of strain on the bands of the anterior bundle may help explain the discrepancies in length between loaded dynamic and static movements especially between 75° and 120°. The anatomical structural information obtained by Dugas and Jackson combined with dynamic movement of this experiment supports the observed clinical efficacy of the MVST as shown by O'Driscoll.¹

CONCLUSIONS

The results suggest that there is a statistically significant relationship between anterior band lengths and varus/valgus angles of the mUCL when comparing loaded dynamic flexion/extension and static trials. The relationship could be a contributing factor to the results seen by the MVST.

REFERENCES

1. O'Driscoll SW, et al. *Am J Sports Med*, **33**, 231–9, 2005.
2. Jackson T, et al. ESSKA, December, 2014.
3. Dugas JR, et al. *J Shoulder Elbow Surg*, **16**, 657–660, 2007.

THE EFFECTS OF MILITARY BODY ARMOR ON KNEE MECHANICS DURING BOX DROP AND PRONE TO STANDING TASKS

¹ Megan P. Phillips, ¹Robert Shapiro, and ¹Babak Bazrgari

¹ University of Kentucky, Lexington, KY, USA
email: babak.bazrgari@uky.edu

INTRODUCTION

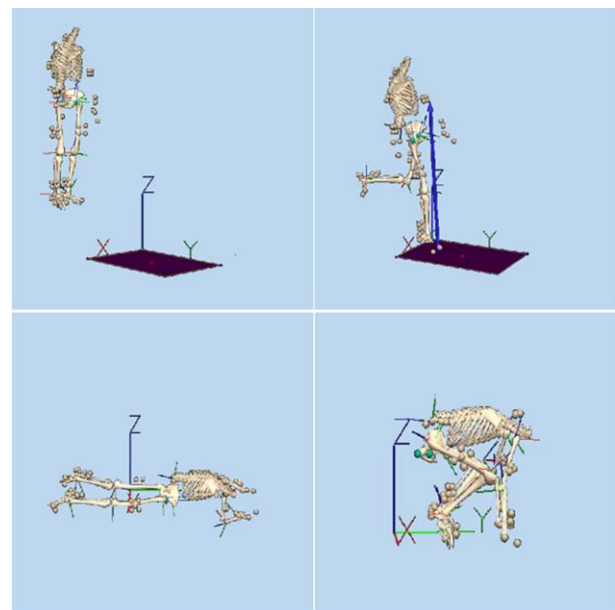
Modern day body armor (BA) has been successful at increasing survivability from previously lethal explosives [1], however, such success has come at the expense of a significant increase to the weight carried by dismounted warfighters. The added weight (106N) of BA has been suggested to reduce warfighter's performance and increase risk of injury. Given the important role of joint biomechanics in performance and risk of injury, the objective of the present study was to quantify BA-induced changes in knee biomechanics. Specifically, the immediate and prolonged effects of wearing body armor on several aspects of knee biomechanics during box drop and prone to standing tasks were investigated. We hypothesized that BA-induced changes in our outcome measures would be consistent with increased risk of injury (e.g., increased loading rate or joint moment) and/or impaired performance (e.g., increased time).

METHODS

A randomized cross-over study design, wherein twelve highly recreationally active (18-35 yrs.), gender balanced, individuals wore BA in one of two sessions, were used to test the effects of BA and wear duration on several measures of knee mechanics. Each session lasted ~2.5 hours and were conducted with a $1 < t \leq 7$ day window [2]. Participants completed prone to standing and box drop tests before and after 45 minutes of treadmill walking (i.e., exposure) with and without body armor.

For the box drop test, participants stood on a box (height: 37.5 cm) located next to an in-ground force platform. The participants initiated the test by stepping down onto the force platform following the

investigators signal to start. They were instructed to step down on the force platform with their dominant foot (i.e., right foot for all subjects in this study) and continue walking in the forward direction off of the force platform (Fig 1). For the prone to standing test, participants started lying prone on the floor. Their feet were plantar flexed with the foot dorsum in contact with the ground. Their shoulders were in 180° of forward flexion, elbows extended with the palmer side of their hand in contact with the ground. When signaled by the investigators to begin the test, in one dynamic movement the participants brought their hands underneath their shoulders, pushed up, jumped their feet in towards their hands and stood upright (Fig 1). Each of the box drop and prone to standing tests were repeated three times for each condition while temporal, knee data (kinematic and kinetic (box drop only)) were collected. Figure 1. 3D model of Box drop (top) and prone to standing (bottom) in Visual 3D software.



Kinematics and kinetics data were collected respectively using a motion capture system (Motion

Analysis, Santa Rosa, CA) and an in ground force platform (Bertec, Columbus, OH). Relevant outcome measures were calculated by an in-house Matlab code (Mathworks, Natick, MA) and using subject specific models, developed in Visual 3D (C-Motion Corp, Germantown, MD).

A REML GEE model (version 9.3, SAS Institute Inc., Cary, NC, USA) was used to examine the effects of armor and sex on pre-exposure measures, and the change in measures from pre-exposure to post-exposure. The pre-exposure model allowed the investigation of the immediate effect of armor and sex alone on risk of injury and performance; where the change model (post-exposure minus pre-exposure) allowed the investigation of the prolonged effect of exposure to BA on risk of injury and performance

RESULTS AND DISCUSSION

The immediate effects of body armor on both tasks were an increase of $\geq 4\%$ ($p \leq 0.02$) in temporal task durations and a decrease of ~ 1.66 N/kg ($p = 0.03$) in normalized peak ground reaction force for the box drop test (Table 1). The significant increase in box drop task duration may be related to the decrease in force, wherein the participants executed the task more cautiously due of the increased load. The decrease in the normalized peak vertical GRF while wearing BA during the pre-exposure BD test

and no significant changes in peak instantaneous loading rate or maximum knee extension moment may be an indication of participants' success in overcoming the BA-induced increase in task demand without a significant increase in risk of injury. The prolonged duration of walking with body armor (i.e., 45 minute) was not found to cause more changes in our measures than walking without body armor. Heavy loads carried by dismounted warfighters, including BA, can adversely impact force generation and sustainment, due to manpower-reducing injuries and impaired warfighter's performance in combat situations. The findings of this exploratory study can guide design of future studies aimed at understanding the underlying mechanisms responsible for the adverse effects of BA on warfighters' performance and risk of musculoskeletal injuries.

REFERENCES

1. Clark, ME, et al. *J Rehabil Res Dev* 44(2): 179
2. Phillips, M et al. *Ergonomics*, 2014

ACKNOWLEDGEMENTS

M.P. acknowledges support from VA Chapter 33 and statistical assistance was provided by the University of Kentucky's CCTS (UL1RR033173 and UL1TR000117).

Table 1: Pre-exposure effects of body armor as well as sex-differences in temporal, kinematics and kinetics outcome measures.

Outcome measures	Armor	No Armor	p value	Male	Female	p value
BOX DROP						
Impact to toe off (s)	0.65 (0.035)	0.62 (0.37)	0.01*	0.67 (0.06)	0.59 (0.037)	0.29
Peak GRF Normalized (N/kg)	24.94 (1.30)	26.60 (1.20)	0.03*	25.36 (1.27)	26.19 (1.78)	0.68
Peak inst. loading rate (N/s)	87064 (7121)	83268 (5474)	0.64	96743 (7235)	73590 (6083)	0.03*
Time peak GRF (% of stance)	10.00 (1.00)	10.00 (1.00)	0.91	9.00 (2.00)	12.00 (1.00)	0.02*
Knee angle at peak GRF (°)	-15.10 (1.62)	-14.91 (1.78)	0.89	-11.68 (2.31)	-18.34 (1.82)	0.04*
Max. knee ext. moment (Nm)	114.33 (5.55)	98.29 (9.87)	0.09	120.90 (7.12)	91.72 (9.50)	0.02*
PRONE TO STANDING						
Foot strike to completion (s)	1.04 (0.07)	0.93 (0.05)	0.02*	0.90 (0.08)	1.07 (0.07)	0.15
Jump distance (m)	0.95 (0.03)	0.95 (0.03)	1.00	1.05 (0.03)	0.85 (0.04)	0.002*
Knee angle at foot strike (°)	-89.44 (5.32)	-82.70 (5.44)	0.01*	-81.64 (8.36)	-90.50 (6.21)	0.41

Notes: * $p \leq 0.05$; values are estimated means (SE).

LOWER EXTREMITY JOINT KINEMATICS IN ALTERNATIVE FOOTWEAR DURING SLIP EVENTS

¹Harish Chander, ²Chip Wade, ¹Adam C. Knight & ³John C. Garner

¹Mississippi State University, Mississippi State, MS, USA

²Auburn University, Auburn, AL, USA

³The University of Mississippi, University, MS, USA

Email: hchander@colled.msstate.edu Web: www.kinesiology.msstate.edu

INTRODUCTION

The Bureau of Labor Statistics reported 15% of a total of 4,693 workplace fatalities and a total of 299,090 cases of non-fatal workplace injuries that were due to slips, trips and falls [1]. Slips occur as a result of failure of normal locomotion and failure of attempts at equilibrium recovery following an induced imbalance [2]. Both extrinsic factors such as the type of footwear [3] and intrinsic factors such as the knowledge or anticipation of a slip [4] have been shown to affect the outcome of a slip event.

The normal gait cycle pattern is disturbed due to the perturbation from a slip. Increased foot-floor angle and plantar flexion angle at the ankle and a greater hip flexion have been demonstrated during slips [4]. However, with perception of slippery conditions, a plantar flexed ankle to achieve a flatter foot strike has been shown previously [4]. Alternative footwear such as flip-flops have been shown to utilize a flat-foot position during heel strike while close-toed shod conditions have greater dorsiflexion [5]. The impact of these alternative footwear under slippery conditions with and without the knowledge of slippery flooring conditions haven't been fully addressed yet. The specific purpose of this paper is to analyze the impact of alternative footwear [cros (CC), flip-flops (FF)] and an industry standard low-top slip resistant shoe (LT)] under multiple gait trials [normal dry (NG); unexpected slip (US), alert slip (AS) and expected slip (ES)] on lower extremity joint angles (hip, knee & ankle) at heel strike.

METHODS AND PROCEDURES

Eighteen healthy male participants [Age: 22.28 ± 2.2 years; Height: 177.66 ± 6.9 cm; Mass: 79.27 ± 7.6 kg] with no history of neuromuscular and vestibular abnormalities participated in this study. The study followed a repeated measures design with participants tested on three separate days wearing a counter-balanced assigned footwear, separated by a minimum of 24 hours. Kinematic and kinetic data were collected with a 12 camera Vicon motion capture system and dual force plates (AMTI & Bertec). Participants were strapped to a harness and a fall arrest track and performed multiple gait trials until normal self-selected pace walking with appropriate foot positioning onto the force plate was achieved. Participants turned away from the walkway and listened to music on head phones for 1 minute between each of these dry normal gait trials (NG). Following these trials, one particular trial was chosen to be the unexpected slip (US) and the contaminant (75% glycerol & 25% water) was applied on the second force plate, without the knowledge of the participant. With the completion of the US and cleaning the floor and footwear, participants performed a similar protocol to complete an alert slip (AS) and an expected slip (ES) with instructions of "may or may not be slippery" and "will be slippery" respectively. Sagittal plane hip, knee and ankle angles at heel strike were determined with the Vicon Nexus software. A 3 (Footwear) x 4 (Gait Trials) repeated measures ANOVA was used to analyze the joint angles at $p = 0.05$.

RESULTS

Significant interaction between footwear and gait trials existed for Ankle Angle at $F(5.237, 89.034) = 2.403$, $p = 0.041$, $\eta_p^2 = 0.124$ (Fig.1). The significant footwear x gait trials interaction was followed up by simple effect analysis. Footwear pairwise comparisons revealed significantly greater dorsiflexion angle in NG compared to US, AS and ES for CC and in NG compared to AS and ES for FF. No significant differences existed for LT across all gait trials. Gait trial pairwise comparisons revealed significantly greater dorsiflexion angle in LT compared to both CC and FF in NG, US, AS & ES trials. No significant differences existed between CC and FF for all gait trials. No significant interaction or significant difference for main effect footwear or gait trials were found in hip or knee angles at heel strike.

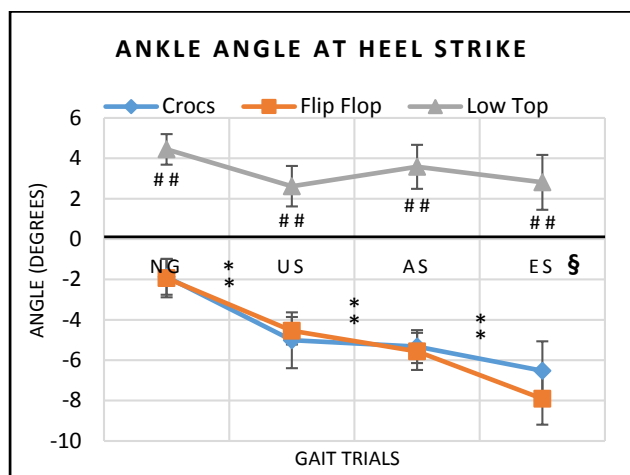


Fig.1: Ankle angle (degrees) at heel strike for Crocs, Flip-Flops and Low Top Slip Resistant Shoe during normal dry gait (NG), unexpected slip (US), alert slip (AS) and expected slip (ES) events. Positive degrees represent dorsiflexion and negative degrees represent plantar flexion. § denotes significant interaction; * denotes significant difference for footwear across gait trials and # denotes significant difference for gait trials across footwear.

DISCUSSION

Modifications in lower extremity joint angles appeared to be present only in the more distal ankle joint, while the proximal knee and hip joint angles showed no significant differences, suggesting the major kinematic changes in response to slips occurred at the distal end of the

lever at heel strike. The incidence of the slips across different slip trials and across types of footwear are reported elsewhere, with significantly greater incidence of slips in alternative footwear (CC & FF) compared to LT and with significantly greater magnitude of slips in US followed by AS and ES compared to NG. The LT appeared to maintain a normal dorsiflexion (close to neutral) ankle joint angle across all gait trials, while alternative footwear exhibited a plantar flexed foot position across all gait trials with significantly greater plantar flexion in slip trials. A greater plantar flexed ankle angle with alternative footwear during normal dry gait trials could be attributed to the different “touch down geometry” associated with these alternative footwear [5], while during slip trials, could be seen as an attempt to make contact with a flatter foot position, and having a greater surface area of the foot and a lesser foot floor angle, thereby preventing slips [4]. The LT had better performance in preventing slips and maintaining a normal gait pattern, and serves to be the choice of footwear for maneuvering slippery floors. Although alternative footwear serves for comfort and easy donning, it might not be the choice of footwear in slippery conditions, especially in hospitals where there is a greater use of crocs. Future research should focus on interactions of these alternative footwear and slippery conditions with an occupational workload.

REFERENCES

1. Bureau of Labor Statistics: US Department of Labor, 2012.
2. Davis, P. R. (1983). Human factors contributing to slips, trips & falls. *Ergonomics*, 26(1), 51-59.
3. Gauchard, G., Chau, N., Mur, J. M., & Perrin, P. (2001). Falls and working individuals: role of extrinsic and intrinsic factors. *Ergonomics*, 44(14), 1330-1339.
4. Cham, R. & Redfern, M.S., (2002). Changes in gait when anticipating slippery floors. *Gait & Posture* 15, 159-171.
5. Shroyer, J. F., & Weimar, W. H. (2010). Comparative analysis of human gait while wearing thong-style flip-flops versus sneakers. *Journal of the American Podiatric Medical Association*, 100(4), 251-257.

EFFECTS OF PROXIMAL AND DISTAL MUSCLE FATIGUE ON REPETITIVE MOVEMENTS

Jeffrey C. Cowley, Rebecka Saunders, and Deanna H. Gates

University of Michigan, Ann Arbor, MI, USA
email: gatesd@umich.edu Web: rehabrobotics.umich.edu/

INTRODUCTION

Upper extremity overuse injuries are a leading cause of lost work days in the United States. During repetitive tasks, muscle fatigue may contribute to the development of overuse injuries. When fatigued, people may alter their movement patterns, but adaptations to fatigue depend on which muscles are fatigued [1]. Due to the different roles of proximal and distal joints in executing movements, fatigue of proximal or distal arm muscles may affect movement differently [2-3]. Movement changes after fatigue can affect the risk of overuse injuries [4]. The purpose of this study was to determine how proximal and distal fatigue affect movement coordination and variability during an unconstrained, repetitive, work-like task. We examined subjects as they manually turned a bolt using a socket wrench. We expected that movement variability would increase after fatigue of the shoulder muscles and decrease after fatigue of the hand muscles.

METHODS

Five healthy, right handed adults (1 male) participated to date. Subjects were screened for medications or conditions which could affect arm movement. Subjects completed two experimental sessions (Fig. 1) to test the effects of proximal (A) and distal (B) muscle fatigue on a repetitive task. Subjects held a wrench in the right hand, reached up and rotated a bolt placed through a board at eye level. The task was repeated at 0.25 Hz for 3 minutes before and 3 minutes after fatigue of either proximal (shoulder flexors) or distal (finger flexors) muscles. Maximal voluntary contractions (MVC) and ratings of perceived exertion (RPE) were obtained at several points during the session to monitor fatigue (Fig. 1). The proximal fatigue protocol (A) is designed to fatigue the shoulder flexors. Subjects repeatedly raised and lowered a weight (~10 % max shoulder

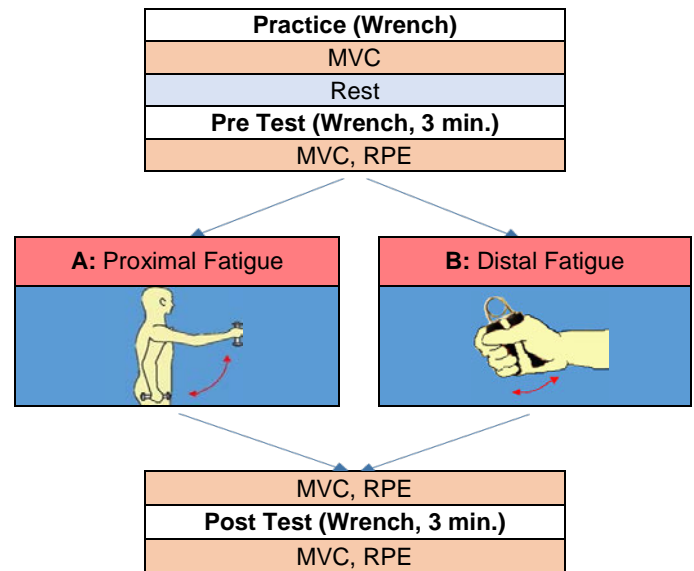


Figure 1. Experimental Session. All subjects completed the same general experimental protocol. Subjects performed two trials of a repetitive wrench task, one pre-fatigue and one post-fatigue. Subjects completed two experimental sessions (A and B).

MVC) to shoulder height in the sagittal-plane with the arm straight at a frequency of 0.5 Hz. The distal fatigue protocol (B) is designed to fatigue the finger flexor muscles. Subjects repeatedly squeezed a spring-loaded grip trainer with their right hand at a frequency of 1 Hz. Subjects were instructed to match each movement phase (up/down, squeeze/release) with a metronome. Subjects performed each fatigue task for 3 minutes or until $RPE \geq 8$. The movement of 47 reflective markers placed on the trunk, arms, and wrench was recorded at 120 Hz using a 16 camera motion capture system (Motion Analysis, Santa Rosa, CA). An 8-segment model was created in Visual3D (CMotion, Germantown, MA). Electromyography instantaneous mean power frequencies were calculated to quantify muscle fatigue. Movement cycles were divided into reaching and torquing phases. The average maximum and minimum angles of the shoulder, elbow, wrist, and

trunk across all movement cycles were obtained and variability was calculated as the median absolute deviation [5]. Results are reported as mean (standard deviation).

RESULTS AND DISCUSSION

During the fatiguing tasks, MVC strength of the targeted muscle group decreased by 25% on average. Subjects completed a similar number of wrench repetitions during all pre- and post-tests.

We noted several differences in upper limb and trunk kinematics after fatigue. After proximal fatigue, subjects exhibited decreased humeral elevation, greater external rotation and forearm supination, and increased trunk movement (Table 1; Fig 2. After distal fatigue, subjects increased wrist extension and ulnar deviation (Table 1). On average these differences were quite small (< 3 deg).

Forearm pronation during the reaching phase of the movement was more variable after proximal fatigue (Pre: $1.7 \pm 0.6^\circ$; Post: $1.9 \pm 0.4^\circ$) and less variable after distal fatigue (Pre: $1.9 \pm 0.5^\circ$; Post: $1.7 \pm 0.6^\circ$). Trunk rotation variability decreased more after distal (Pre: $2.0 \pm 0.4^\circ$; Post: $1.6 \pm 0.4^\circ$) than proximal fatigue (Pre: $1.9 \pm 0.4^\circ$; Post: $1.7 \pm 0.4^\circ$). During torqueing, peak external rotation of the humerus was more variable after proximal (Pre: $3.5 \pm 0.8^\circ$; Post: $4.5 \pm 2.1^\circ$) but not distal fatigue (Pre: $3.1 \pm 0.9^\circ$; Post: $3.3 \pm 1.7^\circ$) (Fig. 2).

CONCLUSIONS

Distinct movement adaptations were observed after fatigue of proximal and distal muscles of the dominant arm during a repetitive task. Compared to pre-fatigue, subjects adopted less variable movement

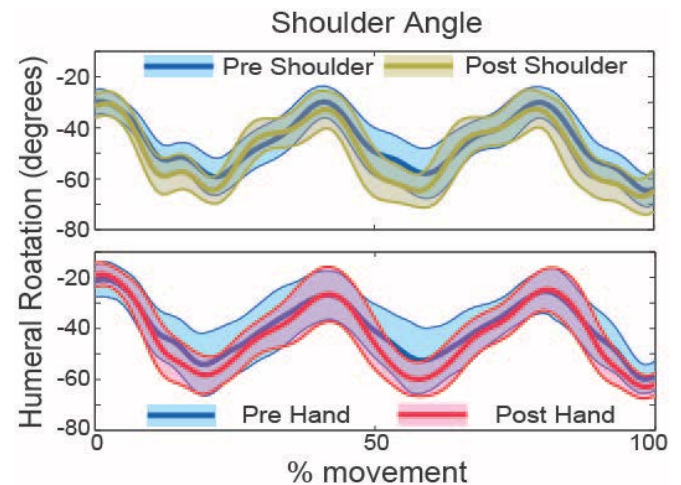


Figure 2. Humeral rotation for one subject during wrench torqueing. Top: Average angle before (blue) and after (tan) shoulder fatigue. Bottom: Average angle before (blue) and after (red) hand fatigue. Shaded areas represent one standard deviation.

patterns after fatigue of the distal muscles and more variable movement patterns after fatigue of the proximal muscles. We observed significant movement redistribution after proximal fatigue, but relatively few changes in joint angles after distal fatigue. The distinct movement strategies may have reduced the effort of fatigued muscle groups, allowing fatigued muscles to recover. A reduction in variability after distal fatigue could accelerate fatigue and affect the risk of injury.

REFERENCES

1. Cowley JC, et al. *Exp Brain Res* **232**, 3939-48, 2014
2. Dounskaia N. *Exp Brain Res* **166**, 1-16, 2005.
3. HufFenus AF, et al. *Exp Brain Res* **170**, 438-47, 2006.
4. Srinivasan D, et al. *Clin Biomech* **27**, 979-93, 2012.
5. Qin J, et al. *J Electromyogr Kines* **24**, 404-11, 2014.

Table 1. Maximum joint angles (mean (SD)) during the wrench task pre and post proximal (shoulder) and distal (hand) fatigue.

		Shoulder		Forearm		Wrist		Trunk	
		Elevation	Rotation	Supination	Pronation	Extension	Ulnar Deviation	Lean	Extension
Shoulder	Pre	99.2 (8.1)	-40.7 (13.9)	-34.3 (6.7)	4.0 (3.9)	-25.6 (11.8)	15.7 (12.6)	-2.6 (3.4)	4.4 (2.5)
	Post	95.2 (10.3)	-46.3 (16.9)	-27.5 (12.1)	7.0 (3.8)	-25.9 (11.7)	16.9 (11.1)	-3.5 (3.7)	5.8 (2.6)
Hand	Pre	101.0 (6.7)	-40.0 (12.8)	-36.8 (5.0)	1.3 (8.1)	-21.8 (9.4)	18.4 (15.2)	-3.0 (3.3)	3.9 (1.3)
	Post	100.2 (7.0)	-40.9 (13.1)	-32.5 (5.8)	1.6 (10.1)	-26.9 (12.6)	20.6 (13.4)	-3.3 (3.2)	4.1 (2.3)

LARGER HORIZONTAL AFFORDANCES FOR PERCEIVED SAFE HANDLING ARE ASSOCIATED WITH INJURY-RISK LIFTING KINEMATICS

¹Jon B. Doan, ²Wayne J Albert

¹University of Lethbridge, Lethbridge AB Canada

²University of New Brunswick, Fredericton NB Canada

email: jon.doan@uleth.ca, Twitter: @DoanJon

INTRODUCTION

Workplaces can be dynamic environments, with variable demands on the physical and cognitive capabilities of workers. Longitudinal studies of different work types have suggested various biopsychosocial worker traits and states that may contribute to an increased injury risk [1,2], but the neuromechanical bases of these differences remains largely unknown [3-5]. The purpose of the current research was to examine affordances and associated kinematics of behaviour in an experimental occupational lifting task. It was hypothesised that participant-workers with high perceived lifting affordance (hyper-affordant) would demonstrate higher injury-risk type kinematics than those with lower perceived lifting affordance (hypo-affordant).

METHODS

One load factor from the National Institute of Occupational Safety and Health (NIOSH) 1991 lifting guideline [6] was tested, specifically horizontal distance to load at start of lift (H Factor in NIOSH 1991 model). Twenty university students (21.4 +/- 2.8 years, 13 females) volunteered to participate in the study, and provided informed consent prior to whole body placement of infrared reflective markers. Participants were positioned with feet on baseline on the floor, with all load starting positions and the load final placement position inside the calibrated volume of a camera-based motion analysis system. The test load was a rigid industrial tote (0.55m x 0.35m x 0.25m) with a fixed mass (4.5 kg) at the centre of its floor, and good bilateral handles. Participants were told they would be choosing the greatest horizontal load placement distance that they felt would be safe for completion of a lift from the floor, using a single forward step with either leg to handle and lift the load. Following this familiarization with the task, the investigator slid the load away from the

participant along the tape measure on the floor. Participants told the investigator to stop at the horizontal affordance threshold (AT) they felt was safe for the lifting task as defined. Participants were given the opportunity to step, forward flex, and place their hands close to the load, without touching or lifting it, to confirm their perceived horizontal AT. Iterative increases or decreases were made to the selected distance by an investigator until the participant was completely satisfied with their AT. Following the recording of this value, each participant completed a series of 21 lifts, three at each of 60%, 70%, 80%, 90%, 100%, 110%, and 120% AT (Figure 1).



Figure 1: Lifting trial. After establishing their safety-based affordance threshold (AT), participants completed multiple flex-to-lift-to-place trials at relative proportions of their AT.

The lifting movement was divided into serial phases (ONSET, ADDRESS, HANDLE, LIFT), and linear and angular kinematic analysis here will focus on the ADDRESS (trunk forward flexion: reach to load on ground) and LIFT (trunk extension: return from ground with load) phases, as the most dynamic aspects of the behaviour. Participants were divided *post hoc* into two groups according to the ratio of their self-selected horizontal lifting affordance threshold (AT) to their stature (H; vertical distance between C7 marker and average ankle marker during quiet standing, as determined from pre-movement motion analysis capture). This dimensionless relationship (AT/H) has previously

been used to represent affordance as a system function of both animal and environment [7]. In this study, lifters who perceived a personal AT/H above the group mean AT/H were defined as hyper-affordant (HYPER; $n = 9$) while those who perceived a personal AT/H at the mean or below were defined as hypo-affordant (HYPO; $n = 11$). This *post hoc* grouping provided an additional serendipitous comparison – the average physical distance for the HYPER group's 80% AT was equal to the HYPO group's average 90% AT, each with a mean real distance of 0.75m. This equality allowed us to develop additional comparisons at a TRUE EQUAL distance. In the current study, we correlated height-normalised lifting affordance perceptions with TRUE EQUAL lifting kinematics, specifically a modified calculation of Burgess-Limerick and Abernethy's "postural index" [8] and a summation of time for dynamic lifting phases (ADDRESS + LIFT) to determine if affordance perceptions were associated with lifting kinematics.

RESULTS AND DISCUSSION

Perceptual and behavioural differences existed between the HYPER and HYPO sub-groups, including significantly different knee flexion angles (smaller values meaning greater knee flexion) during the ADDRESS phase (Figure 2; $F(1,6) = 4.334$, $p = .039$).

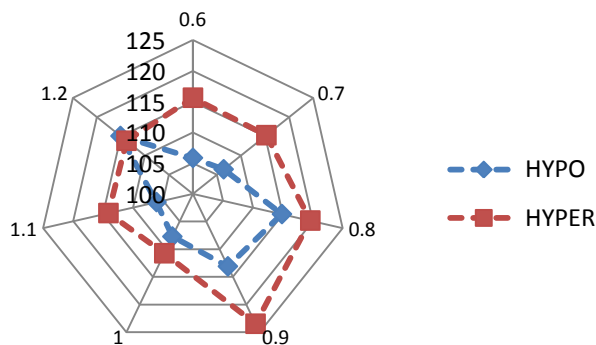


Figure 2: Magnitude of knee flexion during ADDRESS phase. The spokes on the graph are the different lifting distances, from 60 to 120% affordance threshold, while the rings of the graphs are knee flexion angles. HYPO and HYPER affordant lifters differed significantly on knee flexion, with HYPO lifters using greater knee flexion to reach to lift the load.

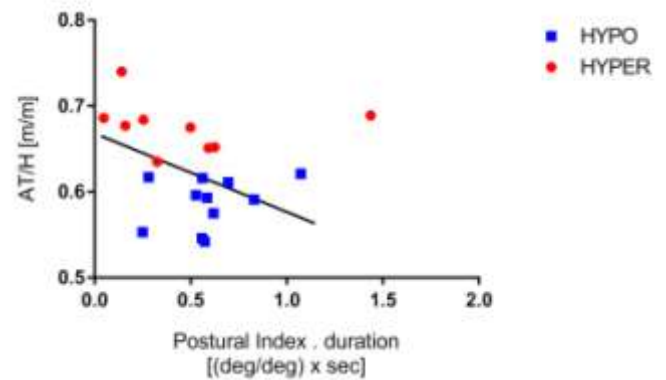


Figure 3: Association between normalized safe lifting affordance perception and lifting kinematics. A significant association existed between height-normalised affordance perception for safe lifting and lifting behaviours, with HYPER affordant lifters using smaller postural index (more stooped lift) at higher rates (shorter duration) than HYPO affordant lifters at TRUE EQUAL distance ($r = -0.47$, $p = .044$).

CONCLUSIONS

These preliminary results suggest that kinematics for lifting are coupled with perceived lifting affordance, at least in the horizontal task context. It is possible that the examination of perceived affordances in valid occupational tasks could identify workplace contexts, worker and organizational states, and worker perceptotypes at increased risk for musculoskeletal injury. Production and manufacturing facilities may benefit from re-examination of their workspaces and manual materials handling tasks, beyond conventional guidelines, and inclusive of affordance-driven concepts of safe and acceptable work behaviours.

REFERENCES

1. Stevenson et al. *Spine* **26**, 1370-1377, 2001.
2. Turner et al. *Spine* **33**, 2809-2818, 2008.
3. Gielo-Periczak & Karwowski. *Ergonomics* **46**, 310 – 326, 2003.
4. Marras. *Ergonomics* **48**, 464 – 477, 2005.
5. Snook. *Scan J Work Env Health* **25**, 13-18, 1999.
6. Waters et al. *Ergonomics* **36**, 746-776, 1993.
7. Fernandez & Marley. *Int J Ind Erg* **44**, 200-206, 2014.
8. Burgess-Limerick & Abernethy. *Human Factors* **39**, 141-148, 1997.

ACKNOWLEDGEMENTS

Thanks to NSERC for separate funding to WJA and JBD.

VALIDITY OF ACCELEROMETERS IN PREDICTING OCCUPATIONALLY RELATED LOWER EXTREMITY EXPOSURES

¹ Mohini Dutt, ¹ Steven A. Lavender, ¹ Ajit M.W. Chaudhari, ¹ Carolyn M. Sommerich

¹ The Ohio State University, Columbus, OH, USA
email: dutt.15@osu.edu

INTRODUCTION

Lower extremity musculoskeletal disorders and injuries affect a number of people in occupational settings. In many occupations, such as manual material handling jobs at distribution centers, there is exposure to prolonged standing, excessive walking on hard surfaces or uneven surfaces, stepping up or down between work surfaces, and there is vibration exposure. Quantifying these occupational exposures and their relationship to injury is necessary to determine thresholds that can be used to identify safe versus unsafe exposures levels for the lower extremities. To understand the force vectors generated at heel strike during walking, previous studies have used transient impulse forces on the tibia, also known as tibial shock [1,2].

The aim of this study was to validate the use of an accelerometer based instrumentation system that measures the transient impulse forces on the tibia, to quantify differences in material handling tasks with varying levels of lower extremity tibial shock exposure. We hypothesized that the measurement system would be able to detect variations in lower extremity tibial shock exposures across three tasks of varying exposure levels.

METHODS

Experimental Design: The study was a repeated measures design consisting of experimental conditions that simulate common types of distribution center work in which there are three different levels of tibial shock exposure as measured via the peak accelerations of the tibia.

Participants: Twenty volunteers, 11 males and 9 females between the ages of 18 and 36 years (mean = 22 years, s.d. = 5 years) participated in this study.

Mean height and weight were 1.71 m (s.d. = 0.09 m) and 69 kg (s.d. = 11 kg). None of the individuals had any lower extremity symptoms or pain 6 months prior to the time of the study. All study participants signed an Institutional Review Board (IRB)-approved consent document. All participants wore some type of athletic shoe.

Instrumentation: Single-axis accelerometers (Vernier – ACC BTA) were attached to the skin on the anterior aspect of the participants' left and right tibia and secured using a self-adhesive wrap. Sensors were attached to a data logging interface (Vernier – Lab Quest Mini) and tablet computer that were placed in a backpack carried by the participant.

Procedures and Data Analysis: Participants were instructed to complete the tasks at 3 exposure levels – Low, Medium and High Exposure. The tasks are described in Table 1 below. The sequencing of the tasks was counter-balanced across subjects and each task was repeated 30 times. The peak positive tibial accelerations were extracted for each task using MATLAB. Data were normalized for individual subjects using the mean value of the peak tibial accelerations of low exposure task and computing a ratio of each peak with the mean value. The distribution of values from each task were compared by obtaining the 50th, 75th and 90th percentile values and overall data analysis was conducted using a one-way ANOVA. Although bilateral tibial acceleration data was collected, only the leg showing the greatest tibial acceleration values was analyzed.

RESULTS AND DISCUSSION

The normalized peak tibial acceleration values for the 3 task exposure levels have been provided in Table 2. At the 50th percentile, the normalized

values of peak tibial acceleration were statistically different for the Low and Medium ($p=0.0021$) and the Low and High Exposure Tasks ($p<.0001$). The differences between the Medium and High Exposure tasks were not statistically significant. This is because the Medium and High tasks were similar apart from the stepping off and on the platform. At 75th and 90th percentile values, the peak tibial acceleration values were statistically different for the Low and Medium ($p=0.0247$ and $p=0.0006$ respectively), the Low and High Exposure Tasks ($p<.0001$) and the Medium and High Exposure Tasks ($p<.0001$). These differences are illustrated in Figure 1.

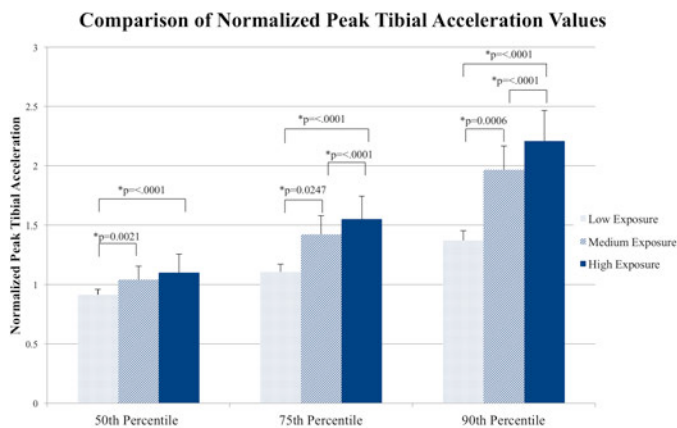


Figure 1: Comparison of Normalized Peak Tibial Acceleration Values across the 3 exposure levels

Though the differences between tasks may appear small, it is important to note that in the context of daily exposure, employees at distribution centers are often working at high speeds, involved in handling heavy cases and walking on average approximately 21000 steps/day or 10 miles/day [2]. Therefore, given the cumulative exposures in material handling occupations within distribution centers, having instrumentation and associated metrics that can differentiate between task exposures could be useful in identifying lower extremity work related musculoskeletal disorder risks.

CONCLUSIONS

The data supported the hypothesis that the instrumentation and associated peak tibial accelerations metrics could differentiate between the tasks at three exposure levels and therefore can be used to develop occupational risk models.

REFERENCES

1. Wosk J and Voloshin AS. *J. Biomech* **12**, 216-267, 1981.
2. Lavender SA, et al. *Applied Ergonomics* **44(5)**, 824-827, 2013.

Table 1: Experimental Tasks.

Task	Description	Type of Distribution Work
Low Exposure	Slow walking, with lifting	Pick to belt operations that are self paced
Medium Exposure	Fast walking, with lifting	Pick to belt operations where productivity is continuously monitored
High Exposure	Fast Walking with lifting and stepping off and on a platform	Pick to pallet operations where workers drive pallet jacks to pick locations and productivity is continuously monitored.

Table 2: Normalized peak tibial accelerations measured for tasks at 3 exposure levels.

Task	50th Percentile		75th Percentile		90th Percentile	
	mean	s.d.	mean	s.d.	mean	s.d.
Low Exposure	0.9151	0.0465	1.1082	0.064	1.3743	0.0827
Medium Exposure	1.0443	0.1131	1.4254	0.1533	1.9655	0.2018
High Exposure	1.1021	0.1558	1.5505	0.1926	2.2083	0.2566

LOW BACK PAIN STATUS AND PROLONGED STANDING ALTER CENTER OF PRESSURE PROFILES DURING CONSTRAINED STANDING

^{1,2} Kaitlin M. Gallagher and ² Jack P. Callaghan

¹ University of Arkansas, Fayetteville, AR, USA

² University of Waterloo, Waterloo, ON, CA

email: kmg014@uark.edu, web: <http://coehp.uark.edu/12889.php>

INTRODUCTION

While approximately 50% of a sample will demonstrate clinical levels of low back pain during prolonged standing[1], few pre-existing variables exist that can distinguish the two groups. The center of pressure (COP) is frequently used to assess the influence of external (vision or a task) and internal (such as pain) changes on a person's balance control. If differences are shown, assessment of the COP could provide a simple way to determine if individuals are susceptible to prolonged standing pain development and track progress in prevention strategies through interventions. Thus, the purpose of this study was to assess the influence of pain development and prolonged standing on balance characteristics during constrained standing.

METHODS

Thirty-one participants between 18 and 35 years were recruited for a prolonged standing occupational simulation. Participants were excluded if they had any previous history of low back pain that required a medical intervention or time off work longer than three days, previous lumbar/hip surgery, employment in a job with prolonged standing during past 12 months, and the inability to stand for 2 hours.

Participants performed two 2-minute constrained quiet standing tasks (with and without vision) before and after a 120-minute prolonged standing occupational simulation where participants completed assembly and sorting tasks. Upon entering the lab, participants filled out a visual analog scale (VAS) to assess their low back pain at that time. Participants then stood on two force plates (AMTI, Watertown, MA, USA) to provide separate 3D kinetics for each foot. Foot position was

standardized by creating a box with dimensions equal to the participant's foot length (with shoes). Participants were instructed to *"look straight ahead, stand as still as possible with your arms by your side and weight evenly distributed between your feet"*. Pain developer status was established using VAS scores during 120 minutes of prolonged standing

The net COP was calculated based on the methods of Winter et al.[2]. Pain developers were categorized if they exhibited a 10 mm or greater increase in their VAS scores relative to their baseline score[1,3]. The COP was filtered at 5 Hz. The mean COP position was subtracted from all data points. Mean power frequency (MPF) and the root mean square (RMS) amplitude (equitable to the standard deviation of the COP position when the mean of the signal is removed) of the COP data were calculated for each 2-minute trial. This was performed for both the medial-lateral (ML) and anterior-posterior (AP) directions.

A four-way general linear model with two between factors (Gender and Pain Group) and two within factors (eyes open/closed, pre/post prolonged standing) was run on each outcome measure. For any significant interactions, simple effects were used to determine the source of the interaction. The level of significance was set at $\alpha = 0.05$ for all tests.

RESULTS AND DISCUSSION

Forty-two percent of participants (13/31) were characterized as pain developers during prolonged standing. There was a significant main effect of pain group for ML MPF ($p=0.0454$). Non-pain developers had consistently greater ML MPF than pain developers. There was also a significant

interaction between time*vision ($p=0.0257$, Figure 1). With vision, ML MPF was significantly higher after 120-minutes of standing than pre-standing and was comparable to the ML MPF measures found with eyes closed. Since prolonged standing uses hip abductor muscles to perform ML weight shifts during standing[4], these muscles may not adequately provide the hip-load unload strategy under normal quiet standing conditions after 120 minutes of standing exposure.

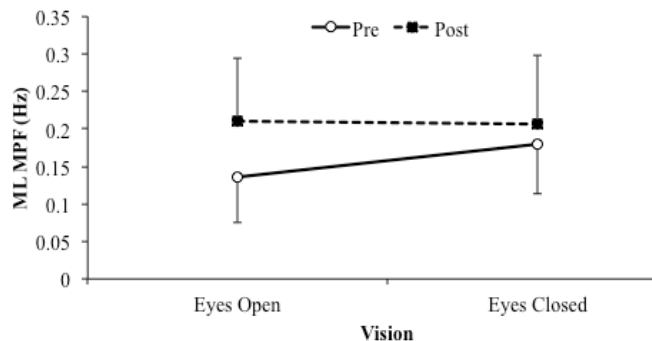


Figure 1: ML MPF compared pre- and post-prolonged standing in the eyes open and closed conditions.

Both AP and ML RMS had a significant interaction of pain group*vision (AP: $p=0.0002$; ML: $p=0.0114$; Figure 2). In general, non-pain developers demonstrated an increase in their COP RMS amplitude when they closed their eyes, while pain developers did not show this change. While there is no difference between the pain groups during normal vision, with the loss of vision pain developers still show a tighter control of the COP. This could be due to the increased gluteus medius co-contraction found previously in pain developers[3]. It may also show that although no differences exist in the two groups during normal vision, the two pain groups may be using different mechanisms to maintain their postural control. For example, the pain developers may show an over-reliance on their gluteus medius muscles to control their center pressure during normal standing.

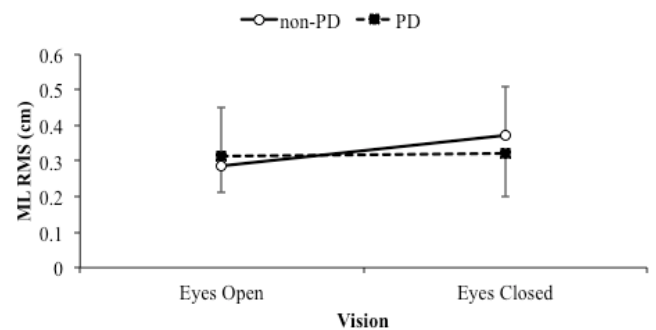


Figure 2: ML RMS amplitude compared between pain (PD) and non-PD in the eyes open and closed conditions.

CONCLUSIONS

Both low back pain development and prolonged standing influenced the amplitude and frequency of the COP movement, respectively. Future work should investigate the lack of change in the COP amplitude with the removal of vision as a predictive test for determining if a person will have prolonged standing induced low back pain development. Second, the potential that prolonged standing could negatively influence a worker's balance over the course of the day should also be studied further.

REFERENCES

1. Gallagher, KM., et al. *Ergonomics*, **57**, 555-62, 2014
2. Winter DA., et al. *Nuero Res Comm*, **12**, 141-8, 1993.
3. Nelson-Wong, E., et al. *Clin Biomech*, **23**, 545-53, 2008
4. Carlsöö, S. *Ergonomics*, **4**, 193-211, 1961.

ACKNOWLEDGEMENTS

The Natural Science and Engineering Research Council and Ontario Graduate Scholarship fund supported KMG. A Tier 1 Canada Research Chair supports JPC.

STANDING IN ANKLE PLANTARFLEXION REDUCES LOW BACK PAIN REPORTS DURING PROLONGED STANDING

^{1,2} Kaitlin M. Gallagher and ² Jack P. Callaghan

¹ University of Arkansas, Fayetteville, AR, USA ² University of Waterloo, Waterloo, ON, CA
email: kmg014@uark.edu, web: <http://coehp.uark.edu/12889.php>

INTRODUCTION

A sloped surface that allows people to work while standing in dorsi- or plantarflexion reduces reports of low back pain (LBP) development in people who report LBP during level ground standing[1]. In the study[1], people were allowed to alternate between the incline and decline surfaces. These findings raised the question of why LBP decreased: the alternating posture that would result in small cyclic flexion and extension of the lumbar spine[1,2] or because the majority of time was spent in dorsiflexion, resulting in mild flexion of the lumbar spine [1,2]. As a result, the purpose of this study was to determine if standing solely on a declining surface during an occupational simulation would decrease LBP reports. A secondary purpose was to determine changes in kinematics caused by standing on the declining surface during both acute and prolonged bouts of standing.

METHODS

Seventeen participants (nine male, eight female) aged 18-35 with no history of LBP that required medical intervention or time off work longer than three days, previous lumbar/hip surgery, employment in a job requiring prolonged standing within the last 12 months, and the inability to stand for at least two hours were recruited for this study.

A motion capture system (NDI Inc., Waterloo, ON, 32 Hz) was used to track kinematics during data collection. Rigid bodies were placed on the spine at T9, L1/L2, and sacral levels. Bilateral rigid bodies were also placed on the thighs and feet. Anatomical landmarks for each segment were tracked within the respective rigid body. A 100 mm visual analog scale anchored with “No Pain at All” and “Worst Pain Imaginable” was presented (e-VAS, University of Waterloo) to the participant on a touch screen tablet (iPad 2) to assess LBP development when they entered the lab, at the start of prolonged standing, and every 7.5 minutes during the protocol.

Standing on level ground and a declining surface (16°) were tested on two separate days. The order the participants saw the conditions were randomized. Participants were instructed to “stand as you normally would if you were required to work at a computer workstation. You can lift up each foot, change your foot position, and shift your weight back and forth. You cannot support your body weight on the table or cross your feet”. During the prolonged standing task, participants worked at a computer performing a standardized typing task.



Figure 1. Level ground (left) and decline (right) standing

Once the participant was instrumented, they performed a static standing calibration trial and a maximum lumbar extension trial to determine relative angles. On the day of the sloped protocol, participants performed two 60-second foot constrained trials prior to prolonged standing to assess the acute kinematic differences between the standing positions. Participants then completed a 75-minute unconstrained standing trial while working at the computer workstation.

Participants were categorized as pain developers (PD) based on visual analogue scale scores provided during the *level ground* standing position if they surpassed a 10 mm increase in their score with respect to baseline[1]. Marker locations were imported into Visual3D (v4, C-Motion, Inc., Germantown, MD, USA) to calculate trunk, lumbar spine, hip angle, and trunk-to-thigh angle were

calculated and expressed with respect to the corresponding angle from maximum extension. The anterior-posterior distance between the location of the trunk center of gravity and joint center of the right angle was also calculated.

For the foot constrained standing trials, outcome measures were entered into a three-way general linear model with between factors of gender, pain group (PD/non-PD) and a within factor of standing condition (level/sloped). For prolonged standing, an additional within factor of time was added to the model. Significance was set at $\alpha = 0.05$.

RESULTS AND DISCUSSION

53% of participants (9/17) were categorized as PD (four males, five females). While standing on the sloped surface, there was a 58% decrease in LBP VAS scores compared to each PD's maximum VAS on level ground (Figure 1).

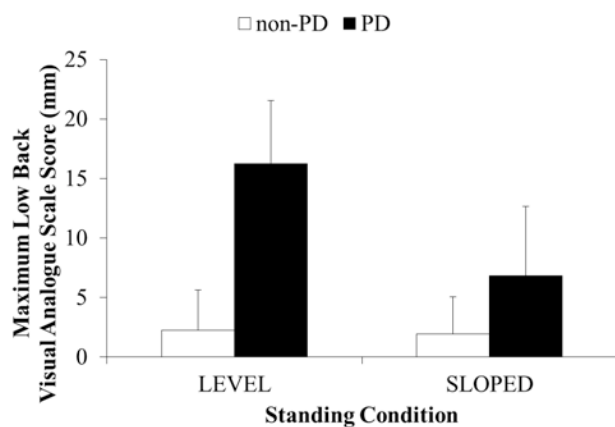


Figure 2: Maximum visual analogue scale scores.

During the foot constrained standing trials, there were no main effects including pain group for the kinematics. The sloped surface induced hip flexion ($p=0.035$), trunk-to-thigh flexion ($p=0.01$), and moved the location of the trunk center of gravity posterior compared to level ground ($p<0.0001$) (Table 1).

During prolonged standing, there was an interaction between pain group and standing condition ($p=0.022$). During level ground standing, the trunk center of gravity of PDs was on average 1.7 cm more anterior to the ankle than in non-PDs. During the sloped standing condition, the location of the center of gravity moved posterior and was aligned with the ankle joint (non-PD = 0.75 ± 1.3 cm; PD = 0.83 ± 1.3 cm).

We hypothesized that when standing on the declining surface the main kinematic change would occur at the lumbar spine[1,2] but this was not the case. Internal measurements while standing on a declining surface corroborate this finding[3]. The sloped surface appears to prompt participants to perform a hip dominant correction, allowing for a postural change without altering the moment induced by the trunk center of gravity at the L5/S1 joint. Also, a more anterior center of gravity with respect to the ankle would result in a greater moment arm with respect to the ankle for the force of the trunk due to gravity in PDs.

CONCLUSIONS

Standing on a sloped surface altered hip and trunk kinematics and may be a reason that self-reports of LBP development are lower in prolonged standing induced PDs when they stand on this surface. These results demonstrate that altering posture that results in mild flexion of the hips and alters the trunk center of gravity location, and not necessarily cyclic movement or isolated postural changes in the lumbar spine, may be responsible for the decreased pain development.

REFERENCES

1. Nelson-Wong, E. et al. (2010). *App Ergo*, **41**, 787-95
2. Gallagher, KM, et al. (2013). *Gait Posture*, **37**, 313-8
3. Gallagher, KM. (2014). *Doctoral Thesis*, University of Waterloo.

Table 1. Kinematic changes during foot constrained standing. Note: mean(SD). Asterisks denote significant differences between the standing conditions. Angle: +=flexion. Trunk COG location: +=anterior to ankle.

Condition	Trunk Angle	Lumbar Angle	Left Hip Angle*	Right Hip Angle*	Left Trunk-Thigh Angle*	Right Trunk-Thigh Angle*	Trunk COG location (cm)*
Level	22.6(10.6)	15.5(10.2)	9.2(10.5)	9.6(10.1)	31.1(14.3)	31.5(14.0)	4.43(1.94)
Sloped	22.8(10.6)	15.4(10.1)	11.0(11.2)	11.3(10.9)	33.0(14.9)	33.3(14.4)	2.55(1.72)

THE INFLUENCE OF INTERACTIONS BETWEEN EXTERNAL TASK DEMANDS IN LIFTING ON ESTIMATES OF *IN VIVO* LOW BACK JOINT LOADS.

Chad E. Gooyers¹, Tyson A.C. Beach², David M. Frost², Samuel J. Howarth³, Jack P. Callaghan⁴

¹ Giffin Koerth Forensic Engineering & Science, Toronto, ON, Canada

² Faculty of Kinesiology & Physical Education, University of Toronto, Toronto, ON, Canada

³ Canadian Memorial Chiropractic College, Toronto, ON, Canada

⁴ Department of Kinesiology, University of Waterloo, Waterloo, ON, Canada

Email: cgooyers@giffinkoerth.com

INTRODUCTION

The most commonly accepted mechanical risk factors linked to low back injury include: (i) high force demands; (ii) frequent repetition; and (iii) awkward postures [1]. However, as noted by Gallagher and Heberger [2] these exposures have typically been examined in isolation, and are often assumed to contribute independently to risk of injury. As such, our understanding of the combined effects of different external task demands (e.g. load, speed, and lift asymmetry) on low back joint loading and injury may be limited. Therefore, the motivation for this study was to evaluate interactions between: (a) external load magnitude, (b) movement speed, and (c) symmetry of initial load placement on estimates of *in vivo* low back joint loading during an occupational lifting task.

METHODS

Thirty-four participants with an average [SD] of 9 [10] years of manual materials handling experience (mean [SD] age = 37 [10] years; height = 1.80 [0.06] m; mass = 86 [10] kg) were recruited. The inclusion criteria for participation specified that participants reported that they were free of any known musculoskeletal injury and pain at the time of testing.

Whole-body, three-dimensional kinematic data were measured at 160 Hz using a 10-camera optoelectronic motion capture system (Vicon, Centennial, CO, USA). Sets of four and five reflective markers, fixed to rigid pieces of plastic were secured to the body with Velcro® straps, and used to track the position and orientation of 15 body

segments that were modeled. Two in-ground force platforms (FP6090; Bertec, Columbus, OH, USA) mounted side-by-side were used to measure reaction forces and moments between the feet and ground. The analog signals from each force platform were synchronized with the kinematic data, and sampled at a rate of 2400 Hz using Vicon software (Nexus version 1.4, Centennial, CO, USA).

Pairs of pre-gelled surface electromyography (EMG) recording electrodes (3 cm inter-electrode spacing; Medi-Trace, Kendall-LTP, Chicopee, MA, USA) were adhered to the skin, bilaterally, over the following six trunk muscle groups: (i) thoracic erector spinae (~T9), (ii) lumbar erector spinae (~L3), (iii) rectus abdominus, (iv) external abdominal obliques, (v) internal abdominal obliques, and (vi) latissimus dorsi. EMG signals were bandpass filtered (10-500 Hz) and differentially amplified (CMRR > 100 dB at 60 Hz; input impedance > 100 MΩ; TeleMyo 2400 G2 Telemetry System, Noraxon Inc., Scottsdale, AZ, U.S.A.) prior to analog-to-digital conversion at 2400 Hz. Surface EMG signals were collected synchronously with the force platform and kinematic data using Vicon software.

Each participant initially performed three lifting trials (box dimensions; 30.5 x 30.5 x 30.5 cm) that represented a low-demand condition (9.3 kg load, preferred movement speed, symmetrical positioning of load). Once these low-exposure trials were collected, the external demands of the lifting task were sequentially modified by manipulating each of the following parameters using a full-factorial design: (a) magnitude of external load – low = 9.3 kg, high = 24.7 kg; (b) movement-speed –

participants were instructed to either perform the lift in a “controlled manner” at their preferred speed or “as quickly as comfortable”; and (c) symmetry of initial load placement – the load was placed either in front of participants or at 45 degrees to the left of participants’ mid-sagittal plane. Each participant completed a total of 24 lifting trials that were evenly distributed across each of the eight experimental conditions.

Reaction forces and moments derived from inverse dynamics analyses, lumbar spine kinematics, and normalized linear envelope EMG signals were incorporated into a three-dimensional, dynamic, EMG-assisted musculoskeletal model of the lumbar spine to quantify L4/L5 joint compression and shear forces [3]. All trial data were truncated to include only the ascending phase of the lifting motion based on the vertical trajectory of participants’ linked-segment model centre-of-mass.

Interactions between the magnitude of the external load, movement speed, and symmetry of initial load placement on peak and cumulative estimates of L4/L5 compressive loading, as well as the normalized peak lumbar flexion angle at the time of peak loading, were evaluated with a within-subject, three-factor general linear model.

RESULTS

Significant two-way interactions between load and speed ($p = 0.0035$), as well as speed and posture ($p = 0.0004$) were revealed in peak measures of L4/L5 compressive loading. Subsequent analyses revealed significantly greater magnitudes of peak compressive loading for fast lifting trials with 9.3 kg of external load compared to the preferred speed ($p < 0.0001$; average difference = 588 N); however, there was no significant difference between the preferred and fast lifting trials performed with 24.7 kg of external load ($p = 0.5586$). Significantly greater magnitudes of peak compressive force were also observed in the high-speed trials with asymmetrical load placement ($p < 0.0001$; average difference = 580 N); however, there was no significant difference observed for the asymmetrical condition ($p = 0.5699$).

A significant three-way interaction between load, speed and posture ($p = 0.0477$) was observed in the cumulative estimate of compressive joint loading at L4/L5. Subsequent analyses of the interaction between load and speed across both symmetrical and asymmetrical load placement trials revealed a significant main effect of load ($p < 0.0001$; average difference = 724.7 Ns) and speed ($p < 0.0001$; average difference = 561.5 Ns) in trials with symmetrical load placement; however, there was a significant interaction between load and speed ($p = 0.0006$) for asymmetrical trials. Tukey’s *post hoc* test revealed that both the low- and high-load conditions were significantly different ($p < 0.0001$), although a more pronounced difference (1030.6 Ns) was observed at the preferred movement speed.

A significant main effect of posture ($p < 0.0001$) was revealed in normalized measures of lumbar flexion angle at the time of peak compressive loading; however, there was no significant main effect of load ($p = 0.4297$) or speed ($p = 0.1963$) found. Tukey’s *post hoc* test revealed that, on average, participants assumed more lumbar spine flexion at the time of peak compressive loading with asymmetrical load placement ($p < 0.0001$; average difference = 8.5% of full flexion).

DISCUSSION & CONCLUSIONS

Results from this investigation provide strong evidence that known mechanical low back injury risk factors should not be viewed in isolation. Rather, injury prevention efforts need to consider the complex interactions that exist between external task demands and their combined influence on internal joint loading. This non-additive response may be especially important to consider when investigating underlying mechanisms of injury.

REFERENCES

1. Bernard BP et al. *NIOSH*, 2007.
2. Gallagher S & Heberger, R. *Human Factors* **55**, 108-124, 2013.
3. Cholewicki J & McGill SM. *Clinical Biomechanics* **11**, 1-15, 1996.

PERCEIVED RISK OF BIOMECHANICAL FACTORS RELATED TO LOW BACK INJURY IN THE WORKPLACE

Chelsea R. Snow¹ and Diane E. Gregory^{1,2}

¹Health Sciences Program, Wilfrid Laurier University, Waterloo, ON

²Kinesiology and Physical Education, Wilfrid Laurier University, Waterloo, ON
email: snow6410@mylaurier.ca; dgregory@wlu.ca

INTRODUCTION

Nearly 80% of the population will encounter a low back problem within their lifetime despite substantial research in the area of low back pain dedicated to the understanding associated risk factors. Risk factors such as repetitive or prolonged twisting, bending, lifting, and sitting have been identified [1]; however, it is not currently known if this has been effectively translated to workers. The aim of this study was therefore to determine worker perceptions of low back injury risk factors.

METHODS

Participant Recruitment and Protocol

109 participants were recruited from four occupations: 50 office/administrative workers, 26 firefighters, 25 university students, and 8 dental workers (dentists and hygienists). Each participant was presented with a series of seven standardized images depicting different spine postures including upright and slumped sitting, lordotic and kyphotic lifting, and twisting (Figure 1) as well as one occupational-specific posture following the seven standard images (Figure 2). Participants were instructed to rate each picture on a scale from 0-10; zero representing no risk and ten representing extreme risk of injury to the low back.

Statistical Analysis

Ratings were statistically compared using a 2-way repeated measures ANOVA with occupation (4 levels: firefighter, student, dental, office) and posture (repeated measure; 7 levels) as the two factors. An alpha level of 0.05 was used to determine significance.



Figure 1: Seven standardized postures (4 lifting postures, 2 sitting postures, 1 twisted posture) presented to each participant. Order was random and participants were not permitted to look back at previous postures or ratings.

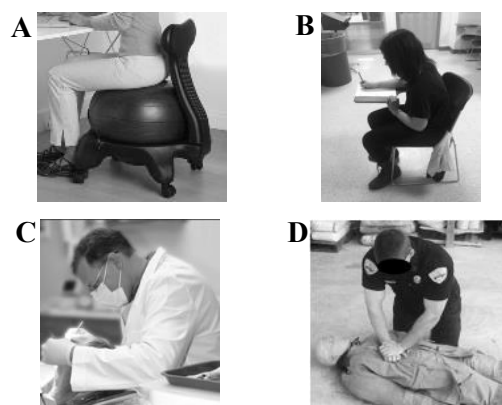


Figure 2: Occupation-specific postures. A) office, B) student, C) dental, D) firefighting.

RESULTS

Collapsed across all of the standardized postures, dental workers had the highest ratings (6.2 ± 1.1)

and firefighters had the lowest ratings (4.8 ± 0.6) (Table 1).

Table 1: Average rating collapsed across the seven standardized postures. Occupations with different letters are significantly different ($p < 0.05$).

Occupation	Average Rating	Standard Error	Significance
Fire	4.8	0.6	a
Student	5.1	0.6	a,c
Office	5.5	0.5	b,c
Dental	6.2	1.1	b

In terms of lifting postures, all four occupations rated kyphotic postures the highest (and therefore most risky), regardless of whether it included a bent or straight knee ($\sim 8/10 \pm 2$). Interestingly, office workers, firefighters and dental workers all perceived lifting with a straight leg as being significantly riskier than with a bent knee when the spine was lordotic ($p < 0.001$), while students perceived the risk to be the same regardless of knee posture ($p > 0.05$). In terms of sitting postures, upright sitting was rated lowest by all occupations ($\sim 2/10 \pm 2$), while slumped sitting was perceived to be approximately twice as risky as upright sitting ($p < 0.001$). Interestingly, firefighters rated both sitting conditions significantly lower compared to the other three occupations ($p = 0.003$). Last, dental workers rated twisted spine postures to be as risky as kyphotic lifting postures, which was significantly higher (and therefore greater risk) than all three other occupation's ratings ($p = 0.003$).

The occupation-specific postures revealed interesting findings that in certain cases complemented the standardized posture findings. In particular, for the students, the slumped sitting posture in a tablet-style desk was rated similarly to the standardized slumped posture. Dental workers rated the slumped twisted posture when working with patients similar to the standardized twisting posture. Interestingly, for the office workers, the stability-ball sitting posture was perceived to have a similar risk to the low back as upright sitting. Last, firefighters rated the CPR posture similar the twisted posture and lordotic straight-knee lifting.

DISCUSSION

Lifting

The differences in posture ratings between office workers, dental workers, firefighters and students demonstrate variance among professions in terms of injury risk perception. All occupations accurately identified lordotic postures, both lifting and sitting, to be less risky than kypohotic. Interestingly, with the exception of students, lifting with bent knees was thought to be less risky than straight knees, even with identical spine postures emphasizing the “lift with your knees” training technique. The student population may not have had experience in occupations where low back injury risk training is incorporated and therefore may not be aware of this common training recommendation.

Sitting

All occupations rated upright sitting as having the lowest risk to the low back. Further, all occupations rated slumped sitting significantly more risky than upright. The more strenuous nature of firefighting may be the reason firefighters rated sitting much lower than the other occupations, which all spend a large proportion of their day sitting. Interestingly, the office workers rated the stability-ball posture to have a similar risk as upright sitting despite published work that has shown otherwise [2].

Twist

The twisted posture rating was most variable across occupations with dental workers rating it highest. Dental workers likely rated twisted postures higher as they spend much of their day in twisted sitting postures when working with patients.

CONCLUSION

The findings from this study can be used to implement new training programs and interventions that are occupation-specific.

REFERENCES

1. Coenen, P., et al . *J Occup Rehabil* **23**,11–18, 2013.
2. Gregory, D., et al., *Hum Factors* **48(1)**:142-53., 2006

ERGONOMIC EVALUATION OF A PROTOTYPE QUICK-RELEASE BODY ARMOR SYSTEM

¹ Brian K. Higginson and ² Jennifer L. Wheeler

¹ Gonzaga University, Spokane, WA, USA

² Montana State University, Bozeman, MT, USA

email: higginson@gonzaga.edu

INTRODUCTION

Most recent military conflicts require that body armor (and associated tactical load) be worn by soldiers during maneuvers and tactical engagements. Due to the weight and bulk of this externally carried load, self-extraction and rescuer-extraction during time-critical emergencies, such as underwater submersions and vehicle rollovers involving fire, can be difficult. In an effort to expedite extractions during time-critical emergencies, a quick-release body armor system was developed.

In addition to facilitating a quicker doffing of the system, the current system also integrates a waist belt that effectively transfers the weight of the body armor and tactical load to the wearer's waist. Most current body armor system designs require that all of the external load be carried on the shoulders, which can lead to shoulder and upper extremity pain and fatigue.

The current system incorporates a 5-point release mechanism that, once activated, allows the front armor plate to fall away via release of two sets of buckles located on the shoulder straps and cummerbunds. The design of the rear armor plate and waist belt interface requires the user to lift the rear plate out of a pocket integrated into the waist belt once the front plate has fallen away.

The purpose of the current study was to perform an ergonomic evaluation of a prototype quick-release system for military body armor and tactical loads in order to facilitate rescue efforts during time-critical emergencies.

METHODS

12 members of the local County Sheriff's SWAT team volunteered to participate in the study (Mean \pm SD: 40.4 \pm 4.3 yrs, 180.3 \pm 6.8 cm, 93.5 \pm 10.3 kg). Each subject was fitted with a five-point quick-release body armor system, Kevlar helmet, and standard tactical load (simulated weight included six 30-round magazines, two fragmentation grenades, hydration system, Improved first aid kit (IFAK), and dump bag). A familiarization period was provided for each subject to practice donning and doffing the armor and load as needed. Upon completion of the familiarization session, a linear force transducer was attached to the quick-release pull lanyard, EMG electrodes were attached to muscles of the upper extremity (anterior deltoid, lateral and long head of the triceps), and an electrogoniometer was attached across the elbow joint.

Once sensor attachment was complete, the subject was asked to utilize the quick-release mechanism to remove the armor and load. This was performed using each hand in the standing and seated positions. Since the release lanyard ran along the left shoulder strap of the armor system, it was expected that outcome measures may be different when using a left vs. right handed release strategy. Each condition was unconstrained and performed three times for each condition, for a total of 12 releases per subject. All outcome measures were averaged over the three releases within a given condition.

Specific outcome measures included linear force required to initiate the quick-release mechanism, linear force required to clear the armor from the integrated waist belt, upper extremity muscle activation during the release, elbow range of motion (RoM), as well as doffing times for each of the

conditions. A 2-factor (release side x release position) Repeated Measures ANOVA was used to detect changes in outcome measures across trials ($\alpha=.05$).

RESULTS AND DISCUSSION

Although muscle activation of the left anterior deltoid tended to be ~25% higher than the right, this difference was not found to be significant ($p=0.270$), nor was there a significant difference in muscle activation as a function of release position ($p=0.764$). Muscle activation of the lateral and long head of the triceps were also similar across release sides ($p=0.460$ and $p=0.334$, respectively) and release positions ($p=0.175$ and $p=0.187$, respectively). Elbow RoM was significantly greater during the left handed release strategy than the right (84.7° vs. 60.6° , respectively, $p=0.005$) and while in the seated position (75.7° vs. 69.4° , respectively, $p=0.018$).

Release force (force at the time of buckle release of shoulder strap) averaged 19.3 N. There were no differences in release force for either position ($p=0.957$) or release side ($p=0.818$). The average applied force during the doffing process was 83.1 N, with no significant differences detected between release position ($p=0.296$) or side ($p=0.612$). Maximum force applied to the release lanyard during the doffing process averaged 139.4 N, and like release force, this force was similar across positions ($p=0.427$) and release side ($p=0.471$).

Overall release time, as defined from movement initiation to rear plate clearance, took 15% longer to perform when using the right hand release strategy than the left (2.2 vs. 1.8 s, respectively, $p=0.012$). There was no significant change in overall release time as a function of release position. The time to maximal force production (from initial applied force on release lanyard) took significantly longer when using the right handed release strategy over the left (0.90 vs. 0.59 s, respectively, $p=0.018$). Similarly, the seated position resulted in longer release times than standing (0.80 vs. 0.68 s, respectively, $p=0.018$). Doff times were also established in which only the time from applied force on the release lanyard to rear plate clearance were considered,

effectively removing variability of time and strategy used from initiation of movement to lanyard pull. As seen with overall release time, the right handed release strategy took longer (26%) than the left (0.93 vs. 0.60s, respectively, $p=0.034$). Unlike overall release times, doff times were 11% greater in the seated position than the standing (0.86 vs. 0.75 s, respectively, $p=0.025$).

Although the increased release time using the right handed release strategy was expected (due to the requirement to reach across the body and clear the arm and release lanyard over the head and helmet, unlike the more direct approach of the left handed release strategy), it was initially unclear as to why the different release positions (standing or sitting) would result in different release times. The primary difference between the seated and standing positions was lower extremity position (~90° of hip and knee flexion), which should have no effect on upper extremity motion required to perform the release task. Upon further investigation it was found that during seated releases, the waist belt would experience vertical motion during rear armor plate clearance, preventing the plate from clearing as quickly as in the standing position. Quantification of waist belt motion, although not an initial measure of interest, revealed that the seated release position resulted in nearly twice the vertical motion as the standing position (10.8 vs. 5.6 cm, respectively, $p<0.001$) before rear plate clearance occurred. This finding also helps explain the increased range of motion seen at the elbow during the seated position. Vertical motion of the waist belt during doffing delayed separation of the rear plate from the belt, requiring greater elbow extension to clear the plate.

CONCLUSIONS

Although a greater elbow range of motion was required to doff the body armor system using the left hand, and muscle activation tended to be greater for this release strategy, release times were consistently lower using the left handed release. Doff times were found to be greater while in the seated position, due primarily to increased vertical motion of the integrated waist belt not seen during the standing conditions.

LOW BACK PHYSICAL DEMANDS DURING A SIMULATED DENTAL HYGIENE TASK

¹Samuel Howarth, ¹Diane Grondin, ¹Jocelyn Cox, ²Nicholas LaDelfa, and ²Jim Potvin

¹Canadian Memorial Chiropractic College, Toronto, ON, Canada

²McMaster University, Hamilton, ON, Canada

email: showarth@cmcc.ca

INTRODUCTION

The annual prevalence of low back pain amongst dental hygienists has been estimated to be up to 67%, and has been cited as the primary reason that dental hygienists either modified their work, or left the profession [1,2]. Previous work has suggested that the prevalence of low back pain in these professionals is likely related to the seated posture that dental hygienists adopt while performing their occupational duties [3]; however, no investigation to date has quantified the low back physical demands for dental hygienists. Thus, our primary goal was to describe the low back physical demands within a population of practicing dental hygienists during a simulated dental hygiene task (manual scaling).

METHODS

A total of 19 female registered dental hygienists were recruited for this study (Age = 30.6 ± 5.5 years, Height = 1.66 ± 0.09 m, Weight = 63.1 ± 15.2 kg, Years in practice = 4.9 ± 3.7 years). All participants were free of pain in their upper extremities as well as the upper and lower back. Technical difficulties experienced during data collection of two participants precluded their inclusion in subsequent data analyses. The protocol was approved by the Research Ethics Board at the Canadian Memorial Chiropractic College, and all participants signed an informed consent document prior to data collection.

Surface electromyographic (sEMG) recordings were obtained bilaterally, at a rate of 2048 Hz, from the lumbar and thoracic portions of the erector spinae (LES, TES) along with the cervical erector spinae, pectoralis major, anterior deltoid, posterior deltoid, upper trapezius, and lower trapezius (Bagnoli-16, Delsys Inc., Boston, MA, USA). For the purposes of this abstract, only data pertaining to the LES and

TES will be discussed. Kinematics of the dental hygienist's upper arms, head, thorax, and pelvis, along with kinematics of the stool on which dental hygienists sat and worked from during our simulated task were monitored at a rate of 32 Hz with an optoelectronic motion capture system (Optotrak Certus, Northern Digital Inc., Waterloo, ON, Canada). Finally, seat pressures were recorded at a rate of 8 Hz using a pressure mat (CONFORMat, Tekscan Inc., South Boston, MA, USA) affixed to the seat pan of the stool. Seat pressure data will not be discussed further due to the scope of this abstract.

After instrumentation, participants performed a series of maximal isometric voluntary contractions (MVICs) and spine range of motion trials followed by a 30-minute manual scaling task. The scaling task required participants to manually debride nail polish that had been painted on the teeth of a dental manikin (M-1R-DA-8, Columbia Dentoform Corp., Long Island, NY, USA) to simulate plaque. All participants used the same set of instruments for the manual scaling task. Participants were given an opportunity to adjust the height of their stool, the dental chair, and the location of the overhead light prior to data collection.

All kinematic and sEMG data were initially post-processed using Visual3D (C-Motion Inc., Germantown, MD, USA). All raw sEMG data were full-wave rectified, digitally filtered with a dual pass Butterworth filter with a cutoff frequency of 2.5 Hz, and normalized to a percentage of the maximum amplitude from the MVIC trials. Relative orientations between the pelvis and thorax defined lumbar spine angular kinematics that were normalized to a percentage of each participants active range of motion in flexion/extension, lateral bend, and axial rotation. Amplitude probability distribution functions (APDFs) were derived for the

normalized sEMG and kinematic time-series data (Matlab, The Mathworks Inc., Natick, MA, USA). Dependent measurements corresponding to the 10th, 50th, and 90th percentiles were obtained from the APDFs. Since lateral bend and axial rotation kinematics could span a range between $\pm 100\%$, the 10th and 90th percentile values effectively reflected peak angular deviations in both the left and right directions.

RESULTS AND DISCUSSION

Our data demonstrated that in addition to forward flexion, dental hygienists are often required to axially rotate their spine away from a neutral posture while performing a manual scaling task (Table 1). Combined flexed and rotated spine postures may present a different risk factor in dental hygienists that is not prevalent in other occupations where the seated posture has been linked to the incidence of lower back pain (e.g. occupational driving, deskwork). Furthermore, activity in both the left and right TES at the 10th percentile exceeded Jonsson's proposed maximally acceptable threshold for static work of 2% MVIC (Fig. 1) [4].

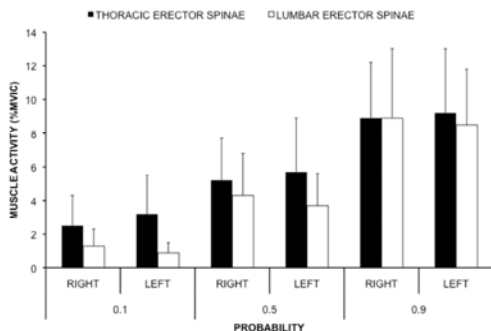


Fig 1: Muscle activity of the TES and LES at the 10th, 50th, and 90th percentiles.

Thus, it is possible that tonic low-level activity of the TES could lead to muscular fatigue and low back pain; however, it is important to note that we did not obtain measurements from the sEMG data that could be a direct indicator of muscular fatigue (e.g. shifts in median power frequency).

CONCLUSIONS

Based on our findings from the simulated manual scaling task, it is possible that the prevalence of low back pain amongst dental hygienists may be related to sustained activity of the spine extensor musculature, and adopting an axially rotated position while seated. Manual scaling is one of many occupational duties performed by dental hygienists, and future work should be conducted to evaluate low back physical demands in these individuals over an entire 8-hour workday.

REFERENCES

1. Anton D, et al. *Am J Ind Med* **42**, 248-257, 2002.
2. Liss GM, et al. *Am J Ind Med* **28**, 521-540, 1995.
3. Marklin RW and Cherney K. *J Calif Dent Assoc* **33**, 133-136, 2005.
4. Jonsson B. *Electroencephalogr Clin Neurophysiol Suppl-34*, 417-428, 1978.

ACKNOWLEDGEMENTS

Funding for this project was provided by the Ontario Ministry of Labour (Grant #12124).

Table 1: Amplitude probability distribution function (APDF) percentiles from normalized spine kinematics. Values in parentheses represent standard deviations of the mean. Positive values represent extension, right lateral bend, and left axial rotation. ROM = range of motion.

	APDF Percentile		
	10 th	50 th	90 th
Flexion/Extension (%ROM)	-33.5 (13.1)	-42.3 (15.5)	-52.5 (16.7)
Lateral Bend (%ROM)	-15.9 (14.0)	-0.7 (9.4)	11.4 (11.2)
Axial Rotation (%ROM)	-18.6 (16.7)	5.5 (16.1)	25.2 (19.9)

EFFECTS OF FATIGUE AND ASYMMETRIC LOAD CARRIAGE ON FIREFIGHTER OBSTACLE CROSSING PERFORMANCE

¹ Michael J. Angelini, ² Richard M. Kesler, ¹ Matthew N. Petrucci, ³ Karl S. Rosengren,
^{1,2} Gavin P. Horn, and ¹ Elizabeth T. Hsiao-Wecksler

¹ The University of Illinois at Urbana-Champaign, Urbana, IL, USA

² The Illinois Fire Service Institute, Champaign, IL, USA

³ The University of Wisconsin at Madison, Madison, WI, USA

email: angelin1@illinois.edu, web: hdel.mechanical.illinois.edu

INTRODUCTION

Slip, trip, and fall related injuries are among the most prevalent encountered on the fireground. These injuries commonly occur while navigating obstacles. Fatigue and load carriage are two intrinsic factors which often lead to difficulty in crossing obstacles, and thus increased risk of injury [1]. However, it is difficult to analyze firefighter fatigue in a lab setting due to an inability to replicate the fireground environment and fatigue. As such, the aim of this study was to quantify the effects of three different simulated firefighting exercise protocols and their resulting fatigue, as well as the carriage of an asymmetrical hose load, on firefighters' ability to cross obstacles.

METHODS

Twenty-four firefighters (23 male) completed three simulated firefighting activities: (1) treadmill walking in an environmental chamber (ECTM) – (14 min. at 4.5km/h, 2.5% incline, 47°C, 20% humidity); (2) simulated firefighting tasks in environmental chamber (ECFF) - 2 min. each of stair climb, hose advance, secondary search, and ceiling pull with 2 min. rest between tasks; and (3) simulated firefighting tasks performed in a live-burn building environment (BBFF) – avg. temp ~85°C. Tests were separated by a minimum of 24 hours.

Before and immediately after each exercise protocol, participants performed a set of four trials of a five-station obstacle course – one station of which involved traversing a 30-cm tall stationary obstacle. During the first two trials in each set, participants wore standard firefighting personal protective equipment of bunker gear, helmet, gloves and self-contained breathing apparatus pack (No Load condition). For the remaining two trials, each participant also carried an 11.3kg hose on the right shoulder (Load condition).

Obstacle contact errors and foot clearances were recorded and analyzed for each trial. Motion data were tracked (Qualisys, Oqus100; 200 Hz) using an arrangement of four markers on each boot, as well as on the top four corners of the obstacle. An error was recorded any time a subject contacted the obstacle. Horizontal and vertical clearances were calculated for each foot [2]. Trailing horizontal clearance (HCT) was defined as the horizontal distance from the trailing toe to the front of the obstacle at trailing foot midstance. Lead horizontal clearance (HCL) was measured from the lead heel to the back of the obstacle at lead foot midstance. The vertical clearances for each foot (VCT, VCL) were defined as the minimum of four vertical distances: between the toe and front obstacle markers, heel and front obstacle marker, toe and back obstacle marker, and the heel and back obstacle marker. Contact errors were totaled based on exercise protocol, the presence of the load, and fatigue. Clearances were analyzed via a three-way repeated measures MANOVA ((3) Protocol \times (2) Load \times (2) Fatigue) at a significance level of $\alpha=0.05$.

RESULTS AND DISCUSSION

Both clearances and errors appeared to be dependent on exercise protocol. Slightly fewer post-activity errors occurred following ECTM compared to ECFF and BBFF (9 vs. 12 in both cases). Significant interaction effects of protocol \times fatigue were observed on HCL and VCL (Fig. 1, $p \leq 0.036$). HCL decreased from pre to post activity for ECFF and BBFF, but did not change following ECTM. This result suggests decreased step length following simulated firefighting task exercise protocols, perhaps a compensatory strategy for decreased lower limb control [3]. VCL remained consistent from pre to post activity for ECFF and BBFF, but

increased following ECTM. These results may indicate that the levels of fatigue induced by the ECFE and BBFE protocols are similar, and are both greater than those induced by the ECTM protocol. Ultimately, these results may suggest that the ECFE protocol represents a reasonable simulation of firefighting in a live-burn environment with the benefits of greater safety and climate control.

Fatigue was shown to significantly affect obstacle crossing behavior. More errors occurred post-activity versus pre-activity for the ECTM and ECFE protocols, which may suggest that fatigue resulted in increased frequency of errors. Most errors (92%) were committed by the trailing foot, so it is likely that the lack of visual feedback during trailing foot early swing phase becomes more detrimental to obstacle crossing performance when fatigued [4]. Significant main effects of fatigue were also observed on HCL and VCT, resulting in respective decreases of 1.8cm and 1.6cm ($p \leq 0.025$). The decrease in HCL may indicate reduced step length, with subjects tending to cross the obstacle later in the lead foot swing phase, perhaps allowing for increased visual feedback to compensate for a decrease in lower limb control [3-4]. The decrease in VCT agrees with the high occurrence of trailing foot errors, and supports the conclusion that a lack of visual feedback compounded with fatigue can increase risk of obstacle contact [4].

Load carriage significantly affected clearances as well, but did not heavily impact contact error totals. Approximately equal numbers of contact errors were committed with and without the hose. Significant main effects due to load carriage were observed on HCL and VCL ($p \leq 0.043$). HCL decreased an average of 3.1cm, while VCL increased 0.9cm. The increase in VCL may be a compensatory strategy employed at the expense of dynamic stability to ensure obstacle clearance when

the perceived difficulty in clearing the obstacle is greater [3]. Significant interaction effects of load \times fatigue on VCT and VCL were also observed ($p \leq 0.024$). VCT remained fairly consistent from pre to post activity without the hose load, but decreased from pre to post in the presence of the hose. VCL increased from pre to post activity without the hose load, but decreased from pre to post in the presence of the hose, perhaps suggesting that it was more difficult to employ the compensatory strategy mentioned above while fatigued. These results suggest that the decreases in dynamic stability brought on by fatigue are compounded by the carriage of an asymmetrical hose load.

CONCLUSIONS

Exercise protocol, fatigue, and asymmetrical load carriage had significant effects on obstacle crossing behaviors. In general, fatigue caused contact errors to increase and clearances to decrease, with more pronounced decreases following protocols involving simulated firefighting tasks, suggesting that ECFE represents a reasonable simulation of live-burn activity. Load carriage was found to amplify the effects of fatigue, with larger decreases in clearances following exercise while carrying the hose. These findings highlight potential factors that could relate to fall risk for firefighters on the fireground.

ACKNOWLEDGMENTS

US Dept of Homeland Security (#EMW-2010-FP-01606).

REFERENCES

1. Park K, et al. *Safety Sci* **49**(5), 719-26, 2011.
2. Ramachandran AK, et al. *Gait & Posture* **26**(2), 248-55, 2007.
3. Said CM, et al. *Arch Phys Med Rehab* **82**(12), 1712-19, 2001.
4. Patla AE, et al. *Adv Psych* **114**, 257-77, 1996.

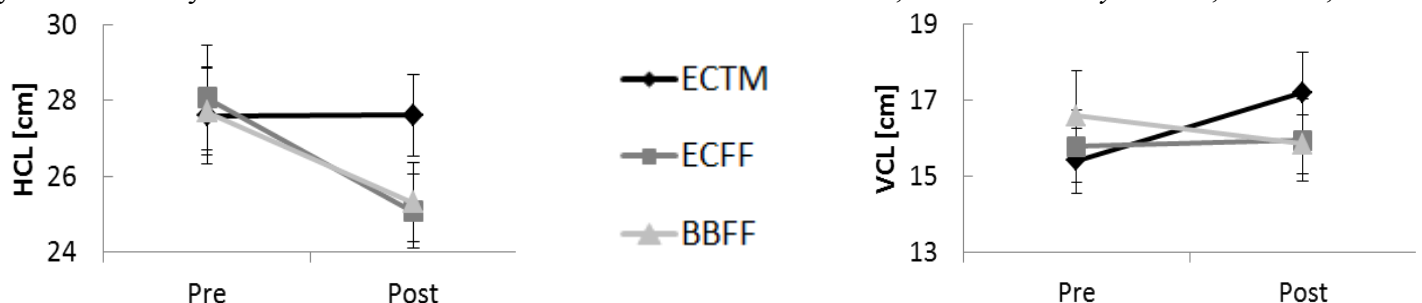


Figure 1: Horiz and vert clearances of the lead foot due to exercise protocol \times fatigue. Error bars = SE.

CONTRIBUTORY FACTORS TO MUSCULAR DEMAND IN CASHIERS

¹Jacquelyn M. Maciukiewicz, ¹Angelica E. Lang, ¹Meghan E. Vidt,

²Sylvain G. Grenier, and ¹Clark R. Dickerson

¹Department of Kinesiology, University of Waterloo, Waterloo ON, Canada

²School of Human Kinetics, Laurentian University, Sudbury ON, Canada

email: jmmaciuk@uwaterloo.ca web; <http://ahs.uwaterloo.ca/kin/research/diesel/>

INTRODUCTION

Cashiers commonly report musculoskeletal discomfort in the shoulder, neck and upper extremities [1]. In 2009, cashiers accounted for 35% of work-related injuries, with 51% of those injuries being a strain or sprain [2]. The underlying factors contributing to injuries in the cashier population include the adoption of awkward and static postures, task repetition, insufficient rest, and fluctuations in customer demands [3]. A recent emphasis for customers to use enviropackaging has caused cashiers to handle greater loads, as typical shopping bag weight has increased from ~10lbs for plastic bags to 28-38lbs for environmental bags and bins [3]. The postural demands and loads intrinsic to cashier tasks likely contribute to increased muscle effort and subsequent injury, although the role of these factors has not been explicitly evaluated in this group. The goal of this study is to evaluate the effects of packaging, workspace geometry, and work load and their interactions on muscular demand during the performance of cashier tasks.

METHODS

Twenty-five experienced cashiers (10M/15F) performed scanning and packaging tasks. A previous field study identified various key factors in a cashier environment, such as fluctuations in customer numbers and orders, types of packaging, and workstation height. Each of these factors was then evaluated in the laboratory study, in which EMG measurements were acquired to assess muscular demand. Workload intensity was evaluated at two levels which small and large orders, represented by 6 and 12 items, respectively. Three packaging types, including bins, reusable bags, and plastic bags, and three workstation heights (66cm, 78cm, 90cm) were evaluated. The low and high workstation heights

corresponded with the minimum and maximum possible heights of cashier workstations. The high workstation height is the standard height in grocery stores, in which the bagging area is flush with the scanner. All combinations of intensity, package, and height parameters were evaluated in a randomized order for a total of 36 trials per participant. Cashiers were instructed to replicate their personal bagging styles and pace in the laboratory setting.

Surface EMG (Noraxon, Inc., AZ, USA) was recorded bilaterally for upper trapezius, middle trapezius, serratus anterior, anterior deltoid, middle deltoid, upper (T9) and lower (L3) erector spinae, and external oblique. EMG data was full wave rectified, normalized by MVC data, integrated, and totaled using custom a Matlab program (The MathWorks Inc., Natick, MA, USA). Total integrated EMG, which gives an assessment of overall muscular demand, was calculated by summing the individual muscle EMG signals.

Mixed effect ANOVA was used to assess the influence of gender, intensity, package type, and workstation height on total muscular demand. Post-hoc Tukey HSD was used to confirm significant differences. Analyses were performed using JMP software (v.11.2.1, SAS Institute Inc., Cary, NC, USA) with significance considered as $p \leq 0.05$.

RESULTS AND DISCUSSION

Intensity, packaging type, and workstation height (all $p < 0.0001$) all influenced total integrated EMG. Higher muscular demand was observed in female participants than in male participants in all tasks ($p = 0.0126$). Interactions between packaging type and workload intensity (Figure 1) ($p < 0.0001$) and workstation height and workload intensity (Figure 2) ($p = 0.0011$) were also influential.

In all task configurations, the 6-item tasks required less total muscular effort than the 20-item tasks (Fig.1). Packaging type had a significant effect on total integrated EMG measures, whereby plastic bags and reusable bags required similar muscular demands, which were 40% higher than the muscular demand used for trials with the bins. The smallest total muscle effort was measured when 6 item trials were packaged with the bins, while the highest muscle effort was recorded when 20 items were packaged with either reusable bags or plastic bags.

During the higher intensity trials, the greatest muscular effort was seen during the highest workstation configuration (Fig.2). There was no effect of workstation height on workload intensity for 6 item trials. Working at low and middle heights elicited 20% lower total muscular demands than tasks performed at the highest workstation height.

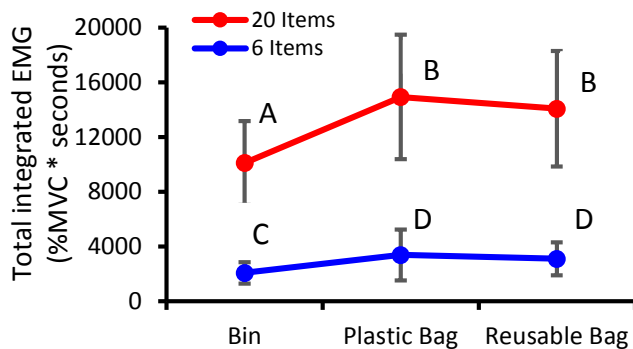


Figure 1: Interaction between packaging type and workload intensity for total integrated EMG. Points not connected by the same letter are significantly different ($p < 0.001$).

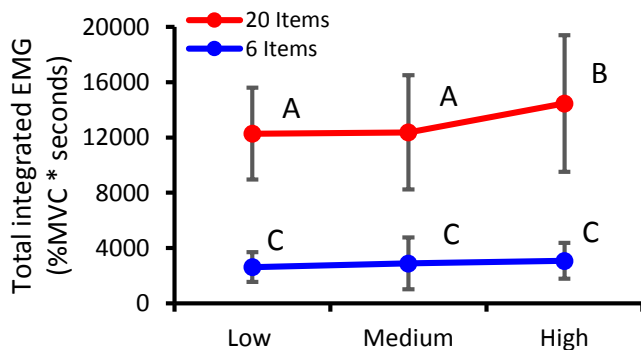


Figure 2: Interaction between workstation height and workload intensity for total integrated EMG. Points not connected by the same letter are significantly different ($p = 0.0011$).

Total integrated EMG, which is an indicator of overall muscular effort, depended on workstation configuration, packaging type, and intensity. These results demonstrate that smaller workloads, lower bagging area heights, and the use of bins reduce the total muscular demand of cashiers. However, these results are in contrast to the current standards of the cashier environment. For example, the highest workstation height is the standard height used in grocery stores. Workstation height is adjustable, but cashiers are potentially not aware of this bagging station feature, and should be instructed on how to lower the station to a more appropriate height.

Total muscular demand of cashiers is highest when processing large orders. Therefore, to reduce the muscular demand, and thereby reduce the musculoskeletal injury risk, adequate opportunities for recovery are crucial. Regular rotation through express and regular checkout lanes would reduce the muscle demands cashiers experience. Total muscle demand was assessed here, but further work is needed to characterize the role of individual and groups of muscles in the shoulder and low back during the performance of cashier work tasks.

CONCLUSIONS

Total muscular demand in cashiers can be lessened when performing work at a low intensity, with the workstation at a low height, and when packaging items in bins. The interactions identified here highlight the complex role of workspace parameters on total muscle demand, and we present steps which can be made to mitigate these demands to reduce the risk of musculoskeletal injury in this group.

REFERENCES

1. Johansson A. *Appl Ergon*, **29**, 261-266, 1998.
2. Health & Safety Ontario. Reusable Bag Guidelines, 2011
3. Lehman R. *Ergonomics* **44**, 719-738, 2001.

ACKNOWLEDGEMENTS

CRE-MSD; NSERC; Canada Foundation for Innovation; Ontario Research Fund.

EFFECT OF UNILATERAL AND BILATERAL LOAD CARRIAGE ON GAIT AND TRUNK ORIENTATION IN HEALTHY YOUNG ADULT FEMALES

¹ Kevin M. McGinnis, ¹ Laura Van Der Post, ¹ Jill S. Higginson

¹ University of Delaware, DE, USA

email: kevinmcg@udel.edu

INTRODUCTION

The majority of the population carries some type of bag to transport their personal items, such as a backpack, one-shoulder tote bag, or briefcase. Carrying a backpack daily has been found to cause back pain in adolescents and pain was correlated with carrying time [1]. It has also been shown that those who carry heavy loads for extended periods of time can experience blisters on the feet, knee pain, back pain, and stress fractures, among other injuries [2]. Coupled with the fact that backpack loads have been consistently increasing over the past two decades makes everyday load carriage an important issue in order to avoid chronic pain and/or injury [3]. College students often carry heavy loads over long distances and long periods of time throughout the day. However, there is little, if any, literature on how this population adapts to increased load carriage during gait. The objective of this study was to determine the alterations in the spatio-temporal parameters and trunk orientation of healthy, college-age females due to unilateral and bilateral load carriage.

METHODS

Nine healthy female college students were recruited from the local community to participate in this study. Spatio-temporal parameters (velocity, step length, stride length, stance time, and double-support percentage) were measured using a Zeno walkway pressure mat (ProtoKinetics LLC, Havertown, PA). Trunk side-to-side lean and trunk forward tilt were measured using an 8-camera motion capture system (Motion Analysis Corporation, Santa Rosa, CA). Reflective markers were placed on the shoulders, iliac crests and sternum to model and track the trunk. Subjects were instructed to make two passes across the gait mat, at a self-selected pace, and 4-5 gait cycles were used

in the analysis. Four scenarios were tested: normal walking, 20% body weight added to the left shoulder, 20% body weight added to the right shoulder, and 20% body weight in a two shoulder backpack. A repeated measures ANOVA was used to determine significant differences with an alpha of 0.05.

RESULTS

Subjects walked significantly slower in the bilateral condition ($1.17\text{m/s} \pm 0.15$) compared to control and both left and right unilateral conditions ($1.26\text{ m/s} \pm 0.15$, $1.23\text{m/s} \pm 0.15$, $1.24\text{m/s} \pm 0.15$ respectively; $p < 0.05$). Subjects carrying the bilateral load had a significantly reduced stride length ($1.30\text{m} \pm 0.076$) compared to the control condition ($1.36\text{m} \pm 0.079$, $p = 0.005$), but not left and right unilateral conditions ($1.32\text{m} \pm 0.102$, $1.32\text{m} \pm 0.082$ respectively).

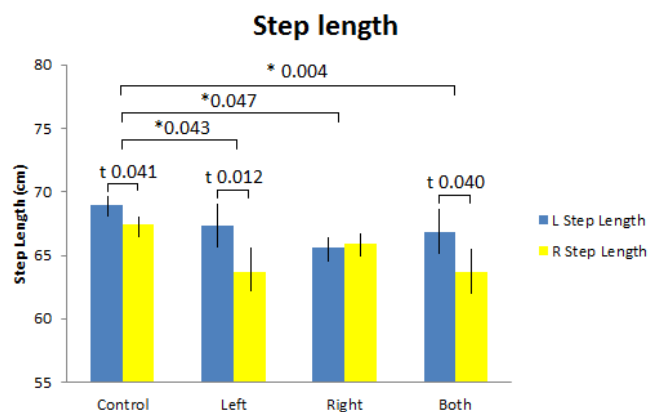


Figure 1: Step length (cm), * indicates between condition difference, t indicates between side difference.

Double support percentage increased for all conditions compared to control ($26.6\% \pm 3.8$), although only the left unilateral ($28.6\% \pm 3.8$, $p = 0.019$), and bilateral conditions ($29.4\% \pm 4.2$, $p = 0.001$) were significant increases. Significant

differences existed between left and right step length at all conditions ($L > R$) except for right unilateral load carriage. When the left and right step lengths were averaged, there were significant decreases between control ($68.2\text{cm} \pm 4.1$) and left unilateral ($65.5\text{cm} \pm 4.7$), right unilateral ($65.8\text{cm} \pm 4.8$), and backpack ($65.2\text{cm} \pm 4.2$) conditions ($p < 0.05$; Figure 1). No differences were found for stance time.

During the control condition, subjects had an average side-to-side trunk lean of $0.90^\circ \pm 1.36$ to the left. When the weight was placed on the left shoulder the subjects leaned $3.09^\circ \pm 2.00$ to the right, and when the weight was placed on the right shoulder the subjects leaned $5.27^\circ \pm 2.59$ to the left. In the bilateral condition, subjects leaned $0.57^\circ \pm 1.42$ to the left. Differences were significant between both unilateral load carriage conditions and all other conditions ($p < 0.05$).

During the control condition, subjects had an average trunk tilt of $-3.55^\circ \pm 2.53$ (negative indicates a backward tilt). The left and right unilateral conditions also had trunk tilts of $-2.16^\circ \pm 2.10$ and $-0.93^\circ \pm 2.38$ respectively. The bilateral condition had a forward tilt of $2.02^\circ \pm 4.18$ and was significantly different from the control ($p = 0.002$) and the left unilateral condition ($p = 0.01$).

DISCUSSION

There were multiple spatio-temporal alterations made due to adding 20% body weight both unilaterally and bilaterally. Subjects walked slower and had increased double support percentage. Singh et al. found similar changes in bilateral load carriage of middle school-aged children and hypothesized that these changes could be a result of the body trying to minimize instability and/or mechanical strain of carrying the added weight [3].

Subjects also had decreased step length with any type of load carriage as well as decreased stride length between bilateral and control conditions. This also supports the compensation strategy mentioned above. Subjects were taking slower and smaller steps and increasing double support in order to support the extra weight.

Subjects also compensated for the extra weight using the orientation of the trunk. They would lean away from the application of the weight, for example: leaning left when the weight was placed on the right shoulder and forward when it was centered on their back. Adding the weight causes the center of mass to move towards the application site (left, right, or back). The subjects adjust to this by leaning in the opposite direction. While this adjustment may lead to less energy expenditure during gait, it may also lead to increased pain and/or injury over time.

These changes highlight an important issue that could affect anyone who carries extra weight as part of their daily routine. It is important to determine whether alterations to normal unloaded gait put individuals at risk for pain and/or injury due to excessive load carriage, even with weights of up to 20% of a person's body weight.

REFERENCES

1. Chiang HY, et al. *Work (Reading, Mass)* **26**(1), 19-28, 2006.
2. Knapik J, et al. *Applied Ergonomics* **27**(3), 207-216, 1996.
3. Singh T, Koh M, *Gait & Posture* **29**(1), 49-53, 2009.

ACKNOWLEDGEMENTS

Special thanks to Ryan Pohlig for the statistical analysis. Funded by NIH P30 GM103333.

THE EFFECT OF EARLY AND FREQUENT SEATED BREAKS ON LOW BACK PAIN DEVELOPMENT DURING PROLONGED STANDING WORK

Colin D. McKinnon¹, Daniel Martel¹, Jack P. Callaghan¹

¹Department of Kinesiology, University of Waterloo, Waterloo, ON

Email: colin.mckinnon@uwaterloo.ca

INTRODUCTION

Known pain developers (PD) will develop low back pain (LBP) during constrained, prolonged standing work tasks and tend to have muscle activation recruitment patterns that differ from non-pain developers (NPD). These pain classifications are predictable from bilateral gluteus medius co-activation profiles [1], and have been further isolated as a predisposing factor, rather than an adaptation to pain [2]. Within the first 15-45 minutes of a standing exposure, PD show a steady increase in low back pain, while NPD remain close to baseline levels of pain. While intermittent seated breaks from prolonged standing exposures create a short-term reduction in pain scores [3], these breaks do not allow complete return to pre-exposure levels and do not prevent known pain developers from reaching the PD threshold. The purpose of this study was to evaluate if early and frequent sitting breaks from prolonged standing work could effectively slow down and/or reduce LBP development in known pain developers.

METHODS

Sixteen participants (8M, 8F) performed 124 minutes of prolonged standing work with intermittent seated breaks at a 3:1 stand-to-sit ratio with increasing durations – 3 minutes:1 minute, 6:2, 12:4, 24:8, 48:16. Participants were classified as PD/NPD in a separate 2-hour prolonged standing trial. Low back perceived pain was recorded during each trial on a 100 mm visual-analog scale. Pain rating scale ranged from ‘No

pain’ to ‘Worst pain imaginable’. Participants were instrumented with surface EMG bilaterally over gluteus medius (GMED). EMG signals were low-pass digitally filtered (single pass, 2nd order Butterworth, 1.0 Hz cutoff frequency), and normalized to maximum voluntary contraction amplitudes. Cross-correlation and corresponding phase lag (τ), were calculated between the left and right GMED signals. A maximum phase lag of ± 500 ms was used to extract the maximum cross-correlation for 1-minute blocks across the session duration. Co-contraction index (Equation 1) was also calculated for left-right GMED activation in 1-minute blocks.

Equation 1:

$$CCI = \sum_{i=1}^N \left(\frac{EMG_{low_i}}{EMG_{low_i}} \right) (EMG_{low_i} + EMG_{high_i})$$

where EMG_{low} and EMG_{high} are the signals with the lower and higher magnitude, respectively, at each sample

Two-way mixed GLM assessed the influence of pain group (between factor) and time (within factor) on all response measures.

RESULTS AND DISCUSSION

Significant pain group-by-time interaction effects were observed for low back pain ($p = 0.0007$). Further, pairwise comparisons between pain groups showed no differences at any time point (minimum $p = 0.06$). No pain group main effects were observed ($p = 0.133$), and low back pain reached a maximum of 7.71 ± 7.54 mm for either pain

group over the entire 124 minute session protocol (Figure 1).

No pain group-by-time interaction effects, pain group main effects, or time main effects were observed for cross-correlation ($p = 0.56$; $p = 0.59$, 0.47) or co-contraction index ($p = 0.41$; $p = 0.92$, $p = 0.23$) of the right and left GMED. Mean GMED cross-correlations collapsed across the entire session were 0.17 ± 0.37 and 0.27 ± 0.40 for PD and NPD, respectively. Similarly, mean co-contraction indices were 1066.0 ± 1217.1 %MVC and 2045.7 ± 2505.0 %MVC.

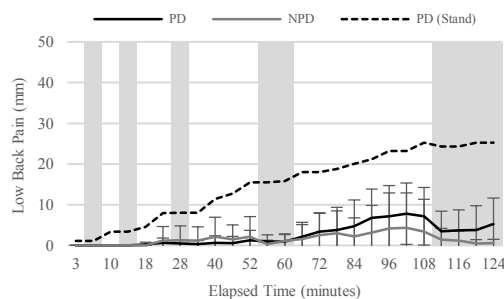


Figure 1: Low back pain showed no difference between pain groups and did not exceed 10 mm over the duration of the protocol. The dashed line shows scores from the same participants in a standing-only protocol.

Early and frequent sitting breaks were effective in reducing and delaying the onset of LBP in known pain developers during standing work. Pain measures did not exceed 0.5 mm for either pain group in the first 60 minutes of the sit-stand protocol, and did not exceed the 10 mm clinically significant change threshold [1,2,3]. GMED co-contraction has been suggested as a predisposing factor in LBP development during standing. The stand-sit protocol in this study showed no difference between pain groups for either cross-correlation or co-contraction index, and reduced both measures for PD to levels of NPD seen in previous studies of standing alone [2]. This

evidence suggests that a reduction in co-contraction may lead to an associated reduction in low back pain among known pain developers during prolonged standing work.

While the co-contraction to pain mechanism is not fully understood, experimental evidence has shown some clear trends between pain groups. Early exposures to greater than 30 minutes of long duration standing can lead to aggravation of tissues surrounding the lumbar spine which cannot be resolved with a short duration seated break [3]. With continued exposures to prolonged standing, this tissue aggravation accumulates and worsens, leading to increasing levels of low back pain [1,3]. Pain group co-contraction differences are greatest during these early exposures, specifically the first 30 minutes of a standing exposure [1]. This appears to both support co-contraction as a predisposing factor for low back pain and drive the early pain generation mechanism. The intervention implemented in this study aimed to target this time period directly, and removes the co-contraction differences between groups.

CONCLUSION

These findings indicate that a stand-sit protocol involving early and frequent seated breaks from standing work may decrease hip muscle co-contraction and the resulting onset of LBP during prolonged standing.

References

- [1] Nelson-Wong, E., Callaghan, J.P. (2010). *JEK* 20: 256-263.
- [2] Nelson-Wong, E. *et al.* (2008). *Clin Biomech* 23: 545-553.
- [3] Gallagher, K., Campbell, T., Callaghan, J.P. (2014). *Ergonomics* 57(4): 555-562.

Novel Assessment of Trunk Regional Peak Torque and Range of Motion in Healthcare Workers

¹Alyssa Kiahara, ¹Marie Zipp, ¹Martin Rice and ²Edward Nyman, Jr.

¹Department of Rehabilitation Sciences, The University of Toledo, Toledo, OH, USA

²Engineering Center for Orthopaedic Research Excellence (E-CORE), University of Toledo, Toledo, OH USA

email: edward.nyman@utoledo.edu

INTRODUCTION

Extensive patient handling is a daily requirement in many healthcare industry professions. Eight out of ten polled healthcare workers reported having a musculoskeletal injury at one point in their career (1). Healthcare workers are particularly susceptible to lower-back injuries which ultimately cost the health care industry \$20 billion per year as a result of treatment and lost work days (2). Development of evidence-based techniques to proactively address the growing number of injuries in the healthcare field is critical. The objective of this study was to examine isometric torque generation and range of motion (ROM) trends in healthcare workers as the initial component in a longitudinal study which will prospectively examine workplace injury at 6 and 12 month time intervals.

METHODS

Healthcare workers at University of Toledo Medical Center (UTMC) were recruited for voluntary participation. To be included, consenting subjects must have had no previous or current acute or chronic musculoskeletal or neurological injury, be between 18-70 years of age, 1.58-1.98 m tall, weigh less than 127 kg, and not be pregnant. A musculoskeletal range of motion and isometric strength testing protocol was based on a standard assessment protocol provided with the equipment (4.0 Rotational Spine System™, Turning Point Biotechnology, Toledo, OH, USA). The testing system (Fig. 1) allows pure transverse plane rotation independently at the hips (pelvis) and shoulders. Transverse plane (axial) range of motion can be measured, and isometric torque generation evaluated, at the shoulders (thoracic spine) under static pelvis position (locked), as well as at the hips (lumbar spine / pelvis) with a static shoulder (thoracic spine) position. Additionally, the pelvis or shoulders can be axially rotated to any fixed point to the left or right wherein isometric torque generation measurements can be made (rather than from a neutral position only). Peak

axial rotation for the shoulders and for the hips, each measured independently to the left and right was performed under volitional control for all subjects. Peak isometric torque measurements were collected for the shoulders in both directions at 25° of right



Figure 1. Turning Point Rotational Spine System

and left rotation as well as in both directions at 0° (neutral). Additionally, peak isometric torque measurements were collected for the hips in both directions at 15° of right and left rotation as well as in both directions at 0° (neutral). ROM data were measured and recorded in degrees and isometric torque output in foot-pounds. Participant subsequent injury history data, via a single blinded approach, will later be regressed onto musculoskeletal performance measurements at 6 and 12 month intervals after testing, as part of ongoing work.

RESULTS AND DISCUSSION

A total of 146 subjects (39.3±11.6 years, 73.7±15.2 kg, 1.67±0.1 m) participated in the study. 80% (117/146) of the subjects enrolled were female.

Peak ROM at the shoulders was 82.6±15.0° to the right and 78.6±13.9° to the left (Fig. 2). Peak ROM at the hips was 42.8±10.2° to the right and 46.6±9.2° to the left (Fig. 2).

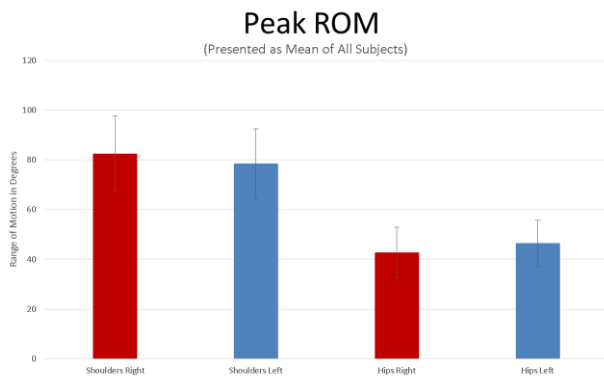


Figure 2. Peak ROM for the pelvis and shoulders (right rotation- red, left rotation – blue)

There were no statistically significant differences in hip or shoulder ROM between left and right sides, nor between sexes when all subjects were grouped accordingly. However, when the data were further interrogated, patterns of asymmetry *within* subjects were discovered. ROM asymmetry, herein defined as greater than 10% deviation to one side from calculated within subject mean ROM, as adapted from Crenshaw (3), was present for 42% (61/146) of subjects at the shoulder level and for 55% (80/146) at the hip level. Peak isometric torque generated at the shoulders was 32.2 ± 16.5 ft-lbs to the right and 34.6 ± 18.0 ft-lbs to the left from neutral position (0°), 34.3 ± 17.8 ft-lbs to the right and 32.6 ± 16.3 ft-lbs to the left from 25° rotation to the right, and 33.9 ± 15.7 ft-lbs to the right and 33.6 ± 17.3 ft-lbs to the left from 25° rotation to the left (Fig. 3). Peak isometric torque generated at the hips was 33.4 ± 16.2 ft-lbs to the right and 29.9 ± 16.8 ft-lbs to the left from neutral position (0°), 33.0 ± 17.8 ft-lbs to the right and 26.8 ± 14.8 ft-lbs to the left from 15° rotation to the right, and 27.0 ± 13.0 ft-lbs to the right and 29.5 ± 16.4 ft-lbs to the left from 15° rotation to the left (Fig. 3).

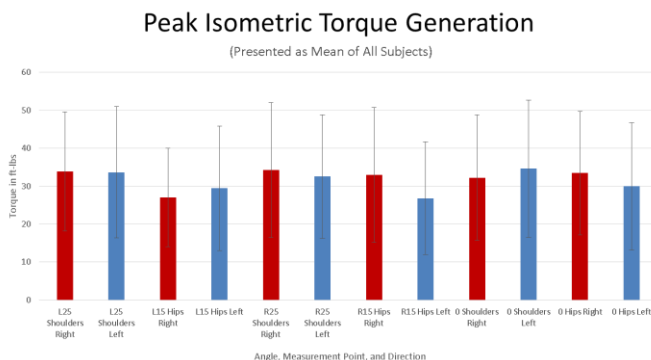


Figure 3. Isometric torque generation for the pelvis and shoulders (right rotation- red, left rotation – blue)

There were no statistically significant differences in hip or shoulder peak isometric strength between left and right sides, nor between males versus females when all subjects were grouped as respective cohorts. Again, however, when the data were further interrogated, patterns of asymmetry *within* subjects were discovered. As measured from the neutral position (0°), significant peak isometric strength asymmetry, defined herein as greater than 10% bilateral difference, within subjects was present for 63% (92/146) of subjects at the shoulder level and for 69% (100/146) at the hip level.

Overall, asymmetry was both marked and contralateral for many subjects with respect to both peak ROM and peak isometric strength. Of obvious concern is the inherent increased risk of musculoskeletal injury, particularly to the lower back, in individuals who present with ROM or peak isometric strength asymmetry.

CONCLUSIONS

This work and that of previous publications support evidence of musculoskeletal ROM and strength asymmetry in healthcare workers with patient handling responsibilities. Future work will evaluate correlations between both range of motion and isometric torque generation and incidence of musculoskeletal injury occurring at the 6 and 12 month time intervals.

REFERENCES

1. B.L.S. (2013). Nonfatal occupational injuries and illnesses requiring days away from work, 2012. Bureau of Labor Statistics Retrieved from <http://www.bls.gov/news.release/pdf/osh2.pdf>.
2. Passier, L., & McPhail, S. (2011). Work related musculoskeletal disorders amongst therapists in physically demanding roles: qualitative analysis of risk factors and strategies for prevention. BMC musculoskeletal disorders, 12(1), 24.
3. Crenshaw, S.J. & Richards, J.G. (2006). A method for analyzing joint symmetry and normalcy, with an application to analyzing gait. Gait & Posture, 24, 515-521.

ACKNOWLEDGEMENTS

Work supported in part by the NSF Industry / University Cooperative Research Center at the University of California at San Francisco and University of Toledo, Toledo (www.nsfcdmi.org).

EXTERNAL FORCE AND DELTOID SURFACE EMG RELATIONSHIP DURING RELEVANT AND ABSOLUTE ISOMETRIC RAMP CONTRACTIONS AT THREE ANGLES

¹ David Phillips and Andrew Karduna

¹Orthopedic Biomechanics Laboratory, Department of Human Physiology, University of Oregon, Eugene, OR
email: dphilli2@uoregon.edu, web: <http://biomechanics.uoregon.edu/obl/>

INTRODUCTION

The deltoid and the supraspinatus muscles are the primary abductors at the shoulder joint. There is a direct relationship between muscle EMG amplitude and muscle force. However this relationship is not linear and one variable cannot predict the other unless they are simultaneously measured. A single muscle's EMG may also not be able to predict externally measured force [1]. The EMG profile may also be affected by the rate at which force is developed. A more rapid rate of force development has a different EMG profile compared to a slower rate of force development due to different motor unit recruitment patterns [2]. Because of this, it is not known whether an absolute rate of force development would produce a more reliable EMG profile than a relative rate of force development for an individual. At different joint angles, a muscle's mechanical advantage may differ due to a changing angle of insertion, fiber length and a changing moment arm and therefore needing less activation to produce the same level of force [3].

The purpose of this study is to determine the EMG profile of the deltoid muscle during absolute and relative ramp isometric contractions at three different angles of abduction as well as the reliability of the EMG profile.

METHODS

Four subjects (2 male and 2 female) volunteered for the study. Subjects stood upright throughout the experiment. Participants were positioned so that the styloid process of the ulna was directly above the lower edge of the load cell with the elbow in full extension and the arm in the scapula plane. The arm was in the neutral, 'thumbs up' position. Three trials for the two rates of loading were conducted at each abduction angle 30°, 60° and 90°. Absolute loading

rate was 15N/s and relative loading rate was determined by the rate needed to reach 50% of subject's MVC force in 3.5 seconds. Subjects maintained the required loading rate through a real-time feedback display programmed with custom Labview (National Instruments, Austin, TX) software. The protocol was repeated after a 15 minute rest period to test for reliability.

EMG data were collected using a Myopac Jr. Electromyography unit (Run Technologies, Viejo, CA). EMG data were sampled at 1000Hz and smoothed using a 300ms RMS sliding window. Deltoid EMG data were normalized to MVC at its relative angle of abduction. Force data were collected from a uniaxial load cell (Lebow Products, Troy, MI) and was sampled at 1000Hz. Force data were normalized to maximum external abduction force relative to each shoulder abduction angle.

RESULTS AND DISCUSSION

At all angles and rate of force application, force output steadily increased as deltoid EMG increased (Fig 1). At smaller shoulder abduction angles more force was generated with less deltoid EMG. This is likely due to greater supraspinatus contribution at lower abduction angles.

Differences between rate of force development and EMG level were analyzed using 2-way repeated measures ANOVA at each shoulder abduction angle. There was no significant main effect for rate of force development at any angle. The difference between absolute and relative rate of force development appears to be minimal at these submaximal and relatively slow rate of force development for both conditions. It must be noted that with the small sample, statistical power is likely insufficient to detect a difference between the rate of force development conditions. Another

consideration is that subjects that had a maximum force MVC of 105N would have had the same absolute and relative rate of force development.

A significant main effect was found for EMG level at 30° ($p < .05$), 60° ($p < .05$) and 90° ($p < .05$). This is to be expected as increasing force output with increasing EMG amplitude has been well documented.

Intraclass correlation coefficients were calculated for deltoid EMG at 10%, 20%, 30% and 40% MVC to indicate reliability (Table 1). ICC values above 0.75 are considered excellent, 0.4-0.74 good and below 0.4 are poor. ICC values demonstrated a high level reliability between the 2 sessions of measurement for 10%, 20% and 30% deltoid EMG MVC.

However, at 40% deltoid EMG, ICC values varied greatly depending on angle and rate of force development. The reason for the inconsistent reliability of external force at 40% deltoid EMG may be the point at which an additional level of motor unit is recruited resulting increased EMG amplitude. It should be noted that some subjects reached 50% force MVC before 40% deltoid EMG MVC.

Table 1: Intra class correlation coefficients for external force at different deltoid EMG levels through sub-maximal range.

Condition	Deltoid EMG Amplitude %			
	10	20	30	40
30° ABS	0.92	0.88	0.91	0.63
30° REL	0.96	0.04	0.65	0.18
60° ABS	0.98	0.78	0.75	0.75
60° REL	0.98	0.86	0.36	0.44
90° ABS	0.95	0.95	0.97	0.71
90° REL	0.75	0.66	0.96	0.84

Note: REL = relative rate and ABS = absolute rate

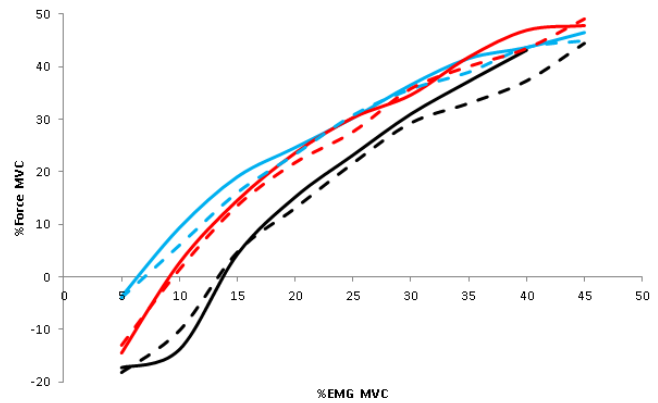


Figure 1: Deltoid EMG and external force relationship. 30° is blue, 60° in red and 90° in black. Absolute rate of force is represented by solid lines with relative rate of force represented by dashed lines.

CONCLUSIONS

A consistent relationship exists between deltoid EMG and external measured force. More force is generated with less deltoid EMG amplitude at lower abduction angles likely due to greater supraspinatus contributions. Currently, a relative rate of force development does not produce a different EMG profile to an absolute rate of force when performed at submaximal loading rates.

Importantly, external force is consistent with deltoid EMG amplitude within the same subject and testing session up to 30% of deltoid EMG MVC. However, the level of reliability of external force becomes inconsistent between angles at 40%

REFERENCES

1. Kuriki HU, Takahashi LS, Filho R. *Relationship between EMG and muscle force*. Intech, Croatia. 2012.
2. Ricard et al. *Int J Sports Med* **26**, 66-70. 2005.
3. Baechle T, and Earle R. *Essential of strength training and conditioning*. Human Kinetics. 2000.

BIOMECHANICAL EFFECTS OF CRANIO-CERVICAL POSITIONS ON CERVICAL MUSCULOSKELETAL DISORDERS

¹ Sicong REN ^{1 2} Wenhao LI and ¹ Ming ZHANG

¹ The Hong Kong Polytechnic University, Hong Kong

² Shandong University, Jinan, China

Email: ming.zhang@polyu.edu.hk, Web: <http://www.polyu.edu.hk/bme/>

INTRODUCTION

Cervical musculoskeletal disorders have been becoming a global health problem which disturbs an increasing number of people [1]. Cranio-cervical position during computer use can be various due to frequent posture adjustment. Poor postures may give rise to abnormal stress on the muscles and joints leading to the development of cervical musculoskeletal disorders. Several studies based on computational models showed that optimal ergonomic design of workstation could minimize load-carrying along cervical spine [2]. A number of studies through experiment measurement suggested that there was a positive correlation between non-neutral cranio-cervical positions (e.g neck flexion, neck lateral bending, and forward head posture) and pain syndromes [3, 4]. Although considerable research has been devoted to normal movement of cervical spine, rather less attention has been paid to coupling motion of head and neck. Particularly, biomechanical characteristics of cranio-cervical protraction position are currently lacking. Therefore, the aim of this study is to determine the biomechanical effects of cranio-cervical positions on cervical musculoskeletal disorders.

METHODS

One male adult (Height: 190.3 cm; Weight: 82.2 kg; BMI: 22.6 kg/m²; Age: 23 years old) with an experience of computer operation for 8 hours was recruited in this study. The support forces were measured using two force platforms.

Participant was asked to wear lycra pants without T-shirts or shoes, and then to do warming up of head and neck to minimize the effects of tissue creep along the cervical spine. An 8-camera,

infrared motion analysis system (Vicon MX, Oxford, UK) was used to capture the three-dimensional posture of seated human. After a set of markers were attached to landmarks, participant was instructed to sit on one force platform and to step on the other one with hips and knees at 90°. The feet positioned shoulder width apart, and arms relaxed at the side of body. This study utilized repeated measure design with participant performing six sitting postures randomly. The six experimental conditions included cranio-cervical neutral position; cranio-cervical protraction; and cranio-cervical flexion. Finally all these three conditions were repeated with upright and slump sitting postures.

A generic human model with detailed neck was established using AnyBody Modelling System. The size of the model was scaled according to the participant's anthropometry. The kinematic data from motion capture was used to drive various motions. The model can calculate joint and muscle forces under each experimental condition. A preliminary model validation was performed by comparing the simulated muscle force of trapezius and muscle activity measured by electromyography.

PRELIMINARY RESULTS AND DISCUSSION

There were obvious differences in muscle recruitment among three cranio-cervical positions with upright and slump sitting postures (Figure 1 and Figure 2). For cranio-cervical protraction, trapezius-scapular muscle during slump generated 46% more force than that during upright sitting. While trapezius-clavicular muscle force was 1.5 times greater than that in upright sitting. Trapezius-scapular muscle in protraction generated 15% more force than that in flexion and neutral position in both upright and slump sitting. Moreover,

this type of superficial muscle shared more load than other parts.

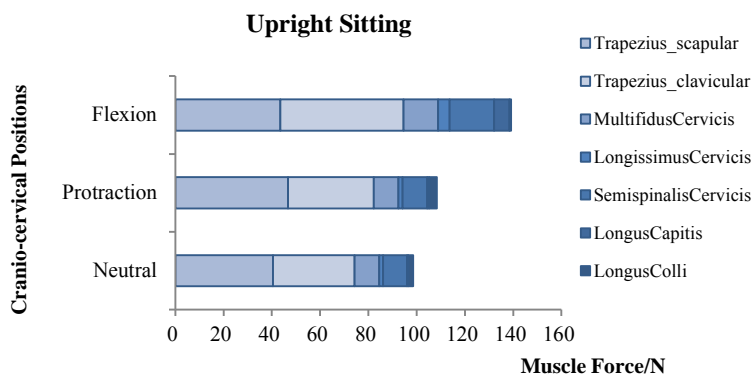


Figure 1. Cervical muscle forces in three cranio-cervical positions during upright sitting.

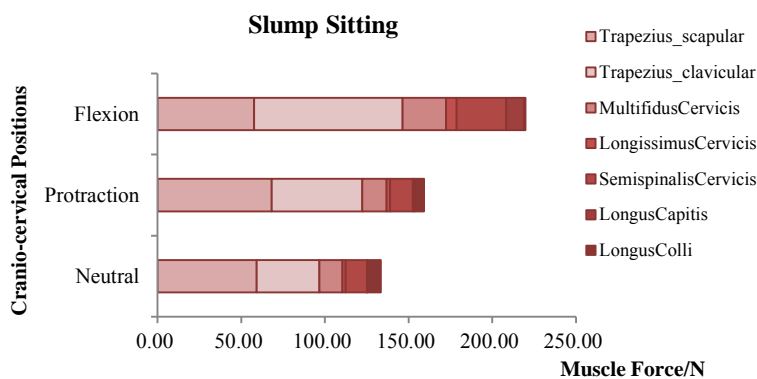


Figure 2. Cervical muscle forces in three cranio-cervical positions during slump sitting.

Muscle force generated by deep muscles such as multifidus and semispinalis along cervical spine, at approximately 12N, was 70% less than superficial muscles such as upper trapezius muscle. It suggested that deep muscles may bear low static loading in cervical motions.

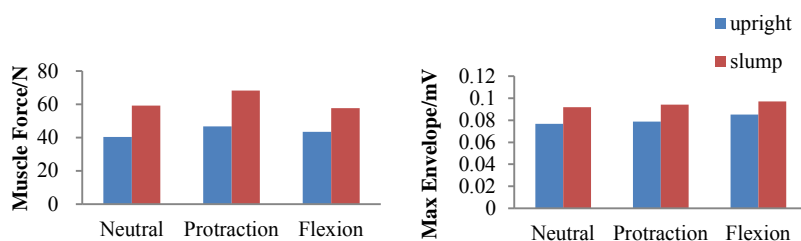


Figure 3. Comparison results between simulated trapezius-scapular muscle forces and EMG envelope.

In order to examine the validity of the simulation, a comparison of trapezius muscles between the simulation results and EMG envelope was performed (Figure 3). From the EMG, trapezius muscles became more active in slump than in upright sitting. This finding can be seen in the simulation, indicating that three cranio-cervical positions with slump sitting required more muscle forces than that with upright sitting.

CONCLUSIONS

Our model simulated three cranio-cervical positions under two major sitting conditions which are commonly adopted during high-tech devices use. These results showed the static behavior of cervical spine as different types of load act on the muscles. It was concluded that extensor muscles including trapezius and multifidus muscles played an important part in maintaining cranio-cervical positions, especially for protraction position. Moreover, superficial muscles were found to be more responsive to positional changes of head and neck than deep muscles. This work may provide insight into understanding the mechanism of cervical musculoskeletal disorders caused by cranio-cervical positions.

REFERENCES

1. Hoy DG, et al. *J Best Pract Res Clin Rheumatol* **24**, 783-792, 2010.
2. Rasmussen J, et al. *J Int J Ind Ergon* **39**, 52-57, 2009.
3. Straker L, et al. *J Ergon* **54**, 539-546, 2011.
4. Quek J, et al. *J Man Ther* **18**, 65-71, 2013.

THE EFFECT OF SUBMAXIMAL HAND FORCE EXERTION ON SHOULDER MUSCLE ACTIVATION

¹ Meghan E. Vidt, ¹ Kimberly A. Meszaros and ¹ Clark R. Dickerson

¹ University of Waterloo, Waterloo, ON, Canada

email: mvidt@uwaterloo.ca, web: <http://ahs.uwaterloo.ca/kin/research/diesel/>

INTRODUCTION

Upper extremity injuries are common sequelae of fatigue and over exertion in the workplace [1]. Hand location and muscular activity influence the muscular effort required to perform upper limb tasks. The intrinsic complexity of the shoulder and upper limb preclude experimental measurements on all possible hand locations in the upper limb workspace. Quantitative description of the effect of hand location, load magnitude, and direction would facilitate the assessment of the individual and total muscle activity required to perform upper limb tasks, which are commonly performed with submaximal loads [2]. The overall goal was to characterize individual and total muscle responses to submaximal workloads at hand locations in the upper limb workspace and develop predictive equations describing the spatial- and load-dependencies of muscle activity.

METHODS

Twenty right-hand dominant males (mean age 21.6±2.7 years) participated. Muscle activation was recorded at 1500 Hz from 14 muscles (anterior, middle, and posterior deltoid, biceps brachii, triceps brachii, supraspinatus, infraspinatus, clavicular and sternal insertions of pectoralis major, latissimus dorsi, serratus anterior, upper, middle and lower trapezius) using surface EMG (Telemetry 2400R T2, Noraxon, Scottsdale, AZ). Maximal voluntary contractions were performed for each muscle to normalize recorded muscle activity.

Participants performed submaximal exertions at five different hand locations within the upper limb workspace. The umbilicus served as the origin, with +X-axis to the right, +Y-axis anterior, and +Z-axis superior. All hand locations were defined in a single plane 30cm anterior to the umbilicus. The five hand

locations included: 1) neutral (X=20cm, Z=20cm); 2) upper right (X=40cm, Z=60cm); 3) lower right (X=40cm, Z=-20cm); 4) upper left (X=-20cm, Z=60cm); 5) lower left (X=-20cm, Z=20cm). Five trials were collected at each location for all combinations of 4 hand force exertion levels (20N, 30N, 50N, 60N) in 6 directions (upward, downward, left, right, forward, backward), for a total of 120 trials. Each trial was 7sec, allowing the participant to ramp up to the desired force level; 1min of rest was given between trials to reduce the effect of fatigue. Hand forces were measured using a 6-degree of freedom transducer (MSA-6, AMTI, Watertown, MA) fixed on a robotic arm (Motoman HP50N, Motoman Inc., West Carrollton, OH).

EMG was processed by removing DC bias, then high pass filtered with a 4th order Butterworth filter with a 30Hz frequency to remove heart rate contamination. Signals were linear enveloped, full wave rectified, and low pass filtered with a 4th order low pass Butterworth filter with a 4Hz cutoff frequency. EMG signal for each muscle was normalized by its corresponding MVC. To represent each static hand force, average EMG was calculated over a 1sec window. Signal during time 5-6sec of the trial was selected to avoid any ramping to the desired force level. Total muscle activity, which is an assessment of overall muscular effort, was calculated by summing individual muscle activities.

Six one-way repeated measures ANOVAs were used to evaluate differences between total muscle activation across different force magnitudes for each exertion direction. Bonferroni corrections were applied and post-hoc Tukey HSD tests were used to confirm significance at $p \leq 0.0083$. Multiple linear regression using a forward stepwise method ($p=0.1$ to enter; $p=0.05$ to leave) was used to develop prediction equations for each muscle for each hand exertion direction; equations included a term for

force magnitude and linear, quadratic, and cubic terms for each X and Z location. All analyses were performed using JMP software (v.11.2.1; SAS Institute Inc., Cary, NC).

RESULTS AND DISCUSSION

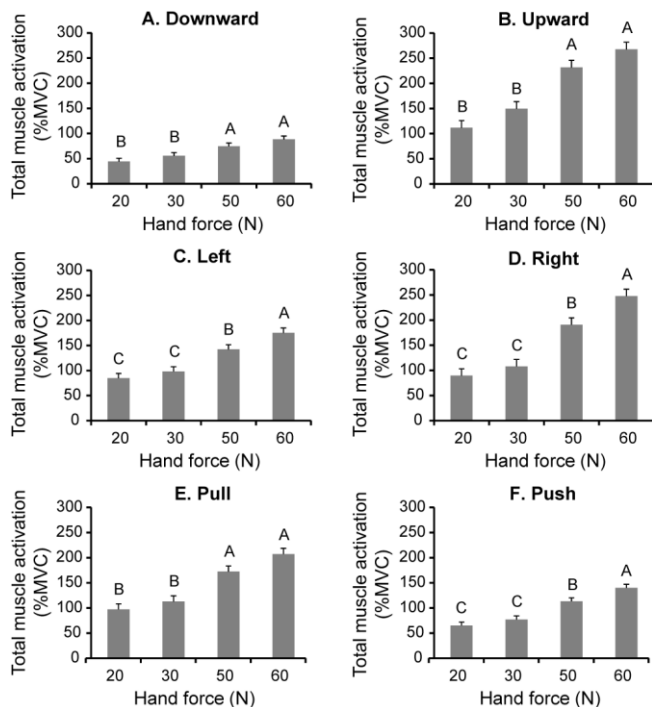


Figure 1: Least squares mean \pm SEM for total muscle activity for A) downward, B) upward, C) left, D) right, E) pull, and F) push exertions at different hand force loads. Different letters within each subplot denote significant differences.

Total muscle activity was smallest for the 20N load and greatest for the 60N load for all exertion directions (Fig.1). The results indicate that force magnitude has a nearly linear effect on total muscle effort. The greatest total effort was seen for upward exertions, which oppose gravity, and the smallest total effort was observed for downward exertions, which correspond with the direction of gravity.

Predictive equations developed for each individual muscle and total muscle activity demonstrated a dependence on force magnitude and linear, quadratic, and interaction terms for X and Z hand positions in the Y=30cm plane (Fig.2). Individual and total muscle activity was not dependent on cubic terms of spatial hand location for exertions in any direction. Previous work has identified a spatial

dependency of muscular demand for three-dimensional hand locations within the upper limb workspace for 40N [3,4] and maximal [5] exertions and the current work corroborates this spatial dependency. Notably, total muscle activation increased linearly with increased hand force magnitudes for all exertion directions, indicating that hand force is directly related to total muscle effort. These results can be leveraged by healthcare workers and ergonomists to evaluate the muscle effort required for tasks across the upper limb workspace requiring various force magnitudes.

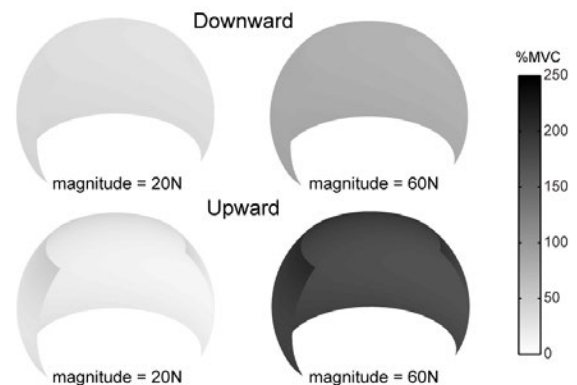


Figure 2: Spheres depicting spatial dependency of total muscle activity for downward (top row) and upward (bottom row) exertions of 20N and 60N magnitudes.

CONCLUSIONS

Muscular demand is influenced by spatial location, load, and direction of exertion. The spatial and load dependency relationships reported here provide a valuable tool to predict approximate muscular demands in the upper limb without the need for lengthy experimentation.

REFERENCES

1. Keyserling WM. *AIHAJ* **61**, 231-243, 2000.
2. Snook SH. *Ergonomics* **34**, 1197-1213, 1991.
3. McDonald A. *Appl Ergon* **43**, 971-978, 2012.
4. McDonald AC. *J Appl Biomech* **30**, 1-11, 2014.
5. LaDelfa NJ. *Ergonomics* **57**, 254-261, 2014.

ACKNOWLEDGEMENTS

NSERC Discovery Grant 311895-2011; Canada Foundation for Innovation; Ontario Research Fund.

EFFECTS OF ERGONOMIC FACTORS ON STAIR NAVIGATION IN OLDER ADULT MULTIFOCAL LENS GLASSES WEARERS

Eric Weston¹, Patrick Sparto¹, Joseph Furman², Scott Drexler², Mark Redfern¹ and Kurt Beschorner¹

¹ University of Pittsburgh, Pittsburgh, PA, USA

² University of Pittsburgh Medical Center, Pittsburgh, PA, USA

Corresponding Author's Email: eric.weston417@gmail.com

INTRODUCTION

Multifocal lens glasses (MfLs), commonly worn by middle-aged and older adults, are known to reduce contrast sensitivity and depth perception [1], alter gait biomechanics [2] and increase fall risk [3]. Existing research on the biomechanics of MfL wearers has focused on single step navigation under a constant set of environmental conditions [2, 3]. Because MfLs affect functional vision, environmental conditions that make steps easier to see (e.g., through better step edge contrast or lighting) may provide benefits in this population. Furthermore, the use of handrails may provide alternative sensory information and reduce the need for vision when navigating stairs, which may also benefit MfL wearers.

This study aims to quantify the effects of certain ergonomic factors and the use of hand rails on the biomechanics of multiple stair negotiation in MfL wearers. This study focused specifically experienced older adult MfL wearers (70-80 years), representing a population at high risk of falling in the community. In addition, this study considered multiple stairs, in contrast to previous single-stair study designs, since multiple stairs require accurate foot placement and may be more challenging for MfL wearers.

METHODS

Five older adults (4 male, 1 female; age 72.8 ± 2.7 years, height 1.76 ± 0.68 m, mass 84.2 ± 18.8 kg) who are experienced bifocal ($n=3$) or progressive lens glasses wearers ($n=2$) were tested. Subjects did not have self-reported balance, gait or vision abnormalities, and each subject was screened for abnormal otolith and vestibular-ocular reflex (VOR) functioning. Subjects provided informed consent, and the study was approved by the University of Pittsburgh Institutional Review Board.

Subjects completed a gait assessment while wearing their current MfLs and a pair of single lens glasses that matched the upper portion of their prescription. Motion capture was used to track the following markers bilaterally at 120 Hz: anterior and posterior head markers, anterior and posterior superior iliac spine, second metatarsal head, anterior most point on the first toe, posterior and inferior-most point of the heel.

Subjects ascended a set of three stairs (19.0 cm tall and 28.0 cm deep), while their spectacles (MfL or single lens glasses), lighting (high or dim), step contrast (high or low) and use of handrails were systematically modified. Step contrast levels were achieved using an angle bar attached to the corner of the steps matching the color of the surrounding stair (low contrast) or contrasting with the stair (high contrast) (Fig. 1). Subjects completed three trials for each handrail x contrast x lighting condition for one lens before switching to the other lens condition; within a single trial, all steps were either high or low contrast. Lens order and the order of each condition were randomized.



Figure 1. Staircase shown in high contrast (bottom stair) and low contrast (top stair) configurations.

Leading and lagging toe clearance values were calculated by taking the minimum perpendicular distance between the toe markers and the step edge as the foot crossed over a stair. Step position was calculated as the distance between the stair edge and the heel marker at heel contact. Heel contact on the stairs was calculated at the local maxima of vectors calculated from the positions of the sacral marker

(midpoint of posterior iliac spine markers), consistent with methods from Zeni et al. [4]. Head angle was calculated using Euler angles relative to the global reference frame. The local coordinate system was established using vectors calculated from the midpoint of the back head markers to the midpoint of the front head markers (y-axis) and from the midpoint of the left head markers to the midpoint of the right head marker (z-axis was perpendicular to the plane formed by this vector and the y-axis). Head angles during the static trial (when subjects looked straight ahead) were offset from the dynamic trials to account for subtle differences in marker placement. The minimum, mean and maximum sagittal plane head angle (head pitch) were reported during the entire step preceding foot contact during the second stair. Repeated-measures ANOVA methods were applied to determine how these biomechanical variables were affected by lens type, environmental conditions (lighting and contrast), the use of handrails, and all first order interactions. Just the results from the second stair (when the subject was walking in steady state) are presented. The alpha value was set to 0.05.

RESULTS & DISCUSSION

The use of MfLs compared with single lens increased minimum leading toe clearance on the second stair from 5.4 ± 2.6 cm to 6.2 ± 2.7 cm ($p=0.025$). As failure to clear the stair edge would result in a trip or fall, an increased leading toe clearance while wearing MfLs could be an attempt to increase the subjects' factor of safety during stair ascent. Increased leading toe clearance has also been observed in single stair or curb ascent while wearing MfLs [3]. The finding that increased leading toe clearance occurs on the second stair suggests that MfLs might affect individuals in the same way whether they are navigating one or multiple stairs.

Subjects increased head pitch minimum, mean and maximum angles when they were not using the hand rail (Figure 2). The observed effect suggests that railings reduce the need for visual information since the subjects did not look down as much when using handrails. The use of handrails may provide subjects alternative sensory information that is used to locate their position relative to the stairs, which may reduce the need for increasing head angle.

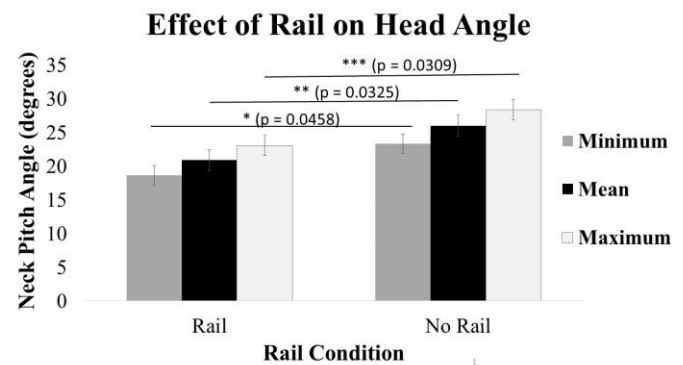


Figure 2. Effect of handrail use on minimum, mean, and maximum head angles during stair ascent.

Subjects also placed their foot more posterior when stepping on step with a low contrast edge (8.4 ± 3.7 cm) than a high contrast edge (7.7 ± 3.7 cm). This shift in step placement suggest that a safer foot placement is used when good contrast is provided. Providing good contrast on each stair edge may reduce the risk of “missed edge of step accidents,” which are prevalent among MfL-wearers [5].

No other main or interaction effects were statistically significant, nor were interaction effects observed between the multifocal lens glasses and environmental effects or use of hand rails. Preliminarily, it appears that certain environmental factors may compensate for the negative effects of MfLs, but that these effects act independently and not interactively. These results may need to be viewed with caution, however, as a larger subject pool will provide the necessary power to identify more subtle interaction effects (this study aims to increase the number of subjects to 20).

REFERENCES

1. Brayton-Chung, A. et. al, 2013 *Phys & Occ Therapy Geriatrics* **31**:47-60
2. Johnson, L. et al, 2007, *Inv. Ophth. & Vis. Sci* **48**: 1466-70.
3. Beschoner, K. et al. 2013. *Gait & Posture* **38**(4): 1015-20.
4. Zeni, J. et al., 2008. *Gait & Posture* **27**: 710-714.
5. Davies J, et al, 2001, *Safety Sci.* **38**: 211-226.

ACKNOWLEDGEMENTS

This study was funded by a Pepper Center Grant (P30 AG024827).

THREE DIMENSIONAL FINITE ELEMENT MODEL OF THE BRAIN RESPONSES TO THE TOP IMPACTS OF A CONSTRUCTION HELMET

*John Z. Wu, Christopher S. Pan, and Bryan M. Wimer

National Institute for Occupational Safety and Health, Morgantown, WV, USA.

*Email: jwu@cdc.gov

INTRODUCTION

Traumatic brain injuries (TBI) are among the most common severely disabling injuries in the U.S. Approximately 1.7 million cases occurred in civilians annually during 2002-2006 [1]. Construction helmets are considered as essential personal protective equipment to reduce TBI risks at work sites. Despite wide applications of the finite element (FE) modeling in the study of the injury mechanisms of TBI [2] and in the design of sport [3] or military helmets [4], there is limited analytical study of the construction helmet [5]. In the current study, we proposed a practical FE modeling approach that would be suitable for engineers to optimize construction helmet design.

METHODS

The FE meshes of the head-brain-neck complex were developed by using a commercially available data base (Materialise, Leuven, Belgium). The FE models were constructed using FE software ABAQUS (version 6.9). The surface scans of the skin, skull, and brain were applied to generate the FE meshes. The head-brain-neck complex consisted of scalp, skin tissues, skull, cervical vertebra (C1, C2, and C3), discs, brain, brain stem, cerebrospinal fluid (CSF), and spinal cord (Fig. 1). The brain tissues included the cerebrum and cerebellum; the brain stem contained the midbrain, pons, and medulla oblongata. The spinal cord included the surrounding pia mater. The CSF was considered to cover over the entire external surface of the brain, brain stem, and the spinal cord. The discs contained both annulus fibrosus and nucleus pulposus. The CSF was constructed using membrane elements, whereas all other components were constructed using 3D continuous elements. The helmet model consisted of a shell and a suspension system. The shell geometry was obtained by the scanning of a representative, commercially available construction helmet (Model: V-Gard, MSA Safety Inc., Pittsburgh, PA, US). The geometry of the suspension system was constructed using a graphic software Inventor (Autodesk, San Rafael, CA, US). The materials of the scalp, skull bone, cervical discs, and vertebral bone were considered as linearly elastic, whereas the skin, brain, brain stem,

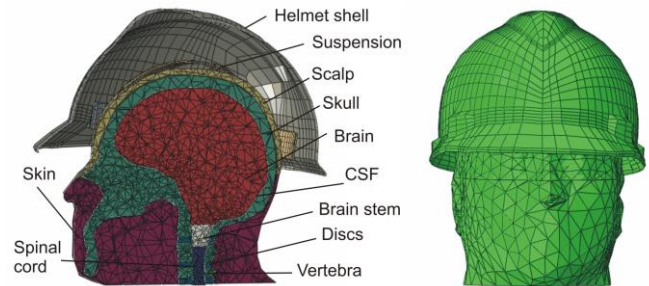


Figure 1. FE model of the head-helmet complex. The head model contains brain, brain stem, spinal cord, CSF, skin, skull, vertebra, and discs.

and spinal cord were considered as hyperelastic and viscoelastic.

The simulations were performed using an implicit dynamic procedure. Initially, a cylindrical object (2 kg) was at a height of 3.27 m above the helmet top. For $t > 0$, the object was released and fell due to the gravity; it reached a speed of 8 m/s just before impacting with the helmet (Fig. 2). The falling object made the contact with the helmet shell at the center. The FE model was applied to analyze the effects of the neck and body mass on the brain responses during the impact by applying three neck boundary conditions: (1)-“Free” (no constraints were applied at the neck, i.e., the effect of the neck and body mass became negligible), (2)-“Mass” (a point mass of 10 kg was attached to the neck bone), and (3)-“Fix” (the neck was constrained).

RESULTS

The head FE model has been calibrated using the experimental data in literature. The predicted brain pressures at four locations agree well with the experimental measurements (results not shown). The peak contact force between the helmet and scalp was found to be 6119.9, 7328.7, and 7345.8 N, and the corresponding head acceleration peaked at 1350.9, 1244.9, and 1188.1 m/s^2 , respectively, for the “Free”, “Mass”, and “Fix” neck boundaries, respectively. The maximal and the minimal brain pressures during the impact were found at the parietal and posterior fossa regions, respectively, and around 3.65 ms, when the accelerations reached

the maximums. The time histories of the brain pressures at the parietal and posterior fossa locations are shown in Fig. 3.

DISCUSSION AND CONCLUSIONS

In a majority of the head-brain models that are used for frontal impacts in automobile crashes, the neck is not included. It is believed that the effects of the neck on the brain responses are negligible [2]. However, the head-helmet stiffness in the top impact, which is primarily considered in the design of the construction helmet, is substantially greater than that in the frontal impact. Therefore, the effect of the neck and body mass during impact could be a non-negligible factor in the helmet design. Our analysis indicated that the exclusion of the effects of the neck and body mass can cause overestimations of HIC (Head Impact Criteria) and the peak head acceleration by 33% and 12%, respectively, whereas an underestimation of the peak impact force by 17%. Excluding the effects of the neck and body mass would not only cause an overestimation of the peak brain pressures at the parietal and posterior fossa locations by 6-12%, but also vary the patterns of the time-histories of the brain pressures (Fig. 3).

For biomedical engineering applications, it is difficult to precisely account the effects of the neck and body mass on the dynamic responses of the head-brain in FE analysis, because FE model usually does not include the entire human body. In the current study, we have established reasonable upper and lower bounds of the precise solutions for this particular problem. The stiffness of the neck for

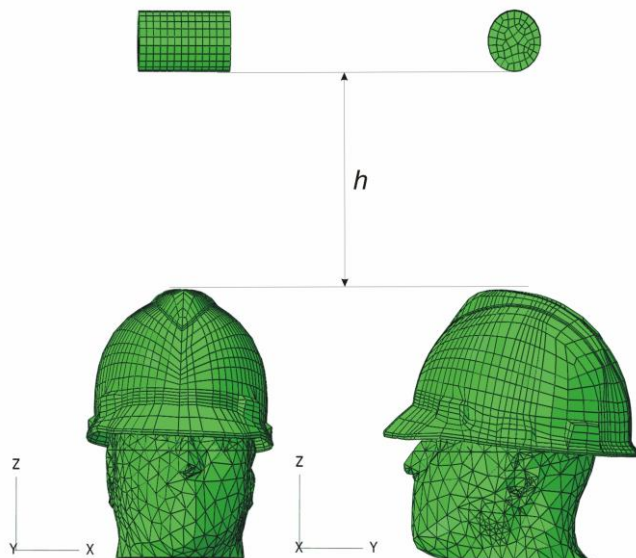


Figure 2. Set-up of the helmet impact test.

a real person should be higher than that for the model with the concentrated mass at the boundary (i.e., “Mass”), whereas lower than that for the model with a fixed boundary (i.e., “Fix”). Our analysis indicated that the first peaks of the acceleration and impact force of the head obtained by using these two models differ by less than 1% (Fig. 3, tests “Mass” and “Fix”). Therefore, a good estimation for the precise solution is obtained by an average of the solutions obtained using these two models.

REFERENCES

- [1] CDC, 2007. Traumatic Brain Injury in the United States – Emergency Department Visits, Hospitalizations, and Deaths 2002-2006. <http://www.cdc.gov/traumaticbraininjury/>.
- [2] Willinger, R., Kang, H. S., Diaw, B., 1999. Ann Biomed Eng 27 (3), 403–10.
- [3] Teng, T., Liang, C., Nguyen, V., 2012. Proc Inst Mech Eng, Part L: J Mater Des Appl 227, 82–88.
- [4] Yang, J., Dai, J., 2010. Comput-Aided Des Appl 7 (1), 59–73.
- [5] Long, J., Yang, J., Lei, Z., Liang, D., 2015. Comput Methods Biomech Biomed Engin 18 (1), 24–37.

DISCLAIMER

The findings and conclusions in this report are those of the authors and do not necessarily represent the official position of the National Institute for Occupational Safety & Health. The mention of trade names, commercial products, or organizations does not imply endorsement by the US Government.

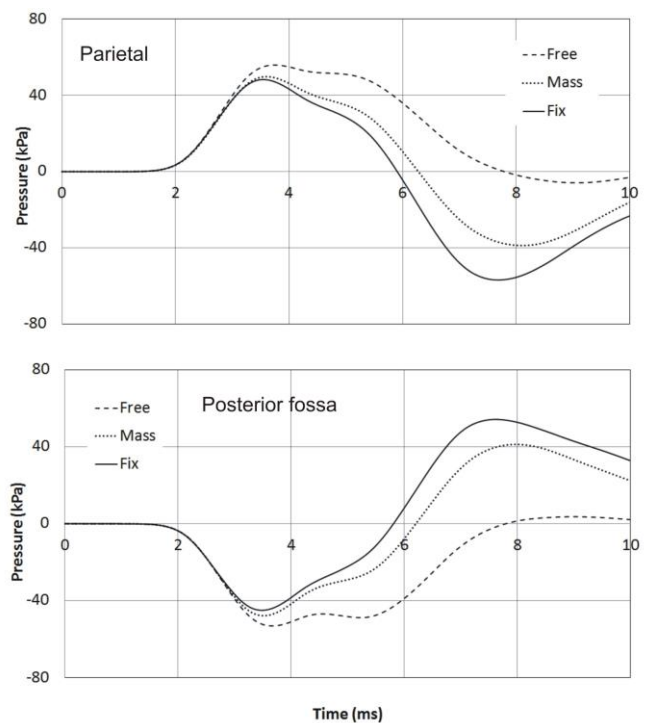


Figure 3. The predicted time histories of the brain pressures at the parietal (upper) and posterior fossa (lower) locations during the impact for different neck boundary conditions.

EFFECTS OF WORKING ENVIRONMENT FACTORS ON UPPER EXTREMITY MECHANICAL PROPERTIES DURING POWERED HAND TOOL USE

¹Xu Xu, and ²Jia-Hua Lin

¹Liberty Mutual Research Institute for Safety, Hopkinton MA, USA

²Safety & Health Assessment & Research for Prevention (SHARP), Olympia WA, USA

email: xu.xu@libertymutual.com

INTRODUCTION

Powered hand tools are widely used for fastening screws and nuts during assembly operations. Compared with manual tools, whose output torque is directly adjusted by the operator, powered hand tools are driven by power sources such as high pressure air or electricity. If the build-up torque exceeds the operator capacity, displacement of the tool occurs and results in upper extremity movement and eccentric muscle exertion of the operator, which is related to muscle damage and muscle soreness. Working environment factors, such as working height, working distance, and joint hardness, have been found to significantly affect hand displacement during powered hand tool use. In the current study, the mechanical properties of the upper extremity were identified under various working environment factors. The goals of the study were to understand whether those working environment factors affect the mechanical properties of the upper extremity during actual tool use.

METHODS

Thirty male participants with no chronic or existing musculoskeletal disorders participated in the study (mean age = 38.4, S.D. 13.3). The experimental protocol was approved by the local institutional review board, and informed written consent was obtained from each participant. The tool operation configuration of a pistol grip tool on a vertical surface was examined. The pistol grip tool had an automatic shutoff mechanism. Two joint (J) simulators (soft and hard) were used to represent typical assembly tasks. The joint hardness was defined as the angle of joint rotation from joint contact to tool shutoff. The working heights (V) were 30 cm below, 30 cm above, and at shoulder

height; the horizontal distances (H) were 25, 50, and 75% of the maximum forward reaching distance. A task platform consisting of two joint simulators was designed to provide the tool operation configuration (Figure 1). A potentiometer (174-0321T, Space Age Control, Palmdale, CA, USA) was used to record the rotational displacement of the handle. A torque transducer (TQ503-63, Omega Engineering, Stamford, CT, USA) was placed between the joint and the tool to measure the torque generated by the tool (Figure 1). All signals were collected at 1000 Hz by an A/D converter.

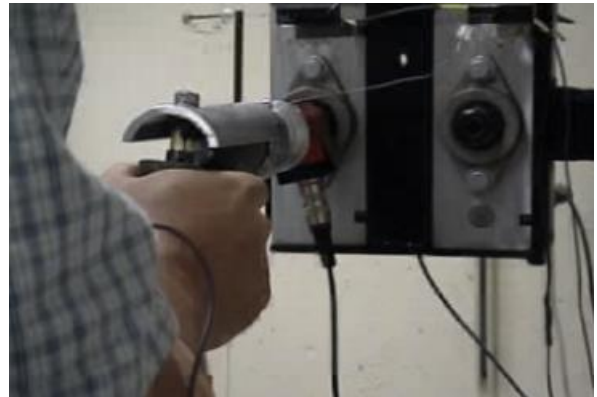


Figure 1: Experiment setup

The torque generated by the tool (T) and the rotational displacement (θ) of the tool during the build-up period were first extracted for each trial. The rotational velocity ($\dot{\theta}$) and rotation acceleration ($\ddot{\theta}$) during the build-up period were then calculated using first order and second order finite differences of θ . For a second order linear system, the dynamic equation can be written as:

$$T = K\theta + C\dot{\theta} + J\ddot{\theta}, \quad (1)$$

where K and C are torsional stiffness and torsional damping coefficient for the upper extremity, and J is the effective moment of inertia of the upper extremity combined with the tool. T , θ , $\dot{\theta}$, and $\ddot{\theta}$ are all column vectors with same number of rows,

which is the number of samples during the build-up time period. The value of K, C, and J were then estimated by the least squares method (Konczak et al., 1999)

RESULTS AND DISCUSSION

For the pistol grip tool on a vertical surface, the mean stiffness, damping coefficient, and effective mass of the upper extremity were 5.55×10^3 N/m, 80.0 Ns/m, and 2.22 kg, respectively. Joint type was a significant factor for all mechanical properties (Figure 2). The mean stiffness increased 12% and 131% for inexperienced and experienced operators, respectively. For the hard joint, the mean stiffness, damping coefficient, and effective mass were 4.07×10^3 N/m, 103.3 Ns/m, and 1.27 kg, respectively, while for the soft joint, those values were 7.03×10^3 N/m, 56.7 Ns/m, and 3.16 kg, respectively.

The hard joint was associated with less stiffness and effective mass, as well as a greater damping coefficient. Such effects could be a result of the nonlinearity of human movement dynamics. The current study modeled the upper extremity as a linear system and the mechanical properties represent the mean values across a fastening sequence. However, because of reflex delay and electromechanical delay between the stimulus and muscle force generation, the stiffness of the upper extremity at the very initial phase during powered hand tool use can be assumed to be zero (Ay, 2011). Although the length of this initial period needs to be further studied, it is clear that the shorter the total fastening time, the more the mechanical properties in a linear model would be affected by the initial phase.

CONCLUSIONS

Mechanical properties of the upper extremity can be used to describe the displacement of powered hand tools. The results suggest that joint type has significant influences on mechanical properties in the tested operating configuration. The results of this study suggest that joint type needs to be considered during the design of a powered hand-tool workstation.

REFERENCES

1. Konczak, J., Brommann, K., Kalveram, K.T., 1999. Identification of time-varying stiffness, damping, and equilibrium position in human forearm movements. *Motor Control* 3, 394-413.
2. Ay, H., 2011. Linear and Nonlinear Models of Human Hand-Arm Dynamics and Torque Tool Interaction. The Ohio State University.

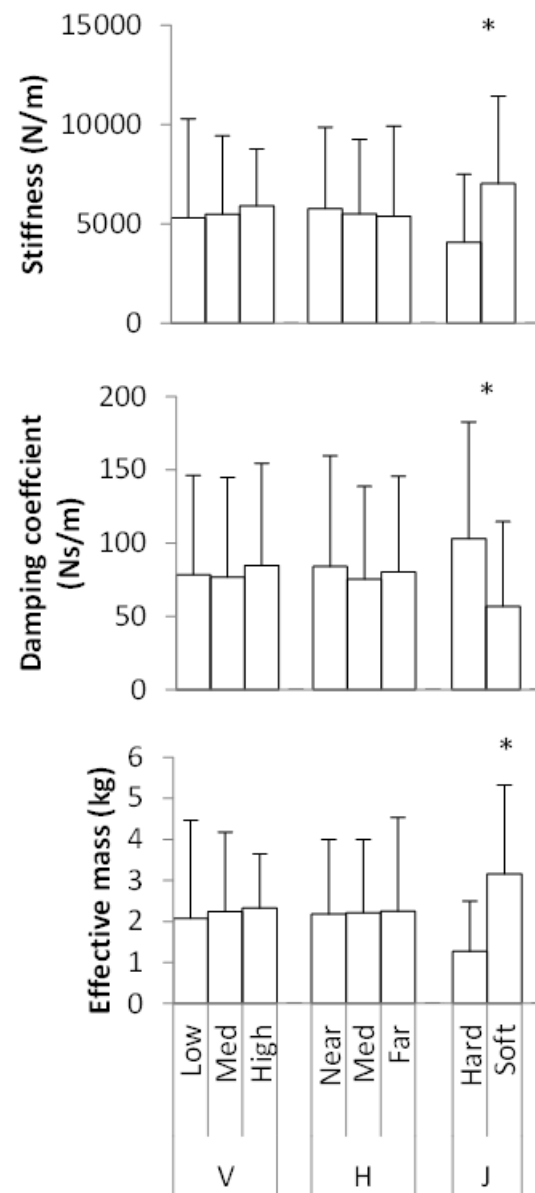


Figure 2: Main effects of task conditions on stiffness, damping coefficient, and effective mass during pistol grip tool use on a vertical surface. Asterisks (*) indicate significant effects.

LOWER EXTREMITY JOINT STRATEGY VARIES WITH STEP WHEN TRANSITIONING ONTO DIFFERENT STAIR RISERS WITH AND WITHOUT ANKLE LOAD

^{1,2}Toyin Ajisafe & ¹Jianhua Wu

¹Texas A&M University, Corpus Christi, TX, USA. Email: toyin.ajisafe@tamucc.edu

²Georgia State University, Atlanta, GA, USA.

INTRODUCTION

Muscle power bursts indicate joint strategy during locomotion [1]. Previous research has outlined important power bursts around toe-off (late stance to early swing) that are associated with surface accommodation and avoidance: A3 (ankle plantarflexor power generation burst) upwardly accelerates the lower extremity and body prior to toe-off; K3 (knee extensor power absorption burst) decelerates the rapidly flexing knee after midstance; H3 (hip flexor power generation burst) is associated with pulling off the lower limb into swing; K5 (knee flexor power generation burst) occurs during swing and was previously thought to only emerge during surface avoidance [1]. Transitions between level and stair walking have been linked to increased mishaps [2], and external ankle load has been suggested as a potentially effective neurofacilitatory tool; however, despite their potential to reveal joint strategy, no studies have investigated the relativity of the foregoing power bursts when transitioning onto stairs of different heights with and without external ankle load. This knowledge may help further guide task-specific gait rehabilitation and inform fall prevention programs.

METHODS

Participants: Twenty young adults (21.68 ± 2.49 years; 169.70 ± 9.56 cm; 63.91 ± 9.62 kg) participated in this study: seven males (21.71 ± 1.25 years; 177.43 ± 7.53 cm; 69.92 ± 8.34 kg) and 10 females (21.75 ± 3.45 years; 163.82 ± 6.36 cm; 60.5 ± 7.59 kg).

Experimental design: Participants (fitted with 15 retroreflective markers) walked barefoot overground and negotiated an intervening three-step staircase (Fig. 1). There were three stair heights: low stairs (LS) (17 cm riser), medium stairs (MS)

(24 cm riser), and high stairs (HS) (31 cm riser), and two external ankle load conditions: no load (NL) and bilateral ankle load (AL) (1.92 ± 0.29 kg). Lower extremity power bursts around toe-off, i.e., A3, K3, H3 and K5 were calculated.

Data collection:

Eight conditions (3 stair height x 2 step x 2 ankle load) were tested. The order of conditions was randomized using a block design. Five trials were collected for each condition. Kinematic data was captured using a 7-camera 3-D Vicon motion capture system (100 Hz) and a Sony 120x digital zoom reference video camera. Two adjoining AMTI force plates (Fig. 1) registered ground reaction forces. A trial was deemed valid, if the lead and trail feet fully contacted the force plates in succession and transitioned onto the stairs successfully.

Data analysis: The interval between initial contact on the second force platform (FP2) and contralateral initial contact on the first stair was delineated as the first floor-to-stair transition step (TS1) (Fig. 1). The interval between initial contact on the first stair and contralateral initial contact on the second stair was delineated as the second floor-to-stair transition step (TS2) (Fig. 1). It is noteworthy that TS2 has been considered both a transition and a steady-state step [3, 4]. Ensemble mean and standard deviation (SD) values were calculated for A3, K3, H3, and K5 bursts across five trials for each condition.

Statistical analysis: A series of 3 stair height x 2 step x 2 ankle load ANOVA with repeated measures was calculated to determine the effects of the factors on the outlined power bursts. Post-hoc pairwise comparisons with Bonferroni adjustments were conducted when appropriate. Statistical significance was set at $p < .05$.

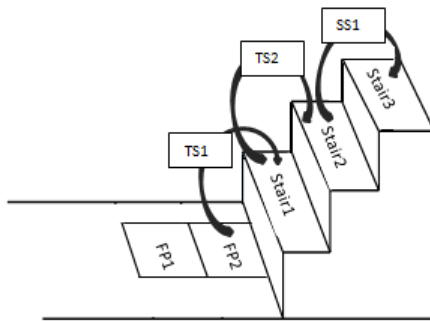


Figure 1: Floor-to-stair transition steps. TS1: interval between initial contact on second force plate (FP2) to initial contact on stair 1; TS2: interval between initial contact on stair 1 to initial contact on stair 2.

RESULTS AND DISCUSSION

There were three-way interactions of stair height, step and ankle load on A3, H3 and K5 ($F_{2,32} = 197.12$, $p < .001$; $F_{2,32} = 34.35$, $p < 0.001$; $F_{2,32} = 10.81$, $p < .001$), respectively. H3 and K5 power bursts were both observed at TS1 and TS2 in the current study suggesting a deliberate strategy to both accommodate and avoid the stair edge. While there was greater reliance on A3 power generation at TS1 in the medium stairs, the low and high stairs were characterized by greater reliance on H3 burst. Conversely, while there was greater reliance on H3 power generation at TS2 in the medium stairs, the low and high stairs were characterized by greater reliance on A3 power generation. Also, the medium stairs was associated with the most diminutive K3 power bursts, suggesting a level of exteroceptive familiarity such that there was not as much need to decelerate the rapidly flexing knee prior to toe off. Relatedly, the presence of ankle load seemed to have increased the need to decelerate the rapidly flexing knee only when ascending the medium stairs.

CONCLUSIONS

Although stair ascent is considered a surface accommodation task, K5 bursts can emerge to help avoid the stair edge. Surface accommodation seemed less of a priority at TS2 when ascending less familiar riser heights, i.e., low and high stairs.

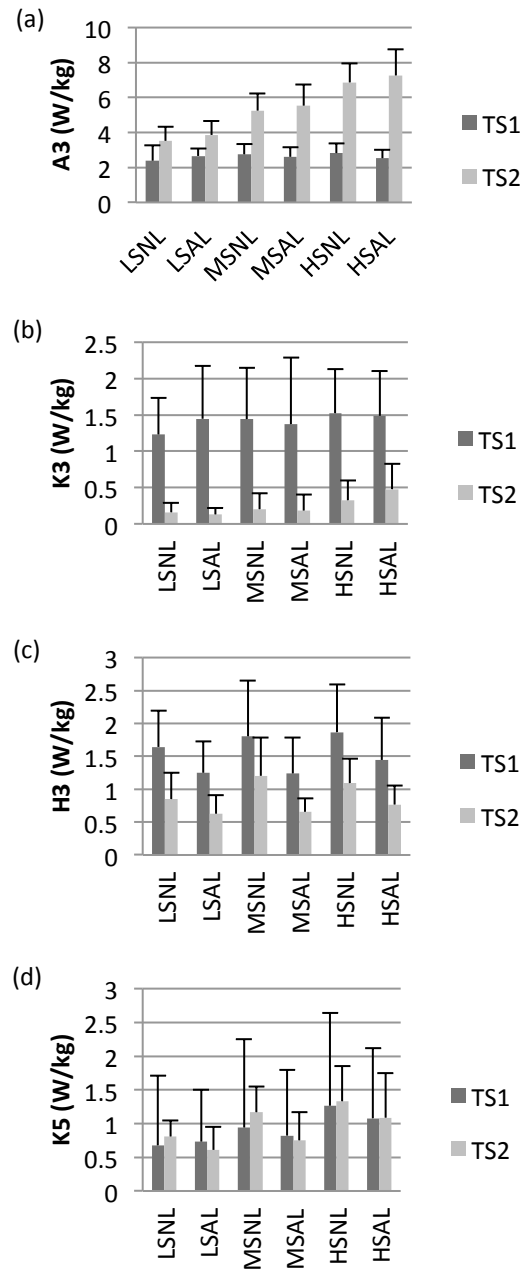


Figure 2: Mean lower extremity power bursts around toe-off: (a) A3, (b) K3, (c) H3, (d) K5; LSNL (low stair without ankle load); LSAL (low stair with ankle load); MSNL (medium stair without ankle load); MSAL (medium stair with ankle load); HSNL (high stair without ankle load); HSAL (high stair with ankle load)

REFERENCES

- [1] McFadyen BJ, Carnahan H. *Exp Brain Res*, **114**, 500-6, 1997.
- [2] Jackson PL, Cohen HH. *J Safety Res*, **26**, 151-9, 1995.
- [3] Andriacchi T. et al. *J Bone & Joint Surg*, **62**, 749-57, 1980.
- [4] Lee HJ, Chou LS. *J Biomech*, **40**, 2530-6, 2007.

AVERAGE MINIMUM TOE CLEARANCE MAY NOT CONTRIBUTE TO INCREASED FALL RISK IN PATIENTS WITH CHRONIC OBSTRUCTIVE PULMONARY DISEASE

¹Andrew Arnold, ¹Eric Pisciotto, ²Stephen Rennard and ¹Jennifer Yentes

¹University of Nebraska at Omaha, Omaha, NE, USA

²University of Nebraska Medical Center, Omaha, NE, USA
email: andrewarnold@unomaha.edu, web: cobre.unomaha.edu

INTRODUCTION

Despite decades of multidisciplinary research, one out of every three older adults will fall each year [1]. In 2013, this amounted to over 2.5 million non-fatal fall injuries with 734,000 of these patients being hospitalized [2]. There is a need to find measures that can analyze fall risk to identify potential fallers and one potential measure is minimum toe clearance (MTC). MTC occurs during swing phase when the toe is at maximum velocity and the distance between the toe and the ground is at a minimum. The chances of having a trip related fall are highest at the MTC [3]. Fallers have a significantly lower toe clearance compared to non-fallers [4]. One disease that leads to a higher susceptibility to falls is chronic obstructive pulmonary disease (COPD) [5], currently the third leading cause of death in the United States and prevalent in older age groups [6]. Patients with COPD have weaker and more fatigable muscles [7], as well as, impairments in balance [8], which could lead to their higher fall risk.

The purpose of this study is to investigate MTC in patients with COPD to potentially identify a reason why patients with COPD are at a higher risk of falling. We hypothesized that patients with COPD would have lower MTC compared to healthy controls for both a rested and a post-activity tests. MTC could be decreased in patients with COPD compared to healthy controls due to patients with COPD having distal leg muscles that are both weaker and have increased fatigability [7]. We also hypothesized that there would be a reduction in the MTC for the COPD group when going from rested to post-activity tests and no change in the control group. As leg muscles get tired from activity it should become harder for patients with COPD to lift the foot as high, but controls should be able to compensate and maintain normal MTC.

METHODS

Sixteen patients with COPD (9 male, 63.8 ± 8.8 yrs, 88.3 ± 24.6 kg, 171.1 ± 11.6 cm) and 21 healthy control subjects (10 male, 66.1 ± 7.0 yrs, 80.61 ± 18.3 kg, 166.0 ± 16.5 cm) were recruited for this study. There were two walking tests that were performed, rested and post-activity. All the patients with COPD and controls performed the rested test. All patients with COPD and four controls performed the post-activity test.

Test 1 – Rested: Subjects walked across a 10 meter walkway at their self-selected pace. Marker trajectories were collected using data from three-dimensional motion capture (Motion Analysis Corp., Santa Rosa, CA; 60 Hz). One minute of rest was taken for all subjects between trials to prevent muscle tiredness or breathlessness. A total of five trials were collected.

Test 2 – Post-activity: Subjects walked at their self-selected speed on a treadmill at a 10% incline until the self-reported onset of muscle tiredness or breathlessness. Controls walked for 15 minutes. Once either symptom was elicited or 15 minutes was reached, the subject was immediately removed from the treadmill and the subject completed five walking trials without any rest between trials.

Minimum Toe Clearance: A virtual toe marker was built in Cortex (Motion Analysis Corp., Santa Rosa, CA) based on the heel, toe, and lateral metatarsal markers placed on the foot. Using custom Matlab code, MTC was calculated from the swing leg as the minimum distance from the toe to the ground during mid-swing. For each walking trial the MTC was calculated for the right leg and averaged across all steps for the trial. For each subject all five trials were averaged to get an average MTC for each of the two

tests. Group means for COPD vs controls rest and post-activity tests were compared using independent t-tests. Group means from the COPD and control groups rest vs post-activity tests were compared using dependent t-tests.

RESULTS AND DISCUSSION

There were no significant differences in COPD rest vs control rest ($p = 0.57$), COPD post-activity vs control post-activity ($p = 0.84$), control rested vs control post-activity ($p = 0.41$), and COPD rested vs COPD post-activity ($p = 0.17$). There was an increase, not significant, in the MTC of the patients with COPD when compared to the control group in the rest tests, which is opposite to what was hypothesized (Figure 1). The patients with COPD could be raising their foot higher to exaggerate lifting their foot to not have the foot catch the ground.

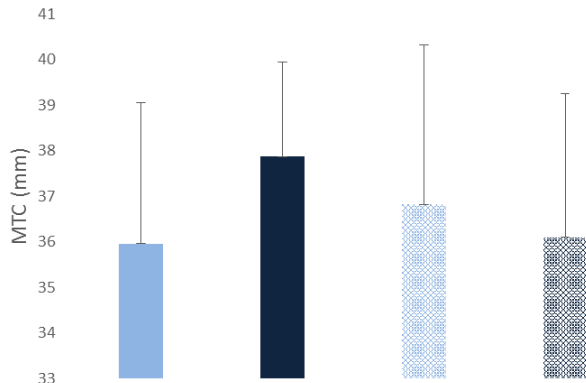


Figure 1. Mean minimum toe clearance for each condition for controls (light blue) and COPD patients (black) in the rested (solid) condition and the no rest (pattern) condition.

When performing the post-activity test, the patients with COPD had lower MTC values, not significant, compared to controls (Figure 1). Therefore patients with COPD had higher MTC values at rest, but lower MTC values during the post-activity test. The decrease in the MTC of the patients with COPD in the post-activity test as compared to the rested test, although not significant, partially supports the second hypothesis. The decrease could be due to tired muscles in the legs causing the toe to be slightly closer to the ground during swing phase. Patients with COPD not only have weaker dorsiflexors and quadriceps compared to age-matched healthy controls, but they also have increased fatigability [7]. Weakness and fatigability in these muscles would cause the foot to be lower during swing phase. A larger difference was expected especially if the

COPD subjects were truly walking with an altered gait due to tired muscles. If the patients with COPD were putting in more effort to raise their foot higher to avoid contact of the toe with the ground during swing phase, then it would be expected that their ability to raise their leg higher would be diminished when they were tired from activity.

Although MTC has been used in previous literature [3,4], the lack of significant differences seen between the average MTC in patients with COPD and controls could be an indication that other measures should be utilized to determine what causes the patients with COPD to have higher fall risk. One potential measure is MTC variability. The variability of MTC was greater in elderly compared to young men and may increase the risk of tripping in the elderly [9].

CONCLUSIONS

There were no significant differences between controls and the patients with COPD for the rest and post-activity tests. There was an increase in the MTC in the patients with COPD as compared to the controls during the rested tests, although this did not reach statistical significance. The MTC of the patients with COPD decreased in the post-activity test as compared to the rested tests however this also did not reach statistical significance. The decrease could have been due to the muscles being tired from activity and a larger study may have more power to detect a statistically significant difference. Other measures (i.e., MTC variability) may provide larger and significant differences between patients with COPD and controls.

REFERENCES

1. Tromp A, et al. *Jrnl of Clin Epidem.* **54**, 2001.
2. CDC. *Web Inj Stat Quer Rep Syst.* 2013.
3. Barrett R, et al. *Gait Posture.* **32**, 2010.
4. Chiba H, et al. *Geriatr Gerontol Int.* **5**, 2005.
5. Roig M, et al. *Respir Med.* **105**, 2011.
6. CDC. *Morb Mort Wkly Rep.* **61**, 2012.
7. Gagnon P, et al. *Jrnl of COPD.* **10**, 2013.
8. Beauchamp M, et al. *Respir Med.* **103**, 2009.
9. Mills P, et al. *Gait Posture.* **28**, 2008.

ACKNOWLEDGEMENTS

We would like to thank Jordan Freeman for his assistance with tracking data for this abstract.

Factors Influencing Frontal Plane Kinematics and Kinetics Before and After Total Knee Arthroplasty

¹Rachel Baker, ¹Gregory Freisinger, ¹Jacqueline Lewis, ¹Laura Schmitt, ¹Xueliang Pan, ¹Jeffrey Granger,
¹Andrew Glassman, ²Matthew Beal, ¹Ajit Chaudhari and ¹Robert Siston

¹The Ohio State University, Columbus, OH, USA

²Northwestern University, Evanston, IL, USA

email: rkbaker1216@gmail.com, web: <https://nmb1.engineering.osu.edu/>

INTRODUCTION

Knee osteoarthritis (OA) is associated with increased varus knee alignment, altered gait kinematics and kinetics, quadriceps weakness, and high muscle co-contraction indices (CCI), all of which negatively affect joint integrity [1-4]. Total knee arthroplasty (TKA) generally improves function and relieves pain associated with severe knee OA. However, even after TKA, more patients have difficulty with daily activities than age-matched controls (52% versus 22%) [5]. Studies have investigated changes in strength, muscle activity, knee alignment and gait before and after TKA, but they primarily studied sagittal plane kinematics or made comparisons to controls [4,6]. To assess potential contributing factors of suboptimal TKA outcomes, it is important to understand how kinematics and kinetics may be affected by CCI, strength, and knee alignment before and after TKA.

The purposes of this study were to investigate: 1) how frontal plane knee kinematics and kinetics during gait are related to CCI, knee flexion and extension strength, and standing knee alignment both before and 6 months after TKA, and 2) if preoperative variables can be used to predict postoperative kinematics or kinetics.

METHODS

19 subjects (21 knees: 4 M / 17 F, age 57.6 ± 7 y, height 1.67 ± 0.9 m, weight 93.8 ± 16 kg, BMI 34.2 ± 5.4 kg/m²) awaiting TKA provided IRB approved consent to participate in this study. Movement analysis was performed during gait at a self-selected speed approximately 1 month before and 6 months after surgery. Knee flexion and extension strength were estimated by maximum voluntary isometric contraction measured on a Biodex System 3 Dynamometer [Biodex Medical Systems; Shirley, NY]. A

modified Point Cluster Technique was used with ten motion capture cameras [MX-F40: Vicon, Oxford UK] at 150 Hz to calculate kinematics [7]. Standing knee varus alignment was extracted from static calibration trials, as similar methods have shown good correlation with radiographic alignment [8]. Ground reaction forces were sampled at 1500 Hz from Bertec 4060-10 force plates [Bertec Corp; Columbus, OH], and lower extremity joint loading was estimated with inverse dynamics. Weight acceptance (WA) was defined as the time period from heel strike to peak knee flexion angle. Peak and mean knee adduction angles and moments (pKAA, mKAA, pKAM, & mKAM) were found over WA for the involved limb.

EMG was collected at 1500 Hz for rectus femoris (RF), vastus lateralis (VL), vastus medialis (VM), semimembranosus (SM), biceps femoris (BF), lateral gastrocnemius (LG) and medial gastrocnemius (MG). EMG was filtered with a zero lag, 4th order, 10 Hz low-pass Butterworth filter and full wave rectified. EMG was normalized to the maximum EMG measured during submaximal reference exercises, as this technique is suggested for use in pathological populations [9]. Trials with poor EMG were removed from further analysis. Average CCI for the involved limb over WA were calculated for total, medial and lateral quadriceps-hamstring (QH, MQH, and LQH), and total, medial and lateral quadriceps-gastrocnemii (QG, MQG, and LQG) co-contractions (Eq. 1) [3].

$$avgCCI = \frac{1}{n} \sum_{i=1}^n \left(\frac{lower\ EMG_i}{higher\ EMG_i} \times (lower\ EMG_i + higher\ EMG_i) \right)$$

Equation 1. Average CCI over n samples during WA.

Statistical analysis was completed using Minitab 17 Statistical Software [Minitab Inc., State College, PA]. Depending on the distributions of the variables, paired t-tests or Wilcoxon Rank-Sum tests were used

to test for differences between the paired preoperative and postoperative variables. Similarly, Pearson's correlation or Spearman's rank-order coefficients were calculated to estimate the association between selected pairs of independent variables.

RESULTS AND DISCUSSION

Before TKA, increased standing varus alignment was associated with increased preoperative pKAA and mKAA (Table 1). CCI and strength were not related to frontal plane knee kinematics or kinetics.

Six months after TKA, increased LQH, QH and standing varus alignment were associated with increased mKAA (Table 1). Increased LQH and standing varus alignment were also associated with increased pKAA. When standing alignment was used as a covariate, LQH remained significantly related to both mKAA and pKAA ($p = 0.025$), but QH was no longer significantly related to mKAA ($p=0.178$). Other CCI and strength were not related to frontal plane knee kinematics or kinetics.

Preoperative variables were not found to predict postoperative kinematics or kinetics. Preoperative standing varus alignment was not significantly related to postoperative pKAA or mKAA ($p = 0.453$). All frontal plane knee kinematics and kinetics, QH, LQH, and standing alignment significantly decreased after surgery ($p = 0.004$). Other CCI and strength were not significantly different before and after TKA.

CONCLUSIONS

While studies may disagree on whether knee varus alignment and muscle co-contractions are related, our results suggest that both factors may be related to

frontal plane knee kinematics after TKA [3,6]. We did not find a relationship between preoperative standing alignment and pKAM, which contrasts previous work that found varus alignment and pKAM are related in subjects with knee OA [10]; this relationship should be further investigated in a TKA population. Regarding the second purpose of this study, significant preoperative variables were not associated to postoperative kinematics. Interestingly, standing alignment was the only variable associated with knee angles both before and after TKA, while 2 CCI parameters emerged after surgery. Since a surgeon corrects preoperative deformity during TKA, our results may suggest an interplay between postoperative limb alignment, CCI, and kinematics that warrants further investigation and could suggest an ability to leverage intraoperative measurement to predict postoperative functional outcomes of TKA.

REFERENCES

1. Brouwer, et al., *Arth & Rheum*, **56**(4), 1204-11, 2007.
2. Andriacchi, *J Biomech* **115**, 575-81, 1993.
3. Schmitt and Rudolph, *J Orth Res*, 1180-85, 2008.
4. Benedetti, et al., *Cl Biomech*, **18**, 871-76, 2003.
5. Noble, et al., *Cl Orth & Rel Res*, **431**, 157-65, 2005.
6. Fallah-Yakhdani, et al., *Cl Biomech*, **27** 485-94, 2012.
7. Andriacchi, et al., *J Biomech*, **120**, 743-49, 1998.
8. Blazek, et al., *J Orth Res*, **31**(9), 1414-22, 2013.
9. Lehman & McGill, *J Man & Phys Ther* **22**(7), 1999, 444-46.
10. Specogna, et al., *Am Sport Med*, **35**, 65-70, 2007.

ACKNOWLEDGEMENTS

Funding from NIAMS, award number R01AR056700 supported this study.

Table 1. Significant Correlations to pKAA, mKAA, pKAM, and mKAM Before and After Surgery.

	Sample Size	pKAA		mKAA		pKAM		mKAM	
		coefficient	p-value	coefficient	p-value	coefficient	p-value	coefficient	p-value
Preoperative Variables									
Standing alignment, °	n = 21	0.597**	0.004	0.726†***	0.000	-0.232	0.311	-0.306	0.178
Postoperative Variables									
Standing alignment, °	n = 21	0.679***	0.001	0.792***	0.000	0.217	0.344	0.307	0.176
QH	n = 15	0.466	0.080	0.543*	0.036	-0.101	0.719	-0.042	0.881
LQH	n = 16	0.566**	0.002	0.535*	0.033	0.237	0.376	0.221	0.411
Footnotes: †indicates Spearman correlation. *(p<0.05) **(p<0.01) ***(p<0.001).									

Footnotes: †indicates Spearman correlation. *($p \leq 0.05$) **($p \leq 0.01$) ***($p \leq 0.001$).

THE EFFECTS OF VARUS AND VALGUS MIDFOOT ORTHOTIC POSTING ON ANKLE AND MIDTARSAL JOINT ANGLES DURING WALKING: A MULTI-SEGMENT FOOT ANALYSIS

¹Joaquin A. Barrios and ¹Hilary F. Feskanin

¹University of Dayton, Dayton, OH, USA
email: jbarrios1@udayton.edu

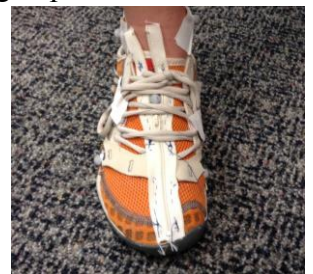
INTRODUCTION

The use of varus and valgus posting in foot orthotic devices has received considerable attention in the biomechanical literature as a conservative means to treat a variety of lower limb disorders. Based on previous research on foot orthoses, nearly all testing has been conducted on devices under the rearfoot. While rearfoot eversion is a key component of the overall foot pronation mechanics, there has been almost no direct research on the kinematic effects of posting aimed at the midfoot (Ferber & Benson, 2011). This paucity of research is largely due to historical limitations in kinematic foot modeling, and can be partly addressed with the growing use of multi-segment foot models. Therefore, the purpose of this study was to assess three-dimensional ankle and midtarsal joint kinematics during shod walking with either varus or valgus posting to the midfoot region using a multi-segment foot model. We hypothesized that varus posting would decrease eversion mechanics at the rearfoot and midfoot compared to the stock orthoses, and valgus posting would increase eversion mechanics.

METHODS

Twenty healthy female subjects were recruited for the study (Table 1). Potential subjects were excluded if they reported any history of spinal or lower extremity pathology in the previous year. Standing Arch Height Index was recorded. To prepare for data collection, subjects were fitted with an established reflective marker set to the right lower extremity and pelvis, which was supplemented with a modified version of a recently established three-segment foot model (Bruening et al., 2012). New Balance Minimus running shoes were used. The shoes have been custom modified with marker cut-outs in the upper, as well as a

midline zipper in the upper from the distal tip of the shoe up through the tongue (see figure). Finally, commercially available foot orthoses (Vasyli Medical, San Rafael, CA, USA) were used. The base orthotic device served as the control condition, and 6 degree varus and valgus posts were added to the same stock device for the posted conditions. Due to the novel zipper modification, a marked foot could be removed without disturbing the marker configuration.



Data collection commenced with a static calibration and functional hip motion trial. Walking trials were then collected along a 23 m walkway at a self-selected speed, using average sacral marker velocity along the line of progression while the subject traversed the volume. All trials were controlled at the established speed within 5%. The control condition was collected first, followed by the two posted condition in random order.

Video data were captured using an 8-camera VICON (Oxford Metrics, Oxford, UK) Nexus system (100 Hz), and kinetic data using a Bertec (Columbus, OH, USA) force platform (1000 Hz). Five usable trials were labeled and trimmed to stance in Nexus, exported in C3D format, and post-processed in Visual 3D (C-Motion, Bethesda, MD, USA). Cardan joint angles (X (Sagittal) – Y (Frontal) – Z (Transverse)) were calculated. Custom Labview software code (National Instruments, Austin, TX, USA) was used to extract the target variables of interest from the array data. The target variable list was comprised of the 3D ankle and midtarsal angles at initial contact, peak deflections, and the corresponding excursions, expressed in degrees. SPSS (v20.0, IBM, New

York, USA) was used to perform repeated measures analyses of variance using an alpha level set to 0.05, with planned comparisons between the posted conditions to the control condition.

RESULTS AND DISCUSSION

Table 1: Mean (SD) subject descriptive data (N = 20)

Age (y)	Height (m)	Weight (kg)	BMI (kg/m ²)	Standing Arch Height Index
22.0 (1.7)	1.7 (0.1)	62.9 (8.9)	23.2 (3.4)	0.33 (0.03)

In general, the purpose of this foot orthotic study was to evaluate the effects of 6-degree varus and valgus midfoot posts on 3D midtarsal and ankle joint angles during walking in healthy females. A three-segment foot model and a shoe customized with a longitudinal zipper were used to facilitate a novel assessment of midtarsal joint mechanics in different orthotic conditions. The female subjects in this study were young, healthy, and presented with normal arch height structure in standing (Table 1).

At the rearfoot, neither the varus nor valgus midfoot post elicited changes in any plane (Table 2). This is a novel finding suggesting that midfoot-targeted orthotic devices have localized effects to the midfoot region, and that more proximal rearfoot kinematics are not secondarily affected by such devices. Future testing for the influence of changes to midfoot mechanics on kinetic parameters is warranted, as is evaluating for effects at more proximal body regions such as at the knee and hip.

At the midfoot, changes by condition were observed in all three planes of motion. All subjects landed with midtarsal plantarflexion, inversion, and slight abduction. Valgus posting elicited increases in midtarsal dorsiflexion total motion, peak eversion and total eversion motion, and peak abduction. These increases are anecdotally in line with greater midfoot pronation in response to lateral posting.

The varus posting to the midfoot did not affect the midtarsal joint in the sagittal plane. However, we unexpectedly observed a small increase in midtarsal eversion. However, at approximately half a degree of motion, this finding may be within the error of the measurement. Decreased abduction excursion was also observed, which supports the notion that less pronation is occurring at the midfoot region, for which abduction is considered a component motion.

CONCLUSIONS

In summary, the multi-segment foot kinematic data support the notion that midfoot posting strategies affect the midtarsal joint but not the rearfoot, and that varus or valgus posting largely introduce changes that reduce or increase pronatory mechanics in the midfoot region, respectively.

REFERENCES

1. Ferber R et al., (2011). *J Foot Ankle Res* 4:18.
2. Bruening D et al., (2012). *Gait Posture* 35:529-534.

Table 2: Means and standard deviations for the 3D variables of interest for the 3 foot orthotic conditions

Rearfoot Angles (degrees)		Control	Valgus	Varus	Midtarsal Angles (degrees)		Control	Valgus	Varus
	Dorsiflexion at IC	3.0 (6.7)	3.0 (6.5)	3.4 (8.0)		Plantarflexion at IC	13.7 (4.7)	14.5 (5.2)	14.0 (7.6)
	Dorsiflexion Peak	13.9 (4.5)	13.6 (4.3)	14.4 (4.6)		Dorsiflexion Peak	-9.0 (3.9)	-8.3 (4.5)	-8.5 (7.3)
	Dorsiflexion Excursion	10.8 (7.8)	10.6 (8.2)	10.9 (8.7)		Dorsiflexion Excursion	4.7 (2.9)	6.2 (2.7)*	5.5 (3.2)
	Inversion at IC	5.7 (5.5)	5.9 (5.5)	5.3 (6.2)		Inversion at IC	7.2 (4.6)	7.1 (4.8)	8.1 (5.2)
	Eversion Peak	0.8 (5.8)	1.2 (7.2)	0.9 (5.2)		Eversion Peak	-3.2 (4.4)	-1.7 (4.3)*	-3.5 (4.1)
	Eversion Excursion	6.5 (4.2)	7.2 (5.0)	6.2 (2.5)		Eversion Excursion	4.0 (2.6)	5.3 (2.9)*	4.6 (2.9)*
	Abduction at IC	5.6 (6.3)	5.2 (6.7)	4.5 (7.5)		Abduction at IC	1.0 (4.3)	1.9 (4.6)	2.5 (5.1)
	Abduction Peak	11.1 (7.0)	11.0 (7.2)	10.3 (7.0)		Abduction Peak	4.5 (5.1)	5.4 (4.7)*	5.1 (5.1)
	Abduction Excursion	5.5 (1.8)	5.7 (2.3)	5.8 (2.7)		Abduction Excursion	3.4 (2.0)	3.5 (2.1)	2.6 (1.5)*

Significance denoted by (*) at or below the 0.05 alpha level in comparison to control condition. IC = Initial Contact

MUSCULAR AND METABOLIC CHANGES IDENTIFIED DURING PROLONGED LOAD CARRIAGE ON VARIABLE GRADES

Jessica Batty, Meghan O'Donovan, Carolyn K. Bense, and Leif Hasselquist

Natick Soldier Research, Development and Engineering Center, Natick MA

E-mail: jessica.m.batty.civ@mail.mil

INTRODUCTION

The negative consequences of prolonged load carriage on soldiers' physical status continue to be a major concern for military services worldwide. However, there is little research into the effects on soldiers of prolonged load carriage and the research that has been done has focused primarily on changes in energy cost as a function of load weight and time marching on a level grade [1]. In one study [2], muscle function was recorded before and after a 2-h march at either a 0% or a -8% grade with a 25-kg backpack load. The two grades resulted in similar decrements in muscle force production. The current research was designed to mimic the physical demands of a more realistic load carriage scenario by varying grade during a prolonged march and including a load typical of the weight soldiers carry. Oxygen consumption ($\dot{V}O_2$) was also recorded during the march. The purpose was to determine the muscular and metabolic effects of a load carriage paradigm with 1 h (H1) of uphill walking followed by 1 h (H2) of downhill or of variable graded walking, for a total march distance of 9.6 km.

METHODS

Eleven soldiers (Age, 23 ± 3 yrs; Ht, 179.3 ± 8.0 cm; Wt, 86.2 ± 12.5 kg; $\dot{V}O_{2peak}$, 49.2 ± 4.4 ml·kg⁻¹·min⁻¹) conducted 2-h treadmill marches at 1.34 m·s⁻¹ under 4 combinations of load and grade (I: 6-kg load, H1 at 4% grade, H2 at -8% grade; II: 6-kg load, H1 at 4% grade, H2 at variable grade; III: 40-kg load, H1 at 4% grade, H2 at -8% grade; IV: 40-kg load, H1 at 4% grade, H2 at variable grade). The variable grade conditions consisted of 10-min of walking at each of three grades (-8%, 0%, and 4%, in order), followed by another 10 min at each of the grades. $\dot{V}O_2$ data (ml·kg⁻¹·min⁻¹ adjusted for body weight) were averaged over 2-min collection samples taken

at 10- min intervals during the march (COSMED, Chicago, IL). The average $\dot{V}O_2$ values for H2 were obtained and used in subsequent analyses. Isokinetic lumbar muscle flexion and extension data were collected immediately before and after the march for 5 maximal muscle contractions at $20^\circ \cdot s^{-1}$ and 21 maximal muscle contractions at $60^\circ \cdot s^{-1}$ (Biodex, Shirley, NY). A mean was obtained over each set of trials and a difference was calculated as the pre- minus the post-march measure. Separate repeated measures analyses of variance (ANOVAs) were done to assess muscle strength differences and average $\dot{V}O_2$ values for each of the 4 march conditions. In those instances in which an ANOVA yielded a significant main effect ($p < .05$), post hoc analyses were performed with a Bonferroni correction applied.

RESULTS AND DISCUSSION

Lumbar pre- minus post-march muscle strength scores revealed: a) Significant differences in isokinetic lumbar extension at $20^\circ \cdot s^{-1}$ between the 6- and the 40-kg loads, reflecting larger decreases in power ($p < .005$) and total work ($p < .005$) and a smaller decrease in peak torque ($p < .01$) for the heavier load condition; b) A significant difference in isokinetic lumbar extension at $20^\circ \cdot s^{-1}$ between constant downhill and variable grades, reflecting a larger increase in time to peak torque ($p < .05$) for the constant grade condition; c) For $60^\circ \cdot s^{-1}$ isokinetic lumbar extension, significantly larger decrements in power ($p < .05$) and total work ($p < .05$) with the heavier load at the variable grade (IV) compared with the constant grade (III), and essentially no differences between constant and variable grades with the lighter load (I and II, respectively; Fig. 1).

$\dot{V}O_2$ responses for H2 of the march demonstrated: a) No significant interaction between the load and the grade variables ($p > .05$); b) A significant difference between the 6- and the 40-kg loads, reflecting higher metabolic cost ($p < .001$) for the heavier load condition; c) A significant difference between constant downhill and variable grades, reflecting higher energy cost for the variable grade ($p < .001$; Fig. 2).

Study results indicate that neuromuscular impairment, displayed as reduced strength of lumbar muscles, can be identified upon completion of a 2-h loaded march. Muscle strength is affected by load weight carried and grades traversed during the march. However, results for slow ($20^\circ \cdot s^{-1}$) and fast ($60^\circ \cdot s^{-1}$) isokinetic test velocities of lumbar extension, likely requiring different patterns of slow- and fast-twitch muscle fiber recruitment, differed somewhat from each other. The $20^\circ \cdot s^{-1}$ data indicated strength decrements for the 40-kg compared with the 6-kg load and for the variable compared with the constant downhill grade, but the interaction between load and grade was not significant ($p > .05$). The $\dot{V}O_2$ data results for the second hour of the march were similar insofar as oxygen cost was higher for the heavier load and for the variable terrain, and there was not a significant interaction between load and grade ($p > .05$). In contrast, the $60^\circ \cdot s^{-1}$ test velocity did reveal a significant interaction ($p < .05$). For the lighter load, there was little change in muscle strength as a function of grade condition. However, strength decrements were substantial for the heavier load carried on the variable compared with the downhill grade. Considering the lumbar muscle strength and the metabolic results, it can be posited that the fast isokinetic test velocity revealed generalized, whole-body muscle fatigue induced by carrying a heavy load on a variable grade, which required uphill and level as well as downhill walking, whereas the slow test velocity reflected a more localized fatigue of the lumbar muscles.

CONCLUSIONS

Reduction in lumbar muscle strength over a prolonged march appears to be linked to the load carried and the variability of the grade of the march.

Variable grade traversals may contribute more substantially to soldiers' loss of mission effectiveness than a downhill traversal.

REFERENCES

1. Knapik JJ, et al. *Mil Med* **169**(1), 45–56, 2004.
2. Blacker SD, et al. *Aviat Space Env Med* **81**(8), 745–753, 2010.

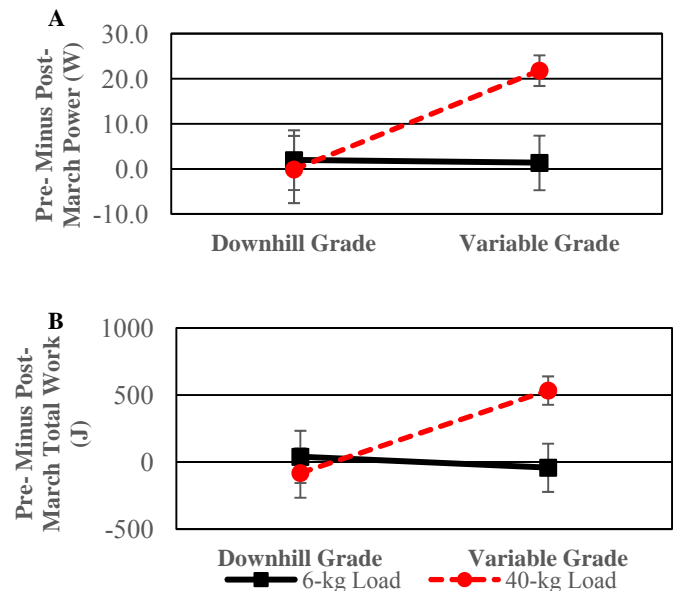


Figure 1: Means (SE) for significant interactions of load and grade on the (A) power and (B) total work measures of isokinetic lumbar extension at $60^\circ \cdot s^{-1}$.

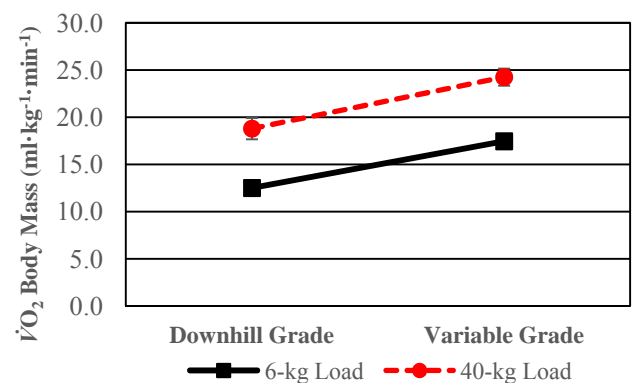


Figure 2: Means (SE) for load and grade effects on $\dot{V}O_2$ adjusted for body mass.

EFFECT OF PLANTAR FASCIA STIFFNESS ON FOOT ENERGY ABSORPTION DURING OVERGROUND WALKING

¹Erica A. Bell, ²Kota Z. Takahashi, ¹Patrick M. Rider, ²Gregory S. Sawicki, and ¹Zachary J. Domire

¹ East Carolina University, Greenville, NC, USA

² North Carolina State University, Raleigh, NC, USA

email: beller10@students.ecu.edu

INTRODUCTION

The foot plays a vital role in locomotion, providing support and standing balance as well as aiding in shock absorption and propulsion. The foot-to-ground interaction during locomotion allows for the modulation of the force generating capacity of the ankle plantar flexor muscle-tendon unit and recent studies have shown the foot's ability to shift ankle muscle operating conditions during ground contact to influence locomotion [1, 2]. The ankle joint has been implicated for its importance in providing energy to propel the body forward. However, the functions of the foot structures in locomotion are less clear. Intrinsic foot structures play a role in foot movement that can affect gait and local changes in these structures can have significant effects on movement and balance. While the ankle provides positive (propulsive) energy, the metatarsal-phalangeal (MTP) joint causes negative (dampening) energy to be done by the foot [3], where mechanical energy is absorbed during forward propulsion (Figure 1).

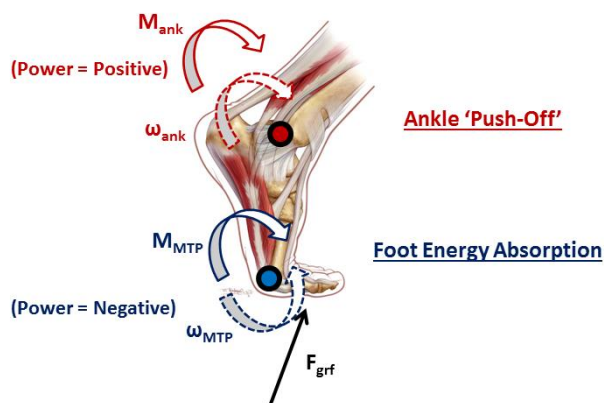


Figure 1: Diagram of the foot and ankle during late stance, where rotation of the MTP joint acts to dampen (i.e., perform negative work) the ankle push-off work.

We anticipate that a stiffer foot will decrease the mobility of the MTP joint and deformation ability of the foot, thereby decreasing the magnitude of energy absorption. The plantar fascia is a key structure in regulating MTP joint mobility during locomotion and may regulate the magnitude of foot energy absorption. **Therefore, the overall goal of this study is to investigate the effects of plantar fascia stiffness on foot mechanics.**

METHODS

Four healthy subjects (two males and two females, ages 24.0 ± 2.2 yrs, height 1.75 ± 0.07 m, and body mass 75.0 ± 19.2 kg) with no previous foot surgery, current plantar fasciitis, osteoarthritis, or musculoskeletal injuries that would compromise walking ability participated in gait analysis and ultrasound scans. All subjects gave informed consent for this protocol approved by the Institutional Review Board at East Carolina University. An eight camera 3D motion capture system (Qualisys, Gothenburg, Sweden) and an embedded force plate (AMTI, Watertown, MA) were used to collect kinetic and kinematic data during overground walking. Subjects walked at four speeds (1.2 m/s, 1.3 m/s, 1.5 m/s, and 1.7 m/s), where 1.5 m/s is considered a normal walking speed. An Aixplorer ultrasound system (SuperSonic Imagine, Aix-en-Provence, France) was used to perform ultrasound elastography scans of the plantar fascia while subjects were lying prone, with feet hanging just off of an examination table. Elastography is a cutting edge medical imaging technology that can be used to non-invasively examine tissue material properties in vivo.

Walking data was processed and analyzed using Visual3D software (C-Motion Inc., Germantown, MD). Elastography measurements were taken by selecting a 1mm diameter circular region of interest located centrally in the tissue, and calculating the mean shear modulus of this region. Regression analysis was used to determine relationship between peak negative power and plantar fascia stiffness across the four walking speeds.

RESULTS AND DISCUSSION

The regression analysis of average peak negative power as a function of plantar fascia stiffness is shown in Figure 2. Foot energy absorption, as measured by peak negative power, increased with walking speed, and was more dramatic at higher speeds (Figure 3). Plantar Fascia stiffness had a strong, positive relationship with foot energy absorption at all walking speeds. There is a moderate relationship of body mass and plantar fascia stiffness (Figure 4).

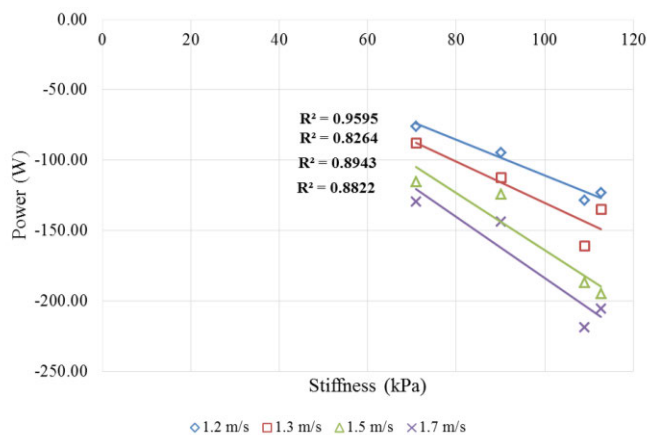


Figure 2: Linear regression analysis of plantar fascia stiffness and average peak negative power across all walking speeds.

We did not make an actual measure of deformation of the MTP joint. However, given that power absorption increased with stiffer feet, it is likely that the deformation stayed the same, as foot stiffness varied across individuals.

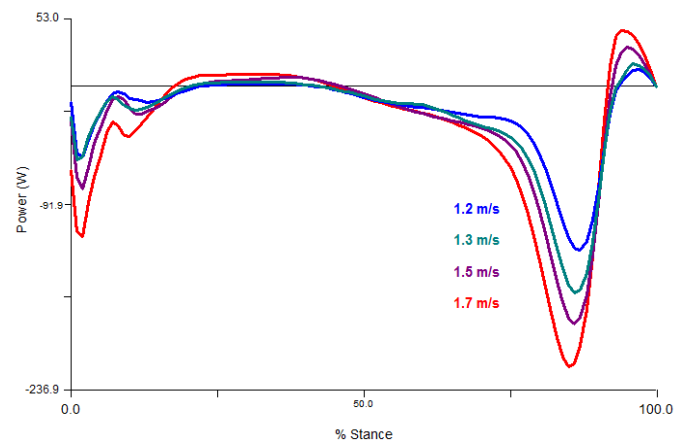


Figure 3: Distal foot power curves across all speeds for a representative subject.

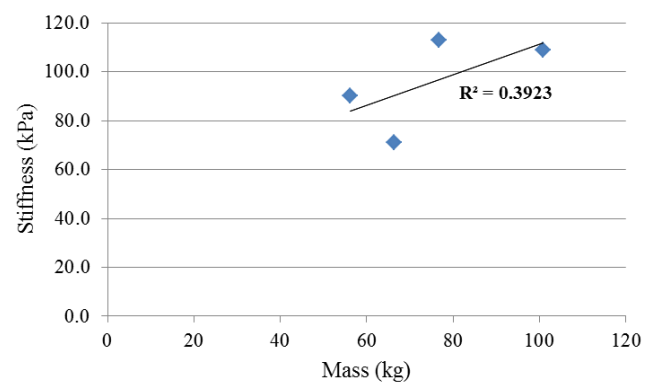


Figure 4: Relationship between body mass and plantar fascia stiffness.

CONCLUSIONS

The results are contrary to our hypothesis. It seems as though increased stiffness of the foot results in greater energy absorption by the foot. This might increase the energy costs of locomotion. However, it could potentially be advantageous in terms of performance. Further research is needed to clarify this relationship.

REFERENCES

1. Baxter, JR et al. *Proceedings of the Royal Society B: Biological Sciences*, **279**(1735), 2018-2024, 2012.
2. Lee, SS & SJ Piazza. *Journal of Experimental Biology* **212**(22), 3700-3707, 2013.
3. Takahashi, KZ & SJ Stanhope. *Gait & Posture*, **38**, 818-823, 2013.

PLANTAR REGIONAL PEAK PRESSURE AND MINIMAL SHEAR STRESS PROFILES IN DIABETIC AND NON-DIABETIC PATIENTS

¹ Visar Berki and ¹ Brian L. Davis

¹ The University of Akron, Akron, OH, USA

Email: vb20@uakron.edu, Web: <http://www.uakron.edu/engineering/BME/>

INTRODUCTION

The measurement of plantar pressure and shear stress profiles is increasingly being applied to the problem of skin tissue breakdown and ulceration in diabetic patients. The complex nature of plantar pressure and shear stress profiles during gait presents a multitude of possibilities for their assessment. Our current objectives were to determine (i) the instantaneous regional peak pressures in diabetic and non-diabetic patients, (ii) the instantaneous regional points of minimal shear stress, and (iii) the relationship, if any, between the two data sets. If there was a significant relationship between peak pressures and low shear, this would lend support to the idea that tissue is “squeezed” radially outwards from points of peak pressure, with zones of almost no shear stress at the center of these regions. Our goal was to investigate these relationships for diabetic patients with peripheral neuropathy and non-diabetic control patients.

METHODS

Pressure and shear stress data were collected on 29 human subjects: 16 control patients (9M, 7F; Age: 47.6±5.8 years; Weight: 824 N) and 13 neuropathic, diabetic patients (8M, 5F, Age: 61.6±14 years, Weight: 944 N). Each subject walked barefoot across a custom built shear and pressure collection system that is aligned in the center of a 3 m. x 0.6 m. platform. The center of the walking platform contains a 40 x 58 x 0.17 cm³ surface stress sensitive film (S3F) [1] that the subject was required to step on with the second of three steps. Four separate steps were recorded for each subject at a sampling rate of 50 Hz. Every step data set consisted of multiple 2-D arrays for pressure, medial-lateral shear, and anterior-posterior shear stress data, representing each sampled timeframe.

Each array contains pressure and shear stress data for every 1.6 mm x 1.6mm area of contact between the plantar and ground surfaces.

For every time frame, regional pressure peaks that correspond to the highest pressure in any 4.8mm by 4.8mm region of pressure values were recorded, along with their respective location coordinates. Simultaneously, shear stress coordinates were recorded, on the condition that the values corresponded to shear stress magnitudes of less than 25 Pa in all four directions (medial, lateral, anterior, and posterior). The distances between all minimal shear stress and regional peak pressure points were calculated, for all time frames.

Two sets of relationships between regional peak pressure and regional minimal shear stress points were then generated. The first set investigated each regional pressure peak, and calculated whether that peak occurred near any point that was considered as a minimal shear stress. The second relationship set investigated each regional minimal shear stress, and calculated whether that value occurred near any regional peak pressure point. Two points were considered to be nearby if they occurred within the same 4.8mm by 4.8mm neighborhood of coordinates. The final results indicated (i) the total number of regional peak pressure points, and how many of those points were near a minimal shear, and (ii) the total number of minimal shear points, and how many of those points occurred near a regional peak pressure point.

RESULTS AND DISCUSSION

For every time frame that contained pressure and shear stress data from any given patient, we observed that there were multiple instantaneous pressure peaks occurring on the plantar contact

surface. There were also numerous points of minimal shear during the same time frames. The total number of points occurring throughout the entire stance phase (multiple time frames) was summed and compared between diabetic and non-diabetic patients (Table 1). The results show that on average, diabetic patients have a higher number of regional peak pressure points (718 vs. 460) and also a higher number of minimal shear stress points (140 vs. 92) on the plantar surface. It is also evident that there were far more points of peak pressure as compared to points of minimal shear over the course of the entire stance phase. These findings are consistent with the concept that neuropathic diabetic patients have arches that flatten more than control subjects. As an arch flattens, there are concomitantly increased sites where local pressures increase. Of note is the fact that for diabetic and control subjects there was little difference in (i) the ratio of regional peak pressure points occurring near minimal shear points, and (ii) the ratio of minimal shear points occurring near regional peak pressures.

CONCLUSIONS

The current study has revealed that diabetic patients with peripheral neuropathy experience more instantaneous pressure peaks as the plantar skin surface makes contact with the ground. We believe

that this is in fact an indication of a collapse in the supporting arch structure of the foot, as is often the case in diabetic patients with foot pathologies. The increased number of peak pressure points means that there is likely a greater surface area that makes contact with the ground, which also explains the increased number of minimal shear stress points. In this scenario, both peak pressures and minimal shear stresses would be more widely distributed.

Previous studies have tried to predict shear stresses based on vertical loading parameters, given the absence of commercial plantar shear force platforms [2]. We examined our results for a possible relationship between regional peak pressure points and points of minimal shear. We conclude that we can safely predict minimal shear points with more than 84% certainty by observing the locations of peak pressures. But we cannot necessarily predict peak pressure points by observing minimal shear locations, as the occurrence rate is less than 19%.

REFERENCES

1. Stucke S, et al. *J Biomech* **45(3)**, 619-622, 2012.
2. Yavuz M, et al, *J Biomech Eng* **131(9)**, 2009.

Table 1: Means that indicate the total number of regional peak pressure and minimal shear stress points. Also shown are means indicating how many (i) pressure peaks, or (ii) minimal shear points, are close in proximity to the other value, and the respective percentage of occurrence.

	Number of Regional Peak Pressure Points (P)	P points near Minimal Shear Points (τ)	Percentage of P near τ	Number of Minimal Shear Points τ	τ , Near Regional Peak Pressure Points P	Percentage of τ near P
Control Patient Means	460	92	18.8%	94	83	86.8%
Diabetic Patient Means	718	140	17.5%	146	119	84.3%

GAIT AFFECTS BOTH KINESTHETIC AND VISUAL PERCEPTION OF DISTANCE TRAVERSED

¹Brandon Bischoff, ¹Nicholas Reynolds, ^{1,2}Nicholas Stergiou, ¹Steven J. Harrison

¹University of Nebraska Omaha, NE, USA

²University of Nebraska Medical Center, Omaha, NE, USA

email: bbischoff@unomaha.edu, web: www.unomaha.edu/college-of-education/cobre/index.php

INTRODUCTION

Humans and animals alike possess capacity for path integration. This capacity allows them to navigate the world around them by perceiving how their body is moving relative to the environment [1]. Path integration can underwrite basic adaptive behaviors such as foraging for food and the capacity to return to one's home location.

Path integration is based upon the use of sensory information to perceive the angles turned and distances traversed by the body as it moves through the world [1]. Perception of the distances traveled during navigation is known to depend upon sources of visual and non-visual information. Non-visual information has been shown to principally rely upon information derived from the movements of the limbs during locomotion (i.e. kinesthetic perception)[2]. In the absence of visible landmarks, vision and kinesthetic perception have been shown to have an approximately equal impact on human path integration [3].

Investigations of kinesthetic distance perception have shown that perception of distance traveled while blindfolded depends upon the way in which the legs are coordinated [2]. In this research, manipulating the gait patterns employed by participants across the outbound and return phases of a simple homing task was found to result in systematic biases in task performance. The two principal gait patterns employed in this research were a walk and a gallop-walk. The gallop-walk involves stepping forward with the right foot, bringing the feet together to parallel, and then repeating this process. While performing a simple homing task, participants who used a gallop-walk as the outbound gait in the homing task, followed by walking in the return phase of the homing task, produced a systematic underestimation bias. Alternatively, either walking or running outbound

followed by walking in the return phase produced no bias [1].

We hypothesized that visual information specifying distance traveled, unlike kinesthetic information for distance traveled, would not depend upon the gait patterns used by participants to complete the task.

METHODS

Eleven subjects, who are healthy individuals between the ages of 19 and 36, were recruited. Participants performed variants of a simple distance matching task consisting of a study phase and a test phase. In the study phase participants either walked or gallop-walked a set distance, and were instructed to get a sense of the distance they had traversed. In the test phase participants were asked to reproduce the studied distance from the study phase by walking a matching distance.

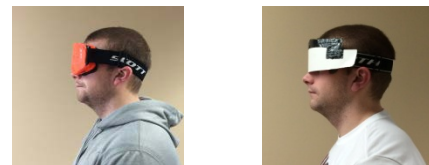


Figure 1. Complete (left) and partial (right) blindfolds used in experiment.

The potential contribution of kinesthetic and visual information in the distance matching task was investigated by manipulating the distances traversed in the study phase (6.5, 13, or 19.5m), the gait pattern employed in the study phase (walk, gallop-walk), and the availability of visual information in both study and test phases (complete blindfold, partial blindfold). The complete blindfold occluded all vision. The partial blindfold, similar to a visor, allowed the subjects to see only the immediate ground surface in front of them (about 2m). The partial blindfold prevented the subjects from getting any distance cues from visual landmarks. Experimental trials consisted of randomly presented combinations of the 3 independent variables (2

vision x 3 study phase distances x 2 study phase gait patterns).

On each experimental trial subjects put the blindfold on. They were instructed which gait pattern to employ in the study phase, which was either a walk or a gallop-walk. Participants then walked or gallop-walked a straight-line path until instructed to stop by the experimenter. While leaving the same blindfold on, subjects were then given instructions to walk a matching distance to that traversed in the study phase by continuing to walk in the same direction until they perceived a matching distance had been traversed.

RESULTS and DISCUSSION

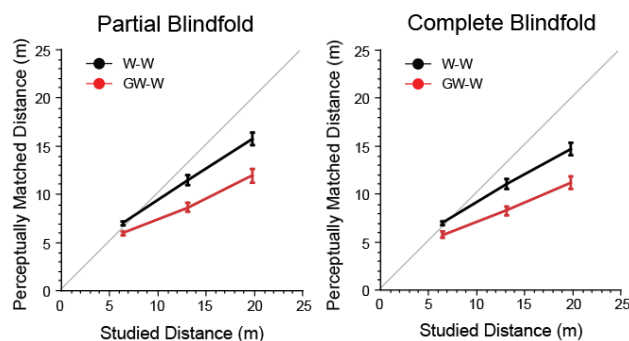


Figure 2. Distances of walked reports in the test phase as a function of distance traversed in the study phase, study phase gait, and the availability of visual information.

A systematic bias in reports was observed as a function of manipulating the study phase gait ($F(1,10) = 26.91$, $p < 0.001$). Although a main effect of vision was observed in the distance-matching task ($F(1,10) = 15.00$, $p < 0.01$), the presence or absence of vision did not diminish the systematic bias resulting from the manipulation of study phase gait patterns ($F_s < 1$). These results are not consistent with our original hypothesis that the availability of visual information across the study and test phases would attenuate the bias resulting from manipulating study phase gait patterns.

CONCLUSIONS

In attempting to interpret these findings, we noted particular characteristics of the results we obtained. We observed that the magnitude of bias resulting from manipulation of the study phase gait was significantly greater than what has previously been observed in the investigation of kinesthetic homing

tasks [2]. Additionally, a general bias towards underestimation of all distances was observed in our data that again is not observed in previous studies. Given these differences, a possible interpretation of our results is that participants in our experiment did not perceive distance in the same way as in previous homing task research. One possibility is that their reports may be biased by other variables such as effort. Effort is known to affect distance perception in some task contexts but not others [4]. Specifically, this research shows that effort affects attempts to reproduce the distance traveled along a recently traveled route (i.e. a distance matching task), but does not affect the ability to return to a fixed location in the environment (i.e. a homing task). In light of recently observed differences in the cost of transport for walking and gallop-walking [5], our results are consistent with the participants matching the following relation [6]:

$$\text{Study} \left(\frac{\text{Metabolic Effort}}{\text{Specified Distance}} \right) = \text{Test} \left(\frac{\text{Metabolic Effort}}{\text{Specified Distance}} \right)$$

We are planning to run a second experiment identical in design to our first experiment with the exception that participants will be asked to perform a homing task rather than a distance matching task.

REFERENCES

1. Loomis J. M. et al. *Wayfinding: Cognitive Mapping and Spatial Behavior*, 125-151, 1999. Baltimore, MD: Johns Hopkins University Press.
2. Turvey M. T. et al. *J Exp Psychol Hum Percept Perform* **38**, 1014-1025, 2012.
3. Kearns, M. J. et al. *Perception*, **31**, 349, 2002.
4. Harrison, S. J. et al. *Neurosci Lett*, **462**(2), 140-143, 2009.
5. White, E.J. Unpublished Doctoral Dissertation. *University of Connecticut*, 2012.
6. White, E. et al. *Psychol Bull Rev*, **20**(6), 1371-1377.

ACKNOWLEDGEMENTS

This work was supported by the Center for Research in Human Movement Variability of the University of Nebraska Omaha, NIH (P20GM109090, R01AG034995, and R01GM105045), and a FUSE grant from the University of Nebraska Omaha.

KNEE JOINT IMPULSE WHILE RUNNING WITH VARIED STEP LENGTHS

Collin D. Bowersock¹, Paul DeVita¹, and John D. Willson²

Departments of ¹Kinesiology and ²Physical Therapy, East Carolina University, Greenville, NC
Email: Bowersockc14@students.ecu.edu

INTRODUCTION

Exercise is important for cardiovascular health and overall well-being. Running is a popular mode of exercise that is associated with repetitive loading of the lower limb joints. Repetitive mechanical loading of the knee may accelerate cartilage degenerative changes, particularly when administered in large doses [1] or when administered to cartilage previously exposed to injury [2]. Knowledge of interventions to minimize exposure to knee joint contact forces during running may be advantageous in the management of people at risk for knee joint osteoarthritis, such as individuals with a history of knee joint injury. Reducing step length leads directly to reduced patellofemoral joint (PFJ) force per step and per kilometer [3]. However, the influence of step length during running on tibiofemoral joint (TFJ) kinetics are less well known. The purpose of this study was to test if the reductions in PFJ force per step and per kilometer are also observed at the TFJ.

METHODS

Twenty subjects who ran at least twice per week for no less than 16 km/week volunteered to participate in this study (10 males, 10 females, 22.6 years). All participants were asymptomatic in their lower extremities during the last 2 months and had no history of lower extremity surgery. Following acclimation to the treadmill, participants ran at their preferred pace (2.84 m/s) and step length. Step length then was then manipulated by increasing and decreasing step rate by 10% using audio cues provided by a metronome while running at the same velocity. After 2 minutes of practice in each condition, lower extremity kinematics (240 Hz, Qualysis AB, Gothenburg, Sweden) and ground reaction forces (2400 Hz, Bertec Corp, Columbus,

OH) were recorded. Foot strike pattern was held consistent between step length conditions.

Knee joint contact forces were estimated using a biomechanical model with inputs of hip, knee, and ankle angles, net joint moments, and joint reaction forces calculated using an inverse dynamics approach [4]. Muscle cross sectional area, line of action, and moment arms as a function of joint position at each joint were derived from the literature to estimate quadriceps, hamstrings, and gastrocnemius muscle forces during the stance phase of 5 steps. PFJ force was determined using quadriceps force after adjusting for cocontraction of the knee flexors. TFJ force was estimated as the sum of knee joint reaction forces and muscle force components applied through an 8.8° posterior tibial slope [5]. Medial TFJ contact forces were estimated as the force necessary to balance the frontal plane knee joint moment and total knee compression forces around contact points at 25% and 75% of subject-specific knee joint width [6].

Variables of interest included total PFJ, TFJ, and medial TFJ impulse per step and total PFJ, TFJ, and medial TFJ impulse per km. Impulse per kilometer was derived as the product of impulse per step and steps required to run a km in each condition. Separate repeated measures ANOVAs were used to test for differences in these variables between each step length condition ($\alpha = .05$)

RESULTS

A 10% shorter step length reduced TFJ impulse per step by 12.5% ($p < .001$), medial compartment TFJ impulse by 13.1% ($p < .001$), and PFJ impulse by 19.0% ($p < .001$). A 10% greater step length increased TFJ impulse per step by 17.3% ($p < .001$), medial compartment TFJ by 17.1% ($p < .001$), and PFJ impulse by 25.8% ($p < .001$).

A 10% shorter step length did not reduce TFJ impulse per km ($p=.246$) or medial compartment TFJ impulse per km ($p=.187$). However, a shortened step length reduced PFJ impulse per km by 10.3% ($p=.014$) despite the increased number of steps per km (Fig. 1). Conversely, a longer step length increased TFJ impulse per km by 6.9% ($p=.003$), TFJ medial compartment impulse per km by 6.7% ($p=.003$), and PFJ impulse per km by 14.8% ($p<.001$) despite the decreased number of steps per km. Post hoc analysis of muscle forces revealed greater gastrocnemius impulse but lower quadriceps impulse per kilometer with each decrease in step length (Figure 2).

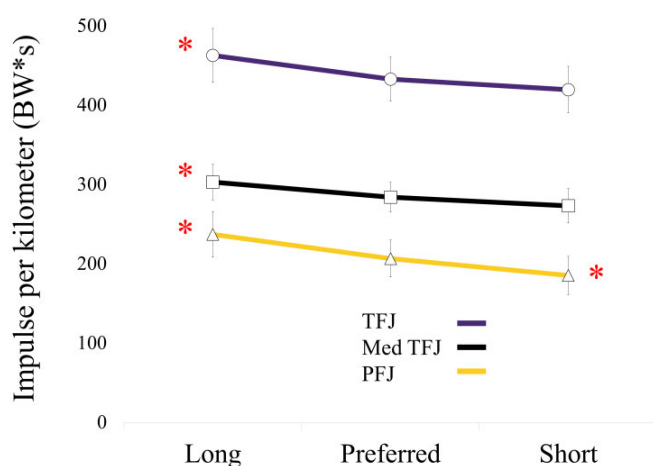


Figure 1: Total tibiofemoral joint (TFJ), patellofemoral joint (PFJ), and medial compartment tibiofemoral joint (Med TFJ) impulse per kilometer. Error bars represent the 95% confidence interval. BW=body weights

* $p<.05$ compared to preferred step length

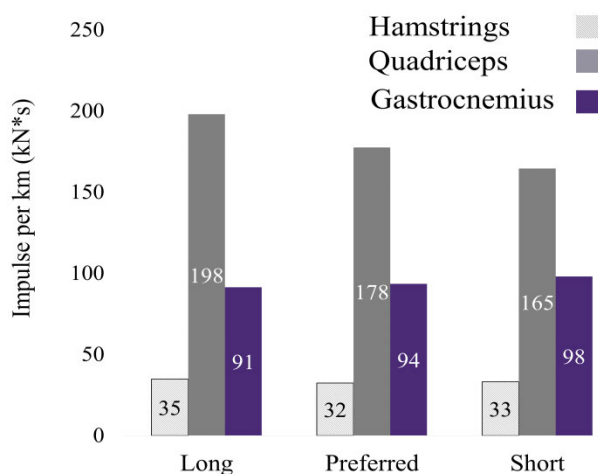


Figure 2: Total hamstrings, quadriceps, and gastrocnemius muscle impulse per km during step length conditions.

DISCUSSION

The purpose of this study was to examine simultaneous effects of step length changes on PFJ and TFJ kinetics during running. We observed a significant increase in both PFJ and TFJ impulse per step and per km with an increase in step length. Increasing step length resulted in 30 additional body weights per km in the TFJ and 31 additional body weights per km in the PFJ. Interventions to decrease step length among runners who demonstrate a particularly long step length may facilitate some knee joint injury prevention and treatment efforts.

Decreasing step length from the preferred condition reduced PFJ and TFJ impulse per step and PFJ impulse per km. However, TFJ impulse per km was not reduced with a shortened step length. This was due to increased gastrocnemius impulse per km. Gastrocnemius force increases TFJ impulse but has little effect at the PFJ due to a relatively small moment arm to the knee joint. PFJ impulse is a function of quadriceps impulse, which was reduced per km while running with a shorter stride. Running with a foot strike closer to the center of mass tends to decrease the braking ground reaction force and negative work of the quadriceps [7].

CONCLUSIONS

We observed increased PFJ and TFJ impulse per km with increased step length. A shorter step length reduced PFJ impulse per km. For people who chose running as a mode of exercise, modifications to reduce step length may be beneficial, particularly among individuals at increased risk for knee joint injuries exacerbated by or associated with repetitive cyclical loading. Future studies will investigate cumulative PFJ and TFJ loads while running with varied step lengths among runners at risk for premature PFJ and TFJ osteoarthritis such as individuals with a history of ACL reconstruction.

REFERENCES

1. Horisberger et al. *Clin Biomech* **28**, 536-43, 2013
2. Lohmander et al. *Arthritis Rheum* **50**, 3145-52 2004
3. Willson et al. *Clin Biomech* **29**, 243-247, 2014
4. DeVita et al. *J Appl Biomech* **17**, 297-311, 2001
5. Giffin et al. *Am J Sports Med* **32**, 376-82, 2004
6. Draganich et al. *J Orthop Res* **5**, 539-47, 1987
7. Heiderscheit et al. *Med Sci Sports Exerc* **43**, 296-302 2011

TIBIAL CHARACTERISTICS OF HABITUAL MID/FOREFOOT AND REARFOOT STRIKERS

¹ Elizabeth R. Boyer, ¹ Alyssa Gantz, and ¹ Tim R. Derrick

¹ Iowa State University, Ames, IA, USA

email: ehageman@iastate.edu, web: <http://www.kin.hs.iastate.edu/>

INTRODUCTION

The purpose of this study was to quantify differences in the distal tibia bone geometry and properties between habitual rearfoot strikers (hRF) and habitual midfoot/forefoot strikers (hFF).

METHODS

Male and female runners who consistently ran 10+ mi/wk were recruited, age 18-35. All were free of injury in the prior 3 months, had not switched foot strike styles within the past 2 years, were not previous or current tobacco users, and did not have a history of amenorrhea.

A 2-mm thickness CT scan (Toshiba Prime 40) was obtained for each participant's right leg 1/3 of the way from the ankle to the knee using the following settings (120 kV, 50 mAs 100 mA with 0.5 sec/rotation). Based on the relationship between the Hounsfield scale and apparent bone density, the elastic modulus of all elements were determined from the CT image. Dependent variables included: cross-sectional area (CSA), inner diameter for the AP (AP_i) and ML (ML_i) directions (see Fig 1), outer diameter for the AP (AP_o) and ML (ML_o) directions, peak elastic modulus (E), average E across the entire cross section, area moment of inertia about the AP (I_{AP}) and ML (I_{ML}) axes, and section modulus (Z). Z was calculated for both AP (Z_{AP}) and ML (Z_{ML}) axes as moment of inertia divided by its respective width.

Data were analyzed with a MANOVA. Significance was assessed at $\alpha < 0.05$. Because of the small sample size, we also calculated effect sizes.

RESULTS AND DISCUSSION

Subject characteristics are shown in Table 1 for 5 hRF and 7 hFF who have completed their CT scans. Bone data are shown in Table 2.

The two groups did not differ based on age, height, mass, BMI, or running mileage (all $p \geq 0.49$).

None of the univariate analyses were significantly different between groups because of the small sample size (all $p \geq 0.563$). However, based on the effect sizes, there was a medium to large E.S. for both AP and ML inner diameters being smaller in hFF. If outer diameter is held constant, a smaller inner diameter would increase I, so this is beneficial for hFF. There was a small/medium E.S. for peak E being larger in hFF, indicating they have stiffer bones in at least one area of their tibia, but this trend was not observed for average E. There were several small effect sizes for I and Z about both axes, being slightly larger for hRF. Since bending predominates the loading in the tibia during running (Meardon & Derrick, 2014), hRF may have slightly more resistance to these stresses. Perhaps the larger ground reaction force loading rates associated with rearfoot striking partially explain the larger I and Z, since we found bone stresses are actually higher in shod mid/forefoot striking than rearfoot striking (data presented in another abstract).

CONCLUSIONS

Since the majority of bone properties were similar or only marginally different between groups (excluding inner diameters), the loading differences hRF and hFF experience solely due to how they run does not seem to distinguish their bone geometry and properties from one another. Other variables, such as gender, mass, other physical activity that participants currently or previously engage in, diet, or genetics may play a larger role in the large variability seen within and between groups. Perhaps

if we included only runners who ran 40+ miles/wk and running was their predominant form of exercise, more distinct bone differences would have been observed.

REFERENCES

1. Meardon SA & Derrick TR. *J Biomech* **47**, 2738-44, 2014.

ACKNOWLEDGEMENTS

Thank you to ASB for the Grant-In-Aid 2014 Award to fund this research.

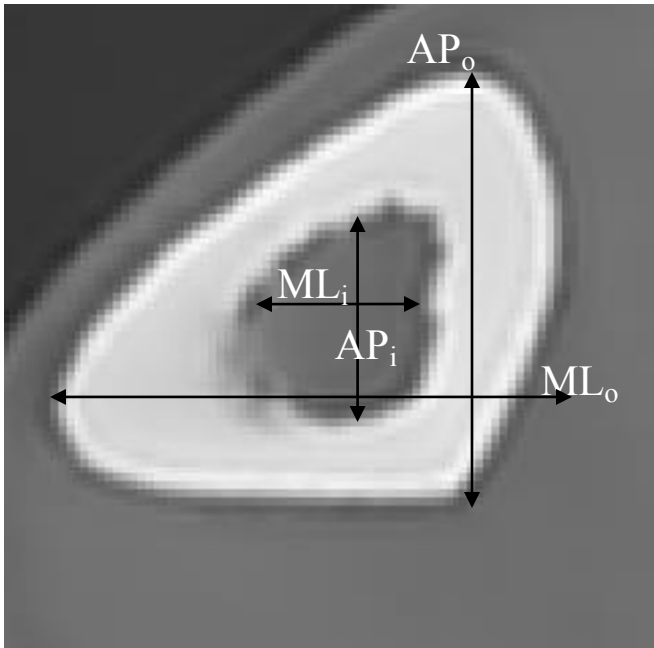


Figure 1: Example tibia cross-section with AP and ML inner (i) and outer (o) diameter definitions.

Table 1. Subject characteristics for habitual rearfoot strikers (hRF) and habitual mid/forefoot strikers (hFF). Mean \pm SD for the men (M) and women (W).

	hRF			hFF		
	3 M	2 W	Mean	4 M	3 W	Mean
Age (yr)	26 \pm 6	21 \pm 3	24 \pm 5	26 \pm 26	25 \pm 7	26 \pm 6
Height (m)	1.85 \pm 0.04	1.60 \pm 0.04	1.75 \pm 0.14	1.77 \pm 0.08	1.66 \pm 0.06	1.73 \pm 0.09
Mass (kg)	73.0 \pm 0.8	50.1 \pm 6.1	63.9 \pm 12.9	66.1 \pm 14.1	61.5 \pm 10.8	64.2 \pm 12.0
BMI	21.3 \pm 1.2	19.5 \pm 1.5	20.6 \pm 1.5	21.0 \pm 2.9	22.2 \pm 2.3	21.5 \pm 2.5
Running Mileage (mi/wk)	34 \pm 39	21 \pm 16	29 \pm 20	48 \pm 46	30 \pm 18	40 \pm 36

Table 2: Bone properties for habitual rearfoot strikers (hRF) and habitual mid/forefoot strikers (hFF). Mean \pm SD for the men (M) and women (W). The effect size (E.S.) compares group means, averaged across sex.

	hRF			hFF			Between group E.S.
	3 M	2 W	Mean	4 M	3 W	Mean	
CSA (mm ²)	379 \pm 44	237 \pm 58	322 \pm 89	328 \pm 48	304 \pm 48	318 \pm 46	0.06
AP _o (mm)	24.2 \pm 0.4	20.8 \pm 0.5	22.9 \pm 1.9	23.3 \pm 2.1	21.9 \pm 0.7	22.7 \pm 1.7	0.11
ML _o (mm)	26.9 \pm 0.8	22.4 \pm 3.0	25.1 \pm 2.9	25.7 \pm 1.6	24.8 \pm 3.5	25.3 \pm 2.4	0.08
AP _i (mm)	12.1 \pm 1.6	11.4 \pm 2.1	11.8 \pm 1.6	11.0 \pm 0.7	10.9 \pm 0.6	11.0 \pm 0.6	0.66
ML _i (mm)	11.3 \pm 0.5	10.4 \pm 2.5	11.0 \pm 1.4	9.9 \pm 0.9	9.9 \pm 1.0	9.9 \pm 0.9	0.90
Peak E (GPa)	26.8 \pm 2.8	30.2 \pm 0.5	28.1 \pm 2.7	29.0 \pm 0.3	28.5 \pm 1.2	28.8 \pm 0.8	0.35
Average E (GPa)	19.6 \pm 1.0	21.4 \pm 0.3	20.3 \pm 1.2	20.4 \pm 1.1	20.7 \pm 0.4	20.6 \pm 7.7	0.05
I _{AP} (mm ⁴) $\times 10^3$	21.6 \pm 2.6	10.1 \pm 4.0	17.0 \pm 6.8	16.3 \pm 3.8	14.7 \pm 5.8	15.6 \pm 4.3	0.25
I _{ML} (mm ⁴) $\times 10^3$	17.0 \pm 2.0	7.7 \pm 0.7	13.2 \pm 5.3	13.0 \pm 3.7	11.0 \pm 2.0	12.2 \pm 3.0	0.23
Z _{AP} (mm ³)	883 \pm 114	482 \pm 182	723 \pm 251	694 \pm 126	669 \pm 257	684 \pm 174	0.18
Z _{ML} (mm ³)	623 \pm 60	343 \pm 13	511 \pm 159	501 \pm 121	446 \pm 45	478 \pm 94	0.25

IDENTIFICATION OF COMPENSATORY MOVEMENT PATTERNS IN PATIENTS WITH AMPUTATION USING SEPARATION OF ANGULAR MOMENTUM

¹ Brecca M. Gaffney, ² Cory L. Christiansen, ¹ Bradley S. Davidson

¹ University of Denver, Denver, CO, USA

² University of Colorado Denver, Aurora, CO, USA
email: brecca.gaffney@gmail.com

INTRODUCTION

Rehabilitation practice following amputation uses gait training to improve ambulation and reduce adverse effects of overloading the musculoskeletal system [1]. These patients exhibit compensatory movement patterns, which are difficult to treat, and are prone to misidentification through observation. Quantitative biomechanics provides a combination of variables that identify movement compensations (e.g. kinematics, inverse dynamics) [2], which lacks the standardization needed for clinical translation.

Assessing individual angular momentum components of each segment within the context of total angular momentum is a potential method for describing clinical movement compensations. The principal of angular momentum separation indicates two components of total momentum [3]:

1. Transfer Momentum: angular momentum of the segment with respect to the point of reference.
2. Rotational Momentum: angular momentum of the segment with respect to its center of mass (COM).

Referencing transfer momentum to the foot mimics inverted pendulum dynamics, which accurately represent the stance period during gait [4]. Within this framework, these components indicate the ability to achieve forward progression and coordination of segmental rotations.

The objective of this investigation was to assess compensatory movements in patients with amputation using angular momentum separation. We hypothesized that patients with amputation would have similar performance (transfer momentum), but with different segmental strategies (rotational momentum) in all three planes compared to controls.

METHODS

Seven male participants with dysvascular transtibial amputation (age: 54.5±3.8 years, BMI: 27.9±1.0 kg/m²) and seven healthy male control participants (age: 63.7±6.7 years, BMI: 26.1±2.6 kg/m²) performed three gait trials at 1.0 m/s. Motions were recorded from 64 skin markers (100 Hz) and used to create a 15-segment model (Figure 1). Inertial properties of the amputated limb were modified [5].

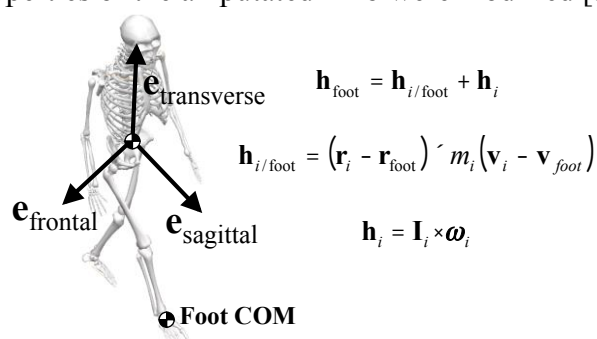


Figure 1. Total angular momentum (\mathbf{h}_{foot}), transfer momentum ($\mathbf{h}_{i/\text{foot}}$), and rotational momentum (\mathbf{h}_i) with respect to the amputated foot COM (right foot for controls) was calculated for each segment (i). All vectors are expressed in path coordinates ($\mathbf{e}_{\text{frontal}}$, $\mathbf{e}_{\text{sagittal}}$, and $\mathbf{e}_{\text{transverse}}$) defined by the velocity vector of the body COM.

Segment momenta were scaled by participant mass, body height, and walking speed for visualization. Peak (minimum and maximum) transfer momentum during stance period and rotational momentum during entire gait cycle were compared between groups using an ANCOVA (covariates: mass and height) and level of significance set as $\alpha=0.05$.

RESULTS AND DISCUSSION

The transfer momentum had similar waveforms across segments and progressively larger magnitudes associated with superior segments

(Figure 1), which corresponds well with the inverted pendulum model of forward progression during gait. Sagittal plane transfer momentum was not different, which corresponds to the similar rate of forward progression (functional performance) between groups (Figure 1a). In the frontal and transverse planes, maximum peak momentum of the pelvis was smaller in patients with amputation compared to controls ($P=0.02$, $P=0.01$, respectively) (Figure 2b), and occurred during weight acceptance (0-12% of gait cycle). Smaller momentum during weight acceptance may be a protective strategy adopted at the hip to increase stabilization by reducing segmental speed with respect to the involved limb.

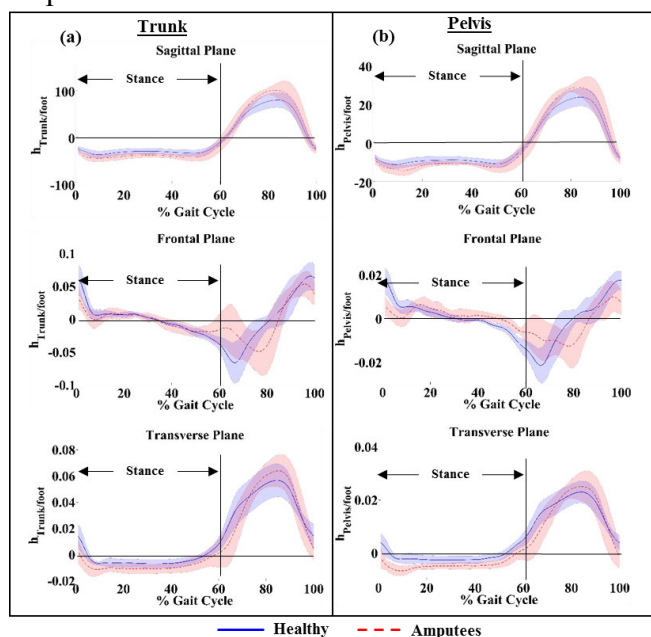


Figure 2. Transfer component of angular momentum of the (a) trunk and (b) pelvis in the sagittal, frontal, and transverse planes (analyzed for *stance* period only).

The rotational momentum waveforms were dissimilar across segments (Figure 3). In the sagittal plane, peak momentum of the pelvis was larger in patients with amputation in comparison to controls ($P=0.01$), and occurred during weight acceptance and contralateral heel strike (Figure 3b). Higher momentum of the trunk during weight acceptance is consistent with Trendelenburg gait and increased momentum at contralateral limb heel strike may be a result of impactful loading (exaggerated braking) caused by the lack of the ankle plantarflexor muscle function on the amputated limb. In the transverse

plane, peak momentum of the trunk was larger in patients with amputation in comparison to controls ($P=0.02$) (Figure 3a), which is likely a result of decreased rotational stabilization at the hip and pelvis.

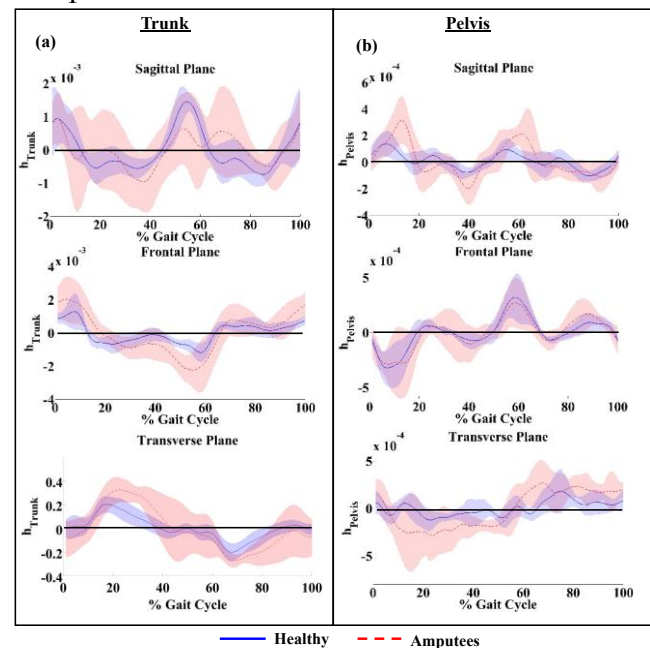


Figure 3. Rotational component of angular momentum of the (a) trunk and (b) pelvis in the sagittal, frontal, and transverse planes.

CONCLUSION

This investigation demonstrates the segmental contributions of transfer and rotational components of total angular momentum taken with respect to the stance foot in patients with amputation and healthy controls during gait. These results indicate that the loss of the ankle plantarflexor muscle function resulted in altered trunk and pelvis momentum in all three planes. Compensatory movement patterns observed at the pelvis and the trunk likely indicate coordination between the hips and low back during gait, which is consistent with previous findings [6]. The compensatory strategies used by patients with amputation may have long-term adverse effects caused by asymmetric and abrupt loading patterns.

REFERENCES

1. Franchignolo F. *Arch Phys Med Rehabil*, **85**, 743-748, 2004.
2. Norvell D. *Arch Phys Med Rehabil*, **86**, 487-493, 2005.
3. Hay J. *J Biomech*, **10**, 269-277, 1977.
4. Hof A. *J Biomech*, **40**, 451-457, 2007.
5. Silverman A. *J Biomech*, **44**, 379-385, 2011.
6. Sagawa Y. *Gait Posture*, **33**, 511-526, 2011.

A SIMULATED INVERTED PENDULUM APPLIED TO HEMIPLEGIC CEREBRAL PALSY GAIT

^{1,2} Frank L. Buczek Jr., ² Kevin M. Cooney, ³ Michael J. Rainbow, ⁴ James O. Sanders

¹ Lake Erie College of Osteopathic Medicine (LECOM), Erie, PA, USA

² Shriners Hospitals for Children, Erie, PA, USA, ³ Queen's University, Kingston, Ontario, Canada

⁴ University of Rochester Medical Center, Rochester, NY, USA

E-mail: fbuczek@lecom.edu

INTRODUCTION

Children with hemiplegic cerebral palsy exhibit diminished motor control, range-of-motion, and strength, not only of the affected lower extremity, but also of the ipsilateral upper body (Winters Type I, II, III, and IV). An inverted pendulum (IP) model of gait can be used to understand the role of gravity in propulsion [1,2], within a framework of biomechanical studies, including joint power patterns [3]. Forward dynamic simulations of an IP [4], applied to normal gait during single support, previously demonstrated predictive value for gait velocities and horizontal ground reaction forces (GRF), but not for vertical GRF. McGrath et al. [5] suggested that a simplified head-arms-trunk (HAT) segment may be stabilized by hip musculature near mid-stance in healthy subjects, but this may not fully represent normal or pathological gait. We hypothesized that our previous findings would extend to patients with hemiplegic cerebral palsy.

METHODS

After informed consent approved by the human subjects committee, seven pediatric patients with hemiplegic cerebral palsy (mean age, height, mass: 11.6 yr, 1.4 m, 36.1 kg), were enrolled in the study. They presented as Winters Type I, II, and IV (n = 3, 1, 3, respectively). Kinematic data were collected at 120 Hz (Vicon 612 system). A thirteen-segment, full-body model was implemented in Visual3D, and the instantaneous center-of-mass (COM) was calculated. Horizontal and vertical GRF (F_h , F_v) were collected at 1560 Hz using three AMTI force plates. Subtracting average center-of-pressure (COP) coordinates from those of the instantaneous COM at mid-stance provided the length of a rigid IP for the

affected side, used in forward dynamic simulations [4]. Bonferroni-adjusted dependent t-tests assessed differences across key points in forward velocity (V_{min} , V_{final}), timing (tV_{min} , tV_{final}), and force profiles (F_{h-min} , F_{h-max} , F_{v-max1} , F_{v-min} , F_{v-max2}) [4].

RESULTS AND DISCUSSION

The rigid IP accurately simulated all key points, apart from F_{v-max1} ($P \leq 0.002476$), which coincided with a mean sagittal hip power burst (Fig 1, Col A). Patient 03 (Type II) exhibits nearly zero hip power, with conflicting knee and ankle power patterns (Fig 1, Col B). Patient 07 (Type IV) exhibits an early onset forward F_h (Fig 1, Col C), with a slightly decreased F_v , a large hip extensor power generation burst, and nearly zero knee and ankle power; these are similar to five other patients.

CONCLUSIONS

We conclude that a rigid IP suggests these patients relied, in part, on gravity for propulsion during single support. A companion study suggests a tele-scoping IP may also reveal the use of joint powers.

REFERENCES

1. Mochon S, McMahon TA. *J Biomechanics*, **13**, 49-57, 1980.
2. McGeer T. *Intl J Robotics Research*, **9**, 62-82, 1990.
3. Ounpuu S, et al. *J Pediatr Orthop*, **11**(3), 341-349, 1991.
4. Buczek FL, et al. *Clin Biomech*, **21**, 288-296, 2006.
5. McGrath M, et al. *Gait & Posture*, Epub, 2014.

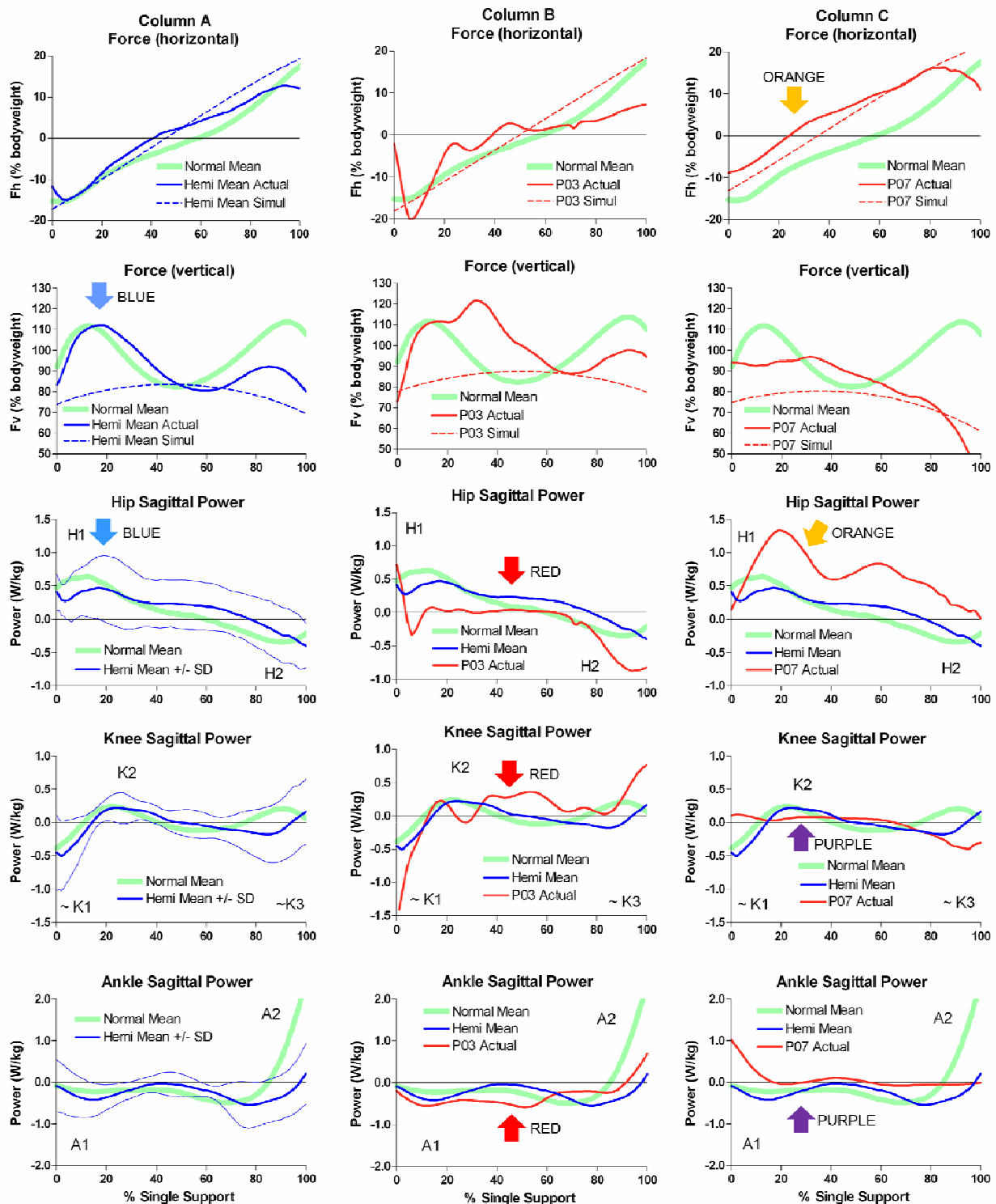


Figure 1. Hemiplegic GRF and Power Patterns. Column A: Mean GRF and joint power patterns for normal children (n=25) and hemiplegic cerebral palsy patients (n=7); **blue arrows** indicate hip extensor power generation coincident with the significant difference between actual and simulated $Fv-max1$. Column B: Patient 03 demonstrates nearly zero hip extensor power generation, with knee extensor power generation in opposition with ankle plantarflexor power absorption (**red arrows**). Column C: Patient 07 demonstrates an early onset forward Fh coincident with a large hip extensor power generation burst (**orange arrows**), with nearly zero joint power at the knee and ankle (**purple arrows**). NOTE: Power bursts H1, H2, K1, K2, K3, A1, and A2 are after Winter DA (Biomechanics and Motor Control of Human Gait, 2nd Ed, 1991).

A TELESCOPING INVERTED PENDULUM APPLIED TO HEMIPLEGIC CEREBRAL PALSY GAIT

^{1,2} Frank L. Buczek Jr., ² Kevin M. Cooney, ³ Michael J. Rainbow, ⁴ James O. Sanders

¹ Lake Erie College of Osteopathic Medicine (LECOM), Erie, PA, USA

² Shriners Hospitals for Children, Erie, PA, USA, ³ Queen's University, Kingston, Ontario, Canada

⁴ University of Rochester Medical Center, Rochester, NY, USA

E-mail: fbuczek@lecom.edu

INTRODUCTION

Children with hemiplegic cerebral palsy exhibit diminished motor control, range-of-motion, and strength, not only of the affected lower extremity, but also of the ipsilateral upper body (Winters Type I, II, III, and IV) [1]. Patients in this study exhibited mild to severe hemiplegic gait (Figure 1).

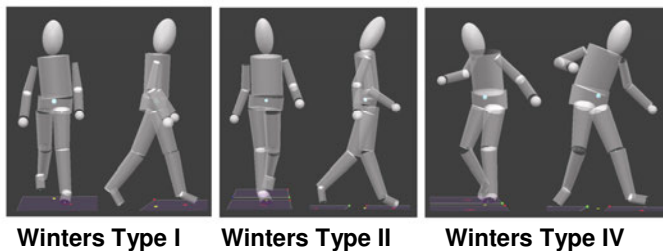


Figure 1. Hemiplegic Types. Winters Type I: left foot drop in swing, mild left internal foot progression angle. Winters Type II: equinus induced right knee recurvatum, with increased hip extension. Winters Type IV: right upper and lower extremity deviations in sagittal, coronal, and transverse planes.

An inverted pendulum (IP) model of human gait can be used to understand the interplay between gravity and joint powers in propulsion. Dynamic walking models have shown that human-like gait can be achieved on downward slopes through gravity alone [2,3]; yet, additional sources of propulsion are needed for level gait [4,5]. Such an analytical finding was supported by inverse dynamics of a telescoping IP directly applied to normal gait [6]. Here, pendulum radial kinematics (telescoping) improved the prediction of both horizontal and vertical ground reaction forces (GRF). Without telescoping, GRF predictions deviated significantly from actual values, during sagittal power bursts at the hip, knee, and ankle joints. We hypothesized that these findings would extend to patients with hemiplegic cerebral palsy, despite a range of mobility disabilities and prior treatment.

METHODS

After informed consent approved by the local human subjects committee, seven pediatric patients (mean age, height, mass: 11.6 yr, 1.4 m, 36.1 kg), diagnosed with hemiplegic cerebral palsy, were enrolled in the study. They presented as Winters Type I, II, and IV ($n = 3, 1, 3$, respectively). Five patients had prior heelcord lengthenings, one had concurrent hip adductor and iliopsoas lengthenings, one had gastrocnemius BOTOX injections, one had no prior treatment. Kinematic data were collected at 120 Hz using a ten camera Vicon 612 system. A thirteen-segment, full-body model was implemented in Visual3D (C-Motion Inc.), and the instantaneous full-body center-of-mass (COM) was calculated. Horizontal and vertical GRF (F_h , F_v) were collected at 1560 Hz using three AMTI force plates. Subtracting average center-of-pressure (COP) coordinates from those of the instantaneous COM provided an IP with optional telescoping action [6]. Affected-side inverse dynamics in Visual3D provided lower extremity joint powers. Five repeated measures ANOVAs with Tukey HSD *post hoc* tests detected differences ($P \leq 0.05$) among actual and predicted minima and maxima in F_h and F_v , with and without telescoping. Root mean square (RMS) errors quantified differences between actual and predicted F_h and F_v .

RESULTS AND DISCUSSION

Telescoping across all patients (mean 2.1 cm) improved the fidelity of F_h and F_v in single support, compared to non-telescoping (Table 1; Figure 2 a, b with RMS values). Mean joint power curves (Figure 2 c) demonstrated an increased and extended hip power generation burst, coincident

with knee power absorption and generation, and ankle power absorption. Movement strategies varied across patients, as in these examples: Patient 03 (Winters Type II) presented with hip, knee, and ankle power absorption during early single support, coincident with a 2.9 cm compression of the telescoping IP. Patient 07 (Winters Type IV) presented with a large hip power generation burst throughout single support, coincident with the onset of a 3.9 cm extension of the telescoping IP and simultaneous forward F_h . Without telescoping, F_h and F_v deviated substantially from actual values for both of these patients.

CONCLUSIONS

Despite their varied mobility disabilities, a telescoping IP improved the fidelity of F_h and F_v during single support, as compared to the non-telescoping action. The mean magnitude for telescoping was 2.1 cm across all patients, with examples of compression (Patient 03, Winters Type II, 2.9 cm) and extension (Patient 07, Winters Type

IV, 3.9 cm) highlighting the effects of Winters Type in hemiplegic cerebral palsy gait. As found previously in normal and diplegic cerebral palsy gait [5,6,7], a telescoping IP reveals, at least in part, the use of joint powers in propulsion.

REFERENCES

1. Winters TF, et al. *J Bone Joint Surg Am* **69**, 437-441, 1987.
2. Mochon S, McMahon TA. *J Biomechanics* **13**, 49-57, 1980.
3. McGeer T. *Intl J Robotics Research* **9**, 62-82, 1990.
4. Winter DA. *Physiotherapy Canada* **37**(4), 245-252, 1985.
5. Ounpuu S, et al. *J Pediatr Orthop* **11**(3), 341-349, 1991.
6. Buczek FL, et al. *Clin Biomech* **21**, 288-296, 2006.
7. Buczek FL, et al. *American Society of Biomechanics*, Aug 26-29, 2009.

Table 1. Repeated measures ANOVAs, with Tukey Honest Significant Difference (HSD) post hoc tests.

Variable	ACT		TEL1		TELO		ACT-TEL1	P values	
								ACT-TELO	TEL1-TELO
<i>Fh-min</i>	-16.1	(6.1)	-7.1	(3.8)	3.8	(5.6)	0.009068*	0.000195*	0.002520*
<i>Fh-max</i>	14.1	(3.8)	11.0	(3.5)	2.1	(4.9)	0.126156	0.000193*	0.000311*
<i>Fv-max1</i>	114.5	(16.4)	109.4	(10.8)	80.7	(5.3)	0.602355	0.000254*	0.000494*
<i>Fv-min</i>	65.6	(17.8)	83.7	(21.3)	83.7	(4.4)	0.160792	0.161860	0.999991
<i>Fv-max2</i>	97.2	(10.4)	93.2	(11.2)	80.7	(5.3)	0.560949	0.002796*	0.017227*

For each kinetic variable (% bodyweight), maxima and minima in actual data were compared with inverse dynamics data predicted after Buczek et al. [6] at the same relative time (i.e., percent of single support). ACT = actual data, TEL1 = inverse dynamics with telescoping, TELO = inverse dynamics without telescoping. Data are means and (standard deviations) with $n = 7$. (*) indicates significant at $P \leq 0.05$.

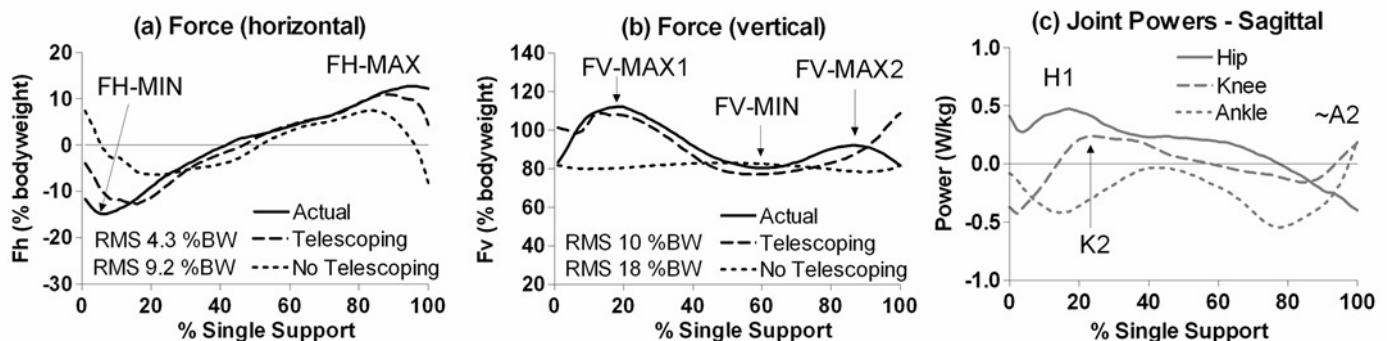


Figure 2. Illustrated Statistical Results for GRF and Joint Powers. For all panels, one walking trial for each of seven hemiplegic cerebral palsy patients were averaged across single support. Panels (a) and (b) include actual (solid), predicted with telescoping (dashed, average length change 2.1 cm), and predicted without telescoping (stippled) horizontal and vertical ground reaction forces; RMS errors are % bodyweight. Panel (c) includes mean sagittal joint powers at the hip, knee, and ankle. Power bursts H1, K2, A2 are after Winter DA (Biomechanics and Motor Control of Human Gait, 2nd Ed., 1991).

THE EFFECT OF HIP ABDUCTOR FATIGUE ON FRONTAL PLANE KINEMATICS DURING WALKING AND RUNNING

¹ Steven E Capehart, ²Michael Baggaley and ¹Michael B Pohl

¹ University of Kentucky, Lexington, KY, USA. ² East Carolina University, Greenville, NC, USA
email: steven.capehart@uky.edu, michael.pohl@uky.edu, baggaleym14@ecu.edu

INTRODUCTION

Female runners are reported to be twice as likely to sustain lower extremity overuse injuries compared to their male counterparts. Moreover, females with certain overuse injuries demonstrate excessive hip frontal plane motion during the stance phase of running (1). Reduced hip abduction strength has also been observed in the aforementioned population, and it has been suggested that excessive hip motion may be the result. However, the potential relationship between strength and kinematics examined during walking remains unclear. For example, patients with knee osteoarthritis have been reported to display weaker hip abduction strength but similar frontal plane hip and pelvis kinematics when compared to controls (2). Thus, it may be possible that the muscular demand of the task may influence the relationship between strength and kinematics. The greater vertical ground reaction forces (GRF) during running should place a higher demand on the hip musculature to stabilize the hip/pelvis during motion. During walking, however, the GRF may not be great enough to exceed the force generating capacity of the musculature even in the presence of reduced strength. Therefore, the purpose of this study was to determine the effects of reduced hip abductor strength on the frontal plane kinematics of the hip and pelvis during walking and running. A fatigue protocol was used to simulate a reduction in hip abduction strength. It was hypothesized that following the hip abductor fatigue protocol, hip adduction and pelvic drop would increase in the running condition but not during walking.

METHODS

Participants included 29 healthy female runners (age: 28 ± 6 yrs; height: 1.66 ± 0.06 m; mass:

61.35 ± 11.35 kg). Lower extremity kinematic data were collected while participants walked (1.1 m/s) and ran (2.7 m/s) on a treadmill before (prefatigue) and after (postfatigue) a hip abductor fatigue protocol. Retroreflective markers were placed bilaterally on bony landmarks of the pelvis and lower extremity and 3D co-ordinate data were collected at 200 Hz (Motion Analysis Corp, Santa Rosa, CA). Joint/segment angles were calculated in Visual 3D (C-Motion Inc, Germantown, MD). Isometric hip abductor strength measurements were conducted with the participants in a side-lying position using a dynamometer (Biodex III, Shirley, NY). Strength measurements were recorded prefatigue and postfatigue. The fatigue protocol was conducted with the participants in a side-lying position performing lateral leg raises to a target bar set at 20° of hip abduction. Each participant was instructed to raise, hold, and lower the leg at a pace of 40 beats per minute (1 beat for each phase) until failure of the set (unable to reach the bar on 2 consecutive occasions). Participants performed 3 sets with a 30 second rest period in between sets, after which isometric strength was assessed. Fatigue was defined as a minimum 20% reduction in hip abduction torque. Variables of interest included peak hip adduction and pelvic drop during stance. A two-way repeated measures ANOVA was conducted comparing peak angles in both prefatigue and postfatigue (fatigue) conditions during walking and running (task). The primary hypothesis was assessed by analyzing the interaction effect (task*fatigue).

RESULTS

Peak isometric hip-abduction strength (52.1 ± 12.1 Nm/kg) was reduced 33% (35.8 ± 11.1 Nm/kg) at the end of the fatigue protocol. Peak hip adduction angle yielded significant main effects for both task

effect ($p < .05$) and fatigue effect ($p < .05$). However, a significant interaction was not found between task and fatigue. Peak contralateral pelvic drop angle yielded no significant effects. The descriptive data are reported in Table 1. Average time to fatigue was 435.8 (164.7) seconds.

Table 1: Mean (SD) kinematic values before and after fatigue during walking and running.

	Prefatigue	Postfatigue
Pelvic Drop (°)		
Walking	5.7 (1.7)	5.6 (1.8)
Running	5.8 (2.7)	5.8 (2.5)
Hip Adduction (°)		
Walking	11.1 (3.0)	9.6 (3.0)
Running	17.9 (4.4)	15.4 (4.1)

DISCUSSION

In contrast to the hypothesis, this study found no significant interaction effect (task*fatigue) for either hip adduction or pelvic drop. We had expected to see an increase in hip adduction following fatigue during running but not during walking. However, the analysis of the main effects revealed that hip kinematics were altered following fatigue in both the walking and running tasks. Surprisingly, fatigue resulted in a reduction in hip adduction during both tasks. It is difficult to offer an explanation for this finding. However, Dierks et al. (3) postulated that ipsilateral pelvic tilt or ipsilateral trunk lean could be used as strategies to control hip adduction in the presence of hip abductor muscle fatigue. Indeed, Smith et al. (4) reported that when comparing groups with either weak or strong hip abductors during a hopping task, the weak group displayed significantly greater ipsilateral trunk lean and ipsilateral pelvic tilt. Our findings show that ipsilateral pelvic tilt was not used as a compensatory strategy in the present investigation. However, ipsilateral trunk lean was not measured in this study and may have been adopted as a compensatory strategy to offload the hip abductor musculature.

Although differences were noted in peak hip adduction following fatigue, subjects may also have landed with less adduction. Evidence for this can be seen in figure 1 in which the angle-time plot is provided for the entire stance. This suggests that the participants may have attempted to land with the hip in a less adducted position to reduce the load placed on the hip abductor muscles after impact. Further analysis of the gait cycle prior to initial contact may lend insight into anticipatory strategies.

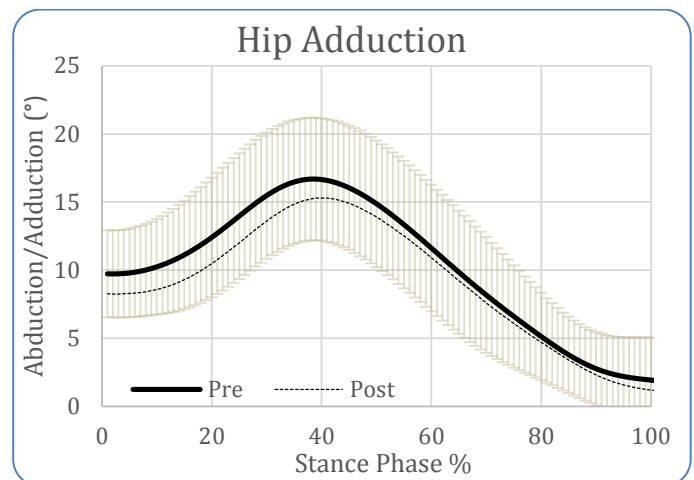


Figure 1: Hip adduction ensemble curve during running

CONCLUSIONS

A reduction in hip abductor muscle strength following a fatigue protocol resulted in no changes in pelvic drop. However, hip adduction during both walking and running was reduced following the fatigue protocol.

REFERENCES

1. Ferber, R, et al. (2003). Clin Biomech, 18(4), 350-357.
2. Pohl, MB et al. (2013). Gait Posture, 37(3), 440-444.
3. Dierks, TA et al. (2008). JOSPT, 38(8), 448-456.
4. Smith, JA, et al. (2014). JOSPT, 44(7), 525-531.

ACKNOWLEDGEMENTS:

We would like to thank Jeff Mettler and Jill Estes for their assistance with data collection.

DOES THE ADDITION OF PERTURBATION TRAINING IMPROVE GAIT ASYMMETRIES IN ATHLETES AFTER ACLR WITH DIFFERENT MECHANISMS OF INJURY?

Jacob J. Capin, Mathew Failla, Elizabeth Wellsandt, Lynn Snyder-Mackler
University of Delaware, Newark, DE, USA
email: capin@udel.edu

INTRODUCTION

Upwards of 250,000 anterior cruciate ligament (ACL) injuries occur annually in the United States [1], with the majority of these injuries occurring through a noncontact mechanism of injury (MOI) [2]. Although many athletes undergo ACL reconstruction (ACLR) to restore normal function and biomechanics, gait asymmetries commonly persist. Even among those who achieve symmetrical strength, gait asymmetries may persist up to 2 years after ACLR [3], which may predispose athletes to an increased risk of ACL re-injury [4]. Despite persisting asymmetries, most physicians utilize temporal guidelines for return to sport decisions rather than objective, functional criteria [5]. Moreover, faulty mechanics are associated with a noncontact MOI; thus athletes who sustain noncontact ACL injuries may demonstrate greater asymmetries as compared to those with contact injuries, and potentially be at even greater risk for re-injury or the development of negative sequelae such as post-traumatic osteoarthritis. It is unclear, however, if athletes after ACLR with different initial mechanisms of injury will benefit from different post-operative training programs.

The purpose of this study is to compare the effects of a type of specialized neuromuscular training rehabilitation program, perturbation training, on gait biomechanics of athletes after ACLR who sustained either a contact or noncontact MOI. We hypothesize that athletes with noncontact injuries who receive perturbation training will demonstrate the greatest improvements in correcting gait asymmetries from pre- to post-training.

METHODS

This study is a secondary analysis of prospectively collected data. Forty-seven level I and II athletes [6]

(78.7% male, 22.9 ± 8.40 years) with a unilateral ACLR (22.3 ± 7.69 weeks) were included in this study. Patients were randomly assigned to a strengthening control group or strengthening plus perturbation training group (PERT), and classified as having a contact (N=19) or noncontact (N=28) MOI via self-report data verified by a licensed physical therapist.

Gait kinematic and kinetic data were collected at baseline (time 1) and after training (time 2) using an embedded force plate and 8-camera Vicon 3-D motion capture system with retro-reflective markers to track the pelvis and lower extremities. Gait variables were analyzed at peak knee flexion (PKF) during stance phase, including: hip flexion angle (HFA) and moment (HFM), hip adduction angle (HAA) and moment (HAM), knee flexion angle (KFA) and moment (KFM), and knee adduction angle (KAA) and moment (KAM). A 2x2x2 ANOVA was used to compare each gait variable with respect to time, MOI, and group. Alpha level was set to ≤ 0.05 .

RESULTS AND DISCUSSION

Significant interactions or main effects (see table 1) were not found for any of the 8 gait variables analyzed at PKF. Our hypothesis that the non-contact group receiving perturbation training would show the greatest improvement in gait asymmetries was not supported. The findings suggest that there is no difference in biomechanical benefits to post-operative perturbation training between treatment groups with respect to MOI and time.

Baseline differences between the strength and PERT groups within the noncontact cohort exceeded MCID values [7] for KFA and KFM and approached MCID values [7] for HFA and HFM. These findings indicate that within the noncontact

cohort, the strength group may have been initially more asymmetric and thus had greater room for improvement, which could have influenced our lack of significant findings. Rigorous inclusion criteria, pre-enrollment physical therapy, similarity between training programs (i.e. all subjects received strengthening, agilities, hops, and jumps), and small sample sizes of these preliminary data may also contribute to our non-significant findings. Finally, it is possible that gait may be too simple an activity in these higher-level athletes to detect asymmetries that may exist during more demanding, sport-like activities and may have improved with a post-operative perturbation training program.

Inter-limb asymmetries did exist among frontal and sagittal plane hip and knee gait biomechanical data regardless of MOI or treatment at both time intervals. KFAs and KFM's at PKF exceeded the MCIDs of 3° and 0.04 N*m/Kg*m [7], respectively, across all 4 groups at time 2. Further research is necessary to identify appropriate training methods to ameliorate inter-limb asymmetries among athletes after ACLR.

CONCLUSIONS

Gait asymmetries exist across various cohorts within the ACLR population during the time-frame at which most athletes begin return to sport activities, but do not differ between patients with noncontact versus contact MOI. Moreover, these

asymmetries still persist in a relatively simple task (i.e. walking) despite neuromuscular training in addition to traditional rehabilitation. Even greater asymmetries likely exist across these groups in higher-level activities. Clearly, there is continued need to study training programs to address these deficits that predispose athletes to increased risk for further knee pathology and osteoarthritis.

REFERENCES

1. Griffin LY, et al. *Am J Sports Med* **34**(9), 1512–1532, 2006.
2. Hughes G, et al. *Sports Med* **36**(5), 411–428, 2006.
3. Roewer BD, et al. *J Biomech* **44**, 1948-1953, 2011.
4. Paterno MV, et al. *Am J Sports Med* **38**(10), 1968-1978, 2010.
5. Myer GD, et al. *Am J Sports Med* **40**(10), 2256–2263, 2012.
6. Hefti F, et al. *Knee Surg, Sports Taumatol, Arthroscopy* **1**, 226-234, 1993.
7. Di Stasi SL, Snyder-Mackler L. *Clinic Biomech* **27**, 360-365, 2012.

ACKNOWLEDGEMENTS

Thanks to Martha Callahan and the UDPT clinic. Funding provided by the National Institute of Health grants R37-HD037985, P30-GM103333, and 5T32HD007490-15.

Table 1: Differences in angles (°) and moments (N*m/Kg*m) between involved and uninvolved limbs at PKF.

	Noncontact (N=28)				Contact (N=19)				
	Strength (N=11)		Perturbation (N=17)		Strength (N=11)		Perturbation (N=8)		
Gait Variable	Time 1	Time 2	Time 1	Time 2	Time 1	Time 2	Time 1	Time 2	p-value
HFA	-4.47 ± 6.63	-2.05 ± 3.71	-1.67 ± 3.42	-1.57 ± 3.43	-0.53 ± 2.84	-0.15 ± 2.75	-1.39 ± 2.75	-2.27 ± 3.71	0.631
HFM	0.037 ± .10	-0.005 ± .09	-0.032 ± .13	-0.053 ± .11	-0.054 ± .09	-0.042 ± .07	0.006 ± .06	0.012 ± .10	0.695
KFA	6.84 ± 7.33	4.37 ± 5.98	2.95 ± 4.64	4.60 ± 4.47	4.09 ± 3.45	3.77 ± 4.13	0.08 ± 4.44	4.25 ± 3.14	0.887
KFM	-0.134 ± .22	-0.157 ± .20	-0.122 ± .14	0.130 ± .13	-0.122 ± .14	0.066 ± .14	-0.026 ± .11	-0.053 ± .08	0.083
HAA	0.80 ± 4.72	1.99 ± 2.82	-0.10 ± 4.12	-0.46 ± 4.33	1.64 ± 3.72	0.78 ± 2.94	2.01 ± 6.26	1.19 ± 3.99	0.416
HAM	0.013 ± .15	0.024 ± .12	0.021 ± .11	-0.012 ± .11	-0.008 ± .11	-0.018 ± .15	-0.104 ± .14	-0.058 ± .10	0.111
KAA	-1.05 ± 5.20	-1.83 ± 3.61	-1.20 ± 3.51	-1.74 ± 3.10	0.51 ± 3.77	-0.16 ± 2.41	-1.10 ± 3.80	-0.28 ± 4.77	0.620
KAM	0.019 ± .08	0.009 ± .10	0.015 ± .08	0.016 ± .10	0.002 ± .08	-0.007 ± .06	0.016 ± .08	0.003 ± .07	0.994

ASSOCIATION OF SPINAL DEFORMITY AND PELVIC TILT WITH GAIT ASYMMETRY IN ADOLESCENT IDIOPATHIC SCOLIOSIS PATIENTS: GROUND REACTION FORCE INVESTIGATION

¹Edward Chu, ²Yang-Sun Park, ³Young-Tae Lim, ¹Kyung Koh, ³Jong-Moon Kim, ¹Hyun-Joon Kwon, ¹Ross H. Miller, and ^{1,4}Jae Kun Shim

¹University Maryland, College Park, USA

²Hanyang University, Seoul, South Korea

³Konkuk University, Chungju, South Korea

⁴Kyung Hee University, Yongin, South Korea

email: edchux@umd.edu, web: <http://www.sph.umd.edu/neuromechanics>

INTRODUCTION

Adolescent idiopathic scoliosis (AIS) is a prevalent orthopedic problem in children between 10 and 16 years of age [1]. If left untreated, scoliosis can lead to asymmetry of the trunk, which may lead to more serious cardiorespiratory and other orthopaedic problems [2]. Gait asymmetry of ground reaction force (GRF) in AIS has been frequently investigated; however, previous studies have reported conflicting results, with some studies reporting a significant relationship between gait asymmetry in GRF and the severity of the spinal deformity, and some studies reporting no significant relationship [3,4].

The goal of this current study is to provide greater insight into gait asymmetry in AIS patients. This study specifically investigated whether the asymmetry of the GRF magnitude and timing in AIS patients would be associated with spinal deformity and pelvic tilt.

Spinal deformity is the primary orthopaedic characteristic in AIS and the degree of asymmetry ostensibly affects the degree of gait asymmetry. GRF reflect the whole-body motion and are sensitive to individual body segment kinematics. Previous studies have shown that pelvic tilt is correlated with leg-length inequality, and leg length inequality can affect GRF phase times [5,6]. We therefore hypothesized that (i) between-leg asymmetry of GRF magnitude variables would increase with spinal deformity, and (ii) asymmetry

of GRF time variables would increase with pelvic tilt (PT).

METHODS

Nine adolescents (3 male and 6 female; ages = 15 ± 1.24 years) with AIS participated and all participants provided written consent. The study was approved by Chungju Konkuk University Hospital.

Frontal plane spinal radiographs were taken. The degree of spinal deformity was quantified using two measures:

- The maximum Cobb angle (MCA; [7]), calculated as the largest angle in the frontal plane among the absolute values of all existing Cobb's angles greater than 10° .
- A new exploratory measure, the adjusted Cobb angle (ACA), calculated as the sum of Cobb's angles in the frontal plane considering the direction of the angle, with the ACA being positive if the angle is going counter-clockwise with respect to the perpendicular line of the vertebrae at the bottom of the curve, and negative when the angle is going clockwise.

PT was also quantified and was calculated as the angle between the line connecting the right and left iliac crest and the horizontal line in the frontal plane.

In the gait data collections, participants were instructed to walk naturally, at a self-selected, comfortable speed along a 20-m walkway. GRF were measured from two force platforms embedded in the middle of the walkway. Starting position was adjusted so that subjects stepped consecutively on the platforms with the right and left feet without deliberately targeting the platforms.

To assess the gait asymmetry between legs, the Asymmetry Index (AI) was calculated using the following formula:

$$AI = \frac{R - L}{0.5 * (R + L)}$$

Where R and L represent the values of a specific GRF component from the right foot and the left foot, respectively [8]. AI was calculated for selected peak and average magnitudes of the vertical and anterior-posterior GRF, as well as the timing of peaks and the braking/propelling phases of stance. Correlations between AIs and the spinal deformity measures were calculated by linear regression ($\alpha = 0.05$).

RESULTS AND DISCUSSION

The average walking speed of the subjects (1.22 ± 0.17 m/s) was similar to previously reported walking speeds for this age group [9].

There were significant correlations between the AI of average vertical GRF over the stance phase (Fz_{AVG}) with MCA and ACA, but not with PT (Table 1). The GRF timing results such as AI of the average stance phase contact time (T_{stance}), indicated that there was an association between the

asymmetry of T_{stance} and PT, while there was no significant association of T_{stance} with ACA or MCA (Table 1).

Our study used a new index, the adjusted Cobb's angle, which considers multiple directions of scoliosis curvatures in addition to maximum Cobb's angle. Both the maximum and adjusted Cobb's angles showed significant correlation coefficients with the asymmetry of GRF magnitude.

CONCLUSIONS

In general, our study shows that the gait asymmetry of both magnitudes and time variables of GRF are associated with the severity of the spinal deformities and pelvic tilt: the spinal deformity is generally associated with the between-leg asymmetry in GRF magnitudes, while the pelvic tilt is associated with the asymmetry of the time variables.

REFERENCES

1. Weinstein SL, et al. *Lancet* **371**, 1527-1537, 2008.
2. Roubal PJ, et al. *Physiotherapy* **85**, 259-268, 1999.
3. Yang JH, et al. *Eur Spine J*. **22**, 2407-2413, 2013.
4. Schizas CG, et al. *Eur Spine J*. **7**, 95-98, 1998.
5. Hoikka et al. *Arch Orthop Trauma Surg* **108**, 173-175, 1989.
6. Delacerda et al. *J Orthop Sports Phys Ther* **3**, 105-107, 1982.
7. Cobb JR. *Instr Course Lect* **5**, 261-275, 1948.
8. Robinson RO, et al. *J Manipulative Physiol Ther* **10**, 172-176, 1987.
9. Mahaudens P, et al. *Spine J* **5**, 427-433, 2005.

Table 1: Linear regression results ($\alpha = 0.05$) for AI of average vertical GRF over the stance phase (Fz_{AVG}) and AI of stance phase contact time (T_{stance}) with maximum Cobb's angle (MCA), adjusted Cobb's angle (ACA), and pelvic tilt (PT). Correlation coefficient (r) and p-values (p) are provided. Statistically significant correlations are bolded.

Variable	MCA		ACA		PT	
	r	p	r	p	r	p
Fz_{AVG}	0.79	0.011	0.697	0.037	-0.476	0.196
T_{stance}	-0.452	0.172	-0.379	0.315	0.715	0.03

A PRINCIPAL COMPONENT ANALYSIS-BASED CORRECTION METHOD FOR ANATOMICAL FRAME VARIATION IN GAIT ANALYSES

Allison Clouthier and Kevin Deluzio

Mechanical and Materials Engineering, Queen's University, Kingston, ON, Canada
email: allison.clouthier@queensu.ca, web: <http://hmrc.engineering.queensu.ca/HMRL/>

INTRODUCTION

Multicentre studies are rare in the area of three dimensional gait analysis due to the challenges associated with combining gait waveform data from different laboratories. One of the largest contributors to the differences that occur between laboratories is inconsistencies in marker placement [1] resulting in discrepancies in anatomical coordinate systems. Principal component analysis (PCA) is a statistical technique that can be applied to waveform data to identify and quantify group differences [2]. Therefore, we propose a PCA-based method that can be applied to identify and correct for the effect of anatomical frame variation on gait kinematic and kinetic data.

METHODS

The proposed correction technique begins with the application of principal component analysis (PCA). For a matrix containing waveform data, \mathbf{X} , PCA extracts features or loading vectors, \mathbf{U} , that are associated with variation and assigns scores, \mathbf{z} , for each loading vector to each subject such that $\mathbf{X} = \mathbf{z}\mathbf{U}$. It is then possible to identify differences between datasets by comparing mean z-scores. This correction method essentially ensures that the data from both sets have similar scores for all principal components. This is accomplished by adding the difference in mean z-scores between the two datasets multiplied by the loading vector to the waveform for each subject from one dataset for all principal components where the two datasets differ significantly:

$$\mathbf{x}_{corr} = \mathbf{x} + \sum_{i \in S} (\bar{z}_{Ai} - \bar{z}_{Bi}) \mathbf{u}_i$$

where \mathbf{x} is the waveform for one subject, \bar{z}_{Ai} and \bar{z}_{Bi} are the mean scores for the i th principal component for datasets A and B, and \mathbf{u}_i is the loading vector

for the i th principal component. The summation is carried out over the principal components that differ significantly between the two datasets (S).

The correction technique was demonstrated on the knee kinematics of 24 healthy subjects walking overground at the Human Mobility Research Laboratory in Kingston, ON. The knee joint angles were perturbed by rotating the thigh coordinate system about its long axis by -5° , 5° , and 10° (Figure 1) thus creating three additional sets of angles for each subject. The resulting differences in joint angles were then corrected using the PCA-based method. A correction was applied for a principal component if a significant difference ($p < 0.05$) was identified using Student's t-test. No knowledge regarding the source of the induced error was used in the correction process.

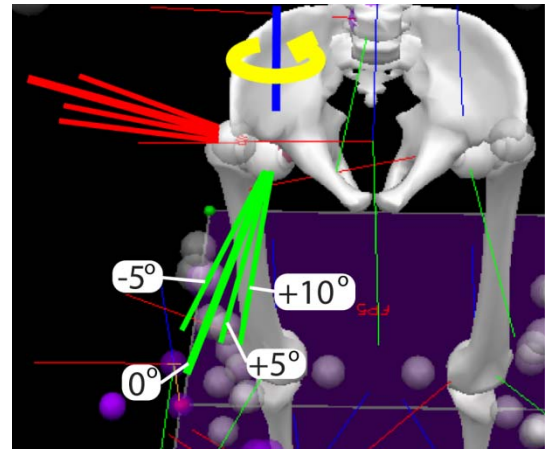


Figure 1: The rotated thigh coordinate systems used to create the perturbed data sets.

RESULTS AND DISCUSSION

The perturbed knee adduction angles are shown in Figure 2A and the resulting waveforms following the correction of the rotated coordinate system angles are shown in Figure 2B.

In this example, corrections were only applied for principal components found to differ significantly from the 0° case. However, this criteria could be modified depending on the level of agreement desired. In theory, if the data was corrected for every PC, the resulting means from the two datasets should be equivalent, while the variation in each dataset is preserved.

These data with joint angle errors induced by a misaligned thigh coordinate system was used to demonstrate the correction method because the source of error (crosstalk) is exactly known and well understood [3] and it is therefore possible to ensure the correction that is applied is appropriate. In verification of this, the applied correction was found to be very similar to the analytically calculated error induced [4]. In addition, since the four datasets were obtained from the same subjects, it is clear that the joint angles should be the same. However, this technique can also be applied to data collected on different subjects in different laboratories, providing the population demographics are similar. Because variation is maintained using this method, differences between laboratories will

be corrected while any effect of pathology, surgical intervention, etc. should be unaffected, providing it is the same at both centres. Therefore, application of this technique may enable synthesis of inter-laboratory 3D gait data and therefore multicentre studies in this field.

CONCLUSIONS

The ability of the proposed PCA-based method to identify and correct for differences in data caused by variation of the anatomical reference frame was demonstrated on a dataset where differences were induced by a known perturbation.

REFERENCES

1. Della Croce U, et al. *Gait Posture* **21**(2), 226-237, 2005.
2. Deluzio KJ, et al. *Hum Mov Sci* **16**(2-3), 201-217, 1997.
3. Piazza SJ, et al. *J Biomech* **33**, 1029-1934, 2000.
4. Brennan A, et al. *J Biomech* **44**(16), 2838-2842, 2011.

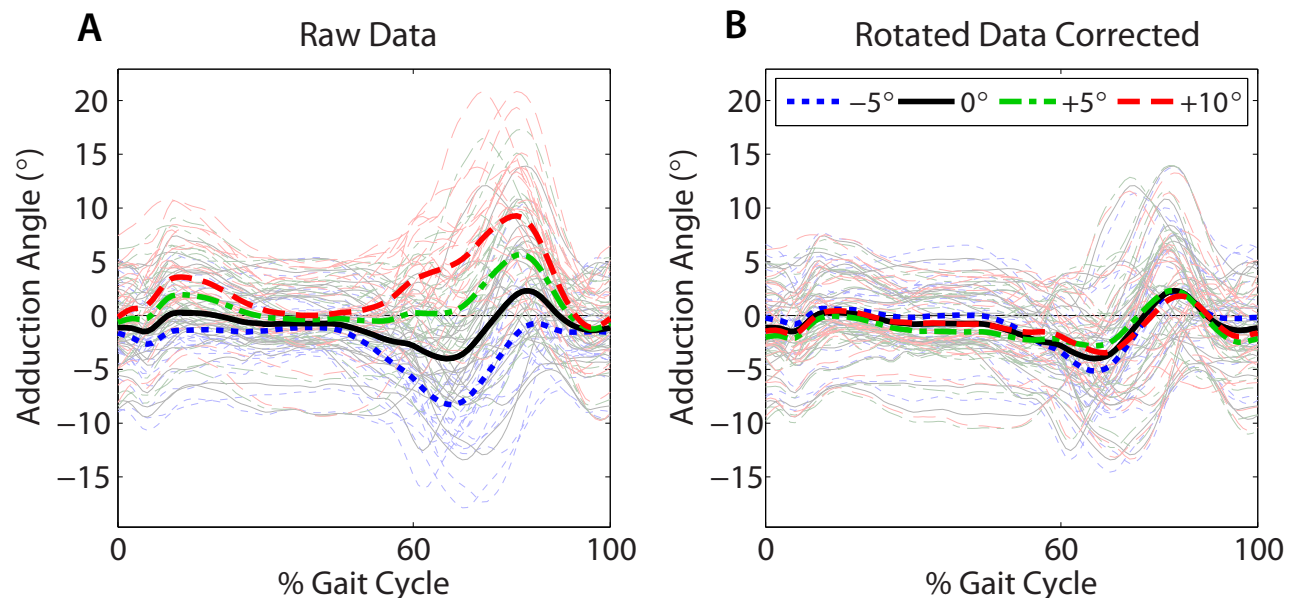


Figure 2: A) Knee adduction angles resulting from the four thigh coordinate systems. B) The knee adduction angles from each coordinate system following the correction of the three data sets obtained by rotating the coordinate system. Mean waveforms for each coordinate system are shown with thick lines.

PREDICTION OF MEDIAL KNEE CONTACT FORCE USING EXTERNAL MEASURES IS POPULATION DEPENDENT

¹ Allison L Clouthier, ² Scott CE Brandon, and ¹ Kevin J Deluzio

¹ Mechanical and Materials Engineering, Queen's University, Kingston, ON, Canada

² Institute of Biomedical Engineering, University of New Brunswick, Fredericton, NB, Canada
email: allison.clouthier@queensu.ca, web: <http://hmrc.engineering.queensu.ca/HMRL/>

INTRODUCTION

The severity and progression of medial knee osteoarthritis (OA) has been linked to increased loading in the medial compartment of the knee. Because this load is difficult to measure *in vivo*, the knee adduction moment is often used as a surrogate measure. Despite this, the strength of the relationship between these two measures has been questioned and it has been found that a combination of adduction moment and flexion moment is a better predictor of medial knee loading [1]. Other factors may also affect joint loading however. Increased varus alignment has been found to be a risk factor for OA [2] and the gastrocnemii provide a large contribution to the knee contact force [3]. Additionally, previous studies relating medial loads to gait parameters have generally included limited numbers of participants from a total knee replacement population. Therefore, the goal of this study was to determine the contribution of static alignment and external moments to the prediction of medial knee contact loads for healthy and OA populations.

METHODS

18 participants with knee OA diagnosed by an orthopedic surgeon and 18 healthy controls walked at a self selected speed at the Human Mobility Research Laboratory in Kingston, ON while marker trajectories and ground reaction forces were recorded. A standing full length radiograph was taken for each participant. A generic musculoskeletal model [4] was scaled for each participant based the radiograph and anatomical markers. Inverse kinematics, inverse dynamics, residual reduction, and muscle analysis were completed in OpenSim 3.2. Static optimization was

performed to estimate muscle forces and resulting tibiofemoral contact loads were calculated [4]. Static alignment was defined by the hip-knee-ankle (HKA) angle which was measured on each radiograph. Varus and valgus alignment were defined by negative and positive values of the HKA angle, respectively.

A stepwise multiple linear regression analysis was carried out to determine the ability of external measures to predict the medial compartment force. Inputs to the regression model included the HKA angle ($^{\circ}$), knee adduction moment (Nm/kg), knee flexion moment (Nm/kg), and ankle plantar flexion moment (Nm/kg). The first and second peak medial contact forces (BW) and the impulse (integral of force with respect to % gait cycle) were predicted. The timing of the first and second peak was based on the first and second peak in the knee adduction moment (Figure 1) and parameters used to predict contact force were all taken at these instants. Similarly, the impulses of the moments were used as inputs when predicting the contact force impulse.

RESULTS AND DISCUSSION

The resulting coefficients for the multiple linear regression models are shown in Table 1. A coefficient of 0 (represented by a "-" in the table) indicates that the input did not significantly improve the contact force prediction and is not included in the model.

A large portion of the variation in medial knee contact force was explained by the model, with better predictions for the peak forces than the impulse. The adduction moment was an important predictor of medial knee contact force for all measures and both groups. For the second peak, the

ankle plantar flexion moment aided in predictions. This is likely due to the large contribution of the gastrocnemii to the contact force at this point in the gait cycle. The knee flexion moment has previously been shown to be important in predicting medial loading, but was only significant for the first peak in the control group in this study. This may be a result of the increased variability and decreased magnitude of the knee flexion moment at peak 1 in the OA group.

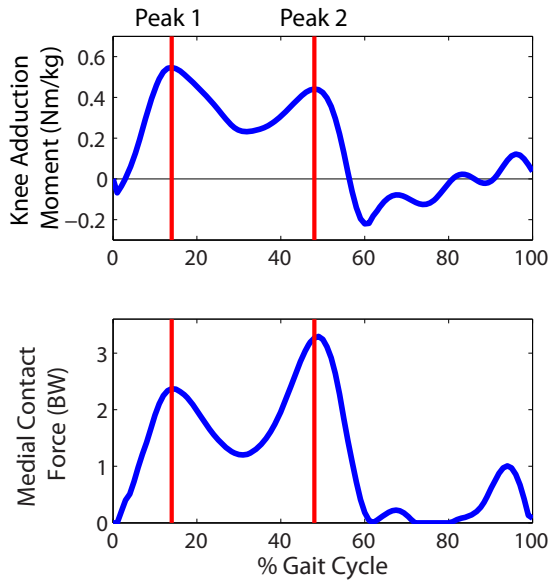


Figure 1: Knee adduction moment and medial contact load for a representative subject. The timing for peaks 1 and 2 was based on the adduction moment and generally corresponded with peaks in the contact force.

An important finding here is that the models for the control and OA groups are not equivalent. The regression coefficients were different for the two groups and the HKA angle was an important predictor for the OA group, but not the control group. It was expected that increased varus

alignment would be correlated with larger medial loads; however, this likely was not significant for the control group due to the small range of HKA angles (-4.5 to 3.2°) compared with the OA group (-19 to 4.5°).

One limitation of this study is that the contact loads were calculated through static optimization using some of the same external moments that were used as inputs to the regression model. However, contact forces and R^2 values were similar to those obtained using in vivo measurements of joint loading [1].

CONCLUSIONS

The multiple linear regression model was able to explain a large percentage ($>70\%$ for peaks 1 and 2) of the variation in medial knee contact forces for participants with knee OA and healthy controls using static alignment and external moments. However, the models used for these two groups differed. Therefore, it may be important to use population specific models when creating surrogate measures for medial knee loading.

REFERENCES

1. Walter J, et al. *J Orthop Res* **28**(10), 1348-1354, 2010.
2. Sharma L, et al. *J Am Med Assoc* **286**, 188-195, 2001.
3. Shelburne KB, et al. *J Orthop Res* **24**(10), 1983-1990, 2006.
4. Brandon SCE, et al. *J Biomech* **47**, 1409-1415, 2014.

Table 1: Coefficients for multiple linear regression model $F_{med} = c_0 + c_{HKA}HKA + c_{Add}M_{Add} + c_{Flx}M_{Flx} + c_{AkFlx}M_{AkFlx}$, R^2 values, and root mean square error (RMSE). A dash indicates a coefficient of 0.

Measure	Group	c_0	c_{HKA}	c_{Add}	c_{Flx}	c_{AkFlx}	R^2	RMSE
Peak 1	Control	0.71	-	1.59	0.93	-	0.88	0.15
	OA	0.89	0.06	2.65	-	-	0.71	0.30
Peak 2	Control	0.14	-	1.19	-	1.50	0.89	0.17
	OA	0.70	0.03	2.05	-	1.03	0.90	0.15
Impulse	Control	88.99	-	1.44	-	-	0.77	5.94
	OA	77.96	2.05	2.49	-	-	0.62	9.28

DYNAMIC THICKNESS CHANGE OF RECTUS FEMORIS MUSCLE DURING GAIT MEASURED USING ULTRASOUND IS RELATED TO HIP AND KNEE JOINT MOMENTS AND MUSCLE ELECTRICAL ACTIVATION

¹ Oladipo O. Eddo, ¹ Siddhartha Sikdar, ¹ Nelson Cortes

¹ George Mason University, Manassas, VA, USA
Email: ncortes@gmu.edu, web: <http://smartlab.gmu.edu>

INTRODUCTION

Quantifying human movement is essential for understanding normal function, which allows the ability to distinguish and characterize movement abnormalities. Recently, researchers have successfully investigated dynamic muscle function with the aid of imaging techniques such as magnetic resonance imaging and ultrasound imaging (USI). These image-based methods can complement existing methods for quantifying human movement based on indirectly estimated joint loads and muscle electrical activity [1], and might provide a more direct assessment of physiological muscle function. Imaging can separately assess different deep-seated muscle groups directly, overcoming the limitations presented by cross talk with traditional electromyography (EMG) [1,2]. Concurrently assessing muscle function and joint mechanics using USI, EMG and 3D motion analysis during a dynamic task such as gait possesses the potential for further understanding the pathophysiology of poorly understood joint diseases. The goal of this study was to investigate the reproducibility of dynamic ultrasound measurements and relate them to conventional biomechanical measures during gait in healthy volunteers.

METHODS

Eighteen healthy participants (23 ± 2 years; 1.7 ± 0.1 m; 65.9 ± 9.4 kg) completed 3 gait trials at a self-selected pace (1.06 ± 0.17 m/s). Lower extremity joint moment, EMG values and *rectus femoris* (RF) muscle function were assessed concurrently during the stance phase of gait from the dominant leg. USI measures were collected in a longitudinal view while the ultrasound (Ultrasonix Sonix) cart traveled alongside study participants over a custom-

built track system. Intra-class correlation coefficients assessed inter-trial reliability of ultrasound measures, whereas Pearson Product-Moment Correlations investigated relationships between hip and knee joint moments and EMG with USI muscle function measures. Standard Error of Measurement (SEM) and Minimum Detectable Difference at 95% (MDC₉₅) were calculated. Statistical significance was assessed at $p < 0.05$.

RESULTS AND DISCUSSION

Table 1 provides descriptive statistics, ICC, SEM, and MDC₉₅ for the muscle function variables of interest. USI measures of peak and average muscle thickness during loading and full stance showed excellent reliability, with low SEM and Minimum Detectable Difference. Figure 1 represents the relationship between peak muscle thickness and *rectus femoris* muscle activation during the load absorption phase.

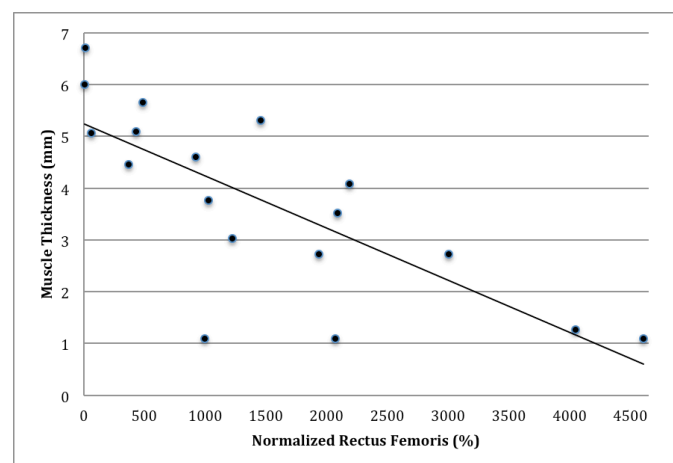


Figure 1: Relationship between *rectus femoris* muscle activation and muscle thickness ($R^2 = .568$) measured via ultrasound during the load absorption phase. It denotes that decreased thickness (stronger contraction) relates with greater muscle activation.

During stance, significant relationships existed between hip and knee joint moments and USI measures of dynamic muscle function ($p < 0.05$). *Table 2* depicts the relationships between muscle function and hip and knee joint moments. Higher peak hip abduction, extensor and external rotation moment were associated with larger *rectus femoris* muscle thickness. A significant negative relationship was found between *rectus femoris* muscle activation and muscle thickness ($-0.714 < r < -0.541$, $p < 0.05$), except with average muscle thickness during terminal stance.

CONCLUSIONS

Our results demonstrate that peak and average muscle thickness can be confidently quantified using imaging techniques during gait. Our results further determine that *rectus femoris* muscle

thickness changes are strongly related to hip and knee joint moments, and the eccentric contraction of the RF is associated with increased activation of the same muscle as well as other muscles of the lower extremity. Our findings are the first to our knowledge investigating the relationship between movement biomechanics and dynamic ultrasound-based measures of muscle function. Future studies should consider applying similar methods to patients with pathological conditions.

REFERENCES

1. Sikdar S, et al. *Exerc. Sport Sci. Rev.*, **42**(3): 126-135, 2014
2. Petterson S, et al. *Med. Sci. Sports Exerc.*, **43**(2): 225-231, 2011

Table 1: Descriptive statistics (Mean \pm standard deviation, ICC, SEM and MDC₉₅) of measures of muscle function measure with ultrasound imaging. Peak and average muscle thickness measured in millimeters.

	Mean	SD	ICC	SEM	MDC ₉₅
Average muscle thickness - absorption phase	3.32	2.30	0.88	0.78	2.17
Average muscle thickness - terminal stance	2.81	1.25	0.87	0.46	1.26
Average muscle thickness - full stance	2.95	1.40	0.88	0.48	1.33
Peak muscle thickness - absorption phase	4.00	2.47	0.89	0.81	2.24
Peak muscle thickness - terminal stance	4.93	2.23	0.87	0.82	2.27
Peak muscle thickness - full stance	5.00	2.23	0.87	0.82	2.27

Table 2: Pearson Product Moment Correlations between measures of muscle function and hip and knee joint moments. *r*-value provided with significance level in parenthesis.

	Hip Abductor Moment at Peak Knee Adductor	Hip Adductor Moment at Peak Knee Abductor	Peak Hip External Rotation moment	Knee Internal Moment at Peak Flexion Angle
Average muscle thickness - absorption phase	.386 (N.S.)	-.468* (0.05)	.465 (N.S.)	.597 (0.009)
Average muscle thickness - terminal stance	.545* (0.019)	-.552* (0.017)	.599* (0.009)	.565* (0.015)
Average muscle thickness - full stance	.516* (0.028)	-.553* (0.017)	.576* (0.012)	.586* (0.011)
Peak muscle thickness - absorption phase	.490* (0.039)	-.502* (0.034)	.483* (0.042)	.642* (0.004)
Peak muscle thickness - terminal stance	.541* (0.02)	-.499* (0.035)	.540* (0.021)	.560* (0.016)
Peak muscle thickness - full stance	.548* (0.018)	-.506* (0.032)	.549* (0.018)	.560* (0.016)

* Statistically significant correlation ($p < 0.05$) / N.S. – Not statistically significant correlation

DIFFERENCES IN STANCE PHASE KINEMATIC AND MUSCLE ACTIVITY AFTER EIGHT WEEKS OF INSOLE USE

Brendan Cotter and Janessa D.M. Drake

Department of Kinesiology and Health Science, York University, Toronto, ON
cotterbd@yorku.ca

INTRODUCTION

Between 60-85% of individuals experience low back pain (LBP) at least once in their lives (1). One method currently used to alleviate and prevent LBP, is the use of insoles designed to affect change in the kinematic and/or kinetic chain by reducing pronation during stance phase (1). While changes in shank and foot motion supporting the kinematic change have been observed during walking, these changes appear to have little effect on the knee, hip, or pelvis (2). In addition to correcting posture, insoles may act to protect the chain by increasing the strength and reaction time of muscles involved in spine stabilization, such as gluteus medius (3). While previous research implies that inserts may reduce LBP through a reduction of shock absorption and/or foot realignment, most orthoses-related LBP research is solely questionnaire based, and there is little known behind the mechanism that makes them a successful treatment for LBP. The purpose of this study is to examine and quantify whether a neuromuscular training insole can alter surface EMG, and joint kinematics, during the stance phase of walking following eight weeks of use.

METHODS

Eight males and eight females were given a neuromuscular training insole and were observed walking prior to the insertion and eight weeks after insertion. The insoles are designed for arch support that changes in height and stiffness. The adjustable aspect allows users to follow a progression, moving from the softest/shortest, to the hardest/tallest insert over the eight week period. Participants were equipped for passive reflective markers for motion capture. Electrodes were placed on a variety of

torso and lower limb muscles, in order to capture surface EMG. Participants angular range of motion, mean, maximum and minimum angle were observed pre-post intervention, in addition to their average muscle activation.

RESULTS AND DISCUSSION

While the insoles did not appear to have a large effect on surface EMG or lower limb and lumbar spine kinematics, they did appear to have an effect on thoracic spine movement. Thoracic spine mean, maximum and minimum flexion angle (\pm sem) was initially observed as 7.23° (2.55), 10.81° (2.56) and 3.64° (2.59), respectively (Fig. 1). Following the intervention a mean of 1.20° (2.37), a maximum of 4.38° (2.53), and a minimum of -1.79° (2.31), was observed. In addition to the thoracic spine, lumbar spine and trunk flexion also appeared to be reduced, although these differences did not appear to be significant. Additional differences were found in other segments when the data was subdivided into male and female populations, as well as left and right limb stance phase.

No differences were found to support a reduction in spinal flexion as a result of the kinematic chain. While a reduction in thoracic flexion was found post intervention, there was no indication this was a result of differences found in lower limb kinematics. There was no trend of the knee or hip displaying less internal rotation, or the pelvis displaying less anterior tilt, post intervention.

While the intervention did result in slight changes in surface EMG, considering the magnitude of the change and the observed kinematics, they did not

appear to alter the biomechanics of walking. Due to the change in thoracic spine sagittal plane motion, it is possible that there were initial changes in EMG that were no longer present following the eight week intervention. Future research should also examine the immediate effects of these insoles on kinematics and surface EMG, to further our understanding on how insoles could possibly reduce low back pain.

CONCLUSIONS

Following the intervention participants displayed less thoracic spine flexion during stance phase. This change in kinematics could help to relieve some off the stress placed on the spine during walking. There was no evidence to support that this

reduction in thoracic spine flexion was a result of changes in pelvis, hip, or knee kinematics. Similarly, the insoles appeared to have little effect on muscle activation following eight weeks of use. Considering the reduction in spinal flexion without any major side effect being detected, these insoles may be beneficial for individuals suffering from LBP.

REFERENCES

1. Bird AR. and Payne CB. *The Foot*, 9, 175-180. 1999`
2. Nester CJ, et al. *Gait & posture*, **17(2)**, 180-187. 2003
3. Ogon M. et al. *International journal of sports medicine*, **22(6)**, 414-419. 2001

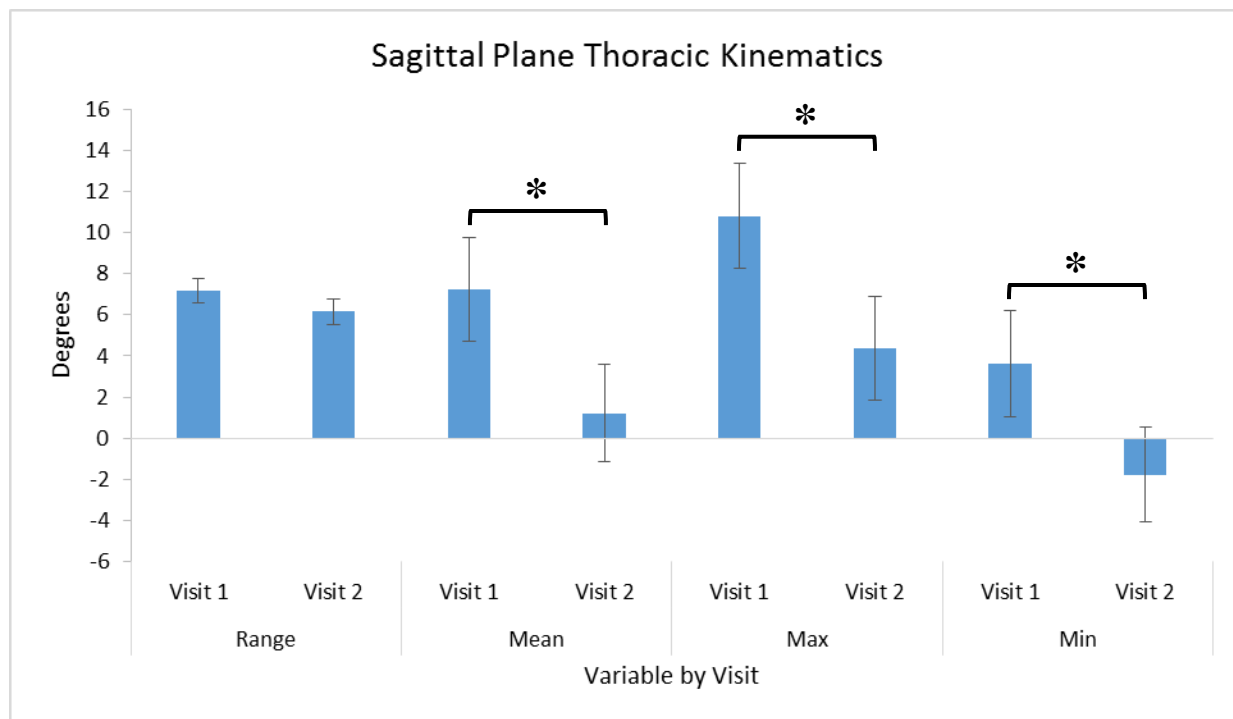


Figure 1: Displays thoracic spine sagittal plane angular range of motion (range), mean, maximum and minimum (\pm SEM) for visit 1 and visit 2, with * denoting $p < 0.05$.

APPROXIMATE ENTROPY OF TRUNK AND FOOT ACCELERATIONS DURING WALKING

¹ Jordan J.W. Craig, ¹ Adam Bruetsch, and ¹ Jessie M. Huisinga

¹ Human Performance Laboratory, The University of Kansas Medical Center, Kansas City, KS, USA
email: jcraig2@kumc.edu

INTRODUCTION

Gait instability is indicative of fall risk, and is commonly characterized by irregular frontal plane motion of the center of mass [1]. Frontal plane instability is reflected in variable step width, as foot placement is constantly adjusted to keep the head and trunk stable and upright [2]. Unfortunately, step width and medial-lateral trunk motion are not easily measured outside of a research or gait laboratory setting. Wireless accelerometry measurement methods have been gaining popularity for their ability to gather information about human gait outside of the laboratory setting [1]. These portable sensors provide a means of measuring relevant parameters to quantify instability in the motion of the trunk and feet, without the need for motion capture or force plate systems. However, these methods don't allow for direct measurement of step width which is related to fall risk and lateral postural control [1].

Approximate entropy (ApEn) quantifies the repeatability of a time series and has previously been utilized to quantify variability during gait [3]. ApEn is of particular interest in this study for analyzing how foot placement is constantly altered in order to stabilize trunk motion during walking.

The aim of this study was to examine whether accelerations at the trunk are more tightly controlled, and thus more repeatable, than accelerations at the feet. We hypothesized that accelerations at the trunk would be more repetitive and less variable than accelerations at the feet.

METHODS

Twenty healthy adult subjects participated in this study (mean 43.5 years, range 27 – 58 years). Participants walked on a treadmill at a self-selected

pace for 3 minutes while wearing tri-axial accelerometers (Opal, APDM, Portland, OR) on their right ankle and sternum. Accelerations of the trunk and foot were recorded at 128 Hz for the duration of the trial. Previous literature has shown that accelerations are attenuated inferiorly to superiorly within the trunk segment [4]; thus, we chose to place the trunk accelerometer over the sternum rather than the lumbar spine in order to measure what is theoretically the more stable position on the trunk. ApEn and root mean square (RMS) values were calculated for the acceleration time series from the foot and trunk sensors in frontal and sagittal planes which resulted in four ApEn and RMS values for each subject – trunk sagittal, trunk frontal, foot sagittal, and foot frontal. A custom MATLAB code was used to calculate ApEn [5] and RMS values. To calculate ApEn, we chose a vector length of $m = 3$, and calculated time delay (τ) for each individual subjects' data sets. Optimizing τ for each individual time series helped ensure accurate ApEn calculations for each time series. A 2x2 ANOVA was performed on the ApEn and RMS values and Pearson's correlations were used to assess the relationship between sensor locations within the same plane.

RESULTS AND DISCUSSION

ApEn values showed a main effect of location ($F = 322.996$, $p < 0.01$), and a main effect of plane ($F = 66.218$, $p < 0.01$). Similarly, RMS values showed a main effect of location ($F = 38.295$, $p < 0.01$), and a main effect of plane ($F = 195.902$, $p < 0.01$). Post-hoc paired t-tests between locations revealed that ApEn values were significantly lower for the accelerations at the foot compared to the trunk ($p < 0.01$) in both the frontal and sagittal planes, and that RMS values were significantly higher for the accelerations at the foot compared to the trunk ($p < 0.01$) in both the frontal and sagittal planes (Table

1). There was a significant positive correlation between foot and trunk acceleration ApEn values within the sagittal plane only ($r = 0.565$, $p = 0.009$) (Figure 1).

Table 1: Mean (standard deviation) for ApEn and RMS values, significance for paired t-tests.

	Foot	Trunk	<i>P</i> - value
ApEn Frontal	1.327 (0.109)	1.700 (0.121)	< 0.01
RMS Frontal	5.213 (2.053)	1.915 (1.159)	< 0.01
ApEn Sagittal	1.096 (0.137)	1.647 (0.140)	< 0.01
RMS Sagittal	6.930 (2.864)	1.977 (1.266)	< 0.01

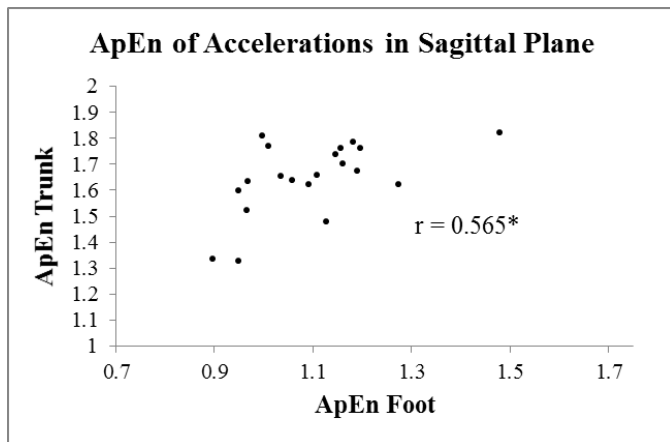


Figure 1: Correlation between ApEn of acceleration time series of foot and trunk in sagittal plane (* denotes $p < 0.01$).

Our results show that ApEn of foot acceleration was less than that of the trunk, indicating that accelerations at the foot are less variable, or more repeatable, than accelerations at the trunk. This is seemingly in contrast to previous findings which showed inferior to superior decreases in variability [4], the acceleration of the foot was not considered in the previous study [4], and it is important to keep in mind that the magnitudes of acceleration at the feet are much larger than that of the trunk. Thus, the overall finding is that greater movement repetition, as identified by ApEn, is higher at the

feet. Also, RMS showed higher variability at the feet compared to the trunk which would indicate overall greater amounts of variability at the feet. Finally, as indicated by a lack of significant correlation in the frontal plane, some subjects may be able to stabilize their trunk independent of foot placement and thus have more repeatable foot accelerations, while other subjects may rely more heavily on foot placement to stabilize their trunk and thus have less repeatable foot accelerations. Taken together, these results indicate that the body may aim to reduce overall motion at the trunk, rather than specifically reducing the variability of the oscillatory movement pattern during gait.

CONCLUSIONS

The results of this study illustrate the utility of objectively measuring motion of the body during gait, specifically with the use of small portable accelerometer available for use outside of a research laboratory. Since common gait parameters relating to stability (ie. step width) are not easily measured outside of a research laboratory, it is important to explore the application of these portable tools for objective gait measurements. The findings of this study highlight significant patterns in steady-state gait, with a methodology that could be performed nearly anywhere.

REFERENCES

1. Toebes MJ, et al. *Gait Posture* **36**, 2012.
2. Hurt CP, et al. *Gait Posture* **31**, 2010.
3. Kavanagh JJ. *J Neuroeng Rehabil* **6**, 2009.
4. Kavanagh JJ, et al. *Gait Posture* **20**, 2004.
5. Pincus SM. *Academy of Sciences of the United States of America* **88**, 1991.

ACKNOWLEDGEMENTS

This work was supported by the National Multiple Sclerosis Society RG 4914A1/2 and the NIH National Center for Advancing Translational Science 1KL2TR00011.

BAREFOOT VERSUS SHOD: EFFECTS OF BACKPACK LOADS ON WALKING MECHANICS

Kevin D. Dames and Jeremy D. Smith

Biomechanics Laboratory, University of Northern Colorado, Greeley, CO

Email: kevin.dames@unco.edu; website: www.unco.edu/biomechanics

INTRODUCTION

Minimally supportive shoes intended to mimic the barefoot condition are a popular form of footwear. With a lack of cushion under the foot, changes in walking gait are evident. Differences such as greater peak loading rate, reduced lower limb joint ranges of motion, and shorter steps have been observed in barefoot walking [1, 2]. Backpack loads also promote altered kinetic, kinematic, and spatiotemporal walking patterns [3, 4]. Increased ground reaction forces (GRFs) experienced while loaded [5] may exaggerate adaptations made to reduce discomfort of barefoot walking. The purpose of this study was to investigate the effects of loading and footwear on walking patterns in young, healthy individuals.

METHODS

Twelve participants (7 female, 5 male; 22.64 ± 2.77 yrs., 1.73 ± 0.11 m, 70.9 ± 12.67 kg) walked overground at $1.5 \text{ m} \cdot \text{s}^{-1}$ under four conditions: Barefoot Unloaded (BU), Shod Unloaded (SU), Barefoot Loaded (BL), and Shod Loaded (SL). A backpack load (15% of body mass) was worn during loaded conditions, but not included in total body mass when normalizing data. Motion (100Hz) and ground reaction force data (2000Hz) were combined through inverse dynamics to estimate joint reaction forces and moments, which were then used to estimate joint powers. Spatiotemporal and peak GRF data were also included as dependent variables. GRFs and joint powers were normalized to body weight and mass, respectively. Trial peaks were averaged and used in statistical analyses. Differences between conditions were assessed via a series of 2x2 ANOVAs with repeated measures. Alpha was set at .05 for all tests.

RESULTS

Loading increased the first and second vertical GRF (VGRF) peaks (Figure 1). Minimum VGRF between peaks was greater while barefoot and loaded, respectively. Greater braking and propulsive GRFs were observed while shod and while loaded (Figure 1). Ankle power absorption increased

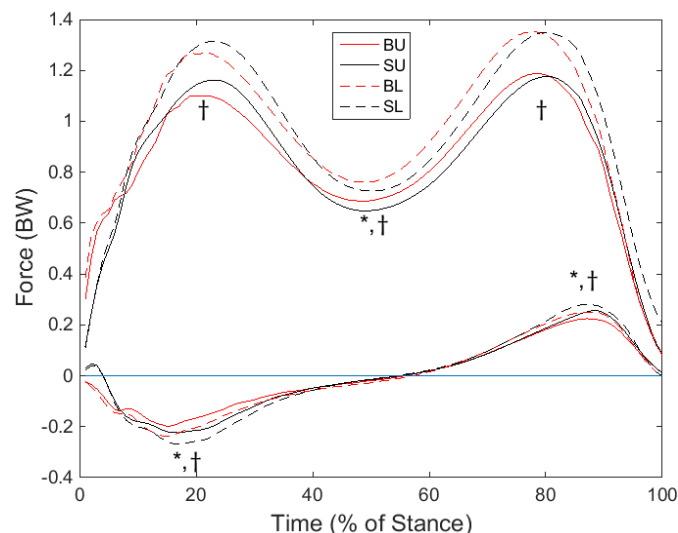


Figure 1. Mean vertical and AP GRF according to condition. * indicates significant footwear effect. † indicates significant load effect.

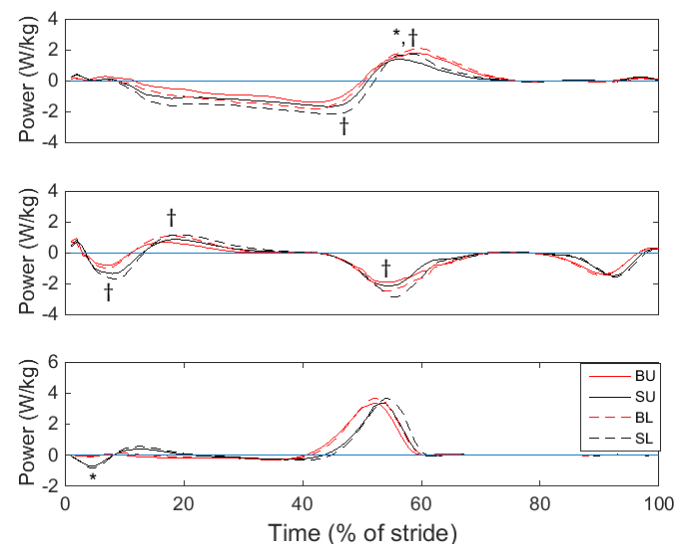


Figure 2. Mean joint powers normalized to body mass for the hip (top), knee (middle), and ankle (bottom). * indicates significant footwear effect. † indicates significant load effect.

immediately after ground contact (0-10% of the gait cycle) while walking shod, but was not altered for the remainder of the gait cycle or by load. At the knee, greater power absorption occurred during early stance (~0-10 % of stride) and just prior to toe-off (~50-60% of stride), whereas power generation increased after the initial loading response (~20% of stride) while walking with a

backpack load. Only load lead to increased power absorption at the hip during stance (40-50% of stride), whereas both loading and walking barefoot increased power generation at the hip prior to toe off (50-60% of stride) (Figure 2). Walking shod resulted in increased stride lengths, stance times, swing times, and double support times. However, loading only increased stance and double support times (Table 1).

Table 1. Spatiotemporal data means (\pm standard deviation).

	BU	SU	BL	SL
Stride Length (m)	1.48* (.12)	1.60 (.07)	1.45*,† (.09)	1.59† (.07)
Stance Time (s)	0.56* (.02)	0.59 (.03)	0.57*,† (.02)	0.60† (.03)
Swing Time (s)	0.40* (.05)	0.41 (.01)	0.38* (.02)	0.40 (.02)
Double Support Time (s)	0.16* (.02)	0.18 (.03)	0.18*,† (.02)	0.20† (.03)

* indicates significant footwear effect. † indicates significant load effect.

DISCUSSION AND CONCLUSIONS

The data presented here highlight that young, healthy adults increase peak knee and hip powers during stance at a fixed walking speed while loaded. Spatiotemporal data agree with the literature for the barefoot [1, 2] and loading conditions [3]. Loading exaggerates the shorter strides observed while barefoot. Barefoot walking elicited decreased peak braking/propulsive GRFs compared to shod walking, which disagrees with previous work [1]. A proportional increase in GRFs with incremental load magnitudes has been shown [5]. The 15% increase in mass while loaded in the present study resulted in 12.5%, 13.7%, 10.1% and 14.17% increases in initial VGRF, second VGRF, braking and propulsive peaks while shod. However, these increased to a lesser extent while barefoot: 11.9%, 11.8%, 9.3%, and 11.99%. Thus, walking barefoot promotes a strategy to reduce peak GRFs while loaded.

During early stance, walking barefoot promoted a reduction in braking GRF and ankle power absorption. The latter is attributed to a less dorsiflexed ankle at foot strike and smaller dorsiflexor moment [1]. No footwear effects were noted in knee power, but hip power generation was increased at toe off while barefoot. This strategy represents a pull-off from the hip rather than increased push-off with the ankle to initiate swing.

Overweight/obese individuals walking barefoot may also exhibit similar responses to those observed here. However, if sensitivity to plantar pressures promotes the altered barefoot walking mechanics, the decreased sensitivity of plantar surface mechanoreceptors in obese individuals [6] may attenuate the observed responses seen here with added load. Comparison between normal weight and overweight individuals is necessary to determine if the changes observed here by adding 15% of body mass while barefoot are also evident between groups whose body masses are 15% different.

An attempt to minimize discomfort while barefoot is evidenced by reduced braking and propulsive GRFs and an increased VGRF at mid-stance. These GRF changes resulted in a greater reliance on the hip for power generation during stance and less reliance on the ankle for power absorption immediately after impact with the ground. This data suggests that the hip was exposed to higher loads during barefoot walking and while carrying a backpack load, which may have implications on joint health over the long term.

REFERENCES

1. Zhang, X, Paquette, MR, & Zhang, S, *J Foot Ankle Res*, **6**:45, 2013.
2. van Engelen SJ, et al., *Clin Biomech* **25**, 809-815, 2010.
3. Wang, YT, Pascoe, DD, & Weimar, W, *Ergo*, **44**(9),858-869, 2001.
4. Majumdar, D, Pal, MS, Majumdar, D, *Ergo*, **53**(6), 782-791, 2010.
5. Tilbury-Davis, DC & Hooper, RH, *Hum Mov Sci*, **18**, 693-700, 1999.
6. Wu, X & Madigan, MI, *Neuroscience Letters*, **583**, 49-54, 2014.

AVERAGING TRIALS VERSUS AVERAGING TRIAL PEAKS: IMPACT ON STATISTICAL TESTS

Kevin D. Dames, Jeremy D. Smith & Gary D. Heise
Biomechanics Laboratory, University of Northern Colorado, Greeley, CO
Email: kevin.dames@unco.edu; website: www.unco.edu/biomechanics

INTRODUCTION

Gait data is commonly displayed in figures as an average of many trials and/or averaged across participants. Smoothing the data in this way reduces the impact of inter-trial variability inherent in the data [1]. However, discrete data points, such as peaks, are used in statistical tests to define differences (i.e. an increase or decrease) between groups. The magnitudes of differences in means, sample sizes, and standard deviations are meaningful components of these statistical models [2]. However, it is often unclear how authors identify a dependent variable from multiple trials. Thus, the purpose of this study was to determine whether identifying dependent variables from an average trial profile versus identifying dependent variables from an individual trial and then averaging influences statistical outcomes.

METHODS

Twelve participants (7 female, 5 male; 23 ± 3 yrs., 1.73 ± 0.11 m, 70.9 ± 12.7 kg) walked overground at $1.5 \text{ m} \cdot \text{s}^{-1}$ under four conditions: Barefoot Unloaded (BU), Shod Unloaded (SU), Barefoot Loaded (BL), and Shod Loaded (SL). A backpack load (15% of body mass) was worn during loaded conditions, but not included in total body mass when normalizing data. Motion (100 Hz) and ground reaction force data (2000 Hz) were combined through inverse dynamics to estimate joint reaction forces and moments, which were then used to estimate joint powers. Peaks were defined according to the conventions described by Winter [3]. Ground reaction forces (GRFs) and joint powers were normalized to body weight and mass, respectively. Dependent variables were identified from each individual trial and then averaged across the three trials and by first averaging the three trials to create an average profile and then identifying the peaks from this average profile. The mean difference and a percent change in the means between the two methods were determined. Differences between conditions were assessed via a series of 2×2 ANOVAs with repeated measures ($\alpha=0.05$). These

statistical tests were repeated for each method of identifying dependent variables.

RESULTS

Figure 1 presents vertical and anteroposterior (AP) GRFs for a subject. Note the time shift in the mean curve versus the trial curves. Figure 2 displays ankle powers of another subject who also shows this time shift. The average percent change in means and the magnitude of the difference between using the two methods are shown in Table 1. Table 2 presents statistical contrasts (i.e., p -values) for the dependent variables according to the method used.

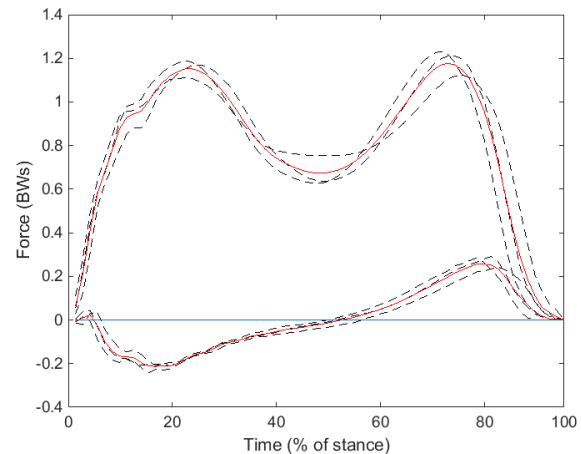


Figure 1. Vertical and AP GRFs for three trials (black dashed lines) and their mean (red solid lines).

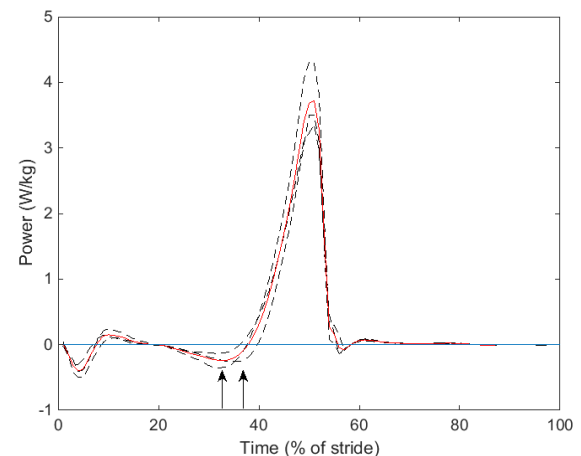


Figure 2. Ankle power curves for three trials (black dashed lines) and their mean (red solid line). The arrows indicate when the minimum occurs – 32% of stride for two trials; 35% for the other trial. The mean curve minimum occurred at 33% of stride.

Table 1. Comparison of differences in average peak values obtained from the two methods.

DV	Magnitude of Difference in Means	Percent Change in Means
A1	0.24625	-143.98
A2	-0.74185	-24.55
K1	-0.0331	2.73
K2	0.001275	0.34
K3	-0.270075	8.26
K4	-0.2473	11.32
H1	0.0796	11.83
H2	-0.0988	5.04
H3	0.202325	8.26
PGRF	-0.000325	-0.07
BGRF	0.007875	-2.98
EVGRF	0.0094	0.78
LVGRF	0.00035	-0.01

PGRF= propulsive GRF, BGRF= braking GRF, EVGRF= early vertical GRF (weight acceptance), LVGRF= late vertical GRF (push-off)

Table 2. P-values for main effects based on the two methods of identifying dependent variables.

DV	Average of trial peaks		Peaks chosen from average trial	
	Footwear	Loading	Footwear	Loading
A1	0.569	0.664	0.282	0.682
A2	0.119	0.92	0.305	0.226
K1	0.059	0.04	0.016	0.013
K2	0.266	0.003	0.165	0.009
K3	0.126	<.0001	0.609	<.0001
K4	0.315	0.142	0.225	0.997
H1	0.137	0.224	0.223	0.33
H2	0.15	0.001	0.104	<.0001
H3	<.0001	0.002	0.001	<.0001
PGRF	0.001	<.0001	<.0001	<.0001
BGRF	0.004	<.0001	0.006	<.0001
EVGRF	0.079	<.0001	0.032	<.0001
LVGRF	0.144	<.0001	0.327	<.0001

Bolded values indicate variables for which the two methods did not result in the same decision about whether to accept or reject the null hypothesis. Abbreviations are the same as in Table 1.

DISCUSSION AND CONCLUSIONS

For some dependent variables, the two methods resulted in <1% difference in means (see Table 1). Additionally, most decisions from the ANOVA did not change despite *p*-values differing (see Table 2). However, two dependent variables that were significant when chosen from the average profile peaks were not significant when peaks were chosen from the individual trials (see Table 2). To further test these two methods using non-experimental data, we simulated data by creating various sine waves of differing amplitude and phase relationships in MATLAB. In addition, we investigated the effects of the time interval between data points on the mean value obtained for a peak. Two observations were made: (1) introducing a phase shift in the sine waves resulted in misrepresentation of the peak amplitude when selected from the average curve, but no error was made when the individual trial peaks were averaged; (2) decreasing sampling frequency (i.e., increasing the time interval between points) caused error in both methods. The first observation supports the notion that an average data profile can mask true trial peaks due to the phase shift that occurs when trials are combined. This shift occurs even with normalization, as presented in the power and GRF data here. The second observation underlines the importance of Nyquist's theorem for choosing adequate sampling rates. Overall, the results of our analysis suggest that for statistical analysis, discrete dependent variables should be chosen from the individual trials rather than from an average data profile.

REFERENCES

1. Schwartz, MH, Trost, JP, & Werve, RA, *Gait Posture*, **20**, 196-203, 2004.
2. Dufek, JS, Bates, BT, & Davis, HP, *Med Sci Sports Exer*, **27**(2), 288-295, 1995.
3. Winter, DA, *The Biomechanics and Motor Control of Human Gait*, 1987.

THE EFFECT OF STEP HEIGHT PERTURBATION ON HUMAN GAIT

^{1,2} Osman Darici, ² Hakan Temeltas and ¹ Arthur D. Kuo

¹ The University of Michigan, MI, USA

² Istanbul Technical University, Istanbul, TURKEY
email: odarici@umich.edu

INTRODUCTION

A minor step height disturbance can potentially disrupt human walking, especially for an inattentive person. Prior awareness such as from vision can help to plan and adjust for a disturbance, but the compensation technique and mechanical consequences of a bump are largely unknown. A simple inquiry confined only to two dimensions may thus yield insight. We therefore sought to explain basic strategies for a single small bump encountered during steady walking, limited to the sagittal plane.

The expectations for a bump are as follows. A small, single-step change in ground height—the bump—may have relatively minor effect on stability, but it will generally slow at least one walking step. If average walking speed is to be recovered, the body must be accelerated accordingly. If the bump is anticipated, there is opportunity to speed up ahead of time, and perform other pre- and post-bump compensations for the step onto and off of the bump. An unanticipated bump can potentially be more disruptive, because it allows compensations to take place only after the fact, perhaps requiring more effort. In the present study, we used a simple model to make these expectations more explicit, and predict some of the mechanical effects of a bump. We also conducted an experiment to examine how humans actually compensate.

METHODS

The experimental paradigm entailed steady treadmill walking interrupted by occasional single bumps. These were applied (Fig. 1) as foam boards, 3 cm thick (height change) placed before the subject episodically. Bumps were either anticipated with vision (termed Visible), or unanticipated due to visual obstruction of the bump (termed Not-Visible). Compensations were evaluated through measured changes in gait parameters such as step length and

period, and with estimates of work performed on the body center of mass (COM).

As a simple model, we considered a point mass for the pelvis with rigid, pendulum-like legs taking fixed step lengths. This is similar to the “rimless wheel” [1], except walking on level ground powered by either an impulsive push-off from one leg prior to the opposite leg’s heel strike collision, or a torque applied to the stance hip to accelerate during stance. This model predicts that an unanticipated bump will cause the heel strike to occur unexpectedly early, shortening that step’s period and length. The bump will also cause a reduced and early collision, with the trailing leg push-off occurring relatively late. To regain lost speed, the model should immediately accelerate by applying stance hip extension torque. This will be followed by an amplified collision stepping back down, again to be compensated for with stance-phase acceleration.

There are several advantages to the anticipated case. It is particularly economical to speed up before the bump, and apply a pre-emptive push-off prior to the collision. This then requires less speed-up after the bump, although some extra hip extension would still be expected for the stance phase on bump and perhaps the subsequent step after the collision.

We measured the effect of bumps on the gait of 8 healthy adults. In the Visible cases, subjects could see the perturbation coming, and hear the foam slid-

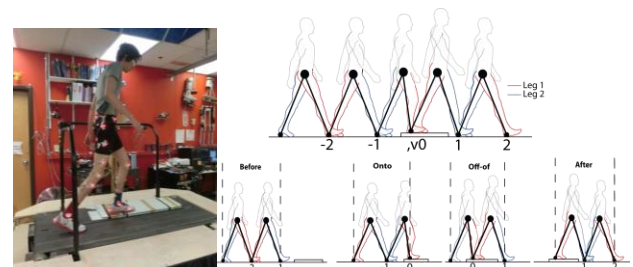


Figure 1: The experiment (left) and model (right) for bump and surrounding steps.

ing on the treadmill before it was released. In Not-Visible tests they wore basketball dribbling glasses (obstructing lower part of vision) and headphones to impede hearing. The steps were termed Before, On-to, Off-of, and After bump; On-to refers to the step ending with a heel strike on bump. The heel strikes were numbered sequentially, with 0 denoting the heel strike onto the bump. We quantified step parameters and COM work rates.

RESULTS AND DISCUSSION

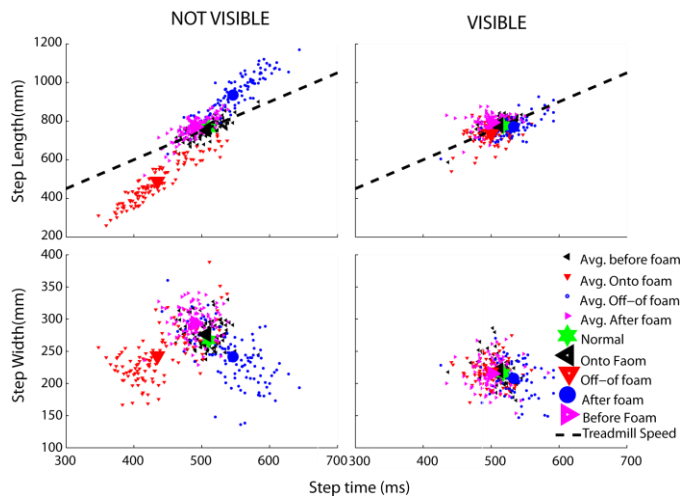


Figure 2: Step lengths and widths of steps onto, and off of bump, vs. step periods (time). Dashed line shows treadmill speed. Not-visible (left column) and Visible (right column) conditions are shown.

Step lengths and periods largely followed model predictions (Figure 2). With the Not-Visible bump, the steps onto bump were significantly shorter in length and period ($P < 0.05$), because of the unexpectedly early heel strike. The off-of bump steps were also longer in length and period due to the slower stance phase and later heel strike. Visible bumps resulted in much smaller effects, with step length differences of no more than 5%, suggesting a considerable effect when the bump is anticipated.

Work performed on the COM also largely agreed with predictions (Figure 3). These are summarized in three phases: positive Push-off work, negative Collision work with the other leg, Middle-stance work, the latter occurring in the stance phase between Collision and next Push-off (Figure 3, before bump step). With Not-Visible bumps, the onto

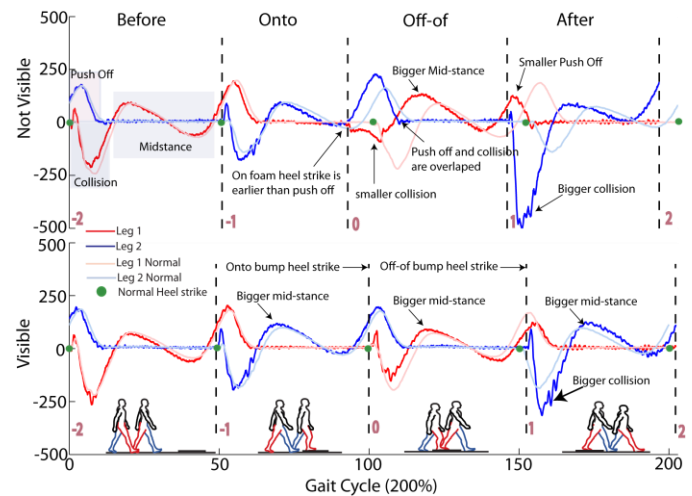


Figure 3: COM work rate vs. time for steps surrounding bump. The step ending with heel strike 0 onto bump is labeled “Onto”, with leg 1 landing on the bump.

bump heel strike (Figure 3, vertical bar 0) started early relative to Push-off, unlike normal walking [2], and with less Collision work. The middle-stance work was greater than normal in the ensuing stance phase, consistent with active speed-up originating from the hip. The Collision off the bump onto level ground was also greater, due to the downward fall of the COM. With Visible bump, the onto push-off was earlier to anticipate the early Collision. The middle-stance work was only slightly greater than normal, indicating a smaller speed-up. The same was true for the Middle-stance work in post-bump step, suggesting continued speed-up after the amplified Collision due to the stepping off the bump.

Anticipation of a minor bump in the road allows for better and smaller gait adjustments than the unanticipated case. Basic effects of a bump in the road, and the proper compensations, may be explained by a very simple dynamic walking model.

ACKNOWLEDGEMENTS

This work was supported in part by DoD (W81XWH-09-2-0142), ONR (ETOWL), NIH (AG030815).

REFERENCES

- [1] McGeer, T., 1990, *Int. J. Robot. Res.*, **9**: 68–82.
- [2] A.D. Kuo, et al. *Exerc. Sport Sci. Rev.*, **33**

DEVELOPMENT OF AN ELASTIC FORCE-FIELD TO INFLUENCE MEDIOLATERAL FOOT PLACEMENT DURING WALKING

¹Jordan Broadway, ¹Elizabeth T. Nyberg, and ^{2,1}Jesse C. Dean

¹Medical University of South Carolina, Charleston, SC, USA

²Ralph H. Johnson Veterans Affairs Medical Center, Charleston, SC, USA

email: deaje@musc.edu

INTRODUCTION

Active control of mediolateral foot placement is an important contributor to bipedal walking stability. Results from human walking experiments (1) and model simulations (2) indicate that appropriate foot placement is a relatively simple, economical strategy for stabilizing gait. Recently, we found direct evidence that uninjured humans actively modulate their mediolateral foot placement based on the mechanical state of their center of mass (3).

However, this gait stabilization strategy may be disrupted in clinical populations. For example, stroke survivors often walk with their paretic leg placed quite far laterally (4), likely due in part to a reduced ability to accurately control their foot placement (5). This disruption of the mechanically-appropriate control over foot placement may contribute to the increased fall risk among this population.

While the importance of mediolateral foot placement during human walking is generally accepted, it has thus far been difficult to investigate this topic through direct experimental manipulation. Instead, previous work has typically observed gait behavior in various contexts, and used trends in foot placement location to provide insight into the underlying mechanical principles.

Based on the current limitation in our ability to experimentally manipulate foot placement during human walking, we have developed a simple elastic force-field. The purpose of these initial experiments was to determine whether our force-field is able to influence mediolateral (ML) foot placement without altering the anteroposterior (AP) gait progression required for normal walking.

METHODS

We built an elastic force-field designed to exert controllable ML forces on the swing leg while walking on a treadmill. The force-field (Fig. 1) consists of two nylon-coated steel wires running parallel to the treadmill belts, in series with extension springs. The wires are secured to load cells on rolling trolleys, which can be quickly repositioned using linear actuators. The wires pass through vertically-oriented slots on leg cuffs strapped laterally to the participants' legs, a setup with minimal friction during AP leg motion.

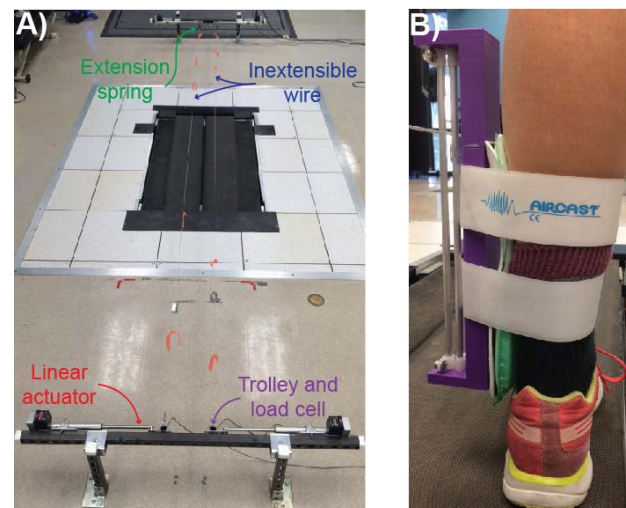


Figure 1. Force-field (A) and leg cuff (B).

We quantified the AP and ML forces exerted by the wires on the leg cuffs, using a calibration frame to position the cuff around a grid above the treadmill. Net AP forces were always small ($<1.4\text{N}$), while net ML forces clearly varied with ML position (Fig. 2A), forming a “channel”. The depth of this channel (indicative of how strongly deviations from the central ML position are resisted) was slightly influenced by the series spring stiffness, and more strongly by the initial spring pre-load (Fig. 2B).

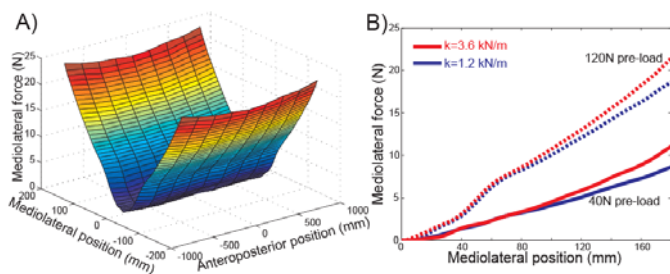


Figure 2. ML forces varied with ML position (A), as modulated by spring pre-load and stiffness (B).

We tested whether the force-field (pre-load=120N; stiffness=3.6 kN/m) had the desired effect of influencing ML foot placement without altering AP progression. Six control participants (3M/3F; age=23.2±0.4 yrs; height=1.77±0.11 m; mass=72±14 kg; mean±s.d.) performed seven 3-minute trials while walking on a treadmill at 1.25 m/s. In the first and last trials, participants walked normally. In the other randomized-order trials, participants walked with the force-field set to one of five positions (encouraging step widths of 0, 10, 20, 30, or 40 cm).

We calculated average step width and length based on LED markers placed on the left and right heels. We used repeated-measures one-way ANOVAs to determine whether walking in the force-field influenced either of these spatiotemporal metrics.

RESULTS AND DISCUSSION

Walking in the force-field significantly ($p<0.0001$) influenced step width (Fig. 3A). As expected, participants walked with wider steps when the force-field channels were far apart and narrower steps when the force-field channels were closer together. In contrast, the force-field had no apparent effects on step length ($p=0.60$; Fig. 3B). These initial results indicate that our simple elastic force-field can influence ML foot placement during walking without interfering with AP progression.

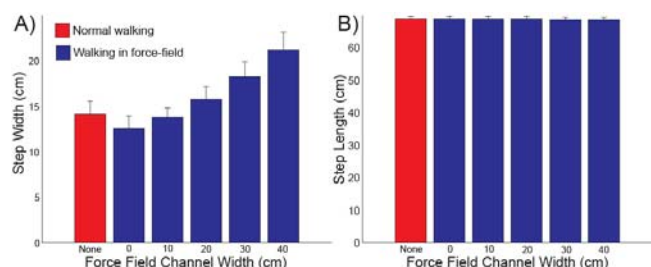


Figure 3. Walking in the force-field influenced step width (A) but not step length (B).

While the force-field influenced step width, participants did not simply adopt the step width encouraged by the force-field. Instead, step width appeared to be a compromise between the normal step width and the prescribed force-field width (Fig. 4). Based on these initial results, participants may have been more reluctant to walk with the narrower-than-normal step widths encouraged by the force-field, although this requires further investigation.

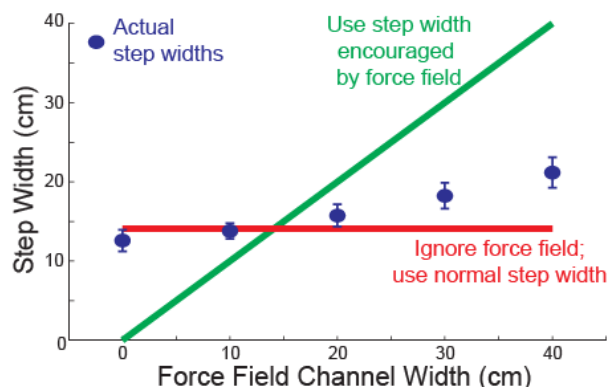


Figure 4. Actual step widths fell between normal values and those encouraged by the force-field.

CONCLUSIONS

We have developed a force-field which can be used to alter ML foot placement without affecting AP progression. Our device will allow us to conduct controlled experimental investigations of how ML foot placement contributes to bipedal gait stability among both controls and clinical populations.

REFERENCES

1. Bauby CE, Kuo AD. *J Biomech* **33**, 1433-1440, 2000.
2. Kuo AD. *Int J Robot Res* **18**, 917-930, 1999.
3. Rankin BL, et al. *J Neurophysiol* **112**, 374-383, 2014.
4. Balasubramanian CK, et al. *Clin Biomech* **25**, 483-490, 2010.
5. Zissimopoulos A, et al. *Gait Posture* **39**, 1097-1102, 2014.

ACKNOWLEDGEMENTS

This work was partially funded by Department of Veterans Affairs grant #IK2 RX000750.

DYNAMIC RELIABILITY AND VALIDITY OF PRESSURE-MEASURING INSOLES

¹ Jessica DeBerardinis, ¹ Mohamed B. Trabia, Ph.D., ² David Samson, and ² Janet S. Dufek, Ph.D.

¹ Department of Mechanical Engineering, University of Nevada Las Vegas, Las Vegas, NV, USA

² Department of Kinesiology and Nutrition Sciences, University of Nevada Las Vegas, Las Vegas, NV, USA
email: deberj1@unlv.nevada.edu

INTRODUCTION

Several commercial insole systems are available for measuring plantar pressure during dynamic activities. Researchers have typically tested the reliability and/or validity of these systems by using static weights or by selecting specific anatomical sites such as, the heel pad region or the metatarsal heads of the foot [1, 2]. We argue that the dynamic validity of these systems should be evaluated by the inclusion of all active sensors in the system during walking. The purpose of the study was to examine the reliability and validity of pressure measuring insoles across the entire plantar surface of the foot during walking.

METHODS

Thirty volunteers (15M, 15F, 26.3±5.9 yrs., 73.1±21.2 kg) granted institutionally approved written consent to participate. After demographic data was obtained, participants were fitted with insoles that closely matched their foot size. The insoles (Medilogic; Schönefeld, Germany; 60 Hz) were placed inside their socks, next to the skin. The subjects were then asked to perform the following: sit and lift their feet off the floor (~2-4 cm) for five seconds, stand stationary for 15 seconds, sit again and lift their feet off the floor for five seconds, and finally, stand and walk approximately five meters at a self-selected pace over two consecutive force platforms (Kistler, Winterthur, Sweden; 1000 Hz), placing only one foot on each platform. Each subject repeated this task until three successful trials were obtained, which was defined as having full contact by each foot with each force platform.

The force and pressure data were filtered using a low pass Butterworth filter with a cutoff frequency of 1/8 of the sampling frequency. The pressure data were

transformed into force data by multiplying the pressure measured by each sensor by the area of the sensor (1.125 cm²). Then, DC bias for the insole data was removed by subtracting the average of the first no load (feet in air) measurements from all subsequent force values.

Insole force data were next calibrated by dividing the average force measured while fully loaded (subject standing) by the recorded weight of the subject. This calibration factor was then applied to the insole force measurements. The insoles only measure pressure in the sagittal plane. Thus, to provide comparison, we excluded the measured force component that was normal to the sagittal plane:

$$F_N = \sqrt{F_y^2 + F_z^2} \quad Eq(1)$$

where, F_y and F_z are the anterior-posterior and vertical components of the ground reaction force, respectively.

Dependent variables (DVs) included bilateral assessment of the first ($F1$) and second ($F2$) vertical ground reaction force maxima and the local minimum (FM) between these two maxima for the F_N curve. Support time (ST) was also identified. The time of occurrences of the force platform and insole variables were matched. The insole force values at the times of occurrence of the three force variable were used to represent force measured by the insoles. The effect of limb on the force insole variables was also considered. It was observed that the force-time curves of the force platforms and insoles qualitatively matched in only 25% and 32% for the left and right feet respectively (Figure 1). Data were statistically evaluated using a two-way (instrument x limb), repeated measures ANOVA (SPSS, version 22; $\alpha=0.05$).

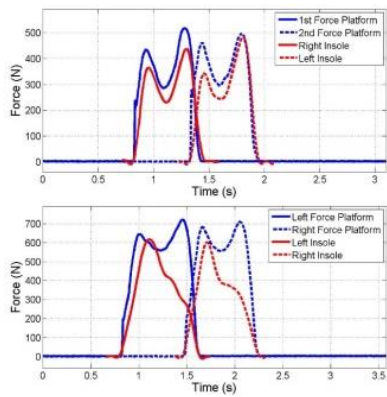


Figure 1. An exemplar qualitatively strong (top) and weak match (bottom) between the insoles and the force platforms.

RESULTS AND DISCUSSION

Descriptive data are given in Table 1 while ANOVA summary is shown in Table 2. The results showed that there was no significant interaction or limb main effects. However, there was a significant main effect for instruments, suggesting that the force platforms and the insoles were not measuring the same force values during walking, which was additionally supported by the observed qualitative differences in the force curves.

Table 1. Main effect (Instrument, Limb) mean and standard deviation values for all DVs. Each instrument includes both left and right limb while the limbs (left and right) include both instruments.

	Force Platform	Insole	Left	Right
F1 (BW_s)	1.06±0.09	0.69±0.23	0.87±0.02	0.83±0.02
FM (BW_s)	0.86±0.10	0.74±0.16	0.83±0.02	0.76±0.02
F2 (BW_s)	1.09±0.12	0.65±0.15	0.89±0.02	0.85±0.02
ST (s)	0.81±0.12	0.86±0.13	0.84±0.02	0.83±0.02

CONCLUSIONS

The objective of this research was to dynamically assess the reliability and validity of pressure-sensing insoles. Reliability was supported, by lack of between-limb-differences. The small effect size for limb (average $\delta^2 = 0.046$), suggested bilateral internal consistency between matched insole pairs. Differences were observed in the force values

measured across the entire plantar foot surface between force platforms and pressure-sensing insoles, with the insoles underestimating the forces, suggesting lack of validity between forces measured with force platforms versus these insoles. Qualitative differences in the shape of the time-force curves were also observed. A possible explanation may be the dampening characteristics of the insoles; being incapable of relaxing to normal at a fast enough rate. Therefore, one should be cautious when using these insoles to represent plantar forces during gait. Further research may explore help better understand the insoles characteristics.

Table 2. ANOVA summary for main effects and interactions for each dependent variable.

	F	p	δ^2
F1			
Instrument	196.15	0.001	0.772
Limb	1.47	0.231	0.025
Instrument x Limb	0.09	0.771	0.001
FM			
Instrument	40.75	0.001	0.413
Limb	7.59	0.008	0.116
Instrument x Limb	8.89	0.004	0.133
F2			
Instrument	400.19	0.001	0.873
Limb	2.41	0.126	0.040
Instrument x Limb	2.93	0.092	0.048
ST			
Instrument	122.40	0.001	0.678
Limb	0.20	0.660	0.003
Instrument x Limb	0.22	0.641	0.004

REFERENCES

1. Kernozek TW, et al. *Foot and Ankle International*, **17**, 204-209, 1996.
2. Price C, et al. *J Foot and Ankle Research* **7**, A67: 1-2, 2014.

ACKNOWLEDGEMENTS

The authors would like to acknowledge the support provided to the first author by the University of Nevada, Las Vegas in the form of a Doctoral Graduate Research Assistant Award.

FEMORAL NECK LOADS IN YOUNG AND OLDER ADULTS DURING STAIR ASCENT AND DESCENT

¹Chen Deng, ¹Jason C. Gillette, ¹Timothy R. Derrick

¹Iowa State University, Ames, IA, USA

email: chend@iastate.edu ; web: [http:// www.kin.hs.iastate.edu/](http://www.kin.hs.iastate.edu/)

INTRODUCTION

Hip pain is a daily occurrence in 14.3% of adults 60 years and older [1] and is a risk factor for falls and hip fractures in older adults [2]. The femoral neck is of particular concern with hip fractures since 50% of femoral fractures occur at this site [3]. The loading environment of the femoral neck can be analyzed to estimate how bone loads are changed by age and physical activities, which may provide further understanding of hip pain and cumulative damage to the femoral neck for older adults. In this study, femoral neck stresses were estimated during stair ascent and descent for both healthy young and older adults. Greater femoral neck stresses were expected for older adults due to bone loss in this area. This may help explain the increased hip pain and fall risk among older adults.

METHODS

seventeen older adults (7 males, age: 60 ± 6 yr, body mass: 75 ± 14 kg, height: 1.73 ± 0.05 m; 10 females, age: 57 ± 5 yr, body mass: 67 ± 8 kg, height: 1.67 ± 0.05 m) and twenty young adults (10 males, age: 23 ± 3 yr, body mass: 80 ± 14 kg, height: 1.76 ± 0.07 m; 10 females, age: 23 ± 3 yr, body mass: 62 ± 10 kg, height: 1.70 ± 0.07 m) with no lower limb injuries volunteered to participate. All subjects performed 5 successful trials of stair ascent and 5 successful trials of stair descent with a 3-stair staircase. Motion capture data (160 Hz, Vicon MX, Vicon, Centennial, CO, USA) and force data (160 Hz, AMTI, Watertown, MA) were collected during each trial.

Raw force data and motion capture data were input into Matlab programs and low-pass filtered at 6 Hz. Inverse dynamics with rigid body assumptions was used to calculate 3-D joint moments and reaction forces at the hip, knee and ankle joints of the right leg. A musculoskeletal model was used to obtain maximal dynamic muscle forces, muscle moment

arms and orientations for 44 lower limb muscles at each time point. Static optimization was used to select a set of muscle forces that minimized the sum of the squared muscle stresses and balanced the sagittal plane hip, knee and ankle moments, frontal plane hip moment, and the transverse plane hip and ankle moments with the external moments for each frame of data. Muscle forces, joint reaction forces and joint moments were used to estimate the 3-D moments and forces at the midpoint of the femoral neck. These loads were applied to an individualized elliptical model of the bone structure to estimate the stresses on the periphery of the anterior, posterior, inferior, and superior portion of the femoral neck. The outer and inner diameters were estimated by the age and gender specific quadratic prediction equations [4] and the ratio of maximal to minimal diameters [5].

MANOVA was used to compare maximum femoral neck stresses between young and older adults for stair ascent and descent. Experiment-wise alpha was set as 0.05. The univariate ANOVAs used alpha = 0.05 if MANOVA was significant. Statistical analyses were performed using IBM SPSS Statistics 22.

RESULTS AND DISCUSSION

MANOVA indicated a significant main effect on maximum femoral neck stresses for young vs. older adults during stair ascent ($p = 0.011$) and descent ($p = 0.011$).

Figure 1 shows that femoral neck stresses were predominantly compressive on the anterior, posterior and inferior aspects and mostly tensile on the superior aspect. There were generally two peaks (P1 and P2) on the stress curves.

As shown in Table 1, young adults had a higher maximum tensile stress at the superior femoral neck site for P1 ($p = 0.01$). Older adults had higher

compressive stress at the posterior femoral neck site for P2 ($p = 0.007$). No significant differences were found during stair ascent for the other maximum stresses at the anterior (P1: $p = 0.572$; P2: $p = 0.791$), posterior (P1: $p = 0.371$), superior (P2: $p = 0.171$), and inferior (P1: $p = 0.478$; P2: $p = 0.577$) sites. There were no differences during stair descent for maximum stress at the anterior (P1: $p = 0.784$; P2: $p = 0.912$), posterior (P1: $p = 0.073$; P2: $p = 0.131$), superior (P1: $p = 0.209$; P2: $p = 0.541$), and inferior (P1: $p = 0.113$; P2: $p = 0.511$) site.

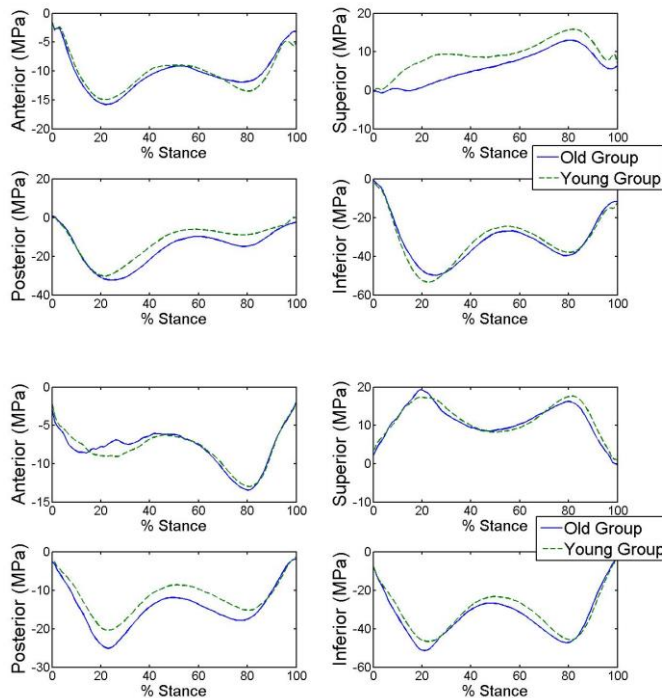


Figure 1. Ensemble averages of femoral neck stresses at 4 sites during stair ascent (upper graph) and descent (lower graph). Positive values indicate tension, negative values indicate compression.

Most femoral neck stresses were statistically similar when comparing young and older adults during stair ascent and descent. One comparison where older adults had significantly higher maximum femoral neck stresses was at the posterior site during stair ascent. The increased compressive stresses at the posterior femoral neck may be of interest in terms of potential effects on cumulative bone structure damage and hip joint pain for older adults.

CONCLUSIONS

With one exception, comparisons did not support the research expectation that older adults would have higher femoral neck stresses in stair ascent and descent, which are activities associated with hip joint pain and fall risk. Greater compressive stresses in the posterior femoral neck during stair ascent are of potential concern. Femoral neck models for older adults that incorporate individualized bone mineral densities, accumulated micro-damage merit further investigation.

REFERENCES

1. Christmas C, et al. J FAM PRACTICE 51(4), 345, 2002.
2. Leveille SG, et al. JAMA-J AM MED ASSOC, 302(20), 2214-2221, 2009.
3. Niva MH, et al. JBJS 87-B, 1385-1390, 2005.
4. Beck TJ, et al. J BONE MINER RES 15, 2297-2304, 2000.
5. Bell, KL, et al. J BONE MINER RES 14(1), 111-119, 1999.

Table 1. Means (SD) of peak stresses (MPa) at 4 sites of the femoral neck for young and older adults during stair ascent and descent. P1 indicates peak 1, P2 indicates peak 2. Values in bold indicate significant differences for older adults as compared to young adults.

Stress Sites	Stair ascent				Stair descent			
	Young		Old		Young		Old	
	P1	P2	P1	P2	P1	P2	P1	P2
Superior	13.20 (6.15)	17.71 (7.64)	8.51 (3.82)	14.68 (5.01)	21.80 (3.64)	19.61 (7.20)	24.79 (9.70)	18.03 (8.39)
Inferior	-55.73 (13.33)	-40.95 (11.81)	-52.89 (10.23)	-42.95 (9.36)	-50.73 (10.11)	-48.17 (12.14)	-57.50 (15.06)	-51.06 (14.33)
Anterior	-16.51 (4.58)	-14.83 (5.22)	-17.66 (7.57)	-14.24 (7.96)	-12.49 (5.52)	-14.75 (6.11)	-12.99 (5.54)	-14.96 (5.32)
Posterior	-31.63 (9.83)	-11.36 (5.02)	-34.78 (11.30)	-17.71 (8.23)	-21.97 (9.15)	-16.74 (4.39)	-27.81 (10.08)	-19.86 (7.69)

Gender Differences in the Association Between Acute Articular Cartilage Metabolism and Ambulatory Kinetics

W. Matt Denning^a, Michael Becker Pardo^b, Jason G. Winward^b, Iain Hunter^b,
Sarah Ridge^b, J. Ty Hopkins^b, Allen C. Parcell^b, Matthew K. Seeley^b

^aWeber State University, Ogden, UT, USA; ^bBrigham Young University, Provo, UT, USA

Email: mattdenning@weber.edu

INTRODUCTION

Females have an increased prevalence of knee articular cartilage (AC) degradation [1]. Serum cartilage oligomeric matrix protein (COMP) has emerged as a reliable biomarker that reflects AC turnover. In able-bodied individuals, serum COMP concentration increases in response to physical activity, and this increase is thought to represent AC metabolism due to exercise-induced load [2]. Baseline serum COMP concentration and the acute COMP increase due to physical activity differ between males and females [3, 4]. It is unclear, however, if certain ambulatory mechanical variables are associated with acute serum COMP concentration increase, and if this correlation varies between genders. Identifying which mechanical variables are most closely associated with acute serum COMP concentration increase, due to physical activity for each gender, may provide further insight regarding possible mechanisms leading to AC degradation differences. The purpose of this study was to evaluate gender differences in the associations between serum COMP change and ambulatory kinetics.

METHODS

Eighteen able-bodied subjects (Table 1) completed three data collection sessions (slow, medium, fast) in a counterbalanced order, separated by 24 hours. For the slow session, subjects walked at a preferred speed. For the medium and fast sessions, subjects ambulated at speeds of 50% and 100% greater than the preferred walking speed. For each session, subjects ambulated 4000 steps. Ten high-speed video cameras (240 Hz) and an instrumented treadmill (1200 Hz) captured synchronized video and ground reaction force data for five stance phases at 1000, 2000, 3000, and 4000 steps. Several discrete mechanical variables that have been linked to knee

load during ambulation were averaged across these 20 stance phases. Also, 3-ml blood samples were collected immediately pre- and post-ambulation for each session. COMP was determined using an enzyme-linked immunosorbent assay. A stepwise multiple linear regression analysis, for each gender, was used to evaluate the associations between serum COMP change (post-walk concentration minus pre-walk concentration) and the discrete mechanical variables, which included peak vertical ground reaction force (vGRF), vGRF load rate (LR), and peak net internal hip flexion (HF), hip extension (HE), hip abduction (HAB), knee flexion (KF), knee extension (KE), knee abduction (KAB), plantarflexion (PF) and ankle inversion (AI) moments. Further, an independent *t*-test was used to compare change in serum COMP concentration, due to ambulation, between genders ($\alpha = 0.05$).

Table 1. Subject demographics (mean \pm SD)

	N	Age (yrs)	Mass (kg)	Height (m)
Male	9	24 \pm 1	75.7 \pm 6.7	1.76 \pm 0.07
Female	9	22 \pm 2	61.0 \pm 5.6	1.64 \pm 0.05

RESULTS AND DISCUSSION

For male subjects, the multiple regression analysis produced a model that explained 78% of the total variance in serum COMP change (adjusted $R^2 = 0.72$). This model included the following significant predictor variables: LR ($p = 0.01$), PF ($p < 0.01$), vGRF ($p < 0.01$), HAB ($p = 0.03$), and HE ($p = 0.05$). The relationship between these predictor variables and serum COMP change, due to ambulation, was defined by the following prediction equation:

$$\Delta COMP = 5.6 + 1.9 (LR) + 40.6 (PF) + 48.6 (vGRF) + 24.5 (HAB) - 29.0 (HE)$$

For female subjects, the resulting model explained 24.5% of the total variance in serum COMP change

(adjusted $R^2 = 0.23$). This model included only KE as a significant predictor ($p = 0.01$) and defined by the following prediction equation:

$$\Delta COMP = -8.16 + 12.4 (KE)$$

Additionally, when pooled between all speeds, average serum COMP concentration change, due to ambulation, was significantly greater for males ($30.3 \pm 20.2 \text{ ng}\cdot\text{ml}^{-1}$), relative to females ($12.5 \pm 19.1 \text{ ng}\cdot\text{ml}^{-1}$; $p = 0.002$).

Our findings indicate that an increased KE is associated with greater increase in serum COMP change for females (Figure 1). For males, increased LR, PF, HAB, and vGRF, and decreased HE is associated with a greater increase in serum COMP change due to ambulation.

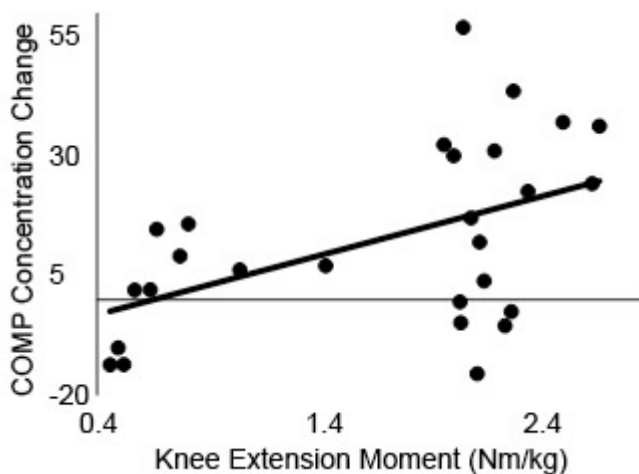


Figure 1. Regression plot and line depicting the relationship between serum COMP change and KE for females.

These findings corroborate other data that indicate compressive knee load is related to ground reaction force characteristics and lower-extremity joint moments, and that these forces and moments may

contribute to AC breakdown [5]. It is difficult to explain the regression model differences between genders. One possible explanation may be the difference in ambulation speed. On average, ambulation speed for female subjects was 23% less than male subject's speed. The difference in speed could be one reason why males generally had higher peak kinetic variables (Table 2) and greater serum COMP concentration change. Further studies need to be conducted to address this issue.

CONCLUSIONS

Acute articular cartilage metabolism, due to physical activity, can be partially explained by ambulatory kinetics. For males, increased serum COMP change correlated with the joint moments of the ankle and hip and ground reaction force characteristics, while the internal knee extension moment partially explains acute serum COMP change in females.

These data could provide useful information for researchers and clinicians who measure either ambulatory mechanics or serum COMP in efforts to learn more about the effects of physical activity on articular cartilage. Further examination of these significant predictor variables, for each gender, is warranted within populations who suffer from joint pathologies involving AC degradation.

REFERENCES

1. Srikanth V, et al. *Osteoarthritis Cartilage*, **13**, 769-781, 2005.
2. Niehoff A, et al. *Eur J Appl Physiol*, **110**, 651-675, 2010.
3. Kersting U, et al. *Osteoarthritis Cartilage*, **13**, 925-934, 2005.
4. Denning M, et al. *Med Sci Sport Exer*, **47:5** Supplement, 2015.
5. Herzog W, et al. *Langenbecks Arch Sug*, **388**, 305-315, 2003.

Table 2. Mean (SD) values for vGRF (BW), LR (BW·s⁻¹), and lower extremity moments (Nm·kg⁻¹).

	vGRF	LR	PF	AI	KF	KE	KAB	HF	HE	HAB
Male	2.00 (0.59)	14.4 (6.9)	2.31 (0.63)	0.33 (0.10)	0.41 (0.11)	1.94 (0.92)	0.66 (0.24)	0.58 (0.13)	0.89 (0.23)	1.32 (0.34)
Female	1.93 (0.56)	12.63 (5.87)	2.01 (0.53)	0.30 (0.13)	0.30 (0.10)	1.67 (0.77)	0.71 (0.32)	0.65 (0.18)	0.68 (0.23)	1.43 (0.41)

SAMPLE ENTROPY OUTPERFORMS APPROXIMATE ENTROPY FOR HOUR-LONG OVERGROUND AND TREADMILL WALKING

¹ William C. Denton, ¹ Eric J. Pisciotto and ¹ Jennifer M. Yentes

¹ University of Nebraska at Omaha, Omaha, NE, USA
email: wdenton@unomaha.edu, web: cobre.unomaha.edu

INTRODUCTION

Entropy provides a measurement of how much information is present in a system [1]. The amount of information relates to the predictability of a time series: how periodic or random it is [2]. Approximate entropy (ApEn) and sample entropy (SampEn) are two commonly used entropy measures in biomechanics. Both measures use a vector length m , which compares each vector to all other vectors of the same length throughout a time series to see if they fall within a tolerance r ; however, SampEn removes the bias of self-matches for each vector and is generally preferred to ApEn [1]. The last parameter of SampEn and ApEn is the length of data N , which has been shown to have a larger affect on ApEn in short biological data sets [2]. Typically, biomechanical data sets are very short (e.g., <200 data points) and it has been found that SampEn is more reliable than ApEn for shorter data sets [2]. Further, SampEn has relative consistency for short data sets because the entropy value does not ‘flip’ based on the data length. Therefore, the primary aim of this study was to investigate the relative consistency and independence to N of both ApEn and SampEn when larger biomechanical data sets are available. It was hypothesized that SampEn will maintain relative consistency across multiple data lengths whereas, ApEn will demonstrate issues with relative consistency as data length changes.

Furthermore, there have been quite a few studies that have found differences in kinematic [3, 4], kinetic [4], and other biomechanical measures [4] between overground and treadmill walking. However, the set speed of the treadmill may have a much larger effect on nonlinear measures (such as entropy) when compared to a variable speed while walking overground. The secondary purpose of this experiment was to determine the effect on entropy

of walking overground versus on a treadmill. It was hypothesized that overground walking will have a larger entropy value (less periodic) than treadmill walking (more periodic) for both ApEn and SampEn.

METHODS

Fourteen volunteers (age: 25 ± 4.2 years, height: 170.8 ± 11.9 cm, weight: 69.4 ± 16.9 kg) participated in this research. No one reported lower extremity injuries or pathology that would affect normal gait.

Each participant was required to make two separate visits. They were instrumented with footswitches (Trigno™ 4-channel FSR Sensor, Delsys Inc., Natick, MA) during both visits to record heel strikes while walking. The first visit consisted of the participant walking on an overground (eighth-mile) track for one hour. The second visit was completed on a treadmill, walking at a self-selected speed, for one hour. The data from both trials was processed using MATLAB code that detected heel strikes and output step times: a temporal measure of the time from heel strike to the following heel strike of the opposite foot.

SampEn(m, r, N) and ApEn(m, r, N) were calculated on the two trials of step time data. The following parameter ranges were used for a total of 80 parameter combinations:

- Vector length to be compared – m : 2 and 3.
- Similarity tolerance – r : 0.15, 0.2, 0.25, and 0.3 times the standard deviation of the entire data set.
- Data length – N : 500, 1000, 1500, 2000, 2500, 3000, 3500, 4000, 4500, and 5000.

For ApEn and SampEn, a value of 0 indicates a perfectly repeatable time series. For perfect white noise, ApEn will result in a value of 2 and SampEn has no upper limit. Independent t-tests were used to determine the effect of mode (overground vs

treadmill) for ApEn or SampEn. Dependent t-tests were used to determine the effect of parameter choice on ApEn and SampEn.

RESULTS AND DISCUSSION

Supporting our first hypothesis, SampEn maintained relative consistency across all data lengths and for all combinations of parameters. However, ApEn demonstrated issues with relative consistency. As can be seen in Figure 1, when $r=0.20$, ApEn for the treadmill condition is less than that of the overground condition at a N of 500 but as the data length increases, the ApEn values ‘flip’ and the treadmill entropy value becomes greater than the overground value at $N=2500$. SampEn also demonstrated independence of data length. The entropy value using ApEn grew much faster than SampEn (Figure 1). Furthermore, due to the elimination of the self-matching in the SampEn calculation, for every parameter combination SampEn was significantly greater than ApEn (Figure 1). The differences in SampEn values using different tolerances (r) are illustrated in Figure 2. The condition with greater entropy value switched between treadmill and overground for tolerance values $r = 0.2$ and 0.25 for all data lengths.

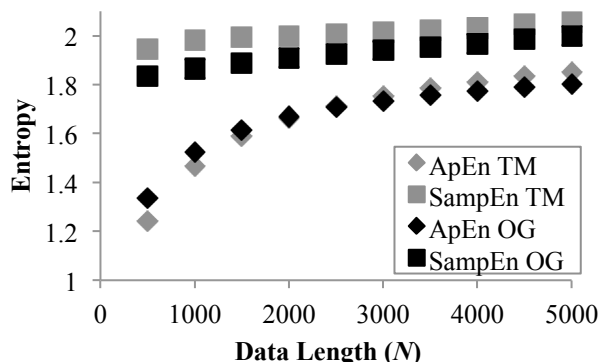


Figure 1. ApEn vs. SampEn in both overground (OG) and treadmill (TM) walking using a tolerance of $r = 0.2$ and vector length $m = 2$.

Treadmill entropy values for SampEn were always greater than the overground entropy values, although this was never significant. This was opposite of the hypothesis and may be caused by the need to adapt normal walking speed fluctuations to maintain position on the treadmill belt. On the other

hand, using ApEn, the treadmill had larger entropy only after 2500 steps and smaller entropy for overground trials, demonstrating a lack of relative consistency.

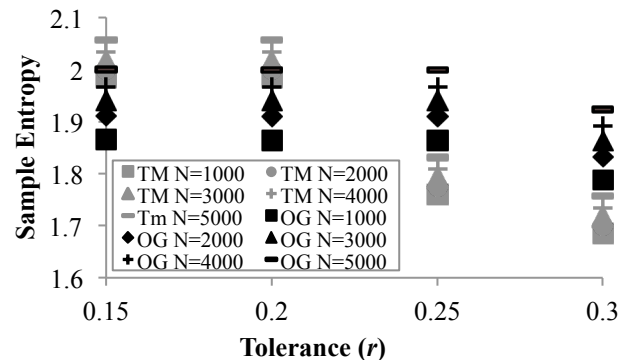


Figure 2. Effect of data length and tolerance on SampEn using vector length $m = 2$.

CONCLUSIONS

SampEn should be used over ApEn for all biological data lengths, as it is consistent and independent across all data lengths. Further emphasis is put on the selection of the tolerance r for both SampEn and ApEn and data length N for ApEn. Using an improper parameter combination may result in reporting findings that are an artifact of parameter selection. Entropy should be calculated at a large range of different parameter selections and analyzed fully before a final set of parameters is selected to ensure relative consistency.

REFERENCES

1. Bravi, A et al. *Biomed Eng Online*, **10**, 1-27, 2011.
2. Yentes, JM et al. *Ann Biomed Eng*, 349-365, 2013.
3. Alton, F et al. *Clin Biomech*, 434-440, 1998.
4. Lee, SJ and Hidler, J. *J Appl Physiol*, 747-755, 2008.

ACKNOWLEDGEMENTS

We would like to thank Joshua Pickhinke, Mike Hough, and Casey Caniglia for their assistance in this project. Funding for this project was provided by NASA Nebraska EPSCoR.

The effect of leg retraction on stability during running

Nihav Dhawale and Madhusudan Venkadesan

Department of Mechanical Engineering and Material Sciences, Yale University, USA

Email: nihav.dhawale@yale.edu, Web: <http://mvlab.yale.edu>

1 Introduction

Simple models of running with spring-like and mass-less legs (SLIP models) show improved stability when the swing leg is retracted at higher speeds [1], and experimental data show increased rate of retraction of the swing-leg when running on terrains with steps [2]. Recent work [3] with robots and detailed models of that robot suggest that there is a trade-off between energetics and stability, and not the simple relationship between stability and swing-leg retraction that was predicted by spring-legged inverted pendulum (SLIP) models of running. However, the mechanical basis for how swing-leg retraction affects stability versus energetics remains unknown. Here, we analyze an alternative model for running [4], which includes many realistic features including dissipative collisions, active-push-off, swing-leg retraction, and yet remains mathematically tractable and generalizable across running animals. We find that instabilities associated with loss of balance in the sagittal plane (*tumbling*) are the major source of instability on uneven terrains. Importantly, truly open-loop running is most stable when retraction rate is zero. In contrast, an optimal leg retraction speed exists if the runner estimates the slope of the terrain at touchdown in planning a leg retraction strategy. On uneven terrains, this once-per-step sensory strategy shows far superior performance than any open-loop runner by stabilizing the orientation of the runner.

2 Methods

Following [4], we approximate the runner as an impulsive bouncing disc in the sagittal plane. Drag-free projectile flight phases are punctuated by stance when an impulse redirects the disc's momentum. Stance is modeled as an impulse-rigid response where the total

impulse (force integrated over time) during stance is prescribed by an appropriate collision law. The collision consists of two sub-phases, a passive collision that is modeled by two coefficients of restitution (normal ϵ_n and tangential ϵ_t) applied at the point of contact, and an active impulse (two force-impulses and one torque-impulse), applied in a constant direction with respect to the lab frame. Sensors detect contact and determine when to apply an impulse against the ground, but no other knowledge of the terrain or ball's state is used. In that sense, this model is open-loop. The constant impulse is chosen such that the bouncing mass will execute a perfectly periodic trajectory on flat ground. Where the tangential collision is inelastic, we include a torque-impulse term that would maintain a constant orientation on flat ground.

The normal coefficient of restitution, ϵ_n , models elastic energy storage, and the tangential coefficient of restitution models swing leg retraction. We assume that the foot does not slip on the ground, and therefore the tangential coefficient of restitution should always equal to 0. However, retracting the leg at a constant rate, reduces the tangential collision. Consider a runner of leg length r_{ball} (equal to the disc's radius) that moves on a flat ground with a forward speed v_x , and a leg retraction rate of ω_{ret} . When ω_{ret} is exactly equal to v_x/r_{ball} , there is no longer any tangential collision, equivalent to $\epsilon_t = 1$, because the foot is moving forward at zero speed at the instant of contact. Following this logic, ϵ_t for a runner whose speed in the direction tangential to the terrain is v_t is given by,

$$\epsilon_t = \frac{\omega_{ret} r_{ball}}{v_t} \quad (1)$$

Therefore maintaining a constant ϵ_t requires knowledge of the tangential speed with respect to the terrain,

i.e. both the forward speed, and the slope of the terrain at the oncoming point of touchdown. A constant leg retraction rate will cause ε_t to vary with changes in the terrain's slope and with speed fluctuations. Using a constant ω_{ret} is therefore an open-loop strategy, while a constant ε_t is a once-per-step sensing and anticipatory strategy.

Simulations used $\varepsilon_n = 0.6$ ($\sim 40\%$ elastic energy storage for human running), speed = 3m/s, ensemble size = 10^5 , orientation bounds = $\pm\pi/6$ from vertical, based on angle between legs at typical step length.

3 Results and Discussion

The optimal open-loop runner, with a constant leg retraction speed, is one with no leg retraction at all (figure 1). However, the number of steps to failure depends only weakly on the leg retraction strategy used, varying from 6–10 steps (median of 100,000 runners) at the extremes of leg retraction rates. By comparison, the closed-loop strategy that incorporates the oncoming slope of the terrain in selecting a leg retraction rate, performs nearly an order of magnitude better. The optimal closed loop strategy consists of retracting the leg at the exactly the speed that would minimize the tangential collision, and runs for 36 steps. However, not retracting the leg fast enough, or too fast, are both detrimental for the closed-loop runner, and at the extremes, the performance is as bad as the open-loop runner.

In open-loop operation, almost all ($> 99\%$) of failures are due to violations of orientation bounds (headhits). The optimal closed-loop runner fails only due to a violation of speed bounds, and with increasing suboptimality of the retraction strategy, the proportion of headhits (stumbling forward or backward) increase.

Because we only consider impulses, and not detailed time history of forces, the results of our simulation are more generally applicable than models which assume specific mechanisms for force transmission. However, unlike SLIP models, our model can address realistic ground collisions, energy consumption, and rough terrains with slope variations. Therefore, we propose this model as a generalized template to understand the mechanics of running, and perhaps as a design guide for robotic runners.

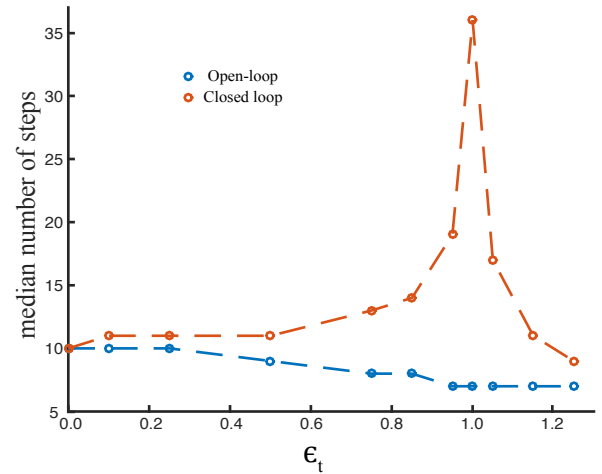


Figure 1. Median number of steps for the open and closed-loop ε_t strategies on uneven terrain.

4 Conclusions

Leg retraction benefits the runner who uses sensory feedback once per step to plan a strategy. Any retraction at all is detrimental for the purely open-loop runner, but only marginally so. Therefore, under imperfect sensory feedback, our results suggest the use of a retraction policy that does not entirely eliminate tangential collisions, and relies on sensory information on the slope of the terrain to plan an optimal retraction rate.

5 Acknowledgements

The work was supported by HFSP grant RGY0091.

References

- [1] Seyfarth A, Geyer H, Herr H. Swing-leg retraction: a simple control model for stable running. *Journal of Experimental Biology*, 206, pp.2547-2555, 2003.
- [2] Birn-Jeffery AV and Daley M. Birds achieve high robustness in uneven terrain through active control of landing conditions *J Exp Biol*, 215: 2117-2127, 2012
- [3] Karssen JGD, Haberland M, Wisse M, Kim S. The effects of swing-leg retraction on running performance: analysis, simulation, and experiment. *Robotica*.
- [4] Dhawale N and Venkadesan M. Unsteady running on uneven terrains. *Dynamic Walking*, 2014.

STUDYING THE PROGRESSION OF COMPENSATION CHANGES DURING SIMULATED RECOVERY FROM INJURY

¹ Louis A. DiBerardino III, ² Harry Dankowicz and ² Elizabeth T. Hsiao-Weckslers

¹ Ohio Northern University, Ada, OH, USA

² University of Illinois at Urbana-Champaign, Urbana, IL, USA

email: l-diberardino@onu.edu

INTRODUCTION

Walking is a fundamental task most people rely on throughout their daily routine. Patients suffering from many different injuries or pathologies strive to maintain their walking ability, developing compensatory strategies to maintain a successful gait [1]. There is clinical evidence that normal gait kinematics can be retained even while the kinetic patterns are significantly different than normal [2]. While there is great interest in how patients compensate for particular injuries, much of the focus is specifically placed on the healing process in order to refine rehabilitation methods and track recovery. For example, certain populations have shown better adoption of successful compensation strategies than others during functional tasks after anterior cruciate ligament repair [3]. These results suggest a need to more fully understand the compensation strategies developed by the neuromuscular control system (NCS) throughout recovery from injury.

The underlying goal of this study was to examine the progression of changes to compensation strategies during recovery from injury. Recovery from ankle injury was simulated using a custom ankle-foot orthosis (AFO) with adjustable bidirectional resistance to ankle motion. The ankle was chosen due to its importance to gait propulsion [4], and the AFO provided a controlled experimental environment for simulating abnormal gait with known conditions [cf. 5]. Our hypothesis was that some of the compensations employed during the full perturbation would *not* change at a comparable rate with the reductions in stiffness; rather they would exhibit relative discontinuities at certain points during reduction in perturbation, or switch between coexisting strategies.

METHODS

Ten able-bodied male subjects (25.5 ± 5.1 yr, 77.4 ± 11.4 kg, 1.77 ± 0.05 m) participated after giving

informed consent. A custom AFO was fabricated for the left lower limb, outfitted with a linear pneumatic cylinder (DSNU-5/8"-5"-P; Festo, Hauppauge, NY) to restrict ankle motion by pressurization. Force produced by the cylinder was measured with a bi-axial load cell (LC202-100; Omega, Stamford, CT). The protocol encompassed two consecutive days. On the first day, subjects were fitted with the AFO and walked *without* the cylinder on a Bertec Instrumented Treadmill (Columbus, OH) to identify a comfortable walking speed and allow acclimation to the AFO. On the second day, to record motion using a three-dimensional motion-capture system (460 Datastation; Vicon, Oxford, UK), reflective markers were attached to the pelvis, lower limbs, and AFO.

The following walking assessments were then performed on the treadmill: **NC**- seven minutes wearing the AFO with zero resistance (no cylinder); **p100**- 15 minutes with the cylinder attached and pressurized to 100 psig; **p60**- seven minutes at 60 psig; **p20**- seven minutes at 20 psig; **NC2**- condition NC repeated for 15 minutes. In order to study *steady-state* compensations, marker locations, ground reaction forces, and cylinder force (for **p100**-**p20**) were recorded for the final 30 seconds of each assessment. Sagittal-plane joint angles, net muscle moments, and cylinder torque were computed using custom MATLAB code (R2012a; Mathworks, Natick, MA). To facilitate averaging, pertinent gait events were aligned using piecewise linear length normalization [6].

Each subject's average behaviors in conditions **p100** through **NC2** were compared against their normative data in **NC** *throughout* the gait cycle using the regions of deviation method [7]. Briefly, the deviation from **NC** of each subject's average behavior in each condition was computed as the distance it lay outside one standard deviation of that subject's **NC** average for each point in the cycle.

These deviations were statistically compared against zero (i.e., no deviation) with a one-sample t test at every time point in the gait cycle ($\alpha = 0.05$) [8]. All points proving significantly different were then considered *regions of deviation* from the NC condition for the group.

RESULTS AND DISCUSSION

Compensations to the increased ankle stiffness occurred throughout the gait cycle, affecting both gait event timing and joint kinematics/kinetics. Perhaps the most interesting compensations were in response to impaired plantarflexion during loading response: 0-15% of the gait cycle (Fig 1). During p100, subjects responded with a slight reduction in dorsiflexor moment. However, this compensation alone was not sufficient to return to normal ankle kinematics, leading subjects to develop a secondary compensation of increased hip and knee flexion (Fig 2). This combination of distinct strategies helped subjects maintain a symmetric gait in the presence of reduced ankle plantarflexion.

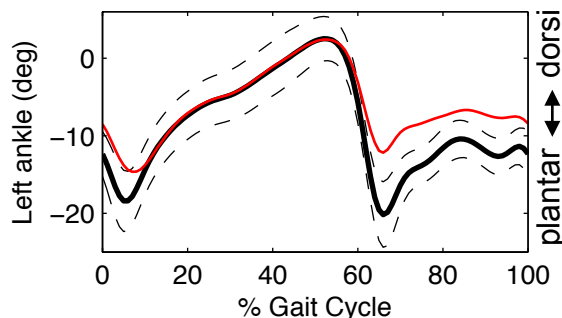


Fig 1: Group averages of left ankle angle during NC (black) and p100 (red).

During recovery from the perturbation (p60-NC2), the reduced plantarflexion gradually diminished, becoming statistically insignificant by NC2. However, the distinct kinetic and kinematic compensation strategies found in p100 returned to normal at *different* rates. The biological ankle moment returned to normal gradually, but the kinematic compensations at the hip and knee disappeared by p60. This result suggests that after a certain point in recovery, subjects were able to overcome the ankle perturbation in loading response by solely adapting their ankle kinetics; they no longer required the additional kinematic hip and knee compensations to maintain a successful gait.

The observed recovery compensations during loading response support the existence of discontinuous changes to neuromuscular adaptations during continuous recovery from an injury, as well as coexisting compensation strategies. This information can inform clinicians to the need for different rehabilitation strategies throughout a patient's recovery, depending on the compensations present at the time. It should be noted that the overall scope of this work was much broader, and could not be conveyed here. Several other adaptations were present throughout the gait cycle, with similar findings of discontinuous or coexisting adaptations during recovery. One major shortcoming of this work was the inability to record truly *continuous* recovery data through more intermediate ankle stiffness conditions. Thus, discussion of *discontinuous* adaptations above must be taken in context, relative to the stiffness changes.

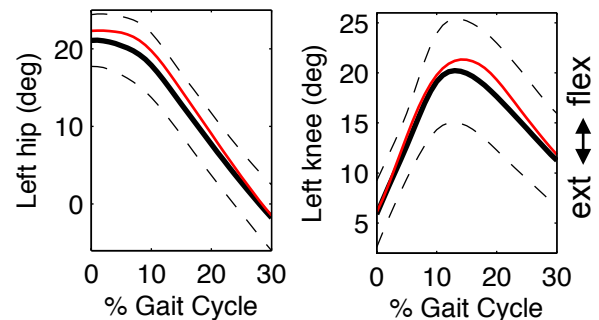


Fig 2: Group averages of left hip and knee angles during NC (black) and p100 (red) for 0-30% of the gait cycle.

CONCLUSIONS

The results from this study show the possibility of coexisting neuromuscular compensations due to injury, which return to normal at different rates. This nonlinear behavior could have major potential implications for the design of rehabilitation protocols, and should be studied in more depth.

REFERENCES

1. Perry J. *Gait Analysis*, Slack, 1992.
2. Lindstrom M, et al. *Knee Surg Sport Traum Arthro* **18**, 106-114, 2010.
3. Wojtys EM, et al. *Am J Sport Med* **28**, 336-344, 2000.
4. Neptune RR, et al. *J Biomech* **34**, 1387-1398, 2001.
5. DiBerardino LA, et al. *Clin Biomech* **25**, 552-556, 2010.
6. Helwig NE, et al. *J Biomech* **44**, 561-566, 2011.
7. Shorter KA, et al. *Clin Biomech* **23**, 459-467, 2008.
8. DiBerardino LA, et al. *J App Biomech* **28**, 210-214, 2012.

Changes in Walking Kinematics Following Bilateral Isolated Lower Extremity Joint Fatigue

¹ Sarah Hovey, Seth Higgins, Kimberly Dahl, Natasha Francksen, Jonathan Foster and D. Clark Dickin

¹ Biomechanics Laboratory, Ball State University, Muncie, IN, USA
email: biomech@bsu.edu, web: www.bsu.edu/biomechanics

INTRODUCTION

In the human body, muscular fatigue is characterized by a reduction in the force generating capacity of a muscle [1]. Alterations of movement patterns often occur following muscular fatigue as compensation for the impairment in the muscle's ability to produce and control force. Fatigue-related changes in normal gait patterns result in a shift in muscle activation from fatigued to less fatigued muscles in order for the body to continue performing the task [2]. Often times these changes occur at the expense of proper biomechanics, which may lead to elevated risk of musculoskeletal injury in the lower extremity [1, 2]. During locomotion, and other whole body tasks, general fatigue of the lower extremity is typically the result. While the whole lower extremity may be fatiguing the resistance to fatigue is variable across the joints [3]. The ankle has been identified as less fatigable than the knee, however reduced function in any joint may compromise joint mechanics at all lower extremity joints [1]. It was therefore the purpose of this study to determine the impact of bilateral fatigue at individual joints of the lower extremity on joint kinematics during walking.

METHODS

Eleven male participants (21.4 ± 3.1 years) walked on a treadmill at 1.39 m/s for 2-minutes: prior to fatigue, immediately following fatigue, and 10-minutes post fatigue. Fatigue of the flexor and extensor muscles of the ankle and knee was induced on separate days using 3-bouts of isokinetic fatiguing contractions at 60°/s until a 50% reduction in peak force occurred. Joint kinematics were captured using a 14-camera Vicon motion capture system (VICON Inc., Denver, CO, USA) collecting at 120 Hz and an AMTI force plate instrumented treadmill (AMTI Inc., Watertown, MA, USA) collecting at 2400 Hz with a modified Plug-In Gait marker set that included marker clusters on the thigh and shank of each leg.

Dominant leg ankle, knee and hip kinematics were calculated at initial impact and at maximal joint excursion during mid-stance using Visual 3D software (Version 5.0, C-Motion, Germantown, MD, USA) and data were analyzed using a repeated measures analysis of variance in SPSS. Alpha level was set at $p \leq .05$.

RESULTS AND DISCUSSION

Significant main effects were revealed for time, but not between for the joint fatigued or time x joint interaction. At initial ground contact, the hip was more extended at 10 minutes post fatigue compared to both pre-fatigue and 2 minutes post fatigue ($F(1,30)=4.22$, $p=.013$). While the ankle angle demonstrated greater dorsi-flexion at pre-fatigue than in all three post fatigue conditions ($F(3,30)=22.7$, $p<.001$) (Table 1). At the knee ($F(3,47.83)=4.56$, $p=.030$) and ankle joints ($F(3,30)=16.04$, $p<.001$) greater maximum flexion and dorsi-flexion angles were seen for both the pre-fatigue and at the end of the 2-minute post fatigue walk than for immediate post and 10-minute post fatigue (Table 1).

Inducing bilateral fatigue at isolated joints in the lower body altered joint motion at all three major joints. The results suggest that while bilateral lower extremity fatigue, at either the ankle or knee, alters walking kinematics the individual joints did not exhibit a differential effect in walking kinematics. At the ankle joint, a reduction in initial contact dorsi-flexion angle was seen following fatigue that did not recover across the 10-minute post-fatigue recovery period. Similar patterns emerged at the hip at initial impact in that fatigue impaired hip flexion immediately post fatigue and although hip flexion angle returned to pre-fatigue levels at the end of the immediate post fatigue walking trial it was again reduced at the 10 minute post fatigue walk. At the

knee and ankle joint fatigue caused an immediate reduction in knee maximum knee flexion and ankle dorsi-flexion that returned at the end of the 2-minute walk period but then was again impaired at the 10-minute post fatigue time. This pattern suggests that lower extremity kinematics may return to normal levels after continuous walking following muscular fatigue but can return during rest. Given a period of rest the individual experiences a general restriction in joint motion that closely resembles the levels experienced immediately after the period of fatigue. Importantly, allowing the individual time to activate and move following fatigue appears to have a restorative effect on joint motion. Overall, the findings suggest a more rigid limb following the fatiguing contractions, potentially reducing the ability to attenuate the forces from landing and increasing the risk of musculoskeletal injury. Although normal joint function seems to return relatively quickly once the individual is permitted to walk and movement joints.

CONCLUSIONS

The study findings confirmed the negative impact of muscular fatigue on joint performance during locomotion and extended them to walking.

Interestingly changes in joint kinematics were not significantly different between isolated bilateral ankle and knee fatigue. These findings suggest that although each individual joint may fatigue differently the impact of its fatigue is relatively similar in terms of joint kinematics. This study demonstrated both the importance and impact of the knee and ankle joints to overall lower extremity functioning.

REFERENCES

1. Kellis, E., A. Zafeiridis, and I.G. Amiridis, *Muscle Coactivation Before and After the Impact Phase of Running Following Isokinetic Fatigue*. Journal of Athletic Training, 2011. 46(1): p. 11-19.
2. Kellis, E., et al., *Muscle architecture variations along the human semitendinosus and biceps femoris (long head) length*. Journal of Electromyography and Kinesiology, 2010. 20(6): p. 1237-1243.
3. Frey Law, L.A. & Alvin, K.G., *Endurance time is joint specific: A modeling and meta-analysis investigation*. Ergonomics, 53(1) p. 109-129.

Joint	Plane of Motion	Angle	Pre-Fatigue	Immediately Post Fatigue	2 Min. Post Fatigue	10 Min Post Fatigue
Hip	Sagittal (Flex +)	Initial Impact Angle	28.63(1.25)	27.95(1.25)	28.41(1.33)	27.09(1.51)
		Maximum Angle	-9.18(1.38)	-7.07(1.42)	-9.31(1.24)	-8.15(1.22)
Knee	Frontal (Adduct +)	Initial Impact Angle	-.58(.80)	-.97(.77)	-.86(.74)	-.82(.65)
		Maximum Angle	-4.17(.76)	-4.46(.75)	-4.49(.66)	-4.40(.72)
	Sagittal (Flex +)	Initial Impact Angle	-.51(.96)	-1.40(1.02)	-.23(1.26)	-.59(1.54)
		Maximum Angle	48.09(.97)	44.04(1.89)	47.23(1.01)	43.22(1.83)
	Transverse (Int.Rot +)	Initial Impact Angle	.68(1.04)	1.36(1.01)	.59(1.02)	1.42(1.02)
		Maximum Angle	8.73(1.08)	8.61(.91)	8.93(1.01)	8.71(.86)
Ankle	Sagittal (Dorsi +)	Initial Impact Angle	6.53(.77)	4.43(.92)	4.22(.80)	4.28(.77)
		Maximum Angle	13.48(.99)	11.30(1.12)	13.20(1.05)	12.04(1.07)

Table 1: Resultant lower extremity joint angles Pre- and Post-joint fatigue at initial contact and at the point of maximum excursion during walking. Values are mean (SD).

COMPLEXITY OF GAIT POST STROKE

^{1,2}Eric L. Dugan, ³Stephanie A. Combs-Miller, Jeff Eggleston, Cara M. Masterson, and ²Cassidy M. Berlin

¹ Seattle University, Seattle, WA, USA

² Boise State University, Boise, ID, USA

³University of Indianapolis, Indianapolis, IN, USA

email: dugane@seattleu.edu, web: <http://www.seattleu.edu/artsci/sport-exercise/>

INTRODUCTION

Determining how individuals will respond to therapeutic interventions focused on improving gait function after stroke is challenging. Some individuals demonstrate improvements in walking speed via the recovery of pre-stroke gait patterns, while others may increase speed through the strengthening of compensatory movement patterns [1]. Traditional measures of gait function derived from spatio-temporal parameters, such as gait speed, do not delineate between recovery of pre-stroke patterns or compensation, and thus, do not provide information about a patient's ability to adapt their gait to different tasks and environmental constraints. There is a critical need to develop methods that differentiate among capacities for adapting movement patterns in individuals with stroke.

One approach to understanding the health and adaptability of biological systems is through the measurement of complexity. Since complexity represents the adaptability of the biological system in question, the assessment of complexity of movement parameters is particularly attractive when attempting to better understand the recovery processes after events such as stroke.

Therefore, the primary purpose of this study was to determine whether the complexity of gait in persons with hemiparesis due to stroke is different to that of individuals without disability during a gait task. Based on the previous work documenting the decrease in complexity [2, 3] of biological signals with age and disease, our hypothesis was that the complexity would be significantly lower in the group with stroke compared to the group without disability.

METHODS

Participants with chronic stroke and participants without disability were enrolled in this case-control study. Participants with stroke had to meet the following inclusion criteria: 1) minimum of 6 months post stroke, 2) able to walk for at least 10 meters on level surfaces without physical assistance or use of an assistive device and/or lower extremity orthosis, 3) continue to experience residual deficits from the stroke that affects walking ability. Participants without disability were included if they were able to walk without physical assistance or use of an assistive device or orthosis during all home and community activities. Exclusionary criteria for the participants without disability included: 1) known neurological condition or any neurological deficits such as prior stroke, 2) current musculoskeletal condition outside typical age-related changes, and 3) complications from health conditions that influence walking.

All participants completed a 2-minute walk at their preferred pace around a level, tiled indoor walking track. During the walking tasks, three dimensional accelerometer data from wireless inertial measurement units (IMUs) (InterSense Inertia Cube BT) worn on each lower extremity segment [foot, shank, thigh] and pelvis were collected (60 Hz) using MotionMonitor software (Innovative Sports Training, Inc.).

These data were used to determine the complexity of the gait patterns using the multivariate, multiscale entropy (MMSE) algorithm developed by Ahmed and colleagues[4]. The calculation of MMSE results in a measure of complexity across multiple time scales and provides a means for comparing the movement complexity across groups

and/or conditions. The complexity index was calculated from the MMSE results and represents the area under the MMSE curve and provides a way of comparing the physiological complexity of gait across multiple time scales.

Two-tailed, independent t-tests with a significance level of $p < .05$ were used to test the hypothesis that the complexity index for each limb segment would be lower in the participants with stroke compared to that of the healthy participants.

RESULTS AND DISCUSSION

A total of 22 participants were enrolled in this case-control study (11 with chronic stroke and 11 participants without disability). Participants with chronic stroke had significantly ($p < 0.05$) lower complexity at every lower limb segment and the pelvis compared to healthy controls during overground walking, see Table 1.

The results of this study support the hypothesis that in individuals with stroke would exhibit lower levels of gait complexity compared to that of healthy participants and are consistent with previous studies of the temporal variability of upper extremity movement in individuals with stroke [5].

Greater complexity is thought to signify the overall health of a system and its underlying physiological capacity to adapt to everyday stresses. Healthy biological systems exhibit complex behaviors while

age and disease reduce this complexity [2, 3]. The results of this study support this paradigm.

CONCLUSIONS

The reduced complexity of gait after stroke represents a decrease in the adaptability in the neuromotor system. This information may discern between those patients who are more likely to respond to therapeutic interventions and those who will not. Ultimately this information could allow therapists to tailor interventions in such a way to optimize function.

REFERENCES

1. Levin, M.F., et al. *Neurorehabilitation and Neural Repair*, **23**(4), 313-319, 2009.
2. Lipsitz, L.A., et al. *JAMA*, **267**(13), 1806-1809, 1992.
3. Costa, M., et al. *Physical Review Letters*, **89**(6), 2002.
4. Ahmed, M.U., et al. *Physical Review E*, **84**(6), 2011.
5. Sethi, A., et al. *Clinical Biomechanics*, **28**(2), 134-139, 2013.

ACKNOWLEDGEMENTS

Joanne Mangun, PT and Jane Spencer, APRN, ACNS-BC for assistance with participant recruitment. Funding source: NIGMS, NIH grant U54GM104944-01A1

Table 1: Complexity Index per Segment

	Complexity Index						
	Paretic Foot	Non-Paretic Foot	Paretic Shank	Non-Paretic Shank	Paretic Thigh	Non-Paretic Thigh	Pelvis
Stroke	3.59 ± 0.58	3.12 ± 0.91	8.47 ± 2.22	6.61 ± 2.93	8.97 ± 3.04	7.71 ± 2.25	12.91 ± 2.34
Healthy	4.71 ± 1.06	4.75 ± 1.00	10.78 ± 2.52	11.22 ± 2.21	12.04 ± 2.54	11.52 ± 2.08	15.52 ± 2.19

ENERGY SUBSTRATE USE DURING WALKING AS A FUNCTION OF STEP RATE

Farzad Ehtemam, Ryan M. Sapp, James M. Hagberg, and Ross H. Miller

University of Maryland, College Park, MD, USA
email: rosshm@umd.edu, web: <http://sph.umd.edu>

INTRODUCTION

Humans can walk at a given speed using a range of mechanically feasible step rates. When the choice of step rate is unconstrained, we tend to choose a moderate rate near the center of this range. The mechanisms behind this subconscious choice are unknown, but a popular hypothesis [1] supported by data [2] is that the preferentially chosen step rate minimizes the rate of metabolic energy expenditure.

An implicit assumption of this “minimum energy” hypothesis is that the nervous system monitors and regulates muscle energy metabolism. Repeated activation of muscles during movement requires energy consumption (e.g. the ATP used in powering the crossbridge cycle), which must be matched by energy production through substrate metabolism. Energy consumption as an optimality criterion in human gait has been widely studied, but the energy production side of this relationship has received minimal attention [3].

In this study, we examined energy production (substrate oxidation of fat and carbohydrates) when walking at a range of step rates. Since this was a preliminary/exploratory investigation, no specific hypotheses were formed, but due to the traditionally observed U-shaped relationship between step rate and energy rate in walking, we expected the oxidation rate of the substrate producing the majority of energy to also be U-shaped.

METHODS

Ten healthy young adult subjects participated in accordance with institutional guidelines. Subjects fasted for at least three hours, and were asked to refrain from alcohol for 24 hours before their test and to not exercise on the day of the test. Subjects walked on a level motorized treadmill at 1.25 m/s.

The subject’s preferred step rate (PSR) was first determined by counting the number of steps taken in a minute. Subjects then walked for five minutes at each of seven different step rates: PSR and ± 5 , 10, and 15% of PSR (randomized order with breaks between trials). Step rate was primed using a metronome, and subjects were instructed to match the timing of their heel-strikes with the beat.

Breath-by-breath rates of oxygen consumption and carbon dioxide production were measured using a metabolic cart (Oxycon Pro, CareFusion, San Diego, CA) and averaged over the final 2 min of each step rate. Mass-specific rates of gross energy expenditure, carbohydrate oxidation, and fat oxidation were calculated assuming protein produced 12.5% of the energy consumed [4,5].

RESULTS AND DISCUSSION

Repeated-measures ANOVA showed no significant effect of step rate on carbohydrate oxidation ($p=0.374$, Fig 1b) and significant effects on metabolic rate and fat oxidation ($p<0.05$, Figs 1a, 1c). The gross metabolic rate was significantly greater at $\pm 15\%$ PSR than at PSR (Fig. 1a). Both the gross metabolic rate and the fat oxidation rate were well fit as functions of step rate by 2nd-order polynomials ($R^2 = 0.89$ and 0.95 , with significant quadratic terms ($p<0.001$). The carbohydrate oxidation was invariant with respect to step rate (Fig. 1b) and was not well fit by the 2nd-order polynomial ($R^2 = 0.26$).

In summary, we saw that the U-shaped relationship between metabolic rate and step rate was explained by fat oxidation, which was also U-shaped, unlike carbohydrate oxidation. Protein oxidation was also U-shaped with respect to step rate, but this relationship was assumed, not measured. Thus, when subjects walked at non-preferred step rates,

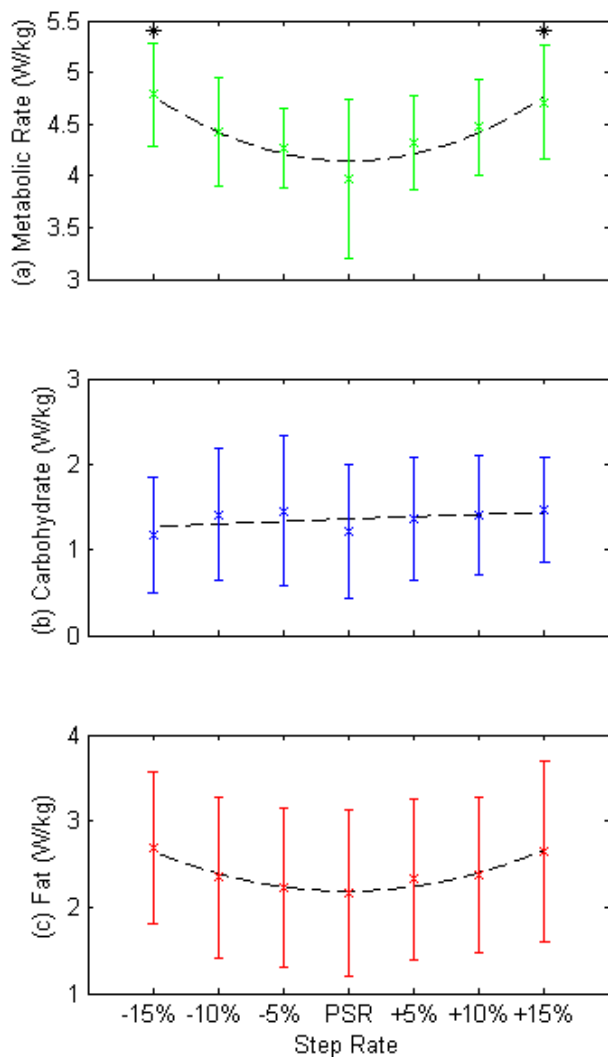


Figure 1. Means and standard deviations for (a) gross metabolic rate, (b) rate of carbohydrate oxidation and (c) rate of fat oxidation, when walking at different step rates. Dashed lines are 2nd-order polynomial fits. * = significantly greater than the value at the preferred step rate.

energy expenditure increased, and fat was used as the fuel to provide this additional energy.

One possible explanation for these results is that humans have evolved to prefer gaits that minimizes fat utilization, sparing consumption of an energy source that has historically been difficult to obtain. For example, prior to animal domestication, obtaining fat required hunting, while carbohydrates could be obtained more consistently and safely through foraging. Obtaining fat elsewhere would require availability of forageable oil-rich foods (e.g. nuts).

A conceptually related notion, the “thrifty gene” hypothesis, has been suggested as an explanation for the high prevalence of diet-related conditions such as obesity, type 2 diabetes, and metabolic syndrome [6]. Measurement of protein use, which was not done here, could further examine the theory that the preferred step rate spares substrates primarily obtained through hunting and meat consumption.

Another possible explanation is that adjustments to the step rate of walking rely on fat in order to spare carbohydrates for use in more intense physical activities such as running. Carbohydrates are less energy-dense than fats, but can supply their energy more quickly, and are thus relied upon as fuel more and more as the intensity of physical activity increases [7]. During low-intensity activities such as walking, humans may prefer to modulate our energy expenditure using primarily fat, saving carbohydrates for situations where energy is needed quickly (e.g. fleeing from danger).

CONCLUSIONS

This study suggests minimization of fat oxidation drives the shape of the energy-step rate relation in human walking. This result provides an energy-production perspective on decision-making in the gait mechanics of humans. Evolutionary studies of movement might also find this substrate minimization important in the context of ecological constraints that shaped our gait prior to agricultural revolutions. Further studies are needed to investigate the effects of abundance of nutrients in modern societies on this minimization process.

REFERENCES

1. Srinivasan M. *Chaos* **4**, 026112, 2009.
2. Zarrugh MY & Radcliffe CW. *Eur. J. Appl. Physiol.* **38**, 215-223, 1978.
3. Willis WT, et al. *Metab.* **54**, 793-799, 2005.
4. Weir JBV. *J. Physiol.* **109**, 1-9, 1949.
5. Frayn KN. *J. Appl. Physiol.* **55**, 628-634, 1983.
6. Neel JV. *Hum. Genet.* **14**, 353-362, 1962.
7. Romijn JA, et al. *Am. J. Physiol.* **265**, E380-E391, 1993.

GROUND REACTION FORCE COMPARISON OF PREDICTION-BASED AND DIRECT FORCE MEASUREMENT SYSTEMS

¹ Portia Flowers and ¹ Trent M. Guess

¹ University of Missouri, Columbia, MO, USA

email: flowerspp@health.missouri.edu, web: www.mizzoumotioncenter.com

INTRODUCTION

Accuracy in ground reaction force measurements is critical to gait analysis interpretation. The current gold standard in ground reaction force (GRF) data collection is the use of force plates. While accurate, force plates are expensive and restrictive. However, markerless, plateless motion capture systems may provide a less expensive and easier method for kinetic data collection and analysis, allowing for less preparation time and restricted movement. Previous studies have described the use of plateless motion capture techniques to obtain GRF [1, 2]. The purpose of this study was to compare GRF obtained via force plate and plateless systems.

METHODS

After providing written informed consent approved by the institution's human subjects review board, all subjects performed 5 trials of a vertical jumping task. Data was collected via two force plates (AMTI Optima) synced with Vicon Nexus 2.0 software and with an 18-camera markerless motion captures system (Organic Motion BioStage). Force plate GRF were collected for each leg independently at 1000Hz. Resultant force magnitudes were determined from the vertical and shear forces and reported. Using a visual hull reconstruction method of tracking segment motion [3], markerless kinematic data were sampled at 120Hz and processed via third party software (Dynamic Athletics DARI, Vault software). In addition to joint angles, DARI also predicted GRF magnitudes for each leg from the markerless kinematics. GRF magnitudes during the landing phase of vertical jump were time normalized. Average GRF throughout the jump cycle and peak GRF during landing for each limb was used in this analysis. Landing phase was determined as the

instant after foot contact with the ground until end of motion. Trials were collected simultaneously, with subjects performing a single elbow flexion motion before each task to sync the two systems.

Coefficients of multiple correlations (CMC) and root mean square (RMS) error were used to determine relationship and accuracy of GRF waveforms for the entire jump cycle. Between-system agreement was assessed by calculating the mean difference within 95% confidence intervals (CI) to determine consistency of peak forces across all trials, and two-way, mixed effects, average, Intraclass Correlation Coefficient (ICC) with 95% CI to determine absolute agreement of peak force between methods. Intra-session reliability of both methods were assessed via Cronbach's alpha to determine consistency of peak forces across all trials, and ICC to determine absolute agreement of peak force between the first and last trials.

RESULTS AND DISCUSSION

Ten healthy adults (5F/5M, age = 26.1 ± 3.7 yrs, height = 1.71 ± 0.1 m, weight = 69.1 ± 12.3 kg) were recruited for this study. Between-system averaged CMC values revealed good agreement throughout the jump cycle (Table 1). However, ICCs revealed moderate agreement in peak GRF between the two methods under the left ($ICC(3,k)=0.493$) and right sides ($ICC(3,k)=0.423$) (Table 2). Large average RMS error revealed an absolute discrepancy between the two methods, further evidenced by a consistent trend toward less DARI predicted peak GRF on both limbs (left limb mean difference=400.2N, right limb mean difference=337.4N) (Table 2, Figure 1).

For intra-session reliability, Cronbach's alpha revealed excellent agreement for all measures

across 5 trials in both the direct (0.875-0.872) and predicted (0.950-0.968) force measurements (Table 3). Agreement of peak force between the first and last trials were moderate for direct ($ICC(3,1)=0.471-0.501$) and predicted ($ICC(3,1)=0.622-0.871$) force measurements.

Table 1: Mean CMC and RMS error comparing between-system waveforms of GRF magnitudes for each limb.

Limb	CMC	RMS error
Left	0.86	106.5 N
Right	0.86	110.1 N

Table 2: Mean peak GRF during vertical jump landing.

	Left limb	Right limb
ATMI GRF (N)	1160.7±295.9	1134.7±447.9
DARI GRF (N)	760.5±205.9	797.3±187.4
Mean Diff (95% CI) (N)	400.2 (264.1, 536.4)	337.4 (64.2, 610.7)
ICC(3,k) (95% CI)	0.493 (-0.19, 0.87)	0.423 (-0.42, 0.83)

Table 3: Intra-session reliability measures

		ATMI	DARI
Cronbach's Alpha	Left	0.875	0.950
	Right	0.872	0.968
ICC (3,1)	Left	0.471 (-0.12, 0.84)	0.622 (0.08, 0.89)
	Right	0.501 (-0.12, 0.85)	0.871 (0.57, 0.97)

With an overall error of nearly one body weight (based on the study sample average), this discrepancy may be a reflection of the sampling rate of the markerless motion capture system. With a maximum sampling rate of only 120Hz, it is possible that the markerless system is unable to accurately track dynamic movement such as jump landing, resulting in a consistent underestimation of peak GRF. However, with excellent within-system agreement, relative measurements may be appropriate for the plateless system.

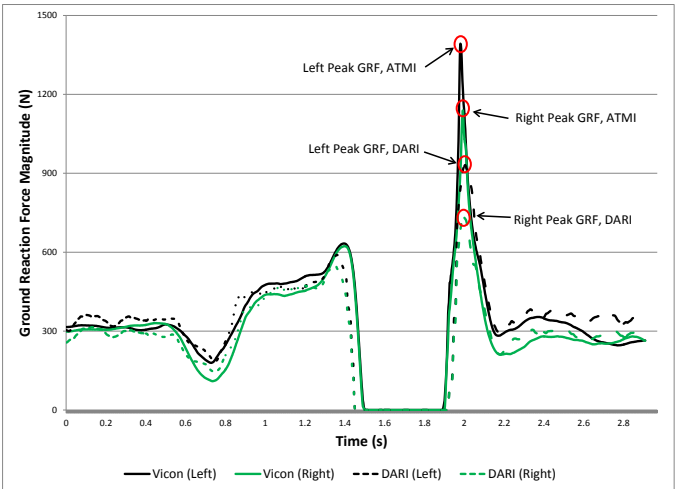


Figure 1: Representative mean GRF in forceplate (ATMI) and plateless (DARI) systems for one subject.

CONCLUSIONS

The potential for using DARI predicted GRF measurements via markerless motion capture is promising, as average force magnitudes were consistent across trials, which was comparable to the gold standard of force plate methods. However, a consistent underestimation of GRF, possibly due to undersampling and inaccurate motion tracking, makes DARI predicted GRF data reliably inaccurate, particularly for high frequency dynamic events. Additionally, DARI predicted GRF is limited by its ability to only provide force magnitudes without direction. Without knowing the components of GRF, it is difficult to identify and diagnose pathologic movement, making clinical use impractical at this time. Future studies should seek to develop equations to account for the difference in force between the two methods.

REFERENCES

1. Corazza, S. & Andriacchi, T. P. J Biomech, **42**, 370-374, 2009.
2. Oh, SE, et al J Biomech, **46**, 2372-2380, 2013.

KINEMATIC COMPARISON OF MARKER-BASED AND MARKERLESS MOTION CAPTURE SYSTEMS

¹Portia Flowers, ¹Swithin Razu, ¹Kaylin Bean, and ¹Trent M. Guess

¹ University of Missouri, Columbia, MO, USA

email: flowerspp@health.missouri.edu, web: www.mizzoumotioncenter.com

INTRODUCTION

Accuracy in motion analysis systems is critical to gait analysis interpretation. The current standard in kinematic motion capture is a marker-based system, using passive or active markers placed on specific anatomical locations to track human movement. However, marker-based methods are highly dependent on marker placement accuracy and require long preparation times. Markerless motion capture systems may provide an easier method for motion analysis, allowing for less preparation time and restricted movement. Previous studies have described the use of markerless motion capture systems [1-3]. The purpose of this study was to compare hip, knee, and ankle joint kinematics outcomes between marker-based and markerless systems.

METHODS

After providing written informed consent approved by the institution's human subjects review board, all subjects performed 5 trials of a Right-Left-Right side cutting maneuver (Figure 1). Markerless motion was collected using 18 cameras (Organic Motion BioStage). Subjects wore a fitted blue short sleeved shirt, fitted black long pants and orange ankle socks to ensure segment identification in the markerless motion capture system. Holes were cut out of the clothing to accommodate placement of 14 retroreflective markers placed on the clavicle, sternum, and C7 & T10 vertebrae, and bilaterally on the acromioclavicular joint, upper arm, lateral humeral epicondyle, forearm, ulnar and radial styloid processes, 2nd metacarpal joint, anterior & posterior superior iliac spines, thigh, lateral femoral condyle, shank, lateral malleolus, heel, and 2nd metatarsal joint. Thigh and shank marker clusters were added for the functional joint calibrations.

Markers were placed by a single tester with good reliability (Intracorrelation Coefficient=0.754).

Marker-based motion was collected using a Vicon MX-T40S 8-camera motion capture system (Vicon, Oxford, UK). Marker-based kinematic data were sampled at 100Hz, processed using Vicon Nexus 2.1 software, and filtered at 6Hz using a 4th order Butterworth filter. Vicon's Plug-In Gait skeletal model with functional joint calibration was used to determine joint angles. The Symmetrical Center of Rotation Estimation (SCoRE) [4] was used to estimate the hip joint center and Symmetrical Axis of Rotation Analysis (SARA) [5] was used to estimate the knee joint axis. Using a visual hull reconstruction method of tracking segment motion [3], markerless kinematic data were sampled at 120Hz and processed via third party software (Dynamic Athletics DARI, Vault software). Trials were collected simultaneously (Fig. 1), with subjects performing a single elbow flexion motion before each task to sync the two systems. Hip and knee angles in the sagittal, frontal, and transverse planes, and ankle angles in the sagittal plane were calculated for the planting limb (left). Using peak elbow flexion as the point of synchronization, data obtained from the markerless system were time synchronized to the marker system.

Coefficients of multiple correlations (CMC) and root mean square (RMS) error were used to determine relationship and accuracy of joint angle waveforms from 1st right heel strike to 2nd right toe-off.

RESULTS AND DISCUSSION

Eight healthy adults (3F/5M, age = 26.6 ± 4.0 yrs, height = 1.72 ± 0.09 m, weight = 71.8 ± 12.3 kg) were recruited for this study. Between-system

averaged CMC values were largest in the sagittal plane, with strongest relationships at the hip and knee (Table 1). Between-system relationships were weakest in the frontal and transverse planes, particularly at the knee. It is possible that such weak correspondence may be due in part to limited range of motion in those planes. RMS errors were smallest in the frontal plane, which reflects a smaller range of motion in that plane. Despite the strongest relationship between systems at the hip in the sagittal plane, average RMS error was also the largest, indicating an absolute discrepancy between the two systems. Once normalized to joint range of motion, RMS errors were largest at the hip in the non-sagittal planes, indicating a possible difficulty in identifying hip joint kinematics. In addition, while joint centers and axes were defined in the marker-based system using a functionally relevant determination, joint centers and axes as defined by the markerless system are unclear. Therefore, a possible disagreement in such definitions may have contributed to the weak between-system relationships, particularly in the non-sagittal planes of movement.

CONCLUSIONS

The potential for using markerless motion capture methods may be limited by the joint of interest as well as the plane of motion. Analysis of joint motion in the sagittal plane may have the best potential for application. However, the viability of a markerless system such as Organic Motion is ultimately dependent on a full understanding of joint center and axes definitions in the markerless system, which is critical to joint angle determination, particularly in non-sagittal planes. Future studies should include day to day repeatability to assess the use of markerless systems in longitudinal testing.

REFERENCES

1. Yang SXM, et al *Comput Methods Biomech Biomed Eng Imaging Vis*, **2**, 46-65, 2014.
2. Mündermann L, et al *J Neuroeng Rehabil*, **3**, 2006.
3. Corazza S, et al *Ann Biomed Eng*, **34**, 1019-1029, 2006.
4. Ehrig RM, et al *J Biomech*, **39**, 2798-2809.
5. Ehrig RM, et al *J Biomech*, **40**, 2150-2157.

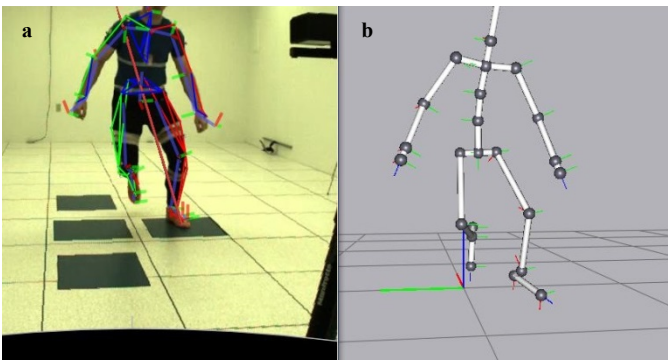


Figure 1: Side cut motion model output in (a) Vicon and (b) Organic Motion systems.

Plane of Motion	Joint	CMC	RMS error	Normalized RMS error
Sagittal	Hip	0.92	23.0°	0.38
	Knee	0.93	11.5°	0.14
	Ankle	0.71	12.7°	0.26
Frontal	Hip	0.67	7.9°	0.70
	Knee	0.06	10.6°	0.32
Transverse	Hip	0.37	13.6°	0.65
	Knee	0.01	18.0°	0.41

Table 1: Average CMC and RMS error comparing between-system waveforms of joint angles on left limb.

FOOT AND ANKLE KINEMATICS DURING DESCENT FROM VARYING STEP HEIGHTS

¹Emily Gerstle, ¹Kristian O'Connor, ¹Kevin Keenan, and ¹Stephen Cobb

¹The University of Wisconsin-Milwaukee, Milwaukee, WI, USA
email: egerstle@uwm.edu

INTRODUCTION

Ankle injuries account for approximately two million emergency room visits in the US annually. An estimated 26% of those injuries occur due to a fall from steps [1]. A study utilizing random population surveys found the total incidence of ankle injuries to be up to five times greater than the emergency room visit estimates [2].

Previous research has modeled the foot as a single rigid segment and focused on hip, knee and ankle movement during multiple step descent [3-5]. However, a study by Yu, 1997 reported the stepping mechanics of descending a single step differed from multiple step descent. Furthermore, recent studies have shown there is significant motion within the distal articulations of the foot during gait [6, 7].

The purpose of this study was to identify foot and ankle kinematics of uninjured individuals during descent from varying step heights.

It was hypothesized that landing strategy would transition from the rearfoot to the forefoot as step heights increased. These changes were anticipated to be accomplished through significant kinematic differences in the rear-, mid-, and forefoot both at initial contact and during weight acceptance. Regarding initial contact in the sagittal plane, the rearfoot, midfoot and medial forefoot were predicted to become more plantarflexed while the lateral forefoot would become more dorsiflexed. In the frontal plane a more inverted position was expected at both the rear and midfoot. We further hypothesized that the rearfoot and medial forefoot ranges of motion during the weight acceptance phase of the step down would be increased when initial contact was made with the forefoot versus the rearfoot. Finally, we proposed that the midfoot and lateral forefoot range of motion would be decreased

during weight acceptance to facilitate foot stability when initial contact was made with the forefoot.

METHODS

Participants:

15 participants (8 female, 7 male; age = 25.6 ± 5.4 years; height = 173 ± 9.7 cm; mass = 70.8 ± 13.4 kg) were recruited for the study. All subjects had weight bearing ankle dorsiflexion ROM $\geq 25^\circ$, did not wear bifocals, and had no history of lower extremity surgery or recent injury.

Gait analysis:

A 10 camera motion analysis system was used to capture 3D positions of clusters of retroreflective markers placed on the foot and leg to define five functional articulations [Rearfoot complex (RC), Lateral midfoot (LMF), Medial midfoot (MMF), Medial forefoot (MFF), and Lateral forefoot (LFF)].

At a self-selected pace, participants walked along a level 5 m walkway, stepped down a height of 5, 10, 15, 20 or 25 cm and continued walking. After completing practice trials to establish a consistent self-selected pace 10 trials were recorded for each step height.

The calibrated anatomical systems technique was used to reconstruct 3D segment positions and orientations. Joint angles between adjacent segments were calculated using the joint coordinate system technique.

Data analysis:

Univariate RM ANOVAs were performed with five within subject factors (step height) to investigate sagittal plane RC, MMF, LMF, MFF, and LFF initial contact angles and ranges of motion during weight acceptance. Frontal plane RC, MMF, and LMF initial contact angles and ranges of motion

during weight acceptance were also calculated. Pairwise comparisons with Bonferroni adjustments were performed to investigate significant RM ANOVA results. Significance level for all tests was set at $\alpha = 0.05$.

RESULTS AND DISCUSSION

Initial contact angles

In the sagittal plane the LMF was significantly more plantarflexed at the 25-cm step compared to the 5-cm ($p=0.003$) and 10-cm ($p=0.026$) steps.

In the frontal plane, the RC at the 25-cm step was significantly more inverted than the 20-cm height ($p=0.023$). While at the 20-cm step the LMF was significantly less everted than at the 10-cm height ($p=0.022$).

Range of motion

The sagittal plane RC ROM differed significantly between the 5-cm and the 20 and 25-cm heights as well as between the 10-cm and 25-cm steps. During weight acceptance, the RC plantarflexed at the 5 and 10-cm steps but dorsiflexed at the 20-cm and 25-cm steps. The LMF went through significantly greater dorsiflexion ROM at the 25-cm step compared to the 5-cm step ($p=0.008$). Finally, the LFF went through significantly more dorsiflexion at the 25-cm step compared to the 5-cm ($p=0.013$) and 15-cm ($p=0.038$) steps.

The frontal plane RM ANOVA for the RC was also significant ($p=0.049$), however the pairwise comparisons did not show any significant differences between any of the step heights.

CONCLUSIONS

The kinematics during negotiation of a single step are influenced by step height. At higher step heights, the more inverted RC and less everted LMF initial contact positions may act to stabilize the foot during the forefoot landing. The increased RC dorsiflexion ROM during weight acceptance as height increased, was consistent with the transition from a heel to forefoot landing strategy. The

increased LMF and LFF dorsiflexion ROM during weight acceptance may have been due to the ground reaction force location associated with a forefoot landing strategy. The change in landing strategy preference may be clinically relevant due to the fact that the plantarflexed position of the ankle joint during the forefoot landing strategy results in decreased bony joint stability thus placing greater dependency upon ligaments and muscles (dynamic stabilizers) of the ankle and foot. This may be especially important in groups that may have compromised strength and/or ligamentous stability such as older adults or patients with chronic ankle instability.

REFERENCES

1. Waterman, B.R., et al., *The epidemiology of ankle sprains in the United States*. J Bone Joint Surg Am, 2010. **92**(13): p. 2279-84.
2. Kemler, E., et al., *Ankle injuries in the Netherlands: Trends over 10-25 years*. Scand J Med Sci Sports, 2014.
3. McFadyen, B.J. and D.A. Winter, *An integrated biomechanical analysis of normal stair ascent and descent*. J Biomech, 1988. **21**(9): p. 733-744.
4. Bosse, I., et al., *Dynamic stability control in younger and older adults during stair descent*. Hum Mov Sci, 2012. **31**(6): p. 1560-70.
5. Karamanidis, K. and A. Arampatzis, *Altered control strategy between leading and trailing leg increases knee adduction moment in the elderly while descending stairs*. J Biomech, 2011. **44**(4): p. 706-711.
6. Lundgren, P., et al., *Invasive in vivo measurement of rear-, mid- and forefoot motion during walking*. Gait Posture, 2008. **28**(1): p. 93-100.
7. Nester, C.J., et al., *In vitro study of foot kinematics using a dynamic walking cadaver model*. Journal of Biomechanics, 2007. **40**(9): p. 1927-1937.

ACKNOWLEDGEMENTS

This study was partially funded by a grant from the University of Wisconsin-Milwaukee College of Health Sciences.

Foot Placement Optimization During Lateral Maneuvers

¹ Julian Acasio, ¹ Mary Wu, ^{1,2} Nicholas Fey, and ^{1,3} Keith Gordon,

¹ Northwestern University, Chicago, USA

² Rehabilitation Institute of Chicago, Chicago, USA

³ Edward Hines Jr. VA Hospital, Hines, USA

Email keith-gordon@northwestern.edu

INTRODUCTION

The ability to safely maneuver through one's environment is crucial for community ambulation. However, for many impaired populations, changing direction during gait challenges both balance and endurance. The purpose of this study was to examine how changing foot placement during a simple "lane-change" walking maneuver affects performance, stability, and energetic cost. We hypothesized that as foot placement of the leading limb (the limb used to initiate the maneuver) increased from narrow (during a cross-over step) to wide (during a lateral side-step), both lateral stability and total lower limb joint work performed during the maneuver would increase. Thus, we expect a trade-off exists between stability and joint work when choosing between foot placement positions in lateral maneuvers.

METHODS

Ten healthy subjects performed overground walking maneuvers. During each maneuver trial, subjects initially walked straight for 5 meters (m) within a 0.36 m wide lane. At the end of this path, subjects were instructed to place their right foot on the ground and maneuver as quickly as possible to a parallel walking lane beginning 0.38 m left of the near border of the initial walking lane. Four conditions were tested in which the mediolateral position of the right foot placement at the maneuver location was varied. The four conditions were:

Step In – Right foot placement 0.25 m left of the center of the initial walking lane, resulting in a "cross-over" step maneuver.

Middle – Right foot placement centered laterally in the initial walking lane, resulting in a "side-step" step maneuver.

Step Out – Right foot placement 0.25 m right of the center of the initial walking lane, resulting in a "side-step" step maneuver.

Unrestricted – Lateral right foot placement was freely chosen by the subject.

All trials were performed at subjects' preferred overground walking speed. Speed was monitored via infra-red sensors to ensure consistency across conditions. Subjects practiced each condition before data were collected from five trials. Motion capture cameras recorded lower limb kinematics and force plates measured ground reaction forces.

Maneuver performance was quantified by maneuver time and peak lateral velocity. To examine lateral stability, we calculated the minimum lateral margin of stability (MoS) [1] during the gait cycles of the trailing limb (from left limb heel strike before the maneuver began to the following left limb heel strike, which was the first step within the new walking lane) and leading limb (from right limb heel strike at one of the four maneuver condition locations to the following right heel strike). A smaller MoS will increase susceptibility to external perturbations, suggesting a decrease in lateral stability. To examine mechanical energy cost, we calculated total work (sum of absolute values of positive and negative work) performed in both the frontal and sagittal planes of the hip, knee, and ankle joints of the Trailing Limb and Leading Limb. We then calculated total work performed by the lower limb by summing across all joints.

RESULTS AND DISCUSSION

As expected, step width at heel strike of the leading limb increased significantly (ANOVA; $p < 0.0001$) as foot placement became more lateral from the **Step In** to the **Step Out** conditions. **Unrestricted** step

width was not significantly different from the **Middle** condition (post hoc; $p > 0.05$).

Maneuver Performance

There were no significant differences between conditions for total maneuver time or peak lateral velocity during the maneuver (ANOVA; $p = 0.9210$ and $p = 0.0510$ respectively).

Lateral Stability

During the trailing limb gait cycle, there were significant differences between conditions in MoS (ANOVA, $p < 0.0001$) (Figure 1). For the **Step In** condition, MoS was significantly smaller than all other conditions ($p < 0.05$) and was negative, indicating that the extrapolated center of mass position crossed outside of the base of support during this step. There were no differences between conditions in MoS during the leading limb gait cycle (ANOVA, $p = 0.2047$).

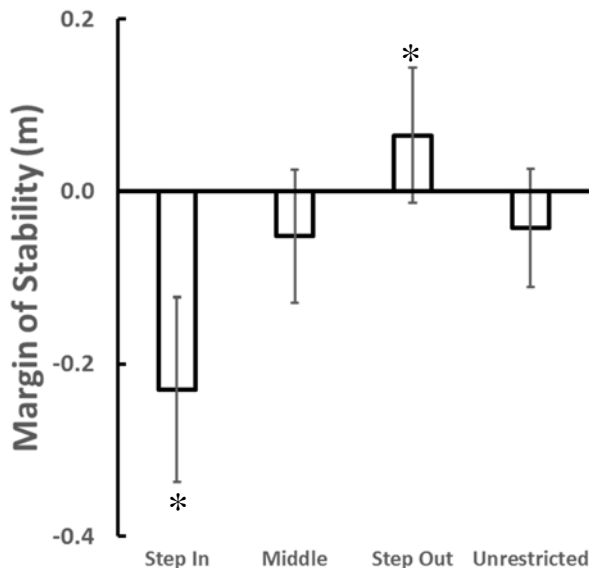


Figure 1: Minimum Lateral Margin of Stability in the trailing limb across conditions. * indicates significantly different from **Middle** condition.

Mechanical Energy

Total lower limb joint work in both the sagittal (ANOVA, $p = 0.0370$) and frontal (ANOVA, $p = 0.0289$) plane was significantly different between conditions for the leading limb, with the greatest total work done during the **Step Out** condition and least work done during the **Step In** condition (Figure 2). For the trailing limb, there were no significant differences between conditions in either sagittal

(ANOVA, $p = 0.4464$) or frontal (ANOVA, $p = 0.8239$) plane total joint work.

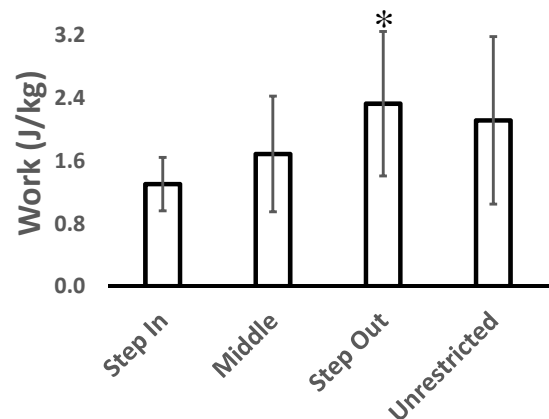


Figure 2: Total Sagittal Plane Work for the Leading Limb. * indicates significantly different from **Step In** condition.

CONCLUSIONS

During a simple “lane-change” maneuver, lateral foot placement of the leading limb affects both lateral stability and energetic cost. As steps become wider, both passive lateral stability and total lower limb joint work increase. Given free choice of foot placement, subjects choose a position similar to the **Middle** condition. While it would require less mechanical energy to perform a **Step In** (cross-over) maneuver and be more passively stable to use a wide **Step Out** (side-step) maneuver, subjects choose a **Middle** step position, suggesting they optimize for both stability and energetic cost. Quantifying these trade-offs in a control population informs future interpretations of data from patient populations.

REFERENCES

- Hof, A.L. et al.. J Biomech., **38**(1): p. 1-8. 2005

ACKNOWLEDGEMENTS

This work was supported in part by Career Development Award #1 IK2 RX000717-01 from the United States Department of Veterans Affairs, Rehabilitation Research and Development Service, and the Northwestern University Undergraduate Research Assistant Program.

THE RELATIONSHIP BETWEEN VARIABILITY AND ASYMMETRY DURING GAIT

Robert W. Gregory

Southern Connecticut State University, New Haven, CT, USA
E-mail: gregoryr3@southernct.edu, Web: <http://www.southernct.edu/>

INTRODUCTION

The mechanics of running have been studied extensively for the past 30 years. However, the etiology of running injuries continues to elude both researchers and clinicians; 27%-70% of distance runners can expect to be injured during any 1-year period [1]. Two factors that have recently been implicated in the development of running-related overuse injuries are movement variability and asymmetry.

Variability has been linked to the health of biological systems in a variety of contexts. This observation led to the formulation of the variability and overuse injury hypothesis: the likelihood of overuse injury is greatest at small magnitudes of variability and the potential for injury decreases as the variability increases [2]. Very high variability can also result in injury and there must be a window of 'higher variability' in which non-injured athletes function [3]. In addition, asymmetry has also been linked to overuse injuries in runners. Asymmetry in gait is often described as a difference in a kinematic or kinetic parameter between the right and left sides. While some level of asymmetry is normal in uninjured runners [4], recent research suggests that injured runners have less asymmetry than non-injured runners [5].

To date, there has been no examination of the link between movement variability and asymmetry during gait. Intuitively, it seems reasonable to hypothesize that increased levels of asymmetry will result in higher variability. Consequently, asymmetry may contribute significantly to the role of functional variability in preventing overuse injuries in runners. Therefore, the purpose of this study was to determine if there is a relationship between variability and asymmetry in recreational distance runners during walking and running.

METHODS

Thirteen healthy recreational runners (5 M, 8 F; age: 31.3 ± 11.0 yr, height: 1.69 ± 0.09 m, mass: 68.7 ± 18.6 kg) participated in this study. All participants ran at least 20 miles per week and were injury-free at the time of the study. All participants provided informed consent according to the procedures established by the Institutional Review Board at Southern Connecticut State University.

The same type of running shoe (Nike Air Pegasus 30+; Beaverton, OR) was worn by all participants. Participants walked (4 km/hr) and ran (10 km/hr and 12.5 km/hr) on an instrumented treadmill (Zebris FDM-T; Isny im Allgäu, Germany). The three conditions were presented in random order. For each condition, the participants walked or ran for six minutes. Kinematic and kinetic data were collected during the last minute of each trial at a sampling rate of 300 Hz and filtered using a 4th order, low-pass Butterworth filter with a cutoff frequency of 25 Hz.

For each participant, a minimum of 30 strides were analyzed. The following kinematic variables were measured: step length, step time, stance phase %, and swing phase %. The following kinetic variable was measured: peak vertical ground reaction force. Descriptive statistics (mean and standard deviation) were calculated for all variables. Variability was assessed using the coefficient of variation and asymmetry was evaluated as the difference in a kinematic or kinetic parameter between the right and left sides. A repeated-measures MANOVA was used to estimate the differences in variability and asymmetry for all variables across the three gait conditions; the Pearson product moment coefficient of correlation was used to estimate the relationship between variability and asymmetry for all variables for each of the three gait conditions.

RESULTS AND DISCUSSION

The results for the kinematic and kinetic variables measured in this study are shown in Table 1. The values presented are those for the right (dominant) side. There were significant increases in step length ($F_{2,24} = 112.6$, $p < 0.0001$), swing phase % ($F_{2,24} = 197.1$, $p < 0.0001$), and peak vertical ground reaction force ($F_{2,24} = 33.0$, $p < 0.0001$) with increasing gait velocity. There were significant decreases in step time ($F_{2,24} = 64.8$, $p < 0.0001$) and stance phase % ($F_{2,24} = 197.1$, $p < 0.0001$) with increasing gait velocity.

Movement variability was larger during running as compared to walking for step time ($F_{2,24} = 4.62$, $p < 0.05$) and stance phase duration ($F_{2,24} = 14.2$, $p < 0.0001$), but smaller for swing phase duration ($F_{2,24} = 18.0$, $p < 0.0001$) (see Table 1). The variability of step length and peak vertical ground reaction force did not change across gait conditions.

The levels of asymmetry for the kinematic and kinetic variables measured in this study were similar to those found in previous studies [4, 5]. Asymmetry did not vary across gait conditions for all measured parameters. While there were several exceptions, the relationship between variability and asymmetry during gait was not significant for the measured parameters (see Table 1).

CONCLUSIONS

High levels of asymmetry are typically thought to be associated with injury or gait inefficiency; symmetrical lower extremity movement patterns during running are often a goal. However, some level of asymmetry is normal in uninjured runners [4, 5]. In addition, there is a window of 'higher variability' in which non-injured athletes function [3]. Intuitively, it seems reasonable to hypothesize that increased levels of asymmetry will result in higher variability. However, there is not a strong relationship between variability and asymmetry during gait. Therefore, it is unlikely that natural levels of asymmetry contribute significantly to the role of functional variability in preventing overuse injuries in runners.

REFERENCES

1. Hreljac A. *Phys Med Rehabil Clin N Am* **16**, 651-657, 2005.
2. James CR, et al. *Med Sci Sports Exerc* **32**, 1833-1844, 2000.
3. Hamill J, et al. *Sports Med Arthrosc Rehabil Ther Technol* **4**, 45, 2012.
4. Zifchock RA, et al. *J Biomech* **39**, 2792-2797, 2006.
5. Bredeweg SW, et al. *Gait Posture* **38**, 847-852, 2013.

Table 1: Average, coefficient of variation (COV), symmetry index (SI), and coefficient of correlation (r) values for kinematic and kinetic variables. [Note: * = significant correlation between COV and SI ($p < 0.05$)]

Gait Condition		Step Length	Step Time	Stance Phase	Swing Phase	Peak vGRF
Walk (4.0 km/hr)	Avg.	0.63 ± 0.04 m	0.57 ± 0.05 s	$65.1 \pm 1.0\%$	$34.9 \pm 1.0\%$	1.13 ± 0.17 BW
	COV	$2.1 \pm 0.7\%$	$1.8 \pm 0.1\%$	$1.2 \pm 0.5\%$	$2.3 \pm 0.9\%$	$2.5 \pm 0.6\%$
	SI	$2.1 \pm 1.8\%$	2.0 ± 1.9	$1.1 \pm 1.0\%$	$2.1 \pm 1.8\%$	$2.8 \pm 2.0\%$
	r	-0.37	-0.61*	-0.41	-0.42	0.22
Run (10.0 km/hr)	Avg.	1.00 ± 0.06 m	0.36 ± 0.02 s	$39.2 \pm 2.8\%$	$60.8 \pm 2.8\%$	2.14 ± 0.23 BW
	COV	$2.1 \pm 0.7\%$	$2.3 \pm 1.1\%$	$2.0 \pm 0.4\%$	$1.3 \pm 0.3\%$	$2.8 \pm 0.7\%$
	SI	$2.0 \pm 2.1\%$	$2.8 \pm 1.7\%$	$2.2 \pm 2.1\%$	$1.6 \pm 1.7\%$	$3.3 \pm 3.2\%$
	r	0.60*	-0.03	-0.15	0.12	-0.11
Run (12.5 km/hr)	Avg.	1.18 ± 0.07 m	0.35 ± 0.02 s	$35.5 \pm 2.9\%$	$64.5 \pm 2.9\%$	2.25 ± 0.27 BW
	COV	$1.7 \pm 0.5\%$	$2.7 \pm 0.8\%$	$2.0 \pm 0.4\%$	$1.1 \pm 0.2\%$	$2.9 \pm 0.4\%$
	SI	$1.4 \pm 1.4\%$	$2.2 \pm 1.8\%$	$2.1 \pm 1.5\%$	$1.2 \pm 0.9\%$	$2.5 \pm 2.2\%$
	r	0.45	-0.15	-0.56*	-0.23	-0.29

PARTIAL LEAST SQUARES FOR DISCRIMINANT ANALYSIS OF KINEMATIC AND KINETIC DATA

¹ Elizabeth A Hassan and ¹ Kevin J Deluzio

¹ Dept. of Mechanical Engineering, Queen's University, Kingston, ON, Canada
email: elizabeth.hassan@queensu.ca

INTRODUCTION

Studies of human movement often demand simultaneous analysis of multiple quantities, such as joint angles and moments from several joints. Multiple comparisons can be challenging to interpret using multi-way ANOVAs or ANCOVAs. Linear discriminant analysis, in combination with Principal Component Analysis has been proposed as an improvement that allows for information from multiple complete waveforms to be analyzed [1]. This abstract proposes that additional discriminant performance enhancements can be achieved by combining Partial Least Squares with discriminant analysis.

Partial Least Squares (PLS) is a generalized form of PCA. PLS has been applied extensively to analysis of multivariate chemometric data [2] but has not yet been widely applied in biomechanical analysis. The only known applications of PLS to gait data are short examples in [3,4].

The primary difference between PLS and PCA is that PCA extracts components that explain the maximum amount of *variance* in the data (X) but PLS extract latent variables that explain the maximum amount of *covariance* between the data (X) and the grouping variable (Y). If the between group variance is larger than the within group variance, the techniques are equivalent, but if they are equal or the within group variance is large PLS is superior for group discrimination [5]. This advantage is particularly useful in cases with large subject-subject variability and when group differences are subtle, which are often the case in biomechanical analysis.

METHODS

To evaluate the performance of PLS-DA for gait compared with PCA-LDA, it was tested on an already published data set. The data set includes knee kinematic and kinetic data from 63 asymptomatic control subjects and 50 subjects with severe osteoarthritis; the details of the data collection are summarized in Deluzio and Astephen [1]. These techniques were compared using the misclassification rate, along with misclassification rates using the peak and PC scores of the knee adduction moment.

This data was preprocessed with PCA using MATLAB code written by our lab group. A 90% trace criterion was used to evaluate the correct number of components to extract. The remaining PC scores composed the data (X) matrix, with control and osteoarthritis being coded as 0-1 respectively as Y.

The PLS analysis was conducted using MATLAB code written by the author, based on the algorithm outlined in Abdi [6]. Discriminant analysis and cross-validation was conducted with built in MATLAB functions. The number of columns in X was reduced to a more parsimonious set of 5 variables using the criteria described in Andersen and Bro [7]. Model validity was checked using a randomization test in which the Y indices were randomized, according to the procedure described in Szymanska et al [8].

RESULTS AND DISCUSSION

The PLS procedure described above yielded 2 Latent Vectors, (LVs) extracted from 5 input variables (X columns). Using the scores of these two LVs, it was possible to separate the groups with

a linear discriminant function, as shown in Figure 1. The misclassification rate was 7% using a leave one out procedure, which is equivalent to that achieved by Deluzio and Astephen [1], 8%, but both techniques were much better than peak knee adduction moment alone, or a single set of principal component scores, as shown in Figure 2. The variable selection procedure resulted in similar variables being identified as most important to the prediction as shown in Table 1.

With PLS analysis, the selection of number of inputs to include and number of variables to extract can be somewhat subjective. In this analysis, we evaluated the discriminant performance over a range of possible inclusion criteria and found that for this data set, the performance is similar over the range of 3 to 13 input variables, ranging from 5.3 to 10% misclassification, and chose 5 variables as being close to the approach in the original paper [1]. Extracting a third LV did not improve the prediction; therefore the analysis used two LVs for parsimony.

CONCLUSIONS

The results of the PLS and LDA analysis suggests that PLS as a processing step prior to LDA can at least equal that of PCA-LDA, but with the advantage of automatic variable selection. In cases of highly collinear data, this selection process is likely more stable than stepwise procedures, and the extracted PLS latent variables are orthogonal, which is the ideal case for LDA performance. Additionally, there are opportunities for enhanced interpretation, which will be discussed in future work.

Table 1: Comparison of variable importance extracted from PCA-LDA and PLS-LDA

PCA-LDA [1]	PLS-LDA (Current Analysis)
Flexion Moment PC2	Flexion Moment PC2
Flexion Angle PC2	Flexion Angle PC2
Flexion Moment PC1	Adduction Moment PC1
Adduction Moment PC1	Adduction Moment PC2
	Flexion Angle PC1

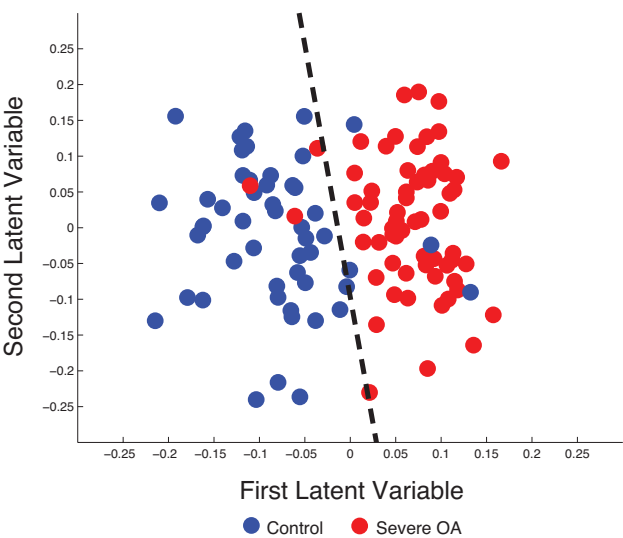


Figure 1: Each point corresponds to one observation’s scores of that observation on the two extracted latent variables. Blue dots are normal subjects, red are severe OA. The linear discriminant function is shown as a black dashed line. Misclassification rate 7%.

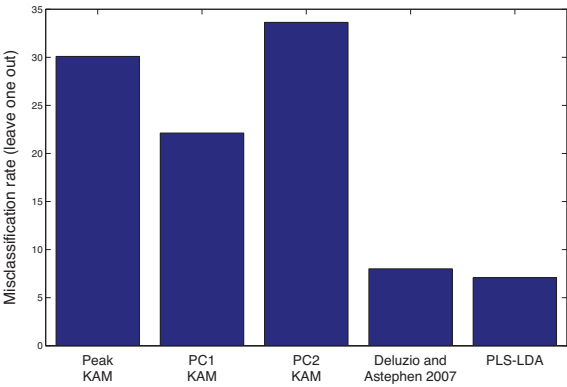


Figure 2: Misclassification rate based on leave one out procedure for peak, PC1 and Pc2 scores of the knee adduction moment, the rate quoted by Deluzio and Astephen for PCA-LDA and PLS-LDA with variable selection.

REFERENCES

1. Deluzio KJ & Astephen JL. *Gait & Posture* **25**, 86-93, 2007.
2. Wold S & Sj  str  m. *Chemometrics and Intelligent Laboratory Systems* **58** 109–130 2001
3. Bourriez J et al. *Gait & Posture* **21**, s144, 2005.
4. Kaptein RG et al. *J. Neuroeng. Rehabil.* **11**, 120, 2014.
5. Barker M & Rayens W. *J. Chemom.* **17**, 166–173. 2003.
6. Abdi, H. *WIREs Comp Stat.* 2010.
7. Andersen, CM & Bro, R. *J. Chemom.* **24**, 728–737. 2010.
8. Szymanska E et al. *Metabolomics.* **8** ,S3-S16. 2012.

FOOT DISSIPATION DURING ANKLE PUSH-OFF: HUMAN WALKING INSIGHTS FROM A MULTIARTICULAR EMG-DRIVEN MUSCULOSKELETAL MODEL

Eric C. Honert, Karl E. Zelik

Vanderbilt University, Nashville, TN, USA
eric.c.honert@vanderbilt.edu, karl.zelik@vanderbilt.edu

INTRODUCTION

Humans perform a burst of push-off work with their trailing limb during the step-to-step transition in walking. This push-off helps redirect the body's center-of-mass, reducing collisional energy losses after heelstrike and enabling economical gait [1]. However, the foot performs negative work during this phase of gait [2], which counteracts a fraction of the positive push-off work of the ankle. These conflicting ankle and foot behaviors are difficult to reconcile with previous findings on energy-saving mechanisms used during gait, and dynamic walking principles emphasizing the importance of center-of-mass push-off [1].

This study sought to investigate one plausible explanation for the conflicting ankle and foot behaviors during push-off. We hypothesized that our current understanding of ankle and foot function is obscured by methodological limitations in commonly-used biomechanical estimates. A key assumption in inverse dynamics and other segment-based kinetics estimates [2] is that joint moments and powers originate from monoarticular sources (e.g., muscle-tendon units). These estimates do not account for multiarticular muscles, such as the flexor digitorum and hallucis longus (FDHL) muscles, which articulate across the ankle and toe joints.

The purpose of this study was two-fold. First, we sought to develop a data-driven musculoskeletal model of the ankle and foot that allowed us to approximate muscle-specific contributions to gait. Second, we aimed to estimate the magnitude of work and power errors that may be inherent in conventional biomechanical estimates which neglect multiarticular muscles, and determine if these errors might impact our current interpretation of ankle and foot function during push-off in walking.

METHODS

Three healthy male subjects (24 ± 5 years, 88 ± 14 kg, height: 1.8 ± 0.1 m) participated in this gait analysis study. All subjects gave informed consent to the protocol. Subjects walked at 1.25 m/s on a split-belt instrumented treadmill (Bertec). Six degree-of-freedom kinematics and kinetics of the shank and foot were derived from a ten camera motion tracking system (Vicon) in conjunction with post-processing via C-Motion Visual3D. Prior to walking, four surface EMG sensors (Delsys) were placed on muscles that contribute to ankle plantarflexion: soleus, medial gastrocnemius, lateral gastrocnemius, and the FDHL (measured together due to limitations in surface EMG). Marker and force data was filtered at 10 Hz and 25 Hz, respectively. EMG data was demeaned, high-pass filtered at 150 Hz, rectified, and low-pass filtered at 10 Hz. All filters used were 3rd order, zero-lag Butterworth filters.

We developed a sagittal plane musculoskeletal model in order to estimate the individual ankle and foot muscle contributions to push-off during walking. To do so, we used a simple EMG to force mapping algorithm and integrated it with conventional gait analysis measurements, using techniques and simplifying assumptions similar to previously published musculoskeletal models [3, 4].

To estimate the potential errors in conventional ankle and foot power calculations due to neglecting multiarticular muscles, we assumed the FDHL muscle-tendon units performed no mechanical work. In other words, we assumed the multiarticular FDHL acted isometrically during push-off, effectively like a cable across the ankle and toe joints. Using our model we then computed how much the FDHL contributed to the conventional ankle and foot power calculations (i.e., the inaccuracy error inherent in

these measures if the multiarticular muscle were acting isometrically). Subtracting these multiarticular power contributions from the conventional ankle and foot estimates yielded updated estimates for ankle and foot power, which may better reflect the underlying physiology.

RESULTS and DISCUSSION

We found that our EMG-driven musculoskeletal model was able to reproduce inverse dynamics based sagittal plane ankle power with high fidelity ($R^2 = 0.98 \pm 0.01$, Fig. 1A).

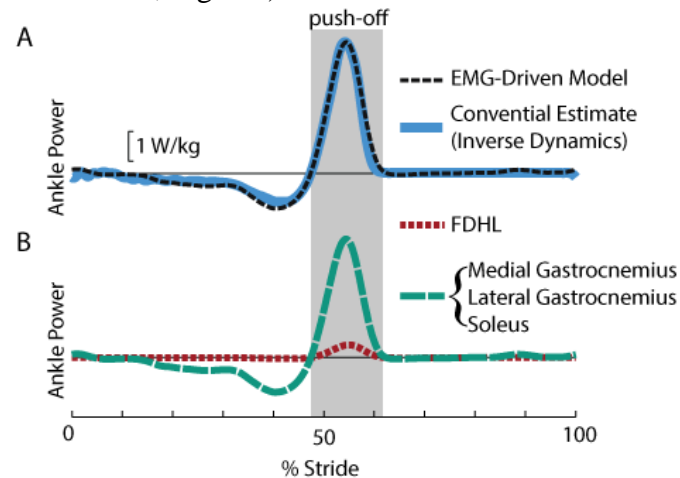


Figure 1: Ankle power at 1.25 m/s for one subject. (A) EMG-Driven Model power reproduced the sagittal plane inverse dynamics estimate. (B) Muscle group contributions to plantarflexion power based on EMG-Driven model. The FDHL are the multiarticular muscle tendon units acting about both the ankle and toe joints.

Next, we estimated the errors that might result from neglecting the multiarticular ankle-toe (FDHL) muscles in inverse dynamics. We found that inverse dynamics may over-estimate sagittal ankle push-off work by about 1.9 ± 0.9 J (Fig. 1B: area under FDHL muscle tendon unit power curve), or about 6% of ankle push-off work, at 1.25 m/s.

We also discovered that the foot may not dissipate as much energy as previously estimated (Fig. 2). On average, we found that there is -9.3 vs. -10.5 J (updated vs. conventional estimate) of negative foot work during push-off, and 2.2 vs. 1.5 J of positive foot work during push-off at 1.25 m/s.

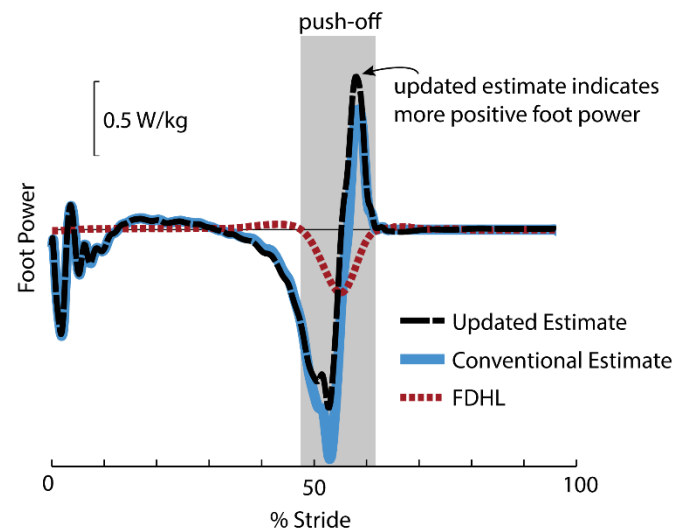


Figure 2: Updated Estimate of foot power was calculated by subtracting the multiarticular muscle tendon unit power (FDHL assuming isometric contractions) from the Conventional foot power estimate based on a deformable foot model [2].

The musculoskeletal model presented provides an estimate of muscle-specific power contributions to ankle plantarflexion push-off during walking, which can then be used to account for multiarticular muscle function. Preliminary findings suggest that the positive ankle work may be over-estimated, and positive foot power under-estimated, by about 1.9 J. Rather than purely dissipating energy during push-off, these findings suggest that the foot may also undergo a cycle of viscoelastic energy storage (~ 9 J) followed by energy return (~ 2 J), which may have implications for prosthetic foot design. However, the foot still appears to absorb more energy during push-off than it returns as positive work in terminal stance. This simple musculoskeletal modeling approach provides an updated estimate of muscle-specific contributions to gait, and could potentially be applied to other joints to improve our fundamental understanding of biological movement.

REFERENCES

1. Donelan JM, et al., *J Exp Biol.*, **205**, 3717-3727, 2002.
2. Takahashi KZ, et al., *Gait Posture*, **38**, 818-823, 2013.
3. Buchanan TS, et al., *J Appl Biomech*, **20**, 367-395, 2004.
4. Farris DJ, et al., *PNAS*, **109**, pp. 977-982, 2012.

ACCURACY OF RUNNING DATA FROM THE GARMIN FORERUNNER

Iain Hunter, James Tracy, Shaquille Walker, and Jordan Eatough

Brigham Young University, Provo, UT, USA
email: iain_hunter@byu.edu, web: <http://biomechanics.byu.edu>

INTRODUCTION

Measurements of running mechanics are prevalent in a variety of studies [1]. Recent advances in running watches have provided increased possibilities for obtaining data related to the mechanics of running. The Garmin Forerunner 620 (GF) with heart rate monitor (HRM) displays and stores stride rate (SR), vertical oscillation (VO), ground contact time (GT), heart rate, distance, pace, and elevation. As with any new technology, these data will only be useful if they are correct.

Typically, the measurements listed above are recorded in a lab setting on a treadmill. If the Garmin watch provides accurate data, these measurements will be available for running outside of a lab where speed is not constrained, surfaces are not fixed, and a more natural environment can be used for data collections.

This study performed a comparison between the GF and a Vicon Nexus motion analysis system in measuring stride rate, ground contact time, and vertical oscillation.

METHODS

A Garmin Forerunner 620 with a heart rate/accelerometer strap was attached to each of 8 experienced runners. They ran at five speeds including: 3.35, 3.84, 4.47, 5.36, and 6.70 m/s (8:00, 7:00, 6:00, 5:00, and 4:00 per mile paces). The running was completed on a force instrumented treadmill (AMTI, Watertown, MA).

While running, measurements were taken using motion capture software (Vicon Nexus 2.1, Oxford, UK) running at 250 Hz. The Vicon Plug-in Gait model provided positions of the feet and center of mass which were used for calculating the same

parameters that the GF exported (stride rate, ground contact time, and vertical oscillation).

After a three minute warm-up, subjects ran at each speed in the order listed above for 30s. During the final 20s of each stage, measurements were simultaneously recorded from both the watch and Vicon system. Ground time was measured through the motion analysis software by observing the ground reaction forces and positions of the feet. Vertical oscillation was taken from the low to high points of the center of mass within each step using the outputs from the Plug-in Gait model. Stride rate was measured from foot-strike events. The GF reported these same measurements using the accelerometers in the watch and chest strap. The methods of calculation used in the GF are understandably not documented; therefore, it is not possible to explain here how GT and VO are calculated.

Three univariate ANOVA were completed (one for each dependent variable) with condition and speed as fixed factors.

RESULTS AND DISCUSSION

The Garmin Forerunner 620 matched the motion capture system very well on stride rate. However, it overestimated ground contact time and vertical oscillation by 15% and 20% respectively (Figure 1 and Table 1). This is encouraging for those interested in using the GF for research purposes outside of a lab setting as improvements come in future software and hardware releases of the GF.

There were no significant interactions for condition by speed. This tells us that the differences between the GF and the motion analysis system are not different between different speeds. So, if a method can be determined for adjusting the output at one

speed, the same adjustment should be possible across all speeds. Since this is the first device to perform these measurements, the GF may be improved over time to become more accurate.

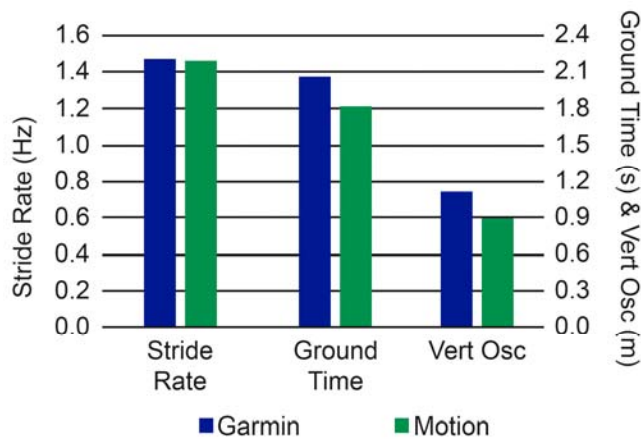


Figure 1. Average stride rate, ground time, and vertical oscillation between conditions.

The expected trends of stride rate, ground time, and vertical oscillation with increases in running speed were observed with the GF. So, even if the values of each measurement from the GF are not exactly correct, they were increasing or decreasing with speed in the same pattern as the motion capture data showed.

This study did not collect enough measurements for an investigation into the variability of the GF data. However, it is possible that since the variability of certain running characteristics increase with fatigue,

the watch may be useful for analyzing how variable these measures are as a run progresses. Over a 20-s measurement, a good understanding of the variability of the steps could not be completed. Future studies could investigate how well the watch estimates variability of the outputted measurements over extended running for studies [2]. That would serve as a method for using the watch outside of a lab setting for extended running.

It is possible that with additional information from the GPS signal, providing a more accurate pace estimation, may improve that ground contact time and vertical oscillation estimations. Since this study was performed in an indoor laboratory, an outdoor setting might lead to more accurate data.

CONCLUSIONS

The Garmin Forerunner 620 with HRM is accurate at measuring stride rate, but overestimates ground contact time and vertical oscillation. The overestimations are often by a consistent percentage, but not in every case. As a research tool, the potential is there for accurate data in the future, but some improvements are still needed.

REFERENCES

1. Williams P, et al. I J Sports Med, **8**, 107-118, 1987.
2. Nakayama Y, et al. Gait Posture, **31**, 331-333, 2010.

Table 1: Data showing stride rate, ground contact time, and vertical oscillation across speeds for the GF and motion capture system. Data are displayed as means \pm standard deviation.

Speed	3.35	3.84	4.47	5.36	6.70
Stride Rate (Hz) Garmin	1.37 \pm 0.03	1.38 \pm 0.03	1.42 \pm 0.05	1.49 \pm 0.07	1.62 \pm 0.09
Stride Rate (Hz) Motion	1.37 \pm 0.03	1.38 \pm 0.03	1.44 \pm 0.05	1.52 \pm 0.06	1.65 \pm 0.07
Ground Time (s) Garmin	0.240 \pm 0.014	0.224 \pm 0.016	0.212 \pm 0.014	0.193 \pm 0.015	0.168 \pm 0.025
Ground Time (s) Motion	0.224 \pm 0.017	0.201 \pm 0.021	0.185 \pm 0.015	0.167 \pm 0.020	0.133 \pm 0.020
Vert Oscillation (m) Garmin	0.119 \pm 0.013	0.120 \pm 0.011	0.115 \pm 0.011	0.108 \pm 0.015	0.091 \pm 0.016
Vert Oscillation (m) Motion	0.091 \pm 0.008	0.103 \pm 0.025	0.092 \pm 0.007	0.087 \pm 0.006	0.076 \pm 0.008

VALIDATION OF DETERMINING STANCE TIME USING ACCELEROMETER DATA

¹⁻³ Steve T. Jamison and ²⁻³ Irene S. Davis

¹ The University of Delaware, Newark, DE, USA

² Harvard Medical School, Boston, MA, USA

³ Spaulding National Running Center, Cambridge, MA, USA

email: sjamison@udel.edu, web: <http://runsnrc.org/>

INTRODUCTION

Patients with unilateral transtibial amputation often exhibit asymmetries in their gait pattern, even after receiving gait training during their rehabilitation [1-2]. Asymmetries have been associated with increased risk of back pain, as well as knee pain and osteoarthritis of the intact limb and osteoporosis in the affected limb [2-4].

Previous work involving individuals with amputation has shown that stance time asymmetry feedback using a force treadmill is effective at improving symmetries during a single session of walking [5]. While gait retraining using real-time feedback from a force treadmill may be effective, these treadmills are cost prohibitive for most clinics. A low-cost, mobile system would be more suitable for clinical- as well as home-use.

Accelerometers which communicate via Bluetooth are becoming readily available and have the potential to be used in the community. However, the accuracy of the information from these devices compared with that from an instrumented treadmill is unknown. Therefore, as a first step, the purpose of this study was to determine whether accurate unilateral stance times could be obtained from acceleration data using an instrumented treadmill as the standard.

METHODS

Five healthy individuals (age: 24.8 ± 4.3 yrs; height: 1.75 ± 0.1 m; mass: 73.0 ± 15.3 kg) walked normally for 1 minute at four speeds (1, 1.2, 1.4, and 1.6 m/s) on an instrumented treadmill (AMTI Inc., Watertown, MA) wearing standard lab shoes (Nike Air Pegasus). One marker placed on the lateral

aspect of the right forefoot was used to determine right from left ground reaction forces. Force (1,000Hz) and marker (100Hz) data were collected using the same system (Vicon Motion Systems Ltd., Oxford, UK).

Force data were filtered using a 45Hz low pass, zero-phase shift Butterworth filter. A dual linear fit algorithm was used to determine force-based foot strike and toe off events. The dual linear fit algorithm iteratively fits a straight line to data just before and after potential event samples. The sample at which these two lines have the lowest residuals becomes the event index.

A tri-axial accelerometer (IMeasureU, Auckland, NZ) collecting at 1,000Hz to an onboard SD card was placed on the medial distal tibia (Fig. 1). A custom algorithm was developed to identify patterns in the x-component of the acceleration data corresponding to heel strike and toe off (Fig. 2). The x-axis of the accelerometer is approximately aligned with the anterior-posterior axis of the shank.



Figure 1: Accelerometer placed on the distal tibia.

Before walking, subjects tapped their heel on the front belt of the treadmill. This provided a clear spike in both the acceleration and force data for time synchronization. Stance times computed from the force data were compared to corresponding stance times computed from the acceleration data.

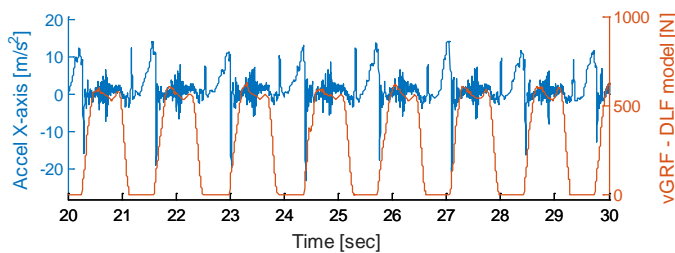


Figure 2: Synchronized vertical ground reaction force (orange), which used the dual linear fit (DLF) model to determine heel strike and toe off events, and x-component acceleration (blue) for 10 seconds of walking for a subject.

RESULTS AND DISCUSSION

1029 stance times were compared over a total of 20 1-minute walking trials (5 subjects x 4 speeds; Fig 3). 969 of the 1029 (94.2%) matched force- and accelerometer-based stance times were less than 3% different from each other. The mean stance time difference was 6 ± 9.5 ms while the mean absolute stance time difference was 11 ± 7.9 ms. The two measurement techniques were also highly correlated, having a 99% confidence interval for the criterion-referenced reliability interclass correlation of [0.956, 0.996].

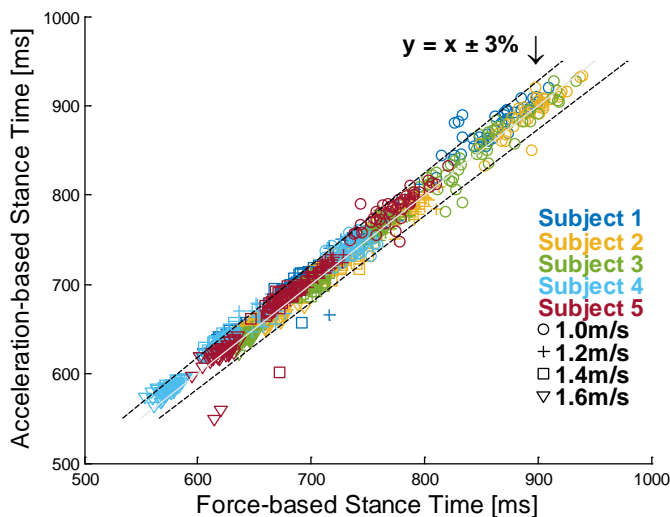


Figure 3: Scatter plot of all compared stance times. Subjects are color-coded while speed is indicated by symbol. Lines indicating an exact match as well as $\pm 3\%$ difference from force-based stance time calculation are also shown.

The acceleration-based stance time algorithm was not able to determine stance times for only 5 of 1034 possible steps (all for Subject 4). Subject positioning on the treadmill resulted in force-based stance time data not being available for 3 steps.

It is important to note that this investigation was done with a convenient sample of healthy individuals on an instrumented treadmill. It is not known if this algorithm would be robust enough for the ambulation of individuals with amputation. Further, instrumented treadmills inherently produce noisy data. Force data were filtered and a dual linear fit model was used to determine stance times as accurately as possible, but even these times could include some level of error.

Determining accurate stance times using an accelerometer is the first step in developing a clinically viable mobile system that provides feedback to improve stance time symmetry. This type of feedback system will have clinical- and home-use applications to a broad range of individuals, including those with amputations and total joint replacements.

CONCLUSIONS

Stance times calculated using an accelerometer attached at the ankle are highly correlated with stances times calculated using force data from an instrumented treadmill.

REFERENCES

1. Sanderson DJ, et al. *Gait Posture* **6**, 126-36, 1997.
2. Gailey R, et al. *J Rehab Res Dev* **45**, 15-30, 2008.
3. Kulkarni J, et al. *Clin Rehabil* **12**, 348-53, 1998.
4. Kulkarni J, et al. *Clin Rehabil* **19**, 81-6, 2005.
5. Dingwell JB, et al. *POI* **20**, 101-10, 1996.

ACKNOWLEDGEMENTS

The authors gratefully acknowledge infrastructure and salary support from the BADER Consortium (DoD OR100017). We also thank IMeasureU and RunKeeper Inc for loaning the sensors used during this investigation.

QUANTITATIVE ASSESSMENT OF MOVEMENT SMOOTHNESS DURING EMOTIONAL GAIT

Gu Eon Kang^{1,*} and Melissa Gross¹

¹University of Michigan, Ann Arbor, MI, USA

*Email: guekang@umich.edu

INTRODUCTION

Emotion changes movement pattern. Movement smoothness is one such thing that is likely to be altered by feeling emotions. The effect of emotion on movement smoothness has been assessed in gestural movements [1], and more energetic gestures (angry and happy) were correlated with greater jerk than less energetic gestures (sad), as might be expected since jerk was not normalized. Recently, jerk analysis (normalized for movement duration and amplitude) has been applied to the whole body center-of-mass (COM) and movement smoothness has been quantified during sit-to-walk performed with emotions [2]. The study reported jerkier sit-to-walk for sadness than for anger or joy. Emotional gait is associated with alterations in kinematics [3] but movement smoothness has not yet been quantified. The purpose of this study was to examine the effect of emotion induced by autobiographical recall on movement smoothness during gait. We quantified movement smoothness during emotional gait using jerk analysis.

METHODS

Eighteen healthy adults (11 women; 20±2 years; 167±7 cm) participated after giving informed consent. Gait data were collected from 41 markers using an 8-camera motion capture system (60 Hz), and were low-pass filtered (6 Hz).

For each gait trial, we asked participants to recall autobiographical episodes for inducing four target emotions: joy (high arousal, positive), anger (high arousal, negative), sadness (low arousal, negative), and neutral emotion. After recalling each emotion, participants walked across the laboratory (10 m). Participants performed three trials with each emotion in a block. After each trial, they rated the intensity of the four target emotions that they felt in

the preceding trial using a 5-point Likert scale (0, 1, 2, 3 and 4). Angry, sad and joyful trials were trials with score ≥ 2 for anger, sadness and joy, respectively. Neutral trials were trials with neutral emotion with score ≥ 2 , and anger, sadness and joy with score < 2 .

We used Visual3D software to compute gait parameters, linear jerk for the whole body COM, head, and wrist in antero-posterior (AP), medio-lateral (ML) and vertical (VT) directions, and angular jerk for the hip, knee and ankle in the sagittal plane during one gait cycle. For normalizing jerk, the sum of the squares of jerk was multiplied by the fifth power of gait duration, and was divided by two and the second power of linear or angular displacement covered during the gait duration. Finally, linear jerk score (NJS) and angular jerk score (AJS) were considered as the square root of the normalized jerk [4]. A higher jerk score indicated a more jerky movement.

A mixed model with random effects of participants and fixed effects of emotion and gender was used to evaluate effects on outcomes. Bonferroni correction was applied for post-hoc pairwise comparison between emotions and genders ($p < .05$).

RESULTS AND DISCUSSION

Gait parameters differed among the target emotions (all $p < .001$). Pairwise comparison indicated that gait parameters differed between neutral emotion and the high arousal emotions (joy and anger), and between sadness and the high arousal emotions (all $p < .05$) (Table 1). Between sadness and neutral emotion, only cadence was different ($p < .05$) (Table 1). Cadence was greater for women (59.9 strides/min) than for men (55.4 strides/min) ($p < .01$).

Both NJS and AJS differed among the target emotions (all $p < .01$). Head AP-NJS was greater for sadness than neutral emotion ($p < .05$) (Table 1). COM and head AP-NJS and VT-NJS, wrist VT-NJS, were greater for sadness than anger and joy (all $p < .05$) (Table 1). Lower limb AJS was also greater for sadness than anger ($p < .05$). Head ML-NJS was greater for women (1505) than for men (1209) ($p < .05$).

CONCLUSIONS

Emotion induced by autobiographical recall was associated with changes in movement smoothness during gait. Our findings demonstrated that linear movement of the whole body COM and head in AP and VT directions, and linear movement of the wrist in the VT direction was jerkier for sadness than for anger and for joy. Angular movement of the lower

limb in the sagittal plane was jerkier for sadness than for anger. To our knowledge, this is the first to quantify movement smoothness during emotional gait. In line with a recent study [2], this study confirmed the importance of assessing movement smoothness in embodiment of emotion.

REFERENCES

1. Pollick FE, et al. *Cognition* **82**, B51-B61, 2001.
2. Kang G and Gross MM. *Hum Movement Sci* **40**, 341-351, 2015.
3. Gross MM, et al. *Hum Movement Sci* **31**, 202-221, 2012.
4. Ketcham CJ, et al. *J Gerontol B Psychol Sci Soc Sci* **57**, P54-P64, 2002.

Table 1: Mean gait speed, stride length, cadence, NJS for the whole body COM, head and wrist, and AJS for the hip, knee and ankle in gait trials with each target emotion across participants.

	Neutral Emotion	Sadness	Anger	Joy
Gait Parameters				
Gait Speed (m/s)	1.25 (0.03) ^{A***J***}	1.18 (0.05) ^{A***J***}	1.41 (0.05) ^{N***S***}	1.41 (0.04) ^{N***S***}
Stride Length (m)	1.30 (0.03) ^{A***J***}	1.28 (0.03) ^{A***J***}	1.40 (0.04) ^{N***S***}	1.41 (0.03) ^{N***S***}
Cadence (strides/min)	57.4 (0.8) ^{S*A**J*}	55.3 (1.1) ^{N*A***J***}	60.1 (1.0) ^{N**S***}	59.8 (1.1) ^{N*S***}
Whole Body COM				
AP-NJS (no unit)	85 (5)	92 (5) ^{A*}	76 (4) ^{S*}	84 (9)
ML-NJS	1661 (137)	1508 (99)	1703 (175)	1780 (182)
VT-NJS	5494 (191)	6268 (518) ^{A**J*}	4655 (160) ^{S**}	4847 (276) ^{S*}
Head				
AP-NJS	53 (4) ^{S*}	71 (8) ^{N*A*J**}	53 (5) ^{S*}	48 (3) ^{S**}
ML-NJS	1386 (87)	1330 (73)	1464 (79)	1380 (97)
VT-NJS	4922 (218)	5718 (496) ^{A**J**}	4357 (161) ^{S**}	4342 (184) ^{S**}
Wrist				
AP-NJS	137 (9)	155 (13)	138 (11)	145 (12)
ML-NJS	1499 (114)	1689 (162)	1505 (121)	1442 (104)
VT-NJS	2767 (181)	3445 (417) ^{A*J**}	2437 (190) ^{S*}	2216 (195) ^{S**}
Lower Limb				
Hip AJS (no unit)	2552 (112)	2891 (209) ^{A**}	2347 (117) ^{S**}	2567 (201)
Knee AJS	3803 (208)	4429 (331) ^{A*}	3502 (203) ^{S*}	4152 (347)
Ankle AJS	10354 (457)	11558 (528) ^{A**}	9757 (244) ^{S**}	10240 (639)

Note: Values in parentheses mean standard errors. Superscript letters represent significant differences between target emotions: N=neutral emotion, S=sadness, A=anger, J=joy. * $p < .05$, ** $p < .01$, *** $p < .001$.

OBESITY IS ASSOCIATED WITH INCREASED JOINT TORQUES AND RELATIVE EFFORT DURING GAIT: PRELIMINARY FINDINGS

¹Hoda Koushyar, ²Dennis E. Anderson, ¹Maury A. Nussbaum, and ³Michael L. Madigan

¹Virginia Tech, Blacksburg, VA, USA

²Harvard Medical School, Boston, MA, USA

³Texas A&M, College Station, TX, USA

email: koushyar@vt.edu, web: <http://www.biomechanics.esm.vt.edu/>

INTRODUCTION

Obesity has been linked to altered gait kinematics and kinetics. For example, individuals who are obese walk with less hip and knee flexion and more ankle plantar flexion during stance [1]. They also exhibit higher hip and knee extensor torques [2], and higher ankle plantar flexor torque [1, 2]. Increased joint loading with obesity may increase the risk of musculoskeletal pathology.

Altered lower extremity strength may explain the differences in gait kinematics and kinetics between obese and healthy-weight individuals [2]. To better understand the importance of lower extremity strength during gait, earlier work investigated relative effort, or joint torques expressed as a percentage of maximum available joint torque [3]. Higher relative effort among obese individuals may help explain their altered gait.

To better understand the obesity-related changes in joint load during gait, and to assess the importance of muscle strength, the purpose of this study was to investigate whether and to what extent lower extremity joint torques and relative effort during gait differ with obesity.

METHODS

Participants included seven healthy-weight (HW, age: 22.3 ± 3.4 years, BMI: 22 ± 2 kg/m²) and seven obese (OB, age: 23.6 ± 3.8 years, BMI: 31.7 ± 3.8 kg/m²) females. Participants with any self-reported history of neurological, cardiac, or musculoskeletal disorders were excluded from the study.

Gait trials were performed at a self-selected speed on a 10-meter walkway. Ground reaction forces were sampled at 1000 Hz from a force platform (Bertec Corporation, Columbus, OH) embedded in the middle of the walkway, and kinematics were sampled at 100 Hz using a six-camera motion analysis system (MX-T10, Vicon Motion Systems Inc., L.A, CA).

Strength measures included isometric and isokinetic (concentric and eccentric) maximum voluntary contractions (MVCs) of the right lower extremity. Torques were sampled at 200 Hz using a Biodex System 3 dynamometer (Biodex Medical Systems, Inc., Shirley, NY), in plantar flexion (PF), dorsiflexion (DF), knee extension (KE), knee flexion (KF), hip extension (HE), and hip flexion (HF).

A sagittal plane, rigid-link model was created, and inverse dynamics analysis was used to estimate resultant joint torques at the ankle, knee, and hip during the stance phase of gait. Relative effort was determined using the method reported by Anderson and Madigan (2014) [3]. At the instants of peak torques, relative effort was calculated as:

$$Relative\ Effort = \frac{T}{A + P} \times 100$$

where T is the peak resultant joint torque, and A and P are the respective active and passive components of available strength determined using a model relating joint torque, angle, and angular velocity [4, 5]. Peak absolute torques and relative effort were compared between groups using unpaired t tests. Statistical analyses was performed using JMP Pro 10 (SAS Institute, Inc., Cary, NC).

RESULTS AND DISCUSSION

Joint torques (Figure 1) and relative effort (Table 1) during gait differed with obesity. Peak torques were higher for the OB group in HF (30%; $p=0.011$), KE (101%; $p=0.006$), and PF (53%; $p<0.001$). Relative effort during gait was 70% higher in KE ($p=0.033$; Table 1). The mean gait speed was 1.33 m/s, and did not differ between groups ($p=0.071$).

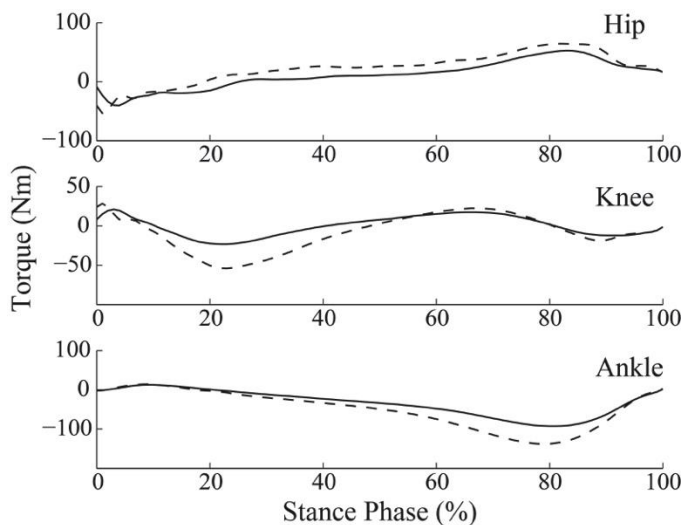


Figure 1: Ensemble averaged sagittal plane torques during stance for OB (dashed) and HW (solid) participants. Positive values are flexor/dorsiflexor torques and negative values are extensor/plantar flexor torques.

The higher HF torque among obese participants during gait has not been reported previously, though the higher knee extensor torque in this group is consistent with earlier evidence [2], as is the higher plantar flexor torque [1, 2]. In general, the current findings suggest that obese individuals walk with higher joint loads.

The higher KE relative effort among obese participants, despite them having higher KE absolute strength [6], suggests that obese individuals are more likely to be limited by knee extensor strength during gait. Furthermore, high muscle forces to produce large KE torques may increase knee loading beyond the increase due to higher weight. The large (>1) value for PF relative effort in both healthy-weight and obese groups suggests that both groups walk near the limits of their available PF strength during gait.

This large PF relative effort, though, may have been influenced by participants not generating true maximum strength during strength measurements or to underestimation of maximum available torque using the torque model.

Table 1: Peak Torque (Nm) and Relative Effort (mean \pm SD)

	Peak Torque during gait (Nm)		Relative Effort	
	HW	OB	HW	OB
HE	49.3 \pm 19.1	61.1 \pm 19.2	0.51 \pm 0.31	0.55 \pm 0.24
HF	53.4 \pm 9.5	69.8 \pm 10.9*	0.61 \pm 0.17	0.59 \pm 0.09
KE	27.1 \pm 14.8	54.6 \pm 15.9*	0.5 \pm 0.26	0.85 \pm 0.28*
KF	18.3 \pm 5.7	24.2 \pm 15.7	0.4 \pm 0.16	0.53 \pm 0.33
PF	92.9 \pm 14.2	142.3 \pm 18.5*	1.29 \pm 0.36	1.93 \pm 0.74
DF	13.5 \pm 6.3	14.1 \pm 5.3	0.45 \pm 0.17	0.4 \pm 0.18

* indicates a significant difference between HW and OB groups ($p<0.05$)

CONCLUSIONS

Obese individuals exhibited higher joint torque at HF, KE, and PF which suggests elevated joint loads in this group. Furthermore, higher KE relative effort among obese individuals may indicate greater likelihood of gait limitations due to KE strength, as well as excessive knee loading that can adversely affect the knee joint.

REFERENCES

- DeVita, P., and Hortobagyi, T. *Journal of Biomechanics*, **36**:9, 1355-1362, 2003.
- Browning, R. C., and Kram, R. *Medicine and Science in Sports and Exercise*, **39**:9, 1632, 2007.
- Anderson, D. E., and Madigan, M. L. *Journal of Biomechanics*, **47**:5, 1104-1109, 2014.
- Anderson, D. E., et al. *Journal of Biomechanics*, **40**:14, 3105-3113, 2007.
- Anderson, D. E., et al. *Journal of Biomechanics*, **43**:6, 1220-1223, 2010.
- Koushyar, H., et al. *Midwest ASB Regional Meeting*, March 4 -5, 2014 in Akron, OH.

ACKNOWLEDGEMENTS

This work was supported by grant R01OH009880.

KNEE JOINT MOMENTS DURING SINGLE-LEG FORWARD HOPPING

Rebecca L. Krupenevich and Ross H. Miller

University of Maryland, College Park, MD

Email: rlkrup@umd.edu

INTRODUCTION

Hopping is not often performed by healthy adults, but is common in amputees when not wearing their prosthetic leg, and in individuals who have their leg in a cast. Many physicians advise against hopping for ambulation in lower-extremity amputees, but recognize that in some situations it is unavoidable, for example, when maneuvering around the home before being fitted for a prosthesis [1], or simply when wearing the prosthesis is not convenient.

The prevalence of knee osteoarthritis (OA) in the intact limb of lower-extremity amputees is nearly twice that of non-amputees [2]. Increased loading of the intact limb is thought to be a contributing factor to the higher rate of OA in amputees compared to non-amputees [2]. However, to our knowledge there have been no studies investigating knee joint loading during single-leg forward hopping, in any population. Therefore, assessing the loads on the knee joint during single-leg forward hopping would enable us to make recommendations on whether frequent single-leg hopping is safe and healthy for the knees.

The purpose of this study was to compare the knee joint mechanics, specifically frontal and sagittal plane joint moments, of healthy adults during walking, running, and single-leg forward hopping. We hypothesized that knee joint moments would be greater in hopping than in walking or running.

METHODS

Six healthy adults (2 males, 4 females) participated after giving written informed consent. Participants completed three different locomotion conditions: running for three minutes at 3.0 m/s and walking for five minutes at 1.0 m/s around a 50-m indoor track, and three trials of hopping forward on one leg across a 12-m platform at 2.0 m/s. The target

speeds were chosen because they were close to self-selected speeds in pilot testing.

Kinematic data were captured using a 12-camera Vicon motion capture system, and force data were captured using eight Kistler force plates embedded in the platform. Knee joint moments were calculated by inverse dynamics using Visual3D. A one-way repeated measures ANOVA ($p < 0.05$) tested for the effect of locomotion condition on the external knee adduction moment's (KAM) peak, impulse, and loading rate (LR), and the peak knee flexor moment (KFM). These variables were selected due to their prior association with OA [3-5]. Post-hoc testing was performed using Tukey's LSD.

RESULTS AND DISCUSSION

Average performed speeds for each condition were: hopping (1.93 ± 0.11 m/s), running (2.87 ± 0.05 m/s), and walking (0.99 ± 0.08 m/s). Average stride lengths were: hopping (0.88 ± 0.25 m), running (1.80 ± 0.30 m), and walking (1.01 ± 0.30 m). The mean values of joint moment time series for all locomotion conditions are presented in Figure 1.

The ANOVA revealed a main effect for locomotion condition on all outcome variables, with several significant post-hoc differences, all with $p < 0.01$:

For KAM impulse

- Between hopping and running (0.92 ± 0.31 vs. 0.54 ± 0.18 %BW*Ht*s)

For peak KAM

- Between hopping and running (4.44 ± 2.06 vs. 2.48 ± 0.89 %BW*Ht)
- Between hopping and walking (4.44 ± 2.06 vs. 2.57 ± 0.39 %BW*Ht)

For peak KFM

- Between hopping and running (20.02 ± 3.99 vs. 17.2 ± 2.96 %BW*Ht)

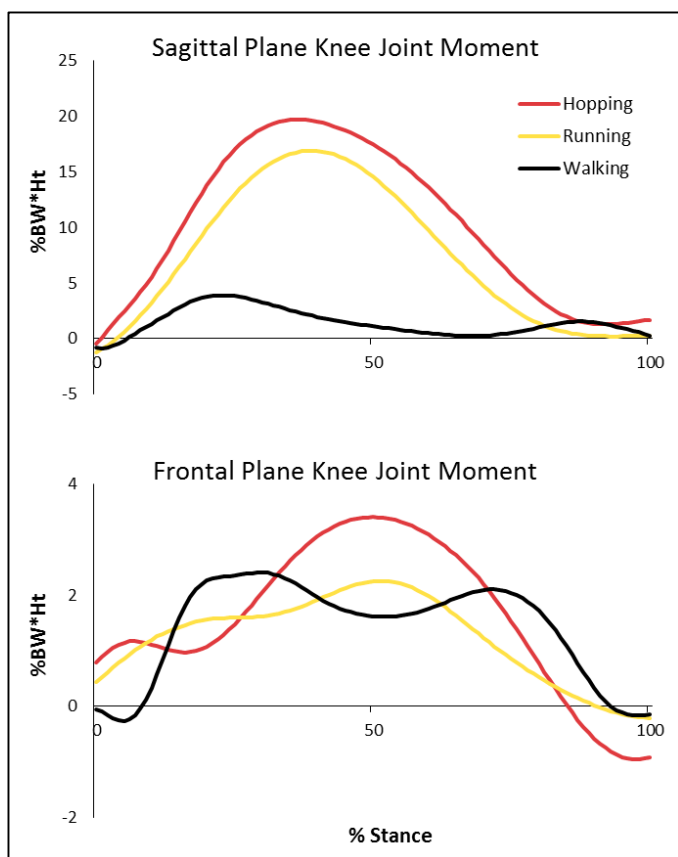


Figure 1: Mean joint moments for the sagittal (top) and frontal (bottom) planes during the stance phase. Positive values are external flexor or adduction moments.

- Between hopping and walking (20.0 ± 3.99 vs. 3.98 ± 1.26 %BW*Ht)
- Between running and walking (17.2 ± 2.96 vs. 3.98 ± 1.26 %BW*Ht)

For KAM LR

- Between hopping and walking (0.52 ± 0.14 vs. 0.25 ± 0.04 BW*Ht/s)
- Between running and walking (0.40 ± 0.05 vs. 0.25 ± 0.04 BW*Ht/s)

Hopping therefore increased the assessed features of the knee joint moments (peaks of KFM and KAM, impulse of KAM, and KAM LR) compared to walking and/or running. Peak KFM, peak KAM, and KAM impulse have been previously associated with the longitudinal initiation and/or progression of knee OA [3,4], and KAM LR has been associated

cross-sectionally with poorer tibiofemoral cartilage health scores [5]. These differences in moments would presumably be manifested internally as increased or otherwise abnormal mechanical loading of the articulating tibiofemoral surfaces. In particular, the rapid horizontal starting and stopping motion of hopping likely places high shear forces on the knee, especially if the compressive loading presumably reflected by these joint moments is also high.

The relatively high risk of OA in intact limb of amputees is thought to result from increased loading due to overreliance on this limb in performing activities of daily living. Therefore, hopping as a form of ambulation may contribute to the development of knee osteoarthritis by placing loads on the cartilage that it is not accustomed to sustaining, and warrants further investigation in the amputee population.

CONCLUSIONS

Single-leg hopping is often performed by lower-extremity amputees when ambulating without a prosthesis. However, hopping places large loads on the knee joint, and increased knee joint loading may be a contributing factor in the development or progression of knee OA. Therefore, it may be advisable to limit single-leg hopping as a form of locomotion in amputees.

REFERENCES

1. Stokes D, et al. *Int J Ther Rehabil*, **15**(12), 551-560, 2008.
2. Morgenroth DC, et al. *PMR* **4**, S20-S27, 2012.
3. Chehab EF, et al. *Osteoarthr Cartilage* **22**, 1833-1839, 2014.
4. Amin S, et al. *Arthritis Rheum*, **51**(3), 371-376, 2004.
5. Morgenroth DC, et al. *Clin Biomech*, **29**, 664-670, (2014).

MECHANICAL WORK PERFORMED BY THE LEGS OF CHILDREN WITH HEMIPLEGIC CEREBRAL PALSY

James E. Gehring and Max J. Kurz

Munroe Meyer Institute, University of Nebraska Medical Center, Omaha, NE, USA

Email: mkurz@unmc.edu, web: <http://www.unmc.edu/mmi/>

INTRODUCTION

Cerebral palsy (CP) results from a brain insult that occurs before or slightly after birth. Children with CP who have a hemiplegic presentation have an insult that affects one hemisphere of the brain, which results in more noticeable impairments on one side of the body. Prior experimental work has shown that the impaired leg of these children generates uncharacteristic external mechanical work for redirecting and lifting the center of mass during gait [1,2]. It has been suggested that the atypical external mechanical work may be the reason that these children often have a greater metabolic cost for walking than their typically developing peers. Although these insights are enlightening, we still have limited understanding on the mechanical work performed by the individual joints of the impaired and unimpaired legs during the double and single support phases. Fulfilling this knowledge gap may provide further insight on which joints are producing a greater positive work for a higher metabolic cost. Furthermore, these new insights may help in the design of physical therapy paradigms that are directed at improving the gait efficiency of these children. The purpose of this investigation was to evaluate the mechanical work performed by the individual joints of the impaired and unimpaired legs of children with CP who have a hemiplegic presentation.

METHODS

15 children with CP who had a spastic hemiplegic presentation (Age = 10.1 ± 2 yrs.) and a Gross Motor Function Classification Score (GMFCS) level of II participated in this investigation. All of the children routinely wore prescribed ankle-foot-orthosis (AFO) for community ambulation, but did not require an assistive mobility device (*i.e.*, forearm crutches, wheeled walker). For the experiment, the children walked barefoot at a self-selected pace along a 16-

meter walkway as the three-dimensional bilateral lower extremity joint kinematics were captured with an 8-camera motion capture system (120 Hz). Concurrently, a series of four force platforms were used to measure the ground reaction forces for the individual legs (1200 Hz). Inverse dynamics were used to calculate the respective joint moments during the stride, and the joint powers were calculated from the product of the joint moments and joint angular velocities. The positive and negative mechanical work performed by the ankle, knee and hip joints was calculated by integrating the respective power curves. The calculated mechanical work was normalized by the child's body mass.

The net mechanical work performed by the impaired and unimpaired legs was evaluated separately during the double and single support phases. This involved summing the positive and negative work during the respective phase. During double support, the mechanical work was evaluated when the leg was in either the lead or trailing positions. The lead position indicated that the leg was in a position ahead of the center of mass during double support, while the trail position indicated that the leg was in a position behind the center of mass during the double support. Separate repeated measures ANOVAs (Leg X Joint) were used to evaluate the mechanical work performed during the single support phase, and double support phase when the leg was in the lead or trail positions.

RESULTS & DISCUSSION

During double support, we did not find a Leg main effect for the mechanical work performed by the impaired and unimpaired legs while they were in the lead position. This indicated that the negative work performed by the respective legs was similar ($P=0.70$; Unimpaired = -0.03 ± 0.01 J/Kg; Impaired = -0.04 ± 0.01 J/kg). As the lead leg, the ankle and knee of both the legs produced negative mechanical work,

while the hip generated positive work. However, we did not find a significant Leg x Joint interaction ($P=0.12$), indicating that the mechanical work performed by the joints of the respective legs were similar in the lead position.

There was a significant Leg main effect for when the legs were in the trail position during double support ($P=0.004$; Unimpaired = 0.24 ± 0.03 J/kg; Impaired = 0.10 ± 0.01 J/kg), indicating that the unimpaired leg produced more positive work than the impaired leg. We also found a significant Leg x Joint interaction ($P<0.001$). Our follow-up post-hoc analyses indicated that the ankle ($P=0.002$) and hip ($P=0.0002$) joints of the unimpaired leg produced more positive work than the impaired leg. In addition, the knee joint of the unimpaired leg also generated more negative work than the impaired leg (Figure 1, $P=0.0002$).

We did not find a significant Leg main effect during the single support phase ($P=0.645$), which indicated that the positive work produced by the unimpaired and impaired legs was similar (Unimpaired = 0.12 ± 0.04 J/kg; Impaired = 0.10 ± 0.03 J/kg). During single support, the ankle and hip of both legs produced positive work, while the knee generated negative work. Despite these observations, we did not find a significant Leg X Joint interaction ($P=0.093$), indicating that the work produced by the joints of the respective legs was similar during single support.

Our results show that the primary differences in the mechanical work performed by the impaired and unimpaired legs occurred during double support when the respective legs were in the trailing position. The unimpaired leg produced 58% more positive work than the impaired leg while acting as the trailing leg during double support. Evaluating the amount of positive work performed by the respective joints indicates that the difference in the amount of positive work performed was primarily due to the ankle joint, and secondarily due to the knee and hip. We suspect that the larger amount of positive work performed by the unimpaired leg likely represents a compensation strategy that was used to offset the diminished positive work performed by the impaired leg during the preceding double support phase. Potentially, this compensation strategy may play a large role in the higher metabolic cost seen in children with CP who have a hemiplegic

presentation. We suggest that gait training strategies that focus on improving the work performed by the muscles of the impaired leg while in the trailing position of double support may improve the gait efficiency of these children. Possibly this may be accomplished with similar biofeedback devices that have been successfully used to improve the double support propulsive forces generated by the legs of the elderly [3].

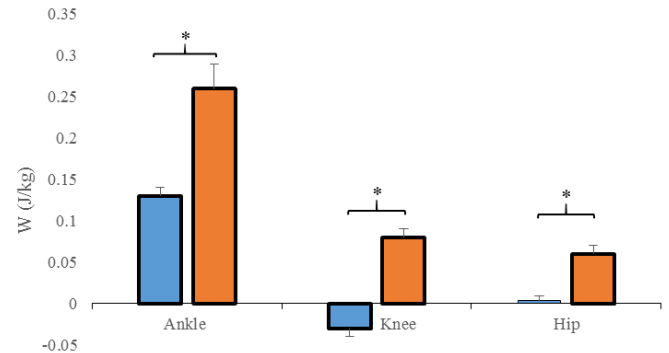


Figure 1: Mechanical work performed for each leg as the trail leg during double support. Blue = Impaired Leg, Orange = Unimpaired Leg. Asterisk signifies $P \leq 0.05$.

Many of the participating children wore AFOs on their impaired leg during their daily ambulatory activities. We selected to not have the children wear their AFOs during our experiment to eliminate the potential differences in the AFO construction on the mechanical work performed by the joints. It is possible that the mechanical work profiles seen in this investigation may be quite different and beneficial if the children wore their AFOs. However, we are somewhat cautionary with these speculations because many of the AFO designs used by the children included a plantarflexion stop that may further hinder the positive mechanical work produced by the impaired ankle while in the trailing leg position. This may require the contralateral leg to produce even more positive work during the double support phase. These speculations remain to be challenged by future investigations on the mechanical work produced by children with CP.

REFERENCES

1. Kurz MJ et al., *Gait & Posture*, **31**, 347-350, 2010.
2. Feng J et al. *Gait & Posture*, **39**, 570-576, 2014.
3. Franz J et al., *Clin Biomech*, **29**, 68-74, 2014.

THE EFFECT OF SHOE HEEL ELEVATION ANGLE ON STRIKE PATTERN

¹Hyun Joon Kwon, ¹Kyung Koh, ²Hiroaki Hobara, ¹Edward Chu, ¹Siyeon Kim,
¹Ross H. Miller, and ^{1,3}Jae Kun Shim

¹Neuromechanics Research Core, University of Maryland, College Park, MD, USA

²Digital Human Research Center, AIST, Tokyo, Japan

³Kyung Hee University, Yong-in, South Korea

email: hjk213@umd.edu, web: <http://www.sph.umd.edu/neuromechanics>

INTRODUCTION

Running is a very popular physical activity that has many cardiovascular and muscular health benefits, but running can also be a source of musculoskeletal injuries such as stress fractures that are mainly caused by repetitive high vertical impact [1].

A possible contributor to running related stress injuries is the foot strike pattern. Previous barefoot running studies have consistently shown that rear foot strike patterns induced greater vertical impact peaks and vertical ground reaction force loading rates (LR) to the skeletal system when compared to a more midfoot or forefoot strike pattern. However, the efficacy of altering shoe structure to change foot strike patterns, vertical impact peaks, and LR during shod running is not as clear [2].

Previous studies have found that heel height and heel drop seems to be a critical factor in altering running behavior; however, these studies examined heel height and heel drop independently of each other, while ignored heel elevation angle. The heel elevation angle (HEA) is important because the heel height and heel drop do not take into consideration the shoe size, which will affect the overall angle of the shoe [3,4].

To the best our knowledge, the HEA has never been studied regarding its influence on the running behaviors. The goal of this study was to investigate the influence of HEA on strike index (SI), foot strike angle (FSA), anatomical foot angle (AFA), and loading rate (LR). See Methods for details of these measures.

METHODS

Nine female volunteers between 18 to 28 years of age (shoe size = 235 mm) participated in the study. All subjects were healthy habitually shod rearfoot strikers without any history of neuromuscular disorders, who ran at least twice a week for a total weekly distance of at least 16 km.

Four pairs of customized shoes, provided by a shoe manufacturer, were used for this study. All shoe characteristics were identical except the shoe HEA. All shoes had the same metatarsus height (7.5 mm) but different heel heights. The heel height differences were carefully manufactured to make 4 different HEA's (0°, 1°, 2°, and 3°). HEA was defined as the angle between the ground and line from heel to metatarsus in the insole [5].

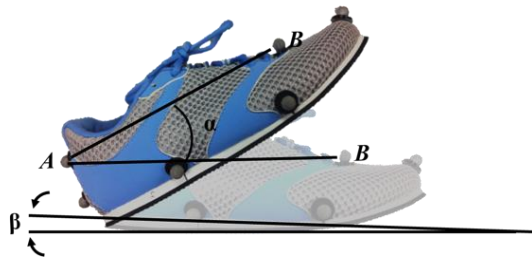
Eight retro-reflective markers were placed on the shoe as depicted in the Fig. 1. Kinematic data were recorded using 10 Vicon cameras (Vicon motion systems, Oxford, UK). Ground reaction force and center of pressure data were collected using 10 force plates positioned in series (Kistler Instrument Corp., NY). Running speed was monitored using customized photoelectric sensors.

The subjects were asked to run around a 60-m track at a controlled speed of 2.6 m/s ($\pm 5\%$) for 15 minutes in each shoe. Data was collected throughout the whole 15 minutes, and the first 10 minutes were used as an adaptation period, while the last 5 minutes were used for data analysis.

The SI was calculated as the location of the center of pressure at initial contact in the percentage of the total foot length [6]. The FSA was defined as the

angle formed by the line of markers A and B between at quiet resting and at initial contact during running as shown in Figure 1 [7]. Anatomical foot angle (AFA) was calculated by subtracting the HEA from FSA. The LR was calculated the slope of the line from 20% to 80% of stance time to impact peak of the vertical GRF.

A one-way repeated measures ANOVA was used to examine the effect of HEA on these dependent measures. Statistical significance was set at $p < 0.05$.



$$AFA(\theta) = FSA(\alpha) - HEA(\beta)$$

Figure 1: Reflective marker placement and schematic illustration of FSA (α) and HEA (β) measurement. AFA (θ) was represented by subtracting HEA (β) from FSA (α).

RESULTS AND DISCUSSION

There was a main effect for HEA on SI (Figure 2). At the two higher HEAs (2° and 3°), the COP at initial ground contact was significantly closer to the heel compared to the 0° HEA condition. In addition, three out of nine participants changed their foot strike pattern from rearfoot strike at 3° and 4° HEA to midfoot strike at 0° HEA. These results suggest that changes in HEA of shoes can alter running strike pattern.

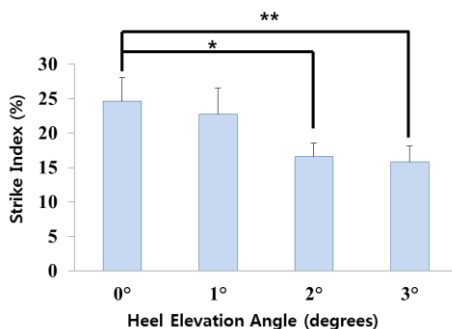


Figure 2: Strike index for four different heel elevation angles.

Similarly, FSA increased as HEA increased (Figure 3). The FSA were significantly greater for the 3°

HEA as compared to the 1° HEA ($p < 0.01$) and 2° HEA ($p = 0.02$) HEA. FSA was correlated with SI, $R = 0.89-0.98$ ($p < 0.01$) according to HEA. Regression coefficients among HEA were not different ($p = 0.3$). This result is consistent with a previous finding which demonstrated that the FSA was significantly correlated with SI ($R = 0.92$ ($p < 0.01$)) from forefoot, midfoot and heelfoot strike pattern [7]. However, AFA were not significantly different among the shoes ($p = 0.3$). Moreover, no differences in the impact peak and LR were found (not shown in figure). These results indicate that altering strike pattern was not caused by adaptations of foot strike patterns, rather the differences were due to the structure of the shoes.

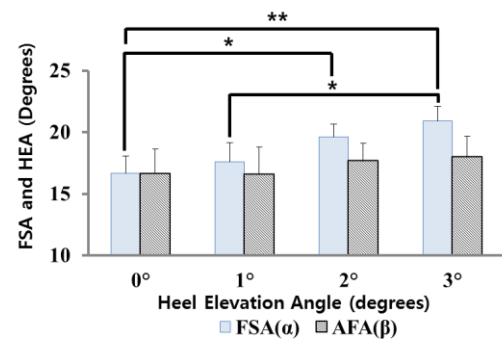


Figure 3: Foot strike angle and Anatomical foot angle for four different heel elevation angles.

CONCLUSIONS

The main finding of the study was the correlation of HEA with SI. It seems that lower HEA shoe have induced more anterior strike pattern; however, this change in the strike pattern was not associated with the AFA, impact peak and LR during stance.

REFERENCES

1. Giandolini M, et al. *European journal of applied physiology* **113**, 2077-2090, 2013.
2. Lieberman DE, et al. *Nature* **463**, 531-535, 2010.
3. Horvais N, et al. *Footwear Sci* **5**, 81-89, 2013.
4. Hamill J, et al., *Footwear Sci* **3**, 33-40, 2011
5. Reinschmidt C, et al. *Med Sci Sports Exerc* **27**, 410-416, 1995.
6. Cavanagh P, et al. *J Biomech* **13**, 397-406, 1980.
7. Altman A, et al. *Gait Posture* **35**, 298-300, 2011.

THE RELATIONSHIP BETWEEN CLINICAL MEASURES AND STAIR CLIMBING BIOMECHANICS IN PATIENTS WITH TOTAL KNEE ARTHROPLASTY

Jacqueline Lewis, Gregory Freisinger, Laura Schmitt, Robert Siston and Ajit Chaudhari
The Ohio State University, Columbus, OH, USA
email: lewis.1127@osu.edu

INTRODUCTION

Total knee arthroplasty (TKA) is a generally successful surgical procedure to treat end-stage knee osteoarthritis; however, suboptimal outcomes, including difficulty stair climbing, do occur [1]. Clinicians use the stair climbing test (SCT) to track functional status, where a patient ascends and descends a flight of stairs as fast as possible and a faster time suggests better function and increased mobility capabilities. Decreased (faster) SCT time is associated with increased knee extension strength in TKA populations [2].

Although SCT time gives an estimate of a TKA patient's function, the relationship to stair climbing biomechanics and underlying knee function is not well defined. It is possible that patients introduce negative adaptations to their gait in order to climb stairs faster, rather than restoring biomechanical function to match those of healthy populations. These adaptations could include increased loading or altered movement patterns at the knee, hip or low back, which may be detrimental in the long term. We hypothesized that faster SCT times and increased knee extension strength of the involved limb would be associated with increased peak knee and hip flexion moments (pKFM, pHFM), of the involved limb, and decreased trunk lean.

METHODS

Twenty-two patients (7 male/15 female, age: 59.9 ± 6.9 y, mass: 94.8 ± 17.1 kg, ht: 1.7 ± 0.1 m) with predominantly medial compartment osteoarthritis were recruited by three orthopedic surgeons at The Ohio State University Wexner Medical Center and provided IRB-approved informed consent. All participants underwent a primary TKA, using a posterior stabilized prosthesis. (Zimmer NexGen LPS Flex, Warsaw IN). Biomechanical and clinical

assessments were completed approximately 6 months following surgery.

During the biomechanical assessment, each patient performed stair ascent and descent trials on a custom made 3-step staircase (tread depth: 25.5 cm, tread rise: 20 cm). The first two steps of the staircase were attached to force plates (Bertec 4060-10, Bertec Corp; Columbus, OH) embedded in the floor to capture stair climbing ground reaction forces at 1500 Hz. Marker data were collected at 150 Hz by 10 cameras [Vicon MX-F40; Oxford, UK]. A modified point-cluster marker set was used to calculate kinematics [3]. Inverse dynamics were calculated using custom Bodybuilder (Vicon; Oxford, UK) and MATLAB scripts. Marker and force data were filtered with fourth order low-pass Butterworth filters at a cutoff frequency of 6 Hz. All moments were expressed as externally applied to the joint of interest and were normalized by body weight times height. Peak forward trunk lean during stance phase was calculated using the markers placed on 10th thoracic and 7th cervical vertebrae, by determining the peak angle relative to global vertical axis in the sagittal plane.

Each patient completed the SCT on a 12 step, carpeted staircase (tread depth: 28 cm, tread rise: 16.5 cm). Patients were instructed to ascend, turn around and immediately descend the staircase as fast as possible, in a safe manner. The use of one handrail was allowed if necessary. Isometric knee extension strength was measured with a Biodex System 3 dynamometer [Biodex Medical Systems; Shirley, NY] with the involved limb held at 60 degrees of knee flexion. The resulting maximal knee extension torque was normalized by each participant's mass (Nm/kg).

Spearman rank order correlation coefficients were used to test the association between the

biomechanical and clinical measures. An alpha of 0.05 was used to denote significance.

RESULTS AND DISCUSSION

pKFM during ascent and pHFM during descent were significantly associated with knee extension strength; however, SCT time was not associated with any biomechanical measures (Table 1). Increased trunk lean was associated with increased pHFM, but not pKFM (Table 2).

Table 1: Spearman correlations between clinical and biomechanical variables.

		SCT		Ext Strength	
Ascent	pKFM	r=-0.24	p=0.28	r=0.42	p=0.05*
	pHFM	r=0.34	p=0.12	r=-0.37	p=0.09
	Trunk Lean	r=0.26	p=0.24	r=-0.25	p=0.26
Descent	pKFM	r=-0.14	p=0.53	r=0.38	p=0.09
	pHFM	r=0.41	p=0.06	r=-0.53	p=0.01*
	Trunk Lean	r=0.37	p=0.09	r=-0.35	p=0.11

Table 2: Spearman correlations between trunk lean and flexion moments at the hip and knee.

	Ascent		Descent	
	pKFM	pHFM	pKFM	pHFM
Trunk Lean	r=-0.212 p=0.344	r=0.643 p=0.001*	r=-0.116 p=0.608	r=0.503 p=0.017*

The purpose of this study was to evaluate the relationships between clinical and biomechanical measures during stair climbing in a population after TKA. Knee extension strength was associated with pKFM during ascent and pHFM during descent, which suggests that the demand on the knee joint is greater during ascent, while demand on the hip joint may be greater during descent. Although increased knee extension strength is associated with faster SCT times [2], biomechanical measures were not significantly associated with SCT time. There was a trend between pHFM and SCT time, where pHFM

increased with increasing speed. A forward trunk lean is often used by TKA patients and is thought to minimize demand on the quadriceps [4]. However, increased trunk lean was not associated with decreased pKFM in this study, suggesting that increased trunk lean may not reduce load at the knee joint. Increased trunk lean was associated with increased pHFM, indicating that trunk lean may increase load on the hip joint. This could put the hip at risk for joint degeneration or injury.

There were several limitations associated with this study. The biomechanics were measured on a 3 step staircase and not during the SCT. Also, this was a cross-sectional study and we did not control trunk angle or test patients at multiple trunk angles.

CONCLUSIONS

The findings of this study suggest that patients with faster SCT time did not have larger pKFM compared to patients with slower SCT times. SCT time was not associated to any of the investigated biomechanical variables, so further study is needed to fully understand how demand on the hip and knee joints change with faster SCT speed in a TKA population. More trunk lean was associated with increased pHFM, so clinicians must be wary that improving a patient's SCT time does not have a detrimental effect on other joints. Focus on decreasing trunk lean during stair climbing may be beneficial to TKA patients. Further study testing individual subjects at different trunk lean angles is necessary to fully understand this relationship.

REFERENCES

1. Weiss JM, et al. *Clin Orthop Relat Res* **404**, 172-88, 2002.
2. Yoshida et al. *Clin Biomech* **23** 320-8, 2008.
3. Jamison ST, et al. *J Biomech* **45**, 1881-5, 2012.
4. Andriacchi TP. *J Arthroplasty*, **1**, 211-219, 1986.

ACKNOWLEDGEMENTS

Funding from award number R01AR056700 from National Institute of Arthritis and Musculoskeletal and Skin Diseases supported this study.

Effects of Prolonged Walking at Preferred Speed in Individuals with Multiple Sclerosis

¹ Joshua J. Liddy, ² Stephanie Jones, ² Michael A. Busa, and ² Richard E. A. van Emmerik

¹ Purdue University, West Lafayette, IN, USA

² University of Massachusetts Amherst, Amherst, MA, USA

email: jliddy@purdue.edu web: <https://www.umass.edu/sphhs/kinesiology>

INTRODUCTION

Alterations to spatiotemporal gait parameters such as increased stride width and dual support time, and decreased stride length, stride time, and gait speed, are characteristic of preferred walking speed (PWS) gait in Multiple Sclerosis (MS) [1] and are generally considered to be reflective of gait instability. Maintaining gait stability in dynamic, cluttered environments is essential for accomplishing tasks of daily living.

Individuals with MS often report elevated levels of symptomatic fatigue, a combination of reversible motor and cognitive impairment, which appears to be unrelated to disease status or patient disability [2] and can be exacerbated by prolonged activity. Furthermore, symptomatic fatigue has been associated with postural instability [3]. However, it is currently unclear how symptomatic fatigue influences gait stability in individuals with MS.

The purpose of the present study was to assess the impact of an induced physical fatigue through a prolonged walking bout on PWS gait parameters in individuals with and without MS. We hypothesized that individuals with MS would display a more stable gait pattern, demonstrated by increased dual support and decreased swing times in response to induced fatigue.

METHODS

Eight participants with mild to moderate MS (7 female, age = 43.5 years, height = 1.67 m, mass = 74.2 kg, PDDS < 3) and eight age, gender, height, and weight matched controls (7 female, age = 42.1, height = 1.69 m, mass = 73.5 kg) participated. Controls (CON) were required to be free of neurological impairment.

PWS was determined on a treadmill by self-selection of walking speed as belt speed was systematically increased and decreased. The protocol consisted of three minutes of PWS followed by 24 minutes of imposed speed walking

(range 0.6 - 1.4 ms⁻¹), and finally three minutes of PWS. Overall fatigue was assessed at baseline and, pre- and post-walking using the Visual Analog Fatigue Scale (VAS-F) [4] with scale anchors of “no fatigue” and “exhaustion”.

Stride length, width, duration, cadence as well as stance, swing, and dual support percentage were computed across gait cycles for each PWS trial. Variability was assessed with the coefficient of variation (CoV). Dependent variables were compared using a mixed-model, repeated measures ANOVA with time as the repeated factor and disease status as the grouping factor ($\alpha = 0.05$). Trends towards significance ($\alpha < 0.1$) are discussed due to the relatively small sample sizes.

RESULTS AND DISCUSSION

Fatigue

Comparison of baseline, pre-walking, and post-walking VAS-F scores revealed significant main effects of group and time. Post-hoc comparisons revealed significantly higher levels of fatigue in the MS group (~ 17%, $p < 0.029$). Both groups reported increased fatigue post-walking compared to baseline (~15%, $p < 0.001$) and pre-walking (~8%, $p < 0.02$). Fatigue rates of change between baseline/pre-walking and pre-walking/post-walking were not significantly different between groups.

Gait Parameters

No significant difference in PWS was found between the MS (1.03 ± 0.39 ms⁻¹) and CON groups (1.21 ± 0.21 ms⁻¹). Alterations to spatiotemporal gait parameters were observed in both groups following the walking bout. In particular, stride time (trend, $p < 0.06$), stride length ($p < 0.02$), stance % (trend, $p < 0.07$), and dual support % ($p < 0.04$) increased while cadence ($p < 0.02$) and swing % (trend, $p < 0.07$) decreased following prolonged walking. A trend for greater dual support % ($p <$

0.09) was observed for the MS group relative to controls.

Gait Variability

Gait parameter variability was not impacted by prolonged walking in either group. However, trends for group differences were observed. The MS group displayed increased CoV for stride width ($p < 0.06$), stance time percentage ($p < 0.07$), swing time percentage ($p < 0.09$), dual support percentage ($p < 0.08$), and cadence ($p < 0.09$).

CONCLUSION

In contrast to previous work [1], gait parameters of the MS group were not found to be significantly different than healthy individuals. This may reflect relatively low levels of disease-related impairment (PDDS < 3). One exception was a trend for increased dual support percentage in the MS group, a finding consistent with earlier reports [1]. Greater dual support percentage represents a reduction in the amount of time spent in single support where the COM is more likely to be located outside of the stability boundaries. Additionally, fatigue-related alterations to gait parameters were seen in both groups following prolonged walking. In general, these changes reflected tendencies of both groups to favor more stable gait identified by increased stance and dual support percentages and shorter swing percentages post-walking.

Finally, the increased variability in stride width observed in the MS group could be a signature of a less controlled gait pattern and associated with the increased rate of falls in this population. An important question is how changes in coordination and coordination variability of the lower extremities, trunk and arms are linked to this increased stride width variability.

Fatigue levels, as measured by the VAS-F, were overall greater in the MS group, consistent with previous findings [3]. Fatigue increased similarly in our MS cohort compared to controls in response to prolonged walking, which may explain the similar response to the walking protocol in both groups.

REFERENCES

1. Benedetti MG, et al. *Multiple Sclerosis*, **5**, 363-368, 1999.
2. Mills R & Young C. *Multiple Sclerosis Journal*, **17**, 604-612, 2011.
3. Van Emmerik REA, et al. *Gait and Posture*, **32**, 608-614, 2010.
4. Krupp LB, & Elkins LE. *Neurology*, **55**, 934-939, 2000.

ACKNOWLEDGEMENTS

National Multiple Sclerosis Society Grant RG 3974A2

Table 1. Gait parameters (mean \pm SD) at PWS for MS and CON groups.

	Pre		Post	
	MS	CON	MS	CON
stride width (m)	0.15 \pm 0.03	0.14 \pm 0.03	0.15 \pm 0.03	0.13 \pm 0.03
stride length (m)	1.08 \pm 0.43	1.32 \pm 0.16	1.10 \pm 0.43	1.34 \pm 0.15
stride time (m)	1.16 \pm 0.25	1.10 \pm 0.14	1.17 \pm 0.22	1.13 \pm 0.16
dual support time (%)	38.3 \pm 5.78	34.2 \pm 2.50	39.0 \pm 6.35	34.4 \pm 2.63
stance time (%)	69.5 \pm 2.91	67.1 \pm 1.27	69.5 \pm 3.22	67.2 \pm 1.29
swing time (%)	30.8 \pm 2.91	32.9 \pm 1.27	30.5 \pm 3.22	32.8 \pm 1.29
cadence (steps/min)	106 \pm 17.8	110 \pm 14.7	105 \pm 16.1	108 \pm 15.9

Table 2. Gait parameter variability measured by CoV (mean \pm SD) at PWS for MS and CON groups.

	Pre		Post	
	MS	CON	MS	CON
stride width (%)	12.55 \pm 4.60	8.05 \pm 2.04	12.59 \pm 5.52	9.09 \pm 2.91
stride length (%)	4.42 \pm 5.31	1.71 \pm 0.84	3.64 \pm 0.43	1.50 \pm 0.42
stride time (%)	0.453 \pm 0.16	0.379 \pm 0.07	0.464 \pm 0.15	0.393 \pm 0.08
dual support time (%)	8.03 \pm 4.69	4.80 \pm 1.82	6.39 \pm 2.71	4.59 \pm 0.99
stance time (%)	3.41 \pm 2.34	1.84 \pm 0.53	2.67 \pm 1.34	1.78 \pm 0.39
swing time (%)	4.59 \pm 3.52	2.36 \pm 0.86	4.01 \pm 2.88	2.06 \pm 0.53
cadence (%)	3.36 \pm 2.02	2.02 \pm 0.67	2.72 \pm 1.42	1.87 \pm 0.42

HEEL ROCKER MECHANICS IN GAIT ARE DIFFERENT BETWEEN LIMBS AND COMPARED TO CONTROLS FOLLOWING ACL RECONSTRUCTION

Paige E. Lin, Kristamarie A. Pratt, Ming-Sheng Chan, Susan M. Sigward

Human Performance Laboratory

Division of Biokinesiology and Physical Therapy

University of Southern California, Los Angeles, CA, USA

email: paigeeli@usc.edu, web: <http://pt.usc.edu/labs/hpl/>

INTRODUCTION

Normalization of gait is a primary goal of early rehabilitation following anterior cruciate ligament reconstruction (ACLR), which is expected to be achieved 8-12 weeks post-ACLR [1]. However, between limb asymmetries in knee extensor moment can persist 6-24 months post ACLR [2], suggesting that strategies used to restore gait during early rehabilitation are not effective at restoring loading mechanics. Their long-term persistence is of concern as they have been attributed to the progression of knee osteoarthritis in this population [3].

Reduced peak knee flexion angle, range of motion, extensor moment, and power absorption in the surgical limb compared to the nonsurgical limb have been identified during loading response (LR) of gait (first 20% of stance phase) [2]. During this phase, the knee flexes to accept body weight in LR just after heel strike using a heel rocker mechanism to decelerate and progress the body over the stance limb [4]. The heel rocker is characterized by forward shank progression after initial contact, resulting in knee flexion, eccentric quadriceps contraction and peak knee extensor moment [4]. Decreased knee extensor moment and knee flexion range of motion in the surgical limb during loading response suggests that individuals are altering ground reaction forces (GRF) and heel rocker mechanics to reduce knee extensor loading.

The purpose of this study was to compare heel rocker mechanics during gait between limbs in individuals following ACLR and to healthy controls.

METHODS

Seven individuals (4 females, 25.1 ± 11.4 years) status post-ACLR (84.7 ± 15.0 days post-op) and six healthy controls (4 females, 22.8 ± 5.0 years)

performed 3 walking trials across a 10 meter walk way at a self-selected speed.

Three-dimensional kinematics (250 Hz) were collected using a 11-camera motion capture system (Qualisys, Inc. Sweden). Ground reaction forces (GRF; 1500 Hz) were quantified using AMTI force platforms (Newton, MA, USA). Laser timing gates (Brower, UT, USA) were used to determine gait velocity. Three dimensional joint kinematics, ground reactions forces and anthropometrics were used to calculate net joint moment using standard inverse dynamics equations. Kinetic data were normalized to body mass. Sagittal plane shank angle and angular velocity were calculated. Shank angle was measured relative to the horizontal, such that a positive angle refers to when the proximal portion of the shank is more posterior than the distal portion. Similarly, a negative angular velocity indicates that the proximal portion of the shank is progressing anteriorly relative to the distal end.

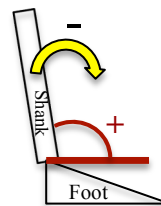


Figure 1: Shank conventions. Positive shank angle (red) and negative shank angular velocity (yellow).

Knee range of motion (initial contact to peak knee flexion), peak knee extensor moment, peak vertical and posterior GRFs, average shank angle (initial contact to 50% stance), and peak negative shank angular velocity were identified during LR. Data were averaged between limbs to represent healthy control mechanics.

Paired sample t-tests were used to compare differences between the surgical and nonsurgical limbs in individuals following ACLR. Gait velocity and differences between the control data and the surgical and nonsurgical limbs of ACLR were

compared using independent samples t-tests. Significance $p \leq 0.05$. Effect sizes were calculated.

RESULTS AND DISCUSSION

On average, individuals following ACLr had a 56% decrease in knee extensor moment and an 8° difference in knee range of motion in the surgical compared to the nonsurgical knee. The between limb differences in these participants 3 months post ACLr are larger but consistent with previous studies reporting decreased sagittal plane knee loading in individuals 6-24 months following ACLr. While peak vGRF were not significantly different between limbs, a 25% decrease in pGRF was observed in the surgical limb compared to the nonsurgical, suggesting that LR strategies may work to reduce braking forces more than vertical forces to limit extensor moments in the surgical knee.

Between limb differences were noted in shank kinematics indicating that individuals following ACLr also modulate components of the heel rocker mechanism during LR to reduce knee flexion and the demand on the knee extensors. On average, throughout LR individuals maintained a shank position that was angled more posteriorly in the surgical knee compared to the nonsurgical knee. A greater posterior angle will shorten the lever arm for the already reduced braking forces (pGRF), further decreasing knee extensor moments. In addition to a more posteriorly rotated shank throughout LR, individuals following ACLr also demonstrated decreased peak shank angular velocity in the surgical compared to nonsurgical limb. Rapid knee flexion during LR is facilitated by rotation of the shank over the foot. Decreased angular velocity of the shank likely further reduces the demands for eccentric quadriceps action contributing to between limb differences in knee extensor moments.

When comparing ACLr to healthy controls, no differences were found in gait velocity ($p=0.416$; $ES=0.45$). Similar to between limb comparisons in ACLr, significant differences were observed between ACLr surgical limbs and controls for all variables except peak vertical ground reaction force ($p=0.06$). The only difference noted between ACLr nonsurgical limb and controls was observed in knee range of motion. Larger knee flexion range of motion was observed in ACLr nonsurgical limbs than controls suggesting that individuals following ACLr may be altering mechanics of the nonsurgical limb to normalize gait.

CONCLUSIONS

Despite the observable normalization of gait at 3 months post ACLr, subtle alterations in LR variables related to loading (GRFs) and heel rocker mechanics result in lower knee extensor moments in the surgical knee. These preliminary data suggest that individuals alter braking forces and shank position and velocity to reduce sagittal plane loading of the knee. It is likely that these kinematic and kinetic variables are related to an overall strategy aimed at shifting the demands away from the knee extensors in the surgical limb. Furthermore, it is not known if these strategies are driven by underlying joint impairments or learned motor adaptations. Future work with larger samples sizes investigating these relationships will inform interventions aimed at improving these mechanics.

REFERENCES

1. Manal TJ & Snyder-Mackler L. *Oper Tech Orthop* 6, 190–196, 1996.
2. Roewer BD, et al. *J Biomech* 44(10), 1948–1953, 2011.
3. Andriacchi TP, et al. *J Bone Jt Surgery, Am Vol* 91 Suppl 1, 95–101, 2009.
4. Perry J & Burnfield JM. *Gait Analysis: Normal and Pathological Function*, SLACK, 2010.

Table 1: Comparison of heel rocker mechanics between ACL reconstructed limbs

Variable	Surgical Limb	Nonsurgical Limb	Effect Size
Peak knee extensor moment (Nm/kg)	-0.35 (0.21)**	-0.79 (0.14)	1.85
Knee range of motion (deg)	9.80 (4.27)**	17.79 (2.86)	1.75
Vertical GRF (N/kg)	11.25(1.05)	1.96 (1.03)	0.70
Posterior GRF (N/kg)	-1.83 (0.36)**	-2.44 (0.49)	3.25
Average shank angle (deg)	98.1 (2.21)*	95.0 (2.63)	0.98
Maximum shank angular velocity (deg/s)	-146.8 (31.3)**	-179.4 (31.7)	1.72
Average (SD); * $p \leq 0.05$; ** $p \leq 0.01$			

A PLANAR DUAL-SLIP MODEL OF INCLINE AND DECLINE WALKING

¹ Yiping Liu, ² James P. Schmiedeler, ³ Patrick M. Wensing, and ¹ David E. Orin

¹ The Ohio State University, Columbus, OH, USA

² University of Notre Dame, Notre Dame, IN, USA

³ Massachusetts Institute of Technology, Cambridge, MA, USA

email: liu.805@osu.edu

INTRODUCTION

The planar Dual Spring-Loaded Inverted Pendulum (Dual-SLIP) or bipedal spring-mass model [1] is known to reproduce the vertical oscillations of the center of mass (CoM), the double-peak ground reaction force (GRF) pattern, and the finite duration of double support in human walking on level ground. This conservative model consists of a point mass and two massless spring legs of equal stiffness and produces stable, symmetric gaits across a range of speeds. To extend the model to incline and decline walking, however, mechanisms to allow for asymmetric steps and for injecting/absorbing energy are required since the potential energy necessarily changes with each step. A recent extension of the planar Dual-SLIP model to 3D [2] introduces such mechanisms by allowing touchdown and liftoff to occur at leg lengths less than the free length, (thereby exhibiting ground impact and toe-off characteristics) and by allowing the free lengths of the legs to vary linearly between gait events. This paper investigates how these same mechanisms can be introduced in the planar Dual-SLIP model to reproduce the sagittal plane motion and GRF characteristics of human incline/decline walking.

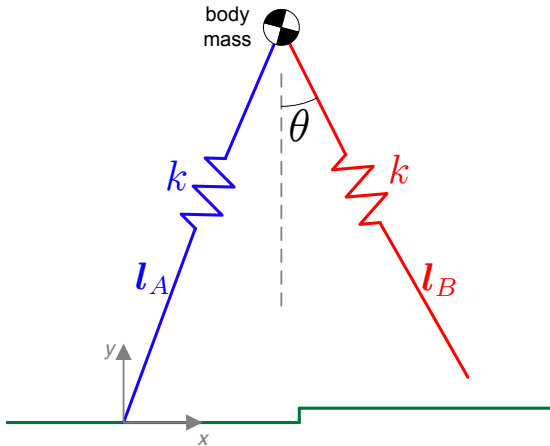


Fig. 1: Planar Dual-SLIP model of incline walking.

MODEL DESCRIPTION

Figure 1 depicts the planar Dual-SLIP model, which has leg stiffness k , instantaneous stance and swing leg lengths l_A and l_B , and swing leg angle with the vertical θ , walking up an inclined surface indicated by a small step. Figure 2 depicts the internal leg “actuation” scheme for this model, which alters when in the gait the energy is stored and released compared to a passive spring. Beginning the cycle at midstance (MS) of single support of the trailing leg A (SS_A), defined as the instant of zero vertical CoM velocity, the free length of leg A, $\ell_A(t)$, initially ℓ_{MS} , changes linearly with a slope of β_A until liftoff (LO). At LO , the length of leg A (L_{LO}) is less than its free length ℓ_{LO} at that instant, so the GRF immediately before LO is non-zero, similar to the effect of toe-off. Likewise at touchdown (TD), the length of the leading leg B (L_{TD}) is less than its free length ℓ_{TD} at that instant, so the GRF is non-zero immediately after TD , similar to the effect of ground impact if the leg had mass. From TD to MS , the free length of leg B, $\ell_B(t)$, changes linearly with a slope of β_B , returning to ℓ_{MS} at MS to ensure periodicity. With this scheme, energy can be injected/absorbed for walking on inclines/declines.

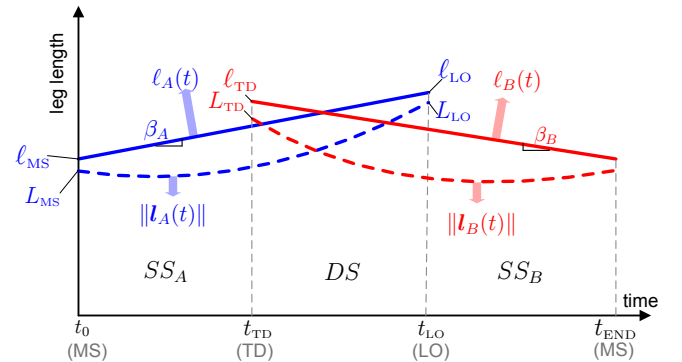


Fig. 2: Illustration of the actuation variables for the leading leg B (red) and trailing leg A (blue). Solid/dashed lines are free/actual leg lengths.

Gaits are generated via a nonlinear optimization to identify the parameters $\{L_{TD}, L_{LO}, \ell_{TD}, \beta_A, \beta_B, \theta_{TD}\}$ that produce a 2-step periodic walking gait at 1 m/s for an 80 kg mass with a leg spring stiffness of 20 kN/m and a nominal leg length of 1 m. (ℓ_{LO} is omitted from the list because it can be computed from the other parameters.) Constraints require each leg's length to remain less than its free length and the vertical GRFs at *MS* to be at least 60% of body weight. Cost functions serve to minimize the GRFs immediately before touchdown and immediately after liftoff and to achieve human-like double support ratios of about 0.2. A multiple-shooting strategy is used to solve the optimization problem by dividing it into three phases: single support of the trailing leg, double support, and single support of the leading leg.

RESULTS AND DISCUSSION

Figures 3 and 4 show the motion of the Dual-SLIP model and the vertical GRFs in ascent and descent. In ascending an incline, the leading leg (red in Fig. 3 left) touches down with a reduced leg length, representing the increased knee flexion found in humans at *TD* on inclines [3]. Also, the vertical GRF peak after *MS* (blue in Fig. 3 right) is increased compared to the peak before *MS*, as is the case in human incline walking [4]. In descending a decline, the trailing leg (blue in Fig. 4 left) has a reduced leg length at *TD* of the leading leg, representing the increased knee flexion humans exhibit in late stance on declines [5]. Likewise, the vertical GRF peak before *MS* (red in Fig. 4 right) is greater than that after *MS*, similar to what is found in human decline walking [6]. Comparing the values of β_A and β_B for incline and decline walking highlights the greater significance of eccentric muscle activity in the weight acceptance phase [7] of decline walking.

CONCLUSIONS

This paper demonstrates that modifying the traditional planar Dual-SLIP model of human walking to allow changes in the free length of the leg spring during a stride and touchdown/liftoff at leg lengths less than the instantaneous free length enables accurate matching of the key characteristics of human walking on inclines and declines.

REFERENCES

1. Geyer H, et al. *Proc R Soc B*, **273**, 2861-2867, 2006.
2. Liu Y, et al. *Proc IEEE ICRA*, to appear, 2015.
3. Leroux A, et al. *Exp Brain Res*, **126**, 359-368, 1999.
4. McIntosh AS, et al. *J Biomech*, **39**, 2491-2502, 2006.
5. Leroux A, et al. *Gait Posture*, **15**, 64-74, 2002.
6. Redfern MS and DiPasquale J, *Gait Posture*, **6**, 119-125, 1997.
7. Worthen-Chaudhari L., et al. *Gait Posture*, **39**, 588-592, 2014.

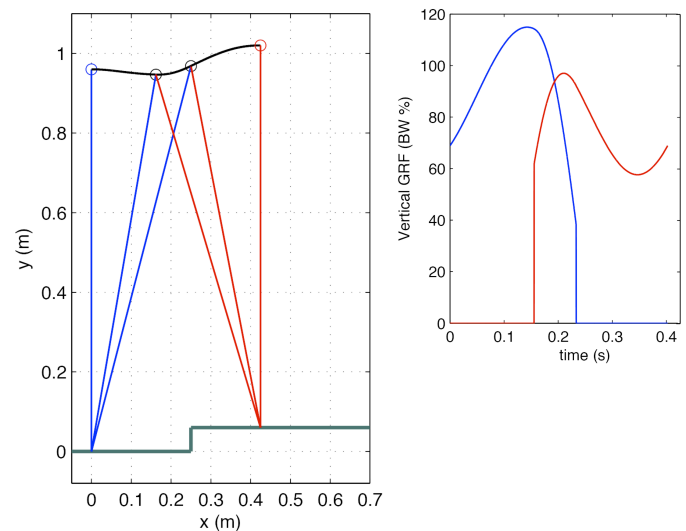


Fig. 3: Motion (left) and vertical GRFs (right) in ascent with the Dual-SLIP model of walking.

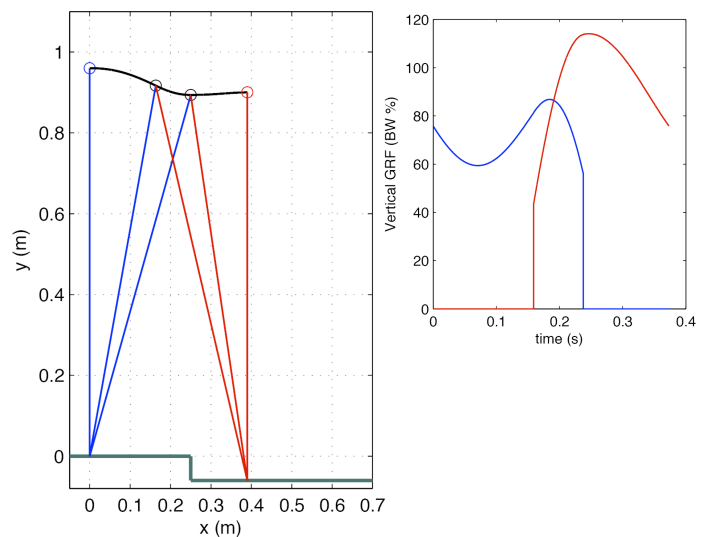


Fig. 4: Motion (left) and vertical GRFs (right) in descent with the Dual-SLIP model of walking.

INDIVIDUAL LIMB TRANSITION WORK DURING WALKING IN SERVICE MEMBERS WITH TRANSFEMORAL AMPUTATION

Caitlin E. Mahon^{1,2}, Brad D. Hendershot^{1,3}, Erik J. Wolf^{1,2}, Alison L. Pruziner^{1,2}

¹Department of Rehabilitation, Walter Reed National Military Medical Center

²DoD-VA Extremity Trauma and Amputation Center of Excellence

³The Center for Rehabilitation Sciences Research, Uniformed Services University of Health Sciences
email: caitlin.e.mahon.civ@mail.mil

INTRODUCTION

The transition between limbs during healthy gait is characterized by [1,2]: trailing limb positive work generation, and leading limb negative work absorption. Past studies examining asymmetric gait have shown that when one affected limb generates less positive trailing work due to ankle weakness, the contralateral (intact) limb will absorb greater negative leading work [3,4]

Greater negative leading intact limb work is suggested to be compensation for affected limb weakness and has been positively correlated to greater metabolic energy consumption in persons with transtibial amputation [3]. The majority of negative work from the leading limb is absorbed at the knee and through soft-tissue [5].

To date, little is known about transition work in persons with unilateral transfemoral amputation (TFA), although prosthetic ankle weakness is present and metabolic consumption during walking is higher than controls. The objective of this analysis was to examine individual limb transition power and work in persons with TFA. We hypothesized that persons with TFA will produce significantly less positive trailing prosthetic limb work and significantly greater negative leading intact limb work compared to controls. Additionally, joint-level transition power was examined to provide more insight into leading limb transition work [5].

METHODS

A retrospective analysis, approved by the Walter Reed National Military Medical Center Institutional Review Board, was performed for 12 male persons

with TFA (30.3±5.4 years, 1.81±0.06 m, 97.2±13.4 kg) and 12 speed-matched male controls (31.0±7.6 years, 1.82±0.05 m, 90.9±10.6 kg). All persons with TFA were evaluated ≥6 months post-injury and wore the microprocessor-controlled C-leg (Otto Bock, Duderstadt, Germany).

Data were collected at the Walter Reed Army Medical Center and Walter Reed National Military Medical Center Biomechanics Laboratories. Individuals walked at a self-selected velocity along a 15 meter walkway. Kinematics were tracked (120 Hz) via retro-reflective markers using a 23-camera motion capture system (Vicon, Oxford, UK) and ground reaction forces were collected (1200 Hz) from 6 force platforms (AMTI, Watertown, MA, USA) embedded in the walkway. Data was processed in Visual3D (C-Motion, Germantown, MD, USA).

Individual limb transition work was calculated using the individual limbs method [2]. First, instantaneous external mechanical power was calculated for each limb by taking the dot product of center of mass velocity and each limb's ground reaction force. Second, trailing prosthetic and leading intact limb external mechanical work were calculated by integrating instantaneous external mechanical power for each respective limb during transition (intact limb foot-strike to prosthetic limb foot-off). Joint-level transition power was calculated using inverse dynamics.

Two independent t-tests ($p < 0.05$) were used to compare transition work between the: (1) trailing prosthetic and trailing control limbs, and (2) leading intact and leading control limbs, using SPSS version 21.0 (IBM, Armonk, NY, USA).

RESULTS AND DISCUSSION

Persons with TFA and controls walked at 1.30 ± 0.01 m/s and 1.33 ± 0.01 m/s, respectively. Mean limb power and work produced by persons with TFA and controls are shown in Figure 1.

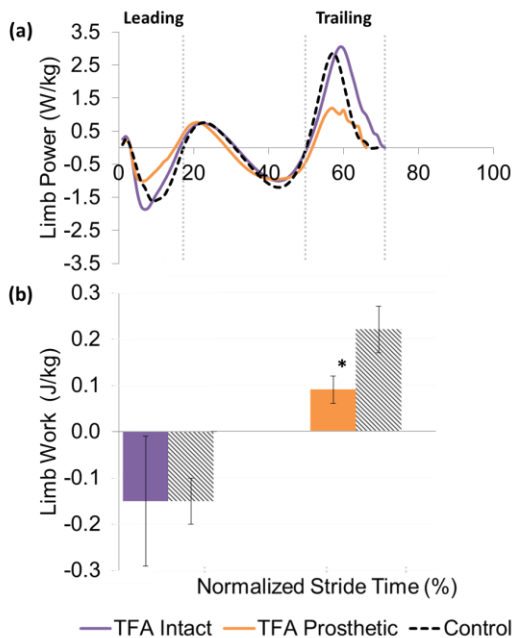


Figure 1: Mean limb (a) power over 1 stride and (b) work calculated during the transition from intact limb foot-strike to prosthetic limb foot-off. Error bars display ± 1 standard deviation. *Indicates significant difference from control.

As expected, the lack of propulsion and ankle plantar-flexion provided by passive prosthetic ankles [1] attributed to significantly less ($p < 0.001$) positive trailing prosthetic work generation by persons with TFA compared to controls. However, unlike other patient populations that exhibit unilateral ankle weakness [3,4], persons with TFA did not absorb greater negative leading intact work compared to controls ($p = 0.979$).

Mean knee joint power produced by persons with TFA and controls is compared in Figure 2. Interestingly, the standard deviations in leading intact limb work and leading intact knee power, the joint that absorbs a majority of leading work [5], were relatively large compared to controls. These variations may indicate differences in walking strategies regarding compensation for prosthetic

limb weakness in persons with TFA. Further analyses should be performed to determine factors contributing to these variations.

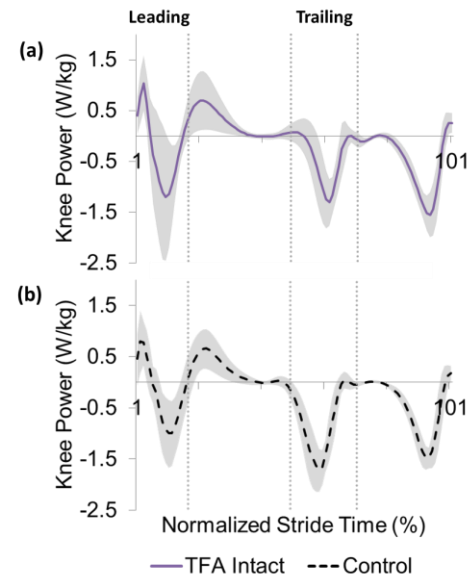


Figure 2: Mean knee power over 1 stride for the (a) TFA intact and (b) control limbs. Grey shading displays ± 1 standard deviation.

REFERENCES

1. Herr HM and Grabowski AM. *Proc. R. Soc* **279**, 457-64, 2012.
2. Donelan JM, et al. *J Biomech* **35**, 77-24, 2002.
3. Houdijk H, et al. *Gait & Posture* **30**, 35-40, 2009.
4. Doets HC, et al. *Hum Movement Sci* **28**, 786-97, 2009.
5. Zelik KE and Kuo AD. *J Exp Biol* **213**, 4257-64, 2010.

ACKNOWLEDGEMENTS

This work was supported, in part, by: the DoD-VA Extremity Trauma & Amputation Center of Excellence (EACE), US Army Medical Command Headquarters, Fort Sam Houston, TX under Public Law 110-417, National Defense Authorization Act 2009, Section 723; the Center for Rehabilitation Sciences Research, at the Uniformed Services University of the Health Sciences; and the BADER Consortium. The views expressed in this abstract are those of the authors and do not necessarily reflect the official policy of the Departments of the Army, Navy, Defense, nor Veteran's Affairs.

AUDIO AND VISUAL BIOFEEDBACK AS METHODS OF GAIT RETRAINING TO REDUCE TIBIAL ACCELERATION UPON FOOT STRIKE

Alexander M. Morgan, Christopher F. Geiser, Philip J. Malloy, Kristof Kipp

Marquette University, Milwaukee, WI
Email: alexander.morgan@marquette.edu

INTRODUCTION

About 15% of all injuries that occur in runners are stress fractures [3]. Nearly half of these stress fractures occur at the tibia. Larger tibial peak positive accelerations (PPA's) at foot strike during running have been associated with a higher risk for stress fracture [2, 4]. Visual and audio biofeedback have both effectively reduced these PPA's in real-time [1, 2, 4, 5]. However, the comparative effectiveness of these two has not been established. While visual biofeedback can be used clinically in the laboratory as a means of decreasing PPA's, this is neither portable nor realistic. Audio biofeedback, however, can be used in a realistic setting through the use of portable technology. As such, audio biofeedback could provide constant feedback during running on a more consistent basis and in a setting that is common to each individual.

PURPOSE

To compare the effectiveness of audio versus visual biofeedback on tibial PPA's during running.

METHODS

Twenty-one healthy, recreational runners (11 female and 10 male) between the ages of 18 and 25 were recruited to run for this study. Subjects were required to be currently running at least 10 miles per week and identify as a heel-striker. A tri-axial accelerometer was placed on the distal, anteromedial aspect of the right tibia. Lower extremity kinematic data were collected via a 14 infra-red camera system. A treadmill was placed within the capture volume of the cameras. Biofeedback was provided via a custom LabVIEW program. The program provided visual biofeedback by displaying continuous accelerometer data on a

TV screen in real-time. Furthermore, the program provided audio biofeedback via a continuous, real-time sound. The sound was a "beep" that linearly increased in pitch and volume as the PPA increased. A five minute warm up was used to determine baseline PPA and a comfortable running speed. Subjects ran at this speed for the remainder of the test. A target threshold was then set at 50% of the baseline PPA, and was used as the goal for one of the following two running conditions: 1) 5 minutes of visual biofeedback, or 2) 5 minutes of audio biofeedback. The assigned condition for each subject was randomized such that a nearly equal number of subjects received visual biofeedback as opposed to audio biofeedback. Data were collected for ten seconds during the last 30 seconds of each interval without subjects' knowledge. Acceleration data were recorded in LabVIEW. Kinematic data were recorded in Vicon Nexus. Data were analyzed using repeated measures ANOVAs to compare between conditions (Audio & Visual) and across time (Warmup & Biofeedback). Data were determined to be significant if $p < 0.05$ and are presented as Mean \pm SD.

RESULTS

There were no significant interactions between biofeedback type and time for PPA. Main effects indicated that PPA values decreased significantly ($p = 0.001$) from the warmup phase to the biofeedback phase for each biofeedback condition (Table 1). Similarly, main effects showed that cadence increased significantly ($p = 0.006$) across time for both audio and visual biofeedback. Kinematic data showed no significant changes between conditions or across time.

DISCUSSION

This study builds upon previous literature that has examined biofeedback as a tool to decrease tibial PPA's. The significant reduction in PPA values from the warmup condition to each biofeedback condition found in the current study is comparable to those decreases found by other authors using visual or audio biofeedback. Crowell and Davis's examination of the effect of visual biofeedback on PPA used a 50% threshold, as performed in this study, and displayed a significant decrease of 48% [1]. In comparison, the current study's averaged data displayed a significant decrease of 18.7%. One reason for this discrepancy may be that Crowell and Davis only accepted runners with initial PPA's above 8g, whereas the current study accepted all heel strikers [1]. As such, those runners in Crowell and Davis' study had more opportunity to decrease their PPA. Furthermore, Wood and Kipp investigated the effect of audio biofeedback on PPA using a threshold of 10-15%, and found a significant decrease in PPA of 11.9% [5]. The greater percent decrease found in the current study is likely due to the lower threshold that is used. Finally, while these two studies presented data regarding changes in PPA in response to biofeedback, this current study is novel in that it also presents data on changes to cadence and kinematics resulting from biofeedback use. This study suggests that an increased cadence without changes in lower extremity kinematics can

produce significantly decreased PPA's. Further research is necessary to determine the longitudinal effect of audio biofeedback on tibial PPA's and on the rate of injury in recreational runners who use this biofeedback.

CONCLUSIONS

Subjects were able to successfully decrease tibial PPA values while running with audio and visual biofeedback. No difference in PPA value reduction was found between the two biofeedback types. In order to achieve this reduction, subjects on average increased their cadence without making any other observed kinematic changes to their gait.

REFERENCES

1. Crowell HP, Davis IS. *Clin. Biomech.* **26**, 78–83, 2011.
2. Crowell HP, Milner CE, Hamill J, Davis IS. *J. Orthop. Sports Phys. Ther.* **40**(4), 206-13, 2010.
3. Matheson GO, Clement DB, McKenzie DC, Taunton JE, Lloyd-Smith DR, MacIntyre JG. *Am. J. Sports Med.* **15**, 46–58, 1987.
4. Milner CE, Ferber R, Pollard CD, Hamill J, Davis IS. *Med. Sci. Sports Exerc.* **38**, 323–328, 2006.
5. Wood CM, Kipp K. *J. Biomech.* **47**, 1739-1741, 2014.

Table 1: PPA, Cadence and Kinematic values for AF and VF conditions

Dependent Variables	Audio		Visual	
	Warmup	Biofeedback	Warmup	Biofeedback
PPA (g)	4.72 ± 1.28	3.93 ± 0.80*	4.79 ± 1.15	3.81 ± 0.61*
Global IC Ankle Angle (°)	18.91 ± 7.08	19.24 ± 7.97	17.46 ± 5.10	16.09 ± 10.07
Global IC Tibia Angle (°)	12.11 ± 4.09	12.19 ± 4.38	10.12 ± 3.11	11.22 ± 3.19
Relative IC Knee Angle (°)	6.41 ± 6.45	6.35 ± 9.10	13.08 ± 6.52	11.96 ± 2.79
Relative Absorption Knee Angle (°)	39.85 ± 5.41	37.83 ± 7.01	44.27 ± 6.94	44.37 ± 6.48
Knee ROM (IC - Absorp) (°)	33.44 ± 2.98	31.48 ± 7.00	31.19 ± 6.27	32.41 ± 5.94
Cadence (steps/min)	164.68 ± 11.36	166.94 ± 11.48*	161.08 ± 10.27	167.13 ± 12.89*

* $p < 0.05$ for Biofeedback vs. Warmup

GAIT BIOMECHANICS IN PATIENTS WITH PERIPHERAL ARTERIAL DISEASE CAN BE PREDICTED BY FUNCTIONAL MEASURES USING STEPWISE REGRESSION

¹ Lauren Bowman, ^{2,3} Jason M. Johanning, ^{2,3} Iraklis I. Pipinos and ^{1,2} Sara A. Myers

¹ The University of Nebraska at Omaha, Omaha, NE, USA

² Omaha Veterans' Affairs Medical Center, Omaha, NE, USA

³ The University of Nebraska Medical Center, Omaha, NE, USA
email: samyers@unomaha.edu, web: cobre.unomaha.edu

INTRODUCTION

For patients with peripheral arterial disease (PAD), the most limiting symptom is physical activity induced pain in the legs known as claudication. Clinically, little is done to assess function other than physicians interviewing them or walking with them to observe the patient's limitations firsthand. Quality of life questionnaires and treadmill and overground maximum walking distance tests are commonly used in research settings. Both types of assessments could potentially be implemented to understand functional limitations in a clinical setting. However, there is no consensus on the best functional walking test to use on these patients^{1,2} and neither type of test has been directly compared with gait biomechanics, which is the gold standard for testing functional limitations³. Biomechanics testing cannot easily be performed on all patients in a clinical setting due to the cost, time, and equipment restraints. Therefore, this study sought to determine whether common research measures of quality of life and maximum walking distance could accurately predict gait biomechanics measures. We hypothesized that distances and quality of life parameters together would be predictors of gait variables in patients with PAD. If true, clinicians could confidently implement these methods into the clinical setting to better understand functional status in patients with PAD.

METHODS

One hundred and six patients diagnosed with PAD (age: 64.4 ± 6.7 years; ht: 174.3 ± 9.2 cm; mass: 86.9 ± 19.2 kg) were referred to the study by vascular surgeons. Consent was documented and the patients were given two different questionnaires: the Walking Impairment Questionnaire (WIQ)⁴ and the

Medical Outcomes Survey Short Form 36 (SF-36)⁵. The WIQ is a questionnaire specific to patients with claudication and it includes component scores for pain, distance, stairs, and speed. The SF-36 has been validated in multiple populations as a measure of quality of life and includes eight domain scores. The walking distance scores were determined by having subjects complete the Gardner treadmill test⁶. Subjects walked on a treadmill set at 0.86 m/s (2.0mph) at 0% grade. The grade of the treadmill was increased 2% every 2 minutes. The initial claudicating distance is the distanced walked prior to the first indication of pain and the absolute claudication distance is the distance walked until the patient cannot walk any further and must stop the test. Additionally, the 6 minute walk test (6MWT) was performed, which is the distance patients can walk overground in 6 minutes⁶.

For the gait biomechanics testing, 27 reflective markers were placed at anatomical positions³. Marker position data was recorded using a twelve camera motion capture system (Motion Analysis Corp., Santa Rosa, CA; 60 Hz). Ground reaction forces were captured by force plates in the overground runway (AMTI, Watertown, MA; 600 Hz). Subjects performed five trials through the overground walkway during a pain free condition. The position data was tracked in Cortex software (Motion Analysis Corp., Santa Rosa, CA) and then processed for gait biomechanics variables in MATLAB (Mathworks Inc., Boston, MA) and Visual3D (C-Motion, Germantown, MD) custom software. Dependent gait biomechanics variables include peak joint angles, moments, and powers of the ankle, knee, and hip during the stance phase. Statistical analysis included a stepwise linear regression analysis using gait variables as the dependents and the quality of life and walking

distances as predictors. For this analysis, the probability level for entry in to the model was set at 0.20 and the significance level of removal from the model set at 0.25. This analysis allowed multiple components of the quality of life measures to be used to predict the gait biomechanics variables. The primary gait outcome variables were ankle plantarflexor moment and ankle plantarflexor power due to previous work in our laboratory identifying the ankle as consistently deficient in patients with PAD. However, prediction models were developed for all ground reaction force, joint angle, joint torque, and joint power peak points from the stance phase.

RESULTS AND DISCUSSION

The models using quality of life questionnaires and walking distances to predict values were significant in 31 of 33 gait parameters tested. Very importantly, the 6MWT was a predictor in 21 of the 31 significant models. For all variables in which the 6MWT was included in the model, as the distance walked increased, the value of the gait parameter was also improved, meaning it moved closer to healthy control values from our previous work⁸. These findings suggest that the 6MWT distances are the best representative of gait parameters from all of the quality of life and walking distance parameters.

An important consideration when interpreting prediction models is the strength of the relationship, or the amount of variance in gait parameters that could be explained by the model. In this study, the significant relationships had r-squared values ranging from .108 to .383, which are not strong relationships. Thus, clinicians should be cautious in thinking that quality of life questionnaires and walking distances could provide the same knowledge as gait biomechanics parameters in patients with PAD. Rather, models of this strength can explain between approximately 10 and 40% of the variance in the specific gait variables and while the models may provide insight into functional status, they are insufficient to describe gait in these patients.

The purpose of this study was to determine whether or not clinicians could rely on quality of life

questionnaires and walking distances to evaluate and understand the gait and function of patients with PAD. Previous studies have demonstrated that gait biomechanics are important outcome measures in assessing treatment efficacy in patients with PAD^{7,8}. Furthermore, there is an argument in the literature regarding whether the treadmill or 6MWT is optimal for assessing functional outcomes for clinical trials^{1,2}. Based on the current study, the 6MWT is the better of the two tests, but neither adequately represents the gold standard for lower extremity function, gait biomechanics. Importantly, this study emphasizes the need for more sophisticated, objective, and accurate methods that could provide stronger models with which to represent function in these patients. Limitations of these studies are they all represent a snapshot in time rather than long-term monitoring of the patient.

CONCLUSIONS

Our results demonstrated that quality of life questionnaires and walking distances can explain between 10-40% of variance in gait biomechanics variables in patients with PAD. Future research should evaluate whether gait parameters assessed through portable devices like accelerometers and inertial sensors are more representative of gait biomechanics in these patients.

REFERENCES

1. Hiatt W, et al. *Circulation*, 69-76, 2014.
2. McDermott M, et al. *Circulation*, 61-68, 2014.
3. Vaughan C, et al. *Dynamics of human gait*. Kiboho Publishers, 1999.
4. Coyne KS, et al. *J Vasc Surg*. **38**, 296-304, 2003.
5. Ware JE. *Spine* **25**, 3130-3139, 2000.
6. Gardner AW, et al. *Med Sci Sports Exerc*. **23**, 402-408, 1991.
7. Liu X. *Proceeding of WCB'14*, Boston, MA, USA, 2014.
8. Yentes J. et al. *J Appl Biomech*. **28**, 184-191, 2012.

ACKNOWLEDGEMENTS

Funding by NIH (R01AG034995 and P20GM109090), VA RR&D RX000604, and UNO FUSE.

THE RELATIONSHIP BETWEEN PERCEIVED HEALTH STATUS AND GAIT IMPROVEMENT FOLLOWING SURGICAL INTERVENTION IN PERIPHERAL ARTERIAL DISEASE.

¹ Madeline Holscher, ^{2,3} Iraklis I. Pipinos, ^{2,3} Jason M. Johanning, and ^{1,2} Sara A. Myers

¹ The University of Nebraska at Omaha, Omaha, NE, USA

² Omaha Veterans' Affairs Medical Center, Omaha, NE, USA

³ The University of Nebraska Medical Center, Omaha, NE, USA

email: samyers@unomaha.edu, web: cobre.unomaha.edu

INTRODUCTION

Health attitudes regarding quality of life and the potential for recovery of function are related to treatment improvement levels in some populations[1]. Patients with peripheral arterial disease (PAD) experience reduced quality of life and physical function from insufficient leg blood flow. The limited blood flow is caused by atherosclerotic blockages in the arteries in the legs. Muscular ischemia causes pain during walking, eventually forcing patients to stop to rest. The standard treatment to improve blood flow in patients with PAD is surgery. In this population, it is unknown how perceived health status prior to surgery influences surgical outcomes. Thus, this project will determine whether a relationship exists between perceived health status, assessed through questionnaires, and improvement in gait biomechanics and maximum walking distances following surgery. If perceived health status is positively related with improvements post surgery, educational and counseling programs to inform patients about the potential for improved outcomes could potentially lead to better restoration of gait function and walking distances post surgery.

METHODS

Twenty-seven patients diagnosed with PAD (age: 61.8 ± 5.63 years; ht: 174.20 ± 7.35 cm; mass: 84.92 ± 17.14 kg) were consented for this study. Patients were having surgery as the standard of care and they participated in additional research evaluations before and six months following revascularization intervention. Perceived health status was assessed using the Walking Impairment Questionnaire (WIQ)[2] and the Medical Outcomes

Study Short Form 36 Healthy Survey (SF-36)[3] The WIQ is a disease-specific questionnaire for individuals with claudication that includes component scores for distance, pain, speed, and stairs. The SF-36 questionnaire evaluates health status across eight physical, emotional, and social domains and has been validated in multiple populations. The scores from each component of the instruments are included as reflective of separate areas of perceived health status.

Walking distance measures included initial and absolute claudication distances as determined by the Gardner treadmill test and the 6 minute walk test (6MWT), the research standards to measure function in patients with PAD. In this test, patients walked on a treadmill set at 0.89 m/s (2.0 mph) and 0% grade, increased by 2% grade every two minutes until patients stopped walking due to claudication pain[4]. The first indication of pain was recorded as the initial claudication distance and the total distance the patients walked on the treadmill before stopping because of pain was the absolute claudication distance. The 6MWT is the maximum distance patients can walk in 6 minutes. For gait biomechanics, five trials of overground walking data were collected using a 12- camera motion capture system (60 Hz; Motion Analysis, Santa Rosa, CA, USA) synchronized with force plates (600 Hz; AMTI, Watertown, MA, USA). Data were collected prior to the onset of claudication pain. Kinematic and kinetic data were calculated using the methods of Nigg et al and Vaughan utilizing Visual 3D (C-Motion, Germantown, MD)[5,6].

Improvements in walking distances and gait biomechanics discrete points were calculated by subtracting baseline data from post surgery data. Pearson's correlations were used to determine the

strength, direction, and significance of relationships between perceived health status variables and gait and walking distance outcome variables.

RESULTS AND DISCUSSION

Significant relationships were found for 7 comparisons ($p < .05$) using Pearson's correlations. Specifically, absolute claudication distance, 6MWT, ankle plantar flexor moment and knee power absorption were related to five of eight domain scores from the SF-36 and one of four WIQ domain scores (Table 1). Only moderate relations were found. Negative correlations mean that as baseline questionnaire scores increase, improvement in the respective gait variable decreases. Positive values indicate that as baseline questionnaire scores increase, gait parameters improved more post surgery.

The direction of the relationships is interesting in that patients who had high baseline scores, meaning fewer perceived physical limitations, did not improve in gait parameters. However, as patients' baseline scores increased in perceived social and general health, increases in absolute walking distances were seen. Perhaps the patients with poor perceived health did not think they would be able to improve. However, they had the most room for improvement and actually benefitted more than patients with positive baseline perceived physical health. Similarly, those who perhaps did not have as severe of symptoms thought they would get a lot better and had a more positive outlook, but the surgery did not help them as much, which could

mean they did not have as much room for improvement in biomechanical parameters.

CONCLUSIONS

The purpose of this study was to examine the relationships between patients' perceived health status and gait and walking distance performance following surgical revascularization. Based on these results we saw differences in level of improvement depending on the area of perceived health. Poor perceived baseline physical health was associated with gait improvements, while positive perceived social and general health was also associated with gait improvements post surgery. Results support the notion that those with poor perceived physical health and those with positive social health can benefit from surgery. Based on the presence of moderate relationships, clinical factors such as restoration of blood flow, extent of muscular myopathy, and presence of co-morbidities are likely greater determinants of surgical outcomes than perceived quality of life in patients with PAD.

REFERENCES

1. Chung K, et al. *Clin Rheumatol*, **34**, 641-51. 2014.
2. Coyne K, et al. *J Vasc Surg*. **38**, 296-304, 2003.
3. Ware JE. *Spine* **25**, 3130-3139, 2000.
4. Gardner AW, et al. *Med Sci Sports Exerc*. **23**, 402-408, 1991.
5. Vaughan C, et al. *Dynamics of human gait*. Kiboho Publishers, 1999.
6. Nigg B, et al. *J Biomech*, **26**, 909-16, 1993.

Table 1: Pearson's correlation coefficients for significant variables.

	ACD	SMWT	Ankle PFM	Knee PowAbs
SF 36: Physical Function			-0.443	
SF 36: Limitation due to Physical Health		-0.562	-0.460	
SF 36: Emotional Well Being				0.429
SF 36: Social Functioning	0.456			
SF 36: General Health	0.422			
WIQ: Distance		-0.394		

Modified falls short-form 36 (SF-36); Walking Impairment Questionnaire (WIQ); Absolute claudication distance (ACD); Six minute walk test (6MWT); and Peak ankle plantarflexor moment (Ankle PFM).

PEAK EMG CHARACTERISTICS OF LOWER-EXTREMITY MUSCULATURE INDICATE UPCOMING LOCOMOTOR TRANSITION

¹ Bryson H. Nakamura, ²Deepak Joshi, and ¹Michael E. Hahn

¹ University of Oregon, Eugene, OR, USA

² Graphic Era University, Dehradun, India

email: bnakamur@uoregon.edu, web: <http://bssc.uoregon.edu>

INTRODUCTION

Transitioning between different forms of locomotion is crucial for functioning in everyday environments. Few studies have identified the characteristic differences in electromyographic (EMG) activation during periods of transition between ramps [1] or stairs [2] and level ground. Recent attempts to develop controllers for classification algorithms in active prostheses have utilized EMG during locomotion [3]. Understanding how locomotor transitions affect peak EMG characteristics would allow for safer ambulation in amputees. The purpose of this study was to determine characteristic difference in peak lower limb muscle activation during transitions between level-ground and ramp/stair locomotive states.

METHODS

Thirteen able-bodied subjects, eleven male (23.5±4.7years; 1.76±0.08m; 76.9±10.kg) and two female (22.5±0.5years; 1.58±0.51m; 59.8±4.3kg), were recruited for this study. Surface EMG data were collected from seven muscles of the right leg. Passive surface electrodes (Ag/Ag-Cl) were placed on the tibialis anterior (TA), medial gastrocnemius (MG), rectus femoris (RF), vastus lateralis (VL), biceps femoris (BF), gluteus maximus (Gmax), and gluteus medius (Gmed), using common placement protocols. Footswitch insoles inserted into the subjects' shoes were used to collect the gait events of foot contact and toe off.

Subjects were asked to complete three successful trials at a self-selected normal walking pace in eight different transition types: LG to ramp ascent (RA), LG to ramp descent (RD), RA to LG, RD to LG, LG to stair ascent (SA), LG to stair descent (SD),

SA to LG, and SD to LG. Three gait cycles per trial were analyzed in this study. Gait cycles were defined from heel-strike to heel-strike of the right leg. The gait cycle beginning three heel-strikes before transition (Pre2), two heel-strikes before transition (Pre1), and one heel-strike before transition (Tr) were analyzed. Each gait cycle was sectioned into one event and two phases: Heel Strike (HS; 0% gait cycle), Stance (ST; first 60% of gait cycle), and Swing (SW; last 40% of gait cycle). The EMG and foot switch data were collected at a sampling frequency of 1500 Hz. The EMG signals were band-pass filtered (3-500 Hz), full wave rectified, and smoothed using a 4th order Butterworth low-pass filter (6 Hz) to generate a linear envelope. Each trial was then amplitude normalized to the maximum peak amplitude of that trial, which was considered to be 100% activation. Relative peak amplitude (AMP) and timing of AMP (GC) were then extracted for each trial, gait cycle and phase.

Two -Way ANOVAs, Phase x Cycle ($\alpha < .05$), were used to determine main effects between cycles and phases of the same transition. Follow-up analyses (adjusted $\alpha < .017$) isolated phases and compared differences between cycles within a single transition.

RESULTS AND DISCUSSION

All eight transitions exhibited significant main cycle effects in either AMP or GC in at least one muscle. Significant changes in shank musculature were found in all transitions. Ramp transitions elicited fewer significant changes than stair transitions.

LGRA: Overall MG AMP increased as subjects moved toward the transition. This may suggest that

MG is increasing overall activation in anticipation of the upcoming RA locomotion which may necessitate increased plantar flexor moments for propulsion.

LGRD: Earlier activation in RF may indicate awareness of the impending transition, while the increased AMP at HS in the VL is utilized to overcome increased external knee flexion moment. In combination, these muscles provide enhanced stability to the subjects as they prepare to transition to RD locomotion.

LGSA: The SW phase showed the greatest evidence of the upcoming LGSA transition. A combination of TA and MG effects suggest a primary goal for toe clearance, followed by stability. The combination of increasing Tr-AMP and earlier Tr-GC during SW was present in VL and Gmax, which may indicate anticipation and manipulation of stride length to transition to stair locomotion.

LGSD: The LGSD transition elicited significant changes to peak activation characteristics in all seven muscles. Shank musculature showed changes during SW phase with earlier TA Tr-GC and increased MG Tr-AMP. The combined effect allows the toe to clear over the edge of the stair and have ample anticipatory activation for stair landing. Further, the combined effects of reduced RF AMP, earlier VL GC, a switch in phase of peak AMP in BF, increase in Gmax AMP at HS, and increase in Gmed AMP during SW, may aid the shank musculature in aiming and control of foot contact.

RALG: The primary change in the RA to LG transition occurred in the gluteal musculature. The Pre1 gait cycle showed a significant, but minimal, change in overall Gmax GC with earlier peak activation.

RD LG: The MG and BF were found to have significant AMP main cycle effects, while TA showed AMP changes in ST phase. In MG, progressive increases in AMP were observed in HS and ST, while AMP in SW remained the same. Similarly in ST, TA increased in Pre1-AMP over Pre2- levels. Alternatively, in BF, progressive increases in AMP were observed in SW, while HS

and ST AMP were not altered. The increases in AMP during the ensuing ST phase may indicate that MG is pushing off the ramp to alter the downward momentum of the body into a more horizontal path, while TA sustains preemptive activation to ensure proper toe clearance during the ensuing SW phase.

SALG: Though part of the same muscle group, the VL and RF acted in opposition. While VL AMP increased in Pre1, RF AMP decreased. This could be a result of bi- vs. mono-articular musculature, which would allow RF to decrease AMP and allow VL to control knee extension.

SDLG: Activation patterns changed during the Tr gait cycle in TA, MG, and Gmax. While subjects were performing SD locomotion, ST phase activation of the MG and Gmax provided sufficient plantar flexor moment and hip extensor moment, respectively. For TA, decreased Pre1-AMP during ST and SW were observed, seemingly in an effort to reduce potential co-activation in the shank and allow the toes to move into a plantar flexed position for ensuing stair contact.

CONCLUSIONS

Peak EMG activation characteristics change as subjects approach a locomotor transition. Unique patterns observed in this study could be used to enhance classification algorithms in active, mechanized prostheses.

REFERENCES

1. Sheehan RC and Gottschall JS. *J. Appl. Biomech.* **28**, 738-745, 2012.
2. Sheehan RC and Gottschall JS. *J. Electromyogr.* **21**, 533-541, 2011.
3. Huang et al. *IEEE Trans Biomed Eng.* **58**, 2867-2876, 2011.

ACKNOWLEDGEMENTS

This work was funded by a grant from the Department of Defense (W81XWH-09-2-0144). Thanks to Daniel Jones and Eileen Deming for assistance in data collection and post-processing.

VARIABILITY OF SHEAR STRESSES ON THE PLANTAR SURFACE OF THE FOOT DURING GAIT

Marisa Papp¹, Visar Berki¹, Brian L. Davis¹

¹Department of Biomedical Engineering, University of Akron, Akron, Ohio 44325, US

Email: mjp117@zips.uakron.edu

INTRODUCTION

Despite the fact that the plantar foot experiences three dimensional force vectors during gait, only the vertical component has been studied thoroughly in association with diabetic neuropathy. There is evidence supporting the existence of a strong association between diabetic neuropathy and higher plantar shear loads that may be responsible for foot ulceration and re-ulceration. No study to date, however, has examined the reliability of shear measurements. For this study, all forces—anteroposterior (AP) and mediolateral (ML) shear, and pressure—were measured simultaneously. The Coefficient of Variation (CV) was then calculated (as the ratio of standard deviation to mean stress) for these groups across multiple regions of the foot.

METHODS

Shear and pressure data during walking were collected on 29 volunteers (16 Males/13 Females) none of whom had gross foot deformities (minor clawing of the toes was permissible), prior foot surgeries, or foot pain. The study included three groups: a control group (CG) that consisted of 16 subjects with no known diabetic symptoms, 7 older diabetic neuropathy patients (ODN), and 6 younger diabetic neuropathy patients (YDN). Subjects walked at a self-selected pace without any sock or shoe apparel on the shear and pressure evaluating camera system (SPECS). The plantar surface was divided into ten areas, based on the schematics of Cavanagh's work in reference to anatomical structures of the foot [1] (Figure 1). The coefficient of variation percentage (CV) was calculated for all plantar pressure and shear variables in order to observe data variability.

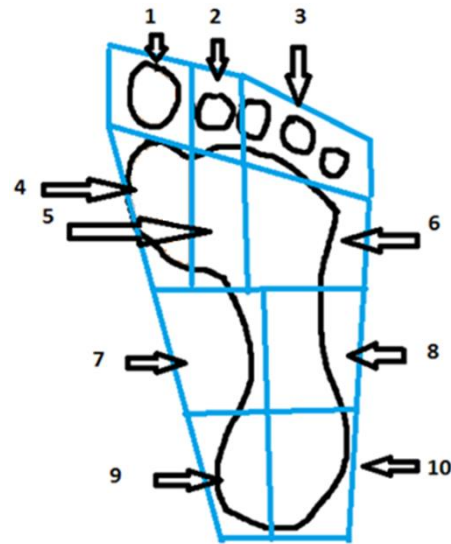


Figure 1. Shear and pressure regions of the foot.

RESULTS AND DISCUSSION

The pressure CV values (Table 1) in the current study were consistently lower, indicating less variability, in all areas except for the midfoot (A7 and A8) when compared to Bacarin et al and Cavanagh et al [1]. Reasons for this could include differences in sensor sizes (the SPECS system has sensors 1.6mm x 1.6mm while Cavanagh et al used a 1.0cm x 1.0cm sensor), differences due to gait speed and/or subjects.

Some theories suggest that patients with neuropathy tend to walk with more variability due to their diminished afferent feedback, while others propose that the neuropathic patients adopt a “robot-like” gait pattern with little variability. In the forefoot regions (A4, A5 and A6), the variability values in diabetic patients seemed slightly lower than for the control group, however, in the toe region (A1) the pressure variability is highest in ODN (Table 2). As expected,

among all testing groups the CV of A7 (medial side of arch) was extremely variable.

This study expands upon the previous research of Cavanagh et al., (1998) who showed there was no significant difference in variability of pressure values in neuropathic diabetic patients [3]. In our study, mean lateral shear CV values were significantly higher in region A4 among CG and YDN compared to ODN ($p_{A4}=0.002$), while mean medial shear CV in A5 was significantly higher when comparing CG and ODN with YDN ($p_{A5}=0.027$). Mean anterior shear CV values for the hallux (A1) were significantly higher in ODN and YDN than in control subjects ($p_{A1}=0.044$). Meanwhile, A5 had significantly lower values among ODN and YDN compared to CG ($p_{A5}=0.045$). Mean posterior shear CV was significantly lower among CG and YDN in A5 compared with ODN ($p_{A5}=0.016$). The heel area did not hold significant variability comparing the diabetic groups to the CG,

most likely because these shear values are more dependent on heelstrike mechanics rather than intrinsic muscle control. The fact that neuropathic diabetic patients have less variability in shear in the medial forefoot region is interesting because this is a high risk area for ulceration. The issue of repetitive moderate shear stresses in this region is a topic that warrants further investigation due to potential implications in the etiology of foot ulceration.

REFERENCES

1. Bacarin TA, Sacco ICN, Hennig EM. Plantar pressure distribution patterns during gait in diabetic neuropathy patients with a history of foot ulcers. *Clinics*. 2009;64:113-20.
2. Cavanagh, P., Rodgers, M., Iiboshi, A., 1987. *Pressure distribution under symptom-free feet during barefoot standing*. *Foot & Ankle* 7(5),262-276.
3. Cavanagh PR, Perry JE, Ulbrecht JS, Derr JA, Pammer SE. 1998. Neuropathic diabetic patients do not have reduced variability of plantar loading during gait. *Gait Posture*. 1;7(3):191-199.

Table 1. Compare Pressure CV Data (%) of given areas, current study, Bacarin et al, and Cavanagh et al [1].

	M5(A1)	M4(A4-A5)	M3(A6)	M2(A7-A8)	M1(A9-A10)
Bacarin	36.0	25.0	20.0	54.0	28.0
Cavanagh	113.2	52.1	40.8	61.3	23.5
CG	17.5	27.9	18.9	59.2	18.4
ODN	46.8	23.4	13.9	59.0	22.4
YDN	21.2	22.9	13.0	74.4	17.1

Table 2. CV values (%) for areas comparable to Table 1.

		M5(A1)	M4(A4-A5)	M3(A6)	M2(A7-A8)	M1(A9-A10)
Shear Lateral	CG	20.7	44.2	18.4	66.8	23.0
	ODN	49.3	27.6	17.7	64.7	21.1
	YDN	27.6	34.9	15.0	74.5	29.7
Shear Medial	CG	17.1	32.1	25.7	53.7	23.7
	ODN	47.2	25.3	23.2	59.6	21.1
	YDN	26.4	22.1	16.0	70.9	22.2
Shear Anterior	CG	19.0	45.2	29.0	55.1	24.2
	ODN	36.7	20.2	17.2	65.2	18.8
	YDN	29.0	19.2	18.1	64.7	20.9
Shear Posterior	CG	16.2	19.1	16.3	70.2	22.5
	ODN	53.3	21.2	14.4	62.0	32.8
	YDN	26.1	18.8	9.2	78.3	16.1

CONTROL STRATEGIES DURING A STEP UP AND OVER TASK IN PATIENTS SIX MONTHS AFTER TOTAL KNEE ARTHROPLASTY AND HEALTHY CONTROLS

¹Federico Pozzi, ^{1,2}Adam Marmon, ¹Lynn Snyder-Mackler and ¹Joseph Zeni

¹ University of Delaware, Newark, DE, USA

² Christiana Health Care System, Wilmington, DE, USA

email: fpozzi@udel.edu

INTRODUCTION

Compared to healthy controls, subjects after total knee arthroplasty (TKA) exhibit less total support moment (TSM), less knee flexion moment, and a greater contribution from the hip when climbing stairs.¹ Similarly, previous work from our lab has shown that patients after TKA perform a step up and over task with reduced knee moment and increased hip joint moment and power generation.² After surgery, biomechanical asymmetries during functional tasks are related to poor functional performance and impaired quadriceps strength.³ Although quadriceps is weaker, and the kinetic and kinematic strategies are abnormal and after TKA, the underlying muscle activation patterns are unknown. Therefore the purpose of this study was to examine the TSM, the relative joint contribution to the TSM, and muscle activation patterns during the step up and over task in patients six months following TKA and healthy older adults.

METHODS

Nineteen patients 6 months following unilateral TKA and 19 healthy older adults participated in this study (Table 1). Participants stepped up and over a wooden box that was mounted to a force plate. They were instructed to step onto the box with one limb, traverse over the step to clear the swinging limb, land on the force plate in front of the box with the contralateral limb, and continue walking.

EMG data were collected using double differential preamplified electrodes placed over seven muscles of the lower extremity (lateral hamstring, vastus lateralis, vastus medialis, tibialis anterior, soleus, and the medial and lateral heads of the gastrocnemius). Maximum volitional isometric contractions (MVIC) were performed to determine the maximum levels of voluntary contraction and used for normalization.

Markers trajectories and kinetic were collected at 120Hz and 1080Hz and smoothed using a low-pass filter (6Hz and 40Hz, respectively). EMG data were collected at 1080Hz, bandpass filtered (20-350 Hz), rectified, and low pass filtered (6 Hz) to create a linear envelope. Dynamic muscle activity was normalized to maximal activity either from the MVIC trial or dynamic trials. Kinematic, kinetic, and EMG data were calculated separately for the stance phase of each limb; these data were time normalized to 100% of stance. For each subjects, EMG data were inspected prior to the analysis; signals that were deemed not usable were excluded from the analysis.

Joint moments were calculated using inverse dynamic and normalized to body mass (Kg). TSM represents the magnitude of the extensor synergy, and was calculated by summing the internal extensor moments at the ankle, knee, and hip joints. The stepping portion of the task was divided into two phases (propulsion and lowering) using the peak vertical position of a marker on the pelvis. During the propulsive phase, time to peak TSM was determined using the interval between foot contact on the step and 1st peak of TSM. During the lowering phase, time to peak TSM was determined using the interval between the highest vertical position of the pelvis marker and the 2nd peak of

Table 1. Demographic characteristics.

	TKA group		Control group	
	Mean	SD	Mean	SD
Sex, male/female	9/11		10/9	
Age, years	69.8	6.2	68.5	7.3
Height, m	1.68	0.7	1.68	0.9
Mass, Kg	85.96	17.39	74.23	16.75
BMI, kg*m ²	30.12	4.96	26.08	3.87

TSM. During landing, time to peak TSM was calculated using the interval between foot contact on the ground and the 3rd peak of TSM. Average EMG for each muscle was calculated during each interval. Each joint's specific contribution to each peak TSM was calculated by dividing the joint specific moment by the relative TSM peak.

One of the limbs of the control group was randomly assigned as surgical limb. For each phase, TSM, time to peak, specific joint contribution, and EMG average activation were compared between surgical limb of the TKA and control groups using an independent sample t-test.

RESULTS AND DISCUSSION

During the propulsive phase, the TKA group had smaller TSM (-18%, $p = 0.01$, Figure 1), longer time to peak interval (+0.08s, $p < 0.01$, Table 2), smaller contribution of the knee joint (-11%, $p < 0.01$), and greater contribution of the hip joint (+8%, $p = 0.02$) compared to the control group. EMG activation for all muscles was similar between both groups.

During the lowering phase, the TKA group had longer time to peak interval (+0.04s, $p < 0.04$, Table 2) and smaller contribution of the knee joint (-10%, $p < 0.01$) compared to the control group. EMG activation for all muscles was similar between groups.

During the landing phase the TKA group had smaller TSM (-22%, $p < 0.01$, Figure 1), greater contribution of the ankle joint (+8%, $p < 0.02$, Table 2), and greater average activation of the lateral gastrocnemius (+38%, $p < 0.01$) compared to the control group. Greater activation was also found for the medial gastrocnemius (+7%) and soleus muscles (+31%), but these results were not significantly different between groups ($p > 0.5$).

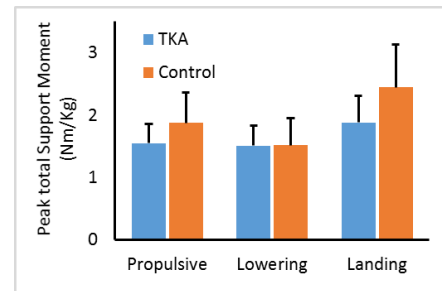


Figure 1. Total support moment during the step up and over task. Error bar represent 1 standard deviation.

CONCLUSIONS

During the step up and over task, patients 6 months following TKA took longer time peak TSM and the peak values were significantly lower than the control group. Factors such as weakness, dynamic stiffness, pain, and slower movement speed may be responsible for the lower TSM. Patients with TKA also exhibited altered joint contribution to the support of the body, as demonstrated by significantly smaller percentage contribution from the knee joint. Similar to stair ascent,¹ the reduction in knee joint contribution is compensated for by increased reliance on the hip. In contrast, during the landing phase, patient after TKA rely more on the ankle joint to support the body, while simultaneously reducing the contribution demands on the knee and hip joints. This landing strategy appears to require greater activation of the triceps surae. Future work should identify the physical impairments that contribute to these altered neuromuscular strategies.

REFERENCES

1. Mandeville D, et al. *Clinic Biomch*, **22**, 787-94, 2007.
2. Pozzi F, et al. *Clinic Biomch*, **30**, 78-85 2015.
3. Christiansen C et al., *Arch Phys Med Rehabil*, **92**, 1624-9.

	Propulsive				Lowering				Landing			
	time to peak	Ankle %	Knee %	Hip %	time to peak	Ankle %	Knee %	Hip %	time to peak	Ankle %	Knee %	Hip %
TKA	0.33 ± 0.11	22.7 ± 10.6	34.7 ± 11.8	42.5 ± 12.7	0.28 ± 0.07	73.5 ± 12.3	46.2 ± 10.5	-19.8 ± 15.3	0.12 ± 0.03	63.9 ± 12.6	18.2 ± 15.0	17.9 ± 20.9
Control	0.25 ± 0.05	20.4 ± 6.0	46.0 ± 8.4	33.6 ± 9.6	0.24 ± 0.04	74.8 ± 10.3	56.5 ± 10.8	-31.3 ± 15.5	0.10 ± 0.02	55.0 ± 11.4	23.0 ± 11.9	22.0 ± 13.4
p-value	0.01*	0.4	<0.01*	0.02*	0.04*	0.73	<0.01*	0.02*	0.06	0.02*	0.28	0.47

*, indicates significant differences between groups

Table 2: Time to peak support moment, and ankle, knee, and hip joint contribution of the TKA and control groups during the three phases of the step up and over task.

COMPARISON OF THREE PLUG-IN-GAIT PROTOCOL VARIATIONS IN GAIT ANALYSIS

¹ Swithin S. Razu and ¹ Trent M. Guess

¹ The University of Missouri, Columbia, MO, USA

email: swithinr@health.missouri.edu, web: www.mizzoumotioncenter.com

INTRODUCTION

Gait analysis is recognized as an important diagnostic tool for the management of patients with gait pathologies. The Vicon® motion capture system is one of the most sophisticated systems used for gait analysis and the Plug-in-Gait (PiG) [1] skeletal model is widely used. As compared to other models, PiG results are reliable in the sagittal plane but show increasing variability in the frontal and transverse planes [2]. The PiG model relies heavily on the capability of the clinician to identify anatomical landmarks and hence is prone to errors. To overcome this drawback, Vicon® has incorporated a functional calibration method (PiG-FJC) to estimate the hip joint center position and knee rotation axes by moving the associated segments through their functional range of motion. This study evaluates the inter-protocol variability of hip and knee angles using three variations of the Plug-In Gait protocol during gait. The first protocol (PiG) is the conventional PiG model based on the original 'Newington model' [1, 3]. The second method, PiG-FJC, uses optimum common shape technique (OCST) [4] to create virtual rigid bodies. The method then uses symmetrical center of rotation estimation (SCoRE) [5] to estimate the hip joint center and symmetrical axis of rotation analysis (SARA) [6] to estimate the knee joint axes. SCoRE and SARA are then combined into the conventional PiG model. The third protocol (PiG-MED) uses medial knee and ankle markers to estimate the thigh rotation offset, shank rotation offset and tibial torsion to be adapted into the conventional PiG model.

METHODS

After providing informed consent approved by the institution's human subjects review board, one female (22 years, 1.68 m, 63.7 kg) and two male subjects (23 and 33 years, 1.75 m and 1.83 m,

80.6kg and 94 kg) participated in this study. A comprehensive marker set was designed by combining individual markers and clusters as required by the three protocols to allow simultaneous data capture. The subjects were marked in accordance to the PiG for the lower body with additional markers on the knee (medial epicondyles) and ankle (medial malleolus) which are necessary for the PiG-MED protocol. For the

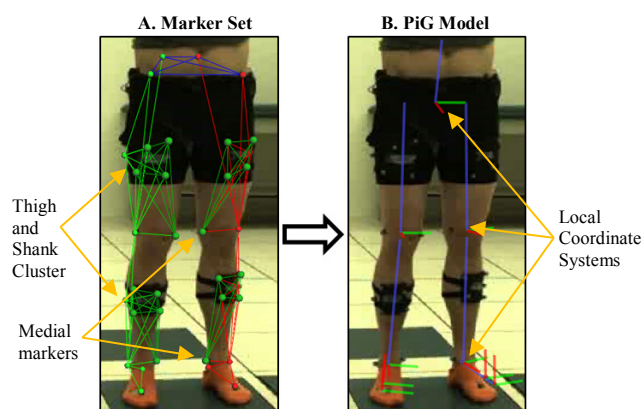


Figure 1: Marker locations and skeletal model.

PiG-FJC, four-marker clusters were attached to the anterior-lateral aspect of the thigh and shank. 3-D marker trajectories were acquired at 100 Hz by an 8 camera motion capture system (VICON MX-T40S, Oxford Metrics, UK) and the data was processed independently according to each protocol.

The PiG and PiG-MED protocols require the same static calibration to be performed where the subjects stands in a static up-right posture. The medial markers were removed after static capture. The PiG-FJC uses functional calibration to estimate the hip joint center and knee joint axis. To estimate the hip joint center using SCoRE the subjects performed a star arc pattern consisting of flexion-extension, abduction-adduction and internal-external rotation while standing on the contralateral limb. For the SARA procedure the subjects performed a knee flexion movement pattern while standing on the

contralateral limb. Relevant anthropometric measures were taken as required by the PiG protocol. The subjects were asked to walk barefoot at their natural speed, and five walking trials were recorded. After data acquisition, 3D marker trajectories were reconstructed and the right and left stride phases identified for all five trials.

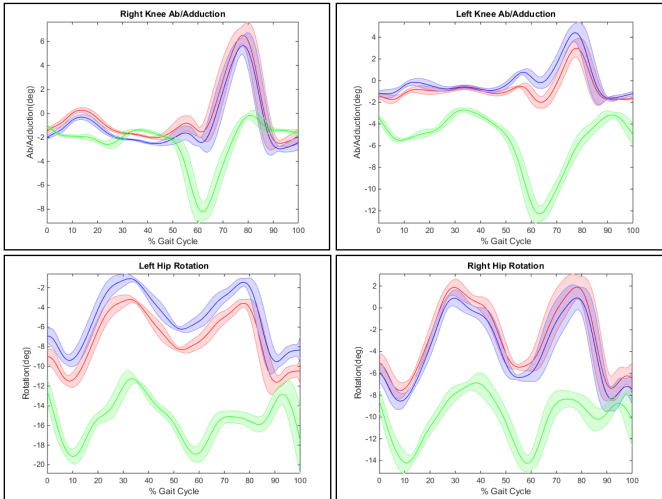


Figure 2: Five trial averages and standard deviations for joint angles with the lowest correlation coefficients. PiG (red), PiG-MED (blue) and PiG-FJC (green).

RESULTS AND DISCUSSION

The intra-subject kinematic variability observed was good over the five trials and within a maximum standard deviation of 6.43° for PiG, 6.39° for PiG-MED and 6.64° for PiG-FJC. Good waveform correlation was also observed for hip and knee flexion/extensions for all three protocols.

Table 1: Walk cycle correlation coefficients.

Protocols	Right			Left		
	PiG vs. PiG-MED	PiG vs. PiG-FJC	PiG-MED vs. PiG-FJC	PiG vs. PiG-MED	PiG vs. PiG-FJC	PiG-MED vs. PiG-FJC
Hip flexion/ extension	1.000	0.999	0.999	1.000	1.000	1.000
Hip abduction/ adduction	1.000	0.997	0.997	1.000	0.999	0.999
Hip internal/ external	1.000	0.311	0.311	1.000	0.257	0.257
Knee flexion/ extension	1.000	1.000	1.000	1.000	1.000	1.000
Knee abduction/ adduction	0.998	-0.433	-0.436	0.975	-0.406	-0.543
Knee internal/ external	0.999	0.986	0.989	1.000	0.968	0.968

The PiG and PiG-MED show similar results for all kinematics. Out-of-sagittal plane rotations, especially hip internal/external rotation and knee abduction/adduction revealed poor waveform correlation for PiG-FJC when compared to PiG and PiG-MED as indicated in red (Table 1). The largest variability was observed at the knee abduction/adduction where opposite trends were

observed (Fig. 2). The PiG-FJC hip joint centers were found to be consistently posterior and lateral relative to the PiG hip joint center (Fig. 3). In all three cases the flexion/extension axes for PiG-FJC were externally rotated (Table 2).

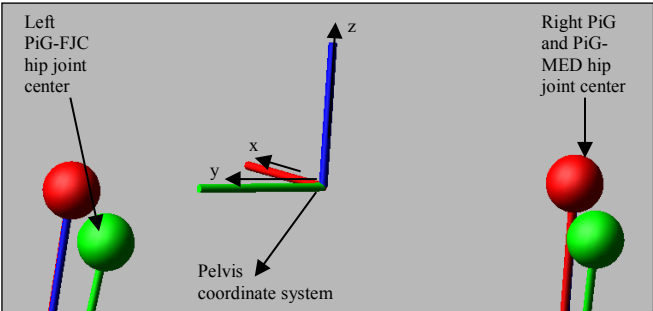


Figure 3: Hip joint center locations with respect to the pelvic coordinate system.

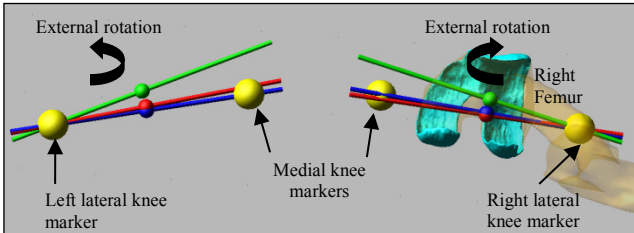


Figure 4: Flexion/extension joint axes for PiG in the transverse plane; (red), PiG-MED (blue) and PiG-FJC (green).

Table 2: Angle on transverse plane between PiG-FJC and line connecting medial-lateral knee marker.

	Right	Left
Subject 1	13.1°	10.74°
Subject 2	14.64°	12.36°
Subject 3	8.54°	12.11°

REFERENCES

1. Davis Iii, R.B., et al., Human Movement Science, 1991. **10**(5): p. 575-587.
2. Ferrari, A., et al., Gait Posture, 2008. **28**(2): p. 207-16.
3. Kadaba, M.P., Ramakrishnan, H.K. & Wooten, M.E. , Biomechanics of Normal and Prosthetic Gait, 1987: p. 87-92.
4. Taylor, W.R., et al., Gait Posture, 2010. **32**(2): p. 231-6.
5. Ehrig, R.M., et al., J Biomech, 2006. **39**(15): p. 2798-809.
6. Ehrig, R.M., et al., J Biomech, 2007. **40**(10): p. 2150-7.

BILATERAL VERTICAL STIFFNESS ASYMMETRY DURING A LOW-INTENSITY RUN IN YOUTH MALE ATHLETES

Joong Hyun Ryu, Dino Palazzi

Aspire Academy, Sport Science Dept., Doha, Qatar
email: joong.ryu@aspire.qa, web: <http://www.aspire.qa>

INTRODUCTION

A stretch-shortening cycle (SSC) during the lower limbs rebound against the ground such as running, jumping, and sprinting is governed by the ability of the musculo-tendon unit to yield against the eccentric stretching of the muscle [1]. Vertical stiffness, calculated as the ratio of the vertical leg spring compression and peak vertical ground reaction force (GRF), often represent SSC mechanically. Although the majority of literature examining vertical and leg stiffness has focused on adults, some studies investigated developmental aspect of neural regulation of stiffness in childhood [2,3]. These studies suggest that as children grow older they improve their ability to use SSC as a result of growth and maturation. The improvement stiffness can be beneficial in sports related tasks performance such as running and jump since we take advantage of the storage and release of elastic energy.

In a developmental context, assessments of bilateral asymmetry, describing functional performance differences between limbs, are also important because the ability to produce stable coordination reflect development of the central controlling structures [4]. In addition, excessive deviations create compensatory movements, modify loading patterns, and may lead to injury or to decline of sporting task performance. Therefore, the aim of current study was to investigate potential age-related difference in bilateral vertical stiffness asymmetry during the running performance as a function of development in adolescent athletes.

METHODS

124 healthy, male student-athletes from 12 to 18 years-old, training up to 8 times a week in 10

different sports, participated for this study. They were well experienced in treadmill running. The age of the participants was calculated on the day of testing. The data allocated into the age range 12-14, 14-16, and 16-18 (table 1).

After warm-up, all participants performed 2-minutes running at 12 km/h on the instrumented treadmill (ADAL3D-WR, France). Three-dimensional GRF were sampled at 1000 Hz over the 30 seconds at the middle of 2-minutes running period. GRF time series were digitally filtered at 30 Hz cut-off, using a zero phase-lag forth-order Butterworth low-pass filter. Vertical GRF of each contact period (vertical GRF above 10 N) were measured for calculating vertical stiffness of the 40 consecutive steps. Vertical stiffness K_{vert} was calculated as:

$$K_{\text{vert}} = F_{\text{max}} / \Delta \text{COM}$$

where F_{max} is the vertical GRF peak and ΔCOM is maximum vertical displacement of the center of mass (COM), which was calculated by integrating the vertical acceleration twice with respect to time. The symmetry index (SI) of bilateral vertical stiffness was calculated using following formula:

$$SI = \frac{|X_{\text{left}} - X_{\text{right}}|}{\text{avg}(X_{\text{left}}, X_{\text{right}})} \times 100$$

One-way ANOVA was performed to determine whether there were significant differences among age groups. A post hoc multiple comparison test (Tukey HSD) was performed if as significant main effect was observed. Statistical significance was set at $p < 0.05$.

RESULTS AND DISCUSSION

Significant main effects in vertical stiffness between age group were reported ($F(2,121) = 6.250, p=0.003$). Significantly greater vertical stiffness were reported for the 14-16 age group (39.2 ± 6.7 kN/m) and the 16-18 age group (40.5 ± 6.2 kN/m) in comparison to the 12-14 age group (35.2 ± 7.2 kN/m). There was a significant difference between groups in the SI of vertical stiffness ($F(2,121) = 3.610, p=0.030$). A post-hoc test revealed that the SI of vertical stiffness for the 12-14 age group was significantly higher (10.6 ± 7.4 %) compared to the 16-18 age group (6.9 ± 4.9 %). There was no significant difference between the 12-14 age group and 14-16 age group although a trend towards significance ($p=0.069$). There was no significant difference between the 14-16 age group and 16-18 age group ($p=0.894$).

The results of the current study seem to highlight that the trend in the development of utilizing SSC in multi joint task is dependent on age in youth male athletics. This maybe due to accelerated limb growth during that age and a greater rise in body mass, which is likely to impact on coordination and motor control. Furthermore, the ability to produce stable coordination and to take advantage of using elastic energy stored in the musculo-tendon structures may be acquired during the period between 14 and 16 years of age. If bilateral asymmetry is related to less optimal performance, it maybe important for sport professional to emphasize bilateral movements in training programs for within these periods of growth athletes. In addition, monitoring of bilateral asymmetry in running routinely may help to identify potential running related injuries. Although this finding is from a cross sectional study at present, follow-up

longitudinal studies will incorporate in order to confirm finding current study.

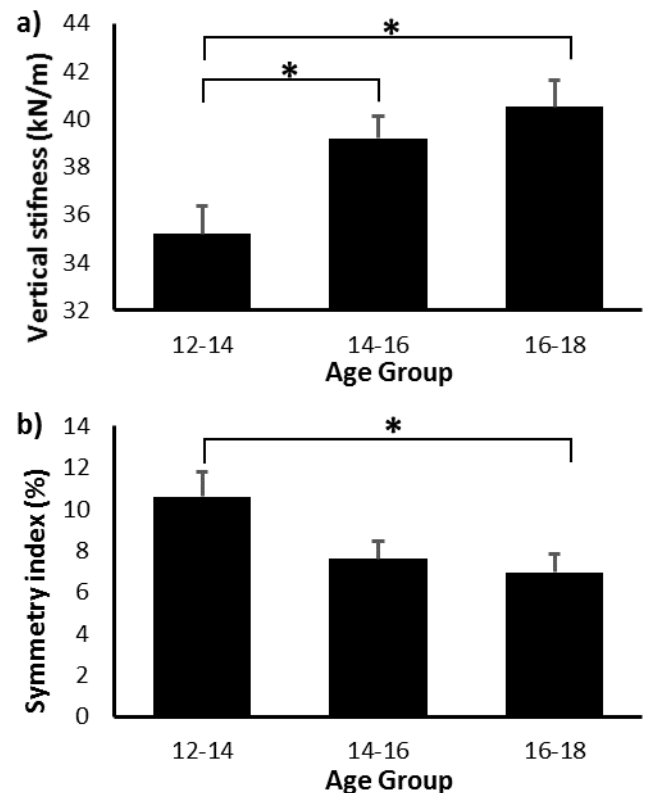


Figure 1: Age group differences in a) vertical stiffness and b) the bilateral symmetry index of vertical stiffness.

REFERENCES

1. Komi PV. *J Biomech*, **33**, 1197-1206, 2000.
2. Lloyd RS, et al., *J Electromyogr Kinesiol* **22**, 37-43, 2012.
3. Korff T, et al., *J Exp Bio*, **212**, 3737-3742, 2009.
4. Cavallari P, et al., *Exp Brain Res*, **141**, 398-409, 2001.

Table 1: Mean (s) values for descriptive details per age group.

Group	12-14	14-16	16-18
N	40	52	32
Age (yrs)	13.2 ± 0.5	15.0 ± 0.5	16.7 ± 0.5
Body mass (kg)	45.8 ± 12.1	57.6 ± 12.0	61.5 ± 9.7

GAIT ALTERATIONS IN PERIPHERAL ARTERIAL DISEASE ARE NOT WORSENER BY THE PRESENCE OF DIABETES

¹Molly N. Schieber, ¹Allison N. Kalina ^{2,3}Iraklis I. Pipinos, ^{2,3}Jason M. Johanning, ¹Sara A. Myers

¹University of Nebraska at Omaha, Omaha, NE, USA

²Omaha Veterans' Affairs Medical Center, Omaha, NE, USA

³University of Nebraska Medical Center, Omaha, NE, USA

email: samyers@unomaha.edu, web: cobre.unomaha.edu

INTRODUCTION

Peripheral arterial disease (PAD) is a vascular disease where atherosclerotic blockages restrict blood flow to muscles in the lower extremities. The primary symptom of PAD is intermittent claudication, or pain during walking that results from ischemia of the leg muscles. Claudication is a mechanism not only of pain, but gait dysfunction and those inflicted experience reduced mobility, reduced physical functioning, and decreased quality of life. PAD affects approximately 8.5 million people in the US and 20-30% of those individuals have diabetes [1, 2]. An abnormal metabolic state associated with diabetes affects multiple cell types within the vascular wall adversely and has been found to directly contribute to atherosclerosis [2, 3]. Thus, diabetes is a common co-morbid condition in PAD and has been shown to increase the risk of lower extremity amputation compared to PAD without diabetes [2]. Although there is a clear pathological relationship between diabetes and PAD, the gait mechanics involved remain indistinct. Therefore, the purpose of this study was to determine whether the presence of diabetes in addition to PAD results in greater functional impairment during ambulation. It is hypothesized that the biomechanical adaptations caused by PAD will be to a greater magnitude in individuals also inflicted with diabetes. Additionally, there is an expected effect of condition in PAD groups as the onset of claudication pain will cause further alterations in gait.

METHODS

Twenty-three subjects with PAD and twelve controls consented to participate in the research.

The subjects were divided into three groups: PAD and no comorbidities (PAD-NC, 12; age (years): 62.4 ± 5.4 ; height (cm): 178.0 ± 8.3 ; mass (kg): 86.8 ± 14.8); PAD with diabetes (PAD-D, 11; age: 62.7 ± 5.2 ; height (cm): 174.63 ± 5.7 ; mass (kg): 85.6 ± 13.9); and healthy controls (12; age (years): 64.4 ± 7.7 ; height (cm): 178.0 ± 5.1 ; mass (kg): 89.8 ± 16.6). All diabetic patients were without neuropathy. Reflective markers were placed in anatomical locations captured with a 12 camera motion capture system (Motion Analysis Corp, Santa Rosa, CA). Kinematics (60 Hz) and kinetics (600 Hz) were captured using Cortex software (Motion Analysis Corp, Santa Rosa, CA) while subjects walked over ground in pain free and pain conditions. Subjects walked over force plates (AMTI, Watertown, MA, USA) for 5 trials in each condition. After baseline lower extremity biomechanics were captured, subjects performed the 6 minute walk test to induce claudication pain. Following this test, subjects immediately began the pain condition where the walking over the force plates was repeated without rest between trials. Marker position data was exported and analyzed using MATLAB (Mathworks, Inc., Natick, MA) and Visual 3D (Germantown, MD, USA). A mixed ANOVA was used to determine the main effect for group (PAD-NC and PAD-D) and condition (pain free and pain) and Bonferroni was used in the case of significant interactions. Additionally, independent t-tests were used to compare means between control and PAD groups at baseline. Dependent gait variables include spatiotemporal variables (stride time, stride length, step width) and peak kinetic discrete points (ankle plantar flexor, knee extensor, and hip flexor moments; ankle, knee, and hip power generation) affected by PAD[4, 5].

RESULTS AND DISCUSSION

In the comparisons with PAD patients, an effect of condition was found for stride length, ($F_{1, 20}=4.75$, $p=0.041$), and ankle power generation, ($F_{1, 21}=8.15$, $p=0.009$) for PAD groups where both values decreased from the pain free to pain condition (Table 1). Contrary to the hypothesis, no main effect of group or any interaction of group and condition were found. PAD has been shown to cause severe myopathy, including altered muscle morphology and mitochondrial function in those afflicted. Therefore, in combination with our findings, it is likely that these problems would dominate any gait deficits caused by diabetes, especially in those without neuropathy.

Regarding the comparisons to controls, ankle power generation was greater in controls with significant differences ($M=2.59$, $SE=.13$) from PAD-NC ($M=2.04$, $SE=.42$, $p=.007$) and PAD-D ($M=1.96$, $SE=.58$, $p=.009$). Hip flexor moment was also greater in controls ($M=-0.93$, $SE=0.06$) but was only significantly different from PAD-D ($M=-0.67$, $SE=0.08$, $p=0.012$). Another significant difference between controls ($M=-0.45$, $SE=0.05$) and PAD-D ($M=-0.25$, $SE=0.06$, $p=0.017$) was found for knee power (Table 1). These results suggest that the PAD-D group has more differences than PAD-NC from healthy controls during pain-free ambulation. The difference in kinetic variables between control and PAD groups are in agreement with previous literature reported by our lab [4, 5].

CONCLUSIONS

Lack of significant group effects between PAD-NC and PAD-D indicates that the mechanisms driving gait deficiencies in patients with PAD are larger than the addition of diabetes on biomechanical variables during locomotion. Significant differences in ankle power generation, hip flexor moment, and knee power between control and PAD groups at baseline in addition to our previous work that found baseline gait deficits prior to the onset of pain further support the idea that gait problems are the results of a known myopathy in these patients. Future research should determine the contribution of these muscular abnormalities to gait alterations and investigate whether improvements in muscular function from treating PAD lead to successive improvements in gait in these patients.

REFERENCES

1. American Heart Association. *About PAD*, 2014.
2. Marso S, et al. *J American College of Cardiology* **47**, 921-929, 2006.
3. Jude EB. *Diabetes Care* **24**, 1433-1437, 2001.
4. Wurdeman SR, et al. *J Gait and Post* **36**, 506-509, 2012.
5. Koutakis BS, et al. *J Vasc Surg* **52**, 340-7, 2010.

ACKNOWLEDGEMENTS

Funding by NIH (R01AG034995 and P20GM109090), VA RR&D (1I01RX000604) and NASA Nebraska Space Grant.

Table 1: Group means and standard deviations for all dependent variables

Groups	PAD		Diabetes		Control
	Pain Free	Pain	Pain Free	Pain	Pain Free
Stride Time (m/s)	1.19 ± 0.08	1.17 ± 0.08	1.15 ± 0.11	1.17 ± 0.11	1.15 ± 0.08
Stride Length (m)	1.36 ± 0.18	1.32 ± 0.18	1.33 ± 0.14	1.31 ± 0.18	1.44 ± 0.09
Step Width (m)	0.10 ± 0.03	0.09 ± 0.03	0.09 ± 0.03	0.10 ± 0.03	0.09 ± 0.03
Ankle Plantar Flexor Moment (N*m/kg)	1.30 ± 0.20	1.30 ± 0.21	1.31 ± 0.17	1.20 ± 0.14	1.43 ± 0.14
Ankle Power Generation (W/kg)	2.03 ± 0.41	1.84 ± 0.45	1.96 ± 0.58	1.67 ± 0.56	2.59 ± 0.45
Knee Extensor Moment (N*m/kg)	0.48 ± 0.31	0.47 ± 0.30	0.48 ± 0.48	0.56 ± 0.38	0.78 ± 0.23
Knee Power (W/kg)	-0.29 ± 0.28	-0.26 ± 0.27	-0.58 ± 0.41	-0.49 ± 0.35	-0.45 ± 0.16
Hip Flexor Moment (N*m/kg)	-0.74 ± 0.24	-0.65 ± 0.55	-0.73 ± 0.27	-0.72 ± 0.25	-0.93 ± 0.19
Hip Power Generation (W/kg)	0.58 ± 0.18	0.56 ± 0.30	0.66 ± 0.27	0.58 ± 0.17	0.57 ± 0.18

MUSCLE FUNCTION DIFFERENCES BETWEEN YOUNG AND OLD ADULTS DURING GAIT

¹ Sarah A. Schloemer, ² Julie A. Thompson, ² Amy Silder, ³ Darryl G. Thelen, ¹ Robert A. Siston

¹ The Ohio State University, Columbus, OH, USA; ² Stanford University, Stanford, CA, USA;

³ University of Wisconsin-Madison, Madison, WI, USA

email: schloemer.7@osu.edu

INTRODUCTION

By 2030 there are expected to be over 71 million Americans (19.6% of the population) over age 65 [1], likely resulting in an increased prevalence of chronic diseases, such as coronary heart disease, stroke, and type 2 diabetes. Although walking is the most accessible form of physical activity that can lower the risk of such diseases, 25% of adults over age 55 have difficulty walking one-quarter of one mile [2].

Previous studies have analyzed walking by evaluating muscle function during gait [3-5] (how individual muscles support, brake and propel the body's center of mass (COM)). Only one study has assessed muscle function during gait in healthy older adults rather than young adults [6]. However, their findings may not be representative of all older adults because the walking speed of the older subjects was 1.42 m/s, which is faster than what is typically reported [7].

Older adults walk with altered kinematic and kinetic patterns compared to young adults, even when walking speed is similar [7], which may also suggest altered muscle function in older adults during gait. Thus, the purpose of this study was to determine muscle function during gait in a healthy older adult population and contrast muscle function of healthy older adults with that of a young adult population.

METHODS

Kinematic, kinetic, and electromyography data of the gait of healthy older adults were collected at the University of Wisconsin-Madison as previously described [7]. For this study, a subset of ten healthy older adults (3M, 7F; Age: 73.9 ± 5.3 years; Height: 1.67 ± 0.10 m; Mass: 64.5 ± 10.2 kg) walking at a self-selected speed (1.31 ± 0.11 m/s) was analyzed, based on the suitability of the available data of each subject for simulation analyses.

OpenSim 3.2 [8] was used to generate simulations of one gait cycle for each subject. A generic musculoskeletal model with 27 degrees-of-freedom and 94 musculotendon actuators [9] was scaled to match the anthropometry of the individual subjects. Joint angle trajectories were determined using inverse kinematics [5]. A residual reduction algorithm [8] adjusted model mass properties and joint kinematics slightly to reduce dynamic inconsistency between the ground reaction forces and body segment accelerations. A static optimization (SO) with an objective function that minimized the sum of squared muscle activations [10] was used to estimate muscle activations and forces in all lower extremity muscles. SO muscle activations were compared to experimental EMG to ensure consistency between the simulated and experimental muscle activation patterns. The instantaneous potential for acceleration (IPA) was calculated to determine the potential of individual muscles to contribute to support and progression of the COM over the gait cycle [5]. To determine individual muscle contributions to support, braking, and propulsion, muscle forces estimated by SO were multiplied by the IPA of each muscle for each subject.

Older adult muscle contributions to support and progression were compared to those of young adults walking at a self-selected speed (1.32 ± 0.13 m/s) from previous work performed at Ohio State [5].

RESULTS AND DISCUSSION

Healthy older and young adults use similar muscles to support (Figure 1), brake and propel (Figure 2) their COM during gait. However, older adults use each muscle to a different degree than young adults. To support their body during the first half of stance, both older adults and young adults primarily use their vasti (VAS) and tibialis anterior (TA). In addition to the vasti, older adults use gluteus medius (GMED) and gluteus maximus (GMAX) for support. Young

adults primarily use their TA during weight acceptance and their VAS and soleus (SOL) during the rest of early stance. GMED and GMAX also contribute to support during early stance in young adults, but to a lesser degree than observed in older adults. In late stance, SOL provides a majority of the support in older adults while young adults are primarily supported by gastrocnemius (GAS). VAS contributes to support during late stance in young, but not older, adults.

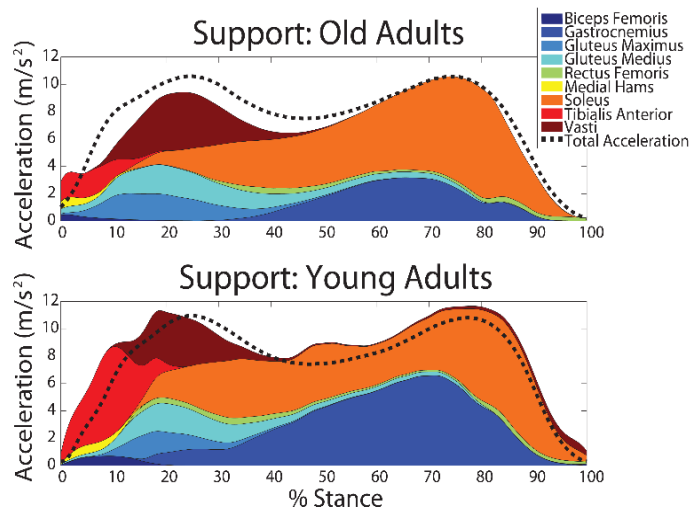


Figure 1: Area plots of muscle contributions to positive support during stance in old and young adults.

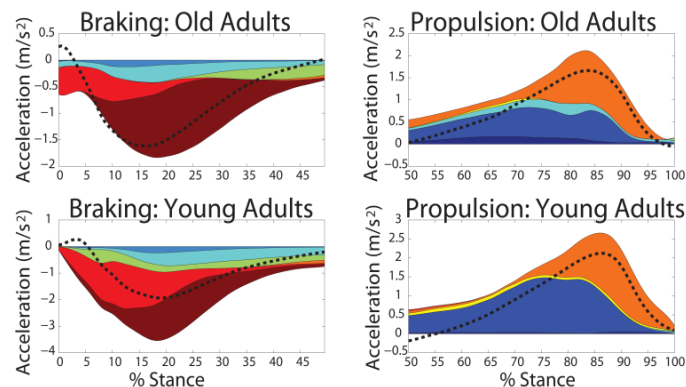


Figure 2: Area plots of muscle contributions to braking and propulsion during stance in old and young adults.

To slow the COM during weight acceptance, the TA and VAS primarily contribute to braking in both groups. However, GMED and GMAX contribute more to braking in older adults, while the rectus femoris provides braking in young adults. To propel the COM, young adults use GAS more than older adults. In contrast, older adults rely more on SOL, biceps femoris (BF) and GMED for propulsion.

CONCLUSIONS

The greater use of muscles about the hip (GMED, GMAX, and BF) by older adults reflects a distal to proximal change in neuromuscular control observed previously [11]. These differences in muscle contributions to COM acceleration between the older and young adults may be due to several factors. Although kinematic differences between age groups have been observed in previous studies [6, 7], this finding is not consistent throughout the literature. In this study, although both groups walked at a similar speed, the older adults walked with a more extended hip, greater knee flexion during stance, and greater plantar flexion at toe off compared to the young adults. Kinematic differences could affect muscle moment arms ($[R]$), a muscle's location on its force-length-velocity curve and thus its force (f), and the orientation and inertial properties of the body segments (the mass matrix: $[M]^{-1}$), which together determine muscle contributions to acceleration (\ddot{q}) [3]:

$$\ddot{q} = [M]^{-1} * [R]f$$

However, age-related changes in muscle-tendon parameters, which could affect muscle forces and moment arms, were not modeled in this study. Future studies should examine the effects of age-related changes to neuromuscular properties on muscle function during gait. Finally, the findings of this study suggest a need to better understand the interplay between neuromuscular control, kinematics, and muscle function during gait in older adults.

REFERENCES

1. Wan H, et al. *Current Population Reports*, 2005, 23-209, 2005.
2. Schoenborn CA and Heyman KM. *National Health Statistics Reports*, 2009.
3. Neptune RR, et al. *J Biomech* **34**, 1387-98, 2001.
4. Liu MQ, et al. *J Biomech* **39**, 2623-30, 2006.
5. Thompson JA, et al. *J Biomech* **46**, 2165-72, 2013.
6. Lim YP, et al. *Gait Posture* **38**, 253-9, 2013.
7. Silder A, et al. *J Biomech* **41**, 1520-27, 2008.
8. Delp SL, et al. *IEEE Trans Biomed Eng* **54**, 1940-50, 2007.
9. Arnold EM, et al. *Ann Biomed Eng* **38**, 269-79, 2010.
10. Crowninshield RD and Brand RA. *J Biomech* **14**, 793-801, 1981.
11. Devita P and Hortobagyi T. *J Appl Phys* **88**, 1804-11, 2000.

A NEW METHOD FOR IDENTIFYING TOE-OFF EVENT RUNNING ON A TREADMILL USING KINEMATIC DATA

^{1,2}Rhiannon M. Seneli, ^{2,3}Robin L. Pomeroy, and ²Stephen C. Cobb

¹ St. Ambrose University, Davenport, IA, USA

² University of Wisconsin-Milwaukee, Milwaukee, WI, USA

³Shiner's Hospitals for Children-Northern California, Sacramento, CA, USA

e-mail: senelirhiannonm@sau.edu

INTRODUCTION

Many running analysis studies are conducted on a runway with a force plate to identify stance phase events. Although running on a treadmill offers the opportunity to evaluate consecutive steps during an uninterrupted run; in the absence of an instrumented treadmill the stance events must be identified using kinematic data. Therefore, several researchers have developed methods for identifying stance phase events of running on a treadmill using kinematic data [1-3]. Several of the algorithms have been shown accurately identify initial contact, however, accurately identifying toe-off has proven to be more challenging. Therefore, the purpose of this study was to investigate a new kinematic method for identifying toe-off during overground and treadmill running using multi-segment foot model data.

METHODS

Twelve runners (≥ 10 miles/week, 26.3 ± 4.85 years) volunteered for the study. Six participants conducted overground running trials on a 25 m platform with a force plate (1000 Hz) and six ran on a non-instrumented treadmill. Each participant was equipped with 6.4 mm retroreflective markers identifying the leg and six foot segments: calcaneus, navicular, first and second metatarsal, hallux, fourth and fifth metatarsal, and cuboid. Three-dimensional positions of markers were captured at 200 Hz with a 10-camera Eagle system.

Three different kinematic methods were used to determine toe-off. The new method identified the toe-off event as the maximum MTP joint extension angle after initial contact (SagM). In addition to the new method, the toe-off event was also identified

using the minimum vertical position of the toe tip (VTOE) proposed by Maiwald, et al. [2]. The third method proposed by De Witt [1] utilizes the local maximum of the vertical acceleration of the toe tip after initial contact and then linearly interpolates the jerk of the toe tip to determine the time at which jerk is equal to zero (ATOE).

For the overground methods, five successful trials of running at 4.0 ($\pm 10\%$) m/s were evaluated. Determinations of the toe-off event using the kinematic methods were compared to identification of the event using a force plate (10 N threshold).

For treadmill methods, subjects ran on a treadmill at 3.3 m/s. Ten seconds of running data were captured. Five consecutive steps during the 10 s period were then used to analyze toe-off timing. Because the treadmill was not instrumented, one corner of the treadmill was positioned on the force plate embedded in the runway. For each participant a ground reaction force baseline and toe-off threshold level was determined. The toe-off events using the kinematic methods were then compared to identification of the event using the force plate method.

All three kinematic methods were then compared to the ground reaction force data methods for each trial and the difference in frames was recorded. The differences were then averaged for each subject's five trials and then mean and standard deviations were recorded for the group (overground and treadmill). Positive frame differences indicated that the kinematic method identified an earlier toe-off while negative numbers identified a later toe-off when compared to ground reaction force. Root

mean square differences (RMS) were then calculated to assess error.

RESULTS AND DISCUSSION

For both overground and treadmill running, the SagM method was the most accurate with a frame error that corresponded to 0.007 s and -0.006 s respectively (Table 1). Small RMS values also indicate that this level of accuracy was consistent for all subjects in each group (Table 2). The use of VTOE was moderately accurate for overground running (-0.04 s, RMS=0.04 s), but not for treadmill running (0.22 s, RMS=0.22 s) (Table 1 & 2). The ATOE also had moderately accurate results for both the overground (-0.03 s, RMS=0.03 s) and treadmill running (-0.07 s, RMS=0.07 s) (Table 1 & 2). The results from the previously published ATOE method is similar to results found by De Witt [1] which reported a difference in contact time of approximately 0.02-0.05 s when using the ATOE toe-off prediction. However, both overground and treadmill results when using the VTOE method were much higher than reported by Maiwald, et al. [2] with overground running.

Although, the maximal MTP extension method provided the most accurate estimate for the toe-off event during running overground and on a treadmill, a disadvantage of the method is that it requires a foot model that defines a first MTP joint/complex. The other methods, VTOE and ATOE, do not

require the additional joint/complex, however, they do not appear to be as accurate and VTOE does not seem adequate for estimating toe-off with treadmill running. One limitation of this study was comparing treadmill running toe-off event via kinematic methods to the ground reaction force data of the treadmill on a force plate rather than the runner. However, error between the ground reaction force and kinematic methods were similar for overground and treadmill running, suggesting that the ground reaction force data from the treadmill on the force plate was an adequate measure.

CONCLUSIONS

Various kinematic methods for determining toe-off during running gait have been developed and found to have varying levels of accuracy. For studies using a multi-segment foot model that identifies a first metatarsophalangeal joint/complex, using maximal extension angle may provide a very accurate option for identifying toe-off when running overground and on a treadmill.

REFERENCES

1. De Witt JK. *J Biomech* **43**, 3067-3069, 2010.
2. Maiwald C, et al. *Footwear Science* **1**, 111-118, 2009.
3. Zeni JA, et al. *Gait Posture* **27**, 710-714, 2008.

Table 1: Mean \pm SD frame error (200 Hz) using SagM, VTOE, and ATOE methods compared to GRF.

	SagM	VTOE	ATOE
Overground	1.31 \pm 1.86	-8.69 \pm 2.57	-5.09 \pm 0.39
Treadmill	-1.19 \pm 1.21	44.5 \pm 2.15	-13.2 \pm 7.07

Table 2: Mean \pm SD RMS frame error (200 Hz) using SagM, VTOE, and ATOE methods compared to GRF.

	SagM	VTOE	ATOE
Overground	2.09 \pm 0.84	8.80 \pm 2.51	5.49 \pm 0.97
Treadmill	1.81 \pm 1.05	44.5 \pm 2.21	13.6 \pm 6.95

COMPARISON OF OVERGROUND, OUTDOOR RUNNING BETWEEN LIMB SALVAGE INDIVIDUALS AND PATIENTS WITH TRANSTIBIAL AMPUTATIONS: INITIAL FINDINGS

Katherine Sharp, Nancy Thesing, Brittney Mazzone, Tatiana Djafar, Trevor Kingsbury, Marilynn Wyatt

Naval Medical Center San Diego, San Diego, CA, USA
email: katherine.sharp.ctr@med.navy.mil

INTRODUCTION

Preparing a traumatically injured service member for return to high-level functional activities is arguably important to promote wellness and improve quality of life. Patients incorporate recreational activities, such as running, into their daily lives, driving the need for more research on the topic. While many studies have been conducted utilizing treadmills, previous research has found significant differences between overground and treadmill running [1]. Due to the disparities between the two, the focus of this effort is on overground running, specifically a comparison between the running biomechanics of patients wearing the Intrepid Dynamic Exoskeletal Orthosis (IDEO) and patients with unilateral, transtibial amputations (TTA). This current work presents initial findings in regard to power, work, and mechanical efficiency calculated from data collected on an outdoor, overground motion capture system.

METHODS

Eight patients (ages 28 ± 6 yrs; height 1.8 ± 0.1 m; weight 89.7 ± 12.9 kg), who had been previously cleared for high-level functional activity by their providers, were studied. Five of the eight patients had undergone limb salvage procedures and wore the IDEO while running. The remaining three were TTA patients using the Össur® Flex-Run™ prostheses.

Kinematic and kinetic data were collected outdoors on the straightaway of a 100m track using 12 Raptor-E infrared cameras (Motion Analysis Corp., Santa Rosa, CA, USA). Frontal and sagittal high-speed videos (Nikon Corp., Tokyo, Japan) were taken for reference purposes. Four portable Kistler force plates (Kistler Group, Winterthur,

Switzerland) were embedded into a portable walkway so they were flush with the running surface. Analog data were sampled at 1800Hz and a fourth order Butterworth filter with a cut-off frequency of 30Hz was applied. After suiting a patients' lower body with 34-reflective markers on specific anatomical landmarks, they were asked to repeatedly pass through a 30m capture volume at their self-selected jogging speed. For IDEO patients, shank clusters were placed on the lateral portion of the proximal cuff of the orthosis. On the affected limb of TTA patients, shank clusters were placed on the lateral portion of the prosthetic socket, and the ankle joint was defined as the apex of the curve on the running prosthesis. Testing ended with successful collection of a minimum of three clean force plate hits per leg and at least six full gait cycles per leg. Kinematic, kinetic, and temporal-spatial data were processed using Visual 3D software (C-Motion Inc., Germantown, MD, USA). Power, work, and mechanical efficiency were calculated using the unified deformable (UD) segment model [2].

RESULTS AND DISCUSSION

Descriptive statistics on initial results can be found in Table 1. Initial results indicate differences between the affected and unaffected limbs of the observed IDEO users. The affected limb generated less positive work and less maximum power compared to the unaffected limb. In this same group, the affected limb was less mechanically efficient than the unaffected limb. There were no large differences in minimum power or negative work between limbs for patients running in the IDEO. Differences between the affected and unaffected limbs of TTA patients were minimal for all UD segment model calculations.

When comparing across groups, initial results also indicated differences. The affected limb of IDEO patients produced less positive work and reduced mechanical efficiency compared to the affected limb of TTA patients. Figure 1 demonstrates how the peak minimum and maximum powers of the affected limbs in each group differ in timing and magnitude with IDEO patients displaying diminished peaks that occur later in stance. Conversely, the power absorption and power generation of the unaffected limb for both patient groups follows a similar pattern. TTA patients within this particular sample appear to be more dynamic runners because they display a more equal distribution of absorption and generation of power compared to IDEO patients.

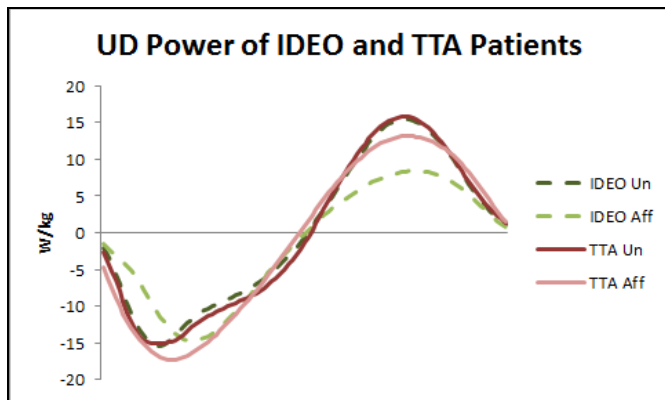


Figure 1: UD power of each limb (Un = unaffected, Aff = affected) presented by IDEO and TTA patients over stance phase of the gait cycle while running.

The main limitation of this initial study is an insufficient sample size. A post-hoc power analysis calculation determined that a sample size of 12 (six patients per group) is necessary to achieve 80%

power. Therefore, the primary immediate goal is to study additional IDEO users and patients with amputation in order to determine if significant differences exist. Future work will also look at kinematics and kinetics of these two patient populations while running.

Presented here are initial findings of running data collected on IDEO and TTA patients in an overground, outdoor environment, the first of its kind for the Navy. Assisting in the transition of our wounded warriors back to high levels of functional activity and increasing their quality of life is a priority. Hopefully, by equalizing the efficiency ratio between affected and unaffected limbs, future overuse injuries and/or injuries due to poor mechanics can be avoided.

REFERENCES

1. Riley PO, et al. *Med Sci Sports Exerc* **40**, 1093-1100, 2008.
2. Takahashi KZ, et al. *J Biomech* **45**, 2662-2667. 2012.

ACKNOWLEDGMENTS

Project was supported by Navy Bureau of Medicine and Surgery, Wounded, Ill, and Injured Program (W239).

DISCLOSURE STATEMENT

All authors have no conflicts of interest to disclose. The views expressed in the abstract do not necessarily reflect those of the Department of the Navy, Department of Defense or U.S. Government.

Table 1: Descriptive statistics for affected and unaffected limbs of IDEO and TTA patients.

		Max UD Power (W/kg)	Min UD Power (W/kg)	Positive Work (N·m)	Negative Work (N·m)	Mechanical Efficiency
IDEO	Affected	8.64±3.43	-15.14±4.01	0.48±0.19	-0.81±0.12	0.63±0.17
	Unaffected	16.20±2.52	-16.38±4.96	0.98±0.11	-0.91±0.23	1.02±0.12
TTA	Affected	13.30±1.04	-17.37±1.48	0.85±0.05	-0.99±0.18	0.91±0.14
	Unaffected	15.87±2.70	-17.57±4.16	0.94±0.19	-1.05±0.01	0.86±0.12

LOWER LIMB TRAUMA IMPAIRS LATERAL WALKING TRANSITIONS IN A VIRTUAL OBSTACLE COURSE

^{1,2} Riley C. Sheehan, ³ Jonathan H. Rylander, ² Jason M. Wilken, and ¹ Jonathan B. Dingwell

¹ The University of Texas at Austin, Austin, TX, USA

² Military Performance Lab, JBSA Ft. Sam Houston, TX, USA

³ Baylor University, Waco, TX, USA

email: rileycsheehan@austin.utexas.edu, web: <http://www.edb.utexas.edu/khe/nbl/>

INTRODUCTION

Lower limb trauma (LLT) leads to significant locomotor impairments [1]. Lateral movements are especially difficult for these individuals [2-3]. Rapid lateral movements are a common occurrence in everyday locomotion, from navigating a crowded sidewalk to avoiding other shoppers at the grocery store. Yet, these specific movements are under-trained and under-researched in clinical populations. Thus, we determined how functional deficits due to LLT affected lateral walking transitions using a virtual reality obstacle course. We hypothesized that individuals with greater functional deficits would require greater time to execute the transitions and would exhibit less smooth transition trajectories.

METHODS

Two able-bodied controls (AB) and 7 individuals with varying levels of LLT (including limb salvage, transtibial amputation, knee disarticulation, and transfemoral amputation) participated. The protocol consisted of a functional assessment and navigating a virtual obstacle course in the Computer Assisted Rehabilitation Environment (Fig. 1A-B). We used the four square step test as a clinically relevant measure of movement function [4]. The obstacle course consisted of the participant walking at 0.9 m/s while navigating an avatar through a series of arches in one of 4 lanes projected on the screen with the goal of hitting as few arches as possible (Fig. 1C). Though participants made 1 and 2 lane transitions, here we only analyzed the more challenging 2 lane transitions.

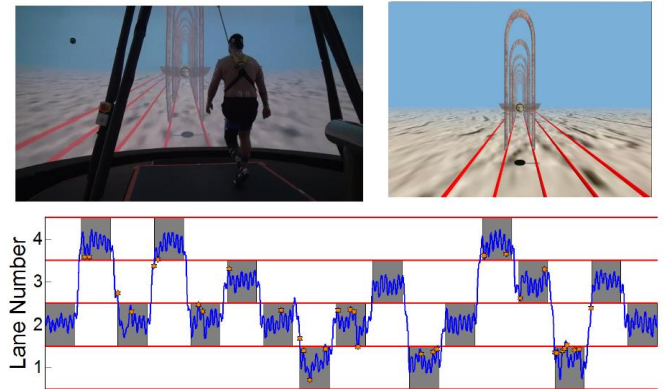


Figure 1: A) Patient walking in the CAREN, B) Example of obstacle course VR scene, C) Pelvis trajectory during typical obstacle course trial.

To measure the timing of the transitions, we calculated the amount of time from exiting the final arch of a set to crossing midway to the next arch set. We quantified the smoothness of the transitions as the sum of the squared jerk across the entire transition zone between arch sets.

To identify how functional abilities influenced lateral transitions, we correlated 4SST times with total number of arches hit, time to midpoint, and summed squared jerk. We tested what differentiated successful and unsuccessful transitions using paired t-tests. We also used paired t-tests to identify differences in transitions toward and away from the injured leg.

RESULTS AND DISCUSSION

As hypothesized, 4SST was positively correlated with total arch hits, time to midpoint, and summed squared jerk (Fig. 2). Thus, more impaired individuals, as measured by greater 4SST times, had a more difficult time completing the transitions.

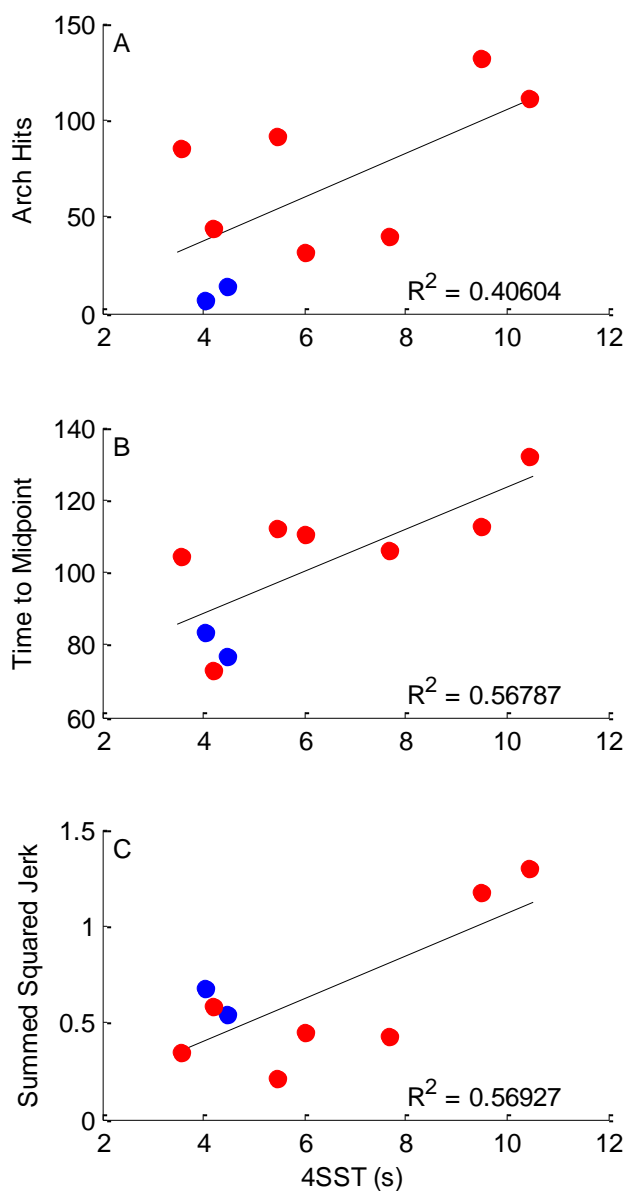


Figure 2: Correlations between 4SST and transition characteristics for AB (blue) and LLT (red) participants. Transition performance worsened with greater lower limb functional deficits.

The only significant difference between successful and unsuccessful transitions was the time to midpoint (Table 1). This suggests that, though more impaired individuals had less smooth trajectories, the ability to quickly move laterally was an important determinate of successful lateral transitions.

Contrary to our hypothesis, there were no significant differences between strategies when transitioning towards or away from the injured leg for the dependent measures quantified here (Table 1). This is likely due to the fact that lateral transitions place

large demands on both legs regardless of direction, with one producing a large lateral force to initiate the transition and the other producing a large, opposing force to slow the lateral movement and return to straight steady walking.

Table 1: Comparison of time to midpoint and summed square jerk for transition success and transition direction. Bold values indicate significant difference at $p < 0.05$.

	Successful	Unsuccessful	Uninjured	Injured
Time to Midpoint	99.44	128.00	111.65	102.95
Summed Squared Jerk	0.64	0.63	0.61	0.67

CONCLUSIONS

LLT significantly impairs the ability to make successful lateral walking transitions and alters the movement patterns used to make them. Due to the ubiquity of these types of movements in everyday life and the potential implications for maintaining stability (i.e., for fall risk), it is important to include lateral transitions in both clinical assessments and in rehabilitation programs. Based on the variables we investigated, the ability to quickly move laterally appears to be an important factor in successful lateral transitions. However, more detailed analyses of these movement patterns may yield additional insights into the strategies these patients use to achieve successful transitions.

REFERENCES

1. Docherty, et al. *Clin J Sports Med* **16**, 203-208, 2006.
2. O'Connor, et al. *J Neurophysiol* **102**, 1411, 2009.
3. McAndrew Young, et al. *J Biomech* **45**, 1053-1059, 2012.
4. Dite & Temple. *Arch Phys Med Rehabil* **83**, 1566-1571, 2002.

DISCLAIMER

The views expressed herein are those of the authors and do not reflect the official policy or position of Brooke Army Medical Center, U.S. Army Medical Department, U.S. Army Office of the Surgeon General, Department of the Army, Department of Defense or the U.S. Government

ATTENTION ALLOCATION ABILITY IN DUAL TASKS AMONG DIFFERENT AGES

Meng Liu, Jerod Post, Ka-Chun Siu

Clinical Movement Analysis (C-MOVA) Laboratory, Physical Therapy Education,
University of Nebraska Medical Center, Omaha, NE, USA
Email: mandy.liu@unmc.edu; web: <http://www.unmc.edu/alliedhealth/research/cmova/>

INTRODUCTION

A growing body of literature investigates the ability to multi-task and to allocate attention between tasks at different age groups [1-3] with a common goal of reducing fall incidences in older population. Increasing complexity of secondary task has more effects on the gait control for older than young group [2,3]. However, middle-aged subjects are not usually tested even though they are the major workforces of our modern society.

Therefore, this study investigated the ability of attention allocation between two tasks among different age groups. We hypothesized that (1) the ability to allocate attention between two tasks would be varied depending on age and complexity of secondary task; (2) dual task performance of middle age subjects would lie between that of young adults and older subjects.

METHODS

Twelve young (19-34), six middle-aged (35-64) and three older healthy subjects (65-80) were included in this study. Subjects crossed two obstacles and performed a secondary task while the gait information was recorded through a pressure-mapping walkway (ProtoKinetics, Havertown, PA). Gait velocity was computed using ProtoKinetics Movement Analysis Software. Secondary task included an easy (7 items) and a hard (20 items) symbol recall test. Number of Responses was recorded. Instructions of five different percentages of attention allocation conditions between walking and secondary task were randomly given to all subjects: 0-100%, 25-75%, 50-50%, 75-25% and 100-0% respectively on walking to secondary task (Conditions 1-5).

Dual Task Cost, $DTC = [(Dual\ task - single\ task) / single\ task]$ was calculated from gait velocity. The Attention Allocation Index (AAI) of gait was computed using $AAI = (P - S) / N$ where P, S and N represent the conditions with 100-0%, 0-100% and 50-50% of attention allocation respectively on walking to secondary task. The AAI of number of responses was computed as $AAI = (S - P) / N$. Three-way repeated measures ANOVA (3 age groups x 5 conditions x 2 tests) was conducted to compare all gait parameters, number of responses of secondary task and DTC of all measures.

RESULTS AND DISCUSSION

The ANOVA indicated that significant interactions between age groups and attention allocation conditions existed in gait velocity ($F=2.728$; $p=0.04$) and the DTC of gait velocity ($F=5.697$; $p=0.001$). Older subjects walked more slowly while focusing more on walking (Figure 1) and their DTC of gait velocity decreased across conditions 1-5. Middle-aged and young subjects did not show such trend in gait, but the dual-task performance of middle-aged group did lie between young and older groups. The reduction of gait performance could be due to the “stiffening strategies” of elder people [4]. When older participants were instructed to allocate more attention to walking, they strategized to slow down their gait. These results indicate that healthy older adults are capable to allocate their attention, but possibly with a paradigm shift using different attention allocation strategies. Such paradigm shift is further confirmed in Figure 2.

The AAI captured the ability to allocate attention between two tasks. Figure 2 illustrates the allocation attention paradigm shift from a positive relation in young adults to a negative relation in elderly. Most

young participants were able to speed up their gait when they allocated their attention to walking and were able to increase the number of responses when they allocated their attention to the secondary symbol recall test. However a paradigm shift begins in middle-age group that the ability of attention allocation becomes less profound. A reversed relation (paradigm shift) was shown in our small sample of older adults.

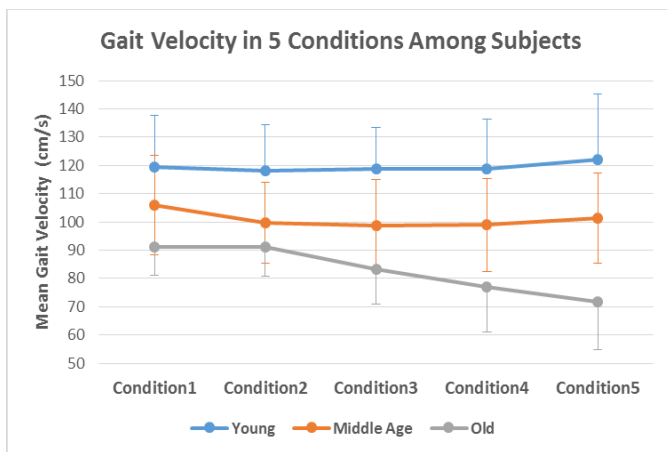


Figure 1. Gait velocity in 5 conditions among three different age groups.

Results of the number of responses showed that significant interactions exist between attention allocation conditions, age groups and tasks ($F=2.8$, $p=0.016$). Young subjects recalled the most numbers in both secondary tasks. Secondary task performance of middle-aged subjects was at the middle level among three groups (Figure 3). This supports our hypothesis and agrees with the result of previous study [5]. The number of responses was similar in older participants regardless of instruction (Figure 3). Older adults might prioritize their attention on walking to reduce the risk of falling [5].

We conclude that the ability of attention allocation varied at different ages. The dual task performance of middle-aged group was at the middle level among three groups. Although the attention allocation instructions (e.g. 25-75%) between two tasks were abstract or even ambiguous, all subjects were able to shift their attention based on instructions, with a paradigm shift of allocation attention ability starting at the middle-aged group. More healthy older subjects are currently studying to confirm our important interpretation.

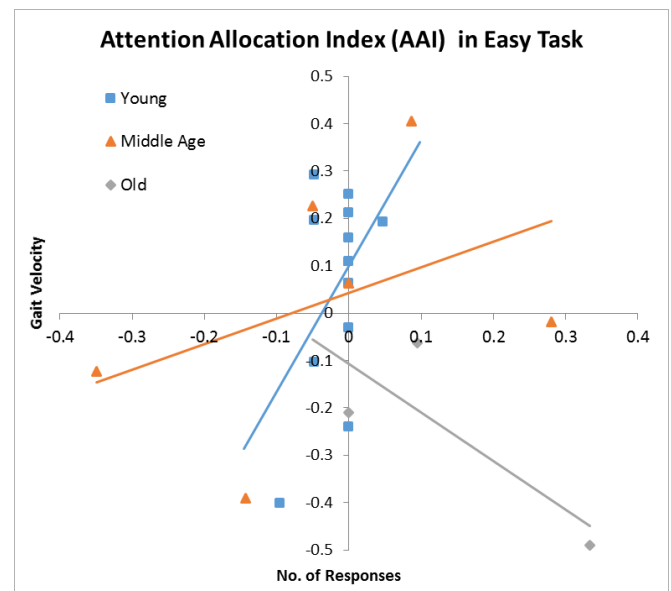


Figure 2. The AAI between gait velocity and number of responses among three different age groups in the easy symbol recall test.

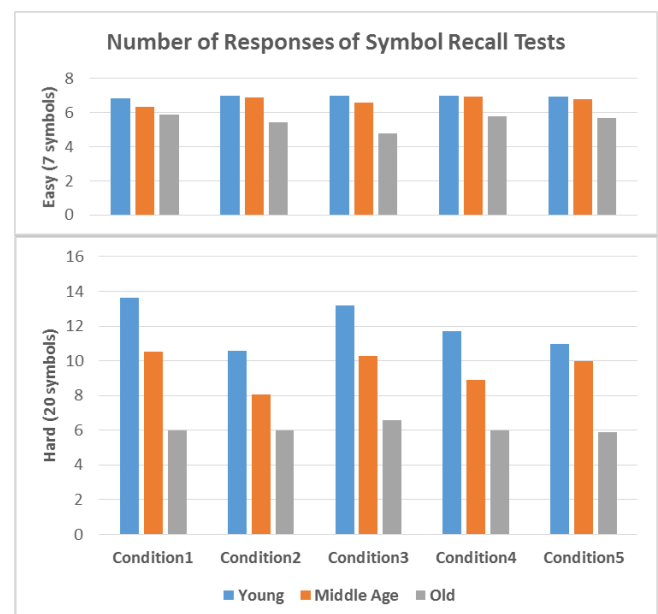


Figure 3. Results of secondary symbol recall tests among three age groups.

REFERENCES

1. Woollacott M, et al. *Gait & Posture* **16**, 1–14, 2002.
2. Kelly VE, et al. *Gait & Posture* **37**, 131–134, 2013.
3. Nijboer M, et al. *PLoS One* **8**(11), 2013.
4. Young WR, et al. *Gait & Posture* **41**, 7–12, 2015.
5. Terrier P, et al. *Gait & Posture* **41**, 170–174, 2015.

INFLUENCE OF HEEL TYPE ON STRIDE LENGTH

Lorraine Smallwood, Adam Jadgodinsky, Christopher Wilburn and Wendi Weimar
Auburn University, Auburn, AL, USA
email: weimarwh@auburn.edu

INTRODUCTION

The introduction of high heeled shoes in the 1600's started a major trend in women's fashion that continues to this day. A myriad of styles including stiletto heeled and wedge heeled shoes have entered the marketplace. Many studies have shown that kinematic changes occur in gait while wearing high heeled shoes. Esenyl et al., found that stride length decreased from 137 to 131 cm when wearing a 6 cm high heeled shoe [1]. Barkema et al., noted women had a significantly shorter stride length while wearing a 9 cm heel when compared to wearing 1 and 5 cm heels when walking at a self-selected pace [2]. When women wore high heels (5 cm) for at least 40 hours per week, Cronin et al., found step length to be significantly shorter than for those who did not habitually wear high heels [3]. These studies looked only at barefoot and stiletto style high heeled shoes. Wedge heeled shoes have been part of the fashion world for many years, but there is little research on the effects of wedge heeled shoes on gait. Walking barefoot while in plantar flexion mimics gait while wearing high heeled shoes, except there is no support for the foot that is normally found in shoes. The purpose of this study is to examine the effects of different styles of high heeled shoes as well as walking barefoot in plantar flexion on spatial gait parameters.

METHODS

Four healthy adult females (age $22.6 \text{ years} \pm 2.21$; height $1.62 \text{ m} \pm 0.04$; weight $63.28 \text{ kg} \pm 4.48$) who were comfortable wearing high heeled shoes and with no lower limb injuries for the past six months volunteered for this study. The participants walked on a 4.75 m instrumented walkway under four randomized conditions: barefoot, barefoot while in plantar flexion (tip toe), stiletto heeled shoes and wedge heeled shoes. Each condition involved three trials of walking at a self-selected pace. Stride

length was compared over the four conditions. Participants wore B-flexible by Bandolino BDINSPIRE stiletto heeled shoes and Forever Doris-22 wedge heeled shoes in the appropriate size. Both styles of shoes were marketed as 3" (7.62cm) heels and were similar in style. The only major difference between the shoes was the heel type. Kinematic data was sampled via Vicon T-Series T40S at 100 Hz, (Denver, Colorado, USA). Reflective markers were placed on the first metatarsophalangeal joint, heel, cuboid, navicular, medial and lateral malleolus, medial and lateral knee, and trochanter on each leg. Kinematic data were extracted from Vicon Nexus. Stride length was calculated through Excel 2013. Prior to statistical analysis stride length was normalized to body height.

RESULTS AND DISCUSSION

Results from the 1 (participant) x 4 (footwear condition) one-way ANOVA failed to reach statistical significance (barefoot to stiletto, $p=0.191$; barefoot to tiptoe, $p=0.206$; barefoot to wedge, $p=0.136$; stiletto to tiptoe, $p=0.956$; stiletto to wedge, $p=0.818$).

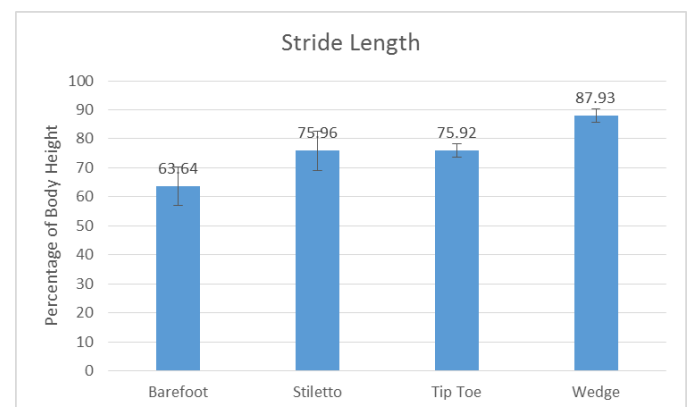


Figure 1. Stride length normalized to body height.

The purpose of this study was to determine if wearing high heeled shoes or walking barefoot while in plantar flexion would influence spatial gait parameters. It was hypothesized that stride length for barefoot gait would be greater than when shod or when walking while in plantar flexion (Figure 1). While not significantly different, stiletto heeled gait did yield a slightly longer stride length. This finding is in contrast to Esenyel et al., who found a decrease in stride length when walking with high heels [1]. Next, it was hypothesized that tip toe gait would result in shorter stride length than barefoot gait since the smaller area of foot contact with the floor leads to a smaller area for the body's base of support. The trend shows a larger stride length while walking in plantar flexion, however, this is not significantly different. Wearing wedge heeled shoes during gait was also hypothesized to result in shorter stride length than when walking barefoot. While not significantly different, the difference between barefoot and wedge heeled gait is the largest amongst all conditions. This leads to question if the additional surface area of the wedge heeled shoe's sole allows the individual to feel more secure in their gait and thus increase their stride length.

Stiletto heeled shoes have a heel surface area of 1 cm². Hence, the surface area of the shoe's sole that makes contact with the ground during gait is greatly reduced when compared to barefoot. It was hypothesized that tiptoe gait would produce a smaller stride length than walking on stiletto heels since walking on tiptoe resulted in even smaller amount of surface area of the foot in contact with the ground than while shod in stiletto heeled shoes. Stride length for both conditions were nearly identical (Figure 1). Since there is more surface area of the wedge heeled shoe's sole making contact with the ground than when wearing stiletto heeled shoes, it was hypothesized that stride length while walking in wedge heeled shoes would differ from walking in stiletto heeled shoes. While no significant differences were found between these conditions, an increase in stride length was seen when individuals shod with wedge heeled shoes were compared to stiletto heeled shoes. Continuing research with a larger population should clarify the trends seen in this pilot study.

REFERENCES

1. Esenyel M, et al. *J Am Pod Med Assoc* **93**, 27-32, 2003.
2. Barkema DD, et al. *Gait & Posture* **35**, 483-488, 2012.
3. Cronin NJ, et al. *J Appl Physiol*, **112**, 1054-1058, 2012.

MODELING THE LEAN RELEASE, LEAN RELEASE WITH WAIST PULLS AND WAIST PULL WHILE WALKING PERTURBATIONS WITH AN INVERTED PENDULUM

^{1,2} Magali Pierre, ³ Kodjo Moglo and ^{1,2} Cécile Smeesters

¹ Research Center on Aging, Sherbrooke QC, Canada

² Department of Mechanical Engineering, Université de Sherbrooke, Sherbrooke QC, Canada

³ Department of Mechanical Engineering, Royal Military College of Canada, Kingston ON, Canada

e-mail: Cecile.Smeesters@USherbrooke.ca web: <http://www.usherbrooke.ca/gmecanique>

INTRODUCTION

Moglo and Smeesters [1] compared large forward lean releases, lean releases with waist pulls and waist pulls while walking in both younger and older adults. Thiaux *et al.* [2] compared large forward lean releases and surface translations in younger adults. Both showed that the angular positions and velocities at reaction time of the threshold of balance recovery trials formed a perturbation threshold line separating falls from recoveries, regardless of the postural perturbation. The perturbation threshold line also declines with age, shifting down and to the left [1].

Thiaux *et al.* [3] showed that a two-dimensional thin rod inverted pendulum mounted on a horizontally moving skid could accurately model the outcome of lean releases and surface translations for younger adults: an unavoidable fall (above perturbation threshold line) or balance recovery (below line).

The purpose of this study was to determine if the inverted pendulum model by Thiaux *et al.* [3] could also simulate the lean releases with waist pulls and waist pulls while walking experiments by Moglo and Smeesters [1] for both younger and older adults.

METHODS

Experimental procedure: The maximum forward initial lean angle from which 10 younger (YA: 20-25yrs) and 10 older (OA: 62-73yrs) healthy adults (50% women) could be suddenly released and still recover balance was determined for 3 waist pull forces including zero [1]. The maximum forward waist pull force that the same participants could suddenly sustain and still recover balance was also determined for 2 walking velocities [1]. The initial

lean angle was increased from 5deg in 2.5deg increments while the waist pull force was decreased from ~600N in ~25N increments, until participants failed to recover balance twice at a given initial lean angle or succeeded in recovering balance at a given waist pull force, respectively. Balance recovery was successful if participants used no more than one step and less than 20% body weight was supported by the safety harness. Angular position (or lean angle), angular velocity, waist pull force and walking velocity were measured from onset of perturbation (OP) to reaction time (RT) using 3 force platforms, 3 load cells and 2 optoelectronic position sensors with 24 markers.

Inverted pendulum model: The maximum perturbations were simulated in Matlab using the inverted pendulum on a skid model by Thiaux *et al.* [3], immobilizing the skid by setting its mass $M=\infty$, pull force $F_2=0$ and coefficient of friction $\mu=0$. The inputs were the mass of the participant (m), height of the participant (h), gravity ($g=9.81\text{m/s}^2$), waist pull force (F_1) and ankle torque ($\tau=0$). The outputs were the angular position (θ), velocity (ω) and acceleration (α) from OP to RT. The initial conditions were θ_o and $\omega_o \approx 0$ for lean releases, and $\theta_o \approx 0$ and ω_o for waist pulls while walking.

Data analysis: The error between the experimental and theoretical angular positions ($\delta\theta$) and velocities ($\delta\omega$) was calculated from OP to RT for trials at the maximum lean angles or pull forces. Single sample t-tests then determined if the errors were different from zero, while repeated measures analyses of variance determined the effect of the postural perturbations on the errors. Linear regressions were also used to establish the relationships between the angular positions and velocities at reaction time for the threshold of balance recovery trials.

RESULTS AND DISCUSSION

For both YA and OA, all RMS errors and errors at RT were significantly different from zero ($p \leq 0.008$), except for $\delta\omega$ errors at RT for waist pulls while walking ($p \geq 0.190$). Nevertheless, errors were all 5% or less of the experimental perturbation threshold line intercepts for YA, except for $\delta\omega$ errors for lean releases with waist pulls which were still 13% or less (Table 1). All RMS errors and nearly all errors at RT were greater for lean releases with waist pulls compared to lean releases and waist pulls while walking ($p \leq 0.049$). Only $\delta\omega$ errors at RT for OA were not significant for postural perturbation effects ($p = 0.081$). The experimental ($\theta_{YA} = -0.250\omega_{YA} + 40.9$, $r^2 = 0.946$ and $\theta_{OA} = -0.202\omega_{OA} + 28.1$, $r^2 = 0.874$) and theoretical ($\theta_{YA} = -0.219\omega_{YA} + 35.7$, $r^2 = 0.885$ and $\theta_{OA} = -0.177\omega_{OA} + 24.1$, $r^2 = 0.732$) angular positions and velocities at RT for the maximum perturbations formed very similar disturbance threshold lines (Figure 1).

CONCLUSIONS

The inverted pendulum on a skid model by Thiaux *et al.* [3] can not only accurately model the outcome (fall or recovery) of lean releases and surface translations for YA, but can also accurately model the outcome of lean releases, lean releases with waist pulls (to a lesser extent) and waist pulls while walking for both YA and OA. This reduces the need for time consuming and dangerous experiments,

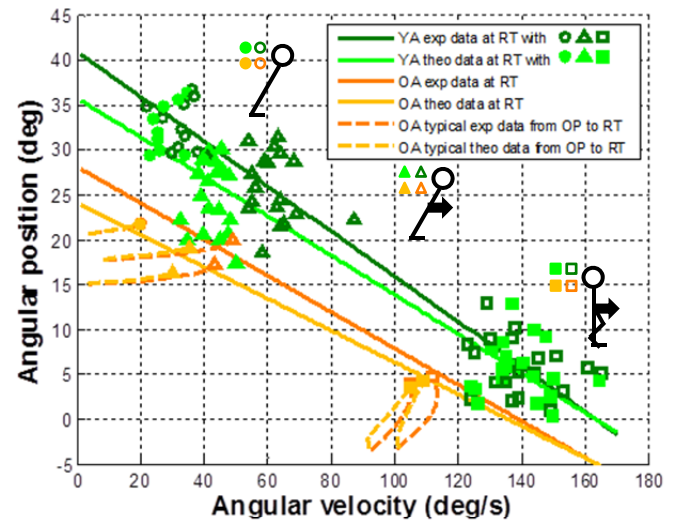


Figure 1: Perturbation threshold lines.

For clarity, typical data from OP to RT lines for YA and data at RT points for OA are not shown.

especially if large postural perturbations are used and avoiding a fall is not always possible.

REFERENCES

1. Moglo KE and Smeesters C. 30th Annu Meet Am Soc Biomech, Blacksburg VA, 2006.
2. Thiaux V, *et al.* 37th Annu Meet Am Soc Biomech, Omaha NE, 2013a.
3. Thiaux V, *et al.* 37th Annu Meet Am Soc Biomech, Omaha NE, 2013b.

ACKNOWLEDGEMENTS

Victorien Thiaux for knowledge transfer as well as NSERC grant 2014-06175 for financial support.

Table 1: Error (mean \pm SD) between the experimental and theoretical angular positions ($\delta\theta$) and velocities ($\delta\omega$)

Postural perturbation	RMS error from OP to RT				Error at RT			
	$\delta\theta$ (deg)		$\delta\omega$ (deg/s)		$\delta\theta$ (deg)		$\delta\omega$ (deg/s)	
	$\delta\theta/y_{intercept}$	$\delta\theta/x_{intercept}$	$\delta\omega/y_{intercept}$	$\delta\omega/x_{intercept}$	$\delta\theta/y_{intercept}$	$\delta\theta/x_{intercept}$	$\delta\omega/y_{intercept}$	$\delta\omega/x_{intercept}$
	YA	OA	YA	OA	YA	OA	YA	OA
Lean Release	0.1 \pm 0.1	0.1 \pm 0.1	4.2 \pm 1.4	3.2 \pm 2.2	0.3 \pm 0.2	0.3 \pm 0.2	4.3 \pm 4.0	3.5 \pm 2.9
(Waist Pull Force = 0N)	0 \pm 0%	0 \pm 0%	3 \pm 1%	2 \pm 1%	1 \pm 0%	1 \pm 1%	3 \pm 2%	2 \pm 2%
Lean Release with Waist Pull	0.6 \pm 0.3	0.6 \pm 0.3	15.3 \pm 6.2	14.7 \pm 5.2	1.2 \pm 0.5	1.3 \pm 0.6	14.7 \pm 10.0	12.5 \pm 11.2
(YA: 426N, OA: 373N)	1 \pm 1%	2 \pm 1%	9 \pm 4%	9 \pm 3%	3 \pm 1%	3 \pm 1%	9 \pm 6%	8 \pm 7%
Lean Release with Waist Pull	0.7 \pm 0.2	0.8 \pm 0.4	18.1 \pm 5.8	19.0 \pm 8.3	1.4 \pm 0.4	1.5 \pm 0.7	21.7 \pm 9.9	16.2 \pm 13.8
(YA: 604N, OA: 563N)	2 \pm 1%	2 \pm 1%	11 \pm 4%	12 \pm 5%	3 \pm 1%	4 \pm 2%	13 \pm 6%	10 \pm 8%
Waist Pull while Walking	0.3 \pm 0.1	0.3 \pm 0.2	7.0 \pm 3.3	8.7 \pm 3.9	0.6 \pm 0.3	0.6 \pm 0.5	1.6 \pm 7.6	5.8 \pm 13.6
(YA: 1.80m/s, OA: 1.31m/s)	1 \pm 0%	1 \pm 0%	4 \pm 2%	5 \pm 2%	1 \pm 1%	1 \pm 1%	1 \pm 5%	4 \pm 8%
Waist Pull while Walking	0.3 \pm 0.2	0.2 \pm 0.2	7.4 \pm 3.8	6.1 \pm 4.2	0.5 \pm 0.4	0.5 \pm 0.4	-1.3 \pm 8.8	3.3 \pm 7.3
(YA: 2.06m/s, OA: 1.54m/s)	1 \pm 0%	1 \pm 0%	5 \pm 2%	4 \pm 3%	1 \pm 1%	1 \pm 1%	-1 \pm 5%	2 \pm 4%
Pperturbation	<0.001	0.001	<0.001	<0.001	<0.001	0.004	<0.001	0.081

OP: Onset of Perturbation, RT: Reaction Time, YA: Younger Adult, OA: Older Adult. The x and y intercepts are from the experimental perturbation threshold line for YA from Moglo and Smeesters [1]. Significant perturbation effects are **bolded**.

The Sensitivity of Predicted Knee Contact Mechanics during Gait to Variations in Ligament Properties

¹Colin Smith, ¹Rachel Lenhart and ¹Darryl Thelen

¹ University of Wisconsin-Madison, Madison WI, USA
email: dgthelen@wisc.edu, web: <http://uwnmbi.engr.wisc.edu/>

INTRODUCTION

Subject-specific multibody models of the knee joint provide valuable insight into the mechanics of the healthy and pathologic knee during movement. However, the quality of the predictions of these models is directly dependent on the accuracy of the model parameters. While knee model geometries can be segmented from magnetic resonance (MR) images, other parameters such as ligament stiffness and reference strains must be estimated. As a result, the uncertainty in these ligament parameters can propagate into the predicted knee mechanics. The objective of this study was to use a probabilistic approach to evaluate the propagation of variations in ligament properties onto knee kinematics and cartilage contact pressures.

METHODS

A three body, 12 DOF knee model was developed from MR images of a healthy adult female (1.65 m, 61 kg). Fourteen ligaments were represented by bundles of nonlinear elastic springs, with wrapping surfaces included to prevent penetration of bony geometries. Articular cartilage surfaces were segmented from the MR images and represented by high resolution meshes. Cartilage contact pressures were calculated by detecting overlap between the articulating surfaces and using an elastic foundation model to determine pressure based on the depth of penetration. The knee model was integrated into an existing lower extremity musculoskeletal model [1], which included 43 muscles acting about the hip, knee and ankle joints. The predictive capacity of the model was validated by comparing simulated passive and active knee kinematics with *in vivo* 3D knee kinematics measured with dynamic MRI [2].

Whole body kinematics and ground reactions were recorded while the subject walked overground in a

motion analysis laboratory. At each frame of a gait cycle, an enhanced static optimization (ESO) routine [3] was used to calculate muscle forces, patellofemoral kinematics and secondary tibiofemoral kinematics that minimized a weighted sum of squared muscle activations while satisfying overall dynamic constraints. The constraints required that the muscle forces and internal knee loads (contact pressures, ligament forces) produced by the optimized knee kinematics generate the measured hip, knee (flexion) and ankle accelerations.

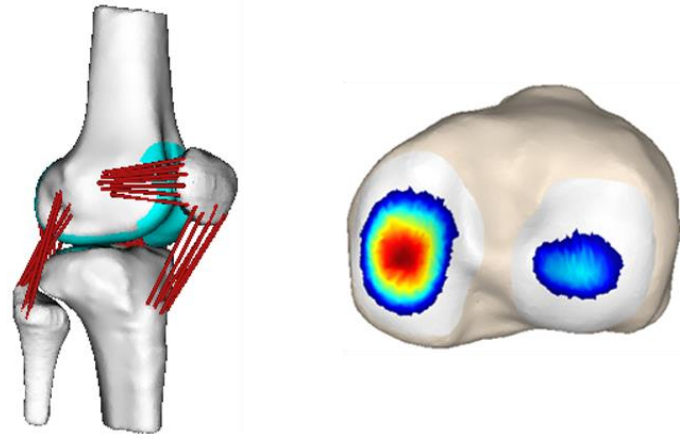


Figure 1: Multibody 12 degree of freedom knee model and representative pressure map

We performed a monte carlo analysis to evaluate the propagation of uncertainty in ligament stiffness and reference strain values into predicted joint mechanics. Nominal values were determined from previous models [4] and tuned to ensure predicted passive kinematics reproduced measured passive kinematics. In the probabilistic analysis, ligament stiffness and reference strains were represented by normal distributions centered at the nominal values with standard deviations of 30% of the mean and 0.2, respectively [5]. A total of 2000 simulations were performed using a high throughput computing grid using randomly selected values from the parameter distributions.

RESULTS AND DISCUSSION

The predicted tibiofemoral kinematics showed variability in each of the degrees of freedom. Internal-external rotation showed the most variability with the maximum standard deviation (5.6°) occurring during swing phase. The superior-inferior translation and medial-lateral translations showed similar variability to the anterior-posterior translation.

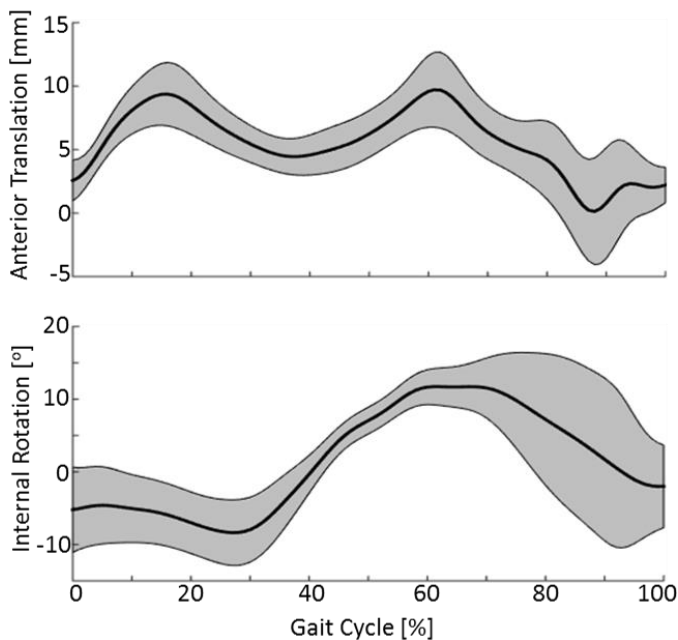


Figure 2: Anterior translation and internal rotation of the tibiofemoral joint during gait. The black line and shaded area represent the mean \pm 2 standard deviations of the monte carlo simulations.

Metrics of articular contact such as mean pressure and contact area also showed substantial variability. The mean pressure on the medial and lateral tibial plateaus had a maximum standard deviation of 0.52 MPa and 0.86 MPa, respectively. The medial and lateral contact areas showed maximum standard deviations of 45.9 mm^2 and 48.0 mm^2 .

Further analysis will reveal the individual ligaments which contribute the most to the variability in the predicted results. This will provide valuable insight into the function of specific ligaments during walking.

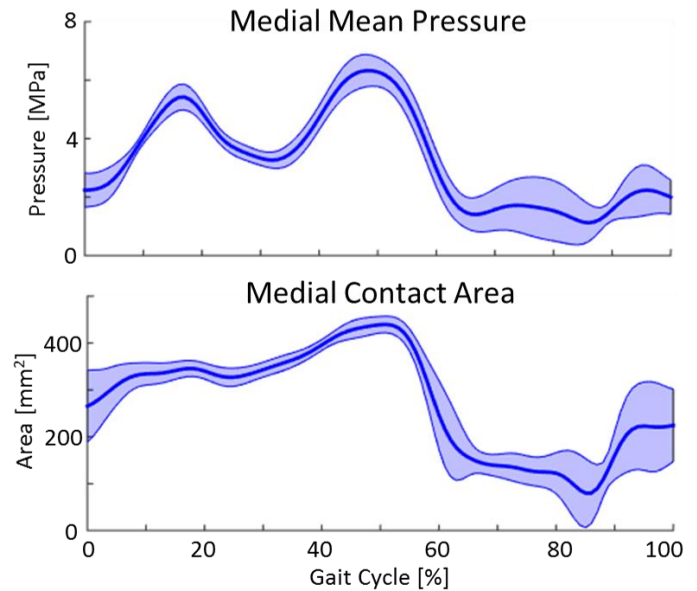


Figure 3: Mean pressure and contact area of the medial tibial plateau over a gait cycle. The blue line and shaded area represent the mean \pm 2 standard deviations of the monte carlo simulations.

CONCLUSIONS

The probabilistic analysis showed that variations in ligament stiffness and reference strains produce substantial variability in the predicted tibiofemoral kinematics and contact mechanics. This indicates that future work is required to accurately determine the values of the ligament parameters.

REFERENCES

1. Arnold, EM, et al. *Ann of Biomed Eng* **38**, 269-79, 2010.
2. Lenhart, RL, et al. *Ann of Biomed Eng* submitted, 2014.
3. Lenhart, RL, et al. *J Biomech* submitted, 2014
4. Blankevoort, L, et al. *J Biomech Eng* **113**, 263-269, 1991
5. Baldwin, MA, et al. *Comput Methods Biomech Biomed Engin* **12**, 651-659, 2009

ACKNOWLEDGEMENTS

NIH EB015410

Figures and tables may be incorporated within the document and must be referenced in the text (Fig. 1). Make sure to use contrasting colors and/or different “dash” types when selecting line styles.

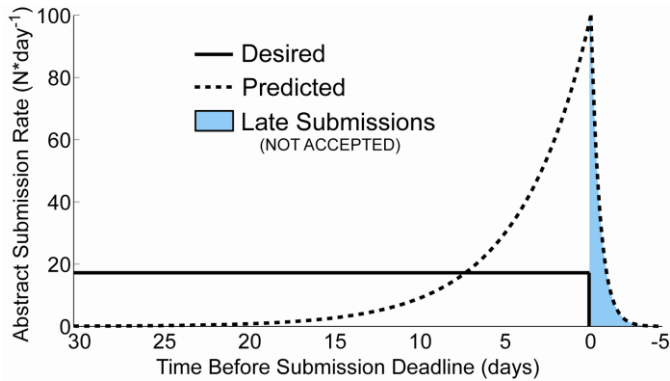


Figure 1: Ensure text is readable. Color can be used, and will display in the online version of the abstract.

Captions must be legible and placed below each Figure, and above each Table. Tables may extend across two columns when needed (Table 1). If your table and/or figure is two columns wide, it will probably be easier to format the abstract correctly if you put the column and/or figure at the end of the abstract. Insert Section Breaks and use “Format -> Columns” to control which parts of the text are in single column format. Note that the contact info for the meeting provided with the sample abstract does not put you in contact with a Technical Assistance expert. Problems with creating columns, converting to a PDF file, creating figures and/or tables, and other software glitches will not be resolved by communicating with the Program Chair.

Optimize the number of citations used in your abstract, referring only to the most relevant works. Reference citations within the text are to be made with numbers [1, 2]. References are to be formatted as illustrated at the end of this sample abstract. Place the journal or book title in italics, with volume numbers in bold [3].

General questions about the conference program should be addressed to:

Rick Neptune, PhD
ASB 2015 Program Chair

Questions regarding the meeting venue or from exhibitors/sponsors should be addressed to the meeting chair:

Ajit Chaudhari, PhD
ASB 2015 Meeting Chair
asb2015@osu.edu

CONCLUSIONS

Abstracts for the 39th ASB meeting must be submitted electronically via our website and received by March 15, 2015. Recall the old adage (slightly modified) that “Failure to plan on your part does not constitute an emergency on ASB’s part”. In the event that a submission is incomplete or received after the submission deadline, the abstract will not be reviewed and considered for the conference program.

At the time of submission, please indicate your preference for a podium, poster or thematic poster presentation. Thematic posters involve presenting a research poster, providing a short (3 min or less) summary of the research and participating in an active discussion among the audience participants. If we are unable to accommodate your preference, your abstract will still be considered for other presentation types. Also, if a student is the first author, please indicate this on the abstract submission page of the website.

REFERENCES

6. Sawicki GS. *Proceedings of NACOB’08*, Ann Arbor, MI, USA, 2008.
7. Gardner JG, et al. *J Biomech* **38**, 1861-1868, 2004.
8. Holzapfel GA. *Nonlinear Solid Mechanics*, John Wiley & Sons, Ltd., 2000.

ACKNOWLEDGEMENTS

Table 1: Tables may extend across both columns, and those should be included at the bottom of the abstract.

Joint Angle (deg)	Running Speed (m*s ⁻¹)					
	3	3.5	4	4.5	5	5.5
Knee Flexion	23.1 ± 2.3	27.2 ± 2.6	28.5 ± 3.3	31.3 ± 4.1	35.1 ± 2.8	38.7 ± 7.3
Hip Flexion	30.1 ± 2.7	33.2 ± 3.3	33.5 ± 1.9	35.9 ± 3.6	36.1 ± 4.5	39.2 ± 2.3

JOINT MOMENT PATTERNS DURING A FATIGUING RUN

Nathaniel I. Smith and Brian R. Umberger

University of Massachusetts, Amherst, MA, USA

email: nathanis@umass.edu, web: <http://www.umass.edu/locomotion>

INTRODUCTION

The vast majority of research on running biomechanics involves brief runs of moderate intensity, such that participants experience minimal fatigue. Because fatigue is an inevitable consequence of strenuous running, addressing its effects naturally leads to a more complete understanding of "real world" running scenarios. Previous work has found that when fatigued, runners use altered kinematics and experience reduced impact attenuation, increased metabolic cost and greater susceptibility to overuse injuries [e.g., 1-3]. In addition, the capacity of leg muscles to produce force is impaired after runs as short as twenty minutes [4]. Research in this area has thus far not addressed gait variables that lie functionally between muscle forces and kinematics.

A better understanding of the kinetic changes that underlie these fatigue effects could lead to improved training and rehabilitation protocols. As a first step toward achieving these goals, the current investigation aims to characterize changes in lower extremity joint moment profiles occurring over the course of an exhaustive run.

METHODS

Participants were eight recreational runners (four male, four female; 24.6 ± 5.8 years; 1.70 ± 0.10 m; 69.6 ± 15.1 kg; 42 ± 14 km/wk). All participants were habitual rearfoot strikers and were uninjured for at least three months prior to testing. All methods were approved by the university's Institutional Review Board.

In order to standardize the speed of the exhaustive run, participants' speed at lactate threshold was determined by means of a speed-based incremental treadmill test, conducted three to seven day prior to

the exhaustive run. Speed of lactate threshold, determined by two independent reviewers, was defined as the speed of the fastest stage prior to a sharp and sustained increase in blood lactate concentration.

Exhaustive runs were completed on the same force-instrumented treadmill used for the incremental tests (Bertec Corporation, Columbus, OH). The speed of the run was set such as to elicit 95% of the oxygen consumption recorded at lactate threshold. Three-dimensional (3-D) kinematics were recorded using a motion capture system while force data were measured using the instrumented treadmill. Marker trajectories and force data were recorded for ten seconds each minute, and perceived exertion (Borg scale) was reported by participants every two minutes throughout the test. Due to the varied durations of the exhaustive runs, trials coinciding with 20, 40, 60, 80 and 100% of the run duration were selected for analysis.

3-D joint angles and moments were calculated using Visual 3-D, and dependent variable values were calculated using custom-written Matlab software (The MathWorks, Natick, MA).

Statistical analysis was conducted using SAS software (SAS Institute Inc., Cary, NC). One-way analyses of variance were used to test for significant differences in variable values across percent of run duration. Trends in variables that showed significant change were described with linear or polynomial regression curves.

RESULTS AND DISCUSSION

Despite a significant increase in rate of perceived exertion ($p < 0.001$, 12.2 ± 0.6 at 20% vs. $19.1 \pm 0.8\%$ at 100%), no significant changes in joint moment or joint angle variables were seen between

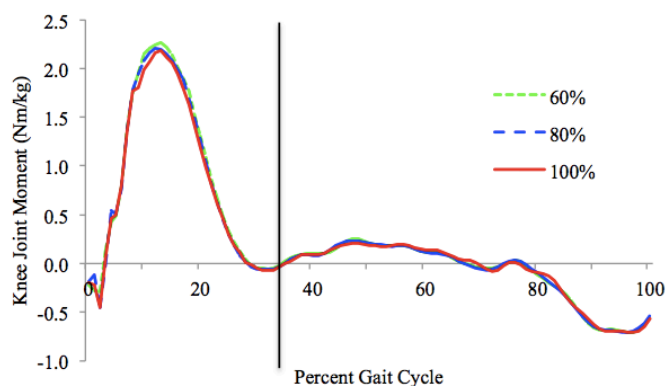


Figure 1: Group mean sagittal knee joint moments at 60, 80, and 100% of run duration. Vertical line indicates toe-off.

the beginning and end of the run. Figure 1 exemplifies the remarkable consistency in the joint moment profiles evaluated. Temporal variables indicated that participants maintained their stride length ($p = 0.79$) and stance time ($p = 0.56$). Frontal plane kinematics and kinetics were also relatively unaffected by fatigue, as participants used similar peak hip abductor moments ($p = 0.80$) to achieve similar peak adduction angles ($p = 0.13$). The standard deviation of gait variables within individual trials was evaluated as a means of detecting changes in variability accompanying fatigue, but these measures did not change significantly during the exhaustive run.

The changes in peak joint moments between the middle and end of the run for the two fastest runners (lactate threshold speeds of 4.30 and 4.57 m/s) and the two slowest runners (lactate thresholds at 3.27 and 3.21 m/s) are presented in Table 1. These groups demonstrated similar changes in peak moments during this period with the exception of the hip flexion moment. This difference could suggest that as their hip flexors fatigued, faster runners adjusted their patterns of muscle activation in order to reduce peak muscle force demands while maintaining the hip range of motion necessary to prepare the foot for ground contact. Alternatively, psychological differences between faster and slower runners could have resulted in higher levels of muscular fatigue before faster participants reached volitional exhaustion. Reductions in peak moments occurring non-uniformly across joints may imply

differences in the rates at which fatigue develops between muscle groups.

Table 1. Changes in selected peak joint moments occurring between 60% and 100% of run duration in the fastest and slowest participants.

	Fastest Runners	Slowest Runners
Peak Hip Flexion Moment	- 8.3%	+ 1.4%
Peak Hip Abduction Moment	+ 6.6%	+ 4.3%
Peak Knee Extension Moment	- 0.8%	- 0.8%
Peak Ankle Plantarflexor Moment	+ 0.5%	+ 1.3%

The duration and relative intensity of the exhaustive run utilized in the present study likely impaired the force-producing capacity of participants' leg extensor muscles [4]. The lack of change in the present results may imply that the muscle forces required to accomplish submaximal running gait are moderate enough to remain unaffected by mild muscular fatigue. Alternatively, net joint moments could be maintained while reducing individual muscle forces by altering patterns of co-contraction, which could be addressed in future studies using electromyography. Lastly, it should be acknowledged that motion capture during an exhaustive run introduces many factors which may have increased somatic stress and caused participants to end the test for reasons other than fatigue, including but not limited to the enforcement of a constant running speed and the hardness of the treadmill, itself.

REFERENCES

1. Derrick, TR, et al. *MSSE* **34**, 998-1002, 2002.
2. Xu, F & Montgomery, DL *IJSM* **16**, 309-15, 1995.
3. Clansey, AC, et al. *MSSE* **44**, 1917-23, 2012.
4. Skof, B & Strojnik, V *BJSM* **40**, 219-22, 2006.

ACKNOWLEDGEMENTS

The authors wish to acknowledge Dr. Julia Choi for the use of her instrumented treadmill.

Effects of Transcutaneous Electrical Nerve Stimulation on Gait Kinetics in Individuals with Experimentally Induced Knee Joint Pain

Seongjun Son, Hyunsoo Kim, Matthew K. Seeley, and J. Ty Hopkins

Brigham Young University, Provo, Utah, USA

Email: seongjunson@gmail.com

INTRODUCTION

Knee joint pain (KJP) is a very common problem in the United States. KJP alters motor function, muscle coordination, and gait mechanics. These alterations may contribute to the progression of structural knee joint disease [1]. Restoration of neuromuscular function and KJP relief is a primary goal for rehabilitative clinicians. While transcutaneous electrical nerve stimulation (TENS) mitigates motor function deficits, due to KJP, it is unclear how TENS might acutely affect ambulatory mechanics in the presence of KJP. The purpose of this study was to examine (i) the effects of experimental KJP on ankle, knee and hip frontal plane joint moments during walking, and (ii) the immediate effects of TENS on the aforementioned joint moments. We hypothesized that (i) experimental KJP would reduce ankle eversion, knee valgus, and hip abduction moments during loading response and push-off, and (ii) TENS treatment would mitigate these mechanical alterations effectively.

METHODS

Participants: Two groups of 30 asymptomatic volunteers participated in the study (10 men, 5 women per group). We randomly selected 15 participants from an initial 75 volunteers for the TENS group (Mean \pm SD; age = 24 ± 3 yrs, mass = 71 ± 12 kg, height = 178 ± 7 cm). For the placebo group, 15 participants were matched to the TENS group by gender, age, mass and height, selected from the remaining 60 volunteers (age = 23 ± 2 yrs, mass = 72 ± 14 kg, height = 177 ± 9 cm). The study was approved by the appropriate institutional review board, and informed consent was obtained prior to participation. **Experimental KJP Procedures:** Two groups of all 30 participants underwent 3 different experimental sessions (hypertonic, isotonic, control)

in a counterbalanced order, two days apart. Session order was blinded to investigators and subjects. A 20-gauge flexible catheter was inserted into the right infrapatellar fat pad, and a portable infusion pump infused a continuous saline solution flow of $0.154 \text{ mL} \cdot \text{min}^{-1}$ for 50 min (total = 7.7 mL). No infusion was administered during the control session. **Therapeutic Intervention:** A TENS protocol was set at a continuous asymmetric biphasic square-pulse wave with a pulse width of 120 μs and a pulse rate of 180 Hz. The treatment session lasted 20 min in a seated upright position. TENS treatment was given to all 15 participants in the TENS group, consistently across all 3 different experimental sessions. In order to blind placebo treatment, all 15 participants in the placebo group was told that an electrical stimulation had been set to sub-sensory level, and the indicator light was on during the placebo treatment. **Gait kinetics:** Synchronized high-speed video (240 Hz) and an instrumented treadmill (1200 Hz) were used to measure gait mechanics throughout the first five observed stance phases of walking at each time interval (baseline, infusion, treatment). **Statistical Analysis:** Functional analysis of variance (FANOVA) were used to evaluate mean differences between TENS and placebo groups over each time interval for joint moments. To perform the FANOVA, the mean curve is represented by polynomial functions, showing us the entire gait cycle, rather than identifying isolated one or two peak joint moments as required for traditional parametric analyses of variance (ANOVA) [2]. Pairwise comparison functions, with 95% confidence intervals were plotted to determine specific differences during the stance phase of gait. If 95% confidence intervals did not cross the zero line in red, statistical significant difference existed ($P < 0.05$; Fig. C and F).

RESULTS AND DISCUSSION

A TENS Group Frontal Knee Moment

B Placebo Group Frontal Knee Moment

C Knee Frontal Moment Group \times Treatment Interactions

D TENS Group Frontal Hip Moment

E Placebo Group Frontal Hip Moment

F Hip Frontal Moment Group \times Treatment Interactions

These findings show that experimental KJP acutely changes frontal knee and hip kinetics during gait. TENS treatment acutely and effectively mitigated the alterations, due to KJP, for frontal-plane knee and hip moments. Since it is difficult to induce chronic KJP, our novel experimental KJP model could allow us to evaluate neuromechanical gait adaptations to KJP. Experimental KJP caused by the hypertonic saline infusion leads to release of substance P, a substance that is released through the c-fiber pathways from sensory nerve terminals in the brain and spinal cord, which is commonly seen in musculoskeletal pain [3]. As we observed decreased knee valgus moment during painful walking, similar gait strategies were also reported in previous literature using patients with early stage of knee osteoarthritic pain [4]. These similar reducing moment gait strategies may result from the immediate gait adaptations to KJP through (i) an unloading strategy [5], (ii) muscle inhibition [5,6], and/or (iii) altered muscle coordination [6]. If altered motor strategies persist, it may increase the risk of changes in normal gait mechanics over the long-term, and possibly accelerate structural changes in knee articular cartilage [1], by shifting the normal load to a location of the knee that does not typically bear load [7]. The present results indicate that TENS treatment might work as a rehabilitation tool to control mechanical alterations due to KJP. Attempting to increase motor neuron excitability through TENS might promote gains in muscle force production and motor neuron activation, which in turn, help overcome deficits in knee and hip joint moment.

1. Segal NA, et al. *Osteoarthr Cartil* 18(6):769-775, 2010.
2. Andrade AG, et al. *J Appl Biomech* (2)30:348-352, 2014.
3. Arendt-Nielsen L, et al. *J Pain* 64:231-240, 1996.
4. Henriksen M, et al. *Arthritis Care Res* 62(4):501-509, 2010.
5. Seeley MK, et al. *J Athl Train* 48(3):337-345, 2013.
6. Hodges PW, et al. *Arthritis Rheum* 61(1):70-77, 2009.
7. Andriacchi TP, et al. *Ann Biomed Eng* 32:447-457, 2004.

DANCE ALTERS SUBJECTIVE AND OBJECTIVE BIOMECHANICAL GAIT AND BALANCE MEASURES IN PARKINSON'S DISEASE: A CASE STUDY

Kristen L. Sowalsky, Jill Sonke, Lori Altmann, and Chris J. Hass

The University of Florida, Gainesville, FL, USA

email: ksowalsky@hnp.ufl.edu

INTRODUCTION

Parkinson's disease (PD) is a progressive neuro-degenerative brain disorder leading to motor and non-motor deficits. Characterized by an overall paucity of movement, PD is classified as a hypokinetic disorder in which there are four hallmark motor signs; tremor, rigidity, bradykinesia, and postural instability. These impairments manifest into gait and balance disturbance which affect mobility and may ultimately lead to a decrease in quality of life [1]. Current treatments including pharmacological therapies, surgery, and physical therapy aim to alleviate symptoms and potentially slow the progression of the disease [2]. Dance training is a relatively new, yet increasingly popular therapy for people with PD [3, 4]. Aside from being an enjoyable activity, dance combines a number of factors already known to benefit those with PD; auditory cueing, aerobic exercise, strengthening exercise, stretching, and a supportive social community. A recent review of the literature demonstrates that dance has been shown to improve UPDRS motor scores, berg balance, gait speed, and quality of life in persons with PD [3]. It was our goal to add to this body of literature by investigating the effects of dance training on various objective and quantitative biomechanical parameters of balance and gait in addition to subjective measures. This case study is to be used as pilot data for a larger and more comprehensive study on the effects of dance therapy on gait, balance, and ultimately mobility in PD.

METHODS

The participant was a 66 year old male with a diagnosis of PD from a fellowship-trained movement disorders neurologist. He was diagnosed at the age of 53 with his symptoms predominantly

on the right side of his body. Intake forms and assessments included an IRB approved informed consent, medical history questionnaire, Activities-specific Balance Confidence Scale (ABC), Tinetti's Falls Efficacy Scale, Functional Gait Assessment, 6 Minute Walk test, and Timed Up and Go gait task. Balance testing was performed on a Bertec force plate for 3 conditions, 3 trials per condition at 360 Hz: 1) Eyes Open (120s), 2) Eyes Closed (20s), and 3) Narrow Stance (60s). Gait performance was captured using an 8 camera Vicon motion capture camera system. Spatiotemporal gait parameters were assessed bilaterally while walking over ground; forward, backward, and while counting (a dual-task activity). After testing, the participant completed a 16 week "Dance for Life" training intervention at the UF Center for Arts in Medicine. Dance training occurred in three 75-minute sessions per week for 16 weeks. Each session included a 15 minute seated warm-up, 15 minute barre segment, 5 minute break, 15 minute floor segment, 20 minute performance or social dance, and 5 minute cool-down. Upon completion of the 16 week dance intervention program, the participant was re-tested in all of the assessments and conditions described above. SPSS software program was used for statistical analysis.

RESULTS AND DISCUSSION

The results for the clinical assessments and gait task (Table 1) were mixed with an improvement in falls efficacy, 6 minute walk distance, and timed up and go speed. Significant differences were found between pre and post balance parameters (Table 2). Center of pressure path length, velocity, sway area, and approximate entropy increased for all balance conditions. As bradykinesia and reduced complexity of movement are associated with PD [5], the increase in the above balance measures may

plausibly be considered an improvement. Pre and post gait assessment (Table 3) revealed significant improvements in both spatial and temporal parameters for forward and backward walking. In the counting condition, a dual-task activity, there were mixed results.

CONCLUSIONS

This case study demonstrates the potential impact dance training may have on persons with PD. There were significant measureable changes in clinical assessments, balance measures, and gait parameters. Future research on a larger sample size is warranted.

REFERENCES

1. Hass CJ, et al. *PLoS One*, 7(8): e42337, 2012.
2. Ondo WG and Young RY, *American Academy of Neurology, Gait and Movement Disorders* 8, 2013.
3. Sharp K and Hewitt J. *Neuroscience and Biobehavioral Reviews*, 47:445-56, 2014.
4. McGill A, et al. *Complementary Therapies in Medicine*, 22, 426—432, 2014.
5. Powell DW, et al. *Motor Control*, 18, 263-277, 2014.

Table 1: Clinical assessments and gait task before and after a 16 week dance training program for PD.

Assessment	Pre Score	Post Score	Change
ABC Scale (%)	82.8	80.6	-2.2
Tinnetti's Falls Efficacy Scale	23	12	-11
Functional Gait Assessment	22	20	-2
6 Minute Walk (m)	446.23	461.77	15.54
Gait Task	Pre (Avg ± SD)	Post (Avg ± SD)	P-value
Timed Up and Go (s)	9.95 ± 0.53	8.57 ± 0.36	< 0.01*

Table 2: Balance parameters during 3 conditions before and after a 16 week dance training program for PD.

CONDITION	Eyes Open			Eyes Closed			Narrow		
Balance Parameter	Pre (Avg ± SD)	Post (Avg ± SD)	P-value	Pre (Avg ± SD)	Post (Avg ± SD)	P-value	Pre (Avg ± SD)	Post (Avg ± SD)	P-value
COP_PathLen(cm)	32.0 ± 3.57	57.7 ± 11.14	< 0.001*	42.7 ± 3.52	67.4 ± 9.22	< 0.05*	37.3 ± 2.93	72.6 ± 11.2	< 0.001*
COP-VEL_X (cm/s)	0.831 ± 0.118	1.44 ± 0.417	< 0.001*	0.995 ± 0.001	1.61 ± 0.20	< 0.05*	1.075 ± 0.131	2.10 ± 0.451	< 0.001*
COP-VEL_Y (cm/s)	1.20 ± 0.142	2.20 ± 0.348	< 0.001*	1.69 ± 0.212	2.69 ± 0.392	< 0.05*	1.28 ± 0.115	2.51 ± 0.311	< 0.001*
SWAY AREA (cm^2)	665.3 ± 216.0	1310.1 ± 879.4	< 0.05*	852.8 ± 413.6	1106.8 ± 257.8	0.45	779.5 ± 202.7	1494.1 ± 452.8	< 0.001*
ApEn_X	0.190 ± 0.076	0.272 ± 0.068	< 0.01*	0.19 ± 0.079	0.403 ± 0.030	< 0.05*	0.190 ± 0.048	0.305 ± 0.067	< 0.01*
ApEn_Y	0.230 ± 0.064	0.343 ± 0.054	< 0.001*	0.298 ± 0.130	0.370 ± 0.0366	0.4	0.294 ± 0.071	0.414 ± 0.083	< 0.01*

Table 3: Spatiotemporal gait parameters during 3 conditions before and after a 16 week dance program for PD.

CONDITION	Over Ground			Backwards			Counting		
Gait Parameter	Pre (Avg ± SD)	Post (Avg ± SD)	P-value	Pre (Avg ± SD)	Post (Avg ± SD)	P-value	Pre (Avg ± SD)	Post (Avg ± SD)	P-value
L Velocity (m/s)	1.32 ± 0.029	1.43 ± 0.041	< 0.001*	—	—	—	1.3 ± 0.052	1.2 ± 0.065	< 0.05*
R Velocity (m/s)	1.31 ± 0.037	1.44 ± 0.04	< 0.001*	—	—	—	1.3 ± 0.041	1.2 ± 0.055	< 0.01*
L Cadence (steps/min)	118.1 ± 2.11	121.78 ± 1.82	< 0.001*	101.6 ± 1.84	109.1 ± 2.88	< 0.01*	123.0 ± 1.2	113.9 ± 2.38	< 0.001*
R Cadence (steps/min)	118.1 ± 1.82	122.16 ± 1.83	< 0.001*	101.2 ± 1.57	106.6 ± 5.06	0.079	123.2 ± 0.86	113.7 ± 2.74	< 0.01*
L Stride Length (m)	1.35 ± 0.027	1.41 ± 0.028	< 0.01*	0.919 ± 0.0339	0.822 ± 0.0371	< 0.05*	—	—	—
R Stride Length (m)	1.33 ± 0.038	1.41 ± 0.024	< 0.01*	0.906 ± 0.0447	0.833 ± 0.047	0.052	—	—	—
L Stride Time (s)	1.02 ± 0.018	0.986 ± 0.0147	< 0.001*	1.182 ± 0.022	1.1 ± 0.03	< 0.01*	0.976 ± 0.0095	1.055 ± 0.022	< 0.001*
R Stride Time (s)	1.017 ± 0.015	0.983 ± 0.0149	< 0.001*	1.188 ± 0.0177	1.14 ± 0.061	0.133	0.974 ± 0.0068	1.056 ± 0.026	< 0.01*
L Step Length (m)	0.603 ± 0.013	0.638 ± 0.0163	< 0.01*	—	—	—	0.556 ± 0.021	0.596 ± 0.018	< 0.05*
R Step Length (m)	0.633 ± 0.021	0.66 ± 0.011	< 0.05*	—	—	—	0.58 ± 0.023	0.591 ± 0.031	0.508
L Step Time (s)	0.505 ± 0.0077	0.483 ± 0.0075	< 0.001*	0.629 ± 0.0092	0.60 ± 0.052	0.373	0.49 ± 0.005	0.525 ± 0.015	< 0.01*
R Step Time (s)	0.512 ± 0.0106	0.5 ± 0.0097	< 0.01*	0.554 ± 0.013	0.533 ± 0.0227	< 0.05*	0.486 ± 0.0049	0.53 ± 0.012	< 0.01*
L Single Support (%)	31.8 ± 0.349	33.4 ± 0.364	< 0.001*	31.04 ± 1.46	35.37 ± 0.69	< 0.01*	30.42 ± 0.6	33.72 ± 1.85	< 0.05*
R Single Support (%)	31.7 ± 0.8	32.0 ± 0.576	0.269	33.5 ± 1.17	36.1 ± 0.36	< 0.01*	30.55 ± 0.624	33.18 ± 3.86	0.229
Double Support (%)	35.7 ± 0.933	33.7 ± 0.69	< 0.01*	34.78 ± 1.87	27.8 ± 0.78	< 0.01*	38.18 ± 1.07	32.32 ± 5.64	0.083
L Stance Time (s)	67.7 ± 1.02	67.7 ± 0.8	0.865	66.2 ± 1.47	63.9 ± 0.52	< 0.05*	68.77 ± 0.886	66.62 ± 3.86	0.323
R Stance Time (s)	68.05 ± 0.6	66.02 ± 0.72	< 0.001*	68.5 ± 1.52	64.05 ± 0.50	< 0.01*	69.41 ± 0.556	65.65 ± 1.8	< 0.01*
L Swing Time (s)	32.3 ± 1.02	32.25 ± 0.8	0.865	33.8 ± 1.47	36.1 ± 0.52	< 0.05*	31.23 ± 0.886	33.38 ± 3.86	0.323
R Swing Time (s)	32.0 ± 0.6	34.0 ± 0.72	< 0.001*	31.46 ± 1.52	35.95 ± 0.50	< 0.01*	30.59 ± 0.556	34.35 ± 1.80	< 0.01*

LOW STRENGTH INCREASES FUNCTIONAL DEMAND DURING WALKING IN OLDER WOMEN

¹ Deborah H. Spinoso, Nise R. Marques, ² Camilla Z. Hallal and ³ Mauro Gonçalves

¹ São Paulo State University, UNESP, Marília, Brazil.

² Uberlândia Federal University, UFU, Uberlândia, Brazil.

³ São Paulo State University, UNESP, Rio Claro, Brazil.

Email: deborahebling@yahoo.com.br

INTRODUCTION

Walking is the most performed activities of daily living and is a complex motor task, which requires an integration of motor, sensorial and cognitive information [1]. The age-related strength loss has been pointed as one of the main factors which leads to biomechanical abnormalities during walking [2].

Also, the lower limb strength loss increases the functional demand (FD) during mobility tasks, which may result in an elevated cost of walking, increased perception of effort and the early onset of fatigue [3]. Increments on FD in older adults are also associated with a reduction to produce maximum strength and it has an important impact on mobility, specially, when it affects the lower limb muscles, such as knee extensor muscles [4].

Thus, the objective of the present study was to identify the FD of lower limb joints (ankle, knee and hip) during the gait in older adults with lower strength and normal strength.

METHODS

Data of thirty older adult women, recruited from community-based physical activity groups, between the ages of 60 and 80 years were considered for this study. The participants were separated into two groups: group with normal strength (knee extensor maximal voluntary isometric torque $> 1.5 \text{ Nm.kg}^{-1}$) and group with lower strength (knee extensor maximal voluntary isometric torque $< 1.5 \text{ Nm.kg}^{-1}$), based on having knee extensor maximum voluntary isometric strength higher than 1.5 Nm.kg^{-1} [5].

Maximal voluntary joint torques were measured isometric for the hip, knee, and ankle for both flexion and extension movements using a isokinetic dynamometer (BIODEX®, New York, USA). The order of joint testing was randomized. Three submaximal repetitions were performed for familiarization purposes, and three maximal repetitions were collected for analysis. Strong verbal encouragement to obtain maximal effort was provided.

The biomechanical assessment of gait was recorded using a 3-D motion analysis system (Vicon®, Oxford, UK) synchronized with a force plate (AMTI®, Watertown, USA). The gait assessment was held on a walkway measuring 14 meters length and 2 meters wide. The volunteers were instructed to walk on the walkway at the speed that they perform their activities of daily living. Each volunteer walked on the walkway for 10 consecutive times.

Data were processed using a fourth-order Butterworth filter with a cut-off frequency of 6 Hz. A purpose written program in Excel was used to amalgamate the data on the knee, ankle and hip angles and moments produced during the gait.

The muscle strength data were combined with the biomechanical moment and angle data to determine the FD placed on the muscles during the gait. FD for a muscle group was defined as the muscle moment required at a particular joint angle, divided by the maximum isometric muscle strength available at that joint angle (expressed as a percentage) [6].

PASW 18.0 (SPSS Inc.) was used for statistical analyses and means and standard deviations were

used to summarize participant characteristics. Then, the comparison of FD between groups was tested using a MANOVA and the significance level for statistical tests was set at $p < 0.05$.

RESULTS AND DISCUSSION

MANOVA demonstrated a significant main effect on the FD between groups ($F = 15.190$, $p < 0.001$). The pos hoc analysis showed that older adults with lower strength had 36 and 67% higher FD of knee flexor and extensor than older adults with normal strength ($p = 0.003$ and $p < 0.001$). Also, the older adults with lower strength had 36% higher FD of hip flexor than older adults with normal strength ($p = 0.004$; Table 1).

Our findings demonstrated that lower limb joint (knee and hip) FD during flexion and extension movements is higher in older adults with lower strength. All subjects that composed the group of older adults with lower strength had knee extensor weakness, which predispose them to have higher knee extension FD than older adults considered with normal strength. However, what deserves to be highlighted in the current study is that the subjects with knee extensor muscles weakness also had increased FD at knee and hip flexor.

According to Reeves et al. (2008) and Samuel et al. (2012), older adults that perform their mobility activities in high levels of lower limb FD have a reduction on their physiological muscular reserve, which represents that if a balance perturbation occurs these people are unable to generate strength to correct the position of the center of mass. Also,

Rowe et al. (2005) suggested that the threshold for an acceptable FD is lower than 80%. In the present study both groups had FD higher than 80% for several joint movements. Thus, based on our results the older women of our sample, especially people with lower strength, may have an increased risk of falling.

CONCLUSIONS

The older women with lower strength had higher hip and knee FD during walking. Our findings demonstrated that older adults with lower strength might be at an increased risk for the early onset of fatigue and falls.

REFERENCES

1. Jahn K, et al. *Dtsch Arztebl Int.* **107**, 306-316, 2010.
2. Taylor ME, et al. *Gait Posture* **37**, 126-130, 2013.
3. Rowe PJ, et al. *Proc IASTED Biomech* 485-420, 2005.
4. Samuel D, et al. *Age and Ageing* **41**, 224-230, 2012.
5. Ploutz-Snyder LL, et al. *J Gerontol* **57**, 144-152, 2002.
6. Samuel D, et al. *Gait Posture* **34**, 239-244, 2011.
7. Reeves ND, et al. *J Electromyogr Kinesiol* **18**, 218-227, 2008.

ACKNOWLEDGEMENTS

This study received funds from Sao Paulo Research Foundation. (FAPESP, process number: 2012/21278-4).

Table 1: Comparison of functional demand during hip, knee and flexion and extension movements in gait between older adults with lower strength and normal strength

Functional Demand	Groups	
	Low Strength	Normal Strength
Hip Flexor	118.58 \pm 7.03	86.98 \pm 7.06*
Hip Extensor	104.85 \pm 6.89	85.86 \pm 6.83
Knee Flexor	83.60 \pm 4.89	61.25 \pm 4.84*
Knee Extensor	116.6 \pm 4.28	69.89 \pm 4.27*
Ankle Flexor	107.48 \pm 5.28	94.43 \pm 7.16
Ankle Extensor	76.16 \pm 5.19	62.77 \pm 5.06

* denotes significant difference ($P < 0.05$)

WALK-TO-RUN TRANSITIONS ON A SPLIT-BELT TREADMILL

Jan Stenum and Julia T. Choi

University of Massachusetts Amherst, Amherst, MA, USA
email: jtchoi@umass.edu, web: <https://blogs.umass.edu/jtchoi/>

INTRODUCTION

The walk-to-run transition in humans has been studied extensively using a range of methods and theoretical perspectives [1, 2, 3, 4]. However, the exact nature of the transition, or the trigger for the transition, has proved elusive so far. Here we present a novel paradigm for studying the walk-to-run transition in humans using a split-belt treadmill. The speed and direction of each leg can be controlled independently, thus allowing us to decouple the normal inter-limb relationship, and probe direction- and leg-specific effects on gait transitions. We studied how subjects walk and run with one leg forward and one leg backward (i.e., hybrid locomotion). The walk-to-run transition speeds were measured for three different conditions: forward locomotion, backward locomotion and hybrid locomotion.

METHODS

Subjects. 4 subjects (2M/2F; 24.5 ± 2.6 yrs; average leg length 0.90 ± 0.03 m) were tested.

Experimental setup. A split-belt treadmill (Bertec) was used to test 3 different conditions: forward, backward and hybrid locomotion. In the hybrid condition the left and right treadmill belts moved in opposite directions (e.g., left leg moved backward and right leg moved forward).

Data collection. Qualisys Track Manager was used to collect and process kinematics data. 11 reflective markers were attached to left and right fifth metatarsal, malleolus, tibial plateau, greater trochanter and anterior superior iliac spine and C7. Ground reaction forces for each leg were sampled at 2000 Hz, and synced to kinematics data sampled at 100 Hz.

Walk-to-run transition. To determine the *preferred* walk-to-run transition speed, subjects walked at

increasing belt speeds. The initial treadmill speed was set at 0.8 m/s. Subjects were instructed to use the preferred gait (most comfortable) at each speed as the belt speed was increased, in steps of 0.1 m/s for forward and backward conditions and 0.05 m/s for the hybrid condition. The process was repeated until the walk-to-run transition occurred. The duration for each belt speed step was 15 seconds. After the transition, the belt speed was increased for three additional steps. The order of the three conditions and the direction of each belt for the hybrid condition were randomized across subjects.

We defined walking as an inverted-pendulum gait, and running as a “bouncing” gait (spring-loaded inverted pendulum). We verified the recorded walk-to-run transition speeds by visual inspection of kinetics data offline, identifying a single peak in the vertical ground reaction forces as running.

RESULTS AND DISCUSSION

The walk-to-run transition occurred at different belt speeds across the three conditions. On average, subjects transitioned at speeds of 2.00 ± 0.20 m/s during forward walking and 1.47 ± 0.15 m/s during backward walking. When one leg walked forward, and one backward, both legs transitioned to running together at a lower speed. We did not observe walking on one leg, and running on the other leg during hybrid locomotion for the tested speed combinations. The average walk-to-run transition speed in hybrid locomotion was 1.17 ± 0.16 m/s.

The joint kinematics of the forward leg in hybrid walking resembled a forward walking pattern (i.e., both legs walking forward), while the backward leg in hybrid walking resembled a backward walking pattern (i.e., both leg walking backward). **Figure 1** shows overlaid trajectories of hip, knee and ankle angles at a walking speed of 1.0 m/s, comparing the joint kinematics of the backward leg during

backward walking and hybrid walking (**Fig. 1A**), and the forward leg during forward walking and hybrid walking (**Fig. 1B**).

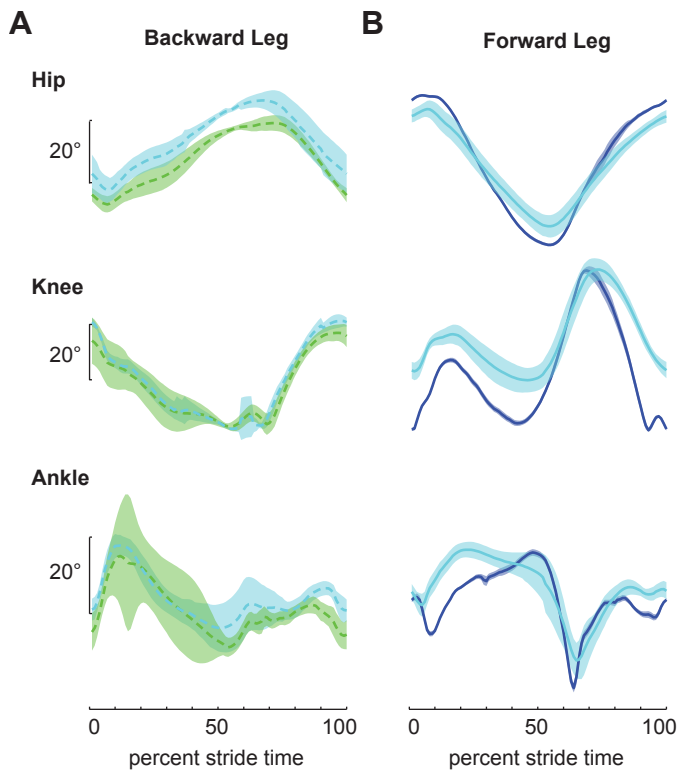


Figure 1: Mean (\pm SD) hip, knee and ankle angles plotted as a function of stride time for a typical subject walking at 1.0 m/s. **A:** The backward leg showed similar kinematics during backward (green) and hybrid (cyan) gait conditions. **B:** The forward leg during forward (blue) and hybrid (cyan) gait conditions.

We calculated peak hip extension, peak hip flexion, peak knee flexion, and peak ankle plantarflexion.

Figure 2 shows the group averaged peak angles across speeds, relative to the walk-to-run transition speed for each gait condition. To average data across subjects, the two walking speeds before the walk-to-run transition in each condition and the two running speeds after the transition in each condition were included.

In summary, our preliminary data suggests that walk-to-run transition speeds are direction-specific. Moreover, the transition speed depends on differences in inter-limb directions. However, intra-limb kinematics for a given walking direction was less dependent on the direction of the opposite leg.

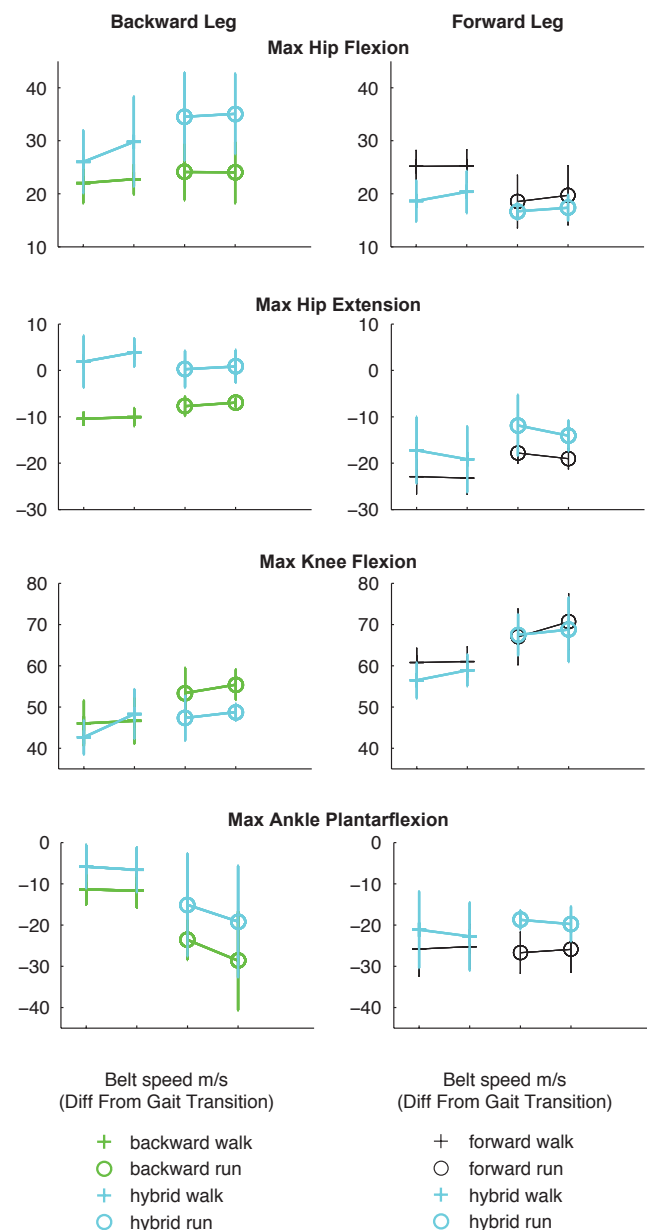


Figure 2: Mean (\pm SD) max hip flexion, hip extension, knee flexion and ankle plantarflexion across subjects for the backward leg during backward and hybrid gaits and for the forward leg during forward and hybrid gaits for walking before the walk-to-run transition and for running after the transition.

REFERENCES

1. Diedrich FJ, Warren WH. *J Exp Psych* **21**, 183-202, 1995.
2. Kram R, et al. *J Exp Biol* **200**, 821-826, 1997.
3. Prilutsky BI, Gregor RJ. *J Exp Biol* **204**, 2277-2287, 2001.
4. Neptune RR, Sasaki K. *J Exp Biol* **208**, 799-808, 2005.

FRACTAL SCALING EXPONENT OF SPATIO-TEMPORAL VARIABLES DUE TO THREE TYPES OF BELT SPEED CONTROL MODES DURING TREADMILL WALKING

Jin-Seung Choi, Jeong-Woo Seo, Dae-Hyeok Kim, Seung-Tae Yang and Gye-Rae Tack*

Konkuk University, Chungju, Chungbuk, South Korea
email: grtack@kku.ac.kr, web: http://kkubme.kku.ac.kr

INTRODUCTION

Long-range correlation of stride time has been used in gait dynamics studies. The scaling exponent α of detrended fractal analysis (DFA) is widely used for quantifying the relationship [1]. Previous study reported that long-range correlation of stride time during metronomic walking disappeared while that of stride velocity during treadmill walking disappeared [2]. This result indicated that the constant rhythm with a metronome and fixed treadmill belt speed limited the stride time and stride velocity, respectively. Recent study using a feedback-controlled treadmill reported that long-range correlation was persisted in the stride velocity as well as stride time and stride length [3]. These results are similar to those of the ground walking condition [4]. Therefore, the purpose of this study was to evaluate and compare the changes in fractal scaling exponent in spatiotemporal variables when the treadmill walking speed was controlled by the visual presentation and the feedback-controlled treadmill.

METHODS

Nine male healthy subjects participated in this experiment (age: 23.3 ± 2.3 years, height: 175.6 ± 3.1 cm, weight: 66.4 ± 4.0 kg). All subjects walked on the treadmill with three kinds of belt speed control modes for 10 minutes or more, such as conventional treadmill (CTM, fixed belt speed), feedback-controlled treadmill (FTM, automatically controls its belt speed depending on the walking speed of the walker, i.e. self-paced) [5], and FTM+Vision (FTM walking while showing current subject's walking speed and target speed on the screen) (Fig. 1). All subjects were asked to maintain the target speed (pre-determined subject's preferred walking speed) throughout the experiment

and were also asked to keep their eyes focused straight ahead.

To acquire spatiotemporal gait variables (stride time, stride length, stride velocity), three-dimensional motion capture system (Motion Analysis System Inc. USA) was used. The mean and fractal dynamics of all variables were calculated. The fractal dynamics were represented by using the scaling exponent α of the detrended fluctuation analysis [1].

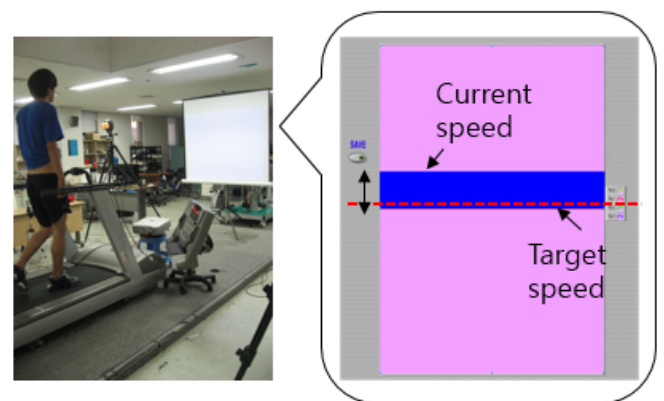


Figure 1: Experimental setup and composition of the screen for presenting subject's current walking speed (The blue bar that moves up and down, and red dotted line represent current speed at each moment and target speed for reference, respectively.)

Asymmetric index (SI) was used to compare asymmetry of gait variables (SI=0: perfectly symmetry, larger SI is the more asymmetry) [6].

$$SI(\%) = \frac{|X_R - X_L|}{X_R + X_L} \times 100$$

X_R and X_L are right and left data, respectively. Matlab R2013b (Mathworks, Inc., USA) were used for calculating all variables.

RESULTS AND DISCUSSION

There was no significant difference in the mean of all variables among three kinds of treadmill walking conditions (average stride time 1.11~1.18sec, average stride length 0.96~1.01m, average stride velocity 0.83~0.92m/sec). Their asymmetric indices were also small values of about 0.5% or less. In results of fractal dynamics, the scaling exponent α from DFA of all variables of CTM and FTM+Vision walking were very similar. Especially the scaling exponent α of stride velocity in both conditions were close to 0.5 value (in other words, long-range correlation of stride velocity in both conditions almost disappeared). The scaling exponent α of stride length and stride velocity in both conditions showed large asymmetry (SI>9% and SI>15%, respectively) as shown in Table 1. On the other hand, in FTM walking, all variables showed long-range correlation ($\alpha>0.5$) like a case of ground walking and represented that the asymmetric indices (SI<5%) were lower than those of the other two conditions.

CONCLUSIONS

The results of this study showed that although the control mechanism of walking speed was different in CTM and FTM+Vision (changing belt speed

itself and adjusted self-paced by looking at current walking speed, respectively), the characteristics of gait dynamics in spatiotemporal variables were quite similar to each other. This result might be due to the same purpose of walking, regardless of the way or variable to control. Further study is necessary to identify the effect of the constrained and unconstrained walking by using various limitations and conditions.

REFERENCES

1. Hausdorff JM. *Hum Mov Sci* **26**, 555-589, 2007.
2. Dingwell, JB & Cusumano, JP. *Gait Posture* **32**, 348-353, 2010.
3. Choi JS, et al. *J Biomech*, In press.
4. Terrier, P., et al. *Hum Mov Sci* **24**, 97-115, 2005.
5. Choi, JS & Tack, GR. Proceedings of ISBS'13, Taipei, Taiwan, 2013.
6. Echeverria JC, et al. *Physica A* **389**, 1625-1634, 2010.

ACKNOWLEDGEMENTS

This research was supported by the National Research Foundation of Korea (NRF) Grant funded by the Korea government (MSIP) (Nos. 2013R1A2A2A03014511 & No. 2013R1A1A10095 71).

Table 1: Scaling exponent α of DFA in spatiotemporal variables while walking on three kinds of treadmill modes. (SI: asymmetric index)

DFA (α)		CTM		FTM		FTM+Vision	
		Right	Left	Right	Left	Right	Left
Stride time		0.84 (0.13)	0.84 (0.14)	0.93 (0.17)	0.92 (0.15)	0.86 (0.14)	0.86 (0.14)
	SI(%)	0.47 (0.40)		0.77 (0.68)		0.59 (0.64)	
	Total	0.86 (0.14)		0.92 (0.15)		0.86 (0.14)	
Stride length		0.74 (0.15)	0.61 (0.15)	0.92 (0.12)	0.85 (0.13)	0.76 (0.09)	0.64 (0.07)
	SI(%)	9.72 (6.05)		5.32 (4.35)		9.26 (4.60)	
	Total	0.84 (0.13)		0.88 (0.11)		0.70 (4.60)	
Stride velocity		0.55 (0.08)	0.40 (0.06)	0.98 (0.05)	0.90 (0.09)	0.75 (0.13)	0.53 (0.10)
	SI(%)	15.79 (7.67)		4.99 (4.17)		17.42 (6.30)	
	Total	0.48 (0.06)		0.93 (0.07)		0.64 (0.11)	

ANTERIOR LAXITY IN HEALTHY YOUNG WOMEN WITH KNEE HYPEREXTENSION

¹ Patricia Teran-Yengle and ² H. John Yack

¹ University of South Florida, Tampa, FL, USA

² University of Iowa, Iowa City, IA, USA

Email: pterany@health.usf.edu

INTRODUCTION

Knee hyperextension, an underrepresented and insidious condition mainly seen in women [1-4], can contribute to abnormal accumulated knee stressors resulting in pathology. Movement of the knee into hyperextension of more than five degrees, is associated with a ground reaction force vector that acts anterior to the knee joint[5]. The anterior location of the ground reaction force vector places increased contact stress on the tibiofemoral cartilage [6] and considerable tension stress on the passive restraining structures that resist further knee extension (e.g. posterior knee capsule and Anterior Cruciate Ligament)[5]. Chronic hyperextension may stress connective tissues resulting in adaptive lengthening of the structures that resist knee hyperextension and consequently contribute to a more unstable joint. The purpose of this study was to investigate joint laxity in women with and without knee hyperextension. We hypothesized that knee laxity, measured by the anterior displacements at specific loadings and the stiffness changes in the knee joint, were different among women with and without hyperextension.

METHODS

Healthy female, 18-39 years of age, with and without knee hyperextension greater than 5° at rest were invited to participate. Participants were screened for: knee extension passive range of motion (PROM); lower limb muscular strength; and general joint laxity using the Beighton and Horan Joint Mobility Index (BHJMI). To determine leg dominance, participants were instructed to kick a ball. The knee ligament arthrometer KT-2000 (MedMetric Co., San Diego, CA, USA) was used to evaluate knee laxity by measuring anterior displacement of the knee joint. Participants were placed in a supine position. KT-2000 device was

placed on participant's lower leg and knee was positioned in 30° of flexion. EMG electrodes were attached to selected lower limb muscles to ensure participant's complete relaxation during the KT-2000 testing. Three successful trials of laxity were obtained to calculate the mean value of anterior displacement bilaterally. Data was collected on knee joint laxity in anterior direction applying 45, 67, 89, and 134 N. The applied force and corresponding displacement data were continuously recorded into a computer via an acquisition card (DaqCard 216b, IOtech, USA) at 1,000 Hz. Intra and inter-session tester reliability was determined (ICC=0.9) prior to data collection.

The recorded force and displacement output data were analyzed using Excel to identify the anterior displacement in millimeters (mm) at each load for further analysis. Stiffness was defined as the ratio of the force to the displacement. The initial stiffness was the stiffness calculated in the initial loading phase (45-67N) and the terminal stiffness was in the terminal loading phase (89-134N). All statistical testing was performed using SAS 9.3 (SAS Institute Inc., Cary, NC, USA).

RESULTS AND DISCUSSION

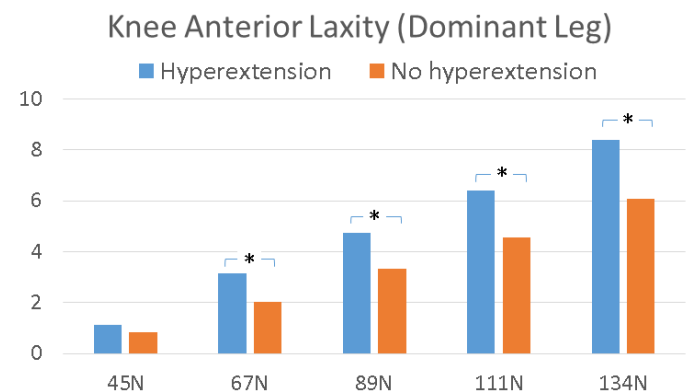


Figure 1: The dominant leg of women with hyperextension showed greater displacement.

Twenty two healthy women: twelve women (mean + SD age, 20.4 ± 2 ; mass, 59 ± 6 kg; height, 1.6 ± 0.1 m) with knee hyperextension greater than five degrees at PROM and ten women (mean + SD age, 21 ± 3 ; mass, 59.3 ± 10 kg; height, 1.7 ± 0.1 m) took part in this study. Mean + SD knee passive range of motion was $8.5^\circ + 1.7^\circ$ (range 6° to 11°) and $3.4^\circ + 1.5^\circ$ (range 0° to 5°) in women with and without knee hyperextension, respectively.

The results of this study showed that the dominant side of the hyperextension group had significant greater anterior displacement that that of the no-hyperextension group ($p < 0.05$) (Figure 1). No significant difference was found in the non-dominant side. Pearson correlation coefficients (Figure 2) showed a moderate correlation between the degree of knee extension at PROM and anterior displacement. The dominant side of the hyperextension group had significantly smaller initial stiffness than that of the non-hyperextension group (Figure 3).

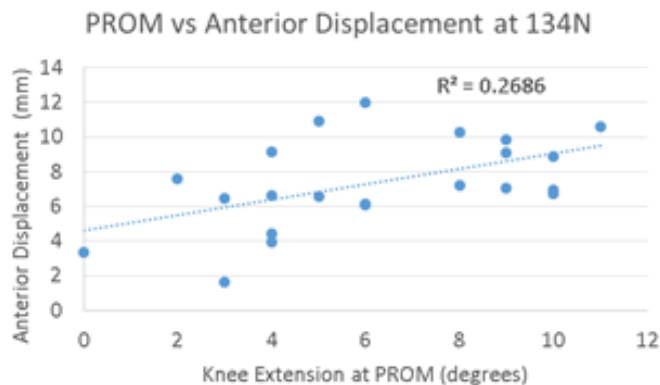


Figure 2: There was a weak correlation between PROM and anterior displacement in the dominant leg across in both groups.

CONCLUSIONS

The results of this study seem to indicate that knee hyperextension places the posterior capsule of the knee joint and Anterior Cruciate Ligament under considerable tension stress. Chronic knee hyperextension may stress connective tissues

resulting in adaptive lengthening of the structures that resist knee hyperextension and consequently contribute to a more unstable joint. These findings may explain why hyperextension knees are at greater risk of injury. Further investigation on knee mechanics in women with knee hyperextension should be performed.

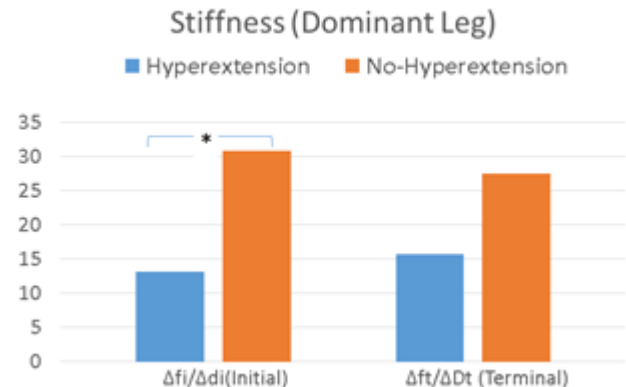


Figure 3: The dominant leg of women with hyperextension had significantly smaller initial stiffness.

REFERENCES

1. Loudon, J.K., H.L. Goist, and K.L. Loudon, Genu recurvatum syndrome. *JOSPT*, 1998. **27**(5):361-7.
2. Nguyen, A.D. and S.J. Shultz, Sex differences in clinical measures of lower extremity alignment. *J Orthop Sports Phys Ther*, 2007. **37**(7): 389-98.
3. Nguyen, A.D. and S.J. Shultz, Identifying relationships among lower extremity alignment characteristics. *J Athl Train*, 2009. **44**(5): 511-8.
4. Medina McKeon, J.M. and J. Hertel, Sex differences and representative values for 6 lower extremity alignment measures. *Journal of athletic training*, 2009. **44**(3):249-255.
5. Levangie, P.K. and C.C. Norkin, *Joint Structure and Function: A Comprehensive Analysis Fifth Edition*. 2011: F.A. Davis Company. 640.
6. Meyer, E.G., T.G. Baumer, and R.C. Haut, Pure passive hyperextension of the human cadaver knee generates simultaneous bicruciate ligament rupture. *Journal of Biomechanical Engineering*, 2011. **133**(1): p. 011012.

Differences in Synergistic Control of Muscles During Treadmill Walking in Anterior Cruciate Ligament Reconstructed Legs

¹ Emily Churchwell ¹ Jaimie Roper, ¹ Matthew J. Terza, ² Ryan Roemmich, ¹ B.J. Fregly ¹ Chris J. Hass

¹ The University of Florida, Gainesville, FL USA, ² Johns Hopkins University, Baltimore, MD USA
email: mjt023@ufl.edu

INTRODUCTION

Individuals who have suffered an anterior cruciate ligament (ACL) injury and undergone a surgical reconstruction show a high incidence of reinjury and osteoarthritis even with extensive physical therapy and return to sports [1, 3]. The progression to further joint issues highlights the need to investigate possible changes in the muscular control of the reconstructed leg to better understand the underlying reasons for these risks. This understanding can help to develop and improve rehabilitation strategies. One study has looked at the complexity of movement patterns of ACLR knees as compared to healthy knees during treadmill walking showing deviations from healthy knee that could underlie progressive joint issues [2]. However, in order to investigate more deeply the neural control mechanisms behind these differences we looked at the synergistic organization of muscle control in ACL-R legs versus healthy legs using muscle synergy decomposition analysis techniques. We hypothesized the total variability accounted for (VAF) by using these synergies would be higher for ACL-R versus healthy legs at the comparable number of modules which would indicate reduce complexity in the ACL-R leg. We also hypothesized that that the ACL-R legs would exhibit altered activation timing of these synergies compared to the healthy legs.

METHODS

In this study we collected electromyography (EMG) (sampled at 1200 Hz) on 16 lower body muscles (eight each leg) in six unilateral ACL-R post rehabilitation individuals while they walked on a treadmill at 1.5 m/s for five minutes. The EMG signals were demeaned, rectified, and filtered using a 6 Hz butterworth filter. Each gait cycle was separated using ground reaction forces to identify

foot contact events. The data for each cycle was normalized to a percent of the gait cycle. Nonnegative matrix factorization (NMF) was used to decompose these eight EMG signals across the gait cycles into lower dimensional components (modules/synergies each with a paired activation profile) for each leg separately [4]. We analyzed our data first assuming three distinct muscle modules, then four muscle modules, and then five muscle modules. Instead of setting a threshold of 95 percent VAF to determine the number of synergies present, we instead compared the VAF at three, four, and five modules. We compared the VAF between the healthy leg and the ACL-R leg of the individuals using independent t-tests. We also calculated the effect size on the timing and magnitude of the main peak in each activation profiles of the synergies under the assumption of three modules.

RESULTS AND DISCUSSION

Our results suggest that there may be altered control of lower body muscles during treadmill walking in persons after ACL-R... The analyses revealed important differences in VAF at 3 modules between healthy legs and ACL legs and effect of ACL-R on the peak timing and magnitude of the activation profile for selected modules.

The convergence of VAF between the ACL-R and the healthy leg as more muscle synergies are assumed is expected. The notable result is that there is significant difference in total VAF at three modules. As shown in Fig. 1 ACL-R legs demonstrate a larger amount of VAF which indicate diminished complexity in coordination of muscle activations during walking.

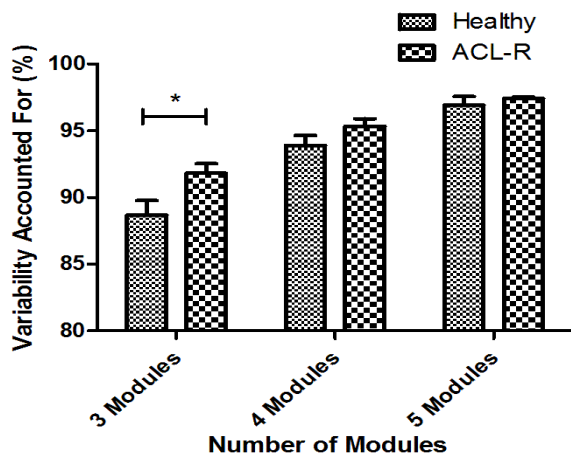


Figure 1: Total VAF of the healthy and ACL-R legs when assuming three, four, and five muscle synergies. * $P < 0.05$

Because of the significant difference in VAF between ACL-R and Healthy legs at three modules, we further investigated the activation profiles for the assumption of three modules. The results of this analysis are shown in Table 1. When evaluating the effect size of ACL-R on the timing and magnitude of the most prominent peak in the activation of each module, Module 1 showed a large effect size on the timing of the peak, Module 2 showed a large effect size on the magnitude of the peak, and Module 3 showed large effects on the timing of the peak. The results point to an altered usage of muscle synergies

that may reveal one way in which deficits in ACL-R legs persist.

CONCLUSIONS

The differences in the total VAF at three modules and the effect of ACL-R on the synergy activation profiles indicate differences in the control of walking movement in the ACL-R leg. It is possible that recruiting more subjects could help detect differences under the assumption of a higher number of modules as well as differences in the VAF for each specific muscle. Although these early results point towards altered control of muscle synergies in ACL-R legs, further investigation of these differences is required to fully characterize changes in neuromuscular control and understand why specifically these individuals are at heightened risk of further joint problems in the reconstructed knee.

REFERENCES

1. Culvenor AG. et al. *Arthritis & Rheumatology* 2015.
2. Decker LM, et al. *Knee Surg Sports Traumatol Arthrosc.* 2011.
3. Salmon L, et al. *Arthroscopy.* 2005.
4. Tresch, M.C. et al. *Journal of Neurophysiology,* 2006.

Table 1: The table shows the timing magnitude with standard error of the on average most pronounced activation peak of each activation profile for each of the three modules determined using NNMF. The effect size of the ACL-R is presented for both the timing and magnitude.

Activation Profile Peaks						
	Peak Time (% of Gait Cycle)			Peak Magnitude		
	Healthy	ACL-R	Effect Size (Cohen's d)	Healthy	ACL-R	Effect Size (Cohen's d)
Module 1	9.17±1.25	6.00±1.26	1.03	0.42±0.07	0.49±0.04	0.57
Module 2	42.83±1.08	43.33±0.71	0.22	0.53±0.03	0.59±0.02	1.00
Module 3	93±0.26	95.67±1.67	0.95	0.54±0.05	0.51±0.09	0.15

CO-CONTRACTION INDEX DURING GAIT AND RELATIONSHIP TO QUADRICEPS STRENGTH IN INDIVIDUALS WITH FOCAL CARTILAGE DEFECTS IN THE KNEE

Louise M. Thoma, Michael P. McNally, Ajit M.W. Chaudhari, Robert A. Siston, Thomas M. Best, David C. Flanigan, Laura C. Schmitt
The Ohio State University, Columbus, OH, USA
email: thoma.24@osu.edu

INTRODUCTION

Greater muscle co-contraction about the knee has been commonly reported in individuals with knee pathology such as anterior cruciate ligament injury and osteoarthritis. Previous work indicates co-contraction is higher in individuals with more severe osteoarthritis [1], and increases potentially injurious compressive forces in the knee. [5] Despite being younger in age, individuals with focal cartilage defects (FCD), or isolated articular cartilage lesions, of the knee present with impairments similar to osteoarthritis, including considerable quadriceps weakness. [2] To our knowledge, there are no reports of muscle activation strategies in individuals with FCDs during dynamic activity. The primary purpose of this exploratory study in individuals with FCDs was to test the hypotheses that (1) co-contraction index (CCI) is higher on the involved limb than the uninvolved limb during gait and (2) weaker quadriceps strength is correlated with greater CCI during gait. We also explored when during the gait cycle CCI is the highest, to inform future research questions.

METHODS

Fourteen individuals (7F:7M, 29.5±6.0 years old, 25.8±3.5 kg/m²) with FCDs in the knee (Grade 3-4) provided IRB-approved informed consent prior to participation. Defect location varied per participant: 5 patellofemoral only, 6 tibiofemoral only, 3 mixed.

Quadriceps strength was quantified as the peak torque produced during 3 maximal isometric knee extensions at 60° knee flexion (Biodex System 3, Shirley, NY), normalized to mass and height.

Five gait trials at each subject's self-selected speed were captured with three-dimensional motion capture (10-camera, Vicon MX-F40, Oxford, UK)

and electromyography (EMG) concurrently. Ground reaction force data were collected for two consecutive foot strikes by independent force plates (Bertec FP4060, Columbus, OH). Motion capture and forces plate data were used to identify initial contact and toe-off to define the stance phase.

A 16-channel telemetric surface EMG system (Noraxon Telemetry DTS, Scottsdale, AZ) measured muscle activation of the right and left vastus lateralis (VL), vastus medialis (VM), biceps femoris (BF), and semitendinosus (ST). EMG signals were filtered using a 50-500Hz 4th order band-pass Butterworth filter and rectified. A 50 millisecond running average was used to create a linear envelope and normalized to the highest signal amplitude during a maximal volitional isometric contraction (MVIC). The normalized linear envelopes for VL and VM, and for BF and ST, were summed to create a single activation curve for the quadriceps and hamstrings respectively.[5] CCI was calculated for each time point during stance phase with Equation 1.[3,4]

Equation 1

$$CCI_i = \frac{\text{lower } EMG_i}{\text{higher } EMG_i} \times (\text{lower } EMG_i + \text{higher } EMG_i)$$

The stance phase of gait was divided into ten 10% epochs (ie. subdivision of stance phase) for analysis (Epoch 1-10 consecutively, with Epoch 1 beginning at heel strike, and Epoch 10 ending at toe off). The average CCI was calculated over each Epoch. We evaluated the average CCI with a 2x10 repeated measures analysis of variance, with Limb (involved, uninvolved) and Epoch (Epochs 1-10) as within-subject factors ($\alpha=0.05$). Limb, Epoch, and the Limb*Epoch interaction violated the sphericity assumption (Mauchly's test), thus the Greenhouse-Geisser correction was used. Significant interactions or main effects were evaluated post-hoc with pairwise comparisons and a Bonferroni correction. Spearman's Rank Order Correlation was used to

evaluate the relationship between quadriceps strength and the average CCI for the stance phase, as quadriceps strength was non-normal.

RESULTS AND DISCUSSION

There was a main effect for limb (Figure 1, $p = 0.013$). CCI was higher in the involved than the uninvolved limb, supporting the first hypothesis. There was also a main effect for epoch ($p < 0.0005$). Post-hoc pairwise comparisons between phases indicated CCI was highest in early stance. Phase 1 was significantly different than Phases 2-9 ($p = 0.000-0.005$) and Phase 2 was different than Phases 1, 4, 5, 9, and 10 ($p = 0.005-0.042$). All other phases were similar to each other. There was no interaction effect of between limb and phase ($p = 0.065$).

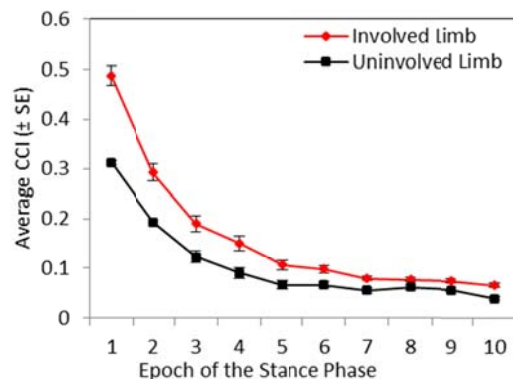


Figure 1: Average CCI per epoch during the stance phase of gait for the involved and uninvolved limb

Our second hypothesis was also supported. Involved limb quadriceps strength was negatively correlated to average CCI during the stance phase (Figure 2, $p = -0.73$, $p = 0.003$). There was no relationship on the uninvolved side ($p = -0.27$, $p = 0.4$).

Previous work suggests co-contraction is a harmful muscle activation strategy, as it increases tibiofemoral compressive forces [5], which may further damage compromised knee cartilage. However, this assertion is dependent on the assumption that muscle activation is related to muscle force production. The common practice of normalizing EMG during gait to MVICs may be inappropriate in individuals with quadriceps inhibition [6], and may lead to an over-estimation of muscle activity. It is likely that many individuals with FCDs also demonstrate quadriceps inhibition.

With future studies, we will investigate if the high CCIs resulted in increased joint compressive forces, or were over-estimated resulting in minimal impact on compressive forces. This study was limited by a small sample size and heterogeneous FCD location.

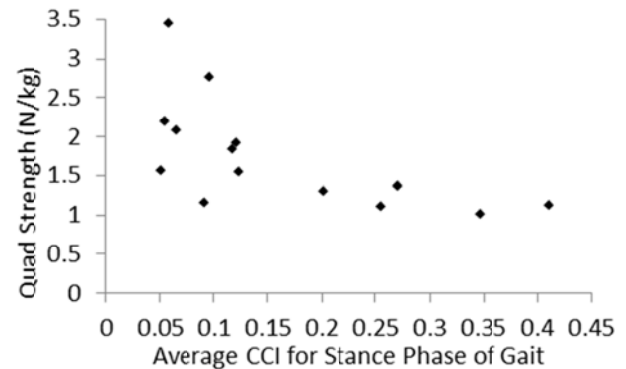


Figure 2: Scatterplot of involved quadriceps strength vs. involved CCI

CONCLUSIONS

Individuals with FCDs demonstrate higher CCI on the involved compared to the uninvolved limb. Given the inverse relationship between quadriceps strength and CCI, future work considering the detrimental effect of higher CCI, especially in early stance, on compressive joint forces must consider the potential over-estimation of CCI in individuals with quadriceps strength deficits.

REFERENCES

1. Hubley-Kozey CL, et al. *Clin Biomech.* **24**, 407-414, 2009.
2. Thoma LM, et al. *J Sports Rehab.* **23**, 259-269, 2014.
3. Lewek MD, et al. *Osteoarthritis Cartilage.* **12**, 745-751, 2004.
4. Schmitt LC, Rudolph KS. *Arthritis Rheum.* **57**, 1018-1026, 2007.
5. Tsai LC, et al. *J Orthop Res.* **30**, 2007-2014, 2012.
6. Soderberg GL and Knutson LM. *Phys Ther.* **80**, 485-498, 2000.

ACKNOWLEDGEMENTS

Partial funding provided by the Sports Health and Performance Institute, OSU Sports Medicine.

Cognitive Influence on Obstacle Avoidance: Auditory and Structural Interference

¹Lori Ann Vallis, ¹Matthew Mendes, ¹Timothy A. Worden and ¹Pratham Singh

¹University of Guelph, Guelph, ON, Canada
email: lvallis@uoguelph.ca, tworden@uoguelph.ca

INTRODUCTION

Throughout our daily lives we are constantly interacting with and moving through our environment, completing concurrent motor and cognitive tasks in a smooth and efficient manner [1]. While gait was once thought of as an automatic task, we now know that use of the cognitive system, and more specifically executive function [2], is vital for the successful planning and executing goal directed actions, e.g. obstacle avoidance [3]. The ability to perform more than one task at a time has been well studied using dual task paradigms, some of which involve cognitive tasks that result in structural interference [e.g. tasks requiring assessment of visual information for task completion; 4] and other tasks which result in capacitance interference [e.g. tasks requiring rapid/intense mental processes; 5].

The **purpose** of this study was to investigate how each type of interference (structural and capacitance) affects executive function strategies used to plan the adaptive locomotor patterns for a complex motor task, obstacle avoidance.

METHODS

Thirteen healthy university students were recruited (aged 20.6 ± 1.6 years) for this study. Exclusion criterion included visual perception problems (e.g. strabismus), hearing problems and history of recent musculoskeletal injuries (e.g. sprain within last 2 months). The experimental paradigm is outlined in Figure 1. Gait velocity, minimum foot clearance, takeoff and landing distance from the obstacle were calculated. Data was analyzed at the instant of heel contact 2 steps before (OBS-2), 1 step before (OBS-1) and at crossing (OBS-xing) the obstacle. Response accuracy and response time for the auditory and visual Stroop task was calculated from a microphone fixed to the subjects' thorax.

Dual task cost (DTC) was also processed for both kinematic and cognitive measures [5]:

$$\frac{(\text{Dual task} - \text{Single task})}{\text{Single task}}$$

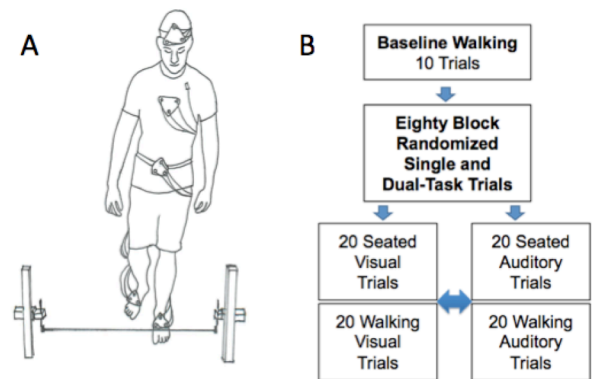


Figure 1(A). Subjects were instrumented with rigid triads of iREDs (100 Hz) and anatomical points were digitized (e.g. heels, toes). A lapel microphone recorded participants audio response times (3000 Hz). **(B).** First, participants completed 10 baseline walking trials where they stepped over an obstacle set to a height of 30% of their lower limb length with *no cognitive task*. They then completed 4 different blocks of experimental trials (seated trials always preceded walking over obstacle trials). Half of the participants completed the visual Stroop task prior to the auditory Stroop task (*10 congruent/10 incongruent*).

A Pearson Chi Square was performed to examine if cognitive accuracy and response time differed between cognitive tasks. A multivariate ANOVA (Stroop Condition X Trial Type) was conducted on mean and variability of obstacle avoidance parameters. A single variable ANOVA was conducted for cognitive measures and another single variable ANOVA was conducted for dual task cost. Significance level was set to $p < 0.05$.

RESULTS AND DISCUSSION

Cognitive task performance. An effect of accuracy for Stroop type was observed with subjects significantly less accurate at identifying the auditory Stroop cue compared to the visual Stroop cue. There was no effect for congruency. For mean response latencies, a main effect of Stroop test was observed; subjects identified the visual Stroop cue significantly faster than the auditory Stroop cue (Figure 2), however no changes in DTC were detected.

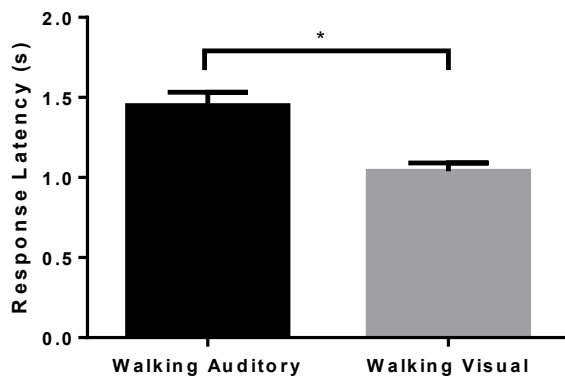


Figure 2: Response latency (s) for the two Stroop tests; visual Stroop cue responses were significantly faster than auditory Stroop responses.

Dual Task performance. Recall that a larger dual-task cost is indicative of an increase in a given obstacle parameter compared to baseline values. Interestingly, there were no detectable differences in gait velocity or takeoff distance across conditions, though a main effect of trial type was observed for *minimum lead foot clearance* DTC (Figure 3).

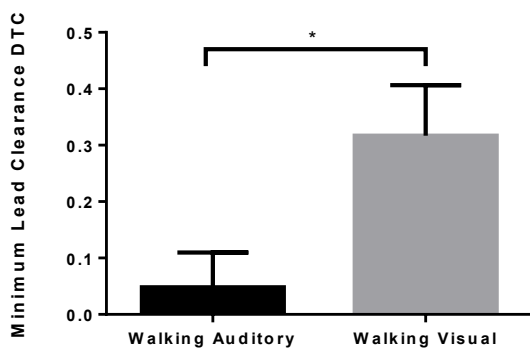


Figure 3: Significantly larger dual-task costs for the visual Stroop cue were observed for minimum lead toe clearances ($p < 0.05$).

Similarly, a main effect of cognitive task was observed for *trail toe clearance*; larger dual-task costs were observed for the visual Stroop cue compared to the auditory Stroop cue (Figure 4).



Figure 4: Significantly larger dual-task costs for the visual Stroop cue were observed for trail toe clearances ($p < 0.05$).

For landing distance, a trend for greater dual-task cost caused by the visual Stroop task was also observed, although this was not statistically significant ($p = 0.069$). It appears that a secondary visual task caused subjects to adopt a more cautious obstacle crossing strategy.

CONCLUSIONS

Our results indicate that a more cautious control strategy is used when performing tasks involving visual (structural) interference compared to tasks involving auditory (capacitance) tasks. These results highlight that researchers should carefully consider the impact of structural interference when selecting cognitive tasks for dual task paradigms during gait.

REFERENCES

1. Botvinick MM, et al., *Psychol. Rev.* **108**, 624-652, 2001.
2. Sheridan L, Hausdorf J., *Dementia and Geriatric Cognitive Disorders* **24**, 125-137, 2007.
3. Chen H, et al., *J Gerontol* **51A**, 116-122. 1996.
4. Berg W, Murdock L, *Age Ageing* **40**, 324-329, 2011.
5. Kelly V, et al., *Exp Brain Res* **207**, 65-73, 2010.

Foot Pressure Masking Differences With and Without Kinematic Data for Unilateral Clubfeet

¹JJ Wallace, ¹Sam Augsburger, ¹Hank White, ^{1,2}Henry Iwinski, and ^{1,2}Janet Walker

¹Shriners Hospitals for Children – Lexington, KY

²The University of Kentucky Department of Pediatric Orthopedics

Email: jwallace@shrinenet.org

INTRODUCTION

The use of pedobarography has been proven to be a reliable measure when assessing normal and pathological feet [1, 2]. When using pedobarography to assess clubfoot deformity, the accuracy of foot pressure data is dependent upon the software's ability to identify regions of interest (ROI) on the foot print. However, built-in software is not always precise when masking the ROI when foot deformity is present. Inaccuracies in masking ROI can be due to the severity of the foot deformity and/or the absence of plantar pressure in different regions of the foot due to problems such as dynamic supination. Therefore, manual corrections have to be made to the ROI in order for data output to be accurate for both clinical and research applications [2]. Differences seen within the data will depend on the experience and subjective interpretations of the data collector [1, 2].

Recent research has reported that the use of 3D kinematic multi-segment foot models in conjunction with pedobarography is a valid and reliable outcome tool to evaluate typically developing and pathological feet [1]. Using kinematic assessment simultaneously with pedobarography may allow for more precise ROI masking and negate the variability that is present in ROI masking for feet with deformity that require manual correction. Therefore, the purpose of this study is to assess the differences between a 10 area pedobarographic ROI mask in children with unilateral clubfeet with and without the use of kinematic data.

METHODS

Twenty-six children, ages 2.6-12.9 years, diagnosed with unilateral clubfoot underwent simultaneous pedobarographs and kinematic data collection. Foot pressure analysis was collected for both the involved and uninvolved sides using Novel emed-x

platform and Novel Database Pro M v.23.3.52. Kinematic data was collected for both feet using 12 Motion Analysis Eagle cameras and Cortex software v.5.0.1.1496. Three trials per subject per side were collected for a total of 156 foot pressure trials. Nine markers were placed on each foot according to the Oxford foot Model [1]. Kinematic data was exported as a .c3d format and loaded into the Novel Automask program where marker coordinates were projected onto the transverse plane [3]. Post processing of the data consisted of masking the foot into 10 ROI with and without the kinematic data using the Automask; hallux, 2nd toe, 3rd-5th toes, 1st metatarsal, 2nd metatarsal, 3rd-5th metatarsal, medial midfoot, lateral midfoot, medial heel and lateral heel [3]. One investigator, with 5 years' experience using Novel software, performed all post processing and evaluation of foot pressure ROI differences.

Differences in masking techniques were expressed as a percentage of the total number of trials that would have required manual corrections. The decision for manual corrections was based on visual assessment of the 10 ROI superimposed onto the maximum pressure picture. If a trial was deemed to need manual corrections it was rated as inaccurate. Manual corrections were based on the following criteria: 1. ROI was misidentified: Ex. Big toe was included in the 1st metatarsal mask; 2. ROI was displaced laterally/medially: Ex. The 1st metatarsal was not in contact with the ground due to dynamic supination; therefore the 1st metatarsal mask was superimposed laterally onto the 2nd metatarsal; 3. The ROI was externally rotated about the vertical (Z) axis. The line dividing the heel was rotated medially and the medial/lateral heels were not divided accurately based on the predefined parameters [3]. In addition to visual differences in ROI, t-tests were used to assess significant

differences between the peak pressure (PP) and contact area (CA) of the total foot and the 10 ROI with and without the kinematic data ($p < .05$).

RESULTS AND DISCUSSION

Of the 156 total pedobarographic trials, 2 were discarded due to the inability to post process kinematic data, resulting in 154 usable trials for data analysis. Differences in masking ROI and changes in CA and PP were assessed in the involved and uninvolved sides of 26 children with unilateral clubfoot.

When masking the foot without kinematic data, compared to the uninvolved side the ROI of the involved side demonstrated a significant increase in PP in both the lateral midfoot and the 3rd-5th metatarsals. When masking ROI with kinematic data these ROI are no longer significantly different between sides (Table 1). For CA in ROI masked without kinematic data the involved side demonstrated significant decreases in the medial midfoot, 1st metatarsal and hallux. When masking ROI with kinematic data the 1st metatarsal difference is lost and new differences are noted in the lateral hindfoot (Table 1). More statistical differences are noted in the medial and lateral feet when masking the ROIs without kinematic data than with kinematic data (Table 1).

When visually assessing the ROI differences between masking techniques, more trials required manual correction when applying kinematic data to the pedobarograph. Masking ROI without kinematic data on the uninvolved side required manual corrections in only 4% of trials, whereas the involved side required manual corrections in 25% of the trials. When masking the ROI with kinematic data, the uninvolved side required manual corrections in 50% of trials and the involved side required manual corrections in 55% of trials. For both masking techniques the involved side required more manual corrections to the ROI. This is contrary to previous research conducted on masking with and without kinematic data which reported kinematic data was more reliable when masking the foot using a 5 area ROI mask for typically developing children and children with clubfeet [1]. However, the 5 area ROI mask previously utilized is

not as widely used in the clubfoot population as the more complex 10 area ROI mask utilized by Jeans et al [2].

We believe the primary reason our findings are not consistent with previous research is that we defined more ROI's (10 as opposed to 5), resulting in smaller regional areas and increased variability due to their definitions. However, the 10 area ROI mask used in this study is more clinically relevant in assessing changes in clubfeet over time and due to surgical intervention since it provides a greater number of detailed regions of interest that we believe are necessary for adequate pre-post intervention comparisons [2].

REFERENCES

1. Stebbins JA, et al. *Gait & Posture* 22, 372–376, 2005.
2. Jeans KA, et al. *J Pediatr Orthop* 34(5), 552-8, 2014.
3. Novel electronics Inc. *Novel Scientific Manual v.24*, St. Paul, MN, USA, 2014.
4. Giacomozzi C, et al. *Journal of Foot and Ankle Research*, 7(Suppl 1), A25, 2014.

Table 1.	Mask without Kinematics		Mask with Kinematics	
	PP	CA	PP	CA
Total Foot	0.04	0.34	0.04	0.50
Medial Hindfoot	0.00	0.42	0.00	0.86
Lateral Hindfoot	0.00	0.18	0.00	0.05*
Medial Midfoot	0.71	0.00	0.96	0.03
Lateral Midfoot	0.01*	0.42	0.16	0.72
1st Metatarsal	0.00	0.03*	0.00	0.46
2nd Metatarsal	0.29	0.11	0.18	0.06
3rd-5th Metatarsal	0.02*	0.13	0.10	0.47
Hallux	0.00	0.00	0.01	0.02
2nd Toe	0.03	0.79	0.02	0.57
3rd-5th Toes	0.81	0.65	0.73	0.65

Table 1: Shaded boxes denote (PP) and (CA) differences between the affected and unaffected sides ($p < .05$). *Denote differences between masking techniques.

EFFECTS OF CUSTOMIZED KNEE REPLACEMENT SURGERIES ON WALKING MECHANICS

Henry Wang, Jonathan Foster, Natasha Francksen, Jill Estes, and Lindsey Rolston
Biomechanics Laboratory, Ball State University

INTRODUCTION

It is reported that 70% of the Knee OA patients have cartilage degeneration isolated to the medial and patellofemoral compartments [1]. Majority of these patients undergo total knee replacements (TKR). The iDuo system is a customized, individually made bi-compartmental knee replacement (BKR) treating OA at medial/lateral and patellofemoral compartments [2]. The BKR features the following benefits: an intact contralateral compartment, retained anterior and posterior cruciate ligaments, anatomical knee geometry, and a good knee alignment. It is surmised that the BKR knee will have similar knee mechanics to that of a normal healthy knee during daily activities. To date, there is no information regarding the knee mechanics during level walking with a BKR. There are no *in vivo* biomechanical comparisons between a BKR limb and a limb with an off-the-shelf TKR. The purpose of the study was to examine the differences in knee mechanics between three groups of participants during level walking: (1) patients with customized BKR, (2) patients with off-the-shelf TKR, and (3) healthy controls.

METHODS

23 participants were recruited in the study. Seven patients (63 ± 10 yr.; 100 ± 43 kg; 1.73 ± 0.12 m) received TKRs (Persona, Zimmer Inc.) (post-op: 14 ± 5 mo.). Four patients (63 ± 7 yr.; 93 ± 18 kg; 1.66 ± 0.06 m) received BKR (iDuo, ConforMIS Inc.) (post-op: 19 ± 4 mo.). Twelve healthy participants (57 ± 6 yr.; 82 ± 12 kg; 1.75 ± 0.11 m) served as controls. Participants walked at a self-select speed in a gait laboratory. A VICON motion capture system was used to collect 3D walking motion at 100Hz. Three AMTI forceplates were used to collect ground reaction forces at 2000Hz. Visual 3D was used to perform model based computations. Knee joint kinematics and kinetics were calculated during the stance of walking. MANOVA was performed. $\alpha = 0.05$.

RESULTS AND DISCUSSION

Table 1 shows the means and SDs of the walking speed, knee mechanics in the sagittal, frontal, and transvers planes of the three groups. No significant differences in walking speed between the BKR and control group ($P > 0.05$). No significant differences were observed in peak knee extensor moment, peak knee power absorption and production, peak knee abduction moment, and peak knee internal and external moments between the BKR and control groups ($P > 0.05$). In addition, the peak internal rotation angle was not significantly different between the BKR and control knees ($P = 0.096$). Compared to the control group, the TKR group showed slower walking speed, less peak knee extensor moment, less peak knee power absorption and production, smaller peak internal rotation angle, less peak knee abduction moment, smaller peak external and internal rotation moments ($P < 0.05$); Compared to the BKR limbs, the TKR limbs demonstrated less peak knee power absorption and production, less peak knee abduction moment, smaller peak external and internal rotation moments ($P < 0.05$); In addition, the TKR group showed a trend of less peak knee extensor moment than that of the BKR group ($P = 0.08$).

Close to normal walking speed and 3D knee mechanics appear to be achievable outcomes with customized BKR surgeries. In this study, the BKR patients demonstrated comparable walking speed and peak knee extensor moment and power to the healthy control participants during stance of walking. Off-the-shelf TKR patients walked significantly slower than healthy controls with less knee extensor moment and power produced. In addition, compared to the BKR knees, the off-the-shelf TKR showed deficits in peak knee extensor moment and power during walking. It is possible that the reduction in TKR knee strength may be associated with the traditional off-the-shelf TKR design. Furthermore, when secondary plane knee mechanics were examined, the BKR limbs revealed

no differences in key variables of knee mechanics from the healthy limbs. On the contrary, the TKR limbs exhibited reductions in the peak internal rotation angle, peak abduction moment, and peak internal and external rotation moments when compared to the control limbs. The deviations in secondary plane knee mechanics displayed by the TKR limbs may be related to alterations of the knee geometry introduced by the off-the-shelf TKRs. Future studies should examine the long-term effects of the customized BKR on knee biomechanics during daily activities to establish its long-term benefits and functionality.

CONCLUSIONS

A customized BKR design could provide adequate support to knees to perform normal walking.

REFERENCES

- [1] McAlindon, et al. J Rheumatol, 1992
- [2] www.conformis.com

ACKNOWLEDGEMENTS

ConforMIS Inc.

Table 1. Means (SDs) of walking speed and key knee mechanical variables of the BKR, TKR, and control groups.

Gait variables	BKR	TKR	Control
Walking speed (m/s)	1.34(0.04)	1.18(0.3)	1.48(0.18)
Peak knee extensor moment (Nm/kg)	0.64(0.11)	0.50(0.15)	0.81(0.22)
Peak knee power absorption (W/kg)	-1.60(0.29)	-1.18(0.22)	-1.80(0.39)
Peak knee power production (W/kg)	0.83(0.44)	0.54(0.23)	1.04(0.28)
Peak knee abduction moment at push-off (Nm/kg)	0.25(0.03)	0.17(0.05)	0.27(0.08)
Peak knee internal rotation angle (deg)	4.1(2.4)	2.7(2.4)	6.7(3.1)
Peak knee external rotation moment (Nm/kg)	0.09(0.03)	0.07(0.01)	0.12(0.03)
Peak knee internal rotation moment (Nm/kg)	0.18(0.03)	0.09(0.06)	0.19(0.05)

EFFECTS OF WALKING SPEED ON THE STUMP-SOCKET INTERFACE IN TRANSTIBIAL AMPUTEES

¹ Ryan D. Wedge, ² Andrew K. LaPre, ² Frank Sup, ¹ Brian R. Umberger

¹ Department of Kinesiology, University of Massachusetts, Amherst, MA, USA

² Department of Mechanical and Industrial Engineering, University of Massachusetts, Amherst, MA, USA
email: umberger@kin.umass.edu, web: www.umass.edu/locomotion, www.ecs.umass.edu/mie/mrrl

INTRODUCTION

The number of amputees continues to rise in the United States, and it is expected that by 2050 there will be 3.6 million people with limb loss [1]. The most common pathway for limb loss is dysvascular pathology, such as diabetes [1]. People with diabetes have difficulties maintaining skin integrity and skin breakdown is a common problem experienced by amputees due to the motion and forces between the stump and socket. The stump soft tissues were not designed to withstand the forces they are exposed to inside of the socket, which can lead to pressure ulcers.

The motion and forces of greatest concern are socket pistoning and flexion-extension. Pistoning refers to translation in the axial direction, while flexion-extension is the rotation that occurs about a mediolateral axis due to a bending moment created by the ground reaction force. Studies have utilized various x-ray and motion capture techniques to statically and dynamically quantify pistoning, with reported values from 1.1 to 7.5 cm, depending on the type of socket [2]. However, the actual magnitudes and patterns of loading at the stump-socket interface (SSI) over a continuous gait cycle have not been fully characterized. The SSI is typically considered to be a rigid connection in musculoskeletal modeling studies [3]. Knowledge of the actual motions and forces at the SSI would lead to more realistic and informative simulations. Our long-term goal is to develop new prostheses that reduce SSI loads and decrease the incidence of soft tissue injury. The specific purpose of this study was to examine the stump-socket kinematics and kinetics during walking across a range of speeds in transtibial (TT) amputees.

METHODS

Data were collected for three subjects, two with a left-side TT amputation and one with a right-side TT amputation. Each subject had a shuttle lock connecting the sleeve and socket, standard pylon and a split toe flex foot. The subject demographics and walking speeds are listed in table 1.

Table 1: Subject demographics and speeds of trials.

Subject	1	2	3
Height (m)	1.88	1.70	1.80
Mass (kg)	104.3	80.7	68.0
Preferred (m/s)	1.26	1.35	1.27
Slow (-20%)	1.02	1.14	1.05
Fast (+20%)	1.47	1.67	1.57

Data analysis was performed using a three-dimensional unilateral TT amputee model that we created [4] by modifying one of the standard gait models provided with OpenSim (gait2354). A residual tibia/fibula (stump) segment articulated with the socket via a joint at the most distal aspect of the stump, representing the SSI. The socket and pylon were connected to a model of a split-toe flex foot via a pin joint. The entire model has 25 degrees of freedom, including pistoning and flexion-extension at the stump-socket joint.

Kinematic data were captured using a full-body marker set and were synchronized with ground reaction forces measured using three force platforms. Inverse kinematics and inverse dynamics analyses were performed in OpenSim and results were averaged over three trials per subject for each speed, and then averaged across subjects within a speed. Data from some non-consecutive gait cycles were joined, resulting in a small discontinuity at approximately 80% of stance (Figure. 1).

RESULTS AND DISCUSSION

The amount of pistoning ranged from 2.42-2.69 cm which is within the range reported in the literature [2] (Figure 1, Table 2). The peak pistoning force occurred in the first half of stance and ranged from 0.94-1.05 bodyweights (Table 2). The peak pistoning force occurred earliest and had the greatest magnitude at the fast gait speed (Figure 1). There was 11-16° of socket flexion-extension at the SSI, with the greatest amount of motion occurring with the fast gait speed (Figure 1, Table 2). The peak extension moment occurred at approximately 80% of stance and was greatest for the slow gait speed (Figure 1). At the slower speed, the subjects limited the amount of socket flexion moment at the beginning of stance (Figure 1). At the preferred speed there was the greatest flexion moment at the beginning of stance, but the smallest extension moment at the end (Figure 1).

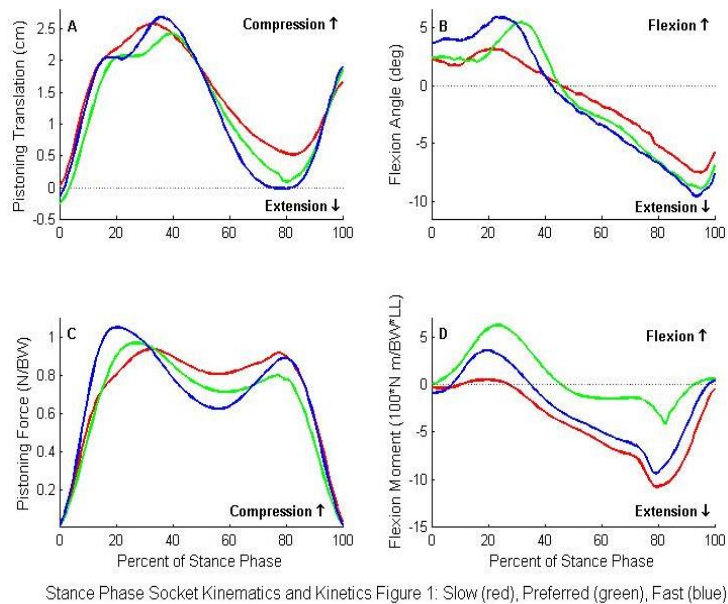


Figure 1: Stance phase socket kinematics and kinetics. Slow speed (red), preferred speed (green), and fast speed (blue).

Table 2: Peak socket kinematic and kinetic values averaged across subjects.

	Pistoning Motion (cm)	Pistoning Force (N/BW)	Socket Flexion (°)		Socket Moment (100*N m/BW*LL)	
			Flexion	Extension	Flexion	Extension
Slow	2.57 ± 0.74	0.94 ± 0.04	3 ± 4	8 ± 4	0.49 ± 0.95	10.74 ± 0.95
Preferred	2.42 ± 0.63	0.97 ± 0.05	5 ± 4	9 ± 4	6.22 ± 2.99	5.01 ± 2.99
Fast	2.69 ± 0.64	1.05 ± 0.08	6 ± 4	10 ± 4	3.56 ± 1.13	9.34 ± 1.13

The pistoning force was around one body weight and the bending moment at the SSI exceeded typical hip and knee joint moment magnitudes. Unlike the case for typical joint kinetics (e.g., knee joint forces and moments), the relatively large pistoning force and bending moment at the SSI are borne by a small area of soft tissue that was not meant to withstand such loading. Interestingly, the peak extension moment, which will correspond with a high pressure concentration on the proximal anterior stump, had the smallest magnitude at the preferred speed (Figure 1, Table 2). Amputees may have difficulty coordinating their movement patterns in such a way as to minimize this loading when walking at non-preferred speeds.

The data demonstrated amputees potentially make compensations with the amount of motion and loading at the SSI when walking at non-preferred speeds. The compensations made may increase stump loading at a susceptible site for skin lesions in late stance. More subjects with different types of prosthetics and diverse preferred speeds need to be collected to increase the generalizability of the findings.

REFERENCES

1. Ziegler-Graham K, et al. *Arch Phys Med Rehabil* **89**, 422-429, 2008.
2. Eshraghi A, et al. *Pros Orthot Int* **36**, 15-24, 2012.
3. Fey NP, et al. *J Biomech Eng* **134**, 111005, 2012.
4. Wedge RD, et al. *Congress of the International Society of Biomechanics*, Glasgow, UK, 2015.

ACKNOWLEDGEMENTS

Supported by a Grant from the National Center for Simulation in Rehabilitation Research.

INDIVIDUALS USING AN ANKLE-FOOT ORTHOSIS HAVE MINIMAL GAIT DEVIATIONS WHEN ACCOMMODATING TO WALKING ON A CROSS SLOPE

^{1,2}Jennifer M. Aldridge Whitehead, ^{1,2}Christopher A. Rábago, and ^{1,2}Jason M. Wilken

¹Center for the Intrepid, Department of Orthopaedics and Rehabilitation, Brooke Army Medical Center,

²DoD-VA Extremity Trauma and Amputation Center of Excellence, JBSA Ft. Sam Houston, TX, USA

email: Jennifer.m.whitehead7.civ@mail.mil

INTRODUCTION

Individuals regularly negotiate non-level terrain during their daily activities. Walking on non-level surfaces, such as cross slopes, requires altered lower extremity biomechanics compared to level ground walking [1]. Dixon and Pearsall [1] observed that while walking on a cross slope healthy individuals increased downslope limb extension and upslope limb flexion in order to functionally lengthen and shorten the downslope and upslope limbs, respectively. Additionally, they observed that the downslope ankle was more inverted while the upslope ankle was more everted to allow the foot to conform to the cross slope walking surface.

Walking on a cross slope may be more difficult for military personnel who are often required to traverse non-level surfaces while carrying loads. The task may become increasingly more challenging for military personnel who have sustained a lower extremity injury resulting in the use of a semi-rigid passive dynamic ankle-foot orthosis (AFO) [2]. AFO use may limit the ability of the foot/ankle to accommodate to the cross slope walking surface. The purpose of this study was to characterize lower extremity kinematic responses made by uninjured individuals and identify gait deviations in individuals utilizing a passive dynamic AFO when walking on a cross slope during a simulated military patrol task.

METHODS

Eleven uninjured service members (33.2±7.0yrs, 1.80±0.06m, 87.9±7.9kg; CONT) and twelve service members prescribed a custom AFO for a unilateral lower extremity musculoskeletal injury (35.4±5.8yrs, 1.83±0.08, 90.0±16.5kg; AFO) participated. All participants wore a standard issued military kit consisting of a Kevlar vest and helmet

and carried a mock M4 rifle. Participants walked in a Computer Assisted Rehabilitation Environment (Motek Medical, Amsterdam) on a 6-degree-of-freedom platform with embedded treadmill during a reality-based simulated patrol. They walked for one minute at a controlled speed, based on leg length, during three platform conditions: 1) level ground, 2) 5° tilt to the left, and 3) 5° tilt to the right (Fig. 1).

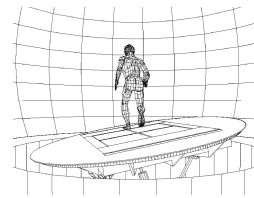


Figure 1. Representative illustration of a cross slope with the platform tilted to the left.

A 24 camera motion capture system (120 Hz; Vicon Peak, Oxford, UK) tracked 61 markers located on 13 body segments, the helmet, and rifle. Marker data were filtered with a low pass Butterworth filter (6 Hz) and lower extremity kinematics were calculated within Visual 3D (C-Motion Inc., Germantown, MD). AFO data was grouped by a tilt toward the AFO limb or the uninjured limb, and compared to the right limb of CONT during the same platform condition. A 2x2 ANOVA compared between groups and within limbs ($p<0.05$). Paired t-tests were used to compare the right limb during each platform condition within the CONT group ($p<0.05$).

RESULTS AND DISCUSSION

Similar to previous reports of cross slope walking, CONT functionally lengthened their downslope limb while shortening their upslope limb. Compared to level ground walking, the downslope limb was more extended throughout the gait cycle to include reduced midstance and swing ankle dorsiflexion ($p<0.03$), greater push-off ankle plantarflexion ($p<0.001$), reduced swing knee and hip flexion ($p<0.03$), and greater late stance hip extension

($p=0.003$). Alternately, the upslope limb was more flexed to include greater midstance ankle dorsiflexion ($p<0.001$), reduced push-off ankle plantarflexion ($p=0.002$), greater stance and swing knee flexion ($p<0.02$), reduced late stance knee extension ($p=0.013$), greater early stance and swing hip flexion ($p<0.001$), and reduced stance hip extension ($p<0.001$) (Fig. 2).

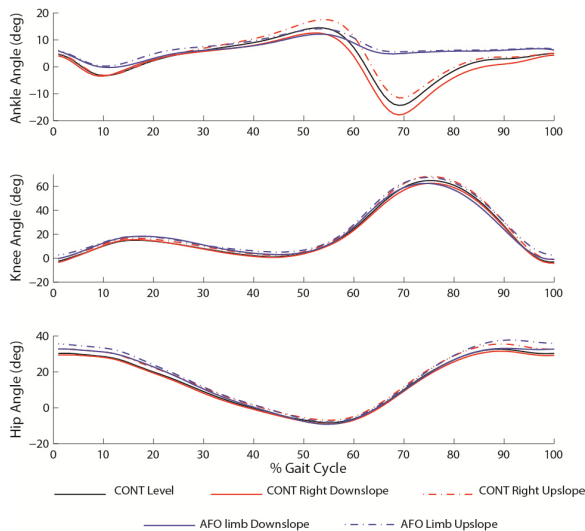


Figure 2. Sagittal plane ankle, knee, and hip kinematics during level walking in CONT and the upslope and downslope limb for both CONT and AFO.

Additionally, the frontal plane tilt of the treadmill elicited kinematic changes within the frontal plane when CONT walked on a cross slope. Compared to level ground walking, CONT had greater downslope limb ankle inversion ($p<0.001$) and greater upslope limb ankle eversion ($p<0.001$). Throughout the gait cycle the pelvis was more rotated in the frontal plane toward the downslope limb than during level walking ($p<0.05$) (Fig. 3).

However, the AFO group did not make the same biomechanical changes at the ankle to the cross slope as CONT. AFO had significantly less movement at the AFO ankle in all planes ($p<0.05$) compared to CONT during all platform states due to the semi-rigid nature of the device and the medio-lateral support that the device is designed to provide. As a compensatory response to the reduced AFO ankle mobility the AFO group had greater frontal plane pelvic rotation towards the AFO limb regardless of platform state than was observed in CONT. The limited AFO ankle motion

did not result in differing sagittal plane responses at the ipsilateral knee and hip or the contralateral limb to the cross-slopes between groups (Fig. 2).

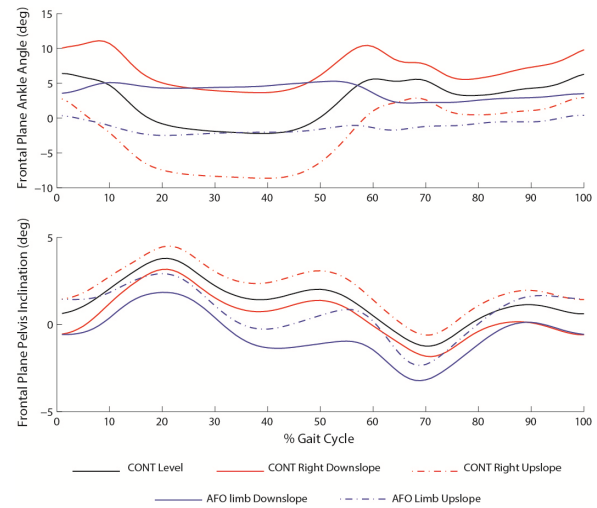


Figure 3. Frontal plane ankle angle and pelvic inclination angle during level walking in CONT and the upslope and downslope limb for both CONT and AFO.

CONCLUSIONS

Both injured and uninjured military personnel used greater downslope limb extension and greater upslope limb flexion while walking on a cross slope during a simulated military task. Service members with traumatic lower extremity musculoskeletal injuries requiring a passive dynamic AFO had limited ankle motion in all three planes. The limited motion at the ankle joint did not result in any significant differences in the sagittal plane at the ipsilateral knee and hip or contralateral limb between injured and uninjured participants. However, the inability of the AFO foot to conform to the tilted surface because of limited frontal plane ankle motion elicited changes in frontal plane pelvic motion.

REFERENCES

1. Dixon, PC and Pearsall, DJ. *J Applied Biomech* **26**, 17-25, 2010.
2. Patzkowski, JC., et al. *J Surg Orthop Adv* **20**, 8-18, 2011

ACKNOWLEDGEMENTS

Support for this study was provided by the Center for Rehabilitation Sciences Research, Dept. of Physical Medicine and Rehabilitation, Uniformed Services Univ. of Health Sciences, Bethesda, MD.

COPD PATIENTS EXHIBIT SIMILAR JOINT ANGLE VARIABILITY COMPARED TO OLDER, HEALTHY CONTROL SUBJECTS

¹ Casey Wiens, ¹ John McCamley, ² Stephen I. Rennard, ¹ Jennifer M. Yentes

¹ University of Nebraska - Omaha, Omaha, NE, USA
University of Nebraska Medical Center, Omaha, NE, USA
email: cwiens@unomaha.edu, web: cobre.unomaha.edu

INTRODUCTION

Chronic obstructive pulmonary disease (COPD) is a syndrome characterized by expiratory airflow limitation; however, the effects of the disease reach further than just the respiratory system. For example many patients report muscle fatigue as the main limiting factor to activity as opposed to dyspnea, indicating muscular limitations [1]. Another possible limitation may be gait; however, an investigation of biomechanics of gait in COPD patients revealed only moderate changes to their ankle mechanics as compared to healthy controls [2]. Moreover, COPD patients walk with a more periodic step length and step width at their preferred walking speed than healthy controls [3]. COPD patients walk with greater mediolateral variability than healthy controls and this walking variability was associated with functional capacity [4]. Therefore, it is feasible that variability measures of gait may be more sensitive to discriminating gait dysfunction in patients with COPD versus healthy controls.

Variability is an inherent characteristic in all physiological systems and the level of variability has two extremes. On one end of the spectrum, a highly variable, yet irregular system is uncoordinated; whereas a highly regular, invariable system is unable to adapt to perturbations. According the optimal movement variability theory, a healthy system is a highly variable system, in which the fluctuations have deterministic properties [5]. A diseased physiological system is characterized by a level of variability away from the optimal level, either too variable and irregular or too periodic. Thus, healthy physiological systems present a moderate level of predictability (i.e. regularity) and a high level of complexity.

Therefore, our aim was to compare the joint angle variability in patients with COPD to healthy, older control subjects using the Lyapunov exponent. It was hypothesized that patients with COPD would exhibit an increase in variability of the ankle joints compared to healthy controls as deficits in ankle mechanics in patients with COPD have been determined previously [2].

METHODS

A total of nine healthy controls (70.2 ± 7.1 yrs; 176.9 ± 8.7 cm; 80.1 ± 17.0 kg) and nine patients with COPD (66.3 ± 9.3 yrs; 176.2 ± 14.3 cm; 101.8 ± 36.5 kg) participated in this study. A spirometry test revealing a $FEV_1/FVC > 0.7$ categorized the subjects into the COPD group. Both groups reported no lower extremity injuries or pathologies that would alter normal gait. The groups were speed matched (post hoc) to attenuate speed as a factor (COPD = 0.88 ± 0.21 m/s; Control = 1.00 ± 0.27 m/s).

Subjects walked for four minutes at a self-selected speed on a treadmill while three dimensional marker trajectories were recorded (MAC, Santa Rosa, CA; 60Hz). The kinematic data were tracked in Cortex (MAC, Santa Rosa, CA) and were unfiltered, providing the true fluctuations over time. Visual 3D (C-Motion, Germantown, MD) was used to calculate the joint angles. Using Wolf's algorithm [5], the Lyapunov exponent of the ankle, knee, and hip joints was calculated in MatLab (MathWorks, Natick, MA). The Lyapunov exponent was calculated from 14400 frames of continuous joint angle data. The lag and embedding dimension used for each subject's Lyapunov exponent calculation was specific to each individual. Lag ranged from 9-53 in the COPD group and 8-30 in the control group, while the embedding dimension ranged from 5-9 in the COPD group and 5-8 in the control group. Group mean Lyapunov

exponent values for each joint were compared using an independent t-test.

RESULTS AND DISCUSSION

Contrary to our hypothesis, the Lyapunov exponent for the ankle angle was not different between the two groups ($p=0.99$; Table 1). In fact, no significant differences were found between the groups at any joint (knee: $p=0.40$; hip: $p=0.35$). The ankle angle demonstrated the greatest Lyapunov exponent value across all three joints. The Lyapunov exponent quantifies the rate at which an attractor is diverging. A larger Lyapunov exponent value indicates larger stride-to-stride fluctuation in the joint angles, while a smaller Lyapunov exponent value represents a more organized and consistent system. As can be seen in Figure 1, although there were no significant differences in the group means, a few patients with COPD did demonstrate a less consistent attractor. It is feasible that some patients with COPD have greater variation in movement and some have less, this is consistent with heterogeneity and the presentation of phenotypes in the patient population.

Although not significant, it is interesting to note that the patients with COPD exhibited decreased knee and hip Lyapunov exponent values as compared to the controls. A smaller number would indicate that the attractor is diverging at a slower rate and possibly maintaining a more consistent pattern. This would indicate an altered organization of the neuromuscular system compared to older healthy control, with the possibility of the knee and hip compensating for the ankle.

CONCLUSIONS

These results do not support our hypothesis that COPD patients would exhibit an increase in ankle joint angle variability compared to older, healthy controls. Although COPD patients alter gait in the

mediolateral direction [4], these results suggest that it does not affect joint angles in the anteroposterior plane. Although no significant differences were found in this study, further investigation into the effects of COPD on gait variability should be done due to variability's association with functional capacity.

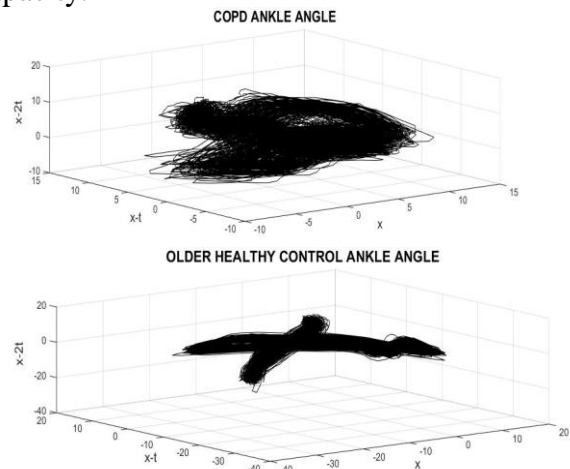


Figure 1: Top: The relative phase of the right ankle joint for a representative COPD subject. Bottom: The relative phase of the right ankle joint for a representative healthy control subject.

REFERENCES

1. Coronell C, et al. *Euro Respiratory J* **24**, 129-136, 2004.
2. Yentes J, et al. *Respir Res.* **16**, 31, 2015.
3. Yentes J, et al. *Proceedings of WCB '14*, Boston, MA, USA.
4. Annegarn J, et al. *PlosOne.* **7**, 1-6, 2012.
5. Stergiou S, *J Neuro Phys Ther* **30**, 120-29, 2006.
6. Wolf A, et al. *Physica D* **16**, 285-317, 1985.

ACKNOWLEDGEMENTS

We would like to thank Jenny Kent for her assistance throughout this project.

Table 1: Calculated Lyapunov exponent values for both groups and all three joints.

Joint Angle (LyE)	Joint		
	Ankle (bits/sec)	Knee (bits/sec)	Hip (bits/sec)
Patients with COPD (n = 9)	1.798 ± 0.91	0.917 ± 0.23	0.725 ± 0.18
Older, Healthy Controls (n = 9)	1.793 ± 0.73	1.030 ± 0.32	0.860 ± 0.38

KINEMATIC PREDICTORS OF TIBIOFEMORAL AND PATELLOFEMORAL JOINT IMPULSE DURING RUNNING

John D. Willson¹, Richard W. Willy¹, Stacey A Meardon¹, Joaquin A. Barrios²

¹ East Carolina University, Greenville, NC

² University of Dayton, Dayton, OH

Email: willsonj@ecu.edu

INTRODUCTION

Elevated tibiofemoral joint (TFJ) and patellofemoral joint (PFJ) contact forces are believed to contribute to the etiology and exacerbation of knee joint symptoms [1, 2]. To promote participation in regular exercise it is important to minimize or avoid these symptoms. Evaluation and treatment of knee joint injuries that are sensitive to elevated knee joint contact forces may be facilitated by development of methods to estimate these parameters in a clinical setting. In this way, clinicians could identify individuals who are likely to benefit from interventions to reduce knee joint contact forces as well as evaluate the effectiveness of their interventions. Kinematic gait analysis is a feasible clinical assessment that is routinely performed in many settings. The purpose of this study was to test for a set kinematic measurements to predict total TFJ and PFJ contact force (impulse) during running.

METHODS

A total of 56 individuals (26 males, 30 females: 22.6 years) participated in this study. All participants reported regular participation in recreational activities that include running or jumping at least twice per week. Three-dimensional lower extremity joint kinematics (200 Hz) and ground reaction forces (1000 Hz) were recorded as participants ran at 3.3 m/s using their preferred foot strike pattern. These data were used to derive hip, knee, and ankle sagittal plane angles, net internal joint moments, and joint reaction forces using an inverse dynamics approach. Muscle cross sectional area, line of action, and moment arms as a function of joint position at each joint were derived from the

literature to estimate quadriceps, hamstrings, and gastrocnemius muscle forces during the stance phase of 5 steps for each participant [3]. Patellofemoral joint contact force was determined using quadriceps force after adjusting for co-contraction of the knee flexors. Tibiofemoral joint contact force was estimated as the sum of knee joint reaction forces and muscle force components parallel with the long axis of the tibia. Total PFJ and TFJ force (impulse) per step was calculated as the integral of these forces curves. Estimated TFJ impulse using this model is within 7% of *in vivo* TFJ joint impulse recorded from an instrumented prosthesis during walking [4].

Six different kinematic measurements during running were evaluated as possible predictors of average TFJ and PFJ impulse: peak trunk flexion angle, peak knee flexion angle, peak ankle dorsiflexion angle, vertical excursion of the participant center of mass during stance, knee angle at initial contact, and step length. Following tests for multicollinearity among the predictor variables, the most parsimonious set of kinematic predictors was determined using separate stepwise multiple linear regressions to predict TFJ and PFJ impulse with a bidirectional elimination approach.

RESULTS

Mean TFJ impulse of the sample was 1.24 (0.17) BW*s. Five kinematic variables (all except peak trunk flexion angle) were found to predict over 75% of the variability in TFJ impulse ($\text{Adj } R^2 = .76$, $P < .001$). Using these kinematic predictors it is possible to predict TJF impulse to within 0.165 BW*s, resulting in an estimate that is expected to be within 13% of the measured TFJ impulse (Figure 1).

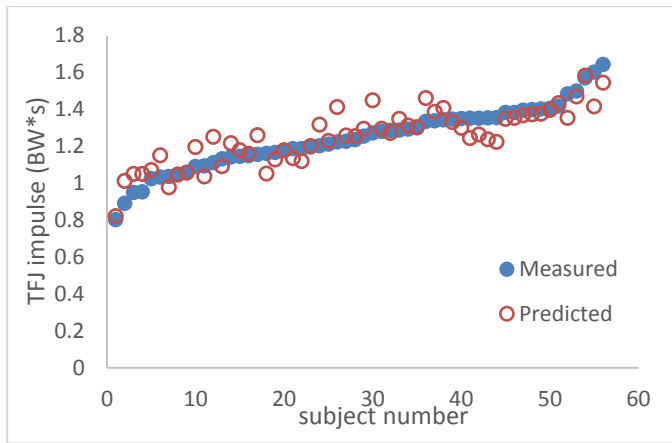


Figure 1. Predicted tibiofemoral joint (TFJ) impulse during running using only kinematic data (predicted) and TFJ impulse estimated using a biomechanical model with kinematic and kinetic inputs (measured).

Mean PFJ impulse of the sample was 0.51 (0.13) BW*s. Peak knee flexion, vertical excursion of the center of mass, and peak ankle dorsiflexion were found to predict over 75% of the variability in PFJ impulse ($\text{Adj } R^2 = .76$, $P < .001$). These kinematic variables alone predicted PFJ impulse to within 0.13 BW*s, which is within 25% of the mean PFJ impulse in our sample (Figure 2).

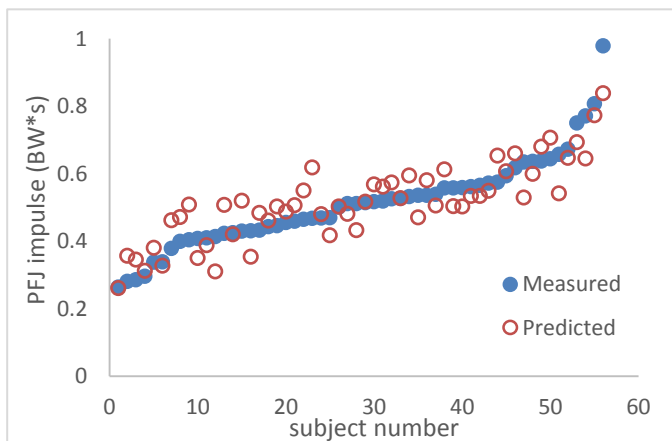


Figure 2. Predicted patellofemoral joint (PFJ) impulse during running using only kinematic data (predicted) and PFJ impulse estimated using a biomechanical model with kinematic and kinetic inputs (measured).

DISCUSSION

The purpose of this study was to test for a set of kinematic variables that could be used to predict TFJ and PFJ impulse during running. We determined that sagittal plane kinematic data alone can be used to generate fair estimates of both TFJ and PFJ impulse during running. Efforts to refine and improve model accuracy in the future may

incorporate frontal and transverse plane kinematics, as these also affect TFJ and PFJ impulse and are often implicated in running related injuries.

The accuracy of the TFJ impulse prediction exceeded that for PFJ. This suggests that sagittal plane kinematics may be particularly suitable for analysis of TFJ disorders during running. In light of the growing popularity of running as exercise among people with TFJ OA and people with risk factors for TFJ OA, these results offer some clinical utility. PFJ impulse prediction was less accurate and would benefit from further refinement of the kinematic predictors. It should be noted that increased peak knee flexion, vertical excursion of the center of mass, and peak ankle dorsiflexion made significant contributions to the prediction of both PFJ and TFJ impulse. Further refinement of the kinematic predictors may improve prediction of both PFJ and TFJ impulse.

Towards clinical utility of biomechanical models, further testing of these predictor variables, acquired with three dimensional motion analysis, is needed. Two dimensional technologies are more pervasive in clinical settings. Theoretically, each predictor variable used in this study could be quantified using a single video camera positioned lateral to a standard treadmill, representing an area for future study.

CONCLUSIONS

Kinematic variables alone produce a fair prediction of TFJ impulse and, to a lesser extent, PFJ impulse during running. The ability to estimate knee joint loads using kinematic data offers promise as a clinical tool for analysis of interventions to reduce TFJ and PFJ loads during running as well as in the identification of people at risk for injury associated with elevated joint loads. Identification of kinematic variables to increase the predictive validity of the model will further improve the clinical utility of these results.

REFERENCES

1. Farrokhi et al. *Osteoarthritis Cartilage* 19:287-294, 2011.
2. Peeler et al. *Clin J Sport Med*, [epub], 2015.
3. DeVita et al. *J Appl Biomech* 17:297-311, 2001.
4. Fregly et al. *J Orthop Res* 30:503-513, 2012.

ANKLE KINEMATICS OF SERVICE MEMBERS WITH AND WITHOUT TRANSTIBIAL AMPUTATION WHILE WALKING ON A SPLIT BELT TREADMILL

^{1,2}Erik J. Wolf, ^{1,3}Devjani Saha, ^{4,5}Benjamin J. Darter

¹Department of Rehabilitation, Walter Reed National Military Medical Center

²DoD-VA Extremity Trauma and Amputation Center of Excellence

³BADER Consortium, University of Delaware

⁴Department of Physical Therapy, Virginia Commonwealth University

⁵Department of Research, Hunter Holmes McGuire VA Medical Center

email: erik.j.wolf6.civ@mail.mil

INTRODUCTION

Temporal-spatial, kinematic, and kinetic asymmetries during gait in persons with unilateral amputation have been well documented [1]. Existing evidence suggests split-belt treadmill based interventions have potential to improve gait symmetry. Specifically, a single session case study of a split-belt treadmill walking intervention showed improved gait symmetry in an individual with a transfemoral amputation [2]. The potential of a multi-session training study to improve gait symmetry in persons with an amputation can be substantiated by research in stroke survivors [3]. However, descriptions of potential training benefits beyond temporal-spatial symmetry are lacking.

Research to quantify the adaptive responses of persons with lower limb amputation when exposed to a split-belt treadmill walking intervention is needed to inform the design of a potential training intervention. Therefore the overall goal of this study was to examine adaptability to a split belt treadmill walking intervention for persons with lower limb amputation. This report focuses on the ankle kinematic strategies used when uninjured participants and those with transtibial amputation (TTA) walk during a split belt treadmill intervention. We hypothesized that participants with TTA would use different strategies at the ankle to walk on a split belt treadmill, specifically indicating greater reliance on the intact limb as defined by peak flexion angles.

METHODS

Eight participants, 4 TTA and 4 uninjured, were enrolled in the study. All participants provided written informed consent, and all study procedures were approved by the local IRB.

Participants were fit with up to 70 retro-reflective markers and data was collected with a 27 camera motion capture system (Vicon, Oxford UK). Participants were asked to walk on a split-belt instrumented treadmill (Bertec, Columbus, OH) for 4-minute to serve as an acclimation period. Foot marker data from the acclimation period were used to quantify step length (heel strike to contralateral heel strike) of each limb which was used to assign belt speeds during the subsequent split-belt intervention conditions; the limb with the shorter step length was assigned to the fast pace (1.5 m/s) condition whereas the limb with the longer step length was assigned to the slow pace (0.5 m/s) condition [3]. Participants then completed 4 walking conditions in order: belts tied at a slow pace for 5 minutes, belts tied at a fast pace for 2 minutes, belts split at a slow and fast pace for 15 minutes, and belts tied at a slow pace for 5 minutes. Ankle kinematics and stance times were created using Visual 3D (C-motion, Germantown, MD).

RESULTS AND DISCUSSION

TTA had a step length difference of greater than ± 4 mm (two standard deviations outside of uninjured population [4]). All uninjured participants had slightly shorter step lengths on their left limb, while all TTA had shorter step lengths on their intact limb.

The stride length of the intact limb for participants with TTA is very consistent with the left limb of uninjured participants. During the split condition, the intact limb plantar flexion prior to toe-off was slightly increased in the TTAs ($-16.7\{7.4\}$ vs. $-13.8\{6.2\}$ degrees). Additionally, the TTA spend less time in stance compared to the uninjured group (Table 1).

Table 1 – Stance time (s) for uninjured participants and TTA while walking in 4 conditions

Condition	LEFT / INTACT		RIGHT / PROSTHETIC	
	Control	TTA	Control	TTA
Before Split 0.5 m/s	1.06s±0.06s	1.20s±0.07s	1.07s±0.05s	1.15s±0.05s
Before Split 1.5 m/s	0.62s±0.02s	0.61s±0.03s	0.62s±0.02s	0.60s±0.02s
Split Belt Condition	0.62s±0.03s	0.60s±0.03s	0.91s±0.05s	0.84s±0.08s
After Split 0.5 m/s	1.11s±0.13s	1.19s±0.08s	1.13s±0.13s	1.13s±0.07s

TTA prosthetic limb differences appear to be limited when compared to uninjured participants. TTA prosthetic dorsiflexion setting was at 6.9{2.1} degrees. TTA tended to have higher peak dorsiflexion during fast walking compared to uninjured participants (22.2{3.7} vs. 16.9{3.5} degrees), while this trend was reversed in the split belt condition (18.6{3.6} vs. 21.2{3.6} degrees).

Limited differences were seen in the sagittal ankle kinematics of uninjured participants and TTA when walking on a split belt treadmill. This may have occurred because the intact limb of the TTA was assigned to the fast belt in the split condition for all participants. The results may have been different had the prosthetic foot had to compensate to greater belt speeds. When examining the stance times however, this paradigm may provide a potential training benefit as it forces increased stance times on the prosthetic limb. However, this result does not carry over once the split belt condition is removed, implying that repetitive training would be required for retention.

CONCLUSION

Ankle kinematics change in a similar manner for TTAs and uninjured participants when exposed to split-belt walking. Mechanical limitations of the prosthetic device (decreased range of motion compared to the intact limb) have a greater effect than any potential difference in adaptive capacity. Kinetic changes at the ankle should be further explored to determine strategies that may be occurring in the intact limb to aid in walking.

REFERENCES

- [1] Sanderson DJ, et al. Gait Posture, 6(2), 126-136, 1997
- [2] Kim SH, et al. AAOP Annual Meeting and Scientific Symposium. Feb. 20-23, 2013. Orlando, FL
- [3] Reisman DS, et al. Neurorehab Neural Re, 27(5), 460-468, 2013
- [4] Reisman DS, et al. Neurorehab Neural Re, 23(7), 735-44, 2009

ACKNOWLEDGEMENTS

This work was supported by the Bridging Advanced Developments for Exceptional Rehabilitation (BADER), Clinical and Translational Science Awards (CTSA) No. KL2TR000057 from the National Center for Advancing Translational Sciences, and the DoD-VA Extremity Trauma & Amputation Center of Excellence (Public Law 110-417, National Defense Authorization Act 2009, Section 723). The views expressed in this abstract are those of the authors and do not necessarily reflect the official policy of the Departments of the Army, Navy, Defense, the United States Government nor National Institute of Health.

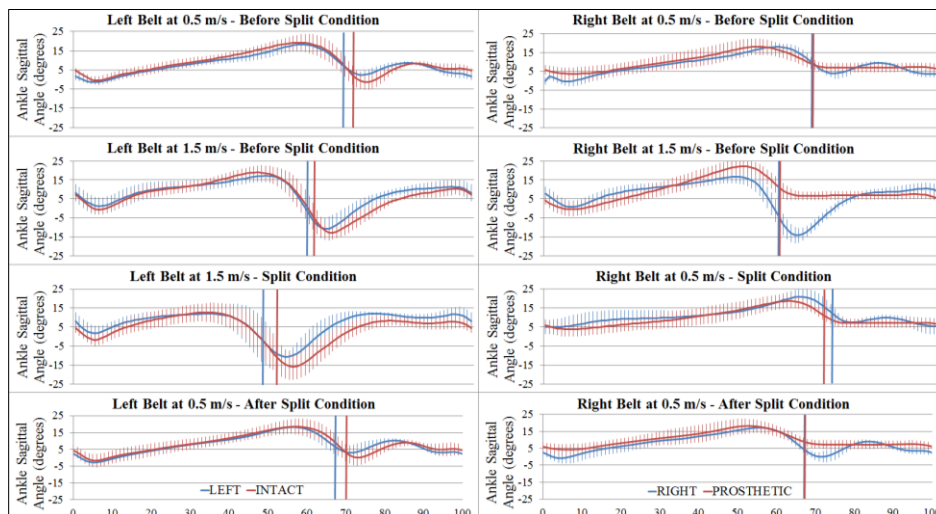


Figure 1 – Ankle kinematics for uninjured participants (blue) and TTA (red) while walking in 4 conditions.

The Effects of Longitudinal Training on Walking Navigation Through a Complex Environment

¹ Timothy A. Worden and ¹ Lori Ann Vallis

¹ University of Guelph, Guelph, ON, Canada
email: tworden@uoguelph.ca, lvallis@uoguelph.ca

INTRODUCTION

Dual-task interference occurs when the cognitive resources shared between two attentionally demanding tasks (e.g. concurrent walking and backwards counting) exceed the available capacity of attentional resources. Research indicates that the amount of dual-task interference increases as tasks require more attention (such as navigating a complex and sensory rich environment) [1]. Dual-task training has been shown to improve dual-task performance in simple reaction time paradigms [2] likely due to optimization of cognitive processes, however the effects of training on complex dual-task situations remain unknown.

The **purpose** of this study was to examine the efficacy of training healthy young adults with concurrent walking and cognitive tasks to improve dual-task performance in a complex environment. We hypothesized that the concurrent training of walking while performing cognitive tasks would improve the sharing efficiency of attentional resources, and thus improve dual-task performance. Furthermore, we believed that duration of training would affect results, with individuals who receive training for a longer duration (four weeks) demonstrating larger improvements than shorter training sessions (one week) or no training at all.

METHODS

Healthy young adults were randomly assigned to either a no training control group (N=9), a one week training group (N=10) or a four week training group (N=12). Participants were tested at baseline (Visit A), one week following the cessation of training (Visit B) and again 6 weeks later to test for learning retention effects (Visit C). Each testing session was the same design, with participants performing a total of 40 randomized dual-task trials. The

cognitive task performed was an auditory Stroop task, and the walking task involved stepping over a dynamic obstacle scaled to 50 % of lower leg length that either moved from a low to high position as subjects approached, or remained stationary [1]. Training was twice a week for 30 minutes; and involved walking tasks (e.g. walking in a pattern) while simultaneously performing various cognitive tests (e.g. backwards counting).

Kinematic data was collected at 60 Hz to quantify stepping patterns. Kinematic outcome measures calculated were minimum lead foot clearance (MLC), minimum trail foot clearance (MTC), take off distance (TOD) and landing distance (LD). Furthermore, mediolateral (ML) dynamic margin of stability (MOS) was calculated for two steps before obstacle crossing, one step before obstacle crossing and the obstacle crossing step [3]. Accuracy for correctly answering the cognitive task was also recorded. A Pearson's Chi Square test was performed to determine differences in cognitive test accuracy. A between-groups repeated measures ANOVA design was performed to identify any changes in outcome measures across the three Visits; statistical significance level was $p < 0.05$.

RESULTS AND DISCUSSION

Participants in the four week training group improved their response accuracy from Visit A to Visit C (92 % to 95 %), while the other training groups showed no change in their ability to accurately answer the auditory Stroop task. In contrast to expected results, improvements in cognitive task performance were not observed directly following training in any group.

Examining MLC, there were no significant differences between groups or testing sessions. For MTC, there was an effect of group, with both

training groups significantly increasing MTC for Visit C as compared to Visit A, while the control group decreased MTC on Visit C, as illustrated in Figure 1. These results indicate that all trained participants adopted a more cautious obstacle clearance strategy with the trailing foot.

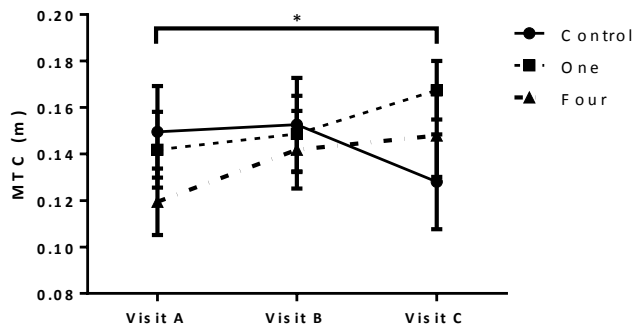


Figure 1: MTC values for the three groups; MTC was increased for all trained individuals in Visit C compared to Visit A ($p < 0.05$).

When examining foot placement before obstacle crossing, the Control group maintained a consistent TOD over the three testing sessions, while both training groups significantly increased their TOD from Visit A to Visits B and C (Figure 2; $p < 0.05$). However, due to differences between groups in takeoff distances in Visit A, it is difficult to conclude if training increased TOD or if, by chance, the control group naturally began with an more optimal takeoff distance, which both trained groups converged upon following training.

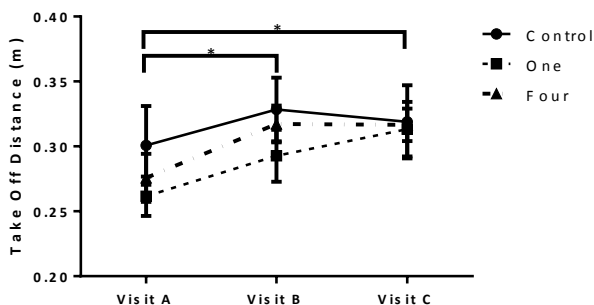


Figure 2: TOD values for the three training groups; TOD increased for all trained individuals in Visits B & C compared to Visit A ($p < 0.05$).

There were no significant effects, for landing distance measures indicating participants landed at the same distance from the obstacle regardless of testing session and training group.

ML MOS increased in only the trained groups, and only for two steps before the obstacle crossing. There was a trend for increasing MOS at obstacle crossing, although it was not significant. These results suggest that training can improve stability in less challenging steady state walking, however when stability becomes more challenged (as is the case for the step before obstacle crossing and the crossing step), training durations of one or four weeks were unable to increase dynamic stability.

CONCLUSIONS

Through short-term training, we were able to alter the performance of individuals as they navigated a complex environment by adopting a more cautious obstacle stepping strategy. Furthermore, trained individuals adapted a more stable walking strategy during over-ground walking, however stability returned to Visit A values during the more challenging obstacle avoidance and cognitive test. Interestingly, only the four week training group improved cognitive test accuracy, suggesting that as participants were trained, prioritization went to implementing more cautious locomotor strategies, with no significant improvements in the cognitive tests (until Visit C with the four week training group). These results suggest participants prioritized the adoption of strategies to improve postural efficiency with our training protocol, with no real improvements in cognitive task performance [4].

REFERENCES

1. Worden TA & Vallis LA. *J Motor Behav* **46**(5), 357-368, 2014.
2. Van Selst MA, et al. *J Exp Psychol: Hum Percept and Perform* **25**, 1268-1283, 1999.
3. McAndrew Young PM & Dingwell JB. *Gait & Posture* **36**, 219-224, 2012.
4. Siu K & Woollacott MH. *Gait & Posture* **25**, 121-126, 2007

WALKING PATTERN IN CHILDREN WITH AND WITHOUT DOWN SYNDROME VIA AN FORCE-DRIVEN HARMONIC OSCILLATOR MODEL

¹Jianhua Wu, ¹Matthew Beerse, ²Toyin Ajisafe, and ¹Huaqing Liang

¹Georgia State University, Atlanta, GA, USA. Email: jwu11@gsu.edu

²Texas A&M University, Corpus Christi, TX, USA

INTRODUCTION

Children with Down syndrome (DS) display poorer kinematic and kinetic patterns of walking than children with typical development (TD). It is generally suggested that low muscle tone and joint laxity contribute to motor deficits in children with DS. However, little is known on neuromuscular control in children with DS during locomotion. A force-driven harmonic oscillator (FDHO) model sheds light on general muscular activation with respect to the gravitational load of the thigh-shank-foot system. The K/G ratio derived from this model represents a scaling between the elastic restoring torque from muscles and soft tissues and the gravitational torque from the weight of the leg during walking. Clinically, this ratio was previously used to show different muscular function in infant walkers [1] and children with cerebral palsy [2]. This study aimed to compare the K/G ratio between children with and without DS while walking overground and on a treadmill.

METHODS

Participants: Twenty six children with and without DS aged 7-10 years completed overground walking at lab visit #1, and 20 children completed treadmill walking at lab visit #2. Of the 26 subjects, the DS group was 9.0 ± 1.3 years in age, 1.24 ± 0.08 m in height, and 30.6 ± 5.6 kg in body mass; the TD group was 9.1 ± 1.4 years in age, 1.33 ± 0.07 m in height, and 29.6 ± 5.1 kg in body mass.

Experimental design: At the first visit, participants walked barefoot overground at two speeds: normal (NS) and the fastest speed (FS). At the second visit, participants walked barefoot on a treadmill at 75% (NS) and 100% (FS) of the preferred overground speed. Two load conditions were manipulated at both visits: no load (NL) and ankle load (AL) that

was equal to 2% of body weight on each side. Average AL condition was 6.0 N in the DS group and 5.9 N in the TD group.

Data collection:

A total of four conditions (2 treadmill speed by 2 ankle load) were tested at both lab visits. The order of condition presentation was mostly randomized across the two groups. A 7-camera Vicon motion capture system was used to register reflective markers attached bilaterally to the subjects. Four trials were collected for each condition during overground walking. A Zebris FDM-T instrumented treadmill was used to register vertical ground reaction force during treadmill walking. Two 60-second trials were collected for each condition.

Data analysis: Customized Matlab programs were used to determine gait events such as heel contact and toe off for overground and treadmill walking trials. An FDHO model [3] represents a hybrid pendulum-spring system that consists of a single pendulum and a spring attached to the pendulum. The simple pendulum represents the gravitational contribution of the thigh-shank-foot system facilitating the passive dynamics of the system, and the spring represents the contribution of muscles and soft tissues facilitating the active dynamics of the system during walking. When ankle load is added, it becomes the thigh-shank-foot-ankle load system. For small amplitude of oscillation during walking, the periodic duration (i.e., stride time) can be predicted as below:

$$\tau = 2\pi \sqrt{\frac{mL^2}{mLg + kb^2}}$$

where τ is stride time, m is the mass, L is equivalent leg length of the system, g is gravitational acceleration (9.81 m/s^2), mL^2 is the moment of inertia of the system about the hip joint, mLg is the gravitational restoring torque associated with the

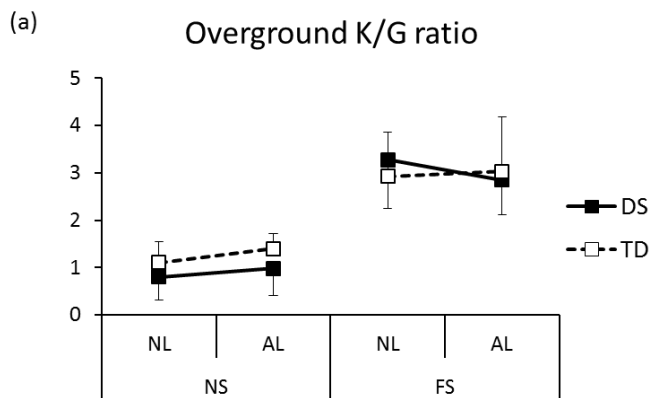
size and mass of the system, and kb^2 is the elastic restoring torque from muscles and soft tissues. This equation can be reduced as below:

$$\tau = 2\pi \sqrt{\frac{L}{g + \frac{kb^2}{mL}}} = 2\pi \sqrt{\frac{L}{(1 + K/G)g}}$$

Statistical analysis: Two 3-way (2 group x 2 speed x 2 load) ANOVA with repeated measures on the last two factors were conducted on the K/G ratio for overground and treadmill walking separately. Post-hoc pair-wise comparisons with Bonferroni adjustments were conducted when appropriate. Statistical significance was set at $p < 0.05$.

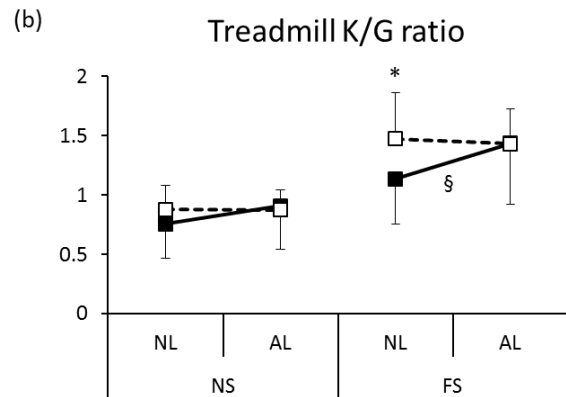
RESULTS AND DISCUSSION

During overground walking, the K/G ratio across the two groups was 1.07 in the NS condition and 3.02 in the FS condition. In other words, the ratio between the elastic and gravitational torques was about 1:1 in the NS condition and 3:1 in the FS condition for the two groups regardless of external ankle load (Fig. a). There was a speed effect on the K/G ratio ($p < 0.001$) such that both groups increased the K/G ratio from the NS to the FS condition.



During treadmill walking, the K/G ratio across the two groups was 0.85 in the NS condition regardless of external ankle load. In the FS condition, the DS group produced a lower K/G ratio of 1.14 compared to 1.47 in the TD group without ankle load, but a similar K/G ratio of 1.44 compared to 1.43 in the TD group with ankle load (Fig. b). There was a speed effect on the K/G ratio ($p < 0.001$) such that both groups increased this ratio from the NS to the FS condition. Also, there was a group by load interaction on the K/G ratio ($p = 0.007$). No

difference in the K/G ratio was observed in the NS condition between the two groups. However, in the FS condition, the DS group increased the K/G ratio from the NL to the AL condition while the TD group maintained the K/G ratio regardless of external ankle load. The DS group produced a lower K/G ratio at the fast speed of treadmill walking without ankle load, but the inclusion of ankle load helped children with DS produce a similar K/G ratio as their healthy peers.



Although no specific muscle was identified, the FDHO model demonstrates that children with DS are able to produce a similar general muscular activation as their healthy peers while walking overground, an important daily motor activity. However, children with DS may have difficulty in performing a novel task such as walking on a treadmill at a fast speed due to the limitations of their physical characteristics.

CONCLUSIONS

The inclusion of external ankle load appears to improve general muscle activation in children with DS, and it may be a promising training component when designing an intervention protocol to improve motor function in children with DS.

REFERENCES

1. Holt KG, et al. *Phys Ther* **87**, 1458-1467, 2007.
2. Jeng SF, et al. *J Mot Behav* **28**, 15-27, 1996.
3. Holt KG, et al. *Hum Mov Sci* **9**, 5-68, 1990.

ACKNOWLEDGEMENTS

We would like to thank the funding support from the Jerome Lejeune Foundation.

CHILDREN DISPLAY ADULT-LIKE KINETIC PATTERN IN THE TIME DOMAIN BUT NOT IN THE FREQUENCY DOMAIN WHILE WALKING WITH ANKLE LOAD

¹Jianhua Wu, ²Toyin Ajisafe, ¹Matthew Beerse, and ¹Huaqing Liang

¹Georgia State University, Atlanta, GA, USA. Email: jwu11@gsu.edu

²Texas A&M University, Corpus Christi, TX, USA

INTRODUCTION

Regulation of locomotion is highly related to control of gravitational load. While external load is added during locomotion, humans increase the activation of extensors during stance and suppress the initiation of flexors during swing [1]. External load at the ankles, rather than on the waist or thigh, elicits higher activities from ankle extensors, and increases stride length and decreases cadence in adults [2]. In contrast to many studies with adults, few have studied the effect of gravitational load on gait patterns in children. It is generally recognized that spatiotemporal and kinematic patterns become adult-like in children aged 5-8 years. However, little is known if children show adult-like kinetic patterns while walking with additional load. A frequency domain analysis of vertical ground reaction force (GRF) helps reveal gait abnormalities in children with cerebral palsy and Down syndrome. The purpose of this study was to investigate differences in kinetic patterns between children and adults while walking with external ankle load using both time- and frequency-domain analyses.

METHODS

Participants: Twenty two children and 20 adults participated in this study. The children group was 11M/11F, 9.2 ± 1.3 years in age, 1.33 ± 0.09 m in height, and 28.8 ± 5.5 kg in body mass. The adult group was 10M/10F, 23.7 ± 2.4 years in age, 1.69 ± 0.11 m in height, and 68.9 ± 12.9 kg in body mass.

Experimental design: Each subject walked three times across the 10-m walkway at their self-selected preferred speed and the average speed was used for treadmill walking. Treadmill speed was normalized to the subject's leg length: $\hat{v} = v/\sqrt{gl_0}$, where g is gravitational acceleration and l_0 is leg length.

Three bilateral ankle loads were manipulated: no load, low load (2% of body mass on each side), and high load (4% of body mass on each side). The order of load presentation was randomized across the two groups. A Zebris FDM-T instrumented treadmill was used to register vertical GRF during treadmill walking. Two 60-second trials were collected for each load condition.

Data analysis: Vertical GRF data were normalized to the subject's body weight (BW). Customized Matlab programs determined gait events (heel contact and toe off), and the timing and magnitude of the first peak force F_{Z1} after heel contact and the second peak force F_{Z2} before toe off. The timing was presented in % of stance and the magnitude was in multiples of BW.

A Fourier transform mathematically transforms vertical GRF into harmonics and each harmonic represents the contribution of certain anatomical components [3]. A discrete periodic signal $F(t)$ can be presented as the sum of a finite number of sine and cosine terms:

$$F(t) = A_0 + \sum_{n=1}^{N/2} [A_n \cdot \cos(n\omega_0 t) + B_n \cdot \sin(n\omega_0 t)]$$

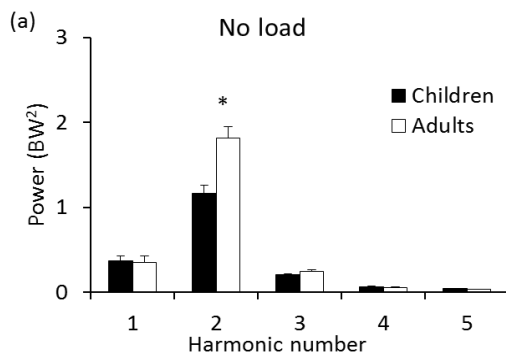
where N is the total number of data points, A_0 is the mean value of the signal, n is harmonic number, A_n and B_n are harmonic coefficients, and ω_0 is fundamental frequency which is equal to 2π divided by the period of the signal. Stance time was used to define the periodicity of vertical GRF. The Matlab programs calculated power of the harmonics in each stance phase. We compared the power of the first five harmonics between the two groups as these harmonics reconstruct the shape of the GRF curve.

Statistical analysis: Average treadmill speed was 1.3 m/s across the two groups. Normalized treadmill

speed \hat{v} was 0.54 ± 0.04 m/s in children and 0.45 ± 0.04 in adults. Since GRF variables show a linear correlation with \hat{v} , 2-way ANCOVAs (2 group x 3 load) with repeated measures and a covariate of \hat{v} were conducted on GRF variables. Post-hoc pairwise comparisons with Bonferroni adjustments were conducted when appropriate. Statistical significance was set as $p < 0.05$.

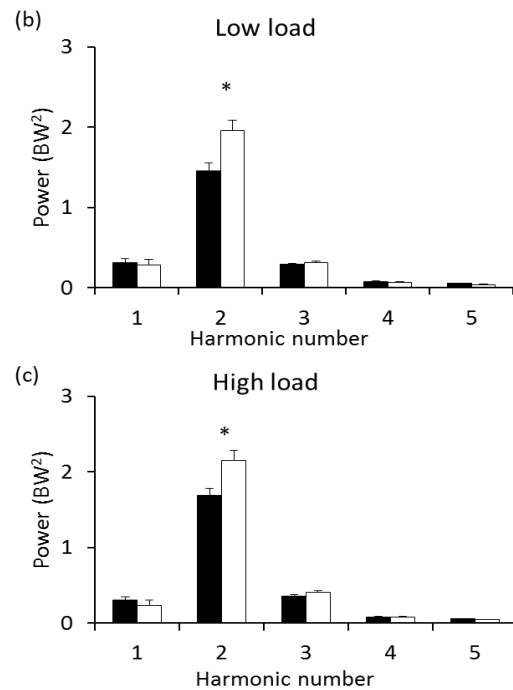
RESULTS AND DISCUSSION

Children produced a similar timing and magnitude of peak vertical GRFs as adults in each condition after adjusting for \hat{v} (Table 1). There was a group by load interaction on F_{Z1} timing ($p = .005$) and a load effect on F_{Z2} timing ($p < .001$). There was a load effect on F_{Z1} magnitude ($p < .001$) and a group by load interaction on F_{Z2} magnitude ($p < .001$). Children at the age of 7-10 years display adult-like spatiotemporal control of foot falls and foot-floor kinetic interaction during walking with ankle load.



Children produced a lower power from the 2nd harmonic than adults in each condition after adjusting for \hat{v} (Fig. a-c). Both groups had the highest power from the 2nd harmonic and increased this power with ankle load. There was a group by load interaction on the 2nd harmonic power ($p = .004$), where children increased the power to a greater extent than adults from no load to both load conditions. There was a load effect on the first five harmonics (all $p < .001$). Both groups increased the

2nd to 5th harmonic power, but decreased the 1st harmonic power with the load.



CONCLUSIONS

Children aged 7-10 years display adult-like kinetic pattern in the time domain but not in the frequency domain. A frequency analysis helps reveal kinetic differences between children and adults. Neuro-muscular development continues into adolescence.

REFERENCES

1. Duysens J et al. *Physiol Rev* **80**, 83-133, 2000.
2. Browning RC et al. *Med Sci Sports Exerc* **39**, 515-525, 2007.
3. Schneider E, Chao EY. *J Biomech* **16**, 591-601, 1983.

ACKNOWLEDGEMENTS

We thank the Jerome Lejeune Foundation for the funding support.

Table 1: Mean (SEM) of GRF variables adjusted for \hat{v}	Children			Adults		
	No load	Low load	High load	No load	Low load	High load
F_{Z1} timing (% stance)	21.5 (0.6)	20.5 (0.6)	20.1 (0.6)	21.6 (0.9)	20.1 (0.9)	19.2 (0.9)
F_{Z2} timing (% stance)	76.2 (0.5)	77.1 (0.5)	77.3 (0.5)	76.7 (0.6)	77.2 (0.6)	77.1 (0.6)
F_{Z1} magnitude (BW)	1.10 (0.02)	1.16 (0.02)	1.21 (0.02)	1.15 (0.03)	1.18 (0.03)	1.26 (0.03)
F_{Z2} magnitude (BW)	0.99 (0.02)	1.10 (0.02)	1.17 (0.02)	1.03 (0.03)	1.11 (0.03)	1.17 (0.03)

2DOF EXTERNAL FIXATOR AND SURGICAL SYSTEM FOR CLUBFOOT CORRECTION

¹ Ying Ying Wu, ² Anton Plakseychuk, and ¹ Kenji Shimada

¹ Carnegie Mellon University, Pittsburgh, PA, USA

² Bone and Joint Center, UPMC, Pittsburgh, PA, USA
email: yingyingwu@cmu.edu

INTRODUCTION

Clubfoot is a complex three-dimensional (3D) deformity of the foot presented at birth. The deformed foot is rigidly held in supination and equinus (an inwards and downwards twist). In the US, clubfoot affects 1 in 1,000 live births and may affect only one or both feet. Even though most recover with initial soft tissue manipulation (Ponseti method), between 11% to over 30% of *fully treated* clubfeet relapse during early childhood [1, 2]. Relapsed and neglected clubfoot is a persisting issue within and beyond the United States.

External fixation is a less destructive and highly effective technique for clubfoot correction [3, 4]. An *external fixator* is a frame that surrounds the leg and is attached to the tibia, first metatarsus and calcaneus via bone pins in a minimally invasive surgery. Adjusting joints on this frame pushes the bones into the correct pose. After surgery, the patient is discharged and instructed to adjust the joints *gradually* (2mm/day) to prevent soft tissue damage. The fixator is worn for another 4-12 weeks to maintain the correction. Although complications such as pin infections were observed, they were mild and without lasting effects [3]. Studies that simultaneously correct angulations in all three planes did not observe “rocker bottom” [5, 6].

Current external fixators are bulky and obstruct patient mobility for the entire treatment period of about 12-18 weeks. Constructing a fixator for 3D deformity based on 2D radiographs is a complex task and surgeons face a steep learning curve [7]. Thus, surgeries tend to be long, averaging 2.5hours and up to 4.5hours or even 8hours for less experienced surgeons [8]. Errors in fixator setup may result in residual deformities that require the whole process to be repeated.

We propose a fixator system consisting of a compact two degrees of freedom (2DOF) external fixator and a surgical system, to correct a *full 3D clubfoot deformity*. This system will improve patient outcome by enabling patient mobility, and reduce surgery time and learning curve by assisting the setting up of the fixator during surgery.

METHODS

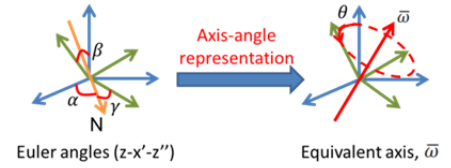


Figure 1: Axis-angle representation.

We define clubfoot deformity correction as a *3D rigid body transformation* of the first metatarsus. The 6DOF bone deformity problem is simplified to only 2DOF: (1) translation along the vector sum of the x, y, z translations, and (2) rotation by θ about an equivalent axis, \bar{w} , as shown in Fig. 1:

$$\theta = \arccos\left(\frac{\text{trace}(R)-1}{2}\right), \quad (1)$$

$$\bar{w} = \frac{1}{2 \sin(\theta)} \begin{bmatrix} r_{3,2} - r_{2,3} \\ r_{1,3} - r_{3,1} \\ r_{2,1} - r_{1,2} \end{bmatrix}. \quad (2)$$

where R is the desired 3×3 rotation matrix, and $r_{i,j}$ is the element in the i -th row and j -th column of R .

To achieve a compact configuration for patient mobility, the magnitude of translation was minimized to minimize the size of the prismatic joint and thus the overall size of the fixator. Fixator components were also constrained to above the foot.

To optimize the rates of adjustment of each joint so that soft tissues are stretched by approximately

2mm/day, we fit Bezier curves to the foot and interpolated intermediate splines during the correction so that the length of neighboring splines differs only by 2mm. Bezier curves are used as they give naturally changing curves. The positions of the first metatarsus across the interpolated splines form the ideal path. Joint adjustments are optimized by minimizing the error between actual and ideal paths.

RESULTS AND DISCUSSION

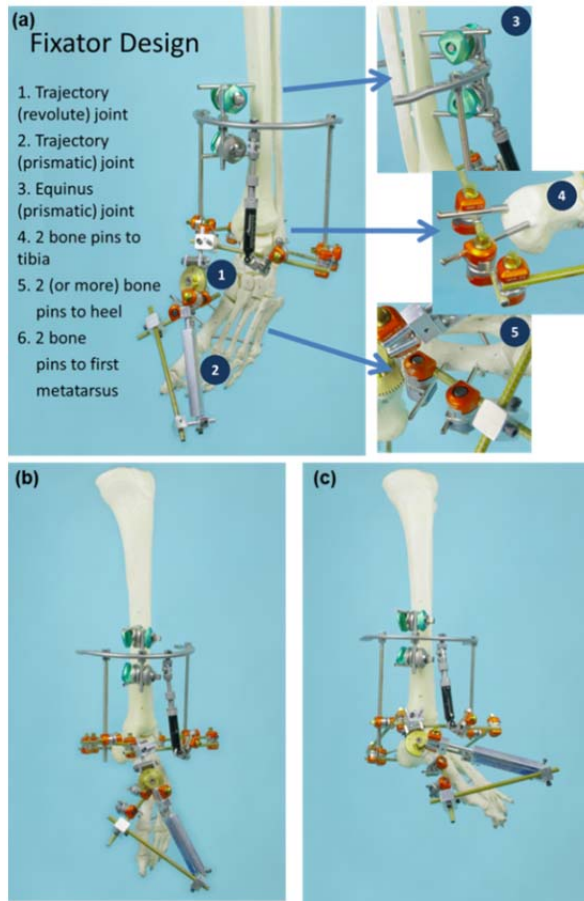


Figure 2. (a) Prototype of our 2DOF external fixator. (a) Before correction. (b) After correction.

A computer-assisted design (CAD) model of clubfoot was created based on our knowledge of clubfoot deformity. The axis-angle representation was applied and the fixator configuration was optimized for the correction of this clubfoot. On a sawbone foot model, we built a compact prototype. Fig. 2 shows the correction on sawbone model.

Using Bezier curves to approximate tissue stretch, we achieved a soft tissue stretch of 2mm/day on both the medial and lateral sides (figure not shown).

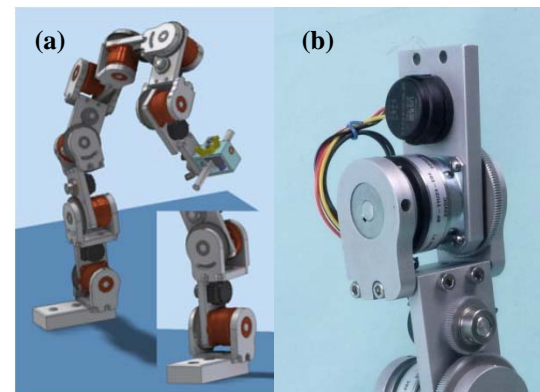


Figure 3. (a) CAD design of passive positioning linkage. Insert: close up of a single joint of linkage. (b) Prototype of a single joint.

The key to this method is to place these joints accurately at the calculated poses. To achieve this, we are designing a passive positioning linkage, as shown in Fig. 3, with no motors, but with electromagnetic brakes that can hold the joints in place while the surgeon set up the fixator.

CONCLUSIONS

We developed a compact 2DOF external fixator that is able to correct a full 3D clubfoot deformity. Our surgical system is able to optimize the joint adjustments to avoid soft tissue damage. Further verifications using real patient data or via patient testing are necessary to fully validate the system.

REFERENCES

1. Dobbs MB, et al. *JBJS. American Volume* **86**, 22-27. 2004.
2. Richards BS, et al. *JBJS. American Volume* **90**, 2313-2321, 2008
3. Makhdoom A, et al. *Indian Journal of Orthopaedics* **46**, 326-332, 2012.
4. Ganger R., et al. *Journal of Pediatric Orthopaedics* **21**, 52-58, 2012.
5. Oganessian OV, et al. *JBJS. American Volume* **78**, 546-556, 1996.
6. El-Sayed M. *Foot and Ankle Surgery : Official Journal of the European Society of Foot and Ankle Surgeons* **19**, 177-181, 2013.
7. Hassan A. *Journal of Pediatric Orthopaedics* **32**, 85-92, 2012.
8. Hosny GA. *Journal of Pediatric Orthopaedics* **11**, 121-128, 2002.

SHOD VS. BAREFOOT WALKING: WHY DO HUMANS CHANGE THEIR STEP FREQUENCY?

Matthew B. Yandell, Karl E. Zelik

Vanderbilt University, Nashville, TN USA

email: matthew.yandell@vanderbilt.edu, karl.zelik@vanderbilt.edu, web: <https://my.vanderbilt.edu/batlab/>

INTRODUCTION

Humans value economy of locomotion and seem to adopt a step frequency while shod that minimizes metabolic cost at a given walking speed [1]. It has also been observed that humans increase their step frequency when walking barefoot (as compared to shod) [2,3]; however, the reason for this increase has not been explained.

Taken together, these empirical observations indicate that either: (1) removing the shoes changes gait dynamics sufficiently such that it shifts the metabolic minimum step frequency for a given walking speed, or (2) humans adopt a new step frequency when walking barefoot that does not minimize metabolic expenditure.

The goal of this study was to determine which of these two possibilities better explains the shift in step frequency when walking barefoot versus shod. We performed an experiment that compared shod versus barefoot walking, and estimated metabolic power as well as the relative effects of shoe-specific properties (e.g., mass, height) on step frequency. A secondary goal was to investigate changes in center of mass (COM) mechanics for shod versus barefoot gait.

METHODS

We studied 5 subjects (mean \pm SD, 23 ± 4.3 years old, 72.3 ± 16.0 kg, 177.4 ± 11.0 cm height) during level walking on an instrumented split-belt treadmill (Bertec). All subjects gave informed written consent prior to participation. Three footwear variants were tested: shod (using each subject's personal athletic shoes), barefoot, and weight-matched (WM) barefoot (ankle mass was added to match shoe mass). Each subject performed acclimation trials at 1.25 m/s to determine their baseline self-selected step frequency for each footwear variant.

Next, each subject was asked to walk at 1.25 m/s while matching a metronome frequency for the five

testing conditions in Table 1. A Cosmed K4b² system measured metabolic data for six minutes, and ground reaction force (GRF) data was collected during the last minute of each trial. Average metabolic power during the last 2.5 minutes of each trial was calculated from the equation given by Brockway [4]. GRF data was low-pass filtered at 25 Hz (Butterworth, 3rd order, zero lag) and used to compute individual limb COM power [5] for each limb. Statistical comparisons between conditions were performed using analysis of variance with Holm-Sidak step down correction ($\alpha = 0.05$).

Table 1: Conditions for each footwear variant

<u>Step Frequency</u>	<u>Footwear Variant</u>		
	<u>Shod</u>	<u>Barefoot</u>	<u>Barefoot WM</u>
Shod SS	X	X	X
Barefoot SS		X	
Barefoot WM SS			X

We also estimated the effect of leg length difference (barefoot vs. shod, due to shoe height) on step frequency using regression equations reported in literature [2,6].

RESULTS AND DISCUSSION

We found that the barefoot and barefoot WM self-selected step frequencies were significantly higher than the shod self-selected frequency ($P < 0.01$, Table 2). No significant difference in step frequency was observed between barefoot and barefoot WM ($P = 0.62$). Mean shoe mass in this study was 296 g.

We observed from metabolic data that 4 out of 5 subjects exhibited a lower gross metabolic power when walking barefoot at the shod self-selected step frequency (~112 steps/min, Table 2) than barefoot at the barefoot self-selected frequency (~121 steps/min). This difference did not reach statistical significance, likely due to the low number of subjects. However, through ongoing testing of additional subjects we will attempt to distinguish if sta-

tistically significant differences exist.

The height of the shoe sole added 20 ± 6 mm (mean \pm SD) to each participant's leg length, as compared to walking barefoot. Based on the published speed-step length relationship [2,6], we estimated this 20 mm decrease in leg length when walking barefoot would result in a 1.9 step/min increase in step frequency. The predicted increase in step frequency was substantially smaller than the empirical increase of 8.4 step/min (Table 2) observed in this study.

Differences were also observed in COM power for barefoot vs. shod gait, specifically in terms of a reduced transient immediately following heelstrike during barefoot walking.

Table 2: Self-selected (SS) step frequency for each footwear variant

	Subject SS Step Frequency (steps/min)					
Variant	1	2	3	4	5	AVG
Shod	112	123	103	112	111	112.2
Barefoot	118	130	118	119	118	120.6
Barefoot WM	117	130	118	120	117	120.4

There are multiple factors which could contribute to the increase in step frequency when a person transitions from shod to barefoot walking. In this study we sought to determine if properties of the shoe could account for the altered dynamics.

We found that the addition of shoe mass to barefoot walking had little to no effect on self-selected step frequency, and thus did not account for the observed barefoot vs. shod changes. Similarly, we estimated that the reduction in leg length when walking barefoot (due to the loss of shoe height) was only expected to lead to a small increase in step frequency (~ 1 -2 steps/min), but this accounted for less than 25% of the observed barefoot vs. shod step frequency increase, which was >8 steps/min.

Since these intrinsic shoe characteristics failed to account for the observed change in step frequency, other factors must be considered. One of these is shoe length (and its effect on effective foot length), which will be investigated in ongoing/future trials. Another factor may be related to the subjective comfort/discomfort experienced as a result of not having shoe cushioning when walking barefoot.

Although it is difficult to define comfort, the lack of cushioning when walking barefoot could have a marked effect on a user's subjective preference and lead to altered behavior.

In summary, we found indications that when walking barefoot, people may choose a self-selected step frequency that is metabolically sub-optimal. The increased step frequency observed for barefoot (as compared to shod) walking was not well explained by the mass or height properties of the shoe. We speculate that cushioning provided by the shoe and/or subjective user comfort may be significant factors in the choice of self-selected barefoot walking frequency, factors which are generally not integrated into biomechanical walking models or our theoretical understanding of gait. Shoe characteristics could potentially be manipulated to encourage desired locomotor behaviors, such as more favorable biomechanics or reduced joint loading associated with long-term injury risk.

REFERENCES

1. Zarrugh MY, et al. *Eur. J. Appl. Physiol.* **33**, no. 4, pp. 293–306, 1974.
2. Grieve DW, et al. *Ergonomics* **9**, no. 5, pp. 379–399, 1966.
3. Lythgo N, et al. *Gait and Posture* **30**, no. 4, pp. 502–506, 2009.
4. Brockway JM. *Hum. Nutr. Clin. Nutr.* **41**, no. 6, pp. 463–471, 1987.
5. Donelan JM, et al. *J. Biomech.* **35**, no. 1, pp. 117–124, 2002.
6. Kuo AD. *J. Biomech. Eng.* **123**, no. 3, pp. 264–269, 2001.

BODY MASS AND HEIGHT ARE NOT GOOD PREDICTORS OF PLANTAR SHEAR STRESS

Hiral Master¹, Linda Adams¹, Stephen Reider¹, Joseph Udofia¹, Michael Canales², Metin Yavuz¹

¹ University of North Texas Health Science Centre, Fort Worth, TX, USA

² College of Podiatric Medicine, Kent State University, USA

Email: metin.yavuz@unthsc.edu, web: <https://sites.google.com/site/dryavuzlab>

INTRODUCTION

Peak pressure has been long considered a risk factor for diabetic foot ulceration. Recent studies also indicated shear as a significant pathological factor. Cavanagh et al (1991) demonstrated a significant correlation between body mass and peak pressures in diabetic patients [1]. However, Ahroni et al (1987) claimed that peak pressure values of heavier individuals may not necessarily be abnormally high [2].

Another physical body attribute, body height, has been associated with step length [3] and step length depends on anteroposterior ground reaction forces [4].

To our knowledge the literature does not contain any reports that discuss a potential correlation between peak plantar shear stress and body measures such as body mass and height or presence of neuropathy. The purpose of this study was to explore these relationships in three subject cohorts.

METHODS

The study was approved by the Institutional Review Board at Kent State University and UNT Health Science Center. Subjects gave informed consent before participation. We studied three groups: (DN) consisted of 14 diabetic neuropathic patients, second - (DC) comprised 14 diabetic patients without neuropathy and third - (HC) healthy control group, which included 11 subjects. Peripheral neuropathy was tested with a Biothesiometer. Vibration perception threshold (VPT) was measured in terms of voltage on a 0-50 volt scale. Each subject walked multiple times at self-selected speeds on the custom-built Cleveland Clinic stress plate, which was installed on a 12-ft walkway and set flush. Data from three trials were averaged and used in statistical analysis. Two shear stress and pressure variables were identified in each subject; peak shear (PS), peak shear time integral (STI),

peak pressure (PP) and peak pressure time integral (PTI). These were correlated against the patients' body mass, height and vibration perception threshold (in DN subjects only).

RESULTS AND DISCUSSION

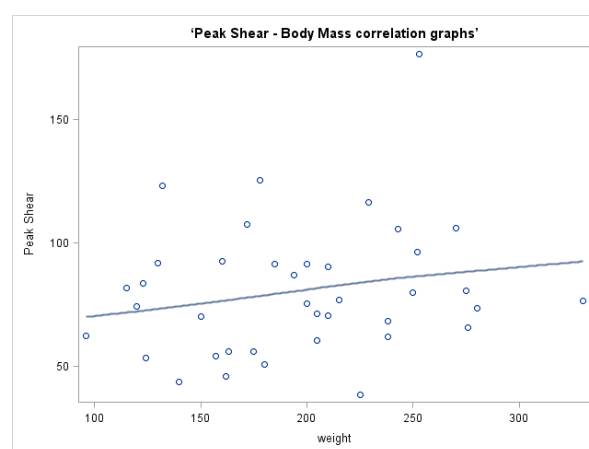


Figure1: PS-Body Mass correlation graphs.

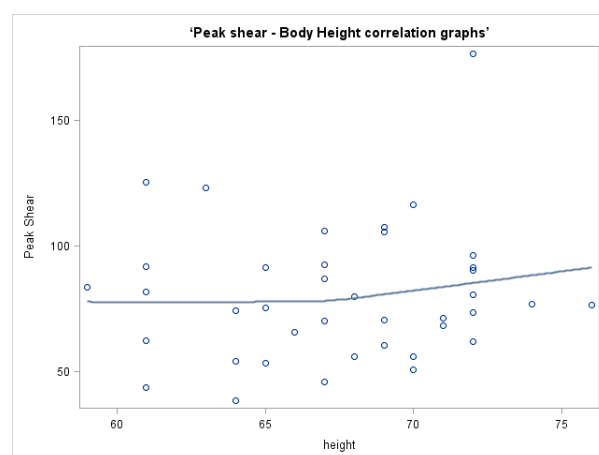


Figure2: PS-Body Height correlation graphs.

Normality assumption was satisfied. Shapiro-Wilk values for the stress variables were >0.1. Pearson correlation analysis was carried out for each group and each stress and pressure variable. No correlation was statistically significant. Body mass and body weight could not account for any degree

of variance in PS, STI, PP and PTI. This indicated that plantar shear and pressure under the foot do not depend on body mass or height. In addition, plantar shear and pressure variables do not correlate with VPT in DN subjects. Table 1 displays the calculated r and respective p values.

The reason to the lack of a strong relationship might be variations in the structure of the foot. For example, in diabetic patients with peripheral neuropathy, compromised plantar fat may lead to bony prominent areas, where high stress values can be seen. Also, the proportional dimensions of the human body and foot may present great variation, which would also lead to substantial variations in the plantar surface area. This study revealed that, PS, PP, PTI and STI may vary regardless of body mass and body height. These results also confirm an earlier report that showed that plantar shear stresses cannot be easily predicted based on normal plantar loads [4]. It was also found in this study that PS, PP, PTI and STI may vary independent of VPT in DN patients.

It is thought that effective load bearing area, gait speed, muscle activity, frictional properties and moisture content of the skin, and other intrinsic factors might influence local shear stresses as well

as body mass and height. Such a complicated relationship needs to be further investigated in a large sample study. The purpose of this study was to present preliminary data on the potential association of plantar shear stress and plantar pressures and physical body measures.

CONCLUSIONS

Thus, plantar shear stresses do not depend on body weight and body height and they need to be measured rather than estimated.

REFERENCES

1. Cavanagh PR, et al. Diabetes Care 14 (8), 750-5,1991.
2. Ahroni JH, et al. Diabetes Care 22 (6), 965-72, 1999.
3. Hof AL. Gait & Posture 4, 222-3, 1996.
4. Martin PE, et al. J Biomechanics 25, 1237-9, 1992.

ACKNOWLEDGEMENTS

This study was possible due to funds from the NIH grant 1R15DK082962.

Table 1: Pearson Correlation Coefficients (p values) of Group DN, DC and HC correlations.

	Group DN (N = 14)			Group DC (N = 14)		Group HC (N = 11)	
	Mass	Height	Vibration	Mass	Height	Mass	Height
PS (kPa)	0.0356 (0.90)	0.0386 (0.9)	-0.0991 (0.74)	0.2175 (0.44)	-0.0412 (0.89)	-0.4263 (0.19)	-0.4011 (0.22)
STI (kPa.s)	0.0500 (0.87)	0.1358 (0.64)	-0.1221 (0.68)	0.2891 (0.32)	0.0354 (0.90)	0.4387 (0.18)	-0.0384 (0.91)
PTI	0.2254 (0.44)	0.2483 (0.39)	0.2223 (0.45)	0.4314 (0.12)	-0.1056 (0.72)	0.0381 (0.91)	-0.2857 (0.39)
PP	0.2410 (0.41)	0.1497 (0.61)	0.2472 (0.39)	0.3956 (0.16)	-0.1399 (0.63)	-0.3839 (0.24)	-0.3170 (0.34)

MORE ULCERS DEVELOP AT PEAK SHEAR LOCATIONS THAN AT PEAK PRESSURE LOCATIONS. A CALL TO REVISIT ULCERATION PATHOMECHANICS

¹Metin Yavuz, ¹Linda Adams, ¹Hiral Master, ¹Allan Garrett, ²Georgeanne Botek

¹ University of North Texas Health Science Center, Fort Worth, TX, USA

² Dept of Orthopedic Surgery, Cleveland Clinic

email: Metin.Yavuz@unthsc.edu

INTRODUCTION

Approximately 100,000 lower extremity amputations need to be performed every year in the US due to diabetic foot ulcers (DFU). In the world, a foot is lost to diabetic ulceration every 20 seconds. Estimated cost of DFU and related amputations to the US Healthcare System is \$30 billion. Amputations place a substantial burden on the quality of lives and families of patients. Foot ulceration has long been associated with plantar pressures. However, only 38% of DFU occur at the location of peak pressure (PP) [1]. Moreover, ulcers may not develop at high pressure values that are considered harmful or they may develop at pressures that are not considered harmful. Therefore, sensitivity and specificity of foot pressure is not high enough to accurately predict developing ulcers [2].

Rationale for DFU prevention is centered on pressure relief. However, studies have revealed limited results from the use of pressure-reducing preventive footwear [3]. Studies from the past decade have shown increased plantar shear in diabetic patients with neuropathy when compared to non-neuropathic diabetic patients and healthy individuals [4, 5]. In addition, peak plantar pressure and shear do not usually occur at the same site in diabetic and healthy subjects [6]. Pollard and Le Quesne reported that peak pressure and shear occurred at the same sites, which were also the sites of a previous ulceration in 100% of the patients (N=5) [7]. However, the equipment used by the authors had major drawbacks such as attachment of thick sensors on the plantar surface and a need for separate sensors for pressure and shear components. The purpose of this ongoing study was to

investigate a site-wise association between healed ulcers and plantar shear loading, using the Cleveland Clinic pressure and shear device.

METHODS

Four neuropathic diabetic subjects (3 F, 1M) with 5 recently healed plantar ulcers were recruited after signing an IRB approved consent form. The ulcers had healed within the past three months of study participation. Peripheral neuropathy was tested by a Biothesiometer and 5.07 Semmes-Weinstein monofilaments. The foot was examined and any calluses noted. Subjects walked on the Cleveland Clinic device, which can quantify triaxial plantar stresses. The stress plate was set flush in the middle of a 4-meter walkway. Data were collected implementing the two-step method, and were analyzed after determining averages from three trials. Locations of peak pressure and resultant shear stress were identified based on the averaged data. The data was then compared to ulcer site locations for descriptive analysis.

RESULTS AND DISCUSSION

In 2 subjects, locations of PS and PP didn't overlap, and the PS site coincided with an ulcer (Figure 1). A third DFU coincided with the location of PP. In the remaining 2 subjects, PS and PP overlapped and coincided with the ulcer site. In summary, 40% of the ulcers had occurred at peak shear site only and 20% had occurred at peak pressure site only. Furthermore, 80% of ulcers had occurred at a location coincident with PS, half of which were coincident with PP as well.

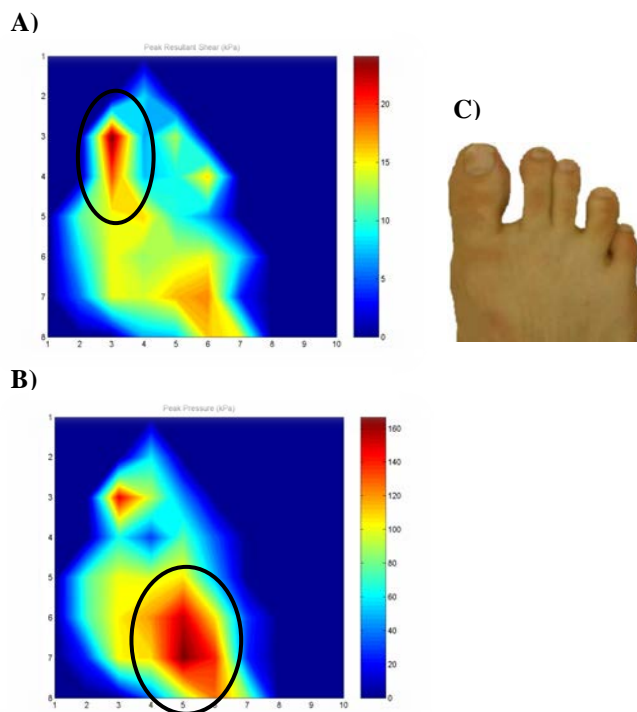


Figure 1: A) Peak plantar shear on the right hallux of a neuropathic diabetic patient, B) Peak pressure in the midfoot and C) Representative foot placement on the stress plate. Note: peak shear had a magnitude of 24 kPa and peak pressure was 167 kPa. Peak shear and pressure sites did *not* coincide and peak shear occurred where a diabetic ulcer had healed a month before assessment.

CONCLUSIONS

The preliminary results of this ongoing study support the previous findings that indicate the clinical significance of plantar shear in diabetic ulceration. The biphasic character of plantar shear stresses is believed to play a major role in ulceration pathomechanics, subjecting soft tissue to cyclic loading that may result in fatigue failure. Shear stresses were also shown to cause hyperkeratosis and hence callus formation in soft tissue. It is a clinical fact that many ulcers are preceded by callosities. Blood occlusion also occurs faster if a soft tissue is subjected to both pressure and shear simultaneously. High temperatures in the diabetic foot are thought to further contribute to ulcer development by increasing metabolic rate of the tissue; this increased metabolic rate might not be compensated by impaired blood circulation which is

often seen in diabetic patients. Frictional shear stresses contribute to elevated plantar temperatures particularly in the presence of kinetic friction. Shear stress couplings observed on the foot-ground interface, such as bunching, twisting and stretching may further damage plantar tissue. Interestingly, one ulcer occurred at a site that experienced only 167 kPa of pressure and 24 kPa of shear stress (Figure 1). This also indicates that other factors might be in play along with plantar stresses that make a foot susceptible to ulceration.

Diabetic ulceration has a multifactorial etiology and oversimplifying the pathology by focusing on only certain factors such as foot pressure will most likely hamper the provision of effective healthcare to patients who are at risk for ulceration. Given that most diabetic ulcers do not develop at peak pressure locations and pressure-reducing therapeutic footwear cannot effectively reduce ulcer incidence, it is crucial to further explore the clinical implications of plantar shear as well as other factors such as physical activity. Better understanding of these factors will lead to designing more effective preventive footwear and methods.

REFERENCES

1. Veves et al. *Diabetologia*, **35**(7), 660-3, 1992.
2. Lavery et al, *Diabetes Care*, **26** (4), 1069-1073, 2003.
3. Bus et al. *Diabetes Metab ResRev*, **24**(S1), 162-180, 2008.
4. Yavuz, M. et al. *Journal of Biomechanics*, **41**, 556-559, 2008.
5. Yavuz, M. et al. *Clinical Biomechanics*, **29**, 223-229, 2014.
6. Yavuz, M. et al. *Diabetes Care*, **30**, 2643-2645, 2007.
7. Pollard, J.P., Le Quesne, L.P. *British Medical Journal*, **286**, 436-437, 1983.

ASSOCIATION BETWEEN HIGH TEMPERATURES AND TRIAXIAL PLANTAR LOADING IN DIABETIC PATIENTS

¹Metin Yavuz, ¹Hiral Master, ¹Linda Adams, ¹Allen Garrett, ²Georgeanne Botek

¹ University of North Texas Health Science Centre, Fort Worth, TX, USA

²Dept. of Orthopedic Surgery, Cleveland Clinic

Email: metin.yavuz@unthsc.edu, web: <https://sites.google.com/site/dryavuzlab>

INTRODUCTION

Many foot disorders have a biomechanical etiology. Ground reaction forces and related stresses that act under the foot are associated with complications such as diabetic ulceration, rheumatoid foot, hallux valgus and foot blistering. The normal component of the 3D plantar stresses, i.e., pressure, can be easily quantified by commercially available barefoot or in-shoe systems. However, few investigators have access to equipment capable of measuring 3D loading under the foot since measuring plantar shear stresses remains to be quite challenging.

Brand has suggested that temperature can be used to predict tri-axial loading under the foot [1]. Studies have also revealed that diabetic patients have increased plantar temperatures when compared to control subjects [2]. It is thought that diabetic feet experience elevated stresses that lead to inflammation within the foot, which can be observed as temperature increase on the plantar aspect of the foot. Unfortunately, this theory has not been validated before. The purpose of this study was to explore a site-wise association between peak plantar temperature and peak pressure and shear stresses obtained from diabetic patients using a thermal camera and a custom-built pressure-shear plate. In addition, peak pressure and shear magnitudes were correlated against peak temperature in order to reveal a magnitude-wise association. The study examined these factors in both diabetic neuropathic patients (DN) and diabetic non-neuropathic control patients (DC).

METHODS

The study was approved by the Institutional Review Board. Subjects gave informed consent before participation. Group DN consisted of 14 diabetic

neuropathic patients (2 F, 64.8±6.8 years, 32.0±5.1 BMI). The second group (DC) comprised 14 diabetic patients (9 F, 52.4±12.9 years, 28.9±7.4 BMI) without neuropathy. Vibration perception threshold (VPT) was tested using a Biothesiometer. 5.07 Semmes-Weinstein monofilaments were used to assess presence of sensation. Each subject waited ten minutes while barefoot in order to ensure the plantar temperatures reached steady-state conditions. After this period, resting plantar temperatures were recorded using an infrared thermal camera. Subjects then walked at self-selected speeds on the stress plate, which was installed on a 12-ft walkway and set flush. Data from three trials were averaged and used in statistical analysis. Data were collected implementing the two-step method. Subjects' feet were masked into five forefoot (FF) regions; hallux, lesser toes, medial forefoot (1st metatarsal head), central forefoot (2nd and 3rd MTH) and lateral forefoot (4th and 5th MTH). Four major stress variables were identified in each subject; peak pressure (PP), peak shear (PS), peak pressure-time integral (PTI) and peak shear-time integral (STI). Peak values of the stress variables and peak temperature (PT) were found in five forefoot regions. Separately, locations of global peak values of all variables were determined for each person. Linear regressions were used to explore the value of temperature in predicting pressure and shear. Differences in temperature by group and site were analyzed by ANOVA. For all analyses alpha was set at 0.05.

RESULTS AND DISCUSSION

Mean temperatures were significantly higher in the DN group by 1.3 °C (31.1 °C vs 28.8 °C, SD=3.3 vs 3.9, p=.001). Temperatures were not different by group and site (Table 1). Significant linear regressions were observed between PS and

temperature at the hallux, but not at other regions. Peak plantar temperature sites matched the site of peak shear in 57% of the DN subjects and in 71% of the DC subjects (Table 2). Figure 1 displays the peak shear stress plantar temperature profiles of a representative DN subject.

Table1. Measured plantar temperature values (°C). Values are means (standard deviations).

Site	DN	DC
Hallux	30.7 (4.0)	28.2 (4.4)
Lesser Toes	30.1 (4.2)	27.7 (4.2)
Medial FF	31.2 (2.7)	29.5 (3.7)
Central FF	31.7 (2.4)	29.5 (3.4)
Lateral FF	31.6 (2.9)	29.2 (3.6)

Table 2: Site-wise correlation percentage values for peak stress and temperature.

	Group DN	Group DC
PP - PT	14% (2/14)	86% (12/14)
PS - PT	57% (8/14)	71% (10/14)
PTI - PT	14% (2/14)	71% (10/14)
STI - PT	57% (8/14)	50% (7/14)

Results indicated that plantar temperature can predict triaxial plantar loading at the hallux but not at other foot sites. As revealed by this study, temperature alone is not an excellent predictor of plantar pressure and shear stress. Plantar temperature values may vary depending not only on plantar loading, but also blood circulation, internal loading and the presence of kinetic friction at the foot-ground interface. Compromised fat layer in diabetic feet, which is a natural heat insulator, might also influence how heat is dissipated on the plantar surface. On the other hand, particularly in group DC, peak temperature values achieved a moderate success in identifying the location of peak stress values. This success was quite lower in group DN.

In a previous study we observed a 5.3 °C increase on the plantar foot of healthy subjects, after ten minutes of walking [3]. This increase may be higher in DN subjects given that elevated stresses are experienced by such feet. Whether caused by activity or inflammation, high temperatures in the diabetic foot are thought to further contribute to ulcer development by increasing metabolic rate of the tissue; this increased metabolic rate might not be compensated by impaired blood circulation which is often seen in diabetic patients.

We believe that the potential relationship between the magnitudes of stresses and temperature has a complicated, non-linear character. Appropriate modeling schemes can be implemented to explore such complicated potential relationships. The results of this study are thought to warrant further investigation on this topic.

REFERENCES

1. Brand PW. *Foot Ankle Int.* **24**, 457-61, 2003.
2. Papanas N, et al. *Exp Clin Endocrinol Diabetes* **117** (1), 44-7, 2009.
3. Yavuz M, et al. *J Biomech*, **47** (15), 3767-70, 2014.

ACKNOWLEDGEMENTS

This study was possible due to funds from the NIH grant 1R15DK082962.

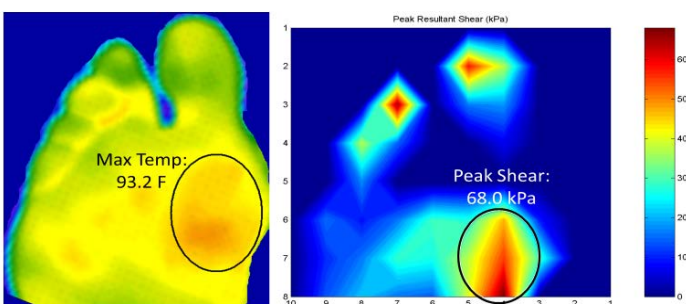


Figure 1: Resting plantar temperature (left) and peak plantar shear (right) profiles of a representative DN subject. Note the match between the sites of peak temperature and peak shear (first MTH)

Gait Patterns Following Anterior Cruciate Ligament Reconstruction Differ With Graft Type

¹ Ryan Zarzycki, ² David Logerstedt, ¹ Lynn Snyder-Mackler

¹ University of Delaware, Newark, DE, USA

² University of the Sciences, Philadelphia, PA, USA
email: rzar@udel.edu

INTRODUCTION

After anterior cruciate ligament reconstruction (ACLR), subjects demonstrate persistent altered movement asymmetries during gait that may increase the risk of osteoarthritis (OA) development¹ and predict re-injury². Graft type can influence kinematics and kinetics during gait although most studies have only explored sagittal plane movement³. The purpose of this investigation was to determine if differences in sagittal, frontal, and transverse plane kinematics and kinetics exist between subjects undergoing ACLR with hamstring (HS) autograft and subjects with bone-patellar tendon-bone (BPTB) autograft.

METHODS

Thirty five subjects following ACLR were included in this analysis. Twenty six subjects underwent ACLR with a HS autograft (mean age 19.1 years, 17 male, 9 female) while 9 underwent ACLR with a BPTB autograft (mean age 20.8, 8 males, 1 female). Subjects were enrolled after they met the following criteria following post-operative physical therapy (mean 22.5 weeks post surgery, standard deviation (SD) 7.7 weeks): full joint range of motion, greater than 80% quadriceps index, minimal/no effusion, and the subjects must have started a running progression. Standard motion capture was performed during gait at the subject's preferred walking speed. Knee and hip joint angles and moments were calculated through inverse dynamics in all three planes of motion at initial contact (IC), peak knee flexion (PKF), and peak knee extension (PKE). A 2 x 2 analysis of variance was utilized to detect differences between limb and group (HS, BPTB).

RESULTS

Significant group x limb interactions were found with knee adduction angle at peak knee flexion (see table 1 for all means, SD's, and p values). The BPTB group had greater asymmetry resulting from a greater mean adduction angle of the uninvolved limb. There was no significant interaction with external knee flexion moment at peak knee flexion although the mean difference between limbs was greater than the minimal clinically important difference of .04 Nm/kg*m. The BPTB group's knee flexion moment asymmetry was .08 Nm/kg*m greater than the HS group. There were no significant interactions with all other variables.

DISCUSSION

In this analysis the BPTB group displayed greater asymmetry between limbs in external knee flexion moment and knee adduction angle at peak knee flexion compared to HS group. The BPTB group were likely underloading their surgical knee as evident by the decreased external knee flexion moment at PKF. Furthermore, the uninvolved knee in the BPTB group had an increase in knee adduction angle at PKF, likely reflecting compensation due to underloading their surgical side. Altered loading following ACLR may increase the likelihood of knee OA. Based on these findings, subjects with BPTB autograft may be more likely to develop knee OA. Special attention during rehabilitation should be given to restoring symmetrical loading.

References

1. Andriacchi TP, Mundermann A, Smith RL, Alexander EJ, Dyrby CO, Koo S. A framework for the in vivo pathomechanics of osteoarthritis at the knee. Ann Biomed Eng. 2004;32(3):447-57.

2. Paterno MV, Schmitt LC, Ford KR, et al. Biomechanical measures during landing and postural stability predict second anterior cruciate ligament injury after anterior cruciate ligament reconstruction and return to sport. Am J Sports Med. 2010;38(10):1968-78.

3. Webster KE, Wittwer JE, O'Brien J, Feller JA. Gait patterns after anterior cruciate ligament reconstruction are related to graft type. Am J Sports Med. 2005;33(2):247-54.

Table 1: Mean Values of Gait Variables and Interaction Significance

	Knee Flexion Moment at PKF		Knee Adduction Angle at PKF	
	HS Group	BPTB Group	HS Group	BPTB Group
Mean/SD Uninvolved Limb	0.50 ± .13	0.51 ± .10	2.2 ± 2.7	5.3 ± 4.2
Mean/SD Involved Limb	0.40 ± .12	0.33 ± .17	2.2 ± 3.2	2.4 ± 2.6
Uninvolved-Involved Limb	0.1*	0.18*	0	2.9
p Value (interaction)	0.065		0.05	

*Greater than .04 Nm/kg*m difference between groups

KNEE JOINT LOADS AND SURROUNDING MUSCLE FORCES DURING STAIR ASCENT IN TOTAL KNEE REPLACEMENT PATIENTS AND HEALTHY CONTROLS

¹Songning Zhang, ¹Robert Rasnick, ¹Tyler Standifird, ²Jeffrey A. Reinbolt, ³Harold E. Cates

¹Biomechanics/Sports Medicine Lab, The University of Tennessee, Knoxville, TN, USA

² Mechanical, Aerospace, and Biomedical Engineering, The University of Tennessee, Knoxville, TN, USA

³Tennessee Orthopedic Clinics, Knoxville, TN, USA

email: szhang@utk.edu, web: web.utk.edu/~sals/resources/biomechanics_laboratory.html

INTRODUCTION

Total knee replacement (TKR) is commonly used to correct end-stage knee osteoarthritis (OA) of the knee joint. Unfortunately, difficulty with stair climbing often persists and prolongs the challenges of TKR patients. Stair climbing is a common activity of daily living and utilized in all clinical recovery assessments after a TKR.

Experimental studies of stair ambulation after TKR reported that peak knee extension moment appears to be reduced following TKR compared to healthy subjects during stair ascent [6]. Studies utilizing an instrumented TKR have shown that compressive loads at the knee during stair ascent were ranged between 2.5 and 3.1 bodyweight (BW) in stair ascent [2, 3]. Only a limited number of studies have utilized musculoskeletal simulations to investigate knee joint loading in stair negotiation in healthy subjects. However, no studies have investigated the knee joint loading and muscle forces in TKR patients during stair ascent using musculoskeletal simulation. Therefore, the purpose of this study was to determine if the knee joint reaction force (JRF) following TKR are recovered to the level of healthy individuals, and determine the differences in muscle forces causing those loadings during stair ascent.

METHODS

Five patients (63.6 ± 8.7 yrs, 1.7 ± 0.1 m, 87.0 ± 8.9 kg, 14.6 ± 3.4 months post-surgery) who received a posterior stabilized TKR and five healthy participants (57.8 ± 10.0 yrs, 1.8 ± 0.1 m, 89.0 ± 6.6 kg) participated in the study. A 9-camera motion analysis system (240 Hz, Vicon Motion Analysis), and two force platforms and an instrumented staircase (1200 Hz, AMTI) were used to obtain 3D kinematic and ground reaction force data for five trials during stair ascent at a self-selected speed.

Kinematic and kinetic data were initially processed in Visual3D (C-Motion, Inc.) and then exported to OpenSim (3.0.1, SimTK, Stanford, CA, USA) to perform musculoskeletal simulations. A generic musculoskeletal model (Gait 2392 Model) was scaled to the height and weight of each individual participant to generate subject-specific models. In order to improve the accuracy of the simulations a residual reduction algorithm (RRA) was used to minimize virtual residual forces added to the model to account for dynamic inconsistency. Kinematic changes from RRA were all kept below 5.5 cm of translation and 3.5 degrees of rotation. Peak residual forces and moments were each kept below 14% of body weight and 1.6 Nm/kg, respectively. Individual muscle excitations and resulting muscle forces were calculated using computed muscle control to drive simulations of the stair ascent trials. Joint reaction forces were computed using the JRF Tool in OpenSim.

In order to compare differences between TKR patients and healthy individuals, a paired samples t-test was used for each variable (21.0, IBM SPSS, Chicago, IL) with an alpha level set at 0.05 a priori.

RESULTS AND DISCUSSION

Peak knee extensor moment was reduced in TKR patients compared to healthy controls (Table 1), which is consistent with findings reported in the literature [1, 5]. Although no differences of both earlier and late peak knee joint compressive forces were found, the late-stance peak compressive knee contact force showed a trend of elevated compressive JRF for TKR patients compared to controls ($p = 0.051$). The magnitudes for compressive JRF seen in this study were elevated slightly over those seen in the literature for stair ascent [2, 3, 4].

The late stance peak rectus femoris muscle force was reduced while the late stance peak vastus medialis force was greater in TKR patients compared to healthy controls (Table 1). No differences were found for the late stance peak hamstring muscle forces. However, the peak late stance medial gastrocnemius muscle force was smaller and the late stance peak lateral gastrocnemius muscle force was greater in TKR patients compared to controls.

It appears a different strategy was utilized by TKR patients to produce similar levels of muscle forces compared with to healthy controls. It can be seen that the majority of muscle force during the push-off phase is from the rectus femoris in healthy individuals. However, TKR patients utilized the vastus medialis more during push-off than healthy controls. Similarly, TKR patients utilized the medial and lateral gastrocnemius differently than healthy individuals. The underlying biomechanical factors causing these differences and the influence they have on JRF remain unclear. TKR patients may be utilizing the muscles differently as a compensatory strategy for the reduced knee extensor strength that remains after rehabilitation. It is possible that gait compensation strategies seen in knee OA patients to relieve pain linger after the TKR rehabilitation is completed.

CONCLUSION

TKR patients showed a trend of having higher late stance peak compressive JRF. Some muscle force compensatory strategies appear to be present in the push-off phase; however, the differences in muscle forces do not clearly explain the trend present in compressive JRF during the second half of stance. Future research utilizing musculoskeletal modeling and simulation is necessary to investigate differences in muscle forces dependent on rehabilitation strategies and differences existing at the ankle.

REFERENCES

1. Berti, L., et al. (2006). *Clin Biomech*, **21**, 610-616.
2. D'Lima, D. D., et al. (2005). *Clin Orthop Relat Res*, **440**, 45-49.
3. D'Lima, D. D., et al. (2006). *J Arthroplasty*, **21**, 255-262.
4. Heinlein, B., et al. (2009). *Clin Biomech*, **24**, 315-326.
5. Mandeville, D., et al. (2007). *Clin Biomech*, **22**, 787-794.
6. Standifird, T. W., et al. (2014). *J Arthroplasty*, **29**, 1857-1862.

Table 1. Peak knee extensor moment and late stance joint contact forces and related muscle forces: mean \pm SD.

Variable	Healthy	TKR	P-value
Peak Extensor Moment (Nm)	119.9 \pm 25.9	77.1 \pm 16.5	0.014
Late Stance Peak Compressive JRF (N)	-2774.3 \pm 456.5	-3560.6 \pm 609.6	0.051
Rectus Femoris (N)	730.7 \pm 127.2	322.3 \pm 310.4	0.026
Vastus Medialis (N)	92.6 \pm 45.6	722.3 \pm 415.5	0.027
Vastus Intermedius (N)	102.5 \pm 53.5	63.1 \pm 23.6	0.186
Vastus Lateralis (N)	184.8 \pm 112.5	76.6 \pm 29.3	0.098
Total Quadriceps (N)	996.3 \pm 227.2	1091.0 \pm 271.2	0.566
Semimembranosus (N)	359.6 \pm 57.6	439.2 \pm 116.3	0.207
Semitendinosus (N)	42.2 \pm 18.5	43.4 \pm 15.0	0.913
Bicep Femoris Long Head (N)	148.5 \pm 77.1	129.7 \pm 31.3	0.628
Bicep Femoris Short Head (N)	322.3 \pm 45.8	398.4 \pm 100.3	0.177
Medial Gastrocnemius (N)	847.5 \pm 207.2	244.7 \pm 296.7	0.006
Lateral Gastrocnemius (N)	242.7 \pm 76.0	906.9 \pm 446.8	0.028
Total Flexor Force (N)	1367.3 \pm 214.1	1587.5 \pm 272.0	0.193

VALIDITY OF THE TWO-DIMENSIONAL SAGITTAL PLANE ASSUMPTION IN MODELING THE STANDING LONG JUMP

¹ Lauren J. Hickox, ¹ Blake M. Ashby, and ¹ Gordon J. Alderink

¹ Grand Valley State University, Grand Rapids, MI, USA
email: ashbybl@gvsu.edu, web: <http://www.gvsu.edu/engineering>

INTRODUCTION

Most standing jumping studies include the assumption that jumping is a sagittal plane activity in order to use a two-dimensional model (2D) instead of a three-dimensional (3D) model. However, the 2D assumption may not always be acceptable for jumping activities, particularly those that include arm movements. To investigate the validity of this assumption, a human subject study was designed that compared the results of kinematic and inverse dynamic analyses using both 2D and 3D full-body models.

METHODS

A Vicon motion capture system (Vicon Motion Systems Ltd., Los Angeles, CA) was used to record positions of markers on the bodies of six adult male volunteers (mean \pm standard deviation, mass: 90.3 ± 12.0 kg and height: 182.0 ± 6.3 cm). Reflective markers were placed on the upper and lower body in locations that allowed for the creation of both 2D and 3D models. The 2D model was single-sided and contained seven segments: foot, shank, thigh, pelvis, trunk, upper arm, and forearm. The 3D model contained 12 segments, including upper and lower extremities on both sides of the body. The anatomical reference frames for the 3D model were based on Ren et al. and recommendations by the International Society of Biomechanics (ISB) [1-3].

The participants performed leg and arm rotations that were collected for determination of the hip and shoulder joint centers using the SCoRE method [4]. Two in-ground force plates (Advanced Mechanical Technology Inc., Watertown, MA) were also used to collect 3D force and center of pressure data during takeoff. For the jumping trials, the subjects were instructed to stand with one foot on each force

plate. After familiarizing themselves with the motion, the participants performed eight standing long jumps for maximum distance with no restrictions on takeoff position or arm motion during the jump. The participants were allowed to rest as long as desired between jumps.

Inverse dynamics analyses were performed for the 2D and 3D models and joint moments, powers, and work values were found using Matlab R2013a (Mathworks, Natick, MA). The use of force plate data resulted in an over-determined system for both models. In order to solve the systems, the trunk equations were not used and the models were solved from the ground up to the lower back and from the hands “down” to the shoulders. The differences between these models were compared using a one-way ANOVA model in SAS JMP 10.0 (SAS Institute, Cary, NC).

RESULTS AND DISCUSSION

The results from this study showed good agreement between the 2D and 3D models for the lower body, with only insignificant differences in the moments, power (Figure 1), and work for the ankle, knee, and lower back. The 2D hip analysis resulted in a slightly higher peak power than the 3D analysis. For the upper body joints, the differences between the two models were more significant, particularly in power generation. The differences at the hip and shoulder were expected as they are ball and socket joints that are not physically constrained to sagittal plane motion, and the planar assumption in the 2D model caused the effects of adduction-abduction to be ignored at these joints. Differences at the elbow are explained in part by the planar assumption's inability to account for the elbow axis of rotation often not being perpendicular to the sagittal plane.

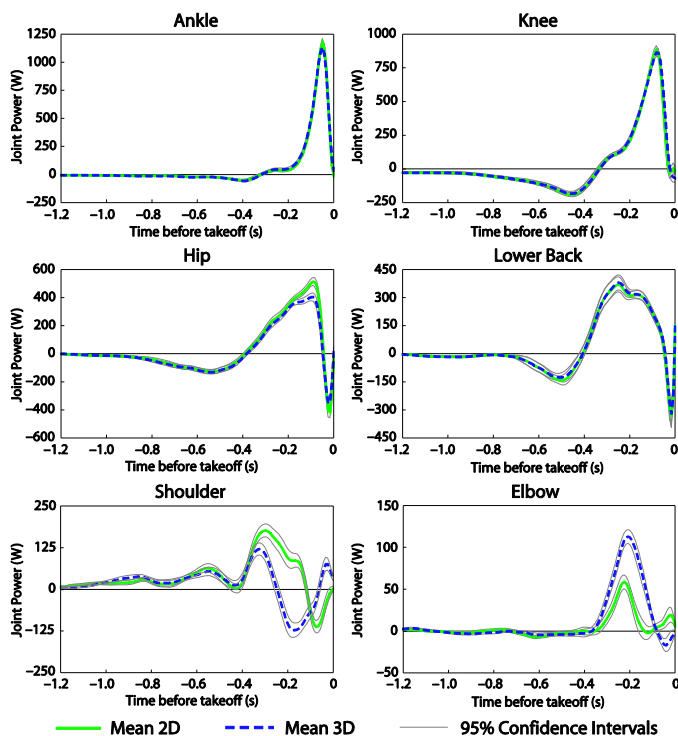


Figure 1: Comparison of Net Joint Power about the Flexion-Extension Axes for 2D and 3D Analyses for the Right Side (+ extension/plantarflexion).

In order to further analyze any non-planar activity that occurred during the jumps, the components of the 3D moments, power, and work were determined. The moments and power generation about the flexion-extension axes were found to be dominant in the lower body, confirming the agreement between the 2D and 3D models. The hip was the only joint in the lower body that showed significant moment and power generation (Figure 2) about the adduction-abduction axis, however flexion-extension was still overwhelmingly the dominant motion. In the upper body, significant moments and power generation were seen about both the adduction-abduction and flexion-extension axes at the shoulder joint (Figure 2). This was expected as more out-of-plane motion was observed in the upper body than in the lower body during the jump trials. Separating the total work at the right shoulder into components, 45.3% was found to be performed about the adduction-abduction axis and 53.6% was found to be performed about the flexion-extension axis. This distinction is not possible with a 2D analysis.

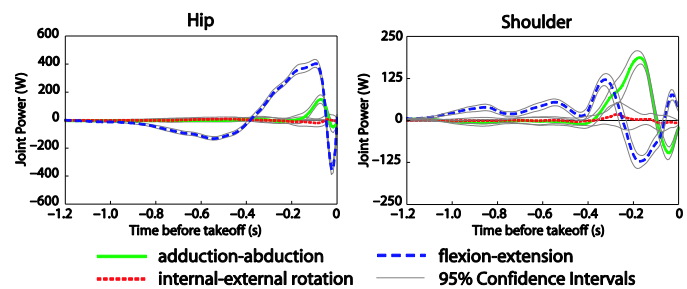


Figure 2: Components of Joint Power for the 3D Analysis for the Right Side Hip and Shoulder (+ abduction, extension, and external rotation).

CONCLUSION

3D models may more accurately represent the motion being studied but add complexity that comes at the cost of processing and analysis time. Gaining a better understanding of the differences between the two types of models should help with correct model selection for specific applications in future studies. When choosing a model for the analysis of the standing long jump, the value added by a 3D model needs to be considered with respect to the goals of the study. The results of this study showed that a planar motion assumption with a 2D model should be appropriate for most studies of the standing long jump, particularly when overall performance is considered and details of the upper body motion are not a concern. In cases where upper body motion is being studied or small increases in performance are vital, a 3D model may be more appropriate as it more accurately represents the motion of the upper body.

REFERENCES

1. Ren L, et al. *J Biomech* **41**, 2750-2759, 2008.
2. Wu G, et al. *J Biomech* **35**, 543-548, 2002.
3. Wu G, et al. *J Biomech* **38**, 981-992, 2005.
4. Ehrig RM, et al. *J Biomech* **39**, 2798-2809, 2006.

ACKNOWLEDGEMENTS

Special thanks is given to Nathaniel Vlietstra for his help in the data collection, data processing, and statistical analysis for this study.

Using a Dynamic Musculoskeletal Model to Explore Human Pinch

¹Alexander Barry, ¹Dan Qiu, and ^{1,2}Derek Kamper

¹ Department of Biomedical Engineering, Illinois Institute of Technology, Chicago, IL, USA

² Sensory Motor Performance Program, Rehabilitation Institute of Chicago, Chicago, IL, USA
email: abarry@hawk.iit.edu

INTRODUCTION

The act of pinching is fundamental to a variety of everyday tasks. The act of pinching involves a transition from dynamic movement to application of a precise isometric force at the tip of the digit. The transitions from movement to force and force to movement are complex [1] and incompletely understood. Computer modeling could help to identify important parameters in the pinching task. This information would further knowledge of hand motor control and guide rehabilitation.

Thus, building on previous models of the index finger [2] and thumb [3-5], we are developing a dynamic model of pinch. This study describes development of the model and preliminary validation testing of isometric force production of individual muscles. Simulation values are compared with cadaver results.

METHODS

The model was developed using OpenSim (SimTK, Stanford, CA). To replicate the structure of the hand in OpenSim the bone geometry was first imported from the OpenSim website [3]. The muscle attachment points and wrapping surfaces for the muscles were adapted from a previous study [2]. The thumb in this simulation was represented as a 5 DOF system, which has not been done before for this kind of simulation. The 5 DOF observed were abduction/adduction (A/A) at the Carpometacarpal (CMC) and Metacarpal (MCP) joints, and there was flexion/extension (F/E) at CMC, MCP, and Interphalangeal (IP) joints. These joints were represented using non-orthogonal axes as found by Hollister [6-7]. The index finger was represented by a 4 DOF system, with A/A at the MCP joint only, and F/E at MCP, Proximal Interphalangeal (PIP),

and Distal Interphalangeal (DIP), represented by non-orthogonal axes [2]. Each joint was provided with limits, to ensure that the joints did not rotate outside of their range during simulation. Initial joint angles were represented in the key or lateral pinch posture for the individual muscle activation simulations. These angles are defined by Valero-Cuevas 2003, to be: CMC A/A=0°, CMC F/E=-30°, MCP A/A=0°, MCP F/E=17°, and IP F/E=23°. For the Index finger the joints were set at: MCP F/E=30°, MCP A/A=0°, PIP F/E=45°, and DIP F/E=15° to coincide with previous studies [2]. Figure 1 provides a visual representation of the model used in simulation.

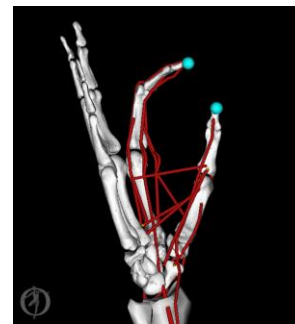


Figure 1: OpenSim model of hand with muscle attachments of the index finger and thumb

Individual muscle properties, specifically the peak force, optimal fiber length, and pennation angle, were obtained from previous studies [2,8]. These values were then used to calculate the tendon slack lengths for each muscle, assuming a 0.033% strain. All 8 muscles were included for the thumb: extensor pollicis longus (EPL), abductor pollicis longus (APL), flexor pollicis longus (FPL), Extensor Pollicis Brevis (EPB), Abductor Pollicis Brevis (APB), Flexor Pollicis Brevis (FPB), Opponens Pollicis (OPP), and Adductor Pollicis (Add). Six muscles were included for the index finger: flexor digitorum profundus (FDP), Flexor Digitorum Superficialis (FDS), Extensor Digitorum Communis

(EDC), First Palmar Interosseous (FPI), Extensor Indicis (EI), and Lumbrical (LUM).

For the individual thumb muscle simulations an activation was applied to produce a force of 10N for each muscle, i.e., if the muscle's peak force were 100N, the activation level would be 10%. This was done to allow a comparison with reported values in literature [8]. For the index finger an activation of 10% was used in every simulation to compare with previous studies [2]. With these activation levels and the initial angular positions a Forward Dynamics Simulation was performed to compute the motion of the model. Obtaining the isometric forces was accomplished by placing a small massless sphere on the fingertip and creating a contact with a ground oriented in the direction of the distal phalanx.

RESULTS AND DISCUSSION

The magnitudes of the forces produced were compared to the values from previous cadaver studies for the thumb [8] and index finger [2].

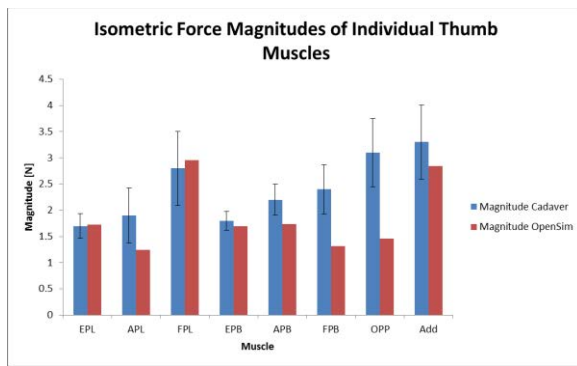


Figure 2: Comparison of the forces simulated in OpenSim to those from a cadaver study [Towles], all forces were generated from 10N of muscle force. Bars represent 95% confidence interval.

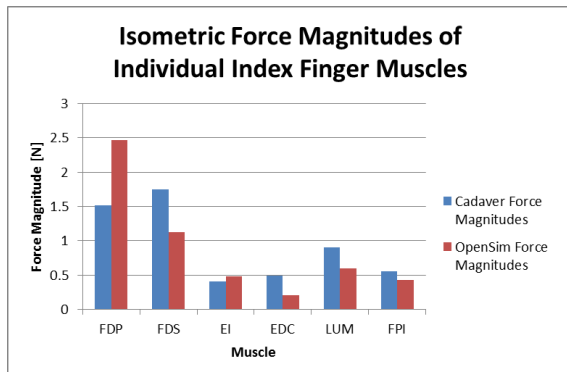


Figure 3: Comparison of force magnitudes from OpenSim and a cadaver study [Dan] in the index finger with 10% activation.

It can be seen that the thumbtip force magnitude closely matches (within 95% confidence interval) the magnitude seen in cadavers for EPL, FPL, EPB, and Add (Fig. 2). Those magnitudes are also shown to be a more accurate representation of the force than the old mathematical model. The forces for APL, FPB and OPP are not significantly close to the cadaver values which may be due to anatomical variations between the cadavers and the definition of the muscle insertions in the model.

For the index finger, the greatest deviations between the model and cadaver results were seen in the long flexors (Fig. 3). Model performance may be improved in the future by adjustments to the contact surfaces used to obtain the forces in the OpenSim model and by routing of the flexor tendons.

CONCLUSIONS

OpenSim can generate an accurate model of the forces generated in the human thumb and index finger. Increasing the accuracy of the model may be accomplished with different muscle wrapping surfaces, improved muscle insertion points, or by adding damping components to each of the joints. Putting these two components together gives a very promising possibility for the simulation of dynamic pinching.

REFERENCES

1. Venkadesan M, Valero-Cuevas F. *J Neurosci* **28**, 1366-1373, 2008.
2. Qiu D. *Dissertation*, Illinois Institute of Technology, 2013
3. Holzbaur KRS, et al. *Ann biomech eng* **33**, 829-840, 2005.
4. Wohlman SJ, et al. *J Biomech* **46**, 1014-1020, 2012.
5. Valero-Cuevas FJ, et al. *J Biomech* **36**, 1019-1030, 2003.
6. Hollister A, et al. *J Orthop Res* **10**, 454-460, 1992.
7. Hollister A, et al. *Clin Orthop Relat R* **320**, 188-193, 1995.
8. Towles JD, et al. *Clin Biomech* **23**, 387-394, 2008.

INVESTIGATION OF THE STRESSES INDUCED IN BONE DURING WALKING AND STAIR CLIMBING PRE AND POST THR

¹ Mohamed Z. Bendjaballah and ¹ Wissal Mesfar

¹ Biomedical Technology Department, College of Applied Medical Sciences, King Saud University
Riyadh, Saudi Arabia
email: bendja@ksu.edu.sa

INTRODUCTION

The total hip replacements (THR) present a high clinical success rate but it presents a number of complications as well especially among the younger patients. The main complication is attributed to the loosening of the stem due to osteolysis and stress shielding, both leading to bone resorption [1]. The stress shielding is defined as bone density loss due stress reduction following THR. While many solutions attempted to minimize the stress reduction between the intact and prosthetic case by exploring, amongst other on the effects of the stem material and shape. The influence of physical activities on the stress shielding reduction is not yet sufficiently explored. The aim of this study is; first, to explore the effect of two common daily activities, walking and stair climbing, on the stress distribution in the femoral bone before and after THR and second, to investigate whether the performance intensification of a particular physical activity reduces the stress shielding rate or not.

METHODS

Series of CT-scan images of a left intact femoral portion of a healthy female subject have served as an essence of the three-dimensional (3D) computer assisted design (CAD) model. The segmentation procedure performed in MIMICS 14.0 has aimed to isolate in a predefined mask only pixels that represent the cortical bone layer. Within this layer, the bulk of the cancellous bony tissue is intuitively determined based on CT images and anatomical data. The design of the femoral stem geometry is inspired from an anatomical cementless commercial design that has neck-shaft angle of about 130°, an oval cross-section proximally and an almost circular one distally. The prosthetic CAD model is then

generated by sectioning the head of the intact femur to accurately house the prosthesis.

A 3D finite element (FE) model is developed to predict the stress induced in the bone during walking and stair climbing. As shown in figure 1, the cortical, cancellous and prosthesis part instances were all meshed with quadratic hexahedral elements.

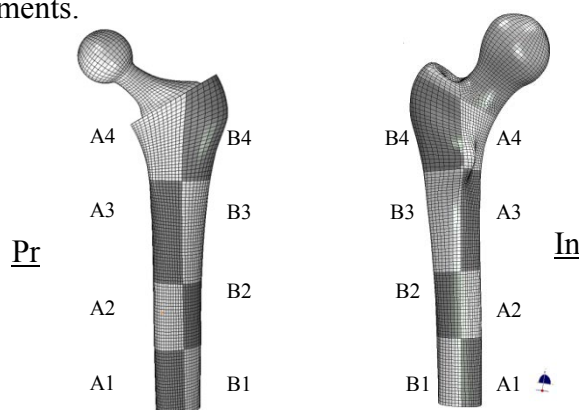


Figure 1: FE hexahedral meshes of the intact (In) and prosthetic (Pr) models showing the zones A1-4 and B1-4 repeatedly and accurately demarcated in both models for comparison purposes.

Orthotropic material property was assigned to the cortical bone and isotropic material properties were assigned to the cancellous bone and the prosthesis (Ti-6Al-4V) [2]. A bounded contact is considered to simulate the fully osseointegration condition that rises between the prosthesis and bone as well as the junction of the cortical and cancellous bone tissues. While the distal face of the cortical bone was set fixed in the subsequent nonlinear FE analyses, the loading applied consists of the action of up to four hip muscles as well as their resulting hip contact forces during walking (Wk) and stair climbing (Sc) loading cases, respectively. The lines and points of applications of the above-mentioned loads were

derived from the study of Heller et al. [3] considering a body weight of 700N. The stress shielding rate η was calculated based on the equation $1 - \sigma/\sigma_0 \times 100\%$, where σ and σ_0 correspond to the maximum of Von-Mises stress in each zone, A1-4 and B1-4, before and after THR, respectively. The analyses were performed using ABAQUS 6.10 FE package program.

RESULTS AND DISCUSSION

The response of the femoral cortical bone shows that the maximum Von-Mises stress increase substantially from Wk and Sc loading cases in both intact and prosthetic cases in the all zones except in the A4 and B4 regions where only a slight variation was predicted (Figure 2). The maximum Von-Mises stress was predicted to be in the intact case under Sc loading case in A1, A2, B1 and B2 regions ranging from 81.3 - 85.7 MPa. The max Von-Mises stress in the A4 zone after a THR is the only one that it decreases from the Wk to Sc case.

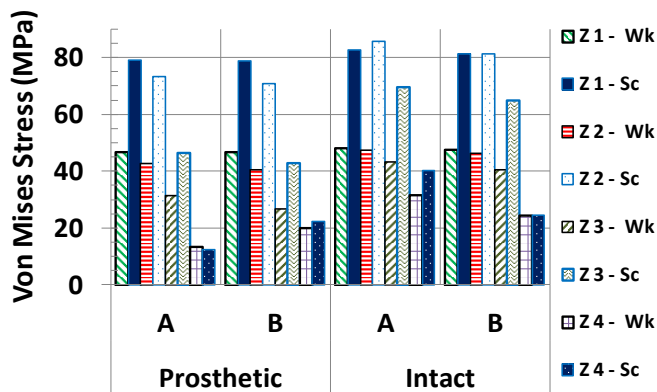


Figure 2: Von-Mises stress in the cortical bone for the Prosthetic and Intact cases for both walking (Wk) and stair climbing (Sc) loading cases.

In regions A1-4, the stress shielding rate increased from the A1 to A4 zones for the both considered loading cases. In Wk and Sc loading cases, the rate of stress shielding (η) reaches in A4 the highest magnitudes of 58% and 70%, respectively (Figure 3). Under the two loading cases, the stress shielding rate is maximum in A4, then in B3 and A3 regions. From B1-B4, the B3 region is the only one that it presents a rate of stress shielding greater than 30% equivalent to the rate in A3.

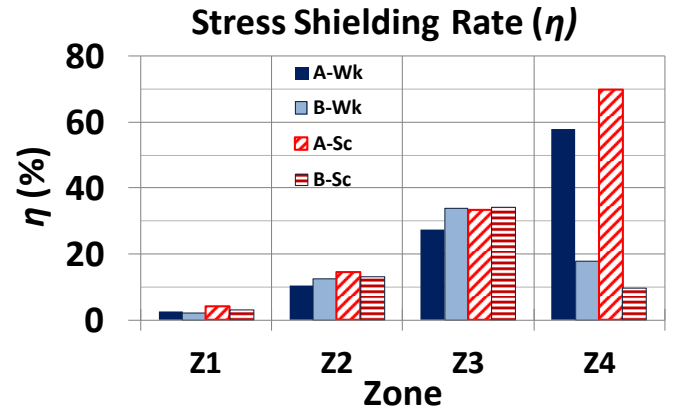


Figure 3: Stress shielding rate η calculated for the different zones and loading cases walking (Wk) and stair climbing (Sc) loading cases.

The zone A4 is found to be the most vulnerable region in the femur post THR. If we consider that walking is the most common daily activity before THR, the stair climbing activity after THR cannot increase the stress in the A4 region, where η is maximum, to its level in this region before the THR. However, stair climbing activity after a THR may be beneficial to reduce the stress shielding in A3 and B3 zones since the max Von-Mises stress in those zones under Sc loading activity is in the same order of magnitude of those recorded under the Wk loading before THR. This study may be of great benefit to provide a comprehension on how the femoral bone responds under common daily activities and how the stress shielding rate is going to be affected by activity intensification.

REFERENCES

1. Berry, D. J et al. *J. Bone Joint Surg. Am.*, **84A**, 171-177, 2002.
2. Caouette et al. *Proc Inst Mech Eng H*. **225(9)**, 907-919, 2011.
3. Heller et al. *J Biomech.*, **38(5)**, 1155-1163, 2005.

EFFECT OF JUMP IMPACT LOAD ON MENISCI, FEMORAL, TIBIAL AND PATELLAR CARTILAGES DURING FULL JOINT KNEE FLEXION

Sohaila El Sagheir, KodjoMoglo

Department of Mechanical and Aerospace Engineering
Royal Military college of Canada, Kingston, Canada,
email: sohaila.el-sagheir@rmc.ca

INTRODUCTION

Menisci and Cartilage degeneration in the knee joint is mainly caused by elevated stress level and high contact forces resulting from impacts. Landing from a jump impact on the knee joint muscles and ligaments has been discussed in previous studies [1] but there was no thorough investigation of its effect on the femoral, tibial and patellar cartilages, as well as menisci, which is presented in this study. The objective of this study is to investigate the effect of ground reaction force due to landing from a jump impact on the knee joint cartilages and menisci and compare results with those before impact to determine the elevation in stress and contact values.

METHODS

A Full Finite Element knee joint model was used to conduct this study. The model was created based on MRI scans of the right knee (Male:45 yr-70 kg) which were used to extract the 3D geometry of the knee joint model. The 3D geometry of the skeletal knee skeletal was built using Mimics and Abaqus. Articular cartilages and menisci were considered to behave as linear elastic isotropic as reported in the literature [2]. Ligaments and Quadriceps muscles were modeled as axial spring connectors which have an elastic nonlinear behaviour [3]. Muscles orientation and insertions were adapted from Sakai et al [4]. Since bone stiffness is much higher than the soft tissues, bones are modeled as rigid bodies represented by a reference node and meshed with tetrahedral elements. Menisci and cartilages were meshed with 8 node hexahedron elements. Frictionless non-linear contact with finite sliding was assumed in all articulations. Model was validated using results reported in previous studies [3] and [5] as shown in (Figure 1) for ACL forces at Quadriceps load of (3N). Boundary conditions of

the presented study was to flex the femur to 33 degrees then apply load of 1265 N to the tibia to simulate the vertical ground reaction force first peak as illustrated in the study of Pflum et al [1]. Parameters of interest are contact pressure, contact area and patella tendon forces at the moment of impact and comparing it with results just before impact. Total contact forces after impact will be measured as well.

RESULTS AND DISCUSSION

As shown in Table (1), contact pressure increased substantially after the impact loading was applied. It was noticed that more contact pressure resulted in the lateral compartment as shown in the contour plot of femoral cartilage (Figure 3). Contact Area results showed the same trend except for medial menisci which remained almost the same. Patella tendon forces before applying the load (5N) reflected the forces given to the Quadriceps muscles (3N) in addition to forces resulted from rotation, however after at the moment of impact load, patella tendon forces increased to (65N). At the moment of impact, total contact forces were (1200N), (320N) and (310N) for the tibial cartilages, menisci and patella cartilage respectively.

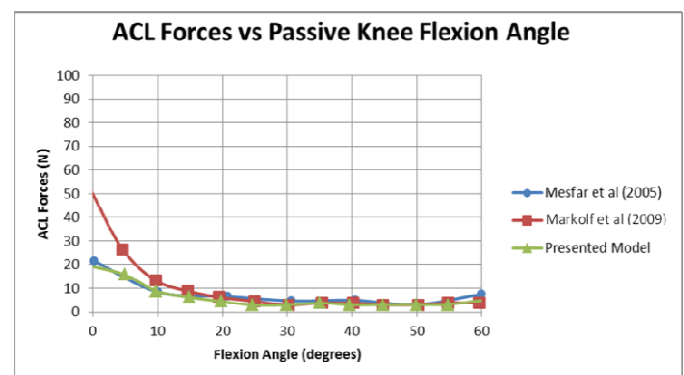


Figure 1: Presented model validation curve

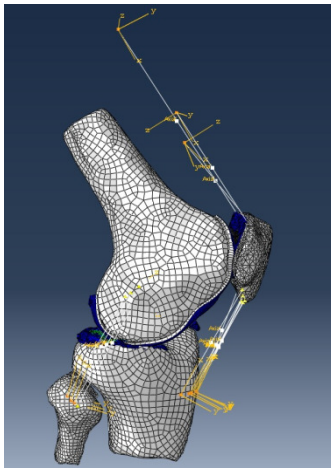


Figure 2: Rotated Model showing contact pairs, Patella tendon and Quadriceps muscles connectors

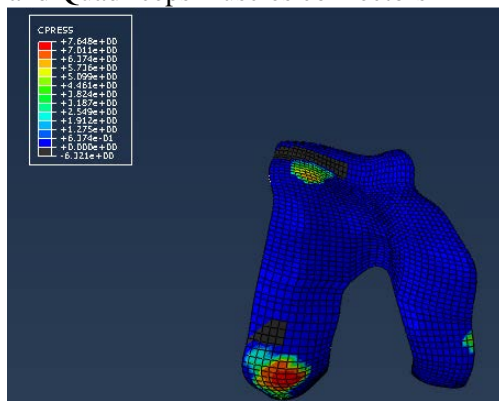


Figure 3: Contact Pressure contour plot on femoral cartilage at 33 degrees flexion and impact loading of 1265 N.

CONCLUSIONS

Results show that most of the load bearing was concentrated on the lateral compartment which requires more investigation. Contact forces results shows the tibial cartilages to be the most impacted in the knee joint at the moment of load impact which indicates more prone to injury and degeneration. The excessive increase in contact pressure due to landing from a jump and impacting with ground reaction force can cause meniscal and cartilage failure. Future work should focus on the design of safer landing technique to avoid joint degeneration.

REFERENCES

1. Pflum M, et al. Model prediction of anterior cruciate ligament force during drop landings. *Journal of Medicine and Science in Sports and Exercise* 36:1949-1958 (2004).
2. Pena B, et al. 3D FE. Analysis of the combined behaviour of ligaments & menisci in healthy human knee joint. *Journal of Biomechanics* 39, 1686-1701 (2006).
3. Mesfar W, et al. Biomechanics of the knee joint in flexion under various quadriceps forces. *The Knee* 12 424-434 (2005).
4. Sakai N, et al. Quadriceps forces and patellar motion in the anatomical model of the patellofemoral joint. *The Knee* 3: 1-7 (1996).
5. Markolf et al. Anterior-posterior and rotatory stability of single and double bundle anterior cruciate ligament reconstructions. *Journal of Bone and Joint Surgery* 91, 107-118 (2009).

ACKNOWLEDGMENTS

This work is supported by Academic Research Program (ARP) and Aerospace Research Advisory Committee (AERAC)

Table 1: Results just before applying impact loading and at the instant of applying it

Parameter	Part or contact pair	Just before Impact loading	At the instant of Impact load (1265N)
Contact Pressure (MPa)	Femoral cartilage	2.58	7.648
	tibialcartilages=	2.6	5.7
	lateralmenisci	2	6.83
	Medialmenisci	1.8	5.45
	Patella cartilage	2.75	5.99
Contact Area (mm ²)	Femoral cartilage /lateral tibial cartilage=	85	225
	Femoral cartilage /Medial tibial cartilage=	80	185
	Femoral cartilage/lateralmenisci	35	75
	Femoral cartilage/Medialmenisci	10	10
	Femoral cartilage/Patella cartilage	89	130
Patella Tendon forces (N)	5		65

MODELING THE AGING ACHILLES TENDON: INTER-FASCICLE ADHESIONS AND TENDON COMPLIANCE AFFECT PLANTARFLEXOR BEHAVIOR DURING WALKING

Jason R. Franz^{1,2} and Darryl G. Thelen¹

¹University of Wisconsin, Madison, WI, USA

²University of North Carolina and North Carolina State University, Chapel Hill, NC, USA
email: jrfranz2@wisc.edu, web: <http://uwnmb1.engr.wisc.edu>

INTRODUCTION

The Achilles tendon (AT) consists of distinct fascicle bundles arising from the gastrocnemius and soleus muscles that intertwine and twist before inserting onto the calcaneus [1]. Current musculoskeletal models simplify this architecture by representing the gastrocnemius and soleus as independent muscle-tendon actuators [2], which may be an appropriate assumption if the fascicles freely slide relative to one another. However, this assumption may not hold with aging, as inter-fascicle adhesions form and reduce sliding between adjacent tendon fascicles [3]. This adaptation could explain our recent finding that depth-dependent variations in AT deformations during walking are much smaller in old vs. young adults (Fig. 1A) [4]. A reduced capacity for sliding in old tendons may couple gastrocnemius and soleus muscle-tendon behavior, which could in turn alter muscle force production.

Tendon also undergoes microstructural changes with aging that are believed to increase its compliance,

consistent with ultrasound imaging studies of the Achilles tendon in walking [4,5]. Tendon compliance systematically influences muscle fiber kinematics and mechanical power production [6], and could modulate the effects of inter-fascicle adhesions in the aging Achilles tendon. Thus, we developed simple models of the plantarflexor muscle-tendons (Fig. 1B) to investigate the independent and combinatory effects of inter-fascicle adhesions and tendon compliance on plantarflexor muscle fiber kinematics and the performance of mechanical work in walking.

METHODS

10 young adults walked at their preferred speed down a 10 m walkway (mean, 1.33 m/s). 3D motion capture recorded pelvis and lower extremity kinematics at 200 Hz. For each subject, we estimated gastrocnemius and soleus muscle-tendon unit (MTU) lengths over one stance phase from scaled, seven segment, 18 degree-of-freedom musculoskeletal models [2]. MTU lengths then served as boundary conditions in models composed of (i) independent

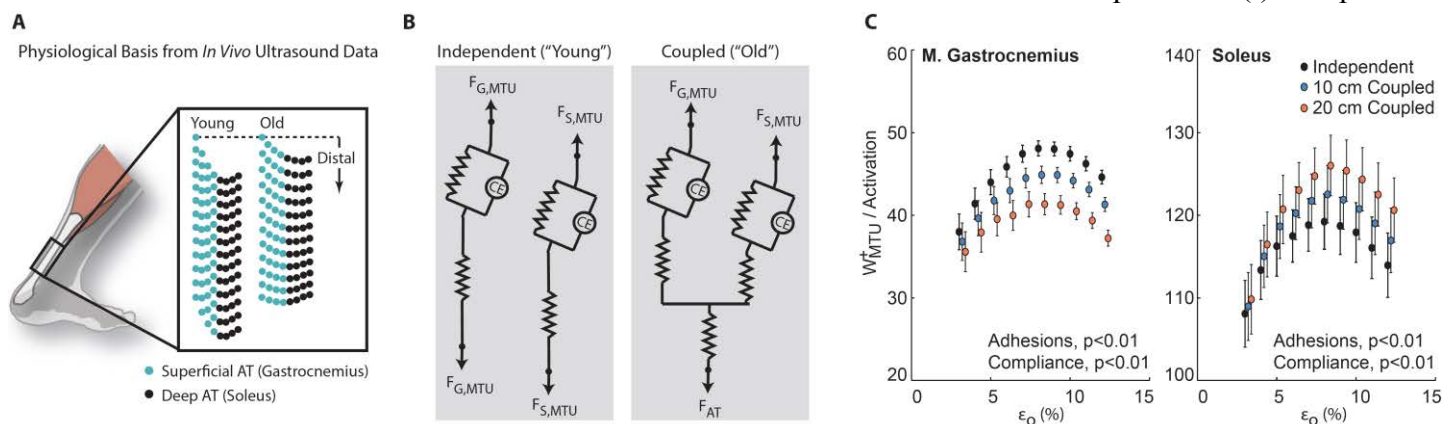


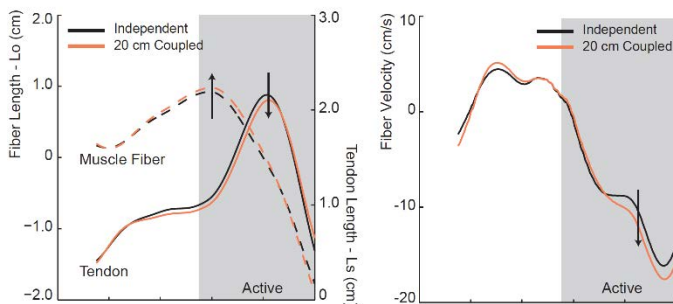
Figure 1. (A) Superficial and deep free AT tissue displacements, tracked using 2D speckle tracking, reveal smaller depth-dependent variations in AT deformations in old vs. young adults [4] which may arise from inter-fascicle adhesions. (B) We simulated inter-fascicle adhesions by coupling the gastrocnemius (G) and soleus (S) via a shared AT of two lengths (10 cm, 20 cm) across range of compliances. (C) Simulating tendon adhesions redistributed stance phase positive work (mean ± SE) from the gastrocnemius to the soleus, with progressively larger changes observed with increasing tendon compliance.

and (ii) coupled gastrocnemius and soleus Hill-type muscle-tendon actuators [7] implemented in Simulink (Fig. 1). We modeled inter-fascicle adhesions (i.e., MTU coupling) by simulating two shared AT lengths (10 cm and 20 cm). In models composed of independent muscle-tendons, we derived muscle excitations that maximized stance phase MTU positive work per unit activation. These excitations were prescribed for models composed of coupled muscle-tendons. We repeated all simulations using a range of tendon compliances, from 3 to 12% strain at maximum isometric force (ϵ_0).

RESULTS AND DISCUSSION

Simulating inter-fascicle adhesions altered muscle and tendon kinematics, with opposing changes evident in the gastrocnemius (longer fiber lengths, faster shortening velocities, less tendon stretch) and soleus (shorter fiber lengths, slower shortening velocities, more tendon stretch) compared to independent MTUs driven by the same excitations (Fig. 2). Functionally, these changes elicited up to a 16% decrease in gastrocnemius positive work

M. Gastrocnemius



Soleus

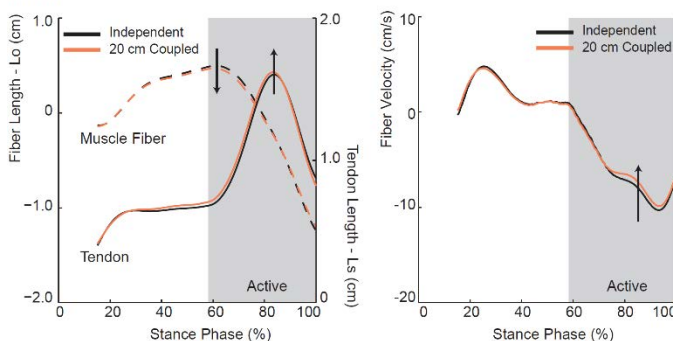


Figure 2. Group mean muscle and tendon kinematics for simulated independent and coupled gastrocnemius and soleus MTUs at 8% tendon strain (L_0 : optimal length, L_s : slack length). Arrows highlight the effects of simulating tendon adhesions, which allude to changes in force generating capacity consistent with changes in the performance of positive work shown in Figure 1.

coupled with a nearly proportional increase in soleus positive work during stance ($p < 0.01$) (Fig. 1C). Thus, inter-fascicle adhesions redistributed positive work from the gastrocnemius to the soleus in a manner consistent with changes in fiber kinematics.

Like prior studies [6], we found a significant relation between tendon compliance and muscle-tendon performance (Fig. 2), wherein an optimum elasticity maximized gastrocnemius and soleus MTU positive work per unit activation ($p < 0.01$). Moreover, tendon compliance modulated the effects of inter-fascicle adhesions, with progressively larger changes in muscle-tendon behavior arising with increasing tendon compliance (interaction, $p < 0.01$) (Fig. 2). Thus, we observed the most substantial changes in muscle-tendon dynamics when co-simulating a reduced capacity for inter-fascicle sliding and an increase in tendon compliance.

CONCLUSIONS

Our *in vivo* ultrasound data suggest a link between smaller depth-dependent variations in AT tissue deformations and reduced ankle joint kinetics during walking with age [4]. Here, we found that a reduced capacity for sliding between AT fascicle bundles can couple gastrocnemius and soleus muscle-tendon behavior. Specifically, we show that this coupling would redistribute positive work from the gastrocnemius to the soleus during walking. This adaptation, exacerbated by increasing tendon compliance and consistent with changes in fiber kinematics, may help to explain the age-related reduction in forward propulsion [4], an important function of the gastrocnemius muscle.

REFERENCES

1. Szaro et al., *Ann Anat* 2009; 6:586-93.
2. Arnold et al., *Ann Biomed Eng* 2010; 38(2):269-79.
3. Thorpe et al., *Eur Cell Mater* 2013; 25:48-60.
4. Franz and Thelen, *J Appl Physiol* (In Revision).
5. Panizzolo et al., *Gait Posture* 2013; 38(4):764-9.
6. Lichtwark and Wilson, *J Theor Biol* 2008; 252:662-73.
7. Zajac FE, *Crit Rev Biomed Eng* 1989; 17:359-411.

ACKNOWLEDGEMENTS

Funded by a grant from NIH (F32AG044904).

PERFORMANCE OF A VERSATILE IN VITRO JOINT SIMULATOR WITH KINETIC CHAIN TESTING CAPABILITIES

Joshua Green, Paul Power, Jerome Hausselle, and Roger V. Gonzalez

Joint Lab, The University of Texas at El Paso, El Paso, TX, USA

email: rvgonzalez@utep.edu, web: <http://jointlab.utep.edu>

INTRODUCTION

Musculoskeletal diseases and disorders (e.g. osteoarthritis, neck and back pain), joint injuries (e.g. ligament failures), and natural aging of joint tissue are among the most prevalent, debilitating, and painful medical conditions. Although tremendous advances have been made in biomedical engineering, potential breakthroughs are hindered by limitations in acquiring reliable *in vivo* measurements such as internal joint contact forces. It is nearly impossible to collect *in vivo* data without using instrumented implants [1], which disrupt the biomechanics of the natural joint and cause altered loading conditions.

Attempting to circumvent this critical barrier, several *in vitro* knee simulators [1-5] have been developed to replicate the complexity of the *in vivo* joint biomechanics. However, existing simulators are limited in their predictive capabilities, lacking synchronously loaded individual muscle forces, external ground reaction forces, and joint kinematics in the three planes. In particular, muscle force control varies tremendously: nonexistent muscle loading [2], grouped flexor and extensor muscle loading [3], and individual muscle force control [4]. Since each individual muscle crossing a specific joint uniquely contributes to internal load and joint stability [5], grouping individual muscle forces or failing to represent muscle forces altogether can significantly influence the joint kinematics and thus introduce errors with respect to the *in vivo* loading conditions. Moreover, to our knowledge, all existing simulators target a single joint, *i.e.* do not simulate movements of kinetic chains consisting of several joints.

To address these limitations and provide reliable experimental data, we sought to develop a versatile

in vitro multi-joint simulator capable of replicating highly dynamic activities such as running, jump landing, and cutting.

METHODS

Simulator design requirements were based on motion analyses of highly dynamic knee motions including jumping, braking, and cutting maneuvers. Twelve electromagnetic actuators control twelve degrees of freedom of the simulator, *i.e.* six for the upper “hip” joint, and six for the lower “ankle” joint, in analogy with current knee joint simulators. The use of electromagnetic actuators ensures accurate and precise control of positions and forces in real-time.

The control system was developed using a Real-Time LabVIEW environment (National Instruments Corporation, TX, USA) to provide controller

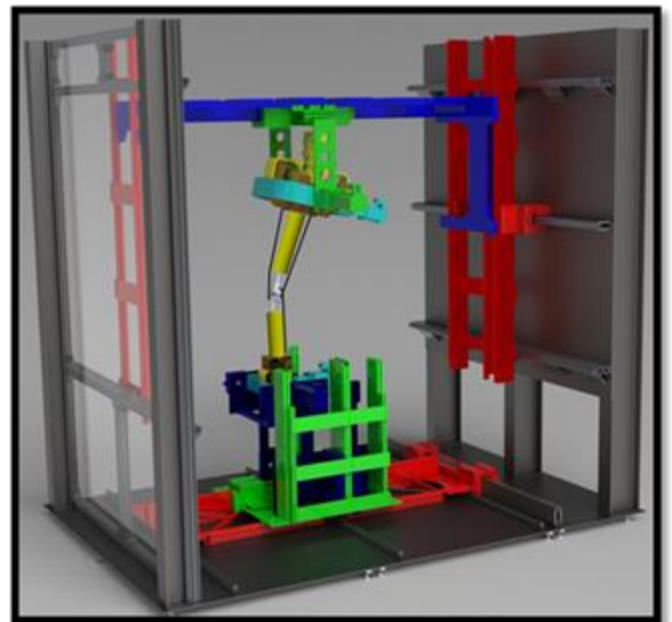


Figure 1: 3D schematic overview of the UTJLS with a mounted cadaver knee specimen.

centralization and flexibility during diverse applications. In order to operate with a variety of system input combinations, each control loop can be configured to react to position or force feedback with standard PID algorithms on top of a second-order system model.

The current muscle actuation system is designed to replicate eight individual muscles acting on a cadaver knee, and each actuator is located with respect to the knee joint center as computed to match a specific muscle in a generic musculoskeletal knee model [6]. The muscle actuators consist of rotational servo motors, pulleys, steel cables, ultra-light miniature load cells, and tendon connectors, which are capable of recreating highly-dynamic muscle forces (maximum force range: 750N to 1170N and maximum velocity range: 180mm/s to 490 mm/s).

RESULTS AND DISCUSSION

We have developed the Joint Load Simulator (UTJLS) (Fig. 1) to be capable of dynamically controlling twelve kinetic and kinematic conditions and eight individual muscle forces. By including control of twelve degrees of freedom instead of only the six necessary for recreating internal joint conditions, the UTJLS is capable of prescribing the entire movement of the cadaver specimen, as compared to the relative bone to bone motion replicated by other simulators.

Design of the UTJLS included the use of high quality electromagnetic actuators in order to reproduce highly dynamic motions (maximum translational velocity range: 1.4 to 4.8m/s, maximum rotational velocity range: 5.0 to 7.5rad/s). These actuators also ensure an accurate and precise control of position and force in real-time (approximate response time of 3ms). During a real-time, 9-axis squatting maneuver, all axes operated with position control and had standard deviations less than 0.49mm and 0.45deg (Fig. 2), and during a 6-axis force test, each axis had standard deviations less than 9.49N and 1.05N*m.

Although it is originally configured to test cadaveric knee specimens, this simulator has been specifically

designed to be easily modified to accommodate a wide range of joints and even entire kinetic chains.

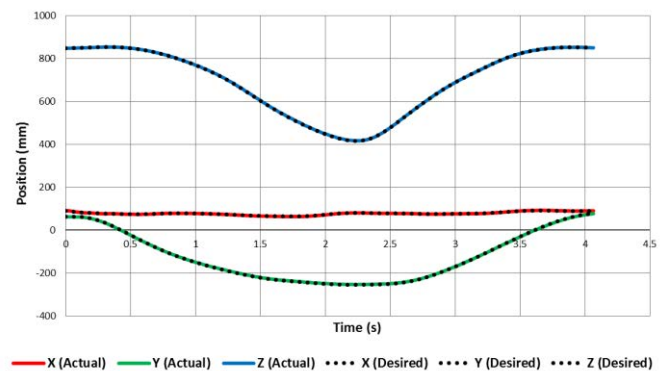


Figure 2: Graph of hip position vs. time during a position controlled squat. Colors correspond to surrogate hip linear axes designated in Figure 1.

CONCLUSIONS

The sophistication of the UTJLS significantly expands our ability to (1) conduct non-invasive clinical and surgical procedures before *in vivo* assessment and (2) to provide an open-source database of reliable *in vitro* measurements for the validation of computational models. The specific design of this simulator allows for multi-joint testing, thus pushing the boundaries of *in vitro* testing capabilities to enhance our knowledge of multi-joint biomechanics.

REFERENCES

1. Kim HJ, et al. *J Orthop Res* **27**, 1326-1331, 2009.
2. Noble LD, et al. *J Biomech Eng* **132**, 025001, 2010.
3. Maletsky LP, et al., *J Biomech Eng* **127**, 123-133, 2005.
4. Muller O, et al. *Biomed Eng* **54**, 142-149, 2009.
5. Wunschel M, et al. *Knee Surg Sports Traumatol Arthrosc* **19**, 1099-1106, 2011.
6. Hausselle J, et al. *Comput Methods Biomech Biomed Engin* **17**, 480-487, 2014.

ACKNOWLEDGEMENTS

This research was supported, in part, by the NSF (BES 0966398), The University of Texas at El Paso Start-up Funds, and Advanced Motion Controls.

MULTI-SEGMENT FOOT MODELING TO MAXIMIZE RELIABILITY AND CLINICAL RELEVANCE

¹ David J. Gutekunst, ¹ Krista Coleman-Wood, and ¹ Kenton R. Kaufman

¹ Mayo Clinic, Rochester, MN, USA

email: Gutekunst.David@mayo.edu web: mayo.edu/research/labs/motion-analysis

INTRODUCTION

A commonly used multi-segment foot (MSF) model uses the ankle joint center to define the hind foot segment axes [1] (Figure 1).

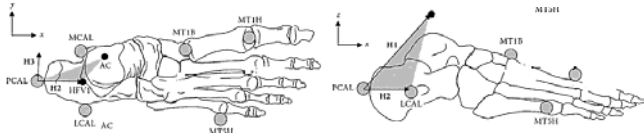


Figure 1: (A) superior, and (B) lateral views of Shriner's Hospital for Children – Greenville landmarks to define hindfoot axes.

Ideally, hindfoot axes would be defined using landmarks placed only on calcaneus, and without anatomical registration from X-ray or goniometry [2] (Figure 2). However, this model has been shown to have poor reliability, with inter-session and inter-therapist errors up to 11° [3].

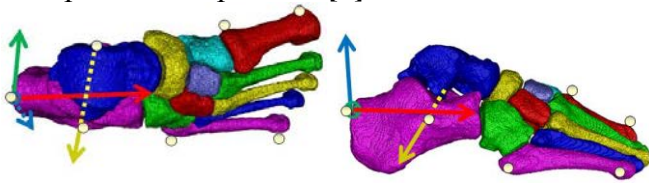


Figure 2: (A) superior, and (B) lateral views of proposed hindfoot axes, based on the Leardini MSF model [2].

Ultrasound imaging can be used to identify anatomical landmarks. This approach could provide a safe, clinically applicable way to improve MSF reliability without X-ray or goniometry. Therefore, the purpose of this study was to assess the effects of adding ultrasound imaging (US) to standard palpation (PALP) on inter-session kinematic reliability of a MSF model. We hypothesized that the combined technique (US+PALP) technique would result in improved inter-session reliability compared to the standard PALP method.

METHODS

8 healthy volunteers with no history of foot deformity (5 female, 3 male, Age = 32.0±5.6 yrs, Height = 170.9±10.0 cm, BMI = 23.4±3.4 kg/m²) agreed to participate and provided written informed consent. Volunteers underwent two sessions of 3D gait analysis on separate days. A single experienced physical therapist placed landmarks bilaterally on the shank, hindfoot, and forefoot. Volunteers completed 3 walking trials at self-selected walking speed per session. One limb was randomly assigned the standard palpation technique (PALP); the other limb was assigned the ultrasound technique (US+PALP). The assigned technique was maintained for both testing sessions.

Segmental motions were computed in Visual3D (C-Motion, Germantown, MD). A Cardan YX'Z" sequence was used, reflecting motion in the sagittal, frontal, and transverse planes. A total of 6 angular measures (X, Y, and Z angles for Hindfoot:Shank and Forefoot:Hindfoot) were computed for a full gait cycle within each walking trial. All angular measures were normalized to 100% of the gait cycle in 1% increments. For each angular measure, inter-trial and inter-session reliability were assessed using the method described by Schwartz *et al.* [4].

RESULTS AND DISCUSSION

Inter-trial error was similar (~1°) for both methods, for Hindfoot:Shank and Forefoot:Hindfoot angles, and in all planes of motion (Figure 3, red bars). Inter-session reliability varied by foot segment (Figure 3, blue bars):

- *Hindfoot:Shank angles* : both techniques demonstrated average inter-session of 3° across the 3 planes of motion. For dorsi/plantarflexion, US+PALP resulted in 1° lower inter-session error than PALP alone (2.5° vs. 3.5°).

- *Forefoot:Hindfoot angles*: the highest inter-session errors for both techniques were seen in dorsiflexion-plantarflexion (5.2° for US+PALP and 7.1° for PALP alone). Inter-session errors were similar between the techniques in the frontal plane (3.6° vs. 3.2°) and transverse plane (3.0° vs. 3.1°).

CONCLUSIONS

Appropriate clinical decisions and assessment of treatment outcomes depend upon reliable MSF measurements that accurately reflect skeletal motion. With the exception of Forefoot:Hindfoot dorsi/plantarflexion, both techniques showed better reliability than previously reported using anatomically-relevant segment axes [3].

Contrary to our hypothesis, the addition of ultrasound did not result in a substantive reduction in inter-session error. Still, the results suggest that it is possible to achieve low inter-session error using clinically-relevant MSF segmental axes *without X-ray or goniometric registration*. Additional preliminary results for multiple therapists indicate that there is a learning curve for kinematics reliability, especially using ultrasound imaging.

Further work is planned to determine (1) kinematics reliability in children and individuals with foot deformity, (2) the effects of therapist experience on reliability using palpation with or without US, (3) kinematics reliability when defining hindfoot axes using the calcaneal sulcus as a lateral hindfoot anatomical landmark, and (4) the ideal forefoot marker setup to maximize reliability and clinical relevance.

REFERENCES

1. Davis RB *et al* (2008). In: *Foot and Ankle Motion Analysis*: 425-44.
2. Leardini *et al* (2007). *Gait & Posture* **25**:453-62.
3. Caravaggi P *et al.* (2011). *Gait & Posture* **33**:133-5.
4. Schwartz MH *et al* (2004). *Gait & Posture* **20**(2):196-203.

ACKNOWLEDGEMENTS

Funding support provided by the Mayo Clinic Foundation and NIH T32 AR056950 (Westendorf). Levi Talbert assisted in data processing and code development.

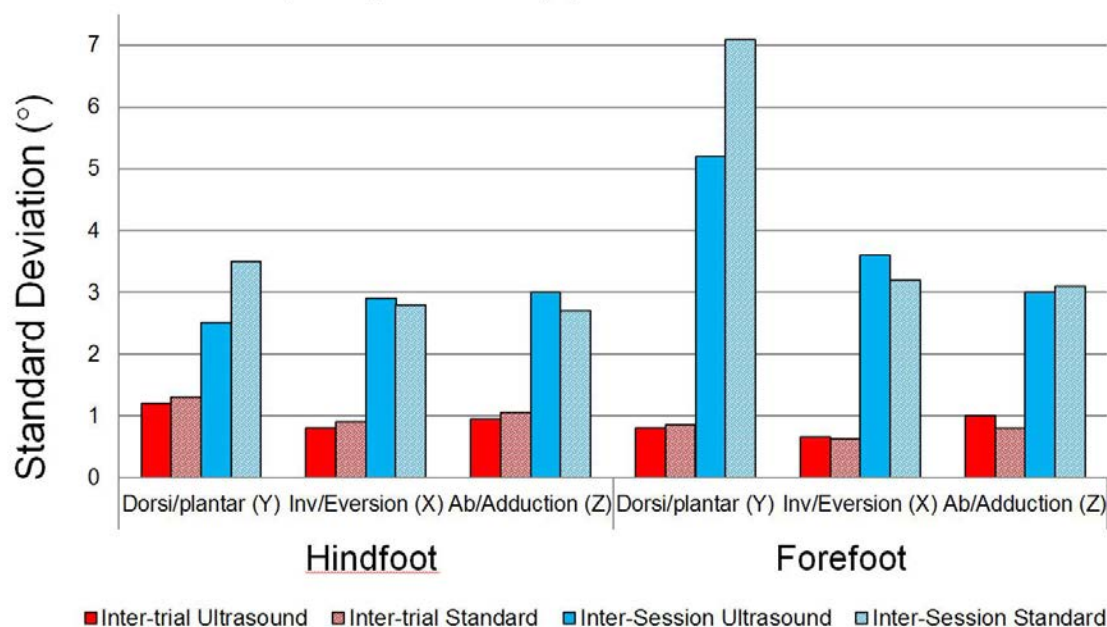


Figure 3: Inter-trial and inter-session error averaged across the gait cycle for **(left)** Hindfoot:Shank sagittal, frontal, and transverse plane angles; **(right)** Forefoot:Hindfoot sagittal, frontal, and transverse plane angles.

Effect of Morphology, Cross-section Type, and Apparent Density on the Elastic Properties of Open-Cell Structures

Reza Hedayati*, Mojtaba Sadighi, Mohammad Mohammadi Aghdam

Mechanical Engineering Department, Amirkabir University of Technology, Hafez Ave, Tehran, Iran,

*Corresponding author, Email: rezahedayati@aut.ac.ir

Abstract

Metallic foams are known as biocompatible materials which are good candidates for being used in orthopedic implants. This is because their open-cellular structure permits the ingrowth of the new bone tissues and the transport of the body fluids. It is especially attractive that the strength and the Young's modulus of the cellular materials can be adjusted through the adjustment of the porosity to match the strength and the Young's modulus of the nature bone which prevents stress shielding which can then lead to aseptic loosening of the implant inside body. Advent of new novel additive manufacturing techniques make it possible to create implants with arbitrary micro-geometrical features. Generally, the properties of open-cell foams depend on three main parameters: first, the material which the foam is made of; second, the morphology of the cells, and third the geometry of the struts. Not many investigations have been carried out on the explicit comparison of static properties of open-cell porous structures having different morphologies, cross-section dimensions, cross-section geometry, and apparent densities. Providing detailed comparison between the elastic properties of structures in terms of their geometrical parameters can be useful for applications in which low/high stiffness in axial/shear loadings is required. In this study, Finite Element simulations have been implemented to investigate the effect of structure morphology, cross-section type, strut length, and apparent density on the elastic modulus, shear modulus, yield stress, shear yield stress, and Poisson's ratio of open-cell tessellated cellular structures to find the appropriate configuration for applications with low-stiffness or high-stiffness requirements. Five different morphologies, namely cube, rhombic dodecahedron, Kelvin, Weaire-Phelan, and diamond were considered. For each morphology, a relationship relating the strut length, cross-section dimension, and apparent density is provided according to which 135 simulations are carried out and their results are compared in terms of different elastic properties. It was seen that the strut cross-section type does not have a considerable effect on the structure elastic modulus while its effect on the structure yield stress is significant. For all the morphologies, the triangular and the circular cross-sections lead to the highest and lowest elastic moduli, respectively. It was seen that the cube morphology has an elastic modulus and yield stress much higher than other morphologies while the diamond structure has the lowest corresponding values. It was also observed that the circular rhombic dodecahedron structure has a high yielding strength (second among all the cases) while its elastic modulus is relatively low. Therefore it is the best choice for applications with low stiffness requirements. This structure is also the strongest morphology in shear loading.

Keywords: Additive manufacturing, Open-cell biomaterials, Finite Element, Rhombic Dodecahedron, Weaire-Phelan, Diamond, Kelvin, Morphology, Apparent Density

KINETIC VALIDATION OF A LINK-SEGMENT TRUNK MODEL

Laura Hutchinson¹, David M. Bazett-Jones², Eric M. Paulos², Kevin J. Deluzio¹, Michael J. Rainbow¹

¹Mechanical Engineering, HMRC, Queen's University, Kingston, ON

²Physical Therapy, Carroll University, Waukesha, WI

email: laura.hutchinson@queensu.ca

INTRODUCTION

Recent evidence suggests that the kinematics of the torso play an important role in lower extremity musculoskeletal syndromes such as patellofemoral pain[1]. In clinical gait analysis, the thoracic and lumbar spines are commonly modelled as a single trunk segment and there is no consensus on the ideal marker set to track the trunk. Importantly, Leardini *et al.* demonstrated that different marker sets for defining and tracking the trunk yielded different joint angles for the same motion[2]. Furthermore, it is unknown how tracking errors vary with specific activity. The purpose of this study was to introduce a method for determining the optimal tracking markers for the trunk. Our method quantifies the error of a trunk model by comparing accurate ground reaction force (GRF) measurements to GRF's computed from the motion of the link-segment model's whole body centre of mass (COM). We hypothesized that trunk errors would vary as a function of tracking markers as well as choice of task.

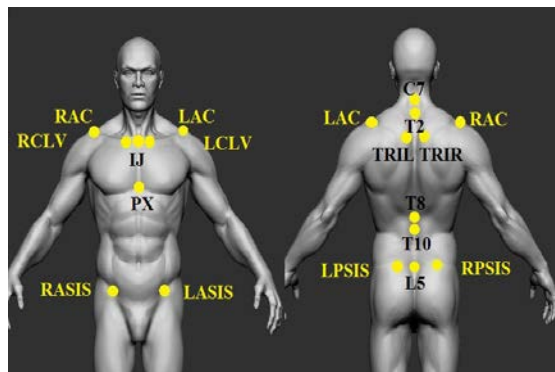


Figure 1: Trunk marker set.

METHODS

The trunk accounts for ~35% of the body's total mass; therefore, we assumed that errors

in tracking the trunk will result in errors in the ground reaction force computed from the model's COM (GRF_{KM}). Our approach compares GRF_{KM} to force plate measurements, (GRF_{FP}). A full body biomechanical model was constructed from reflective markers. Different trunk models were tested by changing the trunk's tracking markers. We tested seven trunk models using combinations of the trunk markers as seen in Figure 1 and Table 1. IRB approval was obtained and informed consent was given from twelve subjects (7 male and 5 female). They performed 4 activities: single leg hop, single leg squat, double leg hop, and double leg squat. Markers were recorded with a motion capture system (Qualysis, 10-camera, 250 Hz). GRF_{FP} was acquired from a force plate (AMTI, 2000 Hz). Marker trajectories and ground reaction forces were filtered at 10 Hz. The model's COM position was computed in Visual3D (C-Motion inc.). GRF_{KM} was computed as the second derivative of COM position multiplied by mass (Fig 2A). Root mean square (RMS) errors were computed between vertical GRF_{KM} and GRF_{FP} . A 2-way repeated measures ANOVA determined whether errors varied as a function of model or task. We also performed a Holm-Sidak post hoc analysis to determine pairwise differences among models and tasks.

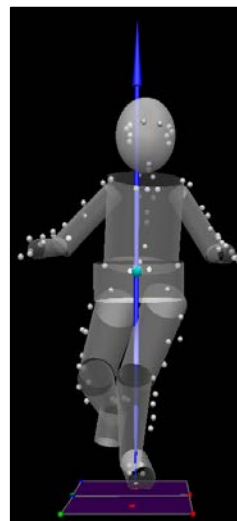


Figure 1: Visual 3D link-segment

RESULTS AND DISCUSSION

COM error varied as a function of both model ($p < 0.001$) and task ($p < 0.0001$), and there was a significant interaction between model and task ($P < 0.004$). Pairwise analysis revealed that error varied among all tasks ($p < 0.02$). Regardless of model choice, the 2 leg jump resulted in 38% larger error compared to other tasks. This task required larger GRF's and a larger trunk range of motion, which may have caused the higher errors. There was no single model that resulted in lower or higher errors across all tasks.

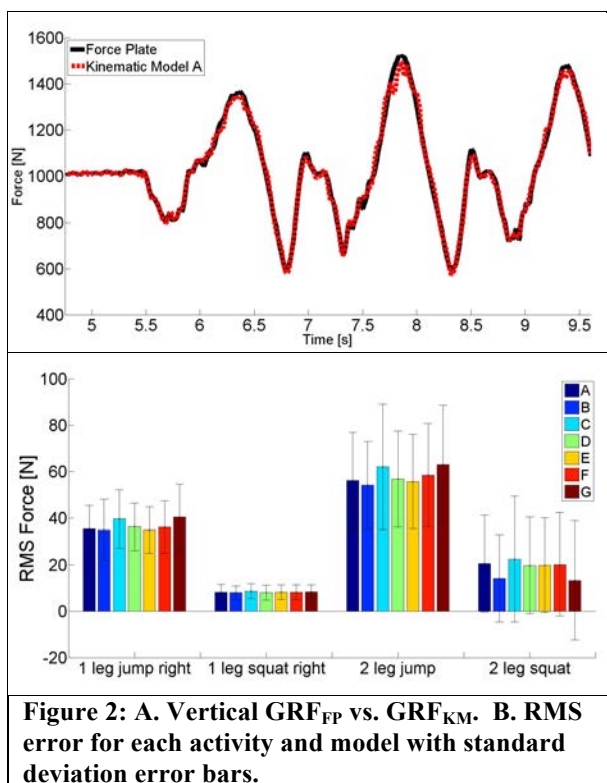


Figure 2: A. Vertical GRF_{FP} vs. GRF_{KM} . B. RMS error for each activity and model with standard deviation error bars.

CONCLUSIONS

We have introduced a promising method for evaluating link-segment trunk models. Error varied as a function of model and task; however, task had a much larger effect on errors than model. Future work will include trunk models with 2 and 3 segments as well as an analysis of the medial-lateral and antero-posterior components. We will also investigate model errors during running and walking. An accurate trunk model may

provide a greater understanding of compensatory strategies used by individuals with musculoskeletal diseases.

REFERENCES

- [1] D. M. Bazett-Jones et al., *Med. Sci. Sports Exerc.*, vol. 45, no. 7, pp. 1331–1339, Jul. 2013.
- [2] A. Leardini et al., *Clin. Biomech. Bristol Avon*, vol. 24, no. 7, pp. 542–550, Aug. 2009.
- [3] Nguyen, T.C. et al., 2004. *Clin. Biomech.* 19, 1060–1065.
- [4] Fantozzi, S et al., 2003. *Gait Post.* 17, 225–234.
- [5] Wu, G. et al., 2005. *J. Biomech.* 38, 981–992.

Table 1: List of the models analyzed and relevant markers.

Model	Markers Utilized
A[2][3]	C7, LAC, RAC, LASIS, RASIS,
B	LAC, RAC, TRIL, TRIR
C	LASIS, RASIS, LCLV, RCLV, LPSIS, RPSIS
D [4]	C7, L5, RAC, LAC, RASIS, LASIS, RPSIS, LPSIS
E[3]	C7, PX, RAC, LAC, RASIS,
F [5]	C7, T8, IJ, PX, RASIS, LASIS,
G [2]	T2, T10, IJ, RPSIS, LPSIS

DESIGN AND VALIDATION OF A TDNN HUMAN WALKING MODEL

¹ Kamran Iqbal and ² Alaa M. Abdulrahman

¹ University of Arkansas at Little Rock, Little Rock, AR, USA

² University of Sulaimania, Iraq
email: kxiqbal@ualr.edu

INTRODUCTION

Stroke, spinal cord injury, traumatic brain injury, and neurodegenerative diseases like Parkinson result in impairment of natural gait in humans [1]. Gait restoration and improvement constitute primary rehabilitation goals whose assessment requires estimation of muscle forces and joint moments. Inability to directly measure the biomechanical variables necessitates reliance on computational musculoskeletal models [2, 3].

Due to their universal mapping capabilities, Neural networks (NN) have been used to predict the kinematics and kinetics of human locomotion. Feed-forward NN trained with anthropometric data, kinematics, ground reaction forces (GRF), and electromyography (EMG) of seven prominent muscles was used to estimate joint moments [4]. The results lacked generality as data from specific subjects was used to train the network; moreover, same data was used for training and testing.

In this paper we present a time delay neural network (TDNN) model for computer simulation of human walking. The input to the model comprises desired generalized variable profiles (joint angles and the trajectories of a stable reference point, i.e., the position of the vestibular center). The model output includes feedforward and feedback components of generalized forces (joint moments). These are used in forward dynamic simulation of human walking. Our TDNN simulation results compare favorably to those obtained from OpenSim software (NCSRR, Stanford, CA), thus validating our model.

METHODS

To facilitate the model development, dynamics of a seven segment human body model (HBM) were

considered with head-arm-and-trunk (HAT), upper legs, lower legs, and feet segments. The generalized degrees of freedom (DoF) of the model included seven joint angles, and x,y positions of head, denoting the vestibular center. For simplicity, only revolute joints were included; hence, the model only analyzed motions in the sagittal plane.

NN with tapped delay line (TDL) were used to model the forward and the inverse dynamics of the human body. Two time-delay NN (TDNN) were developed, one that captured human forward dynamics and acted as identifier (TDNN_i), and a second TDNN that captured the inverse dynamics during walking, and acted as controller (TDNN_c) for the HBM. The identifier network was validated against joint torques captured in a laboratory experiment of walking. The actuator network was validated against optimized muscle activation data obtained for walking from the OpenSim software.

We used multi-sine formula proposed by [5] to implement a persistent excitation signal generator for the human body model. The input frequencies were randomly selected in the range 1Hz-25Hz based on frequencies of rotation of human body segments while walking. The limits in the angle range of human walking were taken into account and embedded into the persistent excitation formula. A total of 5000 samples data was generated for each of the generalized variables associated with walking.

The model used for the forward dynamic identifier (TDNN_i) was of NARMAX type. The TDNN_i had two TDLs at the input, one each for torques and feedback elements. The network was built with linear input and output layers and a nonlinear hidden layer. It was trained using Levenberg-Marquardt (LM) back-propagation algorithm. The training took 19 epochs with a performance goal of 10^{-6} for the error.

The torque controller for the model consisted of feed-forward u_{ff} and feedback u_{fb} components ($\tau = u_{ff} + u_{fb}$), both generated via TDNN (Fig. 1). Due to linearity, a single TDNN with 9 inputs (2 delays each) and 12 outputs (5 delays each) could generate both terms. The lags were chosen with the help of correlation function from the MATLAB NN toolbox. A single hidden layer with 50 neurons with sigmoid activation function was used with linear output layer. Training the NN took 14 epochs in batch processing using Levenberg-Marquardt back-propagation algorithm with recorded error of 10^{-27} .

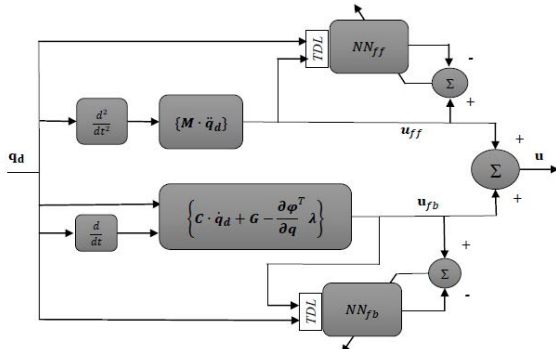


Fig. 1: TDNN model used to generate joint torque components

The TDNN_c employed a total of 74 inputs: 42 inputs from the muscles activation data, 14 from feeding back the seven controller outputs with unit delays, and 18 inputs from feeding back the nine HBM outputs with one delay each. Its output constituted the generated torques required to derive the HBM such that it could track the reference model outputs.

Walking data for model validation were recorded in the laboratory using 10 VICON cameras, NEXUS software, and 2 AMTI force platforms. The marker data were used to construct the desired variable profiles (q_d), which were then used to develop the inertial and nonlinear torques that were input to the TDNN_c that generated $\tau = NN_{ff} + NN_{fb}$ at the output.

RESULTS AND DISCUSSION

Fig. 2 shows the comparison between the output of the TDNN_i and the laboratory trajectories of joint torques for one stride. The maximum root mean squared error (MSE) during one stride was 2.7×10^{-3} . The small error obtained was attributed to the ability of the TDNN to learn human body dynamics.

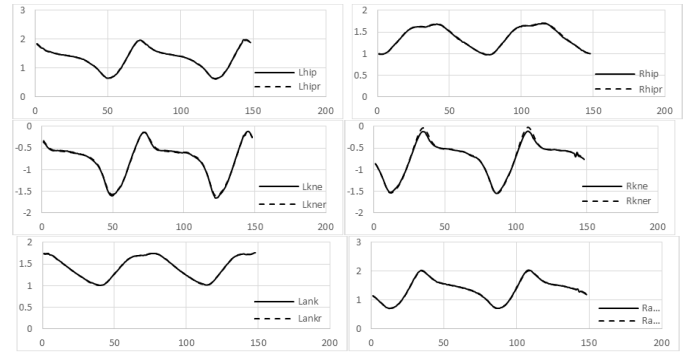


Fig. 2: A comparison of the identifier NN output with joint torques recorded in the laboratory.

Fig. 3 shows the simulation output (joint angles) as the HBM was simulated driven by joint torques generated from the TDNN_c. For comparison, the joint trajectories obtained from OpenSim simulation of same stride are also shown. The maximum joint torque and trajectory errors were less than 0.5%.

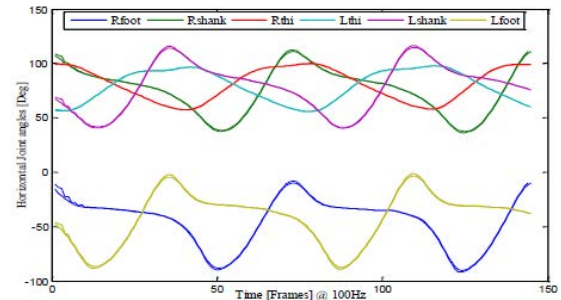


Fig. 2: TDNN output (joint angles) superimposed on OpenSim output during simulation of two strides of walking.

In conclusion, TDNN_i exhibited excellent capacity to learn human body dynamics during walking. The controller, TDNN_c, correctly generated muscle activation commands and joint torques to simulate the HBM in walking mode. These results can be extended to simulation of complex movements.

REFERENCES

1. Steele KM, et al., *J. Biomech.*, 43, 2099-2105, 2010.
2. Delp S, et al., *IEEE Trans. Biomed. Eng.*, 54, 1940-1950, 2007.
3. Silverman AK, Neptune, RR, *J. Biomech.*, 45, 2271-1178, 2012.
4. Hahn ME and O'Keefe KB, *J. Musculoskeletal Research*, 11, 117-126, 2008.
5. Ljung L, *System Identification Theory for the User*, 2nd Ed., Prentice Hall, NJ, 1999.

EFFECT OF AGE ON BODY SEGMENT PARAMETERS IN NORMAL WEIGHT FEMALES

Molly Knewton, Zachary Merrill, Rakie Cham, April Chambers

University of Pittsburgh, Pittsburgh, PA, USA

email: mek122@pitt.edu, web: <http://www.engineeringx.pitt.edu/hmb/>

INTRODUCTION

The population of adults over 55 years old in the United States increased over 15% from 2000 to 2010 [1]. Adults in this age group are more susceptible to injuries resulting from falls, including over 10,300 fatal fall-related injuries in 2000 [2]. In order to understand the mechanisms of falls and resulting injuries in the older adult population, biomechanical research is required. Biomechanical gait analysis and injury prevention research relies on anthropometric tables to give accurate approximations of body segment parameters (BSPs) of subjects. These parameters include mass, center of mass, and radius of gyration of the common body segments: upper arm, lower arm, torso, thigh, shank, and head.

Current anthropometric tables were developed with college-aged adults and are proven to be inaccurate in predicting BSPs of other age groups [3, 4, 5]. There are many proven ways to create predictive models such as cadaver-based studies and imaging [3, 6], but each method has disadvantages such as monetary cost, time-intensiveness, and/or delivery of high doses of radiation to the participant. Dual energy X-ray absorptiometry (DXA) is a validated in-vivo method of determining BSPs [7]. It is a quick, inexpensive, low-radiation, full-body scan that can differentiate densities of bone, muscle, and fat tissue, allowing for accurate mass calculations. This study uses DXA scanning and analyzing techniques to compare BSPs of normal-weight, young females against those of normal-weight, old females, focusing on the largest segments of the body: the torso and the thigh.

METHODS

The young subgroup corresponds to ages 21 to 40, while the old subgroup corresponds to ages 55 to

70. Thirteen young and thirteen old females, with BMI $18.5\text{--}25\text{ kg m}^{-2}$, were recruited for participation in this study. Height and weight of each participant was recorded to confirm BMI and eligibility. Each participant was scanned with a Hologic Discovery DXA System to gather a full body, frontal plane image.

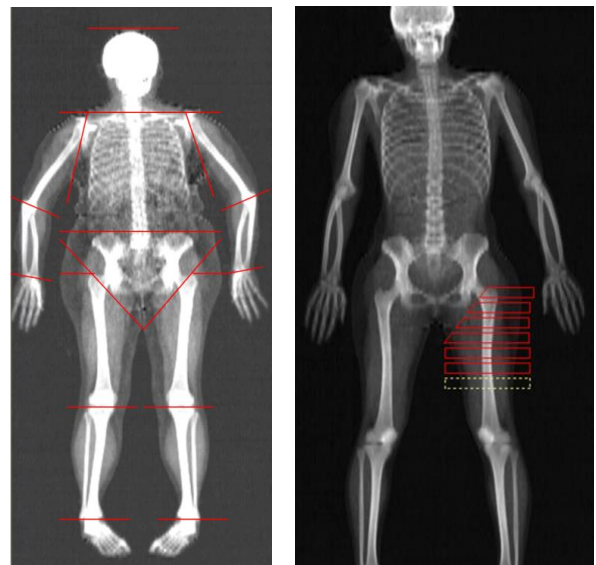


Figure 1: *left:* Whole body DXA scan with segmental boundaries designated by red lines *right:* sub-regions of the thigh segment indicated with red boxes.

Bony landmarks were used to define boundaries between body segments in analysis of each DXA scan (Fig. 1). The segments of interest were the torso and the thigh. The torso extended from the acromion to the greater trochanter. The torso's lateral boundaries were defined with a line through the medial acromion to the axilla and a line just lateral to the anterior superior iliac spine and the ischial tuberosity of the pelvis. The thigh segment began at the greater trochanter and extended to the center of the knee joint.

Each body segment was then divided into sub-regions that spanned the width of the segment and were 2-3 pixels (2.6-3.9 cm) tall (Fig. 1). Masses were calculated for each sub-region and used to determine BSPs for the whole segment.

Sub-region and segment measurements were used to determine segment mass as a percent of body mass (SM), longitudinal distance from the proximal end to the center of mass of the segment as a percent of segment length (COM), and frontal plane radius of gyration as a percent of segment length (RG). A two-tailed t-test was run to compare BSPs between the two age groups. Statistical significance was set at 0.05.

RESULTS AND DISCUSSION

Age was found to significantly affect SM for both the torso and thigh segment and RG for the torso. Thigh and torso parameters for the young and old age groups are presented in Table 1. Thigh SM was smaller in the older age group, while torso SM was larger in the older age group. Torso RG was smaller in the older age group. These differences represent a variation in mass distribution across age groups. Young females have a higher percent of overall body mass in the thigh segment, and old females have a higher percent of overall body mass in the torso. This trend continues in old and elderly populations as well, as examined in Chambers et al. [8]. Elderly subjects were found to have a significantly higher torso SM than old subjects [8], confirming the finding that torso SM increases with age. The torso segment was found to have a more concentrated mass for the older subgroup, as indicated by a smaller RG. No significant differences in COM locations in any of the segments were found.

CONCLUSIONS

Current anthropometric tables were developed using measurements of young, normal weight adults. However, significant differences were found in the torso and thigh segments between normal-weight, young females and normal-weight, old females, indicating the commonly-used tables do not accurately model subjects in every age category. The difference in thigh SM and torso SM are of particular interest as these segments are commonly used in gait analysis and other biomechanical research. This study underlines a need for age-specific anthropometry tables.

REFERENCES

1. U.S. Census Bureau. *Statistical Abstract of the United States:2012*, 2012.
2. Stevens JA, et al. *Inj Prev* **12**, 290-295, 2006.
3. de Leva, P. *J Biomech* **29**(9), 1223-30, 1996.
4. Ganley KJ, et al. *Gait Posture* **19**, 133-140, 2004.
5. Durkin JL, et al. *J. Biomech Eng* **125**, 515-522, 2003.
6. Dempster, WT. *Wright-Patterson Air Force base*, 55-159, 1955.
7. Durkin JL, et al. *J Biomech* **35**(12), 1575-80, 2002.
8. Chambers AJ, et al. *Clin Biomech*, Bristol, Avon, 2010.

ACKNOWLEDGEMENTS

Funding Source: NIOSH grant No. R01 OH010106. Special thanks to the Osteoporosis Prevention and Treatment Center.

Table 1. Mean and standard deviation of torso and thigh segment parameters of young and old females.

*** indicates statistically significant values (p<0.05)**

Age	Segment Mass (% of total body mass)		Center of Mass Location (% of segment length)		Radius of Gyration (% of segment length)	
	Torso*	Thigh*	Torso	Thigh	Torso*	Thigh
Young	41.5 ± 1.5	11.9 ± 1.0	54.0 ± 0.8	45.6 ± 1.0	28.4 ± 0.5	25.6 ± 0.3
Old	43.4 ± 2.7	11.1 ± 1.0	54.8 ± 1.1	45.6 ± 2.0	27.5 ± 0.7	25.8 ± 0.7

ESTIMATION OF IMPACT FORCES ON HUMAN HIP AND WRIST JOINTS BASED ON REAR-SIDE FALLING SIMULATION USING A MUSCULOSKELETAL MODEL

¹Taesoo BAE, ²Taemin BYUN, and ²Cheolwoong KO

¹Jungwon University, Goesan, Korea

²Korea Institute of Industrial Technology (KITECH), Cheonan, Korea

email: cheko@kitech.re.kr web: <http://www.kitech.re.kr>

INTRODUCTION

As people get older, their motion speeds generally tend to get slower in walking motions on flatland or stairs as well as the motions sitting and standing up. Especially, for the people over 65 years old, the frequency of injuries from fall accidents is very high enough that one-third of the aged persons experience some injuries resulting from fall accidents every year, and the number of the elderly dying or suffering from the fall injuries is gradually increased.

The R&Ds developing safety devices against fall accidents, detecting the fall events, and reducing the amount of impact based on the detected falling events by various complex sensors are actively performed. However, there are still few studies on quantitatively analyzing the influences of actual fall's impact on the human body as the basic information for the development process of safety devices. Given the fact that there is very possible to be injured at conducting a fall experience, an actual experiment targeting human subjects is extremely limited, so most experiments have utilized corpses or dummies until now.

This research aimed to make a three-dimensional musculoskeletal dynamic simulation model to overcome the limits of experiments in previous studies to analyze a fall influence on the human body injuries.

METHODS

2.1 Subject Selection

In order to make a computational model for simulation of falling situation, we selected one Korean adult man who is healthy without any orthopaedic disability or injury history in the musculoskeletal system and the nerve system (28-years old, 177cm, 76kg).

2.2 Motion Analysis Experiment

In order to obtain the human body's falling motions on space, we utilized a motion analysis system. After attaching reflective markers on the subject in an experimental space where 10 infrared cameras (6 Raptor-E cameras, 4 Osprey cameras, Motion Analysis Inc. USA) and 2 force plates (FP4060, Bertec Inc. USA) were installed, rear-side falling experiments were conducted. A program for the motion analysis (Cortex version 4.0, Motion Analysis Inc. USA) was used in collecting and analyzing the data of kinematics and kinetics (Figure 1).

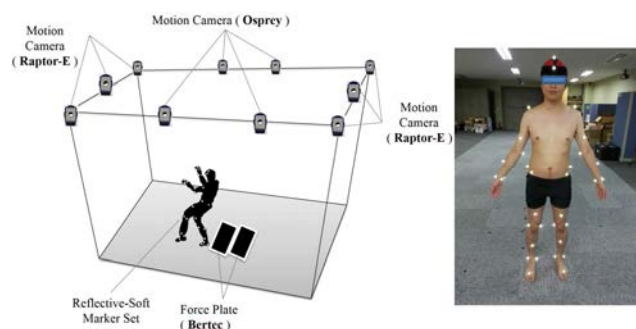


Figure 1. Experimental space for analyzing falling motions and subject with reflective markers

2.3 Construction of Musculoskeletal Model and Dynamic Simulation

In order to the subject-specific musculoskeletal model, the total 42 reflective markers (Helen Hayes Marker Set) were attached on the subject's body (upper limbs: 21 markers, lower limbs: 21 markers), and the static pose was taken by the 10 cameras. Also, full-body musculoskeletal model was scaled by utilizing the conversion programs (Motion module, Motion Analysis Inc., CA, USA). Especially, each vertebra in the neck and lumbar spines was defined separately with three degrees of freedom.

To conduct the dynamic simulations by the musculoskeletal model, several dynamic parameters including the center of mass and the moment of inertia for each skeleton were defined based on the previous references.

The initial values for every joint were set up based on the standing pose, and motions of all joints were not restricted to reproduce the falling situation. Besides, the data of kinematics and kinetics captured from the motion analyses were inputted as the prescribed motions. For the physical parts colliding onto the ground, the user-defined contact forcemattes were defined to calculate the contact force to the ground. The DLL (Dynamic Linking Library) was made with the SD FAST (B.2, Symbolic Dynamics Inc, USA) of the dynamic solver. After setting the DLL used as the basic library, the dynamic simulations were conducted (Figure 2).

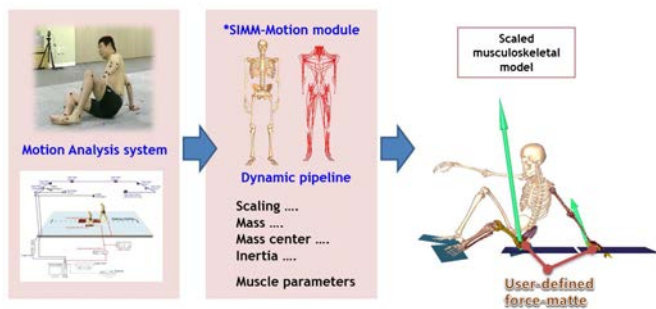


Figure 2. Three-dimensional musculoskeletal modeling of dynamic simulation for falling events

RESULTS AND DISCUSSION

We carried out the side-rear falling simulations using a three-dimensional musculoskeletal model, and calculated the contact force on the human body by the user-defined contact forcemattes. In the falling simulations, the maximum contact force was primarily calculated (1.90 times of the subject's weight) when the hip was collided with the ground. And the maximum contact force was secondarily calculated (0.57 times of the subject's weight) when the wrist was touched to the ground.

While the falling experiment generally showed similar patterns as the simulation results, the former showed a little higher values (2.21 times of the subject's weight at the hip, 0.63 times of the subject's weight at the wrist) (Figure 3). It is considered that the difference could be caused from

the insufficient information on the soft tissue thickness in the hip and the wrist parts.

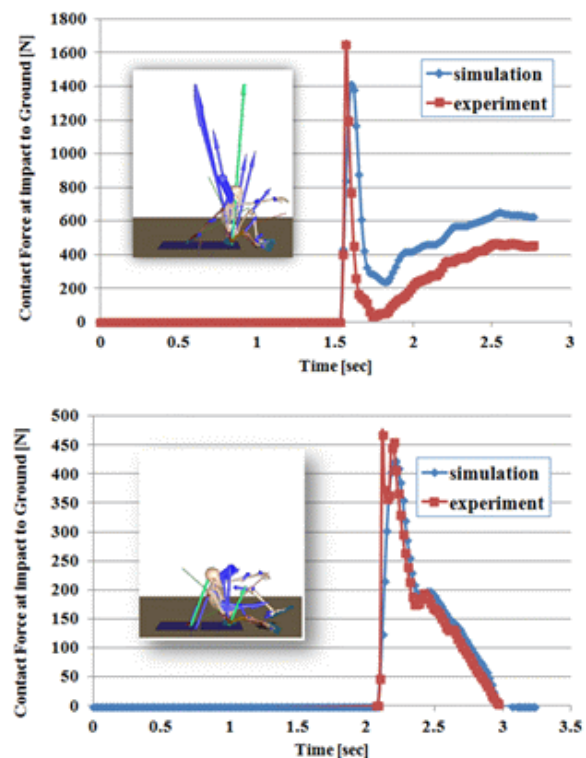


Figure 3. Results of falling simulation for the hip (up) and the wrist (down) joints

CONCLUSIONS

This research constructed a motion analysis-based three-dimensional musculoskeletal dynamic simulation model to estimate a falling influence on human body which can't directly be measured. It is considered that the 3D musculoskeletal dynamic simulation model will be effectively utilized to acquire basic information on the falling-injury studies using the various conditions of human body and environment in future.

ACKNOWLEDGEMENTS

This research was supported by Korea Institute of Industrial Technology (KITECH) & Basic Science Research Program through the National Research Foundation of Korea funded by the Ministry of Science, ICT & Future Planning (2013R1A1A1005740).

DYNAMIC STABILITY OF STRUCTURES FOR AN ELECTRIC HANDBIKE BY MOTION ANALYSIS DURING DURABILITY TEST

¹Tae Soo BAE, ¹Dae Dong KIM, ¹Hee Su PARK, ²Hyungtae KIM, ³Joonhmm LEE, ²Cheolwoong KO

¹Department of Biomedical Engineering, Jungwon University, Republic of Korea

²Korea Institute of Industrial Technology (KITECH), Cheonan, Republic of Korea

³OX Korea Co. Ltd., Cheonan, Republic of Korea

email: cheko@kitech.re.kr web: <http://www.kitech.re.kr>

INTRODUCTION

For most of the disabled people who use manual wheelchairs, they often experience shoulder pain due to steering wheelchairs with only the upper limb muscles for a long time. Some disabled people need medicine treatments, and also have a surgical treatment in serious cases. To alleviate these potential musculoskeletal disorders, several types of electric handbikes have been recently introduced, in which docking method is easy and it is possible to easily move by using the electric system after docking.

In case of a relatively high speed on various terrain after easy installation using a connector, the mechanical loads are continuously applied to the connecting parts between the manual wheelchair and the electric handbike, and the resultant force accumulated at the connecting parts is determined to affect the structural stability of the connection parts. However, related researches on this area are still rare. Therefore, this study aims to implement a three-dimensional dynamic model that can simulate the durability test through computational analysis, and to evaluate the dynamic structural stability of the parts between the manual wheelchair and electric handbike during durability experiment by verifying the model through motion analysis.

METHODS

To implement a computation analysis model for durability experiment, we constructed a three-dimensional wheelchair-handbike assembly model using a Solidworks software program (ver.2012, Dassault Systems, USA). In addition, the durability test device was modeled referred to its actual size (Korean Industrial Standards) (Figure 1).

To make a multi-flexible dynamic model for the whole system, the connection parts (snatch lock,

connecting rods, etc) between the electric handbike and wheelchair that have high possibility of mechanical failure in terms of structural stability, have been implemented as the finite element model to calculate mechanical loads (von-mises stresses). Other structures have been assumed as rigid bodies.

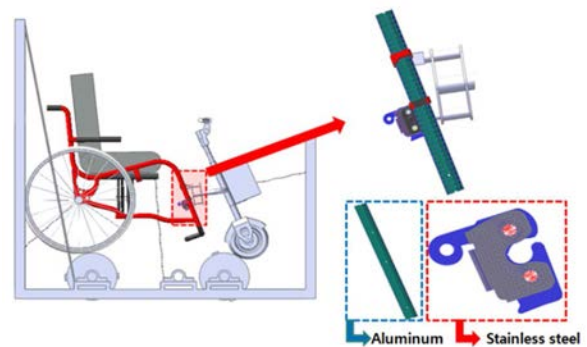


Figure 1: Multi-flexible dynamic model including a wheelchair, a handbike with snatch lock, and a drum tester.

To perform dynamic analyses, a commercial analysis program (Recurdyn V8R2, FunctionBay, South Korea) was used. Referred to KS standards for an electric wheelchair, we set the rotation speed of the drum so as to rotate at 1m/s with a rotational joint [1], and fixed a 75kg human dummy model onto the wheelchair's seat top parts [2].

To verify a computational model, the motion analysis system was used in this study including 8 infrared cameras (Eagle 4, Motion Analysis Inc., USA), 10mm-reflective markers attached to the handle, electric wheels, connectors, rotation axis of the wheelchair, and the rotation cylinder of the drum tester, respectively. We calculated kinematical data by using three-dimensional coordinates of each reflective marker (Figure 2).

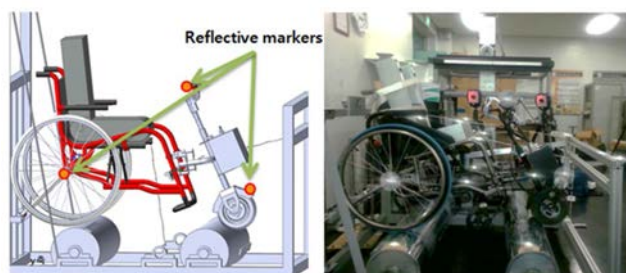


Figure 2: Motion analysis model of marker position

Through motion analysis on the durability test, the trajectories of each marker were measured in real-time. After that, we compared kinematical results between experiments and computation analyses to verify the computational model.

RESULTS AND DISCUSSION

Through comparison of kinematical data between experiments and motion analyses at the same locations, it was found that the maximum difference of the markers were about 13mm. However, it was also confirmed that they showed similar movements with similar tendency in general (Figure 3). After verifying, we performed the stress analysis for connecting parts including snatch lock, connecting rod of both sides. The results showed that maximum von-mises stress was about 216MPa (Yield stress 552MPa) for the snatch lock and 1.1MPa for the frame part (Yield stress 185MPa). By considering that the stress level of the connecting part was lower than yield stress of each structure, it was expected that the structural stability would be secured for the connecting parts during durability experiment (Figure 4).

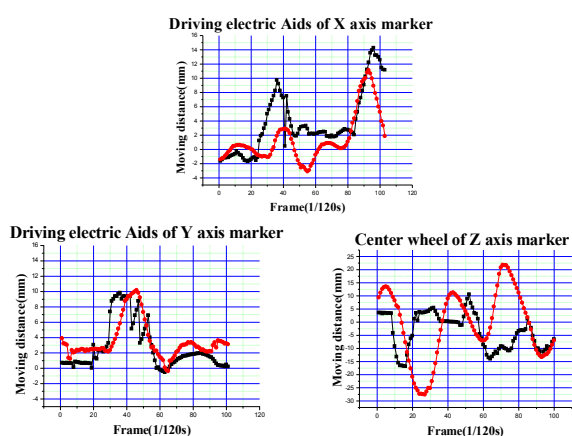


Figure 3: Comparison of simulation (red circle) and experiment (black circle) for center wheel marker



Figure 4: Distributions of von-mises stress in snatch lock and wheelchair frame

CONCLUSIONS

In this study, we established an effective process to give the validity of computational analysis on actual durability test for wheelchair-handbike assembly system by motion analysis. Although there was a slight kinematical difference between two results, the movements of each part in the system generally showed a similar tendency.

Based on the verification for a computational model, lower stress value were calculated at the snatch lock and the frame parts of the wheelchair's major connecting parts also showed a lower stress value than yield stress.

From these results, we could estimate that this system would be dynamically stable during durability test. Afterwards, it is believed to be necessary to improve the safety for electric handbike through usability evaluation like field test in various terrain.

REFERENCES

1. KS P ISO 7176-8 Wheelchair, section 8: Requirements and test methods for the strengths of static loads, impacts and fatigues
2. KS P ISO 7176-11 Wheelchair- The model of a human body A

ACKNOWLEDGEMENTS

This study was conducted with research funds of Small and Medium Business Administration (S2145061).

COMPARISON OF BONE STRENGTH BETWEEN OSTEOPOROSIS AND NORMAL MOUSE FEMORA USING FE ANALYSIS

¹Sang Kuy HAN, ²Dong-hyun SEO, ²Ji hyung PARK, ²Changsoo CHON,
²Han sung KIM, ¹Keyoungjin CHUN and ¹Cheolwoong KO

¹Korea Institute of Industrial Technology (KITECH), Cheonan, Korea

²Yonsei University, Wonju, Korea

email: cheko@kitech.re.kr web: <http://www.kitech.re.kr>

INTRODUCTION

Osteoporosis is defined by a decrease in bone mass and density which can cause an increased risk of fracture. Especially in the elderly population osteoporosis is treated as the significant medical problem, because the bone fracture from osteoporosis can lead to the fatal issue of patients. Therefore, the biomechanical understanding of osteoporosis has been extensively investigated [1-2].

Previous studies of osteoporosis using medical images, such as DEXA scan and Micro-CT, mainly focused on the changes of bone density. However, the bone density analysis based on 2D (dimensional) images can limit the result because each bone has inhomogeneous distributions of bone density in a 3D structure. In particular, to precisely understand bone fracture it is required to analyze mechanical behavior with bone density and bone strength in a 3D structure. Since experimental methods to understand structure and mechanical behavior of bone have technical limitations, finite element method has been effectively utilized to better understand a sophisticated bone structure.

The purpose of this study is to utilize the finite element analysis based on 3D bone structural images of Micro-CT for understanding the spatial degradation of bone strength in osteoporosis mouse femora.

METHODS

Osteoporosis Mouse Model

A surgical removal of ovaries (Ovariectomy, OVX) in mouse was used for osteoporosis animal model (Osteoporosis, OP, N=3) in this study. For the comparison, non-surgical mouse was included in a separate group (Control, Con, N = 3). At the 4 and 8 weeks after ovariectomy, mice from each group were anesthetized for Micro-CT imaging.

Micro-CT Imaging and 3D Reconstruction

Femora from each group were scanned by Micro-CT (SKYSCAN 1076, Brucker, Germany). Image resolutions were $18 \times 18 \mu\text{m}$. A 3D femur reconstruction was conducted by using a 3D image process software (Mimics 16.0, Materialise) (Figure 1). For the finite element modeling, the material properties of femur were calculated based on pixel image intensities. The grey value (GV) of each pixel was linearly converted to the Hounsfield Units (HU). For the simplicity, the average Hounsfield Units was calculated for the 3D reconstructed local model for the analysis. The average Young's Modulus was finally calculated based on the conversion formula from the previous study [3].

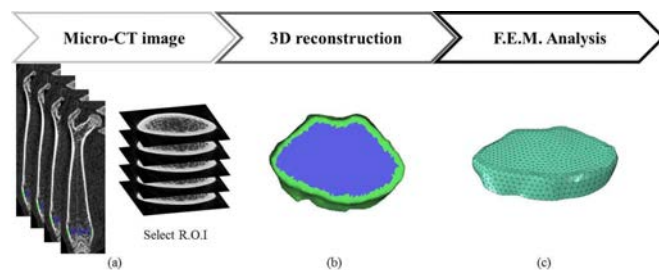


Figure 1: 3D reconstruction of femur FE model: (a) Segmentation of femur on the MRI slides and selection of R.O.I, (b) 3D reconstruction, (c) 3D Finite Element Model.

Finite Element Analysis

Finite element analysis using a commercial solver (ABAQUS 6.10) was conducted on the local model including the region closed to the condyle where the trabecular bone showed bone density loss. Concentrated loads of 2, 4, 6, 8, and 10 N were axially applied to the plate on the top of the local model (Fig. 2).

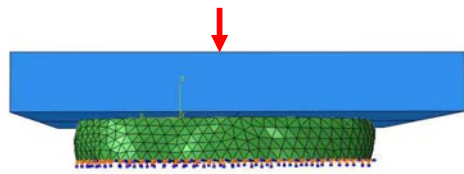


Figure 2: Finite element model including load and boundary conditions.

RESULTS AND DISCUSSION

At 4 weeks after ovariectomy in mouse model, there is no large difference on average bone density for the entire femur. However, the bone density in the trabecular bone decreased and that in the cortical bone increased (Table 1). Under 2-10N of external force on the local model, osteoporosis group at 8 weeks had more stress and displacement compared to 0 week (Fig. 3). Under 10 N load, a maximum displacement in the axial direction decreased about 11%, and increased 67%, and stress increased about 29%, and 84% for 4 weeks and 8 weeks after OVX, respectively compared to 0 week (Fig. 3 and 4).

CONCLUSION

Based on the results, the early osteoporosis of mouse model decreased bone densities in trabecular region but increased them in cortical region.

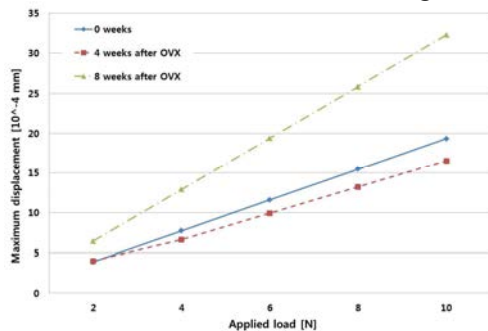


Figure 3: Maximum displacements in the axial direction with respect to the applied forces.

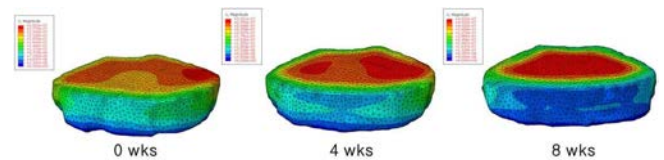


Figure 4: Results of finite element analysis for axial deformations between 0, 4 and 8 weeks.

Therefore, we anticipated that osteoporosis model using mouse should consider its bone degradation behavior depending on measuring time point. Early osteoporosis in mouse model may have compensation effect on cortical bone while trabecular bone loses its bone density. Although bone density is highly inhomogeneous, an average bone density was used in this study for the simplicity of numerical calculations. Further study will aim to implement inhomogeneity of bone density to represent the intrinsic behavior of material properties and structure of bone.

REFERENCES

1. Rietbergen BV, et al. J Biomech **28**, 69-81, 1995.
2. Joshua M. and Steven B. Bone **42**, 1203-1213, 2008.
3. Rho, JY, et al. Med Eng Phys **17** 347-355, 1995.

ACKNOWLEDGEMENTS

This study was funded by grants from the KITECH. This research was also supported by the Leading Foreign Research Institute Recruitment Program through the National Research Foundation of Korea (NRF) funded by the Ministry of Science, ICT & Future Planning (2010-00757)

Table 1. Comparisons of femur bone densities and Young's Moduli in osteoporosis animal model

Bone densities				Young's Modulus			
	0 weeks	4 weeks	8 weeks		0 weeks	4 weeks	8 weeks
trabecular	715	595	480	trabecular	2,204	1,571	1,087
cortical	1,057	1,180	1,159	cortical	4,804	6,004	6,356

[kg/m³]

[MPa]

EFFECT OF INCREASED BODY MASS INDEX ON BODY SEGMENT PARAMETERS IN MALES

Zachary Merrill, Molly Knewton, Rakié Cham, April Chambers

University of Pittsburgh, Pittsburgh, PA, USA
email: zfm1@pitt.edu, web: <http://www.engineering.pitt.edu/hmbl/>

INTRODUCTION

Over the last 30 years, the obese population has grown to over 60 million people in the US. Along with obesity, the associated risk of injury related to biomechanical factors also increases [1,2]. In order to understand these mechanisms of obesity-related risk of injury, accurate body segment parameter (BSP) measurements are required to model joint contact forces and muscle forces applied during a given task.

Current anthropometry tables, which show the mass of each body part as a percent of total body weight (BW), and center of mass (COM) and radius of gyration (R_G) locations as percent of segment length were compiled using healthy, college-age adults, however these parameters have shown to be inaccurate in predicting BSP's in subjects with an increased body mass index (BMI), as well as in different age groups [3-6]. Several methods exist for determining BSP's including cadaver-based studies, magnetic resonance imaging, computed tomography, and measurements based on bony landmarks [7-10], however these methods have some issues as far as cost, time required, and high doses of radiation. Dual energy x-ray absorptiometry (DXA) is a validated method of determining BSP's in vivo that avoids these common problems. DXA scans are commonly used to determine bone density and body composition [11], as well as mass calculations. The scan itself is an inexpensive, low radiation scan that can differentiate between bone, muscle, and fat.

The goal of this study is to determine differences in segment masses, COM's, and R_G 's in normal weight (NW), overweight (OW), and obese (OB) young males. We will focus on the differences in the torso and dominant-side thigh.

METHODS

The subjects in this study were all between the ages of 21 and 40, and the weight groups are defined by body mass index (BMI); the normal weight group covers BMI's between 18.5 and 24.9, overweight group is between 25.0 and 29.9, and obese group is between 30.0 and 39.9 kg m^{-2} (Table 1). Thirteen subjects were recruited for each weight category.

Table 1: Mass, height, and BMI for each group. Values are shown as mean \pm standard deviation.

Group	Mass (kg)	Height (cm)	BMI (kg m^{-2})
Normal Weight	66.8 \pm 6.2	178.4 \pm 5.0	22.6 \pm 1.4
Overweight	77.7 \pm 7.9	175.2 \pm 6.3	27.0 \pm 1.1
Obese	96.4 \pm 11.2	178.5 \pm 6.4	32.3 \pm 2.6

During the single study visit, the height and weight of each participant were recorded in order to calculate BMI to confirm eligibility and then each participant was then scanned using a Hologic Discovery DXA System (Hologic, Bedford, MA, USA) to collect a frontal plane, full body image.

Predetermined anatomical landmarks were used to define the boundaries between BSP's in each DXA scan. The head segment covered the most superior point of the head to the base of the mandible. The torso extended from the acromion to the superior border of the greater trochanter, with lateral boundaries defined by a line connecting the acromion through the axilla, and another line connecting the greater trochanter and ischial tuberosity. The thigh segment extended from the superior greater trochanter to the knee joint center, lateral to the inferior portion of the torso section. Lastly, the shank segment started at the knee joint center, and ended at the lateral malleolus.

In order to calculate segment COM's and radii of gyration, each segment was separated into small slices. Each slice covered the width of the segment, and had a height of 2-3 pixels, corresponding to 2.6-3.9 cm tall. The analysis determined the mass of each sub-region, and used the masses and known slice height to calculate the segment parameters. For each segment, COM and R_G were expressed as percent of the segment length, and mass was expressed as a percent of the total body mass. A two-tailed t-test was used to compare each BSP of interest between each of the three groups, with significance set at $\alpha = 0.05$.

RESULTS AND DISCUSSION

Significant differences were found for the thigh and torso radii of gyration (Figure 1), with the normal weight group having more distally located R_G 's. While the differences appear relatively small, they are all highly statistically significant.

The normal weight group also has statistical trend toward lower torso and thigh masses as a percent of body weight compared to the overweight and obese groups, however these differences are not statistically significant (Table 2). As would be expected, no significant differences were determined for any of the segment lengths.

CONCLUSIONS

Current anthropometry tables were designed using young, normal weight adults as the measurement standard, however these parameters are not accurate in people with varying age and BMI. Significant differences were found between young normal weight, overweight, and obese males in the torso and thigh radii of gyration. These differences demonstrate that the current anthropometry sets cannot be applied across all body types, especially when analyzing gait. This study highlights the need to develop age and size specific anthropometry sets.

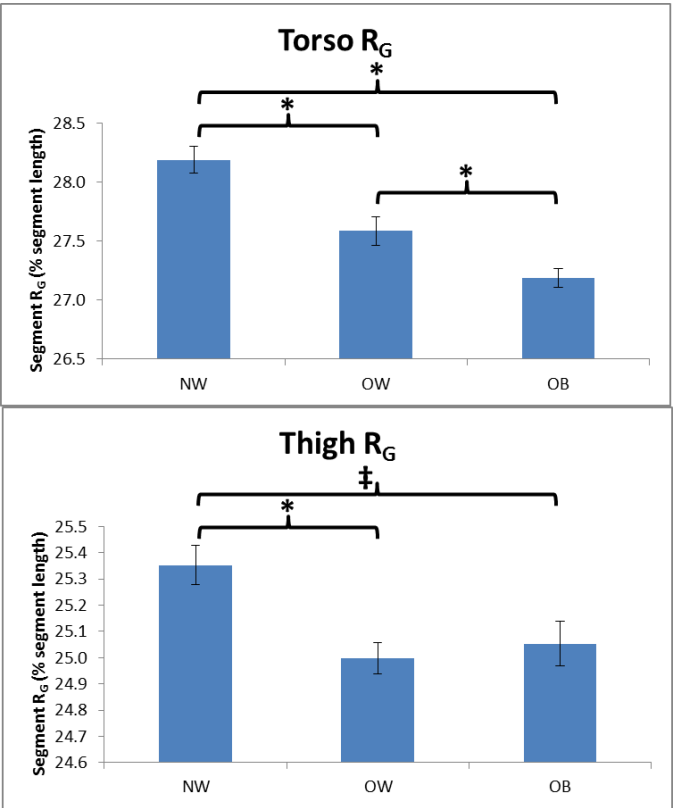


Figure 1: Torso and thigh R_G values, expressed as distance from proximal joint. * indicates $p < 0.01$, and ‡ indicates $p < 0.02$. Error bars show standard error.

REFERENCES

1. Ranavolo A, et al. *BioMed Res Int*, ID 142323, 2013.
2. Hergenroeder AL, et al. *Cardiopulm Phys Ther*, **22**, 11–20, 2011.
3. de Leva, P. *J Biomech* **29**(9), 1223-30, 1996.
4. Durkin JL, et al. *J. Biomech Eng* **125**, 515-522, 2003.
5. Ganley KJ, et al. *Gait Posture* **19**, 133-140, 2004.
6. Knewton ME. *Ingenium: Undergrad Res SSOE* 2015.
7. Clauser CE, et al. *AMRL-TR-69-70*, 1969.
8. Pearsall DJ, et al. *Ann Biomed Eng* **24**, 198-210, 1996.
9. Martin PE, et al. *J Biomech*, **22**(4), 367-369, 1989.
10. Cheng C-K, et al. *Clin Biomech*, **15**, 559-566, 2000.
11. Ganley KJ, Powers CM. *Clin Biomech* **19**, 50-56, 2004.

ACKNOWLEDGEMENTS

Funding Source: NIOSH grant No. R01 OH010106

Table 2: Torso and thigh mass and center of mass values. Mass is shown as percent BW, and COM is shown as percent segment length. * indicates $p < 0.10$ between NW and OB groups. Values shown as mean \pm standard deviation.

Group	Torso Mass (%)	Torso COM (%)	Thigh Mass (%) *	Thigh COM (%) *
NW	41.78 \pm 0.52	51.96 \pm 0.26	11.50 \pm 0.18	46.82 \pm 0.35
OW	41.91 \pm 0.72	52.41 \pm 0.21	11.69 \pm 0.25	46.34 \pm 0.30
OB	42.15 \pm 0.75	52.41 \pm 0.34	11.94 \pm 0.17	46.00 \pm 0.24

IMPACT OF MASS REDISTRIBUTION ON LOWER EXTREMITY BIOMECHANICS DURING SLIPPING

Zachary Merrill, April Chambers, Rakié Cham

University of Pittsburgh, Pittsburgh, PA, USA

email: zfm1@pitt.edu, web: <http://www.engineering.pitt.edu/hmbl/>

INTRODUCTION

Anthropometry is commonly found in tables containing measurements of body segment parameters (BSP's) such as the mass of each body part as a percent of body weight (BW) and center of mass location (COM) within each segment as a percent of segment length (SL). These tables contain values compiled from healthy, college-age adults, however they have shown to be inaccurate in predicting BSP's in subjects with increased body mass index (BMI), as well as in different age groups, therefore not properly representing real-life parameters and mass distributions [1-3]. In order to understand potential injury mechanisms in a given task, accurate BSP's are required to model joint contact forces and muscle moment contributions.

Several methods exist for determining subject specific BSP's, including magnetic resonance imaging, computed tomography, and measurements based on bony landmarks [4-7], however these methods have some issues as far as cost, time required, and high doses of radiation. Dual energy x-ray absorptiometry (DXA) is a validated method of determining BSP's in vivo that avoids these common problems. DXA scans are commonly used to determine bone density and body composition [8], as well as mass calculations. The scan is an inexpensive, low radiation scan that can differentiate between bone, muscle, and fat.

The goal of this study is to quantify the relative effects of incorrect BSP's, specifically segment masses and center of mass locations, on lower extremity biomechanics during slipping. In order to quantify the impacts of these BSP's on joint contact force and muscle moment contributions, traditional BSPs and parameters previously determined via DXA scan analysis of overweight young males were

applied to a biomechanical analysis of slip during gait in an overweight young male.

METHODS

The subject used in this study was an overweight 25 year old male (stature: 182 cm, mass: 88.2 kg, BMI: 26.6 kg m⁻²). Motion tracking data were collected by a 14-camera Vicon motion tracking system (Vicon Motion Capture, Oxford, UK), and force data with a Bertec force plate (Bertec, Columbus, OH). Data were collected during a slip event that occurred during gait [9].

Following the single study visit, data were analyzed using custom kinematic modeling software [10], with a standard anthropometry set from deLeva [1], and then again with a BMI-specific anthropometry set for young, overweight males (Figure 1). The body segments were altered for the shank, thigh, and HAT (head, arms, and torso). Because ankle moments and forces were not observed for the purpose of this study, standard foot mass and center of mass were applied for both models.

Parameters calculated include hip and knee forces in the superior-inferior (SI), medial-lateral (ML), and anterior-posterior (AP) directions, and hip and knee moments about the SI, ML, and AP axes. Forces and moments were both normalized to body weight, given as N kg⁻¹ and N m kg⁻¹, respectively. The forces and moments were calculated between left heel strike (LHS) and the end of the slip, defined by the heel shear velocity decreasing to zero.

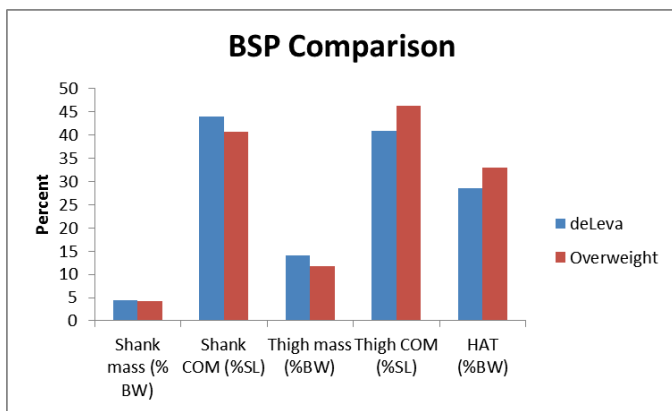


Figure 1: Mass and center of mass comparison between standard deLeva parameters and custom overweight, young male parameters derived from DXA scans. Values are given as percent of body weight or segment. $p < 0.0001$ for shank and thigh COM, and thigh and HAT mass.

RESULTS AND DISCUSSION

When comparing knee joint contact forces or muscle moments, the differences between the BSP sets were less than 0.05 N kg^{-1} and 0.01 N m kg^{-1} , respectively, throughout the slip and reaction, corresponding to less than 1% error relative to the deLeva parameters. There were larger relative errors (6.6-19.4%) in hip muscle moments and contact forces (Figure 2), with the largest errors occurring between 210 and 290 ms following slip initiation. While maximum hip forces in the ML direction were nearly identical, they had the largest average error over the full course of the slip. When comparing the maximum flexion, extension, adduction, abduction, and internal and external rotation moments at the hip, the values for both BSP sets were nearly identical, with less than 1% difference relative to the deLeva parameters.

The largest errors for adduction moment occurred at approximately the same time as the maximum errors in hip joint contact forces, however the largest errors in flexion and external rotation moments occurred between 250 and 350 ms following slip initiation.

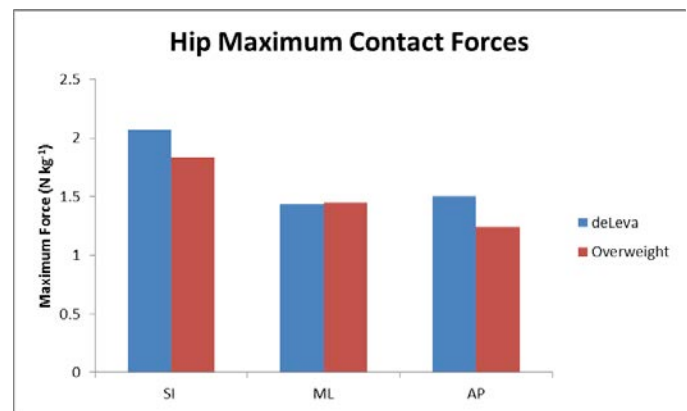


Figure 2: Maximum normalized hip joint contact forces in the SI, ML, and AP directions using deLeva and overweight BSP's. Average errors relative to deLeva were 8.9%, 19.4%, and 6.6%, respectively over the course of the trial.

CONCLUSIONS

This study shows that different assumptions regarding mass distribution and body segment parameters have negative impacts on joint contact force and muscle moment calculations. Because the difference between standard and BMI-specific parameters increases with obesity and BMI, BMI-specific parameters are necessary in order to accurately determine joint kinetics. While the calculated errors appear to be relatively small, these errors due to incorrectly applied standard BSP's will increase with BMI [11] and levels of dynamic movement within the activity being observed.

REFERENCES

1. de Leva, P. *J Biomech* **29**(9), 1223-30, 1996.
2. Durkin JL, et al. *J. Biomech Eng* **125**, 515-522, 2003.
3. Ganley KJ, et al. *Gait Posture* **19**, 133-140, 2004.
4. Clauser CE, et al. *AMRL-TR-69-70*, 1969.
5. Pearsall DJ, et al. *Ann Biomed Eng* **24**, 198-210, 1996.
6. Martin PE, et al. *J Biomech*, **22**(4), 367-369, 1989.
7. Cheng C-K, et al. *Clin Biomech*, **15**, 559-566, 2000.
8. Ganley KJ, Powers CM. *Clin Biomech* **19**, 50-56, 2004.
9. Cham R, Redfern MS. *J Biomech* **34**(11), 1439-1445, 2001.
10. Moyer BE, et al. *Ergonomics* **49**(4), 329-343, 2007.
11. Knewton ME. *Ingenium: Undergrad Res SSOE* 2015.

ACKNOWLEDGEMENTS

Funding Source: NIOSH grant No. R01 OH010106

MULTISCALE COMPUTATIONAL MODELING OF SHOE-FLOOR FRICTION

Seyed Reza M. Moghaddam and Kurt E. Beschorner

The University of Pittsburgh, Pittsburgh, PA, USA

Email: sem162@pitt.edu , web: <http://www.engineeringx.pitt.edu/hmbl/>

INTRODUCTION

Slip and fall accidents present a major health and occupational hazard. Increased shoe-floor coefficient of friction (COF) has been demonstrated to be indicative of reduced slipping risk [1].

Previous research by our group has shown that a microscopic finite element model can predict COF of shoe-floor samples by considering roughness and material properties [2]. However, that study did not consider macroscopic interactions and few other studies have attempted to model whole-shoe friction against walkway surfaces [3]. Current study builds on previous research by expanding the model to consider macroscopic (i.e., whole-shoe) interactions with the floor surface. As a first step towards a comprehensive shoe-floor-contaminant COF model, this study focuses on hysteresis friction, since it is the dominant friction mechanism on lubricated shoe-floor surfaces [2].

METHODS

The model consists of a microscopic model that simulates the interaction between shoe and floor asperities and a macroscopic model that determines contact pressure across the shoe surface. The microscopic model yields hysteresis COF as a function of contact pressure and macroscopic model uses this relationship and the predicted contact pressure to calculate the overall COF.

The microscopic model consists of a rough shoe material sliding against a rigid floor surface (Figure 1 (Left)) [2]. The asperity heights of these blocks were set to achieve a desired peak to valley roughness (R_z) and spacing between asperities was selected to achieve a desired average slope (Δ_a). Shoe material was modeled as a viscoelastic material, which causes energy loss as shoe

asperities deform and relax, while sliding over floor asperities. The hysteresis COF for micro-model was determined as the ratio of shear to normal force. Three different shoe materials were simulated against a single floor surface. Surface parameters were measured and averaged across four scans using a two dimensional stylus profilometer (Taylor-Hobson Surtronic S100 ®, Leicester, UK) (Scan length: 6.2 mm; low-pass cutoff filter: 0.8 mm). The boots had a consistent roughness ($R_z = 24.5 \mu m$, $\Delta_a = 29^\circ$) across the three materials. The flooring's roughness was also recorded and applied to the model ($R_z = 9.5 \mu m$, $\Delta_a = 24^\circ$). Shore A Hardness of the three boots was measured and used to characterize material properties of the three boots i.e. short-time shear modulus, G_0 , long-time shear modulus, G_∞ , and decay constant, β , using relationships introduced in [4] (Table 1). Microscopic simulation was repeated over several contact pressures to produce an exponential fit model between contact pressure and COF.

Material geometry for macro-model was determined using 3D scan of a shoe (Faro ScanArm ®) (Figure 1(Right)). Contact simulations were performed using explicit analysis (LS-Dyna, LSTC, Livermore, CA, USA). Vertical displacement of the shoe was applied until reaching a normal force level of 250 N, while the sliding velocity was 0.3 m/s and shoe-floor angle was 7° . Shoe material was modeled as linear elastic for computational efficiency since viscoelastic contributions to hysteresis friction were already accounted for in microscopic model (Table 1).

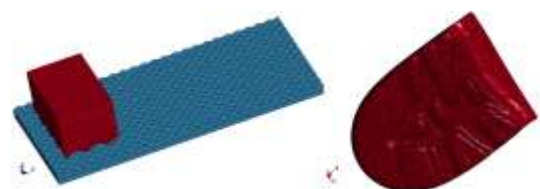


Figure 1. Micro (Left) and macro- model (Right)

Table 1. Material parameters used for boots

Shore A	G_0 (MPa)	G_∞ (MPa)	β (s ⁻¹)	E(MPa)
85	4.39	1.84	0.022	13.18
76	2.48	0.99	0.017	7.44
64	1.41	0.92	0.2	4.24

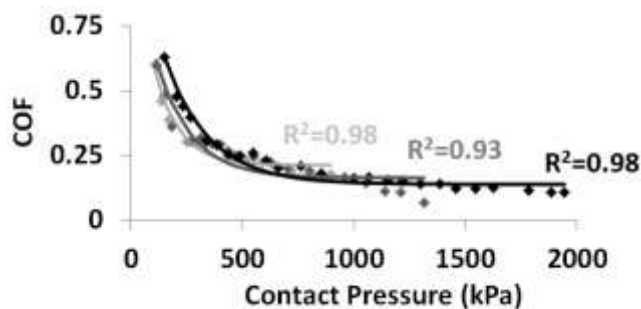
Friction force was calculated based on the contact pressure (p_i) and area (A_i) for each element from the macro-model, and the COF values as a function of contact pressures ($COF(p_i)$) from the micro-model (Eq.1). COF was calculated as the ratio of average friction force to normal force (Eq. 2).

$$F_{Friction} = \sum COF(p_i) * p_i * A_i \quad Eq. 1.$$

$$COF = F_{Friction} / F_{Normal} \quad Eq. 2.$$

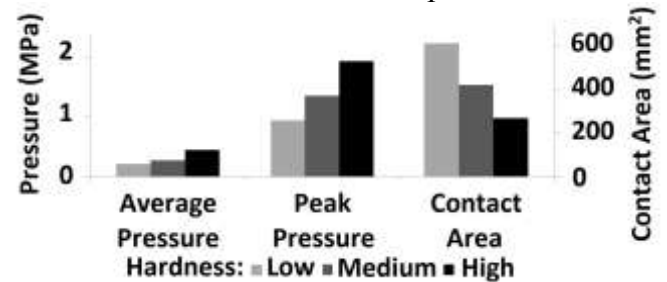
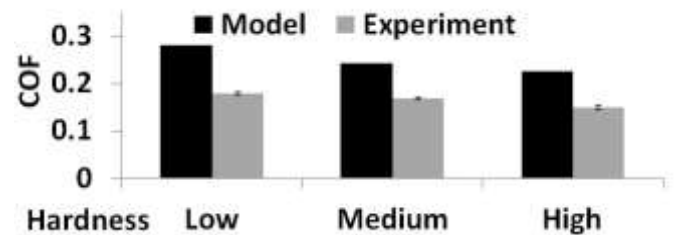
RESULTS AND DISCUSSION

An exponential fit described the relationship between predicted COF and contact pressure with an R^2 of greater than 0.93 for all three materials (Figure 2). The micro-model revealed that the hardest material experienced the greatest level of hysteresis COF and the medium and low hardness material had similar but less hysteresis COF.

**Figure 2.** Curve fitting for materials. Hardness: Low(Light Gray), Medium(Gray) and High(Black).

The macro-model revealed that pressures were typically along the posterior portion of the shoe. Increasing shoe hardness was found to increase average and peak pressures and reduce contact area (Figure 3.). Increased contact pressures of the hard shoe led to an overall reduction of hysteresis COF (Figure 4.). This finding was consistent with experimental measurements of shoe-floor COF (Figure 4.) and with slipping risk during unexpected human slips [5]. The model did overestimate hysteresis COF since it predicted COF values

between 0.25 and 0.3 whereas experiments found COF values between 0.15 and 0.2. This discrepancy may be due to the fact that the floor was modeled as rigid, which may have overestimated the hysteresis COF between the floor asperities and the shoe material. Overall, this study demonstrates the potential for using finite element analysis to model shoe-floor friction in a way that predicts slipping risk. The model suggests that the mechanism behind increased COF for soft shoe material is increased contact area and reduced contact pressures.

**Figure 3.** Contact pressure and contact area across the three materials.**Figure 4.** COF obtained from model versus experiments.

REFERENCES

1. Hanson JP, et al. *Ergonomics*, **42**, 1619-1633, 1999.
2. Moghaddam SRM, Master's Thesis, University of Wisconsin-Milwaukee, 2013.
3. Beschorner KE, PhD Thesis, University of Pittsburgh, 2008.
4. Mix AW and Giacomini AJ, *Journal of Testing and Evaluation*, **39**,1-10, 2011.
5. Beschorner KE, et al. Submitted to *Ergonomics*, 2015.

ACKNOWLEDGEMENTS

This work was supported by funding from National Institute of Occupational Safety and Health (NIOSH R01 OH008986). Custom footwear was provided by Timberland®.

VALIDATING A COMPUTATIONAL MODEL OF REVERSE SHOULDER ARTHROPLASTY

Vijay N. Permeswaran, Carolyn M. Hettrich, Jessica E. Goetz, Donald D. Anderson

The University of Iowa, Iowa City, IA, USA

email: vijay-permeswaran@uiowa.edu, web: <http://tinyurl.com/UIOBL>

INTRODUCTION

Reverse shoulder arthroplasty (RSA) is indicated for treating end-stage arthritis when the rotator cuff is compromised. In RSA, the native anatomy of the ball-in-socket joint is reversed by implanting a cup onto the humerus and a sphere onto the glenoid (Figure 1). A common complication is impingement between the humeral cup and inferior scapular ridge, which causes scapular bone erosion (notching). In order to prevent notching, surgeons lateralize the center of rotation of the glenosphere. We previously presented a finite element (FE) analysis of the effect of lateralization on range of motion and stress at the impingement site [1]. This study aimed to validate that prior FE analysis by measuring the contact stress at the impingement site in a cadaveric model.

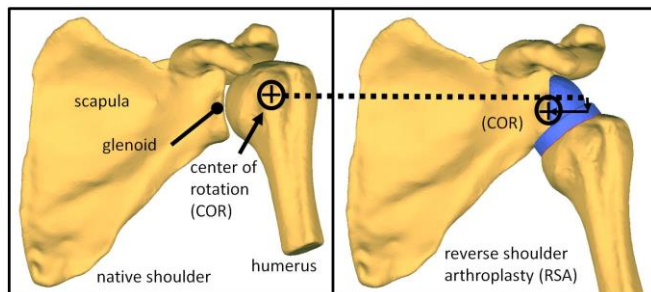


Figure 1: The image on the left shows a native shoulder, while that to the right shows a shoulder after RSA.

METHODS

A cadaveric shoulder was dissected and prepared using the bony increased offset (BIO) technique [2]. The proximal humerus was transected 5 cm distal to the deltoid insertion. The medial edge of the scapula and distal end of the humerus were both potted in PMMA. A Tornier Reversed Aequalis RSA system (Tornier, Amsterdam, Netherlands) was implanted. Metal spacers replicating BIO offsets were used to study lateralizations of 0, 2.5, 5, 7.5, and 10 mm. A

custom loading frame was constructed to secure the scapula. The humerus was held in place by a cable representing the deltoid muscle. This cable was clipped onto an eyehook screwed into the distal humerus PMMA block, routed through a pulley to replicate the wrapping of the deltoid, and attached to the load frame by a turnbuckle, which facilitated adjustment of tension in the deltoid cable.

CT scans were obtained for the cadaveric specimen before and after RSA implantation. The scapula, humerus, and implant components were segmented using Seg3D software (CIBC, Salt Lake City, UT). The FE model was generated from these surfaces.

A Tekscan ankle sensor (model #5033; Tekscan, South Boston, MA) was selected to measure the impingement contact stress because of its high spatial resolution (sensel resolution of 0.834 mm x 0.834 mm). A hole was punched in the sensor in order to secure it to the post of the glenosphere. The sensor was then pinched between the glenosphere and metal spacer. A portion of the sensor around the punched hole was trimmed to eliminate major wrinkling (Figure 2). During testing, a 5 lb. load

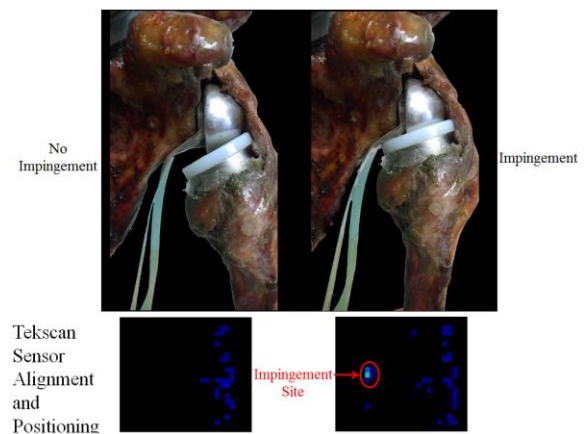


Figure 2: Tekscan sensor alignment and positioning. The lateral end of the tekscan sensor was modified and pinched between the glenosphere and lateralization spacer.

was hung from the humeral PMMA block. The deltoid cable was tensioned to prevent subluxation. In addition, a Qualisys Oqus motion tracking system (Qualisys AB, Gothenburg, Sweden) was used to record the position of the scapula and humerus at impingement.

The FE analysis was done using Abaqus/Explicit (Dassault Systèmes, Vélizy-Villacoublay, France). The global model included deformable glenoid and BIO bone, a rigid glenosphere, a deformable polyethylene cup, a rigid humeral component, and a rigid humerus. In addition, a series of cable and pulley elements were used to model the deltoid muscle, and spring elements were used to represent the joint capsule. The humerus was adducted until impingement and then fixed in position. Due to the highly focal nature of the contact patch, a high-resolution submodel of the impingement site was created. Boundary node displacements were applied using the submodel option. A custom Matlab (MathWorks, Natick, MA) script was used to analyze and compare the Tekscan results to the results of the FE analysis. Contact stress, area, and recovered load values were analyzed as well as location and contact patch morphology.

RESULTS AND DISCUSSION

Only results for the 7.5 mm implantation are here reported. The FE-computed maximum contact stress was 30.9 MPa, while the maximum contact stress for the Tekscan sensor was 21.2 MPa. The FE-computed contact area was 1.05 mm². The contact area of the two primary Tekscan sensels was 1.4 mm². The load transferred across the FE-computed contact patch was 39.9 N. The Tekscan sensor provided a loading of 42.3 N.

Figure 3 shows how the Tekscan sensor and FE model locations and areas correspond. The FE analysis reported a small contact patch indicative of the edge contact that occurred between the humeral cup and inferior ridge of the glenoid. The Tekscan sensor reported two sensels with contact significantly higher than all surrounding sensels (21 and 19 MPa vs. 2-5 MPa). When overlaid, the FE-computed contact patch aligned well with the two highly loaded sensels. This result provides a potential explanation for why the two sensels

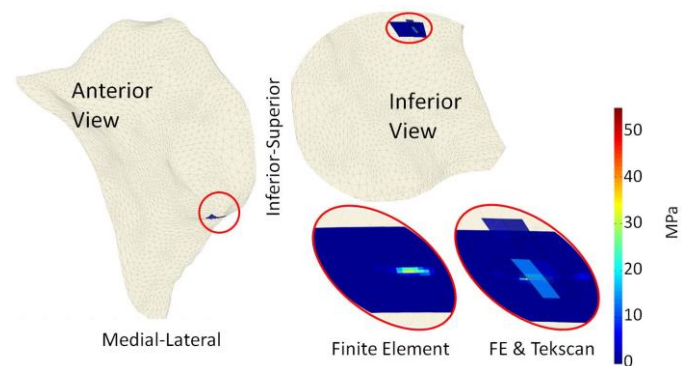


Figure 3: Anterior and inferior view of glenoid region of the scapula with FE-computed and Tekscan-measured contact stresses overlaid. A close-up view of the inferior view is inset below the inferior view. Tekscan sensels reporting zero contact stress were removed for visualization.

measured a smaller contact stress than that computed in the FE analysis. In addition, the FE model would be expected to create smaller contact area than the Tekscan due to the difference in spatial resolution. Finally, the Tekscan sensor can wrinkle around load application sites, yielding artifactually low contact stress readings. The similarity in contact load calculated is an indication that difference in contact area is likely the cause for dissimilar maximum contact stress.

CONCLUSIONS

In conclusion, a finite element analysis of the mechanical consequences of lateralization in RSA was successfully validated against cadaveric measurement of contact stress. This FE model can be used to computationally assess novel implantation procedures prior to clinical application.

REFERENCES

1. Permeswaran et al. 37th ASB Annual Meeting, 201, Omaha, NE, USA, 2013
2. Boileau et al. *Clin Orthop Relat Res* **469**, 2558-2567, 2011

ACKNOWLEDGEMENTS

This work was partially funded by a New Investigator Grant from the Orthopaedic Research and Education Foundation.

Simulation of Reduced Ankle Torque During the Anticipatory Postural Adjustments for Gait Initiation

¹Matthew N. Petrucci, ²Louis A. DiBerardino, ³Colum D. MacKinnon and ¹Elizabeth T. Hsiao-Wecksler

¹University of Illinois Urbana-Champaign, Urbana, IL, USA

²Ohio Northern University, Ada, OH, USA

³University of Minnesota, Minneapolis, MN, USA

email: mpetruc@illinois.edu, web: hdel.mechanical.illinois.edu

INTRODUCTION

Up to half of the Parkinson's disease (PD) population eventually suffers from freezing of gait, a term used to describe episodic disruptions in walking, turning and gait initiation. Impaired gait initiation may be related to an inability to properly coordinate the anticipatory postural adjustments (APAs) that are required for stability with forward locomotion. APAs in persons with PD are usually prolonged in duration and attenuated in amplitude compared to healthy controls [1].

The appropriate sequence of an APA begins with initial bursts of the tibialis anterior (TA) muscles on both legs and a simultaneous loading of the stepping foot and unloading of the stance foot (loading-unloading phase). Then, activation of the plantarflexor muscles of the stepping leg generates the forces necessary to accelerate the center of mass forward and toward the stance foot. This phase is followed by another TA burst of the stepping leg as it comes off the ground, resulting in a step [2]. An essential component of the loading-unloading phase of an APA is the magnitude of the initial TA burst of the stepping leg, which has been shown to be correlated with gait initiation velocity [3]. In PD, the initial TA burst can be diminished or absent, resulting in a decreased excursion of the center of pressure in the sagittal plane [1,4]. However, the neuromechanical significance of this diminished or absent TA burst has yet to be fully understood.

In the current study, we utilized an inverted pendulum model to investigate the consequences of reduced dorsiflexor torque to overall body lean angle during gait initiation.

METHODS

To study the effects of reduced dorsiflexion, the upright body during gait initiation was modeled as a single-link inverted pendulum. It was assumed that both ankles pivoted around the same point; thus torque was a combined value from both ankles. The

resulting transfer function from applied ankle torque (T_A) to body lean angle (θ) was derived as

$$\frac{\theta(s)}{T_A(s)} = \frac{1}{Js^2 - mgL} \quad (1)$$

where m was body mass, g was acceleration due to gravity, $J = \frac{1}{3}mL^2$ was the moment of inertia about the ankles, and L was body length divided by 2 (estimated position of center of mass). It was assumed that the body was a uniform rod.

In order to simulate proper gait initiation, a nominal trajectory θ_{ref} was generated from the average behavior of 10 self-initiated right leg gait initiation trials collected from one participant (age 30, ht. 180 cm, wt. 86 kg). Markers were placed on the lateral malleolus and acromion of both sides to generate the body segment.

The T_A term in equation 1 included multiple components representing different parts of the neuromuscular system. The first was a feed-forward torque (T_F), which would produce θ_{ref} in ideal conditions:

$$T_F = J\ddot{\theta}_{ref} - mgL\theta_{ref}$$

The second component of the T_A term was related to corrective torques driven by the feedback from the combined sensory systems detecting body lean angle. Both stiffness (K_p) and damping (K_d) terms were included (Fig 1).

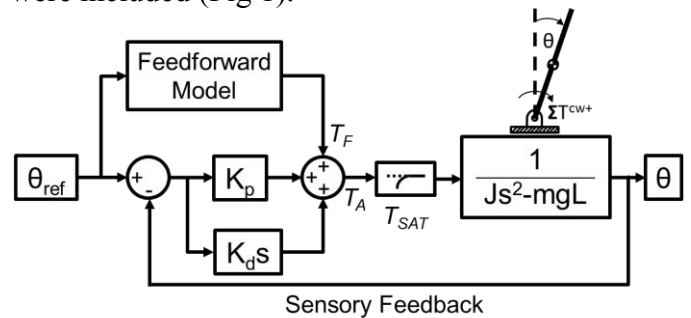


Fig 1: Inverted pendulum model of gait initiation

Diminished TA activity and reduced dorsiflexor torque during the loading-unloading phase of an APA (time from APA onset to peak loading) through heel-off of the stepping foot were simulated by limiting the torque generated at the ankle via a saturation function (T_{SAT} in Fig 1). The saturation magnitude was decreased in increments of 2 Nm, with each condition simulated using Simulink (MathWorks Inc., Natick, MA). Prior to varying the saturation block value, the feedback gains were heuristically tuned to reduce the sum of squared error between experimental and simulated data. These gains were $K_p = 6500$ and $K_d = 0$.

RESULTS AND DISCUSSION

Application of the saturation block revealed a possible threshold for decreased body lean angle and an improper torque sequence (Fig 2). From an initial plantarflexor torque of -33 Nm, the model achieved a peak dorsiflexor torque (most positive value) at -22 Nm. Thus, saturation values of -22 Nm to -28 Nm did not result in large differences in body lean angle or torque. However, when the dorsiflexor torque was limited to -30 Nm, decreases in body lean angle became apparent and the model went into plantarflexion later than the unsaturated torque profile. When dorsiflexor torque was almost fully limited to -32 Nm, the body lean angle was more than half of a degree less than the no saturation condition, and the model never went back into plantar flexion. Even though the difference in overall body lean angle was small, these results suggest that there may be a threshold of the initial dorsiflexor torque where the neuromuscular system is unable to generate a sufficient forward lean at the ankle.

Although preliminary, these results provide insight into the mechanisms behind impaired gait initiation for persons with PD. Experimentally, it has been shown that persons with PD still plantar flex their stepping foot without first dorsiflexing, further inhibiting forward progression [4]. This aberrant activation requires further adaptations in the sequence of muscle activation, which can be difficult for persons with PD [5]. It is possible that these neuromechanical alterations may underlie the symptoms of freezing of gait or start hesitation.

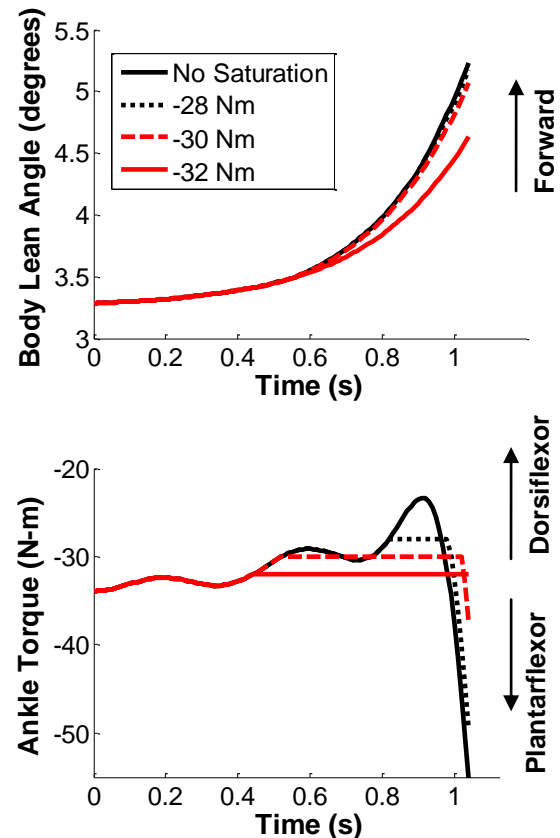


Fig 2: Body lean angle and ankle torque at different dorsiflexor torque saturation values.

CONCLUSIONS

Our preliminary findings highlight the possible consequences of reduced dorsiflexor torque during the initial phase of the APA. Future studies will focus on parameter optimization to more accurately model the neuromuscular system with additions such as time delays and noise. Ultimately, this model could be used to better understand freezing of gait and inform strategies for alleviating these symptoms.

REFERENCES

1. Burleigh-Jacobs et al. *Mov Disord* **12**, 206-215, 1997
2. Carlsoo, S. *Acta anat.* **65**: 1-9, 1966
3. Crenna et al. *J of Physiol* **437**, 635-653, 1991
4. Elble et al. *Brain* **119**, 1705-1716, 1996
5. Benecke et al., *Brain* **110**, 361-379, 1987

ACKNOWLEDGEMENTS

This material is based upon work supported by the National Science Foundation Neuroengineering IGERT under Grant No. 0903622

EVALUATION OF THE TRANSVERSE METATARSAL ARCH OF THE FOOT

¹ Sayed Cyrus Rezvanifar, ¹ Brian L. Davis

¹ The University of Akron, Akron, OH, USA

Email: sr106@zips.uakron.edu, Web: <http://bme.uakron.edu>

INTRODUCTION

The existence of the transverse metatarsal arch (TMA) of the foot is controversial, with some researchers [1, 2, 3] historically describing either an arch, or a foot that rests on the floor on the heel, 1st and 5th metatarsal heads. Biomechanically, this configuration has been considered to be a shock absorber. More recently – largely due to the emergence of pressure measurement technologies – researchers have disputed the arch concept by showing that during gait the highest pressures are found at the 2nd - 3rd metatarsal heads (MTH's) and the heel in midstance [4]. According to these researchers, there cannot be a “tripod” if there are no significant pressures under the 1st and 5th MTH's.

In this study, we developed a model that could reconcile both the existence of a TMA and the fact that pressure values can be elevated under the 2nd and 3rd MTH's.

METHODS

A 2D finite element (FE) model was prepared in Abaqus 6.13 based upon a simplified cross-sectional view of the foot at the metatarsal heads (Figure 1). The considered model includes two beams having the mechanical properties of bone tied together at the apex and free to slide horizontally at the medial and lateral edges of the foot.

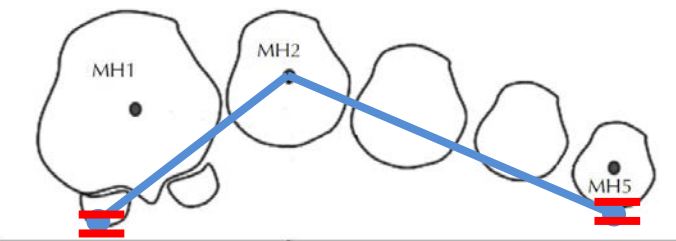


Figure 1. The TMA was modelled as a simplified arch, with the apex coinciding with MTH2.

The triangular free space between these two beams was filled with an elastic material representing soft tissue. Material properties used for different parts are listed in Table1.

Table1. Mechanical properties of elements used in the model

Material	Density(kg/m ³)	Young's Modulus (MPa)	Poisson's ratio
Bone Beams	1750	7300	0.3
Soft Tissue	1050	2000	0.33
Ground	7800	200,000	0.3

Fillets were applied at all edges of the soft interior portion of the model in order to avoid excessive distortions. The coefficient of friction between the soft triangle and ground was set 0.5 [5]. Moreover, the angled sides of the soft tissue were tied to the beams leading to ensure no relative movement. A 10 mm vertical displacement was applied to the apex for observing the effect of applying bodyweight to the forefoot. Boundary conditions were established by setting the lower horizontal surface of the rectangular modeled ground to have no displacement or rotation in any direction. Furthermore, the beam ends in contact with the ground were constrained to translate only in the horizontal (medio-lateral) direction.

Meshing involved using beam elements for the “bone” structures and plane stress elements for soft tissue and ground since the assumed cross section with a small thickness would have negligible stresses in the perpendicular direction. Finally, the conducted analysis was modelled as Dynamic-Explicit. Of note is the fact that for quasi-static problems, Dynamic-Explicit analysis requires attention to the static status of the problem during

the iterative modelling process. Accordingly, the values of internal and kinetic energies were compared throughout the loading process. Finally, in order to verify the meshing process, a convergence study was performed to assess the influence of element sizes.

RESULTS AND DISCUSSION

The model was assessed and found to exhibit consistently lower magnitude of kinetic energy in comparison with internal energy. This implies the model was acceptable from a quasi-static point of view.

The convergence validation showed that predicted pressures at the ground-foot interface changed by only 1% when the elements were increased by a factor of four (i.e., from 2mm to 0.5mm). These results supported the decision to select elements 1mm in size.

The primary finding of this study is that the model showed that pressures can be elevated in the MTH2 and MTH 3 regions – simply by virtue of the fact that as the arch flattens, the soft tissue is compressed in a matter that leads to pressure build-up in the central forefoot region (Figure 2).

CONCLUSIONS

This study has shown that a “controversy” in whether or not there is a transverse arch can be reconciled through the use of a simple model. What the model shows is that pressures can be elevated in MTH2 and MTH3 regions even when there is a bony “tripod” made up of osseous elements within the foot. The fact that loads may be distributed through the calcaneus and 1st and 5th rays may not be at odds with elevated pressures in the central forefoot region.

REFERENCES

1. Kapandji LA (1970) The physiology of the joints. E & S Livingstone, Edinburgh
2. Henle, J (1858). Handbuch der systematischen Anatomie des Menschen (p. 292). Braunschweig : Druck und Verlag von Friedrich Vieweg und Sohn.
3. Dickson FD, Diveley RL (1953) Functional disorders of the foot, 3rd ed. Lea & Febiger, Philadelphia
4. Kanatli U, Yetkin H, Bolukbasi S. Evaluation of the transverse arch of the foot with gait analysis. Arch Orthop Trauma Surg 2003; 123:148 –150.
5. Lemmon D, Shiang TY, Hashmi A, Ulbrecht JS, Cavanagh PR. (1997). The effect of insoles in therapeutic footwear--a finite element approach. J Biomech. 30(6):615-20.

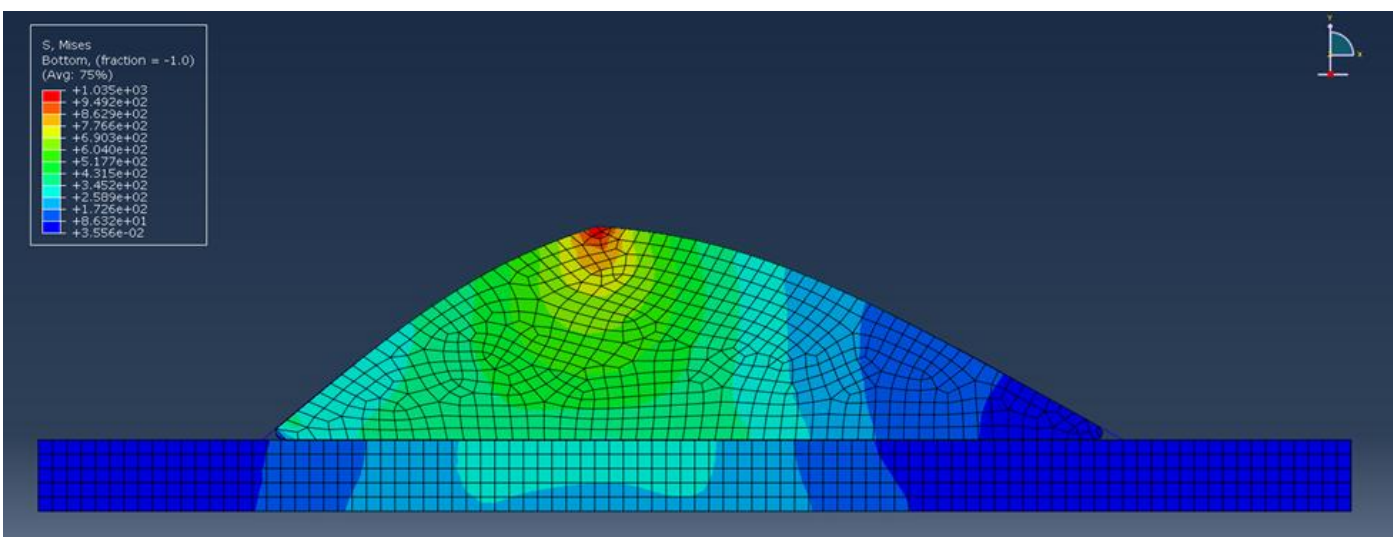


Figure 2: Results showing elevated pressures at the foot-ground interface at the MTH2 and MTH3 region. Mesh Size: 1 mm, maximum MTH pressure = 309 Pa

GLENOHUMERAL ABDUCTION AND FLEXION MUSCLE MOMENT ARMS: A VERIFICATION STUDY OF A NEW MUSCULOSKELETAL MODEL OF THE SHOULDER

¹ R. Tyler Richardson, ² Brian A. Knarr, ¹ Jill S. Higginson, and ¹ James G. Richards

¹ Biomechanics and Movement Science Program, University of Delaware, Newark, DE, USA

² Delaware Rehabilitation Institute, University of Delaware, Newark, DE, USA

email: trich@udel.edu

INTRODUCTION

Musculoskeletal modeling possesses the capability to estimate internal muscle forces that cannot be directly measured [1]. However, the validity of the results must first be assessed to ensure that the model is sufficiently robust to recreate the mechanics that occur in vivo. Moment arms define the function of a muscle about a joint and dictate the mechanical advantage with which it operates. Accordingly, evaluation of moment arms represents a particularly important step in the model verification process as they strongly influence simulation predictions. Existing upper extremity models [2, 3] possess limitations that compromise their ability to replicate scapulothoracic kinematics and estimate the associated underlying muscle forces. In an effort to overcome these limitations, a new shoulder model (UDSM) has been developed. This study compared the UDSM glenohumeral (GH) abduction and flexion muscle moment arms with published cadaveric data [4]. It was hypothesized that the UDSM GH abduction and flexion moment arms would be similar in both function and magnitude to the established values.

METHODS

The UDSM possesses 16 degrees of freedom allowing for physiological motion of the thorax, clavicle, scapula, humerus, and forearm. Thirty-five muscle actuators have been employed to represent 18 muscles which span the shoulder and elbow joints. Continuous GH abduction and flexion moment arms for the deltoid, latissimus dorsi, pectoralis major, teres major, and rotator cuff muscle actuators were calculated for the model using OpenSim [1]. The model GH abduction and flexion muscle moment arms were assessed during in vivo shoulder abduction (10°-120°) and flexion

(2.5°-120°), respectively. Dynamic orientations of the trunk and upper extremity segments were recorded with motion capture for one healthy subject. Each motion trial permitted unprescribed scapular kinematics which were estimated by an acromion marker cluster [5]. Joint kinematics were calculated using inverse kinematics. The GH abduction and flexion moment arms estimated using these kinematics were qualitatively compared with cadaveric data from Ackland et al. [4].

RESULTS AND DISCUSSION

UDSM GH abduction moment arms accurately reflected the functional role of each muscle. The anterior and middle deltoid, infraspinatus, and supraspinatus operated as abductors throughout the motion (Fig. 1). The posterior deltoid, latissimus dorsi, sternal and costal heads of pectoralis major, subscapularis, and teres major acted primarily as adductors (Fig. 1). Teres minor and the clavicular head of pectoralis major functioned as both abductors and adductors within the motion.

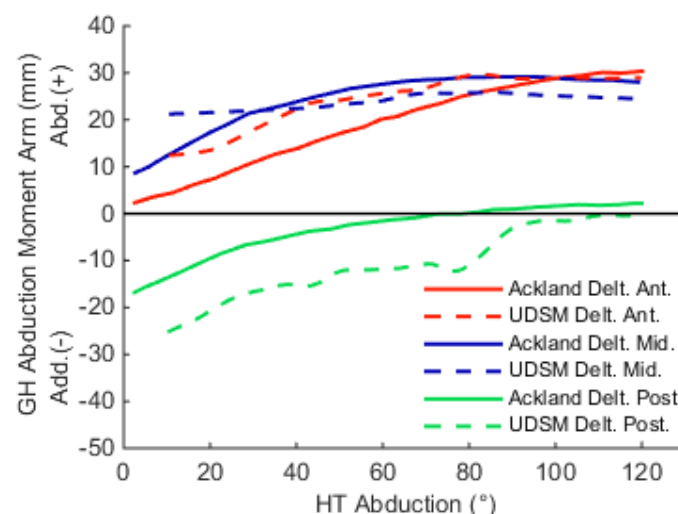


Figure 1: GH abduction moment arms of the deltoid. (+) values indicate abduction.

The magnitudes of the UDSM abduction moment arms also compared favorably with cadaveric data [4]. The anterior and middle deltoid and supraspinatus had the greatest mechanical advantages for abduction while the posterior deltoid, latissimus dorsi, teres major and pectoralis major possessed the largest mechanical advantages for adduction (Fig. 1).

Glenohumeral flexion moment arms of the UDSM corresponded with the functional role of each muscle. The anterior and middle deltoid, superior subscapularis, clavicular head of the pectoralis major, and supraspinatus operated as flexors throughout the motion (Fig. 2). The posterior deltoid, middle and inferior latissimus dorsi, costal head of pectoralis major, inferior infraspinatus, teres minor, and teres major acted primarily as extensors (Fig. 2). The sternal head of pectoralis major, inferior subscapularis, superior infraspinatus, and superior latissimus dorsi functioned as both flexors and extensors at different portions of the motion. The magnitudes of the UDSM flexion moment arms were also similar to cadaveric data [4]. The anterior and middle deltoid possessed the greatest mechanical advantages for flexion while the posterior deltoid, latissimus dorsi, and teres major had the largest mechanical advantages for extension (Fig. 2).

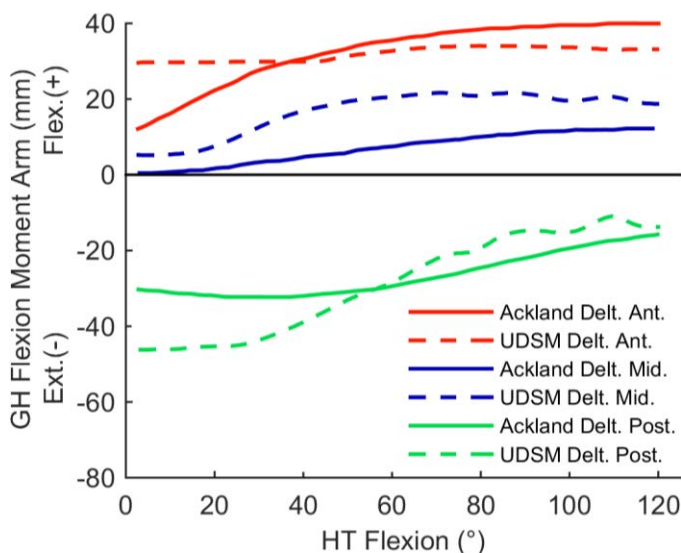


Figure 2: GH flexion moment arms of the deltoid. (+) values indicate flexion.

While the general functional roles of all the muscle actuators of the model were in agreement with published cadaveric data, there were a few muscles displaying appreciable differences in moment arm pattern and magnitude. Conditional differences between the motions used for the model analysis and the kinematics prescribed in the cadaveric experimental setup [4] are likely responsible for these discrepancies. For both the abduction and flexion trials the model was driven with in vivo motion which involved unprescribed scapular motion with three degrees of freedom while the cadaveric experiments [4] were performed with a prescribed scapular rhythm with only one degree of freedom. Additionally, the cadaveric study [4] fixed the clavicle in a neutral position during each motion, while the kinematics used in the model's analysis permitted physiological motion of the clavicle. The observed minor variations in pattern and magnitude of GH moment arms are to be expected and can be explained considering these conditional differences in the kinematics between the cadaveric and model analyses.

CONCLUSIONS

This analysis establishes that the UDSM GH abduction and flexion moment arms are similar to cadaveric data while also allowing for unprescribed scapular motion. Continued research comparing the model's properties and predictions to published data is warranted to provide a more complete verification of the UDSM.

REFERENCES

1. Delp SL, et al. *IEEE Trans Biomed Eng* **54**, 1940-50, 2007.
2. Saul KR, et al. *Comput Methods Biomech Biomed Eng* **18**, 1445-58, 2015.
3. van der Helm FC. *J Biomech* **27**, 551-69, 1994.
4. Ackland DC, et al. *J Anatomy* **213**, 383-90, 2008.
5. van Andel C, et al. *Gait & Posture* **29**, 123-8, 2009.

ACKNOWLEDGEMENTS

NIH National Center for Simulation in Rehabilitation Research Pilot Project Award

DEVELOPMENT OF AN OPEN-SOURCE, DISCRETE ELEMENT KNEE MODEL

Anne Schmitz

Gannon University, Erie, PA, USA; email: schmitz005@gannon.edu

INTRODUCTION

Osteoarthritis, the most common form of arthritis, occurs more in the knee than any other joint [1]. Therefore, knee models are valuable tools that can be used to study normal joint function, simulate potential strategies to prevent injury, and assess the effect of treatment programs. These models range in complexity from a hinge joint [2,3] to a complex continuum representation using finite element analysis [4]. Discrete element models offer a balance between simplified and finite element models by providing soft tissue loads at a low computational cost. Uses of these models include the estimation of immeasurable forces (i.e. muscle forces and soft tissue loads) and the performance of ‘what-if’ studies. For example, a discrete element model of the knee, which included cartilage loads and spring representations for ligaments, has been used to predict hamstring and quadriceps forces that could be used to restore normal joint function in a knee without an anterior cruciate ligament [5]. However, there is not an open-source, discrete element knee model available in the literature. Therefore, the goal of this work was to develop a discrete element model of the knee that is open-source.

METHODS

The right femur and tibia of a generic musculoskeletal model (i.e. gait2392 model [6]) were scaled for a 77.5 kg female in the open-source software OpenSim [7]. A six degree-of-freedom (dof) tibiofemoral joint and one dof patellofemoral joint were created that included tibiofemoral contact, ligaments, and vastii muscles (Figure 1). The patellofemoral joint was modeled as a one dof joint where the patella moved in a constrained path about the distal femur subject to vastii and patellar tendon forces. Contact was modeled between the femur and tibia using an elastic foundation model [8]. The geometry of the distal femur articular cartilage was based on an open-source finite element knee model [9]. The tibial plateaus were

modeled as two planes: the lateral plateau sloped 7 degrees posteriorly and 2 degrees laterally while the medial plateau sloped 2 degrees posteriorly and medially [5,10]. Eighteen ligament bundles were included in the model: anterior cruciate ligament (ACL, 2), posterior cruciate ligament (PCL, 2), medial collateral ligament (MCL, 5), lateral collateral ligament (LCL, 1), popliteofibular ligament (PFL, 1), posterior capsule (4), and patellar tendon (3). The origins and insertions were based on the literature and modeled as nonlinear elastic springs with properties adapted from the literature [5,11]. The properties were minimally tuned to match the model behavior to literature measures of passive motion, anterior-posterior stiffness, and axial rotational stiffness. The developed model is available from <https://simtk.org/home/kneemodel> and can be freely downloaded and recreated using OpenSim.

To validate the model, its passive behavior was compared to cadaveric literature. First, the model was passively flexed while the other five dof were compared with [12]. Next, an anterior and posterior force of 100N was applied to the tibia with the amount of anterior-posterior translation measured [13]. Then, an axial rotation torque of 5Nm was applied to the tibia with the resulting rotation measured [14,15].

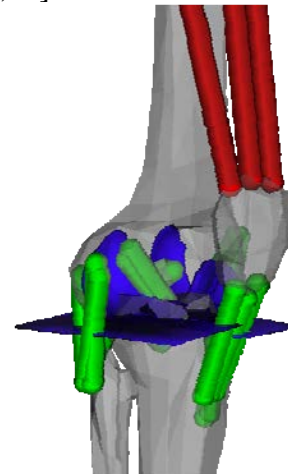


Figure 1: Discrete element knee model created in OpenSim

RESULTS AND DISCUSSION

Passive motion and stiffness properties of the model mostly agreed with the range presented in the literature (Figure 2). This provides a comprehensive description of the passive behavior of the model and highlights its physiological relevance. However, there are some exceptions to note. When the model was flexed, the tibia did not translate as much superiorly as the literature suggests. This may be largely governed by the contact geometry. Also, anterior translation of the model under an applied anterior force was on the low side of the literature range. However, further loosening of the ligaments to increase this translation caused intercondylar lift-off during the passive flexion motion.

This model has many applications: (1) investigate the sensitivity of passive motion and stiffness to ligament properties and placements, (2) investigate the effect of scaling on passive behavior, (3) used to create a surrogate model, and/or (4) used in a cosimulation or serial (e.g. [16]) approach to predict soft tissue loading during movement.

CONCLUSIONS

In summary, a discrete element knee model has been presented. Through a comparison with the literature, the model has shown physiologically reasonable passive behavior. A novel element of the model is that it is open-source. This enables more researchers to add to the refinement of the model as well as providing modeling as an accessible tool to a wider audience.

REFERENCES

1. Oliveria, S. A., et al. *Arth and Rheu* **38**, 1134-1141, 2005.
2. Asano, T., et al. *J Arthro* **20**, 1060-1067, 2005.
3. Reinbolt, J. A., et al. *J Biomech* **38**, 621-626, 2005.
4. Dhaher, Y. Y., et al. *J Biomech* **43**, 3118-3125, 2010.
5. Shelburne, K. B., et al. *Med Sci Sports Exerc* **37**, 642-648, 2005.
6. Delp, S. L., et al. *IEEE Trans on BME* **37**, 757-767, 1990.
7. Delp, S. L., et al. *IEEE Trans BME* (in press), 2007.
8. Sherman, M. A., et al. *Procedia IUTAM* **2**, 241-261, 2011.
9. Sibole, S., et al. *Proc of 34th Annual Meeting of the American Society of Biomechanics*, Providence, RI, 2010.
10. Garg, A., et al. *J Biomech* **23**, 45-53, 55-58, 1990.
11. Shin, C. S., et al. *J Biomech* **40**, 1145-1152, 2007.
12. Wilson, D., et al. *J Biomech* **33**, 465-473, 2000.
13. Gollehon, D. L., et al. *J Bone Joint Surg Am* **69**, 233-242, 1987.

14. Griffith, C. J., et al. *Am J Sports Med* **37**, 1762-1770, 2009.
15. Coobs, B. R., et al. *Am J Sports Med* **38**, 339-347, 2010.
16. Shelburne, K. B., et al. *J Biomech* **37**, 797-805, 2004.

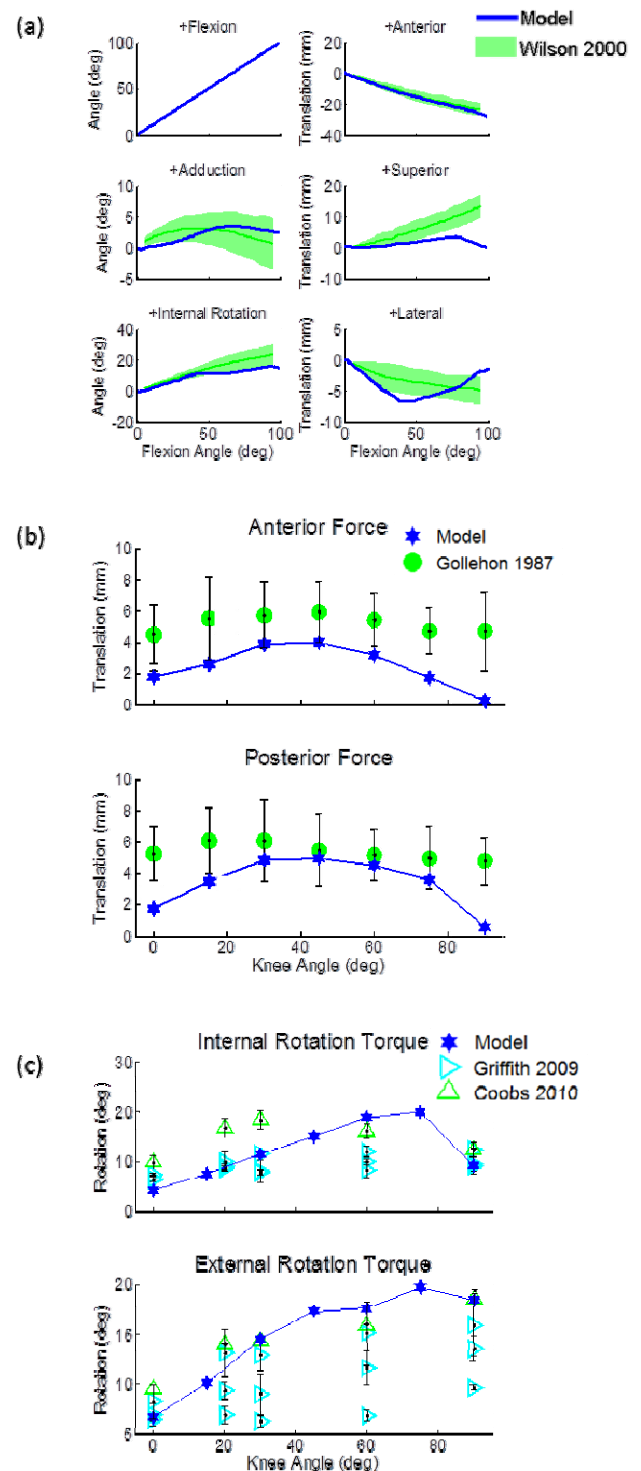


Figure 2: (a) Passive motion of the tibiofemoral joint compared to [12]. (b) Anterior-posterior translation of the tibia resulting from application of 100N. Results compared to [13]. (c) Axial rotation of the tibia with 5Nm torque applied. Results compared to [14,15].

IMPROVING PATIENT SIMULATOR UPPER ARM BIOMECHANICS

¹ K. Dyer, ¹ A. Merlino, ¹ N. Bouaynaya, ¹ T. Merrill, ¹ D. Podolin, ^{1&2} A. Singh

¹ Rowan University, Glassboro, NJ, USA

² Widener University, Chester, PA, USA

email: singh@rowan.edu

INTRODUCTION

Patient simulators (SIMs) have been used effectively to teach basic science and clinical knowledge as well as clinical skills, teamwork, and communication to both undergraduate and graduate medical students [1,2]. Despite costs ranging from \$30,000 to \$200,000, existing high-fidelity mannequin simulators are limited in their capabilities. There is a critical need for SIMs with extremities that move realistically and respond with normal muscle tone when educating healthcare students. This functionality would allow students to learn: a) appropriate methods to move and position patients and b) neuromuscular examination techniques. Improper skill in patient positioning can result in patient injury, particularly among geriatric, obese, and immunocompromised patients. To meet this critical unmet need, this study aims to improve the biofidelity of the upper extremity by i) including normal degrees of freedom (DOF) in the elbow joint, ii) incorporating muscle tone in the upper arm, and iii) automatically controlling the upper arm to simulate different muscle tones and neuromuscular disorders

METHODS

SimMan 3G (Laerdal, NY) offers some realism as the arms rotate at the shoulder joint in a circular motion, but they do not bend at the elbow. We used mechanical design principles to incorporate required DOF at the elbow joint as shown in Figure 1.

Designing Elbow Joint: Using the anatomical details obtained from the existing SimMan 3G arm, solidwork models of the upper and lower arm was created. The final arm configuration was then

fabricated after taking the degrees of freedom at the elbow joint, arm weight (<10 lbs) and biceps and triceps muscles attachment points into consideration as shown in Figure 2.

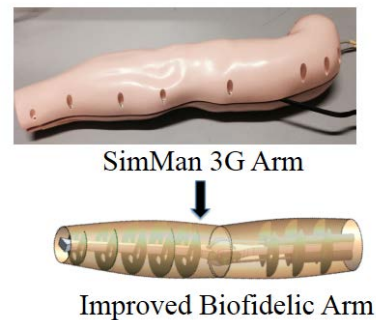


Figure 1: Sim-Man 3G Arm and the newly designed bio-fidelic arm.

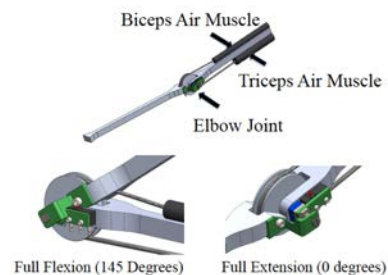


Figure 2: Solidworks rendering of the biofidelic arm with human like range of motion at the elbow joint.

Designing Muscle Tone in a SimMan Arm: A real arm is a highly redundant complex system made of muscle, tendons, bones and nerve. Simulating arm with changes in any of these components has always remained a challenge for simulator manufacturers. No one mannequin offers a system that replicates a limb under the effect of an abnormal muscle, tendon or bone function. In this study, we incorporated the biceps and triceps muscles using an air-muscle model as shown in Figure 3. Muscle tone, a continuous, passive, partial contraction of the muscles is affected in patients,

such as older individuals, individuals with dementia display paratonia, patients with extrapyramidal disease, particularly Parkinson's. In the designed system, we could simulate changes in muscle tone by regulating the pneumatic pressure inside each air muscles.

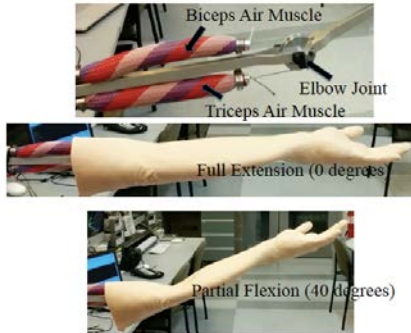


Figure 3: Air Muscles simulating the Biceps and Triceps Muscles.

Controlling the upper arm of SimMan: The pneumatic artificial muscles are controlled through proportional valves used to control the pressure and resultant displacement. To simulate muscle tone, the angular position of the arm must be controlled. A potentiometer is used to determine angular position and provide feedback to the control system. In addition, strain gauges are placed on each muscle 'tendon' to determine the amount of force that muscle is exerting. This feedback also allows the user to be notified that they are 'hurting' the patient when too much force is applied. The block diagram of the control system can be found in Figure 4. The system uses three PID controllers for bicep tension, tricep tension, and angular position. The output of the position controller is tuned to be in the range of strain gauge feedback. If the position controller is attempting to increase angle (flexion), the output is such that the bicep controller should increase tension while the tricep controller releases tension. In order to simulate muscle tone, the position setpoint responds to the external force applied to the mannequin arm. External force is detected when the position exceeds the operating bounds of the control system. The bounds control the response of the arm and therefore the muscle tone. By responding later (bounds are larger), the control system will try to resist movement. On the contrary, when the bounds are small, the system will quickly change its setpoint, resulting in little to no resisting.

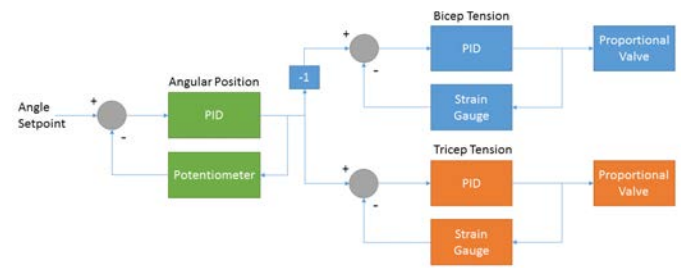


Figure 4: Block diagram of control system using multiple integrated PID controllers

RESULTS

The newly fabricated arm offers a range of motion between 0 and 100 degrees. The two air muscles simulate the biceps and triceps muscles and precisely control the range of motion at the elbow joint. Furthermore, by regulating the pneumatic pressure within the air muscle, the muscles can be pre-strained to offer various muscle tone in the forearm. Currently, the modified biofidelic forearm is being attached to a mannequin to carry out clinical validations and establish the efficacy of this improved arm in the medical education.

CONCLUSIONS

In the current teaching setting, the most common mannequin used to teach physiologic points lacks limb mobility and/or offer unrealistic mobility. By adding DOF in these joints, incorporating the air-muscles for muscle tone, and controlling the arm, we will offer a much more realistic teaching tools for patient positioning [3].

REFERENCES

1. Cooper JB, Taqueti VR. Qual Saf Health Care 2004; 13 (suppl 1): I11-18
2. Gaba DM. Qual Saf Health Care 2004; 13 (suppl 1): i2-10
3. Rosen AK, Rivard PE, Zhao S, Loveland S, Tsilimingras D, Christiansen C, Elixhauser A, Romano PS. Medical Care. 2005;143(9):873-84

ACKNOWLEDGEMENTS

This study was funded by Rowan University Robert Wood Johnson Foundation.

THE EFFECTS OF ADDED FOOT STIFFNESS ON SOLEUS MUSCLE FASCICLE BEHAVIOR DURING HUMAN WALKING

¹Kota Z. Takahashi, ²Michael T. Gross, ³Herman van Werkhoven, ⁴Stephen J. Piazza and ¹Gregory S. Sawicki

¹North Carolina State University, Raleigh, NC, USA, ²The University of North Carolina, Chapel Hill, NC, USA,

³Appalachian State University, Boone, NC, USA, ⁴The Pennsylvania State University, University Park, PA, USA
email: ktakaha@ncsu.edu

INTRODUCTION

Understanding the interplay between foot and ankle structures may help uncover the fundamental principles governing the mechanics and energetics of human locomotion. The structure of the foot, for example, defines the input and output lever arms that set the mechanical advantage of the plantar flexors during push-off in walking and running [1]. The foot and ankle can also interact in a rather unintuitive manner; while the muscles and tendons crossing the ankle do positive work during push-off, the foot may counteract the ankle by absorbing or dissipating energy [2,3]. We explored this functional interplay by adding stiffness to the foot (through footwear) and evaluated ankle plantar flexor (soleus) muscle fascicle behavior and whole-body energy cost during walking.

Prior studies involving footwear have shown that a stiffer shoe increases the gear ratio (the ratio of ground reaction force lever arm to ankle plantar flexor moment arm) and also increases the mechanical energy returned by the foot [4,5]. The effects of altered shoe stiffness on ankle plantar flexor function, however, remain unclear. In theory, increased gear ratio could enhance muscle force production through slower shortening velocity [6]. In addition, increased foot energy return may decrease the mechanical work demands elsewhere (such as from structures crossing the ankle), as net work done by the body is conserved during steady-state locomotion.

We hypothesized that adding stiffness to the foot would increase soleus fascicle force while decreasing the fascicle shortening velocity and positive work. Additionally, we hypothesized that these altered muscle mechanics would decrease the whole-body metabolic energy cost of walking.

METHODS

Kinematic and kinetic gait data were collected from 5 healthy subjects (2 females and 3 males). We fabricated carbon fiber foot insoles with four different thicknesses (0.8, 1.6, 2.4 and 3.2 mm) to vary insole stiffness. Subjects walked at a fixed speed of 1.25 m/s on an instrumented treadmill under six different foot conditions (barefoot, shod, and shod with four different insole thicknesses). The shod and shod+insole conditions corresponded to an added stiffness of 16.3, 24.3, 27.1, 30.8, and 64.1 N/mm relative to barefoot, respectively. We note that the shoe and insoles were intended to *add* stiffness to the anatomical foot, and not necessarily to modify the stiffness of the foot itself.

Soleus muscle fascicle length and pennation angle during walking were estimated using B-mode ultrasound (Telemed, Lithuania), while fascicle velocity was computed by differentiating the length with respect to time. Soleus fascicle force was estimated by dividing the total ankle joint moment (computed from inverse dynamics) by the Achilles tendon moment arm, scaled to cross sectional area of the soleus relative to all plantar flexor muscles, and then corrected for pennation angle. Work done by the soleus muscle fascicle was estimated by integrating the fascicle power (product of fascicle force and velocity) over time.

The effects of different foot conditions were analyzed using a 1-way repeated measures ANOVA for the following variables: (1) peak soleus fascicle force, (2) soleus fascicle velocity at the time of peak force, (3) soleus fascicle positive work, and (4) whole-body net metabolic power (estimated from indirect calorimetry). If a significant main effect ($p < 0.05$) was detected, we used a paired t-test to perform pairwise comparisons. Because of the

current low sample size, we opted not to adjust for multiple comparisons to control for Type I errors.

RESULTS AND DISCUSSION

With added foot stiffness, soleus fascicle peak force increased ($p < 0.01$). Furthermore, the fascicle velocity was decreased across several foot conditions ($p < 0.05$), with shod, shod+0.8mm, and shod+1.6mm having slower fascicle shortening velocity (at the time of peak force) compared with barefoot. These preliminary findings are consistent with previous findings that footwear can alter gear ratio [4], increasing plantar flexor force by reducing contraction velocity. Despite these changes in force and velocity profiles, there was no significant change in fascicle positive work ($p = 0.22$). Lastly, added stiffness was found to influence whole-body metabolic cost ($p < 0.05$). The barefoot condition had the least metabolic power (2.80 ± 0.38 W/kg) while the shod+3.2mm (stiffest condition) had the greatest metabolic power (3.08 ± 0.29 W/kg).

CONCLUSION

Our preliminary data indicate altered force-velocity behavior of the soleus muscle fascicle with varied foot stiffness conditions. We are currently collecting data from more subjects to confirm these initial observations.

REFERENCES

1. Carrier DR et al. *Science* **29**, 651-653, 1994.
2. Rolian C, et al. *J Exp Biol* **212**, 713-721, 2009.
3. Takahashi KZ and Stanhope SJ. *Gait Posture* **38**, 818-823, 2013.
4. Willwacher S, et al. *J Appl Biomech* **29**, 583-592, 2013.
5. Willwacher S, et al. *Gait Posture* **40**, 386-390, 2014
6. Baxter JR, et al. *Proc Biol Sci* **79**, 2018-2024, 2012.

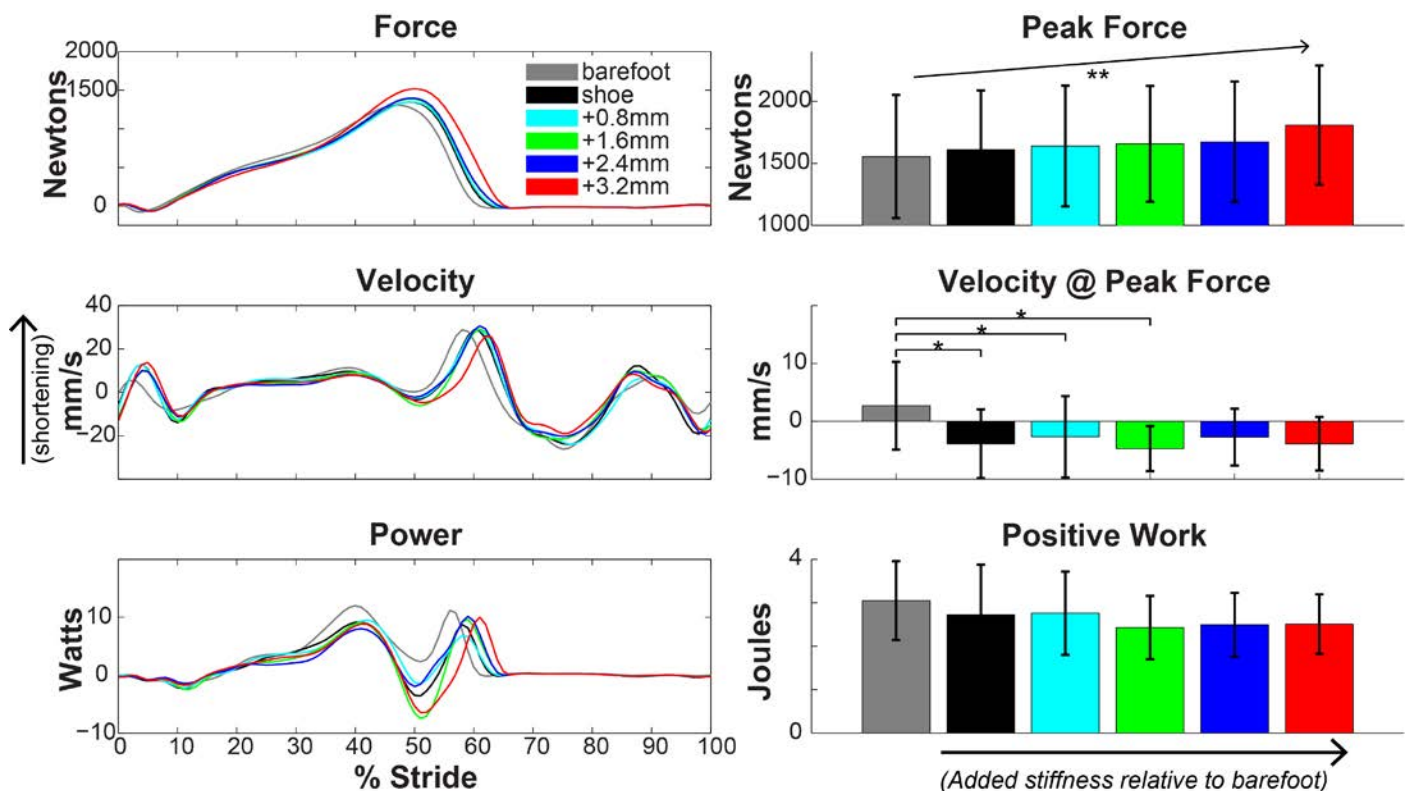


Figure: Averaged soleus muscle fascicle data (N=5) of force, velocity, and power (time-normalized to stride cycle) and magnitudes (mean \pm SD) of peak force, velocity at the time of peak force, and positive work. There was a significant effect of added foot stiffness on peak force ($p < 0.01$, denoted by **), and velocity at the time of peak force ($p < 0.05$, with significant pair-wise comparisons denoted by *), but there was no significant effect on positive work ($p = 0.22$).

ASSESSING WIRE NAVIGATION PERFORMANCE IN TREATING HIP FRACTURES

Leah Taylor, Colleen Rink, Steven Long, Geb W Thomas, Matthew D Karam, and Donald D Anderson

The University of Iowa, Iowa City, IA, USA
email: leah-taylor@uiowa.edu, web: <http://tinyurl.com/UIOBL>

INTRODUCTION

One of the most common procedures performed by orthopaedic surgeons is the fixation of a hip fracture involving the proximal femur [1]. A sliding hip screw is one preferred fixation device. Its failure is most often due to cut-out of the implant from the femoral head [2]. The cannulated implant is placed after using fluoroscopy to navigate a guide wire into the femoral head. The Tip-Apex Distance (TAD) measures the accuracy of implant placement from AP and lateral radiographs or fluoroscopic images (Figure 1). A larger TAD carries with it a greater cut-out risk, especially when it exceeds 25 mm [1].

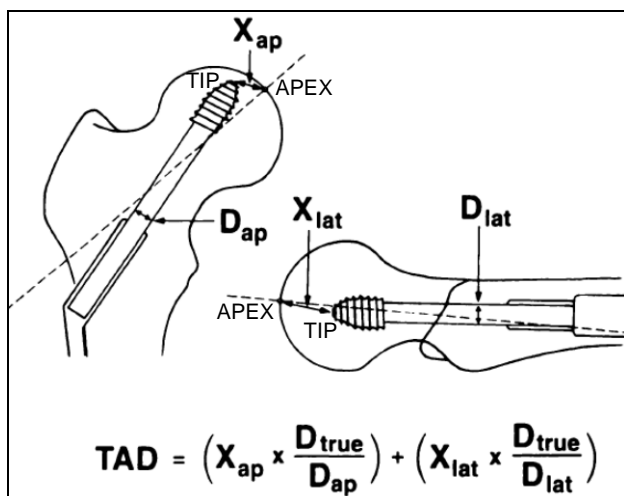


Figure 1: Technique for calculating the TAD. The D (diameter) values are used to adjust for radiographic magnification [3].

The TAD measure is obtained directly from two orthogonal projections, not from a 3D distance [3]. The methods for measuring TAD are ambiguous [1, 2], relying on precise radiographic landmark point definitions, the fitting of an ellipse to the femoral head, the angles at which the x-ray images are acquired, and the patient position. All of these factors contribute to calculations of TAD that are inconsistent and imprecise. The purpose of this work was to begin to develop a more reliable metric of wire navigation performance.

METHODS

Twelve first-year orthopaedic residents performed fluoroscopy-guided wire navigation on a hip bone/soft tissue surrogate (Figure 2). Their task was to insert a K-wire from the lateral cortex centrally through the neck to the apex of the femoral head.



Figure 2: A resident is shown performing the wire navigation task.

Each resident repeated the exercise three times. The position of the fluoroscopy unit was controlled to limit variability in the projection angles. The final AP and lateral fluoroscopic images were analyzed independently. To account for intra- and inter-observer variability, each evaluator measured the TAD twice (72 fluoro images, 288 measurements) using methods previously described [3] (Figure 3).

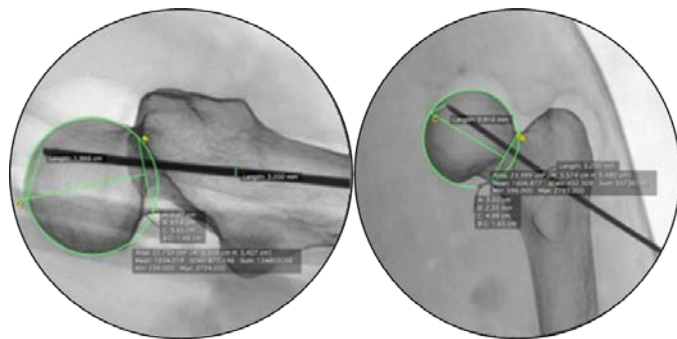


Figure 3: TAD measurements on the lateral (left) and AP (right) fluoroscopic images.

RESULTS AND DISCUSSION

The degree to which an ellipse of best fit was able to encompass the femoral head on the fluoro images depended on the anteversion of the femur. The size, shape, and location of the ellipses were subjectively assigned by the evaluator. The lateral image was more susceptible than the AP to uncertainty of how and where the ellipse should be placed, as a slight degree of rotation would skew the image. Depending on the angle of the femoral shaft, the point where the head and neck intersection occurred was more or less difficult to identify.

The inter-observer standard deviation in TAD measurement was found to be 0.89 mm, with values ranging from 0.21 to 3.1 mm. Similarly, the average intra-observer standard deviation was found to be 0.74 mm, with values ranging from 0.0 to 3.8 mm.

Baumgaertner et al. similarly analyzed their measurements of TAD from actual surgical cases. Their results showed an average inter-observer standard deviation of 1.7 mm, with measurements ranging from 0.3 to 5.1 mm. Their intra-observer standard deviation averaged 1.2 mm, with measurements ranging from 0.0 to 5.7 mm.

With current methods, a “non-ideal” lateral image can move the apex from the outermost point of the subchondral bone inward and vertically. This reasons that this way of establishing the apex does not accurately represent the actual location from various rotations and views (Figure 4). As residency programs consider moving towards a competency-based assessment protocol, measurements such as TAD will play a role in evaluating a resident’s surgical skill. As an assessment parameter the method, variability, and accuracy within a technique must be minimized.

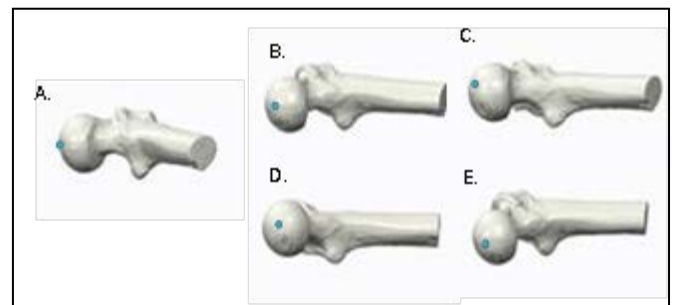


Figure 4: Image (A) represents an ideal lateral position; images B to E represent less ideally rotated views and corresponding apex location designated by a blue dot.

CONCLUSIONS

The variation in methods of calculating TAD, as well as the variability and inaccuracy in its measurement, calls for a standardized, consistent measurement technique. It is undesirable to have research teams referencing a TAD, when one group is using an alternate method and in turn may actually be calculating a different distance. For the TAD to remain a universal standard a single, an improved technique is needed.

REFERENCES

1. Herman et al. *Injury* **43**, 856-863, 2011.
2. Johnson et al. *Injury* **39**, 787-790, 2008.
3. Baumgaertner et al. *J Bone Joint Surg* **77**, 1058-64, 1995.

ACKNOWLEDGEMENTS

This work was partially supported by grants from the American Board of Orthopaedic Surgery and the Agency for Healthcare Research and Quality. The residents from the Mayo Clinic participated as a part of the Midwest Orthopaedic Surgical Skills (MOSS) Consortium.

TRACKING THE TRUNK SEGMENT: BACKPACK VS. ELASTIC STRAP

Nienke W. Willigenburg and Timothy E. Hewett

The Ohio State University, Sports Health and Performance Institute, Columbus, OH, USA
Mayo Clinic, Departments of Orthopaedics, Physiology & Biomedical Engineering and PM & R
email: nienkewilligenburg@gmail.com, web: <http://sportsmedicine.osu.edu>

INTRODUCTION

Impaired trunk control may be associated with low back pain and lower extremity injuries [1, 2]. Tracking movement of the trunk segment in a motion capture setting can be challenging, as placing markers directly on the skin is not feasible in certain populations. Therefore, several studies have used a small backpack with three integrated reflective markers, which can be worn over a T-shirt or tank top, to track 3D motion of the trunk during athletic tasks. Limitations of this method are that the backpack can move with respect to the trunk, especially when the arms and shoulders move, and that the backpack is not rigid, so the markers can move with respect to each other. To overcome these issues, we developed and tested an alternative marker setup. The present study compares 3D trunk angles, as measured during athletic tasks with these two different marker configurations.

METHODS

Eight subjects (6m, 2f) performed 3 repetitions of a drop vertical jump (DVJ), a well-established symmetric task, and a cross over drop (COD), which requires frontal plane displacement and a single leg landing (Figure 1). We analyzed the landing and flight phase of the DVJ, as well as the first 0.5 second of the COD landing.

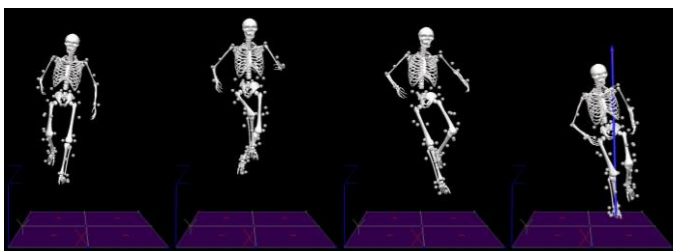


Figure 1. Cross over drop

The pelvis segment was tracked by markers on the left and right anterior superior iliac spines, iliac crests, and sacrum. The trunk segment was tracked by A) a backpack with 3 integrated markers, and B) an elastic strap surrounding the trunk just below the chest with a dorsal rigid marker cluster and a ventral marker on the xiphoid process (Figure 2).

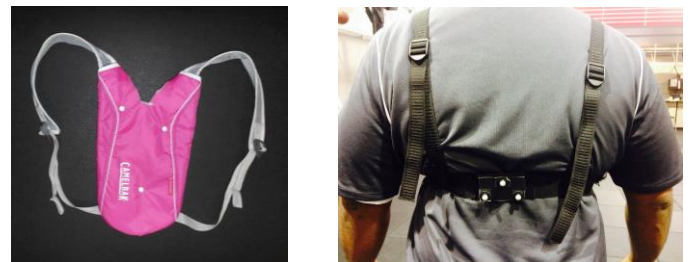


Figure 2. Marker configurations for tracking the trunk.

3D trunk angles were calculated with respect to the pelvis segment, and time series were averaged over 3 repetitions per subject. To compare time series between the different marker configurations, we calculated the coefficient of multiple correlation (CMC) [3] for each subject and plane of motion.

RESULTS AND DISCUSSION

When averaged over subjects, the backpack tended to overestimate trunk flexion during most of the landing phase, but trunk extension during the flight phase (Figure 3). This is likely related to arm movement, which can cause the backpack to move with respect to the trunk.

Additional differences between marker configurations were observed in the transverse plane during the COD landing (Figure 4). Specifically, the backpack consistently overestimated trunk rotation in this asymmetric athletic task.

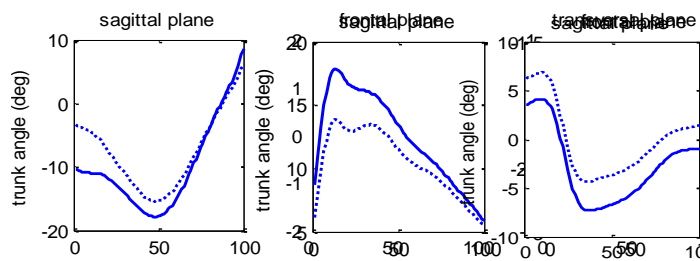


Figure 3. Sagittal plane trunk angle averaged over subjects for the backpack (solid) and elastic strap (dotted), in the DVJ landing (left) and flight phase (middle), and in COD landing (right).

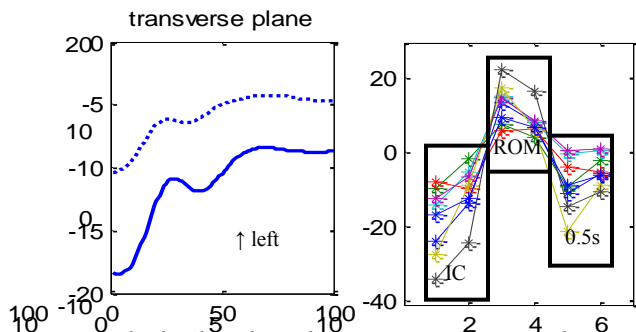


Fig4. The backpack tended to overestimate trunk rotation; this pattern was consistent between subjects.

We observed substantial variation between subjects in the two trunk angle time series. Individual subjects' CMCs in the sagittal plane ranged from 0.63 to 0.98 in the landing phase of the DVJ. In the flight phase, differences between methods were larger, with CMCs ranging from 0.39 to 0.96, or yielding imaginary results. Frontal and transverse plane excursions were small in this symmetric task, but differences between methods were substantial. In the asymmetric COD landing task, individual subjects' CMCs ranged from 0.52 to 0.99 for the sagittal and frontal plane trunk angles. Time series curves were less similar in the transverse plane, with imaginary CMCs for half of the subjects, while the remaining CMCs ranged from 0.46 to 0.88.

These findings indicate that different trunk marker configurations yield different results. The overestimation of trunk flexion during DVJ landing, extension during the DVJ flight phase, and rotation during the COD landing indicate that the backpack method may be more affected by arm movement. Additional individual differences between methods may depend on spinal curvature, as the backpack is typically located higher on the thoracic spine.

CONCLUSIONS

The backpack and elastic strap trunk marker configurations yield different trunk angle measures during athletic tasks. Some differences were consistent between tasks and subjects, but others were not. The elastic strap method may be more accurate, because it seemed less affected by arm movement, and it allows for an additional xiphoid marker. However, for longitudinal studies we recommend to adhere to the original choice of marker configuration in order to obtain reproducible measures over time.

REFERENCES

1. Willigenburg et al. *Hum Mov Sci* **32**, 228-39, 2013.
2. Zazulak et al. *Am J Sports Med* **35**, 1123-30, 2007
3. Kadaba et al. *J Orthop Res* **7**, 849-60, 1989.

ACKNOWLEDGEMENTS

The authors wish to acknowledge the entire Sports Health and Performance Institute's research team for collecting these data.

SPECIFICS OF A LOWER EXTREMITY BIOMECHANICAL MODEL THAT YIELDS RELIABLE KINEMATICS AND KINETICS DURING LANDING IN ATHLETES.

¹Nienke W. Willigenburg, ²Kevin R. Ford, ³Gregory D. Myer, and ^{1,4}Timothy E. Hewett

¹The Ohio State University, OSU Sports Medicine, Sports Health and Performance Institute, Columbus, OH, USA

²High Point University, School of Health Sciences, Department of Physical Therapy, High Point, NC, USA

³Cincinnati Children's Hospital Medical Center, Division of Sports Medicine, University of Cincinnati, Department of Pediatrics, Division of Sports Medicine, Cincinnati, OH, USA

⁴Departments of Physiology and Cell Biology, Orthopaedic Surgery, Family Medicine, and Biomedical Engineering
nienkewilligenburg@gmail.com, <http://sportsmedicine.osu.edu>

INTRODUCTION

Three-dimensional (3D) motion capture and biomechanical modeling are powerful tools to identify motor control behavior and injury risk deficits in athletes. In the past decennia, several linked-segment models have been developed and optimized for use in specific motor tasks or subject populations. Some standard models are well documented [1-3], but the specifics of tailored biomechanical models are sometimes not fully described in the literature. As biomechanical models continue to advance based on technological improvements and changes in software it is critical to detail the progression of modeling parameters. The present study describes the specifics of our model that has demonstrated reliability in recording dynamic athletic tasks for identification of injury risk and motor behavior in athletes [4].

METHODS

The lower extremity model was originally developed in Kintrak (Motion Analysis Corporation, Santa Rosa, CA, USA), and then transitioned to Visual3D (C-Motion Inc, Germantown, MD, USA). Key priorities in development and advancement of this model were 1) test-retest reliability of dynamic tasks for longitudinal cohort studies in athletes, and 2) consistency with previous model versions, to allow for comparisons with previous results.

The model employs a minimum of three retro-reflective tracking markers per segment, and its proximal and distal ends of each segment are defined by a combination of markers and/or virtual landmarks. Virtual landmarks are created relative to

marker positions from a static T-pose, with the joint coordinate systems aligned with the lab coordinate system [5]. Foot placement was standardized during the static trial while the subject was instructed to stand in anatomical position.

RESULTS AND DISCUSSION

The figures below present the pelvis, thigh, shank and foot segments with the locations of the markers and virtual landmarks that (directly or indirectly) define the proximal and distal ends of the segments.

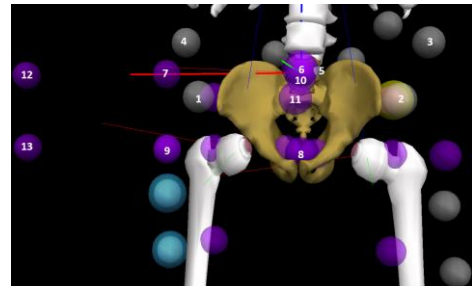


Figure 1. Pelvis markers on the 1) RASIS, 2) LASIS, 3) LiliacCrest, 4) RiliacCrest, and 5) Sacrum. Virtual landmarks are 6) PelvisJC, 7) PelvisLatProx, 8) MidHip, 9) PelvisLatDist, 10) MidHipZ, 11) MidASIS, 12) PelvisJCLabY, and 13) PelvisDistLabY.

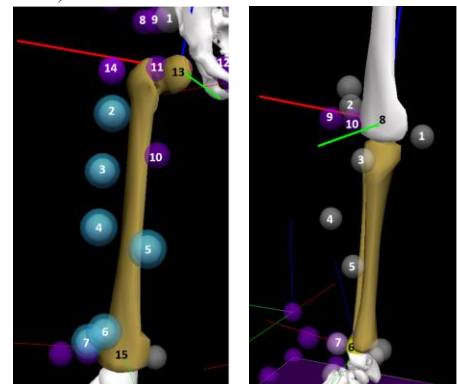


Figure 2. Thigh markers on the 1) ASIS, 2) GrTroch, 3) ThighPost, 4) ThighMid, 5) ThighAnt, 6) ThighDist, and 7) EpicLat. Virtual landmarks are 8) ASISLabX, 9) HipJC_ML, 10) HipJCTmpZ, 11) HipJCAx, 12) HipJCTmpY, 13) HipJC, 14) HipJCLat, and 15) KneeJC. Shank markers on the 1) EpicMed, 2) EpicLat, 3) TibTub, 4) TibLat, and 5) TibDist. Virtual landmarks are 6) AnkleJC, 7) AnkleLatProx, 8) KneeJC, 9) KneeTmpY, and 10) KneeLatProx.

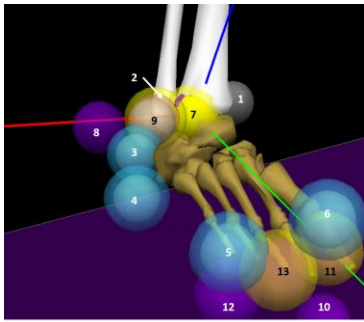


Figure 3. Foot markers on the 1) MalMed, 2) MalLat, 3) Heel, 4) PostFoot, and 5) Toe, and virtual landmarks 7) AnkleJC, 8) AnkleTmpY, 9) AnkleLatProx, 10) ToeFloor, 11) DistFootJC, 12) DistFootTmpY, and 13) FootLatProx.

To estimate the location of the hip joint center, this model uses Bell's regression equations for the medio-lateral and superior-inferior directions [6], and the marker on the greater trochanter for the anterior-posterior direction [7]. More recently we have utilized a motion trial to calculate the functional hip joint center that could replace estimations based on pelvic width. The mass and inertial properties for each segment are based on De Leva's sex-specific parameters [8]. The subject's height and body mass are included in each model.

The lack of a 'gold standard' for calculation of joint angles and moments during athletic task performance may limit adequate validation of any biomechanical model. However, both within and between-session reliability of most kinematic and

kinetic variables obtained with this model were good to excellent in athletes during the landing phase of a drop vertical jump [4]. Moreover, the present model allowed for identification of knee abduction moment as biomechanical risk factor for anterior cruciate ligament injuries in a large-scale prospective study [9].

CONCLUSIONS

The specifics of a biomechanical model used in multiple longitudinal cohort studies assessed kinematics and kinetics during athletic tasks were detailed. Sharing the details of model parameters across multiple laboratories will help to interpret differences between previously reported findings, and facilitate future large scale multi-center collaborative studies [10].

REFERENCES

1. Wu G. et al. *J Biomech* **35**, 543-8, 2002.
2. Wu G. et al. *J Biomech* **38**, 981-92, 2005.
3. C-motion.com/v3dwiki/index.php/Tutorials/BuildingModels
4. Ford et al. *Am J Sports Med* **39**, 2021-8, 2007.
5. Ford et al. *Med Sci Sports & Exerc* **42**, 1923-31, 2010.
6. Bell et al. *Hum Mov Sci* **8**, 3-16, 1989.
7. Kirkwood et al. *Clin Biomech* **14**, 227-35, 1999.
8. De Leva et al. *J Biomech*, **29**:1223-30, 1996
9. Hewett et al. *Am J Sports Med* **33**, 492-501, 2005.
10. Myer et al. *Int J Sports Phys Ther* **9**, 289-301, 2014.

Table 1. Segment definition in Visual3D for the pelvis, thigh, shank and foot.

	Lateral	Joint center	Radius
PELVIS			
Proximal	PelvisLatProx	PelvisJC	Distance between Pelvis_Lat_Prox and Pelvis_JC
Distal	PelvisLatDist	MidHip	Distance between Pelvis_Lat_Dist and Mid_Hip
THIGH			
Proximal	HipJCLat	HipJC	Distance between Hip_JC_Lat and Hip_JC
Distal		KneeJC	Distance between Knee_JC and Knee_Lat_Prox
SHANK			
Proximal	KneeLatProx	KneeJC	Distance between Knee_Lat_Prox and Knee_JC
Distal		AnkleJC	Distance between Ankle_JC and Ankle_Lat_Prox
FOOT			
Proximal	AnkleLatProx	AnkleJC	Distance between Ankle_Lat_Prox and Ankle_JC
Distal	FootLatProx	DistalFootJC	Distance between Foot_Lat_Prox and Distal_Foot_JC

PREDICTIVE SIMULATION OF ROWING EXERCISE USING GPOPS II

Milad Zarei and Antonie J. van den Bogert

Department of Mechanical Engineering, Cleveland State University, Cleveland, OH, USA

Email: m.zarei@vikes.csuohio.edu, Web: <http://hmc.csuohio.edu/>

INTRODUCTION

An exercise machine presents a specific geometrical and mechanical environment to the user. The design parameters affect how the user performs the exercise and which forces are generated in musculoskeletal tissues. If we are able to predict these effects during the design process, exercise outcomes can be improved. Current approaches aim at presenting simple conditions such as constant load or constant speed, or replicate existing sports-related exercise conditions such as rowing, weightlifting and bicycling. There is, however, much more design freedom which remained unexplored.

To predict human execution and optimize machine parameters, human musculoskeletal dynamics and adaptive neuromuscular control should be taken to account. Here we will use a computational method based on musculoskeletal modeling and optimal control to predict how mechanical parameters alter human performance [1]. The specific purpose of this research is to investigate the effects of resistance parameters on movements and forces generated by the arm during periodic arm flexion exercise.

METHODS

System dynamics

We will consider a one-degree of freedom arm flexion exercise, where resistance is similar to that found in a rowing machine. The rowing machine model has two phases in which there are different dynamics. In the first phase (power phase), resistance is provided by a spring (k_1), a damper (b) and a mass, which is the total effective mass of the user (m_h) and the rowing machine (m_r) (Fig 1). In the second (recovery) phase, the resistance mechanism is disengaged, except for a weak spring (k_2) which winds up the cable (Fig 2). The user's action is represented by a force (F_{arm}) which is generated by the arm.

The rowing machine inertia was assumed to be 40 kg and the human inertia was assumed to be 10 kg. Also k_1 , k_2 and b were set to 120 N/m, 10 N/m and 20 Ns/m, respectively.

A Hill-based muscle model (Fig 3) was used to model the dynamics of muscle contraction in which the contractile element (CE) represents the muscle fibers, the series elastic element represents the tendon that transfers force from muscle fibers to the skeleton [2]. A small amount of parallel damping was added to the contractile element for numerical reasons. The connection between muscle and the machine was a simple lever where d is moment arm at elbow is and L is the total length of forearm and hand.

Muscle properties and other model parameters were obtained from both heads of the biceps brachii muscle in an existing arm model, and combined into one equivalent muscle [3].

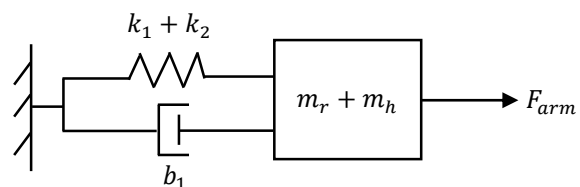


Figure 1: Dynamic model for the power phase.

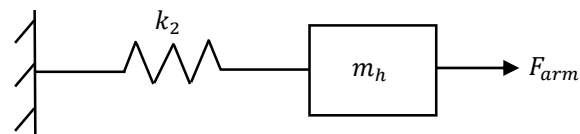


Figure 2: Dynamic model for the recovery phase.

Simulation

The predictive simulation was formulated as an optimal control problem, to find the force profile that produces a periodic movement with an amplitude of 0.2 m with minimal effort. Effort was defined as the integral of the squared neural control. Duration of the

entire movement fixed at 4 seconds; however the duration of each of two phases (power phase and recovery phase) was predicted.

GPOPS II [4] (MATLAB optimal control software) was used to solve the two-phase optimal control problem.

Preliminary results will be presented with a simplified static muscle model in which there was no series elastic element and no length or velocity dependence in muscle force generation. In this model, the muscle force was directly controlled by the neural control signal u .

$$F_{muscle} = uF_{max} \quad (1)$$

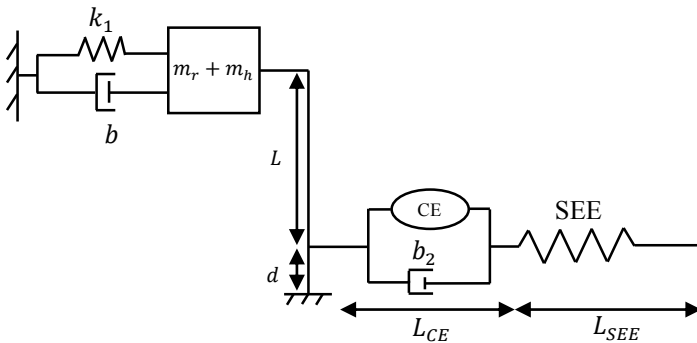


Figure 3: Dynamic model for the muscle model in power phase .

RESULTS AND DISCUSSION

GPOPS II required about 10 seconds of computation time to solve the problem. The optimal phase 1 occurred in 1.84 s and phase 2 had a duration of 2.16 s (Fig 3). As expected, the model starts from the initial position and moves towards the final position with positive velocity in first phase. In the second phase, the model goes back to the initial position with a negative velocity.

The optimal control profile for the phase one shows that the muscle applies about 70% of its maximal force during the power phase. During the return phase, the mass-spring dynamics rewinds the system and muscle controls the system with a small force to avoid overshooting the starting point.

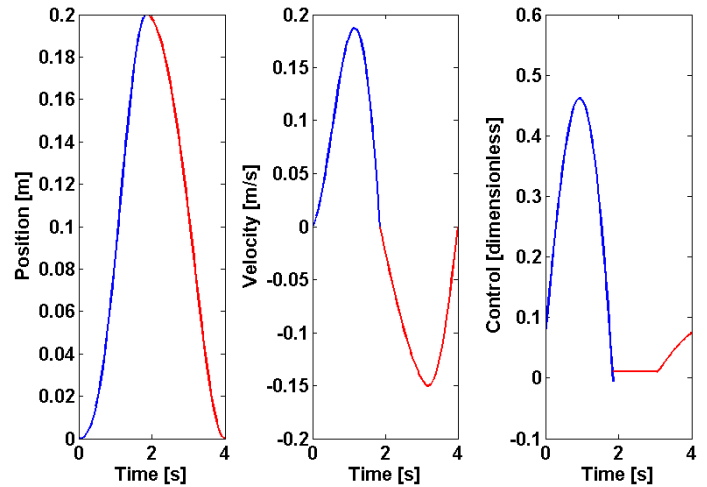


Figure 4: Predicted movement, velocity and control.

CONCLUSIONS AND FUTURE WORK

GPOPS II was able to solve the optimal control problem quickly and accurately. The predicted motions and forces seem realistic. A non-linear dynamic muscle model will be added to the model to examine how it affects the results.

REFERENCES

1. van den Bogert, AJ, et al. *Proc Inst Mech Eng, Part P: J Sports Eng Technol* 226, 123-133, 2012.
2. van den Bogert, AJ et al. *Procedia IUTAM* 2, 297-316, 2011.
3. Chadwick, EK, et al. *IEEE Trans Biomed Eng* 61, 1947-1956, 2014.
4. Patterson, MA, et al. A general-purpose MATLAB software for solving multi-phase optimal control problems, University of Florida (<http://www.gpops2.com>), 2014.

ISOMETRIC AND DYNAMIC ACTIVATION CHARACTERISTICS OF THE HUMAN LATISSIMUS DORSI MUSCLE

¹ Shawn M. Beaudette, ¹ Rudy Unni and ¹ Stephen H. M. Brown

¹ University of Guelph, Guelph ON, CAN
email: sbeaudet@uoguelph.ca

INTRODUCTION

The latissimus dorsi (LD) muscle has a unique design with an origin spanning the thoracic and lumbar spine and a common insertion point on the anterior humerus. Due to the LD muscle having a large surface area, broad spine attachment, obliquities in fiber direction and variability in neurovascular supply, previous researchers have suggested possible compartmentalization of its primary functions [1]. Furthermore, from an anatomical standpoint, functional differences between the thoracic and lumbar portion of the LD have been identified in cadaveric specimens; these differences include variation in physiological cross-sectional area and fascicle length [2]. The purpose of the current study was to identify the isometric and dynamic activation characteristics of the LD muscle. Based on previous works it was expected that the thoracic and lumbar components of the muscle would show different temporal and spatial electrical activation characteristics during both isometric and dynamic tasks.

METHODS

Eight male (mean age 23 ± 1.8 years; height 1.8 ± 0.04 m; and mass 76.9 ± 10.6 kg) and eight female (mean age 22 ± 1.2 years; height 1.7 ± 0.09 m; and mass 61.6 ± 8.6 kg), recreationally active, right hand dominant individuals participated in this study. The LD muscle was characterized about four separate compartments with reference to their spinal origin (two thoracic and two lumbar compartments, see Fig. 1). Surface EMG (sEMG) was obtained from each of these T10, T12, L1 and L4 compartments.

LD activation was obtained during both maximal isometric, as well as submaximal dynamic tasks.

Isometric activation tasks included a) humeral adduction (ADD), b) humeral adduction and internal rotation (ADD + INT), c) chest-supported row (ROW) and d) humeral extension (EXT) maximal voluntary isometric contractions (MVICs). Dynamic activation tasks included sagittal lifting/lowering movements spanning the a) floor to knee (FK), b) knee to hip (KH) or c) hip to shoulder (HS). Male and female participants lifted an absolute load of 12 kg and 8 kg, respectively.

sEMG data were linear enveloped by rectifying and low-pass filtering (2nd order Butterworth, 2.5 Hz cut-off). MVIC techniques were compared to determine which technique elicited the true participant MVIC (tMVIC). All other isometric and dynamic sEMG were normalized to tMVIC. LD compartments were compared during both isometric and dynamic activations for differences in normalized, linear-enveloped sEMG magnitude, and relative activation timing (cross-correlation; r_{xy}). Differences in sEMG magnitudes for isometric and dynamic activations were assessed using separate two, and three way ANOVAs respectively ($\alpha = 0.05$). Post hoc pairwise comparisons were made using a Tukey adjustment within each ANOVA.

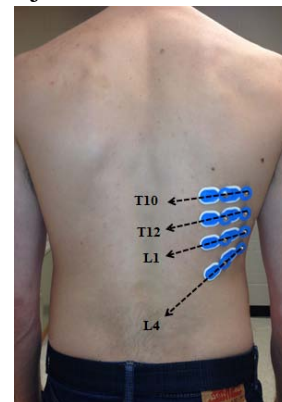


Figure 1: LD muscle compartments showing T10, T12, L1 and L4 sEMG electrode sites from superior to inferior.

RESULTS AND DISCUSSION

For the MVIC tasks there was no significant difference in sEMG signal magnitude between LD compartments ($p = 0.6116$). Significant differences between MVICs ($p < 0.0001$) showed that the ROW and EXT techniques elicited larger activations than the ADD or ADD + INT techniques ($p < 0.0001$). Relative sEMG activation magnitudes for each MVIC (across all LD compartments) can be seen in Fig 2A. No temporal activation differences were observed for any LD compartment throughout any of the MVIC tasks ($r_{xy} = 0.9607$).

Peak dynamic sEMG magnitudes were observed to differ significantly with main effects of dynamic lift type (FK, KH, HS) ($p = 0.0470$) and LD compartment ($p = 0.0002$). Specifically, larger peak sEMG activation was seen in the T10 ($p = 0.0002$) and L4 ($p = 0.0076$) compartments relative to the T12 compartment. Mean dynamic sEMG magnitudes were observed to differ significantly with main effects of lifting versus lowering ($p < 0.0001$) and LD compartment ($p = 0.0002$). Larger mean sEMG activation was seen in the T10 ($p = 0.0001$) and L4 ($p = 0.0146$) compartments relative to the T12 compartment. Relative peak and mean sEMG activation magnitudes for each LD compartment (across all lifting types) can be seen in Fig 2B. No temporal activation differences were observed for any LD compartment throughout any of the dynamic tasks ($r_{xy} = 0.9114$).

CONCLUSIONS

For MVIC-style activations of the LD muscle, compartmentalization of function is not apparent. For all MVIC types LD compartment activation was uniform in sEMG magnitude and timing. During dynamic activations differences in activation magnitude may suggest some compartmentalization of the LD; however activation timing was always uniform. Additionally, from this work it was determined that the optimal sEMG normalization-electrode site combination was the ROW task at T12. Similar LD EMG normalization suggestions have been made previously [3].

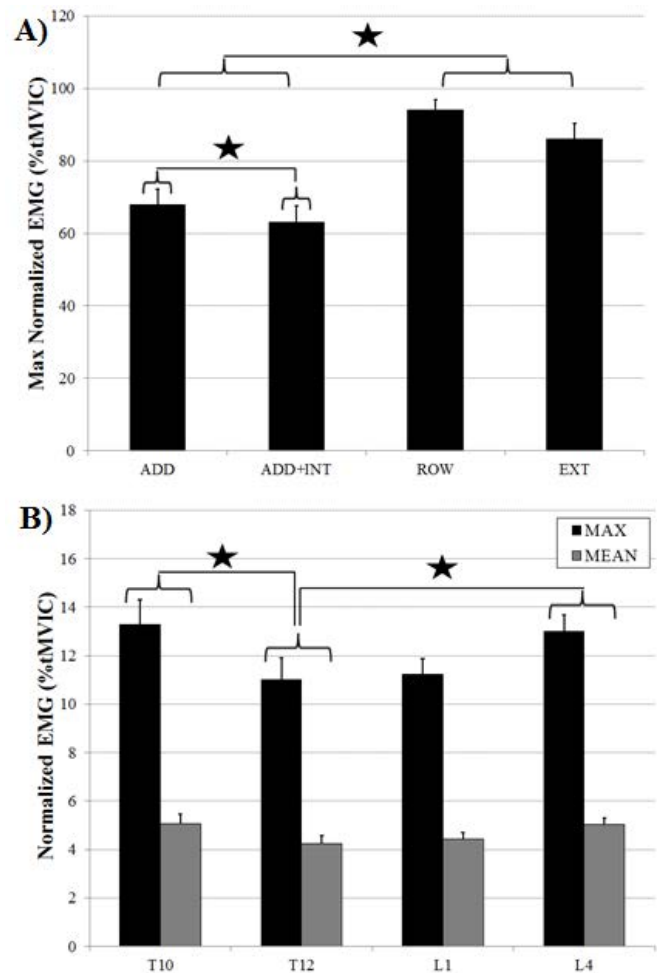


Figure 2: A) Normalized LD sEMG activation magnitude between MVIC types, pooled across all compartments. B) Peak and mean normalized LD sEMG activation magnitude between LD compartments, pooled across dynamic movement. Stars represent significance at $p < 0.05$.

REFERENCES

1. Brown JMM, et al. *J Electromyogr Kinesiol* **17**, 57-73, 2007.
2. Gerling ME and Brown SHM. *J Anat* **223**, 112-22, 2013.
3. Park S and Yoo W. *J Electromyogr Kinesiol* **23**, 1350-5, 2013.

RELATIONSHIPS BETWEEN CLINICAL AND BIOMECHANICAL MEASURES OF CORE STABILITY

¹Courtney M. Butowicz, ²Brian Noehren, ¹D. David Ebaugh, ¹Sheri P. Silfies

¹Drexel University, Philadelphia, PA, USA

²University of Kentucky, Lexington, KY, USA

Email: cmb524@drexel.edu

INTRODUCTION

Emerging evidence suggests that poor core stability is a risk factor for low back and lower extremity injuries in athletes [1-3]. Core stability is the ability to control trunk position and motion for the purpose of optimal production, transfer, and control of forces to and from the terminal segments during functional activities [4]. Optimal neuromuscular control and muscle capacity (strength and endurance) are critical components of core stability. Frequently used clinical tests to assess core stability include the unilateral hip bridge, trunk extensor endurance, and Y-Balance tests [5,6]. Recently the trunk control test was developed to clinically assess core stability in a manner that closely resembles a biomechanical method of assessing isolated core stability [7]. Although these and other clinical tests of core stability exist, how well they assess core stability when compared to biomechanical measures of isolated core stability has not been thoroughly evaluated. Furthermore, relationships amongst clinical tests of core stability are not well understood. The purposes of this study were to determine relationships between 1) clinical measures of core stability, and 2) clinical and biomechanical measures of core stability.

METHODS

Twenty healthy active individuals (11 males; age 23.5 \pm 1.7 years; height 173.0 \pm 8.3 cm; weight 71.9 \pm 15.5 kg) completed the unilateral hip bridge endurance (UHBE (s)), Y-Balance test (YBT (reach as % leg length)), trunk extensor endurance tests (TEE (s)), and trunk control test (TCT (errors)). The TCT is performed with the subject sitting on a Swiss ball, one foot is lifted, eyes closed (EC), and attempting to balance for 30s (Fig 1A). The number of errors (plant foot moving, uncrossing the arms, elevated foot touches ground) are recorded. Recent

work suggests the ability of the TCT to detect possible trunk control impairments in an ACL rehabilitation population [7]. Three trials/side of TCT were observed by a trained clinician and scored based on errors [7]. The biomechanical test of isolated core stability [3] was developed to reduce contribution from the lower extremities, by using an unstable chair situated on a force plate (Fig 1B). Two 60s balance trials, where subject was asked to move as little as possible with their eyes closed (EC), were used to assess core stability. Center of pressure (COP) data was quantified using the 95% confidence ellipse area (CEA) (CEA, mm²) and average displacement of the COP per second (MVEL) (mm/s). For the biomechanical measures of core stability, higher values represent poorer core stability. UHBE and TEE tests were completed 2 times with ability to maintain control of position recorded in seconds. Y-balance was completed 3 times in each direction. Averaged trials for each test were used for analysis. Spearman's rho and Pearson's correlations were used to determine the association between measures. Correlations were interpreted according to Cohen [8].

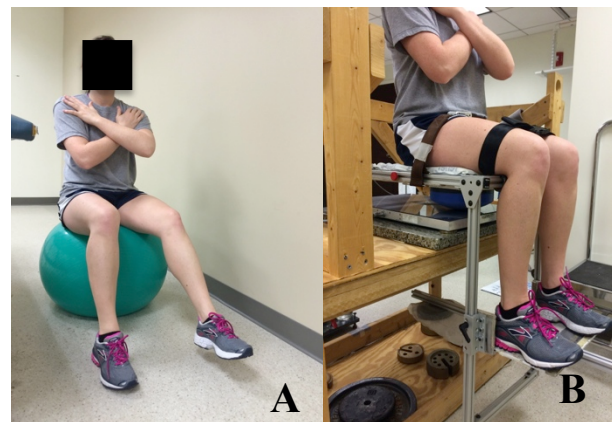


Figure 1. A) Clinical trunk control test (TCT). B) Biomechanical measure of isolated core stability.

RESULTS AND DISCUSSION

Mean (SD) values for clinical measures: UHBE (s) = 23.01 (17.83), TEE (s) = 78.58 (24.15), TCT (errors) = 5.81 (3.94), YBT ANT (%LL) = 81.66 (6.25), YBT PM (%LL) = 96.10 (8.16), YBT PL (%LL) = 90.29 (7.73). Means for YBT and TEE were similar to those previously reported [6,9]. TCT means were slightly higher than previously reported, however that study recruited competitive athletes [7]. There was little to no correlation between TCT and biomechanical measures of core stability ($\rho = 0.2 - 0.22$), thus it appears they are testing different aspects or regions of core stability. Biomechanical measures of isolated core stability demonstrated a moderate to large correlation to with the core endurance tests and the anterior YBT (Table 1). Our data suggest that clinical core endurance of trunk and hip muscles captures 15-33% of the variance in our biomechanical measure of isolated core stability. The TCT was moderately correlated to dynamic unilateral standing balance, but not core muscle endurance (Table 2).

CONCLUSIONS

These findings support use of the UHBE and TEE as clinical measures of core stability; however, further work is needed to develop or determine if other clinical tests can assess the neuromuscular control aspect of core stability. While the TCT was not correlated with biomechanical or core stability

measures emphasizing core muscle capacity, the TCT demonstrated a significant relationship to dynamic unilateral standing balance as assessed by the YBT. Analysis of the location of the errors recorded in the TCT revealed that approximately 89% of the errors were related to lower extremity movements while 11% were related to the trunk or upper extremity. This may suggest that the TCT captures more lower extremity control than trunk control or core stability. However, further research is needed to evaluate this relationship.

REFERENCES

1. Cholewicki J, et al. *Spine* **30**, 2614-1620, 2005.
2. Ireland ML, et al. *J Orthop Sports Phys Ther* **33**, 671-676, 2003.
3. Cholewicki J, et al. *J Biomech* **33**, 1733-1737, 2000.
4. Kibler WB, et al. *Sports Med* **36**, 189-198, 2006.
5. Okubo Y, et al. *J Orthop Sports Phys Ther* **40**, 743-750, 2010.
6. Pilsky PJ, et al. *J Orthop Sports Phys Ther* **36**, 911-919, 2006.
7. Noehren B, et al. *J Orthop Res* **32**, 1305-1310, 2014.
8. Cohen, J. *Statistical power analysis for the behavioral sciences*, Lawrence Erlbaum, 1988.
9. McGill SM, et al. *Arch Phys Med Rehabil* **80**, 941-944, 1999.

Table 1. Relationship between clinical and biomechanical measures of core stability

	<u>L UHBE</u>	<u>R UHBE</u>	<u>TEE</u>	<u>Y ANT</u>
EC CEA	-0.44	-0.39	-0.45	-0.45
EC MVEL	-0.6	-0.39	-0.47	-0.45

Table 2. Relationship between novel and common clinical measures of core stability

	<u>L UHBE</u>	<u>R UHBE</u>	<u>TEE</u>	<u>YBT ANT</u>	<u>YBT PM</u>	<u>YBT PL</u>
L TCT	-0.14	-0.25	-0.18	-0.11	-0.42	-0.36*
R TCT	0.13	-0.15	-0.24	-0.08	-0.39	-0.35*

Pearson's or Spearman's reported as appropriate.

Shaded Bold Italics indicates significance at $p \leq 0.05$

*Indicates significant trend at $p \leq 0.10$.

THE EFFECT OF STRUCTURED RHYTHMIC AUDITORY STIMULI ON THE PERFORMANCE OF A REPETITIVE HAMMERING TASK

¹Megan Catlett, ³Peter C. Raffalt, ¹Diderik Jan Eikema, ^{1,2}Nicholas Stergiou, and ¹Steven J. Harrison

¹University of Nebraska at Omaha, Omaha, NE

²University of Nebraska Medical Center, Omaha, NE

³University of Copenhagen, Denmark

email: mcattlett@unomaha.edu, <http://www.unomaha.edu/college-of-education/cobre/index.php>

INTRODUCTION

Rhythmic stimuli such as auditory metronomes have been used therapeutically to improve the walking patterns of individuals that have been affected by Parkinson's Disease [1]. The walking patterns of older adults and individuals affected by motor pathologies are known to differ from young healthy adults in terms of the variability structure of their stride-to-stride intervals [2]. In general, fractally structured movement variability has been found to be associated with healthy motor behavior [2]. Specifically, it has been shown that optimal healthy movement patterns are most closely associated with a variability structure containing pink noise structure. Pink (fractally structured) noise differs from white (random) noise in that persistent trends (i.e. long range correlations) are observed in the time series (Fig. 1).

Recent research has explored the possibility that the variability structure of human movements could be manipulated with structured auditory stimuli. This research has investigated young healthy adults listening to structured auditory stimuli while walking [3, 4]. In this research, stimuli were based upon a simple fixed period metronome with pitch changes [3] that were embedded in the tune Für Elise [4]. In the case of structured stimuli either random white noise or structured pink noise was added to the stimulus (Fig. 1). These stimuli produced white and pink variability structures in the movements studied.

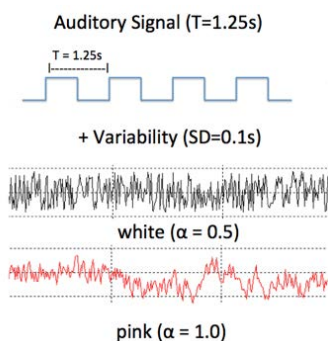


Figure 1: Creating fractal auditory stimuli

Following this previous research we hypothesized that we would also be able to manipulate the movement variability of upper extremity movement patterns, such as hammering, that neurologically are controlled differently, using structured auditory stimuli. We hypothesized that coordinated hammering movements performed in time to a metronome would show a variability structure that reflects the variability structure of the auditory stimuli used.

METHODS

Eleven healthy young adults (age 21.2 ± 3.7) participated in the study. Each participant was asked to strike a force plate with a hammer in



Figure 2: Experiment setup

synchronization with an auditory stimulus that was delivered via headphones (Fig. 2). There were four conditions presented in a randomized fashion. The conditions included a no metronome (control) condition, a metronome with no variability (regular metronome) condition, a metronome with unstructured variability

(white noise) condition, and a metronome with fractal variability (pink noise) condition. Each condition lasted 3 minutes during which participants performed continuous repetitions of right-hand hammering movements (with the start of the motion beginning from head height and ending with the hammer contacting a force plate. Each participant was provided with the option of having received a

1-minute break between trials. Participants' movements during the experiment were recorded with an NDI 3D Investigator system. Participants performed two tasks per condition. They were asked to either hammer anywhere on the force plate for 4 of the trials or to strike a dot in the center of the force plate for the other 4 trials. Detrended Fluctuation Analysis (DFA) was used to measure the fractal scaling (α) of the hammering movements of participants. A 4X2 (condition by task) repeated measures ANOVA was performed on the results.

RESULTS AND DISCUSSION

Overall effects of both auditory stimulus ($F(3,10) = 14.52, p < 0.001$) and task ($F(1,10) = 5.33, p < 0.05$) were observed. No interaction of the effects of task and auditory stimulus was observed ($F(3,30) = 2.25, p = 0.10$). Post-hoc tests with corrections for multiple comparisons were performed. For the **non-aiming task** α was higher for the no-metronome (free hammering) condition compared to the other conditions (p 's < 0.05), and the pink noise condition was found to differ from the regular metronome condition (Fig. 3). For the **aiming task** α was higher for the no-metronome condition compared to the regular and white noise conditions, and the pink noise condition was found to differ from the regular metronome condition (Fig. 3). A difference in α between tasks (aiming vs. non-aiming) was observed for the no-metronome condition (Fig. 3).

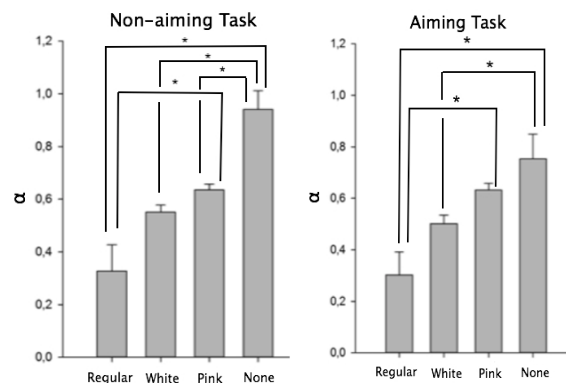


Figure 3: Analysis for the inter strike time variability for each of the four stimulus conditions for both aiming and non-aiming tasks. * indicates significant difference from the non-stimulus condition within each task.

Consistent with previous work in this research area, [3] we found that the variability structure of human

movement could be manipulated through the use of auditory stimuli. While the different auditory stimuli did affect the variability structure of the hammering behavior investigated, the results were not as clean as the results of similar previous studies [3]. Possible reasons for this include methodological differences between this study and previous research. For example in our research the number of hammer strikes performed by each participant was limited (i.e. 3 minutes of hammering as opposed to 15 minutes of tapping). This difference will impact the precision of the Detrended Fluctuation Analysis performed. Given this possibility we plan to run a follow up study with longer trials. Alternatively the nature of the hammering task both from a mechanical and a neuro control perspective may impact the efficacy of auditory stimuli to manipulate the variability structure of human movement.

CONCLUSIONS

This study was a variation of studies that have been recently been performed in our lab. It aimed to extend research findings from lower extremity actions like walking to upper extremity coordinated actions like hammering. It is presently unclear to what degree structured auditory stimuli can be used to manipulate the variability structure of complex motions such as that represented by hammering.

REFERENCES

1. Rochester L, et al. *Mov Disord* **24**, 839-845, 2009
2. Stergiou N, & Decker LM. *Hum Mov Sci* **30**, 869-888, 2011
3. Kaipust JP, et al. *Ann of Biomed Eng* **41**, 1595-1603, 2013
4. Hunt N, et al. *Sci Rep* **4**, 5879 (2014).

ACKNOWLEDGEMENTS

This work was supported by the Center for Research in Human Movement Variability of the University of Nebraska Omaha, NIH (P20GM109090, R01AG034995, and R01GM105045), and a FUSE grant from the University of Nebraska at Omaha.

VISUALIZING THE STRUCTURE OF HIGH DIMENSIONAL FEASIBLE ACTIVATION SETS FOR STATIC FORCE PRODUCTION

¹ Brian A. Cohn, ³ Hordur F. Ingvason, ^{1,2} Francisco J. Valero-Cuevas

¹ Department of Biomedical Engineering, ² Division of Biokinesiology and Physical Therapy University of Southern California, Los Angeles, CA, USA.

³ Swiss Federal Institute of Technology-Zurich, Zurich Switzerland
email: brianaco@usc.edu, web: <http://bbdl.usc.edu>

INTRODUCTION

We present a novel ‘vectormap’ transformation to visualize the features of feasible force and feasible activation sets. Visualizing the polyhedra and high-dimensional polytopes corresponding to these feasible sets, respectively, is challenging. Prior work [1] used their bounding boxes, which overestimate their volume, and oversimplify their shape. Understanding the structure of these feasible sets is critical to inform the central debates in motor control such as muscle redundancy, synergies and motor learning.

METHODS

The ‘vectormap’ is a radial projection of these polytopes onto the surface of their enclosing ball, where the resulting color-mapped sphere represents the size of the polytope in that direction (Fig. 1). As an example, we present the feasible force set of a feline hind limb, and its associated 31D feasible activation set. The parameters from the musculoskeletal model were shared with us by [2].

Extending Fig. 1 to higher dimensions, a similar idea applies. A vectormap sphere can display a muscle’s activation solution across all maximal forces, as shown on the right in Fig. 2. The production of a given sub-maximal force magnitude in a particular direction can be achieved by multiple coordination patterns [4,5]. Therefore, two vectormap spheres can be created for each muscle to provide a color map of the minimal and maximal activation for endpoint forces in all possible 3D directions.

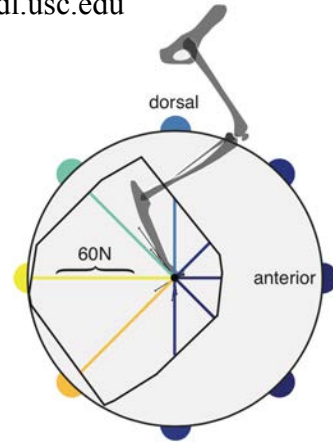


Figure 1: 2D description of vectormap for the feasible force set of feline hind limb in the sagittal plane. The polygonal feasible force set represents the maximal static force in each radial direction. That maximal force value is encoded as the color of the surface of the enclosing circle in that same direction. This same approach is extended to higher dimensions.

RESULTS AND DISCUSSION

Figure 1 shows a 2D slice of a vectormap for the feasible force set, and Figure 2 shows the activation at different levels of force magnitude for *vastus lateralis* and *medial gastrocnemius* as sample muscles. http://bbdl.usc.edu/vector_mapping/ shows the vectormaps of feasible activation for all 31 muscles. The left side of Fig. 2 shows those two vectormap spheres for different levels of force output, revealing how redundancy of activation is lost for each muscle as we march towards the maximal feasible force. These plots provide a detailed view of the structure of the 31D feasible activation set, one muscle at a time. For example, note that the lower and upper bounds naturally converge for maximal output, but they converge at different rates across muscles (vectormap progressions for all 31 muscles are not illustrated here) and directions of force output.

Interestingly, we find that the upper and lower bounds are more sensitive to than expected, with the bounds changing dramatically between vectors less than a degree apart in direction. We find that activation vectormaps can show strong discontinuities depending on the direction of output force, even at low magnitudes. Common tasks like locomotion require changes in force direction, thus muscle redundancy, synergies, and motor learning must be considered from a spatiotemporal perspective [3]. The vectormap approach allows us to pose and test musculoskeletal hypotheses for generalized force outputs, even for high-dimensional musculoskeletal systems.

REFERENCES

1. Kutch, Jason J., and Francisco J. Valero-Cuevas. "Muscle redundancy does not imply robustness to muscle dysfunction." *Journal of biomechanics* 44.7 (2011): 1264-1270.
2. McKay, J. Lucas, and Lena H. Ting. "Functional muscle synergies constrain force production

during postural tasks." *Journal of biomechanics* 41.2 (2008): 299-306.

3. Rácz, Kornelius, and Francisco J. Valero-Cuevas. "Spatio-temporal analysis reveals active control of both task-relevant and task-irrelevant variables." *Frontiers in computational neuroscience* 7 (2013).
4. Sohn, M. Hongchul, J. Lucas McKay, and Lena H. Ting. "Defining feasible bounds on muscle activation in a redundant biomechanical task: practical implications of redundancy." *Journal of biomechanics* 46.7 (2013): 1363-1368.
5. Ting, Lena H., and Jane M. Macpherson. "A limited set of muscle synergies for force control during a postural task." *Journal of neurophysiology* 93.1 (2005): 609-613.

ACKNOWLEDGEMENTS

Research supported by NIAMS of the National Institutes of Health under award numbers R01AR050520 and R01AR052345 grants to FVC. We thank Lena Ting for generously sharing her cat hindlimb moment arm data with us.

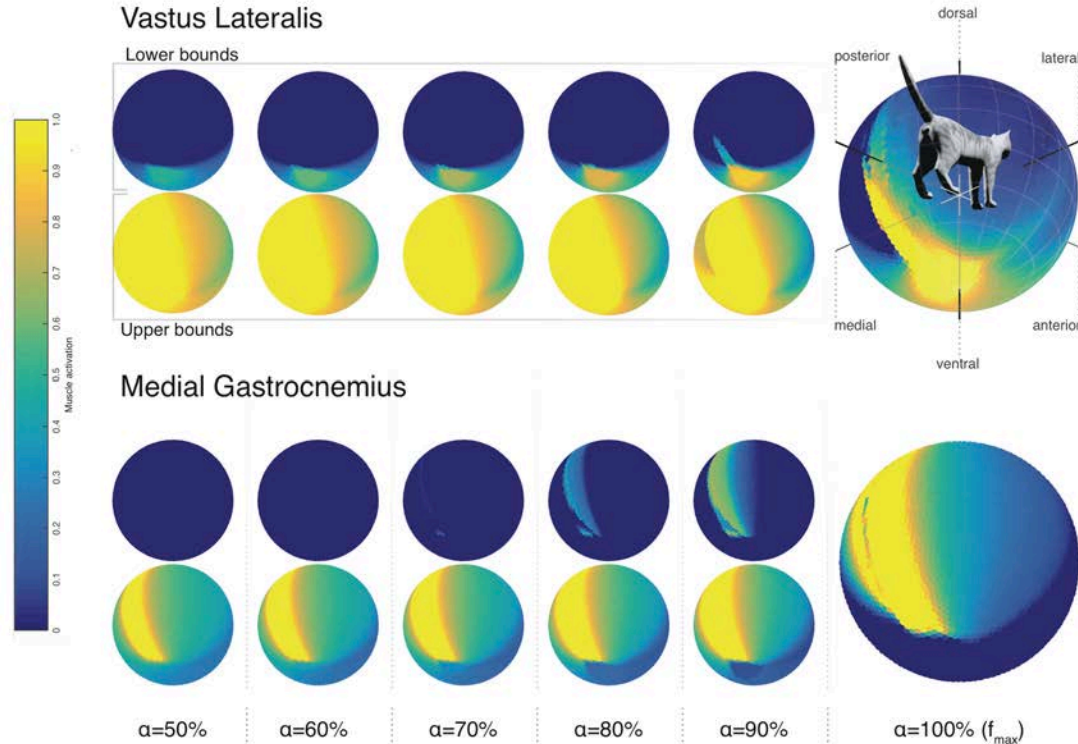


Figure 2: Vectormap visualization of one cat's feasible activation space for *vastus lateralis* and *medial gastrocnemius*. Activation lower (top) and upper bounds (bottom) are shown for 50%, 60%, 70%, 80%, 90% and 100% of maximal force (from left to right). Vectormap visualizations exist for the other 29 muscles in the same format. A muscle activation of 1.0 is 100% MIC.

LUMBAR ANGLE AND MUSCLE ACTIVATION TIME SERIES ARE STRONGLY RELATED IN INDIVIDUALS ASYMPTOMATIC FOR LOW BACK PAIN

¹ Brian C Nairn, ² Alison Schinkel-Ivy and ¹ Janessa DM Drake

¹ York University, Toronto, ON, CAN

² Toronto Rehabilitation Institute – University Health Network, Toronto, ON, CAN
email: jdrake@yorku.ca

INTRODUCTION

Previous studies utilizing cross-correlation (R_{xy}) analysis have typically involved correlating the same signal type, such as kinematics [1], and electromyography (EMG) [2]. The extent to which different signals have been correlated (e.g. EMG and centre of pressure [3]) is limited. The relationship between lumbar motion and lumbar muscle activation during typical forward flexion remains unclear. Therefore, the purpose of this study was to quantify the spatial and temporal relationship between angle and muscle activation in the lumbar region in asymptomatic individuals.

METHODS

Thirty right-hand dominant participants, asymptomatic for low back pain (LBP) were recruited from a university aged population. Data were collected as part of a larger study. Reflective clusters were placed on the spine at the level of T₁₂ and L₅, and EMG electrodes were placed over the erector spinae at the L₃ level. Electromyographical data were collected using two AMT-8 amplifiers (Bortec, Calgary, Canada) and synchronized with the kinematic data using a seven camera Vicon motion capture system (Vicon Systems, Ltd., Oxford, UK). Five forward trunk flexion trials randomly distributed throughout the protocol were selected for analysis. The arms were crossed over the chest and the head was flexed forward followed by initiation of trunk flexion [1].

Both kinematic and EMG data were processed using Visual3D v.4.0 software (C-Motion, Inc., Germantown, USA). Lumbar angles were calculated as the relative angle between the clusters at T₁₂ and L₁ and expressed in degrees, with positive

indicating flexion. Right side EMG data were expressed as a percent of a maximum voluntary contraction (%MVC) and down sampled to 50 Hz to align with the kinematic data. The R_{xy} time series between lumbar angle and EMG data for each trial were calculated using MATLAB (The Mathworks Inc., Natick, USA), and the maximum R_{xy} and time of maximum R_{xy} (time lag) were identified. An R_{xy} value between 0.40-0.59, 0.60-0.79, and 0.80-1.00 were considered to be moderate, strong, and very strong, respectively [4]. A negative time lag indicated that the lumbar angle motion preceded the EMG activation. Both maximum R_{xy} and time lags were averaged across the five trials for each participant.

RESULTS AND DISCUSSION

The mean (*SD*) R_{xy} was 0.670 (0.046) ranging from 0.512 to 0.881 (Figure 1). The mean (*SD*) time of R_{xy} was -1.19 s (0.43) ranging from -3.19 s to 0.88 s. A pattern was found in individual trials when the R_{xy} value was in the ‘very strong’ category, where the EMG data in these trials did not show a reduction in EMG activity (Figure 2).

To the authors’ knowledge this is the first direct quantification of the relative timing between lumbar kinematic and EMG data using cross-correlation analysis. Relationships were generally found in the ‘strong’ category; however, some variation was found between and within individuals.

The strong positive R_{xy} and negative time lag indicated this occurred when both the angle and EMG were increasing after the initiation of flexion, which corresponded to the first “burst” of EMG activity (Figure 2A). In the cases where the R_{xy} was in the ‘very strong’ category (such as Figure

2B), the EMG showed a continual increase/maintenance of activation throughout the flexion phase. This was opposed to the typical reduction of EMG activity typically found in asymptomatic individuals.

These preliminary results suggest that strong cross-correlation magnitudes may be representative of the relationship between muscle activation and motion in asymptomatic individuals. A ‘very strong’ R_{xy} magnitude tends to show a distinctly different pattern, which could have implications for clinical applications in characterizing movement differences in individuals with LBP.

REFERENCES

1. Schinkel-Ivy A and Drake JDM. *J Electromyogr Kinesiol* **25**, 239-246, 2015.
2. Nelson-Wong E, et al. *Clin Biomech* **23**, 545-553, 2008.
3. Sozzi S, et al. *Clin Neurophysiol* **124**, 1175-1186, 2013.
4. Swinscow TDV. *Statistics at Square One*, BMJ Publishing, 1997.

ACKNOWLEDGEMENTS

Natural Sciences and Engineering Research Council of Canada (NSERC), and York University.

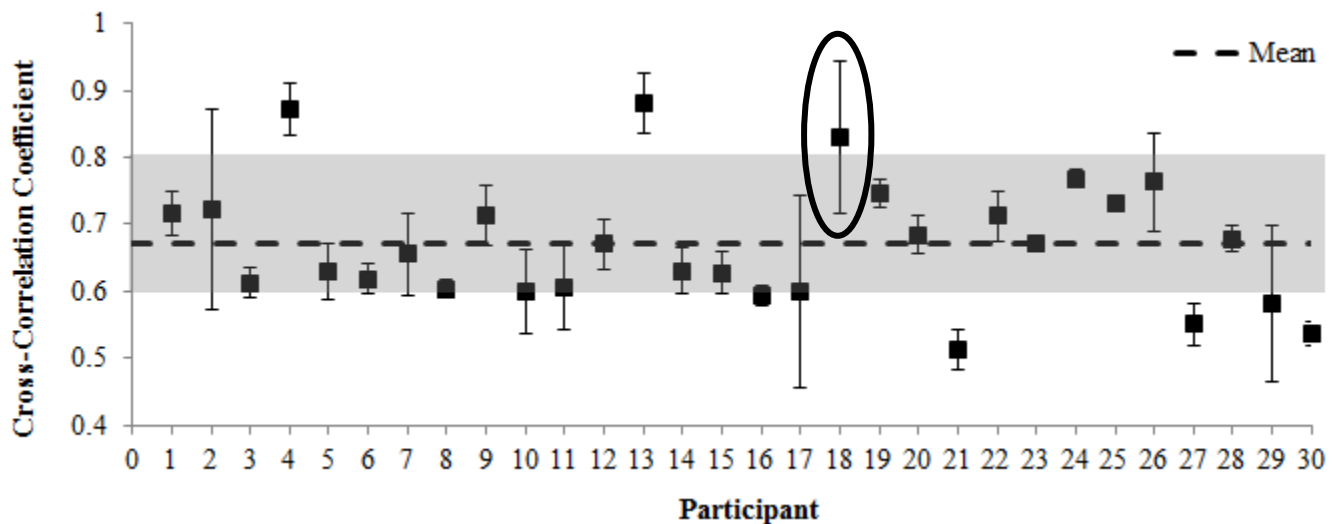


Figure 1. Mean (SD) cross-correlation coefficients for each participant. The shaded region represents the ‘strong’ category; the dashed black line indicates the grand mean. Circled point indicates participant in Figure 2.

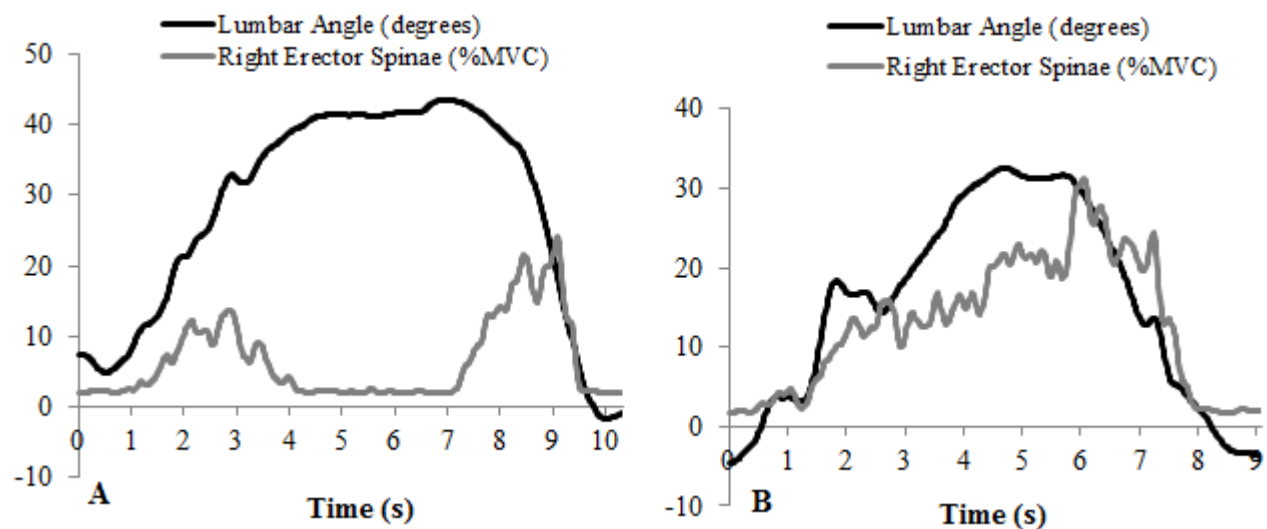


Figure 2. Two trials from Participant 18. A) represents a ‘strong’ relationship ($R_{xy} = 0.724$) with the typical muscle quieting. B) represents a ‘very strong’ relationship ($R_{xy} = 0.972$) with a lack of muscle quieting.

DECREASED DYNAMICAL COMPLEXITY DURING QUIET SITTING IN CHILDREN WITH AUTISM SPECTRUM DISORDERS

¹ Kimberly Fournier, ²Shinichi Amano, ³Hyo Kuen Lee and ³Chris Hass

¹ The University of Rhode Island, Kingston, RI, USA

² Ohio University, Athens, OH, USA

³ The University of Florida, Gainesville, FL, USA

email: kimfournier@uri.edu

INTRODUCTION

Movement impairments are a ubiquitous symptom in children diagnosed with Autism Spectrum Disorders (ASD) [1]. Purposeful movements necessary for functional independence, first require an ability to control one's posture. Children with ASD have been reported to exhibit impairments in their control of posture [2] and non-linear analyses of the center of pressure (COP) data during quiet stance has revealed their control to be more regular or restrictive [3]. In an effort to further explore the link between postural control and the characteristic repetitive and stereotyped behavior associated with this population, detrended fluctuation analysis (DFA) was applied to quiet, unsupported sitting posturography data in children with ASD.

METHODS

Posturographic data for sixteen children diagnosed with ASD (age: 6 ± 1 years, height: 1.2 ± 0.1 m, mass: 23.8 ± 6.2 kg, Leiter-R Brief IQ: 81.5 ± 25.0) and sixteen age-matched typically developing (TD) children (age: 6 ± 1 years, height: 1.2 ± 0.1 m, mass: 20.6 ± 2.90 kg, Leiter-R Brief IQ: 115.2 ± 13.9) were analyzed. Ground reaction forces (GRF) and moments were recorded (360 Hz) from a forceplate (Type 4060-10, Bertec Corp., Columbus, OH). During quiet sitting trials, children sat on a stool that was positioned on the forceplate. During each trial, children viewed a video that contained vibrant images and music for 120 s. Each 120 s trial was subdivided into smaller 20 s trials. Trials where the participant was moving and not attending to the video were discarded. GRF and moments were used to calculate the location of the COP in a time-series and these data were then filtered using a second order, low pass frequency Butterworth filter

(cut-off frequency of 20 Hz). The filtered locations of the COP were then outputted for further analyses.

The time-dependent structure of sway variability during sitting was examined by means of DFA. This approach provides a measure of the rate of growth in the fluctuation of variance as a function of increasing time scales, and the slope of this rate of growth (α -value) provides an index of the breadth of fluctuations across the range of time scales [4]. The robustness of this technique to non-stationarity underscores the appropriateness of its use for postural sway data [5]. A larger rate of growth or steeper slope (larger α -value) indicates fluctuations occur over relatively few time scales indicating a more predictable system (decreased complexity). A smaller growth rate or gradual slope (smaller α -value) indicates fluctuations dispersed more evenly across a range of time scales and thus indicative of a more random system (increased complexity) [5]. In general, the motor patterns of mature, healthy adults are represented with an α -value of approximately 1. Alternatively, α -values for less mature systems, such as those of children, would likely be greater than 1 and would gradually decrease over their development [4].

Growth rates in the fluctuation of variance (α -value x , α -value y) were calculated for the anteroposterior and mediolateral directions based on previous methodology [4]. Additionally, the movement present in the COP time series was characterized by the traditional linear measures of COP range in the anteroposterior and mediolateral directions and the elliptical sway area containing 95 % of the COP data ($COP_{RANGE-X}$, $COP_{RANGE-Y}$, and $Area_{CE95}$). Independent t-tests were used to identify differences in the dependent variables (Linear: $COP_{RANGE-X}$, $COP_{RANGE-Y}$, $Area_{CE95}$, Nonlinear: α -value x , α -value

γ) between children diagnosed with ASD and TD children. An a priori alpha level of 0.05 was set for all statistical tests and all statistical tests were performed using SPSS 16.0 for Windows (Chicago, Illinois).

RESULTS AND DISCUSSION

Children with ASD exhibited significantly larger α -values in both the anteroposterior and mediolateral directions ($p < 0.05$). The α -values were 14.5% larger in the anteroposterior direction (α -value x) and 16.8% larger in the mediolateral direction (α -value y). Additionally, the three linear measures for movement present in the COP time series were significantly larger in children with ASD when compared to TD children (76.4 % larger, 135.5 % larger, and 271.9 % larger for $COP_{RANGE-X}$, $COP_{RANGE-Y}$, and $Area_{CE95}$ respectively, $p < 0.05$ for all 3 measures) (Table 1).

Linear and nonlinear analyses of the COP time series during quiet, unsupported sitting support previous postural control findings reported in the literature. As hypothesized, children diagnosed with ASD displayed larger linear measures ($COP_{RANGE-X}$, $COP_{RANGE-Y}$, $Area_{CE95}$) when compared to TD children [2]. Similar to previous findings for quiet stance [3], DFA analyses revealed that children with ASD had a more predictable control of posture. Growth rates in the fluctuation of variance approached values previously reported for behavior with predictive patterns or reduced complexity [4].

Unsupported sitting, when compared to quiet stance, is believed to require less control and/or coordination (fewer degrees of freedom). Previous reports suggest postural impairments may be the

result of abnormalities and dysfunction in the underlying neural networks responsible for coordinated activity [3]. However, abnormalities in these same areas have also been associated with restricted, repetitive behaviors (RRBs), a cardinal feature of ASD [6]. While quiet sitting is more readily accomplished as a research task in this population, the restricted control of posture observed during the less coordinated task lends support to a global impairment associated with ASD and an underlying central rigidity that result in a lack of complexity in the control of a broad range of stereotypic behavior, including motor behavior. [3]

CONCLUSIONS

The main finding of this work is that children with ASD exhibit reduced dynamical complexity in their control of posture, over a range of behaviors that now includes unsupported sitting. Results further support the links between restricted control of posture, stereotypic behavior and the neurobiology of ASD.

REFERENCES

1. Fournier, K.A., et al., *J Autism Dev Disord*, 2010. **40**(10): p. 1227-40.
2. Fournier, K.A., et al., *Gait Posture*, 2010. **32**(1): p. 6-9.
3. Fournier, K.A., et al., *Gait Posture*, 2014. **39**(1): p. 420-3.
4. Hong et al., *Dev Psychobiol*, 2008. **50**(5): p. 502-10.
5. Newell, K.M., et al., *Gait & Posture*, 1997. **6**(1): p. 56-62.
6. Turner, M.A., *J Child Psychol Psychiatry*, 1999. **40**(2): p. 189-201.

Table 1: Means and standard deviations (SD) for measures of COP variability during quiet, unsupported sitting.

Measure of Variability	ASD (n=16)		TD (n=16)		p value
α -value _x	1.26	(0.13)	1.10	(0.14)	0.002*
α -value _y	1.25	(0.16)	1.07	(0.12)	0.001*
$Area_{CE95}$	12.31	(10.10)	3.31	(4.57)	0.004*
$COP_{RANGE-X}$	4.57	(2.43)	2.59	(1.92)	0.016*
$COP_{RANGE-Y}$	3.98	(2.79)	1.69	(1.09)	0.005*

*Significant at $p < 0.05$

MUSCLE ACTIVATION STRATEGIES OF STEPPING ONTO A COMPLIANT SURFACE IN HEALTHY ADULTS

Alexa K. Johnson, Jasmine L. Mirdamadi, Nicole C. Gervasi, and Deanna H. Gates

The University of Michigan, Ann Arbor, MI, USA

email: gatesd@umich.edu, web: <http://rehab-biomech-lab.kines.umich.edu>

INTRODUCTION

Walking on uneven terrain may contribute to instability, especially in those who are at higher risk of falling, such as older adults [4] or people with lower limb amputation [1]. To adjust for the potentially destabilizing surface, people increase step width [1,3]. This kinematic adaptation likely indicates altered muscular control. Gluteus medius activity has been shown to increase with step width [2]. There are peak activation differences during the transition step onto a foam surface in the biceps femoris, tibialis anterior and the medial gastrocnemius [3]. Similarly, it has been shown that there is an anticipatory effect of muscle activation in the peroneus longus, peroneus brevis, medial and lateral gastrocnemius and soleus when walking on a treadmill with a random inversion step [5]. In contrast to a single plane perturbation such as inversion, when walking over sand, there are multiple stabilization techniques the body may have require. The purpose of this study is to determine if healthy individuals utilize different muscle activation strategies when stepping into a sand pit, as opposed to a regular stride on level ground. This includes anticipatory muscle activation and peak activation strategies. We hypothesize there will be an increase in lower extremity activity when stepping into the sand as compared to a level ground stride to improve stability. The timing of muscle activation patterns on a compliant surface could be beneficial in understanding and preventing falls.

METHODS

Five healthy young adults completed this study (age 20 ± 2 years; height 1.73 ± 0.08 m; mass 66.8 ± 11.6 kgs). Subjects were instructed to walk at a self-selected speed on hard level ground as a control condition. Subjects then started on a hard level surface and stepped into a pit (12ft x 3 ft x 7 in) filled with sand and continued to walk. Full body

kinematics were collected using 53 reflective markers and a 16 camera optoelectric camera system (Motion Analysis, Inc., Santa Rosa, CA). Surface electromyography (EMG) (Delsys, Natick, MA) measured muscle activity bilaterally from nine lower limb muscles. Here, we focus on five of the nine muscles; biceps femoris (BF), vastus lateralis (VL), gluteus medius (GLM), medial gastrocnemius (MG) and tibialis anterior (TA). The stride analyzed was indicative of a transition stride from the over ground into the sand pit (Fig. 1). The cycle began with heel contact on the hard level surface and with the subsequent heel strike on the same leg, in the sand pit.

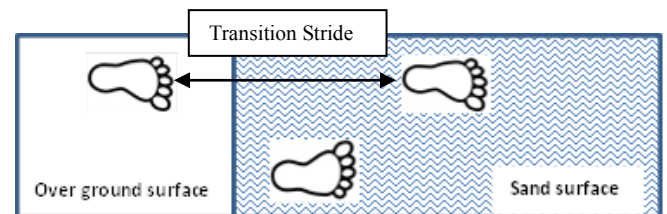


Figure 1: A diagram of how the transition stride is defined, stepping from an level over ground surface to a compliant (sand) surface.

EMG data was filtered with a 6th order Butterworth filter to a band width of 20-400 Hz, full wave rectified and enveloped via a 6 Hz low-pass Butterworth filter. Finally a custom Matlab (MathWorks, Natick, MA) code was used to determine muscle activation differences between the level ground and sand conditions, of right and left BF, VL, GLM, MG, and TA.

RESULTS AND DISCUSSION

During the sand condition, there was earlier activation of the BF in pre-swing, in the left leg, when compared to a stride on level ground (Fig. 2). This 52.8% increase in BF activity during pre-swing, and earlier activation may have to do with the contralateral heel strike into the sand. As the contralateral foot sinks into the sand, the decrease in level of the step requires greater knee flexion and

BF activity. On the right leg, during the first step into the sand, there was 41.9% less activation in the BF when compared to a level ground step.

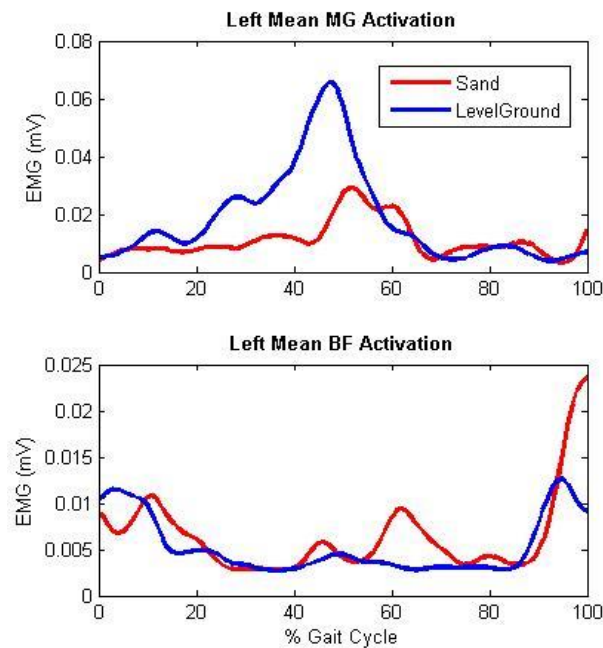


Figure 2: Mean muscle activation of BF and MG on the left leg of a stride. A transition from level ground to a compliant surface is indicated in red. Blue indicates a normal, level ground stride.

In the sand condition, during stance phase on level ground, the left GLM reached 108% greater activation than in left stance on level ground. An increase in GLM activity may have to do with individuals anticipating a greater step width for a greater base of support on a compliant surface.

The MG had decreased peak activation in both legs during the sand condition when compared to the level ground condition. In the left leg, during toe off, peak activation of the MG was 47.8% lower than toe off on a regular level ground step. This decrease may be caused by less of a push off, and greater knee flexion, as indicated by the BF activity

Table 1: A positive percent is represented as a, increase in peak muscle activation in the sand condition compared to the peak activation in the level ground walking condition. A negative percent is a decrease in peak muscle activation in the sand condition compared to the level ground condition.

Percent Activation	Muscles				
	GLM	MG	BF	VL	TA
Right Leg	-4.77%	-15.9%	-41.9%	4.04%	
Left Leg	108.4%	-47.8%	52.8%	-6.4%	-33.4%

in pre-swing. In the right toe off in the sand, the MG activated 15.9% lower than the level ground toe off. This decrease, likely occurs as the force produced by the MG dissipates into the sand. This indicates that there need to be further compensations to accelerate the leg into swing. There was also a later peak in the MG activation during toe off, when stepping onto the sand (Fig. 2). Additionally, there was a 33.4% decrease in TA peak activation in the sand condition, compared to the level ground condition. All other muscles showed less than 10% change in peak activation.

CONCLUSION

Muscle activation strategies changed when individuals step onto a compliant surface. Changes can be seen as decreased muscle activation at toe off, and decreased activity during stance on level ground in anticipation of stepping into the sand pit. Future analysis will address timing of muscle activation patterns to understand if the central nervous system adjusts to instability through anticipatory or compensatory mechanisms. Future research about how older adults or those with pathology may interpret and maneuver the same transition stride may be beneficial to reducing their risk of falling and further injury.

REFERENCES

1. Gates, DH, et al. (2013) *Gait Posture*, **38**, 570-5.
2. Kubinski, SN, et al. (2015). *Gait Posture*, **41**, 130-5.
3. MacLellan, MJ., & Patla, AE. (2006) *Exp brain res.*, **173**, 521-530.
4. Marigold, DS., & Patla, AE. (2008) *Gait Posture*, **27**, 689-96.
5. Nieuwenhuijzen, PH., & Duysens, J. (2007) *J neurophysiol*, **98**, 2266-73.

MOVEMENT QUALITY DURING UNIMANUAL AND BIMANUAL FUNCTIONAL REACHING MOVEMENTS

Hari Sriram, Jeffrey C. Cowley and Deanna H. Gates

The University of Michigan, Ann Arbor, MI, USA

Email: gatesd@umich.edu Web: <http://rehab-biomech-lab.kines.umich.edu/>

INTRODUCTION

In our everyday life, we often require the simultaneous use of both hands to perform tasks (e.g. buttoning up shirts, tying shoelaces). Bimanual (two-handed) tasks require a higher degree of complexity compared to unimanual tasks due to the coordination required to control both hands [1]. Unconstrained bimanual tasks, such as in activities of daily living, may enforce temporal and spatial coordination across both arms. Constrained reaching movements or simple rhythmic movements have often been used to study bimanual coordination, but these are not representative of tasks in daily life [2 3]. Improving our understanding of how people perform unconstrained bimanual tasks, may provide a basis for the assessment of pathologies associated with bimanual coordination. Therefore, the purpose of this study is to assess movement quality of healthy individuals performing unimanual and bimanual unconstrained daily life reaching tasks. We hypothesize that the bimanual tasks will be performed slower and smoother compared to unimanual tasks and that the dominant arm will perform smoother movements than the non-dominant arm.

METHODS

Seven healthy young adults (4 male, 3 female) participated. Subjects were screened for medications or conditions that could affect arm movement. All subjects were right hand dominant. Trials began with the subject standing in front of a shelf (head height) with their hands resting at their sides. Subjects were instructed to stand 100% of arm's length away from the shelf. Subjects retrieved a can from the top of the shelf and placed it on a lower shelf. The task was completed separately with each hand as well as simultaneously using both

hands. Subjects completed five successful trials of each task and the reach phase of each trial was analyzed.

The motion of reflective markers placed on the radial and ulnar styloids was tracked at 120Hz using Cortex (Motion Analysis, Santa Rosa, CA). Wrist joint center was calculated by finding the midpoint of the distance between the two wrist styloids, and the wrist joint center data was analyzed. The onset and termination of the reach phase was calculated by using a velocity threshold of 2% of maximum velocity. Index of curvature (IOC) was calculated by dividing the arc length of the wrist joint path by the straight line distance between the movement start and end points. For each trial, smoothness was calculated by integrating jerk and normalizing the value to peak speed [4]. Movement time, curvature, and smoothness were analyzed using Matlab (MathWorks, Natick, MA). A two-factor within subjects ANOVA was used to test for differences between tasks (unimanual/bimanual) and limbs (dominant/non-dominant). Significance was set at $p \leq 0.05$.

RESULTS AND DISCUSSION

For movement curvature, there was a significant main effect for task ($p=0.04$). Bimanual reaches were more curved (IOC: 1.045 ± 0.003) compared to unimanual reaches (IOC: 1.052 ± 0.003) (Figure 1). There was no significant difference between arms ($p=0.603$). For movement time, there was no significant main effect for task ($p=0.225$) or arms ($p=0.661$) (Figure 2).

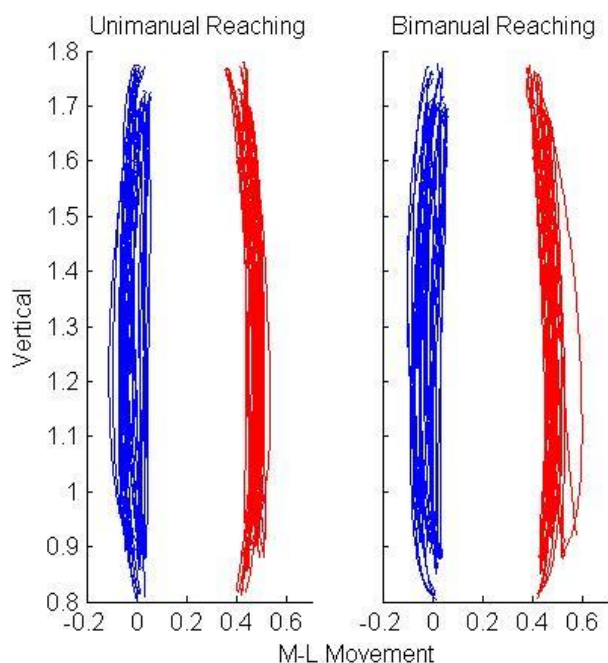


Figure 1: Mediolateral movement (m) of dominant and non-dominant arm during reaching. Left arm (blue), Right arm (red).

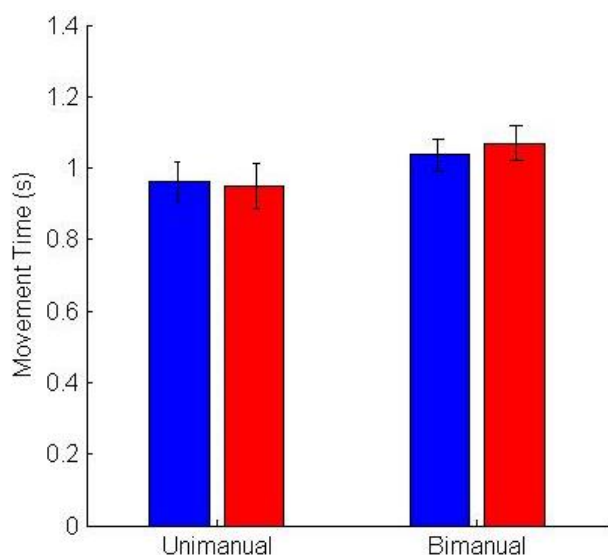


Figure 2: Movement time during bimanual and unimanual tasks. Left Hand (blue), Right Hand (red). Error bars represent 95% confidence interval.

For smoothness, there was no significant main effect for task ($p = 0.321$) or arms ($p = 0.312$) (Figure 3).

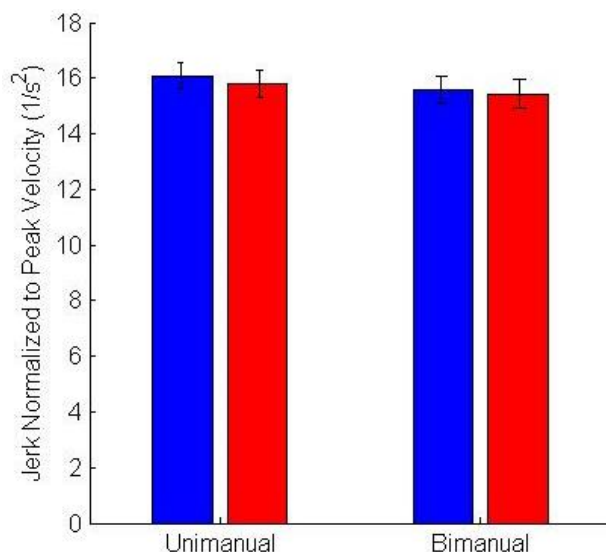


Figure 3: Smoothness of bimanual and unimanual reaches. Left Hand (blue), Right hand (red). The smaller the value, the smoother the movement is. Error bars represent 95% confidence interval.

CONCLUSION

There were significant differences in the curvature of reaching between unimanual and bimanual tasks. While the differences in movement time and smoothness were not significant, this could be due to the small sample size of data collected. Additional data will be collected in the future. The results of this study show how healthy individuals perform unconstrained tasks that mimic everyday life. This can be beneficial in understanding the role bimanual coordination plays in everyday life tasks.

REFERENCES

1. Wiesendanger M., and Serrien D.J. *Progress in Brain Research*, vol. 143, 2004
2. Neely., et al. *Brain and Cognition*, vol. 57, 2005
3. Forrester L., and Whittall J. *J Mot Behav*, vol 32, 2000
4. Rohrer et al., *J. Neurosci.*, vol 22, 2002.

Motor Cortex Activation and Landing Neuromuscular Control after Anterior Cruciate Ligament Reconstruction

¹Dustin R. Grooms, ¹Stephen J. Page, ¹Deborah Nichols-Larsen, ¹Ajit M.W. Chaudhari, ¹James A. Onate

¹The Ohio State University, Columbus, OH, USA
email: grooms.dusty@gmail.com, web: <http://medicine.osu.edu/hrs/at/research>

INTRODUCTION

Anterior cruciate ligament (ACL) injury and reconstruction may induce brain motor control adaptations that influence neuromuscular function and potentially, future injury risk. Traditional neuromuscular control assessment and therapy may not adequately address this neuroplasticity. Functional magnetic resonance imaging (fMRI) provides a detailed method to assess brain changes to bridge this gap in knowledge. The purpose of this work is to determine the relationship between biomechanically measured neuromuscular control during drop landing and brain activation during a knee motor control task in those with ACL reconstruction and matched controls

METHODS

Participants were matched on height, mass, extremity dominance, education level, history and current physical activity level. Eight left anterior cruciate ligament reconstructed (ACLR) (25.5±1.37 years, 1.70±0.13 m, 75.6±19.2 kg, Tegner activity level 6.0 ± 1.5, 23±18 months post-surgery) and 8 matched healthy controls (23.6±3.14 years, 1.75±0.05 m, 73.5±12.24 kg, Tegner activity level 6.0 ± 1.5) participated. The brain fMRI was



Figure 1: Knee motor control task: Four sets of 30 seconds of rest followed by 30 seconds of 45° extension-flexion completed at 1.2 Hz.

collected during a unilateral knee motor task consisting of repeated cycles of extension and flexion while lying supine in the MRI scanner (figure 1). The brain activation pattern for knee movement was completed on a subject-specific level on the contrast between knee movement and rest with a general linear model fixed-effects analysis *a priori* threshold at $p < 0.01$ corrected (figure 2) with the Oxford Centre software package FSL. The motor cortex was selected as an *a priori* region of interest and the voxel cluster with the peak activation was extracted for analysis.

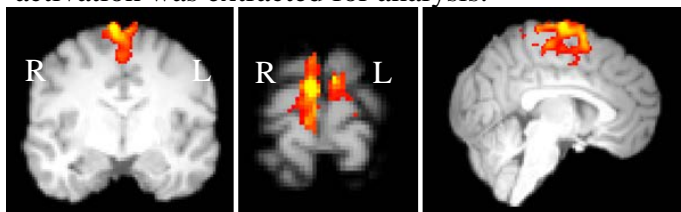


Figure 2: Typical sensorimotor brain activation for left knee movement.

A drop vertical jump task was completed to assess functional neuromuscular control. Participants were fitted with a full body point cluster marker set to track 3D kinematics via a Vicon passive optical motion capture system. Participants then completed three drop vertical jumps consisting of leaning forward from a 30.5 cm plyometric box until falling, landing and then immediately jumping up to a target for maximum height. Data were processed using Visual 3D software to assess peak knee flexion during the initial landing from the box.

A Pearson correlation was completed on the relationship between motor cortex activation during knee extension-flexion and peak knee flexion angle during landing.

RESULTS AND DISCUSSION

Motor cortex brain activation in participants with ACL reconstruction was significantly correlated with peak knee flexion during landing ($r = -0.717$, $p = 0.034$). There was no correlation for the control group ($r = 0.275$, $p = .509$) or the combined group ($r = -0.211$, $p = 0.433$). There was no difference in peak knee flexion or motor cortex activation between groups.

Table 1: Mean and standard deviations of peak motor cortex activation (percent signal change) and peak knee flexion (degrees) for each group

Group	Variable	
	Motor Cortex Activation	Peak Knee Flexion
ACL	1.243 ± 0.245	82.0 ± 14.0
Control	1.6 ± 0.677	76.15 ± 7.37

The ACL reconstructed cohort had a strong negative correlation between motor cortex activation and knee flexion during landing. This suggests that, as demand on the motor cortex increases to complete knee movement, the relative amount of knee flexion during landing decreased. Knee flexion was selected as it is a common metric of neuromuscular control during drop landing, with more knee flexion indicating increased ability to control the landing and decreased sagittal plane moments [1]. In contrast, a landing with decreased knee flexion is associated with increased injury risk, poorer neuromuscular control and increased sagittal plane moments [1]. The association of motor cortex activation indicates there is likely a relationship between how the brain generates knee motor control and the neuromuscular control displayed during drop landing after ACL reconstruction.

The lack of a relationship in the control group between motor cortex activation and knee flexion may indicate that the fMRI task does not offer sufficient physical demand for controls. While the

relative activation level of the motor cortex between cohorts was similar, previous work has indicated greater motor planning and sensory area activation in those with ACL injury, possibility indicating the task is neurologically more challenging in this cohort [2]. It may be that, in a healthy population, a more challenging motor control task is required to be related to the more functional drop landing.

Additionally, this being a retrospective analysis, it is unknown if this relationship was present prior to the injury and may have played a role in the initial loss of neuromuscular control associated with the ACL injury mechanism or developed due to the injury. Also, the intensive unilateral rehabilitative therapy after injury may induce a greater cortical-functional relationship after ACL injury. The great deal of training to restore muscular function post injury may increase the level of cortical vs. sub-cortical or spinal cord contribution to knee neuromuscular control [3].

CONCLUSIONS

ACL reconstruction may induce specific neuroplastic adaptations in motor control within the brain that translate into neuromuscular control during landing.

REFERENCES

1. Pollard CD, et al. *Clin Biomech* **25**, 142-146, 2010.
2. Kapreli E, et al. *Am J Sports Med* **37**, 2419-2426, 2009.
3. Park JW, et al. *NeuroRehab*, **26**, 95-103, 2010.

ACKNOWLEDGEMENTS

The authors gratefully acknowledge support for this study from the National Athletic Trainers' Association and National Strength and Conditioning Association doctoral student grants and The Ohio State University College of Medicine pilot award.

Dual-Task Effects on Motor Performance in Healthy Younger Adults

Sean Wehry, Tiphany Raffegau, Lori J.P. Altmann, Chris J. Hass¹

¹ The University of Florida, Gainesville, FL, USA

Email: sawehry@ufl.edu

INTRODUCTION

Daily activities often require that we perform two tasks concurrently, termed dual-task behavior. Traditional views of cognitive-motor interaction suggest that when two things are done simultaneously, performance on one or both tasks declines. However, our laboratory recently observed that performing cognitive tasks while pedaling on a stationary bicycle led to enhanced cycling speeds. This study's purpose was to determine whether this phenomenon extends to similarly rhythmic modalities with increased balance demands. Herein we compared dual-task behavior during stationary cycling and elliptical walking. We hypothesize that with an increase in cognitive complexity there will be a decrease in the facilitation of motor performance across tasks.

METHODS

Sixteen healthy young adults (9 males, 20 ± 1 yrs) were tested on three separate occasions. Participants were evaluated during two separate motor tasks, cycling and elliptical exercise, and during a battery of 14 cognitive tests spanning 5 cognitive domains including verbal fluency, working memory, controlled processing, response time, and executive function [1]. Participants performed the motor and cognitive task in isolation and during dual task conditions where the cognitive challenges were done while walking/pedaling. In each modality, subjects pedaled/walked at a self-selected pace for two minutes to measure baseline performance. Then they performed the same task while concurrently performing the cognitive battery. Reflective markers placed on the foot were tracked using a six-camera motion capture system. Cycling and elliptical cadence, measured in revolutions per minute (RPM), were calculated from the marker data using custom written software.

The primary outcome variable, changes in RPM from single to dual-task exercise, is represented by Dual-Task Effects (DTE). DTE's were calculated as follows:

$$\text{DTE} = \text{dual task RPM} - \text{baseline RPM}$$

If the difference is negative, the change is interpreted as a "dual-task cost". Alternatively, if the values are positive, it is interpreted as a "dual-task benefit." Subject's DTEs were compared between cycling and elliptical modalities using paired t-tests in SPSS (version 12.2).

RESULTS AND DISCUSSION

Cadence increased significantly during dual-tasks in both modalities ($p < 0.05$). However, those dual-task benefits were significantly greater during cycling than during elliptical walking (all $p < 0.05$).

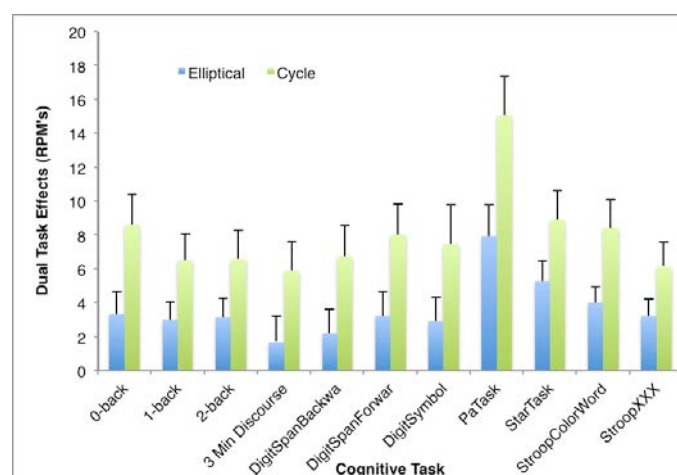


Figure 1: DTE observed during cycling and elliptical. All comparisons were statistically significant.

The data above provide clear evidence that concurrent cognitive tasks facilitated performance in both modalities. This is indicated by the positive DTE values reflecting dual-task benefits during each cognitive test (Figure 1). However, the degree in which motor output improved differs significantly. Facilitation of performance by the concurrent cognitive challenge in cycling was significantly greater than that observed during elliptical walking. We suggest that walking on the elliptical is a more demanding motor task due to the increased coordination and balance demands. As the motor complexity increases, these dual-task benefits are reduced.

Previous research suggests that performing a motor and cognitive task concurrently results in depreciation in one or both factors [2]. There are multiple theories suggested to explain the decrease in dual-task performance, such as the bottleneck and capacity theory [3], but these cannot explain the observed dual-task benefits in this study. Recently, we have proposed the Arousal and Attentional Demands (AAD) model to explain the increase in motor performance due to cognitive stimuli [4]. The AAD model proposes that the cognitive task has an arousal effect, which ultimately leads to an increase in attentional resources in order to maintain motor performance [4]. If the cognitive task stimulates an optimal arousal level and the motor demands are managed, there appears to be a dual-task benefit.

The AAD model supports the DTE results during cycling and elliptical use. The cognitive arousal level was maintained across both modalities, however cycling exhibited a greater dual-task benefit than the elliptical. Cycling is rhythmic, non-weight bearing, and minimal coordination is

involved, thus the attentional demands are considered low. However, elliptical use requires additional motor skills such as maintaining upright balance while pedaling and coordinating arm extension. This complexity increases arousal and attentional demands beyond the optimal levels observed in cycling, comparatively reducing the dual-task benefits.

CONCLUSIONS

This study presented unique results regarding a positive dual-task effect. The addition of concurrent cognitive tasks to cycling and elliptical exercise increased motor performance, a dual-task benefit. The increase in motor complexity from cycling to elliptical use decreased this dual-task benefit, fitting the AAD model. Further investigation should observe additional motor tasks with increasing complexity, such as treadmill walking.

REFERENCES

1. Al-Yahya E et al. (2011) *Neurosci Biobehav Rev* 35: 715-728.
2. Verhaeghen P et al. (2003) *Psychol Aging* 18: 443-460.
3. Pashler H et al. (1998) *Attention* 4: 155-189
4. Altmann, LJP et al. (submitted). *PLOS-1*

SYNCHRONIZATION OF GAIT WITH FRACTAL MUSICAL STIMULI OCCURS DIFFERENTLY AT SHORT AND LONG TIME SCALES

¹Michael L. Hough, ¹Steven J. Harrison and ^{1,2}Nicholas Stergiou

¹University of Nebraska at Omaha, Omaha, Nebraska, USA

²University of Nebraska Medical Center, Omaha, Nebraska, USA

email: mlhough@unomaha.edu, web: <http://www.unomaha.edu/college-of-education/cobre/index.php>

INTRODUCTION

Lately, attention has been given to synchronization of movement with auditory stimuli containing the fractal temporal structures commonly found in nature. These stimuli are locally unpredictable, but still afford synchronization of another type, termed “strong anticipation” [1]. Strongly anticipatory systems are hypothesized to achieve synchronization through the coupling of behavior to global regularities in the environment. Research typically relies on detrended fluctuation analysis (DFA) to demonstrate the coupling of auditory input and motor output. Strong coupling is shown as a high correlation between the fractal temporal structure of variability of the auditory and motor signals. Specifically, experiments have shown this relationship between auditory stimuli and tapping [1] or gait [2]. It is clear that the presence of long-term correlations in the stimulus affect the structure of the coupled movement, however, the nature of coupling at shorter time scales is still largely unexplored [3].

Recently, Marmelat et al presented participants with metronomes exhibiting various levels of fractal structure, and assessed synchronization over short and long time scales [3]. They found significant correlation only over the long-term scaling regions, implying that the synchronizing behavior with fractal signals is dominated mainly by the long-term persistence in these stimuli.

Our previous experiments have demonstrated strong correlations between fractal auditory input and movement using a musical stimulus, rather than a metronome [2]. Synchronizing movement with music is a near-universal component of an individual’s experience, and using a familiar

melody (Beethoven’s “Für Elise”) with rhythmic structure matched to a participant’s natural cadence potentially affords stronger coupling than the single tones used by others. Importantly, preliminary experiments using musical stimuli with a tapping task seem to indicate strong coupling at both short and long time scales. Thus, in the present study investigating gait, we hypothesized that the richer information in the musical signal would allow participants to be more sensitive to short-term regularities, resulting in strong correlations across a wider range of time scales.

METHODS

Ten participants walked on a treadmill at a self-selected speed for 15 minutes. We then created musical stimuli matched to each participant’s cadence (at 2 beats/step, or 4 beats/stride) and amount of variability in cadence. Each stimulus consisted of an identical melody, but varying temporal structures - a constant, isochronous rhythm, and rhythms perturbed by white noise, pink noise, and brown noise. Participants repeated the walk while listening to each stimulus, having been given the instruction, “While this may be difficult, I want you to try to walk in step with the rhythm of the music. Try to imagine playing the notes with your heels.” The times of each note onset and each heel strike were recorded with a Delsys footswitch system.

The resulting inter-beat interval and inter-stride interval time series were trimmed to include the middle 630 strides and the accompanying beats. These series underwent DFA to determine the fractal scaling exponent α in each of three scaling regions: overall (10 - 300 strides), short-term (10 - 50 strides), and long-term (50 - 300 strides). We

also calculated mean intervals, mean asynchrony (time of heel strike minus time of the associated beat onset) and mean accuracy (absolute value of asynchrony) for each condition.

RESULTS AND DISCUSSION

Repeated measures ANOVA revealed no significant differences due to condition in inter-beat interval, inter-stride interval, mean asynchrony, or mean accuracy (Table 1). A main effect of condition was found for overall α , and in the long-term scaling region. No differences were found in the short-term region (Figure 1).

These findings agree with Marmelat et al., in that strong coupling behavior was demonstrated in all conditions, but that this behavior was primarily occurring at the longer time scales. This remained the case despite our use of a musical signal. This differs from the behavior observed in our tapping experiment. These differences may be due to the pendulum-like swing phase in gait that places an additional physical constraint on stride-to-stride timing.

CONCLUSIONS

While our initial hypothesis was not supported, the question of whether musical stimuli lead to stronger coupling than metronomes remains to be determined. Our results suggest a direct test of this assumption is required. In addition, the differential coupling seen at different time scales suggests that synchronization with complex stimuli may not be fully characterized using DFA. Another approach to quantify coupling may be warranted.

REFERENCES

1. Stephen DG, et al. *Phys A*, 387(21), 5271-5278, 2008.
2. Hunt N, et al. *Nature Sci Rep*, 4, 5879, 2014.
3. Marmelat V, et al. *PloS One*, 9(3), 2014.

ACKNOWLEDGEMENTS

This work was supported by the Center for Research in Human Movement Variability of the University of Nebraska Omaha, NIH (P20GM109090 and R01GM105045).

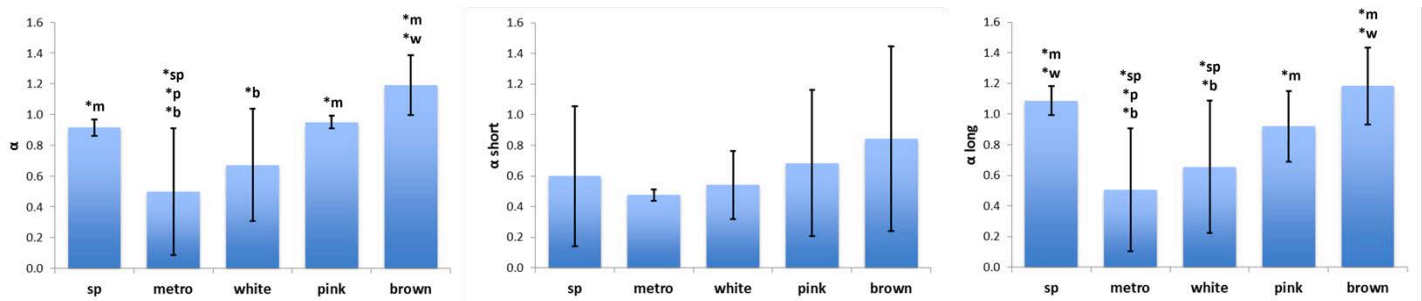


Figure 1: Significant differences in variability between conditions reflect findings of previous work. This study reveals that with a musical stimulus, these differences occur over long time scales. (Note: ***sp** - significantly different from self-paced; ***m** - significantly different from metronome; ***w** - significantly different from white noise; ***p** - significantly different from pink noise; ***b** - significantly different from brown noise; $p < 0.05$.)

Table 1: Musical stimuli were constructed to differ between conditions only in temporal structure of variability. This resulted in musically paced conditions differing only in temporal structure. Asynchrony and accuracy were also not significantly affected by condition.

	Stimulus Type				
	self-paced	metronome	white noise	pink noise	brown noise
Inter-beat interval (s)	n/a	0.29 ± 0.00	0.29 ± 0.02	0.30 ± 0.02	0.29 ± 0.02
Stride interval (s)	1.18 ± 0.06	1.17 ± 0.07	1.19 ± 0.08	1.16 ± 0.08	1.15 ± 0.07
Mean asynchrony (s)	n/a	-0.01 ± 0.01	-0.01 ± 0.03	0.01 ± 0.01	0.01 ± 0.02
Mean accuracy (s)	n/a	0.06 ± 0.02	0.07 ± 0.01	0.06 ± 0.01	0.07 ± 0.01

SIMULTANEOUS TURN AND STEP TASK FOR INVESTIGATING CONTROL STRATEGIES IN HEALTHY YOUNG AND COMMUNITY DWELLING OLDER ADULTS

¹ Andrew H. Huntley, ¹ John L. Zettel and ^{1,2} Lori Ann Vallis

¹ Human Health and Nutritional Sciences, University of Guelph, ON, Canada

² Schlegel-UW Research Institute for Aging, ON, Canada

Email: ahuntley@uoguelph.ca

INTRODUCTION

Reorientation of the body is an important component of many activities of daily living, i.e. turning to reach for an object on a shelf, or changing travel direction when walking along a busy sidewalk. While it may seem simple, reorienting to a new direction is actually a complex task that requires the transfer of body segments in a coordinated way. In older adults, incorrect weight transfers have, in fact, shown to be a serious cause of falls in both community dwelling and institutionalized settings [1, 2]. Past research has explored stepping and turning tasks executed during on-going gait (e.g. step and quick turn from Neurocom Balance Master; 3]. Few studies have examined the dynamic action of performing a turn and step simultaneously from a standing position though this task may, arguably, be more representative of an activity of daily living performed by older adults.

The **purpose** of our study was to investigate age related changes when performing a simultaneous turn and step task from quiet standing balance. We expected an increase in variability of the COM motion with aging, indicating a decrement in control strategies employed by older adults to complete this challenging task.

METHODS

Nine healthy young adults (5 females and 4 males; 22 ± 2.088 years) and ten healthy, community dwelling older adults (5 females and 5 males; 79.9 ± 6.315 years) were instrumented with reflective markers placed on anatomical landmarks (e.g. head, trunk) and captured using an Optitrak 3D motion analysis system. All participants were right arm and

right leg dominant and older adults had never experienced a fall. Falls Efficacy Scale (FES) data was collected as a measure of balance confidence.

Both groups performed a simultaneous turn and step task (STS) from a quiet stance in two directions (towards dominant or non-dominant limb) under two self-select speed (normal and as quickly and efficiently as possible; Figure 1). Two task speeds were employed as previous work has shown many older adults report trying to rush or hurry to complete a given task just prior to experiencing a fall [4].

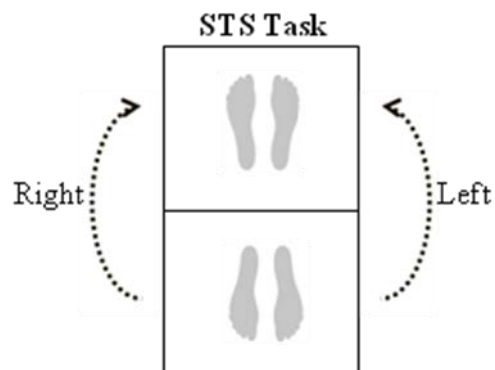


Figure 1. Simultaneous turn and step (STS) task performed by both healthy younger and community dwelling older adults. As illustrated, the task involves a 180 degree rotation (turn) as well as a translation (step) of the center of mass to complete.

Whole-body center of mass (COM) was estimated (modified Winter model [5]). Peak COM velocity, Coefficient of Variation (CoVa) of the COM velocity, and number of steps were recorded to characterize performance during the turning task. Cross correlation analysis of the COM velocity was also conducted to characterize the repeatability of this novel, dynamic task.

RESULTS AND DISCUSSION

A significant main effect of task speed ($F(1,74)=4.969$, $p = 0.029$) was observed for the CoVa of the STS task (Figure 2A) and a significant main effect of age ($F(1,74) = 13.953$, $p < 0.001$) was observed for the CoVa of the STS task (Figure 2B).

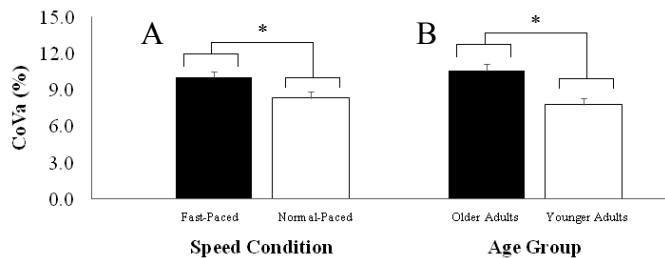


Figure 2: Coefficient of Variation (CoVa) of the center of mass velocity for **A)** fast-paced trials (filled bars) and normal-paced trials (unfilled bars), and **B)** healthy older adults (filled bars) and healthy younger adults (unfilled bars). Mean and standard error values are illustrated (*, $p < 0.05$).

A significant main effect of age was also observed for Peak COM velocity ($F(1,75) = 42.142$, $p < 0.001$), cross correlation analysis ($t(73) = -7.844$, $p > 0.001$), and steps to complete the STS task ($F(1,75) = 81.502$, $p < 0.001$) (Table 1). No significant main effect of direction of the STS task was observed for any of the measured variables.

Previous work on the 180 degree turn in place task in older women showed increased variability due to aging, in addition to significant differences between turn directions [6]. However no differences due to age were observed for maximum pelvic rotational velocity. Our STS task demonstrates similar variability but no preferential difference in turn direction, as well as significant differences in peak COM velocity. This suggests the STS task equally discriminates between turn directions while presenting a more difficult challenge to older adults

(e.g. decreased peak COM velocity during trials under self-selected speeds). Interestingly, while cross-correlation analysis exhibited significant main effects due to age, we observed a high rate of repeatability by older adults completing the STS task, which is critical for test-retest situations.

CONCLUSIONS

In conclusion, the STS task challenged the control strategies of healthy older adult participants. Increased variability, along with decreased peak COM velocity, exemplified potential decrements in postural control in older adults even when performing the task at a slower rate. Furthermore, this decrease in performance was coupled with a high repeatability, exemplifying that subjects were still able to consistently execute the STS task. The present study provides evidence that a turn coupled with a simultaneous step may be a better discriminator of the quality of control strategies than just a simple turn in place task.

REFERENCES

1. Berg WP, et al. *Age Ageing* **26**, 261-268, 1997.
2. Robinovitch SN, et al. *Lancet* **381**, 47-54, 2013.
3. Naylor ME, et al. *J Sport Rehabil* **15**, 326-337, 2006.
4. Nachreiner NM, et al. *J Women's Health* **16**, 1437-1446, 2007.
5. Winter DA, et al. *J Neurophy* **80**, 1211-1221, 1998.
6. Meinhart-Shibata P, et al. *Gait Posture* **22**, 119-125, 2005.

ACKNOWLEDGEMENTS

The authors would like to thank Lukas Linde for his assistance with data collection, as well as Michael Smith and Joel Winsor for assistance with analyses.

Table 1: Falls efficacy scale (FES) score, number of steps, peak COM velocity and cross correlation analysis for both younger and older adults. Means and standard error is presented, with the exception of FES score, where mean and standard deviation is presented. * $p < 0.05$, significant main effect of age.

	FES	Steps*	Peak COM Velocity* (m/s)	Cross Correlation*
Younger Adults	10.33 ± 0.707	2.933 ± 0.088	0.644 ± 0.012	0.959 ± 0.004
Older Adults	10.90 ± 1.375	4.025 ± 0.083	0.539 ± 0.011	0.834 ± 0.015

SHARED AND TASK-SPECIFIC MUSCLE SYNERGIES DURING NORMAL WALKING AND SLIPPING

Mohammad Moein Nazifi¹, Han U. Yoon¹, Kurt Beschorner² and Pilwon Hur¹

¹Department of Mechanical Engineering, Texas A&M University, College Station, TX, USA

²Department of Bioengineering, University of Pittsburgh, Pittsburgh, PA, USA

email: {moeinnazifi, hanulyoon, pilwonhur}@tamu.edu, beschorn@pitt.edu, web: <http://hurgroup.net>

INTRODUCTION

The CNS controls motor tasks using a low-dimensional modular organization of muscle activation (muscle synergies) [1] and some synergies might be shared across different behaviors [2]. Studying slip, as a leading cause of falling accidents that occur on the same level ground is of importance. A comprehensive knowledge about the slip-related muscle synergies in healthy subjects may lead to better understandings of the motor strategy to recover from slip and could be used as a gauge in diagnosis and rehabilitation in future studies.

The objective of this study is to study the muscle synergies during slip initiation while walking and how these synergies are compared with those during normal walking. Specifically, muscle synergies and the corresponding time courses of coefficients will be extracted during both normal walking and slip. Synergies during both normal walking and slipping will then be compared to study if some of the synergies are shared. Similarly, the corresponding coefficients will be compared to learn if they are similar or not during both normal walking and slipping.

METHODS

Eleven healthy young adults (6 male and 5 female, age=22-33yrs) were asked to walk on a floor with four force plates embedded, and informed that the floor would be dry. They were fitted with surface electromyography (EMG) electrodes and donned with a harness to prevent falling due to slipping throughout the trials. Starting location was chosen in a way that subjects hit their right foot on the first and third plates.



Figure 1: The side and top view of the experiment. Red plate shows the slippery surface for slip trials.

The experiment had five normal walking trials followed by an unexpected slip trial. During the slip trial, the third force plate was contaminated by applying a thin layer of a diluted glycerol (90% glycerol and 10% water). All subjects gave informed consent prior to their participation and this research was approved by the University Institutional Review Board. The EMG signals were collected during the task at 1000 Hz from eight

different muscles: medial hamstring (MH), tibialis anterior (TA), rectus femoris (RF), and medial gastrocnemius (MG) on both legs. The EMGs for the first 300ms after the heel strike on the third plate were processed off-line using MATLAB (v2014a, Mathworks, Natick, MA). The EMG data of each channel were normalized by dividing the data with the maximum recorded activity of that channel during all trials for each subject, then rectified and low-pass filtered (4th order Butterworth, 30 Hz as cut-off frequency).

To extract muscle synergies, the EMG data were averaged for each 10ms (300ms resulted in 30 time steps). Using a nonnegative optimization algorithm [3, 4], muscle synergies (W) and the activation coefficients (C) were estimated. Considering the variability curve versus number of synergies [3], four synergies were picked for both normal walking and slipping for each subject. Since the order of subject-specific synergies does not match across the subjects, rearranging of synergies for all subjects were performed as described in the following paragraph.

To rearrange the order of synergies across all subjects for each condition, the following method was used. A reference subject was chosen for each condition, (one for normal walking and one for slipping) that showed the highest similarity with all the other subjects. Specifically, correlation coefficients (r) for every combination of synergies of an arbitrary subject and all other subjects' synergies were calculated. Then, a subject who has the greatest number of shared synergies (i.e., $r > 0.632$ [5]) with the other subjects was defined as a reference subject. Then the order of synergies (W) and the corresponding coefficients (C) were arranged in each subject to have the best matching synergies according to the order of the reference subject. This process was repeated for the other condition as well.

Once synergies and the corresponding coefficients were reordered across all subjects for both conditions, shared synergies and coefficients between both conditions were determined in the following ways. Correlation coefficients for all possible combinations of the four reordered normal walking synergies and four reordered slip synergies (sixteen " r " values for each subject) was calculated. One sample t -test was used to check if $r \geq 0.632$ (for shared synergies) and $r \geq 0.4$ (for marginally shared synergies) (SPSS v21, IBM, Chicago, IL). The significance level was set to $\alpha = 0.05$.

The same procedure was done for activation coefficients (C) only for the first 200ms because the corrective moments on the leading foot initiates about 200ms after the heel contact onto the slippery surface [6]. Assessment of the correlation between activation was restricted to the shared synergies and only the first 200ms after heel strike.

RESULTS AND DISCUSSION

Synergies and coefficients for both normal walking and slipping were successfully extracted (Fig. 2, 3). One sample *t*-test found one share synergy (W1 in Fig.2a, $r=0.82\pm0.13$, $p=0.002$) and one marginally shared synergy (W2 in Fig.2a, $r=0.62\pm0.23$, $p=0.024$) between two conditions. The first shared synergy (W1, Fig.2a) seems to be responsible for ankle dorsiflexion, knee flexion, and hip extension on the leading foot in gait as it activates *TA_R* and *MH_R*. The second shared synergy is knee extensor and hip flexor of the leading foot, since *RF_R* is the main activated muscle. The rest of the two synergies (Fig. 2b) did not seem to be shared and could be considered as task-specific synergies.

The third and fourth normal walking synergies are responsible for the propulsive power of the support leg (as *MG_L* is activated) and dorsiflexion on the support leg (*TA_L* is activated), respectively (Fig.2b, W3 and W4 walk). The function of the third slip synergy seems to stabilize the leading foot (as it activates all muscles almost equally), while the fourth slip synergy creates a dorsiflexion on the support leg (Fig.2b, W3/W4 slip).

For the first shared synergy, the activation coefficient showed a significant correlation between normal waking and slipping for the first 200ms (C1, Fig.3a, $r=0.84\pm0.17$, $p=.004$). For the second shared synergy, the activation coefficient showed a marginally strong correlation (C2, Fig.3a. $r=0.59\pm0.21$, $p=.026$). This agreed with the expectation of having the same activation pattern in the shared synergies before reaction of the CNS (Fig.3a, before 20 time steps). However, after 200ms, the peaks of activation for slip can be considered as the primary and secondary response of the CNS to slip. The primary response (see the first peak after 200ms in C1 slip, Fig 3a) is to dorsiflex the ankle for delayed foot flat, and to flex knee to bring body COM forward into base of support [6]. The secondary response of the CNS to slip (see the second peak after 200ms in C2 slip, Fig 3a) is to extend knee and flex hip [5], which is achieved by the second shared synergy.

CONCLUSIONS AND FUTURE WORK

In this study, shared and task-specific synergies and their corresponding activation coefficients were examined for normal walking and slipping. Two shared synergies and two task-specific synergies were found for

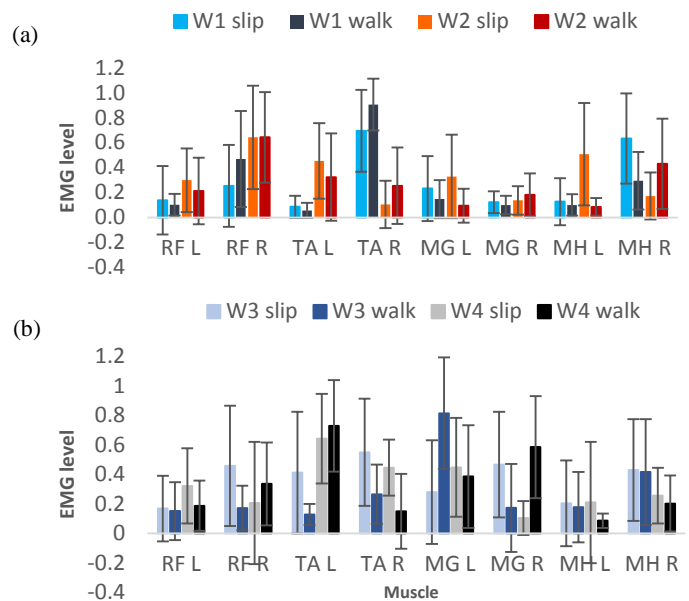


Figure 2: Four synergies for both normal walking and slipping conditions. a) Two shared synergies between both conditions. b) Task-specific (non-shared) synergies between both conditions. Error bar is one standard deviation.

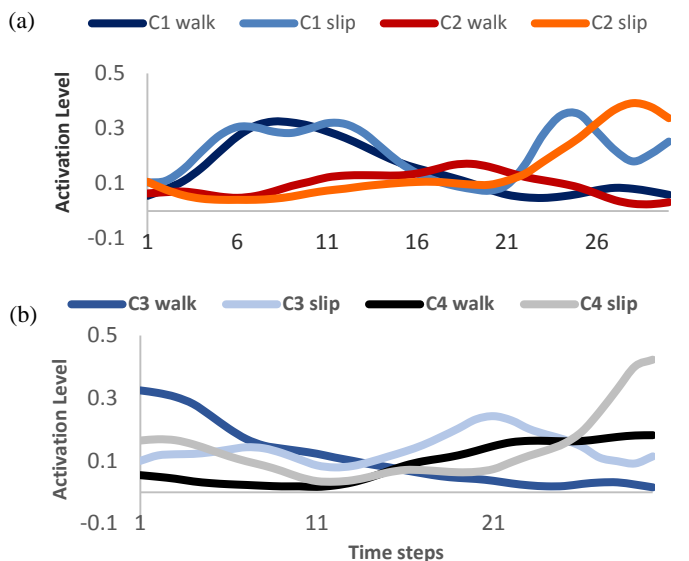


Figure 3: Activation coefficients of the corresponding 4 synergies in Fig. 2. a) Activation coefficients for the 2 shared synergies. b) Activation coefficients for the 2 task-specific synergies. One time step corresponds to 10ms.

normal walking and slipping tasks. Future work will include investigating the shared/task-specific synergies based on slip severity. Comparing synergies and coefficients of both severe and mild slip groups may help identify and intervene factors responsible for severe slips.

REFERENCES

1. d'Avella A, et al. *Nature neuroscience* **6**, 300-308, 2003.
2. d'Avella A, et al. *PNAS* **102**, 3076-3081, 2005.
3. Ting LH, et al. *J Neurophysiology* **93**, 609-613, 2005.
4. Neptune RR, et al. *Journal of Biomechanics* **42**, 1282-1287, 2009.
5. Chvatal SA, et al. *Frontiers in computational neuroscience* **7**, No. 48, 2013.
6. Chambers AJ, et al. *Gait and Posture* **25**, 565-572, 2007.

HIGH KNEE FLEXION AND LOWER LIMB MUSCLE ACTIVATION: DOES MOVEMENT PATTERN MATTER?

David C. Kingston, Helen C. Chong, Liana M. Tennant, Stacey M. Acker

The University of Waterloo, Waterloo, ON, Canada

E-mail: david.kingston@uwaterloo.ca

INTRODUCTION

Industrial occupations or activities of daily living require kneeling and squatting movements. Limited work has measured lower limb muscle activation during high flexion movements and no study has reported the relationship of activation and knee flexion angle. Considering the similarities in range of motion during these movements, muscle activation strategies may be alike. In addition, the use of muscle synergistic patterns can improve model optimization [1] and, should these movements be similar, these high knee flexion movements may be represented using similar synergistic patterns. Therefore, the purpose of this study was to compare muscle activation waveforms between squatting and symmetric kneeling to full flexion. We tested the hypothesis that there would be no difference in lower limb muscle activation between kneeling and squatting when normalized to knee flexion angle.

METHODS

Thirteen female participants (age 22 ± 2 yrs; height 1.64 ± 0.1 m; mass 62.0 ± 9.1 kg) were instrumented with lower limb motion tracking (Certus, NDI, Waterloo, ON) and electromyography (Wave Plus, Cometa srl, Milan, IT) equipment. Data from the right leg were assessed. EMG activity was recorded from the lateral and medial gastrocnemius, semitendinosus, biceps femoris, vastus lateralis and medialis, and rectus femoris. EMG signals were linear enveloped using a low-pass unidirectional 2nd order digital Butterworth filter with a 2 Hz cutoff to replicate an 80 ms phase shift seen in lower limb muscle neuromuscular delay [3]. These activations were normalized from 1° to 137° of knee flexion (in 1° increments) for each of the descending and ascending phases of squatting and symmetric kneeling. The upper limit of 137° was selected from the maximum range of motion of the least flexible

participant. Principal component analysis (PCA) was performed for each muscle using 26 (13 participants x 2 activities) x 137 matrices for descending and ascending separately. Principal components (PCs) which discerned between squatting and kneeling movements by showing a clear delineation of z-scores on bi-plots were assessed using a student's t-test with alpha set to 0.05. The discerning PCs were categorized by operator type [2].

RESULTS AND DISCUSSION

Within muscles, PCs that discerned between squatting and kneeling are listed in Table 1. All discerning PCs were difference operators, indicated by biphasic loading vectors that peaked at the same time as mean activation profiles [2]. Only the PCs which would be retained using a 90% trace criterion were inspected.

During descent, only the biceps femoris muscle had a different normalized activation profile ($p = 0.001$) between movements. However, from 75° to 137° of flexion the squatting movement activation was, on average, only 1.2% MVC greater than the symmetric kneel. Similarly, when ascending the biceps femoris had a discerning PC ($p = 0.003$), but from 5° to 50° of flexion squatting was an average of 1.1 % MVC higher and from 70° to 105° of flexion kneeling was 1.2 % MVC higher in activation. For the purposes of this study, we have deemed these changes not biologically meaningful.

When ascending from full flexion PC2 could separate the activation profiles of the semitendinosus between movements (Table 1 and Figure 1, $p = 0.004$). From 12° to 28° of flexion the symmetric kneel activation was an average of 3.6% MVC higher. As well, from 118° to 137° of flexion, the symmetric kneel activation was 10.4% MVC higher. The only range of semitendinosus activation where

the squat movement required higher activation than the symmetric kneel was from 28° to 50° of flexion, which was 8.6 % MVC higher. For the purposes of this study, changes in ascending semitendinosus activation are considered biologically meaningful.

Considering the lack of differences in nearly all muscles for either the descending or ascending phase of these movements we have highlighted that these closed kinetic chain activities may be interchangeable. The small differences in biceps femoris activity is compounded by the variability within the data, a result inherent to EMG of dynamic high range of motion activities.

These data could be useful as input to a mathematical model as the similarities in activation profiles may allow them to be mapped to knee flexion angle. We acknowledge that an increased sample size and number of collected cycles would be required for these activities before confidence in activation mapping by flexion angle could be realized [1].

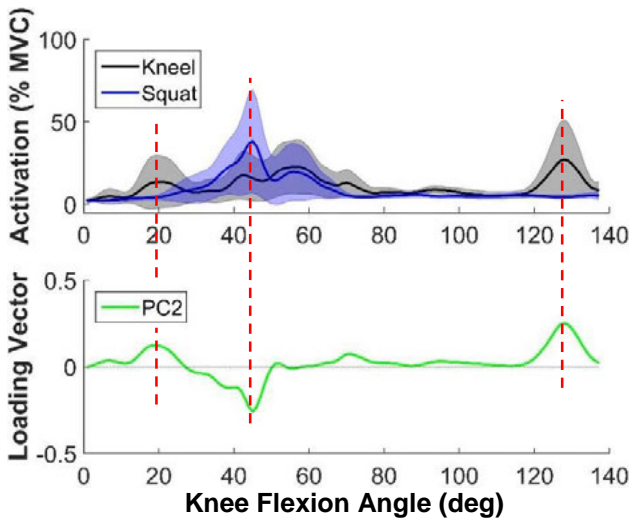


Figure 1: Right: Ensemble average muscle activation of the ascending semitendinosus with 1 SD shaded and PC 2 loading vector for these data with peak differences highlighted. Left: The PC1 vs. PC2 bi-plot of participant z-scores which delineate the symmetric kneel and squatting movements into separate groups.

Table 1: Principal components (PC) which differentiated movement pattern muscle activations. Variance is the percent of variance explained by that PC between group ensemble waveforms. Type is an interpretation of that PC’s operator function [2].

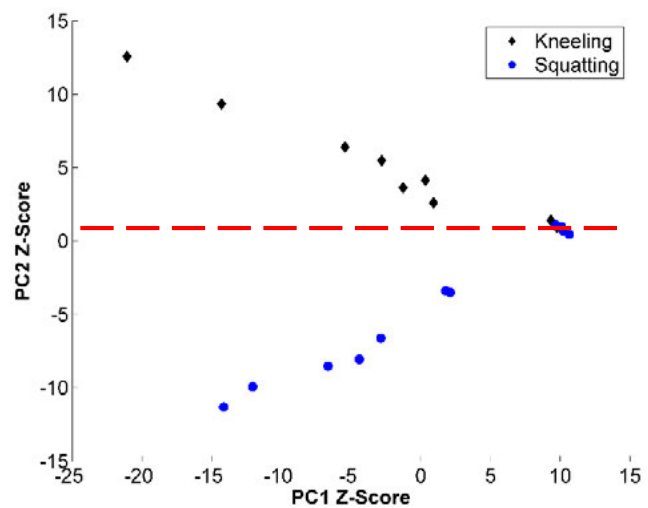
Muscle	Descending			Ascending		
	PC #	Type	Variance %	PC #	Type	Variance %
Biceps Femoris	2	Diff	18.7	4	Difference	3.9
Semitendinosus	-	-	-	2	Difference	27.2

CONCLUSIONS

Using PCA we objectively identified ranges of knee flexion where activation strategies differed. These findings suggest that, when normalized to knee flexion angle, descending to high flexion postures has no meaningful differences between symmetric kneeling and squatting and only the semitendinosus requires separate activation profiles while ascending. Therefore, these movements may be generalized to a single activation profile with respect to flexion angle within each muscle. Future work may explore synergistic patterns of high flexion activities.

REFERENCES

1. Walter, et al. *J Biomech Eng* **136**, 1-9, 2014.
2. Brandon S, et al. *JEK* **23** (6), 1304-1310, 2013.
3. Shultz S, et al. *J Athl Train* **36** (1), 37-43, 2001.



DISTINCTIVE CONTROL STRATEGY OF DYNAMIC FINGERTIP FORCE IN INDIVIDUALS WITH MILD TO MODERATE PARKINSON'S DISEASE AND ITS CLINICAL IMPLICATIONS

¹Na-hyeon Ko, ²Akira Nagamori, ¹Andrew Hooyman, ³Analiese Diconti, ³Jonathan Lerner, ^{1,3}Beth Fisher, and ^{1,2}Francisco J Valero-Cuevas

¹Division of Biokinesiology and Physical Therapy, University of Southern California, Los Angeles, CA, USA

²Department of Biomedical Engineering, University of Southern California, Los Angeles, CA, USA

³Keck school of Medicine, University of Southern California, Los Angeles, CA, USA

INTRODUCTION

Individuals with Parkinson's disease experience progressive impairment of sensorimotor control in fingers, which impacts on dexterous manipulation [1]. Basal ganglia are important neural substrates for grip force control [2]. Damage in basal ganglia might result in different behavioral strategies of grip force control. Using PD model, we may be able to study roles of basal ganglia in grip force control, investigating impairment of sensorimotor control of grip force in PD. However, measuring subtle changes of sensorimotor control in the hands for PD has been challenging because of the low sensitivity and specificity of commonly used clinical assessments, such as the Unified Parkinson's Disease Rating Scales (UPDRS). The Strength-Dexterity (S-D) test has been validated to measure sensorimotor control of dynamic fingertip force at one's maximal instability that he or she has to control [3]. The S-D test requires compressing a spring prone to buckling, and great involvement of basal ganglia was found during the spring task [4]. Therefore, the goal of study is 1) to investigate distinguishable control strategy of dynamic fingertip force in individuals with mild to moderate PD at one's maximal instability and 2) how the findings will correlate with their motor impairment level for its clinical implications.

METHODS

A total of 22 individuals with mild to moderate PD (Hoehn and Yahr stages 1-3) (68.6 ± 7.5 yrs, 11M, 11F) and 41 age-matched individuals without disability (67.0 ± 9.2 yrs, 18M, 23F) participated in the study. The S-D test was used to measure dynamic sensorimotor control of fingertip force from the thumb and index finger. The spring is

prone to buckling, and designed to be impossible to compress fully. Full compression requires $< 3\text{N}$, or about 6-7 % of the maximal voluntary contraction of the thumb and index pinch grip ($\sim 10\text{lbs}$ or 44.5N). The participants compressed the spring to its solid length as much as they could, sustained the compression for 5 seconds, and release the compression. Both affected and less-affected hands were measured for the PD group (PD_{aff} and $\text{PD}_{\text{less-aff}}$), and both dominant and non-dominant hands were measured for the control group (C_{dom} and $\text{C}_{\text{non-dom}}$). Customized miniature load cells (ELB4-10, Measurement Specialties, Hampton, VA, USA) at the end caps measured fingertip force in the compression direction. Force signals were sampled at 400Hz, down-sampled to 100Hz, and low pass filtered at 25Hz. The top three-sustained compression was selected for data analysis. Outcome measures were the maximal sustained compression force level (F) and force dynamics: the 1st derivative of F (F') and its root mean square (RMS) variability from the mean sustained compression. The MDS-UPDRS motor examination was used to measure motor impairment for 14 participants from a subset of the PD group. Spearman rho coefficient was used to test association between the force outcome measures and motor impairment level.

RESULTS

Individuals with mild to moderate PD were able to compress the spring as well as the control group, revealing no significant difference in the group average maximal sustained compression level among four hands. However, how they controlled the instability at their maximal level was distinctive; force variability measured by F' and RMS of the PD_{aff} was significantly greater than those of the

C_{dom} . The greater force variability showed no correlation with the group compression force level in the PD group: F' vs. F ($\rho=0.07$, $p=0.74$) and RMS vs. F ($\rho=-0.03$, $p=0.90$) while force variability increased with the group compression force level in the control group: F' vs. F ($\rho=0.37$, $p=0.031$) and RMS vs. F ($\rho=0.37$, $p=0.031$). Interestingly, the greater F' and RMS in PD_{aff} was negatively associated with the low UPDRS motor score (the lower the score, the less the motor impairment) and the low UPDRS hand-only motor score while no correlation was found between F and the UPDRS motor scores (Table 1).

Table 1: Correlation between UPDRS motor scores and S-D test outcome measures.

	UPDRS_motor	UPDRS_hand_only
F	$\rho = -0.042$, $p = 0.887$	$\rho = -0.192$, $p = 0.512$
F'	$\rho = -0.526$, $p = 0.053$	$\rho = -0.479$, $p = 0.083$
RMS	$\rho = -0.561$, $p = 0.037^*$	$\rho = -0.667$, $p = 0.008^{**}$

* $p < 0.05$, ** $p < 0.01$

The results of the correlation showed that the PD participants with less motor impairment exhibited higher F' and higher RMS. As an example of differences in motor strategies, two PD participants with the same UPDRS hand-only motor score as 12 showed distinctive force control strategies as shown by the phase portraits of F , the 1st derivative of F (F'), and the 2nd derivative of F (F'') plotted during a sustained hold phase (Figure 1).

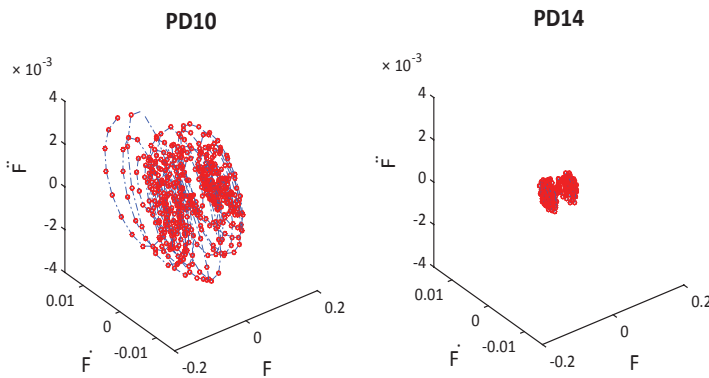


Figure 1: Distinctive fingertip force control strategy in two participants with the same UPDRS hand-only motor score.

CONCLUSIONS AND DISCUSSIONS

Individuals with mild to moderate PD were capable of performing the challenging spring task at a similar level of instability as the control group. But they exhibited greater force variability in the PD_{aff} as described by F' and RMS. Damages in basal ganglia and its sensorimotor cortical closed loop in PD might result in greater force variability because the neural structures are involved in stimulus-response control including rapid automatic corrections [5]. The statistically significant correlation between higher force variability and less motor impairment as per the UPDRS motor scores suggests that force variability is compatible with healthy neurophysiological control of movement in an aging population [6]. Our methodology may be able to detect the progress of the disease as the gradual loss of this variability, which may be related to the loss of mobility in later stages of the disease seen as freezing, bradykinesia, and akinesia. Therefore, measuring changes of force variability with this unstable manipulation task might provide a higher resolution to quantify the progression of motor impairment than the UPDRS motor examination. This could be beneficial to determine a dosage of medication and parameters for deep brain stimulation; or measure motor fluctuations throughout the day.

REFERENCES

1. Lukos et al. *Hand function*, 133-149, 2014.
2. Prodoehl et al. *Neurosc and Biobehav Rev* **33**(6), 900-908, 2009.
3. Valero-Cuevas et al. *J Biomech* **36**, 265-270, 2003.
4. Mosier et al. *J Neurophy* **105**(3), 1295-1305.
5. Redgrave et al. *Nat Rev Neurosc* **11**(11), 760-772, 2010.
6. Lipsitz et al. *Jama* **267**(13), 1806-1809, 1992.

ACKNOWLEDGEMENTS

Supported by NIH-NIAMS under award numbers R01AR050520 and R01AR052345 grants to FVC.

INTRA-AUDITORY INTEGRATION IN A CONSTANT FORCE PRODUCTION TASK

¹Kyung Koh, ¹Hyun Joon Kwon, ¹Ross H. Miller, and ¹²Jae Kun Shim

¹Neuromechanics Research Core, University of Maryland, College Park, MD, 20742, USA

²Kyung Hee University, Yongin-si, Syeonggi-do, 446-701, Korea

Email: kyungkoh@umd.edu, Web: www.sph.umd.edu/neuromechanics

INTRODUCTION

Humans can combine multiple sources of sensory information to estimate the state of the body and environment. Several empirical studies have shown that sensory information is integrated in a statistically optimal (i.e., minimum-variance) fashion following Bayesian rules or maximum likelihood estimation (MLE) [1]. Most of these studies have focused on the optimal integration between different sensory systems (e.g. visual and auditory, visual and tactile, or visual and proprioceptor), called inter-sensory integration [1, 2]. However, our knowledge on integration of different modalities within one sensory system (i.e. intra-sensory integration) is limited [3].

Previous studies on intra-sensory integration have primarily examined vision (e.g. color and shape). Despite the fact that auditory perception is critical in our day-to-day living, very little is known about how the central nervous system (CNS) integrates multiple features of auditory sensation (e.g. frequency and intensity) to guide motor performance (i.e. intra-auditory integration).

Therefore, our purpose was to determine if Bayesian inference can explain intra-auditory integration in a finger force-production task. We hypothesized that intra-auditory integration would follow Bayesian inference supported by improved motor performance when both frequency and intensity modalities are used for auditory feedback as compared to a single modality condition.

METHODS

Ten right-handed adults (age 27.3 ± 5.3) participated. The subjects were instructed to produce a constant target isometric force of 18 N for 20 s by pressing individual force sensors with 2nd to 5th digits.

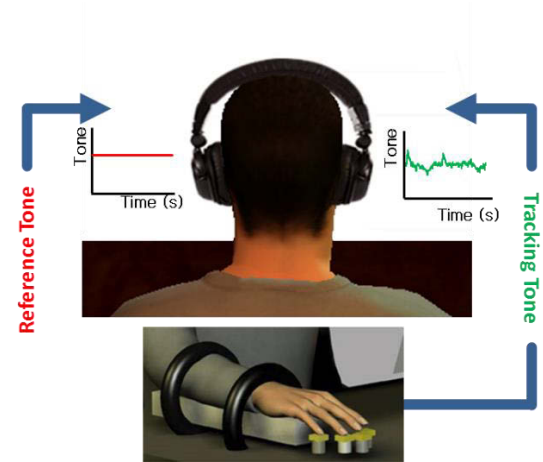


Figure 1. Experimental setup.

Participants completed fifteen 20-s trials in each of three conditions, with 30 s rest between trials. During the task, the reference force (18N) was provided as an auditory signal, a sinusoid signal with frequency 1000 Hz and intensity 70 dB (i.e. reference tone), played to the subject's left ear. The force generated by the subject was also provided as a sinusoid signal (i.e. tracking tone) to their right ear. The tracking tone had three feedback conditions:

- 1) Frequency condition (F): the frequency of the tracking tone changed depending on the deviation of the subject's sum of finger forces from 18 N, with a constant intensity of 70 dB.
- 2) Intensity condition (I): the intensity of the tracking tone changed depending on the deviation of the subject's total finger force from 18 N, with a constant frequency of 1000 Hz.
- 3) Frequency & Intensity condition (FI): both frequency and intensity of the tracking tone changed depending on the sum of finger forces.

The rate of changes of frequency and intensity per Newton were set as 7Hz/N and 0.7dB/N,

respectively, according to minimum detectable differences previously reported [4, 5].

Motor performance was quantified using the average mean-squared error ($AMSE$) between the sum of finger forces and the target 18-N force:

$$AMSE = \frac{1}{N} \sum_{i=1}^N \left\{ \frac{1}{\tau} \int [f_T - y_i(t)]^2 dt \right\}$$

where $y_i(t)$ is the sum of individual finger force at trial i , f_T is the target force, and τ is the duration of $y_i(t)$. Data were collected for 20 s, but only the data between 6 s and 17 s (11 s total) were analyzed. We also compared the experimentally obtained $AMSE$ to the $AMSE$ predicted by Bayesian inference (MLE) [6] as follows:

$$AMSE_{FI} = \sigma_{FI}^2 + b_{FI}^2$$

where variance is calculated as $\sigma_{FI}^2 = \frac{\sigma_F^2 \sigma_I^2}{\sigma_F^2 + \sigma_I^2}$ and

systematic error is $b_{FI}^2 = \left(\frac{\sigma_F^2 b_F}{\sigma_F^2 + \sigma_I^2} + \frac{\sigma_I^2 b_I}{\sigma_F^2 + \sigma_I^2} \right)^2$.

RESULTS AND DISCUSSION

Repeated measures ANOVA revealed that $AMSE$ was lower ($p < 0.005$) with combined FI feedback than with F or I feedback alone (Fig. 2). The reduction of $AMSE$ with FI feedback was mainly due to the reduction of variance ($p < 0.01$) while the systematic errors remained unchanged across the feedback conditions ($p=0.153$; Fig. 3).

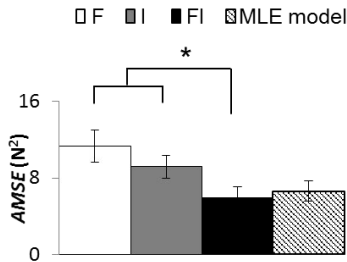


Figure 2: The overall mean squared error ($AMSE$). Means and standard errors across subjects. Asterisk indicates significant differences among feedback conditions ($p < 0.05$).

No significant differences ($p > 0.05$) between experimental measurements (in FI condition?) and the MLE predictions were found for $OMSE$ (Fig. 2), variance, and systematic error (Fig. 3).

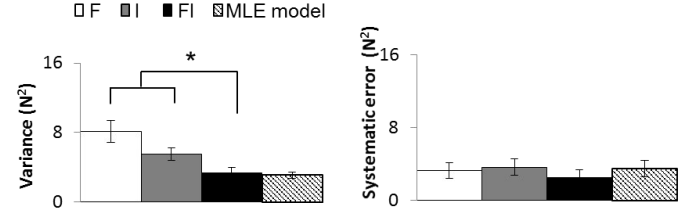


Figure 3. The variance and systematic error. Means and standard errors across subjects. Asterisk indicates significant differences among feedback conditions ($p < 0.05$).

The results suggest that Bayesian inference can accurately predict observations of intra-auditory integration during isometric multi-finger force production. Notably, the target finger force was produced with reduced force variation when multiple auditory modalities were presented as auditory feedback (FI condition), as compared to single auditory modality conditions (F condition and I condition). These results are consistent with previous studies of inter- and intra-sensory integration across visual modalities [1-3]. Thus, our research supports the hypothesis that humans have the ability to optimally integrate intra-auditory modalities, enhancing motor performance.

CONCLUSIONS

Intra-auditory integration leads to the enhancement of constant finger force production, following maximum likelihood estimation. The data support the Bayesian inference in intra-auditory integration for motor performance in humans.

REFERENCES

1. Ernst MO, Banks MS., *Nature* **415**, 429-33, 2002.
2. Alais D, et al. *Curr Biol.* **14**, 257-62, 2004.
3. Hillis JM, et al. *J. Vis* **4**, 967-92, 2004.
4. Moore BC, et al. *J. Acoust Soc Am* **54**, 610-9 1973.
5. Ozimek E, et al. *J. Acoust Soc Am* **100**, 3304-20 1996.
6. Scarfe P, Hibbard PB. *J. Vis* **11**, 1-17, 2011.

REPRESENTATION OF WRIST MOTION CHARACTERISTICS USING THE AXIS OF ROTATION

Mahmood Lahroodi and Ilhan Erhan Konukseven

Middle East Technical University (METU), Ankara, Turkey
email: lahroodi@gmail.com, web: http://metu.edu.tr

INTRODUCTION

Since the motion of wrist is almost pure rotation, spherical coordinate system is a compatible reference frame for analyzing the motion of wrist. Kinematically, human wrist can be modeled by 3DOF (FE, RUD, PS) manipulator with 2DOF (FE, RUD) in universal-like joint of wrist and additional DOF (PS) which comes from forearm[1]. Dynamically, it is shown that passive wrist stiffness is dominant dynamic of wrist [1] and depends nonlinearly on the position of wrist [2]. The present study shows that similar to passive stiffness, level of wrist noise depends on the position as well. For modeling the noise of wrist, we have studied the variation of Axis Of Rotation (AOR). Behavior of AOR not only depends on noise but also the biomechanical properties of wrist [3]. The results of experiment imply that fast changes of AOR is most probably because of internal noise (in actuation and sensing) and systematic patterns produced intentionally according to the dynamic of task and wrist.

METHODS

In this study, new approach has been followed for analyzing the wrist motion by adding a fixed link to the multi DOF joint. In fact, the new manipulator, let us call it wrist manipulator has a spherical-like joint in the origin of spherical coordinate system and a link which connects the origin to the surface of sphere with the radius of the length of link. The Jacobian matrix of new-defined manipulator can be easily obtained by finding the relation between rotational velocity at joint and translational velocity on the surface of sphere. The position of tip point of wrist manipulator can be written in vector form as

$$\vec{L} = L_x \vec{i} + L_y \vec{j} + L_z \vec{k} \quad (1)$$

The rotational velocity of link can be written in vector form as well. The translational velocity of tip point can be obtained by cross product of rotational and position vectors.

$$\vec{V} = \vec{\omega} \times \vec{L} = (\omega_y L_z - \omega_z L_y) \hat{i} + (\omega_z L_x - \omega_x L_z) \hat{j} + (\omega_x L_y - \omega_y L_x) \hat{k} \quad (2)$$

By writing in matrix form and comparing with $\vec{V} = J \dot{\Theta}$, we obtain the Jacobian matrix of this manipulator. By finding the projection of displacement vector in each axis we obtain the matrix with respect to angles.

$$\begin{cases} L_x = L \cos(\alpha) \\ L_y = L \cos(\beta) \\ L_z = L \cos(\gamma) \end{cases} \Rightarrow J = \begin{bmatrix} 0 & L \cos(\gamma) & -L \cos(\beta) \\ -L \cos(\gamma) & 0 & L \cos(\alpha) \\ L \cos(\beta) & -L \cos(\alpha) & 0 \end{bmatrix} \quad (3)$$

The Jacobian matrix of this manipulator is skew symmetric matrix and its determinant is zero. In fact, since we can show any vector in spherical coordinate system with just two angles (Azimuth and Elevation) in comparison with three angles of wrist in FE, RUD and PS directions, then it is expectable to have Jacobian matrix which is not invertible. Since we do not have an access to wrist robot [4] for measuring the angles of wrist and at the same time the Jacobian is not invertible, we had to capture the motion of tip point of wrist manipulator and utilize AOR notion for our analysis. In addition, AOR technique magnifies the deviations at wrist motion and makes it possible to capture the small and sometimes hidden dynamic of wrist. For doing so, we used following experiment with Omni Haptic device. We asked subjects to track a pre-determined circle (10 cm diameter) on space with two different positions for 4 times with just wrist motion. Figure 1 shows the connection of human wrist and pen of Omni haptic device. The link of wrist manipulator is defined from the location of wrist to the tip point of Omni pen which is shown by Orange vector.

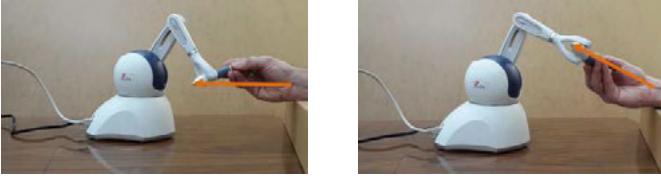


Figure 1: Human wrist holds the pen of Omni haptic device for doing the task: first position (left), second position (right)

RESULTS AND DISCUSSION

Axis of rotation of a perfect circle is a fixed line, however when human tries to produce a circle because of noisy sensory inputs and motor commands and biomechanical properties of wrist it will not be a perfect circle. Producing a perfect circle even for a skillful person may not be possible. It is important to note that producing a circle can be done in two different ways; drawing a circle (mostly engaged with internal model of this task in nervous system) and tracking a circle (mostly engaged with internal optimal control system). The distribution of axis of rotation is a good criterion for measuring a performance of operator in producing circular motions. It is obvious that producing circular motion is just a primitive example for generation versatile kinds of motions like writing a letter and doing deburring with so many curvature motions. The probabilistic model of producing circular motion reveals the performance and impairment of a subject. Figure 2 shows the distribution of elevation and azimuth angles of AOR for two different positions of wrist produced four times for one subject. It denotes that AOR is more noisy for second position in Azimuth direction.

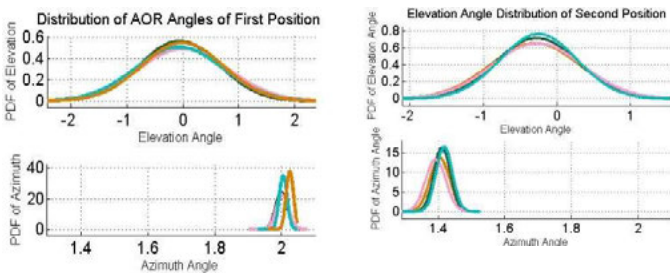


Figure 2: Gaussian distribution of AOR for position one (left diagrams) and position two (right diagrams)

As it is shown in Figures 3 and 4 (left ones), the special region of ROM are more noisy than other

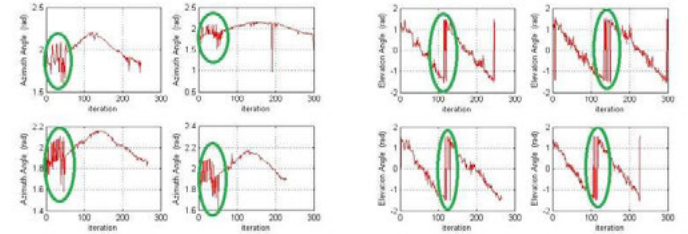


Figure 3: Behavior of AOR for first position

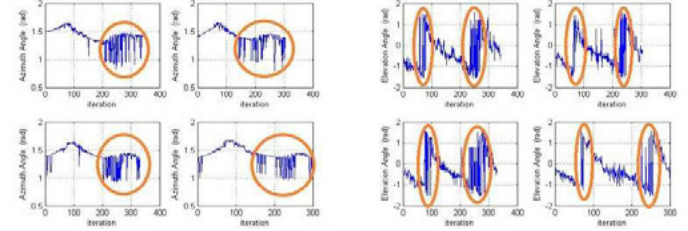


Figure 4: Behavior of AOR for second position

regions and this pattern is almost same for a same position and different cycles. It shows that wrist noise is position- depended signal. On the other hand, there are some sharp changes of elevation angles (right ones) which are same again for different cycles. The systematic pattern of behavior of AOR reveals that noise is not the only source of this pattern. The biomechanical properties of wrist and the dynamic of task may determine the shape of those patterns. In this study we showed that the variance of noise is changing during task; moreover; the unique behavior of elevation and azimuth angles of AOR denotes that there should be a systematic pattern for this task. However the mathematical and biomechanical reasons behind this phenomenon are not represented here. The advantage of this study is that it will help us to create a comprehensive map of wrist noise in entire range of motion.

REFERENCES

1. A. W. Peaden and S. K. Charles, *J. Biomech.*, vol. 47, no. 11, pp. 2779–2785, 2014.
2. A. L. Pando, H. Lee, W. B. Drake, N. Hogan, and S. K. Charles, *IEEE Trans. Biomed. Eng.*, vol. 61, no. 8, pp. 2235–44, Aug. 2014.
3. S. K. Charles and N. Hogan, *Exp. brain Res.*, vol. 203, no. 1, pp. 63–73, May 2010.
4. B. T. Volpe, J. Celestino, and S. K. Charles, *IEEE Trans. Neural Syst. Rehabil. Eng.*, vol. 15, no. 3, pp. 327–335, 2009.

ACKNOWLEDGEMENTS

This study is supported by the TUBITAK, 114E274.

MODULATION OF TREMOR DURING ISOMETRIC FORCE TRACKING

¹ Christopher Laine*, ² Strahinja Dosen, ² Jakob Dideriksen, ¹ Francisco Valero-Cuevas, ² Dario Farina

¹ The University of Southern California, Los Angeles, CA, USA

² University Medical Center Göttingen, Göttingen, Germany

* Email: claine@usc.edu

INTRODUCTION

To investigate neural control of fingertip forces, subjects are often asked to track a target using visual feedback of their exerted force level. In the context of such tasks, measures of tracking error and force tremor can reveal a wealth of information relevant to understanding closed-loop neural control. However, it is often difficult to disambiguate central (cognitive) vs. peripheral (reflexive or mechanical) contributions to task performance. For example, both attentional [1] and mechanical [2] aspects of a task can influence the magnitude and gain of afferent feedback from muscles, and therefore both can affect the amplitude of physiological tremor [3,4,5].

While psychosensory factors influencing tremor amplitude have received much attention, mechanical/muscular factors such as the magnitude, velocity, and dynamics of force production have not been well characterized. In this investigation, we quantified the modulation of tremor amplitude during the visually-guided production of sinusoidal forces.

METHODS

Eleven healthy participants used a 3-finger pinch grip to produce force against a transducer during visually-guided tracking tasks. Participants were asked to track sinusoidal target trajectories of either 0.1 or 0.25 Hz, each with a mean value (offset) of 7% of their maximal force and an oscillation amplitude of 1%. Each 40s target trajectory was displayed on a 19-inch computer monitor, with the vertical axis (displaying force magnitude) spanning from 5 to 9% of the maximal grip force. Subjects used a feedback cursor to trace the targets from left

to right across the screen. Each subject completed 5 trials tracking each of the two target sinusoids.

Because frequencies of force tremor under 5 Hz are thought to relate to voluntary visuomotor error corrections, the force signals were high-pass filtered at 5 Hz (second-order zero-phase-shift Butterworth filter) prior to assessing involuntary physiological tremor. Wavelet analysis characterized the magnitude of force fluctuations at each frequency over time. A cross-cycle median tremor amplitude was derived for each frequency (bin size = 0.5 Hz), at each ms of the sinusoidal target cycle (Fig 1). We also assessed low frequency force fluctuations (1-5 Hz) in the same way (not shown).

RESULTS AND DISCUSSION

The magnitude of tremor was highly and consistently dependent upon the phase of sinusoidal force production. The most striking feature was a burst of ~10 Hz tremor when the target force was lowest, at the transition from isometric relaxation to contraction.

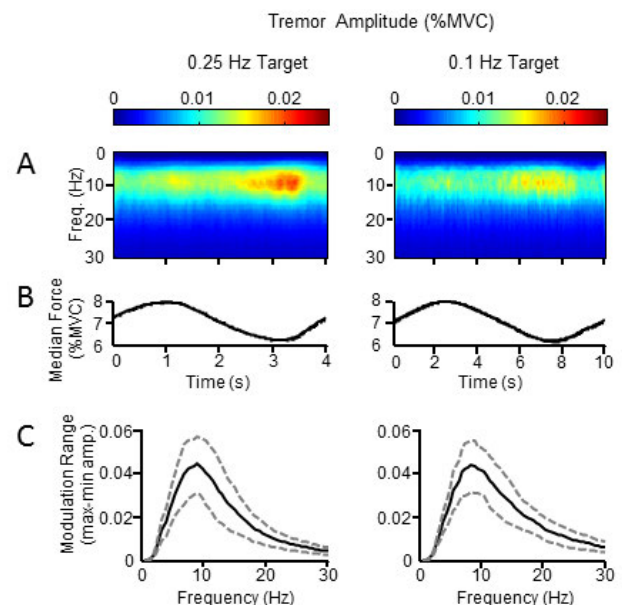


Figure 1: Tremor modulation during sinusoidal tracking.

Panel A (left) shows the spectrogram of force fluctuations occurring during the tracking of a 0.25 Hz target oscillation. The tremor amplitude at each time-frequency pixel represents the median amplitude over all cycles, and all subjects. To the right, the results of the same analysis are shown for the 0.1 Hz sinusoidal target. Beneath each spectrogram (Panel B) are the median forces produced at each time point shown in the above spectrograms. Panel C represents the median (black line) amplitude modulation range per frequency. This range was calculated for each cycle of the target sinusoid as the difference between the maximum and minimum tremor amplitude at a given frequency. The dashed lines represent the interquartile range (25th – 75th percentile) surrounding the median.

Tremor amplitude did not appear to be strongly determined by the overall magnitude or velocity of force at any given phase of the target cycle. Rather, a gradual buildup of ~10 Hz tremor during periods of declining force was observed prior to the large burst at the trough of the target sinusoid. The 0.1 and 0.25 Hz sinusoidal targets produced similar patterns of tremor amplitude modulation, and the degree of cross-cycle tremor modulation at ~10 Hz was nearly identical for both frequencies. Although the degree of ~10 Hz tremor amplitude modulation was similar for both target sinusoids, the faster target was generally associated with larger tremor amplitudes across all phases. An analysis of low frequency force fluctuations (not shown in Fig. 1) revealed the existence of a consistent fluctuation (~3 Hz in frequency) in force tracking which occurred simultaneously with the burst of ~10 Hz tremor. On the basis of their common timing with

respect to the phase of the target cycle, the two phenomena may share a similar neural origin.

We speculate that the tendon stretch at the transition from isometric relaxation to contraction may disrupt ongoing control of force, possibly via feedback from Golgi tendon organs and/or muscle spindles. Additional factors may include cycle-dependent alterations of reflex sensitivity [2] or changes in motor unit synchronization [4,5].

CONCLUSIONS

The amplitude of physiological force tremor depends upon the temporal dynamics of force production. The transition between isometric relaxation and contraction appears to be of particular importance, and may represent a disruption of smooth (feed-forward) force control by a sudden change in peripheral feedback.

REFERENCES

1. Ribot-Cisar E. et al. *Journal of Neurophysiology*, **101**, 633-640, 2009
2. Xia R, et al. *Journal of Physiology* **564.3**, 941-951, 2005
3. Young RR, Hagbarth K, *Journal of Neurology*, **43**, 248-256, 1980
4. Christakos CN et al. *Journal of Neurophysiology*, **95**, 53-66, 2006
5. Laine CM, et al. *Acta Physiologica* **211**, 229-239, 2014

ACKNOWLEDGEMENTS

Funding from the Commission of the European Union (Grant ICT-2011-287739, NeuroTREMOR) to DF and by NIH-NIAMS under award numbers R01AR050520 and R01AR052345 to FVC.

CARPAL TUNNEL SYNDROME IMPAIRS FINGER RESPONSES TO UNPREDICTABLE PERTURBATION

¹Kaihua Xiu, ¹Tamara L. Marquardt, ¹Chengliu Li, ²Peter J. Evans, ²William H. Seitz Jr., ^{1,2,3}Zong-Ming Li

Hand Research Laboratory, Departments of ¹Biomedical Engineering, ²Orthopaedic Surgery, and ³Physical Medicine and Rehabilitation, Cleveland Clinic, Cleveland, OH, USA

email: liz4@ccf.org, web: <http://www.handlab.org>

INTRODUCTION

Successful object manipulation requires effective integration of sensory information and motor commands. Carpal tunnel syndrome (CTS), a prevalent entrapment neuropathy, is caused by chronic compression of the median nerve in the carpal tunnel. CTS patients experience sensory deficits, such as numbness, paresthesia, and reduced sensation. However, the effects of these CTS-associated sensory deficits on finger responses are not well understood. The purpose of this study was to investigate finger muscle and force responses to unpredictable perturbations in patients with CTS. We hypothesized that CTS patients would demonstrate impaired finger responses to perturbations.

METHODS

Seven CTS patients (48 ± 16 years) and seven asymptomatic control subjects (52 ± 12 years) participated in this study. The experimental setup for the perturbation-induced finger response task is depicted in Fig. 1.

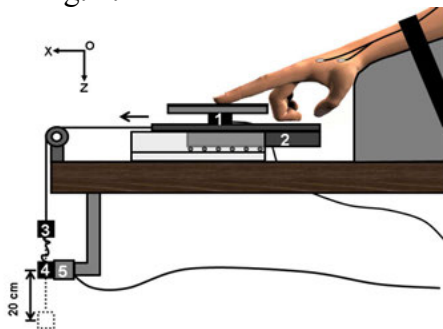


Figure 1: Schematic of experimental setup: (1) transducer; (2) slide; (3) baseline weight; (4) perturbation weight; (5) electromagnet.

The wrist and forearm were rested on a wedged-support with the index finger parallel to the

inclination surface of the support. At the beginning of each trial, the subject pressed a plate with the index finger and maintained a 3N baseline force according to provided visual feedback. The unpredictable perturbation was implemented by releasing a 100g weight from a height of 20cm at a random instant in the 20-40s time window. The subject was instructed to stop the slide from moving as quickly as possible. The activity of the first dorsal interosseous (FDI) muscle was recorded by a surface electromyography (EMG) system and the forces from the index finger were collected by a six-component force/torque transducer. A total 15 trials were completed and 9 trials were used for analysis.

Muscle and force responses to the perturbation were quantified based on latency, duration, and intensity. For each trial, the onset of perturbation was identified as the time point when the tangential force (x-direction) exceeded 3 standard deviations (SD) of its baseline (mean of the signal 5s prior to the release of the perturbation weight). Then, the signals from individual trials were synchronized according to the onsets of perturbation and averaged for each subject. From the averaged trial, the EMG/normal force signal was used to determine the onset of muscle/force response as the time point when the EMG/normal force exceeded 3SD of its respective baseline. The muscle/force response latency was defined as the time period between the onset of perturbation and the onset of muscle/force response. The time point and magnitude of the peak EMG/normal force response were also obtained. The muscle/force response duration was the time interval between the onset of muscle/force response and the time point of peak muscle/force response. Additionally, the muscle/force response intensity was defined as the ratio of the peak EMG/normal force response magnitude to the baseline EMG/normal force. The moving duration of the

slide was also derived to determine the consequence of the finger's responses on the object. It was quantified as the time interval between the onset of perturbation and the time instant when the plate stopped sliding (i.e. when the velocity of the center of pressure measured by the transducer was zero). Independent t-tests were performed on variables between groups. A $p < 0.05$ was considered statistically significant.

RESULTS AND DISCUSSION

For the CTS and control groups, finger responses were characterized by activation of the FDI muscle followed by increased applied normal force (Fig. 2).

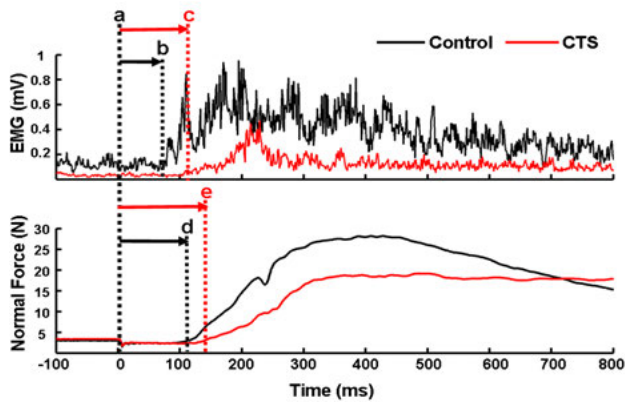


Figure 2: Muscle (top) and force (bottom) responses for representative control and CTS subjects: a-onset of perturbation; b/d-onset of muscle/force response (Control); c/e-onset of muscle/force response (CTS).

Muscle and force response latencies, durations, and intensities are presented in Table 1. In comparison to the control group, the CTS group demonstrated 22.0% prolonged muscle response latency ($p < 0.05$) and 11.7% prolonged force response latency ($p < 0.05$). No statistical differences were found between groups for duration or intensity of the muscle or force responses. The duration of plate sliding for the CTS group (140.6 ± 3.5 ms) was significantly longer than that of the control group (135.6 ± 3.6 ms, $p < 0.05$).

In current study, the CTS group demonstrated prolonged response latencies to unpredictable perturbations. CTS-associated changes of the cutaneous sensory function and/or adaptations of the central nervous system may have contributed to the slower responses. In particular, decreased stimulus encoding by cutaneous mechanoreceptors or deteriorated central information processing could slow down the sensorimotor integration process, resulting in the delayed responses. Although significant differences were not found for response intensities between groups (muscle: $p = 0.079$; force: $p = 0.057$), the CTS group displayed trends of lower response intensities. With a larger sample size, we expect this difference will be significant. If CTS patients respond less forcefully than controls to unpredictable perturbations, then this expected result is in contrast to previous studies which have reported that CTS patients use increased grip force during static precision pinch [1]. This discrepancy may be attributable to the different strategies used to complete each task [2]. Specifically, precision pinch tasks rely predominantly on anticipatory mechanisms from previous sensorimotor memories, whereas unpredictable perturbation tasks depend more on instantaneous sensory feedback from the perturbations. Together, the delayed and decreased responses may indicate a different pattern of inefficient object manipulation by CTS patients. The deteriorated efficiency of the index finger's responses likely contributed to the prolonged duration of plate sliding, and may help to explain why CTS patients tend to drop objects.

REFERENCES

1. Lowe BD and A Freivalds. *Ergonomics* 42(4), 550-564, 1999.
2. Nowak DA and J Hermsdorfer. *Eur J Appl Physiol* 89(2), 127-133, 2003.

ACKNOWLEDGEMENTS

NIH/NIAMS R01AR056964

Table 1: Finger responses to perturbations from control and CTS group (Mean \pm SD, * $p < 0.05$)

	Muscle Latency (ms)	Muscle Duration (ms)	Muscle Intensity (ratio)	Force Latency (ms)	Force Duration (ms)	Force Intensity (ratio)
Control	77.1 \pm 9.6*	166.7 \pm 22.4	9.6 \pm 3.5	103.7 \pm 6.7*	233.6 \pm 31.3	8.0 \pm 2.4
CTS	94.1 \pm 17.1*	181.3 \pm 53.6	6.6 \pm 2.1	115.9 \pm 12.5*	263.9 \pm 32.5	5.4 \pm 2.0

POSTURAL STABILITY, MOTOR SKILLS, AND REPETITIVE BEHAVIOIRS IN CHILDREN WITH AUTISM SPECTRUM DISORDER

¹ Melissa A. Mache and ² Teri A. Todd

¹ California State University, Chico, CA, USA

² California State University, Northridge, CA, USA

email: mmache@csuchico.edu

INTRODUCTION

Postural stability is believed to be a prerequisite for the performance of mature patterns of fundamental motor skills. It has been reported that the development of postural stability is delayed among individuals with autism spectrum disorder (ASD); further, it may never reach mature levels [1]. Individuals with ASD also commonly exhibit poor motor skills when compared to typically developing peers [2]. Recent comparisons of postural stability in children and adults with ASD have indicated postural stability and motor skill difficulties may not be uniform across individuals with ASD [3]. At present it is not clear how postural stability and motor skill deficits may be related to ASD severity.

The purpose of this pilot study was to compare postural stability and motor skills among children with and without ASD. Additionally, relationships between postural stability, gross motor skills, and repetitive behaviors was examined in children with ASD.

METHODS

Twelve age-matched boys (6-12 years; 6 with ASD) provided assent to participate in the present study. Informed consent was also provided by a parent or guardian.

Postural sway and motor skills data were collected during a single testing visit. A parent or guardian completed the Repetitive Behavior Scale – Revised (RBS-R) for each child.

In order to assess postural stability participants completed three quiet standing trials. All trials were 20 seconds in duration. During the quiet standing trials participants were asked to stand quietly on the force plate, with their hands at their sides, their feet a comfortable width apart, while looking at a 'smiley face' on the wall at eye-level approximately 5 meters in front of them. Center of pressure (COP) data were sampled at 60 Hz with a Kistler force plate (Kistler, Amherst, NY, USA) or Neurcom Balance Manager Long Force plate (Neurocom, WA, USA).

In the same laboratory visit participants also completed the Test of Gross Motor Development, 3rd Edition (TGMD-3). The TGMD-3 is a criteria-based assessment consisting of 13 fundamental motor skills, including run, jump, and throw. For each skill a researcher provided a demonstration of the skill and the child then performed the skill twice. Performance of the motor skills was videoed and analyzed subsequently using the TGMD-3.

The following variables were computed for analysis: (1) Postural stability was assessed during the quiet standing trials by computing postural sway area which was defined as the smallest ellipse that included 95% of the COP data points; (2) motor skills were evaluated using the TGMD-3 total score; and (3) the RBS-R total scores were computed to assess severity of ASD. Paired, one-tailed t-tests were used to assess differences between children with and without ASD. Simple linear correlation was used to explore relationships between variables (i.e., sway area, TGMD-3 score, and RBS-R score) among children with ASD. To account for the

small sample size and multiple statistical comparisons, the alpha level was set at 0.025 for all statistical analyses.

RESULTS AND DISCUSSION

There were no differences in postural sway among children with and without ASD ($t = -1.54$, $p = 0.092$) (Table 1). This contrasts some previous work, however, it supports the idea that children with ASD may not exhibit uniform deficits in postural stability [1, 3]. Children with ASD did score significantly lower on the TGMD-3 ($t = 3.32$, $p = 0.011$) than their peers without ASD (Table 1). The deficits in motor skills observed in the present population are in agreement with previous findings [2]. Furthermore, these results highlight the need for appropriate means of identifying children with ASD who may be affected by motor skill deficits and developing effective interventions to target these deficits [2].

There was no relationship between postural sway area and motor skills in children with ASD ($r = -0.588$, $p = 0.110$) (Figure 1). When considered in light of the fact that this cohort did not exhibit deficits in postural stability compared to their peers it is possible that postural stability is not the limiting factor for motor skill development in this group of children with ASD. Similarly, severity of repetitive behaviors was not related to postural stability ($r = -0.571$, $p = 0.118$) or fundamental motor skills ($r = 0.341$, $p = 0.23$) in this group of children with ASD. Based on the present findings it does not appear that the RBS is a suitable tool for identifying children with ASD who may be affected by deficits in postural sway or motor skills.

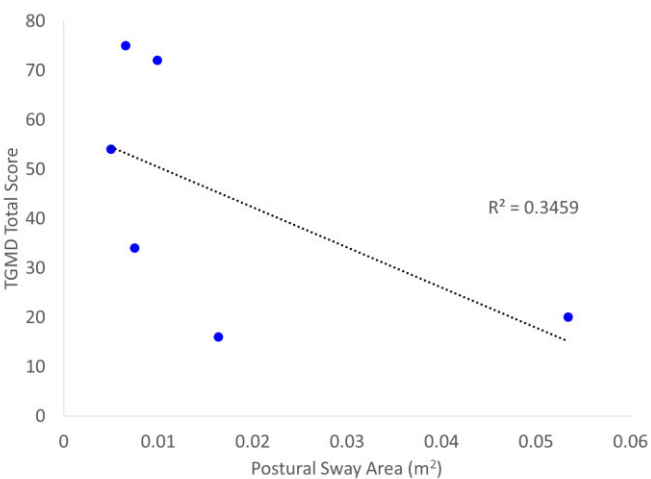


Figure 1: TGMD-3 total score Vs. Postural sway in children with ASD.

CONCLUSIONS

Though, motor skill deficits were greater among children with ASD than among their peers without ASD this was not a predictor of postural stability. The present study is somewhat limited by the small number of participants. Differences between children with and without ASD and relationships between repetitive behaviors, motor skills, and postural stability among children with ASD may become more evident in a larger group of participants or under conditions of reduced sensory input (e.g., eyes closed or modified proprioceptive input).

REFERENCES

1. Radnovich, KJ, et al. *Front Integr Neurosci* **7**, doi: 10.3389/fnint.2013.00028
2. Fournier, KA, et al. *J Autism Dev Disord* **40**, 1227-1240, 2010.
3. Travers, BG, et al. *J Autism Dev Disord* **43**, 1568-1583.

Table 1: Test of gross motor development (TGDM-3), postural sway area, and repetitive behavior scores (RBS-R) for children with and without ASD (Mean ± SD).

Variable (units)	Children With ASD	Children Without ASD
Sway Area (m ²)	0.00942 ± 0.005	0.01161 ± 0.012
TGMD-3 Total Score	44.0 ± 23.6*	72.3 ± 21.5
RBS-R Total Score	22.6 ± 13.0	4.6 ± 5.5

* $p < 0.025$ vs. children without ASD

PATIENTS WITH SYMPTOMATIC FEMOROACETABULAR IMPINGEMENT (FAI) DEMONSTRATE DIFFERENT LOWER EXTREMITY JOINT COORDINATION COMPARED TO HEALTHY CONTROLS DURING A DOUBLE LEG SQUAT TASK

¹ Philip Malloy, ¹ Alexander Morgan, ¹ Michael Kiely, ¹ Christopher Geiser, ² John T Heinrich, ¹ Kristof Kipp

¹ Marquette University, Milwaukee, WI USA

² Milwaukee Orthopedic Group

email: Philip.malloy@marquette.edu

INTRODUCTION

Femoroacetabular impingement (FAI) is a skeletal deformity that has been linked to intra-articular hip injuries, such as acetabular labral tears and early onset osteoarthritis [1, 2]. Often times these hip injuries occur through overuse type mechanisms. FAI patients typically demonstrate losses of terminal hip flexion, internal rotation, and adduction range of motion [1]. Therefore, compensations in adjacent joints may be observed because of structural abnormality that constrains joint motion.

Alterations in joint coordination patterns have been linked to overuse type injury [3]. Kinematic changes associated with lower extremity injury can constrain movement patterns of the injured limb thereby altering the coordination of movement between all joints of the lower extremity. Principal components analysis (PCA) is a useful analytic technique for identifying kinematic pattern differences between pathologic and healthy populations [4, 5].

The purpose of this study was to investigate lower extremity joint coordination patterns in symptomatic FAI patients and healthy controls during a double leg squat task. It was hypothesized that compared to healthy controls, symptomatic FAI patients would use a more constrained joint coordination pattern in the frontal and transverse planes of motion, but not in the sagittal plane.

METHODS

Five symptomatic FAI subjects (3 male/2female) and five healthy matched controls (3 male/2 female) were included in this study. Symptomatic FAI

subjects were diagnosed by a board certified orthopedic surgeon (JTH). Symptomatic FAI was confirmed by standard radiographs, MRI/A, and an intra-articular injection. Control subjects were included if they were free of hip symptoms and demonstrated a negative hip examination by a licensed physical therapists (PM).

All subjects performed five repetitions of a double leg squat task. Kinematic data were collected with a 14 camera motion capture system (Vicon Ltd, London, UK) at a sampling rate of 100 Hz. Marker position data were tracked in Vicon Nexus and processed using visual 3D software. Raw position data were filtered with a 4th order low pass Butterworth filter with a cutoff frequency of 6 Hz. Relative joint angles for all lower extremity joints were calculated in Visual 3D based on segment positions defined in a static standing trial that was collected prior to movement testing.

Principal components analysis (PCA) was used to quantify the patterns of joint coordination for the relative angle curves of the lower extremity joint. Three separate PCAs were performed for each plane of motion using the 5-trial ensemble averages of the relative joint angles for each subject. The input matrices for the PCA thus contained 3 row vectors (i.e., one for each of 3 joints) with 101 time points. Eigenvector decomposition was performed on the covariance matrices to extract the eigenvectors (i.e. principal components) and eigenvalues for plane of motion. The eigenvalues demonstrate the percent variance explained by each PC for each subject and were used as proxies to represent the degrees of freedom for the joint coordination pattern of the lower extremity for each of the respective planes of motion. To evaluate differences in the coordination

strategies between FAI and control subjects one-tailed, paired samples *t*-test were used to compare the eigenvalues for each plane of motion.

RESULTS

Although, no statistical differences in any of the mean eigenvalues were found, the results of the current study demonstrated a trend towards statistical difference between the FAI and control subjects for the eigenvalues of the first and second PC in the frontal plane (Table 1).

DISCUSSION

The results of the current study demonstrate differences in the coordination strategy of frontal plane motions between FAI and control subjects. Specifically, the differences in eigenvalues for frontal plane joint motions between the groups point toward a more constrained and simpler coordination pattern in the FAI group. This result is consistent with previous studies that suggest injured individuals tend to constrain kinematic degrees of freedom of the lower extremity [3]. Hip joint injury associated with FAI most often occurs during repetitive movements that involve end range motions as during squatting. Therefore, it seems reasonable that symptomatic FAI patients would adopt a movement strategy that constrains the degrees of freedom of the lower extremity joints so as to avoid potentially painful motions that reproduce or exacerbate symptoms.

Although previous researchers reported no differences in frontal plane hip kinematics during a double leg squat task in symptomatic FAI patients [6], it is interesting to note that these authors also reported that one third of their patients used an alternative frontal plane kinematic squat strategy characterized by greater hip adduction compared the hip abduction pattern used by the majority of the subjects [6]. These observations suggest that FAI patients may adopt alternative movement strategies to accomplish tasks that require end terminal ranges of hip motion, such as a double leg squat task.

Although the effect of FAI on movement patterns is not well understood, the current study demonstrates support for movement pattern differences in patients with symptomatic FAI. More research is needed to understand the interaction between movement patterns and FAI morphology to understand the specific mechanisms of hip joint injury associated with this pathology.

REFERENCES

1. Ganz R et al. *Clin Orthop Relat Res* **417**, 112-120, 2003
2. Lung R et al. *Clin Rheumatol* **31**, 1239 – 1242, 2012
3. Hamill J et al. *Clin Biomech*, **14**, 297 -308, 1999
4. Daffertshofer A et al. *Clin Biomech*, **19**, 415 -428, 2004
5. Kipp K et al. *Clin Biomech*, **27**, 706 -710, 2011
6. Lamontagne M et al. *Clin Orthop Relat Res* **467**, 445 -450, 2009

Table 1: PC eigenvalues for each plane and group.

		FAI	Control	<i>p</i> -value
Sagittal	PC 1	99.9	99.9	.49
	PC 2	1.9	8.5	.07
Frontal	PC 1	98.4	93.0	.07
	PC 2	1.9	8.5	.07
Transverse	PC 1	96.9	93.3	.22
	PC 2	3.1	7.5	.22

REDUCTIONS IN STRUCTURAL AND FREQUENCY COUPLING BETWEEN POSTURE AND SURFACE MOTION ARE FACILITATED BY PLANTAR TACTILE STIMULATION

¹Kimberly Lueders, ¹Diderik Jan Eikema, Pradeep Ambati, Nicholas Stergiou, ²Jacob Bloomberg and ¹Mukul Mukherjee

⁻¹University of Nebraska at Omaha, Omaha, NE, USA

²Johnson Space Center, Houston, TX, USA

email: mmukherjee@unomaha.edu, web: <http://cobre.unomaha.edu/>

INTRODUCTION

Human locomotor adaptation requires feedback and feed-forward control processes to maintain dynamic balance while exposed to external perturbations such as a moving or unstable support surface. When exposed to such conditions, the system's initial instability is reduced over time as a function of adaptation, thereby reducing the amount of movement variability, enhancing dynamic stability. Effective postural adaptation is characterized by a decoupling of the environmental perturbation and concurrent multisegmental movements of the trunk [1]. The efficacy of this type of adaptive behavior is dependent on the ability to use integrated sensory input to decompose environment and body movement dynamics and correct for deviations in postural stability [2]. The involved sensory systems provide specific contributions to the control of posture. Lower limb proprioception provides information on the orientation of the body with respect to the support surface. This is then used as a reference for the control of posture [3]. As the support surface becomes unstable, information provided through this modality becomes inaccurate. Through a process of sensory reweighting, the subsequent sensory contribution is reduced and alternate sensory signals are used as references [3]. Cues that reduce accuracy of a sensory modality can therefore facilitate sensory reweighting. For example, high frequency tactile vibration may reduce tactile sensitivity [4], thereby facilitating the down-weighting of this modality. In this study we investigated postural coupling and the effect of plantar tactile vibration on adaptation to a continuously rolling treadmill.

We hypothesize that plantar tactile vibration facilitates the down-weighting of proprioceptive information, which in turn enhances postural decoupling by allowing the system to rely more on

alternative sensory inputs such as vision and vestibular perception.

METHODS

Twenty healthy young adults (9 male, 11 female) performed a walking task on a continuously rolling treadmill (Fig 1). Participants were separated into 2 groups. The control group received no tactile stimulation (NT) whereas the tactile group (TC) received vibratory stimulation (250Hz, 17.5dB), provided through tactors embedded in insoles placed in the shoes (Fig 1). The participants were asked to walk on a treadmill, which was stationary, performed a random roll motion or a sinusoidal roll motion, depending on the condition (Fig 2). In all treadmill roll conditions, the roll frequency was centered around 0.3Hz with a peak to peak amplitude of 10 degrees.

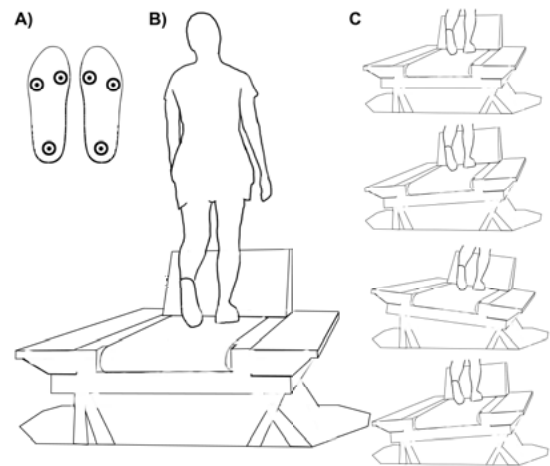


Figure 1: A) Participants wore insoles with 3 embedded tactors. B) Participants walked on a stock treadmill placed over a six degrees of freedom motion base. (C) The motion base allowed for a random or sinusoidal roll of 5 degrees to either side.

Posture control was quantified as the roll motion of the trunk in degrees, as recorded by a motion capture system. Postural coupling was quantified as

the spectral distribution (CFR) and cross recurrence quantification (RR) of treadmill and trunk roll motion. All variables were analyzed using mixed model RM ANOVA, separately for each variable.

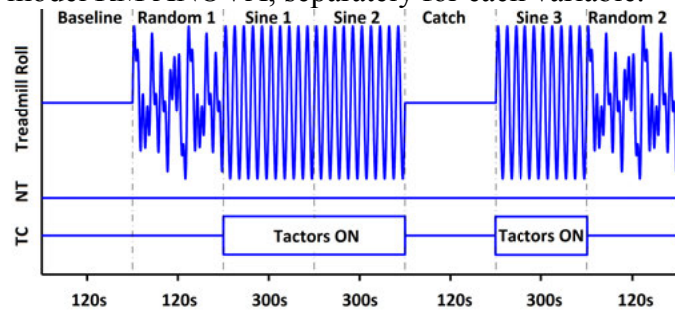


Figure 2: Stimuli in the groups and conditions. The condition durations are provided in seconds.

RESULTS AND DISCUSSION

The spectral distributions of trunk and treadmill motion indicated that the roll movement of the treadmill significantly affected the frequency distribution of the trunk roll motion (Fig 3).

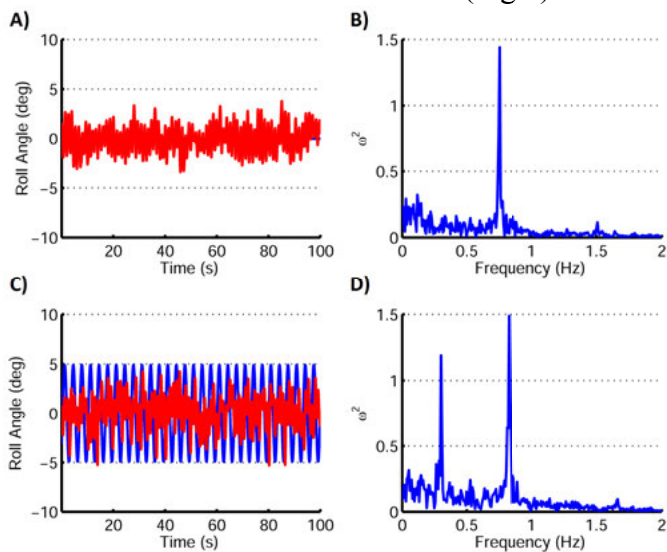


Figure 3: A) Trunk roll (red) and treadmill roll (blue) time series in the baseline trial. B) The corresponding spectral distribution. The peak corresponds with the walking frequency at 0.8Hz. C) Trunk and treadmill roll during adaptation. D) The effect of treadmill roll can be observed in the additional peak at 0.3Hz.

The reductions in both CFR (Fig 4) and RR (Fig 5) coupling measures indicate that, as a function of adaptation to the sinusoidally rolling support surface (Sine 1, 2, 3), trunk-treadmill coupling decreases. This time-dependent reduction in coupling is significantly greater in the TC group. When exposed to a new roll environment post-training, coupling rates are significantly lower than

pre-training, however here no difference between NT and TC is noted.

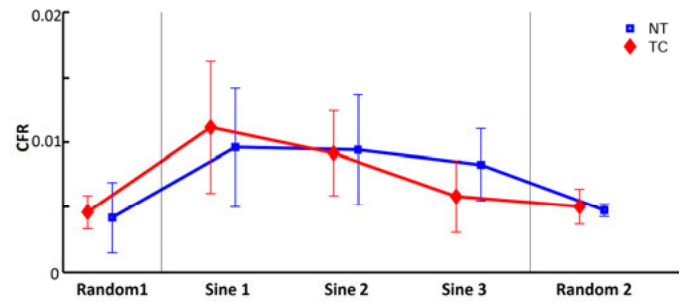


Figure 4: CFR in the treadmill roll conditions. The blue lines and symbols represent NT, the red lines represent TC. Means \pm SD are shown.

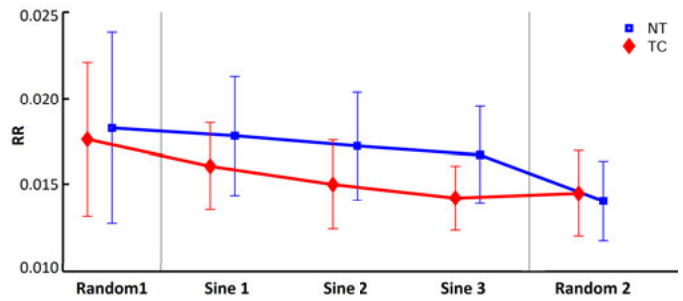


Figure 5: RR in the treadmill roll conditions. The blue lines represent NT, the red lines represent TC. Means \pm SD are shown

CONCLUSIONS

Characteristic roles for postural and locomotor processes during adaptation to support surface roll oscillations while walking on a treadmill were demonstrated. The postural control component required integrated sensory contributions which are updated based on the accuracy of sensory inputs [2]. Improvements in balance through noisy plantar stimulation may be potentially useful for sensorimotor training in special populations by driving the system towards using a more appropriate sensory gain configuration [3].

REFERENCES

1. Brady RA, et al. *Gait Posture*, **29**, 645-649, 2009.
2. Dokka K, et al. *PLoS Comput Biol*, **6**, 2010.
3. Peterka RJ. *J Neurophysiol*, **88**, 1097-1118, 2002.
4. Collins, et al. *Phys Rev E*, **56**, 923-926.

ACKNOWLEDGEMENTS

This study was supported by NASA EPSCoR grant number NNX11AM06A, the Center of Biomedical Research Excellence grant 1P20GM109090-01 from NIGMS/NIH and the NASA Nebraska EPSCoR Research Mini-Grant.

The ability to dynamically regulate instabilities with the leg is susceptible to repetitive eccentric contractions.

¹ Akira Nagamori, Emily L. Lawrence, ¹James M. Finley, ¹Francisco J Valero-Cuevas

¹University of Southern California, Los Angeles, USA.
Email: nagamori@usc.edu

INTRODUCTION

Controlling continuous instabilities with the legs (as per the Lower Extremity Strength-Dexterity (LED) paradigm [1]) is likely a product of a hierarchical organization of neural control [2]. This ability, therefore, likely requires continuous fine-tuning of motor output through intricate interactions among afferent signals, descending commands and muscle mechanics.

A pilot study suggested that LED performance deteriorates with 20-minutes of downhill walking, despite subjects reporting no evidence of fatigue. This result compelled us to investigate whether or not repetitive eccentric contractions can disrupt the fine motor control required for this task. However, studying this in walking remains ambiguous because concentric and eccentric phases coexist during downhill walking. Therefore, we investigated the effect of purely eccentric contractions of the *soleus* muscle on LED performance.

afferents (i, Figure 1). The H-reflex is a practical means to quantify spinal excitability to afferent signals (ii, Figure 1). Therefore, we hypothesized that purely eccentric contractions of the *soleus* muscle would induce changes in H-reflex.

METHODS

Nine young adult male subjects (25.4 ± 3.8 yrs) participated in this study. They attended two separate sessions. In the first session, we quantified resting H-reflex amplitude of the *soleus*, LED performance, and electromyographic (EMG) activities of the *soleus* and *tibialis anterior* (TA) during the LED test bilaterally before and after exposure to unilateral eccentric exercise. The ankle dorsiflexion eccentric exercise consisted of 500 eccentric contractions of the *soleus* at 15% maximal voluntary contraction (MVC). The subjects were seated with the knee joint at 90° flexion during eccentric contractions and MVC trials in order to minimize the contribution of other plantarflexors. In the second session, those measurements were obtained unilaterally after level treadmill walking of duration required for each subject to complete 500 eccentric contractions (i.e., steps).

Note the LED test requires low forces $< 25\%$ of body weight, where the maximal compression force indicates the maximal level of instability that can be controlled. The maximal compression force was quantified as a mean of three best trials that achieved maximal mean compression force during the hold phase of the LED test.

RESULTS AND DISCUSSION

There was no measurable fatigue after eccentric contractions as per objective MVC measurements (mean percentage increase of $18.8 \pm 23.6\%$) and the

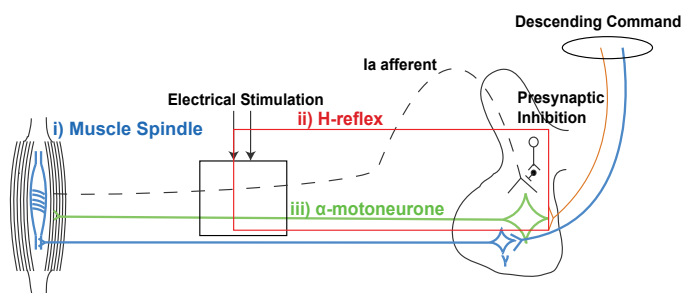


Figure 1: Schematic diagram of neurophysiological components likely responsible for the LED test performance. The original figure was obtained from Pierrot-Deseilligny and Burke (2012).

The hierarchical control of instabilities is likely mediated in part by short-latency, “low level” sub-cortical or spinal circuitry [3]. Such short-latency control is often mediated by tunable spindle

subjective Borg scale (mean value of 2.0 ± 0.7 out of 10).

There was a statistically significant increase in contralateral control ($p=0.029$), while a decrease in the LED compression force was observed only in eccentric contraction condition (non-significant, $p=0.106$). In order to account for a difference in baseline LED performance among conditions, changes in LED compression force in different conditions were normalized to respective baseline LED compression forces (normalized relative change). There was a significant difference ($p=0.026$) in normalized relative change of the LED compression force between contralateral control and eccentric contraction condition (Figure 2).

Finally, there were no statistically significant effects of conditions on H-reflex amplitude or EMG activities of the *soleus* and the TA (average root mean square and mean or median power frequency of EMG signals) during the LED test.

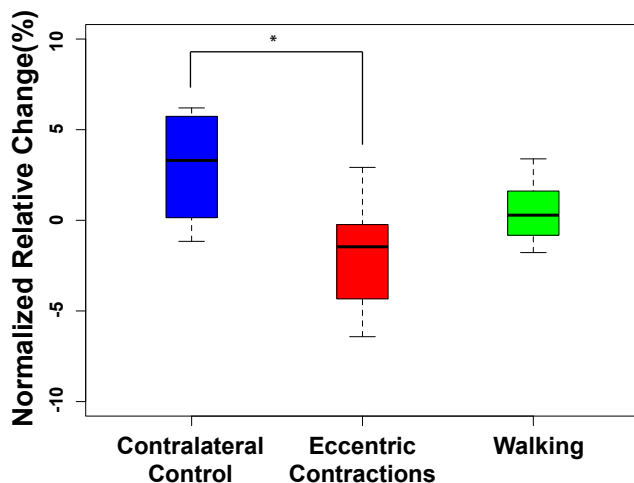


Figure 2: Normalized relative change for LED compression force. There was a significant difference between contralateral control and eccentric contraction conditions. * denotes $p < 0.05$.

Although additional subjects are needed to corroborate these trends, the results confirm that eccentric contractions likely degrade the ability to control instabilities with the leg. In this case, eccentric contractions seemed to override the positive exposure effect observed in the contralateral leg. The isolated eccentric contractions

of one muscle may also induce a smaller effect than eccentric contractions across multiple leg muscles in downhill walking.

Importantly, the hypothesis of modulation of spinal excitability due to eccentric contractions was falsified, as they did not affect resting H reflex (**ii**, Figure 1). These results, alongside retained neural drive to the involved muscles measured by EMG signals (**iii**, Figure 1), suggest the decreased LED performance did not stem from a deficit in the central neural drive to the motor units or spinally modulated gain of afferent signals. Therefore, eccentric contractions likely tend to degrade the ability to control instabilities via other mechanisms. Specifically, eccentric contractions could affect the passive and active properties of muscle, or spindle sensitivities (**i**, Figure 1) [4]. These results motivate future work to disambiguate the contributions of peripheral mechanisms involved in the short-latency corrections needed to continuously stabilize the leg at low force levels—and may have implications to injury prevention in sports activities.

CONCLUSIONS

The ability to control dynamics instabilities in the lower limb is susceptible to non-fatiguing, repetitive eccentric contractions. The neuromechanical mechanisms responsible for this effect warrant further investigation.

REFERENCES

- [1] Lyle et al. *J Biomech* 46(5), 998-1002, 2013.
- [2] Loeb et al. *Exp Brain Res*, 126(1), 1-18, 1999.
- [3] Lawrence et al, *Front Neurol*, 15, 5-53, 2014.
- [4] Avela et al, *J Appl Physiol*, 86(4), 1283-1291, 1999.

ACKNOWLEDGEMENTS

This study was supported by NIH-NIAMS under award numbers R01AR050520 and R01AR052345 grants to FVC and by NIH-NICHD under award number K12HD073945 to JMF.

CAN PARAVERTEBRAL FACET INJECTION IMPROVE MOTOR PERFORMANCE IN PATIENTS WITH DEGENERATIVE FACET OSTEOARTHROPATHY?

Nima Toosizadeh, Tzu-Chuan Yen, Michael Dohm, Cindy Fastje, Bijan Najafi

College of Medicine, University of Arizona, Tucson, AZ, USA
email: bnajafi@surgery.arizona.edu

INTRODUCTION

Low back disorder (LBD) is the fifth most common reason for medical treatment and costs up to \$50 billion annually in the United States alone [1]. One such LBD is degenerative facet osteoarthropathy (DFO), which has a high prevalence of 57% DFO in younger adults (20-29 years) and can increase up to ~95% in older populations (40-59 years) [2]. Corticosteroid injections are commonly requested treatments for patients with various LBDs, especially for DFO; however, no study uses motor performance assessment to evaluate the efficacy of facet spine steroid injections. Hence, the purpose of this study was to assess immediate improvements in motor performance following facet spine injection in patients with DFO.

METHODS

Thirty DFO participants were recruited from the University of Arizona Medical Center after screening based on CT and MRI images. Exclusion criteria were previous spine, hip, or lower extremity surgeries within a one month time-window of the spine injection, along with severe comorbidities (e.g., Parkinson's and Stroke). A sample of 10 healthy, age-matched adult controls were recruited from the University of Arizona Geriatric clinic. DFO Participants were treated with 1% lidocaine plain, 0.25% marcaine plain and 40 mg per cc triamcinolone for a medial branch block, intermediate branch block, pericapsular and intracapsular injection [3]. Data were collected pre- and post- surgery, with baseline measures collected within three days prior to the injection and follow-up measurements taken immediately after the procedure. The Oswestry Disability Index and the 10-point Visual Analog Scale (VAS) were used to assess patient reported disability and pain, while wearable sensor technology were utilized to assess

gait, postural balance, and Timed Up & Go (TUG) (Table 1). Gait was evaluated with a minimum of 25 steps under four conditions of normal single task, normal dual task, fast single task, and fast dual task. In all dual tasks, participants were asked to count backwards by one from a number between 1 and 100. As for balance assessment, two trials were conducted for the eyes open and eyes closed conditions, where participants crossed their arms and minimized the distance between their feet. In the TUG test, the walking distance was three meters and the same chair was used every time. A total of five sensors, each with a triaxial accelerometer and gyroscope were placed on the shanks, thighs, and back to track lower extremities and hip motion (LEGsys, MA). Analysis of covariates were used to compare outcomes between DFP pre-injection and healthy controls, considering age, gender, and body mass index as covariates. Comparison between pre- and post-surgery data was performed using the paired *t*-test or Mann-Whitney U test for non-parametric samples (Significance: $P < 0.05$).

RESULTS AND DISCUSSION

Mean age and body mass index of DFO participants were 50 ± 14 years and 32.5 ± 6.6 kg/m², respectively; corresponding values for healthy controls were 46 ± 15 years and 25.2 ± 4.1 kg/m². Before injection the Oswestry Disability Index scores ranged between 4% and 70% (mean = $44 \pm 16\%$), and the mean pain score was 5.6 ± 2.6 at the moment of measurement among DFO participants. A significant improvement of 50% was determined when comparing immediate pre- and post-surgery pain ratings (post-injection pain = 2.8 ± 2.7 ; $P < .0001$).

Within the gait analysis, gait velocity, stride length, medial-lateral sway, and shin mid-swing velocity were 38%, 20%, 51%, and 27% larger, respectively, while gait cycle time and double support percentage were 16% and 51% smaller in healthy controls

compared to DFO participants on average among all conditions ($P<0.04$, Figure 1). After injection, significant improvements were observed in all gait parameters, except stride length ($P>0.5$, Figure 1). More noticeable changes were observed in gait cycle time and shin mid-swing velocity after injection ($P<0.03$). Double support percentage reduced 10% after injection only in the single task fast walking ($P=0.03$). Balance results demonstrated a higher amount of sway in DFO participants compared to healthy controls in both anterior-posterior (60%; $P<0.05$) and medial-lateral (43%; $P<0.05$) directions, on average among two conditions. However, no noticeable reduction in body sway was observed in DFO group after injection ($P>0.34$). Finally, for TUG, duration of sit-to-stand (82%), walking (121%), turning (80%), stand-to-sit (114%), and total TUG duration (101%) were significantly smaller ($P<0.04$) while trunk velocity within sit-to-stand (64%), turning (77%), and stand-to-sit (47%) transitions was significantly larger in healthy controls compared to DFO participants ($P<0.02$). After injection a significant reduction of 14% in the total TUG duration was observed ($P<.001$), which mainly resulted from a reduction in walking duration (21% reduction in walking speed; $P=0.03$). Although not significant, improvements in sit-to-stand, turning, and stand-to-sit performance were observed ($P>0.08$).

In agreement with previous studies [4,5], our results demonstrated a compromised motor performance caused by DFO. Furthermore, our results demonstrated that pain reduction after spine injection led to instantaneous improvement in motor performance. Improvements were more pronounced within the gait assessments, and mainly for parameters related to agility of movement. Interestingly, improvement in gait speed also caused a reduction in TUG duration. Additionally, the range

Table 1: Parameter definitions

Gait	Definition
Stride Length	Distance travelled by the same limb between two successive heel contacts
Medial-lateral Sway	Range of angular rotation of the trunk in the medial-lateral direction
Shin Mid-swing Velocity	Mean value of shin angular velocity peaks during each swing
Gait Cycle Time	Time interval starts when one foot makes contact with the ground and ends when that same foot contacts the ground again
Double Support	Time that both feet are on the ground as a percentage of the gait cycle time
Postural Balance	Definition
Anterior-posterior or Medial-lateral Sway	Range of center of gravity sway in the anterior-posterior or medial-lateral direction
TUG	Definition
Trunk velocity	Mean angular velocity of the trunk during turning, rising from a chair, or sitting on a chair

of medial-lateral sway during walking was significantly different between the two groups, which was improved after injection. The DFO group showed a smaller range of medial-lateral sway during walking, probably to alleviate pain by restricting medial-lateral motion. Turning ability was also compromised in the DFO group; DFO participants required more time to perform a turning task, which may happen due to poorer balance and lack of hip flexibility. Although not significant, improvements in turning ability was noticeable after injection in the DFO group. In summary, for the first time, we assessed the association between pain reduction and improved motor performance in DFO using innovative wearable sensor technology.

REFERENCES

1. Waterman BR, et al. *Spine J* **12**, 63-70, 2012.
2. Eubanks JD, et al. *Spine* **32**, 2058-2062, 2007.
3. Manchikanti L, et al. *Pain Phys* **12**, 699-802, 2009.
4. Al-Obaidi A, et al. *Int J Rehab Res* **26**, 101-8, 2003.
5. Ruhe A. et al., *Eur Spine J* **20**, 358-68, 2011.

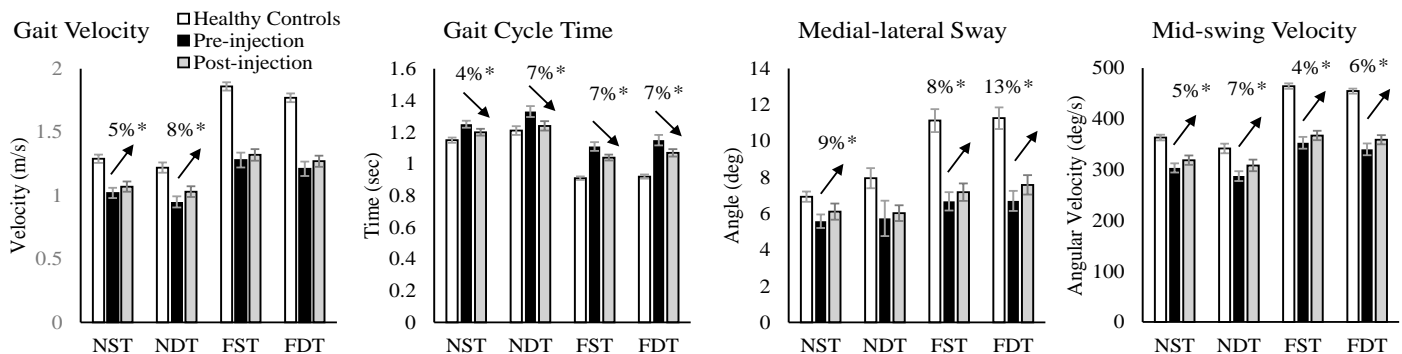


Figure 1: Gait parameters in healthy and DFO (pre- vs. post-injection) groups. (NST = normal single task, NDT = normal dual task, FST = fast single task, FDT = fast dual task.)

SUBJECT-SPECIFIC LANDING STRATEGIES IDENTIFY CHANGES IN MOVEMENT CONTROL

Andrew D. Nordin and Janet S. Dufek

University of Nevada, Las Vegas, Las Vegas, NV, USA
email: nordin@unlv.nevada.edu

INTRODUCTION

Single-leg landing injuries from a jump or an elevated surface are well documented in scientific literature, leading to explorations of overuse and acute injury mechanisms [1,2,3]. Within-subject movement variability across task repetitions has therefore been used in assessing musculoskeletal health and motor system flexibility [2]. In contrast, inter-subject variation confounds human movement analyses, a consequence of the large pool of motor solutions available to a performer [1]. As a result, the load accommodation strategies model has been used in classifying performer strategies following alterations in landing height and subject mass [1]. The conversion of gravitational potential to kinetic energy allows Newtonian predictions of kinetic parameters, including landing impulse [1].

The purpose of this investigation was to examine changes in movement control following alterations in mechanical task demands via external load and landing height. Single-subject analyses were used in identifying subject-specific strategies and changes in movement variability in the context of factors related to landing injuries. Two hypotheses were tested. With greater mechanical task demands: (1) within-subject movement variability would decrease; (2) subject-specific strategies would demonstrate lesser load accommodation capacity.

METHODS

Nineteen healthy volunteers (15M, 4F, age: 24.3 ± 4.9 y, mass: 78.5 ± 14.7 kg, height: 1.73 ± 0.08 m) provided informed consent prior to participation, as required by the Institutional Review Board at the affiliated institution. Subjects completed 10 preferred limb single-leg landing trials (9 analyzed) in each of 6 experimental conditions; 3 load and 2 height conditions, computed as percentages of subject

bodyweight (BW, BW+12.5%, BW+25%) and height (12.5%H & 25%H). Condition order was counterbalanced.

Twelve variables were assessed in each trial, including lower extremity sagittal joint angles and moments (hip, knee, & ankle), vertical ground reaction force (GRFz), and electrical muscle activity (gluteus maximus, biceps femoris, vastus medialis, medial gastrocnemius, & tibialis anterior muscles). Kinematic, kinetic, and EMG data were collected using a 10-camera motion capture system (Vicon Plugin-Gait; MX-T40S; 200Hz), synchronized force platform (Kister Type 9281CA; 2000Hz), and 16-channel EMG system (dual surface Ag/AgCl electrodes; Noraxon Myosystem 2000; 2000Hz).

Kinematic and kinetic data were low-pass filtered (15Hz & 50Hz cutoffs, respectively). Joint moments were calculated with matched cutoffs (15Hz). EMG data were band-pass filtered (15-300Hz), full-wave rectified, and low-pass filtered (15Hz), preserving the pattern of muscle activation in landing [3]. Data were analyzed (Matlab R2012a) in each trial from the time of ground contact (GRFz > 20N) to the time the vertical center of mass velocity reached zero. GRFz data were normalized to subject BW, sagittal joint moments were normalized to subject BW and height (BW•H), and EMG data were normalized to mean dynamic baseline activity for each subject (lowest task demands: BW, 12.5%H).

Within-subject variability was assessed using the 95% confidence interval (CI) of the integrated time-series for each subject-condition-trial-variable. Changes in within-subject variability across conditions were assessed using a 3x2 repeated measures factorial MANOVA, with follow-up 3x2 repeated measures factorial ANOVAs and pairwise comparison for each variable ($\alpha = 0.05$). Degrees of freedom were adjusted via Huynh-Feldt corrections

as necessary, with Bonferroni adjusted pairwise comparisons.

Collective within-subject movement variability was assessed using single-subject principal component analyses (PCA). Prior to PCA the time series of each variable and trial was normalized to 101 data points via cubic spline interpolation. Time series variables were converted to z-scores, subtracting the subject's baseline mean and normalizing to baseline standard deviation. Analyses were carried out on 108x101 dimension matrices (12 variables x 9 trials = 108) for each subject-condition. The number of PCs explaining 90% of the variance in each condition was used in subsequent inferential testing. Main effects were examined using Friedman tests and follow-up Wilcoxon signed-rank tests due to the ordinal nature of the extracted PCs ($\alpha = 0.05$). The interaction of load and height was explored in a 3x2 repeated measures ANOVA ($\alpha = 0.05$).

Landing strategies were identified using the load accommodation strategies model and 95% confidence intervals (CI) for the impulse ratio of each subject relative to baseline. Impulse ratios defined predicted (Newtonian) increases in landing impulse relative to baseline. Landing strategy classifications included: (1) Newtonian: CI containing the predicted impulse ratio (2) Fully-Accommodating: CI containing impulse ratio of 1.0, (3) Positive Biomechanical: CI greater than 1.0 and less than the Newtonian predicted impulse ratio, (4) Negative Biomechanical: CI less than impulse ratio of 1.0, (5) Super-Newtonian: CI exceeding the Newtonian impulse ratio [1]. Associations among conditions and observed strategy frequencies were assessed using Fisher's exact tests ($\alpha = 0.05$). Separate tests were carried out at each load and landing height.

RESULTS AND DISCUSSION

Within-subject variability and subject-specific landing strategies differed by load and landing height. Within-subject variability decreased with greater load ($F[12,26]=8.1$, $p<.001$, $\eta^2=.79$), demonstrating decreases among sagittal angle and moment variability at the hip, knee, and ankle

($p\leq.016$). Total medial gastrocnemius muscle activity variability also decreased with greater load ($p<.048$). Collective within-subject movement variability decreased with greater load ($\chi^2[2]=36.1$, $p<.001$) and landing height ($Z=-5.1$, $p<.001$), demonstrating fewer extracted PCs.

Subject-specific strategies were associated with load and landing height adjustments ($p<.001$). Landing strategies were more frequently Negative Biomechanical with greater load at 12.5%H, and more frequently Positive Biomechanical with greater load at 25%H ($p<.001$). Landing strategies were more frequently Positive Biomechanical with increased landing height at BW+12.5% and BW+25% ($p<.001$).

CONCLUSIONS

The influence of mechanical task demands on subject-specific landing strategies identified changes in movement control during single-leg landing. The observed load accommodation strategies highlight movement control adjustments as mechanical task demands outpace neuromuscular accommodation capabilities [1]. Alongside observed decreases in within-subject movement variability, the application of greater loads with fewer available motor solutions may underscore potential injury mechanisms in landing activities [2].

Combined use of the load accommodation strategies model, within-subject variability, and single-subject PCA demonstrated utility in examining subject-specific movement control adjustments across changes in mechanical task demands.

REFERENCES

1. James CR, et al. *JAB*, **19**(2), 106-118, 2003.
2. James CR, et al. *MSSE*, **32**(11), 1833-1844, 2000.
3. Kipp K, et al., *JAB*, **30**, 262-268, 2014.

ACKNOWLEDGEMENTS

The UNLV Foundation and UNLV Graduate College financially supported this research.

THE EFFECTS OF VIBRATORY STIMULI ON CORTICAL AND SPINAL NEURON EXCITABILITY: IMPLICATIONS FOR OSTEOARTHRITIS TREATMENT AND PREVENTION

¹Derek N. Pamukoff, ¹Brian Pietrosimone, ¹Eric D. Ryan, ¹Paul S. Weinhold, ¹Michael D. Lewek, ¹J. Troy Blackburn

¹The University of North Carolina at Chapel Hill, Chapel Hill NC
email: pamukoff@live.unc.edu

INTRODUCTION

Vibration acutely enhances neuromuscular function [1], but the mechanism of improvement is unclear. Past research suggests that heightened motor neuron excitability within the spinal cord is responsible for improved muscle function following vibration [2]. However, reflexive activity is often depressed following vibration [3], and the response of supraspinal structures – such as the motor cortex – to vibration is unclear. Vibratory treatments could have implications for individuals with deficits in quadriceps muscle activation, such as patients with knee pathologies [4]. Whole body (WBV) and local muscle vibration (LMV) both improve quadriceps function [5], but the efficacy of treatment may vary. Furthermore, WBV is cost prohibitive, and LMV may provide an alternative treatment tool. However, there are few investigations that have compared the effects of WBV and LMV. The purpose of this study was to compare the effects of whole body and local muscle vibration on three measures of quadriceps function including: corticomotor excitability, spinal neuron excitability, and voluntary activation.

METHODS

We recruited 60 healthy subjects into a single blinded randomized control trial. Subjects were randomized into 1 of 3 different groups following pretest assessments of quadriceps function: WBV (n = 20, age = 20.2±0.9 years, height = 172.1±10.8 cm, mass = 66.4±10.4 kg, males = 9), LMV (n = 20, age = 19.5±1.4 years, height = 168.3±9.0 cm, mass = 65.5±10.7 kg, males = 8), Control (n = 20, age = 20.5±1.2 years, height = 171.1±8.8 cm, mass = 69.4±12.9 kg, males = 10).

Corticomotor excitability was assessed via active motor threshold (AMT), spinal neuron excitability was assessed using Hoffman's (H) reflex, and voluntary activation was assessed using the central activation ratio (CAR). Subjects completed 3 testing visits (Vastus medialis H-reflex, vastus medialis AMT, and quadriceps CAR) in a random order separated by 1-week washout periods, each lasting 1.5 hours. On each day, subjects completed a baseline assessment of H-reflex, AMT, or CAR and then received the WBV, LMV, or Control intervention. Following the intervention, subjects completed a follow-up assessment of H-reflex, AMT, or CAR immediately, 10 minutes, and 20 minutes following the treatment. H-reflex measurements of the vastus medialis were collected with surface electromyography (EMG) in the dominant limb. The ratio of maximal H-wave to a maximal M-wave was used for analysis. AMT was defined as the minimum transcranial magnetic stimulating intensity required to elicit a motor evoked potential greater than 10mv in at least 5 out of 10 trials. The ratio of voluntary torque to additional torque produced from a superimposed electrical stimulus during a maximal voluntary isometric contraction was used for analysis (CAR). H-reflex, AMT, and CAR were compared via separate 3x4 (group x time) analyses of variance.

RESULTS AND DISCUSSION

The group by time interaction was significant for AMT (Table 1, $F_{2,57} = 13.39$, $p < 0.001$) and CAR (Table 2, $F_{2,57} = 2.86$, $p = 0.011$), but not for H-reflex (Table 3, $F_{2,57} = 1.36$, $p = 0.619$). Post hoc analyses revealed a significant increase in CAR immediately post-treatment in the WBV group

(+2.9%, $p<0.01$), and a significant reduction in AMT immediately post-treatment in the WBV (-2.6%, $p<0.001$) and LMV (-2.3%, $p<0.001$) groups. The reduction in AMT was significant 10 minutes following WBV (-2.3%, $p<0.001$) and LMV (-2.3%, $p<0.001$), and 20 minutes following WBV (-2.4%, $p<0.001$) and LMV (-1.6%, $p<0.001$).

CONCLUSIONS

These results suggest that both WBV and LMV improve voluntary quadriceps function via a reduction in AMT rather than from enhanced spinal reflex activity. Interestingly, we found no change in spinal reflex activity, indicating that the effect of vibratory stimuli on spinal neuron activity may be limited to the time while treatment is applied, rather than persisting following it. Furthermore, the effects on quadriceps function may be more pronounced following WBV compared to LMV as there was a greater reduction in AMT, and an increase in voluntary quadriceps activation (CAR) in the WBV group only. Next, the effects on muscle vibration on AMT may persist for up to 20 minutes following treatment. As such, vibratory stimuli – particularly WBV – may provide a suitable treatment for those individuals with deficits in quadriceps function. Future studies should investigate the effects of vibratory stimuli in pathologic populations, as the

magnitude of effect could be larger in those with underlying neuromuscular deficits.

REFERENCES

1. Rittweger J. Vibration as an exercise modality: how it may work, and what its potential might be. *European journal of applied physiology*. 2010;108(5):877-904.
2. Burke D, et al. The responses of human muscle spindle endings to vibration during isometric contraction. *The Journal of physiology*. 1976;261(3):695-711.
3. Ritzmann R, et al. The effect of whole body vibration on the H-reflex, the stretch reflex, and the short-latency response during hopping. *Scandinavian journal of medicine & science in sports*. 2013;23(3):331-339.
4. Hart JM, et al. Quadriceps activation following knee injuries: a systematic review. *Journal of athletic training*. 2010;45(1):87-97.
5. Blackburn JT, et al. Whole body and local muscle vibration reduce artificially induced quadriceps arthrogenic inhibition. *Arch Phys Med Rehabil*. 2014.

ACKNOWLEDGEMENTS

This study was supported by the American Society of Biomechanics Grant-in-aid program.

Table 1: AMT Results (mean (SD))

AMT (%)	Pre	Post	10 min Post	20 min Post	<i>P</i> (group x time)
Control (n=20)	42.7 (8.6)	42.7 (9.0)	43.0 (8.9)	43.1 (8.6)	<0.001
WBV (n=20)	45.4 (7.7)	42.9 (8.2)	43.1 (8.3)	43.4 (7.9)	
LMV (n=20)	46.3 (11.5)	44.0 (11.5)	44.0 (11.3)	44.7 (11.3)	

Table 2: CAR Results (mean (SD))

H-Reflex (H:M)	Pre	Post	10 min Post	20 min Post	<i>P</i> (group x time)
Control (n=20)	93.1 (3.9)	90.9 (5.7)	90.4 (6.6)	89.7 (6.4)	0.011
WBV (n=20)	91.9 (4.6)	94.4 (3.9)	90.9 (6.5)	92.0 (5.9)	
LMV (n=20)	91.9 (3.2)	92.2 (3.9)	87.5 (8.8)	87.4 (8.7)	

Table 3: H-Reflex Results (mean (SD))

CAR (%)	Pre	Post	10 min Post	20 min Post	<i>P</i> (group x time)
Control (n=20)	0.27 (0.19)	0.26 (0.16)	0.25 (0.16)	0.25 (0.14)	0.619
WBV (n=20)	0.26 (0.15)	0.20 (0.15)	0.23 (0.17)	0.23 (0.17)	
LMV (n=20)	0.28 (0.17)	0.23 (0.15)	0.24 (0.15)	0.23 (0.15)	

INFORMATION ABOUT HOW ANOTHER PERSON IS MOVING THROUGH THE ENVIRONMENT IS CONVEYED IN THE MOVEMENTS OF THEIR LIMBS

¹Nicholas Reynolds, ¹Brandon Bischoff, ^{1,2}Nicholas Stergiou, and ¹Steven J. Harrison

¹ University of Nebraska at Omaha, Omaha, NE, USA

² University of Nebraska Medical Center, Omaha, NE, USA

email: nrreynolds@unomaha.edu, web: www.unomaha.edu/college-of-education/cobre/index.php

INTRODUCTION

By watching the movements of another person it is possible to know many things about them. Just by seeing how another person is moving we can perceive their age, gender, and even mood.[1] Here we investigate if it is possible to perceive how another person is moving through an environment, just based upon seeing how their lower limbs (hips, knees, ankles) are coordinated in locomotion. The way in which the limbs are coordinated in locomotion has been found to affect kinesthetic distance perception.[2,3] Kinesthetic distance perception concerns perceiving one's own movements during locomotion based upon the sensory information that is generated from coordinated body movements. Research into kinesthetic distance perception has employed simple homing tasks in which blindfolded participants travel outbound from a "home" location for a certain distance, before being told to stop and turn around, and then attempting to travel the same distance to return to "home". Depending on the gait patterns used in the outbound and return phases of simple homing tasks, systematic biases are observed.[3] For example, gallop-walking (Fig. 1) outbound followed by walking in the return phase

produces a systematic underestimation bias. Alternatively, running outbound followed by walking produced no bias.[2] This study investigates if an individual's visual perception of distances travelled by other people is affected by the way in which that person's limbs are coordinated. We hypothesized that the patterns of bias observed in our experiments would match those found in previous investigations of kinesthetic perception.

METHODS

Four experiments were conducted. Twenty participants aged between 19 and 65 took part in each experiment (n = 80). Each participant read and signed a consent form prior to taking part in this study. Motion capture recordings were used to create animations of a stick figure (Fig. 1) employing various gaits to complete a simple homing task. The animations were constrained so that the hips of the stick figure always stayed in the center of the screen. The animation was used to simulate the outbound and return phases of a homing task performed by another person. Participants attempted to perceive the distances travelled by the stick figure. Outbound distances were set as 3m, 6m, and 9m. Outbound gait performed by the stick figure was manipulated across the four experiments to be either a walk (W), gallop-walk (GW), or hesitation-walk (HW) (see Fig. 1). The return gait was always a walk. All conditions were randomized and programmed into the test prior to the participant arriving. In the outbound phase of the homing task, participants watched as the stick figure moved towards the right of the screen. The stick-figure would then stop and turn around once it had reached its predetermined distance and turn around. It would then begin moving towards the left of the screen. Participants were asked to press a button on a keyboard when

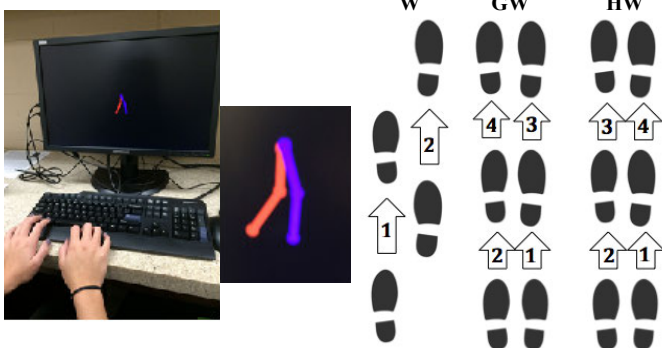


Figure 1: A) Experiment setup and stimulus. B) Gait patterns used in this experiment.

they perceived the stick figure had returned to where it started out.

RESULTS AND DISCUSSION

In all experiments, participants reported longer return distances as a function of increasing outbound distances (p 's < 0.001). Results of all experiments are shown in figures 2 and 3.

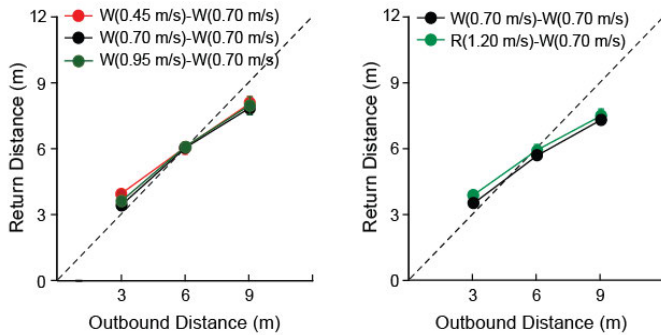


Figure 2: Results from experiments 1 and 2.

In **experiment 1**, we manipulated the speed of the outbound gait. We found that participants were able to perceive the outbound distances independent of outbound speed (F 's > 1).

In **experiment 2**, we manipulated the outbound gait being displayed; it could either be a walking or a running pattern. We observed no effect of outbound gait ($F(1,19) = 1.62, p = 0.22$), nor an interaction of outbound gait and outbound distance ($F < 1$). In this case the participants were able to perceive the outbound distances independent of outbound gait.

In **experiment 3**, we manipulated the outbound gait to be either a gallop-walk or a walk pattern. In this case there was a significant difference in perceived return distances as a function of the outbound gait ($F(1,19) = 11.86, p > 0.01$). A significant interaction of outbound gait and outbound distance was observed ($F(2,38) = 4.65, p < 0.05$). Paralleling previous studies of kinesthetic distance perception the results show that when employing the gallop-walk, participants came up significantly shorter than when they began with the walk.

In **experiment 4**, we manipulated the outbound gait being displayed to either a gallop-walk or a

hesitation-walk pattern. The results showed that participants were able to perceive the outbound distances independent of outbound gait (F 's > 1).

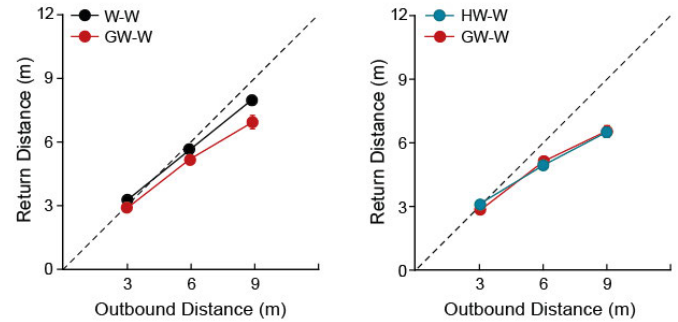


Figure 3: Results from experiments 3 and 4.

CONCLUSIONS

We found that people are able to accurately perceive the distance travelled by another person from information obtained by watching the movements of their legs. We also found that the ability to perceive another person's movements depended upon the way the seen person legs were coordinated in movement. The results showed that the pattern of results observed for perceiving other's movements matched those for non-visually perceiving one's own movements. We are currently investigating further into the possible visual mechanisms underlying this interesting phenomenon.

REFERENCES

1. Shiffrar M. *Cognitive Science*, **2**, 68-78, 2011.
2. Turvey MT, et al. *J. Exp. of Experimental Psychology: Human Perception and Performance*, **38**, 1014-1025, 2012.
3. Turvey MT, et al. *Proceedings of the Royal Society B: Biological Sciences*, **276**, 4309-4314, 2009.

ACKNOWLEDGEMENTS

This work was supported by the Center for Research in Human Movement Variability of the University of Nebraska at Omaha, the NIH (P20GM109090, R01AG034995, and R01GM105045), and a FUSE grant from the University of Nebraska at Omaha.

ADAPTATION STRATEGIES OF INDIVIDUALS WITH ANTERIOR CRUCIATE LIGMENT RECONSTRUCTION

Jaimie A. Roper^a, Mathew J. Terza^a, Mark D. Tillman^b, Chris J. Hass^a

^a The University of Florida, Gainesville, FL; ^b Troy University, Troy, AL
email: jaimier@ufl.edu

INTRODUCTION

Even after ACL reconstruction (ACL-R), lengthy rehabilitation, and return to sport, asymmetry and alterations in gait and neuromuscular control persist. Interventions that may reduce the alterations and asymmetries in gait associated with ACL-R could produce improved walking patterns. Insight into whether and to what extent individuals with ACL-R can modify their movement patterns is essential for designing successful rehabilitation. Yet a lack of understanding remains regarding whether people with ACL-R are capable of adapting to gait perturbations and storing new gait patterns.¹ Therefore, the purpose of this study was to observe the ability of individuals with ACL-R to adapt and store novel gait patterns walking on a split-belt treadmill (SBT).

METHODS

Locomotor adaptation was investigated as 20 participants with ACL-R and 20 healthy matched-controls (HYA) walked on a split-belt treadmill. We assessed locomotor adaptation by 1) the magnitude of asymmetry persisting in late adaptation and 2) the magnitude of the asymmetry during de-adaptation.

After a 5 minute warm-up period of walking at self selected speed, participants walked at a slow speed (0.75 m/s) for 2 minutes (BASELINE).² Treadmill speeds were then adjusted such that the belt under the non-dominant leg in HYA and the belt under the reconstructed leg in the individuals with ACL-R sped up to 1.5 m/s. The belt under the contralateral leg remained at 0.75 m/s. Participants walked under these conditions for thirteen minutes (ADAPT 1). Next, the belt moving at 1.5 m/s was returned to the slow speed and participants walked for five minutes

with both belts moving at 0.75 m/s (DE-ADAPT 1). The last 30 second period of DE-ADAPT 1 was used for the second BASELINE for the following adaptation conditions. Following the DE-ADAPT condition, participants continued walking on the SBT with the belts moving in the opposite configuration of ADAPT 1. That is, the belt under the dominant leg in HYA and the belt under the uninjured leg in the individuals with ACL-R was sped up to 1.5 m/s while the belt under the contralateral leg remained at 0.75 m/s. Participants walked under these conditions for thirteen minutes (ADAPT 2). Then the belt moving at the fast speed was returned to the 0.75m/s and the participants walked for an additional five minutes, (DE-ADAPT 2). The order of ADAPT 1 and ADAPT 2 conditions were randomized between all participants.

Kinematic (120 Hz; Vicon Nexus, Oxford, UK) and kinetic data (1200 Hz; Bertec Corporation, Columbus, OH) were recorded for the first and last 30 seconds of all conditions. For clarity, all variables calculated for the leg on the belt moving at 1.5 m/s are henceforward referred to as the “fast” leg, and the leg on the belt moving at 0.75 m/s referred to as the “slow” leg. Stride length was defined as the anterior posterior distance traveled by the ankle marker from heel-strike to toe-off.² Stance time was defined as the percent of the gait cycle between heel-strike and subsequent toe-off of the same limb. Step length was defined as the anterior posterior distance between the ankle markers at heel-strike. Slow double-limb support refers to the time from fast leg heel-strike to slow leg toe-off and fast double-limb support refers to the time from slow leg heel-strike to fast leg toe-off. Symmetry was defined in each spatiotemporal gait parameter using the following asymmetry index:

$Asymmetry = (fast\ leg\ parameter - slow\ leg\ parameter) / (fast\ leg\ parameter + slow\ leg\ parameter)$.³

RESULTS AND DISCUSSION

Healthy individuals adapted a new walking pattern and stored the new walking pattern equally in both the dominant and non-dominant limb. Conversely, individuals with ACL-R displayed impairments in locomotor adaptation and significant differences in behavior between the reconstructed and uninjured limb (Figures 1-3). Indications of significant effects of leg and walking condition are omitted for clarity.

CONCLUSIONS

This investigation supports that after surgical reconstruction and physical therapy fundamental features of motor control remain altered. Following ACL-R, participants display an altered ability to learn and store functional gait patterns. Thus, sensorimotor integration may underlie the prolonged deficits in locomotor performance and control in this population.

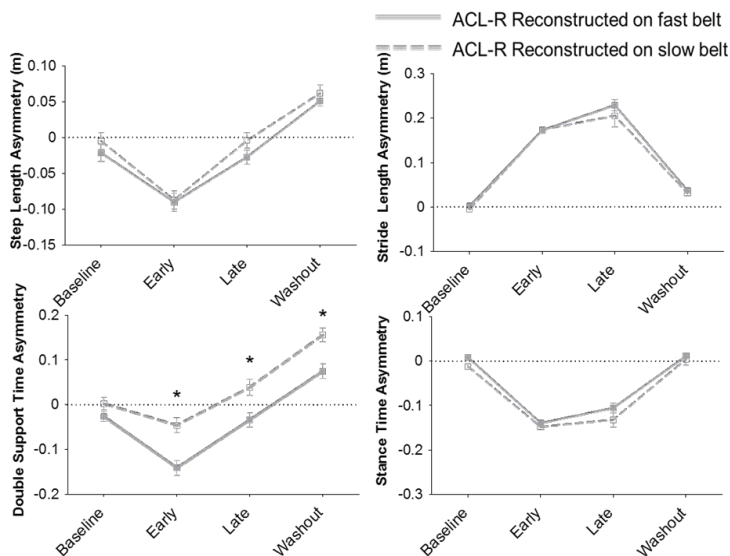


Figure 1. ACLR leg asymmetry scores on the slow and fast belt. Error bars indicate standard error. *indicates $p < .05$ differences between limbs.

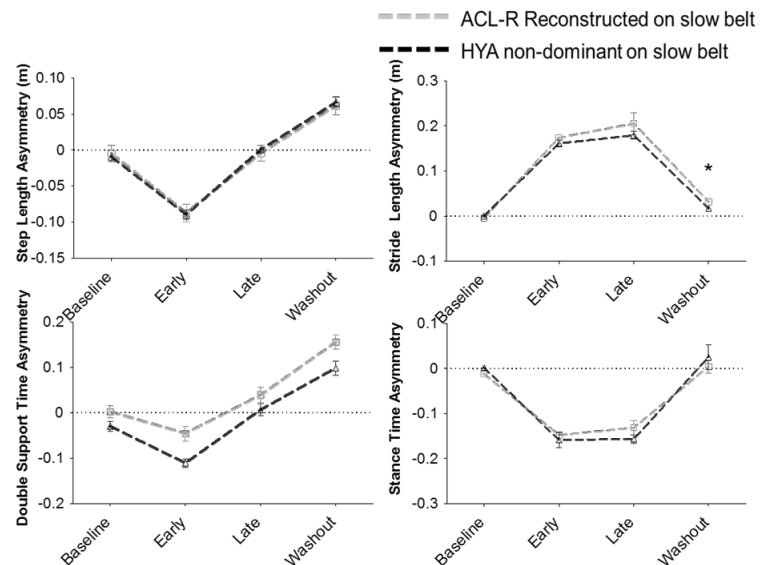


Figure 2. ACLR leg compared to the HYA nondominant leg on the fast belt. Error bars indicate standard error. *indicates $p < .05$ difference between groups.

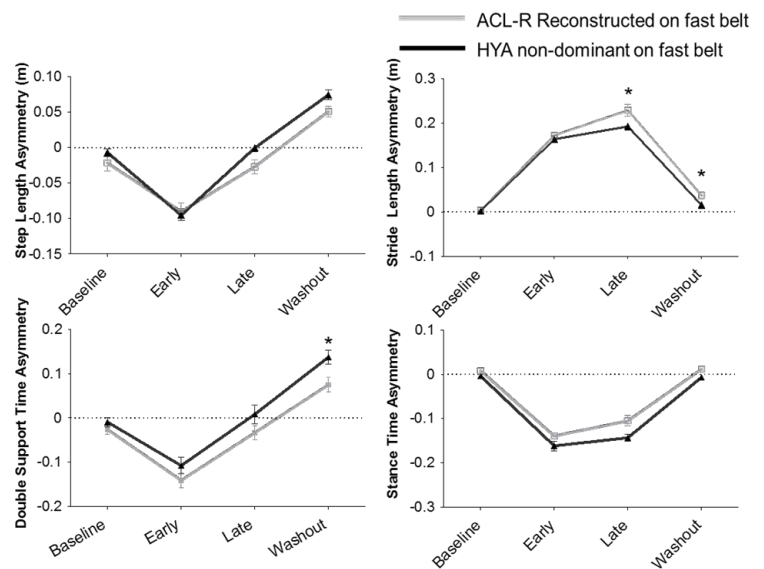


Figure 3. ACLR leg on the slow belt compared to the HYA nondominant leg on the slow belt. Error bars indicate standard error. *indicates $p < .05$ difference between groups.

REFERENCES

1. Gokeler A, et al. *J Orthop Res* **31**, 458-464, 2013.
2. Reisman DS, et al. *Phys Ther* **90**, 187-195, 2005.
3. Roemmich et al. *Clin Neurophysiol* **125**, 313-319.

Hamstring Strength Deficits Three Years after Anterior Cruciate Ligament Reconstruction in Individuals with Hamstring Autografts Alter Knee Mechanics during Gait and Jogging

Matthew N. Abourezk¹, Matthew P. Ithurburn¹, Michael P. McNally¹, Louise M. Thoma¹, Matthew S. Briggs¹, Kurt P. Spindler², Christopher C. Kaeding¹, Timothy E. Hewett¹, Laura C. Schmitt¹

¹The Ohio State University, Columbus, OH; ²Cleveland Clinic, Cleveland, OH

Corresponding author email: Laura.Schmitt@osumc.edu

INTRODUCTION

Anterior cruciate ligament reconstruction (ACLR) using hamstring tendon autografts may result in hamstring muscle weakness in the involved limb [1]. Altered mechanics are also observed during gait and jogging following ACLR for up to two years [2]; however, to our knowledge, the impact of hamstring strength asymmetry on involved limb gait mechanics has not been reported. The purpose of this preliminary study was to test the hypothesis that individuals with hamstring strength asymmetry would demonstrate altered involved limb knee mechanics during walking and jogging compared to those with symmetric hamstring strength two years after ACLR with hamstring tendon autograft.

METHODS

Participants (n=40; age=22.7; 21F/19M) were a subset of individuals that participated in the Multicenter Orthopaedic Outcomes Network (MOON) ACLR Two-Year Follow-up cohort. All participants had undergone a primary, unilateral ACLR with hamstring tendon autograft at least 2 years prior (mean=34.5mo.; range=27.9-42.7mo.). Hamstring strength was quantified as peak isometric knee flexion torque on an isokinetic dynamometer (Biodex) at 60° knee flexion. Limb-symmetry indices (LSI) were calculated for isometric hamstring strength using: $LSI = \frac{\text{involved value}}{\text{uninvolved value}}$. Hamstring strength LSI were used to divide the participants into a symmetric hamstring strength (SH) group ($LSI \geq 0.90$) and a weak involved limb hamstring (WH) group ($LSI < 0.85$) [3], resulting in 18 participants per group. 4 individuals had LSI from .85-.90 and were not included due to small group size. Involved knee mechanics were quantified by tracking 46 retroreflective markers using a 10-camera three-dimensional motion analysis system (Vicon Nexus; 300 Hz) during walking and jogging

across embedded force plates (Bertec; 1500 Hz). Visual3D software was used to calculate peak sagittal, frontal, and transverse plane knee kinematics, moments, and powers during each phase of walking and jogging. Gait phases included initial contact, weight acceptance (initial contact to peak knee flexion), mid-stance (peak knee flexion to peak knee extension), push-off (peak knee extension to toe-off), and toe-off. Jogging phases included initial contact, weight acceptance, push-off (peak knee flexion to toe-off), and toe-off. Marker trajectories and force-plate data were filtered with a low-pass Butterworth filter at 6 Hz. Joint moments and powers were normalized by body mass. Independent samples *t*-tests were used to compare involved knee kinematic and kinetic variables between the SH and WH groups across each phase of gait and jogging ($p < .05$; 2-tailed). Given the preliminary nature of this study in guiding future work, multiple comparisons were not controlled for.

RESULTS AND DISCUSSION

There were no differences in sagittal and frontal plane knee kinematics between the WH and SH groups during any phase of gait or jogging. During jogging, the WH group demonstrated increased tibial external rotation at initial contact ($p = .02$) and during weight acceptance ($p = .02$) compared to the SH group (Figure 1A). During gait, the WH demonstrated decreased tibial internal rotation during weight acceptance ($p = .011$) (Figure 1B).

In addition, the WH group demonstrated decreased internal knee flexion moment at initial contact ($p = .012$) and during weight acceptance ($p = .011$), decreased internal knee extension moment at toe-off ($p = .007$), and decreased peak knee power during mid-stance ($p = .001$), during push-off ($p = .026$) and at toe-off ($p = .005$) during gait compared to the SH group. (Table 1).

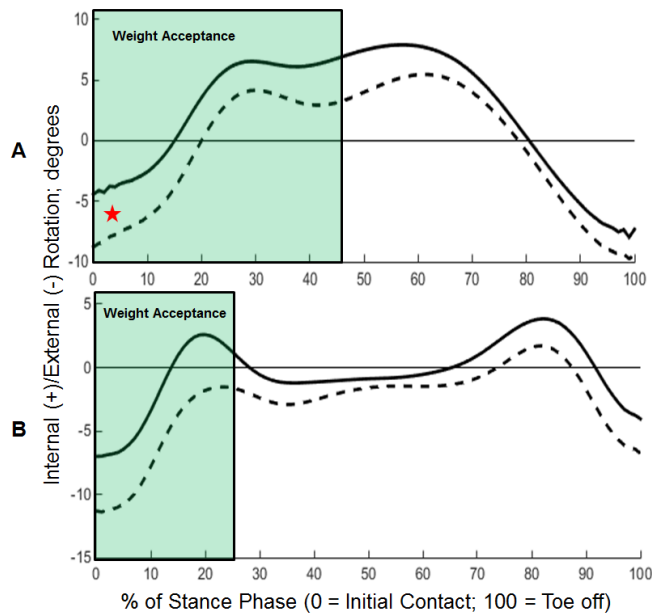


Figure 1. SH vs. WH transverse plane knee angles during jogging (A) and gait (B). (Solid = SH; Dashed = WH; Star indicates differences at initial contact)

These preliminary findings demonstrate that decreased involved hamstring strength often persists over two years after ACLR, as nearly half of our sample was in the WH group. These strength deficits may contribute to differences in involved limb knee mechanics, due to persistent morphological deficits from hamstring graft harvest during ACLR [4]. Previous work has illustrated that strength contributions must be increased from the lateral portion of the hamstring to prevent strength loss due to medial hamstring harvest for the graft [5]. This may contribute to altered transverse plane knee kinematics during gait and other functional tasks. Additionally, the findings of increased

involved tibial external rotation in the WH group were consistent with previous work comparing the involved limb to the uninvolved limb during gait post-ACLR, regardless of hamstring strength [6]. In addition, the current data demonstrated differences in sagittal plane knee moments and power between the SH and WH groups. This is similar to previous work demonstrating that individuals after ACLR with quadriceps strength deficits also demonstrate reduced sagittal plane knee moments during gait [7].

CONCLUSIONS

Two years after ACLR with hamstring tendon autograft, participants with deficits in involved hamstring strength show altered knee mechanics in the sagittal plane during gait and in the transverse plane during jogging compared with individuals with symmetric hamstring strength. Given these preliminary findings, future work will further examine the impact of persistent hamstring strength deficits on mechanics during functional and dynamic tasks after ACLR.

REFERENCES

1. Ardern CL, et al. *Orthop Rev*, **1**, e12, 2009.
2. Bush-Joseph CA, et al. *Am J Sports Med*, **29**, 36-41, 2001.
3. Schmitt LC, et al. *J Orthop Sports Phys Ther*, **42**, 750-759, 2012.
4. Segawa H, et al. *Arthroscopy*, **18**, 177-182, 2002.
5. Maeda A, et al. *Am J Sports Med*, **24**, 504-509, 1996.
6. Scanlan SF, et al. *J Biomech*, **43**, 1817-1822, 2010.
7. Lewek M, et al. *Clin Biomech*, **17**, 56-63, 2002.

Table 1. Involved Sagittal Plane Knee Moments and Knee Powers During Gait

	SH (n = 18)	WH (n = 18)	P-Value
Moment at Initial Contact	.351 ± .061	.295 ± .064	.012
Peak Moment during Weight Acceptance	.359 ± .059	.303 ± .067	.011
Moment at Toe-Off	-.078 ± .040	-.045 ± .027	.007
Peak Power during Mid-Stance	-.397 ± .207	-.196 ± .089	.001
Peak Power during Push-Off	-1.999 ± .494	-1.624 ± .471	.026
Power at Toe-Off	-.489 ± .258	-.272 ± .166	.005

All values: mean ± SD; All moments and powers normalized to mass in kg (Nm/kg; W/kg, respectively); Positive sagittal plane moment represents internal flexion moment, negative sagittal plane moment represents internal extension moment; Positive power represents power generated, negative power represents power absorbed

EFFECTS OF SIMULATED SURGICAL REPOSITIONING OF THE TIBIAL TUBERCLE ON PATELLOFEMORAL KINEMATICS IN KNEES WITH PATELLOFEMORAL MALALIGNMENT

¹ A. Amerinatanzi, M. Ingels, E. Nyman, K. Deep, A. Agarwal, V. Goel

¹ Engineering Center for Orthopaedic Research Excellence (E-CORE), The University of Toledo, Toledo, OH, USA
email: anand.agarwal@utoledo.edu

INTRODUCTION

Maltracking of the patella is a major cause of anterior knee pain and patellar instability. It is widely accepted that maltracking causes elevated patellofemoral contact pressures resulting in anterior knee pain and subsequent arthrosis [1,2]. Most patients with patellofemoral symptoms experience improvement with conservative treatment. However, a subset of these patients fail to respond to such interventions and ultimately require surgery. Surgeons can perform medialization and anteriorization of the tibial tubercle to correct abnormal patellar tracking. However, there is little experimental evidence regarding patellar kinematics after realignment procedures. As anteromedialization of the tubercle is surgically difficult, and associated with elevated risk of post-operative fracture, experimental insight will benefit the clinician [3]. The objective of this study was to evaluate the effects of medialization, anteriorization, and anteromedialization of the tibial tubercle on patellar tracking.

METHODS

A lower extremity finite element model was developed based on MRI and CT images of a female subject with no history of knee injury. 3D geometries of hard and soft tissues were digitized using Mimics v15.0 (Materialise, Leuven, Belgium). Geometries were converted into solid 8-node hexahedral elements for the patella, ligaments (ACL, MCL, LCL, and PCL), and menisci. The geometries of the femur, fibula, and tibia were constructed with an outer layer of wedge C3D6 elements for cortical bone and tetrahedral C3D4 elements for cancellous bone. Cartilage utilized tetrahedral C3D4 elements. Meshes were imported into ABAQUS 6.11-2 (SIMULIA, Providence, RI, USA). Capsules, muscles, tendons, and remaining ligaments were simulated using uniaxial truss elements.

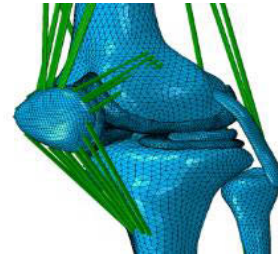


Figure 1 – ABAQUS Knee Joint Model

The material properties of the ACL, PCL, and MCL were modeled with hyperelastic properties. Material properties of all other tissues were modeled as linear elastic with different moduli assigned to the corresponding tissue. The femur, fibula, and tibia were defined as non-deformable rigid bodies. All uniaxial truss elements were defined as incompressible. The resultant model was validated against cadaveric testing with respect to ligament strain in quasi static motion. Cadaveric specimens underwent loading conditions to simulate tibial rotation, anterior shear, and valgus/varus moments during knee flexion.

RESULTS

Patellar kinematics were plotted for comparison (Figs. 2-7). Anteriorization of the tibial tubercle decreased patellar flexion (herein defined as sagittal plane gliding with respect to femur) 27% and 63% for 1 and 2 cm anterior elevation, respectively (Fig. 2). Medialization resulted in medial tilting of the patella up to 34% in the 20-45 degree flexion range. At higher levels of knee flexion, anteromedialization increased medial tilting up to 52%. Medialization decreased patella rotation in the coronal plane to the medial side while anteriorization had no discernible effect on rotation. Patellar medial translation is affected by medialization of the tibial tuberosity (i.e. 6.26 mm medial translation in normal vs. 0.12 mm in lateralization). Proximal patellar motion, defined herein as superior translation of the patella with respect to the femur in the sagittal plane, decreased by 10% and 23% as a result of anteriorization and medialization, respectively.

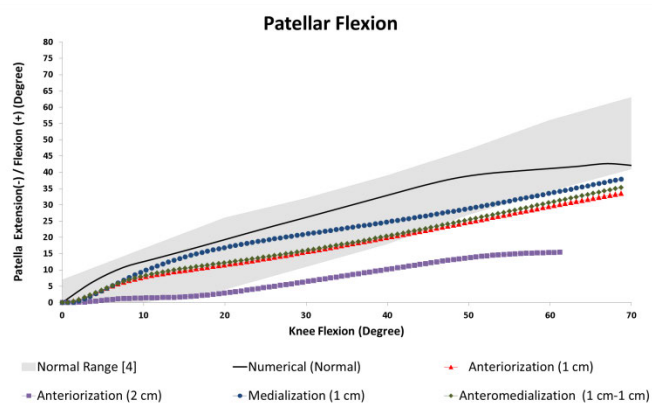


Figure 2 – Patellar flexion for different simulated cases

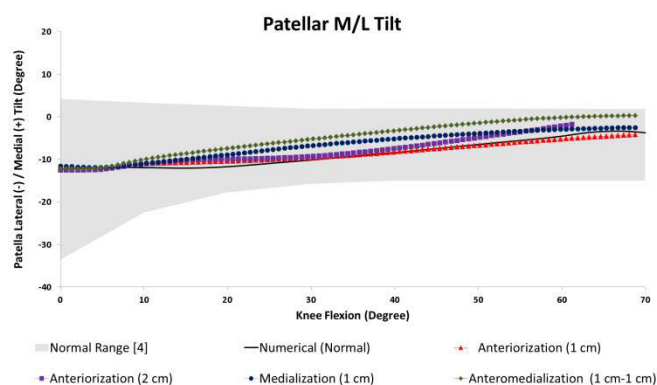


Figure 3 – Patellar medial/lateral tilt for different simulated cases

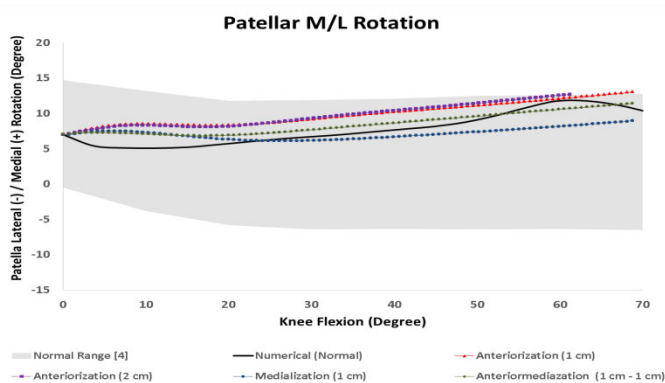


Figure 4 – Patellar medial/lateral rotation for different simulated cases

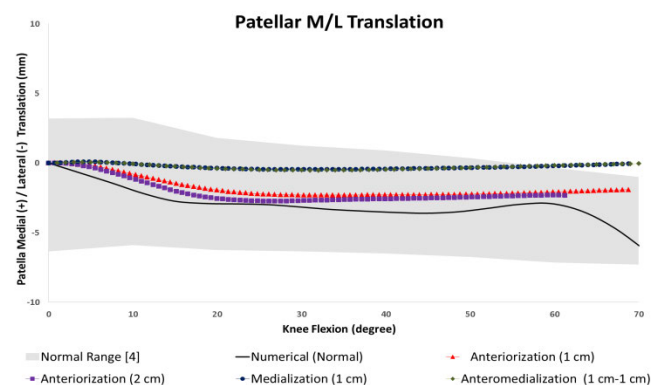


Figure 5 – Patellar Medial/Lateral translation for different simulated cases

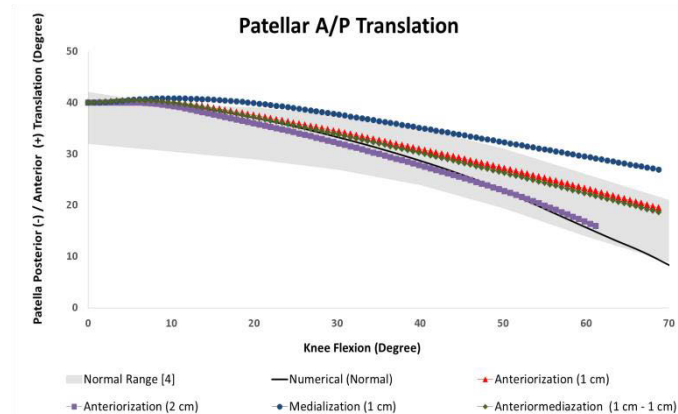


Figure 6 – Patellar anterior/posterior translation for different simulated

cases

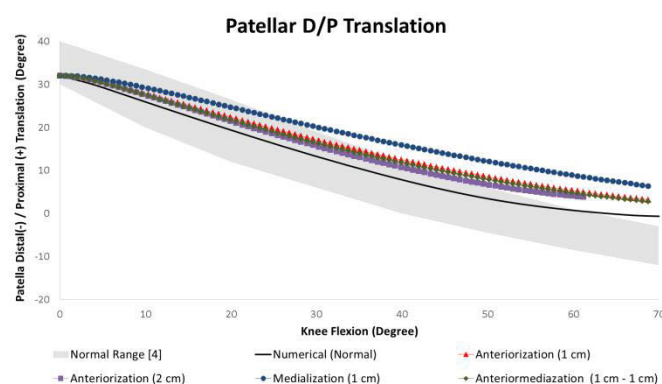


Figure 7 – Patellar Distal/Proximal translation for different simulated cases

DISCUSSION

This study directly compared the effects of contemporary patellofemoral joint realignment procedures. While both anteriorization and medialization can alter patellar kinematics, medialization decreased patellar lateral motion more than anteriorization or anteromedialization. An enhanced understanding of the resultant kinematics can influence clinical decision making with respect to surgical correction of patellar malalignment.

REFERENCES

1. Ramappa, A., et al. 47th Annual Meeting of the Orthopaedic Research Society. 2001.
2. Fulkerson JP, AJSM 1990, 490-6.
3. Bellemans J, AJSM 1998, 300-2.
4. C. Belvedere et al., springer (2014) 22:1719–1727

ACKNOWLEDGEMENTS

Work supported in part by the NSF Industry/University Cooperative Research Center at the University of California at San Francisco and University of Toledo, Toledo (www.nsfcdmi.org)

EFFECTS OF FOLLOWER LOAD AND RIB CAGE ON INTERVERTEBRAL DISC PRESSURES IN STATIC TESTS OF CADAVERIC THORACIC SPINES

¹ Dennis E. Anderson, ² Erin M. Mannen, ² Hadley L. Sis, ² Benjamin M. Wong, ² Eileen S. Cadel
² Elizabeth A. Friis, and ¹ Mary L. Bouxsein

¹ Beth Israel Deaconess Medical Center – Harvard Medical School, Boston, MA, USA

² The University of Kansas, Lawrence, KS, USA

email: danders7@bidmc.harvard.edu

INTRODUCTION

Cadaveric testing indicates that the rib cage adds significantly to thoracic stiffness. However, only a few studies have examined the in vitro mechanics of the full thoracic spine with the rib cage attached [e.g. 1, 2], or of the thoracic spine under a follower load [e.g. 3]. No study has previously done both simultaneously. Furthermore, it is not clear whether or how the rib cage might alter spinal loading. While the loading of a particular vertebral level cannot be measured directly, pressure within intervertebral discs is known to correlate strongly with compressive loading [4]. Thus, the purpose of this study was to determine whether the rib cage alters intervertebral disc pressure in static, upright loading conditions. We hypothesized that disc pressure would increase with increasing follower load, would decrease by artificially stiffening the rib cage, and would increase by the removal of the rib cage from the spine. We also assessed differences in disc pressure between two vertebral levels (T4/T5 vs T8/T9).

METHODS

Five full human cadaveric thoracic spines (T1-T12) with the rib cage intact were obtained (3 female and 2 male, mean age 65 years, range 61-71). Follower loads were applied by means of cables running lateral to the spine, connected to the spine by a rod inserted through each vertebral body with an eye nut at each end (Fig. 1). The specimen was positioned upright, and weights hung from the cables to apply follower loads. Five follower load levels were tested: 0 N, 200 N, 400 N, 600 N, and 800 N. Disc pressures were measured using pressure transducers side mounted on 1.3 mm diameter needles (Gaeltec, Isle of Skye, Scotland) inserted in the T4-T5 and the T8-T9 discs (Fig. 1).

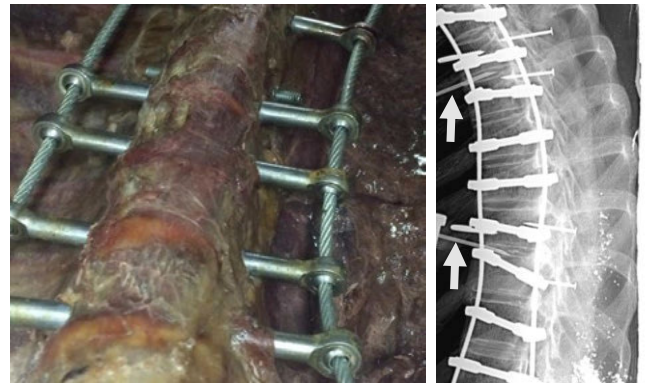


Figure 1: Follower load was applied by bi-lateral cables running through eye nuts attached to rods through the vertebral bodies (left). Radiograph showing specimen with follower load hardware attached and pressure transducer needle insertions (arrows) in the T4-T5 and T8-T9 intervertebral discs (right).

Measurements were performed under three testing conditions: normal intact rib cage, “stiffened” rib cage, and removed rib cage (Fig. 2). Rib cage “stiffening” was achieved by attaching plates that bridged the costal cartilage and sternocostal joints for ribs 2-5.

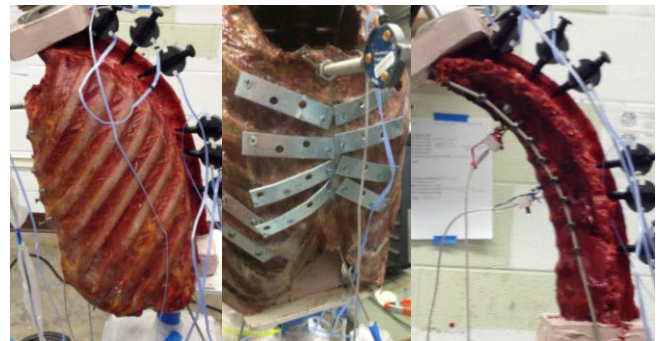


Figure 2: Testing conditions included normal intact (left), stiffened rib cage (center), and rib cage removed (right).

The effects of follower load and testing condition on disc pressure were examined with a mixed effects model for each level measured (T4-T5 and T8-T9), adjusting for specimen as a random variable. The difference in pressure between levels (T4-T5 vs. T8-T9) was similarly examined for effects of load and testing condition. Significance was set at $\alpha = 0.05$, and analyses were performed in JMP (SAS Institute Inc., Cary, NC).

RESULTS AND DISCUSSION

Disc pressure at both T4-T5 and T8-T9 increased significantly with increasing follower load magnitude ($p < 0.001$, Fig. 3), from a mean of about 180 kPa with no follower load to 1,040 kPa with 800 N follower load. The testing conditions did not influence disc pressure at T8-T9, but T4-T5 pressures without ribs were about 100 kPa lower than in the intact condition ($p = 0.010$). There was no difference in pressure between vertebral levels with no follower load, but the difference between T4-T5 and T8-T9 increased with increasing follower load ($p = 0.032$).

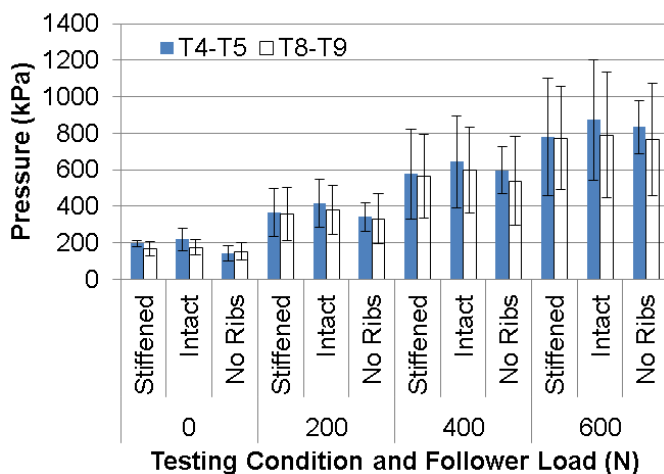


Figure 3: Measured pressures in the T4-T5 and T8-T9 intervertebral disc under different testing conditions and follower loads from 0 to 600 N. Error bars show ± 1 SD.

The pressures measured here and trends with follower load compare well to previous reports. For example, an average pressure of 1,270 kPa was reported for T8-T9 motion segments under a direct compressive load of 1,000 N [5]. Extrapolating the trend found here predicts a T8-T9 pressure of 1,155 kPa at a follower load of 1,000 N. Thus, the follower load approach used here successfully produces similar disc pressures to comparable directly applied compressive loads.

The effect of test condition was limited, but the significant pressure reduction at T4-T5 with rib cage removal was counter to our hypothesis. It is possible that removal of the ribcage produced kinematic differences that tend to reduce pressure, and this could be examined in future analyses. Furthermore, this analysis was limited to pressures in a static, upright position, and it is likely that the results are not representative of disc pressures in dynamic or kinematically different conditions.

CONCLUSIONS

A static follower load applied to a full cadaveric thoracic spine with the rib cage produces intervertebral disc pressures proportional to the follower load. Stiffening or removal of the rib cage minimally affects disc pressures.

REFERENCES

1. Mannen EM, et al. *Spine*, epub ahead of print (DOI: 10.1097/BRS.0000000000000879), 2015.
2. Watkins R, et al. *Spine* **30**, 1283-1286, 2005.
3. Stanley SK, et al. *Spine* **29**, E510-E514, 2004.
4. Pollintine P, et al. *J Biomech* **37**, 197-204, 2004.
5. Dolan P, et al. *Spine* **38**, 1473-1481, 2013.

ACKNOWLEDGEMENTS

This study was supported by the National Institute on Aging (K99AG042458) and by a Mentored Career Development Award from the American Society for Bone and Mineral Research.

DETERMINANTS OF APONEUROSSES SHAPE CHANGE DURING MUSCLE CONTRACTION

¹ Christopher J. Arellano, ² Nicholas J. Gidmark, ¹ Nicolai Konow, and ¹ Thomas J. Roberts

¹ Brown University, Providence, RI, USA

² University of Washington, Friday Harbor, WA, USA

email: christopher_arellano@brown.edu

INTRODUCTION

Aponeuroses are sheet-like tendons that connect in series with muscle fibers. The mechanical behavior of aponeuroses differs from that of free tendons because free tendons are loaded uniaxially, while aponeuroses experience loads in more than one direction. During a shortening contraction, aponeuroses increase in both length and width [1, 2]. It has been proposed that forces generated from muscle bulging as fibers shorten and expand radially cause an increase in aponeurosis width [1], but this idea has not been tested directly.

We tested the hypothesis that changes in aponeurosis width are governed by two forces: 1) forces resulting from radial expansion (i.e. bulging) of shortening muscle fibers, and 2) the force acting along the muscle's line of action (longitudinal axis). Fiber bulging due to shortening should increase aponeurosis width, whereas increases in longitudinal force should decrease aponeurosis width, as expected for a biaxially loaded material. To test this hypothesis, we measured muscle force, aponeurosis length, and aponeurosis width during isotonic muscle contractions.

METHODS

Small (0.8-1.0 mm diameter) radiopaque markers were surgically implanted along muscle fibers and into the aponeurosis of the lateral gastrocnemius (LG) muscle of wild turkeys, *Meleagris gallopavo* (Fig. 1A-B; $n=3$). Following established *in-situ* methods [1], the muscle's distal tendon was rigidly attached to a lever of a servo-controlled motor that regulated force and length (Aurora Scientific, Inc).

In-situ measurements of muscle force were combined with high-speed biplanar x-ray video for

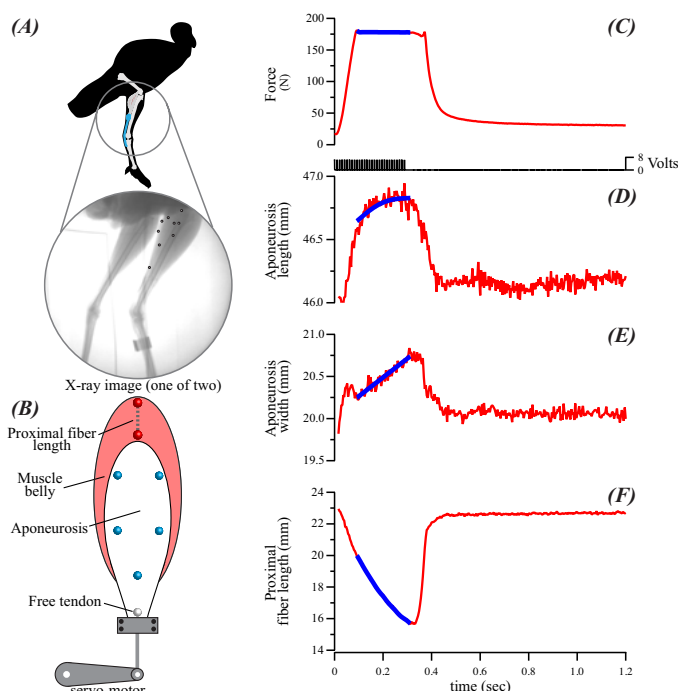


Figure 1: (A) In combination with x-ray video, an *in-situ* preparation (B) allowed us to quantify the effects of muscle fiber shortening on aponeurosis width and length changes (C-F) during an isotonic (constant force) contraction at maximal activation. Blue lines indicate isotonic period used for analysis.

a series of isotonic contractions. For each contraction, the positions of the radiopaque markers were tracked using an established marker-based workflow (www.xromm.org). Changes in muscle fiber length, aponeurosis width, and aponeurosis longitudinal length were quantified from the 3D marker coordinates (IGOR Pro 6, Wavemetrics).

We isolated the influence of fiber shortening on aponeurosis width by plotting the two during the time when the muscle produced a constant force (Fig. 1C-F; Fig. 2). The linear slope of aponeurosis width strain versus fiber shortening strain during each contraction was calculated to give the *relative strain ratio* (Fig. 3).

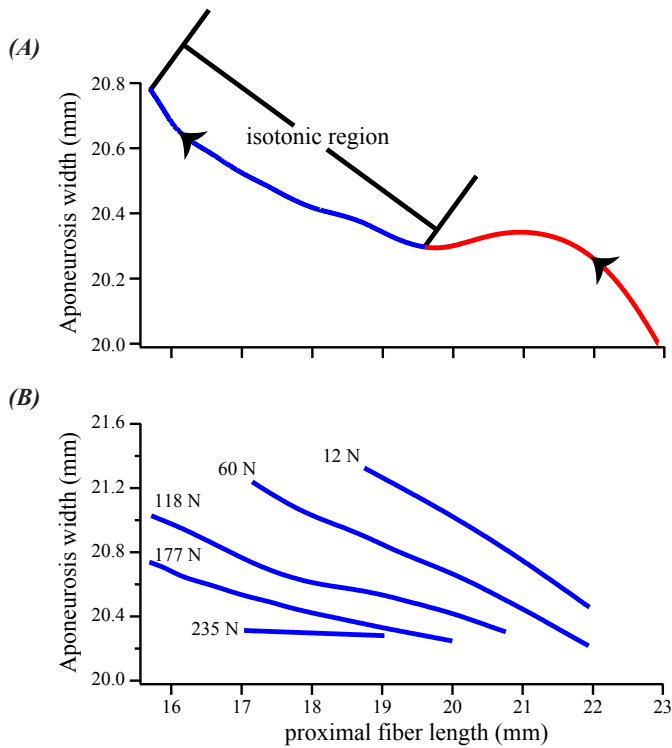


Figure 2: (A) Data for a single contraction showing the increase in aponeurosis width as muscle fibers shorten. Arrowheads indicate direction of fiber shortening during the contraction. (B) For a series of contractions, increases in aponeurosis width depend on both magnitude of fiber shortening and longitudinal muscle force. Representative data from several isotonic contractions measured from a single LG muscle.

RESULTS AND DISCUSSION

Influence of muscle fiber shortening and force: During periods of constant force, aponeurosis width increased as the muscle fibers shortened (Fig. 2A). Across contractions, the amount of increase in aponeurosis width also depended on longitudinal force. At higher forces, aponeurosis width increases to a lesser extent with fiber shortening (Fig. 2B). For example, when the muscle produced 12 N of constant force, 3 mm of fiber shortening coincided with a 0.8 mm increase in aponeurosis width (Fig. 2B). At 177 N, the same amount of fiber shortening coincided with only a 0.3 mm increase in aponeurosis width.

Relative strain ratio vs. relative force: Aponeurosis width increases more for a given amount of fiber shortening at low compared to high force levels. Overall, the ratio of aponeurosis strain to fiber strain

decreased as force increased. As seen in Fig. 3, increases in aponeurosis width were negligible when the fibers shortened at the highest constant force contractions.

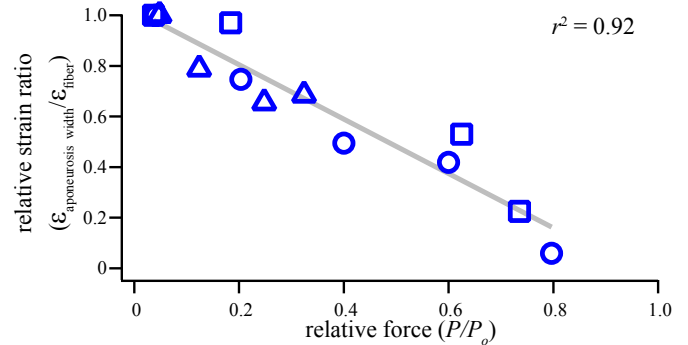


Figure 3: Relative strain ratio decreases as relative force increases indicating that shape change is force dependent ($n = 3$). Data are fitted with a linear least-square regression analysis (gray line). Symbols distinguish data from individual birds.

CONCLUSIONS

Our findings support our hypothesis that aponeurosis width is governed by two forces. The radial expansion of fibers associated with muscle shortening drives increases in aponeurosis width, while longitudinal forces on the aponeurosis tend to limit increases in aponeurosis width. The biaxial strain patterns in aponeuroses depends upon the relative magnitude of these two forces during a muscle contraction. These results demonstrate that muscle shape change influences the mechanical behavior of aponeuroses and highlight the mechanism for modulating aponeurosis stiffness.

REFERENCES

1. Azizi and Roberts. *J Physiol* **17**, 4309-4318, 2009.
2. Scott and Loeb. *J Morph* **224**, 73-86, 1995.

ACKNOWLEDGEMENTS

The authors thank Trovay Walker, Drew Schmetterling, and Benjamin Scott for their assistance on this project. The National Institutes of Health research grant [AR055295] awarded to TJR supported this research.

REMOVABLE ANCHORING PEDICLE SCREW RESTORES PULL OUT STRENGTH IN AN OSTEOPOROTIC VERTEBRA TO NORMAL BONE VALUE - A FINITE ELEMENT ANALYSIS

M. Saeid Asadollahi, Anand K. Agarwal, Vijay K. Goel

Engineering Center for Orthopaedic Research Excellence (E-CORE)

Departments of Bioengineering and Orthopaedic Surgery, University of Toledo, Toledo, OH, USA

Email: vijay.goel@utoledo.edu, web: <http://www.eng.utoledo.edu/ecore/>

Introduction:

Pedicle screws are the foundations in a posterior fixation system for an effective stabilization of the spinal segment(s). These have been in use for more than 25 years. However, the fixation efficacy is suboptimal in osteoporotic vertebrae. Various designs concepts have been floated to enhance their pull out strengths, but each design has some limitations [1]. Krenn et al. [1] have defined a parameter, flank overlap area – FOA, which shows the contact area between screw and bone to predict the fixation of screw in bone of poor quality. Increased FOA will lead to increase in the pullout strength. We have designed a pedicle screw whose FOA can be increased *in situ* through an anchor and which can be collapsed for ease of removal, if need arises. The biomechanics of this screw in a normal and an osteoporotic FSU are evaluated using the finite element technique.

Methods:

An experimentally validated 3-D FE model [2] of the L4-5 FSU was modified to simulate the new concept pedicle screw, a cage, and a rod posterior system. Expanding anchoring pedicle screw was drawn in solidworks with a 6mm outer diameter [3]. Wings were drawn in 30° position. An inner screw with a 2mm diameter was drawn. This screw passes through the cannula of the anchoring screw and expands the anchor *in situ*. Screw assembly was imported to Abaqus in STEP file format. Screws were put in pedicles such that expanded part was located within the cancellous bone. For anchoring screw, surfaces of the wings were tied to cancellous bone. Screw head also was tied to rod. All implants were titanium with 115GPa

Young's modulus and 0.34 Poisson's ratio. Two models were prepared, one for normal cancellous bone (100MPa Young's modulus and 0.2 Poisson's ratio), and a 69.7MPa Young's modulus and 0.2 Poisson's ratio was assigned to cancellous bone for the osteoporotic bone model. Lower end plate of L5 was fully constrained and a 10 N.m moment was applied to the upper end plate of L4. For flexion and extension cases, a 400N compressive connector pre-load was applied as well. An elasto-plastic material property was considered for cancellous bone for pullout strength; 100MPa Young's modulus and 1MPa Yield stress for normal bone and 69.7MPa Young's modulus and 0.697MPa Yield stress for osteoporotic bone. For pullout strength test axial load was applied to the screw in only L4 vertebra and load-displacement curve was computed, including the yield load values in all of the model types.

Results:

Pullout strength results showed 84% improvement for anchoring screw (with wing) in osteoporotic bone compared to normal screw (without wing), and even 33% compared to normal screw in normal bone. This shows that anchoring design could successfully restore pullout strength in osteoporotic bone (Fig. 1). On an average, RoM showed 15.6% improvement in stability. RoM decreased for anchoring screw compared to normal screw in Flexion (16%), Extension (16%), LB (21%), LR (8%), Flex with pre-load (22%) and Ext with pre-load (11%) in 10N.m moment (Fig. 2). Use of anchoring screw decreased the end plate stress (73.1 MPa for anchoring screw vs 79.9MPa for normal screw), (Fig. 3).

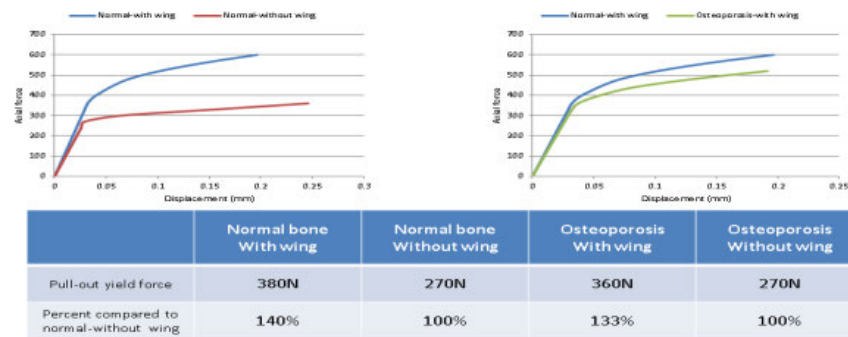


Figure 1: Pullout strength results for anchoring screw (with wing) and normal screw (without wing) in normal and osteoporotic bone



Figure 2: RoM results for L4-L5 at 10N.m for anchoring screw (with wing) and normal screw (without wing) in normal and osteoporotic bone

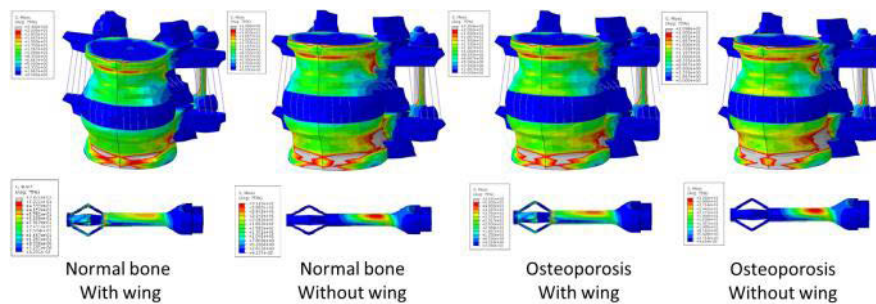


Figure 3: Stress distribution on whole FSU and screw in normal and osteoporotic bone

Discussion:

FE study on anchoring screw showed that increased FOA could increase the pullout strength and make it more stable in a normal and osteoporotic bone, compared to normal screw. A slight improvement in the stability of the construct was also predicted, although not significant from a cadaver test perspective.

Conclusion:

Since loosening is a challenging issue for pedicle screws, anchoring screw can improve anchorage of screw in an osteoporotic vertebra and thus may reduce loosening.

References:

- [1] Krenn, M H et al: *Journal of Neurosurgery*, vol. 9, no. 1, pp. 90–95, 2008.
- [2] Gilbertson, Lars G., et al: *Critical Reviews™ in Biomedical Engineering* 23, no. 5-6 (1995)
- [3] Goel, Vijay K., and Aaron Matyas. "Removable anchoring pedicle screw" U.S. Patent 8,734,497, issued May 27, 2014.

ACKNOWLEDGEMENTS:

Work supported in part by the NSF Industry/University Cooperative Research Center at the University of California at San Francisco and University of Toledo, Toledo (www.nsfcdmi.org)

IMPROVED ROD FIXATION REDUCTION IN LOOSENING OF THE PEDICLE SCREWS DUE TO PEEK/TITANIUM SCREW CONCEPT- A FINITE ELEMENT ANALYSIS

M. Saeid Asadollahi, Manoj K. Kodigudla, Amey Kelkar, Anand K. Agarwal, Vijay K. Goel

Engineering Center for Orthopaedic Research Excellence (E-CORE)

Departments of Bioengineering and Orthopaedic Surgery, University of Toledo, Toledo, OH, USA

Email: vijay.goel@utoledo.edu, web: <http://www.eng.utoledo.edu/ecore/>

Introduction:

Pedicle screws are the foundations for an effective stabilization of the spinal segment(s). These have been in use for more than 25 years. However, the fixation efficacy is suboptimal in osteoporotic vertebrae. Various designs concepts have been floated to enhance their pull out strengths, but each design has some limitations [1-4]. CT-scans show a halo around the loose screw. This we feel is due to significant difference between material properties (Young's modulus) of Titanium as implant material and the bone (115GPa for Ti and 0.1GPa for cancellous bone). We propose use of Polyether ether ketone's (PEEK) pedicle screws since its Young's modulus of 3.6GPa is closer to that of bone. A pilot cyclic loading of the construct with PEEK screw showed no loosening till 100,000 cycles. However tulip at the screw head couldn't provide effective fixation between rod and screw. Thus, 5 hybrid designs of PEEK/Ti pedicle screws were compared in FE to determine an optimal design.

Methods:

An experimentally validated 3-D FE model [5] of the L4-5 FSU was modified to simulate the new concept pedicle screw, a cage, and a rod posterior system. Five hybrid multiaxial pedicle screws consisting of PEEK and Titanium components (Fig. 1) were simulated. The results were compared to PEEK or Titanium only screw models. In the hybrid designs, tulip consisted of two parts with different materials (as shown in Fig. 1). Screws were drawn in Solidworks with a 6mm outer diameter and 40mm length.

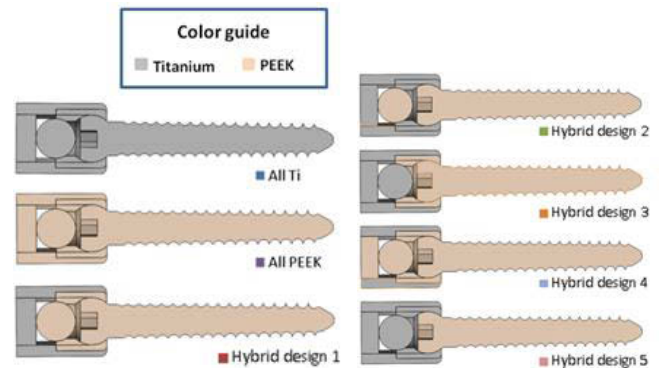


Figure 1: Seven proposed pedicle screws with different materials for the tulip section.

Screw assembly was imported to Abaqus in STEP file format. Screws were put in pedicles and connected to each other with a 5.5 mm rod. Screw threads were tied to cancellous bone, as well as rod to tulip. Screw head also was tied to tulip and washer, as well as washer to rod. A 115GPa and 4.6GPa Young's modulus and 0.34 and 0.38 Poisson's ratio were assigned for Titanium and PEEK, respectively. For each screw, two models were prepared; one with normal cancellous bone (100MPa Young's modulus and 0.2 Poisson's ratio), and one with osteoporotic bone (69.7MPa Young's modulus and 0.2 Poisson's ratio). Lower end plate of L5 was fully constrained and a 10 N.m moment was applied to the upper end plate of L4. For flexion and extension cases, a 400N compressive connector pre-load was applied as well. Also, as a parameter for rod fixation, tulip expansion at the rod/tulip interface was computed and compared.

Results:

RoM showed comparable stability for all cases in both normal and osteoporotic bone in Flexion, Extension, Left bending and rotation,

as well as Flexion and Extension with simulated body weight (Fig. 2). All Titanium provided the most stability, though all PEEK was the least stable. Results also point out that rod's stiffness has a big effect on the stability of implanted level, while screw's stiffness doesn't affect that much. Expansion of tulip was larger than all

Titanium compared to all PEEK, confirming the preliminary study showing rod loosening for all PEEK pedicle screw construct (Fig. 3). But Expansion of tulip for hybrid designs was considerably lower than all PEEK and closer to all Titanium pedicle screws.

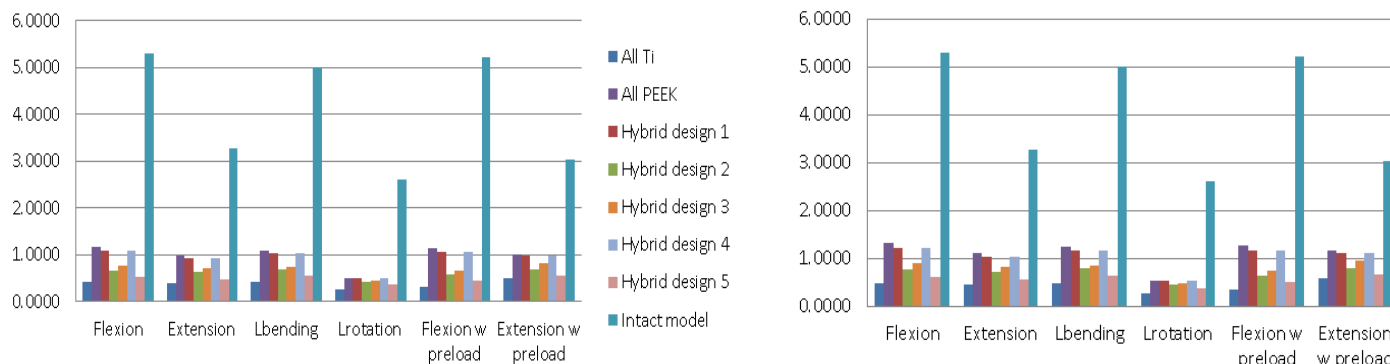


Figure 2: RoM results for L4-L5 at 10N.m for all designs with normal bone (Left) and osteoporotic bone (Right)

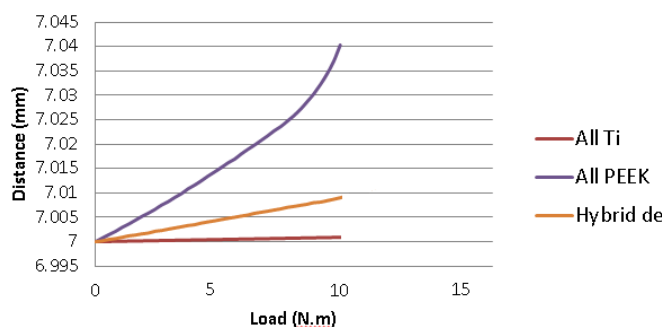


Figure 3: Expansion of tulip for all Titanium, all PEEK, and hybrid design1 in Flexion with normal bone

Discussion:

Preliminary work showed that PEEK pedicle screw can successfully decrease the loosening of screw, while it is not strong in rod fixation. Combining the metal to metal interaction of rod and tulip from traditional pedicle screws, and taking the advantage of PEEK as a material with stiffness close to bone, we propose different hybrid designs that is effective in stabilizing the construct. RoM for hybrid designs showed similar stability to traditional screws (All Titanium screws) and improvement of rod fixation compared to all PEEK screws.

References:

- [1] Wu, Zi-xiang, et al: *Clinical & Investigative Medicine* 33, no. 6 (2010): E368-E374.
- [2] Shea, Thomas M., et al: *BioMed research international* 2014 (2014)
- [3] Krenn, M H et al: *Journal of Neurosurgery*, vol. 9, no. 1, pp. 90–95, 2008.
- [4] Goel, Vijay K., and Aaron Matyas. "Removable anchoring pedicle screw" U.S. Patent 8,734,497, issued May 27, 2014.
- [5] Gilbertson, Lars G., et al: *Critical Reviews™ in Biomedical Engineering* 23, no. 5-6 (1995)

ACKNOWLEDGEMENTS:

Work supported in part by the NSF Industry/University Cooperative Research Center at the University of California at San Francisco and University of Toledo, Toledo (www.nsfcdmi.org).

ROBOTIC SIMULATION OF IN VIVO KINEMATICS ON CADAVERIC LIMBS EXHIBIT MINIMAL MECHANICAL DIFFERENCES BETWEEN CONTRALATERAL PAIRS

Nathaniel A. Bates^{a,b,c}, April L. McPherson^b, Rebecca J. Nesbitt^b, Jason T. Shearn^b,
Gregory D. Myer^{a,c}, Timothy E. Hewett^{a,b,c}

^aOSU Sports Medicine Sports Health & Performance Institute, Ohio State University, Columbus, OH, USA

^bUniversity of Cincinnati, Cincinnati, OH, USA

^cCincinnati Children's Hospital Medical Center, Cincinnati, OH, USA

email: batesna@gmail.com website: <http://sportsmedicine.osu.edu/>

INTRODUCTION

In vivo investigations have identified side-to-side limb asymmetries as a biomechanical precursor to primary and secondary ACL injury.[1] Recently, novel methods of *in vitro* simulation driven by *in vivo* recorded kinematics have been developed to directly investigate knee mechanics during athletic tasks that may relate to ACL injury.[2] However, it remains unknown whether side-to-side limb asymmetries persist exhibit between contralateral specimen pairs exposed *in vitro* articulations of the knee joint driven by identical kinematics. The objective of this study was to determine if mechanical side-to-side asymmetries observed *in vivo* persist in contralateral pairs during *in vitro* simulation testing.

METHODS

In vivo kinematics were recorded for male and female drop vertical jump (DVJ) tasks using 3D motion capture. Kinematics were filtered and processed to be usable in robotic simulation.[2] 14 cadaveric lower extremities from seven unique donors were obtained from an anatomical donations program (age = 47.2 ± 8.9 years; mass = 876 ± 201 N; BMI = 29.6 ± 5.8). A six-degree-of-freedom robotic arm and custom mechanical fixtures were used to drive each specimen through male- and female-specific DVJ simulations. Throughout each task, joint forces and torques were recorded by a six-axis load cell aligned with the tibial axis and ligament strains were recorded by differential variable force transducers implanted on the ACL and MCL. For each task, data was analyzed for significance ($\alpha < 0.05$) between contralateral pairs using paired t-tests.

RESULTS AND DISCUSSION

Comparison for biomechanical differences between contralateral limb pairs exhibited a lack of mechanical differences between limb sides. There were no statistically significant side-to-side differences in the peak forces or torques generated throughout each simulated task, nor were there significant differences at initial contact ($P > 0.05$). Mean forces and torques generated by each limb of a contralateral pair exhibited similar patterns of behavior throughout each simulation (Figure 1).

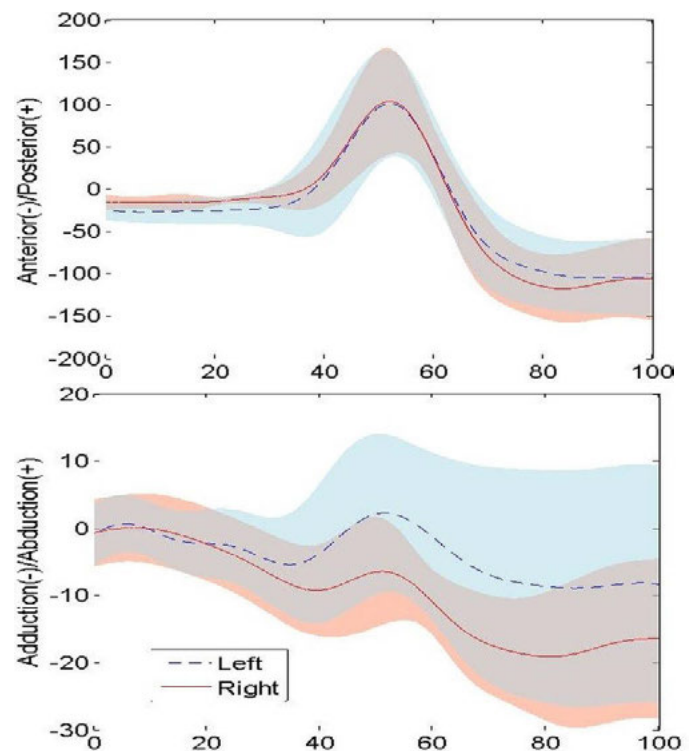


Figure 1: Mean anterior force (top) and abduction torque (bottom) generated at the knee by separate limbs from a contralateral pair during simulated female DVJs. These degrees of freedom represent those most associated with ACL loading and injury.

Table 1: ACL and MCL strain values as recorded throughout each simulated task.

	FEMALE DVJ		MALE DVJ	
	LEFT	RIGHT	LEFT	RIGHT
ACL				
IC	4.24 ± 3.28%	4.43 ± 3.22%	3.34 ± 3.28%	3.16 ± 3.53%
Peak	7.27 ± 4.14%	6.33 ± 4.70%	7.67 ± 4.48%	6.33 ± 5.34%
MCL				
IC	0.21 ± 1.69%	0.40 ± 2.96%	0.46 ± 1.77%	0.82 ± 3.15%
Peak	1.90 ± 1.71%	1.04 ± 3.25%	1.12 ± 1.62%	0.91 ± 3.15%

* indicates statistically significant difference between sides ($P < 0.05$)

Similar to the forces and torques, neither simulated task exhibited side-to-side differences in ligament strains for the ACL or MCL at peak value or initial contact (Table 1). The range of strain values observed in the MCL was statistically greater in the left limb for both the female (1.76% vs. 0.75%) and male (0.95% vs. 0.34%) DVJs. However, the clinical relevance of a 1% change in ligament strain remains unclear. This is especially true as peak ligament strain values observed during the current study were consistent with those found in previous *in vitro* simulations of drop landing tasks, which are well below reported failure magnitudes of the ACL and MCL.[3,4]

Previous literature found that removing a specimen and reinstalling it for further testing resulted in clinically significant differences.[5] That side-to-side variability between contralateral specimens expressed fewer statistical differences than repeated biomechanical testing on a single, re-potted specimen was surprising. The consistency of the present data therefore reinforced the reproducibility of our testing methodology and further validated the concept that right and left contralateral pairs can be used interchangeably in cadaveric simulations.

The present study utilized identical kinematics to simulate articulation in both limbs of a contralateral pair. *In vivo* studies would yield unique kinematics for each limb as known differences exist between dominant and non-dominant limbs, [6] but dominance information was not provided for the specimens used. However, this study was an investigation of asymmetries present in contralateral limbs for *in vitro* simulations, not asymmetries *in vivo*. Anatomical geometry was analyzed for effect on mechanical differences during simulation.

CONCLUSIONS

There was a lack of mechanical differences between limb sides in biomechanical simulations, which supported the null hypothesis that side-to-side asymmetries would not persist during *in vitro* tests. This finding suggested that contralateral knee joints are representative of each other in biomechanical tests. In future *in vitro* simulations, specification of limb side should not be a dependent variable impacting the test results. Results of this study indicated that during *in vitro* simulation, specification of left or right knee joint does not alter biomechanical outcomes during athletic movements. This finding will help to further develop protocols for robotic simulation. Contralateral limbs can be used interchangeably in cadaveric simulations. Furthermore, direct comparisons can be made between structural behaviors in one knee and between its contralateral partner for isolated conditions.

REFERENCES

1. Paterno MV, et al. *Clin J Sport Med.* **17**, 258-62. 2007.
2. Bates, N.A., et al. *Submitted for Publication.* 2015.
3. Withrow TJ, et al. *Clin Biomech.* **21**, 977-83. 2006.
4. Levine JW, et al. *Am J Sport Med.* **41**, 385-95. 2002.
5. Goldsmith MT, et al. *Med Eng Phys.* **36**, 1331-7. 2014.
6. Lanshammer, K., et al. *Phys Ther Sport*, **12**, 76-9. 2011.

ACKNOWLEDGEMENTS

Funding from NIH Grants R01-AR049735, R01-AR05563, R01-AR056660, and R01-AR056259.

TIBIAL SLOPE CORRELATIONS WITH PEAK KNEE JOINT LOADS AND ANTERIOR CRUCIATE LIGAMENT STRAIN DURING SIMULATIONS OF CONTROLLED ATHLETIC TASKS

Nathaniel A. Bates^{a,b,c}, Rebecca J. Nesbitt^b, Samuel C. Wordeman^a, Jason T. Shearn^b,
Gregory D. Myer^{a,c}, Timothy E. Hewett^{a,b,c}

^aOSU Sports Medicine Sports Health & Performance Institute, Ohio State University, Columbus, OH, USA

^bUniversity of Cincinnati, Cincinnati, OH, USA

^cCincinnati Children's Hospital Medical Center, Cincinnati, OH, USA

email: batesna@gmail.com website: <http://sportsmedicine.osu.edu/>

INTRODUCTION

Tibial slope has been identified as a non-modifiable risk factor for anterior cruciate ligament (ACL) injury as ACL injury patients exhibit higher tibial slopes than matched healthy controls.[1,2] Despite these findings, limited work has been done to assess how tibial slope affects ACL strain and joint loading during athletic tasks related to non-contact ACL injury. Recent advancements in robotic simulation have made it possible to create *in vitro* simulations of knee articulation using *in vivo* kinematics recorded from athletic tasks.[3] The purpose of this investigation was to quantify the influence of tibial slope on knee mechanics during an *in vitro* simulated drop vertical jump (DVJ). The primary hypothesis was that increased posterior tibial slope would be associated with increased knee loads in the frontal and sagittal planes.

METHODS

A 6-degree-of-freedom robotic manipulator articulated 18 cadaveric knees from 11 unique donors (age = 47.6 ± 7.3 years; mass = 829 ± 199 N) through simulations of kinematics recorded from *in vivo* DVJs.[3] DVJs from both male and female subjects were used to articulate separate simulations while forces and torques were recorded by a 6-axis force sensor that was aligned with the long axis of the tibia. A coordinate measuring device was used to digitize landmarks on the articulating surface of the tibial plateau at the anterior and posterior aspects of the midline in the medial tibial compartment as well as the lateral tibial compartment. These landmarks correspond with the points that were selected in previously documented methods of radiographic-based tibial slope

calculation.[2] Posterior tibial slope was then calculated via these same previously published techniques using the points specified.[2] Pearson correlations were used to assess the significance of linear relationships between tibial slope and joint forces and torques. All torques are presented as internally-generated within the knee joint.

RESULTS AND DISCUSSION

During the simulated DVJs for both sexes, increased posterior tibial slope in the lateral compartment was significantly correlated with increases in peak knee adduction torque (female: $r = 0.65$, $P = 0.02$; male: $r = 0.60$, $P = 0.04$), peak knee flexion torque (female: $r = 0.64$, $P = 0.03$; male: $r = 0.66$, $P = 0.02$), and peak lateral knee force (female: $r = 0.69$, $P = 0.01$; male: $r = 0.57$, $P = 0.05$). During simulations of male DVJs, increased tibial slope in the lateral compartment corresponded with increased peak external rotation torque ($r = 0.72$, $P = 0.01$) and decreased peak internal rotation torque ($r = -0.79$, $P < 0.01$). Across sexes, increased posterior tibial plateau slope in the medial compartment was only correlated with an increase in peak knee flexion torque (male: $r = 0.69$, $P = 0.01$; female: $r = 0.64$, $P = 0.02$).

The data confirmed the *a priori* hypothesis that increased posterior tibial slope was associated with larger magnitudes of knee loading in directions that correspond with larger demand on the ACL. Previous investigations have shown that externally generated knee abduction, extension, and internal rotation torques strain the ACL or are associated with injury risk.[4-5] These degrees of freedom correspond with the internally generated torques documented in the present results. (Figure 1 & 2)

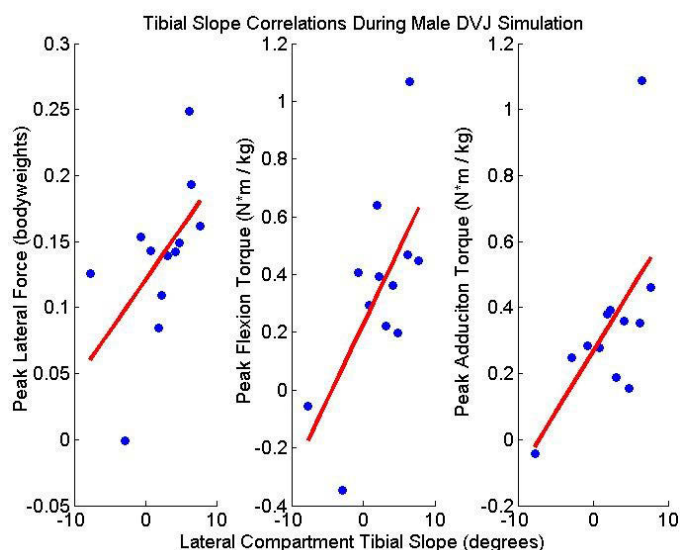


Figure 1: Significant correlations between posterior tibial slope in the lateral compartment and knee loading relative to the male DVJ.

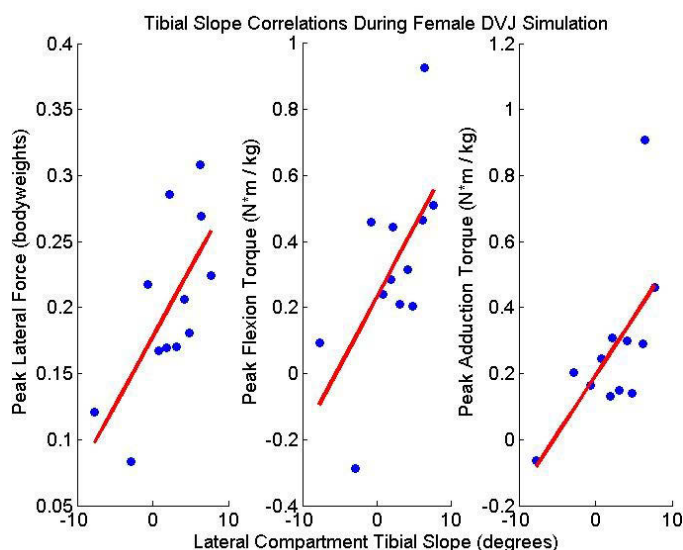


Figure 2: Significant correlations between posterior tibial slope in the lateral compartment and knee loading relative to the female DVJ.

Published literature has traditionally shown that tibial slope in the lateral compartment is more closely related with ACL injury risk than the medial compartment.[1-2] These findings corroborate the present data, as only lateral compartment slope was correlated with the frontal and transverse plane torques most associated with altering ACL strain.

Athletes who land with greater knee extension and greater externally-generated knee extension torques

increase strain on the ACL and are therefore more susceptible to injury. [6] The present data indicated that increased posterior tibial slope may drive this kind of loading in the knee as internally-generated flexion torques were moderately correlated with posterior tibial slope angle in both compartments.

It was surprising that tibial slope did not correlate with antero-posterior forces in either the male or female simulation. *In vitro* studies demonstrate that increased tibial slope generates anterior tibial translation and correspondingly anterior tibial force in the knee.[7] The present *in vitro* simulations are governed by recorded kinematics and a high-precision robotic arm.[3] Therefore, it is possible that the stiffness and precision of the manipulator only permitted minimal bone bending, despite anatomical differences, and inadvertently inhibited any antero-posterior shift that may otherwise be naturally induced with higher tibial slope.

CONCLUSIONS

Data from this investigation demonstrated that increased posterior tibial slope angle, especially in the lateral compartment, is correlated with increased knee joint loading during simulated landing in degrees of freedom that are known to place additional mechanical demand on the ACL. The mechanical data presented confirms that alterations in tibial slope angle have the potential to influence ligament loading; and thus, may be related to injury risk.

REFERENCES

1. Wordeman SC, et al. *Am J Sp Med.* **40**,1673-81. 2012.
2. Hashemi J, et al. *Knee.* **17**,235-41. 2010.
3. Bates NA, et al. *Ann Biom Eng.* In-press. 2015.
4. Hewett TE, et al. *Am J Sp Med.* **33**,492-501. 2005.
5. Shin CS, et al. *Med Sci Sp Ex.* **43**,1484-91. 2011.
6. Heijne, et al. *Med Sci Sp Ex.* **36**, 935-41. 2004.
7. Giffin JR, et al. *Am J Sp Med.* **32**, 376-82. 2004.

ACKNOWLEDGEMENTS

Funding from NIH Grants R01-AR049735, R01-AR05563, R01-AR056660, and R01-AR056259.

THE INFLUENCE OF INTERNAL AND EXTERNAL TIBIAL ROTATION OFFSETS ON KNEE JOINT AND LIGAMENT BIOMECHANICS DURING SIMULATED ATHLETIC TASKS

Nathaniel A. Bates^{a,b,c}, Rebecca J. Nesbitt^b, Jason T. Shearn^b,
Gregory D. Myer^{a,c}, Timothy E. Hewett^{a,b,c}

^aOSU Sports Medicine Sports Health & Performance Institute, Ohio State University, Columbus, OH, USA

^bUniversity of Cincinnati, Cincinnati, OH, USA

^cCincinnati Children's Hospital Medical Center, Cincinnati, OH, USA

email: batesna@gmail.com website: <http://sportsmedicine.osu.edu/>

INTRODUCTION

Following anterior cruciate ligament (ACL) injury, transverse plane tibiofemoral rotation becomes underconstrained, while subsequent reconstruction leaves it overconstrained.[1,2,3] That ligament deficiency and repair cause alterations in the transverse-plane orientation of the tibiofemoral joint would suggest that the ACL is a mechanical restraint to knee motion within this plane. However, the effect of isolated internal tibial torques on knee loading has been evaluated via biomechanical testing and the current literature is conflicted.[1] The objective of this investigation was to determine the mechanical effects of transverse plane tibial rotation offsets on knee kinetics and ligament strains during *in vitro* simulations of *in vivo* kinematics recorded from athletic tasks.

METHODS

In vivo kinematics were recorded for male and female athletic tasks using 3D motion capture. *In vivo* kinematics were filtered and processed to be usable in robotic simulation.[4] 11 cadaveric lower extremities from 9 unique donors were obtained from an anatomical donations program and accepted for use in this study (age = 46.1 ± 7.7 years; mass = 861 ± 203 N). A six-degree-of-freedom robotic arm and custom mechanical fixtures were used to articulate each specimen through male- and female-specific simulations of recorded drop vertical jump (DVJ) and sidestep cutting tasks. The robotic manipulator then applied isolated $\pm 4^\circ$ rotational offsets to the tibia in the transverse plane and rearticulated the same kinematic simulations. Throughout each simulated articulation, joint forces and torques were recorded by a six-axis load cell

aligned with the long axis of the tibia and ligament strains were recorded by differential variable force transducers implanted on the ACL and MCL. Each motion condition was analyzed individually with a 3x1 ANOVA with Bonferroni post-hoc analysis was used to determine significantly different ($\alpha < 0.05$) forces, torques, and strains between each of the three simulation offset conditions.

RESULTS AND DISCUSSION

Transverse plane rotational offsets had a significant effect on peak posterior force for female motion simulations ($P < 0.01$), on peak lateral force for most simulated tasks ($P < 0.01$), and on peak anterior force, internal torque, and flexion torque for sidestep cutting tasks ($P \leq 0.01$). Rotational offsets did not influence significant differences on peak ACL strain ($P > 0.05$) or MCL strain ($P > 0.05$) for any task (Figure 1). With that consideration, during the sidestep cutting tasks, the peak magnitude of ACL strain did increase linearly as the initial orientation offset orientation shifted from and externally rotated to internally rotated position. A similar linear, but non-significant, change in peak MCL magnitude was noted. Transverse plane rotational offsets comparable to those observed in ACL deficient and reconstructed patients alter knee kinetics without significantly altering ACL strain.

Internal and external tibial rotation offsets were able to effect significant changes on the loading profile at the knee joint without effecting significant changes on ACL strains. A 4° internal offset did generally increase the peak ligament strain; however, the magnitude of this change was not great enough to be statistically significant.

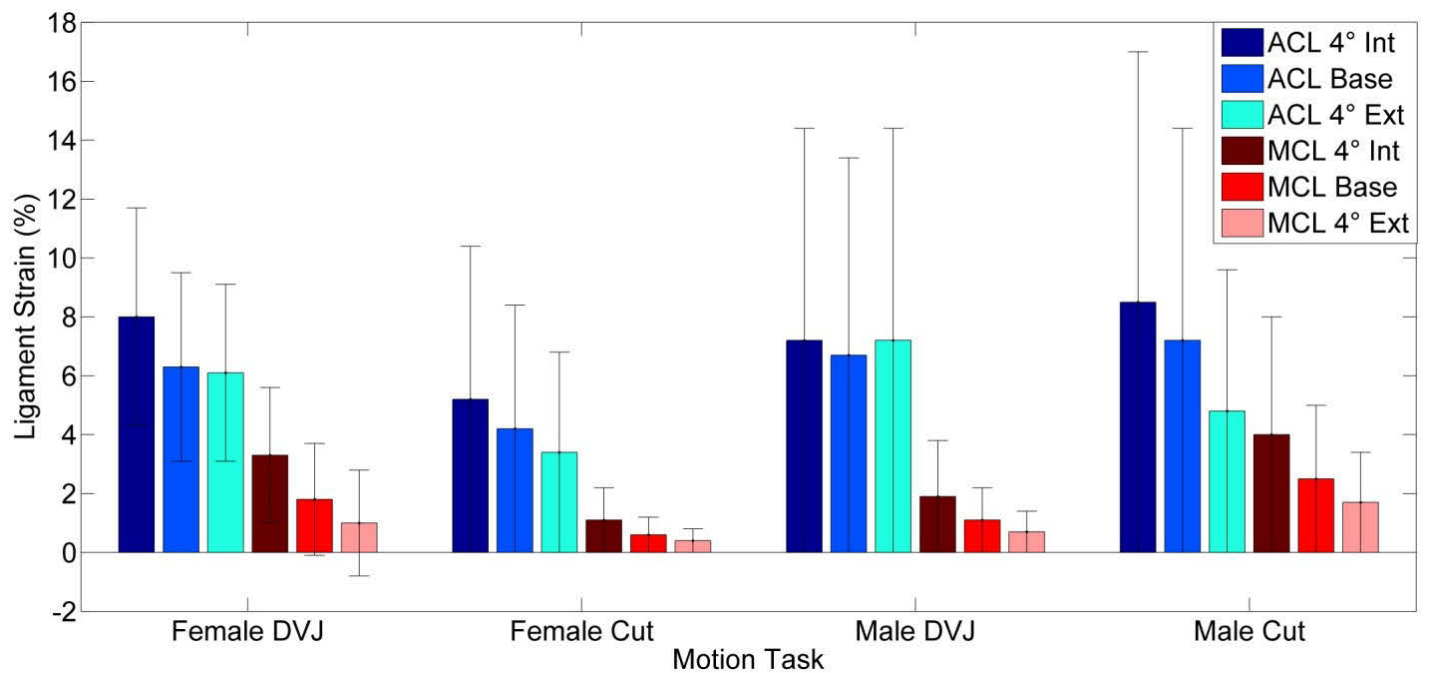


Figure 1: Depiction of peak ACL and MCL strain values and standard deviations for all three rotational offset conditions for each motion task simulated. For both ligaments, there were no statistically significant differences in peak strains between offset conditions.

Kinematic changes following ACL-deficiency and ACL-reconstruction imply that the ACL has an important role in transverse plane stabilization of the knee.[2,3] However, the present results indicate that the role of the ACL in this regard is limited. Not only did magnitude changes in ACL strain lack statistical significance (1.1% mean increase for internal offset; -1.9% mean decrease for external offset), but the peak strains achieved were approximately half of previously reported failure values in the ACL.[5]

ACL reconstructions may overconstrain the joint as reconstructed patients have demonstrated 4° greater external tibial rotation during gait than healthy controls.[3] Similarly, the magnitude of mean ligament force in reconstructed ACLs can often exceed that of the native ligament tissue. [1] In the present study, ACL strain magnitudes were generally smaller in the 4° externally rotated offset condition. Therefore, it is conceivable that this external offset induced by ACL reconstructions would stress shield native ACLs from natural loading.

CONCLUSIONS

As knee degeneration is attributed to abnormal loading profiles, altered transverse plane kinematics may contribute to this. However, the data demonstrated that transverse plane perturbations on the magnitude of those applied in the present investigation likely play a limited role in ACL loading. These physiologic offsets failed to significantly influence ACL strain during tasks commonly associated with ligament loading.

REFERENCES

1. Bates NA, et al. *Clin Biomech.* **30**, 1-13. 2015.
2. Andriacchi TP & Dyrby CO. *J Biomech.* **38**, 293-998. 2005.
3. Tashman S. *Am J Sports Med.* **32**, 975-83. 2004
4. Bates NA, et al. *Submitted for Publication.* 2015.
5. Levine , et al. *Am J Sports Med.* **41**, 385-95. 2013.

ACKNOWLEDGEMENTS

Funding from NIH Grants R01-AR049735, R01-AR05563, R01-AR056660, and R01-AR056259.

SCREW PULL OUT UNDER CYCLIC FATIGUE LOADING IN SYNTHETIC AND CADAVERIC BONE

Molly Baumann and Alan S. Litsky

Ohio State University, Columbus, OH, USA

email: Baumann.113@buckeyemail.osu.edu

INTRODUCTION

There are about 6 million bone fractures in the United States every year [1]. Fracture fixation devices are often used in these fractures to reduce recovery time and allow the injured individuals to regain their function sooner [2]. Many preliminary tests on new fracture fixation devices are done on composite bones as they are more readily available and more mechanically consistent than cadaveric bones. Zdero, et al., have studied the screw pull-out, shear stress, and energy to failure in composite bones (Sawbones®) and cadaveric bones finding that there is no statistical difference between the two bone types for these properties [3]. To our knowledge there has been no study comparing screw pull-out in cadaveric and composite bone under cyclic loading which is a clinically relevant mode of failure for these screws.

METHODS

Bicortical anterior-posterior holes were drilled 3 cm apart in both the composite and the cadaveric bones. These holes were tapped for 3.5 mm cortical bone screws which were inserted bicortically into the bone. Each test construct was loaded into a servohydraulic materials test frame [Bionix 858, MTS Corp, Eden Prairie, MN] with a custom-designed screw grip to assure axial alignment of the force and the screw. The straight pull-out force was collected under displacement control at 0.1 mm/sec. This was performed on 5 composite bones and 4 cadaveric bones.

After the straight pull-out tests were performed, the cyclic loading tests were performed. A 20 N pre-load was applied followed by a tensile cyclic load of 200 to 1000 N applied at 7 Hz for 200,000 cycles.

This approximates twelve weeks of post-fixation ambulatory activity, a clinically relevant time frame for having a fracture fixation device in place. This process was repeated on 17 cadaveric bones and 19 composite bones.

RESULTS AND DISCUSSION

The straight pull-out force results are consistent with the results of Zdero's study (Table 1); there is no statistical difference between the cadaveric and composite bones in terms of straight pull-out force ($p > 0.05$).

Table 1: Straight Pull-Out Force in Composite and Cadaveric Bone	
	Mean \pm Standard Deviation
Cadaveric n = 4	4746 \pm 553 N
Composite n = 5	3865 \pm 571 N

The cyclic load data was collected continuously for 200,000 cycles. The displacements at initial peak load, at 100,000 cycles, and at 200,000 cycles were analyzed and used to compare failure in composite and cadaveric bone. The results are presented in Table 2 as the mean and standard deviation, in millimeters.

Table 2: Mean and Standard Deviation of Pull-Out Length in Cyclic Loading			
	Entire Run	First 100,000 Cycles	Second 100,000 Cycles
Cadaveric n = 17	0.094 ± 0.030 mm	0.084 ± 0.030 mm	0.0099 ± 0.0040 mm
Sawbone n = 19	0.057 ± 0.026 mm	0.051 ± 0.027 mm	0.0065 ± 0.0043 mm

Results were compared using a two sample t-test between the cadaveric and the composite bones. The results were compared over the entire 200,000 cycles as well as the first 100,000 cycles and the last 100,000 cycles. These results are shown graphically in Figure 1. There was statistical significance for each comparison – $p = 0.001$ over the first 100,000 cycles; $p = 0.021$ for the second 100,000 cycles; $p = 0.00$ for the entire 200,000 cycles. There was also a statistical difference between the first half and the second half in terms of amount displaced. The displacement leveled off after some initial displacement.

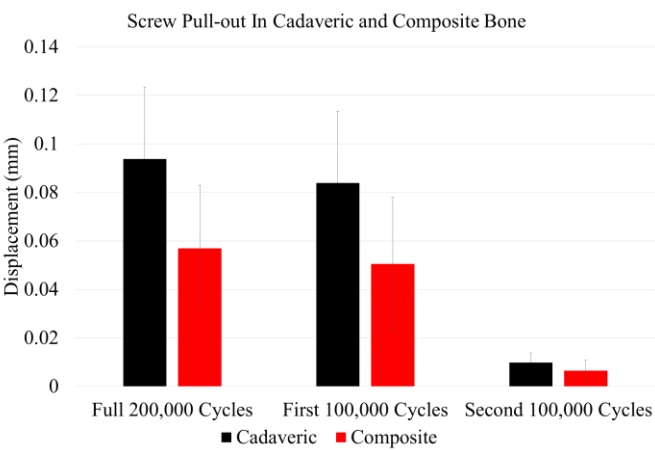


Figure 1: Screw Pull-out in Cadaveric and Composite Bone. Screw pull-out distance is shown as mean ± standard deviation. $p < 0.05$ in all cases comparing cadaveric and composite within the same time frame.

CONCLUSIONS

This study shows that there is a statistical difference between composite and cadaveric bone screw failure under cyclic loading. This difference is not thought to be of clinical significance as the average pull-out of 0.1 mm is not enough to cause failure or clinical concern over the time frame that a device is typically implanted. This does cause some concern as to whether or not other properties of the composite bone are the same as the cadaveric bone.

Moving forward, tests can also be performed to compare the composite constructs to other bone types such as canine or equine bones. A substantial amount of veterinary research and testing is reported using the composite human bones as a model for their animal bones of interest. Studies are underway to ascertain whether these composite bones are accurate representations of the animal bones. Additional testing could also be performed with a different cyclic loading pattern (i.e. 2000 N instead of 1000 N) to determine if a different loading pattern has a different result in terms of failure.

REFERENCES

1. Orthoinfo. AAOS. Oct. 2002. Web. <http://orthoinfo.aaos.org/topic.cfm?topic=A00279>
2. Orthoinfo. AAOS. Aug. 2007. Web. <http://orthoinfo.aaos.org/topic.cfm?topic=A00196>
3. Zdero R, et al. *Journal of Biomechanical Engineering* **131**, 094503, 2009.

ACKNOWLEDGEMENTS

We appreciate Synthes Corp. for donating the screws and the OSU Department of Orthopaedics for supplying the drill bits and tap. Thank you to the OSU College of Engineering for their support.

Comparisons of Three Hip Joint Center Estimation Methods in Estimating Knee Mechanical Axis using Motion Capture

Hunter J. Bennett, Guangping Shen, Songning Zhang

Biomechanics/Sports Medicine Lab, The University of Tennessee, Knoxville, TN, USA

email: hbennet4@vols.utk.edu

INTRODUCTION

The knee mechanical axis has been utilized in assessment of frontal plane knee alignment in knee osteoarthritic and total knee replacement populations, and associated with frontal plane knee joint loading, osteoarthritic disease severity, and progression. The mechanical axis is the angle between lines drawn from the center of femoral head to the center of the tibial spines and down to the center of the talus, measured using radiographs [1]. As an alternative measure, the mechanical axis can be approximated utilizing hip joint centers and centers of the femoral epicondyles and malleoli with a three-dimensional motion capture system [2]. Although epicondylar and malleolar centers can be found more easily and accurately, determining hip joint centers is more challenging.

The three commonly used hip joint center methods are the Bell (BELL) [3], functional (FUN) [4] methods, and a method using 25% distance between the greater trochanters (TROCH) [5]. As these methods have been previously shown to differ slightly in hip joint center locations [5], it is important to determine if these differences affect knee mechanical axes estimated from motion capture data. Therefore, the purpose of this study was to validate estimations of the knee mechanical axis using the three hip joint center methods with the mechanical axis measured on a long standing lower limb radiograph.

METHODS

Seven healthy subjects (aged: 26 ± 3 yrs, mass: 78.9 ± 19.2 kg, height: 1.77 ± 0.1 m) were included in this study. Each subject had a full limb anteroposterior radiograph, while standing barefoot with tibial tuberosities facing forward [1,2]. Knee mechanical axes of each limb were determined with the previously defined standardized measures using

the radiograph [1, 2]. The center of the femoral head was measured through fitting a circle to the head. A nine-camera motion capture system (240Hz, Vicon) was used in determining joint centers during static and dynamic trials. Anatomical markers were placed bilaterally on the anterior superior iliac spine (ASIS), posterior superior iliac spine (PSIS), iliac crest and greater trochanter, femoral epicondyles, and malleoli. Tracking markers on rigid shells were placed on the posterior pelvis, thighs, and shanks. One static trial was captured with the subject in the same standing position used during x-ray data collection. Two functional hip trials were performed (one for each limb) using an arc motion, which included flexion/extension, ab/adduction, and circumduction of the hip [6]. All data were processed and analyzed using Visual3D (5.0, C-Motion, Inc.). The marker data were filtered using a low pass fourth-order Butterworth filter at a cutoff frequency of 8 Hz. Each anatomical marker was corrected for the diameter of the marker and its base.

Both BELL and TROCH methods were computed using the static trial. The BELL hip joint centers were determined using the CODA pelvis (determined by ASIS and PSIS) in Visual3D. The TROCH hip joint centers were determined using 25% distance between the trochanters. The FUN hip joint centers were determined based on the methods of Schwartz and Rozumalski [4] using the functional trials. All three hip joint centers were applied to the static trial and subsequently used to determine the respective knee mechanical axes.

The differences between mechanical axes measured with x-rays and the three hip joint center methods using motion capture were used for comparisons per limb. A 2×3 (limb \times method) ANOVA was used to detect variations between hip joint center methods and x-ray scores.

RESULTS AND DISCUSSION

The difference scores for each hip joint center method are provided in Table 1. There was no significant limb by method interaction ($p=0.54$) or main effects for limb ($p=0.75$) or method ($p=0.54$). All three methods overestimated the x-ray mechanical axis by less than 2.3° on average. On an individual subject basis, mechanical axes varied as high as 4.6° and as low as 1.0° between hip joint center methods (Table 2).

Overall, the differences between x-ray and motion capture knee mechanical axes, on average, were quite small. These results assist in solidifying motion capture as a non-invasive alternative to x-ray assessments of the knee mechanical axis. The lack of significant differences between each method and the x-ray mechanical axes provides further evidence for the validity of each method in determining hip joint centers. As these methods are commonly utilized in biomechanics research, and variations in epicondylar and malleolar centers are likely to be much smaller, validation of these methods is important when considering knee frontal plane alignment using motion capture systems.

While we found no significant differences between methods for the knee mechanical axis, significant variations of the hip joint center locations have been found in the frontal plane [5]. It is possible that the hip joint center locations could still be different between methods, but they did not seem to contribute significantly to the variations of the motion capture knee mechanical axis.

A larger sample size is needed to strengthen the results. Further research is warranted to determine the validity of these methods in all three anatomical planes as well as assess their accuracy in diseased populations. Additionally, further research should focus on how each method affects lower limb biomechanics during dynamic movements.

CONCLUSIONS

Knee mechanical axes measured using motion capture were shown to differ from x-ray based mechanical axes by less than 2.3° . Comparisons of the three common hip joint center methods were shown to produce similar frontal plane knee alignment measures as the gold standard x-rays. Therefore, all three hip joint center methods seem to be valid choices when used in motion capture assessments of the frontal plane knee alignment.

REFERENCES

1. Sharma L, et al. *JAMA* **286**(2), 188-195, 2001.
2. Vanwanseele B, et al. *Clin Orthop Relat Res* **467**, 504-509, 2009.
3. Bell AL, et al. *J Biomech* **23**(6), 617-621, 1990.
4. Schwartz, MH & Rozumalski. *J Biomech* **38**(1), 107-116, 2005.
5. Weinhandl J, et al. *J Biomech* **43**, 2633-2636, 2010.
6. Camomilla V, et al. *J Biomech* **39**(6), 1096-1106, 2006

Table 1. Averaged Mechanical Axis Differences between Three Hip Joint Center Methods: mean \pm STD.

	LEFT LEG Mechanical Axis			RIGHT LEG Mechanical Axis		
	TROCH	BELL	FUN	TROCH	BELL	FUN
Difference ($^\circ$)	1.84 \pm 1.79	1.79 \pm 2.15	2.19 \pm 3.29	2.05 \pm 2.47	1.95 \pm 2.51	2.30 \pm 2.53

Table 2. Largest and Smallest Individual Mechanical Axis Differences between Three Hip Joint Center Methods.

Subject	LEFT LEG Mechanical Axis			RIGHT LEG Mechanical Axis		
	TROCH	BELL	FUN	TROCH	BELL	FUN
3	3.24	2.15	2.35	4.63	3.32	1.96
4	1.01	1.79	1.36	1.02	1.87	1.66

EFFECT OF ROTATION ANGLE ON DISC TORSIONAL MECHANICS

Semih E. Bezci and Grace D. O'Connell

Department of Mechanical Engineering, University of California, Berkeley
email: g.oconnell@berkeley.edu

INTRODUCTION

The primary function of the intervertebral disc is to absorb and distribute large complex loads placed on the spine, including combinations of compression, tension, bending, and torsion. While extensive research has been performed on compressive mechanics of the disc, there remains a lack of information about its torsional or axial-torsional properties.

Previous studies have indicated that combinations of torsion and compression can lead to disc degeneration, back pain, and disc injuries [1, 2]. The surrounding boney architecture of the disc joint, including the facets, may absorb part of the torsional loads placed on the spine. However, these loads may also result in rim lesions, which are tears between the disc and adjacent vertebral body, and result in neovascularization and nerve ingrowth [3]. Therefore, the disc's mechanical function under torsional loading is crucial for understanding the onset and progression of disc degeneration, back pain, and injury. The objective of this study was to evaluate the torsional properties of healthy intact bovine discs under various rotation angles.

METHODS

Caudal spine sections were acquired from skeletally mature bovines from the local abattoir (~18 months). The surrounding musculature and facet joints were removed and motion segments were prepared by making a parallel cut through the vertebrae and potted in bone cement (n = 10 samples). All samples were hydrated overnight in 0.15 M saline solution and allowed to equilibrate to room temperature prior to testing. Motion segments were attached to custom-designed fixtures with screws evenly spaced 60° to ensure that samples did not slip during torsion. Samples were aligned with the center of the testing machine to ensure that the applied moment arm was similar for all samples. Then, samples were preloaded under axial compression (300 N) for 10 minutes, and 10 cycles

of axial rotation was applied at 0.05 Hz to ± 1, 2, 3, 5 or 7°. Maximum rotation angle was applied in a random order with full recovery between experiments. Axial force, axial displacement, torque, and rotation were recorded throughout the experiment.

Following mechanical testing, discs were removed from vertebral bodies using a scalpel. Disc geometry (i.e. disc height and cross sectional area) was measured using a custom-written algorithm in Matlab (Mathworks, Inc.) [4]. The disc's polar moment of inertia was calculated using Eqn. 1 [5]. Disc geometry and polar moment of inertia were used to normalize mechanical properties.

$$J = \frac{\pi(W_{AP}W_L^3 + W_{AP}^3W_L - N_{AP}N_L^3 + N_{AP}^3N_L)}{64} \quad (1)$$

Torque-rotation data were analyzed using the last cycle of torsional loading. Axial displacement range (DR), torque range (TR), torsional stiffness (k_T), and energy loss (E_h) were computed. Torsional stiffness was defined as the slope of the most linear region of torque-rotation curve at rotation range of 0-1°. Energy loss was defined as the area between loading and unloading torque-rotation curve. DR was calculated by computing the difference between maximum and minimum axial displacement. Disc height (h) and the polar moment of inertia (J) were used to calculate the normalized torsional stiffness (MPa/deg), T , using Eqn. 2. Displacement range, torque range and energy dissipation were assumed to be zero under no rotation.

$$T = k_T * \frac{h}{J} \quad (2)$$

One-way ANOVA with a Bonferroni post-hoc analysis was used to determine the effect of rotation angle on torsional mechanics. Significance was set at $p \leq 0.05$. A Pearson's correlation was performed between disc geometry and torsional mechanical

properties. Correlation results that demonstrated $|r| \geq 0.7$ and $p \leq 0.05$ were considered to be strong and significant.

RESULTS AND DISCUSSION

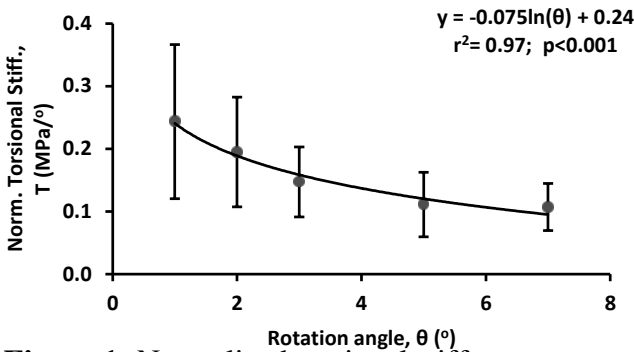


Figure 1: Normalized torsional stiffness.

There was a nonlinear decrease in the normalized torsional stiffness with rotation angle (Fig. 1). Normalized torsional stiffness appeared to plateau at approximately 0.1 MPa/° for healthy discs. In contrast, there was a nonlinear increase in hysteresis, or energy loss during torsion, with rotation angle (Fig. 2). Normalizing energy loss (N-mm) by the displacement range (DR, mm) demonstrated a constant value of 28 kN for all rotations greater than 2°. The direction of rotation (i.e. + or - rotation) did not show any difference in mechanical properties, as previously reported [5].

Torsional stiffness, a solid-like property of the disc was strongly correlated with disc height, while the energy loss, a fluid-like property of the disc, was strongly correlated with disc cross-sectional area and the polar moment of inertia (Fig. 3). However, torsional stiffness was only strongly correlated with disc height at high angles of rotation. The correlation between torsional stiffness and disc height increased with rotation angle ($|r| = 0.09, 0.39,$

0.44, 0.73 and 0.71 at $\pm 1, 2, 3, 5$ and 7° , respectively), which may suggest separate mechanisms absorbing torsional loads at very low angles versus higher angles. That is, as the disc experiences higher torsional loads, the collagen fibers become more engaged and have been shown to contribute to the highly nonlinear behavior of the disc under compression.

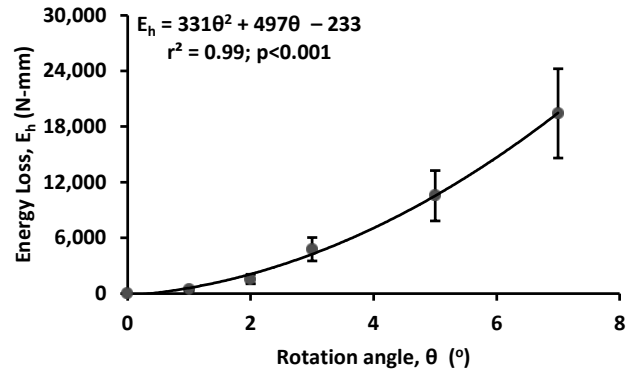


Figure 2: Energy loss with rotation angle.

The findings of this study demonstrate a functional difference between the elastic solid-like properties and fluid-like properties of the disc in axial rotation. The data in this study will be valuable in accurately describing the viscoelastic function of healthy discs. Further studies will examine the effect of torsional loading on healthy, degenerated, and injured human discs.

REFERENCES

1. Farfan HF, Cossette JW, Robertson GH, et al. *J Bone Joint Surg* **52A**:468-497, 1970.
2. Marras WS, Lavender SA, Leurgans SE, et al. *Spine* **18**(5):617-628, 1993
3. Osti O. *J Bone Joint Surg* **84-B**: (SUPP III) 210-211, 2002
4. O'Connell, GD. *Spine* **32**(3), 2007
5. Showalter, BL. *Spine* **37**(15), 2012

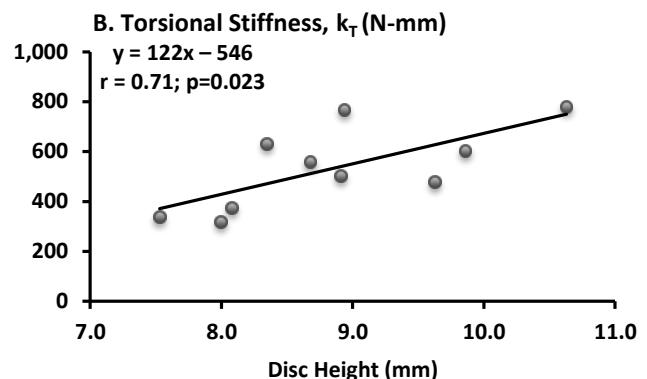
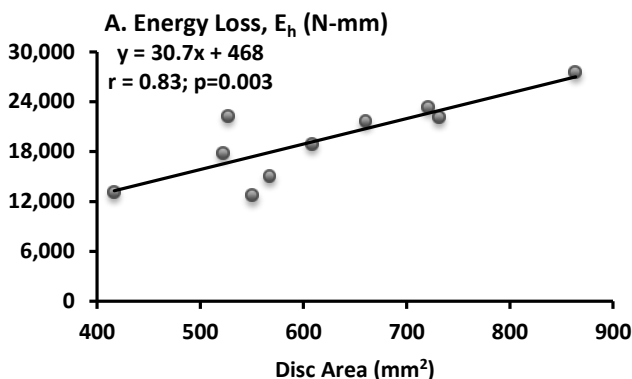


Figure 3: A) Energy loss with respect to disc area at 7° B) torsional stiffness with respect to disc height at 7°

OPTIMIZATION OF THE DIGITIZED GROOD AND SUNTAY KNEE JOINT COORDINATE SYSTEM

¹Tara F. Bonner and ¹Robb W. Colbrunn

¹Cleveland Clinic, BioRobotics Core, Cleveland, OH, USA

email: Bonnert2@ccf.org, web: <http://mds.clevelandclinic.org/Services/BioRobotics.aspx>

INTRODUCTION

In robotic testing of cadaveric knees, the reported values of measured and applied motions and loads are dependent on the defined joint coordinate system (JCS) that describes the three-dimensional translations and rotations of the tibia with respect to the femur. The International Society of Biomechanics standard for describing tibiofemoral kinematics is reported by Grood and Suntay [1], relying on the locations of anatomical landmarks to define the axes about which flexion/extension, varus/valgus and internal/external rotations occur. While calculating coordinate systems (CSs) based on anatomical landmarks allows for specimen-specific descriptions of motion, the method is not ideal for comparing kinematics of many specimens, as the representation of kinematic responses will vary with uncertainty in locating the anatomical landmarks. This variability is evident when observing the range of off-axis translations and rotations during passive flexion. Grood and Suntay recognized this issue and recommended a method for translating the tibia and femur CSs to reduce off-axis translations during passive flexion. However, off-axis rotations were not considered and no detailed methodology exists to describe how to perform the necessary transformations [1]. While the tibiofemoral joint is not truly a hinge joint, and some off-axis motion is expected, choosing a JCS that will minimize these motions might better regularize the manner in which tibiofemoral kinematics are measured, allowing for a more standardized representation that allows for tibiofemoral kinematic responses to be compared amongst specimens. Many have recognized a need for a more consistent JCS for describing tibiofemoral kinematics [1-3], but no established method has been adopted by the scientific community.

METHODS

Anatomical landmarks from six legs were digitized to define the tibiofemoral JCS reported by Grood and Suntay [1]. The JCS kinematics are reported as three translations (medial (M), posterior (P), superior (S)) and three rotations (flexion (F), valgus (V) and internal rotation (I)).

Each knee was rigidly secured to a custom testing apparatus and mounted to the Universal Musculoskeletal Simulator (UMS) [4] controlled with simVITROTM software programmed using LabVIEW software (National Instruments, Austin TX). The system is capable of manipulating in six degrees of freedom (DOF) with six-axis force-torque control applied to the tibia CS. Each knee was positioned on the UMS at a neutral position and offsets were applied so that all JCS translations and rotations were zero. Each knee underwent a passive flexion profile ramping from 0-90 degrees flexion. A constant 50N compression load was applied and all other off-axis loads were set to zero.

The representation of the JCS was optimized ($JCS_{opt}(M_{opt}, P_{opt}, S_{opt}, F_{opt}, V_{opt}, I_{opt})$) such that the tibia CS remained the same, but an offset transformation was applied to femur CS ($F_{offset}(X, Y, Z, R, P, W)$) to minimize off-axis motions during passive flexion. Eq. 1 displays the transformation chain equation.

$$T_{fem_{opt}, tib}(JCS_{opt}) = T_{fem_{opt}, fem}(F_{offset}) * T_{fem, tib}(JCS) \quad (1)$$

Tibiofemoral kinematics were considered at each 15 degree flexion increment during the passive flexion profile and optimization was performed in two parts using the LabVIEW NI_Gmath.lvlib: Constrained Nonlinear Optimization.vi. The rotational femur offsets (R, P, W) were initially set to zero and translational offsets were optimized by minimizing the cost function in Eq. 2 subject constraints ($|X, Y, Z| < 30 \text{ mm}$), where i represents each flexion angle considered.

$$f(X, Y, Z) = \sum_{i=1}^{N=7} (|M_{opt}(i)| + |P_{opt}(i)| + |S_{opt}(i)|) \quad (2)$$

With the translational offsets calculated, the rotational offsets were optimized by minimizing the cost function in Eq. 3, subject to constraints ($|R, P, W| < 29 \text{ degrees}$).

$$f(R, P, W) = \sum_{i=1}^{N=7} (|F_{opt}(i) - F(i)| + |V_{opt}(i)| + |I_{opt}(i)|) \quad (3)$$

With the optimized femur CS, offsets were reapplied at the neutral position and the knee underwent the passive flexion profile with measured motions represented based on the optimized JCS.

RESULTS AND DISCUSSION

The optimized femur CS position differed from the original position by 5 to 34 mm and the resultant orientation differed by 1 to 18 degrees for the six specimens. Table 1 displays the femur CS offsets for all specimens.

Table 1: Femur CS Offsets

Spec. #	Femur CS Offsets					
	$X \text{ (mm)}$	$Y \text{ (mm)}$	$Z \text{ (mm)}$	$R \text{ (}^\circ\text{)}$	$P \text{ (}^\circ\text{)}$	$W \text{ (}^\circ\text{)}$
oks_001	1.0	-21.3	8.4	-1.6	2.2	-17.2
oks_002	1.0	-6.7	5.3	0.0	7.1	4.7
oks_003	1.0	-12.0	-0.7	0.1	-2.0	-2.8
oks_004	1.0	-14.1	30.0	0.0	-0.6	1.6
oks_006	1.0	-13.2	6.8	-0.9	6.8	-2.1
oks_007	1.0	-1.3	-5.4	-0.4	8.8	3.6

Note: The X offset optimized to 1.0 mm for all specimens due to the optimization requiring a non-zero initial estimate. The default value was 1 mm and the X offset, being aligned with the medial direction, likely did not vary from the initial estimate. In the future, the initial estimate should be set to closer to zero.

Figure 1 displays an example of the off-axis translations and rotations with motions represented based on the anatomical and optimized JCSs for specimen oks-001. Off-axis motions decreased substantially with the optimized JCS. However, there are still some, which supports the notion that the tibiofemoral joint is not a true hinge.

Figure 2 displays the ranges (averages and standard deviations) of off-axis motions for the six specimens undergoing passive flexion calculated based on both JCS representations. The average motions decreased when represented with the optimized JCS for all DOF. In addition, the standard deviations decreased for all DOF, indicating that as a JCS better aligns with the mechanical axes of the tibiofemoral joint, off-axis motions will converge to values within a threshold, allowing for kinematics to be compared across specimens.

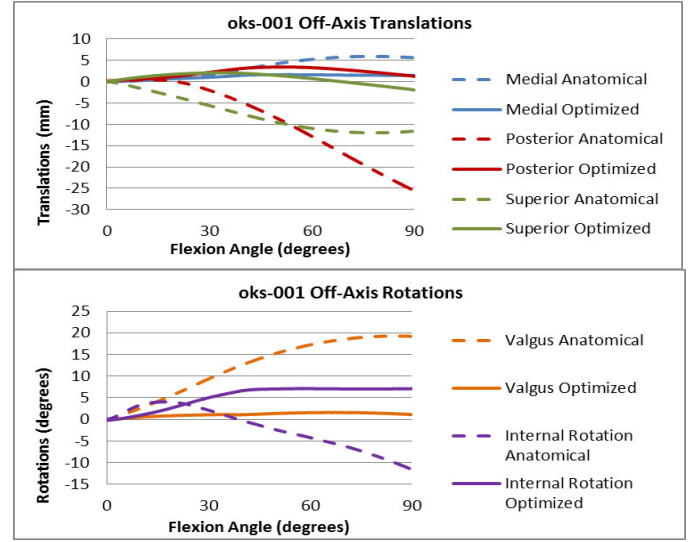


Figure 1: oks-001 Off-Axis Motions during Passive Flexion.

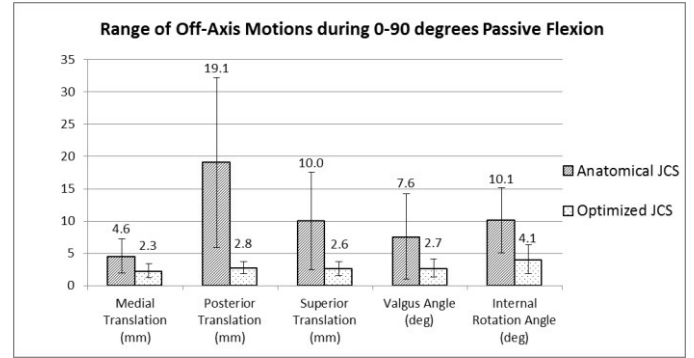


Figure 2: Average and Standard Deviations of the Ranges of Off-Axis Motions during passive flexion from 0-90°

A JCS optimized for minimal off-axis translations and rotations during passive flexion can facilitate a better baseline for comparing kinematics across specimens. The results in Figure 2 provides adequate evidence that our proposed methodology for optimizing the location of the femur CS decreases the off-axis motions of all knee specimens to a comparable amount during passive flexion.

REFERENCES

1. Grood and Suntay. *J. Biomech. Eng.*, **105**(2), 1983.
2. Piazza SJ, et al. *J. Biomech.*, **33**(8), 2000.
3. Morton NA, et al. *J. Ortho. Res.*, **25**(9), 2007.
4. Noble LD, et al. *J. Biomech. Eng.*, **132**(2), 2010.

ACKNOWLEDGMENTS

Specimens for this study were funded by Open Knee(s) Project, NIGMS, NIH (R01GM104139, PI: Erdemir). Assistance from Ahmet Erdemir is appreciated.

INTER-SEGMENTAL SPINE JOINT REACTION FORCES DURING ACTIVITIES OF DAILY LIVING

^{1,2} Scott P. Breloff and ² Li-Shan Chou

¹University of Oregon, Eugene, OR, USA

²The University of Scranton, Scranton, PA, USA

email: scott.breloff@scranton.edu

INTRODUCTION

Spine inter-segmental joint reaction forces have rarely been calculated in high resolution and it is unclear if activities of daily living will influence these inter-segmental joint reaction forces.

Direct measurements of intervertebral discs are the most accurate to fully quantify the forces associated with motions in the spine. However, these procedures are very invasive and would be difficult to apply to a large clinical population.

Therefore, the purpose of this study is to explore the feasibility of an in-vivo multi-segment spine marker set used to quantify the joint reaction forces at various spinal joints during different activities of daily living in young adults. It is hypothesized that unique ambulatory activities of daily living will effect joint reaction forces at specific joints of the spine.

METHODS

Fourteen healthy young adults (7 males/7 females; mean age: 27.9±5.9 years, mean height 176.0±27.7cm, mean mass 67.8±17.2 kg) were recruited from the university community to participate in the study.

A total of 65 markers, modified from Pruess et al. [1], were placed on the subject. Participants then preformed four different activities: level walking (W), obstacle crossing (OC), stair ascent (SA) and stair descent (SD).

A MATLAB® program was used to calculate three-dimensional peak joint reaction forces between each pair of adjoining spinal segments: Sacrum-to-Low Lumbar (SLL), Lower Lumbar-to-Upper Lumbar (LLUL), Upper Lumbar-to-Lower Thorax (UPLT), Lower Thorax-to-Lower Middle Thorax (LTLMT), Lower Middle Thorax-to-Upper Middle Thorax (LMTUMT) and Upper Middle Thorax-to-Upper Thorax (UMTUT) from heel strike (HS) to toe off (TO).

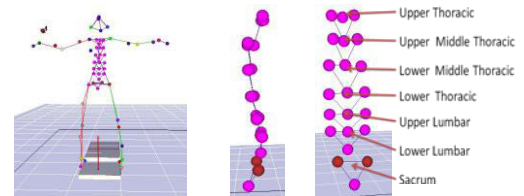


Figure 1: Anterior view of motion capture marker set with enhancements of the spine tracking markers. Sagittal view 2nd and posterior 3rd moving left to right.

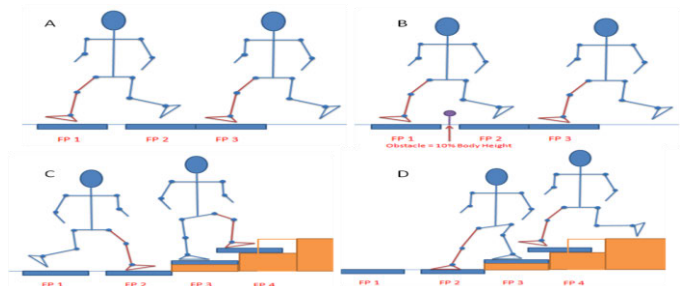


Figure 2: Definition of each task. (A) Level walking (W) – ipsilateral heel strikes, (B) Obstacle Crossing (OC) – Leading limb ipsilateral heel strikes, (C) Stair Ascent (SA) - ipsilateral heel strikes, (D) Stair Descent (SD) - ipsilateral heel strikes.

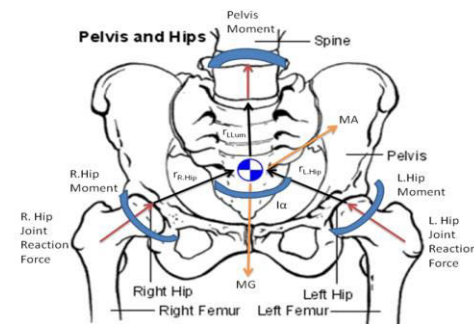


Figure 3. Free body diagram of the pelvis. Showing how lower extremity forces will be handled to continue the summation of forces into the spine.

Segmented spine joint reaction forces were calculated using the Inverse Dynamics algorithm through a rigid body linkage starting with the lower extremities. Lower extremity forces are transferred to the spine through the hip joints and pelvic segment, which includes the femur

heads, where hip joint reaction forces are well documented, and the 1st sacral vertebra [4].

$$\overrightarrow{Jrf_{S1}} = m\vec{a}_{pelvisCOM} - m\vec{g}_{pelvis} - \vec{f}_{r,hip} - \vec{f}_{l,hip}$$

Equation 1. Vector form equation for reaction force at sacral joint.

$$\overrightarrow{Jrf_{proximal\ spine\ segment}} = m\vec{a}_{pelvisCOM} - m\vec{g}_{pelvis} - \vec{f}_{distal\ spine\ segment}$$

Equation 2. Vector form equation for reaction force at subsequent spine segments

Peak joint reaction forces were normalized by body mass and assessed using a two-way within factor ANOVA. If the two-way interaction was non-significant, then main effects of task and spine level were examined. In all cases, adjusted p-values (Greenhouse-Geisser) were used to evaluate within subject effect ($p < 0.05$).

RESULTS AND DISCUSSION

The task * spine level interaction for the anterior-posterior segmental force peaks was non-significant ($p = 0.429$). Similarly the anterior-posterior main effects for task ($p = 0.628$) and spine level ($p = 0.952$) were also non-significant. The medial-lateral task * spine level joint reaction force interaction was non-significant ($p = 0.999$). Likewise the main effects for both task ($p = 0.536$) and spine level ($p = 0.772$) in relation to the medial-lateral force peaks were not-significant.

The two way interaction for vertical inter-segmental force peaks of task and spine level was not significant ($p = 0.842$). However, there was a significant main effect for task ($p < 0.001$). Post-hoc pairwise comparisons of the task marginal means showed the level walking ($M=8.05\pm3.19$ N/kg) task had significantly smaller peak reaction forces than the stair decent ($M=12.12\pm1.32$ N/kg) task ($p = 0.007$).

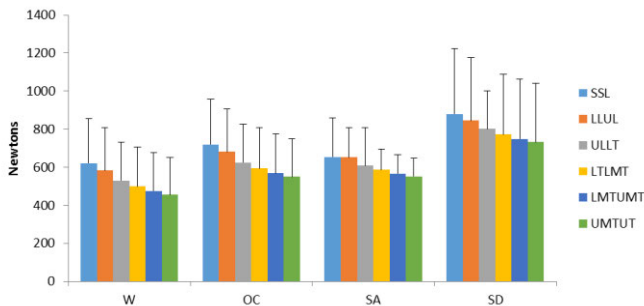


Figure 3. Vertical peak non-normalized spine joint reaction forces for spine level and multiple tasks.

Additionally, it should be noted the obstacle crossing ($M=9.43\pm0.76$ N/kg) task was trending to have larger reaction forces than level waking, ($p = 0.009$).

This study sought to compare peak spine joint reaction forces of a multi-segmented spine marker set during four distinct ambulatory activities of daily living. All of the interaction tests were non-significant, therefore only a general discussion relating how the factor (task or spine level) would influence the observed peak force is appropriate.

All tasks were completed at the subjects own comfortable pace, which generally indicates an average walking speed of approximately 1.36 m/s for young adults [2]. It has been shown a slow jog, or speeds greater than 2.0 m/s are required before changes in vertical ground reaction forces are observed [3]. Thus the self-selected speeds of the individuals in this study might not have induced changes in the ground reaction force which in turn would have induced a change in the peak spine joint reaction forces.

CONCLUSIONS

Though the hypothesis was not fully supported, the results found the main effect of peak reactions forces in the segmental spine can be influence by task. This was a new observation from previous studies and is therefore encouraging. Nevertheless, further validation is important with the inclusion of a larger and more diverse sample set and should include testing with multiple speeds. One future direction for application of this model would to investigate sports applications which involve more inter-trunk motion than walking based tasks

REFERENCES

1. Preuss RA. & Popovic MR *J. of Electro and Kinesiology* **20**, 823-832, 2010.
2. Perry J. & Burnfield JM. *Gait Analysis: Normail and Pathological Function*. 2nded. SLACK Incorp, 2010.
3. Keller MP, et al. *Clinical Biomechanics* **11**, 253-259, 1996.
4. Winter DA. *Biomech and Motor Cont. of Hum. Move*. Wiley, 2009

ACKNOWLEDGEMENTS

This work was funded in part thanks to the Eugene & Clarissa Evnouk Memorial Graduate Fellowship in Stress Physiology.

FRONTAL PLANE TRUNK AND KNEE ANGLES DURING UNILATERAL LANDING TASKS ONE YEAR AFTER ANTERIOR CRUCIATE LIGAMENT RECONSTRUCTION

¹Matthew S. Briggs, ¹Joshua T. Hoffman, ¹Samuel C. Wordeman, ¹Laura C. Schmitt, ²Mark V. Paterno, ¹Timothy E. Hewett

¹The Ohio State University, Columbus, OH, USA

²Cincinnati Children's Hospital Medical Center, Cincinnati, OH, USA
email: Matt.Briggs@osumc.edu

INTRODUCTION

Increased frontal plane trunk and knee motion are prospectively validated predictors of anterior cruciate ligament (ACL) injury.[1-3] In addition, risk of second injury after ACL reconstruction (ACLR), to either the involved or uninvolved knee, is dramatically higher than risk of initial injury.[4,5] However, previous investigation into trunk control and stability after ACLR during dynamic tasks is limited. The objectives of this study were to identify asymmetries and quantify relationships between frontal plane trunk and knee angles in patients following ACLR during two single-leg landing tasks.

METHODS

Sixteen patients [11 males; 5 females; mean (SD) age: 20(9)years] 12 months following ACLR [53(2)weeks] were included in this study. Fifty-five retro-reflective markers were adhered to the skin at anatomical and tracking landmarks. Three-dimensional motion capture data was collected bilaterally for 3 successful single leg drop (SLD) and cross over drop (COD) landings off a 31cm tall box. During the SLD, patients balanced on one leg, dropped from the box and landed on the same limb. For the COD, patients stood on one leg and dropped forward at a diagonal angle off the box towards their stance limb, but landed on their opposite limb. Frontal plane trunk and knee angles were analyzed for the first 100 milliseconds after initial contact for each task. Discrete variables were taken from each subject's individual data and time series averages were calculated on a time-point by time-point basis. Statistical analyses included paired t-tests and

Pearson's correlation coefficients to identify asymmetries between the involved and uninvolved limbs, and the relationships between trunk and knee angles, respectively.

RESULTS AND DISCUSSION

During the COD, patients demonstrated greater peak frontal plane trunk angles away from the stance limb [8.70°(4.02), 5.09°(5.19); p=0.04] and greater total frontal plane trunk excursion [5.20°(2.28), 4.07°(1.63); p=0.03] in the involved compared to uninvolved limb (Fig. 1A). Significant differences in frontal trunk motion between limbs were not observed for the SLD. Significant differences were not observed in frontal plane knee angles between limbs for either task or frontal plane trunk motion between the tasks. However, the involved limb, during COD compared to SLD, had greater knee adduction at initial contact [1.46°(2.22), 0.13°(2.33); p=0.003], greater peak knee adduction angles [3.58°(1.96), 2.48°(2.47); p=0.02], and decreased knee abduction angles [0.12°(2.38), -1.29°(2.29); p=0.001] during landing (Fig. 1B). During the COD, total frontal plane trunk excursion negatively correlated with peak knee adduction ($r=-0.58$; p=0.02) and positively correlated with peak knee abduction angle ($r=0.62$; p=0.01) on the involved but not the uninvolved lower extremity. We did not observe any significant relationships between frontal plane trunk displacement and frontal plane knee motion during the SLD task.

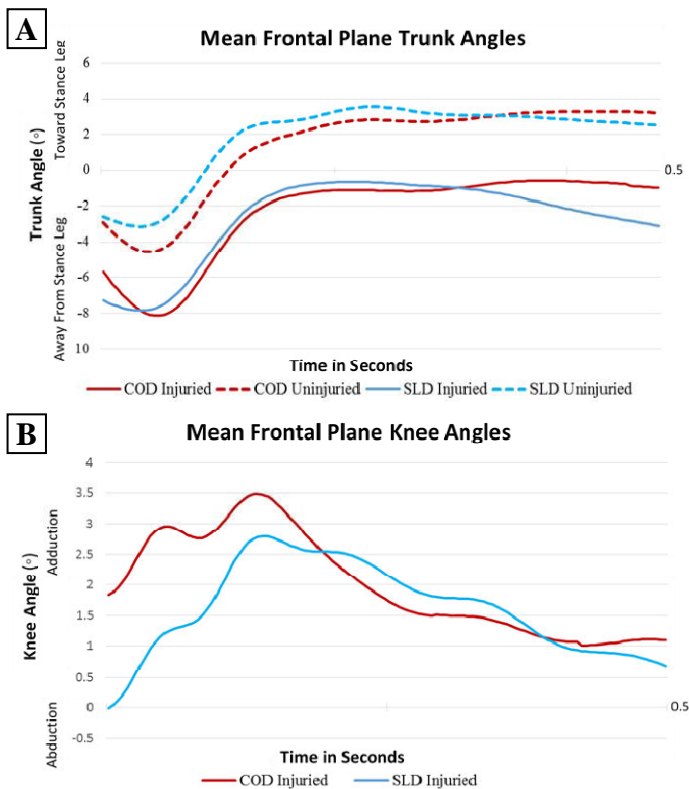


Figure 1: A) Mean Frontal Plane Trunk Angles during the first 500 milliseconds of landing; B) Mean Frontal Plane Knee Angles during the first 500 milliseconds of landing. Cross Over Drop (COD); Single Leg Drop (SLD).

To the authors' knowledge, this is the first study to evaluate the relationships between frontal plane trunk and knee motion following ACLR. These findings are somewhat contradictory to other reports of frontal plane trunk motion and ACL injury risk in healthy controls. Jamison et al.[6] demonstrated that greater lateral trunk motion toward the stance limb was associated with greater knee valgus during a cutting task in healthy controls. While Frank et al. [7] did not demonstrate a relationship between frontal plane trunk displacement and frontal plane knee joint loading during a side-cutting task in healthy controls.

Differences between this study and previous investigations may be attributed to our use of ACLR patients and the difference between landing and cutting tasks. Limitations of this study include a small sample size and limited numbers of female patients, who have been shown to be at a higher risk of initial and second ACL injury.[4,5] Further, the

differences noted in the frontal plane knee angles between the COD and SLD tasks are small ($1-2^{\circ}$) and may be attributed to measurement error associated with three dimensional motion analysis.[8] These statistical differences may not be clinically relevant.

Further evaluation of kinetics and kinematics of the lower extremity, including the hip and ankle, will provide additional insight into joint loading patterns during SLD and COD. Finally, comparison of these results to a healthy population will provide valuable insights into frontal plane trunk and knee mechanics and potentially secondary ACL injury risk.

CONCLUSIONS

One year after ACLR, patients demonstrate asymmetries in frontal plane trunk movement during a COD task. Moreover, increased knee abduction angles on the involved limb positively correlate with total frontal plane trunk excursion. Understanding the relationships between frontal plane trunk and knee movement after ACLR may assist in designing interventions focused on minimization of the risk of second injury.

REFERENCES

1. Hewett TE, et al. *Exerc Sport Sci Rev.***39**:161-166, 2011.
2. Hewett TE, et al. *British journal of sports medicine.***43**:417-422, 2009.
3. Zazulak BT, et al. *Am J Sports Med.***35**:1123-1130, 2007.
4. Paterno MV, et al. *Clin J Sport Med.***22**:116-121, 2012.
5. Paterno MV, et al. *Am J Sports Med.* 2014.
6. Jamison ST, et al. *J Biomech.***45**:1881-1885, 2012.
7. Frank B, et al. *Am J Sports Med.*2676-2683, 2013.
8. Benoit DL, et al. *Gait Posture.***24**:152-164, 2006.

ACKNOWLEDGEMENTS

Marissa Hunter, Joseph Panos, and Robert Gregg for their assistance with data processing. DJO Global for funding assistance to conduct the study.

KNEE ADDUCTION MOMENT IMPULSE AT BASELINE PREDICTS CHANGE IN MEDIAL TIBIAL CARTILAGE VOLUME OVER 2.5 YEARS IN KNEE OSTEOARTHRITIS

¹ Nicholas M. Brisson, ¹ Emily Wiebenga, ² Saara Totterman, ^{2,3} José G. Tamez-Peña, ¹ Monica R. Maly

¹ School of Rehabilitation Science, McMaster University, Hamilton, ON, Canada

² Qmetrics Technologies, Rochester, New York, USA

³ Escuela de Medicina, Tecnológico de Monterrey, Nuevo Leon, Mexico
email: mmaly@mcmaster.ca

INTRODUCTION

Osteoarthritis (OA) is the most debilitating musculoskeletal condition among older adults [1]. Mechanical factors, particularly increased medial knee joint loads, play a crucial role in the structural progression of knee OA [2–4]. The external knee adduction moment (KAM) is a valid and reliable estimate of the mechanical load incurred by the medial knee compartment, relative to the lateral, during weight-bearing activities such as walking [5]. The impulse of the KAM waveform accounts for both the magnitude and the duration of medial loading during stance [6].

In cross-sectional work, the KAM impulse correlated with the severity of medial tibial cartilage defects noted on magnetic resonance imaging (MRI) scans [7] and discriminated between radiographic knee OA severities [6,8]. Longitudinal studies implicate the KAM in the progression of knee OA [2–4]. For example, higher baseline KAM impulse was associated with greater loss of medial tibial cartilage volume over 12 months in individuals with knee OA [2]. While the KAM impulse appears to be an important marker of structural disease progression [2,6–8], there is a paucity of evidence supporting a causal link between these variables [9]. Thus, longitudinal investigations with longer follow-up times are required to corroborate and clarify the existing relationships between the KAM impulse and the progression of knee OA.

The purpose of this study was to evaluate whether greater KAM impulse during walking at baseline would be associated with greater loss of medial tibial cartilage volume over 2.5 years in individuals with knee OA.

METHODS

A subset of data (n=36/53) from a cohort of older adults with knee OA was used for interim analysis. Participants were diagnosed with symptomatic and radiographic knee OA according to the criteria set by the American College of Rheumatology and the Kellgren-Lawrence classification, respectively.

At baseline and follow-up, MRI scans of the knee were acquired with a 1.0 Tesla peripheral scanner (General Electric Healthcare, USA) using a coronal fat-saturated spoiled gradient recalled acquisition in the steady state. Medial tibial cartilage volume was segmented from the scans using a highly automated, atlas-based method [10].

At baseline, barefoot walking trials at a self-selected speed were collected with a motion capture system (3 Optotrak Certus banks, Northern Digital Inc., ON, Canada) and synchronized force plate (OR6-7-1000, AMTI, MA, USA). Marker and force plate data were filtered using a 2nd order low-pass Butterworth filter (6 Hz cut-off). A validated musculoskeletal model (three-dimensional floating axis coordinate system) and inverse dynamics were used to obtain external KAM waveforms (Visual 3D, C-Motion Inc., MD, USA). For each participant, the impulse of the stance phase was calculated for 5 non-normalized KAM waveforms using trapezoidal integration, and then averaged.

Multiple linear regression assessed the relationship of baseline KAM impulse and change in medial tibial cartilage volume over 2.5 years. Regression analyses were performed unadjusted, and adjusted for the covariates sex, age and body mass index [11–13]. The independent variables were entered simultaneously in the multivariate regression equation. The level of statistical significance was set at $\alpha=0.05$.

RESULTS AND DISCUSSION

At baseline, the sample (30 women; 6 men) had a mean (SD) age of 61.1 (6.7) years, body mass index of 28.0 (5.1) kg/m², knee axis angle of 182.1 (3.9) degrees (>180 degrees = valgus knee alignment), Kellgren-Lawrence grade II=12; III=12; IV=12, and medial tibial cartilage volume 1657 (397) mm³. The mean follow-up time was of 2.59 (0.53) years. Compared to baseline, the mean medial tibial cartilage volume at follow-up was reduced to 1543 (402) mm³ ($P=0.002$).

Both the unadjusted results (Fig. 1) and adjusted results showed that a higher KAM impulse at baseline was independently associated with significantly greater loss of medial tibial cartilage volume over 2.5 years (Table 1). Both the univariate and multivariate regression models significantly explained part of the variance in medial tibial cartilage volume change over 2.5 years (Table 1).

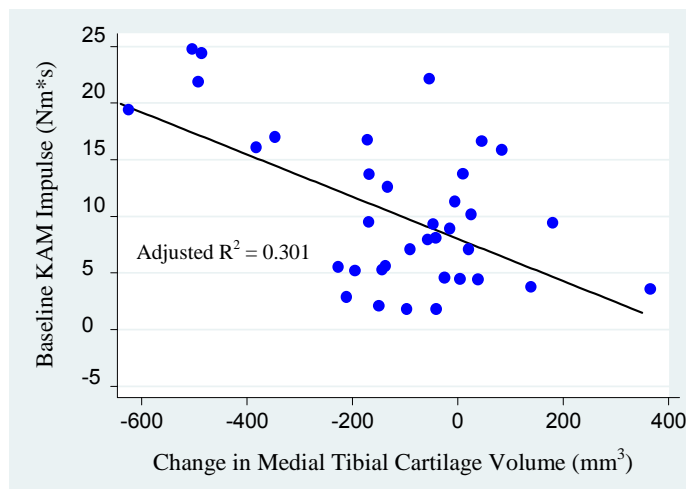


Figure 1: Correlation of unadjusted baseline KAM impulse and change in medial tibial cartilage volume over 2.5 years.

CONCLUSIONS

In this interim analysis, higher KAM impulse at baseline predicted the loss of medial tibial cartilage volume over 2.5 years in individuals with knee OA. These findings corroborate previous work [2]. Analysis of the whole sample ($n=53$), including knee axis angle and baseline medial tibial cartilage volume as covariates, may provide more in-depth insight into the relationship between baseline KAM impulse and change in medial tibial cartilage volume over time. Since knee loading parameters are modifiable, tailored treatment strategies may potentially slow OA disease progression.

REFERENCES

1. Badley E. *J Rheumatol* **72**, 39–41, 2005.
2. Bennell K, et al. *Ann Rheum Dis* **70**, 1770–4, 2011.
3. Miyazaki T, et al. *Ann Rheum Dis* **61**, 617–22, 2002.
4. Chehab E, et al. *Osteoarthritis Cartil* **22**:1833–9, 2014.
5. Zhao D, et al. *J Orthop Res* **25**, 789–97, 2007.
6. Thorp L, et al. *Arthritis Rheum* **54**, 3842–9, 2006.
7. Creaby M, et al. *Osteoarthritis Cartil* **18**, 1380–5, 2010.
8. Kean C, et al. *Clin Biomech* **27**, 520–3, 2012.
9. Henriksen M, et al. *BMJ Open* **4**, e005368, 2014.
10. Tamez-Peña J, et al. *IEEE Trans Biomed Eng* **59**, 1177–86, 2012.
11. Jones G, et al. *Arthritis Rheum* **43**, 2543–9, 2000.
12. Wluka A, et al. *Arthritis Res Ther* **8**, R90, 2006.
13. Ding C, et al. *Obes Res* **13**, 350–61, 2005.

ACKNOWLEDGEMENTS

Joint Motion Program, a CIHR Training Program in Musculoskeletal Health Research and Leadership (NB); Ontario Graduate Scholarship (NB); CIHR Operating (102643) and New Investigator Awards (MRM); Canadian Foundation for Innovation and Ontario Ministry of Research & Innovation (MRM)

Table 1: Relationship of baseline KAM impulse and change in medial tibial cartilage volume over 2.5 years.

Dependent Variable	Predictor	Unstandardized Coefficient (95% confidence interval)	P value	Adjusted R ² for Model	P value for Model
Change in medial tibial cartilage volume (mm ³) over 2.5 years	Unadjusted			0.301	< 0.001 [†]
	<i>KAM impulse</i>	-17.21 (-25.94 to -8.48)	< 0.001 [†]		
	Adjusted			0.324	0.003 [†]
	<i>KAM impulse</i>	-14.45 (-24.48 to -4.43)	0.006 [†]		
	<i>Sex</i>	70.22 (-87.82 to 228.26)	0.372		
	<i>Age</i>	1.72 (-6.98 to 10.42)	0.690		
	<i>Body mass index</i>	-10.68 (-23.64 to 2.28)	0.103		

[†] Indicates statistical significance ($p<0.05$).

THE EFFECT OF DIFFERENT RANGES OF MOTION ON LOCAL DYNAMIC STABILITY OF THE ELBOW DURING UNLOADED REPETITIVE FLEXION-EXTENSION MOVEMENTS

Kelsey Gsell¹, Shawn Beaudette¹, Ryan Graham², and Stephen Brown¹

¹Department of Human Health and Nutritional Sciences, University of Guelph, Guelph, ON, CAN

²School of Physical & Health Education, Nipissing University, North Bay, ON, CAN

email: kgsell@uoguelph.ca

INTRODUCTION

Local dynamic stability (LDS) is represented by the equilibrium of a movement trajectory about an intended path [1, 2]. When confronted with small kinematic disturbances or neuromuscular control errors, a stable system will remain close or return to the original intended trajectory, whereas an unstable system will diverge away from this stable norm [1, 2]. LDS is controlled primarily by active muscles, and is known to be influenced by factors such as movement speed and inertial load [1, 3]. Other factors such as muscle length, the length of the target trajectory, and the resistance of passive tissues through ranges of motion (ROM) may also influence LDS. This study was designed to examine the effect of ROM, which impacts each of the aforementioned factors, on LDS of the elbow. It was expected that movements over a smaller ROM and at end-ROMs would be more stable due to a smaller distance over which a movement could deviate from its intended trajectory and due to increased proprioceptive input at end-ROM.

METHODS

Sixteen healthy, right-hand dominant participants took part in the study (eight male and eight female; mean age (\pm SE) = 21.8 ± 0.44 years, height = 1.75 ± 0.024 m, mass = 69.8 ± 2.21 kg). Participants performed 30 unloaded, repetitive flexion-extension movements of the elbow with varying 1) angular displacement magnitudes: 40° and 80° ; 2) locations of ROM: mid-range, flexion end-range, and extension end-range; and 3) rotated position of the forearm: pronated and supinated. Movements were paced to the beat of a metronome, with the 40° at twice the speed of the 80° trials to ensure constant velocity between conditions.

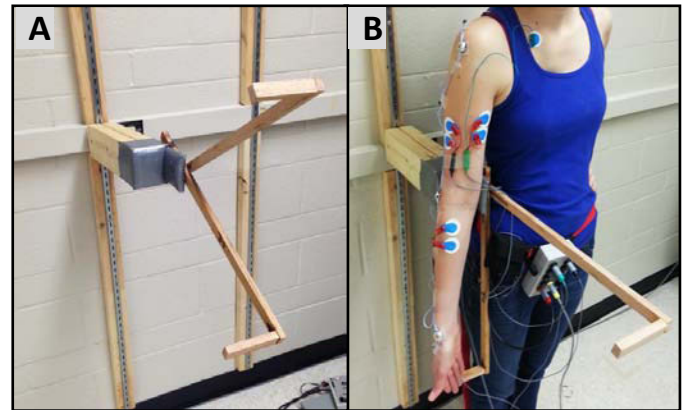


Figure 1: Pictures of the custom built apparatus (A) used to control ROM magnitude and ROM location during repetitive flexion-extension of the elbow. A participant is shown using the apparatus (B) with the kinematic and sEMG electrodes placed on the right arm.

The experimental set up can be seen in Figure 1, with surface EMG (sEMG) collected at 2048 Hz from the biceps brachii (BB), the lateral head of the triceps brachii (TB), and the brachioradialis (BR) of the right arm. Optoelectronic kinematic data were collected at 64 Hz from 4 markers placed at the approximated glenoid joint centre of the shoulder, the lateral epicondyle of the elbow, and the medial and lateral wrist at the level of the carpal bones. LDS was calculated using a finite time Lyapunov analysis of angular elbow flexion-extension kinematic data [1, 3]. EMG-based muscle activation and co-contraction data were also included to examine possible mechanisms of stabilization. The statistical analyses were a three-way repeated measures ANOVA with ROM magnitude, ROM location, and forearm rotated position as independent variables and LDS, individual muscle activation, mean flexor activation (FA_{mean}), and co-contraction index (CCI) as dependant variables. Post-hoc analyses were performed using a Tukey's adjustment ($\alpha=0.05$).

RESULTS AND DISCUSSION

There were no changes in LDS with any movement condition; however there were significant main effects of ROM location on muscle activation, quantified individually (Figure 2) (BB: $p<0.0001$, BR: $p<0.0001$, and TR: $p=0.0004$), and as mean elbow flexor activation ($p<0.0001$), as well as the ratio of co-contraction (CCI) between the elbow flexor and extensor muscles ($p<0.0001$) (Figure 2).

Flexion end-ROM demonstrated the highest magnitudes of flexor muscle activation while extension end-ROM demonstrated the lowest. This is explained as BB activation increased significantly from extension end-range to mid-range to flexion end-ROM, with BR activation significantly higher only at flexion end-ROM. TR activation was also significantly higher in flexion end-ROM, generating a balanced co-contraction as can be seen by a CCI close to 50. As CCI is a ratio of the activation of the extensors to the sum of the average flexors and extensors, numbers larger than 50 demonstrate greater extensor activation than flexor activation and vice versa. With both an increase in muscle activation and a balanced co-contraction, movements at flexion end-ROM experience a potential stiffening strategy. Conversely, while extension end range had the highest CCI this simply indicates that the flexors were less active than the extensors, and with a low level of muscle activation, any stiffening effect of co-contraction is limited. These differences in muscle activation patterns likely served to help maintain LDS of the elbow at consistent levels during the different ROM conditions. This has been seen previously, where LDS was maintained at consistent levels in response to decreases in the stability of the external environment while lumbar spine muscle stiffness increased [4].

It should be noted that movements over 40° and 80° demonstrated no differences in muscle activation along with no differences in LDS. This may simply be due to a lack of difference in the overall challenge of performing this movement over these two different ranges of motion.

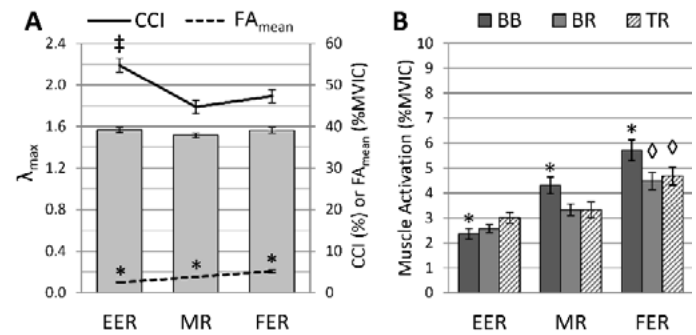


Figure 2: (A) Local dynamic stability (λ_{max}), average elbow flexor activation (FA_{mean}), and co-contraction indices (CCI), as well as individual muscle activation (B) during repetitive flexion-extension movements of the elbow through different ROM locations. * indicates significant differences between all levels within a condition; ‡ indicates EER is greater than each of MR and FER; † indicates FER is greater than each of MR and EER. Data are shown as means \pm SEM. EER = extension end-ROM; MR = mid-ROM; FER = flexion end-ROM.

CONCLUSIONS

LDS of the elbow was maintained at consistent levels through varying magnitudes of ROM, locations of ROM, as well as forearm rotated position. Flexion end-ROM demonstrated the highest magnitudes of flexor activation of any ROM location while extension end-ROM demonstrated the lowest. As flexion end-ROM also demonstrated the most balanced level of co-contraction this suggests a potential stiffening strategy was employed. These differences in muscle activation patterns, while driven by mechanical and physiological factors, likely act as a contributing mechanism to enable the maintenance of LDS. In the future it would be beneficial to assess the effect of ROM on more challenging (loaded) movements, as well as to fully consider the interplay of the active (muscle) and passive tissues on LDS.

REFERENCES

1. Granata K & England S. *Spine*, **31**(10), E271-276.
2. Reeves et al. *Clin Biomech*, **22**(3), 266–274.
3. Graham R & Brown S. *J Biomech* **45**(9), 1593-1600.
4. Beaudette et al. *J Biomech*, **47**(2), 491–496.

INVESTIGATING THE RELATIONSHIP BETWEEN HIP POSITION AND LUMBAR SPINE RANGE OF MOTION

¹ Grace O. Glofcheskie, ¹ Kaitlyn S. Bertram and ¹ Stephen H.M. Brown

¹ University of Guelph, Guelph, ON, Canada
email: shmbrown@uoguelph.ca

INTRODUCTION

There is a clear anatomical relationship between the spine and the hip joint, as they are connected via the pelvis. However, the relationship between hip position and lumbar spine range of motion (ROM) is not yet well understood. The top of the sacrum forms the base for the L5 vertebrae, therefore changing the position of the pelvis will also affect the movement of the lower lumbar spine. Relaxed standing normally causes the pelvis to rotate slightly posteriorly, resulting in erect posture without active muscular control due to the strong iliofemoral ligaments on the anterior hip joint resisting further rotation [1]. The resting position (mechanical neutral zone [2]) of the hip is defined as the position where the capsule and ligaments surrounding the joint are in their most slack position, therefore resulting in the least resistance to movement. In the hip joint, this occurs at approximately 30° of both flexion and abduction, with slight external rotation [3]. This suggests that changing the hip position from standing neutral posture, to positions such as abduction and external rotation, has the potential to alter the relationship between the hip joint, pelvis and lumbar spine. The purpose of this study was to determine the relationship between various hip positions and the ROM exhibited in the lumbar spine. It was hypothesized that adopting an abducted and externally rotated hip position would lead to the greatest increase of ROM at the lumbar spine, while abduction alone and external rotation alone would lead to less of an increase compared to a neutral hip position.

METHODS

Healthy young adult participants (n=12, 6 male and 6 female) were recruited from the university population and exhibited no current or history of hip

or back pain or associated injuries. All participants demonstrated at least 120° of active hip flexion, which has been stated in previous literature as the minimum degree of flexion for healthy ROM [4]. An active marker motion capture system (Optotrak™ Northern Digital Inc., Ontario, Canada) was used to record body segment and joint movement. Markers were placed in rigid body clusters on the lumbar spine at vertebral levels T12 and S1, on the lateral aspect of the left thigh and lateral aspect of the left shank. Rigid bodies located on the leg were placed at 50% of segment length. Electromyography (EMG) was recorded to measure muscle activity bilaterally of the thoracic (T9) and lumbar (L3) erector spinae, gluteus medius and biceps femoris (AMT-8™ Bortec Biomedical Ltd., Alberta, Canada). Maximum voluntary contractions were performed according to standard procedure in previous EMG literature [5,6]. Participants performed full trunk flexion and extension, trunk lateral bend and trunk axial twist ranges of motion in four different hip positions. Neutral hip position was self-selected by the participant, with the instruction to stand in a comfortable neutral width stance and feet facing forward. Hip abduction was defined as twice the distance of their self-selected neutral width stance. Hip external rotation was defined as the participant's forefoot on a 45° angle outward, while the heel remained in the same position. The fourth position was combined hip abduction and external rotation (as described above). Participants were instructed to go to their end trunk range of motion, while keeping their hips facing forward. Three trials of each movement were completed in each of the four hip positions. The dependent variables (3D lumbar spine motion, EMG amplitudes) were compared between all hip positions within each task. A significance level of $\alpha < 0.05$ was used for all statistical comparisons.

RESULTS AND DISCUSSION

Lumbar spine angles were normalized to the average maximum ROM angle each individual achieved in the neutral hip position. Therefore, a value of 1 is indicative of no change in ROM from the neutral position, as the average over three trials would be equal to the average ROM in neutral hip position. Significant increases in lumbar spine flexion were observed in the abducted and combined abducted and externally rotated hip positions when compared to neutral; however no differences were observed between abduction, external rotation, and combined abduction and external rotation (Figure 1). Significant increases in lumbar spine extension were observed when the hips were positioned in abduction, and combined abduction and external rotation when compared to neutral hip position. In lumbar spine flexion and lumbar spine extension, no significant differences were noted between abduction alone and combined abduction and external rotation, which suggests that either hip position increases lumbar spine ROM when moving in the sagittal plane.

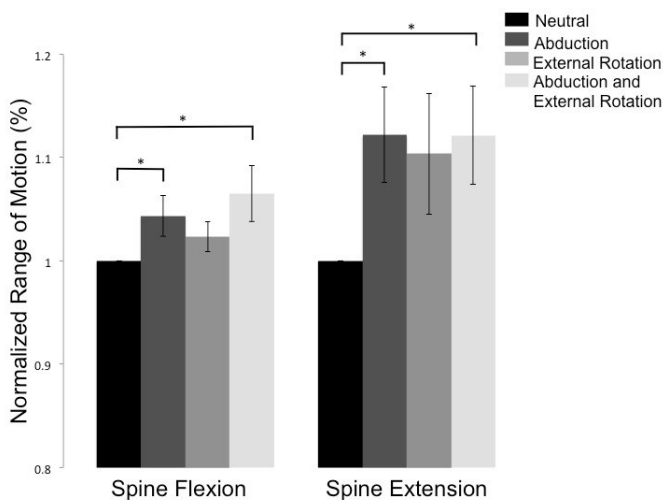


Figure 1: Normalized lumbar spine flexion and lumbar spine extension ranges of motion in each hip position: neutral, abduction, external rotation and combined abduction and external rotation.

No significant differences were observed during lumbar spine lateral bend (Figure 2). This suggests that potentially during neutral stance, the hip joint is in the best position for the greatest amount of ROM when moving in the frontal plane. Significant increases in lumbar spine axial twist were observed

when the hips were positioned in abduction, and combined abduction and external rotation compared to neutral (Figure 2). The increases of ROM demonstrated during abduction were also significantly greater than external rotation, suggesting that abduction is the best hip position for movements in the transverse plane for the greatest increase in lumbar spine ROM.

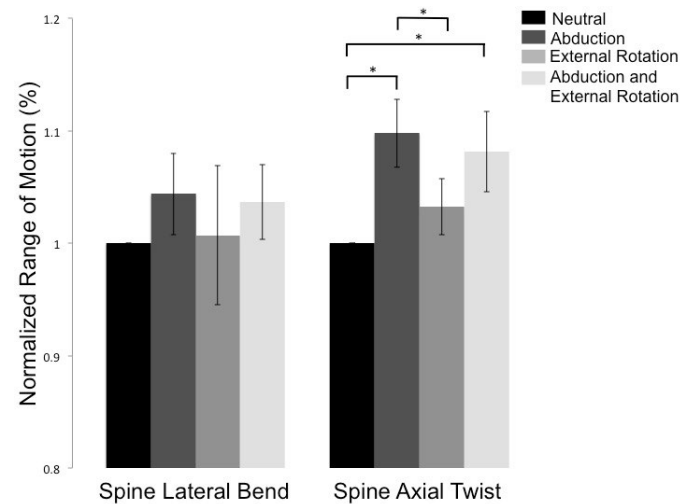


Figure 2: Normalized lumbar spine lateral bend and lumbar spine axial twist ranges of motion in each hip position: neutral, abduction, external rotation and combined abduction and external rotation.

CONCLUSIONS

Altering hip position is one potential way to increase ROM in the lumbar spine. Increases in lumbar spine ROM were observed when the hips were positioned in abduction, and combined abduction and external rotation during lumbar spine flexion, extension, and axial twist. This suggests these hip positions increase ROM the most during sagittal plane and transverse plane movements.

REFERENCES

- [1] Aspden RM, et al. *J Biomech* **39**, 1757 – 1759, 2006.
- [2] Panjabi, MM *J Electromyography* **13**, 371 – 379, 2003.
- [3] Gray H. *Gray's Anatomy*, 1974.
- [4] Kerrigan DC, et al. *Arch. Phys. Med. Rehabil* **82**, 26 – 30, 2001.
- [5] Brown SHM, et al. *Clin Biomech* **18**(9), 812-820, 2003.

A BIOMECHANICAL MECHANISM TO EXPLAIN HIGH INCIDENCE OF THORACOLUMBAR VERTEBRAL FRACTURES

^{1,2}Alexander G. Bruno, ^{1,2,3}Mary L. Buxsein, and ^{2,3}Dennis E. Anderson

¹Harvard-MIT Health Sciences and Technology Program, Cambridge, MA, USA

²Center for Advanced Orthopaedic Studies, Beth Israel Deaconess Medical Center, Boston, MA, USA

³Department of Orthopedic Surgery, Harvard Medical School, Boston, MA, USA

email: agbruno@mit.edu, web: <http://www.buxseinlab.org/>

INTRODUCTION

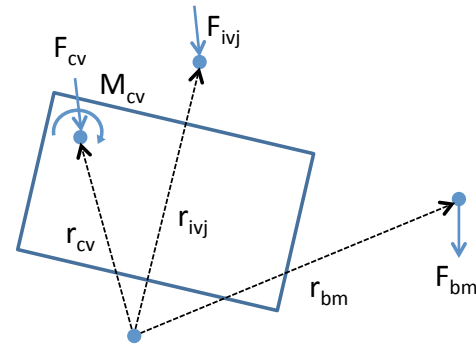
Vertebral fractures occur most frequently in the thoracolumbar region of the spine (T11-L1), but the mechanisms underlying this site-specific prevalence are not known [1]. One possibility is that this region of the spine experiences relatively high loading, increasing the risk of fracture. To investigate this possibility, we have developed an anatomically detailed and fully articulated musculoskeletal model of the full thoracolumbar spine and rib cage to estimate patterns of spine loading for a large variety of daily activities. Loading estimates from this model frequently produce a peak in compressive loading around T11-L1, supporting the idea that the high prevalence of vertebral fracture in this region may be due to high compressive loads *in vivo*. The goal of this study was to examine the mechanics of spinal loading more closely to explain why the model predicts high loads in this region.

METHODS

We used an anatomically detailed model of the fully articulated thoracolumbar spine and rib cage (implemented in OpenSim) to predict trunk muscle forces and spine loading for three activities: 1) neutral standing, 2) trunk flexion at 70°, and 3) reaching forward to open a window (40 N downward force applied to each hand). The model was previously validated against *in vivo* measures of intradiscal pressure, vertebral loading from telemetrized implants, and trunk muscle activity from EMG. The model uses a static optimization routine to predict the pattern of muscle forces required to balance moments from body weight and any externally applied loads, while at the same time

minimizing the sum of cubed muscle activations (equivalent to maximizing muscle endurance).

To investigate vertebral compressive loading patterns predicted by the model, and to understand why the model generally predicts high thoracolumbar spinal compression, we calculated the flexion/extension moments applied to each vertebral body by 1) the body weight (bm) associated with that vertebra, 2) the adjacent intervertebral joint (ivj) reaction forces, and 3) the adjacent left and right costovertebral joint (cv) reaction forces and moments (only in the thoracic spine) (Fig. 1). These moments must be balanced by the pull of muscles directly attached to that vertebra.



$$\Sigma M = M_{cv} + r_{cv} \times F_{cv} + r_{ivj} \times F_{ivj} + r_{bm} \times F_{bm} = M_{muscles}$$

Figure 1: The intervertebral joints are modeled as ball joints and the costovertebral joints are modeled as pin joints. The sum of flexion/extension moments was computed about the inferior intervertebral joint of each vertebra.

RESULTS AND DISCUSSION

For all three activities, our musculoskeletal spine model predicted a peak in thoracolumbar compressive loading (T11/T12) (Fig. 2). The erector

spinae and multifidus were the primary muscle groups activated during these activities, with the other trunk muscle groups generally producing less than 50N of tension. The multifidus activated strongly in the thoracolumbar region of the spine, contributing to the peak in thoracolumbar vertebral compressive loading (Fig. 3). Results were similar for all activities, and are only shown for neutral standing.

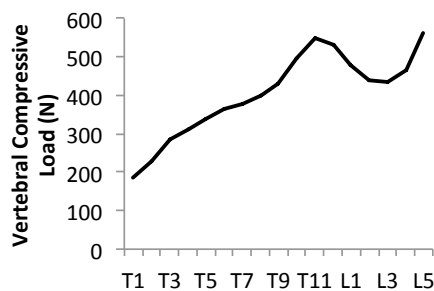


Figure 2: Vertebral compressive loading during neutral standing.

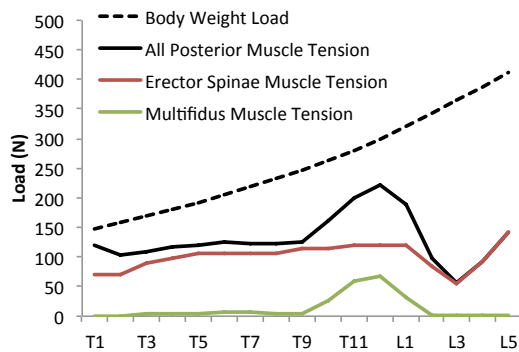


Figure 3: The contribution of body weight and muscle tension to vertebral compression during neutral standing.

The moments applied to each vertebra during neutral standing are shown in Figure 4. It appears that the reason for strong activation of the multifidus, and thus high thoracolumbar compressive loads, is the requirement that the muscles apply extension moments to T11, but flexion moments to T12 and L1 (dashed line in Fig. 4). The only way for this requirement to be met is for the multifidus muscle group to activate. The multifidus consists of short fascicles posterior to the spine that connect adjacent vertebrae. When contracting, the multifidus will pull down and apply an extension moment to its superior vertebra (ie: T11), and pull up and apply a flexion moment to its inferior vertebra (ie: T12). The reason for this

different requirement is that at T11 the muscles must balance flexion moments applied by the costovertebral joint reaction forces, whereas at T12 and L1 the dominant moments the muscles must balance are extension moments applied by the intervertebral joint reaction forces. The pattern of moments produced by the intervertebral joint reaction forces are likely driven by the curvature of the spine and the moment arms between adjacent intervertebral joints. Interestingly, this analysis also showed that the moments from the costovertebral and intervertebral joint reaction forces largely balanced each other in the upper thoracic spine (T1 to T6), resulting in low muscle loads and spine compression, illustrating a unique mechanism for thoracic load sharing between the ribs and spine.

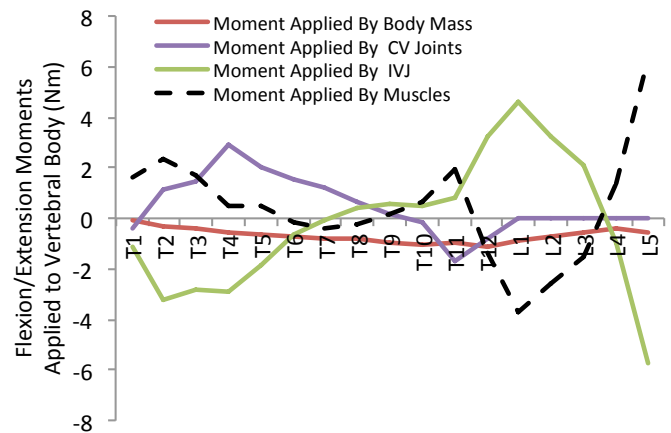


Figure 4: Moments applied to each vertebra by body mass, and the costovertebral (CV) and intervertebral joint (IVJ) reaction forces, all of which must be balanced by equal and opposite moments generated by the muscles (dashed line). Negative values are flexion moments.

CONCLUSIONS

Using a unique model that accounts for the complex anatomy of the spine and rib cage, we demonstrated that the multifidus muscle group applies large compressive forces to the thoracolumbar vertebrae (T11-L1) in an effort to balance competing moments applied by the intervertebral and costovertebral joint reactions. The resulting high loading could contribute to the high prevalence of vertebral fractures in this region.

REFERENCES

1. Cooper C. *JBMR* 7, 221-227, 1992.

BIOMECHANICAL EVALUATION OF PATELLAR FRACTURE RISK AFTER TENDON GRAFT HARVEST FOR CRUCIATE LIGAMENT RECONSTRUCTION: A FINITE ELEMENT STUDY

¹Robert E. Carey, ¹Liying Zheng, ¹Tom H. Gale, ²Christopher D. Harner, ¹Xudong Zhang

¹University of Pittsburgh, Pittsburgh, PA, USA

²University of Pittsburgh Medical Center, Pittsburgh, PA, USA

Email: xuz9@pitt.edu

INTRODUCTION

Anterior cruciate ligament reconstruction is one of the most common orthopaedic procedures performed in the United States. Two common types of grafts are quadriceps tendon and bone-patellar tendon-bone (BPTB) autografts. They both require bone block harvest of the patella, which may weaken the latter and lead to increased risk of fracture – this in fact has been reported as one of the major complications following ACL reconstruction. Previous cadaveric biomechanical studies of patellar fracture risk were limited, yielding inconsistent or incomplete guidelines for safe patellar bone harvest [1,2]. In this study, we applied a finite element (FE) modeling approach to biomechanically evaluate the effect of the shape, size and location of the patellar graft harvest on the risk of patellar fracture.

METHODS

A 3D model of a patella was developed from an MRI of the healthy right leg of a single subject. The location of the patellar tendon, patellar ligament and patellar cartilage were also determined from the MRI. Material properties were taken from the literature [3]. Non-Uniform Rational B-Splines (NURB) surface models were generated on the 3D geometric models of the patella bones with different bone block removals and automatically meshed to approximately 100,000 tetrahedral elements. The FE models were set to simulate a patella-injury-prone knee flexion posture (90-degree squat). The quadriceps tendon force (2700 N; 5 x BW) was applied at the location of quadriceps tendon insertion sites in both the proximal and distal locations of the patella. This value was within the range of bipedal squat forces in the literature (4.8-6.9 x BW) [4,5].

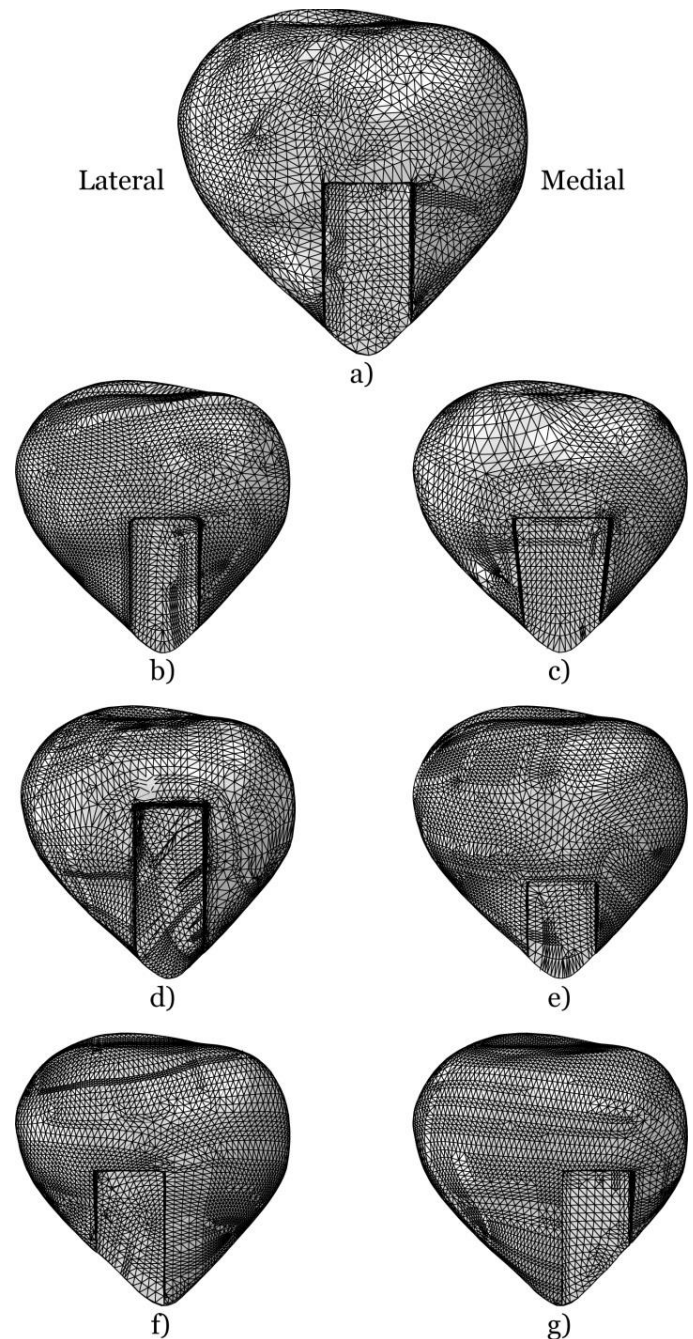


Figure 1: Patellar bone block cuts: a) regular cuboid cut; b) through g) alternative cuts.

Based on a cut commonly used for graft harvest – cuboid, extending to the transverse midline with a proximal depth of 10 cm (Fig. 1a) – we explored several alternatives with different shapes, lengths and locations: cuboid with rounded corners (Fig. 1b) and trapezoidal cuboid (Fig. 1c); long, above the transverse midline (Fig. 1d), and short, below the midline (Fig. 1e); medial (Fig. 1f) and lateral (Fig. 1g) shifts from the sagittal midline. The maximal stress associated with each cut was determined and its ratio to the maximal stress from the regular cuboid cut (Fig. 2a) was calculated to evaluate the risk of patellar fracture.

RESULTS AND DISCUSSION

We found that the maximal stress on the patella was near the cut. The different shapes did not show a great impact on the stress ratio on the patella: 0.96 for the rounded-corner (Fig. 2b) and 0.97 for the trapezoidal (Fig. 2c). The cut located below the midline (Fig. 2e) had a lower ratio than the long cut (Fig. 2d), with respective ratios of 0.81 and 1.22. The medially shifted cut (Fig. 2g) increased the stress (1.17), while the laterally shifted cut (Fig. 2f) had minimal effect (0.99).

CONCLUSIONS

The preliminary results of this on-going study demonstrate the ability and capacity of FE modeling to biomechanically evaluate the risk of patellar fracture. The models will be verified by experimental data and more thorough simulations will be carried out to provide the optimal graft harvesting plan. The simulation tool described here can be adapted for other surgical procedures to “digitally” and cost-effectively address clinical problems that otherwise would be difficult or impossible to study.

REFERENCES

1. Moholkar K. *J Bone Joint Surg Am* **84**, 1782-1787, 2002.
2. Sharkey NA. *Arch Phys Med Rehabil* **78**, 256-263, 1997.
3. Fitzpatrick CK. *J Orthop Res* **29**, 232-239, 2011.
4. Dahlkvist NJ. *Eng Med* **11**, 69-76, 1982.

5. Van Haver A. *Proc Inst Mech Eng H* **227**, 229-233, 2013.

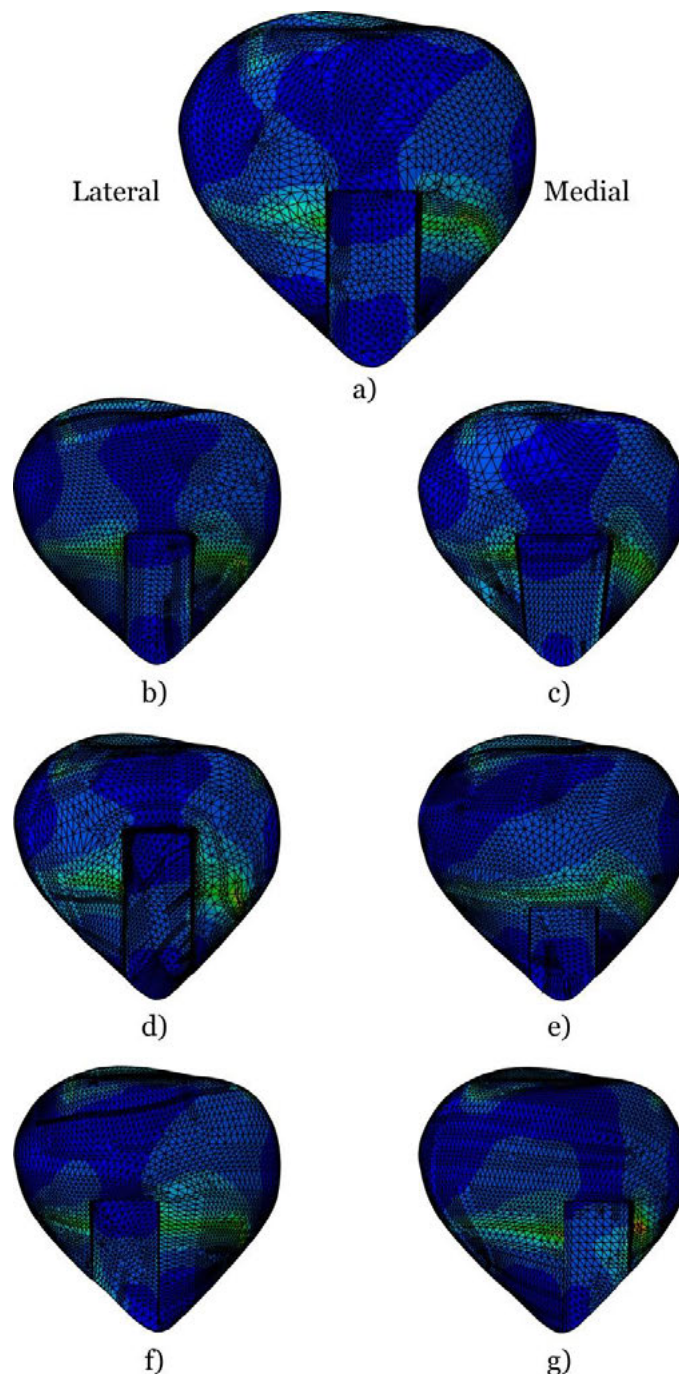


Figure 2: von Mises stress results for a) standard cuboid cut; b) through g) alternative cuts.

ACKNOWLEDGEMENTS

Albert B. Ferguson Jr. M.D. Orthopaedic Fund (MR2013-66648)

EVALUATION OF A SIMPLE METHOD FOR DETERMINING MUSCLE VOLUME *IN VIVO*

John H. Challis¹ and Benjamin W. Infantolino^{1,2}

¹Biomechanics Lab, Pennsylvania State University, University Park, PA, USA

²Division of Science, Pennsylvania State University, Berks Campus, Reading, PA, USA

email: jhc10@psu.edu

INTRODUCTION

The assessment of muscle architecture *in vivo* is an important way to augment the more detailed knowledge of muscle which can be obtained from muscle architecture in cadavers. Modern imaging methods make the measurement of various aspects of muscle architecture *in vivo* feasible but data collection and processing can both be time consuming. Albracht *et al.* [1] suggested that muscle volume can be estimated from measurements of muscle cross-sectional area and muscle belly length only, thus reducing the time for data collection and processing. This method was evaluated by Mersmann *et al.* [2] for the *Triceps Surae*, where muscle volumes were estimated with errors less than 8.5% of the criterion magnetic resonance imaging determined values.

It was the purpose of this study was to further evaluate this method for the determination of muscle volume based on a limited set of measurements. It extends the analysis of Mersmann *et al.* [2] in four ways,

1. It examines two different muscles, the *Vastus Lateralis* and *First Dorsal Interosseous*.
2. It uses direct measurement of muscle volume using cadaver dissection.
3. Uses the more generally available method of ultrasound to estimate muscle cross-sectional area and muscle length.
4. Uses a statistically optimal procedure for the estimation of the scaling parameter required in the method.

METHODS

Two sets of muscles were analyzed: the human *First Dorsal Interosseous* (FDI), and *Vastus Lateralis* (VL).

The cross-sectional area and length of the FDI was imaged using ultrasound in 22 cadaver hands (mean age at death: 64 years \pm 18, mean height: 172 cm \pm 8). The FDI muscles were scanned using a 7.5 MHz ultrasound probe (SSD-1000, Aloka, Japan) in B-mode. To enhance FDI image quality, by decreasing echo reverberations, a stand-off pad (2 cm thick and 9 cm in diameter) and a small amount of ultrasound gel was used. Following ultrasound scanning, the FDI muscles were dissected from the hand. Muscle volume of the FDI was determined using the water displacement technique; prior to testing it was ensured the water and muscle were at the same temperature. Test objects ranging in volume from 1 mL to 10 mL were measured in the apparatus with an accuracy of estimation of 0.01 \pm 0.01 mL.

The cross-sectional area and length of the VL was imaged using ultrasound in 8 cadaver legs (mean age at death: 64 years \pm 12, mean height: 171 cm \pm 11). In a similar fashion to the FDI the muscles of the VL were scanned prior to dissection and determination of muscle volume via underwater weighing.

To estimate muscle volume the following equation was used [1, 2],

$$V_m = p \text{ ACSA } L_m$$

Where V_m – muscle volume, p – scaling parameter, ACSA - muscle anatomical cross-sectional area, and L_m is the muscle belly length. Given the cadaver measurements the scaling parameter must be estimated for each of the muscles. To estimate the scaling parameter a robust linear regression was performed using a bivariate least squares method [3, 4]. This approach accounts for their being errors influencing both variables (V_m , and the product of ACSA and L_m) rather than assuming one variable is error free.

The sample size was small for the VL (n=8), therefore to circumvent the problem of model evaluation when there are no additional data with which to evaluate the model a cross-validation procedure was used [5]. An unbiased estimate of error was obtained by calculating the scaling parameter for sub-sets of the complete data set; the sub-set was achieved by removing one of the cadaver samples from the original data set; these removed values then served as an independent sample on which to evaluate error. By doing this sequentially for each of the muscles in turn it was possible to get multiple estimates of error from which a mean value was then computed. In addition Bland-Altman plots were also used to assess the model [6].

RESULTS AND DISCUSSION

The two sets of muscles analyzed, VL and FDI, reflect muscles of contrasting sizes (Table 1), and are representative of the larger and smaller muscles which are found in the human body [7].

Table 1: Means (\pm standard deviation) of length, anatomical cross-sectional area, and volume of the two sets of muscles analyzed.

	VL	FDI
Length (cm)	8.5 ± 1.5	5.7 ± 0.7
ACSA (cm ²)	33.8 ± 3.28	1.73 ± 0.40
Volume (mL)	239.4 ± 23.2	4.5 ± 1.0

For the VL the percentage root mean square error in the estimation of muscle volume was 5.0%. In the Bland-Altman plot all volume estimates were within the 95% confidence interval, with no proportional bias or relative bias in the volume estimates ($p > 0.05$); indicating no change in measurement accuracy with size of specimen, or the presence of a constant deviation in all estimate measures compared with the criterion. For the FDI the percentage root mean square error in the estimation of muscle volume was 18.8%. The results for the Bland-Altman plot had some predictions outside of the 95% confidence interval and the presence of proportional bias (Figure 1).

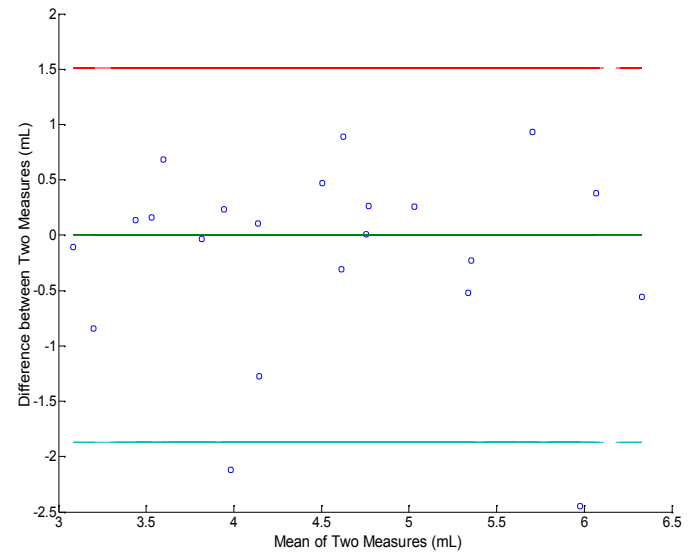


Figure 1: Bland-Altman plot of ultrasound volume estimation versus water displacement volume for the FDI.

CONCLUSIONS

The results of the current study suggest that with two measures of muscle dimensions, ACSA and length, ultrasound can be used for the estimation of muscle volume for the VL but not the FDI. Other simplified approaches should be explored for the FDI. Such analysis might be useful for tracking the changes in muscle volume of the VL with aging [8], or tracking the changes due to strength training [9]. Such applications of this method warrant further examination.

REFERENCES

1. Albracht K, et al. *J Biomech* **41**, 2211-18, 2008.
2. Mersmann F, et al. *J Biomech* **47**, 1348-52, 2014.
3. Rousseeuw PJ, & Leroy AM. *Robust Regression and Outlier Detection*. John Wiley & Sons. 1987.
4. Van Huffel S, & Vandewalle J. *The Total Least Squares Problems: Computational Aspects and Analysis*. SIAM Publications. 1991.
5. Allen DM, *Technometrics* **16**, 125-7, 1974.
6. Bland JM, & Altman DG. *Stat Methods Med Res* **8**, 135-60, 1999.
7. Yamaguchi GT, et al. In *Multiple Muscle Systems*. Springer, pp. 717-73, 1990.
8. Trappe TA, et al. *J Appl Physiol* **90**, 2070-4, 2001.
9. Aagaard P, et al. *J Physiol* **534**, 613-23, 2001.

COMPARING FAILURE RATES OF AUTOGRAFTS AND ALLOGRAFTS IN ANTERIOR CRUCIATE LIGAMENT RECONSTRUCTION: A SYSTEMATIC REVIEW

¹Albert J. Chen, ²Julie A. Stephens, ²Mahmoud Abdel-Rasoul, ¹Joshua T. Hoffman, and ¹Timothy E. Hewett

¹OSU Sports Medicine Sports Health & Performance Institute, Ohio State University, Columbus, OH, USA

²OSU Center for Biostatistics, Ohio State University, Columbus, OH, USA

email: Albert.Chen@osumc.edu, web: <http://sportsmedicine.osu.edu>

INTRODUCTION

With an annual healthcare expenditure of approximately \$625 million, anterior cruciate ligament (ACL) rupture is one of the most costly injuries among active individuals. Injuries to the ACL are not only associated with a large financial burden, but also result in the loss of participation in athletics for at least six months. [1] Therefore, it is crucial for the patient to undergo the best treatment option so that he or she may safely return to pre-injury levels of activity.

The most effective treatment for ACL rupture is ACL reconstruction (ACLR). Arden et al have reported that 90% of patients report normal or nearly normal knee function 41 months after ACLR. [2] ACLR involves replacing the injured ACL with an autologous or allogenic graft. Common graft choices are the hamstrings tendon autograft (HST), bone-patellar tendon-bone autograft (BPTB), or allograft. Despite numerous studies comparing reconstruction results among graft types, there is no consensus as to which graft type has the lowest likelihood of failure. In addition to patient reported functional scores, graft outcomes can be objectively determined either through laxity measurements or whether or not the graft has ruptured. These objective measures provide for a clear determination of graft integrity and function and can reveal which graft is the optimal choice.

The goal of this review is to compare failure rates across all three graft types in order to determine the ideal graft choice for ACLR. Graft failure rates based on various objective criteria will be utilized in this review. We hypothesized that all three graft types would demonstrate similar outcomes.

METHODS

A literature search was performed in the PubMed/MEDLINE, SPORTDiscus, and Scopus databases in August 2014. The search terms used were (ACL OR anterior cruciate ligament) AND (reconstruction OR surgery) AND (autograft or allograft). To be included, studies must have had sample sizes of 16 or more and at least a 2 year follow up. Furthermore, only comparative studies with level of evidence 1 or 2 were included in this review. After excluding all papers that did not meet our inclusion criteria, outcome data were extracted including Lachman and pivot shift scores, knee laxity measurements, and incidence of graft ruptures. Failure was defined as having a Lachman or pivot shift score of 1+ or more, and having a side to side laxity difference of more than 3 mm. Random effects meta-analyses were conducted for each outcome separately.

RESULTS AND DISCUSSION

Of the initial 1768 papers, 39 met the inclusion criteria and had relevant outcome data extracted. The odds of having a laxity measure greater than 3 mm was 1.624 times higher for the single bundle HST than the BPTB (95% CI: 1.158-2.278, $p = 0.005$) (Figure 1). In addition, the odds of having a pivot shift grade of 1+ or more was 2.934 times higher for the single bundle HST than the double bundle (95% CI: 1.030-8.358, $p = 0.044$), but only two studies were used for this estimate. The estimate for clinical failures comparing single bundle HST to BPTB was trending toward significant, with the odds of rupture for single bundle HST being 1.53 times higher than BPTB (95% CI: 0.96-2.42, $p = 0.07$). Other comparisons

of remaining outcomes were not observed to be statistically significant at the 0.05 level.

The increased incidence of greater than 3mm of laxity with the single bundle HST is not unexpected. Studies have reported a significant differences in laxity between the two graft types, especially as the time from reconstruction increases. [3] While increased laxity may be an indicator of graft failure, these studies found that there were no functional deficits reported by the HST patients.

Given that we found no other significant treatment comparisons among all the other outcomes, it may be necessary to consider other outcome measures. Some of these may include activity scores, incidence of anterior knee pain, pain when kneeling, etc. Some studies have reported a significant difference between HST and BPTB patients when reporting knee pain post-reconstruction. [4] These symptoms are generally a result of the graft harvesting process rather than the performance of the graft itself. Donor site morbidity, or lack thereof, may be a more meaningful factor to success of ACLR. In addition, pain and extensor/flexor

weakness could affect a patient's decision to return to sport. A review of subjective outcomes will be the topic of future work.

CONCLUSIONS

After a systematic review and meta-analysis of the relevant literature, it was observed that the single bundle HST had greater odds of failure, as measured by 3 mm or more on the knee laxity test, than BPTB. Because overall knee function depends on objective and subjective measures, future work is needed to explore the influence of graft type on subjective outcomes.

REFERENCES

1. Hewett TE, et al. *Am J Sports Med.* **34**, 490-498, 2006.
2. Ardern CL, et al. *Br J Sports Med.* **45**, 596-606, 2011.
3. Beynnon BD, et al. *J Bone Joint Surg Am.* **84-A**, 1503-1513, 2002.
4. Feller JA, et al. *Am J Sports Med.* **31**, 564-573, 2003.

Studies	Estimate (95% C.I.)	Ev/Trt	Ev/Ctrl
Beynnon et al 2002	4.080 (1.108, 15.020)	12/22	5/22
Denti et al 2006	5.512 (0.215, 141.215)	1/22	0/39
Feller et al 2003	3.478 (0.359, 33.727)	4/27	1/21
Gifstad et al 2012	1.773 (0.279, 11.255)	3/36	2/41
Ibrahim et al 2005	1.289 (0.375, 4.439)	7/45	5/40
Laxdal et al 2005	1.954 (0.633, 6.030)	10/39	6/40
Leys et al 2012	1.889 (0.740, 4.823)	17/51	9/43
Pinczewski et al 2002	1.736 (0.777, 3.875)	19/67	13/70
Sajovic et al 2011	0.696 (0.164, 2.951)	4/27	5/25
Shaieb et al 2002	2.713 (0.830, 8.870)	12/35	5/31
Taylor et al 2009	0.571 (0.090, 3.641)	4/11	4/8
Tow et al 2005	1.688 (0.414, 6.878)	9/15	8/17
Wagner et al 2005	0.401 (0.116, 1.390)	4/55	9/55
Zaffagnini et al 2006	1.909 (0.620, 5.876)	14/25	10/25
Overall ($I^2=0\%$, $P=0.571$)	1.624 (1.158, 2.278)	120/477	82/477

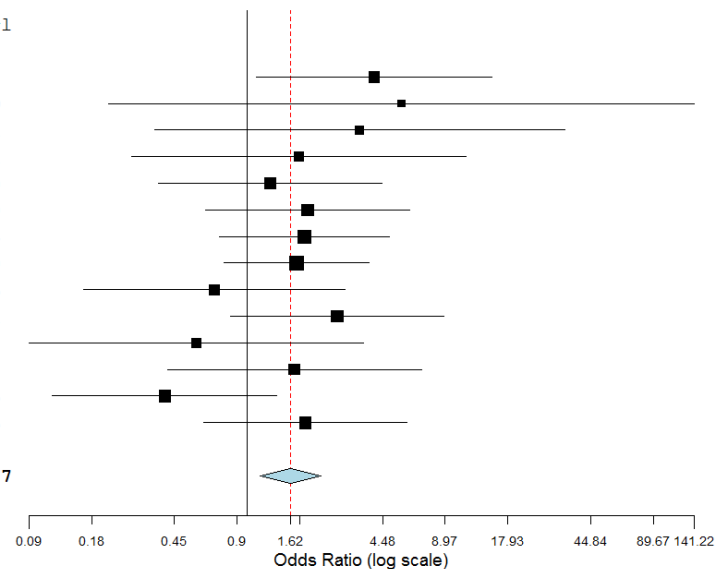


Figure 1: Forest plot showing the odds ratio for the comparison of single bundle HST and BPTB. We estimated that the HST had a 1.624 times greater likelihood to have a side-to-side laxity difference of greater than 3 mm versus BPTB. ($p = 0.005$, 95% CI (1.158-2.278))

COMPARISONS OF COORDINATION PATTERNS BETWEEN LUMBAR SPINE VERSUS LEADING AND TRAILING HIP IN GOLF DOWNSWING

Ahnryul Choi and Joung Hwan Mun

Sungkyunkwan University, Suwon, Republic of Korea

email: avery@skku.edu and jmun@skku.edu

INTRODUCTION

Golf swing is one of complex activities that require well-coordinated movement between body joints [1]. Maximally coiled trunk in the backswing top event enables the release of the stored energy during downswing phase due to a rapid axial rotation of the trunk, leading to a transfer of the energy into the ball [2]. Specifically, the lumbar spine and hip joints have primary roles in the axial rotation in golf swing and are known to have a close relationship with each other in their movement [3]. The inner-joint coordination represents the relationship of the movements among the neighboring joints, and it provides a basic insight into how the central nervous system organizes the joints in order to perform a particular movement from a neuromuscular systematic perspective [4]. In this study, therefore, we have investigated the kinematics (angular displacements and velocities) and inner-joint coordination of rotational movement at the lumbar spine and hip joints during golf downswings.

METHODS

A total of 21 right-handed male golfers participated in this experiment. All participants were professional golfers who is affiliated with Korea Professional Golf Association. Physical characteristics of the participants were 177.5 ± 8.7 cm height and 79.2 ± 10.0 kg weight; and self-reported handicaps scores were all under 0. Each golf swing motion was captured using six infrared cameras, and recorded images were synchronized by using a VICON 460 system. Twelve optical markers (upper torso: 4, pelvis: 4 and each thigh segment: 2) were attached on each participant to extract kinematic information, and two additional markers were located on the club head and lower part of grip to

determine downswing phase (Figure 1). Average of the best two shots among five trials of each participant based on the 3D reconstructed data quality was used for data analysis [5]. The anatomical coordinate system, angular displacement and velocity of the upper torso, pelvis and each thigh segment were calculated from similar methodologies of the previous studies [6, 7]. The inner-joint coordination was calculated using continuous relative phase (CRP) method [8]. All data was limited to the downswing phase, and underwent 100% normalization utilizing cubic spline technique.

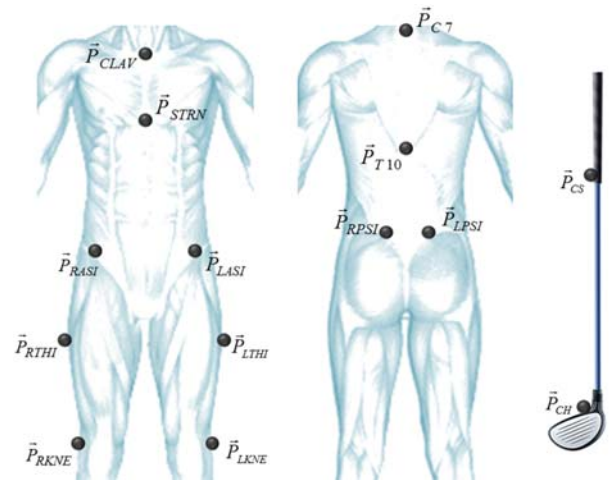


Figure 1: The locations of optical markers attached on the body and golf club

RESULTS AND DISCUSSION

The average angular displacement demonstrated an increasing pattern in all three joints during downswing phase. Particularly, the lumbar spine and trailing hip joints showed a similar pattern, but the angular displacement pattern of the leading hip joint revealed a markedly different shape compared to those of other joints. In angular velocity, the lumbar spine demonstrated a steadily

increasing pattern, while the leading and trailing hip joints showed their peaks in the early and late downswing phase, respectively. These results indicated that each joint complete their rotational movement during downswing phase by coordinating each other in different patterns. It is believed that the lumbar spine works constantly throughout the downswing phase, whereas the leading hip in early phase of downswing and the trailing hip joint in late downswing phase.

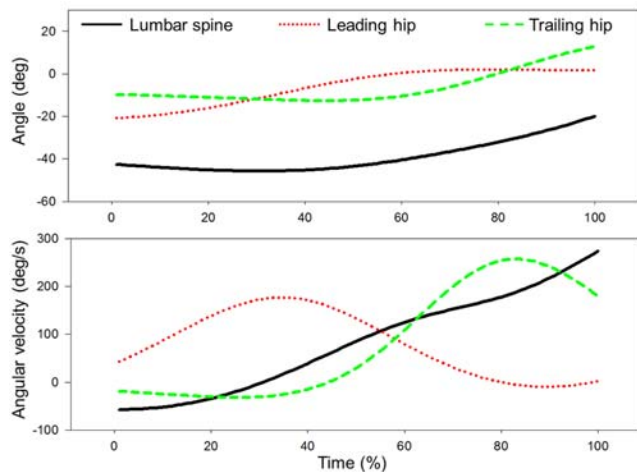


Figure 2: Average rotational angular displacements and velocities of lumbar spine, leading hip, and trailing hip joints

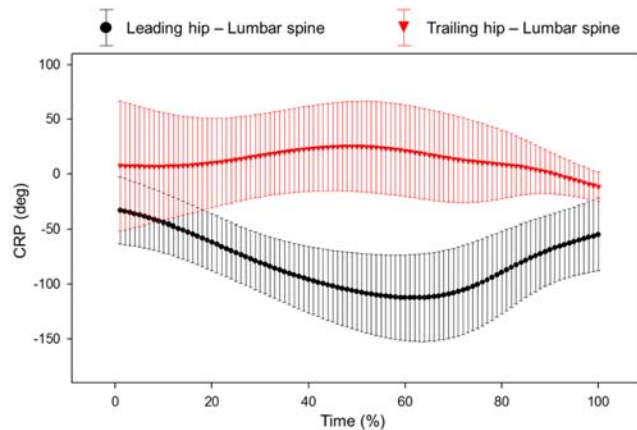


Figure 3: Average and standard deviation of CRP curves between lumbar spine versus leading and trailing hip joints

The inter-joint coordination between lumbar spine and leading hip joints demonstrated a typical ‘V’ pattern, and the minimum CRP value was found at approximately 60% of the downswing phase. A

faster rotational movement of the leading hip joint was observed in the early downswing phase compared to the lumbar spine, while lumbar spine joint rotated faster in the late downswing phase. On the other hand, the inter-joint coordination between lumbar spine and trailing hip joints revealed an average CRP close to 0 degree with no clear pattern. Therefore, it is considered that a clear coordination strategy exists between lumbar spine and leading hip joints rather than between lumbar spine and trailing hip joints.

CONCLUSIONS

Based on these results, we could confirm that the axial rotational movement during golf downswing is closely associated with leading and trailing hip joints as well as lumbar spine. We could also found that there were clear differences between the leading and trailing hip joints in terms of angular displacement, velocity and inter-joint coordination. Particularly, a significant inter-joint coordination strategy between lumbar spine and leading hip joints exists in professional golfers. This study will provide useful guidelines to improve swing proficiency of amateur golfers.

REFERENCES

1. McNally MP, et al. *Int J Sports Med* **35**, 785-788, 2014.
2. Myers J, et al. *J Sports Sci* **26**, 181-188, 2008.
3. Lee RYW, et al. *Hum Mov Sci* **21**, 481-494, 2002.
4. Scholz JP. *Phys Ther* **70**, 827-843, 1990.
5. Choi A, et al. *J Sports Sci*, 2015 (In Press).
6. Choi A, et al. *Biomed Eng Online* **13**, 20, 2014.
7. Beak SH, et al. *Biomed Eng Online* **12**, 13, 2013.
8. Li L, et al. *Hum Mov Sci* **18**, 67-85, 1999.

ACKNOWLEDGEMENTS

This work was supported by the National Research Foundation of Korea (NRF) grant funded by the Korea government (MSIP) (No. NRF-2013R1A2A2A03068269).

EVALUATION OF ROTATIONAL QUASI-STIFFNESS IN THE HIP JOINTS DURING GOLF DOWNSWING OF EXPERIENCED GOLFERS

Ahnryul Choi and Joung Hwan Mun

Sungkyunkwan University, Suwon, Republic of Korea
email: avery@skku.edu and jmun@skku.edu

INTRODUCTION

Golf is an activity that involves a predominant axial rotation with both feet fixed on the ground [1]. Golf swing in general applies biomechanical principles that deliver a drastic power to the ball by ejecting a stored energy from the coiled trunk during downswing phase [2]. Human hip joints allow rotational movement, while the excessive rotation of hip joints can cause the sports injury such as acetabular labral tears [3]. Kinematics and kinetics of the hip joints during golf downswing can provide a basic insight into the golf swing-specific injury mechanisms as well as quantitative and objective guidelines for improving swing skills [4]. Specifically, the joint quasi-stiffness, which is represented by the relationship between the given load and deformation, allows to further understand the complexities of joint dynamics [5]. In this study, therefore, we evaluated the rotational angles, moments, and quasi-stiffness of the leading and trailing hip joints in the transverse plane during golf downswing phase.

METHODS

Twenty-one tour professional golfers (height: 177.5 ± 8.7 cm, weight: 79.2 ± 10.0 kg) registered on Korea Professional Golf Association were recruited for the study. All golfers were right-handed, so left and right was determined to be leading and trailing direction, respectively. Their self-reported handicap scores were all below zero. The experimental apparatuses including six MCam2 cameras and two AMTI force platforms were prepared, and VICON 460 system was used to synchronize between devices in time domain. The modified Helen Hayes markerset protocol was employed to record the swing motion (sixteen markers on the lower extremity of each participant

[6]). Also, downswing phase was decided by an additional markers located on the clubhead and shaft region [7]. The anatomical coordinate system of pelvis and both thigh segments and the locations of joint rotation center were constructed using the markers attached on the lower body based on the previous study [8]. The anatomical angles and moments of each hip joint were calculated by the Euler angle and inverse dynamics techniques, respectively. All kinematic and kinetic data during downswing phase were normalized to 100%. Quasi-stiffness of the leading and trailing hip joints were defined as the instantaneous slope of angle-moment plot; the positive and negative slope were determined as 'resistance' and 'facilitation', respectively [9]. Additionally, the ratio of resistance and facilitation duration in a complete downswing cycle were calculated. In order to compare the difference between leading and trailing hip joints, a paired t-test was used, and the level of significance was set to $p < 0.05$.

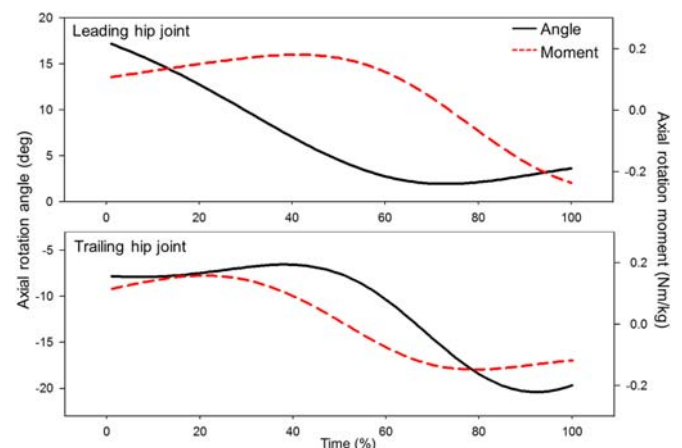


Figure 1: Axial rotation angles and moments of leading and trailing hip joints during downswing phase for a typical participant

RESULTS AND DISCUSSION

During downswing phase, the leading hip joint rotated internally, while the trailing hip joint rotated externally. Additionally, the rotational moments were observed in the same direction with angle (Figure 1). The leading hip joint markedly rotated at the beginning of the downswing, while a change of angle of the trailing hip joint revealed in approximately 50% of the downswing. The difference of plot pattern between the angle and moment was greater in the leading hip than the trailing hip joint.

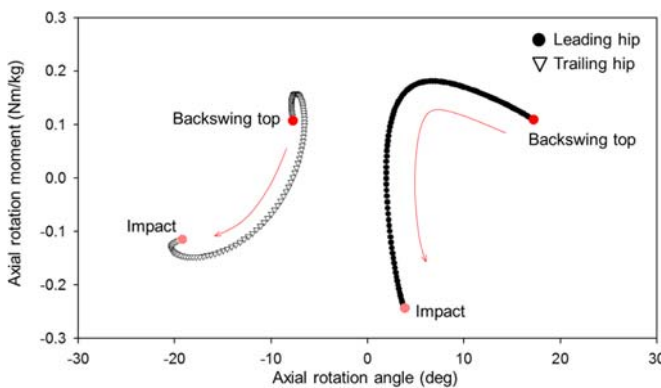


Figure 2: The angle-moment plots for the leading and trailing hip joints for a typical participant

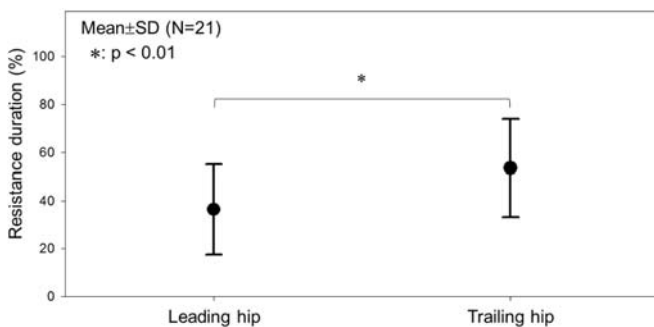


Figure 3: Average normalized resistance duration during downswing phase of all experienced golfers

The angle-moment pattern in the trailing hip joint generally displayed a linear positive slope shape, while no typical pattern was observed in the leading hip joint (Figure 2). The average and standard deviation of the positive quasi-stiffness (resistance) duration in the leading and trailing hip joints are demonstrated in Figure 3. The resistance

duration in the leading hip joint was 36% of the complete downswing cycle, and this was 18% lower than that in the trailing hip joint ($p < 0.009$). This implies that the leading hip has a different biomechanical roles from the trailing hip joint of the experienced golfers during downswing. In particular, the leading hip joint of the experienced golfers has a higher rotational flexibility than the trailing hip joint.

CONCLUSIONS

In this study, we have evaluated the axial rotation angle, moment and quasi-stiffness in the leading and trailing hip joints during golf downswing phase. We concluded that the rotational movement of the leading hip joint has a more flexible strategy compared to that of the trailing hip joint in the experienced golfers, and this could speculate as the effects of repetitive training. These results will be utilized as coaching guidelines to improve swing skills, and basic knowledge to identify golf swing injuries.

REFERENCES

1. Gulgin H, et al. *J Sports Sci Med* **8**, 296-299, 2009.
2. Myers J, et al. *J Sports Sci* **26**, 181-188, 2008.
3. McCarthy J, et al. *Clin Orthop Relat Res* **406**, 71-74, 2003.
4. Farrally MR, et al. *J Sports Sci* **21**, 753-765, 2003.
5. Butler RJ, et al. *Clin Biomech* **18**, 511-517, 2003.
6. Choi A, et al. *Biomed Eng Online* **13**, 20, 2014.
7. Beak SH, et al. *Biomed Eng Online* **12**, 13, 2013.
8. Choi A, et al. *J Mech Sci Technol* **23**, 64-74, 2009.
9. Choi A, et al. *J Sports Sci*, 2015 (In Press)

ACKNOWLEDGEMENTS

This work was supported by the National Research Foundation of Korea (NRF) grant funded by the Korea government (MSIP) (No. NRF-2013R1A2A2A03068269).

EFFECTS OF PELVIS IMPACT ANGLE AND HIP MUSCLE FORCES ON HIP FRACTURE RISK DURING A FALL USING AN ADVANCED HIP IMPACT SIMULATOR

¹ Woochol Joseph Choi and ² Stephen N. Robinovitch

¹ Department of Physical Therapy, Chapman University, Irvine, CA, USA

² Department of Biomedical Physiology & Kinesiology, Simon Fraser University, Burnaby, BC, CANADA

Email: wchoi@chapman.edu

INTRODUCTION

Over 90% of hip fractures in older adults are caused by falls [1]. Whether a given fall will cause hip fracture depends on bone strength, and on the impact force and stress applied to the bone during impact [2]. Improved understanding is required on how peak bone stresses during a fall depend on the mechanics of a fall, and on the state of contraction at the moment of impact of the muscles spanning the hip. Recently, Choi et al showed that, for lateral impact to the hip, peak stresses decrease with increases in hip abductor muscle force [3]. In the current study, we used an advanced hip impact simulator to examine the independent and interacting effects of both hip muscle force and pelvis impact angle on peak bone stresses during a fall.

METHODS

A second-generation “SFU hip impact simulator” was developed, consisting of a surrogate pelvis and pendulum [3]. The system allowed us to measure total force over the hip and 3D forces at the femoral neck (at 1000 Hz) under various levels of gluteus maximus and medius muscle forces, and pelvis impact angles, during simulated falls (Figure 1a). We used the system to simulate sideways falls involving an impact velocity of 2 m/s, and initial hip abductor muscle forces 300 or 700 N in each of the two abductor muscles. We also conducted trials for seven different impact configurations of the pelvis, including direct impact to the lateral aspect of the greater trochanter (zero degree), and impact to the pelvis when rotated (about the long axis of the pendulum) 5, 10 and 15° posterior or anterior to the frontal plane (Figure 1b and 1c).

Outcome variables (Figure 2) included the peak values at the femoral neck of: (a) axial force (F_z ; aligned with the femoral neck axis), (b) shear force (vector sum of F_x and F_y), (c) bending moment, (d) shear stress, (e) compressive stress and (f) tensile stress (see inset to Figure 2a for equations used to calculate these parameters).

ANOVA was used to test whether each outcome variables associated with muscle force (2 levels), and pelvis impact angles (7 levels). All analyses were conducted with SPSS using a significance level of $\alpha = 0.05$.

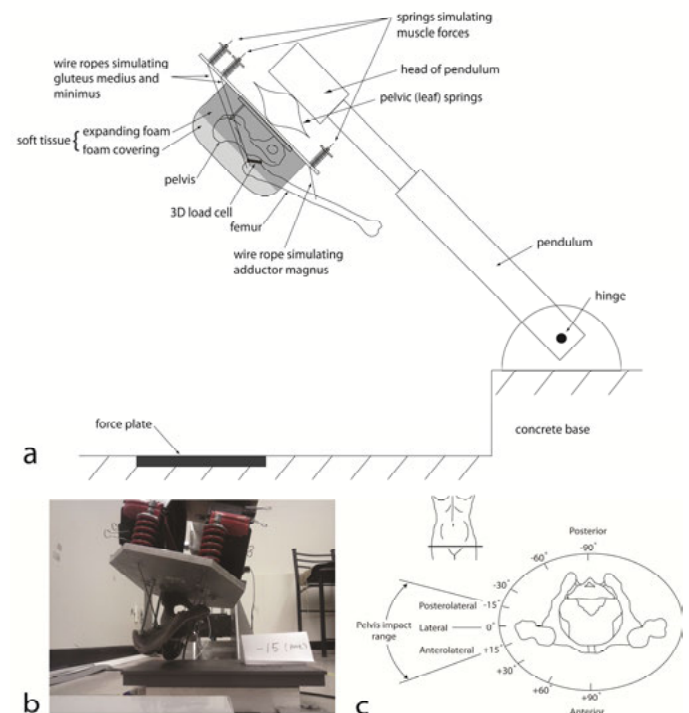


Figure 1. SFU Hip impact simulator, showing (a) schematic of the system, and (b) snapshot of surrogate pelvis (soft tissue covering removed) before impact with a pelvis rotation of 15° posterior along with (c) range of pelvis impact angle tested.

RESULTS AND DISCUSSION

We found that pelvis impact angle associated significantly with all of our outcome variables ($p<0.0005$), but had a more dramatic effect on peak tensile than peak compressive force (Table 1). On average, peak compressive and tensile stresses decreased 27% and 68%, respectively, when the pelvis impact angle changed from 15° posterior to 15° anterior. These results agree with previous findings from cadaveric studies and finite element modeling that posterolateral hip impact carries highest risk of hip fracture during a fall [4,5].

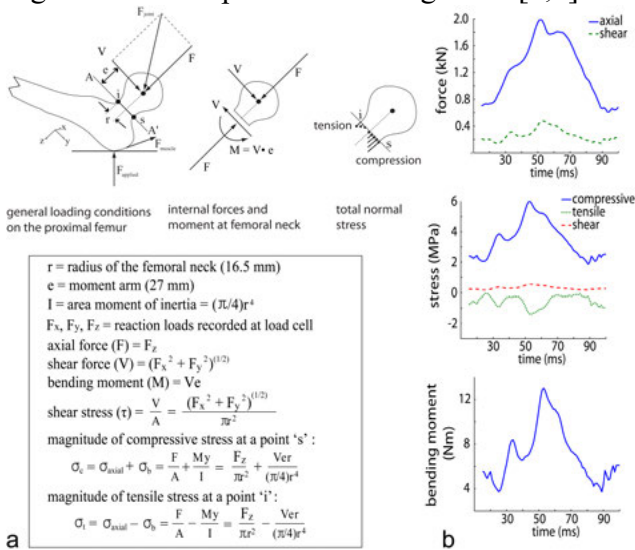


Figure 2. Experimental measures and calculated outcome variables. (a) Free body diagram and stress analysis at the proximal femur at impact from a fall. (b) Sample force and stress traces for 300 N with zero degree of pelvis rotation (lateral impact).

We also found that the hip abductor muscle force associated significantly with all of our outcome variables ($p<0.018$). Furthermore, there was a significant interaction between muscle force and pelvis impact angle for all outcome variables ($p<0.02$). Overall, peak tensile and compressive stresses were 25% lower and 5% greater, respectively, with 700 N than 300 N hip abductor muscle force. When the pelvis impact angle was zero, peak tensile and compressive stresses averaged 73% and 8% lower in the 700 N than 300 N muscle force condition. These results are similar to our previous findings for lateral impacts under a variety of knee boundary conditions [3].

In general, increases in muscle force were protective (caused a reduction in bending moment, and peak compressive and tensile stress) at zero degree and anterior impact angles, and dangerous (caused an increase in bending moment and peak stresses) for posterior impact angles. This likely relates to the muscle force having a greater protective “tension band” effect when the impact force and muscle force are aligned to create moments about a similar axis.

REFERENCES

1. Grisso JA et al., *J Am Geri Soc* **12**, 1326-31, 1991
2. Bouxsein ML et al., *JBM* **22**, 825-31, 2007
3. Choi WJ et al., *Osteoporos Int* **26**, 291-301, 2015
4. Keyak JH et al., *J Orthop Res* **19**, 539-544, 2001
5. Pinilla TP et al., *Calcif Tissue Int* **58**, 231-5, 1996

Table 1: Average values of outcome variables (with SD shown in parentheses).

muscle force (N) pelvis impact angle (deg)	300 N							700 N						
	posterior ← lateral → anterior							posterior ← lateral → anterior						
	-15	-10	-5	Zero	5	10	15	-15	-10	-5	zero	5	10	15
peak axial force (N)	1418 (1)	1515 (175)	1850 (3)	2004 (15)	2138 (17)	2161 (32)	1899 (19)	1709 (96)	1906 (5)	2177 (16)	2228 (45)	2284 (16)	2314 (28)	2005 (163)
peak shear force (N)	484 (1)	445 (75)	513 (2)	489 (13)	454 (3)	378 (9)	326 (17)	584 (29)	542 (13)	451 (9)	388 (23)	355 (46)	283 (9)	332 (13)
peak bending moment (Nm)	13.1 (0.0)	12.0 (2.0)	13.8 (0.1)	13.2 (0.3)	12.2 (0.1)	10.2 (0.2)	8.8 (0.4)	15.8 (0.7)	14.6 (0.3)	12.1 (0.2)	10.5 (0.6)	9.6 (1.2)	7.7 (0.2)	9.0 (0.3)
peak shear stress (MPa)	0.56 (0.00)	0.52 (0.08)	0.60 (0.00)	0.57 (0.01)	0.53 (0.00)	0.44 (0.01)	0.38 (0.02)	0.68 (0.02)	0.63 (0.01)	0.52 (0.01)	0.45 (0.02)	0.41 (0.05)	0.33 (0.01)	0.38 (0.01)
peak compressive stress (MPa)	5.35 (0.01)	5.16 (0.80)	6.08 (0.01)	6.06 (0.09)	5.96 (0.02)	5.38 (0.08)	3.89 (0.14)	6.47 (0.29)	6.46 (0.03)	6.00 (0.05)	5.57 (0.23)	5.54 (0.08)	5.17 (0.05)	4.73 (0.22)
peak tensile stress (MPa)	2.09 (0.01)	1.66 (0.33)	1.78 (0.01)	1.43 (0.10)	0.99 (0.03)	0.41 (0.04)	1.10 (0.11)	2.52 (0.10)	2.03 (0.05)	0.90 (0.09)	0.38 (0.14)	0.41 (0.09)	0.46 (0.02)	0.39 (0.06)

INFLUENCE OF PELVIS IMPACT ANGLE DURING A FALL ON THE PROTECTIVE BENEFIT OF HIP PROTECTORS

¹ Woochol Joseph Choi and ² Stephen N. Robinovitch

¹ Department of Physical Therapy, Chapman University, Irvine, CA, USA

² Department of Biomedical Physiology & Kinesiology, Simon Fraser University, Burnaby, BC, CANADA

Email: wchoi@chapman.edu

INTRODUCTION

Over 90% of hip fractures are due to falls [1]. Laboratory measures have shown that wearable hip protectors reduce impact forces to the proximal femur during a simulated sideways fall on the hip [2, 3]. However, clinical evidence suggests that hip fractures still occur when hip protectors are worn [4]. Furthermore, while falls in real life result in a variety of impact configurations, biomechanical tests to date have focused only on lateral impact to the pelvis. In the current study, we examined how the force reduction provided by wearable hip protectors is affected by pelvis impact configuration during simulated sideways falls.

METHODS

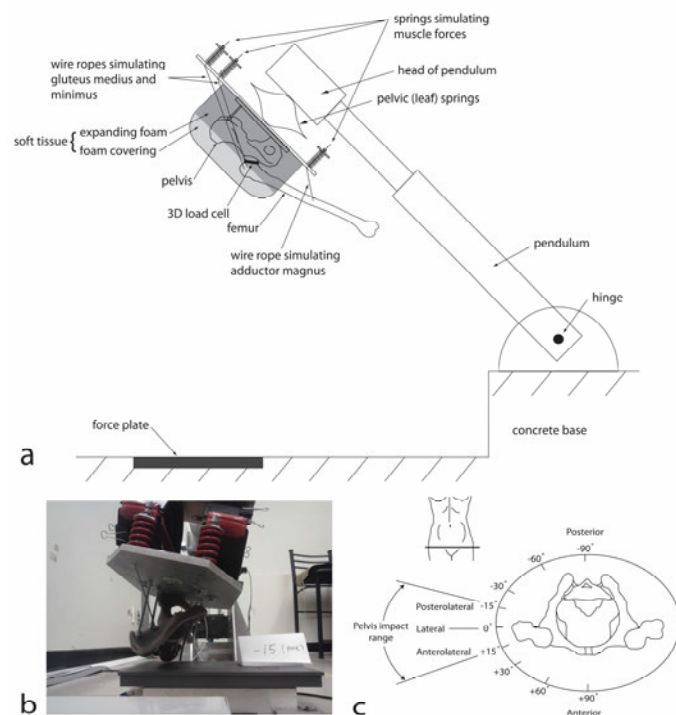


Figure 1. SFU Hip impact simulator, showing (a) schematic of the system, and (b) snapshot of surrogate pelvis (soft tissue covering removed)

before impact with a pelvis rotation of 15° posterior along with (c) range of pelvis impact angle tested.

We conducted experiments with a second-generation “SFU hip impact simulator” consisting of a surrogate pelvis and pendulum [5]. The system (Figure 1a) allowed us to simulate falls involving different magnitudes of gluteus maximus and medius muscle forces, and pelvis impact angles, and systematically examine how these factors affect total force over the hip and 3D forces at the femoral neck (measured at 1000 Hz).

We used the system to simulate sideways falls involving an impact velocity of 2 m/s, and initial hip abductor muscle force of 700 N in each of the two abductor muscles. Trials were acquired for seven different impact configurations of the pelvis: (a) direct impact to the lateral aspect of the greater trochanter, and (b) impact to the pelvis when rotated (about the long axis of the pendulum) 5, 10 and 15° posterior or anterior to the frontal plane (Figure 1b and 1c). Trials were also acquired with no pad applied (unpadded) and with two commercially available hip protectors (HipSaver and SafeHip).

Our main outcome variable was the percent attenuation in peak compressive stress at the femoral neck provided by the padding devices, when compared to the unpadded condition:

$$\%attenuation = 100 \times \left(1 - \frac{\sigma_{padded}}{\sigma_{unpadded}}\right)$$

Secondary outcome variables (Figure 2) included the peak values at the femoral neck of: (a) axial force (Fz; aligned with the femoral neck axis), (b) shear force (vector sum of Fx and Fy), (c) bending moment, (d) shear stress, (e) compressive stress and (f) tensile stress (see inset to Figure 2a for equations used to calculate these parameters).

We used ANOVA to test whether the outcome variables associated with the padding devices (3 levels), and pelvis impact angle (7 levels). All analyses were conducted with SPSS using a significance level of $\alpha = 0.05$.

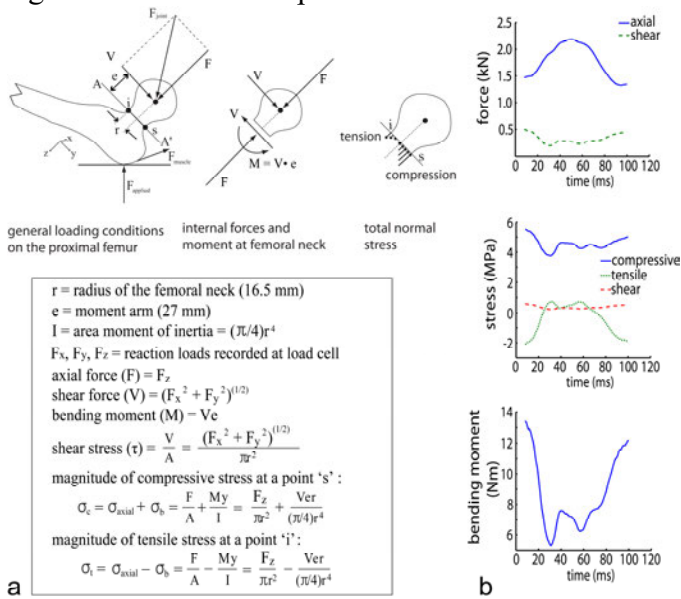


Figure 2. Experimental measures and calculated outcome variables. (a) Free body diagram and stress analysis at the proximal femur at impact from a fall. (b) Sample force and stress traces for SafeHip with +15° of pelvis rotation (anteriolateral impact).

RESULTS AND DISCUSSION

Our main outcome variable (percent compressive stress attenuation at the femoral neck) associated with padding device ($p < 0.0005$) and pelvis impact angle ($p < 0.0005$). On average, the percent stress attenuation was greatest while falling with HipSaver (30.7%) than SafeHip (20.9%) (Figure 3). Furthermore, the percent attenuation was greatest while impacting slightly anteriorly (+5 or +10°; 35%) and least while impacting anteriolaterally or posteriolaterally (+15 or -15°; 17~18%) (Figure 3). There was a significant interaction between padding device and pelvis impact angle ($p < 0.0005$).

All of other outcome variables associated with padding device ($p < 0.0005$) and pelvis impact angle ($p < 0.0005$). Furthermore, there were significant interactions between padding device and pelvis impact angle for all outcome variables ($p < 0.0005$).

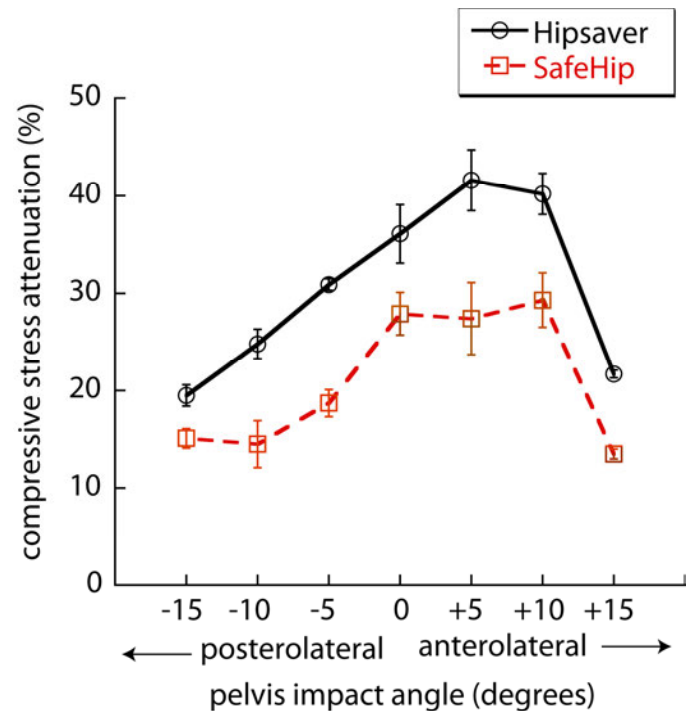


Figure 3. Effect of pelvis impact angle on percent compressive stress attenuation.

Our results confirm that padding devices help to reduce risk of fall-related hip fracture during a fall by attenuating peak compressive stress at the femoral neck up to 42%. However, our results also suggest that the protective effect may be compromised by pelvis impact configuration during fall impact, especially at the extremes of anteriorly and posteriorly directed impacts, where the point of contact was outside or at the edge of the padding device. These results agree with Choi et al (2010) who reported that performance of padding devices declines with poor positioning, for laterally-directed impacts [6]. These results should help to inform the design of improved padding devices that provide protection over a greater range of fall impact configurations [4].

REFERENCES

1. Grisso JA et al., *J Am Geri Soc* **12**, 1326-31, 1991
2. Choi WJ et al., *Clinical Biomech* **25**, 63-69, 2010
3. Laing AC and Robinovitch SN, *Accid Anal Prev* **41**, 642-650, 2009
4. Santesso N et al., *Cochrane Data Syst Rev*, 2014
5. Choi WJ et al., *Osteoporos Int* **26**, 291-301, 2015
6. Choi WJ et al., *J Biomech* **43**, 818-825, 2010

EFFECT OF MUSCLE CONTRACTION ON IMPACT VELOCITIES OF THE HEAD DURING BACKWARD FALLS IN YOUNG ADULTS

¹ Woochol Joseph Choi, ²Stephen N. Robinovitch, ¹Daniel Cipriani and ¹Jimmy Phan

¹ Department of Physical Therapy, Chapman University, Irvine, CA, USA

² Department of Biomedical Physiology & Kinesiology, Simon Fraser University, Burnaby, BC, CANADA

Email: wchoi@chapman.edu

INTRODUCTION

Falls are a direct cause of head injuries in older adults, and 60% of traumatic brain injuries are due to a fall, accounting for 32% of hospital admission and 50% of death from falls [1,2]. Most head impacts in older adults in long term care occur from backward falls [3], and a recent kinematic analysis of video-captured real-life falls in older adults suggested that contracting the core and neck muscles during decent and impact may help to prevent, or lessen the severity of head impact during backward falls [4]. In this study, we have conducted falling experiments with young adults to determine how muscle contraction during a fall influences the impact velocity of the head during backward falls.

METHODS

Healthy young adults (n=8) aged between 19 and 35 participated in falling experiments. Participants were taught and trained to mimic older adults backward falls on the buttock, back and head, captured by surveillance cameras installed in long-term care facilities [5] (Figure 1). The experiment was approved by the IRB of Chapman University, and all participants provided written informed consent.

For all falls, participants were instructed, “fall naturally while imagining you are falling on a hard surface”, and were not allowed to use their arms to arrest fall. Participants were also instructed to fall in three different ways: a. “fall backward and prevent your head from impacting the ground”, b. “fall backward and allow your head to impact the ground, but with minimal impact severity”, and c. “fall backward and allow your head to impact the ground, while inhibiting your efforts to reduce head impact severity”. All participants wore wrist guards

and helmets, and fell onto a padded mattress.

Reflective markers were placed on bony landmarks of the body to monitor participants’ fall kinematics through 10 Raptor motion analysis cameras (Motion Analysis Corp, Santa Rosa, CA) at a sampling rate of 250 Hz. Muscle activation of the core and neck muscle was monitored through electromyography (EMG) electrodes placed bilaterally on the skin over the rectus abdominis and sternocleidomastoid muscles, at a sampling rate of 2,000 Hz (Noraxon EMG DTS system, Scottsdale, AZ).



Figure 1. Self-initiated backward fall on a 12” thick gymnastics mat. Participants mimicked older adults’ backward falls and head impacts, based on video-captured backward falls in long term care.

Outcome variables included the vertical and horizontal velocities of the head at impact, and the integrated EMG (IEMG; a measure of the intensity of muscle activity) over the time period a. between fall initiation and head impact for falls resulted in head impact, or b. between fall initiation and a moment when the head marker was at its lowest point in z axis for falls involved no head impact. The time of fall initiation was defined as 10 frames (40 ms) after the instant when the greater trochanter started to move downward. The time of head impact was defined as the moment that the head marker

passed a threshold height 240 mm above the mat surface [6]. EMG data were full-wave rectified and low-pass filtered with a cut-off frequency of 20 Hz (4th order Butterworth algorithm). IEMG data from right and left sides were averaged for each muscle.

ANOVA was used to test whether our outcome variables associated landing type during backward falls (3 levels). We also conducted a regression analysis to test whether impact velocity associated muscle activity. All analyses were conducted with SPSS using a significance level of $\alpha = 0.05$.

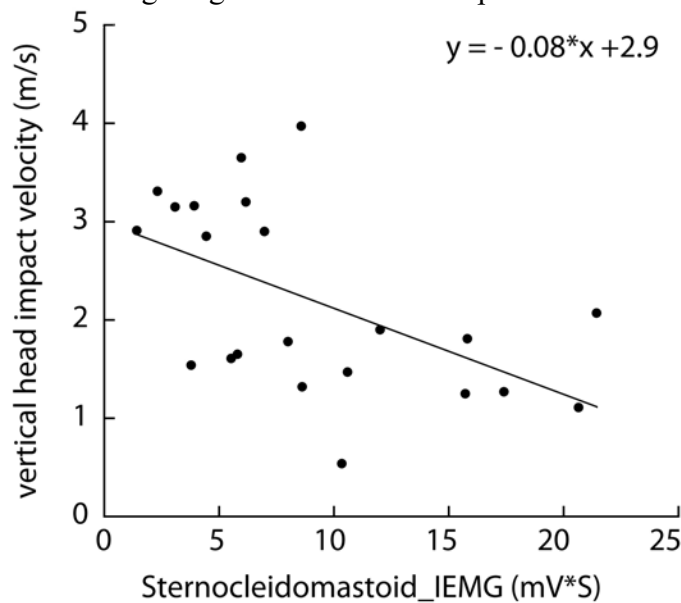


Figure 2. Association between vertical head impact velocity and neck muscle activity during backward falls.

RESULTS AND DISCUSSION

The experimental instruction associated with neck muscle activity ($p=0.009$), but not with core muscle activity ($p=0.14$). On average, neck muscle IEMG was 197% greater in falls where participants attempted to avoid head impact when compared to falls where they allowed head impact, while

inhibiting efforts to reduce impact severity (13.4 versus 4.5 mV*S) (Table 1). The falling instruction also associated with vertical head impact velocity ($p<0.0005$) and horizontal impact velocity ($p<0.0005$). Overall, vertical head impact velocity was 82% greater in falls where participants inhibited efforts to reduce impact severity versus impacted softly (3.24 versus 1.78 m/s). Furthermore, our regression analysis indicated that vertical head impact velocity associated neck muscle activity ($p=0.01$, $R^2=0.28$) (Figure 2). Our average value of vertical head impact velocity in falls where participants inhibited protective responses (3.24 m/s) is similar to the mean value (2.91 m/s) we recently observed from analysis of real-life falls in older adults captured on video in long term care [4].

Our results provide novel measures of head impact velocities during backward falls in humans, to inform the design and testing of protective gear (helmets, crash mats). Our results also indicate the essential role, in reducing the frequency and severity of head impacts in backward falls, of neck and core muscle activation during the descent and impact phases of falling. Further research is required to understand age-related changes and the role of neck and core strengthening exercises to prevent fall-related head injuries in older adults.

REFERENCES

1. Harvey LA et al., *Injury* **43**, 1821-6, 2012
2. Bouras T et al., *J Neurotrauma* **24**, 1355-61, 2007
3. Schonnop R et al., *CMAJ* **185**, 803-10, 2013
4. Choi WJ et al., *J Biomech* published online 24Feb2015. doi: 10.1016/j.jbiomech.2015.02.025
5. Robinovitch SN et al., *Lancet* **381**, 47-54, 2013
6. Hsiao ET and Robinovitch et al., *J Biomech*, 1998

Table 1: Average values of outcome variables (with SD shown in parentheses).

	Backward fall		
	No head impact	Minimize impact severity	Inhibit protective responses
Sternocleidomastoid_IEMG (mV*S)	13.4 (6.2)	10.1 (5.3)	4.5 (2.4)
Rectus Abdominis_IEMG (mV*S)	12.8 (7.3)	10.4 (4.0)	7.1 (3.8)
Vertical head impact velocity (m/s)	...	1.78 (0.6)	3.24 (0.4)
Horizontal head impact velocity (m/s)	...	1.50 (0.5)	2.73 (0.5)

COMPARISON OF RECTUS FEMORIS FORCE OUTPUT AND ACTIVATION IN SEATED VS. PRONE EXTENSION

¹ Gabrielle Colucci, ² Meghan M. Miller, ² Kristen Looman, ² Jared Seidel, ² Daniel Clifton, ² Dustin Grooms, ² Michael P. McNally, ² Eric Schussler, ² Cambrie Starkel, ² James A. Onate

¹ Youngstown State University, Youngstown, OH, USA

² The Ohio State University, Columbus, OH, USA

email: Colucci.Gabrielle@gmail.com, web: <http://medicine.osu.edu/hrs/at/research/moves/>

INTRODUCTION

The comparison of the force production and muscle activation of seated and prone positioning when testing a commonly measured muscle, the rectus femoris (RF) is currently unknown. The RF is a biarticular muscle crossing both the knee and hip joint and its force output can be altered by different positions of the hip for a given knee angle [1]. The amount of force a muscle can generate is dependent on its length and velocity [2]. In the seated position, the RF is shorter than in its prone counterpart which allows for a mechanical advantage in the seated position. We hypothesize there will be a significant difference in both force production and muscle recruitment of the RF when testing in the seated position and prone position.

METHODS

Thirteen subjects (8 male, 5 female; age 24 ± 5.1 yr; height 175.05 ± 7.46 cm; mass 72.67 ± 8.77 kg) participated in the study which involved a unilateral test of their dominant leg. All subjects were free from musculoskeletal injury at the time of testing and volunteered their participation. Informed consent was given through a process approved by The Ohio State University's Institutional Review Board. Electromyography (EMG) was used to compare muscle activation of the RF. The skin was prepared by abrading and cleansing it with alcohol pads prior to placing the electrodes as per Surface Electromyography for the Non-Invasive Assessment of Muscles (SENIAM) recommendations. For load cell (BTE Technologies, Inc., Hanover, MD) testing, subjects laid on a table in a prone position and Velcro straps were used to secure the subject above the knee and across the lumbar region. The load cell was



Figure 1A: Seated Position



Figure 1B: Prone Position

rigidly attached to a wall at ankle height and an ankle cuff was attached to the subject after their knee was placed in 90° flexion and hips at 0° flexion (Figure 1B). A Biodex System III isokinetic dynamometer (Biodex Medical Systems, Shirley, NY) was used to assess isometric strength while seated. Subjects were placed in a seated position with the hips and knees in 90° flexion with straps around the dominant ankle and thigh to isolate knee motion, and around the waist and trunk to limit whole body involvement (Figure 1A). Three trials of the leg extension task were completed on the self-selected dominant leg. Activity from the RF was captured via EMG (1500 Hz). Prior to testing, maximum voluntary isometric contraction (MVIC) of the RF was recorded to normalize task EMG. RF MVIC testing involves placing the participant in a seated position and instructing them to provide a maximal effort isometric hip flexion contraction. Both MVIC and task isometric contractions were held for five seconds. Raw EMG data underwent full wave rectification, band-pass filter of 50-500Hz, and moving RMS smoothing window of 150ms. Recruitment output was normalized to % MVIC.

Peak force from each trial was normalized to % body weight of each subject. A students *t*-test with *a priori* $\alpha=0.05$ was utilized to examine differences between force production in seated Biodex and prone load cell positions. A second students *t*-test was utilized to test the differences in muscle activation in the same positions.

RESULTS AND DISCUSSION

There were significant differences between force production ($p<0.01$) and RF activation ($p<0.01$) in the seated and prone position. The average force output of the RF was 78.2 ± 12.7 lbs. in seated testing and 49.6 ± 11.6 lbs. in prone testing as seen in Figure 2A. The average activation of the RF was $182.3 \pm 128.9\%$ of MVIC was seen in seated testing and $88.4\% \pm 45.2\%$ of MVIC in prone testing as seen in Figure 2B.

CONCLUSIONS

Testing the RF in a seated position and in a prone position does not produce comparable results in muscle activation or force output. Therefore, the tests are not interchangeable and can't be used in place of one another. The length-tension relationship plays an

essential role when it comes to muscle function [2]. In the prone position, the RF is at a greater length than at its seated counterpart which causes a mechanical disadvantage producing less force output and activation [1]. The seated testing position is commonly used and has standardized normative values for strength testing. Different testing positions yield different force outputs and muscle activation patterns having both advantages and disadvantages.

REFERENCES

1. Maffiuletti NA and Lepers R. *Med Sci Sports Exerc.* 2003; **35**(9): 1511-1516.
2. Brughelli M and Cronin J. *Sports Medicine.* 2007; **37**(9): 807-826.

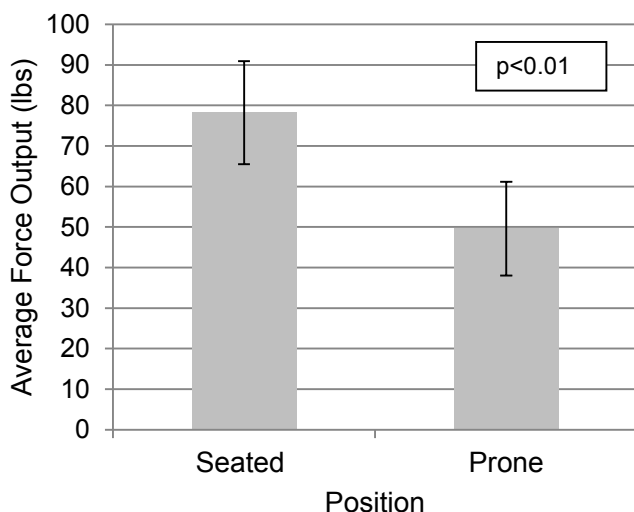


Figure 2A: Average Force Output of RF

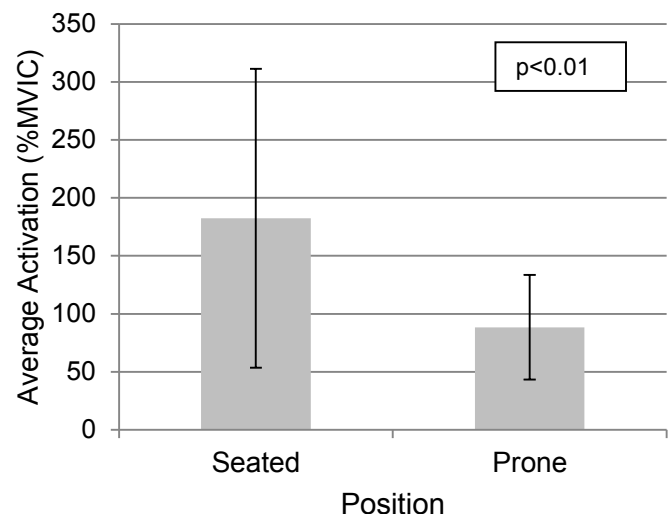


Figure 2B: Average Activation of RF

AGE AND SEX EFFECTS ON FORCE ASYMMETRY DURING JUMP AND PUSH-UP TASKS IN YOUTH SOCCER PLAYERS

Mara J. Cosgrove, Mitchell L. Stephenson, Taylour J. Hinshaw, Kathryn L. Overton, Austin L. Roberts, Elizabeth A. Meyer, and Boyi Dai

University of Wyoming, Laramie, WY, USA
email: mcosgrov@uwyo.edu, web: <http://www.uwyo.edu/kandh/>

INTRODUCTION

Playing soccer is associated with improved health but also risks for injuries. Previous studies have suggested that increased asymmetry in lower extremity bilateral strength is associated with increased risks for lower extremity injuries and decreased sports performance [1]. Several factors including injury history, asymmetry in lean mass, and muscle activation have been identified as contributors to asymmetry in bilateral strength. Understanding how strength asymmetry changes as a function of age and sex may inform injury prevention and performance training in soccer [1].

One validated tool to quantify asymmetry in lower extremity bilateral strength is a countermovement jump for a maximum height [2]. Similarly, a maximum push-up task may be used to assess asymmetry in upper extremity bilateral strength. A previous study has quantified the performance asymmetry between the preferred and non-preferred legs in soccer players aged 6 to 10 years old [3]. A recent study has examined the force asymmetry between the dominant and non-dominant legs during squat in soccer players aged 13 to 17 years old [4]. The strength asymmetry during jump and push-up tasks in youth soccer players, however, has not been investigated.

The purpose of this study was to investigate the effects of age and sex on force asymmetry during jump and push-up tasks in youth soccer players aged 7 to 14 years old. It was hypothesized that force asymmetry would be present and different between males and females and increase as age increases in youth soccer players.

METHODS

Thirty male and 29 female youth soccer players (age: 10.6 ± 2.0 years; mass: 36.9 ± 11.0 kg; height: 141.7 ± 20.7 cm) participated in the current study. The dominant leg was defined as the preferred leg to kick a ball and the dominant arm was defined as the preferred arm to throw a ball. Participants performed three trials of a countermovement jump and a maximum push-up with each limb on a Bertec force plate. The vertical ground reaction force was sampled at a frequency of 1000 frames/second. The maximum force produced by the dominant and non-dominant legs and arms during jump and push-up tasks were extracted for analysis and normalized to body weight (BW). The bilateral force asymmetry index between the dominant and non-dominant limbs was calculated and expressed as a percentage of the stronger limb. Paired t-tests were used to compare the maximum force between the dominant limb and non-dominant limbs during jump and push-up tasks. Regression analysis with age as a continuous variable and sex as a dummy variable was used to predict the force asymmetry index as a function of age and sex. A type I error rate was set at 0.05 for statistical significance.

RESULTS AND DISCUSSION

With regard to force asymmetry in lower extremity strength during the jump, t-tests indicated that the dominant leg (1.26 ± 0.19 BW) tended to demonstrate increased maximum force compared with the non-dominant leg (1.24 ± 0.18 BW, $p=0.08$). The bilateral force asymmetry index (Figure 1), however, was not significantly correlated with age ($p=0.77$), nor different between the sexes ($p=0.36$) (Fig. 1).

With regard to force asymmetry in upper extremity strength during the push-up, t-tests indicated that the dominant arm (0.48 ± 0.06 BW) demonstrated increased maximum force compared with the non-dominant arm (0.46 ± 0.04 BW, $p=0.01$). The bilateral force asymmetry index (Figure 2), however, was not significantly correlated with age ($p=0.441$), nor different between the sexes ($p=0.431$) (Fig. 2).

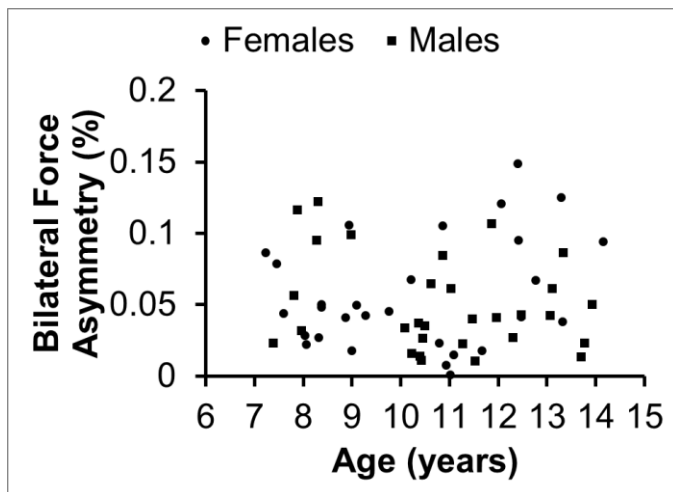


Figure 1: Bilateral force asymmetry during the jump as a function of age and sex

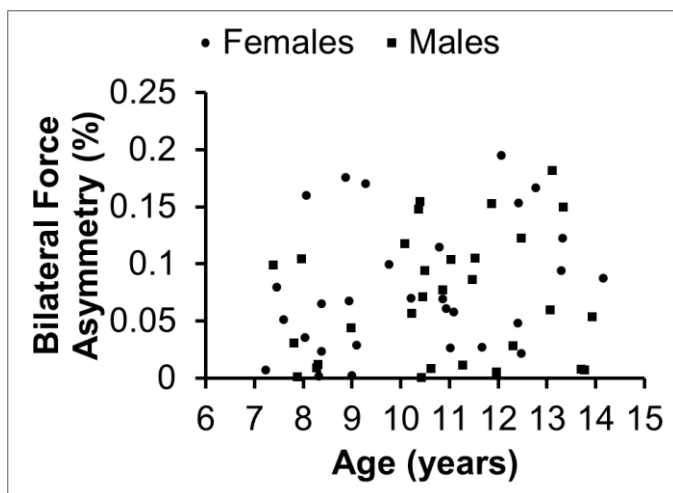


Figure 2: Bilateral force asymmetry during the push-up as a function of age and sex

Our first hypothesis was supported that force asymmetry would be present in youth soccer players. For both jump and push-up tasks, participants tended to demonstrate greater force on the dominant limb compared with the non-dominant limb. The findings were consistent with the findings

by Teixeira and Teixeira [3], who observed greater velocities when youth soccer players kicked with their preferred leg. On the other hand, Atkins et al. [4] observed bilateral force asymmetry during a squat task in youth soccer players, but the non-dominant leg demonstrated greater force compared with the dominant leg. The discrepancy between the findings of the current study and the study by Atkins et al. [4] may be due to the high physical demand of the jump task versus the relatively low physical demand of the squat task.

Our second hypothesis, however, was not supported. It was expected that older individuals were more likely affected by limb dominance and history of injury and therefore may demonstrate increased force asymmetry. The findings of the current study did not support the notion of a general increase in force asymmetry as age increases in youth soccer players. The findings were generally consistent with the findings by Atkins et al. [4], who did not observe increased force asymmetry as age increased.

CONCLUSIONS

Preliminary results from this study indicate potential asymmetry in lower and upper strength between the dominant and non-dominant limbs in youth soccer players aged 7 to 14 years old. The asymmetry, however, did not tend to change as age increased. Males and females also demonstrated similar asymmetry. The findings suggest that screening for asymmetry in lower extremity strength should be initiated in childhood and adolescence in soccer players. An individual-based strategy may be needed for screening and injury prevention instead of simply using age and gender to classify the injury risk.

REFERENCES

1. Dai, B, et al. *Proceedings of ISBS Annual Meeting*, Johnson City, TN, USA, 2014.
2. Impellizzeri, FM et al. *Med Sci Sports Exerc*, **39**, 2044-2050, 2007.
3. Teixeira MC and Teixeira LA. *Dev Psychobiol*, **50**, 799-806, 2008.
4. Atkins, SJ et al. *J Strength Cond Res*, in press.

AUTOMATED CALCULATION OF LONG BONE BENDING STIFFNESS FROM CT SCANS AND ONE-DIMENSIONAL FINITE ELEMENT ANALYSIS

¹Eric Arnold and ^{1,2}John Cotton

¹Mechanical Engineering, ²Biomedical Engineering, Ohio University, Athens, OH, USA
email: cotton@ohio.edu

INTRODUCTION

Traditional CT-based finite element (FE) modeling of long bones uses 3D models that require a skilled user, specialized software for model creation and solution, and moderate to large resources for solution and data storage. The goal of this project was to create an alternative, lean and fast method that reads serial transverse CT images and automates creation of a 1D FE model that can be solved with minimal resources and user experience. We then test the accuracy of this method against experimental data and 3D FE results for 18 cadaveric ulnae.

METHODS

CT images of cadaveric ulnae and results from quasistatic mechanical tests (QMT) in three-point bending were provided by Bowman [1]. Transverse slices spaced 2.5 mm apart were rotated with the mid shaft interosseous crest pointed downward (Figure 1) to match QMT orientation.

We wrote MATLAB code (Mathworks, Natick, MA) that read each transverse CT slice, and for every pixel assigned a value for Young's modulus, E , in MPa according to

$$E = (k \cdot im)^B$$

where im is the pixel brightness in Hounsfield units and k and B are tunable parameters. With E mapped for each pixel in the slice, the centroid of each section was found. Then the section modulus EI was calculated about the horizontal axis through the centroid according to

$$EI = \sum_i \sum_j E_{ij} (y_j - \bar{y})^2 \Delta x \Delta y$$

where i and j represent the pixel indices, \bar{y} is the centroid location, and Δx and Δy are the pixel dimensions.

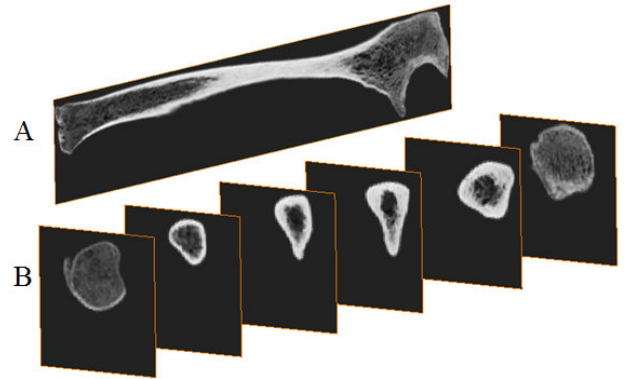


Figure 1: CT scan of a representative ulna, with lateral view (A) and six transverse slices (B), shows geometric and bone density changes in the ulnar shaft. Actual simulations examined approximately 100 slices per model.

These section moduli were used to create a 1D FE model with Hermitian beam elements and one element per slice. End conditions of a simply supported beam were assigned and deflection calculated under a 1 N mid-span load modifying and extending code from [2]. We then calculated the bending stiffness k_b as the mid-span load divided by the mid-span deflection.

Results of our 1D FE models were compared to stiffness values generated from QMT [1] and 3D FE models [3]. The parameters k and B were optimized using a Nelder-Mead algorithm to minimize the sum of the square of the residuals compared to QMT. This was done on a subset of ulnae randomly selected from three equal subsets of high, medium, and low QMT stiffness values. These results are referred to as *tuned* values. To separate geometric from tuning effects of material properties, simulations were also run where all pixels above a threshold value were assigned the same cortical bone stiffness used by the 3D models. These results are referred to as *standard* E .

RESULTS AND DISCUSSION

The results of the optimization found parameters of $k = 1.064$ and $B = 1.27$. Figure 2 shows results of a single ulna's calculated EI variations and the simulated displacement. All FE simulation results are compared to QMT measurements in Figure 3.

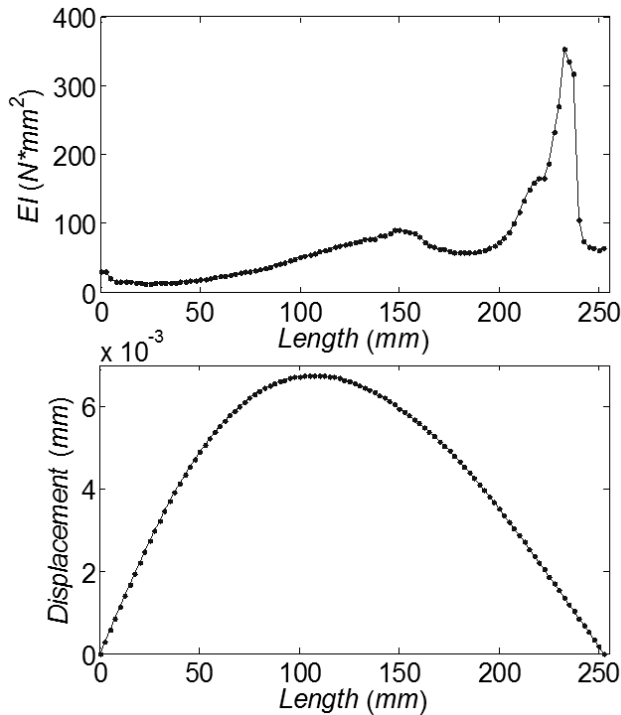


Figure 2: Results for a representative ulna.

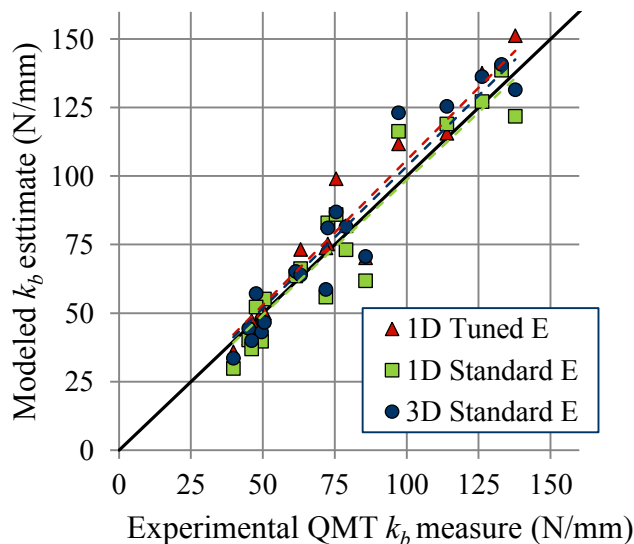


Figure 3: Comparison of experimental stiffness against three FE modeling methods. Dark line represents identity line, $y = x$.

A linear regression of all three FE methods compared to QMT experiments showed that the intercept was not significantly different from 0. Slopes were not significantly different from one at the 95% confidence level model for the 3D Standard E and 1D standard E methods. Table 1 shows results of the regression analysis.

Table 1. Data from regression analysis of the three FE methods compared to experimental QMT data.

Method	Slope [95% C.I.]	R ²	SEE (N/mm)
1D Tuned E	1.06 [1.01-1.11]	0.93	8.1
1D Standard E	0.99 [0.92-1.05]	0.92	11.1
3D Standard E	1.03 [0.97-1.09]	0.93	10.0

CONCLUSIONS

We have implemented a fast technique to create 1D FE models to estimate the stiffness of long bones. This method produces comparable results to a more complex process of 3D FEA, but takes less than 1 second to read the scans, mesh, and solve the problem. While experiences vary, 3D FE modeling and analysis from a set of CT scans in our lab would take a trained user two to four hours.

Our results indicate that optimizing material property relations add little accuracy. Somewhat surprising was the deviation from the *1D standard E* and the *3D standard E* models as these had similar geometric information and the same material properties. Differences in these cases may indicate the importance of precise 3D boundary conditions, and torsional or shear deformation neglected in the formulation of the 1D case.

REFERENCES

1. Bowman, L. Dept. of Biological Sciences, Ohio University. Unpublished data, Nov. 20, 2014.
2. Kwon, Y.W. and Bang, H., **The Finite Element Method Using MATLAB**, CRC Press, 1997.
3. Garven, B., M.S. Thesis, Ohio University, August, 2014.

ACKNOWLEDGEMENTS

Eric Arnold was supported by the Russ Vision Fund for undergraduate research. We thank Lyn Bowman for many helpful suggestions to the study.

THE EFFECTS OF MEDIAL AND LATERAL WEDGES ON ILIOTIBIAL BAND STRAIN DURING OVERGROUND RUNNING

¹ Evan M. Day and ¹ Jason C. Gillette

¹ Iowa State University, Ames, IA, USA
email: eday@iastate.edu

INTRODUCTION

Iliotibial band syndrome (ITBS) is an overuse injury that is the second most prevalent running injury behind patellofemoral pain syndrome [1]. Excessive hip adduction and internal knee rotation have been linked to individuals with ITBS [2,3], but not without confounding results [4,5]. Iliotibial band (ITB) strain and strain rate have been observed to be higher in individuals with ITBS, suggesting that a high strain rate could be the underlying factor for development of ITBS [6]. Orthotics are commonly used in clinical settings to alter gait mechanics to prevent injury. The goal of this study was to manipulate ITB strain and strain rate by using medial and lateral wedges to influence foot motion and change other kinematic parameters that affect the length of the ITB. Our hypotheses were that lateral wedges would increase strain and strain rate of the ITB, where as medial wedges would reduce strain and strain rate.

METHODS

Fifteen males (21 ± 2 years, 71 ± 3 in., 158 ± 11 lbs.) and fifteen females (21 ± 2 years, 65 ± 3 in., 124 ± 11 lbs.) were recruited for this study. Participants were healthy runners. Subjects completed five running conditions using a lateral 7° wedge, lateral 3° wedge, no wedge, medial 3° wedge, and medial 7° wedge. Wedges were made of EVA and extended from the back of the shoe to the base of the metatarsals. Subjects wore their own running shoes. Subjects completed 5 trials per condition at their preferred running speed $\pm 5\%$. Order of conditions was randomized between subjects. Subjects ran on a treadmill for 1 minute between conditions. Stance phase kinematics of the knee and hip in the sagittal, frontal, and transverse plane were input to a custom MATLAB program

that calculated strain and strain rate of the ITB. The ITB model was created using dimensions from OpenSim. Data were analyzed using MANOVA tests in JMP.

RESULTS AND DISCUSSION

There were no significant differences in strain ($p > .05$) or strain rate ($p > .05$) in males. There were no significant differences in strain ($p > .05$) or strain rate ($p > .05$) in females. Strain and strain rate were observed to be higher in females than males.

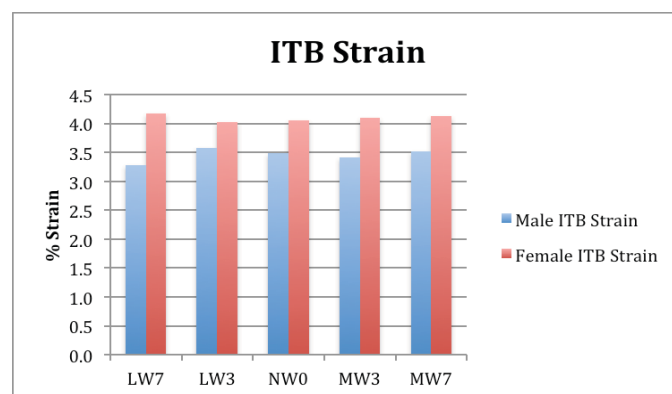


Figure 1: Average maximum ITB strain in males and females

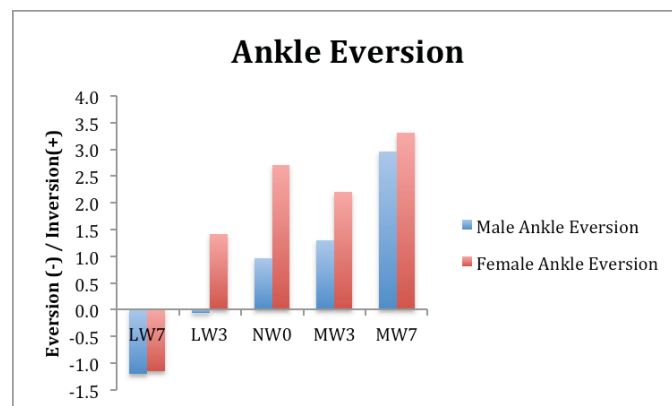


Figure 2. Average maximum ankle eversion in males and females

The wedges produced systematic results in influencing ankle eversion. Other kinematic variables associated with lengthening the ITB were analyzed. Control condition results differed between genders. Knee internal rotation was greater in males (11.3° vs. 2.5°), knee flexion was greater in males (48.8° vs. 45.1°), knee valgus was greater in females (3.6° vs. -0.3°), and hip adduction was greater in females (15.3° vs. 13.8°). No significant differences in kinetics were observed between conditions in either males or females.

Our hypotheses were that strain and strain rate would be greater when using the lateral wedges than the medial wedges. Contrary to our hypotheses, strain rate was greater in females using the medial wedges, although not statistically significant.

Failure to produce significant differences in strain and strain rate could be due to using a wedge insert that extends to the base of the metatarsals, and not a rigid or full foot orthotic. The wedges did produce systematic results for peak ankle eversion, but failed to influence differences at the knee and hip. A rigid or full foot orthotic has potential to have a greater influence on skeletal motion.

Subjects using their own footwear could have dampened the effects of the wedges. Shoes with a softer midsole will absorb the effects of the wedge more than shoes with a firm midsole. Controlling footwear would increase internal validity and potentially influence greater differences between conditions.

A limitation of this study is that the subjects were healthy individuals that do not wear orthotics. By inserting wedges into the running shoes we essentially created a problem for the subject. This could result in the subjects fighting the effects of the wedges. However, no significant differences were

observed in plantarflexion or ankle inversion moments for males or females ($p > .05$).

It has been previously reported that individuals with ITBS exhibit greater ITB strain and strain rate than healthy individuals [6,7]. By redoing this study with groups of healthy runners and runners with ITBS, we could gain further insight into how wedges affect ITB strain and strain rate in injured individuals as they are the target demographic of this study.

Conclusions

The wedge inserts used did not have a significant effect on ITB strain and strain rate in healthy individuals. The goal of this study was to manipulate strain and strain rate of the ITB as a high strain rate is theorized to be the underlying factor for development of ITBS [6]. Using a semi rigid or full foot orthotic and a subject pool including individuals with ITBS could result in different results.

REFERENCES

1. Taunton, J. et al. *British Journal of Sports Medicine* **36**, 95-101, 2002.
2. Ferber, R. et al. *Clinical Biomechanics* **18**, 350-357, 2010.
3. Noehren, B. et al. *Clinical Biomechanics* **22**, 951-956, 2007.
4. Grau, S. et al. *Scan. J. of Med. And Sci. in Sports*. **22**, 184-189, 2011.
5. Noehren, B. et al. *Journal of Orth. & Sports Physical Therapy*. **44**, 217-222, 2014.
6. Hamill, J. et al. *Clinical Biomechanics*. **23**, 1018-1025, 2008.
7. Miller, R. et al. *Gait and Posture* **26**, 407-413, 2007.

Table 1: Strain Rate in Males and Females (%/s)

Gender	Wedge Condition				
	LW7	LW3	NW0	MW3	MW7
Male	32.9 ± 10.8	35.0 ± 14.0	32.2 ± 11.8	31.8 ± 11.2	32.2 ± 11.6
Female	36.4 ± 9.3	34.3 ± 9.3	47.8 ± 3.4	50.7 ± 5.2	44.2 ± 7.3

TIBIAL STRESS DURING LANDINGS FROM TWO HEIGHTS

¹Steve Dado, ¹Elizabeth R. Boyer, ¹Timothy R. Derrick

¹Iowa State University, Ames, IA, USA

email: tderrick@iastate.edu ; web: [http:// www.kin.hs.iastate.edu/](http://www.kin.hs.iastate.edu/)

INTRODUCTION

It has been suggested that subjects can maintain levels of strain in the tibia while landing from varying drop heights [1]. The suggested mechanism is an increase in the range of motion at the joints when the height is increased. Data providing evidence for this come from strain gages that are mounted to staples that are embedded within the bone of human subjects. Questions persist as to the normalcy of the landing under these conditions and the limitation of measuring the strain at a single point on the tibia. The purpose of this study was to estimate the peak stresses in landing from two heights using non-invasive techniques. It was hypothesized that there would be no difference in peak compressive, tensile and shear stresses between the two heights.

METHODS

Nine young adults (5 males, age: 25.6 ± 5.0 yr, body mass: 68.3 ± 8.1 kg, height: 1.81 ± 0.07 m and 4 females, age: 20.8 ± 1.7 yr, body mass: 57.0 ± 12.0 kg, height: 1.64 ± 0.06 m) with no lower limb injuries volunteered to participate. All subjects landed 5 times by stepping off a box with both feet hitting the ground at the same time. This was repeated for two heights (28 cm and 48 cm). Kinematic data were collected at 200 Hz (Vicon MX, Vicon, Centennial, CO, USA) and force data at 1000 Hz (AMTI, Watertown, MA).

A succession of 3 models were used to estimate tibial stresses during the landing. First, a rigid body model was used to estimate 3D joint moments and reaction forces at the ankle, knee and hip joints during the first 500 ms after contact with the force platform. Second, a musculoskeletal model was used to estimate length and velocity adjusted maximal muscle forces and moment arms of 44 lower extremity muscles. Muscle parameters for this model were derived from Arnold et. al, [2]. Static optimization was used to estimate the dynamic muscle forces using an optimizing criteria that minimized the sum of the muscle stress

squared. The muscle forces were constrained to equal the sagittal plane ankle, knee and hip moments and the frontal plane ankle and hip moments that were estimated using the rigid body model. They were also bound by zero and the maximal muscle forces estimated by the musculoskeletal model. Third, a bone model was used with beam theory and finite element methods [3] to derive stresses in a cross section of the tibia located approximately 67% of tibial length from the knee joint. Bone parameters were derived from CT scans (Toshiba Prime 40, 120 kV, .4 mm resolution) and used to create a 600 element (60 circumferential and 10 radial nodes) mesh for each subject.

Peak compressive, tensile and shear stresses were located in the tibial cross section and recorded during each landing. Paired t-tests were done on each variable and p-values were compared to an alpha criterion of 0.016 (0.05/3 variables) to determine statistical significance.

RESULTS AND DISCUSSION

Peak compressive stress was located on the posterior medial aspect of the cross section while the peak tension was located on the anterior lateral region (Figure 1). Peak shear was inconsistently located from subject to subject. Peak compression, peak tension and peak shear all occurred about 100 ms after contact with the ground. Most of the normal stress (82% at peak compression) was caused by muscular contraction – predominantly triceps surae. This caused the tibia to bend concave posterior. The reaction force was responsible for the remainder of the stress and it caused a concave anterior bending during the first 50 ms followed by a concave posterior bending during the second 50 ms. Bending of the tibia resulted in much more stress on the bone than did the axial forces (89.1% at peak compression). Peak compressive stress increased from the low landing height to the high landing height (low: -146.7 ± 27.0 MPa, high: -174.9 ± 33.5 MPa, $p < .001$). Peak tensile stress also increased (low: 152.5 ± 40.4

MPa, high: 179.9±47.8 MPa, $p<.001$). However there was not a significant difference in the peak shear stress (low: 8.6±2.4 MPa, high: 9.4±3.3 MPa, $p<0.424$).

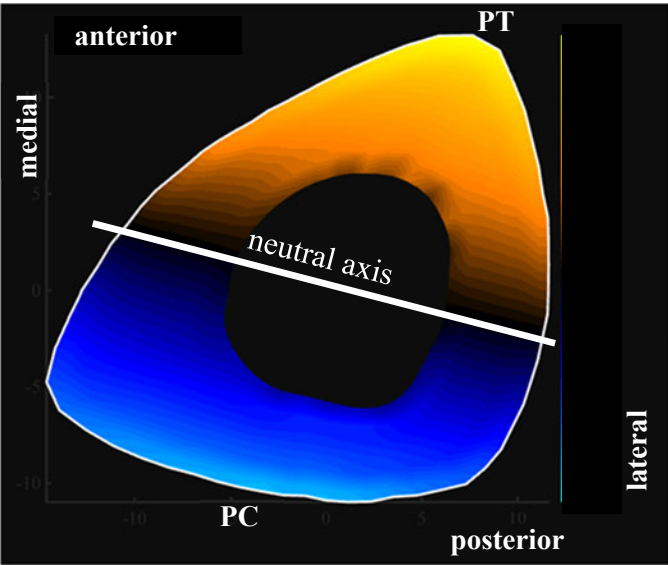


Figure 1. Stresses during peak compression of a drop landing. PT indicates the location of peak tensile stress and PC indicates the location of peak compressive stress averaged across subjects.

CONCLUSIONS

The evidence provided by these data did not fully support the hypothesis that landing height would not affect stresses. Tensile and compressive stresses increased with landing height, however, shear stresses did not change significantly.

Table 1. Peak compressive, tensile and shear stresses in a cross section of the tibia located at 67% of the tibial length from the knee. Drop landings were from low (28 cm) and high (48 cm) heights.

Variable	Landing		p-value
	low	high	
Peak Compressive Stress (MPa)	-146.7 ± 27.0	-174.9 ± 33.5	0.000
Peak Tensile Stress (MPa)	152.5 ± 40.4	179.9 ± 47.8	0.000
Peak Shear Stress (MPa)	8.6 ± 2.4	9.4 ± 3.3	0.424

One difference between these data and previous research is that Milgrom et al. [1] mounted strain gages to the anterior medial aspect of the tibia. This would result in strain measurements close to the neutral axis (Figure 1) and thus may have underestimated the loading in the tibia.

Compressive stresses at the distal 1/3 of the tibia were generally not as high during these landings as they would be during running. This is likely due to both feet making contact with the ground at the same time. The tensile stresses were relatively higher during the high drop height compared to running. This may indicate that athletes performing a lot of jumping may be more susceptible to anterior tensile stress fractures while runners might be more susceptible to posterior compressive fractures.

REFERENCES

1. Milgrom C et al. *Br J Sports Med*, **34**, 195-199. 2000.
2. Arnold EM et al. *Annals Biomed Eng*, **38**, 269-279. 2010.
3. Kourtis LC et al. *Computer Meth Biomech Biomed Eng*, **11**, 463-476. 2008.

SELF-REPORTED HIP FUNCTION IS RELATED TO ANKLE JOINT MOMENT ASYMMETRY DURING LANDING IN INDIVIDUALS WITH FEMOROACETBULAR IMPINGEMENT

^{1,2} Stephanie Di Stasi, ³ Michael McNally, and ^{1,3} Timothy E. Hewett

¹ The Ohio State University, Sports Health and Performance Institute, Columbus, OH, USA

² Department of Orthopaedics, The Ohio State University, Columbus, OH, USA

³ School of Health and Rehabilitation Sciences, The Ohio State University, Columbus, OH, USA
email: stephanie.distasi@osumc.edu

INTRODUCTION

Femoroacetabular impingement (FAI) is an increasingly recognized source of hip pain and disability in active individuals [1]. In an attempt to maintain their level of sport participation, 71% of athletes report modifying their technique [2]. Only one published study to date has characterized the biomechanical adaptations of a small group of individuals with FAI during a sports-related jump-landing task [3]. Importantly, the association of biomechanical adaptations to self-reported hip function has not previously been evaluated, but could provide valuable insight into why some athletes are able to maintain a high level of sports participation in spite of a painful hip joint. The purpose of this study was to evaluate the relationship between sagittal plane joint moment asymmetries during a drop vertical jump and self-reported hip function. The hypothesis tested was that higher self-reported function in athletes with symptomatic FAI would be associated with smaller involved hip moments and larger moments of the uninvolved knee and ankle.

METHODS

Thirty-six highly active individuals with symptomatic FAI scheduled to undergo hip arthroscopy (19 females; age: 25 years \pm 10; mass: 72.9kg \pm 16.9; height: 1.70m \pm 0.10) were recruited from The Ohio State University Hip Preservation practice. The Institutional Review Board approved this study and all subjects provided written, informed consent prior to participation. All subjects underwent standard three-dimensional motion analysis testing (Motion Analysis, Santa Rosa, CA). Kinematic data during three drop vertical jump

(DVJ) trials were sampled at 240Hz and ground reaction force data (1200Hz) were simultaneously collected from embedded force platforms. Marker trajectories and ground reaction force data were low pass filtered at 15Hz with a bidirectional Butterworth filter. Inverse dynamics were used to calculate external joint moments with custom Visual 3D (C-motion Inc., Germantown MD) and Matlab (Mathworks Inc. Natick, MA) coding. Ensemble averages were generated for both the involved and uninvolved limbs. Peak joint moments were identified during the landing phase of the DVJ (initial contact to lowest center of mass point), normalized to body mass and height (Nm/kg*m) and then used to calculate an asymmetry value (involved - uninvolved limb). Positive asymmetry values denoted larger joint moments in the involved limb.

Subjects were also asked to complete the Hip Outcome Survey Sports subscale (HOS-S), which is a reliable and valid questionnaire of hip function in patients with non-arthritic hip pain. Higher HOS-S scores reflect better hip function. Spearman rank correlation was used to test the association between HOS-S and sagittal plane joint moment asymmetries during the landing phase of the DVJ. A priori significance level was set at 0.05.

RESULTS AND DISCUSSION

The HOS-S scores ranged from 12.5% to 83.3% (52.4% \pm 20.4). Hip and knee joint moment asymmetries were not significantly associated with HOS-S scores (Hip: $r = -0.151$, $p = 0.380$; Knee: $r = -0.244$, $p = 0.151$; **Figures 1 and 2**). Only ankle joint moment asymmetry was associated with HOS-S scores ($r = 0.410$, $p = 0.013$; **Figure 3**). Specifically, higher ankle moments on the involved

limb (positive asymmetry values) were associated with higher HOS-S scores.

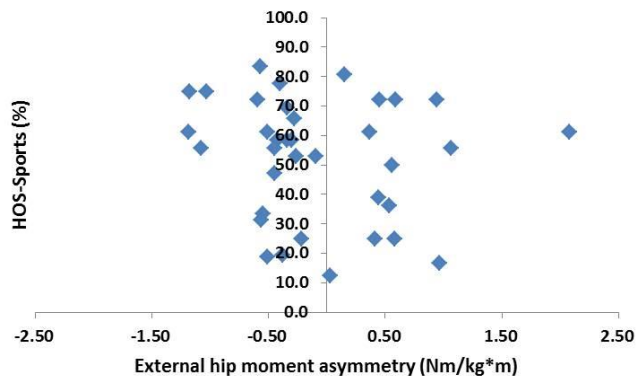


Figure 1: Scatter plot of HOS-S scores and external hip joint moment asymmetry during the landing phase of the DVJ.

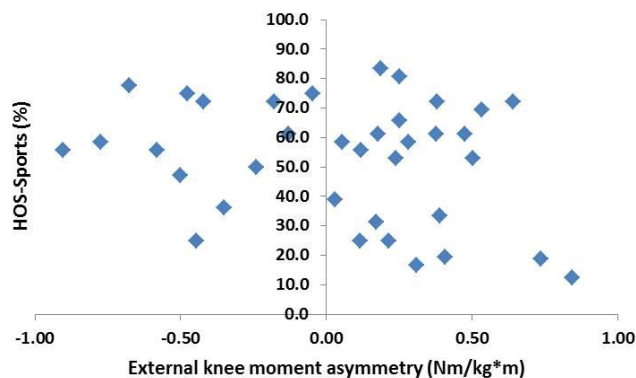


Figure 2: Scatter plot of HOS-S scores and external knee joint moment asymmetry during the landing phase of the DVJ.

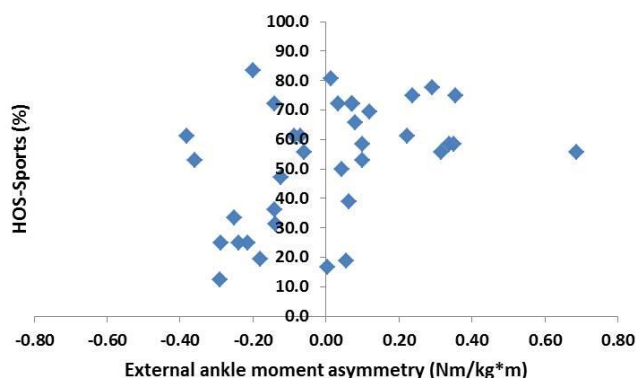


Figure 3: Scatter plot of HOS-S scores and external ankle joint moment asymmetry during the landing phase of the DVJ.

The wide range of HOS-S scores reflects the established variability in self-reported function previously reported in this population. In partial support of our *a priori* hypotheses, higher ankle joint moments on the involved limb were identified in individuals with higher self-reported hip function. This ‘ankle strategy’ may reflect a neuromuscular compensation that allowed individuals to maintain a high level of sports participation. Ultimately however, this strategy was not an adequate, sustainable compensation; at the time of testing, all subjects were scheduled to undergo hip arthroscopy after failed attempts at conservative treatment.

CONCLUSIONS

Active individuals with FAI demonstrated kinetic asymmetries at the hip, knee, and ankle during a DVJ task. However, only ankle joint moment asymmetry was associated with self-reported hip function, and may be indicative of a compensatory strategy of athletes who maintain the highest levels of sport-related function despite painful hip symptoms.

This study was limited to sagittal plane kinetics during a bilateral landing task. We did not examine multiplanar compensatory strategies, which are known to occur during activities of daily living in this population. Future work is also required to determine whether hip arthroscopy allows athletes to achieve more symmetrical joint loading strategies, or if these adaptations require special attention during post-surgical rehabilitation efforts.

REFERENCES

1. Clohisy JC, et al. *Am J Sports Med* **41**, 1348-56, 2013.
2. Philippon MJ. *Knee Surg Sports Traumatol Arthrosc* **15**, 1041-1047, 2007.
3. Kumar D, et al. *PM R* [epub ahead of print] 2015.

ACKNOWLEDGEMENTS

This study was funded in part by the Legacy Fund of the Sports Physical Therapy Section of the American Physical Therapy Association

Comparison of objective fracture severity measures in tibial plateau and pilon fractures

¹ Kevin N. Dibbern, ² Laurence B. Kempton, ³ Thomas F. Higgins, ² Todd McKinley, ¹ J. Lawrence Marsh, and ¹ Donald D. Anderson

¹ The University of Iowa, Iowa City, IA, USA

² Indiana University Health, Indianapolis, IN, USA

³ The University of Utah, Salt Lake City, UT, USA

email: Kevin-Dibbern@uiowa.edu , web: <http://tinyurl.com/UIOBL>

INTRODUCTION

Intra-articular fractures of the proximal tibia (plateau) have lower rates of post-traumatic osteoarthritis (PTOA) compared to those of the distal tibia (pilon). PTOA following joint injuries has been strongly correlated with mechanical factors, such as initial damage at the time of injury and repetitive damage from changes in joint congruity, alignment, and/or stability.

Differences in PTOA incidence between these fracture types may result from different impact energies absorbed by the joint surface. Differences in articular fracture edge lengths (AFELs), edges along which chondrocyte death is elevated [1], may also play a role. In this study, novel objective CT-based measures of fracture energy and of AFELs were used to describe differences between tibial plateau and tibial pilon fractures.

METHODS

Thirty-seven patients with intra-articular tibial plateau fractures and 32 with pilon fractures were enrolled from three different medical centers. A validated CT-based assessment was used to objectively measure fracture energy [2]. When bone is fractured, new surface area is liberated. This fracture-liberated (interfragmentary bone) surface area, scaled by its CT-derived bone density, provides an estimate of fracture energy [3,4]. Newly developed methods for measuring AFEL were used to analyze all of the fractures of the tibial pilon and 17 of the plateaus.

Custom software was utilized to identify fracture edges on CT-segmented bone fragments and to classify interfragmentary surface area for each fragment (Figure 1). AFELs were then measured directly at the intersections between subchondral and interfragmentary bone surfaces. Fracture

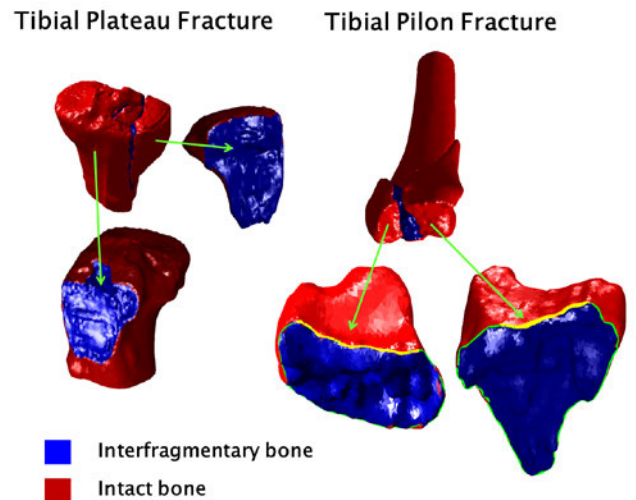


Figure 1: Views of tibial plateau and pilon fractures in the custom software. The left panel demonstrates the classification of a tibial plateau fracture into intact and interfragmentary bone. The right panel demonstrates two intra-articular fragments of a tibial pilon fracture, with the measured articular fracture edge lengths (AFELs) highlighted in yellow (bottom right images).

energies and AFELs measured from tibial plateau and pilon fractures were then compared.

RESULTS AND DISCUSSION

Fracture energies for tibial pilon fractures ranged from 6.43 to 37.95 J and for tibial plateau fractures from 3.55 to 39.63 J (Figure 2). The range of AFELs for tibial pilon fractures was from 56 to 289 mm and for tibial plateau fractures from 68 to 385 mm (Figure 3).

The fracture energy for tibial pilon fractures was 15.88 ± 8.71 J (mean \pm standard deviation) and for tibial plateau fractures was 15.33 ± 9.16 J. There was no statistically significant difference between these groups.

The AFEL for tibial pilon fractures was 130 ± 55 mm and for tibial plateau fractures was 204 ± 82 mm. There was a statistically significant difference between these findings at a P-value of 0.003.

There were minimal differences in fracture energy between the two fracture types. There was a difference in articular fracture edge length, however. The injury mechanisms that produce these fractures are similar, but prior clinical studies have shown that PTOA develops in substantially fewer plateau cases. Anecdotally, orthopaedic surgeons believe there to be more crush in the tibial plateau fractures, potentially explaining the increased AFEL found in these cases.

CONCLUSIONS

PTOA is a complex disease. The underlying mechanical factors are poorly understood and likely joint specific. The data reported here suggest that fractures of the tibial plateau involve equivalent fracture energy as do fractures of the tibial pilon,

but they generate larger AFELs. The reported discrepancy in PTOA incidence may be better explained through differences in joint anatomy such as cartilage thickness and the presence of a meniscus, mechanics of load distribution, or a combination of additional factors.

REFERENCES

1. Lewis JL, et al. *J Orthop Res* **21**:881-7. 2003.
2. Thomas TP, et al. *J Orthop Trauma* **24**:764-8. 2010.
3. Beardsley CL, et al. *J Biomech* **35**:331-8. 2002
4. Anderson DD, et al. *J Orthop Res* **26**:1046-52. 2008.

ACKNOWLEDGEMENTS

The research reported in this abstract was supported by the National Institute of Arthritis and Musculoskeletal and Skin Diseases of the National Institutes of Health under award number R21 AR061808. The research was also aided by a grant from the Foundation for Orthopaedic Trauma.

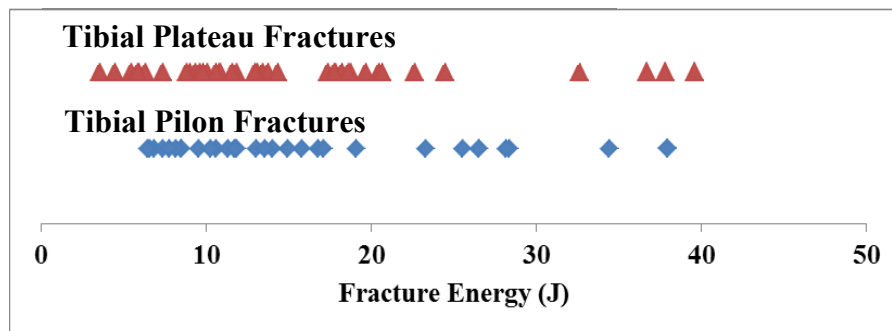


Figure 2: Tibial plateau and pilon fracture energy distributions.

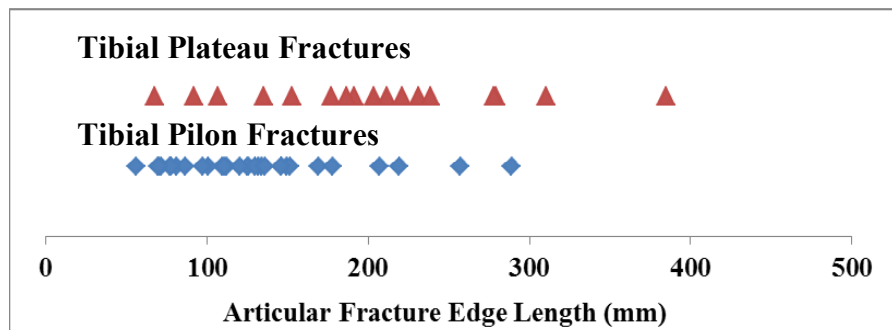


Figure 3: Tibial plateau and pilon articular fracture edge length distributions.

DYNAMIC SIMULATION OF PATELLAR TRACKING FOR KNEES WITH INSTABILITY

¹ Michael J. Kelly, ² Alexis K. Schlosser, ³ Andrew J. Cosgarea, ⁴ Danielle E. Filipkowski, ⁴ John J. Elias

¹ University of Akron, Akron, OH, USA, ² Northeast Ohio Medical University, Rootstown, OH, USA, ³ Johns Hopkins Medicine, Baltimore, MD, USA, ⁴ Akron General Medical Center, Akron, OH, USA
email: john.elias@akrongeneral.org

INTRODUCTION

Patellar dislocation is the most common acute knee disorder in children and adolescents. Numerous surgical options are available for treatment of recurrent lateral patellar instability, with limited consensus on how to optimize treatment based on the pathology of an individual patient. In vitro and computational evaluations of surgical options have consistently been based on normal knees. The current study focuses on development of a technique for dynamic computational simulation of patellar tracking for knees with instability that can be used to evaluate surgical options.

METHODS

Computational models were developed to represent knees of four patients with recurrent patellar instability who participated in an IRB-approved study to quantify the influence of tibial tuberosity realignment on patellar tracking [1]. Both pre-operatively and post-operatively, each patient performed a 10 second knee extension exercise against gravity within the bore of a dynamic CT scanner (Aquilion ONE, Toshiba Medical Systems). Bone models were reconstructed from the CT images to represent the femur, patella and tibia at 5 or more time points. Shape matching techniques were used to represent each position of knee extension with a single model of each of the three bones. Patellofemoral and tibiofemoral kinematics were characterized based on anatomical coordinate axes using the floating axis convention. Cartilage surfaces and bone models were also reconstructed from MRI scans of the knees, and shape matching techniques were used to align the cartilage surfaces to the bone models developed from CT.

Each knee model was individually imported into a multibody dynamics simulation platform

(RecurDyn, Function Bay Inc). The ACL, PCL, MCL, LCL, posterior capsule, patellar tendon, and lateral retinaculum were represented with multiple springs and dampers, with anatomical attachment points [2]. Medial retinacular structures were not modeled as they are damaged by recurrent dislocation. Nonlinear force-strain relationships were assigned to the ligaments [2]. Pre-operative and post-operative (following tibial tuberosity realignment) patellar tendon attachment positions on the tibia were established based on the respective CT scans. Quadriceps forces representing the vastus medialis obliquus, vastus lateralis, and the vastus intermedius were applied through springs representing the quadriceps tendon, with a total force of 600 N (Fig. 1). Hamstrings forces were applied with a total force of 100 N. The mass of the lower leg was represented with structures extended from the proximal tibia. With the femur fixed and no other degrees of freedom constrained, dynamic extension from flexion was induced with application of the muscle forces. Cartilage contact was governed by a compliant model based on simplified Hertzian

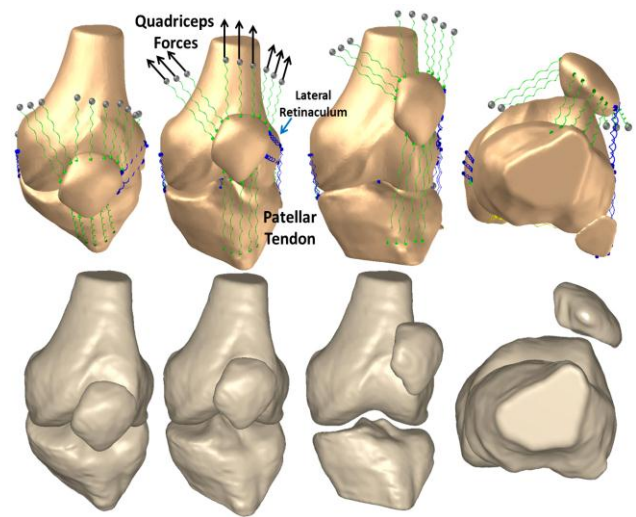


Figure 1: Dynamic knee motion for one knee: computational simulation (top) and in vivo motion (bottom). The computational model includes cartilage embedded within the bone surfaces.

contact [2], allowing for simulation of knee extension in less than 15 minutes. Knee kinematics were quantified using the same coordinate systems used for the computational reconstruction of in vivo motion. Linear regressions were performed to relate simulated patellar tracking to the in vivo data at the knee flexion angles recorded for in vivo motion.

RESULTS AND DISCUSSION

Simulation produced kinematics trends similar to those measured in vivo (Fig. 1). For both the multibody dynamics models and the in vivo data, pre-operative patellar lateral shift and tilt tended to increase dramatically near full extension, and tibial tuberosity realignment tended to reduce both parameters near full extension (Figs. 2, 3). The in vivo data and the data from the simulations were significantly correlated ($p < 0.001$) with r^2 values of 0.71 and 0.61 for lateral tilt and shift, respectively. With the regression line passing through the origin, the slope of the regression was 0.98 for lateral tilt and 0.57 for lateral shift, indicating that lateral shift tended to be underpredicted, with more accurate predictions for patellar tilt.

The strengths of the modeling technique include an ability to represent unstable motion patterns, incorporate abnormal anatomy associated with instability, and rapidly characterize dynamic motion. Additional development is needed to improve the accuracy of representation of lateral shift and to represent functional activities more likely to induce patellar instability.

CONCLUSIONS

The multibody dynamics simulation models can be used to simulate in vivo patellar tracking patterns representative of knees with patellar instability. Tracking changes induced by surgical stabilization procedures can also be simulated. The modeling technique will be used to evaluate treatment options for patients with patellar instability while accounting for initial maltracking and abnormal anatomy.

REFERENCES

1.Elias et al., *Knee Surg Sports Traumatol Arthrosc*

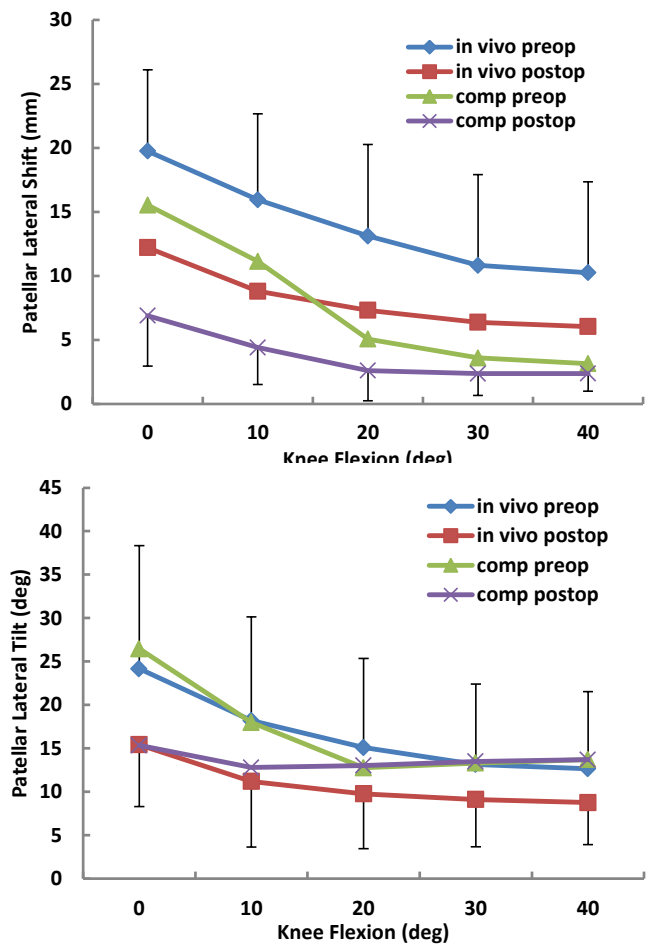


Figure 2: Average (\pm standard deviation) values of patellar lateral shift and tilt in the pre-operative and post-operative conditions.

Following Tuberosity Realignment

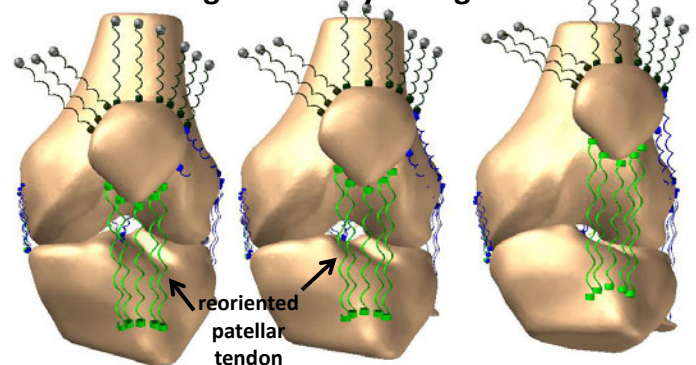


Figure 3: Simulated post-operative tracking for knee from Figure 1.

22:2350-6

2.Purevsuren et al., *Comput Methods Biomech Biomed Engin* 18:1606-10.

ACKNOWLEDGEMENTS

Funding was provided by MedShape, Inc.

THE BIOMECHANICAL ADVANTAGE OF LOCKED VERSUS NON-LOCKED SYMPHYSEAL PLATING OF UNSTABLE PELVIC RING INJURIES

¹Ryan Godinsky, ¹Gregory Vrabec, ¹Loredana M. Guseila, ¹Danielle E. Filipkowski, and ¹John J. Elias

¹Akron General Medical Center, Akron, OH, USA
email: john.elias@akrongeneral.org

INTRODUCTION

Symphyseal plate systems for treating pubic symphysis diastasis in unstable pelvic ring injuries are available with locked and non-locked capabilities. Locked plating systems were developed to improve post-operative stability and reduce the risk of failure, although a biomechanical advantage for locked symphyseal plating has yet to be experimentally demonstrated. The current study was performed to characterize the stiffness provided by locked and unlocked screws used for anterior pelvic ring internal fixation.

METHODS

In vitro testing was performed with pelvis models (Sawbones model 1301 full pelvis, foam with cortical shell). Each model was disarticulated at one sacroiliac joint and stabilized with S1 sacroiliac screws (Synthes 7.3 mm, cannulated, partially threaded) inserted via standard technique under direct visualization and real-time fluoroscopy. Anterior fixation consisted of symphyseal plating (Synthes 3.5 mm, 6-hole, locked symphyseal plate) used in either a locked (7 models) or non-locked (7 models) fashion.

The setup and loading protocols were adapted from previous in vitro studies simulating the single limb stance phase of gait [1-3]. The affected hemipelvis was supported by an articulating femoral head oriented at an angle of 15° adduction and steel cables secured to the iliac wing and the testing frame to recreate the effects of the abductor musculature (Fig. 1). A contralateral load of 80 N was applied through pulleys to represent the weight of the contralateral limb. Each model was cyclically loaded through the sacrum from 150 N to 350 N at 1 Hz for a total of 1000 cycles.

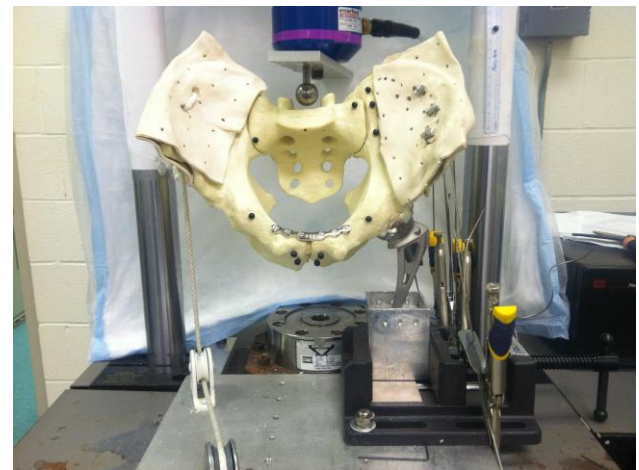


Figure 1: Experimental testing setup.

Opening at the symphysis was measured with a three dimensional video tracking system (MaxTRAQ 3D). Three pairs of markers were placed across the pubic symphysis, with several other markers distributed along the pelvis. Following calibration of the three cameras with a standardized frame, the position of each marker could be tracked as a function of time with an error of 0.1 mm (Fig. 2). The marker data was read in custom written software (Matlab). The software created a local coordinate system at the symphysis

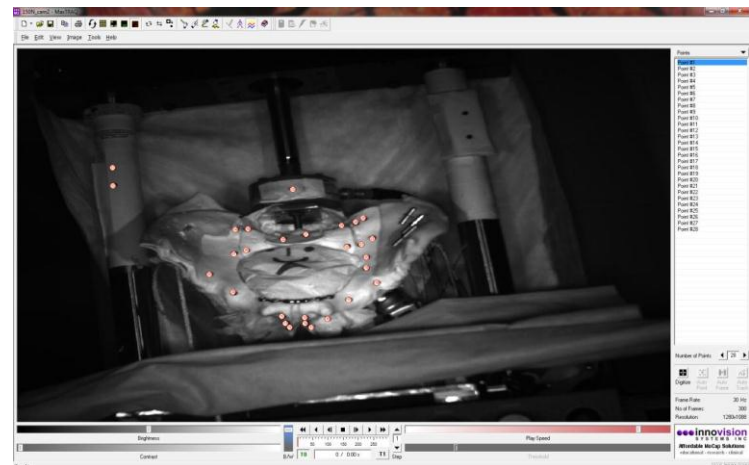


Figure 2: Markers identified on a specimen.

that moved with the markers on the hemi-pelvis supported by the hip stem. The software applied a Gaussian filter to the cyclic motion of the markers and averaged data for 3 successive cycles at every 100 cycles of loading. Relative motion was measured between opposing markers across the symphysis in regards to medial-lateral gap formation, shear along the symphysis, and along an axis perpendicular to the other two (distal translation of the unsupported hemi-pelvis at the symphysis). For each cycle number evaluated, data was compared between the locked and non-locked conditions with t-tests.

RESULTS AND DISCUSSION

At the symphysis, distal translation during cyclic loading was larger for the non-locked models than the locked models. For the non-locked models, the translation tended to increase from cycle 1 to 100, and hold steady until 1000 cycles, while the motion did not tend to increase after the first cycle for the locked plates. For the markers closest to the plate (top markers) the translation was approximately 0.4 mm larger for the non-locked than locked models, compared to approximately 0.7 mm at the bottom markers (Fig. 3). At the onset of loading, average (\pm standard deviation) distal translations at the bottom markers for the non-locked and locked models were 1.6 ± 0.5 mm and 1.2 ± 0.5 mm, respectively ($p = 0.182$). At 1000 cycles, the distal translations for the non-locked and locked models were 2.3 ± 0.6 mm and 1.4 ± 0.6 mm, respectively ($p = 0.015$). No significant differences were identified for gap formation or shear motion ($p > 0.3$).

CONCLUSIONS

The data indicates that symphyseal plating performed with locked screws provides more rigid stability than plating with non-locked screws. The primary mode of increased motion was the unsupported hemi-pelvis moving in a direction perpendicular to the symphysis, close to the direction of loading, with respect to the supported side. Reduced motion with locked screws could potentially allow earlier mobilization after injury

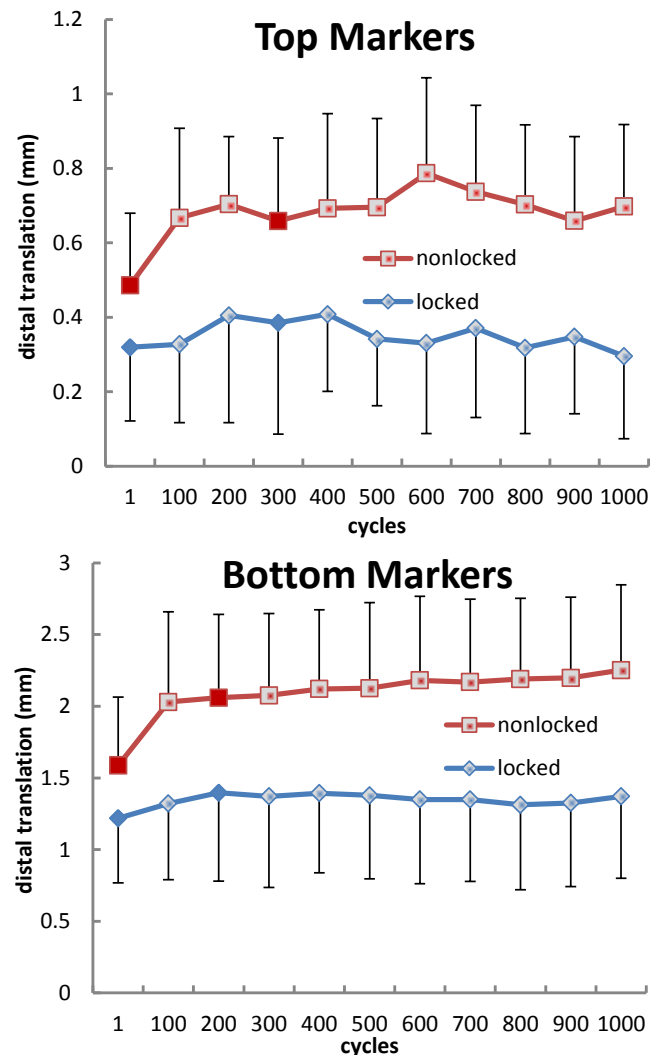


Figure 3: Distal translation for the top markers (closest to the plate) and bottom markers at the symphysis. Significant ($p < 0.05$) differences occurred at the cycles with nonsolid symbols.

with reduced risk of destabilization due to repetitive motion.

REFERENCES

1. Berber O et al. *J Bone Joint Surg*, 93-B, 237-44, 2010.
2. MacAvoy MC et al. *J Orthop Trauma*, 11, 590-3, 1997.
3. Schildhauer TA et al. *J Orthop Trauma*, 17, 22-31, 2003.

ACKNOWLEDGEMENT

Funding was provided by Synthes.

AGREEMENT BETWEEN 3D RECONSTRUCTIONS FROM FLUOROSCOPIC CONE BEAM AND CONVENTIONAL HIGH RESOLUTION CT FOR TRACKING NATIVE KNEE KINEMATICS

Arin M. Ellingson, Ryan Breighner, Joseph D. Mozingo, Dixon J. Magnuson,
Mark W. Pagnano, and Kristin D. Zhao
Mayo Clinic, Rochester, MN, USA
email: zhao.kristin@mayo.edu

INTRODUCTION

Kinematic assessment is a critical aspect of understanding normal and pathological joint function. Traditional analysis methods using surface based markers are inherently prone to error due to skin motion, which is exacerbated by high velocity motion.

Fluoroscopy offers a solution by directly capturing dynamic radiographic images of the bones and when combined with a 3D model of the bony anatomy, can properly quantify motion *in vivo*. The method uses a 2D/3D shape-matching approach, where the projection of a bony model is aligned with fluoroscopic image frames obtained dynamically during movement (Fig. 1). These models are generally created from a high resolution CT, which are costly, irradiative, and time consuming – as the patient or subject must be imaged by another scanner in a different location than the fluoroscope.

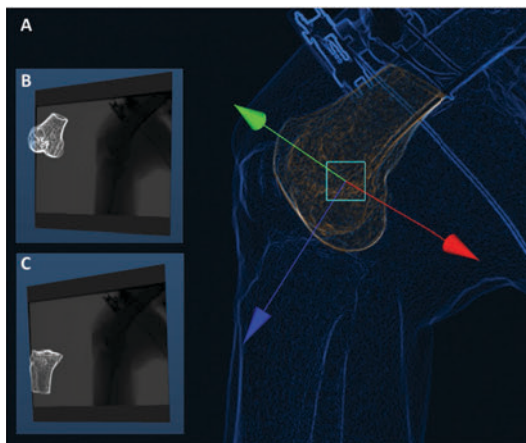


Figure 1: Shape-Matching Software. A- Screenshot of femur being tracked in Autoscoper. B- World view of 3D geometric model of femur. C- World view of 3D geometric model of tibia.

Fluoroscopic cone-beam CT (CBCT) – a volumetric acquisition capability on many fluoroscopes – overcomes these limitations since the bony geometry can be collected during the same session on the same device used for dynamics fluoroscopy acquisition. This ability portends a potential

economical, radiation dose, and a clinical translation improvement over conventional CT.

Therefore, this research effort aimed to assess the comparative accuracy of surface models (femur and tibia) generated from a conventional multi-detector CT to a flat-panel cone beam acquisition via a fluoroscope. Additionally, these models were applied to a 2D/3D shape-matching protocol of a lower extremity during a flexion-extension activity and the limits of agreement between the kinematics outcomes were assessed.

METHODS

A fresh-frozen cadaveric lower extremity was obtained from Mayo Clinic Bequest Program and imaged using conventional multi-detector CT (0.57 x 0.57 x 0.7mm) and fluoroscopic cone-beam (1 x 1 x 1mm) 3D models of the femur and tibia were generated from each modality using simple thresholding techniques (Analyze 12.0 Mayo Clinic Biomedical Imaging Resource). Anatomical landmarks were digitized to define local coordinate systems for each bone [1]. Additionally, comparison of surface geometries was performed by first co-registering the mesh surfaces using a surface matching algorithm and then computing the Euclidean distances between the vertices on the CT reconstructed surface and the CBCT surface [2].

The femur and tibia of the intact lower extremity were secured in a custom apparatus that allowed for unconstrained knee flexion at a manually guided rate. The knee was centered in the imaging field of view of the 48 cm flat-panel Multi-Diagnost Eleva C-arm single-plane x-ray system (Philips Medical Systems, Best, Netherlands). X-ray (63 kV, 160 mA) images were acquired at 30 Hz with a Pulse Width of 1ms while performing a flexion-extension activity. A custom cube with evenly spaced tantalum beads was imaged to calibrate the image volume.

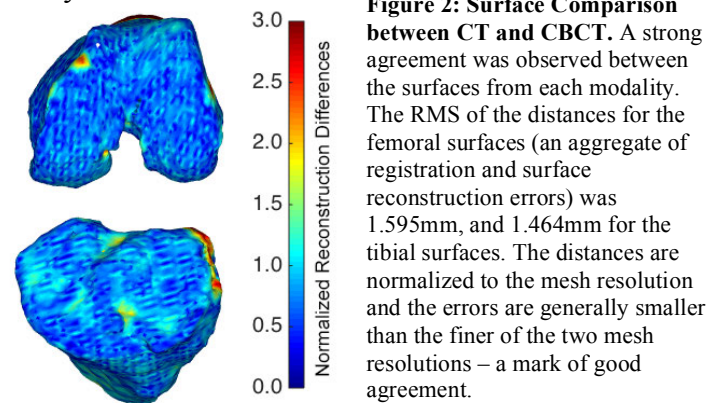
An open-source software, Autoscooper (Brown University www.xromm.org) was utilized to perform the 2D/3D shape-matching and relative tibia to femur kinematics defined using Euler angles (Z-X-Y sequence; flexion, abduction, external rotation) was measured for the flexion-extension activity from sets of bones generated from each image acquisition technique [3]. The limits of agreement for the relative 3D position and orientation between each technique were defined using a Bland-Altman approach.

RESULTS AND DISCUSSION

Effective dose between conventional CT and CBCT was 0.128 mSv and 0.022 mSv, respectively. A strong agreement between the surfaces of both femur and tibia was observed when comparing CT to CBCT reconstructed surfaces. As shown in Figure 2, the articular surfaces of the femur and tibia show surface reconstruction differences smaller than the mesh resolution (~1.685mm). On the femoral surface, 91.8% of CBCT vertices were within sub-resolution proximity of their respective neighbors on CT surface. This figure is 88.5% for the tibia, owing largely to the simplicity of the segmentation approach. The RMS of the distances for the femoral surfaces (an aggregate of registration and surface reconstruction errors) was 1.595mm, and 1.464mm for the tibial surfaces.

The average mean kinematic differences were 0.8°, 0.7°, and 0.4° (flexion, abduction, external rotation) and 0.3mm, 0.4mm and 1.4mm (anterior, superior, and lateral). Figure 3 displays a Bland-Altman plot quantifying the limits of agreement between the two models. As anticipated, the largest mean differences

were in medial-lateral translation. The error is associated with in-plane subjectivity with a single fluoroscope and the software's inability to view both the femur and tibia simultaneously during the analysis.



CONCLUSIONS

In conclusion, segmented 3D models generated from fluoroscopic cone beam and high resolution CT resulted in comparable surface geometries and sufficient kinematic agreement – similar to other reports [4,5].

REFERENCES

1. Grood ES. *J Biomech Eng*, **105**(2), 136-144, 1983
2. Breighner R. *Comput Meth Biomech Biomed Eng*, 1-8, 2014
3. Miranda DL. *J Biomech*, **46**(3)567-573, 2013
4. Dennis DA. *J Biomech*, **38**(2) 241-253, 2005
5. Acker S. *J Biomech*, **44**(4), 784-787, 2011

ACKNOWLEDGEMENTS

Funding was provided through NIH/NIAMS grant T32AR56950 and Minnesota Partnership and Medical Genomics. Also, we thank Gregory Michalak and the CT Clinical Innovation Center.

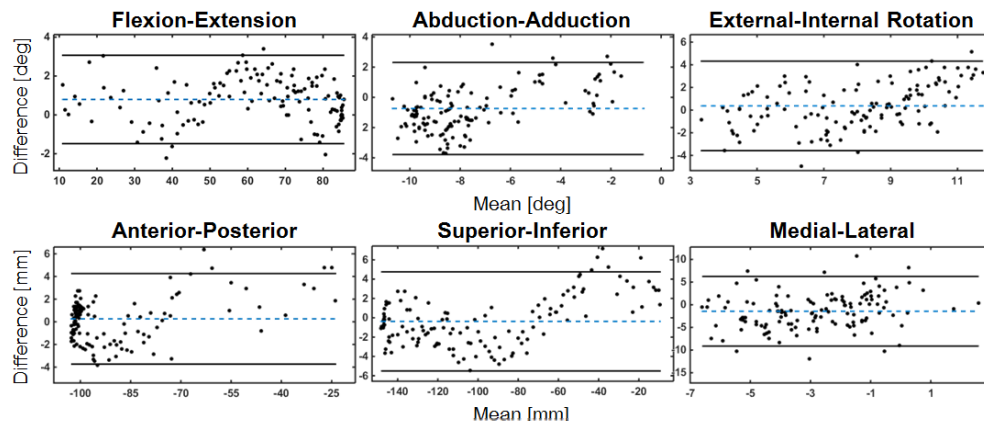


Figure 3: Bland-Altman Plots. The limits of agreement in relative tibia to femur knee kinematics measured between 3D geometric models generated from conventional CT and cone beam CT. Each point represents the mean and difference of relative joint angles (top row) and translations (bottom row) between each method, at a given frame. The dashed and solid lines are the mean difference between methods, and the 95% confidence intervals respectively.

EFFECT OF LONG-TERM USE OF HIGH-HEELED SHOES AND KNEE POSITION ON CALF MUSCLE ISOKINETIC STRENGTH

¹Walaa H. Elsayed and ²Ahmed T. Farrag

¹University of Dammam, Dammam, Saudi Arabia

²Cairo University, Cairo, Egypt

email: ahmedfarrag@cu.edu.eg, whelsayed@uod.edu.sa

INTRODUCTION

Wearing high-heeled shoes (HHS) was reported to negatively impact different body structures [1]. Few studies examined the effect of long-term use of HHS on the muscular performance of the calf muscle [2, 3]. Furthermore, none of them tested how knee position would influence the calf muscle performance in high heels users. The importance of this study comes from the fact that the knee joint position was reported to significantly affect torque productivity of the calf muscle in non high heels users [4]. We thought that it is essential to explore that effect in high heel users as well. Therefore, the aim of this study was to test the combined effect of habitual wear of HHS and knee position on the calf muscle isokinetic torque productivity and the ankle joint active range of motion (ROM).

METHODS

A sample of 24 healthy young females was recruited (age: 23.4 ± 2.9 y, weight: 58.5 ± 0.8 Kg, height: 1.6 ± 0.1 m). Participants had to have never suffered from major musculoskeletal or neurological disorders of the lower limbs. Participants were assigned to either the high-heel (HH) group or the control (CTRL) group. The HH group consisted of 12 participants who must have worn HHS of at least 5 cm high for a minimum of 40 h/week and for at least a year before joining the study. Participants who have worn HHS for less than 10 h/week were assigned to the control group.

A Biodex 4 pro dynamometer (Biodex Medical Systems Inc., Shirley, NY, USA) was used to measure the peak torque of the calf muscle. System calibration was performed each session prior to data collection. The movement velocity was set at $60^\circ/\text{s}$ and the ROM was set between 15° of dorsiflexion and 30° of plantar flexion. After signing a consent

form, subjects were seated and secured in the Biodex chair with the back support inclined to 80° . According to the test condition performed, the knee joint was positioned in either full extension or 90° flexion. The knee was supported and secured in place using a knee pad and velcro straps. Participants were secured by trunk and pelvic straps in addition to a thigh strap to limit body and lower limb rotations. Positional adjustments ensured the alignment of the ankle joint axis with that of the dynamometer. After that, the ankle joint ROM was measured using a BASELINE digital inclinometer. The inclinometer was placed along the fifth metatarsal bone. Participants were instructed to avoid non-sagittal plane movement of the foot and to move the foot from full dorsiflexion to full plantar flexion. Measurements were recorded in both testing positions. The foot was then secured to the foot plate. Following familiarization trials, participants were instructed to move the foot throughout the pre-set range as fast and as strong as possible. This was followed by a 2 minutes rest, during which the lower limb position was changed to fit the other knee position. Then, the participants performed the task under the new arrangement. This was followed by a 5 minutes rest. Then, the entire procedures were repeated for the contralateral side. Order of the test conditions was randomized.

Three repetitions were performed for each condition. Data were averaged for statistical analysis. An unpaired t-test was used to test the effect of high heels long-term use (HH \times CTRL). A paired t-test was used to test the knee position effect (Flex. \times Ext.). The alpha level was set at $p \leq 0.05$.

RESULTS AND DISCUSSION

Knee joint position significantly impacted torque measurements in both groups ($p < 0.001$). The extended knee position resulted in a 37% and 27.8%

greater peak torque for the HH and CTRL groups, respectively, compared with the flexed knee position (Figure 1).

The calf muscle is primarily composed of the biarticular gastrocnemius and the uniarticular soleus muscles. Therefore, manipulating the knee position could be mechanically disadvantageous for the gastrocnemius muscle. According to the length-tension relationship, flexing the knee joint can limit force productivity of the gastrocnemius muscle. Interestingly, flexing the knee decreased torque measurements in the HH group (37%) more than it did in the CTRL group (27.8%). Furthermore, Torque measurements in the flexed knee position were significantly different between the two test groups ($p=0.04$). The CTRL group exerted a 22.5% greater torque compared to the HH group. This would imply the likelihood of structural changes that might have occurred in the soleus muscle of the HH group.

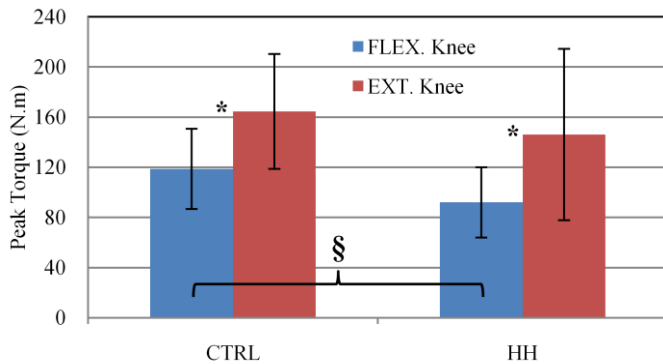


Figure 1: Peak torque measurements as a function of group and knee position. * indicates significant paired t-test. § indicates significant unpaired t-test.

Shortening of the gastrocnemius fascicle length in long-term users of HHS was previously reported. It was concluded that it could have been compensated by the observed increase in the achilles tendon size and stiffness [2]. This resulted in an insignificant difference in torque measurements between high heels users and non-users. However, this conclusion was based on measurements performed in an extended knee position only. In our study, it seems that such structural changes of the achilles tendon could not produce a similar compensatory effect when the knee joint was flexed. This could be attributed to the increased slack of the musculo-

tendinous unit and the limited contractility of the gastrocnemius muscle in the flexed knee position.

The CTRL group performed a significantly greater ankle joint ROM ($p<0.001$) in the flexed knee position compared with the extended position (Figure 2). Furthermore, ROM of the CTRL group was significantly greater (15.8% difference) than that of the HH group, only in the flexed knee position ($p<0.001$). This would reflect a decreased flexibility of the muscular and connective tissue structures of the calf muscle, which is further evidenced by the insignificant difference observed between the two test positions for the HH group.

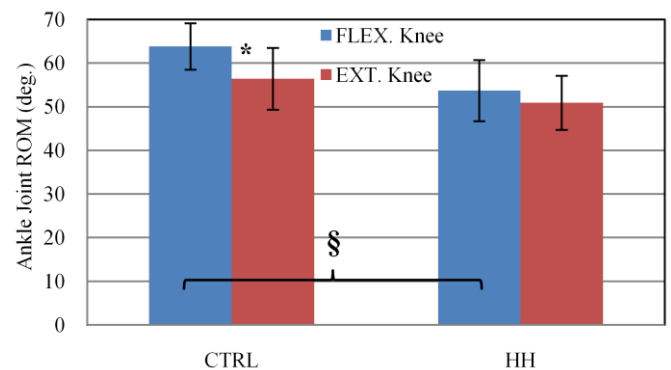


Figure 2: ROM measurements as a function of group and knee position. * indicates significant paired t-test. § indicates significant unpaired t-test.

CONCLUSIONS

The results suggest that knee flexion has a more profound effect on plantar flexion torque in habitual high heel users compared to non-users. This may indicate that the contractile properties of the soleus muscle could be significantly affected, even more than the gastrocnemius muscle, by the long-term use of high-heeled shoes. Therefore, it is recommended that upon evaluating the effects of prolonged use of HHS, evaluators should consider the test position of the knee in order to properly assess the functional capacity of the calf muscle.

REFERENCES

1. Cowley EE, et al. *J Am Podiat Med Assn* **99**, 512-518, 2009.
2. Csapo R, et al. *J Exp Biol* **213**, 2582-2588, 2010.
3. Kim Y, et al. *Foot Ankle Int* **34**, 414-419, 2013.
4. Dalton BH, et al. *Eur J Appl Physiol Occup Physiol*, **113**, 1431-1439, 2013.

A NOVEL PLANNING PARADIGM FOR AUGMENTATION OF OSTEOPOROTIC FEMUR

¹ Amirhossein Farvardin, ¹ Ehsan Basafa and ^{1,2} Mehran Armand

¹ Department of Mechanical Engineering, Johns Hopkins University, MD, USA

² Johns Hopkins University Applied Physics Laboratory, MD, USA

email: farvardin.amirhossein@gmail.com, web: <http://bigss.lcsr.jhu.edu/>

INTRODUCTION

The one-year mortality rate after osteoporotic hip fracture in elderly is 23% [1]. Current preventive measures commonly do not have a short-term (less than one year) effect. Moreover, the risk of a second hip fracture increases 6-10 times in elderly with osteoporosis [2]. Osteoporotic hip augmentation (femoroplasty) is a possible preventive approach for patients at the highest risk of fracture and who cannot tolerate other treatment modalities. Recent computational work and cadaveric studies have shown that osteoporotic hip augmentation with Polymethylmethacrylate (PMMA) can significantly improve yield load and fracture energy [3]. However, higher volumes of PMMA injection may introduce the risk of thermal necrosis. In this study, we introduce a modified planning approach to lower the injection volume as compared to the previous work [3]. This will likely reduce the risk of thermal necrosis caused by exothermic polymerization of PMMA. The method was preliminarily tested in a pilot experiment where we also monitored the surface temperature of bone tissue during the procedure.

METHODS

A pair of frozen osteoporotic femora (neck T-score of -2.0 left and -3.8 right sides) was acquired from Maryland Board of Anatomy. The PMMA injection was computationally planned on the weaker specimen using the method discussed in the following. Invasive bone fracture experiments were then performed and the results were compared to the plan.

The modified planning paradigm involves three steps: 1) finite element (FE) optimization of the PMMA distribution, 2) geometric optimization for

approximating the FE-optimized model geometry with spheroids, and 3) hydrodynamic simulation to predict the resulting PMMA distribution in the bone. FE models of the femora were created using CT scans obtained from the specimens following the procedure described earlier [4]. The boundary conditions simulated a fall to the side. For the first step of planning, three injection patterns were optimized utilizing the Bi-directional Evolutionary Optimization (BESO) method [5].

In the second step, the FE-optimized injection pattern was approximated by a number of spheroids (realistic injection volumes) along a single injection path. During this step the size and location of the spheroids along the injection path was optimized to find the best match between FE model and the spheroid alignments (Fig. 1). Finally, we used a particle based simulation to predict the resulting pattern of cement diffusion inside the bone.

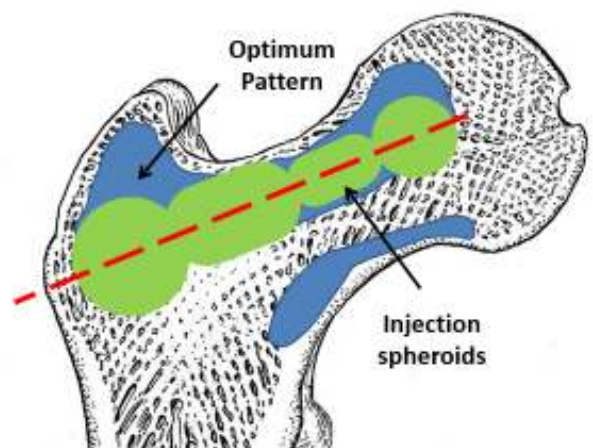


Fig. 1: Schematic of the optimized injection pattern by BESO (blue), practical injection volume (green) and line of injection (red)

To accurately inject PMMA in selected regions of the bone, we used a previously developed navigation system along with a custom-made injection device [3]. Surface temperature of the

bone was recorded utilizing 3 k-type thermocouples placed at neck, greater trochanter, and trochanteric crest of the femur.

Finally, mechanical testing was performed to fracture the bones in a configuration that mimics a fall to the side on the greater trochanter [3]. The mechanical strength of the femora was determined from these invasive tests.

RESULTS AND DISCUSSION

From planning, it was determined that only 7.7 cm³ of bone cement is sufficient to increase the yield load of the specimen by 67% (from 1350 N to 2256 N). Adding to the volume of cement did not significantly increase the predicted yield load. The calculated amount of bone cement was 23% less than the 9.5 cm³ average volume used in the previous method of augmentation planning [3].

Mechanical testing showed that the yield load for augmented specimen was 59% higher than that of control (Fig. 2). Also yield energy was 161% higher for the augmented pair (2897 vs. 7549 N.mm). These results show significant improvements in bone strength with a reduced amount of PMMA.

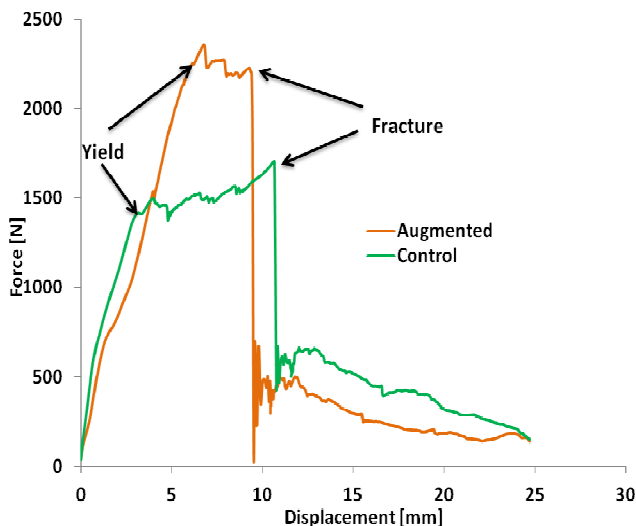


Fig. 2: Force-Displacement curves obtained from mechanical testing

The measured profiles (Fig. 3) show that maximum temperature-rise of 10 °C occurs at 12 minutes after the injection. The 10 degrees temperature-rise was maintained for less than 30 seconds which is well

below the level causing osteonecrosis [6]. Of note, for this preliminary study the exact distance of the thermocouple from the bone-cement interface was not determined.

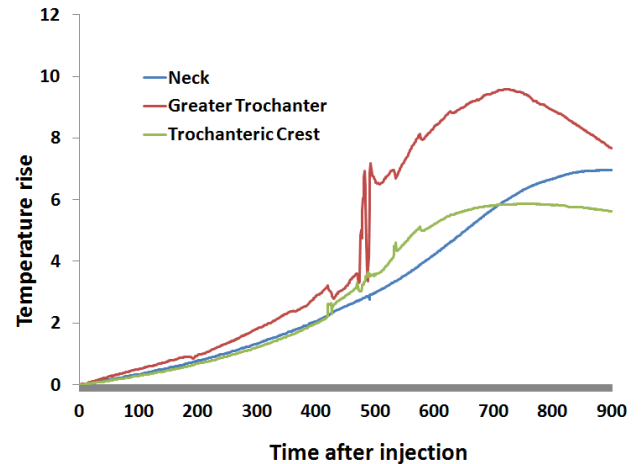


Fig. 3: Recorded temperature rise of bone surface at different locations.

CONCLUSIONS

Both simulation and experimental results suggest that the modified planning for bone cement injection remains effective while reducing the cement volume and the number of required injection paths. Reduced volume of bone cement can lead to a lower risk of thermal necrosis a potential challenge associated with bone augmentation. Future work will include additional experiments to fully validate the findings of this study.

REFERENCES

1. Cummings S, *Clin Orthop*, **252**,163-166, 1990
2. Dinah A, et al. *Injury* **33**, 393-394, 2002
3. Basafa, E, et al. *J Biomech* **48**, 59-64, 2015
4. Basafa, E, et al. *Med. Eng. Phys.* **35**, 860-865, 2013
5. Basafa, E, et al. *J Biomech* **47**, 2237-2243, 2014
6. Boner V, et al. *BMJ* **90**, 842-848, 2009.

ACKNOWLEDGEMENTS

The work was supported with grant R21AR06315. We would like to thank Mr. Demetries Boston and Dr. Stephen Belkoff of Johns Hopkins Bayview Medical Center for their help with preparing the specimens and mechanical testing.

EXPLORING THE REGIONAL RESPONSE OF THE INTERVERTEBRAL DISC UNDER POSTURAL VARYING LOADS

¹Kayla M. Fewster, ¹Mamiko Noguchi, ²Chad E. Gooyers, ³Alexander Wong, ¹Jack P. Callaghan

¹Department of Kinesiology, University of Waterloo, Waterloo, ON

²Giffin Koerth Forensic Engineering & Science, Toronto, ON

³Department of Systems Design Engineering, University of Waterloo, Waterloo, ON

INTRODUCTION

This investigation examined differences between the anterior and posterior radial displacement (*i.e.* bulging) of the annulus of the intervertebral disc. Generally, there have been very few studies that have quantified the magnitude of IVD disc bulging on the posterior aspect of the disc. This is attributable to bony structures and passive tissues that occlude a direct line-of-sight to the posterior-lateral region of intact functional spinal units (FSUs). Recent work [1], has characterized the effect of posture on IVD bulging on human lumbar FSUs. With the posterior elements removed, results from this investigation revealed that the median IVD bulge in the anterior and posterior-lateral regions was altered, when a 7.5 Nm flexion moment was applied. However, to the best of the author's knowledge the combined effects of increasing magnitude of compressive load and posture on IVD bulging have yet to be investigated. Therefore, to better understand how the structural responses of the anterior portion of the IVD may be related to the posterior portion, this study quantified the magnitude of anterior and posterior-lateral radial displacement in the IVD across different postural conditions and magnitudes of compressive load. In-line with this objective it was hypothesized that a negative correlation between anterior and posterior bulging would emerge. Results from this study may elucidate a link between radial displacement on the anterior side of the IVD that would facilitate inferences on the structural changes on the posterior side on intact specimens with the posterior element intact.

METHODS

Six cervical porcine FSUs were tested. A modified servo-hydraulic materials testing system was used to apply flexion/extension motion and compressive

loading to intact specimens. A 3D non-contact laser displacement sensor (LJ-V7080, Keyence Corporation, Osaka, Japan) was used to measure annulus fibrosus (AF) radial displacement across four levels of compressive load (10 N, 300 N, 600 N and 1200 N) and two posture conditions (neutral and flexion). The anterior aspect of the six FSUs were scanned during all conditions with the posterior elements intact (*i.e.* anterior-intact condition). Then the posterior elements from these specimens were removed, leaving a reduced FSU. Both the anterior and posterior sides of the IVD were scanned during all remaining conditions (anterior-reduced and posterior). A total of 24 scans (load x4, posture x2, location x3) were collected from each specimen. The primary dependent measure analyzed was peak AF radial displacement across conditions, which was computed from the 3D IVD surface profiles measured using a using a computer-aided bulge analysis software platform produced by the Vision and Image Processing research group, designed to track and quantify AF radial displacement (Version 8.5, Matlab, Mathworks Inc., Natick, MA, USA) (Figure 1).

To facilitate a comparison of peak AF bulging measurements between specimens and to improve anatomical interpretation of the measure, the maximum bulge perpendicular to a vector defined by the endpoints of the superior and inferior endplates has been reported [2]. To determine whether the removal of posterior elements had any effect on the bulge size, a paired t-test was employed to compare the anterior and anterior-reduced AF bulge measurements. A Pearson's *r* correlation analysis was also conducted on the anterior and posterior AF bulge measurements. Initially, a paired t-test was used to determine if there was a significant difference in the slopes of the posterior-anterior bulge comparisons across magnitudes of compressive load. There was no significant difference that emerged therefore all

loading conditions were collapsed into one correlation analysis.

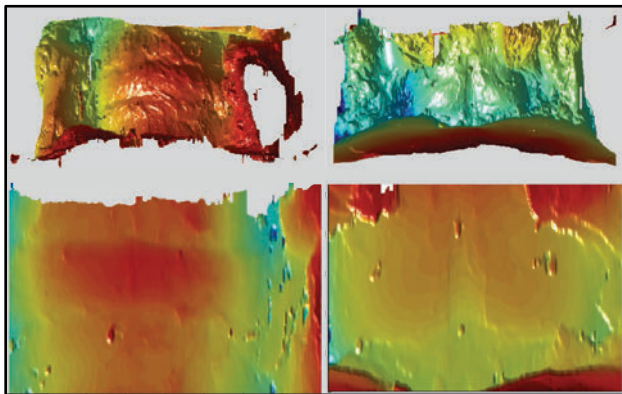


Figure 1: Anterior (left) and Posterior (right) 3D surface profiles of radial displacement measured from the surface of an IVD.

RESULTS AND DISCUSSION

No significant difference was observed between anterior-intact and anterior-reduced peak AF bulge ($p = 0.312$). Therefore, anterior-reduced surface scans were utilized to make comparisons to peak posterior AF bulge. A significant negative correlation between anterior-reduced and posterior bulge measurements was observed in a flexed posture (Pearson's $r = -0.432$; $p = 0.018$). As posterior AF bulging increases anterior AF bulging decreases. (Figure 2).

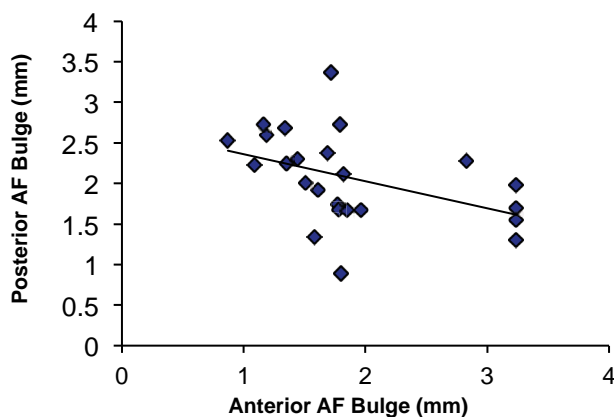


Figure 2: Scatter plot illustrating a negative correlation between anterior-reduced and posterior AF bulging in a flexed posture.

Results also demonstrated that in a flexed posture, as the magnitude of compressive loading increased,

there was a trend that emerged of an increased posterior AF radial displacement and a decrease in anterior AF bulge (Figure 3). No significant correlation was observed between anterior-reduced and posterior radial displacement measurements in a neutral posture ($p = 0.312$).

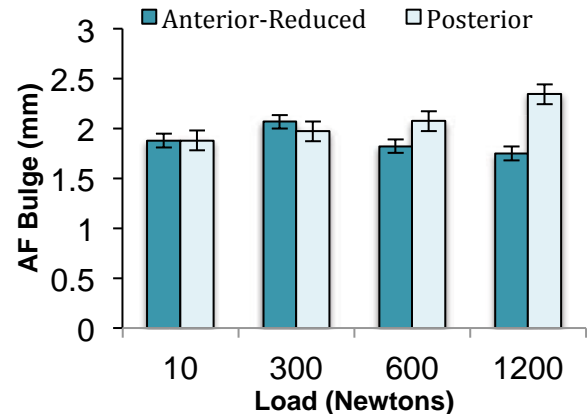


Figure 3: Average anterior-reduced and posterior peak AF radial displacement in a flexed posture across loading conditions. Standard error bars are displayed.

CONCLUSIONS:

The preliminary results from this investigation elucidate a link between measured AF bulge on the anterior and posterior side of the IVD. Understanding how the AF responds under various loads in flexion and extension postures has clinical relevance, as IVD herniation has been observed with repeated flexion-extension under modest amounts of compressive load. The magnitude of posterior AF bulge increased in flexion as the magnitude of the applied compressive load increased. As such, the magnitude of strain and risk of tissue damage in the AF is expected to follow a similar trend.

REFERENCES:

1. Heuer, F et al. (2008b). *J Biomechanics*, **41**(5), 1086-94.
2. Gooyers, C.E. & Callaghan, J.P. (2015). *J Biomech*, Submitted.

PRELIMINARY FINITE ELEMENT ANALYSIS OF SUBCHONDRAL BONE CYSTS IN THE STIFLE OF THE HORSE

¹ Lance L. Frazer, ¹ Kenneth J. Fischer, and ² Elizabeth M. Santschi

¹ The University of Kansas, Lawrence, KS, USA

² Kansas State University, Manhattan, KS, USA
email: fischer@ku.edu

INTRODUCTION

Medial femoral condylar (MFC) bone cysts (SBC) develop in the trabecular subchondral bone of the MFC of young horses (Fig. 1), and can cause lameness and limit performance.¹ Experimental MFC defects demonstrate progressive changes (void enlargement and MFC collapse) very similar to equine natural disease, and mechanical alterations that negatively affect the bone repair process due to the voids have been hypothesized, but not proven.² Recent clinical evidence in the horse indicates that lag screw placement across the MFC promotes bone healing and lameness resolution³, but little is known about the biomechanics of an intact or damaged MFC, or how mechanics can optimize healing. The objective of this preliminary study was to develop a finite element model of the equine stifle joint and to describe stress in the medial femoro-tibial joint with an intact MFC, with two sized of MFC voids, and with sclerotic trabecular bone, which is present before cyst development.

METHODS

Using Simpleware™ software, a finite element model was generated using a CT scan of a cadaveric normal yearling equine stifle joint (Fig. 2). Bone was semi-automatically segmented by thresholding with manual adjustment, and the soft tissues were manually segmented. Segmented structures included: femur, tibia, and associated articular cartilage, medial and lateral meniscus, and menisco-tibial and menisco-femoral ligaments. The final mesh contained 336,000 linear, tetrahedral elements with the highest concentration of elements in the MFC. Bone material properties were assigned using the grayscale properties from the CT. The range of apparent density was 0.007 to 1.82 g/cm³, and the equation $E = 6000\rho^{2.5}$ was used to relate density to

Young's Modulus (YM), resulting in YM up to 20 GPa for cortical equine bone, and a Poisson's ratio of 0.3 was also assigned. The mesh and bone material properties were then imported into ABAQUS finite element analysis software. Approximate relaxation soft-tissue material properties were assigned also based on prior published studies.^{4,5,6} Thus, a YM of 4 MPa was assigned for cartilage, 20 MPa for meniscus, and 345 MPa for ligaments, each with a Poisson's ratio of 0.2. The model was analyzed under four MFC conditions; 1) intact, 2) with 1000 mm³ of stiffened subchondral trabecular bone (sclerosis) (YM raised to 20 GPa), 3) a subchondral void of 80 mm³ and, 4) a 1000 mm³ void in the central weight bearing surface of the MFC.

The models were tested in extension (approximately 155°), and all tissues were modeled as isotropic and linear elastic. Contact surfaces were established for all exterior surfaces to fully allow normal meniscal sliding. The friction coefficient between these surfaces was set to 0.02. Displacements were fully constrained for the distal tibia. In the cystic models, the void was assigned a YM of 0.001 MPa. All 4 models underwent the same testing procedure with a normal pressure loading at the proximal femur (1000N resultant load).

RESULTS AND DISCUSSION

Max principal stress values for each model are summarized in Table 1. Figure 3 illustrates that the intact model yields negligible Von Mises stresses. The sclerotic model shows increased stress distribution in the superior and inferior aspects of the sclerotic region; SBCs originate at the inferior aspect of sclerotic subchondral bone. The 80 mm³ MFC causes large stress concentrations caudal and cranial to the lesion as well as tensile stress above

the lesion, not present in the intact model (Table 1). The 1000 mm³ void results in severe stress alterations around the void with high tensile stress in the bone just below the cyst region (Table 1).

CONCLUSIONS

This preliminary study provides insight into the biomechanics of the yearling stifle joint under 4 MFC conditions: intact, with sclerotic subchondral bone, and with 2 sizes of subchondral voids. Under load, the MFC with sclerotic bone and 80 mm³ or 1000 mm³ voids demonstrates stress increases around the void, suggesting a biomechanism for formation of subchondral lucencies, an explanation for their frequent failure to heal, and a justification for the use of a transcondylar MFC screw. The increase in tension under any condition may suggest a formation mechanism as trabecular bone is weakest under tensile force. Understanding the biomechanics of the intact MFC and the MFC with a void and will help direct the development of future therapies for treatment of SBCs in the horse. Future models will examine bone stress and strain

with variations in load, flexion angle, and cyst size. The model itself will also be improved by implementing viscoelastic properties for the various soft tissues, using quadratic elements, and gaining a better understanding of tissue property changes before and during cyst development.

AKNOWLEDGEMENTS

We acknowledge technical assistance from Garret Noble for initial segmentation of tissue structures.

REFERENCES

1. Jeffcott, LB et al., *Equine Vet J.*, 15(4):304-11, 1983.
2. Jackman et al. *JBJS*, 83-A:53-64, 2001.
3. Santschi, E et al., *Vet Surg.*, 10.1111/j.1532-950X, 2014.
4. Buttler et al., *J Biomech*, (19):425-432, 1986.
5. Chahine et al, *J Biomech*, (37):1251-1261, 2004.
6. Brown, Load-Bearing Role of the Human Knee Meniscus, *Doctoral Dissertation*, MIT, 1990.

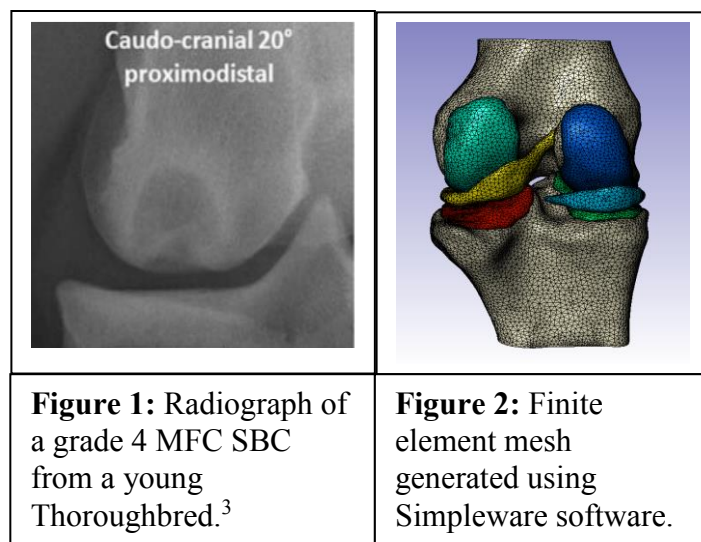
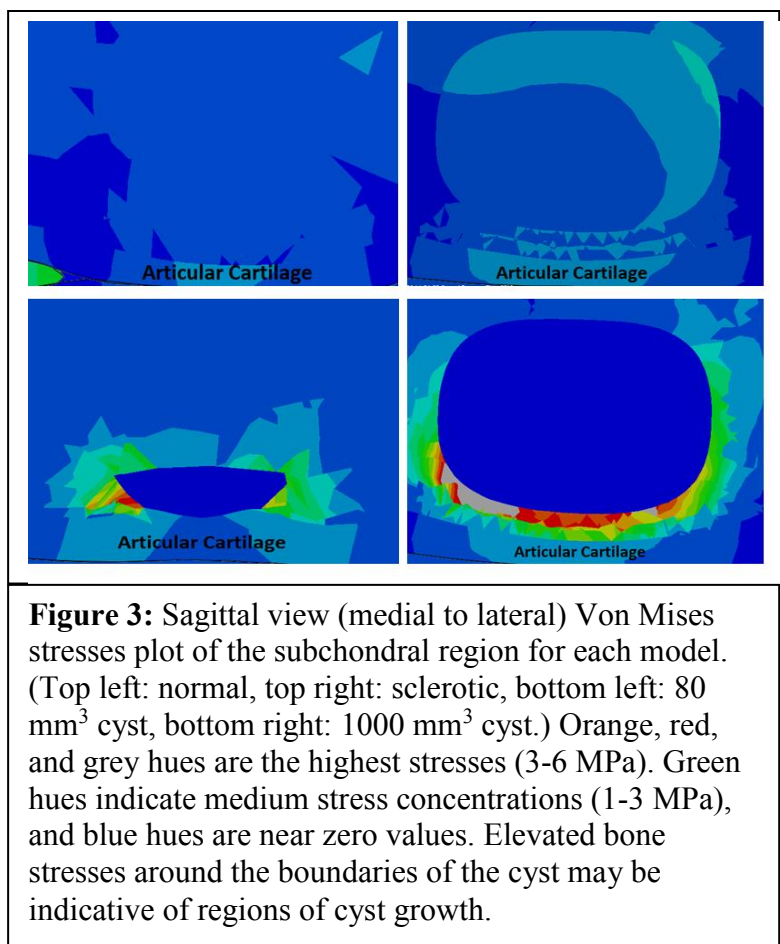


Table 1: Shown are the max principal stresses found in the subchondral region of each model.				
Max Principal Stress	Models			
	Intact	Sclerotic	80 mm ³	1000 mm ³
Compression (MPa)	0.55	0.83	1.14	2
Tension (Mpa)	negligible	0.62	0.62	2.5



VALIDATION OF A FINITE ELEMENT MODEL OF THE HUMERUS FOR FRACTURE RISK ASSESSMENT DURING ASSISTED AMBULATION

^{1,2} Jessica M. Fritz, ^{1,3} Prateek Grover, ⁴ Nicole M. Grosland,
^{1,5} Carolyn Albert, ² Linda McGrady, ^{1,2} Mei Wang, and ^{1,2,5} Gerald F. Harris

¹ Marquette University, Milwaukee, WI, USA

² The Medical College of Wisconsin, Milwaukee, WI, USA

³ Washington University School of Medicine, St. Louis, MO, USA

⁴ The University of Iowa, Iowa City, IA, USA

⁵ Shriners Hospitals for Children, Chicago, IL, USA

email: jessica.fritz@marquette.edu

INTRODUCTION

Finite element (FE) modeling provides an established, useful tool for assessing biomechanics without invasive testing. One important and emerging application is the use of FE models to assess the risk of long bone fractures, which are prevalent in populations with bone fragility due to aging, osteoporosis, and various genetic and metabolic disorders. For example, FE modeling can be used to assess bone strength and fracture risk in individuals with osteogenesis imperfect (OI), a heritable bone fragility disorder [1, 2]. Children with OI have an especially high prevalence of long bone fractures. As the major load-bearing bones during ambulation, current models of OI have focused on lower extremity bones [1, 2]. However, the upper extremity bones, including the humerus, experience weight-bearing loads during assisted ambulation with crutches and walkers. Analysis of children walking with instrumented Loftstrand crutches showed they experienced shoulder forces up to nearly 35% of their body weight [3]. It has also been shown that assisted ambulation can cause a 24Nm bending moment at the shoulder joint [4]. However, to date, no study has examined how loads sustained during assisted mobility may put patients with OI at risk for upper extremity fractures.

This project focused on the development and validation of a humeral FE model subjected to physiologic bending loads such as those seen during assisted ambulation [3, 4]. This model is appropriate for application to various populations at increased risk for humeral fractures who use assistive devices for ambulation.

METHODS

Fourth-generation composite humeri (named H-VHP model; Sawbones Worldwide, Pacific Research Lab, Inc., Vashon, Washington, USA) were manufactured for this project based on the humerus geometry of the National Institutes of Health (NIH) Visible Human Project (VHP).

A composite humerus was instrumented with two stacked rectangular strain gage rosettes (Vishay Micro-Measurements, Raleigh, North Carolina, USA) and subjected to bending loads. The center gage of each rosette was aligned with the anatomic axis on the anterior and posterior side of the humerus. A four-point bending setup was used, in which the support rollers were on the anterior side, 92 mm distally and proximally from the gage rosettes. Loading was applied on the posterior side; each roller positioned 28 mm on either side of the gage rosette (Fig. 1a). The humerus was loaded with 200 N through a servo-hydraulic materials testing machine (MTS 809, Eden Prairie, Minnesota, USA). This load was selected in order to simulate a 24 Nm bending moment about the shoulder joint axis that an individual would experience during assisted ambulation with Loftstrand crutches [4]. Strains were recorded from each gage and the principal strains were calculated for each rosette.

The testing conditions were then replicated in a three-dimensional (3D) FE model of the humerus (Fig. 1b) and processed in Abaqus 6.10 (Dassault Systèmes Americas Corp.; Waltham, MA). The 3D model geometry was defined from a CT scan of the composite humerus and then imported into IA-

FEMesh software [5]. The humerus was meshed with 59,852 eight-noded linear hexahedral elements (C3D8) with an average element size of 1.25 mm. Meshing of both the cortex and cancellous layers of the humerus was performed using the multi-block approach in IA-FEMesh [5]. Cortical bone was defined with a Young's modulus (E) of 10.6 GPa (based on experimental data of tensile testing) and a Poisson's ratio (ν) of 0.3 (from composite bone manufacturer). Cancellous bone regions were assigned material properties provided by the composite manufacturers: $E = 0.160$ GPa and $\nu = 0.26$. A set of elements corresponding to the locations of each strain gage rosette was defined. These elements were used for the FE model analysis in order to correspond with the testing data since the rosette locations may not coincide with overall maximum and minimum principle strain locations.

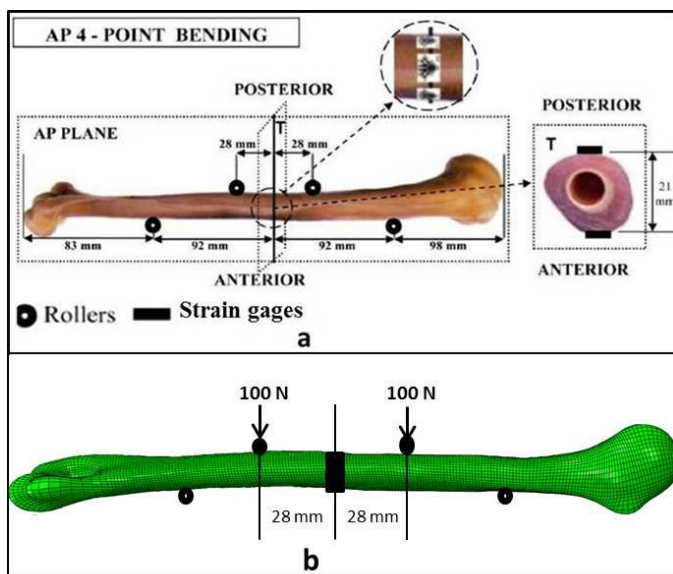


Figure 1: Four-point bending of humerus models during a) experimental bending test of the composite humerus in the anterior-posterior (AP) plane and b) finite element (FE) model analysis. The FE model also shows the location of the strain gages (SG) from experimental testing.

RESULTS AND DISCUSSION

The FE analysis showed excellent agreement with the experimental data during AP bending in maximum principal strain with a difference of 1.4% (Table 1). The difference in minimum principal strains between the experimental and FE results showed good agreement with a difference of 10.8% (Table 1). Limitations in this study include some variability between the three experimental trials and the inherent assumptions in FE modeling and analysis. Despite these limitations, there was good agreement between the FE model results and experimental data.

CONCLUSIONS

The high level of agreement between the two results validates the use of the FE model of the humerus to examine biomechanical responses to loading. This model has potential applications in populations such as the elderly or those with OI. These populations may use assistive devices for ambulation and would, therefore, be loading their upper extremity long bones, such as the humerus, with a percentage of their body weight.

REFERENCES

1. Fritz JM, et al. *Med Eng Phys* **31**(9), 1043-1048, 2009.
2. Caouette C, et al. *J Musculoskelet Neuronal Interact* **14**(2), 205-212, 2014.
3. Slavens BA, et al. *J Biomech* **44**, 2162-2167, 2011.
4. Grover P, et al. *Proc Inst Mech Eng H* **225**, 1169-1176, 2012.
5. Grosland NM, et al. *Comput Methods Programs Biomed* **94**, 96-107, 2009.

ACKNOWLEDGEMENTS

Funding for this work was provided by the following NIDRR sponsored grants: ARRT grants H133P080005 and H133P100008 and RERC grant H133E100007. Contents do not necessarily represent the policy of the Department of Education, and you should not assume endorsement by the federal government.

Table 1: Maximum and minimum principle strains for the finite element (FE) model and experimental testing.

Applied Load	Max Prin $\mu\epsilon$ FE Model	Max Prin $\mu\epsilon$ Experimental	Max % Difference	Min Prin $\mu\epsilon$ FE Model	Min Prin $\mu\epsilon$ Experimental	Min % Difference
200 N	1414	1394	1.4	-1134	-1271	10.8

FINITE ELEMENT ASSESSMENT OF PEDIATRIC FEMORAL RESPONSE TO LOADING DURING AMBULATION: NORMAL VS. OSTEOGENESIS IMPERFECTA (OI) BONE

^{1,2} Jessica M. Fritz, ^{1,3} Carolyn I. Albert, ⁴ Nicole M. Grosland, ³ Peter A. Smith and ¹⁻³ Gerald F. Harris

¹ Marquette University, Milwaukee, WI, USA

² The Medical College of Wisconsin, Milwaukee, WI, USA

³ Shriners Hospitals for Children, Chicago, IL, USA

⁴ The University of Iowa, Iowa City, IA, USA

email: jessica.fritz@marquette.edu

INTRODUCTION

Osteogenesis imperfecta (OI) is a heritable disorder characterized by skeletal deformity and bone fragility. While the mechanisms are not fully understood, the fragility is believed to stem from a combination of bone mass deficiency and compromised bone material properties [1, 2]. Poor bone quality poses unique orthopaedic and rehabilitation challenges for treating persons with OI. Risk of fracture becomes a major consideration not only for prescribing physical therapy but also for activity restrictions and modifying activities of daily living (ADLs). Unassisted ambulation may result in a high enough load to cause a fracture in persons with moderate to severe OI. Due to these challenges, fracture risk quantification can be an invaluable tool in OI management and fracture rehabilitation. Finite element (FE) models have recently been applied to quantitatively assess *in vivo* loads experienced by long bones in persons with OI [3, 4]. Material properties reflective of the mechanical response of OI bones to loading are imperative to accurate fracture risk assessment [5]. A recent study confirmed that cortical bone material strength of OI bone is substantially lower than normal pediatric bone, indicating that reduced mechanical tissue quality is a contributing factor to fracture risk in this population [6].

The present study examined the response of an FE model of pediatric femurs with normal, mild-moderate OI and severe OI material properties under ambulatory loads (i.e., joint forces and moments and intrinsic muscle activation forces).

METHODS

Three-point bending tests were performed on bone specimens obtained from the femoral diaphysis of

three donors: 1) an 11-year-old male (cadaveric) with no known bone disorder, 2) a 10-year-old male with OI type I (mild-moderate), and 3) an 11-year-old male with OI type III (severe). The OI specimens were acquired and tested under informed consent/assent and following a protocol approved by our Institutional Review Board (IRB). Longitudinal and transverse Young's modulus (E) and yield strength (σ_y) were determined for each specimen.

A previously developed hexahedral FE model of a pediatric femur was used for this study (Fig. 1) [7].

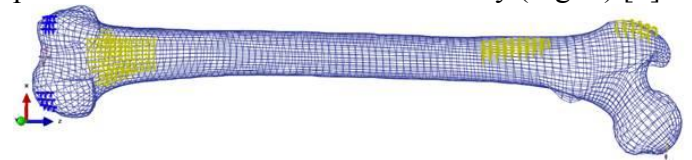


Figure 1: Finite element (FE) model of the femur with boundary conditions (condyles) and representative loading during mid-stance.

Three models were created, corresponding to the material properties of each cortical bone specimen (Table 1). Young's modulus for cancellous bone was conservatively modeled as being 60% of cortical bone [8]. Shear modulus was estimated assuming transversely isotropic material behavior. Each model was loaded based on forces experienced during the mid-stance phase of gait. Gait data was previously collected under IRB approval from a 12-year-old with OI type I [3]. All three femurs were modeled with normal geometry (no bowing). The geometry and loading were kept constant among the three models in order to solely focus on the effects of the bone material properties (Fig. 1). Maximum longitudinal stresses and strains were analyzed. Results were compared between models as well as against yield strength from the mechanical analyses.

RESULTS AND DISCUSSION

The model's material properties and the resulting maximum stresses and strains are presented in Table 1. While the analysis did not show major differences in the maximum longitudinal stress values between bone types, these values are much closer to a level of stress causing yield for the OI bones than for a normal pediatric femur. This can be clearly seen by looking at the maximum longitudinal stress as a percentage of σ_y , which provides a metric for proximity to fracture level. Maximum transverse stresses only reached a maximum of 13.5 % of transverse yield strength for OI type III bone, with lower values in the other two models. However, the severe OI (type III) reaches about 80% of its longitudinal yield strength. It must also be kept in mind that persons with OI often have deformed long bones. Increases in lateral bowing of the femur have been shown to cause a linear increase in maximum stress results [5, 7].

CONCLUSIONS

This study demonstrates the need to not only understand the difference in mechanical properties, such as Young's modulus, seen in OI bone, but also their failure loads and mechanisms. Finite element modeling and analysis has the capabilities to estimate safe loading levels from activities such as

walking, running and jumping in which children with OI may want to participate. The current work, combined with previous analyses, shows the multifactorial requirements for subject-specific FE analysis of material properties, loading and geometry to provide the most accurate assessment of femoral loading during ADLs [5, 7, 8].

REFERENCES

1. Rauch F & F Glorieux. *Lancet* **363**, 1377-1385, 2004.
2. Albert C, et al. *Bone* **66**, 121-130, 2014.
3. Fritz JM, et al. *Med Eng Phys* **31**, 1043-1048, 2009.
4. Caouette C, et al. *JMNI* **14**, 205-212, 2014.
5. Fritz JM, et al. *Proceedings of ASB '13*, Omaha, NE, USA, 2013.
6. Albert C, et al. *Proceedings 7th WCB '14*, Boston, MA, USA, 2014.
7. Fritz JM, et al. *Proceedings of ASB '11*, Long Beach, CA, USA, 2011.
8. Fritz JM, et al. *Biomed Sci Instrum* **45**, 316-321, 2009.

ACKNOWLEDGEMENTS

Funding for this work was provided through RERC grant H133E100007. Contents do not necessarily represent the policy of the Department of Education, and you should not assume endorsement by the federal government. The study was also supported by a research fellowship from Shriners Hospitals.

Table 1: Material properties for the finite element model of the femur; Young's modulus (E), shear modulus (G), and Poisson's ratio (ν). The three right columns show the maximum longitudinal stresses and strains for each femur as well as the maximum longitudinal stress as a percentage of yield strength (σ_y) to represent a fracture (FX) risk value.

		Longitudinal Properties				Transverse Properties				Results		
		E (GPa)	G (GPa)	ν	σ_y (MPa)	E (GPa)	G (GPa)	ν	σ_y (MPa)	Max Stress (MPa)	Max Strain (%)	FX Risk (Max Stress as % of σ_y)
Normal	Cortical	15.0	5.8	0.3	157	8.2	3.1	0.3	75	55.0	0.36	35.0
	Cancellous	9.0	3.8	0.2		4.9	2.1	0.2				
OI Type I	Cortical	7.4	2.8	0.3	85	4.6	1.8	0.3	47	56.0	0.74	65.9
	Cancellous	4.4	1.9	0.2		2.8	1.2	0.2				
OI Type III	Cortical	5.7	2.2	0.3	72	3.7	1.4	0.3	37	56.7	0.98	78.8
	Cancellous	3.4	1.4	0.2		2.2	0.9	0.2				

PTH SIGNALING MEDIATES PERILACUNAR REMODELING DURING EXERCISE

¹Joseph D. Gardinier, ¹Salam Al-Omaishi, ¹Michael D. Morris, ¹David H. Kohn

¹ The University of Michigan, Ann Arbor, MI, USA

email: josephdg@umich.edu

INTRODUCTION

The structural integrity of bone is constantly adapting in response to dynamic loading and calcitropic hormones, specifically parathyroid hormone (PTH) [1]. The transient increase in PTH levels during short-term treadmill exercise contributes to the increase in structural and tissue-level properties of bone despite no significant changes in mineral content or overall geometry [2]. Un-like osteoblasts, osteocytes are ideally located throughout cortical bone to augment its intrinsic properties by modifying the perilacunar tissue through osteocytic osteolysis [3]. Given that the osteocytes' ability to modify the perilacunar tissue is also mediated by PTH signaling [3], we hypothesize that PTH signaling during exercise contributes to changes in the perilacunar tissue composition. Therefore, the purpose of this study is to (1) establish that changes in perilacunar composition occur following short-term exercise and (2) demonstrate the influence PTH signaling has on perilacunar adaptation during exercise.

METHODS

16 week old male C57Bl/6J mice were used along with an exercise regimen involving 30 minutes of running on a treadmill at 12 m/min and 5° incline for 21 consecutive days. Mice were divided into four weight-matched groups: sedentary + vehicle, sedentary + PTH(7-34), exercise + vehicle, and exercise + PTH(7-34). Each mouse received a subcutaneous injection of either 60µg/kg of PTH(7-34) to inhibit PTH signaling or vehicle control each day over the course of 21 consecutive days. On day 22, each mouse was sacrificed and tibiae were removed. One tibia was used for ex-vivo micro-CT scans and then mechanical testing, which applied four-point bending with the medial side in tension. The second tibia was embedded in PMMA, sectioned at the mid-diaphysis, polished to a thickness of 200 µm, and then imaged using a locally constructed Raman microprobe with a line

focused 785-nm diode laser (Invictus, Kaiser Optical Systems) and 40X/0.75DIC objective (Plan Fluor, Nikon Instruments). Raman spectroscopic signatures were taken across the perilacunar (< 5 µm from an osteocyte) and non-perilacunar regions (>15 µm from an osteocyte) regions of 3 to 4 osteocytes within the medial cortex of each tibia. The carbonate-to-phosphate ratio (CPR) was calculated based on the carbonate (1071 cm⁻¹) and phosphate (959 cm⁻¹) band intensities. The mineral-to-matrix ratio (MMR) was calculated based on the phosphate and hydroxyproline (855 cm⁻¹) intensities. Peak fitting was implemented using GRAMS software and the MMR and CPR for each group was the average of 4 samples, where each sample was the average of 3 to 4 representative perilacunar or non-perilacunar regions. Two-way ANOVA with a post-hoc Tukey-Kramer test was used to establish interactions between groups.

RESULTS AND DISCUSSION

Across the vehicle treated groups, exercise caused a significant increase in the mechanical properties at the structural and tissue levels: stiffness (105.1 ± 13.7 N/m vs. 84.3 ± 4.6 N/m), post-yield displacement (171.8 ± 34.4 mm vs. 96.9 ± 6.4 mm), modulus (12.6 ± 0.6 GPa vs. 9.8 ± 0.6 GPa), ultimate stress (206 ± 6 GPa vs. 180 ± 6 GPa), and post-yield toughness (2.6 ± 0.4 MPa vs. 1.3 ± 0.1 MPa) compared to sedentary controls, along with a decrease in pre-yield work (1.8 ± 0.1 mJ vs. 2.5 ± 0.2 mJ). Despite these changes in mechanical properties, there were no significant differences in cortical area, moment of inertia, or bone mineral density. However, there were significant changes in tissue composition, which included an overall increase in the CPR (0.14 ± 0.01 vs. 0.12 ± 0.01 , p-value < 0.001) compared to sedentary controls (Fig 1). The largest increase in CPR was found in the perilacunar region (0.12 ± 0.01 vs. 0.15 ± 0.01 , p-value = 0.08) compared to the perilacunar region of sedentary controls. Exercise also caused a

significant decrease in the perilacunar MMR compared to sedentary mice, and as a result exhibited the same MMR as the non-perilacunar tissue (Fig 2). In contrast, sedentary mice exhibit a significantly higher MMR in the perilacunar tissue compared to the non-perilacunar.

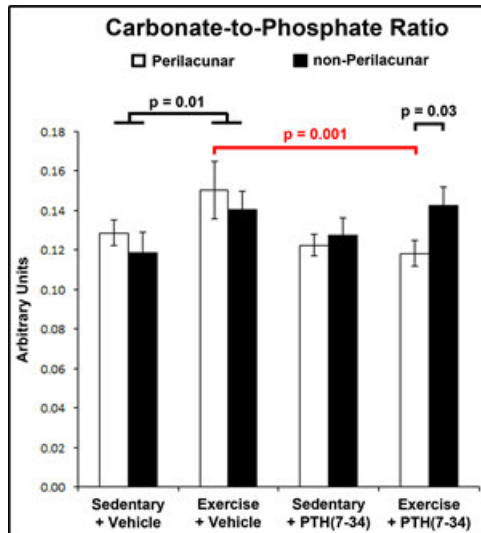


Figure 1: Exercise had a main effect on the CPR. Significant differences in perilacunar CPR between exercise + vehicle and exercise + PTH(7-34) indicates that PTH signaling mediates perilacunar remodeling during exercise. (mean \pm SEM, n = 4).

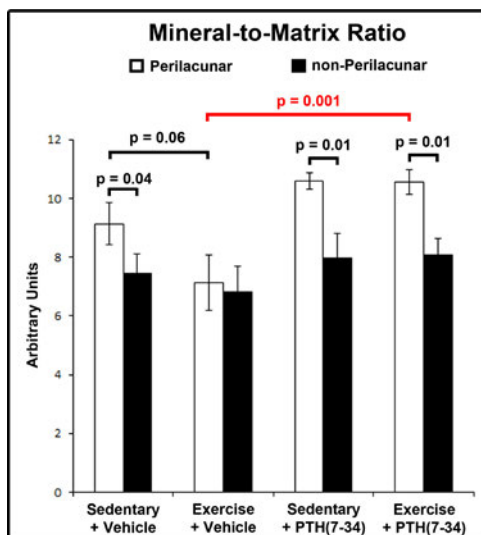


Figure 2: In response to exercise, adaptation to the MMR only occurred in the perilacunar region. PTH signaling during exercise mediated changes in perilacunar MMR given the significant differences between exercise + vehicle and exercise + PTH(7-34). (mean \pm SEM, n = 4).

Comparisons between sedentary and exercise groups treated with PTH(7-34) revealed no significant changes in the mechanical properties of the tibia (stiffness, post-yield displacement, modulus, ultimate stress, pre-yield work, and post-yield toughness). In addition, the perilacunar tissue did not exhibit significant changes in the CPR or MMR during exercise and PTH(7-34) treatment compared to sedentary controls treated with PTH(7-34) (Fig 1 & 2). However, significant differences in the perilacunar MMR and CPR were found between exercise + vehicle and exercise + PTH(7-34).

CONCLUSIONS

Exercise induced significant changes in the mechanical properties of bone in coordination with significant changes in tissue composition without altering its geometry, size or bone mineral density. As a result, the increase in stiffness and ultimate stress due to exercise were attributed to the increase CPR, given that an increase in carbonate substitution increases tissue stiffness [4]. Similarly, the increase in post-yield displacement and toughness were considered a function of a decrease in MMR [5], due to a potential increase in collagen synthesis during exercise [6]. Adaptations in MMR and CPR during exercise were localized predominately within the perilacunar regions, and dependent upon PTH signaling at the cellular-level. In response to lactation, the osteocytes ability to remodel the lacunae structure is mediated by the PTH/PTH-related protein receptor [3]. In this study, the use of PTH(7-34) revealed that PTH signaling during exercise mediates changes in the perilacunar tissue composition, which also corresponded with changes in the mechanical properties at the whole bone level.

REFERENCES

1. Iwamoto J, et al. *J Bone Miner Metabol*, 22, 26-31, 2004.
2. Gardinier J, et al. *J Bone Miner Res*, 2014
3. Qing H, et al, *J Bone Miner Res*, 27, 1018-1029, 2012.
4. Morris MD, et al. *Clin Orthop Relat Res*, 469, 2160-2169, 2011.
5. Burstein A, et al. *J Bone Joint Surg*, 57, 956-961, 1975.
6. Scott J, et al. *J Appl Physiol*, 110, 423-432, 2011.

LUMBAR SPINE KINEMATICS FOR END-RANGE TRUNK POSITIONS IN HEALTHY INDIVIDUALS USING UPRIGHT MRI

¹Jenna L. Rubin, ²David B. Berry, ²Samuel R. Ward, ¹Sara P. Gombatto

¹ San Diego State University, San Diego, CA, USA

² University of California San Diego, San Diego, CA, USA

email: ptresearch@mail.sdsu.edu

INTRODUCTION

Low back pain (LBP) is a problem that affects up to 80% of people at some point in their lives [1]. Poor posture and movement abnormalities have been identified as contributing factors to the problem.

Researchers have measured spine kinematics using imaging technologies such as x-ray, dual fluoroscopy, and magnetic resonance imaging (MRI) [2-4]. Prior MRI studies have examined kinematics during unloaded positions, including rotation [2]. Studies using x-ray and dual fluoroscopy have been limited in their ability to measure a wide variety positions and axial plane mobility. A recent study by Rodriguez-Soto et al has used upright MRI to measure lumbar spine kinematics in military personnel during different loading conditions [5], however, only sagittal plane motion was measured. The purposes of the current study are: 1) to quantify end range lumbar spine kinematics in healthy individuals using MRI, and 2) to determine which intervertebral segments contribute most in each plane of movement. Examining kinematics across a variety of positions with MRI will help researchers and clinicians better understand normal mobility in the lumbar spine with physiologic movements and provide a basis for comparing these to measurements in people with spine disorders.

METHODS

Sagittal T2-weighted images were acquired using a 0.6T upright MRI scanner (Fonar Corporation, Melville, NY). Eight healthy individuals (3 male and 5 female), with an age range of 18-33 years, height 67.0 ± 3.9 in, and weight 144.0 ± 3.9 lb were imaged in eight different static positions (standing, sitting flexion, prone on elbows, prone extension, sitting right and left rotation, standing right and left lateral bending) in blocked random order based on position (Figure 1). Global and local measurements

were used to quantify the alignment of the lumbar spine using a validated endplate-based joint coordinate system [6].

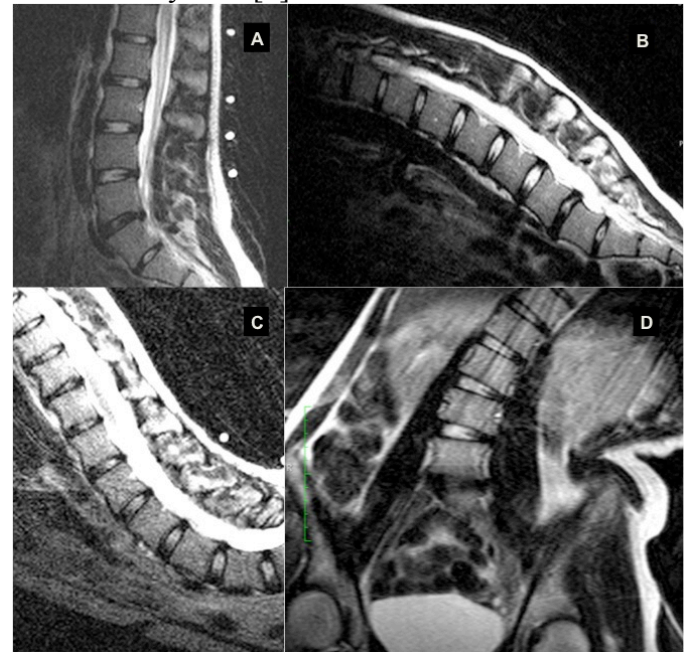


Figure 1: Sample T2-Weighted MRI of Standing (A), Sitting Flexion (B), Prone Extension (C), and Left Lateral Bending (D).

Briefly, the endplates and posterior elements of each vertebra (L1-S1) were marked on each slice using the region of interest (ROI) tool in OsiriX. ROI's were imported into a custom-written Matlab program to calculate three-dimensional rotations and translations of the whole lumbar spine and each intervertebral segment. Global measures of lumbar spine alignment were: angle with respect to the horizontal and sagittal and coronal Cobb angles. Local measures were lumbar intervertebral angles. To determine differences in global measures of lumbar spine alignment in each plane, repeated measures ANOVA tests were conducted to determine the effect of position on sagittal and coronal Cobb angles. To determine which vertebral segments contributed most to kinematics in each

plane, separate repeated measures ANOVA tests were conducted to examine the effect of level (L1-S1) and position on intervertebral kinematics.

RESULTS AND DISCUSSION

There was a significant effect of position on angle with respect to the horizontal and sagittal Cobb angle ($P < .01$) for **sagittal plane** positions, with larger Cobb Angles associated with more extended positions ($61.9-74.0^\circ$). For sagittal intervertebral angles, there were significant main effects of position and level, and a position x level interaction effect (Figure 2, $P < .01$). The greatest degree of change between positions occurred at L5-S1.

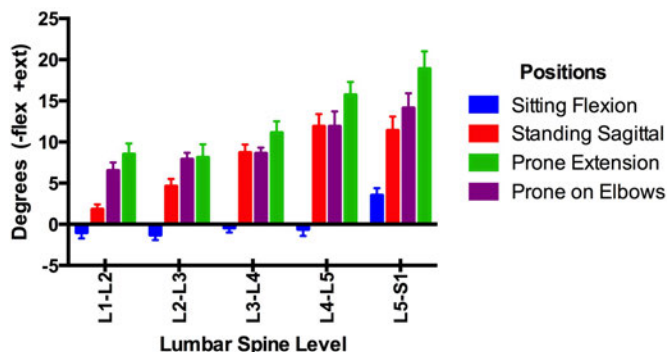


Figure 2: Sagittal Intervertebral Kinematics

For **coronal plane** positions, there was a significant effect of position on coronal Cobb Angle ($P < .01$). For coronal intervertebral angles, there was a significant effect of position ($P < .01$), no effect of level ($P = .9$), but a significant position x level interaction effect (Figure 3, $P < .01$).

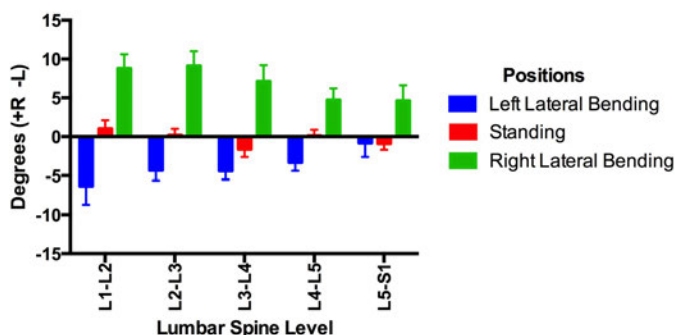


Figure 3: Coronal Intervertebral Kinematics

Greater movement occurred in the upper lumbar spine segments and to the right with lateral bending. For **axial plane** positions, there was a significant effect of position on coronal Cobb Angle ($P < .01$), indicating that participants displayed coronal plane movement with sitting rotation positions. For axial

intervertebral angles, there was a significant main effect of position ($P < .05$), but no level ($P = .25$) or level x position ($P = .89$) interaction effects (Figure 4).

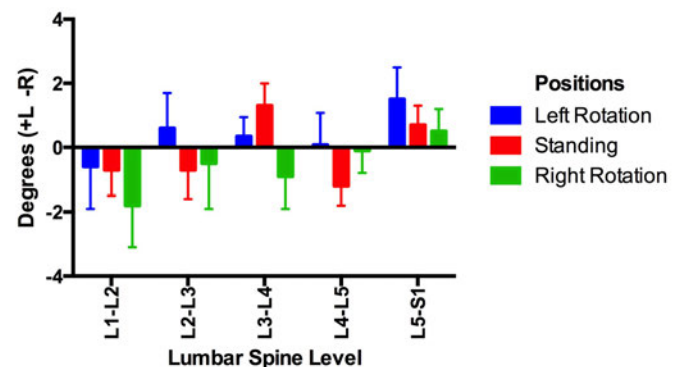


Figure 4: Axial Intervertebral Kinematics

CONCLUSIONS

The greatest degree of movement in the lumbar spine occurred in the sagittal plane, followed by the coronal plane, with the least mobility in the transverse plane. The greatest degree of sagittal plane movement occurred in the lower lumbar segments, while more coronal plane movement occurred in the upper lumbar segments. Minimal rotation movement was observed with positions of loaded, sitting rotation. These data provide information on lumbar spine kinematics during end-range, loaded positions using upright MRI and can provide a basis for comparing people with low back pain.

REFERENCES

1. Andersson, G. B. et al, *The Lancet* **354**, 581-585, 1999.
2. Fujii, R, et al. *European Spine Journal* **16**, 1867-1874, 2007.
3. Hashemirad, F, et al. *Journal of Bodywork and Movement Therapy*, **17**, 46-52, 2013.
4. Breen, AC, et al. *Adv Orthop*. 2012.
5. Rodriguez-Soto, A.E, et al. *Spine*, **38**, E783-91, 2013.
6. Berry, DB, et al. *Journal of Applied Biomechanics*. In Review.

ACKNOWLEDGEMENTS

This project was funded by the University Grants Program at San Diego State University.

THE EFFECT OF AGE ON THE MECHANICAL PROPERTIES OF PORCINE INTERVERTEBRAL DISCS FOLLOWING A CYCLIC LOADING PROTOCOL

¹ Kristina M. Gruevski*, ¹ Mamiko Noguchi, ² Chad E. Gooyers and ¹ Jack P. Callaghan

¹ University of Waterloo, Waterloo, ON, Canada

² Giffin Koerth Forensic Engineering & Science, Toronto, ON, Canada

*Corresponding author email: kmgruevs@uwaterloo.ca

INTRODUCTION

The North American working population is aging. American workers over 55 comprised 19% of the labour force in 2010 [1] and the proportion of Canadian workers over 55 increased by 21.7% between 1997 and 2010 [2]. Occupational injuries sustained by American workers 65 and older resulting in a lost-time claim increased by 6.4% between 2007 and 2008 [3]. The low back was the body location ranked highest in number of injuries sustained among Ontario workers in 2013, accounting for 17% percent of all lost time claims, with the leading demographic group 50-54 year old males [4]. A mechanistic understanding of the age-related responses to loading in spinal tissues is essential to the prevention of low back injury throughout the aging process. Known age-related changes to the intervertebral discs (IVDs) of the spine include; the denaturation of collagen fibres [5], reduction/alterd distribution of proteoglycans [6] and an increased propensity to form microstructural clefts in response to tensile loading when compared to more juvenile samples [7]. The formation of clefts is a known mechanism of initiation and propagation of an IVD herniation [8]. The aim of this investigation was to quantify the effect of age on the mechanical properties of annulus fibrosis tissue following exposure to cyclic loading.

METHODS

A total of 8 (4 mature, 4 young) cervical functional spinal units (FSUs) were obtained fresh-frozen from mature (aged ~3 years) and immature (aged ~6 months) porcine spines. The FSUs included two adjacent vertebral bodies with the intervening disc and were tested in a modified servohydraulic testing system (Model 8872, Instron Canada, Burlington, ON, CAN). To counteract post-mortem swelling,

specimens were loaded with 300 N of compression for 15 min while the zero moment posture about the flexion/extension axis was determined. Following the preconditioning phase, specimens were loaded with 1400 N of compression and cyclically loaded at 1 Hz to a range of motion 8.5 degrees in flexion and extension around the midpoint of each specimen's neutral zone for 3000 cycles.

Following the cyclic loading protocol, specimens underwent further biaxial mechanical testing to determine how age impacts the mechanical properties of the annulus following loading exposure. A total of 12 (6 mature, 6 young) anterio-lateral annular specimens were excised from the intermediate layers of the IVD with an average (SD) thickness of 0.9 (0.2) mm and comprised of 3-5 annular layers. The specimens were tested in a humidity and temperature-controlled environment of 30 (1.4) degrees Celsius and 94.3 (1.5) % humidity to prevent dehydration. Specimens were dissected to dimensions of approximately 5 mm x 5 mm and mounted into a biaxial tensile (BioTester 5000, CellScale, Waterloo Instruments Inc., Waterloo, ON, CAN) testing system by puncturing the edges with sharpened tungsten wires. Following the mounting procedure, specimens were preloaded in the axial and circumferential directions with 10-15 mN, followed by preconditioning of 5 cycles of 10% actuator stretch at a rate of 1%/s and subsequently loaded to 20% actuator stretch for 100 cycles at a rate of 2%/s.

Dependent measures of interest included neutral zone range (degrees) and neutral zone stiffness (Nm/degree) both pre and post loading protocol for intact FSUs. Additionally, peak stress (MPa) in the circumferential and axial directions for excised annular samples during cycles 1, 50 and 100 were examined.

RESULTS AND DISCUSSION

Of the 8 FSU specimens tested; sagittal plane radiographs indicated that 2 of the specimens (1 young, 1 mature) sustained a herniation due to the loading protocol. There was a significant effect of age on neutral zone range ($p=0.0448$) where mature specimens had a smaller range before and after the loading protocol compared to the younger specimens (Figure 1). There was a main effect of age on neutral zone stiffness ($p=0.0446$) where mature FSUs had greater stiffness compared to younger specimens (Figure 2). There was no main effect of the loading protocol on neutral zone range or neutral zone stiffness.

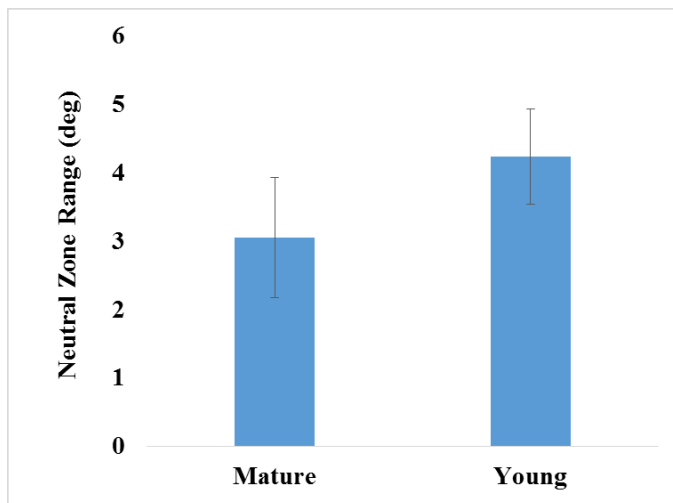


Figure 1: Neutral zone range by age across time point

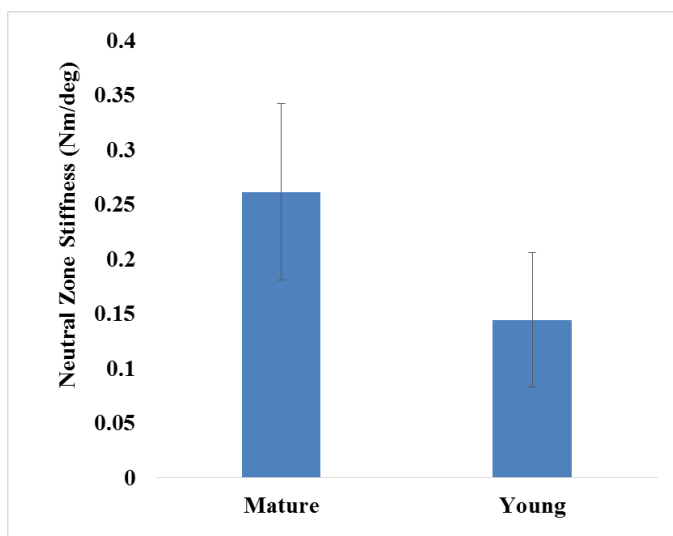


Figure 2: Neutral zone stiffness by age across time

Decreased specimen flexibility among the mature FSUs is consistent with previous work [9]. There was no main effect of age or cycle on the peak stress. While not statistically significant, Figure 3 depicts a trend consistent in both loading directions of higher peak stress in the mature specimens compared to the young specimens with an overall reduction in peak stress with a more cycles.

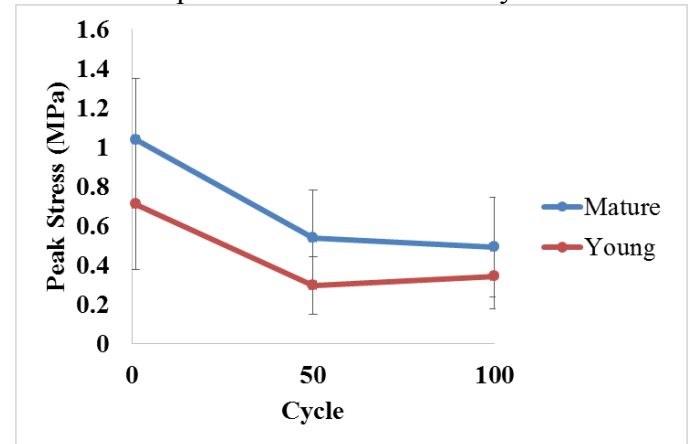


Figure 3: Peak stress in the circumferential direction by age and cycle

Ongoing work continues on samples excised from the postero-lateral location of the annulus and on mature and young annular samples in the absence of cyclic loading in order to isolate any innate differences due to aging alone. The results from this work will provide insight into differences in the responses to loading due to age. The biological changes and the cumulative exposures that occur throughout the aging process are important to understanding the mechanisms of injury given an aging workforce.

REFERENCES

- [1] Toosi, M *Mon Labour Rev*, Oct 2010, 3-16 [2] Carrière Y & Galarneau D *Statistics Canada* 2011; Cat No: 75-001-X, 3-16 [3] Rice, J et al. 2008 *Bureau of Labor Statistics*, Report 1028 [4] WSIB Statistical Report, 2013, *Schedule 2*, Toronto, ON, CAN [5] Antoniou J et al. *J Clin Invest* 1996; 98(4):996-1003 [6] Taylor, TKF et al. *Spine*, 2000; 25(23): 3014-3020 [7] Schollum, ML et al. *J. Anat*, 2010; 216: 310-319 [8] Tampier, C et al. *Spine*, 2007; 32(25): 2869-2874 [9] Park, C et al. *Spine*, 2005; 30(10): E259-E265

THE EFFECTS OF A FIVE-WEEK EXERCISE INTERVENTION USING EMG BIOFEEDBACK ON SCAPULAR KINEMATICS AND SCAPULAR STABILIZER MUSCLE ACTIVATION

¹ Samantha R. Gunderson, ¹ Jun G. San Juan, ¹ Wren L. Cunningham, and ¹ David N. Suprak

¹ Western Washington University, Bellingham, WA, USA
email: Samantha.Gunderson13@gmail.com

INTRODUCTION

Research on utilizing electromyography (EMG) biofeedback training as a preventative tool is limited. It is well documented that EMG biofeedback has become a useful tool with rehabilitation of subacromial impingement syndrome. Biofeedback gives patients a better sense of the activation of different muscles that are involved in the movement of the shoulder girdle [1]. With the muscle activation patterns shown on a projected screen, patients are able to get a visual representation of the proper firing of the muscles [2]. However, research on utilizing EMG biofeedback as a preventative tool in the reduction of the risk of onset subacromial impingement is limited. The purpose of this study is to investigate changes in scapular kinematics as a result of changes in muscle activation patterns in a healthy population.

METHODS

Twenty-one healthy subjects (12 females, 9 males) participated in this study. The mean age was 22.3 ± 1.92 years old, mean height was 1.71 ± 0.11 m, and a mean weight of 67 ± 10.28 Kg. Those who had shoulder pain within a year, were diagnosed with impingement, who had shoulder surgery, or previously participated in EMG biofeedback were excluded. The subjects were randomly assigned to two different groups that consisted of an exercise only group, and an exercise with biofeedback group. Both groups participated in exercises that targeted activation of the lower trapezius. The scapular stabilizer exercises (I, W, T, Y) were performed three times a week at 1 set of 10 repetitions. The exercise with biofeedback group participated in an EMG biofeedback session once a week. To measure muscle activation, a Noraxon Desktop DTS (Gain 500, CMRR > 100dB, input impedance > 100Mohm) was

utilized and sampled at 1500 Hz. The EMG data were normalized using maximum voluntary isometric contraction for all the muscles tested. Bi-polar Ag/AgCl surface electrodes were placed parallel to the muscle fibers of the upper and lower trapezius, serratus anterior, and lumbar paraspinals of the dominant arm with an inter-electrode distance of 1.7 cm (Figure 1 A).

A Polhemus Fastrak magnetic tracking device was used to measure 3-dimensional scapular kinematics. The receivers were attached to the spine of the scapula using a customized scapular tracker, thorax, and distal humerus (Figure 1 B). A Polhemus sensor pen was utilized to digitize the spinous process of C7, T1, T7, and T8, the sternal notch, the sternoclavicular joint, and lateral and medial epicondyles of the humerus to set-up the coordinate system following the standard set by the International Society of Biomechanics.

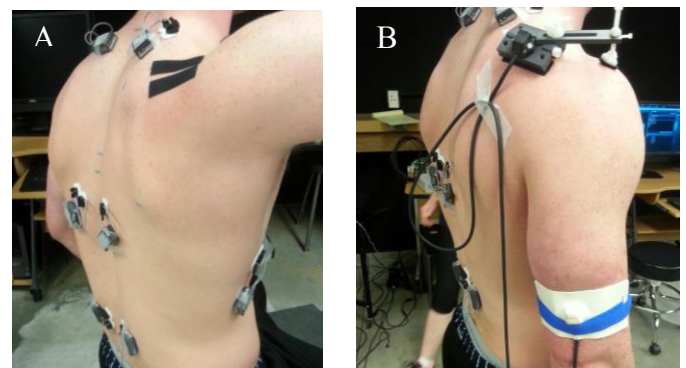


Figure 1: (A) Set up of the EMG electrodes on UT, LT, SA and LPS and (B) set up of the Polhemus Fastrak 3D kinematics system.

The EMG data were displayed on a stationary overhead projector connected to a PC-type of computer using MR3.4 MyoMuscle software (Figure 2). Subjects were told to actively try and reduce the

muscle activation shown on the screen for the upper trapezius during the exercises.

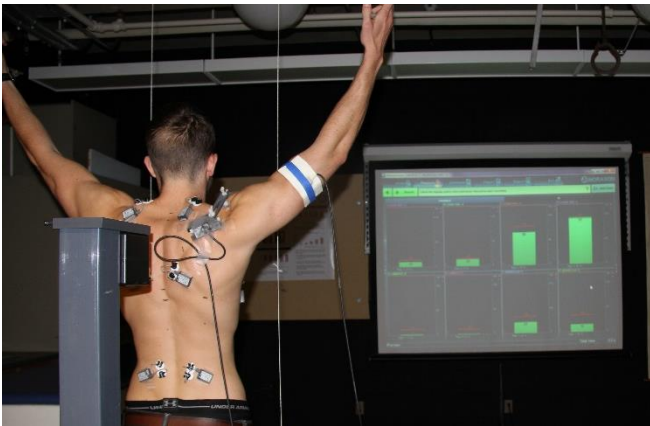


Figure 2: EMG muscle activation patterns projected on a screen during a biofeedback session.

A three-way mixed ANOVA was utilized to compare scapular kinematics, and mean EMG amplitude at baseline, week 6, and week 8. The independent variables were humeral elevation (30°, 60°, 90° & 110°), group, and time (baseline, week 6, and week 8). The dependent variables were scapular kinematics (upward rotation, external rotation, and posterior tilt), and EMG amplitude. Alpha level was set to 0.05.

RESULTS AND DISCUSSION

One subject dropped out due to injury that was unrelated to this study. There was a statistically significant interaction between time and elevation during scapular posterior tilt ($p < 0.001$), for the exercise only group (Figure 3). After the exercises, the scapula was in a less posteriorly tilted orientation. There were no significant differences found for scapular upward rotation, nor for scapular external rotation at all humeral elevation angles between times, and group. There was no significant difference found between the groups for mean EMG amplitude, at baseline, week 6, or week 8. The decrease in posterior tilt that was observed with the exercise only group could lead to a decrease in subacromial space. A decreased subacromial space brings the subacromial bursa, biceps brachii long head tendon, and supraspinatus tendon closer to the coracoacromial arch [3].

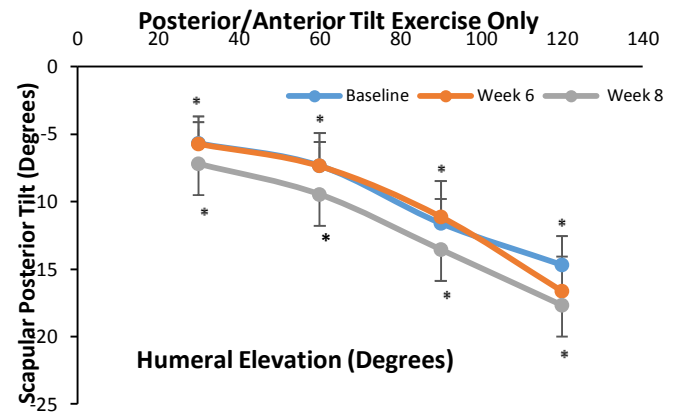


Figure 3: Scapular posterior tilt for the exercise only group at baseline, week 6, and week 8. An asterisk denotes statistical significance.

Electromyography biofeedback intervention training does not seem to have an impact on altering scapular kinematics or scapular stabilizer muscle activation patterns in healthy individuals. However, the exercises that were performed by both the exercise only group, and exercise with biofeedback group may alter scapular kinematics. Moving toward a more functional type of exercise may be more beneficial in altering the scapular kinematics and muscle activation patterns. Utilizing EMG biofeedback with a more functional type of task could improve the muscle activation patterns and scapular kinematics.

CONCLUSIONS

Exercises focusing on activation of the lower trapezius, and serratus anterior may alter scapular kinematics in healthy individuals. A less posteriorly tilted scapula might result in a decrease in subacromial space, which can help in the development of shoulder pathologies such as subacromial impingement. The exercises performed in this study did not elicit the desired alterations in muscle activation patterns and scapular kinematics.

REFERENCES

1. Holtermann A, et al. *J Electro and Kines*, **20**, 359-365, 2010
2. Paine, R, et al. *Int J Sport Phys Ther*, **8**, 617-629, 2013.
3. Solem-Bertoft, E, et al. *Clin Orthop Relat Res*, **26**, 99-103, 1993

USING DIGITAL IMAGE CORRELATION TO INVESTIGATE THE EFFECT OF IMPACT VELOCITY ON THE RESPONSE OF A VERTEBRA

¹ Hannah Gustafson, Kohle Merry and Peter Crompton

¹ Department of Mechanical Engineering and ICORD, The University of British Columbia, Vancouver, BC, Canada

email: gustafson.30@gmail.com, web: www.sites.mech.ubc.ca/~injury/

INTRODUCTION

Vertebrae exhibit rate dependent behavior with a stiffer response observed at higher displacement rates [1-3]. Therefore, it would be expected that the strain would be lower at higher loading rates. However, the full-field strain response at different loading rates has not been quantified.

We propose investigating strain on cadaveric vertebrae at varying impact rates using digital image correlation (DIC), an optical method which provides full-field non contact strain measurements on the bone surface. We hypothesize that with increasing impact rates, the deformation and strain magnitude at a given force will be lower; furthermore, we predict the strain magnitudes at one impact rate will be predictive of the strain magnitudes at other impact rates.

METHODS

A custom built impactor rig with a mass of 1.6 kg was attached to a drop rail. One fresh frozen cadaveric L1 vertebra was used for initial testing. All soft tissue and the posterior elements were removed from the bone. The bone was potted in polymethylmethacrylate (PMMA) to create parallel surfaces for loading. For the DIC, the bones were painted white and speckled with black paint using an airbrush. Images of the anterior surface during loading were captured with two high speed cameras (Phantom V12s, Vision Research, USA) at 11,000 fps (Figure 1). The forces and moments were collected with a six-axis load cell placed below the specimen. The bone was impacted 30 times at heights of 2 cm, 5 cm, and 10 cm. These heights correspond to nominal velocities of 0.62, 0.99 and 1.40 m/s. During testing, no visible damage was

observed. Furthermore, the 2 cm drops at the start and end of testing had similar force-deformation responses and peak forces indicating that the overall response of the bone was similar with time and no significant structural damage occurred which may have contributed to changes in the bone's mechanical response.

The DIC was processed using commercial software (Strainmaster, LaVision Inc., Germany). The displacement was measured on the anterior surface in the superior-inferior direction and the strain was analyzed over a region in the center of the anterior surface (Figure 1).

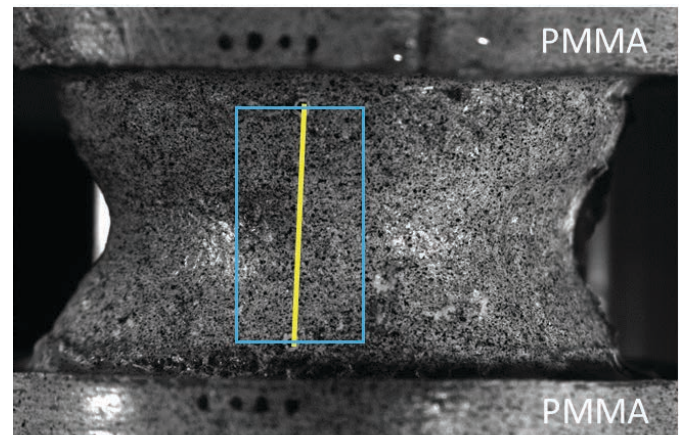


Figure 1: High-speed camera image of the anterior surface of the bone potted in PMMA. The line indicates the location where the displacement was measured. The box indicates the location over which the DIC pattern was compared

RESULTS AND DISCUSSION

The force-displacement curves of 14 (of the 30) tests are presented along with the average curves for the three drop heights (Figure 2).

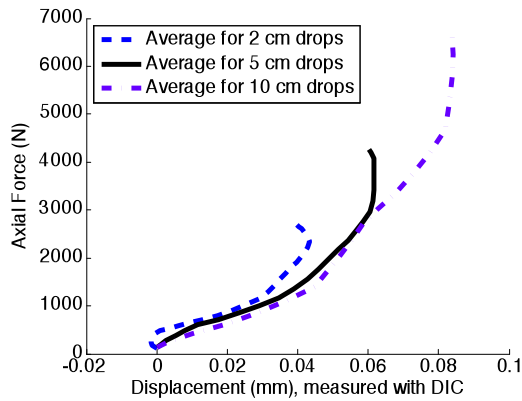


Figure 2: Average force-displacement response. Displacement was measured on the anterior surface of the bone (Fig 1); force was measured in the axial direction.

The patterns of DIC strain were compared using regressions in which the minimum principal strain magnitude on the anterior surface of the bone was plotted against the strains measured at the same locations on the bone surface at another drop height and at similar applied force values (Figure 3).

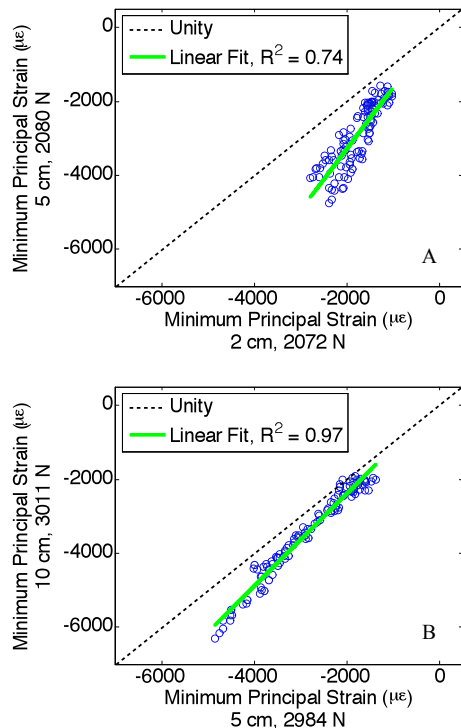


Figure 3: Strain regressions comparing the DIC-measured strain from (A) 5 cm drop height to 2 cm drop height at ~2080 N and (B) 10 cm drop height to 5 cm drop height at ~3000 N. Each dot represents the strains at a particular location.

As impact velocity increased, a greater displacement was measured at a given force. This result does not support the hypothesis that the bone would deform less at higher impact velocities. Furthermore, in the strain patterns we similarly observed more strain at the higher impact velocity for a particular force value. The strain patterns at lower impact velocities predicted the strain patterns at higher impact velocities ($R^2 = 0.74$ and 0.97). Since strain is related to failure, this result suggests that vertebral failure locations on the anterior surface of the bone are similar at different impact velocities.

In contrast to previous research and our expectations, the tested vertebra did not behave viscoelastically. This may be a result of the quality of the bone or a result of inertia-driven impact loading instead of loading with a driven actuator such as in a materials testing machine.

CONCLUSIONS

The tested vertebra did not behave viscoelastically, based on the force-displacement curves and strain results. Although the strain at lower velocities was strongly correlated with the strain at higher velocities, the magnitudes were larger for the higher velocity impacts. Understanding of the strain on the bone surface at varying impact rates helps us better understand bone fracture initiation and failure mechanics and can be used to validate computational models.

REFERENCES

1. Ochia RS, et al. *J Biomech*, **36**, 1875-1881, 2003.
2. Stemper BD, et al. *J Mech Behav Biomed Mater*, **41**, 271-279, 2015.
3. Yingling VR, et al. *Clin Biomech*, **12**, 301-305, 1997.

Finite Element-Based Adjacent Level Intersegmental Rotation and Intradiscal Pressure Analysis after Lumbar Fusion for Scoliosis

¹Ram Haddas, ²Ming Xu, ³Isador H. Lieberman, ²Brandon J. Snailer, and ²James Yang

¹Texas Back Institute Research Foundation, Plano, TX, USA

²Texas Tech University, Lubbock, TX, USA

³Texas Back Institute, Plano, TX, USA

Email: rhaddas@texasback.com; james.yang@ttu.edu

INTRODUCTION

Degenerative adult scoliosis results from age related changes leading to segmental instability, deformity and stenosis.[1] Spinal fusion is a standard method of surgical treatment for deformity.[2] Loss of native lumbar lordosis, abnormal loading and increased mobility in adjacent segments, may alone or in combination explain the development of adjacent level deterioration.[3] Finite element (FE) model studies have made important contributions to the understanding of functional biomechanics of the lumbar spine.[4] In comparison to in vitro or in vivo approaches, computational methods eliminate the issues with cadaver use, animal use and clinical human studies, in addition to being cost efficient, time efficient, and an accurate surrogate.[5] The purpose of this study was to develop a finite element model of a lumbar scoliotic spine, and investigate the effect of adjacent load transfer before and after fusion surgery.

METHODS

Two three-dimensional nonlinear finite element models of the lumbosacral spine were created from a 73-year old male subject's pre and post scoliosis surgery CT scans (Fig. 1). Pedicle screws and rods were implanted during surgery at the L₂ to S₁ levels. The FE spine models were developed encompassing the T₁₂ to S₁ levels, along with the screws and rods for the post surgery model (Fig.2). 3D Slicer software was used to generate the outer shell virtual model of each individual vertebrae and disc. This was followed by a smoothing process to smooth these outer surfaces and fill in holes using Geomagic Studio software. These modified virtual models from T₁₂ to S₁ were imported into Truegrid

and Hyperworks software to form 3D solids and these solids were meshed. Finally these meshed models were input into LS-DYNA for FE analysis under different loading conditions.



Figure 1. Pre and post scoliosis fusion surgery scans.

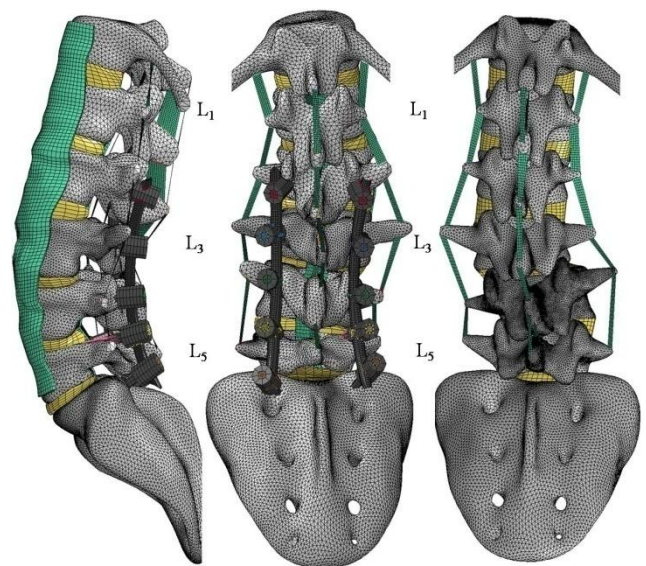


Figure 2. Pre and post fusion surgery finite element models of scoliosis spine from T₁₂-S₁ level with pedicle screws and rods at L₂-S₁.

For the analysis the S₁ level of the model was fixed. Seven ligaments and local muscle forces were added to this model.[6] A 500N compressive follower load and six different moments were applied to this model: (1) flexion bending moment; (2) extension bending moment; (3) right lateral bending moment; (4) left lateral bending moment; (5) right axial rotation moment; and (6) left axial rotation moment. The compressive follower load was applied to represent the subject's upper body weight. The six types of bending moment represent the six movements of the spine. The following values for pre- and post-surgery were compared for each load condition: intradiscal pressure and intersegmental rotation (flexion, extension, lateral bending, and axial rotation) at the L₁₋₂ level.

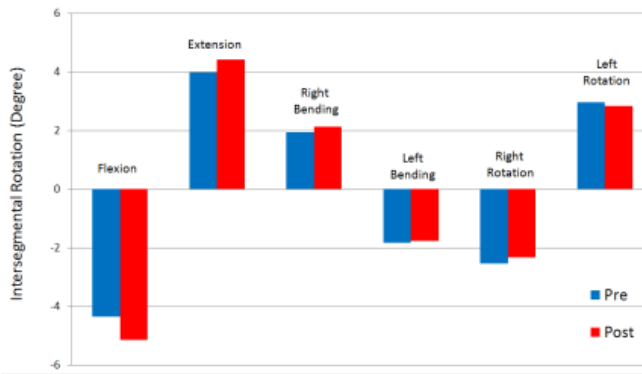


Figure 3. Pre and post fusion surgery intersegmental rotation of scoliosis spine at the L₁₋₂ level.

RESULTS AND DISCUSSION

The extent of intersegmental rotation in degrees and the extent of the intradiscal pressure at the L₁₋₂ level post surgery increased or stayed the same under the six loading conditions compared to the pre surgery condition (Fig. 3, Table. 1). The post surgery pressure contours on the L₁₋₂ intervertebral disc varied with the different applied moments for the pre-and post-surgery (Table 1).

CONCLUSIONS

With this study we were able to develop a finite element model of a lumbar scoliotic spine, and investigate the effect adjacent load transfer before and after fusion surgery. The results of this study will help define the variables contributing to adjacent level deterioration in the clinical environment. With this information a surgeon can plan the most appropriate surgical strategy pre surgery to prevent mid and long term adverse outcomes associated with adjacent level deterioration.

REFERENCES

1. Kotwal S. *HSS J* **7**(3), 257-64, 2011.
2. Kuklo TR, *Spine* **31**(19), S132-8, 2006.
3. Barrey C, et al. *World J Orthop* **6**(1), 117-26, 2015.
4. Dreischarf M, et al. *J Biomech* **47**(8), 1757-66, 2014.
5. Bloemker KH, et al. *Open Biomed Eng J* **6**, 33-41, 2012.
6. Rohlmann A, et al. *J Biomech* **39**, 2484-90, 2006.

	Flexion	Extension	Right Bending	Left Bending	Right Rotation	Left Rotation
Pre intersegmental rotation (Degree)	-4.347	3.984	1.937	-1.824	-2.547	2.965
Post intersegmental rotation (Degree)	-5.154	4.427	2.122	-1.7795	-2.324	2.837
Pre intradiscal pressure (Mpa)	1.486	0.809	0.435	0.438	0.324	0.387
Post intradiscal pressure (Mpa)	1.548	0.633	0.525	0.453	0.274	0.436

Table1. Intersegmental rotation and intradiscal pressure at level L₁₋₂ follower by 500N compressive load and six different types of moments.

Lifting Risk after Lumbar Fusion in Scoliosis

¹Ram Haddas, ²Ming Xu, ³Isador H. Lieberman, and ²James Yang

¹Texas Back Institute Research Foundation, Plano, TX, USA

²Texas Tech University, Lubbock, TX, USA

³Texas Back Institute, Plano, TX, USA

Email: rhaddas@texasback.com; james.yang@ttu.edu

INTRODUCTION

Lifting is a ubiquitous activity, where individuals are required to manually handle materials and loads while engaged with occupational tasks and activities of daily living.[1] Asymmetric lifting, including flexion and rotation, is the most frequently reported culprits associated with low back disorder.[2] Degenerative adult scoliosis resulting from age related changes leads to segmental instability, deformity and stenosis.[3] Spinal fusion is a standard method of surgical treatment for deformity.[4] Loss of native lumbar lordosis, abnormal loading and increased mobility in adjacent segments, may alone or in combination explain the development of adjacent level deterioration.[5] Finite element (FE) model studies have made important contributions to the understanding of functional biomechanics of the lumbar spine.[6] In comparison to in vitro or in vivo approaches, computational methods eliminate the issues associated with cadaver use, animal use and clinical human studies, in addition to being cost efficient, time efficient, and an accurate surrogate.[7] The purpose of this study was to develop a finite element model of a lumbar scoliotic spine and then investigate the effect of asymmetric loading as is common with lifting, on the adjacent segment after lumbar fusion surgery.

METHODS

A post operative CT scan of a 73-year old male scoliosis subject was used. Pedicle screws and rods were implanted at L₂-S₁ levels. A FE spine model was developed encompassing the T₁₂-S₁ level along with the screws and rods (Fig.1). 3D Slicer software used to generate the outer shell virtual model of each individual vertebrae and disc. This was followed by a smoothing process to smooth these

outer surfaces and fill in holes using Geomagic Studio software. These modified virtual models from T₁₂-S₁ were imported into Truegrid and Hyperworks software to form 3D solids and these solids were meshed. Finally these meshed models were input into LS-DYNA for FE analysis under different loading conditions. All screws that were used to fuse the spine from L₂-S₁ were built into the FE model as well.

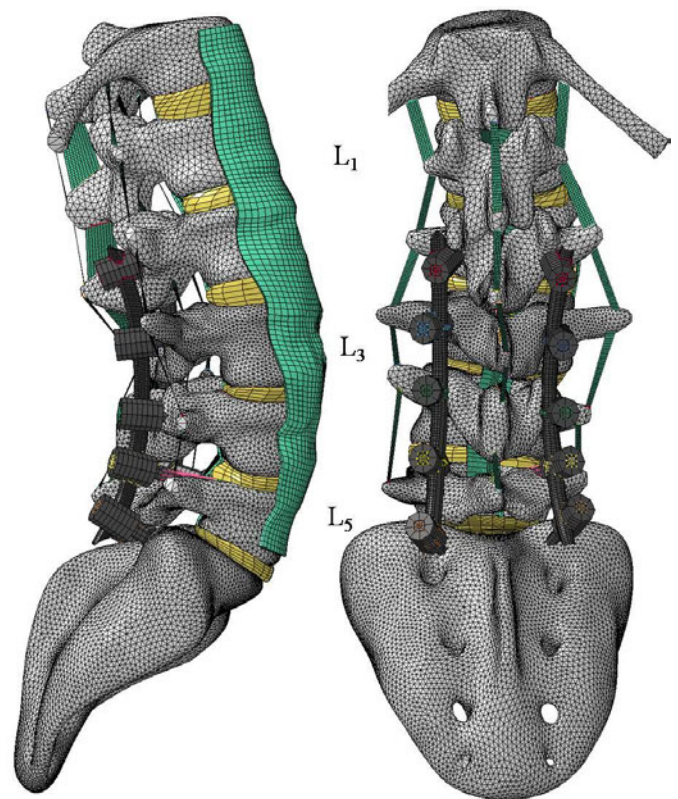


Figure 1. Post fusion surgery finite element model of scoliosis spine from T₁₂-S₁ level with pedicle screws and rods at L₂-S₁.

For this subject the S₁ vertebral level of the model was fixed. Seven ligaments and local muscle forces were incorporated into this model.[8] Two types of

combined loads were applied to this model: (1) 7.5 Nm flexion and right axial rotation moments and (2) 7.5 Nm flexion and left axial rotation moments with compressive follower loads of: 500N, 750N, 1000N, 1250N, and 1500N, respectively. The compressive follower load was applied to represent the subject's upper body weight. The FE analysis was conducted and compared for post-surgery for each load condition: intersegmental rotation and intradiscal pressure at the L₁₋₂ level, the L₂₋₃ level pedicle screws and rod forces.

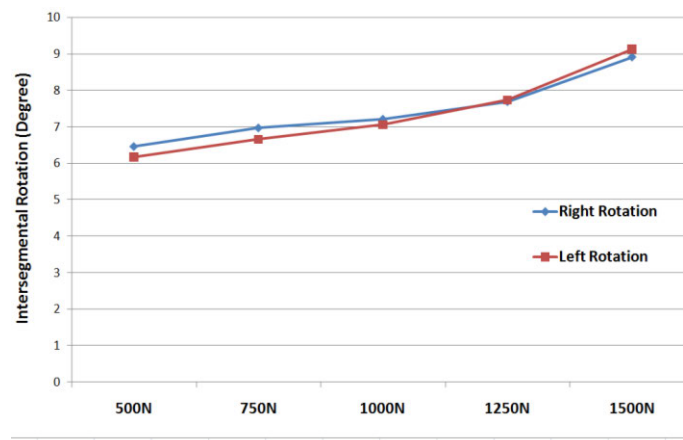


Figure 2. Post fusion surgery finite intersegmental rotation at L₁₋₂ for right and left rotation along with flexion moment and five different load conditions.

RESULTS AND DISCUSSION

The intersegmental rotation angle and the intradiscal pressure at level L₁₋₂ were recorded for each of the five loading conditions (Table 1, Figure 2). The maximum resultant forces in the pedicle screws and rods at the L₂₋₃ level were recorded under each loading condition as well (Table 1.) Increasing the amount of compression load increased the intersegmental rotation and the intradiscal pressure nonlinearly. As the compression

force increased, the pedicle screws and the rod were subject to higher stresses.

CONCLUSIONS

With this study we have developed a FE model of a lumbar scoliotic spine in an effort to determine the adjacent level stress and strain as well as the stress and strain on the pedicle screws and rods. The results of this study will help define the variables contributing to adjacent level deterioration in the clinical environment. With this information a surgeon can plan the most appropriate surgical strategy pre surgery to prevent mid and long term adverse outcomes associated with adjacent level deterioration.

REFERENCES

1. Kuijer P, et al. *Ann Occup Environ Med* **26**(16), 2014.
2. Coenen P, et al. *J Occup Rehabil* **23**(1), 11-18, 2012.
3. Kotwal S. *HSS J* **7**(3), 257-64, 2011.
4. Kuklo TR, *Spine* **31**(19), S132-8, 2006.
5. Barrey C, et al. *World J Orthop* **6**(1), 117-26, 2015.
6. Dreischarf M, et al. *J Biomech* **47**(8), 1757-66, 2014.
7. Bloemker KH, et al. *Open Biomed Eng J* **6**, 33-41, 2012.
8. Rohlmann A, et al. *J Biomech* **39**, 2484-90, 2006.

	500N		750N		1000N		1250N		1500N	
	Right Rotation	Left Rotation	Right Rotation	Left Rotation	Right Rotation	Left Rotation	Right Rotation	Left Rotation	Right Rotation	Left Rotation
IntersegmentalRotation (Degree)	6.465	6.168	6.974	6.654	7.214	7.056	7.694	7.731	8.915	9.128
Intradiscal Pressure (Mpa)	1.606	1.656	1.729	1.836	1.947	1.918	2.082	2.145	2.315	2.286
Pedicle Screw (N)	79.7	68.5	96.4	86.1	140.5	178.2	284.3	291.7	308.3	352.4
Rod (N)	25.4	28.9	37.5	33.4	46.1	37.7	70.5	62.9	93.4	110.6

Table1. Intersegmental rotation and intradiscal pressure at level L₁₋₂, pedicle screw and rod forces at level L₂₋₃ under 7.5 Nm flexion and axial rotation moments and with a five conditions of compressive follower load.

Peak Knee Joint Contact Force Increases with Body Borne Load During Run-to-Stop Task

¹Clifford L. Hancock, ^{1,2}John W. Ramsay, and ¹Tyler N. Brown

¹U.S. Army Natick Soldier Research, Development and Engineering Center, Natick, MA, USA

²Oak Ridge Institute for Science and Education (ORISE), Belcamp, MD, USA

email: Clifford.L.Hancock4.civ@mail.mil

INTRODUCTION

Musculoskeletal injury, particularly of the lower extremity, is a serious military issue that increasingly leads to long-term disability and discharge of the soldier [1]. These injuries often result from repetitive forces that impact the lower limbs during military-relevant tasks, such as the run-to-stop (RTS). Performing the RTS requires rapid deceleration which potentially places large compressive forces on the knee. These compressive forces may further increase with the addition of body borne loads commonly worn during military training, e.g., 20 kg or greater, and potentially lead to musculoskeletal injury. However, to date, the effect of body borne load on knee joint contact force during the RTS is unknown. Unexpected stops, i.e., performing an unplanned, reactive RTS, may further elevate these compressive forces and the subsequent risk of musculoskeletal injury. Therefore, the purpose of this study was to determine if peak knee joint contact force (PKJCF) increases with the addition of body borne load during anticipated and unanticipated RTS tasks.

METHODS

Seven males (21.7 ± 4.2 years; 1.8 ± 0.1 m; 71.7 ± 9.1 kg) had lower limb biomechanical data recorded during a series of RTS maneuvers. Each participant performed the RTS with three military-relevant body borne loads: no load (NL; 6.2 kg), fighting load (FL; 20.0 kg) and approach load (AL; 40.0 kg). While wearing each load, participants performed three anticipated (AN) and unanticipated (UN) RTS maneuvers with their dominant limb. Each RTS required the participant to run at $3.5 \text{ m/s} \pm 5\%$ on a walkway, plant their dominant limb on a force platform (AMTI) embedded in the floor, and immediately stop in a low-ready position. For the AN maneuver, each participant responded to a visual stimulus delivered ~ 5 s prior to initiation of the

movement. During the UN task, each participant responded to a visual stimulus triggered ~ 600 ms prior to force platform contact.

For each RTS maneuver, sagittal plane limb biomechanics were quantified from the 3D coordinates of 36 reflective skin markers recorded using twelve high-speed (240 Hz) optical cameras (Qualysis AB). The marker trajectories were low-pass filtered with a fourth-order Butterworth filter (12 Hz) by Visual 3D (C-Motion). Biomechanical data (kinematics, kinetics and GRF) were imported into OpenSim [2] to estimate lower limb joint moments, segment positions and muscle forces. The force estimation process entailed generation of an anthropometrically scaled subject-specific model, residual reduction analysis and static optimization. The FL configuration was modeled with a 20 kg point mass applied at the torso center of mass, while the AL included the FL mass and an additional 20 kg attached to the posterior torso. PKJCF was estimated using the Joint Reaction tool and was defined as the force acting on the tibial plateau parallel to the longitudinal tibial axis [3]. Limb stiffness (k) was defined as the ratio of peak vertical ground reaction force (vGRF) to change in leg length (ΔL) [4].

For analysis, PKJCF, peak vGRF, knee flexion moment at PKJCF, ΔL , and k were assessed during the stopping phase (from initial contact of the dominant limb to contact of the non-dominant limb) of each RTS maneuver. Subject-based means for both the AN and UN maneuvers were calculated. The subject based mean for each dependent variable was submitted to a repeated measures ANOVA to test the main effects of and possible interactions between body borne load (NL, FL and AL) and movement type (AN and UN). Where statistically significant ($p < 0.05$) differences were observed, Bonferroni pairwise comparisons were used.

RESULTS AND DISCUSSION

The biomechanical results of the RTS tasks are presented in Table 1. During the RTS, adding body borne load increased the PKJCF ($p<0.001$) and the potential for musculoskeletal injury. Specifically, participants exhibited a significant 1.15 N/kg increase in PKJCF with the AL compared to the NL configuration ($p=0.006$), but a similar increase was not evident compared to the FL (0.54 N/kg; $p=0.107$), or between the NL and FL configurations (0.61 N/kg; $p=0.063$).

The increased PKJCF evident with body borne load may stem from a simultaneous increase in vGRF ($p=0.002$) and knee flexion moment ($p=0.025$). During the RTS, peak vGRF was significantly greater (0.5 N/kg; $p=0.014$) during the AL compared to NL configuration. Yet, similar increases of peak vGRF were not evident between the AL and FL (0.3 N/kg; $p=0.114$), or between the FL and NL conditions (0.2 N/kg; $p=0.156$). To prevent musculoskeletal injury, the vGRF needs to be attenuated through lower limb (e.g. knee) joint moments. The fact that participants exhibited significantly larger knee flexion moment with the AL compared to NL ($p=0.010$), but not compared to the FL ($p=1.000$), or between the NL and FL configurations ($p=0.147$), supports this contention. The larger external knee flexion moment, which must be counterbalanced by eccentric quadriceps activation to prevent lower limb collapse, potentially increases compressive force and subsequent injury risk of the knee joint, particularly with the heavy (i.e. 40 kg) body borne load.

To prevent collapse of the lower limb and successfully perform the RTS, participants exhibited a significant increase in k ($p=0.015$) with the addition of body borne load. However, after controlling for Type I error, k was not significantly different

($p>0.05$) between any of the load configurations, which may be attributed to the fact that ΔL did not change ($p=0.899$) when adding body borne load [3]. As such, future research is warranted to determine if varying ΔL (i.e. greater lower limb flexion) while performing military-relevant tasks helps soldiers attenuate the larger compressive forces exhibited on the knee joint with the addition of body borne load.

Performing an unplanned RTS did not further elevate the potential for musculoskeletal injury. Specifically, PKJCF did not significantly differ ($p=0.693$) between the UN (3.05 N/kg) and AN (2.96 N/kg) maneuvers. The insignificant increase in PKJCF during the UN task may be attributed to the fact that participants failed to exhibit a significant increase of peak vGRF ($p=0.280$), knee flexion moment ($p=0.864$), k ($p=0.463$), or ΔL ($p=0.398$) as compared to the AN maneuvers.

CONCLUSIONS

The addition of body borne load during military-relevant tasks likely increases the risk of musculoskeletal injury. This elevated risk results from greater compressive force on the knee joint that may be attributed to the increased peak vGRF and knee flexion moment evident with the heavy (40 kg) body borne load. Yet, performing an unplanned task did not result in greater knee joint force and risk of musculoskeletal injury. Future research should determine the lower limb mechanical patterns necessary to decrease the compressive force on the knee joint, particularly with heavy body borne loads.

REFERENCES

1. Jones BH, et al. Amer J Prev Med. 38(1):S42-S60
2. Delp S, et al. IEEE. TBME. 54(11):1940-1950
3. Lerner Z, et al. Med & Sci Sport & Ex. 46(6):1261-1267
4. Silder A et al. J of Biomech. Run with Load Leg Stiff.

Table 1: Biomechanical Results for each Load and Movement Type

	NL		FL		AL	
	AN	UN	AN	UN	AN	UN
PKJCF (N/kg)*	2.40 ± 0.41	2.44 ± 0.60	2.91 ± 0.46	3.14 ± 0.71	3.58 ± 0.62	3.56 ± 0.47
vGRF (N/kg)*	1.72 ± 0.42	1.82 ± 0.45	2.01 ± 0.38	2.08 ± 0.39	2.31 ± 0.39	2.31 ± 0.19
Knee Moment (Nm/kg)*	2.06 ± 1.19	1.35 ± 1.67	2.55 ± 1.70	2.54 ± 2.08	2.98 ± 1.36	3.33 ± 2.86
k *	10.30 ± 4.59	10.56 ± 3.98	10.02 ± 3.82	11.40 ± 2.94	12.36 ± 1.43	13.00 ± 2.17
ΔL (m)	0.20 ± 0.05	0.21 ± 0.05	0.21 ± 0.03	0.21 ± 0.03	0.21 ± 0.03	0.20 ± 0.03

*significant ($p<0.05$) effect of body borne load

MEASURING CAPULOHUMERAL RHYTHM WITH SUPRASPINATUS IMPAREMENT: A PRE- AND POST-OPERATIVE COMPARISON

¹ Ashley N. Hannon and ^{1,2} Thomas R. Jenkyn

¹ Western University, London, ON, CANADA, Dept. of Kinesiology

² Western University, London, ON, CANADA, Dept. Mechanical Engineering
email: ahannon@uwo.ca

INTRODUCTION

A common clinical measurement of glenohumeral kinematics is the evaluation of scapulohumeral rhythm. Inman[1] measured this motion in-vivo through bone pins and x-rays. Observations of scapulohumeral motion after the initial stabilization period, which is variable, lead to a 2:1 ratio of glenohumeral motion to scapulothoracic motion.

Improvements in technology allows for non-invasive in-vivo measurements to be observed. Giphart[2] used biplanar fluoroscopic radiostereometric analysis (RSA) in healthy normal subjects and noted results similar to Inman¹ for abduction, but slightly lower in forward flexion.

Quantifying the motion during abduction (ABD), flexion (FF), and compound motion (arm across chest (AAC) using a biplanar fluoroscopic RSA technique in subjects with healthy, normal shoulders as well as pre- and post- surgical repair supraspinatus muscle uses a very accurate technique to describe motion in 3D and gains further insight for clinicians.

METHODS

Five healthy normal subjects were recruited. The subjects performed one trial of right arm ABD to 90°, FF to 90° and the compound motion of moving the right hand to the left shoulder (AAC). These were completed at a self-selected pace. One subject with medium sized supraspinatus tear determined by MRI by operating clinician also completed the movement trials, 7 days prior to surgical intervention, and 6 weeks post-surgical intervention.

Biplanar fluoroscopy was collected at 30 Hz on all subjects and was matched with a Sawbone® generic shoulder model CT scan according to Hannon[3] RSA technique was employed in Rhinoceros® 3D modeling software. Once each frame of motion was matched in both planes, ISB recommended[4] landmarks of the scapula and humerus were exported, as seen in Figure 1, below.

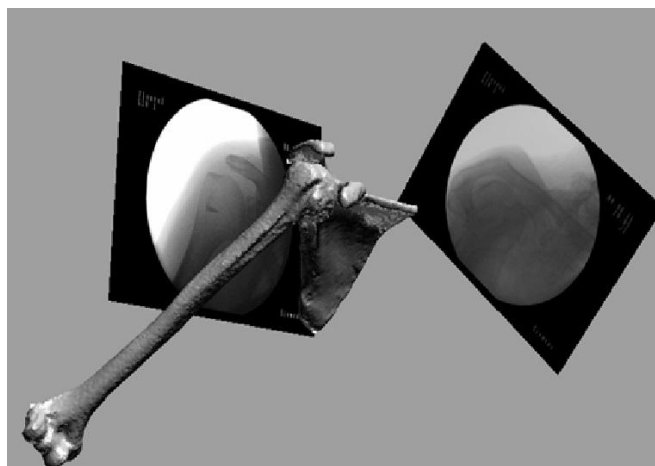


Figure 1: Virtual 3D biplanar fluoroscopic laboratory set up in Rhinoceros® with Sawbone® imported.

The measurements of the humerus in relation to the scapula for the motions were calculated. Data was filtered with a 4th lowpass Butterworth filter with a cutoff frequency of 3Hz. Data was normalized to 100% of motion. Standard error was calculated to determine excursion from the mean. Descriptive statistics were determined for all three rotations of the humerus in relation to scapula.

In order to obtain scapulohumeral rhythm measurements, glenohumeral motion was subtracted from total scapulohumeral motion, calculating the scapular motion component of ABD, FF and ACC motions.

RESULTS AND DISCUSSION

Results for this study illustrate that there is a large variability within all scapulohumeral motion. Figure 2 illustrates the glenohumeral motion during abduction. It is evident that the healthy population has a large variability as the humerus reaches 90° in relation to the midline. The trial of the subject prior to surgical intervention shows that there is a larger component of humeral motion. Finally, post-surgical intervention, the subject has a slightly lower component of glenohumeral abduction during this motion.

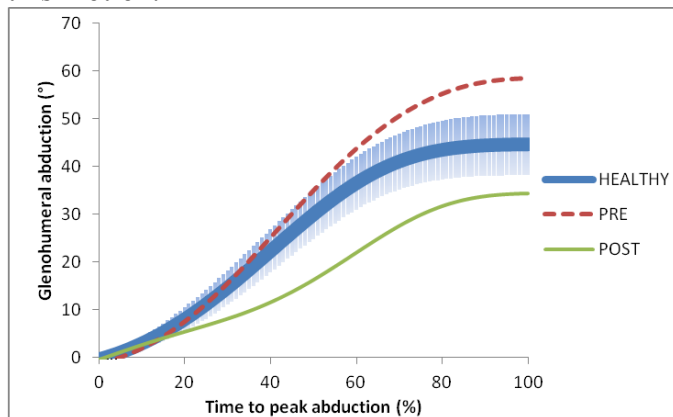


Figure 2: Glenohumeral abduction during ABD in healthy (with SEM), pre and post intervention

The increased glenohumeral motion could be due to increased activation of associated humeral abductor muscles including deltoids as a compensatory mechanism for the weakness in the injured supraspinatus.

Table 1 illustrates that there is slightly less motion during the overall movement in the injured population, prior to surgical intervention, while the healthy population maintained the approximate 2:1 ratio of humerus to scapula found prior [1, 2]. The post-operative group could have increased humeral motion in relation to the scapula due to the other

muscles of the rotator cuff compensating for the injured supraspinatus for a period prior to intervention, and with the repair, all abductors are activated, increasing the humeral component of abduction. Additional changes in variability could be due to the calculation accounting for the entire range of motion as opposed to only the portion above 30° in ABD or 60° FF, in addition to attempting to quantify motion of the AAC compound motion[1].

CONCLUSIONS

It is evident that scapulohumeral motion is variable. Further work is needed to quantify motion for individuals with rotator cuff impairments, to create a body of knowledge for clinicians to determine success of invasive interventions for repair of supraspinatus tear and investigate causes for increased humeral motion.

REFERENCES

1. Inman et al. *Observations on the Function of the Shoulder Joint*, J Bone Joint Surg, 1944.
2. Giphart et al. *Effect of Plane of Arm Elevation on Glenohumeral Kinematics: A Normative Biplane Fluoroscopy Study*. J Bone Joint Surg Am, 2013.
3. Hannon, A. & Jenkyn, T.R. *Measuring In-Vivo 3D Glenohumeral Joint Motion During Forward Flexion and Abduction of the Humerus Using Subject-Specific Markerless Biplanar Fluoroscopic Radiostereometric Analysis*. World Congress on Biomechanics, Boston, MA, 2014.
4. Wu et al. *ISB recommendation on definitions of joint coordinate systems of various joints for the reporting of human joint motion—Part II: shoulder, elbow, wrist and hand*. J. Biomech, 2005.

Table 1: Ratio of humeral motion compared to scapular motion in 3 movements

Motion	Scapulohumeral ratio		
	Healthy	Pre	Post
ABD	2.71 ± 0.41	0.09 ± 1.66	3.75 ± 0.34
FF	2.72 ± 0.38	1.26 ± 0.95	3.83 ± 0.48
AAC	2.03 ± 1.68	1.22 ± 1.35	1.56 ± 1.62

Changes in muscle work with disease progression during gait in Duchenne muscular dystrophy

¹ Kent Heberer, ² Susan Sienko, ² Cathleen Buckon, ¹ Loretta Staudt, ³ Anita Bagley, ² Michael Sussman, ¹ Eileen Fowler

¹ The University of California, Los Angeles, Los Angeles, CA, USA

² Shriners Hospitals for Children Portland, Portland, OR, USA

³ Shriners Hospitals for Children Northern California, Sacramento, CA, USA
email: kheberer@mednet.ucla.edu

INTRODUCTION

Duchenne muscular dystrophy (DMD) is a genetic disorder that primarily affects males. The hallmark of disease is proximal weakness with a gradual loss of ambulation in the second decade of life. While basic kinematic deviations have been documented, the purpose of this study is to determine how the ability of individual muscles to perform eccentric and concentric work changes with disease progression, and compare this with fatty infiltration as reported in the literature [1, 2]. We hypothesized that work production would decrease in the proximal thigh muscles and increase in the distal shank muscles with disease progression in DMD.

METHODS

Overground gait data were collected at self-selected walking speeds from a participant with DMD over three visits at 1 year intervals beginning at 9 years of age and compared to normative data (n=8). Experimental data were collected with Cortex (Motion Analysis Corp., Santa Rosa, California, USA) and analyzed with a scaled 92 muscle model in OpenSim [3]. Individual muscle velocity, force, power and work were normalized and calculated as described by Hu and Blemker [1]. This study focused on the stance phase of gait.

RESULTS AND DISCUSSION

Eccentric and concentric work generated by individual muscles is shown in Figure 1. The same 22 muscles used in the previous paper [1] have been separated by location and ordered by fat fraction rank as reported by Wokke et al [2].

Eccentric work was below the normal average in the one boy with DMD at all time points for most proximal and all distal muscles. Exceptions to this came from the rectus femoris, which was within the normal range at the baseline visit only, and the adductor longus and adductor magnus, which were both above the normal average at all time points.

Concentric work was below average at all time points for most proximal muscles. Exceptions to this came from the semitendinosus, which was above normal at baseline, and the semimembranosus (SM), which was above average at all time points, but trended toward the normal average with disease progression. For the distal muscles, the dorsiflexors were within the normal range initially, but progressively decreased with disease progression. However, the plantar flexors progressively increased concentric work with disease progression. While the medial and lateral gastrocnemii were below the normal average at baseline, concentric work increased markedly with increasing disease progression.

Our data agree with Hu and Blemker [1] in that muscles that normally generated more eccentric work had higher fat fractions in DMD [2]. However, the eccentric work of the biarticular hamstring muscles were much lower in the present study, which can be attributed to the exclusion of the swing phase. In DMD, muscles with a higher fat fraction are less able to generate force, resulting in reduced mechanical work as evident in the reduced eccentric work in the quadriceps and triceps surae and the reduced concentric work in the adductor magnus, long head of the biceps femoris (LHBF), and the tibialis anterior.

Results for the SM and triceps surae suggest possible compensatory mechanisms. The SM had a lower reported fat fraction and initially provided excessive concentric work (in contrast to the LHBF, which had a higher fat fraction and showed decreased concentric work). Interestingly, Hu and Blemker [1] reported that in normative gait, the SM had a larger eccentric demand than the LHBF, which they hypothesized would result in more fatty infiltration. The results of our study suggest that the SM is less affected by stresses associated with eccentric work as shown by the increased concentric work production. Physiological differences between the SM and LHBF may explain why the former has a lesser fat fraction in response to similar eccentric demands and should be studied further to better understand this potential compensatory mechanism. The triceps surae showed progressively increasing concentric work with disease progression despite having nearly the highest fat fraction of the distal muscles. Kinetic changes associated with toe walking, which occurred after baseline, explain the shift from eccentric to concentric work. Toe walking eliminates the eccentric requirement of the triceps surae to control the forward progression of the tibia over the foot. The ankle plantar flexes into single limb support, during which the associated plantar flexor moment would be supplied concentrically. This action adds energy and work to the stance limb to support and propel the center of mass and would compensate for the decreased work production of the proximal muscles. Fatty infiltration data as reported previously [2] were not available for the gluteal muscles; however, we did find a marked reduction in both eccentric and concentric work production for these muscles.

CONCLUSIONS

With disease progression in DMD, the demands placed on individual muscles changes as compensatory gait patterns arise in response to muscle weakness. Based on the muscle work simulation, proximal extensor muscles provide less concentric work and distal extensor muscles provide more concentric work. In general, muscles that have greater fat fraction are those that have a greater eccentric demand, especially for the proximal group. Compensatory mechanisms reflect changes

in muscle use, as distal muscles transition from eccentric to concentric work production, which may alter muscle stresses and fatty infiltration in mid to late disease states.

REFERENCES

1. Hu X and Blemker SS. *Muscle and Nerve* Accepted Article, 2015. DOI: 10.1002/mus.24607
2. Wokke BH, et al. *Neuromuscular Disorders* **24**, 409-416, 2014.
3. Delp SL, et al. *IEEE Transactions on Biomedical Engineering* **54**, 1940-1950, 2007.

ACKNOWLEDGEMENTS

Funded by Shriners Hospitals grant 79115.

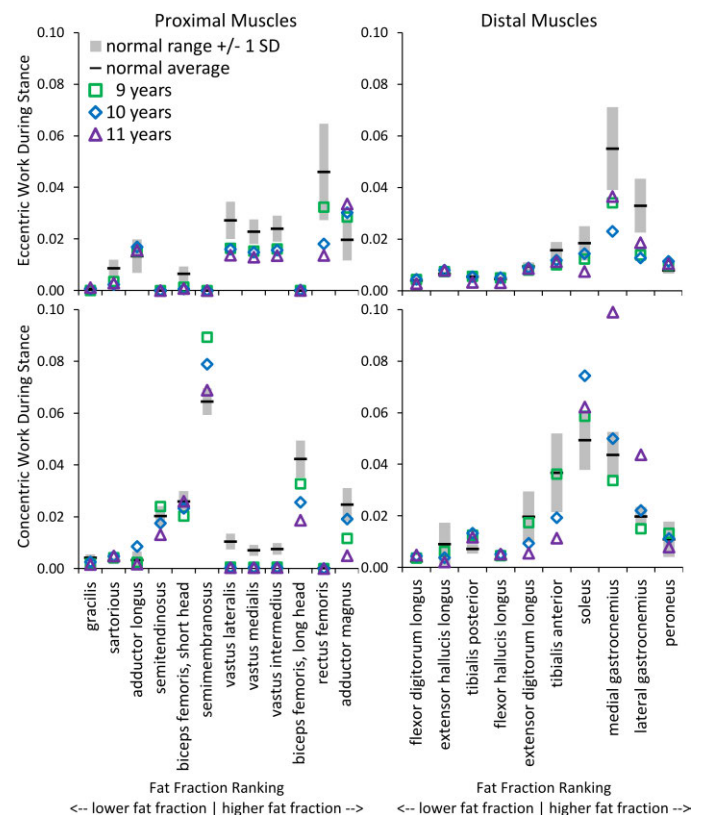


Figure 1: Total normalized eccentric (top row) and concentric (bottom row) work for individual proximal (left column) and distal (right column) muscles during stance. Normative average and range is denoted by the black lines and grey regions. Data for one boy with DMD is shown at age 9 by the green squares, age 10 by the blue diamonds, and age 11 by the purple triangles. Muscles are ranked in order of fat fraction, increasing from left to right.

EFFECTS OF A LONG TERM STRETCHING INTERVENTION ON THE MATERIAL PROPERTIES OF MUSCLE: PRELIMINARY RESULTS

Jamie E. Hibbert, Zachary J. Domire

East Carolina University, Greenville, NC, USA
email: hibbertj12@students.ecu.edu

INTRODUCTION

Muscle strength is a significant predictor of mortality [1]. Additionally, decreased muscle mass and strength, or sarcopenia, is also associated with decreased independence for older adults. This occurs because as they become weaker, activities of daily living become more difficult to perform without assistance. Decreased muscle size and strength are also associated with increased instance of falls and fractures [2], and strongly correlated with quality of life in older adults [3].

It is reasonable to recommend resistance training as a potential means of combating age-related muscle mass loss. However, there have been many studies that have found that older adults have a diminished response to exercise when compared to their younger counterparts [4, 5]. The observed decreased response to exercise seen in the aged population indicates that the hypertrophic response is impaired. There are many levels of the hypertrophic response at which the impairment may occur, but evidence suggests that the impairment occurs at or near the level that the mechanical signal is sensed [6]. A possible explanation is the mechanotransduction is impaired as a result of extracellular matrix stiffening. The overarching hypothesis for this study is that the attenuated response to exercise seen in older adults is caused by an impaired ability to sense mechanical stimuli as a result of increased muscle stiffness.

In order to conduct an experimental study of our hypothesis, a means to manipulate muscle stiffness in vivo was needed. Stretching has been shown to be an effective intervention to increase range of motion. We examined changes in muscle material properties, rather than simply changes in range of motion, as a result of a stretching intervention.

METHODS

The participants were three generally healthy women aged 70+ years with BMIs of less than 30 kg/m². All participants were free of neurological illness, cardiovascular disease, lower extremity musculoskeletal dysfunction, peripheral artery disease, cancer, type II diabetes, and high blood pressure. Men were not recruited for this study because the prevalence of sarcopenia is greater in women. It is also currently unknown if there are gender differences in muscle stiffness values.

Ultrasound elastography (Supersonic Imagine, Aix-en-Provence, France) was used to measure muscle stiffness of both heads of the gastrocnemius. A 10 second clip was collected to allow for stabilization. At the 5 second mark of the clip, a 2mm region of interest was placed in the center of the muscle and shear modulus was calculated as the average across this region.

The participants were taken through a series of contract-relax Proprioceptive Neuromuscular Facilitation (PNF) stretches for the lower body. Each stretch began with the subject passively taken to the end of their range of motion or the point at which they begin to feel a stretch, but no pain. They were held in this position for 20 seconds then told to push against resistance for 7 seconds, activating the agonist muscles. They were then instructed to relax and the stretch was taken to a new end point and held for an additional 20 seconds. Each stretch was performed three times bilaterally, alternating between sides. Subjects will participate in this stretching routine 3 days a week for 8 weeks. The data presented in this abstract are from the first 4 weeks of the intervention.

RESULTS AND DISCUSSION

Due to the small sample size, at this point, data for each participant is presented individually rather than mean values for the group. This provides a more clear illustration of the observed changes.

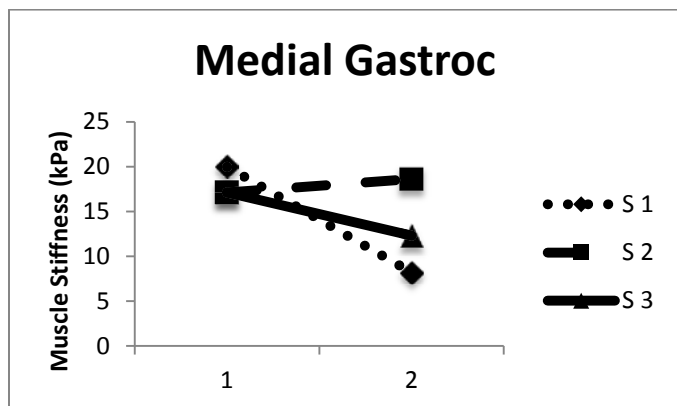


Figure 1: Changes in medial gastroc stiffness from baseline to the beginning of week 5

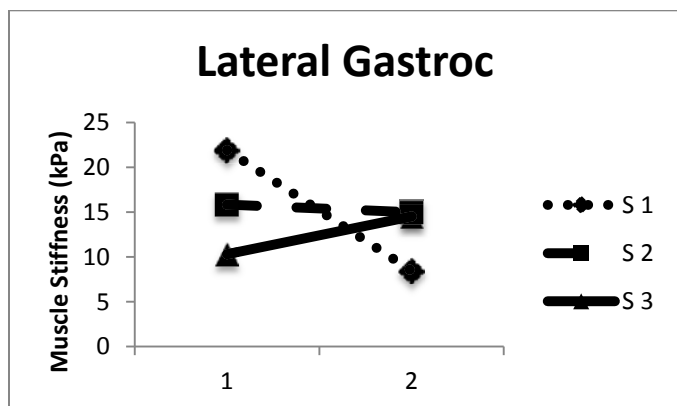


Figure 2: Changes in lateral gastroc stiffness from baseline to the beginning of week 5

Based on the data, it appears that each of the participants to this point has a slightly different response compared to the other two participants. The participant listed as S 01 has shown a large decrease in stiffness in both the medial and lateral

gastrocnemius muscles. S 02 has not exhibited much change in either muscle with one increasing slightly and one decreasing slightly. S 03 also increased in one portion of the muscle and decreased in the other, but these changes were larger than the changes exhibited by S 02.

CONCLUSIONS

It is still early in the intervention and the sample size is too small to draw many conclusions based on the current data, but it does appear that at least in some subjects stretching has the capacity to change muscle stiffness.

Interestingly the oldest participant is the one who has exhibited the greatest change in muscle stiffness at this time. Additionally she was also the subject who was stiffest in the pre-test. Further research may show changes in stiffness may be dependent on the initial stiffness. As this study continues, the relationship between age and response to the intervention will also be investigated further.

REFERENCES

1. Rantanen T. *Scand J Med Sci Sports*. **13**, 3-8, 2003.
2. Short KR. *Int J Sport Nutr & Ex Metab*. **11**, S119, 2001.
3. Ozcan A, et al. *BMC Public Health*. **5**, 90, 2005.
4. Raue et al, *J Appl Physiol*. **106**, 1611-17, 2009.
5. Dennis et al, *Physiol Genomics*, **32**, 393-400, 2007.
6. Rice, et al. *Biogeront*. **8**, 257-267, 2007.

ACKNOWLEDGEMENTS

The authors would like to acknowledge funding from the American Society of Biomechanics Graduate Student Grant-In-Aid.

	Age (years)	Pre- Test Stiffness (kPa)	Week 5 Stiffness (kPa)	Change in Stiffness (kPa)
S 01 MG	87	19.97	8.23	-11.74
S 01 LG		21.9	8.43	-13.47
S 02 MG	73	17.13	18.63	1.5
S 02 LG		15.83	14.97	-0.86
S 03 MG	70	17.13	12.3	-4.83
S 03 LG		10.3	14.5	4.2

Table 1: Changes in muscle stiffness over 4 weeks

Matrix stiffness affects human mesenchymal stem cell differentiation uniquely in 2D and 3D culture

¹ Nathaniel Hogrebe and ¹ Keith J. Gooch

¹ The Ohio State University, Columbus, OH, USA
email: nathaniel.hogrebe@gmail.com

INTRODUCTION

Matrix stiffness has been shown to be an important regulator of cell behavior. For example, given the same biochemical environment, soft matrices induce human mesenchymal stem cells (hMSCs) to become adipocytes, while stiff matrices with a modulus similar to bone sends them down an osteogenic lineage [1]. It is still unclear, however, how these effects translate to more physiologic 3D culture. In this study, we investigated how matrix stiffness affected hMSC differentiation differently in 2D and 3D culture using a biomimetic self-assembling peptide (SAP) hydrogel system that allowed for independent control of stiffness and RGD binding site concentration.

METHODS

To study the effects of stiffness and culture dimensionality on hMSC differentiation, we used a SAP hydrogel system with a fibrous microstructure similar to collagen. This system allowed for non-spherical morphologies similar to those observed within collagen matrices in 3D culture without the drawbacks of heterogeneous natural matrices, such as the lack of controllable biochemical functionality. We altered matrix stiffness ($G' = 0.25, 1.25, 5, \text{ and } 10 \text{ kPa}$) while maintaining a constant RGD binding site concentration, and hMSCs were either grown on top of (2D environment) or encapsulated within (3D environment) these gels. Either growth medium or a 1:1 mixed adipogenic/osteogenic induction medium was used to investigate the possibility that stiffness and culture dimensionality alone are able to induce differentiation, or alternatively if these physical parameters work synergistically with biochemical factors to direct differentiation. For experiments involving ROCK inhibition, $10 \mu\text{M}$ of Y-27632 was added to the culture medium every 24 hours.

After 26 days of culture, cell morphology was assessed with differential interference contrast (DIC) microscopy. Differentiated cells were stained with either Oil Red O for lipids, Alizarin Red for calcium deposition, or with BCIP/NBT substrate for alkaline phosphatase, and all were imaged with a brightfield microscope. Quantitative RT-PCR was performed to test for markers of differentiation, including PPAR γ -2 for adipogenesis and alkaline phosphatase for osteogenesis.

RESULTS AND DISCUSSION

As illustrated by Figure 1, both matrix stiffness and dimensionality heavily influenced cell morphology, which is of note since cell shape has been strongly correlated with its function [2].

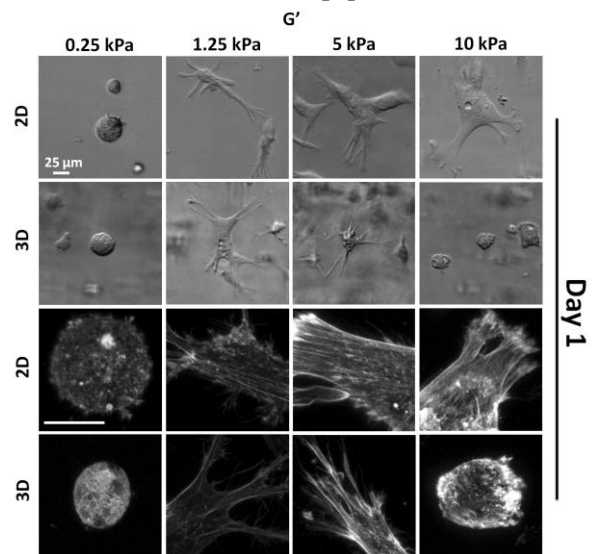


Figure 1: hMSC morphology is strongly influenced by both stiffness as well as whether the cells are grown on top of or encapsulated within the gels. Cells in the bottom half of figure were stained for F-actin. Scale bars = $25 \mu\text{m}$.

After 24 hours, hMSCs cultured on top of the gels progressively spread with increasing stiffness and

had an increasingly more organized actin structure. Cells within the gels spread greatest at intermediate stiffness, adopting stellate morphologies. As time progressed while using growth medium, the cells within the 1.25, 5, and 10kPa gels took on an elongated, spindle morphology as they do within collagen gels. Cells cultured on top of the gels continued to spread and increase in area.

Using growth medium, no visual signs of differentiation appeared after 26 days in culture, and this lack of differentiation was confirmed with qRT-PCR (Fig 2A-B). With a 1:1 adipogenic/osteogenic induction medium, however, overt differentiation was observed as indicated by adipogenic lipid vacuoles that stained with Oil Red O as well as osteogenic mineralization that stained with Alizarin Red (Fig 2C). QRT-PCR after 26 days in induction medium confirmed this differentiation. In addition, correlating PPAR γ -2 gene expression with the percentage of cells possessing lipid vacuoles showed good agreement between gene expression and visual indications of differentiation.

While stiffness and culture dimensionality alone were unable to induce differentiation, they both acted synergistically with induction factors to direct differentiation. Specifically, low stiffness promoted higher adipogenic gene expression as well as lipid formation, while increasing stiffness drove cells toward a more osteogenic phenotype as indicated by higher alkaline phosphatase activity and mineral

deposition (Fig 2A-D). Interestingly, there were notable differences between 2D and 3D culture at a given stiffness. For example, PPAR γ -2 expression was higher in 3D than in 2D at a particular stiffness. In contrast, alkaline phosphatase was much higher in 2D than 3D at a given stiffness. Thus it seems that 3D culture is more conducive to adipogenesis, while 2D facilitates osteogenesis more efficiently at a given matrix stiffness.

Rho-kinase (ROCK) is vital to a cell's ability to respond to matrix stiffness. Inhibiting ROCK increased adipogenesis and decreased osteogenesis, consistent with the work of others [2]. Much of the differences between stiffness seemed to be abrogated by ROCK inhibition, but notably differences between 2D and 3D at a given stiffness persisted (Fig 3). Thus there seems to be another mechanism independent of the ROCK pathway that is contributing to the variations in differentiation observed between 2D and 3D culture.

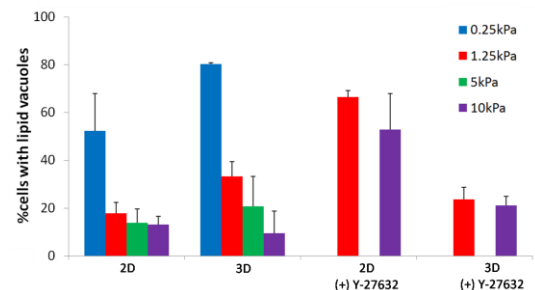


Figure 3: ROCK inhibition eliminates much of the variation in hMSC differentiation between stiffness, but differences between 2D and 3D remain.

CONCLUSIONS

Matrix stiffness is now widely recognized as an important determinant of cell behavior, but how these effects translate to a 3D environment is not fully understood. In this study, we observed that while the general trends seen with changes in matrix stiffness appear to be the same in 3D culture, the magnitude of this effect differs. Specifically, 2D culture appears to be more conducive to osteoblast formation while 3D culture is better at facilitating adipogenesis at a given stiffness.

REFERENCES

1. Zhao, W et al. *Materials Science and Engineering C* **40** (2014), 316-323.
2. McBeath R, et al. *Developmental Cell* **6** (2004), 483-95.

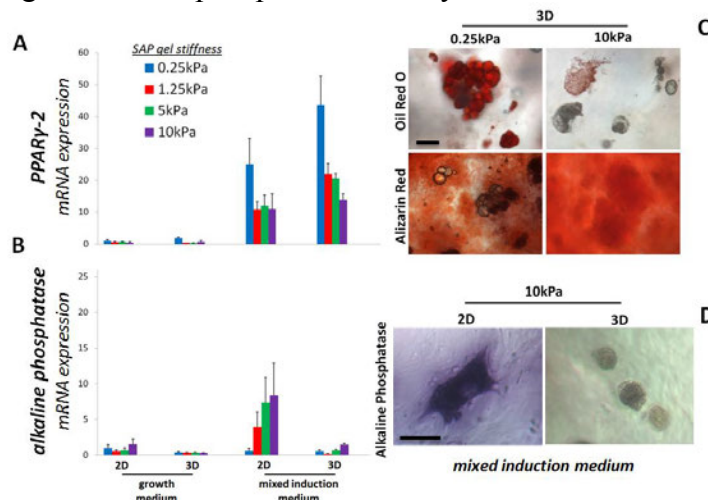


Figure 2: Induction medium, substrate stiffness, and culture dimensionality regulate hMSC differentiation. Scale bars = 50 μ m

A PROBABILISTIC MODEL OF THE SUBACROMIAL SPACE: IMPLICATIONS FOR SUBACROMIAL IMPINGEMENT SYNDROME

¹Jaclyn N. Chopp-Hurley, ²Joseph E. Langenderfer, ¹Clark R. Dickerson

¹Department of Kinesiology, University of Waterloo, Waterloo, ON

²School of Engineering and Technology, Central Michigan University, Mount Pleasant, MI

INTRODUCTION

Glenohumeral (GH) and scapulothoracic (ST) kinematic relationships, as well as morphological characteristics of the scapula and humerus affect the dimensions of the subacromial space [1-2]. Each measure varies considerably across the population, which can lead to misestimation of mechanical impingement of the subacromial space (SAIS). Further, the relative influence of each parameter on the size of the subacromial space is unclear.

There were three primary objectives:

1. To predict the distribution of the minimum subacromial space width (SAS) among a young, healthy male population due to variability in morphological and fatigue-related kinematic parameters across humeral elevation and fatigue state conditions.
2. Determine the relative importance of each parameter for modifying the size of the SAS.
3. Calculate the probability that measured subacromial tissue thicknesses would exceed this predicted SAS for each condition.

METHODS

A deterministic subacromial geometry model was developed that enabled calculation of the SAS based on modifying acromial, glenoid, and humeral morphology, and GH and ST kinematic parameters.

Morphological Model Parameters:

- Glenoid inclination (GI)
- Lateral acromial angle (LAA)
- Acromial anterior slope (AS)
- Acromial tilt (AT)
- Acromion index (AI)

GH/ST kinematic model parameters:

- Superior-inferior humeral head translation (HHT)
- Upward-downward scapular rotation (SR)
- Posterior-anterior scapular tilt (ST)
- Scapular protraction-retraction (SPR)

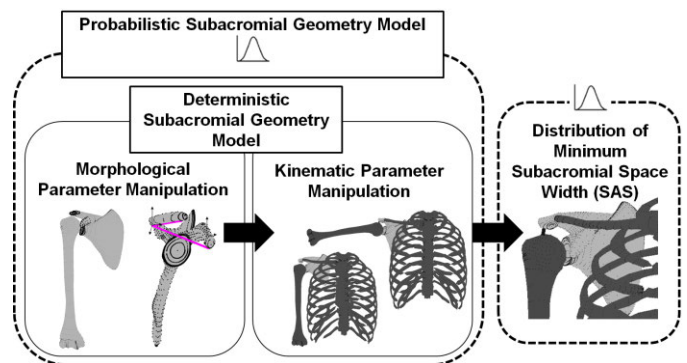


Figure 1: Overview of subacromial geometry model: morphological and kinematic model parameters were modified using empirically measured input distributions, from which the distribution of SAS could be obtained.

A probabilistic subacromial geometry model was then developed (NESSUS, SwRI, San Antonio, TX) which, using input distributions obtained from empirical data for each of the described model parameters, predicted the distribution of SAS for ten conditions (Figure 1).

- Humeral elevation angle (0, 30, 60, 90, 120°)
- Fatigue state (pre-fatigue, post-fatigue)

Using the AMV probabilistic method, importance factors (α) were calculated to evaluate the relative contribution of each parameter to predicted outputs.

A second probabilistic subacromial impingement risk model was then constructed. This model calculated the probability that experimentally measured subacromial tissue thicknesses (supraspinatus tendon, subacromial bursa) would

exceed the SAS predicted from the subacromial geometry model, thereby generating an estimate of the SAIS risk.

RESULTS AND DISCUSSION

Across all conditions, the SAS was highly variable, as evidenced by wide 1-99% confidence intervals (spanning a mean of 8mm) (Table 1). The SAS was not influenced by fatigue, but reduced considerably with arm elevation (4.5-5mm) within each fatigue state. Morphological parameters, notably glenoid inclination ($\alpha = 0.57$ [range, 0.33 – 0.71]), had consistently high relative importance in modulating the size of the SAS across all conditions, while the influence of kinematic parameters was modulated by elevation angle and fatigue state (Figure 2). While targeted interventions for morphological characteristics which predispose an individual to SAIS are challenging, glenoid inclination has been associated with superior humeral head translation [3-4]; this in turn promotes rehabilitation strategies that target GH stability maintenance.

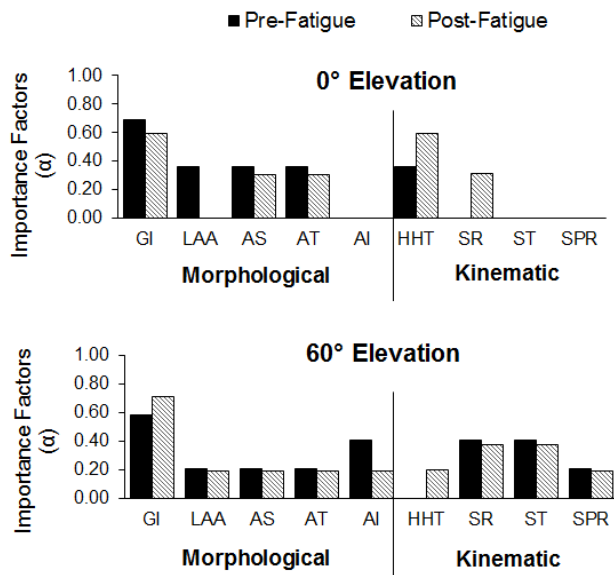


Figure 2: Importance Factors (α -levels): pre- and post-fatigue states at 0° and 60° humeral elevation angles.

The probability that subacromial tissue thicknesses would exceed the SAS (causing mechanical tissue impingement) was <5% at low elevation angles. At mid-range elevation, the probability was between 46.1% and 68.6%, while at 120° of elevation, the probability was as high as 73.6%. However, previous research has concluded that at elevation angles >90° (and possibly even >72°) the SAS vector passes lateral to the supraspinatus tendon [5-6]. This indicates that mid-range elevation likely poses the highest risk for mechanical SAIS.

CONCLUSIONS

The highly variable SAS suggests that solely considering the population average may strongly underestimate SAIS risk. The high probability of tissue compression at critical elevation angles (60-90°) implicates repetitive elevation that includes overhead arm postures as a likely contributor to rotator cuff degeneration and pathology. Additionally, the high relative importance of glenoid inclination across all conditions indirectly suggests high importance for superior humeral head translation. This finding supports glenohumeral stability maintenance and rotator cuff strengthening to alleviate the risk of SAIS and additional shoulder pathologies.

REFERENCES

1. Chopp JN and Dickerson CR. (2012). *Hum Movement Sci* 31(2); 448-60.
2. Michener LA et al. (2003). *Clin Biomech* 18; 369-79.
3. Flieg NG et al. (2008). *Clin Biomech* 23; 554-61.
4. Wong AS et al. (2003). *J Shoulder Elbow Surg* 12(4); 360-4.
5. Graichen H et al. (1999). *Surg Radiol Anat* 21(1); 69-64.
6. Giphart JE et al. (2012). *J Shoulder Elbow Surg* 21; 1593-1600.

Table 1: Minimum subacromial space width (SAS) [50% [1-99%] Confidence Interval] across the range of scapular plane elevation for both pre- and post-fatigue states.

Elevation Angle (°)	0	30	60	90	120
Pre-Fatigue SAS (mm)	9.5 [6.2 – 12.8]	9.3 [5.9 – 12.6]	6.3 [1.9 – 10.6]	5.1 [0.7 – 9.5]	4.8 [0.5 – 9.2]
Post-Fatigue SAS (mm)	9.7 [6.2 – 13.1]	9.4 [6.0 – 12.9]	6.3 [2.0 – 10.7]	5.3 [0.9 – 9.7]	4.9 [0.5 – 9.4]

PREDICTING PATELLOFEMORAL CONTACT MECHANICS: A COMPUTATIONAL STUDY

¹Hamidreza Jahandar, ¹Swithin Razu, ²Seth L. Sherman and ^{1,2}Trent M. Guess

¹The University of Missouri, Columbia, MO, USA

²Missouri Orthopaedic Institute, Columbia, MO, USA

Email: jahandarh@health.missouri.edu, web: <http://www.mizzoumotioncenter.com>

INTRODUCTION

Cartilage contact force, congruency, and contact area affect cartilage contact stress and high stresses in the patellofemoral joint are associated with cartilage degeneration. Cadaveric studies have been conducted to evaluate patellofemoral contact mechanics. However, physiological loading of a healthy patellofemoral joint may not be evaluated accurately using cadaveric methods [1]. A musculoskeletal computational model capable of accurately predicting cartilage contact pressures may serve as a valuable tool to orthopaedic surgeons. In this study, patellofemoral contact mechanics were studied in four different cases:

1. Normal model
2. Increased tibial tuberosity – trochlear groove distance (TT-TG) of 20mm
3. Patella alta – patella abnormally high
4. Patella baja – patella abnormally low

METHODS

With institutional approval and informed consent, magnetic resonance imaging (MRI) and gait lab measurements (motion capture and ground reaction forces) were obtained for one healthy subject (female, 20 years, 159.5 cm, 59.0 kg). MRI measurements were used to determine the TT-TG distance (12mm) and the Caton-Deschamps index (1.09) of the subject's right knee. The MRI and gait data were previously used to develop a subject specific computational musculoskeletal model (Fig. 1) as described in [2]. For the model, bone, cartilage and meniscus geometries were created from the MRI. Patellofemoral and tibiofemoral joints were defined as deformable contacts. Ligaments were defined using anatomical insertion and origin points on the bone geometry and the force was calculated using a non-linear force-length relationship [3]. Zero-load lengths for the ligaments were derived

from experimental laxity tests. The menisci were modeled as wedge shaped rigid bodies connected by 6 x 6 stiffness matrices as previously described [4]. The muscle forces were calculated using a feedback control loop to duplicate the experimental motion measurement in the gait lab. The foot segment was divided into five segments to calculate the ground reaction force [3].

The current project looks at the contact pressure distribution of the patellofemoral joint by discretizing the patella cartilage into 3mm x 3mm elements and defining contact between each element and the femoral cartilage. Four different models were developed. One normal condition (the original model based on the MRI measurements) to be compared against three pathological conditions:

1. TT-TG value of 20mm: TT-TG is increased by moving the Patellar tendon insertion points (tibial Tuberosity) 8 mm laterally.
2. Patella Alta: Caton-Deschamps index value is increased to 1.2 by increasing patellar tendon length.
3. Patella Baja: Caton-Deschamps index value is decreased to 0.8 by decreasing patellar tendon length.

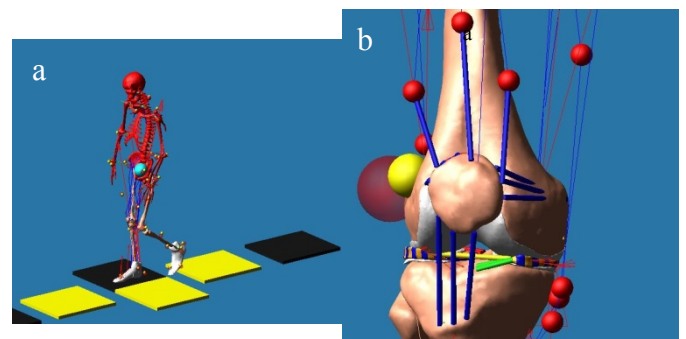


Figure 1: Muscle force driven model during gait (a.) and the anatomical right knee model (b.).

RESULTS AND DISCUSSION

Maximum vasti activation occurs at loading phase of the gait cycle. The pressure distribution and location of maximum pressure were measured for each model during the loading phase (21% of gait cycle). Predicted contact parameters are presented in Table 1. The contact pressure and area are comparable to that of experimental studies under similar loading conditions [5]. The increase in contact area with patellar tendon shortening (Patella Baja) matches the experimental results for knee flexion at 15° [6]. Predicted contact area for the normal model agrees with measured female contact area in an MRI based study [1].

The region of high contact pressure area moved distally in the Patella Alta case as the patella rode higher on the femoral trochlear groove due to longer patellar tendons. The Patella Baja model predicted the opposite outcome with the contact area occurring more proximally on the patella. It should be noted that the Patella Baja model predicted a lower maximum contact pressure at the loading phase mainly due to higher contact area. Moving the Tibial tuberosity distally leads to a more lateral contact distribution and also higher contact areas on

the lateral side. The maximum contact pressure was also increased.

Table 1: Patellofemoral contact parameters at loading phase

	Maximum Contact Pressure (MPa)	Contact Area(mm ²)	Average Contact Pressure (MPa)
Patella Alta	3	162	0.61
Patella Baja	1.7	324	0.29
Normal	2.2	225	0.49
TT-TG 20	2.7	189	0.70

CONCLUSIONS

Patellofemoral contact pressure was predicted during the loading phase of a gait cycle using a computational model of a healthy female subject. The model predicted changes in the contact mechanics of the patellofemoral joint in response to modification of tibial tuberosity location and patellar tendon length.

Future work will include models in other anatomical variations such as trochlea dysplasia as well as more movement simulation activities such as a dual limb squat.

REFERENCES

1. Besier TF, et al. Journal of Orthopaedic Research **23** (2005) 345-350.
2. Guess, T.M., et al., Predicted Loading on the Menisci during Gait: The effect of Horn Laxity. Journal of Biomechanics, In Press
3. Guess TM, et al., J Biomech Eng, 2014. **136**(2): p. 021032-021032.
4. Guess TM, et al., Med Eng Phys, 2010. **32**(5): p. 505-15.
5. D'Agata SD, et al., AM J Sports Med, 1993. **21**(2):212-9.
6. Upadhyay N, et al. AM J of Spots Med, 2005. **33**(10):1565-74.

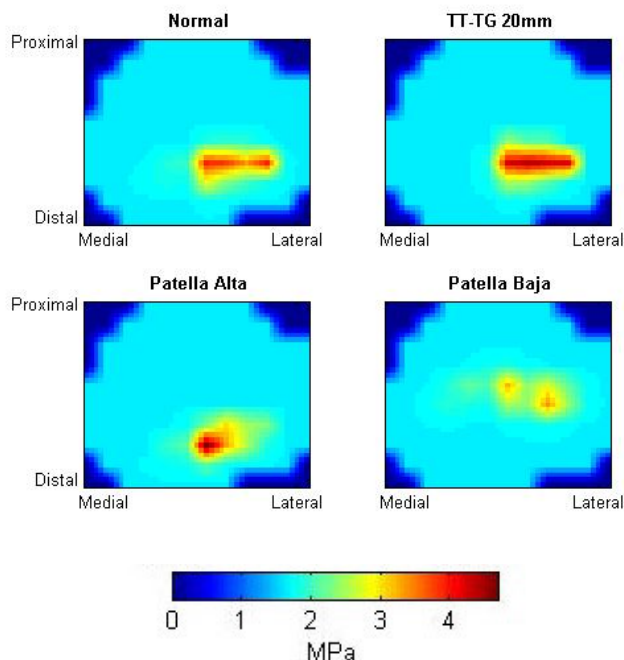


Figure 2: Pressure distribution in different models during the loading phase of gait.

LOWER EXTREMITY KINETICS DURING STOP-JUMP OF INDIVIDUALS WITH ADOLESCENT IDIOPATHIC SCOLIOSIS AFTER SURGICAL FUSION OF SPINE.

¹Rumit Singh Kakar, ²Yumeg Li., ²Cathleen Brown-Crowell, ³Yang-Chieh Fu and ²Kathy J. Simpson

¹Ithaca College, Ithaca, NY, USA

²The University of Georgia, Athens, GA, USA

³The University of Mississippi, MS, USA

email: rkakar@ithaca.edu

INTRODUCTION

Spinal fusion for individuals with adolescent idiopathic scoliosis (SF-AIS) is aimed at correcting the three dimensional deformity of the spine. Consequently, pelvic alignment would be expected to improve, thereby leading to more typical lower limb mechanics. However, whether spinal fusion influences pelvic dynamics thereby influencing lower limb and inter-limb mechanics during physical activities is not known. Therefore, the objective of the study was to compare the lower extremity kinetics displayed during the stance phase of stop-jump (Figure 1) between SF-AIS and healthy matched controls (CON) and inter-limb mechanics within the groups.

METHODS

The stop-jump task was performed by 10 SF-AIS (physically active; posterior-approach spinal fusion: 11 ± 2 fused segments; post-op time: $2.0 \pm .6$ yrs), and 10 CON individuals, pair matched for gender, age (17.4 ± 1.3 yr, 20.6 ± 1.5 yr, respectively), mass (63.5 ± 12.2 kg, 66.4 ± 10.9 kg), height (1.7 ± 0.1 m, 1.7 ± 0.1 m) and level of physical activity participation (International Physical Activity Questionnaire [1]).

The locations of the 18 reflective markers placed on the pelvis and lower extremities were recorded via 7-camera VICON motion capture system when the participants performed 5 acceptable trials of the stop-jump. Vertical ground reaction forces (vGRF) were measured (Bertec 4060-NC[®]; Sampling Frequency: 1200Hz) and joint moments were calculated for the stance phase using inverse dynamics and Euler's equations of motion using joint centers, segmental mass, ground reaction forces and kinematics of the joint. 2 (Group: SF-AIS or CON) x 2 (Limb: dominant leg or non-

dominant leg) mixed-model ANOVA ($p < .05$) and Tukey's HSD posthoc test were used to compare peak vGRF and peak joint moments normalized to body mass of both lower extremities in the three planes of motion displayed in the stance phase. Jump heights between the two groups were compared using a one-way ANOVA ($p < .05$).

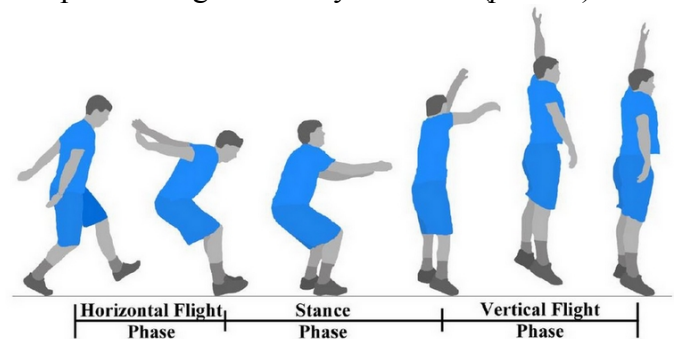


Figure 1: Stop-jump task and phases.

RESULTS AND DISCUSSION

Several main effects and no interactions were detected (Tables 1a and 1b). At the hip joint, for peak internal rotation moment, SF-AIS generated significantly greater moment (mean difference main-effect: 0.06 Nm/kg; $p = .015$) than CON, and the dominant limb displayed a tendency of greater moment than the non-dominant limb (range: $0.02 - 0.06$ Nm/kg; $p = .096$).

At the knee joint, a lower peak extensor (0.39 Nm/kg; $p = .011$) and greater abduction moment ($.40$ Nm/kg; $p = .032$) were displayed by SF-AIS than CON.

At the ankle joint, SF-AIS produced a greater peak internal rotation moment (0.03 Nm/kg; $p = .033$) and tendency for greater peak plantarflexion moment ($.18$ Nm/kg; $p = .065$). Jump height was not significantly different between the two groups ($p = .872$).

No significant interactions or main effects were observed for vGRF. Jump height was not different between groups.

Greater hip internal rotation moments coupled with greater knee abduction moments could predispose SF-AIS to knee injuries. This along with lower knee extensor moments coupled with greater knee abductor moments for SF-AIS compared to CON during the stance phase of the jump could potentially increase strains on the anterior cruciate ligament [2].

The lack of inter-limb differences for the sagittal plane and frontal plane joint moments suggests that SF-AIS may have acceptable inter-limb symmetry for joint moments, contrary to asymmetries reported for gait [3]. Another explanation may be within-group variability influenced by the participants' experience with jumping movements.

CONCLUSIONS

SF-AIS display mostly comparable lower limb kinetics to that of CON to prepare and propel their

body vertically to a similar jump height. Clinically, these results suggest that spinal fusion does positively influence lower extremity mechanics, and physically-active AIS individuals who have had spinal fusion surgery, can successfully produce typical lower limb kinetics similar to healthy controls during high-effort tasks such as the stop-jump.

REFERENCES

1. Hagströmer M, et al. *Public Health Nutr* **9**(6):755-762, 2006.
2. Chappell JD, et al. *Am J Sports Med* **30**(2):261-267, 2002.
3. Schizas CG, et al. *Eur Spine J* **7**(2):95-98, 1998.

ACKNOWLEDGEMENTS

Funding source: Scoliosis Research Society
Small Exploratory Research Grant (#046051-01)

Table 1a: Mean \pm standard deviation of peak joint moments (Nm/kg) for the group main effects control (CON) and individuals with adolescent idiopathic scoliosis post spinal fusion (SF-AIS) groups.

		Extensor	Flexor	Abductor	Adductor	External Rotator	Internal Rotator
Hip	SF-AIS	1.92 \pm 0.77	0.95 \pm 0.64	0.62 \pm 0.19	1.00 \pm 0.61	0.24 \pm 0.16	0.16 \pm 0.09*
	CON	1.95 \pm 0.50	0.81 \pm 0.27	0.53 \pm 0.32	0.92 \pm 0.55	0.28 \pm 0.13	0.10 \pm 0.05*
Knee	SF-AIS	1.45 \pm 0.39*	0.57 \pm 0.20	1.36 \pm 0.57*	0.31 \pm 0.23	0.22 \pm 0.10	0.04 \pm 0.03
	CON	1.83 \pm 0.44*	0.61 \pm 0.23	0.95 \pm 0.49*	0.31 \pm 0.27	0.19 \pm 0.09	0.05 \pm 0.05
Ankle	SF-AIS	1.81 \pm 0.30^T	0.10 \pm 0.14	0.56 \pm 0.34	0.13 \pm 0.10	0.18 \pm 0.15	0.07 \pm 0.06*
	CON	1.63 \pm 0.25^T	0.21 \pm 0.27	0.40 \pm 0.22	0.08 \pm 0.10	0.20 \pm 0.11	0.04 \pm 0.03*

Table 1b: Mean \pm standard deviation of peak joint moments (Nm/kg) for the limb main effects dominant (Dom) and non-dominant (NDom) legs.

		Extensor	Flexor	Abductor	Adductor	External Rotator	Internal Rotator
Hip	Dom	2.08 \pm 0.67	0.80 \pm 0.47	0.56 \pm 0.25	1.03 \pm 0.58	0.23 \pm 0.16	0.15 \pm 0.07^T
	NDom	1.79 \pm 0.59	0.96 \pm 0.51	0.60 \pm 0.28	0.89 \pm 0.57	0.29 \pm 0.12	0.11 \pm 0.08^T
Knee	Dom	1.61 \pm 0.50	0.64 \pm 0.22	1.21 \pm 0.60	0.35 \pm 0.27	0.23 \pm 0.10	0.05 \pm 0.04
	NDom	1.66 \pm 0.42	0.55 \pm 0.20	1.09 \pm 0.53	0.28 \pm 0.21	0.19 \pm 0.09	0.04 \pm 0.03
Ankle	Dom	1.76 \pm 0.29	0.15 \pm 0.20	0.20 \pm 0.13	0.07 \pm 0.06	0.48 \pm 0.26	0.11 \pm 0.09
	NDom	1.69 \pm 0.29	0.16 \pm 0.24	0.18 \pm 0.13	0.04 \pm 0.05	0.47 \pm 0.33	0.11 \pm 0.11

* represents statistically significant main effect difference ($p < .05$) and ^T represents tendency for statistical significance ($p = .05 - .10$).

COMPARISON OF MEDIAL-LATERAL CONTACT FORCE BALANCE IN KNEE JOINT BEFORE AND AFTER HIGH TIBIAL OSTEOTOMY FOR OSTEOARTHRITIS

Tserenchimed Purevsuren, Won Man Park, Kyungsoo Kim and Yoon Hyuk Kim

Kyung Hee University, Yongin, Korea
Email: yoonhkim@khu.ac.kr

INTRODUCTION

The opening wedge high tibial osteotomy (HTO) has been usually recommended for a young and active population for treatment of medial knee osteoarthritis (OA). Its main principle is to shift the weight-bearing line from medial compartment to lateral compartment of the knee and decompress the degenerated cartilage [1]. Relatively good outcome of HTO has been reported in clinical short-term, mid-term, and long-term studies [2, 3]

The joint forces on human knee during normal walking are dominant on medial compartment due to external knee adduction moment [1]. Therefore, the conventional gait analysis based on three-dimensional (3D) limb motion has been usually performed to evaluate surgical outcome of HTO. Previous studies demonstrated that the HTO successfully reduce the varus angle and decrease the knee adduction moment which characterizes osteoarthritic gait [3]. However, the reduction of contact loading on the medial compartment and shift of those loading into lateral compartment of knee after medial opening-wedge HTO are also necessary to fully understand mechanism of HTO to the OA knee.

In this study, the effect of medial opening wedge HTO on medial-lateral contact force balance in tibiofemoral joint was quantitatively evaluated during stance phase of gait. Since the muscle force is determinant to calculation of contact force, we also tried to demonstrate difference between muscle forces in OA patient and subject with HTO surgery. The muscle forces and joint contact forces were obtained by two-step modeling technique that combined with conventional inverse dynamic analysis and multibody dynamic simulation (Fig. 1).

METHODS

Five patients, who have moderate medial knee OA (Mean age: 57.6 years, weight: 67.4 kg, and height: 157.2 cm), participated in this study. 3D motion data of lower extremity was recorded by motion analysis system (Hawk[®] Digital Real Time System, Motion Analysis System, Santa Rosa, CA, USA) using ten cameras and reflective skin markers. The external ground reaction forces were measured by four force plates (MP4060, Bertec Corporation, Columbus, OH, USA) during walking. The participants performed 5 trials of motion with a self-selected walking speed along six meter walk-way. All procedure described above was repeated for each individuals 12 month after the HTO surgery.

At the first step, the muscle forces, joint forces and moments were calculated based on the recorded joint motion and ground reaction forces using an inverse dynamic lower extremity model [4]. The lower extremity was modeled as a 6-segment, 18 degree of freedom (DOF) articulated linkages actuated by 52 muscles. The output of inverse dynamic model such as predicted muscle forces, ankle joint forces and moments were used as the input to the multibody lower limb model with anatomical representation of the knee joint.

At the second step, a multibody lower extremity model of each subjects before and after HTO were developed in a dynamic analysis software (RecurDyn ver.7, Function Bay Inc., Korea). The previously developed and validated knee joint model [5] with bones (femur, tibia and patella), cartilage layers, non-linear ligaments, and deformable contact in both medial and lateral tibiofemoral compartment was placed in the symptomatic leg.

For the contact force estimation, the quasi-static analysis was run at the time step of 0.05 second during the stance phase of gait. The muscle forces from inverse dynamic analysis were applied constantly via muscle force actuators and ankle joint forces/moments which calculated in inverse dynamic analysis were applied as external forces on the distal tibia. The compressive contact forces on the medial compartment, lateral compartment as well as the total tibiofemoral joint force were investigated. The contact force result of each subject was normalized to the body weight and the results for OA subjects were compared to those of post-HTO. The estimated quadriceps and hamstring muscle forces, and medial to lateral compartment load ratio were also analyzed.

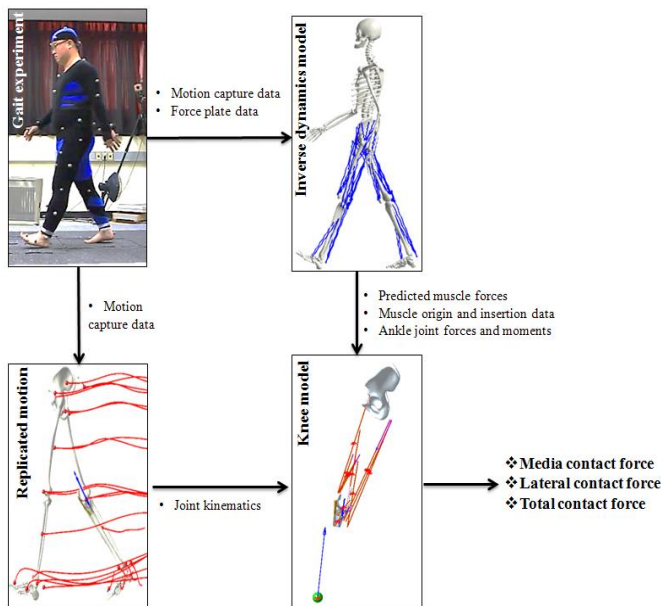


Figure 1: Diagram to explain the procedure for the estimation of tibiofemoral loading as well as muscle forces during normal walking

RESULTS AND DISCUSSION

Medial opening wedge HTO dominantly decreased the compressive contact force on the medial compartment during stance phase of gait (Fig. 2). The reduction in the first and second peaks of contact curve were about 0.8 BW. HTO increased the compressive loads on the lateral compartment, however the lateral compartment contact force was not higher than the medial contact force (Fig. 2).

The total tibiofemoral compressive force decreased after HTO due to reduction of quadriceps muscle activation. The medial to lateral load ratio showed that HTO significantly balanced the knee joint loading during normal walking. Our result indicates that the HTO surgery could improve the tibiofemoral contact force balance.

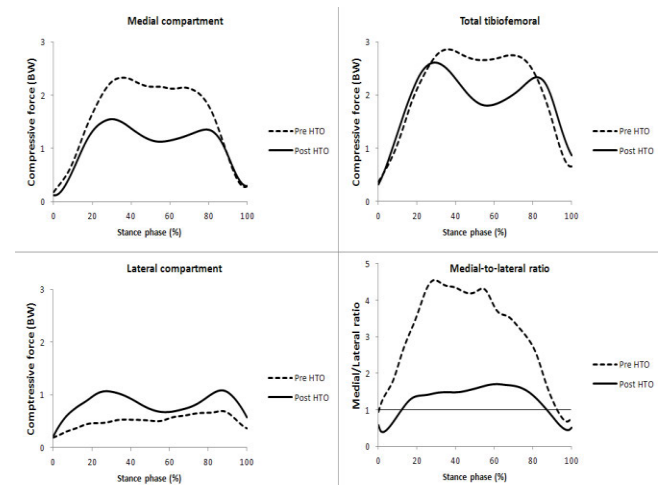


Figure 2: Mean compressive contact forces on medial compartment, lateral compartment and total tibiofemoral joint as well as medial-to-lateral load ratio before and after HTO during normal gait

REFERENCES

1. Amis AA. *Knee Surg Sports Traumatol Arthrosc* **21**, 197-205, 2013.
2. Hui C, et al. *Am J Sports Med* **39**, 64-70, 2011.
3. DeMeo PJ, et al. *Am J Sports Med* **38**, 2077-2087, 2010.
4. Nha KW, et al. *Comput Math Methods Med* **2013**, 314280, 2013.
5. Purevsuren T, et al. *Comput Method Biomech Biomed Engin* **15**, 1-5, 2014.

COMPARATIVE ANALYSIS OF STRESS AND STRAIN OF SPINAL CORD IN VARIOUS POSTERIOR DECOMPRESSION EXTENTS FOR CERVICAL OSSIFICATION OF THE POSTERIOR LONGITUDINAL LIGAMENT

Batbayar Khuyagbaatar, Won Man Park, Kyungsoo Kim and Yoon Hyuk Kim

Kyung Hee University, Yongin, KOREA
email: yoonhkim@khu.ac.kr

INTRODUCTION

Ossification of the posterior longitudinal ligament (OPLL) is a common cause of cervical myelopathy due to compression of the spinal cord. Patients with multiple levels of OPLL usually require the posterior decompression surgery. Clinical studies have reported that the decompression extent play an important role in the clinical outcomes [1, 2]. Thus, there is a need to better understand the optimal surgical extent with which sufficient decompression without excessive posterior shifting can be achieved. However, few quantitative studies have clarified this optimal extent for decompression of cervical OPLL. In this study, we used finite element (FE) modeling of the cervical spine and spinal cord to investigate changes in stress, strain, and posterior shift of the spinal cord for posterior decompression extent that occur with three different surgical methods.

METHODS

The FE model of the human C2-C7 cervical spine was reconstructed from the CT images. The FE model of spinal cord consisted white matter, gray matter, dura mater with nerve roots, denticulate ligaments (DLs), and a cerebrospinal fluid (CSF) layer (Fig 1). Material properties of white and gray matter obtained from Ichihara's study [3] then fitted to hyperelastic model. A single tangent modulus for dura mater derived from the Persson's study [4]. The DLs were modeled as 22 triangular extensions, using link element at each spinal level that attached laterally from the cord to the dura mater, and material property was obtained from a previous study [5]. The CSF layer was demonstrated Newtonian fluid characterized by viscosity of CSF derived from previous literature [6].

Three type of posterior decompression models for laminectomy, laminoplasty and hemilaminectomy were developed based on conventional surgical protocols with different extent of decompression (Fig 2a). The extent of decompression ranged from one- to five- levels: C5, C4-C5, C4-C6, C4-C7, C3-C6, and C3-C7 for each types of model, where the continuous OPLL placed through the C4 to C6 vertebral bodies (Fig 2b). The OPLL was modeled as simple rigid body model, and an OPLL occupying ratio of 20% to 60% was imposed to the spinal cord based on plain radiographic findings. Under various OPLL occupying ratios, the von-Mises stress and maximum principal strain in the spinal cord as well as the posterior spinal cord shift were analyzed for pre-operative and various posterior decompression models using FE analysis (ABAQUSTM, ABAQUS Inc., Providence, RI, USA).

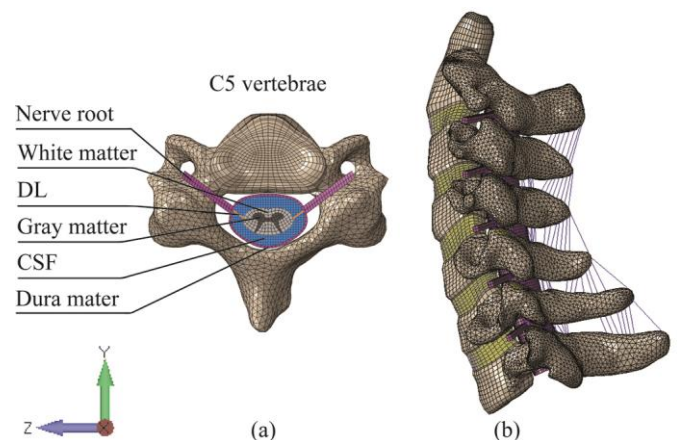


Figure 1: FE model of the cervical spine and spinal cord. (a) axial view and (b) sagittal view.

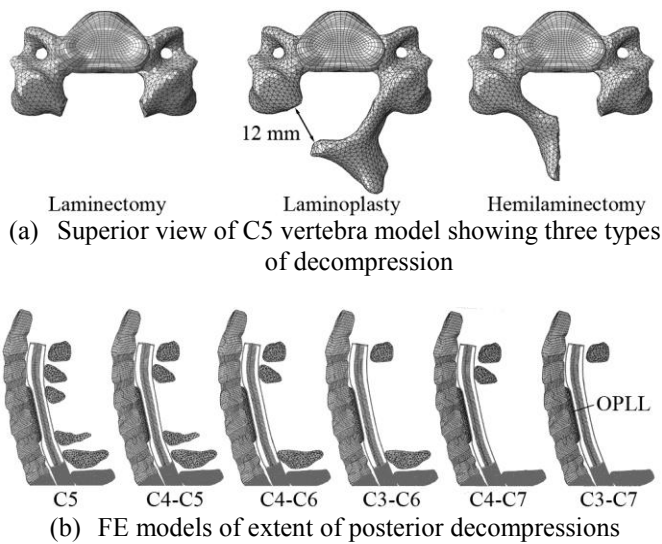


Figure 2: FE models and types of posterior approaches

RESULTS AND DISCUSSION

The von-Mises stress and maximum principal strain in the cord decreased as the extent of posterior decompression increased, regardless of the occupying ratio and the type (Table 1). The maximum stress in the cord was decreased by 30% to 90% from 1- to 5-levels of decompression by laminectomy and laminoplasty. The C3-C6 and C3-C7 in the laminectomy and laminoplasty at the 60% occupying ratio of OPLL had a maximum posterior shift of greater than 3 mm, which was associated with positive clinical outcomes after laminoplasty [2] and which showed substantial reductions in stress and strain. In contrast, the stress and strain reductions of hemilaminectomy differed from the values of laminectomy and laminoplasty due to

maximum values at the lateral column arising from lateral decompression of the spinal cord. Our results showed that hemilaminectomy is inferior to laminectomy and laminoplasty in terms of cord decompression.

In conclusion, stress and strain in the spinal cord decreased and posterior shifting of the cord increased as posterior decompression extended. The location of the decompression extent also influenced shifting, depending on the patient's anatomy. Laminectomy and laminoplasty were very similar in terms of decompression results, and both were superior to hemilaminectomy in all parameters tested. Decompression to the extents of C3-C6 and C3-C7 of laminectomy and laminoplasty could be considered sufficient with decompression itself. Our findings provide fundamental information regarding the treatment of cervical OPLL and can be applied to patient-specific surgical planning in the future.

REFERENCES

1. Kong Q, et al. *Spine* **36**, 1030-1036, 2011.
2. Sodeyama T, et al. *Spine* **24**, 1527-1531, 1999.
3. Ichihara K, et al. *J Neurotrauma* **18**, 361-367, 2001.
4. Persson C, et al. *Ann Biomed Eng* **38**, 975-983, 2010.
5. Greaves CY, et al. *Ann Biomed Eng* **36**, 396-405, 2008.
6. Bloomfield JG, et al. *Rediatr Neurosurg* **28**, 246-251, 1998.

Table 1: von-Mises stress, maximum principal strain, and posterior shift in the cord at the 60% occupying ratio of OPLL in the pre-operative model and posterior decompression models.

	Pre-op.	Laminectomy						Laminoplasty						Hemilaminectomy					
		C5	C4-C5	C4-C6	C4-C7	C3-C6	C3-C7	C5	C4-C5	C4-C6	C4-C7	C3-C6	C3-C7	C5	C4-C5	C4-C6	C4-C7	C3-C6	C3-C7
Stress (kPa)	210	139	60	22	15	7.3	5.7	150	54	19	20	8.9	7.8	162	101	67	66	50	52
Strain	0.41	0.38	0.33	0.26	0.26	0.17	0.17	0.38	0.32	0.26	0.26	0.17	0.18	0.4	0.38	0.34	0.34	0.33	0.34
Shift (mm)	-	0.5	2.2	2.6	2.6	3.1	3.0	0.5	2.1	2.7	2.7	3.1	3.1	0.3	1.3	1.5	1.5	1.6	1.5

DYNAMICAL FINITE ELEMENT ANALYSIS TO REPRODUCE THE TYPICAL PATTERNS OF PELVIC INSUFFICIENCY FRACTURES

¹Yoshimori Kiriyaama, ¹Kazuaki Nojima, ²Fumihiro Yoshimine, ³Yoshiaki Toyama and ³Takeo Nagura

¹Kogakuin University, Tokyo, JAPAN

²Ohkubo Hospital, Tokyo, JAPAN

³Keio University, Tokyo, JAPAN

email: kiryama@cc.kogakuin.ac.jp

INTRODUCTION

Pelvic insufficiency fracture (PIF) is caused by the reduction of bony elastic resistance due to aging. It is known that there are many typical fracture patterns [1]. The relations between the patterns and static loading conditions have been analyzed by using finite element model [2]. However, dynamical analysis of stress is needed to simulate the actual *in vivo* conditions. The purpose of this study is to analyze dynamical stress changes and to elucidate the relation between the fracture patterns of PIF and loading conditions.

METHODS

The model was based on the CT images of a female suffering from L1 vertebral compression fracture (76 years old). The sacrum, hip bones, and pubic symphysis were modeled with tetrahedral meshes (HyperMesh 10.0, Altair, USA). The sacroiliac joints were filled with soft elastic meshes to model the micro motion due to the joints and surrounding ligaments. Although PIF is caused by the bony porosis, the distribution of the bone material property in the pelvis is not necessarily clear. Thus, the isotropic materials as healthy model were used to reproduce the typical fracture patterns of PIF in this study.

The material properties were referred to the previous literatures (Cortical Bone ($E=18000$ MPa, $\nu=0.3$), Cancellous Bone (150 MPa, 0.3), Pubic Symphysis (5 MPa, 0.3), Sacroiliac Joint (1000 MPa, 0.3)) [3, 4]. Also, the sacrospinous ligaments were modeled because they are large and work to transmit loads the pelvis. Therefore, the ligaments were modeled as to generate force only when they were extended (spring constant: 45.0 N/mm) [5].

In this study, the base of sacrum was constrained completely. Also, total of 16 loading conditions were simulated as shown in Figure 1. The loads were applied to the iliac crest, acetabular surface and the ischial tuberosity. To generate surface loads, rigid surfaces were attached to those parts and the loads were applied to the rigid surfaces. The load of 2000 N was applied to the each of the iliac crest and acetabulum, while 1000 N was applied to both sides of the ischial tuberosity. In this study, RADIOSS (Ver.12, Altair, USA) was used as an explicit solver.

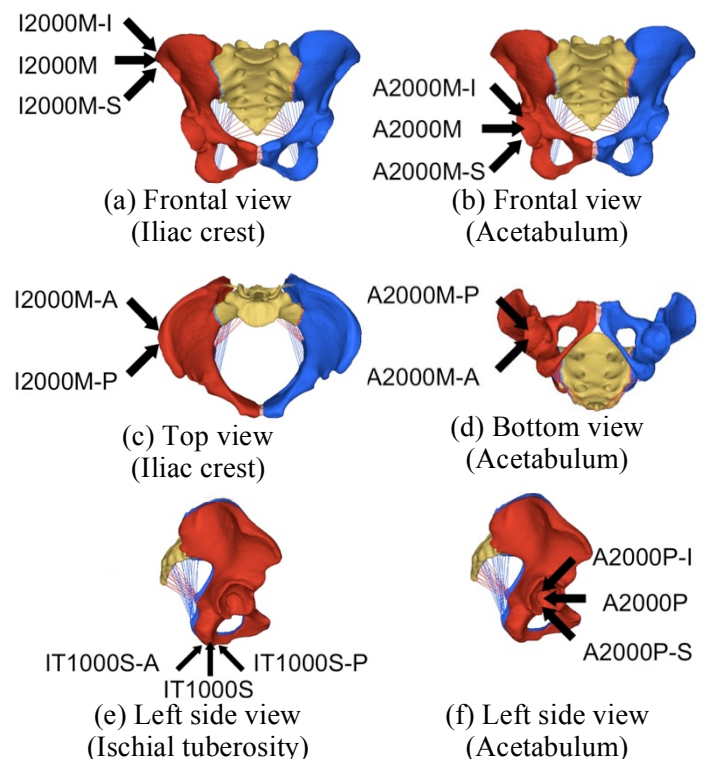


Figure 1: Loading condition in this study. The model is consisted of the sacrum (yellow) and hip bones (red and blue), and sacrospinous ligaments (lines). Total of 16 conditions were simulated. Here, arrows show the loading directions.

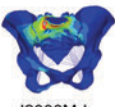
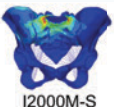

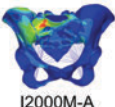
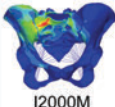
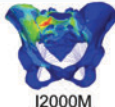
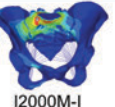
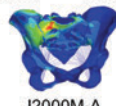
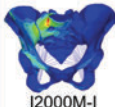
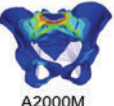

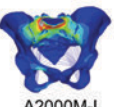
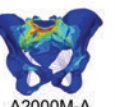
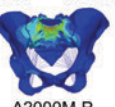
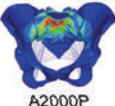
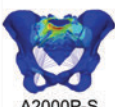
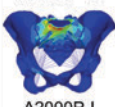
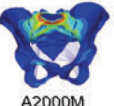

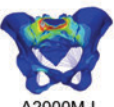

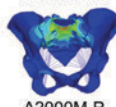
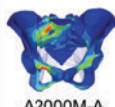
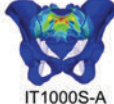
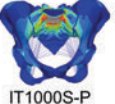



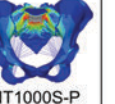
		Typical fracture patterns							
		Sacrum				Hip bone			
		H type	U type	L type	Unilateral vertical fracture	Bilateral vertical fracture	Pubic fracture	Supraacetabular fracture	
Load conditions	Iliac crest	 I2000M-I	 I2000M-S  I2000M-P		 I2000M-A	 I2000M	 I2000M  I2000M-I  I2000M-A	 I2000M-I	
	Acetabulum	 A2000M  A2000M-S  A2000M-I  A2000M-A  A2000M-P		 A2000P  A2000P-S  A2000P-I			 A2000M  A2000M-S  A2000M-I  A2000M-A  A2000M-P	 A2000M-A	
	ischial tuberosity	 IT1000S-A  IT1000S-P	 IT1000S				 IT1000S  IT1000S-A  IT1000S-P		

Figure 2: Classification between fracture patterns of PIF and loading conditions.

RESULTS AND DISCUSSION

The simulated fractures patterns were classified as shown in Figure 2. All loading conditions had stress concentration on the sacrum and pubic rami. This means that the combination fractures of the sacral and pelvis could be happened regardless of the loading conditions.

The fracture patterns of H, U and L characters on the sacrum were looked like each other well, and this could mean that it is difficult to identify a mechanical cause of PIF from the sacrum fracture. This also shows that a slight difference of loading condition could change the fracture patterns.

The superior area of the acetabular roof showed the stress concentration only under the conditions of I2000M-I or A2000M-A. This agrees with the clinical findings in which that the fracture of the area is observed rarely. Therefore, the starting point of the fracture on the superior area of the acetabular roof could be identified when the fracture is diagnosed.

While the classification showed the most of the typical fracture patterns of PIF, the inferior

horizontal fracture pattern was not confirmed with our model [1, 3]. Actually, through whole of the loading conditions, the lower part of the sacrum did not show the stress concentration. The reason for this was that the finite element model did not necessarily simulate the distribution of the material property, muscle loads and realistic loading conditions. These are limitations in this study, and the model might be modified in the future work.

Although our study had some limitations, the simulated fracture patterns were almost similar to clinical patterns of PIF. Therefore, the model and loading conditions could be constructed adequately. Also our model and the results of this study could be useful to elucidate the mechanism of PIF.

REFERENCES

1. Yoshimine F, *J Japan Soc. Fract. Rep.* **34**, 827-831, 2012 (in Japanese).
2. Kiriyama Y, et al. *Proceedings of 7th WCB 2014*, Boston, MA, USA, 2014.
3. Linstorm NJ, et al. *SPINE* **34**, 309-315, 2009.
4. Richard AM, et al. *J Osteoporosis* **2010**, 2010.
5. Zhao Y, et al. *Injury* **43**, 490-494, 2012.

HIGH-DIMENSIONAL ANALYSIS REVEALS PATTERNS OF LOWER LIMB MUSCLE VOLUME DISSIMILARITIES ACROSS CLINICAL AND ATHLETE POPULATIONS

¹ Katherine R. Knaus, ¹ Geoffrey G. Handsfield, and ¹ Silvia S. Blemker

¹ The University of Virginia, Charlottesville, VA, USA
email: ker4e@virginia.edu

INTRODUCTION

Muscle volume is a major determinant of force generating capacity. Recent *in vivo* measurements demonstrate that in healthy individuals, lower limb muscle volumes scale linearly with the product of height and mass [1], making it possible to compare body-size-independent muscle sizes between different subjects. We have used this normative database in order to identify differences in body-size normalized lower limb muscle volumes between a healthy normative database and subjects ranging in functional capacity from children with cerebral palsy (CP) [2] to collegiate athletes [3]. In all these (and other similar studies), analyses of muscle volumes are performed on a muscle-by-muscle (or functional group) basis. The goal of this work was to explore the applicability of high-dimensional data analysis approaches that would allow a more holistic understanding of how muscle volumes across the entire limb vary across populations.

METHODS

Using high resolution MRI, we imaged the lower limbs of 23 active healthy individuals [1], 10 patients with cerebral palsy [2], and 35 collegiate athletes [3], of who competed in track and field (10), football (5), baseball (5), and basketball (10). We manually segmented 35 unique muscles in these images to compute volumes, which were normalized for body size differences by dividing by height*mass. Z scores were computed by comparing the normalized volumes for each subject to the mean and standard deviation of the healthy normative database.

Using hierarchical clustering to calculate the multi-dimensional Euclidean distance between each vector of normalized volumes, individual subjects and muscles were sorted based on statistically similar patterns of muscle size. Principal

component analysis was used to reduce the data to only two dimensions that captured the most significant portion of the original variance. Subjects were plotted in these dimensions, defined by the first principal component, which described 52% of the original variance, and the second component, which described 9% of the variance. Finally, the contribution of each muscle to the different components was computed.

RESULTS AND DISCUSSION

Clustering along the subject “axis” resulted in three main groupings [Fig. 1A]: the first group (top) included athletes, the second group (middle) included primarily healthy non-athletes, and the third group (bottom) included primarily cerebral palsy patients, revealing the intrinsic differences in the muscle volume patterns between these subject populations. Furthermore, when plotted along the first two principal components, regional similarity was observed in subject groups, including athletes competing in the same sport [Fig. 1B].

Clustering along the muscle “axis” revealed that four subgroups of muscles contributed to this organization of subjects [Fig. 1A]. The first group included mostly distal ankle muscles, which tend to be small in CP patients and relatively normal in athletes. Group 1 muscles had average contributions to the first principal component, and large positive contributions to the second principal component [Fig. 1C]. The next group included gluteal muscles and small hip and ankle muscles, which tended to be normal in both CP patients and athletes. Group 3 muscles had small contributions to both first and second principal components [Fig. 1C]. The following group included mainly hip and knee extensors, which tended to be very large in athletes, and relatively normal in CP patients. Group 4 muscles had large contributions to the first principal component, and negative contributions to the second principal component [Fig. 1C]. The last

group included miscellaneous “other” muscles, which tended to be small in CP patients and large in athletes. Group 2 muscles had average contributions to the first principal component, and a small mostly negative contribution to the second principal component [Fig. 1C].

High-dimensional clustering and principal component analysis revealed patterns of muscle volumes across individuals and muscles. The subgroups of muscles that contribute most to the principal components and distinguish the CP patients or athletes from the healthy subjects corresponded with several of the reported modules of co-activation during walking [4]. For example, muscles in Module 1 that were responsible for body support during stance were primarily members of Group 4. The muscle clustering results demonstrate

regionally specific variations in muscle size that would be indicative of certain muscles and regions showing altered functional capacity. Future work will reveal if these regions of diminished capacity correlate with muscle functional demands relevant to these subject populations (such as high speed running in the athlete populations [5] and movement abnormalities in the cerebral palsy population [6]).

REFERENCES

1. Handsfield G, et al. *J Biomech* **47**, 631–38, 2014.
2. Handsfield G, et al. *Mus & Ner*, (in review), 2015
3. Knaus KR, et al.. *ACSM Annual Meeting*, San Diego, CA, USA, 2015.
4. Neptune RR, et al. *J Biomech* **42**, 1282–87, 2009.
5. Dorn TW, et al. *J Exper Bio* **215**, 1944–56, 2012.
6. Steele KM, et al. *J Biomech* **45**, 2564–69, 2012

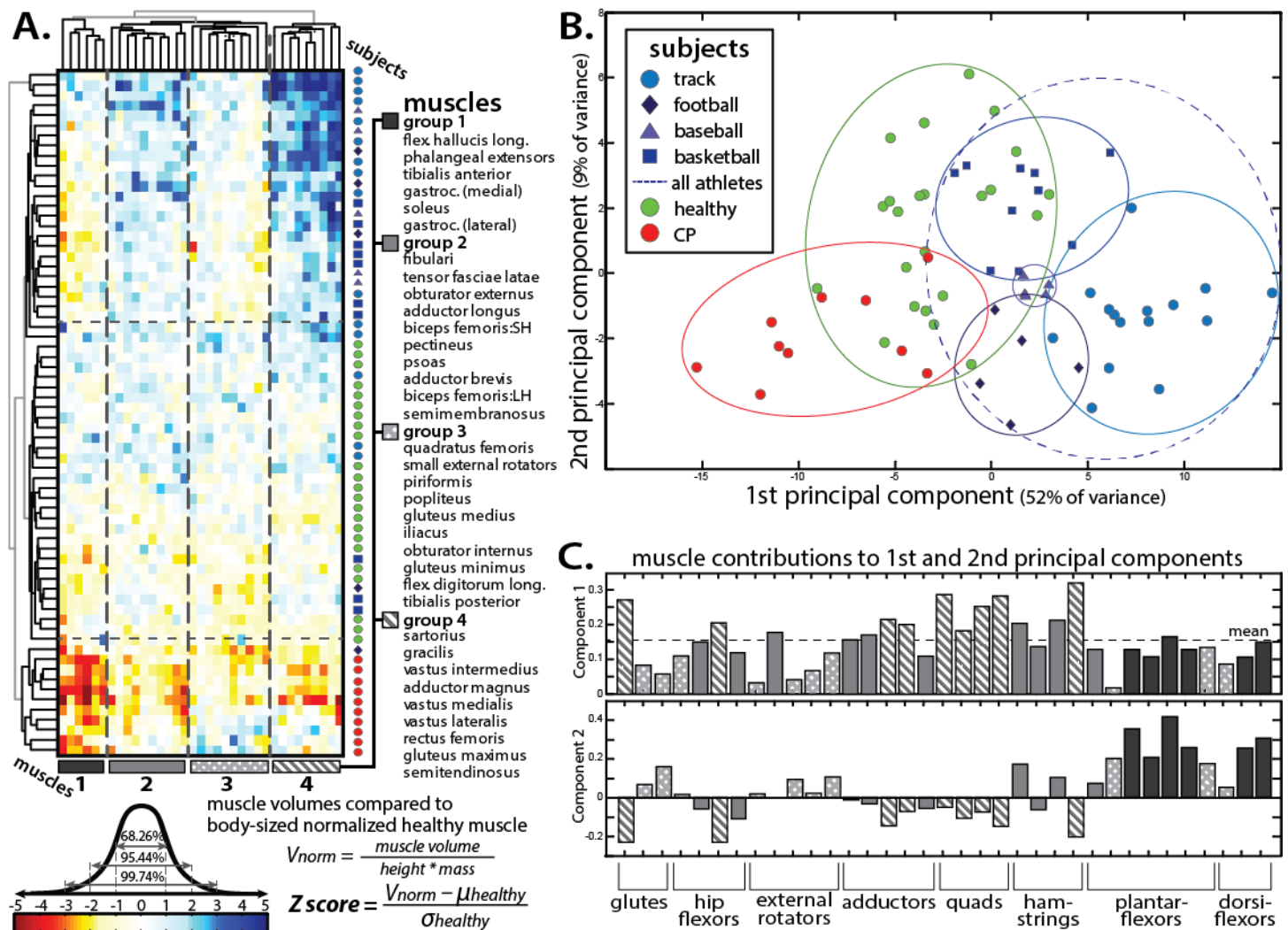


Figure 1: A) Hierarchical clustering and B,C) principal component analysis were used to compare patterns of muscle volume dissimilarities between 35 lower limb muscles in 68 healthy, impaired, and athletic individuals.

ANALYSIS OF 3D STRAIN IN MEDIAL MENISCAL ALLOGRAFT TRANSPLANTS FOLLOWING TWO SURGICAL TECHNIQUES

¹Kolaczek, S; ²Hewison, C; ²Catterine, S; ²Ragbar, MX; ²Getgood, A¹Gordon, K;

¹School of Engineering, University of Guelph;

²Fowler Kennedy Sport Medicine Clinic, 3M Centre, University of Western Ontario
email: kgordon@uoguelph.ca

INTRODUCTION

At present, there is a deficiency in the understanding of the biomechanical characteristics of meniscal tissue in meniscal allograft transplantation (MAT), and how these may be affected by surgical techniques.[1, 2] A novel in-vitro loading device capable of applying physiologically relevant loads has been developed, enabling 3D strain measurements in meniscal tissue.[3] The objectives of this study were to investigate the 3D strain in intact and transplanted medial menisci, with and without an additional peripheral 3rd point of fixation on the tibial plateau.

METHODS

Ten human cadaveric knees (average age approximately 67, 5 male, 5 female) were evaluated. Eight teflon beads (0.8 mm) were inserted in two tetrahedral formations in the middle 1/3 and posterior 1/3 of the medial meniscus under arthroscopic guidance. The joint was positioned at 5° flexion and loaded to 1x body weight (650 ±160 N) during CT image acquisition using the custom loading device. MicroView 3D image viewer was used to obtain 3D bead coordinates to calculate the principal strains.[4] The same process was repeated for a medial MAT, utilizing soft tissue anterior and posterior root fixation via transosseous suture, and a 3rd transosseous suture tied over a button providing peripheral fixation on the tibial plateau. Strain data was collected for loaded and unloaded menisci, with and without the peripheral fixation.

Statistical analysis using repeated measures ANOVA (IBM SPSS Statistics 22) was conducted to determine differences in strain results between intact or MAT with either surgical technique.

RESULTS AND DISCUSSION

Figures 1-3 show the average 3D strain found in 10 knees for the middle 1/3 and 8 knees for the posterior 1/3 of the meniscus. Medial-Lateral (ML), Anterior-Posterior (AP) and Superior-Inferior (SI) principal strains are shown. Directions ML/AP, ML/SI and AP/SI indicate shearing strains.

In the intact knee, ML (-0.94% Middle, -6.62% Posterior) and SI (0.09% Middle, -8.14% Posterior) are both negative (compressive) strains while AP (8.44% Middle, 10.05% Posterior) is positive (tensile). These results are expected as tibiofemoral loading of the meniscus causes hoop stresses, resulting in, fibres in the ML direction to be compressed and fibres in the AP direction to be pulled as the meniscus is mainly anchored at the anterior and posterior horn attachments. [7]

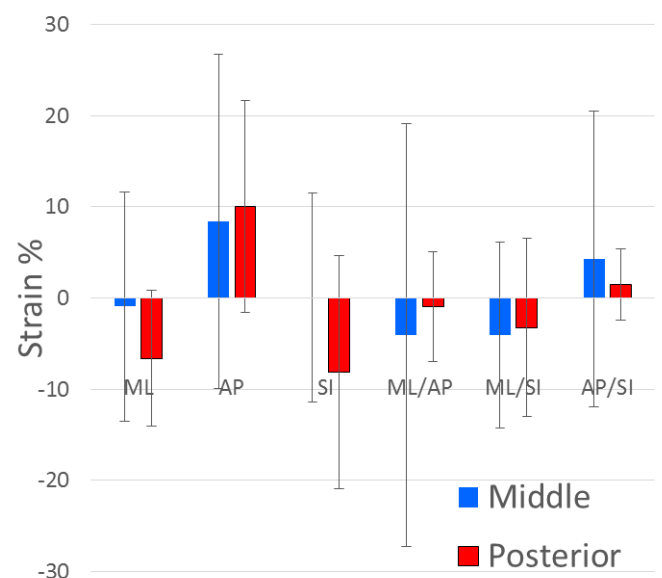


Figure 1: Strain profile in an intact meniscus

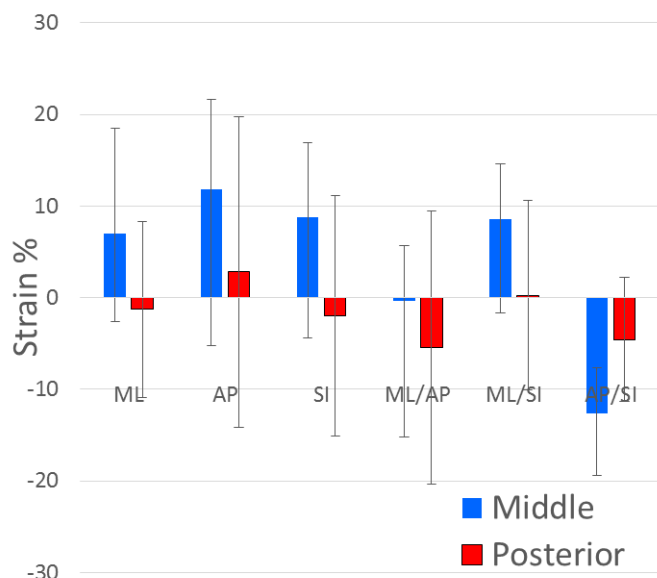


Figure 2: Strain profile in a MAT using soft tissue anterior and posterior root fixation via transosseous suture

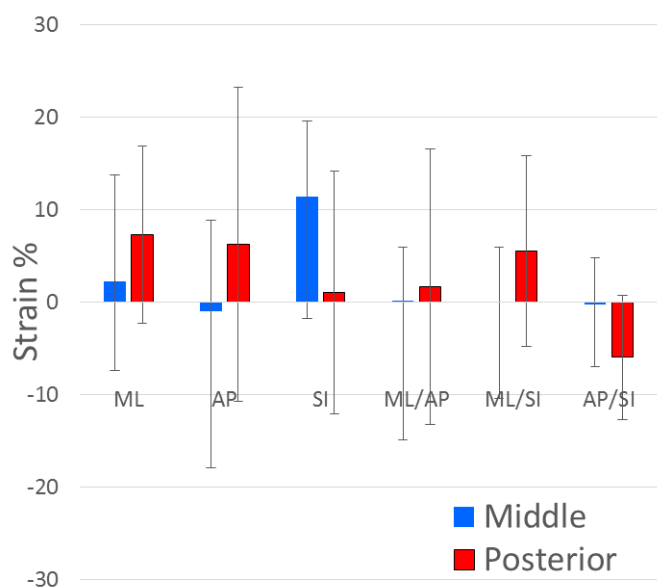


Figure 3: Strain profile in a MAT using soft tissue anterior and posterior root fixation via transosseous suture, and a 3rd transosseous suture tied over a button

This is the first study to quantitatively study regional 3D meniscal strain in a large number of human knees under simulated physiological loading regimes. The values obtained are within reason of previous literature where strain was quantified through linear strain gauges or elongation tests of resected tissue. [5, 6]

The strain profile is changed following allograft replacement, but due to the high variability in these measurements no statistical difference has been uncovered. The current results indicate no differences in strain measurement between any of the surgical conditions tested and the intact meniscus. The efficacy of the peripheral anchor may require a cyclic loading protocol rather than static as was conducted in this study. More testing is required to assess differences in strain between these fixation techniques.

CONCLUSIONS

There is no significant difference in strain between the native meniscus and a MAT without an additional peripheral anchor. The addition of a peripheral anchor conferred no significant benefit in this model. These results suggest that a peripheral anchor in medial MAT may not be necessary to replicate native tissue strain or improve the chondroprotective effect of MAT.

REFERENCES

1. Roos H, et al. *Arthritis Rheum* **41-4**, 687-93, 1998.
2. Xu C, et al. *Knee Surg Sports Traumatol Arthroscop* **23-1**, 164-7, 2013.
3. Chen L, et al. *Med Eng Phys* **36-10**, 1346-1351, 2014.
4. Waldman LK, et al. *Circ Res*. **57-1**, 152-63. 1985.
5. Spencer Jones R, et al. *Clin. Biomech* **11-5**, 295-300, 1996.
6. Tissakht M, et al. *J. Biomechanics* **28-4**, 411-422, 1995.
7. Makris EA, et al. *Biomaterials* **32**, 7411-7431, 2011.

ACKNOWLEDGEMENTS

Supported in part by the Joint Motion Program – A CIHR Training Program in Musculoskeletal Health Research and Leadership.

COMPARATIVE EVALUATION OF MORPHOMETRIC AND BIOMECHANICAL PROPERTIES OF THE CERVINE FEMUR

Morgan A. Libruk, Mark J. Hegdland, Nicole C. Corbiere, Mario J. Ciani, and Laurel Kuxhaus

Clarkson University, Potsdam, NY, USA

email: lkuxhaus@clarkson.edu, web: <http://www.people.clarkson.edu/~lkuxhaus/>

INTRODUCTION

The morphological and biomechanical evaluation of the musculoskeletal structures of animals is essential to the evaluation of orthopedic devices. Bones of various animal species have been used in biomechanical research, including the femur, tibia and vertebrae [1-6]. Ovine, porcine, bovine and canine models are commonly used, but there has been little research on cervine (deer) species as a suitable animal model. A recent study in New Zealand assessed the red deer (*Cervus elaphus*) femur as a potential model [4]. Given that tibiae and vertebrae of white-tailed deer (*Odocoileus virginianus*) have been shown to be appropriate models for human tibiae and vertebrae [2, 5], and are regionally abundant in North America, the objective of this study is to quantify and compare the morphometric and biomechanical properties of the *Odocoileus virginianus* femur to those of the human femur and other animal models.

METHODS

Sixteen pairs (10 male, 6 female) of fresh frozen *Odocoileus virginianus* femora (average age 2.1 ± 0.9 years) were obtained from Nolt's Custom Meat Cutting (Lowville, NY). Right femora were used for the morphometric study while left femora were used for biomechanical testing. Dimensions measured (Figure 1) include total and biomechanical lengths (L_T , L_B), anteversion and cervicodiaphyseal angles (AV, CD), head diameter in AP and SI planes (HD_{AP} , HD_{SI}), head offset and position (H_O , H_P), outer and medullary diameters (OD, MD) in AP and ML planes, cortical cross-sectional area (CSA), cortical thickness (CT), AP and ML dimensions of lateral and medial condyles (LAP, LML, MAP, MML) and intercondylar height and width (ICH, ICW). MD, OD, CSA and CT were reported as the average of the values measured at 40%, 50% and

60% of L_B . L_T , AV, CD, HD, H_O , H_P and CSA were measured via scaled photos (Fujifilm FinePix Z33WP camera) of specimens in ImageJ (ImageJ 1.48, nih.gov) while the other dimensions were measured by hand with inside/outside calipers with the exception of L_B , which was measured with a flexible tape measure to the nearest mm. MD dimensions were measured at incremental percentages of the total length by transecting the bone at each of these locations with a hacksaw. Each dimension was measured three times by three different people and recorded in mm (lengths) or degrees (angles).

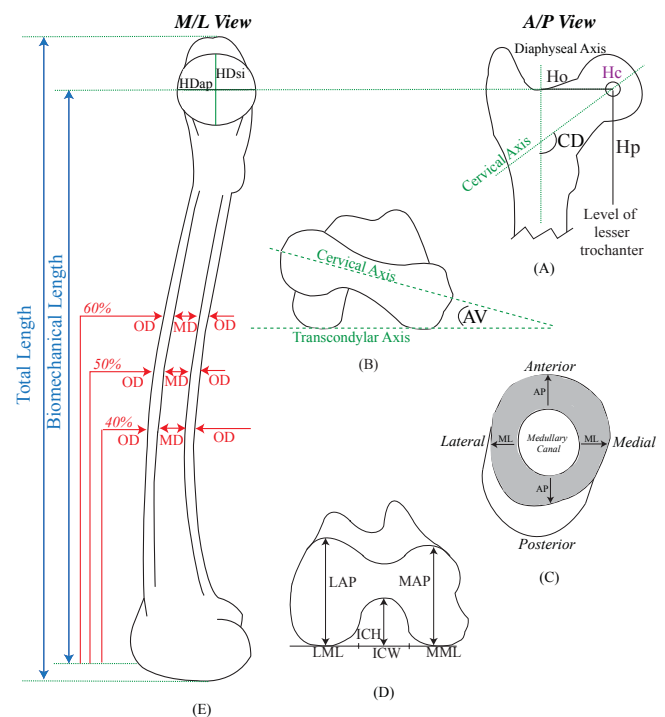


Figure 1: Morphometric dimensions. (A) AP view of proximal femur showing H_O and H_P relative to H_C (head center), and CD angle; (B) AV angle; (C) Cross-sectional view of diaphysis showing CT in AP and ML planes; CSA is also represented by the shaded area; (D) Distal femoral dimensions; (E) ML view showing L_T and L_B as well as head diameter in AP and SI planes, and OD and MD at each % of L_B .

The diaphysis of the 16 left femora were potted in Bondo™ (Auto Body Filler, 3M, St. Paul, MN) at a 10° angle in the frontal plane [3, 6]. Half were monotonically compressed and the other half were torqued to failure in a load frame (MTS 809 Axial/Torsional Test System, Eden Prairie MN). Rates of compression and torsion were 0.1 mm/sec and 0.2°/sec respectively. Stiffness and ultimate strengths were calculated ($K_{\text{Axial}} = \Delta F / \Delta \delta$ & $K_{\text{Torsional}} = \Delta M / \Delta \theta$) using a custom MATLAB code (R2012b, MathWorks, Natick, MA).

RESULTS AND DISCUSSION

Although markedly shorter than the human femur, the cervine femur has a length closer to that of the human femur than other species [3, 4] (Fig. 2). Average cervine AV and CD angles were closer to human values than canine species [1]. Average values for HD_{AP} , HD_{SI} , H_O and H_P were all smaller than human dimensions [1]. This is expected, as the cervine pelvis is much smaller than the human pelvis, and thus requires smaller head dimensions overall [1].

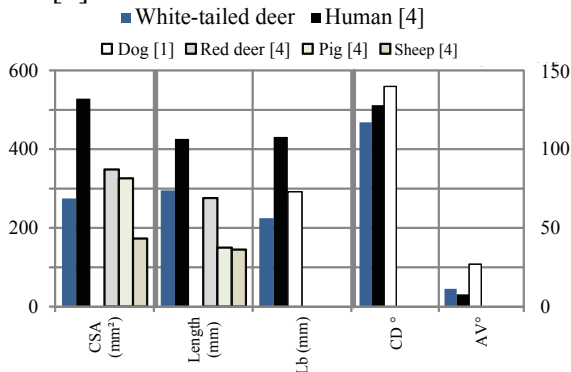


Figure 2: CSA, length, and head angles

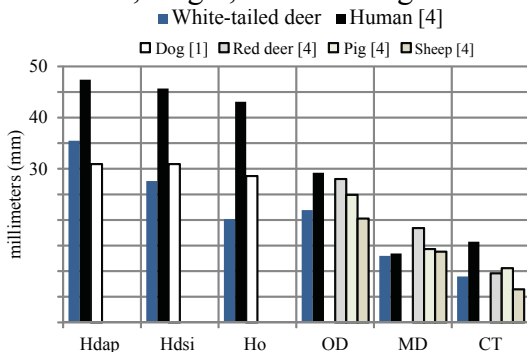


Figure 3: Diaphyseal and shaft dimensions

Figures 2 and 3 compare mid-diaphyseal averages for CSA, CT, MD and OD. The average LML, ICH and ICW were smaller than human values but

follow similar trends to other animals. The cervine femur has a greater torsional stiffness than the human femur, which has a higher torsional ultimate strength: 106.83 Nm for cervine compared to 170.00 Nm for human femurs (Fig. 4). In addition, the cervine femur was found to have an axial stiffness within range of previously-reported human values [4,6].

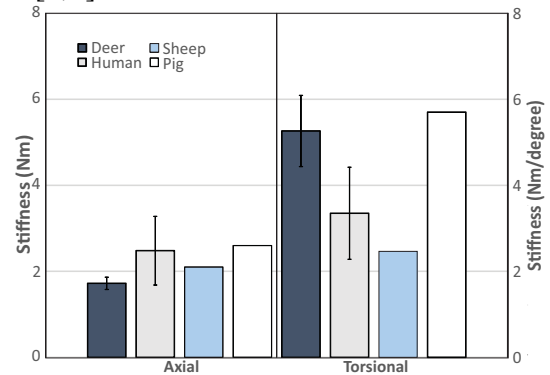


Figure 4: Axial and torsional stiffness of deer femora compared to human, pig, and sheep femora [4]

CONCLUSIONS

Cervine femora have average length, angular, distal femoral and endosteal values closer to human values than some other animal models and also have similar biomechanical properties. Therefore they may be suitable analogs for human bone in the testing of orthopaedic devices. These results may have important implications for orthopaedic device development and may offer an inexpensive, locally-abundant and sustainable source of suitable animal models for the human femur.

REFERENCES

1. Bloebaum RD, et al. *J Biomed Mat Research*, **27**(9), 1993.
2. Corbiere NC, et al. *J Biomech Eng*, **136**, 2014.
3. Cristofolini L, et al. *J Biomech*, **29**, 1996.
4. Kieser DC, et al. *Biomed Mat Eng*, **24**, 2014.
5. Throop AD, et al. *J Biomech Eng*, **137**, 2015.
6. Heiner AD & Brown TD. *J Biomech*, **34**, 2001.

ACKNOWLEDGEMENTS

The authors thank Elizabeth Miele for her help potting specimens. The authors have no conflict of interest.

ADJUSTING THINKING ABOUT IM NAILS: MECHANICAL EVALUATION OF AN ADJUSTABLE INTRAMEDULLARY NAIL PROTOTYPE

¹Mark J. Hegdeland, ¹Alexander D.W. Throop, ²Alexander Martin Clark Jr., and ¹Laurel Kuxhaus

¹Clarkson University, Potsdam, NY, USA

²Canton Potsdam Hospital, Potsdam, NY, USA & Sharon Hospital, Sharon, CT, USA

email: lkuxhaus@clarkson.edu web: <http://people.clarkson.edu/~lkuxhaus/>

INTRODUCTION

The fixation of a long bone fracture via intramedullary (IM) nailing is a common orthopaedic surgical procedure. To ensure rigid fixation, the IM nail must be the proper length for the patient's bone [1]. Improperly sized IM nails can lead to complications such as non-union which can eventually result in mechanical failure [1]. The currently available IM nails come in discrete sizes, (up to 98 sizes for one model) which often do not fit a patient's IM canal length exactly [1]. Alternatively, an adjustable-length nail would offer improved patient outcomes. In addition, the adjustable nail would reduce hospitals' need to stock many discrete sizes of nails, and therefore reduce stocking costs and procedure time. This work aims to improve on the four previously designed adjustable tibial IM nail prototypes' stiffness values with a new design and compare these values to currently-in-use nails. This will be done in cervine tibiae, which have already been shown to be suitable models for human tibiae [1].

METHODS

A new adaptation to previous IM nail prototypes was designed in Creo Parametric 3.0 (PTC, Needham, MA) and SolidEdge (Siemens PLM Software, Plano, TX) and then machined from surgical stainless steel (316L). The machined "Prototype 5" was able to extend through its full range of adjustability (approximately 290-410 mm) and lock into place securely with a flattened locking nut and thread-locking set screw. To provide greater torsional resistance than previous prototypes, the new design also incorporated a thicker overall structure. Prototype 5 had the largest total cross-sectional area of any of the prototypes thus far, but



Figure 1: X-ray of Prototype 5 inserted into a cervine tibia.

was still comparable to the size of currently-in-use nails[1]. Prototype 5 was then tested in torsion and four-point bending according to the ASTM standard to determine its stiffness values [2]. For torsion testing, Prototype 5 was inserted into three right cervine tibiae specimens (2 male and 1 female, 2.1 ± 0.6 years) according to standard surgical procedures and under the direction of a certified orthopaedic surgeon [AMC] (Figure 1). The tibiae were from white-tailed deer donors, *Odocoileus virginianus*, obtained from Nolt's Custom Meat Cutting (Lowville, NY). After insertion, the tibia/Prototype construct was potted vertically in Bondo™ (Auto Body Filler, 3M, St. Paul, MN) for support around the diaphysis. They were then tested in torsion at a rate of 0.1/sec at 1° increments up to 10° (MTS 809 Axial/Torsional Test System, Eden Prairie MN). The bending test was performed in a non-articulating four-point

bending fixture. Prototype 5 was tested alone (not inserted into a tibia) at a rate of 1 mm/sec until 5 mm of displacement had been reached. The load-displacement data from each trial of torsion and bending tests were analyzed, and the stiffnesses of each construct were calculated as in Equations 1 and 2 using a custom MATLAB code (R2012b, Mathworks, Natick, MA).

$$K_{Torsional} = \Delta M / \Delta \theta \quad (1)$$

$$K_{Bending} = \frac{(L+2c)(\Delta F / \Delta \delta)s^2}{12} \quad (2)$$

where L, s, and c are based on roller geometry [2]

RESULTS AND DISCUSSION

The device performed better than its predecessors in bending stiffness (Figure 2). Note that its bending stiffness is much greater than the currently-in-use nail, Synthes (Tibial Nail EX, Johnson & Johnson, New Brunswick, NJ), and within range of human tibia values [3,5]. In addition, the torsional stiffness of Prototype 5 is within the range of the Synthes nail.

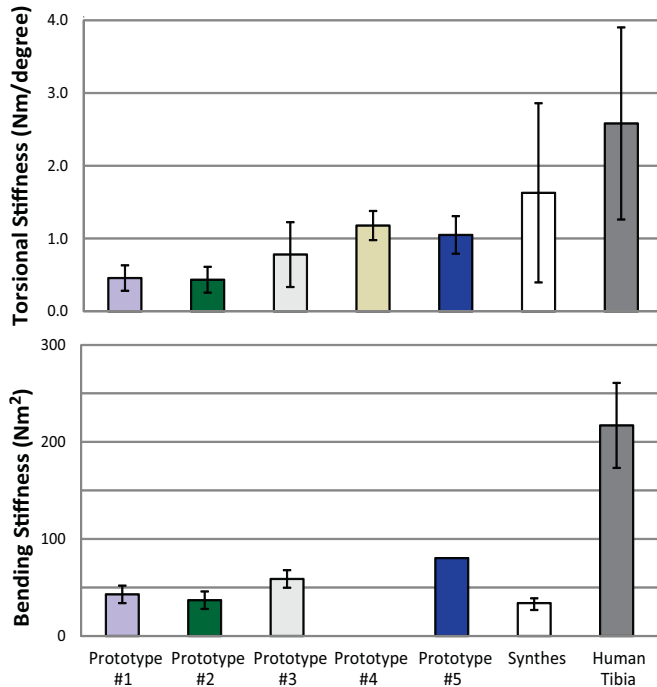


Figure 2: Torsional and bending stiffness of Prototype 5 compared to previous prototypes [1], the currently-in-use Synthes [4], and human tibia [5].

CONCLUSIONS

The higher bending stiffness of Prototype 5 is not surprising as it has the largest overall cross-sectional area of any of the previous prototypes. The aforementioned prototypes employed a design which consisted of a single threaded rod screwed into a bent proximal end with adjustability at the distal end. These designs were locked by nut, set screw, or pin, but never a combination of these [1]. The high torsional stiffness of Prototype 5 indicates that the combination of the locking nut and set screw as a locking mechanism, coupled with the rearrangement of the Prototype's region of adjustability, better resists rotational forces while implanted in the tibia. Prototype 5 also more closely resembles the overall structure and appearance of currently-in-use nails. Future work will include axial compression, and a larger sample size. These initial findings indicate that this device may be comparable in mechanical behavior to that of currently-in-use devices.

An adjustable IM nail that could serve as a viable alternative to current discretely-sized models would have significant positive clinical impacts. The addition of adjustability to IM nailing, made possible by a device such as this, could improve patient outcomes from fracture fixation surgeries and drastically reduce healthcare costs associated with the procedure by eliminating the need to stock several dozen discretely-sized nails.

REFERENCES

1. Throop, A. D. et al., (In Press), *J. Med. Dev.*
2. ASTM International, 2007. F 1264.
3. Synthes, 2012. Expert Tibial Nail.
4. Dailey H., et al. *Clin Biomech* 28, 579-585, 2013.
5. Cristofolini L., et al. *J Biomech* 33, 279-88, 2000.

ACKNOWLEDGEMENTS

The authors would like to thank Nicole Corbiere for her help in preparing and testing specimens, and Douglas Leonard and Travis Leggue for machining the Prototype. The authors have no conflicts of interest to declare.

ACTIVITIES OF DAILY LIVING INDUCE VERTEBRAL FRACTURES DESPITE HEALTHY BMD

Nicole C. Corbiere, Stacey L. Zeigler, Kathleen A. Issen, Arthur J. Michalek, and Laurel Kuxhaus

Clarkson University, Potsdam, NY, USA

email: lkuxhaus@clarkson.edu, web: <http://www.people.clarkson.edu/~lkuxhaus/>

INTRODUCTION

Osteoporotic vertebral compression fractures are a growing problem and the micromechanical origin of these fractures remains unclear. Patients with osteoporosis often can't recall an extreme event that caused a compression fracture, suggesting that activities of daily living (ADLs) could contribute to these fractures. Repetitive small movements during ADLs affect the vertebrae; the study of these movements could provide insight on fracture initiation. The effects of lower angle motion ADLs on vertebral compression fracture development is unknown, despite the fact that flexion of less than 15° is the most common motion of the lumbar spine during ADLs [1].

This work will mechanically simulate vertebral fractures under low-load low-angle loading conditions in cervine lumbar vertebral motion segments. Cervine vertebral motion segments have a similar mechanical response to human vertebral motion segments [2-4]. Characterizing the hysteresis loops from loading that simulates ADLs is an important first step towards quantifying the effects of ADLs on fracture initiation and propagation.

METHODS

Six 5-vertebra motion segments (male, 2.67 ± 0.52 years) were harvested from cervine donors (Nolt's Custom Meat Cutting, Lowville, NY). X-rays (Multix X-Ray System, Siemens, Berlin, Germany) and DXA scans (Lunar Prodigy Advance DXA System, GE Healthcare, Little Chalfont, Buckinghamshire, United Kingdom) were performed at Canton Potsdam Hospital to rule out any bone pathologies and obtain bone mineral density (BMD). The average BMD for all

specimens was $1.182 \pm 0.155 \text{ g/cm}^2$, comparable to healthy human bone. Specimens were potted in Bondo™ (Auto Body Filler, 3M, St. Paul, MN) to create end-caps to interface with a pinned end loading fixture.

Cyclic loading with this fixture simulated repeated flexion; the pinned end conditions more accurately represent physiologic loading conditions than fixed end conditions. Eccentric compressive loading of the fixture (eccentricity of 10mm) induced flexion (Figure 1). Specimens were cyclically loaded at 2Hz between displacements corresponding to approximately 0° and 15° flexion for 40,000 cycles. Periodically, the loading rate was slowed to 0.1Hz to capture images for digital image correlation (not discussed here) and motion analysis. A 4-camera Qualisys (Oqus 500 cameras, Qualisys Inc., Sweden) motion capture system, with an accuracy of 0.1mm and a capture rate of 120Hz, was used to measure the intervertebral flexion angles; for this, four retroreflective markers were secured to each vertebral body with cyanoacrylate adhesive.

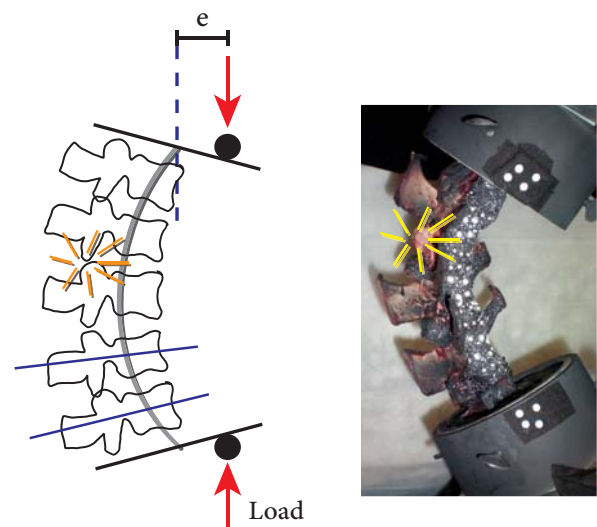


Figure 1: Pinned end conditions.

After 40,000 cycles of loading, specimens were monotonically compressed to further failure at a rate of 25.4 mm/min [5] and again X-rayed. These data were processed to compute the intervertebral angles (during the motion capture), load-displacement during monotonic compression, and peak load during the cyclic compression. Number of cycles to first observable failure and monotonic compression failure loads were also determined.

RESULTS AND DISCUSSION

All specimens failed at the articular facet joints (Figure 1); the fracture continued through the intervertebral disc interface. In 5 of the 6 specimens, facet fracture was observed prior to monotonic compression as early as 1,400 cycles (range: 1,400-35,000 cycles). During this cyclic flexion, the peak load decayed nonlinearly by an average of 73% (range: 57-84%), indicating that damage occurred. During monotonic compression to catastrophic failure, the average failure load was $240 \pm 146\text{N}$, substantially smaller than previously-reported failure loads ($7,244 \pm 1,795\text{N}$) using fixed end conditions [6]. These results demonstrate that fractures can be created under cyclic low-angle flexion (e.g., during ADLs).

As expected, the early cycle hysteresis loops (not shown) exhibit relaxation of the motion segment: the load decreases with increasing cycles. Figure 2 shows the hysteresis loops for a representative specimen for the 500th and 40,000th cycle of loading. This specimen failed at both the L2/L3 and L3/L4 articular facet joints. The peak compressive load decreased 84% during the cyclic loading and the intervertebral flexion angles (not shown) changed markedly after fracture occurred, indicating that the structure accumulated considerable damage.

In addition to decreased peak load, the difference in hysteresis loops from the 500th to the 40,000th cycle shows accumulation of damage: the shapes of the loops change. The specimen shown in Figure 2 visibly failed at approximately 7,000 cycles. The articular facet failure caused this change in mechanical response as evidenced by the undulations in the 40,000th cycle hysteresis loop.

Given the known articular facet joint fracture, the change in shape and slope of the last loop suggests that the facet joints may be catching, causing the undulations in this loop.

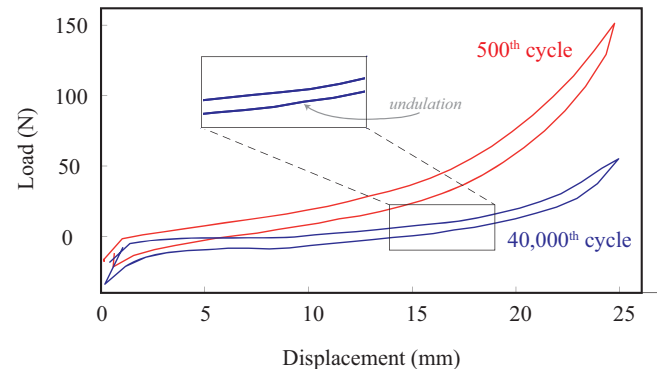


Figure 2: Hysteresis loops for the 500th and 40,000th cycles from a representative specimen.

CONCLUSIONS

These preliminary data suggest that the cyclic loading of small movement ADLs can contribute to fracture formation, despite healthy BMD. Future analyses, including calculating cortex surface strain and intervertebral angles during cyclic loading, may elucidate vertebral fracture mechanisms. Despite the limitations of a small sample size and the use of cervine specimens, these results suggest that health care providers may need to consider small movement ADLs in fracture prevention education.

REFERENCES

1. Cobian D, et al. *J of ASTM Int* **9**, 2011.
2. Corbiere N, et al. *J Biomech Eng* **136**, 2014.
3. Kumar N, et al. *The Anat Record* **266**, 108-117, 2002.
4. Wasinpongwanich K, et al. *J Spine* **3**, 187, 2014.
5. McCubbrey D, et al. *J Biomech* **28**, 891-899, 1995.
6. Corbiere N, et al. *Proceedings of WCB*, Boston, MA, USA, 2014.

ACKNOWLEDGEMENTS

The authors have no conflicts of interest, and thank Mark J. Hedgeland for experimental testing support and Sandra Thitten, Arlene Roach, and Canton Potsdam Hospital for the X-Ray and DXA scans.

MONITORING ACOUSTIC EVENTS IN BONE DURING SCREW INSERTION

¹ Evan R. Langdale and ¹ Stephen M. Belkoff

¹ The Johns Hopkins University, Baltimore, MD, USA
email: sbelkoff@jhmi.edu

INTRODUCTION

No objective standard exists for optimal bone screw tightening during the application of fracture plates. Proper tightening is necessary to maintain fracture reduction and prevent malunions and nonunions, yet surgeons strip up to 20% of screws in osteoporotic bone [1]. The patient dependent variation in the material properties of bone has made previous attempts at predicting optimal screw purchase difficult. Loss of screw purchase is likely a result of bone failure in the bone-screw-thread interface. Damage to the bone has been identified by acoustic emissions [2]. The goal of the current study is to use acoustic emissions as a measure of bone damage and a predictor of subsequent loss of screw purchase.

METHODS

Cadaveric humeri were stripped of soft tissue and mounted in a custom testing fixture. Pilot holes were drilled to their appropriate size and a 1/3 tubular bone plate instrumented with strain gages was placed on the bone. The plate was calibrated to measure the force that a screw applies to the plate and has been used previously to measure screw purchase [3]. A 3.5mm cortical bone screw (Synthes) was inserted into the bone manually until the screw head was close to seating in the plate. Further screw tightening was achieved using a servohydraulic testing machine that rotated the screw at 20°/s until the screw was stripped and lost purchase.

During the test, a piezoelectric transducer, attached to the bone, recorded acoustic data at 200 kHz. Torque, angle and plate strain were recorded at 1 kHz.

An acoustic event was defined as any signal that was ≥ 2 times the average noise that was recorded during manual screw insertion. Cumulative acoustic events and force on plate were plotted against screw angle of rotation to identify a relation between the number of acoustic events and loss of screw purchase as indicated by loss of plate compression against the bone.

RESULTS AND DISCUSSION

Acoustic events began occurring at the end of the linear region of the plate strain vs. angle of screw rotation curve (Fig. 1).

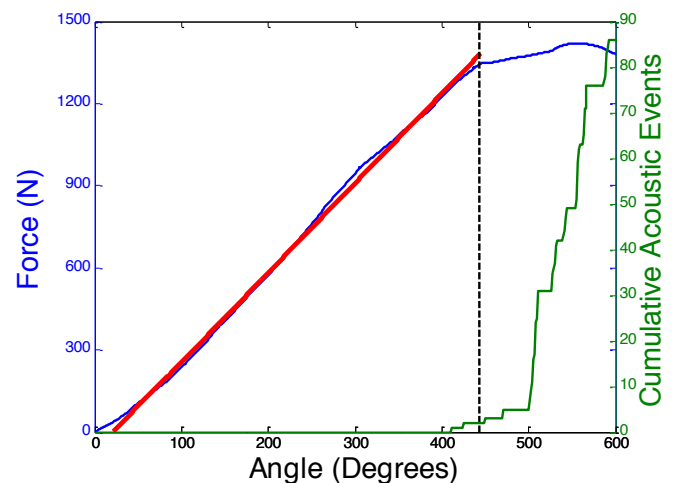


Figure 1: Plate strain and cumulative acoustic events plotted as a function of angular rotation. Dashed vertical line signifies end of linear region.

The onset of acoustic events initiated at 89% of peak compression.

As plate compression versus screw rotation continued beyond the linear region, the additional screw rotation did not result in an appreciable increase in plate compression. The results suggest that the onset of acoustic events may be indicative

of bone failure leading to loss of screw purchase and concomitant loss of screw force applied to the plate. These findings are consistent with acoustic events observed in bone loaded in compression [4].

CONCLUSIONS

Acoustic events correlate with loss of screw purchase in bone and may indicate damage at the bone-screw interface.

REFERENCES

1. Dinah AF, et al. *Geriatric orthopaedic surgery & rehabilitation*, **2**(3), 86-89, 2011.
2. Thomas RA, et al. *Ultrasonics Symposium, IEEE*, 237-241, 1977.
3. Thakkar SC, et al. *Journal of orthopaedic trauma*, **28**(4), 195-199, 2014.
4. Zioupos P, et al. *Medical engineering & physics*, **16**(3), 203-212, 1994.

VALIDATION OF THE SUBJECT-SPECIFIC FINITE ELEMENT ANALYSIS UNDER QUASI-STATIC AND DYNAMIC GAIT CONDITIONS

^{1,2}Vara Isvilanonda, ^{1,2}Joseph M. Iaquinto, ¹Matthew W. Kindig, ¹Bruce J. Sangeorzan and ^{1,2,3}William R. Ledoux

¹RR&D Center of Excellence for Limb Loss Prevention and Prosthetic Engineering, Department of Veterans Affairs, Seattle, WA, USA; Departments of ²Mechanical Engineering and ³Orthopaedics & Sports Medicine, University of Washington, Seattle WA, USA
email: wrledoux@uw.edu Web: <http://www.amputation.research.va.gov>

INTRODUCTION

Finite element (FE) foot modeling is a useful tool for investigating foot and ankle biomechanics. Such models can provide insight into internal soft tissue behavior of the foot and are ideal for conducting parametric analyses [1, 2]. Many of the previous FE foot models simulated quasi-static loading and imposed major simplifications on anatomy and material properties [1, 2], which could compromise their accuracy and usefulness. The purpose of this study was to develop and validate a subject-specific FE foot model of a healthy normal subject capable of accurately simulating both quiet stance (quasi-static loading) and the stance phase of gait (dynamic loading), and to explore the plantar pressure and internal soft tissue stress distribution under these two loading conditions.

METHODS

A right foot of a 43-year-old male (945 N body weight (BW)) subject was scanned using high resolution partially-loaded computed tomography (CT) and unloaded magnetic resonance imaging (MRI). The scan data were segmented to obtain subject-specific bone, skin, muscle and fat anatomy using custom software. Boolean operations were performed using ScanIP (Simpleware, Exeter, UK) to generate joint capsules and skin thickness, and eliminate gaps and volume overlaps (Figure 1). Models were meshed with linear tetrahedral elements using ANSYS ICEM CFD (ANSYS Inc, Canonsburg, USA) and preprocessed in LS-Prepost (Livermore Software, Livermore, CA). Bones were assumed rigid due to their small deformation relative to the soft tissue. Subject-specific Ogden hyperelastic material properties of the skin, fat,

muscle and generic soft tissue (Table 1) were determined from inverse FE analysis of gated MRI compression experiments [3, 4]. A total of 102 ligaments, 9 extrinsic muscle tendons [5], and joint cavities were accurately modeled based on the medical images. The plantar aponeurosis component was divided into four different regions, with non-linear material properties obtained from cadaveric mechanical testing [3].

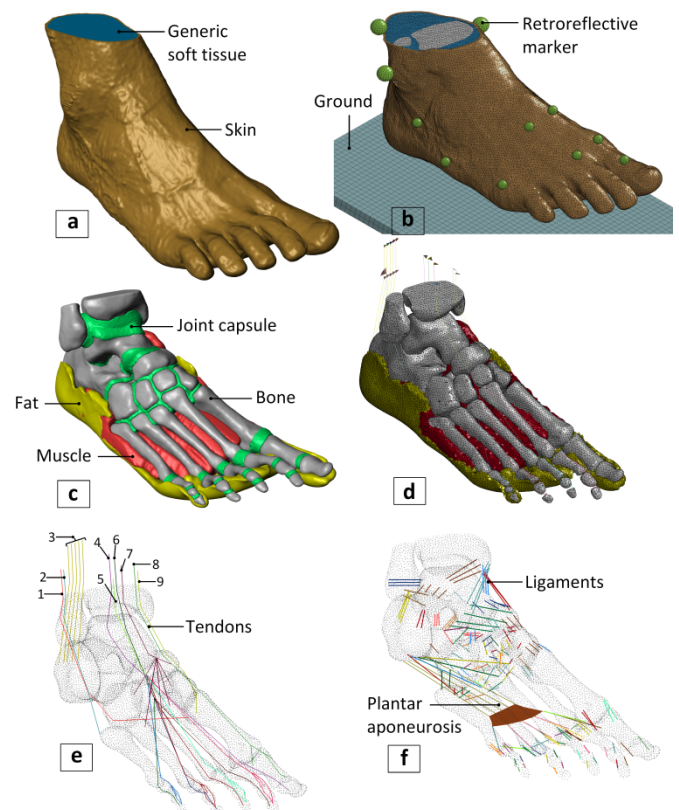


Figure 1: (a, c) Surface model of the foot showing skin (brown), generic dorsal soft tissue (blue), plantar fat (yellow), intrinsic muscle (red), bones (gray) and joint capsules (green). (b, d) Solid model components. (e) 9 extrinsic muscle tendons, (f) 102 ligaments and the plantar aponeurosis.

The models were validated under three loading conditions: passive 10% BW compression, quiet stance, and the stance phase of gait. The passive compression loaded the tibia and Achilles tendon (zero and 20% BW) in the vertical direction such that the GRF was 10% BW. In quiet stance, the tibia was oriented based on *in vivo* motion capture data collected in-house for this subject. The model was loaded by the tibial force, Achilles tendon force (54.5% BW) and gravitational acceleration to apply 50% BW at the ground. For gait simulation, the tibial kinematic time history from motion capture was prescribed, as were eight tendon force-time histories (taken from literature [6]). The initial ground position and Achilles tendon force were tuned to achieve physiologic vertical ground reaction force (GRF). All models were solved in LS-DYNA (v971d R5.1.1 explicit analysis). Bone kinematics, dynamic GRF, plantar pressure, plantar aponeurosis force and ankle joint force were compared with the *in vivo* experimental data for this subject and with literature data [7, 8].

Table1: Material models and properties.

Material	Model	Properties [†]
Bone	Rigid	$\rho = 0.449\text{e-}6 \text{ kg/mm}^3$, $E = 20,100 \text{ MPa}$, $\nu = 0.3$
Skin	Hyperelastic	$\rho = 1.142\text{e-}6 \text{ kg/mm}^3$, $\mu = 0.158 \text{ kPa}$, $\alpha = 185.20$, $\nu = 0.4990$
Fat	Hyperelastic	$\rho = 0.916\text{e-}6 \text{ kg/mm}^3$, $\mu = 1.874 \text{ kPa}$, $\alpha = 8.29$, $\nu = 0.4999$
Muscle	Hyperelastic	$\rho = 1.047\text{e-}6 \text{ kg/mm}^3$, $\mu = 0.161 \text{ kPa}$, $\alpha = 31.95$, $\nu = 0.4999$
Dorsum tissue	Hyperelastic	$\rho = 1.000\text{e-}6 \text{ kg/mm}^3$, $\mu = 0.787 \text{ kPa}$, $\alpha = 21.11$, $\nu = 0.4999$

[†] Density (ρ), modulus of elasticity (E), Poisson's ratio (ν), Ogden hyperelastic coefficients (μ_i and α_i). Poisson's ratios were estimated from tissue properties: longitudinal ultrasound speed, density and elastic modulus. Detailed calculations (Poisson's ratio) and data references (ligament, tendon and plantar aponeurosis) are listed in [3]

RESULTS AND DISCUSSION

The subject-specific model was capable of simulating physiologic compression, quiet stance and dynamic gait conditions. The difference between the simulated and experimental data from passive compression validation ranged from 0.4% to 52.3%. The quiet stance experimental and simulated plantar pressure distribution were similar, but did not exactly match (Figure 2).

The simulated gait vertical GRF (Figure 3) agreed with our *in vivo* data (RMS error of 13%), partially due to tuning. The predicted anteroposterior and

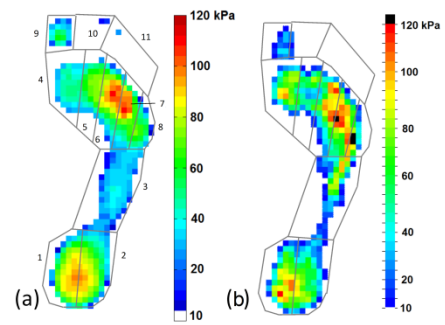


Figure 2: Quiet stance plantar pressure (divided into 11 regions) from (a) experimental measurement and (b) FE simulation.

mediolateral progression of the center of pressure, mean pressure, contact force and contact area also agreed with *in vivo* data. Peak pressure was over-predicted, possibly due to numerical artifacts. The bone-to-ground and segment-to-segment angles showed physiologic movements in the sagittal plane, but implied an overly stiff transverse deformation. The pattern and magnitude of the simulated plantar aponeurosis force and ankle joint resultant force were comparable to the literature.

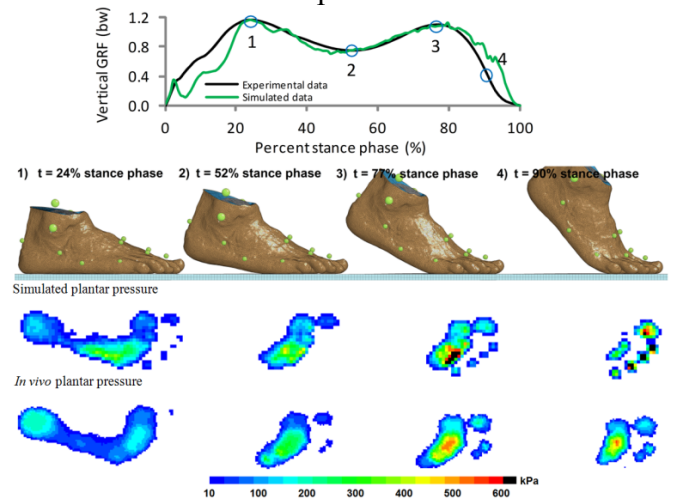


Figure 3: Predicted foot deformation and plantar pressure distribution compared to the corresponding *in vivo* plantar pressure measurement at four instances of gait.

REFERENCES

1. Chen WP, et al. *Med. Eng. Phys.* **32**, 324-331, 2010.
2. Cheung JT, et al. *J. Biomech.* **38**, 1045-1054, 2005.
3. Isvilanonda V. University of Washington, 2015 (in preparation).
4. Williams ED. University of Washington, 2015 (in preparation)
5. Isvilanonda V, et al. *Clin. Biomech.* **27**, 837-844.
6. Aubin PM, et al. *IEEE T. Robot.* **28**, 246-255.
7. Erdemir A, et al. *J. Biomech.* **86**, 546-552, 2004.
8. Sanford BA, et al. *Computational Biomechanics for Medicine*, Springer New York, 2014.

ACKNOWLEDGEMENTS

This work was supported by the VA Grant A6973R.

PATIENT-SPECIFIC MECHANICAL PROPERTIES OF DIABETIC AND HEALTHY PLANTAR SOFT TISSUE FROM GATED MRI

Williams, ED^{1,2}, Stebbins, MJ^{1,2}, Cavanagh, PR^{2,3}, Haynor, DR⁴, Chu, B⁴, Fassbind, MJ¹, Isvilanonda, V^{1,2} and Ledoux, WR^{1,2,3}

¹RR&D Center of Excellence, Department of Veterans Affairs; Departments of ²Mechanical Engineering, ³Orthopaedics and Sports Medicine, ⁴Radiology, University of Washington, Seattle, WA USA.
email: wrledoux@uw.edu

INTRODUCTION

The Hydraulic Plantar Soft Tissue Reducer (HyPSTR) is an MRI compatible device that applies dynamic loading profiles to a subject's foot while gated MRI captures soft tissue deformation. The combination of force and image data is used to calculate plantar soft tissue stiffness, which has been shown to be significantly different in subjects with/without diabetes [1]. Diabetes mellitus can lead to ulceration in the foot, and eventually amputations [2]. Ulcers may form at regions of high internal stress, which motivates the use of MRI to obtain volumetric information, as opposed to external deformation measurements [3,4] or one-dimensional ultrasound probing [5,6]. Finite element (FE) models can use this force and three-dimensional image data to conduct inverse FE analyses to determine patient-specific material properties, which in turn can be used to improve foot simulations under a variety of loading scenarios.

METHODS

Verification data and calibration curves were obtained to ensure that the motor and control electronics could accurately transmit displacements through plastic, water hydraulic tubing to the loading platen in the MRI core. Applied force was measured indirectly from system pressure and matched with the appropriate MRI time stamps for 16 loading/unloading phases during a periodic (5s) sine-wave displacement protocol. Gated MRI was synchronized with a peripheral pulse unit signal so that cardiac MRI gating protocols could be used to obtain 16 images of the tissue deformation at custom rates. Distances between anatomical

landmarks were measured in pixel units with segmentation software and converted to mm.

An ankle foot orthosis (AFO) was designed from carbon fiber and leather to secure the foot and lower leg to the loading apparatus during testing (Figure 1). The HyPSTR can be fitted with an ultrasound adapter, for pilot testing or adjusted to test forefoot tissue properties, or left or right feet.

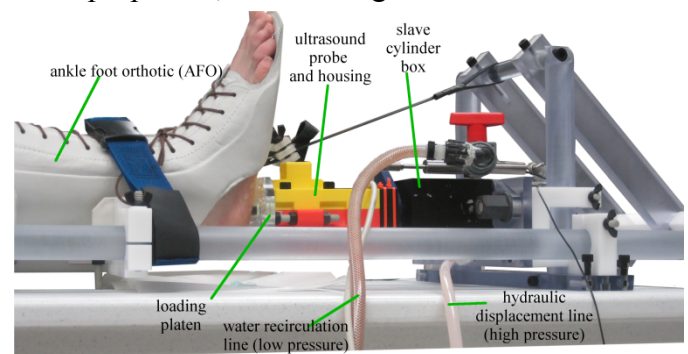


Figure 1: HyPSTR slave cylinder (black) and loading jig. The ultrasound probe adapter (bicolor, yellow/red) is connected to the loading platen.

Two subjects were tested. Subject A had no history of diabetes and was 93 kg in mass, 180 cm tall, and 43 years old. Subject B had type II diabetes and was 70 kg in mass, 170 cm tall, and 31 years old.

RESULTS AND DISCUSSION

Image data (Figure 2) for Subject B shows maximum tissue compression near the tenth acquisition phase. The first three phases appear to be unloaded (force data from the HyPSTR was 0N). This is due to the heel preconditioning that occurs after the subject is secured in the AFO. The gap that forms between the platen and foot is not completely avoidable, without pre-loading the subject.

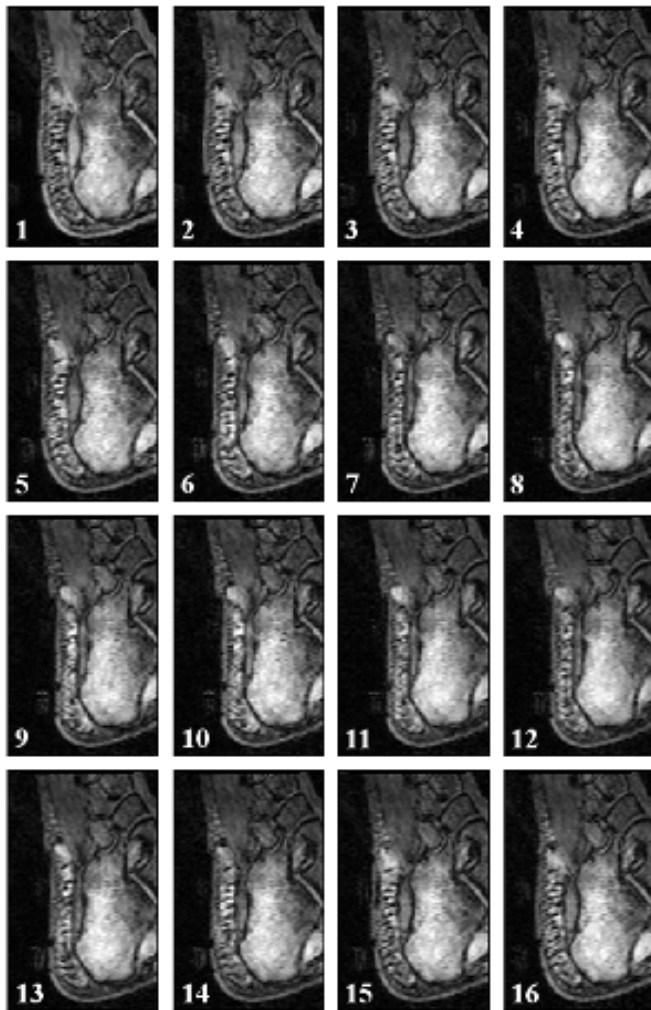


Figure 2: Subject B (diabetic) center slices of the calcaneus from each of the 16 image volumes.

A loading/unloading stiffness curve was obtained for both subjects (Figure 3 for subject B, subject A not shown). The magnitude (approx. 200N) and velocity (approx. 3.5 mm/s) of the deformation was mostly elastic (i.e., there was no significant hysteresis, Figure 3). Fat pad stiffness is generally thought to increase exponentially with strain [3], which could still be true for these subjects at higher strains. Subject B tissue was 2.65 times more stiff than Subject A (data not shown here) in the final 0.06 mm of compression. This agrees with trends in the cadaver sample data from Pai and Ledoux [1].

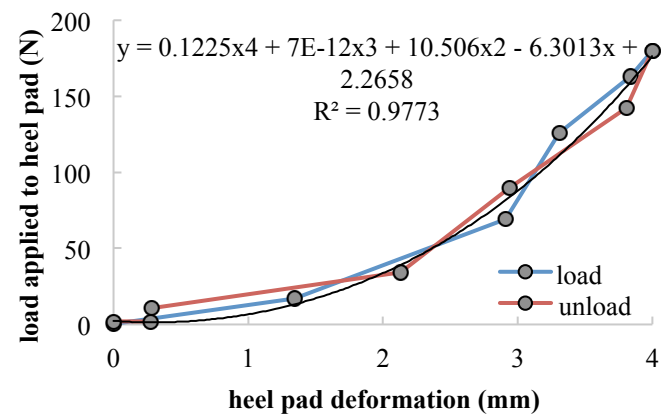


Figure 3: Stiffness curve for Subject B with polynomial fit.

CONCLUSIONS

The HyPSTR represents progress toward measuring patient-specific, dynamic heel pad stiffness. Currently there are limitations in platen velocity (0.2 Hz) that need to be addressed in order to test compressibility at a more physiologic rate (1 to 10 Hz). Still, the data indicate that the HyPSTR can differentiate between dynamic stiffnesses of subjects with and without diabetes.

REFERENCES

1. Pai S, Ledoux WR. *J Biomech* **43**, 1754-1760, 2012.
2. National diabetes fact sheet. *Centers for Disease Control and Prevention*, 2014.
3. Aerts P, De Clercq D. *J Sports Sci* **11**, 449-461, 1993.
4. Kinoshita H, et al. *Int J Sports Med* **14**, 312-319, 1993.
5. Cavanagh PR. *J Biomech* **32**, 623-628, 1999.
6. Erdemir A, Viveiros ML, Ulbrecht JS, Cavanagh PR. *J Biomech* **39**, 1279-1286, 2006.

ACKNOWLEDGEMENTS

This work was supported by VA RR&D Grant A6973R.

QUANTIFYING MUSCLE MATERIAL PROPERTIES OF PASSIVE AND ACTIVE STROKE-IMPAIRED BICEPS BRACHII

^{1,2} Sabrina S.M. Lee, ²Sam. Speer, and ^{1,2} William Z. Rymer

¹ Northwestern University, Chicago, IL, USA

² The Rehabilitation Institute of Chicago, Chicago, IL, USA

email: s-lee@northwestern.edu, web: <http://www.feinberg.northwestern.edu/sites/pthms>

INTRODUCTION

Individuals who have had a stroke routinely experience long-term motor and sensory impairments. Decreased strength and range of motion contribute greatly to decreased mobility. In conjunction with neurological changes, muscle properties, including architecture and material properties such as stiffness, may also progressively change. Prior descriptions of muscle material properties in stroke survivors have observed increased muscle stiffness [1]. However, these previous measures are estimates derived from individual joint stiffness or whole muscle groups. In addition, current standard clinical examinations cannot readily distinguish between active reflex and passive tissue components [2]. Thus, the purpose of this study was to compare material properties, by measuring shear wave velocity (SWV) which is related to shear modulus, in spastic paretic muscles at rest and at different activation levels with contralateral muscles in stroke survivors and in age-matched control subjects.

METHODS

Fourteen stroke survivors participated in this study (age: 58.9±7.4yrs; height: 1.68±0.10m; body mass: 85.5±18.2kg; time post-stroke: 11.4±11.6yrs.; Fugl-Meyer: 4-48, 19±15). We tested nine subjects who were gender and age-matched to the stroke survivors (age: 57.9±7.1yrs; height: 1.64±0.10m; mass: 74.4±11.2kg;).

Subjects were seated upright with their upper arm resting on a plastic support, the forearm secured in a fiberglass cast, and the wrist and forearm held in a neutral position in a ring-mount interface mounted to the table. The shoulder was positioned so that the humerus was abducted 45 degrees and the elbow

positioned at 90 degrees. Subjects performed a series of isometric elbow flexion contractions at different activation levels (0, 10, 25, 50, 75, 100% maximum voluntary contraction (MVC)) while force and torque were measured at the wrist (load cell). During each trial, muscle activity (electromyography), and ultrasound images (Aixplorer, SuperSonic Imagine) of the biceps brachii were captured. Mean SW velocity was calculated from a 12mm by 12mm region of the ultrasound images. Here we use shear wave ultrasound elastography which measures the velocity at which shear waves propagate through the tissue [3]. Shear waves will propagate faster in a tissue that has a higher elastic shear modulus:

$$\mu = \rho v^2$$

where μ is the elastic shear modulus, ρ is the muscle mass density ($\rho \approx 1000 \text{ kg m}^{-3}$), and v is the SW velocity. We calculated the slope and r^2 of the linear fit between SWV and % MVC until 50%MVC as the SWV at 75% and 100%MVC reached the maximum the ultrasound system is capable of measuring (16m/s). An Analysis of Variance was used to compare the SWV at the different % MVC levels, slope, and r^2 of the non-paretic and paretic muscles, and those of the gender, age-matched controls.

RESULTS AND DISCUSSION

Our main findings show that at rest, the SWV was on average 40% greater in the paretic muscle compared to either the contralateral non-paretic muscle or the muscle of control subjects (Fig.1, $p=0.003$, $p=0.002$), and no significant difference in SWV between the non-paretic muscle and control muscle. In active muscle (10, 25, 50%), there was no significant difference in SWS between the non-paretic, paretic, and control muscles (Fig.1). The

slope of SWV versus %MVC (up to 50%MVC) and R^2 values was 10% and 15% greater, respectively, in the non-paretic muscles compared to that of the paretic muscle, but was not significant (Table 1, $p = 0.06$).

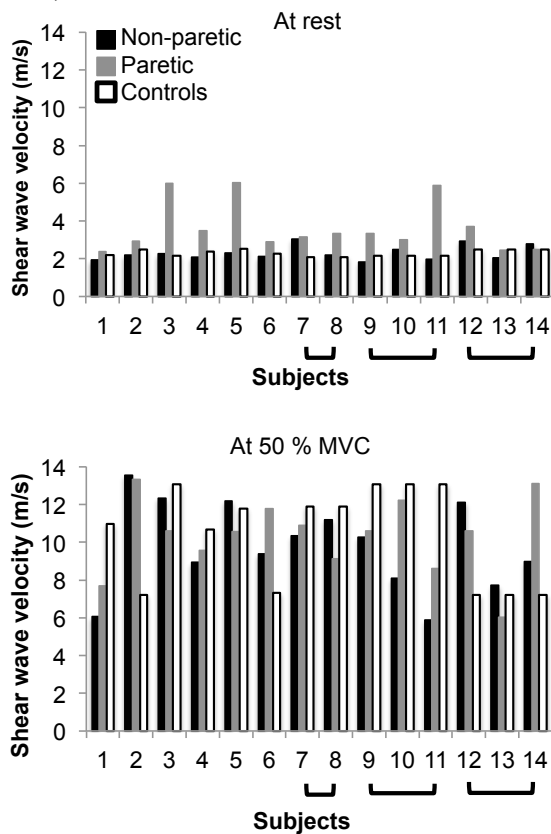


Figure 1: Mean shear wave velocity at rest and at 50 %MVC (force) for the non-paretic (black) and paretic (gray) muscle of individuals who have had a stroke and muscle of gender, age-matched controls (white). Brackets indicate the same control subject.

CONCLUSIONS

We demonstrate that SW velocity is faster in the biceps brachii of the paretic limb than in the contralateral non-paretic limb of stroke survivors and age-matched individuals with no neurological impairments when the muscle is at rest. This

suggests that paretic muscles have potentially altered muscle material properties, specifically stiffness in both passive and active muscles, but primarily in passive states. This can be a result of increased collagen in the perimysium and abnormal accumulation of the extracellular matrix[4].

Interestingly, this difference in SWV between three muscle groups disappears once the muscle was active. One source of active stiffness is short-range stiffness. Thus, it is possible that the non-contractile elements contribute minimally to stiffness in active muscle and the active short-range stiffness is not altered in stroke-impaired muscle.

These results offer us insight and a first look into active and passive stiffness of stroke muscle. Quantitative measurements of muscle material properties, in particular stiffness, in individual muscles is important for accurately evaluating muscle function and for understanding the fundamental mechanisms of impairment that occur after a stroke. This knowledge has the potential for aiding clinical decisions, and for guiding rehabilitation interventions that may specifically target altered passive and active stiffness.

REFERENCES

1. Katz RT, et al. *Arch Phys Med Rehab* **70**, 144-155, 1989.
2. Burke, D et al. *Neurology* **80**, S20-S26, 2013
3. Bercoff J, et al. *Ultra Ferro Freq Contr, IEEE Trans* **51**, 396-409, 2004.
4. Lieber RL, et al. *Am J Physiol* **305**, C241-C252, 2013

ACKNOWLEDGEMENTS

We would like to acknowledge our funding source H133P110013 and K12HD073945.

Table 1: Mean shear wave velocity at rest and at 50%MVC, slope of SW velocity and % MVC, and R^2 . Mean (SD).

Muscle	SW velocity at rest	SWV at 50%MVC	Slope ($\text{ms}^{-1} \% \text{MVC}^{-1}$)	R^2
Paretic	3.65 (1.31)	10.33 (2.03)	0.12 (0.04)	0.73 (0.12)
Non-paretic	2.30 (0.38)	9.79 (2.36)	0.15 (0.05)	0.81 (0.12)
Control	2.29 (0.18)	10.42 (2.28)	0.13 (0.05)	0.89 (0.16)

PRINCIPAL COMPONENT ANALYSIS OF THE 3D STRUCTURAL STIFFNESS OF THE WRIST

^{1,4}Joseph N. Gabra and ^{1,2,3,4}Zong-Ming Li

Hand Research Laboratory, Departments of ¹Biomedical Engineering, ²Orthopaedic Surgery, and ³Physical Medicine and Rehabilitation, Cleveland Clinic, Cleveland, OH, USA

⁴Department of Chemical and Biomedical Engineering, Cleveland State University, Cleveland, OH, USA
Email: liz4@ccf.org, Web: <http://www.handlab.org>

INTRODUCTION

The wrist structure is primarily composed of irregularly shaped carpal bones interconnected by numerous ligaments, resulting in complex structural mechanics. The mechanical characteristics of the wrist have an immense impact on wrist stability and function. Previous studies of wrist biomechanics were mainly limited to uniaxial and planar experimentation but the mechanical properties in 3D are not well understood. The purpose of this study was to examine the 3D stiffness characteristics of the wrist with displacement perturbations applied to the carpal arch.

METHODS

A custom stationary apparatus held five ($n = 5$) cadaveric hands in a vertical position (Fig. 1). For each specimen the hamate was fixed to the stationary apparatus and the trapezium was free to be displaced in 3D. An instrumented 6 DOF robot arm displaced the ridge of the trapezium and

measured 3D reaction forces. A ball-socket interface between the trapezium and robot allowed for free rotation without torque constraints. The displacement perturbations were implemented with various magnitudes (0.5, 1.0, 1.5, and 2.0 mm) from its initial position towards 14 directions that were equally spaced in 3D with respect to an anatomically defined coordinate system – X, Y, Z axes corresponded to the lateral(+), distal(+), and volar(+) directions, respectively. Prior to data collection, the carpal arch was preconditioned by displacing the trapezium 2 mm in each direction ten times. The force-displacement data were used to determine a stiffness matrix K according to $\mathbf{f} = K\mathbf{d}$, where \mathbf{f} and \mathbf{d} are force and displacement vectors, respectively. The matrix was determined by fitting the force-displacement data with least-squares optimization procedures.

The stiffness matrix was separated into symmetric (K_S) and antisymmetric (K_A) components, where $K_S = (K + K^T)/2$ and $K_A = (K - K^T)/2$ (T denotes matrix transpose). The determinates of K and K_S , $\det(K)$ and $\det(K_S)$ respectively, were calculated to provide a scalar quantity of the overall stiffness values. K_A was a 3x3 skew-symmetric matrix and subsequently $\det(K_A) = 0$. An elastic index was calculated as $\det(K_S)/\det(K)$ where an elastic index of 1 indicates pure elasticity, i.e. spring-like behavior. Eigendecomposition of K_S was then used to determine the magnitudes and directions of principal stiffness components.

RESULTS AND DISCUSSION

The optimization procedures to determine the stiffness matrix resulted in a goodness of fit of $R^2 = 0.815 \pm 0.070$. The stiffness matrix and its decomposed symmetric and antisymmetric matrices were:

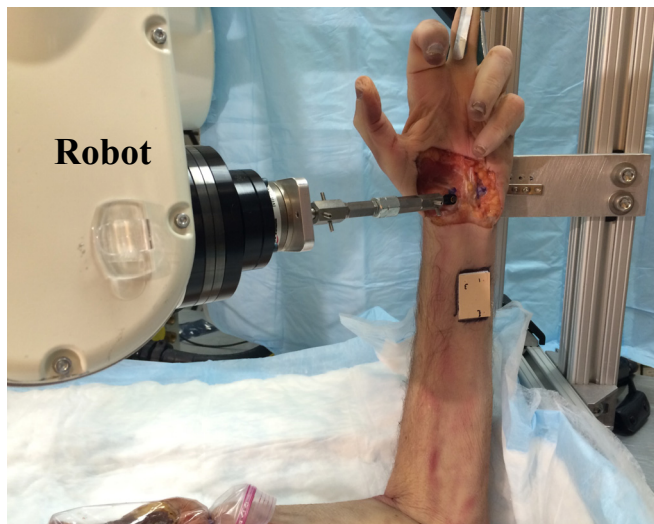


Figure 1: Experimental setup for applying displacement perturbations to the trapezium.

$$K = \begin{bmatrix} 11.7 \pm 2.4 & 0.5 \pm 0.9 & 5.7 \pm 1.0 \\ -0.9 \pm 0.7 & 2.9 \pm 0.5 & -0.6 \pm 0.6 \\ 6.7 \pm 1.5 & 0.5 \pm 0.6 & 7.4 \pm 1.0 \end{bmatrix} \text{ N/mm}$$

$$K_s = \begin{bmatrix} 11.7 \pm 2.4 & -0.2 \pm 0.7 & 6.2 \pm 1.2 \\ & 2.9 \pm 0.5 & 0.0 \pm 0.5 \\ & & 7.4 \pm 1.0 \end{bmatrix} \text{ N/mm}$$

$$K_A = \begin{bmatrix} 0 & 0.7 \pm 0.4 & -0.5 \pm 0.4 \\ -0.7 \pm 0.4 & 0 & -0.6 \pm 0.2 \\ 0.5 \pm 0.4 & 0.6 \pm 0.2 & 0 \end{bmatrix} \text{ N/mm}$$

The determinates of K and K_s were $151.3 \pm 70.4 \text{ N}^3/\text{mm}^3$ and $146.1 \pm 67.0 \text{ N}^3/\text{mm}^3$, respectively. The subsequent elastic index was $97.0 \pm 2.0\%$. Eigendecomposition of K_s resulted in the three principal components of 16.2 ± 2.9 , 3.1 ± 0.6 , and $2.8 \pm 0.5 \text{ N/mm}$ (Fig. 2, Table 1).

The wrist structure had a high elastic index demonstrating a spring-like characteristic. In other words, the force vector field for the displacement perturbations was essentially conservative. Generally, the specimens varied in stiffness magnitude (See Determinant of K_s , Table 1), but their principal directions and relative principal component magnitudes were more comparable. The principal stiffness components of the wrist structure differed in magnitude indicating that the wrist had an anisotropic stiffness behavior. Specifically, the maximum principal stiffness component was 5.8 times greater than the minimum principal stiffness.

The direction of the wrist's maximum principal stiffness was within the transverse plane and was pronated 36° relative to the medial-lateral axis. This may be due to wrist ligament orientation and the tightly bound distal carpal row that is predominately within the transverse plane. The minimum principal

stiffness occurred in a direction oblique to the anatomical axes and was situated in the plane of dart thrower's motion, i.e. radial-extension to ulnar-flexion.

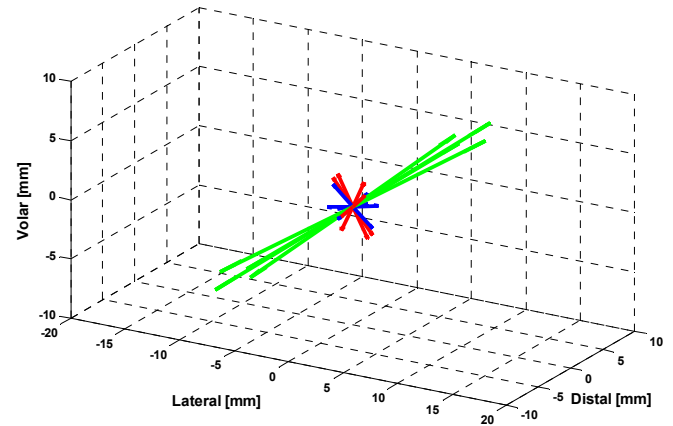


Figure 2: Specimen specific principal stiffness components. The 1st, 2nd, and 3rd principal components are shown (green, red, and blue respectively) with length corresponding to stiffness magnitude.

CONCLUSIONS

The wrist structure exhibited spring-like and anisotropic stiffness behaviors. The maximum principal stiffness occurred in the transverse plane while the minimum principal stiffness was situated in the plane of dart thrower's motion. This study provides advanced characterization of the wrist's 3D structural stiffness for improved insight into wrist biomechanics, stability, and function.

ACKNOWLEDGEMENTS

NIH/NIAMS R21AR062753 and the Cleveland State University's Dissertation Research Award

Table 1: Parameters of the symmetric stiffness matrix, K_s , in N/mm unless otherwise noted

Specimen	1	2	3	4	5
1 st Principal Component	20.5	17.1	12.7	16.1	14.5
2 nd Principal Component	3.6	3.1	3.3	3.4	2.2
3 rd Principal Component	3.3	3.0	2.5	2.8	2.1
Determinant of K_s [N^3/mm^3]	243.2	162.5	104.7	154.4	65.7

CARPAL TUNNEL CREEP DURING EXTERNAL COMPRESSIVE FORCE APPLICATION

¹Scott A. Galey, ¹Tamara L. Marquardt, ¹Joseph N. Gabra, ^{1,2,3}Zong-Ming Li

Hand Research Laboratory, Departments of ¹Biomedical Engineering, ²Orthopaedic Surgery, and ³Physical Medicine and Rehabilitation, Cleveland Clinic, Cleveland, OH, USA

email: liz4@ccf.org, web: <http://www.handlab.org>

INTRODUCTION

The carpal tunnel is comprised of eight carpal bones held together by a network of interosseous ligaments. Previous studies have demonstrated relative movement of the carpal bones with force application on aspects of the wrist [1, 2]. Narrowing of the carpal arch width (CAW), measured from the hook of the hamate to the ridge of the trapezium, has been demonstrated by applying force across the wrist [3, 4]. However, the time dependent effects of applying compressive force across the wrist on CAW narrowing have not been studied. Therefore, the purpose of this study was to investigate the change in CAW over time while external compressive force was applied across the wrist *in vivo*. Given the viscoelastic nature of the soft tissues that bind the carpal bones, we hypothesized that prolonged force application to the carpal tunnel would result in creep of the carpal tunnel deformation, which would be manifested by increased CAW narrowing over time.

METHODS

Fourteen (n=14) female participants (24.5±4.2 years old) participated in this study. Study exclusion criteria included history of musculoskeletal or neurological disorders affecting the hand and wrist. Each subject placed the hand in a splint in a supinated position, and an ultrasound probe was placed on the volar aspect of the wrist at the level of the hamate and trapezium. A carpal compression device powered by linear air pressure actuators and a surgical tourniquet provided an external compressive force across the wrist of 15 N for 5 minutes. The device and setup are demonstrated in Fig. 1. Ultrasound video was captured throughout the 5 minutes of wrist compression.

The ultrasound video was decomposed into individual frames and analyzed using a custom

LabVIEW program to track the most volar aspects of the hook of the hamate and the ridge of the trapezium over time. The CAW magnitude for each frame was then calculated based on the coordinates of the hamate and trapezium (Fig. 2). Then, a creep function of the CAW was determined by fitting a standard linear solid (SLS) viscoelastic model. The model consisted of a spring (K_1) in parallel with a Maxwell element that included a spring (K_2) in series with a dashpot (η) (Fig. 3). The creep function of the SLS model was of the form

$$\varepsilon(t) = \varepsilon_0 (1 - Ae^{-Bt})$$

where $\varepsilon_0 = \frac{F}{K_1 L_0}$, $A = \frac{K_2}{K_1 + K_2}$, $B = \frac{K_1 K_2}{[\eta(K_1 + K_2)]}$, F was the applied compression force, L_0 is the initial CAW, and $\varepsilon(t)$ was the strain at time t .

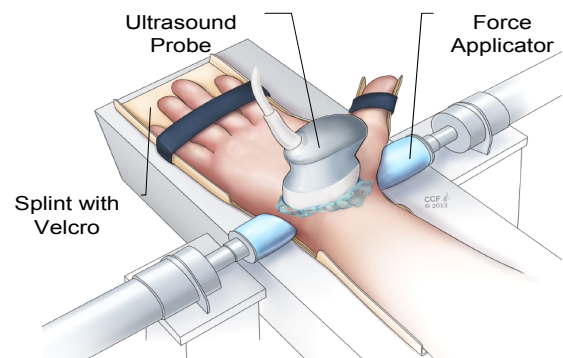


Figure 1: Experimental setup of ultrasound imaging and wrist compression to narrow the CAW.

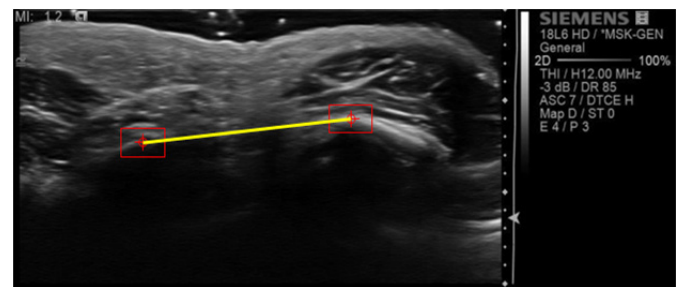


Figure 2: Representative ultrasound image with the hook of the hamate and ridge of the trapezium identified for tracking (red boxes), and the CAW (yellow line) between the two bony landmarks.

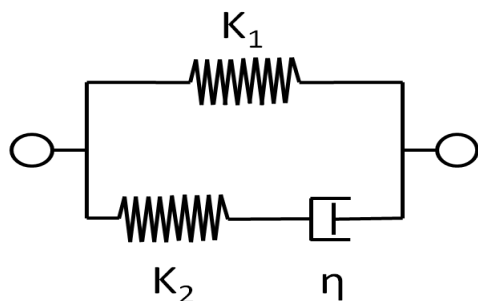


Figure 3. Schematic of the SLS model.

RESULTS AND DISCUSSION

Data from 11 of the 14 subjects were analyzed; the remaining three subjects were unable to be used due to poor image quality. Over the 5 minutes of force application, the mean CAW increasingly narrowed as time increased (Fig. 4). Significant narrowing from baseline CAW was observed after 1, 2, 3, 4, and 5 minutes of force application ($p < 0.05$). The amounts of CAW narrowing were 2.56% (SD 1.8%), 3.6% (SD 1.95%), 4.07% (SD 1.91%), 4.26% (SD 2.0%), and 5.15% (SD 2.44%) from baseline, at times of 1, 2, 3, 4, and 5 minutes, respectively. The best-fit of the viscoelastic model to the average CAW data produced a curve with a R^2 value of 0.938 (Fig. 4). The values for the springs and dashpot in the SLS model fit were $K_1 = 0.526 \times 10^6$ N/m, $K_2 = 6.74 \times 10^5$ N/m, $\eta = 70.3 \times 10^6$ Ns/m.

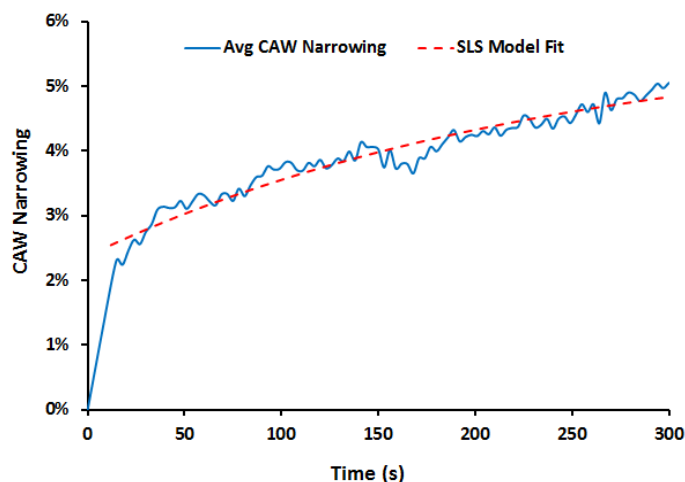


Figure 4. Average CAW narrowing from all subjects over the 5 minutes of compression and the SLS model fit curve ($R^2=0.938$).

During the 5 minutes of continuous compressive force application across the wrist, the CAW

progressively narrowed over time. This suggests that when external forces are used to manipulate the carpal bones, time dependent effects should be taken into account to ensure accurate manipulation of these bony structures. To better characterize this viscoelastic pattern of observed deformation, the data was fit to an SLS viscoelastic model. This model characterized the observed narrowing of the CAW well. Using this model, it was further predicted that the maximum amount of CAW narrowing would be 5.8% as time approached infinity when the wrist is under 15N of compressive force application. Therefore, at 5 minutes of force application the CAW had narrowed by 88.8% of its maximum predicted narrowing at this force level.

CONCLUSIONS

CAW narrowing due to external compressive forces occurs in a viscoelastic fashion over time. Future studies looking into manipulation of the carpal structures from external force application should account for this time dependent deformation.

REFERENCES

1. Gabra JN, et al. J Biomech Eng. 2012; 134(10): 101004.
2. Xiu K, et al. Clin Biomech. 2010; 25(8):776-80.
3. Li ZM, et al. Clin Biomech. 2013.
4. Marquardt TL, et al. Clin Biomech. In Press. doi:10.1016/j.clinbiomech.2015.01.007.

ACKNOWLEDGEMENTS

NIH/NIAMS R21AR062753

CARPAL ARCH COMPRESSION DECREASES MEDIAN NERVE FLATTENING IN CARPAL TUNNEL SYNDROME PATIENTS

¹Tamara L. Marquardt, ²Peter J. Evans, ²William H. Seitz, Jr., ^{1,2,3}Zong-Ming Li

Hand Research Laboratory, Departments of ¹Biomedical Engineering, ²Orthopaedic Surgery, and ³Physical Medicine and Rehabilitation, Cleveland Clinic, Cleveland, OH, USA
email: liz4@ccf.org, web: <http://www.handlab.org>

INTRODUCTION

The carpal tunnel in the wrist is formed by the interconnected carpal bones and the transverse carpal ligament (TCL). The tunnel contents include the median nerve, which is susceptible to entrapment in the space-limited tunnel leading to carpal tunnel syndrome (CTS). CTS patients have increased flattening of the median nerve which is alleviated after surgically transecting the TCL to increase carpal tunnel space and decrease tunnel pressure [1]. Recent studies support that the carpal tunnel space can be augmented by narrowing the carpal arch width [2-4]. Furthermore, it has been shown that applying radioulnar compression to the wrist decreases median nerve flattening in asymptomatic controls [4]. However, the implications of wrist compression on the carpal tunnel and median nerve in CTS patients have not been examined. Therefore, the purpose of this study was to investigate the morphological changes of the carpal arch and median nerve in response to wrist compression in CTS patients.

METHODS

Five (n=5) female volunteers diagnosed with CTS (54.6 ± 7.5 years; 4 right, 1 left) participated in this study. Each patient placed the arm in a custom compression system, palm side facing up (Fig. 1). The system applied radioulnar compressive forces of 10 N and 20 N across the distal carpal tunnel level for 3 minutes and then three cross-sectional ultrasound images at this level were acquired. Three unloaded (0 N) ultrasound images were also captured prior to each force application. Each force condition was repeated four times in a randomized order. A 5-minute rest was provided between consecutive trials.

The three unloaded (0 N) and three loaded (10 N or 20 N) ultrasound images from one trial for each load condition were analyzed. *ImageJ* was used to determine the coordinates of the most volar point of the hook of hamate and the ridge of trapezium, as well as the volar boundary of the TCL. Additionally, *ImageJ* was used to trace the median nerve's border and calculate its shape descriptors including perimeter, area, and flattening ratio (major axis/minor axis of fit ellipse). The *ImageJ* coordinates were transformed into an anatomically relevant coordinate system, and carpal arch width (CAW) and carpal arch area (CAA) were calculated. CAW was defined as the distance between the hamate and trapezium. CAA was the area bounded by the volar TCL boundary and the CAW line.

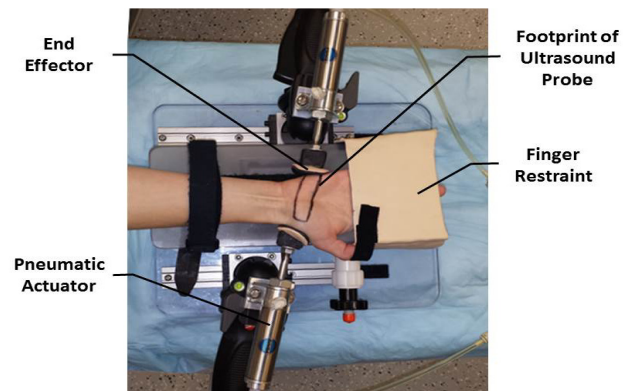


Figure 1: Experimental setup with the compression system and outline of ultrasound probe footprint indicating the location of imaging.

One-way repeated measures ANOVAs were performed to investigate the effect of force magnitude (0, 10, and 20 N) on CAW and CAA, as well as the median nerve's perimeter, area, and flattening ratio. Post-hoc Tukey's tests were used for pairwise comparisons and $p < 0.05$ was considered statistically significant.

RESULTS AND DISCUSSION

Ultrasonography captured changes of the carpal arch and median nerve in response to compressive force applied across the wrist of CTS patients (Fig. 2). CAW and the nerve's flattening ratio were significantly affected by force ($p<0.01$).

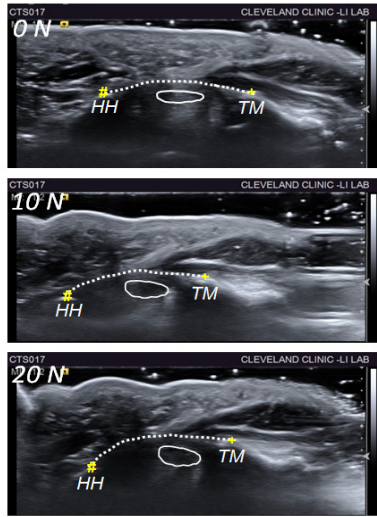


Figure 2: Representative images at 0, 10, and 20 N with the hamate (HH, #), trapezium (TM, +), TCL boundary (dotted line), and nerve (solid line) identified.

Specifically, CAW decreased by $0.9\pm0.5\text{mm}$ with 10 N of applied force and by $2.0\pm1.3\text{mm}$ with 20 N of force, relative to the initial CAW of $22.7\pm2.4\text{mm}$ at 0 N (Fig. 3). Pairwise comparisons revealed a significant difference between CAW at 0 N and 20 N ($p<0.01$). Although CAW decreased, CAA remained relatively constant ($17.6\pm6.2\text{mm}^2$ at 0 N) when compressive forces were applied ($17.4\pm6.6\text{mm}^2$ at 10 N and $18.2\pm5.6\text{mm}^2$ at 20 N), and the changes were not statistically significant ($p=0.88$).

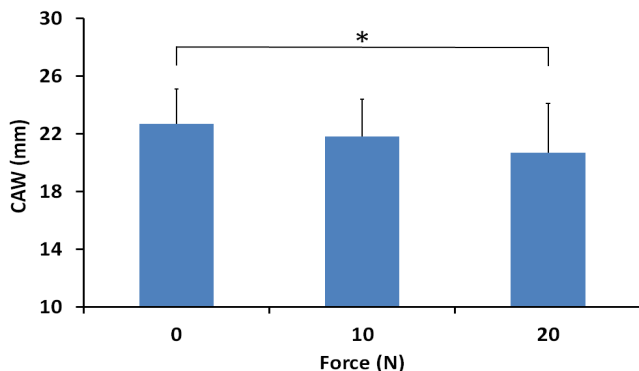


Figure 3: Carpal arch width (CAW) at force magnitudes of 0, 10, and 20 N. * $p<0.01$

Force did not significantly affect the nerve's perimeter ($p=0.07$) or area ($p=0.68$) which were initially $16.3\pm0.9\text{mm}$ and $11.1\pm1.3\text{mm}^2$, respectively. However, the nerve's shape became more round (Fig. 4) as reflected by decreases in its flattening ratio with force application ($p<0.01$). The flattening ratio of the nerve was 3.90 ± 0.79 at 0 N, and it decreased by 0.54 ± 0.57 at 10 N and by 1.06 ± 0.44 at 20 N. Pairwise comparisons found that the flattening ratio was significantly different between 0 N and 20 N ($p<0.01$).

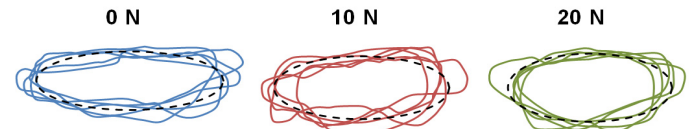


Figure 4: Median nerve outlines for individual patients at 0, 10, and 20 N with the dashed line indicating the average fit ellipse.

This study revealed that radioulnar compressive force applied across the wrist affected the morphology of the carpal arch and the median nerve in CTS patients. Previous studies have demonstrated that CAW can be narrowed [2, 3], and that this narrowing can be achieved *in vivo* [4]. The changes in CAW of CTS patients from wrist compression in the current study agree with the findings from a previous study with control subjects [4]. Even though CAA did not increase with force application, flattening of the median nerve decreased. It has been shown that the nerve undergoes shape changes to minimize insult within the tunnel space [5]. Nerve flattening in CTS patients also decreases after carpal tunnel release surgery. Therefore, radioulnar wrist compression may provide relief of nerve compression in patients with CTS.

REFERENCES

1. Horch RE, et al. 1997. Neurosurgery 41(1):p 76-83.
2. Li ZM, et al. 2009. J Biomech Eng 131(8):p. 081011.
3. Li ZM, et al. 2013. Clin Biomech 28(4): p.402-7.
4. Marquardt TL, et al. In Press. Clin Biomech: doi:10.1016/j.clinbiomech.2015.01.007.
5. Wang Y, et al. 2014. Ultrasound Med Biol 40(1):p. 53-61.

ACKNOWLEDGEMENTS

NIH/NIAMS R21AR062753

PREDICTORS OF PATELLOFEMORAL JOINT STRESS: AN EXAMINATION OF PATELLOFEMORAL JOINT MORPHOLOGY

¹ Tzu-Chieh Liao, ² Shawn Farrokhi and ¹ Christopher M. Powers

¹ University of Southern California, Los Angeles, CA, USA

² University of Pittsburgh, Pittsburgh, PA, USA

email: powers@usc.edu, web: <http://pt.usc.edu/labs/mbrl/>

INTRODUCTION

Patellofemoral pain (PFP) is a common condition seen in orthopedic practice, accounting for approximately 25-40% of all knee injuries [1]. A commonly cited hypothesis as to the cause of PFP is elevated patellofemoral joint (PFJ) stress [2] secondary to abnormal PFJ structure. With respect to the morphological factors that influence PFJ stress, previous studies have shown that persons with PFP exhibit altered patella position [3], abnormal femoral morphology [4], and decreased patella cartilage thickness [5] when compared to healthy individuals. However, the influence of the abnormal morphology on PFJ stress is unknown. Using finite element (FE) analysis, the purpose of the current study was to assess the relationship between PFJ morphology and elevated PFJ stress in persons with PFP.

METHODS

Nineteen subjects (10 PFP and 9 pain-free controls) were recruited for this study. Each subject completed 2 phases of data collection: magnetic resonance imaging (MRI) assessment and biomechanical testing. Each subject underwent 4 different scans on a 3.0 T General Electric scanner. These scans were necessary to obtain subject-specific data used for the FE modeling and for the measurement of morphological variables (patella height (Insall-Salvati ratio or ISR), lateral trochlear inclination angle (LTI), and patella cartilage thickness). For the biomechanical testing, kinematic, kinetic, and electromyographic were obtained during a static squatting task (45° of knee flexion).

Patella cartilage stress profiles were quantified utilizing a subject-specific FE model of the PFJ (Fig. 1). Input parameters for the FE model included: (1) joint geometry, (2) quadriceps muscle forces, and (3) weight-bearing PFJ kinematics [2]. Using a nonlinear FE solver, quasi-static loading simulations were performed to quantify patella cartilage stress during the squatting maneuver (45° knee flexion).

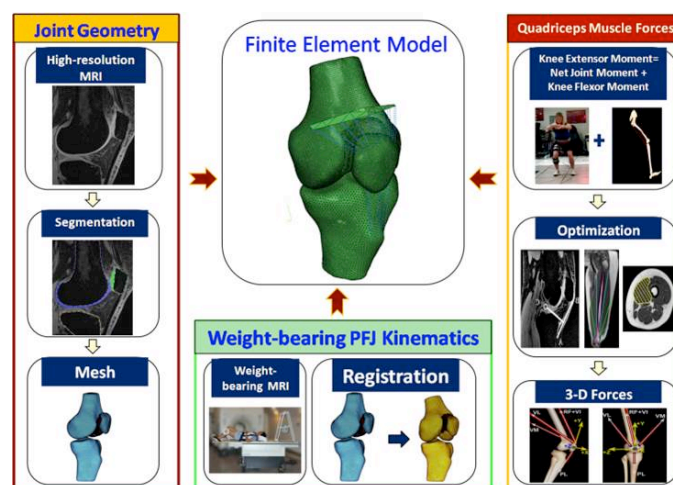


Figure 1: Finite element modeling pipeline.

Pearson correlation coefficients were used to examine the associations between peak hydrostatic pressure between ISR, LTI angle, and patella cartilage thickness. Variables that were significantly correlated with PFJ stress were put into a stepwise regression model to determine the best predictor of elevated PFJ stress.

RESULTS AND DISCUSSION

Pearson correlation coefficients revealed that only patella height ($r=0.48$, $p=0.018$) and patella cartilage thickness ($r=-0.58$, $p=0.005$) were significantly correlated with peak hydrostatic

pressure (Table 1). Results of the stepwise regression analysis revealed that patella cartilage thickness was the single best predictor of peak hydrostatic pressure, followed by patella height. Together, these 2 variables explained 50% of the variance in peak PFJ stress.

Table 1: Relationship between peak hydrostatic pressure and morphological variables of interest.

	Correlation Coefficient
Patella height (ISR)	0.48*
Lateral trochlear inclination	-0.29
Patella cartilage thickness	-0.58*

*p<0.05.

The results of the current study support the premise that PFJ stress is associated with PFJ morphology. Patella height was the best predictor of PFJ stress with greater degrees of patella height being correlated with greater stress. This is logical given that a higher positioned patella articulates with the more shallow portion of the trochlear groove, thus decreasing PFJ contact area [6]. The finding that patella cartilage thickness was negatively correlated with PFJ stress is in agreement with the results of Li et al. [7], who demonstrated that a reduction of cartilage thickness causes increase cartilage stress. Furthermore, our findings revealed that 50% of the variance in PFJ stress could be explained by morphological factors.

CONCLUSIONS

Identifying the underlying factors that contribute to elevated PFJ stress is an important step in developing effective interventions for persons with PFP. Although abnormal morphological may not be correctable through conservative measures, it is important to recognize the role abnormal structure may play in contributing to pain and pathology.

REFERENCES

1. Devereaux MD and Lachmann SM. *Br J Sports Med* **18**(1), 18-21, 1984.
2. Farrokhi S et al. *Osteoarthritis and Cartilage* **19**(3), 287-294, 2011.
3. Ward SR and Powers CM. *Clin Biomech (Bristol, Avon)*, **19**(10), 1040-1047, 2004.
4. Teng HL, et al. *Knee*, **21**(1), 142-146, 2014.
5. Farrokhi S et al. *Am J Sports Med*, **39**(2), 384-391, 2011
6. Ward SR, et al. *J Bone Joint Surg Am*, **89**(8), 1749-1755, 2007.
7. Li G, et al. *J Biomech Eng*, **123**(4), 341-346, 2011.

THE EFFECT OF EXERCISE TRAINING ON SHOULDER KINEMATICS AND MUSCLE ELECTROMYOGRAPHY DURING ARM ELEVATION

Yin-Liang Lin and Andrew Karduna

University of Oregon, Eugene, OR, USA
email: yinliang@uoregon.edu, web: <http://karduna.uoregon.edu/>

INTRODUCTION

Due to the inherent lack of stability provided by the bony, ligamentous, and capsular structures, dynamic control of the muscles plays an important role in stabilizing the shoulder during dynamics motions. The rotator cuff muscles, including the supraspinatus, infraspinatus, teres minor, and subscapularis, serve as the chief stabilizers of the shoulder. The rotator cuff muscles produce compressive forces to center the humeral head in the glenoid fossa, as well as generate inferior and posterior shear forces to counterbalance the superiorly directed deltoid force [1].

Scapular muscles, including the trapezius and serratus anterior, rotate the scapula to coordinate with humerus during arm elevation [2]. The rotator cuff and scapular muscles are essential to producing smooth shoulder movement. While many studies have investigated which exercises result in higher electromyography (EMG) activity during exercises, few studies have focused on if the changes in muscle activation happen after exercise training. The purpose of this study is to assess the effect of exercise training on shoulder kinematics and EMG during arm elevation.

METHODS

Twelve healthy subjects were recruited (4 males and 7 females, 18 – 26 years old). They received exercise training three times per week for four weeks, with an average duration of 30 minutes per session. All training sessions were supervised to ensure compliance with the training protocol. The exercise protocol consisted of six exercises, including full can, prone full can, external rotation in sidelying, diagonal exercise, push up with plus, and push up on exercise ball. The training consisted of three sets of 10 repetitions using variable

resistance: one set at 50% of the 10-repetition maximum (RM), one at 75% of the 10 RM, and one at 100% of the 10 RM [3].

A magnetic tracking device (Polhemus Liberty, Colchester, VT) was used to measure scapular, humeral and thoracic kinematics. The Myopac Jr (Run Technologies, Mission Viejo, CA) was used to collect raw surface EMG data. Paired fine wire electrodes were inserted into supraspinatus and infraspinatus muscles. Surface electrodes were used for the middle deltoid, upper trapezius, lower trapezius and serratus anterior. The subjects were instructed to conduct three arm elevation trials in the scapular plane with their dominant arm (Figure 1). The EMG during the arm elevation was synchronized with the kinematic measures and normalized by a MVC during a five second contraction.



Figure 1. The experimental setting

The scapular kinematics and root mean square EMG data were calculated over four 30° increments of motion during arm elevation from 0° to 120°. A two-way repeated measures ANOVA was used to examine the changes after the training.

RESULTS AND DISCUSSION

Figure 2 and figure 3 show the scapular kinematics and shoulder muscle activation during arm elevation. After training, scapular upward rotation tended to increase at higher humeral elevation angles (interaction effect, $p = 0.06$). The upper trapezius EMG tended to decrease throughout the range of elevation (main effect, $p = 0.07$). No significant difference was found in other parameters.

This study is still ongoing. The preliminary results show the exercises focusing on training rotator cuff and scapular muscles may increase scapular upward rotation and decrease upper trapezius muscle activity during arm elevation.

REFERENCES

1. Yanagawa T, et al. *J Biomech Eng.* **130**, 021024, 2008
2. Ludewig PM, et al. *J Orthop Sports Phys Ther* **39**, 90-104, 2009.
3. Reinold MM, et al. *J Orthop Sports Phys Ther* **39**, 105-117.

ACKNOWLEDGEMENTS

The authors would like to thank Andrew Duchesne, Vikas Mankala, Kirby Tobin, and Katya Trouset for the help of data collection.

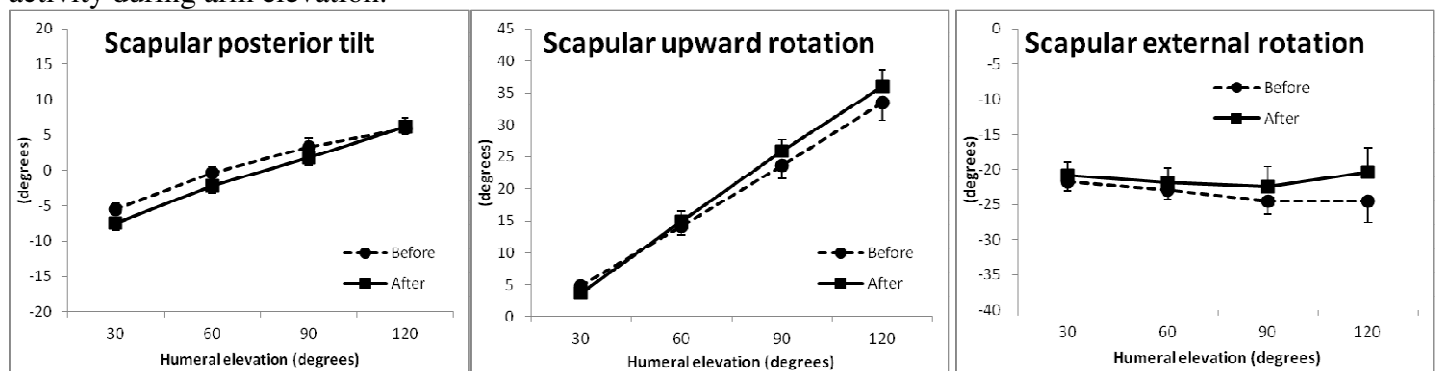


Figure 2. Scapular kinematics during arm elevation

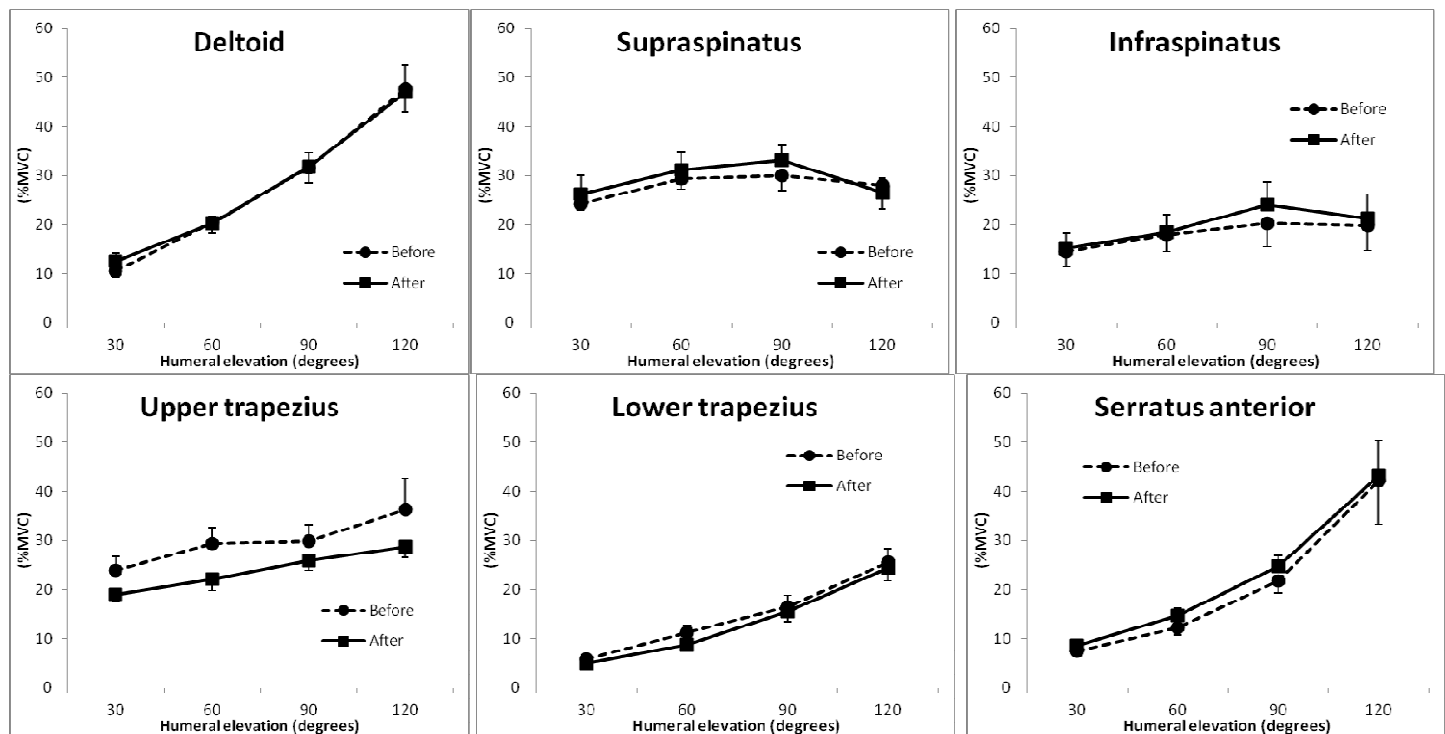


Figure 3. Shoulder muscle activation during arm elevation

THE EFFECTS OF ENTHESEAL SHAPE ON STRAIN FIELDS IN A PLANAR MODEL OF THE ANTERIOR CRUCIATE LIGAMENT

Callan M Luetkemeyer, Ellen M Arruda, James A Ashton-Miller

The University of Michigan, Ann Arbor, MI, USA
email: cmluetke@umich.edu

INTRODUCTION

The posterolateral (PL) bundle of the anterior cruciate ligament (ACL) is susceptible to failure at its femoral enthesis [1,2], where it resembles a ribbon [3]. Dissimilar tidemark profiles of the femoral enthesis were recently described and categorized in a histological study (Figure 1) [2].

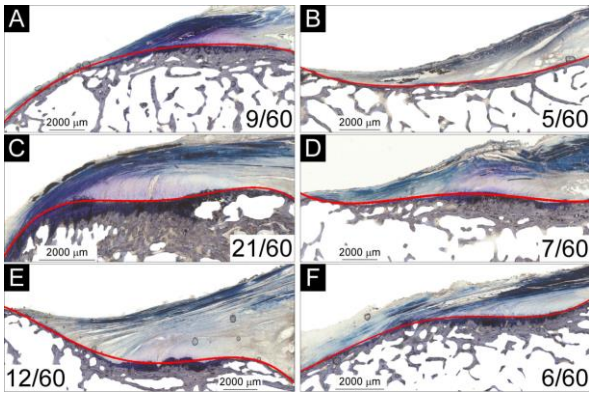


Figure 1: Human ACL femoral enthesis profiles and their respective frequency in 60 sample sections. Reproduced from Figure 5.3 in [1].

A knowledge gap is whether these enthesal profiles affect ligament mechanics. We therefore developed a model to examine the differences in strain fields among these characteristic tidemark profiles in order to determine whether certain profiles may be more advantageous than others.

METHODS

The ACL femoral enthesis was modeled as a 2D trapezoidal body of width w rigidly attached to a fixed curve, $y=A(x)$. This curve characterized the enthesal shape, and had an overall slope of a/w , such that the insertion angle of the enthesis (ϕ) was 30 degrees [1]. The opposite edge of the body ($y=L$) represented the ligament proper, and it underwent a uniform displacement δ .

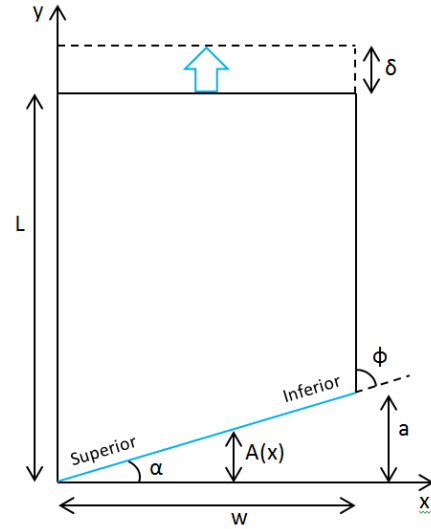


Figure 2: Diagram depicting the relationship among variables used in the model. The open arrow indicates the displacement of the boundary $y=L$.

Assuming homogeneity and no Poisson's effect, the displacement field is characterized by Equation 1.

$$u_y(x, y) = \frac{\delta}{L - A(x)} (y - A(x)) \quad (1)$$

Entheses A-F (Figure 1) were modeled using Equations 2-4.

$$A_{A,B}(x) = \frac{a}{w}x \pm [x^2 - wx] \quad (2)$$

$$A_{C,D}(x) = \frac{a}{w}x \pm [4x^4 - 8wx^3 + 5w^2x^2 - w^3x] \quad (3)$$

$$A_{E,F}(x) = \frac{a}{w}x \pm [2x^3 - 3wx^2 + w^2x] \quad (4)$$

The Lagrangian strain fields and Von Mises strain field were computed for each displacement field.

RESULTS AND DISCUSSION

Contour plots for the Von Mises strain fields are shown in Figure 3 with red indicating the highest strain region and blue, the lowest. The yellow line indicates the fixed enthesis boundary. The area

below this line is not part of the ligament and is not of interest.

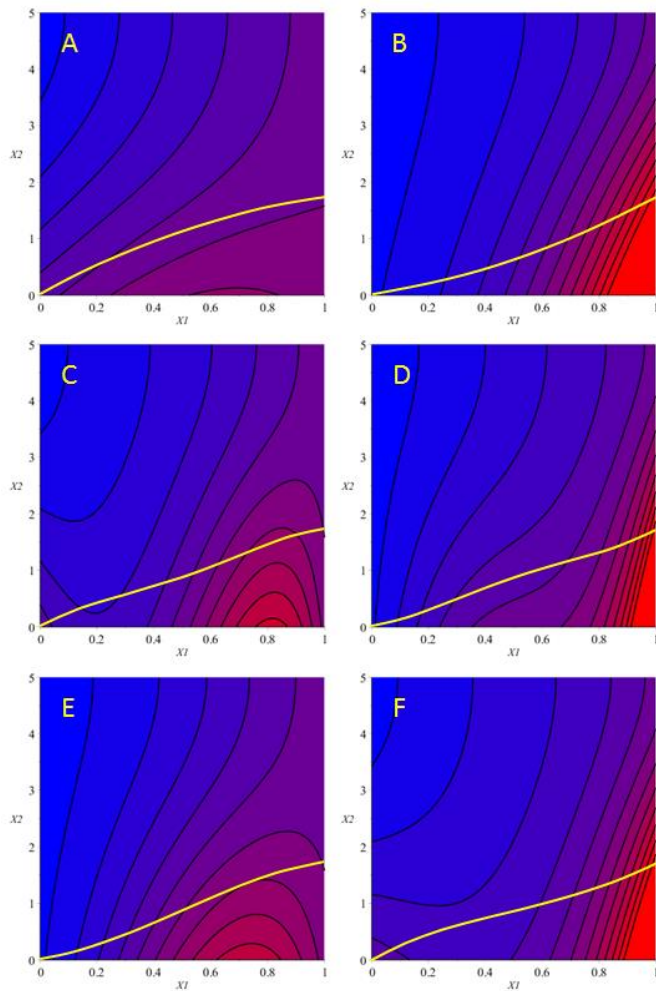


Figure 3: The Von Mises strain fields for enthesal profiles A-F as defined in Figure 1.

While a parabolic convex (A) enthesis increased the longitudinal strain throughout most of the ligament, it simultaneously reduced the maximum Von Mises strain by 32.3% compared to the parabolic concave (B) enthesis. This is due to a shift in the shape of the shear field; the point of maximum shear strain switches from the obtuse angled corner (most inferior attachment point in the ACL) to the acute angled corner (most superior attachment point). Clearly, shear effects play an important part in the concentration of strain within the femoral enthesis.

The most important feature of enthesal shape in determining the maximum Von Mises strain was the convexity near the most inferior attachment point of the ACL. If this part of the curve was convex (as in A, C, and E), the Von Mises strain was reduced.

Maximum Von Mises strain also increased with increasing polynomial order.

A parabolic convex tidemark seems to be the most advantageous shape for an angled ligament enthesis. It likely experiences less shear stress and Von Mises stress than other enthesal shapes. The present results lend insight into why ACL failures often occur at the femoral enthesis [2,3] and suggest the site of failure initiation might lie at the inferior corner. These results are also useful for establishing one of the variables in an ideal ACL enthesis. A future experimental study might examine whether the femoral enthesal shape can be remodeled in response to particular exercises, thereby reducing ACL injury risk. Likewise, tissue engineers might consider optimal enthesal shape when designing artificial ligaments with angled attachments.

This study is limited by the assumptions of homogeneity and zero Poisson's ratio. A finite element study incorporating realistic ACL geometry and a nonlinear, viscoelastic, anisotropic constitutive model or a well-designed experimental study with high imaging resolution would yield more realistic results. Still, there is valuable insight contained in this simple 2D analytical model.

While shear strain clearly plays a critical role in ligament mechanics, most studies have focused on the tensile properties of ligaments. More research is needed to characterize their shear properties and to determine the role of shear in ligament failure.

CONCLUSIONS

The profile of the ACL femoral enthesis affects its strain field and thereby the strain concentration at its most inferior point of attachment. A parabolic convex shape reduces the shear strain at this point and thus reduces the maximum Von Mises strain.

REFERENCES

1. Beaulieu ML. Doctoral Dissertation, School of Kinesiology, University of Michigan, 2014.
2. Lipps DB, et al. *Am J Sports Med* **41**, 1058-1066, 2013.
3. Smigielski R, et al. *KSSTA* June 28, 2014 [ePub].

A COMPREHENSIVE META-ANALYSIS OF SKELETAL MUSCLE ARCHITECTURE IN HUMANS

¹Lydia A. Luu*, ¹Sibo Zhang*, ¹Catherine M. Pelland, ¹BME 4280, ¹MAE 4280, ¹Silvia S. Blemker

¹University of Virginia, Charlottesville, VA, USA

email: lal2ta@virginia.edu, sz2fw@virginia.edu

*These authors contributed equally to this work as first authors.

INTRODUCTION

Skeletal muscles are the motors for all voluntary movements in the body, from walking to speech to breathing. The last few decades of biomechanics research have led to breakthroughs in our understanding of structure and function of individual muscles in the upper and lower limb. However, a holistic understanding of the diversity of muscle structure and function of all skeletal muscles of the human body remains lacking. Studies of muscle architecture have been performed for various groups of muscles such as the upper extremity [1] or lower extremity [2], but there is no comprehensive single source of muscle architecture data for all skeletal muscles in the human body.

This study aimed to perform comprehensive meta-analysis of the architectural properties of the nearly 300 skeletal muscles in the human body in order to (i) explore relationships between muscle form and function across all skeletal muscles across the body, (ii) examine subject demographics (age, gender, etc.) and the experimental means of collecting data across muscle architecture studies, and (iii) identify key gaps in our understanding of muscle architecture that provide future avenues of research.

METHODS

As part of an upper-level undergraduate Movement Biomechanics course, students were instructed to search PubMed and Web of Science for published values (in existing literature) of four skeletal muscle architecture parameters: physiological cross-sectional area (PCSA), optimal fiber length (L_0^M), volume (V), and pennation angle (α). Each muscle was researched by at least two undergraduates independently and their data compiled into a shared document for analysis. The data submitted by the class was examined to verify the values and sources. Data acquired from non-peer reviewed articles, estimations made by students, and modeling studies were omitted. Further research was conducted to fill in missing muscle architecture parameters with data from cadaver or *in vivo* studies. When volume, PCSA, or optimal fiber length was missing in data acquired from the same source, the other two were used to calculate the missing value.

For the purpose of muscle architecture analysis, all non-optimal data points (fiber length, muscle length, anatomical cross-sectional area, etc.) were eliminated from the data set. Average PCSA, optimal fiber length, and pennation angle were calculated for each muscle (with available data);

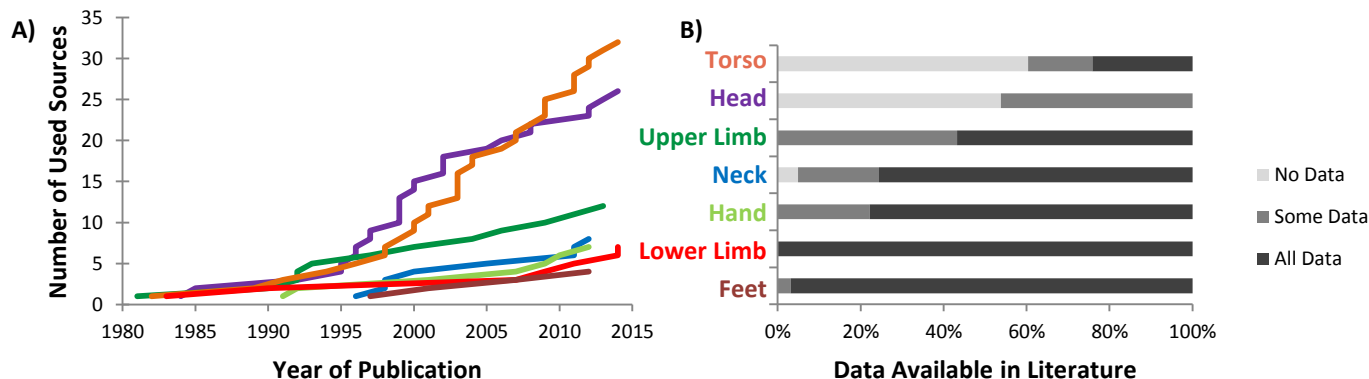


Figure 1 - Muscle Architecture Literature Meta-analysis: A) depicts a timeline of the cumulative number of muscle architecture studies for each muscle region. B) represents the percentage of muscles in each region of the body for which we have found all, some, or none of the four architecture parameters (PCSA, L_0^M , V , and α).

each data point was weighted based on the number of subjects in its respective study. Average volume for each muscle was calculated by multiplying the average PCSA and average optimal fiber length. For comparison between cadaver and *in vivo* studies, only muscles with both cadaver and *in vivo* volume data were included. Lastly, each study was evaluated based on the amount of information provided on subject age, weight, height, and gender.

RESULTS AND DISCUSSION

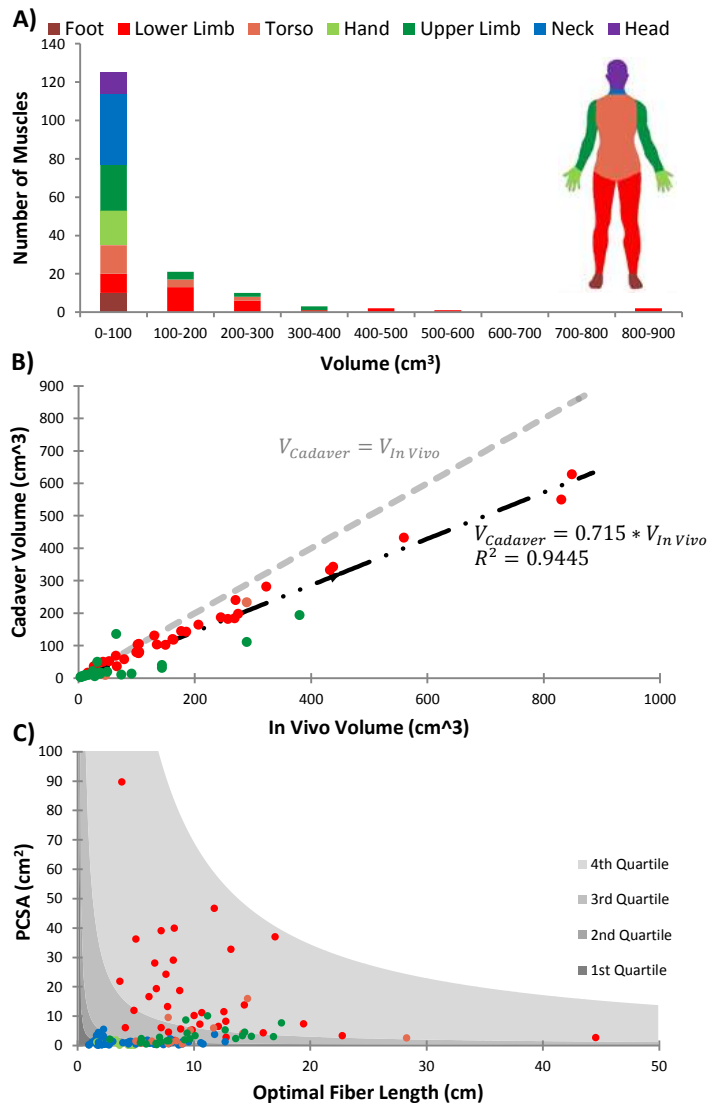


Figure 2 - Muscle Architecture analysis: **A)** a histogram of average cadaver volumes throughout the human body. **B)** is scatterplot of muscles with recorded cadaver and *in vivo* muscle volumes. The fitted trend line shows loss of volume in cadaveric samples when compared to the unity line. **C)** presents the average PCSA and L_o^M of all muscles for which architectural data was found. Shading represents volume quartiles.

A timeline of the cumulative number of muscle architecture sources for each muscle region reveals several key observations concerning muscle

architecture research (Fig. 1A). First, finding head and torso architecture data required searching through a significantly larger number of sources, partly due to the fact that there are more muscles in those regions. However, fewer sources that cover a large number of muscles in those regions exist, compared to the upper and lower extremities. While the studies used to compile the data for this analysis do not necessarily represent all muscle architecture studies, our timeline implies that the emergence of architecture studies has been linear over time for muscles of all body regions. Studies of limb and torso muscles were found at earlier time points as compared to the other regions. The four desired muscle architecture parameters were not found for every single muscle (Fig. 1B). All of the muscles in the upper limb, lower limb, hand, and feet have been measured to some extent with the lower limb being the most thoroughly studied muscle region. Conversely, the head and torso have a large number of muscles for which we no architecture data could be found. Future work should more rigorously characterize muscle architecture in these regions.

Muscles throughout the body range in volume (Fig. 2A). Of the muscles for which data was found the smallest is the interspinalis cervicis in the neck (0.16 cm^3) and the largest is the gluteus maximus in the lower limbs (849 cm^3). Reported muscle volumes in the head, neck, hand, and foot are less than 100 cm^3 , whereas muscles in the torso and upper limbs can be larger (up to 290 and 380 cm^3 , respectively). Muscles of the lower limb encompass the greatest range of volumes (from 16 to 849 cm^3). Volumes collected from cadavers are 71% of *in vivo* MRI volume measurements (Fig. 2B). We observed an inverse relationship between PCSA and L_o^M , and the maximum volume of every muscle falls under a hyperbolic curve (Fig. 2B). The trade-off between PCSA and length was observed for both large muscles (primarily in the lower limb) as well as smaller muscles (e.g. the foot and hand).

REFERENCES

1. Holzbaur KRS, Murray WM, Gold GE, & Delp SL. *J Biomech* **4**, 742-749, 2007.
2. Ward SR, Eng CM, Smallwood LH, & Lieber RL. *Clin Orthop Relat Res* **467**, 1074-1082, 2009.

KINETICS AND KINEMATICS OF THE ANKLE DURING FOOT EXTERNAL ROTATION

¹ Alexander Mait, John Paul Donlon, Adwait Mane, Jason Forman and Richard Kent

¹ The University of Virginia, Charlottesville, VA, USA

email: arm7sb@virginia.edu, web: www.centerforappliedbiomechanics.org

INTRODUCTION

High ankle sprains are a debilitating injury in athletics. They typically involve excessive external rotation of the foot causing diastasis between the fibula and tibia, thus injuring the syndesmotic ligaments [1, 2]. Other motions of the ankle such as dorsiflexion and eversion have also been shown to contribute to the injury [1, 3]. The goal of this study was to collect kinematic and kinetic data of specific ankle bones during external rotation of the foot to better understand high ankle sprains and to refine an existing finite element (FE) model of the ankle.

METHODS

A custom rig was designed to test lower limbs from human cadavers. Preliminary tests were performed with a left lower limb of a male 46 year old cadaver with a stature of 177 cm and mass of 113 kg. The test device was designed to rotate the leg about the long axis of the tibia to $\pm 20^\circ$ of foot rotation. The proximal portion of the tibia was potted in a cylindrical cup which was rigidly attached to an index table that could be rotated internally or externally. In order to not constrain the axes of rotation, the foot was allowed to translate in the x, y, and z directions via a system of rail bearings attached to the calcaneus (Fig. 1). A lockable gimbal device was attached between the calcaneus mount and rail system to provide an ability to pre-set the foot in eversion (10°) and/or dorsiflexion (20°) prior to applying foot rotation.

In order to capture the kinetics of the lower limb, a load cell was rigidly attached to the potted tibia. A quasi-linear viscoelastic (QLV) model [4] was then developed for each test to describe the relationship between the applied rotation and the moment recorded about the long axis of the tibia. From the QLV models, the instantaneous elastic moment (M_{z0}) and steady-state moment ($M_{z\infty}$) were

calculated for external rotation of the foot initially in neutral, eversion, and dorsiflexion.

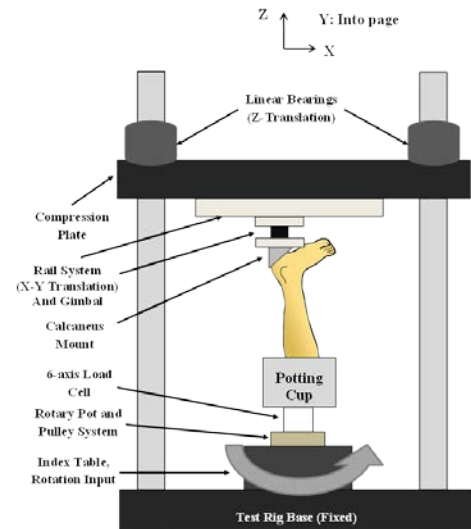


Figure 1: Schematic of experimental test rig.

To capture the kinematics of the bones of the ankle, an aluminum cube was screwed into the fibula and talus using wood screws set a certain distance off the bone with a spacer. For each test these cubes were scanned at the initial position (neutral) and final position (rotated) using a 7-axis, three-dimensional laser scanner (ROMER Absolute Arm, Hexagon Metrology, Inc., Surrey, Great Britain). Based on computed tomography (CT) scans and coordinate transformations [5], the yaw, pitch, and roll angles as well as x, y, and z displacements of each bone were calculated.

RESULTS AND DISCUSSION

When the foot was initially placed in neutral, the instantaneous moment M_{z0} observed under 20° external rotation was 9.87 N-m. This dropped slightly to 8.97 N-m when the foot was initially everted by 10° . When the foot was initially placed into dorsiflexion, the M_{z0} observed under 20° external rotation was 7.03 N-m. For all three foot initial position conditions, $M_{z\infty}$ was approximately

3.0 N-m (Fig. 2). The drop in Mz_0 from neutral foot to everted foot is consistent with [3], where approximately 37 N-m was measured at 20° external rotation for neutral foot and 19 N-m for everted foot; however the magnitudes vary significantly from the current study. The Mz_0 for the neutral foot in Fig. 2 is more consistent with [6], where about 15 N-m was measured for the “strongest” specimen at 20° external rotation.

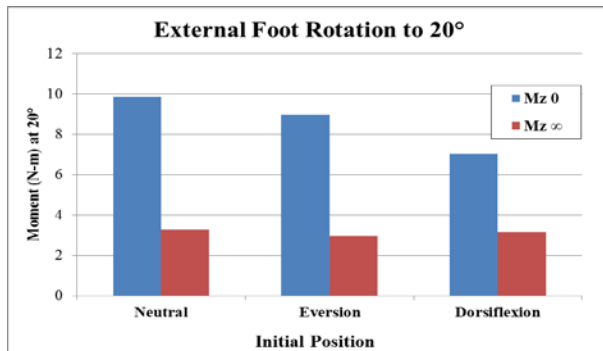


Figure 2: Instantaneous elastic and steady-state moment about tibia axis based on QLV models of each test [4].

The changes in yaw, pitch, and roll angles as well as x, y, and z displacements of the fibula and talus relative to the tibia global coordinate system are listed in Table 1. Talus lateral translation relative to the tibia was found to be 2.88 ± 1.13 mm in [3] at 30° of external foot rotation when the foot is everted 20°, yet the current study found only 0.83 mm of y (lateral) translation. Fibula rotations about all axes (relative to the tibia) were found to be less than 0.6° on average for a neutral foot under 10° of external foot rotation in [7]. The current study, with applying 20° of external foot rotation, found two angles of rotation greater than 1° for the fibula, namely the change in yaw angle at -4.705°.

The differences in the kinetics and kinematics from the current study to previous studies can most likely be attributed to the difference in boundary

conditions for the experiments. Previous studies have typically disarticulated the tibia and fibula at mid-shaft and did not allow the foot to translate when foot rotation was applied [3, 6, 7].

The current study focused on using quasi-static rotation loading of the lower limb. In future studies, a more dynamic loading should be considered to capture the nonlinear kinematics of the ankle bones. Also, the current study focused on one specimen. More specimens should be tested in order to gather a better confidence in the results. To expand the scope of the study, more initial foot motions should be explored, higher degrees of external rotation should be used, and capturing data on other ankle bones should be completed.

CONCLUSIONS

This study demonstrates that capturing detailed kinematics of the bones of the ankle during a combination of foot motions is possible. Using these methods, data may be gathered to refine a computational model of the ankle to accurately reproduce bone kinematics and boundary forces. Such a model may then be used to study effective strains in ankle ligaments that are not accessible to observe experimentally.

REFERENCES

1. Boytim MJ, et al. *Am J Sports Med* **19**, 294-298, 1991.
2. Williams GN, et al. *Am J Sports Med* **35**, 1197-1207, 2007.
3. Wei F, et al. *J Orthop Res* **30**, 1423-1429, 2012.
4. Kent RW, et al. *J Biomech* **42**, 1656-1663, 2009.
5. Shaw G, et al. *Stapp Car Crash J* **53**, 1-48, 2009.
6. Markolf KL, et al. *Clin Orthop Relat Res* **246**, 266-272, 1989.
7. Svensson OK, et al. *Clin Biomech* **4**, 155-160, 1989.

Table 1: Kinematic data for the fibula and talus, relative to the tibia coordinate system, for all initial foot motions after applying 20° of external rotation.

Specimen 616L	External Rotation of 20°											
	Fibula						Talus					
Foot Initial Position	Δ Yaw (°)	Δ Pitch (°)	Δ Roll (°)	Δ X (mm)	Δ Y (mm)	Δ Z (mm)	Δ Yaw (°)	Δ Pitch (°)	Δ Roll (°)	Δ X (mm)	Δ Y (mm)	Δ Z (mm)
Neutral	-4.705	-1.573	-0.653	-4.599	-0.233	-0.003	-15.968	-1.701	2.444	2.303	0.832	-0.750
Eversion (10°)	-4.677	-1.338	-0.420	-4.570	-0.595	-0.091	-14.938	-2.002	4.791	2.408	-0.692	0.215
Dorsiflexion (20°)	-4.339	-0.806	-0.290	-3.347	-0.970	0.158	-14.667	18.126	-5.197	1.598	-1.462	-1.694

BIAXIAL QUANTIFICATION OF TRANSVERSE CARPAL LIGAMENT ELASTIC PROPERTIES BY SEX AND REGION

¹Bryan Mathers, ²Anne Agur, ¹Michele Oliver, ¹Karen Gordon

¹School of Engineering, University of Guelph, Guelph, ON, CA

²Division of Anatomy, Department of Surgery, University of Toronto, Toronto, ON, CA

E-mail: bmathers@uoguelph.ca

INTRODUCTION

Carpal tunnel syndrome (CTS) is a widespread peripheral neuropathy which occurs more frequently in women than in men [1]. While a great deal of research has been conducted, CTS etiology is not clearly understood. The transverse carpal ligament (TCL) makes up the volar border of the carpal tunnel. The TCL acts as a pulley for the flexor tendons running through the carpal tunnel, anchors the thenar and hypothenar muscles and is thought to play a role in the stability of the carpus. As a result of these important roles, the material properties of the TCL are of great interest. Recent studies of the TCL have shown its properties vary with location and depth due to the complex orientation of collagen fibers [2-5]. Brett et al., found that the TCL strains significantly more radially than ulnarly when under uniaxial load [2]. In addition, the study reported a trend that female specimens experienced more strain on the radial side of the TCL compared to male specimens [2]. Given the increased incidence of CTS in women, further work evaluating this trend, specifically a comparison of regional sex based differences in properties, is warranted.

Material properties derived from biaxial loading more closely reflect the in-vivo behavior of tissue. Based on the uneven loading of layers and difficulties in clamping thicker tissues, Sacks et al. [6] recommended that biaxial sample thickness should not exceed 3 mm with 1 mm being the optimal thickness to obtain valid results. As TCL thickness can approach 3 mm, biaxial testing of this ligament can become problematic. Histological and mechanical studies of the TCL have found that load bearing fibers in deep layers of the TCL become more organized, providing greater mechanical strength in comparison to superficial layers [4,5]. Testing only deep layers of the TCL would ensure

that sample thickness approaches the recommended 1 mm and that the TCL fibers contributing to mechanical strength are evaluated.

The purpose of this study was to quantify deep TCL layer biaxial moduli to evaluate differences in between males and females, and radial and ulnar locations. The results of this work could impact our understanding of the etiology of carpal tunnel syndrome, and may improve treatment options, specifically related to non-surgical manipulative therapy.

METHODS

22 (13 Male (71 ± 14.3 years) and 9 Female (81 ± 2.8 years)) cadaveric wrists, were used in this experiment. Human ethics approval to conduct the study was obtained from the University of Toronto as well as the University of Guelph. Visual assessment of the tissue showed no discernible pathologies. Each wrist was dissected to expose the TCL. Two, 7 x 7 mm squares of the TCL were obtained from each specimen, centered through the proximal distal thickness and on either side of the medial lateral midline of the ligament. A layer of superficial tissue was removed from each sample. The final thickness was measured using a custom micrometer. Biaxial testing was performed using a CellScale BioTester (Waterloo, ON). Samples were mounted using four 5 mm rakes such that the predominant medial lateral fibers were aligned with the X axis. Samples were preconditioned over 10 cycles to 9% strain at 1%/s before undergoing biaxial strain to 12% at 1%/s. Axial forces and displacements were collected at a rate to 15 Hz. Cross sectional area was calculated based on tissue thickness and distance between rakes. Cross sectional area, force and rake displacement were used to determine stress-strain relationships for each

axis. The linear region of this plot was identified, and its slope was calculated to generate the elastic modulus. Statistical analyses were conducted using the GLM procedure in Minitab 17.1.0 (Minitab, State College, PA, USA) where specimen was included in the model as a random effect. Moduli were assessed by region (radial or ulnar), testing direction (medial-lateral or proximal-distal) and sex (male or female). When appropriate, differences were assessed using Tukey post-hoc analyses. In all analyses, $p \leq 0.05$ was required to declare a significant difference between means.

RESULTS AND DISCUSSION

The mean thickness of the tested samples was 1.14 ± 0.18 mm. Elastic moduli in the medial-lateral direction were significantly larger than the proximal-distal direction for both radial and ulnar samples ($p=0.013$). Medial-lateral and proximal-distal elastic moduli of the ulnar samples were significantly larger than those of the radial samples ($p=0.001$). No significant differences were found in elastic moduli between male and female specimens for any combination of region and/or direction (Figure 1). This lack of significance suggests that the increased incidence rate of CTS in females may not be a result sex based differences in mechanical properties of the TCL. Significantly lower medial-lateral transverse elastic moduli for radial samples compared to ulnar samples support the findings of Brett et al. [2]. These results may be useful in improving manipulative therapy techniques used to treat CTS. The TCL may stretch more radially than ulnarly so manipulative

therapy may benefit from focusing stretching on the radial side of the TCL.

This study is not without limitations, with an average specimen age of 81 in women and 71 in men, results may differ from results obtained from younger specimens. Sectioning the TCL does disrupt the fibers and may affect results, however, this effect would be consistent across all samples.. Finally, while every effort was taken to keep the tissue moist during sectioning and testing, dehydration of the sample over the course of testing may have impacted results.

REFERENCES

1. Atroshi, I., et al. *Journal of the American Medical Association*. **282** (2), 153–158.
2. Brett, AW., et al. *Clinical Biomechanics*, **29**(6), 601-606. 2014.
3. Holmes, MWR., et al. *Journal of Orthopaedic Research*, **30**(5), 757-763, 2012.
4. Prantil, RK., et al., *Journal of Clinical Anatomy*, **25**: 478–482, 2012.
5. Brett, AW., et al. *60th Annual Meeting of the Orthopaedic Research Society*. Poster **1026**. 2014.
6. Sacks, MS., Sun, W. *Annu. Rev. Biomed. Eng.* **5**, 251-284, 2003.

ACKNOWLEDGEMENTS

Funding for this project was provided by the Natural Sciences and Engineering Research Council of Canada and the Canadian Foundation for Innovation.

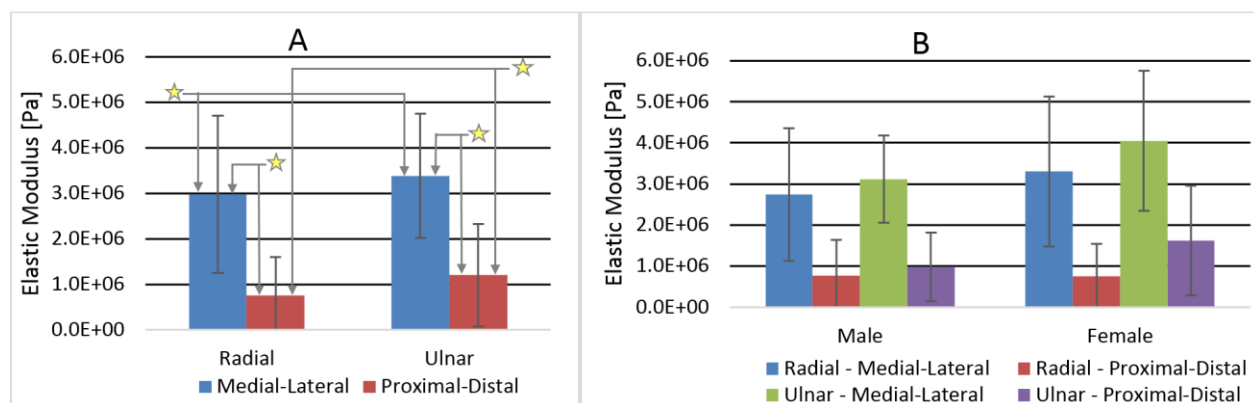


Figure 1: A – Comparison of mean biaxial elastic moduli in medial-lateral and proximal-distal directions between radial and ulnar TCL samples. Connected elements denoted by a star were found to be significantly different. B – Comparison of mean biaxial elastic moduli of radial and ulnar samples of the TCL in medial-lateral and proximal-distal directions between male and female specimens.

AXIAL ROTATION CAUSES BILATERAL DIFFERENCES IN THE SIZE RATIO OF INTERVERTEBRAL FORAMEN TO NERVE ROOT

Graham Mayberry and Janessa Drake

York University, Toronto, ON, CANADA
email: mayberr1@yorku.ca, jdrake@yorku.ca

INTRODUCTION

Axial rotation in the lumbar spine can lead to potential injury and pain development. Therefore, our understanding of transverse spinal rotation is critical to research in functional anatomy disciplines. Previous research has been conducted to measure nerve compression *in vitro* [1] while the foramina heights and widths have been measured *in vivo* [2]. The relationship between the size of the intervertebral foramen (IVF) and the spinal nerve root (NR) that exits through it has not been quantified, though it may play a significant role in how or whether individuals experience low back pain (LBP) [3]. Additionally, it is known that facet joints of the left and right side of the same functional spine unit (FSU) experience different degrees of motion during axial rotation [4]. The purpose of this study was to compare the left and right sides of the spine by quantifying the size ratio between the intervertebral foramen and associated nerve root in supine and axially rotated postures.

METHODS

Two healthy males (24.0 +/- 2.0 yrs) were recruited for this study with no history of LBP over the previous 12 months and successfully pass the MRI screening process. A Siemens MAGNETOM 3T Trio MRI scanner was used to acquire 3D MRI scans, using a T2SPC imaging protocol, with a slice thickness of 0.781mm.

During the imaging session, the participants were asked to lie in a supine position with their shoulders strapped down while 3D MRI scans were acquired. The participants then moved to their maximal axially-rotated position (with their knees pointing to the left). Wedges were placed at the hips and between the knees, and straps were fastened around

the shoulders, knees and hips to ensure they were comfortable and would not move during imaging. The lumbar spine was imaged, focusing on the levels of L4-L5, providing a complete FSU.

The images were analyzed using OsiriX (© Pixmeo Sarl, V 5.0.1) to measure cross-sectional area (CSA) of the NR and IVF from a series of subsampled slices that represent the best view of both features. The CSA for both the NR and IVF of the left and right sides were calculated by averaging the seven smallest CSAs from the entire series of slices along an axis that was manipulated to run directly through the center of the IVF perpendicular to the sagittal plane. The NR:IVF ratio was then calculated and compared for both the left and right sides.

RESULTS AND DISCUSSION

The CSA of the right and left IVF and NR, in addition to the NR:IVF ratio, were quantified for the L4-L5 FSU in both the supine and axially-rotated positions for both subjects (see Table 1). These preliminary results do not suggest any predictability or trend when looking at the IVF and NR independently, though a greater sample size would help verify that claim. However, focus on the NR:IVF ratio reveals that the behavior of the left and right sides are in the same direction though with very different magnitudes. A graphical representation of the NR:IVF ratio allows a much easier comparison (see Figure 1). In both subjects, the NR:IVF decreases on the right side but increases on the left side when going from supine to right axial rotation.

The greater the NR:IVF ratio seen would suggest a greater probability of nerve root compression or impingement which may result in behavioural changes. One study investigated this relationship

in rats and found that the amount of mechanical compression in the nerve root was proportional to amount of behavioural change exhibited in rats [5]. The relatively low NR:IVF ratios acquired in this study would likely lead to the development of low back pain and associated periphery pain, however it has been found that this NR impingement occurs in 50% of patients with LBP [6].

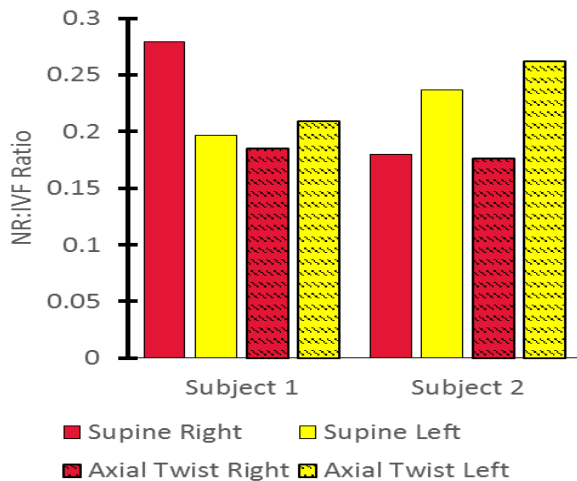


Figure 1: NR:IVF ratio of the left and right side of L4-L5 in the supine and axially rotated positions of two pilot subjects.

The two subjects exhibited different trends of the NR and IVF if analyzed independently, which we attributed to morphological variation and possibly different strategies while rotating, despite being given the same instructions. For instance, if one shifts the hips dorsally or ventrally in an effort to remain comfortable (ie. Following the instruction to maximally rotate while being comfortable) then the left and right IVFs may open or close to accommodate the movement. For this reason, the choice to measure the relationship between the NR and IVF is more functionally appropriate.

CONCLUSIONS

The quantification and comparison of the NR and IVF between sides and positions will aid in our understanding of the left to right behaviour during axial rotation and supplement the *in vitro* work that has been completed to date in that regard. Our results suggest that there is a tradeoff between the left and right sides in terms of NR:IVF ratio and that they do seem to behave conversely to one another.

Due to the fact that this study provides novel data in an area in which our understanding of LBP still lacks a definitive mechanism, this research is extremely valuable. With more subjects currently being scanned, we can provide a database for which asymptomatic baseline measurements can be compared. Future research should examine females, various age groups, and perhaps even patients suffering from LBP to fully understand the left to right behaviour of the NR:IVF relationship during axial rotation in the lumbar spine.

REFERENCES

1. Nowicki, B, et al. *Am J Neuroradiol* **17**, 1605-14, 1996.
2. Senoo, I, et al. *Spine* **39**, 929-35, 2014.
3. Lee, Y, et al. *Am J Neuroradiol*, **30**, 1062-67, 2009.
4. Drake, JDM, et al. *Spine* **33**, 728-34, 2008.
5. Winkelstein, BA, DeLeo, JA. *Brain Res*, **956**, 294-301, 2002.
6. Boos, N, et al. *Spine* **20**, 2613-25, 1995.

Table 1: The cross-sectional area (cm²) of the IVF and NR and the NR:IVF ratio for the two subjects.

		Supine		Axial Twist	
		Right	Left	Right	Left
Subject 1	IVF	1.05	1.36	1.14	1.39
	NR	0.29	0.27	0.21	0.29
	NR:IVF	0.28	0.20	0.19	0.21
Subject 2	IVF	1.00	1.07	0.96	0.90
	NR	0.18	0.25	0.17	0.24
	NR:IVF	0.18	0.24	0.18	0.26

Maximal Biceps Contraction During Supination Causes Proximal Radial Head Translation.

¹Brett Bergman, ¹David Rion, ²Tennyson Lynch, ¹Thomas Maher, ¹Edward Birdsong,
^{1,3}Mark Carl Miller

¹Orthopaedic Surgery, Allegheny General Hospital, Pittsburgh, PA, USA

²Temple University, Philadelphia, PA

³University of Pittsburgh, Pittsburgh, PA, USA

INTRODUCTION

The design of radial head prostheses for cases of comminuted radial head fractures enables a surgeon to restore the native length to the radius and approximate the appropriate kinematic relationships for supination and flexion. Unfortunately, not all patients can tolerate these prostheses and revision surgeries may be required. The current designs of prostheses consider head diameter and length and offer few choices with respect to the foveal radius of curvature. The possible problems of a capitellar-radial head mismatch have been recently considered with respect to the increased pressures on capitellar cartilage.(Kim, 2014) The possible problems related to shear loads on the capitellum have not received the same attention. The current work sought to demonstrate *in vivo* axial and shear loading by quantifying the amount of radial head translation due to a maximal biceps contraction during a supination resistance loading, working from the null hypothesis that at 90 degrees of shoulder abduction and 90 degrees of elbow flexion there would be no difference between the head positions during a maximal supination effort and during a relaxed pose.

METHODS

Institutional Review Board approval was received to obtain six radiographs of the elbow of the dominant arm in 14 men(age 34.8±10) and 14 women(age 39.5±12). Each subject sat in a chair with the shoulder abducted to 90 degrees, the elbow flexed to 90 degrees and with her/his elbow on the surface of an x-ray table.(Expert 4000, Swissray, Piscataway, NJ) Each subject first relaxed the arm musculature with the forearm in neutral rotation while a technician imaged the elbow. The subject then gripped a fixed handle connected to a torsional

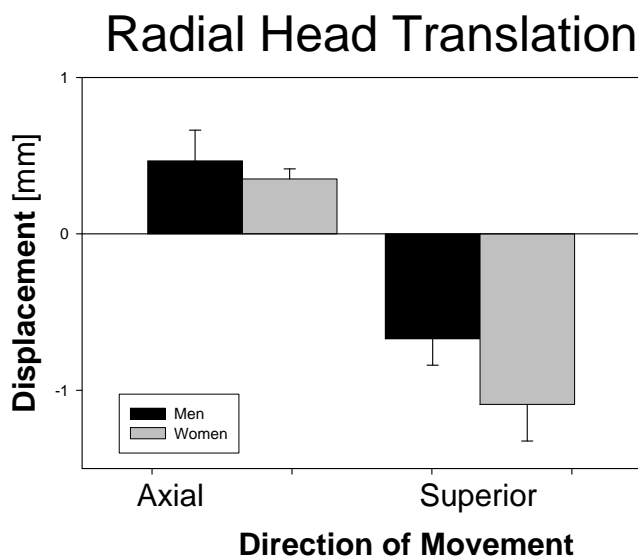
loadcell and performed a maximal supination effort while the loadcell recorded the torque and the technician again imaged the elbow. Two additional trials with accompanying radiographs of the unloaded and loaded elbow were performed.

Each digital radiograph was then processed to find the relative locations of the center of the capitellum and the radial head. Rouleau et al. (2012) used the center of the face of the radial head to locate the radius but the current work judged the centroid of the head to be less sensitive to error. Radiographs were imported into MatLab(MathWorks, Natick, MA). Three trained medical personnel then outlined the capitellum and radial head in each image and identified the center of the radial canal at the canal narrowing of the bicipital tuberosity. A custom MatLab program then established an orthogonal coordinate system by connecting the radial head centroid and the center of the radial canal and finding the perpendicular to this first line segment.

A line segment was formed by connecting the centroids of the radial head and capitellum and this line segment located the capitellum with respect to the radial head. Upon finding the capitellar radial head locations for the unloaded and loaded cases, the averages of each and the differences between them were computed. The difference in the locations between the loaded and unloaded cases represented the displacement of the radial head, with the movement along the radial head axis representing proximal/distal translation and the movement along the perpendicular to the radial axis representing vertical movement, described as superior/inferior translation. The differences of locations of the unloaded and loaded positions and, second, the differences of the displacements for men and for women, were compared with paired t-tests in Minitab(Minitab Inc., State College, PA).

RESULTS AND DISCUSSION

The vertical locations of the radial head with respect to the capitellum in the loaded condition were statistically different than the unloaded locations in both men and women (men, $p < 0.026$; women, $p < 0.001$) while the horizontal positions were not statistically different in men ($p > 0.200$) but were in women ($p < 0.010$). Women had greater vertical movement ($p = 0.040$) but there was no difference in axial movement (proximal-distal) towards the humerus ($p = 0.390$). (s. Figure) A comparison of the findings of three raters with an ANOVA found no differences due to the rater ($p = 0.409$).



The radius moved with respect to the humerus, which one would expect when the directions of the muscle forces acting during maximal supination effort are considered. At 90 degrees of elbow flexion, the biceps pulls the radius upward, while the forearm musculature pulls the radius toward the capitellum. Compression of the cartilage of the capitellar-radial head interface provides one possible measureable movement, but the cartilage on the radial head and capitellum combined is two millimeters thick. Thus in the average, the axial movement of the radius towards the humerus of less than 0.5 mm could be cartilage compression if the load were very large, but the vertical movement of the radius towards the shoulder is more than could occur due to this compression.

The resistance to translation toward the shoulder could be provided by forces from several

sources. Foremost, ligaments of the forearm are likely to contribute, with the annular ligament especially well placed for this purpose. The annular ligament constrains the radius laterally and the fibers should also resist the vertical biceps load under consideration. The load sustained by the annular ligament under these circumstances is not yet carefully quantified, but the fibers at the medial insertion of the annular ligament are not oriented directly toward shoulder. Nonetheless, fibers could certainly resist the load, although not efficiently. The interosseous membrane could also resist the translation in question. Its fibers are most effectively oriented to resist axial movement of the radius, but their obliquity and the central band could play a role in constraint of vertical translation. Muscle activity could also play a direct role, particularly the supinator, which can not only work with the biceps to effect supination: a component of its force on the radius would act in a distal direction. The other muscles act primarily along the longitudinal axis of the forearm. Lastly, the radial head could resist upward movement by contact between the posterior side of the fovea and the capitellum. Given that the radius moved upward, the capitellum certainly adds to the vertical translation constraint on the radius. Force due to this contact would add to the pressure between the radial head and capitellum and create additional design considerations for radial head prostheses. The shear loading could have a particular importance to the ability of the capitellar cartilage to survive radial head replacement. The difference between men and women could be due to larger axial muscle forces which lead to greater capitellar/radial head contact and therefore greater shear loads but no certain evidence currently exists.

CONCLUSIONS

The results show that the radial head does translate towards the shoulder during supination so that both compressive and shear forces are applied to the capitellum, adding to the demands on any radial head replacement.

References

Kim, ISBN 132142924X, 9781321429244
Rouleau et al., JSES, 2012.

Associations between Quadriceps Muscle Strength, Power, and Knee Joint Mechanics in Knee Osteoarthritis: A cross-sectional study

¹ Amanda Murray, Abbey Thomas², Charles Armstrong³, Brian Pietrosimone⁴, and Michael Tevald³

¹ Department of Physical Medicine & Rehabilitation, Physical Therapy Program, University of Colorado

² Department of Kinesiology, University of North Carolina at Charlotte, ³ Department of Kinesiology, University of Toledo, ⁴ Department of Exercise and Sport Science, University of North Carolina at Chapel Hill
email: Amanda.murray@ucdenver.edu

INTRODUCTION

Individuals with knee osteoarthritis (OA) commonly exhibit abnormal mechanics during gait, including altered knee joint angles and moments, which may contribute to the initiation and progression of the disease [1]. Quadriceps weakness is common in individuals with knee OA and has been suggested to contribute to abnormal knee joint mechanics. However, 1) prior studies have found no significant associations between quadriceps strength and knee joint mechanics and 2) quadriceps strengthening has not been shown to influence knee joint mechanics in these individuals [2,3]. Conversely, quadriceps muscle power (force x contraction velocity) has been found to be significantly associated with the peak external knee adduction moment (KAM), a measure of frontal plane knee loading, in patients with knee OA [4]. The association between quadriceps power and sagittal plane knee joint mechanics such as peak knee flexion angle (KFA) and external knee flexion moment (KFM) have not been explored in this population.

The purpose of this study was to examine the contributions of quadriceps strength and power to knee mechanics (peak KFA, KFM, and KAM) during gait in individuals with knee OA.

METHODS

Thirty-three adults (age > 40 years) with physician-diagnosed knee OA and moderate impairment in physical function participated in this study (23 females, 10 males, 59.79±9.02 years; 100.08±24.98kg; 1.70±0.95m; WOMAC function subscale: 29.32±8.06 out of a possible 44 with higher scores indicating greater dysfunction).

Quadriceps strength was quantified as the one repetition maximum (1RM) assessed on a pneumatic knee extension machine with the involved limb positioned at 90° of hip and knee flexion. The resistance from the last full repetition of knee extension was recorded as the 1RM (kg) and normalized to body mass. Quadriceps power was assessed at 40%, 50%, 60%, 70%, 80%, and 90% of 1RM in a random order. The participants were instructed to extend their knee as hard and fast as possible, pause at end range, and return to the starting position over two seconds. Three trials at each resistance were performed and the peak power (W) produced at 40% 1RM (low intensity), 70% 1RM (moderate intensity), 90% 1RM (high intensity), and overall regardless of external load was recorded (W) and normalized to body mass.

Gait trials were collected using a three-dimensional, 12-camera passive marker motion capture system synchronized with an embedded force platform. Participants were outfitted with 35 retroreflective markers on the trunk, pelvis, and lower extremities and walked along a 10m walkway at a self-selected speed. After the gait trials, participants were asked to mark the pain in their knee on a visual analog scale (VAS). Kinematic and kinetic data were normalized to 100% of stance phase. Peak KFA, KFM, and KAM during the first 50% of stance phase were averaged over 3 trials and used in the analysis.

Pearson correlation coefficients were used to examine the relationships between each dependent variable, independent variable, and potential covariates (sex, pain, and gait velocity). If any covariates were significantly associated with the dependent variables, they were entered into the regression analysis prior to the muscle variable.

Separate linear regression analyses were used to assess the amount of variance in peak KFA, KFM, and KAM explained by each measure of quadriceps strength and power.

RESULTS AND DISCUSSION

Quadriceps strength and all measures of power were significantly, positively correlated with peak KFA ($r=0.42-0.56$). Strength explained 15% of the variance in peak KFA while power explained 20-29% of the variance (Table 1). Only quadriceps power at 90% 1RM was significantly correlated with peak KAM, explaining 9% of the variance in peak KAM (Table 1). No measures of quadriceps strength or power were significantly correlated with peak KFM. None of the covariates were significantly correlated with the dependent variables and were therefore not entered into the regression analysis.

A novel finding in the present study is the positive association between quadriceps power and peak KFA, suggesting individuals who generate more power also have greater KFA during stance. These results suggest that not only does the force generating capacity of the muscle influence knee joint position during stance phase of gait, but also the speed at which that force is generated.

Peak KAM was not significantly correlated with quadriceps strength but was significantly correlated

with power at 90% 1RM ($r=-0.35$). These results indicate that individuals who generate greater power at a higher intensity also have higher medial compartment loading. Additionally, all measures of quadriceps power explained more of the variance in peak KFA than strength (Table 1). Taken together, these results suggest that muscle power may play a larger role in knee kinematics than strength alone.

CONCLUSIONS

Quadriceps muscle strength and power both influence knee joint mechanics in individuals with knee OA. Since knee joint mechanics have been associated with the initiation and progression of knee OA, it is important to consider the possible consequences that increasing quadriceps strength and power may have on overall joint health. Future studies should examine the effects of interventions aimed at improving quadriceps strength and power on knee joint mechanics in individuals with knee OA.

REFERENCES

1. Mills, K, et al. *Arthritis Care Res (Hoboken)* **65**, 1643-1665, 2013.
2. Lim, BW, et al. *Arthritis Rheum* **61**, 451-458, 2009.
3. Lim, BW, et al. *Arthritis Rheum* **59**, 943-951, 2008.
4. Calder, KM, et al. *Arthritis Care Res* **66**, 687-694, 2014.

Table 1: Regression analyses of associations of quadriceps strength and power to knee joint mechanics.

Variable	Unstandardized β Coefficient	SE	Adjusted r^2	p
Peak Knee Flexion Angle				
1RM	-19.17	7.52	0.15	0.016*
Power at 40% 1RM	-6.99	2.41	0.20	0.007*
Power at 70% 1RM	-6.41	1.73	0.29	0.001*
Power at 90% 1RM	-6.09	2.09	0.20	0.007*
Peak Power	-6.42	1.94	0.24	0.002*
Peak Knee Flexion Moment				
1RM	0.33	0.23	0.03	0.16
Power at 40% 1RM	0.08	0.08	0.04	0.32
Power at 70% 1RM	0.07	0.06	0.02	0.22
Power at 90% 1RM	0.09	0.07	0.02	0.20
Peak Power	0.07	0.06	-0.01	0.38
Peak Knee Adduction Moment				
1RM	-0.11	0.13	-0.01	0.42
Power at 40% 1RM	-0.05	0.04	0.01	0.25
Power at 70% 1RM	-0.04	0.03	0.01	0.26
Power at 90% 1RM	-0.07	0.04	0.09	0.05*
Peak Power	-0.06	0.03	0.05	0.11

* $p \leq 0.05$

SENSITIVITY OF CARTILAGE PRESSURE TO LIGAMENT STIFFNESS DURING SHOULDER ABDUCTION

¹ Hafizur Rahman and ¹ Mariana E. Kersh

¹ The University of Illinois at Urbana-Champaign, Urbana, IL, USA
email: mrahman3@illinois.edu, web: <http://uitbl.mechse.illinois.edu>

INTRODUCTION

Rotator cuff tears are considered one of the primary causes of shoulder pain and dysfunction in adults [1]. Statistics show that more than 50% of patients over the age of 60 and 80% of patients over the age of 80 have a cuff tear [2]. Unfortunately, the success rate of rotator cuff repair is variable with many resulting in a re-tear. The chance of persistent tears or re-tears has been documented to be 35% for small tears and 94% for larger multi-tendon tears [3-5]. Similarly, revision surgeries can be as high as 30% for isolated supraspinatus tendon tears [6].

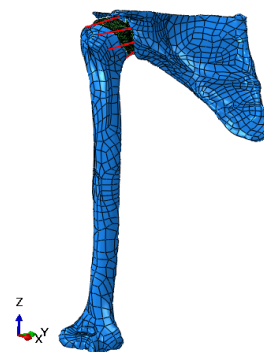
The aim of our research is to provide orthopedic surgeons with specific recommendations that will improve the outcome of rotator cuff surgeries. It is therefore important to understand the biomechanical properties of the ligaments, capsule, and dynamic properties of the muscles of the shoulder joint. Of note from the literature is the variation in the measured stiffness of shoulder joint ligaments [7-8]. It is essential to know how the variation of ligament stiffness affects the cartilage pressure in the glenohumeral joint. To investigate this, we developed a three-dimensional finite element (FE) model of the shoulder joint that includes the major ligaments and glenohumeral cartilage.

METHODS

The geometries of the humerus and scapula were created from computed tomography (CT) data of the shoulder (voxel size: 0.34 x 0.34 x 0.49 mm). The CT files were imported into Amira (v5.6, Visualization Sciences Group, France, and Zuse Institute Berlin, Germany) for segmentation of the bones using a semi-automated method. After segmentation, surfaces were generated and exported as an STL file and then imported into Geomagic Studio (v2014, Geomagic Inc., USA). The bone surfaces were smoothed, refined and noise was reduced. Finally, a solid model was created and exported as an STPAP203.

Construction of the FE model and all simulations were performed using Abaqus (v6.13, Dassault Systems, France). Quadrilateral dominant surface meshes were used for the humerus and scapula ($E=17\text{GPa}$, $\nu=0.35$) [9]. The cartilage mesh was a layer of elements offset from the surface of the proximal and distal ends of the humerus and scapula, respectively. Scapula cartilage was defined as 1 mm thick and the humerus cartilage as 0.5 mm thick ($E=30\text{MPa}$, $\nu=0.45$) [10]. Frictionless contact was defined between the humerus and scapula cartilage.

The coracohumeral ligament (CHL), superior glenohumeral ligament (SGHL), middle glenohumeral ligament (MGHL), and inferior glenohumeral ligament (IGHL) were modeled as axial springs (Fig. 1).



The model was kinematically constrained along the scapula, and a 15 degree abduction was enforced on the humerus while translational components of the humerus were left unconstrained. The simulation was run with ligaments at three stiffness values: (1) the average value reported in the literature, (2) low: the average value minus the reported standard deviation, and (3) high: the average stiffness plus the reported standard deviation (Table 1). No stiffness values were found for the MGHL, therefore the average of the SGHL and IGHL were used. The kinematics of the humerus and cartilage contact pressure was recorded under the three stiffness levels.

Table 1: Stiffness for ligaments, K (N/mm) [7-8]

	CHL	SGHL	MGHL	IGHL
Low	30.8	15.9	15.6	15.4
Avg	36.7	17.4	21.4	25.4
High	42.6	18.9	27.1	35.4

RESULTS AND DISCUSSION

From the simulation results, it is interesting that the translational motion of the humerus remained almost the same for the first 5° of abduction. After 5° of abduction motion, the medial-lateral translation began to change for low, average and high ligament stiffness. By 15°, medial translation for average stiffness ligaments was 16.6% higher than low stiffness ligaments and 7.9% lower than high stiffness ligaments (Fig. 2). On the other hand, at 15° abduction, anterior translation for average stiffness ligaments was 1.7% higher than high stiffness ligaments and 4.3% lower than low stiffness ligaments (Fig. 3).

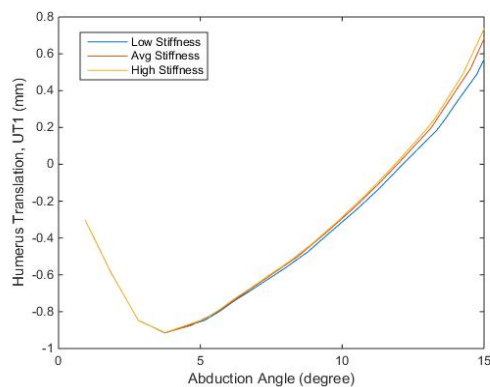


Figure 2: Humerus medial-lateral translation

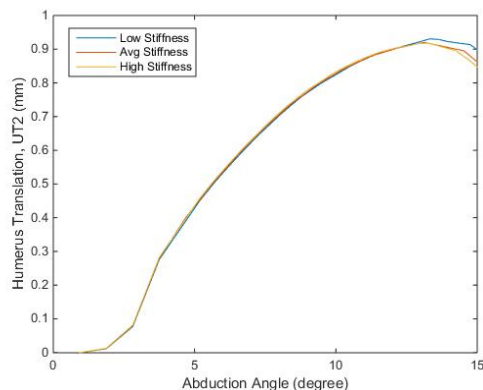


Figure 3: Humerus anterior-posterior translation

The average contact pressure of the scapula cartilage was nearly constant for all stiffness values until 5° of abduction, as expected, since there was no change in translation motion of humerus until 5° of abduction (Fig. 4). But after 5°, the changes in cartilage contact pressure was abrupt – possibly because of differences in the topology of the scapula cartilage surfaces that were in contact. After 13° of abduction, the cartilage contact pressure rose sharply and varied for all three stiffness values. The

medial-lateral and anterior-posterior translation changes observed after 10° might be contributing to the cartilage contact pressure differences. A similar phenomena was also observed for the humerus cartilage contact pressure.

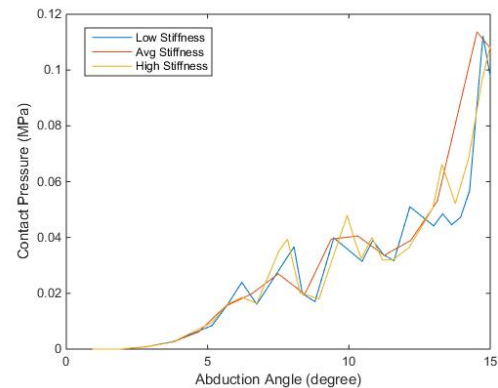


Figure 4: Scapula cartilage contact pressure during abduction

Our results suggest that the translation of humerus can be sensitive to ligament stiffness. This sensitivity of the humerus translation motion also has contributing effects on how the contact pressures are generated in cartilage. This is important for both experimental studies where care should be taken to not disturb the ligaments when measuring cartilage mechanics and modeling studies that make use of this experimental data. To date, we have not validated our model, but experimental procedures are going on to validate the simulation results.

REFERENCES

1. Apreleva M, et al. *Arthroscopy* **18**(5), 519-526, 2002.
2. Milgrom C, et al. *J Bone Joint Surg Br* **77**(2), 296-298, 1995.
3. Harryman DT, et al. *J Bone Joint Surg Am* **73**(7), 982-989, 1991
4. Liu SH, et al. *Arthroscopy* **10**(1), 54-60, 1994.
5. Calvert Pt, et al. *J Bone Joint Surg Br* **68**(1), 147-150, 1986.
6. Goutallier D, et al. *J Shoulder Elbow Surg*, **12**(6), 550-554, 2003.
7. Boardman ND, et al. *J Shoulder Elbow Surg* **5**(4), 249-254, 1996.
8. Bigliani LU, et al. *J Orthop Res* **10**(2), 187-197, 1992
9. Varghese B, et al. *J Biomech* **44**(7), 1374-1379, 2011.
10. Besier, TF, et al. *Journal of Orthopaedic Research* **26**(12), 1627-1635, 2008.

ACKNOWLEDGEMENTS

We would like to thank Stu Warden for the use of the CT data.

ARTHROKINEMATIC EFFECTS OF JOINT MOBILIZATION OF THE TALOCRURAL JOINT: AN IN VITRO STUDY

Anthony R. McNally, Stacie I. Ringleb, Cameron P. Powden and Matthew C. Hoch
Old Dominion University, Norfolk, VA, USA
email: sringleb@odu.edu

INTRODUCTION

Ankle injuries, resulting in damage to the lateral ligamentous complex, are often associated with limited dorsiflexion (DF) range of motion (ROM). Deficits in dorsiflexion ROM may be the result of arthrokinematic restrictions, specifically in posterior talar glide [1]. To restore normal ankle arthrokinematics and ROM, clinicians often use manual therapy techniques referred to as joint mobilization (JM). Anterior-to-posterior joint mobilization techniques are frequently employed to increase dorsiflexion ROM of the talocrural joint [2]. Several studies have identified immediate improvements in dorsiflexion ROM following JM treatment; however, these studies failed to confirm the arthrokinematic alterations that were involved [3, 4]. Therefore, the mechanisms underlying the effect of talocrural JM have not been satisfactorily explored.

Examining the effects of JM using in vitro testing methods may provide a model to capture subtle changes at the arthrokinematic level. Distal tibiofibular JM was simulated in vitro and was able to detect increased ankle dorsiflexion after treatment [5]. However, arthrokinematic changes at the talocrural and subtalar joints remain unclear [3, 4] and an in vitro model examining kinematics following talocrural joint mobilization has not been investigated. Therefore, the purpose of this preliminary in vitro study was to examine changes in talocrural arthrokinematics and dorsiflexion ROM after performing Maitland Grade III anterior-to-posterior JM to the talocrural joint.

METHODS

Three fresh frozen cadaver lower extremities (3 left limbs, age 68.3 ± 8.08 , one male) with no documented history of ankle injury were secured to a custom 6 degree of freedom ankle loading device.

A certified athletic trainer with 3 years of experience performed two sets of Maitland Grade III anterior-to-posterior JM to the talocrural joint with 200 oscillations per set. The Grade III JM was defined as a 1-second large amplitude rhythmic oscillation applied from the mid-range of accessory motion to the area of tissue restriction. Data were collected at baseline and after each set of JM.

A six camera Motion Analysis Eagle System (Motion Analysis Corporation, Santa Rosa, CA) was used in combination with the MotionMonitor (Innovative Sports Training, Chicago, IL) to track and collect 3D motion of retroreflective sensors installed directly to the talus, calcaneus and tibia bones during dorsiflexion and posterior translation of the ankle joint. Kinematic motion of the foot during data collection included neutral to anterior to posterior translation and neutral to maximum dorsiflexion. Two separate data sets were collected at each interval with each data set containing two cycles of rotational and translational motion.

Dorsiflexion data were exported from the MotionMonitor using an Euler sequence of Z-X'Y". Data were post processed using a custom Matlab program (The MathWorks, Inc., Natick, Massachusetts V7.12.0, 2011).

The dorsiflexion ROM and posterior talar translation collected following each set of JM treatment were qualitatively compared to the baseline measures for each specimen. The mean and SD for both variables was calculated across subjects for each time point to examine preliminary data trends.

RESULTS AND DISCUSSION

This preliminary study suggests that talocrural JM did not increase dorsiflexion ROM or posterior talar translation. On the contrary, a slight decrease in dorsiflexion ROM and posterior talar

translation was observed across all three specimens. These results are in opposition to many in vivo studies that determined talocrural JM can effectively increase dorsiflexion ROM [3, 4] and in vitro research which identified dorsiflexion improvements following tibiofibular JM [5].

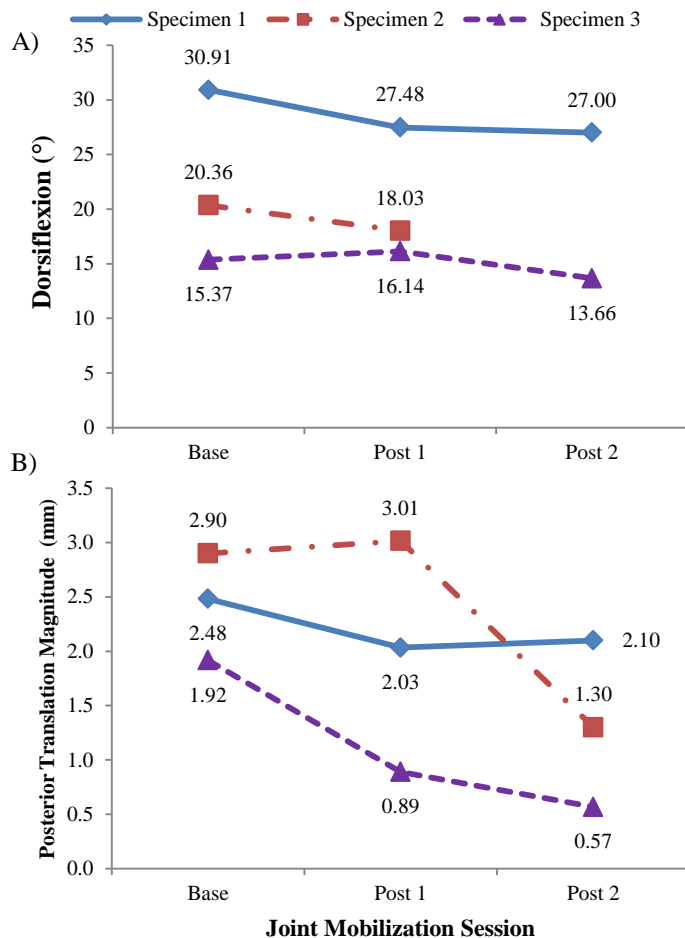


Figure 1: Effects of talocrural JM on ankle dorsiflexion ROM (a) and posterior translation (b). * The talus bone cracked during Post 2 testing in Specimen 2 and was not included in this aspect of the analysis.

Interval Relation	Dorsiflexion (°)	Posterior Translation (mm)
Base to Post 1	1.66±7.07°	0.45±0.83
Post 1 to Post 2	1.48±8.76°	0.66±0.93
Base to Post 2	2.81±10.24°	1.11±0.64

Table 1: Mean \pm SD of dorsiflexion and posterior translation of the talocrural joint. Positive values represent gains in range of motion. Several factors may account for the unanticipated results of this study. The primary explanation for

the decreased posterior translation dorsiflexion ROM may be associated with the open kinetic chain model used for assessing motion in this study. The decrease in posterior translation may actually represent a posterior shift in the location of the talus with each subsequent JM session, creating a new starting point for the beginning motions of dorsiflexion and posterior translation. While we tracked motion of the talus during anterior and posterior glides, we were unable to account for the starting position of the talus between JM treatments. A posterior migration of the talus in an open kinetic chain may alter the contact between the talar dome and ankle mortise which could change the axis of rotation. A weight bearing model observed that JM expanded the range of ankle dorsiflexion[5]. Therefore, if a closed kinetic chain test were implemented, the talus may not shift posteriorly and an increase in dorsiflexion may be observed. Furthermore, the use of an open chain versus a closed chain model may explain the opposing effects of the JM between the two studies. Additional exploration which may include advanced imaging and closed kinetic chain models may clarify relationships between boney positioning and ROM and elucidate the underlying mechanisms of talocrural JM.

CONCLUSION

Further investigation should be performed to clarify the effects of JM including closed kinetic chain in vitro models or radiographic imaging to examine changes in boney positioning.

REFERENCES

1. Denegar C J, et al. J Orthop Sports Phys Ther **32**. 166-173, 2002.
2. Green T, et al. Phys Ther. **81**, 984-994, 2001.
3. Hoch MC, et al. Athl Train Sports Health Care **4**, 237-244, 2012.
4. Loudon JM, et al. Br J Sports Med **48**, 365-370, 2014.
5. Fujii, M., et al. Manual Therapy **15**, 117-121, 2010.

COMPARISON OF TWO FUNCTIONAL SHOULDER JOINT CENTER PROTOCOLS

Clarissa Levasseur, Jacob Howenstein, and Michelle B. Sabick

Department of Biomedical Engineering, Saint Louis University, St. Louis, MO, USA
email: sabickmb@slu.edu, web: <http://parks.slu.edu/departments/bme/>

INTRODUCTION

Although ISB recommendations for reporting shoulder joint motion were published in 2005 [1], these recommendations are difficult to follow using video-based motion capture since they rely on knowledge of the location of the glenohumeral joint center, which is not visible or palpable. As a result, marker sets used to quantify upper extremity motion often vary widely from the ISB proposal.

For years, lower extremity biomechanics studies have used functional methods for identifying joint centers, and the process is standard in some clinical gait protocols. In functional methods, the subject performs a specific movement that allows the joint center of rotation to be inferred from the pattern of motion of one segment relative to the other. In some subjects, accuracy of hip joint center location can be improved significantly compared to regression or anatomical landmark methods [2].

Accurately identifying the location of the glenohumeral joint center could improve both kinematic and kinetic analysis at the shoulder. In this study, we compare two different protocols for functionally locating the glenohumeral joint center. This study is the first step in an attempt to develop an accurate glenohumeral joint center representation for use in video-based motion capture.

METHODS

Trunk and humerus motions were captured using a video-based motion capture system in six adult subjects (4M, 2F) with no existing symptomatic pathology of the right shoulder. A total of 10 retroreflective markers were placed on the trunk (C7, T8, sternal notch, xiphoid process) and right upper arm (acromion, lateral epicondyle of the elbow, medial epicondyle of the elbow, three-

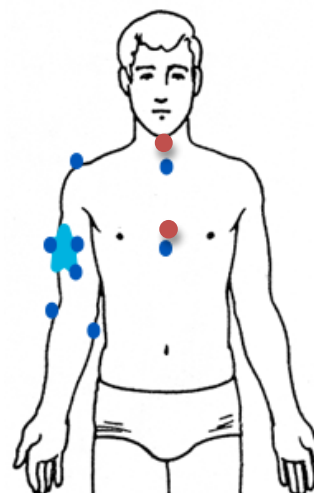


Figure 1: Marker placement for tracking motion of the humerus relative to the thorax. Red markers are placed on the back at C7 and T8.

marker triad). The seven skin-mounted markers were located according to the ISB recommendations for tracking motion of the humerus relative to the thorax [1]. An additional rigid three-marker triad was secured distal to the insertion of the deltoid muscle on a tight Velcro strip (Figure 1).

After performing a calibration in the “T” position (both shoulders abducted 90°, palms facing forward), subjects performed functional calibration movements in two different positions. In the 0° abduction position subjects performed small circumduction motions (approx. 15°) with the arms held in anatomical position. A second functional circumduction motion was performed with the shoulders in 90° of abduction (arm circles). In each case, three to five full cycles of motion were captured. Finally, subjects performed two trials each of full shoulder flexion and full shoulder abduction (both nominally from 0° to 180°).

Motion data were captured at 120 Hz using an eight-camera Vicon Nexus (Oxford, UK) motion capture system and reconstructed marker

trajectories were smoothed using a second order Butterworth lowpass filter with 6 Hz cutoff frequency. Post-processing was completed using Visual3D software (C-Motion, Germantown, MD). For each subject, Euler angles of the humerus relative to the trunk were computed using the plane-elevation-rotation (Z-Y-Z) rotation sequence described by An et al [3]. Location of the functional shoulder joint center relative to the acromion marker was computed using the finite helical axis algorithm [4] for each functional motion. These data are presented below.

RESULTS AND DISCUSSION

Mean computed locations of the functional shoulder joint center were similar for the two functional motion positions (Table 1). The mean position in the A-P direction was essentially the same for the two motions. However, the mean M-L positions were 6 mm apart and the mean S-I positions were 7.5 mm apart.

Both functional motions resulted in computed shoulder joint center locations that were posterior, medial, and inferior to the acromial marker. These results are consistent with the anatomy of the glenohumeral joint. With the shoulder abducted, the functional joint center moved superiorly relative to the acromion by about 7 mm.

Sangeux et al. [2] found that location of the functional joint center at the hip was highly dependent on the range of motion performed and whether the motion was performed voluntarily or with assistance. Therefore, much more work still needs to be done to optimize the specific protocol for functional joint center determination. In this study, subjects were allowed to select a comfortable

range of motion, with no attempt to control either the exact magnitude of the motion or the speed at which it was conducted.

While much more validation data is needed to ensure that the functional joint center computed using this technique corresponds to the true glenohumeral joint center, the technique yielded reasonable results for both different motions, at least in this small group of subjects without shoulder pathology.

CONCLUSIONS

Accurate glenohumeral joint kinetics, and to a smaller extent kinematics, require accurate location of the glenohumeral joint center. This technique, when fully developed, should help improve estimates of glenohumeral joint mechanics. In future studies we will attempt to validate the procedure with medical image data. We will also focus on optimizing the functional joint center protocol. It is likely that the optimal position of the functional motion will depend on the specific motion to be studied, and whether it contains a significant amount of shoulder abduction.

REFERENCES

1. Wu G, et al. *J Biomech* **38**, 981-992, 2005.
2. Sangeux M et al. *Gait & Posture* **40**, 20-25, 2014.
3. An K-N, et al. *J Ortho Research* **9**(1), 1991.
4. Begon M et al. *Gait & Posture* **25**, 353-359, 2007.

ACKNOWLEDGEMENTS

Special thanks to Gretchen Salsich and Angela Reitenbach for their help in data collection and analysis.

Table 1: Mean distance from acromial marker to functional shoulder joint center (mm) in the anterior-posterior (A-P), medial-lateral (M-L) and superior inferior (S-I) directions

Functional Motion Shoulder Position	X (A-P)	Y (M-L)	Z (S-I)	Resultant
0° Abduction	-5.0 ± 7.7	-9.9 ± 11.4	-61.4 ± 8.2	63.8 ± 7.7
90° Abduction	-5.1 ± 10.3	-15.1 ± 8.9	-53.9 ± 21.2	58.4 ± 18.2

VIBRATION OF QUADRICEPS MUSCLE AFFERENTS AFFECTS BOTH IPSILATERAL AND CONTRALATERAL QUADRICEPS AND HAMSTRINGS RATIO OF TORQUE, POWER, AND ACCELERATION TIME

¹ Nathan D. Schilaty, ¹ Christopher V. Nagelli, and ^{1,2} Timothy E. Hewett

¹ OSU Sports Health & Performance Institute, Columbus, OH, USA

² OSU Sports Medicine, Departments of Physiology & Cell Biology, Orthopaedic Surgery, Family Medicine, School of Health & Rehab Sciences, and Biomedical Engineering, Columbus, OH, USA

Email: nathan.schilaty@osumc.edu, Web: <http://sportsmedicine.osu.edu>

INTRODUCTION

Arthrogenic muscle inhibition (AMI) is a devastating side effect to joint injuries such as anterior cruciate ligament (ACL) rupture. A chronic inability to fully activate the ipsilateral quadriceps and subsequent contralateral atrophy of the quadriceps results from AMI [1,2]. Possible mechanisms for these effects of AMI include flexor withdrawal reflex, gamma-loop, or Ib inhibitory pathways.

Previous studies that utilized vibration to affect muscle afferents stimulated the muscle tendon for 20-30 minutes to discharge vesicular release and theoretically block all neurotransmission available from the Ia fibers [3]. However, recent microneurography findings regarding vibration and sensory afferents indicate that vibration will activate Ia, Ib and II afferents to varying degrees and thus caution should be utilized to distinguish the afferent input specifically affected via vibration [4].

The aim of this study was to determine whether real-time inhibition of muscle forces occurred from muscle afferents and to specifically identify whether these afferents can affect contralateral musculature as a basis to model AMI.

METHODS

Ten healthy participants (mean age: 27.7, \pm SD 5.3) were tested bilaterally (4 females, 6 males). We examined the effect of vibration during isokinetic knee extensor and flexor at 60°/s and 300°/s using Biodex dynamometer. Each subject performed 3 sets at each speed and the vibration modality was

randomized to the contralateral, ipsilateral, and control (no vibration) conditions.

Vibration (43 Hz) was applied via a medical-grade percussor to the belly of the quadriceps muscle (localization of Ia and II afferents). Prior to each trial, the subject was permitted two practice reps for familiarization. During each trial, the subjects were given verbal encouragement. Five reps of the isokinetic strength measures were averaged for the 60°/s trial and ten reps averaged for the 300°/s trial. Measures of agonist/antagonist ratio of acceleration time, deceleration time, avg. torque, peak torque, and avg. power of quadriceps and hamstrings in both ipsi- and contralateral vibration were compared to control conditions for statistical analysis. Agonist/antagonist ratios were calculated and utilized in order to determine the holistic effects of vibration on the musculature (hamstring = agonist; quadriceps = antagonist). In addition, data was normalized to control measures for analysis of individual musculature effects. Data was analyzed via paired *t*-tests and multivariate linear regression in JMP Pro 9.

RESULTS AND DISCUSSION

t-tests revealed lack of significance between left and right limbs on similar trials ($p > 0.05$), thus data from both limbs were combined to increase sample size ($n=20$).

At 300°/s, contralateral vibration of the tested leg demonstrated significance of decreasing agonist / antagonist acceleration time ($p=0.0427$), decreasing agonist/antagonist ratio of peak torque ($p=0.0242$), and decreasing agonist/antagonist ratio of avg.

torque ($p=0.0497$). In addition, contralateral vibration of the tested leg demonstrated significance ($p=0.0448$) for increasing agonist/antagonist ratio of deceleration time. This data demonstrates that aberrant afferent input (in this case, from the contralateral limb) can affect efferent output of the other limb. Thus, the aberrant afferent input (vibration) from the contralateral limb moved these values in the opposite direction of desired outcomes, demonstrating that the contralateral limb can influence outcomes of the other limb in both injury and recovery mechanisms. The 300°/s trial speed is a physiologically relevant speed of movement during sporting activity and thus is important for measuring criteria simulating real-world scenarios of acceleration, deceleration, avg. torque, and peak torque.

At 60°/s, ipsilateral vibration of the tested leg only demonstrated a trend toward statistical significance ($p=0.0532$), but this difference may be a clinically significant decrease in the agonist/antagonist ratio of avg. power. This value may reach significance with an increased sample size.

Standard least squares multivariate linear regression with categorical predictors of group, sex, and group*sex revealed significance for control group vs both ipsi- and contralateral vibration ($p=0.0268$) for avg. power of hamstrings at 60°/s normalized to control measures (**Fig. 1**).

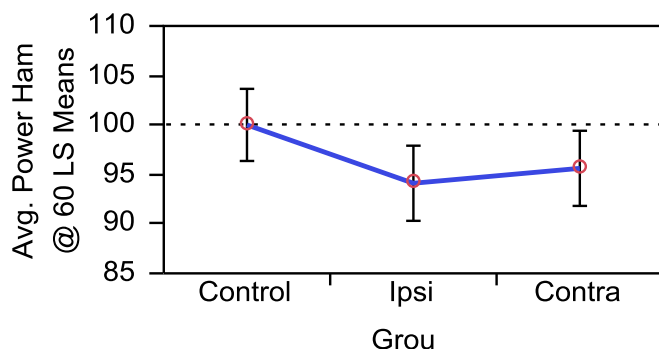


Figure 1: Avg. power of hamstrings at 60°/s decreases with both ipsilateral and contralateral vibration (values normalized to control measures).

CONCLUSIONS

This is the first study to observe effects of real-time vibration (causing aberrant afferent input) on ipsilateral and contralateral muscle efferents, either agonist or antagonist. The current results indicate that contralateral aberrant afferent input is an inhibitory factor of the muscle efferents of the other limb in control subjects. This serves as a possible model for AMI as deafferentation that occurs either post-injury or post-surgery can have a contributing factor on muscle efferents ipsi- or contralaterally. In addition, this data serves as a neuromuscular model for the importance of proprioceptive afferent input to the muscles from both limbs for injury prevention.

Similar to the crossed extensor reflex, interneuron linkage to contralateral alpha motor neuron and subsequent gamma motor neuron co-activation may exist to regulate muscle efferents. Thus, this data provides evidence for a possible model for AMI to pursue the underlying mechanisms of and the relevance of these effects on neuromuscular control in the ACL injured population.

REFERENCES

1. Rice DA, McNair PJ. Quadriceps arthrogenic muscle inhibition: neural mechanisms and treatment perspectives. *Semin Arthritis Rheum*; **40**(3):250–66.
2. Konishi Y, Aihara Y, Sakai M, Ogawa G, Fukubayashi T. Gamma loop dysfunction in the quadriceps femoris of patients who underwent anterior cruciate ligament reconstruction remains bilaterally. *Scand J Med Sci Sport*. 2007; **17**:393–399.
3. Konishi YU. ACL Repair Might Induce Further Abnormality of Gamma Loop in the Intact Side of the Quadriceps Femoris. *Clin Sci*. 2011; **32**:292–296.
4. Fallon JB, Macefield VG. Vibration sensitivity of human muscle spindles and golgi tendon organs. *Muscle and Nerve*. 2007; **36**(July):21–29.

HIERARCHICAL CONTROL IMPROVES JOINT MOTION SIMULATOR PERFORMANCE

¹ Patrick J. Schimoler, ¹ Jeffrey S. Vipperman, and ^{1,2} Mark Carl Miller

¹ University of Pittsburgh, Pittsburgh, PA, USA

² Allegheny General Hospital, Pittsburgh, PA, USA

email: pjs50@pitt.edu

INTRODUCTION

In vitro cadaveric testing allows invasive instrumentation, testing in various states of injury, and application of multiple surgical techniques to the same specimen; but without the central nervous system present, motion requires external actuation. A joint motion simulator (JMS) fixes a cadaveric joint's proximal side and loads the tendons inserting on the joint's distal side. An elbow JMS fixes the humerus and actuates the freely moving radius and ulna through their tendinous insertions. Loads applied repeatably at physiologic levels actuate a cadaveric elbow in as natural a way as possible yielding meaningful insights into elbow behavior.

Specimen variation, muscles affecting multiple degrees of freedom (DOF), and orientation dependent gravitational loading complicate JMS control. Current JMSs use EMG based muscle loading ratios [1], angle dependent muscle activation [2], and specimen specific movement scaling [3] to manage these problems. Specimen specific controller modifications may still be necessary with these methods to achieve highly accurate motion. The purpose of the following work is to show that the addition of iterative learning control (ILC) to antagonist source switching decoupled feedback control achieves highly accurate JMS control with no specimen or orientation specific modifications.

METHODS

The Allegheny General Hospital (AGH) elbow JMS (Figure 1) [4] actuates the elbow's two kinematic DOFs through the insertions of the biceps, brachialis, pronator teres, and triceps. The brachialis and triceps affect the flexion / extension (FE) DOF. The biceps and pronator teres affect both the FE DOF and the pronation / supination

(PS) DOF. Encoders (US Digital) and load cells (Transducer Techniques) feed back joint positions and tendon loads, respectively. The elbow JMS's control system contains three layers: decoupled feedback control, antagonist source switching [5], and ILC [6]. Antagonist tension control is included to prevent tendon slack. Two muscles, maintained at small but positive tensions, are designated antagonists: one for FE and one for PS.

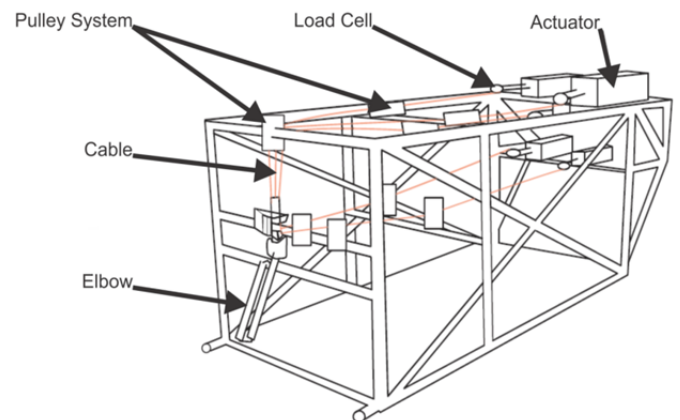


Figure 1: AGH elbow JMS

Decoupled feedback control maps errors in FE position, PS position, FE antagonist tension, and PS antagonist tension into combinations of tendon velocities. For example, FE position error creates simultaneous triceps extension and biceps, brachialis, and pronator teres retraction. Moment arms and stiffnesses determine the decoupling map.

Motion with low antagonist tension precludes a dedicated antagonist tension source. For instance, moving from full supination to full pronation with a vertical humerus and horizontal forearm is impossible with a small antagonist biceps tension. When the gravitational moment changes from aiding supination to aiding pronation, a low biceps tension and accurate position control require the pronator teres to reduce its tension, but tension in

the pronator teres can only be reduced so far. Switching the antagonist tension source to the smaller of the two tensions solves this problem. In this case, the source closing the tension control loop switches from the biceps to the pronator teres.

ILC, a method using past errors to reduce future errors, is used here to overcome specimen specific dependence. The current decoupled feedback controller's dependence on moment arms and stiffnesses, both of which vary between specimens, prevents accurate control for all but the parameter sourcing elbow. With ILC, an average elbow's decoupling map suffices for any elbow. As more trials are run, the ILC modifies the inputs improving joint position and tendon tension accuracy.

An ILC generating references for an antagonist source switching decoupled feedback controller was implemented and evaluated over three cyclic motions using a mechanical elbow: a 60° flexion motion with fixed 30° of pronation, a 120° pronation motion with fixed 90° of flexion, and a simultaneous 60° flexion and 120° pronation motion. Antagonist tension references were set to one pound. The three motions were performed with the humerus and flexion plane both horizontal and vertical. Five second periods were used for all motions. Performance was quantified with maximum absolute error and RMS error.

RESULTS AND DISCUSSION

Forty control iterations reduced maximum errors for all motions below 1° in position control and 0.3 lbs in antagonist tension control (Figure 2, Table 1). For comparison, a successful, validated elbow JMS [2] designed for motion in all orientations tracked

FE motions from 10° to 120° at 10°/s with RMS errors of 1.7° (vertical) and 2.2° (horizontal).

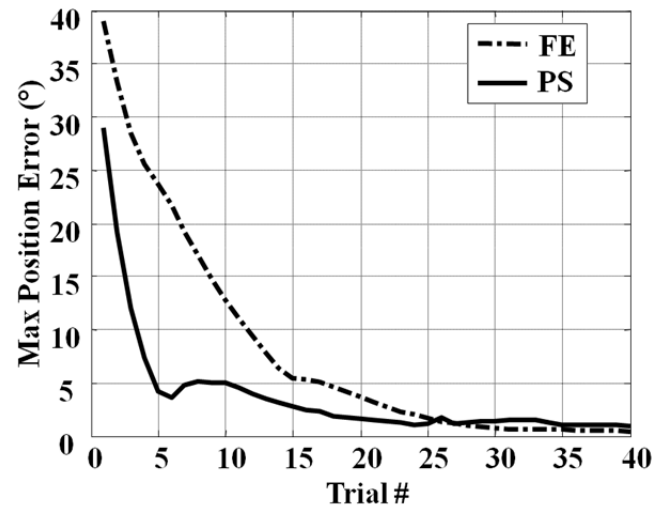


Figure 2: Maximum position error reduction over 40 trials during horizontal, simultaneous motion

CONCLUSIONS

A combination of ILC for specimen variation, decoupled feedback control for actuator interaction, and antagonist source switching for varying gravitational loading achieves accurate JMS control. Future work will apply the approach to a range of real elbows proving it manages specimen variation.

REFERENCES

1. Dunning CE. *JOR* **21**, 405-11, 2003.
2. Ferreira LM. U Western Ontario PhD, 2011.
3. Hoskins AH. Penn State PhD, 77-85, 2006.
4. Kuxhaus L. *J Med Dev* **3**, 1-7, 2009.
5. Potkonjak V. *Int J Adv Rob Sys* **8**, 143-55, 2011.
6. Moore KL. *ILC for Det Sys*, Springer, 1993.

Table 1: Joint position and antagonist tension tracking errors - maximum absolute and (RMS)

Humerus / Flexion Plane	Movement	Position (°)		Tension (lbs.)	
		FE	PS	FE	PS
Horizontal	60° FE at fixed 30° PS	0.46 (0.13)	0.22 (0.07)	0.11 (0.04)	0.16 (0.04)
	120° PS at fixed 90° FE	0.09 (0.06)	0.65 (0.18)	0.05 (0.01)	0.19 (0.04)
	Simultaneous 60° FE and 120° PS	0.47 (0.15)	0.92 (0.24)	0.15 (0.05)	0.14 (0.05)
Vertical	60° FE at fixed 30° PS	0.41 (0.13)	0.72 (0.24)	0.16 (0.06)	0.26 (0.06)
	120° PS at fixed 90° FE	0.26 (0.12)	0.78 (0.21)	0.04 (0.01)	0.14 (0.04)
	Simultaneous 60° FE and 120° PS	0.54 (0.15)	0.83 (0.29)	0.19 (0.06)	0.26 (0.07)

CHANGES IN TIBIOFEMORAL CONTACT FORCES FOLLOWING ALTERATIONS IN JOINT CAPSULE STIFFNESS

¹Anne Schmitz, ²Zahra Abbasi, ²Srinath Kamineni, and ²Babak Bazrgari

¹Gannon University, Erie, PA, USA; email: schmitz005@gannon.edu

²University of Kentucky, Lexington, KY, USA

INTRODUCTION

Post-traumatic osteoarthritis (OA) affects the knee more than any other joint in the human body [1]. While the cause of this disease is multifactorial, one component may be abnormal tibiofemoral joint loading that occurs after knee injury or surgery [2,3]. The number of joints that become arthritic as a direct consequence of traumatic events is unquantified within the literature, due to the difficulty of collecting such data. One common surgery, for a traumatically unstable knee, is reconstruction of the anterior cruciate ligament (ACL), with over 200,000 of these reconstructions occurring each year in the United States [4]. In fact, in some studies, OA occurs in over 50% of these ACL reconstructed individuals 10-20 years after surgery [5].

The effect of ACL graft placement and tension on tibiofemoral function is well-studied. In contrast, the effect of anterior capsule properties on joint loading is largely understudied. This anterior restraint is important to investigate because the structural integrity of the capsule is altered during the initial trauma to the knee joint and secondarily changes during the post-surgical course. To aid in minimizing OA, it is important to understand the effect of joint capsule properties on tibiofemoral loading. Therefore, the goal of this work was to investigate the effects of knee joint capsule stiffness on tibiofemoral loading. We hypothesized that increased capsule stiffness would lead to increased joint loading.

METHODS

A parametric modeling study was conducted on a previously developed discrete element model of the knee [6] implemented in the open-source software OpenSim [7]. The tibiofemoral joint contained six degrees-of-freedom (dof) while the patellofemoral joint contained one dof. Twenty-two ligaments were

included as non-linear springs, as well as an elastic foundation model for tibiofemoral contact.

The knee joint capsule was added using four non-linear springs in the anterior portion of the knee joint. These elements included two parallel elements running from the distal femoral metaphysis to the proximal tibial metaphysis, along with two crossing elements connecting the insertions of the parallel elements to each other (Figure 1). The knee joint capsule springs were constrained by a cylindrical wrapping surface to simulate sliding of the knee capsule on the femur distal surface during knee flexion. The capsular elements were modeled with stiffness values equal to 30% of the stiffness of other ligaments.

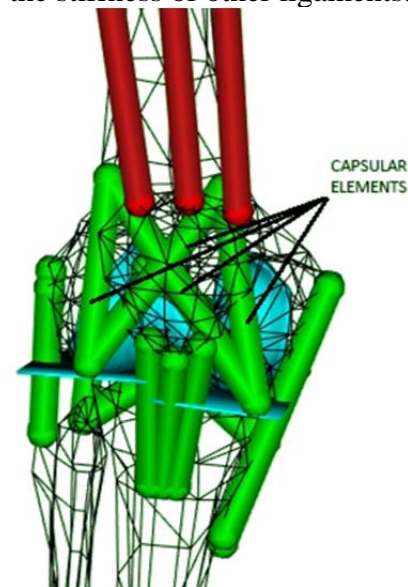


Figure 1: Discrete element knee model in OpenSim

A forward dynamic simulation was used to passively flex the knee joint from an extended position to 75 degrees of flexion for two cases: 1) normal condition and 2) stiff condition where the stiffness of the capsule was increased by 20%. For each of these simulations, the tibiofemoral contact force was calculated as the vector sum of the forces

in the muscles and ligaments (expressed in the femoral reference frame) [8]. The simulation was run at a speed such that inertial forces were negligible.

RESULT AND DISCUSSION

The magnitude of the tibiofemoral contact force (i.e. resultant force) increased with knee flexion, reaching its maximum at peak knee flexion (Figure 2). Our hypothesis was supported in that a 20% increase in joint capsule stiffness caused a 16% increase in maximum contact force. This implies that increased joint capsule stiffness may be a factor in OA progression.

There are some limitations and study design factors that should be considered when interpreting this work. First, the tibiofemoral contact force was not decomposed into the medial and lateral compartments. Therefore, it is unclear which compartment is more sensitive to changes in joint capsule stiffness. Second, the joint capsule stiffness was set to 30% of the stiffness of the other ligaments. This was approximated due to the paucity of literature data on joint capsule properties. This would affect the quantitative results of the study but not the trend or interpretation.

CONCLUSIONS

Clinically, increased joint capsule stiffness may occur either as a consequence of an original traumatic insult to this structure or due to secondary changes subsequent to a surgical intervention. The quantifiable change, in either circumstance, to the joint capsule commonly appears to be a stiffer joint capsule. Our results show this increase in stiffness may lead to increased tibiofemoral cartilage loading, thus predisposing the joint to OA. Therefore, preserving the structural integrity and minimizing scar tissue in the knee joint capsule may be an important consideration when treating a traumatic injury to the joint and when considering the rehabilitation following an ACL reconstruction.

REFERENCES

- 1.Oliveria, S. A., et al. *Arth and Rheu* **38**, 1134-1141, 2005.
- 2.Andriacchi, T. P., et al. *Ann Biomed Eng* **32**, 447-457, 2004.
- 3.Andriacchi, T. P., et al. *Curr Op Rheum* **18**, 514-518, 2006.
- 4.Owings, M. F., et al. *Vital Health Stat 13* **1**, 1-119, 1998.
- 5.Lohmander, L. S., et al. *Am J Sports Med* **35**, 1756-1769, 2007.
- 6.Schmitz, A. *Biomedical Engineering PhD*, 2012.
- 7.Delp, S. L., et al. *IEEE Trans BME* **54**, 1940-1950, 2007.
- 8.van Arkel, R. J., et al. *J Orthop Research* **31**, 1172-1179, 2013.

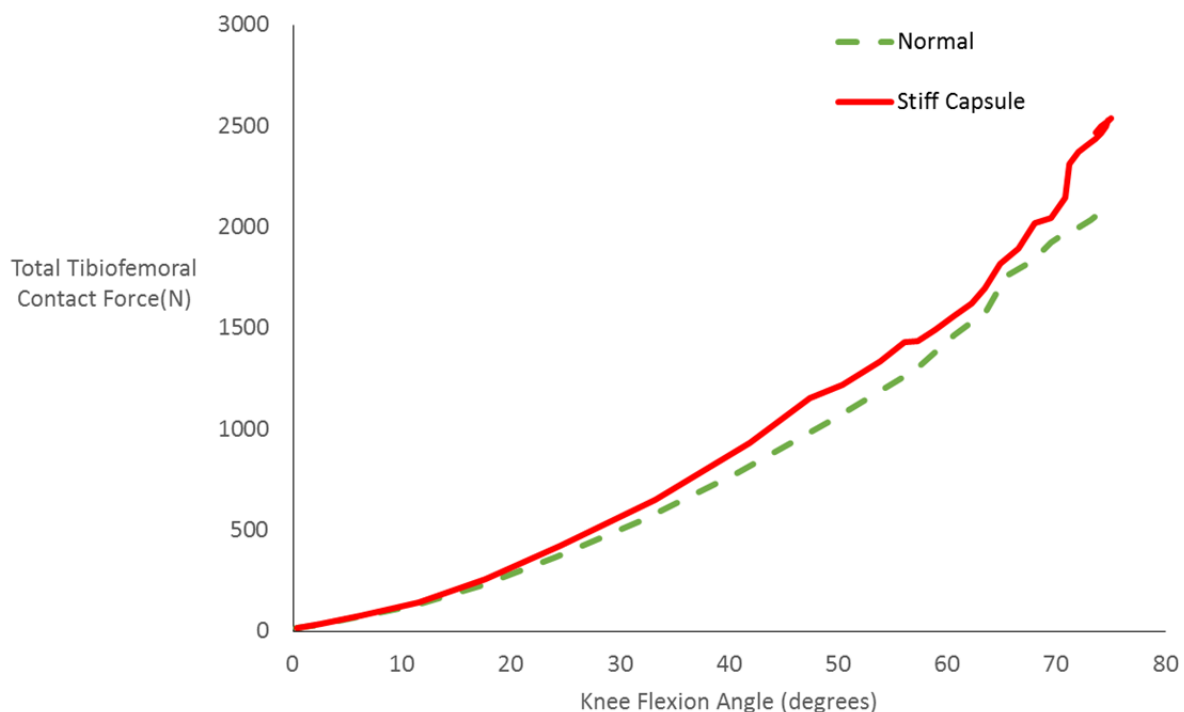


Figure 2: Total tibiofemoral contact force for the normal and stiff capsule scenarios.

EXPERIMENTAL ANTERIOR KNEE PAIN AFFECTS ACTIVATION OF CERTAIN MUSCLES DIFFERENTLY DURING LANDING AND JUMPING

¹Matthew K. Seeley, ¹Jordan D. Pitt, ²Jihong Park, ³W. Matt Denning, ⁴Devin Francom and ¹J. Ty Hopkins

¹Brigham Young University, Provo, UT, USA; ²Kyung Hee University, Yongin, Korea;

³Weber State University, Ogden, UT, USA; ⁴University of California at Santa Cruz, Santa Cruz, CA, USA
email: matthewkseeley@gmail.com; web: biomech.byu.edu

INTRODUCTION

Anterior knee pain (AKP) is a common problem that is associated with abnormal lower-extremity movement neuromechanics [1]. The independent effects of AKP are difficult to study due to other simultaneous effects of knee pathology (e.g., knee effusion or degradation). The purpose of this study was to evaluate the independent effects of AKP during landing and jumping on activation of lower-extremity muscles during two land and jump tasks performed at two different intensities.

METHODS

Thirteen healthy subjects (7 males, 6 females; mass = 70 ± 15 kg; height = 1.74 ± 0.11 m; age = 22 ± 2 yrs) gave informed consent and completed a control and pain data collection session, 48 hours apart. For each session, subjects performed two land and jump tasks at a low and high intensity: a forward double-leg land and jump task (FDJ) and lateral single-leg land and jump task (LSJ). The FDJ task required subjects to jump off of two legs, forward over an obstacle, and land on two legs, on a force platform; then, immediately jump forward off of two legs over a second obstacle. Low and high intensities for this task involved obstacle heights that were standardized to each subject. The LSJ task required subjects to jump off of the left leg, laterally, and land on the right leg on a force platform; then, immediately jump back to the beginning location, landing on the left leg. Low and high intensities for this task involved lateral jump distances that were standardized to each subject. Surface electromyography (EMG; 1000 Hz) was recorded for the right gastrocnemius (GA), vastus medialis (VM), medial hamstrings (MH), gluteus medius (GMD), and gluteus maximus (GMX) while

subjects contacted the force platform during each trial. First and second halves of the time that subjects contacted the force platform defined landing and jumping.

For both sessions, subjects first completed three trials of both tasks, at both intensities, to provide reference EMG values. Next, for the pain session, 1 ml of hypertonic saline (5.0% NaCl) was injected into the right-leg infrapatellar fat pad, to induce experimental AKP, and subjects performed three more trials of both tasks at both intensities; these were the experimental trials. The control session was the same as the pain session, except the injection was omitted. Subject perceived AKP was measured every two minutes of both sessions using a 10-cm visual analog scale.

Functional linear models were used to evaluate the effect of session and intensity on normalized EMG amplitude throughout the time that the subjects contacted the force platform for each trial. Also, mixed-model repeated measures ANOVA and Tukey-Kramer *post hoc* tests were used to compare subject perceived AKP between sessions. All alpha levels were set to 0.01.

RESULTS AND DISCUSSION

Subject perceived AKP was greater for the pain-session trials, relative to the control-session trials (Figure 1; $p < 0.01$). The AKP significantly altered EMG amplitude for all of the observed muscles, at varying parts of both tasks, except for the VM during the FDJ ($p < 0.01$). Effects of the experimental AKP on EMG amplitude were admittedly varied, in direction and timing, and did not reveal a consistent pattern, and the space required to describe all of these effects is not

presently available. Three muscles (GA, MH, and GMD), however, did display a similar interesting pattern, for both tasks, that we wish to emphasize here. This pattern is demonstrated by MH EMG amplitude during the LSJ (Figure 2): as a result of AKP, muscle activation decreased during landing and increased during jumping. This pattern was also observed for the GA and GMD, however, we do not now have space enough to present these data.

The cause of this inhibition and subsequent facilitation is unclear and will require additional research to elucidate. We now speculate, however, that the decreased muscle activation during landing could be due to greater reliance on force contributions from passive muscle components [2] or the skeletal system (i.e., a more upright landing position). We further speculate that the increased muscle activation during jumping could reflect an attempt to compensate for the preceding inhibition during landing and/or increased neural drive, via the group Ib pathway, resulting from the high forces associated with landing [3]. Regardless of the cause(s) of the observed inhibition and facilitation, these EMG alterations are important because they

likely result in altered tibiofemoral and patellofemoral joint loads.

REFERENCES

1. Patil S et al. *Knee*, **18**, 329-332, 2011.
2. Padulo J et al. *Springerplus*, 2:520, 2013.
3. Grey MJ et al. *J Physiol*, **581**, 99-105, 2007.

Figure 1. Mean subject perceived AKP for both sessions. Asterisks indicate between-session differences ($p < 0.01$).

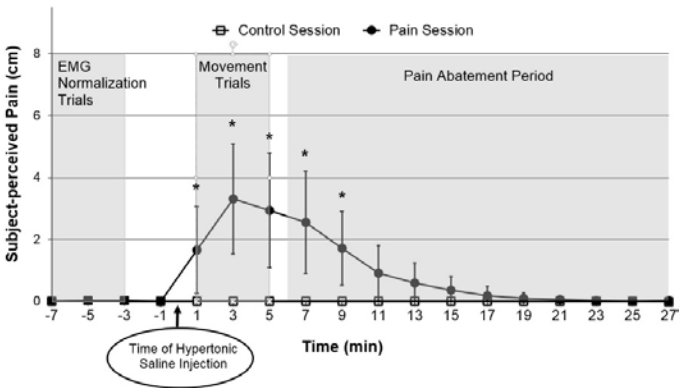
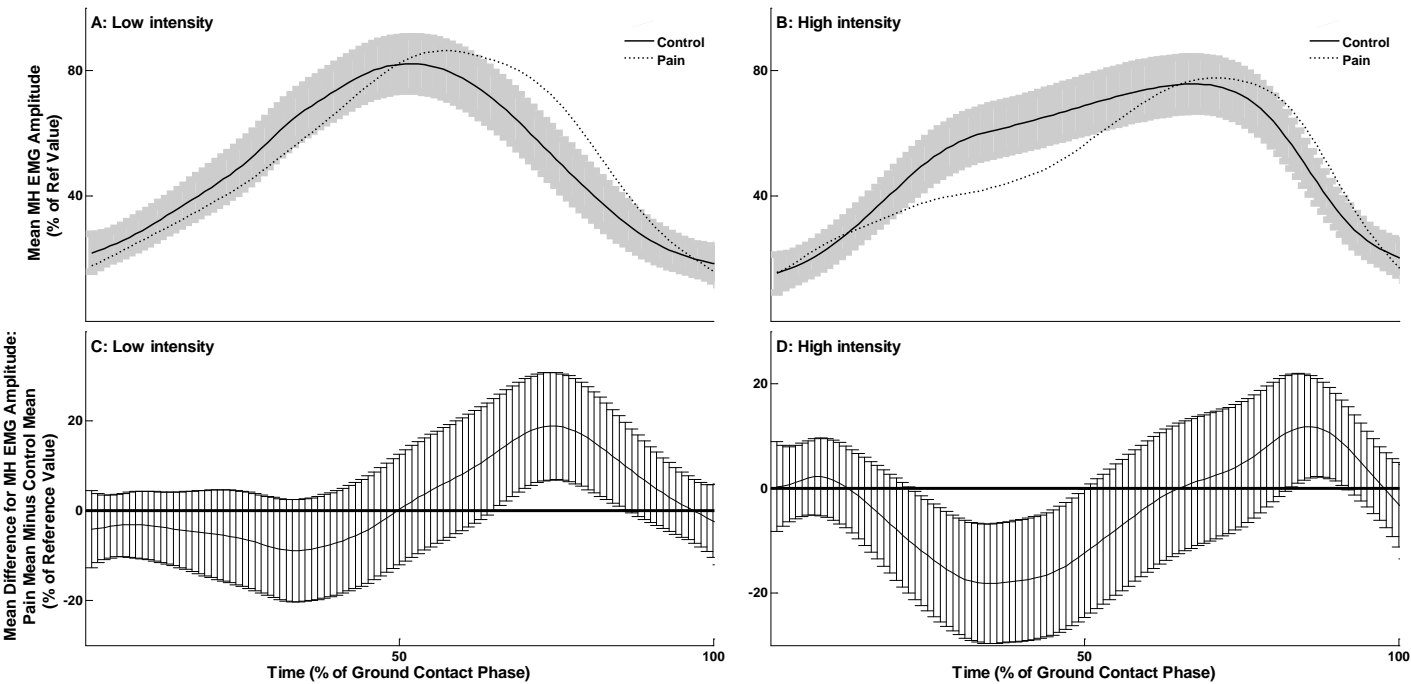


Figure 2. Subplots A and B: mean right MH EMG during ground contact of the LSJ. Subplots C and D: mean between-session differences for right LSJ MH EMG during ground contact of the LSJ. 95% confidence intervals (vertical bars) that do not overlap the zero lines indicate a significant effect of AKP on MH EMG amplitude. Negative mean differences indicate MH EMG that was greater for the control session, while positive mean differences indicate MH EMG that was greater for the pain session.



Reduced Rate of Proximal Junctional Fractures Above Long-Segment Instrumented Constructs Utilizing a Tapered Dose of Bone Cement for Prophylactic Vertebroplasty – A Biomechanical Investigation

¹Shah Anoli, ²Zavatsky J, ³McGuire R, ⁴Serhan H, ¹Kelkar A, ¹Kodigudla M, ¹Goel VK

¹Engineering Center for Orthopaedic Research Excellence (E-CORE)

Departments of Bioengineering and Orthopaedic Surgery

Colleges of Engineering and Medicine

University of Toledo, Toledo, OH 43606

²Florida Orthopaedic Institute, Tampa, FL 33617

³University of Mississippi Medical Center, Jackson, MS 39216

⁴DePuy Spine Inc., Raynham, MA 02767

INTRODUCTION

Proximal junctional kyphosis (PJK) and proximal junctional failure (PJF) are an increasingly recognized complication after long-segment instrumentation for the correction of kyphosis and scoliosis. Vertebral compression fractures (VCFs) at the upper instrumented vertebra (UIV) and the UIV + 1 have been described. Prophylactic vertebroplasty has been advocated to reduce the rate of VCFs but still results in the creation of a stiff “super vertebra”. We hypothesize that utilizing a tapered dose of bone cement in the UIV, UIV + 1, and UIV + 2 eliminates the creation of a “super stiff” vertebra further decreasing the rate of VCFs and PJK.

METHODS

A biomechanical cadaveric study along with finite element analysis (FEA) was utilized.

Fifteen fresh-frozen ligamentous T6 - pelvis specimens were used. The spines were equally divided into three Groups of 5 specimens each: Group 1 - Bilateral pedicle screw and rod instrumentation from T10 to S1, no cement; Group 2 - Instrumentation + 4cc of cement injected into T10 (UIV) and 4cc into T9 (UIV + 1), 2cc of cement injected through each pedicle; & Group 3 - Instrumentation + 4cc total in T10 (UIV), 3cc total in T9 (UIV + 1), and 2cc total in T8 (UIV + 2). Dual-energy X-ray absorptiometry (DEXA) was obtained on all specimens. The pelvis and T6

vertebra of each specimen were fixed in bondo epoxy resin. The spines were mounted on a MTS biaxial load actuator and axial compression was applied eccentrically, 10 mm anterior to the center of the T6 vertebra, until failure occurred. Maximum load to failure was measured in Newton (N). The spines were also analyzed visually, fluroscopically, along with computed tomography (CT) scans for the presence of VCFs.

Finite element analysis (FEA) was utilized to simulate similar scenarios for the three groups as the cadaveric study using normal and osteoporotic bone models. An axial compressive load was applied perpendicular to the top of T6 vertebra, 10 mm anterior to its center just like the cadaver study. Stresses at the endplates and the posterior ligaments were analyzed.

RESULTS

Cadaveric Data

There was a significant reduction in the number of fractures (Fig. 1) observed in Group 3 vs. Groups 2 and 1 (p=0.0019). There was only one fracture in one specimen observed in Group 3; all five specimens suffered a fracture in Group 2; and five in Group 1. Posterior ligamentous rupture occurred in four specimens in Group 3; three in Group 2; and only one in Group 1. The mean peak load-to-failure values showed an increasing trend from Groups 1 to 3, but were not significant (p=0.38). Load vs. deformation plots in specimens that failed exhibited a peak load (inflection point) followed by an

obvious loss of structural integrity (Figure 2). There was no difference in DEXA values among the specimens in the three Groups ($p=0.71$). There was no hardware failure in any Group.

Finite Element Analysis (FEA) Data

Load to failure in normal bone was higher in comparison to osteoporotic bone, which followed the same trend as the cadaveric data. Specimens with higher bone mineral density (BMD) were stiffer and the maximum load to failure increased from Group 1 to Group 3. The T8 (Figure 3) and T9 (Figure 4) endplate stresses were reduced by 20% and 33%, respectively in Group 3. The stresses observed at the supraspinous (SSL) and interspinous ligaments (ISL) in Group 3 were higher at T6-T9 as vs. Groups 1 and 2. At T9-T10, the stresses observed in the SSL and ISL in Group 3 were lower as compared to Groups 1 and 2.

CONCLUSIONS

There was a significant reduction in VCFs in those specimens treated with a tapered dose of vertebral cement in the UIV, UIV + 1, and UIV + 2 (Group 3) as compared to spines treated with instrumentation only (Group 1), and those treated with the same amount of cement at the UIV and the UIV + 1 (Group 2). This tapering technique of cement increases the load required for failure decreasing the risk of VCF, the precursor of PJK.

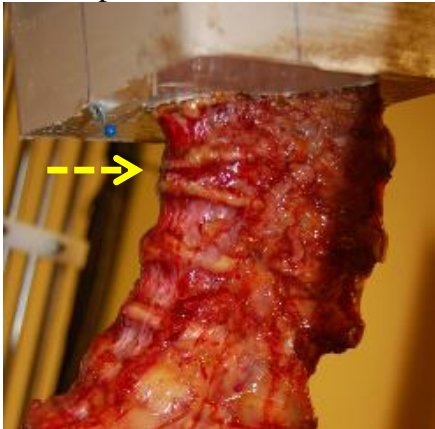


Figure 1: Failure observed in the anterior column (T8) during compressive loading of a specimen in Group 1.

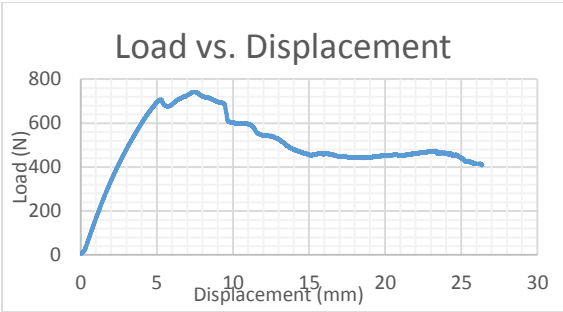


Figure 2: Load vs. displacement plot of a specimen exhibiting an inflection point (peak) indicating the failure load.

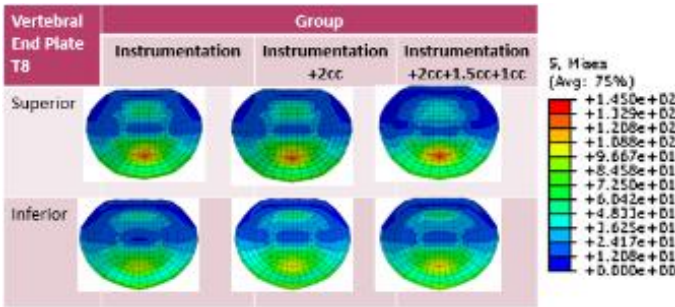


Figure 3: T8 endplate stresses

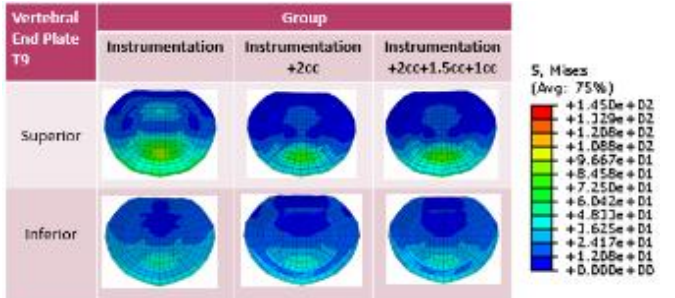


Figure 4: T9 endplate stresses

In both cadaveric and FEA models, this novel technique of using the tapering dose of prophylactic vertebroplasty cement in the UIV, UIV + 1, UIV + 2 decreased the endplate stresses, increased the load required for failure, and reduced the incidence of VCFs above long-segment instrumented constructs. Clinically, this technique may reduce the risk of PJK and PJF. Further biomechanical and clinical analyses are required.

ACKNOWLEDGEMENTS

Work supported in part by the NSF Industry/University Cooperative Research Center at the University of California at San Francisco and University of Toledo, Toledo (www.nsfcdmi.org) and AOSpine TK, AO Foundation, Davos.

THREE-DIMENSIONAL HUMERAL SHAPE MORPHOLOGY THROUGHOUT THE PEDIATRIC AGE SPECTRUM IN CHILDREN WITH UNILATERAL OBPP

¹Jennifer N. Jackson, PhD, ²Michael L. Pearl, MD, ¹Jesi Kim,
¹Katharine E. Alter, MD, ¹Frances T. Sheehan, PhD

¹ Rehabilitation Medicine Department, National Institutes of Health, Bethesda, MD, USA

² Kaiser Permanente, Los Angeles, CA, USA

email: gavellif@cc.nih.gov

INTRODUCTION

To understand the relationship between humeral morphology and pathology, developmental shape changes must be understood. Little data exist in regards to how pathology and development influence three-dimensional (3D) humeral shape. A pediatric cadaver study established that the humeral head anteverts through development [1], but the lack of an ossified head in younger children prevented direct measures of humeral head orientation. Closing this knowledge gap is crucial for treating pathologies such as obstetrical brachial plexus palsy (OBPP), where the current trend supports earlier intervention (physical therapy, botulinum toxin injections, surgery) to help prevent functional losses.

The purpose of this study is to quantify the 3D humeral morphology in children across the pediatric age span (6 months to 18 years old) with unilateral OBPP and internal rotation contractures in order to test the following hypotheses: 1) development is correlated with 3D humeral shape changes in the unaffected arm; 2) the impaired arm has significant multi-planar shape deformities, relative to the unimpaired arm, which increase with age.

METHODS

In total 29 bilateral 3D axial MR images of children/adolescents with unilateral OBPP were included in this study. The first set ($n = 17$, age = 1.5 ± 1.2 years) was acquired as part of a pre-surgical evaluation protocol (author MLP). The second set of 12 subjects (age = 11.8 ± 3.3 years), was taken from a previously published study [2]. Both centers had IRB approval.

The humeral head and shaft/elbow were segmented by manually outlining the outer cartilage and cortical bone surface, respectively [2]. The resulting point cloud was fitted with a 3D mesh and aligned to its principal axes. The epicondylar axis and the lesser tuberosity (LT) were identified on the 3D model (Fig 1).

The model was then converted back to a point cloud and imported into a customized Matlab program. This program determined the best-fit ellipsoid and cylinder to the humeral head and central shaft, respectively. From these data the inclination angle and two retroversion angles, V1 and V2 were calculated (Fig 1). Paired t-tests were used to identify significant ($p < 0.05$) differences between sides. Pearson's correlations were run to determine the relationship of specific variables to age.

RESULTS AND DISCUSSION

The humeral head was significantly less retroverted ($\Delta V1 = -10.3^\circ$ and $\Delta V2 = -16.9^\circ$, $p < 0.008$), more elliptical ($p < 0.001$), and smaller in all three dimensions ($p < 0.001$) for the unimpaired arm. The decreased retroversion disagrees with the past 2D study in younger children [3], whereas all other results are supported by past 2D work [4]. Although V1 was strongly correlated to V2 ($r = 0.83$, $p < 0.001$), the variation in $\Delta V1$ and $\Delta V2$ and the more elliptical humeral head on the impaired side demonstrates that retroversion is associated with both the orientation between the humeral head and elbow and the shape of the humeral head itself. The level of pathology increased with age ($r = 0.507$, $p = 0.012$), which may explain the discrepancy in retroversion when comparing to past work [3]. A

longitudinal study is needed to identify how shape changes with age in individual subjects, yet the results indicate that intervening early may help prevent larger musculoskeletal pathologies later in life.

Although the inclination angle was not significantly different between sides, the results are noteworthy when analyzing patient-specific changes. Six and five subjects showed declination and inclination, respectively, greater than one standard deviation away from the control average. This discrepancy suggests that patient-specific, 3D morphometric analyses will support optimal treatment.

There was a significant correlation between humeral morphology and age for the control side (V1: $r = -0.57$; V2: $r = -0.711$; and inclination: $r = -0.477$, $p < 0.05$). Numerous factors such as increases in the variety of tasks performed and changes to the external forces on the arm (e.g., the initiation of crawling) may influence the relationship between shape and age on the control side. These natural developmental changes must be taken into account when assessing pathology. In addition, these

changes in shape likely influence the musculotendon moment arms [5], confirming the concept that musculoskeletal models must be tailored to the pediatric population and not be derived by simply scaling adult models.

CONCLUSIONS

This study is the first to evaluate 3D humeral shape changes in OBPP across the full pediatric age span. It provides novel findings in terms of inclination. The increased understanding of 3D morphologic changes in both the control and impaired arms of children with OBPP can lead to improvements in determining the unique and optimal treatment options for an individual based on subject-specific 3D morphological analyses.

REFERENCES

- 1 Edelson (2000) J Should & Elb Surg
- 2 Sheehan et al (2014) J Should & Elb Surg
- 3 van der Sluijs et al (2002) JBJS
- 4 Pearl et al (2014) J Should & Elb Surg
- 5 Voight et al (2011) J Ortho Trauma

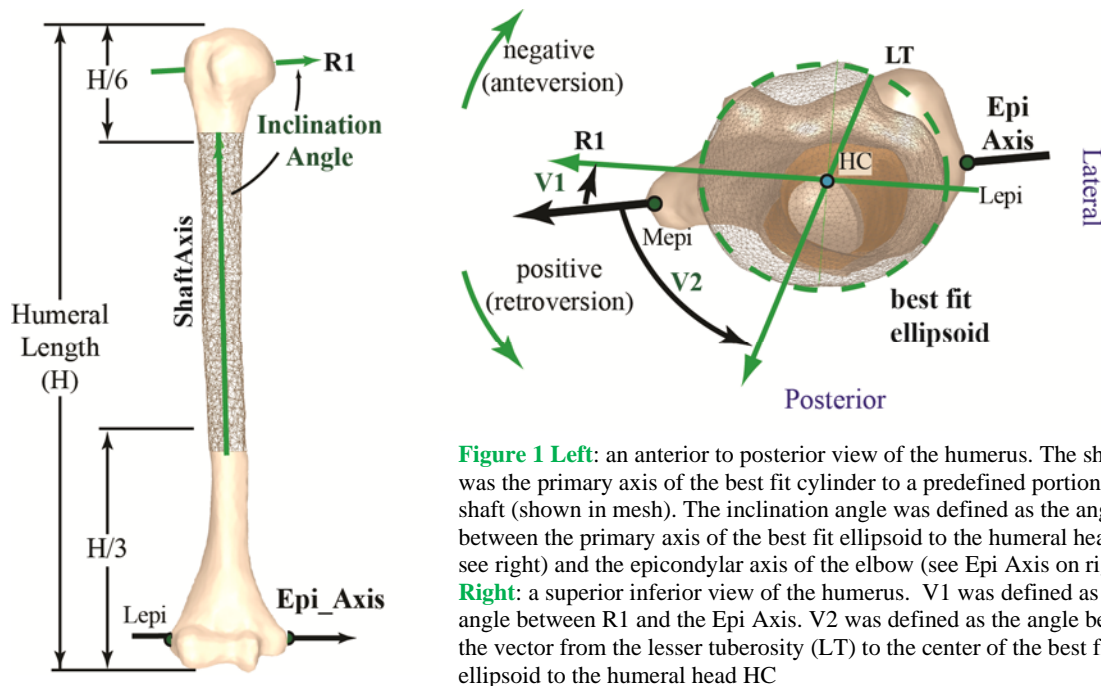


Figure 1 Left: an anterior to posterior view of the humerus. The shaft axis was the primary axis of the best fit cylinder to a predefined portion of the shaft (shown in mesh). The inclination angle was defined as the angle between the primary axis of the best fit ellipsoid to the humeral head (R1: see right) and the epicondylar axis of the elbow (see Epi Axis on right). **Right:** a superior inferior view of the humerus. V1 was defined as the angle between R1 and the Epi Axis. V2 was defined as the angle between the vector from the lesser tuberosity (LT) to the center of the best fit ellipsoid to the humeral head HC

INFLUENCE OF AGE AND GENDER ON LUMBAR SHEAR TOLERANCE

¹Sean Shimada and ¹Nicholas Merrier

¹Biomechanical Consultants of California, Davis, CA, USA

email: sean@motionsandforces.com

INTRODUCTION

A review of literature examining shear tolerance of the lumbar spine revealed that minimal research has been performed regarding the failure mechanism to external loading situations. Studies have been conducted on lumbar functional spinal unit tolerances; however, this method is not representative of the dynamic failures typically seen in a motor vehicle collision. The Hybrid III Anthropometric Test Device (ATD) lumbar spine has been designed to be biofidelic. Despite this fact, the ATD family assumes that the mass densities and elastic moduli of human tissue are the same for all individuals, regardless of size, age and gender. Additionally, biomechanical studies report that males on average are stronger and have higher injury tolerances than females. Furthermore, variables such as age and gender need to be considered as maintained by the literature in order to increase the biofidelity of ATDs. This study proposes a method to calculate the lumbar spine shear tolerance for any size occupant of varying age and gender for accidental injury reconstruction. If implemented, the methodology and result can benefit biomechanists and injury reconstructionists by providing higher physiological specificity to injury tolerance models.

METHODS

A review of the current literature revealed that the number of studies concerning lumbar shear tolerance is very limited; much of the specimens are older males and a constrained number of female specimens are reported. To the best of our knowledge, the only study that tested whole cadaver specimens was Begeman et al. (1994). Begeman et al. reported that anterior lumbar failure began at 1292 N and 1767 N for 0.5 mm/s and 50 mm/s, respectively. Complete failure of the posterior ligaments was defined as soft tissue failure. Pathologic examination revealed that the

predominant injuries were tearing of the interspinous and supraspinous ligaments as well as the ligamentum flavum. Taking into consideration the Hybrid III spine was designed to duplicate a 50th percentile male spine, data points from the spine comparison tests by Begeman et al. (1994) were also utilized for the subject study. An analysis of the load-deflection curve of the complete Hybrid III lumbar spine matched quite well with that of the average unconstrained cadaver specimen with maximum forces of 1560 N for a loading rate of 0.5 mm/s and 2225 N for 50 mm/s.

The lumbar soft tissue properties for males and females were additionally deduced from the literature. Compilations of data related to the effect of age and gender on spinal muscle and ligament strength were used to establish linear regressions.

The lumbar shear tolerances for the 50th percentile male were assessed to the 5th percentile female by adopting the anthropometric scaling procedure expressed by Mertz et al. [1]. Geometric properties such as height and weight were used to determine proportional sizes and tolerance. Linear regressions of 1st percentile, 50th percentile and 99th percentile population representatives of each gender were used to establish erect sitting height. The mass ratio and sitting height were used to determine the scaling factors. Regressions of age and gender were applied to the current Mertz et al. anthropometrically scaled models injury tolerance in order to determine their effects. The models altered with age and gender were then quantitatively compared to the impact and injury tolerance of the Mertz et al. anthropometrically scaled models.

RESULTS AND DISCUSSION

The influences of age and gender on lumbar shear impact response and injury tolerance were compared to the current anthropometric scaling of Hybrid III ATDs. Conservatively, the average soft

tissue failure is expected to occur at 1430 N at 0.5 mm/s and 2000 N for 50 mm/s for a 50th percentile male. The 5th percentile female shear tolerance for soft tissue injury was determined to be approximately 785 N at 0.5 mm/s and 1100 N for 50 mm/s. The effect of age and gender on the 50th percentile male and 5th percentile female soft tissue shear failure is presented in the following figures.

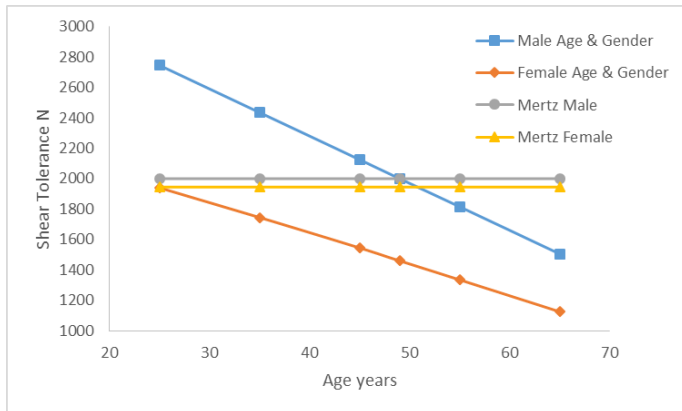


Figure 1: Comparison of 50th percentile male injury tolerance between the anthropometrically scaled models and the influence of aging and gender.

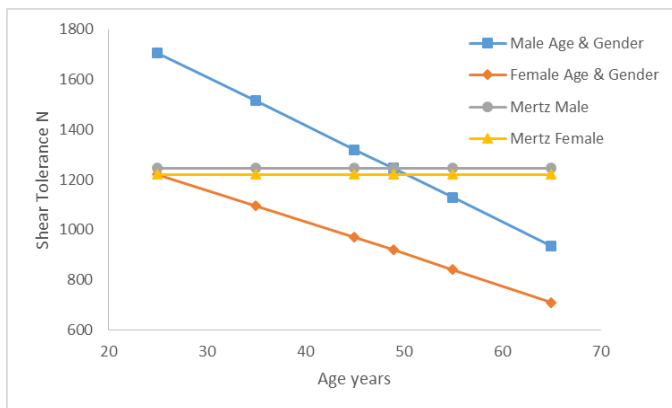


Figure 2: 5th percentile female anthropometrically scaled impact and injury tolerance with the influence of aging and gender.

The existing anthropometric scaling technique for a female and male of the same height and weight results in nearly identical tolerances. The small variation seen in the anthropometric scaling tolerance is a result of females having naturally taller erect sitting heights. Implementing the regressions revealed that tolerances have higher variation when accounting for the differences in age and gender. The regressions demonstrated that the female strength was approximately 75 percent of the male counterparts; however, strength decreased with age for both genders. Strength decreased more so for males and most rapidly after middle age.

CONCLUSIONS

Low back pain is one of the most common and growing health problems. The information and method proposed in the subject study will provide a basis for determining the likelihood of lumbar injury due to shear loading. These tolerance values and the ability to scale to numerous individuals will provide a higher physiological specificity to injury tolerance models, as well as present a foundation for assessing the likelihood of lumbar shear injury given the loading dynamics during a motor vehicle collision. Low back pain costs billions in health care and a basis for determining the likelihood and prevention of lumbar shear injury could advance biomechanical and injury analysis.

REFERENCES

1. Mertz H, et al. SAE 1989, SAE Paper No. 890756.
2. Begeman, P. C., et al. Viscoelastic shear responses of the cadaver and Hybrid III lumbar spine. No. 942205. SAE Technical Paper, 1994.

AGE-RELATED DIFFERENCES IN MECHANICAL RESPONSE OF LOWER BACK TISSUES AND THE RESULTANT SPINAL LOADS DURING LIFTING

¹Iman Shojaei, ¹Milad Vazirian, ¹Emily Croft, and ¹Babak Bazrgari

¹University of Kentucky, Lexington, KY, USA

Email: shojaei.iman@uky.edu

Introduction

Among identified risk factors for low back pain (LBP), age is becoming increasingly important due largely to the increasing population of older workers in the US. Given the important role of lower back biomechanics in development of LBP, the objective of this study was to investigate differences in the active and passive mechanical responses of lower back tissues and the resultant spinal loads when persons of different age complete the same manual material handling (MMH) task.

Method

Experimental procedure

53 individuals between 22 and 68 years old participated in this study after completing an informed consent procedure approved by the University of Kentucky IRB. During experimental session, participants completed a symmetric MMH task by lowering a 10 lb load from upright standing posture to their knee height and lifting it back to their initial upright posture. Each participant also completed a maximum voluntary isometric trunk extension (MVE) test and a passive trunk stress relaxation test as explained elsewhere [1].

Trunk kinematics and electromyography (EMG) of select trunk muscles were collected using respectively accelerometers (Xsens Technologies, Enschede, Netherlands) and surface electrodes (DE-2.1

Differential EMG sensor, Delsys, Natick, MA). Trunk kinetics during MVE and stress-relaxation tests, was collected using a load cell (Interface, Scottsdale, AZ) while ground reaction force during MMH task was collected using a force plate (AMTI, Watertown, MA). The raw collected data were filtered according to literature recommendations.

Modeling procedure and analysis

Active tissue response to task demand was calculated using a simple EMG-assisted model including a single extensor and a single flexor muscle with respective fix moment arms of 6 cm and 10 cm with respect to L5-S1 joint. Active muscle response was calculated using the following relation

$$F_a = \frac{EMG}{EMG_{max}} * G * f(l) * f(v) \quad \text{wherein}$$

EMG denotes mean EMG of four extensor/flexor muscles, EMG_{max} denotes the maximum mean EMG of the same four muscles during MVE test, $f(l)$ and $f(v)$ represent length-tension and velocity-tension coefficients. G , as a gain factor, is calculated for each person such that the error between the moment of predicted active force and measured moment during MVE is minimized. Passive tissue response at any given angle was considered to be the required force in the extensor muscle of the model such that its moment around L5-S1 to be the same as the measured passive moment for the same angle during stress-relaxation test. The

resultant spinal loads (i.e., compression and shear forces) were calculated using both active and responses. A multivariate analysis of variance (MANOVA) was used to determine the effects of age on the maximum values of the ratio of active to passive tissue responses, and estimated compression and shear forces.

Results and discussion

For younger participants, sum of moments from the active and passive responses of lower back tissues with respect to the L5-S1 joint matched well with the net external moment obtained using a link-segment model (Table 1). For older participants, though, the error between the aforementioned moments increased due to inability of our model to account for active response of abdominal muscles; an event that was present at larger trunk flexion of older participants. To account for such contribution from abdominal muscles to active tissue response and the resultant spinal loads, the difference between the aforementioned moments were

considered as the contribution of abdominal muscles. Compared to younger participants (Table-1), older individuals (20s, 30s and 40s vs. 50s and 60s) developed higher ratio of passive to active moments in the extensor muscles ($P=0.0174$). Further, older versus younger individuals completed the task such that a similar compression force ($P=0.1286$) but higher shearing demands ($P=0.0393$) were imposed on their lower back.

Increased shearing demand of task with aging was due to higher/lower contribution of pelvis/lumbar spine to trunk flexion among older vs. younger participants and may result in a higher risk of LBP due to excessive pressure on the facet joints.

REFERENCES

1. Toosizadeh N, et al. *PLOS ONE* 7, e48625, 2012.

ACKNOWLEDGEMENT

This work was supported by CDC-NIOSH grant number R21OH010

Table 1: The estimated maximum moments at the L5-S1 predicted by the link-segment model (M_s) and EMG-driven model (M_E). AEM/PEM represents active/passive extensor moments

Age range	Segment model	EMG-assisted model				Error (%)
	M_s (N.m)	AEM (N.m)	PEM (N.m)	PEM/AEM	M_E (N.m)	
22-28	96(9)	48(6)	56(7)	1.16(0.15)	92(8)	3
32-38	105(23)	56(14)	75(17)	1.33 (0.23)	111(26)	6
42-48	86(16)	52(11)	59(10)	1.13(0.14)	92(18)	7
52-58	82(18)	42(13)	73(15)	1.74(0.23)	103(24)	26
62-68	90(11)	48(7)	81(9)	1.69(0.20)	113(16)	26

Table 2: Estimated spinal loads

Age range	Moment (N.m)	Compression (N)	Shear (N)
22-28	96(9)	1997(283)	705(105)
32-38	105(23)	2143(308)	609(99)
42-48	86(16)	1877(245)	672(107)
52-58	82(18)	1935(277)	874(142)
62-68	90(11)	2079(301)	866(129)

ADVANCES IN HYPERELASTIC FINITE ELEMENT MODELING OF BIOLOGICAL TISSUES: EXPLICIT STRAIN ENERGY FUNCTION SPECIFICATION

¹ Joshua M. Inouye and ¹ Silvia S. Blemker

¹ University of Virginia, Charlottesville, VA, USA
email: ssblemker@virginia.edu

INTRODUCTION

Finite element modeling (FEM) is a suitable method to study the mechanics of biological tissues, but its utility for studying soft tissues has been limited by problems with numerical stability at large, complex deformations. Here, we describe a new paradigm for finite element tissue modeling that greatly increases numerical stability: explicit specification of a strain energy density function using SefeaTM (Strain-Enriched FEA, AMPS Technologies). This method relies on numerical differentiation of the strain energy function to calculate the stress and tangent tensors for each integration point (instead of using complex analytical expressions). We create an image-based model of a hamstring musculotendon unit—the biceps femoris longhead—to demonstrate this method's utility and stability.

METHODS

Typically, FEM of hyperelastic materials relies on a strain energy density function. For example, a simple isotropic, quasi-incompressible hyperelastic material model is a Mooney-Rivlin solid, whose strain energy function is given by the expression

$$W = C_{10}(\bar{I}_1 - 3) + C_{01}(\bar{I}_2 - 3) + W(J)$$

Where W is the strain energy (a scalar), C_{10} and C_{01} are material constants, \bar{I}_1 and \bar{I}_2 are scalar deviatoric invariants that are functions of the deformation tensor, and $W(J)$ is a volumetric strain energy term of the relative volume J in order to enforce a nearly-incompressible material response. More complex strain energy functions can be used for transversely isotropic biological tissues. Most solvers require calculation of the stress and tangent tensors that are functions of the derivatives of the strain energy density with respect to the right Cauchy-green deformation tensor C :

$$\sigma = f\left(\frac{\partial W}{\partial C}\right)$$

$$C = f\left(\frac{\partial^2 W}{\partial C^2}\right)$$

where σ is the Cauchy stress and C is the tangent tensor. These tensors are typically calculated analytically, but SefeaTM calculates them with numerical differentiation of the strain energy density function.

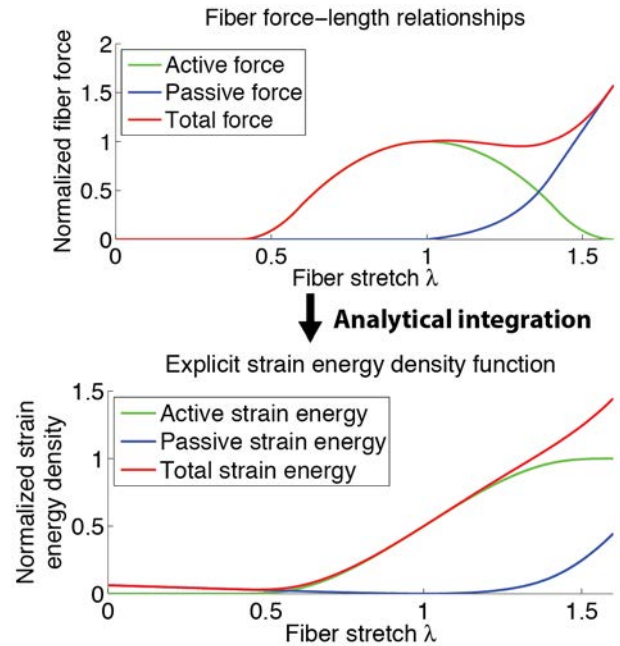


Figure 1: We integrate the force-length relationship of muscle [1] to obtain an explicit strain energy function for muscle.

The advantages of SefeaTM include i) using enhanced 4-node tetrahedral elements to enable automatic meshing and ii) specifying an explicit strain energy density function rather than the stress and tangent tensors. We determine the along-fiber strain energy function of muscle by integrating the force-length curve of muscle [1] (Figure 1). The active force curve scales with muscle activation. The same operation is performed to determine the

tendon strain energy function. We used material parameters for muscle and tendon from a previous study [1].

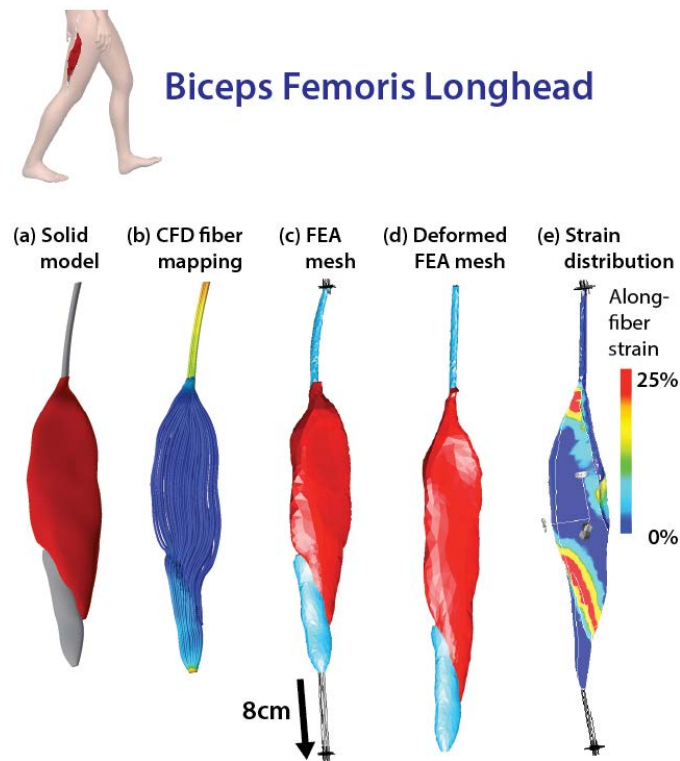


Figure 2: (a) MRI-based solid model of the biceps femoris longhead [2]. (b) Computational fluid dynamics determines the fiber directions for the transversely isotropic formulation [3]. (c) The solid was meshed automatically with enhanced 4-node tetrahedral elements and the distal tendon was displaced by 8cm. (d) The deformed mesh reaches full convergence. (e) Strain distributions within the muscle are non-uniform.

We created a 3D model of the biceps femoris longhead based on MRI data [2] (Figure 2a). We used computational fluid dynamics to specify fascicle trajectories for the transversely isotropic material models [3] (Figure 2b). We used automatic tetrahedral meshing and simulated a long eccentric

contraction by ramping the muscle activation from 0 to 1 while displacing the distal tendon by 8cm (well above the stretch during sprinting of 5cm [4]) (Figure 2c).

RESULTS

The model was numerically stable using SefeaTM, reaching full convergence (Figure 2d). The deformed model at a physiological 2cm displacement (approximately 40° of knee extension [2]) shows non-uniform strain distributions (Figure 2e). Non-uniform strain distributions have been shown characteristically in previous finite element studies of eccentric contraction [1,2,4].

DISCUSSION

Our new finite element modeling paradigm of explicit strain energy function specification within SefeaTM significantly enhances numerical stability. Furthermore, it enables fully automatic meshing of biological tissues of arbitrary shape and complexity using 4-node tetrahedral elements. These elements are also stable in contact scenarios—typically not the case for non-linear elements. This new paradigm and technology will empower hyperelastic finite element studies of biological tissues that would be otherwise unfeasible.

REFERENCES

1. Blemker SS, et al. *J Biomech* **38**, 657-665, 2005.
2. Rehorn MR and Blemker SS. *J Biomech* **43**(13), 2574-2581, 2010.
3. Inouye JM, Handsfield GG, et al. *Submitted to Proc. Am. Soc. Biomech*, Columbus, OH, USA, 2015.
4. Fiorentino NM, et al. *Med Sci Sport Exer* **46**(4), 776-786, 2014.

ISOMETRIC SQUAT PEAK FORCE IN RANGE OF KNEE FLEXION ANGLES STRONGLY RELATED TO COUNTERMOVEMENT JUMP PEAK FORCE

Mitchell L. Stephenson, Harry Fisher, Kyle K. Graves, Taylour J. Hinshaw,
and Boyi Dai

University of Wyoming, Laramie, WY, USA
email: mitch.stephenson@gmail.com, web: <http://www.uwyo.edu/kandh/>

INTRODUCTION

The one-repetition maximum (1RM) is considered the gold standard of dynamic peak strength, commonly used in squat competition and training. Due to the methodology, 1RM testing has a relatively large time requirement and poses injury risks to the athlete. In comparison, isometric squat (IS) testing has often been proposed as an alternative that would reduce the time requirement and risk to the athlete. While both performances are strongly related, IS testing was found to introduce error in the 1RM predictions [1].

Previous research has identified the importance of the specificity in testing when relating IS to squat 1RM, as the removal of the dynamic movement in IS testing only allows for the quantification of strength at a single knee flexion angle (KFA) of the 1RM range of motion [2]. A similar phenomenon should also exist when relating IS force testing to countermovement jump (CMJ) force output; as an athlete moves through a range of motion in a CMJ, testing a single angle in an isometric test may not best reflect CMJ peak force [3].

The purpose of the current study was to assess the relationship between isometric force output at a range of KFAs in a squat and the peak force during a CMJ. It was hypothesized that the force output at deeper KFAs in the IS would be positively correlated with the peak force output in the CMJ.

METHODS

Thirty-one physically-active, uninjured recreational athletes (sex: 14 males and 17 females; age: 20.2 ± 1.7 years; height: 1.73 ± 0.12 m; mass: 72.8 ± 17.7 kg) participated in the current experiment.

Participants provided informed consent and then performed a warm-up protocol. Participants completed three trials of a countermovement jump task and then four maximal isometric squats. Vertical ground reaction force (GRF) data were collected by one FP4060 force plate (Bertec Corporation, OH, USA) sampling at 1600 Hz and subsequently filtered with a 100 Hz low-pass filter.

For the jump, participants stood with the testing leg on the force plate, performed a countermovement jump with an arm swing for maximum height and landed back in the initial position. Participants then performed an isometric squat (Figure 1) for maximal effort against a weighted squat rack while standing with the testing leg on the force plate in each of four external KFA ranges: 35-45°, 55-65, 75-85, and 95-105, set by manipulating the top catch pin of the rack and identified by 2D kinematics. Each isometric squat was performed for a total of 5 seconds, with a minimum of 3 minutes of rest between trials. The order of different isometric squats was randomized.

Pearson correlation tests were used to assess the relationship between the peak 1s average vertical GRF from the squat and the peak takeoff force in the CMJ with using SPSS v21 (IBM Corporation, Armonk, NY, USA) with a type I error rate of 0.05.



Figure 1. Isometric squat with different knee flexion

RESULTS AND DISCUSSION

Significant and strong correlations were found between the IS peak force and CMJ peak force in all IS KFAs (Table 1). The peak force at 80° KFA in the IS was most strongly correlated with the peak force in the CMJ.

The current results are consistent with previous research that has investigated fewer IS KFAs' relationship with a dynamic squat [2]. The current finding of the strongest correlation at 80° KFA is possibly explained by the proximity of this KFA to just above the “sticking region” in a squat and CMJ movement [4], as this may be related to the muscle stretch-shortening cycle and represent the critical performance instance in the CMJ.

The current results contrast with previous research investigating a similar relationship with an isometric leg press, in which the investigators did not find a significant relationship between isometric peak force at 90° knee flexion and jump performance [3]. This is possibly due to the necessity of specificity in testing similar postures between the movements [5] and a small sample size in the previous study [3]. Furthermore, as research [6] has indicated that squat depth, not barbell load, predominantly loads the knee, kinematic assessment of CMJ KFAs as they relate to peak force and IS peak force at specific KFAs may better illuminate the dynamic relationship between these variables and the value of IS performance in predicting CMJ kinetics and kinematics.

CONCLUSIONS

Strong, positive correlations were observed between IS peak force at a range of KFAs and CMJ peak force, with the IS peak force at 80° relating the

strongest to CMJ peak force. This is possibly due to the relation of this KFA and the sticking point in the movement. The findings provide implications in using isometric squat for assessing jumping performance and lower extremity strength. Subsequent kinematic analysis of both the IS and CMJ is necessary for elucidating individual differences in this relationship and how it is associated with the maximum knee flexion angle during the CMJ.

It should be noted that the relationship between the investigated variables only accounts for 26-43% of the variability in performance, and as such utilizing one to predict the other may introduce error in estimation. As the IS does not allow for expression of other factors such as the utilization of muscle stretch-shortening cycle, muscle coordination, and differing motor control programs, it represents only one perspective of assessment.

REFERENCES

1. Blazevich, AJ, et al. *J Strength Cond Res*, **16**, 298-304, 2002.
2. Bazyler, CD, et al. *J Strength Cond Res*, **Accepted**, 2014.
3. Marcora, S, et al. *J Sports Sci*, **18**, 313-319, 2000.
4. Paulus, DC, et al. *Biomed Sci Instrum*, **40**, 277-282, 2004.
5. Wilson, GJ, et al. *Eur J Appl Physiol*, **73**, 346-352, 1996.
6. Bryanton, MA, et al. *J Strength Cond Res*, **26**, 2820-2828, 2012.

ACKNOWLEDGEMENTS

Research was funded by the University of Wyoming College of Health Sciences Student Research Grant.

Table 1: Pearson product-moment correlation coefficients and p values between the peak 1s force production during IS and average instant peak takeoff force during the CMJ.

	IS Peak Force @ 40° KFA	IS Peak Force @ 60° KFA	IS Peak Force @ 80° KFA	IS Peak Force @ 100° KFA
CMJ Peak Force (r)	0.511	0.562	0.661	0.613
Correlation p-value	0.0033	0.0010	0.0001	0.0003

THE EFFECTS OF STIMULUS TIMING ON THE KINETICS OF A DIRECTED JUMP LANDING

Mitchell L. Stephenson, Taylour J. Hinshaw, Tyler Trumble, Qin Zhu and Boyi Dai

University of Wyoming, Laramie, WY, USA

email: mitch.stephenson@gmail.com, web: <http://www.uwyo.edu/kandh/>

INTRODUCTION

Tearing the anterior cruciate ligament (ACL) has been identified to be a significant threat to athletes, resulting in the implementation of intervention programs to counter the threat. However, most current programs are based on investigations with unrealistic research environments that do not reflect the dynamic nature of sport performance.

Previous investigations attempted to contend with this by introducing an unanticipated component in their protocols, resulting in increases of biomechanical factors associated with ACL loading [1]. But these investigations did not control the timing of the directional stimulus. Further research manipulated the timing of the stimulus in regards to landing, but found no difference in ACL loading factors between the unanticipated conditions [2]. It is possible that participants sacrificed performance to counter ACL loading [3].

As the previous research only investigated manipulating the timing of the stimulus 600ms to 400ms before landing [2] while evidence indicates lower extremity reactions can be significantly faster [4], the current research proposes to investigate the change in injury and performance kinetics when manipulating the timing of directional stimulus through a range of 0ms to 400ms.

METHODS

Thirteen physically-active, uninjured recreational athletes (sex: 11 males and 2 females; age: 20.6 ± 1.7 years; height: 1.77 ± 0.07 m; mass: 76.2 ± 11.7 kg) participated in the current experiment. Participants provided informed consent and then performed a warm-up protocol. They then performed a series of successful practice trials before 45 block-randomized recorded trials.

Participants jumped forward from a 30cm tall block, instrumented with a Bertec forceplate (FP4060-05-PT, Bertec Corporation, Columbus, OH, USA) sampling at 1000hz, landing bilaterally with the dominant foot on a second Bertec FP4060-10-2000 forceplate sampling at 1600hz. In a fluid motion, participants jumped forward and upon landing either performed a vertical jump for maximum height or a left/right jump at 90° for maximum distance depending on the directional stimulus.

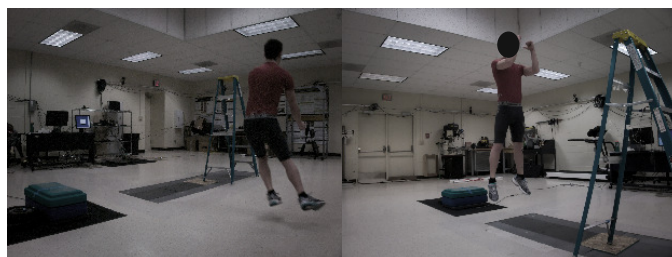


Figure 1: Example of right lateral jump (posteriorlateral perspective) and vertical jump (anteriolateral perspective).

The directional stimulus was presented by three LEDs mounted in front of the landing forceplate: Left and right yellow LEDs indicated their medial and lateral jumps relative to their dominant leg and a center red LED indicated the vertical jump. Stimuli were sent in one of four conditions: 1) anticipated (AN) condition, well before movement was initiated; 2) classically unanticipated (CU) condition, the moment the participant left the jump block; 3) timed unanticipated condition at 300ms (TU300) and 150ms (TU150) before landing; and 4) at the instant of landing (LA). Stimuli and timing were controlled via an Arduino Uno microcontroller (Smart Projects, Strambino, Ivrea, Italy) connected to the forceplates.

Participants performed three trials in each direction at each stimulus timing condition. Peak vertical landing force (FZ_{LA}) and peak vertical takeoff force (FZ_{TO}) were identified, averaged between the three trials, and normalized to bodyweight (BW). Contact

time (CT) was also extracted and averaged amongst the three trials. A one-way repeated measure analysis of variance was performed to analyze differences in dependent variables amongst the stimuli timing, with a Type I error rate of 0.05. Greenhouse-Gesier corrections were used for sphericity violations. Bonferroni-corrected pairwise comparisons were performed when significant main effects were detected.

RESULTS AND DISCUSSION

Results are presented in Table 1. Differences in FZ_{LA} and FZ_{TO} were found in the lateral jump condition, with stimuli presented at LA resulting in a larger FZ_{LA} than the other conditions and a smaller FZ_{TO} with stimuli presented at TU150 than AN and CU. These differences only in the lateral jump may be due to a unilateral reliance on the tested limb in this direction. Respectively, these results indicate a possible increase in ACL loading and decrease in performance. Significant differences in CT were found in all three jump directions, with LA resulting in a longer duration CT than all other stimuli timings.

No significant kinetic differences were found between the AN and CU conditions for any jump direction, contrasting with previous literature [2]. An increase in sample size may be necessary to better elucidate possible differences. Generally, FZ_{TO} decreased and CT increased as available time for reaction before landing was reduced via the stimulus timing. This implicates a reduction in performance as time for reaction is reduced. Further

research is necessary to determine whether performance was sacrificed to specifically reduce ACL loading, however.

Error in the exact timing of each stimulus was not quantified with the current statistical technique and the exact timing may better determine possible effects on the kinetic variables. Furthermore, the current results are limited to ground reaction force; kinematic analysis would provide a more holistic analysis when performed in conjunction.

CONCLUSIONS

Preliminary data from the current research indicates an increase in vertical landing force before a lateral jump when directional stimuli are presented at the instant of landing, as well as an increase in contact time for any directional jump as available time for reaction before landing decreases. This decrease in performance may be countered with reaction time training, but further research on the changes of combined kinetics and kinematics is necessary before intervention programs are implemented.

REFERENCES

1. Sell, TC, et al. *Am J Sports Med*, **34**, 43-54, 2006.
2. Brown, TN, et al. *Br J Sports Med*, **43**, 1049-1056, 2009.
3. Dai, B, et al. *Am J Sports Med*, **43**, 466-474, 2015.
4. McLean, SG, et al. *Clin Biomech*, **25**, 563-569, 2010.

Table 1: Averages (standard error) of dependent variables for each jump direction relative to stimuli timing.

		AN	CU	TU300	TU150	LA
Lateral	FZ _{LA} (BW)*	2.17 (0.25) ^e	2.19 (0.26) ^e	2.37 (0.26) ^e	2.72 (0.14) ^e	3.23 (0.14) ^{a,b,c,d}
	FZ _{TO} (BW)*	1.15 (0.05) ^d	1.11 (0.04) ^d	1.08 (0.04)	1.02 (0.03) ^{a,b}	1.06 (0.05)
	CT (s) *	0.48 (0.03) ^{d,e}	0.50 (0.03) ^{d,e}	0.53 (0.03) ^{a,d,e}	0.59 (0.02) ^{a,b,c,e}	0.71 (0.03) ^{a,b,c,d}
Medial	FZ _{LA} (BW)	3.38 (0.18)	3.53 (0.17)	3.52 (0.17)	3.39 (0.16)	3.12 (0.18)
	FZ _{TO} (BW)	1.53 (0.11)	1.50 (0.10)	1.42 (0.08)	1.39 (0.07)	1.39 (0.07)
	CT (s) *	0.42 (0.03) ^{c,d,e}	0.45 (0.02) ^{d,e}	0.48 (0.02) ^{a,d,e}	0.53 (0.03) ^{a,b,c,e}	0.70 (0.03) ^{a,b,c,d}
Vertical	FZ _{LA} (BW)	3.07 (0.17)	3.02 (0.14)	2.86 (0.13)	3.06 (0.12)	3.13 (0.13)
	FZ _{TO} (BW)	1.36 (0.08)	1.31 (0.07)	1.32 (0.07)	1.28 (0.05)	1.25 (0.06)
	CT (s) *	0.45 (0.03) ^{d,e}	0.48 (0.03) ^e	0.48 (0.03) ^{d,e}	0.52 (0.02) ^{a,c,e}	0.62 (0.02) ^{a,b,c,d}

*Significant main effect; ^asignificantly different than AN; ^bsignificantly different than CU;

^csignificantly different than TU300; ^dsignificantly different than TU150; ^esignificantly different than LA condition.

ALTERED TRABECULAR MICROARCHITECTURE IN BRACHIAL PLEXUS BIRTH PALSY: A RAT MODEL STUDY

^{1,2} Carolyn M. Stolfi, ^{1,2} Dustin L. Crouch, ^{1,2} Katherine R. Saul, and ^{1,2} Jacqueline H. Cole

¹ North Carolina State University, Raleigh, NC, USA

² The University of North Carolina at Chapel Hill, Chapel Hill, NC, USA

email: cmstolfi@ncsu.edu, web: www.mae.ncsu.edu/ksaul & http://www4.ncsu.edu/~jcolehu

INTRODUCTION

Brachial plexus birth palsy (BPBP) is a peripheral nerve injury affecting about four in 1,000 births annually [1], leading to impaired function of the neonatal upper limb. The resulting denervation of muscles often causes gross morphological changes in surrounding bone structures, exacerbating limb impairment that is observed clinically [2]. Effects to bone due to altered musculoskeletal loading requires an in-depth understanding of changes in bone mineralization and microstructure in developing joints, which is currently not well understood. Examining changes in bone will provide clinicians with additional information to optimize treatment plans and minimize or circumvent onset of permanent shoulder deformity.

The purpose of this study was to determine whether changes in cancellous bone mineralization and microarchitecture of the proximal humerus occur with the altered musculoskeletal loading characteristic of BPBP injuries using a rat model.

METHODS

Sixteen male Sprague-Dawley rat pups were separated into two groups ($n=8$ each). Group 1 (neurectomy) underwent neurectomy of the left brachial plexus upper trunk, representative of the C5 and C6 nerve root injuries most commonly observed in clinical cases of BPBP [3]. Group 2 (sham) received a sham surgery including division of the left pectoralis major with no injury to the nerve. Surgical interventions were applied five days after birth and approved by the Institutional Animal Care and Use Committee. Animals were sacrificed eight weeks post-operatively, and the left (affected) and right (control) humeri were excised and imaged

using micro-computed tomography (micro-CT) (SCANCO μ CT 80). One animal from each group was excluded from analyses due to specimen damage following excision.

Micro-CT scans were reconstructed at a 10- μ m isotropic voxel size, and a global threshold of 441 mg/cm³ of calcium hydroxyapatite (HA) (3891 Hounsfield units, or HU) was applied. A region of interest (ROI) equal to 5% of the overall humeral length was selected in the proximal metaphysis immediately distal to the growth plate. The ROI was evaluated using the SCANCO proprietary software to assess tissue mineral density (TMD) and 3D trabecular thickness (Tb.Th), separation (Tb.Sp) and number (Tb.N), as well as trabecular connectivity and orientation. Two-tailed t-tests ($\alpha=0.05$) were used to compare bone mineralization and microstructure between groups (SAS 9.4).

RESULTS AND DISCUSSION

The affected limbs in the neurectomy group experienced trabecular thinning with a tendency for reduced tissue mineral density relative to sham affected limbs (Fig. 1). Tb.Th was reduced by 12% ($p=0.046$) in the neurectomy group (Fig. 2).

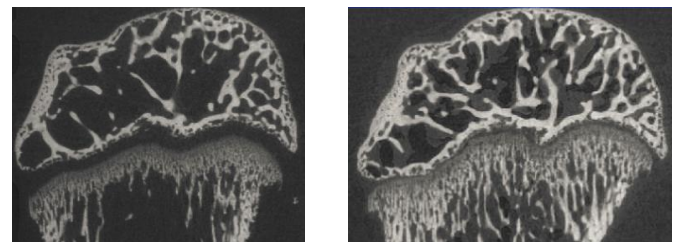


Figure 1: Sagittal view of the proximal metaphyseal region (bottom half of the bone profile, separated from the top by the dark curvature representing the growth plate) shows reduced trabecular thickness with neurectomy (left) compared to sham (right).

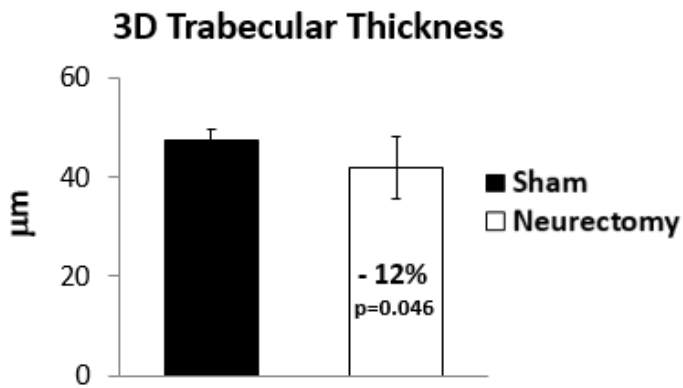


Figure 2: Trabecular thickness decreased with neurectomy (white) versus sham (black).

Clinically, radiographic evidence of muscle atrophy in all rotator cuff muscles following BPBP injury has correlated with anterior humeral head subluxation and changes in glenoid shape [5]. Prior analyses using the same animals from our study showed postural (reduced external rotation) and osseous (glenoid declination, inferior humeral head translation) deformity of the glenohumeral joint for animals experiencing neurectomy. Deformity was significantly correlated with reduced optimal fiber length for muscles, including teres major and subscapularis, thereby simulating mechanical conditions capable of altering normal bone growth [4]. Other studies have also suggested that impairment to the longitudinal growth of muscles can induce postural constraints, causing increased passive forces of muscles crossing the glenohumeral joint [6].

In addition to gross changes in bone morphology, altered musculoskeletal loading with disuse has been associated with trabecular thinning in mice [7]. The present study suggests that altered mechanobiological effects on bone following peripheral nerve injury, compounded with the resulting changes in load transferred from paralyzed muscle to bone, may disrupt normal bone remodeling processes. We are currently examining bone cell activity in histologic sections from these humeri. Simulations of load distribution in cancellous bone have shown that changes in trabecular microarchitecture lead to reduced stiffness [8]. Likewise, changes in bone tissue

mineralization represent significant alterations in cancellous bone tissue that are associated with large changes in bone elastic modulus and resistance to loading [9]. While not a direct indicator of bone strength, reduced bone mineral density has been associated with higher fracture risk clinically [10]. Currently, we are analyzing the right (control) humeri to assess trabecular differences between the unaffected (right) and affected (left) limbs in the same animal. Future computational and animal model studies are necessary to isolate the extent of changes in trabecular mineralization and microarchitecture associated with limited use of the affected limb alone and in the presence of denervated muscle. While the etiology of osseous deformity in BPBP remains unclear, understanding changes in bone microstructure resulting from injury may present a foundation for understanding the progression of deformity and offer targets for interventions and treatments.

REFERENCES

1. Pearl ML. *J Am Acad Orthop Surg* **17**, 242, 2009.
2. Li Z. *J Bone Joint Surg Am* **92A**, 2583, 2010.
3. Hale HB. *J Hand Surg Am* **35A**, 322, 2010.
4. Crouch DL. *J Bone Joint Surg Am* (in review).
5. Hogendoorn S. *J Bone Joint Surg Am* **92A**, 935, 2010.
6. Nikolaou S. *J Bone Joint Surg Am* **93**, 461, 2011.
7. Wagner EB. *J Appl Physiol* **109**, 350, 2010.
8. van der Linden JC. *J Bone Miner Res* **16**, 457, 2001.
9. Carter DR. *J Bone Joint Surg Am* **59A**, 954, 1977.
10. Cummings SR. *Lancet* **341**, 72, 1993.

ACKNOWLEDGMENTS

Funding was provided by OREF/POSNA (KRS), NCSU Research Innovation Seed Funding (KRS, JHC), UNC/NCSU Rehabilitation Engineering Center Seed Grant (KRS, JHC), and NIH (K12HD073945, JHC). The authors thank Dr. Z. Li for clinical support, Dr. T. Bateman for micro-CT support, and J. Antoniono, C. Hudson, E. Livingston, and A. Murray for help with data collection and analyses.

Influence of Fatigue on Lower Extremity Biomechanical Variability during Forward Lunge

Amanda E. Stone, Diana M. Alonso, Kyle C. Norder, Austin C. Norden, Kaitlyn T. Girard, and Chris J. Hass

University of Florida, Gainesville, FL, USA

email: stonaman@ufl.edu; web: <http://apk.hhp.ufl.edu/index.php/departments-centers/center-for-exercise-science-ces/applied-neuromechanics-laboratory/>

INTRODUCTION

Soft tissue injuries to the knee stabilizers most often occur during landing and cutting types of activities where the knee flexes under eccentric control of the quadriceps muscles. Fatigue of the stabilizing muscles is also thought to contribute to an increased injury risk. Investigations implementing applied dynamic fatigue protocols have shown that high fatigue levels cause significant alterations in lower limb kinematics [1]. Additionally, changes in performance after fatigue may be attributed to alterations in force generation capacity, as well as changes in muscle coordination patterns [2]. Several studies argue that fatigue may be an integral component of some sports-related injuries [3, 4, 5]. During rehabilitation, lunge exercises are often used as a perceived safe exercise to train the muscles in a manner that mimics the lower extremity mechanics observed during sport-related injuries. It is unknown, however, how fatigue may affect the ability to safely perform lunge exercises. Thus, the purpose of this study was to investigate which, if any, biomechanical changes occur during a fatigued state when completing a forward lunge task.

METHODS

Eight healthy subjects (age 19 to 24 years) comprised of four males (age 21 ± 2 , weight 73 ± 9 kg, height 177 ± 8 cm) and four females (age 21 ± 1 , weight 56 ± 4 kg, height 162 ± 4 cm) were recruited to participate in this study. At the time of recruitment, all subjects were physically active as defined by at least 30 minutes of physical activity at least three times per week. Subjects were excluded from the study if they had any surgery to their back or lower extremity, or an injury within the last six months that limited their physical activity for more than three days. Subject were required to have previous experience performing a lunge.

Reflective markers were placed bilaterally over the lower extremities in accordance with the Vicon Plug-in Gait marker set. Three dimensional kinematics (eight camera Vicon Motion System, 120 Hz) and ground reaction forces (Bertec, 360 Hz) were collected while participants completed lunge repetitions until a maximum state of fatigue was reached; maximum fatigue was defined as a 9 out of 10 on the modified BORG rating of perceived exertion scale for two consecutive trials (Figure 1). The first and last two trials were used to analyze pre- and post-fatigue data. Three-dimensional kinematics were calculated for the lower extremity joints and angle variability was calculated at the hip, knee and ankle in the frontal plane using the root mean square error (Equation 1); this variable was chosen because it is a strong indicator of instability.

$$Variability = \sqrt{\frac{1}{N} \sum_{i=1}^N (x_i - \bar{x}_i)^2} \quad (1)$$

Rating of Perceived Exertion (RPE)- Modified Borg Scale	
0	Rest
1	Really Easy
2	Easy
3	Moderate
4	Sort of Hard
5	Hard
6	
7	Really Hard
8	
9	Really Really Hard
10	Maximal effort

Figure 1. Modified BORG rating of perceived exertion scale.

Dependent samples t-tests were used to determine if behavioral changes were present in the dependent variables of interest between pre- and post-fatigue conditions (SPSS, $P \leq 0.05$).

RESULTS AND DISCUSSION

Results revealed an increase in variability in the frontal hip and ankle angles ($P=0.04$ and $P=0.02$, respectively), as well as decreased variability in the frontal knee angles ($P=0.03$) from pre- to post-fatigue when the non-dominant leg was forward (Table 1). Lower extremity kinematics and kinetics revealed no significant trends between pre- and post-fatigue for hip, knee, and ankle angles and moments.

Table 1. Mean \pm SD of pre- and post-fatigue variability for hip, knee and ankle joints.

	Pre-Fatigue	Post-Fatigue	<i>P</i>
Variability ($^{\circ}$)			
Frontal Hip	4.7 ± 1.6	5.6 ± 2.1	0.04*
Frontal Knee	12.2 ± 9.1	10.9 ± 8.5	0.03*
Frontal Ankle	3.1 ± 1	3.5 ± 1	0.02*

*Indicates trend between pre- and post-fatigue conditions, $P \leq 0.05$

Previous studies have suggested insufficient proprioception caused by muscle fatigue may increase postural instability [6]. Furthermore, hip and ankle fatigue have been specifically shown to decrease postural control [7]. Related to postural stability, joint angle variability is also affected by muscle fatigue and may be a contributing factor to increased injury in a fatigued state.

These findings demonstrate that certain biomechanics are compromised in a fatigued state while performing a forward lunge task. When ignored, these changes in variability could potentially lead to injury.

CONCLUSIONS

This study is one of few to investigate biomechanical changes due to muscle fatigue and is the first to provide an analytical comparison pre- and post-fatigue during a commonly used rehabilitation exercise, the forward lunge. Our findings have identified an increase in frontal hip and ankle angle variability, as well as a decrease in frontal knee angle variability, in the non-dominant leg during the lunge task. These changes in variability may be a target for rehabilitation interventions and future investigations to limit frontal angle variability in lower extremity joints and decrease the likelihood of sport-related injuries.

REFERENCES

1. Chappell JD, et al. *Am J Sport Sci* **33**, 1022-1029, 2005.
2. Kellis E, et al. *Scand J Med Sci Sport* **16**, 334-344, 2006.
3. Borotikar BS, et al. *Clin Biomech (Bristol, Avon)* **23**, 81-92, 2008.
4. Kernozek TW, et al. *Am J Sports Med* **36**, 554-565, 2008.
5. McLean SG, et al. *Med Sci Sports Excer* **39**, 502-514, 2007.
6. Vuillerme N, et al. *Gait Posture* **24**, 169-172, 2006.
7. Bisson EJ, et al. *Gait Posture* **33**, 83-87, 2011.

Comparison of Standalone PLIF expandable cage and TLIF standard cage: an *in vitro* and finite element study

¹ Sushil P. Sudershan, M. ¹ Saeid Asadollahi, ¹ Manoj Kodigudla, ¹ Dhanvin Desai, ¹ Aakash Agarwal,
¹ Narjes Momeni, ¹ Anand K. Agarwal, ¹ Vijay K. Goel, and ² Christian Schultz

¹ Engineering Center for Orthopaedic Research Excellence (E-CORE), Departments of Bioengineering and Orthopaedic Surgery, Colleges of Medicine and Engineering, The University of Toledo at Toledo, OH, USA

² Apex Spine, Munchen, Germany

Email: sushil.sudershan@rockets.utoledo.edu, website: <http://www.eng.utoledo.edu/ecore/>

INTRODUCTION

Spinal fusion has been the gold standard for treatment of degenerative disc disease. Over the years, numerous surgical techniques and various implants (expandable versus non-expandable) have been developed to increase fusion rates and decrease operative and recovery time. The purpose of this study was to evaluate the stability of TLIF standard surgical technique and cage versus the PLIF surgical technique with expandable cage. Kinematics and endplate stresses will be recorded to evaluate which implant might better promote bone fusion.

METHODS

Six L23 (TLIF) and six L45 (PLIF) ligamentous functional spinal units (FSUs) were used for the study. The caudal end was fixed to the testing apparatus while pure moments up to 10 N*m were applied to the cranial end in extension (Ext), flexion (Flex), left (LB), and right (RB) lateral bending, and left (LR) and right (RR) axial rotation. Specimen motion was recorded using Optotrak motion capture (NDI, Waterloo, Canada). A previously validated whole spine model was used to obtain the necessary L23 and L45 segments for finite element analyses, wherein respective surgeries were simulated. TLIF simulation involved complete facetectomy and nucleotomy. PLIF simulation involved bilateral partial laminectomy and bilateral cage placement. In each surgical simulation, the disc space was distracted until the cage was in contact with both endplates, after which a 10 N*m pure moment was applied. Cadaveric and finite element range of motion results and endplate stresses were compared.

RESULTS AND DISCUSSION

Cadaveric results demonstrated standalone TLIF increased motion in extension, left and right bending, left and right rotations, and flexion with pre-load

(Fig. 1). Finite element analysis revealed that the TLIF group showed increased extension, flexion, left and right bending, extension with preload, and flexion with preload but decreased axial rotation. The PLIF group demonstrated decreased motion in all loading conditions (Fig. 2) as was further substantiated by finite element analysis. The differences in motion between cadaver and finite element motion are listed in Table 1.

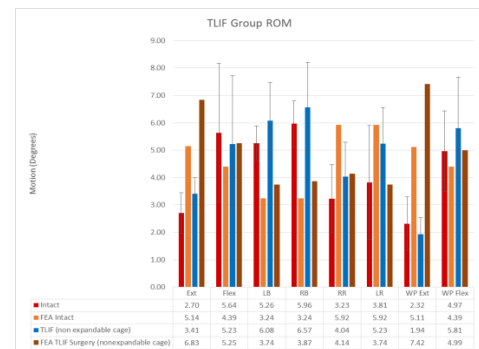


Figure 1: TLIF range of motion results for cadaver and finite element model

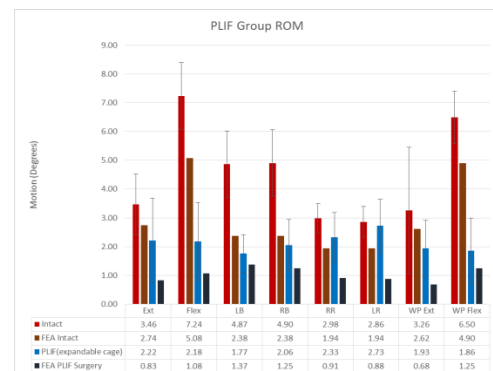


Figure 2: PLIF range of motion results between cadaver and finite element model.

Motion	Ext	Flex	LB	RB	LR	RR	WP Ext	WP Flex
Cadaver TLIF	+21%	-8%	+13%	+9%	+20%	+27%	-20%	+14%
FEA TLIF	+33%	+20%	+15%	+19%	-30%	-37%	+45%	+14%
Cadaver PLIF	-36%	-70%	-64%	-58%	-22%	-5%	-41%	-71%
FEA PLIF	-70%	-79%	-42%	-47%	-53%	-55%	-74%	-74%

Table 1: Table below shows the reduction in motion for all of the loading conditions between cadaver and finite element.

Differences in range of motion can be attributed to surgical technique and implant type. The TLIF approach required total facetectomy. As the facets, in conjunction with the capsular ligaments, are responsible for limiting motion in extension, left and right bending, and left and right axial rotation, performing the facetectomy altered the center of rotation for all loading conditions. The bilateral expandable cage placement has two advantages: endplate contact and fit. The cage can be expanded for proper fit with both endplates and provides a greater surface contact area.

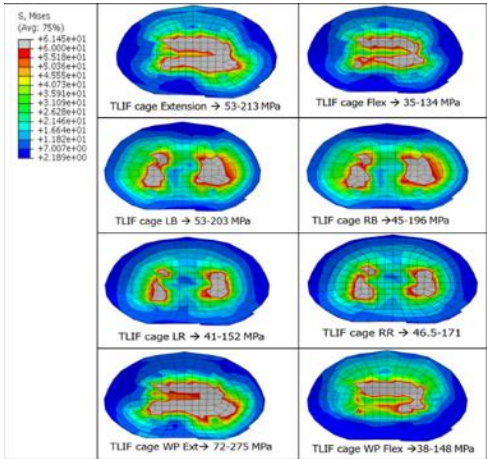


Figure 3: Endplate stresses for TLIF group. Minimum and maximum stress reported were 35 MPa and 275 MPa respectively.

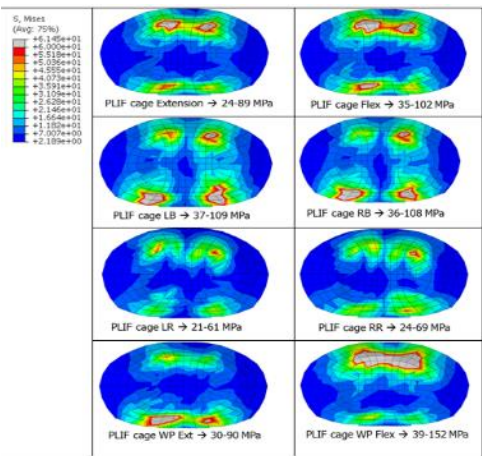


Figure 4: Endplate stresses for PLIF group. Minimum and maximum stress reported were 35 MPa and 275 MPa respectively.

The TLIF group (Fig. 3) demonstrated higher endplate stresses than the PLIF group (Fig. 4). The TLIF model yielded an average stress of 186.5 MPa as compared to 97.5 MPa in the PLIF model. Under higher stresses, bone growth is more likely occur. However, higher stresses may be problematic if the bone is osteoporotic; leading to cage subsidence

CONCLUSIONS

The results showed that the PLIF expandable cage stabilized the functional unit better than the non-expandable TLIF cage. Furthermore, the TLIF non-expandable cage demonstrated higher contact stresses than the expandable PLIF cage. Future work will focus on interrogating the pedicle screw system via a similar approach and on the effect of device contact footprints on the endplate stresses and load transfer.

REFERENCES

1. Kodigudla, M., Desai, D., Agarwal, A., Momeni, N., Goel, VK., Agarwal, AK., Schultz, C., “PLIF Expandable Cages Effectively Stabilizes the Spine Better than TLIF Cage” World Congress of Biomechanics (2014), Boston, MA, USA.

ACKNOWLEDGEMENTS

Work supported in part by Apex Spine and the NSF Industry/University Cooperative Research Center at the University of California at San Francisco and University of Toledo, Toledo (www.nsfcdmi.org)

MODELING OF HUMAN INTENT FOR CLASSIFICATION OF A WEIGHT LIFTING TASK

Deema Totah, Lauro Ojeda, Daniel Johnson, Deanna Gates, Emily Provost, Kira Barton

The University of Michigan, Ann Arbor, MI, USA
email: deema@umich.edu, web: <http://brg.engin.umich.edu/>

INTRODUCTION

Back injury is one of the leading causes of missed work days in the United States, with musculoskeletal disorders forming 33% of all reported work injury and illness cases in 2013 [1]. Lifting is known to be a major cause of these injuries and lifting belts are a common solution for their prevention. Research suggests, however, that these passive braces are biomechanically ineffective at unloading the lower back and merely serve as a reminder to the user to keep an upright posture [2].

To gain a better understanding of these injuries, researchers are using instrumented braces and wearable sensors to collect spinal motion data [3, 4]. Given the limitations of current braces however, robotic assistive devices and adaptive exoskeletons could provide more adequate biomechanical support through actuation and relieve some of the back muscle loading. In particular, the efficacy of these devices would be greatly improved if they are able to alter their level of supplied assistance in time to meet task-specific demands of the user (e.g. trunk motion alone vs with an external load). In order to integrate these devices with the user, better models of human intent must be developed. Human intent models that can recognize a task, and do so earlier, allow devices to have faster response times and more targeted control. In this work, we investigate whether phenomena indicative of anticipatory activity, occurring in muscles prior to loading [5, 6], can be used to predict a human's intent to lift a specific load. While the majority of research in this area investigates anticipatory activity in cases of sudden loading, our pilot study considered anticipatory activity during dynamic lifting of different loads.

METHODS

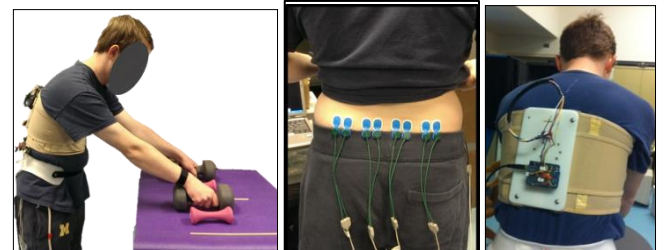


Figure 1: Experimental setup with subject lifting 12-lbs dumbbells (left). EMG sensors (middle). IMU sensor attached to a soft brace around the upper-back (right).

A 33-year old, healthy male subject was recruited for this pilot study and all protocols were approved by the University of Michigan IRB. The subject was positioned in front of a table at hip height. Three pairs of objects were placed on the table (two 12-lbs dumbbells, two 2-lbs dumbbells, and two sticks with negligible weight), as shown in Figure 1. A display screen placed at eye level in front of the table informed the subject which pair of weights he should lift. During each task, which was paced according to audible and visual cues, the subject assumed a series of poses according to a specific sequence (see Figure 2): sagittal flexion of the trunk to 30° with arms hanging vertically, hand contact with the weights while holding the trunk stationary (“pre-onset” of loading), lifting of the weights to the shoulders while holding trunk stationary (“early-onset” and “post-onset” of loading), and extension of the trunk to a neutral erect posture with weights held at the shoulders. The sequence was then reversed, and the subject rested for 10 s. During each experimental session, the subject lifted each pair of weights thirty times (for a total of 90 lifts per session). The order of the weights was randomized. A total of six identical data collections were conducted over 6 days.

Muscle activity of the erector spinae and multifidi muscle groups was collected at 1kHz using four bipolar surface electromyography (sEMG)


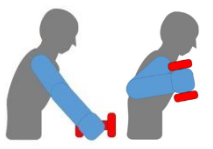

	Pre-onset	Early-onset	Post-onset
			
No weight	47.1%	88.2%	94.1%
2 lbs	35.3%	76.5%	76.5%
12 lbs	44.4%	100%	100%

Figure 2: Successful classification percentages for each weight class are shown for the three neural network models (before and after the onset of weight lifting).

electrodes (Ambu, Copenhagen, Denmark) placed on the subject's lower back at L3 level, with a single reference electrode placed over the right iliac crest. Additionally, motion was tracked using two inertial measurement units (IMUs) (Invensense Inc., Sunnyvale, CA) placed on the upper-back at the middle of the thoracic curvature and sampled at 150 Hz.

sEMG signals were filtered, rectified, and then run through a low-pass filter (4Hz cutoff frequency) to form linear envelopes. We then constructed three-layer neural network models for prediction (pre-onset) and classification (early and post-onset) of a given weight. The first layer consisted of varying time windows of EMG linear envelope data as an input to the network. The second layer contained half the number of units as the input layer. The output layer contained the three weight classes (no weight, 2-lbs, and 12-lbs).

The pre-onset prediction model used a 1-second EMG time window beginning 1 s before the subject lifted the weight from the table, ending at the transition to lifting (i.e. before the onset of lifting). The early-onset classification model used a 100-ms time window starting 300 ms after the onset of weight lifting. This time window was found to be the best window for early-onset identification by performing a 100-ms sweep across the first second of lifting. Finally, the third model, termed 'post-onset' classification, used a 1-second window after lifting was initiated. We leveraged the Matlab Neural Network Toolbox (Mathworks, Natick, MA) to construct the models. Data from three trial days were used to train the network, while data from one

other day and two different days were used to validate and test the models, respectively. This created user-specific, inter-day models.

RESULTS AND DISCUSSION

The 'pre-onset' prediction model obtained 42.3% accuracy. The 'early-onset' classification model obtained 88.5% accuracy. The 'post-onset' classification model obtained 90.4% accuracy. Figure 2 shows success percentages for each weight case along with markers on the torso flexion angle curve showing the time windows of the input data for each model. The light weight class (2-lbs) resulted in the least accurate prediction or classification. Incorrect assignment of this class generally resulted in a classification of no weight.

CONCLUSIONS

This pilot study demonstrates that prediction from anticipatory muscle activity lacks accuracy; yet early load identification is possible with accuracy rates on par with a 'post-onset' classification model. Early-onset classification, achieved within the first 400ms of lifting, shows promise for developing smart assistive and rehabilitative devices with faster response times; a requirement for real-time, user-driven control. Future work should focus on early-onset prediction, as a potential identification model. Further work is needed to validate this model and generalize it with multiple subjects. Incorporating muscle fatigue effects would further improve the performance of this model.

REFERENCES

1. Bureau of Labor Statistics, US Department of Labor, 2013 Nonfatal Occupational Injuries Requiring Days Away from Work. Accessed March 21, 2015.
2. Van Poppel M., et al. *Spine* **25**, 2103-2113, 2000.
3. Marras W, et al. *International Journal of Industrial Ergonomics* **9**, no. 1, 75-87, 1992.
4. O'Sullivan K, et al. *Proceedings of KCMACP Conference*, Edinburgh, UK, 2009.
5. Marras W, et al. *Ergonomics* **30**, 551-562, 1987.
6. Brown M, et al. *Clinical Biomechanics* **18**, no. 9, 812-520, 2003.

ASSESSMENT OF BONE QUALITY BY NOVEL SPECTROSCOPIC BIOMARKERS

¹ Mustafa Unal and ^{1,2,3} Ozan Akkus

¹ Department of Mechanical and Aerospace Engineering

² Department of Orthopaedics

³ Department of Biomedical Engineering

Case Western Reserve University, Cleveland, OH 44106, USA

email: mustafa.unal@case.edu, ozan.akkus@case.edu , web: http://engineering.case.edu/groups/Akkus_Lab/

INTRODUCTION

The research on the effects of matrix water on the fracture resistance of bone is accelerating [1]. This understanding may be central to improving fracture risk assessment. Water in bone exists in unbound state in the pore spaces or in the bound state to the matrix. Recently, we developed a custom designed short-wave infrared (SWIR) Raman spectroscopy to identify the bound and unbound water compartments of bone [2]. Using this novel technique, for the first time, we identified four peaks which associate with various water compartments in bone (Fig. 1). The current study investigated the relationship between various water compartments in bone and the mechanical properties. Distinguishing the contributions of various water compartments on bone's mechanical properties would help to further elucidate the function of water compartments on the bone fracture resistance.

METHODS

Mechanical properties: The cortical bone beams (N=30) with the dimension of 30 mm in length, 3 mm in width and 1.1 mm in thickness were subjected to three-point bending test under displacement control (1 mm/sec) to measure elastic modulus, maximum flexural strength, toughness and post-yield toughness (PYT).

Selective dehydration: Contributions of different water compartments were probed by a sequential dehydration process: 1) drying in ambient condition following by oven drying at 40 °C for 48 h, 2) partial replacement of remaining bound water by ethanol for 36 h followed by a vacuum treatment for

40 h to remove the remnant ethanol. Also, the water loss was recorded by using gravimetric analysis.

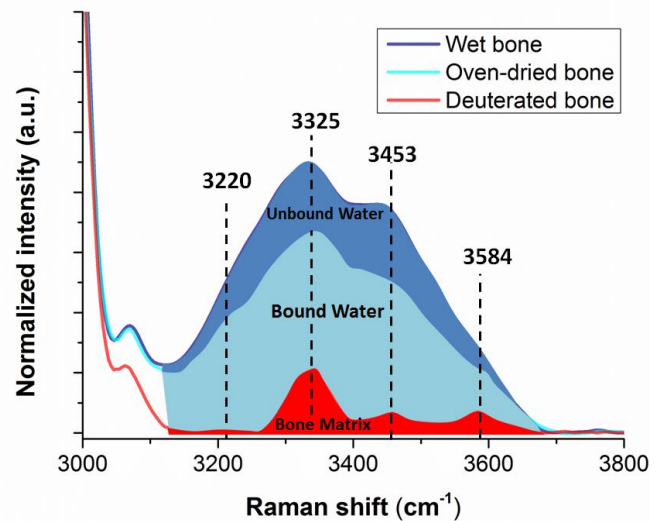


Figure 1: The breakdown of band intensities between bound water, unbound water and bone matrix (see reference for details[2]).

SWIR Raman spectroscopy: Raman spectra were collected immediately after each step of dehydration episode to record the reductions in OH-band intensities using our custom SWIR Raman system. All spectra were normalized to the protein related CH stretch band. Intensity ratios (I_{OH}/I_{CH}) of different OH peaks in the range of 3100-3800 cm^{-1} were qualified in terms of correlation with mechanical properties of bone.

Statistical analysis: Linear regression analyses were conducted to study associations between mechanical properties and Raman biomarkers. Statistical significance was set at $p < 0.05$ for the resulting R^2 value.

RESULTS AND DISCUSSION

Using the four peaks that we previously identified, we developed four new spectroscopic biomarkers: I_{3220}/I_{2949} , I_{3325}/I_{2949} and I_{3453}/I_{2949} reflect status of collagen-related water compartments and collagen portion of bone while I_{3584}/I_{2949} reflects status of mineral-related water compartments and mineral portion of bone (Figure 1). The overall results herein support the notion that there are different sorts of bound water compartments in bone and the bound water layer that was partially removed by ethanol treatment is the critical portion for bone mechanics since R^2 correlation coefficients between mechanical properties and spectroscopic biomarkers mostly peaked after oven dried and decreased after ethanol treatment. We found that two new biomarkers (I_{3220}/I_{2949} and I_{3325}/I_{2949} ; $R^2=0.81$ and $R^2=0.79$, respectively) are appropriate predictors of bone toughness whereas the I_{3584}/I_{2949} had moderately strong positive correlation with strength ($R^2=0.46$) and strong negative correlation with the modulus ($R^2=0.78$), indicating this biomarker can be used to assess bone stiffness and strength.

CONCLUSIONS

As a complementary tool to assess bone fracture risk, Raman-based water measurement can potentially provide risk assessment because even in wet condition of bone (bone's natural condition), 37%, 45% and 39% of total variance of toughness, strength and stiffness, respectively can be explained

independently from bone mineral density (BMD) and porosity.

For the first time, it was revealed that Raman-based water measurement has a strong correlation with mechanical integrity; therefore, this novel approach may help assess bone quality and improve the current diagnosis of those who may be at risk of bone fracture due to aging or disease.

REFERENCES

1. Nyman JS, Ni Q, Nicolella DP, Wang X. *Bone*; 42: 193-9. 2008
2. Unal M, Yang S, Akkus O. *Bone*; 67: 228-236. 2014

ACKNOWLEDGEMENTS

This research is partially supported by think[box] Student Research Fund at CWRU. We also thank to Shan Yang and Bolan Li for their valuable help to set up our customized SWIR Raman system and thank to Cedric Hansen for his help to prepare bone samples.

Table 1: R^2 Pairwise correlations between mechanical properties and Raman biomarkers

Linear Regression Analyses (R^2)	Raman Analysis											
	Wet (Bound, Unbound water and bone matrix)				Oven-dried (Bound water and bone matrix)				Ethanol treatment (Bound water and bone matrix)			
	I_{3220}/I_{2949}	I_{3325}/I_{2949}	I_{3453}/I_{2949}	I_{3584}/I_{2949}	I_{3220}/I_{2949}	I_{3325}/I_{2949}	I_{3453}/I_{2949}	I_{3584}/I_{2949}	I_{3220}/I_{2949}	I_{3325}/I_{2949}	I_{3453}/I_{2949}	I_{3584}/I_{2949}
Toughness	0.37 [#]	0.23*	0.22*	NS	0.81 [#]	0.79 [#]	0.28*	NS	0.48 [#]	0.47 [#]	0.39 [#]	0.43 [#]
Post-Yield Toughness	0.32 [#]	0.17*	0.19*	NS	0.65 [#]	0.73 [#]	0.18*	NS	0.44 [#]	0.48 [#]	0.40 [#]	0.47 [#]
Elastic Modulus	NS	NS	NS	0.39 [#]	NS	NS	NS	-0.78 [#]	NS	NS	NS	NS
Max. Flexural Strength	0.23*	0.18*	0.20*	0.45 [#]	0.40 [#]	0.29*	0.48*	0.46 [#]	NS	NS	NS	0.15*

* $p<0.05$, [#] $p<0.001$, NS= not significant

SPECTRAL EVIDENCE FOR ASSOCIATION BETWEEN COLLAGEN DENATURATION AND BONE TOUGHNESS

¹Mustafa Unal, ¹Hyungjin Jung and ^{1,2,3}Ozan Akkus

¹Department of Mechanical and Aerospace Engineering

²Department of Orthopaedics

³Department of Biomedical Engineering

Case Western Reserve University, Cleveland, OH 44106, USA

email: ozan.akkus@case.edu, web: http://engineering.case.edu/groups/Akkus_Lab/

INTRODUCTION

Raman spectroscopy has become a powerful tool in the assessment of bone quality. However, the use of Raman spectroscopy to assess collagen quality is less established than mineral quality. The only specific spectroscopic biomarker for collagen quality in bone is the ratio of underlying sub-bands of amide I region ($1660/1690\text{ cm}^{-1}$) corresponding to enzymatic collagen cross-links [1]; however, the validation of this ratio is still controversial [2]. Toughness and post-yield toughness (PYT) of bone are mostly determined by collagen rather than the mineral phase. Therefore, it is essential to identify new spectroscopic biomarkers which help infer the status of collagen quality in bone and other collagen-rich tissues. The first aim of this work was to identify the regions of amide bands in collagen to determine new spectroscopic biomarkers which are sensitive to denaturation. The second aim was to assess whether there is an association between the new spectroscopic biomarkers and toughness of cortical bone.

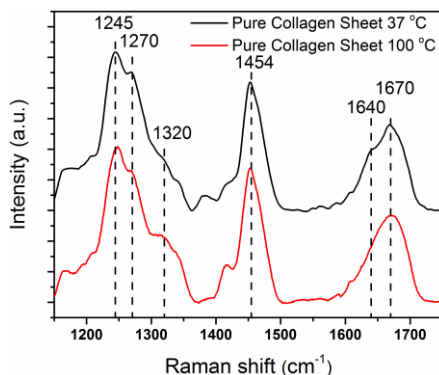


Figure 1: Changes in Raman peaks of pure collagen sheets due to the thermal denaturation.

MATERIALS AND METHODS

Sample set 1: Pure collagen sheets were prepared from bovine collagen type I solution at 37°C as the reference. Sheets were kept at 100°C for 2 h to induce thermal denaturation. *Sample set 2:* Cortical bone wafers from bovine femur with V-notch were used in thermal and mechanical denaturation experiments ($N=3$ in each experimental group). *Sample set 3:* Cortical beams for three-point bending test ($N=25$) were used to assess the correlation between toughness and new spectral biomarkers. Thermal denaturation of bones was attained by boiling the samples in water for ~ 90 min. Mechanical denaturation was attained by loading notched bone wafers using a miniaturized tensile loading device to induce an extensive damage zone at the notch tip [3].

Raman spectra of pure collagen sheets were collected at 10 randomly selected points using a 785 nm Raman system (Xplora, Horiba). Raman mapping of each cortical bone wafer was conducted before (control) and after the denaturation (thermal or mechanical) on the same area of the notched region to investigate changes in target spectroscopic ratios due to denaturation. On three-point bending specimens, an average of 12 Raman spectra was collected in the vicinity of the region where tensile fracture occurred. Three notched bone wafers were utilized as negative controls from which spectra were collected in a similar time frame with mechanically loaded specimens, but without any mechanical loading. Spectral ratios of experimental groups were compared using one-way ANOVA followed by Tukey's post-hoc test. Linear regression analyses were also performed between Raman

spectroscopic biomarkers and the mechanical properties. Statistical significance was set at $p < 0.05$

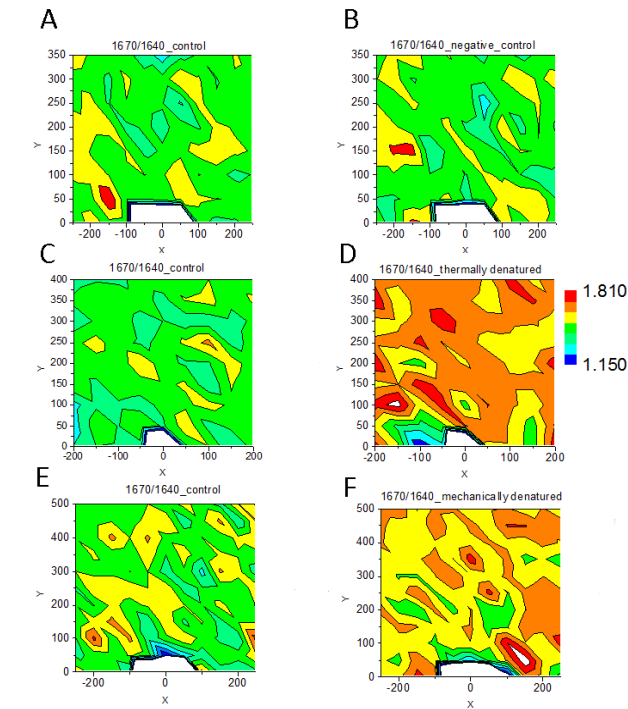


Figure 2: 2D Raman maps of bone wafers corresponding to 1670/1640 ratio. (A-C-E) Control samples before denaturation, and (B) negative control sample assessed secondarily without denaturation, (D) thermally and (F) mechanically denatured samples.

RESULTS AND DISCUSSION

Four intensity ratios were calculated using five peaks (Fig. 1) whose intensities were sensitive to thermal denaturation: 1670/1640, 1320/1454, 1245/1270 and 1245/1454. These ratios were significantly affected by thermal denaturation ($p < 0.001$ compared to pure collagen at 37 °C). Raman analysis of negative controls revealed that there were no significant differences in Raman spectral markers ($p > 0.05$) (Fig. 2A-B).

Table 1: R^2 pairwise correlations between mechanical Properties and Raman biomarkers

Linear Regression Analyses (R^2)	Raman Analysis			
	1670/1640	1245/1454	1245/1270	1320/1454
Toughness	0.38 $p < 0.001$	NS	NS	NS
PYT	0.54 $p < 0.001$	0.22 $p < 0.05$	NS	0.22 $p < 0.05$

NS = not significant

The results of thermal and mechanical denaturation experiments of cortical bone wafers showed that all these four ratios to be sensitive to both thermal and mechanical denaturation in cortical bone samples (Fig. 2C-F). The cumulative result showed the 1670/1640 peak intensity ratio as a novel biomarker to assess collagen quality (Table 1). The changes in this ratio with denaturation may reflect alterations in the collagen secondary structures, specifically a transition from ordered to unordered structure since the Raman study of collagen type I indicated that the peak at $\sim 1640\text{ cm}^{-1}$ is associated with ordered (triple helix or α -helix) structure whereas $\sim 1670\text{ cm}^{-1}$ is associated with random/unordered structure [4]. So far, the literature utilized the ratio of $\sim 1245/1454$ ratio based on FTIR studies. However, current results indicate that 1245/1454 ratio have a weak correlation with PYT and no correlation with toughness (Table 1).

CONCLUSIONS

To the best of our knowledge, the current work is among the first thorough analysis of the Raman amide bands in terms of providing spectroscopic manifestations of collagen integrity and bone toughness. These new spectral information can be used to understand the involvement of collagen quality in the fragility of aging and in diseased bone.

REFERENCES

1. Paschalis E. et al., *Journal of Bone and Mineral Research*;16: 1821-1828, 2001
2. Farlay D. et al., *PLoS One*;6: e28736, 2011
3. Sun X. et al., *Journal of Biomechanics*; 43: 1989-1996, 2010
4. Wisniewski M. et.al., *Journal of Photochemistry and Photobiology A: Chemistry*;188: 192-199, 2007

ACKNOWLEDGEMENTS

This research is partially supported by think[box] Student Research Fund at CWRU and NSF CMMI-1233413.

SHORTER HEELS ARE ASSOCIATED WITH STIFFER PLANTARFLEXOR TENDONS

Herman van Werkhoven, Daniel Lidstone, and Jeffrey M. McBride

Appalachian State University, Boone, NC, USA
email: vanwerkhovenh@appstate.edu

INTRODUCTION

The foot and ankle plays an important role in many activities. Understanding how foot and ankle anthropometry affect ankle musculoskeletal properties allows us to better understand the capabilities of the musculature to successfully perform motor tasks. Previous research have shown that ankle plantarflexor moment arm, or heel length as external estimate of plantarflexor moment arm, is negatively correlated with running economy [1]. Furthermore, it has been shown that sprinters have shorter plantarflexor moment arms compared to controls [2]. Results from these studies suggest that heel length influences the biomechanics associated with better performance in different tasks. Apart from the relationship between heel length and certain performance criteria, it is also reasonable to consider potential relationships between heel length and other musculoskeletal properties of the ankle muscles. Heel length affects the force transmitted by the plantarflexor muscles, as joint moment is a product of muscle force and muscle moment arm. The internal muscle-tendon unit (MTU) therefore experiences different forces dependent on properties associated with the heel length.

Recently, [3] showed that subjects with better running economy have shorter heels and that heel lengths were associated with an external measure of dynamic stiffness. In this study, stiffness was calculated by dividing peak force produced during a straight leg vertical jump by the distance covered during the jump. It is unclear whether a similar association exists between heel length and more direct measures of muscle-tendon unit stiffness. The purpose of this study was to investigate the relationship between heel length and tendon stiffness. We hypothesized that heel length would be negatively correlated with tendon stiffness.

METHODS

Ten healthy male subjects participated in this study. Subjects' height, weight and foot length was recorded. Photographic images were taken of their feet from which heel length (average horizontal distance from lateral and medial malleolus to back of heel), as well as first toe length were calculated.

Subject performed three isometric maximal voluntary contractions (MVC) while standing with a stationary rigid bar across their shoulders and their knees straight. The balls of the subjects' feet were placed on a wooden block and the block was situated on top of a force plate. Isometric maximal voluntary plantarflexor force (MVPF) was estimated by multiplying MVC ground reaction force by ankle gear ratio (forefoot length divided by heel length).

Tendon stiffness was estimated using the free oscillation method [4]. Subjects stood with a bar resting on their shoulders. The bar was able to rotate freely about an axis at the same height as the shoulders. Subjects were instructed to remain in a stationary position without moving as a medicine ball was dropped onto the bar on their shoulders. The impact caused measurable ground reaction force oscillation, similar to a spring-damper system experiencing damped oscillations. The medicine ball drop was repeated over several trials. Spring-damper model parameters were estimated using a least-square curve fitting method. System stiffness was converted to a single-leg MTU-specific tendon stiffness by taking ankle gear ratio into account.

Correlation analyses were performed between heel length and tendon stiffness, tendon stiffness and MVPF, as well as MVPF and other anthropometric measures.

RESULTS AND DISCUSSION

Results showed a significant negative correlation between heel length and tendon stiffness (Figure 1, $r = -0.76$, $p = 0.011$). Tendon stiffness was positively correlated with MVPF (Figure 2, $r = 0.75$, $p = 0.012$). MVPF was not significantly correlated with any of the other anthropometric measures (Table 1)

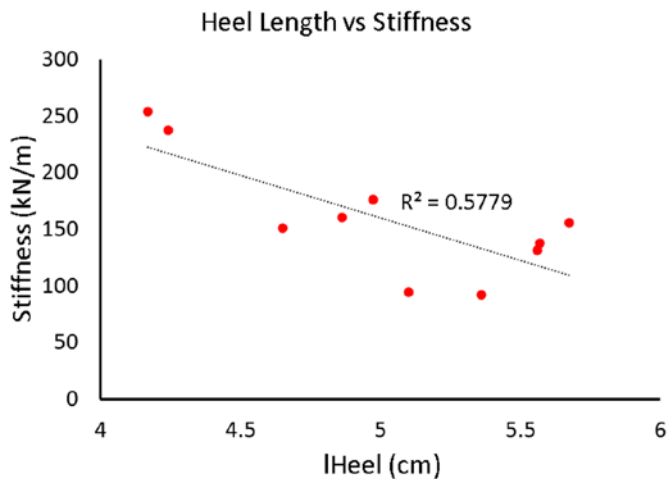


Figure 1: Heel length vs. tendon stiffness. A significant negative correlation was observed.

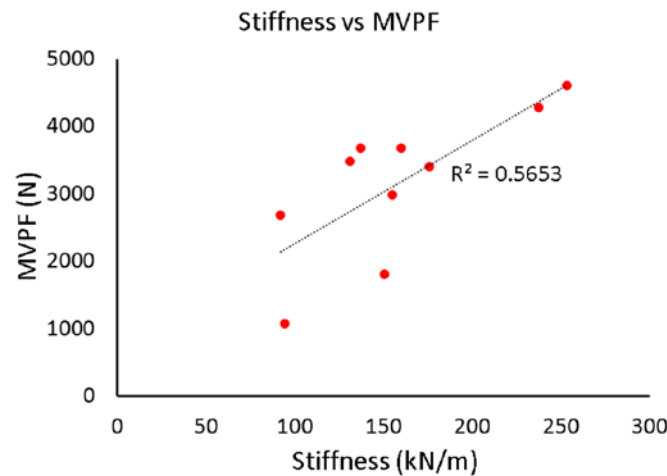


Figure 2: Tendon stiffness vs MVPF. A significant positive correlation was observed ($p < 0.05$).

Previous research have shown the potential link between tendon stiffness and force production, as sprinters appear to have stiffer tendons [5]. The researchers hypothesized that that larger forces might cause adaptations to the tendon allowing it to perform at lower strain values for a given force, reducing the risk of tendon damage [5]. For a specified joint moment related to a given task,

Table 1: Correlations between MVPF and anthropometric measures – no significant correlations

measure	r	p-value
body mass	0.24	0.50
height	0.33	0.35
toe length	0.13	0.72
heel length	-0.32	0.37

shorter heels would also cause larger plantarflexor forces. It could be expected that the tendon adaptations that would occur due to higher forces might similarly reduce the likelihood of tendon damage. A potential link between heel length and tendon damage should be further investigated. Previous studies have shown that more efficient distance runners have shorter heels [1], which given the current findings suggests stiffer tendons. It has also been suggested that muscle stiffness is associated with better running economy [6].

Further analysis of muscle and tendon stiffness, potentially using more direct stiffness measures, such as the ultrasound technique, could give further insight into the relationship between MTU stiffness and anthropometric measures, and their association with performance and injury.

REFERENCES

1. Scholz MN, et al. *J Exp Biol* **211**, 3266-3271, 2008.
2. Baxter JR, et al. *P R Soc B* **279**, 2018-2024, 2012.
3. Barnes KR, et al. *JSCR* **85**, 1289-1297, 2014.
4. Fukashiro S, et al. *Acta Physiol Scand* **172**, 241-248, 2001
5. Arampatzis A, et al. *J Biomech* **40** 1946-1952, 2007
6. Dumke CL, et al. *Int J Sports Physiol Perform* **5** 249-261, 2010

ACKNOWLEDGEMENTS

We would like to acknowledge the following lab members for their significant contribution during data collections: Caitlin Gallagher, Jackson Faught, Zachary Howell, Michael Moore.

RELATIONSHIP BETWEEN ACL GRAFT GEOMETRY AND TIBIOFEMORAL KINEMATICS

¹Michael F. Vignos, ¹Jarred Kaiser, ¹Geoffrey S. Baer, ¹Richard Kijowski, ¹Darryl G. Thelen,

¹The University of Wisconsin-Madison, Madison, WI, USA
email: mvignos@wisc.edu, web: <http://uwnmbi.engr.wisc.edu/>

INTRODUCTION

ACL reconstruction (ACL-r) surgeries are normally successful at restoring knee stability. However, >50% of reconstructed knees exhibit osteoarthritis at long-term follow-up [1]. One theory is that ACL-r is unable to restore normal knee mechanics, resulting in abnormal cartilage loading that leads to tissue degeneration [2]. Indeed, studies have shown bilateral differences in ACL-r knee kinematics, with greater external tibia rotation and progressive anterior tibia translation observed in downhill running [3]. It is important to assess how ACL graft placement may contribute to such asymmetries.

Studies investigating the relationship between graft geometry and knee mechanics have taken two main approaches. The first approach is cadaveric studies. One such study found that anterior femoral attachment location was correlated with anterior tibia translation [4]. However, cadaver studies are inherently limited by an inability to consider functional loading scenarios. A second approach is to bilaterally compare joint level mechanics in ACL-r subjects during locomotion. With this approach, Scanlan et al. found that ACL graft orientation in the frontal plane was negatively correlated with the knee extensor moment [5]. However, the net knee moment is inherently influenced by many factors including knee structure, neuromuscular coordination and movement patterns. Hence, it may be preferable to study links between ACL-r geometry and knee kinematics using simpler tasks.

In this study, we used static and dynamic MR imaging to investigate the relationship between ACL-r graft geometry and tibiofemoral kinematics during an isolated knee flexion-extension task. We hypothesized that graft orientation would be the best predictor of bilateral differences in anterior tibia translation and external rotation.

METHODS

We tested eight subjects that underwent a primary unilateral, isolated ACL-r (4 F, 25.8±4.9 yrs, 86.3±18.2 kg, 2.3±0.6 yrs post-surgery, 5 patellar tendon grafts, 1 partial lateral meniscectomy). Bilateral MR images of the knee were collected using a 3D SPGR sequence (0.37x0.37x0.90 mm resolution) and a 3D FSE Cube sequence (0.31 mm isotropic resolution). We manually segmented femur, tibia, and ACL geometries for both the reconstructed and contralateral knees. We then measured the area and location of the ACL attachments, and the orientation of the ACL relative to the tibia plateau in the sagittal and frontal planes (Fig 1). We computed the bilateral difference for each metric by subtracting the contralateral value from the reconstructed.

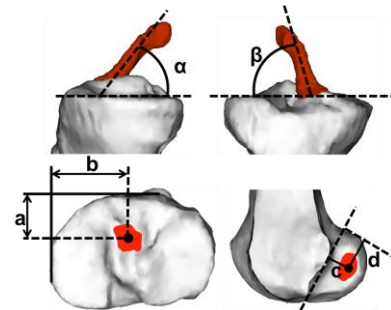


Figure 1: Geometry measurements shown on a representative non-ACL-r knee. (α) Sagittal plane angle, (β) frontal plane angle, (a) anterior-posterior and (b) medial-lateral tibia attachment, and (c) anterior-posterior and (d) cranio-caudal femur attachment.

Each subject then lied supine in the MR scanner with their lower leg secured to a loading device. Subjects performed cyclic knee flexion against an inertial load at 0.5 Hz, which induced quadriceps loading with knee flexion. Subjects continuously performed this task for 5 min. while SPGR-VIPR images were collected for both knees [6].

Six degree of freedom tibiofemoral kinematics were measured using model-based tracking [6]. The metrics computed were the tibiofemoral translations

and rotations at peak flexion angle, as well as translation and rotation ranges over a motion cycle. Bilateral differences in kinematic metrics were computed for each subject. We then computed the correlation between the bilateral difference in ACL geometry metrics and the bilateral difference in kinematic metrics. Significance was set at $p < 0.05$.

RESULTS AND DISCUSSION

We found that bilateral differences in kinematics were most significantly correlated to differences in the sagittal plane ACL orientation (Table 1). At peak knee flexion, an increase in the sagittal plane ACL orientation was positively correlated with anterior and medial tibia translation and internal tibia rotation. Sagittal plane orientation was also correlated with internal tibia rotation range of motion over a motion cycle (Fig 2). These results suggest that an ACL graft that is oriented more vertically than the native ACL may be associated with greater anterior-posterior and rotational laxity, such that the quadriceps induce greater anterior tibia translation and internal rotation with contraction.

We also found that bilateral differences in the femoral attachment area was negatively correlated with anterior tibia translation and internal tibia rotation. A bigger femoral footprint may reflect a larger graft cross-section, and hence greater resistance to anterior tibia translation and rotation.

The initial results in this study suggest that ACL geometry may be predictive of knee kinematic behavior under simple *in vivo* loading conditions. However, increased subject numbers are needed to

assess the robustness of the relationships observed. Further analysis is also needed to consider potential multifactorial interactions between graft types, geometry metrics and kinematics.

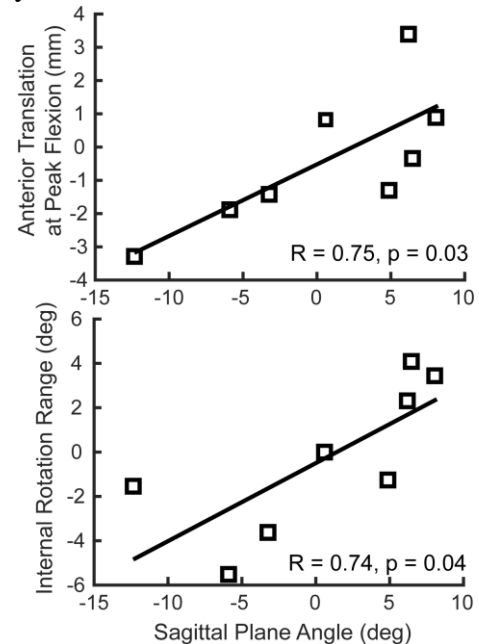


Figure 2: Correlations between bilateral differences in anterior translation at peak flexion and internal rotation range with differences in sagittal plane angle.

REFERENCES

- [1] Linden, M et al. *Arthroscopy* **24**: 10, 2008.
- [2] Andriacchi, TP et al. *Ann Biomed Eng* **32**:11, 2004
- [3] Tashman, S et al. *Am J Sports Med*, **32**:4, 2004
- [4] Zavras, TD et al. *Knee Surg, Sports Traumatol, Arthro* **13**:2, 2005
- [5] Scanlan, SF et al. *Am J Sports Med* **37**:11, 2009
- [6] Kaiser, J et al. *MRM* **7**, 2013.

ACKNOWLEDGEMENTS

Oliver Wieben, Arezu Monawer, Kelli Hellenbrand, NIH EB015410 and AR06273

Table 1: Correlations between bilateral differences in ACL geometry and knee kinematics. Correlation coefficients (R) given only for significant correlations ($p < 0.05$). Adduction angle and superior translation at peak flexion and lateral and anterior translation range were not significantly correlated with any geometry metrics. Labels (a, b, etc.) are from Fig 1.

		Tibia Attachment Geometry			Femur Attachment Geometry			Angles Relative to Tibia	
		Area	AP Distance (a)	ML Distance (b)	Area	AP Distance (c)	CC Distance (d)	Sagittal Plane (α)	Frontal Plane (β)
Values at Peak Flexion	Internal Rotation				R = -0.78			R = 0.78	
	Medial Translation							R = 0.84	
	Anterior Translation				R = -0.79		R = -0.76	R = 0.75	
Ranges	Adduction					R = 0.71	R = 0.76		
	Internal Rotation							R = 0.74	
	Superior Translation		R = -0.80	R = 0.83					

BICEPS BRACHII AND BRACHIALIS CROSS-SECTIONAL AREAS ARE MAJOR DETERMINANTS OF MUSCLE MOMENT ARMS

¹ Andrew D. Vigotsky and ² Bret Contreras

¹ Arizona State University, Phoenix, AZ, USA

² Auckland University of Technology, Auckland, New Zealand
email: avigotsk@asu.edu

INTRODUCTION

Changes in strength are often attributed to changes in muscle morphology and architecture [1-4], in addition to neural adaptations [5]. However, changes in muscle moment arm (MA) as a result of hypertrophy are less described. Sugisaki, et al. [6], Akagi, et al. [7], and Akagi, et al. [8] described the positive correlation between muscle cross-sectional area (CSA) and muscle MA, and Sugisaki, et al. [9] noted a small increase in triceps brachii moment arm following hypertrophy. Therefore, the purpose of this paper is to develop a two-dimensional mathematical model to describe how changes in muscle architecture of the biceps brachii (BIC) and brachialis (BRA) may influence the MA of each muscle.

METHODS

A position-elbow flexor anatomical CSA (ACSA) hyperbolic cosine regression equation was extrapolated from West, et al. [10], wherein an MRI was taken with the elbow in extension and a neutral radioulnar joint position.

The radius of the proximal elbow flexors was assumed to be the average of the muscle group's force vector field. A coefficient was applied to all equations to represent the degree of hypertrophy (or atrophy) from baseline, which assumes uniform growth.

A tangent line was calculated to represent the distal BIC and BRA tendons, which originated from the distal-most section of each muscle belly. Because the original hyperbolic cosine regression equation was representative of both the BIC and BRA, it was

assumed that both muscles had equal ACSAs, and that the BIC lay directly superficial to the BRA. Previous research has described the similar sizes of the BIC and BRA [3].

The muscle belly of the BIC was set to begin 1.1 cm proximal to the joint center in order to control for insertion point, which was fixed 4.51 cm distal to the axis of rotation (capitulum). This was assumed to be about where the center of the insertion site is, as the capitulum has a 10.6 mm radius [11], the bicipital tuberosity is 25 mm distal from the radial head, and the insertion site is 22 mm long [12].

The muscle belly of the BRA was set to begin 0.69 cm proximal to the joint center in order to control for insertion point, which was fixed 3.17 cm distal to the axis of rotation (trochlea). Like the BIC, it was assumed that this was the center of the insertion site, as the trochlea has a 7.5 mm radius [13], the coronoid process is about 11.0 mm from the trochlea, and the insertion site is about 26.3 mm long [14].

The joint center of the elbow was represented by the origin (0,0), and the perpendicular distance from the tendon to the joint center was then calculated as the MA.

RESULTS AND DISCUSSION

The hyperbolic cosine regression equation showed a strong correlation with the length-ACSA relationship described by West, et al. [10] ($p < 0.001$; $r = 0.911$). The calculated MAs of the BIC and BRA were within previously reported ranges [15] (Figure 1).

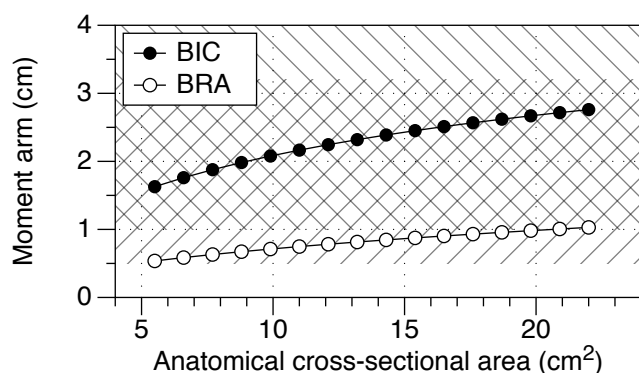


Figure 1: Relationship between biceps brachii anatomical cross-sectional area and muscle moment arm. Negatively sloped lines are normal BIC MAs, and positively sloped lines are normal BRA MAs [15].

To the authors' knowledge, this is the first model to describe the effects of muscle hypertrophy on MA length, which demonstrated remarkable changes in MA of the BIC and BRA with increases in ACSA. Previous research has only attributed increases in torque production to the effects of hypertrophy on muscle force [2, 3], while ignoring potential changes in MA, as described by our model.

Intuitively, this change in MA is a function of the change in insertion angle, as the insertion point cannot shift. This increase in insertion angle occurs when the size of the muscle belly increases, thus shifting the muscle's resultant vector further from the humerus and joint center (Figure 2).

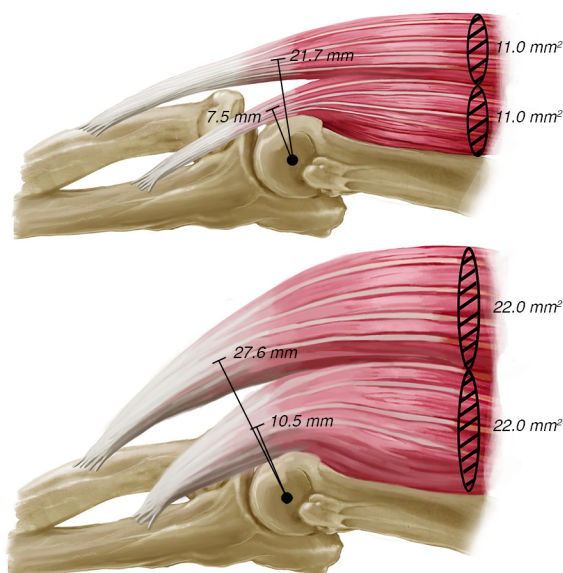


Figure 2: Illustration of the changes in BIC and BRA MAs with increases in ACSA.

The modeled change in MA is proportional to the square root of the change in ACSA ($\Delta MA \propto \sqrt{\Delta ACSA}$). Coincidentally, a similar relationship was observed by Sugisaki, et al. [9], wherein a 33.6% increase in triceps brachii ACSA was accompanied by a 5.5% increase in MA, although the authors did not note this mathematical relationship. More training studies are warranted to examine both the validity of this model and the hypothesis that changes in BIC and BRA MAs are proportional to the square root of changes in ACSA.

REFERENCES

1. Kawakami, et al., *Eur J Appl Physiol Occup Physiol.* **72(1-2)**, 37-43, 1994.
2. Aagaard, et al., *J Physiol.* **534(Pt. 2)**, 613-623, 2001.
3. Erskine, et al., *Eur J Appl Physiol.* **114(6)**, 1239-1249, 2014.
4. Seynnes, et al., *J Appl Physiol.* **102(1)**, 368-373, 2006.
5. Behm, *J Strength Cond Res.* **9(4)**, 264-274, 1995.
6. Sugisaki, et al., *J Biomech*, 2010.
7. Akagi, et al., *J Appl Biomech.* **28(1)**, 63-69, 2012.
8. Akagi, et al., *J Appl Biomech.* **30(1)**, 134-139, 2014.
9. Sugisaki, et al., *J Appl Biomech*, 2014.
10. West, et al., *J Appl Physiol.* **108**, 2009.
11. Shiba, et al., *J Orthop Res.* **6(6)**, 897-906, 1987.
12. Mazzocca, et al., *J Shoulder Elbow Surg.* **16(1)**, 122-127, 2006.
13. Murray, et al., *J Biomech.* **35(1)**, 19-26, 2002.
14. Cage, et al., *Clin Orthop Relat Res*(**320**), 154-8, 1995.
15. Ramsay, et al., *J Biomech.* **42(4)**, 463-473, 2009.

ACKNOWLEDGEMENTS

We would like to thank Dr. Stu Phillips for providing the position-CSA data necessary to complete this model, and Dr. Silvia Blemker for reviewing and critiquing our model.

EFFECT OF SCAPULAR MISALIGNMENT DURING SETUP ON STABILITY OF THE SHOULDER

¹⁻³Piyush Walia, ⁴Ronak M. Patel, ²Lionel Gottschalk; ²Matthew Kuklis, ²Morgan H. Jones, ⁵Stephen D. Fening, and ²Anthony Miniaci

¹Cleveland State University, Cleveland, OH, USA

²Cleveland Clinic, Cleveland, OH, USA

³Summa Health System, Akron, OH, USA

⁴Illinois Bone and Joint Institute, Morton Grove, Illinois, USA

⁵Case Western Reserve University, Cleveland, OH, USA

email: nonupiyush@gmail.com

INTRODUCTION

Multidirectional instability can result due to multiple factors like the increased retroversion, a hypoplastic posteroinferior rim, and decreased scapular abduction during arm elevation [1]. Biomechanical studies are often used to understand the changes in the shoulder biomechanics [1-4]. During a biomechanical study setup misalignment of the scapula can occur leading to anterior or posterior tilt, which is rotation around the glenoid height (superior-inferior axis) as shown in Figure 1. In past only one study has investigated the effect of scapular inclination [1-4]. However, to our knowledge there is no other study that has evaluated the influence of scapular misalignment/tilt. This study aimed to understand the relationship between glenoid tilt/misalignment and glenohumeral joint stability. We hypothesized that the shoulder stability would not change with variation in very small variations of glenoid tilt.

METHODS

Eight fresh-frozen cadaveric specimens were tested using a custom dislocation simulator. The specimens were thawed overnight and dissected before experimentation. All experiments were performed at glenohumeral abduction angle of 60° and 0° external rotation. After potting the scapula in a rectangular box, a line was drawn on glenoid from superior to inferior aspect of the glenoid. This line represented the height of the glenoid and was determined by using circumferences. After the glenoid superior-inferior aspect was aligned parallel to the Y-axis of the simulator, it

was then verified using a microscribe digitizer. However, the accuracy of a microscribe is 0.3mm, so we chose a 3° tilt for both anterior (red) and posterior (blue), because it represented three standard deviation of the error (“d”) that can occur as shown in Figure 1.

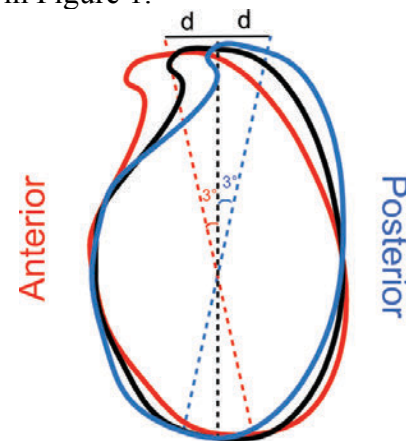


Figure 1: Different orientations of the glenoid fossa tilt, black shows the normal tilt at 0°, red glenoid shows the 3° anterior tilt, and the blue glenoid is the 3° posterior tilt evaluated in this study, d represents the two st.dev of error that occurred on each side.

Distance to dislocation and stability ratio was the primary measurement for every trial. Each experiment comprised of translating the glenoid in a posterior direction to cause an anterior dislocation. Firstly, experiment was performed in the right orientation verified by a microscribe shown as black. Then, both an anterior or posterior tilt was performed at 3° in a randomized manner. A centering medial load of 50N was applied on the humeral head, which was kept constant throughout each trial. This compressive load simulated the

static load of soft tissue that was removed for this study. Translational distance of the glenoid and medial-lateral displacement of the humeral head, along with horizontal reaction force were recorded for every trial. Repeated measures analysis of variance (ANOVA) was performed with statistical significance set at $p < 0.05$.

RESULTS AND DISCUSSION

The distance to dislocation for each specimen was determined as the point at which the tangential reaction force was zero. The distance to dislocation was similar at all three orientations. The results from ANOVA showed no effect on distance to dislocation for change in glenoid orientation (Table I). Similarly, the results for reaction force and stability ratio had same mean values. The stability ratio for normal, 3° anterior, and 3° posterior tilt were 0.25 ± 0.07 , 0.24 ± 0.07 , and 0.25 ± 0.07 , respectively. Change in tilt or glenoid orientation mismatch did not affect any measured variable.

To our knowledge no study has evaluated the effect of glenoid tilt. The present study demonstrated that the small mismatch in the glenoid alignment (tilt) did not affect the shoulder stability in terms of both

translation and stability ratio. These findings were in agreement with our hypothesis. This study examined the sensitivity of the scapula alignment during potting process for a biomechanical experiment. In conclusion, a digitizer device like microscribe can be used to verify the scapula potting.

CONCLUSIONS

This study demonstrated that very small variation in glenoid tilt does not affect the stability of shoulder.

REFERENCES

1. Kikuchi K et al. J Orthop Sci (2008) 13:72–77.
2. Kaar SG et al. Am J Sports Med 2010;38:594-9.
3. Itoi E et al. J Bone Joint Surg Am 2000;82:35-46.
4. Yamamoto et al. Am J Sports Med, Vol. 37, No. 5, 2009.

ACKNOWLEDGEMENTS

Authors acknowledge the funding from NFL Charities and Cleveland Clinic Research Program Grant.

Table 1: Changes in distance to dislocation, reaction force, and stability ratio for different glenoid orientations (mean and standard deviation).

Tilt Orientation	Distance to Dislocation (mm)	Force (N)	Stability Ratio (Force/50)
3° Anterior	10.98 ± 2.12	11.89 ± 3.44	0.24 ± 0.07
0° Normal	11.36 ± 2.16	12.47 ± 3.45	0.25 ± 0.07
3° Posterior	11.09 ± 2.20	12.42 ± 3.73	0.25 ± 0.07
p-value	0.937	0.936	0.937

MINIMAL EFFECT OF COMPRESSIVE LOADING ON THE GLENOHUMERAL JOINT STABILITY RATIO

¹⁻³Piyush Walia, ⁴Ronak M. Patel, ²Lionel Gottschalk; ²Matthew Kuklis, ²Morgan H. Jones, ⁵Stephen D. Fening, and ²Anthony Miniaci

¹Cleveland State University, Cleveland, OH, USA

²Cleveland Clinic, Cleveland, OH, USA

³Summa Health System, Akron, OH, USA

⁴Illinois Bone and Joint Institute, Morton Grove, Illinois, USA

⁵Case Western Reserve University, Cleveland, OH, USA

email: nonupiyush@gmail.com

INTRODUCTION

Anterior dislocation accounts for approximately 98% of all shoulder dislocations [1]. Most common pathologies associated with shoulder dysfunction include rotator cuff tears, labral tears, and bony pathology [2]. Many biomechanical studies and computational studies are often conducted to investigate the changes in shoulder instability due to either bone defects or surgical repair [3-6]. Many cadaveric studies of shoulder instability use stability ratio (peak horizontal force/compressive load) as an outcome measure [4-7]. It is critical for readers to compare and understand results among different studies. However, many of these studies used different axial load for the compressive force [3-7]. This variation in compressive load sometimes poses a challenge to compare force or stability ratio results across past studies. The aim of the present study was to investigate if the stability ratio changes with variation of compressive force. We hypothesized that the shoulder stability ratio would not be affected with increasing compressive force.

METHODS

Eighteen fresh-frozen cadaveric specimens were tested using our custom dislocation simulator. The specimens were thawed overnight and dissected before experimentation. All experiments were performed at glenohumeral abduction angle (ABD) of 60° and 0° external rotation (ER). Each experiment comprised of translating the glenoid in a posterior direction in order to perform an anterior dislocation. Four different medial loads of 50N,

100N, 150, and 200N were applied on the humeral head and were kept constant throughout the trial. These forces were randomized for each specimen. This compressive load simulated the static load of soft tissue that was removed for this study. Translational distance of the glenoid and medial-lateral displacement of the humeral head, along with horizontal (tangential) reaction force were recorded for every trial. Stability ratio is calculated as the ratio of horizontal reaction force to compressive load. Every specimen was tested in an intact condition. One-way repeated measures analysis of variance ANOVA was performed at a significance level of $p < 0.05$ along with post-hoc Tukey HSD test.

RESULTS AND DISCUSSION

The relationship between the compressive force and stability ratio for all shoulders is shown in Figure 1. The repeated measures ANOVA revealed that the force had a significant effect on the stability ratio ($p < 0.001$). Stability ratio decreased significantly for 150N ($p < 0.05$) force and 200N force ($p < 0.05$). The average slope obtained from linear regression for all specimens was -0.00017 ± 0.00017 . R square value for the fit was 0.57.

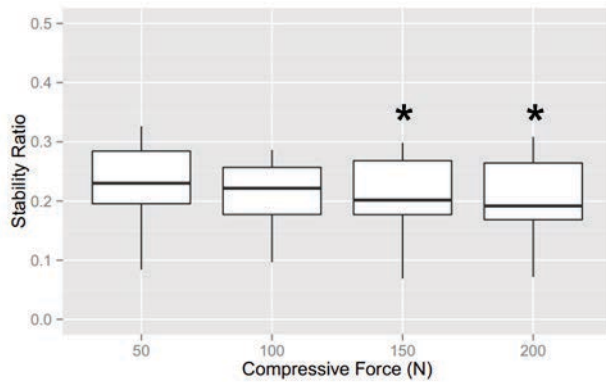


Figure 1: Relationship of stability ratio and compressive force for four different loading cases (50N, 100N, 150N, and 200N), * signifies significant difference from 50N with $p < 0.05$.

This is the first study to show the effect of different compressive loading on the stability ratio of the glenohumeral joint. The important finding of the present study is that the increasing compressive force after 100N leads to significantly reduced values of the stability ratio. Lippitt et al. [7] also showed the decrease in stability ratio in their study, even though these authors were measuring the effect of concavity depth in their study. This decrease in stability ratio shows that stability is reduced in terms of concavity compression after the compressive force surpass 100 N; however the decrease is so small that it should not cause any instability. Moreover, it will be a safe assumption to compare the results for stability ratio across different studies, if the compressive force used in those study were between the ranges of 50-200N.

CONCLUSIONS

The results from this study establishes that the effect of compressive force is minimal on stability ratio, however the stability ratio decreases contrary to the assumption of increasing stability with increasing force.

REFERENCES

1. Camarinos J et al. J Man Manip Ther. 2009; 17(4): 206–215.
2. Burkhart SS, De Beer JF. Arthroscopy 2000;16: 677-94.
3. Kaar SG et al. Am J Sports Med 2010;38:594-9.
4. Itoi E et al. J Bone Joint Surg Am 2000;82:35-46.
5. Yamamoto et al. Am J Sports Med, Vol. 37, No. 5, 2009.
6. Sekiya JK et al. Am J Sports Med. 2009; Vol. 37, No. 12:2459-2466.
7. Lippitt SB et al. J Shoulder Elbow Surg. 1993 Jan;2(1):27-35.

ACKNOWLEDGEMENTS

Authors acknowledge the funding from NFL Charities and Cleveland Clinic Research Program Grant.

Effect of Musculoskeletal Model Choice on Muscle Activations During Landing, Running, and Lateral Cutting

Kevin C. Fontenot, Stacie I. Ringleb, and Joshua T. Weinhandl
email: jweinhan@odu.edu

INTRODUCTION

OpenSim is a platform for analyzing and understanding the effects of human locomotion mechanics through musculoskeletal modeling [1]. The three musculotendon models implemented in OpenSim 3.1 are the Thelen2003 (THE) [2], Millard Acceleration (ACC), and Millard Equilibrium (EQU) [3] models. The Hill-type model was used as the foundation for the models; however, each model utilizes a different approach for computing outputs. It remains unclear how predicted model activations between models vary for different tasks (i.e. landing, cutting, etc...). It is important to provide validation of models during tasks via surface electromyography (sEMG). The purpose of this study was to compare THE, ACC, and EQU musculotendon model activations to sEMG for landing, running, and lateral cutting. It was hypothesized that the Millard EQU model would be the best predictor of sEMG excitations and that the ability for all models to predict muscle excitation would decrease with task complexity.

METHODS

One healthy female (age 19 yr, height 1.63 m, and mass 65.08 kg) volunteered to participate. Data were collected synchronously using an 8 camera Vicon (Oxford Metrics, Oxford, England) motion analysis system (200 Hz), Bertec (Bertec Corporation, Columbus, Ohio) force plate (2000 Hz), and 7 Delsys (Delsys Incorporated, Natick, Maryland) surface electrodes (2000 Hz). Retro-reflective markers were placed bilaterally on anatomical landmarks [4], sEMG electrodes were placed on the vastus lateralis (VL), rectus femoris (RF), vastus medialis (VM), lateral and medial hamstrings (LH and MH respectively), medial gastrocnemius (MG), and tibialis anterior (TA). Electrode placements were confirmed by inspecting muscle excitations while conducting manual muscle tests.

For a single leg landing task the subject was instructed to cross their arms and fall from a box equivalent to their maximum jumping height, land with the dominant leg, return to an upright stance, and hold the landing for approximately one second. Running consisted of moving in a straight line at a speed of 4.5 ± 0.2 m/s. The lateral cutting maneuver required the subject to run in a straight line at a speed of 4.5 ± 0.2 m/s, plant the dominant foot on the force plate, and cut at a 45° angle. Five successful trials were completed for all tasks.

Kinematic and kinetic data were output using Visual 3D (v5.00, C-Motion Incorporated, Rockville, MD). Custom MatLab (MATLAB, Natick, MA) software was used to determine the initial weighting factors for each trial prior to input into a residual reduction algorithm (RRA) [4]. Kinematic and kinetic RMS residuals from RRA were compared to acceptable ranges as suggested by OpenSim before input into computed muscle control (CMC). A modified gait2392 model was utilized. Each model was implemented in CMC for every trial of each task to obtain muscle activations.

Model activations and sEMG excitations were time normalized to 101 data points defined as initial contact to maximum knee flexion for single leg landing and initial contact to toe off for running and lateral cutting. Activation and excitation data were normalized to the peak value of all trials for the respective task and averaged. Root-mean-squared difference (RMSD) was calculated between sEMG excitations and the OpenSim output activations.

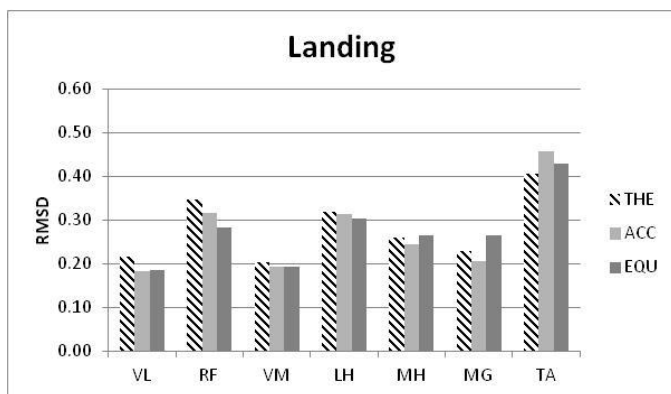


Figure 1: RMSD values of the muscles for THE, ACC, and EQU during a single leg landing.

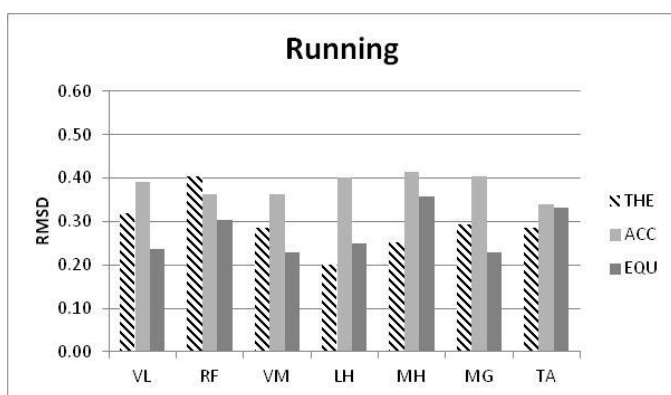


Figure 2: RMSD values of the muscles for THE, ACC, and EQU for running.

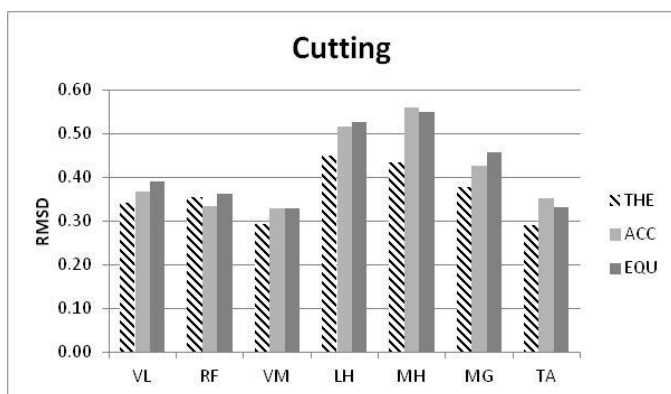


Figure 3: RMSD values of the muscles for THE, ACC, and EQU for lateral cutting.

RESULTS AND DISCUSSION

Model activations followed sEMG excitation patterns during all tasks for all models. During a single leg landing RMSD is lowest ($\text{RMSD} \leq 0.26$)

in the VL, VM, MH, and MG (Figure 1). The ACC model displayed the greatest RMSD values for all muscles except the RF when running (Figure 2). During lateral cutting THE model displayed the lowest RMSD values for all muscles except the RF (Figure 3).

The purpose of the study was to compare the THE, EQU, and ACC musculotendon models; included in OpenSim, to sEMG during a single leg landing, running, and lateral cutting. Although model activations followed sEMG excitation patterns, THE model consistently produced lower RMSD values. An increase in task complexity did correspond to an increase in RMSD values for all models.

Limitations to the study include sample size. One subject was utilized and the study could be stronger with the incorporation of a more diverse population. The use of a one degree of freedom knee reduced model ability to accurately predict muscle activation. A three degree of freedom knee may better predict sEMG [5]. Tasks in the current study were anticipated resulting in pre-excitation. Constraining model activations to sEMG initial contact excitation may increase model accuracy.

Increasing task dynamics reduces model ability to predict sEMG excitation. THE displayed activation patterns which followed sEMG excitation with a lower RMSD than EQU and ACC models. Future research should consider constraining initial contact activation and incorporating a three degree of freedom knee. It is also strongly suggested that model type be reported in order to better understand how different models predict excitation patterns.

REFERENCES

1. Delp et al. *IEEE Trans Biomed Eng* **54**:1940-50, 2007.
2. Thelen et al. *J Biomech* **36**:321-8, 2003.
3. Millard et al. *J Biomech Eng*, 135, 2013.
4. Weinhandl et al. *Clin Biomech* **28**:655-63, 2013.
5. Mokhtarzadeh et al. *J Biomech*, **46**:1913-20, 2013.

The Effects of Squat Depth on Right Leg Kinematics and Kinetics

Zachary A. Sievert, Stacie I. Ringleb, Laura C. Hill & Joshua T. Weinhandl

Old Dominion University, Norfolk, VA, USA
email: zsiev001@odu.edu

INTRODUCTION

The need to increase lower extremity power, strength and coordination can be found in many resistance training programs from Olympic athletes to the everyday exercise enthusiast. Traditionally the squat exercise is performed at four different depths: 45° of knee flexion (partial), 90° of knee flexion (normal), thighs parallel to the floor (parallel), and >120° of knee flexion (deep) [1]. There is a debate in the literature with regards to the optimal knee flexion angle during the squat exercise and how much loading is placed on the lower extremity throughout the various knee angles [1,2,3]. To help determine the optimal knee angle, the effect of squat depth on joint kinematics, moments, muscle activations, and ligamentous loading should be investigated. First, the kinetic and kinematic parameters of the squat exercise at various squat depths should be analyzed.

It is imperative to examine the differences in three dimensional joint kinetics and kinematics between normal and deep squats at bodyweight (BW), 50% one repetition maximum (1RM) and 80% 1RM. It was hypothesized that there would be significant increases in three dimensional peak joint moments about the right knee, hip and ankle during deep squats compared to the normal squats. This study had three hypotheses: 1) there would be significant increases in three dimensional joint moments about the right knee, hip and ankle as load increased; 2) there would be increases in all joint angles during deep squats compared to normal squats; and 3) as external load increased all joint angles would increase as well.

METHODS

Seventeen individuals participated in this study (age: 22.8±1.88 yrs, height: 1.69±0.06 m, mass: 73.5±12.72 kg). All participants were recreationally active, free of injury within the last six months and had no history of lower extremity surgery. Prior to data collection, participants provided written informed consent in accordance with institutional guidelines. The study was conducted over two testing days separated by no more than seven days in-between. On the first day of testing subjects reported to the laboratory for 1 repetition maximum (1 RM) [4].

On the second day of testing, the participants wore spandex shorts, a sports bra or form fitting shirt if applicable, and lab shoes. Eighteen retro reflective markers were placed bilaterally on anatomical landmarks [5]. Once the anatomical markers were placed on the skin, tracking plates with four markers were attached to the back, pelvis, bilateral thighs, shanks and shoes via elastic Velcro straps (McDavid, Woodridge, IL, USA). Three-dimensional marker coordinate data were collected at 200 Hz using an eight-camera motion analysis system (Vicon, Centennial, CO). All force data were collected at 2000 Hz using two Bertec force plates (Bertec Co., Columbus, OH).

When the participant was adequately warmed up they performed normal squats (90 ±10 °) with zero load (NBW), as well as at 50% 1RM (N50), 80% 1RM (N80). They also performed deep squats (120±10 °) with the same loads (DBW, D50, D80). Five repetitions were performed for each condition with 2-4 minutes of rest between conditions. The order of squat condition, normal and deep squats, was counterbalanced between participants. The order of loads, however, was the same for each participant.

Once all data were collected, a kinematic model was created in Visual 3D (v5.00, C-Motion Inc., Rockville, MD) for each participant from the standing calibration trial that consisted of eight segments: a trunk, pelvis, right and left thigh, right and left shank and right and left feet [5]. Marker data and ground reaction force data were filtered with a low-pass fourth order Butterworth zero lag filter with 12 Hz and 50 Hz cut off frequencies, respectively. 3D ankle, knee, and hip angles were calculated using a joint coordinate system approach [6]. After joint angles were estimated three-dimensional joint kinetics were calculated using a Newton-Euler approach [7] with body segment parameters estimated from De Leva (1996) and reported in the distal segment reference frame [8].

To analyze the data, separate two by three (condition (normal and deep) by load (BW, 50%, and 80%)) repeated measures ANOVA were conducted for each of the dependent variables. If two-way interactions were found, *post hoc* pairwise comparisons were conducted with a Bonferroni correction. Significance for all statistical analyses was set at $p < 0.05$.

RESULTS AND DISCUSSION

A weight*condition significant interaction was identified for knee internal rotation angle ($p=0.05$) (Table 2). Post hoc analyses revealed significant differences between NBW-DBW, N50-D50, and N80-D80 ($p<0.001$). No other joint angle had significant interaction of weight*condition. The only significant main effect for weight was observed in knee adduction angle ($p<0.001$), as weight increased knee adduction angle increased. It was also found that there was a significant main effect for condition across all joint angles.

A significant interaction was identified for peak hip extension moment ($p=0.001$) in which post hoc analyses revealed that all load and depth combinations were significantly different ($p<0.001$) (Figure 1). A significant interaction was identified for peak knee extension moment ($p=0.043$). All load and depth combinations were significantly different ($p\leq 0.003$) except for the NBW-DBW, N50-D50 comparisons. Significant main effects for weight and condition were identified for peak hip external rotation, knee external rotation, and plantarflexion moments ($p\leq 0.001$). Knee adduction moments were shown to have a main effect for the condition ($p=0.001$) but not for weight ($p=0.080$).

With regard to joint kinetics, hip extension moments were significantly different at each condition. The increased hip extension moments between normal and deep squat agrees with previous literature [1, 2] and may be explained by the observed increase in hip flexion as squat depth increased as this may place a greater demand on the hip extensors to return the body to an upright position. The increased demand would require increased force production from the hip extensors which would result in increased hip extension moments.

The interaction of the knee extensor moments may be explained by the increased demand the increased external resistance would place on the knee extensors to help return the body to an upright position. The increased depth would result in larger range of motion which may increase the joint moment as the demand increased to return the body to its resting upright position.

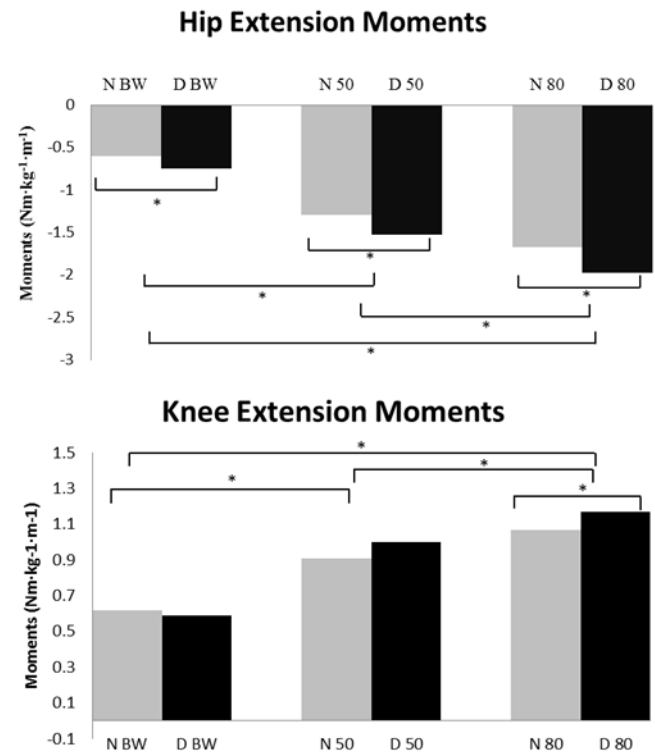


Figure 1. Mean Hip (top) and Knee (bottom) extension moments ($\text{Nm} \cdot \text{kg}^{-1} \cdot \text{m}^{-1}$) during 90° and deep squats at BW, 50% 1RM, and 80% 1RM.

CONCLUSIONS

From this examination of squatting mechanics it is apparent that there are many intricate components that differentiate normal and deep squats. Results of the current study indicate that there are significant changes in 3D lower extremity joint moments and angles as squat depth changes, and as external load increases. Further research is needed to determine if the increased joint loading exhibited during deep squats is harmful to the passive structures of the joints.

REFERENCES

1. Wretenberg et al. *Scand J Med Sci Sports*. **3**:244-50, 1993.
2. Caterisano et al. *J Strength Cond Res*. **16**:428-32, 2002.
3. Escamilla. *Med Sci Sports Exerc*. **33**:127-41, 2001.
4. Baechle and Earle. *Essentials of strength training and conditioning*: Human kinetics. 2008.
5. Weinhandl et al. *J Appl Biomech*. **26**:444-53, 2010.
6. Grood & Suntay, *J Biomech Eng*, **105**:136-44, 1983.
7. Bresler & Frankel. *Trans ASME*. **72**:25-35, 1950.
8. De Leva. *J Biomech*, **29**:1223-30, 1996.

PATIENT-BASED PREDICTORS OF HIGH-RISK BIOMECHANICS IN ANTERIOR CRUCIATE LIGAMENT-RECONSTRUCTED SUBJECTS

¹Samuel C. Wordeman PhD and ^{1,2}Timothy E. Hewett PhD

¹ Sports Health and Performance Institute, The Ohio State University, Columbus, OH, USA

² Departments of Orthopaedics, Physiology and Cell Biology, Family Medicine, and Biomedical Engineering, The Ohio State University, Columbus, OH, USA

Email: Samuel.Wordeman@osumc.edu, **Web:** sportsmedicine.osu.edu

INTRODUCTION

Knee abduction moment (KAM), internal tibial rotation moment (ITR), and anterior tibial shear (ATS) all increase ACL strain, and are reportedly influenced by both modifiable and non-modifiable factors.[1] In recent literature, high medial and lateral tibial plateau slope (MTPS and LTPS, respectively) have gained attention as potential risk factors for noncontact ACL injury.[2] It is unclear whether non-modifiable factors preclude the efficacy of neuromuscular training (NMT) in ACL-reconstructed subjects. The purpose of this study was to determine the relationship(s) between provocative external knee loading and select modifiable and non-modifiable risk factors. We hypothesized that ITR and ATS would be significantly associated with non-modifiable factors, while KAM would be most strongly related to modifiable factors.

METHODS

Eleven ACL-reconstructed subjects were evaluated one year after surgery (7 male, 4 female, 20.5±6.9 years old, 53.3±1.27 weeks post-op). Another group of six subjects (4 male, 2 female, 23.5±10.9 years old) were evaluated prior to and after participation in NMT (31.0±6.5 and 45.0±9.3 weeks post-operative, respectively). Instrumented knee laxity, medial and lateral tibial plateau slope (MTPS and LTPS, respectively), isokinetic quadriceps and hamstrings strength, and three-dimensional motion analysis during drop vertical jump were assessed.

Separate general linear mixed models were created to determine the effects of modifiable and non-modifiable factors on peak KAM, ITR, and ATS, and body-mass normalized values for these variables. Initial models included sex, MTPS, LTPS, LTPS:MTPS ratio, HQ ratios at 60 degrees

per second (HQ₆₀) and 300 degrees per second (HQ₃₀₀), peak hip abduction moment, and peak vertical ground reaction force (vGRF) as predictors. Body-mass normalized values for vGRF and peak hip abduction moment were used in prediction models for body-mass normalized outcome variables. Only data from the uninvolved limb were utilized in the linear regression models. Models were finalized in an iterative fashion. Predictors with p-values below 0.2 from the first iteration were included in the second model. Variables in the second model with p-values below 0.1 were included in the third iteration. Final models for each variable were developed based only on predictors that demonstrated statistical significance at an alpha level of 0.05.

RESULTS AND DISCUSSION

For peak ATS, male sex ($p=0.007$) and MTPS ($p=0.0226$) accounted for 40% of the variance ($R^2=0.422$, $p=0.0037$; **Figure 1a**). LTPS accounted for approximately 30% of the variance in peak KAM ($R^2=0.29$, $p=0.0051$; **Figure 1b**). 80% of the variance in ITR was accounted for by combined measures of laxity ($p=0.0023$), MTPS ($p<0.0001$), LTPS ($p=0.0142$) and peak hip abduction moment ($p<0.0001$; $R^2=0.78$, $p<0.0001$) (**Figure 1c**). *Post-hoc* power analyses revealed greater than 80% power for all models.

The multivariate predictive models for peak internal tibial rotation moment and body mass-normalized peak internal tibial rotation moment were the strongest in this study. While the final models for this variable contained the most predictors of any outcome variable, the generalized linear mixed model for net ITR demonstrated an extremely large effect size of 4.55. This model accounted for nearly 80% of the variance in ITR, and a *post-hoc* assessment demonstrated that the

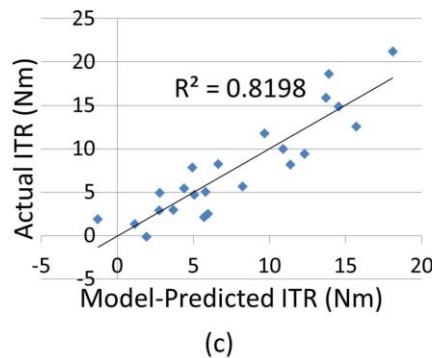
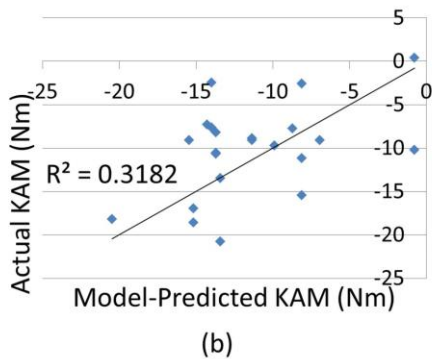
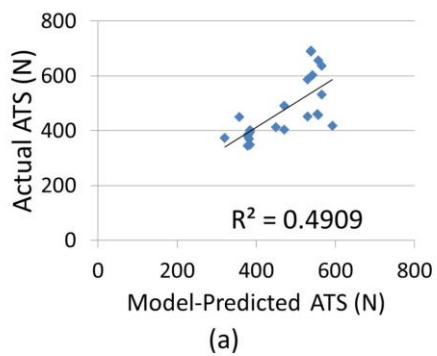


Figure 1: Relationship between model predictions and actual values for peak anterior tibial shear force (a), peak knee abduction moment (b), and peak internal tibial rotation moment (c).

four-predictor model was valid with over 99% statistical power at an alpha level of 0.05.

McLean et al. reported significant associations of MTPS and LTPS to knee kinematics and kinetics in all three planes of motion in active females.[3] Their results showed that LTPS could explain 60.9% of the variance in the inverse-kinetically calculated ATS. Furthermore, they reported that tibial and femoral geometry accounted for 75.4% of the variance in knee abduction angle, and nearly half of the variance in peak tibial internal rotation angle.[3] Further investigation is needed to

determine the effect tibial geometry has on knee abduction and how much that relationship is affected by neuromuscular control strategy.

CONCLUSIONS

LTPS and MTPS predicted relatively small proportions of the variance in KAM and ATS, respectively. Non-modifiable factors accounted for a greater portion of the variance in ITR, though hip abduction moment, a modifiable variable, was also a strong predictor. Despite a relationship with non-modifiable risk factors, KAM, ITR, and ATS are modifiable and may be reduced through NMT in ACL-reconstructed subjects.

Risk of reinjury to the reconstructed limb, or injury to the contralateral limb is anywhere from five-to-twenty fold greater than risk of initial injury.[4] Recently-emerging literature indicates that the likelihood for second injury to occur on the non-reconstructed limb is greater than on the reconstructed limb.[4] The cohort utilized in this study represents a small, heterogeneous sample of ACL-reconstructed subjects. We are also limited by the fact that a handful of these subjects were measured both prior to and after participation in a neuromuscular training protocol. The rationale behind this approach was to utilize all subjects and time points for which we had data on all of our outcome and predictor variables. The relationships delineated by these preliminary models will need to be confirmed through analysis in an independent data set.

REFERENCES

1. Levine JW, et al. *Am J Sports Med* **42**, 312-319, 2014.
2. Hashemi J, et al. *Am J Sports Med* **38**, 54-62, 2010.
3. McLean SG, et al. *Clin Biomech* **25**, 781-8, 2010
4. Paterno MV, et al. *Am J Sports Med* **38**, 1968-78, 2010.

ACKNOWLEDGEMENTS

The authors would like to acknowledge Joshua Hoffmann and the entire staff of the Sports Biodynamics Lab at The Ohio State University for their assistance, as well as NIH 2R01-AR056259.

PROTECTIVE HIP AND KNEE KINEMATICS DURING UNILATERAL AND BILATERAL LANDINGS AFTER NEUROMUSCULAR TRAINING IN ACL-RECONSTRUCTED SUBJECTS

¹Samuel C. Wordeman PhD, ¹Joshua T. Hoffman M.S., and ¹⁻²Timothy E. Hewett PhD

¹ Sports Health and Performance Institute, The Ohio State University, Columbus, OH, USA

² Departments of Orthopaedics, Physiology and Cell Biology, Family Medicine, and Biomedical Engineering, The Ohio State University, Columbus, OH, USA

Email: Samuel.Wordeman@osumc.edu, **Web:** sportsmedicine.osu.edu

INTRODUCTION

Anterior cruciate ligament (ACL) injury leads to significant reductions in patient function, and biomechanical asymmetries that frequently persist for two years or longer after ACL-reconstruction. [1] Recent reports indicate that as many as one in four ACL-reconstructed patients will suffer a second ACL injury to either the affected or contralateral limb within their first year of return to sport. [2] Furthermore, patients who suffer a second injury have significantly poorer short-to-long term outcomes.

Hip, knee, and ankle kinematics are critical modifiable factors that affect ACL injury risk. Previous research indicates that landing with the hip and knee near full extension, and reaching lower levels of peak hip and knee flexion increase the likelihood for injury. In addition, stiffer landings transmit greater forces and torques through the joints, and likely contribute to increased injury risk. Neuromuscular training (NMT) protocols that target high-risk biomechanics and impairments in neuromotor control effectively reduce rates of primary ACL injury. [3] Furthermore, subjects that participate in these training protocols demonstrate a number of associated improvements in functional biomechanical control. [4] Despite success in large, prospective analyses of healthy athletes, few studies have investigated the impact of NMT on functional biomechanics in ACL-reconstructed subjects. The goal of this study was to quantify lower extremity kinematics during unilateral and bilateral landing in ACL-reconstructed subjects prior to and after participation in NMT.

METHODS

Twenty-one (9 males, 12 females, 20.2±7.3 years old) ACL-reconstructed subjects who were recently discharged from supervised physical therapy participated in this study (37.1±17.2 weeks post-

operative). Subjects underwent two biomechanical testing sessions: One prior to participation in a twelve (12) session NMT program (Pre-test), and one after training (Post-test). Biomechanical testing consisted of 3D motion analysis using a 12 camera motion analysis system with marker data sampled at 240 frames per second. Subjects were outfitted with fifty-five (55) retro-reflective markers in a modified Helen Hayes configuration.

Subjects performed three successful trials of a bilateral drop vertical jump (DVJ) task, and a single leg drop landing (SLD) task off a 30.5 cm box in the motion capture volume. Knee, hip, and ankle angles in all three planes were averaged over the three trials. The NMT protocol consisted of twelve (12) training sessions. The program consists of biomechanical feedback from a certified trainer, and a multi-phase progression of task difficulty. The program is described in detail by Di Stasi et al. [5]

Discrete values for maximum and minimum angles, alignment at initial contact (IC), and joint excursions in all three planes were calculated and utilized for statistical analyses using 2x2 (limb-by-session) repeated measures analysis of variance (ANOVA). *Post-hoc* t-tests were used to determine differences between limbs and effects of training.

RESULTS AND DISCUSSION

Nineteen (19) of the 21 subjects performed the DVJ task at both biomechanics sessions. Twenty (20) of the 21 subjects performed the SLD task at both the sessions.

Hip Kinematics: Subjects demonstrated greater hip flexion at IC on the involved limb compared to the uninvolved limb during both tasks (DVJ: INV: 33.9±9.4 deg, UNIN: 31.5±10.1 deg; $p=0.006$), (SLD: INV: 26.2±5.8 deg, UNIN: 21.9±6.3 deg; $p<0.001$). After training, peak hip flexion during SLD increased (Pre-Test: 50.1±12.0 deg, Post-Test: 55.4±10.5 deg; $p=0.02$), as did hip flexion

excursion (Pre-Test: 26.3 ± 8.6 deg, Post-Test: 30.9 ± 9.1 deg; $p=0.02$). Subjects also demonstrated a strong trend toward decreased hip frontal plane excursion (Pre-Test: 17.1 ± 6.0 deg, Post-Test: 15.4 ± 4.8 deg; $p=0.056$).

Knee Kinematics: Knee flexion at IC after training increased for both tasks (DVJ: Pre-Test: -17.1 ± 7.2 deg, Post-Test: -23.9 ± 8.9 deg; $p=0.001$, SLD: Pre-Test: -9.4 ± 4.8 deg, Post-Test: -11.8 ± 5.7 deg; $p=0.014$). Peak knee flexion increased significantly after training for the SLD task (Pre-Test: -60.6 ± 10.8 deg, Post-Test: -66.3 ± 8.4 deg; $p=0.006$), and demonstrated a similar, but statistically insignificant trend during the DVJ task (Pre-Test: -88.0 ± 11.0 deg, Post-Test: -93.1 ± 12.2 deg; $p=0.077$). During the SLD task, subjects also demonstrated increased knee flexion excursion after training (Pre-Test: 51.1 ± 9.6 deg, Post-Test: 54.5 ± 8.67 deg; $p=0.036$).

Ankle Kinematics: Subjects demonstrated a decrease in ankle plantar flexion at IC during the DVJ (Pre-Test: -46.1 ± 7.7 deg, Post-Test: -40.2 ± 8.5 deg; $p<0.001$) and the SLD tasks (Pre-Test: -54.6 ± 7.8 deg, Post-Test: -48.7 ± 12.6 deg; $p<0.001$). Ankle flexion excursion also decreased after training for DVJ (Pre-Test: 51.6 ± 8.4 deg, Post-Test: 46.0 ± 8.7 deg; $p<0.001$) and SLD (Pre-Test: 49.8 ± 8.4 deg, Post-Test: 46.6 ± 6.5 deg; $p=0.01$).

This study demonstrates that the primary kinematic effects of NMT after ACL-reconstruction occur in the sagittal plane. Unpublished pilot data from our group demonstrates that the reported Post-Test hip and knee flexion values for peak and IC are likely greater than those of untrained ACL-reconstructed subjects at one year post-operative. Importantly, the tasks performed during the biomechanics sessions were not the same as the tasks performed during training. Thus, the biomechanical feedback provided to subjects during training appears to carry over into other landing tasks to which the subjects may not be accustomed.

Approximately 70% of ACL injuries occur via a non-contact mechanism, and are most frequently characterized by near full extension of the knee and hip at the time of IC. [6] Landing with the hip and knee in greater initial flexion, reaching deeper peak flexion, and exhibiting greater sagittal

plane excursion are all likely protective of the native ACL and/or graft. [7]

While NMT did not affect coronal or transverse plane landing mechanics, the standard physical therapy regimen for ACL-reconstructed subjects at Ohio State, where most subjects performed their formal rehabilitation, is highly focused on controlled landing mechanics. At the time of Pre-Test, the patients in this study, on average, landed with their knees in slight adduction at IC for DVJ (INV: 1.9 ± 3.4 degrees, UNIN: 1.6 ± 2.0 degrees) and exhibited low values for peak knee abduction (INV: -2.2 ± 3.6 degrees, UNIN: -1.98 ± 3.3 degrees). Similar values were observed after training, and for the SLD task. These are representative of generally low-risk frontal plane mechanics, thus our cohort may not exhibit the frontal and transverse-plane control issues commonly observed in ACL-reconstructed subjects.

CONCLUSIONS

ACL-reconstructed subjects who participate in NMT after completion of formal rehabilitation exhibit ACL-protective adaptations in sagittal plane kinematics at the hip and knee during unilateral and bilateral landing tasks. The effects of NMT in ACL-reconstructed subjects as they pertain to second injury rates and joint kinetics will be investigated further and training programs should be optimized to maximize safe return to sport.

REFERENCES

1. Roewer BD, et al. *J Biomech* **44**, 1948-53, 2011
2. Paterno MV, et al. *Am J Sports Med* **42**, 1567-73, 2014.
3. Hewett TE, et al. *Am J Sports Med* **27**, 699-702, 1999.
4. Chappell JD, et al. *Am J Sports Med* **36**, 1081-6, 2008
5. Di Stasi SL, et al. *J Orthop Sports Phys Ther* **43**, 777-792, 2013.
6. Koga H, et al. *Am J Sports Med* **38**, 2218-25, 2010.
7. Beynon BD, et al. *Am J Sports Med* **25**, 823-9, 1997.

ACKNOWLEDGEMENTS

The authors would like to acknowledge the staff of the Sports Biodynamics Lab at The Ohio State University, as well as NIH 2R01-AR056259.

LACK OF ASSOCIATION BETWEEN SUBJECTIVE AND OBJECTIVE ASSESSMENT OF SPINAL STIFFNESS

¹ Ting Xia, ¹ Maruti R. Gudavalli, ¹ James W. DeVocht, ¹ Robert D. Vining, ² Gregory N. Kawchuk, ¹ Cynthia R. Long, ¹ Wen Che, ³ David G. Wilder, and ¹ Christine M. Goertz

¹ Palmer College of Chiropractic, Davenport, IA, USA

² The University of Alberta, Edmonton, AB, Canada

³ The University of Iowa, Iowa City, IA, USA

email: ting.xia@palmer.edu

INTRODUCTION

Spinal stiffness (SS) is routinely assessed by clinicians and utilized for clinical decision making [1]. However, manual assessment of SS has demonstrated poor reliability [2], likely due to the subjective nature of this procedure. Koppenhaver et al. reported that subjective rating of SS using manual assessment at L3 was uncorrelated with objectively assessed SS using an automated indenter [3]. The purpose of this study was to evaluate subjective SS ratings using 3 objective SS assessments: a clinician's palm with optical marker and force plate measurement, an instrumented hand-held probe, and an automated indenter.

METHODS

This was an observational study nested within a clinical trial on low back pain patients undergoing chiropractic spinal manipulative therapy (SMT). The local institutional review board approved the study protocol [4] and all participants signed a written informed consent document.

We performed 1 subjective and 3 objective assessments of lumbar spine SS before SMT delivery during the first treatment visit. For the subjective procedure, the clinician's impression of SS in the region directly under the assessing hand was rated using the following classifications: rigid (no joint motion), hypomobile (abnormally limited joint motion), normal, or hypermobile (greater than normal motion), for each of 5 lumbar segments.

We next performed 3 sequential objective SS assessment methods (Fig. 1). These methods

included applying force in the posterior-to-anterior direction over lumbar spinous processes using the clinician's palm (P), an instrumented hand-held probe (I), and an automated indenter (A). The applied force was monitored using a force plate during P and a load cell during I and A. Displacement was monitored using an optical motion capture system during P and I and a linear variable differential transformer during A. P and I were performed over each of 5 lumbar segments while A was conducted only over the spinous process at or closest to the most anterior point of lumbar curvature. Details of these methods can be found in the study protocol [4].

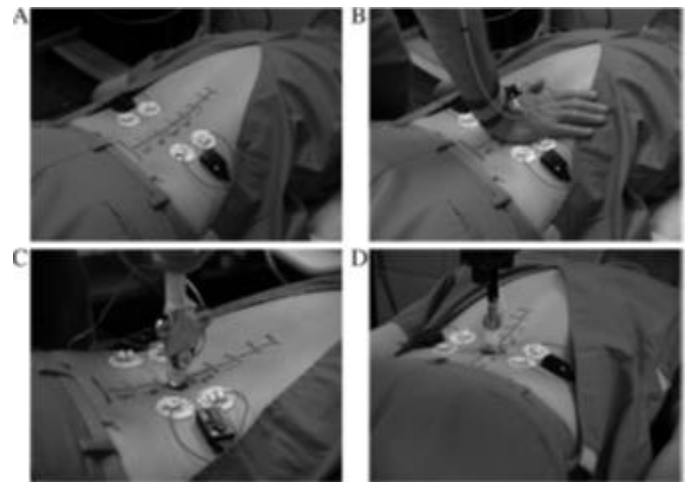


Figure 1: Illustration of skin marks for spinous processes from L1-L5 (A) and 3 types of objective spinal stiffness assessment methods using the clinician's palm (B), an instrumented hand-held probe (C), or an automated indenter (D).

The SS value was calculated from the force-displacement curve using linear regression over the force range of 10 – 60 N. Each objective SS was classified according to the subjective ratings for each

of 5 lumbar segment levels (L1-L5). Mean objective SS differences compared with subjective SS ratings are reported with 95% confidence intervals.

RESULTS AND DISCUSSION

82 participants were enrolled with 39 (48%) as females, mean (SD) age of 44.9 (10.6) years, and a moderate mean pain intensity of 46.1 (18.1) on the visual analog scale (0-100) at baseline. Table 1 summarizes the mean differences between the subjective ratings for each of the 3 objective SS assessments according to the lumbar spine levels. Very few observations were classified as hypermobile or rigid, thus they are not presented. The magnitudes of all the mean differences are small and all 95% confidence intervals span 0.

There are a few limitations in the current study. The P method used a larger surface contact area than I or A measures causing paraspinal soft tissue compression that was not measured. Breathing instructions differed for the P, I, and A methods. The subjective and palm methods assessed stiffness at slightly different angles over different segments, whereas the automated and instrumented stiffness compressed at angles perpendicular to the examination table. Clinically or biomechanically meaningful magnitude of difference in spinal

stiffness is currently unknown making it difficult to interpret measurement variability.

CONCLUSIONS

The results from the current study for A at L3 support the observations made by Koppenhaver et al. [3]. We performed two additional types of objective assessments at all five lumbar segment levels, but did not find evidence of a relationship with subjective SS ratings. Therefore, we conclude that these results have added support to the original work of Koppenhaver in showing that a subjective measures of stiffness do not correlate to other objective measures of stiffness. This work adds to a growing body of evidence that subjective methods of assessing spinal stiffness have important limitations.

REFERENCES

1. Maitland GD. *Vertebral manipulation*. Oxford, 1986.
2. Van Trijffel E et al. *Man Ther* **10**, 256-69, 2005.
3. Koppenhaver SL et al. *Man Ther* **19**, 589-94, 2014.
4. Xia T et al. *BMC Complem Alt Med* **14**, 292, 2014.

ACKNOWLEDGEMENTS

The study was supported in part by NIH/NCCIH. Thank Dr. Stacie Salsbury for editing the abstract.

Table 1: Mean differences between subjective ratings for 3 objective spinal stiffness (N/mm) assessments.

		L1			L2			L3 *			L4			L5		
		n	mean	SD	n	mean	SD	n	mean	SD	n	mean	SD	n	mean	SD
P	Hypo.	28	5.6	2.4	34	5.3	2.2	33	4.7	1.8	33	4.3	1.2	50	3.8	1.2
	Norm.	52	4.9	1.7	46	4.7	1.4	44	4.9	1.8	40	4.5	1.7	27	3.9	1.4
	Mean Diff. (95%CI)	0.71 (-0.32, 1.74)			0.68 (-0.32, 1.74)			-0.14 (-0.98, 0.71)			-0.18 (-0.88, 0.52)			-0.04 (-0.63, 0.56)		
I	Hypo.	26	8.4	2.4	29	7.9	2.1	29	8.1	2.4	33	7.5	2.2	46	7.6	1.9
	Norm.	43	8.3	2	40	8	2.1	39	7.5	1.9	32	7.6	2.4	21	8	3.3
	Mean Diff. (95%CI)	0.04 (-1.03, 1.12)			-0.04 (-1.05, 0.97)			0.54 (-0.52, 1.60)			-0.11 (-1.24, 1.02)			-0.45 (-2.03, 1.14)		
A	Hypo.	2	3.6	1.6	2	3.2	0.7	10	6.1	1.9	3	4.9	1.3	.	.	.
	Norm.	2	5.6	0.7	5	5.1	1.3	27	5.2	1.3	2	4.4	1.2	.	.	.
	Mean Diff. (95%CI)	-1.99 (-7.62, 3.63)			-1.95 (-4.51, 0.62)			0.88 (-0.22, 1.98)			0.49 (-3.22, 4.21)					

A COMPARISON OF TWO SUPERFICIAL MCL RECONSTRUCTION INCLUDING SINGLE-BUNDLE ANTERIOR CRUCIATE LIGAMENT (ACL) RECONSTRUCTION

² Zhu J, ¹ Dong J, ² Marshall B, ¹ Linde-Rosen M, ^{1,2} Smolinski P and, ¹ Fu FH

¹ Department of Orthopedic Surgery, University of Pittsburgh, Pittsburgh, PA

² Department of Mechanical Engineering and Material Science, University of Pittsburgh, PA

INTRODUCTION

Anterior cruciate ligament (ACL) and medial collateral ligament (MCL) are the most commonly injured ligaments in the knee, which serves as the primary medial stabilizer to anterior translation and valgus stress [1]. It is not uncommon for superficial medial collateral ligament (sMCL) damage to occur with ACL injury. While conservative treatment of the MCL injury is often done, in cases of severe injury, reconstruction of the sMCL can be done in addition to the ACL reconstruction. There are two MCL reconstructions (parallel and tri-vector) in clinic. But we don't know which technique can better restore the biomechanics of the intact knee. The objective of the study was to compare knee biomechanics of two sMCL reconstructions combined with single-bundle ACL reconstruction using a porcine model.

METHODS

Twenty (n=20) fresh frozen unpaired adult pig knees were used for biomechanical testing. Specimens with a congenital abnormality or arthritis were excluded from the study and the existence of an intact ACL was confirmed arthroscopically. All specimens were frozen at -20 C⁰, and thawed the night before testing at room temperature. The knees were kept intact and the specimens were kept moist with physiologic saline solution. The tibia and femur were sectioned ~15 cm from the joint line and the ends of femur and tibia were potted in heavyweight epoxy putty.

The specimens were divided into two groups, tested with the robotic testing system (CASPAR Orto MAQUET, Germany) under (1) an 89-N anterior tibial (AT) load at 30° (porcine full extension), 60°, and 90° of knee flexion, (2) 4-Nm internal and external tibial torques at 30° and 60°, and (3) a 7-Nm valgus torque at 30° and 60° of knee flexion [2, 3].

The groups were divided into either parallel or tri-vector group sMCL reconstruction and both groups had single bundle ACL reconstructions. The ACL reconstructions were performed with a 7 mm graft which was fixed with 60 N at 30° of flexion. The sMCL reconstructions were performed with 6 mm grafts and fixed with 44 N at 30° of flexion. The ACL reconstructions were done arthroscopically in an anatomic fashion with hamstring grafts and graft fixation was done with a screw and washer on the tibia and an extra-cortical button on the femur.

Differences in anterior tibial translation (ATT) displacement, internal / external rotation angles, and in situ forces at the different flexion angles were analyzed using one-way ANOVA with repeated measures, and statistical significance was set at $p < 0.05$.

RESULTS AND DISCUSSION

With ACL MCL co-injuries, ACL reconstruction alone can't restore ATT, valgus, internal or external rotation result. With ACL and two different sMCL reconstructions, no significant differences were found between two groups for ATT at 30° flexion, and both method restored intact knee biomechanics. At 60° and 90° of flexion, MCL tri-vector reconstruction can restore the ATT, while parallel MCL reconstruction cannot improve the ATT (Fig.1a). Under valgus loading, ACL reconstruction alone did not restore intact knee stability, the parallel sMCL reconstruction did restore stability while the tri-vector method did not (Fig.1b). Under the external tibial torque, parallel sMCL reconstruction does restore external rotation while tri-vector sMCL reconstruction does not restore (Fig. 1c). Under the internal tibial torque, both sMCL reconstruction techniques restored intact knee internal rotation (Fig. 1d).

REFERENCES

1. Robinson et al., *J Bone Joint Surg* 2004
2. Yuki Kato, Freddie H. Fu1, *Knee Surgery, Sports Traumatology, Arthroscopy*, 2012
3. Brian T. Feeley, et al. *The American Journal of Sports Medicine*, 2009

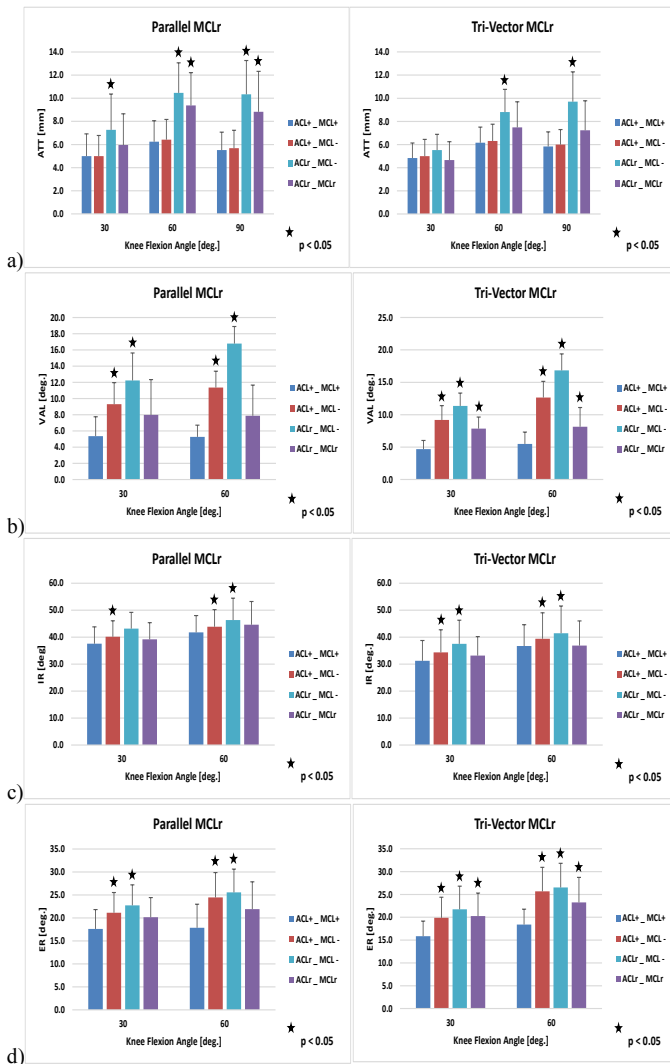


Figure 1: Results comparison of displacement and rotation between two sMCL reconstructions (Tri-vector and Parallel) combined with single-bundle ACL reconstruction a) ATT; b) valgus; c) internal rotation; d) external rotation

THE RELATIONSHIP BETWEEN ARCH HEIGHT AND ARCH FLEXIBILITY

¹ Becky Zifchock, ¹ Christal Theriot, ² Howard Hillstrom, ³ Jinsup Song, and ¹ Michael Neary

¹ United States Military Academy, West Point, NY, USA

² The Hospital for Special Surgery, New York, NY, USA

³ Temple University, Philadelphia, PA, USA

email: rebecca.zifchock@usma.edu

INTRODUCTION

Previous literature suggests that there is a relationship between foot structure and injury patterns [1]. The correlation between arch structure and injury may be related to the fact that foot structure influences its function. Several studies have considered both arch height and arch flexibility to be a defining characteristic of foot structure. In their recent study of high-arched runners, Williams et al [2] found varying levels of arch flexibility, which led to differing lower-extremity movement patterns and loading.

It is often assumed that high arches tend to be stiffer, while low arches tend to be more flexible. However, recent literature suggests that arch height does not necessarily dictate arch flexibility [2]. Therefore, the purpose of this study is to use a proposed arch stiffness classification system to categorize both the arch height and arch flexibility of individuals' feet and determine the tendency for certain arch height types to cluster toward certain arch flexibility types. Based on the assumption that high arches are stiffer while low arches are more flexible, a different distribution of arch flexibility types was expected for each of the arch height categories.

METHODS

Volunteers were drawn from pool of incoming military cadets, of whom 1124 agreed to participate in this study. All procedures were reviewed and approved by the Institutional Review Board, and all subjects gave informed consent prior to participation in the study. After the removal of erroneous data, a total of 1056 subjects, 882 men and 174 women, were included in the study (18.4

±1.4 years, 1.76 ±0.80 m, 76.1 ±12.7 kgs). The right foot was characterized for each participant: Arch height index was measured using the Arch Height Index Measurement System, and arch height index (AHI) was calculated [3]:

$$AHI = \frac{\text{Dorsal Height}_{50\% \text{ Total Foot Length}}}{\text{Truncated Foot Length}}$$

Arch flexibility, (AHF) was defined as the change in arch height (distance from the dorsal surface to the ground) from sitting to standing due to the change in load borne by the arch during these activities [3]:

$$AHF = \frac{AH_{\text{sitting}} - AH_{\text{standing}}}{0.4 \times BW} \times 100 \text{ [m/kN]}$$

The data were then used to create a classification scheme for AHF. Due to the skewness of the AHF data, the median value was established and a system of quintiles was used to classify five AHF categories: Very Stiff, Moderately Stiff, Average, Moderately Flexible, and Very Flexible.

The distribution of AHF types was then compared amongst AHI categories. This was accomplished by identifying the number of individuals of AHF type in each AHI category. AHF type was based upon the classification system proposed in this paper, and AHI category was based upon previous cutoff values for cavus, rectus, and planus proposed by Hillstrom et al. [4]. The distribution was compared using a Chi-Square Test of Goodness of Fit.

RESULTS AND DISCUSSION

The classification scheme based upon the quintiles is shown in Table 1. The median AHF value was 14.75 mm/kN. Of the 1056 feet, an approximately equal distribution (range = 210 – 212 feet/category)

were classified in each of the five AHF types. For the AHI categorization, 68 feet were classified as cavus, 225 were classified as rectus, and 763 were classified as planus. The test of goodness-of-fit suggested that, amongst AHI types, there were a significantly disproportional number of feet that were classified in each of the AHF categories ($p < 0.01$). As shown in Figure 1, the largest proportion of cavus feet was very stiff, and the smallest proportion was very flexible. This was also true of the feet in the rectus arch height category; although a large portion of the rectus feet also demonstrated neutral arch flexibility. Conversely, the largest proportion of planus feet was very flexible, and the smallest proportion was very stiff. The planus group demonstrated a very obvious step-wise increase in the proportion of individuals in each category from very stiff to very flexible. However the distribution of AHF categories within the cavus and rectus feet is less defined.

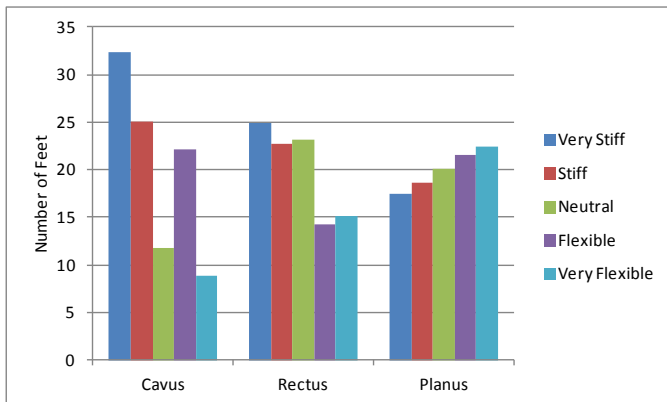


Figure 1: Distribution of arch flexibility types amongst arch height categories

The purpose of this study was to expand our understanding of arch flexibility as a measure of foot structure. From this study, we proposed a five-category classification scheme for arch flexibility.

It is important to note that the classification scheme

Table 1: Proposed cutoff values for arch flexibility categories and distribution of feet ($n = 1056$) amongst arch flexibility and arch height categories

Arch Flexibility Category			Number of Feet		
	Quintile	Cutoff Value, mm/kN	Cavus	Rectus	Planus
Very Stiff	0 – 20%	$AHF < 9.91$	22	56	133
Stiff	20 – 40%	$9.91 \leq AHF < 13.54$	17	51	142
Neutral	40 – 60%	$13.54 \leq AHF < 16.00$	8	52	153
Flexible	60 – 80%	$16.00 \leq AHF < 20.54$	15	32	164
Very Flexible	80 – 100%	$AHF > 20.54$	6	34	171

proposed in the current study is based upon a population of healthy men and women between 18 to 25 years. Future studies should be carried out to determine whether the classification scheme can be applied to children, older adults, or a pathological population.

Despite the skew towards planus feet enrolled in the study, the results supported the hypothesis: there was a significantly different distribution of the arch flexibility types between arch height types. Specifically, the planus feet were much more likely to be very flexible, while the cavus and rectus feet were more likely to be stiffer. This relationship was most evident for the two extreme arch flexibility categories (very stiff and very flexible).

CONCLUSIONS

The results of the current research supports the common belief that cavus feet tend to be very stiff, while planus feet tend to be very flexible. However, the results of this study also demonstrate that there was a distribution of arch flexibility types amongst the arch height types. Therefore, at least two foot classification methods are useful to fully characterize foot structure.

REFERENCES

- Williams DS, et al. *Clin Biomech* **16**(4), 341-347, 2001.
- Williams DS, et al. *J Athl Train* **49**(3), 290 – 296, 2014.
- Zifchock R, et al. *Foot Ankle Int* **27**(5), 367 – 372, 2006.
- Hillstrom HJ, et al. *Gait Posture* **37**(3), 445 – 451, 2013.

Long-range correlations of center of pressure are stronger for AP perturbations than ML perturbations in healthy young adults

¹Venkata Naga Pradeep Ambati, ¹Troy Rand, ¹James Nielsen, ¹Mukul Mukherjee

Biomechanics Research Building, University of Nebraska, Omaha, NE, USA
email: vambati@unomaha.edu, web: <http://cobre.unomaha.edu/>

INTRODUCTION

Control of center of pressure in anterior-posterior and medial-lateral directions use different mechanisms [1]. This is because recovering stability requires activation of different joints in different directions [1]. Biological signals like COP have a fractal structure with long-range correlations (LRCs) such that postural sway at one point of time are related to postural sway at another point in time [2]. Recent studies have shown that the LRC of a healthy system can be driven towards a specific direction by administering a sensory input with the desired temporal structure [3, 4]. Hence we used signals with different temporal structures to perturb the support surface in AP and ML directions and examined the LRCs of resultant COP patterns. Due to the difference in the alignment of body segments and forces required to control stability in AP versus ML, we expected that LRCs for COP in AP perturbations will be greater than the LRCs for COP in ML perturbations. In addition to this, we also hypothesized that the root mean square (RMS) for COP during AP translations will be greater than RMS for COP during ML translations.

We also expected that LRCs and RMS for COP in response to different noise signals would be different because a healthy system shows flexibility in its responses to sensory input signals of varying temporal structures [3].

METHODS

10 healthy young adults stood in a side-by-side stance on a force platform that was subjected to translations in the AP and ML directions (figure 1). There were five separate translation conditions in each direction: no noise, white noise (WN), pink noise (PN), brown noise (BN) and sinusoidal wave

(SW). Each condition other than no noise was created with 1800 data points and the frequency of platform translation was 10 Hz, which resulted in a three-minute trial. The COP data series used for further processing involved only the AP component of COP data during AP translations and the ML component of COP data from trials involving ML translations. We did not include the COP components orthogonal to the direction of perturbation. The COP data was processed using customized Matlab scripts (Mathworks Inc., Natick, MA) to generate root mean square (RMS) and DFA (detrended fluctuation analysis) measures of variability. DFA analysis results in a scaling exponent α that quantifies the long-range correlations in a time series. Repeated measures ANOVA was used to identify the differences in RMS and DFA α of the COP time series due to perturbation direction and noise conditions.

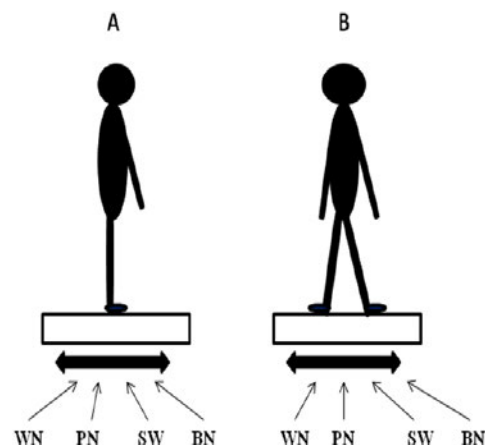


Figure 1. Schematic of experimental set up represent AP (A) and ML (B) perturbations produced in the force platform using waveforms with different temporal structures.

RESULTS AND DISCUSSION

DFA α values for COP during support surface translations in AP and ML directions were significantly different ($p=0.001$). DFA α values for COP were significantly different in the five noise conditions ($p<0.0001$). Post-hoc analysis showed significant differences in the DFA α values of COP from no noise condition when compared to corresponding values from white noise, pink noise and sinusoidal wave translations (Figure 2). Significant differences were also found between brown noise and white noise, pink noise, and sinusoidal wave translations. There was no interaction effect of perturbation direction and noise conditions on the DFA of COP time series.

There was a significant difference in RMS of COP during AP translations when compared to RMS of COP during ML translations ($p=0.001$). A significant difference due to noise conditions was observed in RMS of COP values ($p=0.002$). Post-hoc analysis showed significant differences in RMS values of COP from pink noise translations when compared to corresponding values from white noise and Sinusoidal wave translations. There was no interaction effect of perturbation direction and noise conditions on RMS of COP.

The results of our study strongly support our hypotheses. We observed that the LRCs of COP in AP and ML directions were different. We also observed that RMS for COP during AP translations was greater than ML translations. The linear measure used for analysis complements the findings of our non-linear analysis.

This may be due to differences in the alignment of body segments and muscles required for the activation of forces to maintain stability when perturbed in these directions.

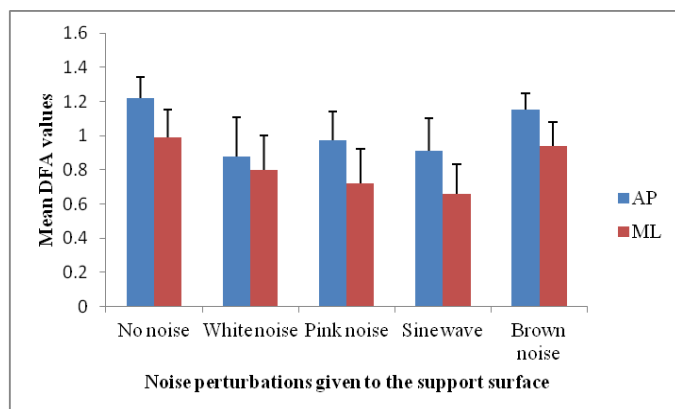


Figure 2. Mean DFA α values of COP during AP and ML perturbations at different noise frequencies

CONCLUSIONS

Exploring the temporal structure of biological processes has provided many new insights into movement control. Because aging and disease are characterized by a degradation of this temporal structure it is important to investigate new ways to restore this highly complex structure. Our previous findings [4] have shown that healthy individuals show adaptive flexibility in their ability to entrain to different support surface inputs in the AP direction where the temporal structures of the inputs are different and alter their COP to match such variable inputs. Our current study shows that such entrainment is also possible in the ML direction. The different strategies used for control of posture in AP and ML directions might result in different temporal structures of COP variability in those respective directions. Future work should explore if the LRCs for COP variability remain different in AP and ML directions with increasing age and clinical conditions.

REFERENCES

- [1] Winter DA, et al. J Neurophysio. 75: 2334-2343. 1996
- [2] Stergiou N, et al. J. Neurol. Phys. Ther. 30:3, 120-9, 2006
- [3] Kaipust J, et al. Ann. Biomed. Eng. 41:8, 1595-603, 2013
- [4] Rand T, et al. Ann. Biomed. Eng. *In Review*.

ACKNOWLEDGEMENTS

This study was supported by the Center of Biomedical Research Excellence grant (1P20GM109090-01) from NIGMS/NIH and the NASA Nebraska EPSCoR Research Mini-Grant.

VIRTUAL TIME TO CONTACT IS MORE STRONGLY RELATED TO DISEASE SEVERITY THAN SWAY EXCURSION IN PEOPLE WITH DIABETES AND DIABETIC NEUROPATHY

¹ Matthew G. Becker, ² Stacey Meardon, ¹ Zachary J. Domire, ³ Sunghan Kim, and ¹ Paul DeVita

¹ Department of Kinesiology, East Carolina University, Greenville, NC, USA

² Department of Physical Therapy, East Carolina University, Greenville, NC, USA

³ Department of Engineering, East Carolina University, Greenville, NC, USA

email: beckerml3@students.ecu.edu , web: <http://www.ecu.edu/cs-hhp/exss/biomechlab.cfm>

INTRODUCTION

Individuals with diabetic neuropathy are significantly less stable during quiet and perturbed standing than individuals without diabetic neuropathy. They exhibit higher center of pressure (COP) sway velocity and sway excursion [1,2]. A second postural measure, Virtual Time-to-Contact (VTC) has been shown to be more sensitive than sway excursion in assessing postural stability in people with other neurological conditions, such as multiple sclerosis and concussions [3,4]. VTC establishes a boundary of support around a person's feet when standing and calculates how long it would take that person's COP to reach that boundary, given current instantaneous position, velocity, and acceleration. If the COP exceeds the boundary of support, the person will either fall or have to catch him or herself. The longer it takes the COP to reach the boundary of support, the greater VTC will be. A higher VTC is associated with greater stability [4]. VTC has not, as of yet, been used to assess postural stability in people with diabetes or diabetic neuropathy. Because of its previous success with other neurological conditions, VTC may provide a more sensitive measure of postural stability for people with diabetes and/or diabetic neuropathy compared to sway-based COP measures. To investigate this concept, we hypothesized that VTC will be more strongly correlated to severity of diabetic neuropathy than sway excursion. The purpose was to compare the relationships of VTC and sway excursion with severity of diabetic neuropathy in anteroposterior (AP) and mediolateral (ML) perturbations in people with diabetic neuropathy.

METHODS

3D motion capture and force plate data were collected on 10 participants (age: 50 yrs; 2 males; 8 females) using markers placed bilaterally on the 1st toe, 5th metatarsal head, and posterior heel. All participants had diabetes with 5 having diabetic neuropathy. Participants were perturbed on a NeuroCom Research Module. Perturbations were at 10 cm/s and 20 cm/s and lasted for 0.5 s. Force plate data were collected at 200 Hz during and 5 seconds following forward, backward, left, and right perturbations.

The severity of diabetic neuropathy was assessed via vibratory threshold using a biothesiometer on both feet. These tests were conducted at 5 plantar sites on both feet: 1st toe; 1st, 3rd, & 5th metatarsal heads; and the heel. The clinical vibratory threshold for neuropathy is 25 V with a biothesiometer.

VTC was calculated using center of pressure force plate data and a boundary of stability, as defined by foot marker locations in MATLAB. Sway excursion was calculated using center of pressure force plate data (Fig. 1). Minimum and average VTC and sway excursion were calculated during the perturbation, for the first 0.5 s after the perturbation, and for 1.0 s after the perturbation. Results for all AP perturbations were averaged for single assessments for VTC and sway variables as were the ML results. Both VTC and sway excursion variables were correlated and regressed with the both left and right vibratory threshold. Correlations greater than 0.632 were significant, $p < 0.05$. The study was approved by the ECU Institutional Review Board and the participants provided written consent.

RESULTS AND DISCUSSION

Four significant and strong correlations were found. During ML perturbations, both average ($r = 0.72$) and minimum ($r = 0.79$) VTC were strongly correlated with vibratory threshold on the right foot and minimum VTC was strongly correlated with vibratory threshold on the left foot ($r = 0.65$). During AP perturbations, average VTC was strongly correlated with vibratory threshold on the right foot ($r = 0.78$, Fig. 2). No significant correlations were found for sway excursion, both during and after perturbation or for VTC after the perturbation (Fig. 3). These data showed neuropathy severity is more strongly correlated to VTC than sway excursion. This is in agreement with research on other neurological conditions, particularly concussions, that VTC is a more sensitive measure of severity of a neurological condition [3,4]. However, the direction of the relationship is completely unexpected. Longer VTC with reduced sensation suggests that people with diabetic neuropathy may employ a safer and more restrained postural control strategy in response to perturbations. Similar findings have been found in gait in people with diabetic neuropathy while walking on different surfaces [5].

CONCLUSIONS

VTC had four significant relationships with severity of diabetic neuropathy, while sway excursion did not have any significant relationships with disease severity. These data suggest that Virtual Time-to-Contact may be more appropriate than sway excursion in assessing severity of neuropathy in people with diabetes and diabetic neuropathy. People with diabetes and diabetic neuropathy may use a more restrained postural control strategy in response to perturbations.

REFERENCES

1. Simoneau et al. *Diabetes Care* **17**, 1411-1421, 1994
2. Boucher P. *Diabetes Care* **18**, 638-645, 1995
3. Gruber et al. *Gait & Posture* **34**, 13-18, 2011
4. Slobounov et al. *Clinical Neurophysiology* **119**, 281-289, 2008
5. Allet et al., *Gait & Posture* **29**, 488-493, 2009.

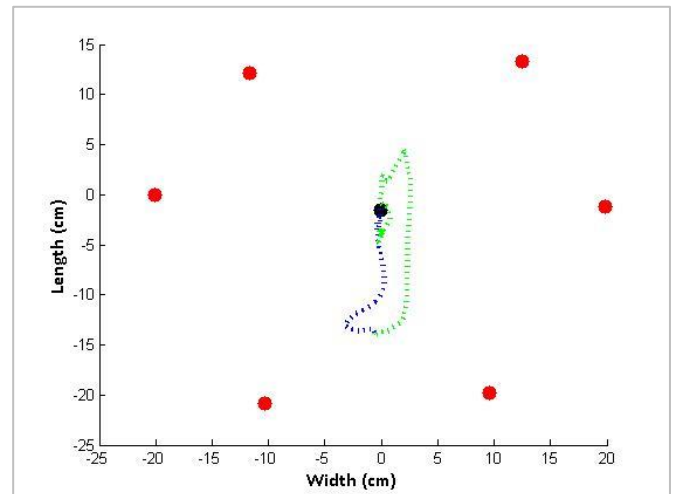


Figure 1. Feet coordinates and COP trajectory during and after a forward perturbation. Black marker indicates starting COP position. Blue, green lines indicate COP trajectory during & after a forward perturbation.

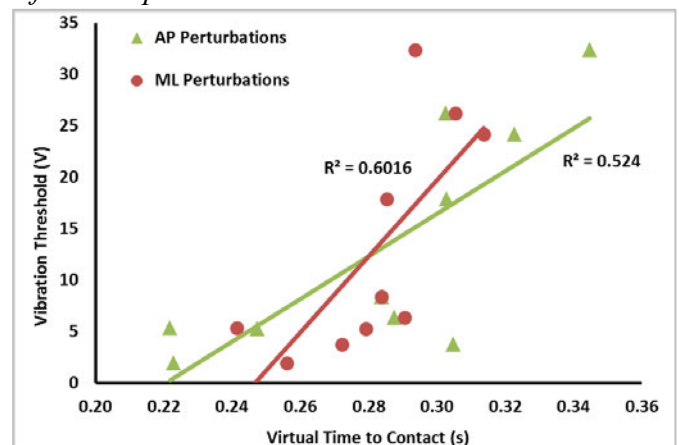


Figure 2. Average VTC during perturbations vs vibratory threshold on right foot.

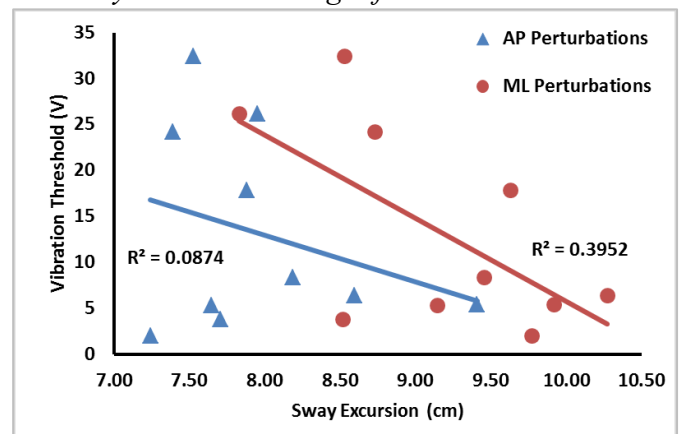


Figure 3. Sway excursion during perturbation vs vibratory threshold on right foot. Neither relationship was statistically significant

LEG STIFFNESS AND POSTURAL CONTROL IN CHILDREN DURING SINGLE-LEG HOPPING

Matthew Beerse and Jianhua Wu

Georgia State University, Atlanta, GA, USA. Email: mbeersel@student.gsu.edu

INTRODUCTION

Hopping, described by a spring-mass model, demonstrates a linear relationship between vertical ground reaction force (GRF) and center of mass (COM) displacement [1]. Leg stiffness, important for movement performance and injury prevention, is commonly calculated from this relationship, but with inconsistent methods. Further, altering hopping frequency away from a preferred frequency requires the manipulation of leg stiffness and increases the demand on the musculoskeletal system [2, 3]. No study has been conducted to investigate how hopping frequency influences movement of the COM in the anterior posterior (AP) and medial lateral (ML) directions in children and adults. This study aimed to compare the kinetic and kinematic calculation methods on leg stiffness and investigate the COM movement in the AP and ML directions in children.

METHODS

Participants: There were 13 preadolescents with typical development (8 M/5 F). Mean (SD) of age, height, and body mass were 8.9 (1.8) years, 1.3 (0.1) m, and 32.7 (8.2) kg, respectively.

Experimental design: The subjects hopped at their most comfortable frequency three times and the average frequency was used to set the four metronome-guided frequency conditions: Preferred, Moderate (20% increase), Fast (40% increase) and Slow (20% decrease). A full body PSIS marker set was attached to the subjects to estimate the COM.

Data collection:

Three 20-second trials were collected for each condition. The order of condition presentation was randomized across the subjects. Because three subjects had an elevated preferred frequency, a fast condition was not possible. An AMTI force plate was used to collect vertical GRF data. A 7-camera

Vicon motion capture system was used to collect kinematic data.

Data analysis: Two methods were used to calculate COM displacement, a kinetic method by double integration of acceleration from the vertical GRF data [1], using the central difference method and adjusted by position of COM at takeoff [4], and a kinematic method using the COM position marker estimated by the full body marker set. Leg stiffness was then calculated as the linear regression slope of the GRF plotted against the COM displacement throughout the entire stance phase (Fig. 1). COM range of motion in the AP and ML were calculated as the difference between the maximum and minimum position during stance phase and flight phase, separately.

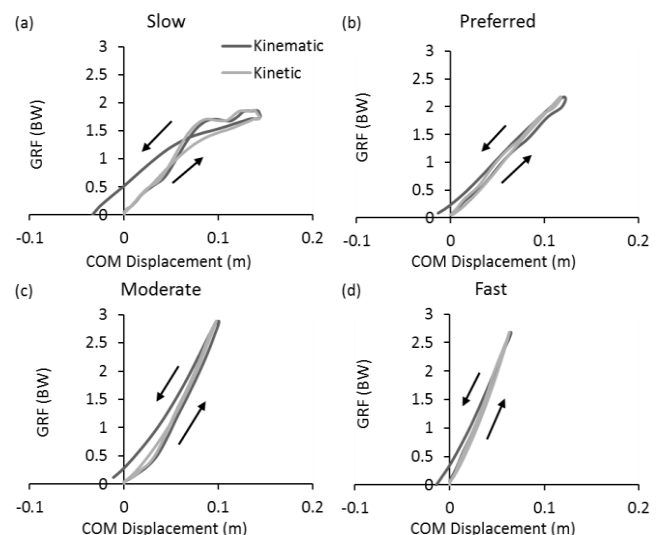


Figure 1: Representative data highlighting similar maximum COM displacement but different COM position at take off between the kinematic and kinetic method.

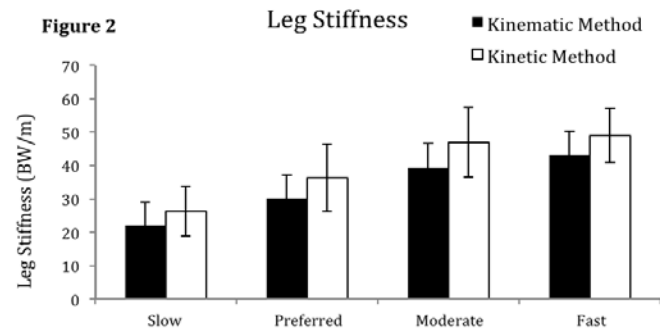
Statistical analysis: Two 2-way (2 method x 4 frequency) ANOVA with repeated measures were conducted on leg stiffness and the maximum COM displacement to compare the kinematic and kinetic methods. Two-way (2 direction x 4 frequency)

ANOVA with repeated measures were conducted on the COM range in stance phase and flight phase. Post-hoc pairwise comparisons with Bonferroni adjustment were completed when necessary. A significance level was set at $p < 0.05$.

RESULTS AND DISCUSSION

The maximum COM displacement during stance phase was similar between the kinematic and kinetic methods and decreased as frequency increased (Fig 1). There was a frequency effect ($F(3,33) = 103.96, p < .001$).

Leg stiffness calculated by the kinematic method was generally lower than that calculated by the kinetic method (Fig. 3). There was a frequency effect ($F(3,33) = 122.46, p < .001$) and a method effect ($F(1,12) = 39.96, p < .001$).



In stance and flight phases, the COM range was smaller in the AP direction than in the ML direction. There was a frequency effect ($F(3,33) = 34.02, p < .001$) and a direction effect ($F(1,12) = 22.84, p < .001$), on the COM range in stance phase (Fig. 4). There was a direction effect ($F(1,12) = 9.01, p = 0.011$) on COM range in flight phase (Table 1).

The maximal COM displacement was similar between the two calculation methods, but leg stiffness calculated from the kinematic method was lower than the kinetic method. The COM calculated

from the kinematic method in Fig. 1 shows that position at takeoff was generally higher than at foot strike in hopping of children. This implies that the trunk was more extended at takeoff compared to landing. Our integration for the kinetic method assumed similar COM position at takeoff and landing resulting in underestimated COM movement after mid-stance. Along with calculating leg stiffness over the entire stance phase using the same vertical GRF, the kinematic method produced lower leg stiffness than the kinetic method.

The COM range during stance increased at lower hopping frequencies challenging the children's balance. The COM movement demonstrated a greater range in the ML direction compared to the AP direction across all conditions. With only one leg supporting the body mass, the COM would need to shift towards the single support in the ML direction, thus causing a higher magnitude of the COM movement in this direction.

CONCLUSIONS

Both kinematic and kinetic methods show that children increase leg stiffness with hopping frequency. Horizontal movement is greater in the ML direction and increases with decreasing frequency requiring greater postural control in children.

REFERENCES

1. Farley CT, et al. *J. Appl. Physiol.* **71**, 2127-2132, 1991.
2. Auyang AG, et al. *Exp Brain Res* **192**, 253-264, 2009.
3. Moran MF, et al. *Front. Integr. Neurosci* **7**, 2013.
4. Hebert-Losier K and Eriksson A. *J Biomech* **47**, 115-121, 2014.

Table 1: Range of the COM	Slow	Preferred	Moderate	Fast
AP, Stance (cm)	1.43 (0.34) ^a	1.11 (0.24) ^b	1.05 (0.33) ^c	0.67 (0.45) ^c
ML, Stance (cm)	1.61 (0.25) ^a	1.32 (0.18) ^b	1.17 (0.23) ^c	1.06 (0.19) ^c
AP, Flight (cm)	4.42 (1.87)	3.89 (2.39)	3.92 (1.03)	3.46 (1.90)
ML, Flight (cm)	6.11 (3.63)	5.74 (4.17)	4.76 (3.13)	5.22 (2.15)

ASSESSMENT OF KNEE MECHANICS AND MUSCLE ACTIVITY DURING BALANCE EXERCISES

Lauren C. Benson and Kristian M. O'Connor

University of Wisconsin Milwaukee, Milwaukee, WI, USA

email: lbenson@uwm.edu

INTRODUCTION

Patellofemoral pain (PFP) is the most common overuse knee injury [1], affecting people in a variety of tasks [2]. Risk factors for PFP are considered to be those that contribute to large patellofemoral joint contact forces at the lateral knee, including increased knee abduction moment [3], and an imbalance between vastus lateralis (VL) and vastus medialis oblique (VMO) [4].

Balance training has been successfully used as protection against recurring ankle sprains [e.g. 5]. The use of balance training to protect against traumatic knee injuries, however, has had conflicting results [6, 7]. Additionally, athletes with a history of knee injury had a greater incidence of overuse knee injury following a balance training program featuring the use of a wobble board [5].

If balance training elicits poor knee mechanics, repeating balance exercises throughout a training program may expose the athlete to large patellofemoral contact forces that, over time, could result in overuse injury. Since the moments at the knee and the timing of the vasti muscles during various balance exercises have not been reported, it is unclear how balance exercises may contribute to mechanics that could put athletes at risk for overuse knee injury. The purpose of this study was to quantify knee abduction moment and relative timing of VMO and VL during balance exercises for recreational athletes.

METHODS

Ten healthy recreational athletes (3 male, 7 female, 28 (4) years, 1.74 (0.12) m, 70.20 (15.40) kg) without functional ankle instability were recruited. Muscle activity of VMO and VL was recorded during maximum voluntary contraction (MVC) trials. Retroreflective markers were applied to the

participants' skin to track the motion of the pelvis, thigh, leg and foot on the dominant side. In addition to muscle activity, three-dimensional kinematic data and ground reaction forces were recorded while balance exercises were performed.

The balance exercises consisted of barefoot, single-legged stance on firm ground with eyes open (EO) and eyes closed (EC), and on a rectangular wobble board allowing only medial-lateral motion (ML), only anterior-posterior motion (AP), and allowing motion in all directions (MULT). For each exercise, the participants completed 5 trials of 40 seconds. At the beginning of the trial, the participant was in bilateral stance, and then stepped forward with their dominant leg onto the balance surface. While balancing, the participants fixated their gaze on a target 2 m away at eye level, but had no restrictions for movement of the arms or the non-dominant leg. All trials of one exercise were completed before moving to the next exercise. The order that each participant completed the exercises was randomized to eliminate a learning effect.

The EMG data were full-wave rectified and root mean square values were calculated using a 120-ms window. The knee frontal plane angle and moment and the processed EMG signals, expressed as a percent of the maximal muscle activation from the MVC trials, were calculated for the final 30 seconds of the balance exercise trials. Each trial was assessed a balance score, defined as the percentage of time in the final 30 seconds of the trial that the participant maintained single-leg balance. Balance scores, peak knee abduction moment, and frontal plane knee moment variability while balance was maintained were averaged across all trials for each exercise. Additionally, the cross-correlation of VMO and VL activity was used to determine the similarity of the muscle activity throughout the balance task, as well as the relative time delay between the activity of the two muscles. The

influence of balance surface on each dependent variable was determined using a repeated measures ANOVA with $\alpha = 0.05$. When a significant effect of task was found, pairwise comparisons between tasks were performed.

RESULTS AND DISCUSSION

The balance score decreased as the instability of the task increased ($F_{(4,6)}=8.379$, $p=0.012$). There was no significant effect of balance surface on the delay ($F_{(4,6)}=1.459$, $p=0.323$) or cross-correlation coefficient ($F_{(4,6)}=0.681$, $p=0.630$) for VMO and VL. Peak knee abduction moment ($F_{(4,6)}=6.441$, $p=0.023$), and frontal plane knee moment variability ($F_{(4,6)}=17.799$, $p=0.002$) were greater for balance board tasks with instability in the medial-lateral direction (EC, ML, MULT). The results of the pairwise comparisons are illustrated in Figure 1.

CONCLUSIONS

Balancing in single-leg stance on surfaces with instability in the medial-lateral direction results in

high knee abduction moment and variability. The goal of this study was to establish the knee loading patterns of healthy recreational athletes across different balance tasks. The next goal would be to determine if individuals with knee pain demonstrate disrupted muscle firing patterns and knee loading during balance tasks.

REFERENCES

1. Taunton JE, et al. *Br J Sports Med.* **36**, 95-101, 2002.
2. Barton CJ, et al. *Sports Medicine.* **40**, 377-395, 2010.
3. Stefanyshyn DJ, et al. *Am J Sports Med.* **34**, 1844-1851, 2006.
4. Neptune RR, et al. *Clin.Biomech.* **15**, 611-618, 2000.
5. Verhagen E, et al. *Am J Sports Med.* **32**, 1385-1393, 2004.
6. Caraffa A, et al. *Knee Surg Sport Tr A.* **4**, 19-21, 1996.
7. Soderman K, et al. *Knee Surg Sport Tr A.* **8**, 356-363, 2000.

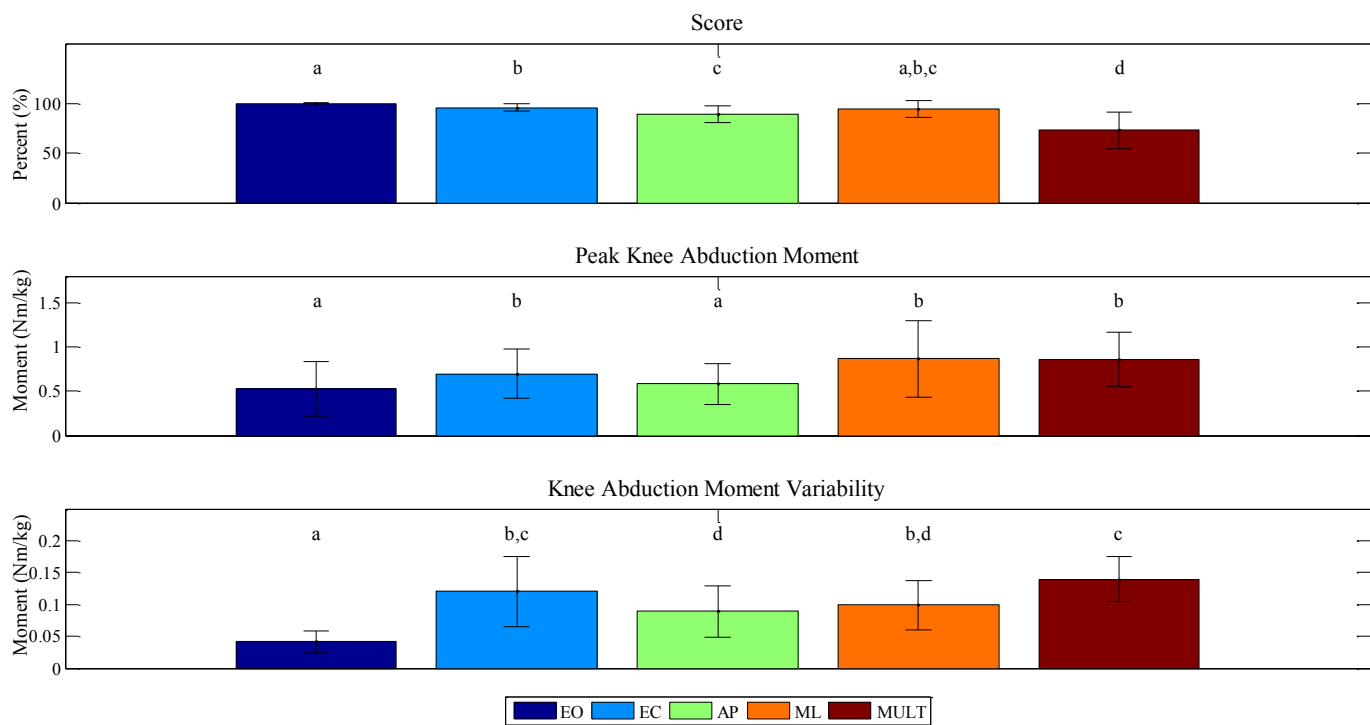


Figure 1: Means and standard deviations (error bars) for each dependent variable. Within each panel, similar letters indicate values are not significantly different from each other; significance determined at $p < 0.05$.

Hand and Foot Responses that Improve Ladder Fall Recovery

¹ Erika M. Pliner, ²Na Jin Seo and ³ Kurt E. Beschorn

¹ The University of Wisconsin-Milwaukee, Milwaukee, WI, USA

² Medical University of South Carolina, Charleston, SC, USA

³ The University of Pittsburgh, Pittsburgh, PA, USA

email: beschorn@pitt.edu

INTRODUCTION

Ladder falls are the leading cause of fatal falls [1]. Previous research has revealed that ladder slip and fall risk is associated with the design of the ladder and climbing biomechanics [2, 3]. Furthermore, preliminary studies by our group have noted that the recovery response to a ladder fall event initially prioritizes reestablishing the hands back on to a ladder followed by the feet [4]. However, there is limited knowledge about the variability in the coordination between hands and feet during ladder climbing and in response to a perturbation. The effect of these different hand and feet strategies on recovery is not well understood. Thus, the purpose of this study is to investigate how hand and foot responses to a ladder climbing perturbation affect recovery.

METHODS

Thirty-five (10 female) participants between the ages of 18 and 29 were recruited for this study. Participant safety protocols were taken with IRB approval, written informed consent, and proper climbing attire which included a safety harness that was equipped with a load cell (1000 Hz). In addition, 47 reflective markers were placed on the participant's anatomical landmarks to record their kinematic data (100 Hz).

Participants climbed a vertical 12-foot custom ladder where they experienced a simulated ladder misstep perturbation. The perturbations were initiated using a rung that was unexpectedly released from under the subject's foot and subjects experienced a perturbation during ascent and descent while wearing high friction gloves, low friction gloves and no gloves. Five to eight unperturbed trials occurred between perturbed trials to reduce anticipation effects.

Recovery to the perturbation was measured based on the amount of weight support that the harness provided after the perturbation. A load cell attached

in series with the harness rope was used to record the maximum force between the start of and end of fall. The start of the fall was determined based on the start of the perturbation and the end of the fall was determined based on when the pelvis reached the first local minimum in the vertical position [5].

Review of videos was used to categorize the hand and foot responses. When analyzing the hand responses, only the hand that was in motion (in the case of 2 points of contact) or the hand that would move next (i.e., the lower hand during ascent in the case of 3 points of contact) was analyzed. Four hand responses were observed: 1-Hand did not move; 2-Hand continued to the next rung as planned (i.e., moved 2 rungs up during ascent or 2 rungs down during descent); 3-Hand interrupted the planned path of motion and grasped the rung before the intended rung (i.e., grabbed one rung above the starting position for ascent or one rung below the starting position for descent); 4-Hand was in contact at the start of fall, but released the rung momentarily before re-grasping the same rung. Trials where the other hand released the rung and grasped a lower rung were excluded (n=4/171). Three types of foot responses from the perturbed foot were observed. A-hit the ladder rail or rung and fell to a hanging position; B-stopped on a lower rung; C-fell to a hanging position.

An ANOVA was performed to determine the effects of the hand response on harness forces. Because previous research had determined that gender was an important factor in ladder recovery, gender and the interaction between gender and hand response were also included. A second ANOVA was performed to assess the foot responses on recovery. This foot response model also included gender and the interaction. Both ANOVAs used harness force as the dependent variable. A Tukey's HSD post hoc analysis was performed on the hand and foot type responses. These ANOVA models were assessed separately for ascent and descent.

RESULTS AND DISCUSSION

The pathway for hand motions were variable across participants during ascent: 1) the hand did not move in 36% of trials; 2) the hand grabbed the target rung in 28% of trials; 3) the hand interrupted the planned path of motion and landed at the next rung in 13% of trials; and 4) the hand left the rung and came back down on to the same rung in 21% of trials. During ascent, harness force varied across hand response type ($p < 0.05$) and were higher for female participants ($p < 0.001$) but was not affected by their interaction ($p = 0.148$). Harness forces were highest when the hand interrupted the planned path of motion and grabbed one rung above the starting position. (Figure 1).

The pathway for hand motions were also variable across participants during descent: the hand did not let go of the rung in 11% of recoveries; the hand grabbed the target rung in 62% of trials; the hand interrupted the planned path of motion to grasp one rung above the target rung in 16% of trials; the hand let go of the rung and then reestablish position on the same rung in 8% of trials. During descent, harness forces varied with hand response type ($p < 0.01$) and were higher for females ($p < 0.05$) but were not influenced by response \times gender interaction ($p = 0.457$). Harness forces were lower when the hand maintained contact with the rung during the entire fall or reestablished position on the rung that was just released than when the hand continued as planned to the next rung. Therefore, maintaining two hands on rungs or reestablishing the hand back to the same rung may offer benefits for ladder recovery during descent.

The response of the foot varied for ascent and descent trials. Specifically, the foot hit the ladder and fell to hanging position in 33% of ascent trials and in 39% of descent trials; stopped on a lower rung in 43% of ascent trials and in 22% of descent trials; and fell to hanging position without hitting the ladder in 22% of ascent trials and 36% of descent trials. Harness force varied between foot response for ascent ($p < 0.01$) and descent ($p < 0.001$) perturbations. In addition, higher harness forces were observed for female participants during ascent ($p < 0.01$) and descent ($p < 0.01$) but no response by gender interactions were observed in either climbing direction ($p = 0.785$ and $p = 0.576$,

respectively). Lower harness forces were observed when the foot reestablished placement onto a lower rung than when the foot hit the ladder side/rung and fell off or when the foot never made contact with the ladder. Therefore, the feet are an important component in recovering from a ladder fall event.

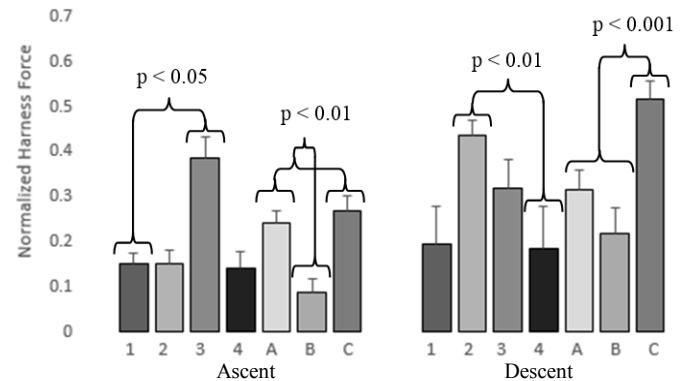


Figure 1: Harness force normalized to body weight for hand (numerical columns) and foot (alphabetic columns) responses during ascent and descent.

CONCLUSIONS

The results of this research indicate that the motion paths of the hands and feet during ladder recovery are important contributors to recovery. Maintaining both hands on the ladder during recovery was effective during ascent and descent. In cases where the hand left a rung, grasping a higher rung (i.e., not interrupting the hand path during ascent and interrupting the hand path during descent) increased recovery. This finding may be explained by previous research that found a more extended arm posture increases upper limb strength [6]. In addition, reestablishing the feet back on the ladder after a fall is critical to recovery. Thus, additional research that identifies means of improving foot placement after a fall may also offer protection against ladder falls.

REFERENCES

1. BLS, *Number of fatal work injuries 1992-2010*, Washington, D.C., '12
2. Shepherd G, et al. *Ergonomics* **49**, 221-234, '06
3. Pliner E, et al. *Ergonomics* **57**, 1739-1749, '14
4. Paul A, et al. *Proc. of ASB*, Omaha, NE, '13
5. Pliner E, et al. *Proc of ASB*, Columbus, OH, '15
6. Salehi S, et al. *Proc. of WCB*, Boston, MA, '14

ACKNOWLEDGEMENTS

This work was funded by NIOSH/CDC (R21OH010038).

CHANGES IN DYNAMIC BALANCE CONTROL AND POSTURAL STABILITY BETWEEN LEVEL AND SLOPED WALKING

^{1,2} Scott P. Breloff and ² Dwight E. Waddell

¹ University of Scranton, Scranton, PA, USA

² The University of Mississippi, University, MS, USA
email: scott.breloff@scranton.edu

INTRODUCTION

Injuries from falls, both fatal and non-fatal, constitute a majority of worksite related injuries each year [1]. In 2013 non-fatal construction falls were 16.1 falls per 10,000 workers [1]. Six hundred and ninety-nine workers lost their lives due to falls, slips, or trips in 2013 while falls from height accounted for 574 (82 percent) of those fatalities [1]. Fatigue induced by abnormal walking has a negative impact on balance control and individuals are less stable after walking along a sloped surface compared to a level surface for a prolonged period of time [2-3]. The purpose of this study was to determine if subjects balance control was compromised following a prolonged time on a non-level surface.

METHODS

Thirteen participants, all college age male students (Mass: 88.06 ± 16.83 kg, Height: 179.60 ± 6.05 cm), who were considered inexperienced walking on sloped surfaces, participated in the study.

Subjects completed two identical procedures on non-consecutive days consisting of one hour of walking on either a level (W) or sloped surface (S). Level walking trials required the subjects to walk on the laboratory floor. For the sloped condition, a pitched roof segment, measuring 24 feet by 8 feet at a 6/12 (26.5°) pitch was constructed for the participants to walk on (Figure 1). Subjects wore steel-toed work boots during all walking conditions.

As a baseline assessment, barefoot subjects completed two NeuroCom EquiTest® balance testing protocols - Sensory Organization Test (SOT) and the Motor Control Test (MCT) [4, 5].



Figure 1. Top: Roof Segment. Bottom: Subject traversing roof segment.

The participants would then put on steel-toed boots and complete a one hour walk for either of the two conditions. Following the one hour walk, subjects would again remove their boots and complete the balance testing protocols a second time. The NeuroCom EquiTest® was in the same room as the walking conditions therefore the transition time from walking to testing was almost instantaneous.

RESULTS AND DISCUSSION

Sensory Organization Test (SOT) and Motor Control Test (MCT) composite scores were statistically analyzed in a 2 x 2 x 2 (Test x Time x Condition) mixed analysis of variance (ANOVA), with repeated measures on the condition to determine if conditions differ between Pre- and Post-Condition composite scores. The SOT composite score is the weighted average of the scores of all sensory conditions which characterizes the overall level of performance. The MCT

composite score is the average of the individual latency scores for the two legs for the medium and large translations [5].

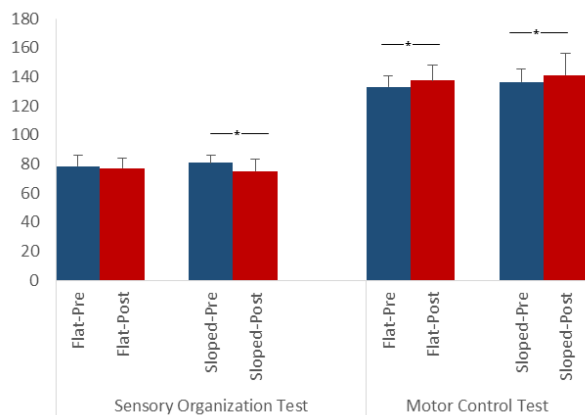


Figure 2: NeuroCom EquiTest® Pre-Condition and Post-Condition composite scores. ‘*’ indicate group differences from post hoc tests

There was significant within subject interaction between Test x Time x Condition, $p < 0.01$; Table 1. Follow up tests revealed no differences in the pre walking scores for either condition (MCT and SOT) indicating that subjects had the same composite postural control prior to the walking intervention. There were significant differences between the pre and post walking composite scores for both the MCT conditions (level and sloped); however the SOT composite scores were significantly different following only the sloped condition (Figure 2). Suggesting, the composite MCT postural control of the walkers who were inexperienced with sloped surfaces was altered due to prolonged walking while the SOT composite scores was altered following only sloped walking.

Walking on a sloped surface for one hour has a significant, detrimental effect on postural control which agrees with previous literature [3]. A decrease in postural control while walking on a sloped surface may be a contributing factor to the construction related falls suggested by the BLS. Data from the BLS did not provide the mechanism of the falls, or how long into a work shift when a fall occurred. Therefore, direct comparisons to deficits in postural may be difficult, but workers

should be educated regarding this change during the work day.

Sensory Organization Test	Mean	Standard deviation
Flat-Pre	78.54	7.41
Flat-Post	77.15	6.56
Sloped-Pre	80.85	5.18
Sloped-Post	74.92	8.58
Motor Control Test	Mean	Standard deviation
Flat-Pre	133.18	7.57
Flat-Post	137.45	11.00
Sloped-Pre	136.45	9.30
Sloped-Post	141.36	14.58

Table 1. Means and Standard Deviations for the Sensory Organization Test and the Motor Control Test for both conditions and over time.

CONCLUSIONS

The study results indicate that a sloped surface can lead to a decrease in composite postural control. The findings demonstrate a decrease in the influence of postural control from both the sensory and motor control systems. A decrease in postural control has been documented in previous literature to be one of the triggering events leading to falls. Balance control is maintained through the integration of sensory and motor control systems and a decrement in either of these systems can lead to a decrease in postural control.

REFERENCES

1. Sawicki GS. *Proceedings of NACOB'08*, Ann Arbor, MI, USA, 2008.
2. Simoneau, M, et al. *J NeuroEngin and Rehab*, **3**, 22-31, 2006.
3. Wade, LR., & Davis. *J. Prof Safety*, **50**, 45-50, 2004.
4. Guskiewicz, KM & Perrin, DH. *J Sport Rehab* **5**, 45-63, 1996.
5. (2012, January 1). Retrieved February 26, 2015, <http://resourcesonbalance.com/neurocom/products/EquiTest.aspx>

ACKNOWLEDGEMENTS

This research was funded by the University of Mississippi's Department of Health, Exercise Science and Recreation Management Graduate Award.

COMPARING TRUNK PROPRIOCEPTIVE ABILITY AND MUSCLE RESPONSES TO SUDDEN TRUNK PERTURBATIONS BETWEEN ATHLETES AND NON – ATHLETES

¹ Grace O. Glofcheskie and ¹ Stephen H.M. Brown

¹ University of Guelph, Guelph, ON, Canada

email: gglofche@uoguelph.ca

INTRODUCTION

Trunk control and stability is essential for athletic performance, as it is the centre of the kinetic chain and the base for all limb movements [1]. Previous studies have found that deficiencies in trunk neuromuscular control can predispose athletes to low back and lower extremity injuries [2, 3]. In order to produce an appropriate muscle response, three levels of motor control must be present. The spinal reflex pathway uses proprioceptive input from both muscle spindles and Golgi tendon organs. The brain stem pathway coordinates both visual and vestibular input using proprioception from joint receptors and mechanoreceptors in the skin [4]. Finally, cognitive programming is based on stored central commands, which lead to voluntary adjustments [5]. Therefore, if a lack of proprioceptive ability was responsible for delayed muscle response to perturbations and poor trunk postural control, a relationship between measures of these three contributors to motor control could be present. The purpose of this study was to determine if differences exist between athletes and non-athletes in neuromuscular response time to perturbations, seated postural control, and sagittal and axial trunk re-positioning ability. It was hypothesized that athletes would exhibit faster response to trunk perturbations, greater postural control and less error in trunk re-positioning tasks when compared to non-athletic controls.

METHODS

Male golfers (athlete group) competing at the collegiate varsity level (n=10), as well as male participants (control group) with no athletic background (n=10) were recruited. These groups were matched based on age, height and weight, with no significant difference between groups. An active marker motion capture system (Optotrak™ Northern Digital Inc., Ontario, Canada) was used to record 3D

lumbar movement, with markers at vertebral levels T12 and S1. Electromyography (EMG) was recorded bilaterally to measure activation levels and response times of the thoracic and lumbar erector spinae, external oblique, and internal oblique muscles (AMT-8™ Bortec Biomedical Ltd., Alberta, Canada). Participants performed three separate testing protocols presented in a random order:

1) seated sagittal and axial trunk re-positioning tests to measure position sense; 2) a seated balance test to measure postural control using a wobble board placed on top of a force plate (True Impulse™, Northern Digital Inc., Ontario, Canada); 3) sudden trunk perturbations, applied with a mass of 10% of their maximum trunk extensor strength, in both the anterior and posterior directions, as well as with combined twist, while kinematic and EMG data were recorded. The dependent variables (3D lumbar spine motion, muscle responses, centre of pressure excursions and velocities, degrees of re-positioning error) were compared between golfers and controls. A significance level of $\alpha < 0.05$ was used for all statistical comparisons.

RESULTS AND DISCUSSION

In sagittal trunk re-positioning tasks, golfers demonstrated significantly less absolute error (absolute difference between positioned target angle and re-positioned angle by participant) and variable error (standard deviation of absolute errors across trials). Significant differences were also observed in sagittal re-positioning to self-selected neutral posture, with less error in both absolute and variable errors in golfers (Figure 1). Similar trends were observed in axial re-positioning, as golfers showed significantly less error in absolute and variable error in both re-positioning to the target angle, as well as neutral posture (Figure 2).

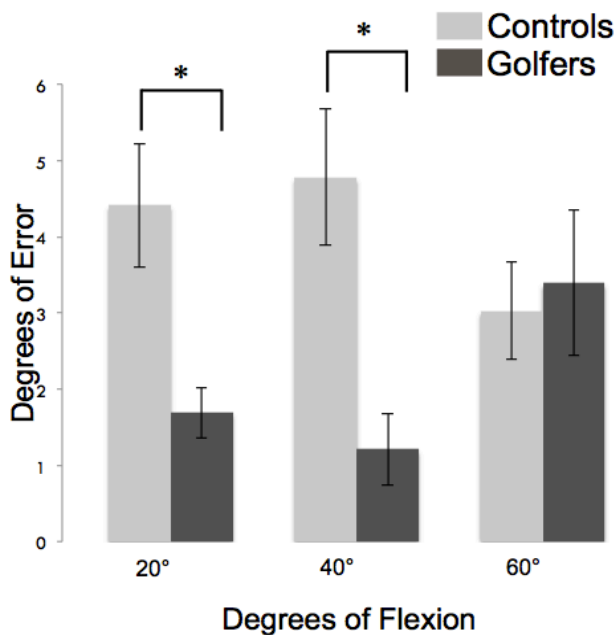


Figure 1: Sagittal re-positioning absolute errors between golfers and controls in repositioning to target angles of 20°, 40° and 60° trunk flexion.

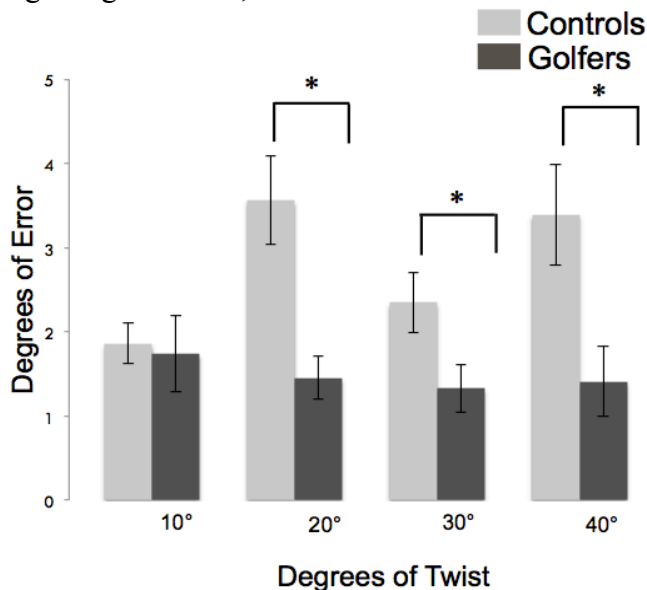


Figure 2: Axial re-positioning absolute errors between golfers and controls in repositioning to target angles of 10°, 20°, 30° and 40° trunk axial twist.

Golfers did not perform sagittal re-positioning at 60° of trunk flexion differently when compared to controls, however demonstrated significantly less error at 20° and 40° flexion. During the training and performance of their sport, golfers consistently adopt a posture of approximately 30° of trunk flexion and rarely position themselves near end ranges of trunk flexion. This is reason to suggest why golfers exhibit

less error at 20° and 40°, yet are no different than controls at 60° of flexion. In axial re-positioning tasks, golfers demonstrated significantly less error at 20°, 30° and 40°, yet no differences from controls at 10° of trunk axial twist. During the golf swing, these athletes are repeatedly twisting to their end ranges of motion in both the backswing and follow through. Due to this repetitive motor pattern that golfers develop, it is possible that they are more comfortable in these ranges of axial twist that are further away from neutral. In the seated balance task, golfers demonstrated significantly smaller ranges of centre of pressure (CoP) deviations in both the anterior-posterior and medial-lateral directions. Golfers also demonstrated significantly shorter cumulative path lengths, as well as significantly less path length velocity. Golfers also demonstrated faster neuromuscular responses to sudden trunk perturbations. This suggests evidence that greater proprioceptive ability is related to faster muscle responses and greater trunk postural control.

CONCLUSIONS

Golfers demonstrated less error in trunk re-positioning tasks, which suggests greater proprioceptive ability compared to non-athletic controls. Greater trunk postural control was also observed in golfers compared to controls in the seated balance task. Finally, faster neuromuscular responses to sudden trunk perturbations were observed in golfers compared to controls. Combined, these data suggest that golfers have enhanced proprioceptive abilities, which potentially lead to faster muscle responses to trunk perturbations, and therefore overall greater postural control compared to non-athletes.

REFERENCES

1. Borghuis AJ, et al. *Med Sci Sports Exerc* **43**(1), 108 – 14, 2011.
2. Cholewicki J, et al. *Spine* **30**(23), 2614 – 20, 2005.
3. Zazulak BT, et al. *Am J Sports Med* **35**(7), 1123 – 30, 2007.
4. Proske U, et al. *J Physiol* **587**(17), 4139 – 46, 2009.
5. Lephart SM, et al. (1997). *Am J Sports Med* **25**, 130 – 37, 1997.

COMPLIANT FLOORING AND ITS EFFECT ON POSTURE: DIFFERENCES BETWEEN YOUNG AND OLDER POPULATIONS

¹Jessica Buschman, ²Samuel Leitkam, PhD, ¹Tamara Reid Bush, PhD

¹Michigan State University, East Lansing, MI, USA

²Ohio University, Athens, OH, USA

email: buschma5@msu.edu, leitkam@ohio.edu, reidtama@msu.edu

web: <http://researchgroups.msu.edu/reidtama>

INTRODUCTION

Thirty percent of older people (65 years and older) fall at least once every year [1]. Although there are many forms of preventative measures for falls, recent studies cite that compliant flooring is a new form of passive intervention for this issue [3]. Research has been conducted to analyze the relationship of flooring compliance and postural stability by measuring sway and/or Center of Pressure [2, 3], but there is currently a lack in research on how flooring compliance affects body kinematics. This study investigated how different flooring types impacted body posture in regards to the ribcage and pelvis orientations for young and older groups of individuals.

METHODS

The subject pool for this exploratory study consisted of 13 healthy participants. These participants were grouped into young and older age brackets: five participants were of the ages 19-29 (ave. 24.2, SD 3.96), and eight participants were over the age of 50 (ave. 69.1, SD 11.1). Qualysis motion capture was used to track markers at the seventh cervical vertebrae (C7), the two anterior superior iliac spine (ASIS) projections, and midway between the two projections of the posterior superior iliac spine (MidPSIS).

Four floorings included in this study were Airex; the flat surface of a force plate; a generic foam-core anti-fatigue mat produced by Hampton Bay; SmartCell; and SofTile. These floorings were labeled “air”, “flat,” “mat”, “smart”, and “soft”, respectively. Airex is a soft foam material used in balance and training; SmartCell is a two inch thick rubber flooring designed to reduce impact and fatigue; and SofTile is playground flooring with a

hollow-core impact pedestal. Participants were seated on a backless stool with no arm supports and their feet placed on the flooring. Seat height was adjusted to ensure a knee angle of 90 degrees for each participant and flooring. The order of the floorings was randomized for each trial and each subject.

When instructed, the participants were asked rise to a standing position, all while keeping a forward gaze. Once in the standing position, participants were asked to maintain the standing posture for twenty five seconds. This method was repeated for all five types of flooring.

Posture was analyzed by evaluating the sagittal orientation of the pelvis and ribcage relative to vertical when standing. The ribcage orientation was defined by a vector starting at the sternum and pointing through the C7 marker. The pelvis orientation was defined by a vector starting at the MidPSIS and passing through the midpoint of the ASIS markers. The ribcage angle was defined as the angle between the ribcage vector and vertical; the pelvis angle was the angle between the pelvis vector and vertical.

RESULTS

Figures 1 and 2 provide the average and standard deviations for the pelvis and ribcage values for both young and older subject groups. A noticeable increase in pelvis angle for the older participants occurred across all floorings. The ribcage angle decreased for the older participants.

A two-way ANOVA was computed to determine whether significant differences in ribcage and pelvis angles between young and older groups existed. The results show that there was a significant difference

(at the 95% confidence interval) between the young and older groups for both the pelvis and ribcage angles. The p values for this significance were 0.0087 and 0.0044, respectively. Between floorings, however, there was no significance found for either the pelvis or ribcage angles for either of the groups.

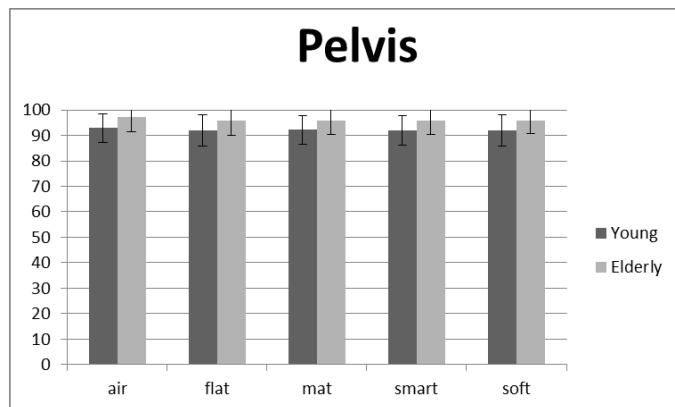


Figure 1: Standing pelvis angles for older and younger groups. All groups showed significance between age groups.

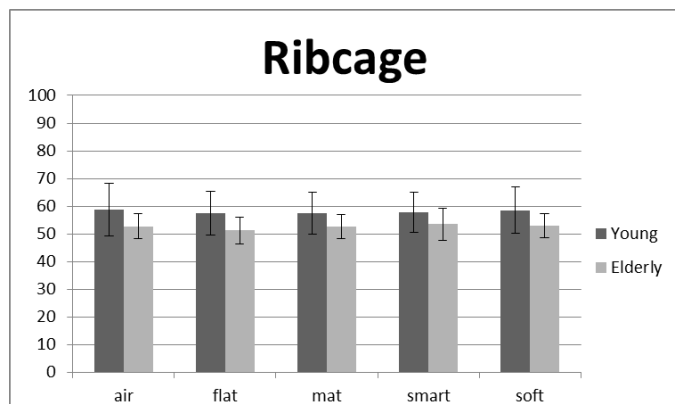


Figure 2: Standing ribcage angles for older and younger groups. All groups showed significance between age groups.

DISCUSSION

Based on the orientation of the pelvis vector, a larger pelvis angle represented a larger anterior rotation of the pelvis; whereas a larger ribcage angle represented a posterior rotation of the ribcage. The results showed that the older group had significantly larger anterior pelvic and ribcage tilt when standing than the younger group. In other words, the older populations rotated their pelvis and ribcage both forwards and downwards when standing, resulting in a “forward lean” of their standing position on the floorings. The lack of significance between

floorings showed that neither group significantly changed their ribcage or pelvis orientations to account for the different floorings.

It was surprising that there were no significant differences seen between the “air” case and the other floorings, as it was a highly compliant flooring. This could be explained by the fact that this study did not look at *movement* of the pelvis and ribcage, but rather average postural angles.

Both Beach et al. and Wright et al. found that compliant floorings have a small but significant effect on postural stability amongst older populations [3, 4]. The forward rotation seen in our study could help explain the significant sway in the anterior/posterior (A/P) direction for these older populations, seen by Beach et al. This is important because this increased sway has been linked to an increase in postural instability, leading to falls [3].

CONCLUSIONS

Significant differences between the older and young postures existed across all floorings. However, no differences existed between floorings. Thus, this research does not indicate a postural difference due to type of flooring; rather the postural differences are age related. Understanding the postural changes in older populations and how different types of flooring compliances affect those postures will help in developing approaches for fall prevention.

REFERENCES

1. Center for Disease Control, 2014
2. Beach et al., Proceedings of ASB ‘13, Omaha, NE, USA, 2013
3. Wright AD, Laing AC and Laing AC. Accident Analysis and Prevention 2011; 43: 1480-1487

ACKNOWLEDGEMENTS

The authors would like to thank Renee Sample and Dr. Kimberly Bigelow with their assistance with data collection; SATECH, Inc. and Sof Surfaces, Inc. for their flooring donations; and Michelle Samalik for her assistance in data analysis.

LOWER EXTREMITY NET JOINT MOMENTS DURING LATERAL LOAD TRANSFERING: DIFFERENCES BETWEEN HIGH AND LOW SURFACE FRICTION

¹ Robert D. Catena and ² Xu Xu

¹ Washington State University, Pullman, WA, USA

² Liberty Mutual Research Institute for Safety, Hopkinton, MA, USA
email: robert.catena@wsu.edu, web: <http://labs.wsu.edu/biomechanics/>

INTRODUCTION

Stress on the lower back is typically the concern in manual material handling tasks. However, when the load and frequency is sufficiently light, balance and falls become a concern. Reports indicate that falls are a leading cause of injury in manual material handling occupations, especially those performed outdoors where conditions aren't as controlled [1].

We have recently endeavored to study balance during the lateral transfer of a load [2]. In our most recent study we reported the differences in lower extremity joint kinematics between two transfer techniques [3]. One technique was successfully used in both high and low surface friction conditions, while another technique was just as successful (determined by transfer distance) in high friction conditions, but increased the likelihood of a fall when the same task and distance were performed on a slippery surface. In this study we sought to retrospectively determine if there is any kinetic benefit to either transfer technique. Toward that goal, we examined the changes in net moments at the lower extremity joints due to surface friction between these two transfer techniques.

METHODS

Thirty-five working aged volunteers with no substantial material handling experience provided informed consent to participate in this study. Participants wore a completely similar wardrobe (including shoes) and were harnessed during testing. Participants completed a 180° transfer of a load at their maximum desired distance (Fig 1). This distance was determined during practice trials in a high-friction ($\mu=0.86$) condition before 6 successful trials were recorded (HCOF). We then changed the

surface to a low friction surface ($\mu=0.16$). Participants performed one trial using the same high-friction start position (LCOF1) before being allowed to practice and change the start configuration if so desired (LCOFp).

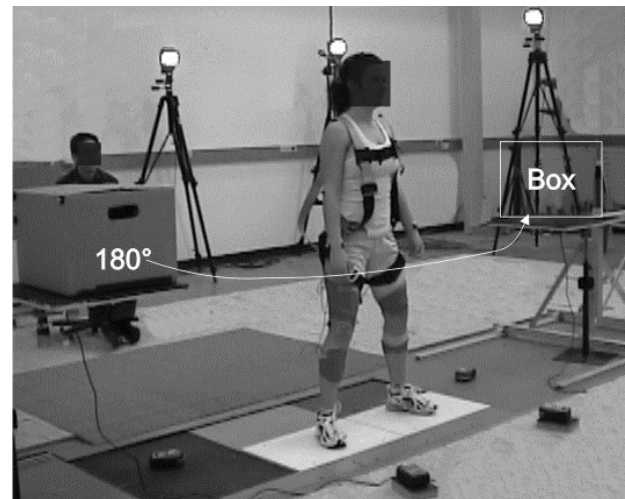


Figure 1: Start position and goal for the lateral load transfer

Participants wore a full-body passive marker set and marker motions were recorded with a 12-camera MotionAnalysis system. Ground reaction forces were recorded with Kistler force plates under each foot. An inverse dynamics method was used to calculate 3D internal net joint moments at the ankle, knee, and hip. Participants were retrospectively grouped by successful (SL) vs. unsuccessful (UL) completion of the LCOF1 trial. Joint moments were statistically compared between 2 groups and 3 tasks using a two-way ANOVA.

RESULTS AND DISCUSSION

There were two unique patterns to achieve the lateral load transfer in high friction conditions [3]. The SL individual used a narrow base that involved

pivoting the entire body, on the feet, towards the load as it was transferred. They did not substantially change their technique after practice in low friction conditions. The UL high friction approach to this task was a wide base of support, with greater motion at the lower extremity joints, but not the feet, resulting in motion of just the upper body towards the load rather than pivoting the whole body. However, after failing to use this technique successfully on a novel low friction surface and subsequent practice, UL individuals modified their transfer technique mostly toward that of the SL technique. The one exception was a newly adopted crouched posture throughout the task.

All subjects increased their starting hip, knee, and ankle adduction moments in low friction conditions compared to high friction conditions (Table 1), but surprisingly the greater UL stance width did not require any more of an increase in hip adduction moments compared to SL. The UL group did require a greater increase in start hip external rotation and extension moments compared to SL. These changes constitute those needed to merely hold a stance on the low friction surface in preparation for the transfer task. Only start moments could be examined in the LCOF1 task because UL individuals failed (fell or gave up) before completion of this task.

Table 1: Starting internal net moments (Nm).

		HCOF	LCOF1	LCOFp
Hip adduction	SL	2.98	22.58	15.48
	UL	9.11	29.24	19.24
Hip external rotation	SL	-0.30	1.64	0.83
	UL	0.59	7.90	4.74
Hip extension	SL	-0.13	7.75	8.09
	UL	7.57	31.30	24.68

While the two group transfer kinematics became more similar following practice on the low friction surface, there were only a few joint moments that became similar between the two groups (Table 2). Hip flexion, knee extension, and ankle adduction moments were originally different between groups in HCOF but converged to similar during LCOFp. Joint moment differences between groups during the transfer in high friction conditions typically

remained even after practice and convergence of the two transfer techniques in low friction conditions. Hip adduction, abduction, and extension moments increased from HCOF to LCOFp. Knee adduction and abduction moments also increased from HCOF to LCOFp. While ankle plantarflexion moment increased, ankle coronal and transverse plane moments decreased from HCOF to LCOFp.

Table 2: Transfer internal net moments (Nm).

C = combined group values.

		HCOF	LCOFp
Max. hip flexion	SL	14.61	12.78
	UL	7.40	11.31
Max. knee extension	SL	20.24	23.76
	UL	19.46	23.82
Max. ankle adduction	SL	21.25	20.36
	UL	23.34	19.73
Max. hip adduction	C	35.12	44.26
Max. hip abduction	C	40.12	49.23
Max. hip extension	C	137.47	145.26
Ave. knee adduction	C	10.40	15.06

CONCLUSIONS

On a low friction surface, the lower extremity muscles are tasked to control the torso position and orientation in the load transfer and do this while avoiding a slip of the foot. The potential for movement at either side of the joint significantly increases many of the net moments at the lower extremity joints. We found that the transfer technique alone, and combined consideration of both transfer technique and surface friction influenced some joint moments. However, surface friction had a much larger effect on joint moments, regardless of the transfer technique used.

REFERENCES

1. B.L.S. report. *US Dept of Labor*, 2012
2. Catena RD, et al. *Ergonomics* **54**, 1060-71, 2011.
3. Catena RD, Xu X. *Ergonomics in press*.

ACKNOWLEDGEMENTS

Funding provided by the Liberty Mutual - Harvard School of Public Health Post-doctoral Program.

EFFECTS OF BLURRY VISION ON STANDING BALANCE

Mitchell Clough, Caitlin O'Connell, Rakié Cham
University of Pittsburgh, Pittsburgh, PA, USA
email: mac306@pitt.edu

INTRODUCTION

Vision loss, specifically the loss of visual clarity, leads to an increased risk of falls [1]. Individuals suffering from vision loss must rely more heavily on other senses to maintain their balance, and in particular the vestibular system and proprioception. These effects are more pronounced in older adults and may decrease their mobility and independence. Previous studies have compared balance between people with normal vision and people who were legally blind, and found a significant difference between balance in people with healthy vision and people with significant vision loss [2]. The purpose of this study is to examine the effect of acute, or sudden, blurry vision on balance of young healthy individuals. This will help determine whether impaired balance in individuals with vision loss is due to just the vision loss or other compounding factors such as age. Our hypothesis is that induced blurry vision in healthy subjects will cause balance impairment.

METHODS

Five subjects (age 20-25, 4 males) with healthy vision were recruited. Individuals with conditions affecting gait or balance were ineligible for the study.

Sensory organization tests (SOT) were conducted using an Equitest posture platform (Neurocom, Inc) [3]. The posture platform allows for sway-referencing of the floor and the visual scene. The platform is implemented with a force plate used to measure the center of foot pressure (COP). The SOT test consisted of 6 trials completed for both normal vision and blurry vision (Table 1). The subjects' eyes were dilated to induce blurry vision. Pupil size was measured before and after dilating drops were instilled to ensure that eyes were dilated.

COP data was collected for 60 seconds at a sampling frequency of 100 Hz for each trial.

Table 1: SOT trial descriptions including eye, vision and proprioception conditions.

Trial	Eyes	Vision	Proprioception
1	Open	Fixed	Fixed
2	Closed	--	Fixed
3	Open	Sway	Fixed
4	Open	Fixed	Sway
5	Closed	--	Sway
6	Open	Sway	Sway

COP data was processed with a low-pass Butterworth filter. The first ten seconds were removed to remove any transient effects. The data was resampled from 100 Hz to 20 Hz. The root mean square (RMS) of the processed COP data was calculated. The mean velocity (MV) of the COP was obtained from the derivative of the processed COP data. Because sway-referencing of the platform is in the anteroposterior (AP) direction, only the RMS and MV in the AP direction were included in analysis (RMS-AP and MV-AP, respectively).

A mixed linear regression model was used to analyze the data, with the outcome variable of interest being RMS-AP or MV-AP. The independent fixed factors included in the model included SOT trial (1-6), the dilation condition (baseline/no dilation, dilated) and the interaction of these effects. Subject was included as an independent random effect. Statistical significance was set at 0.05.

RESULTS AND DISCUSSION

The effect of the dilation on RMS-AP was found statistically significant ($p < 0.05$), with greater

movement noted in the dilated eyes condition. This finding was consistent across all subjects (Figure 1). While the impact of the dilation on MV-AP did not reach statistical significance, a similar trend demonstrating greater sway velocities was noted in the dilated eye condition compared to the baseline condition ($p=0.1$). As expected SOT trial was a statistically significant effect ($p < 0.01$), but the interaction of dilation and SOT trial was not ($p > 0.1$), suggesting the dilation effect was consistent across all SOT conditions (Table 2).

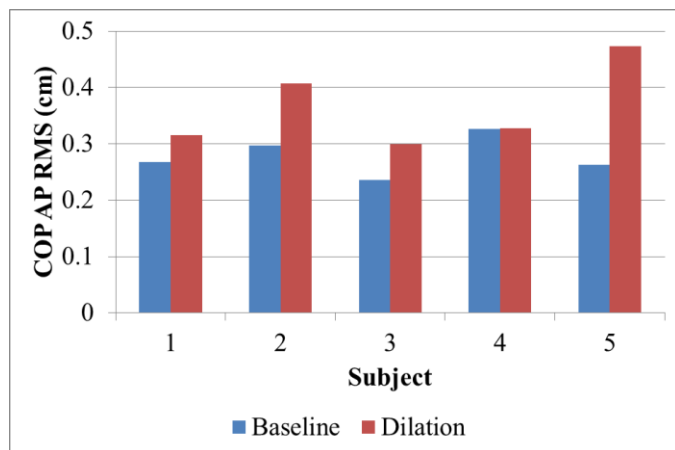


Figure 1: Average RMS-AP across all SOT trials for each subject for normal vision (baseline) and blurry vision (eyes dilated).

Table 2: Average COP RMS-AP across all subjects for each SOT condition.

SOT Trial	AP RMS (cm)	
	Baseline	Dilation
1	0.18 ± 0.04	0.21 ± 0.06
2	0.21 ± 0.05	0.30 ± 0.15
3	0.22 ± 0.06	0.31 ± 0.08
4	0.28 ± 0.10	0.37 ± 0.05
5	0.40 ± 0.10	0.57 ± 0.21
6	0.37 ± 0.08	0.43 ± 0.12

The findings of this study suggest that blurry vision or loss of visual acuity is associated with impaired balance. This finding agrees with epidemiological studies relating visual acuity loss with falls. The within-subject experimental design used in this study is a significant advantage of this study.

There are two potential mechanisms relating blurry vision or reduced visual acuity to falls. The findings of this study suggest that the loss of visual acuity is associated with an inability to rely on available and accurate sensory modalities. The second potential theory is that blurry vision reduces the ability to detect and avoid obstacles while walking, which was not tested directly in this study [4].

A limitation to this study is the small subject group, which limited the power of the statistical analysis. Additionally, all subjects were young and fit and thus may not have been affected by blurred vision to the extent that the elderly, who may have other comorbidities affecting balance, would have been. A future extension of this study could examine the effects of age on balance with blurry vision.

CONCLUSIONS

The differences in balance between the subjects when they had healthy vision versus when they had blurry vision suggest that vision loss does negatively impact balance. Further larger sample size studies are needed in order to understand the potential mechanisms mediating this effect.

REFERENCES

1. Elliot DB et al. *Optometry and Vision Science*. **91**, 593-601, 2014.
2. Ray CT et al. *Gait and Posture*. 2008.
3. Nashner, LM, et al. *J Neurosci*, **5**, 117-124, 1982.
4. Reed-Jones et al. *Maturitas*. **75**, 22-28, 2013.

ACKNOWLEDGEMENTS

Funding provided by the National Institutes on Aging (R03 AG04374).

Principal component analysis of human balance on a tunable balance board

¹Denise Cruise, ²Shirley Rietdyk, ²Jeffrey M. Haddad, ²Howard N. Zelaznik, ^{1,2}James R. Chagdes, ²Joshua Liddy, ¹Arvind Raman

¹School of Mechanical Engineering, Purdue University, West Lafayette, IN, USA

²Department of Health and Kinesiology, Purdue University, West Lafayette, IN, USA
email: drhickma@purdue.edu

INTRODUCTION

Understanding how many degrees of freedom are involved in human posture is important because it forms the basis for mathematical models of upright stance [4]. For quiet standing, it has been argued that one degree-of-freedom (DOF) models capture the dynamics of quiet standing [3,5,7]. Others argue that one DOF models cannot give a comprehensive description of human kinematics in upright posture, and that the model needs to be a multi-segment inverted pendulum [6].

Recently, there has been an interest in balance boards for training and rehabilitation of balance [1]. More recently, mathematical models of human balance on balance boards provided insight into how a person's region of stability (the parameters that lead them to be stable in an upright position) can be identified [2]. Thus mathematical models of humans on a balance board become important; however, little effort has been made to understand if the essential DOF of postural control on a balance board are related to the DOF on a rigid surface.

This work will act as a feasibility study to develop a protocol using principal component analysis (PCA) that will allow us to quantify the DOF of a person standing on a balance board transitioning from a stable to an unstable condition. Our initial results are presented here. Understanding the required DOF to maintain balance on an unstable rotational surface will help strengthen conclusions made about how people balance as they approach an instability, and inform models of human postural control.

METHODS

Participants

Fourteen healthy young university students (mean \pm S.D.: height 171.8 ± 9.1 cm, weight 65.4 ± 10.1 kg), 3 male and 9 female, with no known balance pathology participated in this study.

Equipment

Kinematic data was obtained using 3D wireless sensors (YEI Technology, Portsmouth, Ohio, USA). These sensors use a 2.4 Gz signal to transfer orientation data. The location of each sensor is shown in Figure 1.

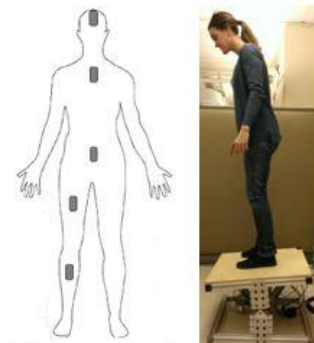


Figure 1: Left: Human diagram showing location of wireless IMU sensors: head, chest, pelvis, thigh, and shin. One wireless sensor was also placed directly on the balance board. Right: Human standing on tunable balance board.

Protocol

Participants were instructed to keep the balance board in a horizontal position, while looking straight ahead at a point on the wall. The torsional stiffness of the board linearly decreased in a continuous fashion, from a high stiffness value (similar to standing on a rigid platform), to no torsional stiffness; each trial lasted 50 seconds. Participants stood on the balance board with their feet side-by-side, approximately shoulder width apart, arms at their sides, and ankles aligned with the pivot point of the balance board.

Data Processing

Segmental angles were extruded from the sensors and used to calculate the following joint angles: ankle (shin – board), knee (thigh – shin), hip (pelvis – thigh), waist (chest – pelvis), and neck (head – chest) angles. The constantly changing demands of the balancing task due to the decreasing torsional stiffness of the balance board required us to analyze small segments of data. After looking at plots for various segment sizes, we chose one second as the length of each segment to analyze. The data were resampled to 30 Hz to ensure a constant sampling rate.

A covariance matrix was created for each second of data, and then PCA was performed on the covariance matrix. This procedure gives information about the modes of movement of the person: which mode is dominant (and by what amount), and which joint angles contribute to each mode.

RESULTS AND DISCUSSION

The PCA analysis provides information on what percentage of total sway motion can be attributed to a dominant mode, secondary mode, tertiary mode, etc. It also provides quantitative information on the contribution of various joints in each mode.

It was found that the movement of a person on a balance board can generally be described with two primary modes; the first mode accounts for the majority of the person's movement (~78% on average), and the second mode can account for 16%. Although there are other modes present, they only represent a small portion of the movement.

The PCA (Figure 2) also tells us what joint movements contribute to each of the modes. For example, at low torsional stiffness (time > 15 seconds), the primary mode features a greater contribution of ankle rotation. The opposite seems to be true of the secondary mode. Investigations into the variability of these modes and the joint contributions are ongoing. In addition, it can be seen that all of the joints contribute to each of the modes, but an analysis needs to be applied to determine which joint movements are statistically relevant.

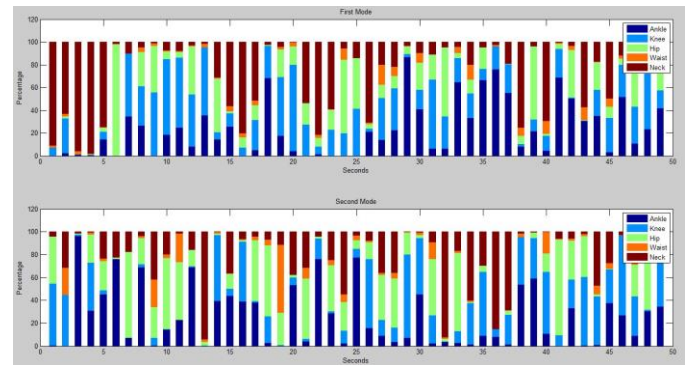


Figure 2: Contributions to the primary (top) and secondary mode (bottom) of postural sway by each of the joints for one participant. Data are plotted as a function of linearly decreasing torsional stiffness of the balance board.

CONCLUSIONS

A feasibility study has been performed using PCA to determine the dominant modes of a human balancing on a balance board with tunable torsional stiffness. Preliminary results indicate that unlike balance on a rigid surface, secondary modes may also be important contributors to balance. The joint rotation contributions to each mode tend to change with board torsional stiffness. Future work will examine the variability of this data with larger populations and trials.

REFERENCES

1. Aaltonen S, et al. *Archives of Internal Medicine* 167, no. 15: 1585-92. Aug. 2007.
2. Chagdes, JR, et al. *Journal of Biomechanics*. 2013.
3. Gage W, et al. *Gait & Posture*, 19, no. 2: 124-32, April 2004.
4. Maurer, C, et al. *Journal of Neurophysiology* 93: 189-200. 2005.
5. Peterka, R.J. *IEEE Engineering in Medicine and Biology Magazine* 22, no. 2: 63-68. 2003.
6. Pinter IJ, et al. *Journal of Neurophysiology* 100, no. 6: 3197-3208. Dec. 2008.
7. Winter, DA, et al. *Journal of Neurophysiology*, 80, no. 3: 1211-21. 1998.

ACKNOWLEDGEMENTS

The authors acknowledge the National Science Foundation for financial support for this project provided through the grant CMMI-1300632.

POSTURAL CHANGES IN YOUNG ADULTS WHEN WEARING A TRADITIONAL BACKPACK VERSUS THE BACKTPACK

Kimberly D. Dahl, D. Clark Dickin, and Henry Wang

Ball State University, Muncie, IN, USA
email: biomech@bsu.edu

INTRODUCTION

Load carriage can be the most convenient way to transport items from point A to point B. Over 40 million students in the United States use backpacks on a regular basis [1]. Poor posture brought on by improper backpack use has led to alignment issues such as forward head posture, rounded shoulders, kyphosis, low back pain, and an asymmetrical axial skeleton during both standing and gait. In 2013 alone, over 28,000 backpack-related injuries were treated at medical practices [2].

The principal purpose of this study was to assess head and trunk position during static stance before and after walking between a traditional backpack and a nontraditional backpack designed to disperse the load across the body and close to the vertical axis. It was hypothesized that the nontraditional backpack would result in a more upright posture showing less forward head posture and forward trunk inclination than the traditional backpack.

METHODS

Following IRB approval, twenty-four healthy young adults (22.5 ± 2.5 years, 12 male) participated in this study. Participants were free from injury and any other condition that would prevent them from carrying 15% and 25% of their body weight in a backpack. Participants also had a history of using a traditional backpack (3+ days/week). An informed consent and a health demographic questionnaire were completed prior to participating.

A 14-camera Vicon infrared motion capture system (VICON Inc., Denver, CO, USA) collecting at 120 Hz and an AMTI force plate instrumented treadmill (AMTI Inc., Watertown, MA, USA) collecting at 2400 Hz were used in conjunction with a modified

Plug-In Gait marker set that included marker clusters on the thigh and shank of each leg. A traditional backpack (BP) and the BackTpack (BTP) (BackTpack LLC, Salem, OR, USA) were used for load carriage. Load was added to the backpacks to equal 15% and 25% of the wearer's body weight and was evenly distributed in the backpacks, placing the heaviest weight closest to the spine for the traditional backpack and balancing the weights between the two pockets for the BackTpack. Each participant was assessed under five conditions: static recordings with no backpack and each of the two backpacks at the two load percentages both before and after walking for 6 minutes at a speed of 1.4m/s. The order in which the backpacks were worn and the load was applied was randomized, although the no backpack condition always came first.

Head angle and trunk angle in the sagittal plane were assessed using Visual 3D software (Version 5.0, C-Motion, Germantown, MD, USA), and pre-to post-walk data was analyzed using two one-way RM ANOVAs to compare the load percentages back to the No Load condition. A two-way RM ANOVA was used to compare the backpack and load percentages to each other. Where appropriate, Bonferroni corrections were utilized. Analyses were conducted in SPSS (Version 22 for Windows, SPSS Inc., Chicago, IL, USA), and the alpha level was set at $p < 0.05$.

RESULTS AND DISCUSSION

For all individual pack conditions (No Load, BTP, and BP) at both load conditions (15% and 25%), there was a significant difference in head angle between pre- and post-walk ($p = .004$, $p = .014$). Both backpacks at 15% and 25% were significantly

different from each other ($p=.002$, $p<.001$) and from the no load condition ($p<.001$).

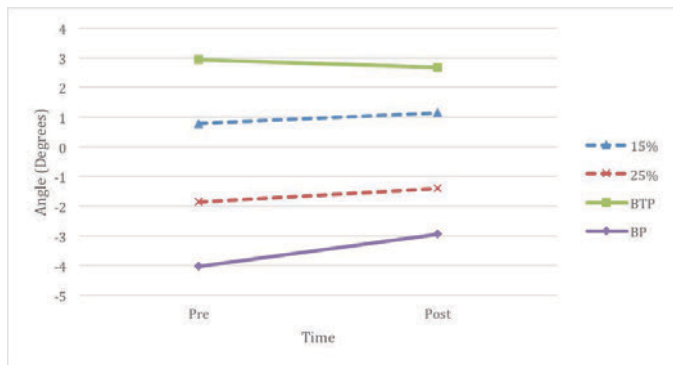


Figure 1: Trunk angle comparison in degrees for interaction effects between time (pre- to post-walk) and load percentage (dashed lines) and backpack type (solid lines). Abbreviations: BTP, BackTpack; BP, traditional backpack.

In comparing the two backpacks during both load percentages to each other, no significant differences were seen between time, load, or pack type for head or trunk angle. However, significant differences were seen in the time x pack interaction ($p=.030$) and in the pack x load interaction ($p=.008$) for trunk angle. These results can be seen in Figure 1.

Head angle was more negative (less hyperextension at the neck) and trunk angle was more positive (less forward flexion) for the BTP than the BP for both the 15% and 25% loads (Table 1). However,

following the walking period, the BP exhibited a slight reduction in trunk flexion while the BTP resulted in a slight increase in flexion. Overall, the more upright posture seen with the BTP may be due to the load placement along the vertical axis in conjunction with the line of gravity rather than being placed behind the wearer as with the BP. The findings supported the hypothesis, which was that the nontraditional backpack would result in a more upright posture than the traditional backpack.

CONCLUSIONS

In conclusion, the BTP more closely resembled the participants' natural stance as determined by the No Load condition for both head and trunk angle. The more upright posture supported by the BTP may help reduce characteristics of poor posture such as forward head positioning and forward trunk lean.

REFERENCES

1. Wang Y, et al. *Ergonomics* **44**, 858-869, 2001.
2. Ip K, et al. *American Academy of Orthopaedic Surgeons*, 2014.

ACKNOWLEDGEMENTS

Thank you to BackTpack for donating the nontraditional backpacks to help support this study.

Table 1: Mean (SD) joint angles of head and trunk in the sagittal plane for all five trial conditions pre- and post-walk. Abbreviations: BTP, BackTpack; BP, traditional backpack.

Joint Angle (deg)		Trial Condition				
		No Load	BTP 15%	BTP 25%	BP 15%	BP 25%
Head	Pre	-30.88(8.36)	-24.20(9.27)	-21.79(9.10)	-19.62(10.13)	-16.40(9.49)
	Post	-29.48(8.85)	-21.60(8.00)	-20.19(8.92)	-17.92(9.46)	-14.60(9.42)
Trunk	Pre	7.43(2.63)	3.69(2.86)	2.19(2.68)	-2.13(4.09)	-5.89(4.76)
	Post	7.95(2.63)	3.26(2.83)	2.07(2.74)	-0.97(3.04)	-4.85(3.09)

EFFECTS OF WHITE NOISE ACHILLES TENDON VIBRATION ON STANDING POSTURE

¹Erin M. Gaffney, ¹Carly C. Sacco and ^{2,1}Jesse C. Dean

¹ Medical University of South Carolina, Charleston, SC, USA

² Ralph H. Johnson Veterans Affairs Medical Center, Charleston, SC, USA

email: deaje@musc.edu

INTRODUCTION

We have proposed that proprioceptive feedback is used in the identification of economical movement patterns (1). Supporting this idea, we recently found that *disrupting* proprioceptive feedback from the plantarflexors during human walking reduces the rate of adaptation to a change in mechanical demand, and increases metabolic cost (2). This result raises the question of whether *enhancing* proprioceptive feedback could have beneficial effects for gait adaptation and economy.

Stochastic resonance, a phenomenon by which noise can increase a system's sensitivity, may hold promise for enhancing proprioceptive feedback. Recent work found that low-amplitude white-noise ankle tendon vibration improved passive movement detection (3). Similarly, low-amplitude electrical noise applied to the plantarflexors reduced postural sway due to enhanced proprioception (4). Such sensory stimulation may improve post-stroke function (5, 6). However, these benefits are strongly dependent on stimulation amplitude (see Fig. 1)

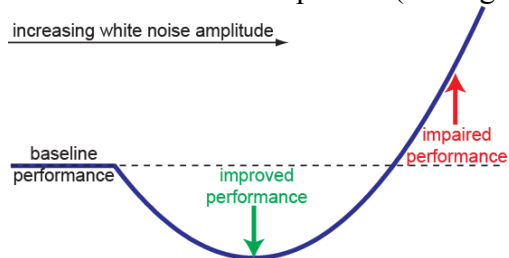


Figure 1. White noise stimulation can improve a system's sensitivity to an input signal, but only within a narrow range of noise amplitudes.

Our long-term goal is to investigate the effects of enhanced plantarflexor proprioception during walking. As a preliminary step, the purpose of these experiments was to test whether Achilles tendon white noise vibration influenced postural control,

and to identify the optimal vibration amplitude. We quantified the effects of such vibration during: 1) quiet standing; and 2) sway toward visual targets, a task requiring more substantial active control of the plantarflexors. We hypothesized that vibration amplitudes just below the sensory threshold would have maximal beneficial effects.

METHODS

Eight healthy females (age=24±3yrs; height=168±7 cm; mass=65±8kg) participated. We applied vibration as 100Hz bandwidth white noise using C-2 tactors strapped over the bilateral Achilles tendons. These vibration characteristics were previously successful in enhancing the sensitivity of plantarflexor muscle spindles (3). For each participant, we determined the sensory threshold (**ST**) for white noise vibration applied to each leg using a standard method of limits technique.

Participants performed 27 quiet standing trials (30s long) on a force plate with their eyes closed, arms crossed, and listening to brown noise, following instructions to stand as still as possible. Participants performed 3 trials for each of 9 vibration conditions: No Vibration and 20%, 40%, 60%, 80%, 90%, 100%, 150%, and 200% ST. These vibration amplitudes were chosen based on the common result that beneficial effects of stochastic resonance occur just below the sensory threshold.

Participants also performed 27 trials using active control of their center of pressure (CoP) location (Fig. 2). Participants used visual feedback of their CoP location to sway to 3 consecutive targets. Once the anteroposterior (AP) CoP location remained within 5mm of the target for 3 seconds, the target moved to the next position. For the fourth target, participants were not provided visual CoP feedback,

and pressed a push-button when they believed they were in the correct position. Participants performed 3 trials at each of the vibration levels listed above.

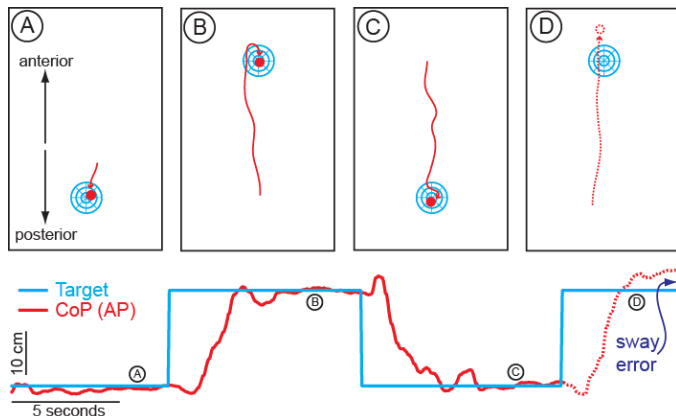


Figure 2. Sample illustration of the visual feedback provided to participants (top row), and CoP location relative to the target positions (bottom). Participants first swayed to a “home” target located relatively posteriorly using visual feedback of their CoP position (A). They then swayed to a variable-location anterior target (B) and back to the home target (C). Finally, participants swayed to the anterior target without visual CoP feedback (D).

Our analyses focused on AP CoP movement, where the effects of plantarflexor proprioception are strongest. For quiet standing, we quantified the CoP location standard deviation. For active sway, we quantified AP error at the final target position. We used repeated measures ANOVA to determine if these metrics were influenced by vibration level.

RESULTS AND DISCUSSION

Sensory thresholds varied widely across participants (range=10-28 μm rms amplitude). Contradicting our hypothesis, vibration amplitude (defined as %ST) did not have a significant effect on sway during quiet standing ($p=0.37$), and did not exhibit clear amplitude dependent modulation (Fig. 3A). Similarly, vibration amplitude did not have a significant effect on repositioning errors during active sway ($p=0.24$; Fig. 3B).

The lack of a clear vibration effect is surprising, as similar stimulation has had beneficial effects for other ankle tasks (3, 4). Our results may be due to the wide variation in the sensory thresholds used to

set individual stimulation intensity, which may be influenced more by cutaneous sensation than plantarflexor muscle spindles. As initial, indirect evidence for this possibility, grouping our results into quartiles of un-normalized vibration amplitude reveals a possible optimum around 20 μm (Fig. 4). Future experiments will test this possibility directly.

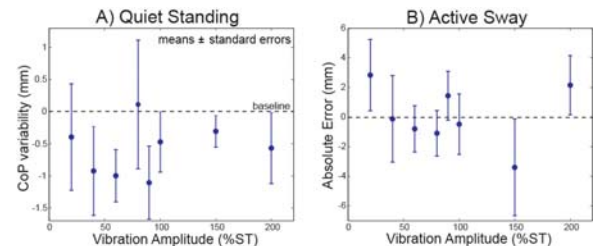


Figure 3. Changes in vibration amplitude did not have the expected effects on postural control during quiet standing (A) or active sway (B).

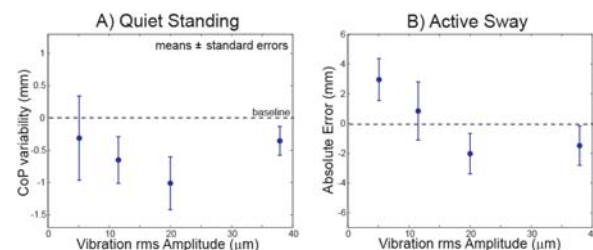


Figure 4. The effects of vibration amplitude may be more apparent if not normalized by threshold.

CONCLUSIONS

We were unable to define an optimal vibration amplitude in terms of the sensory threshold. Using un-normalized amplitude may be more appropriate (3) in order to define a stimulus likely to have future beneficial effects during post-stroke walking.

REFERENCES

1. Dean JC. *Exerc Sport Sci Rev* **41**, 36-43, 2013.
2. Hubbuck JE et al. *J Biomech* In Press.
3. Ribot-Ciscar E et al. *Exp Brain Res* **228**, 503-511, 2013.
4. Magalhaes FH, Kohn AF. *Exp Brain Res* **217**, 175-186, 2012.
5. Lee et al. *Clin Rehab* **27**, 921-931, 2013.
6. De Santis et al. *Front Hum Neuro* **8**, 1037, 2014.

ACKNOWLEDGEMENTS

This work was partially funded by Department of Veterans Affairs grant #IK2 RX000750.

ELECTROMYOGRAPHIC ANALYSIS OF CORE MUSCLE ACTIVATION DURING LUMBAR STABILIZATION EXERCISES: IMPLICATIONS FOR REHABILITATION AND TRAINING

¹ Harshavardhan Deoghare, ² Bhupinder Singh and ² Barbara Chan

¹ Western University of Health Sciences, Los Angeles, CA, USA

² California State University Fresno, Fresno, CA, USA

email: hdeoghare@westernu.edu0

INTRODUCTION

Enhanced core stability, defined as "the ability to maintain or resume an equilibrium position (or trajectory) of the trunk (and pelvis) after perturbation", has been touted to improve injury-prevention in many sports. Additionally, with increasing amounts of evidence showing that neuromuscular activation is delayed in individuals with low back pain, it is important to determine which specific exercises, when utilized as a part of rehabilitation intervention, specifically target those muscles for motor control. There is no consensus as to which exercise elicits the largest activation magnitude for the core muscles, and subsequently, is most appropriate to be included in the exercise-training program for core rehabilitation. Previous EMG studies generally relied on trained eyes to ensure lumbo-pelvic alignment and no objective measure is provided which questions their validity. Using the 'LevelBelt' it is possible to objectively confirm lumbo-pelvic alignment during functional postures/exercises. In female college students with no history of low back pain we investigated activation of Transverse abdominis (TAr), external oblique (EO), multifidus (MF) and quadratus lumborum (QL) during three specific core stabilization exercises including static and dynamic stabilization on a physioball, and planking.

METHODS

15 healthy female subjects between the ages of 22-30 years old, with no recent complaint of low back pain, has normal flexibility of lumbar spine and lower extremity range of motion, were recruited from Fresno State for this study. Subjects were excluded if they reported previous fracture or surgery to the spine and/or lower limbs, gross postural deformities, pregnancy and current low back pain symptoms. All subjects were provided

informed consent to participate. Following skin preparation and EMG instrument set up, all subjects were verbally and visually cued for the following exercises: sitting unsupported on physioball, and progress to dynamic stabilization (lifting a seven pound weight in seated position) followed by planking. 'LevelBelt' was strapped onto each participant across the upper sacrum and secured with the stabilization straps. The level belt was set to provide auditory and vibratory feedback with \geq two degree of pelvic tilt. Each participant had a visual demonstration of the activity before performing a practice trial. EMG recording was collected three times for accuracy for each exercise. The order of the exercise sequence was randomized for each subject to avoid order effect and fatigue. Muscle activity recorded from the three exercises was normalized to MVIC by dividing the raw data by MVIC values. The percentage of all the exercise activity in each of the four muscles was then averaged and imputed into SPSS software to compute a one-way ANOVA.

RESULTS AND DISCUSSION:

Table 1. Level of muscle activation during progressive core stabilization exercises

	High (>60%)	Moderate (21-40%)	Low (<21%)
Static			Multifidus
			Transverse Abdominis
			Quadratus Lumborum
			External Oblique
Dynamic		Transverse Abdominis	Multifidus
		Quadratus Lumborum	
		External Oblique	
	Transverse Abdominis	Quadratus Lumborum	Multifidus
Plank	External Oblique		

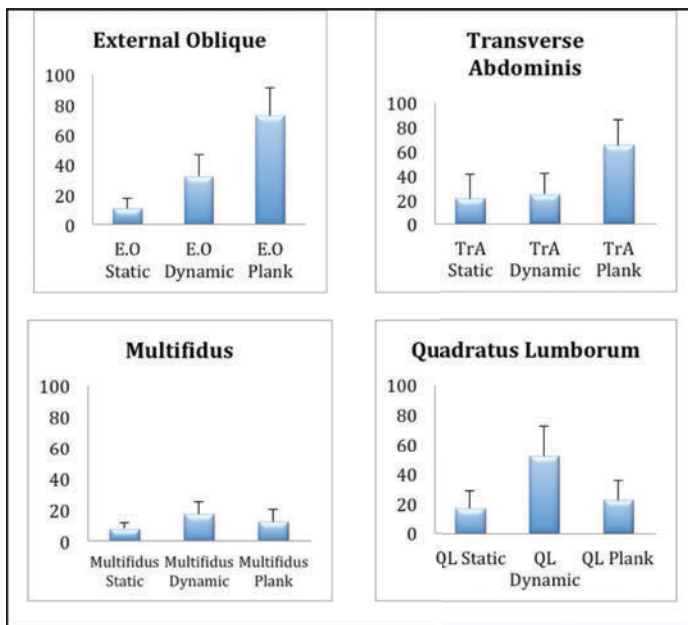


Figure 1: EMG Activity of Core Stabilizers during common physical therapy exercises.

The results suggest that core muscle activity is dependent on the type of core stabilization exercise as some muscles are more heavily activated in one type of exercise than the other. The significant difference between muscle activity during exercise suggest that prescribing static exercise, progressing to dynamic and plank will elicit progressive activation for the TA and EO; however MF and QL are mostly activated with dynamic stabilization type activity and not with planking.

Limitation: The interpretation of this study should be with caution as we examined only healthy female subjects performing the exercises in an attempt to maintain consistency and determine accurate muscle activation, however muscle recruitment pattern will be different in subjects with low back pain and may require additional, if not different, techniques to accurately activate the targeted muscle.

CONCLUSIONS:

Accurate neuromuscular activation of core muscles ensures the stability of the lumbo-pelvic complex, which is required for optimizing sports performance and prevent injuries. This is the first pilot study investigating muscle activation during core

stabilization exercises where lumbo-pelvic alignment is objectively measured and confirmed using a novel device called level belt, a clinical tool that provides real-time biofeedback about the antero-posterior and lateral pelvic tilt.

Tar and EO exhibited the most EMG activity during plank. Whereas, (MF) and QL demonstrated highest EMG activity during dynamic stabilization type exercises.

To construct an exercise regimen for treatment or prevention of low back pain or optimization of sports performance and prevent injury in healthy subjects consideration must be made for the desired target muscle and evidence based exercises that elicit the highest muscle activity must be utilized.

REFERENCES

1. Briggs M, Givens DL, Best TM, Chaudhari AM. Lumbopelvic Neuromuscular Training and Injury Rehabilitation: A Systemic Review. *Clin J Sport Med*. 2013 May;23(3):160-71.
2. MacDonald D, Moseley GL, Hodges PW. Why do some patients keep hurting their back? Evidence of ongoing back muscle dysfunction during remission from recurrent back pain. *PAIN* 2009;142:183-8.
3. Martuscello JM, Nuzzo JL, Ashley CD, Campbell BI, Orriola JJ, Mayer JM. Systematic review of core muscle activity during physical fitness exercises. *J Strength Cond Res*. 2013;27(6):1684-1698.
4. Ekstrom RA, Dontatelli RA, Carp KC. Electromyographic analysis of core trunk, hip, and thigh muscles during 9 rehabilitation exercises. *J Orthop Sports Phys Ther*. 2007 Dec;37(1):754-62.
5. Wong A YL, Parent EC, Funabashi M, Stanton TR, Kawchuk G. Do various baseline characteristics of transverse abdominis and lumbar multifidus predict clinical outcomes in nonspecific low back pain? A systematic review. *Pain*. 2013 Dec;152(2):2589-2602.
6. Hides J, Stanton W, Mendis MD, Sexton M. The relationship of transversus abdominis and lumbar multifidus clinical muscle tests in patients with chronic low back pain. *Manual Therapy*. 2011 Dec

USING MUTUAL INFORMATION TO CAPTURE MAJOR CONCERNS OF POSTURAL CONTROL IN A TOSSING ACTIVITY

¹ Harshvardhan Gazula and ¹ Simon M. Hsiang

¹ Texas Tech University, Lubbock, TX, USA

email: harshvardhan.gazula@ttu.edu

INTRODUCTION

In this study, to analyze the biomechanics of tossing, we hypothesize that an optimal toss is characterized by a sequence of decisions so that certain objective functions are optimized. The relationship among multiple objective functions when accounted for can lead to a greater explanation/control over the tossing behavior. The aim of this study is to show the logical relationship between different objective functions, using mutual information [1], and to provide an overview of how those relationships change as the tossing task comes to a termination under different experimental conditions. When viewed in this manner, differences between the major concerns in each phase of the activity become interesting as they are a reflection how the information is flowing from phase to phase and this information flow helps us identify optimal tossing behavior.

METHODS

10 adults (age: 26.92 ± 1.62 years; height: 166.6 ± 6.8 cm; weight: 64.2 ± 11.6 kg) without any history of musculoskeletal disorders participated in the study. All protocols were approved by Institutional Review Board and written informed consent obtained prior to enrollment. Test conditions were selected to mimic typical tossing tasks often observed in a warehouse. Participants picked a box of varying weights from the ground and tossed it to the target location (on the ground or on to a table right in front of them) in one smooth motion. A $2 \times 2 \times 3 \times 3$ (distance- 1 m, 1.5 m, height- floor, table (set to 53% of the subject's stature, usually waist height), weight- 1 kg, 5 kg, 7 kg, and target clearance- 110%, 150%, 200%, respectively) factorial design was used in this study.

Passive retro-reflective markers on the main joints (wrist, elbow, shoulder, hip, knee and ankle) were affixed to each participant to track whole body motion. In addition, two markers were attached to the side of load. Marker trajectories were collected using a 6-camera motion capture system sampling at 60 Hz. A combination of bony landmarks, measured anthropometry and marker positions was used to calculate each segment position. We use three objective functions (concerns) viz., mobilization (M), stabilization (S) and strength utilization (T) in this study as identified in a previous study [2].

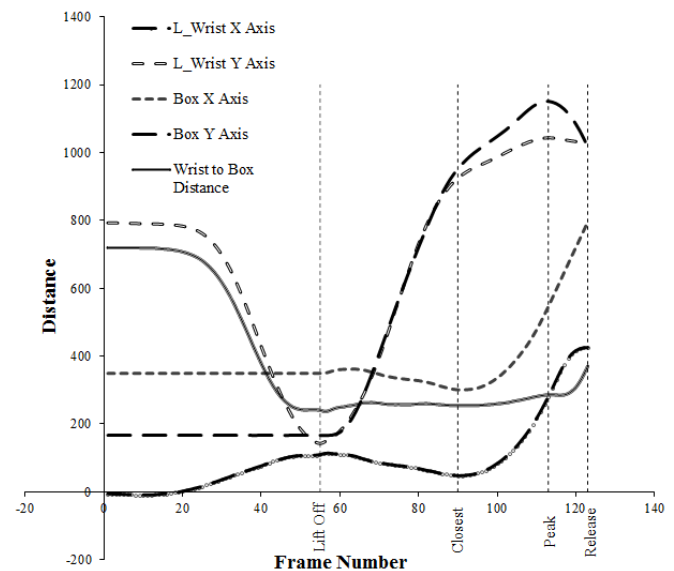


Figure 1: Identification of different phases of tossing using motion capture data.

Each trajectory is divided into three phases marked by four events [3]. These four events were the initial position (lift off), the load closest-to-body-position, the highest position (peak), and the final position (release). We calculated the three objective function values for each phase. To calculate mutual information (MI) we discretized each of the

performance measures into three categories, based on where they fell on the 33.33 (Lo-Low), 66.66 (Med-Medium) and 100 (Hi-High) percentiles scale, so as to build a conditional probability table. This discretization was performed separately for all phases.

MI is a quantitative measurement of how much one random variable tells us about another random variable [1]. In this study, information was thought of as a reduction in the uncertainty of a variable. Thus, more the MI between S and M (I), the less uncertainty there is in S knowing M or M knowing S. The formula to calculate the MI between two random variables S and M is given as follows:

$$I(S;M) = \sum_{s \in S} \sum_{m \in M} p(s,m) \log \left(\frac{p(s,m)}{p(s)p(m)} \right)$$

where p(s,m) is the joint probability distribution function of S and M are the marginal probability distributions of S and M, respectively, all obtained from the conditional probability table.

RESULTS AND DISCUSSION

Results of the study are presented as the primary concerns (pair of objective functions with the highest MI value) among the previously considered objective functions in each phase of the tossing activity under different experimental conditions. Cells with only one objective function mean that there's a tie between two pairs of objective functions and this objective function is common between the two pairs.

No clear patterns were found for Phases 1 and 2 for different load and clearance conditions. During Phase 3 more than 50% of the subjects resorted to a type of tossing pattern that showed 'mobilization' and 'strength utilization' as the most important concern under almost all the experimental conditions. These findings suggest that mobilization and torque utilization are the most important concerns at the moment the load is released from the hand.

Table 1: Major concerns in each phase of the tossing activity under different experimental conditions (with the percentage of subjects)

Condition	Phase 01	Phase 02	Phase 03
Tossing on Floor	MS (40%)	MS (30%)	MT (70%)
Tossing on Table	MT (60%)	ST (30%)	MT (40%)
Distance = 1m	MT (40%)	M (60%)	MT (60%)
Distance = 1.5 m	MS (30%)	ST (30%)	MT (50%)
Weight = 1kg	MT (30%)	M (60%)	MT (60%)
Weight = 5kg	MT (40%)	MS (40%)	MT (70%)
Weight = 7kg	MS (30%)	MS (30%)	M (60%)
Tolerance = 100%	M (60%)	MT (30%)	MT (60%)
Tolerance = 150%	MT (20%)	MT (30%)	MT (50%)
Tolerance = 200%	MS (50%)	T (60%)	MT (50%)

The key is to identify information regarding systematic relations that hold between objective functions that concern behavior and use such information in determining the right input needed to lead to a desired outcome. We hypothesize that knowing the systematic relations between actions and their outcomes in terms of the major concerns, the right action can be chosen at the right time for an effective control.

CONCLUSIONS

In this paper, we introduced a novel uncertainty reduction approach for the identification of body kinematic patterns and their logical organization based on different objective functions at different phases of a tossing task. The proposed research concept based on mutual information provides users with a useful diagnosis of the relevance of different objective functions and of the mutual dependencies in designing the task.

REFERENCES

1. Cover TM, et al. *SIAM Rev.* **36**(3), 509-510, 1994.
2. Hsiang SM & McGorry RW, *Ergonomics* **40**(9), 928-939, 1997.
3. Hsiang SM, et al. *Ergonomics* **41**(3), 239-256, 1998.

ACKNOWLEDGEMENTS

Special thanks to Dr. Chien-Chi Chang at National Tsing Hua University, Taiwan, ROC and Dr. Ming-Lun Lu at NIOSH, Cincinnati, OH, USA.

Relationship Between Thoracic and Lumbar Spinal Curvature During Unsupported Sitting

Deborah L. Givens¹, Gregory M. Freisinger², Jackie Lewis², Michael McNally²,
Steve T. Jamison³, and Ajit M. W. Chaudhari²

University of North Carolina¹, Chapel Hill, NC, USA

The Ohio State University², Columbus, OH, USA

University of Delaware³, Newark, DE, USA

email: deborah_givens@med.unc.edu, web: http://www.med.unc.edu/ahs/physical/faculty/deborah_givens

INTRODUCTION

Maintaining the natural curvature of the lumbar, thoracic, and cervical spine, or “neutral spine” posture while sitting is widely recommended for good spinal segment alignment.[1] A common clinical approach to correcting seated posture is to teach people to reduce posterior rotation of the pelvis in order to improve the lumbar lordotic curve and reduce mechanical stresses on the spine.

Changes in lumbar lordosis while sitting can result in compensatory adjustments in the cervical spine to maintain the orientation of the head, which have the potential to impact the spinal loading.[2] However, little is known of how the curvature and motion of the lumbar region correlates with the adjacent thoracic region while seated. Although the thoracic and lumbar regions have the potential to move independently and, therefore, respond to postural changes differently, we hypothesized that the curvatures of the thoracic and lumbar spine in the sagittal plane would be coupled during sustained, unsupported sitting.

METHODS

Forty individuals at the 37th Annual Meeting of the American Society of Biomechanics in Omaha, NE participated in this study. Study volunteers assented that they were free from back pain while sitting or standing for a period of 15 minutes. Thirty-five participants (21 males, 14 females, mean age=33.8 ± 10.6y) had complete data for analysis.

Each subject sat on a backless stool while wearing a chest harness and belt. Markers with moiré patterns and unique markings on them were placed over the spine and pelvis (Figure 1). Subjects were instructed to maintain an erect sitting posture for 15 minutes

while utilizing a hand-held iPad to play games that challenged the brain. The three-dimensional locations and orientations of each marker were obtained using a moiré pattern motion capture system at 1 Hz [MC 40180; Metria Innovation, Milwaukee, WI]. The Metria system has been validated to provide accuracy within 1mm and 0.05 degree.[3]

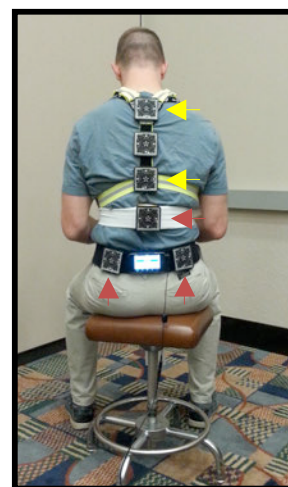


Figure 1. Subject and marker positions

The radius of curvature (RoC) in the sagittal plane for the thoracic spine was estimated using the intersection of vectors normal to the face of each marker, which were located on the proximal and distal aspect of the thoracic spine (yellow in Figs 1, 2a). The lumbar RoC was estimated similarly with a marker on the lumbar spine and the combined orientation of 2 markers on the posterior superior iliac spines (red in Figs 1, 2a). Spinal curvature was calculated from the inverse of each RoC.

RESULTS AND DISCUSSION

The medians and ranges for the thoracic and lumbar curvature were 2.20 [0.26, 4.81] m⁻¹ and 0.70 [-1.85, 5.96] m⁻¹, respectively. A Spearman's rank correlation coefficient (ρ) was calculated between the thoracic and lumbar curvature for each subject (Figure 2b). All ρ were different from 0 ($p < 0.01$), with the exception of subject 6 (blue point in Fig. 1b, $p = 0.12$). The range was from $\rho = -0.74$ to $\rho = 0.86$. When each subject's curvature data was normalized to his/her initial thoracic and lumbar

curvature, the thoracic and lumbar curvature were significantly correlated for the group, though the relationship was weak (overall $r = 0.12$, $p < 0.001$).

These results suggest that thoracic and lumbar curvature may be coupled for most individuals, but the relationship varies widely in both strength and direction, even among these subjects without back pain during unsupported sitting.

CONCLUSIONS

These data suggest that monitoring and correcting the lumbar spine curvature tends to influence the thoracic spine curvature in most individuals without back pain during sustained, unsupported sitting. However, the relationship between lumbar, thoracic, and cervical curvatures is probably more complex than is generally accepted clinically. Lumbar curvature and pelvic rotation should be considered when improvement of thoracic posture is also

desired. Future studies should investigate coupling patterns of the lumbar and thoracic spine in people with back pain during sustained sitting and in patients with musculoskeletal disorders of the spine.

ACKNOWLEDGMENTS

The authors gratefully acknowledge support for this study from the organizing committee of ASB 2013, Metria Innovation for loaning the motion capture system during the meeting, and the members of ASB for participating.

REFERENCES

1. Harrison DD, et al. *J Manipulative Physiol Ther.* 22, 594-609, 1999.
2. Black KM, et al. *Spine.* 21(1), 65-70, 1996.
3. Armstrong B, et al. *2002 IEEE International Conference on Robotics and Automation*, Washington, DC, 2002.

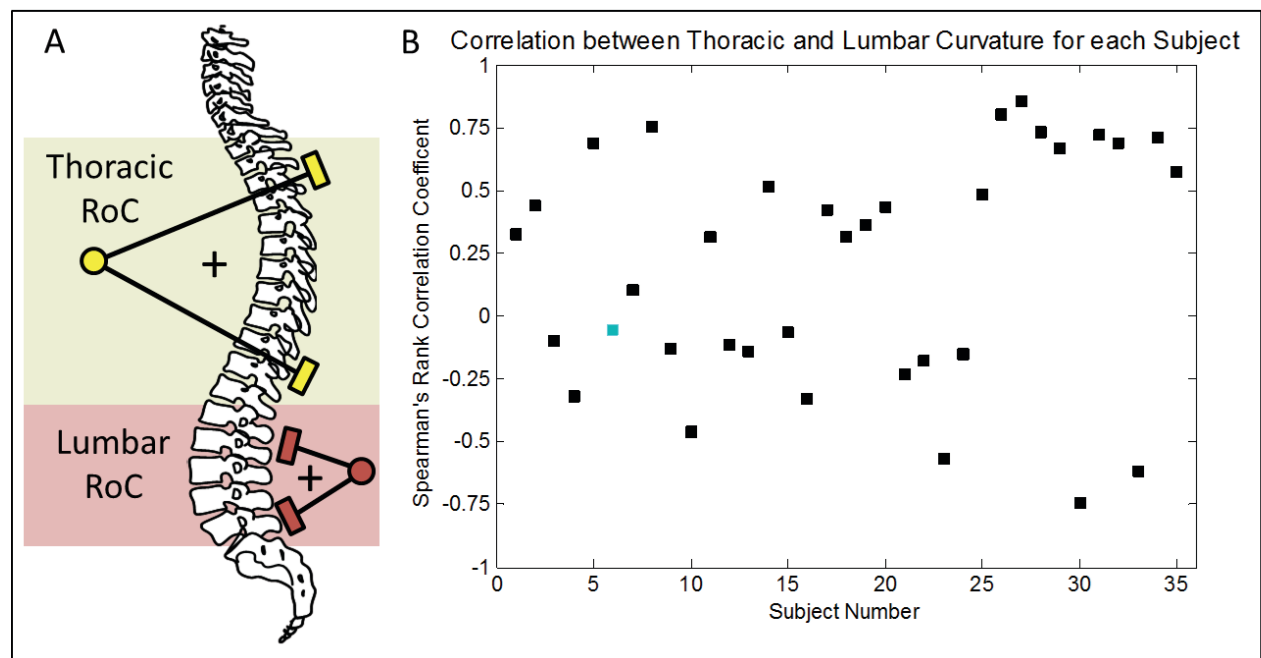


Figure 2. A) Radius of curvature for the thoracic and lumbar spine was found by the intersection point of vectors perpendicular to the moiré marker face. B) Spearman's rank correlation coefficient (!) of the thoracic and lumbar curvatures for each subject individually. The blue point indicates Subject 6, the only participant for whom ! was not significantly different from zero.

THE RELATIONSHIP BETWEEN KNEE PROPRIOCEPTION AND BALANCE IN ANTERIOR CRUCIATE LIGAMENT RECONSTRUCTED INDIVIDUALS

¹ Jared C. Seidel, ¹ Dustin R. Grooms, ¹ Michael P. McNally, ¹ Cambrie D. Starkel, ¹ Ajit M.W. Chaudhari, PhD,
¹ James A. Onate, PhD

¹ The Ohio State University, Columbus, OH, USA
email: grooms.dusty@gmail.com, web: <http://medicine.osu.edu/hrs/at/research>

INTRODUCTION

The anterior cruciate ligament (ACL) of the knee is an important ligament that prevents anterior translation and medial rotation of the tibia relative to the femur. Non-contact ACL tears can occur via poor landing, planting, or cutting mechanics. Injury to this ligament causes changes in the somatosensory and proprioceptive capabilities of the joint [1,2]. Proprioception is the ability to sense the location of parts of the body in space without the use of visual assistance and is vital to maintaining neuromuscular control during movement. The loss of proprioception can result in neuromuscular deficits that may force the nervous system to increase dependence on visual feedback for motion [2]. Increased deficits in the ACL reconstructed (ACLR) leg increase the risk of re-injury [3]. These deficits may be displayed when moving into a complex athletic environment or restricting visual feedback. It is unknown how vision moderates the relationship between proprioception and postural control. The purpose of this study was to determine the relationship between proprioception and static balance in ACLR individuals under varying two visual conditions.

METHODS

2.1 Participants

Thirteen individuals who previously had an ACL reconstruction (6 males, 7 females; age = 25.5 ± 1.37 years, height = 1.70 ± 0.13 m, mass = 75.6 ± 19.2 kg) participated in this study. Inclusion criteria were as follows: 18 to 39 years old, underwent an ACL tendon graft reconstruction, and currently physically active. Participants completed a Tegner activity [4] survey indicating their current levels of activity

(Tegner score = 6.0 ± 1.5). The mean time interval after reconstruction was 23 ± 18 months.

2.2 Measurement of Proprioception

Proprioceptive capability was measured using a Biodex System 3 isokinetic dynamometer (Biodex Medical Systems, Shirley, NY). Active joint position sense (AJPS) and passive joint position sense (PJPS) were performed to determine proprioception. Both methods tested errors associated with movement into flexion and into extension to a knee position of 20° . For both sensing tests, participants were placed at 90° hip flexion, eyes were blindfolded and ears covered. The knee was placed in 45° of flexion and extended to 20° flexion, either by the dynamometer during PJPS, or by the subject during AJPS. The participant's knee was then moved by the dynamometer back to 45° of flexion, and the participant was instructed to mark when they returned to the 20° flexion position. During PJPS, the dynamometer moved at an angular velocity of $2^\circ/\text{s}$, and the leg was allowed to freely move during AJPS. The same procedure was repeated for both PJPS and AJPS, starting from an extended position (0° flexion) and moving into 20° of flexion. Error for proprioception tests was determined to be the absolute difference from 20° .

2.3 Single Limb Balance Measurement

Static single limb balance was performed on a tri-axial force platform (Bertec, Columbus, OH) collecting at 1500 Hz to measure center of pressure (CoP) excursion with eyes open and blindfolded. During testing, participants stood on the uninvolved limb first, and then repeated the task on the involved limb. Participants were instructed to maintain balance on the specified leg for 30 seconds. Processing of balance data was performed

through custom MATLAB scripts (MathWorks, Natick, MA) with all CoP data low-pass filtered at 100 Hz using a 4th order Butterworth filter. CoP excursion was calculated as the total path length of the CoP excursion during the first ten seconds of the balance task.

2.4 Statistical Analysis

Separate Pearson correlations were used to assess the relationship between proprioception and single limb postural control across different vision conditions with a significance level of $p < 0.05$ *a priori*.

RESULTS AND DISCUSSION

There was a significant correlation between CoP excursion during eyes closed balance and AJPS into extension error in the involved limb ($r^2 = 0.34$, $p = 0.038$), meaning decreased single leg stability on the reconstructed limb was correlated with worse proprioceptive ability (**Figure 1**).

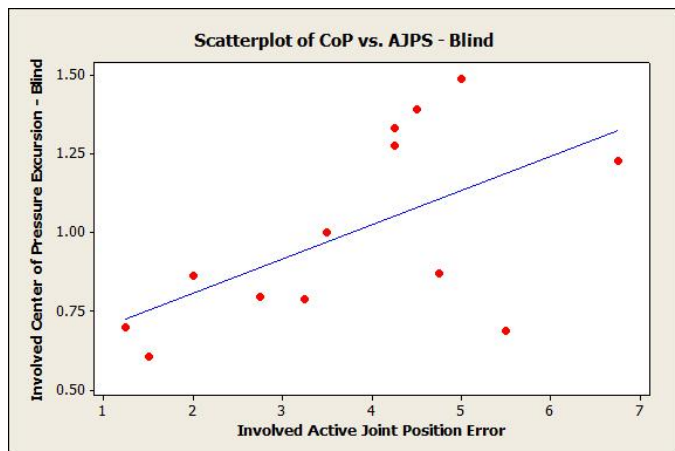


Figure 1: Scatter plot of CoP excursion and AJPS during blindfolded balance ($r^2=0.34$, $p=0.038$).

No significant correlations were found between proprioception and postural control in the involved limb for the eyes open condition. No significant correlations to joint proprioception were found in the uninvolved limb during the eyes open and blindfolded condition. Lee et al. observed that the threshold for detection of passive motion was strongly correlated with dynamic single leg balance after ACL injury [1]. Additionally, literature reviews have concluded that ACL injuries may

cause neuroplastic changes and knee proprioception deficits [2, 5]. As AJPS error decreased in the involved limb, CoP excursion was greater during the eyes closed condition, indicating vision may moderate the relationship between proprioception and static single limb balance on knees with reconstructed ACL's. The moderate r^2 value for this relationship indicates that there may be additional factors that contribute to balance. Some factors may include core control, leg strength, and/or vestibular influence. Future research is needed to further explore what kind of influence, if any, such variables may have.

CONCLUSIONS

After ACL reconstruction, individuals may experience changes or deficits in proprioception and neuromuscular control. To maintain postural stability, ACLR individuals may depend more on vision with decreasing proprioceptive capabilities, but without visual restriction proprioception does not seem to play a role.

These findings suggest that active joint proprioception in ACL reconstructed limbs may be utilized in moderating involved single leg balance when vision is impaired. Improving proprioception under varying visual conditions may be an additional rehabilitation tool to aid in reducing the risk of re-injury.

REFERENCES

1. Lee HM., et al. *The Knee* **16**, 387-391, 2009.
2. Grooms DR., et al., *J of Orthopedic & Sports Physical Therapy*, 1-33, 2015.
3. Paterno MV, et al., *Am J Sport Med* **38**, 1968-1978, 2010.
4. Briggs KK, et al. *Am J Sport Med.* **37**, 890-897, 2009.
5. Relph N, et al. *Physiotherapy* **100**, 187-195, 2014.

ACKNOWLEDGEMENTS

The authors gratefully acknowledge funding support for this study from the National Strength and Conditioning Association doctoral grant and The Ohio State University College of Medicine pilot award.

DEVELOPMENT OF A NOVEL PROPRIOCEPTIVE PERTURBATION DURING STANDING BALANCE

¹Joan R. Guyer, ¹Jarad W. Prinkey, ²Patrick Sparto, ³J. Richard Jennings, ⁴Joseph Furman, ^{1,4}Mark Redfern, ¹April J. Chambers

¹Human Movement and Balance Laboratory, Department of Bioengineering;

²Department of Physical Therapy; ³Department of Psychiatry; ⁴Department of Otolaryngology
University of Pittsburgh, PA, USA

Email: jrg97@pitt.edu, Web: <http://www.engineering.pitt.edu/hmbl/>

INTRODUCTION

Aging has been proven to affect both attentional processes as well as postural control. As falls in the elderly population continue to pose major public health concerns in the United States, investigating relationships between executive controls, stability, and attention becomes increasingly important. Through measurement of sway and reaction time in response to visual and auditory stimuli, many studies have explored the effects of challenging the balance system of young and older adults. These results confirm that attention is involved with sensory integration of visual and auditory stimuli as well as standing balance. Moreover, more attention is required to maintain balance when multiple senses are in conflict compared to a single contradictory sensory input [1]. Increased reaction time and increased sway with age indicate that these attentional challenges to the balance system affect older adults to a greater degree [2].

The effects of challenging attention by other systems, particularly the proprioceptive system, have been previously unexplored. In this study, we will explore the effects of a proprioceptive stimulus on reaction time and sway in younger and older adults. Through the results of dual-task experiments, with information processing and proprioceptive components, we hope to achieve a greater understanding of the mechanisms contributing to the interactions between balance and cognitive processes and how aging affects these mechanisms. The goal of this abstract was to develop a novel proprioceptive stimulus to be used in further evaluating sensory integration during standing balance.

METHODS

Reaction time (RT) trials were collected on a NeuroCom EquiTest platform controlled by a (insert DAQ here). Body sway was calculated using the position of a Polhemus magnetic tracking sensor attached to the subjects' waist compared to a measured baseline distance from the sensor to the top of the EquiTest platform. Subjects were tested in a darkened room and told to focus on a fixed, eye-level target approximately 2 meters in front of them.

Each subject completed a total of three trials in four conditions: fixed floor with eyes open (FIX-EO), fixed floor with eyes closed (FIX-EC), sway referenced floor with eyes open (SRF-EO), and sway referenced floor with eyes closed (SRF-EC). Data were collected for 2.5 minutes per trial. For each condition, two baseline trials were collected without an RT task (one with perturbations and one without). The third trial per condition included a simple reaction time (SRT) test in conjunction with the perturbation. Trial order was randomized for each subject.

The proprioceptive perturbations used for the experiment involve rotation about the ankle invoked by the EquiTest system. The perturbations consist of a random toe up or down ankle rotation of ± 0.5 degrees superimposed on the current rotational position of the platform (Figure 1).

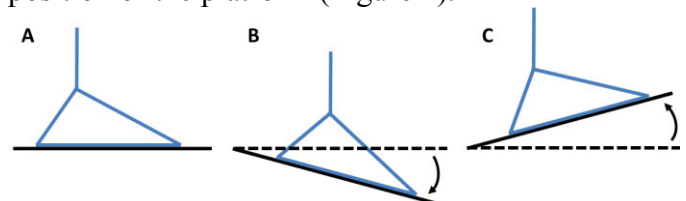


Figure 1. A. No rotation of foot. B. Toes down rotation (5°), C. Toes up rotation (-5°).

To ensure minimal sway at the time of a perturbation, before a perturbation was given, a constraint on the anterior-posterior sway was met. This was termed dwell time and defined as the sway angle of the subject being within ± 2 degrees for at least 2 seconds before the next stimulus was presented (Figure 2). This would mean that the time between stimuli may be higher for subjects that have more unperturbed sway.

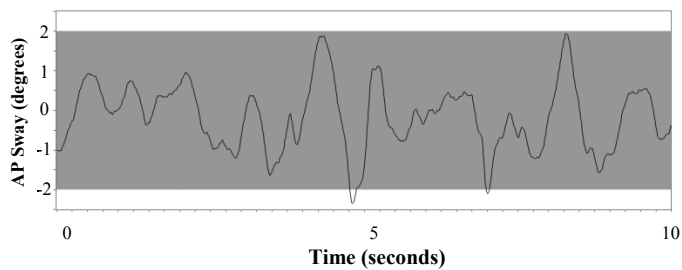


Figure 2. Degrees of subject anterior-posterior sway are shown. Dwell time requires that the subject's sway must be within the shaded area (± 2 degrees) for at least 2 consecutive seconds before the next stimulus is presented.

Proprioceptive perturbations were randomly introduced 3 seconds plus or minus up to 2 seconds after the previous perturbation and once the dwell time constraint was met (Figure 3). The average perturbation was 0.125 seconds in length.

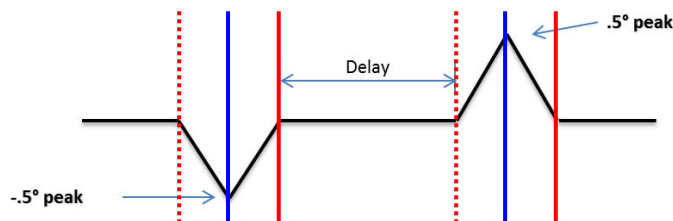


Figure 3. Visual representation of the signal driving the perturbations on the platform. The 0.5 degree triangular wave is added to the current position of the platform. The delay is calculated using a randomized wait period (3 seconds \pm up to 2 seconds) and the subjects dwell time. If the wait period has passed, but the dwell time has not been achieved; the perturbation will commence after the dwell time has been reached. Red dotted line = start of perturbation; blue solid line = maximum perturbation; red solid line = end of perturbation

Over the course of a 150 second trial we expected to see approximately 43 perturbations for a healthy

subject who does not typically sway more than ± 2 degrees.

RESULTS

On average, there were 44 perturbations per 2.5 minute trial. Typical center of pressure time history plots are provided to demonstrate the impact of our novel perturbation on standing balance. Perturbations were averaged within condition, zero-meaned to the initial sway value before each perturbation, and the standard deviation was determined across perturbations within the trial.

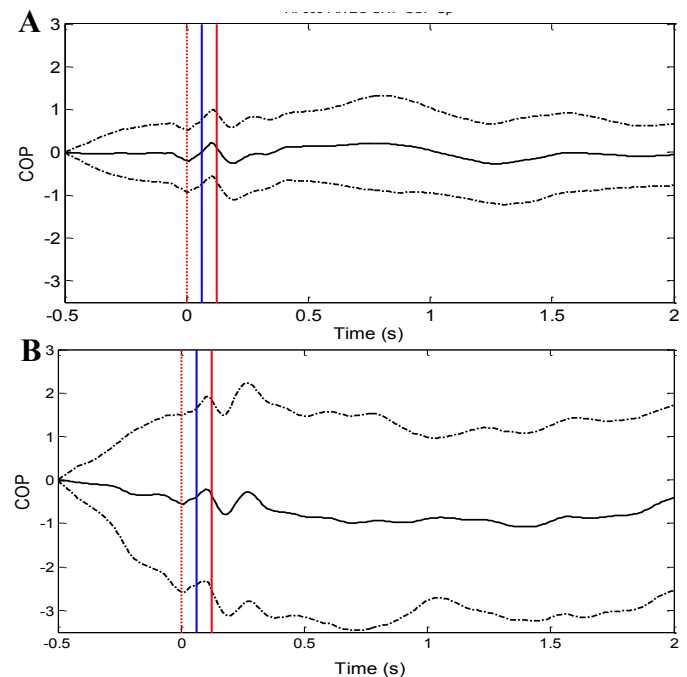


Figure 4. Average COP with standard deviation for an older subject during "down" perturbations of (A) FIX-EO-SRT and (B) SRF-EO-SRT trials. Red dotted line = start of perturbation; blue solid line = maximum perturbation; red solid line = end of perturbation

DISCUSSION

A novel proprioceptive perturbation was developed that does not significantly alter sway. This paradigm will aid in providing a greater understanding of the mechanisms contributing to the interactions between balance and sensory integration as well as how aging affects these mechanisms.

REFERENCES

- [1] Redfern MS et al. G & P. 2001. 14; 211–6.
- [2] Pellecchia GL. G & P. 2003. 18; 29–34.

RELATIONSHIPS BETWEEN HIP ABDUCTOR STRENGTH AND MEASURES OF SINGLE-LEG STABILITY IN FIT, YOUNG ADULTS

Gary D. Heise, Sutton Richmond, Austyn Resek, Brian Garcia, and Jeremy D. Smith

University of Northern Colorado, School of Sport & Exercise Science, Greeley, CO, USA
email: gary.heise@unco.edu, web: <http://www.unco.edu/biomechanics/>

INTRODUCTION

Postural stability, particularly static, whole-body stability in older adults, has received considerable attention in the research literature. Whole-body stability in younger, athletic populations has received less attention, primarily because typical static, two-legged postural assessments do not sufficiently tax a younger person's overall stability. Stability during one-legged standing is more challenging. Dynamic stability, usually tested on one leg, describes the process of transitioning from movement to a quiet, standing posture. Various measures, based on ground reaction forces (GRF) and center-of-pressure (COP) trajectories are often used to assess both types of stability. Clinicians have assessed dynamic stability in athletes with compromised joints (e.g., ACL injuries, ankle instability), but the influence of muscle strength has not been thoroughly examined [1].

Overall muscle strength, especially core and lower extremity muscle strength, is thought to enhance overall stability and reduce the risk of joint injury [2]. Previous work in our lab identified back extensor muscle strength as a significant predictor of static and dynamic stability, but knee and ankle muscle strength were not identified as predictors of static or dynamic stability [3,4]. Weak hip abductors have been associated in runners with iliotibial band syndrome [5], but this muscle group's influence on static or dynamic stability, especially in one-legged standing, has not been examined.

The purpose of this experiment was to explore the relationships between hip abductor muscle strength and various measures of single-leg static and dynamic stability among young, fit adults. It was hypothesized that greater hip abductor strength would be associated with better stability.

METHODS

Twenty people volunteered for this study (9 men; 11 women). All participants were young, healthy, and active (age, 26 ± 5 yr; body mass, 70.9 ± 9.8 kg; height, 173.2 ± 9.3 cm). At the beginning of a single test session, the protocol was explained and informed consent was obtained. Demographic and anthropometric data were collected in addition to some details about the frequency, duration, and intensity of weekly workouts.

Participants performed a brief, 10-15 minute warm-up (e.g., walk, stretch, low-intensity exercise). For static stability, ground reaction force (GRF) data were collected for 30 s at 1000 Hz and center of pressure (COP) coordinates were calculated for analysis. Trials were collected on each leg and for two floor conditions (rigid surface and compliant surface). COP mean velocity, 95% confidence ellipse area, and 95% power frequency were calculated [5]. Four dynamic, single-leg postural stability trials were collected: two from a forward hop; two from a medially directed hop. For dynamic stability, GRF data were collected for 20 s. A stability index (SI), based on root-mean-square values, was computed for both the medial-lateral (ML) and anterior-posterior (AP) GRF components [1]. The SI was calculated over 3 seconds, beginning 0.5 s after impact to avoid inclusion of the impact GRF peak.

Hip abductor muscle strength was determined with an isokinetic dynamometer. Maximal, isometric efforts were measured for right and left sides in a standing position. Correlations were used to evaluate the relationships between hip strength and measures of static and dynamic stability.

RESULTS AND DISCUSSION

Our hypothesis that stronger hip abductor strength would be associated with individuals displaying better one-legged stability was not supported. Two significant correlations that were identified in the present study resulted in the opposite relationship (i.e., greater hip abductor strength associated with greater COP movement). Figure 1 shows a measure of static stability and Figure 2 shows a measure of dynamic stability. These were the only significant correlations.

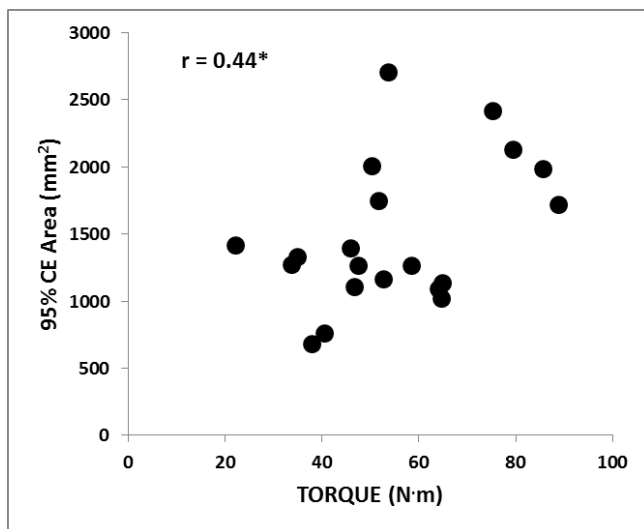


Figure 1: Scatterplot of hip abductor strength and the 95% confidence ellipse (CE) area for a left-footed, static stability trial. $*p < .05$

Previous work in our lab [3,4] investigated isometric muscle strength at the knee and ankle joints, but found no association between those measures, taken from a muscle dynamometer, and measures of static or dynamic stability. Furthermore our previous work identified several significant inverse relationships between back extensor muscle endurance and stability (i.e., longer endurance associated with lower metrics of stability). The only two significant correlations identified in the present study (Figures 1 & 2) show the opposite result. In addition, the significant correlations identified here show that hip abductor muscle strength explains only about 20-23% of the variance in stability.

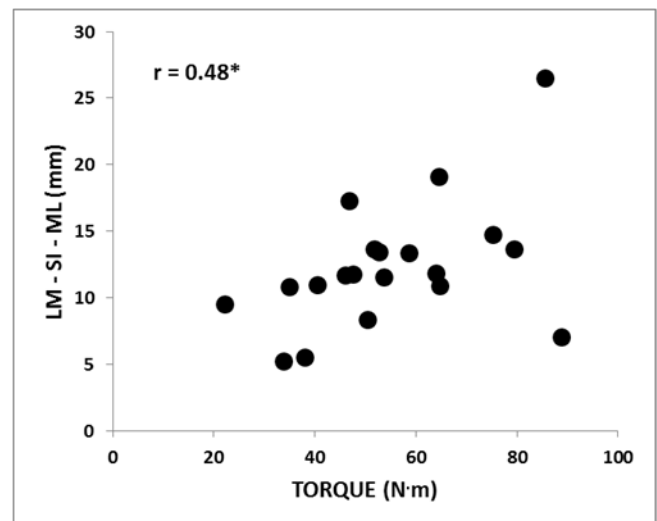


Figure 2: Scatterplot of hip abductor strength and the medial-lateral stability index (SI) for a left-footed, medial landing (lower SI = better dynamic stability). $*p < .05$

Given that stability is governed by the equilibril triad (vision, vestibular apparatus, and proprioception), it is not surprising that muscle strength at a single joint is not strongly related. Taken together with our previous findings, one-legged stability does not seem highly influenced by proximal or distal lower extremity muscle strength.

CONCLUSIONS

Overall, our hypothesis was not supported; individuals exhibiting greater stability in both static and dynamic conditions would be associated with greater isometric hip abductor strength. Only one measure of static stability and one measure of dynamic stability were significantly associated with hip abductor strength, but both relationships were in the opposite direction of our stated hypothesis.

REFERENCES

1. Ross, S et al. *J Athl Training*, **40**, 298-304, 2005.
2. Leetun, DT et al. *Med Sci Sports Exerc*, **36**, 926-934, 2004.
3. Silvernale, C et al. *Proceedings of ASB '13, Omaha, NE, USA, 2013*.
4. Esselman, E et al. *Proceedings of ASB '13, Omaha, NE, USA, 2013*.
5. Fredericson, M et al. *Clin J Sport Med*, **10**, 169-175, 2000.

THE RELATIONSHIP BETWEEN FOOT CONTACT AREA AND SINGLE-LEGGED POSTURAL STABILITY

Sutton B. Richmond, Kevin Dames, Jeremy D. Smith, and Gary D. Heise

University of Northern Colorado, School of Sport and Exercise Science, Greeley, CO, USA
email: sutton.richmond@yahoo.com, web: <http://www.unco.edu/biomechanics/>

INTRODUCTION

Postural stability, particularly static whole-body stability in older adults, has received considerable attention in the research literature. Whole-body stability in younger, athletic populations has received less attention, primarily because typical static, double-legged postural assessments do not sufficiently tax a younger person's overall stability. Stability during single-legged standing is more challenging and, when unshod, may be influenced by the actual contact area between foot and floor during quiet standing. This contact area is influenced by a number of anatomical and mechanical factors.

Hertel et al. [1] studied foot arch height and its influence on single-legged static stability. They reported that greater center of pressure (COP) excursions were found in participants with cavus feet (i.e., high arch height). They suggested that a higher arch height would result in a lower contact area and less range of motion in the subtalar and midtarsal joints. These joints are main contributors to pronation/supination movements, which are critical to single-legged stability. Their conclusions were based on classifying arch height with an approach that used linear and angular anthropometric measurements of the foot and ankle region while a person was lying prone. In addition, Hertel and colleagues only reported COP excursion and velocity as measures of static stability.

The present study addressed the limitations of Hertel et al. [1] by quantifying foot contact area and examining its relationship with single-legged static stability. Specifically, we hypothesized that greater foot contact area would be associated with more stable individuals. We also introduce a novel measure of foot contact area, which takes into account variations in foot morphology.

METHODS

Twenty healthy, active volunteers participated in this study (9 men, 11 women; age, 26 ± 5 yr; body mass, 70.9 ± 9.8 kg; height, 173.2 ± 9.3 cm). The participants were initially given time to stretch or warm-up for 5-10 min before testing began. Prior to stability testing, a physical trapezoidal measurement of the foot was taken using H, B1, and B2 which are shown on Figure 1.

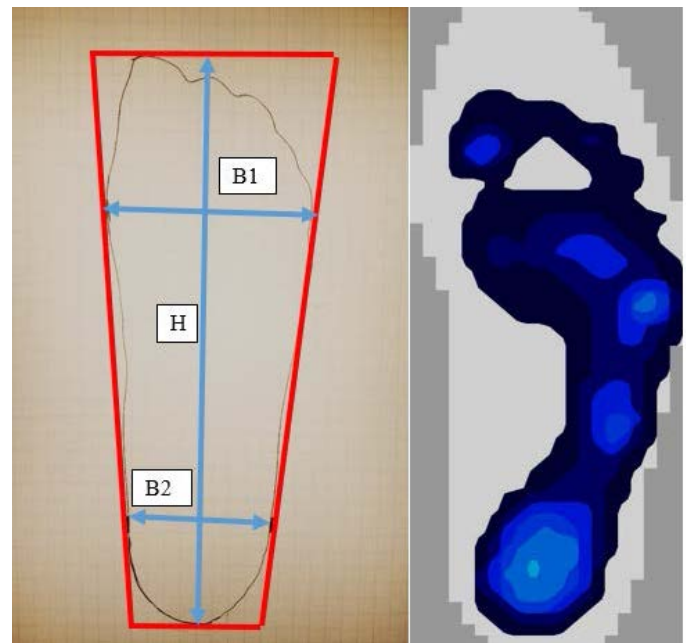


Figure 1: Physical trapezoidal measurement of the foot (left) and pressure scan of the foot (right).

Next, a plantar pressure scan was taken at 50 Hz for 8 s (Tekscan, Boston, MA) while a person stood quietly on one leg. Average contact area was calculated from the Tekscan software. Contact area was divided by trapezoidal area to quantify a foot contact index (FCI). Static, single-leg postural stability trials were collected on each leg and for two floor conditions (rigid surface and compliant surface). Ground reaction force (GRF) data were

collected for 30 s at 1000 Hz and the COP coordinates were calculated for analysis. COP mean velocity, 95% confidence ellipse area, sway area, and 95% power frequency were calculated [2]. Correlation coefficients were used to evaluate the relationships between FCI and all measures of static stability.

RESULTS AND DISCUSSION

The novel measure of FCI yielded similar values for right and left feet with an average coefficient of variability of 8% (SEE Table 1), whereas the variability of the physical trapezoidal area of the foot and the variability of the scanned contact area were higher (~15%).

Table 1: Mean trapezoidal area (MTA), scanned area (SA), and foot contact index (FCI) for right and left feet. Standard deviations are included.

	RIGHT	LEFT
MTA (cm ²)	188.8 ± 25.7	187.2 ± 27.3
SA (cm ²)	140.6 ± 19.3	139.7 ± 20.9
FCI (%)	74.7 ± 5.8	74.8 ± 6.2

There were no significant correlations between FCI and any measure of static stability across all conditions of testing (Table 2). Values of COP mean velocity for the rigid surface found in the present study (3.5 cm·s⁻¹) were similar to those reported by Hertel et al. [1], but values of sway area (108-120 mm²) were much less.

Table 2: Correlation coefficients between measures of static stability (first column) and the foot contact index for all four testing conditions.

	RR	RL	CR	CL
VEL	.35	.33	-.03	.21
ELLIP	.24	-.09	-.18	-.09
SWAY	.40	.16	.34	.09
POWER	.14	.22	.29	.25

VEL= COP mean velocity; ELLIP=95% confidence ellipse area; SWAY= sway area; POWER=95% power frequency; RR=rigid surface, right leg;

RL=rigid surface, left leg; CR=compliant surface, right leg; CL=compliant surface, left leg.

The lack of a significant relationship between FCI and single-legged static stability measures are in contrast to the findings of Hertel et al. [1]. They used a discrete classification system for categorizing arch height, whereas the present study introduced a novel measure of foot contact area, a continuous variable. Although not significant in the present study, the positive correlation coefficients between sway area and static stability is also in direct contrast to Hertel et al. [1]. They found greater sway area in individuals who had high arch height (i.e., low contact area).

Our results question the notion that individuals with a high foot arch are less stable because of decreased contact area between the foot and the ground [1,3]. More specifically, no relationship seems to exist between foot contact area and stability.

Our study is limited to a young, healthy population. In fact, only five participants were considered overweight based on body mass index. In addition, we did not recruit people based on foot arch height or any other distinguishing, anthropometric characteristics. This may explain our relatively low variability in FCI.

CONCLUSIONS

Our hypothesis that greater foot contact area would be associated with better single-legged stability was rejected. This applied to both feet and two surface conditions.

REFERENCES

1. Hertel, J et al. *J Athl Training*, **37**, 129-132, 2002.
2. Prieto et al. TE, et al. *IEEE Trans Biomed Eng* **43**, 956-966, 1996.
3. Cobb, SC et al. *J Ortho Sports Phys Ther*, **34**, 79-85, 2004.

IMPACT OF VISUAL GUIDANCE ON DIABETES' TOE ELEVATION DURING VIRTUAL OBSTACLE CROSSING TASKS

^{1,4}Chun-Kai Huang, ²Vijay Shivaswamy, ³Pariwat Thaisethhawatkul, ²Lynn Mack, ²Amy Neumeister and ^{1,4}Ka-Chun Siu

¹Division of Physical Therapy Education, School of Allied Health Professions, ²Division of Diabetes, Endocrine & Metabolism, College of Medicine, ³Department of Neurological Sciences, University of Nebraska Medical Center, Omaha, NE, USA,

⁴Biomechanics Research Building, University of Nebraska-Omaha, Omaha, NE, USA
email: chunkai.huang@unmc.edu

INTRODUCTION

People with more than 15 years of diabetes mellitus (DM) are at a high risk of suffering from diabetic neuropathy (DPN) with abnormal sensation and sensory loss of their feet [1], which increases the incidence of falling or tripping accidents. To maintain stability during locomotion, the reliance of body-based and visual senses (e.g. perception of self-motion) plays a very important role in DPN population to react on all kinds of external perturbations during walking [2].

Obstacle crossing is a common daily activity that might cause tripping accidents in diabetic population due to the insufficient toe elevation [3]. Our previous study indicated that through the perception of self-motion diabetic population decrease their gait variability during walking [4]; it is expected that toe elevation could be adjusted accordingly to cross obstacles successfully through the appropriate visual guidance that orientates body location related to the environment (i.e. exproprioception).

Therefore, this study investigated the effect of visual guidance on toe elevation during virtual obstacle crossing (VOC) tasks among people with Type 2 DM, DPN and age-matched healthy control. We hypothesized that the mean toe elevation in DPN would be significantly higher than other groups, and would be lowered when visual guidance was offered during VOC.

METHODS

Six subjects (two subjects in each Type 2 DM, DPN and age-matched group; one female; mean age: 50.17

years) were recruited to perform the VOC task, which was projected in the front screens and created with the dimensions of 45cm (width) x 20cm (depth) x 15% subject's leg length (height) using D-flow software (Motek Medical BV, the Netherlands). The virtual obstacles either showed up at the end of the corridor and moved towards subjects (Feedforward condition) or suddenly appeared two steps ahead of subject (Feedback condition). Two virtual markers that represented subject's toes were shown on the screen as their visual guidance. Subjects were instructed to elevate their dominant leg (leading leg) to step over the virtual obstacles (Fig 1). The collision event between virtual markers and the virtual obstacle was defined as the failure of obstacle crossing, and only successful trials were analyzed.

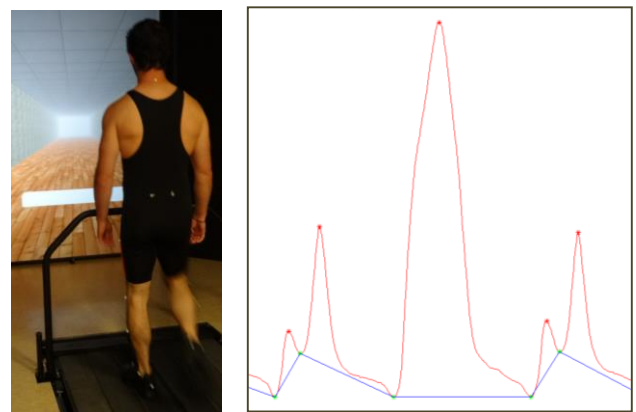


Figure 1: A subject performed a VOC task during treadmill walking (left); the movement of toe marker in sagittal plane during VOC (right).

After the familiarization of six-minute treadmill walking at each individual's self-selected pace, subjects completed four treadmill walking conditions in which consists of Feedforward/ Feedback and

with/without visual guidance conditions (three three-minute trials in each condition).

Three-dimensional spatiotemporal kinematic data were collected using VICON motion capture system at 100 Hz and processed along with Nexus software (Vicon, Oxford, UK). Toe elevation of leading leg during VOC task were calculated using MATLAB program (MathWorks, Inc., Natick, MA) and was defined as the vertical distance between the highest toe marker position and its position during quiet standing (Fig. 1). The mean and variability (coefficient of variance, CV) of toe elevation during VOC task were calculated.

The Kurskal-Wallis one-way ANOVA was conducted to examine the effect of visual guidance on toe elevation among three groups ($\alpha=0.05$).

RESULTS AND DISCUSSION

The preliminary results shown in Table 1 are in line with our hypothesis even though there was no significant finding ($p > .19$). Both DM and DPN lowered toe elevation during VOC without visual guidance which is expected to cause trip and fall; the visual cue assisted in increasing DM and DPN's toe elevation during VOC when compared to age-matched healthy controls in Feedback condition (Fig. 2). These findings are also in agreement that the leading leg is impacted prominently by the visual cue during obstacle-crossing task from a previous study [5]. The increased toe elevation in DM/DPN due to visual guidance can be inferred as the visual perception reliance that is expected to improve the balance during VOC.

More subjects are warranted to examine if the gait alternations found in the DM group is beneficial to stabilize their gait and reduce fall incidence.

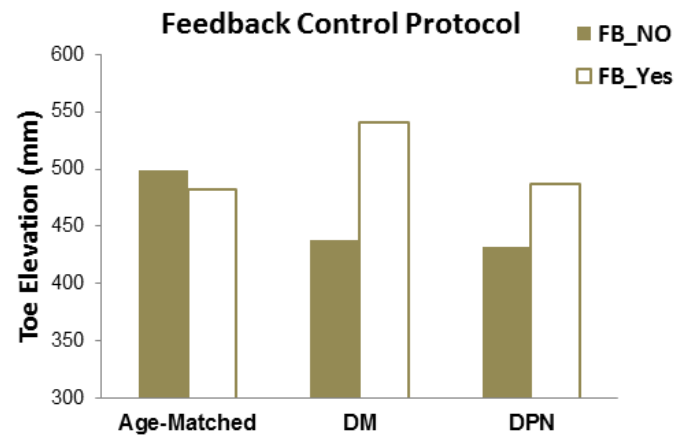


Figure 2: The effect of visual guidance on mean toe elevation (mm) during VOC among age-matched, DM and DPN groups. FB: Feedback.

CONCLUSIONS

Overall, compared subjects with Type 2 DM with their age-matched healthy control, this study provides further evidence that visual guidance which offers the real-time location of individual's toe plays a prominent role on facilitating toe elevation and reducing fall risk in diabetic population during walking.

REFERENCES

1. Simmons RW, et al. *Diabetes Res Clin* **36**, 153-160, 1997.
2. Mohler B, et al. *Exp Brain Res* **181**, 221-228, 2007.
3. Galna B, et al. *Hum Mov Sci* **29**, 843-52, 2010.
4. Huang CK, et al. *Proceedings of ASB*, Omaha, 2013.
5. Rhea CK, et al. *Neurosci Lett* **418**, 60-5, 2007.

ACKNOWLEDGEMENTS

This project was supported by the NASA Nebraska Space Grant & EPSCoR, the UNMC SAHP Pilot Research Grant and Graduate Fellowship.

Table 1.

Condition Group	Age	BMI	A1C (%)	Toe Elevation (FF) [§]		Toe Elevation (FB) [§]	
				No Guidance	Guidance	No Guidance	Guidance
Healthy	51.0	28.71	--	562.05	582.05	498.30	482.60
DM	46.5	30.44	7.1	451.14	517.05	437.50	541.04
DPN	53.0	34.55	7.8	464.96	452.60	431.71	487.19

[§]FF: Feedforward; FB: Feedback

PERCEPTION OF SELF-MOTION IMPACTS THE VARIABILITY OF PLANTAR PROPULSION FORCE IN DIABETES

^{1,4}Chun-Kai Huang, ²Vijay Shivaswamy, ³Pariwat Thaisethhawatkul, ²Lynn Mack, ²Amy Neumeister and ^{1,4}Ka-Chun Siu

¹Division of Physical Therapy Education, School of Allied Health Professions, ²Division of Diabetes, Endocrine & Metabolism, College of Medicine, ³Department of Neurological Sciences, University of Nebraska Medical Center, Omaha, NE, USA,

⁴Biomechanics Research Building, University of Nebraska-Omaha, Omaha, NE, USA
email: chunkai.huang@unmc.edu

INTRODUCTION

Human movement variability generated in the neuromuscular locomotor system contributes to the stability of system, and an excessive movement variability of lower limb is seen as an indicator of fall risk [1].

People with more than 15 years of diabetes mellitus (DM) are at a high risk of suffering from diabetic neuropathy (DPN) with abnormal afferent nerve sensory inputs or efferent motor outputs [2], which causes higher spatiotemporal gait characteristics and increases the incidence of falling/tripping accidents. To maintain stability during locomotion, the reliance of body-based and visual senses (e.g. perception of self-motion) plays a very important role in DPN population to react on all kinds of external perturbations during walking [3].

The increased ground reaction force (GRF) in vertical direction and plantar propulsion force (PPF) in anteroposterior direction that will worsen the formation of plantar ulcer in DM population [4]. In addition, our previous study addressed that through the perception of self-motion (i.e. exproprioception) diabetic population decrease their gait variability during locomotion [5].

Therefore, we speculate that the perception of self-motion will affect DM's plantar force generation by decreasing GRF/PPF and aim to further exam that whether the perception of self-motion will reduce the variability (i.e. coefficient of variation, CV) accordingly during locomotion.

METHODS

We recruited three chronic Type-2 DMs and three healthy controls to walk on an instrumented treadmill (FIT, Bertec Corp., Columbus, Ohio) with their self-selected pace. A six-minute treadmill walking was adopted as familiarization to stabilize the neuromuscular locomotor system. All subjects went through three no self-motion and three self-motion walking trials (120s/trial). The perception of self-motion was generated by presenting a virtual corridor that moved toward subjects with their matched velocity (Fig 1). Three-axis kinetic data during stance phase (heel-contact to toe-off) were recorded at 300 Hz and processed along with MATLAB program (MathWorks, Inc., Natick, MA) in vertical (i.e. GRF) and anteroposterior directions (i.e. PPF) respectively. The peak value and variability (CV) of GRF and PPF during treadmill walking were recorded.



Figure 1: A well-secured subject walks on the treadmill with his self-motion perceived through the rear projected virtual corridor moves toward himself.

Two-factor ANOVA with repeated measures were conducted to examine the role of self-motion impacts GRF/PPF in DM and age-matched healthy; The Bonferroni adjustment was adopted for the following analysis ($\alpha = 0.05$).

RESULTS AND DISCUSSION

The self-motion and group factors show significant interaction on PPF_{Peak} (toe-off) and PPF_{CV} whereas there is non-significant effect of self-motion on GRF. The following comparisons using Bonferroni adjustment show significant visual effect on reducing: (1) PPF_{Peak} in healthy controls; (2) PPF_{CV} in DM patients.

First of all, the decreased PPF_{Peak} and PPF_{CV} founded in this study were in line with previous study and can be explained as the optimization of neuromuscular locomotor system in the anteroposterior direction. Secondly, visual perception of self-motion shows its effect on reducing PPF_{Peak} during toe-off phase and PPF_{CV} in DM and healthy controls. Lastly, the significant decreased PPF_{CV} of DM in the following comparison illustrated that the reliance of exproprioceptive visual information improves to reduce human movement variability and to regain the stability in DM's neuromuscular locomotor system [1].

More subjects are warranted to consolidate if the gait alternations found in the DM group is beneficial to stabilize their gait and reduce fall incidence.

CONCLUSIONS

In summary, compared subjects with Type 2 DM with their age-matched healthy control, this study provides further evidence that the perception of self-motion (i.e. exproprioception) not only decreases gait variability during treadmill walking, but also plays a prominent role on reducing plantar propulsion force that may eliminate the cause of plantar ulcerations.

REFERENCES

1. Masani Kei, et al. *J Appl Physiol* **92**, 1885-1890, 2002.
2. Simmons RW, et al. *Diabetes Res Clin* **36**, 153-160, 1997.
3. Mohler B, et al. *Exp Brain Res* **181**, 221-228, 2007.
4. D'Ambrogi E et al. *Diabet Med* **22**, 1713-9, 2005.
5. Huang CK, et al. *Proceedings of ASB*, Omaha, 2013.

ACKNOWLEDGEMENTS

This project was supported by the NASA Nebraska Space Grant & EPSCoR, the UNMC SAHP Pilot Research Grant and Graduate Fellowship.

ASSESSMENT OF SLIP-RISK USING A PORTABLE SLIP SIMULATOR

Arian Iraqi, Rakié Cham and Kurt E. Beschorner

The University of Pittsburgh, Pittsburgh, PA, USA
email: ari16@pitt.edu, web: <http://www.engineeringx.pitt.edu/hmbl/>

INTRODUCTION

According to the Bureau of Labor Statistics (BLS), falling events account for 25% of non-fatal occupational accidents [1]. A slip is likely to initiate when the friction required (RCOF) to sustain gait is less than the available friction at shoe-floor interface (ACOF) [2]. ACOF can be measured using a slipmeter on different floor surfaces, under both dry and contaminated conditions, whereas RCOF is measured on dry surfaces [3]. ACOF varies across different slipmeters [2], which makes the use of these devices to predict the risk of slips and falls challenging. Hanson et. al. developed a method to evaluate the relationship between slip resistance measurements and actual slips and falls. However, their study involved only one type of shoe. Different shoes have significantly different slip-resistant properties [4] and the ability of slip-testers to assess the slip risk across these shoes has not been sufficiently quantified. An in depth understanding of friction properties of shoes is required to minimize injuries due to falls from slips. The aim of this study is to test the ability of the Portable Slip Simulator, a whole-shoe tester capable of testing shoe-floor-coefficient of friction, to predict the outcomes of slipping accidents.

METHODS

Slip-resistance and slipping risk were characterized for three shoe and three boot conditions. In order to get a robust number of shoe/boot conditions, data from three similarly-conducted studies were combined for this post-hoc analysis [5,6]. The shoes included a standard work shoe (S1), a slip resistant shoe in new condition with full tread (S2T) and one in completely worn condition with not tread (S2NT), and three boot designs with identical tread but different hardness materials (Soft: B1, Medium hardness: B2; and Hard: B3, Table 1). The fluid contaminant was diluted glycerol for all conditions,

however, the concentration varied across the studies (Table 1).

Experiments to quantify ACOF were conducted using the Portable Slip Simulator [7]. This device tests an entire shoe heel and utilizes three vertical electromagnetic motors to apply a normal force and a linear motor to move the shoe across the flooring. Ground reaction forces (GRF) were measured using a 6DOF force plate (Advanced Mechanical Technology, Inc ®, Watertown, MA). Coefficient of friction (COF) values were measured at a sliding speed of 0.3 m/s, normal force of 250 N and shoe-floor angle of 7°. COF was quantified as the average ratio of resultant shear force to normal force during the first 200 ms after the normal force reached 250 N. Each test condition was repeated for 5 cycles.

Table 1: Shoe-floor-contaminant conditions and the number of subjects unexpectedly slipped.

Shoe #	Fluid Contaminant	Floor	n
S1	75% glycerol-25% water	Vinyl	26
S2T	90% glycerol-10% water	Vinyl	7
S2NT	90% glycerol-10% water	Vinyl	7
B1	50% glycerol-50% water	Vinyl	16
B2	50% glycerol-50% water	Vinyl	16
B3	50% glycerol-50% water	Vinyl	18

RCOF was calculated based on a method by Chang, et. al. [3] from baseline walking trials for previous studies conducted by our research group. The RCOF was considered only when the vertical force was above the 100 N threshold. Another criteria was that the longitudinal component of GRF had to be positive at the instant of the RCOF to correspond with the friction required for an anterior slip. Once the first two criteria were achieved, the RCOF was considered only when the instantaneous COF was increasing with time. This criterion bypasses peaks 1 and 2 of the COF data and considers the third peak.

All of the slipping trials were conducted by unexpectedly placing a liquid contaminant on the floor surface (Table 1 for different fluid contaminants) using a consistent method that obstructed the condition of the floor with dim lighting and distracting the subjects (Table 1 for number (n) of subjects for each shoe condition). The first and second unexpected slips were used for each of these studies. Slipping was tracked with a marker placed on the subject's heel. For slipping trials, occurrence of a slip event was considered when a slip distance was more than 1 cm [8].

A logistic regression model was used to determine if the mean difference between ACOF and RCOF (ACOF-RCOF) (Eq. 1) for each shoe was predictive of slip risk. The outcome was the occurrence of a slip and the prediction variable was the mean ACOF-RCOF, respectively.

$$\text{Slip_Risk} = 1/(1+\exp(\beta_0+\beta_1*(\text{ACOF}-\text{RCOF}))) \quad \text{Eq.1.}$$

RESULTS AND DISCUSSION

The logistic regression demonstrates that as the ACOF-RCOF increases, slip risk is reduced ($p<0.0001$) (Fig. 1). The average difference between the logistic fit curve and the actual proportion of subjects who slipped was 3.95 % (standard deviation: 3.422 %).

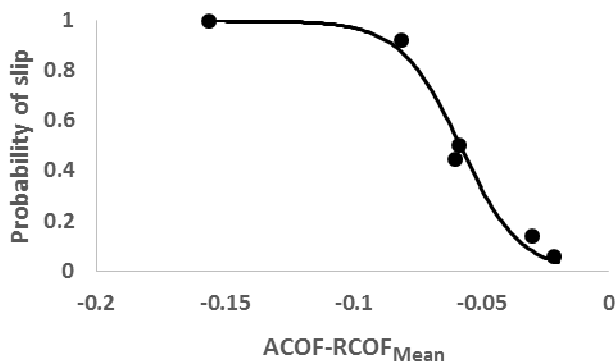


Figure 1: Logistic regression model comparing ACOF-RCOF to the predicted probability of slip.

This study suggests that the average ACOF and RCOF should both be considered when predicting the overall slip risk. For example, Shoes 2T and B2 both had an ACOF (0.151) (Fig. 2) however, shoe 2T had a much lower RCOF (0.181) than B2 (0.209). The difference in RCOF may explain why

shoe 2T had a lower slip risk (14.29%) than B2 (50.00%) despite their similar ACOF values. The Tribometer used in this study showed a bias for slips of -0.058, i.e., ACOF-RCOF point where 50% of slips occur [4].

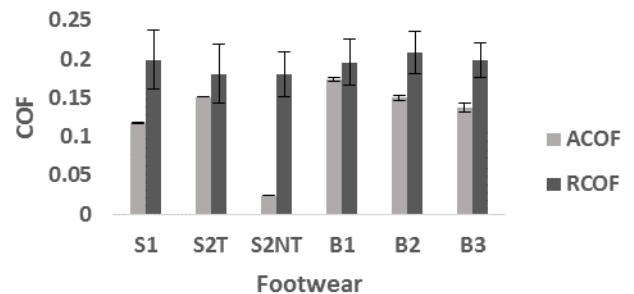


Figure 2: ACOF and RCOF across different shoes.

The Portable Slip Simulator provides valid measurements of slip risk for different shoes. Difference between ACOF and RCOF across the shoes and boots predicted the risk of slipping consistent with a logistic regression fit. Thus, the ACOF values from this slip-tester can be used to predict slipping risk as long as the RCOF for that shoe is known.

REFERENCES

1. U.S. Department of Labor- Bureau of Labor Statistics. Nonfatal Occupational Injuries and Illnesses Requiring Days Away From Work, 2012
2. Hanson JP, et al. *Ergonomics* **42**, 1619-1633, 1999.
3. Chang WR, et al. *Human Factors* **53**, 461-473, 2011.
4. Menz HB, Lord ST. *Gerontology* **47**, 145-149, 2001.
5. Moyer BE, et al. *Ergonomics*, **49**, 329-343, 2006.
6. Beschorner et al., 2014, *J. Biomechanics* **47**, 458-63.
7. Aschan C, et al. *Applied Ergonomics* **36**, 585-593, 2005.
8. Redfern MS, et al. *Ergonomics* **44**, 1138-1166, 2001.

ACKNOWLEDGEMENTS

Funding for this study was provided by the National Institute of Occupational Safety and Health (NIOSH R01 OH008986 and R01 OH007592).

Intrinsic and extrinsic foot muscles have unique roles in functional standing postures

¹ Toshiyuki Kurihara, ² K. Michael Rowley, ² Stephen F. Reischl, ² Lucinda L. Baker, and ² Kornelia Kulig

¹ Ritsumeikan University, Kusatsu, Shiga, Japan

² University of Southern California, Los Angeles, CA, USA

Email: t-kuri-a@st.ritsumei.ac.jp

INTRODUCTION

The longitudinal arch of the human foot is an elastic structure with passive and active connective tissues that allow for energy storage and return during locomotion.¹ Activity of intrinsic muscles such as the abductor hallucis (ABDH) and flexor hallucis brevis (FHB) is necessary for arch support during standing,² and stimulation of these muscles results in arch lift and center of pressure (COP) movement.^{3,4} Extrinsic muscles also activate during external arch loading, but show greater activation in posturally demanding tasks such as tandem stance⁵ and unstable shoe wearing.⁶ It has been proposed that intrinsic foot muscles behave as local stabilizers of the arch and extrinsic foot muscles as primary movers of the foot and ankle,⁷ but it is unknown how these groups of muscles function during stances of varying postural demand and foot positions.

The purpose of this study was to evaluate activity of extrinsic and intrinsic foot muscles during common functional and sport postures of varying balance difficulty. It was hypothesized that these two groups of muscles would function differently, and that extrinsic muscles would be more active in single-leg stances due to the increased balance difficulty.

METHODS

Twenty healthy young adults free from pain and lower extremity injury for the past six months were recruited for the study (7 Males, 13 Females; Age: 27.5 ± 5.6 yrs; Weight: 669.8 ± 149 N) according to guidelines by the Institutional Review Board. The supporting foot, defined as contralateral to the preferred kicking foot, was examined. Paired fine-wire intramuscular electrodes were inserted into ABDH, FHB, flexor hallucis longus (FHL), and

tibialis posterior (TP) muscles in the supporting foot of each subject. Surface electromyography (EMG) was collected from peroneus longus (PER) and tibialis anterior (TA). EMG data were collected using a wireless Noraxon system (Scottsdale, AZ) sampled at 3000 Hz, and bandpass filtered between 30 Hz and 500 Hz for surface data and 30 Hz and 1000 Hz for fine-wire data using a fourth-order Butterworth filter. Root mean square (RMS) signal amplitude was calculated over a 3 second epoch and normalized to the maximal voluntary isometric contractions for dorsiflexion, inversion, and eversion of the ankle, flexion of metatarsal-phalangeal (MTP) joints, and abduction of the first digit during manual muscle testing. Ground reaction force (GRF) data of each foot in each platform were collected with two force plates (Advanced Medical Technology Inc., Watertown, MA) in parallel setting. Sampling rate was 1500 Hz and synchronized with EMG. GRF were low-pass filtered using a fourth-order Butterworth filter with a 6 Hz low-pass cutoff. The postural demands of six balancing tasks were evaluated by COP velocity in a 3 second epoch of same duration for averaging EMG.

Subjects held six standing postures: bilateral stance (BLS), single-leg stance (SLS), bilateral squat (BSQ), single-leg squat (SSQ), bilateral calf raise (BCR), and single-leg calf raise (SCR) – in a random order for five seconds each. This sequence was repeated three times and measures were averaged for each posture. To keep the postures static in the three single-leg postures, the subjects were allowed light-touch on a supporting structure. A two-way analysis of variance (ANOVA) was conducted to compare differences between muscles and postures using Tukey post-hoc tests for pairwise comparisons with significance set at $\alpha=0.05$

RESULTS AND DISCUSSION

The average COP sway velocity of six standing postures were, increasing in order, BLS (1.8 ± 0.9 cm/s), SCR (2.1 ± 1.0 cm/s), BSQ (2.4 ± 0.9 cm/s), BCR (3.4 ± 1.5 cm/s), SSQ (3.9 ± 2.4 cm/s), SLS (4.8 ± 1.6 cm/s). We would expect SCR to be the most challenging of the postures because of the greatly decreased base of support. But COP sway to be slower in SCR, likely because all subjects had to use a light touch cue to retain balance in this position.

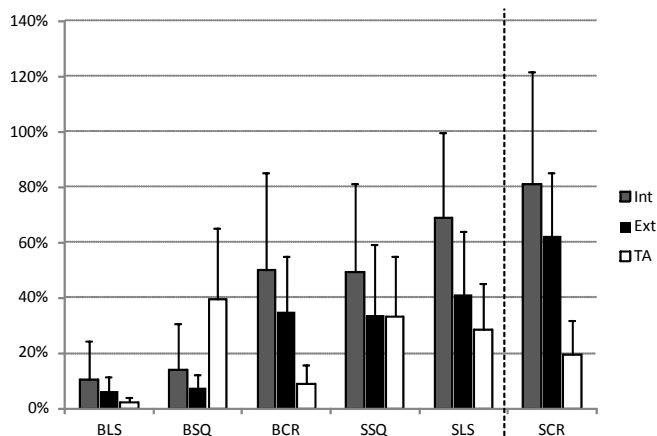


Figure 1: Averaged RMS EMG of three muscle groups in six standing postures. Int: intrinsic foot muscles, Ext: extrinsic foot muscles, TA: tibialis anterior muscle.

RMS of each muscle of six standing postures was summarized in Table 1. The ANOVA revealed significant differences in muscle activation level

across tasks ($F=13.2$, $p<0.001$) with post-hoc testing revealing three groups: (1) ABDH/FHB (intrinsic foot muscles), (2) FHL/TP/PER (extrinsic foot muscles), and (3) TA. Also, significant differences in muscle activation level within postural changes revealed BLS, BSQ < BCR, SSQ < SLS < SCR.

Figure 1 shows RMS EMG of three muscle groups in six standing postures. With increasing postural demand, intrinsic and extrinsic muscle groups increase activity in a similar manner. TA acts as a postural muscle only increasing in postures where it is demanded, primarily squatting.

CONCLUSIONS

Our results indicate the intrinsic and extrinsic foot muscles activate as unique groups. The activity of intrinsic and extrinsic foot muscles increases with postures of increasing balance difficulty in a similar manner.

REFERENCES

1. Verneecke E, et al. *J Exp Biol* **211**, 3661-3670, 2008.
2. Kelly L, et al., *Clin Biomech* **27**, 46-51, 2012.
3. Kelly L, et al., *JR Soc Interface* **11**, ePub, 2014.
4. Tortolero X, et al., *Artif Organs* **32**, 5-12, 2008.
5. Sozzi S, et al., *Clin Neurophysiol* **124**, 1175-1186, 2013.
6. Landry S, et. al., *Gait Posture* **32**, 131-139, 2013.
7. McKeon et. al., *Br J Sports Med* **49**, 290, 2015.

Table.1: Mean (SD) EMG root mean square (RMS) signal amplitude as a % of maximum voluntary contraction during bilateral stance (BLS), single-leg stance (SLS), bilateral squat (BSQ), single-leg squat (SSQ), bilateral calf raise (BCR), and single-leg calf raise (SCR), for abductor hallucis (ABDH), flexor hallucis brevis (FHB), flexor hallucis longus (FHL), and tibialis posterior (TP), peroneus longus (PER) and tibialis anterior (TA).

	EMG (% MVIC)					
	ABDH	FHB	FHL	TP	PER	TA
BLS	12.2 (14.3)	12.2 (17.5)	5.8 (5.6)	9.0 (8.9)	5.7 (4.5)	2.3 (1.2)
BSQ	14.0 (11.9)	18.1 (30.3)	4.2 (4.8)	10.5 (6.9)	7.6 (5.5)	38.5 (23.2)
BCR	53.4 (38.1)	45.6 (31.3)	44.5 (32.9)	24.0 (23.4)	37.1 (15.6)	8.9 (5.1)
SSQ	51.7 (34.4)	43.2 (28.4)	21.9 (19.6)	42.3 (31.3)	36.4 (27.6)	33.0 (18.6)
SLS	74.0 (31.3)	65.2 (42.9)	23.3 (15.0)	53.9 (37.3)	48.2 (24.2)	28.6 (15.9)
SCR	86.3 (52.4)	78.8 (40.5)	69.2 (43.9)	42.0 (35.1)	75.2 (26.1)	19.7 (10.6)

THE EFFECT OF STATIC STIMULUS ON THE NONLINEAR DYNAMICS OF POSTURE IN CHILDREN WITH ASD

¹Zachary Motz, ¹Venkata Naga Pradeep Ambati, ³Josh Haworth, ¹Jordan Grubaugh, ^{1,2}Nicholas Stergiou, ¹Anastasia Kyvelidou

¹Biomechanics Research Building, University of Nebraska at Omaha, Omaha, NE

²Department of Environmental, Agricultural & Occupational Health, University of Nebraska Medical Center, Omaha, NE

³Kennedy Krieger Institute, Center for Autism Related Disorders, Baltimore, MD
email: akyvelidou@unomaha.edu, web: coe.unomaha.edu/biomechanics

INTRODUCTION

Postural stability is a fundamental skill of motor development. Children with Autism Spectrum Disorders (ASD) exhibit repetitive behaviors and difficulties maintaining postural stability [1]. These issues may be apparent from an early age. Current literature quantifies the magnitude of postural sway in anteroposterior (AP) and medio-lateral (ML) directions. However, this does not explain the inherent variability of posture, which has been shown not to be random, but deterministic in origin [2].

Postural variability can be examined using linear (i.e. mean, standard deviation) and non-linear measures (i.e. Lypunov Exponent, Sample Entropy), which aid in the understanding of postural control organization. Non-linear measures complement traditional linear measures and provide further insights when comparing typical and atypical development in children [3]. In the one study that used non-linear measures (multi-scale entropy), Fournier et al. [4] revealed that children with ASD had less dynamical complexity in their center of pressure (COP) when compared with healthy controls. In addition, children with ASD present greater postural sway than typically developing children [5]. Since, stationary stimuli have stabilizing effects on posture in healthy young adults, [6] we also wanted to examine whether a static-point target would have a stabilizing effect on children with ASD.

The purpose of this study was two fold: a) to determine postural control differences between typically developing children and children with ASD using linear and nonlinear measures of center

of pressure (COP) and (b) to determine the effect of static stimulus on the postural sway of typically developing children and children with ASD. We hypothesized that children with ASD would have higher excursions in linear measures of COP when compared with typically developing children. Secondly, we expected to observe lower values of the nonlinear measures in children with ASD due to their restrictive and repetitive behavior. Lastly, we hypothesized that when children were presented with the static-point stimulus, both linear and non-linear measures would be reduced for both groups.

METHODS

Twenty-eight children participated; six diagnosed with autism (5.39 ± 1.01 years old) and twenty-two typically developing children (5.49 ± 0.77 years old). Participants attended a single session during which COP data was collected via force plate (AMTI, OR6) while looking at a blank TV screen or at a TV screen with a static-point target at eye level. Eye tracking equipment (Seeing Machines, faceLAB) was used to verify maintenance of attention during collection, ensuring that the children were looking forward.

Trials lasted for three and a half minutes each; with data recorded at 50 Hz. Post processing involved identifying segments during which the participant was not speaking or making overt motions with their head or arms. The longest common segment across all children was 750 data points, or 15 seconds of continuous data. The anterior-posterior (AP) and medial/lateral (ML) components of COP were further processed using custom Matlab scripts (MathWorks Inc.). The linear measures that we used were the mean, root mean square (RMS) and

velocity, and the nonlinear measures were the Lyapunov Exponent (LyE) and Sample Entropy (SampEn).

A 2x2 (Group x Visual Conditions) repeated measures ANOVA was used for statistical comparisons.

RESULTS AND DISCUSSION

Our analysis showed no significant differences between stationary stimulus versus no stationary stimulus conditions. However, significant differences were observed between the typically developing children and children with ASD with the nonlinear measures. Children with ASD exhibited significantly smaller ($p < 0.05$) LyE and SampEn for COP in AP direction when compared to typically developing children (Table 1). No significant differences were found for LyE and SampEn values for COP in the ML direction. There were also no significant differences found in any of the linear measures (i.e. mean, RMS, and velocity).

Although our initial hypotheses were not fully supported (in that there were no significant differences in our linear measures), the hypothesis that children diagnosed with ASD would have lower LyE and SampEn values was supported ($p = 0.025$ and 0.044 respectively). The lower LyE and SampEn values indicated lower divergence and decreased predictability of posture in children with ASD. This confirms what was found in previous literature [1,3], that children with ASD have restrictive and repetitive movements.

Static-visual stimuli have been shown to have stabilizing effects on postural sway [6]. However, a surprising finding from our data was that providing the static-visual stimulus did not have any significant effect on posture for either group. This result could be due to the experimental set-up. The static stimulus was a small picture of Elmo in the middle of the TV screen while the only difference with the non-stimulus condition was the absence of Elmo. Possibly, the whole TV screen served a static reference point.

CONCLUSIONS

The present data indicates that postural control in children with ASD is more repetitive and dynamically less complex than children without ASD. These differences are particularly noticeable when using non-linear analysis to evaluate posture.

REFERENCES

1. Kohen-Raz R., Volkmar F., Cohen D., *Journal of Autism and Developmental Disorders* **22** 419-432, 1992.
2. Stergiou N., Harbourne R., & Cavanaugh J., *J Neurological Phys Ther*, **30**, 120-129, 2006.
3. Kyvelidou A., Harbourne R., Willett S., Stergiou N., *Pediatr Phys Ther*, **25**, 46-51, 2013.
4. Fournier K., Amano S., Radonovich K., Bleser T., Hass C., *Gait & Posture*, **39**, 420-423, 2014.
5. Molloy CA., Dietrich KN., Bhattacharya A., *J Autism Dev Disord*, **33**, 643-52.
6. Laurens J., Awai L., Bockisch C., Hegemann S., van Hedel H., Dietz V., Straumann D., *Gait & Posture*, **31**, 37-41, 2010.

Table 1. Linear (mean, RMS and Velocity) and non-linear measures (LyE, SampEn) of variability for COP in AP direction.

Measure of Variability	ASD	TD	P value
Mean	0.49±0.06	0.51±0.05	0.27
RMS	0.50±0.06	0.53±0.05	0.28
Velocity	0.40±0.09	1.20±1.9	0.34
LyE	1.63±0.22	2.51±0.89	0.025*
SampEn	0.23±0.05	0.30±0.08	0.044*

* Significance at $p < 0.05$

CHANGES TO FORCE CONTROL STABILITY AFTER ANTERIOR CRUCIATE LIGAMENT RUPTURE AND RECONSTRUCTION

¹ Amelia S. Lanier and ² Thomas S. Buchanan

¹ The University of Delaware, Newark, DE, USA

² Delaware Rehabilitation Institute, Newark, DE, USA

email: alanier@udel.edu

INTRODUCTION

Rupture of the anterior cruciate ligament is a prevalent sports related injury. 70% of ACL injuries occur through a noncontact mechanism during sports requiring running and cutting. After ACL injury and reconstruction, patients experience altered neuromuscular control and reduced proprioception. Additionally, about 25% of those injured will experience a re-tear within the first year after returning to sports [1]. In an effort to reduce re-injury and return patients to activity, physical therapy aims to recover knee joint stability. Joint stability is measured in a number of different ways, including passively and dynamically. Recently, nonlinear analyses have been used to assess stability and have been able to provide valuable insight. These analyses are able to tap into the subtle time varying biomechanical changes that occur stride to stride, that current stability measures are unable to capture. One such example, called the Lyapunov exponent (LyE), utilized during gait analysis has shown reductions to kinematic knee joint stability after initial ACL injury and following reconstruction [2]. These changes to kinematic knee joint stability are present in all reconstruction types and in both the injured and uninjured limbs of patients [2].

However, the consequences of kinetic stability in this population have yet to be evaluated. The ability to stably produce multidirectional GRFs are crucial as patients return to running and cutting sports. Therefore, the purpose of this study was to evaluate force control stability after ACL rupture and subsequent ACL reconstruction using LyE. We hypothesized increased kinetic instability would be present after ACL rupture and ACL reconstruction when compared to healthy uninjured controls. We

also hypothesized all subjects would be less stable when tested in the anterior/posterior (AP) direction when compared to the medial/lateral (ML) direction.

METHODS

For this study we recruited 7 (2M) healthy uninjured individuals, 3(1M) who have experienced ACL rupture, and 2 (1M) who have undergone ACL reconstruction. All subjects were instructed to stand on two force plates with a foot on each force place. They were provided real time visual feedback of their force production, via a screen in front of them. Subjects were instructed alternatively and continuously to produce $\pm 50\%$ of their maximum force production in the AP or ML direction. LyE analysis was performed using the AP and ML force profiles as the variables of interest. To calculate the LyE two parameters were initially determined, time lag (τ) and embedding dimension (m). These parameters transformed our signal of interest into state space. Tau & m were calculated using an average mutual information (AMI) function and a global false nearest neighbor (GFNN) function respectively. Once in state space we used the Wolf algorithm [3] to calculate LyE. Further detail on AMI, GFNN, and Wolf algorithms is described in Stergiou et al. [4]. For this study we reported the maximum LyE value as it corresponds to the maximal instability.

RESULTS AND DISCUSSION

Our results support our first hypothesis that injury leads to reduced force control stability. Both ACL deficient (ACL-d) and ACL reconstructed (ACL-r) subjects had larger LyE values when compared to healthy uninjured controls (Fig.1, 2). However,

there is no difference in stability when comparing directions (Fig.1). Additionally, there appears to be no effect of limb (inv vs. uninv) (Fig 1).

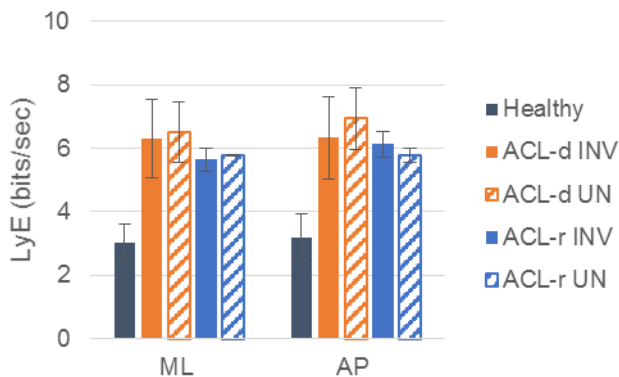


Figure 1: Avg LyE \pm SD (bits/sec) for healthy uninjured (gray), ACL-d (orange), and ACL-r (blue) subjects. Lower values for LyE indicate greater stability.

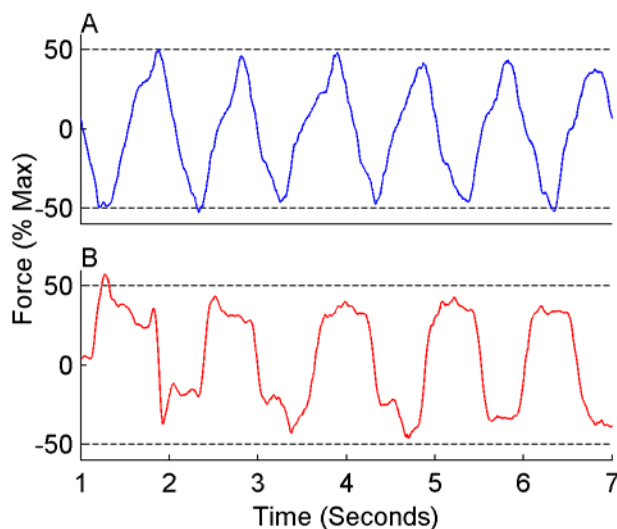


Figure 2: Representative force profile for a healthy subject (Plot A) and ACL-r subject (Plot B) in the anterior (+) and posterior (-) directions.

Being that ACL injury typically leads to muscular changes including quadriceps weakness we initially hypothesized force control stability would be more impaired in the AP direction compared to the ML direction. However, deficits to force control stability are present in both the AP and ML directions. This generalized reduction in force control stability may indicate upper level impairments are influential. Reduced proprioception and neuromuscular control is commonly seen after ACL injury.

Additionally, our results reflect those seen in studies that calculate kinematic stability. Using knee flexion/extension angle during gait Moraiti and colleagues found increased LyE values or reduced stability after ACL reconstruction [2]. Reductions to kinematic stability were equal in both involved and uninvolved limbs. Increased LyE present in both the involved and uninvolved limbs measured from both kinetics and kinematics may also indicate an upper level neuromuscular deficit. Diminished force control stability and kinematic stability in both the involved and uninvolved is important when considering there is a higher rate of re-injury in the contralateral limb [1].

CONCLUSIONS

After initial ACL injury and subsequent reconstruction there a large reductions to force control stability. Reduced force control stability is present in both the AP and ML directions. Our results indicate diminished stability in those with ACL injury and reconstruction when generating multidirectional ground reaction forces in both the injured and contralateral limb. Being that most injuries occur during running and cutting maneuvers a deficit to force control stability may be extremely detrimental. Reductions in force control stability may be contributing to re-injury rates in both contralateral and ipsilateral limbs as patients return to sports as it could lead to reduced running and cutting performance.

REFERENCES

1. Paterno MV, et al., *Clin J Sport Med* **22**, 116-121, 2012.
2. Moraiti, C, et al., *Gait & Posture* **32**, 169-175, 2010.
3. Wolf A, et al., *Physica* **16**, 285-317, 1985.
4. Stergiou N. *Innovative Analysis of Human Movement*, Human Kinetics, 2004.

ACKNOWLEDGEMENTS

NIH R01-AR046386, P30-GM103333, and R01-AR0482

REDISTRIBUTION OF JOINT MOMENTS AND DYNAMIC BALANCE CONTROL OF PERSONS WITH PARKINSON'S DISEASE

Hyo Keun Lee, Jared W. Skinner, Chris J. Hass

The University of Florida, Gainesville, FL, USA
email: leehk82@ufl.edu

INTRODUCTION

One of the cardinal motor symptoms of Parkinson's disease (PD) is postural instability. Postural instability contributes to impaired balance control, ultimately leading to an increased incidence of falls during activities of daily living. Further, such deficits in balance control are especially prominent during challenging motor tasks where the individual transitions from one base of support to another.

The Sit to Stand (STS) is a challenging task for persons with PD because it requires significant momentum generation in the forward and upward direction at a time when the base of support reduces to the span of the feet. Thus, the STS task requires the execution of joint moments to produce the necessary momentum but this momentum must also be able to be constrained to prevent falling forward or backward after rising [1].

Previously, we have reported that individuals with PD have reduced torque generating capacity and express a redistribution of joint torques during locomotor tasks. Herein, we evaluate the torque generating capacity of persons with PD during a STS task and evaluate the contribution of the hip, knee, and ankle to the net support moment in comparison to performance of age-matched healthy older adults. In addition, we examined and compared postural stability during the stabilization period after standing. We hypothesized that persons with PD perform the STS task with redistribution of their lower extremity joint moment along with less dynamic balance control capabilities.

METHODS

Eleven participants with mild to moderate PD (mean \pm SD age: 65 ± 8 years, mean height: $170.5 \pm$

7.2 cm, mean body mass: 77.3 ± 9.9 kg) and 9 age matched HOA (mean \pm SD age: 66 ± 8 years, mean height: 171.2 ± 8.3 cm, mean body mass: 70.3 ± 12.9 kg) volunteered in this study.

Participants were instructed to perform 5 experimental STS trials from a standard height chair. The individuals' feet were positioned uniformly on a force plate in front of the chair. Joint moment data were calculated from inverse dynamics techniques using motion capture (120 Hz, Vicon, Oxford, UK) and force plates data (360 Hz, Bertec Corporation, Columbus, Ohio). The distribution of lower extremity joint moments was also examined as a percentage of the total support moment. The total lower extremity moment (TLEM) in sagittal plane following seat off was determined for STS task by summing the peak hip, knee, and ankle joint moments from both limbs [3]. TLEM provides a quantitative assessment of the support and propulsive effort of the musculature for both legs during the STS task [1].

Dynamic Postural Stability Index (DPSI) was calculated from ground reaction force data during stabilization of the STS task. A 3-sec interval starting from onset of STS was used for the evaluation of dynamic stability. Anterior-posterior, medio-lateral, vertical, and dynamic postural stability indices (APSI, MLSI, VTSI, DPSI) were calculated from ground reaction forces (F_x , F_y and F_z) [2].

All comparisons between groups were evaluated using independent T-tests. A traditional level of significance $p \leq 0.05$ was adopted for the investigation.

RESULTS AND DISCUSSION

Findings showed persons with PD produced smaller peak ankle moment ($p<.05$), while they produced significantly greater peak knee moment ($p<.01$) than HOA during STS. However, there was no significant group difference in peak hip joint moment. This indicates that contribution of the knee to the extension moment is greater while ankle flexor is less in PD, causing a redistribution of joint moments during STS (Fig 1).

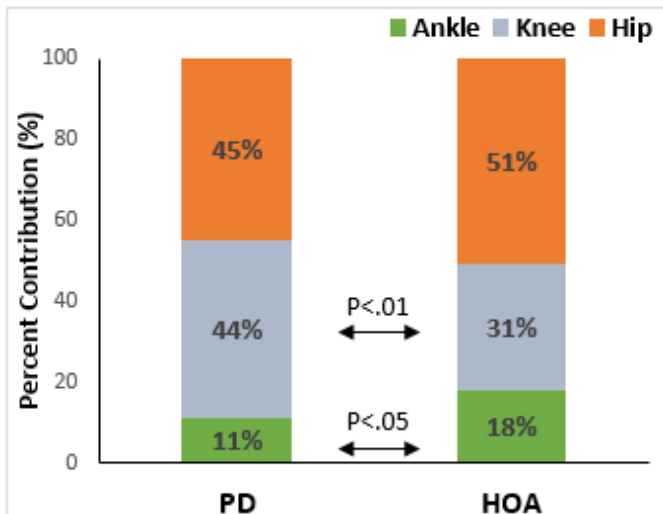


Figure 1: TLEM joint distribution for STS

In addition, persons with PD exhibited similar DPSI score to the score of HOA ($p>.05$) whereas the APSI score was significantly higher in PD ($p<.05$). Our results support evidence from previous studies that PD patients have impaired ankle joint function producing relatively less joint moment during activities of daily living. Given that PD patients showed redistribution of joint moment and decreased balance control in the AP direction during

STS, our result suggest that there may be a close relationship between muscular function and balance control capability in PD.

CONCLUSIONS

Persons with PD use a different strategy in lower extremity joint moment production during STS in comparison to HOA. This finding of redistribution of joint moments may indicate that the deficit of dynamic balance control in PD is closely related to muscular function. In the future study, correlation analyses should be performed to better understand the relationship between muscular function and balance control. This study further proposes the need of intervention like exercise training aimed on improved muscular function.

REFERENCES

1. Margaret KY et al. Joint torques during sit-to-stand in healthy subjects and people with Parkinson's disease. Clin Biomech, 2003; 197-206
2. Wikstrom EA, Hass CJ. Gait termination strategies differ between those with and without ankle instability. Clin Biomech, 2012;27(6):619-624.
3. Skinner JW, Lee HK, Roemmich R, Amano S, Hass CJ. Execution of activities of daily living in persons with Parkinson's disease. 2014;42(1):197-205.

Table 1: Net joint moments and dynamic postural stability indices during STS

Outcome Measures	PD	HOA	P-Value
Ankle joint moment (N/kg)	0.40 ± 0.23	0.59 ± 0.14	< .05
Knee joint moment (N/kg)	1.60 ± 0.42	1.03 ± 0.35	<.05
Hip joint moment (N/kg)	1.65 ± 0.34	1.70 ± 0.59	.40
DPSI	55.14 ± 16.4	53.19 ± 9.7	.38
APSI	4.98 ± 0.73	4.0 ± 1.0	<.05
MLSI	19.2 ± 5.3	21.2 ± 3.5	.18
VTSI	51.2 ± 16.1	48.5 ± 9.25	.34

EFFECT OF WHOLE BODY VIBRATION ON CENTER OF MASS MOVEMENT IN HEALTHY YOUNG ADULTS

Huaqing Liang and Jianhua Wu

Georgia State University, Atlanta, Georgia, USA. Email: hliang2@gsu.edu

INTRODUCTION

Whole body vibration (WBV) has acute effects on postural control strategy. The degree of impact depends on the amplitude, frequency, and duration of WBV, and the difficult level of balance task as well as the reliability of sensory information to the individual [1, 2, 3]. Healthy young adults can return to the baseline level of postural sway for a simple balance task within 20 minutes after repeated exposure to WBV [4]. Still, little is known about the acute and residual effects of WBV on the center-of-mass (COM) movement after a single bout of WBV. The purpose of this study was to understand the COM movements of young adults pre-, during, immediately post-, and 5-minute post 40-second WBV during standing.

METHODS

Participants: Fourteen healthy young adults (6M/8F) participated in the study. Mean (SD) of age was 24.5 (3.9) years, height 1.68 (0.12) m, and body mass 70.6 (13.4) kg.

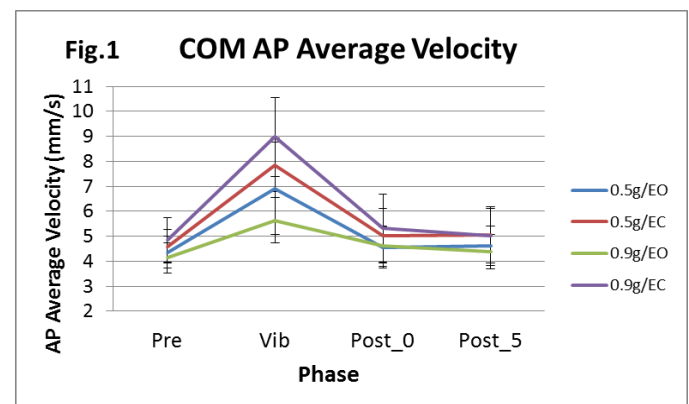
Experimental design: There were two vibration conditions: 0.5g and 0.9g (g is gravitational acceleration). These two vibration conditions represented WBV with amplitude less than 1mm at the frequency of 30 Hz and 50 Hz, respectively. There were two visual conditions: eyes open (EO) and eyes closed (EC). For each condition, data were collected for 40 seconds before vibration (phase *Pre*), during vibration (phase *Vib*), immediately after vibration (phase *Post_0*), and 5 minutes after vibration (phase *Post_5*). A Vicon full-body PSIS model was used to attach reflective markers on the subjects. A 7-camera Vicon motion capture system was used to record these markers.

Data collection and analysis: A total of four conditions (2 vibration x 2 visual) were tested and each condition was repeated twice. The order of the

conditions was randomized and adequate amount of time was given between conditions. Customized MATLAB programs were used to calculate average velocity and range of the COM during each phase in the anterior-posterior (AP) and medial-lateral (ML) directions separately.

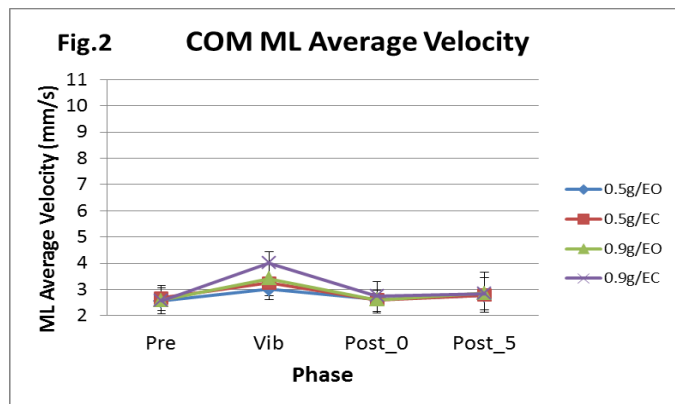
Statistical analysis: A series of 3-way (2 vibration x 2 visual x 4 phase) ANOVA with repeated measures were conducted on dependent variables. Post-hoc pair-wise comparisons with Bonforreni adjustments were conducted when appropriate. Statistical significance was set at $p < 0.05$.

RESULTS AND DISCUSSION

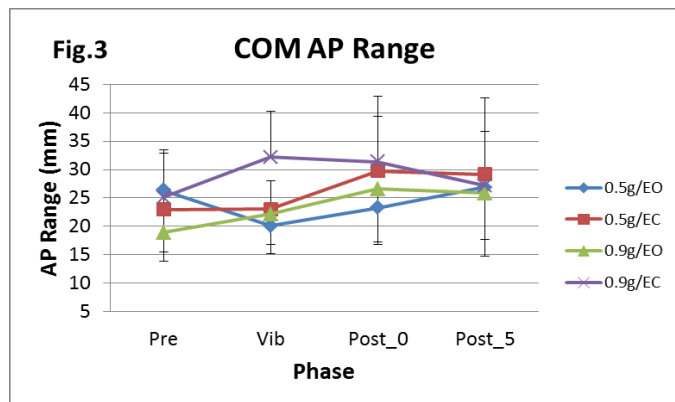


In the AP direction, average velocity increased from *Pre* to *Vib*, and reduced to the *Pre*-level after the vibration (Fig. 1). There was a vibration by visual by phase interaction ($p=0.006$). Post-hoc analysis revealed that average velocity was higher in the *Vib*-phase than the other three phases. Average velocity was higher in the EC than in the EO condition. Additionally, it increased to a greater extent from EO to EC condition in the *Vib*-phase than the other three phases. Average velocity increased from 0.5g to 0.9g in the EC condition, but decreased from 0.5g to 0.9g in the EO condition. For a higher level of vibration, participants may have intentionally restricted their postural sway in the AP direction and successfully did so in the EO

condition, but swayed at a faster velocity when visual information was not available.

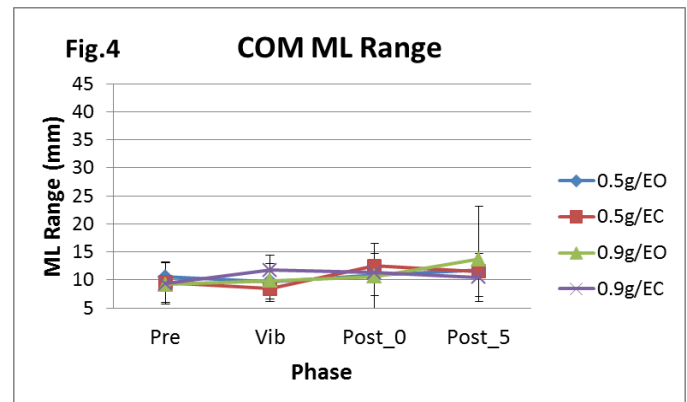


In the ML direction, average velocity increased from *Pre* to *Vib*, and reduced to the *Pre*-level after the vibration (Fig. 2). There was a vibration by phase interaction ($p<0.001$) as well as a visual by phase interaction ($p=0.019$). Post-hoc analysis indicated average velocity was higher in the EC than in the EO condition only in the *Vib*-phase. When the vibration increased from 0.5g to 0.9g, average velocity increased only in the *Vib*-phase. Additionally, average velocity was higher in the *Vib*-phase than the other three phases. A higher level of vibration elicited a faster postural sway in the ML direction, particularly when visual information was not available.



In the AP direction, range was larger after vibration than before and during vibration, and increased from EO to EC condition (Fig. 3). There was a vibration by phase interaction ($p=0.020$) and a visual effect ($p=0.002$). Post-hoc analysis showed that range was larger during the *Post_0* and *Post_5* phases than the *Pre*-phase respectively. It seems that

vibration has an acute and residual effect on the COM range in the AP direction regardless of vibration and visual conditions.



In the ML direction, range was larger 5-minute after vibration than before vibration (Fig. 4). There was a phase effect ($p=0.009$) and post-hoc analysis revealed that range during the *Post_5* phase was greater than the *Pre* phase regardless of vibration and visual conditions, suggesting a residual effect of vibration.

CONCLUSIONS

During vibration, young adults increase average velocity of the COM but maintain its range mostly in both the AP and ML directions regardless of visual conditions. After vibration, young adults return average velocity of the COM to its pre-vibration level in both the AP and ML direction; however, the vibration elicits a residual effect on the COM range in both directions. Young adults may need to constrain the range of sway to maintain balance during vibration, but increase the sway velocity to make sway corrections more frequently.

REFERENCES

1. Torvinen S, et al. *Int J Sports Med* **23**, 374-379, 2002.
2. Pollock RD, et al. *Eur J Appl Physiol* **111**, 3069-3077, 2011.
3. Dickin DC, et al. *Hum Mov Sci* **31**, 1238-1246, 2012
4. Dickin DC, et al. *J Appl Biomech* **30**, 529-533, 2014.

POSTURAL STABILITY IN ADOLESCENTS WITH EHLERS-DANLOS SYNDROME (HYPERMOBILITY TYPE) FOLLOWING AN EXERCISE INTERVENTION

¹ Jason T. Long, ² Bailey A. Petersen, ¹ Cailee M. Caldwell, and ¹ Stephanie F. Sabo

¹ Cincinnati Children's Hospital Medical Center, Cincinnati, OH, USA

² The Pennsylvania State University, State College, PA, USA

email: jason.long@cchmc.org, web: www.cincinnatichildrens.org/mal

INTRODUCTION

Ehlers-Danlos Syndrome (EDS) comprises a group of disorders marked by abnormal collagen function. In the most common form of EDS (type III or Hypermobility Type, hereafter EDS-HT), major diagnostic findings involve joint hypermobility and chronic pain. The prevalence of EDS-HT is up to 10-30% of males and 20-40% of females [1, 2]. Current interventions for chronic pain in EDS-HT consist of physical therapy, orthotic arch supports for postural alignment, neuromuscular and proprioceptive training, joint protection, stability and strengthening [3-5].

Physical therapy has been recognized in practice for its benefits to patients with joint hypermobility. Although the literature focused on these benefits is limited, evidence suggests that mechanical interventions may improve fatigability, pain, and stability [1-4]. Pilot findings from our group suggest that participation in an intensive exercise intervention (IEI) may lead to improvements in joint motion, loading, and symmetry [5, 6]. This IEI is a current care option for these patients at our institution.

Our group has previously reported on changes in biomechanical factors during walking in patients with EDS-HT. While ambulatory parameters demonstrate minimal change following exercise intervention, underlying postural stability parameters have not been assessed. In a pilot study, Greenwood et al. [6] found that strategies for stabilization during balance tasks may be relevant to injury risk in EDS-HT populations. Therefore, the purpose of this study was to assess postural stability metrics in patients with EDS-HT before and after participation in the intensive exercise intervention.

METHODS

Adolescents with EDS-HT or hypermobility disorder were recruited from the roster of IEI participants (ages 6-17 years). Each participant made an initial visit to the Motion Analysis Lab (MAL) immediately prior to starting the IEI, and a second visit within five days of completing the IEI. Between lab visits, participants took part in the IEI. This is a 10-day program involving two hours of intensive therapy per day, focused in neuromuscular re-education, flexibility, strengthening, joint stabilization, and endurance. Therapy sessions are both land-based and pool-based

During each visit to the MAL, participants underwent postural stability testing on an OR6-500 force platform (AMTI; Watertown, MA). Participants were asked to assume a position of comfortable bilateral stance on the platform. Two trials were collected, corresponding to two different visual conditions--Eyes Open (EO) and Eyes Closed (EC). During each trial, ground reaction force data were collected at 1800Hz for 60 seconds and processed to obtain center of pressure (COP) information. Data were subsequently analyzed using custom Matlab software (The Mathworks, Inc.; Natick, MA). Measures of interest included linear (COP excursion, velocity, and standard deviation) and nonlinear (approximate entropy and sample entropy) metrics in the A/P and M/L directions. Data were compared between test conditions using paired *t* tests.

RESULTS AND DISCUSSION

Summary findings are presented in Table 1. Select findings with statistical significance and potential clinical relevance are highlighted in Figures 1 and 2.

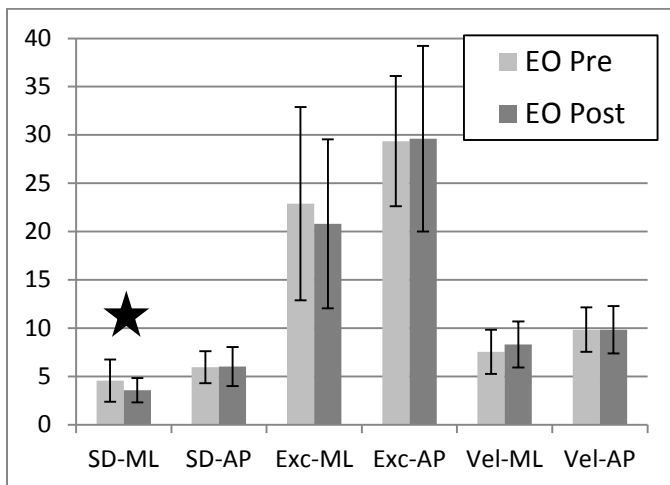


Figure 1: Linear measures of COP excursion in ML and AP directions for EO condition pre- and post-intervention (*SD* standard deviation, *Exc* excursion, *Vel* velocity). Star indicates significant difference ($p<0.05$).

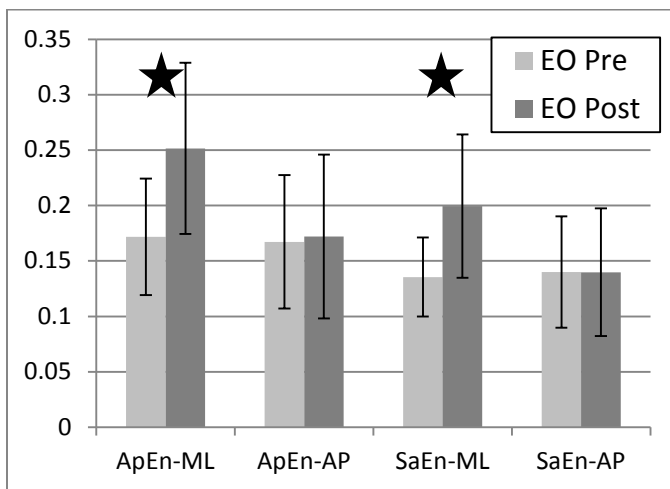


Figure 2: Approximate entropy (*ApEn*) and sample entropy (*SaEn*) of COP location in ML and AP directions for EO condition pre- and post-intervention. Star indicates significant difference ($p<0.01$).

Table 1: Velocity and entropy metrics for COP displacement in all conditions. † denotes significance for EO Pre vs EC Pre ($p<0.01$).

Measure	EO Pre	EO Post
Vel-ML [cm/s]	7.55 ± 2.3	8.3 ± 2.39
Vel-AP [cm/s]	9.84 ± 2.3	9.83 ± 2.46
Tot Vel [cm/s]	13.87 ± 3.24	14.44 ± 3.71
ApEn-ML	6.66 ± 2.08	6.06 ± 1.9
ApEn-AP	3.69 ± 1.22	3.51 ± 1.31
SaEn-ML	0.17 ± 0.05	0.25 ± 0.08
SaEn-AP	0.17 ± 0.06	0.17 ± 0.07

†
†
†
†
†

Significant differences in SD-ML between the EO Pre and EO Post conditions indicate variability of COP excursion that decreases following participation in the IEI, indicating a reduced amount of ML position variability. Significant increases in nonlinear postural control metrics are observed in the ML direction for both approximate and sample entropy, indicating changes in the structure of the ML position variability. These findings are similar to those from studies of adolescent athletes recovering from traumatic brain injury [7, 8]. Collectively, these findings suggest that the patients improved their ability to stabilize in the ML direction, and that their patterns of balance demonstrated increased complexity. This increased complexity of sway control may point to an increase in the patients' postural adaptability, and an improved readiness for perturbation.

Additionally, significant differences between EO and EC conditions for AP velocity and entropy were noted both pre- and post-intervention. While these findings are similar to those in the literature, it may be interesting to assess patients' reliance on visual input for maintaining stability and the effect of the IEI on this.

CONCLUSIONS

Significant improvements in mediolateral postural stability have been observed in adolescents with EDS-HT following participation in an IEI. These findings stand in contrast to the absence of change observed in concurrent studies of gait metrics. Further study is warranted to learn how these changes are affected by patients' baseline characteristics (e.g. pain level, fitness level, etc.) Additional stratification by age and gender may also be useful in delineating the most appropriate intervention strategy for subsets of this population.

REFERENCES

- [1] Hakim A et al. *Best Prac Rsch Clin Rheum* **17**, 989-1004, 2003.
- [2] Sacheti A et al. *J Pain Symp Mgt* **14**, 88-93, 1997.
- [3] Keer R et al. *Cur Op Rheum* **23**, 131-136, 2011.
- [4] Simmonds JV et al. *Man Ther* **12**, 298-309, 2007.
- [5] Simmonds JV et al. *Man Ther* **13**, e1-e11, 2008.
- [6] Greenwood NL et al. *Man Ther* **16**, 623-628, 2011.
- [7] Guskiewicz KM. *Clin Sports Med* **30**, 89-102, 2011.
- [8] Sigurdardottir S et al. *Brain Inj* **23**, 489-97, 2009.

HEAD ACCELERATIONS AFTER SLIPPING AND TRIPPING EXCEED THOSE DURING WALKING

¹Sara L. Arena, ²Julian L. Davis, ³J. Wallace Grant, and ⁴Michael L. Madigan

¹High Point University, High Point, NC, USA

²University of Southern Indiana, Evansville, IN, USA

³Virginia Polytechnic Institute and State University, Blacksburg, VA, USA

⁴Texas A&M University, College Station, TX, USA

email: sarena@highpoint.edu

INTRODUCTION

Slipping and tripping contribute to a large number of falls and fall-related injuries among older adults [1]. Detecting the onset of a loss of balance after a slip or trip is critical in preventing a fall. The vestibular system provides sensory feedback on head orientation and motion. The purpose of this study was to compare peak linear head accelerations after slipping or tripping to those experienced during walking. This information can help determine whether vestibular information may be used to detect the onset of a slip or trip, and may guide the development of fall prevention strategies.

METHODS

Twelve young male adults (mean \pm SD age: 20.9 \pm 2.2 years) performed several walking trials along a 10m walkway at a prescribed gait speed (\sim 1.5 m/s). After a minimum of 20 walking trials, an unexpected slip or trip (but not both) was induced to the dominant (right) foot.

Body segment positions of select anatomical landmarks on the head and feet were sampled at 200 Hz using a Vicon MX motion analysis system with T-10 cameras (Vicon Motion Systems, Inc., Los Angeles, CA). Head acceleration was sampled at 800 Hz using a lightweight six degree-of-freedom inertial measurement unit (IMU) (Memsense, LLC., Rapid City, SD) attached to the forehead. Marker position and acceleration data were low-passed filtered at 5 and 20 Hz, respectively.

Using methods similar to Startzell et al. [2] and Rivera et al. [3], head accelerations were converted to coordinate system aligned with the skull and transformed to an approximate location of the vestibular organ within the skull.

Peak accelerations in each direction (anterior/posterior, rightward/leftward, superior/inferior) were determined over six time intervals following perturbation onset, and compared between tasks (walking, slipping, tripping) and time intervals using a two-way repeated measures analysis of variance on the ranks (due to non-normal distributions). In the event of a significant condition by time interval interaction, contrasts were performed within each time interval. Statistical analyses were performed using JMP Pro 11 (SAS Institute, Inc., Cary, NC) with a significance level of $p \leq 0.05$.

RESULTS AND DISCUSSION

Peak head acceleration after tripping (Fig. 1) and slipping (Fig. 2) both differed from walking. After tripping, (Fig. 1), peak head acceleration during the 0-50ms time interval after trip onset was 0.68 m/s² higher in the anterior direction ($p < 0.001$), 0.47 m/s² higher in the posterior direction ($p = 0.011$), 0.63 m/s² higher in the rightward direction ($p < 0.001$), and 3.88 m/s² higher in the superior direction ($p < 0.001$) compared to walking. Several other differences in peak head acceleration between tripping and walking were found over 50-300ms time interval after trip onset ($p < 0.05$), and the magnitude of these differences tended to increase with time (Fig. 1).

After slipping (Fig. 2), peak head acceleration did not differ from walking until the 100-150ms time interval after slip onset, and was 2.00 m/s² higher in the inferior direction compared to walking. Several other differences in peak head acceleration between slipping and walking were found over the 150-300ms time interval after slip onset ($p < 0.05$), and

the magnitude of these differences tended to increase with time, but the magnitude of these differences was smaller than those seen during tripping.

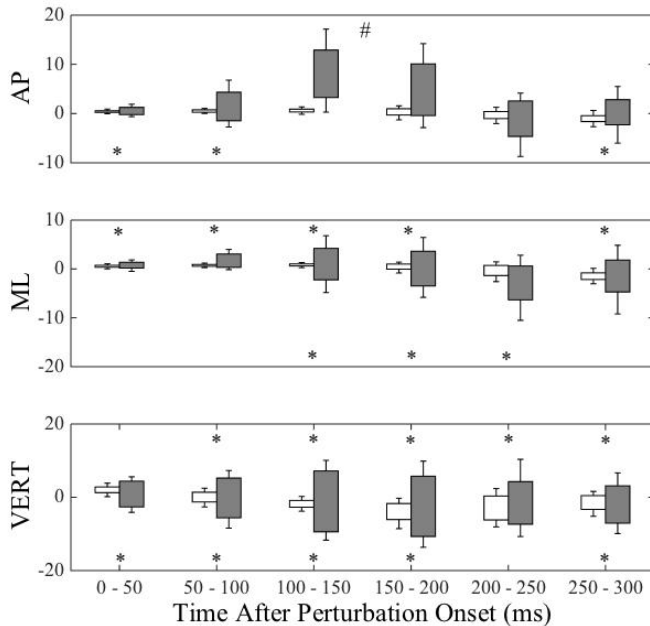


Figure 1: Peak head acceleration (m/s^2) after tripping (dark gray) and during walking (white). Time 0 indicates the instant of trip onset and mid-swing during walking. * denotes a difference between tripping and walking ($p < 0.05$). # denotes a main effect of condition ($p < 0.001$). The top of columns indicate the mean and SD in the positive direction (anterior, right, and inferior), and the bottom of the columns indicate the mean and SD in the negative direction (posterior, left, and superior).

Previous studies have shown muscle latency times of approximately 55-150ms [4] following trip onset. Because differences in head acceleration between tripping and walking were seen within 0-50ms of trip onset, these results suggest that vestibular information may play a role in generating a balance recovery response from a trip. However, previous studies have shown muscle latency times following a slip to be 90-160ms following a slip [5]. Differences in head acceleration between slipping and walking were not seen until 100-150ms of slip onset, suggesting that the vestibular system is less likely involved in the initial neuromuscular response to a slip.

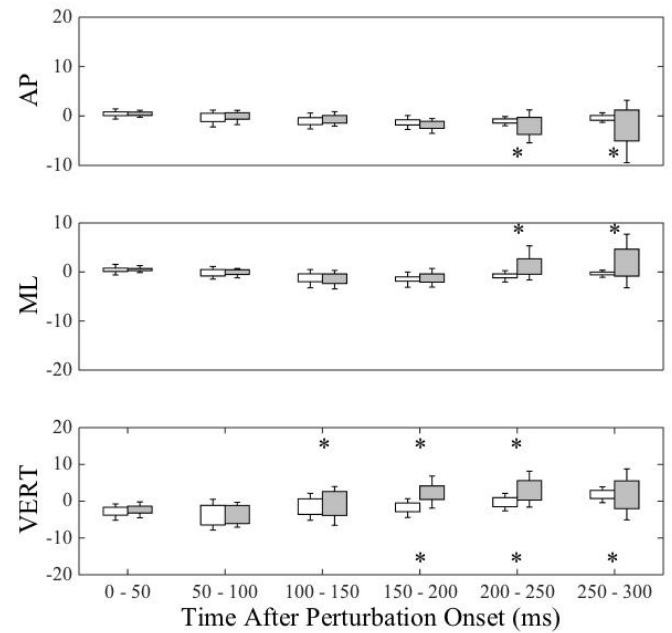


Figure 2: Peak head acceleration (m/s^2) after slipping (light gray) and during walking (white). Time 0 indicates the slip onset at heel contact, and heel contact while walking. * denotes a difference between slipping and walking ($p < 0.05$).

CONCLUSIONS

Peak head acceleration after slipping and tripping differed from those during walking. Differences occurred sooner after tripping compared to slipping, and the magnitude of these differences was larger after tripping than those after slipping. These results suggest that vestibular information may play a role in initiating a balance recovery response to a trip, but it remains unclear if such information contributes to recovery from a slip.

REFERENCES

1. Blake AJ et al. *Age Ageing* **17**, 365-372, 1988.
2. Startzell JK et al. *Hum Mov Sci* **18**, 603-611, 1999.
3. Rivera et al. *J Exp Zool A Ecol Genet Physiol* **317**, 467-480, 2012.
4. Eng JJ et al. *Exp Brain Res* **102**, 339-349, 1994.
5. Marigold DS and Patla AE. *J Neurophysiol* **88**, 339-353, 2002.

ACKNOWLEDGEMENTS

This work was supported by award R01OH009880 from the CDC-NIOSH.

OBESITY DOES NOT INCREASE LIKELIHOOD OF SLIPPING WHILE DESCENDING RAMPS

¹John M. Scanlon, ¹Abigail M. Zadnik, ¹Maury A. Nussbaum, and ²Michael L. Madigan

¹Virginia Tech, Blacksburg, VA, USA

²Texas A&M University, College Station, TX, USA

email: mlm@tamu.edu

INTRODUCTION

Over the past several decades, there has been an increasing prevalence of adult obesity in the U.S. (22.9% in 1988-1994 [1] and 34.9% in 2011-2012 [2]). Obese individuals have a 27% annual fall rate compared to 15% for those of healthy weight [4]. The effects of obesity on the likelihood of slipping during level walking has shown mixed results [5,6]. Descending ramps has been found to increase the likelihood of slipping [7], and may influence how obesity affects the likelihood of slipping.

The purpose of this study was to investigate the effects of obesity on likelihood of slipping during ramp descent. Because obese individuals exhibit a higher annual fall rate [4], we hypothesized that the likelihood of slipping would be higher among obese participants. Understanding how obesity affects slipping could help guide the development of effective fall prevention strategies.

METHODOLOGY

Twenty-three young male adults were recruited from the university population including thirteen healthy weight (age 21.8 ± 2.1 years, BMI 22.1 ± 2.0 kg/m²) and ten obese (age 23.9 ± 3.5 years, BMI 32.0 ± 3.6 kg/m²) individuals. Participants descended five randomly-ordered ramp angles, including 0, 2.5, 5, 10, and 15 degrees, at a walking speed of 1.1-1.6 m/s. Five trials were performed at each ramp angle. Prior to the session, participants donned athletic compression shorts and standardized athletic shoes in their respective size, and were told that they were not at any risk of being slipped.

The ramp was 0.9-m-wide and 1.8-m-long, and covered in vinyl flooring. A force platform (Bertec, Columbus, OH) was integrated in the ramp and located halfway down the length of the ramp. A hand railing was attached to the left side of the ramp for safety, but was not used in any trials analyzed. Ground reaction force data were sampled from the force platform at 1000 Hz and processed using a customized Matlab program (The Mathworks Inc., Natick, MA). Acromion marker data and force platform data were filtered using 4th order low-pass Butterworth filters with cutoff frequencies of 5 Hz and 25 Hz, respectively. Walking speed was calculated as the mean velocity of the acromion marker while traversing the ramp. Resultant RCOF was calculated as the resultant shear force divided by normal force.

A four-way mixed-model ANCOVA was used with walking speed as a covariate. Independent variables included obesity group, ramp angle, ramp order, and trial number (an obesity group x ramp angle interaction was also included). Post hoc pair-wise comparisons were performed using Tukey's Honestly Significantly Different test. Analyses were performed with JMP v7 (Cary, North Carolina, USA), and statistical significance was concluded when $p \leq 0.05$.

RESULTS & DISCUSSION

RCOF exhibited an obesity group x angle interaction ($p=0.043$). Pair-wise comparisons indicated RCOF increased as ramp angle increased within each group, but no effects of obesity group at each ramp angle (Figure 1).

The RCOF values obtained in this study compared well with results from past studies.

Cham and Redfern [8] investigated gait during ramp descent on a vinyl surface for healthy weight subjects, and found RCOF values of: 0.18 (current: 0.19) for 0 deg, 0.26 (current: 0.27) for 5 deg, and 0.32 (current: 0.33) for 10 deg. Redfern and Dipasquale [7] and McVay and Redfern [9] also observed positive trends in RCOF with increasing ramp angles.

It should be noted that slip risk (which requires measuring the difference between the available COF and RCOF) was not directly measured. However, because the available COF was the same in all conditions, RCOF as reported here does indicate relative slip risk.

CONCLUSIONS

Although the risk of slipping increases as ramp angle increases, obese individuals are not at an increased risk of slipping while descending ramps. This result, combined with previous

results [5,6,10], suggest modest, if any, increase in risk of slipping while walking among individuals who are obese.

ACKNOWLEDGMENTS

This work was supported by award R01OH009880 from the CDC-NIOSH.

REFERENCES

- [1] Flegal K, et al. *JAMA* 288, 1723-1727, 2002.
- [2] Ogden C, et al. *JAMA* 311.8, 806-814, 2014.
- [4] Fjeldstad C, et al. *Dyn Med* 7, 4, 2008.
- [5] Wu X et al. *J Biomech* 45, 1042-1047, 2012.
- [6] Liu J. *Int Conf on Fall Prev and Prot*, 2010.
- [7] Redfern S et al. *G&P* 6, 119-125, 1997.
- [8] Cham R et al. *G&P* 15, 159-171, 2002.
- [9] McVay E et al. *Am Ind Hy Assoc J* 55, 626-634, 1994.
- [10] Matrangola SL et al. *ASB Annual Meeting* 2013.

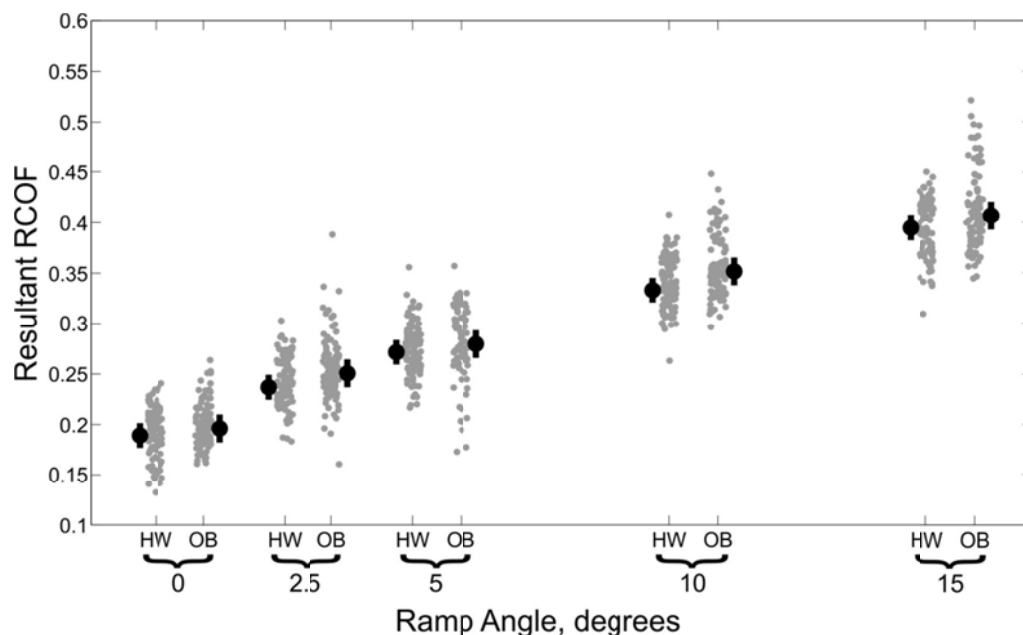


Figure 1: Black dots with black vertical lines represent least squares means and 95% confidence intervals, respectively. Gray dots represent all calculate RCOF values. HW refers to healthy weight participants, whereas OB refers to obese subjects.

Lumbar Spine Movement Patterns During a Clinical Test and a Functional Activity in People With Low Back Pain and People Without Low Back Pain

Marich AV, Bohall SC, Hwang CT, Sorensen CJ, Van Dillen LR

Washington University in St Louis School of Medicine,
Program in Physical Therapy, St Louis, MO, USA
email: maricha@wusm.wustl.edu

INTRODUCTION

Low back pain (LBP) is a common musculoskeletal problem with a complex etiology. One proposed movement-related mechanism contributing to the development and recurrence of LBP is the repeated use of stereotypic movement patterns. Previous research using clinical tests has identified early lumbar motion as one stereotypic movement pattern that is associated with LBP^(1,2). It is proposed that early lumbar motion used repetitively throughout the day results in an accumulation of tissue stress in the lumbar region, leading to microtrauma and eventually LBP symptoms. The movement patterns observed during clinical tests are assumed to reflect the behavior of the lumbar spine during daily functional activities.

The purpose of this study was to examine the lumbar movement patterns in people with LBP and back-healthy (BH) people during a clinical test and a functional activity. We hypothesized that (1) lumbar movement patterns during a functional activity would be similar to those observed during a clinical test, and (2) the amount of lumbar range of motion (ROM) used early in the movement would be greater in people with LBP compared to BH people, and be related to disability in people with LBP.

METHODS

Subjects. 32 people with chronic LBP and 16 age-, height- and weight-matched BH people participated. Subjects were excluded if they were in an acute flare-up or had a history of spinal trauma or certain spinal conditions. Subjects with LBP completed the modified Oswestry Disability Index (mODI). The mODI is a disease-specific disability measure.

Scores range from 0-100%. A score of <20% indicates low disability.⁽³⁾ Thirteen LBP subjects had mODI scores < 20% (LBP-LOW, age 35.08 ± 12.28 yrs, 8 male), and 19 subjects had mODI scores ≥ 20% (LBP-HIGH, age 32.95 ± 8.57 yrs, 9 male).

Instrumentation. An 8-camera, 3-D motion measurement system (Vicon Motion Systems, LTD, Denver, CO) was used. All kinematic data were processed using Visual3D (C-Motion Inc., Germantown, MD) and variables calculated using custom written software in MATLAB (MathWorks Inc., Natick, MA).

Laboratory Based Testing. Kinematics were collected during the clinical test of forward bending (FWB) and the functional activity of picking up an object (PUO). For PUO, an empty plastic container was placed at a height equal to 100% shank length and a distance 50% of the trunk length away from the front of the knee. The variables calculated were maximum ROM of the lumbar spine and lumbar ROM at 25% increments of total movement time.

RESULTS AND DISCUSSION

Forward Bending. There were no differences in maximum lumbar ROM among the 3 groups. The LBP-HIGH group displayed significantly greater lumbar ROM from 0-25% of the movement time compared to the BH group (Table 1). There were no other differences among the groups.

Picking Up an Object. The LBP-HIGH group had significantly greater maximum lumbar ROM compared to the other 2 groups. The LBP-HIGH group also displayed significantly greater lumbar

ROM from 0-25% and 25-50% of movement time compared to the other 2 groups (Table 1).

Relationship of Movement Patterns to Disability:

There was a moderate positive correlation between lumbar ROM in the early part of movement and mODI scores for all LBP subjects for both FWB and PUO (Table 2).

CONCLUSIONS

There were no differences in maximum lumbar ROM among the groups during FWB. Compared to the BH group, the LBP-HIGH group displayed significantly greater lumbar ROM in the early part of the movement (0-25%). Compared to the other 2 groups, the LBP-HIGH group had greater maximum lumbar ROM during PUO, and the differences in lumbar ROM occurred in the 1st 1/2 of the movement (0-50%). The amount of lumbar ROM early in FWB and PUO is positively related to

mODI scores. The data suggest that as the amount of lumbar ROM used increases, particularly early in the movement, the greater the LBP-related disability.

REFERENCES

1. Gombatto, SP, et al. Clinical Biomechanics, 21, 263-271, 2006.
2. Scholtes, SA, Gombatto, SP, & Van Dillen, LR. Clinical Biomechanics, 24, 7-12, 2009.
3. Fritz, JM & Irrgang, JJ. Physical Therapy, 81, 776-788, 2001.

ACKNOWLEDGEMENTS

Funding sources include NIH/NICHD 5R01HD047709-07, the Foundation for Physical Therapy, and the Missouri Physical Therapy Association.

Table 1: Lumbar Maximum ROM (deg) and Lumbar ROM (deg) at Quartiles of Total Movement Time

	BH (n=16)	LBP-LOW (n=13)	LBP-HIGH (n=19)	p-value
Lumbar Maximum ROM				
Forward Bend	33.75 ± 7.10	32.68 ± 10.86	36.82 ± 7.92	0.36
Picking Up an Object	21.25 ± 4.74 ^a	21.55 ± 9.09 ^b	27.23 ± 4.42	0.01
Quartiles of Movement Time: Forward Bending				
0-25%	5.87 ± 2.13 ^a	6.16 ± 2.81	8.58 ± 3.87	0.03
25-50%	13.87 ± 3.42	12.72 ± 4.78	13.34 ± 3.57	0.73
50-75%	9.76 ± 2.78	9.29 ± 3.87	9.48 ± 4.24	0.94
75-100%	4.12 ± 2.09	4.46 ± 3.31	5.32 ± 3.93	0.54
Quartiles of Movement Time: Picking Up An Object				
0-25%	2.76 ± 1.33 ^a	2.39 ± 1.34 ^b	4.21 ± 1.47	< 0.01
25-50%	6.90 ± 2.07 ^a	6.92 ± 3.29 ^b	9.26 ± 1.96	0.01
50-75%	7.79 ± 2.33	8.39 ± 3.26	9.17 ± 2.35	0.31
75-100%	3.87 ± 1.28	3.78 ± 2.16	4.71 ± 1.87	0.26

^a Significant difference between the BH group and the LBP-HIGH group

^b Significant difference between the LBP-LOW group and the LBP-HIGH group

Table 2: Correlation of mODI scores and lumbar ROM at quartiles of movement time during (a) FWB and (b) PUO.

		Percent of movement time						Percent of movement time			
FWB		0-25	25-50	50-75	75-100	PUO		0-25	25-50	50-75	75-100
mODI r-value	.39	.25	.13	.15		mODI r-value	.59	.55	.33	.33	
p-value	.03	.17	.47	.40		p-value	.00	.00	.06	.07	

(a)

(b)

Boldface indicates correlation is significant at the 0.05 level (2-tailed)

STANCE TIME VARIABILITY IS THE BEST PHYSICAL AND GAIT BIOMECHANICAL PARAMETER TO DISCRIMINATE OLDER FALLERS AND NON-FALLERS

¹ Nise Ribeiro Marques, ² Camilla Zamfolini Hallal, ¹ Deborah Hebling Spinoso, ³ Luciano Fernandes Crozara, ³ Mary Hellen Morcelli, ³ Adriane Beatriz de Souza Serapião, ³ Carlos Noberto Fischer, ³ Verônica Oliveira de Carvalho, ³ Mauro Gonçalves

¹ The São Paulo State University, Marília, SP, BRA

² The Uberlândia Federal University, Uberlândia, MG, BRA

³ The São Paulo State University, Rio Claro, SP, BRA

email: nisermarkes@yahoo.com.br

INTRODUCTION

Falls are responsible for reduction of functional independency, institutionalization, fear of falling and loss of confidence in older adults [1]. Previous studies demonstrated that older faller adults have lower strength, an increased energy cost of walking and changes on gait biomechanical, such as an increased gait kinematics variability than older non-faller adults [2-4]. However, to the authors' knowledge the identification of the best physical and gait performance parameter to discriminate older fallers and non-fallers still unknown.

Thus, the current study aimed to identify the best physical (lower limb maximum strength) and gait performance (metabolic and biomechanical) parameter to discriminate older fallers and non-fallers. Also, a second objective of this study was to identify the cut-point of the best physical and/or gait performance parameter to discriminate older fallers and non-fallers.

METHODS

Thirty-seven older female adults participated of this study (age 67.8 ± 7.1 yr). The subjects were separated into two groups: older fallers ($n = 15$) and non-fallers ($n = 22$) based on having fallen or not in the period of 1 year before the evaluation.

The volunteers visited the laboratory on two separate occasions within 24-72 hours. On the first day of data collection the preferred treadmill walking speeds (PTWS), and the hip, knee and ankle maximal isometric voluntary joint torques were measured. During the second day of data

collection, the volunteers were familiarized with treadmill walking at PTWS for 10 min and then the energy expenditure during seated rest was measured via indirect calorimetry. Next the cost of walking at PTWS was measured followed by kinematic assessment of gait.

Kinematic gait parameters, cost of walking, and joint voluntary torques were assessed by: a motion analysis system with seven infrared cameras (Vicon Motus, Oxford, UK®) and an 8-channel, telemetered biological data system (Noraxon®, Phoenix, USA); a metabolic measurement system (Quark PFT, Cosmed®, Rome, ITA); and an isokinetic dynamometer (Biodex®, New York, USA).

For the kinematic gait parameters, 39 markers were fixed on the head, trunk, upper and lower limbs, according to the manufacturer's Plugin Gait Full Body model. The kinematic parameters were recorded at a sample frequency of 100 Hz. Also, heel contact and toe-off were detected by two footswitches (Noraxon®, Phoenix, USA), composed of four sensors attached on both feet at the heel, first and fifth metatarsals, and toe, which were synchronized with the motion analysis system.

The algorithm C4.5 of learning machines was used for the data analysis. Table 1 summarizes the variables used in the categorization.

Table 1. Summary of variables used in the categorization.

Variables
<i>Kinematic</i>
Stance time variability

Swing time variability

Stride time variability

Dynamometric

Hip extensor isometric peak torque

Knee extensor isometric peak torque

Ankle extensor isometric peak torque

Hip flexor isometric peak torque

Knee flexor isometric peak torque

Ankle flexor isometric peak torque

Hip extensor isokinetic peak torque

Knee extensor isokinetic peak torque

Ankle extensor isokinetic peak torque

Hip flexor isokinetic peak torque

Knee flexor isokinetic peak torque

Ankle flexor isokinetic peak torque

Metabolic

Energy cost

Class

Faller

Non-faller

RESULTS AND DISCUSSION

The stance time variability was capable of distinguishing groups of elderly fallers and non-fallers. The accuracy achieved was 97.30%, correctly classifying 36 of 37 samples. Observing the model generated by C4.5, a decision tree was composed of a single node represented by stance time variability, with a discriminant value for the class of older fallers and non-fallers (Figure 1). In this case, the decision tree can be expressed as a single decision rule as follows: *if* (stance time variability ≤ 0.101917); *then* (class = non-faller); and *else* (class = faller).

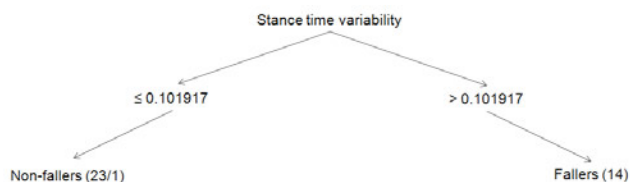


Figure 1: Decision tree using full dataset.

The most novel aspect of this study was that it demonstrated that the best parameter to discriminate older fallers and non-fallers was the stance time variability with 93% of sensitivity, 100% of

specificity and the cut-point of 0.1 seconds. Our findings corroborate with Bruijn et al. (2011)[5] and Toebe et al. (2012)[1] findings which demonstrated an association between step time variability and risk of falls.

The stance is the gait phase that requires more strength, balance and motor control during walking. During the initial stance phase, muscles are activated to maintain joint stability while the ground reaction forces are absorbed [6]. Also, during the final stance phase, while the hip and trunk muscles are activated to maintain balance, the plantar flexors are recruited to accelerate the center of mass to perform the next step [6]. Thus, once older adult fallers would have lower strength and poorer balance than older adults non-fallers the gait variability may be increased by this physical limitations.

CONCLUSIONS

The current study provides new knowledge of the best physical and gait biomechanics parameters to discriminate older fallers and non-fallers. According to our findings, the best gait biomechanical parameter to identify older fallers and non-fallers was the stance time variability (sensitivity of 93% and sensitivity of 100%) and the cut-point found was a variability of 0.1 seconds between the strides.

REFERENCES

1. Toebe MJP, et al. *Gait Posture* **36**, 527-531, 2012.
2. Callisaya ML, et al. *Age Ageing* **40**, 481-48, 2011.
3. Pijnappels M, et al. *Gait Posture* **21**, 388-394, 2005.
4. Peterson DS and Martin PE. *Gait Posture* **31**, 355-359, 2011.
5. Bruijn SM, et al. *J Biomech* **44**, 2401-2408, 2011.
6. LaRoche DP, et al. *Gait Posture* **33**, 668-672 2011.

ACKNOWLEDGEMENTS

Funding for this study was provided by São Paulo Research Foundation (FAPESP).

Role of the Paretic and Nonparetic Limbs to Arrest Forward Momentum Following a Perturbation

¹ Nicholas K. Reimold, ^{1,2} Keith E. Gordon and ¹ Katherine M. Martinez

¹ Northwestern University, USA

² Edward Hines Jr. VA Hospital, Hines, USA

email: k-martinez@northwestern.edu

INTRODUCTION

Stroke survivors often have deficits in gait, balance and postural stability and are at higher risk for falls [1]. Clinically, ambulatory stroke survivors tend to initiate voluntary steps with their paretic leg. In contrast, when stepping is induced by a perturbation, individual less than three months post stroke show a preference to initiate stepping with their nonparetic leg [2]. However, the probability that ambulatory chronic stroke survivors will initiate stepping with their paretic leg in response to a perturbation will increase if the limb is passively unloaded [3]. The purpose of this study was to investigate the ability of community dwelling stroke survivors to use their paretic and nonparetic limbs to control their forward momentum following a significant postural perturbation. Specifically, our goal was to quantify the braking impulse created during the first step after the perturbation. We hypothesized that the braking impulse created when subjects stepped first with their paretic limb would be significantly less than the braking impulse generated by their nonparetic limb and would often be inadequate to stop their forward momentum within a single step.

METHODS

Six individuals post stroke participated in the study. All subjects ambulated independently in the community (mean age 51.5 yrs, 4 males, 4 right side weak, 1-26 years post stroke). Subjects were tested without their ankle-foot orthosis and/or assistive devices.

We measured trunk and lower limb kinematics and ground reaction forces as subjects performed multiple trials in which they were instructed to respond naturally to the perturbation they would

receive. Each trial began with subjects standing quietly with their feet shoulder width apart. Three initial standing conditions were included in which the distribution of the subjects body weight between their two feet was manipulated by providing visual feedback to the subjects about their weight distribution. The three conditions were weight equally distributed, more weight (70%) on the paretic limb, and more weight (70%) on the nonparetic limb. Once subjects achieved and held the target weight distribution for 250-1000 msec they would receive an anterior-directed waist pull perturbation. The perturbations were created by dropping a weight equal to 10% of their body weight connected by a cable attached to the front of a belt worn by the subject. Ten perturbation trials were conducted at the three different weight distribution conditions, and 6 additional catch trials at 2% BW were randomly applied. Rest breaks were given after 18 trials and as needed.

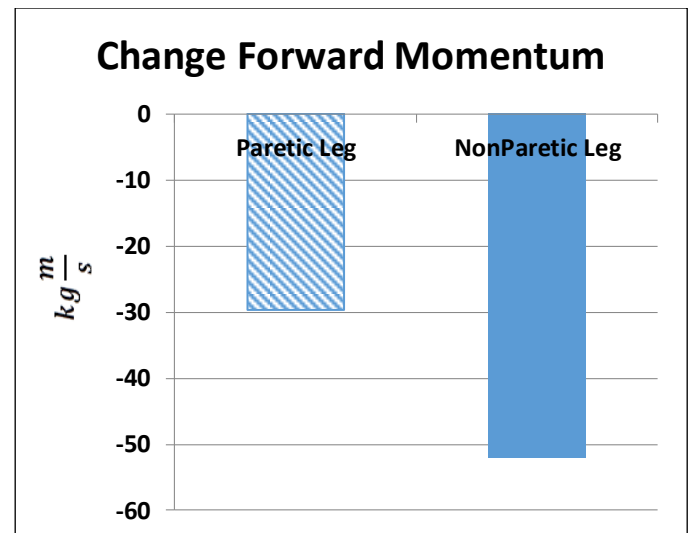
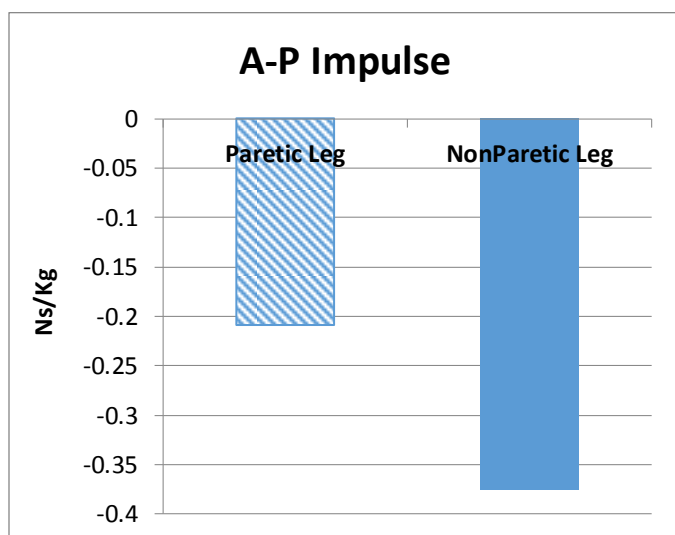
For each trial we first identified which limb subjects stepped with and calculated the number of recovery steps required after the perturbation. We also calculated the anterior-posterior impulse during the period from heel strike of the first step until heel strike of the second step after the perturbation. We estimated forward velocity at heel contact of the first step using the trunk markers. Finally we calculated change in forward momentum during the first step using the two previous values.

RESULTS AND DISCUSSION

All subjects stepped in all of the 10% body weight perturbation. In 83.6% of the trials subjects stepped their nonparetic limb and 16.4% of the trials with their paretic leg. Two subjects made their first response step exclusively with the nonparetic limb.

Across the body weight distribution conditions no significant differences in the anterior-posterior impulse ($F(2, .044)=3$, $p=0.13$) or change in momentum ($F(2, 485.3)=1.25$, $p=0.54$) were observed. Thus, the conditions were combined to increase the number of trials that could be used to compare the first step response between the limbs.

Making a first response step with the paretic or nonparetic limb did not result in a significant difference between the total number of steps taken in response to the perturbation or effect the forward velocity at the first heel strike after the perturbation. While there was a trend for individuals to display a smaller braking impulse (-0.21 Ns/kg vs -0.37 Ns/kg), smaller change in forward momentum (-29.68 $kg \frac{m}{s}$ vs -52.11 $kg \frac{m}{s}$), and shorter duration (.56s vs .79s) when the first response step was made with the paretic limb vs the nonparetic limb these trends were not significant ($z=-1.83$, $p=0.068$). The lack of significance is most likely due to small number of steps with both legs. These results suggest that during the first response step after a perturbation subjects post stroke were better able to decrease their forward momentum when using their non-paretic leg.



CONCLUSIONS

After a forward perturbation, there appears to be a difference between the ability of the paretic and non-paretic limb to produce the braking impulse required to reduce one's forward momentum. In the current study even when the paretic limb was initially unloaded when the perturbation occurred subjects almost always shifted their weight and took their first response step with their nonparetic limb. While this may delay an individual's time to respond to a perturbation, their overall ability to arrest their forward momentum may be improved because of the much greater ability of the nonparetic limb to generate a braking impulse. Task specific perturbation-induced step training with the paretic leg may strengthen the ability to generate a braking impulse with this leg and allow individuals post-stroke the option to slow their forward momentum with either leg.

REFERENCES

1. Weerdesteyn V, et al. *J Rehabil Res Dev* **45**, 1195-1213, 2008.
2. Mansfield A, et al. *Arch Phys Med Rehabil* **7**, 1179-1184, 2012.
3. Martinez KM, et al. *Arch Phys Med Rehabil* **94** 2425-2432, 2013.

ACKNOWLEDGEMENTS

Nathan Brimm, Stephany Thomas, Mary Wu for their assistance with data collection.

A COMPARISON OF TANDEM WALK PERFORMANCE BETWEEN BED REST SUBJECTS AND ASTRONAUTS

¹Chris Miller, ¹Brian Peters, ¹Igor Kofman, ¹Tiffany Phillips, ²Crystal Batson, ¹Jody Cerisano,
¹Elizabeth Fisher, ³Ajitkumar Mulavara, ⁴Alan Feiveson, ⁴Millard Reschke and ⁴Jacob Bloomberg

¹Wyle Science Technology and Engineering Group, Houston, TX, USA

²MEI Technologies Inc., Houston, TX, USA

³Universities Space Research Association, Houston, TX, USA

⁴NASA Lyndon B. Johnson Space Center, Houston, TX, USA

Email: chris.miller-1@nasa.gov

INTRODUCTION

Astronauts experience a microgravity environment during spaceflight, which results in a central reinterpretation of both vestibular and body axial-loading information by the sensorimotor system. Subjects in bed rest studies lie at 6° head-down in strict bed rest to simulate the fluid shift and gravity-unloading of the microgravity environment. However, bed rest subjects still sense gravity in the vestibular organs. Therefore, bed rest isolates the axial-unloading component, thus allowing the direct study of its effects.

The Tandem Walk is a standard sensorimotor test of dynamic postural stability [1]. In a previous abstract [2], we compared performance on a Tandem Walk test between bed rest control subjects, and short- and long-duration astronauts both before and after flight/bed rest using a composite index of performance, called the Tandem Walk Parameter (TWP), which takes into account speed, accuracy, and balance control. This new study extends the previous data set to include bed rest subjects who performed exercise countermeasures. The purpose of this study was to compare performance during the Tandem Walk test between bed rest subjects (with and without exercise), short-duration (Space Shuttle) crewmembers, and long-duration International Space Station (ISS) crewmembers at various time points during their recovery from bed rest or spaceflight.

METHODS

All subjects provided written informed consent before participating in this study, which was

approved in advance by the NASA Lyndon B. Johnson Space Center Institutional Review Board.

This study is part of a larger protocol that uses a suite of physiologic tests and functional tasks to relate physiologic changes to changes in functional performance of mission-critical tasks immediately after flight/bed rest. Subjects groups included: (a) 10 bed rest controls, all of whom completed 70 days of 6° head-down strict bed rest with no exercise countermeasure; (b) 17 bed rest exercisers, all of whom completed the same bed rest but with exercise countermeasures; (c) 6 short-duration crewmembers who completed Space Shuttle missions (12.9 ± 1.5 d) with in-flight exercise countermeasures, and (d) 13 long-duration crewmembers who completed missions aboard the ISS (151.6 ± 17.1 d) with in-flight exercise countermeasures. Data collection sessions occurred twice within a 2-month or 2-week time period before flight or bed rest, respectively (Pre), and four times after flight/bed rest: on the day of landing or end of bed rest (Post+0d), one day post (Post+1d), six days post (Post+6d) and a final session 10 days (bed rest) or 30 days (flight) post (Post+10/30). Due to logistical limitations, data could not be collected from long-duration crewmembers on landing day.

In the Tandem Walk test, the subjects walked in a heel-to-toe fashion at a self-selected speed for 10-12 steps with their arms crossed on their chests and their eyes closed. A spotter walked next to the subject to ensure safety and to monitor the step count. Three Tandem Walk trials were performed per session.

Torso and head linear accelerations (relative to their respective local coordinate systems) were recorded at 50 Hz using triaxial inertial measurement units (Xsens, North America Inc., Culver City, CA). During the analysis, the start and end of the trials were manually selected by inspection of a plot of the vertical head acceleration to get the total trial time. The gravitational acceleration was removed from the Z-component of the torso acceleration. The root-mean-square (RMS) of the resultant linear torso accelerations (TorsoAccR) over the trial was then computed. Video of the trials was reviewed to determine the percentage of heel-to-toe (“correct”) steps during the task. The TWP was then computed for each session as follows:

$$TWP = \ln \left(1 + \frac{PctCorrectSteps}{TotalTime * RMS(TorsoAccR)} \right)$$

The log transformation was used to prevent extreme values from dominating the data analysis. Larger values of TWP reflect better overall performance.

A separate analysis revealed no significant difference between the two Pre sessions, so their data were pooled in the subsequent analysis. A linear mixed model with TWP as outcome and random subject effects was used to estimate group-by-session means and test for pre-post differences between groups for each post session. P-value thresholds for reporting significance were calculated using the Hochberg multiple-comparison procedure [3] to control the family-wise Type I error rate to 0.05.

RESULTS AND DISCUSSION

All groups exhibited lower TWP values (i.e., increased instability) during Tandem Walk immediately after flight/bed rest (Figure 1). Thus, axial-unloading alone – as is the case in bed rest – resulted in decreased Tandem Walk performance immediately after flight/bed rest.

The multiple-comparison analysis of the pre- to postflight/bed rest difference estimates showed that the *change* in TWP for the bed-rest exercise subjects was: (a) significantly less than that of the bed rest controls for Post+0d and Post+1d, (b) significantly less than the long-duration flight group

for Post+1d, and (c) significantly more than the short-duration flight group for Post+6d. Thus changes in TWP in the bed rest exercise group were similar to short-duration astronauts for Post+0d and Post+1d, but similar to the long-duration astronauts at Post+6d. Therefore, exercise countermeasures helped mitigate some of the decrement in TWP after bed rest (exercise vs. control). However, additional balance and/or coordination training during flight/bed rest may be required to maintain TWP at Pre levels on Post+0d.

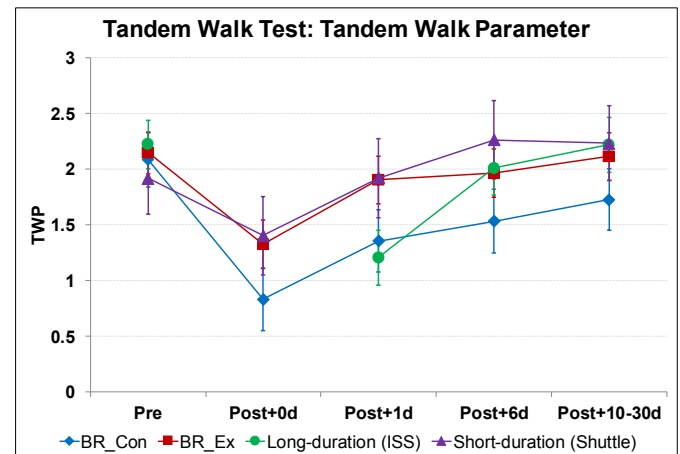


Figure 1: Tandem Walk Parameter ($\pm 2SE$)

CONCLUSIONS

Exercise countermeasures during space flight or bed rest helped mitigate some of the decrements in tandem walk performance immediately after flight/bed rest. But performance deficits remained, thus suggesting an additional sensorimotor countermeasure may be necessary to maintain tandem walk performance on Post+0d at preflight/bed rest levels.

REFERENCES

1. Fregly AR, et al. *Aerospace Medicine* **43**, 395-399, 1972.
2. Miller C, et al. *Proceedings of the 37th Annual Meeting of the ASB*, Omaha, NE, USA, 2013.
3. Hochberg Y. *Biometrika* **75**, 800-802, 1988.

ACKNOWLEDGEMENTS

This study is funded by the National Aeronautics and Space Administration.

USING THE FEASIBLE BALANCE REGION TO ESTIMATE THE STRENGTH REQUIREMENTS OF ONE LEG BALANCE: EFFECTS OF AGE AND DIABETIC PERIPHERAL NEUROPATHY

Payam Mirshams Shahshahani and James A. Ashton-Miller
University of Michigan-Ann Arbor, email: mirshams@umich.edu

INTRODUCTION

In the clinic, balance is often assessed by testing the ability to stand on one leg. An inability to balance for 5 seconds is associated with an increased risk of injurious falls [1]. Prior efforts to assess postural stability have considered the human as a simple inverted pendulum under the control of an ankle torque and then have considered the state space containing center of mass position and velocity [2]. A knowledge gap is how hip torque affects balance, given the importance of hip and ankle strategies [3]. So we considered a double inverted pendulum model of one leg balance via hip and ankle torques and movements. If the ankle and hip each have a displacement and velocity state, then one can hypothesize a “Feasible Balance Region” (FBR) that is the volume within which the states have to remain in order to balance during the balance test. We thought it might be instructive to use this approach to study the quasi-static strength requirements for balancing on one leg.

METHODS

In this planar double inverted pendulum frontal plane model the lower link represents the stance leg with hinge joints at each end representing the ankle and hip. The upper link represented the rest of the body. For simplicity, the foot was assumed fastened to the floor. The link dimensions and masses for a mid-sized male (1.78 m, 81.4 Kgf) were taken from [3]. The torso was assumed rigid, the contra-lateral leg perpendicular to the pelvis, and the arms crossed. The state of the model is then determined with two angles and their angular velocities: the angle that the leg link makes with the vertical (θ_1) and the abduction angle of the ipsilateral hip (θ_2) (Figure 1). Angular accelerations and velocities were assumed negligible.

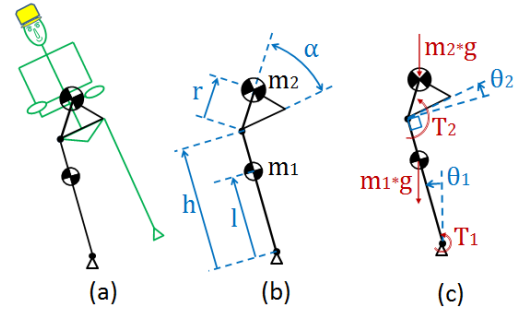


Figure 1: Model of one-legged-balance

The torques (Figure 1c) for holding a quasi-static posture are:

$$T_1(\theta_1, \theta_2) = -(m_1 l + m_2 h)g \sin \theta_1 + m_2 g r \cos(\alpha + \theta_1 + \theta_2) \quad (1)$$

$$T_2(\theta_1, \theta_2) = m_2 g r \cos(\alpha + \theta_1 + \theta_2) \quad (2)$$

$$T_{1min} \leq T_1 \leq T_{1max} \quad (3)$$

$$T_{2min} \leq T_2 \leq T_{2max} \quad (4)$$

where T_{1min} and T_{1max} are the maximum ankle inversion and eversion torques, respectively; and T_{2min} and T_{2max} are the maximum hip ABduction and ADduction torques. θ_1 and θ_2 are also constrained by the physiological ranges of motion for the ankle and hip joints. We can combine equations (1) and (2) with the ranges defined in (3) and (4) to find all the combinations of θ_1 and θ_2 that are achievable by a person for quasi-static balance. We called this region the FBR. The area of the FBR was then calculated (in deg^2) for three different populations: healthy young (HY) and healthy old (HO) subjects, and patients with diabetic peripheral neuropathy (PN). Values for maximum torque capacities and ranges of motion for each group were taken from the literature [5-7]. We used a dynamometer to measure the force-length characteristics of the maximum isometric hip torques over the ROM (Figure 2) [5]. We scaled the data for PN with respect to HO in [5] to obtain HY, HO, and PN values [7].

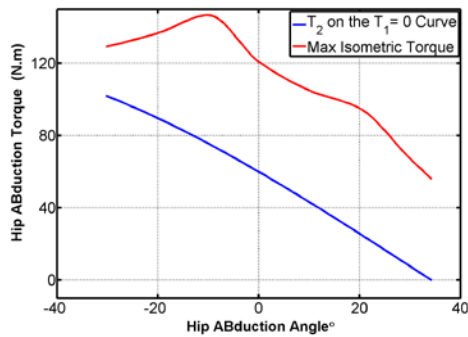


Figure 2. Estimated force-length characteristics on hip abduction torque in a healthy YM. (Red) The hip abduction torque when center of mass is centered over the ankle. (Blue)

RESULTS

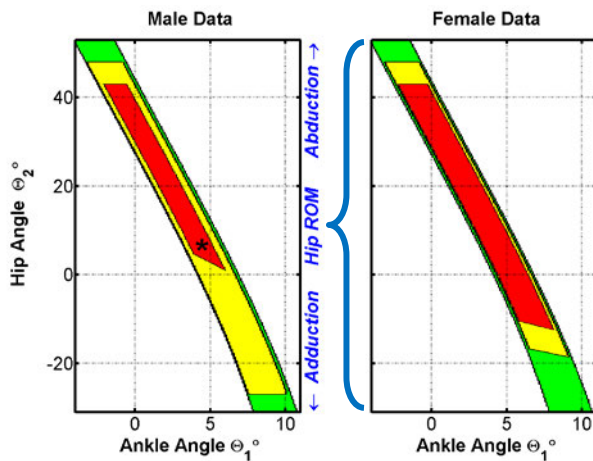


Figure 3. The calculated FBR for HY (green+yellow+red), HO (yellow+red) and PN (red)

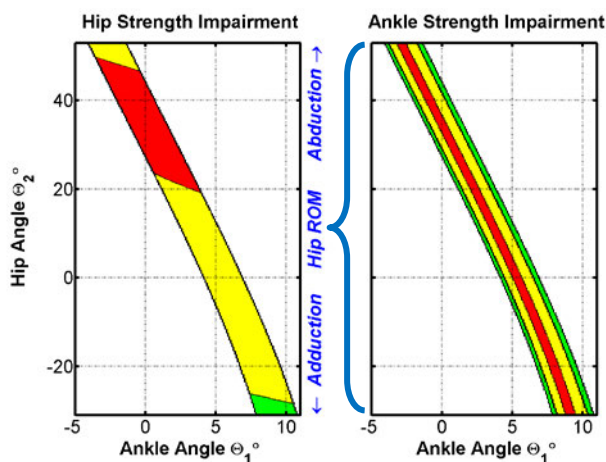


Figure 4. Effect of hip and ankle impairment on the FBR. No impairment (green+yellow+red), 25% impairment (yellow+red), 75% impairment (red)

For the males the calculated FBR area for the HY (222 deg²) was x1.3-times larger than HO (177 deg²); this was 3.8 times larger than PN (58 deg²). For females, the corresponding results were 218, 146 and 104 deg² respectively (**Figure 3**). When ankle and hip strengths were impaired by 25% and 75%, the FBR area was slightly more sensitive to ankle strength impairment (164 and 48 deg²) than hip strength impairment (211 and 69 deg²) (**Figure 4**). The hip abduction torques required to stand on one leg without pelvic tilt ($\theta_2 = 0$, **Figure 2**) were 50%, 56%, 65%, and 80% of maximum hip abduction torques for HY males and females, HO males and females, respectively.

DISCUSSION

These results are the first to quantify the FBR and demonstrate how impairments in ankle and hip strength narrow and shorten the FBR, respectively, to make the balance task more difficult. If a state reaches a boundary of the FBR, T_1 or T_2 must have saturated, so any perturbation of the state beyond the boundary will result in instability. The reduction in FBR area with age correlates well with the decline in unipedal stance times [8]. The limitations of the analysis are (1) its quasistatic nature, (2) constant maximum ankle isometric torques, and (3) simplification to two body segments. The truncated FBR near the asterisk in Figure 3 likely resulted from weaker-than-normal male PN data.

REFERENCES

1. Vellas BJ, *JAGS* **45** (1997): 735-8.
2. Pai YC *J. Biomech.* **30** (1997): 347-354.
3. Horak FB. *J Neurophys.* **55** (1986): 1369-1381.
4. Armstrong HG. *AAMRL TR-88-010* (1988)
5. Allet LE, *Muscle Nerve* **45** (2012): 578-585.
6. Cahalan TD *CORR* **246** (1989): 136-145.
7. Sepic SB, *AJPMR* **65** (1986): 75-84.
8. Morioka S, *Curr. Ger. Ger. Res* 10.1155/2012/516283 (2012)

ACKNOWLEDGEMENTS

Supported by a pilot grant from the CDC grant to the U-M Injury Center, U49/CE002099.

Stride Time Variability and Fall Risk in Persons with Multiple Sclerosis

Yaejin Moon, D. A. Wajda, R. W. Motl, J. J. Sosnoff

Department of Kinesiology and Community Health, University of Illinois at Urbana-Champaign
email: ymoon9@illinois.edu

INTRODUCTION

Multiple sclerosis (MS) is one of the most prevalent chronic disability neurological diseases in young adults and results in conduction delays along neuronal pathways commonly resulting in impairments in gait [1]. There is evidence that gait variability measures may be more sensitive to subtle abnormalities in gait compared to average gait parameters in MS [2]. However, the clinical importance of higher gait variability in MS is not clear.

One potentially important interpretation of gait variability is as a possible indicator of fall risk for people with MS (PwMS) [2]. This investigation examined the relationship between the magnitude and structure of stride-time variability in a 6-minute walking test (6MW) and physiological fall risk in PwMS compared to age-matched healthy controls. It was predicted that 1) stride-time variability will be positively associated with fall risk and 2) the association will be stronger in the MS group.

METHODS

17 PwMS (F=11, M=6, age=62.8 \pm 7.4years) and 17 healthy age matched controls (F=12, M=5, age=62.8 \pm 5.9 years) participated. For the MS group, seven (41%) walked without assistive devices, six (35.3%) used a cane and four (23.5%) utilized a walker during the 6MW. Ten of the MS participants (58.8%) had relapse remitting MS, while four (23.5%) had secondary progressive, and three (17.6%) had primary progressive. None of the control group participants used an assistive device during the 6MW.

Fall risk was measured utilizing the short form of the Physiological Profile Assessment (PPA) [3]. The PPA involves a series of five tests including assessments of vision, proprioception, quadriceps force, reaction time and postural sway on a compliant surface. The outcome of each test was combined to generate an overall fall risk score [3]. Higher values indicate greater fall risk.

All participants performed the 6MW test in a 21 m hallway. Stride-time was assessed with use of Xsens MTx inertial measurement units (Xsens Technologies B.V., the Netherlands) attached to the participants' shanks. Shank angular velocity parallel to the mediolateral axis was obtained at sampling frequency of 150HZ. The stride-to-stride time interval was defined as the time between consecutive heel strikes of the same foot. It was determined using a custom MATLAB script (The MathWorks, Natick, MA) (See Figure 1) [4]. All analyses utilized the first 140 strides of the 6-minute walk based on the minimum number of strides within the sample.

Stride time data series was characterized with average stride time (AVG_{ST}) and with variability calculated by coefficient of variation (CV_{ST} = SD_{ST} / AVG_{ST})

All statistical analyses were performed using SPSS (V19.0, Chicago, IL). To examine group differences of outcomes, independent t-tests were conducted for normally distributed measurements while the Mann-Whitney U test was conducted for non-normally distributed measurements. Due to the small sample size, Spearman rank order correlations were used to test the association between fall risk and stride-time parameters in each group respectively. The difference between the correlation coefficients was tested by Steiger's Z-test. All analyses used two-sided tests with an alpha of 0.05.

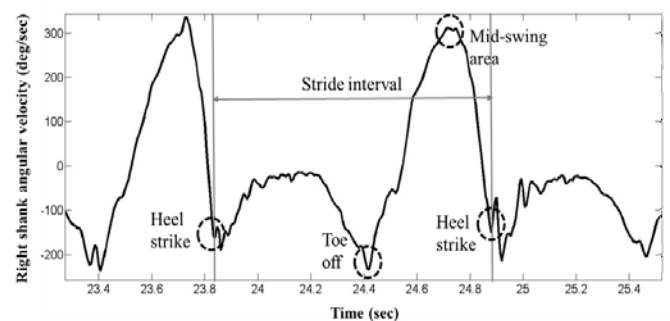


Figure 1: Schematic of shank angular velocity gait events and stride interval.

RESULTS AND DISCUSSION

Analysis of group differences of demographics revealed that there was no difference in age and gender composition between groups (P 's>0.05). Self-reported disability of the MS group had median EDSS score of 6.0 (IQR 4.75 to 6.0). Also fall risk score was significantly higher in the MS group (Mean: 1.4+/-1.5) than in the control group (Mean: 0.1+/-0.7) (p <0.01).

Effect of group on stride time metrics: Stride time parameters as a function of group are presented in Table 1. The MS group exhibited greater average and variability of stride-time.

Table 1: Effect of group on stride-time metrics

Variables	MS	Control	P-value
AVG _{ST} (sec)	1.16 (1.07-1.32)	0.95 (0.88- 0.98)	<0.01
CV _{ST} (%)	3.43 (2.91-7.07)	1.67 (1.37- 2.21)	<0.01

Note: Median (IQR)

Correlation between stride time metrics and fall risk: AVG_{ST} was not correlated with fall risk in either group (p 's>0.05). There was a strong positive correlation between CV_{ST} and fall risk in both groups (MS: ρ =0.71, p <0.01; Control: ρ =0.67, p <0.01) (Figure 2). The association was not different between groups (p 's>0.05).

There are several potential mechanisms underlying the association between increased stride-time variability and fall risk. First, impaired reaction time, proprioception, and lower limb muscle strength might be a mediator of the relationship given that those are related to increased temporal gait variability [5] and have been attribute to falls in MS [6]. Also, considering a more variable gait is believed to be less energetically efficient, fatigue (a fall risk factor) could be another possible mediator [7]. Lastly, it has been suggested that increased gait variability reflects breakdown of the automatic gait rhythm system. Less rhythmic gait is believed to require greater attentional demand which has been related to increased fall risk in MS [6].

Also, although PwMS had higher gait variability and fall risk than the controls, the strong association between the factors might be driven by aging than MS related pathology.

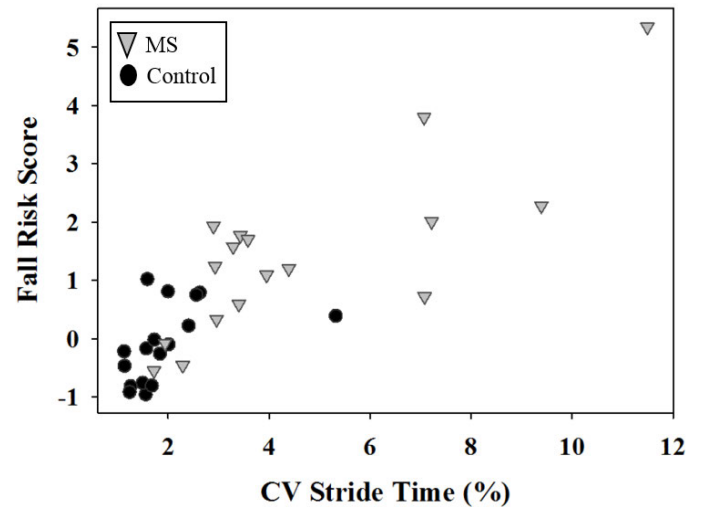


Figure 2: Correlation between CV of stride-time and fall risk as a function of group

CONCLUSIONS

The current investigation demonstrates the amount of stride-time variability (but not average stride-time) is strongly related to physiological fall risk both in PwMS and the controls. The mechanisms underlying the association remain to be elucidated. A major limitation of the study is the small sample size with relatively high level of neurological impairment in the MS group. Also it may limit generalizability of the result that most of the controls had minimum risk of fall. It is possible that variability in other gait parameters may yield distinct results given that other parameters imply different aspects of gait impairment. Future work examining whether gait variability is predictive of future falls in PwMS is warranted.

ACKNOWLEDGEMENTS

This project was funded by National Multiple Sclerosis Society (IL Lot NMSS 006).

REFERENCES

1. Cameron M.H. et al, *Somatosensory motor research*,25, 113-22., 2008
2. Socie, M.J., & Sosnoff J. J. *MS Int.*,645197, 2013
3. Lord, S.R., *Gait Posture*, 83, 237-51., 2003
4. Aminian,K. et al., *J Biomech*, 35, 689-99., 2002
5. Callisaya M.L. et al., *J Gerontology.*, 65A, 386-92, 2010
6. Nilsagard,Y. et al.,*Clin Rehab*, 23,259-69, 2009
7. Paterson,K.L. et al.,*Gait Posture*,33, 251-5, 2009

BIOMECHANICS OF THE FUNCTIONAL REACH TEST

Tulika Nandi, Andrea Du Bois, ¹Nicole Runkle, Kathryn L. Havens and George J. Salem
Jacqueline Perry Musculoskeletal Biomechanics Research Laboratory
Division of Biokinesiology and Physical Therapy
¹ University of Southern California, Los Angeles, CA

Email: nandi@usc.edu Web: www.usc.edu/go/mbrl

INTRODUCTION

Balance refers to the ability to move the center of mass (COM) in a safe and controlled manner. The Functional Reach Test (FRT) is commonly used to assess balance in both clinical and research settings. Though the reach distance is believed to be an indicator of COM and center of pressure (COP) excursions, there are conflicting reports across studies [1, 2]. The correlation of reach distance with COM excursion has been found to be dependent on the biomechanical strategy. Hip strategy (HS) is characterized by ankle plantarflexion and greater than 15° of hip flexion; ankle strategy (AS) is characterized by less than 15° of hip flexion, with or without some ankle dorsiflexion [3]. To the best of our knowledge, the relation between COP excursion and strategy has not been reported.

It may be argued that the reach distance can be driven or limited by different biomechanical factors in HS and AS. Sagittal plane hip and ankle moments are potential variables that can influence the choice of strategy. However, it is currently not known whether moments differ between strategies and whether they are associated with the reach distance.

Thus, the purpose of this study was first, to compare the biomechanics of hip and ankle strategy **within subjects during the FRT**. Secondly, the relations between reach distance and COP COM excursions, and hip and ankle moments were tested.

METHODS

Eight (5 females) healthy young individuals participated. Participants stood with their arms relaxed by the sides. A yardstick was placed parallel to the floor at the level of the acromion. They were

instructed to reach forward as far as possible without taking a step and without raising their heels off the floor. 1-3 trials each were collected with 2 different instructions – do not bend the hip (AS) and bend the hip (HS) (Figure 1).

A full body marker set was used to define and track the following segments - foot, shank, thigh, pelvis, trunk, brachium, forearm, hand and head. Two AMTI force plates (Model #OR6-6-1, Watertown, MA) and an 11 camera motion capture system (Qualisys, Gothenburg, Sweden) were used to collect ground reaction forces and segment coordinates. Subsequently joint angles and moments, and whole-body COM and COP excursions were computed using Visual 3D (C-Motion, Inc., Germantown, MD) and Matlab (The Mathworks, Natick, MA). Reach distance was quantified as the distance between one marker on the distal heel and one on the 3rd metacarpal head at the point of maximum reach. Reach distance and excursions were normalized to body height.

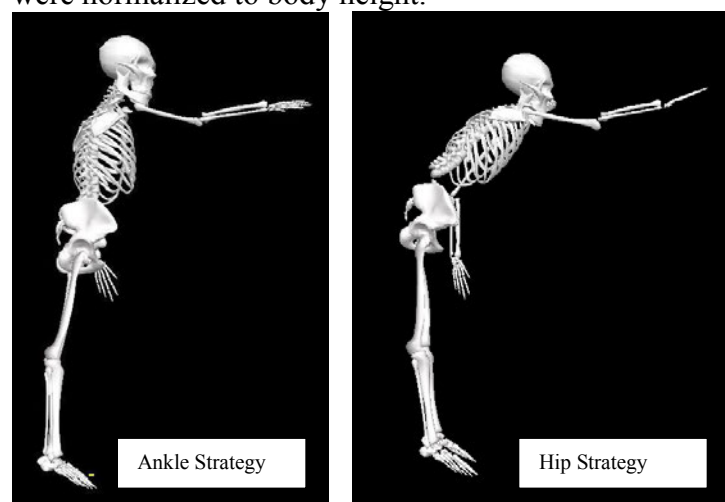


Figure 1

Statistics

Given the small sample size, non-parametric tests (related samples Wilcoxon Signed Ranks Tests and Spearman correlation coefficient) were used. The following outcome variables were compared between HS and AS – reach distance, COM excursion, COP excursion, peak hip extensor moment, peak ankle plantarflexor moment. PASW Statistics 18 (IBM Corporation, NY, USA) was used for statistical analysis and the significance was set at $\alpha=0.05$. The following correlations were tested for each strategy separately –

- Reach distance – COM excursion
- Reach distance – COP excursion
- Reach distance – peak hip extensor moment
- Reach distance – peak ankle plantarflexor moment

RESULTS AND DISCUSSION

When compared to the ankle strategy, reach distance and peak hip extensor moment were significantly greater in the hip strategy. There was no significant difference between strategies for any of the other variables (Table 1). Only the correlation between reach distance and peak hip extensor moment in the ankle strategy ($\rho=0.714$, $p=0.047$) was significant.

Contrary to Liao and Lin [3], no significant correlation between reach distance and COM excursion was found in either strategy. Given that the reach distance is achieved by a combination of movements at multiple joints along the kinetic chain, the relation between COM or COP excursion and reach distance must be interpreted with caution. Reach distance may be driven by strength and/or flexibility at multiple joints and not necessarily by balance.

Given the difference in reach distance and peak hip moments between HS and AS, we hypothesized that the distance may be correlated with hip moment in the HS and ankle moment in the AS. However, this was not found to be true and other explanations must be considered in future research. Reach distance may be influenced by moment measures that incorporate duration (like impulse) rather than peak moments. It may also be driven by other joints or segments – large movements at the trunk and shoulder can have a considerable influence.

The findings of this study may be limited by the small sample size. Further, it must be acknowledged that conflicts across studies may be a reflection of differences in the exact instructions given to participants and differences in the methods used to compute and normalize each variable.

CONCLUSIONS

The use of reach distance during a FRT as a direct indicator of balance must be done with caution, and the biomechanical strategy employed by each individual must be taken into consideration. Also, future research should rule out strength and flexibility limitations before attributing decreased reach distance to poor balance.

REFERENCES

- Duncan PW, et al. *Journal of Gerontology* **45**(6), M192-197, 1990.
- Jonsson E, et al. *J Rehabil Med* **35**, 26-30, 2002.
- Liao CF, Lin SI. *Gait and Posture* **28**, 16-23, 2008.

Table 1: Differences between hip strategy and ankle strategy

N=8	Hip Strategy (Mean±SD)	Ankle Strategy (Mean±SD)	p-value (related samples Wilcoxon signed ranks test)
Reach Distance (percentage body height)*	62.23±1.79	56.86±2.36	0.01
Center of Mass excursion (percentage body height)	6.81±0.85	6.77±1.34	0.89
Center of Pressure excursion (percentage body height)	6.69±1.61	7.12±1.53	0.33
Peak Hip Extensor Moment (Nm/kg)*	0.87±0.23	0.41±0.16	0.01
Peak Ankle Plantarflexor Moment (Nm/kg)	0.67±0.09	0.70±0.19	0.40

* Significantly different at the level of $\alpha \leq 0.05$

ERROR AUGMENTATION FEEDBACK FOR DYNAMIC LATERAL WEIGHT SHIFTING

Kevin O'Brien and James Schmiedeler

The University of Notre Dame, South Bend, IN, USA

email:kobrie23@nd.edu, web: <http://ame-robotics.nd.edu/LAB/Biomechanics/WeHab.php>

Introduction

Regaining motor coordination is an important aspect of rehabilitation following stroke, and balance performance in particular is crucial to prevent injuries from falls. Previous work has shown that the type of visual feedback provided can influence balance performance [3]. Additionally, in arm reaching tasks, augmenting the visual feedback position error has been shown to promote faster learning of new reaching tasks [5]. The effects of such biofeedback in mobility and balance tasks, however, are not entirely known [6]. The current study investigates use of error augmentation in a lateral weight shifting task.

As a relatively inexpensive means by which to provide biofeedback in rehabilitation activities, low-cost gaming peripherals have potential for both clinical and home use. The Nintendo Wii Balance Board has been shown to perform comparably to more sophisticated force plates in terms of balance assessment based on center of pressure (CoP) data [1, 2]. The WeHab software [3] was developed to display visual feedback based on CoP data from the balance board and was extended in this work to include error augmentation capability.

Methods

Eight subjects each completed nine, three minute lateral weight shifting tasks with a period of rest midway through the test. All subjects gave their informed consent prior to the study, and this research received approval from the appropriate Institutional Review Board. Using the WeHab software, the tasks involved subjects laterally shifting their CoPs to lie within target regions presented as shaded rectangular areas, as in [3].

In previous error augmentation studies, the error was calculated relative to a straight line between the starting point and the target [5]. While the ideal path of the CoP may also be a straight line, the CoP exhibits a non-minimum phase (NMP) behavior in lateral weight shifting [4], so calculating the error is non-trivial. To account for this, shift data from a previous study were

averaged to find an idealized CoP path as a function of the time after a target was presented.

The error was found by comparing the true CoP position to the time-dependent, ideal CoP positing in real time. A gain was then applied to the calculated error, and the CoP position displayed as feedback was the true CoP position with the augmented error added to it. To test the effect of this feedback, a perceived weakness was introduced which increased the force necessary to shift the displayed CoP in either direction relative to the center of the balance board.

Time to Target vs. Target # for Task Low Gain/ High Weakness

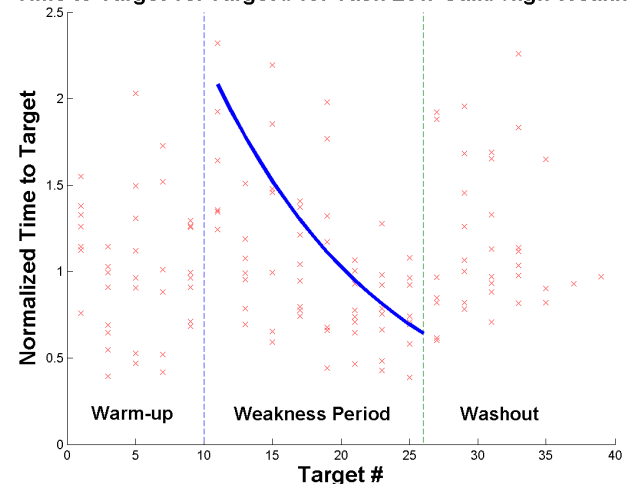


FIGURE 1. Representative result for a single task. Data points represent time-to-target from all 8 subjects for shifts from center outward tasks. An exponential fit is shown for trials with simulated weakness.

The error feedback gain was applied for the entire task, having one of three values: no gain (in which the true CoP was displayed), low gain (33% error gain), and high gain (67% error gain). The gain increases the sensitivity of the CoP to movement when the subject shifts faster than the ideal trajectory, but decreases the sensitivity when the subjects shifts slower than the ideal trajectory. After subjects successfully shifted to 10 targets, an artificial weakness was applied for the next 15 weight shifts, making the targets more difficult to reach

by altering the CoP position. The three weakness conditions were no weakness, low weakness (44% reduction), and high weakness (63% reduction). Each subject experienced the nine possible combinations of gain and weakness in a different order to mitigate the covariance between tasks.

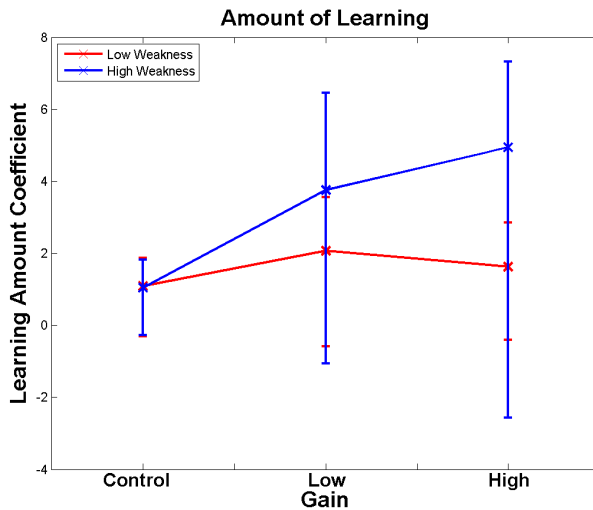


FIGURE 2. Learning amount

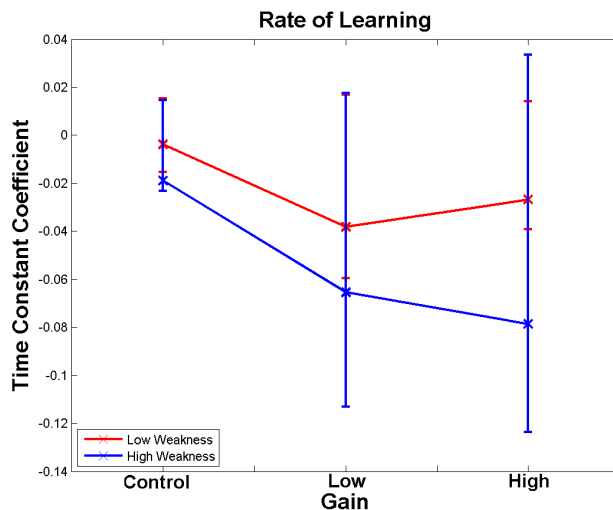


FIGURE 3. Learning rate

From the “No Weakness” tasks, a subject-specific average time-to-target for each gain value was determined. This time was used as a reference to normalize the time-to-target for the “Low” and “High Weakness” tasks. An exponential curve was then fit to the normalized time-to-target data (see Figure 1) to analyze both the rate and

extent of weakness learning for each gain, similar to [5].

$$t_x = A * e^{B*x},$$

where t_x is the approximate time-to-target for each target, x is the target number, A is the amount of learning (change in time-to-target for each task, Figure 2), and B is the rate of learning (time constant associated with each task, Figure 3).

Results and Discussion

Although the results are not statistically significant due to the high variability and small sample size, both the gain and weakness values affected the time to completion for each target. The learning response to each level of weakness also appears to follow an exponential curve (Figure 1). For “High Weakness” cases, the amount of learning increased, and the rate of learning also improved. Meanwhile, for “Low Weakness” cases, the level of weakness was too low to produce clear trends as results were fairly similar regardless of gain.

The results suggest trends that conform with previous learning and rehabilitation studies. The sensitivity to movement appears to help the subjects recognize changes in perceived weakness. This suggests that it may be appropriate to scale gain values according to the level of balance disability.

Conclusions

This study examined the effects that augmenting biofeedback error sensitivity has on a subject’s ability to learn a simulated level of weakness in a lateral weight shifting task. The increased sensitivity provided a stronger feedback signal to the subject that appeared to offer greater benefits at higher levels of simulated weakness. Nonetheless, increasing the gain can make controlling the perceived CoP more difficult and destabilize the balance feedback system. Gain sensitivity in balance rehabilitation activities may require tuning to the impairment level of the patient.

References

- [1] W Chang et. al. *J Phys Ther Sci*, 25(10):1251–1253, 2013.
- [2] RA Clark et. al. *Gait Posture*, 31(3):307–310, 2010.
- [3] MW Kennedy et. al. *Exp Brain Res*, 230(1):117–125, 2013.
- [4] MW Kennedy et. al. *Gait Posture*, 40(1):134–139, 2014.
- [5] JL Patton et. al. *PloS One*, 8(1):e46466, 2013.
- [6] A Zijlstra et. al. *J NeuroEng Rehabil*, 7:58, 2010.

ROLE OF MULTI-SENSORY INTEGRATION RELEVANT FOR BALANCE IN SLIP RECOVERY

Caitlin O'Connell, April Chambers, Arash Mahboobin, Rakié Cham

University of Pittsburgh, Pittsburgh, PA, USA
email: caitlino@pitt.edu, web: <http://www.engineeringx.pitt.edu/hmbl/>

INTRODUCTION

Falls are a leading cause of injury and death, particularly in the elderly, with over one-third of elderly adults experiencing a fall each year [1]. Stepping reactions are important for recovering and maintaining balance after gait perturbations such as slips and trips [2]. The purpose of this study is to determine if balance, specifically sensory integration abilities, play a role in stepping reactions to slips. It is predicted that deterioration in sensory integration abilities is related to delayed stepping reactions.

METHODS

Thirty-six subjects were recruited for participation in this balance and gait study and classified into two age groups: young (N=17, 8 females, age = 24.0 ± 3.2 years) and old (N=19, 9 females, age = 55.9 ± 4.6 years). Written informed consent approved by the University of Pittsburgh Institutional Review Board was obtained prior to participation. Exclusion criteria included orthopedic, neurological, pulmonary and cardiovascular abnormalities clinically hindering normal balance and gait.

For gait testing, participants walked along a vinyl tile pathway wearing a safety harness. Full body motion (120 Hz) and bilateral ground reaction forces (1080 Hz) were collected. EMG data were recorded from the trailing (swing) leg on the vastus lateralis (VL). Data was collected using a 8-channel Noraxon Telemetry EMG system sampled at 1080 Hz with a hardware bandpass filter (10-500 Hz).

Participants were instructed to walk at a comfortable self-selected pace. Several baseline (dry) trials were collected to ensure correct foot placement and consistency in gait. Then without

participant's knowledge, a glycerol contaminant was placed on leading leg force platform. One trial, the unexpected slip (US), was collected with contaminant present. For the US, the start of the slip was defined as heel strike of the leading (slipping) leg. Slip severity is quantified by the peak slip severity (PSV) measured at the heel marker attached on the slipping foot shortly after heel strike onto the contaminated floor [3]. Slip hazardousness was classified into two categories: hazardous (PSV ≥ 1 m/s) and non-hazardous (PSV < 1 m/s) [3].

EMG data was rectified and normalized using the average maximum value of the baseline gait cycles. EMG was not filtered to prevent smoothing of sudden onset of muscle activations. A custom algorithm was used to determine reactive muscle activation of the trailing leg [4]. Activation was calculated as the time when difference between slip and dry EMG signals exceeded 2 standard deviations of the difference during quiet period of gait. Only the VL was considered here due to its main contribution to a stepping reaction.

Standing balance testing consisted of sensory organization tests (SOT) using an Equitest posture platform (Neurocom, Inc). This platform is capable of providing rotations of the floor and/or the visual scene to allow sway-referencing of vision and/or proprioception [5]. Prior to testing, subjects donned a harness and instructed whether to keep eyes open or closed before beginning each trial. The SOT protocol consisted of six trials that were 20 seconds long, repeated twice (see Table 1 for trial descriptions). Only the second trial of each type was considered. The outcome variable of interest was the mean velocity of anteroposterior (AP) sway.

The statistical analyses consisted of a regression model ($\alpha = 0.05$) to determine the effect of age and sway mean velocity, as well as their interaction, on

the activation of the VL after slip. The log transformation of the mean velocity was used in the statistical model in order to normalize the data. Analysis was conducted within each SOT trial type and hazardousness of slip.

Table 1: SOT trial descriptions including eye, vision and proprioception conditions.

Trial	Eyes	Vision	Proprioception
1	Open	Fixed	Fixed
2	Closed	--	Fixed
3	Open	Sway	Fixed
4	Open	Fixed	Sway
5	Closed	--	Sway
6	Open	Sway	Sway

RESULTS AND DISCUSSION

Mean sway velocity was significantly related to VL activation of hazardous slips for SOT condition 4 only. SOT condition 4 provides accurate visual information but unreliable proprioception. Thus, proprioception may be more important than vision in sensing a slip and triggering a stepping recovery response.

An increase in COP sway representing less balance stability correlated to faster muscle activations after slip (Figure 1). This is contrary to the hypothesis that poor balance will be associated with a delayed stepping reaction. A possible explanation for this trend is that individuals with poor balance are more cautious during gait, specifically when they encounter a perturbation such as a slip. Thus, they may interrupt swing phase of the trailing gait more quickly after slipping faster to prevent loss of stability. Alternatively, poor balance may correlate to more severe slips that require a faster reaction to recover balance [6]. The lack of relationship between muscle activation and balance for non-hazardous slips further supports this theory.

Interestingly, there was no age effect on VL activation, nor was there an interaction between age and sway mean velocity for SOT condition 4. This could be explained by the relative fitness and age of the subjects in the older group. The subjects did not

have any comorbidities that typically affect balance performance and fall risk in the elderly.

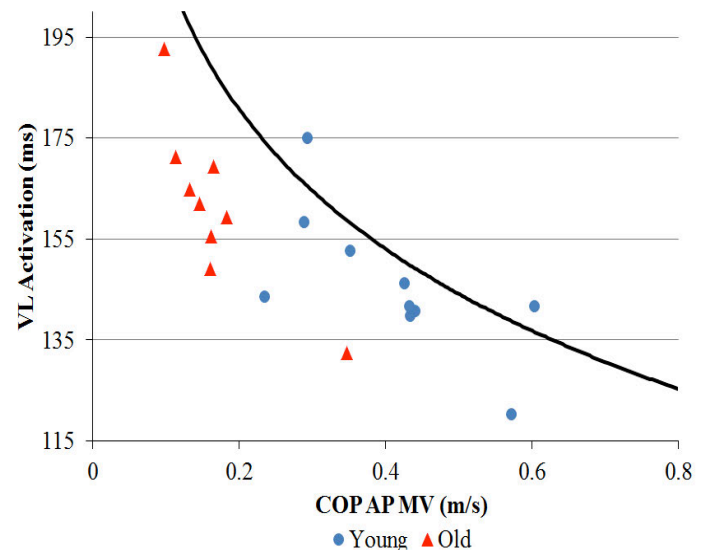


Figure 1: Relationship between reactive activation of the vastus lateralis muscle during hazardous slips and mean velocity of anteroposterior center of pressure sway during SOT condition 4.

CONCLUSIONS

The goal of this study was to determine the role that balance plays in slip recovery. The results suggest that proper integration of proprioception information is important in regaining balance after hazardous slips and that individuals with compromised balance may react more cautiously, and thus faster, to slips than those with normal balance.

REFERENCES

1. Rubenstein LZ. *Age Ageing*, **35**, ii37-ii41, 2006.
2. Bhatt T, et al. *Gait & Posture* **21**, 146-156, 2005.
3. Moyer BE, et al. *Ergonomics*, **49**, 329-343, 2006.
4. Chambers AJ, & Cham R. *Gait & Posture*, **25**, 565-572, 2007.
5. Nashner, LM, et al. *J Neurosci*, **5**, 117-124, 1982.
6. Wyszomierski, S. *U. of Pittsburgh (Master's Thesis)*, 2006

ACKNOWLEDGEMENTS

Funding provided by the National Institute of Occupational Safety and Health (R01 OH007592).

LOW BACK FATIGUE INFLUENCES POSTURAL VARIABILITY

Michael W. Olson and Shelby Kemp

Southern Illinois University, Carbondale, IL, USA

INTRODUCTION

Human bipedal stance requires proprioceptive input from the external environment and successful neuromuscular and musculoskeletal responses to maintain an upright posture. The somatosensory system receives visual, tactile, auditory, and vestibular information which is transmitted to the central nervous system (CNS) for processing. The correct spatiotemporal neural responses (amplitude and firing rates) and the corresponding muscle forces generated must be specific to the constraints of the environmental parameters experienced by the system. Modification of intrinsic factors that influence the neuromuscular responses significantly alter the response of the system to the external environment [1,2]. Fatigue of the trunk extensor muscles, primarily the lumbar paraspinal (LP) muscles, is reported to significantly reduce system stability when external perturbations are applied during stance [3]. Similarly, the muscles surrounding the ankle joints assist in maintaining the postural control of the system. The position and velocity changes of the movements are modified as fatigue is induced, however, the variability of these variables, based upon the standard deviation measures, needs to be researched further to identify how the motor control strategy of the system is being influenced.

Determine how neuromuscular fatigue of the paraspinal muscles influences postural control of the system assists in studying motor control strategies. Therefore, it is hypothesized that the variability of the movement and variability of the EMG signals from the postural muscles will provide insight into the motor control strategy modifications of the system.

METHODS

Eighteen healthy individuals (7 men, 11 women) (74.3 ± 16.8 kg, 1.71 ± 0.12 m, 22.6 ± 4.5 yrs)

participated in this study. Static stance was performed for 30 s prior to and after the fatigue protocol. Participants were instructed to focus on a target (5cm x 5cm) on a wall (placed 3.5m from the participants), while standing with feet shoulder width apart.

Fatigue protocol: Participants were seated in a chair with the lower extremities fixed at the pelvis and thighs. The trunk was positioned 30 deg in flexion from erect posture. A harness system was secured to the trunk at the T6 level and attached through a tethered line to an isokinetic dynamometer (resistance). Three 8 s ramped maximal voluntary isometric contractions (MVIC) in trunk extension were performed to determine each participant's maximal torque output. Participants maintained isometric back extension at 50% of their predetermined voluntary maximum for up to 10 min.

Equipment: A multi-camera system (120 Hz collection rate) was used to track markers positioned bilaterally on acromion processes, posterior superior iliac spines (PSIS), anterior superior iliac spines (ASIS), greater trochanters, lateral femoral epicondyles, lateral malleoli, calcanei, and 5th metatarsophalangeal joints. Additionally, single markers were positioned on the skin over the T6 and S1 vertebrae. It was assumed that an ankle strategy was used by all participants, thus the body sway was calculated as the T6 marker about the left malleolus. From the kinematics data, variability of postural sway in the anteroposterior (AP) and mediolateral (ML) directions could be evaluated. Variability of the sway and sway velocities were analyzed. EMG (band-pass 20-500 Hz, CMRR ratio < 100 dB, input impedance < 10 M Ω , 1200 Hz collection rate) data were collected bilaterally from thoracic (LTP/RTP) and lumbar (LLP/RLP) paraspinal muscle groups along with soleus (LSol/RSol) and tibialis anterior

LTA/RTA) muscle groups using stainless steel electrodes (20 mm center to center distance). EMG data were analyzed for signal variability differences.

A low-pass Butterworth filter set at 10 Hz was used to reduce the kinematics data. The EMG data were full-wave rectified and then a low-pass Butterworth filter set at 10 Hz was used to smooth the data. Variability measures were determined as the standard deviation of respective position sway and sway velocity calculations.

A one way ANOVA was used to analyze the dependent variables of sway variability and sway velocity variability in the AP and ML directions, and EMG activity variability from trunk and leg muscles between pre and post fatigue conditions over 30 s periods. Alpha was set at 0.05.

RESULTS AND DISCUSSION

AP sway variability did not change ($p > 0.05$), but the AP sway velocity variability was significantly greater after fatigue ($F_{1,215} = 2.771$, $p < 0.02$, Table 1). ML sway variability was significantly greater after fatigue ($F_{1,215} = 4.915$, $p < 0.03$, Table 1) while ML sway velocity variability was not modified ($p > 0.05$).

The RLP EMG variability decreased significantly ($F_{1,215} = 5.98$, $p < 0.02$, Table 2) as did the LSol EMG variability ($F_{1,215} = 4.621$, $p < 0.04$, Table 2). No other muscle activities were modified ($p > 0.05$).

CONCLUSIONS

It was hypothesized that variability measures from kinematics and EMG variables would explain modifications in motor control strategies. The mean values of sway and sway velocity did not differ from pre to post-fatigue stances, but the variability in AP sway velocity and ML sway provided additional information regarding how the system was controlled. Muscle activity variability was either decreased or did not change, indicating the proprioceptive components, which determine the parameters of movement for balance, may have been modified to induce modifications in sway variables.

REFERENCES

1. Masani K, et al. *J Neurophysiol*, **90**, 3774-3782, 2003.
2. Wilson EL, et al. *Gait Posture*, **23**, 348-354, 2006.
3. Lin D & Nussbaum MA. *App Ergonomics*, **43**, 1008-1015, 2012.

Table 1. Mean (\pm sd) of the AP and ML sway and sway velocity variability measures during stance.

Condition	AP sway ($^{\circ}$)	ML sway ($^{\circ}$)	AP sway velocity ($^{\circ}\cdot s^{-1}$)	ML sway velocity ($^{\circ}\cdot s^{-1}$)
Pre-fatigue	0.136 (0.14)	0.0409 (0.038)	0.199 (0.13)	0.0977 (0.065)
Post-fatigue	0.154 (0.09)	0.0570 (0.066)*	0.305 (0.64)*	0.282 (1.7)

* indicates a significant difference between pre and post fatigue conditions.

Table 2. Mean (\pm sd) of the EMG variability (in mV) from paraspinal and leg muscles during stance.

Condition	LTP	RTP	LLP	RLP	LSol	RSol	LTA	RTA
Pre-fatigue	0.00155 (0.002)	0.00144 (0.002)	0.00468 (0.018)	0.00705 (0.026)	0.00597 (0.012)	0.00461 (0.007)	0.00288 (0.007)	0.00413 (0.009)
Post-fatigue	0.00161 (0.002)	0.00153 (0.002)	0.00365 (0.014)	0.00392 (0.017)*	0.00315 (0.005)*	0.00520 (0.008)	0.00296 (0.006)	0.00488 (0.008)

* indicates a significant difference between pre and post fatigue conditions.

GAIT ADAPTATIONS TO UNEXPECTED DROP-AWAY FLOORING PERTURBATIONS

¹ Matthew J. Peterson, PhD, ² Manutchanok Jongprasithporn, PhD, and ^{1,3} Stephanie L. Carey, PhD

¹ HSR&D Center of Innovation on Disability and Rehabilitation Research, James A. Haley VAMC, Tampa, FL

² King Mongkut's Institute of Technology Ladkrabang, Bangkok, Thailand

³ University of South Florida, Department of Mechanical Engineering, Tampa, FL

email: Matthew.Peterson1@va.gov

INTRODUCTION

To avoid falling while walking, individuals must be able to recover from unexpected perturbations. Sudden loss of the support surface can cause serious injury if one cannot create a rapid posture response in order to maintain balance. Previous work reported that the rapid response while stepping down into a hole was to extend the perturbed limb to avoid limb collapse and a fall [1]. Moreover, the muscle activity of the perturbed ankle was reported to show a high response for both the ankle plantar-flexor and the dorsi-flexor [2]. Not only is the posture response of the perturbed limb vital to avoid falls, but the trialing limb adaption also plays an important role in successful fall recovery. In this study, a drop-away floor tile was created to investigate the mechanisms of postural control and adaptation of the perturbed limb (PL) and the unperturbed limb (UPL) during unexpected loss of the support surface. We hypothesized that the drop-away floor would result in a rapid recovery process by increasing the maximum toe clearance (MTC, maximal distance between toes and ground during the swing phase), joint angles, and co-contraction indices (CCIs) of the perturbed and unperturbed limbs.

METHODS

Ten young, healthy adult subjects (5 males, 5 females) with a mean age of 24.3 ± 5.0 years participated in this gait study. A 13 camera Vicon MX40 motion analysis system (Denver, CO) was used to collect motion data at 150 Hz and analyze gait parameters. A Noraxon electromyography system (Scottsdale, AZ) recorded muscle activity at 1500 Hz. A Hokuyo scanning laser rangefinder (Osaka, Japan) was used to create a speedometer

displayed on a television screen at each end of the walkway to encourage subjects to walk at their preferred speed. The drop-away flooring was randomly activated to create an unexpected loss of ground support by dropping the walkway surface (8 cm). Kinematic parameters including MTC, joint angles (hip, knee, and ankle), and ankle and knee CCIs of the PL and UPL were recorded and analyzed during and after the drop-away perturbation. Muscle CCIs at the ankle and knee were examined during the stance and swing phases from the ratio of the antagonist/agonist muscles (tibialis anterior/lateral gastrocnemius; vastus lateralis/medial hamstring). CCIs were integrated to calculate the area under the CCI curve [3]:

$$CCI = \int_{start}^{stop} \frac{LowerEMG}{HigherEMG} \times (LowerEMG + HigherEMG)$$

One-way ANOVA, within subject (control v drop perturbation), was performed to test the difference of mean values on each dependent variable. JMP software (SAS Institute, Cary, NC) was used for all statistical analyses, and effects were considered significant at $p < 0.05$.

RESULTS AND DISCUSSION

MTC, joint angles, and CCI results are shown in Table 1. During drop-away perturbations, the PL was in stance phase and UPL was in swing phase. During fall recovery, the PL was in swing phase and UPL was in stance phase. MTC of the PL and UPL increased during the swing phase of the perturbation in order for subjects to avoid tripping over the edge of the hole after stepping into it. Ankle, knee, and hip joint angles of the PL during stance phase were significantly smaller than during normal gait. Ankle and knee CCIs of the PL during stance phase were significantly greater than during normal gait. The

PL creates the rapid response by extending all joints and increasing ankle and knee CCIs (stiffness) to compensate for the unexpected lower support surface and to prevent joint buckling. Ankle, knee, and hip joint angles of the UPL (swing phase) during the drop-away perturbation were significantly larger than those joint angles during the swing phase of normal gait. The results indicate that large joint angles are gait adaptations of the UPL to create higher limb swing in order to avoid unknown hazards. Ankle CCIs of the UPL during the swing phase were significantly greater than ankle CCIs during normal gait.

Table 1: Variable means \pm standard deviations and statistical significances during normal and perturbed gait.

Variables	Normal Gait	Perturbed Gait	P-Value
Maximum Toe Clearance, MTC (m)			
PL	0.11 \pm 0.01	0.20 \pm 0.05	<0.0001
UPL	0.11 \pm 0.01	0.17 \pm 0.04	<0.0001
Joint Angles (degrees)			
<i>PL (Stance)</i>			
Ankle dorsi-flex	12.4 \pm 3.1	9.46 \pm 5.9	0.0162
Knee flexion	45.0 \pm 7.9	24.2 \pm 13.1	<0.0001
Hip flexion	28.9 \pm 1.6	20.6 \pm 2.4	0.0057
<i>PL (Swing)</i>			
Ankle dorsi-flex	4.0 \pm 2.8	8.6 \pm 5.7	0.0002
Knee flexion	66.1 \pm 5.7	90.0 \pm 3.4	<0.0001
Hip flexion	32.3 \pm 1.9	50.0 \pm 12.4	0.0029
<i>UPL (Stance)</i>			
Ankle dorsi-flex	12.9 \pm 4.1	12.6 \pm 6.3	0.8380
Knee flexion	45.7 \pm 8.6	37.8 \pm 11.5	0.0002
Hip flexion	29.9 \pm 12.8	34.3 \pm 13.0	0.2378
<i>UPL (Swing)</i>			
Ankle dorsi-flex	3.7 \pm 3.6	17.2 \pm 4.7	<0.0001
Knee flexion	65.5 \pm 7.4	95.0 \pm 12.1	<0.0001
Hip flexion	31.4 \pm 11.4	59.0 \pm 9.7	<0.0001
Co-Constrictions (CCIs)			
<i>PL (Stance)</i>			
Ankle CCI _{GAS_TA}	21.0 \pm 14.7	34.0 \pm 19.0	0.0104
Knee CCI _{VL_HAM}	43.1 \pm 11.5	72.2 \pm 33.6	<0.0001
<i>PL (Swing)</i>			
Ankle CCI _{GAS_TA}	20.7 \pm 11.2	48.0 \pm 25.1	<0.0001
Knee CCI _{VL_HAM}	25.6 \pm 10.8	78.6 \pm 43.6	<0.0001
<i>UPL (Stance)</i>			
Ankle CCI _{GAS_TA}	20.7 \pm 11.2	53.4.0 \pm 22.4	<0.0001
Knee CCI _{VL_HAM}	25.6 \pm 10.8	139.4 \pm 55.5	<0.0001
<i>UPL (Swing)</i>			
Ankle CCI _{GAS_TA}	21.0 \pm 14.7	32.0 \pm 12.6	0.0124
Knee CCI _{VL_HAM}	43.1 \pm 11.5	47.1 \pm 20.1	0.3681

During fall recovery, ankle, knee, and hip joint angles of the PL during the swing phase were significantly larger than those joint angles during the swing phase of normal gait. Ankle and knee CCIs of the PL during the swing phase were significantly greater than those CCIs during normal gait. The PL during fall recovery tended to flex more and had higher ankle and knee CCIs than during normal gait in order for subjects to lift their limbs and generate a higher MTC to step out of the dropped floor. Only the knee joint angle of the UPL (stance phase) during fall recovery was significantly larger than knee joint angle during the stance phase of normal gait. The larger knee flexion of the UPL occurred during the beginning of fall recovery since the UPL was on the floor but the PL was about to create a toe-off from the hole. Ankle and knee CCIs of the UPL during fall recovery were significantly greater than the CCIs during normal gait. The UPL after perturbation increased joints stiffness to maintain stability while the PL stepped out of the dropped floor.

CONCLUSIONS

As hypothesized, MTC increased to recover from an unexpected drop-away perturbation. Knee angle (UPL, stance), ankle, knee, and hip angles (PL, swing), and ankle and knee CCIs (UPL, PL) increased during fall recovery of this perturbation indicating the importance of the knee joint when developing rehabilitation strategies for fall preventions. Future work is planned to compare these results to older adults with and without a history of falls in efforts to develop interventions to train fall avoidance and recovery ability.

REFERENCES

1. Van Dieen JH, et al. *J Biomech* **40**, 3641-9, 2007.
2. Shinya M, et al. *Gait & Posture* **29**, 483-7, 2009.
3. Rudolph KS, et al. *Knee Surg. Sport Traumatol* **9**, 62-71, 2001.

ACKNOWLEDGEMENTS

Support for this work is funded by a Veterans Affairs Rehabilitation Research & Development Merit Review Award.

DYNAMIC STABILITY DURING SINGLE STANCE IN MULTIPLE SCLEROSIS PATIENTS

^{1,2}Alyson Reinholdt, ²Sunny Ranu, ²Jessie M. Huisinga

¹Department of Bioengineering, University of Kansas, Lawrence, KS, USA

²Human Performance Laboratory, University of Kansas Medical Center, Kansas City, KS, USA
email: aboyer3@kumc.edu

INTRODUCTION

Persons with multiple sclerosis (PwMS) are at a higher risk of falling than healthy persons, and 50% of all falls reported in PwMS have occurred during locomotion [1]. Static postural control is defined by the body's ability to maintain the center of mass (COM) within the base of support (BoS). Due to the dynamic-corrective nature of gait and one's ability to regulate COM motion, it is necessary to assess a person's step-to-step balance control to define their dynamic postural control during walking. To do this, Hof et. al [2] developed a measure of dynamic balance called 'margin of stability' (MoS) which is derived from the extrapolated COM. The extrapolated COM applies the necessity of maintaining the COM within the BOS to dynamic postural control through the addition of a linear velocity component to the COM [2]. The MoS is then able to characterize the discrepancy between the extrapolated COM and the BoS. Although MoS provides postural control information during walking which is advantageous over conventional static measures since most falls happen during walking, little research has been done to understand MoS in PwMS even though they are at high risk for falls [2]. The purpose of this study was to determine if there is a difference in MoS between healthy adults and PwMS with difference levels of disease severity. We hypothesized that healthy adults would have a greater MoS than PwMS regardless of their disease severity.

METHODS

Thirty-nine PwMS and 19 age-matched healthy controls (HC) participated (Table 1). Exclusion criteria for PwMS were an EDSS score greater than 5.5 or inability to walk 25 feet without an assistive mobility aide. To assess general walking disability,

three timed 25-foot walk (25FTW) tests were performed and averaged for each subject. For the purposes of collecting kinematic data, reflective markers on the toe, heel, MTP, calcaneus, bilateral ASIS, and sacrum were used in this analysis to calculate MoS. Kinematic data were collected at 60 Hz using a 6-camera motion capture system (Eagle System; Motion Analysis Corporation, Santa Rosa, CA); ground reaction forces were collected at 600 Hz using a force platform (AMTI 1000; Advanced Mechanical Technology Inc., Watertown, MA). All data were analyzed using Matlab (MathWorks, Inc., Natick, MA). MoS was calculated only during single support by methods previously described by Hof et. al [2].

Five successful overground trials were collected for each foot. Because only single support data were used, MoS was only calculated in the anteroposterior (AP) direction. For analysis, PwMS were separated by 25FTW time into two groups: Mild ($25FTW \leq 5.0$ sec) and Moderate ($25FTW > 5.0$ sec). A 1-way ANOVA with a between-subject design was performed using three groups: HC, Mild PwMS, and Moderate PwMS. Tukey's post-hoc comparison between groups was also performed. Significance was found when $p < 0.05$.

RESULTS AND DISCUSSION

Mean MoS for each group is listed in Table 2. There was a significant main effect of group ($F=43.76$, $p<.001$) on mean MoS. HC and Mild PwMS had a significantly greater mean MoS than Moderate PwMS ($p<.001$), but there was no significant difference between HC and Mild PwMS. This data in part supports our hypothesis that the MoS of healthy controls would be greater than that of PwMS. Not surprisingly, patients with a lower MoS (Moderate PwMS) also had a significantly slower 25FTW time compared to both HC and Mild

PwMS groups ($p<0.001$), whereas there was no significant difference between 25FTW times of HC and Mild PwMS ($p=0.846$) (Table 2). Previous studies have observed that an increased velocity allows the body's COM to be more quickly positioned above a stable BoS and to more effectively transition into the next step, decreasing fall risk and increasing balance [3, 4]. However, with the destabilizing effects of a decreased COM velocity combined with the known motor and muscular deficits in PwMS, the system becomes more unstable. This is evident in the finding of decreased MoS of Moderate PwMS compared to Mild PwMS and HC. It is important to make note of the lack of significant difference in outcome measures between HC and Mild PwMS. Our results show that dynamic stability of PwMS with a 25FTW time less than 5 seconds is no different from that of HC.

Table 2: Average 25-Foot Walk (25FTW) times and Margin of Stability (MoS) for each group.

	25FTW (sec)	MoS
Mild PwMS (n=24)	4.29±0.44	0.275±0.0384
Moderate PwMS (n=21)	6.33±1.50	0.194±0.0332
Healthy Controls (n=19)	4.38±0.44	0.269±0.0461

Velocity of the COM, leg length, and BoS are all used to calculate MoS. In PwMS, decreasing the distance between the COM and the leading limb heel strike during gait, i.e. shorter stride lengths, results in a smaller joint moment about the ankle and hip [5]. When people have an increased fear of falling, they are more likely to walk more slowly [6], decreasing their COM velocity. When walking slowly, strides are shortened, and BOS during double support is shortened which decreases MoS in the AP direction. However, subjects who walk more quickly take longer strides and therefore have a longer BoS which results in an increased MoS.

Table 1: Subject demographics and mean 25-foot walk time (25FTW).

	Gender	Age (yrs)	EDSS	Yrs since diagnosis	Height (cm)	Weight (lbs)	25FTW (sec)
Mild PwMS	7M, 17F	46.2±6.0	1.6±0.6	11.5±8.5	170.81±14.69	183.33±46.36	4.29±0.44
Moderate PwMS	3M, 18F	43.9±9.4	2.7±1.2	10.1±7.6	163.43±7.91	168.45±56.12	6.33±1.50
Healthy Controls	1M, 18F	41.1±8.8	-	-	166.80±7.79	163.34±38.24	4.38±0.44

This may indicate that HC, who are at no risk for falls, and Mild PwMS, who are at a smaller risk for falls than Moderate PwMS, do not fear falling and can therefore have the confidence to walk more quickly [6]. In this study, MoS was only calculated in the AP direction. For future studies, MoS should be investigated during single stance and double stance to determine dynamic stability in both the AP and ML directions during walking.

CONCLUSIONS

Using MoS, a quantitative measure of dynamic stability during walking, we found that mild PwMS (faster 25FTW) and HC had a significantly greater MoS than moderate PwMS (slower 25FTW). However, no difference was found between PwMS with a faster 25FTW time and HC. By investigating dynamic stability, we hope to learn more about the factors that contribute to loss of balance in PwMS and understand which of those factors have the greatest impact on fall risk.

REFERENCES

1. Winter, D.A., *Gait & Posture*, 1995. **3**(4).
2. Hof, A., *Journal of biomechanics*, 2005. **38**(1).
3. You, J.-Y., *Clinical Biomechanics*, 2001. **16**(2).
4. Bhatt, T., *Gait & posture*, 2005. **21**(2).
5. Huisinga, J.M., *Journal of applied biomechanics*, 2013. **29**(3).
6. Menz, H.B., *Gait Posture*, 2007. **25**(2).

ACKNOWLEDGEMENTS

This work was supported by the National Multiple Sclerosis Society RG 4914A1/2 and the NIH National Center for Advancing Translational Science 1KL2TR000119.

COP PARAMETERS FOR ACL REPAIRED INDIVIDUALS DURING STAIR NEGOTIATION

¹ Elizabeth Rullestad, ² Michelle Hall and ¹ Jason Gillette

¹ Iowa State University, Ames, IA, USA

² The University of Melbourne, Melbourne, Australia

INTRODUCTION

Almost 50% of individuals who have undergone anterior cruciate ligament reconstruction (ACLR) display symptoms of knee osteoarthritis within 10-20 years [1]. One proposed mechanism for the development of early onset knee osteoarthritis is reduced postural control in the knee joint. Short-term decreases in reach distance for the star excursion balance test and in jump distance for the single leg hop have been shown during post-ACLR assessment [2]. In the long-term, post-ACLR knee joints have demonstrated reduced postural stability and increased energy dissipation for knee varus and knee internal/external rotation motions [3].

Stair negotiation is a common activity of daily living. During stair ascent, the individual must have knee strength control to lift the weight of the body against gravity. During stair descent, the individual must have knee balance control to lower the weight of the body without falling forward and downward. Center of pressure (COP) velocities may be used to assess overall body postural control by measuring the rate at which body weight is shifting. Time-to-boundary (TTB) may also be used to assess postural control by estimating the time in which a postural adjustment is necessary before the COP leaves the base of support [4].

The purpose of this study was to compare COP velocity and TTB values between: 1) healthy controls, 2) non-injured legs of ACLR individuals, and 3) injured legs of ACLR individuals. It was hypothesized that the ACLR legs would demonstrate higher COP velocities and lower TTB.

METHODS

Seventeen ACLR individuals (7 males, 10 females; age 26 ± 6 yr; height 1.73 ± 0.14 m; mass 73 ± 16

kg) and 17 healthy controls (7 males, 10 females; age 26 ± 4 yr; height 1.70 ± 0.12 m; mass 68 ± 12 kg) participated in this study. Individuals performed three trials each of stair ascent and descent with a right and left leg lead. A three-step staircase was utilized for stair ascent and descent (step height 18.5 cm, tread depth 29.5 cm). Portable AMTI force platforms measured ground reaction forces on the lowest two steps of the staircase. An eight-camera Vicon Nexus motion analysis system was used to track retro-reflective markers placed on the feet.

COP velocities in the anterior-posterior (AP) and medial-lateral directions were calculated using the first central difference method. TTB values were calculated using COP positions, velocities, and accelerations in the AP and ML directions. The base of support for TTB calculations was determined using video marker data and foot anthropometrics. COP velocities and TTB values were calculated during the single stance phase of steps one and two for stair ascent and descent. Mean COP velocities and minimum TTB values were used for statistical comparisons. COP parameters were calculated using a custom-written Matlab code.

Univariate analysis of variance (ANOVA) was performed to test the effect of 'leg' on mean AP COP velocity, mean ML COP velocity, minimum AP TTB, and minimum ML TTB values. When a significant main effect was found, post-hoc Tukey tests were performed to compare control legs vs. non-injured legs and control vs. ACLR legs. Post-hoc paired t-tests were used to compare significant COP parameters for non-injured vs. ACLR legs. As secondary analyses, paired t-tests were used to test stair ascent vs. stair descent and step one vs. step two. The level of significance for all statistical tests was set to $p < 0.05$.

RESULTS AND DISCUSSION

There was significant main effect of 'leg' for mean AP COP velocity during stair descent ($p = 0.035$). Post-hoc comparisons further indicated that the mean AP COP velocity for the ACLR leg was significantly higher than the control leg for the first step of stair descent (Table 1, $p = 0.030$). There were no other significant main effects of 'leg' for other COP parameters ($p = 0.079$ and higher).

Secondary comparisons revealed that mean AP COP velocity (22.5 ± 6.0 cm/s vs. 15.4 ± 4.2 cm/s, $p < 0.01$) and ML COP velocity (8.1 ± 3.0 cm/s vs. 4.7 ± 1.1 cm/s, $p < 0.01$) were significantly higher during stair descent as compared to stair ascent. In addition, minimum AP TTB (0.13 ± 0.02 vs. 0.30 ± 0.06 s, $p < 0.01$) and ML TTB (0.21 ± 0.04 vs. 0.25 ± 0.04 s, $p < 0.001$) were significantly lower during stair descent. When comparing steps, minimum AP TTB values were significantly lower during step two of stair ascent (0.19 ± 0.04 vs. 0.41 ± 0.10 s, $p < 0.001$) and during step one of stair descent (0.12 ± 0.03 vs. 0.14 ± 0.03 , $p = 0.01$).

CONCLUSIONS

The purpose of the study was to test COP parameters between an ACL reconstruction group and a healthy control group during stair negotiation. Our hypothesis that ACLR legs would have higher

mean COP velocities was supported for one variable, while our hypothesis that ACLR legs would have lower minimum TTB values was not supported. Mean AP COP velocity was significantly higher for the ACLR leg than the control leg for step one of stair descent.

In general, COP parameters were not significantly changed in the ACLR leg. Postural stability measures that target the knee joint may be more sensitive than overall body measures. Higher mean AP COP velocity in the ACLR leg during the first step of stair descent is potentially of concern since the repaired ACL acts to restrict anterior translation of the tibia. In terms of assessment, stair descent was the more challenging movement with significantly higher COP velocities and lower TTB values. Testing multiple steps is suggested, with step one of stair descent and step two of stair ascent resulting in significantly higher AP TTB values.

REFERENCES

1. Lohmander LS, et al. *Acta Orthopaedica Scandinavia* **65**, 605-609, 1994.
2. Samaan, MA, et al. *International Journal of Athletic Therapy & Training* **20**, 24-29, 2015.
3. Chandra, A, et al. *Proceedings of the Royal Society A*, In press.
4. Hertel, J, et al. *Gait & Posture*, **25**, 33-9, 2007.

Table 1: COP parameters as a function of control leg, non-injured leg, and ACLR leg. Means \pm SD are displayed. * and bold indicates significantly higher AP COP velocity for ACLR leg vs. control leg.

Stair Ascent	AP COP Vel Step 1 (cm/s)	AP COP Vel Step 2 (cm/s)	ML COP Vel Step 1 (cm/s)	ML COP Vel Step 2 (cm/s)	AP TTB Step 1 (cm/s)	AP TTB Step 2 (cm/s)	ML TTB Step 1 (cm/s)	ML TTB Step 2 (cm/s)
Control Leg	16.0 \pm 5.2	16.0 \pm 5.0	4.9 \pm 1.5	4.7 \pm 1.0	0.44 \pm 0.10	0.19 \pm 0.05	0.24 \pm 0.04	0.26 \pm 0.04
Non-injured Leg	15.7 \pm 5.1	15.1 \pm 4.5	4.7 \pm 1.2	4.7 \pm 1.2	0.37 \pm 0.10	0.19 \pm 0.04	0.26 \pm 0.06	0.24 \pm 0.05
ACLR Leg	14.2 \pm 3.8	15.3 \pm 5.0	4.4 \pm 1.1	4.9 \pm 1.8	0.43 \pm 0.08	0.19 \pm 0.04	0.25 \pm 0.04	0.26 \pm 0.06
Stair Descent								
Control Leg	19.8 \pm 5.1	20.8 \pm 8.2	8.5 \pm 4.3	7.7 \pm 3.7	0.12 \pm 0.03	0.14 \pm 0.03	0.20 \pm 0.05	0.22 \pm 0.07
Non-injured Leg	23.6 \pm 6.1	24.4 \pm 7.4	8.0 \pm 2.2	7.7 \pm 3.4	0.11 \pm 0.03	0.13 \pm 0.03	0.21 \pm 0.06	0.22 \pm 0.05
ACLR Leg	25.6 \pm 7.6*	20.9 \pm 6.4	8.6 \pm 2.8	8.2 \pm 3.3	0.12 \pm 0.02	0.14 \pm 0.04	0.20 \pm 0.03	0.20 \pm 0.05

BALANCE CONTROL DURING COMMON REHABILITATION EXERCISES IN OBESE FEMALES

¹ Bhupinder Singh, ¹ Ashley Van Artsdalen, ¹ Derek Camilleri, and ² H. John Yack

¹ Department of Physical Therapy, California State University, Fresno, CA.

² Program in Physical Therapy & Rehabilitation Sciences, University of Iowa, Iowa City, IA.

Email: bhsingh@csufresno.edu

INTRODUCTION

Obese individuals have difficulties performing basic rehabilitation exercises due to balance problems, an important issue in addition to adipose tissue restriction [1, 2]. The association between obesity and balance deficits has been observed under certain conditions, but no research has been presented about the link between obesity and balance during execution of simple commonly performed exercises like squat and lunge. The purpose of this study was to analyze the balance of adult obese females while performing squat and lunge activities, as measured by center of pressure (CoP) area and root mean square velocity (RMS-V). It is hypothesized that obese females will have poorer balance control than their normal weight counterparts; and that as the difficulty of the exercises increase, the balance control deficits will be more apparent.

METHODS

Ten obese (BMI > 30 kg/m²) female subjects age 37.4±3.7 years, BMI 39.2±3.7 kg/m² and ten normal weight (BMI<23 kg/m²), age matched females, BMI 21.6±2.3 kg/m², volunteered for the study. Infrared marker triads were applied to the lower limbs, pelvis, and trunk to generate an anatomical model using three dimensional motion analysis system (Optotrak, NDI) (Fig 1).



Figure 1: Shows the skeletal model of an obese subject during squat exercise (left), placement of markers (center) and lunge exercise (right).

Testing session included: Quiet standing with eyes open for 30 seconds(s) on the force plate (Kistler). Squatting down, feet shoulder width apart on one force plate, holding for 3s at 3 different knee angles: 60, 70, and 80 degrees. Lunging at 3 different distances, holding for 3s at 1, 1.1 and 1.2 times subject's tibial length with one foot on each force plate (Fig 1). Sway area was defined as area of ellipse (cm²) enclosing 95% of COP points over 3 seconds and RMS-V of sway as mean of anterior-posterior (AP) and medial-lateral (ML) peak velocities over 3 seconds.

DATA ANALYSIS

Visual 3-D (C-Motion) was used to analyze data. The 30 second standing data were analyzed, and seconds 2-5 were used to mimic the squat and lunge data collected (3s). A group (obese vs normal weight) by level of difficulty ANOVA was used to find differences in CoP area and RMS velocity across three levels of difficulty for the squat and lunge. Pearson correlation coefficient was calculated to find relationships between BMI and balance measures. SPSS 21.0 was used for analysis with p-value < 0.05 considered as significant.

RESULTS AND DISCUSSION

For standing, there was a significant difference for RMS-V between obese (1.7±0.3 cm/s) and normal weight females (1.41±0.19 cm/s) (p=0.011), but not for CoP area; 3.92±1.90 cm/s² for obese and 3.63±1.90 cm/s² for normal weight females (p=0.070). For squatting, changing the depth of the squat exercise (60, 70, and 80 degrees) did not result in a change in CoP area (p=0.401) or RMS-V (p=0.057). There was also no significant difference between obese and normal weight females for CoP area (p=0.120) or for RMS-V (p=0.212) (Table 1).

The analysis on squatting determined that the depth of the squat did not significantly alter the sway data, indicating that squat depth changes do not necessarily influence balance control significantly. There was also no significant difference in sway area or velocity between the obese and normal weight groups. There was a medium Cohen's effect size found for CoP area (0.73) and for RMS-V (0.53), indicating that there may be a trend for obese individuals to have increased sway than normal weight females.

The correlation coefficient for BMI and CoP area for squat 60, 70 and 80 degree levels was 0.13, 0.16 and 0.21 respectively. Similar trends were seen for RMS-V with correlation coefficient values of 0.17, 0.22 and 0.43 for the three squat levels. This is likely due to maintenance of the subject's center of gravity over the base of support during the activity, which minimizes challenges to balance control.

For lunge, altering the step distance for lunging did not result in any change in CoP area ($p=0.297$) or RMS-V ($p=0.412$). There was, however, a significant difference between obese and normal weight females for CoP area ($p<0.001$) and for RMS-V ($p=0.005$). The lunge had greater sway area as compared to standing as well as squat activities ($p<0.001$). Strong correlations were seen between BMI and CoP area (0.65, 0.77 and 0.70) and between BMI and RMS-V (0.45, 0.69 and 0.60).

Contrary to the squat, the base of support during a lunge is altered with the staggered step [2]. With increased adiposity, the subject's center of gravity is

displaced, and when an increased demand is imposed by altering base of support, the subjects present with decreased balance control. Previous research on walking biomechanics has demonstrated that obese individuals require a wider base of support to maintain balance during gait [3]. Given this information, clinicians may want to consider the benefits versus concerns prior to prescribing lunging exercises to obese individuals.

CONCLUSIONS

The lunge activity was more challenging for obese females than squatting and standing, as shown by greater CoP sway area and RMS velocity. The results could be attributed to the greater base of support and more effort needed to stabilize the mediolateral shift of the trunk in obese females during lunging. There were no differences in the three squat depths, indicating that squat may be a better exercise choice for obese individuals, especially with fall risk. To conclude, identifying the underlying balance issues in obese individuals may help to better tailor exercise programs for this patient population, which could increase performance and decrease the risk for loss of balance, falls, and injury.

REFERENCES

1. Flanagan SP, et al. *Med Sci Sports Exerc.* **35**, 635-43, 2003.
2. Wilson DJ, et al. *J Sport Rehabil.* **17**, 387-398, 2008.
3. Devita P, et al. *J Biomech*, **36**, 1355-1362, 2003.

Table 1: Mean (standard deviation) CoP area and RMS-V for different levels of squat (60°, 70° and 80° depth) and lunge (1, 1.1 and 1.2 tibial length) exercises. The measures highlighted in bold and italics showed significant differences between obese and normal weight subjects ($p<0.05$).

Group	Squat			Lunge		
	60°	70°	80°	1	1.1	1.2
COP Area (cm ²)	4.85 (2.48)	6.46 (3.37)	6.07 (3.13)	17.31 (5.30)	19.00 (7.71)	20.00 (6.11)
Normal COP Area (cm ²)	4.31 (2.12)	4.50 (2.40)	3.66 (3.11)	7.54 (3.23)	5.93 (2.09)	8.49 (5.01)
Obese RMS-V (cm/s)	2.92 (0.83)	3.10 (1.10)	3.53 (1.26)	<i>13.06 (6.98)</i>	<i>10.79 (4.13)</i>	<i>14.92 (9.38)</i>
Normal RMS-V (cm/s)	2.84 (0.82)	2.67 (0.78)	2.51 (0.80)	<i>6.40 (1.62)</i>	<i>6.32 (1.58)</i>	<i>6.19 (1.74)</i>

LOCOMOTOR CONTROL DURING PLANNED AND UNPLANNED GAIT TERMINATION IN ESSENTIAL TREMOR

¹ Jared W. Skinner, ¹ Hyo K. Lee, ^{2,3} Ryan T. Roemmich, ¹ Jacob R. Suggs and ¹ Chris J. Hass

¹ The University of Florida, Gainesville, FL, USA

² Kennedy Krieger Institute, Baltimore, MD, USA

³ The Johns Hopkins University School of Medicine, Baltimore, MD, USA

Email: jskinner1@ufl.edu

INTRODUCTION

Gait termination (GT) is a destabilizing transitional task that requires a shift from a dynamic state of motion to a static position [3]. GT can either be in response to unanticipated or anticipated stopping. While deficits in gait and gait initiation have been reported in individuals with essential tremor (ET), there is an absence in information regarding GT in those with ET, making it difficult for clinicians to design interventions to improve the ability to terminate gait quickly and efficiently.

ET is one of the most prevalent neurological disorders and yet when it comes to gait dysfunction there appears to be a void. Although, gait abnormality in ET has been documented as milder than that seen in patients with Parkinson's disease and cerebellar ataxia, it does seem to have functional consequences [1]. Recently, investigations of cerebellar dysfunction have supported the manifestation of motor disturbances in ET [1]. These investigations have shown that there is increased gait variability, increased dysfunction during tandem gait and difficulty initiating gait in ET.

However, to date no studies have been performed to analyze and compare planned and unplanned gait termination strategies in ET. In light of the movement control problems reported for patients with ET, the purpose of the study was to examine the lower extremity control strategies, specifically braking and propulsive ground reaction forces, dynamic postural stability and spatiotemporal characteristics during planned (feedforward) and unplanned (feedback) GT.

METHODS

Seventeen individuals with ET (mean \pm SD age: 67.4 ± 9.1 years, mean height: 173.2 ± 3.3 cm, mean body mass: 95.3 ± 19.4 kg) participated in this study. Subjects using a self-selected walking speed, traversed an 8 meter walkway with three force plates (360 Hz; Bertec Corporation, Columbus, Ohio) mounted flush with the walking surface. Kinematic data, time-synchronized to the kinetic collection, were collected using an 8 camera Optical Capture System (120 Hz, Vicon Nexus, Vicon, Oxford, UK).

Subjects completed five planned and unplanned gait termination trials, with normal gait trials randomly mixed in to prevent anticipation of stopping for unplanned trials. This investigation utilized a two-step termination paradigm. Braking and propulsive forces under the lead and trail limb were calculated using the peak ground reaction forces from two force plates. Peak propulsive and braking forces were normalized to the subject's mass. Dynamic postural stability index (DPSI) was calculated from ground reaction force data [3] during a 1-sec interval starting from onset of heel strike on the second force plate (by the trail limb). Additionally, spatiotemporal variables of gait, step length (SL), step velocity (SV) and step time (ST) were measured on the lead limb (terminating limb of GT) as well as the average velocity prior to the terminating step.

Ground reaction forces during the braking and propulsive phases of gait termination were analyzed using a paired sample t-test. Additionally, a paired sample t-test was used to compare the mean differences in spatiotemporal variables, gait velocity and DPSI (and component indices) between conditions (Planned vs Unplanned) with $\alpha=0.05$.

RESULTS AND DISCUSSION

Braking forces were significantly greater during unplanned GT compared to planned GT ($217.74 \text{ N/kg} \pm 67.9$ vs $157.11 \text{ N/kg} \pm 49.5$, $p < .05$). (**Figure 1**). There were no statistical differences in propulsive forces. The analysis revealed there were no differences in DPSI scores between the planned and unplanned condition. However, further analysis revealed significantly higher value in the component indices during unplanned GT; specifically in the AP (81.5 ± 40.8 vs 32.3 ± 9.7 , $p < .001$) and ML (177.6 ± 69.1 vs 90.6 ± 25.8 , $p < .001$) directions. Results of the spatiotemporal variables of the lead limb in GT are found in **Table 1**.

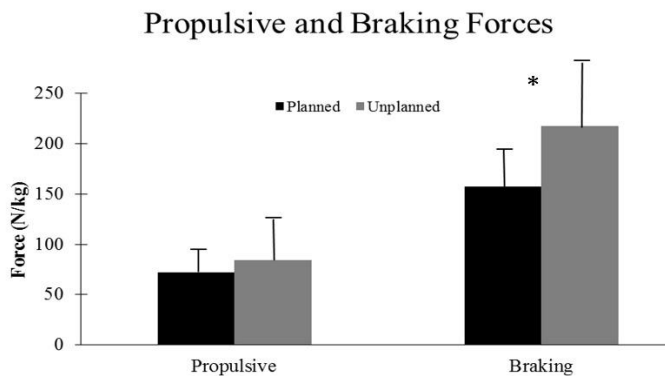


Figure 1: Propulsive and braking forces with standard deviation during planned and unplanned gait termination. (*Denotes significant value $p < .05$)

The current investigation found during unplanned GT performance was characterized by a mild decrease in the propulsive force of the penultimate limb and statistical increase in the braking force of the termination limb. Research has shown that the ability to produce sufficient anterior–posterior ground reaction forces is crucial for stopping efficiently and safely.

It has been shown during tandem gait an increased number of mis-steps and variability during tandem gait is a risk factor for future falls [2]. Gait dysfunction during tandem gait is an apparent issue

in ET [1]. In the current investigation, postural stability scores in ET, specifically in the APSI and MLSI directions, suggested less stability during unplanned GT. The results of the current investigation, in combination with previous literature in tandem gait, suggest ET have impaired postural stability. This investigation indicated less stability during unplanned GT as compared to planned GT and thus more likely to become unstable when forced to terminate gait abruptly and could lead to higher incidence of falls.

The results of the current investigation converge with previous findings, that during unplanned GT, the control strategy is modulated so that the terminal limb would attenuate the forward velocity. This is evidence by the increased step length and velocity in the unplanned condition and the increased time in the planned condition of GT. The lack of statistically difference between the gait speeds prior to the terminal/lead step in planned and unplanned GT may imply that there is an inability to voluntarily adapt gait velocity in preparation for gait termination.

CONCLUSIONS

GT involves a rapid deceleration of the body's forward momentum and requires a complex interaction of the neuromuscular system, it is possible to challenge both the feedforward and feedback neuromuscular control. Inconsequence, we were able to ascertain that patients with ET utilized alternative biomechanical control strategies during planned and unplanned gait termination.

REFERENCES

1. Louis ED, Okun MS. It is time to remove the 'benign' from the essential tremor label. *Parkinsonism Relat Disord* 2011;17(7):516-520.
2. Nevitt M., Cummings S., Kidd S., Black D. (1989) Risk factors for recurrent nonsyncopal falls. A prospective study. *JAMA* 261: 2663–2668
3. Wikstrom EA, Bishop MD, Inamdar AD, Hass CJ. Gait termination control strategies are altered in chronic ankle instability subjects. *Med Sci Sports Exerc* 2010;42(1):197-205.

Table 1: Spatiotemporal variables of terminating limb and gait velocity during planned and unplanned stopping.

Outcome Measures	Planned (\pm SD)	Unplanned (\pm SD)	P-Value
Step Length (m)	.47 \pm .06	.52 \pm .07	.02
Step Velocity (m/s)	.74 \pm .12	.89 \pm .18	<.001
Step Time (s)	.64 \pm .07	.60 \pm .08	<.001
Gait Velocity (m/s)	.73 \pm .14	.77 \pm .11	.26

VALIDATION OF A CLINICAL TEST TO ASSESS HIP ABDUCTOR MUSCLE CONTROL IN PATIENTS WITH HIP ARTHROPLASTY

¹Kathryn G. Thompson, ²Dana L. Judd, ²Jennifer E. Stevens-Lapsley, and ¹Bradley S. Davidson

¹University of Denver, Human Dynamics Laboratory, Denver, CO, USA

²University of Colorado Physical Therapy Program, Aurora, CO, USA

email: katie.thompson@du.edu

INTRODUCTION

Total hip arthroplasty (THA) is a common reconstructive surgery, with approximately 332,000 performed in 2010 and anticipated to reach over 500,000 each year by 2030 [1,2]. Functional deficits still remain after surgery, and are linked to weak hip abductor and knee extensor muscles and compensatory movement strategies developed in the late stages of osteoarthritis [3].

Hip abductor performance can be measured by assessing stability through examining the orientation of the pelvis during single limb stance for 30 seconds [4]. Clinical inference from the single limb stance test may be enhanced by the addition of quantitative postural measures. Trendelenburg angles are important measures in understanding the contribution of hip abductor strength to pelvic stability, but they are difficult to measure. Common measurements of pelvic posture use goniometers [5], which may not be sensitive to detect subtle, yet significant changes [6].

The purpose of this investigation was to assess the validity of using still-frames taken from video recordings to measure Trendelenburg postural angles. We validated these measurements to a criterion standard (motion capture system), and hypothesized that the video-based method would provide an accurate and reliable tool that can be easily incorporated into the clinic to examine contribution of hip abductors to pelvic stability.

METHODS

Eight patients (3 males, 8 females) diagnosed with end stage hip osteoarthritis before total hip replacement performed a single limb stance on their involved limb. Patients were instructed to balance

on one leg for 30 seconds or until they lost balance. Each patient was instrumented with reflective markers on bilateral anterior superior iliac spine (ASIS), patellae, and sternum (Fig. 1). Video (30 Hz) from directly in front of the patient and Vicon motion data (100 Hz) were recorded simultaneously during the entire single limb stance task.

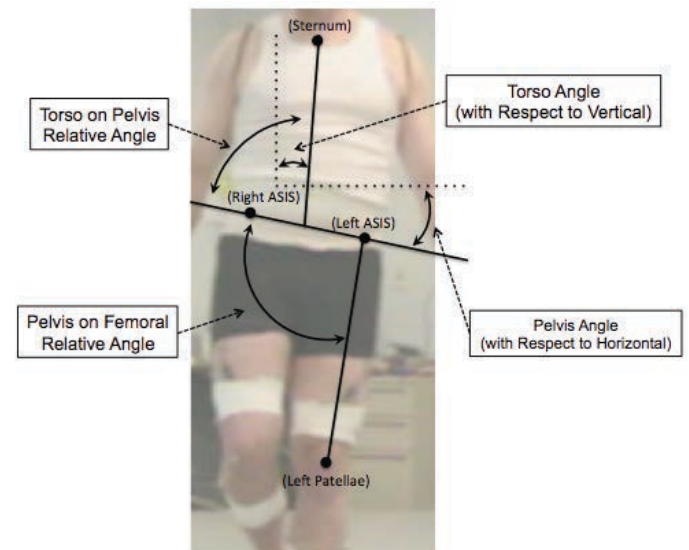


Figure 1: Single-limb stance with absolute and relative angles from reflective marker locations.

Three time points during the task, in which the patient was not visually unstable, were used for comparison between the video and motion capture methods: within the first 10 seconds of initial foot clearance, midtrial, and within the last 10 seconds. A still frame image was taken from the video at each time point of interest, and synchronized with the Vicon recording.

Two absolute angles (torso with respect to vertical, pelvis with respect to horizontal) and two relative angles (torso on pelvis, pelvis on femoral) were calculated at each time point. Still frame images were imported into NIH ImageJ software and the marker coordinates were used to generate angles of

interest. Motion capture coordinates of the reflective markers were used directly for the angle calculations. Differences between the methods (video-based, Vicon) were used to calculate error. 95% limits of agreement were calculated, and visual trends in the agreement were assessed using Bland-Altman plots.

RESULTS and DISCUSSION

Errors in the video-based measurement were smaller in the absolute angles than the relative joint angles (Table 1). All angles except for the torso, were smallest within the first 10 seconds of the trial. Mean error of the video-based method versus the Vicon criterion ranged from 0.1 to 2.5 deg. The smallest error was 0.1 deg (torso angle during last 10 sec) and the largest mean error was 2.5 deg (pelvis on femoral angle during mid trial). Bland-Altman plots demonstrated that errors were uniformly distributed across all angles in all angles except for pelvis on femoral (Fig. 2). The error of the pelvis on femoral angle increased as mean angle increased above 75 degrees, which is associated with the large mean errors in this variable.

Table 1: Measurements error (degrees) for each time point. Mean error [95% limits of agreement].

Angle	First 10 Sec	Mid Trial	Last 10 Sec
Pelvis	-0.2 [-5.7,6.1]	-0.3 [-4.7,5.3]	0.5 [-4.6,3.6]
Torso	0.2 [-3.6,3.3]	1.0 [-7.8,5.8]	0.1 [-7.1,6.9]
Torso on Pelvis	-0.7 [-7.0,8.4]	-1.7 [-7.7,11.0]	-1.6 [-6.9,10.2]
Pelvis on Femoral	-2.3 [-4.2,8.8]	-2.5, [-4.8,9.9]	-2.4 [-5.2,10.0]

The results demonstrate that using video-based still frames to estimate the Trendelenburg angles is a potentially viable method for clinical use. The error limits associated with the angles used in this investigation were centered around zero, and were consistent among time points.

Trendelenburg angles are important measures to understand hip abductor strength, but they are difficult to measure. A goniometer measure is challenging to implement and can affect patient behavior. It is impossible to measure torso on pelvis and pelvis on femoral angles at one time point using

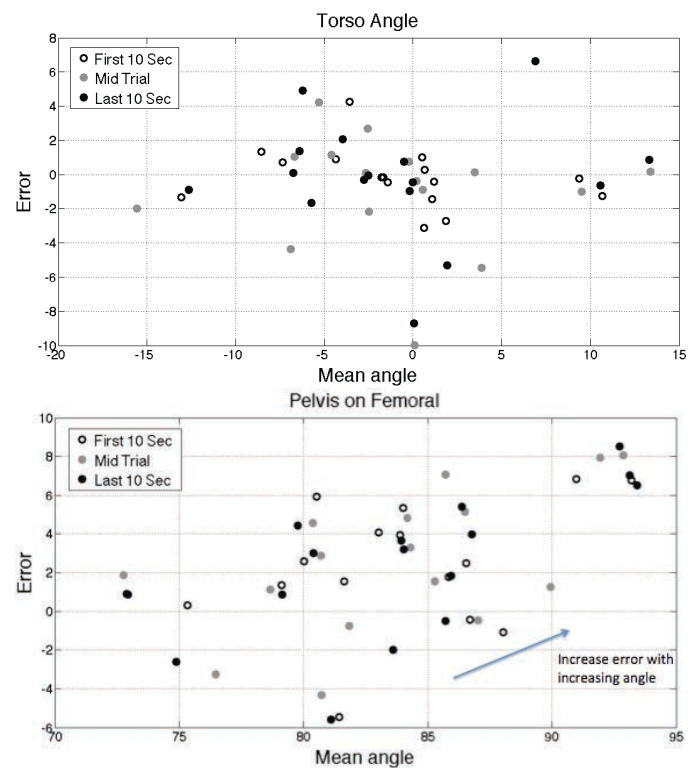


Figure 2: Bland-Altman plot of torso and pelvis on femoral angle.

a goniometer. The video-based method will measure all Trendelenburg angles at the same time point.

The video-based method is easily implemented into a lab or clinic to measure Trendelenburg posture (difficult to quantify). For example, a smartphone, positioned on a tri-pod, can record a 30-sec one-limb stance and still frame images can be processed through NIH ImageJ software and Excel.

CONCLUSIONS

The video-based method was a good estimate of relative and absolute angles of a patient during a single limb stance. This method is easily and inexpensively implemented into the clinic and can help to reduce diagnostic errors associated with clinical observation.

REFERENCES

1. CDC/NCHS, National Hospital Discharge Survey, 201
2. Kurtz *Journal of bone and joint surgery*, **89**,780-85, 2007
3. Judd et al. *Clin Orthop Relat Res*, **472**, 654-64, 2014
4. Kivlan and Martin *Int J Sports Phys Ther*, **7**, 402-12, 2012
5. Hardcastle & Nade. *J Bone Joint Surg Br*. **67**, 741-46, 1985
6. Youdas, et al. *Journal of Sport Rehabilitation*, **16**, 326-35, 2010

EFFECTS OF A COMBINED INVERSION AND PLANTARFLEXION SURFACE ON KNEE AND HIP KINEMATICS DURING LANDING

¹Kevin Valenzuela, ²Divya Bhaskaran, ¹Cicily Hummer, ¹Antonio Schefano, ¹Songning Zhang

¹Biomechanics/Sports Medicine Lab, The University of Tennessee, Knoxville, TN, USA

²University of Minnesota, Twin Cities, Minneapolis, MN, USA

email: kvalenzu@utk.edu, web: <http://krss.utk.edu/centers-labs/biomechanics-laboratory/>

INTRODUCTION

Landing from a jump is an activity commonly associated with many team sports including basketball, volleyball, and soccer. During the landing, assorted motions at the knee and hip have been associated with increased risk of anterior cruciate ligament (ACL) injury (1, 6). While many ACL injuries are non-contact, sports such as soccer and basketball often require jumping with other people in the vicinity and may result in landing on another competitor's foot, providing an altered landing surface.

This altered landing surface often manifests into a lateral ankle sprain as a result of excessive inversion and plantarflexion during landing (4). As a result, it is likely that the knee and hip joints are subsequently affected by this altered position. Most research has not examined the effects of the altered landing surface on the knee and hip joints and how it may further predispose athletes to certain knee and hip injuries such as ACL injuries.

ACL injuries during landing often occur due to increased knee abduction motion (7), hip adduction (6), and reduced hip and knee flexion (1, 3). These joint angles may change as a result of the altered landing surface during jumping, which may further predispose these athletes to ACL injury risk during their landings. Therefore the purpose of this investigation was to examine the effects of landing on a combined inversion and plantarflexion surface on knee and hip kinematics during a drop landing.

METHODS

Twelve healthy recreational athletes (age: 24.4 ± 4.2 years, height: 1.74 ± 0.09 m, mass: 71.4 ± 11.6 kg), ten males and two females, participated in this study. Participants did not have a history of major lower extremity injury and had not suffered a lateral

ankle sprain within 6 months prior to testing. Subjects performed drop landings from a height of 30cm. Five successful trials were performed in three testing conditions (landing surfaces): a flat surface, a 25° inversion surface, and a 25° inversion and plantarflexion (combined) surface. The landing platform consisted of a movable top surface that was held by one ball-and-socket joint and two releasable ball-and-socket joints, allowing for the tilting of inversion only or a combination inversion and plantarflexion on contact (2). The landing trials were performed with the right leg (perturbed) landing on the modified surfaces while the left leg (non-perturbed) always on a flat surface.

A 9-camera motion analysis system (240 Hz, Vicon Motion Analysis Inc., Oxford, UK) was used to obtain 3D kinematic data during the trials. Anatomical and tracking markers were placed on the pelvis, thighs, shanks, and feet of both legs. Pilot data had shown that landing on the combined surface without practice frequently led to loss of balance after landing, therefore for safety reasons, surface conditions were not randomized. The kinematic data were computed using the Visual3D biomechanics analysis suite (4.0, C-Motion, Inc., Germantown, MD). The right-hand rule was used to establish the conventions of 3D kinematics. Marker trajectories were filtered with a zero-lag fourth order low-pass Butterworth filter at 12 Hz. A 2 x 3 (leg x surface condition) repeated measures analysis of variance (ANOVA) was used to examine the effects of the legs and surface conditions on hip and knee kinematics (SPSS 22.0, SPSS Inc., Chicago, IL). Post hoc comparisons with Bonferroni adjustments were performed using a pairwise t-test ($p < 0.05$).

RESULTS AND DISCUSSION

Significant interactions were seen in peak knee flexion ($p < 0.001$), knee flexion ROM ($p < 0.001$), peak hip flexion ($p < 0.001$) and abduction

($p<0.001$), and hip flexion ($p=0.001$) and abduction ROM ($p<0.001$). A significant main effect for leg was seen in the peak hip flexion ($F=16.765$, $p=0.002$). In addition, a main surface effect was seen for knee abduction ROM ($F=8.381$, $p=0.007$), peak hip abduction ($F=62.382$, $p<0.001$), and hip abduction ROM ($F=72.826$, $p<0.001$). Post-hoc comparisons showed that peak knee and hip flexion was significantly lower and peak knee abduction was significantly higher in the perturbed leg on the combined surface compared to the flat and inverted surfaces ($p<0.05$, Table 1). Hip abduction ROM was significantly higher in perturbed leg compared to the non-perturbed leg in the inverted condition ($p=0.024$). On the combined surface, the perturbed leg compared to the non-perturbed leg showed decreased knee flexion ROM, peak knee flexion, hip flexion ROM, and peak hip flexion and increased knee abduction ROM, peak knee abduction, and hip abduction ROM and (Table 1, $p<0.05$).

Increases in knee abduction have been frequently suggested to place athletes at risk for ACL injury (5, 7). Results from this research suggest that landing on the combined surface may increase the risk of ACL injury due to the increased knee abduction seen in the perturbed limb. This result occurred during double-leg landing with the perturbed leg making contact first. But it is important to note that single-leg landing has been shown to further increase the knee abduction and therefore increase the risk of ACL injury (7). It is common for athletes in competition situations such as basketball, soccer, and volleyball to often land on a single limb which may increase the risk factor during landing on a combined surface. Additionally, our results

showed that the perturbed limb landed with a more extended knee, which decreases the ability of the hamstrings to prevent anterior tibial translation and increases ACL injury risk (3). It has also been suggested that hip adduction increases knee abduction. However landing on the tilting surfaces induced hip abduction, which may have been a protective mechanism to limit the amount of knee abduction experienced by the knees during landing.

CONCLUSION

Kinematic differences of the knee and hip between the flat and inverted conditions were few and small. However, when adding the plantarflexion to the inversion tilt, there were many more significant differences which may predispose athletes to ACL injuries during their landings. The increased hip abduction may be a protective mechanism designed to limit the knee abduction occurring during the inverted and plantarflexed landing.

REFERENCES

1. Blackburn, J.T., et al. (2008). *Clin Biom*, **23**, 313-319.
2. Bhaskaran, D. et al. (in press). *J Health & Sport Sci*.
3. Fagenbaum, R., et al. (2003). *Am J Sports Med*, **31**, 233-240.
4. Garrick, J.G. (1977). *Am J Sports Med*, **5**, 241-242.
5. Hagins, M., et al. (2007). *Clin Biom*, **22**, 1030-1036.
6. Hewett, T.E., et al. (2006). *J Ortho Research*, **24**, 416-421.
7. Nagano, Y., et al. (2009). *Knee*, **16**, 153-158.

Table 1. Mean knee and hip kinematic variables (degree): Mean \pm SD.

	Perturbed Leg			Non-perturbed Leg		
	Flat	Inverted	Combined	Flat	Inverted	Combined
Knee Flexion ROM	51.3 \pm 3.5 ^B	51.5 \pm 5.7 ^B	44.7 \pm 7.9 [#]	52.1 \pm 6.3 ^A	47.9 \pm 7.7 ^B	53.8 \pm 6.9
Peak Knee Flexion	73.7 \pm 8.9 ^B	72.1 \pm 5.6	64.5 \pm 10.0 [#]	73.5 \pm 8.0	70.0 \pm 8.2 ^B	75.2 \pm 6.1
Knee Abduction ROM	2.8 \pm 3.3 ^B	3.1 \pm 2.9 ^B	4.7 \pm 2.6 [#]	2.5 \pm 2.6	2.6 \pm 2.6	2.7 \pm 2.6
Peak Knee Abduction	2.9 \pm 6.0 ^B	3.3 \pm 5.0 ^B	4.4 \pm 5.5 [#]	2.3 \pm 3.2	2.5 \pm 3.3	2.5 \pm 3.8
Hip Flexion ROM	28.5 \pm 12.7 ^B	26.4 \pm 8.2 ^B	23.0 \pm 9.1 [#]	29.9 \pm 13.1	23.6 \pm 7.6	25.8 \pm 8.6
Peak Hip Flexion	48.1 \pm 16.6 ^B	44.8 \pm 9.6 ^B	38.1 \pm 11.9 [#]	49.5 \pm 16.5	43.3 \pm 9.9	46.8 \pm 11.7
Hip Abduction ROM	3.2 \pm 3.5 ^{AB}	9.1 \pm 2.6 [#]	8.7 \pm 2.4 [#]	3.2 \pm 5.2 ^A	5.2 \pm 3.8	4.2 \pm 2.9
Peak Hip Abduction	10.9 \pm 6.3 ^{AB}	17.7 \pm 4.9	17.0 \pm 4.9	13.0 \pm 5.7	14.3 \pm 5.0	12.4 \pm 3.7

Note: All differences are significant ($p<0.05$), ^A: different from Inverted of same leg, ^B: different from Combined of same leg, [#]: different from the non-perturbed leg of same surface condition.

EFFECTS OF DIFFERENT PERTURBATION LEVELS DURING FALL RISK ASSESSMENT FOR OLDER ADULTS AT HIGHER FALL RISK

Srikant Vallabhajosula, Jane Freund, Victoria Flood, Lucas Boyd, Mary Cameron Hamilton, Stephen P. Bailey

Department of Physical Therapy Education
Elon University, Elon, NC, USA
email: svallabhajosula@elon.edu, web: www.elon.edu/dpte

INTRODUCTION

A fall is defined as an event which results in a person coming to rest inadvertently on the ground or floor or other lower level. According to the World Health Organization, each year an estimated 424,000 individuals die from falls globally. Particularly, falls are a serious concern among the aging population with one in three adults aged 65 or above experiencing a fall every year [1]. In 2009, more than 2.4 million older adults had to visit emergency room for nonfatal fall-related injuries [2]. These falls cause both morbidity and mortality, resulting in multiple injuries and increased medical costs (estimated to become \$54.9 billion by 2020) [3]. Hence it is critical to identify assessments and mechanisms that increase this risk of falls to design effective fall-prevention programs.

Assessments for risk of falls include examining the motor control strategies when an individual is given an external perturbation. While the use of systems like the Biodex Balance System SD that can provide an external perturbation in a clinical setting is increasing, little evidence exists on the amount and kind of perturbation needed to effectively and quantitatively assess risk of fall. The purpose of the current study is to examine fall risk assessment among older adults using two different conditions of perturbation (LESS and MORE) on the Biodex Balance System SD (Biodex Medical Systems, Shirley, NY). We hypothesized those older adults who are classified to be at higher fall risk will perform poorly than those who are classified to be at lesser fall risk under both the perturbation conditions but the performance will be more similar under the MORE perturbed condition.

METHODS

Twenty two older adults, including 15 females and 7 males were categorized into two groups based upon American Geriatrics Society guidelines for fall risk assessment; lesser fall risk, $n=11$, mean age 72 ± 4.84 years and higher fall risk, $n=11$, mean age of 75 ± 6.86 years.

The Biodex Balance system SD was used for fall risk assessment. The Biodex Balance System SD uses a circular force platform that is free to tilt in the anterior-posterior and medial-lateral directions simultaneously. It is possible to control the degree of perturbation from levels 12 to 1 with a higher level indicating more stable platform. In the current study two levels (conditions) were used: level 8 (LESS perturbation) and level 2 (MORE perturbation). Under each condition, participants performed one standing practice trial followed by two test trials for 30s each. Sufficient rest as desired by the participants was given between the trials and between the conditions. The order of the conditions was randomized among the participants. The force platform records center of pressure data during standing trials. However no visual feedback of the center of pressure was given while the participants tried to maintain their balance on the unstable platform. The recorded center of pressure data was used to calculate several center of pressure based dependent variables such as range, path length, mean velocity, root mean square displacement in medio-lateral and antero-posterior directions. Total path length and elliptical sway area were also calculated. All the calculations were made using customized Matlab scripts. For statistical analysis, independent samples t-tests and Receiver Operating Characteristics (ROC) curve analysis were performed for both the conditions separately as the main purpose of the study was to see the difference

between the groups during each condition. An average of both the test trials was used for statistical analysis.

RESULTS AND DISCUSSION

While all the participants could complete the LESS perturbation condition, 5 participants in the higher fall risk group and 1 participant in the lesser fall risk group could not complete the MORE perturbation condition.

For the LESS perturbation condition, older adults at higher fall risk displayed significantly greater medio-lateral range ($P = 0.044$), antero-posterior range ($P = 0.024$) and antero-posterior root mean square displacement ($P = 0.027$; Table 1). When perturbed MORE, older adults at higher fall risk who completed the task displayed significantly greater antero-posterior root mean square displacement ($P = 0.043$) and a trend towards greater elliptical sway area ($P = 0.057$; Table 1). These results suggest that among those who completed the tasks, older adults at higher fall risk performed poorly during both the conditions compared to those who were at lesser fall risk. More differences were seen when perturbed to a lesser extent as older adults at lesser fall risk group could perform this task better compared to the older adults at higher fall risk. However when perturbed more, perhaps participants in both the groups who could complete the task found it similarly challenging.

ROC curve analysis for the LESS perturbation condition showed that the area under the curve ranged from 0.69 to 0.79 for all the dependent variables. Similarly, ROC curve analysis for the MORE perturbation condition showed that the area under the curve ranged from 0.61 to 0.76 for all the

dependent variables. Results from the ROC curve analysis echo those of the independent samples t-test with a greater area under the curve seen for the LESS perturbation condition compared to the MORE perturbation condition suggesting that the LESS perturbation condition was better at differentiating the two groups.

CONCLUSIONS

Greater percentage of older adults at higher fall risk seemed to be unable to complete a more challenging perturbation task compared to those at lesser fall risk. This could be due to insufficient input from sensory systems to maintain balance when the force platform tilted more. Perturbing to a lesser extent also seemed to be beneficial to differentiate those at higher and lesser fall risk. Results of the current study suggest that older adults who were categorized as at higher fall risk could be further sub-divided during clinical examination into two groups – those who cannot perform the MORE perturbation task and those who can but perform poorly on the LESS perturbation task compared to older adults at lesser fall risk. Greater sample size is required to warrant these findings.

REFERENCES

1. Hornbrook MC, et al. *Gerontologist* **34**(1),16–23, 1994.
2. CDC, National Center for Injury Prevention and Control. WISQARS [online]. Accessed October 25, 2012.
3. Englander F, et al. *J Forensic Sci.* **41**(5), 733–746, 1996.

Table 1: Mean (SE) of dependent variables that showed significant differences between the groups

Older adults group	LESS perturbation condition			MORE perturbation condition	
	Medio-lateral range (cm) *	Antero-posterior range (cm) *	Antero-posterior root mean square displacement (cm) *	Antero-posterior root mean square displacement (cm) *	Elliptical Sway Area (sq. cm) †
At higher fall risk	1.81 (0.31)	2.18 (0.45)	0.018 (0.003)	0.082 (0.015)	68.98 (18.00)
At lesser fall risk	0.97 (0.24)	0.93 (0.23)	0.008 (0.002)	0.045 (0.009)	27.03 (11.57)

* Significant difference ($P < 0.05$); † Trend towards significance ($0.051 < P < 0.07$)

THE INFLUENCE OF LOCOMOTOR TRAINING ON DYNAMIC BALANCE AND ITS RELATION TO INCREASED WALKING SPEED IN POST-STROKE HEMIPARETIC SUBJECTS

Arian Vistamehr¹, Steven A. Kautz^{2,3}, Mark G. Bowden^{2,3} and Richard R. Neptune¹

¹ Department of Mechanical Engineering, The University of Texas, Austin, TX

² Department of Health Sciences and Research, Medical University of South Carolina, Charleston, SC

³ Ralph H Johnson VA Medical Center, Charleston, SC

email: arian.vistamehr@utexas.edu web: <http://www.me.utexas.edu/~neptune>

INTRODUCTION

Slow walking speed and lack of balance control are common impairments post-stroke. Thus, rehabilitation interventions often target improved gait coordination and overall mobility. One intervention that has received much attention is locomotor training, which consists of walking on a treadmill with partial body-weight support [1] and manual assistance from trainers. While numerous studies have reported improved walking speed in subjects post-stroke (e.g., [1-2]), the effect of locomotor training on dynamic balance during walking is unclear.

To maintain dynamic balance, whole-body angular momentum (H) needs to be controlled through proper foot placement and generation of appropriate ground-reaction-forces (GRFs) (e.g., [3]). Thus, poor regulation of H during walking results in higher magnitudes of H , which may indicate a decreased ability to recover balance. However, no study has assessed if locomotor training improves dynamic balance through improved regulation of H . In addition, it is not clear if clinically meaningful increases in walking speed after locomotor training are correlated with improved dynamic balance.

The goal of this study was to assess the influence of a 12-week locomotor training program [2] on dynamic balance in post-stroke subjects during steady-state walking and determine if clinically meaningful improvements in walking speed are associated with improved balance control.

METHODS

Previously collected kinematic and GRF data [2] from 20 post-stroke subjects with hemiparesis (11

left hemiparesis; age: 56 ± 11.7 years) pre- and post-therapy were analyzed. Subjects participated in a 12-week locomotor training program described previously [2]. Three-dimensional kinematics and GRFs were collected within one week of therapy initiation and completion. Subjects walked on a split-belt instrumented treadmill at their self-selected (SS) and fastest-comfortable (FC) walking speeds pre-therapy. During post-therapy data collection, each subject walked at a speed matched to their pre-therapy SS and FC speeds. In addition, SS and FC speeds were determined post-therapy to allow the determination of speed increases from pre- to post-therapy. Kinematic data from ten healthy subjects [4] were used to provide a basis for comparison.

Dynamic balance was assessed using the peak-to-peak range of H in the frontal and sagittal planes as described by Vistamehr et al [4]. The range of H between pre-therapy walking at SS (and FC) speed and post-therapy walking at a speed matched to their pre-therapy SS (and FC) speed were compared for each subject using a paired t-test ($p < 0.05$). In addition, those with clinically meaningful improvements in walking speed (> 0.16 m/s, [5]) were identified as responders and Pearson's correlation analyses were performed to identify relationships between changes in SS walking speed and changes in the range of H walking at fixed speeds pre- and post-therapy. If significant correlations were found, to further understand the mechanisms used for maintaining balance and improving walking speed, GRF peaks and impulses (i.e., time integral of GRFs) were calculated during early (0-50%) and late (51-100%) stance. Also, foot placement was calculated as the vector from the

body center-of-mass to the center-of-pressure. Pearson's correlation analyses were performed between the range of H in each plane and GRFs (peaks and impulses) as well as foot placement.

RESULTS AND DISCUSSION

For the group as a whole, locomotor training did not improve dynamic balance as measured by changes in whole-body angular momentum. The range of H decreased (improved) in only 25% of the subjects and became worse (increased) in 35% of the subjects. The remaining subjects did not have a consistent response, with each subject improving, becoming worse or showing no change in the different planes and walking conditions (Fig. 1 and Table 1). Compared to the healthy control subjects, the range of frontal-plane H was higher in the hemiparetic subjects both pre- and post-therapy, suggesting poorer mediolateral balance control post stroke (Fig. 1). In the sagittal plane, the range of H was generally higher during the nonparetic leg stance than during the paretic leg stance (Fig. 1). This was mainly due to the longer duration of the nonparetic leg stance.

For those subjects who achieved a clinically meaningful improvement in their SS walking speed ($n = 11$), changes in walking speed were correlated with improved dynamic balance in the frontal plane ($r = -0.48$, approaching significance at $P = 0.09$) and sagittal plane during the first half of the paretic gait cycle ($r = -0.55$, $P = 0.05$). Also, changes in the FC walking speed were correlated with changes in the range of H in the sagittal plane during the first ($r = -0.86$, $P < 0.001$) and second ($r = -0.63$, $P = 0.02$) halves of the paretic gait cycle. Further, the improved dynamic balance was correlated with changes in foot placement and generation of GRFs. Specifically, better balance control was associated with a mediolateral paretic foot placement closer to midline, longer anterior nonparetic steps, higher braking GRF peaks and impulses, higher (lower) propulsive GRF peaks and impulses from the paretic (nonparetic) leg, and higher vertical GRF impulses from both legs in the late stance. These relationships highlight the importance of foot placement and appropriate GRF generation to balance control and may assist clinicians with designing effective locomotor therapies that target these biomechanical variables.

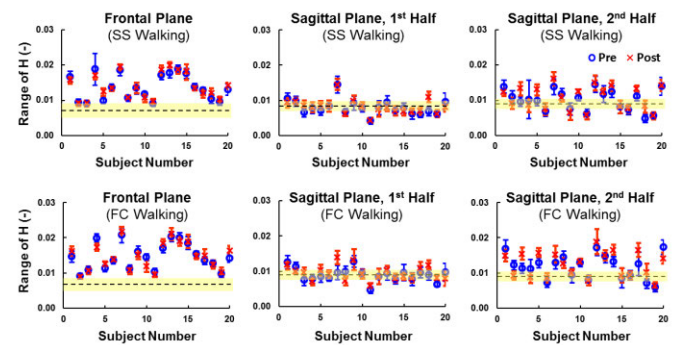


Figure 1: Normalized, mean (\pm SD) range of H for each hemiparetic subject pre- and post-therapy. The range of H in the sagittal plane is shown during the 1st (paretic leg stance) and 2nd (nonparetic leg stance) halves of the gait cycle. The dashed line indicates the group average range of H (shaded region, \pm SD) for the healthy control subjects.

Table 1: Significant changes ($p < 0.05$) in the range of angular momentum (H) between pre- and post-therapy are shown for each subject. Significant decreases in the range of H are shown with '✓' and significant increases are shown with 'x'. '1st' and '2nd' represent the 1st (paretic leg stance) and 2nd (nonparetic leg stance) halves of the gait cycle.

Subject	SS walking speed			FC walking speed		
	Frontal	Sagittal 1st	Sagittal 2nd	Frontal	Sagittal 1st	Sagittal 2nd
1	✓	✓	✓	x		✓
2	✓		✓		✓	✓
3		x	x		x	x
4	✓		✓	✓		✓
5	x	x	x	x	x	x
6	✓			x	x	x
7			x		x	x
8			✓		✓	✓
9						
10	✓		x	✓		
11				✓	x	
12	x			x		
13	x	✓				
14			x	✓		x
15		✓				
16	✓			✓		
17		x	x	x	x	
18		x	x		x	x
19					x	x
20		✓	x	x	✓	✓

ACKNOWLEDGEMENTS

This work was supported by AHA SouthWest Affiliate pre-doctoral fellowship (12PRE12030414) and the Rehabilitation Research and Development Service of the Department of Veteran's Affairs.

REFERENCES

1. Hesse S. *NeuroRehabilitation* **23**, 55-65, 2008.
2. Bowden MG, et al. *Arch Phys Med Rehabil* **94**, 856-62, 2013.
3. Pijnappels M, et al. *Gait & Posture* **21**, 388-94, 2005.
4. Vistamehr A, et al. *Clin Biomech* **29**, 583-589, 2014.
5. Tilson JK, et al. *Phys Ther* **90**, 196-208, 2010.

POSTURAL STABILITY DURING STAIR NEGOTIATION WHILE CARRYING ASYMMETRIC LOADS

Junsig Wang and Jason Gillette

Iowa State University, Ames, IA, USA

INTRODUCTION

Individuals often carry items in one hand instead of both hands during activities of daily living. Asymmetric load carriage is expected to produce a lateral shift of the center of mass. A laterally displaced center of mass during unilateral load carriage results in a challenge to postural stability during walking. Furthermore, asymmetrical load carriage during stair negotiation results in even higher demands on postural stability.

Previous studies have investigated how load carriage affects the biomechanics of human movement as a function of load magnitude and asymmetry. However, no studies exist that evaluate postural stability of asymmetric load carriage during stair negotiation. Therefore, the purpose of this study was to assess postural stability when carrying symmetric vs. asymmetric loads during stair ascent and stair descent. We hypothesized that: 1) postural stability would be decreased during unilateral load carriage as compared to bilateral load carriage, and 2) postural stability would be decreased during stair descent as compared to stair ascent.

METHODS

Twenty-five young healthy adults (13 males, 12 females; age 24.0 ± 4.2 yr; height 171.3 ± 7.7 cm; mass 68.7 ± 13.3 kg) participated in this research. A three-step staircase (step height 18.5 cm, tread depth 29.5 cm) with force platforms on the two lowest steps was used for stair negotiation. The participants were asked to carry three types of loads: no load, 20% body weight (BW) load on one side of the body, and 20% BW load split between both sides of the body. Two hand-held bags were filled with sealed bags of lead shot to match the two loaded conditions.

An eight-camera Vicon motion analysis system was used to collect three-dimensional kinematic data at a

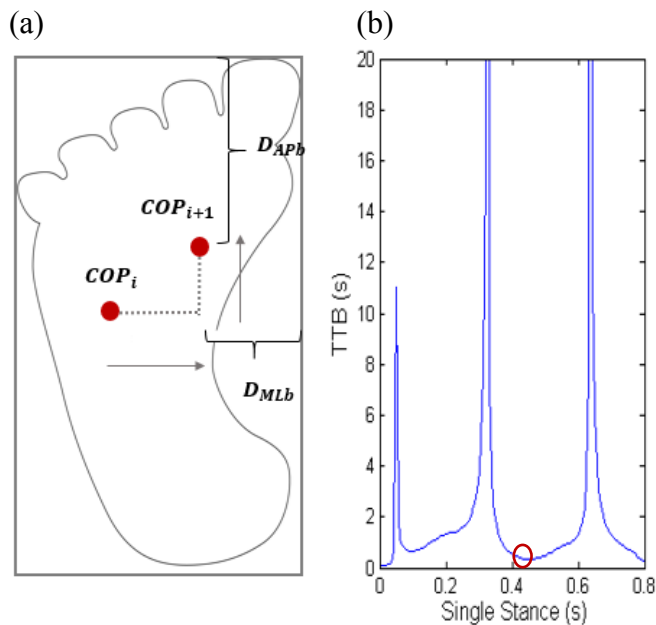
sampling rate of 160 Hz. Five retro-reflective markers were placed on toe, mid-foot, heel, medial malleoli, and lateral malleoli. Force platform data were sampled at 1600 Hz. Kinetic and kinematic data were synchronized using Vicon Nexus.

Center of pressure (COP) based parameters were calculated using custom-made Matlab code. COP velocities were calculated utilizing the first central difference method. Rectangular boundaries of the base of support were modeled from marker data and foot anthropometrics. Anterior-Posterior (AP) and Medial-Lateral (ML) COP position and velocity were then used to estimate Time-to-Boundary (TTB, Figure 1). TTB is the estimated time it takes the COP to reach the boundary of foot [1]. The dependent variables included mean COP AP and ML velocities and minimum AP and ML TTB values during single-leg stance.

Two independent variables were tested: loading conditions (no load, 20% BW bilateral load, 20% BW unilateral load) and stair negotiation (ascent vs. descent). Repeated measures ANOVA with two within factors (3×2) was performed to test the effects of loading conditions and stair negotiation. Holm-Bonferroni post-hoc tests were performed when appropriate. The level of statistical significance for all tests was set at $p < 0.05$.

RESULTS

For mean AP COP velocity, there were significant main effects of load condition ($p = 0.05$) and stair ascent vs. descent ($p < 0.01$, Table 1). Mean AP COP velocity was significantly higher during stair descent as compared to stair ascent, but post-hoc analysis did not detect any significant differences between load conditions ($p \geq 0.11$). For mean ML COP velocity, there was a significant main effect of stair ascent vs. descent ($p < 0.01$). Mean COP ML velocity was significantly higher during stair descent as compared to stair ascent (Table 1).



$TTB_{(i)} = D_{b(i)} / COP_{vel(i)}$
 D_b = displacement from COP to AP or ML boundary
 COP_{vel} = AP or ML COP velocity
 i = each data point (1/160s interval)

Figure 1 Illustration of (a) TTB calculation and (b) the minimum TTB value (in ML direction)

For minimum ML TTB, there were significant main effects of stair ascent vs. descent ($p < 0.01$) and the interaction between stair ascent vs. descent and load condition ($p = 0.01$). Minimum ML TTB was significantly lower for stair descent as compared to stair ascent (Table 1). Exploring the interaction effects, minimum ML TTB was significantly lower for stair descent as compared to stair ascent when carrying no load, 20% BW bilateral load, and 20% BW unilateral load. For minimum AP TTB, there were no significant main effects.

Table 1: COP parameters as a function of load condition and ascent vs. descent. Means \pm SD are displayed.
 * significant main effects. Bold indicates significantly higher COP velocities or significantly lower TTB.

	No Load	20% BW Bilateral	20% BW Unilateral	Ascent	Descent	Load	Ascent vs. Descent	Interaction
AP COP vel (cm/s)	19.2 \pm 6.9	17.7 \pm 5.9	17.9 \pm 5.9	16.3 \pm 5.6	20.2 \pm 6.2	0.05*	< 0.01*	0.08
ML COP vel (cm/s)	6.5 \pm 3.6	6.5 \pm 3.3	6.8 \pm 3.7	4.6 \pm 1.5	8.6 \pm 3.8	0.54	< 0.01*	0.06
AP TTB (s)	0.20 \pm 0.10	0.24 \pm 0.22	0.21 \pm 0.12	0.24 \pm 0.20	0.20 \pm 0.08	0.27	0.36	0.79
ML TTB (s)	0.55 \pm 0.29	0.54 \pm 0.24	0.51 \pm 0.26	0.67 \pm 0.28	0.39 \pm 0.16	0.28	< 0.01*	< 0.01*

DISCUSSION AND CONCLUSIONS

We investigated the effect of different methods for carrying loads on postural stability during stair negotiation in healthy young adults. Our first hypothesis that postural stability would be decreased during unilateral load carriage as compared to bilateral load carriage was not supported. Our second hypothesis that postural stability would be decreased during stair descent as compared to stair ascent was supported for three variables. More specifically, mean AP COP velocity was increased, mean ML COP velocity was increased, and minimum ML TTB was decreased during stair descent.

COP-based parameters measure challenges in postural stability. Specifically, minimum TTB estimates the lowest margin of safety before a postural adjustment is necessary [2-3]. These parameters indicated that stair descent results in decreased postural stability compared to stair ascent, particularly in the ML direction. However, load carriage did not significantly affect these measures of postural stability. Challenges associated with load carriage may be better assessed with musculoskeletal models that estimate structural loading.

REFERENCES

1. Slobounov, S.M. et al. *J Gerontol A Biol Sci Med Sci*, 53 (1), B71-8, 1998.
2. Hertel, J. & Olmsted-Kramer. *Gait Posture*, 25 (1), 33-9, 2007.
3. Wikstrom, E.A. et al. *Gait Posture*, 32 (1), 82-6, 2010.

THE EFFECT OF LOAD MAGNITUDE AND DISTRIBUTION ON LUMBAR SPINE POSTURE IN ACTIVE-DUTY MARINES

¹ Ana E. Rodriguez-Soto, ¹ David B. Berry, ² Laura Palombo, ¹ Emily Valaik, ² Karen R. Kelly and ¹ Samuel R. Ward

¹ University of California, San Diego, La Jolla, CA, USA

² Naval Health Research Center, San Diego, CA, USA

email: s1ward@ucsd.edu, web: www.muscle.ucsd.edu

INTRODUCTION

Lower back pain in the military population has been associated with injuries that result from heavy load carriage during training and operational tasks [1]. As a result, load carriage limits and configuration recommendations have been studied and established based on energy expenditure and situational awareness [2,3]. However, the interaction between load magnitude and distribution on lumbar spine (LS) posture has not been described in detail.

METHODS

A group of 12 active-duty Marines (age 24.42 ± 5.48 years, BMI 24.69 ± 2.53 kg/m², time of service: 57.21 ± 44.72 months) were scanned using a 0.6T MRI scanner (Upright MRI scanner, Fonar Corporation, Melville, NY, USA). This scanner allows for images to be acquired while subjects are standing. The lumbar spine of each Marine was scanned while standing unloaded and loaded with 6 different configurations: carrying 22, 33 and 45 kg, with the load distributed 50% anteriorly and 50% posteriorly and 20%-80%, respectively. The order of the scans was randomized.

The imaging protocol consisted of a 3-plane localizer and sagittal T2 weighted images (TR = 1974msec, TE = 160sec, FOV = 32cm, 224x224 acquisition matrix, 4.5-mm slice thickness, no gap, scan duration 3min) were acquired. Images were used to create a 3D representation of the endplates of each vertebra (L1-S1) by placing seed points on the four corners of each vertebra and posterior elements landmarks using Osirix (Pixmeo, Geneva, Switzerland). Custom software was then used to measure the overall angle of the LS with respect to the horizontal, overall LS lordosis, superior LS lordosis (Sup L1 to Inf L3), inferior LS lordosis

(Sup L4 to Inf S1), and intervertebral angles (L1-S1) [4].

All variables were compared using two-way (load \times configuration) repeated measures ANOVA and *post hoc* Sidak tests to identify significant differences and interactions among these factors ($\alpha=0.05$). All data in plots are reported as means \pm standard deviation.

RESULTS AND DISCUSSION

A significant interaction ($p<0.05$) between load magnitude and distribution was found, meaning that the effect of load on LS posture is distribution dependent. Moreover, loads carried in the 20%-80% configuration induced ($p<0.05$) postural changes through 33kg, while those carried in the 50%-50% configuration did not have an effect on LS posture.

Increased trunk flexion ($p<0.05$) was found when load was carried in the 20%-80% configuration. However, no differences in lumbar flexion were measured between 33kg and 45kg (Fig. 1, solid bars).

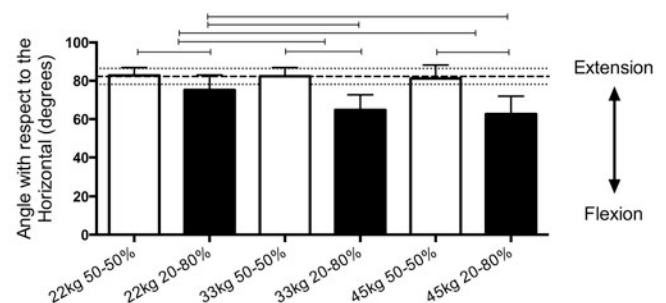


Figure 1: Results for angle with respect to the horizontal. Thick dashed line indicates average value when standing without external load; thin dashed lines indicate one standard deviation. Clear bars: 50-50% load distribution; solid bars: 20%-80% load distribution. Horizontal bars represent statistical significance ($p<0.05$).

Significant ($p < 0.05$) main effects of both load magnitude and configuration on whole LS lordosis were found. However, *post hoc* tests revealed no differences between load magnitudes (Fig. 2A). Furthermore, superior and inferior LS lordoses were measured to identify regional postural response to load magnitude and distribution. A main effect of load magnitude was found ($p < 0.05$) on the superior LS. Overall, superior LS became more lordotic as load magnitude increased from between 22kg to 33kg, while no difference was detected 33kg and 45kg (Fig. 2B). Contrastingly, a main effect of load configuration was detected ($p < 0.05$) on the inferior LS; furthermore, when load was carried in the 20%-80% configuration the inferior LS became straighter ($\sim 5^\circ$) regardless of load magnitude (Fig. 2C).

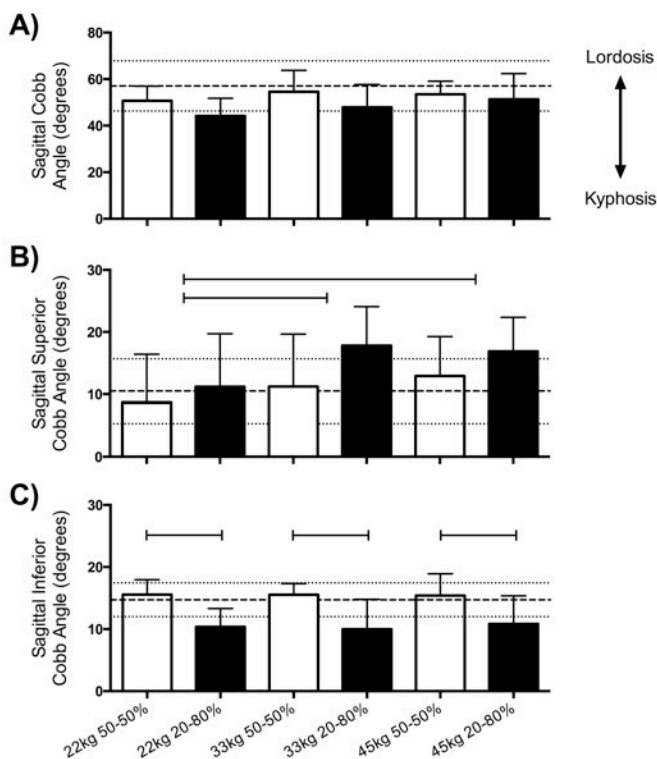


Figure 2: Results for A) whole, B) superior and C) inferior LS lordosis. Thick dashed line indicates average value when standing without external load; thin dashed lines indicate one standard deviation. Clear bars: 50-50% load distribution; solid bars: 20%-80% load distribution. Horizontal bars represent statistical significance ($p < 0.05$).

CONCLUSIONS

Load carriage in the 50%-50% configuration did not induce changes in LS flexion or lordosis. These data suggest that the LS posture while carrying load

equally distributed anteriorly and posteriorly is similar to that while standing without external load. Future work is needed to establish if this may have a positive or negative effect on LS health or operational efficiency.

In this study, we have shown that as load magnitude increases the LS flexes forward when load is carried in the 20%-80% configuration. Additionally, we observed opposing lordosis postures in the superior and inferior LS. The superior LS becomes progressively more lordotic as load magnitude increases, potentially to maintain an upright head position. Surprisingly, we found that the inferior LS became less lordotic regardless of load magnitude.

It has been previously hypothesized that LS postural changes during load carriage are aimed at maintaining the center of mass of the system. Interestingly, global LS postural differences were not found when Marines carried 33kg and 45 kg in the 20%-80% configuration. This may suggest a plateau effect of load induced postural changes with a posterior load-carriage bias. Importantly, lumbar spine postural changes were not observed when loads were balanced anterior to posterior.

REFERENCES

1. Attwells RL. *Ergonomics* **49**:1527-1537, 2006.
2. Heir T. *Scand J Med Sci Sports* **6**:186-191, 1996.
3. Swain DP. *Military medicine* **175**:664-670, 2010.
4. Rodriguez-Soto AE. *Spine* **38**:E783-791, 2013.

ACKNOWLEDGEMENTS

This project was funded by the United States Army Medical Research Acquisition Activity. Award number: W81XWH-13-2-0043.

THE EFFECT OF POSTERIOR FOOT PLACEMENTS ON SIT-TO-STAND KINETICS, ENERGETICS AND MUSCLE ACTIVITY

Eric Pitman, Zachary A. Sievert, Kevin C. Fontenot, Jessica A. Mutchler & Joshua T. Weinhandl

Old Dominion University, Norfolk, Virginia, USA

Email: epitman@odu.edu

INTRODUCTION

The Sit-to Stand (STS) is an activity of daily living (ADL) frequently performed by all people [1]. The ability to accomplish this task is essential to perform other ADLs such as walking and stair climbing [2]. It has been shown that people with movement difficulties will alter their initial seated position to make this task easier [3]. There are a variety of different strategies to make this task easier based off the specific pathology; but, the common goal of the movement change is to reduce dynamic instability of the center of mass (COM).

A common strategy change for the STS is positioning the feet posteriorly by increasing flexion at the knee joint. This reduces the displacement of the COM to the base of support while increasing the joint moment of force at the knee while decreasing it at the hip. [3] However, it is unclear the accumulative effect of the moment of force at each joint in foot positions with varied knee joint angles. Therefore, the purpose of this study was to determine the effects of altered foot positions on joint angular impulse and work, as well as integrated surface electromyography (iEMG) of the dominant lower limb.

METHODS

Ten healthy, recreationally active participants (70.1 ± 8.70 kg, 1.66 ± 0.07 m, 18-30 years) volunteered to perform STS on a force plate. Prior to data collection, participants were informed of study procedures and provided written informed consent in accordance with institutional guidelines. Single reflective markers were placed on specific anatomical landmarks [4] and a static standing calibration trial (neutral position) was collected. Participants were asked to complete five STS with in three foot placements. The knee joint angle was positioned at 90° , 100° and 110° measured by a goniometer. Three-dimensional marker coordinate data were collected at 200 Hz using an eight-camera Vicon motion analysis system. Synchronously, three-dimensional force data and surface EMG of 8 lower extremity muscles were collected at 2000Hz using a Bertec force plate and Delsys trigno sensors, respectively. The lower extremity muscles include:

Tibialis Anterior, Soleus, Gastrocnemius, Rectus Femoris, Vastus Lateralis, Vastus Medialis, Biceps Femoris and Medial Hamstrings.

Raw three-dimensional marker coordinate and GRF data were low-pass filtered using a fourth-order, zero lag, recursive Butterworth filter with cutoff frequencies of 12 Hz and 50 Hz, respectively. The raw EMG data was pre-amplified and high-pass filtered using fourth-order, zero lag, recursive Butterworth filter with a cutoff frequency of 10Hz to remove artifact from movement. The signal was then full-wave rectified. The full-wave rectified signal was low pass filtered with a cutoff frequency of 5 Hz to create a linear envelope and normalized to the MVICs of the individual muscles. The linear envelope was then integrated over duration the rising phase.

A kinematic model comprised of the dominant side pelvis, thighs, shanks, and feet segments was created from the standing calibration trial [4]. Sagittal plane ankle, knee, and hip angles were calculated using a joint coordinate system approach [5]. From here, inverse dynamics was applied to calculate joint moment of force and secondary calculations were made for joint work and angular impulse. [6]

Separate one-way ANOVAs were conducted for each dependent variable with foot positions as the independent variable. Multiple comparisons were performed with the Bonferroni correction method between foot positions and individual kinetic, energetic and EMG dependent variables. Significance was set a priori at $p < 0.05$.

RESULTS AND DISCUSSION

Seven significant differences were found in the dependent variables. The result of a posterior shift of feet ultimately changed the linkages between the ankle, knee and hip joints. As the knee joint flexion angle increased, significant increases in joint work occurred in the ankle and knee with a subsequent significant decrease in the hip. This is indicative that the distribution of joint work for the STS will increase the energetic demand of the knee extensors and ankle plantar flexors while decreasing the demand of the hip extensors. As the feet

shift back, the base of support is now closer to the COM. This may explain why the hip joint experienced a decrease in work since there is a smaller range of motion which requires less time to move the COM over the base of support. As for the ankle joint, it is possible that shifting the feet back increased the initial dorsiflexion angle resulting in the increased range of motion resulting in increased work. As the knee joint increases flexion, there is a greater range of motion to be achieved thus resulting in increased knee joint work. However, the knee joint angular impulse did not follow this pattern entirely.

To clarify joint loading, angular impulse was determined at the ankle knee and hip joints. As the knees flexed from 90-100° and then from 100-110° there were significant increases in ankle angular impulse with subsequent significant decreases in hip angular impulse. As for the knee, there was a mild decrease from 90-100° and then a slight increase from 100-110°. It is possible that the knee joint angular impulse remained constant due to the influence of trunk flexion. Increased trunk flexion will decrease the moment of force about the knee joint. Increasing trunk flexion is a strategy commonly used in those with quadriceps weakness to reduce the force at the knee. [7] The ankle joint experienced increased angular impulse in the negative direction suggesting that its primary role is absorbing force due to increased ankle dorsiflexion.

For iEMG, as the feet were shifted posteriorly, the only significant difference occurred in the biceps femoris and medial hamstring in the 90-100° condition. This is likely the result of the significant decrease in hip joint work and angular impulse. Although not significant, there was an increase in activity in the Soleus and Gastrocnemius with a subsequent decrease in the Tibialis Anterior as the feet shifted back.

The activity of the Vastus Lateralis, Vastus Medialis, and Rectus Femoris followed a similar pattern of the knee joint angular impulse. This may also be explained by the role trunk flexion.

CONCLUSIONS

This study investigated the role of shifting the feet posteriorly from a 90° knee bend to 110° in the STS on the accumulative lower body joint energetics and kinetics along with iEMG. The decrease in joint angular impulse at the hip and increase at the ankle shows similarity with the results of the distribution of joint work. The knee joint work increased accordingly with an increase in knee joint angle; however, this was not the case for knee joint angular impulse. Future work should measure trunk kinematics since the extensor moment arm can be decreased with increased trunk flexion. There were few significant outcomes from iEMG of the lower extremity muscles, revealing the total muscle activity does not necessarily correspond with the total energy and loading contributions. Future research should evaluate the effect of foot position on the ability to improve STS performance in those individuals with movement difficulties.

REFERENCES

1. Alexander et al. *J. Gerontol* **46**: 91-98, 1991.
2. Hirvensalo et al. *J. Am. Geriatr. Soc.* **48**: 493-8, 2000.
3. Khemlani et al. *Clinical Biomechanics* **14**:236-46, 1999.
4. Weinhandl et al. *J Appl Biomech.* **26**:444-53, 2010.
5. Grood & Suntay. *J Biomech Eng*, **105**:136-44, 1983.
6. Bresler & Frankel. *Trans ASME*, **72**, 27-36.
7. Papa & Cappozzo. *J Biomech* **33**:1113-22, 2000.

Table 1 Means and Standard Deviations Energetics and Kinetics				
Work (J/kg)	90 Degrees	100 Degrees	110 Degrees	
Ankle *†	0.049 ± 0.025	0.086 ± 0.039	0.146 ± 0.043	
Knee †**	0.486 ± 0.081	0.615 ± 0.129	0.752 ± 0.143	
Hip †**	0.668 ± 0.145	0.485 ± 0.171	0.351 ± 0.128	
Angular impulse (Nms/kg)	90 Degrees	100 Degrees	110 Degrees	
Ankle *†	-0.139 ± 0.042	-0.179 ± 0.045	-0.269 ± 0.086	
Knee	0.330 ± 0.142	0.312 ± 0.111	0.342 ± 0.097	
Hip ††	-0.395 ± 0.118	-0.266 ± 0.089	-0.215 ± 0.067	
Significant difference between (p<0.05)	† 90-100	* 100-110	‡ 90-110	

Table 2 Means and Standard Deviations Integrated electromyography				
iEMG (%MVIC)	90 Degrees	100 Degrees	110 Degrees	
Tibialis Anterior	0.070 ± 0.065	0.042 ± 0.029	0.036 ± 0.029	
Soleus	0.179 ± 0.101	0.251 ± 0.189	0.301 ± 0.188	
Gastrocnemius	0.088 ± 0.042	0.092 ± 0.055	0.130 ± 0.096	
Rectus Femoris	0.080 ± 0.057	0.074 ± 0.053	0.105 ± 0.081	
Vastus Lateralis	0.233 ± 0.133	0.207 ± 0.116	0.243 ± 0.119	
Vastus Medialis	0.344 ± 0.265	0.296 ± 0.185	0.320 ± 0.189	
Medial Hamstring †	0.064 ± 0.032	0.051 ± 0.031	0.106 ± 0.203	
Biceps Femoris †	0.095 ± 0.578	0.072 ± 0.048	0.074 ± 0.052	
Significant difference between (p<0.05)	† 90-100	* 100-110	‡ 90-110	

ALTERNATIVE FOOTWEAR'S INFLUENCE ON MUSCLE ACTIVATION PATTERNS OF THE LOWER LEG FOLLOWING A ONE MILE WALK

¹ Samuel J. Wilson, ²Harish Chander, ³Cody E. Morris, ¹John C. Garner, ¹Dwight E. Waddell, and ⁴Chip Wade

¹ The University of Mississippi, University, MS, USA

² Mississippi State University, Mississippi State, MS, USA

³ Georgia Regents University, Augusta, GA, USA

⁴ Auburn University, Auburn, AL, USA

email: sjwilso2@olemiss.edu, web: <http://hesrm.olemiss.edu>

INTRODUCTION

Falls are the third leading cause of unintentional death in homes and communities in the United States, causing 27,800 fatalities in 2012 [1]. The ability to maintain proper postural control is an essential part of activities of daily living (ADLs). However, recent types of alternative footwear may be placing the body's postural control system at an increased risk for perturbations to equilibrium and subsequent falls. The purpose of this study was to examine the effects of three forms of alternative footwear (thong style flip-flops (FF), clog style Crocs® (CC), and Vibram® Five-Fingers (MIN)) on postural control.

METHODS

Eighteen healthy male adults (age: 22.9±2.88 years; height: 179±6.0 cm; mass: 81.3±8.8 kg) with no history of neuro-musculoskeletal disorders participated in this study. Static balance measures were recorded using the six conditions of the Neurocom® sensory organization test (SOT) [eyes open (EO), eyes closed (EC), eyes open with sway referenced vision (EOSRV), eyes open with sway referenced support, (EOSRP), eyes closed with sway referenced support (ECSR), and eyes open with sway referenced vision and support (EOSRVP)]. Surface electromyography (EMG) signals were recorded from the right leg musculature: tibialis anterior (TA), and medial gastrocnemius (MG). The EMG signals were recorded using silver/silver chloride monopolar surface electrodes. The ground electrode was placed on the tibial plateau. The EMG was recorded using Noraxon® MyoResearch software (Noraxon U.S.A.

Inc. Scottsdale, AZ.). Raw EMG data were collected at 1,500 Hz, Band-pass filtered (20-250Hz) and rectified prior to analysis. Post acclimatization, participants performed isometric MVC of plantar flexion and dorsiflexion, preceding and after a one-mile self-controlled walk on a treadmill. Muscle Co-contraction index (CCI) (operationally defined as the simultaneous activation of two muscles) was calculated based on the ratio of the EMG activity of antagonist/agonist muscle pairs of the lower leg (TA/MG) using the following equation [2],

$$(\text{EMGS}/\text{EMGL}) \times (\text{LowerEMG} + \text{HigherEMG})$$

where EMGS was the level of activity in the less active muscle, and EMGL was the level of activity in the more active muscle. This ratio was multiplied by the sum of the activity found in the two muscles. This method has been used because it provides an estimate of the relative activation of the pair of muscles as well as the magnitude of the co-contraction. Results were analyzed in SPSS with a predetermined alpha level of 0.05 using a 2 x 3 [2 time measures (pre, post) x three footwear types (FF, CC, MIN)] repeated measures analysis of variance (ANOVA) for each of the SOT conditions. Pairwise comparisons with a Bonferroni correction were used to identify post-hoc differences if interaction or main effect significance were found. If at any point during analysis there was a violation of Mauchly's test of sphericity, a Greenhouse-Geisser correction was used to determine significance.

RESULTS

There is evidence of a significant interaction between footwear and time for CCI in the EOSRVP condition ($F(1.607, 27.322) = 3.684$, $p = 0.047$) (Figure 2). Moreover, plotting of the results suggests a potential reverse interaction, follow-up analyses using simple effects were conducted in an attempt to understand the nature of this interaction. Analyses showed that following the one mile walk, the MIN showed significantly greater CCI than the FF ($F(2,16) = 7.002$), $p = 0.007$) (Figure 3).

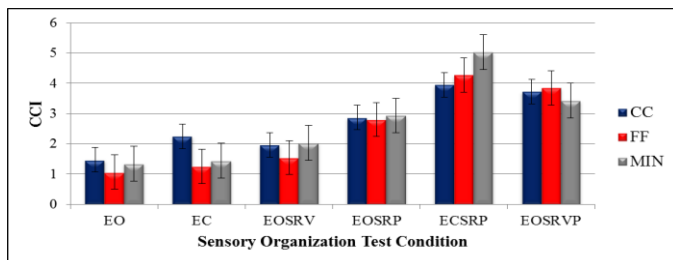


Figure 1: Co-contraction index before the one-mile walk. * represents a significant interaction, error bars represent standard error.

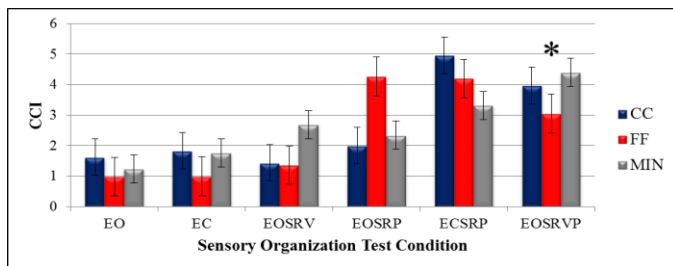


Figure 2: Co-contraction index following the one-mile walk. * represents a significant interaction, error bars represent standard error.

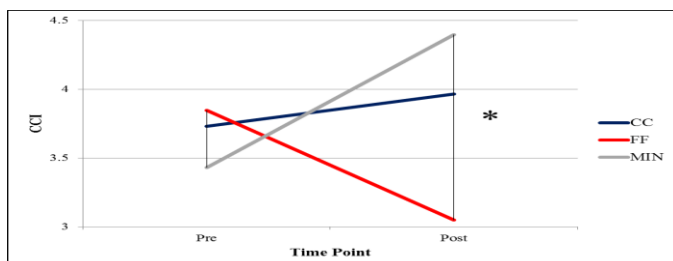


Figure 3: Plotted footwear by time interaction observed in the EOSRVP condition. * represents simple effect significance.

DISCUSSION

Previous literature has suggested that when proprioceptive feedback at the ankle becomes less reliable due to age related effects, there is an adoption of a new co-contraction strategy for maintaining postural stability [3]. This study adds to this notion, and suggests that different footwear characteristics could potentially cause a fatigue effect, and decline in proprioception at the ankle joint after a one-mile walk. This potential fatigue and shift in strategy may be explained in part by the increase in CCI observed currently, and may be exacerbated when other sensory information is also unreliable. This stiffening of the ankle joint, as opposed to relying on multiple sensory sources, may pose more of a threat to the individual's ability to stay stable, and subsequently lead to greater risk of a loss of balance and fall.

REFERENCES

1. National Safety Council. (2014). Injury Facts®, 2014 Edition. Itasca, IL.
2. Rudolph KS, Axe MJ, Buchanan TS, Scholz JP, & Snyder-Mackler L. (2001). Dynamic stability in the anterior cruciate ligament deficient knee. *Knee Surgery, Sports Traumatology, Arthroscopy*, 9(2), 62-71.
3. Benjuya N, Melzer I, & Kaplanski J. (2004). Aging-induced shifts from a reliance on sensory input to muscle cocontraction during balanced standing. *The Journals of Gerontology Series A: Biological Sciences and Medical Sciences*, 59(2), M166-M171.

ACKNOWLEDGEMENTS

Funding for this project was provided by the University of Mississippi Graduate Student Council Research Grant.

A BIOMECHANICAL MODEL TO PERSONALIZE AFO FOOTPLATES TO PROMOTE NATURAL SHANK KINEMATICS WITH LIMITED DORSIFLEXION

Elisa S. Arch, Bretta L. Fylstra, and Travis R. Pollen

University of Delaware, Newark, DE, USA

email: schranke@udel.edu, web: <http://www.udel.edu/chs/facultystaff/arch.html>

INTRODUCTION

A primary purpose of gait is to move the body forward in space. During the stance phase, the kinematics of the shank are critical for achieving sufficient, yet controlled, forward progression [1]. Shank kinematics are a function of ankle angle and foot-to-floor motion [2]. Thus, individuals with limited dorsiflexion range of motion (ROM) often have impaired shank kinematics. Owen developed an algorithm for tuning ankle-foot orthosis (AFO) and footwear alignment to achieve typical shank-to-vertical angle during midstance in an effort to promote forward progression during gait [1]. However, via this technique the ankle is locked in a static position, regardless of if the individual has some dorsiflexion ROM, and forward progression is achieved as the thigh and proximal segments progress over the shank-foot system [1].

As an alternative, AFOs with footplate toe rockers may be able to promote natural shank kinematics by replacing the impaired dorsiflexion with foot-to-floor motion. This approach will still utilize the individual's available dorsiflexion ROM and then engage the toe rocker when maximum dorsiflexion is reached, continuing to enable forward progression as the foot rocks over the ground. Algorithms by Owen include the use of rockers incorporated into the shoes, but proposed rockers are primarily designed for use during late stance with AFOs that inhibit all dorsiflexion [1]. Other studies have explored the influence of various rocker designs on pressure distribution or gait variables [3]; however to our knowledge, no study has proposed a quantitative model to personalize the toe rocker based on an individual's dorsiflexion limitation. The purpose of this study was to develop a biomechanical model to guide AFO footplate toe

rocker personalization to promote typical shank kinematics for individuals with limited dorsiflexion.

METHODS

A biomechanical model was developed to predict ankle joint center (AJC) and knee joint center (KJC) sagittal plane trajectories, which together determine shank kinematics, based on subject anthropometrics and footplate toe rocker design (start location and radius of curvature) (Eq 1-5; Fig. 1). The model predicts AJC and KJC trajectories from the time when the dorsiflexion ROM limit would be reached in typical gait until the end of stance.

$$AJC_y = H \sin \theta + (D + R\theta) - (D + L) \cos \theta \quad (1)$$

$$AJC_z = H \cos \theta + (D + L) \sin \theta \quad (2)$$

$$\text{where } L = 2 * R \sin(\theta/2) \quad (3)$$

$$KJC_y = AJC_y + S \sin(\theta + \alpha) \quad (4)$$

$$KJC_z = AJC_z + S \cos(\theta + \alpha) \quad (5)$$

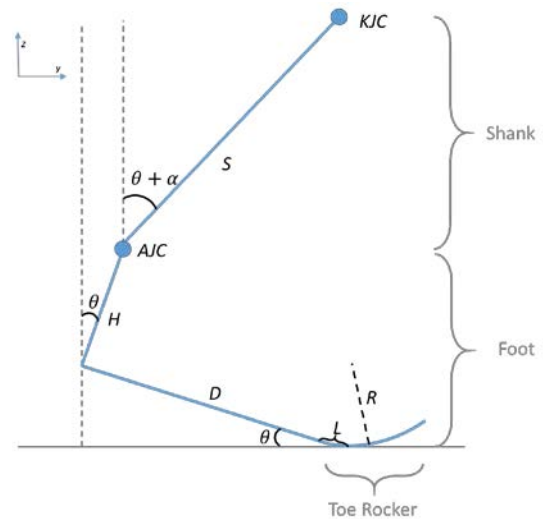


Figure 1: Schematic of shank kinematics with a personalized AFO footplate model.

Using this model, the toe rocker design that enabled the most typical shank kinematics was determined for three limited dorsiflexion ROM conditions (0°, 5°, 10° motion). For each condition, the toe rocker

start location (D) was set to the typical location of the center of pressure when the ankle angle reached its limit. Average typical, adult anthropometrics from our lab's database were used to determine ankle height (H) and shank length (S). Dorsiflexion angle (α) was held constant at its ROM limit (0° , 5° or 10°) until late stance, when it was allowed to decrease back to 0° . The progression angle (θ) was input to move the shank-foot system through a typical excursion. Then, AJC and KJC trajectories were calculated and compared to typical AJC and KJC trajectories for an average, comfortable walking speed (0.8 statures/second) [2]. The toe rocker radius of curvature (R) was iteratively adjusted until the model-predicted AJC and KJC trajectories best mimicked typical trajectories.

RESULTS AND DISCUSSION

The model identified toe rocker designs that are predicted to enable nearly typical shank kinematics for each of the three limited dorsiflexion ROM conditions (Fig. 2). The toe rocker start location was set to approximately 43%, 17% and 10% foot length and the radius of curvature was set to approximately 33%, 61% and 69% foot length for the 0° , 5° and 10° dorsiflexion conditions, respectively.

Future studies will experimentally evaluate model predictions. Furthermore, while this model suggests

that personalized AFO footplates can help preserve natural shank kinematics, it is not yet known how replacing ankle motion with foot-to-floor motion will influence the kinetics and energetics of gait.

CONCLUSIONS

This study successfully developed a model to predict how to personalized AFO footplate toe rockers to promote natural shank kinematics for individuals with varying dorsiflexion ROM limitations. Ultimately, we aim to implement this model to rapidly and effectively personalize AFO footplates to improve gait function for individuals with limited ankle ROM. Combining personalized AFO footplates with AFO bending stiffness [4], which can control the rotational velocity of the shank during available dorsiflexion for individuals who also have plantar flexor weakness, may provide meaningful enhancements in the gait function and mobility for individuals with ankle joint impairments.

REFERENCES

1. Owen E. *Prosthet Orthot Int* **34**, 254-269, 2010.
2. Pollen TR, et al. *Proceedings of ASB 2015*, Columbus, OH, USA, *submitted*.
3. Hutchins S, et al. *The Foot* **19**, 165-170, 2009.
4. Arch ES, et al. *Proceedings of WCB 2015*, Boston, MA, USA.

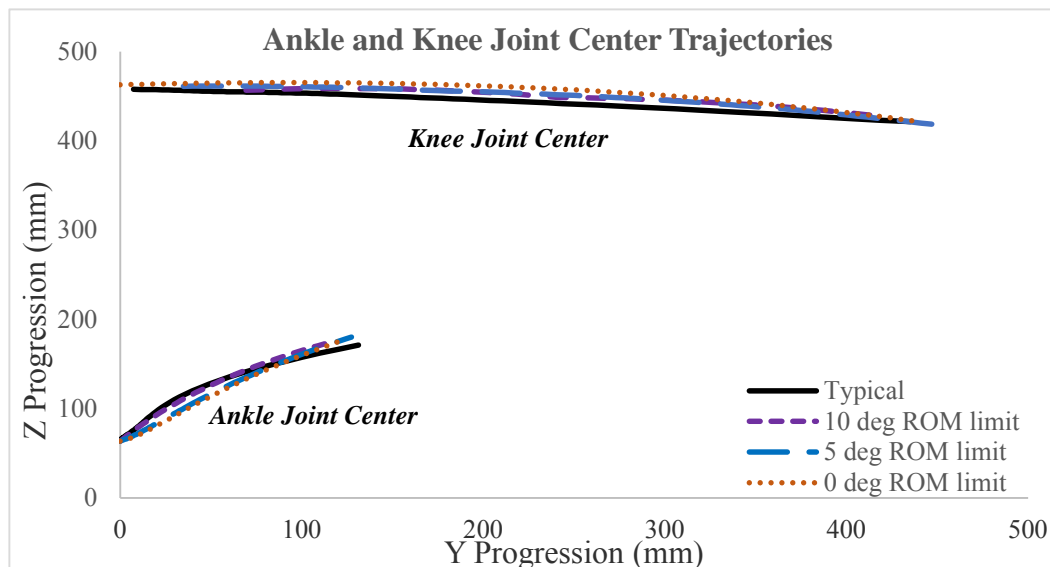


Figure 2: AJC and KJC Trajectory Predictions. With personalized toe rocker characteristics, shank kinematics (AJC and KJC trajectories) were able to be closely mimicked for all three limited dorsiflexion conditions (0° , 5° and 10° ROM).

BIOMECHANICAL ANALYSIS OF TWO NOVEL TAPERED HIP SCREW SYSTEMS

Timothy J. Ashworth¹, Andrew G. Tsai², Patrick Getty³, Randall Marcus², Ozan Akkus^{2,4,5}

¹Case Western Reserve University, School of Medicine, Cleveland, OH, USA

²Case Western Reserve University, School of Medicine, Department of Orthopaedics, Cleveland, OH, USA

³University of Chicago, Chicago, IL, USA

⁴Case Western Reserve University, Department of Mechanical and Aerospace Engineering, Musculoskeletal Materials and Mechanics Laboratory, Cleveland, OH, USA

⁵Case Western Reserve University, Department of Biomedical Engineering, Cleveland, OH, USA

Email: tja40@case.edu

INTRODUCTION

Femoral neck fractures are commonly repaired using percutaneous cannulated lag screws. Unfortunately these fractures are still associated with high rates of complications including osteonecrosis of the femoral head (15-45%), nonunion (10-30%) and iatrogenic subtrochanteric fractures (ISF, 2-4%) [1, 2]. Minimal gaps and good stability are essential to reduce the incidence of osteonecrosis and nonunion [1]. Little is known about the etiology of ISFs other than they typically occur through the lowest screw hole and lower hole placement seems to increase this risk [3]. We postulated that the stress risers caused by lag screw heads impinging on the lateral cortex could lead to ISF. We also hypothesized that these high local stresses could cause a settling effect that would lead to loosening at the fracture surface. The present study investigates the use of two novel tapered screw systems in an attempt to spread the load over a larger area to reduce the stress riser effect and minimize settling of the screw head.

METHODS

Two types of tapered screws were designed based on the geometry of traditional lag screws, the head of the screw being replaced with a conical taper (Fig. 1). One screw had a long, shallow taper (long tapered screw) while the other had a short, steep taper (short tapered screw). These screws were used to create two novel screw systems, both using three screws arranged in an upside-down triangle configuration [4]. One system used long tapered screws at all three positions (3 Long System) while the second system used two short tapered screws at the two superior positions and one long tapered screw at the inferior position (1 Short 1 Long System). These systems were compared to the current standard using three

traditional lag screws (3 Lag System). All screws, including traditional lag screws, were custom manufactured from 316L stainless steel. Ten synthetic, fourth generation Sawbones® femur models were used to test the screws.



Figure 1: The three types of screws in this study are the traditional lag screw (top), long tapered screw (middle) and short tapered screw (bottom).

Each femur was cut 15.5 cm distal to the lesser trochanter and potted in PMMA. Three 5.0 mm holes were drilled in identical locations from the lateral proximal cortex in an upside-down triangle configuration with each hole oriented through the femoral neck. Femurs used for testing tapered screws were reamed using custom reamers with the same angle as the taper on the screws. Femoral necks were cut uniformly using an industrial band saw. Screws were tightened to achieve uniform pretension, which involved each screw type being tightened to a different torque due to unique head geometry. Femurs were loaded at the femoral head using a computer-directed algorithm that consisted of 1) a linear ramp from 20 to 750 N and back, 2) 500 sinusoidal cycles between 188 and 1875 N and 3) a linear ramp from 20 to 750 N and back. Load displacement data were recorded for steps 1) and 3) to evaluate pre and post-cyclic loading stiffness and post-cyclic loading permanent displacement of the femoral head.

Finite element analysis (FEA) mimicking mechanical testing was performed using a femur model with geometry identical to that of the synthetic femurs to predict stiffness values and strain distributions in the proximal femur [5]. Addition of the abductor muscles at the greater trochanter has been shown to yield more accurate FEA results than a joint load alone, so FEA including abductors was performed as a supplement [6].

RESULTS AND DISCUSSION

Results of mechanical tests are shown (Table 1, Fig. 2, Fig. 3). There was no difference in permanent displacement of the femoral head in any system.

Table 1: Results for FEA. Percentages are relative to the 3 Lag System.

FEA: joint force only		
	3 Long	2 Short 1 Long
Stiffness	-10.4%	5.4%
Strain at inferior hole	-9.1%	-4.2%
FEA: joint force + abductors		
	3 Long	2 Short 1 Long
Stiffness	-10.3%	2.9%
Strain at inferior hole	-5.3%	-2.9%

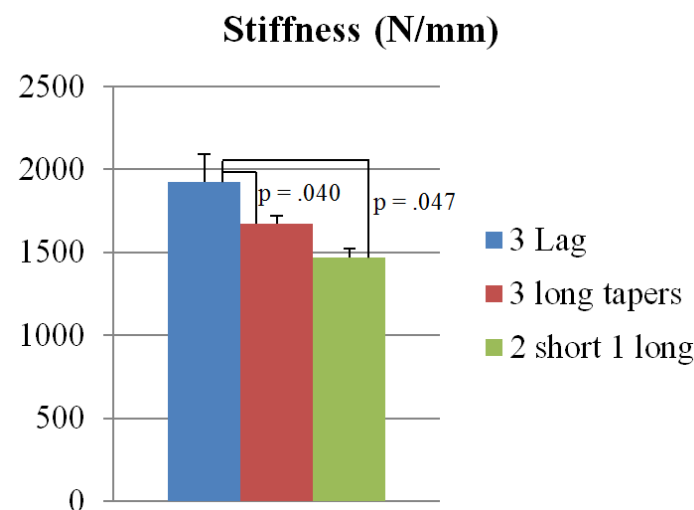


Figure 2: Bar graph showing stiffness following cyclic loading. Standard deviation whiskers and p-values are shown.

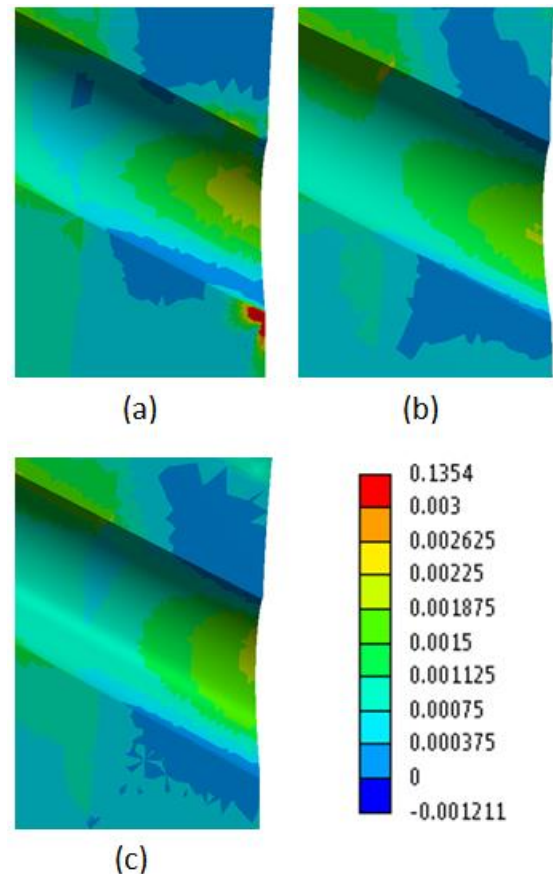


Figure 3: FEA showing a coronal section of first principal strain at the inferior hole in the a) 3 Lag, b) 3 Long and c) 2 Short 1 Long Systems.

FEA showed that the tapered screw systems eliminate the strain riser caused by the impinging traditional lag screw head and decrease strains at the sides of this hole, which may reduce the incidence of ISF. However, they also decrease the stiffness of the repaired femur which may increase the rates of the more common complications of osteonecrosis and nonunion. Therefore neither of these systems can be recommended to replace the current method using three traditional lag screws.

REFERENCES

1. Wu CC. Chang Gung Med J. 2010;33(3):241-251.
2. Yang JJ et al. J Bone Joint Surg Am. 2013;95(1):61-69.
3. Hickey B et al. ANZ J Surg. 2014;84(4):245-248.
4. Oakey JW et al. Clin Orthop Relat Res. 2006;443:302-306.
5. Papini M. 3rd generation composite femur, the solid model, from: the BEL Repos
6. Stolk J et al. J Biomech. 2001;34(7):917-926.

Techniques used to optimize wheelchair propulsion startup

Sarah Bass^{1,2} and Alicia M. Koontz, Ph.D, RET^{1,2}

¹Human Engineering Research Laboratory, Department of Veterans Affairs, Pittsburgh, PA;

²Department of Rehabilitation Science and Technology, University of Pittsburgh, Pittsburgh, PA;

Email: srb94@pitt.edu

INTRODUCTION

Manual wheelchair users with spinal cord injuries (SCI) rely heavily on their upper extremities for independence in their home and community. Wheelchair propulsion along with wheelchair transfers have been linked to upper extremity pain and injury [1]. In addition, wheelchair propulsion has been shown to be generally inefficient with a reported gross mechanical efficiency around 10-12% [2]. Startup is an important aspect of wheelchair propulsion, yet little is known about how to optimize the first strokes to achieve the highest possible efficiency. The average wheelchair user spends more time during the day starting and stopping their wheelchair than in constant propulsion motion [3]. The purpose of this study was to better understand the relationship between terminal velocity and aspects of startup propulsion technique such as pushrim start and release angles, time spent on the pushrim and force variables. Terminal velocity is defined as the highest velocity attained by a person during any one wheelchair stroke.

METHODS

Subjects

Twenty nine subjects were recruited to participate in the study and all signed informed consent forms. The inclusion criteria for the study were: between the ages of 18 and 65, has a neurological impairment secondary to a spinal cord injury, the injury occurring after the age of 18, at least one year post injury, use a manual wheelchair as a primary means of mobility (over 40 hours per week) and the wheelchair has wheels with a 24 or 26 inch diameter. Exclusion criteria for the study were: women of childbearing age who are pregnant, having a history of fractures or dislocations in the arms including the shoulder, wrist and elbow, experience arm pain that interfered with propulsion and a wheelchair without quick release wheels.

Biomechanics Measurement

Kinetic data were collected using a SmartWheel® (Out-Front, Mesa, AZ), an instrumented hand rim

that measures three dimensional forces and moments. The SmartWheel® was placed on the non-dominant side of the wheelchair and a dummy wheel of identical size and tread to maintain symmetry was placed on the dominant side. Kinetic data were collected at 240 Hz and filtered with an 8th order Butterworth low-pass filter, zero lag, and 20 Hz cutoff frequency. Data were down sampled to 120 Hz to align with kinematic data, which were collected at 120 Hz using a 20-camera VICON motion-capture system (Vicon Peak, Lake Forest, CA) surrounding a Figure-8 course. Reflective markers were placed on the center hub of the SmartWheel and on various bony landmarks on the head, trunk and arms to create a coordinate system with respect to the global reference frame.

Experimental Protocol

Participants used their personal wheelchairs to propel over level ground in a figure eight pattern (Figure 1). Each participant started at the center of the figure eight and was instructed to propel around a cone set at 9m from the center. Once back in the center they were told to come to a dead stop before propelling to the opposite cone. Participants propelled for one minute at a maximum self-selected speed while data were collected.

Data Analysis

Data was analyzed using Matlab (Mathworks Inc., Natick, MA, USA). Strokes were identified using a custom Matlab program. The wheelchair stroke was separated into two phases, push and recovery using the forces and moments about the hub as indicators of when the hand was on and off of the pushrim. The first five strokes performed after every dead stop during the one minute trial were analyzed.

Start and release contact angles were calculated for each of the five strokes as well as time spent on and off of the pushrim. Contact angles were measured from the horizontal, with 90 degrees being at the top dead center of the wheel. Additionally, for each push phase peak mechanical effective force (MEF) and total force were calculated. Lastly, peak velocity was calculated during each propulsion

cycle. IBM SPSS version 21 was used for all statistical analysis. Pearson correlation was used to look at the relationship between terminal velocity and the other propulsion variables.

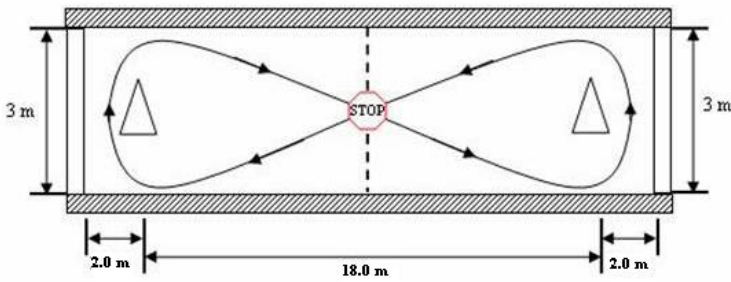


Figure 1. Figure eight course used in the study

RESULTS AND DISCUSSION

Twenty-five subjects, 17 males and 5 females, participated in this study. Their average age, weight, and duration of injury were 36 ± 10 years, 75.9 ± 20.9 kg and 12.9 ± 8.3 years, respectively. The levels of spinal cord injury ranged from C5 to L4.

For the first stroke, less time spent on the pushrim, greater total force, and a greater percentage of force directed tangentially to the pushrim (MEF) was significantly related to higher peak velocities (Table 1). However, for strokes two through four, more time spent on the pushrim and greater total force (strokes 2 and 4) was significantly related to higher

peak velocities. For the second startup stroke, more time in the recovery phase was also significantly related to higher terminal velocity. For stroke two, persons who released the pushrim closer to top dead center achieved higher terminal velocities. Applying more force over a shorter period of time (e.g. impulse) and higher mechanical effective force was significantly related to velocity for the first push stroke only. Greater overall force and longer push times appeared to be important to achieving higher velocities for the remainder of startup (strokes 2-4) while total force seemed to be the only factor linked to higher velocity for stroke 5 (steady-state propulsion). Thus if a person needs to get up to speed as quickly as possible (e.g. to cross a busy intersection or to race across a basketball court), he or she should try to minimize the time spent on the push rim for the first stroke, but increase their time on the pushrim during the strokes that follow. Spending more time on the pushrim allows for more time to impart force which facilitates higher velocities. This strategy may also lessen the impact of loading on the upper limbs [1].

REFERENCES

1. Boninger, M. L., et al. 2000. *Arch Phys Med Rehabil* **81**: 608-613
2. van der Woude LHV et al: *Am J Phys Med Rehabil* 2001;**80**:765-777
3. Tolerico ML, et al.. *J Rehabil Res Dev* **44**(4), 573-580. 2007

ACKNOWLEDGEMENTS Funding provided by VA Grant #B6252R. The contents of this paper do not represent the views of the Department of Veterans Affairs or the United States Government

Table 1: Means, standard deviations, correlation coefficients and p values for key variables calculated

	Stroke 1		Stroke 2		Stroke 3		Stroke 4		Stroke 5	
	M(std)	r p	M(std)	r p	M(std)	r p	M(std)	r p	M(std)	r p
Start Angle (°)	91.5(22.3)	-.072 .733	81.5(9.37)	-.337 .099	83.8(38.8)	-.0671 .75	96.0(45.3)	-.136 .526	87.7(33.4)	-.265 .221
End Angle (°)	.729(27.8)	.333 .103	1.73(19.2)	.406 .039*	-3.66(32.8)	-.160 .454	-8.98(53.8)	.004 .986	-10.8(36.5)	.060 .785
Push Time (s)	1.04(.333)	-.662 <.001**	1.17(.051)	.401 .042*	1.37(.064)	.442 .024*	1.57(.099)	.527 .006**	1.87(.108)	.201 .326
Recovery Time (s)	1.43(.118)	.287 .156	1.38 (.075)	.526 .006**	2.22(.874)	-.200 .327	1.25(.074)	.345 .085	1.28(.132)	.108 .599
Total Force(N)	118.7(41.1)	.542 .004**	107.3(34.5)	.627 .001**	113.9(41.9)	.335 .094	100.8(30.9)	.460 .018*	92.5(29.6)	.415 .035*
MEF	1.53(.162)	.400 .043*	1.53(.262)	-.003 .989	.931(.085)	.042 .840	1.01(.109)	-.146 .477	.907(.094)	.029 .887

*Significant at $\alpha = .05$, **Significant at $\alpha = .001$

RUNNING-SPECIFIC PROSTHESIS MODELING EFFECTS ON JOINT MOMENTS DURING OVERGROUND RUNNING

^{1,2} Brian S. Baum, ³ Hiroaki Hobara, ^{2,4} Jae Kun Shim

¹ Regis University, Denver, CO, USA

² University of Maryland, College Park, MD, USA

³ National Institute of Advanced Industrial Science and Technology, Tokyo, Japan

⁴ Kyung Hee University, Seoul, Korea

email: bbaum@regis.edu

INTRODUCTION

Gait analyses for individuals using running-specific prostheses (RSPs) are often performed by placing tracking markers arbitrarily on the RSP to define joint and segment positions. RSP marker placement affects foot model definitions and can alter lower extremity joint kinetic estimations. Running studies investigating RSPs have estimated the prosthetic limb “ankle” joint to be at the same relative position as the intact limb’s ankle joint [1] or the most acute point on the prosthesis curvature [1-3]. Using only one marker on the RSP may oversimplify keel motion and modeling RSPs as single rigid objects may not be appropriate since these devices can flex throughout their length. Using multiple markers to create multisegmented RSP models is challenging since definitive joint axes may not exist and anthropometric assumptions may induce critical errors. Considering an RSP as a unified deformable segment can accurately estimate the total power of below-knee prosthetic components [4], but this method is limited to stance phase calculations and cannot provide kinetic estimations within the RSP. The aim of this study was to investigate the effect of RSP marker placement on peak lower extremity joint moments during overground running. We hypothesized that marker placement on RSPs would not affect peak knee and hip joint moment estimations, but the RSP “ankle” definition would affect the peak prosthetic “ankle” moments.

METHODS

Eight male subjects with unilateral transtibial amputation volunteered to run around a 100m long track at 3.5m/s. Prior to running, reflective markers were placed on standard lower extremity anatomical

positions for gait analysis. Eight markers were then fixed on the prosthetic keels (Figure 1), including the most proximal (“head”) and distal (“toe”) points of the keel along with the point of most acute curvature. Markers were placed laterally and medially at the base of the most proximal linear segment of each prosthesis. Three markers were evenly distributed on the lateral keels between the most acute point and the RSP toe. Prosthesis subsegments were considered rigid and defined via the keel markers. Body segment anthropometric and inertial properties were estimated with regression equations [5]. RSP inertial properties were measured [6] and RSP subsegment inertial properties were then estimated [7]. A 10-camera motion capture system (Vicon, Centennial, CO) captured marker positional data at 200Hz while 10 forceplates (Kistler, Amherst, NY) embedded in the track collected ground reaction forces at 1000Hz.

Four RSP foot models were defined by different marker combinations (Fig. 1). Model effects on joint moment outputs were compared for each subject. Joint moments were calculated using standard inverse dynamics equations with Visual3D software (C-Motion, Germantown, MD). The resultant “ankle,” knee, and hip joint peak moments were compared across models. A one-way repeated measures ANOVA was used to test for peak moment differences between models with $\alpha=0.05$.

RESULTS

Sagittal plane joint moment profiles are presented in Fig. 2. Model differences were evident between Models 1, 2, and 3 for peak ankle plantarflexion moments ($P\leq 0.006$). No differences were observed between models for stance phase peak knee and hip

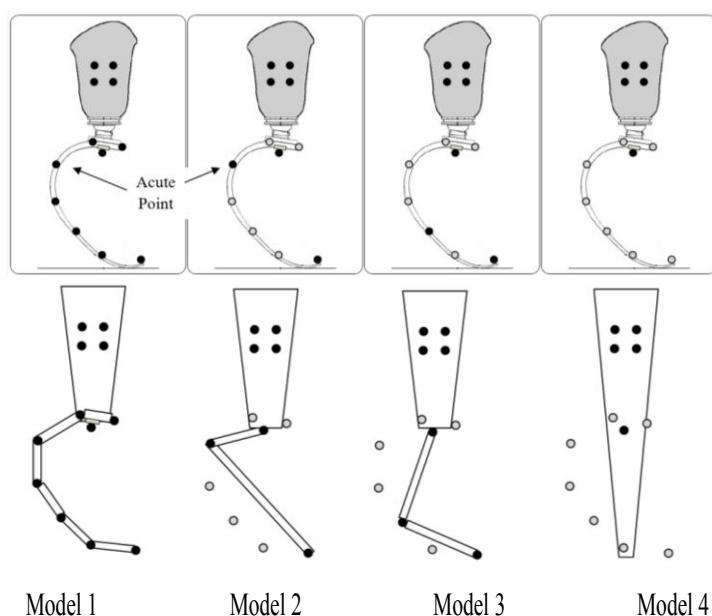


Figure 1: Marker placements and model definitions for running-specific prostheses. Filled dots represent markers used to define each model.

extension moments. For peak swing phase knee flexion and hip extension moments, Models 1, 2, and 3 significantly differed from each other ($P \leq 0.027$). No significant differences existed between any of the models for any peak varus or valgus moments during stance or swing phase. Models 1 and 3 significantly differed for stance phase peak knee external rotation moments ($P = 0.001$) and swing phase knee internal rotation moments ($P = 0.009$). In both cases, these variables differed on average by only 0.003 Nm/kg.

DISCUSSION AND CONCLUSIONS

These data partially support and partially reject the hypothesis that the number of markers and their placement on the keel of RSPs do not significantly affect the residual limb joint moment estimations. With the exception of the peak knee external rotation moment, stance phase moments at the knee and hip joints were not affected by marker placement and modeling of the prosthetic foot. As expected, the RSP “ankle” joint plantarflexion moments during running stance were sensitive to the marker placement and definition of the ankle joint in the prosthetic limb. Marker placement on RSP keels has little effect on knee and hip joint moments, especially during stance phase. “Ankle”

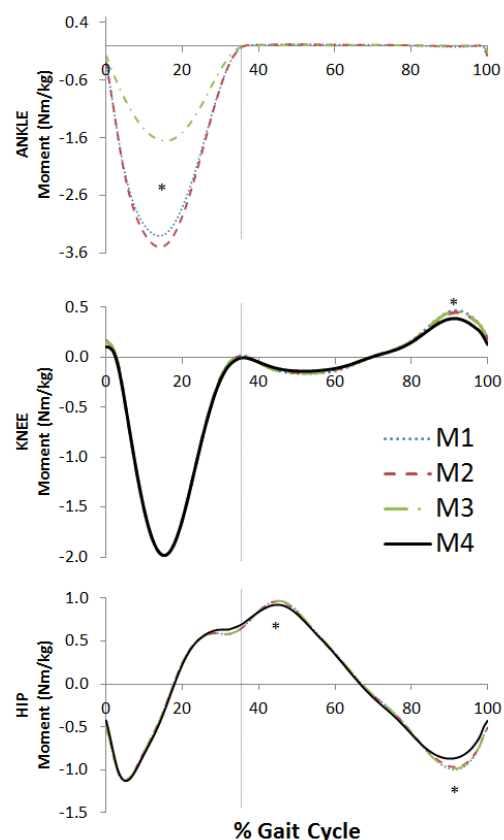


Figure 2: Sagittal plane ankle, knee, and hip joint moment results for each model (M1-M4). Dorsiflexion and flexion moments are positive. * indicates significant model differences for the peak.

plantarflexion moments, however, can differ substantially based on marker placement. For consistency and flexibility in modeling, we recommend placing markers according to prosthesis architecture rather than intact limb architecture.

REFERENCES

1. Buckley JG. *Clin Biomech* **15**, 352-358, 2000.
2. Buckley JG. *Arch Phys Med Rehabil* **80**, 501-508, 1999.
3. Burkett B, et al. *Prosthet Orthot Int* **27**, 36-47, 2003.
4. Takahashi KZ, et al. *J Biomech* **45**, 2662-2667, 2012.
5. Dempster WT. Wright-Patterson Air Force Base, Ohio, 1955.
6. Baum BS, et al. *Arch Phys Med Rehabil* **94**, 1776-1783, 2013.
7. Baum BS. Dissertation, University of Maryland, College Park, MD, 2012.

SPATIOTEMPORAL AND METABOLIC IMPACTS ON GAIT OF A POWERED ANKLE EXOSKELETON IN PERSONS WITH MULTIPLE SCLEROSIS

¹Morgan K. Boes, ²Rachel E. Klaren, ³Richard M. Kesler, ⁴Mazharul Islam, ²Yvonne Learmonth, ^{4,5}Matthew N. Petrucci, ²Robert W. Motl, and ^{1,4}Elizabeth T. Hsiao-Wecksler

¹Dept. of Bioengineering, ²Dept. of Kinesiology and Community Health, ³Illinois Fire Service Institute, ⁴Dept. of Mechanical Science and Engineering, ⁵Neuroscience Program
University of Illinois at Urbana-Champaign, Urbana, IL, USA
email: mboes2@illinois.edu, web: <http://hdcl.mechanical.illinois.edu/>

INTRODUCTION

Traditional ankle-foot orthoses (AFOs) often fail to restore normal ankle function because they lack the ability to actively modulate motion control during gait and cannot produce propulsion torque and power. A test bed of a portable, powered ankle-foot orthosis (PPAFO) has been developed to explore the issues and challenges related to creating mobile actively-powered orthotic devices [1].

In this study, we used the PPAFO test bed to further understand the functional needs and constraints of an active ankle assist device in a population of persons with gait impairment and Multiple Sclerosis (MS). The major disease process of MS is characterized by demyelination lesions of the white matter of the brain stem, cerebellum, and spinal cord [2] resulting in lower limb weakness leading to gait impairment [3]. Passive AFOs are often used clinically to assist with foot drop due to lower limb weakness in persons with MS, but have shown mixed results when analyzed in a research setting [4, 5]. An active AFO that can provide bidirectional powered assistance (dorsiflexor and plantarflexor torque) could be beneficial to persons with MS by helping to overcome their gait impairment.

METHODS

The study included 15 participants with a neurologist-confirmed diagnosis of MS and daily use of a prescribed custom passive AFO for gait assistance (11 Female/4 Males, age: 54.3 ± 5.3 years, Expanded Disability Status Score (EDSS): 5.2 ± 1.1). Approval for the study was granted by the Institutional Review Board and participants gave informed consent.

First, a clinical examination of disability was performed to establish EDSS score. Participants completed three standard 6-minute walk (6MW) tests that were performed over-ground in a hallway with four 90-degree turns. One 6MW was completed per footwear condition: *shoes*, *AFO*, and *PPAFO*. The PPAFO was worn on the affected limb (i.e. the same side as their AFO) with a normal walking shoe on the contralateral limb. Participants first wore the PPAFO for an adaptation period (>10 min) where their gait pattern was programmed into the PPAFO controller. The *shoes* condition 6MW was always completed first as a baseline. The remaining two conditions (*AFO* and *PPAFO*) were randomized between subjects with 10-minute periods of recovery between walks.

Multiple parameters of interest were collected during each 6MW. Spatiotemporal parameters of gait were measured as the participant passed over a 29 ft gait mat (GAITRite, Sparta, NJ) with each lap (≥ 4 passes). Average values of *stride length*, *stride width*, and *stride velocity* for each participant were calculated. The total *6MW distance* traveled was recorded with a measuring wheel. Oxygen consumption (VO_2) was measured breath-by-breath using a commercially available portable metabolic unit (K4b2 Cosmed, Italy). VO_2 (mL/kg/min) was measured as 30-second averages for 1 minute before the 6MW (resting VO_2) and over the entire 6MW. Net steady-state VO_2 was computed from average VO_2 values of the final 3 minutes of the 6 MW and subtracting average resting VO_2 . The *O_2 cost of walking* was then computed by dividing net steady-state VO_2 by walking speed during the 6MW [6].

Since multiple variables (*stride length*, *width*, *velocity*, *6MW distance*, *O_2 cost*) were examined,

repeated-measures MANOVA tests* (SPSS Inc., Chicago, IL) were used to compare parameters across **footwear** conditions (shoes, AFO, and PPAFO) and between EDSS **groups** ($\alpha = 0.05$). Follow-up univariate ANOVAs were performed on significant variables. Post-hoc examination of data suggested distinct differences due severity of disability; therefore participants were binned into two groups based on EDSS (moderate: ≤ 5.5 ; severe: ≥ 6.0). *Accounting for 6MW distance and O_2 cost data missing for one participant.

RESULTS AND DISCUSSION

The MANOVA tests found significant main and interaction effects for all variables ($p < 0.05$, Fig. 1). Significant main effects for **footwear** and **group** were found for *stride length*, *stride velocity*, and *6MW distance*. Only **group** was significantly different for *O_2 cost of walking*. Significant interactions of **group** \times **footwear** were found for *stride length*, and *stride width*.

Follow-up univariate ANOVAs indicated that PPAFO use resulted in shorter *stride length*, slower *stride velocity*, and a shorter *6MW distance* than a custom AFO, especially in the moderate group compared to the severe group. The moderate group also widened their *stride width* in response to the PPAFO, whereas the severe group showed no change based on footwear. Also in agreement with previous research, regardless of footwear, the moderate group had longer and faster strides, and longer *6MW distances* than the severe group [7, 8]. The *O_2 cost of walking* was greater for the severe group than the moderate group, and footwear did

not result in a significant change in the metabolic cost of walking.

CONCLUSIONS

These results indicate that within this study design, the participants did not overcome their gait impairment while using the PPAFO. Yet, the PPAFO did not negatively impact *O_2 cost of walking*. The hypothesized impact of the PPAFO providing gait assistance was not realized in this study and could be due to any number of factors, such as a need for more training and experience walking with the PPAFO, fatigue, or a need for improved device design.

REFERENCES

1. Shorter, KA, et al. *JRRD* **48**: 459-72, 2011.
2. Noseworthy, JH, et al. *New Engl J Med* **343**(13): 938-52, 2000.
3. Motl, RW. *Phys Med Rehabil Clin N Am* **24**(2): 325-36, 2013.
4. Sheffler, LR, et al. *Am J Phys Med Rehabil* **87**(1): 26-32, 2008.
5. Bregman, DJ, et al. *Gait Posture* **35**(1): 148-53, 2012.
6. Waters, RL and S Mulroy. *Gait Posture* **9**(3): 207-31, 1999.
7. Sosnoff, JJ, et al. *Arch Phys Med Rehabil* **92**(12): 2028-33, 2011.
8. Pilutti, LA, et al. *J Neurol Sci* **334**(1-2): 72-6, 2013.

ACKNOWLEDGEMENTS

Funding support was from the NSF Engineering Research Center for Compact and Efficient Fluid Power (0540834) and the Foundation of the Consortium of Multiple Sclerosis Centers' MS Workforce of the Future program. This work was made possible by help from Ziming Wang and undergraduates in the HDCL at UIUC.

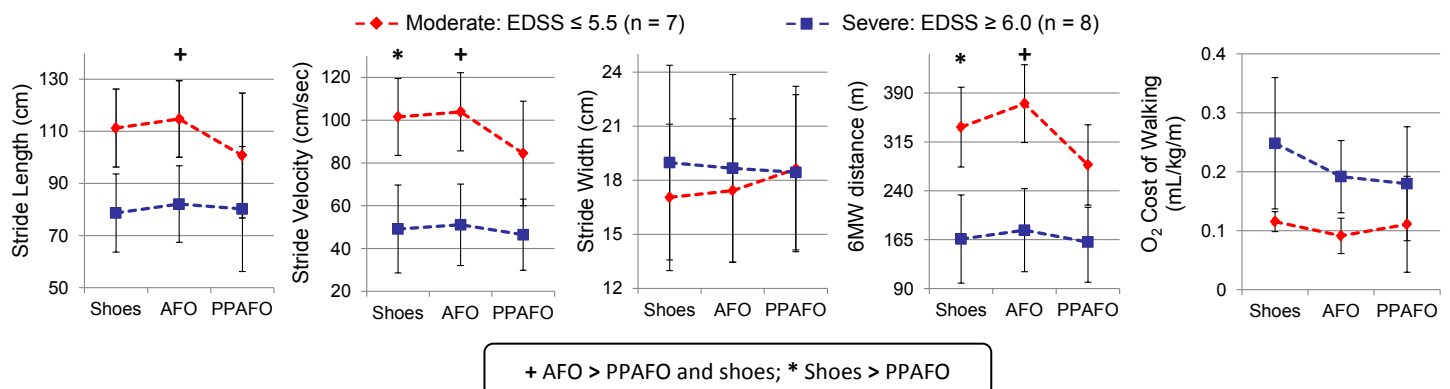


Fig.1. Spatiotemporal gait parameters and 6 minute walk outcomes for 15 persons with MS in three footwear conditions: shoe, AFO, or PPAFO. The *O_2 cost of walking* was not significantly different between **footwear** even though spatiotemporal parameters varied. Disability **group** differences were significant for all parameters except *stride width*.

A STRENGTHENING PROGRAM DESIGNED TO MINIMIZE KNEE LOADS IN WOMEN WITH KNEE OSTEOARTHRITIS: A PROOF-OF-PRINCIPLE STUDY

Elora C. Brenneman, Alexander B. Kuntz, Emily G. Wiebenga, and Monica R. Maly

¹McMaster University, Hamilton, ON, Canada
Corresponding email: mmaly@mcmaster.ca

INTRODUCTION

Exercise prescription is the cornerstone to knee osteoarthritis (OA) management. Physical exercise reduces symptoms and comorbidity while improving function in people with knee OA [1,2]. While strengthening exercise is often prescribed, the type of strength training for knee OA is still unknown.

The knee adduction moment (KAM) represents the ratio of medial (versus lateral) loading in the knee [3] and predicts knee OA progression [4]. Studies suggest that strengthening exercise does not change the KAM in people with knee OA [5,6]. It is probable, however, that using the KAM as a guide to identify appropriate exercise a priori for people with knee OA could reduce load exposure with strengthening exercise while aiming to improve clinical outcomes.

The purpose of this study was to test whether a 12-week strengthening program designed to minimize the KAM could improve symptoms, mobility, and strength in women with symptomatic knee OA. The secondary objective was to evaluate KAM and muscle amplitudes during static squat and lunge exercises from the program as well as peak KAM from gait.

METHODS

Participant eligibility was based on clinical criteria for knee OA from the American College of Rheumatology (ACR) [7]. Participants completed a lower extremity strengthening program designed to minimize the KAM for people with knee OA. Participants were asked to attend a supervised exercise class 3 times per week for 12 weeks. The program focused on lower extremity strengthening and hip mobility using a variety of squats and lunges. Following a warm-up of large range body movements against gravity, weight-bearing isometric exercises emphasizing quadriceps strengthening were used. To balance the targeted focus on the quadriceps, exercises to engage the

hamstrings and ankle plantarflexors were incorporated. Exercise modifications were available from the instructor.

All baseline and follow-up, measures reflected the most symptomatic knee. Self-reported symptoms and physical function were recorded using the Knee injury and Osteoarthritis Outcome Score (KOOS). Mobility was captured using the Six-Minute Walk Test (6MWT; distance covered in metres), the 30-second chair stand test (30-s CST; number of chair stands), and a stair ascent and descent task (timed in seconds). Lower extremity strength was captured during maximum voluntary isometric contractions (MVICs) of the knee extensors and knee flexors performed on a dynamometer (Biodex Medical Systems, Inc., Shirley, NY, USA) at 65 degrees of knee flexion. Values were normalized to body mass and expressed as Nm/kg.

The KAMs and muscle activations during static squats, static lunges, and gait were calculated from motion and force data. All kinematic, kinetic, and electromyography (EMG) data were time synchronized. Motion was captured using a 9-camera motion capture system collected at 100 Hz (Optotrak Certus, Northern Digital Inc., Waterloo, ON). Kinetic data were collected using a floor embedded force plate (OR6-7, AMTI, Watertown, MA) at 1000 Hz. KAM data were expressed relative to body mass (Nm/kg). EMG from the biceps femoris (BF), semitendinosus (S), rectus femoris (RF), vastus lateralis (VL), and the vastus medialis (VM) muscles were collected using a Desktop Telemyo DTS (Noraxon, Scottsdale, AZ). All EMG data had bias removed, were full-wave rectified, and linear enveloped using a 2nd order low-pass zero-lag Butterworth filter with a cutoff of 6 Hz. EMG data were normalized to %MVIC obtained from peak activation during the dynamometer MVICs.

For these motion analyses, squats included a legs-together squat (feet pointed forward and

shoulder-width apart) and a wide-legged squat (feet outside shoulder-width and externally rotated). For lunges, both the leading leg (front bent leg) and trailing leg (back straightened leg with the foot externally rotated on the floor) were examined. Squat and lunge trial data were extracted as a 3-second window of the static portion of the trial. An average of the two best trials were used. The peak KAM during each of the four best gait trials were extracted and ensemble averaged.

Paired t-tests evaluated group changes between baseline and follow-up of self-reported outcomes, mobility, and strength with an adjustment for multiple comparisons made with a Bonferroni correction ($p < 0.005$). Five separate one-factor repeated measures analysis of variance (ANOVA) were conducted to evaluate differences in EMG amplitudes between five muscles and four exercises.

RESULTS AND DISCUSSION

Forty-five women with clinical knee OA (mean age 60.3 ± 6.5 years) enrolled. Six dropouts were recorded. One participant was lost to co-intervention. Therefore data from 38 women were analyzed at follow-up. KAM and EMG data were analyzed for 36 participants due to equipment issues. Mean attendance was 2.6 classes per week.

Improvements were demonstrated in all 5 subscales of the KOOS, ranging from 16.0-42.5% ($p < 0.001$). Participants improved from 535.2 to 573.0 metres covered on the 6MWT ($p < 0.001$). Participants also improved on the 30-s CST but this difference was not significant after adjusting for multiple comparisons ($p > 0.005$). Stair ascent and descent time did not change. Participants improved strength in the knee extensors (1.8 to 1.9 Nm/kg; $p = 0.004$). No significant change occurred between baseline and follow-up in knee flexor strength ($p > 0.005$). KAMs during the four exercises tested were lower than that of normal gait ($p < 0.001$). Muscle activations from the exercises are displayed in Figure 1. Amplitudes ranged from 7.3-31.0 %MVIC across all exercises. There was a main effect of the intervention on the semitendinosus and rectus femoris muscles with decreased activation following the intervention for both muscles [$F(1.0, 506.3) = 4.30$, $p = 0.046$; $F(1.0, 471.0) = 4.51$, $p = 0.041$ respectively]. For all three quadriceps muscles, the squat exercises generated higher amplitudes than the lunge exercises ($p \leq 0.009$).

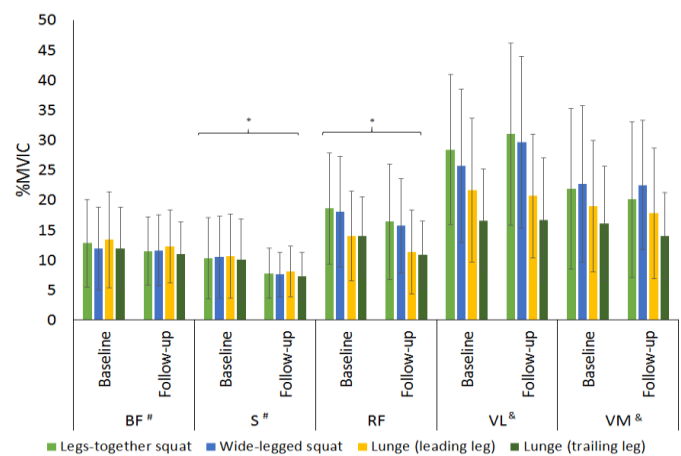


Figure 1: Muscle activations normalized to %MVIC for the four static exercises. Significant main effects are denoted with an asterisk (*).

These data show promise for the design of a strengthening program minimizing medial knee loads in women with knee OA. Our finding that KAM was unchanged after the intervention is consistent with the literature [4]. Although we did not expect KAM to change, we showed that utilizing KAM to guide exercise prescription can result in an improvements in clinical outcomes. Second, we demonstrated that achieving muscle amplitudes lower than those cited in the literature to elicit strength gains can improve isometric strength in women with knee OA.

CONCLUSIONS

This study showed that a strengthening program designed to minimize the KAM resulted in improvements in self-reported outcomes, mobility, and strength while appropriately activating lower limb musculature in women with knee OA.

REFERENCES

- [1] van Baar ME, et al. *Ann Rheum Dis*, 60, 1123-1130, 2001.
- [2] Zhang W, et al. *Osteoarthritis Cart*, 15, 981-1000, 2007.
- [3] Andriacchi TP. *Orthop Clin North Am*, 25, 395-408, 1994.
- [4] Chebab EF, et al. *Osteoarthritis Cart*, 22, 1833-1839, 2014.
- [5] Bennell KL, et al. *Osteoarthritis Cart*, 18, 621-628, 2010.
- [6] Foroughi N, et al. *Clin Biomech*. 26, 167-174, 2011.
- [7] Altman R, et al. *Arthritis Rheum*. 29, 1039-1049, 1986.

A PILOT PROGRAM TO DETERMINE INTRAMUSCULAR FAT PERCENTAGE IN THE QUADRICEPS AND HAMSTRINGS MUSCLES IN WOMEN WITH KNEE OSTEOARTHRITIS

¹Elora C. Brennehan, ¹Michael Davison, ¹Karen A. Beattie, ^{1,2}Jonathan Adachi, and ¹Monica R. Maly

¹McMaster University, Hamilton, ON, Canada

²St. Joseph's Healthcare, Hamilton, ON, Canada

Corresponding email: mmaly@mcmaster.ca

INTRODUCTION

Thigh muscle weakness is a trademark feature in knee osteoarthritis (OA). People with knee OA have demonstrated greater declines in thigh lean muscle mass beyond that typically seen with healthy aging [1]. Given that declines in thigh lean mass alone cannot directly explain OA-related declines in strength, muscle composition must also be considered.

Magnetic resonance imaging (MRI) is a useful tool for visualizing muscle. In the elderly, MRI scans of the lower limb were used to calculate muscle quality, or strength per unit of lean muscle mass. With aging, a loss of lean muscle mass is often accompanied with a concomitant increase in fatty infiltrates in the muscle belly. This issue is exemplified with obese elderly individuals who, despite having greater absolute lean muscle mass, demonstrated poor performance on dynamometer strength tests and mobility on the six-minute walk test [2]. With knee OA, fat in the muscle may play a role in the loss of physical function.

Manual and semi-automated image segmentation methods exist for examining tissue composition from MRI scans. However, there are two major limitations: 1) it is time consuming; and 2) pixel intensity thresholding is often subjectively chosen by the user, with little standardization between participants. Therefore, the primary aim of this study was to create a pilot program for calculating intramuscular fat percentage in the quadriceps and hamstrings muscle groups from MRI scans of the thigh from the most symptomatic knee in older women with knee OA. The secondary purpose was to determine a protocol for objectively choosing a pixel intensity threshold from the MRI image to complete image segmentation.

METHODS

Images of the thigh were used from a previous study explained in detail elsewhere [3]. Briefly, all

participants had radiographic and symptomatic knee OA as defined by the American College of Rheumatology [4]. A fixed-flexion, weight-bearing knee radiograph was acquired of each participant's most symptomatic knee [5]. Next, MRI scans were acquired of the thigh of the same knee using a GE Discovery MR750 3.0T scanner (WATER:AX PD IDEAL, axial plane, 512x512, 75 slices, 280 display of vie, 3mm slice thickness, slice gap 0, TE=31.512 ms, TR=2000 ms, echo train length = 6, bandwidth = 195.3 kHz, 1 NEX, scan time = 7.25 minutes). The most proximal slice was acquired at the 70% site (distance from the knee joint space to the lesser trochanter) and moved 180 mm distally. Post-processing Surface Coil Intensity Correction (SCIC) was used to improve image intensity homogeneity.

Gold Standard: All images were analyzed for intermuscular and intramuscular fat volumes using SliceOmatic 5.0 software by a single rater (MD) using traditional semi-automated segmentation techniques. Intermuscular fat refers to all fat within the fascial lining of the thigh exterior to the muscle and intramuscular fat is all fat present within a muscle belly. Percentage intramuscular and percentage intermuscular fat were calculated for each the quadriceps and hamstrings muscle groups from these volumes.

Pilot Program: The pilot program was created in Matlab (Mathworks, Inc., Natick, MA). Pilot data were compiled from 2 participants using the first 50 proximal slices from their scans (Participant 1 was 71 years and 98.4 kg; participant 2 was 66 years and 75.8 kg). For each slice, a histogram of the pixel intensities from the thigh region was created (Fig 1).

Next, a Lorentzian curve was fit to the muscle intensity spike (first peak of the histogram; Fig 1) and the fat intensity spike (second peak of the histogram; Fig 1). The peaks from each of these curves were extracted and thresholds between each

peak were normalized to 100% to create a new curve (0% as the peak of the muscle spike and 100% as the peak of the fat spike). At each percentage of this normalized curve, fat was separated from each muscle group using the corresponding threshold. A total percentage of fat from each muscle group was calculated creating 100 threshold cutoffs for each muscle group.

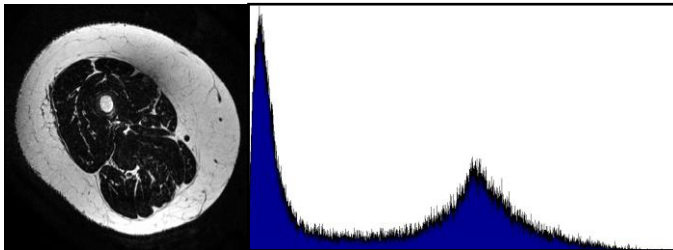


Figure 1: A histogram (right) created from the thigh slice (left).

Percentage fat in the muscle was calculated by a single rater (EB) and compared to the ‘gold standard’. Pearson correlation coefficients and intraclass correlation coefficients were computed for each calculated percentage. Bland-Altman plots were created using the best cutoff for each the quadriceps and hamstrings muscle groups to analyze agreement.

RESULTS AND DISCUSSION

For the quadriceps, Pearson correlation coefficients showed good to excellent agreement across all cutoffs, ranging from 0.77-0.89. The peak ICC value was 0.86 and occurred at the 35% mark of the normalized curve. For the hamstrings, both Pearson correlation coefficients and intraclass correlation coefficients demonstrated low to moderate agreement: Pearson coefficients ranged from 0.31-0.85 and a peak ICC value of 0.85 occurring at 24% of the normalized curve.

A Bland-Altman plot for both muscle groups is displayed in Figure 2. Bland-Altman plots show that the pilot program has a mean difference comparable to output from the SliceOmatic program, with an average mean difference of 0.1% and 0.3% for the quadriceps and hamstrings, respectively. However, estimates for the quadriceps were less variable than hamstrings (± 1.96 SD represents approximately 4% error between programs for the quadriceps and 10% for the hamstrings). These plots suggest that the ability of the pilot program to estimate percent

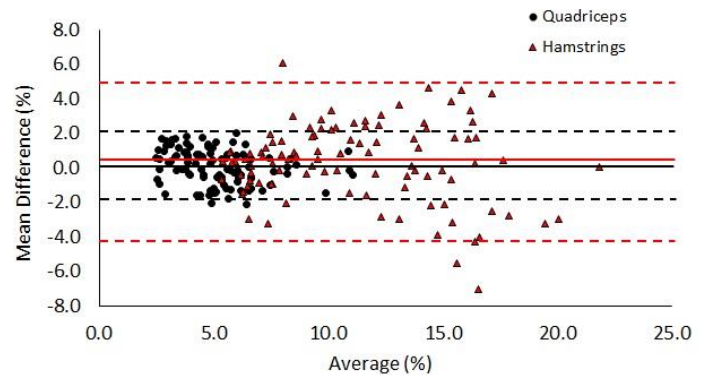


Figure 2: A Bland-Altman plot showing agreement between the pilot program and traditional MRI scan segmentation using SliceOmatic for percentage of intramuscular fat in the quadriceps (black circles) and hamstrings (red triangles) muscle groups. The dotted lines show the mean of the program differences for quadriceps (black) and hamstrings (red). Similarly, the solid lines show ± 1.96 SD of the mean difference.

is better for the quadriceps muscle group compared to the hamstrings muscle group. Differences in estimates for each muscle group may be explained by the increased overall adiposity in the hamstrings group compared to the quadriceps group in these 2 participants. The increased proportion of adipose tissue in this region may make it harder to distinguish borders between muscle and fat, and therefore muscle group estimates are more variable between slices.

CONCLUSIONS

A pilot semi-automated program was created that objectively quantified percentage of fatty infiltration of muscle from axial MRI scans. This program chooses threshold cutoffs based on a pixel intensity histogram. The program showed good to excellent agreement with traditionally segmented data for the quadriceps muscle group, but not the hamstrings. Further piloting and testing is required.

REFERENCES

- [1] Hart HF, et al. *Osteoarthritis Cart.* 20, 863-868, 2012.
- [2] Vilaca KH, et al. *Osteoporos Int.* 24, 1095-1100, 2014.
- [3] Davison MJ. MSc Thesis, McMaster Uni., 2014.
- [4] Altman R, et al. *Osteoarthritis Rheum.* 29, 1039-1049, 1986.
- [5] Kothari M, et al. *Eur Radiol.* 14, 1568-1573, 2004.

EFFECT OF ANKLE FOOT ORTHOSIS ALIGNMENT ON MUSCLE ACTIVITY

¹Starr E. Brown, ^{1,2}Elizabeth Russell Esposito, ^{1,2}Jason M. Wilken

¹ Center for the Intrepid, Department of Orthopaedics and Rehabilitation, Brooke Army Medical Center, JBSA Ft. Sam Houston, TX, USA

²DoD-VA Extremity Trauma and Amputation Center of Excellence
email: starr.e.brown2.ctr@mail.mil

INTRODUCTION

An ankle foot orthosis (AFO) is commonly prescribed to improve walking ability in individuals with lower limb neurological and/or muscular impairments. For example, the Intrepid Dynamic Exoskeletal Orthosis (IDEO), a custom carbon fiber passive-dynamic AFO, has been prescribed to over 600 service members to meet their need to perform a wide range of functional activities [1]. Many factors, to include mechanical properties such as stiffness and alignment angle have the potential to influence an individual's walking ability [2,3] and the demand placed on the muscles of the limb.

To aid in the prescription and design of AFOs, gait biomechanical analysis is used to investigate the effects of various AFO mechanical parameters and the associated patient costs and benefits. For example, AFO sagittal plane alignment can impact patient shock absorption capabilities and energetic cost during gait [4,5]. Associated with these adaptations are muscle activity responses, of which quantitative analyses are limited. Therefore, the purpose of this study was to determine the effects AFO alignment had on muscle activity accompanying biomechanical changes.

METHODS

Nine male subjects with limited unilateral ankle range of motion and plantar flexor weakness due to limb injury participated in the study. Each subject was fit with a custom IDEO in which the neutral alignment was based on the recommendation and experience of the prosthetist/orthotist and the patient's available pain-free ankle range of motion. A 3° wedge placed between the posterior strut and foot plate (Fig. 1) was used to test three distinct alignment conditions: no wedge (Neutral), 3°

dorsiflexion (DF), and a 3° plantarflexion (PF) angle.



Fig. 1: IDEO in dorsiflexed condition (left) and plantarflexed condition (right). A 3° wedge between the strut and footplate changed alignment angle.

Subjects walked at a standardized velocity over level ground while marker (120 Hz, Motion Analysis Corp.) and ground reaction force data (1200Hz, AMTI, Inc.) were recorded. Surface electromyography (EMG) was collected (1200 Hz, Motion Laboratory Systems, Inc.) from the soleus, medial gastrocnemius, tibialis anterior, vastus medialis (VM) and rectus femoris (RF). Sagittal plane knee angles and moments were calculated and time normalized to 100% of the gait cycle for five strides; peak values were averaged across the strides. EMG data were demeaned, high pass filtered (20 Hz), low pass filtered (400 Hz) and smoothed using a root mean square calculation with a 50 ms window. The processed signal was normalized to 100% of the gait cycle. The gait cycle was divided into six phases [6] and the integrated EMG value for each phase was averaged for five strides (MatLAB, The Mathworks, Inc).

Normality was assessed with a Shapiro-Wilk test (SPSS, IBM Corp., $p > 0.05$). A repeated measures

ANOVA ($p < 0.05$) identified significant main effects. Least Significant Difference post-hoc comparisons determined significance between conditions.

RESULTS AND DISCUSSION

A 3° change in the AFO sagittal plane alignment significantly affected muscle activity as well as kinetics and kinematics during 10-30% of the gait cycle (early single leg support). EMG activity of the VM and RF in the DF alignment was 76.5% ($p = 0.046$) and 55.8% ($p = 0.045$) greater, respectively compared to the PF alignment (Fig. 2). Muscle activity differences for the other muscles did not reach significance between conditions.

Consistent with the increase in quadriceps muscle activity, the DF alignment increased the internal knee extensor moment (KEM) by 61.9% compared to the PF alignment ($p < 0.001$). Compared to the Neutral alignment, KEM increased by 21.1% ($p = 0.002$) and decreased by 25.2% ($p < 0.001$) in the DF and PF alignments, respectively (Fig. 2). Maximum knee flexion angle increased by 7.9% ($p = 0.019$) and 13.3% ($p = 0.010$) in the DF alignment compared to the Neutral and PF alignments, respectively (Fig 2). Subjective patient experience was in agreement with the reduced KEM and knee flexion angles and associated decrease in quadriceps muscle activity in the PF alignment. Preference for alignment conditions showed 7/9 subjects preferring PF over DF and Neutral alignments.

In other patient populations, however, potential benefits resulting from a DF alignment have been highlighted [4]. For post-stroke patients, a DF alignment also increased the KEM and knee flexion angle but beneficially increased shock absorption capability [4], suggesting that specific alignments may serve patient groups differently.

A limitation of this study was the non-standardized neutral alignment position used to accommodate patient specific clinical needs. This limits the generalizability of a precise prescription metric for optimal alignment, but the results of this study indicate that erring on the side of a PF alignment may better serve this patient population.

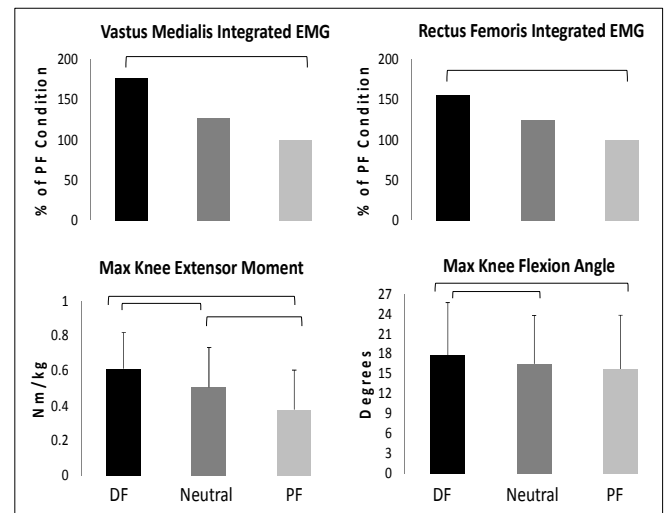


Fig. 2: Mean (SD bars) maximum values at 10-30% of the gait cycle. Horizontal bars indicate significant differences between conditions.

In conclusion, these results highlight the importance of proper alignment in the design and prescription of AFOs. Device alignment angle can be modified to influence joint moments and the demand placed on proximal muscles.

REFERENCES

1. Patzkowski JC, et al. *J Bone Joint Surg Am* **94**, 507-515, 2012.
2. Bergman DJJ, et al. *Gait Posture* **30**, 144-149, 2009.
3. Harper NG, et al. *Clin Biomech* **29**, 877-884, 2014.
4. Silver-Thorn B, et al. *Prosthet Orthot Int* **35**, 150-162, 2011.
5. Ploeger HE, et al. *Gait Posture* **40**, 391-398, 2013.
6. Winter DA. *Physiotherapy Canada* **47**, 245-252, 1985.

ACKNOWLEDGEMENTS

Support for this study was provided by the Center for Rehabilitation Sciences Research, Dept. of Physical Medicine and Rehabilitation, Uniformed Services Univ. of Health Sciences, Bethesda, MD.

The views expressed herein are those of the authors and do not reflect the policy or position of Brooke Army Medical Center, the US Army Medical Department, US Army Office of the Surgeon General, Department of the Army, Department of Defense or US Government.

CLINICAL MEASUREMENTS WITH A DEVICE TO ENABLE WEIGHTBEARING CT IN A HORIZONTAL GANTRY

Bradley C. Campbell¹, Stephen F. Conti, MD; Mark Carl Miller, PhD^{1,2}

¹The University of Pittsburgh, Pittsburgh, PA, USA

²Allegheny General Hospital, Pittsburgh, PA USA

Email: brc57@pitt.edu

INTRODUCTION

Weightbearing imaging can be the most appropriate method for diagnosis of many orthopaedic pathologies¹. Certain deformities, like hallux valgus, are altered by the application of loading and the change in geometry can affect clinical decision-making². Vertical devices for imaging have been developed but are costly and not readily available. Therefore, we designed and developed a computed tomographic imaging system compatible foot and ankle-loading device to be retrofitted to horizontal entry, donut gantry devices. The current goal is to demonstrate the method for device validation and illustrate the change caused by weight-bearing in hallux valgus.

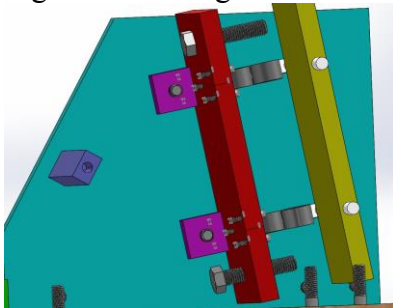


Figure 1: Device for simulated weightbearing in a CT scan. The springs (grey struts) apply a pedal load



which in turn is limited by the darker grey bolts.

Figure 2: Device in use for a CT scan.

METHODS

The main function of the device is to apply a load to a patient's foot during a CT scan in order to simulate full weightbearing. The device should also allow for variation of the pressure distribution between the heel and forefoot.

The device is comprised of a platen with a spring-loaded pedal and a seat at an adjustable distance from the device.(Figures 1, 2) The pedal mechanism abuts polyester-based elastomer rings which function as springs positioned between two plates: one plate is fixed and one is capable of planar movement guided by slots. The deflection of the springs provides a measurable load on the foot and ankle. Calibration of the elastomeric springs is shown in Figure 3. The maximum load is chosen by adjusting two bolts that limit the spring deflection. The patient's foot pushes on the top, moveable plate until it compresses the springs and the top plate is stopped from further movement by the bolts.

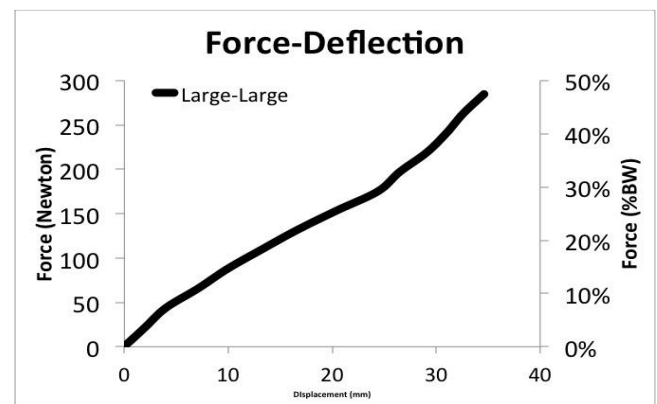


Figure 3 Force-deflection curve for loading of the CT device.

The pedal and adjustable seat are constructed from 3/4-inch thick Delrin and fastened with nylon hardware. Both the pedal and seat are easily detached for portability.

The intent of the device is for use with foot imaging during computed tomography. As a first validation of the device, standing full weightbearing plane film radiographs will be compared with horizontally captured CT scans utilizing the device. Full weightbearing radiographs were taken in the anteroposterior plane at 15°. CT scans, loaded and unloaded, were taken employing the device with the GE Lightspeed scanner with a slice thickness of 1mm. The image was reconstructed and projected onto the anteroposterior plane.

RESULTS AND DISCUSSION

The hallux valgus angles, the angle between the first phalanx and metatarsal³, were compared between a normal patient in a standing radiograph and weightbearing CT scan. The HV angle in the radiograph was 7° while the HV angle in the CT scan was 6°. Weightbearing and non-weightbearing CT scans were also compared in an HV patient. In the non-WB CT, the HV angle scan was 28.8° and, in the WB CT scan, the HV angle was 36.6°.

CONCLUSIONS

The initial tests show that the HV angles in the standing radiograph and in the CT image created while using the device in a normal patient are almost identical. The difference observed for the HV patient demonstrates that the device effects a change due to load application. Further data collection to obtain a sample size more generalizable to the population and to validate simulated full weightbearing equivalence to full weightbearing is underway.

REFERENCES

1. Tanaka, Yasuhito, et al. Clin Orthop Relat Res 336 (1997): 186-194.
2. Fuhrmann, Renée A., Frank Layher, and Wolf D. Wetzel. Foot Ankle Int 24.4 (2003): 326-331.
3. Coughlin, Michael J., Charles L. Saltzman, and James A. Nunley. Foot Ankle Int 23.1 (2002): 68-74.

ACKNOWLEDGEMENTS

Thanks to E. Jensen, J Marcanio, A Pruitt, & R McKenzie of the University of Pittsburgh for significant contributions to this project.

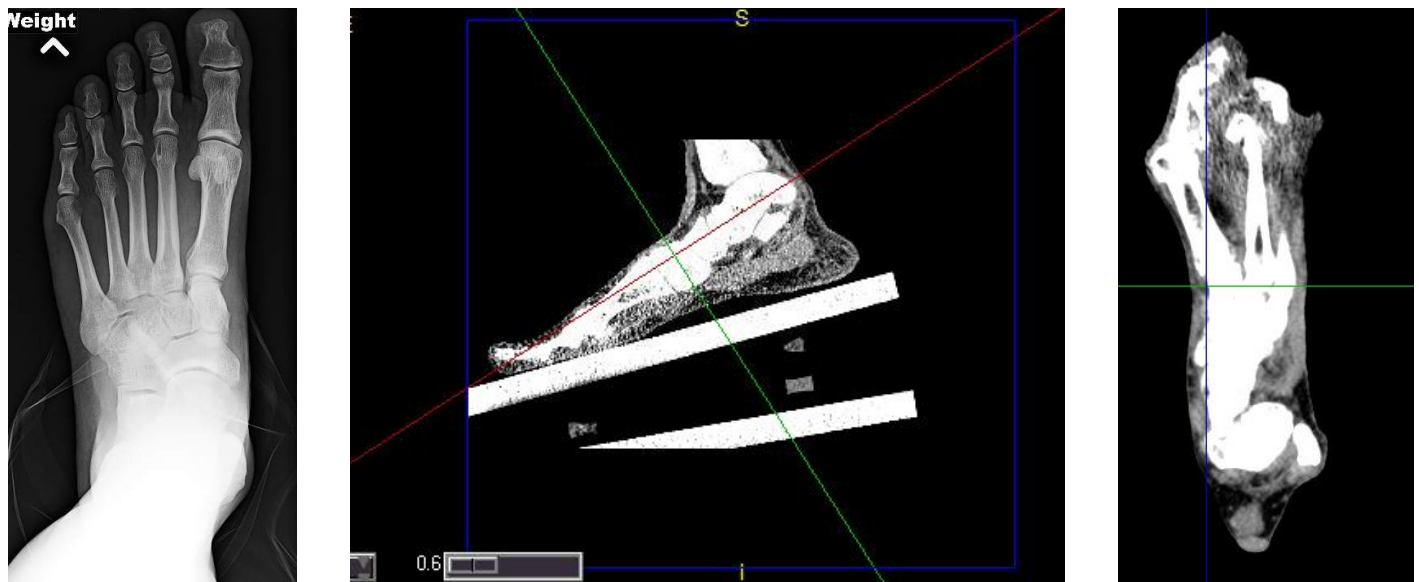


Figure 4 Left: Radiographic image of normal foot taken in the clinical anteroposterior plane. Middle: Lateral-medial plane view of the HV foot. The image is used to show the axes to be used for reconstruction and projection. Right: CT image of HV foot taken in the projected plane created with the ISB recommended second ray axis and tertiary orthogonal axis.

USING HYBRID NEUROPROSTHESES TO IMPROVE STAND-TO-SIT MANUEVER FOR INDIVIDUALS WITH PARAPLEGIA

^{1,4}Chang, Sarah R., ^{2,4}Nandor, Mark J., M.S., ⁴Foglyano, Kevin M.,
²Lesieutre, Maria, ⁴Kobetic, Rudi, M.S., and ^{1,3,4}Triolo, Ronald J., Ph.D.

Departments of ¹Biomedical Engineering, ²Mechanical Engineering, and ³Orthopaedics,
Case Western Reserve University, Cleveland, OH, USA

⁴Advanced Platform Technology Center,
Louis Stokes Cleveland Veterans Affairs Medical Center, Cleveland, OH, USA
email: sarah.r.chang@case.edu

INTRODUCTION

Individuals with paraplegia rank walking as a high priority to improve their quality of life [1]. The ability to perform and control the standing up and sitting down movements is important before walking. These movements can be facilitated with different technologies such as functional neuromuscular stimulation (FNS), powered lower extremity orthoses commonly known as exoskeletons, or hybrid neuroprostheses (HNP). FNS produces strong muscle contractions to coordinate limb movement but lacks stability. Exoskeletons can support an upright user and coordinates limb movements but requires large power consumption. A HNP coordinates muscle contractions generated by FNS with the support and stability of an exoskeleton to create the desired movement. Stand-to-sit (STS) requires eccentric contractions or lengthening of the active quadriceps muscles, which can be difficult to achieve with FNS. STS maneuvers performed with FNS alone result in high knee angular velocities, large impact forces when making initial contact with the chair, high accelerations, and an excessive amount of force placed on the upper extremities [2]. This study evaluates two different hydraulic mechanisms for a hybrid neuroprosthesis to control stand-to-sit maneuvers in participants with spinal cord injury who are using FNS.

METHODS

The first hydraulic approach being evaluated to control the STS maneuver after spinal cord injury is a hip-knee coupling mechanism that locks, unlocks,

or couples the movement of the ipsilateral hip and knee joints. Hydraulic fluid is transferred between cylinders at the hip and knee joints such that hip flexion extends the hip cylinder rod and results in the knee cylinder rod retracting to cause knee flexion via a mechanical transmission. Fluid can also flow between the blind side of the knee cylinder and blind side of the hip cylinder during movement for synchronized joint extension. By coupling the ipsilateral hip and knee joints, subjects with paraplegia should be able to control the speed of their hip angle flexion using a walker and their upper extremities, thus controlling the rate of knee angle flexion.

The second approach is a knee damping mechanism that locks, unlocks, or damps the movement of the knee joint. A proportional valve in the hydraulic circuit directs the fluid flow between the rod and blind sides of the knee cylinder. The knee joint will be locked when the proportional valve is fully closed. However, a damping force will be created at the knee when the proportional valve is partially open. By damping the knee joint, subjects with paraplegia would have a slower knee angular velocity that better controls knee flexion during STS.

The hydraulic mechanisms are bilaterally affixed to the uprights of the exoskeleton as a part of the HNP device. Subjects with paraplegia perform the STS transition using one of the hydraulic mechanisms at a time. Motion capture data are recorded to determine kinematic variables such as joint angles, while a load instrumented walker (AMTI, Inc., Watertown, MA, USA) measures upper extremity

forces. A chair instrumented with a force plate on the seat (AMTI, Inc., Watertown, MA, USA) measures the impact forces and moments when making contact with the seating surface. Measures such as upper extremity effort, knee angular velocity, and impact force are being compared between the two hydraulic mechanisms and between the mechanisms and only using FNS.

RESULTS AND DISCUSSION

The mechanisms have undergone bench testing to ensure safety before clinical evaluation in able-bodied volunteers and subjects with paraplegia. A consistent 1:1 coupling ratio is created with the hip-knee coupling mechanism, where one degree of hip flexion results in one degree of knee flexion. 1:1 hip-knee angle relationships are similar to that seen in able-bodied STS maneuvers and show promise for controlling the STS for subjects with paraplegia [2]. The damping mechanism was used in a preliminary experiment to determine the feasibility in controlling the STS, and it resulted in an impact force at least half of that found in a previous study

when only FNS was used to perform the STS. Both mechanisms are undergoing further testing during STS maneuvers for subjects with paraplegia from spinal cord injury to determine the effectiveness of the mechanisms in controlling the STS transition.

REFERENCES

1. Anderson KD. *J Neurotrauma* 21, 1371-1383, 2004.
2. Chang SR, et al. *J Rehab Res Dev* 51, 1339-1352, 2014.

ACKNOWLEDGEMENTS

This work was supported by Grant B0608-R and W81XWH-13-1-0099 from the Department of Veterans Affairs and Department of Defense, and S. Chang was supported by training grant 5T32AR007505-28 to Case Western Reserve University.

SPINAL CURVATURE AND SHOULDER KINEMATICS DURING WHEELCHAIR PROPULSION: EVALUATING THE IMPACT OF SPINAL CORD INJURY LEVEL

Beth A. Cloud, Kristin D. Zhao, Arin M. Ellingson, and Kai-Nan An

Mayo Clinic, Rochester, MN, USA
email: zhao.kristin@mayo.edu (KD Zhao)

INTRODUCTION

Upper limb pathology is common in individuals who use manual wheelchairs (MWC). Shoulder pain in particular has been reported at rates of up to 70%[1]. To better understand the mechanism of how pain and dysfunction develop, upper limb kinematics have been evaluated during MWC-based activities. However, little is understood about spinal posture and movement during MWC-based activities. Due to reported interactions between posture and shoulder movement [2], postural parameters may contribute to the development of pain and dysfunction and may be a means by which upper limb motion can be influenced.

The overall goal of our research is to quantify the relationship between spine and shoulder movement and determine the influence, if any, spinal curvature has on shoulder kinematics. The purpose of this work was to **(1)** quantify spinal curvature, trunk motion, and shoulder kinematics across the propulsion cycle in MWC users with spinal cord injury (SCI); and **(2)** evaluate differences between high and low SCI level groups.

METHODS

MWC users with SCI (n=13, 10 male: sex proportion comparable to the SCI population) were recruited and provided written informed consent to participate. All participants had been using a wheelchair as their primary mode of mobility for at least one year.

Spinal curvature was captured at 60 Hz with a fiber optic sensor system (ShapeTape, Measurand). The ShapeTape was placed in a flexible sleeve and placed over spinous processes from the first sacral (S1) to seventh cervical (C7) vertebra. The ShapeTape was anchored over S1 but was otherwise free to move with contour changes of the spine. Spinal curvature was defined as regions of lordosis (concave posteriorly) and kyphosis (concave

anteriorly) of the thoracolumbar spine as previously described [3]. Spinal curvature was quantified as the angle created between the normal lines to the curve at the endpoints of each curvature region.

Shoulder and thorax motion were captured at 120 Hz with electromagnetic sensors (Liberty, Polhemus) placed on the thorax at the sternum, scapula at the acromion, and humerus via thermoplastic cuff. The thorax, scapula, and humerus segments were defined according to ISB standards [4]. Motion was quantified with Euler sequences and included thoracic (relative to global, ZX'Y"), humerothoracic (YX'Y"), scapulothoracic (YX'Z"), and glenohumeral (ZX'Y").

Participants propelled in their personal MWC on a custom set of stationary rollers at a self-selected speed. Minimum and maximum values were identified from an averaged propulsion cycle (based on two trials) for all outcome variables (lordosis, kyphosis, thoracic flexion/extension, 3 humerothoracic rotations, 3 scapulothoracic rotations, 3 glenohumeral rotations). Range of motion across the propulsion cycle was determined from the minimum and maximum values.

Minimum, maximum, and range of motion values were compared between individuals with high levels of SCI (T9 and above) and individuals with low SCI (T10 and below) using a Wilcoxon Rank Sum test ($\alpha = 0.05$).

RESULTS AND DISCUSSION

In the high injury group (n=7, 7 male), SCI level ranged from C6/7 to T5, mean age was 36.9 (SD: 9.8) years and years using MWC was 13.8 (12.0). In the low injury group (n=6, 3 male), SCI level ranged from T10 to L1, mean age was 48.8 (5.3) years and years using MWC was 16.6 (8.8).

The low injury group had a significantly higher maximum lordosis ($26.8 \pm 15.8^\circ$ v. $8.1 \pm 9.2^\circ$) and

range of lordosis ($12.4 \pm 9.1^\circ$ v. $4.5 \pm 4.6^\circ$) as well as minimum and maximum kyphosis ($42.4 \pm 5.4^\circ$ v. $53.2 \pm 6.3^\circ$ & $50.0 \pm 4.6^\circ$ v. $62.6 \pm 6.3^\circ$) than the high injury group (Figure 1). There are trends for the low injury group to have less flexion at maximum trunk angle ($-1.6 \pm 7.2^\circ$ v. $-9.6 \pm 10.5^\circ$) and a larger minimum lordosis ($14.4 \pm 13.0^\circ$ v. $3.6 \pm 5.4^\circ$).

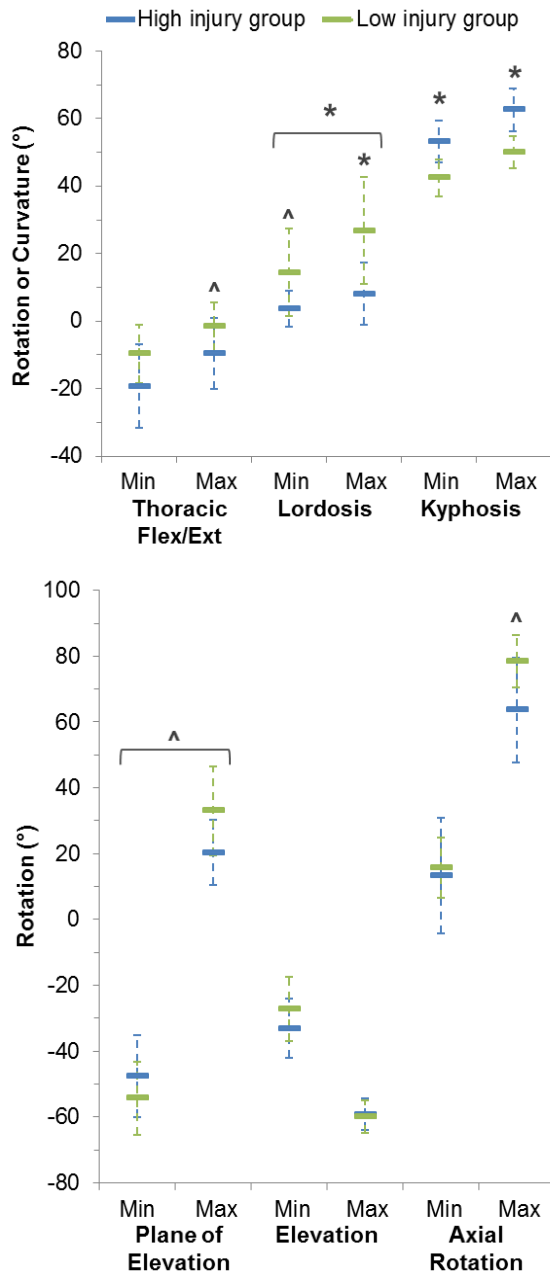


Figure 1. [top] Mean (SD) minimum and maximum thoracic flexion(-)/extension(+), lordosis, kyphosis; [bottom] humerothoracic plane of elevation (+: horizontally adducted), elevation (-: elevated), axial rotation (+, internally rotated); *denotes difference between groups, $p < 0.05$; ^, $p \leq 0.1$; brackets signify difference in range of motion

Differences in shoulder kinematic parameters did not reach significance. However, the low injury group trended toward having a larger range of glenohumeral axial rotation ($20.8 \pm 4.2^\circ$ v. $15.9 \pm 4.1^\circ$) and humerothoracic plane of elevation ($87.3 \pm 23.2^\circ$ v. $68.0 \pm 7.0^\circ$), as well as a larger maximal humerothoracic internal rotation ($78.5 \pm 8.0^\circ$ v. $63.6 \pm 15.8^\circ$, Figure 1).

CONCLUSIONS

Based on our results, individuals with low levels of SCI have greater maximum and range of thoracolumbar lordosis and lower minimum and maximum kyphosis than individuals with high levels of SCI. This occurs with possible differences in thoracic sagittal plane motion, humerothoracic motion and range of glenohumeral axial rotation. Therefore, spinal posture may be influencing the overall motion of the humerus relative to the thorax with various strategies occurring at the glenohumeral and scapulothoracic joints to obtain this effect. Additionally, thoracic motion alone may not be sufficient to describe trunk movement - measures of lordosis and kyphosis are necessary. Though differences were seen between groups with different injury levels, the differences could also be attributed to differences in sex or age, as these characteristics differed between the groups. This work represents an intermediate in understanding the relationship between spine and shoulder motion during propulsion. Additional data collections and analyses are ongoing.

REFERENCES

1. Dyson-Hudson & Kirshblum. *J Spinal Cord Med*, **27**. 4-17, 2004
2. Kebaetse et al. *Arch Phys Med Rehabil*, **80**. 945-50, 1999.
3. Cloud et al. *Gait Posture*, **40**. 369-74, 2014.
4. Wu et al. *J Biomech*, **38**. 981-92, 2005.

ACKNOWLEDGEMENTS

Personnel supported by: PODS II Scholarship, Foundation for Physical Therapy (BAC); NIH/NCATS TL1 TR000137 (BAC); NIH/NIAMS T32AR56950 (AME).

We thank the following for their contributions to data collection and analysis: Christina Webber, Joseph Mozingo, James Hartman, Ryan Breighner, Mayo Clinic Motion Analysis Laboratory.

IDENTIFICATION OF FINGER FORCES OVER RANGES OF MOTIONS: A COMPARISON BETWEEN HEALTHY AND REDUCED HAND FUNCTIONALITY PARTICIPANTS

¹Joshua Drost, ²Sam Leitkam, ¹Tamara Reid Bush

¹Michigan State University, East Lansing, MI, USA

²Ohio University, Athens, Ohio, USA

Email: drostjos@msu.edu, reidtama@msu.edu

Introduction

Diagnosing the amount of hand function lost due to injury, arthritis, or nerve damage is currently task-based and subjective to the clinician [1, 2]. Recently, work has modeled the differences in kinematic finger space between hands with and without reduced functionality due to arthritis [3]. This model includes the full range of motions for each finger; however, the forces that each finger can produce at each posture are not included.

Both motion and forces associated with each finger posture are necessary to generate a comprehensive hand model for clinical use. Such a model will result in a tool for clinicians to easily compare changes in hand function and finger strength pre- and post- rehabilitation, treatment or surgical intervention.

Thus, to achieve this comprehensive model, the forces that can be applied over various finger postures must first be quantified and compared. The goal of this work was to map forces associated with the index finger at different positions and orientations within the kinematic fingertip workspace of participants with and without reduced hand functionality.

Methods

Twelve participants (average age 26.5 years, SD 5.99 years) without any reported injury or arthritis, termed “Healthy”, and fifteen participants (average age 73.5, SD 4.81 years) with doctor diagnosed arthritis, termed “Arthritic”, were included in this study.

The maximum forces of the index finger were measured in two tests. In-plane forces (no adduction

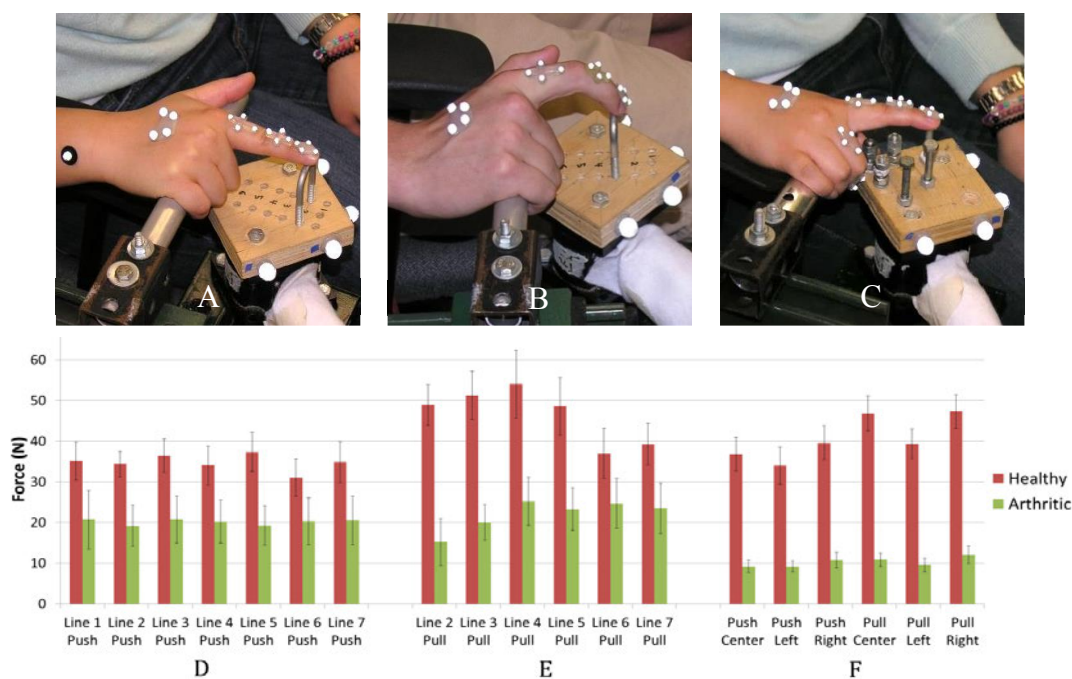


Figure 1: Healthy and Arthritic data. Experimental setup and force data for in-plane push (A, D), in plane pull (B, E) and out-of-plane (C, F) motions with standard error of the mean. For in-plane motions, the U-shaped device was moved in toward the participant resulting in 7 different positions (line 1-7).

or abduction of the finger) measured differences by using a “U-shaped” metal bracket placed in seven positions along a line, each a half inch apart. This set-up was developed to measure the maximum forces related to changes of finger flexion. Each participant was asked to press down on the bracket with their maximum load (Figure 1A) then pull the bracket with maximum load for each position (Figure 1B). During data collection participants were asked to continually grip a cylindrical handle to isolate the finger forces and to maintain a consistent orientation of the wrist.

Out-of-plane maximum finger forces were measured at each of six positions to determine force differences related to abduction/adduction. Three of the positions were at maximum extension and the other three positions were at moderate flexion of the interphalangeal joints (Figure 1C).

Results/Discussion

Using a two-way ANOVA, several differences were identified in the finger forces. Overall, the forces of Arthritic participants were less than those of Healthy participants ($p < 0.001$). Neither the Healthy or Arthritic groups showed differences in the forces perpendicular to the palm (push) with varying amounts of finger flexion or extension, $p = 0.967$ (Figure 1D). While there was no statistical significance, there was a visible trend showing maximum applicable force for the pull motions at position 4 (Figure 1D). Both push and pull forces varied with respect to abduction/adduction. In both Healthy and Arthritic groups, maximum forces were lower with abduction (left) and increased with adduction (right). While not statistically significant ($p = 0.077$), this should be investigated with a larger sample size (Figure 1F).

Models overlaying these force data with the kinematic space were also successfully developed. Figure 2 shows the kinematic fingertip workspace for a single participant with the measured force directions and magnitudes represented by the vectors projected onto the sagittal plane of finger flexion. The color scale represents the sum of possible ways to reach that position with the finger

tip, with red indicating the most possibilities. The forces pointing towards the top left represent the push motions and the forces pointing towards the bottom left represent the pull motions.

Subject specific modeling that includes both force generation and kinematics will allow for clinical comparisons pre-/post interventions. With the combination of motions and forces, these models will be robust tools for clinical assessment of the hand and fingers.

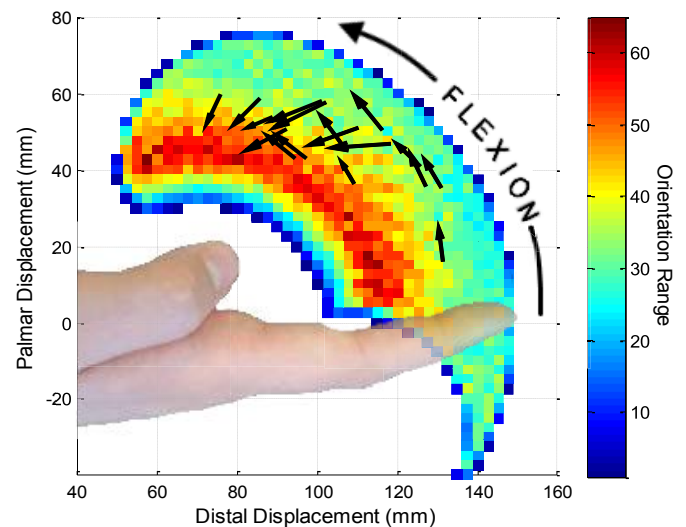


Figure 2: Sagittal plane view of kinematic finger space for the index finger of a healthy participant with overlaid force vectors. The displacements of the workspace and force vector origins were measured from the center of the wrist with the vertical axis normal to the palm.

Acknowledgments

The authors would like to thank the Pearl J. Aldrich Endowment in Aging Related Research for their funding as well as Wu Pan, Jessica Buschman, Jeffrey Hall, Eric Waldron and Anand Saripalli for assistance in capturing and analyzing data.

References

1. Chung K C., et al *The Journal of Hand Surgery*, 575-587. 1998.
2. Katz S, et al. *Journal of the American Medical Association*, 914-919. 1963.
3. Leitkam S, Bush TR. *ASME Journal of Biomechanical Engineering*. 2015.

COMPARISON OF TIBIA STRAIN BETWEEN SIMULATED EXOSKELETON-ASSISTED GAIT AND NORMAL GAIT

¹ Ying Fang, ² Nathan Smith, ¹ Joshua E. Johnson, ¹ Karen L. Troy

¹ Worcester Polytechnic Institute, Worcester, MA, USA

² The University of Massachusetts, Amherst, MA, USA

email: yfang3@wpi.edu

INTRODUCTION

Spinal cord injury (SCI) is associated with rapid bone loss, which can be attributed to the reduction in mechanical strains that are generated through gait and other activities. Recently, the development of exoskeletons such as the Ekso (Ekso Bionics, Richmond, CA), ReWalk (Marlborough, MA) and others has made walking possible among individuals with complete paralysis. Dissimilar to natural walking, where motion is driven by muscle force, the joint torque needed to initiate exoskeleton-assisted gait generally comes from an external actuator that produces a strap force on the mid-thigh and shank. Weight-bearing gait training using exoskeletons may potentially improve bone health through bone adaptation, depending on the strain the bone undergoes during gait. On the other hand, exoskeleton users with SCI are at higher risk of fracture due to their weaker bones. Bone strain occurring during exoskeleton-assisted gait is a critical factor for evaluating both the potential therapeutic benefit, and also patient safety during this task. Here, we compared tibial strain magnitude and distribution between simulated exoskeleton-assisted gait and normal gait at heel strike (HS), midstance, and toe off (TO).

METHODS

Musculoskeletal model

A generic 12-segment, 23-degree of freedom, 54 muscle musculoskeletal model (Gait2354 Model), originally developed by Delp et al. [1] was used and scaled to a subject with height of 1.8 m and mass of 72.6 kg using OpenSim (3.2, SimTK, Stanford, CA, USA).

Previously reported experimental gait data of the subject, which were initially collected by John et al. [2], were applied to the scaled model. Inverse kinematics and dynamics were performed to identify net joint moment and joint reaction forces. Next, individual muscle forces were calculated via

the "Computed Muscle Control (CMC)" tool, and joint contact forces were calculated.

Muscle insertion location and muscle force vectors at HS, midstance, and TO were calculated based on muscle properties provided by OpenSim. All vectors were transformed to the tibia coordinate system.

Finite element model

A finite element (FE) model of a right tibia was generated from the Living Human Digital Library (LHDL) database. Bone was assigned inhomogeneous linear-elastic material properties based on apparent density [3]. As described below, normal and exoskeleton-assisted gait were simulated, and distal nodes of the tibia were constrained for both conditions (Figure 1).

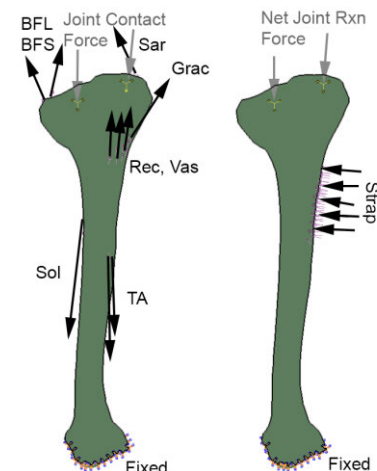


Figure 1: Boundary conditions applied to the right tibia FE models. Left: normal condition with muscle forces and joint contact forces; Right: exoskeleton-assisted condition with strap force and joint reaction forces.

For normal gait, knee contact force vectors and muscle force vectors derived from the musculoskeletal model were applied to the FE model. Knee joint contact forces were applied such that 63% of the total force acted on the medial tibial compartment and 37% on the lateral [4]. Muscle

forces were applied as surface traction with appropriate vector directions. Included muscles were long head of biceps femoris (BFL), short head of biceps femoris (BFS), gracilis, sartorius, rectus femoris, vastus, soleus, tibialis anterior (TA), and tibialis posterior.

For exoskeleton-assisted gait, it was assumed that muscles exerted zero force and the net joint moments resulting from the inverse dynamics calculations were generated via the strap at the tibia. The strap force was modeled as pressure normal to the tibia and located at 22% of the tibia length. The strap area and location were estimated using photographs and measurements of an Ekso suit. The strap force magnitude was set such that the net external moment generated at the knee was the same for exoskeleton-assisted gait and normal gait. Knee reaction force was assumed to be the net joint reaction force at the knee calculated via inverse dynamics.

Von Mises stress and equivalent strain was calculated within the entire tibia and in a 1.5 cm transverse region of interest located 3.5 cm proximal to the distal end. Variables were considered at HS, midstance, and TO.

RESULTS AND DISCUSSION

Peak Von Mises stress within the entire tibia in exoskeleton-assisted gait was 18, 71, 2.5 MPa, which was smaller than 139, 96, 176 MPa in normal gait at HS, midstance, and TO, respectively. The stress distribution was different between conditions; high stress regions were identified medially during normal gait, but posteriorlaterally during exoskeleton-assisted gait. A qualitative comparison of stress distributions at midstance is shown in Figure 2.

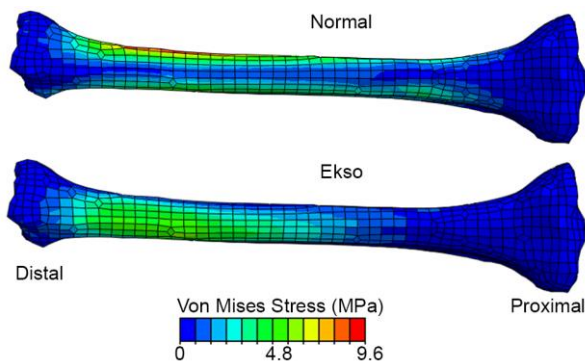


Figure 2: Posteriorlateral view of a right tibia FE model illustrating Von Mises stress (MPa) at midstance for normal and exoskeleton-assisted condition.

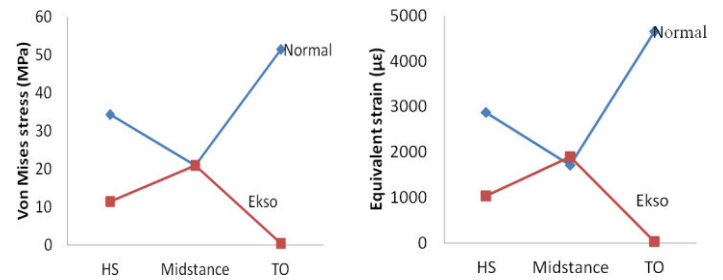


Figure 3: Mean Von Mises stress and mean equivalent strain of the region of interest at HS, midstance, and TO for normal and exoskeleton-assisted gait.

The summed magnitude of forces applied to both models were highest at midstance. It is interesting to note that tibia strain and stress were the lowest for normal gait, and highest for exoskeleton-assisted gait at this time point (Figure 3). This suggests muscles may play an important role in redistributing and decreasing bone stress. Once the muscles are dysfunctional, the protective mechanism disappears.

To validate the simulation, we compared normal gait ankle reaction forces from FE model to those calculated from OpenSim. The error was 58%, 19%, 35% at HS, midstance, and TO, respectively. The larger errors at HS and TO may be attributed to the neglect of segment inertia and acceleration, as we used quasi-static methods in current study. In addition, the net joint moment was assumed to be the same at the knee for both conditions. The FE and gait models were generic and derived from able-bodied subjects. Despite these limitations, the data suggest that tibial stresses and strains during exoskeleton gait are dissimilar to normal gait. Our long term goal is to improve these models with CT-based FE models from individuals with SCI and real exoskeleton-assisted walking data as input.

CONCLUSIONS

The strain distribution and magnitude in the tibia were different for exoskeleton-assisted gait and normal gait. Future study is warranted to determine the degree to which these calculations, which were performed based on able-bodied gait data, are corroborated with experimental data in individuals with SCI.

REFERENCES

1. Delp SL, et al. *IEEE Trans. Biomed. Eng* **37**, 757-67, 1990.
2. John, et al. *Comp Meth Biomech Biomed Eng* **16**, 451-62, 2013.
3. Morgan et al. *J Biomech* **36**, 897-904, 2003.
4. Zhao et al. *J Orthop Res.* **25**, 789-97, 2007

PREDICTING INERTIAL PROPERTIES FOR INDIVIDUALS WITH TRANSTIBIAL AMPUTATION

¹Abbie E. Ferris, ¹Jeremy D. Smith, ¹Gary D. Heise, ²Richard N. Hinrichs, ³Philip E. Martin

¹School of Sport & Exercise Science, University of Northern Colorado

²Department of Kinesiology, Arizona State University

³Department of Kinesiology, Iowa State University

Email: abbie.ferris@unco.edu; website: <http://www.unco.edu/Biomechanics>

INTRODUCTION

Compared to the intact limb, the mass of the prosthetic side of a transtibial amputee (TTA) is consistently 30-40% less, the center of mass location is 25-35% closer to the knee joint, and the moment of inertia is 50-60% less about a transverse axis through the knee joint [1]. Inverse dynamics requires knowledge of the inertial properties of each segment in the model. Although previous research [2] has suggested that changing the inertial properties of a segment by as much as 5% has little to no effect on joint moment magnitudes, Smith et al. [1] recently reported that the reduced inertia of a below-knee prosthesis significantly influences the joint moment magnitudes of swing.

The only method currently available to researchers for estimating prosthesis inertia involves directly measuring the inertial properties of the prosthesis itself. This method measures inertial properties of the prosthesis via oscillation and reaction board techniques [1]. This process is time consuming; it takes as much as 30 minutes to complete these measurements. The purpose of this study was to develop predictions of prosthesis inertial properties based on direct measures obtained from the prosthetic limb. A secondary purpose was to determine the effects of these predictions on joint moment estimates during walking.

METHODS

This study was divided into two phases. The first phase focused on developing an inertial model to predict prosthetic side inertial properties (n=11 TTAs). The second phase assessed the validity of the developed inertial model using an inverse dynamics analysis of walking (n=5; different TTAs). IRB approval and written informed consent were obtained prior to data collections.

In phase one, total body mass and height were measured while participants wore their prostheses. Prosthesis inertia properties were then measured directly. Prosthesis mass (with and without shoe), center of mass location (COM), and moment of inertia about a medial-lateral axis through the prosthesis center of mass were determined using a standard scale, reaction board, and oscillation techniques, respectively [1]. The combined inertial properties of the residual limb and prosthesis were then distributed into a prosthetic shank and foot based on proportions of mass between these two segments for a dismantled prosthesis. The mass, COM, and radius of gyration (ROG) were determined for the shank (including the residual limb) and foot segments of the prosthetic leg. Inertial property estimates of the intact shank and foot were estimated using de Leva [3].

In phase two, participants walked at $1.5 \text{ m}\cdot\text{s}^{-1}$ along a 10 m walkway with embedded force plates. Inertial properties of their prostheses were measured as previously described above. Ground reaction forces (2000 Hz) and motion data (100 Hz) were collected. Using a three segment inverse dynamics model, joint moments at the hip, knee, and ankle were computed with three different inertial models: (1) INTACT – prosthetic leg inertia properties were assumed to match those predicted for the intact leg estimated using de Leva, (2) DIRECT - our direct measures using an oscillation and reaction board technique, and (3) PREDICTED - using the mean percentages from the DIRECT model to estimate the mass of the shank (as a percentage of body mass), COM location (as a percentage of segment length), and ROG about the COM (as a percentage of segment length). ROG was subsequently used to predict the moment of inertia using $I = m\cdot k^2$. A single factor MANOVA was preformed to identify significant differences between the three inertial

models and between peak joint moments during swing ($\alpha=.05$).

RESULTS

Inertial properties of the prosthetic shank and foot obtained from DIRECT measures and used in the PREDICTED model are shown in Table 1. COM and ROG of the foot were based on data from de Leva as a starting point for our predictive model given that the inertial properties of the foot are minimal in comparison to those of the shank. Inertial properties of the prosthetic shank were significantly different between the INTACT and DIRECT models and between the INTACT and PREDICTED models (Table 2). No statistically significant differences in inertial properties were found between the DIRECT and PREDICTED models of the shank. Mass of the foot was significantly greater using INTACT compared with DIRECT and PREDICTED models.

Table 1. Estimates of inertial properties for prosthetic shank and foot for PREDICTED model based on DIRECT measures (n = 11).

	Mass (%body mass)	COM (% segment length)	ROG (% segment length)
Shank	3.3	20.9	17.2
Foot	1.3	^a 44.15m 40.14f	27.9m 24.5f

Note: ^a Estimates based on de Leva were gender specific (M: male, f: female) ; prosthesis inertia values were not.

Moment magnitudes were not significantly different at the ankle regardless of inertia model. Peak joint moments at the knee and hip during swing were significantly smaller for the DIRECT and PREDICTED models compared with the INTACT model (Table 2). There were no significant differences in moment magnitudes between DIRECT and PREDICTED models (Figure 1).

DISCUSSION AND CONCLUSIONS

In phase one, we developed predictions for inertial properties of the prosthetic limb based on direct

measures from 11 TTAs (see Table 1). In phase two, inverse dynamics analyses illustrated that our predictions did not result in significantly different joint moments at the knee and hip compared with direct measures. Thus, our predictions for segment mass, COM location, and ROG should be used by other researchers where direct measurements of prosthesis inertia are unavailable.

Table 2. Inertial properties of the three models and joint moments at the hip and knee during swing.

^a Inertial Properties (n = 11)			
	INTACT	DIRECT	PREDICTED
SHANK	Mean \pm SD	Mean \pm SD	Mean \pm SD
Mass	4.26 \pm 0.69*†	3.16 \pm 0.56	3.19 \pm 0.55
COM	0.20 \pm 0.01 *†	0.09 \pm 0.02	0.09 \pm 0.01
ROG	0.11 \pm 0.01 *†	0.08 \pm 0.03	0.08 \pm 0.01
FOOT			
Mass	1.70 \pm 0.31 *†	1.19 \pm 0.19	1.31 \pm 0.24
Peak Joint Moments (Nm/kg) (n = 5)			
Knee	-0.46 \pm 0.08*†	-0.32 \pm 0.021	-0.26 \pm 0.03
Hip	0.71 \pm 0.13 *†	0.34 \pm 0.086	0.28 \pm 0.03

^a Units: Mass = kg, COM = m, & ROG = m

*Significant difference from DIRECT (p = .05)

† Significant difference from PREDICTED (p=.05)

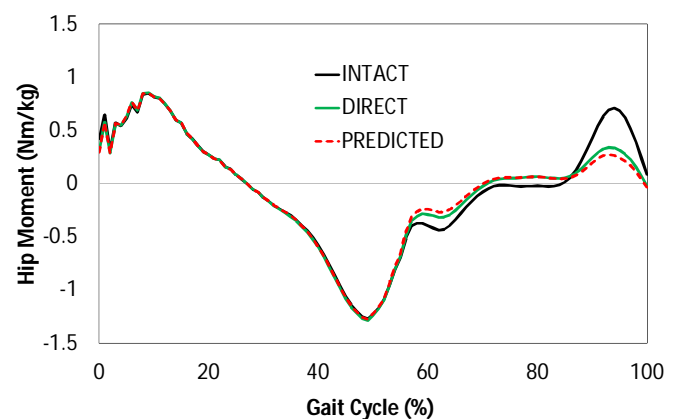


Figure 1. Mean hip joint moment of 5 TTAs using INTACT, DIRECT, and PREDICTED inertial models.

REFERENCES

- Smith, J., et al. (2014). *J Vis Exp*(87), e50977-e50977. doi: 10.3791/50977
- Challis, J. H. and Kerwin, D.G (1996). *J Sport Sci*, 14(4), 219-231.
- de Leva (1996). *J Biomech*, 29(9), 1223 -1230.
- Mattes, S. J., et al. (2000). *Arch of Phys Med Rehab*, 81(5), 561-568.

USE OF MEDICAL IMAGING AND MECHANICS TO QUANTIFY THE STIFFNESS CONNECTING LOWER-LIMB PROSTHESES AND TRANSFEMORAL AMPUTEES

Nicholas P. Fey^{1,2}, Timothy Reissman^{1,3}, Tommaso Lenzi^{1,2} and Todd A. Kuiken¹⁻³

¹Center for Bionic Medicine, Rehabilitation Institute of Chicago, Chicago, IL, USA

²Department of Physical Medicine and Rehabilitation, Northwestern University, Chicago, IL, USA

³Department of Biomedical Engineering, Northwestern University, Chicago, IL, USA

email: nfey@ricres.org web: <http://www.ric.org/research/centers/bionic-medicine/staff/nicholas-p-fey-phd/>

INTRODUCTION

In the design and control of assistive devices for human locomotion, rigid connections between devices and their users are commonly assumed and often do not exist. Yet, the mechanics of these interfaces can constrain device assistance [e.g., 1].

For example, amputees wear prosthetic sockets, which capture bone, muscle and soft tissue of the residual (i.e., amputated) limb and transmit linear and angular loads to the outside of limb. Using radiographic techniques, displacement of the residual tibia and femur inside the sockets of transtibial and transfemoral amputees have been identified decades ago, respectively [2, 3]. Despite these known phenomena and advances in radiography [e.g., 4], large knowledge gaps exist.

Displacement per unit load (i.e., stiffness) in functionally-relevant weight-bearing conditions, stiffness about both linear and angular axes, and the influence of socket technologies are unknown. The purpose of this study was to develop and test a technique to fill these gaps regarding the socket-limb interface of transfemoral amputees. These outcomes are needed to provide quantitative rationale for prescription and engineering of prostheses as well as insights into the underlying mechanisms contributing to abnormal gait mechanics, chronic pain and joint disorders of amputees [for review, see 5].

METHODS

A transfemoral amputee (female, 75.6 kg, 1.64 m, 49 yrs. age and 35 yrs. post-amputation, osteosarcoma etiology) provided informed consent. Residual limb length was 69% of the sound limb. The subject was positioned in front of a digital radiographic system (Phillips, Inc.), including a vertical digital detector

and suspended X-ray tube carrier—capable of imaging a 43 cm by 36 cm window encompassing the residual limb and socket (Fig. 1). The subject wore a custom prosthetic assembly including a flat rigid foot, pylon and 6-axis load cell (AMTI, Inc.) (Fig. 1). Two test sockets (ischial containment and subischial) were fabricated based on a cast of the subject's limb by a licensed prosthetist. These sockets are common clinical options and vary in trim-line height (Fig. 2).

For each socket, a total of eight static radiographic images were captured. Images during unloaded, loaded with body weight in a neutral standing posture, and loaded with medial and lateral as well as anterior and posterior foot placements were taken from corresponding frontal and sagittal-plane views. For loaded conditions, the subject received visual feedback of a corresponding load cell signal (i.e., axial force for loaded in a neutral position, frontal-plane moment for medial/lateral foot placements, and sagittal-plane moment for anterior/posterior placements). She was asked to maintain a maximum constant isometric load for a total of eight seconds.

Multiple pairs of landmarks from the digitized radiographs (Fig. 1) were used to determine changes in axial and angular positions of the socket relative to the residual femur. Stiffness was computed as the change in average force or moment divided by changes in angle or linear position for given unloaded/loaded conditions. Stiffness was computed for repeated pairs of digitized landmarks.

RESULTS AND DISCUSSION

Socket design, loading plane, and foot placement (i.e., loading direction) were all shown to influence the interface stiffness (Fig. 2). Across conditions, the ischial containment socket was found to increase stiffness over the subischial socket. A ~3 fold

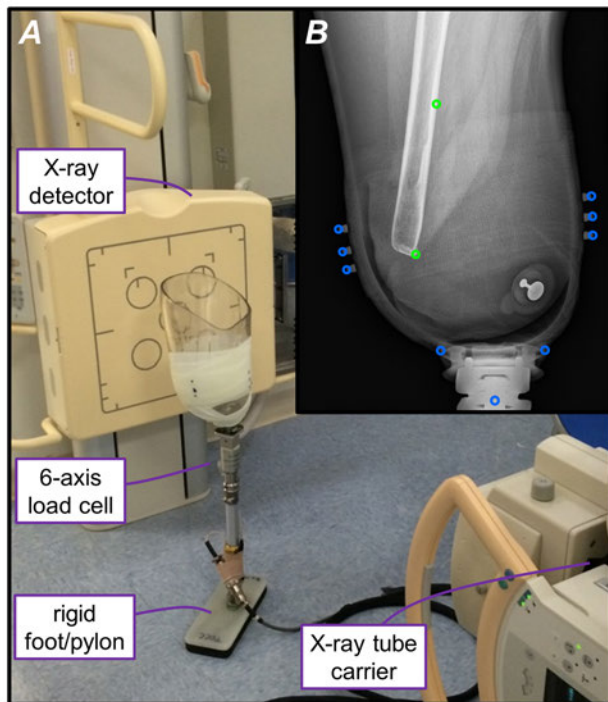


Figure 1: Experimental setup, subject not shown (A); and example radiograph with digitized bone and prostheses landmarks (B).

increase in the axial stiffness, as well as the rotational stiffness in the lateral and posterior foot placement conditions, were observed. Greater than 10 fold increases of rotational stiffness were found in the other conditions. Thus, these trends support the use of ischial containment to increase interface stiffness.

The ischial containment socket has the highest trim-lines on the lateral and posterior aspects of the socket. These geometries correspond with the largest rotational stiffness and largest increases in stiffness relative to the subischial socket occurring with the foot loaded in medial (2100 Nm/rad) and anterior (2000 Nm/rad) positions. In these respective conditions, external abduction and extension moments result in the highest, most proximal, locations of the socket engaging the limb. These data highlight the importance of trim-line geometry and socket height in influencing interface stiffness.

In the subischial socket, the highest trim-lines were also on the lateral and posterior aspects of the socket. Yet, opposite trends were observed with the largest rotational stiffness occurring in lateral and posterior foot positions (Fig. 2). These data suggest that when a bony prominence such as the ischium cannot be engaged, interface stiffness becomes more dependent on the underlying tissue makeup of the limb, as well as contraction level of residual limb muscle associated with weight-bearing.

CONCLUSIONS

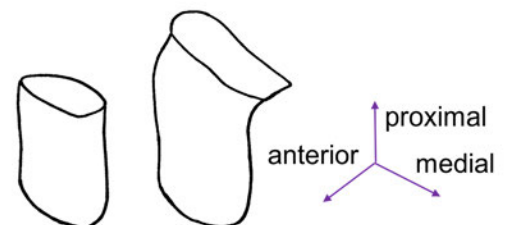
Even in transfemoral sockets with ischial containment, the interface should not be considered rigid. As a reference, the sagittal-plane stiffness of conventional prosthetic feet (~1300 Nm/rad, [6]) are similar to the largest interface stiffness, and higher than the smallest stiffness measured. Thus, irrespective of socket type, the interface likely influences the dynamics of locomotion. These characterizations are increasingly relevant, as biomimetic control approaches of emerging robotic devices seek to emulate able-bodied joint mechanics, and do not account for the mechanics of the interface.

REFERENCES

1. Sensinger JW and Weir RF *IEEE TNSRE* 16(2), 184-90, 2008.
2. Grevsten S and Erikson U *Upsala J Med Sci* 80, 49-57, 1975.
3. Erikson U and James U *Upsala J Med Sci* 78, 203-14, 1973.
4. Papaioannou G, et al. *Comp Vis Med Imag Proc* 91-112, 2011.
5. Gailey R, et al. *J Rehabil Res Dev* 45 (1), 15-29, 2008.
6. Mooney LM, et al. *IEEE EMBC*, 2014.

ACKNOWLEDGEMENTS

This work was supported by U.S. Department of Education grant H133F130034, U.S. Army grant 81XWH-09-2-0020 and NIH grant T32 HD07418. The authors thank Kelly Lee, Lisa Streff and Suzanne Finucane.



	Subischial	Ischial	Units	Isch./Sub.
Axial	19 (0.81)	50 (1.4)	N/mm	2.6
Frontal (medial)	160 (6.5)	2100 (660)	Nm/rad	12.9
Frontal (lateral)	610 (38)	1500 (700)	Nm/rad	2.4
Sagittal (anterior)	170 (5.0)	2000 (620)	Nm/rad	12.0
Sagittal (posterior)	470 (20)	1600 (250)	Nm/rad	3.4

Figure 2: Illustrations of subischial (top left) and ischial containment (top middle) sockets, as well as axial and rotational stiffness metrics (bottom table) for differing sockets, planes of loading (frontal and sagittal), and foot placements conditions, mean (standard deviation). Values are resolved in a local pylon/socket reference frame, which is shown (top right).

ASSISTIVE ANKLE POWER PROMPTS MUSCULAR COMPENSATIONS DURING GAIT

Emily S. Gardinier, Wyatt Felt, Jeffrey Wensman, C. David Remy and Deanna H. Gates

University of Michigan, Ann Arbor, MI, USA

email: egardin@umich.edu, web: <http://rehab-biomech-lab.kines.umich.edu/>

INTRODUCTION

Muscular compensations by both intact and residual limbs have been described for individuals walking with passive elastic ankle prostheses [1, 2]. These devices can only supply about half the power normally provided by the plantarflexors in the intact human ankle. A commercially-available, powered ankle-foot prosthesis that supplies plantarflexor power with each step has shown promise in improving walking economy and normalizing ankle kinematics and kinetics [3, 4]. However, the neuromuscular adaptations that drive these changes are not yet understood. Characterizing these adaptations will help clarify the mechanisms by which powered devices improve walking economy and may inform future device design. Therefore, the purpose of this study was to characterize the muscular compensations exhibited in response to walking with various amounts of prosthetic ankle power.

METHODS

Two (2) males with trans-tibial amputation were fitted with the powered ankle prosthesis (BiOM T2 Ankle System, BiOM, Inc., Bedford, MA) by a manufacturer-certified prosthetist. Subjects were experienced prosthesis-users (44 and 15 yrs post-amputation; ages 59, 24 yrs old; BMI: 28.9, 26.9 kg/m², respectively). Testing consisted of treadmill walking at five ankle power settings in random order: prosthetist-chosen, 0%, 25%, 75% and 100% power (0P, 25P, 75P, 100P). Metabolic cost of transport was measured using a portable gas analyzer. Surface electromyography (EMG) was recorded from gluteus medius (GM), vastus lateralis (VL), rectus femoris (RF), medial/lateral hamstring (MH/LH), medial/lateral gastrocnemius (MG/LG) and tibialis anterior (TA) bilaterally where possible. Treadmill belt speed was set based on leg length

(1.16, 1.23 m/s). The first power setting condition was preceded by a 10-minute accommodation period and subsequent accommodation periods were five minutes each. After accommodation, a 3-minute sample of expired air and a 30-second sample of EMG were acquired. Cost of transport was energy expenditure normalized to bodyweight and distance traveled. After visual inspection of raw EMG signals, linear envelopes were generated by full-wave rectifying and applying a low-pass filter (6 Hz). The resultant envelopes were normalized to peak EMG from the prosthetist-chosen settings. Muscle EMG magnitude variables included peak amplitude (pkEMG) and the integral of muscle activity per gait cycle (iEMG). Muscle co-contraction was assessed for 2 muscle pairs: VL-LH and MG-TA. Co-contraction indices equaled the agonist iEMG divided by antagonist iEMG. For analysis, the gait cycle was divided into discrete phases as outlined by Seyedali et al. [5] (for VL-LH: early mid-stance and late swing, for MG-TA: early stance, late stance and early swing).

RESULTS AND DISCUSSION

Metabolic cost of transport tended to decrease with increasing levels of ankle power (means in J/Nm; 0P = 0.396; 25P = 0.427; 75P = 0.375; 100P = 3.57). For the intact limb, the maximum prosthetic ankle power (100P) was associated with large, consistent decreases in EMG_{pk} and iEMG in muscles of the intact limb, particularly the hamstrings, quadriceps and gluteus medius muscles (Table 1). Increased prosthetic ankle power was associated with inconsistent changes in muscle co-contraction indices (Figure 1). In general, the muscles of the intact limb were less active when additional ankle power was supplied (Figure 2). The largest decreases in muscle activity were seen for the intact limb, which suggests that much of the energetic gains provided by the powered ankle

prosthesis are accomplished by reducing demand on intact limb muscles crossing the hip and knee.

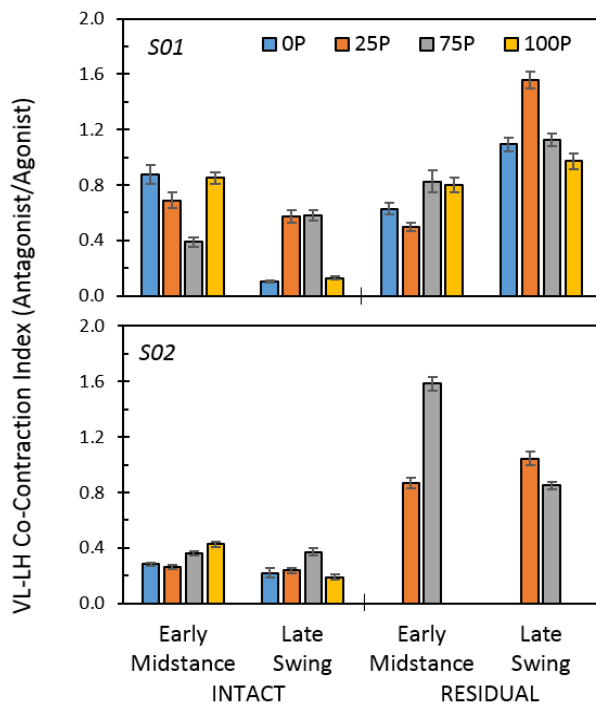


Figure 1. With increased power, co-contraction for residual limb VL-LH increased in early mid-stance and decreased in late swing (means \pm SE). Residual EMG unavailable for S02 at 0P and 100P.

For the residual limb, modest-sized decreases in pkEMG and iEMG occurred for hamstrings (Table 1). Changes in other residual limb muscles were small and inconsistent in direction. Persons using passive elastic ankle-foot prostheses walk with greater residual limb hamstring and hip flexor activity [1, 2]. The addition of ankle power in the present study appeared to decrease compensatory hamstring activity. For the residual limb, VL-LH co-contraction was greater than for the intact limb and tended to increase in early stance with increasing ankle power (Figure 1). Co-contraction on the prosthetic side may indicate a limb stiffening strategy adopted to increase stability early in stance.

Table 1: Sizes of change (Cohen's d) in peak and integrated EMG for 0P vs. 100P. Large negative effects are shaded and represent decreased muscle activity with the addition of more prosthetic ankle power (100P).

	Subject	GM	RF	VL	LH	MH	LG	TA
Intact iEMG	S01	-0.3	-1.3	-0.5	-0.8	-1.4	-1.2	-0.6
	S02	-0.8	0.8	-2.0	-1.8	-1.3	0.2	-0.2
Intact pkEMG	S01	-0.8	-1.3	-1.1	-0.7	-0.5	-1.7	-0.7
	S02	-0.9	0.7	-2.1	-0.8	-0.8	-0.7	-0.5

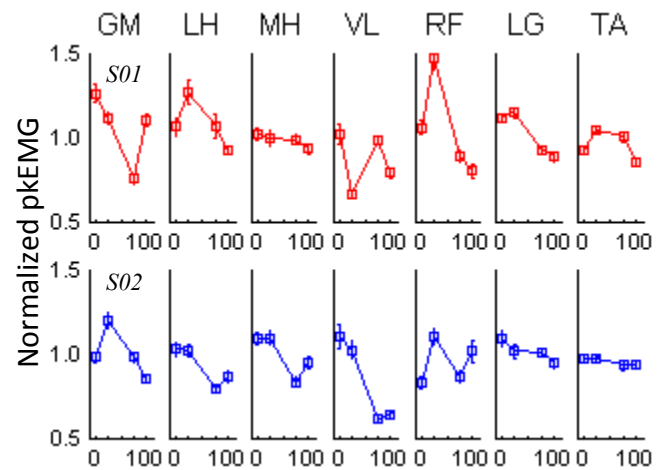


Figure 2. Peak EMG decreased for intact limb muscles of both subjects with increasing power (means \pm SE).

CONCLUSIONS

Data from the two individuals tested in the present study suggest that reductions in energy cost of walking with a powered ankle prosthesis may stem from decreased muscular effort of the intact limb. Additionally, residual limb hamstring muscle compensations appear to decrease when using a powered ankle. Further work with more subjects will clarify the mechanisms by which ankle power can reduce energy expenditure during gait.

REFERENCES

1. Isakov, E. et al. *J Rehabil Med*, **33**: 196-9, 2001.
2. Fey, N. et al. *J Electromyogr Kinesiol*, **20**: 155-61, 2010.
3. Herr, H. and Grabowski, A. *Proc Biol Sci*, **279**: 457-64, 2012.
4. Ferris, AE. et al. *Arch Phys Med Rehabil*, **93**: 1911-8, 2012.
5. Seyedali, M. et al. *J Neuroeng Rehabil*, **9**: 29, 2012.

METABOLIC COST CHANGES WITH THE AMOUNT OF PROSTHETIC ANKLE POWER PROVIDED

Audra Davidson, Wyatt Felt, Jeffrey Wensman, Emily S. Gardinier, C. David Remy, Deanna H. Gates

The University of Michigan, Ann Arbor, MI, USA
email: gatesd@umich.edu, web: <http://rehab-biomech-lab.kines.umich.edu/>

INTRODUCTION

The ankle plantarflexors produce roughly 80% of the mechanical power required for normal gait [1], yet current passive elastic prostheses only produce an eighth of this power [2]. Likely due to this deficit, people with transtibial amputation have a 10-30% greater metabolic cost for walking than non-amputees [3]. Active ankle prostheses that are able to accommodate for the functionally absent plantarflexors have improved metabolic cost during walking [4]. However, it is unclear whether directly matching the power of the intact limb would alleviate this plantarflexor deficit, as higher power outputs might be needed to counteract sub-optimal power delivery of the prosthesis. Therefore, the purpose of this study is to determine how incremental adjustments in prosthetic ankle power affect the metabolic cost of walking.

METHODS

Two males with transtibial amputation (ages 59, 24 yrs; BMI 28.9, 26.9 kg/m²) were fitted with the BiOM T2 powered ankle prosthesis (BiOM, Inc. Bedford, MA) by a certified prosthetist. Subjects walked on a treadmill while the power supplied to the prosthesis was varied. Metabolic costs were measured using a portable gas analyzer (K4b², Cosmed, Rome, Italy). Treadmill speed was determined by subject leg length and remained consistent across conditions.

Each participant was given 10 minutes to accommodate to treadmill walking prior to testing. Subjects were tested at five ankle power setting conditions in random order: prosthetist-chosen (PC), 0%, 25%, 50%, 75% and 100% power. Participants were given five minutes to acclimate to each power setting, after which a 3-minute sample

of expired air was acquired during steady-state oxygen consumption.

In order to determine if changes in metabolic costs were a result of a true metabolic change rather than normal variability, the minimal detectable change (MDC) value for metabolic cost of transport (COT) was determined. This was acquired by collecting steady-state oxygen consumption data on nine healthy subjects (age 23 ± 3 years, 56% male) during treadmill walking. Oxygen consumption was collected for three bouts of walking interrupted by three bouts of seated rest to obtain within-session variability of COT. Testing was performed on two separate days to determine between-session variability. Intraclass correlation statistics were performed on COT within a session and on the average COT between days. The MDC was calculated using the intraclass correlation coefficient [5] and compared to the changes exhibited in the subjects with amputation.

RESULTS AND DISCUSSION

The within-session MDC value determined for cost of transport was 0.016 J/N.m (Table 1). The between-day ICC was 0.878, and the MDC was 0.0543 J/Nm.

Table 1. Reliability of Cost of Transport (COT) Values for COT are given as mean (standard deviation) across nine healthy subjects for each of three bouts of treadmill walking over two days.

	COT (J/Nm)			ICC	MDC
	Bout 1	Bout 2	Bout 3		
Day 1	0.350 (0.077)	0.347 (0.063)	0.331 (0.065)	0.991	0.017
Day 2	0.346 (0.046)	0.350 (0.047)	0.349 (0.050)	0.987	0.015

For subjects with amputation, the COT tended to decrease as ankle power increased (Fig. 1). There were no measurable differences in COT in comparison to 0% power for S01, as this was measured on a separate day (Table 2). COT was measurably diminished at 75% and 100% power for S01, whereas no detectable differences in COT were exhibited in the lower power levels or between 100% and higher power levels. The COT difference between PC (57%) power and 0% power was -0.013 J/N.m, falling below the between-day MDC value.

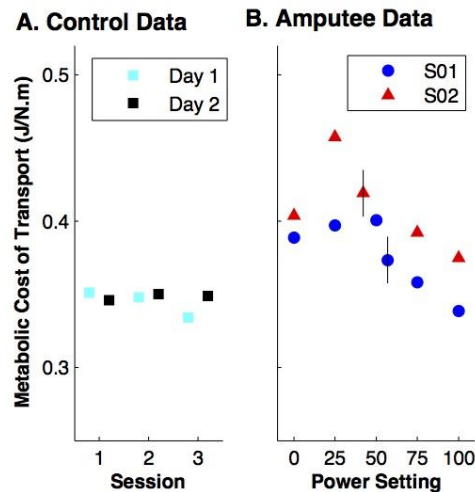


Figure 1: (A) Average COT for healthy subjects over two days over three sessions of walking and (B) COT during three minutes of steady state walking for two subjects with a solid line representing \pm MDC (0.016 J/N.m) on PC power.

Subject S02 demonstrated measurable changes in COT between all power settings except for 75% to 0% power. COT was higher for PC (42%) power when compared to 0% power, and for 25% compared to 0% power (0.027 J/N.m and 0.0650 J/N.m respectively). All other pairings demonstrated measureable decreases in COT (Table 2).

For both subjects, increasing the power supplied by the prosthetic beyond PC power yielded decreases in cost of transport greater than the MDC (Table 1).

Prosthetist-selected power settings were chosen in an effort to match the ankle work done by the intact limb. These data suggest that higher ankle work of the prosthesis may further reduce the metabolic cost of walking. It is possible that the power output of the prosthesis is not only compensating for the loss of plantarflexor power, but also reducing muscular compensations at the hip flexors of the residual limb [6]. Additionally, accommodating for any inefficiencies in power delivery of the device may lead to the necessity of power increases greater than that of the intact ankle. This inefficiency would lead to the dissipation of energy needed to aid powered ground push-off, thereby requiring increased power supply.

CONCLUSIONS

Increased power delivered by the ankle prosthesis was sufficient to reduce COT by measurable amounts. Future directions for this work include an examination of these parameters with a larger sample size. Characterizing the effects of the timing of power delivery on metabolic costs as well as changes in muscular activity will further clarify the mechanisms of these metabolic cost savings.

REFERENCES

1. Winter DA, Sienko SE, *J Biomech* **21**, 361-367, 1988.
2. Zmitrewicz RJ, et al. *J Biomech* **40**, 1824-31, 2007.
3. Fisher SV, Gullickson G Jr, *Arch Phys Med Rehabil*, **59**, 124-133, 1978.
4. Herr HM, Grabowski AM, *Arch Phys Med Rehabil*, **279**, 457-464, 2012.
5. Gardinier ES, et al. *Gait Posture* **38**, 1051-3, 2013.
6. Sadeghi H, et al. *Am J Phys Med Rehabil* **80**, 25-32, 2001.

Table 2. Cost of transport (J/N.m) for two subjects across power settings (0-100%) and at the prosthetist-chosen power (PC). * = data taken on a separate day.

Subject	0%	25%	PC = 42%	50%	PC = 57%	75%	100%
S01	0.389*	0.397		0.401	0.376	0.358	0.338*
S02	0.392	0.457	0.419			0.392	0.375

Developing a Robotic Elbow Joint Controlled by EMG Stimulus

Louis Christensen, Julia Jenks, Cody Johnson, and Craig M. Goehler

Department of Mechanical Engineering, Valparaiso University, Valparaiso, IN, USA
email: craig.goehler@valpo.edu

INTRODUCTION

Prosthetics allow users to regain mobility in limbs that were lost due to trauma or birth defect. Due to the variety of patient needs and capabilities, prosthetics can be categorized as aesthetic, functional, or robotic. Aesthetic prosthetics recreate the limb with little to no functionality while functional prosthetics allow users to regain basic movements, such as grasping objects, by implementing simple systems like pulleys and hooks. Robotic prosthetics provide finer control with a broader range of motion in tasks but can be difficult to use. Although the field of prosthetics has made vast improvements in terms of replicating natural movement, people still stray away from these advancements because they are difficult to use, expensive, or do not have aesthetic appeal.

The goal of this design study was to independently create an elbow joint prototype with an emphasis on simplicity and affordability. The resulting design uses a battery powered worm drive and an EMG control system. This paper describes the process for the joint design along with completed electronic schematics and part drawings for the completed design.

METHODS

To begin the joint design, literary review was conducted to determine a baseline for this design. One design used pneumatics to simulate muscle contractions; however, this design was bulky, inaccurate, and overdesigned for lifting in a typical prosthesis [1]. This led the design towards a more mechatronic approach.

Useful designs were found for a high thrust helical motor joint design [2] and an elbow rehabilitation

device [3]. The helical motor design was a lighter, more compact design that provided the torque necessary for an elbow joint, but the cost for a helical motor was too great to be practical for this study. The elbow rehabilitation design contained an alternative to the helical motor that was similarly compact and significantly reduced the cost involved for the prosthetic. This ultimately led to a final design which implements a worm gear drive to provide thrust for the joint movement.

For the control system, EMG signal processing was found to be the simplest solution that allowed the user the most natural control for the joint. EMG processing circuits have already been developed to convert the muscle stimulus into a usable signal for control [4]. These designs were reconfigured to reduce cost, which resulted in a signal processing system that can be calibrated for the user in real time.

RESULTS AND DISCUSSION

Figure 1 displays the SolidWorks model of the elbow joint. The elbow was built around the motor, gear, and worm. These design parameters keep the product relatively small and allow for future modular construction. The forearm allows for any number of end effectors to be attached, such as a hook, a false hand, or even a robotic alternative. The prosthetic can be attached by fitting a tube into the brackets on the elbow, above the motor. This tube could be clamped onto a static surface, or onto a socket for use on a person. Plastic covers, shown in orange, enclose the worm drive to ensure the user does not contact the high-speed motor. Finally, each part is designed to be simple to machine. This reduces the build time and the cost.

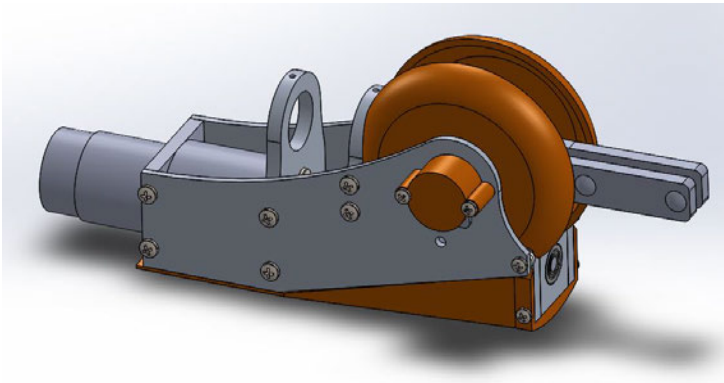


Figure 1: 3D Rendering of the Elbow Joint

The simplicity in the design stemmed from some aspects of human kinematics being ignored. The normal range of motion for a human elbow is 145 degrees, but this design can move up to 180 degrees. This can be accounted for in the control program where a limit of motion is imposed from feedback with a potentiometer. Another aspect that is overlooked is the carrying angle of the elbow. Normally, this is between 5 and 15 degrees, but in this elbow it is 0. This simplified the design because it allowed the device to be symmetric about a middle plane.

The electrical system was similarly designed with a focus on simplicity. The EMG processing circuit, shown in Figure 2, provides a DC analog voltage that can relate to muscle flexion. By rectifying and then envelope filtering the output of the EMG amplifier, the system utilizes a simple method to create a signal usable by a microcontroller.

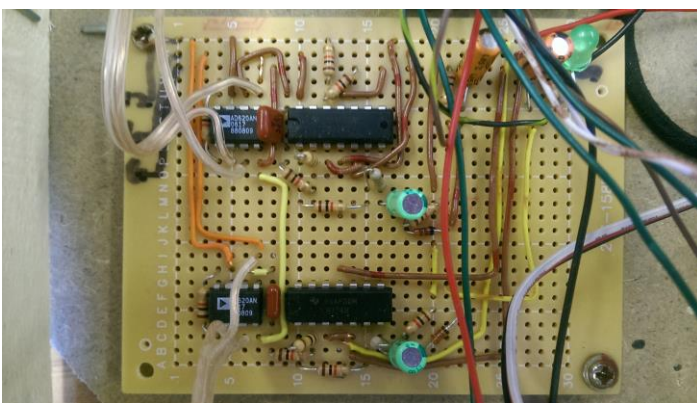


Figure 2: EMG Processing Circuit

The control system then interprets EMG signal from the triceps and biceps to move a set point that the motor will follow. To provide an inexpensive method of elbow feedback, a potentiometer is connected to the elbow joint. By combining position feedback and EMG inputs, the user can move the mechanical elbow up and down by tensing and relaxing muscles in their arm that would have originally been used to move the anatomical elbow.

CONCLUSIONS

The scope of this project can extend to multiple fields. Outside of prostheses, the joint could be implemented as part of a robotic arm for high torque operations. The EMG processing could eventually stem into the fields of virtual reality for finer control by users. For prosthetics, creation of end effectors would be the next step, as a wide variety of end effectors adds functionality to the elbow. These can range from a simple hook to a fully controllable hand. Experiments could also be performed to create calibration curves in order to design a more universal design rather than the current custom calibrated system. Finally, the design could be adapted for mass production by improving the construction techniques for the elbow.

REFERENCES

1. Robinson, R. *Journal of intelligent material systems and structures* **22**, 13, September 2011.
2. Furuya, Y. et al. *IECON proceedings* 5894-5899, 2013.
3. Ripel, T. et al. *International Journal of Advanced Robotic Systems* **11**, 143, 11 July 2014.
4. Al-Faiz, M.Z. et al *Iraq J. Eletrical and Electronic Engineering*, **6**, 2, 2010.

MECHANICAL ENERGY DIFFERENCES IN ARM-CONSTRAINED HUMAN ROLLING

Mahdi Hassan, Linh Q. Vu and Nils A. Hakansson

Wichita State University, Wichita, KS, USA

email: nils.hakansson@wichita.edu, web: <http://www.wichita.edu/thisis/home/?u=bme>

INTRODUCTION

Rolling is a complicated movement that requires the coordinated motion of the entire body. The ability to roll, most commonly executed as turning in bed, is a milestone in human development [1] and is one of the most fundamental activities of daily living. However, the underlying mechanisms, i.e., the neuromuscular coordination and muscular strength requirements, necessary to roll, remain unknown.

Healthy individuals use a wide range of movement patterns when they roll from the supine to side-lying position. The motion of the upper extremities is a primary source of the variability in the movement patterns [2]. A reduction in rolling variability could facilitate a biomechanical analysis and improve our understanding of rolling. Therefore, the goal of the study was to determine whether constraining the arms would alter biomechanical measures associated with rolling. To this end, the objective of this study was to determine whether crossing the arms over the chest changed the energy demands of rolling from the supine to side-lying position.

METHODS

All subjects gave informed consent to participate in the study that was approved by the Wichita State University Human Subjects Review Board. Experimental kinematic data were collected from ten college-aged subjects (male to female ratio 6:4) with no limitations to their ability to roll.

An 8-camera video motion capture system (Motion Analysis Corp., Santa Rosa, CA) recorded (50 Hz) the positions of 32 retro-reflective markers that were used to define the foot, shank, thigh, pelvis, trunk, upper and lower arms, and head segments for each subject for both a standing static pose and the rolling motion.

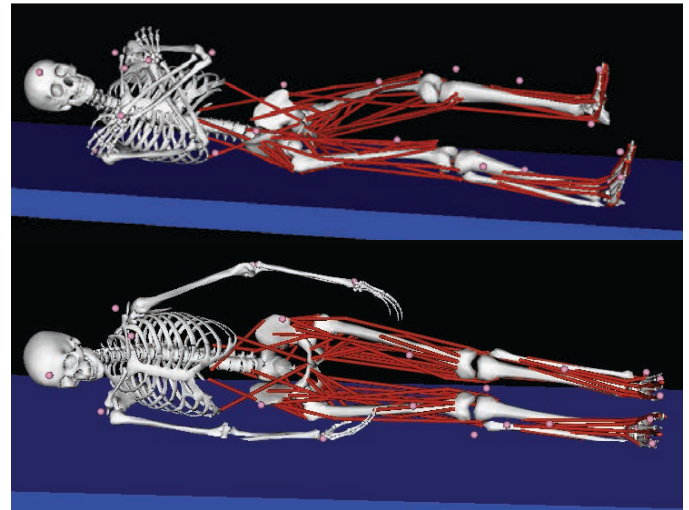


Figure 1: Musculoskeletal model of rolling for the arms crossed (upper figure) and arms uncrossed conditions.

For the rolling trials, subjects laid on a firm surface in the supine position and rolled to their right into a side-lying position. Subjects performed two types of rolling movements: i) arms crossed over the chest and ii) arms uncrossed and free to move naturally. Five trials were collected for each type of rolling and for each subject, resulting in 100 trials total.

Marker position data were imported into OpenSim (v3.2) [3] to calculate the centers of mass (COM), linear (!), and angular velocities (") of the body segments. The parameters of a full body musculoskeletal model consisting of 20 segments and 37 degrees-of-freedom were adjusted to best fit the experimentally measured subject mass and markers positions (Figure 1). The resultant kinematics were low-pass filtered at 4Hz and then analyzed to determine the COM and linear and angular velocities of each body segment.

The potential and kinetic energy of the body segments were calculated to determine the

mechanical energy. The potential (E_p) and kinetic (E_k) energy were calculated as:

$$E_p = mgh$$

$$E_k = \frac{1}{2}mv^2 + \frac{1}{2}I\omega^2$$

where m is the mass of body segment, g is the gravitational constant, h is the height of the segment COM, v is the velocity of the segment COM, I is the mass moment of inertia of the segments, and ω is the angular velocity of the segment. Total energy (E_{tot}) was calculated by summing all positive increments in E_p and E_k [4].

A two-factor repeated measures ANOVA ($\alpha = 0.05$) was performed to identify differences in E_{tot} between the two rolling conditions. The two factors were rolling condition at 2 levels and trials at 5 levels.

RESULTS AND DISCUSSION

The mechanical energy averaged across subjects for rolling with the arms crossed and uncrossed was $60.1 \pm 12.1J$ and $72.6 \pm 13.8J$, respectively. For nine of the ten subjects, the mechanical energy averaged across the five trials was lower for rolling with the arms crossed than with the arms uncrossed (Figure 2). The statistical analysis indicated that there was a significant difference ($p = 0.007$) between the E_{tot} measures for rolling with the arms crossed and uncrossed. There were no identified differences in E_{tot} associated with the trials or the interaction between trials and rolling conditions. The potential energy component comprised the majority of E_{tot} for arms crossed (90%) and uncrossed (87%) rolling.

Based on the results, crossing the arms over the chest changed the energy demands of rolling from the supine to side-lying position. The result that rolling with the arms crossed is associated with less mechanical energy than rolling with the arms uncrossed was not unexpected. Potential energy increases were the primary contributor to E_{tot} for both rolling conditions. Motion of the arms increases both potential and kinetic energy as they are raised and maneuvered to either assist or not

interfere with rolling. However, the motion of the lower extremities was not examined in this study and could have contributed to the observed differences in the E_{tot} measures.

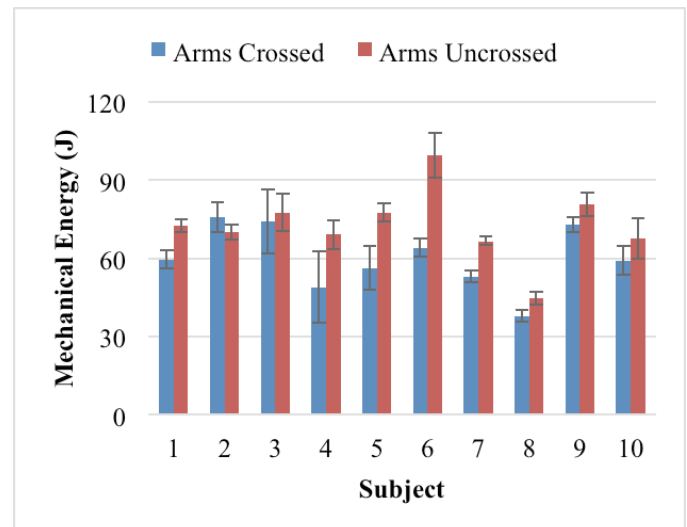


Figure 2: Mean mechanical energy for rolling with the arms crossed and uncrossed. Error bars represent ± 1 standard deviation.

CONCLUSIONS

Rolling is a complicated motor task for which there exist many movement patterns. This study is one of the first to quantify biomechanical measures of human rolling and the first to examine the effects of constraining the arms on generated mechanical energy. The result that crossing the arms over the chest changed the energy demands of rolling could have implications for future biomechanical studies and clinical settings.

REFERENCES

1. Alexander R, et al. *Normal development of functional motor skills: the first year of life*, Therapy Skill Builders, 1993.
2. Richter RR et al. *Phys Ther* **69**, 63-71, 1989.
3. Delp SL, et al. *IEEE Trans Biomed Eng* **54**, 1940-1950, 2007.
4. Cavagna GA et al. *J Physio* **262**, 639-657, 1976.

ACKNOWLEDGEMENT

This work was supported by the Wichita State University Research/Creative Projects (URCA) Award.

VARIABILITY IN TORSO KINEMATICS IN ARM-CONSTRAINED HUMAN ROLLING

Linh Q. Vu, Mahdi Hassan and Nils A. Hakansson

Wichita State University, Wichita, KS, USA

email: nils.hakansson@wichita.edu, web: <http://www.wichita.edu/thisis/home/?u=bme>

INTRODUCTION

Decubitus ulcers (DU), also known as bedsores, are injuries to the skin and underlying tissues. Estimates indicate that 1 to 3 million people develop a DU in the United States each year and at a cost of over one billion dollars per year [1].

Human rolling, most commonly executed as turning in bed, is one of the most fundamental activities of daily living. Rolling in bed serves to improve comfort, circulation, sleep quality, and reduce the risk of DU. Rolling is a complicated movement that requires the coordinated motion of the entire body [2, 3]. Previous research on human rolling has been dependent on observing the rolling motion with constraints to decrease due to the variable nature human rolling [3]. Based on the observations of the aforementioned studies [2, 3], we hypothesized that applying constraints to the rolling motion, for example arms crossed over the chest, would not change the fundamental rolling movement patterns of the torso. Therefore, the objective of this study was to determine whether constraining the upper extremities would alter shoulder and pelvis kinematics when rolling from the supine to side-lying position.

METHODS

All subjects gave informed consent to participate in the study that was approved by the Wichita State University Human Subjects Review Board. Experimental kinematic data were collected from twelve college-aged subjects with no limitations to their ability to roll.

An 8-camera video motion capture system (Motion Analysis Corp., Santa Rosa, CA) recorded (50 Hz) the positions of retro-reflective markers adhered to the left and right acromion of the shoulders and

anterior superior iliac spine (ASIS) of the torso of each subject as they rolled from the supine to side-lying position. Subjects performed two types of rolling movements: i) arms crossed over the chest and ii) arms uncrossed and free to move naturally. All subjects rolled to their right. Five trials were collected for each type of rolling and for each subject, resulting in 120 trials total.

Shoulder and pelvis angles were defined as the angle formed by the vector from the right to left shoulder markers and by the vector from right to left pelvis markers with respect to the horizontal plane, respectively. The angular velocities of the shoulders and pelvis were determined through numerical differentiation (central difference method) of the angle data.

Initiation and cessation of the rolling motion was based on the shoulder and pelvis angular velocities. Initiation of the roll was defined as the earlier occurrence of the last peak before the shoulder or pelvis angular velocity increased monotonically towards its peak velocity. The cessation of the motion was defined by the latter of the shoulder or pelvis angular velocities to reach zero after achieving its peak velocity. All trials were normalized as a percentage of the rolling motion (supine to side-lying) based on the identified initiation and cessation times.

One-factor repeated-measures ANOVA tests were performed to examine the effect of crossing the arms had on the segment that initiated and ended the roll (shoulder or pelvis), the peak shoulder and pelvis angular velocities, the percentage of roll at which the peak velocities occurred, and the duration of the roll. For each test, the independent variable was rolling condition at two levels (arms crossed and uncrossed).

RESULTS AND DISCUSSION

Rolling with arms crossed did not significantly affect the segment that initiated the roll ($p = 0.667$), the segment that concluded the roll ($p = 0.331$), or the timing of peak shoulder and pelvis angular velocities. The rolling condition effects did significantly affect the peak shoulder ($p = 0.001$) and pelvis ($p = 0.004$) angular velocities, and the duration of the roll ($p = 0.044$). In the arms crossed condition, subjects had increased roll completion times by a mean difference of .167 seconds. Across the 60 trials for each rolling condition, the percentage of rolls in which the pelvis or the shoulder started and ended the roll were similar (Table 1).

Table 2: Percent of trials in which the shoulders and pelvis initiated or terminated the motion for the two rolling conditions for the 120 trials.

Sequence order	Rolling Restraint	Segment	Occurrence (%)
Start of roll	Arms crossed	Shoulder	75%
		Pelvis	23.3%
		Both	1.7%
	Arms uncrossed	Shoulder	70%
		Pelvis	26.70%
		Both	3.30%
End of roll	Arms crossed	Shoulder	45%
		Pelvis	40%
		Both	15%
	Arms uncrossed	Shoulder	43.30%
		Pelvis	48.30%
		Both	8.40%

The focus of this study was on torso kinematics because the torso largely controls how the rolling motion is executed. An important finding was that there was no significant change in whether the shoulder or pelvis initiated the roll or whether shoulder or pelvis concluded the roll, when rolling with the arms crossed and uncrossed. These findings are consistent with those presented by Richter et al. [2] who reported that the most common rolling movement initiation involved shoulder movement first. Another important finding was that peak shoulder and pelvis angular velocities

varied as a result of different rolling conditions. However, the time in the roll at which these peaks were observed did not vary. because the occurrence of peak velocity for both the shoulder and peak velocities across conditions was not significantly different, it was inferred that the integrity of the roll was kept and the timing of the rolling motion was similar. The third important finding was that people execute the rolling motion slower when crossing the arms, as compared to arms uncrossed. The increased pelvis and shoulder velocity in arms uncrossed may be due to a momentum increase from the usage of the arms. The extension of the arms could have generated more torque by shifting the center of mass away from the axis of rotation during rolling.

CONCLUSION

Rolling is a fundamental and complicated task. By having subjects roll with their arms crossed, it increased the speed of the roll, yet produced no identifiable difference in their fundamental rolling movement. This finding is very useful because the folding of arms will remove any momentum that can be generated and still keep the integrity of the roll. Studies made using the arms crossed constraint may be more inclusive as persons with physical or neurological limitations may not have use of their arms to assist in the roll. The study provides more information regarding the biomechanics of human rolling that may be useful in the creation of solutions for those persons who cannot roll independently.

REFERENCES

1. Lyder CH, et al. *J Amer Geri Soc* **60**,1603-1608, 2012.
2. Richter RR, et al. *Phys. Ther* **69**:63-71, 1989.
3. Sekiya N, et al. *J. of Jpn. Phys. Ther. Assoc* **7**, 1-6, 2004.

ACKNOWLEDGEMENT

This work was supported by the Wichita State University Research/Creative Projects (URCA) Award.

Human-Exoskeleton Hybrid Model to Produce Stable Gait through Inter-limb Coordination

Duanyi Wei, Ioannis Poulakakis, Jill S. Higginson

University of Delaware, Newark, DE, USA

email: higginso@udel.edu

INTRODUCTION

Robotic gait training has been studied and tested in research labs and clinical settings [1]–[3], and it has shown mixed success in improving the functional ambulation in post-stroke individuals [4,5]. The current state-of-the-art in rehabilitation robots is to encourage subjects' participation in tracking desired trajectories obtained from healthy subjects, by providing feedback about the performance error [5]. As human locomotion is composed by movements of both sides, it clearly involves well-organized inter-limb coordination. But current rehabilitation robots fail to include this cooperative mechanism of locomotion. To address the dynamic interaction between human and exoskeleton, a model is needed to capture key aspects of human locomotion and provide the infrastructure for evaluating different coordination strategies.

Current musculoskeletal models are insufficient to address gait stability over time [6], thus are of limited value when it comes to predicting the interaction between human and exoskeleton. Low-dimensional human-inspired biped models [7]–[9], on the other hand, have proven capable of producing salient human-like gait features and providing tractable measures to ensure gait stability and robustness. The objective of this study is to construct a low-dimensional model to represent the asymmetric, hybrid human-exoskeleton locomotion. We then use this model to propose a control strategy for the robotic limb that accounts for the contralateral human limb dynamics, and test the hypothesis that the proposed control framework can achieve stable gait.

METHODS

Model: To characterize the dynamical asymmetry between the side wearing exoskeleton and the unaffected

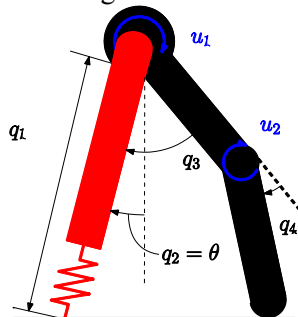


Figure 1: Model of human (red) and robotic (black) limbs.

limb, a hybrid, low-dimension, sagittal-plane model of Fig. 1 is proposed. We adopt the prismatic-leg model in [7] as the representation for “human limb”. Such models have proven successful in capturing key gait features [7,8]. The exoskeleton is represented as a two-link structure. The torso mass is condensed to a point mass at the hip. The human side is actuated by the hip and the robotic actuators are located at contralateral hip and knee joints. To avoid confounding internal interactions, it is assumed that the robot drives the affected human side and behaves as human limb during stance (Fig. 2).

Dynamics: Due to the lateral asymmetry of the model, the cyclicity of gait over a complete stride composed by a left and right step is monitored. Each step consists of swing phase (SW), impact, double stance (DS) and liftoff. Rather than presenting detailed derivations, we highlight the modifications with respect to impact dynamics. The derivation of impact dynamics follows the impact hypotheses and procedure as in [9], except that we enforce the post-impact stance leg to be fixed to the ground in order for the system to enter double stance, which permits the influence of external forces at the stance leg end during impact. See [7]–[9] for more details.

Limb Coordination: Coordinated locomotion is achieved by enforcing output functions that prescribe the motion of the robot relative to the human, to zero. Specifically during robot swing phase, we want to coordinate hip and knee angles according to motions of the human side. We construct output functions that embed the constraints of controlled variables: $h(q) := [q_3, q_4]^T - h_d(\theta)$ where h_d specifies the desired evolution of hip and knee angles, which can be parametrized by polynomials of self-selected order. By choosing θ to be the angle of the human limb (q_2), the movements of the robot hip and knee are coordinated with the states of the human side upon zeroing the outputs. To fulfill the objective, we adopted input-output linearization to compute the torque necessary to maintain the output at zero [9].

Gait Stability: The notion of stability in this work assures that nominal walking motion can be recovered when the system is perturbed. A Poincaré map [10] is defined as a mapping from the starting states to the states when the model returns to the same instance

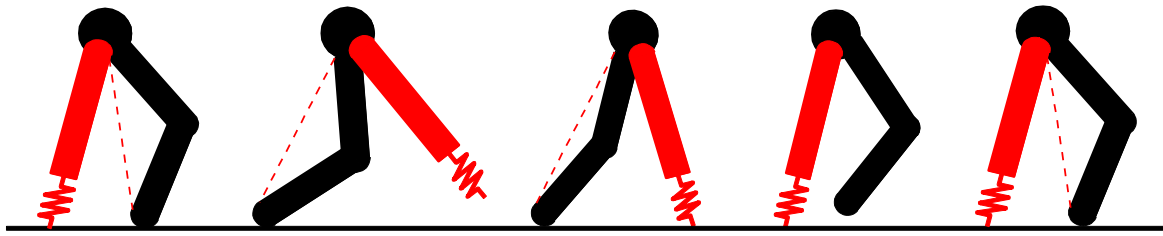


Figure 2: Snapshots of the model over one full gait cycle

after a full cycle. Our model is initialized at the instant of human limb push-off. A periodic gait *exists* if the corresponding initial states can be repeated after the return to the human push-off in the next step. The stability of this gait is further guaranteed by ensuring the eigenvalues of the linearized Poincaré map have magnitude less than 1 [10].

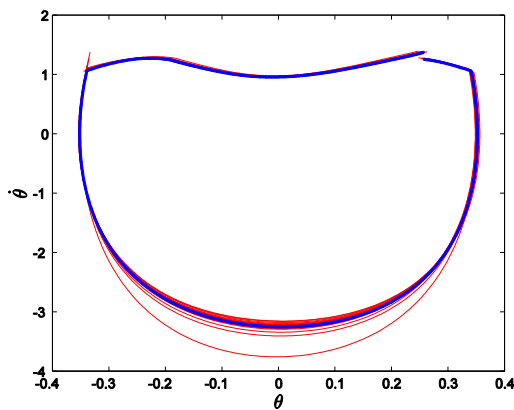


Figure 3: Phase portrait of the system if hip angle (q_3) is perturbed by 2° (10%) away from its initial value. The blue trajectory indicates nominal walking motion.

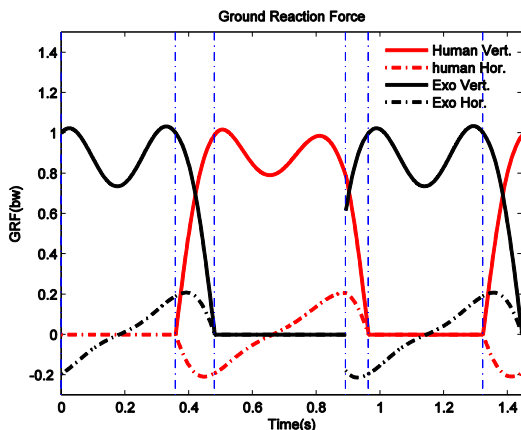


Figure 4: GRF profile of stable gait over three consecutive steps. The step starts after human limb push-off. The vertical lines separate swing and double support phases. All forces are normalized by body weight.

RESULTS AND DISCUSSION

Fig. 3 shows the stability of the obtained gait cycle (magnitude of eigenvalues < 1) after perturbation. The hybrid model eventually returns to its nominal walking

motion (blue) over time. Despite apparent asymmetry in the limbs, the introduction of coordinated exoskeleton motion with respect to human makes the system tolerant to external disturbances. This is due to the fact that exoskeleton can respond to changes in the human gait. In addition, despite the internal complexity of the actual system, this generic hybrid model demonstrates close resemblance in gait kinematics and GRF profile (Fig. 3) to human.

CONCLUSIONS AND OUTLOOK

This work proposed a control framework of enforcing inter-limb coordination. The results have shown the success of such coordination strategy in stabilizing the gait cycle in the presence of moderate disturbances. So far the controller only engages during the swing phase. Future work will identify a control strategy to coordinate the two sides during stance phase. Currently, we are also seeking means to integrate the controller with gait data from human locomotion and implement the control framework to human walking with the assistance of an exoskeleton device. This has potential applications in promoting limb coordination and gait stability for post-stroke subjects.

REFERENCES

1. Vallery J, et al. *IEEE Robot. Autom. Mag* **15**, pp. 60–69, 2008
2. Alex LE et al. *IEEE Trans. neural Syst. Rehabil. Eng* **17**, pp. 2–8, 2009
3. Riener RL et al *J. Rehabil. Res* **43**, pp. 679–94, 2006
4. Husemann B, et al. *Stroke* **38**, pp. 349–54, 2007
5. Kao PC, et al. *Gait Posture* **37**, pp. 113–20, 2013
6. John CT, et al. *Comput. Methods Biomech. Biomed. Engin* **6**, pp. 451–62, 2013
7. Haberland M, et al. *IEEE Int. Conf. Intell. Robot. Syst.*, pp. 3957–3962, 2011
8. Geyer H, et al. *Proc. Biol. Sci.* **273**, pp. 2861–2867, 2006
9. Westervelt ER, et al. *IEEE Transactions on Automatic Control* **48** pp. 42–56, 2003
10. Guckenheimer J, et al. *Nonlinear Oscillations, Dynamical Systems, and Bifurcations of Vector Fields*. Springer Science & Business Media, 1983

WRIST COMPRESSIVE FORCES AFFECT THE MEDIAN NERVE RESPONSE TO WHEELCHAIR PROPULSION AND OTHER MARKERS FOR CARPAL TUNNEL SYNDROME IN PEOPLE WITH PARAPLEGIA

^{1,2}Nathan S. Hogaboom*, ³Yen-Sheng Lin, ^{2,4,5}Lynn A. Worobey, ^{1,2}Alicia M. Koontz, ^{2,5}Michael L. Boninger

¹Department of Rehabilitation Science and Technology, University of Pittsburgh, Pittsburgh, PA

²Human Engineering Research Laboratories, VA Pittsburgh Healthcare System, Pittsburgh, PA

³Sensory Motor Performance Program, Rehabilitation Institute of Chicago, Chicago, IL

⁴Department of Physical Therapy, University of Pittsburgh, Pittsburgh, PA

⁵Department of Physical Medicine & Rehabilitation, University of Pittsburgh, Pittsburgh, PA

*Email: nsh15@pitt.edu

INTRODUCTION

Wheelchair users with paraplegia rely on their arms to perform most activities of daily living, and thus carry a high risk of developing repetitive strain injuries. One common injury in this population is carpal tunnel syndrome (CTS) [1], a compressive neuropathy in the wrist. One CTS risk factor is the repetitive application of external forces to the wrist, especially during movement [1]. Indeed, propulsive handrim kinetics and wrist kinematics are linked to CTS [2,3]; however, joint forces have not been examined in this context. The purpose of this paper was to investigate how propulsive wrist joint forces relate to markers for CTS in a sample of wheelchair users with paraplegia. Higher compressive wrist forces were hypothesized to correlate with subjective symptoms, physical examination findings, and ultrasound markers for CTS.

METHODS

Wheelchair users with non-progressive paraplegia were recruited through research registries and flyers. They were included if they were 18-65 years old; were injured for at least a year and after age 15; spoke English; had no unhealed upper limb fracture or dislocation, upper limb dysthetic pain, or cardiopulmonary problems; had a quick-release axle; and were not pregnant. Participants provided informed consent prior to the study, which was approved by the appropriate Ethical Committees.

Participants completed demographic and CTS symptom questionnaires [4], were weighed on a scale, and underwent a physical examination of the

median nerve (PEMN). This scale is comprised of five clinical tests for median nerve health: Phalen's test, Tinel's sign, thenar muscle atrophy and weakness, and pin-prick along median nerve distribution. Each is scored 0 (no sign), 1 (equivocal), or 2 (sign present). Bilateral scores are summed for a maximum of 20. Quantitative ultrasound (QUS) measurements of the median nerve were taken before and after the propulsion activity; this technique has high reliability when obtaining serial images [5]. A cross-sectional image of the nerve was obtained at the inlet of the carpal tunnel – the level of the pisiform bone – in the non-dominant hand (Fig. 1). A higher cross-sectional area (CSA) indicates a larger nerve proximal to the carpal tunnel, and thus possible entrapment. A MATLAB algorithm utilizes boundary trace to determine CSA of the nerve on the image, while blinding the user to subject and image time point.



Figure 1. *Cross-sectional ultrasound image of the median nerve (MN) at the pisiform bone (arrows).*

Participants propelled down a 15-meter runway over tile and carpet at self-selected and targeted (1.5 meters/second) speeds, then around a figure-8 course at maximum speed (five trials per condition). A 20-camera VICON system captured the runway volume. Participants were equipped with reflective

markers on the acromion, trunk, medial and lateral epicondyles, ulnar and radial styloids, and 3rd metacarpal-phalangeal joint; 8 reference markers were added to the upper- and lower-arm. A SmartWheel, which detects handrim kinetics, was attached to the chair. The SmartWheel and markers were placed on the non-dominant side. Kinematic data were collected at 60 Hz and filtered using a 4th order zero-phase low-pass Butterworth filter with 7 Hz cutoff. Kinetic data were collected at 240 Hz and filtered using an 8th order zero-phase low-pass Butterworth filter with a 20 Hz cutoff, then down-sampled to 60 Hz to match kinematics. Trials were split into start-up (first 3 strokes) and steady-state (all other strokes). All steady-state strokes per trial, and all trials per condition were averaged. Propulsion during the targeted and self-selected conditions was analyzed for the present study (no figure-8 trials). An inverse dynamics model was created to transform handrim kinetics from the SmartWheel to the wrist local coordinate system, which was defined as recommended by the International Society of Biomechanics [6]. Compressive forces are those acting along the long axis of the hand, directed proximally.

Significance was set to $\alpha=.05$. Kinetics from the four conditions were correlated ($p<.05$) and thus averaged to minimize Type 1 error. Body-weight can influence propulsive forces; thus, compressive forces were weight-normalized [2]. Three multiple linear-regression models were built with age, weight, and normalized compressive force as predictors. Outcomes included PEMN and CTS symptom questionnaire scores, and post-propulsion CSA. Baseline CSA was a covariate when post-propulsion CSA was an outcome, which tests how changes in CSA relate to age, weight, and force.

RESULTS AND DISCUSSION

Twenty-three wheelchair users with paraplegia were recruited yet data from 18 were analyzed; 3 did not meet inclusion criteria and 2 had kinematic data that could not be analyzed. Participants were 35.3 ± 10.4 years old with 13.3 ± 8.9 years since injury and weighed 75.5 ± 20.8 kilograms. There were 13 males and 5 females; 14 were white, 3 were black, and 1 was multiracial.

Subjects who propelled with higher compressive forces reported more CTS symptoms ($R^2=.370$, $p<.05$) and PEMN findings ($R^2=.272$, $p<.05$). Greater post-propulsion increases in median nerve CSA were also observed in those who propelled with higher compressive forces ($R^2=.195$, $p<.10$). The wheelchair handrim rests along the palm, approximate to the carpal tunnel. Prolonged exposure to force at this location may cause entrapment of the nerve or cumulative trauma; both of which may cause nerve damage that manifests as pain, weakness, or other symptoms. Although the relationship only trended toward significance ($p<.10$), a medium/large effect was observed. A larger sample size would likely yield significance.

CONCLUSIONS

CTS symptoms and physical examination findings were greater in those who propelled with higher compressive wrist forces. Using higher forces also amplified the median nerve response to propulsion. It is possible reducing the amount of upper limb force during this activity can delay or prevent the onset of CTS in this population.

REFERENCES

1. Yang J, et al. *Am J Phys Med Rehab* **88**, 1007-16, 2009.
2. Boninger ML, et al. *Arch Phys Med Rehab* **80**, 910-15, 1999.
3. Boninger ML, et al. *Arch Phys Med Rehab* **85**, 1141-45, 2004.
4. Levine DW, et al. *J Bone Joint Surg* **75**, 1585-92, 1993.
5. Impink BG, et al. *Muscle Nerve* **41**, 767-73, 2010.
6. Wu G, et al. *J Biomech* **38**, 981-992, 2005.

ACKNOWLEDGEMENTS

This material is based upon work supported by the Department of Veterans Affairs (Grant #B6252R) and NSF Graduate Research Fellowship (#1247842). Any opinion, findings, and conclusions or recommendations expressed in this material are those of the authors and do not necessarily reflect the view of the NSF, Department of Veterans Affairs, or United States Government.

WEEKLY CHANGES IN VASTUS LATERALIS VOLUME AFTER ACL INJURY

¹Kevin Yoh, and ¹Benjamin W. Infantolino

¹Penn State - Berks, Reading, PA, USA

email: bwi100@psu.edu

INTRODUCTION

Anterior cruciate ligament (ACL) injuries are one of the most prevalent injuries in athletics, affecting females at a much greater rate than males. The musculature around the knee is affected in several ways, but the most negative effects occur in the vastii muscle group, and more specifically the vastus lateralis [1]. Muscle volume is indicative of the power a muscle can produce and therefore knowing muscle volume at different points in the process (post injury, reconstruction surgery, and rehabilitation to full participation) can provide insight into how the muscle is effected by injury, surgery, and rehabilitation. Additionally, thigh circumference is used clinically to track muscle volume changes and there is no consensus if this is accurate. Therefore, the purpose of this study was to quantify vastus lateralis volume post ACL injury and throughout the reconstruction surgery and rehabilitation process and to compare volume changes to changes in thigh circumference.

METHODS

The participant was a 20 year old female Division III soccer athlete whose mass was 59kg, and height was 1.63m. Informed consent was obtained in accordance with The Pennsylvania State University Institutional Review Board. The athlete suffered a non-contact ACL injury during a game. The ACL was reconstructed using a bone-patellar-bone autograft approximately 3 weeks post-injury. Weekly measures of vastus lateralis volume (estimated using B-mode ultrasound; EchoBlaster 128, Telemed, Lithuania) and thigh circumference commenced 4 days post injury following the procedures detailed in Infantolino et al. [2]. Briefly, a system of wire guides was placed on the thigh to break up the vastus lateralis on the ultrasound image (Figures 1 and 2).



Figure 1. System of wires on subject's leg.

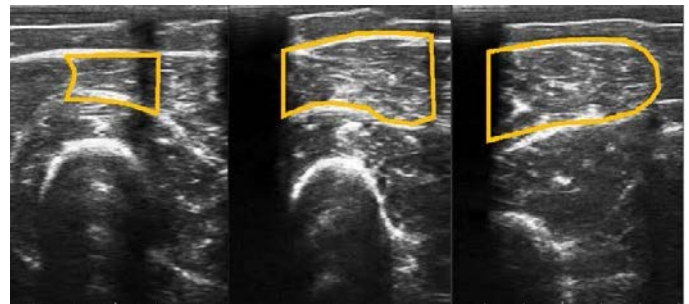


Figure 2. Ultrasound images illustrating one full cross-section of the vastus lateralis. Yellow outlines show the outline of the muscle. The dark vertical artifacts are the wires

The cross-sectional area of the vastus lateralis was measured every 2 cm. Two sequential cross-sectional areas and the distance between the areas was used to calculate the volume of the segment. Segment volumes were added to reach total muscle volume. A schedule of weekly measures was adhered to as closely as possible with 3, week-long academic breaks being the only interruptions in the schedule. Measures were discontinued once the athlete was cleared by her physician to participate in soccer again (8 months post-injury). The athlete participated in a full season of Division III soccer once cleared for full participation. Muscle volume and thigh circumference correlation was assessed using a Pearson's correlation test.

RESULTS AND DISCUSSION

The results of the Pearson's correlation test indicated a correlation between muscle volume and thigh circumference measures ($p < 0.05$). Figure 3

illustrates muscle volume throughout time.

Important points of change in the volume occur at:

- Week 3 – the measurement after ACL reconstruction (volume probably influenced by swelling post surgery).
- Week 5 – volumes illustrate how much volume decreased 2 weeks after surgery (36% from week 1).
- Week 15 – subject stopped attending physical therapy after 30 sessions.
- Week 19 – subject returned to physical therapy.

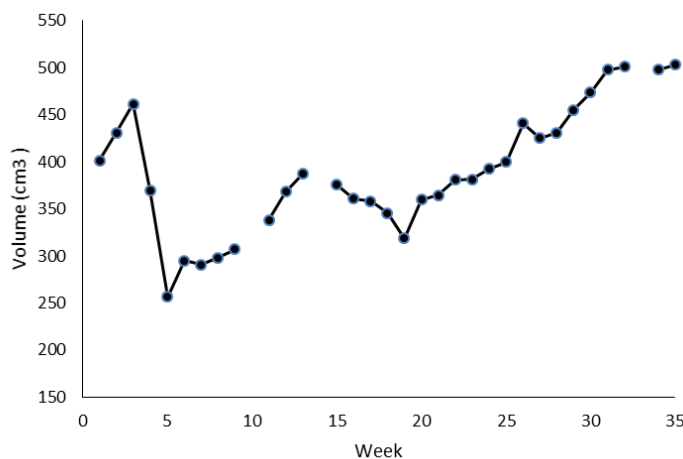


Figure 3. Vastus Lateralis volume throughout time.

CONCLUSIONS

The results of the correlation indicate that thigh circumference is an accurate method for assessing vastus lateralis volume changes during rehabilitation following ACL reconstruction. This is clinically important as thigh circumference measurements are used to track muscle hypertrophy during rehabilitation and are much quicker measurements than measuring muscle volume. Another important finding was how quickly atrophy

ensued following discontinuation of rehabilitation. In this study the subject stopped attending regular physical therapy sessions during the winter break. During this time her vastus lateralis volume decreased by nearly 18%. This demonstrates that consistent rehabilitation is critical to maintaining muscle hypertrophy gains.

Some limitations exist in this study with the largest limitation being sample size. Since the injury, operation, and rehabilitation were not unique there is no reason to believe that these results would not be seen on other individuals. However, without additional subjects it is difficult to categorically state that these findings would generalize to other individuals. Another limitation would be the focus on the vastus lateralis muscle. Given that previous literature has shown decreases in the other quadriceps muscles there is no reason to suspect that these findings would not apply to the other quadriceps.

Clinically, these results indicate that thigh circumference can be used to estimate vastus lateralis muscle volume changes. Muscle volume is an indicator of the power a muscle can produce and therefore can be used during rehabilitation as an independent measure of muscle power production ability. Finally, these results also demonstrate the need for continuous rehabilitation (even months post-op) to continue increasing vastus lateralis muscle volume.

REFERENCES

1. Williams et al. *A J Sports Med* **33**, 402-407, 2005
2. Infantolino et al. *J Appl Biomech* **23**, 213-217, 2007

UPPER EXTREMITY JOINT DYNAMICS AND ELECTROMYOGRAPHY (EMG) DURING STANDARD AND GEARED MANUAL WHEELCHAIR PROPULSION

Omid Jahanian, Alyssa J. Schnorenberg, Lianna Hawi and Brooke A. Slavens

The University of Wisconsin–Milwaukee, Milwaukee, WI, USA
The Rehabilitation Research Design and Disability (R₂D₂) Center, Milwaukee, WI, USA
email: jahanian@uwm.edu

INTRODUCTION

Wheelchairs are the primary mobility device for individuals having difficulty with ambulatory activities [1]. In the U.S. it is estimated that 3.3 million people used a wheelchair in 2010 [2], of which 90% used manual wheelchairs (MWs) [3]. However, MWs often lead to reduced independent function and quality of life [4]. Furthermore, shoulder pain and injuries are commonly associated with MW propulsion [5]. Geared manual wheelchairs (GMWs) may be a promising alternative that reduces the biomechanical demands of the shoulder needed for MW propulsion while maximizing function. However, there is limited scientific evidence supporting the benefits of GMW mobility.

The purpose of this study is to compare the glenohumeral (GH) joint dynamics and shoulder flexors electromyography (EMG) during geared and standard MW propulsion. It is hypothesized that using GMWs will decrease glenohumeral joint range of motion and shoulder muscle activity.

METHODS

Six able-bodied individuals, 4 females and 2 males, ages 18-30, were recruited for this study. This study was approved by the University of Wisconsin-Milwaukee Institutional Review Board (IRB). An acclimation period (30 minutes) was provided to the participants to familiarize themselves with wheelchair propulsion techniques. Subjects were instrumented with 27 reflective markers on the upper body and surface electrodes on the anterior deltoid and pectoralis major muscles. Maximum voluntary contractions (MVCs) were performed against manual resistance for the targeted muscles [6]. Subjects were asked to propel both standard and

geared MWs on a level, carpeted floor, to simulate the home environment. A Breezy MW (Sunrise Medical LLC.) was used with both its standard wheels and Easy Push (IntelliWheels, Inc.) geared wheels (gear ratio of 1:1.6). Motion analysis data was collected using a 14 camera, three-dimensional (3-D) Vicon T-series motion capture system (120 Hz). A custom inverse dynamics model was used to calculate the 3-D upper extremity (UE) joint dynamics [7]. Delsys Trigno wireless surface electrodes were used to record EMG data (2040 Hz). All recorded EMG signals were rectified and their root mean square (RMS) were normalized by their associated MVC. Normalized EMG was used to determine onset, offset [8], peak time, peak EMG and integrated EMG during a wheelchair stroke cycle using Matlab (The Mathworks, Inc.) software. Statistical analyses were completed with IBM SPSS software using a paired samples t-test ($p = 0.05$ significance level).

RESULTS AND DISCUSSION

EMG onset and offset, burst duration, peak time, peak EMG and integrated EMG were calculated for three trials of the wheelchair stroke cycle for five subjects. The results of a representative subject are shown in Figure 1. Peak EMG of pectoralis and anterior deltoid decreased by an average of 7% and 8% during GMW propulsion, but they were not statistically significant. Pectoralis burst duration throughout one stroke cycle decreased by 24% ($p=0.038$) with geared wheels, and integrated EMG for pectoralis and anterior deltoid decreased by 36% and 21%, respectively, but was not statistically significant. When normalized by the distance travelled per stroke cycle, both burst duration and integrated EMG were not significantly different between the two wheel types.

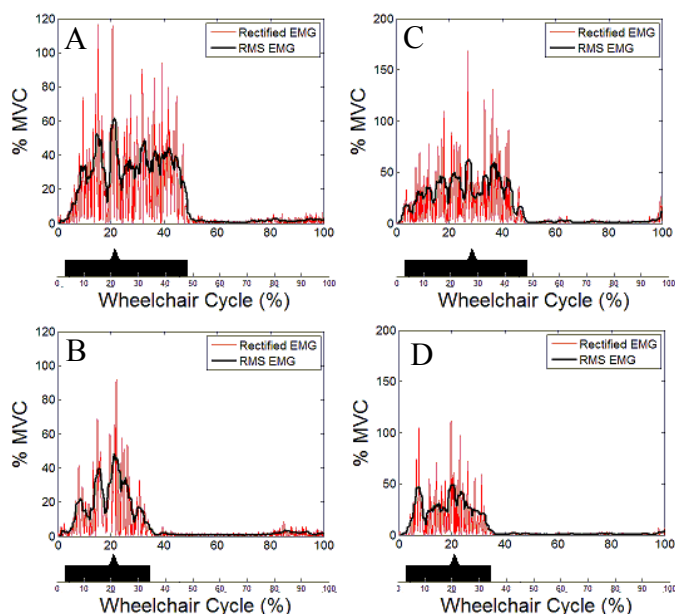


Figure 1: Anterior deltoid and pectoralis major muscle activity during wheelchair propulsion. (A) pectoralis: standard wheel, (B) pectoralis: geared wheel, (C) anterior deltoid: standard wheel, and (D) anterior deltoid: geared wheel.

Glenohumeral joint kinematics of five subjects were not significantly different between geared wheels and standard wheels and SWs. Glenohumeral joint angle mean ranges of motion in the sagittal, coronal and transverse plane are presented (Table 1).

CONCLUSIONS

Preliminary results of this study demonstrate trends between wheel types and showed benefits for GMW mobility based on muscle activity. Reducing peak EMG may be advantageous for wheelchair users during demanding tasks such as propulsion on carpeted floor. Howarth and colleagues [9] reported similar results for using GMWs during ramp ascent. Reduction in muscle energy (integrated EMG) may result in less resultant joint force in the shoulder [8]

which may potentially prevent associated UE pathologies. Further investigation is underway with a larger population of able-bodied persons and persons with spinal cord injury. The results from this study will help us determine the types of mobility tasks and populations of users for which GMWs are beneficial. Ultimately, this work will lead to new multi-gear wheel designs for manual wheelchairs.

REFERENCES

1. Chow J W et al. *Disability and Rehabilitation: Assistive Technology* **6**(5): 365–377, 2011.
2. U.S. Census Bureau. Americans with disabilities in 2010.
3. Kaye H S, et al. *US Dept of Ed, Disability Statistics Report* **14**, 2000.
4. van der Woude LH, et al. *Indian J Med Res* **121**: 719–722, 2005.
5. Alm M, et al. *J Rehabil Med* **40**: 277–283, 2008.
6. Chow J W, et al. *Medicine & Science in Sports & Exercise* **33**(3): 476-484, 2001.
7. Schnorenberg A J, et al. *Journal of Biomechanics* **47**: 269-276, 2014.
8. Dubowsky S R, et al. *Journal of Biomechanical Engineering* **131**: 021015-1 :8, 2008.
9. Howarth SJ, et al. *Clin Biomech* **25**: 21–28, 2010.

ACKNOWLEDGEMENTS

The content of this work were developed under a student research grant from UW-Milwaukee College of Health Sciences, a National Institutes of Health (NIH) SBIR Phase II grant number 2R44HD071653-02, and the Eunice Kennedy Shriver National Institute of Child Health & Human Development Of the National Institutes Of Health Under Award Number K12HD073945. However the contents of this work do not necessarily represent the official views of the NIH.

Table 1: Glenohumeral joint mean ranges of motion and standard deviations during a wheelchair stroke cycle.

Wheel Type	Geared Wheels			Standard Wheels		
Plane	Sagittal	Coronal	Transverse	Sagittal	Coronal	Transverse
GH Joint Angle	60.7 ± 8.7	16.1 ± 4.4	24.4 ± 10.3	58.7 ± 6.2	15.8 ± 3.0	26.7 ± 7.1

EFFECT OF PROSTHETIC FOOT DAMPING ON ANKLE PUSH-OFF WORK IN LATE STANCE

¹ Li Jin, ^{2,3} Peter G. Adamczyk, ¹ Michelle Roland, ¹ Michael E. Hahn

¹ University of Oregon, Eugene, OR, USA

² Intelligent Prosthetic Systems, LLC, and ³ University of Michigan, Ann Arbor, MI, USA
email: ljin@uoregon.edu, web: bssc.uoregon.edu

INTRODUCTION

Lower limb amputation poses many challenges and can lead to secondary impairments such as knee osteoarthritis (OA) in the intact limb. It has been reported that intact limb the 1st peak of knee external adduction moment (EAM) is related to the prosthetic limb push-off work [1]. Different prosthetic foot properties such as stiffness and energy storage and return are related to ankle-foot system push-off work during late stance phase. Little is known regarding the effect of prosthesis damping on the energy return in late stance phase. We hypothesized that use of an energy return foot would increase the ankle push-off work compared to a foot with significant damping.

METHODS

Eight healthy subjects (23 ± 1.9 years, 167.5 ± 7.6 cm, 65.5 ± 10.0 kg) walked wearing a prosthesis simulator boot with two kinds of prosthetic feet (Figure 1): the energy return foot (ERF) and the damping foot (DF). Each foot had three stiffness variations (high, medium and low stiffness), all matched in stiffness, mass and ground contact geometry.



Figure 1: The energy return foot (left) and the damping foot (right).

Subjects walked along a 10 m walkway over four in-ground force plates, using each foot (ERF, DF) in each stiffness condition (high, medium and low), at three walking speeds (self-selected fast, normal and slow). We recorded body motion and ground

reaction forces and performed standard inverse dynamics analysis. We also computed prosthetic ankle power according to a deformable-body model, as the sum of rotational and translational power at the distal shank [1, 2]. It was expressed as:

$$P_{ankle} = M_{ankle}\omega_{shank} + F_{ankle}v_{shank}$$

where P_{ankle} is the power, M_{ankle} and F_{ankle} are the ankle joint moment and joint reaction force, ω_{shank} and v_{shank} are the angular and translational velocities of the distal shank [1]. Prosthetic foot-ankle push-off work was calculated as the positive integral of power during late stance phase (~50-60% of gait cycle) [1, 2]. Parameters were normalized to body mass (Figure 2).

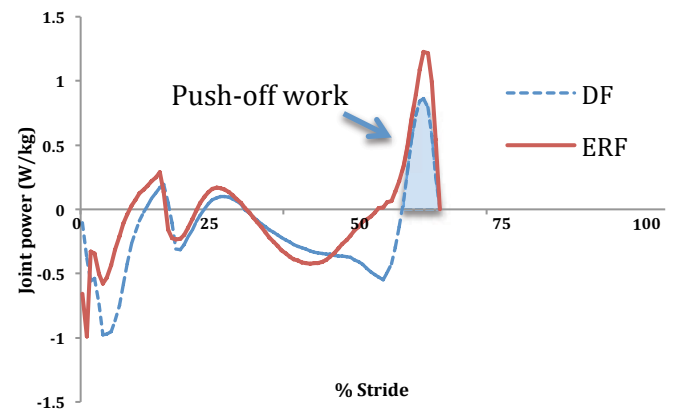


Figure 2: Prosthetic foot-ankle power during gait cycle in high stiffness condition (DF & ERF) at self-selected slow walking speed.

Statistical analysis was performed using a 3-way ANOVA (foot*speed*stiffness) in SPSS (V22.0, IBM, Armonk, NY). Bonferroni procedure was used to reduce pairwise comparisons.

RESULTS AND DISCUSSION

Main effects of foot, speed and stiffness on the prosthetic foot-ankle push-off work were all significant, while the interaction effect between them was not significant. For pairwise comparisons, the energy return foot significantly increased the ankle push-off work compared with the damping foot ($p = 0.001$). Within three different stiffness comparisons, prosthetic ankle push-off work was significantly larger in low stiffness condition than the medium and high stiffness condition ($p = 0.001$); medium stiffness was also larger than the high stiffness condition ($p = 0.01$) (Figure 3). Comparing across walking speeds, fast walking resulted in significantly larger ankle push-off work compared with slow walking ($p = 0.004$).

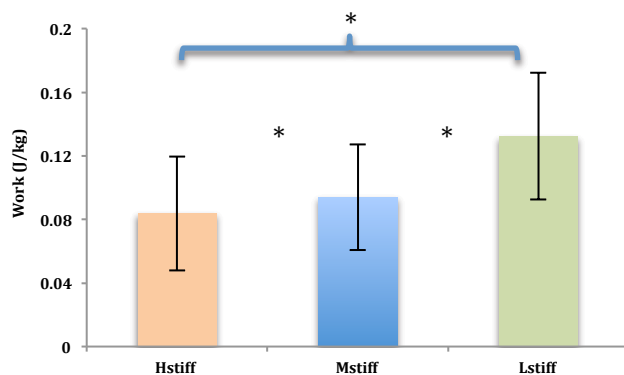


Figure 3: Prosthetic foot-ankle push-off work with high, medium and low stiffness feet. Work was significantly different among stiffness conditions.

CONCLUSIONS

The results of the study support the hypothesis. The damping effect of the prosthetic foot significantly reduced foot-ankle push-off work in the late stance phase of gait, compared with the energy return foot. There was a trend that positive peak ankle power

value is higher by wearing the energy return foot (Figure 2). This is due to the damping effect of foam or rubber cushions in prosthetic systems dissipates some of the energy in the mid stance phase (30-50% of gait cycle) (Figure 2). The damping foot also appears to absorb energy over a longer period of time. All of these contribute to the reduced energy return observed in this study.

Different stiffness levels also play an important role in affecting prosthetic foot-ankle push-off work. The lower stiffness condition led to higher ankle push-off work. When the loading force remains the same, a higher stiffness would result in lower deflection, which subsequently reduces energy storage and resultant energy return [3]. Increased walking speed will result in higher ground reaction force impulse, thus leading to increased foot-ankle system push-off work. Future research should explore the changes of walking speed on the prosthetic foot-ankle energy storage and return efficiency, to better generalize new developments for clinical application.

REFERENCES

1. Morgenroth DC, et al. *Gait Posture* **34**, 502-507, 2011.
2. Geil MD, et al. *J Biomech* **33**, 1745-1750, 2000.
3. Adamczyk PG, et al. *Hum Mov Sci*, in review, 2015.

ACKNOWLEDGEMENTS

This study was funded by the Department of Veterans Affairs (RR&D Grant #N7348R). We thank Alexis Vaughan and David Stephenson for their assistance in data collection and processing.

Table 1: Prosthetic foot-ankle push-off work values over different foot, stiffness and speed conditions (J/kg); Sample Mean (SD).

(n = 8) Stiffness	Energy Return Foot (ERF)			Damping Foot (DF)		
	Fast	Normal	Slow	Fast	Normal	Slow
High	0.12 (0.03)	0.11 (0.04)	0.10 (0.02)	0.07 (0.02)	0.05 (0.01)	0.05 (0.02)
Medium	0.13 (0.02)	0.12 (0.03)	0.11 (0.03)	0.08 (0.01)	0.06 (0.01)	0.06 (0.01)
Low	0.18 (0.03)	0.16 (0.03)	0.15 (0.02)	0.12 (0.02)	0.10 (0.01)	0.09 (0.01)

DESIGN OF SENSORY AUGMENTATION SYSTEM FOR POSTURAL CONTROL REHABILITATION

Yoo-Seok Kim, Yi-Tsen Pan, and Pilwon Hur

Mechanical Engineering, Texas A&M University, College Station, TX, USA
Email: {yooseokteam,yitsenpan,pilwonhur}@tamu.edu web: <http://hurgroup.net>

INTRODUCTION

In activities of daily living (ADL), postural control plays a significant role for people with neurological impairments. Jeka et al. [1] have shown that light touch (contact force less than 1N) of fingers on fixed surfaces contributes to postural control during quiet standing and walking. By virtue of this additional sensory information from skin stretch feedback, people with neurological impairments may reduce their body sway in ADL, which can ultimately lead to improved quality of life.

In recent years, Verite et al. developed a sensory augmentation system for postural control while quiet standing [2]. However, this system is not portable because this system requires force plate and fixed structure of actuators, which in turn limit the usability of device in daily living and have less availability in ADL. Therefore, portability was one of the main concerns in our study. The objectives of this study are to i) design a portable sensory augmentation system for postural control, and ii) estimate the feasibility of our system in postural control application.

METHODS

Fig. 1 shows a schematic diagram of our sensory augmentation system and Fig. 2 shows a fabricated system. Using the gradient descent algorithm [3], the pitch angle in subject's anterior-posterior direction is calculated from the data of inertia measurement unit (IMU) (MPU-9150, InvenSense Inc., San Jose, CA) which is attached at the center of mass (COM) of a subject. Contactor's angular velocity is defined to be proportional to angular deviation of pitch angle from a reference angle. A reference angle is defined as a pitch angle when a subject is standing upright. When a subject tilts forward, the contactor rotates in clockwise direction and vice versa. The contactor is operated by a DC motor (Faulhaber, Germany). An embedded control

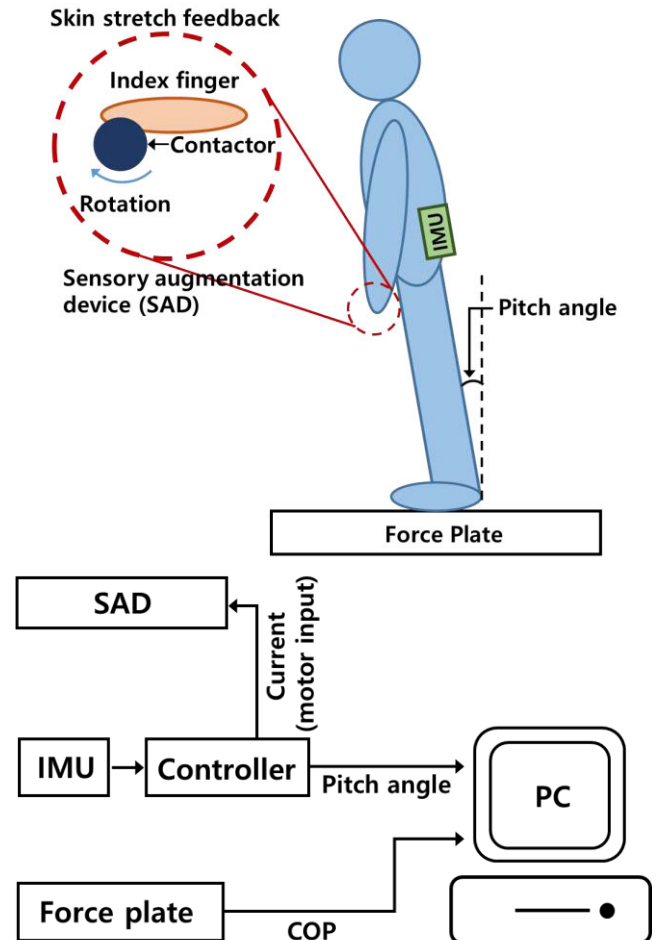


Figure 1: Schematic diagram of sensory augmentation system.

unit (myRIO, National Instruments, Austin, TX) takes the pitch angle of a subject from the IMU as an input, calculates the desired angular velocity, and controls the DC motor so that the contactor will maintain the desired angular velocity. A PID feedback control and an encoder were used to robustly maintain angular velocity of the contactor to a desired value.

The skin stretch is triggered at the index fingertip pad since the distribution of mechanoreceptors sensitive to skin stretch on the hand is concentrated

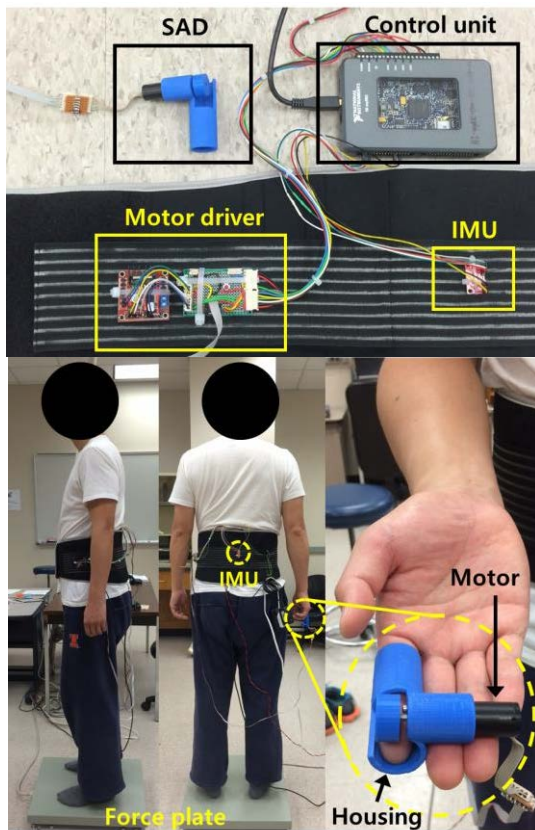


Figure 2: Fabricated sensory augmentation system.

at the index fingertip pad [4]. The DC motor is mounted at the housing of sensory augmentation device (SAD) where subject's index finger is inserted. Several contactors and housings with different size were fabricated using the 3D printer (Replicator 2X, Makerbot, Brooklyn, NY) to accommodate various finger sizes of subjects.

Besides the portable system of SAD and IMU, a force plate (OR6, AMTI, Watertown, MA) and a data acquisition system (DAQ) (USB-6002, National Instruments, Austin, TX) with a PC were prepared to collect center of pressure (COP) and pitch angle data. These data will be used to evaluate the efficacy of the SAD system. The IMU, embedded control unit, and a motor driver are enclosed in a waist belt so that subjects can easily wear the system (Fig. 2). Sampling rates of SAD, IMU and DAQ system were 2kHz, 500Hz, and 1kHz, respectively.

RESULTS AND DISCUSSION

Fig. 3 shows the relationship between contactor's angular velocity and pitch angle. As expected, contactor's angular velocity tracked the desired

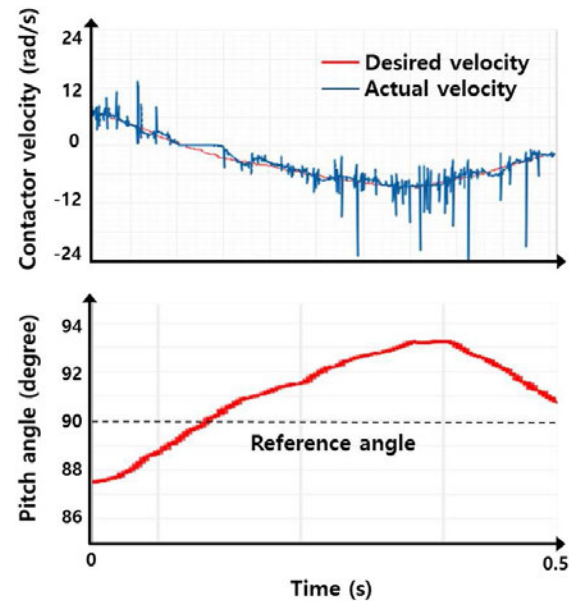


Figure 3: Relationship between contactor's angular velocity and pitch angle of subject.

angular velocity determined by body postural sway (pitch angle). Note that the reference angle was set to 90°.

CONCLUSIONS AND FUTURE WORK

A sensory augmentation system for postural control rehabilitation was developed using skin stretch feedback. This portable system consists of SAD, embedded control unit, motor driver, and IMU. To test the efficacy of the system, a force plate and DAQ was additionally used. By virtue of this device, subjects would receive skin stretch feedback, which may contribute to the reduction of body sway. Currently, only pitch angle was used to determine the motor velocity input. However, time derivative of pitch angle can also be used. Furthermore, battery should be used as a power source for portability. These studies will be included in future work. The efficacy of SAD system will be evaluated by examining the effect of augmented sensation at the fingertip due to SAD on quiet standing balance for various sensory modalities

REFERENCES

1. Jeka JJ et al., *Physical Therapy* 77: 476-487, 1997.
2. Verite et al., *IEEE Trans on Haptics* 7: 150-160, 2014.
3. Madgwick OHS. et al., *Proceedings of Rehab Robotics'11*, Zurich, Switzerland, 2011.
4. Johansson RS. et al., *Nature Reviews* 10: 345-359, 2009

IMPROVING THE MOBILITY AND POSTURAL BALANCE OF INDIVIDUALS WITH MULTIPLE SCLEROSIS

¹ Brenda L. Davies, ¹ David J. Arpin, ¹ Min Liu, ¹ Heidi Reelfs, ² Kathleen G. Volkman, ¹ Brad Corr, ³ Kathleen Healey, ³ Rana Zabad, and ¹ Max J. Kurz

¹ Munroe-Meyer Institute, University of Nebraska Medical Center, Omaha, NE, USA

² School of Allied Health Professionals, University of Nebraska Medical Center, Omaha, NE USA

³ College of Medicine, University of Nebraska Medical Center, Omaha, NE, USA

email: mkurz@unmc.edu, web: <http://www.unmc.edu/mmi/>

INTRODUCTION

Multiple sclerosis (MS) is a demyelinating disease that affects about 570,000 individuals in the United States [1]. These individuals are often faced with muscular impairments that have devastating effects on their mobility and standing postural balance. Traditionally, clinicians have discouraged individuals with MS from participating in exercise programs or intensive physical therapy because it was thought that these types of activities would exacerbate the MS symptoms [2]. However, this notion has been challenged by numerous studies that have shown that exercise and physical therapy does not aggravate the symptoms and can result in postural balance and mobility improvements [3-5]. Outcomes from our recent investigation have shown that an intensive neuro-physical therapy can result in substantial improvements in the mobility and postural balance of individuals with MS [4]. Our protocol was different from prior clinical trials in that it was performed twice-a-day, five days a week. This immersive therapeutic protocol was directed at igniting beneficial neuroplastic changes through a massed practice paradigm that constantly challenged the patient's movements. Exemplar individualized challenging exercises included standing on foam with feet close together and eyes closed, walking sideways on a treadmill, or walking overground while stepping over obstacles. Although the initial outcomes appeared to be quite successful, it is currently unknown if the clinically relevant changes were related to the therapeutic dosage or the novel therapeutic paradigm. The purpose of this study was to test the therapeutic outcomes of our prior study by comparing it with the mobility and postural balance outcomes for a cohort of individuals with MS who participated in an exercise

based training protocol that was conducted at the same therapeutic dosage.

METHODS

Twenty-four adults with relapsing-remitting or secondary progressive MS participated in this investigation (Mean Age: 53.5 ± 1.8 years). The subjects were assigned to either the Therapeutic Challenge Group (TCG) or the Exercise Group (EG). All subjects completed a battery of biomechanical testing before and after the 6-weeks of training. Postural control was measured based on the composite score from the Sensory Organization Test (SOT) (NeuroCom[®] International, Clackamas OR), where a higher score indicated a lower amount of postural sway. The preferred walking pace spatiotemporal kinematics were measured with a GAITRite[®] system (CIR Systems Inc., Sparta, NJ). Two walking trials were completed and averaged together for analyses.

Both groups completed their training five consecutive days each week, two times each day, over a 6-week period. The initial two weeks were completed on the UNMC campus under close supervision of a licensed physical therapist (HR, KGV, or BC). The TCG completed the same training that was conducted in our initial investigation [4]. For this group, each session consisted of 5 minutes of movements isolating the control of joints, 20 minutes of challenging postural balance training and 20 minutes of challenging gait training. The EG completed 15 minutes of strength/flexibility exercises, 15 minutes of postural balance exercises, and 15 minutes of treadmill walking. This group focused more on completing the assigned exercises rather than learning new

motor control strategies. After the initial two weeks of therapy, both groups completed the remaining four weeks of their training at home and were monitored through weekly phone contact from one of the treating therapists. Separate repeated measures ANOVAs (group x Pre/Post Assessment) were used to evaluate the differences in the treatment effects of the respective groups.

RESULTS AND DISCUSSION

For the SOT measures, we found a significant Pre/Post main effect, which indicated that all of the patients reduced their postural sway after the therapy ($p < 0.001$; Fig. 1A). However, we did not find a significant group main effect or an interaction ($p > 0.05$), indicating that the postural sway improvements were equivocal for the two treatment groups. We also found a significant Pre/Post main effect for walking speed ($p = 0.007$; Fig. 1B), indicating that all of the patients walked faster after participating in the therapy. Yet, we did not find a significant group main effect or an interaction ($p > 0.05$); indicating that the walking speed improvements were the same for the two groups. There additionally was a significant Pre/Post main effect for the step length ($p = 0.001$; Fig. 1C), suggesting that all the patients improved their walking speed after therapy by using a longer step length. There was not a significant group main effect or interaction for the step length ($p > 0.05$), once again indicating that there were no differences between the two treatment groups. Lastly, there were no significant differences for the step width or the cadences for both the main effects and interactions ($p > 0.05$).

Our results show that a high dosage of physical therapy over a 6-week period can result in clinically relevant improvements in the mobility and postural balance of individuals with MS. On the other hand, our results also indicated that there were no differences for any of the outcome variables between the respective treatment groups. This suggests that the therapeutic gains in postural balance and mobility were more likely related to the high therapeutic dosage rather than the type of therapy implemented. Potentially, an intensive mass-practice of a motor task may be an important

treatment parameter for promoting clinically relevant improvements in the mobility and posture of individuals with MS. The training conducted with the TCG was guided by the challenge point framework, which states that beneficial changes in motor learning can be augmented by altering the task difficulty. It is possible that there were no differences between the two treatment strategies because a high dosage of activity was sufficient for the patient to work above their challenge point. Alternatively, we suspect that having the patient perform the training at home may be the reason the TCG group did not perform better than the EG. Our rationale is that the patients in the TCG may have not known how to reliably exceed their challenge point without the therapist's daily guidance. Effectively, the TCG home training program may have been relatively similar to the home program of the EG.

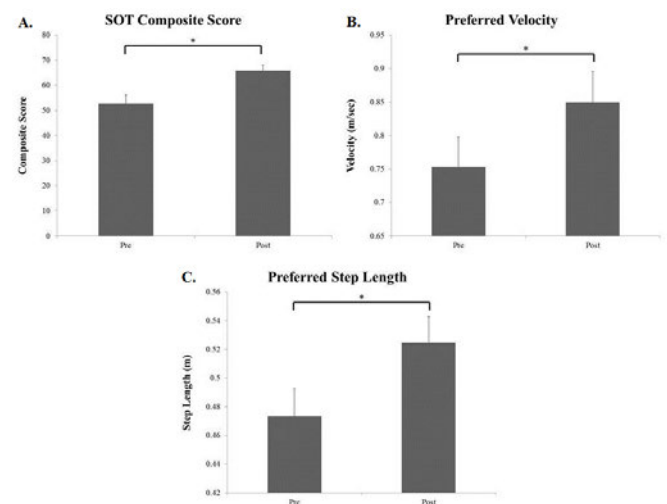


Figure 1: A) SOT composite scores, B) velocity, and C) step length for both therapy groups combined before and after the 6-weeks of therapy.

REFERENCES

1. Campbell JD, et al. *Mult Scler Relat Disord* **3**, 227-236, 2014.
2. Sutherland G, et al. *J Sports Med Phys Fitness* **41**, 421-432, 2001.
3. Hebert JR, et al. *Phys Ther* **91**, 1166-1183, 2011.
4. Davies BL, et al. *J Neurol Phys Ther*, in press, 2015.
5. Motl RW, et al. *J Neurol Phys Ther* **36**, 32-37, 2012

Comparing Effects of Body Weight Supported Treadmill Training on Bone and Muscle Following Complete and Incomplete Spinal Cord Injury

¹ J.P. Loftus, ² J. Kadlowec, ^{1&2} A. Singh

¹ Widener University, Chester, PA, USA

² Rowan University, Glassboro, NJ, USA
email: jploftus@mail.widener.edu

INTRODUCTION

The incidence of lower extremity fractures has been reported to be as high as 46% post SCI (spinal cord injury), as seen in [1-3]. Body weight-supported treadmill training (BWSTT) has been reported to restore muscle mass and prevent bone loss in SCI patients. While the beneficial effect of this therapy is known, the effect of this training paradigm on varying severity of SCI has not been investigated in a single study. The purpose of this study was to investigate the effects of BWSTT on the muscle mass and biomechanical properties of the bone in transected and contused rats.

METHODS

A. Group Set Up

In this experiment 32 female Sprague-Dawley rats were split up into five groups (Fig. 1). Animals in the training group received 8 weeks of BWSTT at 75% BWS and 7 cm/sec speed and 500 steps/day for 5 days/week using a robotic device (Robomedica Inc., CA) (Fig 2). At the end of nine weeks post injury, all animals were euthanized and the right tibia and soleus muscle were harvested. Muscle mass was measured and calculated against the total body weight. The tibial bone was subjected to a three point bending test.

B. 3-Point Bending Test

The tibiae were placed on the lateral surface on two rounded supporting bars with a distance of 20 mm (Fig. 3). A constant displacement rate of 5 mm/minute was applied at the medial surface of the diaphysis by lowering a third rounded bar until failure (shampo, FGS-100PVH/L, Itasca, Illinois) Ultimate failure load (lb) was calculated for each specimen.

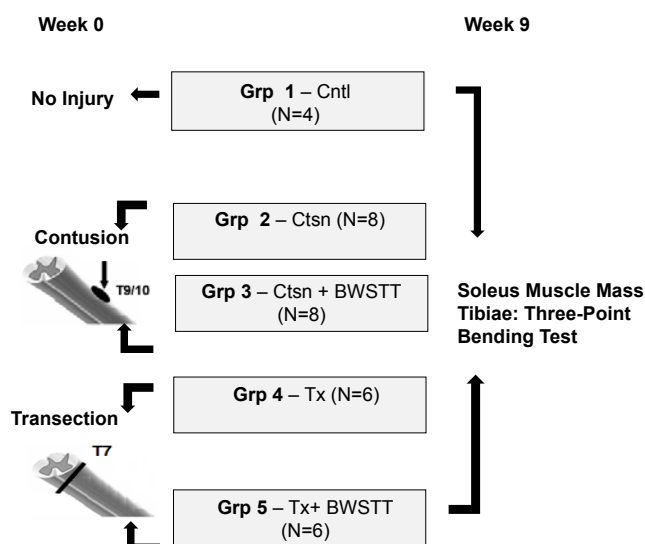


Figure 1: Groups Details

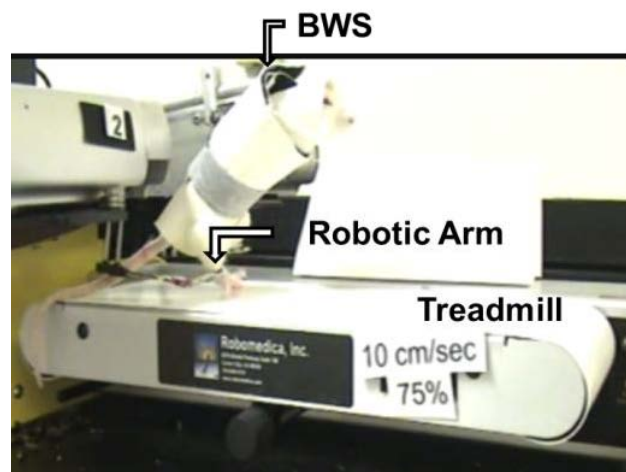


Figure 2: Body Weight-Supported Treadmill Training apparatus.



Figure 3: 3-Point Bending Test

RESULTS

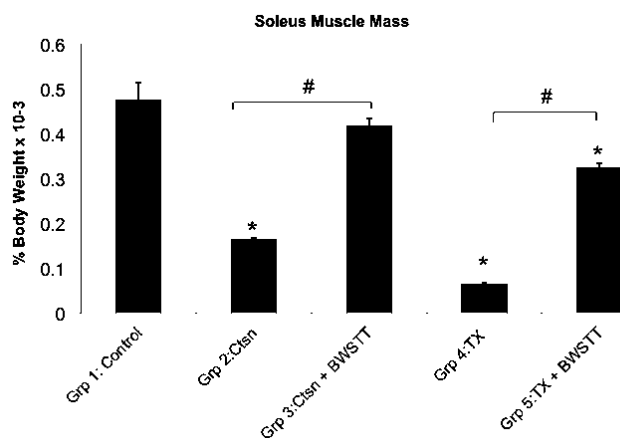


Figure 4: Percent Soleus Muscle Mass for each animal group. Asterisk indicates significant difference from control. Bracket with # indicate significant difference between groups ($p < 0.05$).

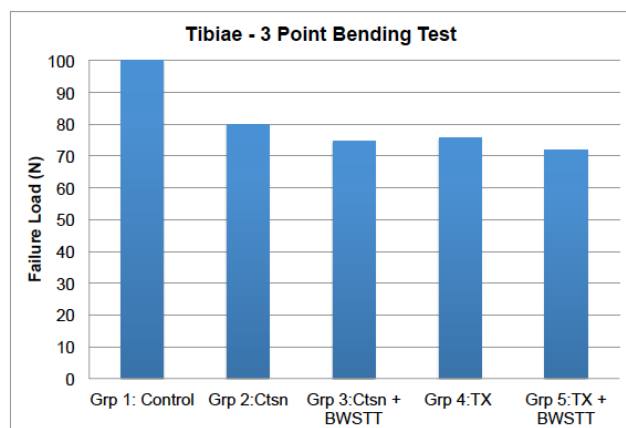


Figure 5: Failure Loads in Tibiae Bone When Subjected to 3-Point Bending Tests .

CONCLUSIONS

BWSTT led to significant improvement in the soleus muscle mass when compared to no training in both contused and transected animals. However, no significant improvement in the biomechanical property of the tibial bone was observed in the BWSTT animals. We attribute this to the severity of contusion injury that results in non-weight supported locomotion in animals in response to injury and also to the 75% BWSTT. Lower body weight support might result in significant improvement in the biomechanical properties of the tibial bone. Future studies are needed to investigate the effects of BWS and bone strength in various SCI models.

REFERENCES

1. Vestergaard P, Krogh K, Rejnmark L, Mosekilde L. Fracture rates and risk factors for fractures in patients with spinal cord injury. *Spinal Cord*. 1998;36:790-796.
2. Ashe MC, Craven C, Krasioukov A, Eng JJ. Bone Health Following Spinal Cord Injury. In: Eng JJ, Teasell RW, Miller WC, Wolfe DL, Townson AF, Aubut J et al., editors. *Spinal Cord Injury Rehabilitation Evidence*. Vancouver, B.C.: SCIRE, 2006: 9.1-9.18.
3. Craven BC, Robertson LA, McGillivray CF, Adachi JD. Detection and treatment of sublesional osteoporosis among patients with chronic spinal cord injury: proposed paradigms. *Top Spinal Cord Inj Rehabil*. 2009;14:1-22.

ACKNOWLEDGEMENTS

This study was partially supported by the New Jersey Commission on Spinal Cord Research – Exploratory Research Grant # CSCR14ERG001 and The Craig Neilson Fellowship Grant.

DETERMINING THE SAGITTAL PLANE FUNCTION FOR A MODEL PROSTHETIC FOOT

Anne E. Martin¹, Jeremy D. Smith², Robert D. Gregg¹, and James P. Schmiedeler³

¹Bioengineering, University of Texas at Dallas, ²Sport & Exercise Science, University of Northern Colorado,

³Aerospace and Mechanical Engineering, University of Notre Dame

Email: aem140630@utdallas.edu

INTRODUCTION

While it is generally believed that the choice of prosthetic components affects amputee gait, systematically quantifying the effects of prosthetic design on amputee walking is difficult [1]. A simulation model capable of predicting human amputee gait could allow for quantitative, systematic investigations. Existing models of amputee gait are either too complex for a predictive study (e.g. [2]) or do not provide any validation that the models can accurately predict amputee walking (e.g. [3]). One successful strategy to limit the complexity of predictive models for healthy human gait is to model the function, not the form, of the foot and ankle complex using a rigid curved foot and revolute ankle joint [4]. The curved foot captures the control of the center of pressure location [5], and the ankle joint helps to capture the change in the whole-body center of mass (CoM) velocity during the step-to-step transition [6]. Without ankle joints, the model exhibits excessively short step durations and large joint angle oscillations [4], both of which are uncharacteristic of healthy human walking. Whether an ankle joint is likewise required to capture the function of a passive prosthetic foot in an analogous model of amputee walking is unclear. Similar to human feet, prosthetic feet help to control the center of pressure location [7], but since passive prostheses cannot generate net positive ankle work, it appears they provide far less control of the CoM velocity than intact ankle joints [2]. Thus, a model prosthetic ankle joint may not be required. Prosthetic feet can, however, store and subsequently release

energy during certain parts of the step. If an amputee model without a prosthetic ankle joint is able to capture amputee gait, this may indicate that amputees do not use this energy transfer to help control the CoM velocity.

METHODS

A planar, five-link, asymmetric bipedal model was developed (Fig. 1) to investigate whether or not the prosthetic foot helps to control the CoM velocity. The amputated leg has a thigh and a combined shank/foot segment, i.e., no ankle joint. The contralateral/sound leg has a thigh, shank, and foot. Both feet are modeled as rigid circular arcs. Because the curved model foot captures some of the motion of the physical ankle, the model and physical ankle motions are not expected to match. The stance foot is assumed to roll without slip. Each stride consists of a finite-time amputated stance phase, an instantaneous transition between stance legs, a finite-time contralateral stance phase, and a second instantaneous transition. The model is controlled using the hybrid zero dynamics control method, which is capable of accurately predicting healthy human walking [4]. Gaits were designed by minimizing the error between the simulation and existing transtibial amputee walking data at the self-selected speed. The experimental data are from overground walking trials of five fully ambulatory amputees (4 male, average age of 44 ± 20 years, average years since amputation of 10 ± 14) wearing their prescribed prosthesis [8].

RESULTS AND DISCUSSION

The model reproduced the kinematics of amputee walking (Fig. 2). In all cases, walking speed error was less than 1%, step period error was less than 2%, and range of motion error was less than 3° , all of which were within the bounds of normal human variation. In particular, the result that the amputee model captured both step periods suggests that a

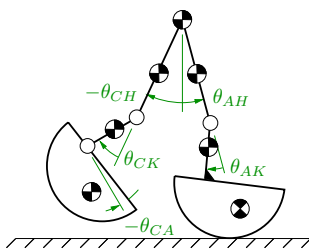


Figure 1: Schematic of the model. The contralateral leg has both knee and ankle joints, while the amputated leg has just a knee joint.

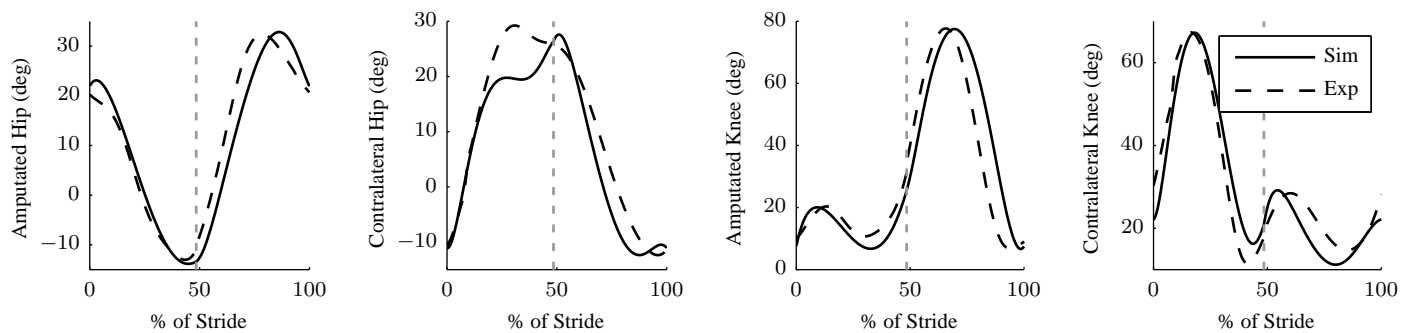


Figure 2: The hip and knee angles for both sides for one representative subject. The amputated stance phase goes from 0 to 48%, and the contralateral stance phase goes from 48% to 100%.

model prosthetic ankle joint may not be needed. The model accurately captured the shape of amputated-side hip motion, but predicted the peak extension of the contralateral hip to occur too early in the gait cycle (error of 15% of the stride). For the amputated-side knee, peak flexion and extension during swing both occurred approximately 5% later in the stride for the model. For the contralateral knee, peak extension during swing occurred approximately 4% later in the stride for the model, but peak flexion was accurately matched. The model was least accurate in capturing the motion of both knees during stance, with the most consistent issues being early peak knee flexion during the weight acceptance phase (errors between 1 and 16% of the stride) for both knees and early peak extension (error of 10% of stride) for the contralateral knee. This difficulty in accurately capturing the knee motion was not surprising because the model allowed for greater variability in stance knee motions compared to the hip motions while still achieving stable, periodic walking. None of the model joint angles exhibited the oscillations observed in the healthy human model when ankle joints were omitted [4]. Since the model was able to accurately match most of the kinematics of amputee walking, it can be concluded that a prosthetic ankle joint is not required in the model. This indicates that the function of the prosthetic foot can be entirely captured using just a curved model foot. Further, it suggests that the energy storage and return capabilities of prosthetic feet do not have a significant effect on the control of the CoM velocity.

CONCLUSIONS

A planar, five-link, asymmetric model is capable of matching the kinematics of transtibial amputee walking for amputees wearing a passive prosthesis. Since a model prosthetic ankle joint is not needed, it appears that the prosthetic foot helps to control the center of pressure location but has minimal influence in controlling the CoM velocity during the step-to-step transition. Using the validated model, an optimization capable of predicting transtibial amputee walking for amputees wearing a passive prosthesis is currently being developed. This predictive model will be used to systematically quantify the effects of prosthetic foot design on amputee gait.

REFERENCES

- [1] van der Linde, H, et al. *J Rehabil Res Dev* **41**, 555–70, 2004.
- [2] Silverman, AK, et al. *Gait Posture* **28**, 602–9, 2008.
- [3] Srinivasan, S, et al. *J Biomech Eng* **131**, 031003, 2009.
- [4] Martin, AE & Schmiedeler, JP. *J Biomech* **47**, 1416–21, 2014.
- [5] Hansen, AH, et al. *Clin Biomech* **19**, 407–14, 2004.
- [6] Donelan, JM, et al. *J Biomech* **35**, 117–24, 2002.
- [7] Hansen, AH, et al. *Prosthet Orthot Int* **24**, 205–15, 2000.
- [8] Smith, JD & Martin, PE. *J Appl Biomech* **29**, 317–28, 2013.

HAND KINEMATICS BEFORE AND AFTER TENDON TRANSFER SURGERY IN HANSEN'S DISEASE PATIENT WITH ULNAR NERVE PALSY

¹ Jéssica de Abreu, Ana Paula Fontana² and ¹ Luciano L. Menegaldo

¹ Biomedical Engineering Program, Federal University of Rio de Janeiro, Brazil

² Medicine School, Federal University of Rio de Janeiro, Brazil

email: jabreu@peb.ufrj.br

INTRODUCTION

Eradicated in many countries, Hansen's disease still presents a challenge for countries like India and Brazil, with 127.195 and 33.955 new cases in 2011, respectively. Patients often experience symptoms like loss of sensitivity, muscular atrophy, paresthesia, erythrocyanosis and nerve pain [1]. One of the most common movement disorders is the ulnar claw, characterized by metacarpophalangeal joints (MCP) hyperextension and interphalangeal joints hyperflexion of the fourth and fifth fingers, as shown in Figure 1.

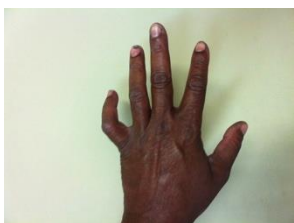


Figure 1: Hansen's disease patient with ulnar claw.

Tendon transfer surgeries followed by rehabilitation therapy can restore hand movement and physiologic posture. The main objective is to improve hand prehension capability by reducing MCP hyperextension. Surgical techniques may vary, normally emulating lumbrical and interossei muscles action. The distal tendon of the long finger flexor superficialis is released, divided in four stripes, and attached to extensor hood, proximal phalanx, A1 pulleys or interossei tendons) [2]. Selection of the surgical technique, tendon tensioning and attachment site is a complex task [2]. Deformities resulting from incorrect surgery decisions, such as swan neck and intrinsic plus, are common. In this study, we provide a framework for kinematic evaluation of tendon transfer surgeries to correct ulnar claw in Hansen's disease patients.

Fifth finger kinematics of a patient with ulnar claw, before and after being submitted to Zancolli-lasso procedure, is shown. We hope the results can provide insight into the biomechanical behavior resulting from the surgical procedure, improving therapeutics and surgical parameters choice.

METHODS

A BTS motion capture system (Milan, Italy) with 8 200Hz infrared cameras was used to measure hand movements of 10 healthy subjects and one Hansen's disease patient with ulnar claw, before and after a Zancolli-lasso tendon transfer surgery. Patient was a 17 year old female teenager with hypermobile joints. Marker protocol includes 23 markers, as shown in Figure 2. Capture sequence includes static posture, flexion/extension and pinch in neutral wrist position and circa 30° forearm rotation. In this paper, subjects are instructed to start in hyperextension, execute pinch involving fingers around a pencil and return to hyperextension immediately after touching the object.



Figure 2: Hand marker protocol. Hand markers are 4 mm and wrist markers 8 mm diameter.

The hand kinematics model adopted in this work considers bones as rigid segments connected by pivot (1 degree of freedom - DoF), Cardan (2 DoF) or spherical joints (3 DoF) [3]. Marker tracks processing includes noise attenuation with a 6 Hz

Butterworth low-pass filter and gaps interpolation. Local reference systems are positioned in each joint according to ISB recommendations [4]. Relative angles between proximal and distal reference systems are estimated. Angle tracks processing includes removal of frames before and after effective movement, according to a trigger of 2.5% of joint angle range. Tracks are normalized and synchronized according to the longest track. Healthy subjects mean and standard deviation are estimated for each frame.

RESULTS AND DISCUSSION

Ulnar claw affects mostly the movement of fourth and fifth fingers, which usually presents the greater joint angle deviations [5]. Figures 3 and 4 show the comparison between patient fifth finger flexion angles during pinch, before and after surgery, referenced to the healthy subjects' average pattern.

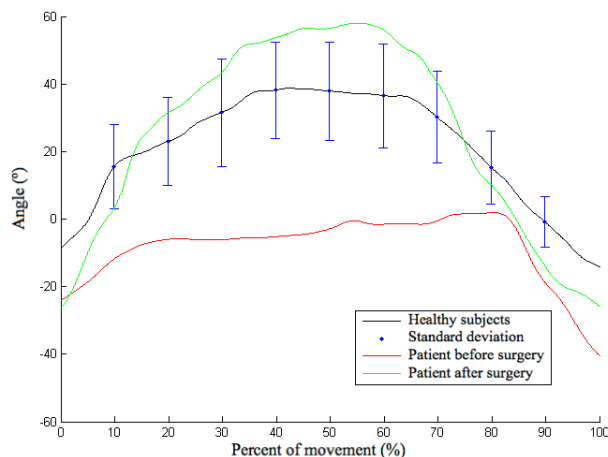


Figure 3: Fifth finger MCP flexion angle during pinch movement.

MCP and distal interphalangeal (DIP) joint angles varies only slightly during pinch movement before the surgery, indicating fifth finger paresis. Figure 3 shows a post surgical MCP movement similar to normal pattern. In Figure 4 significant reduction of distal interphalangeal joint (DIP) hyperflexion can be observed. However, the patient possibly requires greater contact forces in order to detect pencil touching, causing DIP joints to extend slightly in the middle of the movement cycle.

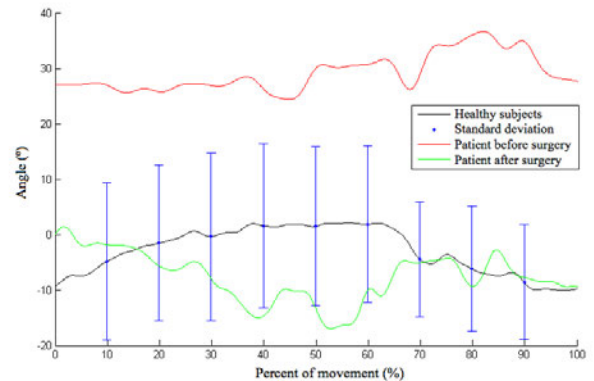


Figure 4: Fifth finger DIP flexion angle during pinch movement.

CONCLUSIONS

A kinematic model of the hand was implemented and joint angles were estimated for a Hansen's disease patient with ulnar claw. Patient's movement was measured before and after a Zancolli-lasso tendon transfer surgery, and compared to the average kinematics of healthy subjects. Results might support qualitative analyses of tendon transfer surgeries outcomes. Further work includes developing methods to characterize pathological movement and quantify surgical improvement.

REFERENCES

1. Rodrigues, LC, Lockwood DN, *Lancet Infect Dis* **11**, 464–70, 2011.
2. Anderson GA, *Journal of Bone Joint Surgery* **88**, 290-294, 2006.
3. Cerveri P, *Annals of Biomedical Engineering* **35**, 1989–2002, 2007.
4. Wu G *et. al*, *Journal of Biomechanics* **38**, 981–992, 2005.
5. Cavalcanti C, *Journal Brasileiro de Neurocirurgia*, 106-108, 2002.

ACKNOWLEDGEMENTS

The authors are acknowledged to FAPERJ, CAPES, FINEP and CNPq for financial support.

KNEE KINETICS AND CONTACT FORCES OF THE INTACT LIMB IN AMPUTEE WALKING

¹Ross H. Miller, ¹Rebecca L. Krupenevich, ^{1,2,3}Alison L. Pruziner, ^{2,3}Erik J. Wolf, and ³Barri L. Schnall

¹University of Maryland, College Park, MD, USA

²DoD-VA Extremity Trauma and Amputation Center of Excellence

³Walter Reed National Military Medical Center, Bethesda, MD, USA

email: rosshm@umd.edu, web: <http://sph.umd.edu>

INTRODUCTION

The prevalence of knee osteoarthritis (OA) is roughly twice as high in the intact limb of lower limb amputees compared to non-amputees [1]. The reasons for this disparity are unknown. However, local mechanical loading is thought to be a major factor in the general OA disease process [2].

Our long-term goals are to better understand how amputee gait mechanics, fitness, and prostheses affect the loading of the intact limb, and if the loads accumulated throughout the day can be modified to mitigate their OA risk. As a first step in these directions, we compared joint loading during self-paced walking between the knee of the intact limb in amputees who have recently begun using their prosthesis, to knees of a non-amputee control group.

Most previous studies on amputee joint loading have assessed loading using peak values of joint moments such as the external knee adduction moment (KAM). Joint moments relate to OA etiology, but do not directly reflect joint contact forces, and can give a misleading picture of how contact forces differ between conditions or subjects [3]. We therefore expected that contact forces summarized using features other than the peak would be greater in amputees than in controls, while peak KAM would be similar between groups.

METHODS

Institutional approval was obtained and consent was granted from each participant. Motion capture and ground reaction force data were measured from 10 unilateral lower limb amputees (five transtibial, five transfemoral). All amputees were Service Members who had sustained traumatic limb injuries in Iraq,

Afghanistan, and related military conflicts, and had been walking independently with their prosthesis for 2 months. Subjects walked overground at self-selected speed (mean 1.25 m/s) and step rate. Knee joint angles, forces, and moments were calculated in Visual3D and averaged over 5 strides. Control data collected elsewhere for 10 non-amputees walking at the same mean self-selected speed were referenced [3] and processed using the same methods.

Knee muscle forces were calculated (custom Matlab code) from the knee extension moment assuming no antagonism, and joint contact forces were then estimated using a frontal plane model to balance the internal and external loads on the joint [4].

Joint loading was quantified using the KAM, the resultant moment (KRM), the medial contact force (Fmed), and the total contact force (Fcon). Summary variables were peak, loading rate in early stance (LR), impulse, and per-unit-distance load (PUD). Forces and moments were scaled by bodyweight (BW) and BW*height (Ht). Results were compared between groups using *t*-tests ($p < 0.05$) and effect sizes ($d > 0.80$).

RESULTS AND DISCUSSION

Compared to controls, the intact limb's knee had:

- Greater KRM peak (5.73 ± 1.63 vs. 4.37 ± 1.11 %BW*Ht, $p = 0.036$, $d = 0.98$)
- Greater KRM impulse (1.89 ± 0.41 vs. 1.43 ± 0.25 %BW*ht*s, $p = 0.007$, $d = 1.36$)
- Greater Fmed impulse (0.71 ± 0.12 vs. 0.60 ± 0.10 BW*s, $p = 0.049$, $d = 0.93$)
- Greater Fcon impulse (1.03 ± 0.16 vs. 0.82 ± 0.08 BW*s, $p = 0.002$, $d = 1.65$)
- Greater Fcon peak (2.74 ± 0.47 vs. 2.15 ± 0.31 BW, $p = 0.042$, $d = 1.47$)

None of the KAM summary parameters, and none of the LR or PUD parameters, were significantly different between groups. The contact force results were robust to 95% of random perturbations to the knee joint model parameters and muscle force distributions, suggesting results were driven by the gait data rather than by modeling assumptions.

The results indicate that conclusions on knee joint loading between amputees and controls depend on (i) the variable chosen to represent loading, and (ii) how that variable is summarized for statistical analysis. For example, if the KAM were chosen, we would conclude no difference in joint loading between groups, regardless of how the KAM is summarized. The same conclusion would be reached for any loading variable summarized using LR or PUD. In contrast, KRM, Fmed, and Fcon all suggest loading is greater in the amputee intact limb's knee joint when summarized with impulse. This latter conclusion is perhaps the expected result if we (ostensibly) assume that knee OA risk in amputees is related to the intact limb's knee joint being mechanically overloaded.

CONCLUSIONS

The choice of how to quantify and summarize joint loading is an important one that can dictate the conclusions reached in a study. The KAM is clearly an important variable in knee OA, but may need to be combined with other gait variables to fully characterize the joint loading environment and risk for mechanics-driven joint degeneration.

REFERENCES

1. Morgenroth DC, et al. *PM R* **4**, S20-S27, 2012.
2. Felson DT. *Osteoarthritis. Cartilage* **21**, 10-15, 2013.
3. Miller RH, et al. *Med. Sci. Sports Exerc.* **46**, 572-579, 2014.
4. Schipplein OD & Andriacchi TP. *J. Orthop. Res.* **9**, 113-119, 1991.

ACKNOWLEDGEMENTS

We would like to acknowledge Jenna Trout for her contribution to this work.

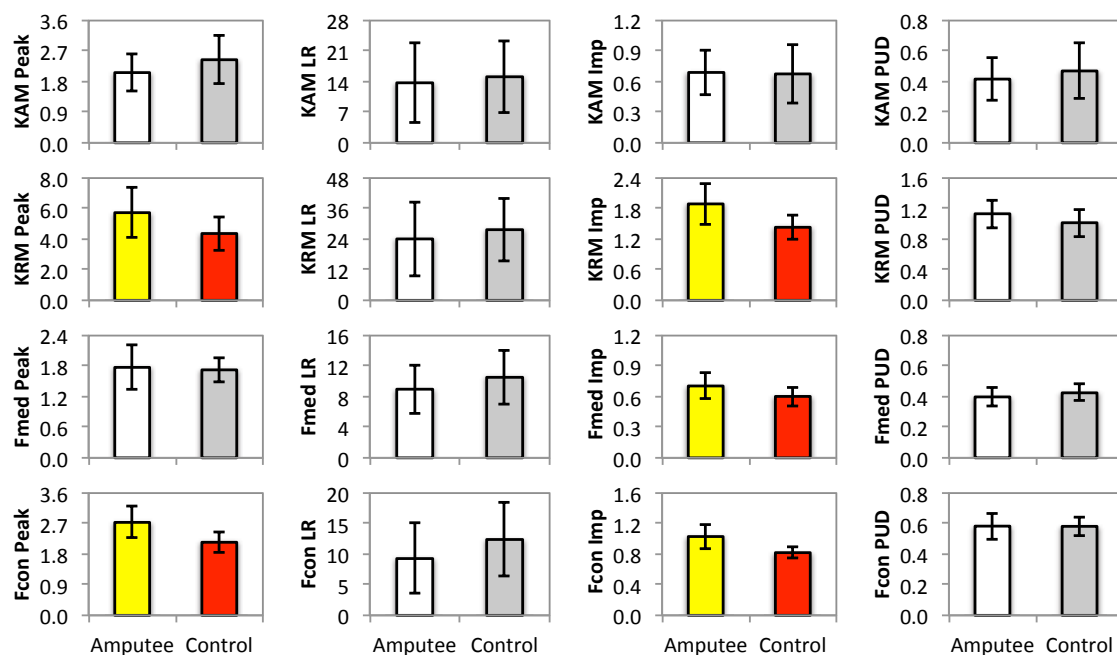


Figure 1: Group means \pm SD for knee adduction moment (KAM), resultant moment (KRM), medial contact force (Fmed), and total contact force (Fcon) summary parameters. Columns 1-4 show the peak, loading rate, impulse, and per-unit-distance loads, respectively. Amputee data are for the intact limb. Moments are scaled by %bodyweight*height. Contact forces are scaled by bodyweight. For graphs shown in color, the group means were significantly different ($p < 0.05$) with large effect size ($d > 0.8$).

DOES UNILATERAL TRANSTIBIAL AMPUTATION AFFECT 90° TURNING STRATEGIES?

^{1,2} Elizabeth M. Nottingham, ³ Nicholas S. Allevato, and ^{1,2} Erik J. Wolf

¹ Walter Reed National Military Medical Center, Bethesda, MD, USA

² DoD-VA Extremity Trauma and Amputation Center of Excellence

³ George Mason University, Fairfax, VA, USA

email: elizabeth.m.nottingham.civ@mail.mil

INTRODUCTION

Advances in prosthetic technology and rehabilitation strategies have allowed ambulation to no longer be an extraordinary task for Service Members (SMs) with unilateral lower extremity amputation (ULEA). Despite locomotion advancements, the majority of research on this population focuses on straight, level-ground walking tasks, which insufficiently defines activities of daily living. Altered gait biomechanics and ambulation strategies while changing direction may contribute to the development of chronic secondary injuries such as osteoarthritis (OA) and low back pain [1].

The task of turning presents a potential challenge to those with ULEA due to increased residual limb pain or discomfort [2]. This pain may lead to gait alterations and decreased stability [3]. Published work has focused on what compensatory strategies are utilized by persons with ULEA as they turn. Limited information regarding turning strategy preference has been documented. Step turning and spin turning are the two main strategies used for 90° turns. Step turning involves a change in direction opposite to the stance limb. Spin turning involves a change in direction toward the same side as the stance limb where the stance limb can pivot or stay rooted throughout the turn [4]. Preliminary analysis of uninjured individuals suggests that the step turn strategy is most commonly selected [4].

This study presents preliminary data obtained as SMs followed laser-guided pathways that consisted of randomly generated transient tasks from a unique system (MITRE, USA). This method of moving freely about the lab space in a controlled manner is called freeform walking (FFW). The concept behind FFW is that participants will walk in a more realistic manner compared to a forced turning

command. This FFW based evaluation allows for the preliminary analysis of how those with ULEA complete non-linear walking tasks, specifically 90° turns. We hypothesize that SMs with a ULEA will adjust turning strategies to favor the sound limb for turning. Therefore, step turns will maintain prominence when turning towards the prosthetic side and spin turns will be favored when turning towards the sound side.

METHODS

Institutional approval was granted by Walter Reed National Military Medical Center to enroll human subjects into this protocol; all subjects provided informed consent prior to participation. Three SMs with unilateral transtibial amputations (TT01, TT02, and TT03) and four uninjured SMs participated in this evaluation. Participants with amputations were preferred prosthetic components and walked without use of other assistive devices. Motion capture data (Vicon, UK; AMTI, USA) were collected as SMs followed five different laser-guided paths conducted in a randomized order (Figure 1). Laser-guided path speed matched pre-determined self-selected walking pace of each SM.

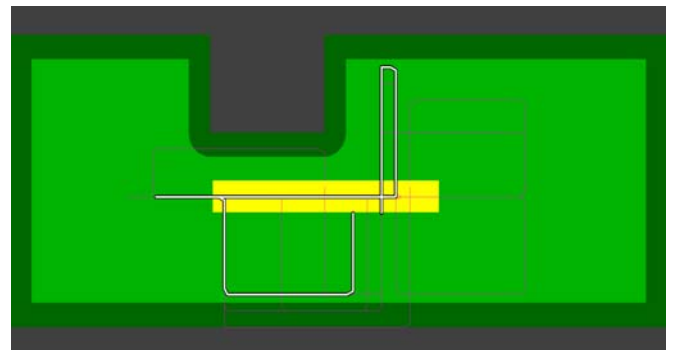


Figure 1: Digital schematic – aerial view of the gait lab area (light green is available area, dark green is the lab perimeter buffer zone), force plate locations (yellow) and an example of laser guided paths (grey / black).

The total numbers of 90° turns were counted and turning strategy was noted for each change of direction.

RESULTS AND DISCUSSION

Results are reported as mean (STD). Control participants averaged a total of 87(2) left turns and 60(5) right turns. SMs with ULEA averaged 71(13) sound side turns and 77(12) prosthetic side turns. Consistent with literature regarding uninjured turning technique preference, all participants were more likely to use a step turn technique than a spin turn strategy when tasked with a 90° turn in a FFW environment [4] (Figure 2).

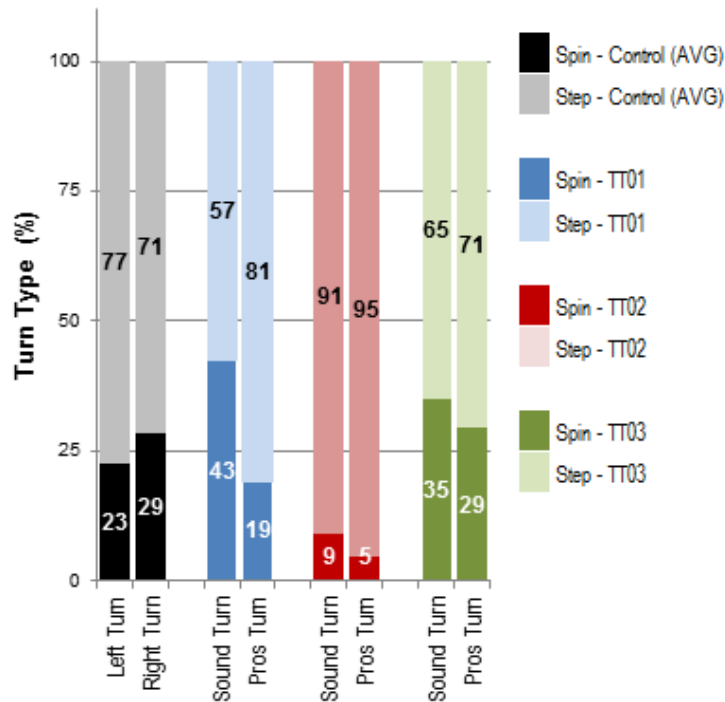


Figure 2: Average self-selected turning techniques of uninjured control group (Control (AVG)) and each SM with amputation (TT01, TT02, TT03).

When turning towards the sound side participants TT01 and TT03 carried out spin turns at a greater rate than the control group. This result indicates that they preferred to change direction while standing on their sound side. When turning towards the prosthetic side TT01 and TT02 implemented step turns at a greater rate than the control group. The greater frequency of step turns to the prosthetic side demonstrates a preference of turning with the

sound limb in stance. Regardless of direction, participant TT02 executed a higher percentage of step turns in comparison with the control subjects. This result may have occurred due to prosthetic fitting or pain associated with spin turns to either direction. This participant was the only SM with ULEA using a powered prosthetic device.

Within participant comparisons between sound and prosthetic side turns indicate that all SM with ULEA performed a step technique more often when turning towards the prosthetic side and utilized spin turns more frequently when turning to the sound side. These observations support the hypothesis that SMs with ULEA adjust their turning strategy to keep the sound limb in stance.

CONCLUSIONS

This observational analysis provides a preliminary comparison of freeform turning techniques used by SMs with and without ULEA. The collection of additional data and further analysis on turning method preference as well as temporospatial, kinematic and kinetic analyses will lead to a better definition of how those with ULEA complete common activities of daily living.

REFERENCES

1. Burke MJ. Ann Rheum Dis, 1978; 37(3): 252-4
2. Segal A.D. JRRD, 2009; 46(3): 375-383
3. Segal A.D. Gait & Posture, 2011; 33(4): 562-567
4. Taylor M.J.D. Hum Movement Sci, 2005; 24: 558-573

ACKNOWLEDGEMENTS

This work was supported, in part, by the DoD-VA Extremity Trauma & Amputation Center of Excellence (EACE), US Army Medical Command Headquarters, Fort Sam Houston, TX under Public Law 110-417, National Defense Authorization Act 2009, and Section 723. The views expressed in this abstract are those of the authors and do not reflect the official policy of the Department of Defense, Army, Navy or United States Government.

DESIGN AND 3D PRINTING OF A DYNAMIC WRIST SPLINT IN THE DART THROW MOTION PLANE

¹ Portnoy Sigal, ² Sayapin Andrey, ¹ Kaufman-Cohen Yael, ¹ Levanon Yafa

¹ Tel Aviv University, Tel Aviv, Israel

² Afeka College of Engineering, Tel Aviv, Israel

Email: portnoys@post.tau.ac.il, web: <http://www.tau.ac.il/~portnoys/>

INTRODUCTION

Rehabilitation following a wrist fracture often includes exercising flexion-extension movements with a dynamic splint. Current studies show that these sagittal wrist movements are not representative of the natural daily wrist movements. We actually perform most of our daily functions, with our wrist moving on a Dart Throw Motion (DTM) plane, also defined as the plane between radial-extension and ulnar-flexion [1]. The DTM may be considered a more stable and controlled motion, since most motion occurs at the midcarpal joint with the proximal row of carpal bones remaining relatively immobile [2]. This might prove advantageous in rehabilitation following wrist fracture, where the ligaments are intact, since minimal pain is expected as a result of minimal bone movement in the proximity of the injured site. To date, no dynamic brace exists which facilitates wrist exercise in the DTM plane. Also, it has not been reported whether the DTM plane angle is similar for the dominant and non-dominant hand. If DTM is similar between hands then the DTM splint can be used for injuries of both dominant and non-dominant hands. Also, we would be able to calculate the individual natural DTM plane of the patient from the uninjured hand and design the splint characteristics according to the calculated plane. Our aims are therefore (1) To characterize the DTM plane in the wrist bilaterally during daily activities, and (2) to design and 3D print a subject-specific dynamic wrist splint that facilitates wrist exercise in the DTM plane.

METHODS

First, the DTM plane was calculated using a wrist electrogoniometer placed on both wrists (Fig. 1a) of healthy subjects (N=36; 28 females; age 30.5±12.8 years), performing twelve activities of daily living

(ADL), e.g. using a hammer, opening a jar, pouring water from a bottle, throwing a ball, and answering the phone. The activities were performed once with the dominant hand and once with the non-dominant hand. The geometry of the splint was designed in Solidworks to fit to a 3D scan of the arm, wrist and hand (Fig. 1b). The brace design comprise of a proximal attachment to the arm and a distal accurate envelope of the palm. An axle with two wheels is attached to the proximal part. Two wires attach the proximal part with the medial-palmar and lateral-ventral aspects of the distal part: when the wrist extends, the medial wire is released and the lateral wire is strained towards the radius. When the wrist flexes, the lateral wire is released and the medial wire is strained towards the ulna. The splint was attached to the wrist using Velcro as two wires attached to two pulleys, situated on a joint axis, pull the hand to move in the desired calculated plane.

RESULTS AND DISCUSSION

As hypothesized, no significant difference was found between the DTM plane angles of the dominant and non-dominant hands, while performing daily activities. In several of the tasks, the angle of the plane of motion was negative DTM plane (radial-flexion to ulnar-extension). The most common ADLs occurred at a DTM plane angle of approximately 20° to 45°. The printed splint fitted the wrist of the subject, was easy to don and doff and constricted movement to the desired DTM plane. The design is adjustable for different DTM planes by calculating the lengths of the wires and the diameter of the two wheels. Hooks were inserted on each part to allow the addition of rubber bands for resistance training towards muscle strengthening.

CONCLUSSIONS

It has been hypothesized that activation of the wrist in the DTM plane following distal radius fracture will accelerate the recovery of the patient and enable him or her improved functionality. Our results show that the DTM angle can be determined from either the dominant or non-dominant wrists. The design of the patient-specific dynamic splint is the first step towards assessing whether DTM splinting is beneficial to the rehabilitation of individuals following distal radius fracture, compared to conventional treatment. The evaluation

of the clinical benefits of this method, compared to conventional rehabilitation methods following wrist fracture, are a part of a PhD work, currently conducted by an occupational therapist (KCY).

REFERENCES

1. Garcia-Elias M, et al. *J Hand Surg Eur*, **39**, 346-352, 2014
2. Crisco JJ, et al. *J Bone Joint Surg Am*, **19**, 169-177, 2011.

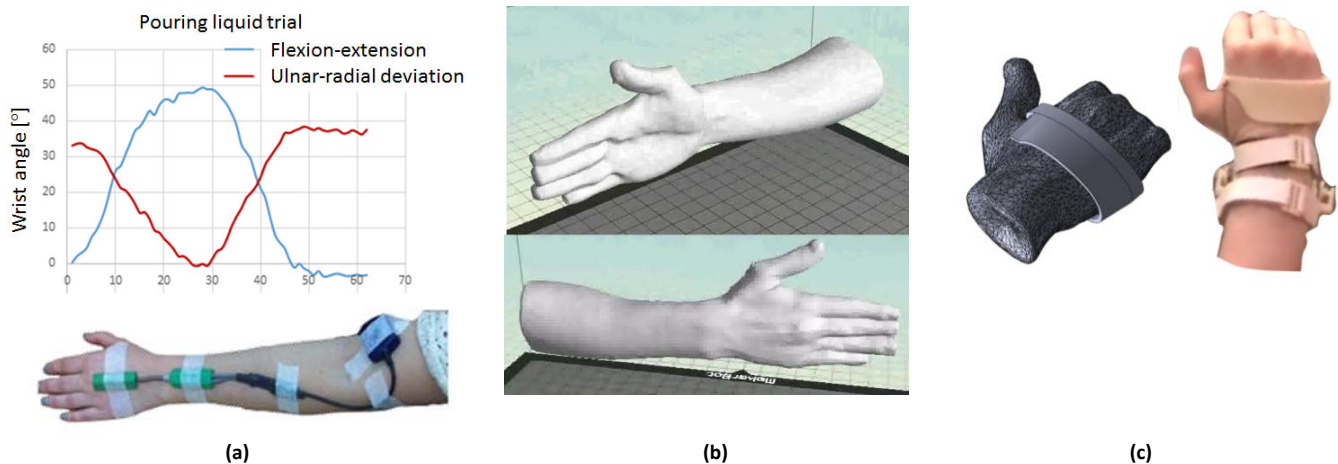


Figure 1: The brace was designed following calculation of the DTM plane during different tasks of daily activities, monitored by an electrogoniometer (a). A 3D scan of the hand and forearm (b) was used to design and print a subject-specific wrist brace (c) according to the wrist geometry of the subject.

OPTIMAL METHOD FOR ESTIMATING SCAPULAR KINEMATICS DURING UPPER EXTREMITY CYCLING

¹Elizabeth A. Rapp, ¹Kristen F. Nicholson, ¹R. Tyler Richardson, ²Therese E. Johnston, and ¹James G. Richards

¹ The University of Delaware, Newark, DE, USA

² Thomas Jefferson University, Philadelphia, PA, USA

email: lizrapp@udel.edu

INTRODUCTION

The scapula plays an important role in the overall function of the shoulder complex, however, accurate dynamic measurements of scapulothoracic (ST) kinematics have proven challenging to obtain. Surface markers fail to capture motion when the scapula translates beneath the skin. Other techniques are either invasive, expensive, or limited to static positions. One of the most widely used estimation approaches, the acromion marker cluster (AMC), is clinically feasible, however loses accuracy at extreme elevations and in pathological populations [1,2]. Improvements in accuracy have been seen from using an interpolated AMC calibration from two different positions [3], however, this validation study was performed on planar motions. An appropriate method for estimating ST kinematics during a cyclic activity such as upper extremity (UE) cycling exercise has yet to be validated. This study aimed to find the optimal method for measuring scapular kinematics during UE cycling. Given the repetitive and constrained nature of cycling, a multi-point calibration of the AMC seemed both promising and feasible. We hypothesized that a four-point AMC calibration would be more accurate in estimating scapular orientation during cycling than a single or double AMC approach.

METHODS

Thirteen healthy adults were recruited. Retroreflective 6mm cube markers were fixed on the trunk and humeri. Additional markers were placed on the cycle to calculate crank position. An acromion marker cluster consisting of three non-collinear cube markers were attached to the acromion process (AP) with the central marker flush to the AP. Subjects moved through eight static

positions in 45° increments of the crank revolution. At each position, markers were placed on the trigonum spinae and the inferior angles of the scapulae. Positions of the markers were recorded at 60 Hz by a nine camera motion capture system and used to define coordinate systems for the trunk, scapula and humerus. Scapulothoracic and humerothoracic (HT) angles were calculated using a helical method and then decomposed into X, Y, Z components to avoid dependence on order of motion [4]. Crank angles were calculated from markers placed on the pedal shaft.

Scapulothoracic angles were calculated via three different methods. The first was the standard single AMC calibration which used the relationship between the AMC and the palpated scapula in the 0° position to create a calibration to estimate scapular orientation from the AMC at other cycle positions. The double calibration approach was similarly created from the 0° and 180° positions, and ST angles were calculated using a weighted average of the two calibrations based on the position of the crank angle. The multiple AMC method repeated the calibration process at three more points: 90°, 180° and 270°. The intermediate positions of 45°, 135°, 225°, and 315° were used to test the accuracy of the three approaches.

Palpation was used as the standard of accuracy for comparison [5]. Paired two-tailed t-tests were used to determine if the three methods were statistically different from palpation. Paired t-tests were run for each method and along each axis of motion for a total of twelve tests. No Bonferroni corrections were performed. Root mean square errors (RMSE) were calculated for each axis for each method.

RESULTS AND DISCUSSION

The root mean square error (RMSE) values of estimated ST angles ranged from 3.8° to 9.2° (Fig. 1). In general, the single AMC calibration produced the highest errors. The paired t-tests showed that the ST angles predicted by the single AMC calibration were significantly different from palpation along the internal/external rotation (Y) and anterior/posterior tilt (Z) axes. Additionally, the ST angles predicted by the double and multiple AMC calibrations were each significantly different from palpation about one axis. Means and standard deviations of the absolute differences between predicted and palpated angles are given in Table 1.

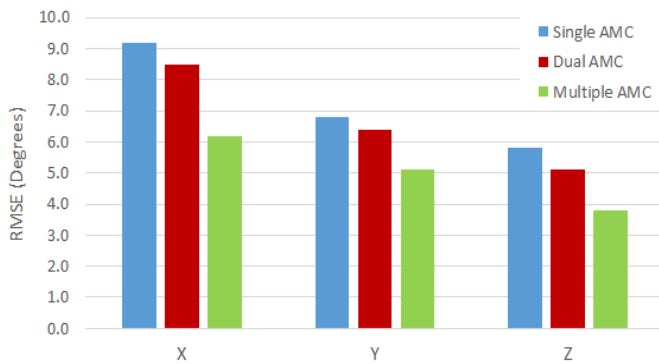


Figure 1: RMSE of ST Angles by Axis and Method

Statistical testing of the new methods demonstrated a marginal improvement upon the single AMC method. For functional application, the RMSE provided an estimate of error independent of directionality and offered a clinically meaningful evaluation of overall accuracy. This study's maximum RMSE under single AMC calibration was 9.2°, which is consistent with previously reported results [3]. For all three methods, the largest RMSE values were found around the X axis (upward rotation). As this is the axis about which

the scapula experienced the most movement, these errors appear to scale within the context of motion. The double and multiple AMC calibration methods both demonstrated improvements in error. The maximum RMSE for the dual AMC calibration was 8.5° and the multiple AMC calibration outperformed both other methods with a maximum RMSE at 6.2° and the smallest RMSEs for each axis. Increasing the number of calibration points notably reduced the errors from AMC estimations of scapulothoracic angles. While additional calibration points could potentially reduce the angle errors even further, the multiple AMC interpolation from four calibrations appears sufficient in both application feasibility and accuracy for UE cycling.

CONCLUSIONS

For cyclic activities such as upper extremity cycling, it appears that the addition of multiple calibration points facilitates the accuracy of scapulothoracic orientation estimates. Looking ahead, we intend to apply this approach to differentiate the scapulothoracic and glenohumeral contributions to shoulder motion during upper extremity cycling therapy in patients with spinal cord injury.

REFERENCES

1. Van Andel, C, et al. *Gait and Posture* **29**, 123-128, 2009.
2. Nicholson, KF, et al. *J Appl Biomech* **30**, 128-133, 2014
3. Brochard, S, et al. *J Biomech* **44**, 751-754, 2011
4. Woltring, HJ, et al. *J Biomech* **18**, 379-389, 1985.
5. Degroot, JH. *Clin Biomech* **12**, 461-472, 1997.

Table 1: Mean (SD) of the absolute value differences between estimations of ST angles and palpation.

METHOD	X	Y	Z
Single AMC	7.3 (5.3)	4.8 (4.1)*	4.5 (3.2)*
Double AMC	6.9 (4.9)	5.0 (3.4)	3.8 (2.9)*
Multiple AMC	4.7 (4.1)	3.3 (2.9)*	2.7 (2.1)

* $p < 0.05$, significant difference between method and palpation

THE EFFECT OF ANKLE-FOOT ORTHOSIS ALIGNMENT ON ROLL-OVER SHAPE IN PATIENTS WITH LOWER LIMB RECONSTRUCTION

¹Mitchell D. Ruble, ^{1,2}Elizabeth Russell Esposito, ^{1,2}Jason M. Wilken

¹ Center for the Intrepid, Department of Orthopaedics and Rehabilitation, Brooke Army Medical Center, JBSA, Ft. Sam Houston, TX, USA, ²DoD-VA Extremity Trauma and Amputation Center of Excellence
E-mail: mitchell.d.ruble.ctr@mail.mil

INTRODUCTION

Injuries requiring limb reconstruction surgery often result in pain and plantar flexor weakness, for which ankle foot orthoses (AFOs) are commonly prescribed. The Intrepid Dynamic Exoskeletal Orthosis (IDEO) is a passive-dynamic AFO created to improve upon conventional AFO designs by utilizing energy storage and return [1]. However, an AFO may compromise how the foot rolls over the ground due to its semi-rigid footplate. Ankle-foot roll-over shape (ROS) is a biomechanical measure which characterizes how the center of pressure (COP) moves relative to the limb. The foot and shoe are viewed as a rocker with a single radius and the COP path relative to the limb is characterized from ipsilateral initial contact to contralateral initial contact [3]. Maintaining an optimal ROS is thought to increase the stability and efficiency of pathologic gait [3]. The ROS technique was initially developed to understand the relationship between device alignment and function [4]. Alignment has been shown to directly influence ROS in prosthetic devices, but its effect on ROS in AFOs is not well understood. The purpose of this study was to measure the effects of the sagittal plane alignment of the IDEO on ROS in patients with lower limb reconstructions.

METHODS

A total of nine male subjects with unilateral limb reconstruction (age 30 ± 6 , height 1.78 ± 0.09 m, mass 87.2 ± 9.7 kg) underwent gait analysis in a motion laboratory (marker data: 120 Hz, Motion Analysis Corp, analog data: 1200 Hz, AMTI, Inc.). Testing was performed with the IDEO aligned in 3 different conditions using a 3° wedge attached to the posterior strut (Fig 1): neutral (determined by

orthotist based on pain-free range of motion), 3° more dorsiflexed, and 3° more plantarflexed.

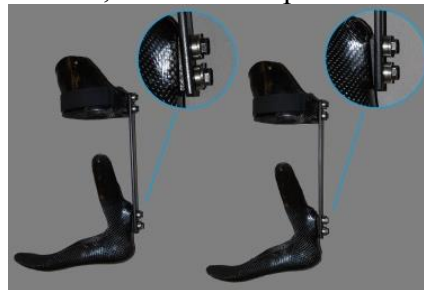


Figure 1: The IDEO aligned in dorsiflexion (left) and plantarflexion (right) using a 3° wedge.

Each subject walked until their affected and unaffected limb each made full contact with a force plate 5 times. To determine ROS, the COP of the ground reaction force was calculated in Visual3D (C-Motion, Inc.), in the shank coordinate system. Ankle-foot ROS was initially calculated from contralateral heel strike to ipsilateral heel strike, then further cropped using only data from forward COP progression and normalized to height. A circle was fit to calculate the ROS radius. A 2-way repeated measures ANOVA (limb x alignment) was performed on the ROS radius values and ankle angle peaks. Paired t-test post-hoc analysis separated main effects ($p < 0.05$).

RESULTS AND DISCUSSION

The 3° modifications in sagittal plane IDEO alignment significantly changed ankle alignment at the stance and swing phases throughout the gait cycle ($p \leq 0.004$ for all comparisons). However, these 3° changes in the alignment from the neutral position did not influence ROS radius in patients with lower limb reconstruction ($p = 0.455$) (Fig 2-3). They also did not affect the ROS of the sound limb ($p = 0.800$). There were no significant interactions ($p = 0.606$).

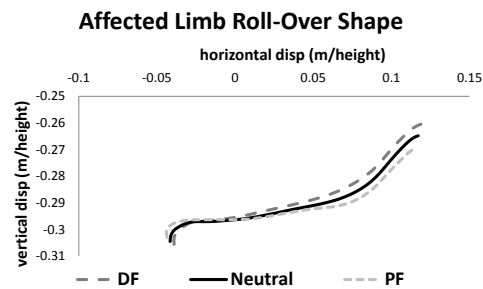


Figure 2: Mean ankle ROS.

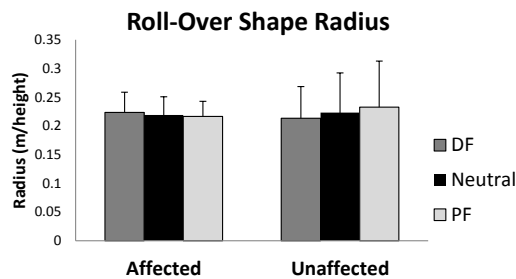


Figure 3: Mean and standard deviation ROS radius.

The mean radii for ROS in the IDEO were found to be consistent with prior studies; Hansen et al. [6] found a range of median ROS radii to be between 0.12-0.28 in healthy controls. Despite the semi-rigid structure of the IDEO, and its impact on ankle biomechanics during walking [6], it did not affect ROS. This may indicate the IDEO maintains an appropriate rocker shape. In addition, the lack of differences between limbs indicates that the limited ankle range of motion permitted by the IDEO [6] did not negatively influence the ability of the intact limb to maintain near-normative ROS radius.

Prior research has studied the effects of other interventions on ROS, such as modifying heel height to change the sagittal plane ankle angle [6]. Similar to the alignment changes about the ankle in the present study, changes to ankle angle by systematically altering heel height also did not change ROS radii from their baseline control levels. The 6-degree range of changes in sagittal plane IDEO alignment were chosen because they were expected to be within the range different orthotists may choose when fitting a patient. Alignment alterations significantly affect the vertical displacement and overall alignment of the ROS ($p < 0.012$). The results of this study indicate that, within this 6-degree range, these modifications to

alignment are not expected to negatively impact the rocker profile of the foot.

One limitation of this study is the lack of a no-IDEO condition, which would identify the acute effects of the IDEO on the rocker shape profile. Multiple subjects were unable to walk pain-free without the use of this assistive device and this condition was necessarily excluded from the study.

CONCLUSIONS

A 6-degree range of changes in the sagittal plane alignment of an AFO influenced the positions of the ROS relative to the leg, but not the radii in patients with lower limb reconstructions. ROS radii values were consistent with previously published literature from able-bodied individuals and did not differ from the unaffected limb. These results indicate that the ROS of the device effectively mimicked that of an intact limb during single limb stance.

REFERENCES

1. Patzkowski JC, et al. *J Bone Joint Surg Am* **94**, 507-515, 2012.
2. Hansen AH, et al. *Disabil Rehabil* **32**, 2201-9, 2010.
3. Hansen AH, et al. *J Rehabil Res Dev* **44**, 11-20, 2007.
4. Hansen AH, et al. *Prosthet Orthot Int* **24**, 205-15, 2000.
5. Hansen AH, et al. *J Rehabil Res Dev* **41**, 547-54, 2004.
6. Harper NG, et al. *J Biomech Eng*. **136**, 091001-7, 2014.

ACKNOWLEDGEMENTS

Support for this study was provided by the Center for Rehabilitation Sciences Research, Dept. of Physical Medicine and Rehabilitation, Uniformed Services Univ. of Health Sciences, Bethesda, MD.

The views expressed herein are those of the authors and do not reflect the policy or position of Brooke Army Medical Center, the US Army Medical Department, US Army Office of the Surgeon General, Department of the Army, Department of Defense or US Government.

BIOMECHANICAL ADAPTATIONS TO ANKLE-FOOT ORTHOSIS STIFFNESS DURING RUNNING

^{1,2}Elizabeth Russell Esposito, ^{1,2}Harmony S. Choi, ¹Johnny G. Owens, ^{1,3}Ryan V. Blanck, ^{1,2}Jason M. Wilken

¹Center for the Intrepid, Brooke Army Medical Center, JBSA, Ft. Sam Houston, TX, USA, ²DoD-VA Extremity Trauma and Amputation Center of Excellence, ³Hanger, Inc., Tacoma, WA, USA
E-mail: erussell.kin@gmail.com

INTRODUCTION

Limb trauma requiring reconstructive surgery commonly results in decreased performance of key functional activities such as walking and running. Ankle-foot orthoses (AFOs) are frequently prescribed to restore limb function by providing mechanical support. To address the desire of patients with injuries requiring lower limb reconstruction to return to running and other high-energy activities, a custom carbon-fiber, passive-dynamic orthosis, the Intrepid Dynamic Exoskeletal Orthosis (IDEO), was developed to improve upon previous AFO designs [1] and facilitate the return to high-energy, performance-based tasks [2]. The customizable nature of the IDEO allows certain features, such as its stiffness, to be tailored to meet the needs of the individual. This mechanical stiffness may also influence the stiffness or compliance of the lower extremity joints [3]. The purpose of this study was to determine the effect of AFO stiffness on lower extremity running biomechanics in individuals with lower limb reconstructions.

METHODS

Ten male subjects with traumatic, unilateral lower limb reconstruction underwent gait analysis (marker data: 120 Hz. Motion Analysis Corp, ground reaction force data: 1200 Hz, AMTI, Inc.) of the lower extremity during overground running at a self-selected speed. All patients were regular users of a custom IDEO (Fig. 1) whose stiffness characteristics were clinically prescribed by the prosthetist/orthotist based on the patient's available range of motion, activity level, body mass and load carriage requirements. Three struts were fabricated using a selective laser sintering technique [4]: 1. Nominal (clinically prescribed stiffness, mean: 832

± 182 Nmm), 2. Compliant (20% less stiff), and 3. Stiff (20% stiffer).



Figure. 1. The Intrepid Dynamic Exoskeletal Orthosis (IDEO) consists of a carbon fiber distal supra-malleolar ankle-foot orthosis, a proximal tibial cuff, and a removable, connective, posterior-mounted strut.

Five trials in which each the affected and unaffected limbs made full contact with one of the force platforms were analyzed. Lower extremity joint angles, moments and powers, and loading rates from the vertical ground reaction force were calculated. At the ankle and knee joints, mechanical work was calculated by integrating the joint power curves and joint stiffness was determined using a torsional spring model during the braking phase of stance. A 2-way repeated measures ANOVA (strut x limb) assessed statistical significance of the dependent measures. Paired t-tests separated main effects. Bonferroni-Holm corrections were used with main effects of strut or interactions ($p < 0.05$).

RESULTS AND DISCUSSION

There was a significant interaction ($p = 0.011$) such that the stiffness of the sound ankle remained unchanged across conditions while the affected ankle was, on average, 152.5% stiffer than the unaffected ($p < 0.001$) and increased joint stiffness with increasing strut stiffness ($p = 0.019$). Specifically, the stiffest strut resulted in an 18% increase in ankle joint stiffness compared to the compliant strut ($p = 0.001$) (Fig 2). Strut stiffness did

not affect temporal spatial measures, preferred running speeds, kinematics or any other kinetics.

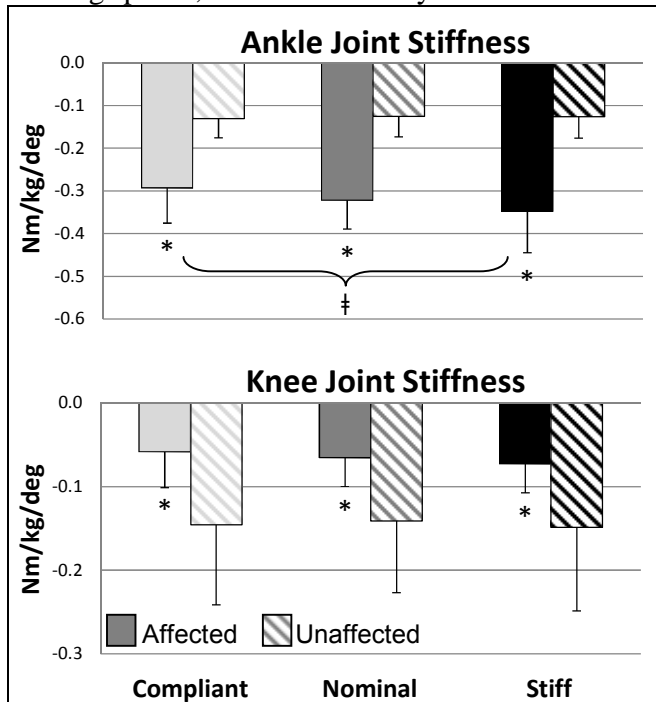


Fig 2. Ankle and knee joint stiffness during the braking phase of stance for the affected (solid bars) and unaffected (dashed bars) limb. † indicates significance between strut stiffness conditions and * indicates significance between groups.

Although the affected ankle was stiffer than the unaffected side, the knee of the affected limb was, on average, 123.2% more compliant ($p=0.007$), potentially in an effort to preserve total limb stiffness [3]. Positive and negative mechanical work were 212.0% and 64.2% greater, respectively, on the unaffected limb for the ankle (pos: $p<0.001$, neg: $p=0.013$) and 62.3% and 124.3% greater for the knee (pos: $p=0.008$, neg: $p=0.003$), respectively.

Limb stiffness is a fundamental component needed for optimal performance [5] and dynamic AFO stiffness can influence the amount of energy storage and return an individual experiences during gait. However, a 40% range in strut stiffness did not influence kinematic and most kinetic mechanics of running. Subjects either readily adapted to the different stiffness conditions or the 40% range of stiffnesses evaluated in this study was not broad enough to elicit significant changes in mechanics. The only exception was that the stiffer strut did

increase the stiffness of the affected biological ankle joint compared to the compliant strut. However, the increase in ankle stiffness did not affect mechanical work or decrease the knee stiffness, which would be expected if total leg stiffness were maintained [3].

CONCLUSIONS

Strut stiffness did not influence joint angles, moments, powers, or mechanical work during running in individuals with unilateral lower limb salvage. However, a stiffer AFO results in a stiffer ankle joint structure which may be particularly useful for patients with limited pain free ankle range of motion. The changes in joint stiffness were not associated with significant changes in mechanical work. It is unknown how these results translate to populations with other injuries and pathologies, but is likely that some adaptation occurs to different stiffnesses. Therefore, a range of stiffness may be clinically appropriate when prescribing ankle-foot orthoses for running activities, while a stiffer AFO may reduce the risk of mechanical failure during high-energy activities other than running.

REFERENCES

1. Patzkowski JC, et al. *J Bone Joint Surg Am* **94**, 507-515, 2012.
2. Bedigrew KM, et al. *Clin Orthop Rel Res* **472**, 3017-3025, 2014.
3. Ferris DP, et al. *J Appl Physiol* **100**, 163-170, 2006.
4. Harper NG, et al. *J Biomech Eng* **136**, 2014, 1-7.
5. Stefanyshyn DJ, Nigg BM. *J Appl Biomech* **14**, 292-9, 1998.

ACKNOWLEDGEMENTS

Nicole Harper and Dr. Richard Neptune at the Univ. of Texas designed, fabricated and tested all struts. Support for this study was provided by the Center for Rehabilitation Sciences Research, Dept. of Physical Medicine and Rehabilitation, Uniformed Services Univ. of Health Sciences, Bethesda, MD.

The views expressed herein are those of the authors and do not reflect the policy or position of Brooke Army Medical Center, the US Army Medical Department, US Army Office of the Surgeon General, Department of the Army, Department of Defense or US Government.

FRONTAL PLANE STEPPING CONTROL IN PERSONS WITH TRANSTIBIAL AMPUTATION

^{1,2,4} Jonathan H. Rylander, ³ Joseph P. Cusumano, ⁴ Jason M. Wilken, and ¹ Jonathan B. Dingwell

¹ University of Texas at Austin, Austin, TX, USA; ² Baylor University, Waco, TX, USA; ³ Pennsylvania State University, University Park, PA, USA; ⁴ Brooke Army Medical Center, Ft. Sam Houston, TX, USA
email: jonathan_rylander@baylor.edu

INTRODUCTION

More than 50% of individuals with lower limb amputation fall at least once/year [1]. Therefore, understanding how these persons regulate walking from step-to-step is critical. In the sagittal plane, unimpaired people walking on treadmills control *speed* from stride-to-stride but not absolute position [2]. However, people are less stable in the mediolateral (M-L) direction [3,4] and it is unknown what control strategies both unimpaired and persons with amputation adopt in this direction. This study characterized the mediolateral step-to-step control strategies of individuals with unilateral transtibial amputation (TTA) and able bodied controls (AB) during un-perturbed and continuously-perturbed walking.

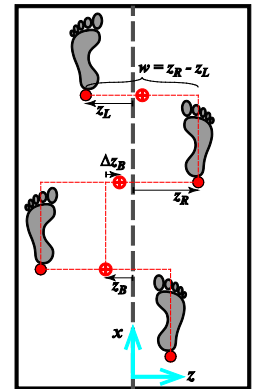
METHODS

Eight physically active traumatic TTAs and 13 ABs (age 22-40) participated. Each participant walked in a “CAREN” virtual environment and completed five, 3-minute trials each for each of 3 conditions: no perturbations (NOP), pseudorandom mediolateral visual field perturbations (VIS), or pseudorandom mediolateral treadmill platform perturbations (PLAT) [3].

For each step, for each trial, we computed absolute mediolateral *position* (z_B), *change* in z_B from the previous step (Δz_B) (i.e., “heading”), and step width (w) (Fig. 1). Mean standard deviations were calculated for z_B , Δz_B , and w . Detrended Fluctuation Analysis (DFA) quantified the level of statistical persistence (reflecting relatively weaker vs. stronger “control”; [2,5]) across steps for each stepping parameter. Lastly, for each stepping parameter, we quantified how deviations from the mean values (e.g., $w'_n = w_n - \bar{w}$, etc.) were directly corrected on the subsequent step (e.g., $\Delta w_n = w_{n+1} - w_n$, etc.). For each plot of the corrections vs. relative deviations, we

computed the slopes and strength of correlation (r^2) values. “Perfect” control of a particular stepping variable would result in a slope ≈ -1 with an $r^2 \approx 1$.

Figure 1: Key parameters for lateral step control: z_B is lateral deviation from some absolute position (e.g., center). Δz_B is change in lateral deviation from previous z_B . w is step width. Humans could control one or more of these three stepping variables while walking.



RESULTS AND DISCUSSION

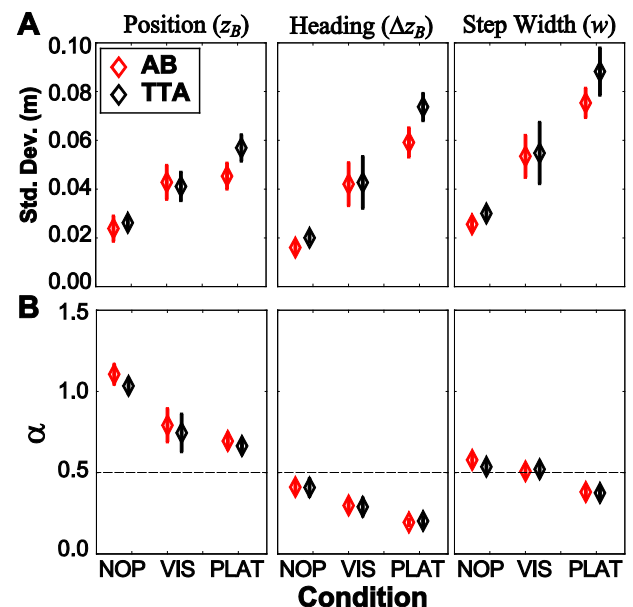


Figure 2: Standard deviations and DFA α values for z_B , Δz_B , and w for AB (red) and TTA (black). Error bars represent a 95% confidence interval.

Standard deviation values for z_B , Δz_B , and w all significantly ($p < 0.001$) increased when visual (VIS) and

platform (PLAT) perturbations were introduced (Fig. 2A). Thus, these perturbations were highly effective in creating a destabilizing environment for both groups [3]. Differences between AB and TTA were only seen in variability of Δz_B and w during PLAT. This may be related to the biomechanical impairment created from the loss of limb.

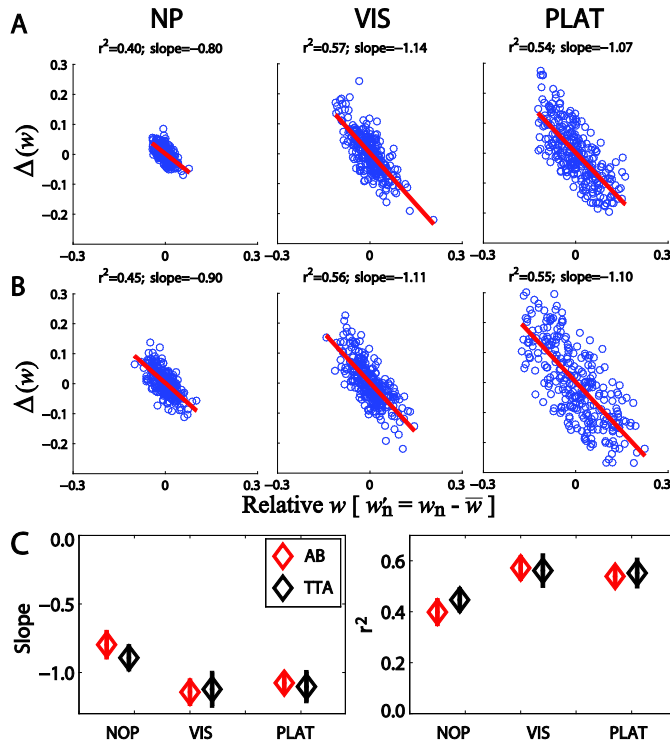


Figure 3: Representative scatter plots of Relative w vs. $\Delta(w)$ for (A) AB and (B) TTA. C: Group means ($\pm 95\%$ CI) for linear regression line slopes and r^2 values for the fitted Relative w vs. $\Delta(w)$ plots.

During all 3 walking conditions, all subjects exhibited anti-persistence for Δz_B ($\alpha < 0.5$), statistically uncorrelated fluctuations ($\alpha \approx 0.5$) for w , and strong statistical persistence ($\alpha > 0.5$) for z_B (Fig. 2). PLAT perturbations significantly increased ($p < 0.001$) the degree of anti-persistence (i.e., as reflected by sharp decreases in α) in all three variables.

Plots of Relative w vs $\Delta(w)$ (Fig. 3A-B) support the idea that subjects strongly controlled step width (i.e., slopes ≈ -1 with high r^2). Under VIC and PLAT perturbations, slopes became steeper with stronger correlations (Fig. 3C), indicating increased step-to-step

corrections. Thus, it appears both AB and TTA tightly control step width through rapid corrections of their step-to-step changes in foot placement and that control increased under perturbed environments.

Findings support the idea of strong prioritization of step width control to maintain lateral balance [4] with far less attention paid to lateral position control [6].

CONCLUSIONS

TTA adopted approximately the same control strategies as AB during both unperturbed and perturbed walking. Higher standard deviation values exhibited by TTA when physically perturbed (Fig. 2A; PLAT) likely indicate that the biomechanical impairments from the amputation make it more difficult for TTA to implement this control strategy. Therefore, when physically perturbed, TTA might have more difficulty adjusting their foot placements, which could lead them to become more unstable.

REFERENCES

1. Miller WC & Deathe AB. *Disabil & Rehabil* 26(14-15): 875-881, 2004.
2. Dingwell JB, John J. & Cusumano JP. *PLoS Comput Biol* 6(7): e1000856, 2010.
3. McAndrew PM, et al. *J Biomech* 43(8): 1470-1475, 2010.
4. Dean JC, Alexander NB, & Kuo AD. *IEEE Trans Biomed Eng*, 54(11): 1919-1926, 2007.
5. Dingwell JB & Cusumano JP. *Gait & Posture*, 32(3): 348-353, 2010.
6. Wang Y & Srinivasan. *Biol Lett*, 10(9): 20140405, 2014.

ACKNOWLEDGEMENTS

DoD/CDMRP/BADER Consortium W81XWH-11-2-0222 (to JBD, JMW, & JPC) and NIH Grant # R01-HD059844 (to JBD & JWM).

DISCLAIMER

The views expressed herein are those of the authors and do not reflect the official policy or position of Brooke Army Medical Center, U.S. Army Medical Department, U.S. Army Office of the Surgeon General, Department of the Army, Department of Defense or the U.S. Government.

Pediatric Joint Dynamics during Manual Wheelchair Mobility

^{1,3} Alyssa J. Schnorenberg, ¹Christine Aurit, ²Joseph Krzak, ²Adam Graf, ⁴Sergey Tarima, ²Lawrence C. Vogel, ^{2,4}Gerald F. Harris and ¹⁻³Brooke A. Slavens

¹ The University of Wisconsin Milwaukee, Milwaukee, WI, USA

² Shriners Hospitals for Children – Chicago, Chicago, IL, USA

³ Marquette University, Milwaukee, WI, USA

⁴ Medical College of Wisconsin, Milwaukee, WI, USA

email: paulaj@uwm.edu

INTRODUCTION

Ten percent of all spinal cord injuries (SCIs) are pediatric cases [1] with an estimated 1455 children admitted for SCI treatment to US hospitals each year [2]. Children with SCIs may achieve functional, home and community mobility through the use of manual wheelchairs (MWCs). The repetitive use of MWCs, however, increases upper extremity (UE) loading demands, and commonly results in pain and injuries which reduce an individual's mobility and quality of life. Studies have examined adult MWC users during mobility tasks including: level propulsion, ramp ascent, start and stop, and weight relief and found significantly different UE joint demands across tasks [3]. Although children are proportionately different than adults, with developing musculoskeletal systems, there is limited research on pediatric wheeled mobility. In order to prevent or slow the development of pain and pathology, a clear understanding of the UE joint dynamics during each mobility task is needed. The purpose of this study is to quantify UE kinematics and kinetics of pediatric MWC mobility during three functional tasks: 1) propulsion, 2) starting from a static position, and 3) stopping from steady state propulsion. We hypothesize that the UE joint dynamics during the start and stop tasks will be significantly greater than during propulsion.

METHODS

Fourteen pediatric MWC users, nine males and five females, with an average age of 13.7 ± 4.8 years, participated at Shriners Hospital for Children – Chicago. Subjects were diagnosed at least one year

prior to the study; average time since injury was 5.3 ± 3.9 years. SCI levels ranged from C3 to T10.

A custom pediatric UE biomechanical model, using 27 reflective markers, defined the acromioclavicular glenohumeral (GH) and wrist, joints (three degrees-of-freedom – DOFs) as well as the sternoclavicular and elbow joints (two DOFs) [4]. Subjects propelled their MWCs along a 15 m level tile walkway using a self-selected speed and propulsion pattern. A 14-camera Vicon MX motion capture system and a SmartWheel system, simultaneously collected bilateral kinematic data at 120 Hz and dominant side kinetic data at the hand-handrim interface at 240 Hz, respectively. During the propulsion task subjects propelled their MWC across the room. Ten stroke cycles were analyzed. To remove acceleration and deceleration effects, the first two and last two strokes were excluded. For the start task subjects began at a static position in the center of the room and propelled to the far side. The first stroke was analyzed for each of three trials. For the stop task subjects propelled into the center of the room and stopped. The last stroke cycle of three trials was analyzed. Three-dimensional (3-D) joint dynamics were determined with the model, normalized to 100% stroke cycle, and processed at 1% increments. Forces and moments were normalized to subject's body weight (% BW) and BW times height (% BWxH), respectively.

RESULTS AND DISCUSSION

Group mean joint forces, and moments (\pm one standard deviation) of the GH, elbow and wrist joints were characterized over the wheelchair stroke cycle. Mean peak forces and moments at the joints

were also computed (Table 1). A one-way ANOVA with linear mixed model analysis determined statistically significantly different biomechanical parameters among tasks ($p < 0.05$).

We found many significantly different parameters across all joints among mobility tasks. All of the significant differences between the propulsion and start task indicate higher forces and moments during the start task. Most of the statistically different parameters were less during the stop task than the propulsion and start tasks, except for the superiorly directed forces for all joints, and the wrist and elbow joint extension moments, which were greater during stop. Functional tasks of start and stop should therefore be of high concern in regards to long-term joint health in children and adolescents.

In a study of adult MWC users with SCI, Morrow et al. reported only GH joint external rotation and extension moments to be greater than propulsion and found no differences among the tasks for GH joint forces. Our results may be attributed to musculoskeletal development and maturation. Research is currently in progress exploring biomechanical differences of task performance between children and adults.

CONCLUSIONS

The study successfully quantified 3-D UE joint dynamics during pediatric MWC mobility tasks. Results indicate that each of the mobility tasks require differing joint demands. Therefore, while propulsion is one aspect of MWC mobility, functional tasks, such as starting and stopping, should also be evaluated due to their importance in community and home mobility. Further investigation into other factors such as duration of load demands, SCI level, and time of MWC use is underway with a larger population. This knowledge may assist in improving training of functional tasks to reduce high joint demands that are causative of pain and pathology.

REFERENCES

- Chien L, et al. , 7, e39264, 2012.
- Vitale M, et al. , 26, 745-749, 2012.
- Morrow M, et al. 20, 61-67, 2010.
- Schnorenberg AJ, et al. 47, 269-276, 2014.

ACKNOWLEDGEMENTS

This work was supported by the Department of Education, NIDRR grant #H133E100007 and also by the NIH NICHD, award #K12HD073945.

Table 1: Mean (stdev) dominant limb joint forces and moments for each task.
* ($p < 0.05$) between that task and propulsion, † ($p < 0.05$) between that task and the start task

Force Direction	Dominant Limb - Mean Peak Force (%Body Weight)								
	GH			Elbow			Wrist		
	Prop.	Start	Stop	Prop.	Start	Stop	Prop.	Start	Stop
Anterior (+)	2.13 (3.26)	2.94 (4.33)	0.20 (3.46)	3.23 (2.32)	3.61 (3.25)	1.47 (3.42)	4.80 (3.48)	5.43 (4.47)	2.58 (3.49)
Posterior (-)	-6.50 (2.05)	-8.14 (3.53)	-4.33 (2.63)*†	-3.37 (2.33)	-4.94 (4.65)	-2.83 (2.40)	-2.02 (1.64)	-3.46 (3.87)	-1.82 (2.42)
Superior (+)	7.04 (1.37)	6.75 (1.48)	10.61 (5.48)*†	3.91 (0.88)	4.48 (1.20)	7.88 (5.92)*†	1.76 (0.74)	2.07 (1.25)	7.07 (5.67)*†
Inferior (-)	-2.43 (3.81)	-4.39 (5.41)	3.96 (1.84)*†	-5.05 (3.97)	-7.68 (5.90)*	1.21 (2.68)*†	-5.39 (4.27)	-8.09 (5.95)*	0.58 (1.633)*†
Lateral (+)	4.85 (2.76)	6.52 (4.59)*	2.23 (2.08)*†	3.88 (2.83)	5.22 (4.69)*	2.25 (2.34)*†	3.19 (2.68)	4.91 (4.88)*	1.39 (1.74)*†
Medial (-)	-2.52 (1.52)	-2.12 (2.08)	-1.11 (1.79)*†	-3.05 (1.59)	-3.07 (2.19)	-1.03 (1.98)*†	-2.10 (1.61)	-2.28 (2.07)	-1.64 (1.64)
Moment Direction	Dominant Limb - Mean Peak Moment (%Body Weight x Height)								
	GH			Elbow			Wrist		
	Prop.	Start	Stop	Prop.	Start	Stop	Prop.	Start	Stop
Adduction (+)	0.81 (0.51)	1.04 (0.72)	0.34 (0.73)*†	0.66 (0.54)	0.89 (0.81)	0.24 (0.75)*†	0.39 (0.35)	0.63 (0.49)*	0.25 (0.56)*†
Abduction (-)	-0.91 (0.57)	-1.29 (1.02)*	-0.50 (0.36)*†	-0.62 (0.49)	-0.73 (0.57)	-0.74 (0.76)	-0.30 (0.31)	-0.35 (0.39)	-0.49 (0.47)
Internal Rot. (+)	0.88 (0.82)	1.13 (0.98)	0.35 (0.56)*†	0.44 (0.60)	0.49 (0.53)	0.33 (0.44)	0.48 (0.41)	0.78 (0.72)*	0.24 (0.29)*†
External Rot. (-)	-0.55 (0.64)	-0.76 (1.07)	-0.34 (0.30)*†	-0.24 (0.32)	-0.25 (0.26)	-0.19 (0.28)	-0.19 (0.22)	-0.28 (0.38)	-0.30 (0.34)
Flexion (+)	0.87 (0.92)	0.98 (1.24)	0.66 (0.65)	1.22 (0.97)	1.76 (1.42)*	0.15 (0.69)*†	0.93 (0.69)	1.54 (1.04)*	0.02 (0.27)*†
Extension (-)	-1.07 (0.55)	-1.11 (0.53)	-0.40 (0.59)*†	-0.44 (0.31)	-0.45 (0.32)	-1.24 (1.13)*†	-0.20 (0.15)	-0.16 (0.13)	-1.26 (1.04)*†

THE INFLUENCE OF SPEED AND GRADE ON WHEELCHAIR PROPULSION HAND PATTERN

¹Jonathan S. Slowik, ²Philip S. Requejo, ²Sara J. Mulroy and ¹Richard R. Neptune

¹The University of Texas at Austin, Austin, TX, USA

²Rancho Los Amigos National Rehabilitation Center, Downey, CA, USA

email: jsslowik@utexas.edu, web: <http://www.me.utexas.edu/~neptune/>

INTRODUCTION

The movement of the hand during manual wheelchair propulsion is closely linked with propulsion mechanics, so the hand pattern (i.e., full-cycle hand path) can provide insight into the user's propulsion technique [1]. However, previous hand pattern analyses have been limited by their reliance on subjective, qualitative characterization methods and/or focus on a single propulsion condition. Pattern characterization has typically involved raters classifying patterns as one of four pattern types (Fig. 1). However, these qualitative methods have difficulty identifying differences between patterns of the same type, and hybrid patterns lead to inconsistencies between raters [1]. In addition, while most hand pattern studies have focused on level propulsion at a self-selected speed, daily living activities can require an individual to propel their wheelchair during different conditions (e.g., at a higher speed or up a graded surface) that may place the upper extremity at a higher risk for injury.

Therefore, the purpose of this study was to develop a set of objective, quantitative parameters to characterize hand patterns and determine the influence of propulsion speed and grade of incline on the patterns preferred by manual wheelchair users.

METHODS

Experimental kinematics and handrim forces were collected from 170 individuals with complete motor paraplegia on a stationary wheelchair ergometer during three conditions [e.g., 2]: level propulsion at self-selected speed (free), level propulsion at fastest comfortable speed (fast), and propulsion at an 8% grade at level self-selected speed (graded). Contact and recovery phase data for each cycle were time-normalized and averaged across cycles. Cadence, contact percentage (CP), and average (F_{avg}) and peak (F_{pk}) resultant handrim forces were also calculated and averaged across cycles. The hand pattern was defined as the path of the third metacarpophalangeal joint projected onto the handrim plane. Each pattern was also objectively characterized by two parameters, net radial thickness (NRT) and total radial thickness (TRT):

$$NRT = \frac{\sum_{i=1}^{nloops} A_i}{r\theta} \quad (1)$$

$$TRT = \frac{\sum_{i=1}^{nloops} |A_i|}{r\theta} \quad (2)$$

where $nloops$ is the number of loops, A_i is the signed area enclosed by the i th loop of the curve, r is the handrim radius, and θ is the contact angle. A set of basic thresholds were then used to ascertain the pattern type (e.g., Fig. 2). For comparison, a multiple rater system was also used to classify each pattern as one of four types (Fig. 1). To determine if propulsion condition affected the hand pattern, differences in the propulsion variables were assessed using a one-factor repeated measures ANOVA with three levels ($\alpha=0.05$), followed by

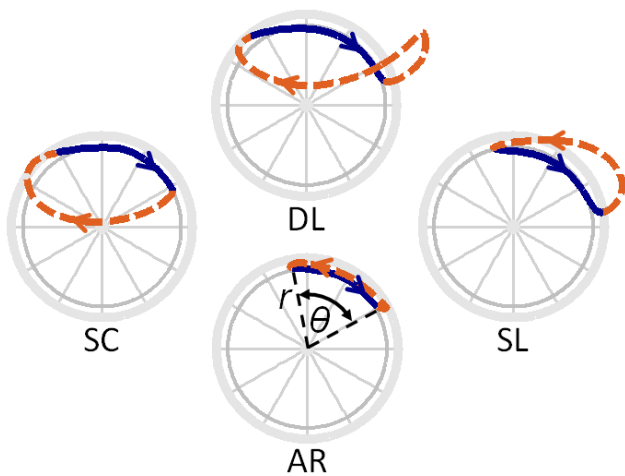


Figure 1: The four hand pattern types: arcing (AR), single loop (SL), double loop (DL) and semi-circular (SC). The solid line denotes contact phase, while the dashed line denotes recovery phase. Also depicted is the handrim radius (r) and the contact angle (θ).

paired t-tests with Bonferroni adjustment if a significant main effect was found.

RESULTS AND DISCUSSION

With pattern type thresholds set at $TRT = 0.03m$, $NRT/TRT = -0.95$ and $NRT/TRT = +0.95$, the objective pattern classification method and the subjective method produced the same results 90% of the time. All variables were found to have a significant propulsion condition main effect. The pairwise comparisons showed that compared to the free condition, the fast condition resulted in significantly higher NRT, TRT, θ , cadence, F_{avg} and F_{pk} and significantly lower CP (Table 1). Compared to the free condition, the graded condition resulted in significantly lower TRT and significantly higher NRT, θ , cadence, CP, F_{avg} and F_{pk} . Compared to the fast condition, the graded condition resulted in significantly lower TRT and significantly higher θ , CP, F_{avg} and F_{pk} .

Increased propulsion speed resulted in a shift away from under-rim hand patterns (e.g., SC), which may be due to the increased velocity of the arm. This would prolong the transition between shoulder flexion and extension at the beginning of the recovery phase and encourage use of a pattern that moves the hand above the handrim. Increased grade of incline resulted in patterns in which the hand remains near the handrim throughout the cycle (e.g., AR), likely because the increased contact percentage requires selection of a short and direct recovery handpath.

The results of the present study suggest that speed and grade significantly influence preferred hand patterns and related parameters. Task-specific

constraints and upper extremity demand requirements likely preclude the existence of a single optimal hand pattern for all propulsion conditions.

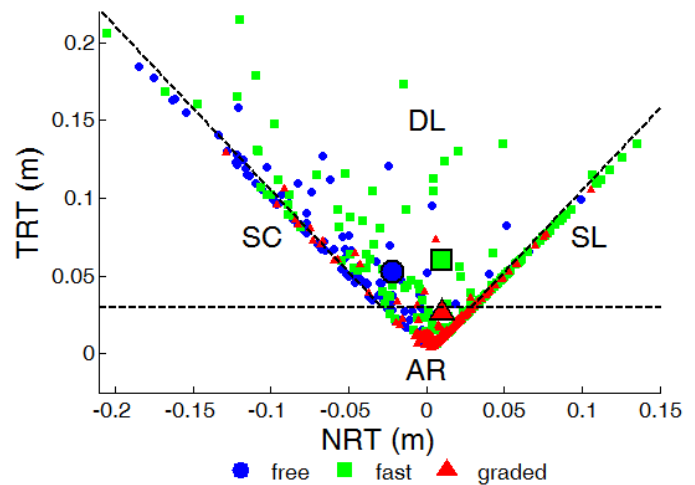


Figure 2: Hand pattern parameter values across conditions. Regions are labeled with the objective pattern type classification. Propulsion condition is indicated as follows: free (●), fast (■) and graded (▲). Small symbols correspond to individuals, while large symbols correspond to across-subject mean values.

REFERENCES

1. Koontz AM, et al. *Arch. Phys. Med. Rehabil.* **90**, 1916-1923, 2009.
2. Lighthall-Haubert L, et al. *Arch. Phys. Med. Rehabil.* **90**, 1904-1915, 2009.

ACKNOWLEDGEMENTS

We thank Shelby Soltau for her assistance in data processing. This study was supported by NIH Grant R01 HD049774 and an NSF Graduate Research Fellowship under Grant DGE-1110007.

Table 1: Mean (standard deviation) values of investigated propulsion variables for each condition. Squares denote significant pairwise comparisons: free to fast (□), free to graded (■) and fast to graded (■).

	NRT [m]	TRT [m]	θ [deg]	Cadence [Hz]	CP [% Cycle]	F_{avg} [N]	F_{pk} [N]
Free	-0.0219 (0.0555)	0.0529 (0.0401)	78.3 (15.7)	0.890 (0.218)	37.6 (7.6)	29.7 (8.0)	46.2 (15.3)
Fast	0.0103 (0.0585)	0.0601 (0.0418)	83.7 (14.2)	1.312 (0.318)	34.0 (7.2)	42.8 (13.0)	79.3 (29.6)
Graded	0.0095 (0.0309)	0.0261 (0.0224)	88.1 (14.2)	1.258 (0.269)	60.0 (6.8)	74.0 (18.0)	124.5 (32.3)
	□■	□■■	□■■	□■	□■■	□■■	□■■

EVALUATING THE ASSUMPTION OF SYMMETRY IN MANUAL WHEELCHAIR PROPULSION

¹Shelby L. Soltau, ¹Jonathan S. Slowik, ²Philip S. Requejo, ²Sara J. Mulroy and ¹Richard R. Neptune

¹The University of Texas at Austin, Austin, TX, USA

²Rancho Los Amigos National Rehabilitation Center, Downey, CA, USA

Email: shelbysoltau@utexas.edu, web: <http://www.me.utexas.edu/~neptune/>

INTRODUCTION

Manual wheelchair propulsion is commonly assumed to be a symmetric task. The rationale is that asymmetry would make straight-line propulsion difficult due to the uncoupled nature of the wheels, and therefore experienced wheelchair users develop symmetrical propulsion mechanics over time [e.g., 1]. However, few studies have tested this assumption. The limited number of studies is partly due to the lack of instrumentation to measure bilateral kinetics. While instrumented wheels are available to measure handrim kinetics, many laboratories are equipped with only one instrumented wheel due to the high cost [3]. Thus, the switching of wheels and multiple trials are required for bilateral measurements.

Despite these challenges, a number of studies have examined side-to-side differences in propulsion mechanics. However, there is a lack of consensus as to whether asymmetry exists. Early studies have suggested that bilateral propulsion mechanics are symmetric [e.g., 1, 2], while more recent studies have suggested they are not [e.g., 3]. Part of the lack of consensus may be due to the limited number of subjects analyzed and conditions under which symmetry was investigated (e.g., at a single speed). Asymmetry may become more prevalent as the task demands increase such as at higher speeds or on a graded surface.

Therefore, the purpose of this study was to evaluate bilateral symmetry in manual wheelchair propulsion with a large number of subjects across different propulsion conditions (self-selected, fast and graded). These results have important implications for the experimental setups in future analyses of wheelchair propulsion mechanics.

METHODS

Data collected from 80 individuals with paraplegia who were free of shoulder pain and used a manual wheelchair at least 50% of the time for community mobility were analyzed (74 men; age: 37.0 ± 9.9 yrs; time from injury: 9.0 ± 6.6 yrs; height: 1.72 ± 0.09 m; mass: 74.5 ± 16.9 kg). Participants propelled a stationary wheelchair ergometer during three conditions [e.g., 4]: level propulsion at their self-selected speed (free), level propulsion at their fastest comfortable speed (fast), and propulsion on an 8% grade at their level self-selected speed (graded).

Subjects acclimated to each condition until they felt comfortable and a 10-second trial was recorded for each condition. Data was collected separately from both the dominant and non-dominant sides, with the side tested first being randomly selected. Handrim forces were collected using an instrumented handrim (SmartWheel, 200 Hz) along with 3D kinematic data (CODA, 100 Hz) from the wheel, trunk and ipsilateral upper extremity. Shoulder and elbow joint ranges of motion (ROMs), peak and average tangential and resultant forces, fraction effective force, cycle time, push percentage and push angle were calculated for each cycle and averaged across cycles for each subject during each condition.

Differences in quantities were compared using two-factor (condition, arm) repeated measures ANOVAs. The condition factor consisted of three levels (free, fast and graded) and the arm factor consisted of two levels (dominant and non-dominant). If an ANOVA had a significant interaction effect, pairwise comparisons were performed using paired t-tests with a Bonferroni adjustment for multiple comparisons. The unadjusted threshold for statistical significance for

all analyses was set at $\alpha=0.05$. Condition main effects and pairwise differences between conditions were not reported.

RESULTS AND DISCUSSION

Elevation angle, shoulder rotation, and elbow flexion ROMs had significant side main effects (Table 1), with larger values in the dominant side. Elevation plane, shoulder rotation and forearm pronation ROMs as well as push angle had significant interaction effects. There were no other side main effects or interaction effects in any of the kinematic, kinetic or spatiotemporal measures. Pairwise comparisons revealed that elevation plane, shoulder rotation and forearm pronation ROM values as well as the push angle were significantly larger in the dominant side during the graded condition. There were no significant differences between sides for these variables during the free and fast conditions. All differences were below 5 degrees except for shoulder rotation ROM during the graded condition.

These results suggest that low levels of asymmetry exist in manual wheelchair propulsion, particularly during graded conditions when the upper extremity demand is high. However, the side-to-side

differences were generally smaller than differences between conditions or between individuals. Thus, the clinical significance of these differences should be carefully considered.

In conclusion, the assumption of symmetry is likely reasonable when analyzing groups of subjects without secondary injury or pain in their upper extremities and the study conclusions are likely not to be influenced by these low levels of asymmetry.

REFERENCES

1. de Groot S, et al. *Med. Sci. Sports Exerc.* **34**, 756-766, 2002.
2. Goosey VL, et al. *Ergonomics* **41**, 1810-1820, 1998.
3. Hurd WJ, et al. *Arch. Phys. Med. Rehabil.* **89**, 1996-2002, 2008.
4. Lighthall-Haubert L, et al. *Arch. Phys. Med. Rehabil.* **90**, 1904-1915, 2009.

ACKNOWLEDGEMENTS

This study was supported by NIH Grant R01 HD049774 and an NSF Graduate Research Fellowship under Grant DGE-1110007.

Table 1: Mean (SD) values for variables with statistically significant differences between sides.

	Side	Free Mean (SD)	Fast Mean (SD)	Graded Mean (SD)
Elevation Plane ROM [deg] ○■	Dominant	72.6 (20.8)	81.3 (21.5)	85.7 (16.3)
	Non-Dominant	72.4 (19.6)	81.6 (17.7)	81.8 (14.5)
Elevation Angle ROM [deg] ▲	Dominant	22.8 (7.2)	22.7 (7.8)	19.8 (7.6)
	Non-Dominant	21.7 (7.5)	21.7 (7.0)	18.8 (7.1)
Shoulder Rotation ROM [deg] ▲○■	Dominant	67.9 (22.5)	73.9 (21.5)	77.5 (17.3)
	Non-Dominant	64.2 (23.1)	70.8 (21.1)	69.5 (19.0)
Elbow Flexion ROM [deg] ▲	Dominant	45.7 (14.7)	52.7 (15.8)	60.3 (16.1)
	Non-Dominant	44.2 (16.2)	51.1 (16.0)	57.7 (16.9)
Forearm Pronation ROM [deg] ○■	Dominant	28.8 (10.5)	32.0 (12.6)	36.9 (15.1)
	Non-Dominant	28.9 (11.1)	31.4 (11.1)	32.4 (13.5)
Push Angle [deg] ○■	Dominant	74.9 (15.5)	79.8 (14.5)	85.4 (14.9)
	Non-Dominant	73.4 (16.2)	80.2 (13.9)	84.0 (15.4)
<p>▲ denotes a significant side main effect. ○ denotes a significant condition*side interaction effect. ■ denotes a significant dominant to non-dominant pairwise comparison for the graded condition.</p>				

PREDICTING ISOLATED LUMBAR MULTIFIDUS ACTIVATION DURING NEUROMUSCULAR ELECTRICAL STIMULATION WITH NEAR INFRARED SPECTROSCOPY

^{1,2} Won Sung, ³ Ardy Wong, ³ Ahmad Pourshogi, ³ Kambiz Pourrezai and ¹ Sheri P. Silfies

¹ Drexel University, Physical Therapy & Rehabilitation Sciences, Philadelphia, PA, USA

² GSPP Penn Therapy and Fitness, Philadelphia, PA, USA

³ Drexel University Biomedical Engineering, Philadelphia, PA, USA

email: won.sung@uphs.upenn.edu

INTRODUCTION

Lumbar multifidus (LM) is considered a key muscle group in spinal stability. Change in muscle quality, contractile properties, and reduced activation has been associated with low back pain (LBP). Reduced LM activation has been associated with higher number of predictors for patients requiring rehabilitative exercises [1]. Larger impairments in muscle quality are predictive of LBP, as well as being thought to play a role in recurrence. LM does not recover automatically and general exercise is ineffective in restoring its function [2]. Neuromuscular electrical stimulation (NMES) provides a method to improve activation of muscle, and thus reverse contractile and quality impairments [3]. However, it is currently unknown if NMES can selectively target LM due to anatomy of the lumbar region, nor if it can provide adequate therapeutic dosage of muscle activity to propagate change. Electrical signal interference of the NMES makes use of EMG in studying muscle activity with NMES difficult. Near infrared spectroscopy (NIR) identifies blood flow patterns associated with muscle contraction, does not have interference making it an option for the study of NMES on the LM. The aim of this study was to determine if 1) NMES activity can be isolated to the LM, and 2) a predictive relationship could be built using an EMG and NIR model, that could demonstrate therapeutic benefit through muscle overload.

METHODS

Ten healthy subjects performed 3 tasks of varying trunk extensor activation: Modified Sorensen, and Multifidus lift tests (MLT) with varying weights [4]. Simultaneous SEMG and continuous wave NIR were collected for LM, lumbar erector spinae (LES)

and thoracic erector spinae (TES). Subjects then received NMES to the LM with NIR collected at LM, LES, and TES.

For NIR, light absorption changes of 730nm and 850 nm were converted to changes in oxygenated hemoglobin (HbO₂) and deoxygenated hemoglobin (Hb) using the Beer-Lambert Law. A logarithmic ratio of absorption for the two wavelengths was used to create arbitrary units (AU) for HbO₂ and Hb with resting values set to 0 AU.

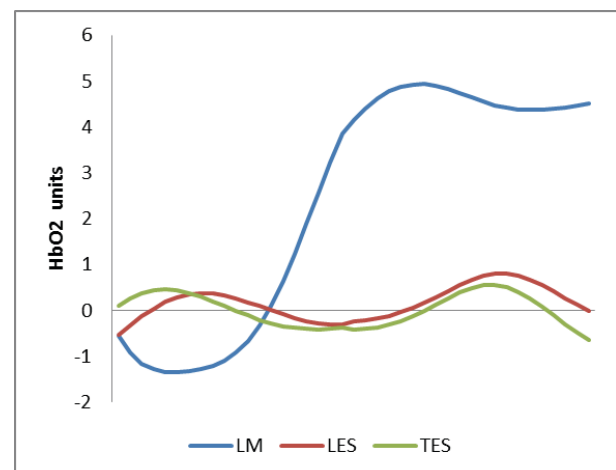


Figure 1: Example of HbO₂ changes of the LM, LES, and TES during administration of NMES to LM for a single subject.

ANOVA of mean LM, LES, and TES AU were performed to determine NMES' ability to isolate activation of LM.

EMG was heart rate stripped, RMS rectified (Tc=30ms) and normalized to the Modified-Sorensen (sMVIC). Pearson correlation was performed between EMG amplitude and NIR variables that were time synchronized during the

MLT lift tests. Results from the linear regression were used to predict a percentage of the sMVIC during NMES across 10 subjects. A paired t-test of the predicted percent sMVIC of the 1st and 5th NMES stimulations were performed to determine if NMES could provide adequate dosage to overload the LM to achieve therapeutic benefit.

RESULTS AND DISCUSSION

An example of HbO2 plot over time, during NMES elicited contraction (**Fig 1**). LM demonstrated significantly greater HbO2 levels (mean=1.15 AU \pm 0.8) compared to the LES (mean=0.3 \pm 0.8) and the TES (mean=0.2 \pm 0.45), $F_{(1,39)}=39.21$, $p<.001$. This supports the ability of NMES to isolate contraction to the LM.

LM HbO2 vs LM EMG yielded the highest correlations ($p<.05$, $r=.81$). Plots of these variables demonstrated a linear best-fit line; therefore, HbO2 and EMG amplitude of the LM were entered into a linear regression to predict the percentage of sMVIC produced by NMES (**Fig. 2**).

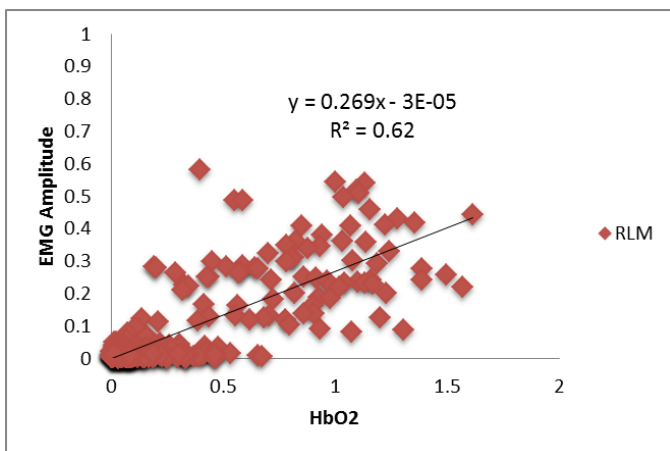


Figure 2: Plot of LM HbO2 and EMG amplitude, with linear regression results (adjusted R^2).

Group average predicted percentage of the sMVIC produced by the NMES (**Fig.3**). Individual subjects produced as high as 100% of the sMVIC in the first trial and as low as 8% of the sMVIC by the 5th trial. There was a significant difference in percent sMVIC produced by the NMES from the 1st to 5th trial, $p<.05$, demonstrating the ability of NMES to produce progressing levels of fatigue in the LM.

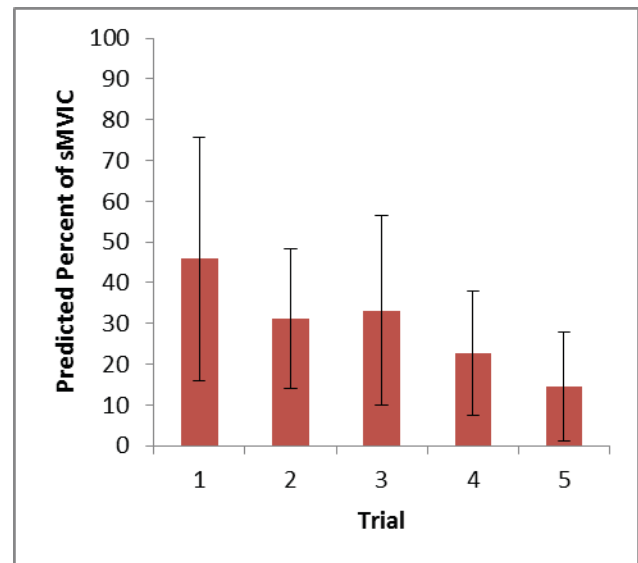


Figure 3: NIR predicted average percentage of LM sMVIC produced by NMES.

CONCLUSIONS

The current study demonstrates that NMES can isolate LM activity to at least 43% of the activation that occurs during a Modified-Biering Sorensen maneuver. It also demonstrates the ability to cause progressive fatigue to the LM within 5 trials. The result suggests that this modality has the potential to cause muscle overloading fatigue with potential to provide a therapeutic effect. This makes NMES a theoretically useful adjunctive treatment in patients with LBP, especially those who have difficulty with voluntary recruitment of this muscle.

Overload of the muscle is required to reverse atrophy and gain muscle hypertrophy. This is not possible in the presence of impairments in muscle activation. NMES has been shown to be effective in reducing these activation impairments and aiding in muscle hypertrophy [3]. In patients with LBP, similar ability to preferentially activate LM to therapeutic levels may be beneficial in recovery of this muscle and reversing changes associated with low back pain.

REFERENCES

1. Hebert J, et al. *Arch Phys Med Rehabil* **91**, 78-85, 2010.
2. Steele J, et al. *Br J Sport Med* **49**, 291-297, 2015.
3. Stevens-Lapsley J, et al. *Phys Ther* **92**, 210-226, 2012.
4. Kiesel K, et al. *Man Ther* **12**, 161-166, 2007.

OPTIMAL RUNNING PROSTHESES FOR SPRINTERS WITH BILATERAL LEG AMPUTATIONS

¹Paolo Taboga, ¹Owen N Beck, ^{1,2}Alena M Grabowski

¹Integrative Physiology Department, University of Colorado Boulder, CO, USA

²Eastern Colorado Healthcare System, Department of Veterans Affairs, Denver, CO, USA

email: paolo.taboga@colorado.edu

INTRODUCTION

To run and sprint, athletes with leg amputations use running-specific prostheses (RSPs), which are comprised of carbon-fiber and intended to replicate the spring-like sagittal plane actions of a biological ankle. RSPs store elastic energy in the first half of stance and release a large portion of this energy in the second half of stance. However, the compliance and passive nature of RSPs impairs the rapid application of vertical force on the ground [1], which is the primary determinant of maximum sprinting speed [2]. Additionally, at speeds ≥ 6 m/s, non-amputee runners progressively increase their normalized leg stiffness (K_{leg}) with speed, while sprinters with unilateral leg amputation maintain the same K_{leg} in their unaffected leg and decrease K_{leg} in their affected leg [1]. Thus, we hypothesized that stiffer RSPs would allow faster top sprinting speed compared to softer RSPs. Since K_{leg} is influenced by the change in total leg length, we hypothesized that increasing RSP height would permit faster top sprinting speed.

METHODS

Three male sprinters with bilateral transtibial amputations gave written informed consent to participate (Table 1). A certified prosthetist fit each athlete with three different models of RSPs. The recommended stiffness category was selected based on each manufacturer's suggestion and the recommended height was set at the maximum allowable height (Ht0) for each runner according to IPC rules [3]. If Ht0 could not be set due to RSP design and residual limb anatomy, the baseline height was set as close to Ht0 as possible.

Each sprinter performed three sprint trials at the recommended, +1, and -1 stiffness categories for each RSP model in a randomized order, while maintaining the baseline height. Then, the category that allowed the top running speed for each model was selected and height was changed (± 2 cm with respect to baseline height) to determine the effect on top sprinting speed.

Each set of sprint trials started at 3 m/s with speed incremented by 1 m/s until subjects approached their top speed. Then, smaller speed increments were employed until subjects reached their top speed, which was defined when subjects could not maintain their position on the treadmill for ten consecutive strides.

All trials were performed on a 3D force-measuring treadmill (Treadmetrix, USA) (1000Hz). We used a custom Matlab program (MathWorks, USA) to condition signals (30Hz low-pass Butterworth filter) and determine contact time (t_c), and peak vertical ground reaction forces ($vGRF_{peak}$). We calculated K_{leg} as:

$$K_{leg} = \frac{vGRF_{peak}}{\Delta L} \left(\frac{L_0}{BW} \right)$$

where L_0 is leg length, ΔL is leg length change during stance and BW is body weight [1].

We used a statistical linear mixed model to determine the effects of RSP model, stiffness, and height on top speed. Then, we used another linear mixed model to predict top speed based on $vGRF_{peak}$, t_c , and K_{leg} .

RESULTS AND DISCUSSION

The linear mixed model showed no significant effect of RSP model or stiffness category ($p = 0.07$ and $p = 0.27$, respectively), but an inverse relationship between prosthetic height and top speed (Fig. 1):

$$TopSpeed = 9.69 - 0.06 \times Ht$$

$$(r^2=0.54, p<0.001)$$

For every centimeter increase in prosthetic height, there was a 0.06 m/s decrease in top speed.

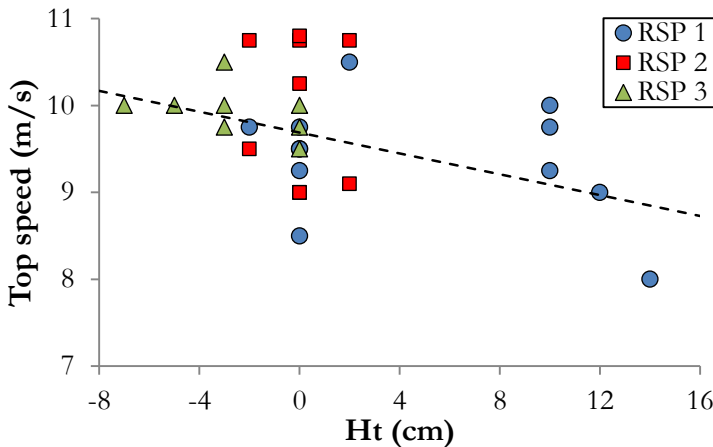


Figure 1: Top speed for each subject and condition relative to Ht. Dashed line is the regression line.

The second linear mixed model showed an inverse relationship between t_c and top speed, but no effect of $vGRF_{peak}$ and K_{leg} ($p=0.83$ and $p=0.81$, respectively) (Fig 2):

$$Top Speed = 13.09 - 29.13 \times t_c$$

$$(r^2=0.15, p=0.02)$$

For every 0.01 s increase in t_c , there was a 0.29 m/s decrease in top speed.

LIMITATIONS

To date, three subjects with bilateral leg amputations participated in our study. We intend to recruit more subjects in order to improve our statistical power. Subject 1's starting height on RSP 1 was set at +10 cm compared to Ht0, due to his long residual limbs; the RSP height was then increased by 2 and 4 cm. Subject 3's starting height

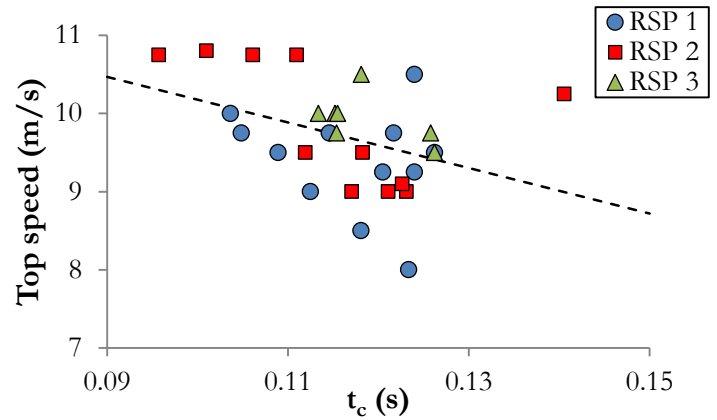


Figure 2: Top speed as a function of contact time (t_c). The dashed line is the regression line

on RSP 3 was set at -3 cm compared to Ht0 due to the dimensions of RSP 3 and the existing attachments on his running sockets; the height was then shortened by 2 and 4 cm.

CONCLUSIONS

Contrary to our initial hypothesis, we found that taller prostheses reduced top sprinting speed, while RSP model and prosthetic stiffness category had no significant effect. Across the different RSP configurations, sprinters with bilateral leg amputations achieved faster sprinting speeds by shortening contact time.

ACKNOWLEDGEMENTS

We thank Freedom Innovations, Ossur, and Ottobock for the donation of RSPs. This project was supported by the BADER Consortium, DoD, CDMRP cooperative agreement (W81XWH-11-2-0222)

REFERENCES

1. McGowan CP, et al. *J R Soc Interface* (9)**73**: 1975-1982, 2012.
2. Weyand PG, et al. *J Appl Physiol* **89**, 1991-1999, 2000..
3. <http://www.paralympic.org/athletics/rules-and-regulations/rules>

Table 1: Subject characteristics, PR = personal record.

Subject	Age (yrs)	Height (m)	Mass (kg)	100 m PR (s)	Cause of amputation
1	25	1.80	70.3	11.66	Congenital
2	18	1.86	75.5	12.36	Congenital
3	23	1.89	78.8	12.45	Congenital

OPTIMAL RUNNING PROSTHESES FOR SPRINTERS WITH UNILATERAL LEG AMPUTATIONS

¹Paolo Taboga, ¹Owen N Beck, ^{1,2}Alena M Grabowski

¹Integrative Physiology Department, University of Colorado Boulder, CO, USA

²Eastern Colorado Healthcare System, Department of Veterans Affairs, Denver, CO, USA

email: paolo.taboga@colorado.edu

INTRODUCTION

To run and sprint, athletes with leg amputations use running-specific prostheses (RSPs), which are comprised of carbon-fiber and intended to replicate the spring-like sagittal plane actions of a biological ankle. RSPs store elastic energy in the first half of stance and release a large portion of this energy in the second half of stance. However, the compliance and passive nature of RSPs impairs the rapid application of vertical force on the ground [1], which is the primary determinant of maximum sprinting speed [2]. Additionally, at speeds ≥ 6 m/s, non-amputee runners progressively increase their normalized leg stiffness (K_{leg}) with speed, while sprinters with unilateral leg amputation maintain the same K_{leg} in their unaffected leg (UL) and decrease K_{leg} in their affected leg (AL) [1]. Thus, we hypothesized that stiffer RSPs would allow faster top sprinting speed compared to softer RSPs. Since K_{leg} is influenced by the change in total leg length, we also hypothesized that increasing RSP height would permit faster top sprinting speed.

METHODS

Three sprinters (2M, 1F) with unilateral transtibial amputations gave written informed consent to participate (Table 1). A certified prosthetist fit each athlete with three different models of RSPs. The recommended stiffness category was selected based on each manufacturer's suggestion and the height was adjusted based on the prosthetist's experience.

Each sprinter performed three sprint trials at the recommended, and ± 1 stiffness categories for each RSP model in a randomized order, while maintaining the baseline height. Then, the category that allowed the top running speed for each model was selected and height was changed (± 2 cm with

respect to baseline height) to determine the effect on top sprinting speed.

Each set of sprint trials started at 3 m/s with speed incremented by 1 m/s until subjects approached their top speed. Then, smaller speed increments were employed until subjects reached their top speed, which was defined when subjects could not maintain their position on the treadmill for ten consecutive strides.

All trials were performed on a high-speed 3D force-measuring treadmill (Treadmetrix, USA). We used a custom Matlab program (MathWorks, USA) to condition signals (30Hz low-pass Butterworth filter) and determine contact time (t_c), and peak vertical ground reaction forces ($vGRF_{peak}$) of UL and AL separately. We calculated K_{leg} as:

$$K_{leg} = \frac{vGRF_{peak}}{\Delta L} \left(\frac{L_0}{BW} \right)$$

where L_0 is leg length, ΔL is leg length change during stance and BW is body weight [1].

We used a statistical linear mixed model to determine the effects of RSP model, stiffness, and height on top speed. Then, we used another linear mixed model to predict top speed based on $vGRF_{peak}$, t_c , and K_{leg} of the UL and AL.

RESULTS AND DISCUSSION

While controlling for other variables, across all conditions, RSP 2 and RSP 3 elicited 8% ($p=0.004$) and 11% ($p<0.001$) faster speeds compared to RSP 1. For RSP 1, every increase in stiffness category reduced top sprinting speed by 5% ($p=0.02$) (Fig. 1), while every 1 cm increase in Ht elicited a 7% decrease in top sprinting speed ($p<0.001$). Stiffness category and Ht showed no statistically significant effect on top speed for RSP 2 and RSP 3.

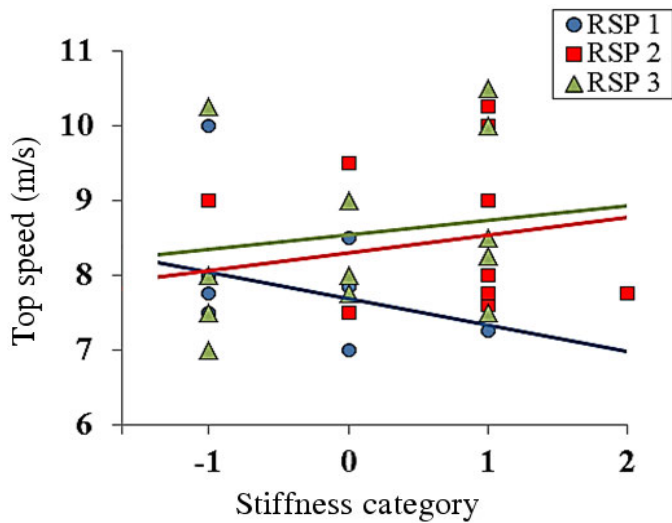


Figure 1: Top speed for each subject and condition relative to Stiffness category. Solid lines are the regression lines for each RSP model.

The second linear mixed model showed that, while controlling for other variables, a 0.01 s increase in t_c for the AL or UL reduced top speed by 4% or 6% respectively ($p < 0.001$) (Fig. 2a), 1 BW increase in $vGRF_{peak}$ for the AL or UL increased top speed by 7% or 6% respectively ($p < 0.001$) (Fig. 2b), and a 1 unit increase in Kleg for the AL or UL, reduced top speed by 1% ($p < 0.001$).

LIMITATIONS

To date, three subjects with unilateral leg amputations participated in our study. We intend to recruit more subjects to improve our statistical power. Subject 3's lowest attainable height on RSP 2 was -1 cm due to the dimensions of the RSP 2 and the length of her residual limb.

CONCLUSIONS

RSP 2 and RSP 3 allowed subjects to reach faster sprinting speeds compared to RSP 1. Stiffness and category showed a statistically significant effect only on RSP 1, with faster top speed achieved with a softer category and lower height. Faster top speeds are achieved, among all conditions, by shortening t_c , increasing $vGRF_{peak}$ and lowering Kleg.

Table 1: Subject characteristics, PR = personal record.

Subject	Sex	Age (yrs)	Height (m)	Mass (kg)	100 m PR (s)	Affected side	Cause of amputation
1	M	31	1.84	76.4	11.55	Right	Traumatic
2	M	25	1.78	90.9	14.26	Left	Traumatic
3	F	21	1.65	56.8	14.58	Left	Traumatic

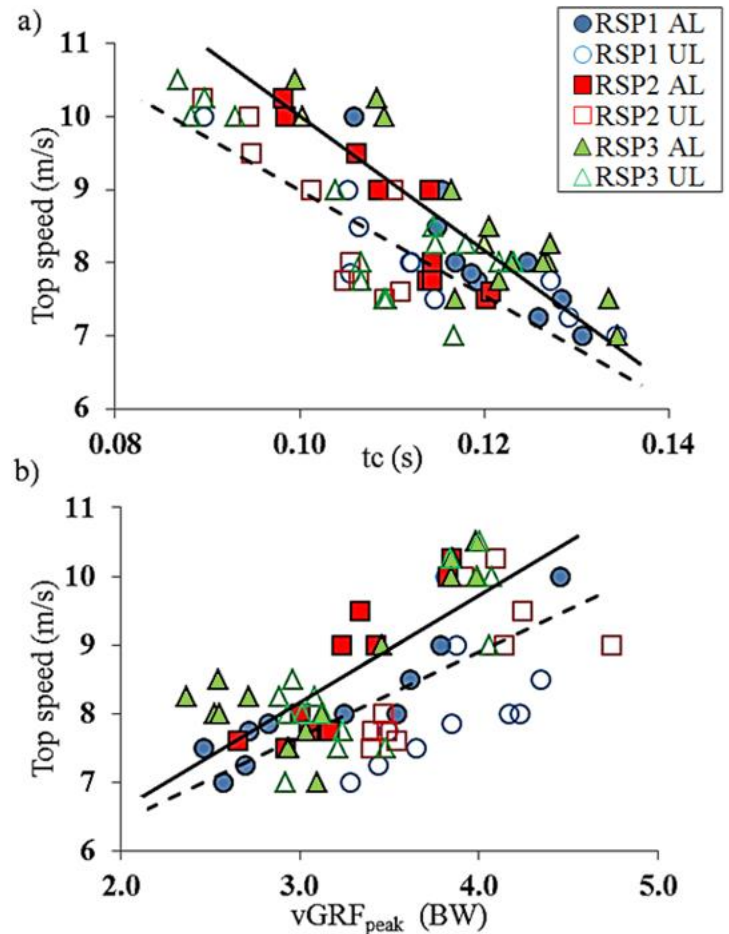


Figure 2: Top speed as a function of (a) t_c and (b) $vGRF_{peak}$, with respective regression lines for the AL (solid) and UL (dashed).

ACKNOWLEDGEMENTS

We thank Freedom Innovations, Ossur, and Ottobock for the donation of RSPs. This project was supported by the BADER Consortium, DoD, CDMRP cooperative agreement (W81XWH-11-2-0222).

REFERENCES

- McGowan CP, et al. *J R Soc Interface* (9)73: 1975-1982, 2012.
- Weyand PG, et al. *J Appl Physiol* 89, 1991-1999, 2000.

Motor learning effects on variability in goal-directed upper limb movements using time warping analysis

¹ Sibylle B. Thies, ²Alaa A. Ahmed and ¹ Laurence P.J. Kenney

¹ The University of Salford, Manchester, UK

² University of Colorado at Boulder, Boulder, Colorado, USA

email: s.thies@salford.ac.uk

INTRODUCTION

We previously introduced a novel methodology, based on dynamic time warping, to calculate measures of timing and amplitude variability over entire movement trajectories [1]. Our methodology has the advantage that it separates out the two elements of trial-to-trial variability: temporal and amplitude variability. As a first demonstration of the method, we established a link between upper limb movement variability calculated using these measures and neurological impairment [1]. A subsequent study built on our approach and used it successfully to identify differences in trajectory variability when comparing stroke survivors with right and left hemisphere lesions to one another as well as to healthy controls [2]. However, while both studies showed that our new methodology identified increased trajectory variability in patients with stroke, compared with controls, the merits of the new methodology for characterizing upper limb movements in relation to motor learning have yet to be explored. Hence it is the objective of this study to determine whether temporal and amplitude variability can serve as metrics for motor learning.

METHODS

Ten young and twelve older adults performed repeated goal-directed reaching movements from a home circle to a target in the horizontal plane (Fig.1). A rehabilitation robot provided corresponding position data that was then assessed for trial-to-trial variability. Temporal variability (Warp Cost) was determined utilizing dynamic time-warping for curve registration since such an approach allows for assessment of signal variations in time. Amplitude variability was defined as the remaining RMS error between signals. Variability was investigated for repeated trials of three

conditions 1) unperturbed reaching: 'Null', 2) immediately after onset of a force perturbation: 'Force 1', and 3) after prolonged exposure to the force perturbation: 'Force 2'. Effects of 'condition' and 'age group' were assessed with General Linear Mixed Effect Models (SPSS), and the accuracy with which variability measures classified subjects to belong to their respective group was determined. Finally, variability measures were compared to a commonly used metric of motor learning, Movement Error (deviation from a straight line), via calculation of Pearson's correlation coefficient.

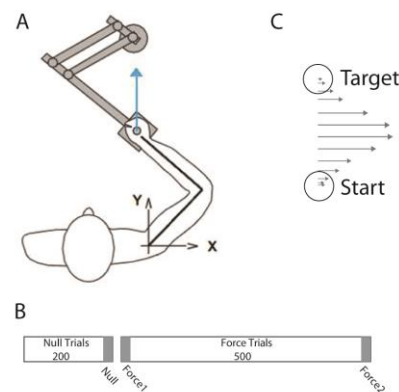


Figure 1: Illustrations of the experimental design. A: Setup. B: Experimental Protocol. Shaded areas represent the trials used for data analysis. C: Schematic of perturbing forces on a forward reach (arrows are equally spaced in time).

RESULTS AND DISCUSSION

An established measure of motor-learning in goal-directed upper limb movements is Movement Error [3,4]. Movement Error typically increases with the onset of a novel perturbation force, and decreases as motor learning progresses with prolonged exposure to the force. In agreement with this we likewise found that for both, young and older adults, both

trial-to-trial variability measures increases with onset of a perturbation force and decreases over prolonged exposure to the force ($p < 0.01$ for all pairwise comparisons) (Table 1). Moreover, both variability measures correlated positively with Movement Error (Fig. 3). Finally, older adults exhibited greater variability than young adults ($p < 0.01$) (Table 1), and Warp Cost classified 80% of young adults and 66.7% of older adults correctly to be in their respective group, while RMS Error classified both, young and older adults with 100% accuracy to belong to their respective groups.

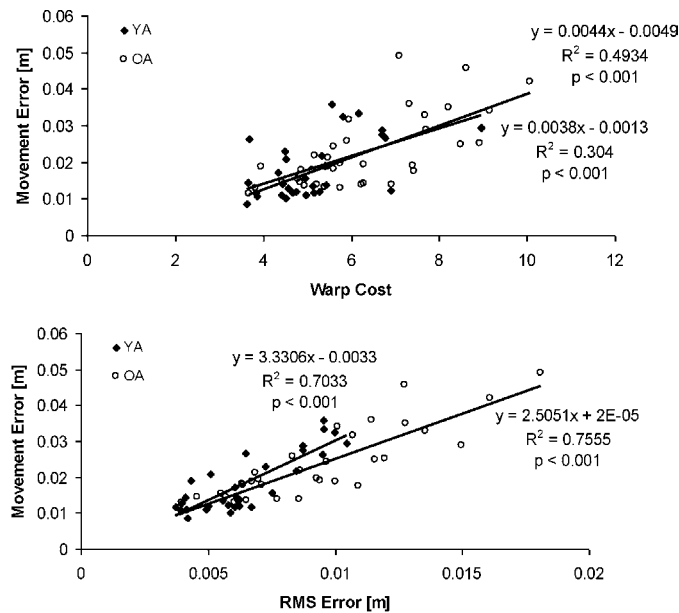


Figure 3: Correlations of Warp Cost (top) and RMS Error (bottom) versus Movement Error. YA: young adults; OA: older adults.

CONCLUSIONS

Considering the healthy test population and the simplicity of the task, a single goal-directed movement towards a target, it is encouraging that variability measures proved informative even

though not many directional changes during task performance were required to complete the task successfully. Hence this study adds to the existing literature [1, 5, 6] on the sensitivity and use of movement variability measures for the assessment of upper limb performance.

This study used data from a motor-learning experiment to investigate the merit of temporal and amplitude variability as a proxy for conventional metrics of motor learning. While in this study trial-to-trial variability was computed from planar position data of an expensive rehabilitation robot, variability could equally be calculated from signal trajectories derived from an alternative, low cost device, such as an accelerometer restricted to move on a low friction planar surface between two targets. Hence we identified the potential for development of an inexpensive clinical assessment method for the upper limb.

REFERENCES

1. Thies SB, et al. *JNER* **6**, 2, 2009.
2. Freitas SM, et al. *Brain Research* **1419**, 19-33, 2011.
3. Shadmehr R, et al. *J Neurosci* **14**, 3208-3224, 1994.
4. Ahmed AA, et al. *J Neurophysiol* **102**, 2816-2824, 2009.
5. Cirstea MC, et al. *Brain* **123**, 940-953.
6. Reinkensmeyer DJ, et al. *Neural Computation* **15**, 2619-2642, 2003.

ACKNOWLEDGEMENTS

Dr. Helen J. Huang (data collection), Dr. Phil Tresadern and Mr. Joel Smith (software design).

Table 1: Group mean±standard deviation of variability outcome measures; $p < 0.01$ for all pairwise comparisons.

	Young Adults		Older Adults	
	Warp Cost [unitless]	RMS Error [m/s ²]	Warp Cost [unitless]	RMS Error [m/s ²]
Null	4.29±0.53	0.0046±0.0008	4.99±0.90	0.0148±0.0016
Force 1	6.01±1.44	0.0089±0.0012	7.41±1.48	0.0338±0.0026
Force 2	5.14±0.71	0.0060±0.0009	6.42±1.40	0.0186±0.0019

MECHANICAL PROPERTIES OF DYNAMIC ELASTIC RESPONSE PROSTHETIC FEET

Christina M. Webber and Kenton R. Kaufman

Mayo Clinic, Rochester, MN, USA
email: kaufman.kenton@mayo.edu

INTRODUCTION

In comparison with basic prosthetic feet, dynamic elastic response (DER) prosthetic feet more closely mimic the native ankle joint, storing and returning energy throughout the gait cycle [1, 2]. This is particularly beneficial to amputee patients who lead active lives.

With countless prosthetic foot manufactures and models, it can be difficult to compare various options when prescribing a prosthetic foot. Both functional and mechanical testing of prosthetic feet provides important information to prosthetists and patients [2]. While many groups have studied the functional characteristics of DER feet, few have focused on the more objective testing of the mechanical properties that is not influenced by intersubject variability [1]. Therefore, the purpose of this study was to test the mechanical properties of DER feet in a standardized and repeatable manner. In particular, the stiffness and hysteresis of the heel and forefoot regions of commercially available DER feet was investigated.

METHODS

DER feet, coded as L5986 and L5987, from four different manufacturers (Table 1) were compared. All feet were 27 cm and recommended for a hypothetical male patient, described as high activity with a right side below-knee amputation, weighing 200 lbs. An MTS 858 Mini Bionix II servohydraulic test system (Eden Prairie, MN) was used to test each specimen in compression. Stiffness testing was conducted adhering to the Static Proof Test detailed in ISO Standard 10328 [3]. Testing was not conducted to failure.

Each foot was tested with the manufacturer-provided foot cover. A compressive load was

applied to the foot at 100 N/s until the load reached 2240 N, per ISO 10328. The system was then completely unloaded at the same rate. Both the heel and forefoot regions of all feet were tested in three successive compression trials. During compression, the load and displacement were measured using a uniaxial load cell and linear variable differential transformer, respectively. Data were collected using Multipurpose TestWare software (MTS, Eden Prairie, MN) at 20 Hz. Heel and forefoot stiffness was observed as the slope of the load-displacement curve for each prosthetic foot. Hysteresis, the difference between the loading input energy and unloading energy, was calculated for the heel and forefoot testing of each DER foot.

RESULTS AND DISCUSSION

There were differences in stiffness for the heel (Fig. 1) and forefoot (Fig. 2) of all DER feet tested. During walking over level ground, a person will experience a peak ground reaction force of approximately 1.2 times body weight [4]. At this loading level, the heel and forefoot of feet A and B were stiffer than feet C and D. If that same patient was to run at a moderate pace, they would experience a peak ground reaction force of approximately 2.5 times body weight [4]. At this loading level, the stiffness was increased, and heel stiffness was greater than forefoot stiffness. The relative rank of stiffness for feet A and B changed for heel loading, but not for forefoot loading. A greater displacement was observed for all DER feet when loaded at the forefoot.

Hysteresis varied between samples under the different loading configurations (Fig. 3). Feet with higher stiffness had greater energy loss at both the heel and forefoot.

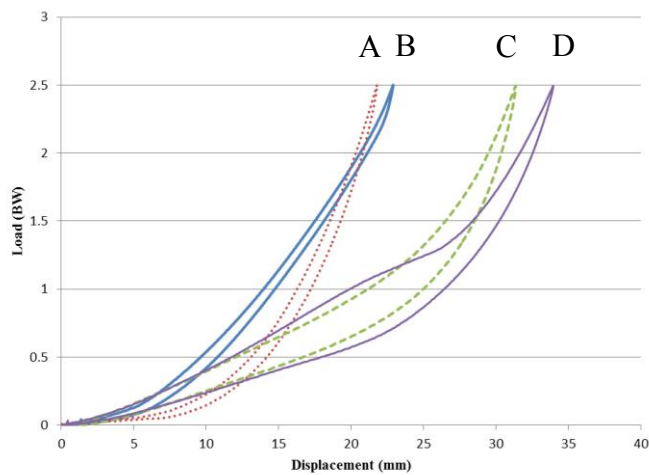


Figure 1: Representative load-displacement curves for heel loading and unloading of DER feet

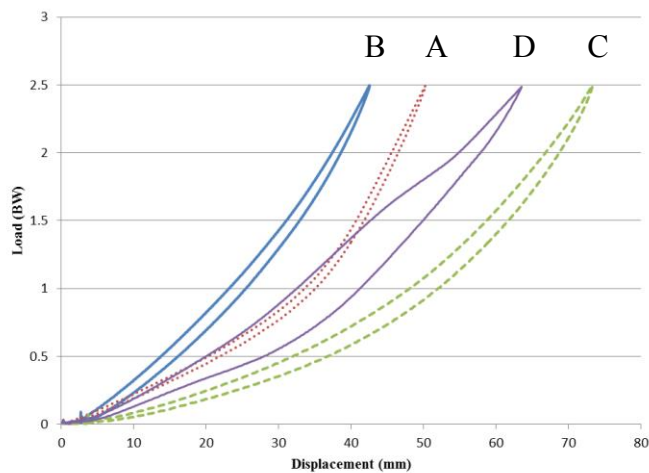


Figure 2: Representative load-displacement curves for forefoot loading and unloading of DER feet

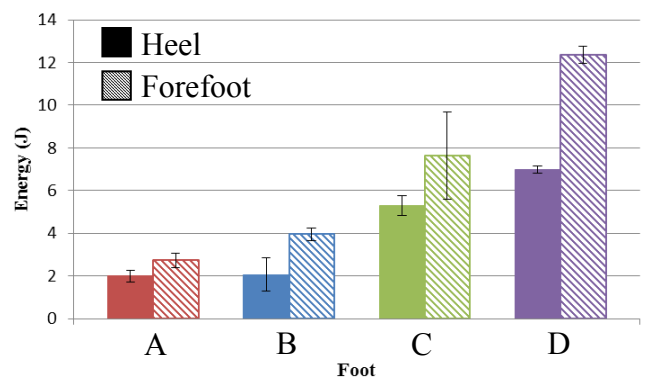


Figure 3: Average hysteresis of heel (solid) and forefoot (crosshatch) of DER feet \pm SD

CONCLUSIONS

When used with the functional kinematic data already present in literature, the stiffness and hysteresis data for commercially available prosthetic feet can be used to guide prosthetic prescriptions of DER feet.

REFERENCES

1. Geil, MD. *JPO* **13**(3), 70-73, 2001.
2. Hafner, BJ et al. *J Rehab R&D*, **39**(1), 1-11, 2002.
3. "ISO 10328: Prosthetics—Structural testing of lower-limb prostheses—Requirements and test methods." ISO, Geneva, Switzerland, 2006.
4. Keller, TS et al. *Clinical Biomech*, **11**(5), 253-259, 1996.

ACKNOWLEDGEMENTS

Fellowship funding (Webber) provided by the Mayo Graduate School.

Table 1: Specific DER feet tested

Foot Code	Manufacturer	Model	Primary Material
A	Ability Dynamics (Tempe, AZ)	RUSH 87	Glass Composite
B	Freedom Innovations (Irvine, CA)	Renegade AT	Carbon Fiber
C	Össur (Reykjavik, Iceland)	Talux	Carbon Fiber
D	Ottobock (Duderstadt, Germany)	Triton 1C61	Carbon Fiber

ELEVATED VACUUM PRESSURE TO QUANTIFY PROSTHETIC SOCKET MECHANICS

¹ Matthew Wernke, ¹ Ryan Schroeder, ¹ Michael Haynes, ¹ Lonnie Nolt, ¹ Jeffrey Denune, ¹ James Colvin

¹ The Ohio Willow Wood Company, Mt. Sterling, OH, USA
email: mattw@owwco.com, web: <http://willowwoodco.com>

INTRODUCTION

The prosthetic socket is a critical component of the prosthesis and greatly impacts comfort, functional performance, and overall user satisfaction with a prosthesis. Therefore, every prosthetic socket is custom made for each amputee in order to create an intimate fit to maximize comfort and create a strong biomechanical connection. Critical parameters to control to achieve these goals are socket geometry/volume and the method of suspension. However, current clinical practices lack quantitative analysis of socket fit, leaving prosthetists with limited tools with which to determine whether appropriate socket fit has been achieved. Prosthetists are currently limited to using feedback from the amputee, visual inspection of movement and skin blanching, as well as previous experience. The socket fitting procedures would greatly benefit from a process to provide prosthetists with empirical data upon which they can base clinical decisions. A few studies have aimed at measuring socket fit and suspension using x-ray techniques^{1,2,3} and optical techniques⁴. Although these techniques were able to measure movement between the socket and residual limb, the techniques themselves were not clinically practical because the data had to be collected at rest or during simulated phases of gait, required large expensive equipment, or required that parts of the socket be removed.

Elevated vacuum suspension creates sub-atmospheric pressure between the prosthetic socket and the interface material. Preliminary work suggests that monitoring the change in sub-atmospheric environment during volitional movement of the amputee can enable a clinically relevant method of assessing socket fit, specifically looking at movement between the limb and socket. The underlying principle stems from Boyle's Law which states that, assuming a closed system,

pressure is inversely related to volume. Therefore, if there is a change in the vacuum pressure, it must be a result of a change in volume between the liner and socket wall, and there must be movement of the residual limb relative to the socket. The purpose of this work is to evaluate the correlation between vacuum pressure fluctuation and distal displacement and to determine the ability of these outcomes to assess socket fit.

METHODS

The testing protocol was divided into benchtop and subject based testing to evaluate the correlation and clinical relevance of vacuum pressure socket fit.

Benchtop Testing: The purpose of this test was to isolate socket fit as the experimental factor. Three different residual limb models were made from a hard plastic core surrounded by a layer of thermoplastic elastomeric material. These models were designed to all fit within a carbon fiber socket.

The amount of vertical displacement and amount of vacuum pressure fluctuation were evaluated for each residual limb model by suspending them across the linkages of a tension-compression machine. The machine was programmed to produce similar amounts of vertical tension and compression in a cyclic pattern for 12 seconds at a frequency of 1.25 Hz. Three different tension and compression values were used in the study, simulating a low, normal, and high force expected during gait. The different residual limb models were placed in the test socket and elevated vacuum suspension applied according to the specified treatment level. Five treatment levels for vacuum setting were used: vacuum set for 5, 9, 13, 16, or 20 inHg. Three repetitions at each treatment were performed. Simultaneous vacuum pressure data measured by the LimbLogic Vacuum System and displacement

data measured by the testing apparatus were collected.



Figure 1: The three models used to simulate socket fit conditions in the benchtop testing.

Subject Testing: Vacuum pressure data was collected from one transfemoral amputee during ambulation. For each trial, vacuum pressure and kinematic data was streamed from the LimbLogic Vacuum System (Ohio Willow Wood, Mt. Sterling, OH).

The ambulation task was repeated for a series of treatment conditions to assess changes in residual limb volume and changes in socket volume. To evaluate changes in residual limb volume, subject testing occurred on two different testing days approximately one month apart. To achieve changes in socket volume, two different sized sockets were made. The subject also wore prosthetic liners with different thicknesses in each of the sockets produce additional changes in fit. Verbal feedback from the patient was also recorded. This was recorded on both testing days as well as after one week of at-home use following the second data collection day.

RESULTS AND DISCUSSION

The benchtop testing demonstrated that the amount of displacement decreased as the vacuum pressure setting increased, consistent with preliminary data. Similarly, distinct trends in the data regarding socket fit were identified. Strong correlations exist between vacuum pressure fluctuation and the amount of vertical displacement, though correlation values and regression results were influenced by

socket fit. Two of the models exhibited similar but slightly different results, while the third model resulted in drastically different data. This third result is not surprising due to the visible difference in socket fit when compared to the other two models.

The subject testing corroborated the benchtop testing. Even though the subject was able to comfortably don both sockets with each liner combination while in the clinic, and reported that each socket felt comfortable, differences were found to exist with the vacuum pressure data. Interestingly, after a week of at-home use, the subject reported that one of the sockets, which corresponded to the socket which had the most movement during the testing days, became uncomfortable after extended periods of use and was rejected. The subject testing also showed that differences in residual limb volume can impact movement of the prosthesis relative to the residual limb. Overall, the socket with the lowest amount of movement was found to be the most comfortable by the patient. Presumably this may be related to a reduction of adverse forces placed on the limb tissues and a superior mechanical connection with the artificial limb.

The technique used in this study to quantify socket mechanics represents a clinically relevant method because it can be supported using existing prosthetic hardware. The ability to assess socket fit can be a useful tool to clinicians to help make more informed decisions. Further research can help identify salient features or trends that can guide the clinical practice of fitting a prosthetic socket. Further work is needed to quantify socket fit in non-elevated vacuum suspension systems which have been shown to exhibit more movement at the socket interface^{4,5}.

REFERENCES

1. Tanner J. J. *Pros Ortho*. 13(1) 14-17 2001.
2. Lilja M. *Pros. Ortho. Int*. 17(1) 21-26. 1993.
3. Narita H. *Pros. Ortho. Int*. 21(3) 175-178. 1997.
4. Sanders J. J. *Pros Ortho*. 43(4) 509-516. 2006.
5. Board W. *Pros. Ortho. Int*. 25 202-209, 2001

DESIGN OF TWO LIGHTWEIGHT HIGH BANDWIDTH, TORQUE-CONTROLLED ANKLE EXOSKELETONS

Kirby Ann Witte and Steven H. Collins

Carnegie Mellon University, Pittsburgh, PA, USA

Email: kwitte@andrew.cmu.edu, web: <http://biomechatronics.cit.cmu.edu>

INTRODUCTION

Lower-limb exoskeletons have the potential to enhance rehabilitation [1], assist walking for people with gait impairments, reduce the metabolic cost of normal and load-bearing walking [2], improve stability and probe interesting questions about human locomotion. Designing effective lower-limb exoskeletons may be simplified by focusing on a single joint. During walking, the ankle produces larger peak torques and performs more positive work than either the hip or the knee [3], thereby making it an effective location for assistance.

The ankle joint experiences a wide range of velocities during walking, with plantarflexion occurring rapidly. It is therefore desirable to have high bandwidth and high torque capabilities to accurately produce a wide variety of torque profiles.

Many exoskeletons have been developed employing different approaches to design, actuation and control, but the most effective mechanical methods of assisting the ankle remain unclear. The process of developing and testing our devices has produced several guiding principles of exoskeleton design that may influence future exoskeleton development.

METHODS

We designed, built and tested two ankle exoskeletons, here called Alpha and Beta, for use with a tethered emulator system (Fig 1 A) described in detail in [5]. Both exoskeletons feature strong lightweight frames, comfortable three-point contact with the leg, series elastic elements for improved torque control [4], modularity, structural compliance in selected directions, and sensors for measuring torque, joint angle, and phase of gait.

Torque is controlled using a combination of proportional feedback, damping injection and iterative learning during walking tests. Series elasticity is provided by leaf springs in the Alpha design and a coil spring in the Beta design. Spring type strongly affected the overall exoskeleton envelopes.

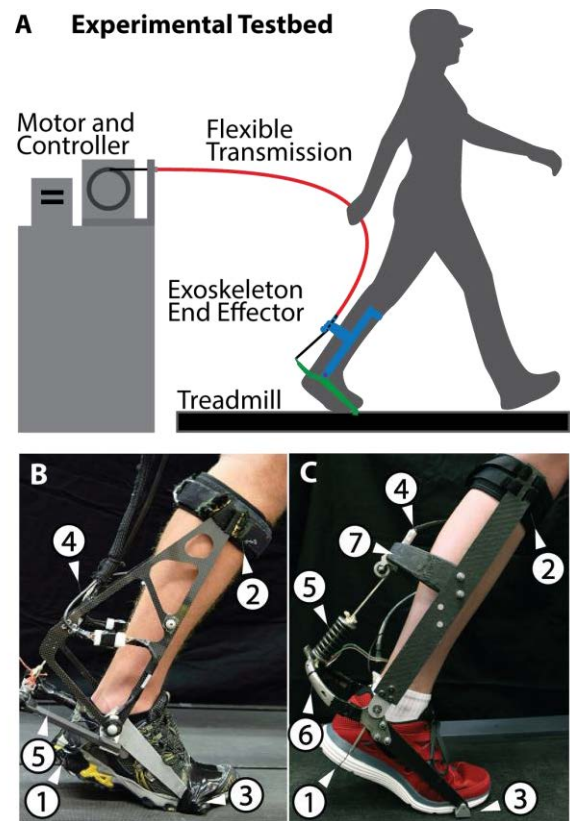


Figure 1: Emulator system and exoskeletons. **A** The testbed comprised a powerful off-board motor and controller, a flexible transmission, and an ankle exoskeleton end-effector. **B** The Alpha design. Each exoskeleton contacted (1) the heel with a string, (2) the shin using a strap, and (3) the ground with a hinged plate embedded in the shoe. The Bowden cable conduit attached to (4) the shank frame, while the Bowden cable terminated at (5) the series spring. **C** The Beta design. In addition to (1-5), this device has (6) a titanium ankle lever made using direct-metal additive manufacturing and (7) a tubular carbon fiber Bowden cable support.

The Alpha device (Fig. 1B) was designed to provide compliance in selected directions. The Beta exoskeleton (Fig. 1C) was designed to reduce overall envelope. Benchtop tests quantified system-wide closed-loop torque bandwidth, and walking trials quantified torque tracking error while verifying that large torques could be comfortably applied. Both ankle exoskeletons interface with the foot under the heel, the shin below the knee, and the ground beneath the toe. The exoskeleton frames include rotational joints on either side of the ankle, with axes of rotation approximately collinear with that of the human joint (Fig. 1 B, C).

The exoskeletons were designed to provide greater peak torque, peak velocity and range of motion than observed at the ankle during unaided fast walking. The Alpha and Beta devices can deliver peak plantarflexion torques of 120 Nm and 150 Nm respectively. The Alpha and Beta devices both have a range of motion of 30° in plantarflexion to 20° in dorsiflexion.

We tested closed-loop torque control by commanding 50 Nm and 20 Nm linear chirps in desired torque while the exoskeletons were worn by human users.

RESULTS

The total mass of the Alpha and Beta exoskeletons were 0.835 and 0.875 kg, respectively. The gain-limited closed-loop torque bandwidths of the Alpha device with 20 Nm and 50 Nm peak torques were 21.1 Hz and 16.7 Hz, respectively. The phase-limited bandwidths for the Beta device, at a 30° phase margin, with 20 Nm and 50 Nm peak torques were 24.2 Hz and 17.7 Hz, respectively. In walking trials with the Alpha device, the peak average measured torque was 80 Nm. The maximum observed torque was 119 Nm. The root mean square (RMS) error for the entire trial was 1.7 ± 0.6 Nm, or 2.1% of peak torque, and the RMS error of the average stride was 0.2 Nm, or 0.3% of peak torque. With the Beta device, the peak average measured torque during walking was 87 Nm. The maximum observed torque was 121 Nm. The RMS error for the entire trial was 2.0 ± 0.5 Nm, or 2.4% of peak

torque, and the RMS error of the average stride was 0.3 Nm, or 0.4% of peak torque.

DISCUSSION

The measured bandwidth, peak torque capability, and mass of both exoskeletons compare favorably with existing devices and with human ankle musculature. In walking tests, we demonstrated robust, accurate torque tracking and the ability to transfer large dynamic loads comfortably to a variety of users. Our results demonstrate that these exoskeletons can be used to rapidly explore a wide range of control techniques and robotic assistance paradigms as the primary elements of versatile, high-performance testbeds.

The three point interface featured in both devices was comfortable and effective. Leaf springs and coil springs were effective series elastic elements. Leaf springs were lighter, but also less robust and more bulky than the coil spring. Strain gauges used in the Beta device were lighter, less expensive, and more effective than the load cell used in the Alpha exoskeleton. The reduced envelope of the Beta exoskeleton was achieved by an acceptable reduction in compliance. These results provide insights into desirable properties of lower-limb exoskeleton hardware, which may inform future designs.

ACKNOWLEDGEMENTS

This material is based upon work supported by the National Science Foundation under Grant No. IIS-1355716.

REFERENCES

1. Aoyagi, D. et al. *Trans. Neural Syst. Rehabil. Eng.* **15**, 387-400, 2007.
2. Malcom, P. et al. *PLoS: ONE* **8**, e56137, 2013.
3. Winter, DA. *The Biomechanics and Motor Control of Human Gait: Normal, Elderly and Pathological*, Waterloo Biomechanics, 1991.
4. Pratt, G. and Williamson, M. *Proceedings of Int. Conf. Intel. Rob. Sys., Pittsburgh, PA, USA 1995*
5. Caputo, JM and Collins, SH. *Biomech Eng.* **136**, 035002, 2014.

SEVERITY OF FUNCTIONAL IMPAIRMENT INFLUENCES REACH KINEMATICS IN PEOPLE POST STROKE

^{1,2}Clinton J. Wutzke, ²Evan Chan, ²Michelle Harris-Love

¹Veterans Affairs Medical Center, Washington DC, USA

²National Rehabilitation Hospital, Washington DC, USA

email: clinton.wutzke@va.gov, web:www.reachingrehab.org

INTRODUCTION

Although people post stroke with severe functional impairment have the greatest need for rehabilitation to attain a higher level of function, few studies have examined reaching movement patterns in this population [1,2]. Differences between levels of functional impairment in people post stroke may indicate a need to optimize rehabilitation paradigms.

The purpose of this study was to determine the influence of functional impairment on seated reaching in people post stroke. We hypothesized people post stroke with severe upper extremity functional impairment have slower movement patterns and greater between subject variability than people with mild functional reaching impairment.

METHODS

Twenty-eight people post stroke (\bar{x} UEFM: 32.9 ± 20.4 , \bar{x} age: 60.1 ± 9.4 years; 19M/9F) participated in this study. Categorization of functional impairment (mild or severe) was determined by score on the Upper Extremity Fugl-Meyer (UEFM, range: 0-66).

Participants were seated in an adjustable chair with chest restraints to limit movement of the trunk. Subjects completed 20 forward reaches with the paretic arm. Trials were initiated from a common starting position. Participants reached forward to 80% of his/her maximal reach to two targets located on a flat, level table. Subjects were asked to reach forward and touch the target as quickly as possible following a visual go stimulus.

Movement of the paretic arm was tracked using an Optotrak (NDI, Waterloo, CAN) motion capture system with a marker placed on the ulnar styloid of

the paretic arm. Temporal (response time, reaction time, movement time) and spatial (peak velocity, initial directional error, and end point error at peak velocity, movement units, path length) variables were calculated for the paretic arm using custom MatLab programs. Between subject variability was calculated as the coefficient of variation within each functional group (mild/severe). A one-way ANOVA (severity) was conducted with significance determined a priori at $\alpha=0.05$.

RESULTS AND DISCUSSION

Fifteen participants (\bar{x} UEFM: 16.0 ± 7.9 , 8M/7F) were identified as severely impaired and 13 participants (\bar{x} UEFM: 52.3 ± 9.7 , 11M/2F) were categorized as mild functional impairment ($p < 0.001$).

Temporal and spatial measures of reaching differed between people post stroke with severe and mild functional impairments. Temporal variables (response time, reaction time, and movement time) were greater for people with severe impairment compared to people with mild impairment (response time: $F=10.8$, $p=0.003$, Table 1; reaction time: $F=22.3$, $p<0.001$; movement time: $F=5.2$, $p=0.031$; Figure 1).

Anterior/posterior peak velocity was greater in people with mild impairment compared to people with severe impairment ($F=18.1$, $p<0.001$, Table 1). Deviation from ideal path at the start (initial error, $F=10.6$, $p=0.003$, Figure 1) and at peak velocity in relation to the target (end point error at peak velocity, $F=14.6$, $p=0.001$, Figure 2) of movement differed between functional groups.

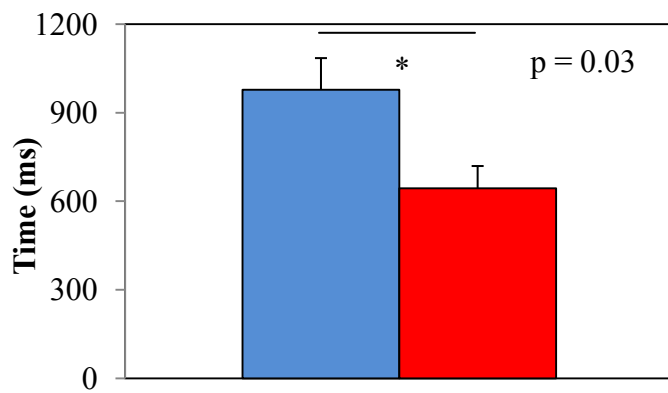


Figure 1: Movement time of forward reach with the paretic arm in people post stroke with severe (blue) and mild (red) functional impairment.

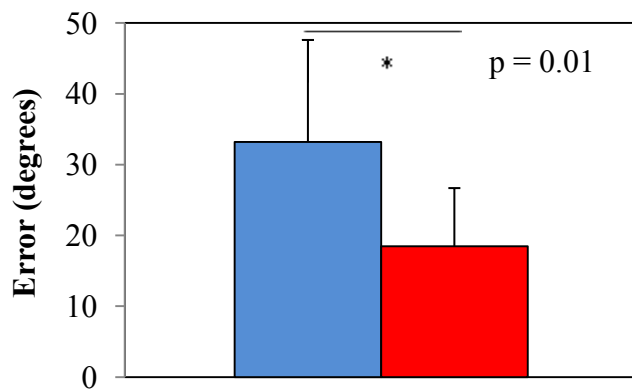


Figure 2: Initial directional Error during forward reach of paretic arm of people post stroke with severe (blue) and mild (red) functional impairment.

Variability of movement units (quantity of oscillations in tangential velocity during reach) within functional groups was greater in the severe functional group compared to the mild functional group when reaching with the paretic arm ($F=7.238$, $p=0.012$, Table 1).

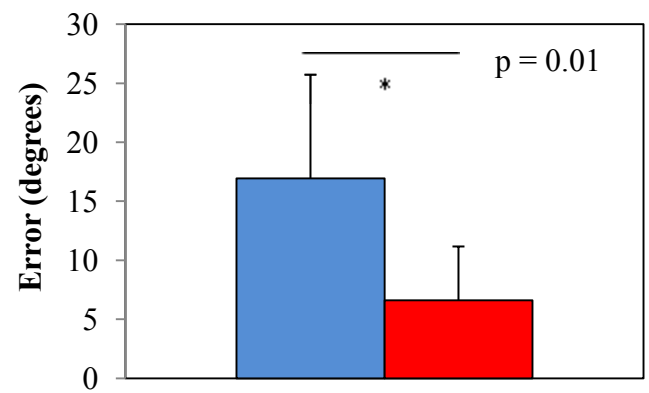


Figure 3: End point error at tangential peak velocity of paretic arm during reaching in people post stroke with severe (blue) and mild (red) functional impairment.

CONCLUSIONS

The results of this study suggest that functional impairment influences reaching movement patterns in people post stroke. People with severe functional impairment have longer duration of movement and increased error compared to people with mild functional impairment. Future studies to identify within subject variability may be beneficial to identify rehabilitation paradigms to improve reach function in people post stroke with severe impairment.

REFERENCES

1. Barker, R.N., et al, *Exp Brain Res*, 221(2): p.211-21, 2012.
2. Harris-Love, M.L., et al, *Neurorehabil Neural Repair*, 25(5): p.398-411, 2011.

Table 1: Mean, standard deviation, and coefficient of variation of temporospatial measures of paretic arm reaching in people post stroke with mild and severe functional impairment (* indicates $p \leq 0.05$).

	Response Time (ms)		Peak Velocity (cm/s)		Movement Units		Ideal Hand Path (m)	
	Mild	Severe	Mild	Severe	Mild	Severe	Mild	Severe
Mean	971.00*	1503.93*	0.90*	0.42*	1.04*	2.07*	0.35*	0.20*
St Dev	204.53	552.93	0.39	0.18	0.14	1.57	0.07	0.09
COV	0.21	0.37	0.44	0.43	0.13*	0.76*	0.19	0.43

EFFECT OF CUSTOMIZED HAPTIC FEEDBACK ON NAVIGATION CHARACTERISTICS AND PERFORMANCE

Han U. Yoon and Pilwon Hur

Department of Mechanical Engineering, Texas A&M University, College Station, TX, USA
email: {hanulyoon,pilwonhur}@tamu.edu, web: <http://hurgroup.net>

INTRODUCTION

Assistive technologies for driving and navigation have been engaged for the past two decades. However, the effectiveness of the outcome of assistive technologies using haptic devices is still debatable. Specifically, determining the level of haptic assistance, e.g., the magnitude and direction of haptic force, is a challenging problem [1]. For instance, an excessive assistance level may degrade user's performance and cause discomfort, whereas a lack of enough assistance may yield task failure.

Previous studies have shown possibilities to enhance human task-performance by adopting control characteristics [2] and to design a controller by mimicking human's driving style via inverse optimal control (IOC) [3]. In this study, subject's control strategy for given tasks was parameterized by IOC. Also, the obtained parameters will serve as metrics to customize haptic feedback for each subject by i) assigning a *coach* whose task-performing characteristics are the desired characteristics for the rest of the subjects, ii) defining a *spine* (guiding path) which guides subjects based on the coach's strategy, and iii) determining the level of assistance. Therefore, the objective of this study is to identify the effect of customized haptic guidance on subjects' task-performance and performing-characteristics.

METHODS

Sixteen healthy young adults (14 male and 2 female, age=20-35 yrs) participated in this study. Subjects were seated at 1.5m from a 105cm-by-81cm (width-by-height) screen as shown in Fig.1. The modified version of Novint Falcon (Novint Technologies, Albuquerque, NM) was used to provide 2D haptic interface [4]. All subjects gave informed consent prior to their participation and this research was proved by the University Institutional Review Board.

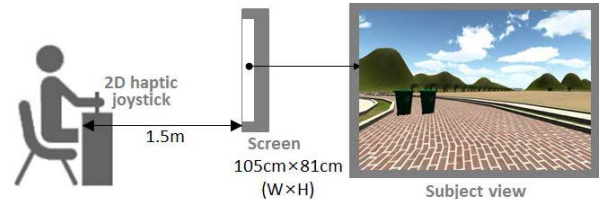


Figure 1: The experimental environment.

The experiment consisted of two separate sessions: the first session for obtaining the baseline data and the second session (one week apart) for identifying the effect of customized haptic feedback based on the baseline data. For both sessions, the subjects were asked to drive a virtual vehicle along four roads each of which had a difference radius of curvature and obstacles. The subjects were instructed to drive the vehicle as fast and safe as possible. Completion time, sampling time, task#, trial#, successes, fails, vehicle's positions and heading direction were recorded from the start line to the finish line. Each task was repeated 3 trials. The sequence of the tasks was randomized. Sampling frequency was 60Hz. This virtual task environment was developed by Unity3D (Unity Technologies, San Francisco, CA).

After the first session, the subjects' strategy for each task was analyzed. A cost function that each subject may have minimized during each task was assumed to be in the following form: $cost = \sum_{i=0}^N c_v v(i)^2 + c_\omega \omega(i)^2 + c_{d_o} d_o(i)^2 + c_{d_f} d_f(i)^2$ where v : linear velocity, ω : angular velocity, d_o : distance from the vehicle to road boundary on obstacle side, and d_f : distance from the vehicle to road boundary on obstacle-free side. As these four variables at each discrete time step $i \in [0, N]$ corresponded to the baseline data, positive coefficients, c_v , c_ω , c_{d_o} , and c_{d_f} , could be estimated by solving an IOC problem [2][3].

Subject's *performing-characteristics* vector q was defined from the estimated coefficients as $q = [c_v, c_\omega, c_{d_o}, c_{d_f}] \times 100 / (c_v + c_\omega + c_{d_o} + c_{d_f})$ where each element represents subject's efforts for *speed control*, *steering*

control, and lane selections for routing and obstacle avoidance as percent, respectively. By clustering the q vectors in \mathbb{R}_+^4 via k-means clustering algorithm, the subjects were classified into 3 groups. As a result, subjects in the same group have similar driving patterns. A subject whose task-completion time was fastest in each group was designated as a *coach* in each group. The *coach*'s baseline vehicle trajectory in the first session was used as a *spine* to guide the rest of subjects in the same group. The level of haptic guidance for each subject was determined proportional to L_1 -norm distance from his/her to the *coach*'s performing-characteristics vector. The resulted guidance is called *customized haptic guidance* (CH). For the second session, CH was applied to assist the subjects. To compare the effect of CH to typical guiding method, another type of haptic guidance that enforced the vehicle to a road center (RH) was applied.

The following 3 parameters were investigated: i) summed average task-completion time, $\sum T_{avg}$, ii) summed standard deviation (std) of T_{avg} , denoted by $\sum T_{std}$, and iii) guided driving characteristics under three assistance modes, NA(no assist), CH, and RH. A repeated measures analysis of variance (rANOVA) was used to identify the effect of haptic guidance on subject's task-performance and performing-characteristics. Significance level was set to 0.05 (SPSS v21, Chicago, IL)

RESULTS AND DISCUSSION

Based on the baseline data during the first session, subjects were grouped into 3 groups (bold is a coach): {**s4**, s2, s5, s7, s8, s13, s14, s15}, {**s9**, s10, s16}, and {**s12**, s1, s3, s6, s11}. The coach data were excluded from statistical analysis since coach data were used as references. First, rANOVA found that $\sum T_{avg}$ was not significantly affected by haptic assistance. Some improvements of $\sum T_{avg}$ could only be observed in slower subjects, e.g., s10, s7, s16, as shown in Fig. 2.

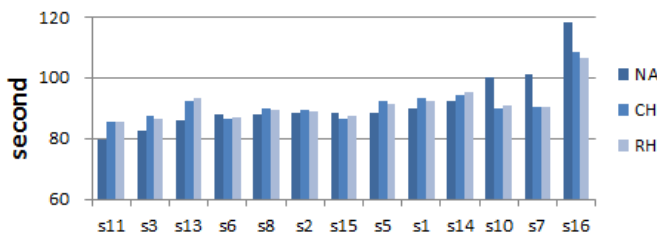


Figure 2: $\sum T_{avg}$ with respect to NA, CH, and RH (From left to right, ordered by $\sum T_{avg}$ under NA).

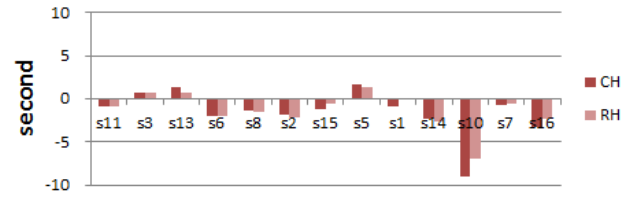


Figure 3: The difference of $\sum T_{std}$ under CH and RH compared with NA.

Next, rANOVA on $\sum T_{std}$ showed tendency for reduction of $\sum T_{std}$ when haptic assistance was provided ($F(2,24)=4.168$, $p=0.061$, with mean of 3.929, 2.430, and 2.658 for NA, CH, and RH, respectively). The mean of variability of subjects' performance reduced the most when CH was provided. Figure 3 depicts the difference of $\sum T_{std}$ for CH and RH compared with NA. However, rANOVA on the guided driving characteristics, which was represented by L_1 -norm distance from the coach under three assistance modes, showed no significant difference.

By direct data observation, several interesting aspects were found. From Table 1, both mean and std decreased in **s12** group for CH. For **s4** group, most subjects' performing-characteristics were already close enough to **s4** as the smallest mean for NA indicated. Hence, applying haptic feedback to **s4** group might work as disturbance. Increased mean in **s9** group might be caused due to small number of subject, but std was reduced under CH. For further statistical analysis on L_1 -norm distance, more data will be collected. Also, task-difficulty will be elevated to investigate the broader range of subjects' performance.

Table 1: Mean(std) of subjects' L_1 -norm distance from the group coach under three assistance modes.

	NA	CH	RH
s4 group	11.95(13.39)	31.34(45.00)	16.44(22.89)
s9 group	27.12(18.38)	67.49(7.53)	37.20(39.58)
s12 group	16.44(6.84)	6.67(3.80)	10.66(9.54)

REFERENCES

1. Feygin D, et al. *Proceedings of IEEE Symp. on HAPTICS*, Orlando, FL, USA, 2002.
2. Suzuki S and Furuta K, *J Control Science and Engineering* **2012**, 1-10, 2012.
3. Lavine S and Koltun V, *Proceedings of ICML*, Edinburgh, Scotland, 2012.
4. Kim Y. et al., *Proceedings of IEEE World Haptic Conf.*, Chicago, IL, USA, 2015.

Proportional Myoelectric Control of a Robotic Hip Exoskeleton

¹ Aaron J Young, ¹ Bridget Cook and ¹ Daniel Ferris

¹ The University of Michigan, MI, USA

email: aayoung@umich.edu, web: <http://kines.umich.edu/lab/human-neuromechanics-laboratory>

INTRODUCTION

Robotic lower limb exoskeletons have significant potential for providing gait assistance and rehabilitation to individuals with lower limb impairment and augmenting human locomotion capability. The objective of this study was to test a hip exoskeleton capable of supplying both flexion and extension torques using proportional EMG control from hip muscles and determine the resulting torque profile. The primary outcome measure was metabolic cost of walking using the powered exoskeleton. We hypothesized that a proportional EMG based controller on the robotic hip exoskeleton would reduce the metabolic cost of walking. We expected the exoskeleton would provide a biological torque profile given that the user can alter the torque based on their muscle recruitment.

METHODS

We designed a hip exoskeleton device to apply torques around the user's hip joint. The design was a modification of a previous exoskeleton frame from our lab [1]. Bidirectional pneumatic actuators (BIMBA) on each leg provided hip flexion and extension assistance. Load cells in line with the actuators measured output force. The exoskeleton attached to the user through straps around the thigh and waist. Only the sagittal plane was actuated but there was passive range of motion in the frontal plane. We placed electrogoniometers (Biometrics, Ltd.) on the exoskeleton to measure hip joint angle.

EMG electrodes on the rectus femoris (RF) and gluteus maximus provided the control signal. The controller used gluteus maximus EMG to activate hip extension assistance. Rectus femoris EMG activated hip flexion assistance. Rectus femoris is

not an ideal muscle for hip flexion assistance because it is biarticular, but other hip flexion muscles (such as the iliopsoas and the sartorius) are hard to record with surface electromyography. To deal with this issue, the controller ignored the rectus femoris burst in early stance.

A single female subject (63.5 kg) wore the exoskeleton during walking at 1.0 m/s. University of Michigan Medical School Institutional Review Board approved the protocol. After fitting the device, she stood for 3 minutes while we measured oxygen consumption and carbon dioxide production using a metabolic analysis system (Max-II, AEI Technologies). The subject walked on a split-belt instrumented treadmill (Bertec) to measure ground reaction forces. The user acclimated to walking with the exoskeleton unpowered for 5 minutes before we collected metabolic data for 6 minutes. The user was given a short resting period before beginning an adjustment period to the powered exoskeleton. The controller applied flexion and extension torque proportional to the myoelectric activity from the control sites. We conducted 6 minutes of walking metabolic data under the powered condition. We calculated metabolic power using the equation from Brockway for each condition, and subtracted standing metabolic power to get net metabolic cost.

RESULTS AND DISCUSSION

When the exoskeleton was powered, the gluteus maximus was active in early stance and turned off by 10-15% of the gait cycle (Fig. 1). The proportional signal was typically between 50-60% of max power. The rectus femoris was active in late stance at a lower proportional signal of between 20-30% of max power, but for a longer part of the gait cycle. The RF was also active in early stance, but

was set to zero as this burst is associated with knee extension activity.

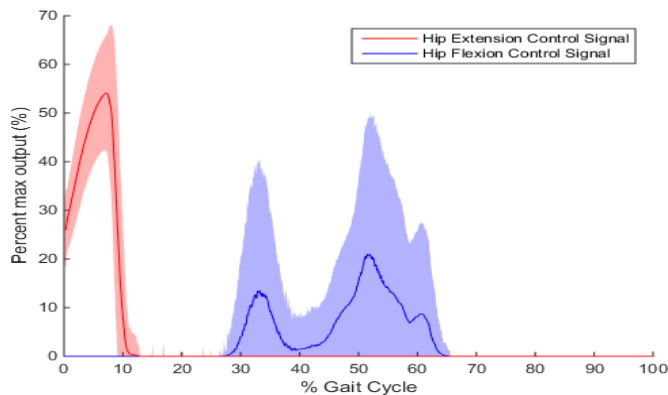


Figure 1: EMG control signals used for applying hip assistance. The hip extension signal (red) was proportionally controlled by the gluteus maximus. The hip flexion signal (blue) was proportionally controlled by the rectus femoris. Data shown are for one subject averaged across 1117 steps (both left and right side).

The exoskeleton device provided torque assistance about the hip that was a small percentage of normal biological torque (Fig. 2). Hip extension torque peaked between 10-20% of the gait cycle, and hip flexion torque peaked between 40-55% of the gait cycle. The average maximum extension torque per stride was 0.477 N*m/kg, and the average maximum flexion torque per stride was 0.280 N*m/kg.

The powered exoskeleton reduced metabolic cost by 9.3% compared to the unpowered condition. Average metabolic cost of walking with the unpowered exoskeleton was 184.2 W. Average metabolic cost of walking with the powered exoskeleton was 167.1 W.

CONCLUSIONS

The max torque generated by the exoskeleton was a relatively small amount of the normal biological torque, but provided a substantive decrease in metabolic cost of walking. The torque profile is roughly consistent to the biological torque profile during stance phase to those required at the hip. The peak extension torque was slightly delayed (due in part to the pneumatic actuation) from normal

walking but otherwise similar. The peak flexion torque typically occurs at 50% and is similar to what was observed in this experiment. The exoskeleton provided nearly zero torque during swing phase, and any torque provided was a result of passive mechanics – except during early swing in which a small amount of flexion torque was provided due to RF activity. EMG-based control may be an effective way to produce biological torque profiles at the hip to help reduce metabolic cost.

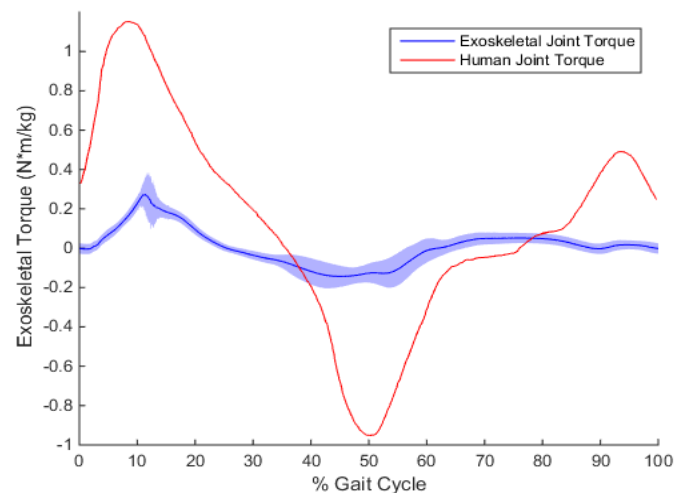


Figure 2: Torque generated by the hip exoskeleton (blue) normalized by body weight. Biological hip torque data from [2] is shown in red as we had not yet calculated inverse dynamics for the subject. Hip extension is positive and hip flexion is negative. Exoskeleton data shown are for one subject averaged across 1117 steps (both left and right side).

REFERENCES

1. Lewis, CA and Ferris, DP. *J Biomech* **44**, 789-793, 2011.
2. Winter DA, et al. In *Human motion analysis: current applications and future directions*, IEEE Press, 1996.

COMPARISON OF TORQUE CONTROLLERS FOR AN ANKLE EXOSKELETON WITH A SERIES ELASTIC ACTUATOR DRIVEN BY A UNI-DIRECTIONAL BOWDEN CABLE DURING WALKING

^{1,2}Juanjuan Zhang, ²Chien Chern Cheah and ¹Steven H. Collins

¹Carnegie Mellon University, Pittsburgh, PA, USA

²Nanyang Technological University, Singapore

Email: juanjuan Zhang@cmu.edu; ecccheah@ntu.edu.sg; stevecollins@cmu.edu

INTRODUCTION

Exoskeletons have been used for human performance restoration and enhancement for many years. Due to the dynamic nature of human locomotion, torque control is widely used in lower-limb exoskeleton assistance during stance phases of walking. In these systems, series-elastic actuators (SEA) are commonly used to provide low error torque tracking in the presence of unknown and changing human dynamics. Good torque tracking performance is important to the fidelity of gait-related biomechanical experiments and the effectiveness of clinical gait recovery training. Control of lower-limb exoskeletons is normally hierarchical, with high level controllers determining behavior-related desired torques and torque control lying at a lower level. Many low-level control methods have been proposed for existing exoskeleton systems. However, relatively little has been reported on the relative performance of different torque controllers on the same platform under practical walking conditions, making differentiation among candidate methods difficult. Moreover, the interactions between high- and low-level controllers are unknown. This study aimed to compare the torque-tracking performance of prominent torque controllers, under realistic experimental conditions, with multiple high-level controllers, in a single exoskeleton platform [1]. These results are expected to help guide the selection and tuning of lower-limb exoskeleton torque controllers for locomotion assistance, which will benefit gait-related biomechanics research and clinical training.

METHODS

The ankle exoskeleton testbed used in experiments consisted of an off-board geared electric motor with real-time driver, a flexible Bowden cable transmission with series compliance, and an exoskeleton that interfaced with the human body (Fig. 1). Motor input

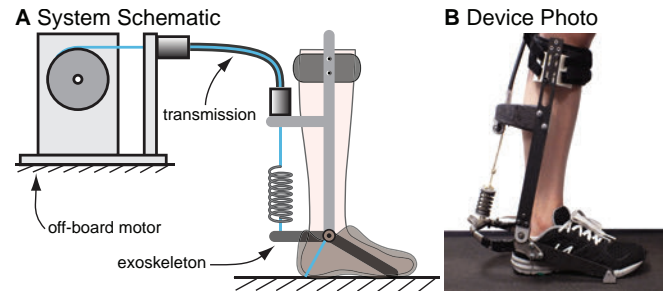


Figure 1: Schematic and photo of the tethered ankle exoskeleton system. (A) Schematic of the system; (B) Photo of the exoskeleton worn by a human.

voltage was regulated by a motor driver running in velocity control mode, which provides smoother torque tracking in series elastic actuators. Desired motor velocity was commanded to a dedicated hardware motor controller for all torque controllers investigated. Nine torque controllers, including variations and combinations of classical feedback control, model-based control, adaptive control and iterative learning, were experimentally compared in this study. Each was tested separately with four high-level controllers that determined desired torque based on time, ankle angle, a neuromuscular model (NMM), or electromyography (EMG). Under each high- and low-level controller combination, the exoskeleton was tested with one subject who walked on a treadmill with 1.25 ms^{-1} for one hundred steady-state steps on a treadmill. The root mean squared torque errors were calculated for each stride (RMSE) and for an averaged stride (RMSE-A).

RESULTS AND DISCUSSION

The best torque tracking performance was observed with the combination of model-free, integration-free feedback control and iterative learning for all high-level controllers, both in real-time and for the average stride. In this study, this type of controller was represented by proportional control and damping injection compensated by iterative learning (PDA+LRN) as described below.

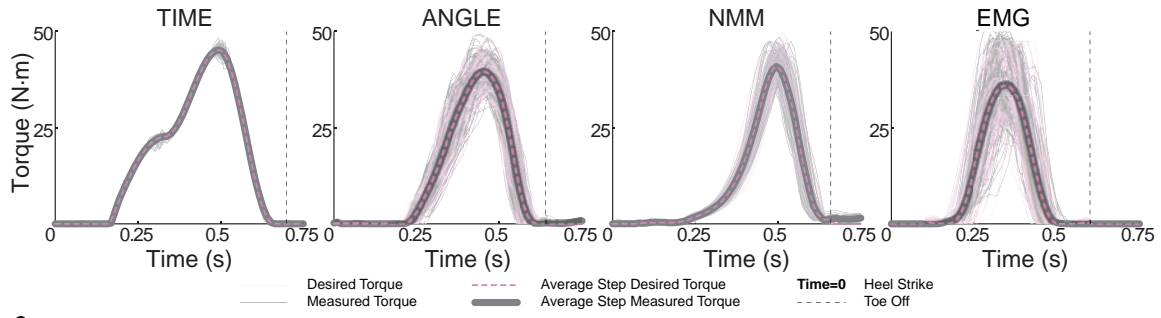


Figure 2: Overlapped trajectories of the desired and measured torques in time for all high level controllers with PDa+LRN

$$\begin{aligned} \dot{\theta}_{m,des}(i,n) = & \underbrace{-K_p e_\tau(i,n)}_{\text{Proportional Control}} + \underbrace{-K_d \dot{\theta}_m(i,n)}_{\text{Damping Injection}} \\ & \underbrace{ + \underbrace{\dot{\theta}_{m,des}^{LRN}(i+D,n)}_{\text{Iterative Learning (LRN)}}}_{\text{PDa}} \end{aligned}$$

In this equation, $\dot{\theta}_{m,des}$ is the desired motor velocity to be commanded, K_p is a proportional gain, e_τ is torque error, K_d is a damping gain, and $\dot{\theta}_m$ is measured motor velocity. $\dot{\theta}_{m,des}^{LRN}$ is the compensation from iterative learning, which is updated by

$$\dot{\theta}_{m,des}^{LRN}(i,n+1) = \dot{\theta}_{m,des}^{LRN}(i,n) - K_L e_\tau(i,n),$$

where i is the time index (number of control cycles elapsed) within this step, n is this step and $n+1$ is the next step, K_L is the iterative learning gain, and D is an estimate of the delay between commanding and achieving a change in motor position. Using this controller, the motor commands arose primarily from feedback control, with iterative learning compensating for consistent tracking errors. Part of the controller is labeled as 'damping injection' instead of 'derivative control' since motor velocity is used instead of the relative velocity between motor and ankle joint. This was to reduce noise while maintaining comparable control performance. The iterative learning part only acts in the next step based on the torque errors of the current one.

Table 1: Tracking errors with PDa+LRN torque control

	RMSE	% τ_{max}	RMSE-A	% τ_{max}
Time	0.57 ± 0.18 Nm	1.3%	0.10 Nm	0.2%
Angle	0.99 ± 0.23 Nm	2.5%	0.11 Nm	0.3%
NMM	0.93 ± 0.32 Nm	2.3%	0.12 Nm	0.3%
EMG	2.14 ± 0.77 Nm	5.9%	0.22 Nm	0.6%

the peak desired torque, τ_{max} , for the average step are given in Table 1. Overlapped desired and measured torque trajectories for one hundred steps with PDa+LRN are shown in Fig. 2. The high variations of torques for Angle- NMM- and EMG-based high level controllers are the result of step-to-step gait variation of the subject. Depending on high-level conditions, the real-time torque errors with this controller were 38%-84% lower than with PDa alone, and average-step torque errors were 91%-97% lower. This approach is effective since it is analogous to the classical proportional-integral-derivative control. The proportional term provides basic tracking; damping injection improves the system stability like derivative control; iterative learning, which is a step-wise integral control, eliminates steady-state errors in cyclic operations.

CONCLUSIONS

A systematic comparison of uni-directional Bowden cable driven exoskeleton torque controllers under walking conditions was conducted, demonstrating that proportional control with damping injection compensated by iterative learning had better torque tracking performance than any other methods tested in this study and in the literature. Implementation of this controller was straightforward, requiring sequential tuning of only four parameters. Our results suggest that this approach can be applied to multiple torque-controlled lower-limb exoskeletons used in cyclic processes like locomotion. The application of this controller in lower-limb robotic devices will improve the precision of interventions and allow better-controlled experiments.

REFERENCES

1. Zhang et al., *Proceedings of ICRA*, Seattle, WA, USA, 2015.

Error values for PDa+LRN and their percentage of

LOWER BODY JOINT KINETICS IN STANDING BROAD, VERTICAL, AND SQUAT JUMPS

¹Kaylin Bean, ¹J. Bryan Mann, and ¹Trent M. Guess

¹ University of Missouri, Columbia, MO USA

email: beank@health.missouri.edu, web: www.mizzoumotioncenter.com

INTRODUCTION

A major interest in athletics is increasing overall power output. A widely accepted way to determine overall athletic ability and power is the vertical jump test [1]. Much research has been conducted on overall jump power in order to determine possible strategies for training [1, 2], but little research has been conducted on the contributions made by the three leg joints (hip, knee, and ankle) and with multiple types of jumps. In order to produce the most powerful movement possible, all three leg joints must work maximally [3] and assessing the joint contributions in jumping power can help determine specific areas of concentration for strength and conditioning.

METHODS

With approval from the institution's human subjects review board, 20 female collegiate soccer players (Mean±standard deviation: 19.6±1.3 yrs; 166±7 cm; 60.4±8.1 kg) participated in the study. All subjects performed five trials for the standing broad jump, vertical jump, and squat jump. The subjects were encouraged to jump maximally and could use their arms as desired on the standing broad and vertical jumps. For the squat jump, the subjects were restricted to keeping their hands on their head to reduce arm contribution to the jump. The best jump by each subject was chosen for analysis; the best referring to the longest standing broad jump and the highest vertical and squat jumps. Before jumping, basic anthropometric data was collected and 16 reflective markers were placed on the lower body using the Plug-in Gait model.

All jumps were measured using an 8 camera VICON MX-T40S retro-reflective motion analysis system synchronized with two AMTI Optima force plates. The motion data was sampled at 100Hz, processed using Vicon Nexus 2.1 software, and filtered at 6Hz using a 4th order Butterworth filter.

The force plate data was sampled at 1000Hz. Joint moments for the ankle, knee, and hip were calculated using inverse dynamics. Data was analyzed from the point of maximum knee flexion (0%) to toe-off (100%), and total maximum power was determined during the propulsion phase (see Figures 1, 2, & 3). A summation of the total joint moments was calculated, and contributions of each joint to the jump were determined as percentages of the sum at the maximum power output during the propulsion phase [3]. Total support jump differences were determined using a repeated measures one-way ANOVA with post hoc t-tests to determine between jump difference. Jump-by-joint differences were determined using a repeated measures two-way 3x3 ANOVA with post hoc one-way ANOVAs to determine between jump differences.

RESULTS AND DISCUSSION

Mean total support power differed significantly between jumps ($F(2, 38)=28.326$, $p<0.001$) (Table 1). Post hoc tests revealed power during the vertical jump was 8.7 W/kg ($p<0.001$) and 3.6 W/kg ($p=0.045$) greater than during squat and broad jumps, respectively, and 5.1 W/kg ($p=0.001$) greater during broad jump compared to squat jump. The difference in mean total joint power in the squat jump can be attributed to the restricted arm movement. The arms act as a driving force, increasing the tension applied to the three leg joints [4]. Thus focusing on the timing of the arm swing with muscle activation of the legs can help produce a greater power output.

There was a significant interaction effect of jump type and joint contribution of total power ($F(4, 38)=28.299$, $p<0.001$). Post hoc tests revealed significant between jump differences at the ankle ($F(2,38)=14.014$, $p<0.001$), knee ($F(2,38)=46.105$, $p<0.001$), and hip ($F(2,38)=17.690$, $p<0.001$) (Table 1). Power during broad jump was significantly

H*2*!F8; I\$.*0!28!5\4\$2\$(0!7*.2F\$&4; I5!\$2X*!
\$(A&! Mh T-TT"+!!I gT-TTWNS(0! CT! Mh T-TT"+!
Ih T-TT"m-42&D*.!\$2X*A(*!MhT-TT"fh T-TTN!
.*5!F27*&! >4FC 0'99*.(F*5 ; \$% .*9&F2 \$!
0'99*.(F*!(!F84(2* ; 87* ; *(252\$2*H404.'(H2C*!
&\$0'(H! IC\$5*! 89! 2C*! <8\$0! G4! ! 28 ;\$ P' ;E *!
98.D\$.0! I. 8I4&58(! M'H4*5! "+!L+QN! 1C*! 24(A!
'(F&*5! \$(2*.'8.&4 2C*! F*(2*! 89 ; \$55! ; 87*5!
98.D\$.0+! *54&(H! '(H*2*!CT! 9&P'8(! \$(0!\$(A&!
08.5'9&P'8(+!DC&4*.*04F(H! A(*! 9&P'8(! '(2C*!
<8\$0!4; I! \$5!F8; I\$.*0!28!2C*!7*.2F\$&\$(0!54\$2
4; I5! JLK! ? &C84HC! 2C*! D\$5! (8! 5'H'9F\$(2!
0'99*.(F*!(!I8D*!F8(2.'<428(! <*D**(! 7*.2F\$&
\$(0!54\$24; I5!\$2X*CT! \$(0! A*+\$(A&!I8D*!
D\$5!5'H'9F\$(2&4H*\$2*!04.'(H7*.'2'F&G4! !2\$(!
04.'(H!54\$24; I! Mh T-TLVN\$4FC0'99*.(F*5! ; \$%
'(0'F\$2! \$! I855<&! '(9&*(F*! 89! .04F*0! \$.; !
; 87* ; *(2!04.'(H!54\$24; I+!& '2(H!2C*!\$(2*.'8!
0'5I&F* ; *(289!2C*!F*(2*! 89 ; \$55!\$(0! .04F(H!
\$(A&!08.5'9&P'8(-

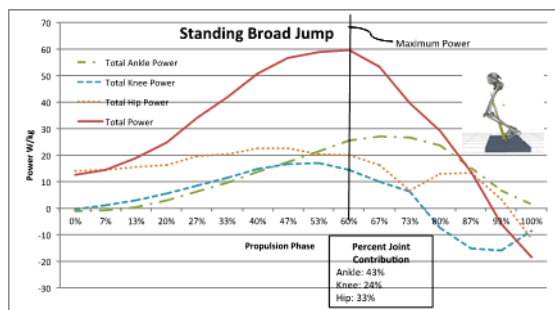


Figure 1 @k *I. *5*(2\$27*!CI+IA(**+\$(A&+\$(0!282&
I8D*!.!04.'(H! I. 8I4&58(! IC\$5*! 89! 52\$(0' (H! <8\$0!
G4! ! 89! 8(*! 9* ; \$&! 54<GF2! D'2C 5A*&2&!
.*F8(524F28(! \$(0! I*.'F*(2! 8'(2! F8(2.'<428(\$2
I8' (2!89;\$ P';4 ;! I8D*.-!!

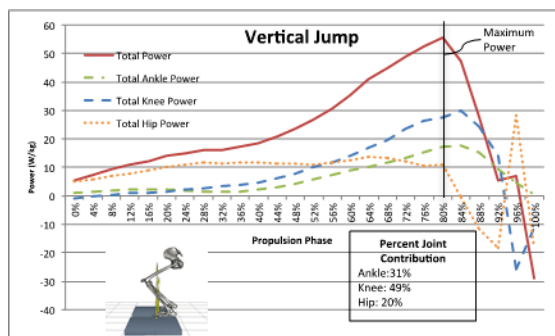


Figure 2 @k *I. *5*(2\$27*!CI+IA(**+\$(A&+\$(0!282&
I8D*!.!04.'(H! I. 8I4&58(! IC\$5*! 89! 7*.2'F&G4! !89!
8(*!9* ; \$&!54<GF2D'2C!5A*&2& *F8(524F28(! \$(0!
I*.'F*(2! 8'(2! F8(2.'<428(\$2 I8' (2! 89 ;\$ P'; 4 ;!
I8D*.-

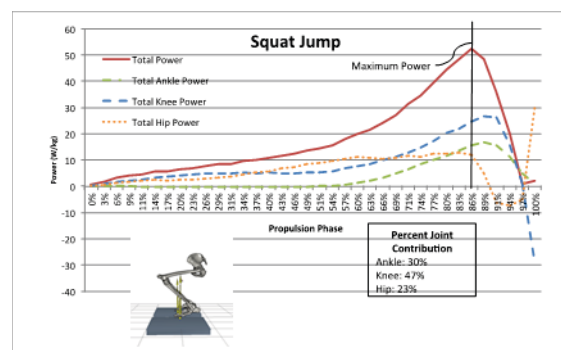


Figure 3 @k *I. *5*(2\$27*!CI+IA(**+\$(A&+\$(0!282&
I8D*!.!04.'(H! I. 8I4&58(! IC\$5*! 54\$24; I! 89!8(*!
9* ; \$&! 54<GF2 D'2C 5A*&2& *F8(524F28(! \$(0!
I*.'F*(2! 8'(2! F8(2.'<428(\$2 I8' (2! 89 ;\$ P'; 4 ;!
I8D*.-

Table 1:!182&\$(0!0'52!<42'8(!89!&D*!*P2* ; 2/4
8'(2! I8D*.'5! 04.'(H! <8\$0+!7*.2F\$&\$(0! 54\$2
4; I5-!M5'H'9F\$(2!0'99*.(F*!9.8 ; !7*.2F\$&4; I+!
m5H'9F\$(2!0'99*.(F*!9.8 ; !54\$24; IN!

,8'(2!	>2\$(0'(H!) .8\$0!4; I!	`.*.2'F&! ,4;I !	>\4\$2 ,4;I !
c 'I!MN!	QZjU" T-Whl	L"-jUVL!	LT-VU-T!
# (*!M N	LYVUT-Qlml	Zj-VUVQ	Z[-UYW
? (A&M N	QYYU-Ylml	QLWUj ml	QTQUW'l !
182&/\$!(,8'(2'8D*! NR iAHN	jL-TUj-[l ml	jj- WUjZml	ZWWUj-Q!

CONCLUSIONS

Q! F8(F&5'8(+!I8D*!F8(2.'<428(5!89!2C*CT!+IA(**+!
\$(0!\$(A&!0'99*!\$F8.0'(H!28!G4! '(H2\$A+D'2C!\$!
CT!\$(0!\$(A&!52\$2*H442&F*0!98!<8\$0!4; I!\$(0!\$!
A*!52\$2*H445*0!98.17*.2F\$&\$(0!54\$24; I5-!!18!
'(F.*5*! ; \$P' ; \$&I8D*!84242+!4; I!0*I*(0*(2+!
8'(2!5I*F'9F!2\$('(H5C84&4!<*!42&F*0-!!]4.2C*!
5240*5! 5C84&4! '(F&40*! G8 2! A(* ;\$ 2'F5! \$(0!
*&F28; %8H\$IC%4 28 0*2* ;(! 2C*! '(9&*(F*! 89!
I8524.*!\$(0! ; 45F&!SF27\$28(!8!I8D*!84242-!!

REFERENCES

- "->\$%&.5!>^+!2\$&Med. Sci. Sports Exerc. **31**(4),!jYLjYY!
"VVV
L-'\$((*2*.HC* ,! ,+2!\$&-J Strength and Condit. Research!
22(3)+YT[Y]ZHLTT-!
Q-k8<*.23(!d 3 n!\$(0!]&* ;'(H!d -!Can. J. Spt. Sci. **12**(1), "V_
LQ-V[Y!
Z-k \$; !d ,+2!\$&-J Strength and Condit. Research!**21**(3)+VWY
VYQITY-

BIOMECHANICAL FACTORS ASSOCIATED WITH MEDIAL TIBIAL STRESS SYNDROME: A PROSPECTIVE STUDY

James Becker, Mimi Nakajima, Wilbur Wu

Center for Sport Training and Research,
Department of Kinesiology, California State University Long Beach, 90840
email: james.becker@csulb.edu

INTRODUCTION

Multiple epidemiological studies over the last thirty years have reported medial tibial stress syndrome (MTSS) as one of the most common overuse running injuries [1,2]. Despite the prevalence of this injury, its etiology is still not well understood. Hip muscle strength [3], passive range of motion [4], and running kinematics [5] have all been suggested as possible factors. While many of these studies have been prospective in nature [3,4,5] each study has focused on a single area such as range of motion, muscle strength, or kinematics, in isolation. It is likely that MTSS results from a combination of all these areas and thus, prospective studies combining all areas are needed.

In relation to foot movement in particular, excessive amounts or velocities of foot pronation are often cited as kinematic factors contributing to MTSS [7]. However, to date, there is conflicting reports in the literature regarding such this relationship. An alternative hypothesis suggests it is not the amount or velocity of pronation which is the issue, rather the time during stance phase over which the foot remains in a pronated position [1]. However, as it relates to MTSS, the idea of prolonged pronation has not yet been investigated.

Therefore, the purpose of this study was to compare flexibility, strength, and kinematics between runners who went on to develop MTSS and a healthy control group. It was hypothesized that compared to controls, the runners who developed MTSS would be weaker, would display limited ranges of motion during a clinical exam, and would have altered hip and foot kinematics during stance phase including higher peak hip adduction and internal rotation, similar amounts but longer durations of

pronation, and a higher tibia varus angle at initial foot contact.

METHODS

These data are part of an ongoing prospective study on relationships between running mechanics, injury, and performance. To date, twenty five runners have participated (sex: 12 female, 13 male; age: 20.2 ± 1.1 years; weekly running mileage: 67.4 ± 18.7). Participants were all members of a collegiate cross country team. All participants underwent an orthopedic exam evaluating lower limb flexibility. Muscle strength for the hip abductors, internal and external rotators, and extensors was measured using a hand held dynamometer (MicroFET2, Hoggan Scientific, LLC). For each muscle group, participants performed three five-second contractions followed by five seconds of rest. Peak force on each trial was recorded and the final value used for each muscle group was the average of the three trials, normalized by body mass.

Participants then completed a three dimensional running gait analysis. Forty two reflective markers were attached to bony landmarks after which participants ran on a treadmill at self-selected speeds approximating their easy training pace. While body kinematics were recorded using a 12-camera motion capture system (Qualisys, Inc.) sampling at 200 Hz. Marker trajectories were exported to Visual 3D (C-Motion, Inc.) where the following specific kinematic variables were calculated: peak amount, velocity, and duration of rearfoot eversion, peak hip adduction and internal rotation, peak contralateral pelvic drop, and shank varus angle at the time of initial foot contact. All variables were calculated over stance phase only.

Runners were followed throughout the course of the cross country season. Diagnosis of MTSS occurred when the injury became severe enough to cause the runner to seek evaluation and treatment from a certified athletic trainer. To date, six participants have been diagnosed with MTSS, forming the injured (INJ) group. Injured participants were matched with a control group (CON) on the basis of sex, and weekly running mileage. Independent samples *t*-tests were used to compare differences in orthopedic exam measures, muscle strength, and kinematic variables between INJ and CON groups.

RESULTS AND DISCUSSION

There was no difference in running speed between the two groups (INJ: 3.5 ± 0.3 m/s; CON 3.4 ± 0.5 m/s, $p = .047$). Compared to the CON group, the INJ group demonstrated tighter hip flexors and IT bands as indicated by lower scores on the Thomas and Ober's tests, reduced passive hip internal rotation range of motion (Table 1), and weaker hip abductors than the CON group (Table 2). While not significantly different, there was also trend towards weaker hip external rotators in the INJ group.

Table 1. Range of motion measurements. SLR: straight leg raise, DF: dorsiflexion range of motion.

ROM Measure (°)	INJ	CON	<i>p</i>
SLR	91.4	87.2	0.616
Thomas	4.2	13.1	0.034
Ober's	9.0	17.0	0.037
Hip IR	34.4	44.6	0.043
Hip ER	43.8	40.5	0.483
DF	12.4	10.2	0.473

Table 2. Hip muscle strength measures. Values are percentage body weight.

Strength Measure	INJ	CON	<i>p</i>
Hip ABD	96.2	124.9	0.036
Hip ER	76.2	75.1	0.926
HIP IR	81.2	90.8	0.350
HIP EXT	117.4	177.1	0.078

For the kinematics the only the differences between INJ and CON groups were in the amount (INJ: $9.2 \pm 2.1^\circ$, CON: $5.5 \pm 1.4^\circ$, $p = .004$) and duration of rearfoot eversion (INJ: 85.4 ± 5.1 % stance, CON: 68.6 ± 7.7 % stance, $p = .001$). Rearfoot eversion-inversion curves are shown in Figure 1.

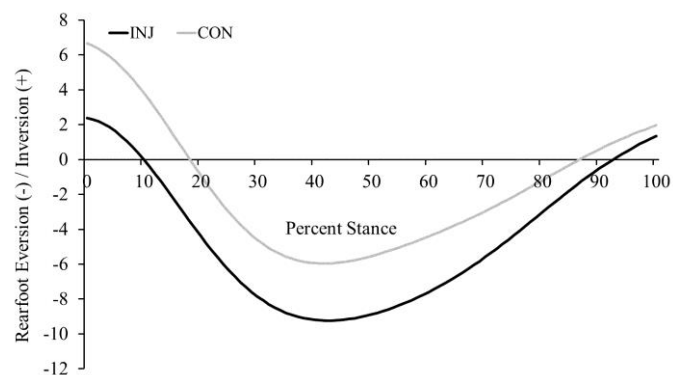


Figure 1. Rear foot eversion-inversion curves for INJ (black) and CON (gray) groups.

CONCLUSIONS

These preliminary results suggest the etiology of MTSS is multifactorial with muscular strength, flexibility, and running kinematics all playing a role. For kinematics specifically, these results suggest distal kinematics may play a more prominent role than proximal kinematics, despite proximal strength deficits. However, since distal kinematics may be influenced by proximal muscle strength, the relative importance of proximal and distal factors as they relate to MTSS still needs to be clarified. The results agree with previous studies documenting increase amounts of rearfoot eversion in runners with MTSS [5]. However, the results also suggest the duration of rearfoot eversion is an important parameter, one which should be considered separately in future studies on this injury.

REFERENCES

- James, S. et al. *Am J Sports Med.* **6**:40-50, 1978.
- Lopes, A.D. et al. *Sports Med.* **42**:891-905, 2012.
- Verrelst, R. et al. *Br. J. Sports Med.* doi:10.1136, 2013.
- Moen, M.H. et al. *Scan J. Med. Sci. Sports.* **22**:34-39, 2012.
- Willems, T.M. et al. *Gait & Posture.* **23**:91-98, 2006.

JOINT MOMENT DIFFERENCES IN DANCERS LANDING IN TURNEDOUT VERSE PARALLEL POSITIONS

Katherine Spitzley, Renae Jackson, Britte Nielsen, Karen Clippinger, and James Becker

California State University Long Beach, Long Beach, CA, USA
email: katespitzley@gmail.com

INTRODUCTION

Dancers incur up to 88% of injuries in their lower limbs, the majority in the hips and knees [3,5]. With 100% of retired dancers, 90% of professional dancers and 63% of student dancers reporting injuries at some point in their career, finding the cause for these injuries should be a priority in research [1]. Studies have shown that classical ballet and professional football are comparable in the amount of physical demand on the body. Yet, little research has been done to sufficiently account for that toll in the ballet world [2].

Knee pain in dancers has been attributed to the repetitive jumping motions which make up many of the most popular ballet movements [3]. Multitudes of studies have investigated the correlation between turnout, external rotation, and injury. These have merely collected static data using manual techniques such as goniometer and inclinometer readings. No research has been conducted to investigate the forces working within the joints during the movements being discussed.

This study will examine joint forces through the hip and knee during a common jumping movement in a turned out ballet position, and compare them to the joint forces through the hip and knee during a jumping motion with the legs in parallel position. This method will give insight into root biomechanical factors contributing to such prevalent hip and knee pain in dancers.

METHODS

Fourteen female college age dancers participated in this study (age: 20.2 ± 1.1 years; 16.1 ± 1.8 years of dance experience). All participants were healthy at the time of testing with no reported injuries.

Participants completed a 10 minute standardized warm up which included aerobic and lower body muscular work. Subjects then performed three sets of three maximal vertical jumps under two different conditions. For condition 1 participants were instructed to perform jumps with feet in turned out first position. For condition 2 participants were instructed to perform jumps with their feet in parallel position. The order of conditions was randomized.

Whole body kinematics were recorded using a 12-camera motion capture system (Qualisys) sampling at 200 Hz while ground reaction forces were recorded using two force plates (Bertec) sampling at 1000 Hz. Marker trajectories and force data were exported to Visual3D (C-Motion, Inc.) where joint moments at the hip, knee, and ankle were calculated. For each joint peak, moments in the sagittal, frontal, and transverse planes were identified. Moments were expressed as internal moments. Differences in moments between conditions were determined using paired *t*-tests.

RESULTS AND DISCUSSION

We observed notable differences in performance between the right and left legs of each dancer. As a result, the data represented here are based on analyzing each leg individually.

Hip extensor, knee external rotator, and ankle external rotator average curves are presented in Figure 1. Hip extensor moments were lower during mid-stance in the turned out position then in the parallel position, but they were not different early or late in stance phase. Knee extensor moments and ankle external rotator moments were higher throughout stance, suggesting higher torsion being applied to the knee in these conditions.

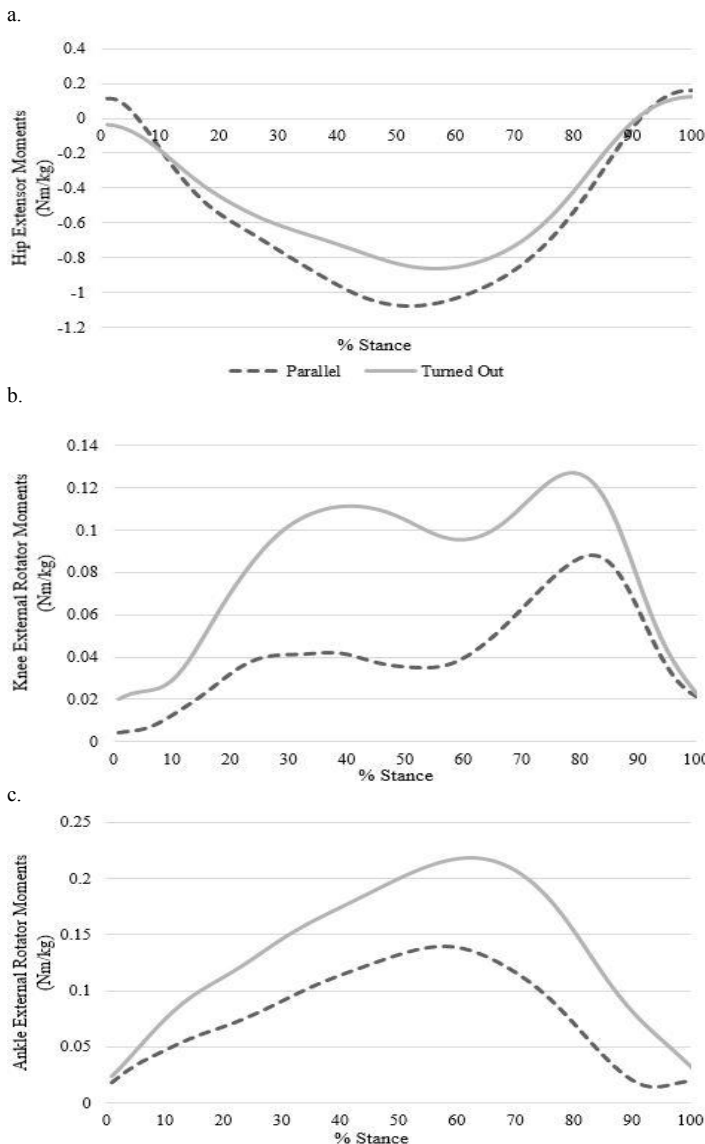


Figure 1: Average moments throughout stance phase comparing parallel and turned out jumps.

Peak moments are shown in Table 1. Peak hip extensor and external rotator moments were lower

in the turned out than parallel conditions, while peak knee and ankle external rotator moments were higher in the turned out than parallel condition.

CONCLUSIONS

As hypothesized, the knees and hips were subjected to higher moments when jumping in a turned out position. As the differences were primarily in the transverse plane, this suggests higher torsional loading being applied to the joints in a turned out position. Previous work has hypothesized that torsional forces could be one contributing factor to knee pain and injuries [4]. Knowing that dance specific movements such as turnout may increase joint loading can be useful for coaches and instructors. This information can aid them in appropriately planning the number of jumps in a given training session. Additionally, the distinction in force generation between extension and external rotation components required to maintain the specific aesthetic involved in turnout should be further examined.

REFERENCES

1. Coplan, JA, *J Orthop Sports Phys Ther*, **32**, 579-584, 2002
2. Hamilton, WG et al, *Am J Sports Med*, **20**, 267-273
3. Milan, KR, *JOSPT*, **19**, 121-129
4. Negus, V, *J Orthop Sports Phys Ther*, **35**, 307-318
5. Reid, DC et al, *Am J Sports Med*, **15**, 347-352

Table 1: Peak moments over both conditions and resulting p values.

	Parallel	Turned Out	p value
Hip Exten.	-77.3 (+/- 18.7)	-59.0 (+/- 20.7)	< 0.001
Hip Abductor	-23.9 (+/- 13.5)	-20.2 (+/- 10.9)	0.10
Hip Ext. Rotator	-25.0 (+/- 10.2)	-12.1 (+/- 10.5)	< 0.001
Knee Exten.	90.6 (+/- 31.1)	91.6 (+/- 29.0)	0.86
Knee Adductor	12.8 (+/- 7.4)	9.6 (+/- 6.0)	0.06
Knee Ext. Rotator	9.3 (+/- 3.7)	11.6 (+/- 5.9)	0.02
Ankle Planarflexor	-83.6 (+/- 21.9)	-88.9 (+/- 22.7)	0.17
Ankle Invertor	19.5 (+/- 10.0)	22.1 (+/- 10.4)	0.54
Ankle Ext. Rotator	10.9 (+/- 5.9)	15.5 (+/- 5.5)	0.000085

TURNOUT GENERATION STRATEGIES AND RESULTING JOINT MOMENTS IN DANCERS

Rena Jackson, Kate Spitzley, Britte Nielson, Karen Clippenger, and James Becker
California State University of Long Beach, Long Beach, CA, USA
email: james.becker@csulb.edu

INTRODUCTION

Turnout is a fundamental component of proper ballet technique. Theoretically perfect turnout requires 90° of external rotation at the hip with the remainder of the limb in a neutral alignment [1]. However, numerous studies have indicated this theoretical ideal is rarely achieved, showing instead, that turnout is a result of summative contributions from the hip, knee, and ankle [1]. Therefore, the term total turnout (TTO) was created to include all of the joint contributions. It has been suggested that the hip contributes approximately 60% of the external rotation while the knee and ankle contribute roughly 40% of the external rotation [1].

Previous research on joint contributions to TTO has primarily been performed under static conditions or quasi dynamic conditions [1]. However, for a truly functional assessment, TTO and relative joint contributions should be measured throughout the entire range of dynamic movements. Therefore the purpose of this study was to characterize the strategies used by collegiate dancers for achieving turnout. Specifically, we examined what percentage of TTO is generated from the hip, knee, and ankle when dancers performed vertical jumps in turned out first position. Additionally, to assess consequences of turnout generation strategies, we examined the relationship between percent TTO which was generated at the hip and peak joint moments during the ground contact phase of the vertical jumps. We hypothesized that dancers with larger TTO contribution from the hip would have lower peak joint moments at the hip and knee than dancers with larger TTO contributions from the knee and foot/ankle.

METHODS

Thirteen female university dancers (Age: 20.2 ± 1.1 years; dance experience: 16.1 ± 1.8 years)

participated in this study. After completing a standardized ten-minute warm-up, participants performed four vertical jumps for maximal height while maintaining turned out first position. Whole body kinematics were recorded using a 12 camera motion capture system (Qualisys AB) sampling at 200Hz while ground reaction forces were recorded by two force plates (Bertec) sampling at 1000Hz.

Marker trajectories were exported to Visual 3D (C-Motion, Inc.) where joint angles and moments at the hip, knee, and ankle were determined. TTO was calculated by summing the external rotation components of the hip, knee, and ankle [2]. At each instant across stance phase, the percent contribution of each joint to TTO was calculated by dividing that joints' external rotation by the TTO.

The percent of TTO originating from the hip was calculated as the average hip contribution to TTO across the ground contact phase of the jump. Linear regression was used to examine the relationship between percentage of TTO originating at the hip and peak joint moments in the sagittal, frontal, and transverse planes. Simply watching the dancers perform the movement during data collection revealed pronounced asymmetry in the amount of turnout on left and right sides. Therefore each limb was treated separately in the analysis.

RESULTS AND DISCUSSION

Across all thirteen dancers the average TTO was 41.3° ($\pm 10.1^\circ$), of which 52.2% ($\pm 16.7\%$) came from the hip. Of the 26 legs analyzed, only 5 achieved 60° of external rotation at the hip, as suggested by previous research [1]. Although many participants achieved the same amount of TTO, their strategies used to achieve it were very different. For example, Figure 1 shows data from two participants who achieved the same amount of TTO, however, participant 1 primarily uses the knee

to achieve turnout, whereas participant 2 predominantly uses the hip and ankle.

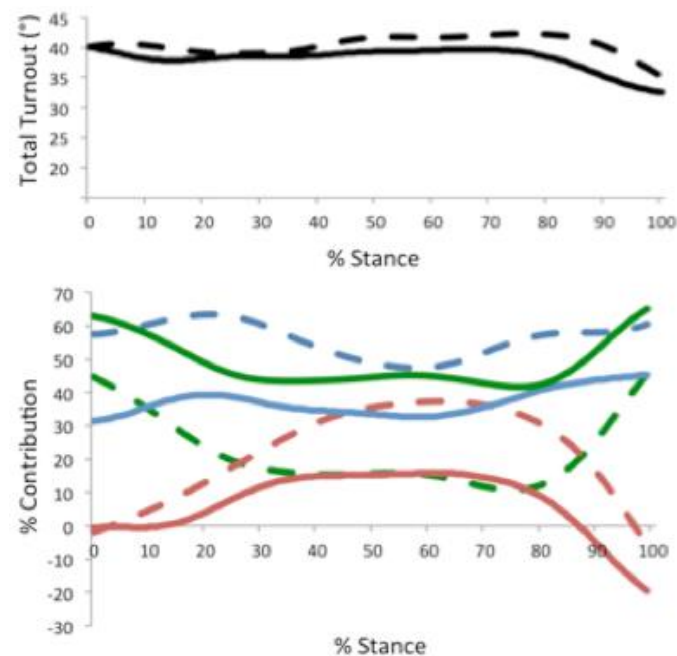


Figure 1: Example Turnout Generate Strategies from Two Dancers. Solid lines represent participant 1 and dashed lines represent participant 2. Black represents TTO achieved in degrees. Blue, green, and red lines represent % contribution to TTO from the hip, knee, and ankle, respectively.

The variation in strategies for generating turnout could be due to a variety of factors including: level of dancer, muscular strength or range of motion limitations, and anatomical variation among the participants. While there are numerous studies investigating how these factors influence turnout under static conditions, there is currently no literature examining how these factors influence turnout in dynamic scenarios. This should be a focal point of future research on dance instruction and dance medicine.

Regression results revealed no relationship between percent TTO generated at the hip and peak hip extensor, hip abductor, or knee adductor moments (Table 1). However, there was a significant relationship between percent TTO generated at the hip and peak hip external rotator and knee extensor moments (Table 1). The greater the hip contribution

to TTO, the higher the peak knee extensor moment and the lower the peak hip external rotator moment. These findings reveal the importance of considering joint contribution when assessing turnout, as different strategies may result in higher or lower loading which overtime could affect the likelihood of overuse injuries.

Table 1. Peak Hip and Knee Moments, R^2 values and p values. Moments are expressed as internal moments and are normalize by body mass.

Moment	Peak Value	R^2	p
Hip Flex.	-1.03 (\pm 0.33)	0.071	0.188
Hip. Abd.	-0.34 (\pm 0.18)	0.136	0.064
Hip Ext. Rot.	-0.21 (\pm 0.17)	0.152	0.048
Knee Ext.	1.62 (\pm 0.39)	0.199	0.022
Knee Add.	0.16 (\pm 0.09)	0.008	0.671

CONCLUSIONS

Turnout plays an important role in performance and injury evaluation, however, the results of the current study suggest dancers vary in both their degree of turnout and strategy used to achieve it. These results also suggest there is a relationship between turnout generation strategies and joint moments, although functional consequences, such as how they relate to injury risk, need to be examined further. Although a higher degree of turnout is sought for optimal ballet posture, the manner in which turnout is produced should be more importantly considered as it relates to increased joint loading. It may be interesting to examine if joint contribution to turnout is a skill that can be taught or if it is a characteristic that is pre-defined by an individual's anatomy. Future studies should examine professional dancers with a similar training background to more clearly define the relationship between joint moments and TTO contributions in dynamic scenarios.

REFERENCES

1. Champion L., et al. *J of Dance, Medicine & Science* **12**, 121-135, 2008.
2. Shippen J. *Arts Biomechanics* **1**, 37-45, 2011.

KINEMATIC DIFFERENCES BETWEEN DROP JUMP, CUTTING, AND REBOUND LANDINGS

¹ Jim Becker ¹ Jonaz Moreno Jaramillo

¹ California State University, Long Beach

email: jim.becker@csulb.edu, jonaz.morenojaramillo@student.csulb.edu

INTRODUCTION

It is well established that non-contact ACL injuries are one of the most common injuries among female basketball players [1]. Predominantly, the risk of non-contact ACL injuries are far greater in sports where athletes perform pivoting and jumping maneuvers [2]–[3].

A common method to estimate the potential an athlete has to obtaining a non-contact ACL injury is through analysis of lower body kinematics during the vertical drop jump (DJ). The DJ has been shown to highlight potential knee valgus on the initial contact, as well as on the second contact that prelude to greater risk of injury [2],[5]. Yet little research has been done comparing lower body kinematics of the DJ to common basketball movements.

The purpose of this study is to determine whether DJ kinematics compare to the basketball movements rebound and cut maneuver. This method will investigate the potential differences of the knee and hip angles between the DJ landings (DJ-1 DJ-2), rebound, and cut maneuver to investigate the potential of alternative methods in predicting ACL injury across athletes.

METHODS

A total of 7 division 1a female basketball players (mean age = 19.9 years), (mean height 178.3 cm), (mean weight 67.8 kg), participated in this study. All participants were healthy and had no prior record of ACL injuries.

Each Athlete performed 3 trials of drop jump, 4 reactive cutting maneuvers, and 3 rebounds. During

the cutting maneuver motion, the player reacted to the movements of another participant to simulate a one-on-one scenario. Both rebound and cutting maneuver were intended to be as close to a game scenario as possible.

Kinematics were recorded using a 12-camera motion capture system (Qualisys) sampling at 200 Hz. Marker trajectories were exported to V3D (C-Motion, Inc.) where joint angles for the hip and knee were calculated.

Knee and hip angles from initial foot contact to max knee flexion were compared through DJ-1, DJ-2, rebound, and the cut maneuver. Differences in joint angles were determined using multiple 1-way ANOVAs with repeated measures. A bonferroni post-hoc was used to find differences between dependent measures.

RESULTS AND DISCUSSION

Results indicated a significant difference of ROM in each movement, for hip external/internal rotation, knee varus/valgus, flexion/extension, and internal/external rotation. Contact angles for hip internal/external rotation, knee varus/valgus, and flexion/extension were also significantly different among movements. Peak angles for hip internal/external rotation, knee internal/external rotation, and knee flexion again showed significant differences between the different movements. Mean angles and standard deviations are indicated in the Table 1.

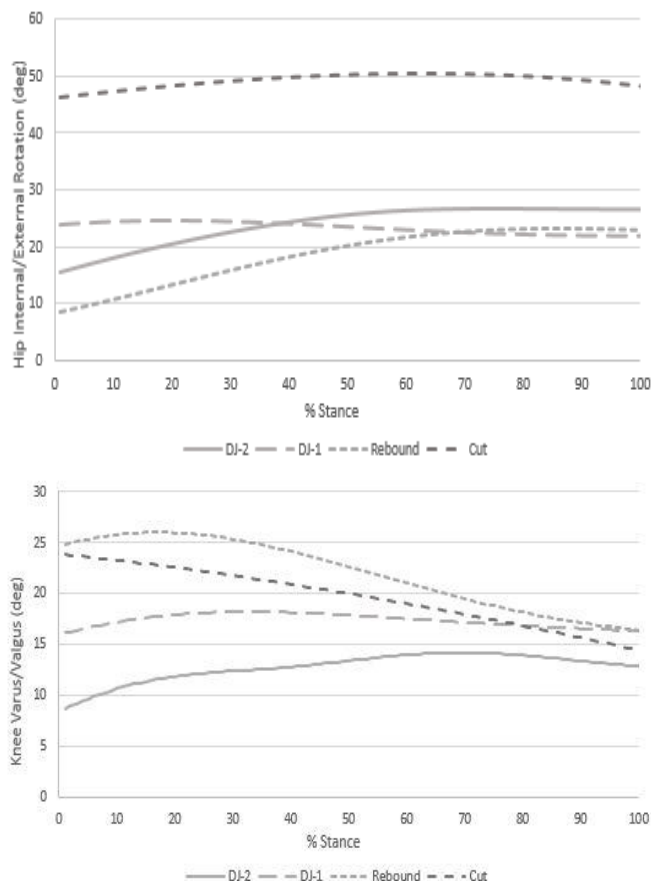


Figure 1. Joint Kinematics throughout the four different movements

CONCLUSIONS

The results indicate that when compared to rebound and cutting maneuvers, the drop jump accurately represents knee varus/valgus and hip ab/adduction values of an individual. However, it was found that hip internal rotation was greater during a rebound and cutting maneuver. The larger ROM of hip internal rotation during these movements could lead greater chance ACL injury if knee valgus and hip abduction are occurring simultaneously. Therefore, it could be beneficial to test athletes not just on a

drop jump but rather a combination of game like dynamic movements to better evaluate and assess an individual's risk to a non-contact ACL injury

REFERENCES

- [1] E. A. Arendt, J. Agel, and R. Dick, "Anterior Cruciate Ligament Injury Patterns Among Collegiate Men and Women," vol. **34**, no. 2, pp. 86–92, 1999.
- [2] T. W. Kernozek, M. R. Torry, H. Van Hoof, H. Cowley, and S. Tanner, "Gender differences in frontal and sagittal plane biomechanics during drop landings," *Med. Sci. Sports Exerc.*, vol. **37**, no. 6, pp. 1003–1012, 2005.
- [3] O.-E. Olsen, G. Myklebust, L. Engebretsen, and R. Bahr, "Injury mechanisms for anterior cruciate ligament injuries in team handball: a systematic video analysis," *Am. J. Sports Med.*, vol. **32**, no. 4, pp. 1002–1012, 2004.
- [4] T. E. Hewett, G. D. Myer, K. R. Ford, R. S. Heidt, A. J. Colosimo, S. G. McLean, A. J. van den Bogert, M. V. Paterno, and P. Succop, "Biomechanical measures of neuromuscular control and valgus loading of the knee predict anterior cruciate ligament injury risk in female athletes: a prospective study," *Am. J. Sports Med.*, vol. **33**, pp. 492–501, 2005.

Table 1: Mean and standard deviation of knee valgus/varus and hip abduction/adduction for each movement

Joint	Variable	DJ-1			DJ-2			Rebound			Cut		
		Contact	PKF	ROM	Contact	Peak	ROM	Contact	Peak	ROM	Contact	Peak	ROM
Knee	Valgus	7.77° ±2.25*	5.70° ±9.6*	-2.07° ±7.5*	2.64° ±4.1*	5.00° ±10.2	2.03° ±9.0*	0.50° ±4.4*	3.19° ±8.9	2.84° ±7.1	8.70° ±8.1	9.24° ±7.3	0.51° ±3.4
Hip	Abduction	-11.58° ±2.7	-13.54° ±4.6	-1.96° ±3.5	-12.77° ±2.8	-16.36° ±4.0	-3.75° ±2.1	-14.84° ±3.5	-16.29° ±4.5	-1.55° ±3.7	-14.26° ±5.3	-22.4° ±6.8	-7.34° ±3.7

*Significance in Post Hoc test. $p < .05$

THE RELATIONSHIP BETWEEN CENTER OF MASS EXCURSION AND ACL INJURY RISK VARIABLES IN THE STATIONARY SINGLE LEG HOP (STASH)

Jack W. Cerne, Dustin R. Grooms, Michael P. McNally, Eric P. Schussler, Ajit M.W. Chaudhari, James A. Onate

The Ohio State University, Columbus, OH, USA

email: cerne.4@buckeyemail.osu.edu, web: <http://medicine.osu.edu/hrs/at/research/moves/pages/index.aspx>

INTRODUCTION

The anterior cruciate ligament (ACL) provides static stability to the knee joint. Non-contact ACL injuries are common in female athletes and are theorized to result from poor neuromuscular control at the knee joint [1]. Variables that have been associated with poor knee joint neuromuscular control include reduced sagittal plane knee excursion and increased normalized vertical ground reaction force (vGRF) [2]. Frontal plane angular knee excursion has also been shown to be higher in females than in males during a single legged hop test [3]. This finding suggests that frontal plane angular knee excursion may play a role in the well-reported increased female injury risk.

The STationary Single Leg Hop (STASH) test is a novel and maximal effort task that can investigate the link between generalized neuromuscular control and neuromuscular control at the knee joint. In the STASH the athlete is required to perform three consecutive hops on one leg, jumping as high as possible while attempting to land in the same place after each hop. They are also required to maintain balance on the same leg after the third landing.

METHODS

Center of mass excursion (COM) is the net distance traveled by the COM during a time interval in the x-y plane (Fig. 1). Typically, the analogous center of pressure (COP) excursion measurement is used to assess postural control in static tasks. In a dynamic task, however, a total COM excursion value quantifies neuromuscular control because COP cannot be assessed whilst athletes are airborne.

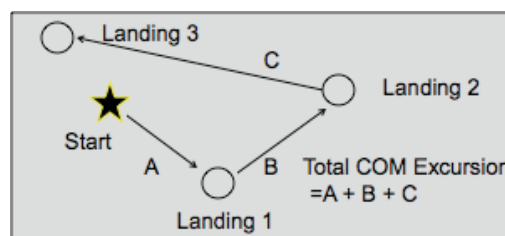


Figure 1: Depiction of total COM excursion calculation

The purpose of this study was to determine the relationship between generalized neuromuscular control, measured as total body COM excursion, and the injury risk biomechanics including vGRF and knee excursion in the sagittal and frontal planes. Prior to testing, Institutional Review Board approval of the protocol was attained and informed consent was provided to all subjects. Eighteen athletes from a Division I university women's soccer team (18.94 ± 0.94 yrs, 1.68 ± 0.054 m, 63.68 ± 6.52 kg) with no current lower extremity injury were recorded performing the STASH using tri-axial Bertec 4060 force plates collecting at 1500Hz and a 10-camera Vicon MX-F40 motion capture system collecting at 300Hz. Each athlete performed two repetitions of the STASH on each leg.

49 retro-reflective markers were placed on each athlete using a modified plug-in-gait model. Pelvic markers were used to estimate the COM location, and total COM excursion was calculated for each trial by tracing the total distance traveled between the time points of peak knee flexion at initial takeoff and peak knee flexion on the third landing. Measurement via this method did not allow the elapsed time to obstruct the measurement, which would have been the case if the distances between starting point and COM were summed at each frame for the duration of the STASH.

Total knee sagittal plane excursion and total knee frontal plane excursion values were calculated by summing the angular excursion differences at each frame during the entire stance phase of each of the three landings. Vertical GRF was normalized by peak potential energy (bodyweight x jump height before landing) to account for force generation and force absorption [4], and the three vertical GRF values were averaged for each trial.

RESULTS and DISCUSSION

Moderate correlations driven by two clusters of data points were found between total center of mass (COM) excursion and total knee frontal plane angular excursion (avg.= $59.37^{\circ} \pm 17.24$; $r=0.62$; $p=0.006$) (Fig. 1), total sagittal plane knee excursion (avg.= $265.39^{\circ} \pm 37.34$; $r=0.48$; $p=0.046$) (Fig. 2), and normalized peak VGRF (avg.= $21.58\text{N/J} \pm 2.862$; $r=-0.44$; $p=0.065$) (Fig. 3).

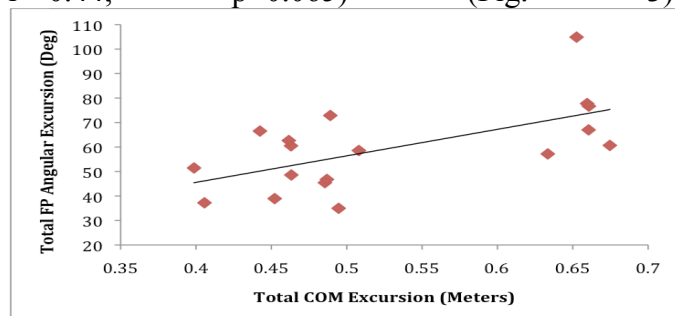


Figure 1: Scattergram of FP Angular Excursion

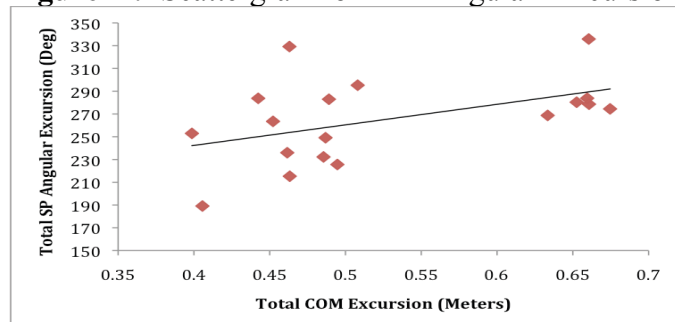


Figure 2: Scattergram of SP Angular Excursion

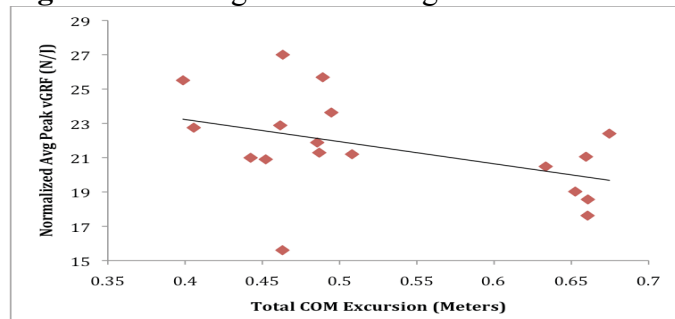


Figure 3: Scattergram of Norm. Avg. Peak vGRF

A limitation of this novel STASH test assessing knee biomechanics is that COM excursion may not have been the ideal way to assess generalized neuromuscular control because it did not take into account the direction of the COM deviation. Other means of assessing generalized neuromuscular control in a static task include COP 95% ellipse area, standard deviation in the anterior-posterior and medial-lateral directions, and root mean square velocity in the anterior-posterior and medial-lateral directions [5]. These measurements can be applied or adapted to the dynamic STASH test, and their relation to knee joint neuromuscular control can be investigated. Further corroboration of the link between generalized neuromuscular control and knee joint neuromuscular control may provide a basis for more effective, targeted interventions for at-risk athletes.

CONCLUSION

The STASH demonstrates that poor overall neuromuscular control, approximated by total COM excursion, is also associated with injury predicting biomechanical variables at the knee joint that may be useful for ACL injury risk detection. Future studies on the STASH and its abilities to assess injury risk prospectively are needed.

REFERENCES

1. Hewett TE, et al. *American J of Sports Med*, **33**, 492-501, 2005.
2. Aerts I, et al. *J of Sports Med and Physical Fitness*, **53**, 509-519, 2013.
3. Ford KR, et al. *Clinical Biomechanics*, **21**, 33-40, 2006.
4. Myer GD, et al. *American J of Sports Med*, **40**, 2256-2263, 2012.
5. Harringe ML, et al. *Gait and Posture*, **28**, 38-45, 2008.

Kinematic and temporal parameters of high school baseball pitchers in different velocity groups

^{1,2} Gautam Kumar, ¹ Michael P. McNally, ¹ James A. Oñate, ¹ Ajit M.W. Chaudhari

¹ The Ohio State University, Columbus, OH, USA

² VU University Amsterdam, Amsterdam, The Netherlands

email: chaudhari.2@osu.edu, web: <http://u.osu.edu/osusportsbiomechanics/>

INTRODUCTION

Throwing velocity is one of the most important components of a successful baseball pitch [1, 2]. Previous work by Matsuo et al. found significant differences in kinematic and temporal parameters between high velocity and low velocity pitchers in collegiate and professional baseball [2]. However, to our knowledge no study has examined the differences in kinematic and temporal parameters between high velocity and low velocity groups in high school pitchers. Additionally, there is a lack of research focusing on the relationship between kinematics and performance in high school baseball pitchers, which may be important for advancing to collegiate or professional baseball. Therefore the aim of this study was to investigate differences in kinematic and temporal parameters between high and low velocity high school pitchers. We hypothesized that there will be significant differences in kinematic and temporal parameters between high and low velocity high school pitchers, and specifically high velocity pitchers would demonstrate greater maximal shoulder external rotation, greater forward trunk tilt at ball release and greater lead knee extension angular velocity at ball release [2].

METHODS

Thirty-two high school male baseball pitchers (height = 1.83 ± 0.07 m, mass = 75.6 ± 10.9) were recruited. The Ohio State University institutional review board approved this study. All participants signed assent forms and permission was obtained from their parents. Before testing, the pitchers were instructed to warm up and prepare themselves just as they would do for an actual game. Once the pitchers were ready, they were instructed to throw 15 fastball pitches from a pitcher's mound towards a target. A passive optical three-dimensional motion

capture system (Vicon Inc., Oxford UK), was used to collect marker trajectories at 300 Hz. Trajectories were filtered using a 4th order Butterworth low-pass filter with a cut-off frequency of 13.4 Hz [2]. Twelve kinematic parameters and nine temporal parameters were calculated to match the previous study done by Matsuo et al [2]. Three representative trials with the most complete trajectory data from each pitcher were selected for further analysis. The 10 pitchers with the greatest hand velocity (23.1 ± 0.83 m/s) and lowest hand velocity (18.9 ± 0.95 m/s) were assigned to the high and low velocity groups, respectively. Student's t tests were used to compare differences between groups for all the parameters, with statistical significance set *a priori* at $p < 0.01$.

RESULTS AND DISCUSSION

Means and standard deviations of kinematic parameters of the two groups are presented in Table 1. To compare the high school pitchers with the low velocity collegiate and professional pitchers, data from Matsuo et al. [2] was added in the Table.

The high velocity group showed significantly greater peak trunk rotation velocity and peak glenohumeral internal rotation angular velocity, and showed trends toward significantly greater peak elbow angular extension velocity and maximum knee extension angular velocity at ball release ($p < 0.02$). No differences were observed between groups for temporal parameters.

Similar to collegiate and professional pitchers, we found that high velocity pitchers trended towards having greater knee extension velocity at ball release [2]. However, contrary to our expectations, we did not find any differences in maximal external shoulder rotation and forward trunk tilt, which have been related to greater ball velocity in professional

and collegiate pitchers [2]. In addition to those variables, we found that glenohumeral internal rotation angular velocity and peak trunk rotation angular velocity were greater in the high velocity group than in the low velocity group. Because the time between strike foot contact and ball release is very short, high angular velocities are required to throw efficiently [1] and it is likely that these significant differences drive the higher ball velocities in that group.

These results suggests that there may be different kinematics distinguishing high velocity pitchers from low velocity pitchers in high school, compared to the more experienced collegiate and professional pitchers who may already have a baseline level of motor expertise. Pitching experience, body maturation, body adaptation and coordination may also play a role in the different kinematic variables affecting performance of high school pitchers as opposed to collegiate or professional pitchers. As shown in Table 1, our groups did not match Matsuo's low velocity group in any of the measured variables, except for lead knee extension angular velocity at ball release.

Understanding the kinematic differences between high velocity and low velocity pitchers may help

determine which pitching mechanics produces maximal ball velocity in high school pitchers. The differences between the groups in our study and those in Matsuo's study suggest that it would also be very valuable to investigate how pitching mechanics change with maturation and experience from youth to elite baseball.

CONCLUSIONS

High school pitchers who throw with high velocity showed greater peak trunk rotation angular velocity, and peak glenohumeral internal rotation velocity, with trends towards greater maximum knee extension angular velocity and peak elbow extension velocity when compared to those who throw with low velocity. These differences do not match the differences between high- and low-velocity groups at elite levels, suggesting that results from adult pitchers cannot be assumed to be generalizable across ages and experience levels.

REFERENCES

1. Werner SL et al. *Journal of Shoulder and Elbow Surgery* 17(6): 905-908, 2008.
2. Matsuo T et al. *Journal of Applied Biomechanics* 17, 1-13, 2001.

Table 1: Means and standard deviations of kinematic parameters between high and low velocity groups. A column with the data from Matsuo et al. [2] of the low velocity collegiate and professional pitchers is added for comparison. *Matsuo et al. reported peak ball velocity, not peak hand velocity.

	High velocity group (n=10)	Low velocity group (n=10)	High v. Low	Matsuo 2001 Low Group
Variable	Mean±SD	Mean±SD	p	Mean±SD
Peak hand velocity (m/s)	23.1±0.8	18.9±0.9	-	33.2±0.9*
Peak trunk rotation angular velocity (°/s)	1019.5±102.4	841.9±96.8	< 0.001	1179±104
Peak elbow extension angular velocity (°/s)	2009.6±116.5	1796.9±232.1	0.018	2353±320
Peak glenohumeral internal rotation angular velocity (°/s)	3920.1±547.7	3218.4±425.9	0.005	7350±1283
Lead knee extension angular velocity at ball release (°/s)	200.5±73.6	109.3±86.0	0.020	124±141
Trunk tilt at ball release (°)	43.7±8.2	46.9±12.3	0.506	28.6±11.1
Maximal shoulder external rotation (°)	142.7±8.7	142.2±16.5	0.939	166.3±9.0

PREDICTION OF FUNCTIONAL MOVEMENT SCREEN™ PERFORMANCE FROM LOWER EXTREMITY RANGE OF MOTION AND CORE TESTS

¹ Nicole J. Chimera, ² Shelby Knoeller, ³ Ron Cooper, ⁴ Nicholas Kothe, ^{4,5} Craig A. Smith and ⁴ Meghan Warren

¹ Daemen College, Amherst, NY, USA

² Binghamton University, Binghamton, NY, USA

³ Morgan State University, Baltimore, MD, USA

⁴ Northern Arizona University, Flagstaff, AZ, USA

⁵ ProActive Physical Therapy, Tucson, AZ, USA

email: nchimera@daemen.edu, web: www.daemen.edu/athletictraining

INTRODUCTION

The Functional Movement Screen™ (FMS) is a clinical tool used to assess 7 fundamental movements. Summing the scores from the fundamental movements creates the FMS composite score (CS). The FMS CS has been linked to injury risk in some studies[1], but not others.[2] Therefore, it is important to begin to investigate the mechanics of the FMS as this area is not well studied and may contribute to the discrepancy in injury risk.

The FMS purports to assess coordination of functional movements [3], which may be related to core function. Further, superior performance on the FMS has been linked to increased hamstring flexibility;[4] however, the role of flexibility in other lower extremity joint motions has not been established. Understanding the association between lower extremity range of motion (ROM) and core function with FMS score may improve the interpretation and intervention for specific scoring.

The purpose of this study was to evaluate the ability to predict FMS performance based on lower extremity ROM and core function. Our first hypothesis was that lower extremity ROM and core function would predict FMS CS. Our second hypothesis was that lower extremity ROM and core function would predict performance on the FMS movement patterns.

METHODS

This was a cross sectional study with the independent variables of lower extremity ROM and

core tests. The dependent variables were FMS CS and movement patterns. Forty recreationally active adults (Table 1) volunteered to participate in this study. Recreational activity was defined as performing 30 minutes of physical activity on at least two days/week. Participants were excluded if they had a current injury that limited activity or they answered “yes” to any question on the Physical Activity Readiness Questionnaire (Par-Q).

Table 1. Means and Standard Deviations (SD)

	N	Age (yr±SD)	Weight (kg±SD)	Height (m±SD)
Female	24	23.2±2.4	64.8±9.7	1.7±0.1
Male	16	24.0±2.7	82.4±10.9	1.8±0.1
Total	40	24.0±2.5	71.8±13.4	1.7±0.1

Following informed consent and screening, all participants completed a 5 minute warm up on a stationary bike. Next, dorsiflexion ROM was measured with an inclinometer during the weight bearing lunge. All additional ROM was measured in the following order using standard positioning and a goniometer: knee flexion (prone); knee extension (90/90 Active Knee Extension Test); hip flexion (supine); hip extension (prone). Three ROM measurements were obtained for each joint motion and the average was used for analysis. Participants then completed two single leg core endurance tests bilaterally: single leg wall sit hold (SLWS) and repetitive single leg squat (RSLS). The SLWS required the participant to sit for as long as possible with the back against a wall in a position of 90° knee and hip flexion; the time began when the one leg was lifted from the ground. The RSLS required the participant to perform repetitive single leg squats, (one repetition every 6 seconds) reaching 60° knee flexion and 65° hip flexion, while

maintaining less than 10° hip adduction/abduction and less than 10° knee varus/valgus, until they could no longer complete the task correctly; the number of squats was recorded.

The fundamental movement patterns of the FMS were performed in the standard order: deep squat, hurdle step, inline lunge, shoulder mobility, straight leg raise, trunk stability, and rotary stability; clearing tests were performed as indicated.[3] The movement patterns were scored using an ordinal scale of (0-3) with a 3 representing perfect movement without compensation; while a 0 was reserved for pain with movement pattern or clearing test.[3] The FMS CS was calculated by summing scores from the movement patterns (max score: 21).

Descriptive statistics were calculated as means \pm SD (Tables 1). Data were checked for outliers ($1.5x < 25^{th}\%$; $1.5x > 75^{th}\%$). Independent t tests were used to assess differences between right and left limb in ROM and core function tests (Table 2). Linear and ordinal logistic regressions were used to determine the best predictors of FMS CS and movement patterns, respectively. Data analysis was completed in SPSS v.20 (IBM, Armork, NY) and SAS 9.4 (SAS Institute, Inc. Cary, NC). The alpha level was set at 0.25 when all predictors were simultaneously entered into the regression equation to determine which variables were most predictive of FMS CS and movement patterns. After which, only those predictive of performance were entered into the final prediction equation; $p < 0.05$.

Table 2. T test for Means [Standard Deviations (SD)] between left and right limb core tests and ROM

	SLWS (sec)	RSLS (reps)	DF (°)	KEXT (°)	KFLEX (°)	HEXT (°)	HFLEX (°)
MeanL (SD)	23.38 (14.78)	22.22 (12.03)	47.78 (9.10)	20.06 (12.07)	135.61 (11.97)	15.48 (6.16)	120.07 (13.70)
MeanR (SD)	26.44 (17.22)	25.76 (17.96)	47.57 (8.65)	20.24 (11.17)	135.83 (12.25)	17.19 (6.61)	119.08 (13.37)
P	0.04	0.12	0.76	0.82	0.65	0.02	0.33

MeanL – mean for left limb; MeanR – mean for right limb; SLWS – single leg wall sit; RSLS – repetitive single leg squat; DF – dorsiflexion; KEXT – knee extension; KFLEX – knee flexion; HEXT – hip extension; HFLEX – hip flexion; n = 37

RESULTS AND DISCUSSION

There were significant differences between right and left limb in SLWS and hip extension (Table 2). Therefore, two separate regression models were developed; one for right predictors and one for left

predictors for each dependent variable. After outliers were removed, 37 data points remained for analysis and indicated, on the left side, that reduced DF and SLWS significantly predicted lower FMS CS ($R^2=0.39$; $p < 0.001$). On the right side only reduced DF significantly predicted lower FMS CS ($R^2=0.27$; $p = 0.001$).

Ordinal logistic regression models for the movement patterns demonstrated that reduced DF ROM (left OR=0.92[CI=0.85-0.98]; pseudo $R^2=0.86$); right OR=0.92[CI=0.85-0.99]; pseudo $R^2=0.78$) was significantly associated with lower performance in deep squat. Reduced left knee extension was significantly associated with better performance in left straight leg raise (OR=1.11[CI=1.04-1.18]; pseudo $R^2=0.85$); while reduced right hip flexion was significantly associated with reduced right straight leg raise (OR=0.95[0.90-1.00]; pseudo $R^2=0.85$). Lower SLWS (left OR=0.92[0.88-0.98]; pseudo $R^2=0.91$; right OR=0.94[0.90-0.98]; pseudo $R^2=0.91$) was associated with reduced trunk stability performance.

CONCLUSIONS

Reduced DF ROM and SLWS resulted in worse FMS CS and the deep squat. The straight leg raise was impacted by hip/knee flexibility; trunk stability was associated with SLWS. Our results suggest that FMS movement patterns are affected by lower extremity ROM and core function. Thus, injury risk may be affected by lower extremity ROM and/or core function, as these appear to affect FMS CS and some movement patterns. Although we did not measure limb dominance, reduced left compared to right SLWS and hip extension ROM may indicate that these two variables are affected by dominance. Researchers should consider evaluating bilateral lower extremity ROM, core function, and limb dominance in addition to FMS to determine implications in injury risk and targeted intervention programs.

REFERENCES

1. Kiesel K, et al. *NAJSPT* 2, 147-158, 2007.
2. Warren M, et al. *J Sport Rehabil* [Epub], 2014.
3. Cook G. *Movement*. On Target Pubs. 2010.
4. Tehyan D, et al. *JSCR* 28, 1272-1283, 2014.

GLUTEAL ACTIVITY DURING PITCHING: COMPARING THE TRADITIONAL LEG KICK AND SLIDE STEP DELIVERIES

¹ Amanda J. Concha, ¹ Marcus A. McClary and ¹ David W. Keeley

¹ New Mexico State University, Las Cruces, NM, USA

email: ajconcha@nmsu.edu, web: <http://hpdr.education.nmsu.edu/index-5/hpdr-research-laboratories/biomechanics-lab/>

INTRODUCTION

The baseball pitching motion is a series of complex dynamic movements that must be properly synchronized. When this is not achieved, the possibility of injury may increase greatly. Currently it is estimated that 1.72 injuries occur per 10,000 athletic exposures [1]. Although there have been a number of studies attempting to identify mechanisms of injury in baseball pitchers, there appears to be no decline in the rate.

The majority of investigations have focused on the upper extremity but there are few that have investigated muscle activity of the lower extremity during pitching. In order to achieve proximal stability for distal mobility, effective and efficient muscle activation of the lower extremity is required, particularly with regard to the role of the gluteal group [2]. Unfortunately, not only have these muscles not been readily investigated, they also have not been investigated regarding the various mechanisms of delivery (e.g. – wind-up, traditional leg kick and slide step). Thus, the purpose of this study is to compare gluteal activity of the stride and drive legs during the two primary stretch deliveries; the traditional leg kick and slide step. It was hypothesized that gluteal activity would differ between the two delivery styles.

METHODS

Eleven male high school baseball pitchers volunteered to participate after completing the fall baseball season. Each pitcher was deemed free of injury and throwing arm dominance was not a limiting factor for participant exclusion. All of the testing protocols were reviewed by the University's Institutional Review Board prior to testing.

Upon arriving, the location of the preferred (drive leg) and non-preferred (stride leg) gluteus maximus and medius were identified by palpation. Adhesive bipolar surface electrodes were attached over the muscle bellies and positioned parallel to the muscle fibers. Manual muscle tests were conducted for each muscle using standard techniques to identify the maximum voluntary isometric contraction for each muscle to establish a comparative baseline for each muscle[3]. Test trials consisted of 5 maximal effort fastball pitches thrown for strikes and surface electromyography (sEMG) data describing muscle activity during test trials were collected via a Noraxon Myopac 1400L 8-channel system (Noraxon USA Inc. Scottsdale, AZ). All sEMG were system amplified with a gain set at 1000 and then processed within MATLAB version 2013B (Mathworks Inc. Natick, MA). Briefly, all sEMG signals were filtered for the removal of 60 Hz noise and then full wave rectified. The data were normalized by their mean to remove any offsets present prior to filtering and filtered using a single lowpass 2nd order Butterworth filter, with a cutoff frequency of 20 Hz. Following data processing, paired sample t-test analyses were conducted to compare muscle activity across the two deliveries.

RESULTS AND DISCUSSION

All data describing lower extremity muscle activity were determined to be normally distributed and the model assumptions of the means test were met. Of the mean comparison tests conducted, three returned significant results.

During the stride phase, the drive leg gluteus maximus was observed to be significantly more active (Fig 1.) during the leg kick delivery ($t_{(11)} = -2.539$; $p = 0.028$). During the arm acceleration phase, the drive leg gluteus medius was observed to

be significantly more active during the leg kick delivery ($t_{(11)} = -2.438$; $p = 0.033$). Finally, during the arm acceleration phase, the stride leg gluteus medius was observed to be significantly more active for the leg kick delivery ($t_{(11)} = -2.264$; $p = 0.045$).

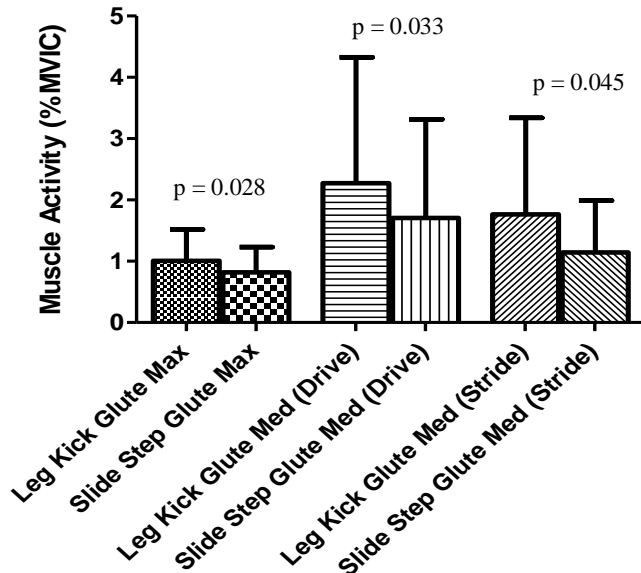


Figure 1: Magnitudes of muscle activity for the muscles observed to differ significantly during the pitching motion.

During the stride phase of the pitching motion, the drive hip extends and laterally rotates. This is done in order to initiate pelvic rotation. During this time the gluteus maximus of the drive leg should be highly active. It is thought peak drive leg gluteus maximus activity occurs just prior to peak pelvis axial rotation velocity during this phase [4]. The differences observed between the two deliveries may be due to increased pelvic instability in the traditional leg kick delivery. At the onset of the stride phase of this delivery, the high leg kick utilized may place the pelvis in a more unstable position as compared to the slide step delivery. This in turn may require greater activation in an effort to stabilize the base on which the trunk sits.

During the arm acceleration phase of the pitching motion, the drive leg medially rotates about the hip. This is done in order to achieve forward trunk tilt allowing more force to be transferred to the upper extremity. During this phase, high muscle activation of the gluteus medius drive leg should occur in an

effort to exert more force onto the ball. At the same time, the stride leg laterally rotates about the hip. This is done in order to support the trunk as it accelerates forward through the pitching motion. The gluteus medius of the stride leg may work to accentuate pelvic rotation and tilt [4]. During the traditional leg kick delivery, the gluteus medius of both the drive and stride legs were significantly more active during arm acceleration. It is possible that this higher activation is the result of differences in the intent of two deliveries. It may be that the main focus when utilizing the traditional leg kick is to exert as much velocity on to the ball as possible but when the slide step is utilized, focus is placed on delivering the ball as quickly as possible. Therefore it may be that not as much conscious effort is placed on imparting maximal force on the ball when the slide step is performed, resulting in lower gluteus medius activation during arm acceleration in comparison to the leg kick style.

CONCLUSIONS

These data indicate that there is greater gluteal muscle activation in the leg kick style of pitching in comparison to the slide step. The underlying reasons for these findings may be a function of differences in both pelvic stability and the primary intent of the two deliveries. This may result in traditional leg kick delivery being a more demanding pitching method when compared to the slide step delivery.

REFERENCES

1. Krajnik, S, et al. *Center for Injury Research and Policy, Research Institute at Nationwide Children's Hospital* **125**,497-501, 2010.
2. Oliver, GD and Keeley, DW. *J Strength Cond Res* **24**, 3015-3022, 2010.
3. Kendall FP, et al. *Muscles: Testing and Function*(4th ed). Lippincott, Williams and Wilkins. 1993.
4. Pujol et al. *Int J Shoulder Surg* **3**, 80-84, 2009.

QUANTIFYING WARFIGHTER PERFORMANCE DURING A PRONE-RUNNING-PRONE MOVEMENT TASK USING WIRELESS INERTIAL SENSORS

¹ Steven P. Davidson, ¹ Stephen M. Cain, ² Ryan S. McGinnis, ¹ Rachel R. Vitali,
¹ Noel C. Perkins, ¹ Scott G. McLean

¹ The University of Michigan, Ann Arbor, MI, USA, ² MC10 Inc., Cambridge, MA, USA
email: stevepd@umich.edu

INTRODUCTION

In a combat scenario, the performance of a warfighter is paramount to the safety and success of a mission. In these situations however, a warfighter is expected to carry over 18kg of advanced armor, weapons, ammunition, and support gear, while simultaneously maneuvering through a complex and often random environment. These additional load constraints often restrict/alter key movements and increase the fatigue rate, contributing to a rapid decay in warfighter performance.

One key aspect of warfighter performance, known as the 'bounding rush,' is the ability to quickly transition from a prone position to a standing/running position, then back to a prone position, which simulates changing cover by exiting one firing position and moving to another. The bounding rush is used in combat scenarios to safely advance upon an enemy position. Increases in load have negative effects on a warfighter's ability to perform the maneuver, specifically regarding the amount of time the warfighter is in an upright position and therefore exposed to enemy fire [1].

An array of wireless inertial measurement units (IMUs) provides the ability to measure 3D segmental dynamics in simulated combat environments where use of traditional motion capture technology is not possible. By employing an array of IMUs, this study aims to quantify differences in warfighter performance metrics during a loaded and unloaded bounding rush task.

METHODS

A pilot group of 6 subjects (4 Male/2 Female, 19.17±1.17 years old) was recruited from an athletic collegiate population. Participants were outfitted

with a sacrum mounted IMU (Opal, APDM, Portland, OR) capable of measuring tri-axial acceleration and angular velocity. Participants wore military issue generation III improved outer tactical vests (IOTV-III), mock-ballistic plates and mock-tactical assault panel attached to the IOTV-III anteriorly (18kg) during the loaded condition. A mock-M4 assault rifle was carried in both load conditions.

The bounding rush task consisted of five cones spaced 4.6m apart in a zigzag pattern (Figure 1) in addition to starting and ending gates. Participants ran to the first cone and dropped into a prone shooting position while aiming at a target down range. After aiming at the target for at least 2 seconds, subjects were given a verbal cue to stand and run to the next cone and to drop to a prone aiming position as before. A synchronized trigger allowed accurate marking of the verbal cues in the data. This method resulted in four distinct prone-to-prone transitions.

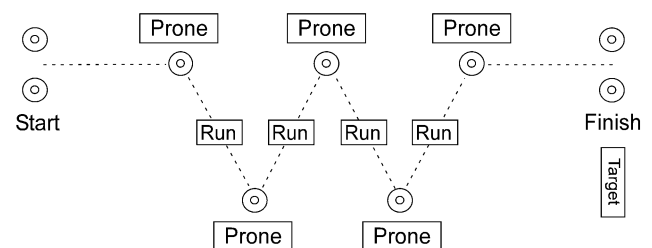


Figure 1: Layout of the bounding rush task. Cones were laid in a zigzag pattern with the participant assuming a prone position at each cone.

Prone-to-prone transitions were analyzed using custom MATLAB software (Mathworks, Natick, MA). Acceleration and angular velocity data were used to calculate three distinct variables: 1) total time between prone positions (total time), 2) time

until maximum vertical displacement of the sacrum (time to standing) and 3) maximum horizontal velocity (running speed). Paired t-tests were used to identify significant differences between loaded and unloaded conditions ($\alpha=0.05$).

Performance degradations were expected to emerge in the data via increases in the total time and time to standing, and decreases in running speed.

RESULTS AND DISCUSSION

As expected, load carriage resulted in performance degradation. The total time of the bounding rush movement increased by an average(std.) of 0.88s(1.20s, $p=0.16$). Running speed decreased significantly with load, dropping by an average(std.) of 0.44m/s(0.31m/s, $p=0.02$). Time to standing increased, though not significantly, with load taking an average(std.) of 0.61s(0.75s, $p=0.13$) longer to reach the standing position. A linear fit was used to reveal how total time relates to with time to standing (Figure 2) and running speed (Figure 3).

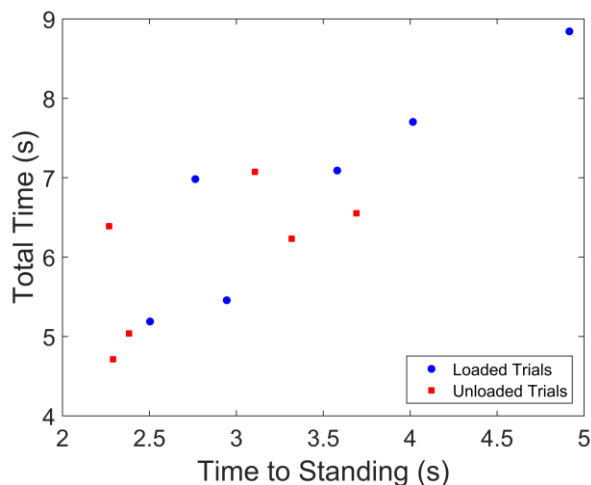


Figure 2: Time to standing versus total time. Linear fit: slope=0.56, $R^2 = 0.72$

Though preliminary, the above results illustrate the potential for deploying a body-worn IMU array to quantify performance and performance degradations in a bounding rush task. Specifically, the correlations between total time and both running speed and time to standing are significant evidence that both time to standing and running speed have the potential to be strong predictors of bounding rush performance.

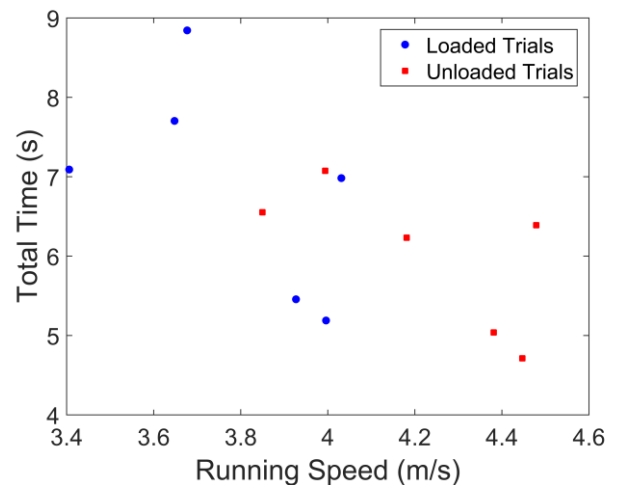


Figure 3: Total time versus running speed. Linear fit: slope=-0.18, $R^2 = 0.43$.

CONCLUSIONS

A body-worn array of IMUs enables the analysis of performance during a bound rush task by providing synchronized kinematic data (accelerations and angular velocities) of the major body segments. Three performance metrics, deduced from the IMU data, reveal performance degradation with added load. In particular, the addition of load increases the total time to execute the maneuver as well as significantly decreasing the running speed. Further analyses may reveal other potential performance predictors as well as potential methods for reducing the negative effects of load.

REFERENCES

1. O'Neal EK, et al. *Military Medicine* **179**, 950-954, 2014.

ACKNOWLEDGEMENTS

Supported by Natick Soldier Research, Development and Engineering Center contract W911QY-13-C-0011.

VALIDATION OF CENTER OF PRESSURE MEASUREMENTS WITH ARTIFICIAL TURF

Andrea M. Du Bois, Tulika Nandi and George J. Salem

Jacquelin Perry Musculoskeletal Biomechanics Research Laboratory
Division of Biokinesiology and Physical Therapy
University of Southern California, Los Angeles, CA, USA
email: amdubois@usc.edu, web: pt.usc.edu/labs/mbrl

INTRODUCTION

Golf swing mechanics have received a lot of attention in the literature as a means to understand swing demands, golf performance and potential golf injury mechanisms, across skill levels and age groups [1-5]. Specifically, many of these studies track the movement of the center of pressure (COP) and/or measure joint moments throughout the swing [1-4]. In order to mimic driving range conditions, artificial grass turf is often fixed to the force plates [1, 2, 5-7]; however, it is unknown how the turf affects the force plate measurement of the COP. Inverse dynamics is dependent upon the location of the applied force (COP) and errors in COP measurement will affect the resulting joint moment calculations [8]. Therefore, the purpose of this study was to assess the validity of COP measurements with artificial turf fixed to a force plate.

METHODS

In order to assess the validity of the COP measurements, force was applied through the handle of a golf club (2.7 cm diameter) at different locations on two separate force plates. Ten locations were arbitrarily picked and marked with tape (Figure 1) on two AMTI force plates (OR6-6-1000; Newton, MA). The location of the marked locations was measured by two separate researchers to the nearest millimeter. These same locations were then marked with tape on Dura Pro™ Tuff-Turf™ (1.25 inch thickness) consisting of a base pad and knitted nylon turf cut to the size of the force plates. To ensure accurate placement of the marks, the X and Y coordinates were measured from the same anterior and lateral edge, respectively for all measures. A second researcher measured the locations on the turf and if the marks were more

than 3 mm different from the corresponding location on the force plate, the location was re-marked and re-verified until all measures on the force plate and the turf were within 3 mm of one another.

To measure the center of pressure location, a researcher placed the center of the club handle at each marked location on the force plate (NoTurf) and applied vertical force for five seconds. Force plate data was collected at 1500 Hz. This same procedure was repeated for all 10 locations on each force plate a total of 4 times at each location. The turf was then fastened to each force plate with Velcro and the anterior and lateral edges were lined up with the respective anterior and lateral edge of the force plate. A turf mat was placed around the force plates to mimic the standard set-up during golf swing analysis (Figure 1). The same procedure was repeated for each of the ten locations on each force plate (Turf). In order to assess the reliability of the assessment, the turf procedure was repeated on a separate occasion by both the same researcher and a second research associate.

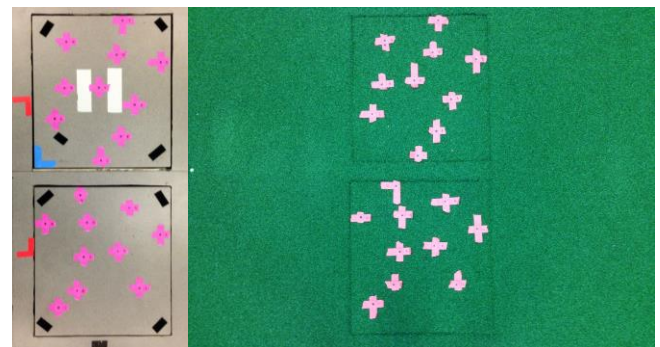


Figure 1. Experimental set-up for the NoTurf (left) and Turf (right).

Data was visually inspected with Qualysis Track Manager Software (Qualysis, Gothenburg, Sweden)

to ensure the direction of the applied force was constant throughout collection. 500 ms of data was extracted from the middle of the five second period. The COP in both the X and Y direction was averaged over the 500 ms and then averaged across the 4 trials for each location. The difference in COP between NoTurf and Turf was calculated for each location.

Pearson product-moment correlations between the NoTurf and Turf COP were calculated to assess the validity of the Turf COP for the X and Y coordinates. The intraclass correlation coefficients were calculated to assess test-retest and inter-rater reliability of the Turf COP for the X and Y coordinates. All statistical calculations were conducted using PASW Version 18.0 (IBM Corporation; New York, USA).

RESULTS AND DISCUSSION

Descriptive statistics for differences in COP location are presented in Table 1.

The Pearson correlation coefficient for COP was high for both the X ($r=0.999$, $p<0.001$) and Y ($r=1.0$, $p<0.001$) coordinates indicating the NoTurf COP is similar to Turf COP. The test-retest reliability was excellent as indicated by high intraclass correlation coefficients for both the X (ICC=0.999) and Y (ICC=1.000) coordinates. Inter-rater reliability was also excellent as indicated by high intraclass correlation coefficients for both the X (ICC=0.995) and Y (ICC=1.000) coordinates.

CONCLUSIONS

Assessment of the COP with artificial grass turf fixed to the force plates is both reliable and valid. While statistically valid, it is important to recognize that there were differences between the NoTurf COP and Turf COP that ranged from 0.348 mm to

13.527 mm. Slight changes in the location of the COP could affect either the magnitude of the calculated joint moment or the direction (extensor/flexor) if the COP is close to the joint axis [8]. It is unknown whether the differences in COP location are the result of errors from the turf being fixed to the force plates or errors due to improper placement of the golf club end. The marked locations on the force plate and turf were within 3 mm of one another. The differences in the COP location between NoTurf and the hand measured location were 1.488 ± 1.173 mm (Range: 0.036 mm – 3.958 mm) and 1.857 ± 0.230 mm (Range: 0.006 mm – 3.530 mm) in the X and Y direction, respectively, demonstrating inherent error within the center of pressure measurements even when turf is not applied. With a small mean difference of 4.414 mm to 7.841 mm in the X and Y direction respectively, it appears that fixing turf to the force plates does not greatly affect the COP location as compared to COP measurements without turf. Therefore, this procedure is a valid method for assessing COP movements and joint moments during the golf swing.

REFERENCES

1. Ball KA, et al. *J Sport Sci*, **25**, 757-770.
2. Brown D, et al. *Science and Golf III*, Human Kinetics, 1998.
3. Foxworth JL, et al. *J Orthop Sports Phys Ther*, **43**, 660-665.
4. Lynn SK & Noffal GJ. *J Sport Sci Med*, **9**, 275-281.
5. McNitt-Gray JL, et al. *Sport Biomech*, **12**, 121-131
6. Williams KR & Cavanagh PR. *Med Sci Sport Exer*, **15**, 247-255.
7. Worsfold P, et al., *J Sport Sci Med*, **8**, 607-615.
8. Winter DA. *Biomechanics and Motor Control of Human Movement*, John Wiley & Sons, Ltd., 2009

Table 1: Descriptive statistics for the differences between the COP measured in the no turf (NoTurf) and turf (Turf) conditions.

	Minimum Difference (mm)	Maximum Difference (mm)	Mean \pm SD (mm)
COP X	0.402	11.917	4.414 ± 3.185
COP Y	0.348	13.527	7.841 ± 3.954

THE COUNTERMOVEMENT JUMP IS MORE FUNCTIONAL THAN THE SQUAT JUMP IN MEASURING ELITE BASKETBALL PLAYER PERFORMANCE

¹ Amarah Epp-Stobbe*, ¹Jenna Dibblee, and ¹Patrick Costigan

¹ School of Kinesiology & Health Studies, Queen's University, Kingston, Ontario, Canada

*Corresponding author's e-mail: 14ajes@queensu.ca

INTRODUCTION

Predicting athletic performance from quantitative tests is of the utmost interest to strength and conditioning professionals, biomechanics, and coaches. For example, sports like basketball host combine events with the goal of highlighting future player performance. However, due to the basketball's multifaceted nature no single test predicts an athlete's abilities [1]. Nevertheless, the force from a player's vertical jump has been linked to increased playing time [2]. The two most commonly tested vertical jump conditions are the countermovement jump and the squat jump [2, 3]. It is argued that the countermovement jump is more sport-specific, allowing for greater vertical height [4] whereas the squat jump is a better measure of lower body power [5]. The various forms of the vertical jump, including squat and countermovement with no arm involvement, one-, or two-arm swings, may be why no one jumping form has been recommender for player testing to date [2, 3, 6, 7].

The purpose of this study is to evaluate the force profiles of the countermovement and the squat vertical jumps in elite basketball players to determine if one jump is superior to the other as a measure of performance.

METHODS

All fifteen players from an elite men's basketball team were recruited to perform six jumps on a portable BERTEC force plate (BERTEC Corporation, Columbus, OH, USA). Three countermovement jumps and three squat jumps were performed, each with an arm swing. A Vertec vertical jump tester (Power Systems Incorporated, Knoxville, TN, USA) was placed 0.25 meters

forward of the force plate at a base height 2.90 meters of to give the players a target. Seven identical data collections took place across the playing season during scheduled practice times, averaging one collection every three weeks. Due to injuries accrued during the season the incomplete data of two players were ignored.

A custom script using MATLAB (The Mathworks Inc., Natick, MA, USA) determined the maximum vertical force, rate of force development, maximum velocity, and maximum power from the ground reaction force.

The data was analyzed using SPSS Statistics (IBM, Corporation, Armonk, NY, USA). The mean values across the season of the maximum vertical force, rate of force development, maximum velocity, and maximum power were calculated for each player by jump type. A bivariate correlation compared the types of jump while a paired sample t-test evaluated the absolute differences of the measured values.

RESULTS AND DISCUSSION

The high correlations of the maximum vertical force, maximum velocity, and maximum power between the jumps demonstrate that the countermovement and squat jump are similar (Table 1). However, the correlation of the rate of force development between the jumps was low ($r = 0.504$). The mean value of the rate of force development of the countermovement jump ($M = 1932$ N/s, $SD = 636$ N/s) was larger than that of the squat jump ($M = 1769$ N/s, $SD = 732$ N/s). This difference may be explained by the initial countermovement before jumping which has been linked to increase force production and muscle activity [4].

In the case of the maximum vertical force (Figure 1), rate of force development, and maximum power, the absolute difference values of the measures did not demonstrate significant differences ($p < 0.01$) between jump types. However, the maximum velocity was higher in the countermovement jump. This difference is due to the increased work produced in the countermovement by the leg muscles [4].

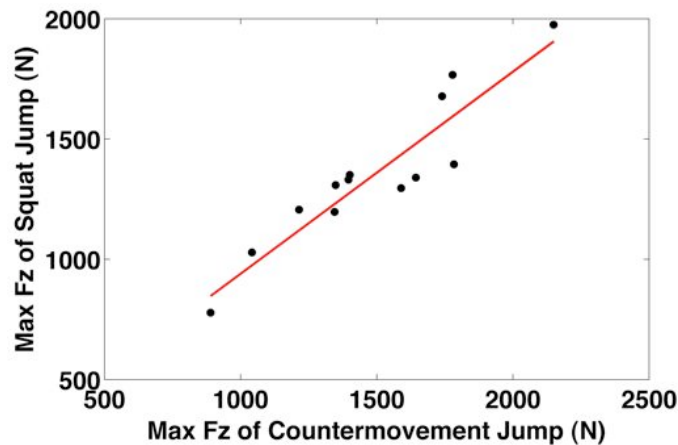


Figure 1: Comparison of maximal vertical forces of the countermovement and squat jumps.

The squat jump is a more direct measure of lower limb strength, as it does not require generating the countermovement with the upper body. Nevertheless, in basketball the squat jump is not common. Players are required to manipulate their upper bodies to achieve a transfer of energy allowing them to successful shoot or to gain possession of a rebound.

Given the high correlations between the squat and countermovement jump suggests that the jumps are similar. However, the increased rate of force

development seen in the countermovement jump suggests that it is the recommended jump to use in basketball field collections.

CONCLUSIONS

In assessing athletic performance, the tactical demands of the particular sport must be assessed ahead of technical considerations [7]. Using the countermovement vertical jump, the lower body power, force, and rate of force development can be assessed while also accounting for a greater vertical jump height than the squat jump. The sport-specific nature of the countermovement jump, combined with an arm swing, may permit basketball players to jump in a manner most natural to them without sacrificing data about the force profile of the jump itself.

REFERENCES

1. Hoffman J.R., et al. *Exercise and Sport Science*, Williams & Williams, 733-744, 2000.
2. Hoffman J.R., et al. *J Strength Cond Res* **10**, 67-71, 1996.
3. Markovic G., et al. *J Strength Cond Res* **18**, 551-555, 2004.
4. Bobbert M.F., et al. *Med Sci Sport Exer* **28**, 1402-1412, 1996.
5. Sayers S.P., et al. *Med Sci Sport Exer* **31**, 572-577, 1999.
6. Floría P., & Harrison A.J. *J Appl Biomech* **29**, 655-661, 2013.
7. Gutiérrez-Dávila M., et al. *Sport Biomech* **13**, 135-143, 2014.

Table 1: Comparisons of correlations of the countermovement and squat jumps.

	Countermovement		Squat		Correlation Coefficient
	Mean	Standard Deviation	Mean	Standard Deviation	
Maximum Force (N)	1486	341	1358	310	$r = 0.93^*$
Rate of Force Development (N/s)	1932	636	1769	732	$r = 0.50$
Maximum Velocity (m/s)	15.6	2.4	14.9	2.1	$r = 0.97^*$
Maximum Power (W)	24736	6614	22940	5616	$r = 0.91^*$

* Significant at $r = 0.01$ level (2-tailed)

THE EFFECTS OF TWO DIFFERENT PULLING STRATEGIES ON BARBELL KINEMATICS DURING THE CLEAN PULL EXERCISE

¹ Travis Ficklin, Natalie Sinnwell, Robin Lund, Ben Thoma, and Ross Curtis

¹ The University of Northern Iowa, Cedar Falls, IA, USA
email: travis.ficklin@uni.edu

INTRODUCTION

In the sport of Weightlifting, research has suggested that a rearward foot displacement and bar trajectory from the start to the catch phase of a clean is advantageous over other techniques. This may be done by shifting the foot center of pressure (COP) rearward toward the heels during the first pull and maintaining a flat-footed position as long as possible before the second pull [1]. Additionally, it is possible that having a center of pressure toward the metatarsophalangeal (MTP) joints pulls the lifter forward and causes a looping effect [2].

Contrary to these suggestions, it has been proposed that the center of pressure during the first pull should never be as far back as the heels [3]. In fact, some recommend that the center of pressure should be through the MTP joints of the feet. The purpose of this study is to compare these two pulling strategies in terms of COP location and barbell kinematics during the clean pull exercise.

METHODS

All methods were approved by the IRB of the university and all subjects signed informed consent agreements before participating in the study. Ten injury-free subjects with at least one year of experience and training in USA Weightlifting technique participated in the study.

Each subject executed four clean pulls each using a load 95% of their self-reported one repetition maximum (1RM). For safety, the subjects were not required to catch the bar at the top of the pull. The subject was instructed to “pull through the heels” during the first pull for two trials and to “pull through the toes” during the first pull for the other two. The order of pulling condition was quasi-randomly counterbalanced between subjects.

The ends of the weightlifting bar were marked with retro-reflective markers for use in a multi-camera motion capture system (Nexus, Vicon, Denver, CO). The 3D locations and velocities of the markers were tracked during each lift at 200 Hz. Additionally, the vertical ground reaction force (GRF_z) and COP location were recorded during each lift using a force platform sampling at 400 Hz (Accupower, AMTI, Watertown, MA).

The first pull was defined as the period of time during which GRF_z was greater than the weight of the lifter-plus-load system as measured in a static calibration, and the second pull was defined as the second such period [4].

Bar height (H) in each frame was calculated as the vertical location of the centroid of the two bar end markers. Its vertical velocity (v) in each frame was calculated as the average vertical velocity of the markers. The peak height (H_{PK}) and maximum upward velocity (V_{MAX}) of the centroid during the whole movement were determined for each trial. H_{PK} was then normalized to subject stature for the purpose of between-subject comparisons.

Fore-aft COP data were used to verify the pulling conditions. The placement of the toes of each subject was standardized to a line marked on the surface of the force platform which was a known distance from the plate's geometric center. Then, the fore-aft location of the COP with respect to this line was calculated during the lift. Using the measured foot length for each subject, fore-aft COP position was normalized to foot length such that a location that was even with the geometric midfoot lines of the feet was zero, a location at a maximum forward limit that was even with the toes being +1.00, and a location at a maximum rearward limit that was even with the heels being -1.00. The average normalized fore-aft location of the COP

was then averaged over the time of the first and second pulls.

Descriptive statistics (mean \pm SD) were calculated for all variables. A multivariate dependent t-test was used to determine the effect of the pulling condition on average fore-aft COP during the first and second pull, peak barbell velocity v_{MAX} , and normalized barbell height H_{PK} . Alpha was set at $p < 0.05$ for all tests.

RESULTS AND DISCUSSION

Descriptive statistics of demographic variables and performance variables by technique can be found in Tables 1 and 2. The multivariate dependent t-test showed a significant pulling condition effect ($F(4,6)=5.27$, $p=0.04$). COP was more forward in the “toes” condition for both the first and second pulls. H_{PK} and v_{MAX} were also both greater for the “toes” condition.

CONCLUSIONS

The COP data confirm that the subjects were in fact using significantly different pulling strategies between conditions. Interestingly, although the COP was more rearward in the “heels” condition, subjects did not actually pull “from the heels” during these trials as indicated by average COP

positions during the pull that were forward of the midline of the feet.

Clearly the subjects attempted to start with the COP further back during the first pull but intuitively shifted the COP forward, perhaps in order to get into a more favorable position for the second pull. Despite the shift of the COP forward for the second pull, the heel pulling strategy most likely resulted in a more simultaneous extension of the hips and knees resulting in significantly less v_{MAX} and H_{PK} . Weightlifters should consider shifting their COP forward, closer to the MTP joint when initiating the clean pull exercise.

REFERENCES

1. Schilling, B. K., et. al. (2002). Snatch technique of collegiate national level weightlifters. *Journal of Strength and Conditioning Research*, 16(4), 551-555.
2. Stone, M.H., et. al. (1998). Analysis of bar paths during the snatch in elite male weightlifters. *Strength Cond. J.* 20(5):30–38.
3. Takano, B. (1993). Coaching optimal technique in the snatch and clean and jerk – part1. *Journal of Strength and Conditioning Research*, 15(1), 33-9.
4. Enoka, R. (1979). The pull in Olympic weightlifting. *Medicine and Science in Sports and Exercise*, 11, 131-137.

Table 1.
Descriptive statistics of demographic variables (n=10).

	Mean	SD
Body mass (kg)	86.7	8.7
Stature (cm)	180.0	5.6
Clean pull load (kg)	118.7	16.1

Table 2.
Descriptive statistics of performance variables by technique.

	“Pull from Heels”		“Pull from Toes”	
	Mean	SD	Mean	SD
COP 1 st Pull	0.01	0.22	0.26*	0.15
COP 2 nd Pull	0.43	0.23	0.57*	0.14
Normalized H_{PK} (stature)	0.62	0.04	0.64*	0.04
v_{MAX} (m/s)	1.52	0.22	1.63*	0.19

*Significantly greater than the heels condition.

THE EFFECT OF DIFFERENT START STYLES ON BASE STEALING KINEMATICS IN DIVISION I SOFTBALL PLAYERS

¹ Keegan Parrott, Brian Rohrbach, Travis Ficklin, Natalie Sinnwell, and Robin Lund

¹ The University of Northern Iowa, Cedar Falls, IA, USA

email: parrottk@uni.edu

INTRODUCTION

There are many advantages associated with the successful steal attempt of a base in the sport of softball [1]. In particular, the advancement to the next base without giving up an out increases the run expectancy for that inning. The rules of softball prohibit leading off, and the baserunner cannot leave the base until the pitcher releases the ball. However, there are no specified constraints regarding the manner in which the baserunner maintains contact with the base before leaving, nor on the manner in which she initiates the takeoff when legally leaving the base to start a steal. Despite the lack of constraint there has been no identifiable research examining the efficacy of different techniques. The purpose of this study is to compare base stealing kinematics when using static and dynamic takeoff styles in base stealing for Division I softball players.

METHODS

All procedures were IRB-approved and all subjects provided their informed consent prior to data collection. Thirteen Division I softball players participated in the study. After a dynamic warm-up period, each subject executed six sprints from first to second base as though executing a steal. The first two trials were executed using their own current game starting style, and were executed before any feedback or instruction were given. These first trials served as the control condition for all subjects. After these control trials, subjects were then taught two other takeoff styles: one from a static ready position and the other from a dynamic countermovement. In order to obtain the best possible time of stealing (t_{STEAL}) for each trial, subjects were not required to

stop at the base but were allowed to run at full speed past it after stepping on it.

Two cameras were used to record each trial (GC-PX1, JVC Corp, Tokyo, JP). The first captured the first 5.0 m of the run at 300 Hz. It was positioned approximately 20 m from the basepath with its optical axis perpendicular to the vertical plane containing the basepath line. The lead edge of first base (closest to second base) was used as the origin and marks at 2.5 m and 5.0 m were used both for distance calibration and for timing purposes. The second camera recorded the entire run at 300 Hz from the time the subject left first base to the time when she touched second base. This camera was allowed to pan to follow the subject throughout the run.

The instant of leaving first base ($t_{START} = 0.0$ s) was determined to be the video frame in which foot contact with the base was broken. Times from start to 2.5 and 5.0 m ($t_{2.5}$ and $t_{5.0}$, respectively) were measured using data from camera 1. To do this, the forwardmost point of the subject's trunk was digitized in each video frame from t_{START} to when the subject had clearly surpassed the 5.0 m mark using MaxTraq software (Innovision Systems, Columbiaville, MI). Additionally, the origin and the marks at 2.5 and 5.0 m were digitized in each trial.

These digitized data were then exported for use in custom Matlab software (Mathworks, Natick, MA) to analyze the batch of trials. For each trial, $t_{2.5}$ and $t_{5.0}$ at which the leading point of the trunk crossed the 2.5 and 5.0 m marks were determined by interpolation between frames of the point's location data for the instant at which it had crossed each mark.

The time of the entire run was calculated using frame number data from camera 2. First, the number of frames captured between t_{START} and the nearest estimated half-frame at which second base was contacted was calculated. Then, this number was multiplied by (1/300 s) to calculate t_{STEAL} .

Descriptive statistics were calculated for all performance variables. A repeated measures MANOVA was used to determine any treatment effect. Mauchley's test was used to test the sphericity assumption. Three repeated variance ANOVAs were administered to determine which variables were affected. Bonferroni-adjusted paired t-tests were used as post hoc analysis. The level of significance was set at $p < 0.05$ for all inferential analyses.

RESULTS AND DISCUSSION

Descriptive statistics of all performance variables can be found in Table 1. The sphericity assumption was tenable for both $t_{2.5}$ ($p = 0.19$) and $t_{5.0}$ ($p = 0.34$) but not for t_{STEAL} ($p = -.001$) resulting in a Greenhouse-Geisser penalty for that variable. The repeated measures MANOVA indicated a significant treatment effect ($F(6,42) = 2.39$, $p = 0.045$). The three repeated measures ANOVA indicated that the observed treatment effect was not significant for $t_{2.5}$ ($p = 0.06$). There were, however, treatment effects for $t_{5.0}$ ($p = 0.002$) and t_{STEAL} ($p = 0.03$). The results of the post hoc analysis are summarized in Table 1.

By the time the player reaches second base, the dynamic takeoff condition has yielded an advantage over both the static and self-selected takeoffs. However, this advantage does not materialize at all

within the first 2.5 m, and only surfaces over the self-selected takeoff after 5.0 m. Due to the stretch reflexes associated with dynamic starts and the subsequent improvement in forward lean and horizontal impulse, it was expected that this strategy would be more effective than the other conditions early in the run but not necessarily as the run progresses [2].

Instead, the effect of dynamically starting the steal seems to continue further into the run than in previous similar studies [2]. This could be because of sport or sex differences, being that the previous similar study examined takeoff technique in male football players. Regardless, the advantages of using the dynamic takeoff style in the present study are realized most fully over the course of the entire steal.

CONCLUSIONS

Practitioners should consider experimenting with dynamic takeoff techniques for base stealing. There may be many ways to adapt dynamic takeoffs for individual players. Coaches should also take into consideration that the dynamic strategies may make it more difficult to time the start accurately with the ball release of a live pitcher. Practice with the timing of the technique must be employed to gain full advantage of its use.

REFERENCES

1. Lund R., Ficklin T., & Reilly-Boccia, C. *The Sport Journal*, 47, 0604.
2. Cusick J, Lund R., & Ficklin, T. *Journal of Strength and Conditioning*, 28(9), 2669-2672.

Table 1: Times at 2.5 m, 5.0 m, and the entire steal between takeoff conditions.

	Control	Static	Dynamic
$t_{2.5}$ (s)	0.37 ± 0.04	0.36 ± 0.04	0.35 ± 0.04
$t_{5.0}$ (s)	0.87 ± 0.05	0.84 ± 0.04	0.82 ± 0.04 *
t_{STEAL} (s)	2.76 ± 0.10	2.72 ± 0.13	2.70 ± 0.11 * #

(*) Denotes that the technique was significantly faster than control. (#) Denotes that the technique was significantly faster than static.

Poster #409 has been withdrawn.

Poster #409 has been withdrawn.

INFLUENCE OF A SELF-INDUCED DROP ON VERTICAL JUMP PERFORMANCE

¹ John W. Fox, ²Adam Jagodinsky, ²Lorraine Smallwood, ²Chris Wilburn, and ²Wendi H. Weimar

¹ Methodist University, Fayetteville, NC, USA

² Auburn University, Auburn, AL, USA

email: jfox@methodist.edu, web: <http://www.methodist.edu/dpt/index.htm>

INTRODUCTION

Countermovements are valuable because of the exploitation of the stretch-shorten cycle. In a traditional countermovement vertical jump athletes lower the center of gravity by flexing the hips and knees, stretching the muscles eccentrically, before changing directions and forcefully extending in the direction of motion. A slight alteration of the countermovement was witness by Angle, Gillette, and Weimar (2012) in canine sprinters. The authors noted that unlike the traditional countermovement (CM) typically seen in humans, canines flexed the elbows and knees to raise the paws 4-8cm from the ground allowing the center of mass to free fall toward the ground. Upon contacting the ground the joints flexed farther prior to take-off [1]. Canines appear to perform a self-induced drop Drops have been associated with higher rate of force development (RFD), which is associated with improved vertical jump performance [2, 3]. Hence, a self-induced drop should lead to increased RFD and increased jump height. Therefore, the purpose of this study was to compare rate of force development and vertical jump height in the self-induced drop (SD) to the countermovement (CM) and squat jump (SJ) conditions.

METHODS

17 males and 17 females were recruited for participation. Participants performed a minimum of 3 maximum vertical jumps utilizing 3 different loading conditions (SD, CM, SJ). Arm swing was not allowed in any of the jumps. The order of the loading conditions was randomized. The SD required participants to lift their feet from the ground without vertical rise in the center of mass, and fall into a countermotion. The second condition was the CM in which the center of mass lowers

prior to the push phase with the feet in contact with the ground. Additionally a SJ condition was performed with the knees pre-flexed to a self-selected depth. Each jump was recorded using a 10-camera Vicon® MX motion capture system (Vicon®, Los Angeles, CA, USA) with a sampling frequency of 200 Hz. Jump height was defined by the difference in maximum height achieved of the greater trochanter marker and its height during the static calibration trial.

RESULTS AND DISCUSSION

A two-way repeated measures ANOVA was used to analyze differences in jump height (Figure 1). The results of the analysis indicated significant differences among conditions ($F(2,64) = 33.738$, $p < 0.001$, $\eta^2 = 0.513$, $Power = 1.000$) and both sexes had the same response to the imposed conditions ($F(2,64) = 2.512$, $p = 0.089$, $\eta^2 = 0.073$, $Power = 0.486$). Pairwise comparisons demonstrated that jump height in the CM was significantly greater than the SD ($p = 0.014$) and the SJ ($p < 0.001$). Additionally, height in the SD was significantly greater than the SJ ($p < 0.001$).

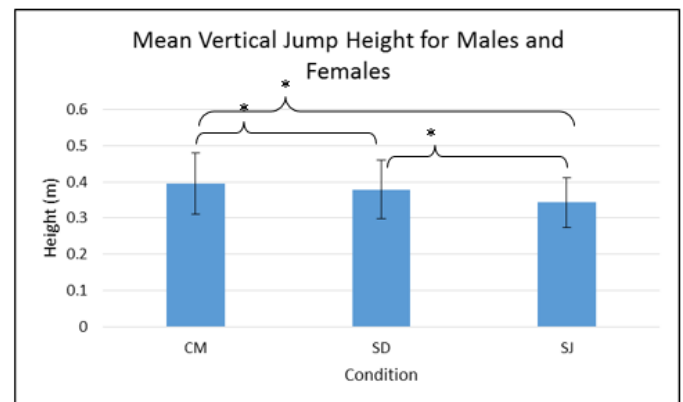


Figure 1: Mean vertical jump height for each SSC condition. * denotes significance at the $p = 0.05$ level.

A two-way repeated measures ANOVA was used to analyze differences in RFD. RFD results violated the sphericity assumption requiring the Greenhouse-Geisser adjustment to the degrees of freedom. The results of the analysis indicated significant differences among conditions ($F(1.297,41.491) = 15.104$, $p < 0.001$, $\eta^2 = 0.321$, $Power = 0.987$) and both sexes had the same response to the imposed conditions ($F(1.297,41.491) = 1.875$, $p = 0.177$, $\eta^2 = 0.055$, $Power = 0.300$). Pairwise comparisons demonstrated that RFD in the SD was significantly greater than the CM ($p < 0.001$) and the SJ ($p = 0.025$). Additionally, RFD in the SJ was significantly greater than the CM ($p = 0.009$).

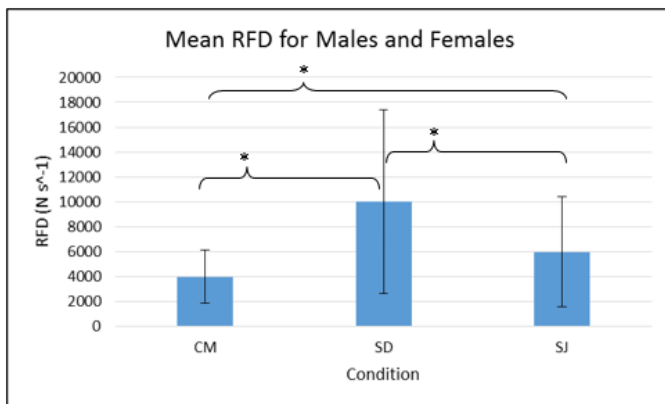


Figure 2: Mean vertical rate of force development for each SSC condition. * denotes significance at the $p = 0.05$ level

Results indicate that the CM is superior to both the SD and SJ conditions in producing maximum jump height. This occurred despite greater rates of force development in the SD condition. It is possible that the rate of force development is too high in the SD condition, especially since the condition was novel to all participants. High rates of force development can lead to muscle fiber lengthening [4]. Muscle fiber lengthening, although it allows for force enhancement, may necessitate greater shortening of the muscle during the concentric phase of the jump. Increased shortening suggests the muscle operates too far to the right on the force-velocity curve, which leads to non-optimal force production.

However, participants did jump higher in SD compared to SJ. The results demonstrate that utilizing the stretch-shorten cycle improves performance.

CONCLUSIONS

This study examined the CM, SD and SJ vertical jump conditions. Utilization of a stretch-shorten cycle improved RFD and vertical jump height. Although the CM appears to be the superior method, this may be due to non-optimal muscle coordination in a novel jumping technique, which could be corrected with training. Furthermore, the efficacy of the SD condition should be examined in horizontal accelerations, since this is the circumstance noted by Angle, Gillette and Weimar (2012).

REFERENCES

1. Angle, T. C., Gillette, R. L., & Weimar, W. H. (2012). Kinematic analysis of maximal movement initiation in Greyhounds. *Australian Veterinary Journal*, 90(3), 60-68.
2. Bobbert, M. F., Mackay, M., Schinkelshoek, D., Huijing, P. A., & van Ingen Schenau, G. J. (1986). Biomechanical analysis of drop and countermovement jumps. *European Journal of Applied Physiology*, 54, 566-573.
3. Laffaye, G., & Wagner, P. (2013). Eccentric rate of force development determines jumping performance. *Computer methods in biomechanics and biomedical engineering*, 16(sup1), 82-83.
4. Ishikawa, M., Komi, P. V., Finni, T., & Kuitunen, S. (2006). Contribution of the tendinous tissue to force enhancement during stretch-shortening cycle exercise depends on the prestretch and concentric phase intensities. *Journal of Electromyography and Kinesiology*, 16, 423-431.

NO ANGULAR SWING KINEMATIC DIFFERENCES IN FEMALE SOFTBALL PLAYERS WITH DIFFERENTLY WEIGHTED WARM-UP BATS

¹ Yang-Chieh Fu, ² Nicole C. Dabbs, and ¹ John C. Garner

¹ The University of Mississippi, Oxford, MS, USA

² California State University, San Bernardino, CA, USA

email: ycfu@olemiss.edu, web: <http://hesrm.olemiss.edu/exercise-science/applied-biomechanics-and-ergonomics/>

INTRODUCTION

Baseball/softball coaches and players display a constant interest in methods to increase bat swing kinematics for competition. A common method to increase swing velocity is utilizing different weighted warm-up bats prior to maximum performance. These warm-up bats may be lighter or heavier than a regular weighted bat used in regular game. However, there is no agreement on efficacy of using the warm-up protocol [1-3], and coaches and players still utilize it based on their own experience or beliefs.

One major concern for this controversy is due to no previous study, up to authors' knowledge, has analyzed the movement using three dimensional (3D) techniques, and no angular swing kinematics has been reported. Therefore, the purpose of this study was to examine the 3D kinematics of three different weighted warm-up bats.

METHODS

Ten female college softball players were recruited (age: 20.1 ± 1.1 yrs; mass: 76.4 ± 21.3 kg; height: 165.7 ± 8.4 cm). All participants were fully informed and signed the consent form. Data collection was conducted in a typical biomechanics laboratory. Seven reflective markers were placed on the bat (1 top marker on the center of the bat top, and 6 on the barrel), and 27 markers were placed on participant's head, trunk, pelvis, and upper limbs. Marker trajectories were recorded by a seven-camera motion analysis system (Vicon, CA, USA) at 100 Hz. Three weighted bats/session (normal weighted, NW, 29 oz.; heavy weighted, HW, 45 oz.; light weighted, LW, 13 oz.) were tested and order was randomized. For each session, each participant

performed a self-selected warm-up protocol (instructed to be consistent with their on-deck routine) using assigned bat and followed by 5 maximal swing with NW bat. There was 3 minutes resting between each condition. The best trial of each condition was analyzed. Marker data was filtered with 4th order Butterworth filter at 6 Hz cut-off prior to subsequent analysis.

Data were analyzed from the beginning of loading phase to the end of the follow through phase of bat swing. Angular kinematics were obtained by steps as followed. First, a best-fitted bat swing plane was generated from the top bat marker at global coordinate system (BAT_g) using least squares method (Figure 1). BAT_g were then projected onto the best-fitted plane (BAT_{g-proj}). Three arbitrary points were selected from BAT_{g-proj} to define a local coordinate system embedded on the plane, and rotation matrix R_{swing} and translation vector V_{swing} were also generated. BAT_{g-proj} were transferred from the global to the local coordinate system by following equation:

$$BAT_{l-proj} = R_{swing}^T * (BAT_{g-proj} - V_{swing})$$

Angular trajectories (BAT_{ang}) were obtained by converting BAT_{l-proj} from Cartesian to polar coordinates. At last, angular velocity of the swing was calculated by differentiation of BAT_{ang} . Plane angle between the best-fitted plane and the ground plane (x-y plane) was also calculated.

Peak angular velocities, time to peak velocity, relative time to peak velocity, and plane angle were tested using a 1x3 (group by condition) repeated measures ANOVA. The significant level was set at $\alpha = 0.10$ for omnibus test due to small sample size and 0.05 for pairwise comparison to minimize familywise errors. All tests were conducted using SPSS (IBM Corp., Version 21.0. Armonk, NY).

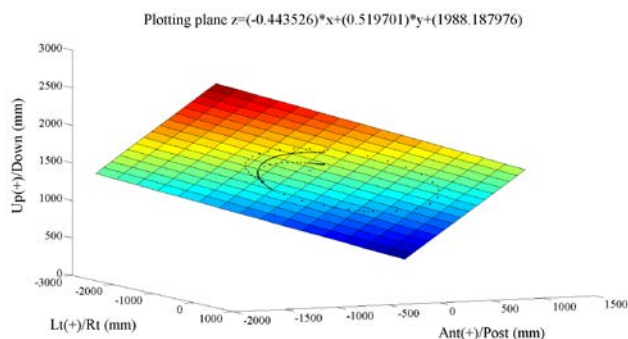


Figure 1: Example of best-fitted swing plane.

RESULTS AND DISCUSSION

For angular kinematics, differences were only found at relative time to peak velocity (Table 1). The HW condition reached peak angular velocity approximately 5% later than the NW condition ($p = 0.014$). No differences were found in other angular variables as well as the plane angle.

Current study aimed to investigate efficacy of using differently weighted warm-up bats by 3D angular kinematic analysis. In general, results do not agree with many coaches and players’ believe: using differently weighted bat warm-up protocol can enhance maximum performance by increasing swing velocity, which agrees with Szymanski’s study [3].

Reason for the delayed relative time to peak angular velocity of HW bat compared to NW is not clear. It was presumed that this delay might be due to the altered rotation axis of the whole body. However, it was partly rejected since there was no difference at the plane angle between conditions. Although the normal axis of the best-fitted plane is not the true axis of rotation of the whole body, theoretically they

are close. Thus, advance study is needed to explain this finding.

Gender and sports type differences might be potential factors affect swing kinematics. Most studies [1-3] recruited male baseball players while female softball players were recruited in current study. Gender differences such as physical strengths might affect swing kinematics. Also, the ‘normal’ bat used in current study is similar to that has been used in regular baseball competition. It might be heavy to female softball players thus affect swing kinematics.

The study is mainly limited by relatively small sample size and selected athletes. Thus, it is recommended that some caution is necessary when interpreting the results and generalize to different sports. Also, camera sampling rate might be low for the high velocity bat swing movement. A higher sample rate is suggested for future study.

CONCLUSIONS

Evidence from our study suggests that there is no notable angular kinematic difference with differently weighted warm-up bats prior maximum performance in female varsity softball players. Further investigation on whole body kinematics as well as kinetic changes of bat swing is necessary to further support finding in current study.

REFERENCES

1. Montoya BS, et al. *J Strength Cond. Res.* 23, 1566-1569, 2009.
2. Southard D & Groomer L *Res. Q. Exerc. Sport* 74(3), 270-276, 2003.
3. Szymanski, DJ, et al. *J Strength Cond. Res.* 26(1), 199-205, 2012.

Table 1: Mean (SD) of peak angular velocity, time to peak velocity, and relative to peak velocity for differenty weighted warm-up protocol.

Bat Weight	Peak Velocity (Deg/s)	Time to Peak Velocity (s)	Relative Time to Peak Velocity (%)	Plane Angle (°)
Heavy	1526.7 (334.9)	0.36 (0.15)	51.3 (23.7)	33.8 (4.1)
Light	1615.5 (455.3)	0.35 (0.16)	50.8 (23.1)	32.7 (5.1)
Normal	1593.2 (354.9)	0.31 (0.15)	46.7 (25.6)	33.7 (4.0)
<i>p</i> value	0.213	0.113	0.058	0.569

DETRENDED FLUCTUATION ANALYSIS OF RUNNING GAIT TRACKS CHANGES IN PERFORMANCE WHEN ATHLETES ARE OVERTRAINED

¹ Joel T. Fuller, ¹ Clint R. Bellenger, ¹ Dominic Thewlis, ¹ Rebecca L. Thomson, ¹ John Arnold ¹ Margarita D. Tsiros, ² Eileen Y. Robertson and ¹ Jonathan D. Buckley

¹ Alliance for Research in Exercise, Nutrition and Activity, Adelaide, SA, Australia

² South Australian Sports Institute, Adelaide, SA, Australia

email: joel.fuller@mymail.unisa.edu.au

INTRODUCTION

Stride-to-stride fluctuations in running stride interval display long-range correlations that breakdown in the presence of fatigue accumulated during an exhaustive run [1]. The presence of long-range correlations in the stride interval of running suggests that small fluctuations in stride interval occur at a high frequency whilst large fluctuations occur at a low frequency [2]. This pattern of scaling is thought to result from motor control processes operating on different time scales. In a healthy state, these processes interact to produce a signal containing long-range correlations [1,3]. However, in the presence of fatigue, injury, aging and pathology the resultant signal is more random, with only weak long-range correlations present [1,3].

Overtraining is a pathological condition that occurs in athletes when training load is too high or recovery from training is too short [4]. Methods for monitoring training status have predominantly focused on measuring changes to heart rate variability and have had mixed success [4]. The recent observation that long-range correlations in stride interval are sensitive to fatigue [1] suggests that the stride interval may provide a new means for monitoring training status. The aim of this study was to investigate whether a state of temporary overtraining, as indicated by a decrease in performance in response to heavy training, is reflected by changes to stride interval long-range correlations measured during sub-maximal running.

METHODS

A prospective intervention design was used to investigate stride interval long-range correlations after two weeks of light training, two weeks of

heavy training designed to induce a temporary state of overtraining and two weeks of subsequent tapering (light) training. Ten trained male runners (Age: 21-53 years; mass: 62-84 kg) completed this study. Stride interval long-range correlations were assessed at the completion of each training phase during 5-min of submaximal running at 8, 10.5 and 13 km/h. Training status was assessed using a 5-km treadmill time trial (5TTT).

Force-sensitive resistors were placed underneath the first metatarsal head and heel regions of each shoe insole during sub-maximal running. This allowed the moment of initial foot contact to be recorded wirelessly at 2000 Hz using a Delsys Trigno system (DelSys Inc, Natick, USA). Stride intervals were calculated as the time between peak forces at initial contact. Peak forces were identified using the findpeaks function in MATLAB (R2013a, MathWorks, Natick, MA). An example stride interval time series is shown in Fig. 1.

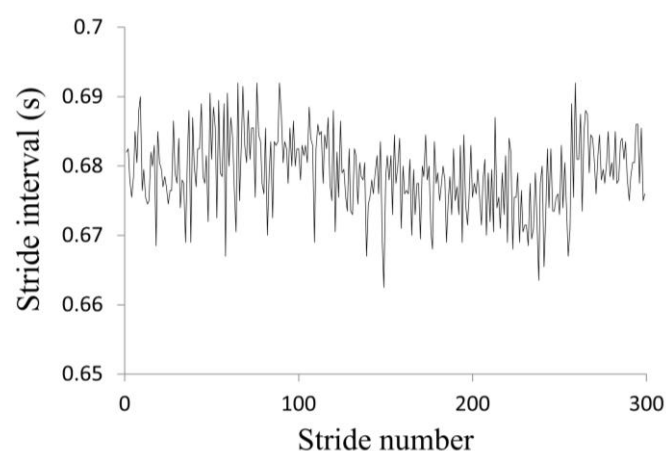


Figure 1: Stride interval time series.

To determine the degree of long-range correlation in each stride interval time series, the initial 30-seconds of data were first removed from each time series. A median filter was then used to remove

values that were outside the inter-quartile range (IQR) by a magnitude of 1.5 times the IQR. A separate detrended fluctuation analysis was then performed on the first 300 strides, for each of the three running speeds [5]. Briefly, the time series (N) was first integrated. Next the integrated times series, $y(k)$, was divided into windows of length n . In each window of length n , a least squares line was fit to the data to represent the local trend, $y_n(k)$. We then detrended the integrated times series by subtracting the local trend in each window. The root-mean-square fluctuation of this integrated and detrended time series was then calculated by:

$$F(n) = \sqrt{\frac{1}{N} \sum_{k=1}^N [y(k) - y_n(k)]^2}$$

This calculation was repeated across all windows sizes from 4 to 75 strides. The coefficient (α) relating fluctuations to window size on a log-log plot was used to assess the degree of long-range correlations [5]. A running stride with long-range correlations across all times in a time-series has a scaling exponent $\alpha=1.0$. In contrast, stride-to-stride fluctuations that occur in an entirely unpredictable sequence have a scaling exponent $\alpha=0.5$.

RESULTS AND DISCUSSION

There was a significant main effect of training on performance ($P<0.01$). The heavy training induced a state of temporary overtraining as evidenced by a decline in 5TTT performance following heavy training and an improvement in performance following taper training ($P<0.03$; Fig. 2).

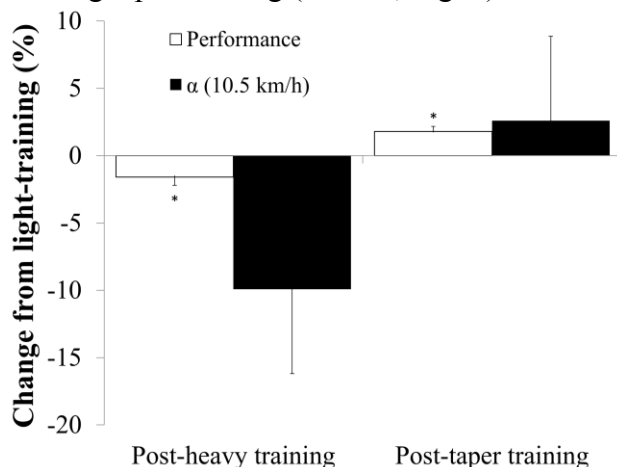


Figure 2: Percentage change in performance and α .
* significantly different to light training ($P<0.05$).

There were no significant main effect of training on α ($P>0.54$). However, changes in α at the 10.5 km/h speed and changes in performance between light and heavy training were moderately correlated ($r -0.41$; $P=0.02$). Stride interval α decreased when time to complete the 5TTT increased (Fig. 3).

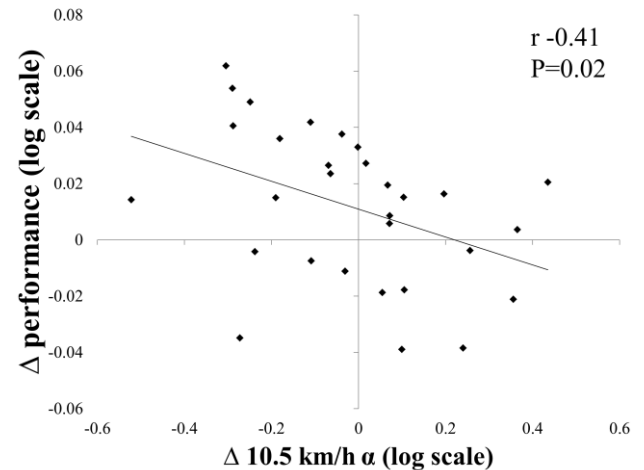


Figure 3: Change (Δ) in performance and α .

Despite not changing significantly in response to alterations in training status, stride interval α shows potential as a marker for tracking changes in training status. The ability of stride interval α to track changes in performance may be improved by using individualised running speeds for assessment of α that are relative to an individual's maximum or preferred running speed. Previous research has shown that gait speed influences α [2] and the fixed running speeds used in the present study would have represented different relative running speeds for each runner. This potential heterogeneity could have made it difficult to detect a consistent effect of training status on stride interval α across runners. Future research should investigate the ability of stride interval α assessed at relative running speeds to monitor training status.

REFERENCES

1. Meardon SA, et al. Gait Posture **33**, 36-40, 2011.
2. Jordan K, et al. Gait Posture **24**, 120-125, 2006.
3. Hausdorff JM, et al. Physica A **302**, 138-147, 2001.
4. Bosquet L, et al. Br J Sports Med **42**, 709-714, 2008.
5. Goldberger AL, et al. Circulation **101**, e215-220, 2000

JUMP PERFORMANCE VARIABLES ARE NOT DIFFERENT IN FEMALE D1 LACROSSE ATHLETES WITH GENERALIZED JOINT HYPERMOBILITY.

Christopher F. Geiser, Carolyn Meinerz, Philip J. Malloy, Michael Kiely, and Kristof Kipp

Marquette University, Milwaukee, WI, USA

email: christopher.geiser@marquette.edu, web: <http://www.marquette.edu/exercise-science/>

INTRODUCTION

Generalized joint hypermobility (GJH) is defined as a form of systemic joint laxity¹ thought to occur from genetic difference in the collagen makeup of these individuals.² Severe forms of hypermobility are a component of Ehlers-Danlos syndrome and Marfans syndrome. Unlike these often debilitating forms of hypermobility, individuals with GJH are generally not impacted during activities of daily living and are often referred to in common vernacular as “double-jointed.” A greater incidence of GJH is found in females and children.² GJH is also reflected in the athletic population, where the incidence of GJH among female athletes is estimated to be as high as 43%.^{3,4}

There is growing evidence that athletes with GJH are at greater risk of knee injury during athletic participation,⁴ that overall they are injured more frequently, and miss participation for longer periods of time.³ Previous investigators have attempted to pinpoint descriptive differences in the movement of individuals with GJH to identify a direction for interventions. Alterations in kinetic variables and muscle activation patterns have been reported in the GJH population during gait and during landing from a jump.^{6,7} Differences in muscle contractile functions have been noted in people with severe forms of hypermobility.⁸ These differences could play a role in increasing injury risk. However investigations to determine if a component of the increased injury risk noted in GJH could be attributable to differences in physical performance, have not been done, or have reported inconsistent findings.⁹

The purpose of this investigation was to evaluate for differences in countermovement jump performance variables in NCAA DI female Lacrosse athletes with GJH and matched controls.

METHODS

After acquisition of informed consent, all healthy uninjured women’s lacrosse players on a NCAA DI University roster were tested for GJH according to the number of positive Beighton’s signs,¹⁰ which are an evaluation of 9 specific movements including hyperextension of the knees and elbows past 10 degrees, dorsal flexion of the 5th digit past 90 degrees, thumb and forearm approximation, and the ability to touch the palms flat to the floor with the knees in full extension. Five or more positive signs were needed for inclusion in the hypermobile group.⁴ The experimental (GJH) group consisted of 8 players (19.4±1.0yrs, 71.0±9.4kg, 165.1±7.1cm) with 5 or more Beighton’s signs (range 5-7, mean 6.0). Eleven matched controls (Ctrl: 19.9±1.2yrs, 65.3±7.0kg, 167.6±3.0cm) were included with zero or one Beighton’s sign (range 0-1, mean 0.1). After a warm up period, participants performed three trials of a countermovement jump (CMJ) standing with each leg on a separate AMTI force plate, with the instructions to keep hands on their hips and jump “as high as they can.” One practice jump was required prior to data collection, more were allowed if the participant wanted. Force data were collected at 960 Hz in Vicon Nexus software and filtered with 4th order Butterworth filter with a cutoff frequency of 12 Hz in a custom Matlab program. Right and left leg vertical reaction forces were summed and the following dependent variables were calculated and exported from Matlab for statistical analysis: Vertical Jump Height, Reactive Strength Index, Peak Vertical Force, Time to Peak Force, Peak Concentric Force, Peak Eccentric Force, Peak Rate-of-Force Development, Peak Rate-of-Force Development normalized to Body Weight, Peak Concentric Rate-of-Force Development, Peak Eccentric Rate-of-Force Development, Take-off Velocity, Peak Power, Force at Peak Power, Velocity at Peak Power, Positive Work, Negative Work, Eccentric Time and Concentric Time. Group comparisons were made between the three trial

averages and the best of the three trials. Independent t-tests were used to compare all means between groups with significance set at $p < 0.05$. As this study was exploratory in nature, no correction for multiple comparisons was made to minimize Type II error possibility.

RESULTS

Data met the assumptions of normality and equal variance for parametric testing. No differences were found between GJH group or controls for anthropometric data.

No differences were noted between groups for any of the CMJ data variables.

DISCUSSION

This exhaustive evaluation of jump performance variables in individuals with GJH failed to identify any differences between those participants with and without GJH. This differs from the work done on isolated muscle fibers in hypermobile individuals where lower peak torque had been reported in isolated muscle fibers, but greater twitch torque⁸ in individuals with a more severe form of hypermobility versus controls. Another single fiber study found that peak force was equal between groups, but that resting tension in the muscle fibers was greater in hypermobile individuals.¹¹ Greater resting tension is thought to be the reason that rate-of-force development was higher in GJH groups⁹ as well as a higher single-fiber twitch torque.⁸

Despite the differences noted at the single level in individuals with hypermobility, the current study did not detect any performance differences between those with GJH and controls during a large, functional movement. This discrepancy is probably due to a task difference. The CMJ task allows for coordinated muscle activity between large groups of muscles. This may allow differences in muscle performance to be compensated for by timing, coordination, or some other factor during the jump. Perhaps future studies of performance variables in GJH should consider a “reactive” component to capture any differences in muscle resting tension or twitch response that a planned CMJ may not have effectively evaluated.

The current results may also be impacted by an underlying selection bias in examining individuals from the same team. The athletes in this study all

play Division 1 Lacrosse, and are therefore different than those evaluated in the single fiber studies. This in itself is interesting, demonstrating that at least some individuals with GJH are capable of jump performance at the same level as their less flexible counterparts. Thus, by demonstrating that athletes with GJH can perform a CMJ equal to non-GJH individuals, this study allows us to move on to considering other variables, including more isolated components of muscle function, that predispose GJH individuals to greater injury risk.

CONCLUSIONS

Participants with GJH participating at a high level in athletics do not appear to exhibit differences during isolated measures of athletic performance when compared to similar level teammates. Thus, the reported differences in injury rates and severity of injury in people with GJH appears be driven by factors other than those related to jump performance. Future studies must examine other variables that could potentially drive the risk of lower extremity injury in hypermobile individuals so that scientifically based effective interventions can be designed.

REFERENCES

1. Carter C, Wilkinson J. *J Bone Joint Surg Br* **46**, 40-45, 1964.
2. Russek LN. *Phys Ther* **79**, 591-599, 1999.
3. Konopinski MD, et al. *Am J Sports Med* **40**, 763-769, 2012.
4. Pacey V, et al. *Am J Sports Med* **38**, 1487-1497, 2010.
5. Simonsen EB, et al. *Clin Biomech* **27**, 573-577, 2012.
6. Shultz SJ, et al. *Med Sci Sports Exerc* **42**, 771-780, 2010.
7. Schmid S, et al. *Clin Biomech* **28**, 1020-1025, 2013.
8. Voermans NC, et al. *Neuromuscul Disord* **17**, 597-602, 2007.
9. Mebes C, et al. *Arthritis Rheum* **59**, 1665-1669, 2008.
10. Juul-Kristensen B, et al. *Rheumatology* **46**, 1835-1841, 2007.
11. Ottenheijm CAC, et al. *J Appl Physiol* **112**, 1157-1165, 2012.

Estimating Joint Contributions in Functional Motions to Create a Metric for Injury Prevention using Motion Capture and OpenSim: A Preliminary Study

¹Alexander Kozlowski, ¹Rebekah Koehn, ¹Lauren Knop, ²Kelly Helm,
³Luis Prato, ⁴Anthony Levenda, and ¹Craig M. Goehler

¹Department of Mechanical Engineering, Valparaiso University, Valparaiso, IN, USA

²Department of Kinesiology, Valparaiso University, Valparaiso, IN, USA

³Incremedical, Portage, IN, USA

⁴Lakeshore Bone and Joint Institute, Chesterton, IN, USA
email: craig.goehler@valpo.edu

INTRODUCTION

A heightened awareness of athletic safety in the field of sports has increased the development of various injury prevention studies. The majority of this research has focused on traumatic injuries, such as concussion prevention and impact related injuries. However, the predominant injury type in sports occurs with overuse and fatigue [1]. Such injuries occur in athletes with repeatedly incorrect biomechanics, improper conditioning and poor stretching. In an attempt to limit injuries, Functional Movement Screening (FMS) and the Landing Error Scoring System (LESS) were developed to identify athletes that are at risk for an overuse injury [2]. Both tests consist of various dynamic movements that are qualitatively scored based upon the athlete's performance. Studies have shown that there is a correlation between the athletes score and the risk the athlete has for an injury [3]. The problems with these tests are that the scores are subjective to each assessor, resulting in human error, inconsistent scoring and misdiagnosis of the motion.

The main objective of this project is to utilize quantitative techniques to measure human movement and develop training protocols that will result in a reduced risk of athletic injury and increased performance. This initial study primarily focuses on injuries related to the lower extremity and will be used as a preliminary training protocol for future work using the LESS test.

METHODS

To develop the testing protocol, one subject participated in the IRB approved study (male, age: 20 years) that utilized quantitative techniques to collect human movement data. Figure 1 shows that the subject was affixed with 23 passive reflective

markers based on the anatomical locations specified in a previously developed musculoskeletal model. Using the VICON Nexus software, a subject-specific model was developed from a generic template of marker locations using the static stance position shown in Figure 1A. Next, rigid bodies were fitted to the marker locations on the individual subject, resulting in Figure 1B. Once this model was complete, the subject performed the LESS test. This test consisted of both vertical and horizontal movements as the subject jumped from a 13.5 inch plyometric box. The subject first jumped to a distance of 50% of their height away from the box, and then immediately jumped as high as they could vertically from that position. The subject was able to practice the test before it was recorded and then four trials were performed.

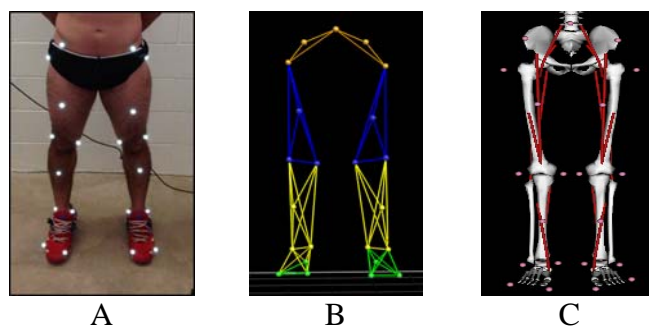


Figure 1: Reflective markers shown on the subject's lower extremity (A) along with the corresponding marker locations on the VICON Nexus model (B) and the corresponding musculoskeletal model in OpenSim (C).

The collected data for the LESS test were processed and filtered in the VICON Nexus software. To process the data, unmarked markers were labeled, gaps in the trajectories were filled using various spline techniques implemented in the software, and unwanted reflective interference were deleted.

The processed files were then exported as ASCII files for further analysis. The ASCII files contained the three-dimensional positioning of each marker throughout the trial and were able to be formatted and loaded into OpenSim. Figure 1C displays the lower extremity model that was scaled using the same static trial previously used for the calibration in the VICON Nexus software. This model was used to determine the inverse kinematics of each jump test.

For the preliminary results, the inverse kinematics determined the angles of hip flexion, hip adduction, hip rotation, lumbar extension, knee flexion, and ankle flexion for each leg. The results were then processed to remove any signal noise using a 4th order low pass Butterworth filter in MATLAB. The results were also normalized with respect to time to compare across trials of the same test, and plotted versus the normalized time. Figure 2 shows the inverse kinematics of the four trials of the LESS test for the single subject.

RESULTS AND DISCUSSION

For the purpose of the preliminary results, the results from the LESS test were analyzed by determining hip flexion, adduction and rotation versus normalized time, lumbar extension versus normalized time, knee flexion versus normalized time, and ankle flexion versus normalized time. By initially examining only this test, it was possible to effectively demonstrate results consistent with prior research, while also not presenting excess information in this exploratory study.

As illustrated in Figure 2, the similar curves shown in each of the plots suggest that the subject performed the jump test in a consistent manner during each trial. There are also noticeable similarities between the right and left legs in the hip flexion and knee flexion plots. These two degrees of freedom are perhaps easiest to visually observe during qualitative analysis of the trials. Differences in the right and left leg exhibited in the remaining plots suggest that the subject favored a leg during the test. This could mean that one leg is stronger and is being used to compensate for stability during the movement, resulting in a potential injury. Because this data represents a small number of

trials, no statistically relevant conclusions can be made.

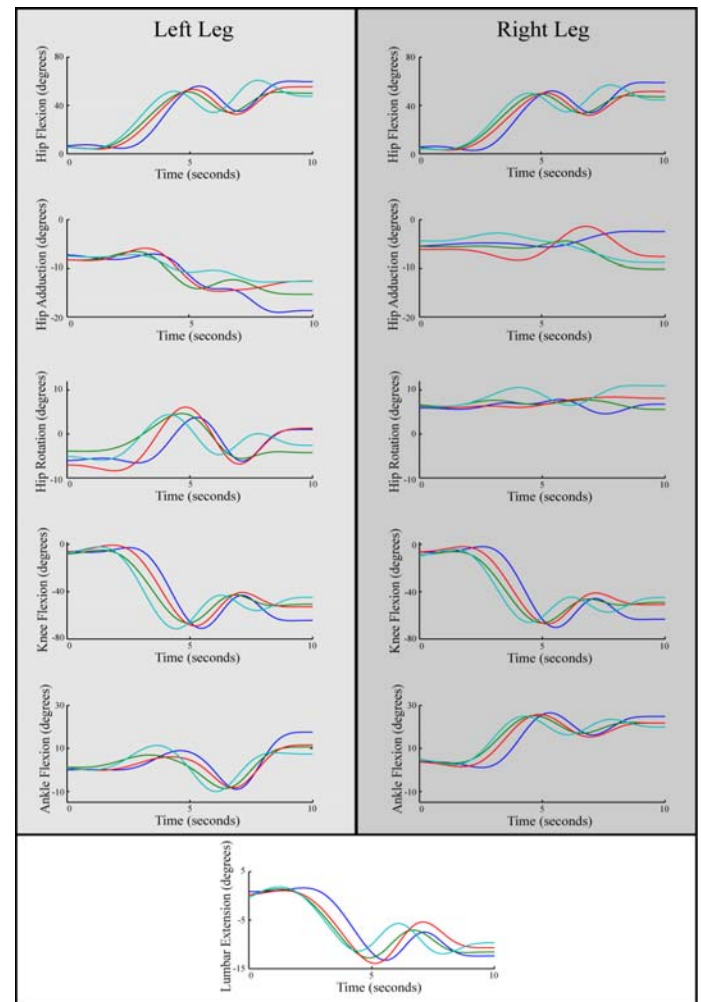


Figure 2 : Initial kinematic results from musculoskeletal simulations of the LESS test.

Future work will build off of this preliminary study and examine a series of functional motions including the LESS test, the FMS tests, and additional jump tests. Once a sufficient library of subject data has been collected, statistical methods will be used to develop the desired metric.

REFERENCES

1. Clarsen B, et al. *British Journal of Sports Medicine* 47, 195, 1 May 2013.
2. Padua D, et al. *The American Journal of Sports Medicine*, 1-2, 2 Sept. 2009.
3. Grooms D, et al. *Journal of Athletic Training*, S79-S82, May 2014.

IMPACT OF ERROR SONIFICATION AUDITORY FEEDBACK FOR NEUROMUSCULAR TRAINING ACROSS TWO DEGREES OF FREEDOM

Rena Hale, Jerome Hausselle, and Roger V. Gonzalez
The University of Texas at El Paso, El Paso, TX, USA
email: rvgonzalez@utep.edu

INTRODUCTION

When performing fundamental maneuvers such as squatting, technique is vitally important as such motions are usually conducted while conducted when lifting weight. Therefore, if performed incorrectly, the risk of joint injury is magnified. Recent studies have demonstrated that neuromuscular training of technique can be beneficial in reducing the risk of anterior cruciate ligament injury through modification of joint kinematics [1-2]. However, the studies tested elite athletes who have access to professional monitoring for proper performance. Such studies cannot be directly applied to the average recreational athlete who suffers from joint injury. Recent studies on visual feedback on multiple degrees-of-freedom (DOF) have shown promising results when training for simple and complex motor control tasks [3]. However, such feedback increases cognitive load and requires the presence of an instructor. Auditory feedback (AF), though only used for one DOF, allows increased quantified instruction while decreasing the cognitive response time needed by athletes to master a motion [3-4]. We propose to investigate the change in individual knee kinematics and kinetics due to error sonification auditory feedback (ESAF) training of proper squat technique. More specifically, our goal is to test the viability of ESAF training over two DOFs in the sagittal plane during a squat maneuver.

METHODS

Six recreationally active males (age 21-35 years old) were selected to participate in this study. IRB approval was obtained and informed consent given by each participant. Subjects were randomly categorized into ESAF and control groups. Subjects participated in two motion capture sessions (pre and post-training), where they performed 40 squats on two tri-axial force plates (Bertec Columbus, OH) while instrumented with a 42-marker set for the

lower body (Northern Digital, Ontario, Canada). The dominant leg of ESAF subjects was also instrumented with an electric goniometer (Biometrics Ltd, Newport, United Kingdom) to measure knee flexion angle. Subjects were informed how to properly squat based on the assessment criteria of Myer et al. [5]. A 'perfect squat' [5] was collected during the Pre training motion capture session where individual Target Maximum Knee Flexion Angle (TMFA) and center of pressure (COP) were determined for each subject. Training sessions consisted of 40 squats per day Monday through Friday for 4 weeks.

During training sessions, ESAF subjects were instrumented with an electric goniometer on their dominant limb and stood one foot on each force plate. Sessions consisted of four sets of five squats with concurrent feedback and five squats with terminal feedback. Concurrent feedback is categorized as any form of augmented feedback during the task and terminal feedback is after the task has been completed. Sets started with a COP calibration during which the location of their heels (0% COP) and toes (100% COP) were recorded on the force plate. Concurrent feedback emitted two sounds simultaneously, a high-pitched sound signaling error regarding TMFA and a low-pitched sound signaling error regarding COP. As the subject descended into his TMFA, volume of each sound proportionally decreased as the deviation from the target decreased. If the subject descended below his target angle an alarm sounded. Terminal Feedback consisted of two sounds after the squat was performed. The first beep informed the subject if 30% COP was achieved and the second beep if the TMFA was achieved within $\pm 4^\circ$. The control group performed 40 squats per day in the lab without any feedback. After the 4-week training period, subjects participated in the post-training motion capture session.

Pre and post-training marker and force data was filtered through a 6Hz low-pass Butterworth filter. Maximum achieved flexion angle was subtracted from the target angle to determine error. Range of COP was determined by calibration and percent of COP range was calculated at the time maximum flexion angle was achieved. Pre and post-training target flexion error and percent of COP were averaged over the 40 trials.

RESULTS AND DISCUSSION

Our results revealed that, post-training, the ESAF subjects were able to shift their COP posteriorly at maximum knee flexion angle when compared to control subjects (Figure 1). The ESAF group also achieved TMFA within $\pm 4^\circ$ (Figure 2).

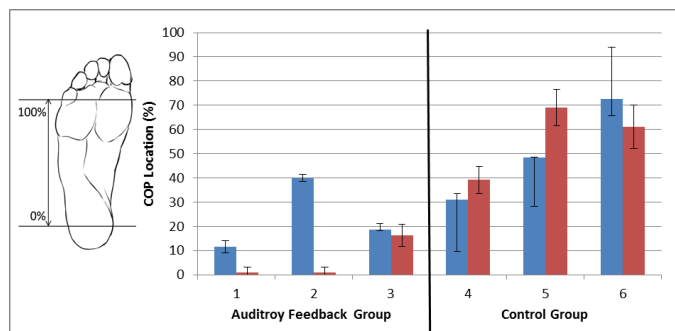


Figure 1 Center of pressure location at maximum knee flexion angle. Pre-training (Blue) and post-training (red) bars represent the average and the whiskers represent ± 1 standard deviation over 40 squats.

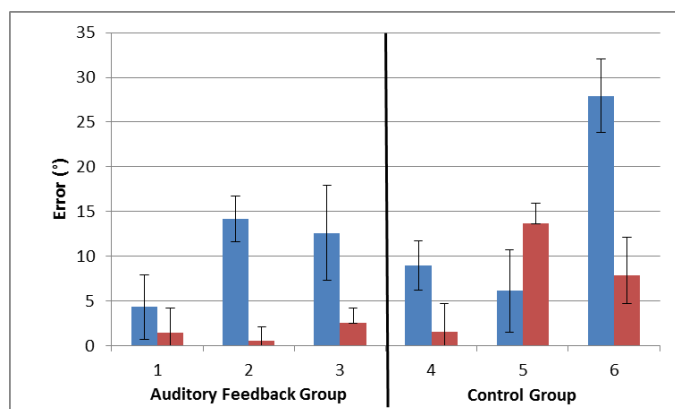


Figure 2 Error from target maximum flexion angle during the squat. Pre-training (blue) and post-training (red) bars represent the average and the whiskers represent ± 1 standard deviation over 40 squats.

These preliminary findings highlighted that error sonification auditory feedback over two degrees of freedom is a viable neuromuscular training modality to further study. Though subjects in the control group also decreased their maximum knee flexion angles after the training period, they also shifted their COP anteriorly, which is not in accordance with proper squatting technique. Thus, the subjects in the control group increased their maximum flexion angle at the expense of proper form, which can lead to joint injuries.

CONCLUSIONS

Over the course of a 4-week fully automated error sonification auditory feedback training protocol, subjects were able to achieve both the target flexion angle and the proper COP location when performing a squat. Results indicated that, for the average 21-35 year-old recreational male, a multiple degree of freedom ESAF neuromuscular training program is a viable training technique for fundamental maneuvers. Further research will address the retention of proper squat terminal position and the effects of neuromuscular squat training on landing phases of complex plyometric maneuvers such as countermovement and depth jumps. Ultimately, these studies could lead to independent individualized neuromuscular training programs to reduce the risk of joint injuries in recreational athletes

REFERENCES

1. Chappell, J. D., & Limpisvasti, O. *The AJSM*, **36**, 1081–6, 2008.
2. Pohl, M, et al *Archives of Physical Medicine and Rehabilitation*, **84**,1760–1766, 2003.
3. Sigrist, R., et al. *Psychonomic Bulletin & Review*, **20**, 21–53, 2013.
4. Riskowski, J. L., *Gait & Posture*, **32**, 242–7, 2010.
5. Myer, G. D., et al. *Strength & Conditioning Journal*, **36**, 4-27, 2014.

ACKNOWLEDGEMENTS

The University of Texas at El Paso STARS Grant (Gonzalez)

The University of Texas Start Up Fund (Hausselle)

PLIÉ FLEXIBILITY IN DANCERS: DIFFERENCE BETWEEN POSITIONS, MEASUREMENT METHODS AND LIMBS

¹Lindsay Harmon-Matthews, PT, DPT; ¹Mariah Nierman, DPT, AT, OCS; ²Nienke Willigenburg, PhD; ²Rachel Tatarski, MS, ATC-L; and ²Timothy E. Hewett, PhD

¹The Ohio State University's Wexner Medical Center, Columbus, Ohio, USA

²The Ohio State University's Sports Health and Performance Institute, Columbus, Ohio, USA
email: Lindsay.Harmon-Matthews@osumc.edu

INTRODUCTION

Since foot and ankle injuries are the most common injuries in dancers [1, 2], understanding ankle biomechanics in dancers is imperative. While dancers regularly utilize maximum ankle plantar flexion, closed chain ankle dorsiflexion is necessary for plié. Plié, a movement similar to a mini squat, involving closed chain knee and hip flexion, is a fundamental dance movement used in nearly every dance genre and is necessary for dancers' jumps and turn preparations. A plié can be performed with neutral hip rotation (parallel plié) or in the turned out position, which involves maximal hip external rotation. Although dancers typically have large plantar flexion ranges of motion, they may lose dorsiflexion with training [3].

Literature on ankle dorsiflexion in dancers is limited. Most studies have limited sample sizes and use either closed chain or open chain measurement methods. Additionally, there have been no known studies that explore dorsiflexion in parallel plié versus turned out plié. Thus, the purpose of this study was to compare ankle dorsiflexion measurement methods by limb. Based on previous literature, greater dorsiflexion angles were expected in closed chain methods. The hypothesis tested was that there would be no difference in angles between parallel and turned out pliés. A second hypothesis tested was that there would be a difference in dorsiflexion between limbs only in open chain.

METHODS

Dorsiflexion was measured three ways during routine screens: open chain with the knee flexed (soleus angle), closed chain in first position plié

(dorsiflexion angle with turnout), and closed chain in parallel plié (dorsiflexion angle in parallel). All angles were measured with a goniometer, which is a reliable method for measuring ankle dorsiflexion in plié [4]. One hundred twenty-six dance academy students gave written informed consent and participated in this study. A 3x2 analysis of variance (ANOVA) compared dorsiflexion measurement methods by limb.



Figure 1: Measurement of ankle dorsiflexion in turned out plié.

RESULTS

As shown in Figure 2, a main effect of ankle dorsiflexion measurement method ($p < 0.001$) was observed. No significant interaction between limb and measurement method ($p = 0.812$) and no significant main effect of limb was observed ($p = 0.495$). Regardless of limb, open chain soleus angle was significantly less than the closed chain dorsiflexion angles both with turnout ($p < 0.001$) and in parallel ($p < 0.001$).

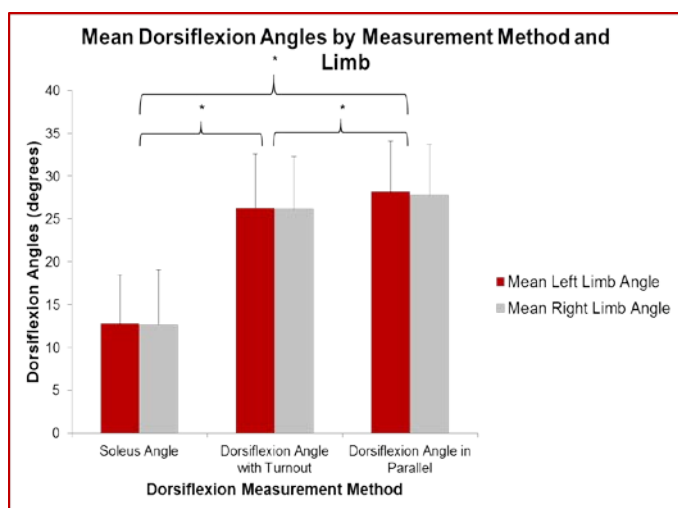


Figure 2: Mean dorsiflexion angles by measurement method and limb.

Specifically, mean soleus angles ($12.8^{\circ} \pm 5.7^{\circ}$ left, $12.7^{\circ} \pm 6.3^{\circ}$ right) were about half the magnitude of both closed chain dorsiflexion angles (turnout: $23.3^{\circ} \pm 6.2^{\circ}$ left, $27.8^{\circ} \pm 5.9^{\circ}$ right and parallel: $28.2^{\circ} \pm 5.9^{\circ}$ left, $27.8^{\circ} \pm 5.9^{\circ}$ right). Also, soleus angles had low significant correlations with both the turned out plié ($r=0.334$, $p=0.004$ left and $r=0.358$, $p=0.002$ right) and the parallel plié ($r=0.31$, $p=0.008$ left and $r=0.434$, $p<0.001$ right) methods (Figure 3).

Non-Weight-Bearing and Weight-Bearing Correlations

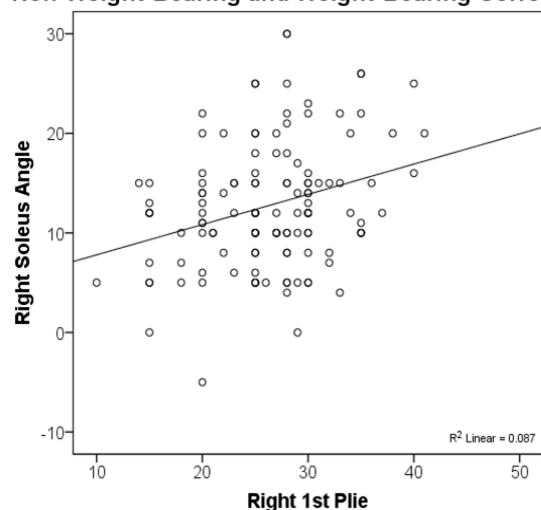


Figure 3: Right soleus angle and right dorsiflexion angle with turnout correlation.

DISCUSSION

These results indicate that measurement of open chain ankle dorsiflexion does not accurately reflect

dancers' plié depths. Although these dancers spend more time training in turnout, the parallel position allows dancers to achieve slightly greater closed chain ankle dorsiflexion than turned out plié and may be a more accurate reflection of their functional flexibility. Consistent with previous literature, soleus angle had a small correlation with the closed chain plié angles, indicating that dorsiflexion should not only be clinically assessed in open chain but also in closed chain positions to understand a dancer's functional plié depth. Future studies should take these differences into account and examine if a relationship exists between ankle dorsiflexion angles and injury occurrence to develop effective injury prevention programs for dancers.

CONCLUSIONS

In dancers, deeper plié dorsiflexion angles could be expected in parallel compared to the turned out position. Non-weight-bearing dorsiflexion angles may not necessarily reflect a dancer's plié depth; therefore, clinical measurement in weight-bearing plié may provide a more accurate representation of the functional closed chain dorsiflexion range of motion utilized in dance movements.

REFERENCES

1. Milan KR. *J Orthop Sports Phys Ther*, **19**, 121-129, 1994.
2. Peer KS, Dubois K. *Athl Ther Today*, **9**, 60-62, 2004.
3. Steinberg N, et al. *Am J Sports Med*, **34**, 814-823, 2006.
4. Russell JA, et al. *Foot Ankle Spec*, **4**, 151-156, 2011.

TURNOUT IN DANCE: EXAMINATION OF MEASUREMENT METHOD AND LIMB ASYMMETRY ACROSS TRAINING LEVELS

¹Lindsay Harmon-Matthews, ¹J. Hope Davis-Coen, ¹Mariah Nierman,
²Nienke Willigenburg, ²Rachel Tatarski, and ²Timothy E. Hewett

¹The Ohio State University's Wexner Medical Center, Columbus, OH, USA

²The Ohio State University's Sports Health and Performance Institute, Columbus, OH, USA
email: Lindsay.Harmon-Matthews@osumc.edu

INTRODUCTION

Turnout in dance requires bilateral lower extremity external rotation, and smaller functional turnout angles may be related to nontraumatic lower extremity and back injuries [1]. While turnout involves active hip external rotation, hip rotation measurements are less than standing functional turnout measurements due to below knee contributions such as tibial version [2]. Dancers who use more functional turnout than available passive hip external rotation have more self-reported lower extremity and back injuries [3]. No gold standard method for measurement of turnout is currently available, although turnout has been previously measured functionally in standing, functionally on rotation discs, and goniometrically in supine and prone [1-5]. Turnout asymmetries have been detected in standing turnout angles when landing jumps [1] and in amounts of tibial torsion [2]. Turnout has not previously been compared between levels of dancers. The purpose of this study was to compare functional standing turnout angles between dancers of different training levels and between floor and disc measurement methods. The hypotheses tested were that 1) dancers would have greater turnout angles on the floor protractor compared to the rotation discs, 2) turnout angles would increase with training level, and 3) right turnout angles would be greater than left turnout angles.

METHODS

Measurements were taken during routine dance screens of 23 professional dancers, 46 academy dance students, and 26 collegiate dance students. Standing functional turnout angles were measured using Functional Footprint® rotation discs and a

floor protractor. Dancers' second metatarsals were aligned with the discs' sagittal plane lines with knees fully extended. Measurements were recorded in degrees from the discs, which allow friction-free external rotation. On the floor protractor, subjects' heels were aligned on the coronal plane line and were asked to turnout as they would in dance class; measurements in degrees were recorded from the line of the second metatarsal. Turnout angles were recorded for left and right limbs, separately. Left and right limb measurements were summed to produce a total turnout angle on the disc and on the floor for each dancer. The absolute difference in turnout angle between limbs was calculated to quantify the magnitude of limb asymmetry. To quantify the direction of limb asymmetry, the right turnout angle was subtracted from the left turnout angle. Three 3x2 analyses of variance (ANOVAs) were used to determine how training group and measurement method affected total turnout angles as well as magnitude and direction of limb asymmetry. A priori alpha level was set at 0.05 to determine statistical significance.



Figure 1: Measurement of functional turnout on floor protractor (background) and Functional Footprint® rotation discs (foreground).

RESULTS

As shown in Figure 2, dancers in each training group demonstrated greater total turnout on the floor compared to the discs ($p < 0.001$), and collegiate dancers had significantly smaller total turnout angles compared to both professionals and academy students ($p < 0.001$). No main effects or interactions of measurement method or training group were observed for magnitude of limb asymmetry. The absolute differences between limbs for each group averaged $4.6^\circ \pm 4.7^\circ$ on the discs and $3.9^\circ \pm 3.4^\circ$ on the floor.

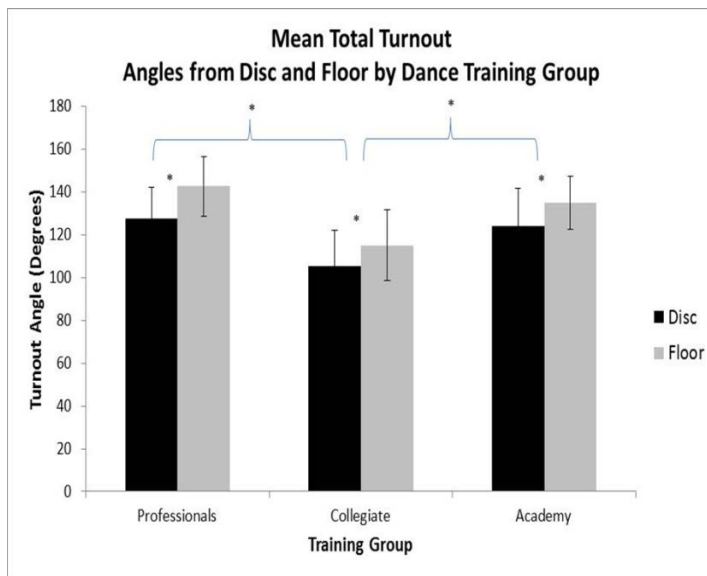


Figure 2: Mean total turnout angles on disc and floor methods for each group.

In the measurement of directional limb asymmetry, a significant interaction between measurement method and training group ($p = 0.047$) indicated that in professionals, left turnout angle was significantly greater than the right turnout angle on the discs ($4.30^\circ \pm 6.64^\circ$) but not on the floor ($0.17^\circ \pm 4.57^\circ$). There was no significant difference in limb asymmetry between methods in academy students ($p = 0.801$) or in collegiate dancers ($p = 0.415$).

DISCUSSION

Regardless of training group, all dancers had $\sim 10^\circ$ greater turnout on the floor compared to the disc measurement method, which is consistent with previous literature [4,5], indicating floor protractor measurements may reflect not only active hip

external rotation but also below knee turnout contributions, compensatory patterns, and use of the friction of the floor to maintain standing functional turnout. Collegiate dancers had smaller turnout angles compared to both the professionals and the academy students, while the professionals and academy students showed similar turnout angles. The only asymmetry that was observed between limbs was detected with the disc method and was shown only in the professional dancers with left turnout angles about 4° greater than right turnout angles; this is in contrast to our hypothesis and to previous studies that found asymmetries in MRI-detected tibial torsion and in total standing turnout following dynamic movements.

CONCLUSIONS

Assessment of functional turnout angles on rotation discs, in addition to on the floor, will provide information about dancers' compensatory patterns below the hip joint when turning out over ground. Turnout did not increase with training level, but was $\sim 20^\circ$ lower in collegiate dancers who primarily trained in modern dance, which may indicate that less turnout can be expected in modern than ballet dancers. Limb asymmetry was observed in professionals on the discs, which may indicate a training effect may lead to limb dominance and limb asymmetry. Future studies will examine if turnout and limb asymmetry are related to injury risk in dancers.

REFERENCES

1. Negus V, Hopper D, Briffa NK. *J Orthop Sports Phys Ther* **35**, 307-318, 2005.
2. Champion LM & Chatfield SJ. *J Dance Med Sci* **12**, 121-135, 2008.
3. Coplan JA. *J Orthop Sports Phys Ther* **32**, 579-584, 2002.
4. Shah S, Weiss DS, Burchette RJ. *J Dance Med Sci* **16**, 17-25, 2012.
5. Grossman G, et al. *J Dance Med Sci* **12**, 142-152, 2008.

RELATIONSHIPS BETWEEN QUADRICEPS STRENGTH SYMMETRY, INTERNAL KNEE AND HIP EXTENSION MOMENT IMPULSE SYMMETRY IS STRONGER IN WOMEN THAN MEN

¹ Erin H Hartigan, ¹ Mike Lawrence, ² Thomas Murray, ² Bernadette Shaw

¹ The University of New England, Portland, ME, USA

² OA Centers for Orthopedics, Portland, ME USA

email: ehartigan@une.edu

INTRODUCTION

Reduced internal knee extension moments are ubiquitous following anterior cruciate ligament (ACL) reconstruction and persist 6 months after progressive rehabilitation in men and women.² The hip joint may compensate for aberrant knee mechanics and the strategy appears to be sex-specific.¹ Preliminary evidence suggests that responses to challenging walking tasks such as walking while towing a weighted sled or wearing a weighted vest are also sex-specific.³ Whether asymmetrical quadriceps strength is related to asymmetrical knee and hip extension moments during normal and challenging walking is unknown. Also unknown is whether asymmetrical knee extension moments is related to the hip extension moment during normal walking and whether knee extension moments during normal gait are related to knee and hip extension moments during challenging tasks. Given the evidence that sexes respond differently to interventions, we chose to investigate these relationships in men and women separately.¹

METHODS

Our 32 subjects (Table 1) met the criteria of an isolated ACL rupture, underwent ACL reconstruction (ACLR) using the hamstring, patella tendon or allograft, were between 5-12 months post ACLR, discharged from physical therapy, and cleared by their surgeon to return to sport.

Testing: Three maximum voluntary isometric quadriceps contractions (MVIQC) were obtained using a Biodex S4 dynamometer set at 90 degrees of knee flexion. The subject's peak torque generated was used for analyses. Gait was analyzed during normal walking and two challenging walking tasks

(load of 50% body weight [BW] while towing a weighted sled attached at the shoulder and wearing a weighted [50% BW] vest). Gait speed was controlled at $1.3 \text{ m/s} \pm 5\%$ for all 3 tasks. Subjects walked normally first and then the order of the two challenging walking tasks was randomized. Motion analysis data were collected using 3D cameras (Qualisys) and force plates with 6 degrees of freedom (AMTI). Data were processed using Visual 3D software (C-Motion). Internal knee and hip extension moment impulses (IKEMI and IHEMI, respectively) were calculated during the initial 25% of the stance phase of gait using inverse dynamics. Five trials of IKEMI and IHEMI were normalized to body weight, and averaged for each limb (Nms/kg). Limb symmetry index [LSI: (involved/uninvolved) *100] were calculated for MVIQC, IKEMI and IHEMI. Descriptive statistics [mean (standard deviations)] were calculated for our variables of interest. Pearson Product-Moment Correlations (PPMC) (r = PPMC coefficient) were used to determine associations between MVIQC LSI and KEMI and HEMI LSI during walking, sled, and vest tasks for men and women. Additionally, PPMC were run to determine whether KEMI LSI is related to HEMI LSI during walking, and if KEMI LSI during walking is related to the KEMI and HEMI during challenging tasks for men and women. Significance was set at $p=.05$. (SPSS, IBM)

RESULTS

Descriptive statistics were run for all variables for men and women (Table 2). For women, MVIQC LSI was associated with HEMI LSI during the sled task only ($r = .58$; $p = .01$). KEMI LSI during normal walking was associated with the KEMI LSI during the sled and vest tasks ($r = .64$ and $.56$,

respectively; $p \leq .01$) and the HEMI during normal walking ($r = -.66$, $p < .01$).

For males, MVIQC LSI did not significantly relate to any KEMI or HEMI LSI for any task. KEMI LSI during walking was associated with the KEMI LSI during the vest task ($r = .60$; $p = .04$).

DISCUSSION

Relationships between variables were different for men and women. For women, asymmetrical quadriceps strength was only associated with HEMI during the sled task. Asymmetrical knee moments used by female subjects during walking were associated with the magnitude of knee asymmetry during more challenging tasks: towing a sled and wearing a weighted vest. For men, no significant relationships between strength symmetry and KEMI and HEMI symmetry were found. For men, the only significant relationship was found between KEMI symmetry when walking normally and KEMI symmetry when wearing a weighted vest.

CONCLUSIONS

Interestingly, relationships between asymmetrical isometric quadriceps force and asymmetrical internal knee extension moments during normal and challenging gait were not found for men or women after ACLR. However, a stronger relationship

between asymmetrical KEMI during walking normally and when challenged existed in women than men.

REFERENCES

1. DeVita P, Hortobagyi T, Barrier J. Gait biomechanics are not normal after anterior cruciate ligament reconstruction and accelerated rehabilitation. *Med. Sci. Sports Exerc.* 1998;30:1481-1488.
2. Di Stasi S, Hartigan EH, Snyder-Mackler L. Sex-Specific Gait Adaptations Prior to and up to 6 Months After Anterior Cruciate Ligament Reconstruction. *J. Orthop. Sports Phys. Ther.* 2015;45:207-214.
3. Hartigan E, Murray T, B. S, M. L. Challenging Walking Increases Knee And Hip Moments In Patients After ACL Reconstruction. *APTA Combined Sections Meeting Indiana*: 2015.

ACKNOWLEDGEMENTS

We acknowledge the University of New England's Patient Population Oriented Research grant for funding this project.

Table 1: Subject Demographics, Mean (SD)

Subjects	Months since surgery	Mechanism of injury	Age (yrs)	Body Mass Index (kg/m ²)
19 Female	7.7 (1.9)	5 contact; 14 non-contact	23.1 (9.3)	24.0 (3.6)
12 Male	7.1 (2.0)	6 contact; 6 non-contact	25.0 (12.6)	25.9 (4.3)

Table 2: Limb Symmetry Index (percentage) for Strength and Moment Impulse Data, Mean (SD)

	MVIQC	Walk KEMI	Walk HEMI	Sled KEMI	Sled HEMI	Vest KEMI	Vest HEMI
Women	64.2 (13.9)	80.3 (29.7)	74.1 (14.8)	85.3 (28.8)	107.0 (25.6)	123.9 (32.5)	104.9 (24.0)
Men	73.3 (12.1)	96.9 (24.7)	82.4 (24.9)	95.1 (33.7)	103.0 (22.7)	113.8 (37.1)	102.5 (20.0)

PERFORMANCE BIOMECHANICS OF RUNNING AND CUTTING TASKS

Kathryn L. Havens, Susan M. Sigward

Human Performance Laboratory

Division of Biokinesiology and Physical Therapy

University of Southern California, Los Angeles, CA, USA

email: khavens@usc.edu, web: www.usc.edu/go/mbrl

INTRODUCTION

The ability to change direction quickly while running is a prerequisite for participation in multi-directional sports. Athletes must be agile, changing direction quickly in response to many types of stimuli. [1] The importance of agility in sports is underscored by its use as an indicator of talent [2] as well as a determinant of player selection into teams. [3]

Many factors have been proposed that may influence the ability of an individual to perform change of direction tasks effectively. Among these factors are anthropometrics, leg muscle quantities, straight running speed, and technique. [4] While some studies have suggested that straight running speed is not related to agility performance, [1,5] others have found the opposite is true. [4] These studies have only studied completion time. However, the biomechanics underlying these relationships has not been investigated.

While changing direction is important for athletic performance, cutting is also associated with non-contact anterior cruciate ligament (ACL) injury. [6,7] Because of this, research has focused on the relationship between change of direction mechanics and potentially injurious knee joint loading. [8,9] However, the biomechanics underlying successful performance of cutting tasks is less well understood.

Performance of cutting tasks likely relies on both effective change of direction mechanics and fast running performance. However, it is currently unclear whether the biomechanics associated with fast cutting performance are the same as those associated with fast running performance.

The purpose of this study was to identify relationships between 3-dimensional (3D) hip, and sagittal plane knee and ankle kinetics and 3D

ground reaction forces (GRF) and performance of running and cutting tasks.

METHODS

Twenty-five healthy soccer players (12 females) with no history of previous knee injury participated. Average age, height and weight were 22.4 ± 3.9 yrs, 1.74 ± 0.1 m and 70.9 ± 9.3 kg, respectively.

Subjects performed a straight running task, and a sidestep cutting tasks to 45° as fast as possible. For the running task, subjects ran for 15 meters. For the cutting task, subjects ran 7.5 meters, planted their dominant foot on the force plate and changed direction away from the plant leg at 45° and continued running for 7.5 meters. (Fig. 1).

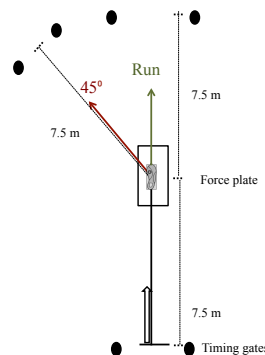


Figure 1: Experimental set-up for right dominate subject. Open arrow indicates original line of progression.

Three-dimensional kinematics were collected using a 10-camera motion capture system (Qualisys, Inc. Sweden), 250 Hz. Ground reaction forces (GRF) were quantified using AMTI force platforms (Newton, MA, USA), 1500 Hz. Laser timing gates (Brower, UT, USA) were used to determine the time to complete the tasks. Inverse dynamics was used to calculate net joint moment and power. Peak 3D hip and sagittal plane knee and ankle moments, peak GRFs and average power were determined. Data was normalized to body weight.

Pearson's correlations were used to determine the relationship between task completion time and variables of interest ($p < 0.05$).

RESULTS AND DISCUSSION

Better performance (shorter completion times) of the 45 degree cutting task was associated with better performance of the run task ($r=0.942$, $p<0.001$), greater average hip sagittal power generation, peak ankle plantarflexor moment, and peak anterior GRF (Table 1).

Better performance of the running task was associated with greater peak hip extensor and external rotator moments, average hip sagittal power generation and peak anterior GRF.

Unlike other studies, [1,5] the results of this study indicate that cutting performance is highly related to running performance. This may be related to the tasks used. While some agility tasks require many changes of direction as well as movement in other planes, [10] this cutting task, with only one change of direction, may be more similar to straight running.

Interestingly, the results showed some but not complete overlap in the mechanics associated with the two tasks. For both tasks, anteriorly directed GRF and hip sagittal plane power generation were related to performance of both tasks. Together, these results suggest the importance of propulsion for fast performance, with athletes using the hip joint to drive the body forward.

Hip engagement may be more beneficial to running, as the majority of mechanics related to run performance were hip variables. In contrast, these data suggest that sagittal plane engagement at the ankle as well as the hip may benefit cutting performance.

This study provides insight into the relationship between the biomechanics associated with running and cutting tasks. More data is needed to understand if these relationships hold with other types of cutting or agility tasks.

REFERENCES

1. Young & Farrow, *Strength Cond*, **28**(5), 24-29, 2006.
2. Reilly et al. *J Sports Sci* **18**(9), 695-702, 2000.
3. McGee & Burkett, *J Strength Cond Res*, **17**(1), 6-11, 2003.
4. Young et al. *J Sport Med Phys Fit* **42**(3), 282-88, 2002
5. Little & Williams *J Strength Cond Res* **19**(1), 76-78, 2005
6. Boden BP, et al. *Orthopadics* **23**, 573-8, 2000.
7. Cochrane JL, et al. *J Sci Med Sport* **10**, 96-104, 2007.
8. Sigward & Powers. *Clin Biomech*, **21**(1), 41-48, 2006.
9. McLean et al. *Clin Biomech* **20**(8) 863-870, 2005.
10. Brughelli et al. *Sports Med* **38**(12) 1045-63, 2008.

Variable	Average \pm SD	Correlation coefficient	p-value
45 degree cutting task			
Completion time (sec)	2.62 \pm 0.22		
Hip sagittal power generation (Watts/kg)	6.66 \pm 3.50	-0.475	0.016
Ankle plantarflexor moment (Nm/kg)	-3.04 \pm 0.53	0.450	0.024
Anterior GRF (N/N)	0.67 \pm 1.0	-0.493	0.012
Run task			
Completion time (sec)	2.69 \pm 0.23		
Hip extensor moment (Nm/kg)	-3.86 \pm 0.98	0.607	0.001
Hip external rotator moment (Nm/kg)	-1.25 \pm 0.59	0.558	0.004
Hip sagittal power generation (Watts/kg)	9.74 \pm 2.82	-0.483	0.015
Anterior GRF (N/N)	0.69 \pm 0.08	-0.535	0.006

Table 1: Biomechanics significantly correlated to completion time of a 45 degree cutting task and run task

Poster #420 has been withdrawn.

Poster #420 has been withdrawn.

ACL INJURY TRENDS BY POSITION AND TEAM ACTIVITY IN THE NATIONAL FOOTBALL LEAGUE BETWEEN 2009-2014

¹Joshua T. Hoffman, MS, ²Christopher Nagelli, BS, ¹Samuel C. Wordeman, PhD, and ¹⁻⁵Timothy E. Hewett, PhD

¹Sports Health and Performance Institute (SHPI) OSU Sports Medicine, ²Department of Biomedical Engineering, ³School of Health and Rehabilitative Sciences, ⁴Department of Orthopaedics, ⁵Department of Physiology and Cellular Biology and Family Medicine, Ohio State University, Columbus, OH

INTRODUCTION

The average National Football League (NFL) player that suffers an anterior cruciate ligament (ACL) rupture requires approximately 10.8 months prior to return to sport (RTS) [3]. While reconstructive surgery and physical therapy after ACL injury cost approximately \$17,000, the time lost by high-profile NFL athletes may amount to millions of dollars in player compensation and a loss of athletic prowess [1]. Most injuries per athletic exposure (AE) occur during games, but the effect of activity (i.e. games and practices) and position on the total number of ACL injuries per season is less clear [3]. Therefore, the purpose of this study was to determine the impact of activity and position on the number of ACL injuries per season.

METHODS

ACL injuries were recorded between the 2009-10 and 2013-14 seasons, for a total of five seasons. A full season was described as the period between the conclusion of the previous Super Bowl to the end of the Super Bowl of the season in question. Several websites (including, but not limited to, <http://www.pro-football-reference.com/>, <http://www.rotoworld.com/> and <http://espn.go.com/>) that list NFL injuries were utilized for this study. A compilation of knee injury listings were investigated to determine whether that injury was an ACL rupture. For each player listed with a knee injury, a Google search that included the athlete's name, year of injury, and keywords, such as "ACL rupture" or "ACL injury", was performed. News articles and team reports were used to confirm injuries. Once an injury was confirmed, the activity and position were recorded.

Activity was divided into game scenario, practice, and not available. The activity associated with not available injuries was unable to be determined. Player position was categorized as skill, lineman, special teams, or other. Skill players included

running backs, wide receivers, quarterbacks, and defensive backs. Offensive and defensive linemen were classified as linemen. Special teams was comprised of kickers, punters, and long snappers. Finally, linebackers and tight ends comprised the 'other' category.

Descriptive statistics for all injury categories were calculated for each of the five seasons. Finally, a pair-wise *t*-test was used to determine if there was a significant difference between game and practice ACL injuries per season.

RESULTS AND DISCUSSION

During the five seasons studied, a total of 253 ACL injuries occurred for an average of (mean \pm standard deviation) 50.6 ± 7.6 per season. Of these, game scenarios and practices were responsible for 37.0 ± 2.4 injuries per year and 12.8 ± 6.0 injuries per year, respectively. Games were responsible for a significantly greater ($p < 0.001$) number of ACL injuries per season. Injuries that could not be attributed to a game or practice accounted for 0.8 ± 0.8 injuries per season. Offensive and defensive skill players accounted for 23.8 ± 4.9 injuries per season, and offensive and defensive linemen suffered 13.0 ± 4.9 injuries per season. Special team players suffered an average of 1.8 ± 1.3 injuries per season, and other players accounted for 12.0 ± 2.5 injuries per season.

Injury surveillance data from the 2009-10 to 2013-14 seasons support previous findings that games are responsible for a greater number of ACL ruptures than practice [2]. However, the current findings indicate that injuries that occur during practice, training camp, and OTA account for nearly all of the variability in total ACL injuries throughout the season. (Figure 1). Therefore, the change in the total number of ACL injuries each season is most likely a result of the nature of team practice. As such, changes in training methods outside of games may be

effective in reducing total ACL injuries throughout the season.

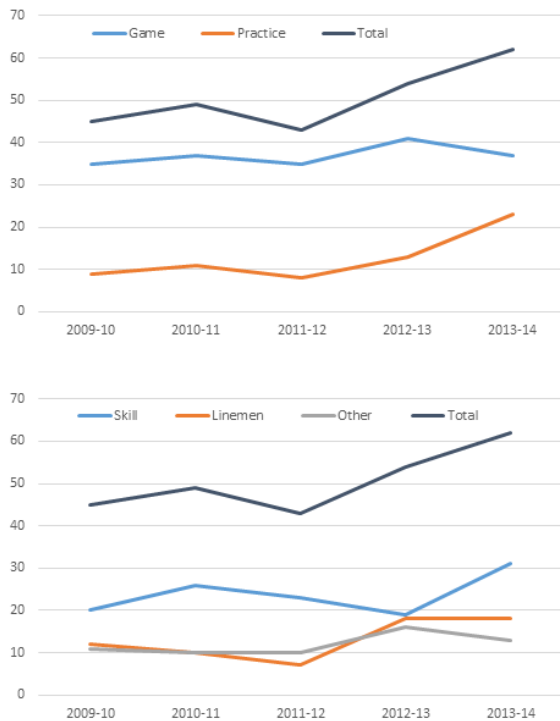


Figure 1. ACL Injuries per Season in the NFL: This figure demonstrates the number of ACL injuries that occur during games and practices [top (a)] and in skill, linemen, other players [bottom (b)] compared to the total number of injuries.

The recent collective bargaining agreement reduced the contact allowed and decreased the time allotted for practice. However, the current data indicates that since the rule change ACL injuries during practice have more than doubled. While these rule changes limit athletic exposures and should prevent contact injuries, approximately 70% of ACL ruptures are caused by a non-contact injury mechanism [2]. Analysis of strength and neuromuscular control can be utilized to identify athletes that are at increased

risk for a non-contact ACL injury. Subsequently, neuromuscular training protocols can be used to improve landing mechanics and decrease risk. Currently, the NFL utilizes several tests, such as the functional movement screen (FMS), to address individual injury risk, but these methods must be improved. Furthermore, proper neuromuscular training should be integrated into team activities to supplement rule changes directed to decrease injuries.

This study was limited by a lack of public access to comprehensive injury reports. While the authors have gone to exhaustive lengths to ensure that our injury data represents all ACL injuries during each season, it is possible that some players were left off the injury lists that we utilized. In addition, injury rates are generally reports per athletic exposures. However, we were unable to attain the number of athletic exposures per activity or position.

Future research should focus on the effects of rule changes on ACL injury rates. In addition, more inclusive injury lists are necessary to determine the total number of ACL injuries. With this information, the NFL can institute proper rules and training programs to reduce ACL injuries.

REFERENCES

1. Hewett, T. E. *Am J Sports Med* **33**, 492-501, 2005.
2. Boden, B.P., et al. *Orthopedics* **23**, 573-8, 2010.
3. Shah, VM, et al. *Am J Sports Med* **38**, 2233-39, 2010.

ACKNOWLEDGEMENTS

The authors would like to acknowledge the OSU Sports Medicine Research Staff.

	2009-10	2010-11	2011-12	2012-13	2013-14	Mean	Std Dev
Game	35	37	35	41	37	37	2.19089
Practice	9	11	8	13	23	12.8	5.38145
Skill	20	26	23	19	31	23.8	4.354308
Lineman	12	10	7	18	18	13	4.38178
Other	11	10	10	16	13	12	2.280351
Total	45	49	43	54	62	50.6	6.829348

Table 1. ACL injuries per season by activity and position in the NFL

Fatigue Effects on Lower Extremity Coordination and Coordination Variability During Multi-joint Ballistic Movement

Adam E. Jagodinsky, Christopher Wilburn, Lorraine Smallwood and Wendi H. Weimar

Auburn University, Auburn, AL, USA

email: aej0015@auburn.edu

INTRODUCTION

Lower extremity multi-joint movements are abundant in sport and sport-related training, often occurring in a repetitive, ballistic nature. When fatigue is evident, understanding coordination strategies adopted by an athlete during ballistic tasks has implications for performance outcomes and injury prevention. As a tenet of dynamic systems theory, variability in coordination patterns is thought to provide information regarding the state of the motor system during a given task and can be used to describe the integrity of a given movement strategy [1]. However, application of such concepts to lower extremity ballistic movements related to sport is lacking. Therefore, the purpose of this project was two fold: (1) to assess coordination and coordination variability (CV) during a repetitive lower extremity ballistic motion; and (2) to investigate the influence of fatigue on lower extremity coordination patterns while performing a ballistic movement.

METHODS

Five healthy and currently resistance training males (age: 23.4 ± 3.4 yrs; weight: 89.73 ± 10.5 kg; height: 1.75 ± 0.1 m) participated in the study, which was approved by the Institutional Review Board. Participants were asked to report on Day 1 for familiarization of the experimental task. During Day 2, participants performed the experimental protocol. The experimental protocol asked the participant to perform kettlebell swings using a 24kg load. The specific movement consists primarily of a loading phase (flexion at the hip, knee, and dorsiflexion at the ankle) followed by a propulsion phase (extension at the hip and knee with ankle plantar flexion), similar to a vertical jump motion. The protocol consisted of one continuous set of repetitions of the experimental

movement until the participant reached self-reported exhaustion. Each repetition represented one cycle of movement and data from each cycle was interpolated to 150 points to allow comparison between cycles. To avoid including unrepresentative cycles related to movement initiation and cessation, the first and last three trials were excluded from analysis. Subsequently, the first ten (T1) and last ten (T2) cycles represented movement from a pre-fatigue and fatigue state respectively.

A ten-camera optical motion capture system (VICON Technology, Los Angeles, CA) was used to obtain kinematic measurements during the experimental protocol. Lower extremity joint angles and velocity were calculated from marker data and used to construct phase portraits (joint angular displacement versus its rate of change) for the hip, knee and ankle joints.

Continuous Relative Phase (CRP) was used to assess the relative motion of the hip, knee and ankle throughout the entire movement cycle [2]. From the phase portrait, phase angles were obtained and relative phase angles were calculated for knee-hip (K-H), ankle-hip (A-H) and ankle-knee (A-K) by subtracting the proximal joint phase angle from the distal joint phase angle at each point within the time series. The relative phase angle represents the spatial/temporal disparity or congruity between joints within a cycle of movement. Mean absolute relative phase (MARP) was calculated as the average absolute value of relative phase mean ensemble. Larger MARP values indicate more sequential or out-of-phase relative motion while smaller values indicate more simultaneous or in-phase relative motion. Deviation Phase (DP) was calculated to assess the stability of the organization of the neuromuscular system and was determined by taking the mean of the standard deviations of the

ensemble relative phase points. Lower DP values indicate a more stable joint coupling relationship while larger DP values suggest reduced stability joint coupling relationship.

RESULTS

Results from paired-samples t-tests indicated that for all joint couplings, changes in coordination (K-H, $p=0.30$; A-H, $p=0.49$; A-K, $p=0.49$) and CV (K-H, $p=0.38$; A-H, $p=0.53$; A-K, $p=0.26$) from T1 to T2 were not statistically significant.

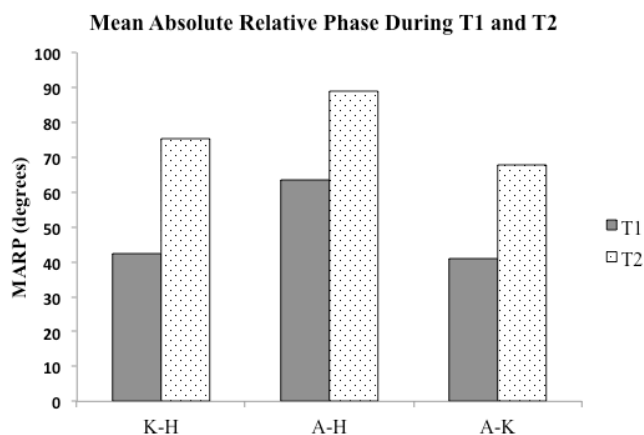


Figure 1: Mean absolute relative phase, as a measure of joint coordination for each joint coupling at T1 and T2.

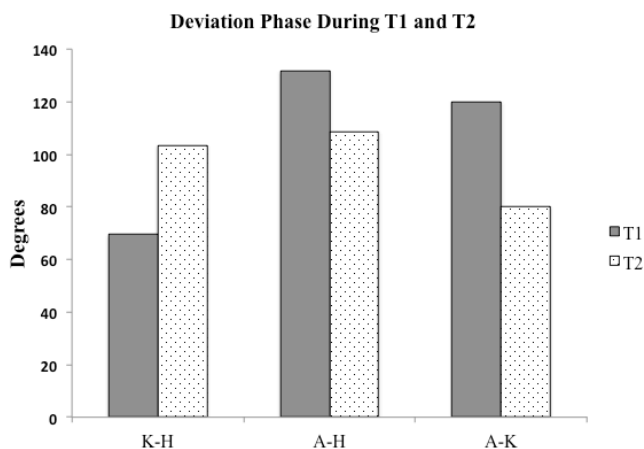


Figure 2: Deviation phase for each joint coupling as a measure of coordination variability at T1 and T2.

DISCUSSION

This project adopted a novel approach to assess coordination and CV during a repetitive ballistic

movement. Although the data failed to reach statistical significance, this project has yielded some interesting findings. First, statistical outcomes suggest that from a pre-fatigued to fatigue state, lower extremity coordination patterns during a ballistic movement are similar. However, for all three joint couplings a considerable difference is noted for the MARP (Figure 1). Data presented in Figure 1 indicates a trend of more in-phase relative motion during pre-fatigue cycles. However, each joint coupling exhibited more out-of-phase behavior with fatigue, suggesting more independent joint motion. In general, lower extremity coordination strategies were highly flexible for each joint coupling (Figure 2), which may be beneficial when high loads are imposed on the system. However, with fatigue A-H and A-K motion became less variable. The less flexible arrangement between A-H and A-K was contrasted by greater variability between K-H during T2. This could be explained by the reduced capacity of the motor system to control more distal joints with fatigue while great flexibility in K-H motion was required for satisfying task requirements.

To account for limitations, expansion of this project will consider the loading and propulsion phases independently in addition to increasing the sample size.

REFERENCES

1. Kelso JA. *Dynamic Patterns*, MIT Press, 1995
2. Burgess-Limerick R, et al. *J Biomch* **26**, 91-94, 1993

UNLOADING REACTIONS DURING SUDDEN ANKLE INVERSION IN INDIVIDUALS WITH FUNCTIONAL ANKLE INSTABILITY

¹Tarang Jain, ^{2,3}Wen Liu, and ³Clayton Wauneka

Department of Physical Therapy and Athletic Training, Northern Arizona University, Flagstaff, AZ, USA

² Department of Physical Therapy and Rehabilitation Science, University of Kansas Medical Center, Kansas City, KS, USA

³ Bioengineering Program, University of Kansas, Lawrence, KS, USA

Email: Tarang.Jain@nau.edu, web: <http://www.pters.kumc.edu/research/neuromuscular-research-lab/index.html>

INTRODUCTION

Functional ankle instability (FAI) is defined as a condition whereby an individual reports feelings of ankle joint instability and/or frequent episodes of ankle “giving way” [1]. The neurophysiological mechanisms causing FAI are unknown, but FAI is considered to be heterogeneous clinical issue that involves multiple factors such as impaired proprioception, neuromuscular control, postural control, and strength deficits [1]. Recently, Santos et al. [2] demonstrated that during a potential injury event, individuals may utilize flexion reflexes, also known as “unloading reactions”, to reduce the vertical load on the supinated foot and thus reduce the risk of ankle sprain injuries. These unloading reactions were characterized by simultaneous movement of the body downwards and a shift of body weight towards the non-stimulated foot. Santos et al. [3] further compared a group of individuals with FAI to a healthy control group and found a hyper-reactivity to unloading reaction in FAI ankles under a normal static ankle stretch. The findings suggested that a static stretched ankle position led to significantly greater unloading reaction in healthy ankles, and ankles with FAI showed greater unloading reaction compared to the healthy ankles. However, the amount of unloading reaction observed was far less than a drastic reaction that usually occurs during ankle giving way. Therefore, the purpose of the present study was to test the sensitivity of unloading reactions in individuals with FAI under a combined sensation of dynamic stretch and nociceptive stimuli. We hypothesized that individuals with FAI would show increased magnitude of unloading reactions on the involved ankle under a combined sensation of dynamic stretch and nociceptive stimuli when compared to uninvolved ankle.

METHODS

We conducted our experiments on twenty-four subjects with FAI (8 males, 16 females; age: 433.9 ± 7.5 years, height: 171 ± 9.24 cm; weight: 75.5 ± 13.4 kg). Participants were at least four weeks but not beyond one year after an unilateral ankle sprain (>grade II), with ongoing ankle giving way incidence during functional activities, and active in exercise. The individuals were excluded if they had severe ankle pain and swelling, ankle surgery, gross limitation in ankle inversion (<15°), lower extremity injuries other than ankle sprain in past 12 weeks, current enrollment in formal rehabilitation program, any severe joint disease, or any previous experience of intolerance to electrical stimulation.

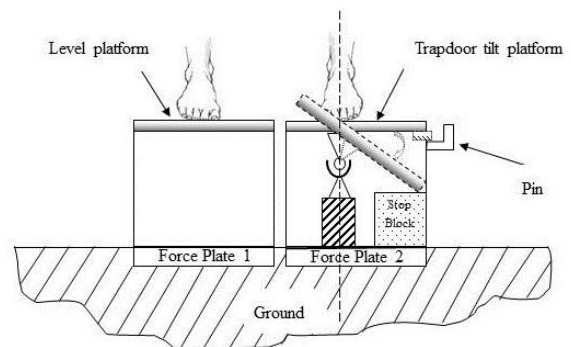


Figure 1: Illustration of the experimental setup.

Two force plates were used to record ground reaction forces of both limbs. Two surface electrodes (3x3 cm) were placed at the lateral aspect of the tested ankle, below and anterior to the lateral malleolus, to deliver nociceptive stimulation. A newly developed trapdoor had a tilt platform held at a level position by a remote-controlled deadbolt which, when released, allowed the platform to rotate 30° before hitting a mechanical stop (**Figure 1**). The subjects distributed equal weight on both feet while keeping one foot on a level wooden box and the tested foot on the tilt platform centered over the pivot joint.

During unloading reaction test, the trapdoor was released without a warning. The subject went through the first five trials of the trapdoor drop test without nociceptive stimulation (“no stim”), followed by five trials of the combined trapdoor drop and nociceptive stimulation (“with stim”). The nociceptive stimuli were delivered to the tested ankle at a level of 20% above the tolerable pain threshold when the trapdoor rotated for about 20-25 degrees. The vertical force variation (VFF) defined as the magnitude of decrease in the combined vertical ground reaction forces was measured for both the involved and uninvolved limb. Paired t-test was used in statistical analysis.

RESULTS

The magnitude of the unloading reactions increased progressively in the following order: (1) Uninvolved ‘no stim’ (54.48 N), (2) Involved ‘no stim’ (57.57 N) (3) Uninvolved ‘with stim’ (61.93 N), and (4) Involved ‘with stim’ (120.63 N) (**Figure 2**). The time to peak VFF on the stimulated foot demonstrated similar values under the four testing conditions. With the number of subjects available ($n = 24$), the VFF magnitude and time to peak VFF were not significantly different between the four conditions ($p > 0.05$).

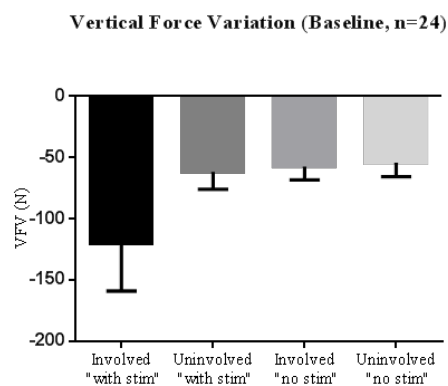


Figure 2: The mean \pm S.E. of the vertical force variations (VFF) during the four conditions.

Based on the video recordings during the testing, seven subjects (age, 38.3 ± 6.6 years; 2 males; weight, 82.0 ± 15.1 kg; height, 171.3 ± 7.5 cm) were identified to have drastic response (hyper-reactivity) to the unloading reaction test. During the trapdoor drop test, these seven subjects were unable to maintain an upright standing position and unloaded their body weight onto the safety harness. The mean magnitude of the unloading reactions in these seven

subjects was greatest during the involved ‘with stim’ condition (325.05 N) when compared to involved ‘no stim’ (111.47 N), uninvolved ‘with stim’ (117.19 N), and uninvolved ‘no stim’ (94.59 N) conditions. The time to peak VFF was similar during the four testing conditions.

DISCUSSION

The magnitude of unloading reactions in the four testing conditions were found to be significantly stronger than the unloading reactions reported by Santos et al. [3]. Although the VFF magnitude did not differ significantly between the four testing conditions, some subjects demonstrated drastic reaction (hyper-reactivity) to the unloading reaction when a combination of dynamic ankle stretching and nociceptive stimuli was applied on their affected ankles (involved ‘with stim’ condition). The video recording during the testing revealed that these subjects were unable to maintain control of upright standing position and unloaded their body weight to the safety harness. Previous studies have indicated that in healthy individuals, hierarchy of postural control is prioritized [4]. During a potential injury event, the flexor reflex is suggested to be modulated in such a way that the primary importance is given to preservation of balance while ensuring an appropriate withdrawal. It appears that in individuals with FAI, modulation of the flexion reflex is affected resulting in impaired descending inhibitory control and/or increased sensitivity to the spinal reflex loop and thus, lack of appropriate use of the unloading reaction.

The drastic reaction (hyper-reactivity) in some subjects may not have occurred because the intensity of ankle stretching or nociceptive stimuli did not reach individual threshold for triggering a drastic reaction. It is also possible that some individuals with FAI might not have hyper-reactivity to unloading reaction. Nevertheless, the drastic reactions showed in involved “with stim” trials indicated a unique reaction pattern in some individuals with FAI.

REFERENCES

1. Hertel J. *J Athl Train*. 2002;37(4):364-375.
2. Santos MJ, Liu W. *Gait & posture*. 2007;26(1):106-112.
3. Santos MJ, et al. *Gait & posture*. 2008;27(4):589-594.
4. Bent LR, et al. *Brain research*. 2001;914(1-2):100-105.

The effects of an exhaustive run on multi-muscle patterns in forefoot runners

¹ Carl Jewell, ² Vinzenz von Tscharnier and ¹ Katherine Boyer

¹ University of Massachusetts Amherst, Amherst, MA 01003

² Human Performance Laboratory, University of Calgary, Calgary, Alberta, Canada
email: cjewell@kin.umass.edu

INTRODUCTION

In recent years, a significant increase in popularity has brought forefoot running into greater prominence in the running community. Despite this popularity, much remains unknown about the effects of forefoot (FF) running on muscle function and mechanics over long distances. Previous literature has indicated that maintenance of a FF strike pattern is impaired during endurance events, and that these changes may indicate fatigue in the plantar-flexor muscles [1]. To combat this plantar-flexor fatigue, an alternative coordination of lower extremity muscles may be used. In the present study, an exhaustive run protocol was used to investigate potential changes in multi-muscle electromyographic (EMG) intensity patterns in forefoot runners to test the hypothesis that there are changes in muscle coordination patterns between the beginning and end of, as well as progressively throughout, the exhaustive run.

METHODS

Thirteen recreational (>22 km/week) habitual forefoot runners were recruited for this study. Each subject performed an exhaustive run on an instrumented treadmill at a pace determined by prior race data (mean run duration: 15.4±2.2 minutes) while EMG data were collected at one-minute intervals using a Trigno Wireless System (Delsys, Inc) sampling at 2000 Hz. Skin and electrodes were prepped and placed according to SENIAM guidelines for the following: Medial and Lateral Gastrocnemius (MGAS, LGAS), Soleus (SOL), Tibialis Anterior (TA), Rectus Femoris (RF), Vastus Medialis (VM), and Biceps Femoris (BF).

EMG signals were decomposed into both time and frequency space using a previously developed

method of wavelet analysis [2]. Foot strike was determined from vertical ground reaction forces and EMG signals were analyzed for 200 ms pre and post-foot strike. Raw EMG from five strides were averaged together to create mean activation patterns for 10 trials evenly spaced in time throughout the run. From these data, each signal was decomposed into 13 wavelets for each muscle and plotted against time [2] (Figure 1). These wavelets were then transformed into a single 1×7371 column vector containing the data from all 7 muscles for each subject and time-point in the run. These column trial vectors were concatenated to create a 130×7371 input matrix for further analyses.

Principal component analysis was performed on the input data matrix as previously described [3]. The eigenvectors, or principal components (PC), and eigenvalues of the covariance matrix were calculated. These represent the primary directions of variation and the amount of variation explained, respectively, in the EMG data. Each of these PC represents a principal pattern (PP) of EMG activation for all lower extremity muscles tested. The PP used in further analyses were selected as those that described at least 1% of the variance in the data. The data vectors for each subject can further be represented as a set of coordinates in a new *pattern space* (*p-space*). Thus, each subjects' trial vector can be represented as a mean waveform plus a weighted linear combination of the PP. Each of these weight factors was determined by projecting the trial vectors onto the respective PP.

Multiple paired t-tests were performed to compare the weight factors of the retained PP between the first and last trials of the run. Linear mixed effects models were used to test for changes occurring throughout the run, varying by trial with subject as a random factor. A X^2 test was used to determine if

time in run had a significant effect on the PP weight factor. The alpha level was set at $p=0.05$.

RESULTS AND DISCUSSION

Ten PP were found explaining at least 1% of variation in the EMG intensity patterns. Together these PP explained 88.1% of the overall variance in the data. The most variation explained by the first principal pattern (PP1) was 57.6%. Of these 10 selected patterns, only PP2, which explained 8.4% of the variance, was found to be significantly different between the weight factor at the beginning and end of the run ($p=0.04$). This supports our hypothesis that coordination patterns of lower extremity muscles were altered by run's end.

A significant effect on time on the weight factors was found for PP1 and PP2, with $X^2 = 4.11$; $p=0.043$ and 9.75 ; $p=0.002$, respectively. The slopes corresponding to these models indicated a reduction in the weight factor over time throughout the run. These results indicate that as the length of time running increased, the contributions of PP1 and PP2 to the original EMG signals were reduced, supporting our second hypothesis that muscle activation changes occurred progressively throughout the exhaustive run.

CONCLUSIONS

The results of this study suggest that forefoot runners experienced a change in patterns of EMG activation of major lower extremity muscles over the course of the exhaustive run. It is likely that these changes in muscle coordination patterns are closely related with changes in joint kinematics previously identified with this same protocol. Further investigations will address the specific nature of the PP changes and the relationship with changes in joint kinematics.

REFERENCES

1. Hasegawa, H. et al. *Journal of Strength and Cond Res*, **21**, 888-893, 2007.
2. von Tscharner, V. *J Electromyography and Kin*, **10**, 433-445, 2000.
3. von Tscharner, V. *J Electromyography and Kin*, **12**, 479-492, 2002.

ACKNOWLEDGEMENTS

The authors would like to thank Dr. Joseph Hamill for his contributions to this project.

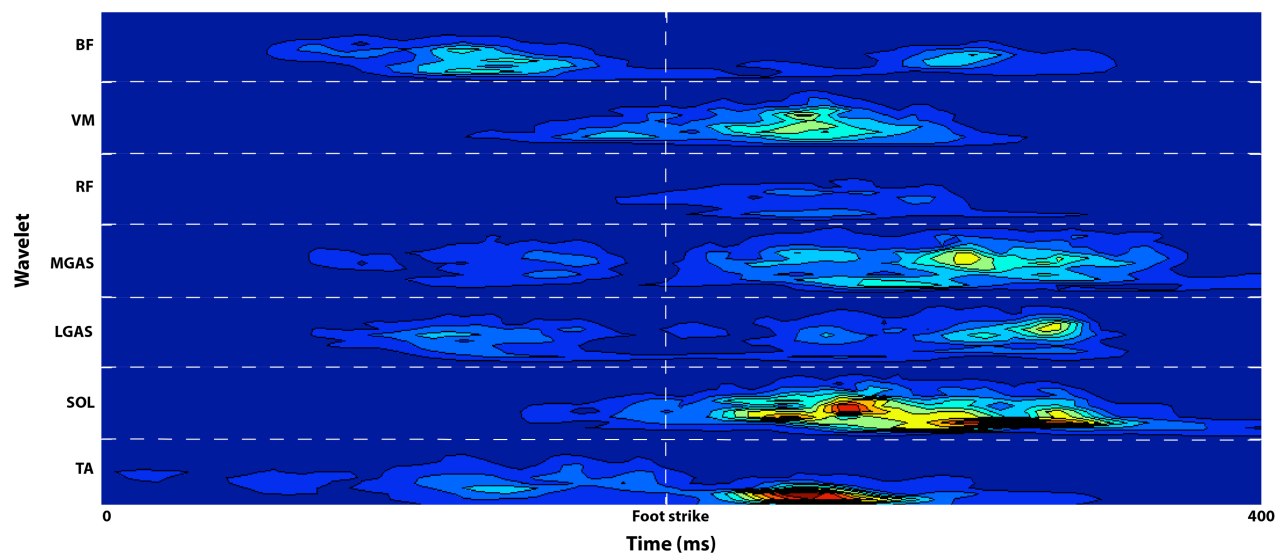


Figure 1. This figure depicts a representative EMG intensity pattern of wavelet versus time at the beginning of the run for one subject. The vertical dashed white line represents foot strike. 200 ms pre- and post- foot strike are shown. On the y-axis, thirteen wavelets are plotted for each of the seven collected muscles, with wavelet 1 at the bottom of each individual muscle section and wavelet 13 at the top.

EFFECTS OF FOOT STRIKE PATTERN AND STEP FREQUENCY ON ACHILLES TENDON STRESS DURING RUNNING

Michael Lyght, Matthew Nockerts, Thomas Kernozek, and Robert Ragan

University of Wisconsin-La Crosse, La Crosse, WI, USA
e-mail: tkernozek@uwlax.edu

INTRODUCTION

Distance running is a common activity for adults with over 29 million in the United States running weekly [1]. Injury to the lower extremities is common in running athletes with Achilles tendon (AT) injuries accounting for 5-18% of all running-related injuries [2]. During running high magnitude forces are transmitted to the AT. The repetitive loading may lead to micro tearing, inflammation and degeneration of the AT.

The human AT may experience greater magnitudes of stress relative to other tendons. Most tendons experience peak stress values below 30 MPa; however, during dynamic activities such as hopping the AT undergoes peak stresses that approach 80 MPa [3]. General running technique influences tendon stress due to the transmission of forces to the AT as it is influenced by the muscle forces of the gastroc-soleus complex and motions at the ankle. Current interventional strategies to reduce the risk or reoccurrence of running-related injuries include altering step rate and foot-strike pattern [4, 5].

The objective of our study was to examine the effects of foot strike pattern and step frequency on AT stress during running.

METHODS

Nineteen female runners (age: 21.5 ± 1.3 yrs; height: 166.4 ± 5.6 cm; mass: 59.5 ± 8.7 kg; weekly mileage: 31.9 ± 18.8 km) participated. Individuals were not eligible to participate if they reported pregnancy, cardiovascular pathology, surgery within the last year, current lower extremity pain and/or less than 5 on the Tegner Activity Level Scale – a measure for regular participation in recreational activities that require running.

Prior to running trials, 2D transverse images of the AT cross-sectional area were measured in prone of the right ankle via ultrasound imaging. Participants were fitted with the same model of footwear and equipped with 47 markers for 3D motion capture. After instruction, participants ran down a 20-meter runway under six conditions including a rearfoot strike (RFS) and non-rearfoot strike (NRFS) pattern at their preferred cadence, +5% preferred cadence and -5% preferred cadence.

Step frequency for each condition was established with a metronome and visually monitored. Speed was controlled to 3.33-3.68 m/s using a photoelectric timing system and foot strike pattern was verified with an inshoe pressure system. Mid- and fore-foot strike indices were combined such that a NRFS pattern was defined as the subject's center of pressure (COP) located on the anterior two-thirds part of the foot at initial contact; RFS was defined as a subject's COP occurring on the rear third. Kinematic data were captured at 180Hz using 15 motion analysis cameras while kinetic data were simultaneously collected using a force platform at 1800Hz. Muscle forces were estimated using static optimization. Strain and strain rate were estimated from the AT elastic properties presented by Wren et al. [6]

Multivariate statistics with repeated measures were used to examine differences between foot strike patterns and cadence ($\alpha=0.05$). Bonferonni post-hoc analyses were used to examine pair-wise comparisons.

RESULTS AND DISCUSSION

Peak AT stress ($p<0.001$, ES= 4.87) and peak force ($p<0.00$, ES=4.59) were different between the NRFS and RFS patterns. Additionally, the RFS pattern exhibited reduced strain ($p<0.00$, ES= 4.91) and strain rate ($p<0.001$, ES= 4.22) compared to the

NRFS pattern with differences of 24% and 15%, respectively. Figure 1 illustrates the time-normalized AT stress in the stance limb over the stance phase during the running cycle for each foot strike pattern.

A reduction in peak AT stress and strain was exhibited with a 5% above preferred step frequency relative to the preferred condition using a RFS ($p<0.001$, ES= 0.16) and NRFS ($p=0.005$, ES= 0.14) pattern. Strain rate was not different ($p>0.05$) between either foot strike condition.

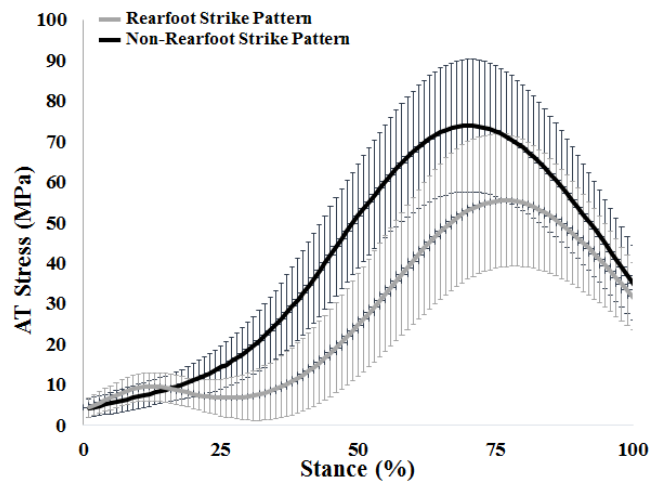


Figure 1: Ensemble average AT stress during stance for RFS and NRFS patterns.

Our findings demonstrate a reduction in peak AT stress and strain between RFS and NRFS patterns. Estimated peak Achilles stress in this study ranged from 57 MPa to 75 MPa at 3.5 m/s (+/- 5%) using subject-specific AT measurements. In comparison, a study performed by Ker [7] measured peak AT stress at 53 MPa while running at 4.5 m/s. Komi [8] reported peak AT stress of 110 MPa in barefoot running at 3.8 m/s in two subjects using buckle transducer data as well as strain values of up to 5% per stride. Our study estimated strain values to be between 6-7%. The difference in values obtained may be attributed to methodological differences including running speed and methods we used for estimating muscle forces.

CONCLUSIONS

Th results suggest that running with a RFS pattern may reduce peak AT stress compared to a NRFS pattern. Increases in step frequency of 5% above preferred, regardless of foot strike pattern, resulted in lowered peak AT stress. The utilization of a RFS pattern and changes to step frequency may be beneficial in the treatment and prevention of AT-related injuries.

Runners may consider altering their foot strike pattern as it has been shown to occur with minimal instruction [9]. We recommend a progressive, transitional period be implemented if changes in foot strike pattern and step frequency is indicated as changes appear to introduce novel loading on the AT during running.

REFERENCES

1. 2014 State of the Sport – Part II: Running Industry Report, 2014.
2. McCrory JL, et al. *Medicine and science in sports and exercise* **31**,1374-1381, 1999
3. Lichtwark GA, et al. *J Experimental Biology* **208**, 4715-4725, 2005.
4. Almonroeder T, et al. *Annals of biomedical engineering* **41**, 1758-1766, 2013.
5. Heiderscheit BC, et al. *Medicine and science in sports and exercise* **43**, 296-302, 2011.
6. Wren TA, et al. *Clinical Biomechanics* **16**, 245-251, 2001.
7. Ker RF, et al. *Nature*, 147-149, 1987.
8. Komi PV, et al. *Clinics in sports medicine* **11**, 521-531, 1992.
9. Williams DS, et al. *J of Applied Biomechanics* **16**, 210-218, 2000.

ACKNOWLEDGEMENTS

This study received funding from a UW-La Crosse Graduate Student Research Grant.

VERTICAL GROUND REACTION FORCE MAGNITUDES AND RATES NOT POSITIVELY CORRELATED WITH PROSPECTIVE RUNNING INJURY

¹Dovin Kiernan, ^{1,2}Jae Kun Shim, and ¹Ross H. Miller

¹University of Maryland, College Park, MD, USA ²Kyung Hee University, Yong-in, South Korea
email: dkiernan@umd.edu web: <http://sph.umd.edu/neuromechanics>

INTRODUCTION

Running is a popular physical activity that can provide numerous health benefits. Running itself is, however, associated with high rates of injury; anywhere from 18.2-92.4% of runners sustain a musculoskeletal injury each year [1]. Thus, identifying the aetiological variables that contribute to running injury is an important goal for injury prediction and prevention.

One relatively easy-to-measure variable proposed to precipitate running injury is vertical ground reaction force (VGRF). High VGRF magnitudes and loading rates during the first, “impact,” phase are theorized to lead to injury. Several studies have examined connections between VGRF and injury, but findings have been equivocal [2].

A limitation of many previous studies on VGRF and running injuries is that they have used cross-sectional and retrospective designs, limiting the ability to infer causality. In the present study, we (1) used a prospective design, and (2) employed a principal component model (PCM) to objectively identify waveforms that contribute to the overall variance in VGRF across participants, along with traditional VGRF measures of impact peak and loading rate.

Given the theoretical connection between VGRF and injury, we hypothesized that – if VGRF does cause injury – greater VGRF magnitudes and/or loading rates at baseline would positively correlate with injury variables (number of injuries, days of training lost due to injury, and pain). Alternatively – if VGRF does not cause injury – no such positive correlations should emerge.

METHODS

Participants were drawn from an ongoing prospective investigation of lower extremity injury causation in running. Participants were over 18 years old, ran three or more times per week, participated in other sport activities two times per week or less, and reported no running-related or lower limb injuries in the past year. Data collection consisted of two phases: (1) baseline biomechanical data collection, and (2) a six-month prospective follow-up period. Forty-four participants (22 male, age 30 ± 10 years), out of a total enrollment of 100, have completed the full six-month prospective period and are included in the present report.

Baseline biomechanical data collection was conducted on a 50-m indoor running track with 8 tandem force plates (Kistler, Amherst, NY) sampling GRF at 1000Hz. Participants ran in their own footwear at a constrained speed where the experimenter provided feedback if the participant deviated from $3.3\text{m/s} \pm 5\%$, and at a self-selected typical speed that participants “ran the majority of their mileage at.” Vertical GRF from 10 left and 10 right steps were used to calculate VGRF impact peak magnitude and loading rate (calculated as the slope between 20-80% of stance onset [VGRF > 15 N] and impact peak). Stance time was then normalized to 101 points and used to create a PCM to identify VGRF waveform features that explained 90% of the total variance in VGRF [3].

Prospective data were collected via 26 weekly online surveys (Qualtrics, Provo, UT). Surveys included a large battery of questions, including: number of injuries, location of each injury, pain caused by each injury (rated from 0 or “no pain” to 10 or “worst pain imaginable” on an 11-point scale), and days of running missed due to each injury.

Using the location data, injuries were categorized as “left” or “right” for the purposes of correlating them with VGRF, assuming contralateral VGRF does not affect injury (bilateral injuries were added to both the left and right injury data pools). The number of injuries reported, pain caused by each injury, and days missed were summed across all weeks for each participant and divided by the number of surveys completed to account for any missing data points (96.5% of surveys were completed successfully).

Pearson product-moment correlations were calculated between ipsilateral VGRF variables (magnitude, rate, and PC scores) and injury variables (number of injuries, pain, days missed). Using a very liberal approach, no adjustments were made for multiple tests and significance for all tests was set at $p < 0.05$.

RESULTS AND DISCUSSION

Results were statistically similar for both speed conditions, so the more ecologically valid condition (self-selected typical speed) results are discussed in detail here. Contrary to our hypotheses, positive correlations between VGRF magnitude or loading rate and injury were not observed. In fact, VGRF loading rate was *negatively* correlated with both the number of injuries reported ($r = -0.31, p < 0.01$) and the severity of pain reported ($r = -0.26, p = 0.01$).

Results from the PCM suggested a similar conclusion. Significance was found only for PC2, which accounted for 18.9% of total VGRF variance and was interpreted as capturing the VGRF impact peak and loading rate, as well as acting as ‘difference operator’ on the size of impact peak relative to overall VGRF peak (Fig. 1). Positive correlations emerged between this PC and both the number of injuries reported ($r = 0.31, p < 0.01$) and the severity of pain reported ($r = 0.25, p < 0.05$).

In summary, when participants had low impact peak magnitudes and rates of loading but higher second peak magnitudes (Fig. 1), they were more likely to report injury or pain. These results are contrary to the notion that high impacts cause injury but are consistent with an earlier prospective study [4].

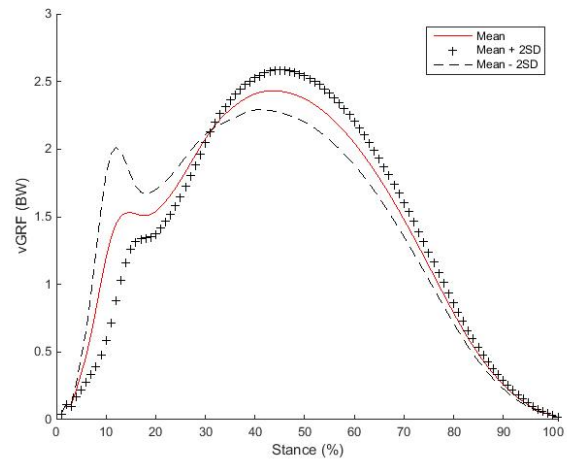


Figure 1: Principal component 2 from the typical speed PCM. High PC scores were associated with lower impact peak magnitudes and rates of loading but higher second peak magnitudes.

CONCLUSIONS

The results of the present PCM suggest this method may be a useful approach for objectively identifying VGRF features that may predict injury. However VGRF parameters alone may be insufficient to accurately and consistently identify runners at risk for injury. Future work will extend the present analysis to additional variables that may be more effective predictors of injury (e.g. kinematics, joint moments, estimates of internal loading).

REFERENCES

1. Lopes AD, et al. *Sports Med* **42**, 891-905, 2012.
2. Zadpoor AA & Nikooyan AA. *Clinical Biomech* **26**, 23-28, 2011.
3. Deluzio KJ, et al. *Hum Mov Sci* **16**, 201-217, 1997.
4. Nigg BM, et al. *J Appl Biomech* **11**, 407-432, 1995.

ACKNOWLEDGEMENTS

Dovin Kiernan was supported by an NSERC PGS-M scholarship and by the University of Maryland Department of Kinesiology Graduate Research Initiative Fund.

Energy Absorption in Subjects with Ankle Instability during a Forward-Side Jump

Hyunsoo Kim, Seongjun Son, Matthew K. Seeley, and J. Ty Hopkins

Brigham Young University, Provo, UT, USA
email: hyunsoo_kim@byu.edu

INTRODUCTION

Lateral ankle sprains are common sport-related injuries which often lead to ankle instability (AI) [1]. Specifically, AI has been shown to impair neuromuscular control and dynamic joint stability of the lower extremity [2]. During the landing phase, an impact force occurs and it is attenuated through the lower extremity joints [3]. These joints contribute to shock absorption via energy dissipation by work performed using eccentric muscle contraction around the joints [4]. Thus, a failure of shock attenuation can place excessive stress on joints, resulting in lower extremity injury such as ligament sprain, articular cartilage damage, and menisci lesions [5]. It is important to examine energy absorption by calculating the amount of work done by the joints to identify how AI affects the absorption strategy adopted by the ankle, knee, and hip joints during functional activity. Therefore, the purpose of this study was to examine the effect of AI on energetic patterns of the lower extremity during a forward-side jump.

METHODS

72 AI (37M, 35F: 22.2 ± 2.3 yrs, 173.9 ± 9.5 cm, 70.0 ± 13.1 kg), and 72 matched healthy control subjects (39M, 33F: 22.0 ± 3.2 yrs, 171.1 ± 14.6 cm, 71.2 ± 20.3 kg) were categorized according to the FAAM (ADL: $82.2 \pm 9.9\%$, Sport: $60.5 \pm 13.0\%$) and MAII (3.7 ± 1.2). Subjects were tested on the dominant limb, and fifty-nine reflective markers were placed over anatomical landmarks to calculate joint powers (W/kg). Subjects performed five trials of a forward-side jump on the force plate, which was to jump forward 1 m to the center of the force plate, land with the dominant leg, and then immediately jump to the contralateral side. Joint power was measured during the landing phase of a forward-side jump which was from initial foot contact (0%) to

peak knee flexion (100%). A functional linear model ($p < .05$) was used to evaluate differences between AI and control groups for lower-extremity joint powers. This analysis compared variables as polynomial functions rather than discrete values. Functions (power curves) were compared between groups. Pairwise comparison functions as well as 95% confidence interval (CI) bands were plotted to determine specific differences. If 95% CI bands did not cross the zero line, we considered the difference significant. Eccentric joint work (J/kg) was calculated as the area under the negative power curve for ankle, knee, and hip joints. Total lower extremity energy absorption was calculated by summing the negative joint work at each joint. Then, relative energy absorption of each joint (%) was calculated as a percentage (each joint work/total lower extremity energy absorption $\times 100$). Independent *t*-tests were used to compare relative energy absorption of each joint during the landing phase of the forward-side jump between the AI and the control groups.

RESULTS AND DISCUSSION

The AI group had less ankle joint power ($p < .05$) during 15-25% and 50-85% of landing phase than the control group (Fig.1-A and B). Compared to the control group, less knee joint power ($p < .05$) was observed during 70-95% of the landing phase in AI group (Fig.1-C and D). Unlike ankle and knee joints, the AI group demonstrated greater hip joint power ($p < .05$) during 15-32% of the landing phase than the control group (Fig.1-E and F). A group difference was found in the relative percentage of hip joint work of total lower extremity energy absorption (AI: $12.3 \pm 7.0\%$ vs Control: $10.1 \pm 6.4\%$; $t_{142} = 2.036$, $p = .044$) (Fig. 2). In the current study, individuals with AI showed decreased ankle energy absorption in the early landing phase of a forward-side jump while increased hip joint energy absorption compared to the control group.

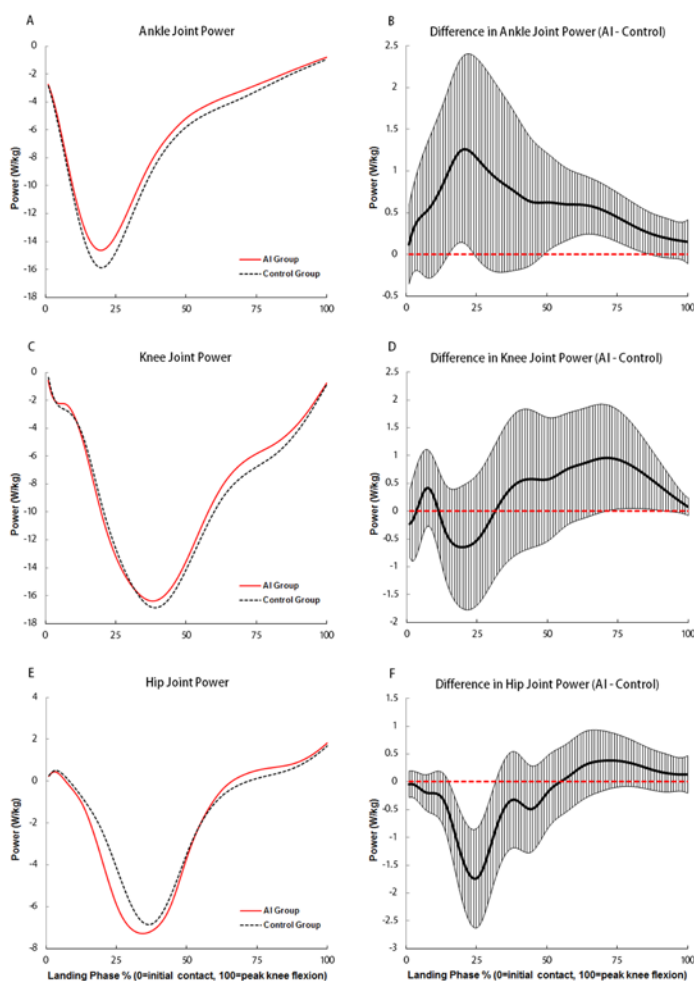


Figure 1: Ankle, knee and hip joint power during the landing phase of a forward-side jump between AI and control groups.

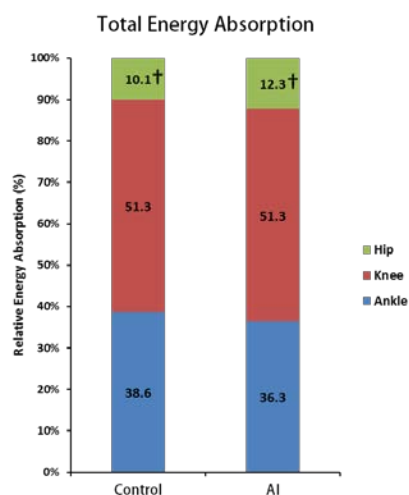


Figure 2: Relative energy absorption of each joint (%) for the AI and the control groups. † indicates significant group difference in hip joint contribution to total energy absorption ($p < .05$).

Less shock attenuation by the ankle joint may place more stress on ankle joint, resulting in ankle injuries such as ligament sprains, and articular cartilage lesions [4, 5]. Thus, this finding suggests that patients with AI focus on improving ankle muscle function to dissipate more shock during landing of functional activities. Overall, the AI group increased the hip joint contribution to the total energy absorption during the landing phase of a forward-side jump. The hip joint has the mechanical advantages of its surrounding musculature (greater cross-sectional area, longer muscle fibers, and relatively shorter tendons) to absorb more energy during landing compared to that of the knee and ankle joint [6]. Increased energy absorption by the hip joint may be an effort to compensate for decreased ankle joint power/work. Subjects with AI altered their energetic patterns, redistributing joint power/work to the hip joint to attenuate shock by dissipating ground reaction force to proximal joints (hip) during a forward-side jump. Our findings suggested that subjects with AI demonstrated altered lower extremity energetic patterns during the landing phase of a forward-side jump. The results of the current study may provide useful information in developing lower extremity muscle training programs and prevention programs for lower extremity injury.

REFERENCES

1. Swenson, D.M., et al., *Epidemiology of U.S. high school sports-related ligamentous ankle injuries, 2005/06-2010/11*. *Clin J Sport Med*, 2013. **23**(3): p. 190-6.
2. Caulfield, B.M. and M. Garrett, *Functional instability of the ankle: differences in patterns of ankle and knee movement prior to and post landing in a single leg jump*. *Int J Sports Med*, 2002. **23**(1): p. 64-8.
3. Coventry, E., et al., *The effect of lower extremity fatigue on shock attenuation during single-leg landing*. *Clin Biomech (Bristol, Avon)*, 2006. **21**(10): p. 1090-7.
4. Devita, P. and W.A. Skelly, *Effect of landing stiffness on joint kinetics and energetics in the lower extremity*. *Med Sci Sports Exerc*, 1992. **24**(1): p. 108-15.
5. Zhang, S.N., B.T. Bates, and J.S. Dufek, *Contributions of lower extremity joints to energy dissipation during landings*. *Med Sci Sports Exerc*, 2000. **32**(4): p. 812-9.
6. Doherty, C., et al., *Single-leg drop landing motor control strategies following acute ankle sprain injury*. *Scand J Med Sci Sports*, 2014.

STANDING VERTICAL JUMPS WITH COUNTERMOVEMENT ACCOMMODATE BIOMECHANICAL CONSTRAINTS

¹ Seyoung Kim, ² Sukyung Park and ¹ Sangkyu Choi

¹ Korea Institute of Machinery & Materials (KIMM), Daejeon, Republic of Korea

² Korea Advanced Institute of Science and Technology (KAIST), Daejeon, Republic of Korea

email: seyoungkim@kimm.re.kr, web: <http://www.kimm.re.kr>

INTRODUCTION

In this study, force-displacement curves (FD curve) of countermovement jumps were obtained from experiments with multiple level heights and the data were examined whether there is any meaningful change that describes the characteristics of each countermovement jump.

METHODS

Subjects

Ten healthy young subjects (mean body parameters: 28 ± 2 yrs, 177 ± 5 cm, 70 ± 6 kg) participated in this study, after signing the consent form approved by the Institutional Review Board of the KAIST.

Experimental protocols

The subjects were instructed to jump straight up to five different levels ranging from 10 % to 35 % of their body heights (Fig. 1). Black colored markers attached to a ceiling pole were used for vertical height guidance. The force data on the center of mass (CoM) were measured using a force plate (Accugait®, AMTI, US), and the data were double integrated to estimate the CoM displacement [1,2].

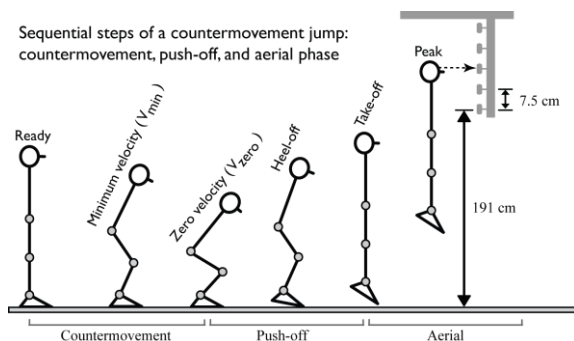


Figure 1: Sequential steps in standing vertical jumping with countermovement.

RESULTS

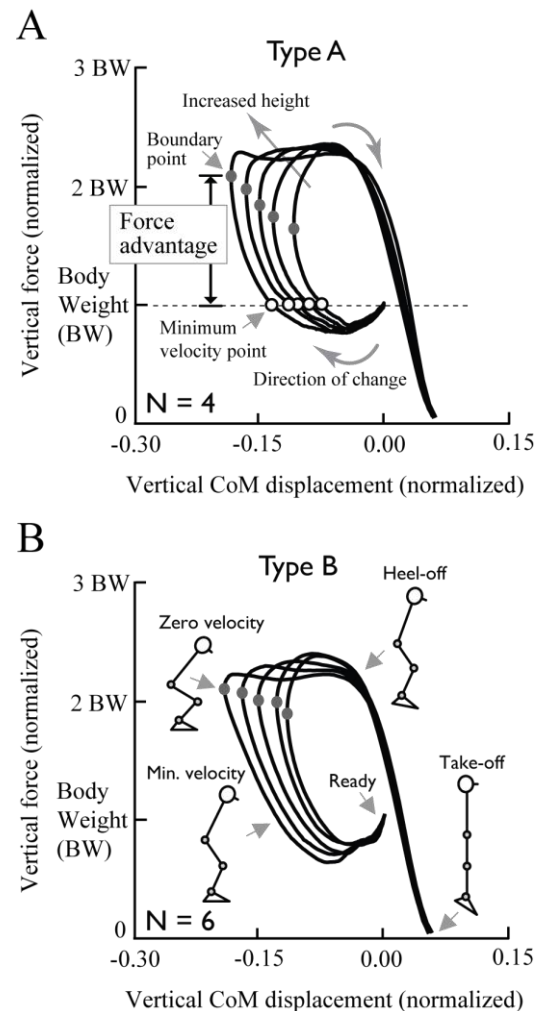


Figure 2: Average force-displacement curves. The trajectories were categorized into two general types of countermovement jumps (A and B), depending on the curve shape.

All subjects generated larger vertical forces compared with their body weights from the countermovement action and gradually lowered

their CoM positions as the vertical jump height increased (Fig. 2).

Particularly, the peak forces appeared to be nearly constant across the range of vertical jump heights and the latter half of the FD curves were almost identical, which means the push-off trajectories between countermovement phase and aerial phase might be roughly estimated when the vertical jump heights were determined (Fig. 2).

The boundary point, which is located between two trajectories of countermovement phase and push-off phase, gradually changed with increasing jump height. The boundary points continuously, as well as progressively, moved toward the left with an upward bend, not discretely or irregularly, on the FD curve (Fig. 2).

DISCUSSION

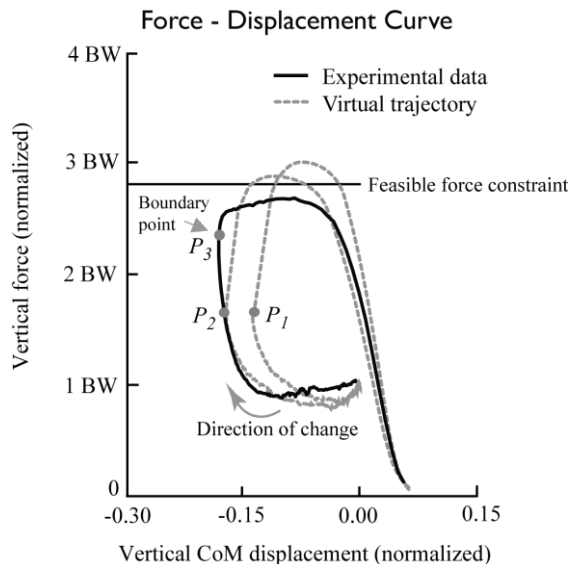


Figure 3: Force-displacement curves of actual data (solid line) and virtual trajectories (dotted lines). The virtual curves were assumed to have the same vertical jump height, which indicates that the positive works done by CoM are exactly same. The black solid circles (P_1 , P_2 , and P_3) represent the boundary points just before the push-off. The arrow indicates the direction of change.

The force-displacement curves obtained from the empirical data and virtual data can be used to better understand the countermovement jump strategy for

the higher elevation (Fig. 3). Assuming that all three pathways, including the boundary points P_1 , P_2 , and P_3 , perform the same amount of positive CoM work, the vertical jump height is the same for all the cases (Fig. 4). However, the subjects have no choice other than to reach point P_3 because of the limited amount of peak force and the limited rate of force generation, i.e., it takes a certain amount of time and distance to attain a high level of force.

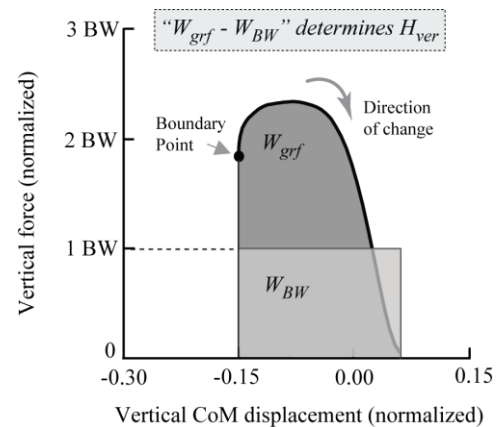


Figure 4: Calculation of vertical jump height from the force-displacement curve. The difference between the work done by ground reaction force (W_{grf} ; dark gray area) and the work done by body weight (W_{BW} ; light gray area) determines the vertical jump height (H_{ver}).

The results may imply that the subjects are aware of body dynamics being subjected to various jump heights and may select appropriate jumping strategies that satisfy feasible force constraints, without violating the maximum allowable force.

REFERENCES

1. Linthorne, N.P. *Am. J. Phys.*, **69**, 1198-1204, 2001.
2. Zelik, K.E. et al. *PloS One*, **7**, e31143, 2012.

ACKNOWLEDGEMENTS

This research was supported by the Unmanned Technology Research Center (UTRC) at the Korea Advanced Institute of Science and Technology (KAIST), the Public Welfare and Safety Research Program through the National Research Foundation of Korea (NRF), and the Korea Institute of Machinery & Materials (KIMM).

MUSCLE ARCHITECTURAL PARAMETERS PREDICT FORCE-VELOCITY PARAMETERS DERIVED FROM LOADED COUNTERMOVEMENT JUMPS

Kristof Kipp, Matthew D. Giordanelli, Philip J. Malloy, Tia M. Jandrin,
Michael T. Kiely, Christopher F. Geiser,

Marquette University, Milwaukee, WI, USA
email: kristof.kipp@marquette.edu

INTRODUCTION

Muscle architectural parameters have been associated with performance parameters measured during the execution of jumping tasks [1, 2]. For example, resting muscle thickness, pennation angle, and fascicle lengths have been associated with jump height, jump power, and rates of ground reaction force development across a variety of jumping tasks [2, 4]. While these studies highlight the associations between muscle architecture and jump performance parameters, it is currently not known if muscle architecture predicts force-velocity parameters across a broad spectrum of movement tasks that require different combinations of force and velocity production, such as during loaded countermovement jumps with different external loads [5].

PURPOSE

To investigate the association between muscle architectural parameters and force-velocity parameters derived from countermovement jumps of different loads.

METHODS

Ten healthy, female volleyball players were recruited from a local NCAA DI team to participate in this study. All players performed multiple countermovement jumps on a force plate (Type 9290BD, Kistler). Jumps were performed at five different absolute loads: bodyweight (BW), BW + 10 kg, BW + 20 kg, BW + 30 kg, and BW + 40 kg. Load was adjusted through dumbbells held in each hand. Each player performed two jumps at each load. Vertical ground reaction forces were sampled at 500 Hz and filtered with a 12 Hz low-pass Butterworth filter. Peak force (F_{\max}) and take-off velocity, which was

derived from the flight time (T_f) of each jump, were calculated from the vertical ground reaction force data (Figure 1), and averaged from the two jump trials that were performed at each absolute weight.

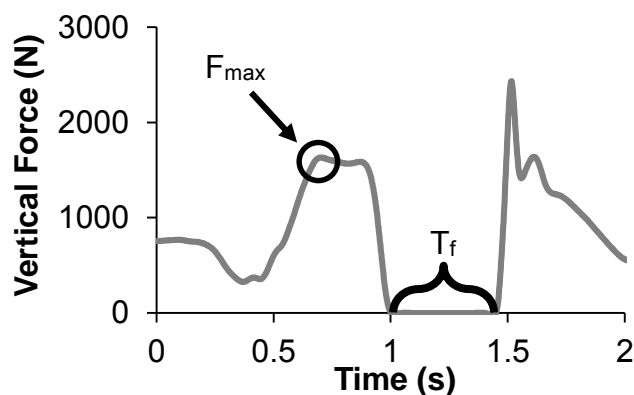


Figure 1: Sample ground reaction force data from a countermovement jump.

After filtering, peak force was normalized to body-mass. Peak force and take-off velocity were then plotted as x-y graphs for each individual. Linear regression lines were fitted to the force-velocity data points through least-squares procedures [3, 5]. The resulting regression lines were then used to extrapolate data to estimate theoretical peak force (F_0) at zero velocity and theoretical peak velocity (V_0) at zero force [3, 5]. In addition, the slope of the force-velocity regression line (S_{F-V}) and the theoretical peak power (P_{\max}) were calculated [3, 5].

Muscle architectural parameters of the vastus lateralis (VL), medial (MG) and lateral (LG) gastrocnemius were determined with B-mode ultrasound at 8 MHz (LS128 EXT-2Z, Telemed). All architectural parameters were measured at pre-determined sites along lines between skeletal landmarks (Figure 2) [1, 2]. Two images were taken at each site. First, muscle thickness (h) and pennation

angle (θ) were measured from ultrasound images, fascicle lengths ($FL = h \cdot \sin\theta^{-1}$) were then calculated from the former two measures [1, 2]. Architectural measures were made twice at each image and averaged for statistical analysis.

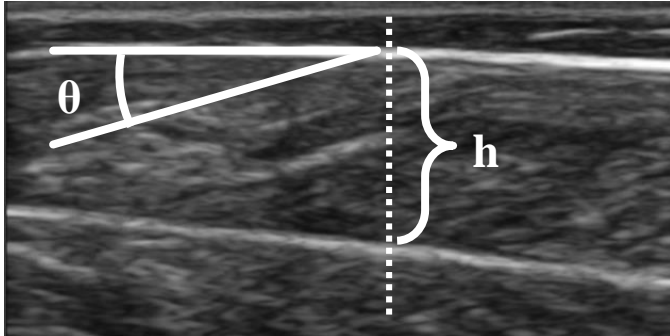


Figure 2: Ultrasound image used to study muscle architectural parameters. The dotted line shows the pre-determined site for architectural measurements.

Simple linear regressions were used to determine the correlations between architectural parameters (h , θ , FL) of the three lower extremity muscles (MG, LG, VL) and force-velocity parameters (F_0 , V_0 , S_{F-V} , P_{max}). The standard of proof for statistical significance was set at an alpha-level of 0.05

RESULTS AND DISCUSSION

The least-squares fits (i.e., r^2) for each players' force-velocity regression line ranged from 0.72 to 0.95, which indicated acceptable model fits.

Several muscle architectural parameters were correlated with force-velocity behavior of countermovement jumps. Specifically, V_{max} was significantly correlated with MG pennation angle ($r = 0.769$; $p = 0.006$). F_{max} was significantly correlated with LG thickness ($r = -0.635$; $p = 0.049$). P_{max} was significantly correlated with MG pennation angle ($r = 0.650$; $p = 0.042$) and LG fascicle length ($r = -0.659$; $p = 0.038$).

Greater peak power outputs were associated with shorter lateral gastrocnemius fascicle lengths. In addition, greater pennation angles of the medial gastrocnemius were associated with greater peak

power outputs and theoretical peak velocities. Overall, these findings are similar to those reported by Earp et al. (2010) who found that greater gastrocnemius pennation angles and shorter gastrocnemius fascicles positively predict vertical jump height and power. Our results extend these findings in that medial gastrocnemius pennation angles predicted both, peak velocity and peak power, from which it could be inferred that peak power is driven primarily by theoretical peak velocities.

Greater theoretical peak force was associated with thinner lateral gastrocnemius muscles. This finding is somewhat surprising because a muscles cross-sectional area, which is related to a muscles force-generating capacity. Further, this finding is also contrary to other reports that have found that muscle thickness is a good overall predictor of absolute power for squat jumps, countermovement jumps, and drop vertical jumps [1]. One contributor to the apparent difference between our finding and those reported in the literature may lie in the fact that our force and power values were normalized to body-weight of the participants whereas those from others were not.

CONCLUSIONS

The results of this study indicate that several muscle architectural parameters are correlated with global force-velocity parameters derived from countermovement jumps that are performed across a spectrum of external loads.

REFERENCES

1. Earp JE, et al. *J Strength Cond Res.* **24**, 722–729. 2010.
2. Earp JE, et al. *J Strength Cond Res.* **25**, 340–347. 2011.
3. Jimenez-Reyes P, et al. *Eur J App Physiol.* **114**, 2281–2288. 2014.
4. Mangine GT, et al. *J Sports Sci Med.* **13**, 904–911.
5. Samozino P, et al. *Int J Sports Med.* **35**, 505–510.

DIFFERENCE IN FORCE GENERATION WHILE DEADLIFTING WITH CHAINS

Michael Lawrence, Chad Lyons, Lara Carlson

The University of New England, Portland ME

Email: mlawrence3@une.edu, web: <http://www.une.edu/wchp/mal>

INTRODUCTION

The primary goal of using accommodating resistances is to help maintain force generation throughout the entirety of the range of movement. When using a normally loaded barbell, force generation decreases and the bar can begin to decelerate at approximately half way through the range of motion in a bench press [1] or between 73-85% of the deadlift [2]. Although deadlifting with chains has not shown to inhibit bar deceleration, this has only been tested with lighter loads (70% of 1 repetition maximum and below [2]. Many strength and conditioning programs routinely use more than 70% when during the strength development phase of training. The utilization of chains may allow an athlete to maintain positive acceleration longer throughout heavier loads and may also have the added benefit of developing greater force and power throughout the movement. Furthermore, research using chains as accommodating resistance usually employs an equation based on bar height in order to calculate how much load the chain was applying to the bar. Regrettably, this method ignores any influence of momentum on the chains. Therefore this investigation will use a load cell to measure the force the chains are applying to the bar.

METHODS

Five male competitive powerlifters (age 26.4 ± 7.9 y, mass 87.6 ± 17.7 kg, height 1.80 ± 0.05 m, 1.8 ± 1.3 y competing in powerlifting, and deadlift one repetition maximum (RM) 234.8 ± 38.7 kg) performed a heavy (3-RM) deadlift using a normally loaded barbell and a barbell loaded with a combination of weights and chains. The amount of chains used was determined from recommendations of the retailer (Elite Fitness Systems, London, Ohio). All participants were loaded with two chains (1.5 m in length, 0.95 cm in diameter, 36.4kg total

load). The chains were attached to each end of the barbell with custom weight clamps. The middle link of each chain was attached to the barbell with the chain completely unloaded at the beginning of the lift and coming off the floor (adding mass to the barbell) as the lift was completed. On one end of the barbell the chains were attached to a linear force transducer (Interface, Scottsdale, USA) to measure resistance provided by the chains. Due to the length of the chains, attachment of the force transducer, and height of the subjects, the chains did not completely come off the ground for all subjects. Subjects were allowed to take their preferred stance on a force plate to perform each lift. Subjects first performed a dynamic warm-up and sub-maximal (25%, 45%, 65%, and 85%) repetitions prior to testing of the 3-RM.

Reflective markers were placed on the ends of the barbell and the position of the markers was tracked with eight Oqus Series-3 Cameras (Qualisys AB, Gothenburg, Sweden). Visual 3D (C-motion, Germantown, USA) was used to calculate peak bar force, peak acceleration and the last point of deceleration (percentage of lift). A repeated-measures analysis of variance was used to determine there were significant differences between the normally loaded barbell and the barbell loaded with weights and chains. The level of significance was set to $p = 0.05$.

RESULTS AND DISCUSSION

The 3-RM with the normally loaded barbell (216.4 ± 27.6 kg) was significantly greater than the barbell loaded with weights and chains (205.5 ± 22.9 kg) ($p = 0.02$). There were no significant differences found between conditions in peak bar force, peak acceleration, or point of deceleration (Table 1); most likely due to the low number of subjects collected in this pilot study. However, there does

seem to be a trend for the point of deceleration to be occurring later in the lift when the chains are attached to the barbell (Figure 1).

The force of the chain increased in a linear fashion until the sudden large decrease in force before the completion of the lift (Figure 2). This may be due to the lifter applying a large amount of force to complete the lift, which imparted a large amount of force to the chains. The momentum of the chains would then cause an upward motion leading to the decrease in force prior to completion of the lift.

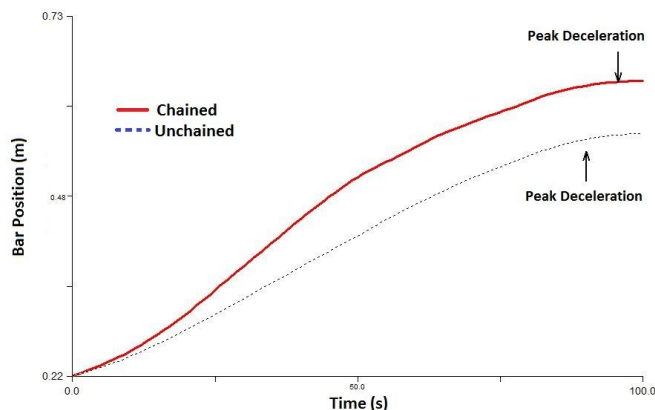


Figure 1: Bar Position vs. Time with Point of Deceleration

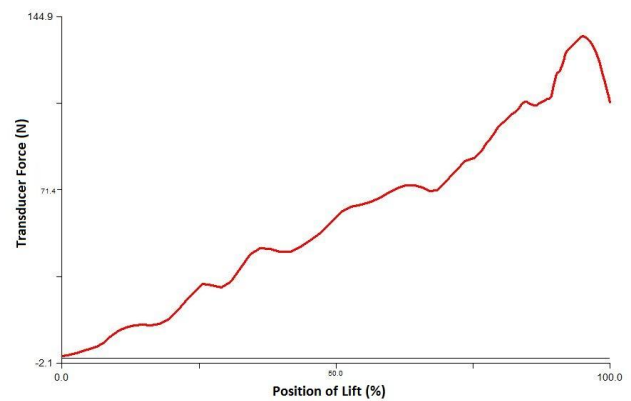


Figure 2: Transducer Force vs. Position in the lift

CONCLUSIONS

Although there were no statistically significant findings, this is likely due to the small number of participants recruited to date. However, the trend with the point of deceleration moving to later in the lift is consistent with previous findings. Also, this study suggests that the chains may be deloading at the top of the lift due to the upward momentum of the chains.

REFERENCES

1. Lander, J.E., et al. *Med Sci Sport Exerc* **3**, 344-53, 1985.
2. Swinton, P.A., et al. *J Strength Cond Res* **11**, 3163-74, 2011

Table 1: Peak Bar Force, Peak Acceleration, and Point of Deceleration in the lift (Mean \pm SD)

Peak Bar Force with Chains (N)	Peak Bar Force (N)	Peak Acceleration with Chains ($\text{m}\cdot\text{s}^{-2}$)	Peak Acceleration ($\text{m}\cdot\text{s}^{-2}$)	Point of Deceleration With Chains (% of Lift)	Point of Deceleration (% of lift)
2488.5 ± 260.4	2442.6 ± 330	1.2 ± 0.4	1.4 ± 0.6	97.7 ± 1.7	90.2 ± 11.5

DIFFERENCES IN LOWER EXTREMITY, PELVIC AND TRUNK KINEMATICS BETWEEN SINGLE LEG SQUAT AND STEP DOWN TASKS

¹ Cara L. Lewis, ² Eric Foch, ¹ Marc M. Luko, ¹ Kari L. Loverro, and ¹ Anne Khuu

¹ College of Health and Rehabilitation Sciences: Sargent College, Boston University, Boston, MA, USA

² Nutrition, Exercise, and Health Sciences, Central Washington University, Ellensburg, WA, USA

email: lewisc@bu.edu, web: <http://sites.bu.edu/movement/>

INTRODUCTION

The single leg squat and the single leg step down are two commonly used functional tasks to assess movement patterns. In the single leg squat, the participant stands on one leg and squats either to a predetermined knee angle or as far as possible. In the step down, the participant stands on the top of a box or step where the height is either fixed or is adjusted based on the participant's height or tibial length. In a controlled manner, the participant lowers him/herself until the non-stance heel touches the ground and then returns to upright standing on top of the box. Both tasks have been found to be reliable and useful in identifying abnormal movement patterns in the trunk, pelvis, and lower extremities. For example, increased ipsilateral trunk lean [1], contralateral pelvic drop [1], hip adduction [1,2], and knee abduction [1] have been noted during the single leg squat in patients with patellofemoral pain (PFP) in comparison to controls. During the step down task, participants with PFP have also demonstrated increased ipsilateral trunk lean, contralateral pelvic drop, hip adduction, and knee abduction when compared to controls [3].

Despite the similarities between tasks, there are differences which may affect the observed movement pattern during the task. For the single leg squat, the goal is to keep the non-stance limb off the ground. In contrast, the goal of the step down task is to touch the non-stance heel to the ground. It is unknown how the kinematics compare between these tasks. The purpose of this study was to identify kinematic differences in the lower extremity, pelvis, and trunk between the single leg squat task and the step down task.

METHODS

Fourteen healthy individuals (females = 10, males = 4; age 23.9 ± 2.0 years; height 1.70 ± 0.12 m; mass 68.7 ± 14.0 kg; UCLA activity score 8.5 ± 1.5) participated in this research and provided informed consent. Kinematic data were collected using a motion capture system (Vicon Motion Systems Ltd, Centennial, CO) while participants performed three different single leg weight-bearing tasks: single leg squat (SLS), step down from a 16 cm step (SD16), and step down from a 24 cm step (SD24). For the single leg squat task, participants held the non-stance limb extended anteriorly, squatted as low as possible, and then returned to the upright standing position. For the step down tasks, participants stood with both feet on top of a wooden box, lowered the non-stance leg until the heel lightly touched the floor, and then returned to the starting position. Participants completed five trials of each task on each limb. Visual3D (C-Motion, Inc., Germantown, MD) was used to calculate knee and hip joint angles, and pelvis and trunk segment angles.

Separate repeated measures analyses of variance (ANOVA) were performed for each dependent variable with task (SLS, SD16, and SD24) as the within-subject factor. The dependent variables were the knee, hip, pelvis, and trunk angles of the right stance limb in the sagittal, frontal, and transverse planes at peak knee flexion and at 60° of knee flexion. Post-hoc paired t-tests with a Bonferroni correction were used to determine significant pairwise differences.

RESULTS AND DISCUSSION

The tasks resulted in kinematics differences at the knee, hip, pelvis, and trunk. At both peak knee

flexion and 60° of knee flexion, the SLS was performed with more knee abduction ($p \leq 0.030$), less hip adduction ($p \leq 0.030$), less anterior pelvic tilt ($p \leq 0.007$), less pelvic drop ($p \leq 0.011$), and more backward trunk rotation ($p \leq 0.004$) than either step down task. Additionally, at peak knee flexion, the SLS had more knee flexion ($p < 0.001$), more hip external rotation ($p = 0.001$), and more trunk flexion ($p = 0.007$) than the SD16. Compared to the SD24, the SLS also had less hip flexion ($p = 0.013$), more backward pelvic rotation ($p < 0.001$), and less ipsilateral trunk flexion ($p = 0.001$). At 60° of knee flexion, the SLS also had more backward pelvic rotation than either step down task ($p \leq 0.011$).

While there were multiple differences in the knee, hip, pelvis, and trunk angles between SD16 and SD24 at peak knee flexion, the only difference at 60° of knee flexion was in trunk flexion ($p < 0.001$) with less flexion in the SD16 than the SD24.

The results of this study highlight the importance of three things: 1) goal of the task, 2) point of comparison, and 3) exercise selection. First, the instructions for the single leg squat and for the step down are fundamentally different and result in different movement patterns. The goal of the SLS is to maximize squat depth while maintaining balance and keeping the non-stance limb off the ground. Hiking the pelvis and minimizing stance hip adduction would help achieve this goal. In contrast, the goal of the step down is to touch the non-stance heel to the ground. This can be achieved with less hip and knee flexion by adducting the stance hip and dropping the pelvis.

Second, the point of comparison between tasks affected the results. The SD16 seemed very different from the SD24 when compared at peak knee flexion, but these differences were almost nonexistent at 60° of knee flexion. This finding indicates that, for a range of step heights, the same movement pattern is used for the step down task. It also indicates that comparisons can be made across studies with slightly different step heights, if analyzed at the same knee angle. Conversely, the single leg squat task continued to be different from the step down tasks at both time points. This finding, again, indicates that the single leg squat

task and the step down task use different movement patterns.

Third, the kinematic differences noted between tasks are important when selecting exercises for a patient. The single leg squat task was performed with more knee abduction (dynamic valgus) while the step down task was performed with more hip adduction. While the rehabilitation goal of the exercise would likely be to reduce both knee abduction and hip adduction, the exercises may have varying degrees of difficulty and could be used in an exercise progression. For example, a single leg squat task might be a more appropriate exercise for a patient with femoroacetabular impingement (FAI), a structural hip condition exacerbated by combined hip adduction and flexion [4,5].

CONCLUSIONS

The results from this study indicate that the single leg squat task and step down task result in different lower extremity, pelvis, and trunk kinematics. The findings from this study provide the clinician with more information when selecting the most appropriate task or exercise for patients with lower extremity movement dysfunction.

REFERENCES

1. Nakagawa TH, et al. *J Orthop Sports Phys Ther* **42**, 491-501, 2012.
2. Willson JD, et al. *Clin Biomech* **23**, 203-211, 2008.
3. Nakagawa TH, et al. *Med Sci Sports Exerc* **44**, 1747-1755, 2013.
4. Nepple JJ, et al. *J Am Acad Orthop Surg* **21**, S16-19, 2013.
5. Ciohisy JC et al. *Clin Orthop Relat Res* **467**, 638-644, 2009.

ACKNOWLEDGEMENTS

Research reported was supported by the Peter Paul Career Development Professorship and the National Institute of Arthritis and Musculoskeletal and Skin Diseases of the National Institutes of Health under Award Numbers R21 AR061690 and K23 AR063235.

DOES MEDIAL KNEE DISPLACEMENT REPRESENT KNEE ABDUCTION ANGLE DURING SINGLE-LEG SQUATS IN FEMALES?

¹ Lukas D. Linde and ¹ Dr. John Z. Srbely

¹University of Guelph, Guelph, ON, Canada

Email: jsrbely@uoguelph.ca

INTRODUCTION

Female athletes are 4-6X more likely to suffer non-contact anterior cruciate ligament (ACL) injuries than males [1]. One of the largest predictors of non-contact ACL injuries is greater knee abduction angle (valgus) and moment during dynamic tasks such as drop jumps [1] or single-leg squats [2]. Identifying individuals prone to greater knee valgus during dynamic tasks is of primary importance in the prevention of ACL injuries, however, the most reliable method of measuring valgus is currently through expensive and technically onerous 3D motion capture technology which is difficult to integrate within a clinical setting. Consequently, cost-effective clinical tools, which can reliably quantify gold standard 3D kinematic measurements, are needed to aid in the clinical diagnosis, rehabilitation, and prevention of ACL injury.

Medial knee displacement (MKD) has recently been used to visually discriminate between individuals with and without knee abduction [2]. While individuals with greater MKD also demonstrate greater knee abduction angle [3], the strength and nature of the relationship between MKD and knee abduction angle has not been quantified.

The primary objective of this study was to examine the statistical correlation between the change in medial knee displacement and knee abduction angle during a single-leg squat task in healthy females. We hypothesized that a strong positive correlation exists between medial knee displacement and knee abduction angle throughout the descent phase of the single-leg squat.

METHODS

Nineteen right-foot dominant healthy females (age: 21.37 ± 1.27 , height 168.91 ± 8.45 cm, weight

63.94 ± 7.35 kg) each performed a total of 30 single-leg squats. Trials consisted of 3 consecutive squats, 6 seconds in duration, to a depth of 65 degrees of knee flexion. All trials were conducted in time with a metronome at 60 bpm. Kinematics of the pelvis, right thigh, and right shank were recorded using an optoelectric motion capture system (Optotrack 3DI: NDI, Waterloo, Canada). Knee abduction angle was calculated using a 6 degrees-of-freedom model constructed in Visual 3D software (Version 5, C-Motion, Germantown, USA). Knee abduction angle was calculated as the angle between the shank and thigh segment about the knee with respect to the Carden rotation to the global coordinate system [4]. MKD was quantified as the horizontal displacement in the frontal plane between two kinematic markers placed on the right kneecap and midline of the foot.

The change in MKD and knee abduction angle was quantified at four time points during the descent phase of each single-leg squat: 25%, 50%, 75%, and 100% of squat depth. The change in MKD and knee abduction angle were normalized to one-legged standing, as the change in knee valgus angle has been shown to have greater validity and reliability than peak angle in visual screening tests [5].

Statistical analyses were performed in SPSS (Version 22, IBM Corp). The Pearson's correlation coefficient (r) and the coefficient of determination from a simple linear regression (r^2) were calculated between the change in MKD and knee abduction angle at squat depth values of 25%, 50%, 75%, and 100% during the descent phase of single-leg squats (Table 1).

RESULTS AND DISCUSSION

A strong positive correlation between MKD and knee abduction angle was observed at all squat depths (Table 1). The strength of the relationship

between MKD and knee abduction angle progressively increased from 25% ($r = 0.725$) to 100% ($r = 0.911$) of squat depth (Table 1).

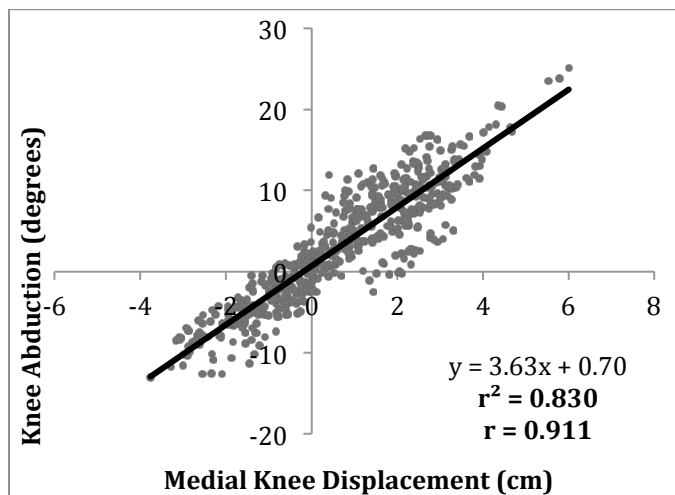


Figure 1: Medial knee displacement and knee abduction angle at 100% squat depth, normalized to one-leg standing. Linear regression equation with the coefficient of determination (r^2) and Pearson's correlation coefficient (r) included.

The strong relationship between the change in MKD and the change in knee abduction angle throughout the single-leg squat further validates and supports the use of MKD as a simple clinical test to screen individuals for knee valgus and ACL injury risk. The strength of the relationship between MKD and knee abduction angle was the highest at the greatest level of squat depth (Table 1; Figure 1).

CONCLUSIONS

The change in MKD throughout a single-leg squat demonstrated a strong linear relationship with the

change in knee abduction angle. Greater knee abduction angles are associated with increased risk of ACL injury [1]. The robust correlation between MKD and knee abduction angle observed in our study provides support for the application of MKD as a reliable clinical measure of knee valgus. The MKD is a simple and cost-effective substitute for expensive and elaborate 3D motion capture technology currently employed in experimental settings to measure knee valgus (abduction angle). The MKD outcome can be routinely employed in the clinical setting to identify individuals at high risk of ACL injury, as well as measuring therapeutic responses to preventative training/rehabilitation programs in the treatment and prevention of ACL injury.

REFERENCES

1. Hewitt TE, et al. *Am J Sports Med* **33**, 492-501, 2005
2. Ageberg E, et al. *BMC Musculoskele Disord*. **11**, 265-273, 2010
3. Mauntel TC, et al. *J Appl Biomech*. **30**, 707-712, 2014
4. Winter DA. *Biomechanics of motor control and human movement*, 4th ed. Wiley, 2009
5. Ekegren CL, et al. *J Orthop Sports Phys Ther*. **39**, 665-674, 2009

ACKNOWLEDGEMENTS

We would like to thank Eve Lampert for her assistance in data collection and Dr. John Zettel for the use of his lab space and equipment.

Table 1: Pearson's correlation coefficient and coefficient of determination from linear regression r^2 values between medial knee displacement and knee abduction angle at 25%, 50%, 75%, and 100% of squat depth during single-leg squat descent.

% Of Squat Depth	Knee Abduction Angle			
	25%	50%	75%	100%
Medial Knee Displacement:				
Pearson's correlation coefficient (r)	0.725	0.856	0.878	0.911
Coefficient of Determination - r^2	0.525	0.733	0.771	0.830

ABDOMINAL MUSCLE ACTIVATION TECHNIQUES REDUCE PEAK KNEE ABDUCTION AND PEAK HIP ADDUCTION DURING SINGLE-LEG SQUATS IN FEMALES

¹ Lukas D. Linde, ¹ Eve C. Lampert, ¹ Jessica Archibald, and ¹ Dr. John Z. Srbely

¹ University of Guelph, Guelph, ON, CANADA

Email: jsrbely@uoguelph.ca

INTRODUCTION

Greater knee abduction (valgus) excursion during dynamic tasks has been associated with an increased risk of non-contact anterior cruciate ligament injury (ACL), especially in females [1]. Greater knee abduction is thought to be the result of increased hip adduction caused by decreased hip strength and neuromuscular control [2]. As a consequence of this, therapeutic exercise programs specifically targeting hip muscle strength and movement coordination have demonstrated improvements in hip adduction and knee abduction during dynamic tasks such as single-leg squats [2]. Many of these hip neuromuscular training programs also include core training and strengthening exercises [2,3], however, the specific impact of core activation techniques on knee abduction is poorly understood. In particular, two common core activation techniques known as abdominal hollowing and bracing selectively increase activation of core muscles [4,5], however, their effect on knee abduction and hip adduction during dynamic activities has not been studied.

The purpose of this study was to investigate the influence of two core muscle activation techniques on knee abduction and hip adduction angles during a single-leg squat task. We tested the hypothesis that both abdominal hollowing and abdominal bracing techniques would reduce peak knee abduction angle and peak hip adduction angle during single-leg squats in females, when compared to no abdominal activation controls.

METHODS

Thirteen females (21.3 ± 0.88 years, 1.68 ± 0.07 m, 58.27 ± 5.46 kg) were trained in the performance of two different abdominal activation techniques, abdominal hollowing and abdominal bracing. Abdominal hollowing selectively activates the

transversus abdominus muscles bilaterally [4] while abdominal bracing involves activation of the entire abdominal wall [5]. Proper application of both techniques was validated through surface electromyography measured from bilateral internal and external oblique muscles and erector spinae muscles at the L3 level. Muscle activation levels for both techniques were maintained at 20% of maximum voluntary contraction throughout single-leg squat trials.

Participants completed single-leg squats under three different conditions of abdominal activation, no instructed activity (control), hollowing, or bracing. Single-leg squat trials consisted of three consecutive 6-second single-leg squats to a depth of 65 degrees of knee flexion. All trials were conducted in time with a metronome at 60 bpm. Five practice trials were completed to familiarize participants with the depth and timing of the squatting procedure, with no feedback on posture or technique given. Participants then completed four blocks of single-leg squat trials, with three trials per block, one control, one hollowing, and one bracing trial, in random order. Rest was given between each trial and block to minimize fatigue.

Knee and hip kinematics during single-leg squats were recorded using an optoelectric motion capture system (Optotrack, NDI, Waterloo, Canada). Rigid body markers attached to segments and imaginary markers were used to construct a 6-degrees-of-freedom model in Visual 3D software (Version 5, C-Motion, Germantown, USA). Peak hip adduction and peak knee abduction were calculated during the descent phase of each squat, normalized to one-leg standing prior to squat descent. A repeated measures ANOVA was performed to compare differences in abdominal activations between abdominal conditions (control, hollowing, bracing) and to assess the influence of abdominal condition

on peak hip adduction and peak knee abduction. Individual post-hoc comparisons (Tukey's) were performed at an alpha of 0.05.

RESULTS AND DISCUSSION

Abdominal hollowing and bracing demonstrated significantly greater activations for all core muscles recorded (Table 1). Abdominal bracing also showed significantly greater activations for all muscles when compared to abdominal hollowing (Table 1).

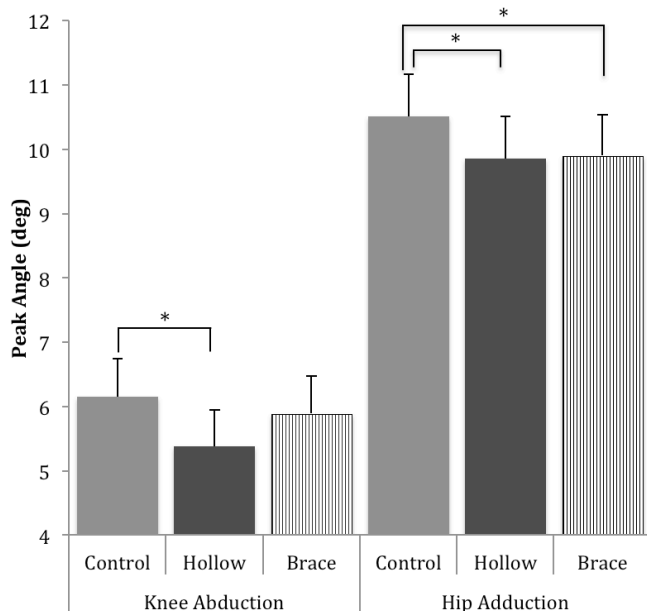


Figure 1: Peak knee abduction angle and peak hip adduction angle during the descent phase of single-leg squat trials across control, hollow, and brace abdominal activation conditions.

* Denotes significance at alpha <0.05.

Both abdominal hollowing and bracing significantly reduced peak hip adduction angle during the descent phase of the single-leg squat when compared with

controls, however, only abdominal hollowing reduced peak knee abduction angle (Figure 1).

CONCLUSIONS

The reduction of knee abduction angle during dynamic tasks is of prime importance in the prevention of ACL injuries, especially in females [1]. Although greater hip adduction and knee abduction both contribute to greater knee valgus, previous research suggests that knee abduction angle is one of the strongest predictors of ACL injury in female athletes [1]. Our data support the notion that core activation techniques may be important in maintaining dynamic stability of the lower limb [5], and suggests that the abdominal hollowing technique may be an important inclusion in ACL injury prevention programs.

REFERENCES

1. Hewitt TE, et al. *Am J Sports Med* **33**, 492-501, 2005
2. Baldon Rde M, et al. *J Appl Biomech*. **27**, 223-232, 2011
3. Myer GD, et al. *Clin Sports Med*. **27**, 425-48, 2008
4. Richardson C, et al. *Aust J Physiother*. **38**, 105-12, 1992
5. McGill SM, et al. *Exerc Sport Sci Rev* **29**, 26-31, 2001

ACKNOWLEDGEMENTS

We would like to thank Dr. John Zettel for the use of his lab space and equipment.

Table 1: Average muscle activity of bilateral internal oblique, external oblique, and erector spinae L3 level during control, hollow, and brace conditions of single-leg squat trials.

* Denotes significance from control, and # denotes significance from hollow both at the alpha 0.05 level.

Condition	Average Muscle Activity (%Maximum Voluntary Contraction)					
	R Internal Oblique Mean ± SE	L Internal Oblique Mean ± SE	R External Oblique Mean ± SE	L External Oblique Mean ± SE	R Trunk Extensor (L3) Mean ± SE	L Trunk Extensor (L3) Mean ± SE
Control	9.25±0.80	11.2±0.79	3.67±0.25	4.17±0.45	5.13±0.51	6.56±0.52
Hollow	18.81±1.46 *	21.09±1.53 *	7.95±0.73 *	7.2±0.64 *	7.59±0.66 *	8.66±0.76 *
Brace	23.08±1.90 *#	23.23±1.45 *#	10.54±0.72 *#	9.79±0.75 *#	9.14±0.77 *#	10.31±0.87 *#

MUSCLE ACTIVATION DURING SINGLE LEG SQUAT IS AFFECTED BY POSITION OF THE NON-STANCE LIMB

Kari L. Loverro, MS, Anne Khuu, and Cara L. Lewis, PT, PhD

College of Health & Rehabilitation Sciences: Sargent College, Boston University, Boston, MA, USA

email: klloverro@bu.edu, web: <http://sites.bu.edu/movement>

INTRODUCTION

The single leg squat (SLS) is a commonly used assessment and treatment tool [1,2]. As an assessment tool, the SLS is used to determine movement patterns of the trunk, pelvis, and lower extremity during single-limb stance. Commonly observed faults include increased ipsilateral trunk lean, contralateral pelvic drop, hip adduction, and knee abduction [3]. As a treatment tool, the SLS is used for both strengthening and neuromuscular retraining to increase control of the hip and knee in the frontal and transverse planes [1]. The majority of this control is thought to come from appropriate activation of the hip abductors and lateral rotators [4]. As with other hip abductor exercises, gluteal muscles are targeted for strengthening while attempting to minimize the use of others (e.g., tensor fascia lata) [4].

There is no widely accepted way to perform the SLS, especially in regard to the position of the non-stance (NS) limb. The three most common positions are with the NS limb in front, in the middle, or behind the stance limb. Different positions may change the neuromuscular demands of the trunk, pelvis, and lower extremity resulting in altered movement and/or muscle activation. No previous studies have evaluated the activation of the gluteals and surrounding muscles during the SLS in the three common NS limb positions. Therefore, the purpose of this study was to compare muscle activation of selected lower extremity muscles during the SLS in the three commonly used positions NS limb: front, middle, and back.

METHODS

A preliminary sample of ten healthy young adults (6 female, 4 male; 23.8 ± 3.7 yrs) were analyzed for this study. Participants completed five trials of the SLS in each of the three NS limb positions: front (hip

flexed/knee extended with NS foot in front: SLS-Front), mid (NS hip and knee flexed with foot held in line with stance ankle: SLS-Mid), and back (NS knee flexed while maintaining vertical thigh position: SLS-Back). Instructions given for each squat were to start from standing, lift the NS limb off the ground to the tested position, do a controlled squat as far as possible on the stance limb, rise back up and place NS foot back on the ground. Both sides were tested.

A surface electromyography (EMG) system (Delsys Inc.) was used to obtain muscle activity. Electrodes were placed over the muscle bellies of gluteus maximus, posterior portion of the gluteus medius, semimembranosus, biceps femoris, rectus femoris, and tensor fascia lata (TFL) bilaterally. Kinematic data of the trunk, pelvis and lower limbs were collected using a 10-camera motion capture system (VICON®). EMG and kinematic data were analyzed using Visual3D. Raw EMG signals were band-pass filtered between 10 Hz and 390 Hz using a 4th order Butterworth filter with zero phase lag. Filtered EMG signals were processed using root-mean squared (RMS) smoothing with a moving window of 100 msec. Average RMS activation of the stance limb was extracted for two phases of movement: descent (start of stance knee flexion to maximum knee flexion) and ascent (maximum knee flexion to return to standing). Participant-based mean activation of the five trials for each side in each position was exported for further analysis.

Repeated measures ANOVA was used to compare mean muscle activation within subjects for SLS position. Additional pairwise comparisons for significant differences of position were completed.

RESULTS AND DISCUSSION

Preliminary analysis indicates that NS limb position significantly affected muscle activation during both

the descent and ascent phase of the SLS (Table 1). Most notably, the TFL exhibited significantly greater average RMS activation in the SLS-Front position during both the descent and ascent phases compared to both the SLS-Mid ($p=0.006$) and SLS-Back ($p\leq 0.013$) positions. NS limb position also significantly increased muscle activation of the gluteus maximus during descent of the SLS-Front compared to SLS-Back ($p=0.012$). There was a main effect for the gluteus medius during descent; however, the pairwise comparisons were not significant. The TFL was the only muscle to have significantly different muscle activation during the ascent phase with the gluteus medius approaching significance.

CONCLUSIONS

Non-stance limb position affects muscle activation of the stance limb during the SLS. This is important information for both clinicians and the general public to facilitate selection of the appropriate SLS variation for individual strengthening goals. This is the first study to indicate specifically that TFL activation is significantly increased during both descent and ascent of a SLS when the NS limb is placed in front. Increased muscle activation of the TFL could suggest that it is being used to control hip

adduction or produce hip flexion during this task, but it may also increase a tendency to internally rotate the hip. Additionally, increased activation of the TFL during SLS-Front may suggest that less focus is being placed on the gluteals (the muscles often targeted during strengthening) to drive the movement. Further analysis is needed to assess if there is a trade-off between gluteal and TFL activation during the SLS.

REFERENCES

1. Willy RW et al. *J Orthop Sports Phys Ther*, **41**, 625-632, 2011.
2. Kivlan BR et al., et al. *Int J Sports Phys Ther* **7**, 402-412, 2012.
3. Nakagawa TH et al. *J Orthop Sports Phys Ther*, **42**, 491-501, 2012.
4. Selkowitz DM et al. *J Orthop Sports Phys Ther*, **43**, 54-64, 2013.

ACKNOWLEDGEMENTS

Research reported was supported by the Peter Paul Career Development Professorship and the National Institute of Arthritis and Musculoskeletal and Skin Diseases of the NIH under Award Numbers R21 AR061690 and K23 AR063235.

Table 1: Participant-Based Average of Average RMS activation (mV) during each phase of the single leg squat.

	SL-Front		SL-Mid		SL-Back		RM ANOVA	
	Mean	SD	Mean	SD	Mean	SD	F	p
Descent								
Gluteus Maximus	0.022	0.021	0.021	0.027	0.012 [^]	0.012	4.542	0.025*
Gluteus Medius	0.050	0.045	0.060	0.058	0.044	0.039	3.697	0.045*
Biceps Femoris	0.029	0.014	0.027	0.013	0.027	0.013	0.659	0.530
Semimembranosus	0.069	0.071	0.069	0.108	0.043	0.057	2.832	0.122
Rectus Femoris	0.052	0.053	0.075	0.102	0.077	0.083	2.415	0.118
Tensor Fascia Lata	0.104	0.084	0.067 [^]	0.059	0.072 [^]	0.065	12.56	0.005*
Ascent								
Gluteus Maximus	0.043	0.044	0.049	0.060	0.037	0.035	1.814	0.211
Gluteus Medius	0.108	0.108	0.128	0.134	0.109	0.112	3.18	0.066
Biceps Femoris	0.032	0.014	0.035	0.021	0.032	0.015	0.539	0.592
Semimembranosus	0.053	0.042	0.071	0.103	0.039	0.025	1.466	0.257
Rectus Femoris	0.054	0.066	0.077	0.123	0.071	0.078	1.418	0.267
Tensor Fascia Lata	0.123	0.112	0.077 [^]	0.075	0.078 [^]	0.069	10.637	0.008*

Note: *Significant main effect $p<0.05$. [^]significantly ($p<0.05$) less than SLS-Front.

Kinetic and Kinematic Based Algorithm for Processing Lateral Cut Maneuver

^{1,2}Adam R. Marmon, ^{1,3,4}Holly Silvers, ¹Amelia Arundale, ¹Ryan Zarzycki, and ¹Lynn Snyder-Mackler

¹University of Delaware, Newark, DE, USA

²Christiana Care Health Systems, Wilmington, DE, USA

³Santa Monica Sports Medicine Foundation, Santa Monica, CA, USA

⁴Institute for Sports Sciences, Los Angeles, CA, USA

email: marmon@udel.edu

INTRODUCTION

The FIFA Medical Assessment and Research Center (F-MARC) developed the FIFA11+ injury prevention program for soccer players. The FIFA11+ is an injury prevention program that combines eccentric, proprioceptive, plyometric and stabilization exercises into a structured warm-up. The program has led to promising results ranging from reduced risk of injury and time loss due to injury in teenage female soccer players [1] and male collegiate players [2] to overall reductions in injury rates in youth players [3] and severe injuries in veteran men [4]. Risk assessments have been reported based on injury rates comparing cohorts who participated in the FIFA11+ to control groups. However, no studies to date have assessed changes in the biomechanics of individuals who participated in the exercise program.

Numerous clinical tests are utilized qualitatively to determine an athlete's likelihood for injury and/or return to play after injury. One of these tests is the lateral cut. Previous biomechanical analyses of a cutting maneuver involved dividing the stance phase of cutting into weight acceptance, peak push off and final push off [5], however the phases were defined as a proportion of the total (e.g. final push off was final 15% of stance).

The purpose of this study was to develop processing algorithms and define variables of interest during a lateral cut maneuver using kinetic and kinematic variables. The developed algorithms will be used to assess changes in kinetic, kinematic, and temporal variables in players who participate in the FIFA 11+ program.

METHODS

Players from a Division I men's collegiate soccer team were invited to participate in the study. Each participant underwent biomechanical testing of six maneuvers, single leg step down, triple hop, deceleration, lateral shuffle, lateral cut, and drop jump prior to and following a 20 game competitive season. The focus of this presentation is on the lateral cut. To complete the lateral cut, players were instructed to run forward, plant their foot on the force plate, complete a 90 degree turn, and continue running (Figure 1). The players were encouraged to complete the movement with speed and explosively, as if they were in a competitive situation and had to quickly change directions. Each leg was tested separately for three trials.

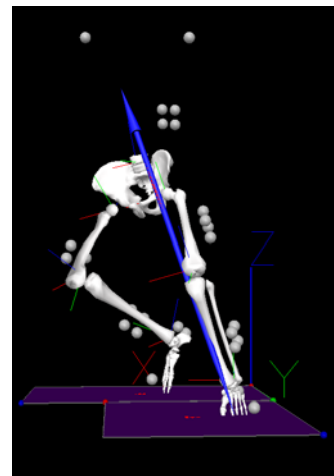


Figure 1. Example biomechanical model of a player performing a lateral cut.

Kinetic and kinematic data were collected during the lateral cut using an 8 camera motion capture system (Vicon, Lake Forest, CA) synchronized with two force plates (Bertec Corp, Worthington, OH).

Retro-reflective markers placed bilaterally on 11 anatomical landmarks and on thermoplastic shells affixed to the thigh, shank, pelvis and torso were tracked and used to create subject specific models. Visual3D software (C-Motion Inc., Germantown, MD) was used to process and calculate kinetic and kinematic variables through inverse dynamics. Marker data were sampled at 240 Hz and force data were sampled at 1080 Hz.

RESULTS AND DISCUSSION

Twenty-four players from a Division I men's soccer team completed the preseason testing (18-25 yrs). All players, but one player who had an ACL injury, completed the cut maneuver with both legs.

Each trial was defined by a stance phase (Figure 2) from Initial Contact (IC, $> 5\text{N}$ threshold of vertical ground reaction force) through Toe Off (TO, $< 5\text{N}$ threshold of vertical ground reaction force). The stance phase was further divided into three phases: Weight acceptance (WtAcc), defined from IC to the first trough in the ground reaction force. Peak push-off (PPO), defined from the first trough in ground reaction force to peak knee flexion. Final push off (FPO), defined from peak knee flexion to TO. Other variables of interest included peak loading rate, peak impact, and the second peak in vertical ground reaction force.

The algorithm was successfully used to process the lateral cut maneuver for numerous players. The algorithm provides a consistent, objective, and automated method for processing this task utilizing kinetic and kinematic variables.

CONCLUSIONS

The kinetic and kinematic variables and regions of interest defined by the algorithm will provide the methodology that will be used to assess biomechanical changes during the lateral cut maneuver in soccer players who participate in the FIFA11+ injury prevention program.

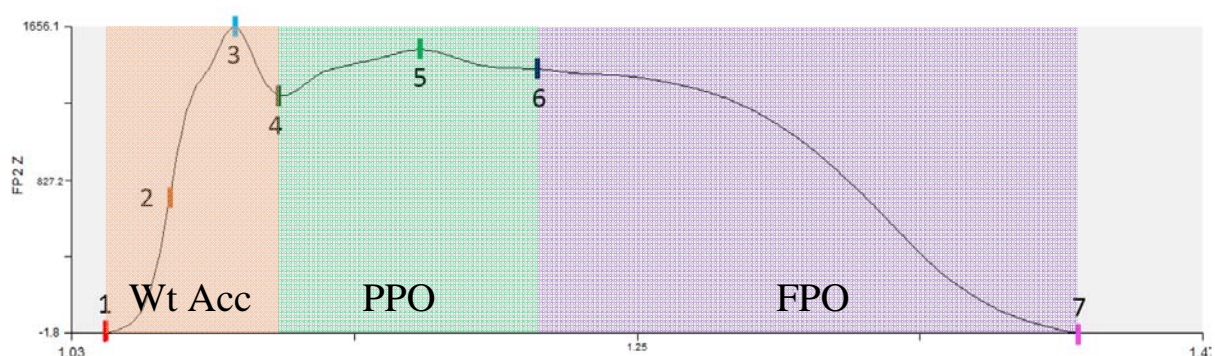
REFERENCES

1. Soligard T, et al. *BMJ*. 2008, Dec **9**;337
2. Grooms DR, et al. *J Athl Training*. 2013, **48**:782–789.
3. Owøye OB, et al. *J Sports Sci Med*. 2014, **13**:321-8.
4. Hammes D, et al. *J Sports Sci*. 2014, **5**:1-9.
5. Besier TF, et al. *Med Sci Sports Exerc*. 2001, **33**:1168-1175.

ACKNOWLEDGEMENTS

We would like to thank the UD athletic training staff and Emily Henderson for your commitment to this project and help administering the FIFA11+.

Figure 2: Kinetic and Kinematic Variables Defined. Sample ground reaction force time-series curve with the key events kinetic and kinematic variables highlighted. 1- Initial Contact, 2- Peak loading rate, 3- Peak Impact, 4- First trough vertical ground reaction trough, 5- Second peak vertical ground reaction force, 6- Peak knee extension, 7- Toe-off. The first phase is weight acceptance (WtAcc), the second phase is peak push-off (PPO), and the third phase is final push-off (FPO).



EYES-CLOSED SINGLE LIMB BALANCE IS NOT RELATED TO HYPERMOBILITY STATUS IN DANCERS

¹Tiffany A. Marulli, ¹Lindsay Harmon-Matthews, ¹J. Hope Davis-Coen, ¹Nienke Willigenburg, ¹Rachel Tatarski, and ¹Timothy E. Hewett

¹The Ohio State University, Columbus, OH, USA
email: tiffany.marulli@osumc.edu

INTRODUCTION

Hypermobility may be associated with decreased lower extremity proprioception, which may be associated with increased injury risk.^{1,2} Joint hypermobility is common in student dancers; however, incidence of hypermobility is lower in professional dancers.³ Although hypermobility may result in deficient proprioception in the general population, it is unclear whether hypermobility affects proprioception and increases injury risk in dancers. If hypermobility increases risk of injury, it could contribute to shorter dance careers for hypermobile dancers and be a possible explanation for decreased incidence of hypermobility among professional dancers.

Single leg stance with the eyes closed is considered a feasible method to evaluate proprioception. It is straightforward to assess since adequate proprioceptive feedback is required to successfully perform such a balance task in the absence of visual input. Thus, the primary aim of this study was to define how hypermobility affects eyes-closed single leg stance balance, as a measure of proprioception in dancers. Our secondary aims were to compare hypermobility and balance between dancer levels. The hypotheses tested were that hypermobility would negatively affect balance time and that students would be more hypermobile than professional dancers.

METHODS

Subjects: Forty-five professional, 11 collegiate, 227 student dancers, and 15 pre-professional dancers consented for this study. Data was collected during routine dance screens.

Hypermobility: Dancer hypermobility status was assessed via the Beighton-Horan Laxity test (Figure 1). Dancers were deemed hypermobile if at least four of eight Beighton-Horan Laxity tests were positive. The forward bend item was excluded as it is not considered to be sensitive to differences in joint mobility in this population. Increased hip flexion range of motion is believed to be acquired through dance training and is common to most dancers.⁴

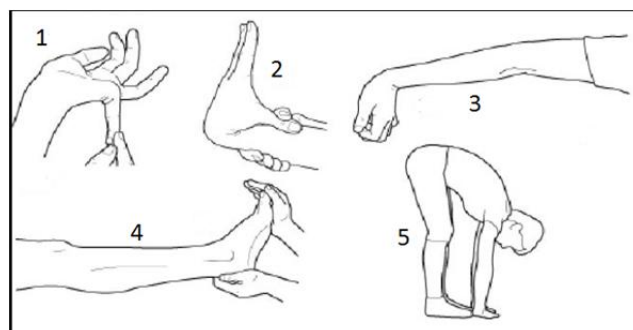


Figure 1: Beighton-Horan Laxity Test⁵ Items 1-4 are performed bilaterally.

Balance/Proprioception: Single limb balance time was assessed in parallel, with the eyes closed and without the non-weight-bearing foot touching the weight-bearing leg. Balance time was measured in seconds, up to a maximum balance time of sixty seconds. Non-weight bearing leg touch down, hopping or torso/hip bending was considered loss of balance. Dancers performed this balance task on both their left and right legs. The average of both balance times was used for further analysis.

Statistical Analysis: We used a t-test to compare balance time between hypermobile and non-hypermobile dancers. An ANOVA with Bonferroni adjusted pairwise comparisons was used to assess the effect of affiliation group (i.e. dancer level) on

hypermobility scores and balance time. The significance level was set to $\alpha=0.05$.

RESULTS

Hypermobile and non-hypermobile dancers showed very similar balance times ($p=0.819$) (Figure 2).

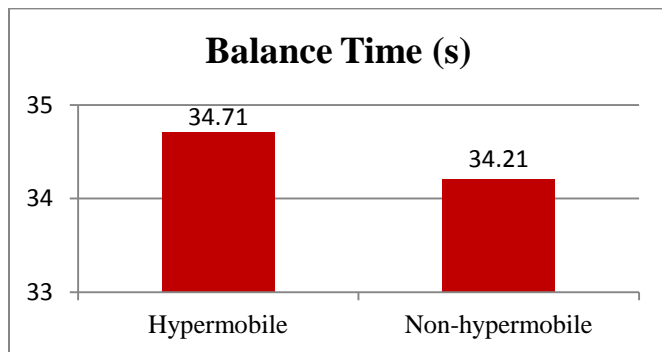


Figure 2: Hypermobile versus non-hypermobile dancer balance times.

Also, incidence of hypermobility was similar across all dancer levels ($p=0.148$) (Table 1). However, a significant difference in balance time was observed between dancer levels. Specifically, professional dancers had almost 20 seconds longer balance times than collegiate dancers ($p=0.018$) (Table 1).

Table 1: Incidence of hypermobility and average balance times by affiliation.

Dancer Affiliation	Incidence of Hypermobility	Average Balance Time (s)
Professional	16 (36%)	39
Collegiate	3 (27%)	21
Pre-Professional	10 (62%)	35
Student	106 (47%)	34

DISCUSSION

In contrast to our hypothesis, hypermobility status did not affect single limb balance time in this large population of dancers. Therefore, single limb static balance with the eyes closed may not be a valid test of dancers' relative proprioception levels. In addition, hypermobile dancers may compensate for proprioceptive deficits through dance and balance training. Furthermore, hypermobility scores did not

differ between students and professionals, which may be due to a relatively limited sample of professional dancers in our population. Another potential limitation is that balance testing may not be a sufficiently sensitive test of proprioception to distinguish differences between these groups. Professional ballet dancers demonstrated enhanced balance compared to collegiate dancers, who trained mainly in modern dance. This may be due to differences in ballet or modern as a primary dance style and differences in training. We recommend that future studies examine dancers' dynamic balance, joint position sense, other sensitive measures of joint proprioception and the relationship to hypermobility and injury occurrence.

CONCLUSIONS

Hypermobility did not affect eyes-closed single leg balance and was similar between age groups of dancers. However, collegiate modern dancers showed lower balance times than professional ballet dancers.

REFERENCES

1. Klemp P, Learmonth ID. Hypermobility and injuries in a professional ballet company. *Brit J Sports Med.* 1984; **18**(3): 143-148.
2. McCormack M, Briggs J, Hakim A, Grahame R. Joint laxity and the benign joint hypermobility syndrome in student and professional ballet dancers. *J Rheumatology.* 2004; **31**: 173-178.
3. Rombaut L, Paeppe AD, Malfait F. Joint position sense and vibratory perception sense in patients with Ehlers-Danlos syndrome type III (hypermobility type). *Clinical Rheumatology.* 2010; **26**: 289-295.
4. Hamilton WG, Hamilton LH, Marshall P, Molnar M. A profile of the musculoskeletal characteristics of elite professional ballet dancers. *Am J Sports Med.* 1992; **20**(3): 267-273.
5. Beighton Score. Physiopedia. http://www.physio-pedia.com/File:Beighton_Score.png Accessed March 6, 2015.

ACKNOWLEDGEMENTS

Thank you to the dancers, physical therapists, athletic trainers, and staff who participated in this study. Special thanks to Ben Roewer, Stephanie Di Stasi Roewer, and Heather Stiff for assistance with database construction and data entry.

INFLUENCE OF FOREFOOT ANTHROPOMETRY ON PAIN IN MINIMALIST RUNNERS

Erica M. Casto, Kyla M. Galbreath, and Jean L. McCrory

¹West Virginia University, Morgantown, WV, USA
email: jlmccrory@hsc.wvu.edu

INTRODUCTION

Distance running is among the most popular exercise activities in society today. However, rate of overuse injury in runners ranges from 19.4 to 79.3% (1). Common running injuries include patellofemoral pain, IT band syndrome, shin splints, plantar fasciitis(PF), Achilles tendinitis(AT) (2), and metatarsal stress fractures(3). Proponents of minimalist running purport it will attenuate injury rates by reducing landing impact forces(4). However, evidence that barefoot running actually reduces injury remains inconclusive(5).

As a counterpoint to this phenomenon, researchers assert barefoot running is not a substantiated preventative measure and should be assessed on an individual basis(6). Several researchers have suggested that a having Morton's foot or hallux valgus may be related to injury(7). Lower extremity anthropometry may influence the type of injury sustained. We have previously reported minimalist runners with pes planus were more likely to sustain a soft-tissue injury(8). However, a search of relevant literature revealed no studies that examined the influence of forefoot anthropometry on running injury in barefoot or minimally shod runners.

The **purpose** of this study was to determine if having a Morton's foot, hallux valgus, or angular splay between the first and second toes are related to type of pain, general location of pain, or specific location of pain in minimally shod runners.

METHODS

Sixteen experienced minimalist runners participated (age: 27.4 ± 10.1 yrs, hgt: 170.3 ± 25.0 cm, mass: 78.1 ± 18.0 kg, gender: 8M, 8F). All subjects reported running > 10 miles/week in minimalist shoes for at least three months. Minimalist shoes were defined as having a midsole drop of 4mm or less.

Informed consent was obtained. Subjects were surveyed about the type and location of pain. Pain at sites of common running injuries was quantified using a validated visual analog scale (VAS)(9). Based on survey data, injuries were then classified as soft-tissue or bony. Subjects were considered to be injured if pain on the VAS >3.

Static forefoot anthropometry measures were taken from superior view photos. While the subject stood in quiet stance with weight distributed equally between both legs, a digital camera (Canon EOS Rebel T2i, Tokyo, Japan) was placed 26 cm directly above the left or right foot. This procedure was repeated for the contralateral foot. The digital images were calibrated using a ruler placed adjacent to the foot in each picture.

Morton's Foot: A foot was classified as Morton's foot if the most distal aspect of the second toe was anterior to the great toe (10) on the digital image.

Hallux Valgus: Using Image-J software (NIH, Bethesda, MD), the angle was determined between a line from the midpoint of the proximal phalanx of the hallux to the midpoint of the first metatarsal head, and a second line drawn from the midpoint of the first metatarsal head to the base of the first metatarsal. Those feet in which the angle was > 15° were classified as having hallux valgus(11).

Toe Splay: To assess the angle of toe splay between the first and second digits, the angle between the line from the interphalangeal joint midpoint of the hallux to the metatarsal line, and a line from the midpoint of the proximal joint of the second toe to the metatarsal line was determined. Those feet with an angle > 45° were classified as having toe splay.

Statistics were performed using IBM SPSS software (v21, Armonk, NY). All data were categorical

(yes/no). Left and right feet were considered separately such that we had 32 total feet from 16 subjects. Independent variables were: Morton's foot, hallux valgus, and toe splay angle. The dependent variables were pain type (soft tissue, bony), general location of pain (foot, ankle, knee /shank, above knee), or specific location of pain (AT, PF, metatarsals, IT band, anterior knee, anterior shank). Chi squared analyses were performed to determine if injury type and location were equally distributed among each category of the independent variables. In this pilot study, our alpha was 0.10.

RESULTS AND DISCUSSION

Of the 32 feet in the study, eight were classified as Morton's feet and 24 as regular feet. Seven of the feet were classified as hallux valgus and 25 were not. Twenty feet had toe splay between the first and second toes and 12 did not.

Several of these forefoot classifications were related to pain in minimalist runners (Table 1). Runners who did not have a Morton's foot were more likely to have soft-tissue pain than runners with a Morton's foot. Seventy-five percent of minimalist runners without a Morton's foot reported soft tissue pain, while only 25% of those with a Morton's foot reported pain. Subjects with a Morton's foot were more likely to experience pain in the foot (100% vs 66%), and less likely to experience pain in the knee and shank (0% vs 33%). The second metatarsal is more mobile in individuals with a Morton's foot(11). This heightened mobility may be related to greater interjoint instability and increased foot pain in those with Morton's feet, but protective of pain at the knee and shank. Subjects with hallux valgus were less likely to experience ankle pain than those without hallux valgus (0% vs 82%). Conversely,

runners with toe-splay were more likely to experience ankle pain (35% vs 8%). Given these two divergent toe alignments, it is not surprising that the results differ. However, because "ankle pain" was defined as having >3 on the VAS scale and the exact nature of the injuries is unknown, the rationale for why individuals with hallux valgus have less ankle pain is elusive.

Our study was limited by the small sample size. Also, our data were based on self-reported pain and not clinical diagnoses. All data were from static photos not dynamic gait parameters. In the future, we plan to increase the sample size to quantify the influence of forefoot anthropometry and specific injury, rather than general location of pain.

CONCLUSION

Forefoot anthropometry is related to pain in minimalist runners. This should be a consideration in the choice to minimalist run as well as in the treatment of running injuries in this group.

REFERENCES

1. van Gent RN et al. *Br J Sports Med* **41**; 469-80, 2007.
2. Brown CR Jr. Ch 72. Common injuries from running. In: Imboden, et al, eds. *Current Diag & Trt: Rheum*. 3rd ed. NY, NY: McGraw-Hill; 2013:
3. Nagel et al. *Gait & Posture*. 27; 152-55, 2008
4. Crowell H and Davis I. *Clin. Bmch*. 26;593-8, 2011.
5. Murphy et al. *Sports Med*. 43:1131-38, 2013
6. Murphy et al. *Sports Med*. 11;1131-8, 2013
7. Rodgers MM and Cavanagh. *MSSE* 21; 23-8, 1989.
8. Galbreath KM, et al. *MSSE*. 46(5): S455, 2014.
9. Stuber J et al. *Foot Ankle Surg*. 17(3): 166-72, 2011.
10. Hlavac, HF. Ch 14: Toes and Metatarsals. *The Foot Book 2nd ed*. World Pubs, Mountain View, CA 1977.
11. Zhou J, et al. *Indian J Orthop*. 47; 278-282, 2013.

Table 1: Results of statistical analysis examining the relationship between anthropometry and pain.

Variable	Soft-tissue	Bony	Foot	Ankle	Knee/Shank	Above knee	AT	PF	Meta-tarsal	IT Band	Ant knee	Ant Shank
Mortons Foot	0.011	0.399	0.059	0.999	0.059	0.399	0.399	0.217	0.399	0.557	0.399	0.160
Hallux Valgus	0.225	0.581	0.459	0.084	0.217	0.440	0.198	0.872	0.440	0.591	0.440	0.912
1-2 Toe Splay	0.706	0.706	0.399	0.092	0.399	0.706	0.379	0.581	0.258	0.190	0.706	0.379

EFFECTS OF LOAD ON THE HIP-TO-KNEE TORQUE RATIO IN A SQUAT EXERCISE

Ben W. Meyer

Shippensburg University, Shippensburg, PA, USA
bwmeyer@ship.edu

INTRODUCTION

A common technique to increase muscular strength involves performing multiple exercise repetitions close to an athlete's maximum muscular tension. The typical method used to increase muscular tensions is to increase the external load used during the exercise. Previous work [1,2] has examined the influence of variations in the external load on lower extremity joint torques during conventional back squats. Although hip and knee extension torque values have been reported in previous studies, limited attention has been given to the hip-to-knee torque ratio. A conventional back squat can be executed in any of the ways shown in Figure 1 (as well as with even more extreme forward leans of the trunk). The hip-to-knee torque ratio gives us information about which muscle groups the athlete is choosing to emphasize in the lift. A conventional back squat with a large hip-to-knee torque ratio emphasizes the relative use of the hip extensors over the knee extensors. Powerlifters (athletes who perform the squat, deadlift, and bench press exercises in competition) tend to emphasize the hip extensor musculature when lifting heavy loads. Therefore, it is expected that powerlifters would exhibit a large hip-to-knee torque ratio (by adopting a larger forward lean of the trunk).

The purpose of this study was to determine the influence of variations in the external load on the hip-to-knee joint torque ratio and trunk angle in conventional back squat exercises (for both powerlifters and non-powerlifters).

METHODS

Five male powerlifters (standing height = 1.72 ± 0.04 m; mass = 93 ± 12 kg) and five male non-powerlifters (standing height = 1.80 ± 0.07 m; mass = 82 ± 13 kg) volunteered for the study. The

subjects performed conventional back squats at 60%, 70%, and 80% of their raw one-repetition maximum. (Raw lifts are those performed without the use of knee wraps or squat suits.)

Each trial was recorded with a Vicon 370 motion analysis system, and the ground reaction forces and torques exerted on the right foot were measured with an AMTI OR6-7-1000 force platform. The sampling rate was 60 Hz for both. Joint torques were computed using the method proposed by Andrews [3,4]. Trunk lean was defined as the angle between the vertical and the line pointing from the midpoint of the two hip joints to the suprasternale. Data were calculated for the low point of the lift, defined as the instant of minimum thigh angle. At the low point, the thigh was approximately parallel to the ground ($5 \pm 8^\circ$). Differences between measures were assessed using ANOVA tests with a cut-off for statistical significance set at $\alpha = 0.05$.

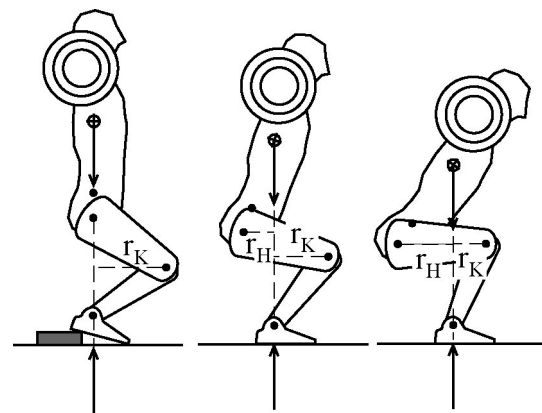


Figure 1: Variations in back squat technique.

RESULTS AND DISCUSSION

Figure 2 shows that the hip-to-knee torque ratio did not significantly change across the loads tested in the study ($p > 0.05$) for either the powerlifters or the non-powerlifters. However, significant

differences in hip-to-knee torque ratio ($p < 0.05$) between the two types of lifters were present at each load tested.

Figure 3 shows that the trunk angle did not significantly change across the loads tested in the study ($p > 0.05$) for either the powerlifters or the non-powerlifters. However, significant differences in trunk angle ($p < 0.05$) between the two types of lifters were present across the range of tested loads.

The present study used a force plate under a single leg and full kinematic and kinetic data to calculate three-dimensional (3D) hip and knee torques, following the kinetic chain of the analyzed leg from the ground upward. The methods used by other authors involve various assumptions and simplifications. Previous work [5] has shown that 2D methods do not properly represent the hip and knee extensor torques during conventional back squats. It is difficult to compare hip and knee torques from different projects, due to variations in body mass, barbell load, body dimensions, relative emphasis of the subjects on hip or knee torque, linear and angular accelerations, and methodological differences.

CONCLUSIONS

The conventional back squat is an effective exercise for working the lower extremity musculature. Powerlifters tend to emphasize the use of the hip extensors, as shown by the large hip-to-knee torque ratio (~1.9) and trunk angle (~41 degrees) in the present study. Non-powerlifters use a more even balance between the hip and knee extensors (hip-to-knee torque ratio ~1.2) as well as a more conservative forward lean of the trunk (~31 degrees).

REFERENCES

1. Hay JG, et al. *Biom Symp Proc*, 286-293, 1980.
2. Hay JG, et al. *Biom VIII-B*, 939-950, 1983.
3. Andrews JG. *Kinesiology IV*, 32-42, 1974.
4. Andrews JG. *Med Sci Sport Exer*, 14, 361-367, 1982.
5. Meyer BW. 7th *World Cong Biom*, M394, 2014.

ACKNOWLEDGEMENTS

The author would like to thank the College of Education and Human Services at Shippensburg University.

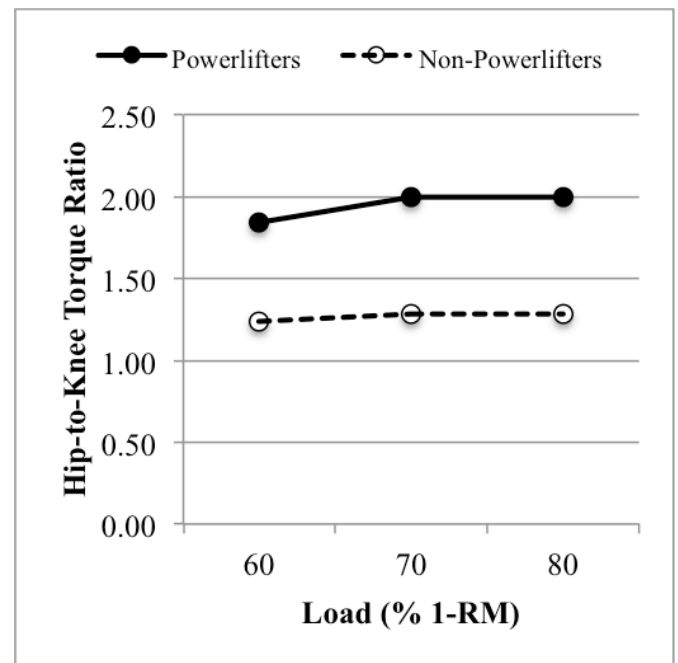


Figure 2: Effects of increasing load on the hip-to-knee torque ratio in a conventional back squat.

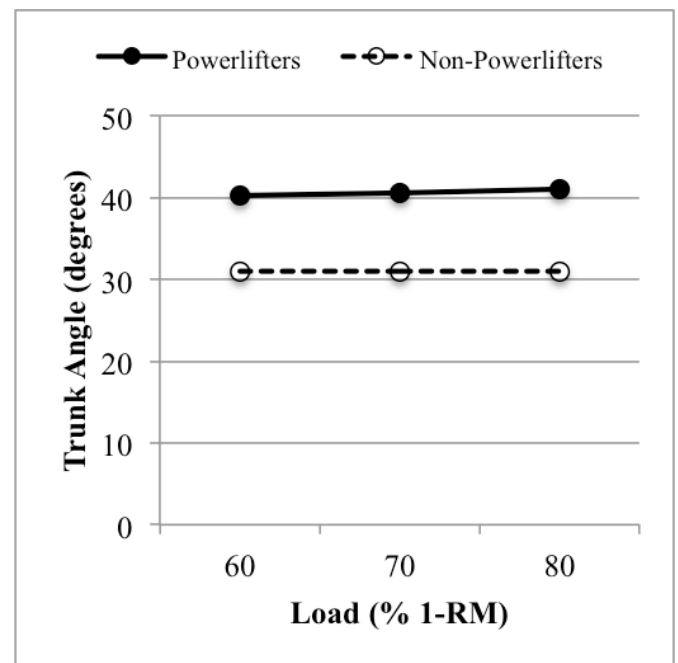


Figure 3: Effects of increasing load on the trunk angle in a conventional back squat.

A GRF COMPARISON BETWEEN LANDING FROM A COUNTERMOVEMENT JUMP AND LANDING FROM HANGING AND DROPPING: A PILOT STUDY

Erin Miranda and Mostafa Afifi Hegazy

Movement Sciences Department, University of Idaho, Moscow, ID, USA

INTRODUCTION

The interest in the biomechanics of landing has increased in the last few decades as injuries from landing are common, especially injuries to the anterior cruciate ligament (ACL) costing approximate \$1.7-2.5 billion annually in the United States alone (Afifi & Hinrichs, 2012). This is a huge concern, especially for female athletes as they are about 4-6 times more likely to injure their ACL than males (Myer et al., 2004). With the introduction of Title IX, the number of female athletes participating in college sports has gradually increased, with approximately 10k participating in sports in the early 70s to more than 107k by the mid-90s (Lewis, 2000) and that number continues to grow.

A common practice when studying landing mechanics is to have individuals step off a box or drop from a hanging bar. The idea behind these techniques is to make sure every individual lands from the same height (Afifi & Hinrichs, 2012). However, as individuals step off a box they tend to lower their foot resulting in a different step-off height for each individual (Afifi & Hinrichs, 2012). In addition, the mechanics of landing are different from that of a countermovement jump (CMJ) with the step-off landing showing greater peak landing ground reaction force (GRF) and maximum loading rate (Afifi & Hinrichs, 2012; Edwards et al. 2010).

To our knowledge, the mechanics of landing when dropping from a hanging bar has never been compared to that of a CMJ. If the mechanics are the same, then hanging and dropping may serve as a model for simulating landing from a jump. Thus, the purpose of this study was to compare the GRF experienced during hanging and dropping to that experienced during a CMJ landing.

METHODS

Seven active female college students (21.8 ± 2.6 years of age and 64.3 ± 9 kg) performed 3 maximal vertical jumps and their highest jump was determined using a Vertec device (Sports Imports, Columbus, Ohio). A bar was then set at 75, 50 and 25% of their maximum jump height in a counterbalanced order. The participants then performed 3 CMJ to high enough to touch the bar and 3 drop landings (Drop) where they hung from and released from the bar height. The order of jumping and dropping was also counterbalanced.

Ground reaction force (GRF) data was collected using two force platforms (1000 Hz, AMTI, Watertown, MA) as participants landed with one foot on a separate platform. The peak GRF, peak normalized ground reaction force (nGRF) and maximum loading rate of the two different landings were measured. Data from each condition's 3 landing trials were averaged. Data from each lower limb and two limb average were statistically compared.

A series of two-way ANOVA with repeated measures (landing type \times height) with both landing type (CMJ vs. Drop) and height (75, 50, and 25 % maximum height) as within subject factors were conducted for each variable.

RESULTS AND DISCUSSION

Our analysis showed a significant main effect of height for peak GRF and maximum loading rate for each lower limb as well as the two leg average ($p < 0.05$). Simple effects did not show significant differences between height pairs for both the CMJ and Drop, however, Drop approached significance for both variables (Table 1). This trend suggests that during CMJ participants were able to adjust their

landing technique to maintain a relatively constant peak GRF at the different heights thus keeping landing impact relatively safe. The gradual increase in peak GRF and maximum load rate during the Drop condition suggest participants were less prepared to the increase of height.

Our analysis also showed a significant main effect of landing type for maximum loading rate for each lower limb as well as the average of both sides ($p<0.05$). Simple effects showed a significant difference between landing types at 75% of maximum height only ($p<0.05$; Figure 1). There may be a height threshold after which the changes in landing mechanics become distinguishable. CMJ and Drop landings were similar at 50 and 25% of maximum height.

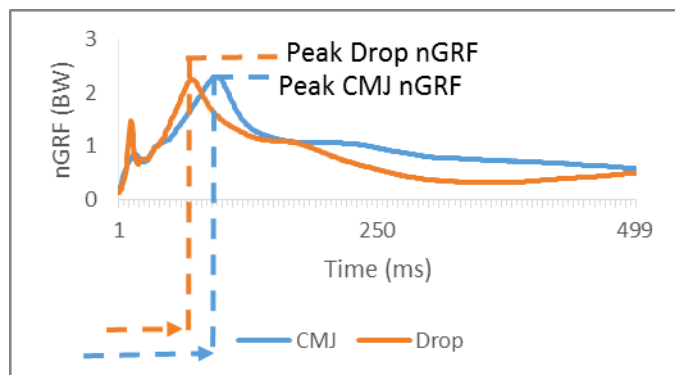


Figure 1. nGRF in BW for the CMJ and Drop landings from 75% peak height for a typical participant. Greater peak nGRF for Drop in a shorter period increasing peak loading rate.

Based on our results, it seems the use of hanging and dropping to study landing mechanics would be an acceptable practice when analyzing submaximal landings of 50% or less of maximum jump height.

The results found in this pilot study warrant a revisit to comparing stepoff landings to CMJ landings.

Afifi and Hinrichs (2012) stated that step-off landings were different from CMJ landings; however, they compared maximum jump landings. Based on our findings, these results may be height specific, but this remains to be tested. Edwards et al. (2010) showed a difference between step-off and CMJ landings from the submaximal height of 33 cm. However, their participants had to hit a ball in the process. Multitasking while landing adds another dimension as central nervous system resources are not just focused on landing.

Any questions about this study should be addressed to:

Mostafa Hegazy, PhD
mhegazy@uidaho.edu

CONCLUSIONS

A comparison was made between vertical GRF when landing from a countermovement jump and drops in female college students. Results suggest that these landings are not similar when the landing height is 75% of maximum jump height but similar at 50% and 25%. These preliminary results suggest that dropping from a height may be used to assess landing mechanics for landings from a height 50% or less but not 75% of maximum jump height. Additional work needs to be done to see how these force differences are reflected in patterns of muscle activity and kinematics of landing.

REFERENCES

1. Afifi MA & Hinrichs RN. *J Appl Biomech* **29**, 1-9, 2012.
2. Edwards S. *Scand J Med Sci Spor* **20**, 516–523
3. Lewis T. *Physiotherapy* **86**, 464-472, 2000.
4. Myer GD, et al. *J Athl Train* **39**, 352–364, 2004

Table 1: Peak Loading rate and Peak GRF at all landing heights for both CMJ and Drop conditions.

	Peak Loading Rate ($N \cdot ms^{-1}$)			GRF (N)		
	Right	Left	Average	Right	Left	Average
CMJ 75 %	178±144	148±64	163±100	1135±278	1225 ±265	1180±261
CMJ 50 %	166±82	167±63	166±73	1209±323	1248±246	1128±272
CMJ 25 %	155±65	151±63	153±73	1206±237	1237±317	1221±259
Drop 75 %	251±117	249±134	250±63	1225±306	1405±277	1315±246
Drop 50 %	163±84	190±74	176±74	1076±165	1279±287	1178±180
Drop 25 %	127±62	147±66	137±59	969±258	1136±234	1052±212

A BIOMECHANICAL PROFILE OF FEAR IN ACL RECONSTRUCTED ATHLETES

Christopher Nagelli, Samuel Wordeman, Stephanie Di Stasi, and Timothy E. Hewett

Sports Health and Performance Institute OSU Sports Medicine, Department of Biomedical Engineering,
The Ohio State University, Columbus, OH USA
email: christopher.nagelli@osumc.edu

INTRODUCTION

Anterior cruciate ligament (ACL) tears are traumatic and devastating knee injuries that frequently occur during sports participation. Most often, ACL-injured athletes undergo ACL reconstruction (ACLR) to regain knee stability and return to sports (RTS) in a timely manner. Despite surgical stability and restoration of normal function, only 65% of athletes return to the pre-injury level of sport at the conservative time point of one year after ACLR¹. Fear of reinjury is the most common reason for a reduction or cessation in sports participation among athletes after ACLR.² Athletes who report less fear of reinjury, and a greater psychological readiness to RTS, are more likely return to their preinjury level of sport after ACLR.³ Furthermore, the athletes who do RTS are at an elevated risk for a secondary ACL injury. Altered biomechanics at the hip and knee have demonstrated to be were predictors of a secondary ACL injury.⁴

Therefore, the purpose of this study was to determine if there is an association between athletes with greater self-reported levels of fear of reinjury after ACLR and biomechanics during a dynamic single-leg landing task. We tested the hypothesis that the magnitude of frontal plane movement in the lower extremities would be associated with the athlete's fear of reinjury.

METHODS

Eighteen athletes approximately 9 months (8.5 ± 4.2 months) from ACLR were recruited for this study. Basic demographics and anthropometrics of the cohort are provided in **Table 1**. The Anterior Cruciate Ligament Return-To-Sport after Injury (ACL-RSI) scale was utilized to measure psychological preparedness and fear or reinjury in the ACLR cohort. There are a total of 12 questions on the ACL-RSI outcome survey and each question is scaled from 0-100. The lower the score the more

fearful or unprepared an athlete felt. Reliability and validity of the ACL-RSI scale to identify athletes who find RTS to be challenging has been demonstrated.⁵

Subsequently, the athletes underwent biomechanical testing using a 12 infrared camera, three-dimensional motion analysis system. The athletes were fitted with 55 retro-reflective markers in a modified Helen Hayes configuration, and completed 5 single-leg landing tasks from a 31 cm box onto two embedded force plates. A trial was deemed successful if the athlete was able to drop off the box unilaterally, land on a single limb, and regain control without adjusting their foot from its initial landing position. Bilateral isokinetic knee extension/flexion strength testing was conducted at 60 °/sec using a dynamometer (Biodex, System 3). A paired t-test was used to evaluate the difference in mean peak knee extensor and flexor torque in the injured and uninjured limb. A multivariate linear regression analysis was used to describe the relationship between fear and lower extremity biomechanics ($p < 0.05$).

Table 1: Demographics of athletes (Mean \pm SD)

<i>Subjects</i>	<i>Age (yrs)</i>	<i>Height (m)</i>	<i>Weight (kg)</i>
Male (n=9)	23.6 \pm 9.0	1.7 \pm 0.07	81.5 \pm 11.8
Females (n=9)	16.3 \pm 2.1	1.6 \pm 0.06	64.0 \pm 10.2

RESULTS AND DISCUSSION

The average ACL_RSI score for the ACLR athletes was 66.7 \pm 22.5. Interestingly, the questions that received the lowest average scores for this cohort were: (1) are you fearful of re-injuring your knee by playing your sport? (56.6 \pm 31.9) and (2) are you afraid of accidentally injuring your knee by playing your sport? (52.7 \pm 30.2). This demonstrates that

regardless of psychological preparedness, a fear of reinjury existed amongst the cohort.

A multivariate linear regression model was built based on frontal plane excursions. For the ACLR limb, the model that included frontal plane excursions at the hip and knee explained a significant portion of the variance in ACL-RSI scores ($p=0.025$, $R^2=0.39$) (**Figure 1a**). However, for the uninjured limb, the same model that included frontal plane excursions at the hip and knee was not significant ($p=0.51$) and only described 8% of the variance (**Figure 1b**).

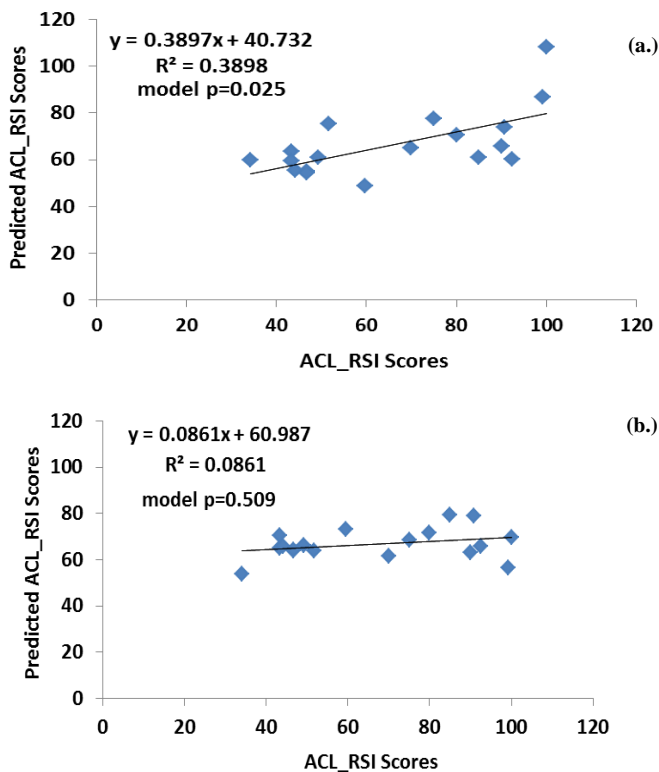


Figure 1: A multivariate linear regression model predicted ACL_RSI scores based on frontal plane excursions at the hip and knee in the injured (a) and uninjured (b) limb during a unilateral landing task.

Isokinetic testing showed significant differences between injured and uninjured limbs in peak extensor (INJ: $.61 \pm .14$ Nm/kg*m; UNINJ: $.67 \pm .16$ Nm/kg*m; $p=0.012$) and flexor (INJ: $.30 \pm .06$ Nm/kg*m; UNINJ: $.33 \pm .06$ Nm/kg*m; $p=0.010$) torque. However, the average LSI for the cohort was 91.2 ± 20.0 . A healthy population with no prior knee injury typically demonstrates quadriceps and hamstrings LSI within the range of 80-100%.

Interestingly, altered neuromuscular control in the frontal plane at the hip and knee during a drop-landing task are predictive of primary and secondary ACL injury. The results of this study indicate that there may be an association between the psychological preparedness of athletes and frontal plane mechanics. An absence of confidence in the ACLR limb may manifest as high-risk biomechanics.

Peak knee extensor and flexor torques were not included in the multiple linear regression model due to the limited sample size in this cohort. The recovery of quadriceps and hamstring strength in the ACLR limb could influence an athlete's confidence in dynamic tasks such as single-leg landing. Furthermore, a unilateral landing task from a 31 cm tall box does not provide an opportunity for compensatory landing strategies by reliance on the uninjured limb. The physical demand of a single-leg task likely requires greater confidence in the injured limb.

CONCLUSION

Current evidence-based ACLR rehabilitation guidelines do not address strategies to build confidence in the ACLR limb of athletes. Fear and its associated biomechanics have not been previously described in an ACLR cohort. High secondary ACL injury rates and the low number of athletes that return to preinjury level of sport indicate that the current rehabilitation guidelines are not sufficient for physical and psychological recovery from the initial injury. Further research is necessary to delineate the effects of fear on biomechanics.

References

1. Ardern et al. Br J Sports Med. 2014. 48.21.1543-1552
2. Ardern et al. Br J Sports Med. 2011. 45.7.596-606.
3. Ardern et al. Am J Sports Med. 2013. 1549-1558.
4. Paterno et al. Am J Sports Med. 2010. 38.10.1968-1678.
5. Webster et al. Phy Ther Sport. 2008. 9.1.9-15

ACKNOWLEDGEMENTS

The co-authors would like to thank the Sports Health and Performance Institute at The Ohio State University.

WEARING A WETSUIT ALTERS ARM MOTION DURING SIMULATED SURFBOARD PADDLING

Jeff A. Nessler, Madison N. Silvas, and Sean C. Newcomer

California State University, San Marcos, San Marcos, CA, USA

email: jnessler@csusm.edu, web: <http://www.csusm.edu/kinesiology/research/nessler.html>

INTRODUCTION

By some estimates over 20 million people participate in the sport of surfing worldwide (International Surfing Association). Growing popularity in the sport has led to an increased demand for surfing related equipment. Wetsuits have become an important piece of surfing equipment, with annual sales exceeding 100 million USD (Board-trac Inc., 2009). However, relatively little is known regarding their effects on human performance.

Wetsuits are primarily utilized for their thermoregulatory properties [1], though surfers may also experience some benefit from increased buoyancy and reduced drag in the water [2]. In addition, there is evidence that wearing a neoprene sleeve may help to enhance proprioceptive acuity [3, 4]. In surfers, improved sensory feedback may lead to beneficial changes in the control of arm motion during repetitive paddling. Control of arm motion has previously been associated with movement variability and complexity [5-7], and measures of entropy and local dynamic stability might lend insight to alterations in the control of repetitive paddling. To date, no study has focused on these aspects of human performance while wearing a neoprene sleeve over any aspect of the body. Therefore, the purpose of this study was to determine the effects of a wetsuit on the complexity and variability of paddling in recreational surfers.

METHODS

Twelve male, recreational surfers were recruited from the local population (age 33.0 ± 8.6 yr, height 1.82 ± 0.07 m, mass 79.9 ± 9.4 kg). All subjects were free of any cardiovascular, musculoskeletal, or neurological condition that might have affected their performance. All procedures were approved

by the Institutional Review Board at California State University, San Marcos and all participants gave their informed consent prior to data collection.

Following a brief orientation and warm-up, each participant paddled at a submaximal level for 2 minutes while wearing a wetsuit and 2 minutes without a wetsuit (in random order). Paddling was simulated in the laboratory using a commercially available swim bench ergometer (VASA Inc., Essex Junction, VT) that was modified by attaching a short surfboard to the top aspect of the bench. Resistance to paddling was provided by a cable and pulley system that actuated a small flywheel. Subjects were instructed to maintain an output of 20 Watts throughout each trial and were given quantitative, verbal feedback every 5 seconds. Subjects were also instructed to align their strokes with an audible metronome at 25 bpm. Arm movement was relatively unrestricted, though subjects were instructed to paddle in a manner that was similar to their normal motion while in water.

An 8 camera motion capture system (Vicon Motion Systems, Oxford, UK) was used to track the motion of a reflective marker placed over the right wrist of each subject at 120 Hz. Long (λ_{long} , 1-10 strokes) and short (λ_{short} , 0-1 stroke) term maximal Lyapunov exponents were then calculated for wrist trajectories in the antero-posterior, cranial-caudal, and medio-lateral directions (with respect to a prone, paddling position) using the method described by Rosenstein et al [8]. The time series data were then reduced by calculating individual stroke lengths, heights, and widths across each 2 minute trial. These data were then analyzed using the approximate entropy (ApEn) technique described by Pincus [9]. Finally, mean stroke lengths, heights and widths were calculated, and paired t-tests were utilized to compare differences between the wetsuit and no-wetsuit conditions.

RESULTS AND DISCUSSION

Wearing a wetsuit resulted in significant increases in average stroke height, stroke variability, and stroke complexity (λ_{short} and ApEn, $p < 0.05$, Table 1). These differences were only noted for motion in the vertical (antero-posterior) direction and not in either of the other directions of movement.

These results suggest that wearing a wetsuit influences the control of arm motion in repetitive paddling. This affect might be related to a change in the sensory feedback that has been reported to occur when a neoprene sleeve is worn [3, 4]. In particular, ApEn values measured here suggest that arm motion in the vertical direction became more complex when additional sensory feedback was provided. Increased complexity has been associated with learning a motor skill [5] and decreased complexity has been associated with aging, injury, and abnormal physiology [6].

Estimates of maximal Lyapunov exponents were significantly increased (λ_{short} only) when a wetsuit was worn. This suggests that wearing a wetsuit leads to an increase in movement variability and/or local dynamic stability, consistent with the observed increase in movement complexity (ApEn). Several studies have provided evidence for the idea of an optimal level of movement variability that is not too low (periodic and inflexible) or too great (noisy or random) [7]. An increase in λ_{short} for surfers may therefore reflect an increase in movement flexibility or divergence from a strict behavioral attractor for paddling. Changes in the variability of repetitive movements may hold implications for

musculoskeletal injury [10] and should be investigated further in paddling surfers.

CONCLUSIONS

Wearing a wetsuit appears to have a beneficial effect on repetitive paddling in surfers by increasing movement complexity and variability. These results may have implications for wetsuit design and for prevention of upper extremity overuse injuries.

REFERENCES

1. Wakabayashi, H, et al., J Phys Anthropol, 25 331-338, 2006.
2. Tomikawa, M, et al., J Sci Med Sport, 11 417-423, 2008.
3. Herrington, L, et al., Res Sport Med, 13 37-46, 2005.
4. Ulkar, B, et al., Br J Sports Med, 38 549-552, 2004.
5. Cordier, P, et al., Hum Mov Sci, 13 745-763, 1994.
6. Khandoker, AH, et al., J Neuroeng Rehabil, 5 1-10, 2008.
7. Stergiou, N, et al., J Neuro Phys Ther, 30 120-129, 2006.
8. Rosenstein, MT, et al., Phys D, 65 117, 1993.
9. Pincus, SM, Chaos, 5 110-117, 1991.
10. Moraiti, C, et al., Knee Surg Sports Traumatol Arthrosc, 15 1406-1413, 2007.

ACKNOWLEDGEMENTS

The authors thank Austin Reeves, Vuk Ekmecic, and Shane Carpenter for their assistance with data collection.

Table 1: Aggregate results for complexity and variability in three dimensions of wrist movement.

Condition	Antero-posterior [Stroke Height]		Cranial-caudal [Stroke Length]		Medio-lateral [Stroke Width]	
	Wetsuit	No Wetsuit	Wetsuit	No Wetsuit	Wetsuit	No Wetsuit
Mean Excursion [mm]	481.5±86.1*	438.5±75.8	970.0±64.2	971.6±76.9	169.9±66.8	171.8±59.4
λ_{short} (0-1 stroke)	1.49±0.26*	1.38±0.28	1.93±0.25	1.91±0.19	1.04±0.30	1.03±0.18
λ_{long} (10 strokes)	0.035±0.036	0.027±0.029	0.047±0.044	0.041±0.030	0.022±0.024	0.021±0.023
Approximate Entropy	0.45±0.05*	0.39±0.09	0.46±0.13	0.43±0.11	0.50±0.11	0.48±0.09

* denotes significant difference between wetsuit and no wetsuit condition ($p < 0.05$)

Multivariate models utilize accelerometers to estimate peak vertical ground reaction force

¹Constantine P. Nicolozakes, ²Joshua Hoffman, ³Kenton Kaufman and ¹⁻⁶Timothy E. Hewett

¹Department of Biomedical Engineering, ²Sports Health and Performance Institute (SHPI) OSU Sports Medicine, ³ Mayo Clinic, Rochester, MN, ⁴Department of Orthopaedics, ⁵Department of Physiology and Cellular Biology and Family Medicine, Ohio State University, Columbus, OH

email: nicolozakes.6@osu.edu, web: <http://sportsmedicine.osu.edu/research/>

INTRODUCTION

Three-dimensional (3-D) motion capture is a valid method to quantify human motion [1]. However, this technique requires expensive equipment and a specialized laboratory that are not available in a clinical or athletics environment. Tri-axial accelerometers pose a portable, cost-effective solution to analyze human motion in the clinic. While previous research indicates that accelerometers can predict peak vertical ground reaction forces (vGRF) during low-impact tasks, such as gait and running, these units have not been validated for dynamic, high-impact landings, like the drop vertical jump (DVJ) and single leg drop (SLD). The objective of this study was to develop a multivariate model that utilized anthropometric measures and peak accelerations to estimate peak vGRF during dynamic jumping tasks.

METHODS

Ten (n=10, males=6, females=4) healthy subjects were recruited for the study. Activity monitors developed at Mayo Clinic (Rochester, MN) were secured bilaterally to the foot, medial tibial surface (shank), lateral femoral epicondyle (thigh), and midpoint between the right and left anterior superior iliac spine (waist). Each monitor incorporated a tri-axial MEMS accelerometer ($\pm 16g$, 100Hz, Analog Devices). Subjects performed 10 DVJ tasks and 10 bilateral SLD tasks off a 31cm tall box onto two floor embedded force plates that recorded ground reaction forces at 1200Hz. All tasks were performed during continuous collection of 3-D motion capture data and tri-axial accelerations.

Peak vGRF was extracted from motion capture data for each DVJ and SLD trial. Acceleration magnitude was calculated from tri-axial acceleration data. The peak acceleration was extracted for each DVJ and SLD trial from the continuous acceleration

magnitude data. Individual trials that did not have continuous vGRF data or acceleration data from all seven activity monitors throughout the task were excluded from the study.

Multivariate linear regression models that incorporated anthropometric data and peak acceleration magnitudes were separately developed to predict peak vGRF for DVJ and SLD trials. R-squared (R^2) values were calculated for each model. Both the DVJ and SLD multivariate models only included significant parameters ($\alpha = 0.05$).

RESULTS AND DISCUSSION

Height, weight, peak waist acceleration, and peak thigh acceleration were significant predictors of vGRF during a DVJ task (Table 1). Peak waist, thigh, and shoe accelerations were significant predictors of vGRF during a SLD task (Table 1). The correlations between recorded vGRF and predicted vGRF for both DVJ and SLD trials were excellent (DVJ: $R^2 = 0.7451$; SLD: $R^2 = 0.7266$) (Figure 1).

Models that utilize anthropometric data and activity monitors to accurately predict vGRF provide a cost-effective method to collect human motion data. Furthermore, clinicians can incorporate testing with activity monitors into current screening strategies conducted both in and out of athletic seasons. The ability to quickly and accurately measure human motion data will provide a portable method to assess athletic health.

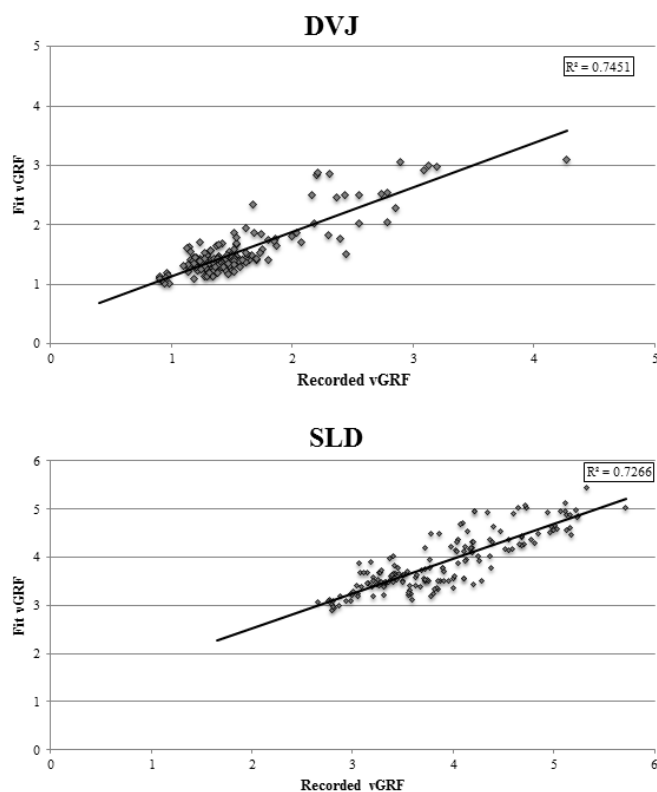


Figure 1: Fit vGRF vs calculated vGRF using parameters from multivariate linear regression

Future work will incorporate sex and task differences into one model. Previous work with running and gait trials has utilized repeated measure mixed effects regression statistics to account for variation between subjects and tasks [2]. Similar models for high-impact landings must be investigated. In addition, future work will attempt to validate activity monitors to measure lower extremity kinetics and kinematics during dynamic tasks.

Limitations to this study include individual activity monitor malfunction, which caused certain acceleration data to be discarded before the final regression analysis. In addition, these models need to be validated with disparate data sets.

CONCLUSIONS

Multivariate models that utilized anthropometric data and peak accelerations successfully predicted peak vGRF. This study is the first to our knowledge to utilize multiple activity monitors to produce these results during dynamic, high-impact landing tasks. Application of this model provides clinicians and performance specialists to expand the environment in which they can measure the forces created by athletes during dynamic tasks. The long-term goal of the study is to validate the use of activity monitors to assess injury risk in a non-laboratory athletic environment while subjects perform sport specific tasks.

REFERENCES

1. Hewett TE, et. al. *Am J Sport Med.* **33**, 492-501, 2005.
2. Neugebauer JM, et al. *PloS One* **7**, e48182, 2012.

ACKNOWLEDGEMENTS

The authors acknowledge funding support from the National Institutes of Health / National Institute of Arthritis and Musculoskeletal and Skin Diseases grants R01-AR049735 and R01-AR056259 (TEH) and the OSU Sports Medicine Sports Health and Performance Institute. The authors would also like to thank OSU Sports Medicine and the Mayo Clinic research staffs.

Table 1: Multivariate regression results

	DVJ		SLD	
	β	p	β	p
Constant	-.619	0.232	1.535	<0.001
Height	.923	0.012	Not Included	Not Included
Mass	-0.007	0.026	Not Included	Not Included
Peak Waist ACC	.123	<0.001	.045	0.035
Peak Thigh ACC	.058	<0.001	.088	<0.001
Peak Foot ACC	Not Included	Not Included	.024	0.002

SOFT TISSUE MOVEMENT OF THE SHANK DURING LANDINGS

^{1,2}Laura-Anne M Furlong, ³Pui Wah Kong and ¹Matthew TG Pain

¹ School of Sport, Exercise, and Health Sciences, Loughborough University, UK

² Institute for Sports Research, Nanyang Technological University, Singapore

³National Institute of Education, Nanyang Technological University, Singapore

email: L.A.M.Furlong@lboro.ac.uk, web: <http://www.lboro.ac.uk/departments/ssehs>

INTRODUCTION

High-speed video has shown that during impacts, the soft tissues of the lower limb move relative to the underlying rigid bone. This movement occurs in a wave-like manner, and Zelik and Kuo (2010) suggested this movement may help dissipate force and energy. By using lightweight surface markers, the characteristics of the wave can be quantified with changes indicative of the mechanical properties of the underlying soft tissues as in comparison to the skin the muscle-tendon complex has high stiffness. Deformation away from the contact site during a landing is hence not due to skin motion as much as it is due to the motion of the underlying muscle because of the low stiffness of the skin at low strains not propagating forces well. The aim of this study was to investigate the characteristics of mechanical waves propagating through the shank during drop landings with the shank highly activated and in a more passive condition.

METHODS

Following university ethical committee approval, six healthy, recreationally active males (age: 23 ± 3 years, height: 1.81 ± 0.08 m, mass: 81 ± 5 kg) provided written informed consent to participate in this study. All were familiar with the performance of a drop jump task. A total of 48 spherical retro-reflective markers, 7.9 mm in diameter, were attached around the shank in a 6x8 array using standard double-sided adhesive tape. A ten-camera motion analysis system (700 Hz, 612 series, 1.3 megapixel cameras, Oxford Metrics Group PLC., Oxford, UK) recorded the position of the 48 marker array on the shank (15-75% of shank length). Two test conditions were utilized. During the active

condition, subjects were instructed to heavily favor landing on the test leg and land on their forefoot. During the passive condition, subjects were instructed to initially land using the control limb and then allow the test limb to land on the force plate heel first. Drops were performed from 0.3, 0.5, 0.7 and 0.9 m onto a force plate sampling at 1200 Hz (Kistler 9281B-11, Amherst, NY, USA). All data pre-processing was completed using Vicon Nexus 1.4.116 with any incomplete marker trajectories reconstructed using the quintic spline gap filling procedure.

Marker data were subsequently analyzed in Matlab (MathWorks, Natick, MA., USA) to calculate the motion of the 48 markers and the 40 sectors defined by the 48 markers (eight columns with five sectors in each) during a 90 ms window surrounding the time of impact, approximately 10 ms prior to impact and 80 ms post-impact. Data were filtered at 50 Hz with a second order, zero lag Butterworth filter. Four of the eight columns were selected for analysis of changes in sector area, those located most anteriorly, medially, laterally and posteriorly. Sector area was calculated from the three-dimensional co-ordinates to account for movement of the soft tissue in all three planes, with percentage changes in area calculated relative to sector area measured during a static trial. Marker velocities were calculated as the difference between the minimum and maximum marker position divided by the time delay between each event after impact. Fast Fourier Transforms were used to determine the frequency content of the signal.

RESULTS AND DISCUSSION

The results support the presence of wave motion in the soft tissues of the shank during a drop landing,

with some characteristics varying dependent on muscle activation conditions. Across all markers, average marker velocity was 10.8 ± 6.1 and $10.6 \pm 6.9 \text{ m.s}^{-1}$ during the active and passive contraction conditions, respectively. Increased muscle activation increases the stiffness of the underlying muscle-tendon unit, with increased stiffness associated with increased speed of wave transmission. The similarity observed is hence unexpected, but it is possible the task was of insufficient difficulty to result in the required activations to produce large enough changes in stiffness.

The dominant frequency of the change in area was approximately 12 Hz during both conditions. This is similar to the frequencies observed during other lower limb motions during impact.

The largest changes in marker sector area were observed at the proximal medial and proximal posterior shank where the muscle: bone ratio is highest (Table 1). The largest increases were 10.5% and 14.4% at the medial and posterior shank, at 30% of shank length. The largest decrease was 12.8% at 15% of shank length, in the posterior sector. Changes are greater than those observed by Pain and Challis (2002) during impacts using the forearm, likely due to the increased soft tissue mass in the shank. Wakeling et al. (2003) proposed

decreased soft tissue movement with increased muscle activation as a strategy to decrease the stress on the body. These results suggest otherwise with larger changes observed with activation. This is potentially due to increased effective mass of the tissues during impact resulting in greater ground reaction forces during this condition which may confound results, or a lower than expected difference in activation between conditions.

CONCLUSIONS

The characteristics of the 3D soft tissue movement during impact can be quantified using motion analysis with similar results to Pain and Challis (2002). Further work is required to determine the relationship between activation and area changes, and to investigate the characteristics of the wave-like motion of the soft tissue during landing to provide insight into the body's response to impact.

REFERENCES

1. Pain, MTG & Challis, JH, *J Appl Biomech*, 231-242, 2002.
2. Wakeling, JM, et al. *J Biomech*, **36**, 1761-1769, 2003.
3. Zelik, KE & Kuo, AD, *J Exp Biology*, **213**, 4257-4264, 2010.

Table 1. Percentage changes in sector area during impact with respect to the static measurement. Top data refers to increases in area, bottom data refers to decreases in area.

	Approximate % of shank length	Active condition % changes				Passive condition % changes			
		Lateral	Anterior	Medial	Posterior	Lateral	Anterior	Medial	Posterior
Percentage increase in area	15	7.2	6.6	10.4	12.0	6.7	7.4	12.4	8.8
	30	7.3	6.7	10.5	14.4	7.7	4.5	7.4	6.4
	45	5.7	7.5	5.4	9.5	6.6	4.0	6.3	6.1
	60	6.6	4.7	5.4	7.8	5.0	2.8	6.0	5.6
	75	3.8	6.6	5.2	3.7	5.1	4.5	5.2	5.3
Percentage decrease in area	15	-6.2	-7.6	-5.5	-12.8	-6.0	-2.6	-6.0	-9.6
	30	-3.8	-7.4	-3.7	-9.2	-3.8	-4.6	-6.1	-7.1
	45	-3.5	-5.3	-5.4	-5.7	-4.0	-4.0	-4.5	-4.1
	60	-3.4	-6.3	-5.1	-5.4	-4.9	-5.9	-4.6	-5.6
	75	-4.1	-5.1	-6.0	-8.0	-3.8	-5.2	-4.1	-5.7

ABSOLUTE AND RELATIVE CMJ PERFORMANCE ACROSS DIFFERENT AGE GROUPS AND SPORTS IN YOUNG MALE ATHLETES

Dino A. Palazzi, Benjamin K. Williams, Jonathan A. Glynn and Philip Graham-Smith

Aspire Academy, Sport Science Dpt., Doha, QATAR
email: dino.palazzi@aspire.qa, web: <http://www.aspire.qa>

INTRODUCTION

Counter movement jump (CMJ) has been extensively used by sport scientists and coaches to assess lower extremity explosive strength in athletes [1, 2]. When CMJs are performed on force platforms (FP) many variables can be obtained such as jump height, force, power, impulse and derivatives of these [3]. The aims of this study were to profile the absolute and relative indices of jumping performance on juvenile athletes, and determine which ones are the most likely to show progress on the performance due to growth and training.

METHODS

236 healthy, male student-athletes from 11 to 17 years-old, training up to 8 times a week in 10 different sports, volunteered for the study. Their performances were tracked 5 times along 16 months, totaling 597 testing sessions. The age of the subjects was calculated on the day of testing and the data allocated into the age ranges 11-13, 13-14, 14-15, 15-16 and 16-17. Group characteristics are shown in Tables 1 and 2.

All subjects practiced a minimum of 3 CMJs for warm-up prior to performing the jumps for analysis. CMJ performances were assessed on two portable FPs (Kistler type 9286AA and Bioware V5.0, Switzerland), sampling at 1000Hz and treated with a 7-point moving average filter.

CMJs started from a stationary position with the subjects' feet symmetrically set about shoulder width apart. CMJ trials were performed with the subjects' hands remaining on their hips throughout the whole movement. A trial was considered successful when both feet clearly landed wholly on their toes on the surface of the FPs. The FPs were zeroed before every trial, and data collection started by measuring the athletes' body weight (BW) on

both FPs to ensure that they registered the same force, prior to performing 3 maximal effort jumps. Following landing, the subjects adjusted the feet position and maintained a stationary position on the FPs for at least a second before jumping; this was to ensure a reliable initial vertical velocity of 0 m/s. The onset of movement was automatically set to the point when the total vertical force deviated -20 N from BW, and the take-off was set to the point when the total vertical force dropped below 10 N. Jump height was calculated using the impulse method with the total vertical force. Results of those 3 jumps were averaged, obtaining a single representative value for every variable in the testing session.

RESULTS AND DISCUSSION

The most relevant general findings related to CMJ performance are shown in Figs. 1 and 2, where moderate relationships between age and absolute measures of jump height ($R^2 = 0.40$, $p \leq .001$) and concentric power ($R^2 = 0.42$, $p \leq .001$) were found.

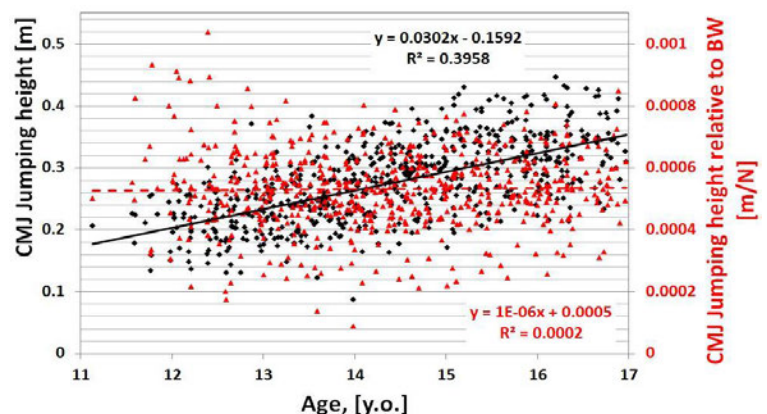


Figure 1: CMJ height in absolute and relative to BW scales, across all ages and sports.

With respect to the specific sports, the athletics group consistently jumped higher than the football players, who in turn outperform the remainder of the sample (Fig. 3).

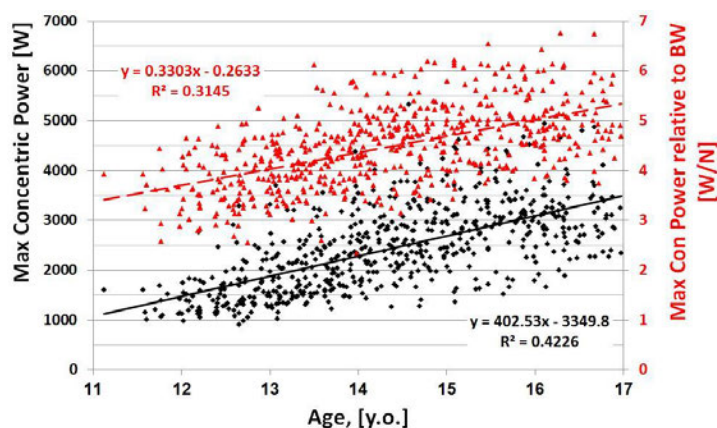


Figure 2: Maximum power during CMJ in absolute and relative to BW scales, across all ages.

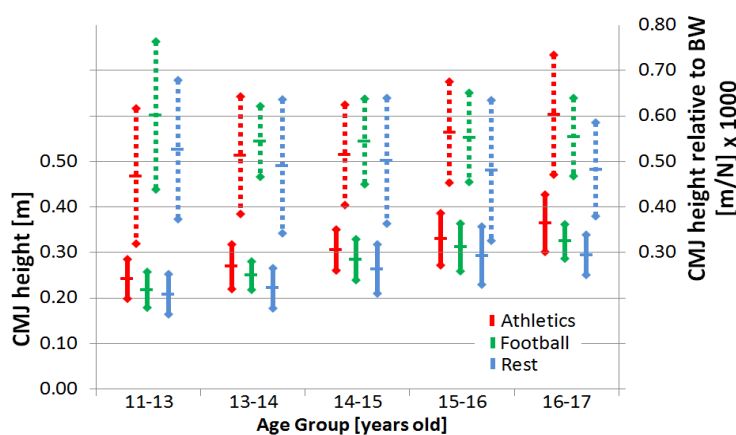


Figure 3: CMJ height (avg. \pm std. dev.), in absolute and relative scales, related to age groups and sports.

The mean football CMJ height is typically one year behind the athletics group, and this may be associated with a different emphasis of training. The athletics group likely devoted more time to power work and work in vertical direction. By the age of 16-17 the athletes jumped 0.37 m and the footballers 0.33 m. In comparison to elite senior

norms, horizontal jumpers would typically jump 0.53 ± 0.07 m [4], and professional football players 0.42 ± 0.04 m [5]. The results found no relationship between CMJ height related to BW and age, when all the data was examined together. However, without the athletics and football groups, the trend revealed a steady rise in CMJ height related to BW from the age of 14-17, increasing from 0.51 to 0.6 m/N x 1000; in contrast, the footballers seemed to maintain an average performance of 0.56 m/N x 1000 through the ages of 13-17.

CMJ relative concentric power produced a slightly lower relationship with age compared to the absolute measure ($R^2 = 0.31$, $p \leq .001$).

CONCLUSIONS

The results highlight that the trend in the development of jump performance is dependent on the sport and the main focus of the training modes adopted. Whilst year on year improvements are seen in youth football players, the relative change in performance is equivocal to increases in BW. Conversely, athletes appear to have performance gains that outweigh their increase in BW.

REFERENCES

1. Tidow G. *NSA*, **1**, 93-110, IAAF, 1990.
2. Young W. *NSA*, **10**, 89-96, IAAF, 1995.
3. Cormie P et al. *J of Strength and Conditioning Research*, **23** (1), 177-186, NSCA, USA, 2009.
4. Graham-Smith P and Brice P. *Proceedings ISBS*, USA, 2010.
5. Brocherie F et al. *Journal of Sports Sciences*, **32** (13), 1243-1254, 2014.

Table 1: Subject's body mass [kg] by sport and age group [y.o.]

Sport	11-13	13-14	14-15	15-16	16-17	Averages
Athletics	57.0 \pm 17.8	56.6 \pm 16.0	62.9 \pm 14.4	61.6 \pm 15.1	63.7 \pm 14.4	60.7 \pm 15.3
Football	38.2 \pm 7.0	47.8 \pm 9.6	54.2 \pm 8.6	58.3 \pm 8.7	60.8 \pm 8.3	52.2 \pm 11.4
Rest*	42.2 \pm 8.8	49.4 \pm 13.4	55.5 \pm 10.5	65.2 \pm 11.6	63.8 \pm 10.3	52.1 \pm 13.8
Averages	41.9 \pm 10.2	51.0 \pm 13.7	57.2 \pm 11.7	61.0 \pm 12.2	62.5 \pm 10.9	54.5 \pm 13.9

(*): Includes fencing, golf, gymnastics, multi-sports, shooting, squash, table tennis and swimming

Table 2: Number of sessions (population) by age group [y.o.]

Age group	11-13	13-14	14-15	15-16	16-17	Total
Sessions	107	147	138	119	86	597

Are Variables Associated With Knee Injuries In Runners Different Before And After A 40min Run?

¹ Max R. Paquette and ¹ Dan A. Melcher

¹ The University of Memphis, Memphis, TN, USA
email: mrpquette@memphis.edu, web: <http://memphis.edu/hss/enl/>

INTRODUCTION

The high frequency of knee injuries in runners has inspired scientists to study a number of running biomechanical variables. A number of discrete variables have been identified as possible risk factors for running knee injuries. Indeed, runners with knee injuries generally exhibit higher peak knee flexion [1], contralateral pelvic drop [2], peak hip adduction [3] and peak internal hip rotation [2] compared to non-injured runners.

To date, the majority of biomechanical studies have assessed injury-related variables during a one-time laboratory test while runners are in non-fatigued states. As postural control is reduced following a fatiguing run [4], the clinical implications of injury-related variables for injury risk may be better understood if studied following a typical training run when runners may be more fatigued.

The purpose of this work was to compare previously identified variables associated with knee injuries at the start and end of a 40min training run in runners with and without a history of knee injury. We expected 1) an increase in the magnitude of injury-related variables following the run and 2) a larger increase in the injury group.

METHODS

Twelve competitive runners who were injury-free (*Healthy*; 8 men; 72.5 ± 12.5 kg; 1.78 ± 0.08 m) and 12 runners who suffered a running-related knee injury in the past year (*Injured*; 7 men; 69.2 ± 17.6 kg; 1.76 ± 0.13 m) participated in the study. Written consent approved by the Institutional Review Board was obtained for all participants before testing began.

All participants filled out an online survey regarding their running and injury history. Before testing, neoprene wraps were secured on both thighs and

shanks and around the waist. Runners then ran at an easy effort on the treadmill for 5 minutes to allow the straps to set into place. An 8-camera motion capture system (120Hz, Qualisys AB, Gothenburg, Sweden) was used to collect kinematic data. Anatomical markers and tracking marker clusters were placed on both lower extremities to define segment coordinate systems. Following a standing calibration trial, only anatomical markers were removed and runners completed a 40-minute treadmill run. The run speed was set to 75% of the runners' best 10 km race time in the past 5 years to ensure a moderate run effort based on running ability. Two 6-second motion capture trials were collected after 10 and 40 minutes to obtain knee and hip angular position data at the start and end of the run.

Visual3D biomechanical software (C-Motion, Germantown, MD, USA) was used to process and analyze all data. Kinematic data were interpolated using a least-squares fit of a 3rd order polynomial with a three data point fitting and a maximum gap of 10 frames. Data were then filtered using a fourth-order Butterworth low-pass filter at 8 Hz. The start and end of stance phase was identified using a kinematic method with the vertical pelvis velocity. Dependent variables included peak knee flexion, peak contralateral pelvic drop, peak hip adduction and peak internal hip rotation. The average of each variable for five consecutive stance phases during the 10 and 40-min collection times was used for analysis.

A two-way (Group \times Time) mixed design analysis of variance (ANOVA) with Time as the within-subject factor and Group as the between-subject factor, was used to evaluate all variables (22.0 SPSS, Chicago, IL, USA). Significance was set at an alpha level of 0.05. Cohen's d effect sizes (ES) were also reported to further assess mean differences.

RESULTS AND DISCUSSION

Peak knee flexion and contralateral pelvic drop showed no interaction or main effects ($P < 0.05$; Table 1). Peak hip adduction showed a Group x Time interaction and a Time main effect (Table 1). *Post-hoc* Paired t-tests showed greater peak hip adduction at 40-min compared to 10-min in the healthy group ($p = 0.014$; $ES = 0.34$) but no time difference in the previously injured group ($p = 0.87$; Figure 1). The time effect for peak hip adduction in healthy runners could suggest the importance of assessing certain biomechanical variables when runners are fatigued.

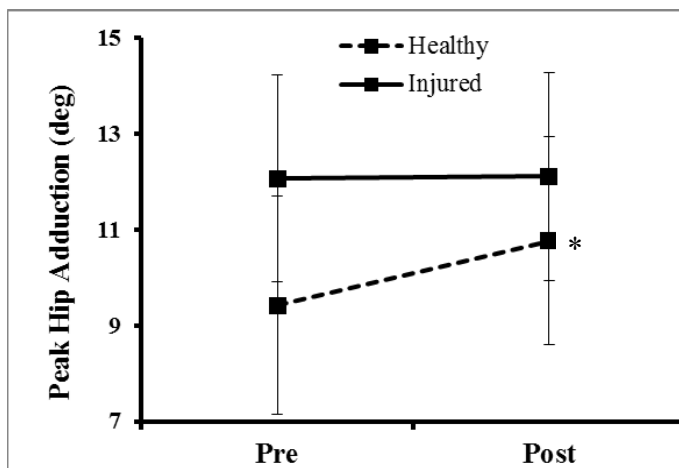


Figure 1: Average peak hip adduction angle during five stance phases of Healthy and Injured runners at 10-min and 40-min points during a run (mean \pm SD). *: Time difference within Healthy group.

Contrary to previous findings, peak knee flexion [1], contralateral pelvic drop [2] and peak hip adduction [3] were not different between groups. However, these studies compared healthy and *currently* injured runners whereas we studied previously injured runners. The current study

included both men and women and it is possible that gender differences masked potential group effects. The small sample size did not allow for statistical adjustments for gender differences.

Peak internal hip rotation showed a Group effect (Table 1). Regardless of testing time during the run, the previously injured group showed greater hip internal rotation compared to the healthy group ($ES = 1.29$). This group difference is consistent with previous findings in currently injured runners [2] and may suggest that runners who suffer a running-related knee injury continue to exhibit increased peak internal hip rotation when symptoms subside. The causal effects of greater peak internal hip rotation on injury risk in runners still remain unknown.

CONCLUSIONS

Findings from this study suggest that differences in most knee and hip kinematic variables between runners with knee injuries and healthy runners are not consistent when comparing healthy and previously injured runners. Peak internal hip rotation was the only variable that showed a similar difference between groups. A time effect within the healthy group for peak hip adduction may suggest that biomechanists should consider assessing joint variables at different time points during a run and not only in non-fatigued states.

REFERENCES

- Ott B, et al. *J Electr Kinesiol*, **21**, 631-637, 2011.
- Dierks TA, et al. *J Orthop Sports Phys Ther*, **38**, 448-456, 2008.
- Noehren B, et al, *Gait Posture*, **36**, 596-599, 2012.
- Steib S, et al, *Clin Biomech*, **28**, 790-795, 2013.

Table 1. Average peak knee and hip joint kinematic variables in the healthy and previously injured group at 10-min and 40-min points of a run (mean \pm SD) with P -values for main and interaction effects.

Variables	10-Min		40-Min		P -values		
	Healthy	Injured	Healthy	Injured	Group	Time	Inter.
Knee flexion ($^{\circ}$)	41.1 \pm 7.5	43.0 \pm 5.0	42.5 \pm 4.8	44.1 \pm 4.8	0.43	0.14	0.89
Contralateral Pelvic Drop ($^{\circ}$)	3.2 \pm 2.9	3.6 \pm 3.4	3.6 \pm 3.1	3.6 \pm 3.0	0.88	0.54	0.52
Hip Adduction ($^{\circ}$) ^{b, c}	9.4 \pm 4.3*	12.1 \pm 4.6	10.8 \pm 4.3	12.1 \pm 4.3	0.27	0.018	0.027
Internal Hip Rotation ($^{\circ}$) ^a	7.3 \pm 5.2	13.1 \pm 4.4	8.2 \pm 5.5	14.0 \pm 4.0	0.011	0.063	0.99

^a: Group main effect; ^b: Time main effect; ^c: Group x Time interaction; *: Time difference within Group

The Effects of MSM Supplementation on Knee Kinetics during Running, Muscle Strength, and Muscle Soreness following Eccentric Exercise-Induced Quadriceps Damage

¹ Shelby A. Peel, ¹ Daniel A. Melcher, ¹ Brian K. Schilling, ¹ Richard J. Bloomer, ¹ Max R. Paquette

¹ Musculoskeletal Analysis Laboratory, The University of Memphis, Memphis, TN, USA

Email: mrpquette@memphis.edu, web: <http://memphis.edu/hss/enl/>

INTRODUCTION

Runners are constantly seeking new approaches to optimize performance and training gains. Delayed onset muscle soreness (DOMS) is elevated following eccentric knee extensor damage (i.e., downhill running) [1]. Along with elevated DOMS, reductions in ankle and knee range of motion (ROM) and knee stiffness have been reported following eccentric knee extensor damage in the 48 hours following damage [1].

Strategies to reduce the duration of DOMS and associated changes in joint biomechanics are important for runners to ensure safe continuity in training. Many strategies have been suggested to speed up recovery. The degree of muscle injury may be influenced by nutritional interventions [2]. Methylsulfonylmethane (MSM) has anti-inflammatory properties [3] that may aid in reducing the duration of DOMS following muscle damage.

The purpose of this study was to investigate the effects of MSM supplementation on knee joint kinetics during running and DOMS following eccentric knee extensor damage. It was expected that the MSM intervention would reduce the negative effects of muscle damage on these variables compared to a placebo.

METHODS

Forty healthy, resistance trained men (age: 25.28 ± 6.31 y, ht: 177.63 ± 6.57 cm, BMI: 26.65 ± 2.47 kg·m⁻²) were recruited to participate. Subjects were randomly assigned in double-blind manner to one of two groups: MSM at 3 grams per day (n=20) or placebo (rice flour; n=20). Subjects underwent a one-month supplementation period prior to testing sessions.

Subjects were tested over a period of five consecutive days: Baseline, 0 hrs, 24 hrs, 48 hrs, and 72 hrs. All daily testing procedures were the same. For the muscle damage protocol subjects performed 10 sets of 10 repetitions (or reps to failure) of eccentric seated knee extension exercise on a 4-second count using 100% of concentric one-repetition maximum. Subjects were given a 2-minute rest period between sets.

Self-reported lower extremity muscle soreness was measured each testing day using a 10-point visual analog scale (VAS) rating for soreness during a body squat and passive knee flexion stretch. Muscle damage was quantified with maximum voluntary isometric knee extensor force using a load cell (MLP-1K, Transducer Techniques). The average of the force plateau of three maximal trials was used for analysis. An 8-camera motion analysis system (120Hz, Qualisys AB,) and a force platform (1200Hz, AMTI, Inc) were used to obtain 3D kinematic and ground reaction force (GRF) data, respectively. Subjects performed three over-ground running trials over a 20 m runway at $3.35 \text{ m} \cdot \text{s}^{-1} \pm 5\%$ contacting the force plate with their right foot. Visual3D biomechanical analysis software suite (C-Motion, Inc.) was used to compute 3D kinematic and kinetic variables of the right limb during running. Sagittal knee stiffness was computed as the ratio of the change in extensor moment and knee flexion ROM. Since dependent variables were different between groups at baseline, data were normalized using the difference between baseline means.

Mixed design repeated measures ANOVA (Group x Time) were used to compare dependent variables. *Post hoc* paired t-tests were used for pairwise comparisons. Mann Whitney U test was used to compare the VAS rating of soreness results between

interventions and test times (i.e., non-parametric data) ($P<0.05$).

RESULTS AND DISCUSSION

Maximal isometric force to assess muscle damage showed no interaction ($P=0.38$) or group effects ($P=0.85$) but showed a time main effect ($P<0.001$; Figure 1). Maximal force was reduced at every time point ($P<0.05$) compared to baseline except for 72hrs post ($P=0.12$). By 72hrs post damage, values returned to baseline for subjects in the MSM condition but remained approximately 8% below baseline for those in the placebo condition (Figure 1); however, the difference was not of statistical significance. DOMS during squat was not different between groups at any time ($P>0.05$) but was different at every time point compared to baseline ($P<0.001$). DOMS during passive stretch was lower in MSM group but remained elevated above baseline. These findings confirm that muscle damage and DOMS persist after 48 hrs [1] and that DOMS remain up to 72 hrs following muscle damage.

No interaction or group effects were found for biomechanical variables. Knee stiffness ($P=0.002$), knee moment ($P<0.001$), knee eccentric power ($P<0.001$) and loading rate ($P=0.02$) all showed time effects. All variables, except for loading rate, did not returned to baseline levels following damage (Table 1). Loading rate was decreased at 24, 48 and 72 hrs compared to 0 hrs, but not compared to baseline. Although not significant, loading rate was slightly higher than baseline at 0 hrs ($P=0.09$)

which likely explains why 24 to 72 hrs were not different than baseline.

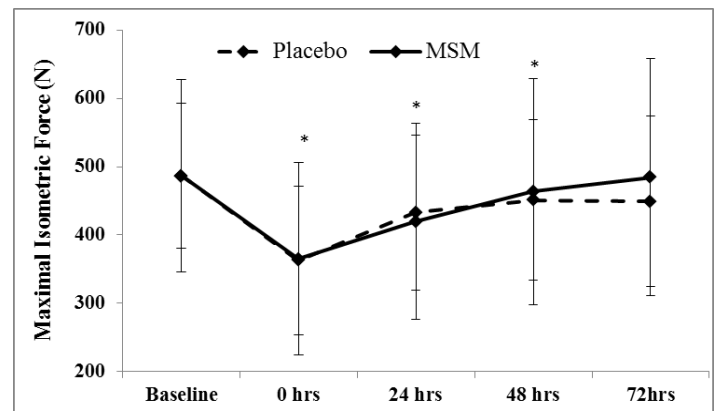


Figure 1. Maximal isometric knee extensor strength at each testing time. *: different than baseline.

CONCLUSIONS

Our findings suggest that MSM does not favorably influence knee biomechanics following eccentric exercise-induced muscle damage using knee extension exercise. MSM supplementation may positively impact muscle force recovery, as well as DOMS during passive stretch.

REFERENCES

1. Dutto DJ. *Med Sci Sp Ex*, **36**(4), 560-566, 2004.
2. Bloomer RJ. *Sports Med*, **37**(6), 519-32, 2007.
3. Kim YH. et. al., *Biological and Pharmaceutical Bulletin*, **32** (4), 651-656, 2009

ACKNOWLEDGEMENTS

This work was supported in part by Bergstrom Nutrition.

Table 1. Knee joint kinetics and peak instantaneous loading rate of the vertical GRF for each group at all five test times (mean \pm SD).

		Baseline	0 hrs post	24 hrs post	48 hrs post	72 hrs post
Knee Stiffness ^{a,b,d} (Nm/kg/ $^{\circ}$)	Placebo	0.10 \pm 0.03	0.08 \pm 0.02	0.09 \pm 0.03	0.09 \pm 0.04	0.09 \pm 0.03
	MSM	0.10 \pm 0.02	0.08 \pm 0.02	0.09 \pm 0.02	0.09 \pm 0.01	0.09 \pm 0.02
Peak Knee Moment ^{a,b,c,d} (Nm/kg)	Placebo	2.74 \pm 0.47	2.30 \pm 0.57	2.57 \pm 0.63	2.46 \pm 0.53	2.52 \pm 0.58
	MSM	2.74 \pm 0.54	2.31 \pm 0.56	2.46 \pm 0.55	2.41 \pm 0.54	2.44 \pm 0.54
Peak Knee Power ^{a,b,c,d} (W/kg)	Placebo	14.5 \pm 3.2	11.8 \pm 5.1	13.1 \pm 4.3	13.3 \pm 4.1	13.59 \pm 4.0
	MSM	14.5 \pm 5.3	12.0 \pm 4.9	12.7 \pm 4.4	12.4 \pm 5.0	12.90 \pm 4.2
Loading Rate ^e (BW/s)	Placebo	86.5 \pm 27.3	88.8 \pm 25.8	84.8 \pm 24.8	86.0 \pm 28.1	84.5 \pm 26.9
	MSM	86.5 \pm 20.4	88.5 \pm 19.0	81.5 \pm 17.8	82.1 \pm 23.2	81.7 \pm 16.8

Notes: Time Main Effects: ^a: 0 hrs different than baseline; ^b: 24 hrs different than baseline; ^c: 48 hrs different than baseline; ^d: 72 hrs different than baseline; ^e: 24, 48 and 72 hrs different than 0 hrs

A Prospective Comparison of Biomechanical Variables Associated With Running-Related Injuries in Collegiate Cross Country Runners

¹ Daniel J. Kuhman, ¹ Daniel A. Melcher, ¹ Shelby A. Peel, ¹ Max R. Paquette

¹ The University of Memphis, Memphis, TN, USA

email: mrpquette@memphis.edu, web: <http://memphis.edu/hss/enl/>

INTRODUCTION

Various biomechanical variables have been linked to runners with a history of injuries. Specifically, runners who use a rearfoot strike (RFS) have shown a higher rate of retrospective injuries compared to mid or forefoot striking (FFS) runners [1]. Greater values of ankle eversion and peak eversion velocity, and smaller ankle dorsiflexion have been observed in currently injured versus non-injured runners [2]. Another study showed a trend for smaller ankle eversion and eversion velocity in previously injured runners. Differences in injury status (i.e., previously vs currently injured) likely explain discrepancies in results between these two studies. Finally, a higher loading rate of the vertical ground reaction force (GRF) has been linked with retrospective injuries in female and male runners [3, 4]. Since these studies compared retrospectively or currently injured runners with non-injured runners, it is difficult to establish causal relationships between these biomechanical variables and running injuries.

The purpose of this collection was to *prospectively* compare biomechanical variables previously associated with injuries in collegiate runners who developed any lower extremity injuries compared to those who did not over the course of a cross country season. We expected higher loading rate, eversion ROM and eversion velocity but smaller dorsiflexion ROM in runners who developed injuries compared to those who did not.

METHODS

Data was collected on 24 non-injured, competitive collegiate runners prior to the start of a Division 1 NCAA cross country season. Written consent

approved by the Institutional Review Board was obtained for all participants before testing began.

At the start of the season, 3D joint kinematics and ground reaction force (GRF) data for both limbs were collected using a motion capture system (240Hz, Qualisys AB) and force platform (1200Hz, AMTI Inc.), respectively. Participants completed a total of 10 over-ground running trials (five trials per leg). Based on preferred training speeds, men ran at 4.5 m/s while women ran at 4.0 m/s ($\pm 5\%$). At the end of the season runners completed a survey regarding, among other training and lifestyle factors, injuries sustained throughout the season. Of the 24 runners who were tested at the start of the season, five sustained injuries that were not running-related (e.g., ankle sprains, falls) and were not included in analyses. Of the other runners, 10 sustained running-related injuries (6 women; 57.8 ± 7.5 kg) and 9 had no injuries (7 men; 66.6 ± 8.9 kg). Data from these 19 runners were analyzed.

Visual3D software (C-Motion, Inc.) was used to compute all variables. Kinematic and GRF data were filtered using a fourth-order Butterworth low-pass filter at 8 and 40 Hz, respectively. Dependent variables included strike index (position of center of pressure at foot contact expressed as a percentage of foot length), peak instantaneous loading rate of the vertical GRF, dorsiflexion range of motion (ROM), eversion ROM and peak ankle eversion velocity. The injured side in injured runners and the right side of non-injured runners were included in analyses.

Independent t-tests were used to compare biomechanical variables between the healthy and injured groups ($P < 0.05$). Cohen's d effect sizes were also computed for mean comparisons.

RESULTS AND DISCUSSION

The ANOVA showed that strike index ($ES=0.24$), peak instantaneous loading rate ($ES=0.28$), and dorsiflexion ROM ($ES=0.04$) were not different between groups (Table 1). Eversion ROM ($ES=1.21$) and peak ankle eversion velocity ($ES=1.26$) were both smaller in injured compared to uninjured runners (Table 1).

Our finding of smaller eversion ROM and peak eversion velocity in injured runners differ from previous findings comparing runners injured at the time of testing to uninjured runners [2]. Their currently injured runners may have altered their running mechanics as a result of pain at time of testing. Further, their study assessed differences between groups for specific types of injuries (e.g., IT band syndrome, shin splints, and plantar fasciitis) whereas all types of injuries were included in the injured group in the current study. Interestingly, our results of frontal plane ankle kinematics are similar to previous findings comparing retrospectively injured and uninjured runners [3]. The authors suggested that a greater eversion velocity may ensure that the foot reaches a stable position prior to mid-stance in preparation for push off. The similar findings of lower ankle eversion and eversion velocity in runners who developed injuries in our prospective study and in their retrospective injury study may indicate that comparisons of retrospective injury rates are more appropriate than comparing currently injured and uninjured runners to assess running injury risk.

Strike index, loading rate and dorsiflexion ROM were not different between groups. RFS pattern yields greater loading rates and lower dorsiflexion ROM than FFS. Thus, since strike pattern (i.e.,

same strike index) were not different between groups, it is unsurprising that loading rate and dorsiflexion ROM were not different between groups.

The current study included a preliminary analysis of prospective data currently being collected on a larger sample of collegiate runners. The small sample size makes it difficult to conclude with confidence that ankle eversion ROM and peak eversion velocity are valid predictors of injury-risk in collegiate runners. In addition, the injury group had twice as many women (6) than men (3). The small sample size made it difficult to assess gender difference with adequate statistical power, but a *post hoc* comparison (independent t-tests) suggested no gender differences for all five variables ($P>0.05$).

CONCLUSION

Our preliminary findings suggest that lower eversion ROM and eversion velocity may be predictive of injury risk in runners. We will continue to use this prospective approach to identify injury risk factors in a large sample of collegiate runners.

REFERENCES

1. Daoud, et al. *Med Sci Sports Ex*, **44**, 1325-1334, 2012.
2. Messier SP and Pitalla KA. *Med Sci Sports Ex*, **20**, 501-505
3. Hreljac, et al. *Med Sci Sports Ex*, **32**, 1635-1641, 2000.
4. Milner, et al. *Med. Sci. Sports Ex*, **38**, 323-329, 2006

Table 1. Average GRF and ankle kinematic variables for the healthy and injured groups (means \pm SD).

Variables	Healthy	Injured	P-values
Strike Index (%)	55.82 \pm 48.69	44.79 \pm 49.95	0.64
Instantaneous Loading Rate (BW/s)	100.30 \pm 19.86	93.52 \pm 30.28	0.65
Dorsiflexion ROM ($^{\circ}$)	22.28 \pm 6.19	22.53 \pm 6.14	0.93
Eversion ROM ($^{\circ}$) ^a	20.35 \pm 3.74	16.73 \pm 2.53	0.029
Peak Eversion Velocity ($^{\circ}$) ^a	478.64 \pm 156.48	326.16 \pm 94.82	0.021

Notes: ^a: Group main effect ($P<0.05$).

Effects of Imposed Foot Strike Before and After a Long Run on Joint Stiffness in Rearfoot Strike Runners

¹ Daniel A. Melcher, ¹ Max R. Paquette, ¹ Brian K. Schilling

¹ Musculoskeletal Analysis Laboratory, The University of Memphis, Memphis, TN, USA

Email: dmelcher@memphis.edu

INTRODUCTION

Biomechanics research has recently focused on the effects of acute foot strike pattern transitions, specifically on the differences in lower extremity joint kinetics and stiffness [1, 2]. Joint stiffness may be related to injury risk in runners [1]. As approximately 75% of recreational and elite runners use a rearfoot strike (RFS) pattern [3], it is worthwhile to study these runners. Since runners often complete long runs as part of their training, it is important to understand potential changes in biomechanical variables during a long run as runners become fatigued.

Here we examine the effects of imposed strike pattern before and after a long treadmill run on ankle and knee joint stiffness in habitual RFS runners. We expected a decrease in joint stiffness following the long run. We also expected a greater decrease in knee joint stiffness following the run during RFS compared to imposed forefoot strike (FFS). Finally, we expected greater knee stiffness during imposed FFS and greater ankle stiffness during RFS.

METHODS

Fifteen experienced male habitual RFS runners were recruited (1.80±0.07m; 74.4±12.0kg; 31.7±9.3yrs; 47.2±14.1mi/wk). Written consent approved by the Institutional Review Board was obtained for all participants before testing.

Runners completed a 5 min running warm-up before testing. Maximal isometric ankle and knee extensor strength was measured while subjects pushed against a strap for 3-4 seconds. The strap was connected via chain to a load cell (Transducer Techniques, Temecula, CA). Ankle and knee joint angle were maintained at 90 degrees. Three trials

for both ankle and knee were collected and averaged over the trials. These data were collected before and after the fatiguing run.

An 8-camera motion capture system (240Hz, Qualisys AB) and force platform (1200Hz, AMTI) were used to collect kinematic and ground reaction force (GRF) data. Anatomical and tracking marker clusters were secured on the right leg. Subjects completed five over-ground running trials with their habitual RFS and imposed FFS pattern over a 20m runway while contacting a force platform with their right foot. Five successful trials were completed using both their habitual strike pattern and imposed FFS, respectively. A speed of ±5% of their long run pace was used. Once markers were removed, all runners then completed a long treadmill run equivalent to 25 % of their average weekly mileage in the past 3 months (11.8±3.5miles; 90.4±23.4min). Immediately following the run, maximal strength and running tests were repeated.

Visual3D software (C-Motion, Inc.) was used to compute all variables. Kinematic and GRF data were filtered using a fourth-order Butterworth low-pass filter at 8 and 40 Hz, respectively. Joint moments were normalized to body mass (Nm/kg). Joint kinetic variables were computed using inverse dynamics and moments were reported as net internal moments. Dependent variables included sagittal plane ankle and knee stiffness. The change in sagittal plane ankle and knee joint moment during stance and joint ranges of motion (ROM) were also measured. Joint stiffness was computed using the following equation:

$$k = \frac{\Delta M}{\Delta \theta}$$

Where k represents joint stiffness, $\Delta \theta$ represents the joint angle range of motion (ROM) from foot strike to peak angle, and ΔM is the change in the joint moment from foot strike to the peak moment. The

average for the five trials of each condition was used in the statistical analyses. A 2X2 within-within factorial repeated measures ANOVA with strike pattern and time were conducted. Alpha level was set at 0.05 for all tests. Cohen's d effect sizes (ES) were calculated for pairwise comparisons using pooled standard deviation.

RESULTS AND DISCUSSION

Knee extensor fatigue following the run was confirmed as knee extensor maximal isometric force was reduced following the long run (ES=0.39; Table 1). Plantarflexor maximal isometric force was not different before and after the run (ES=0.16) (Table 1).

Contrary to our hypothesis, no foot strike and time interaction were found for ankle ($p=0.30$) and knee joint stiffness ($p=0.25$). Ankle ($p<0.001$, ES=1.62) and knee joint stiffness ($p<0.001$, ES=0.91) both showed foot strike effects. Consistent with previous literature [2], knee stiffness was greater during imposed FFS while ankle stiffness was greater during RFS (Figure 1). Sagittal plane ankle ROM was greater during imposed FFS (ES=0.96) while knee ROM was greater during RFS (ES=3.07; Table 1). In addition, knee ROM was reduced following the long run which may explain the unchanged knee stiffness before and after the long run.

Although no interactions were found in sagittal plane joint kinetics, it is possible that fatigue altered frontal and transverse plane ankle and knee joint kinetics between strike patterns. Further biomechanical analyses on the effects of fatigue and strike pattern along with their relationship with injury risk are needed to examine these hypotheses.

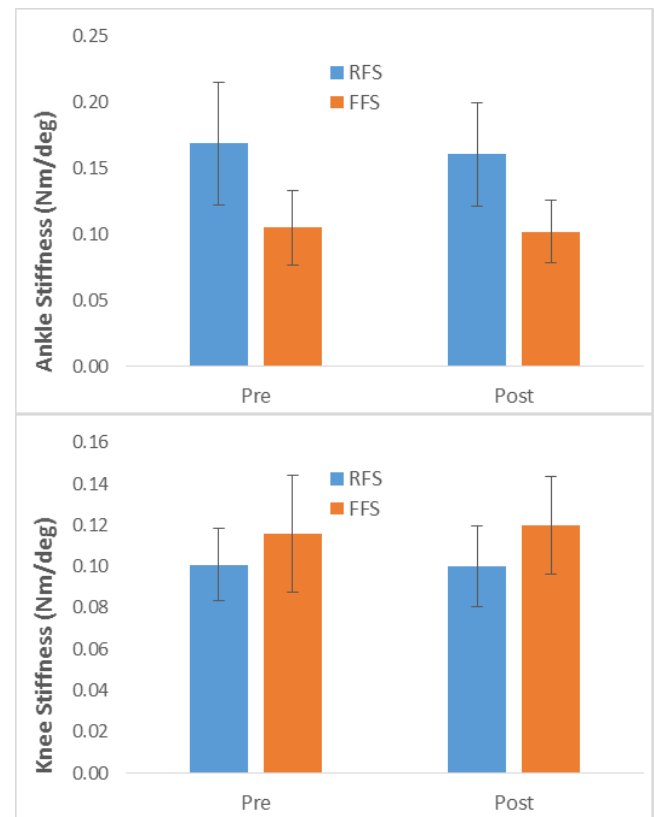


Figure 1: Mean (\pm SD) of sagittal plane ankle and knee stiffness between RFS and imposed FFS pre & post treadmill long run.

CONCLUSIONS

Our findings indicate that changes in ankle and knee joint stiffness between RFS and imposed FFS in habitual RFS runners are independent of fatigue.

REFERENCES

1. Hamill J, et al. *Eur J Sport Sci.* 14(2):130-6, 2014.
2. Derrick TR, et al. *Med Sci Sports Exerc.* 30(1):128-35, 1998.
3. Hasegawa H, et al. *J Strength Cond Res.* 21(3):888-93, 2007.

Table 1. Ankle and knee joint ROM and, plantarflexor and knee extensor maximal isometric strength pre and post fatiguing protocol between strike patterns (mean \pm SD) with P -values for main and interaction effects.

Variables	Pre		Post		P -values		
	RFS	FFS	RFS	FFS	Foot strike	Time	Inter.
Ankle ROM ($^{\circ}$) ^a	19.19 \pm 3.14	32.55 \pm 6.21	19.36 \pm 2.81	32.06 \pm 5.60	<0.001	0.53	0.81
Knee ROM ($^{\circ}$) ^{a, b}	30.18 \pm 4.47	29.66 \pm 4.23	27.46 \pm 4.87	24.57 \pm 4.57	<0.001	0.035	0.053
Plantarflexor Strength (N)	500.7 \pm 187.5		467.9 \pm 223.0		-	0.29	-
Knee Ext. Strength (N) ^b	388.6 \pm 67.6		361.5 \pm 76.5		-	0.018	-

Notes: ^a: foot strike main effect; ^b: time main effect ($P < 0.05$). Inter: foot strike x time interaction.

Does Fatigue And Imposed Forefoot Strike Alter Strike Pattern Variability And Loading Rate In Rear Foot Strike Runners?

¹ Max R. Paquette, ¹ Dan A. Melcher

¹ The University of Memphis, Memphis, TN, USA
email: mrpquette@memphis.edu, web: <http://memphis.edu/hss/enl/>

INTRODUCTION

A higher rate of injuries has been linked with rearfoot striking (RFS) during running [1] but the correct strike pattern for reducing injury risk is highly debated. Many runners have attempted to switch from a RFS to a forefoot strike (FFS) pattern. Clinicians often advise these runners to do so gradually as a sudden increase in stress applied to the Achilles tendon from an imposed FFS may be injurious. Movement variability has been hypothesized to broaden stress distribution on musculoskeletal tissue [2, 3]. As differences in strike patterns alter joint kinetics in running, greater variability in strike pattern could promote greater dispersion of loads and potentially reduce the risk for tissue injury. In addition, higher loading rate of the vertical ground reaction force (LR) have been observed in female runners with a history of tibial stress fractures measured during running trials in a non-fatigued state [4]. Finally, considering most competitive runners often complete longer runs as part of their training (i.e., 60 min or more), it would be insightful to study changes in strike pattern variability and loading rate before and after a long run.

There, the purpose of this study was to compare strike pattern variability and instantaneous loading rate between habitual RFS and imposed FFS before and after a long run. We expected lower strike pattern variability and a higher LR following fatigue. Higher variability and lower LR during imposed FFS compared to RFS was also expected.

METHODS

Fourteen experienced male habitual RFS runners were recruited (1.79 ± 0.07 m; 73.5 ± 11.4 kg; 31.5 ± 9.6 yrs; 48.3 ± 14.0 mi/wk). Written consent approved by the Institutional Review Board was obtained for all participants before testing.

Runners completed a 5 min running warm-up before testing. An 8-camera motion capture system (240Hz, Qualisys AB) and force platform (1200Hz, AMTI) were used to collect kinematic and ground reaction force (GRF) data. Anatomical and tracking marker clusters were secured on the right leg. Subjects completed five over-ground running trials with their habitual RFS and imposed FFS pattern over a 20m runway while contacting a force platform with their right foot. Five successful trials were completed using both their habitual strike pattern and imposed FFS, respectively. A speed of $\pm 5\%$ of their long run pace was used. Once markers were removed, all runners then completed a long treadmill run (11.8 ± 3.5 miles; 90.4 ± 23.4 min) equivalent to 25 % of their average weekly mileage in the past 3 months. Immediately following the run, markers were placed back on the runners and running tests were repeated. Ink marks were used to ensure high reliability in marker placement before and after the long run.

Visual3D software (C-Motion, Inc.) was used to compute all variables. Kinematic and GRF data were filtered using a fourth-order Butterworth low-pass filter at 8 and 40 Hz, respectively. Dependent variables included strike index, its coefficient of variation (CV) and peak instantaneous loading rate of the vertical GRF. Strike index is the ratio of the location of the center of pressure location as a percentage of foot length at time of foot strike. The strike index CV was calculated as a percentage of the ratio of the standard deviation over the mean of five trials. The average values of these variables for the five trials of each strike pattern condition before and after the long run was used in the statistical analyses.

A 2X2 within-within factorial repeated measures ANOVA with strike pattern and time ($\alpha = 0.05$). Paired t-tests were used to compare means when

interaction effects were found. Cohen's d effect sizes (ES) were calculated for pairwise comparisons using pooled standard deviation.

RESULTS AND DISCUSSION

RFS and FFS patterns were confirmed at every time point as strike index was greater for imposed FFS compared to RFS (Table 1). Habitual RFS runners appear to be able to acutely adopt a FFS pattern even following a long fatiguing run.

A strike pattern by time interaction was not found for strike index variability (CV; Table 1). Although stride index variability was reduced by 20% during RFS and 21% during imposed FFS after the long run, no time effect was found (Table 1). Lower strike index variability was found during imposed FFS compared to RFS (Table 1). This finding is unsurprising since runners were likely highly focused on performing the FFS as per their instructions. Changing foot strike pattern may introduce new stresses to musculoskeletal tissue that, if too sudden, may be injurious. Movement variability has been hypothesized to broaden stress distribution on musculoskeletal tissue [2, 3]. Thus, the reduced variability in strike index when RFS acutely adopt a FFS pattern could be linked with injury development potential following an acute strike pattern transition. This hypothesis still needs to be tested using a prospective approach.

A strike pattern by time interaction trend ($P = 0.064$) was observed for loading rate (Figure 1). As expected, loading rate was lower before (ES = 2.21; $P < 0.001$) and after (ES = 2.20; $P < 0.001$) the run during imposed FFS compared to RFS. During RFS, loading rate was slightly higher following the run ($P = 0.064$; ES = 0.17) but the small effect size suggests a non-meaningful change. Finally, loading

rate was unchanged following the long run ($P > 0.05$).

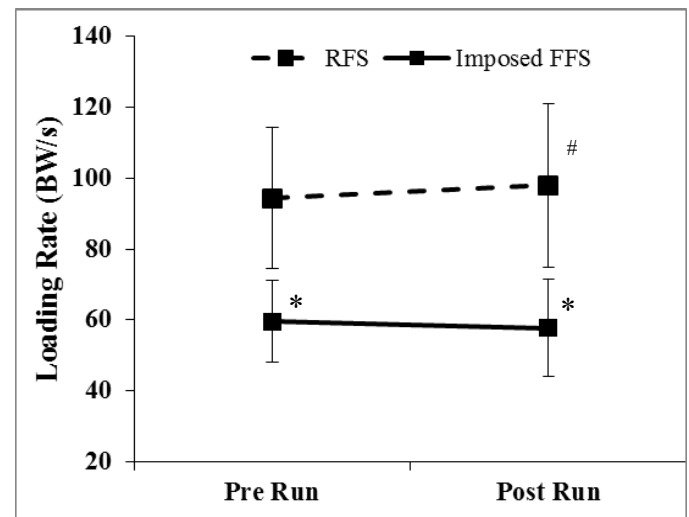


Figure 1: Instantaneous loading rate of the vertical GRF in RFS and imposed FFS pre and post run. Notes: *: difference between strike patterns within test time; #: trend for difference between test times within RFS pattern. Means \pm SD.

CONCLUSIONS

Changes in strike pattern, its variability and loading rate between habitual RFS and imposed FFS appear to be unchanged following a long run. However, the ability and the injury risk of habitual RFS runners to use a FFS pattern for an entire long run remain unknown.

REFERENCES

1. Daoud AI, et al. *Med Sci Sports Exerc*, **44**(7), 1325-34, 2012.
2. Heiderscheit BC, et al. *J App Biomech*, **18**, 110-121, 2002.
3. Hamill J, et al. *Clin Biomech*, **14**, 297-308, 1999
4. Milner, et al. *Med. Sci. Sports Ex*, **38**, 323-329, 2006.

Table 1. Average strike index, and strike index coefficient of variation (CV) of five stance phases for RFS and imposed FFS before and after a long run in habitual RFS runners (mean \pm SD)

Variables	Before Run		After Run		<i>P</i> -values		
	RFS	Imposed FFS	RFS	Imposed FFS	Strike	Time	Inter.
Strike Index (%)	14.9 \pm 6.3	109.4 \pm 11.0	14.2 \pm 5.7	109.4 \pm 8.9	<0.001	0.80	0.75
Strike Index CV (%)	43.3 \pm 22.6	6.9 \pm 9.1	36.1 \pm 16.5	5.7 \pm 2.8	<0.001	0.23	0.13

HIP LOADING DURING FORWARD AND SIDE LUNGES

Jaimee M. Zorn and Michael J. Pavol

Oregon State University, Corvallis, OR, USA
email: mike.pavol@oregonstate.edu

INTRODUCTION

Hip fractures have serious consequences for older adults, and a major risk factor for these fractures is osteoporosis [1]. Encouragingly, exercise can slow aging-related bone loss at the hip, as a result of the associated loading [2]. However, there is little evidence as to what exercises are most effective in this regard. Notably, little is known about femoral loading at the hip during forward and side lunge exercises, despite the common inclusion of these exercises in programs aimed at osteoporosis prevention. This study thus determined the peak joint contact force at the hip during a lunge exercise as a function of lunge direction, limb, and use of a weighted vest for added resistance.

METHODS

Seven healthy, physically active women, aged 38-54 years (mean \pm SD: 44 ± 4 yrs, 165 ± 4 cm, 57 ± 5 kg), gave their informed consent to participate. Participants began with a task-specific warm-up/practice. Next, a set of 26 reflective markers was attached to the lower limbs and torso. Participants then performed two blocks of lunge trials: one with and one without a 5.4 kg weighted vest (CAP Barbell, Houston, TX). Each block included one set each of forward and side lunges, each set consisting of 3-4 trials with a pause between. Orders were counterbalanced. In each trial, participants stepped forward or right with the right foot to a marked position at a step length of 110% of their leg length to execute the lunge. Participants were to lower their hips as far as they felt they safely could during the lunge (without touching the left knee to the ground during forward lunges), then step back to their original position. Each lunge was to be performed in a continuous manner at a self-selected, unhurried pace, the arms crossed across the chest and the back kept straight. A chair was placed

within reach for the participant to grasp if needed. During each lunge, kinematic data were recorded at 60 Hz by a motion capture system (Vicon, Los Angeles, CA) and the ground reactions under the feet were recorded at 600 Hz by three force platforms (Bertec, Columbus, OH). Height, weight, and selected body dimensions were also measured.

Motion capture and ground reaction force data were filtered at 9 and 45 Hz, respectively, and cropped to the period from 0.1 s before foot contact of the right (lunging) limb until 0.1 s after foot-off. Marker positions relative to body segments and joint centers were estimated (BodyBuilder, Vicon), and the pelvofemoral contact force at each hip was then calculated from the data using a rigid-body model of the torso and lower limbs within the AnyBody Modeling System (Aalborg, Denmark). The Twente Lower Extremity Model (AnyBody Managed Model Repository, v1.2) was modified to include a ball-and-socket knee joint with torsional springs for passive restraint. Each lower limb consisted of five segments (thigh, leg, patella, talus, foot) with nine degrees of freedom and 55 muscles divided into 169 fascicles, each modeled by a 3-element, Hill-type muscle model. Dimensions, inertial properties, and strength of the model were scaled to the participant. To solve for the contact forces at the hip, inverse dynamics solutions were found to minimize the sum of the squared muscle fascicle forces, normalized to the fascicle's strength, in each frame of data.

Peak contact forces at the hip were extracted and normalized to body weight (BW), with values averaged across correctly-performed trials within a condition. Effects of lunge direction, limb, and weighted vest use on the peak contact force were identified by a 3-factor repeated-measures ANOVA, with effects considered significant at $p < .05$. Two participants were excluded from the analysis, one as an outlier and the other due to a model singularity.

RESULTS AND DISCUSSION

Consistent patterns of hip loading were observed during forward and side lunges. For forward lunges, the contact force at both hips peaked shortly after the low point of the lunge, as participants propelled upward (Figure 1). A similar pattern was seen in the left (non-lunging) limb during side lunges, but the contact force at the hip of the right (lunging) limb peaked later, as participants propelled medially.

Peak contact forces at the hip were approximately 44% larger for forward lunges than for side lunges ($p=.023$; Figure 2). Peak contact forces were also about two times larger for the right (lunging) limb than for the left (non-lunging) limb ($p=.002$). The addition of a 5.4 kg weighted vest did not affect the peak contact force ($p=.075$). These effects were seen regardless of lunge direction, limb, and/or weighted vest use ($p>.05$ for all interaction effects).

The peak contact forces found for forward and side lunges are larger by factors of about 4 and 2.5, respectively, than femoral forces directly measured during running or jumping [3]. These peak forces found may overestimate the actual contact forces, as model-predicted contact forces are sensitive to assumed muscle moment arms. However, it is also reasonable that lunges would result in large contact forces at the hip. The large distance of the lunging foot from the hip during forward lunges necessitates large hip extensor moments for weight support.

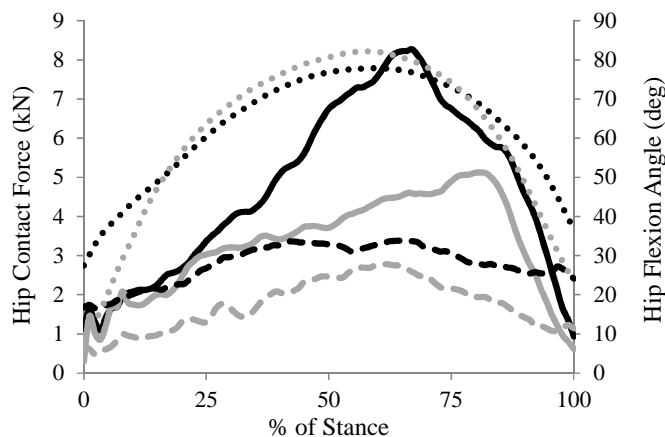


Figure 1: Contact forces acting at the right hip (—) and left hip (---) and the right hip flexion angle (···) during stance of a typical forward lunge (black lines) and side lunge (grey lines) for one participant.

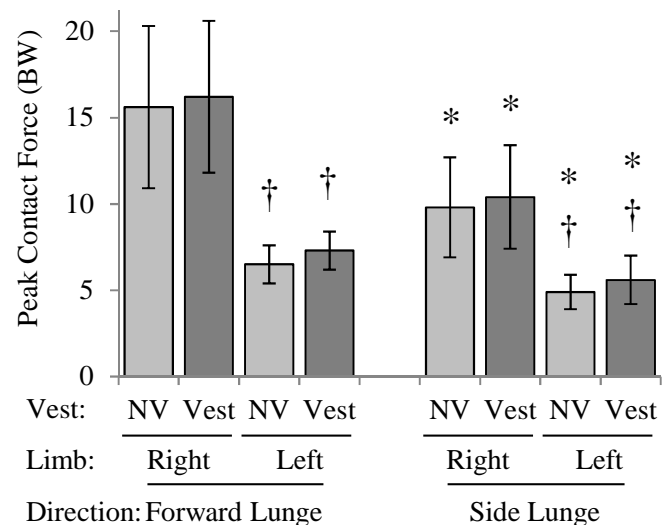


Figure 2: Mean \pm SD peak contact force at the hip during lunges as a function of lunge direction, limb, and weighted vest use. * $p<.05$ vs. Forward Lunge; † $p<.05$ vs. Right (Lunging) Limb. NV = No Vest.

Large hip extensor moments are also needed during side lunges to support the forward-inclined torso, and those will come disproportionately from the lunging limb, as it supports more of one's weight. With the large muscle forces needed to produce these moments and the large hip contact forces that result, the effect of wearing a 5.4 kg weighted vest was neither significant nor meaningful. That hip contact forces were smaller for side lunges than for forward lunges may be due to a smaller distance of the lunging foot from the hip. Differences between limbs likely reflect differences in weight support.

CONCLUSIONS

The present findings suggest that both forward and side lunges produce enough force at the hip of the lunging limb to stimulate bone formation, even without adding a weighted vest, and forward lunges are more beneficial in this regard. The findings thus support the inclusion of lunges, particularly forward lunges, in osteoporosis prevention programs.

REFERENCES

1. Ensrud KE. *J Gerontol A Biol Sci Med Sci* **68**, 1236-1242, 2013.
2. Snow CM, et al. *J Gerontol A Biol Sci Med Sci* **55A**, M489-M491, 2000.
3. Bassey EJ, et al. *J Biomech* **30**, 213-223, 1997.

FACILITATION OF SHORT-LATENCY RATE OF FORCE DEVELOPMENT OF NECK MUSCLES

¹ Lucie Pelland, ¹ Ian Gilchrist, ¹ Yehyah Hamandi, ² Wissal Mesfar, and ³ Kodjo Moglo

¹ School of Rehabilitation Therapy, Queen's University, Kingston, ON, Canada

² College of applied Medical Sciences, King Saud University, Riyadh, KSA

³ Mechanical & Aerospace Engineering, Royal Military College of Canada, Kingston, ON, Canada

email: Lucie.Pelland@queensu.ca; web: <http://www.queensu.ca/>

INTRODUCTION

Increasing neck strength has been promoted as a player-specific strategy for lowering the severity of impacts to the head and the incidence of concussion [1,2]. Specifically, the rate at which neck muscle force (RFD) can be developed prior to or early post-contact is a variable of neck strength which could modify the biomechanics of concussive and upper cervical spine injuries [3]. The sternocleidomastoid (SCM) muscle is a key feature of this protective response as it is the only muscle of the neck that can adjust the position of the head and neck in three-dimensional space to optimize alignment of the response to the line of application of the external force. Therefore, applying principles of motor learning to train athletes to improve RFD of the SCM would, theoretically, be an important outcome of neck strength training programs for contact sports.

The aim of this feasibility study was to evaluate the short-term effects of a motor learning program on the RFD along the line of force of the SCM.

METHODS

This study received clearance from our institution's Faculty of Health Sciences and Affiliated Hospitals Research Ethics Board. Participants were eight physically active males recruited from the university community. The mean (SD) values of relevant characteristics of the study group were: age, 22.5 (1.8) years; height, 1.8 (7.3) m; weight, 80.1 (9.2) kg; neck length, 8.7 (0.8) cm; neck-to-head circumference (NH) ratio, 0.7 (0); and right-hand dominant ($n = 7$).

Static neck strength was measured using the Multi-Cervical Unit (MCU, BTE Technologies; Hanover,

MD, USA). The MCU was retrofitted with a custom head frame assembly system designed and fabricated at Queen's University (Pelland and Gilchrist) for measurement of maximum voluntary efforts (MVEs) along eight directions covering 360° at increments of 45° in the transverse plane of the head, and positioning of the head along the sagittal plane in up to 20° of extension and 20° of flexion (see Figure 1).



Figure 1: Standard positioning for assessment and training in the custom-adapted MCU. The head-neck is held in neutral position along the sagittal plane for all testing and for training.

Maximal voluntary efforts (MVEs) were produced under static conditions and with ballistic intent; on a 'go' signal, participants were asked to push against the force transducer 'as fast and as hard as possible' and to hold their maximum force until the end of the three-second trial. Near-instantaneous visual feedback of force output was provided on a computer screen placed directly in front of participants.

The line of application of force of the SCM was considered to be along the 45° plane of right (R45) and left (L45) forward flexion. The structure of the motor learning program was as follows: baseline measure of MVE, three trials along R45 and L45; 2 sets of 5 MVE contractions, blocked randomized along R45 and L45, the order being randomly selected between participants; 10-minute rest period; post-training measure of MVE, three trials along

R45 and L45, obtained at 10 and 20 minutes and 2 days post-training.

Three variables were calculated from the force-time curve: RFD at 0-50ms and 50-100ms ($\text{Nm} \cdot \text{s}^{-1}$), the area under the force-time curve at 0-50ms (AUMC, Nms), where AUMC is proportional to the short-latency impulse of force [4], and peak force (N). Percent change from baseline was calculated for each variable, and effects of training evaluated by repeated measures 'split-plot' ANOVA, with hand-dominance as the between-subject factor and force variables measured at baseline, post-test 1 (PT1, 10 mins), post-test 2 (PT2, 20 mins), and post-test 3 (PT3, 2 days). All statistical analyses were performed using SPSS (v.21, IBM Corp., Chicago, IL).

RESULTS

There was no effect of hand dominance on calculated outcomes ($P > 0.05$). Overall, performance improved on all measured outcomes ($P < 0.001$) from baseline to PT1. There were no significant differences between measures evaluated post-training (PT1, PT2, PT3; $P > 0.05$). While training effects were significant, calculated coefficients of variation (CV) of outcomes were high, ranging between 13% and 100%. The fit of the data was improved by plotting baseline MVE values against the percent change at PT1 for each of the calculated variables. For RFD at 0-50 ms, the

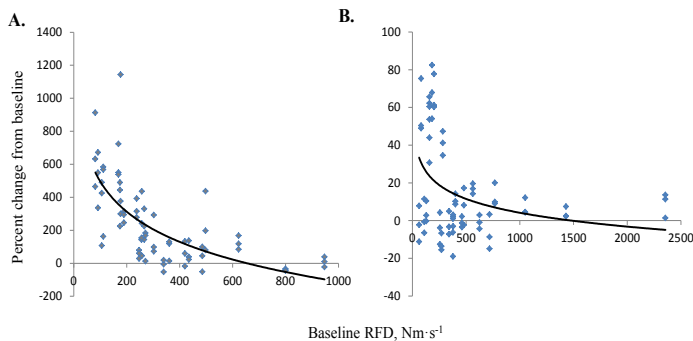


Figure 2: Percent change in RFD (0-50ms) from baseline to PT1 (y-axis) is plotted as a function of baseline RFD (x-axis) for the non-dominant (A) and dominant (B) sides. The best fit curve was logarithmic, with r^2 of 0.49 for non-dominant and 0.13 for dominant side.

A logarithmic curve also predicted training effects on AUMC, with r^2 of 0.21 for non-dominant and 0.51 for dominant side. The resultant effects of facilitated short-latency R45 and L45 force are shown in Figure 3.

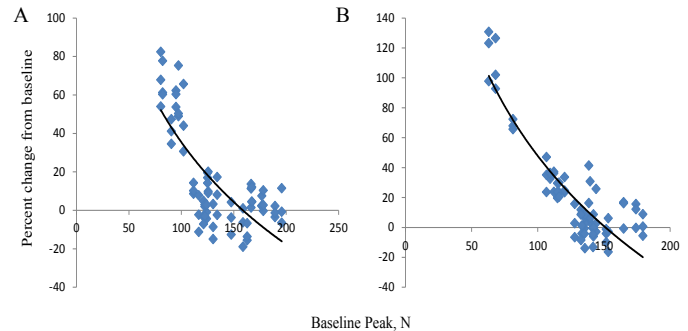


Figure 3: Percent change in peak (N) from baseline to PT1-3 (y-axis) is plotted as a function of baseline peak force (x-axis) for the non-dominant (A) and dominant (B) sides. The best fit curve was logarithmic, with r^2 of 0.59 for non-dominant and 0.81 for the dominant side.

Increases in RFD at 0-50ms were significantly correlated to percent increase in peak force ($p < 0.05$, $r = 0.42$). The training effect was stronger at lower baseline peak neck force.

CONCLUSIONS

This feasibility study yielded good evidence to support the integration motor learning into neck strength training programs for concussion.

REFERENCES

1. Mansell J, et al. *Athl Training* **40**, 310-319, 2005
2. Collins C, et al. *J Primary Prevent* DOI: 10.1007/s10935-014-0355-2, 2014.
3. Saari A, et al. *J Biomech Eng* **135**, 111003-1-11.
4. Aagaard P, et al. *J Appl Physiol* **2002**, 1318-1326, 1985.

ACKNOWLEDGEMENTS

This study was funded, in part, by DTAE - Department National Defence, Canada.

DEVELOPMENT OF A NOVEL PROTOCOL TO TEMPORARILY REDUCE CORE STABILITY

Margaret E. Raabe, Scott M. Monfort, Tom M. Best, Jimmy A. Oñate, and Ajit M.W. Chaudhari

The Ohio State University, Columbus, OH, USA
email: raabe.23@osu.edu, web: <http://u.osu.edu/osusportsbiomechanics>

INTRODUCTION

In recent years, core stability has become an extremely popular topic among clinicians, researchers, and physically active people in general. It is believed that the core musculature (muscles of the abdomen and lower back) contracts to stabilize the spine and provide a solid foundation of movement for the lower extremities [1]. Consequently, this has led to the popular notion that insufficient core stability may lead to inefficient movements that may ultimately lead to injury [2].

The scientific data supporting the relationship between core stability and lower extremity injury is limited and primarily cross-sectional or retrospective [2]. Causal conclusions cannot be drawn from these studies or from the prospective studies that also exist. Therefore a new paradigm is needed to determine causal relationships between core stability and lower extremity movement.

The purpose of this study was to develop a core stability knockdown protocol (CSKP) that reduces one's ability to control movement of the torso. By allowing core stability to be reduced in an isolated, controlled manner this paradigm will permit within-subject analyses during a single testing session. Such a protocol could then be used to determine the influence of core stability on various biomechanical variables.

METHODS

Five subjects (1 female, age = 24.8 ± 2.9 years, height = 1.78 ± 0.08 m, mass = 77.6 ± 18.7 kg) provided IRB-approved informed consent prior to participating in this study. Each subject had their core stability measured before and after the CSKP using a novel unstable quiet sitting test developed by our research team, shown in Figure 1. We

designed this test in order to objectively and quantitatively measure core stability in a way that could also be replicated in the clinical setting. In this test, a participant sat on top of the rounded end of a BOSU ball positioned on a platform high enough so that their feet did not touch the ground. This platform was placed on top of two Bertec 4060-10 force plates embedded in the ground. Participants were instructed to sit as still as possible for 60 seconds with their eyes closed while performing a secondary task of counting backwards in increments of 4. Recent postural control research has utilized a similar secondary task during quiet standing because it may be a more functional measure of stability since typically attention is divided between multiple tasks and not solely focused on postural control [3].



Figure 1. Unstable quiet sitting test used to quantitatively measure core stability.

During the trial, center of pressure (COP) data were recorded and used as measures of core stability. Measured variables included: COP path length, average anterior-posterior (A-P) COP velocity, and average medial-lateral (M-L) COP velocity. For

each condition (baseline/pre-CSKP, post-CSKP) three trials were collected and the median was used for analysis.

After a participant's baseline core stability was measured, they completed the CSKP. The CSKP consists of 4 dynamic and 4 isometric exercises chosen by our research staff to target both the superficial and deep core musculature with minimal involvement from the lower extremity muscles. All subjects completed each exercise to voluntary exhaustion or until proper form could not be maintained in the following order: 1) right side bend on a BOSU ball, 2) left side bend on a BOSU ball, 3) back extension reps on a BOSU ball, 4) sit-ups on a Swiss ball, 5) right side plank, 6) left side plank, 7) back extension hold, and 8) traditional plank. All exercises were completed consecutively with minimal to no rest between each. Following the CSKP, participants were given a 3 minute rest to allow their breathing rate to return to normal. A participant's post-CSKP core stability was measured immediately after this rest as previously described.

Two sided paired t-tests were used with a significance level $\alpha = 0.05$ to test the hypothesis that after the CSKP participants had significantly different COP measures following the CSKP, signifying a change in core stability.

RESULTS AND DISCUSSION

The average change in COP measures from pre- to post-CSKP is shown in Table 1. We found that both COP path length and mean M-L COP velocity were significantly different and mean A-P velocity trended toward significance when tested 3 minutes after the conclusion of the CSKP. Looking at the mean difference in COP measures from pre- to post-CSKP we found all COP measures increased for all subjects, confirming a reduction in core stability. Since the core stability measurements took an additional 3 minutes, this protocol significantly increased these measures for at least 6 minutes following the conclusion of the CSKP. This demonstrates that the CSKP negatively affected postural control of participants indicating that the

knockdown protocol was successful in temporarily reducing a person's core stability.

This approach minimizes confounding variables and eliminates retention and compliance issues that frequently arise in long-term intervention studies. The protocol should allow for causal conclusions to be drawn when studying core stability and has the potential to be used in a variety of settings to further establish the relationship between core stability and lower extremity function. Knowledge gained from studies utilizing this approach will be able to determine the degree to which core stability changes are associated with various biomechanical changes. This knowledge may assist in the development of improved injury prevention and rehabilitation protocols.

Table 1: Average change in COP measures for all subjects (N=5) from pre- to post-CSKP.

* signifies a significant difference at a significance level $\alpha = 0.05$.

	Mean Change \pm SD (Post-CSKP – Pre-CSKP)	P-value
COP path length (mm)	200.17 \pm 123.28	0.0221*
Mean A-P COP velocity (mm/s)	1.92 \pm 1.69	0.0647
Mean M-L COP velocity (mm/s)	2.37 \pm 1.16	0.0105*

REFERENCES

1. Hodges, PW & Richardson, CA. *Phys Ther* **77**, 132-142, 1997.
2. Willson J, et al. *J Am Acad Orthop Sur* **13**, 316-325, 2005.
3. Moghadam M, et al. *Gait and Posture* **33**, 651-655, 2011.

ACKNOWLEDGEMENTS

The authors gratefully acknowledge support from NIAMS R03-AR065215.

BIOMECHANICAL CONSEQUENCES OF RUNNING WITH DEEP CORE MUSCLE WEAKNESS

Margaret E. Raabe, Thomas M. Best, Jimmy A. Oñate and Ajit M.W. Chaudhari

The Ohio State University, Columbus, OH, USA

email: raabe.23@osu.edu, web: <https://u.osu.edu/osusportsbiomechanics>

INTRODUCTION

In recent years core stability has become a popular topic among sports medicine clinicians, physically active people in general, and especially runners. Its popularity is stimulated largely due to the theory that insufficient core stability during physical activity may lead to movements that are less efficient and ultimately lead to injury [1].

The deep core muscles (quadratus lumborum (QL), psoas major (PS), multifidus (MF), and the deep fascicles of the erector spinae (deep ES) are believed to be vital to postural control and stabilization of the lumbar spine [2]. One mechanism by which core musculature contributes to stability of the lumbopelvic-hip complex is through axial compressive spinal loads [3]. Inadequate compressive spinal loads may not stabilize the spine sufficiently, but excessive loads have been associated with low back pain (LBP), so a balance between these extremes is necessary to minimize injury.

The role of the deep core muscles during everyday tasks and especially during running is not well understood. The purpose of this study was to use simulations to identify compensation strategies for weakness of the deep core musculature and changes in spinal compressive loads during running.

METHODS

Three subjects (2 female, height = 1.71 ± 0.03 m, mass = 63.16 ± 4.73 kg) from a healthy population provided informed consent participated in a previously published IRB-approved study [4]. We collected marker trajectory and ground reaction force data during continuous overground running at a self-selected comfortable speed in our motion analysis laboratory. Multiple subject-specific kinematically-driven simulations were generated for

each subject using OpenSim. A full-body generic musculoskeletal model we developed from three previously built OpenSim models was scaled to match each subject's anthropometry. This model is comprised of 21 segments, 30 degrees-of-freedom, and 324 musculotendon actuators. The trunk contains the 8 major muscle groups of the lumbar spine (rectus abdominis (RA) external and internal obliques (EO and IO), latissimus dorsi (LD), erector spinae (ES) which is comprised of the superficial (sf) and deep longissimus thoracis (LT) and iliocostalis lumborum (IL), QL, MF, and PS), each of which is modeled as multiple fascicles. The spine consists of the sacrum, five lumbar vertebrae, and lumped thoracic and cervical vertebrae. After solving for the model's joint angles and moments that best matched the experimental marker data, static optimization (SO) was performed to resolve the net joint moments into individual muscle forces at each time instant. Lastly, a joint reaction analysis was performed to calculate internal joint loads acting on each of the lumbar vertebrae.

A baseline simulation of running was created for each subject. Additional simulations were then created for each subject at progressively higher levels of deep core muscle weakness. The QL, MF, PS, and deep ES were weakened individually and simultaneously from 20-100% weakness in increments of 20%. Trunk muscle force production and axial compressive loads on the lumbar vertebrae were recorded at each level of muscle weakness. When individual muscles were weakened, compensating muscle forces were recorded at the point of the weakened muscle's baseline peak force production. When the four deep core muscles were weakened simultaneously, peak muscle force was reported for compensating muscles.

RESULTS AND DISCUSSION

Compensations for individual and total deep core muscle weakness are shown in Table 1. Based on

the level of required compensations, these results suggest the deep ES may be most crucial to maintain running kinematics, followed by the Psoas, MF, and QL, respectively. Of the weakened deep core muscles, the deep ES produced the highest muscle forces during running and therefore, the largest compensations were necessary, while the contrary was true with the QL. When all deep core muscles were weak, muscles that compensated were those that also attached to the lumbar vertebrae.

For individual muscle weakness, axial spinal loading was most affected when the deep ES was weakened. Axial compressive loads on all lumbar vertebrae decreased when the QL and PS were each individually weakened. In all other cases loading on the higher lumbar vertebrae increased and loading on the lower lumbar vertebrae decreased with muscle weakness. Increased axial spinal loads could be detrimental since elevated loads are believed to be associated with LBP, while decreased loads similarly may also signify a loss of spinal stability. Changes observed in these loads with our simulations suggest that all deep core muscles contribute to maintaining stability of the spine, and the MF and deep ES fascicles may be most influential in minimizing elevation of normal (baseline) axial compressive loads.

One limitation of this study is that running kinematics were forced to stay the same after the muscle weakness was implemented. It is likely some people may choose to alter kinematics rather than muscle forces in order to compensate for muscle weakness. Also, the deep core muscles could successfully be weakened 100% individually and together in the model. This may have occurred because the model has an abundant number of trunk muscle fascicles that are able to compensate and SO is a robust, frame-by-frame solver. It is unknown if this phenomenon is entirely realistic clinically, however these simulations will still provide valuable insight into compensations and consequences of core muscle weakness.

REFERENCES

1. Willson J, et al. *J Am Acad Orthop Sur* **13**, 316-325, 2005.
2. Richardson, C., et al. *Therapeutic Exercise for Lumbopelvic Stabilization (2nd ed)*, 13-28, 2004.
3. Cholewicki J., et al. *Clin Biomech* **11**, 1-15, 1996.
4. Jamison, ST., et al. *J Biomech*, **46**, 2236-41, 2013.

ACKNOWLEDGEMENTS

The authors gratefully acknowledge support from NIAMS R03-AR065215.

Table 1. Primary compensators and altered spinal loading that result when the specified muscles are weakened 100%. Color coding indicates the level of % increase in compensating muscle forces. **blue**=0-9.9%, **orange**=10-24.9%, **red**=25-49.9%, **dark red**=50+%.

Weakened muscle(s)	Compensating muscles										Mean % change in axial compressive load on given spinal vertebrae ± SD					
	deep IL	deep LT	Sf IL	Sf LT	MF	QL	LD	PS	IO	Iliacus	L1	L2	L3	L4	L5	S1
QL	blue	blue		blue							-0.18 ± 0.14	-0.11 ± 0.09	-0.09 ± 0.08	-0.16 ± 0.03	-0.17 ± 0.03	-0.17 ± 0.04
MF	orange	orange	blue	blue							2.50 ± 0.45	2.13 ± 0.87	0.32 ± 0.42	-0.33 ± 0.15	-0.47 ± 0.18	-0.34 ± 0.15
Psoas	orange		red			orange	red			dark red	-0.24 ± 0.38	-1.19 ± 1.97	-1.64 ± 2.72	-1.68 ± 2.74	-1.76 ± 2.88	-1.82 ± 2.97
Deep ES (deep IL, LT)			dark red	dark red	dark red	dark red	orange	dark red			10.29 ± 2.29	5.77 ± 1.41	0.426 ± 0.98	-2.97 ± 1.02	-4.75 ± 1.07	-3.69 ± 2.76
All deep core			orange	red			orange				14.64 ± 4.06	7.95 ± 3.83	-0.51 ± 3.55	-4.97 ± 2.80	-7.20 ± 3.07	-7.97 ± 3.23

ESTIMATING VERTICAL AND LONG JUMP POWER IN FEMALE COLLEGIATE SOCCER ATHELETES

¹Swithin S. Razu, ¹J. Bryan Mann and, ¹Trent M. Guess

¹ The University of Missouri, Columbia, MO, USA
email: swithinr@health.missouri.edu, web: www.mizzoumotioncenter.com

INTRODUCTION

Peak power and average power are essential components in assessing the performance of an athlete. In terms of evaluating sports performance, power is used to evaluate the effectiveness of strength training programs over time, evaluating an athlete's aptitude towards a specific sport. A number of prediction equations [1-3] have been developed to estimate peak and average jump power from jump height. Studies have shown that each population may require a specific regression equation to ensure accuracy of prediction [4]. Hence the purpose of this study was to develop new regression equations for female athletes and to develop a regression equation for long jump power that can be used to assess athletic performance.

METHODS

Twenty female university soccer players (age, 19.3 ± 1.12 years; mean weight 61.30 ± 7.80 kg; and height 1.66 ± 0.07 m) agreed to participate in this study, which was approved by the institution's human subject review board. Anthropometric measurements included body mass (BM), height, inter-anterior superior iliac spine (ASIS) distance, leg length, knee width, and ankle width. All limb measurements were taken from both limbs.

For the motion capture, an 8 camera VICON MX-T40S retro-reflective motion analysis system was used. This system was synchronized with two AMTI Optima force plates. The cameras acquired data at 100 Hz and the force platform at 2000 Hz. Sixteen skin-surface retro-reflective markers were placed with tape on the trunk and legs according to the protocol of the lower body Plug-in-Gait model (PiG) [5]. The kinematic and force plate data obtained were filtered using the Butterworth routine and processed using the VICON Nexus software

that incorporated the PiG model to calculate pelvis center of mass (CoMP) location during each trial.

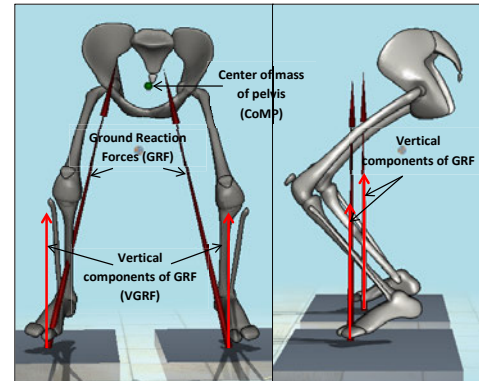


Figure 1: Force components during vertical jump

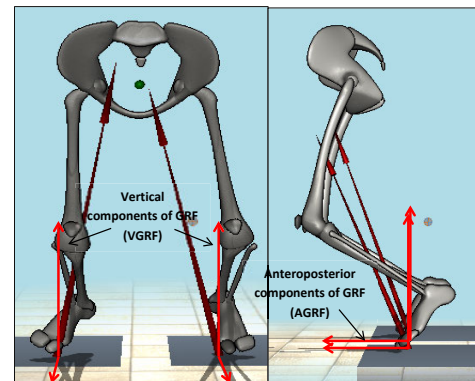


Figure 2: Force components during long jump

The jump techniques were demonstrated to each subject followed by one practice jump. All jumps were performed barefoot and no restrictions for hand position were enforced. Each subject performed 5 maximum effort trials where they stood on force platforms in such a way that each leg was placed on a separate plate. The vertical jump height (VJ_{height}) was the difference between the standing pelvis CoMP height and the maximum height attained by the pelvis CoMP during the vertical jump. The long jump distance (LJ_{distance}) was the minimum distance between the heel motion-capture markers during take-off and landing positions for both feet.

Power output of the subject was calculated as a product of force and velocity [6]. Force exerted by the subjects resulted in vertical ground reaction forces (VGRF) at the feet which are assumed to act at the CoMP. The VGRF is the vertical component of force platform output and CoMP vertical velocity (CoMPVV) is obtained from the result of the PiG model. The resulting equation is:

$$\text{Vertical Jump Power (W)} = \text{VGRF (N)} * \text{CoMPVV (m.s}^{-1}\text{)} \quad (1)$$

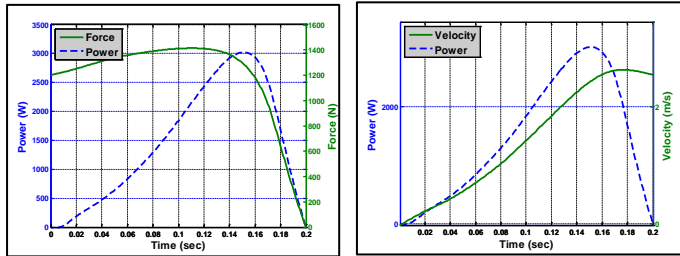


Figure 3: Power versus force and power versus velocity during vertical jump.

Instantaneous power was calculated throughout the jumping movement using Eqn.1 from the loading position to the landing position for all 5 trials. Peak VJ_{pk} was the highest instantaneous power output value achieved; average VJP was calculated by computing the area under the positive instantaneous power output curve achieved during the vertical jump.

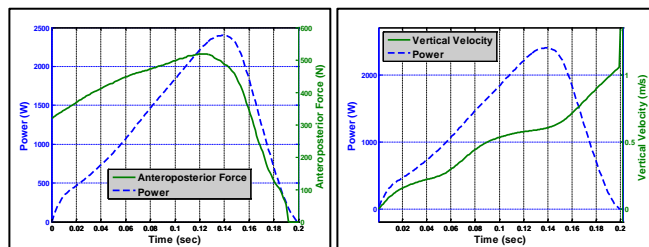


Figure 4: Power versus force and power versus velocity during long jump.

Instantaneous power was calculated throughout the jumping movement using Eq.1 from the loading position to the landing position for all 5 trials. Peak VJ_{pk} was the highest instantaneous power output value achieved; average VJP was calculated by computing the area under the positive instantaneous power and was calculated throughout the jumping movement using Eq. 2 from the loading position to the landing position for all 5 trials. Similarly long

jump peak power (LJ_{pk}) and average power (LJ_{avg}) were calculated.

$$\begin{aligned} \text{Vertical Jump Power (W)} \\ = \text{VGRF (N)} * \text{CoMPVV (m.s}^{-1}\text{)} + \text{AGRF (N)} \\ * \text{CoMP(m.s}^{-1}\text{)} \end{aligned} \quad (2)$$

RESULTS AND DISCUSSION

The purpose of this study was to develop more accurate regression equations to estimate power during long jump and vertical jump for a sport, gender and age specific group as shown below. Both regression models employed vertical jump height, jump distance and body mass (BM) as independent variables.

$$\begin{aligned} VJ_{pk} (W) &= -2259 + 36.49 * BM (kg) + 6983 * VJ_{height}(m) \\ \text{Adjusted } R^2 &= 0.83 \\ \text{RMSE} &= 197.5 \text{ W} \\ VJ_{avg} (W) &= -1831 - 1.753 * BM (kg) + 7510 * VJ_{height}(m) \\ \text{Adjusted } R^2 &= 0.75 \\ \text{RMSE} &= 160.6 \text{ W} \\ LJ_{pk} (W) &= -2722 + 47.03 * BM (kg) + 1423 * LJ_{distance}(m) \\ \text{Adjusted } R^2 &= 0.78 \\ \text{RMSE} &= 247.5 \text{ W} \\ LJ_{avg} (W) &= -1382 + 24.44 * BM (kg) + 837.1 * LJ_{distance}(m) \\ \text{Adjusted } R^2 &= 0.64 \\ \text{RMSE} &= 186.7 \text{ W} \end{aligned}$$

Over the course of an athlete's career, they will most likely gain or lose weight which affects their jumping ability. By calculating the power from the jumps, the practitioner can better evaluate the athlete's power production capability, allowing them to more effectively evaluate their strength training program. Also, the long jump and vertical jump can be more accurately compared as both units are in Watts and more closely related in nature.

REFERENCES

1. Sayers, S.P., et al., Med Sci Sports Exerc, 1999. **31**(4): p. 572-7.
2. Amonette, W.E., et al., J Strength Cond Res, 2012. **26**(7): p. 1749-55.
3. Canavan, P.K. and J.D. Vescovi, Med Sci Sports Exerc, 2004. **36**(9): p. 1589-93.
4. Quagliarella, L., et al., J Strength Cond Res, 2011. **25**(6): p. 1638-46.
5. Kadaba, M.P., H.K. Ramakrishnan, and M.E. Wootten, J Orthop Res, 1990. **8**(3): p. 383-92.
6. Harman, E.A., et al., The Journal of Strength & Conditioning Research, 1991. **5**(3): p. 116-120.

COMPARITIVE EVALUATION OF THE MICROSOFT KINECT WITH THE VICON MOTION CAPTURE SYSTEM TO OBTAIN 3D KNEE ANGLES

¹Swithin S. Razu, ¹Amirhossein Jahandar, and ¹Trent M. Guess

¹ The University of Missouri, Columbia, MO, USA
email: swithinr@health.missouri.edu, web: www.mizzoumotioncenter.com

INTRODUCTION

Various applications for rehabilitation and assistive technologies require quantitative assessment of the specific performed task, such as the measurement of joint motion. Within the clinical or research setting several methods exist to provide such precise estimates. For instance, the Vicon® motion capture system uses IR cameras and markers placed on the subject to estimate joint motion. Organic Motion Biostage is a markerless system capable of delivering positions and orientations for 21 segments which can be further processed into joint angles. These systems are accurate, but are expensive and typically only used in a laboratory setting. More recently wearable sensors such as inertial sensors (accelerometers and gyroscopes) have become more common for kinematic measurements in clinics, athletic training and in home settings as they are small, portable and inexpensive. Despite their advantages, motion estimates from these systems are often inflated with various kinds of errors such as signal noise and drift. Also, sensors must be placed securely and accurately and the measured parameters are limited. More recently, the Microsoft Kinect™ (Microsoft, Redmond, WA) sensor has gained momentum as a tool for quantitative assessment in clinics [1-3] due to its ability to extract a 3-D virtual skeleton, its affordability, and portability.

The first system presented is the affordable Microsoft Kinect™ v2, which is available either bundled with the Microsoft X-Box or as a stand-alone Windows PC device with a supplied SDK and drivers. The second system, which is at the high end of the price range, is an 8 camera motion capture system (VICON MX-T40S, Oxford Metrics, UK), which uses the Plug-in-Gait (PiG) model with functional calibration (PiG-FJC) to estimate 3-D

angles. This study compares joint angles derived from the new Kinect v2 to Vicon PiG-FJC joint angles calculated during simultaneous capture. Absolute segment orientation provided by the Kinect v2 was used to calculate a relative Cardan rotation sequence for the knee.

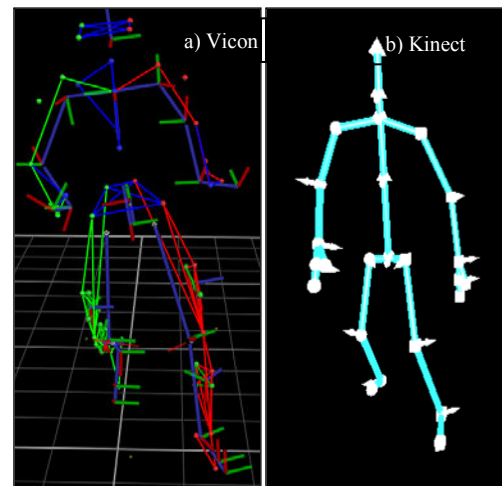


Figure 1 – Side cut motion model output in (a) Vicon and (b) Kinect™ motion capture systems.

METHODS

After providing informed consent approved by the institution's human subjects review board, three females and four male subjects (26.6 ± 4.0 years, 1.72 ± 0.09 m, 71.8 ± 12.3 kg) participated in this study. Data was simultaneously recorded using the Vicon MX motion capture system, sampled at 100 Hz using Vicon Nexus 2.1 software and Microsoft Kinect™ v2, sampled at 30 Hz using Kinect™ Studio. The Kinect™ sensor was positioned directly in front of the subjects at a height of 43 cm above the floor. Retro-reflective markers were placed according to the full body PiG protocol along with four-marker clusters which were attached to the anterior-lateral aspect of the thigh and shank as required by PiG-FJC. Relevant anthropometric

measures were taken as required by the PiG-FJC protocol. The subjects performed 3 trials of a right-left-right side cutting maneuver. Peak knee flexion was used to synchronize data obtained from the two systems.

KINECT PREDICTIVE MODEL

The Kinect sensor and its SDK provide a 3-D virtual skeleton. The virtual skeleton consists of the position and orientation of 25 joints. For each joint, the position is reported using X, Y, Z coordinates and the orientation are reported in terms of a quaternions (w, x, y, z). Each quaternion is the absolute orientation of the parent with respect to the global coordinate system.

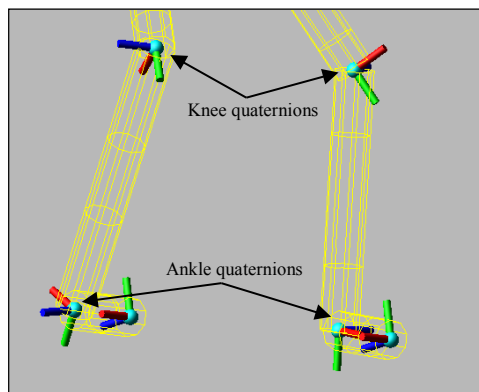


Figure 2 – Kinect™ model displaying absolute quaternions

To obtain the relative 3-D knee angles our method uses the relative quaternion achieved by multiplying the absolute quaternion of the ankle joint by the inverse absolute quaternion (the quaternion conjugate) of the knee joint. The relative quaternion is then converted into Cardan angles to represent flexion/extension, varus/valgus, and internal/external rotation in order to directly compare them with the Vicon acquired knee angles.

RESULTS AND DISCUSSION

The peak flexion angles measured by the Kinect™ were smaller than the Vicon system consistently for all the cases. The peak extension angles were consistently greater for the Kinect™ for all cases indicating that the Kinect often interpreted full knee extension as hyperextension. Knee internal/external

rotation and knee abduction/adduction revealed poor waveform for Kinect™ when compared to Vicon as indicated in Table 1. It may be possible to improve the accuracy of the joint angles by re-orienting the local coordinate systems to represent the anatomical axes of rotation especially in the non-sagittal plane. Before it can be used in the clinical setting several improvements should be made to the predictive model in terms of fixed segment length, anatomically accurate rotation axes, accuracy and smoothness of joint center location. Although some improvements are necessary the Kinect™ v2 displayed promising initial results for use as an affordable tool in the clinical setting.

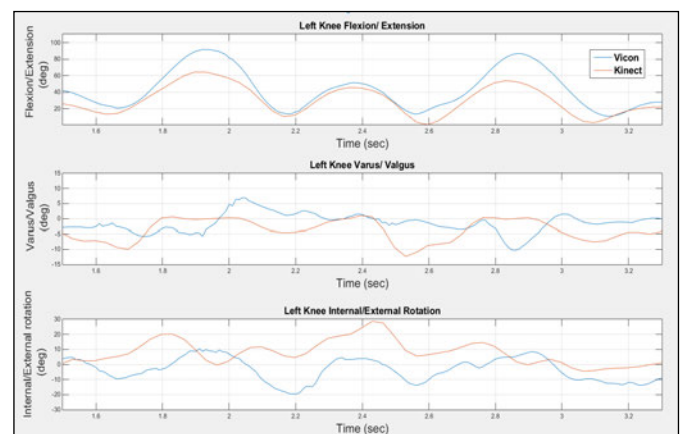


Figure 3 – Left knee angles comparison (Vicon vs Kinect™)

Table 1: Correlation coefficients

	Left Knee Flexion	Right Knee Flexion	Left Knee Valgus	Right Knee Valgus	Left Knee Rotation	Right Knee Rotation
Subject 1	0.91	0.91	0.16	-0.13	0.28	0.07
Subject 2	0.95	0.93	-0.11	-0.31	0.05	0.39
Subject 3	0.88	0.85	0.21	-0.33	0.28	-0.15
Subject 4	0.96	0.96	-0.57	-0.24	0.28	0.18
Subject 5	0.83	0.76	0.17	0.01	0.44	0.51
Subject 6	0.95	0.76	0.17	-0.16	0.32	0.28
Subject 7	0.83	0.77	-0.07	-0.28	0.14	0.33

REFERENCES

1. Yeung, L.F., et al., Gait Posture, 2014. **40**(4): p. 532-8.
2. Gabel, M., et al., Conf Proc IEEE Eng Med Biol Soc, 2012. **2012**: p. 1964-7.
3. Pfister, A., et al., J Med Eng Technol, 2014. **38**(5): p. 274-80.

BILATERAL SYMMETRY DURING A POWER CLEAN IN RECREATIONAL VS. COMPETITIVE WEIGHTLIFTERS

¹Patrick M. Rider, ¹Robert Leonard, ¹Charles Kemble, and ²Joshua Leonardis

¹East Carolina University, Greenville, NC, USA

²National Institute for Occupational Safety and Health, Morgantown, WV, USA

email: riderp@ecu.edu, web: <http://www.ecu.edu/cs-hhp/exss/biomechanics-members.cfm>

INTRODUCTION

High intensity weightlifting has grown in popularity with recreational exercisers. This style of training often includes performing power cleans. Power cleans are bilateral weightlifting exercises that involve explosive generation of lower extremity joint torques to vertically accelerate a heavy load as rapidly as possible. The goal of this lift is to increase an individual's ability to generate lower extremity power [1].

There are concerns towards increased risk of musculoskeletal injury by taking part in this type of exercise [2]. Complex, bilateral movements, such as the power clean, typically exhibit symmetry between left and right limbs in elite weightlifters [1,3], however, joint injuries that occur during these movements are typically unilateral. The relationship between lower limb bilateral asymmetries and level of experience during the power clean has not been fully explored.

The purpose of this study was to compare bilateral lower extremity kinetics during the pulling phase of a power clean between recreational and competitive weightlifters. We hypothesized that competitive weightlifters would show more symmetry than the recreational lifters in all lower extremity joint torques and peak ground reaction force (GRFs) values.

METHODS

Four males and three females between the ages of 18-35 years old participated in this study. Each participant was placed in one of two groups, competitive or recreational weightlifters. Groups were determined using the following criteria: Participants that had received at least 6 months of

power clean training from a qualified coach were placed in the competitive group ($n = 4$). Individuals who had regularly performed power cleans within the past 3 months but had not received consistent coaching ($n = 3$) were placed in the recreational group.

After completing several warm-up trials, each participant completed four single power clean trials at 70% self-reported 1-RM. This percentage was chosen to simulate a typical training load. Full-body, three dimensional biomechanical data were collected using two AMTI force plates (force data captured at 960Hz) and a motion capture system (markers captured at 240Hz). Markers were also placed at each end of the weight bar to track bar movement. Each trial included a 60 second rest period to minimize fatigue. Lower extremity joint torques and peak ground reaction forces were calculated and absolute differences between left and right sides were compared between groups. Percentage differences were calculated by dividing the absolute difference left to right by the average absolute torque produced at each joint.

RESULTS AND DISCUSSION

Peak ground reaction forces showed significantly greater asymmetry in the recreational group (18% vs. 9%). Peak hip joint torque asymmetry was no different between the groups (13.0% Recreational vs. 12.9% Competitive). Peak knee joint torques showed significantly greater asymmetries in the recreational vs. competitive group (30.4% vs. 11.2%). Peak ankle joint torques also showed greater asymmetry in recreational vs. competitive (14.4% vs. 9.5%). Absolute values and associated standard deviations for left and right peak GRFs and torque values are located in Table 1.

CONCLUSIONS

The results partially supported our hypothesis that competitive weightlifters would show less asymmetry in lower extremity joint torques and ground reaction force values. Interestingly, the hip joint showed similar amounts of asymmetry between groups. Individuals may be able to more effectively produce symmetrical motion at the hip joint as each joint is connected through a rigid body (the pelvis). This may provide more proprioceptive feedback for the hip joint.

Although the left to right differences in peak ground reaction forces in competitive weightlifters were small (9%), larger percent differences were observed at the individual joints (11%) within this group. This may indicate kinematic asymmetries at these joints. Lower extremity kinematic and kinetic asymmetries might also impact upper extremity symmetry and weight bar movement and play a role in the higher rates of injury in the shoulder and wrist joint in recreational high-intensity weightlifters. Further investigation should examine if any relationships exist between lower extremity kinematic and kinetic asymmetry and upper extremity and bar path kinematics and kinetics.

The most asymmetrical lower extremity joint was the knee in recreational lifters. This might help explain the relatively high injury rates at the knee joint in participants in high intensity training programs. These data might be especially useful for

exercise practitioners who prescribe power cleans as a method of training to recreational individuals. Coaching has shown to be effective at improving power clean performance [4] and these individuals may consider reducing the power clean load until lifting technique has been mastered to improve symmetry between left and right limbs.

REFERENCES

1. Graham, J. (2000). "Power Clean". *Journal of Strength and Conditioning*.
2. Hak, P. (2013). "The nature and prevalence of injury during CrossFit training." *Journal of Strength and Conditioning Research*.
3. Adelsberger, R. (2013). "Experts lift differently: Classification of weight-lifting athletes," *Body Sensor Networks*.
4. Winchester, J. (2005). "Changes In Bar- Path Kinematics And Kinetics After Power-Clean Training." *Journal of Strength and Conditioning Research*.

ACKNOWLEDGEMENTS

The authors would like to acknowledge the contributions of Tayler Snipes and Jenny Magee in the collection and analysis of these data and their efforts in participant recruitment.

Table 1: Left to right differences in peak ground reaction forces and peak joint torques in recreational vs. competitive weightlifters.

Recreational	Peak GRF	Peak Hip Torque	Peak Knee Torque	Peak Ankle Torque
Left	1005.3N \pm 288.0N	193.3 Nm \pm 52.2Nm	95.4 Nm \pm 19.2Nm	123.5 Nm \pm 52.4Nm
Right	1109.1N \pm 531.4N	212.9 Nm \pm 26.5Nm	70.2 Nm \pm 10.2Nm	139.5 Nm \pm 74.1Nm
Competitive				
Left	1175.6N \pm 234.1N	221.7 Nm \pm 48.3Nm	122.6 Nm \pm 15.8Nm	134.4 Nm \pm 23.8Nm
Right	1231.6N \pm 194.7N	212.3 Nm \pm 28.1Nm	113.9 Nm \pm 21.7Nm	145.6 Nm \pm 23.5Nm

THE EFFECTS OF A FOOT STRENGTHENING PROGRAM ON INTRINSIC FOOT MUSCLE SIZE AND STRENGTH – A PILOT STUDY

¹ Sarah Trager Ridge, ² Irene S. Davis, ¹ Tiffany D. deVries, ¹ J. William Myrer, ¹ A. Wayne Johnson

¹ Brigham Young University, Provo, UT, USA

² Harvard Medical School, Boston, MA, USA
email: sarah_ridge@byu.edu

INTRODUCTION

Recent studies have shown that the transition to running in minimalist or partial minimalist shoes can result in greater incidence of injury than running in traditional running shoes[1,2]. Based on those results, it has been suggested that transitioning to minimalist shoes should be preceded by a preparatory strengthening program.

Intrinsic foot muscles help control motion of the foot, support the medial longitudinal arch, and assist with shock absorption. It has been hypothesized that the structure of traditional or supportive shoes results in weakened intrinsic foot muscles, which may be related to the increased injury rate in runners transitioning from traditional to minimalist running shoes.[3] Stronger intrinsic muscles will be able to better support the metatarsals as well as the plantar fascia, thereby reducing the risk of injury to these structures.

Two studies have shown that performing activities in minimalist shoes increases intrinsic foot muscle size, but the studies did not directly measure increases in strength[4,5]. Therefore, the purpose of this study was to determine whether a foot strengthening intervention alters intrinsic muscle size and strength. It was hypothesized that both size and strength of these muscles would be significantly increased following this program.

METHODS

Ten recreational runners (5 male, 5 female; average age 22 ± 2 years, average mileage 15-30 miles/week) with no experience running barefoot or in minimalist shoes have participated in this ongoing study to date. Runners participated in a pre-training testing session, then performed 8 weeks of strength training. This program included a progression of single and double leg calf raises, foot doming, doming and hopping and

toe flexion exercises. Intrinsic muscle size and strength were measured post-training. Pre- and post-training testing included ultrasound assessment of intrinsic foot muscle size, and strength.

Ultrasound images were recorded from the abductor hallucis (ABDH), flexor hallucis brevis (FHB), flexor digitorum brevis (FDB) and quadratus plantae (QP). Images were recorded using a 10 MHz GE LogiqP5 linear probe. For the FHB the probe was aligned with the shaft of the first metatarsal, using the metatarsal head as a consistent bony landmark. The FDB and QP were recorded after finding the navicular tuberosity, then moving the ultrasound probe to the plantar surface of the foot. The probe was oriented transversely across the sole of the foot. The ABDH was recorded with the probe in the same orientation, using the navicular as a reference landmark. Measurements taken from the images included the thickness of the FHB and cross-sectional areas (CSA) of the ABDH, FDB, and QP.

Muscle strength measurements were recorded using a hand-held ergoFet dynamometer, which was secured to a custom built wooden support system (Figure 1). Strength was assessed during doming (arch flexion) and toe flexor activities. During the doming testing, subjects stood with one foot in a Brannock device and the lower leg strapped to a support beam (Figure 1A). The dynamometer was placed on the dorsum of the foot, above the navicular tuberosity (Figure 1B). The subject performed the doming movement using a maximal voluntary isometric contraction for approximately 3 seconds. Toe flexor strength was assessed from the big toes individually (1Toe Flexor), and the 2nd, 3rd, and 4th toes together (234Toe Flexor). The subject's foot was placed on a raised, flat surface with the heel against a support and the toe(s) gripping either an S-beaner or bar and flexed their toes (Figure 1b). The S-beaner or bar was secured to the dynamometer by

an adjustable turn buckle. Trained researchers observed the motions throughout the testing in an effort to ensure subjects were limiting the recruitment of extrinsic muscles. Strength data were monitored and recorded in real-time.



Figure 1. Foot strength testing devices. A. The doming test with dynamometer on the dorsum of the foot. B. Testing of the 2nd, 3rd, and 4th toe flexion test. The S-beaner used for the 1st toe flexion test can be seen at the bottom right of image B.

Runners were given a set of 5-7 exercises to do at least 5 days/week for 8 weeks. The exercises got progressively more difficult through the 8 weeks. Participants were asked to maintain their typical running in their traditional running shoes. Following

the 8 weeks, the same set of tests were performed again.

Pre- and post-training data for each side were compared using paired t-tests ($\alpha=0.05$), with feet separated into dominant and non-dominant sides.

RESULTS AND DISCUSSION

All muscle sizes on both feet increased significantly from pre- to post-training. Doming and 234Toe flexor strength of both feet also increased significantly from pre- to post-training, while 1Toe flexor strength increased significantly on the non-dominant side only.

Based on these data, this intervention appeared to produce the intended result of significantly increasing intrinsic foot muscle strength. These results are promising for runners who want to transition to minimalist footwear. This type of footwear removes cushioning and arch support, placing greater demands on foot and arch musculature. This type of strengthening may also be beneficial to runners who want to move away from motion control shoes or foot orthoses. Stronger intrinsic muscles may reduce the risk of injuries associated with arch flattening such as plantar fasciitis and stress fractures...

REFERENCES

1. Ryan, et al. *Br J Sports Med* **48**, 1257-1262, 2014.
2. Ridge, et al. *Med Sci Sports Exerc* **45**, 1363-1368, 2013.
3. Robbins, et al. *Med Sci Sports Exerc* **19**, 148-156, 1987.
4. Miller, et al. *J Sports Heal Sci*, **3**, 74-85, 2014.
5. Bruggeman, et al. *Proceedings of ISB XXth Congr*, Cleveland, OH, USA, 2005.

Table 1. Pre- and post-training data for muscle size and muscle strength

	Dominant			Non-Dominant		
	Pre	Post	p	Pre	Post	p
Muscle size						
ABDH CSA (cm ²)	1.89 ± .63	2.09 ± .62	.001*	1.91 ± .47	2.17 ± .48	.002*
FDB CSA (cm ²)	1.74 ± .49	1.98 ± .49	.001*	1.79 ± .51	2.01 ± .48	.000*
FHB thickness (cm)	1.25 ± .13	1.44 ± .25	.012*	1.26 ± .18	1.46 ± .19	.000*
QP CSA (cm ²)	1.77 ± .45	1.98 ± .41	.012*	1.67 ± .39	2.01 ± .34	.009*
Strength (kg)						
1ToeFlex	5.37 ± 2.43	6.84 ± 4.32	.109	5.53 ± 2.22	6.95 ± 3.14	.009*
234ToeFlex	5.45 ± 2.97	7.46 ± 4.03	.027*	5.65 ± 2.71	7.05 ± 3.30	.050
Doming	6.19 ± 4.38	11.02 ± 4.59	.007*	7.87 ± 4.15	11.79 ± 6.14	.014*

RE-EXAMINATION OF THE RELATIONSHIP BETWEEN BI-ARTICULAR MUSCLE COACTIVATION AND RUNNING ECONOMY

Barbara J. Schornstein, Kevin D. Dames, and Gary D. Heise

University of Northern Colorado, School of Sport & Exercise Science, Greeley, CO, USA
email: barbara.schornstein@unco.edu, web: <http://www.unco.edu/biomechanics/>

INTRODUCTION

Running economy (RE) is strongly associated with distance running performance, but researchers from various disciplines have had limited success explaining the inter-individual variability in RE [1]. Biomechanists have identified certain kinematic and kinetic descriptors of the running cycle which are related to RE, but the findings between RE and muscle activity are mixed.

EMG analysis offers great potential in addressing this interindividual variability. Research from our lab showed, in two separate samples, that more economical runners coactivated rectus femoris and gastrocnemius during stance for a longer duration when compared to less economical runners [2,3]. We suggested that greater coactivation during stance may increase joint stiffness, which would allow for efficient use of stored elastic energy.

Recently, Moore et al. [4] examined muscle coactivations during stance at multiple running speeds and, in direct contrast to our previous findings, reported positive relationships between energy cost and muscle coactivations. These results further cloud the issue of muscle activity and its relationship to running economy. Methodological differences play a role in explaining why different results have been reported.

It is with these issues in mind that the present study was designed. We re-examined the relationships between running economy and muscle coactivations during stance at multiple speeds. In order to address methodological concerns, we used the same EMG activity threshold identification procedure as Moore et al. [4] and runners ran on a force-measuring treadmill to better identify stance phase.

METHODS

Nineteen healthy, active adults (6 women, 13 men) free from any existing neuromuscular or skeletal injury volunteered for the study (Mean \pm SD: Age = 34 ± 10 yrs.; Body Mass = 67.4 ± 9.1 kg). A performance inclusion criterion was a 5 km time less than 23 min.

After appropriate skin preparation, electrodes were placed over the lateral head of gastrocnemius (LG), rectus femoris (RF), and the long head of biceps femoris (BF). Participants then completed 5-min running trials at 3.3, 3.5, and 3.7 m/s in a randomized order. Expired gasses were collected during the final 1 min of each trial and analyzed using indirect calorimetry (Parvo Medics). Cost of running (C_r) was then calculated by normalizing $\dot{V}O_2$ to running speed and expressed in mL/kg/km. EMG data (2000 Hz, Delsys Trigno) and ground reaction forces (2000 Hz, AMTI) were simultaneously collected. The vertical component of the ground reaction force was used to determine when stance occurred.

EMG data were full-wave rectified and low-pass filtered ($F_c = 15$ Hz). Thresholds for identifying onset/offset times were set at 20% of max for BF, and 7% of max for RF and LG [4]. Coactivation of muscle pairs (RF & LG, BF & LG, and RF & BF) as a percent of stance were calculated using a custom Matlab script. Correlation coefficients were used to relate C_r and EMG measures ($\alpha = .05$).

RESULTS AND DISCUSSION

The ranges of C_r , expressed as a percent of their mean, for all speeds were 33%, 37% and 37% (3.3, 3.5, and 3.7 m/s, respectively). This is slightly higher than previously reported ranges (20-30%)

from the literature [1]. Values for C_r at each speed are shown in Table 1.

Coactivation ratios of each muscle pair at each speed are shown in Table 1. The largest r-value between a coactivation value and C_r with men and women grouped together was -.37 (RFLG), but this did not reach significance. RFLG had a higher coactivation during stance than the other two muscle pairs. The scatterplot of RFLG against C_r for each speed is shown in Figure 1 (linear trend lines are included). Other scatterplots were similar.

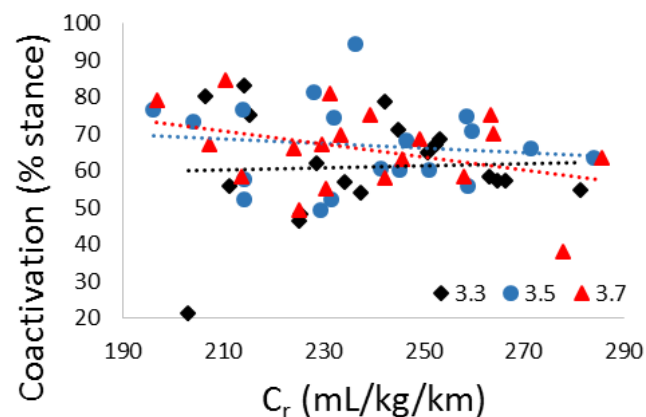


Figure 1. Scatterplot of C_r versus rectus femoris-lateral gastrocnemius coactivation at all speeds.

When men and women are separated (Figure 2), these groups appear to follow trends in opposite directions. However, one male runner exhibited very low coactivation of RFLG, which pulls the trend into the opposite direction of the women. If that participant were removed, the relationship between C_r and RFLG coactivation for men is greatly reduced. These different trends appear across all speeds and muscle pairs in varying strengths. With only six women, we can only call this a trend. It agrees with previous research by Heise, et al. [3], who showed that more economical

women demonstrate a higher coactivation of bi-articular muscles during stance.

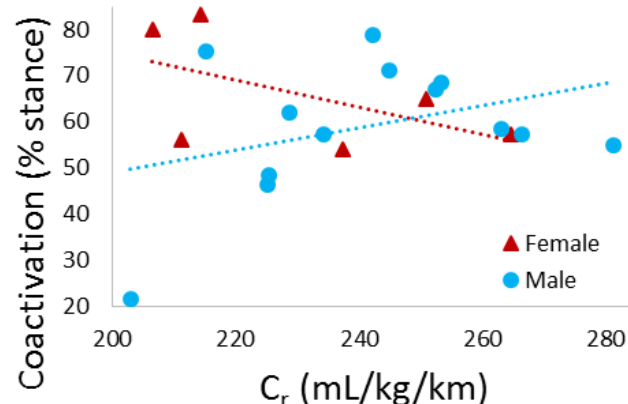


Figure 2. Scatterplot of C_r versus rectus femoris-lateral gastrocnemius coactivation. Data points and linear trend lines are shown for men and women.

CONCLUSIONS

While a strong correlation between C_r and coactivation of bi-articular muscles was not shown in the current study for all participants, several interesting trends emerged suggesting that men and women coactivate lower extremity muscles differently. A trend for women was shown, while not strong enough for significance, that more economical women have higher coactivation ratios across all speeds and muscles tested. Further investigation into the differences of men and women is needed in the area of coactivation of bi-articular muscles and C_r .

REFERENCES

1. Saunders PU et al. *Sports Med* **34**, 466-485, 2004.
2. Heise GD et al. *Int J Sport Med* **17**, 128-133, 1996.
3. Heise GD et al. *Int J Sport Med* **29**, 688-691, 2008.
4. Moore IS et al. *J Sci Med Sport* **17**, 671-676, 2014.

Table 1. Cost of running (C_r) and coactivation ratios for all speeds and muscle pairs (Mean \pm SD).

	3.3 m/s	3.5 m/s	3.7 m/s
C_r (mL/kg/km)	237.9 \pm 22.5	237.7 \pm 23.3	238.9 \pm 23.9
Muscle Pairs	COA ¹ at 3.3 m/s	COA ¹ at 3.5 m/s	COA ¹ at 3.7 m/s
RF-LG ² (% stance)	61.2 \pm 14.3	66.8 \pm 11.6	65.7 \pm 11.3
RF-BF ³ (% stance)	36.3 \pm 22.7	37.2 \pm 20.9	34.7 \pm 23.3
BF-LG ⁴ (% stance)	41.0 \pm 24.2	38.7 \pm 21.1	37.7 \pm 25.8

¹Coactivation of muscle pair as a percent of stance, ² Rectus femoris and lateral gastrocnemius, ³ Rectus femoris and biceps femoris, ⁴Biceps femoris and lateral gastrocnemius

RELATIONSHIP BETWEEN LANDING, TAKING-OFF KINEMATIC VARIABLES AND MAXIMUM RUNNING VELOCITY PERFORMANCE

¹ Zhanxin Sha, Kimitake Sato, Brad DeWesee, Michael H. Stone and ² Bing Yu

¹ The East Tennessee State University, Johnson City, TN, USA

² The University of North Carolina at Chapel Hill, Chapel Hill, NC, USA

Email: shazhanxin@gmail.com

INTRODUCTION

Pursuing faster sprint velocity is one of most interesting topics, but it is also a great challenge for athletes, coaches, and researchers. Previous studies [1, 2, and 3] indicated that fast sprinters showed rapid leg retraction during the terminal swing phase; closer landing distance, greater landing angle, shorter contact distance, greater taking off angle during foot contact phase. However, how these landing and taking off kinematic variables related to maximum running velocity is still not clear at present. Therefore, the purpose of the current cross sectional study was to determine the relationship of those landing and taking-off kinematic variables with maximum running velocity performance.

METHODS

Twelve male (mass: 75.28 ± 6.39 kg, height: 1.79 ± 0.04 m, age: 19 to 21 years old) NCAA Division I sprinters participated in the study.

Two sprints from standing position were performed by each participant. Electronic timing gate system (Brower system, UT, US) were placed at 10 m intervals from the start line for 60 m. The Maximum 10 m interval running velocity (V_{60}) were used for further analysis.

Kinematic data (between 50 m and 57 m) were collected using Vicon Nexus system (Vicon, UK) with six cameras at a sampling rate of 240 frames/s. Reflective markers were placed based on Vicon Full Plug-in-gait marker set. An analyzable trial was a trial in which all kinematics data for two running step were recorded successfully by the system.

Phase of landing, and taking-off kinematic variables determination were according to [4, 5, and 6].

Touch down distance (TD_D), touch down angle (TD_A), contact distance (Con_D), take-off distance (Off_D), take-off angle (Off_A), leg retraction acceleration (Re_A), maximum center of mass velocity (V_{max}), minimum center of mass velocity (V_{min}), and velocity loss during the foot contact phase (V_{loss}) were used for further analysis.

Pearson correlation were used to test relationship of kinematic variables between two steps, no statistical significance was found between them indicating that both limbs were not asymmetrical. Thus, average values of kinematics variables from two steps were used to further analysis. Correlation of kinematics and sprint variables, were performed using Pearson Correlation Coefficient test (SPSS 21). Statistical significance was set at $p \leq 0.05$.

RESULTS AND DISCUSSION

Descriptive statistics were shown in table 1. Correlation of landing and taking-off kinematic variables with maximum running velocity performance were listed in the table 2. Only a few landing and taking-off kinematic variables were correlated with each other. Except center of mass velocity (V_{max} and V_{min}) and leg retraction prior to the foot contact with ground (Re_A), none of the kinematic variables showed correlation with maximum running velocity performance.

Results of the current study consistent with previous studies [1, 2, 3, 7] that horizontal center of mass velocity (V_{max} and V_{min}) highly correlated with maximum running velocity; Moreover, It also supported that landing kinematic variables is

function of the foot speed relative to the ground at landing and the distance between the foot and the CoM (TD_D and TD_A; TD_A and Con_D; Re_A and Off_A). However, among those kinematic variables only Re_A correlated with V_{\max} and maximum running velocity performance. Therefore, those landing and taking-off kinematic variables may not impact maximum running velocity performance as most people believed, however, the current study recruited homogenous group of sprinters, further study need to recruit heterogamous group sprinters to confirm the results from the current study.

REFERENCES

1. Hunter, J. P., et al. *J Appl Biomech* **21**, 31-43. 2005.
2. Mann, R.V., & Herman, J. *J Appl Biomech* **1**, 151-162, 1985.
3. Putnam, C. A., & Kozey, J.W. *Biomechanics of Sports*. CRC Press, Inc., 1-34, 1989.
4. Cicacci, S., et al. *Gait & Posture* **31**, 209-212, 2010.
5. Cunha, L., et al. *Proceedings of ISBS'02*, Caceres, Spain, 2002.
6. Yu, B., et al. *J Biomech* **41**, 3121-3126, 2008.
7. Sha, Z. X., et al. *Proceedings of WCB'14*, Boston, MA, USA, 2014.

Table 1: Descriptive statistics.

Kinematic Variables	Mean	SD
TD_D (m)	0.23	0.06
TD_A (deg)	77.59	2.85
Con_D (m)	0.79	0.15
Off_D (m)	0.55	0.11
Off_A (deg)	62.44	1.89
Re_A (m/s²)	-98.01	20.25
V_{max} (m/s)	9.57	0.46
V_{min} (m/s)	8.97	0.47
V_{loss} (m/s)	0.60	0.16
V₆₀ (m/s)	9.33	0.43

Table 2: Correlation between landing, taking-off kinematic variables and maximum velocity performance.

Kinematic Variables	TD_D	TD_A	Con_D	Off_D	Off_A	Re_A	V_{max}	V_{min}	V_{loss}	V₆₀
TD_D	1									
TD_A	-.989**	1								
Con_D	0.555	-.582*	1							
Off_D	0.222	-0.259	.930**	1						
Off_A	-0.413	0.461	-.725**	-.691*	1					
Re_A	-0.499	0.544	-0.409	-0.31	.655*	1				
V_{max}	0.088	-0.124	0.197	0.218	0.011	-0.567	1			
V_{min}	-0.111	0.085	-0.09	-0.035	0.229	-0.412	.943**	1		
V_{loss}	.590*	-.622*	.851**	.748**	-.653*	-0.445	0.137	-0.199	1	-
V₆₀	0.196	-0.204	0.088	0.055	0.033	-.637*	.946**	.910**	0.079	1
** Correlation is significant at the 0.01 level (2-tailed).										
* Correlation is significant at the 0.05 level (2-tailed).										

EFFECTS OF WEARING TOE CAGE ON KNEE BIOMECHANICS DURING STATIONARY CYCLING

Guangping Shen, Hunter J. Bennett, Songning Zhang

Biomechanics/Sports Medicine Lab, The University of Tennessee, Knoxville, TN, USA
email: gshen1@vols.utk.edu, web: web.utk.edu/~sals/resources/biomechanics_laboratory.html

INTRODUCTION

Studies have shown that the internal knee abduction moment (KAM) in walking is closely associated with the development of medial knee osteoarthritis (OA) [1]. Many non-surgical recommendations for the management of knee OA have been proposed to slow down the progression of the disease. Cycling is frequently prescribed by health professionals to improve physical fitness, muscle strength, and function in rehabilitation programs. During the cycling workout, cyclists are putting most of body weight on the saddle, which allows weight-bearing joints such as knees and hips to experience relatively lower compressive force than in walking and jogging [2].

In cycling, a toe cage is used to stabilize the foot on the pedal to keep the foot in a parallel orientation, while a pedal without toe cage provide a self-selected and float foot alignment. However, it was suggested allowing some freedom of movement between foot and pedal is beneficial to the knee injury prevention during cycling. Furthermore, two patterns of the knee frontal plane movements were observed during cycling where some people tended to cycle with knee adduction while others cycled with knee abduction [3]. It is currently unknown whether wearing toe cages during cycling would adversely affect knee frontal plane biomechanics. Therefore, the purpose of this pilot study was to investigate effects of two foot alignment methods, with and without toe-cage, on knee biomechanics during stationary cycling.

METHODS

Four healthy male subjects (age: 27.3 ± 3.6 years, mass: 77.9 ± 10.2 kg, height: 1.8 ± 0.1 m) were included in this study. Participants did not have any history of major lower extremity injury and surgery. A nine-camera motion analysis system (240 Hz, Vicon Motion Analysis Inc., UK) was used to

obtain the three dimensional (3D) kinematics during the test. Reflective anatomical and tracking markers were placed on both sides of feet, ankles, legs, knees, thighs, and hips during testing.

A Monark cycle ergometer (828E, Monark, Sweden) equipped with a weighted brake system was used in the study. A customized instrumented bike pedal was used on the left side of the cycling ergometer, which records three dimensional pedal reaction forces (PRF). The assembly contained two 3D force sensors (Type 9027C, Kistler, Switzerland) coupled with two industrial charge amplifiers (Type 5073A, Kistler, Switzerland).

The saddle height on the cycle ergometer was adjusted so that the angle of the knee joint was about 30° when the crank was at the bottom dead center. The horizontal saddle position was adjusted so that the knee was in line with the pedal spindle when the crank was in the forward horizontal position. The position of the handlebars was set so that the angle between the subject's trunk and thigh was 90° when the crank is in the forward horizontal position. The participants pedaled in six cycling conditions: pedaling at 80 rpm with workloads of 0.5 kg (40 Watts), 1.0 kg (78 Watts), and 1.5 kg (117 Watts) without (an unrestricted foot position on the pedal) and with toe cage (a restricted foot position). Participants performed a 2-minute cycling in each condition, where five consecutive pedaling cycles were recorded at last 30 seconds. A 2-minute rest was provided between the conditions.

All data were processed and analyzed using Visual3D (5.0, C-Motion, Inc.). Hip joint centers were determined using the CODA pelvis (determined by ASIS and PSIS), where each anatomical marker was corrected for the diameter of the markers and its base. Both kinematic and PRF data were filtered using a low-pass 4th order Butterworth filter with zero lag at a cutoff frequency of 6 Hz. The joint moments were

computed as internal moments. The pedal cycle of a trial is defined from the top dead center (0°) to the following top dead center (360°). Due to the small sample size of this pilot study, paired t-tests were used to examine the effects of the toe cage and workloads on knee biomechanics (SPSS 22.0, SPSS Inc., Chicago, IL) with an alpha level set at 0.05 a priori.

RESULTS AND DISCUSSION

The PRF, foot angle, knee range of motion (ROM) and peak knee moment are provided in Table 1. There were no significant differences in any variables with or without toe cages when cycling at the same workloads ($p>0.05$). In fact, toe cages did not alter the foot alignment on the pedal for the subjects from their self-selected foot alignment position. The peak vertical PRF was significantly greater in the conditions with larger workload when subjects were wearing the toe cage ($p<0.05$). In addition, the peak knee extension moment was significantly greater in workload of 1.5 kg compared to workloads of 0.5 kg and 1.0 kg ($p<0.05$).

Overall, our results showed wearing toe cage during cycling did not affect either knee kinematics or kinetics. This results are similar to the study by Gardner et al. (2015), where 5° and 10° of toe-in angles were applied to the healthy subjects and patients with knee OA during stationary cycling [3]. They showed that increased toe-in angles did not affect the KAM, although it did have influences on

knee flexion and adduction angles. Workloads mainly affected the knee extension moment. However, increased workload did not affect peak knee abduction moment. The lack of differences may be related to the small sample size and a relatively large variability with one subject. As for the knee kinematics, they are barely affected by the workloads (Table 1).

A larger sample size is needed to strengthen the results. Further research is warranted to determine effects of foot fixation on other joints such as ankle and hip during stationary cycling.

CONCLUSIONS

Wearing toe cages during stationary cycling did not affect the knee biomechanics. Therefore, toe cages may or may not be used when cycling is prescribed as a rehabilitation program for patients with knee OA or other knee condition such as total knee replacement.

REFERENCES

1. Mundermann, A., et al. *Arthritis Rheum*, **50**(4), 1172-1178, 2004.
2. Kutzner, I., et al. *J Orthop Sports Phys Ther*, **42**(12), 1032-1038, 2012.
3. Gardner, J., et al. *Clinical Biomechanics*, **30**(3), 276-282, 2015.

Table 1. Mean peak PRF (N), knee ROM (°) and peak knee moment (Nm): Mean±SD.

	Without toe cage			With toe cage		
	0.5 kg	1.0 kg	1.5 kg	0.5 kg	1.0 kg	1.5 kg
Peak Vertical PRF	158.1±50.5 ^B	181.2±73.1	253.9±88.8	161.9±60.8 ^{A B}	204.5±81.5 ^B	254.5±79.7
Peak Medial PRF	44.1±36.9	62.8±52.8	48.0±18.3	36.5±18.0	34.7±17.6 ^B	48.2±16.1
Peak Foot Ext. Rotation Angle	-13.7±3.9	-15.0±4.7	-14.3±5.1	-14.3±4.9	-13.9±4.5	-15.0±4.0
Knee Extension ROM	74.2±6.1	74.3±7.5	74.7±6.2	74.0±6.6	75.1±5.6	75.2±5.8
Knee Abduction ROM	-10.1±4.0	-9.6±3.7 ^B	-10.8±4.0	-10.6±4.5 ^B	-9.8±3.9	-9.6±4.6
Knee Ext. Rotation ROM	-32.1±4.0	-31.8±3.9	-30.7±2.8	-31.9±4.7	-31.8±3.4	-31.4±3.0
Peak Knee Extension Moment	22.9±8.4 ^B	31.6±13.5 ^B	40.5±14.4	25.1±8.3 ^B	31.4±15.3 ^B	41.1±15.3
Peak Knee Abduction Moment	-12.6±11.1	-19.2±17.2	-12.8±5.2	-10.6±4.8	-8.8±5.1	-12.6±6.1
Peak Knee Ext. Rotation Moment	11.4±13.4	16.0±19.8	7.9±1.8	8.6±8.7	5.5±1.0 ^B	8.6±1.9

Note: All differences are significant ($p<0.05$), ^A: different from 1.0 kg of the same foot alignment, ^B: different from 1.5 kg of the same foot alignment, [#]: different from the self-selected foot alignment of the same workload.

PREDICTORS OF LOADING RATE IN HEEL-STRIKE RUNNERS

Yo Shih, Hsiang-Ling Teng, Christopher M Powers

University of Southern California, Los Angeles, CA, USA

email: powers@usc.edu, web: <http://pt.usc.edu/labs/mbrl/>

INTRODUCTION

High loading rates are thought to contribute to lower extremity injuries in runners.^{1,2} It has been reported that loading rates are higher in heel strikers than forefoot strikers during running.³ However, not all heel strikers exhibit high loading rates.⁴ To date, it is not known what kinematic or kinetic factors are predictive of high loading rates in heel strike runners.

METHODS

Twenty male (age, 27.1 ± 7.0 yr) and 20 female heel-strike runners (age, 26.2 ± 5.8 yr) were recruited for this study. Kinematic and kinetic data were collected while participants ran at a controlled speed of 3.4 m/s along a 14 meter runway with a force plate mounted flush to the floor. Average loading rate was quantified as the slope of vertical ground reaction force (GRF) curve from initial contact (IC) to the 1st peak of the GRF (20-80% time frame). Kinematic and kinetic variables of interest included lower extremity joint angles at initial contact, joint angle excursions from IC to 1st peak of the GRF (1PK), joint angle excursions from IC to peak angle, maximum joint moments, joint power from IC to the 1PK and to maximal GRF, leg stiffness and joint angular stiffness from IC to 1PK, maximal GRF and peak sagittal plane joint moments (ankle, knee, and hip). Pearson correlations were used to evaluate the relationships among the average loading rate and all kinematic and kinematic variables of interest. Step-wise multiple linear regression was performed to determine the best predictor(s) of loading rate. Only those variables that were significantly correlated with the loading rate were input to the regression model.

RESULTS and DISCUSSION

Five variables were significantly correlated with the average loading rate (Table 1), however, only 2 entered into the regression equation. Leg stiffness from IC to 1PK was the first variable that entered the stepwise regression model of loading rate (Fig 1, $R^2=0.728$). The second variable that entered was the knee angle excursion from IC to 1PK (Fig 2, $R^2=0.04$) (Table 2). No other variables entered into the final model.

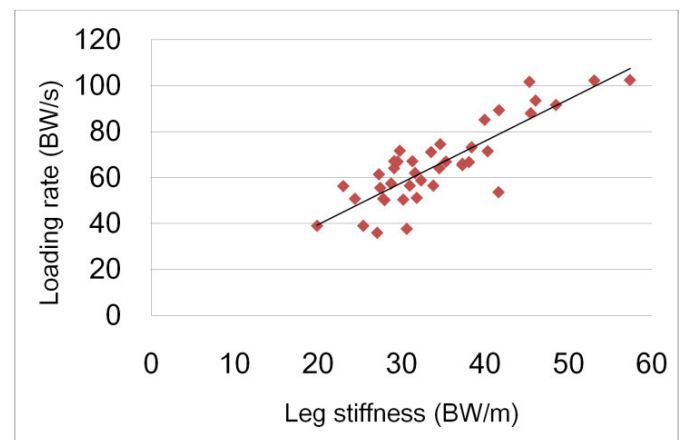


Figure 1: Correlation between loading rate and leg stiffness from IC to 1PK

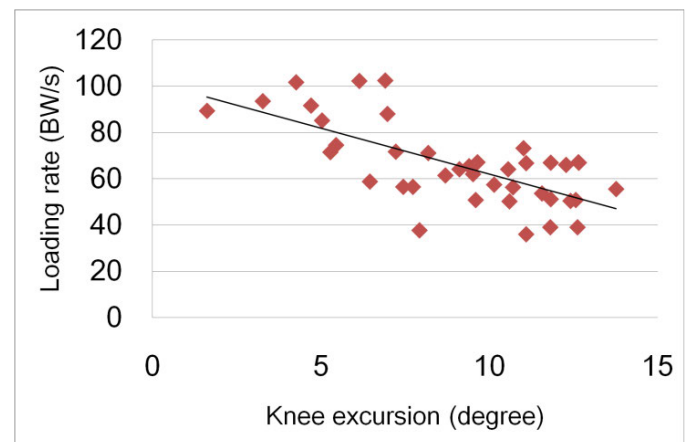


Figure 2: Correlation between loading rate and knee excursion from IC to 1PK

CONCLUSIONS

Our findings suggest that increased lower extremity compliance immediately following initial contact may protect against high loading rates in heel strike runners. Further study is needed to test the feasibility of manipulating leg stiffness and knee excursion immediate following initial contact to minimize loading rates.

REFERENCE

1. Zadpoor AA, Nikooyan AA. (2011). Clin Biomech. 2011 26(1):23-8.
2. Pohl MB, Hamill J, Davis IS.(2009). Clin J Sport Med. 19(5):372-6.
3. Lieberman DE, Venkadesan M, Werbel WA, Daoud AI, D'Andrea S, Davis IS, Mang'eni RO, Pitsiladis Y.(2010). Nature. 28;463(7280):531-5.
4. Milner CE, Ferber R, Pollard CD, Hamill J, Davis IS.(2006). Med Sci Sports Exerc. 38(2):323-8.

Table 1: Variables significantly correlated with average loading rate.

Variable	<i>r</i>	<i>p</i>
Knee angle at IC	0.488	0.001
Knee excursion IC to 1PK	-0.682	<0.001
Hip excursion IC to max flexion	-0.316	0.047
Leg stiffness IC to 1PK	0.854	<0.001
Knee stiffness IC to max moment	0.415	0.008

Table 2: Result of step-wise multiple linear regression to predict loading rate.

Variable	R	R ²	Adjusted R ²	Change in R ²	p
Leg stiffness IC to 1PK	0.854	0.728	0.721	-	<0.001
Leg stiffness IC to 1PK + Knee excursion IC to 1PK	0.877	0.769	0.756	0.040	<0.001

KNEE JOINT LOADS AND SURROUNDING MUSCLE FORCES OF SELECTED KNEE UNFRIENDLY MOVEMENT ELEMENTS IN 42-FORM TAI JI

¹Chen Wen, ²Jeffrey A. Reinbolt, ¹Songning Zhang

¹Biomechanics/Sport Medicine Lab, The University of Tennessee, Knoxville, TN, USA

²Department of Mechanical, Aerospace, and Biomedical Engineering, The University of Tennessee, Knoxville, TN, USA

INTRODUCTION

Tai Ji, as a mind-body therapy, is a traditional Chinese martial art that includes natural postures as well as gentle and smooth movements [1]. The American College of Rheumatology recommended Tai Ji as one of the non-pharmacologic treatments for knee osteoarthritis (OA) [2], but it remains unclear if all Tai Ji movements would be suitable and beneficial for knee OA patients.

Tai Ji movements often require bending the knee to a squatting position, which may place high loads on the knee joint. In addition, repetitions of some Tai Ji deep knee flexion movements (e.g., twisting and single-leg stance) may further increase loading to harmful levels at the knee. A previous study showed a greater knee flexion range of motion (ROM) in Tai Ji gait caused a higher knee extension (rectus femoris) muscle activity compared to normal speed walking [3].

Musculoskeletal modeling and simulation provides an efficient way to estimate joint loading and corresponding muscle forces during a movement. However, no study has utilized musculoskeletal simulations to investigate knee joint loading in Tai Ji movements. Therefore, the purpose of this study was to investigate the knee joint loading of selected unfriendly Tai Ji movement elements performed in high-pose position compared to slow walking.

METHODS

A male subject (23 yrs, 1.78 m, 73.3 kg) with two months of Tai Ji experience participated in this study. He performed three trials of level walking at 0.8 m/s and each of four identified knee unfriendly Tai Ji movement elements: lunge, pushdown and kick performed in high-pose position ($35 \pm 5^\circ$) and pseudo-step[4].

Three dimensional (3D) kinematic data were collected using a nine-camera infrared motion capture system (120 Hz, Vicon Motion Analysis, Inc., Oxford, UK). Anatomical and tracking reflective markers were placed bilaterally on the trunk, pelvis, thighs, shanks and feet. Three force platforms (1200Hz, Advanced Mechanical Technology, Inc., USA) were used to collect ground reaction forces (GRF) with the 3D kinematic data simultaneously using Vicon Nexus software. Maximum knee flexion angle was monitored using an electrogoniometer (Biometrics Inc., Newport, UK) placed on the lateral side of the right knee joint. Visual 3D (C-Motion Inc., USA) was used to compute 3D kinematics and kinetics. Kinematic and GRF data were smoothed at cutoff frequencies of 4 and 50 Hz, respectively, using a fourth-order zero-lag Butterworth low-pass filter. All joint moments were computed as internal moments.

The processed individual trials of each movement condition were exported to OpenSim (version 3.2, SimTK, Stanford, CA, USA) to perform musculoskeletal simulations. A generic 12-segment, 19-degree of freedom, and 92 muscle-actuated OpenSim musculoskeletal model (Gait 2392 Model), originally developed by Delp, et al. [5], was scaled to the height and weight of the subject to generate subject-specific models. Muscle forces were estimated using static optimization minimizing the sum of squared muscle activations. Knee joint reaction forces (JRF) were computed using the joint reaction analysis tool with the muscle forces from static optimization as inputs. The compressive force was the vertical component of the JRF along the long axis of the tibia and the anterior-posterior shear component of the JRF was orthogonal to the axial component.

RESULTS AND DISCUSSION

Lunge, pushdown and kick demonstrated similar peak knee compressive JRF compared to slow

walking. Pseudo-step showed higher compressive JRF than other Tai Ji movement elements. In addition, Tai Ji movement elements showed greater peak knee anterior shear JRF than slow walking. Pushdown showed the greatest peak anterior shear JRF among the Tai Ji movement elements. The peak muscle forces of vastus medialis, vastus lateralis and vastus intermedius, and sum of knee extensor forces were greater for Tai Ji movement elements compared to slow walking. Kick showed the smallest peak muscle forces of vastus medialis, vastus lateralis and vastus intermedius, and sum of knee extensor forces compared with other Tai Ji movement elements. Tai Ji movement elements showed smaller peak sum of knee flexor forces than slow walking. Peak knee extension moments were higher in lunge, pushdown and pseudo-step than slow walking.

Our results are supported by the previous study of Tai Chi gait [3] which demonstrated rectus femoris had a significant higher activity level than semitendinosus. Xu et al. [6] also reported higher rectus femoris muscle activity level than semitendinosus in Brush Knees and Twist Steps, popular Tai Ji movements which include lunges. Our results showed that the anterior shear JRF is relatively high in lunge, pushdown and pseudo-step as knee extensions are more heavily involved in maintaining flexed knee postures.

CONCLUSION

The high-pose lunge, pushdown and kick Tai Ji movement elements demonstrated similar knee compressive JRF as slow walking. Thus, these movements may be suitable for Tai Ji participants with knee OA and other knee pathological conditions to practice. However, high shear loading was found in all of the Tai Ji movement elements and there is cause for serious concerns. Future investigations are necessary to find ways of reducing the shear JRF during Tai Ji and other knee OA treatments.

REFERENCES

1. Zhang, S. (2013). *J Sport Health Sci*, **2**, 158-159.
2. Hochberg, M.C., et al. (2012). *Arthritis Care Res*, **64**, 465-474
3. Wu, G., et al. (2004). *J Electromyogr Kinesiol*, **14**, 343-354
4. Wen, C., (2014), Master's Thesis, University of Tennessee
5. Delp, S.L. (1990), *IEEE Trans Biomed*, **37**, 757-767.
6. Xu, D., et al. (2003). *Int J Sports Med*, **11**, 129-144

Table 1. Peak knee muscle forces (N), peak JRF (N) and knee extension moment (Nm/kg) of the selected Tai Ji movement elements and slow walking: Mean \pm SD.

Variable		Lunge	Pushdown	Kick	Pseudo-step	Slow Walking
Knee extensor muscles	Rectus Femoris	748.1 \pm 112.9	865.2 \pm 90.0	998.0 \pm 96.0	1211.2 \pm 34.1	907.6 \pm 81.7
	Vastus Medialis	454.9 \pm 133.7	552.9 \pm 108.9	241.0 \pm 57.6	376.6 \pm 22.5	101.5 \pm 32.0
	Vastus Intermedius	526.5 \pm 157.7	648.1 \pm 126.9	279.9 \pm 66.8	438.5 \pm 25.2	118.0 \pm 36.8
	Vastus Lateralis	963.9 \pm 278.1	1191.1 \pm 215.2	528.4 \pm 121.7	815.9 \pm 44.9	213.7 \pm 73.0
	Sum	2233.6 \pm 517.9	2928.1 \pm 330.9	1910.4 \pm 145.7	2563.1 \pm 153.0	915.8 \pm 92.7
Knee flexor muscle	Sum	608.1 \pm 34.6	134.6 \pm 126.0	417.6 \pm 22.7	305.2 \pm 135.5	1132.0 \pm 41.4
Peak Anterior Shear JRF		1927.7 \pm 619.5	2281.5 \pm 86.9	1368.1 \pm 221.1	2101.3 \pm 59.7	643.9 \pm 24.2
Peak Compressive JRF		-2369.2 \pm 386.7	-2541.0 \pm 43.7	-2495.5 \pm 103.5	-2905.9 \pm 58.3	-2640.8 \pm 139.7
Peak knee extension moment		1.04 \pm 0.21	1.01 \pm 0.28	0.48 \pm 0.41	1.46 \pm 0.26	0.38 \pm 0.19

WHOLE BODY MECHANICS DURING JAPANESE ELITE AND NON-ELITE MALE WRESTLERS DURING A TACKLE

¹ Daichi Yamashita, ¹ Hiroshi Arakawa, ² Takahiro Wada, ³ Kenichi Yumoto, ⁴ Kotaro Fujiyama, ⁵ Tomoyuki Nagami and ⁶ Seshito Shimizu

¹ Japan Institute of Sports Sciences, Kita-ku, Tokyo, Japan

² Kokushikan University, Tama, Tokyo, Japan

³ Nippon Sports Science University, Yokohama, Kanagawa, Japan

⁴ Japan Sport Council, Tama, Tokyo, Japan

⁵ Waseda University, Tokorozawa, Saitama, Japan

⁶ Japan Wrestling Federation, Shibuya-ku, Tokyo, Japan

email: daichi.yamashita@jpnnsport.go.jp

INTRODUCTION

Wrestling is a man-to-man combat sport and it is described as an intermittent physical event to score points and falls. A technical-tactical analysis of profiles of freestyle wrestling indicated that leg attacks were the most used techniques of winners in international competitions [1]. Besides the importance of tackling to win the competitions, not much is still known about the mechanics of a tackle. The purpose of this experiment is to investigate the biomechanics of the tackling maneuvers of several elite and non-elite wrestlers.

METHODS

Twenty Japanese male wrestlers belonging to the light weight category (former 55-, 60-, or 66-kg) performed double leg tackles to a defender for at least 4 trials each. Eleven participants were elite level including 3 medalists of the 2012 London Olympic Games and nine were collegiate level. A defender was acted by an experienced wrestler throughout this experiment. At first, an attacker and a defender made contact in the hand fighting position while slightly touching each other's shoulders. Before tackling, the height of the defender's markers (shoulders and great trochanters) were monitored and adjusted to a predetermined height. Then, the attacker tackled the defender in the same way as a competition. For each wrestler, the trial with the highest subjective score was selected for detailed analysis.

Three-dimensional coordinates of the anatomical landmarks were acquired using a 3D optical motion capture system with 20 cameras (200 Hz; Vicon, Oxford, UK). Forty-six reflective markers were placed on each subject's body. The whole body centre of mass (COM) position was calculated as the weighted sum of the 14-segment model. The ground reaction force (GRF) at the trailing limb was recorded (1000Hz; Kistler, Winterthur, Switzerland). All GRF data were normalized by body weight. The start of the tackle and the contact were determined from the COM velocity data. COM and GRF data were rotated in order to align it with the local coordinate system using a rotation matrix. Axis alignment was determined using the COM trajectory because it in the horizontal plane during tackle was almost linear. Comparison between groups was performed using the unpaired t-test.

RESULTS AND DISCUSSION

Vertical displacement of the COM was lesser for elite wrestlers than for non-elite wrestlers ($p = 0.025$, 0.18 ± 0.07 m vs 0.25 ± 0.06 m in elite and non-elite, respectively) (see Fig.1). Peak forward velocity of the COM tended to be slower for elite wrestlers than for non-elite wrestlers ($p = 0.086$, 2.27 ± 0.18 m/s vs 2.43 ± 0.17 m/s, respectively). Duration of tackle was shorter for elite wrestlers than for non-elite wrestlers ($p = 0.0499$, 401 ± 60 ms vs 458 ± 61 ms, respectively).

Peak forward GRF did not differ significantly between groups ($p = 0.186$, 1.00 ± 0.17 N/N vs 0.89 ± 0.19 N/N, respectively). However, time-to-peak forward GRF was faster for elite wrestlers than for non-elite wrestlers ($p = 0.026$, 243 ± 60 ms vs 322 ± 87 ms, respectively).

During a tackle, it seems important that an attacker move quickly and provided high momentum to a defender to score a takedown. However, Peak forward velocity of the COM for elite wrestlers tended to be slow than for non-elite wrestlers. They tackled quickly with a smaller downward movement. Therefore, it is suggested that to move forward quickly is effective for a successful tackle and to score points.

Further study is needed to focus on the interpersonal tackling mechanics because of the intragroup variability of the COM (see in Fig.1).

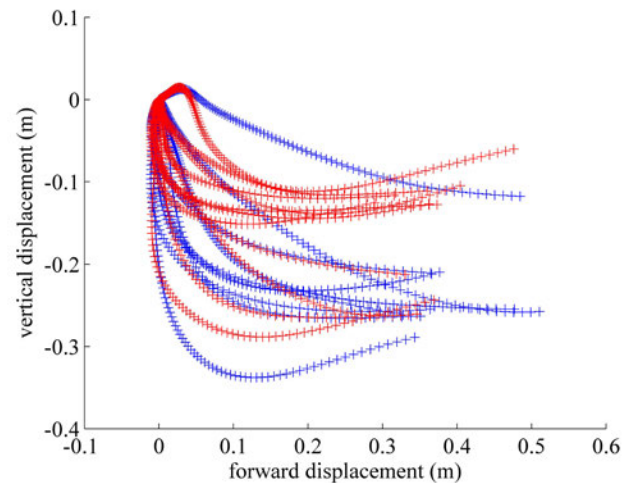


Figure 1: COM trajectory from the beginning of the tackle to the contact. Red and blue colors represent each trial of elite and non-elite level wrestlers, respectively.

REFERENCES

- [1] Tunnemann H, *Int J Wrestling Sci*, **3**, 94-104

Thromboelastographic Clot Parameters of Autologous Blood Products

Sasan Ghassab¹, MAE, MS, Jennifer Dulin², DVM, MS, DACVS, and Alicia L. Bertone², DVM, PhD, DACVS, DACVSMR

¹Department of Mechanical and Aerospace Engineering, The Ohio State University, Columbus, OH

² The Ohio State University, Columbus, OH, USA
email: bertone.1@osu.edu

INTRODUCTION

Tissue repair in musculoskeletal injuries is often slow, incomplete, and refractory to conventional therapies.^{1,2} Regenerative therapies aimed at delivering growth factors, bioactive molecules, and accelerating healing locally has been a recent focus of scientific evaluation^{3,4} The purpose of our study was to compare the clot strength and efficiency of platelet- rich plasma (PRP) and concentrated platelet-poor plasma (cPPP) to citrated whole blood when activated by autologous thrombin, bovine thrombin or calcium chloride (CaCl₂). Our study assessed the dynamic mechanical properties of fibrin and platelet bonding for surgery or injection when clot holding is desired.

METHODS

Six healthy horses were used as blood donors. PRP and cPPP were prepared by commercial devices and tested against autologous whole blood. Autologous blood, PRP and cPPP were activated by each of 3 clotting agents (autologous thrombin, bovine thrombin and CaCl₂) and compared for clotting parameters using a thromboelastograph. Clotting tests were performed to establish normality of test subjects. Platelet counts of whole blood and PRP were measured.

RESULTS AND DISCUSSION

Whole blood, PRP, and cPPP clotted with all agents. Among blood products, PRP

demonstrated the greatest clot strength and quickest clot rate; cPPP had the weakest clot strength, slowest clot rate, and longest clot initiation time. Among clotting agents, bovine thrombin had the shortest clot initiation time, quickest clot rate and tied CaCl₂ for greatest clot strength; CaCl₂ had the longest clot initiation time and time to reach maximum clot strength; autologous thrombin had the lowest clot strength.

CONCLUSION

When combined with either bovine thrombin (rapid clot) or CaCl₂ (slow clot), PRP provided the top combination for clinical use. Autologous thrombin was suboptimal, but would be an autologous alternative to commercial fibrin for clinical application. As prepared here, cPPP had inefficient clotting, but may be sufficient for plasma spray indications.

REFERENCES

1. Sophia Fox AJ, Bedi A, Rodeo SA: The Basic Science of Articular Cartilage: Structure, Composition, and Function. Sports Health 2009;1(6):461-468
2. Textor JA, Tablin F: Intra-Articular Use of a Platelet-Rich Product in Normal Horses: Clinical Signs and Cytologic Responses. Vet Surg 2013;42(5):499-510
3. Kakudo N, Minakata T, Mitsui T, et al: Proliferation-Promoting Effect of Platelet-Rich Plasma on Human Adipose-Derived Stem Cells and Human Dermal Fibroblasts. Plast Reconstr Surg 2008;122(5):1352-1360
4. Smith RG, Glassmann CJ, Campbell MS: Platelet-Rich Plasma: Properties and Clinical Applications. Lancaster, PA, Journal of Lancaster General Hospital (www.jlgh.org), 2007;2(2):73-78

WALKING-MEDIATED UPREGULATION OF FOLLISTATIN-LIKE 3 EXPRESSION IS INSUFFICIENT TO INCREASE MUSCLE CONTRACTILE FORCE

¹ Alisa D. Blazek, Eric Beck, Jackie Li, Kevin E. McElhanon, Timothy E. Hewett, Sudha Agarwal, and Noah L. Weisleder

¹ The Ohio State University, Columbus, OH, USA
email: blazek.16@buckeyemail.osu.edu

INTRODUCTION

Molecular mechanisms coordinating muscle and bone strength and growth following exercise (EX) remain undefined. We have identified a TGF- β family protein, follistatin-like 3 (FSTL3), which is upregulated in mouse and human skeletal muscle, bone and serum in response to low intensity walking EX. We have previously determined by mineral apposition rate analysis of *Fstl3*^{-/-} mouse bone that FSTL3 is required for EX-driven bone formation [1]. FSTL3 is known to bind and inhibit myostatin [2]; thus, this study was to determine if FSTL3 increases muscle hypertrophy and force generation through this mechanism to collectively regulate musculoskeletal function.

METHODS

C57/Bl6 mice (n=20, 10 male, 10-12 wks), wild-type (WT, n=5) or *Fstl3*^{-/-} (FSTL3 knock-out, "FSTL3KO," n=5), were treadmill walked for 45 min/day at 8 m/min for 6 weeks, a protocol that increases bone formation. Ten mice (male n=5) were used as NonEX controls. Intact extensor digitorum longus (EDL) and soleus (SOL) muscles were dissected and mounted vertically between two stimulating platinum electrodes and immersed in bathing chambers containing modified Ringer solution. A constant stimulatory voltage was applied to equilibrate muscles at maximum force, followed by stimulation at frequencies from 1-150 hz to generate force vs. frequency curves.

RESULTS AND DISCUSSION

No differences in stimulated force were observed in WT EX and WT NonEX mice, indicating that the walking EX protocol used was not sufficiently rigorous to produce a training effect on muscle force production (Fig.1). Interestingly, no force differences were observed in FSTL3KO EX and FSTL3KO NoEX groups (Fig. 2). These results indicate that endogenous FSTL3 may not be sufficient to alter muscle contractile force generation in response to walking EX training.

CONCLUSIONS

FSTL3 regulates bone health in response to low intensity, low impact walking EX; however, the walking protocol used here is insufficient for increasing muscle force and hypertrophy. This study provides information on the efficacy of walking to increase muscle strength that may be applied to designing EX programs in a clinical setting. While walking may be prescribed as a treatment regimen for increasing bone growth in humans, clinicians should be aware that walking may need to be supplemented with a resistance EX program to increase muscle strength/hypertrophy. *In vitro* and human studies to address FSTL3 mechanisms are ongoing.

REFERENCES

1. Nam J, et al. *Bone*, in press, 2015.
2. Lee SJ, et al. *Mol Endocrinol* **24**, 1998-2008, 2010.

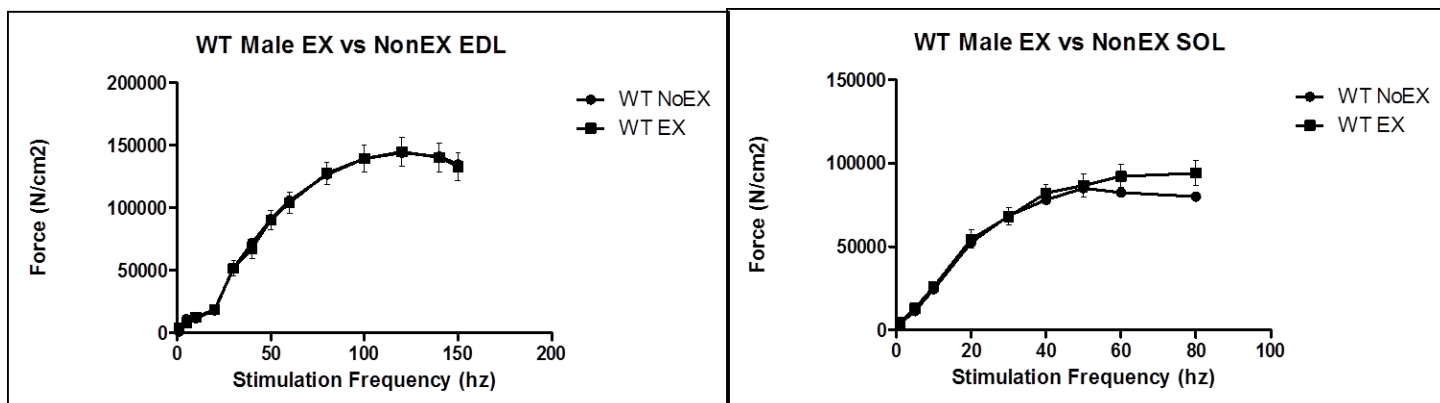


Figure 1: No differences in stimulated muscle force in walking WT EX and NonEX mice. Representative graph from male mouse EDL and SOL muscles. The walking exercise protocol used, although sufficient for producing bone growth in WT mice, was not sufficiently rigorous to produce a training effect on muscle force production.

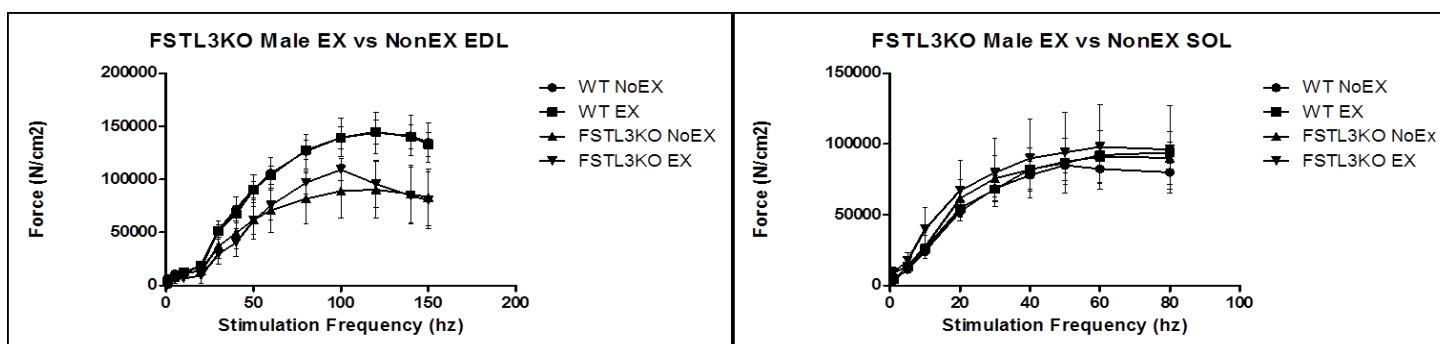


Figure 2: No differences in stimulated muscle force in walking FSTL3KO EX and NonEX mice. Representative graph from male mouse EDL and SOL muscles.

TEMPORAL GENE EXPRESSION PATTERNS REVEAL THAT WALKING-GENERATED BIOMECHANICAL SIGNALS MAINTAIN CARTILAGE HEALTH AND REGULATE GENES ASSOCIATED WITH OSTEOARTHRITIS

¹ Alisa D. Blazek, ² Jin Nam, ¹ Rohan Gupta, ¹ Meera Pradhan, ¹ Priyangi Perera, ¹ Noah L. Weisleder, ¹ Timothy E. Hewett, and ¹ Sudha Agarwal

¹ The Ohio State University, Columbus, OH, USA

² University of California Riverside, Riverside, CA, USA
email: blazek.16@buckeyemail.osu.edu

INTRODUCTION

The beneficial effects of exercise on bone and muscle tissues of the musculoskeletal system are well established [1, 2]. Biomechanical signals generated by exercise induce a multitude of physiological changes required for homeostasis of cartilage [3] that may ultimately play a critical role in exercise-mediated prevention or progression of osteoarthritis (OA). However, gene expression in healthy cartilage in response to these signals has not been comprehensively assessed. The objective of this study was to examine the stable alterations in gene expression of healthy rat articular cartilage in response to low intensity walking exercise.

METHODS

Sprague Dawley rats (n=15, 12-14 wk old females, Harlan Labs, IN) were exercised by treadmill walking at 12 m/min for 45 min daily for 2, 5, or 15 days. Rats were sacrificed 2 hours after the last exercise regimen, and femurs were harvested and snap-frozen in liquid nitrogen. RNA from cartilage was extracted using Trizol and analyzed using Affymetrix GeneChip Rat Gene 1.0 ST Array. This temporal, transcriptome-wide analysis on the cartilage of the walking rats was compared to the transcriptome of sham control rat cartilage. Gene networks activated by exercise were analyzed via Ingenuity Pathways Analysis (IPA).

RESULTS AND DISCUSSION

IPA analysis revealed five distinct categories of gene expression patterns: I), Tissue development and function (extracellular matrix (ECM) and

proteases); II) Cell metabolism; III) Cell growth (growth factors and signals), IV) Inflammation, V) Cell Cycle (Fig. 1). Exercise significantly upregulated matrix associated genes (Cluster I) involved in cartilage scaffolding, synthesis of elastin fibers, cell-matrix interactions, and proteins involved in keratin sulfate, heparin, and proteoglycan synthesis. Importantly, expression of extracellular proteins not associated with cartilage was dramatically suppressed, and genes regulating proteins that degrade collagens and proteoglycans were significantly suppressed. Conversely, several inhibitors of proteolytic enzymes involved in cartilage degradation were dramatically upregulated. A significant number of genes involved in cell signaling and metabolism (Cluster II) were regulated by biomechanical signals generated by exercise. These included serine/threonine kinases, molecules associated with membrane lipid and proteins metabolism, Krebs cycle enzymes, ion channels, and genes affecting cytoskeletal arrangements. Signals generated by exercise also induced several growth factors involved in chondrocyte growth and differentiation (Cluster III), but inhibited cell cycle progression (Cluster IV). Anti-inflammatory activities of exercise were also apparent by the suppression of a significant number of genes that are upregulated during acute and chronic inflammation (Cluster V).

CONCLUSIONS

The exercise stimulus was found to be a strong cartilage regenerative signal that induced cell metabolism, ECM synthesis, and cell growth. Similarly, pathways regulating cellular structure and biomechanics were upregulated. Cell proliferation

and cell cycle genes, many of which are involved in pathological conditions, were suppressed by exercise. Importantly, exercise also suppressed many inflammation associated genes, some of which have been shown to be upregulated in osteoarthritic cartilage. While it has long been suspected that exercise is beneficial for cartilage health, these results indicate that exercise effectively maintains cartilage matrix homeostasis by increasing cell metabolism while decreasing potentially detrimental proteolytic and inflammatory processes. These results may provide a potential mechanism for the protective effects of

exercise against the onset of OA in healthy articular cartilage.

REFERENCES

1. Turner CH, et al. *Sig Science* **28**, 3, 2009.
2. Robling AG, et al. *Crit Rev Eukaryot Gene Exp* **19**, 319-338, 2009.
3. Anghelina M, et al. *Biorheology* **45**, 245-256, 2008.

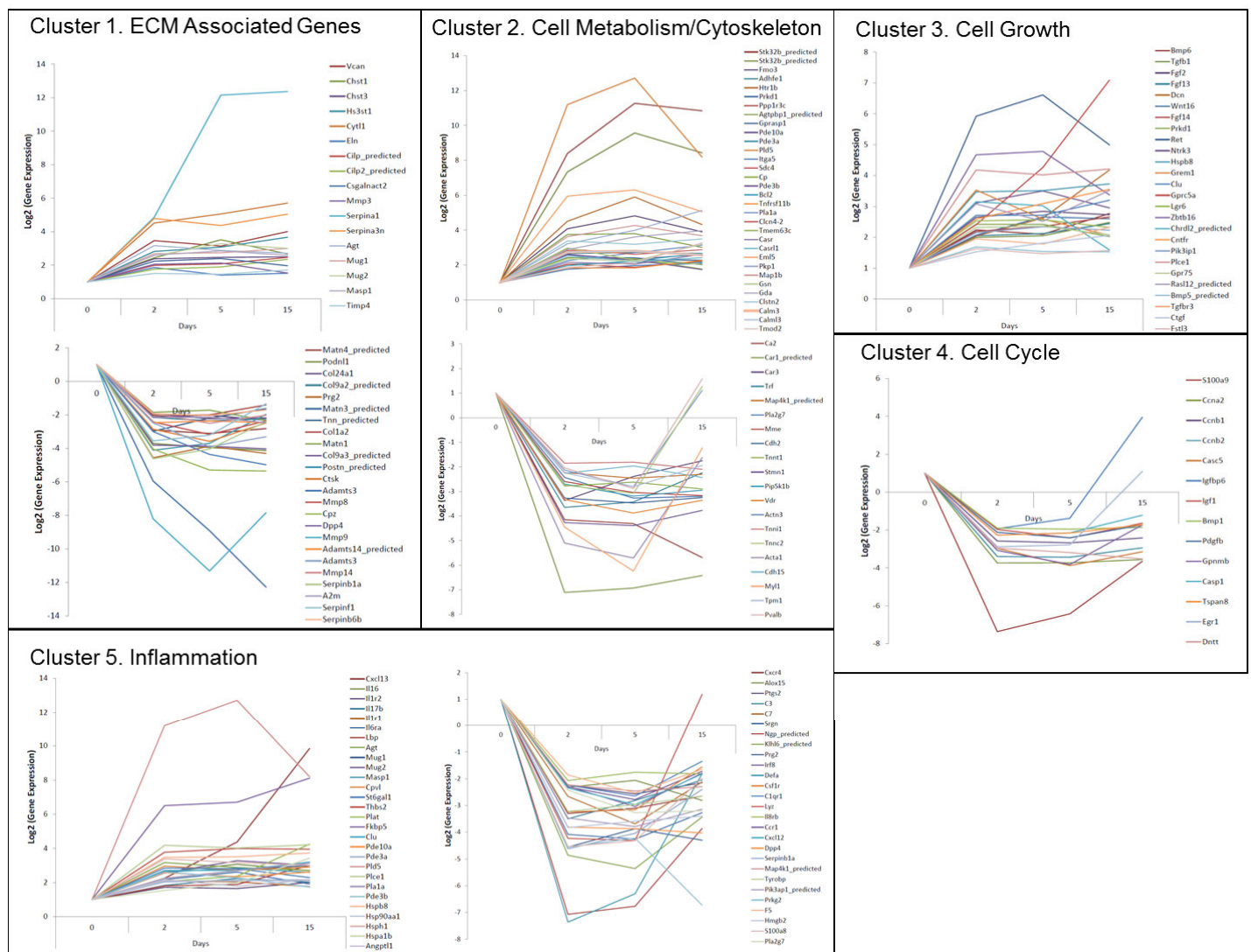


Figure 1. Gene expression clusters generated by IPA from transcriptome wide analysis of walking rat cartilage. The graphs show the major expression changes of walking rat genes compared to control rat genes.

Full field in vivo characterization of skin deformation under pressure loading

W. J. Bong¹, S. Daly^{1,2}, and K. A. Shorter¹

¹ Department of Mechanical Engineering, University of Michigan, Ann Arbor, MI, USA

² Department of Materials Science and Engineering, University of Michigan, Ann Arbor, MI, USA

Email: kshorter@umich.edu

INTRODUCTION

Skin is the largest organ in the body. It plays an important role in the sensory system and is vital for thermoregulation. This multirole functionality is maintained all while providing a critical line of defense against the external environment. In general, the detailed characterization of skin's mechanical properties facilitates a better understanding of the tissue and advances fields such as disease diagnosis [1], tissue modeling, medical device design, cosmetics, and surgery. Full field deformation and strain measurements are key for the characterization of this viscoelastic composite. However, experimental techniques that provide these types of measurements for skin in vivo are currently lacking.

Digital image correlation (DIC) tracks unique features on the surface of a material during deformation to extract shape, deformation and motion measurements of the substrate. Recently, 3D DIC has been used to capture full-field measurements of deformation over relatively large test areas for a variety of substrates. This technique has been used in ex vivo bulge inflation tests to identify material parameters and perform stress-strain analysis for excised skin [2]. However, there are currently no methodological examples that use DIC to make in vivo measurements of intact skin. In this work, a portable device that combines pressure loading and DIC (termed here as PDIC) is used to compare the mechanical properties of skin at two different sites on the body.

METHODS

The experimental setup (Fig. 1) consists of two cameras rigidly mounted to a sealed housing that is evacuated using a venturi vacuum pump. The pump creates a partial vacuum in the housing while a pressure sensor logs pressures inside the housing at 20Hz. The housing is made up of four main components – a machined nylon cap; printed ABS

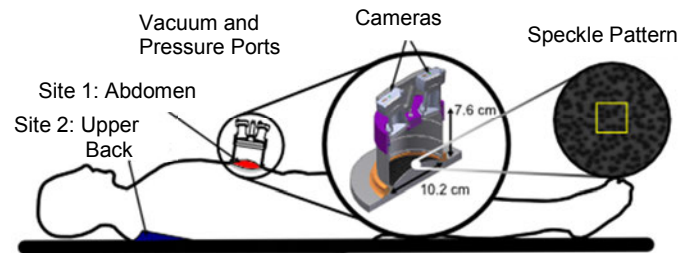


Figure 1: Experiments were conducted on the skin over the abdomen and on the upper back between the shoulder blades. The yellow box shows a representative subset size.

camera supports; a machined main PVC cylinder; and a silicone lip. The silicone lip provides a compliant interface and enhances the seal between the cylinder and the tissue. Each camera assembly is comprised of a camera lens (3.5 mm focal length, aperture range of f/2.4 to f/8) attached to a 1.3 megapixel monochrome USB digital video camera. The camera setup provides a near limit for depth of field of about 2 in from the cameras. Quartz glass inserts are set between the camera lens and the nylon cap to protect the lens and provide a good vacuum seal. Illumination for the cameras is provided by LED lights seated in a groove cut in the PVC housing.

The PDIC system was used to characterize the deformation response of skin from two test subjects at two anatomically distinct sites – the abdomen and the upper back between the shoulder blades. The two male test subjects were 29.5 (s.d. 7.8) years old, 72.0 (s.d. 4.3) in tall, and weighed 153 (s.d. 8.7) pounds. In this work the unique features for the DIC technique consisted of a speckle pattern printed onto temporary tattoo paper. Following preparation and cleaning of the sites, speckle pattern tattoos were applied and allowed to dry before testing.

The cameras were calibrated with a 12x9 grid before the start of each experiment. A preprogrammed cyclic pattern was used to apply

pressure loading over a range of magnitudes to the tissue. Each loading condition lasted for 30 s, and a set of preconditioning cycles of the same magnitude and duration were applied before data were collected. Maximum pressure was kept below 0.1 bar (73 N) for the abdomen and 0.12 bar (96 N) for the upper back. These limits ensured that the subjects did not experience discomfort as a result of the pressure loading. During the trials, pressure data were used to control the pump to achieve the desired loading profile. Images of the skin were captured using Correlated Solution's Vic-Snap 2012 software, at about 7 FPS, after the preconditioning phase. Images were analyzed using Correlated Solution's Vic-3D software to obtain full-field displacements, which were in turn analyzed using MATLAB.

RESULTS AND DISCUSSION

The shape of the average response obtained in our experiments agrees with load-deformation curves for collagenous tissues [3]. Peak displacements increased with increasing peak load, and hysteresis was evident during unloading for all trials at both sites. The energy dissipated during each cycle was quantified using the area within each hysteresis loop and was present during all loading conditions. Figure 2A compares the load-deformation curves from the two sites for one subject at similar loading conditions.

Both peak skin displacement and energy absorption were further characterized with linear fits. Peak out-of-plane skin displacements and the energy dissipated over each cycle increased linearly with force for the skin at both the abdomen and the upper back. Figure 2B illustrates the linear relationship between peak force and peak displacement. The r-squared value of the abdomen fit was 0.893 while the fit for the upper back fit was 0.710. While both are relatively good fits, data from the upper back differed more between the two subjects. Figure 2C presents the energy absorbed by the skin as a function of peak force. The r-squared value for the abdomen fit is 0.948 while that for the upper back fit is 0.839. Similarly, data for the upper back differed more between the two subjects, resulting in the lower r-squared value. Both figures present data from the two subjects at both sites.

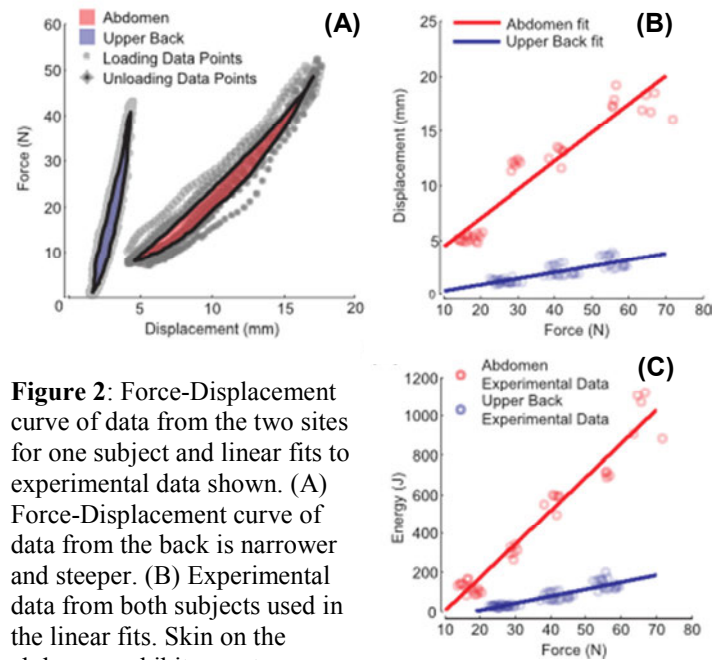


Figure 2: Force-Displacement curve of data from the two sites for one subject and linear fits to experimental data shown. (A) Force-Displacement curve of data from the back is narrower and steeper. (B) Experimental data from both subjects used in the linear fits. Skin on the abdomen exhibits greater displacements for the same pressure. (C) Experimental data from both subjects used. The skin in the abdomen area dissipates more energy than the skin on the upper back.

The anatomy under the skin at the two sites was very different, and this significantly affected the resulting measurements. The lack of a boney substructure below the skin at the abdomen resulted in a softer loading response with more hysteresis (Figure 2A). This in turn created larger deformations with more energy absorption during all cyclic loading conditions (Figures 2B and C).

CONCLUSIONS

The PDIC system enables the capture of full-field in vivo deformation of skin under pressure loading. Future work will involve the use of this approach to characterize skin properties at multiple sites for a range of age groups. We will also explore the use of this device for medical device design and disease diagnostics.

REFERENCES

1. Nightingale K, et al. *Ultrasound in Medicine and Biology* **28**, 227-335, 2002
2. Tonge T, et al. *Acta Biomaterialia* **9**, 5913-5925, 2013
3. Viidik A, *Journal of Biomechanics*, **1**, 3-11, 1968

STOPPED TEACHING PHYSICS, STARTED TEACHING BIOMECHANICS AND FLIPPED THE CLASSROOM

¹ Scott P. Breloff

¹ University of Scranton, Scranton, PA, USA
email: scott.breloff@scranton.edu

INTRODUCTION

Team Based Learning (TBL) is a student centered ‘flipped-classroom’ teaching style which requires the students to work together in small teams on real life application activities during class time. A flipped classroom necessitates students to prepare for content prior to coming into lecture. Lecture time is then used to apply and build on the content students obtained on their own outside of the class.

TBL was developed by Larry Michaelsen in the 1970s [1]. The purpose was to have students learn by doing (i.e. active learning), rather than simply receiving all content via lecture. Adoption of TBL into the biomechanics course at the University of Scranton arose for several reasons; first, this style seemed like a logical fit with a difficult class like biomechanics. Second, with teaching three sections of the same course, it was difficult to lecture in all three sections. Third, the addition of TBL was to improve the students’ learning by reducing lecture time and providing a more relaxed atmosphere where the students feel comfortable with discussion and asking questions.

The first iteration of TBL in biomechanics was spring 2013. The class was then completely overhauled for spring 2014. Physics is a pre-requisite for biomechanics at the University of Scranton and the first eight chapters of the text used in 2013 was essentially a physics review. Many student comments suggested to ‘not simply repeat physics’. Biomechanics at the University of Scranton now uses a custom text which draws from ten different sources to allow students to learn what biomechanics is and how to apply biomechanical concepts in several different situations. This is how the classroom was flipped, teaching physics stopped and teaching biomechanics began.

METHODS

Team Based Learning is a modular learning style divided into three phases: Preparation, Readiness Test and In-class Application Activities. The Preparation phase requires students to complete specific reading in order to prepare for phase two. The second phase, readiness assurance process (RAP), is separated into four sub-sections:

- i. individual readiness assurance test (iRAT)
- ii. team reading assurance test (tRAT)
- iii. appeals process
- iv. mini-lecture.

The iRAT assesses how well the students comprehended the readings by themselves. The students then gather in their teams and take the same test to further their understanding of the material (tRAT). If students feel any of the selected answers are not correct, they are allowed to appeal that question through a previously approved process. Finally, a mini-lecture is provided to touch on the important and/or difficult concepts from the reading.

After the mini-lecture, students enter phase three which is in class application activities. Students work in teams to use their foundational knowledge to solve problems, prepare arguments and provide explanations.

A BIOMECHANICS TBL COURSE

Learning modules are designed to focus on one or two particular concepts. The modules for this course were chosen with the understanding the students have completed a ‘Physics I’ course which generally discusses mechanics, forces, etc. In addition, students are provided with a physics review of the concepts they are expected to know from the pre-requisite physics course.

The learning modules for the TBL course in Biomechanics:

- **Module 1: Orientation**
- **Module 2: Intro. Biomech. & Biomech. Tech.**
- **Module 3: Fluid Mechanics & Anthropometrics**
- **Module 4: Ground Reaction Forces**
- **Module 5: Inverse Dynamics**
- **Module 6: Clinical Biomechanics**
- **Module 7: Ergonomic Biomechanics**
- **Module 8: Forensic & Sport Biomechanics**

Students are assessed with the use of modular examinations, modular homework projects, the RAP, and team maintenance. Team maintenance allows each individual student in a team to rate the contributions of their fellow team members during the end of the term. This portion of the grade (usually 5%) does not come from the instructor, but from the students themselves.

TECHNOLOGY/LEARNING AIDS

Many improvements and additions have been made to increase student learning and improve course effectiveness. These improvements range from technology to teaching assistants.

- *iClicker*: is a student response system used in RAP.
- *WhiteBoards*: a 2'x 3' whiteboard instead of an 8.5"x 11" sheet of paper.
- *Teaching Assistants*: former undergraduate students to help with in class activities.
- *Practice Problems*: Excel spreadsheets with modifiable input parameters.
- *Custom Book*: a custom packet developed from several sources.
- *iRAT recorder sheet*: to help with recall between the iRAT and tRAT.

BENEFITS AND CHALLENGES

Some of the benefits of this approach to biomechanics:

- More interaction with the students.

- Lecture time is more enjoyable for the students and professor.
- Students learn by doing (i.e. active learning).
- Though anecdotally, this approach has allowed the students to have a better understanding of biomechanics (not enough data to run statistics).
- Students come back later to tell the instructor how much they appreciated the style and how much they retained.

This format has had some challenges. Many of these have been addressed in the improvements:

- An unfamiliar system makes the students nervous.
- Students are uncomfortable with a student centered classroom.
- It has been documented that TBL will have better student learning as demonstrated by higher test scores but lower student evaluations [2].
- Students feel the instructors are not teaching, and making the students do all the work.
- As with any team based work, individual contributions are always a concern.

CONCLUSIONS

This approach to teaching biomechanics has been a welcome change to the instructor. It allows for more interaction with the students and reduces overall time spent on lecture by requiring the students to prepare content outside of classroom and learn by doing in the classroom. Currently, in the second semester using this approach, students are beginning to accept and embrace it. As with any new style of teaching, there have been challenges, but they have been addressed and the course continues to improve.

REFERENCES

1. Michaelsen, LK et al. *Team-Based Learning*, Stylus Publishing, LLC. 2004.
2. Fatmi M, et al. *Medical Teacher* **35**, 1608-1624, 2013.

ACKNOWLEDGEMENTS

The University of Scranton's teaching enhancement grant and all the student feedback for improvements to better the course.

MODELING REPERFUSION RESPONSES IN PATIENTS WITH LEG WOUNDS

Wu Pan, Josh Drost, Amy Lenz, Seungik Baek PhD, Tamara Reid Bush PhD

Department of Mechanical Engineering, Michigan State University, East Lansing, MI, USA
email: reidtama@egr.msu.edu, web: <http://researchgroups.msu.edu/reidtama>

INTRODUCTION

Skin ulcers are a significant health problem affecting millions of people in U.S including the elderly, those with vascular deficiencies, and people with a reduction in mobility, such as wheelchair users [1]. These skin wounds take months to heal, are prone to infection, and can lead to amputation or death.

Reperfusion injury, which is the blood reflux back to tissues, usually results in inflammation and leads to tissue damage. In the study of skin ulceration, reperfusion injury has been investigated as an important factor in chronic skin wounds [2]. Currently, a model does not exist that can completely characterize the occlusion of blood flow and the reperfusion process. Development of a model that can characterize this process will provide insight into the pathophysiology of wound formation which will lead to improved treatment and care, benefiting the millions of patients who experience these painful, debilitating wounds.

In this study, a mathematical model using a Windkessel approach was developed to replicate and predict the capillary blood flow during reperfusion process in subjects with and without lower limb deep tissue wounds. The model was then evaluated by comparing output to experimental results obtained by testing healthy individuals and patients with wounds.

METHODS

Experimental methods: Patients with skin ulcers (“wounded”) in their lower legs and healthy subjects (“healthy”) were recruited for this study. A customized load applicator was built to allow normal and shear forces to be applied on the skin of lower legs of test subjects (Fig.1). A laser Doppler system was used to monitor and record the blood

perfusion responses of the skin where the loads were applied. The perfusion-time history data were analyzed using three different phases: a) baseline, where no load was applied; b) under loading, either normal loading or combined normal and shear loading; c) recovery, where the blood reperfusion had a spike of hyperemia after load was removed and then returned to baseline.

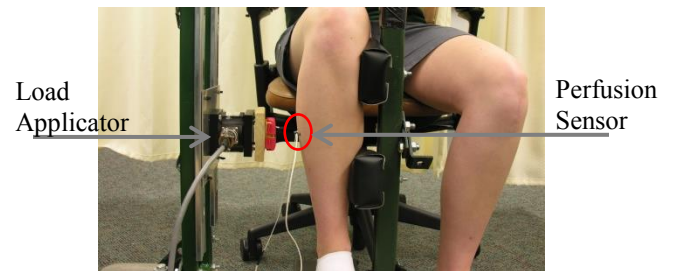


Figure 1: Perfusion test configuration. A six axis load cell was mounted on a vertical frame, allowing force to be measured in the medial and vertical directions. The Perfusion sensor was attached to the lower leg skin of the subject.

Modeling method: Using the analogy of an electrical circuit, Ohm’s law for electricity is equalized with Poiseuille’s law for fluid dynamics of the blood vessel. In a Windkessel circuit, the voltage supply represents the hydraulic pressure of the vessel. Our model (Fig. 2) was proposed based on models developed by De Mul [3] and Vo, T. Van [4] and modified to represent the experimental procedure.

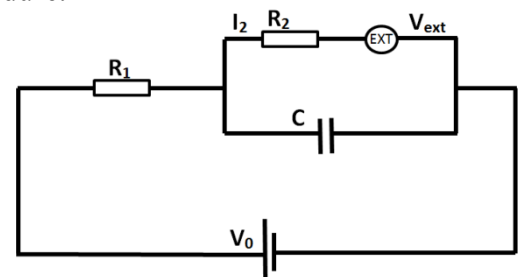


Figure 1: Model developed for reactive hyperemia. R_1 and R_2 represent the arterial and venous resistance respectively, C is the capillary capacitance. V_0 is the hydrostatic arterial pressure; V_{ext} is the external pressure (shown as a voltmeter EXT), I_2 represents venous blood flow.

The hydrostatic arterial pressure (V_0) was calculated as the arterial pressure at the heart plus the hydrostatic pressure with respect to the vertical distance between the heart and where the measurement was taken on the lower leg (Eq.1). The external pressure (V_{ext}) was calculated and normalized as the applied force over the contact surface area of the customized load applicator. The governing equation for this circuit was derived as Eq. 2.

$$V_0 = 100\text{mmHg} + 77.7\text{mmHg/m} \times 0.55\text{m} \quad (1)$$

$$(R_1 + R_2)I_2 + CR_1R_2 \frac{dI_2}{dt} = V_0 - V_{ext} - CR_1 \frac{dV_{ext}}{dt} \quad (2)$$

In our model, the V_{ext} served as the input and I_2 the output. Empirical values for parameters such as R_1 , R_2 and C were obtained from literature and used as initial values for iteration. Iterations of the model were run until RCR values were obtained that could reproduce the experimental curve for that specific patient.

RESULTS AND DISCUSSION

Numerical simulation in MATLAB was used to perform the blood flow of the Windkessel circuit model. The experimental perfusion data (blue) are presented along with model results (red). The comparison between experimental data and the numerical simulation for two different patients and under different loading conditions are shown in Fig.2 and Fig. 3.

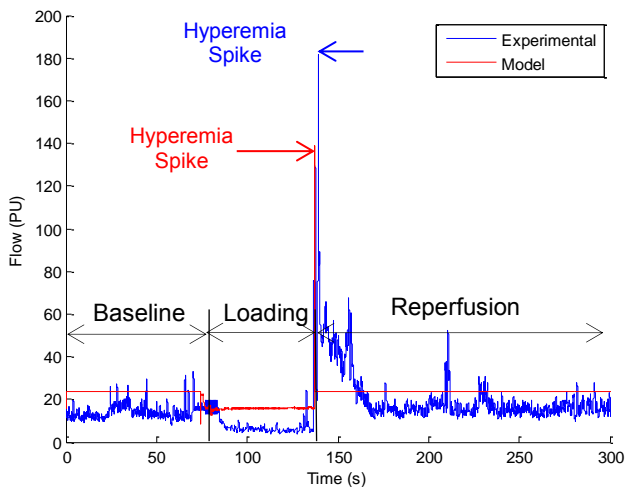


Figure 2: Comparison of blood flow of leg with skin ulcers under normal loading.

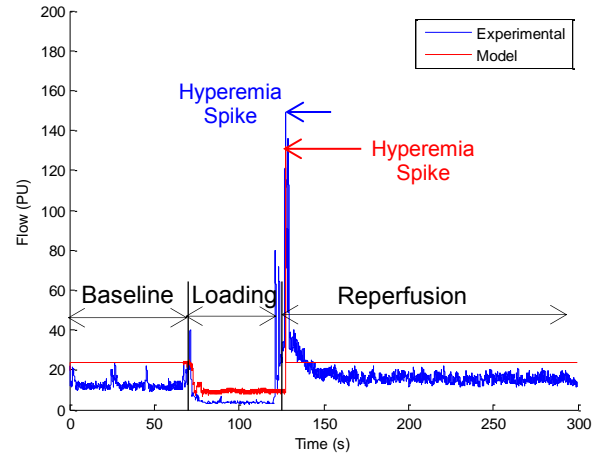


Figure 3: Comparison blood flow of a healthy leg under combined normal and shear loading.

It can be seen from Fig. 2 and Fig. 3 that the current circuit model represents the *general* trend of a decrease in blood flow under loading and the hyperemia spike at the beginning of the reperfusion period upon the release of external loading. However, further modification and development of the model are required to better represent the magnitude of the hyperemia spike, as well as to accommodate the decaying trend from the hyperemia spike to the baseline value during the reperfusion period after the load was removed.

CONCLUSIONS

The model developed in this study aimed to address a computational solution to understanding blood flow occlusion followed by the reperfusion process in capillary flow of lower limbs. The proposed model successfully replicated the blood flow during loading and the hyperemia spike. A current limitation is the inability to characterize the hyperemia recovery slope (period right after the spike) during reperfusion. With further work in this area, the model has great potential to be an improvement on previous reported models in the literature and provide insight for the complex physiological problem of ulcers.

REFERENCES

- [1] S. Tsuji, et al, *Wound Repair Regen.*, 2005.
- [2] D. L. Carden and D. N. Granger, *J. Pathol.*, Feb. 2000.
- [3] F. F. M. De Mul, et al, *IEEE Trans. Biomed. Eng.*, 2005.
- [4] T. Van Vo, et al *IEEE Trans. Biomed. Eng.*, Apr. 2007.

BLOOD PERFUSION RESPONSES OF LOWER LEGS: STUDY OF VENOUS STASIS ULCERS

¹Wu Pan, ¹Joshua P. Drost, ²Marc D. Basson, and ¹Tamara Reid Bush

¹Department of Mechanical Engineering, Michigan State University, East Lansing, MI, USA

²Department of Surgery, Michigan State University, East Lansing, MI, USA
email: reidtama@egr.msu.edu, web: <http://researchgroups.msu.edu/reidtama>

INTRODUCTION

Venous stasis ulcers are skin wounds that occur most commonly on the lower leg. These chronic wounds are painful, can lead to infection, amputation and even death. They affect 2.5 million patients annually in the United States. Stasis ulcers also have high recurrence rates, resulting in multiple visits to wound clinics or hospitals [1].

Ulcer formation has been linked to external loads on the skin which impair blood circulation and the high blood flow that occurs after the loads are removed (called reactive hyperemia). Little work has been conducted to identify differences in perfusion responses (blood flow) between healthy individuals and individuals with stasis ulcers. **The goal of this work** was to identify differences in perfusion responses to force (both normal and shear forces) between legs with existing venous stasis ulcers and healthy legs.

METHODS

Eighteen individuals with wounds on their lower leg and twenty healthy individuals with no vascular issues participated in the testing. A total of seventy five legs were evaluated resulting in three groups: 20 legs with wounds (“wounded”), 15 non-wounded legs but from patients with leg wounds (“non-wounded”) and 40 “healthy” legs.

Load was applied with a custom built device (Fig. 1). The normal loading was applied in the medial direction on the lateral portion of the calf; approximately 25 cm above the ankle. Shear load was applied to the skin when the load cell was shifted vertically while still applying a normal force so the load cell did not slip on the skin. Loading was never directly applied over a wound. If a

wound was located at the test site; the test site was shifted slightly so loading was at least one inch away from the edge of the wound.

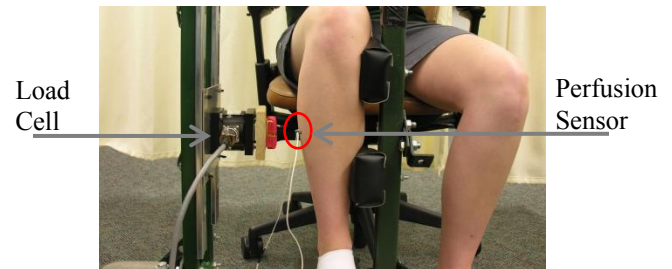


Figure 1: Perfusion test configuration with load cell. A six axis load cell was mounted on a vertical frame and was constrained to two degrees of freedom, allowing force to be measured in the medial and vertical directions.

The magnitude of normal loading was 75% of the subject's lower leg weight which was 4.5% of the subject's whole body weight[2]; shear loading, in the combined loading condition, was 50% of the applied normal loading. The forces used were comparable to those that the leg might experience intermittently during normal living, such as crossing one's legs or resting one's legs on a couch.

A Laser Doppler Perfusion Monitor was used to monitor and record the blood perfusion of the skin during the entire test period. Loading was applied around the region of the sensor with a customized device surrounding the sensor. Each perfusion test consisted of 5 phases: baseline (no load), normal loading, recovery from normal loading, combined normal and shear loading, and recovery from combined loading. The order of normal load or combined loads was altered across the subject pool.

RESULTS AND DISCUSSION

Baseline Comparisons: A sample blood perfusion curve is provided in Figure 2. Statistically significant differences occurred between wounded

legs and healthy legs during baseline study ($p=0.02$). Wounded legs had the highest perfusion values during baseline while healthy legs had the lowest baseline perfusion values.

Perfusion during loading: Two different approaches were used to evaluate the perfusion changes. The first examined the difference with regard to the initial baseline data set ($\bar{A}_0 - \bar{B}_i$ $i=1, 2$); while the second treated the period immediately prior to the trial as the “new baseline” and compared perfusion data to this value ($\bar{A}_{i-1} - \bar{B}_i$ $i=1, 2$). Perfusion values of wounded legs decreased the most when loading was applied regardless of the approach used for comparison. Each approach yielded significant and similar differences between the wounded and healthy legs for the combined loading condition. ($p=0.02$ for $\bar{A}_0 - \bar{B}_i$; $p=0.0007$ for $\bar{A}_{i-1} - \bar{B}_i$). Note: all individuals showed a 90% level or higher recovery after loads were removed and prior to the start of the next test.

Reactive Hyperemia: The reactive hyperemia value (C_1 and C_2) were compared. One-Way ANOVA and Tukey tests demonstrated significant differences between wounded and healthy legs for reactive hyperemia values ($p=0.006$ for normal loading; $p=0.02$ for combined loading).

Medium effect sizes (range 0.3~0.5) were found in comparison between non-wounded legs and healthy legs for blood perfusion values during baseline loadings. In addition, medium effect sizes were also

shown between wounded legs and non-wounded legs for blood perfusion decrease under normal and combined loadings. This finding suggested that statistically significant differences might be expected for higher sample sizes when comparing reactive hyperemia between wounded and non-wounded legs; as well as for the comparison of perfusion values during baseline and loadings between non-wounded legs and healthy legs.

CONCLUSIONS

These data show that the legs with existing venous stasis ulcers are significantly different from healthy legs when comparing reactive hyperemia, baseline perfusion and the perfusion decrease under loading, whereas the non-wounded legs exhibited an intermediate trend between wounded and healthy legs. A progressive trend from healthy to non-wounded to wounded legs exists and the fact that individuals eventually develop an ulcer in the “non-wounded” leg [3] supports the possibility that changes in force-perfusion responses could serve as predictor of ulcer formation.

REFERENCES

- [1] T. E. Arnold, et al. “Prospective, multicenter study of managing lower extremity venous ulcers.” *Ann. Vasc. Surg.*, vol. 8, no. 4, pp. 356–62, Jul. 1994.
- [2] D. B. Chaffin and G. B. J. Andersson, *Occupational Biomechanics*, 2nd ed. Wiley-Interscience, 1991, pp. 83–89.
- [3] L. P. F. Abbade and S. Lastória, “Venous ulcer: epidemiology, physiopathology, diagnosis and treatment.” *Int. J. Dermatol.*, vol. 44, no. 6, pp. 449–56, Jun. 2005.

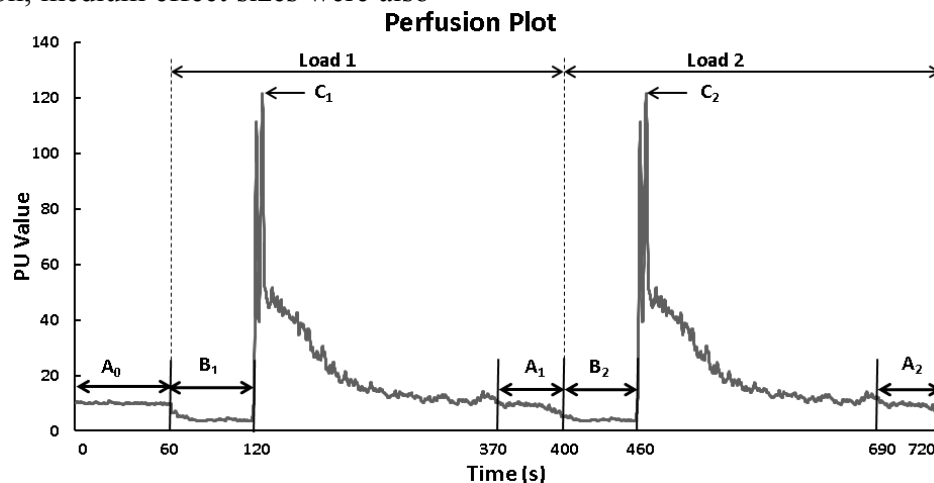


Figure 2: Blood perfusion curve with parameters identified: A_0 is the original pre-loading baseline; A_1 and A_2 are the last 10% during recovery after load 1 and 2 respectively; B_1 and B_2 are the loading periods; C_1 and C_2 are the hyperemia after load is released. PU is perfusion unit (y axis).

MECHANICAL WORK OF MASSAGE AFTER ECCENTRIC EXERCISE IN A RABBIT MODEL

¹ Scott K. Crawford, ¹Yi Zhao and ¹Thomas M. Best

¹ The Ohio State University, Columbus, OH, USA

email: crawford.606@osu.edu

INTRODUCTION

Skeletal muscle damage, often a result of unaccustomed eccentric exercise (EEC), is a common problem in sports medicine. One popular treatment utilized to accelerate recovery of muscle function following EEC is massage [1]. This therapy is theoretically based on the principles of mechanotransduction, wherein externally applied forces trigger production of molecular signals that modulate specific physiological responses. However, the forces applied to tissues during human massage are not quantified, which makes comparing results between studies difficult. Additionally, human massage typically involves a combination of both compressive and transverse (along the tissue) forces. We have investigated the magnitude of forces applied during massage, but have focused on compression and transverse forces in isolation rather than in combination [2,3]. This current analysis attempts to account for total loading during massage by analyzing the mechanical work performed on the muscle.

METHODS

Twenty-four skeletally mature New Zealand White rabbits were instrumented with bilateral peroneal nerve cuffs for consistent external stimulation of the tibialis anterior [2]. One hindlimb from each animal was randomly selected to undergo an intense bout of EEC. Animals were randomized for massage commencing immediately after or 48 hrs after EEC. Massage was applied using a customized mechanical device for 4 consecutive days. Each massage bout was approximately 24 hrs apart and utilized a previously determined optimal set of parameters for restoring ankle joint torque (10 N compressive force, 0.5 Hz, 15 min) [2]. A 300 second compressive ramp-and-hold stress relaxation test estimated the muscle's passive mechanical

properties. Mechanical properties were measured pre- and post-massage for all days.

Mechanical work was defined as

$$W = \int F(z) dz \quad (1)$$

where W was work, $F(z)$ was force as a function of displacement, and dz was the displacement in the direction of the applied force. Compression work (W_c) was calculated as

$$W_c = W_0 + W_{\text{massage}} \quad (2)$$

where W_0 was the initial work input into the system by manually lowering the massage tip. W_{massage} was the work done during massage due to the massage tip traveling deeper into the muscle as a result of tissue relaxation. The transverse forces, expressed as a function of time $F(t)$, were transformed and expressed as a function of displacement along the muscle belly $F(x)$. This function was then integrated (Eq. 1) to determine the work performed along the muscle belly (W_t). The total work was calculated as

$$W_{\text{total}} = W_c + W_t \quad (3).$$

All variables had non-normal distributions therefore the data were transformed for subsequent ANOVA tests. Bartlett's test was performed and determined equal variance for all analyses ($p > 0.05$).

RESULTS AND DISCUSSION

Average daily values of W_c , W_t , and W_{total} are shown in Table 1. The average values of mechanical work in the immediate and delayed massage groups are shown in Table 2. W_0 was very small and on the order of 30 mJ. There was a difference in W_0 between groups ($p = 0.024$), but day (i.e. massage bout) ($p = 0.072$) and the interaction of day and group ($p = 0.356$) had no significant effect. ANOVA

showed no differences in W_c due to any factors ($p=0.336$). Day ($p=0.010$) and group ($p=0.009$) had a significant effect on W_t , but their interaction did not ($p=0.732$). *Post hoc* Tukey tests showed differences between days 1 and 2 ($p=0.041$), days 1 and 3 ($p=0.015$), and days 1 and 4 ($p=0.040$), as shown in Figure 1. All other comparisons were not significant ($p>0.05$). There was a difference in W_{total} between groups ($p=0.002$), but day ($p=0.055$) and the interaction of day and group did not have a significant effect ($p=0.492$).

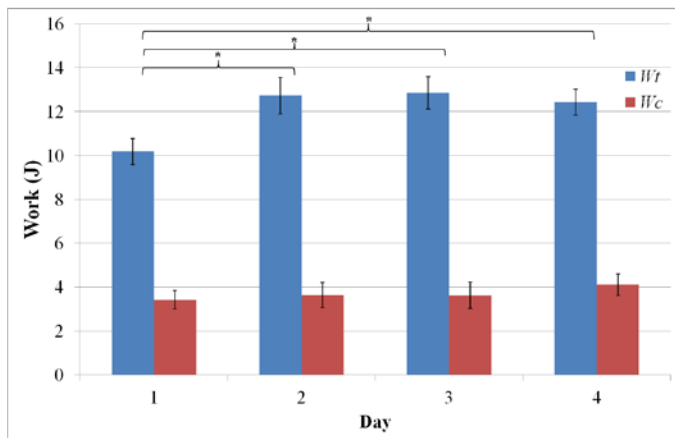


Figure 1: Daily average transverse (W_t) and compression (W_c) work performed during massage.

The observed differences in W_0 between groups indicated that initial work input into the tissue was different between groups, which is not completely unexpected since the initial work was performed by manually lowering the massage tip to a 10 N compressive force. Moreover, any differences in W_c would be due to tissue relaxation, and previous work has shown that massage had no effect on

altering the muscle's relaxation response [4]. Interestingly, W_t was an average 3.25 times greater than W_c despite compressive forces being an average 2.9 times greater than transverse forces [3]. The finding that W_t was less in the delayed group compared to the immediate massage group is perhaps not surprising since transverse forces were higher in the immediate group compared to the delayed group [3] and the total displacement along the muscle is the same in all massage bouts. W_{total} was greater in the immediate group compared to the delayed group, which is most likely due to the differences in W_t . Taken in conjunction with previous work [2-4], we conclude that acceleration of functional recovery due to this particular massage protocol following EEC is primarily a result of work due to loading along the muscle belly rather than muscle compression. These findings may provide guidance to inform clinical practice and the use of massage.

REFERENCES

1. Farr, T, et al. *J Sci Med Sport* **5**, 297-306, 2002.
2. Haas, C, et al. *BJSM* **47**, 83-88, 2013.
3. Best TM, et al. *BMC Complement Altern Med* **14**, 393, 2014.
4. Crawford SK, et al. *Clin Biomech* **29**, 671-678, 2014.

ACKNOWLEDGEMENTS

Supported by NIH NCCAM R01AT004922 (TMB).

Table 1: Daily averages of W_c , W_t , and W_{total} . Differences between Day 1 indicated by * ($p<0.05$).

	Day 1	Day 2	Day 3	Day 4
Compression (W_c)	3.4 ± 0.4 J	3.6 ± 0.6 J	3.6 ± 0.6 J	4.1 ± 0.5 J
Transverse (W_t)	10.2 ± 0.6 J	12.7 ± 0.8 J*	12.9 ± 0.7 J*	12.4 ± 0.6 J*
Total (W_{total})	13.6 ± 0.65 J	16.4 ± 1.2 J	16.5 ± 0.9 J	16.5 ± 0.8 J

Table 2: Average initial, compression, transverse, and total work between groups (* denotes $p<0.05$).

	Immediate	Delay
Initial (W_0)	35.8 ± 1.2 mJ*	32.4 ± 1.0 mJ*
Compression (W_c)	4.3 ± 0.4 J	3.1 ± 0.3 J
Transverse (W_t)	13.0 ± 0.6 J*	11.0 ± 0.4 J*
Total (W_{total})	17.3 ± 0.7 J*	14.2 ± 0.5 J*

INVESTIGATION OF NECK AND HEAD INJURY POTENTIAL DURING INERTIAL LOADING OF THE PEDIATRIC HEAD: IMPLICATIONS TO SHAKEN BABY SYNDROME CHARACTERIZATION

¹ Mark A. Davison, BS, ¹ Brian Weaver, MS, PE, ¹ Steven A. Rundell, PhD, PE
¹ Explico Engineering Co., Ann Arbor, MI, USA
email: steve@explico.com, web: www.explico.com

INTRODUCTION

It has been suggested that violent shaking of a child, in the absence of head impact, can result in closed head injury. Specifically, the symptoms associated with shaken baby syndrome (SBS) are relegated to the head, and include retinal hemorrhaging, cerebral hemorrhaging, and encephalopathy. Careful characterization of the injuries resulting from shaking is critical when determining a potentially abusive situation. Unfortunately, a paucity of real-world or empirical validation exists to confirm the SBS injury pattern.

Both real-world and empirically derived data from automobile collisions provides valuable information related to pediatric injury patterns during pure inertial loading of the head, which is similar to violent shaking. These data indicate the presence of cervical spine trauma in the absence of closed head injury [1,2].

Therefore, the objective of the current study was to evaluate pediatric neck and head injury potential during purely inertial loading of the head. Given the anatomical and biomechanical properties of the pediatric cervical spine, we hypothesized that inertial loading of the pediatric head provides a greater risk of injury to the cervical spine when compared with closed-head injury.

METHODS

Publicly available sled and full-scale crash testing was downloaded from The National Highway Traffic Safety Administration's website.

Frontal sled tests were performed at an approximate change in velocity (delta-V) of 30 mph. The full-scale crash tests were performed at a barrier equivalent speed of 35 mph. Both of these modes of

testing utilized forward-facing Hybrid III, 3 year-old anthropomorphic testing devices (ATDs) restrained in age-appropriate child restraint systems.

Head Injury Criterion 15 (HIC₁₅) and upper neck peak tension force was documented for each of the ATD's (n=107). The published Hybrid III 3 year-old injury assessment reference values (IARVs) for HIC₁₅ and upper neck peak tension force were 570 and 1,430 N, respectively [3]. The percentage of data points that exceeded either IARV was calculated. Additionally, HIC₁₅ was plotted against peak neck tension in order to investigate the presence of a correlation, and graphically depict each data point in relation to the IARV (see Fig. 1 and 2)

Statistical outliers were identified and removed using the Tietjen-Moore method for multiple outliers. Any crash test that resulted in direct head contact was also removed. Pearson correlation coefficients were calculated to determine correlations between HIC and peak neck tension.

RESULTS AND DISCUSSION

Data from a total of 34 ATDs was obtained from the 30 mph sled tests. The average HIC₁₅ was 305.3 (SD = 117.3). The average upper neck peak tension force was 1719.2 N (SD = 328.5). The Pearson Test indicated a positive correlation between HIC₁₅ and upper neck peak tension force, $r = 0.74$, $p < 0.05$, with a $R^2 = 0.55$. Of the 34 data points gleaned from the sled testing reports, 27 (80%) exceeded the upper neck tension IARV while only 1 test (3%) surpassed the HIC₁₅ IARV (Fig. 1).

Data from a total of 73 ATDs was obtained from the 35 mph full-scale crash tests. The average HIC₁₅

was 506.2 (SD = 174.2). The average upper neck peak tension force was 1935.5 N (SD = 248.5). The Pearson Test indicated a positive correlation between the HIC₁₅ and upper neck peak tension force, $r = 0.46$, $p < 0.05$, with a $R^2 = 0.22$. Of these tests, 72 (99%) exceed the upper neck peak tension IARV and 17 (23%) exceed the HIC₁₅ IARV (Fig. 2).

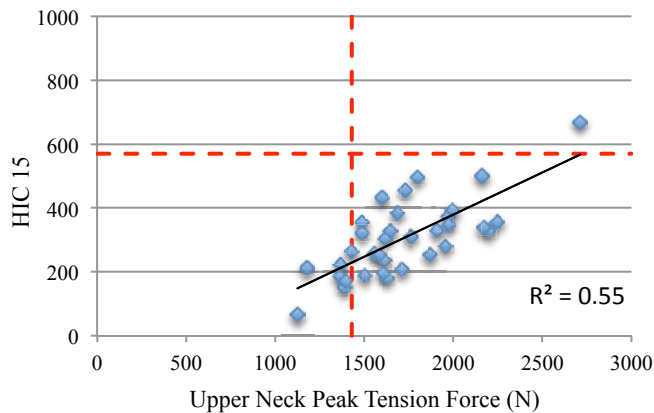


Figure 1: Sled testing of the Hybrid III, 3 year-old ATD compared to the head and neck IARVs.

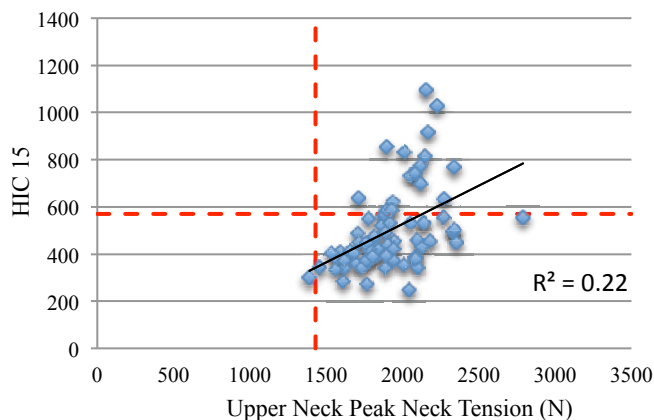


Figure 2: Full-scale crash testing of the 3 year-old ATD compared to head and neck IARVs.

Results from the current study indicate generally injurious levels of neck tension. Conversely, HIC₁₅ values tended to remain below the IARV. These findings support the hypothesis that inertial loading of the head provides a greater risk of injury to the cervical spine when compared with closed-head injury. At minimum, these data indicate a clear coupling of head and neck injury risk for the pediatric population in the absence of head impact.

The results from this study help corroborate and support the current IARV for three-year-old peak neck tension. Specifically, previously reported

cervical injury patterns for restrained young children during frontal collisions include atlanto-occipital dislocation. The mechanism for this type of injury involves a high level of tensile forces in the cervical spine. These data indicate good bio-fidelity of the HIII three-year old dummy.

Unfortunately, similar real-world validation does not typically exist in instances involving child abuse. Specifically, the injury pattern associated with violent shaking of a child has been suggested, but never reliably, empirically verified. Results from the current study provide valuable insight into the injury pattern associated with inertial loading of the head. Specifically, the results indicate a high risk of neck injury when compared with the risk of head injury. Moreover, the results indicate a statistically significant correlation between head and neck loading, which suggests a coupling of injury potential. Therefore, the injury pattern associated with violent shaking should be altered to include the presence of cervical spine injury. Moreover, during instances in which abusive shaking is suspected, special consideration should be paid to the cervical spine.

The current study shares the limitations associated with all ATD studies. Additionally, the current study relied upon IARVs to determine the relative risk of injury between the neck and the head. While this comparison provides insight into the general pattern of injury, it does not provide reliable information related to the relative severity of the injuries. Finally, the current study utilized HIC₁₅ to evaluate the risk of closed-head injury. Ideally, rotational acceleration and velocity would have been included.

REFERENCES

1. Huelke, DF, et al. *Accid. Anal. And Prev.* **25**(6), 731-743, 1993
2. Arbogast, KB, et al. *Annu Proc Assoc Adv Automot Med.* **46**, 213-230, 2002
3. Mertz, HJ, et al. *Stapp.* **47**, 155-188, 2003

USING A HYBRID COURSE FORMAT TO TEACH BIOMECHANICS RESEARCH METHODS

Erin Feser

Arizona State University, Phoenix, AZ, USA
email: enharper@asu.edu

INTRODUCTION

Hybrid courses (also known as blended learning) are courses that replace a portion of the traditional in-person class time with online learning [1]. Often, the hybrid course format is utilized to address an access or convenience issue [2]. For example, a traditional class that meets in-person twice per week during the semester could be re-designed such that it is offered 50% in-person and 50% online. The students would meet for the in-person session one day per week, thus freeing up classroom space for the other day of the week.

The hybrid course structure can be utilized for reasons other than scheduling convenience. For many, designing or re-designing a course to a hybrid format allows one to incorporate the advantages that come from in-person course delivery with the advantages of online course delivery to provide a course that is most beneficial for the learner. This type of hybrid course is referred to as transforming, as the design intention is to allow for student learning experiences that are not possible without the incorporation of online course delivery [2].

The Kinesiology degree program at Arizona State University was met with the challenge of offering an undergraduate, senior level elective course on biomechanics research methods and technology. At the time of onset, elective courses were offered for enrollment of 40 students. However, there was not a formal biomechanics lab space that could accommodate large groups of students and equipment was limited. Therefore, a transforming-type hybrid course format was adopted to meet the course objective needs.

Many universities, with limited space and equipment, might also be encountering the challenge of offering undergraduate or graduate students hands-on laboratory experiences, and would therefore benefit from learning more about our experience with utilizing a hybrid course format to meet this challenge.

COURSE DESIGN

This course, entitled KIN 418 Experimental Neuromechanics, is delivered as two components, lecture and laboratory. The lecture component of the course serves to discuss the theory behind quantitative biomechanical analysis techniques, proper equipment usage, and the connection to biomechanical and motor control concepts. During the laboratory component, students gain hands on experience with the equipment by performing experiments. During these experiments, the students alternate their roles as both a technician and participant. Following laboratory experiences, students gain practice in analyzing, reporting, interpreting, and presenting data.

The course now has a maximum enrollment of 24 students, so there are a total of six experiments planned for the semester. Each experiment demonstrates a different concept and equipment usage. The class is divided into six groups, each assigned a different experiment. Experiments are scheduled throughout the semester and occur as the lecture material progresses.

When an experiment is scheduled for the class period, only the group that has been assigned to that experiment attends class for the entire period. Three other groups are assigned to different segments of the

class period to attend as a participant, while the other two groups are not required to attend.

The time of the groups that are not required to attend, or are required to attend for only a small segment of the class period, is instead allocated towards independent work online or small group project work. Having these students occupied outside of the formal class session allows the instructor to work one-on-one with the lab group. Additionally, it allows for only a small group of students to be in the lab at a time, which further allows for the students to be hands-on with the equipment.

Utilization of the hybrid class structure has provided the flexibility to largely transform the experience students receive when learning about biomechanics technology. Instead of simply observing, the students are able to be fully involved in all aspects of an experiment, from designing the methods to troubleshooting when something unexpected arises while carrying out their experiment. Naturally, this reinforces lecture material and permits higher level learning objectives.

BEST PRACTICES

When designing a hybrid course, there are many design considerations [3]. Once the learning objectives are set, the main point of focus should be on how and when the students will interact with the instructor. Currently, there is no standard ratio for how much of the course instruction is received by the student online versus in-person [1]. Students in KIN 418 Experimental Neuromechanics receive about 63% of the course in-person. This percentage was not decided on in advance; instead, how much class time was allocated for each group to spend on their experiments with the instructor was decided. Also, it was taken into consideration what material the other students would be able to work on asynchronously and independently.

It is essential when designing a hybrid course that a course outline is built to clearly communicate the expectations of when, where, and how the students will be actively engaging in course material. A course outline is especially important for this course, considering the asynchronous nature of some of the

assignments. To address this, a table is provided to the students, in addition to the course schedule to indicate what will occur in the classroom (e.g., lecture, equipment demonstrations, exams, particular assignment instructions) and what will occur outside of the classroom (e.g., assignment instructions, materials presented online, small group work). This helps the students recognize the interaction of the in-person and online course components and stay informed as to what is expected of them during the duration of the course.

Lastly, the instructor must imbed opportunities for students to self-monitor progress. This is important to support online course component success. A variety of methods can be employed. Examples include guided reading questions, post-online lecture quiz, writing assignment examples, and breaking a group project down into phases with separate graded submissions.

CONCLUSIONS

While most Kinesiology degree program students do not continue to research careers, most do continue into careers that require use of evidence based practice. Their understanding of the research process is invaluable to their ability to critique research literature in the future. Therefore, it is important for students to receive learning experiences that support and bring forth a knowledge base of research methods for their respective discipline. A hybrid format course design allows for an active learning environment which has been identified and empirically validated for increasing student performance and recommended over traditional lecturing as a teaching method [4].

REFERENCES

1. Blended Learning ToolKit, <https://blended.online.ucf.edu>, retrieved 2015.
2. Bonk C & Graham C. *Handbook of Blended Learning: Global Perspectives, Local Designs*. Pfeiffer Publishing, 2005.
3. McGee P & Reis A. *J of Async Learning Networks*, **16**(4), 7-22, 2012.
4. Freeman et al. *Proceedings of the NAS*, **111**(23), 8410-8415, 2014.

A JOINT COORDINATE SYSTEM TO DESCRIBE RELATIVE 3D MOTION BETWEEN THE REAR AND FRONT BODY SEGMENTS OF RODENTS: APPLICATION IN THE STUDY OF NEURODEGENERATIVE DISEASES

^{1,2} Tasos Karakostas, ³ Lawrence Middaugh, and ³ Ann-Charlotte Granholm

¹ Rehabilitation Institute of Chicago, Chicago, IL, USA

² Northwestern University, Chicago, IL, USA

³ Medical University of South Carolina, Charleston, SC, USA

email: tkarakosta@ric.org

INTRODUCTION

Walking safely and smoothly requires intact visual, vestibular, proprioceptive and musculoskeletal systems information processing and integration at the brain. Aging and neurodegenerative disorders not only affect the quality and quantity of the information, but also the integration at the brain. Therefore, loss of motor function and gait has been found to parallel cognitive impairment, eventually leading to dementia [1]. On this basis, quantitative instrumented gait has been found a sensitive and measurable tool for determining risk for frailty and progression of dementia [2]. Parkinson disease (PD) is another such neurodegenerative disorder where only recently instrumented motion analysis has been used to track progression of the disease as well as the effects of surgical or pharmaceutical treatment paradigms [3]. However, because most drug trials for PD and dementia involve pre-assessment in models of the disease, translatable and accurate motion capture methods also need to be developed for mouse and rat models.

To the best of our knowledge, our group was the first to report, firstly on the feasibility of using an optical motion capture system to study aging-related changes on a mouse while walking [4], and secondly on a three body-segment rodent model comprised of the head, the anterior and hind body segments [5] with application to PD. This model provided the ability to quantify and study the distinct 3D motion patterns of each body segment between each body-segment's coordinate system and the laboratory coordinates, using an Eulerian approach, i.e., such that angular displacement data are not sequence dependent, unlike when they are derived directly from rotation matrices.

However, much like when human motion is considered, it may be of greater interest if the

motion of the rodent's body-segments are described relative to each other. Consequently, the purpose of this study is to expand on our previous work and propose a model to describe the 3D motion of the anterior body-segment of the rodent relative to its rear body-segment.

METHODS

The development of the model has been described previously [5]. Briefly, for the purposes of this report, one GDNF^{+/-} mouse and a wildtype littermate (WT) were anesthetized with isoflurane and 2mm diameter retro-reflective markers were fixed to their hair via hypoallergenic double-sided tape. The markers were placed on the anterior rim of the pelvis bilaterally (RR, RL), the greater tubercle bilaterally (FR, FL), and the middle of the back at the level of L4 (S) to define the posterior © and anterior body-segments (B) (Figure 1).

A 6-camera VICON optical capture system (ViconMotion Systems Inc, Lake Forest, CA) recording at 240Hz captured the 3D position of each marker as a function of time. Each marker trajectory was low-passes filtered with a zero lag 6th order butterworth filter. Rodents walked freely in a 4 feet constrained walkway, 1 foot wide and 5 inches high walls. Our kinematic model was implemented in a custom computer program. For the purpose of this report, the model ultimately determined the relative angles between the rear and anterior body-segments assessing flexion/extension, tilting and rotation or spin. The overall velocity of forward progression of the rodent's body was estimated from the marker positioned at L4 on the back.

Construction of each body-segment coordinate system and description of its 3D motion in space has been described previously [5]. To determine

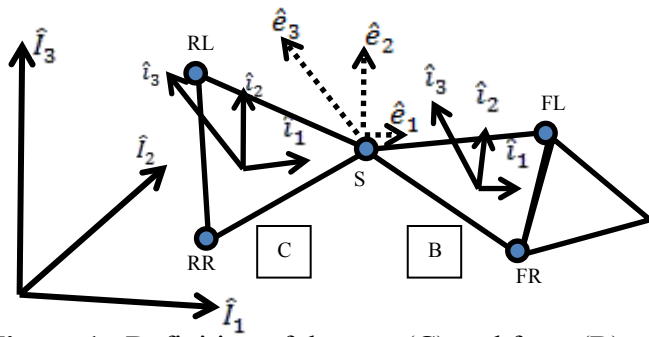


Figure 1: Definition of the rear (C) and front (B) body-segments and coordinate systems. Motion was previously described with respect to the global coordinate system $\hat{i}_1, \hat{i}_2, \hat{i}_3$ representing the posterior-anterior, medial-lateral and vertical directions respectively. Relative motion between the two body-segments is described from the joint coordinate system with unit vectors \hat{e}_1, \hat{e}_2 , and \hat{e}_3 .

now the relative motion between (B) and (C), a joint coordinate system was constructed from the two body-segment coordinate systems with unit vectors \hat{e}_1, \hat{e}_2 , and \hat{e}_3 . We selected \hat{e}_2 to coincide with the (medio-lateral) coordinate of the front body-segment coordinate system, and \hat{e}_3 to coincide with the (vertical) direction of the rear body-segment coordinate system. When the general motion of the two body segments is considered, \hat{e}_2 cannot be assumed to be perpendicular to \hat{e}_3 , and, therefore, the joint coordinate system will not be an orthogonal system. In addition, there will not be a common origin. The third joint coordinate is chosen to be an axis which is mutually perpendicular to both of the other two coordinates:

$$\hat{e}_1 = \frac{\hat{e}_2 \times \hat{e}_3}{|\hat{e}_2 \times \hat{e}_3|}$$

Rotation about the \hat{e}_2 axis represents flexion/extension of the body segment; rotation about the \hat{e}_3 axis represents rotation in the transverse plane which quantifies the body-segment tilting that is taking place; and rotation about the \hat{e}_1 axis represents rotation in the frontal plane which quantifies the amount of spin.

RESULTS AND DISCUSSION

Table 1 demonstrates the results from the implementation of the model and the joint coordinate system to quantify the relative 3D motion between the rear and front body-segments of the rodent. The normal aging rodent walked almost twice as fast as its parkinsonian type counterpart. In the sagittal and transverse planes the motion of the WT rodent was also greater than that of the $GDNF^{+/-}$.

These results correlate very well with the current knowledge about the motor deficits of individuals with PD.

CONCLUSIONS

The model we have presented is the first to treat distinctly the rear from the front body-segments. The body-segment coordinate systems along with the joint coordinate system “ride” with the rodent and the angular displacement data are not sequence dependent. Finally, our results appear to be clinically valid.

REFERENCES

1. Montero-Odasso M., et al. *J. Am Geriatr Soc* **60**, 2127-2136, 2012.
2. Karakostas T., et al. *J Comp Nonlinear Dynamics* **8**, 210171-210176, 2013
3. Dias S., et al. *IEEE EMBS*, Boston, MA, USA, 2011
4. Karakostas T., et al. *Cell Transplant* **17**, 468, 2008
5. Karakostas T., et al. *J. Neurosci Methods* **231**, 31-37, 2014.

ACKNOWLEDGEMENTS

Supported by NIH grant AG023630 and partly by the South Carolina Spinal Cord Injury Research Fund. Thanks are due to Ms. Claudia Umphlet and Mr. Alfred Moore for expert technical assistance.

Table 1: Relative 3D motion between the rear and front body-segments in the $GDNF^{+/-}$ and wildtype rodents

Parameter	Sagittal/Pitch (Degs) Max Flex(+)/Ext(-)	Frontal/Yaw (Degs) Max Spin Right (+)/Left(-)	Transverse/Roll (Degs) Max Tilt Right (-)/Left (+)	Velocity (max): m/sec
$GDNF^{+/-}$	50/58	10/-4	-18/-2	0.13
Wildtype	54/76	8/-22	-13/21	0.24

CHARACTERISTICS OF PERI-IMPLANT BONE QUALITY WITH GUIDED BONE REGENERATION

Trenton Johnson¹, Ben Siderits¹, Erin Kosel¹, Seth Nye¹, Yong-Hoon Jeong¹,
Jung-Suk Han², Do-Gyoon Kim¹

¹ Orthodontics, The Ohio State University, Columbus, OH, USA

² Prosthodontics, Seoul National University, Seoul, Korea

e-mail: kim.2508@osu.edu

INTRODUCTION

Peri-implant bone quantity has been measured to determine success of guided bone regeneration (GBR). However, there is a lack of research assessing how bone quality affects the ability of local bone tissues to resist mechanical damages around the implant in function. Thus, the objective of this study was to examine the mechanical properties of bone tissue at different regions of the dental implant system and to compare multiple GBR treatment methods at peri-implant bone defects.

METHODS

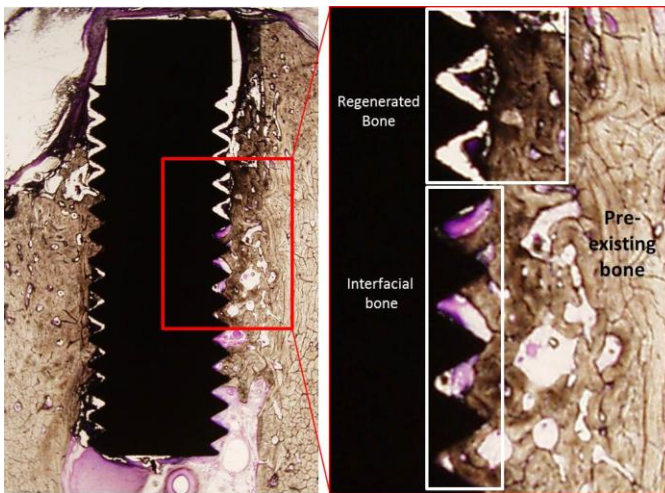


Fig. 1. Representative image of the indent locations as regenerated bone, pre-existing bone, and interfacial bone

Following IACUC approval, 38 dental implants were bilaterally placed into buccal dehiscence defects in mandibles of beagle dogs following 3 months of post-extraction healing. The implant

systems were randomly assigned to 3 groups of GBR surgeries including: no treatment (control), demineralized bone matrix, and bone morphogenetic protein-2 groups. After 4 and 8 weeks of post-implantation healing, bone-implant constructs were dissected for nanoindentation. Total of 1921 indentations were performed for new bone tissue regenerated in the defects, bone adjacent to the implant, and old bone tissue away from the implant. Plastic hardness (H), elastic modulus (E), and brittleness (E/H) were obtained to assess the fracture resistance of bone tissue. ANOVA was tested ($p < 0.05$).

RESULTS

Averaged values of E, H, and E/H for regions of each implant were not significantly different between new bone tissues in the defect sites and adjacent to the implant ($p > 0.14$). Those of E and H of old tissue region were significantly higher than those of other regions ($p < 0.003$). The regional variation of those values was significant dependent on the tissue age and treatments ($p < 0.043$).

CONCLUSIONS

The less mineralized newly formed bone next to the implant had comparable quality independent of the peri-implant regions, which is different from the more mineralized pre-existing old bone tissue away from the implant. Treatments to stimulate bone regeneration could alter the regional variation of peri-implant bone quality.

REFERENCES

1. T. Johnson, et al. *J Dent Res* **93** (B), 556, 2014.

2. DG Kim, et al. *J Biomech Eng*, **132**, 024502, 2010.
3. DG Kim, et al. *J Biomech*, **46**, 110-115, 2013.

ACKNOWLEDGEMENTS

The project described was supported by Award Number Grant UL1TR001070 from the National

Center for Advancing Translational Sciences. The content is solely the responsibility of the authors and does not necessarily represent the official views of the National Center for Advancing Translational Sciences or the National Institutes of Health.

Table 1: Nano-indentation results of regenerated bone, pre-existing bone, and interfacial bone for Elastic modulus, Hardness, and Brittleness. (average \pm standard deviation)

	Elastic Modulus (GPa)	Hardness (GPa)	Brittleness (E/H)
Regenerated	10.24 \pm 2.01	0.38 \pm 0.07	28.77 \pm 5.04
Pre-existing	13.53 \pm 4.44	0.52 \pm 0.08	27.12 \pm 7.51
Interface	11.32 \pm 2.50	0.40 \pm 0.08	30.74 \pm 7.17

Table 2: Nano-indentation results at each location at 4 and 8 weeks for Elastic modulus, Hardness, and Brittleness. (average \pm standard deviation)

	Elastic Modulus (GPa)	Hardness (GPa)	Brittleness (E/H)
Regenerated (4 wks)	10.17 \pm 2.00	0.39 \pm 0.07	28.17 \pm 5.75
Regenerated (8 wks)	10.32 \pm 2.07	0.37 \pm 0.06	29.43 \pm 4.17
Pre-existing (4 wks)	13.98 \pm 4.50	0.50 \pm 0.07	28.31 \pm 7.46
Pre-existing (8 wks)	13.02 \pm 4.45	0.53 \pm 0.08	25.81 \pm 7.56
Interface (4 wks)	12.21 \pm 2.60	0.41 \pm 0.10	32.87 \pm 7.43
Interface (8 wks)	10.33 \pm 2.01	0.40 \pm 0.03	28.38 \pm 6.25

Table 3: Nano-indentation results after treatment of BMP, DBM, and control (CTR) for Elastic modulus, Hardness, and Brittleness. (average \pm standard deviation)

	Elastic Modulus (GPa)	Hardness (GPa)	Brittleness (E/H)
Regenerated (BMP)	10.83 \pm 2.13	0.39 \pm 0.07	29.20 \pm 3.09
Regenerated (DBM)	10.07 \pm 1.87	0.40 \pm 0.06	26.98 \pm 6.14
Regenerated (Control)	9.58 \pm 1.94	0.35 \pm 0.06	30.43 \pm 5.59
Pre-existing (BMP)	14.38 \pm 4.31	0.52 \pm 0.04	28.18 \pm 7.75
Pre-existing (DBM)	13.14 \pm 4.51	0.52 \pm 0.10	26.15 \pm 6.90
Pre-existing (Control)	12.75 \pm 4.78	0.49 \pm 0.10	26.80 \pm 8.46
Interface (BMP)	11.37 \pm 2.02	0.40 \pm 0.06	30.19 \pm 4.00
Interface (DBM)	11.55 \pm 2.50	0.42 \pm 0.07	29.46 \pm 6.65
Interface (Control)	10.93 \pm 3.09	0.38 \pm 0.11	33.23 \pm 10.86

MEASUREMENT OF CONTACT PRESSURE OF FEMORAL FRACTURE FIXATION PLATE MADE OF SHAPE MEMORY ALLOY

¹Taemin BYUN, ²Namgu KIM, ²Shinhyouk YIM, ²Shingoo HUR, ²Changyun HWANG,
³Seungbaik KANG, and ¹Cheolwoong KO

¹Korea Institute of Industrial Technology (KITECH), Cheonan, Korea

²SMA Co., Ltd., Kwangju, Korea

³Seoul National University Boramae Hospital, Seoul, Korea

email: cheko@kitech.re.kr web: <http://www.kitech.re.kr>

INTRODUCTION

Recently, Korea has already become an aging society at the fastest rate in the world and approximately 12.7% of the entire population is 65 and older. As the proportion of the elderly continues to rise, prevalence of femoral fracture of the elderly caused by fall and other accidents is increasing as well. According to National Health Insurance Service, between 1999 and 2003, the number of femoral fracture cases in people aged 50 and older increased by 114% for men and 164% for women. Particularly, even though it is treated, 15% to 20% of patients die within a year. And, even after full recovery, many patients tend to suffer disability.

Generally, surgeons use different types of medical treatment for femoral fracture according to the fracture conditions. For instance, intramedullary nails can be inserted inside bone-marrow cavity for fixation, or a metal plate can be fixed on the bone fracture surface by nails. However, these methods could damage the bones and cause secondary bone fracture, which is fatal to the elderly. Therefore, it is recommendable to use a metal plate suitable for the patient's femur shape, and desirable to fix the metal plate on the bone fracture surface without screws.

In this study, we newly developed a prototype of a femoral fracture fixation plate made of shape memory alloy which has no screws for the fixation of the plate. Also, we fabricated test equipment to measure contact pressure of the plate using the test equipment.

METHODS

Femoral Fracture Fixation Plate made of Shape Memory Alloy

In this study, according to our previous studies on the anthropometrical measurement of Korean femurs using Korean Cadaver CT images, a prototype of a femoral fracture fixation plate made of shape memory alloy was newly developed, which is capable of providing clamping force based on reaction to body temperature (Figure 1). The clamping force can produce contact pressure between the plate and the bone surface.

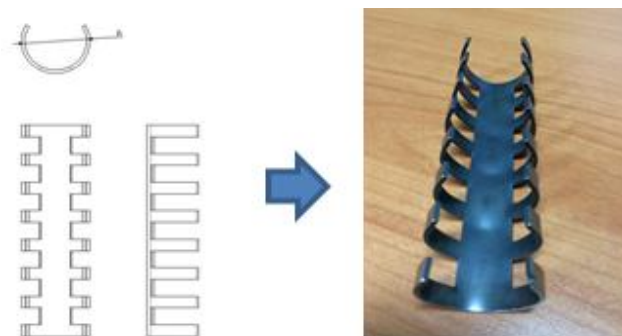


Figure 1. Prototype of Femoral Fracture Fixation Plate made of Shape Memory Alloy based on Anthropometrical Information on Korean Femurs

Contact Pressure Test Equipment

In this study, we newly fabricated test equipment to measure contact pressure of the plate (Figure 2). The test equipment included a water tank, circulating pump, temperature sensor, and bone clamp, to secure behavior of the plate according to temperature change (cold water temperature to body temperature).

The test was performed using the pressure sensitive paper (MS, Fujifilm, Japan), the composite cylinder (Length: 500mm, Diameter 30mm, Sawbone, USA), the plate, and the test equipment.

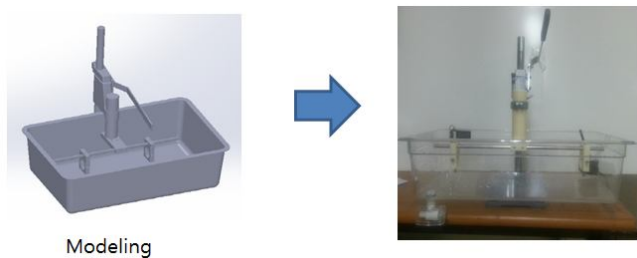


Figure 2 Fabrication of Contact Pressure Test Equipment

Procedure of Contact Pressure Test

The procedure of the contact pressure test was as follows. First, the plate was immersed in cold water (4°C ice water) and the open area of the plate was transformed to the outside. A pressure sensitive paper was attached onto the composite cylinder before fixing it inside the test equipment. The tank was filled with hot water and the water temperature was set to human body temperature, 37.5-40°C. Finally, the transformed plate was placed on the composite cylinder with the pressure sensitive paper and completely immersed in the water tank. In this study, contact pressure was measured by repeating this process five times for the plates of 26mm and 28mm in diameter, respectively (Figure 3).

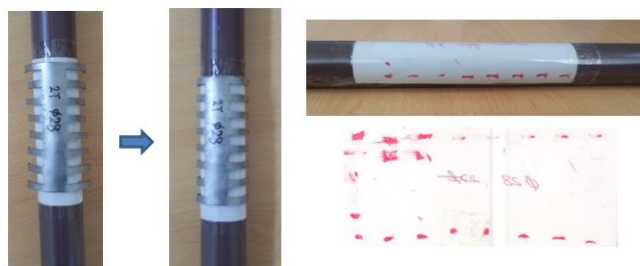


Figure 3 Contact Pressure Test of Femoral Fracture Fixation Plate made of Shape Memory Alloy

RESULTS AND DISCUSSION

In order to quantitatively analyze the measured contact pressure between the plate and the composite cylinder, a software of Pressure Distribution Mapping System (FPD-8010E, Fujifilm, Japan) was utilized. In case of the 26mm-diameter plate (Thickness: 2.4mm), the contact pressure range on the pressure sensitive paper was

between 35MPa and 45MPa. Meanwhile, for the 28mm-diameter plate (Thickness: 2.4mm), the contact pressure range was confirmed between 30MPa and 40MPa (Figure 4).

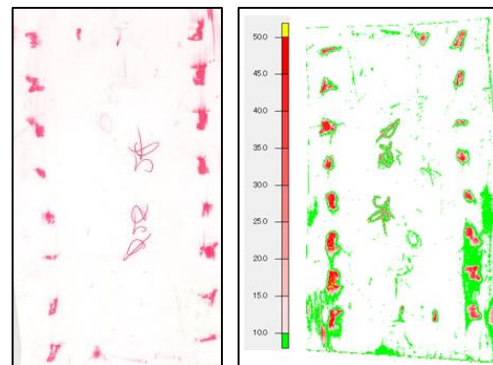


Figure 4 Analysis Results of Contact Pressure on Pressure Sensitive Paper (28mm-diameter Plate)

CONCLUSIONS

In this study, contact pressure test equipment was developed to measure the contact pressure of a prototype of a femoral fracture fixation plate made of shape memory alloy. Based on the acquired results of the contact pressure of the plate, we will plan to conduct the same test using human femur sawbones for the next step. The measurement data of contact pressure are expected to provide important and basic design information for the development of the femoral fracture fixation plates made of shape memory alloy (Figure 5).



Figure 5 Application of Femoral Fracture Fixation Plate made of Shape Memory Alloy

ACKNOWLEDGEMENTS

This study was conducted with research funds of Small and Medium Business Administration (S2127785).

ACTIVITIES TO PROMOTE REFLECTIVE LEARNING IN THE BIOMECHANICS CLASSROOM

Laurel Kuxhaus

Clarkson University, Potsdam, NY, USA

email: lkuxhaus@clarkson.edu, web: <http://people.clarkson.edu/~lkuxhaus/>

INTRODUCTION

The basic premise behind reflective learning is that student reflection on educational experiences informs future actions and choices both in and outside of the classroom. For example, reflecting on a difficult homework assignment, a student might conclude that s/he is not well-suited to an engineering career. When asked to consider the challenge of the assignment relative to their motivation for studying engineering, the same student may conclude that engineering is just the challenging career they seek. Encouraging reflection in the classroom coaches students to view their learning experiences from different perspectives and influences their future actions, learning, and careers. Reflection in the engineering classroom is growing. [1, 2]

Given that undergraduate biomechanics course often attract students with diverse mechanics backgrounds, the pace of the technical content is often perceived as 'too fast' or 'too slow' by students in the same classroom. Reflective activities can help all students to articulate the value of both the technical content and skills learned through the course and help form broad-thinking habits which will be carried throughout these young students' careers. This abstract presents some ready-to-implement strategies to promote reflective learning in an undergraduate Biomechanics class, intended to be customized as needed.

METHODS

The activities described below have been implemented in six years of teaching biomechanics, and can be used as graded or ungraded activities.

In-class Reflective Writing.

5-10 minutes (can also a take-home activity).

Inspired by "Emergency Assessments" [3], this technique guides students to reflect on their course-

related experiences through the 'lens' of their future selves. Students spend a few minutes writing in response to a prompt, such as:

You've applied for a job as a technical consultant for the next Batman movie. They have called you in for an interview. The person doing the hiring says "I see that you have taken a course in Biomechanics. How will a background in that make you a better member of our crew?" What will you reply? (modified from [3])

Journal Club.

Variable time; the author uses 25 minutes per week. Journal Club helps students locate, read, analyze and discuss current biomechanics research topics. Briefly, students have structured discussions of self-chosen journal articles in groups of 3-4. During in-class discussion time, the instructor(s) spends a few minutes with each group to clarify student questions and offer insights. To maximize effective discussions, students choose one of the following roles for each discussion (see [4] for more detail):

- Gatherer: Chooses the article, shares it with the group in advance, and summarizes the article prior to discussion.
- Questioner: Brings several questions about the chosen article to the discussion.
- Answerer: Reports answers to the questions after discussion.
- Historian (groups of 4 only): Brings information about the authors and their previous work on the topic to the discussion.

Assessment of students can be performed via the quality and timeliness of preparation posts to Moodle (course management software) and participation during the in-class discussion time. Journal Club encourages students to reflect on the course topics relative to contemporary biomechanics research. Furthermore, students often choose articles pertaining to areas of personal interest (for example, students who have had ACL

replacement may choose read about kinematics following the procedure), [4] and may alter their future behavior based on their reading.

Pyramid Exams

Can be completed in standard exam time.

Pyramid, or Cooperative, Exams [5] demand that students immediately reflect on their exam-taking experience. In essence, students take an exam individually and then immediately retake the exam in a small group setting (2-3 students per group). Scores are computed as a combination of the Individual and Group scores. (The author typically uses the higher of the Individual Exam Score, or $90\% * \text{IndividualScore} + 10\% * \text{GroupScore}$.) Anecdotally, the author observes lively discussions among students during the Group Exam; on course evaluation surveys, students overwhelmingly report that they both like and learn from the Group Exams.

To effectively implement this technique, the author uses frequent short exams to permit completion of both Individual and Group Exams in the allotted time. There is an obvious increase in the number of exams to grade; it is noted that the Group Exams tend to be more accurate than the Individual Exams, minimizing the increase in grading time.

Dedicated Reflective Assignment.

Completed outside of class.

Dedicated assignments may guide students to reflect on their learning experiences. For example, a “Popular Press” assignment encourages students to reflect on the portrayal of scientific results in the media. Students identify a news story published during the current semester which reports the results of a biomechanical study. They must also read the original journal article before writing a 1-2 page discussion of how the results were accurately (or not) portrayed in the media.

Resubmission of Homeworks and Projects

No additional class time.

The author permits students to redo homework assignments at any point in the class to encourage students to reflect on and learn from their mistakes immediately. Redo assignments must include a reflective description of the previous errors or they are returned to the student without review. There is

a penalty (-10 points out of 100) for students who delay the submission of a Redo beyond the class period immediately after an assignment is returned, and an additional penalty (-10 points) for delaying the Redo submission beyond the next Exam. In the authors’ experience in an undergraduate Statics class, approximately 15% of homework assignments are resubmitted, which requires time to grade. However, like the Pyramid Exams, the additional grading time is minimized because the resubmission assignments tend to be more accurate.

A similar process can be implemented in student projects and reports. For example, consider a student report which analyzes a failed fracture fixation device and describes a possible failure mechanism. The author then requires students’ reports to undergo peer review, where fellow students must reflect on the technical content and presentation of their colleagues’ work. All students may then reflect on their colleagues’ reflections and have the opportunity to revise their own report prior to grading by the instructor.

DISCUSSION

Reflective learning encourages broad thinking skills and deepens the learning experience for students. Simple activities, such as those described above, can encourage reflection both in and outside of the biomechanics classroom. They are generally well-received by students. Future work may assess the pedagogical benefits of these techniques on student outcomes. Furthermore, instructors can also benefit by using the feedback from students in the reflective exercises to inform their own teaching.

REFERENCES

1. Turns, J. et al., 2014; *ASEE Conference*.
2. <http://depts.washington.edu/celtweb/cpree/>
3. Huston, T., 2012. “Teaching what you don’t know.” Harvard University Press. 320pp.
4. Corbiere and Kuxhaus, 2012; *ASEE St. Lawrence Regional Mtng.*
5. Cohen and Henle, 1998. *Faseb J.*

ACKNOWLEDGEMENTS

The author thanks her students for their willingness to try these activities in class.

VALIDATION OF INERTIAL SENSORS FOR USE IN SHOOTING EVENT DETECTION

Lindecker, PR, Higginson, BK
Gonzaga University, Spokane, WA USA
email: plindecker@zagmail.gonzaga.edu

INTRODUCTION

In tactical and competitive shooting it is common for the shooters and coaches to utilize an optical targeting system such as Noptel Sport II shooting training system. These systems can be extremely helpful for training purposes as they are able to measure and display shot data in real time. Some of the variables that are possible to collect are shot times, time on target, stability of hold, and placement of shots on target. One limitation of these systems is the lack of resolution for timing between shots. These measures are provided only in whole seconds. For applications such as rapid-fire events in competitive shooting, and multiple-shot, multiple-target tasks in tactical shooting, a greater resolution is required. Inertial sensors mounted to the weapons platform can be effectively used to quantify this measure with greater resolution, yet it is still unknown whether these inertial sensors can reliably provide other shooting outcome measures such as time on target.

The purpose of this study was to determine if inertial sensors can be reliably used to quantify shooting events, such as time on target, during tactical shooting applications.

METHODS

For this study 8 male novice shooters with little to no shooting experience were recruited to take part in the study. Each shooter participated in three different shooting conditions. In each condition subjects wore tactical body armor. In the first condition, only body armor was worn during the shooting task. In the second condition, a 35 lbs backpack was worn over the body armor. The third condition was the same as the second, only with load stabilizers added to the pack to improve pack contact with the armor system.

Then, using a weight matched airsoft M-4's, each subject completed a tactical shooting scenario in

which they engaged three targets, one directly in front of them, one 60 degrees to the right and left of the center target. Shooters engaged the center target and then moved to the second target immediately following an auditory cue, and then engaged the remaining target.

Inertial sensors and the optical targeting system were attached to the rifle. Acceleration data was then collected using an inertial sensor system as well as an optical targeting system. Times between shots and target engagement times were collected using both systems.

RESULTS AND DISCUSSION

There was a moderate level of agreement between the two measurements techniques in detecting time on target (engagement times) during the tactical shooting tasks ($ICC=.506$, $p<0.001$) with a slopes approaching unity ($\beta_1=0.770$) and intercept values of ($\beta_0=0.258$) shown in Figure 1.

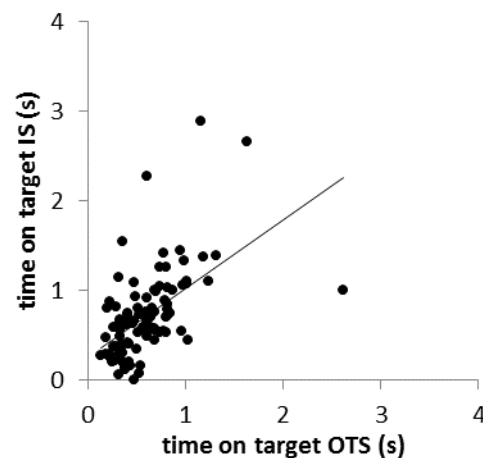


Figure 1. Scatterplot of time on target from the optical targeting system (OTS) versus the inertial sensor system (IS).

Given the moderate level of agreement between the optical targeting system and the inertial systems it is concluded that the use of inertial sensors maybe valid instruments for detecting time on target for tactical shooting tasks

CONCLUSIONS

The moderate levels of agreement between optical targeting system and the inertial sensor system indicates that inertial sensors could be used to

determining the time subjects spend on the target during tactical shooting tasks. It is believed that the correlation could be improved with the use of trained shooters who are able to settle on target faster and more accurately than the untrained population used in this study.

THE EFFECT OF SKIN MOTION ON DYNAMIC ULTRASOUND OF THE VASTUS LATERALIS

^{1,2} David B. Lipps, ^{1,2} Allison B. Wang, ^{1,2} Eric J. Perreault and ^{1,2} Sabrina S. Lee

¹ Northwestern University, Evanston, IL, USA

² Rehabilitation Institute of Chicago, Chicago, IL USA

email: dlipps@ricres.org

INTRODUCTION

Muscles generate force and movement through contractions, with resultant length changes occurring at the whole muscle level and fascicle level. Quantifying these length changes provides insight into muscle function and mechanics. Musculoskeletal ultrasound is commonly used to quantify muscle strain and muscle architecture non-invasively and in real-time in healthy and impaired populations during passive and active dynamic movements [1, 2]. The transducer is primarily affixed to the skin such that movements of structures underlying the skin are measured as displacements relative to the skin (Fig. 1). Thus, errors in estimates of muscle displacement occur if there is skin motion. Our objective was to quantify how skin motion alters ultrasound estimates of muscle movement for the vastus lateralis (VL) in a static posture, as well as passive and active sagittal-plane knee flexion and extension.

METHODS

Five subjects (3 M, 2 F; mean±SD age 29±4 yrs, mass 73±13 kg, height 178±4 cm) seated in an adjustable chair were attached to a high-precision rotary motor centered at the knee (Fig. 2).

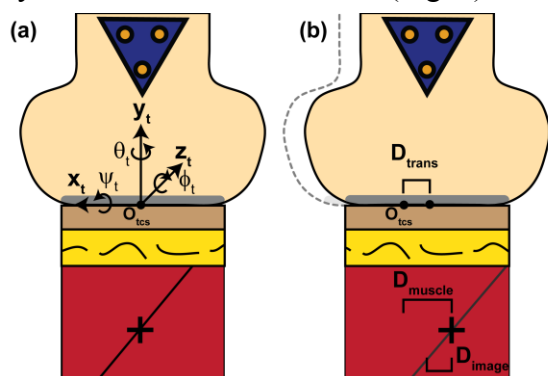


Figure 1. Illustration of the movement of a trackable muscle feature (+) as both the transducer and underlying muscle move to the right. (a) Ultrasound transducer with corresponding coordinate system. (b) The raw displacement of the muscle feature on the ultrasound video and the 3D movement of the ultrasound transducer can be summed to find the true displacement of the muscle feature.

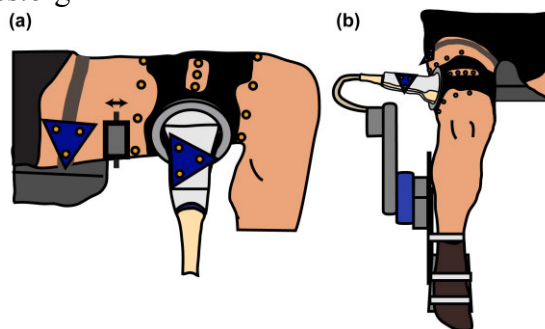


Figure 2. (a) Static condition: Subjects remained stationary as the skin was pulled with tape. (b) Dynamic condition: Subjects were attached to a rotary motor for passive and active movements. Infrared markers recorded the 3-D kinematics of the transducer to correct for skin motion errors.

The effect of skin motion was investigated both statically and dynamically. The static condition investigated the effect of skin motion on ultrasound videos when no underlying muscle movement is present (Fig. 2a). The dynamic condition investigated the effect of skin motion on ultrasound videos as the underlying VL moves (Fig. 2b). Subjects relaxed their VL while the motor flexed and extended the knee (range: 35°–80°) with a constant velocity (40 °/s). Subjects also actively moved their knee through a similar range and velocity to an audible cue. There were 10 movement cycles per subject for each movement condition.

In both conditions, dynamic ultrasound was collected (25 Hz) from the VL using a 49-mm transducer (Supersonic Imagine Aixplorer) aligned to the fascicle plane and secured around the thigh with a custom holder. A custom algorithm estimated local displacements of the VL's mid-belly and superficial adipose tissue on the ultrasound video, ad modum [2]. Movement of the transducer was quantified using infrared markers (Optotrak, 60 Hz). The 2D displacements estimated with ultrasound were transformed to 3D with respect to the transducer's initial position, allowing the observed muscle displacement to be corrected by the amount of transducer translation in the x-direction (Fig. 1). For each testing condition, paired t-tests compared the raw and corrected muscle displacements.

RESULTS AND DISCUSSION

The static condition allowed the effect of skin motion to be studied independent of muscle movement. Skin motion led to errors in the estimation of muscle motion, as the stationary muscle appears to move on the ultrasound videos while the superficial adipose layer was stationary (Fig. 3a,b). By correcting for the 3D kinematics of the ultrasound transducer, the muscle remained stationary (Fig. 3c,d). These results show tracking the adipose layer is not sufficient for assessing skin motion (contrary to [1]). Instead, tracking the 3D kinematics of the transducer is needed to correct for skin motion errors on ultrasound.

The effect of skin motion on ultrasound was further explored as the VL moved during passive and active knee flexion. Passive and active movements produced similar 3D transducer kinematics (Fig. 4a,b). Active displacement of the VL estimated from the ultrasound videos was significantly lower than the muscle displacement corrected for skin motion ($p < 0.001$) (Fig. 4c,d). No significant difference was found for the passive condition ($p = 0.14$), as both over- and under-estimation of muscle displacements were observed.

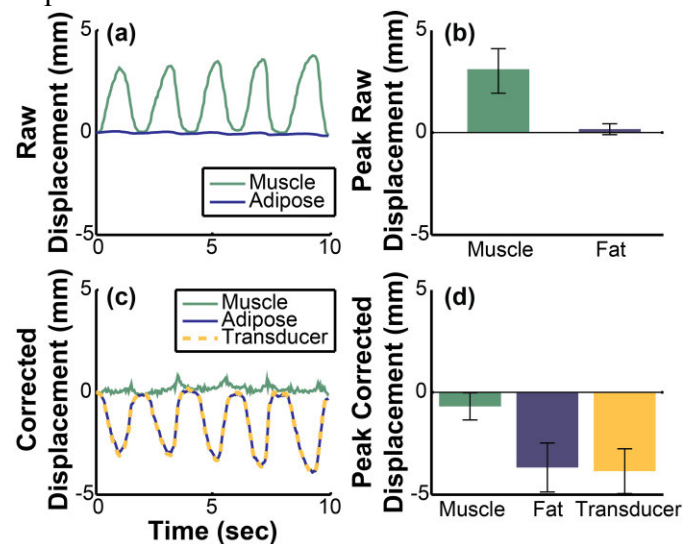


Figure 3. (a) Exemplar trial and (b) group results showing the raw displacement of adipose layer and VL's mid-belly on the ultrasound video as the skin is pulled above the static muscle. The raw ultrasound video gives the impression that the muscle is moving while the adipose is stationary. The displacements recorded with ultrasound were then corrected for the 3D kinematics of the transducer. (c) The exemplar trial and (d) the group results indicate the muscle was stationary as expected, while the adipose layer moves a similar amount as the transducer.

This is the first study to explore the effect of 3D skin deformations on ultrasound measurements; prior work has been limited to isometric conditions [3]. These results have important implications for musculoskeletal ultrasound since inaccurate estimations of muscle displacement will occur if these skin motion errors are not properly corrected. Future work will explore if the observed inter-subject variability was due to differences in adipose tissue and thigh circumference.

CONCLUSIONS

Estimated measures of vastus lateralis muscle displacement using dynamic ultrasound are affected under passive and active conditions by skin motion; these errors are correctable using motion analysis of the ultrasound transducer.

REFERENCES

- [1] Bojsen-Moller et al. (2010) *J Appl Physiol* 109, 1608-18.
- [2] Darby et al. (2012) *J Appl Physiol* 112, 313-27.
- [3] Maganaris et al. (1999) *J Physiol*. 521, 307-13.

ACKNOWLEDGEMENTS

Funding: NIH T32-HD07418 & T32-EB009406

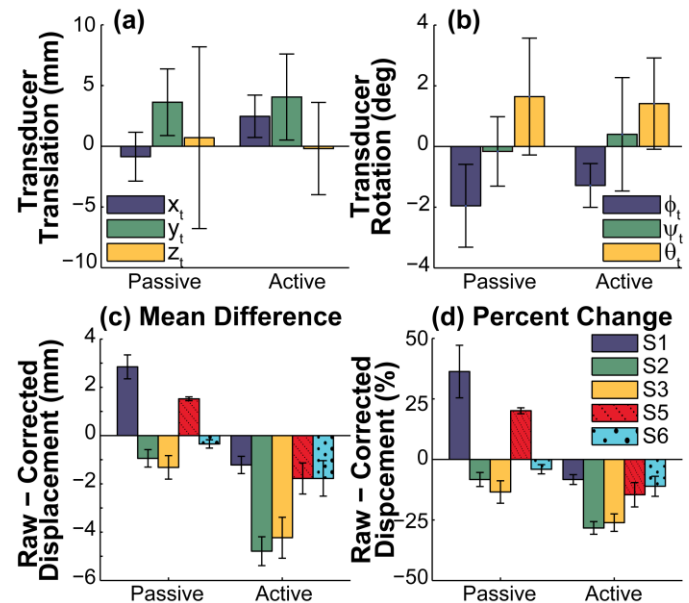


Figure 4. Mean 3D (a) translation and (b) rotation of the ultrasound transducer during passive and active knee flexion across subjects, relative to the transducer's initial position. Refer to Fig. 1 for coordinate system. The kinematics of the transducer were used to correct the raw displacement of the vastus lateralis from the ultrasound videos. The (c) mean difference and (d) percentage change between the raw and corrected muscle displacements for each subject are shown.

A Vision-Based, Hybrid-Reality, Wire Navigation Simulator

Steven A. Long, Geb W. Thomas, Leah K. Taylor, Colleen E. Rink, Don D. Anderson

¹ The University of Iowa, Iowa City, IA

Email: steven-long@uiowa.edu; web: <http://tinyurl.com/UIOBL>

INTRODUCTION

Advancements in simulation, particularly for laparoscopic surgery, have moved surgical skill acquisition from the operating room (OR) to safer environments. Orthopaedic surgical skill training, however, has remained largely unchanged for the past century. Orthopaedic residency training still relies on novices first observing expert surgeons performing a task, then attempting the task on a live patient under supervision. This training method is costly because it extends the amount of time in the OR and puts the patient at risk. Wire navigation is an important orthopaedic surgical skill in which the surgeon directs a wire to a target position in a bone, while visualizing the position with a fluoroscope. With approximately 247,000 hip fracture cases each year¹, trochanteric neck fractures often provide an important opportunity for junior residents to develop this skill. The simulator presented here helps residents develop the wire navigation skill in the context of directing a surgical wire (a K-wire) towards the tip of the femoral head, a common first step in performing surgery for a trochanteric neck fracture.

METHODS

The simulator has five main components: a pair of USB web-cams, a plastic foam bone surrogate, a K-wire driver, a laser-etched K-wire, and a laptop computer (Figure 1). The cameras, located above and on either side of the workspace, capture a stereo image pair that is used to determine the position, angle and depth of the wire relative to the bone. The flowchart in Figure 2 illustrates how the data is gathered, processed, and presented back to the user.

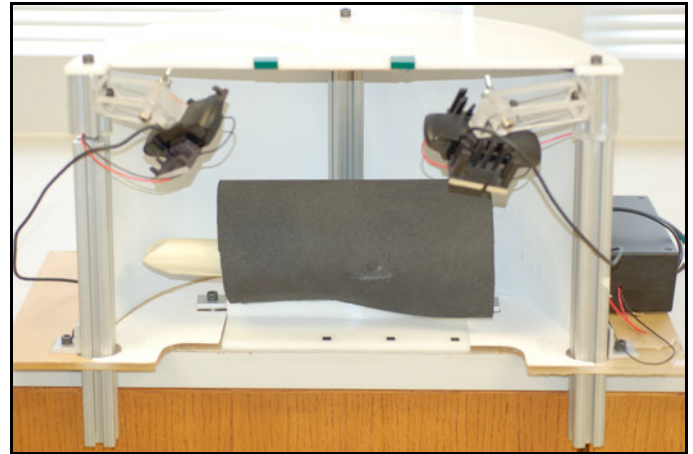


Figure 1 – A Display of the simulator. The laptop is not shown here.

The image processing proceeds in three stages: gross edge detection, fine edge detection, and address assessment. The gross edge detection stage finds the wire edges within both images. It relies on the difference between (a) the image including the current wire position and (b) a previously stored image of the empty working space. This difference image isolates the wire. A Canny edge detection algorithm is then applied to a binary version of this image. A Hough algorithm then finds the best-fit position for the edge-enhanced images.

Once the edges of the wire have been found, the original image is then cropped and rotated so that the long edges of the wire are vertical. A horizontal edge detection filter then isolates the etched, horizontal lines. A Hough algorithm marks these lines in the image, which are then represented by a series of points along the center of the wire. In this way, each horizontal line then has one point at its start and one at its end. Once these reference points are located in each stereo image, they are matched across the images. Their corresponding positions in each image are input into a Direct Linear Transform algorithm (DLT). The DLT uses a previously calibrated relationship between the 2D space of the

images with the 3D space of the surrogate bone. The DLT algorithm provides the output of the fine edge detection stage: the wire's axis in 3D space relative to the bone. The only remaining degree of freedom to define is where the tip of the wire sits inside the bone, which is hidden from view.

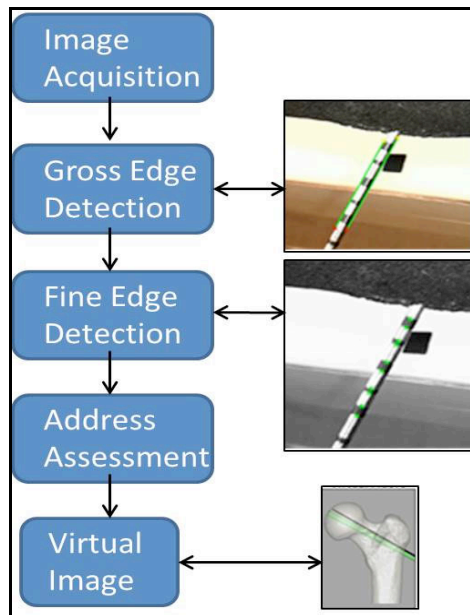


Figure 2 - A flowchart describing the sequence of algorithms used to generate a virtual fluoro image.

The address assessment stage uses a normalized, cross-correlation algorithm to determine the position of the wire tip within the bone. The algorithm takes the section of wire seen by a camera and compares it to a template of the complete wire address. The location of the markings on the wire, its address, is determined by the position of maximum agreement between the template and visible wire section. This information, coupled with the wire's axis relative to the bone that was determined in the previous stage, is sufficient to calculate the position of the tip within the bone.

The accuracy of the simulator was determined by placing the K-wire at known locations in the workspace and comparing the calculated tip location to the known tip location.

Table 1 - Accuracy measurements of the simulator

	Point 1	Point 2	Point 3	Point 4
Calculated Point	38.52, 99.22, 31.11	-14.62, 103.88, 28.59	-7.36, 103.38, 29.21	42.95, 98.96, 32.86
Known Point	37.11, 98.82, 31.75	-14.86, 102.89, 30.63	-8.74, 102.85, 30.75	40.22, 98.86, 34.17
Difference (mm)	1.66	2.28	2.14	3.03

RESULTS AND DISCUSSION

The proposed simulator for this work has been successfully tested with orthopaedic surgical residents at three training institutions. The system displays the virtual fluoro images after a 2 second lag and users indicate that they trust the veracity of the result. As can be seen in Table 1, the accuracy of the simulator in controlled tests varies from approximately 1.66 to 3.03 mm. Occasionally in field tests, obviously wrong position estimates are produced, with errors of several centimeters. We believe these are the result of software errors and a more accurate estimate is generally produced on a second request in the same position. A previously developed simulator reported on by Thomas et al. showed similar accuracy values ranging from 1.5 to 3.6 mm of error². In that simulator, the virtual images were generated through the use of a costly device that generated an electromagnetic field. As the image processing algorithms continue to develop, it is expected that the error and run time of the proposed simulator will only decrease with time. Furthermore, given that the simulated experience depends more on the internal and relative consistency than on absolute consistency, it is unlikely that absolute accuracies greater than 1 mm would have a large impact on training effectiveness.

REFERENCES

- [1] J. L. Kelsey and S. Hoffman, New England J Med, 404:406-316 1987.
- [2] G.W. Thomas, et al. IEEE Trans Human-Machine Systems, 119:125-45, 2015.

ACKNOWLEDGEMENTS

This work was partially supported by grants from the Orthopaedic Research and Education Foundation, the American Board of Orthopaedic Surgery, and the Agency for Healthcare Research and Quality.

RELIABILITY OF A MRI-BASED TECHNIQUE FOR QUANTIFICATION OF DYNAMIC MOTION OF SOLID BODIES

^{1,2}Niladri K. Mahato, ^{1,2}Stephane Montuelle, ^{1,3}Craig Goubeaux, ^{1,3}John Cotton, ^{1,2}Susan Williams, and ^{1,2,4}Brian C. Clark

¹Ohio Musculoskeletal and Neurological Institute (OMNI),

²Department of Biomedical Sciences,

³Department of Mechanical Engineering, and

⁴Department of Geriatric Medicine at Ohio University, Athens, OH 45701

email: nm620511@ohio.edu

INTRODUCTION

Abnormal motion patterns between constituent bony elements of a joint have been etiologically linked to arthropathies in general and to the occurrence of back pain, in particular [1]. Current methods of quantification of inter-vertebral motion is associated with exposure to ionizing radiation, and are mostly restricted to two dimensional analysis [2]. The technique reported here is being developed with the long-term goal of using it to detect and quantify complex motion of spine segments. The proposed technique uses (i) a series of images acquired using a dynamic MRI sequence that can scan objects in motion, (ii) a 3D segmentation software to create virtual models of solid body objects, and (iii) an animation software that re-creates and permits quantification of displacements between 3D models in six degrees of freedom of motion.

METHODS

MRI compatible solid-body objects (two, 4 cm cubes of solid wood) were constructed with cylindrically hollowed-out centers. The adjacent edges of two sides of these cubes were marked at 0.5 cm increments so that one cube could be manually translated relative to the other over a range 2 cm on either side of a neutral position (zero displacement between the mid-line of the cubes). Customized 3D models of the solid bodies were segmented using the 3D segmentation software AVIZO (Hillsboro, OR) from transverse scans obtained using a T₁ weighted sequence (TR=810 ms, TE=30 ms) in the neutral position prior to initiating the trials. The solid bodies were placed in

a 0.3 Tesla open-MRI (Esaote G-scan Brio, Genoa, Italy) coil after the imaging volume of the coil was calibrated with a custom built calibration grid. A camera-view was created in Autodesk MAYA animation software (San Rafael, CA) using the information from the coil volume calibration. The objects were scanned at different displacements between 0.5 to 2 cm in a random order (n=32 trials; each respective displacement having 8 trials) (Table 1) between the solid bodies, across several scanning sessions on multiple days. A dynamic 2D HYCE S[®] sequence was used to scan the static displaced positions (slice thickness=7 mm). The series of 2D HYCE S DICOM images of the solid-body objects were then processed in AVIZO and converted into JPEG files. The camera-views were used to import the scanned images and the 3D models of the solid-bodies into MAYA. Next, the virtual 3D models were manually positioned (rotoscoped) [3] to align and fit into the images captured during the trials. The rotoscoping process was assisted by using the margins and hollowed core of the solid bodies as anatomical cues. This process was repeated for all trial image frames. A joint co-ordinate system between the solid-body elements was created using a semi-automated process in MAYA. The animation software quantified the inter-body translation in one plane, as performed in the experiment. The rotoscoping and quantification processes for all images were performed twice at two different week-long sessions separated by a week. Obtained data from the two sessions (S1 and S2) was analyzed for reliability (correlation coefficient) (Figure 1) and variability (coefficient of variation, CV) (Table 1) by a single observer.

RESULTS AND DISCUSSION

The technique exhibited a high degree of reliability between the measurements from the two sessions ($r=0.978$; Figure 1), and low variability as observed from the CV's ranging between 5-9% (Table 1). A paired T-test comparing the measurement of each displacement from the two sessions did not show any significant difference ($p \geq 0.21$).

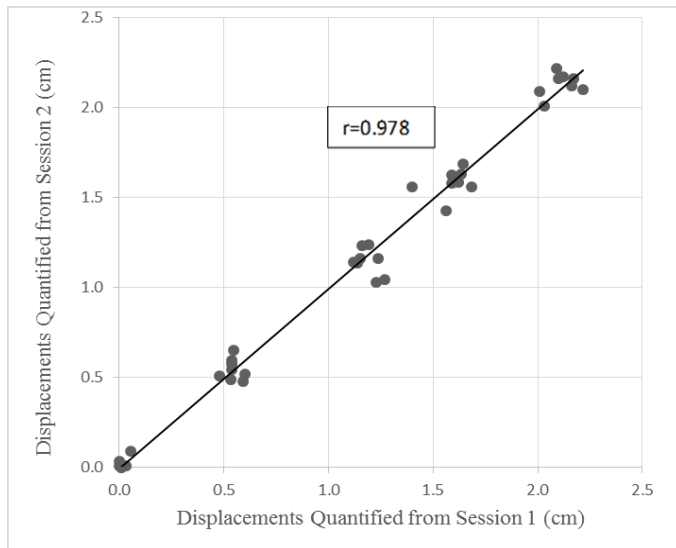


Figure 1: Correlation between quantified displacements from two measuring sessions ($n=32$ for each session).

Our work shows that quantification of solid-body displacements can be achieved with use of the 2D HYCE S[®] dynamic sequence. Accordingly, the use of the reported technique can be used to quantify motion in dynamically moving elements in human joints. While our observed reliability was very high,

it is probable that higher levels of accuracy are obtainable using higher field magnets, using motion control devices that could move solid-bodies through pre-determined displacements with greater precision and/or with the use of improved multi-planar dynamic sequences. The animation software is capable of quantifying 3-dimensional angular and linear displacements, and we are currently exploring modalities of imaging and quantifying multi-planar spine motion using the same technique. Additionally, we are currently investigating the accuracy of this technique.

CONCLUSIONS

Our results provide basic proof-of-concept for a reliable non-ionizing radiation based inter-body motion quantification technique that can be safely used to identify and characterize pathological behavior between elements in bony articulations. This technique can also be applied for biomechanical analysis of complex joint system such as the human spine.

REFERENCES

1. Wu M, et al. *Eur Spine J* **23**, 2350-2358, 2014.
2. Shaffer WO, et al. *Spine (Phila Pa 1976)* **15**, 741-750, 1990.
3. Gatesy SM, et al. *J Exp Zool A Ecol Genet Physiol*, **313**, 244-261, 2010.

Table 1: Descriptive statistics derived from the scanned images from two different quantification sessions (S1 and S2).

Scanned Displacements ($n=8/\text{displacement}$)	Mean \pm SD for S1	Mean \pm SD for S2	CV (%)
0.5 cm	0.55 \pm 0.04	0.55 \pm 0.06	9.32
1.0 cm	1.25 \pm 0.10	1.14 \pm 0.07	9.51
1.5 cm	1.59 \pm 0.09	1.58 \pm 0.07	8.66
2.0 cm	2.11 \pm 0.07	2.13 \pm 0.07	5.47

METHODOLOGY, VALIDATION AND TESTING OF AN INEXPENSIVE OPTICAL PLANAR-MOTION CAPTURE SYSTEM

¹ Joseph M. Mahoney, ¹ Jacob D. Weir, ¹ Courtney M. Jankowski, and ¹ Benjamin W. Infantolino

¹ The Pennsylvania State University, Berks College, Reading, PA, USA

email: jmm694@psu.edu, web: <http://www.personal.psu.edu/jmm694/>

INTRODUCTION

Full 3D motion-capture systems (e.g. Motion Analysis, Vicon) can cost well over \$100,000. However, for classroom demonstrations and undergraduate research, a full system may not be needed. If joint angles are desired, electric goniometers can be employed, but are intrusive and also expensive. Furthermore, it is hard to find angles for some joints (e.g. hip) with a goniometer.

We present and validate, via a pilot experiment, a motion capture system and method for planar motion for less than \$500 (not including software). The hardware is available off the shelf and the software runs in Matlab. The system was tested while capturing knee and ankle angles of a participant walking on a treadmill. A pilot validation of the method was performed by comparing the angle found with the camera system to that found by an electric goniometer.

METHODS

Six green markers were affixed to locations on the right leg of a participant: proximal and distal medial thigh, proximal and distal medial shank, lateral calcaneus and the base of the fifth metatarsal. For later calibration, the ankle was set perpendicular to the ground and the knee was set to 180° and a still image was captured. The knee and ankle angle found in this image are used as the 0° values.

As a proof of concept, the system was set up to capture knee and ankle angles in the sagittal plane. A participant walked on a treadmill (Quinton TM65, Milwaukee, WI) at a comfortable walking pace of 2 mph for 30 s. The right sagittal plane (See Fig. 1) was filmed with digital video camera (Canon r500) at a high resolution of 1920x1080 at 60 fps.

The first frame of video is used to initialize the program. Here, the six markers are manually identified for their position and color. The program iterates one frame at a time, to identify the marker positions. First, markers are found by color-thresholding the image using previously identified marker color. Next, a *k-means clustering* routine is run on the image to identify the six largest clusters, using the previous image as a starting point for their location. Each cluster is then associated with the appropriate marker by calculating which previous marker it was closest to. All marker centroid coordinates are saved and the data is fed forward to the next frame and repeated through all frames.

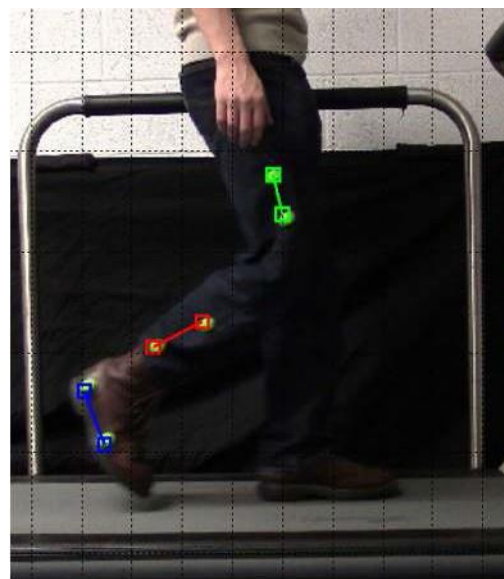


Figure 1: Vector overlay of limb segments on typical screenshot of video. A black sheet was placed behind the treadmill to increase contrast.

The pairs of markers on each limb segment are used to calculate a vector describing the limb's direction (see line overlays on Fig. 1). The angle between limbs is then found using the dot product operation. Since the markers are not aligned with the limbs themselves, the angles found in the calibration are subtracted off to find the angle

between limbs rather than the angle between markers.

Gait cycles are automatically identified from the joint angle data. We define the cycle beginning *near* heel strike (specifically when the shank and ankle are 90° after the heel strike). For each stride, the time is normalized to 100% and data is resampled using a cubic-spline interpolation. For each point in the cycle, the mean (μ) and standard deviation (σ) is calculated.

To validate the optical method for finding joint angles, a test was performed to compare the angle found by video to an angle determined by an electric goniometer (Biometrics Ltd, Ladysmith, VA). Four markers and the electric goniometer were affixed to an analog goniometer. Data capture began and the analog goniometer was moved from 70° to 180° in 10° increments. This test was repeated at distances from the camera lens of 70 cm to 370 cm.

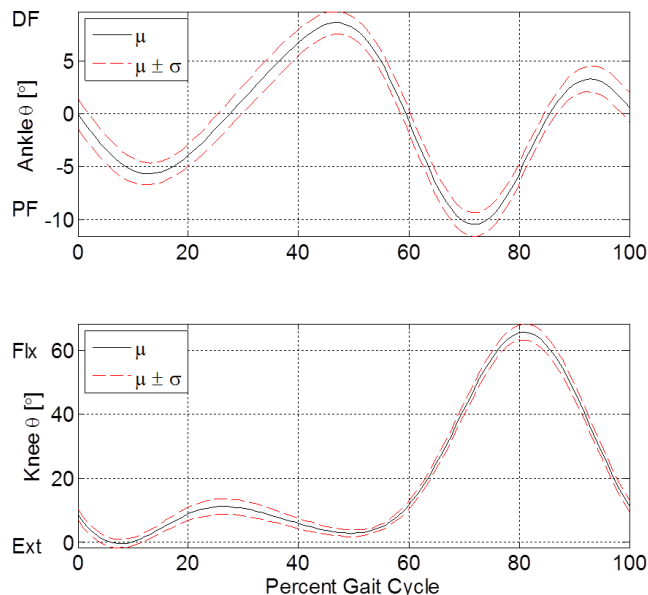


Figure 2: Gait cycle created from video analysis on pilot participant. For the ankle angle, positive values indicate dorsiflexion, negative are plantar flexion. For knee angle, negative values indicate extension, positive are flexion.

RESULTS AND DISCUSSION

The original video was overlaid with the identified markers and limb-segment vectors for visual inspection of the automated method. A

typical screenshot is shown in Fig. 1.

The average knee and ankle angles of one participant over 20 strides are shown in Fig. 2. By visual inspection, the data look similar to normative gait data for ankle and knee presented in Kadaba [1].

For the validation test, a typical result – taken from the 250 cm test – is shown in Fig. 3. Using the electric goniometer as the “true” measure, the difference between the measurements was calculated. The standard deviation was at most 0.571°.

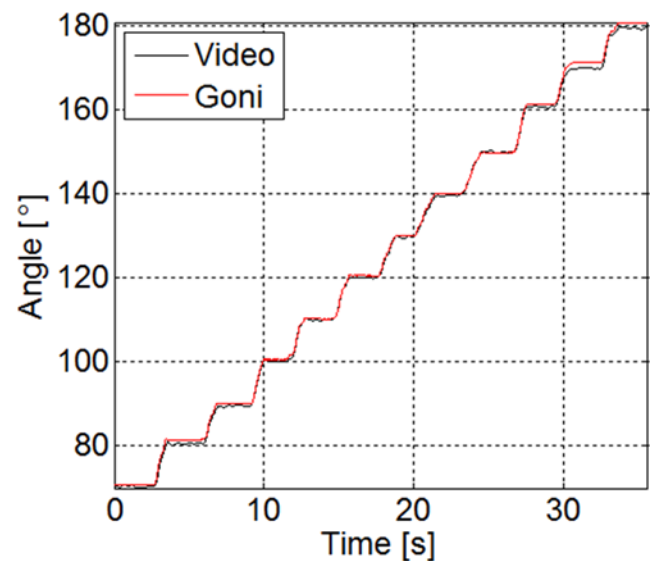


Figure 3: Comparison of angle determined by video and by electric goniometer in pilot test (250cm from camera lens)

CONCLUSIONS

The system gives reasonably accurate ($\pm 0.58^\circ$) joint angles when compared to data captured from an electric goniometer. Based on this validation pilot, the error is certainly small enough for classroom use and potentially research as well. The joint angles measured for the pilot participant matches reasonably well to published results. Based on these promising early results, the system will be used further for testing on larger participant pools.

REFERENCE

1. Kadaba MP, et al. *J Orthopaedic Research*, Vol. 8, No. 3, 1990.

Between day reliability of markerless versus traditional marker based motion capture during a stepdown task

¹Kristin Morgan, ¹Mao Ye, ¹Ruigang Yang and ¹Brian Noehren

¹University of Kentucky, Lexington, KY, USA
email: kmo242@uky.edu

INTRODUCTION

Marker based motion capture analysis enables researchers to measure dynamic motion to assess movement abnormalities. However, this technology is cumbersome to use, requires a large space, is expensive to purchase and requires significant expertise to operate limiting its ability to be translated to a clinical setting or be used in a natural environment (e.g. playing field). Clinicians could benefit from a system that allows them to evaluate changes in joint biomechanics in their office or on the playing field to be able to better tailor rehabilitation programs and assess their outcomes.

Markerless motion capture analysis has the ability to address this need. Markerless motion capture has been shown to measure joint kinematics with similar levels of accuracy as motion capture system [1]. The next step in markerless motion capture analysis is to assess the day-to-day reliability of this system and its post processing algorithm. This is particularly critical to evaluate as clinicians are interested in being able to assess day to day changes due to the patient and not the variability in the system.

Thus this study investigated the day-to-day reliability of the Microsoft Kinect markerless motion capture system [1]. To assess this, we evaluated individuals during a stepdown task over two different days using both the markerless (Kinect) and marker-based systems. The objective of this research was to determine if a markerless motion capture system could measure joint angles with the same level of precision and reliability as the marker based motion capture system.

METHODS

Five participants (4 males, 1 female; height 1.8 ± 0.1 m; mass 75.8 ± 10.4 kg; age 25.2 ± 2.8 yrs) were recruited to perform the study protocol. The study had the participants conduct a series of five single-leg stepdown tasks on a small box three inches high on two different days with a minimum of 24 hours between each session. Twenty-eight reflective markers were placed on the participants' lower extremity to track their movement via the 10-camera motion capture system (Motion Analysis Corp, Santa Rosa, USA) that were sampled at 200Hz [2].

A single Kinect camera was used to record the participants at the same time as the marker based system during the stepdown task [3]. Color images and depth maps were extracted from the Microsoft Kinect image data and an iterative closest point (ICP) algorithm was used to align the initial scan of the participant with the extracted images [4]. Joint angles were obtained from these extracted images using MeshLab [5] and a custom Matlab code (MathWorks Inc., Natick, MA).

Peak joint angles were obtained from the motion capture and Kinect generated waveforms of the hip and knee in the sagittal, frontal and transverse planes. The between day reliability of the motion capture and Kinect measured peak joint angles was assessed using intraclass correlation (ICC).

RESULTS AND DISCUSSION

The between day reliability of both the markerless and marker based techniques was comparable for many of the measurements (Table 1). The Kinect displayed high day-to-day reliability in the sagittal (0.95) and frontal (0.93) plane at the hip (Table 1).

The between day knee and hip ICC values for the Kinect though were lower (0.67 knee 0.53 hip) Lastly, the ICC for the Kinect was 0.53 and 0.49 in the transverse plane for the hip and knee, respectively.

Differences in day-to-day mean peak joint angles for the Kinect were approximately 1° for hip and knee in the sagittal and frontal planes. Furthermore, the Kinect measured peak joint angles that were within 5° of the marker based motion capture system in all three planes for the hip and in the sagittal and frontal planes for the knee. Analysis of the markerless system waveforms showed similar patterns to the marker based system and between the two days (Fig. 1).

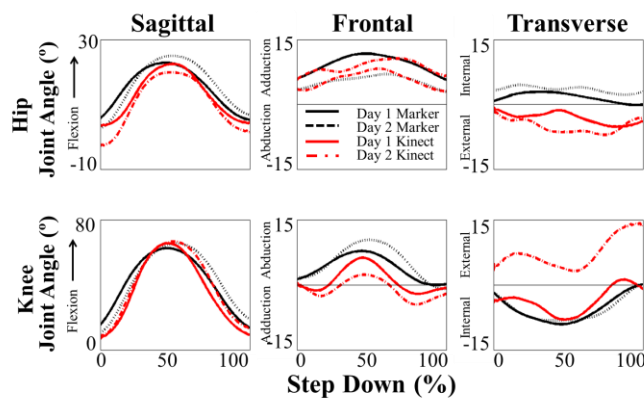


Figure 1. Comparison of the day-to-day hip and knee waveforms between the marker based (red) and markerless (black) systems for one participant. Day 1 waveforms are represented by the solid lines while day 2 waveforms are represented by the dashed lines.

CONCLUSIONS

These findings indicate that the markerless system possesses the day-to-day reliability to assess joint kinematics with similar precision as the marker based system in the sagittal plane. The markerless

system also displayed high reliability in the frontal plane at the hip.

The day-to-day reliability of the markerless system was weaker in the transverse plane at both the hip and knee. Future assessments will include adjusting how anatomical landmarks are denoted on the initial registration of the markerless motion capture system. Additionally, improvements tracking transverse plane motion may be found in using a higher resolution markerless camera.

These results highlight the potential ability of the markerless system as an application in clinical settings to measure and document changes in motion due to rehabilitation. Further we have shown reliability in a task that is common for clinicians to assess when evaluating a patient with lower extremity dysfunction, increasing the systems external validity. Further work is needed though assessing the system during high speed movements and during more complicated tasks that patients commonly engage in such as a side cut run task.

REFERENCES

1. Schmitz, A. et al., *Journal of Biomechanics*, **47** (2), 587-591, 2014.
2. Noehren, B. et al., *Gait & Posture* **36**, 596-599, 2012.
3. Microsoft. <http://www.microsoft.com/en-us/kinectforwindows/>
4. Rusinkiewicz, S. et al., Third Int'l Conf. on 3-D Digital Imaging and Modeling, 2001.
5. Cignoni, P., et al., *ERCIM News* **73**, 45-46, 2008.

ACKNOWLEDGEMENTS

This research was funded by NSF IIS 1231545.

Table 1. Comparison of the day-to-day peak hip and knee angles obtained from the marker-based and Kinect systems and the associated intraclass correlation analysis.

	Marker based			Kinect		
	Day 1	Day 2	ICC	Day 1	Day 2	ICC
	Degrees	Degrees		Degrees	Degrees	
Hip Flexion	25.5 ± 5.0	24.9 ± 7.4	0.91	21.4 ± 7.6	21.9 ± 7.0	0.95
Hip Adduction	10.1 ± 3.7	8.9 ± 4.5	0.67	7.5 ± 7.7	7.7 ± 5.5	0.93
Hip Internal Rotation	8.2 ± 7.2	8.7 ± 5.0	0.91	2.0 ± 3.3	7.7 ± 14.4	0.53
Knee Flexion	62.1 ± 2.8	63.3 ± 3.2	0.96	66.0 ± 4.3	65.8 ± 2.7	0.67
Knee Abduction	11.4 ± 4.0	11.6 ± 1.7	0.74	7.4 ± 1.0	8.1 ± 9.7	0.14
Knee External Rotation	-0.7 ± 3.6	-1.7 ± 3.4	0.83	4.1 ± 4.8	12.8 ± 10.9	0.49

POST PROCESSING TECHNIQUE FOR APPROXIMATING PROJECTILE TRAJECTORY IN 3D SPACE

¹ C.M. Pfeifer, ^{1,3} J.M. Burnfield, ² M.H. Twedt, ¹ J.A. Hawks, ³ R.M. Hasenkamp, ³ G.M. Cesar

University of Nebraska-Lincoln ¹ Dept. of Mechanical & Materials Engineering,

² Dept. of Biological Systems Engineering, ³ Nebraska Athletic Performance Lab

Email: ChasePfeifer@gmail.com

INTRODUCTION

Understanding the three-dimensional (3D) trajectory of ball flight and its relationship to environmental (wind, humidity, temperature) and human factors (kinematics and EMG) is essential to optimizing elite athlete performance. Unfortunately, existing technology is often too expensive (\$15,000-\$100,000), has limited accuracy, and/or lacks the versatility required to track diverse objects (e.g., soccer ball vs. football vs. baseball). The purpose of this study was to develop and validate an affordable post-processing method that uses computer-vision to track the 3D trajectory of a ball.

METHODS

A golf ball was selected as the initial object for algorithm development. One camera (Panasonic HC-V100, 1080p, 24 Hz), oriented perpendicular to the x -axis (Figure 1), produced data relevant to the projectile's motion along the x and z -axis (longitudinal and vertical position). A second similar camera, oriented parallel to the x -axis, produced data relevant to the projectile's motion along the y -axis (lateral position). To create a "sight triangle" which was subsequently used to evaluate the projectile's movement in the y -direction, a set of calibration lines (40x10 mm) was affixed to the ground 0.762 m apart in the expected direction of projectile motion (x -axis) to calibrate the video data in the x - z plane. A second equidistant set (in the x -direction) was placed 0.305 m apart in the y -direction for calibration of the camera directed down the x -axis.

An *uncompensated* 2D motion trajectory of the golf ball's flight was calculated for each camera by measuring position with a pixel to distance ratio (Tracker software) [1]. Data from the two cameras

were time-synched through identification of the ball to ground impact.

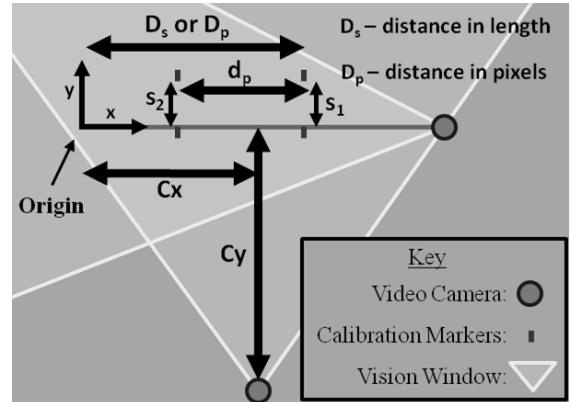


Figure 1 - Data Collection Set-Up/Explanation of Variables

To accommodate for the distortion arising from out-of-plane motion for each camera, coordinate data were adjusted using the following methodology.

The y -position was adjusted using equations 1-3:

$$y'_i = \frac{s_1}{s_1 - y_{c(i)}} * y_i \quad \text{[Eq. 1]}$$

$$y_{c(i)} = \frac{\frac{D_p * D_s}{s_1} - x_{p(i)}}{\left(\frac{d_p * d_s}{s_1 - s_2} \right)} \quad \text{[Eq. 2]}$$

$$x_{p(i)} = \frac{D_p}{D_s} * x_i \quad \text{[Eq. 3]}$$

where y_i is the uncompensated y -position, s_1 and s_2 are the distance between the two calibration markers in pixels from the view of the parallel camera (see Figure 1), $y_{c(i)}$ is the correcting y -factor, D_s is the distance from the origin of the reference frame to the furthest set of calibration markers, D_p is the distance D_s in pixels from the view of the parallel camera, x_i is the uncompensated x -position, $x_{p(i)}$ is the x_i position in pixels, d_s is the distance between the two sets of calibration markers, d_p is the distance d_s in pixels from the view of the parallel camera, and y'_i is the compensated y -position.

Next, y'_i was used to calculate the compensated z and x -positions, z'_i and x'_i respectively. These compensated positions were calculated using equations 4 and 5:

$$z'_i = \frac{z_i - h}{C_y} * (C_y + y'_i) + h \quad \{\text{Eq. 4}\}$$

$$x'_i = C_x - (C_y + y'_i) * \frac{C_x - x_i}{C_y} \quad \{\text{Eq. 5}\}$$

where h was the viewing height of the camera, C_y was the distance from the perpendicular camera to the x - z plane (see Figure 1), C_x was the longitudinal distance the perpendicular camera was from the coordinate origin, and z_i is the uncompensated z -position.

Algorithm validation was performed using a “gold standard” 3D motion analysis system (3 Qualisys Oqus 300 series cameras, 200 Hz, calibration residuals < 1mm). A golf ball (42.67 mm in diameter), covered with retro-reflective tape, was simultaneously tracked during flight through a 3x3x3 m capture volume by the 2D Panasonic cameras and the 3D motion capture technology. Ten repetitions were performed (Table 1).

RESULTS AND DISCUSSION

The *uncompensated* coordinate data resulted in an average percent deviation from the *gold standard* 3D trajectory of $10.37 \pm 3.88\%$. After applying the presented geometrical adjustment technique, the average percent deviation of the *compensated* from the *gold standard* trajectory was reduced to $4.20 \pm 1.35\%$. These findings demonstrate that the compensated technique was over 240% more accurate than the uncompensated approach at golf ball trajectory tracking.

The error presented relates to the average overall error in the system with respect to the distance

traveled by the projectile. Calibration markers must be accurately positioned and the cameras need to be directed to clearly view the x - z and y - z planes to obtain the most accurate position measurements.

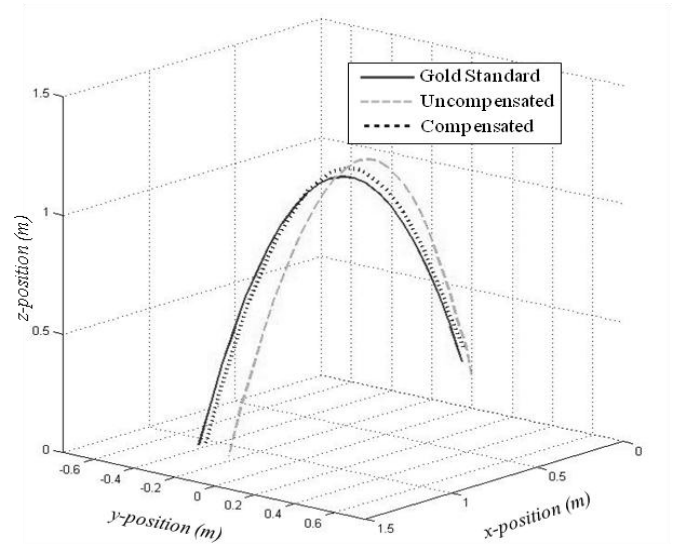


Figure 2 - Example result displaying the *Gold Standard*, *Uncompensated*, and *Compensated* trajectories. (Trial 05)

The low frame rate (24 Hz) of the 2D cameras used in the current study resulted in projectile blurring in a number of frames. In these instances the center of the blurred projectile was approximated and assessed as the data point. Cameras recording at a higher frequency would be expected to reduce the amount of error resulting from video processing and time-based compiling.

In summary, this work developed and validated an affordable (estimated at \$400), accurate (<5% average error) technology for tracking 3D ball flight. Current work is aimed at validating range and versatility of use with other projectiles (e.g., a football).

REFERENCES

1. D. Brown. *Tracker-Video Analysis and Modeling Tool*, www.cabrillo.edu/~dbrown/tracker

Table 1 - Average resultant deviation from the control for uncompensated and compensated position.

		Trial 01	Trial 02	Trial 03	Trial 04	Trial 05	Trial 06	Trial 07	Trial 08	Trial 09	Trial 10	Average*	STDEV*
Uncompensated Position	Error (mm)	62.6	253.8	325.9	254.9	109.8	61.6	192.5	169.2	201.2	243.1	172.1	77.4
	Error (%)	6.77%	14.40%	19.30%	12.08%	10.12%	3.21%	9.61%	8.97%	15.99%	12.14%	10.37%	3.88%
Compensated Position	Error (mm)	39	88	314.8	140.3	47.2	50.1	40.8	70	60.9	88.6	69.4	32.4
	Error (%)	4.22%	4.99%	16.11%	6.65%	4.34%	2.61%	2.04%	3.71%	4.84%	4.43%	4.20%	1.35%

*Trial 03 was determined an outlier and is not included in the average and standard deviation calculations.

THE EFFECT OF FORCEPLATE DATA ERROR ON JOINT TORQUES DURING RUNNING

¹Anne Schmitz and ²Jaclyn Norberg

¹Gannon University, Erie, PA, USA; email: schmitz005@gannon.edu

²Salem State University, Salem, MA, USA; email: Jnorberg@salemstate.edu

INTRODUCTION

Joint torques have been used to elucidate muscle function in injured subjects. For example, people with a reconstructed anterior cruciate ligament have been shown to exhibit a decreased knee extensor moment, which has been interpreted as avoidance of the quadriceps muscles [1]. Errors in these torque calculations can arise from many sources: segmental parameters, marker movement, ground reaction force data, and joint center location [2]. These errors can range from 6-232% of the torque magnitude where the proximal joints are more adversely affected than distal joints [2]. Although the effects of these errors on joint torques are well documented, walking has been the focus [2-8].

Running has gained much interest over the last decade as a form of exercise. This has also led to a large prevalence of running injuries as up to 70% of runners get an overuse injury [9]. Therefore, the evaluation of joint torques during running has gained much clinical interest to investigate the causes of these injuries. For example, patellofemoral pain patients have been shown to exhibit a decreased peak knee extensor moment but greater hamstring co-activation during running when compared to healthy controls, which may result in greater patellofemoral contact forces and pain [10]. Although [11] have shown that sagittal plane hip, knee, and ankle torques can vary by 7-14% during running due to errors in the center of pressure measurement, it is unclear how non-sagittal angles are affected. Since forceplate data has been shown to have the largest effect on joint torques [6], the purpose of this study was to determine how errors in force and center of pressure measurements propagate to three-dimensional hip, knee, and ankle joint torques during running.

METHODS

One subject (mass 53.2 kg, height 1.63 m, age 31 years) ran across a runway at 4.35 m/s. Data was

collected from two Bertec forceplates sampling at 1000 Hz while trajectories of 61 retroreflective markers were also collected at 200 Hz using an 11 camera MotionAnalysis system.

A Monte Carlo analysis was performed using sixty simulations with Visual 3D (C-motion, Germantown, MD, USA) as the dynamics engine. In each simulation, the forceplate data was first perturbed by adding an offset of 0 ± 1 N to each direction of the ground reaction force (GRF) data and 0 ± 3.5 mm to each direction of the center of pressure (COP) data [12]. The perturbation levels were chosen at random, assuming a normal distribution. Next, the marker trajectories were filtered at 10 Hz and perturbed forceplate data at 26 Hz using a lowpass, zero-lag, fourth order Butterworth filter. The cutoff frequencies were determined from a residual analysis of the data [13]. Then, joint torques of the hip, knee, and ankle were calculated. The distal segment was referenced to the proximal segment and the torque resolved into the proximal segment coordinate system. Joint torques were also calculated for the unperturbed data.

Custom Matlab code (MathWorksInc., Natick, MA) was used to extract joint torques during the stance phase of running, where stance was defined as when the vertical GRF was greater than 10 N. Next, the peak joint torques were calculated as: maximum transverse plane hip torque, maximum knee torque in all planes, maximum non-sagittal ankle torques, minimum non-transverse hip plane torques, and minimum sagittal plane ankle torque. Then, the maximum differences between the peak torques calculated from the perturbed simulations and the unperturbed original data were calculated. Pearson's product moment correlation coefficients were also calculated to quantify the relationship between each perturbed variable and the peak joint torques. The correlations provide an estimate of Sobol indices [14] and thus a way to rank the effects of each

variable on peak joint torque (i.e. greater correlation means greater sensitivity to that variable). To justify the use of Pearson's coefficients, the normality of the peak joint torques was verified using the Lilliefors test.

RESULTS AND DISCUSSION

During walking, joint torque uncertainty has been shown to be larger for proximal joints compared to the distal joints [2]. Our results show this also extends to running. The maximum error induced by forceplate error was 4.8 (4%), 3.6 (3%), and 0.9 (3%) Nm for the sagittal, frontal, and transverse plane peak hip torques, respectively. These errors decreased at the knee, which were 2.5 (2%), 1.7 (7%), and 0.1 (1%) Nm for the sagittal, frontal, and transverse plane. These errors decreased even further at the ankle with errors of 0.5 (<1%), 0.4 (1%), and 0.1 (2%) Nm for the sagittal, frontal, and transverse plane. This may occur due to the bottom-up approach used to calculate joint torques. For example, the ankle torque is calculated using a free body diagram of the foot. Then, this ankle torque is applied to the distal end of the tibia and used in conjunction with the tibia's mass and kinematics to calculate the torque at the proximal end (i.e. knee joint torque). Hence, this may lead to the propagation of torque errors from distal to proximal joints.

Errors in joint torques were due more to inaccuracies in the GRF magnitude than the COP measurements (Table 1), which agrees with a previous sensitivity study of torques during walking

[6]. The torque the GRF produces about any joint can be calculated as GRF magnitude times its moment arm about the joint center. It is likely that joint torques were more sensitive to GRF magnitude than location because the GRF magnitude is much greater than the moment arm value, thus dominating this term.

CONCLUSIONS

Forceplate errors had a larger effect on proximal joint torques than on the distal joints, with torque errors ranging from 0.1 – 4.8 Nm (<1%-4%). Therefore, forceplate accuracy may be an important aspect to report in studies investigating more subtle torque differences (<4%) between clinical populations. The main contributors to torque error were inaccuracies in the GRF magnitudes, as opposed to the location of the center of pressure.

REFERENCES

1. Hart, J. M., et al. *Clin Biomech* **25**, 277-283, 2010.
2. Riemer, R., et al. *Gait & Posture* **27**, 578-588, 2008.
3. Reinbolt, J. A., et al. *IEEE Trans BME* **54**, 782-793, 2007.
4. Rao, G., et al. *J Biomech* **39**, 1531-1536, 2006.
5. Ganley, K. J., et al. *Clin Biomech* **19**, 50-56, 2004.
6. Silva, M., et al. *Gait & Posture* **19**, 35-49, 2004.
7. Pearsall, D., et al. *Gait & Posture* **9**, 173-183, 1999.
8. Holden, J. P., et al. *Gait & Posture* **5**, 217-227, 1997.
9. Hreljac, A. *Med Sci Sports Exerc* **36**, 845-9, 2004.
10. Besier, T. F., et al. *J Biomech* **42**, 898-905, 2009.
11. McCaw, S. T., et al. *J Biomech* **28**, 985-988, 1995.
12. Collins, S. H., et al. *Gait & Posture* **29**, 59-64, 2009.
13. Winter, D. A. *Biomechanics and motor control of human movement* John Wiley & Sons, 2009.
14. Glen, G., et al. *Environ Model Soft* **37**, 157-166, 2012.

Table 1: Correlation between forceplate errors and peak joint torques during running

Peak Torque	COPx	COPy	COPz	GRFx	GRFy	GRFz
Hip						
Sagittal	r= 0.097, p=0.459	r=-0.166, p=0.206	r=-0.075, p=0.569	r=-0.981, p<0.001	r=-0.152, p=0.247	r=-0.075, p=0.567
Frontal	r= 0.049, p=0.713	r= 0.196, p=0.134	r=-0.266, p=0.040	r=-0.058, p=0.657	r=-0.998, p<0.001	r=-0.012, p=0.929
Transverse	r=-0.010, p=0.938	r=-0.267, p=0.039	r= 0.226, p=0.083	r=-0.374, p=0.003	r= 0.907, p<0.001	r= 0.008, p=0.954
Knee						
Sagittal	r= 0.017, p=0.899	r=-0.265, p=0.040	r=-0.001, p=0.995	r=-0.959, p<0.001	r= 0.164, p=0.211	r= 0.259, p=0.046
Frontal	r= 0.023, p=0.861	r= 0.152, p=0.246	r=-0.272, p=0.035	r=-0.163, p=0.213	r=-0.988, p<0.001	r= 0.157, p=0.230
Transverse	r= 0.063, p=0.635	r=-0.174, p=0.183	r=-0.100, p=0.448	r=-0.985, p<0.001	r=-0.223, p=0.087	r= 0.118, p=0.369
Ankle						
Sagittal	r= 0.181, p=0.167	r=-0.071, p=0.590	r=-0.017, p=0.897	r=-0.720, p<0.001	r=-0.033, p=0.800	r=-0.629, p<0.001
Frontal	r=-0.036, p=0.785	r= 0.159, p=0.224	r=-0.258, p=0.047	r= 0.038, p=0.772	r=-0.938, p<0.001	r= 0.367, p=0.004
Transverse	r= 0.050, p=0.705	r= 0.018, p=0.894	r=-0.243, p=0.062	r=-0.623, p<0.001	r=-0.809, p<0.001	r= 0.164, p=0.209

AUTOMATIC CLASSIFICATION OF MOUSE MOTOR FUNCTION FROM MARKERLESS MEASUREMENTS

¹ Alison L. Sheets, ² Susan E. White, ^{2,3} Lesley C. Fisher and ^{2,3,4} D. Michele Basso

¹ Sheets Consulting, Portland, OR, USA

² School of Health and Rehabilitation Sciences, The Ohio State University, Columbus, OH, USA

³ Center for Brain and Spinal Cord Repair, The Ohio State University, Columbus, OH, USA

⁴ Neuroscience Graduate Studies Program, The Ohio State University, Columbus, OH, USA
email: Alison.sheets@gmail.com

INTRODUCTION

Many biomechanics researchers aim to move out of the lab and quantitatively evaluate function in natural environments for a variety of movements. While many focus on this goal for humans, techniques may initially be developed for mice because they use numerous behaviors, and small variations in movement reflect differences in functional capability. Also, mice are used as experimental models to identify mechanistic targets for treating persons with neuromuscular disorders; therefore, distinguishing the continuum of pathological movement patterns from normal would advance the understanding of locomotion control and enable development of more effective treatments for human disability.

Spinal cord injury (SCI) in mice produces variable patterns of disability similar to humans, and resulting motor deficits are well characterized [1]. Animals of all functional ability are evaluated using the Basso Mouse Scale (BMS), a 10-point semi-quantitative, observation-based, locomotor rating scale [1]. The BMS is limited to visually detectable behaviors during a 4-min trial. For animals capable of stepping, marker-based motion capture has been used to assess limb kinematics and motor function following SCI. Limitations to this approach include accuracy due to skin movement artifact [2], and the biological relevance of straight line, steady-state locomotion to unconstrained movements [3].

This research aims to automatically classify motor function in rodents with SCI using markerless motion tracking data. This approach would address many limitations in current methods used to characterize rodent motor function.

METHODS

Markerless tracking methods were used to reconstruct each mouse 3D volume throughout a 2-min trial [4]. Animals moved freely in a 2' diameter environment while 10 synchronized cameras recorded at 100 Hz. Every animal's 3D shape was reconstructed with and without a tail from each set of 10 video images using background subtraction and shape-from-silhouette techniques (Fig. 1) [4].

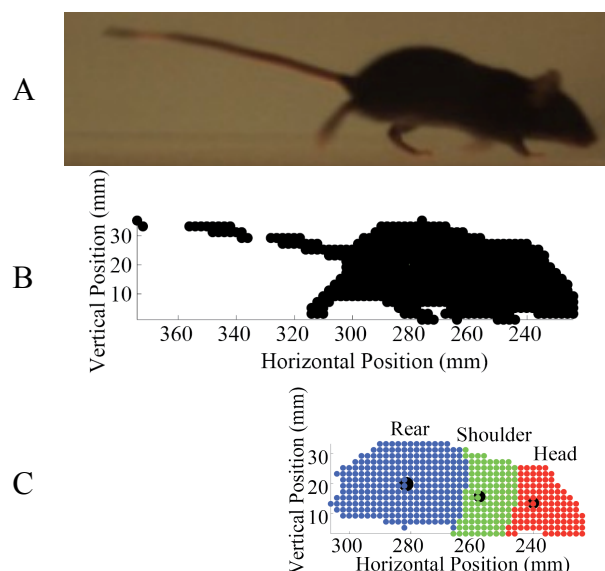


Figure 1: (A) Video frame, (B) 3D reconstructed mouse volume, (C) Volume with tail removed, then divided into 3 segments. Black dots are CoV positions.

Thirty-two animals with a wide spectrum of motor capabilities were tested 1-3 times each throughout recovery following SCI. Sixty trials were used to develop the two-step motor function classification algorithm consisting of movement segmentation and parameter identification. The algorithm's predictive capability was evaluated using the BMS.

First, center of volume (CoV) position and speed were used to segment the continuous 2-min trials into periods containing five different movements: directed and exploratory locomotion, meandering, standing, and rearing [4]. Directed locomotion was defined as CoV displacement faster than 60mm/s, and longer than 200mm. Animals must have directed locomotion and standing to be classified.

Next, parameters describing CoV positions of three segments roughly representing the head, shoulders, and rear were calculated by dividing the mouse volume into 3 clusters (Fig. 1). The animal was divided into equal front and rear clusters at the CoV mean, perpendicular to the volume's first principle component. A head and shoulder were segmented at the center of the front cluster, perpendicular to the same first principle component. Median, minimum, maximum, 25% and 75% percentile values were calculated to describe an animal during directed locomotion and standing. The 160 parameters included: CoV speed (10), locomotion path straightness (10), three eigenvalues of the volume PCA (30), absolute and relative CoV height of each segment (60), distance between each segment CoV (30), and body straightness defined as angles between vectors connecting the three CoV (20).

A stepwise linear regression was performed to identify parameters best predicting the BMS score. A post hoc analysis ensured that linear modeling assumptions were satisfied and that the model did not contain parameters with multicollinearity.

RESULTS AND DISCUSSION

A model with 4 parameters from directed locomotion, and 1 from standing predicted the BMS score with an $r^2=0.89$ (Fig. 2). Errors in the predicted BMS score have a slight bias toward overestimating the lower functioning animals, and underestimating higher ones. Parameters included:

- directed locomotion – straightness of path, median
- directed locomotion – head height, 25th percentile
- directed locomotion – rear height, 75th percentile
- directed locomotion – height difference between the shoulder and rear, 25th percentile
- standing – body straightness in the animal's sagittal plane, 75th percentile

These parameters indicate that mice with varying motor capabilities had different movement patterns and distinct body positions during directed locomotion and standing. The higher functioning animals had straighter locomotion paths, lower head CoV positions, higher rear CoV positions, and the shoulder CoV height was lower than the rear CoV. Also, when standing higher functioning animals had a larger back arch than lower functioning animals (i.e. the head is lifted upward).

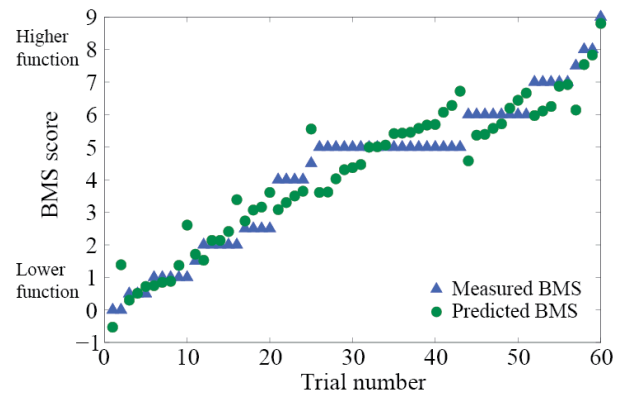


Figure 2: Measured and predicted BMS scores

CONCLUSIONS

The method and classification parameters identified here represent a fundamental shift in behavioral and kinematic analysis of animal locomotion. The increased precision, sensitivity, and repeatability address many limitations of current research methods, while including continuous data and more behaviors when classifying function. This 2-step framework could also be applied to human functional assessments in order to include a wider variety of unconstrained movements.

REFERENCES

1. Basso, DM et al., *J Neurotrauma*, **23**:635-659, 2006.
2. Bauman, JM and Chang, YH, *J NeurosciMeth*, **186**:18-24, 2010.
3. Herbin, M et al., *Behav Brain Res*, **181**:173-179, 2007.
4. Sheets AL, et al. *PLoS One*, 2014.

ACKNOWLEDGEMENTS

NIH 1R21NS077446-02

pyCellAnalyst: A robust, open-source tool for 3D image segmentation and deformation analysis

^{1,2} Scott C. Sibole and ¹ Walter Herzog

¹ The University of Calgary, Human Performance Laboratory, Calgary, AB, Canada

² The University of Calgary, Schulich School of Engineering, Calgary, AB, Canada
email: ssibole@ucalgary.ca

INTRODUCTION

Recent advances in multi-photon laser scanning microscopy allow for the three-dimensional (3D) imaging of live cells embedded in native tissue. When coupled with controlled mechanical testing systems, the multiscale problem of how mechanics are transferred between the tissue and cellular scales can be investigated [1]. This is accomplished by comparing the geometry of cells in a state in which the tissue boundaries are unloaded to the geometry of cells in some loaded tissue state. The nature of this load transfer is crucial to understanding the mechanical environment of cells, and their biological response resulting from mechanical stimuli.

Analysis of these 3D image data is challenging in both the image segmentation and characterization of the deformation. Historically, image segmentation has been performed using simple threshold-based methods [2]; however, these often fail when objects are in close proximity. To characterize the deformation, objects were typically approximated as ellipsoids and changes in the ellipsoid axes lengths were taken to reflect strains. This approach has two major drawbacks: 1) it cannot distinguish rigid body rotation from shear strain, and 2) it degrades as the object's true shape diverges from ellipsoidal. To address these limitations, new software was developed that provides robust image segmentation and more complete deformation analysis.

METHODS

Custom software for 3D image segmentation and kinematics (deformation) analysis, pyCellAnalyst, was developed in Python employing the Insight and Visualization Toolkits (Kitware Inc.) An array of image segmentation strategies are implemented in pyCellAnalyst including thresholding (statistics-,

entropy-, and intensity-based) and active contour models. Likewise, numerous smoothing/denoising filters are also provided. This extensive functionality allows for segmentation of images acquired with different modalities where the object of interest can appear in either the foreground or the background. Cells in close proximity can typically be resolved as single objects with the proper selection of tool(s). A support vectors machine algorithm is provided as a fallback measure for resolving clustered objects.

Three methods are included for kinematics analysis.

- 1) The traditional ellipsoidal approximation measures can still be acquired allowing users to compare with past analyses. This ellipsoidal approximation is calculated from the reconstructed object's principal moments of inertia.
- 2) In addition to this, the complete deformation gradient can also be calculated using an iterative closest point algorithm included in *VTK* and the reconstructed objects in reference and deformed frames. The complete Green-Lagrange strain tensor is then calculated from this deformation gradient.
- 3) Finally, a non-uniform deformable image registration can be performed using a diffeomorphic demons registration algorithm provided in *ITK* [3]. This returns the displacement field that maps the reference state object to the deformed state object. Additionally, a finite element mesh is automatically generated with *TETGEN* and the displacement fields are interpolated to the surface nodes of this mesh to serve as boundary conditions for a finite element analysis of the cellular deformation. All necessary information for such an analysis is

saved in a Python *pickle* binary file. A utility to perform a finite element simulation employing this information to do finite element analysis in the open-source software, FEBio, is provided.

The software can be imported into any Python script as a module, and its functionality can be applied as needed. Additionally, a graphical user interface (GUI) has been developed to ease usage (Figure 1).

RESULTS AND DISCUSSION

The software exhibited robust segmentation performance for datasets acquired with different modalities (second harmonic generation, confocal, and dual photon fluorescence). Furthermore, it was capable of reconstructing cells in very close proximity. The novel tools for deformation analysis showed good performance in verification/validation studies. The iterative closest point algorithm was able to calculate strains for objects with known large deformations and rotations with little error. Likewise, the deformable image registration calculated correct displacement fields for image pairs of known deformation.

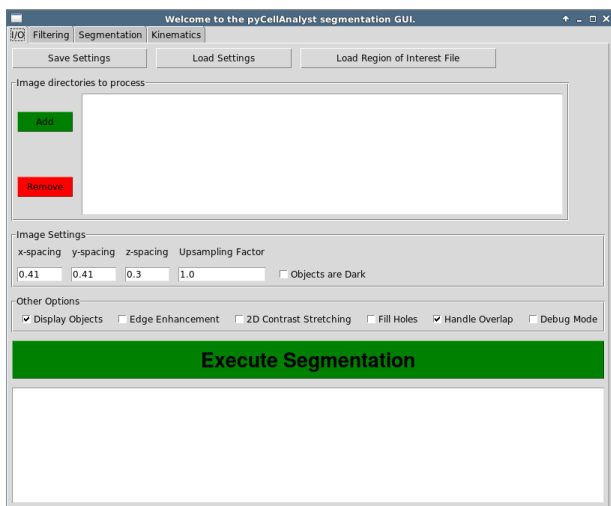


Figure 1: The graphical user interface utility for pyCellAnalyst. Note the four tabs to present all tools in an organized, easy-to-follow manner.

CONCLUSIONS

pyCellAnalyst supplies the user with powerful tools for 3D image segmentation and kinematics analysis.

It is capable of resolving cells in close proximity into individual objects, allowing users to consider most cells in the field of view rather than simply the ideal, isolated ones. For kinematics analysis, it can return the traditional ellipsoidal approximation based measures used in many studies, but additionally offers the ability to calculate the complete Green-Lagrange strain tensor assuming uniformity across the cell. Furthermore, by employing the deformable image registration tools the user can also calculate the non-uniform displacement field that best maps the cell between reference and deformed states. This information can be used to drive finite element models, providing a powerful avenue for analysis of the complete stress-strain state of the cell (Figure 2). A utility to do this with the popular open-source finite element software, FEBio, is included.

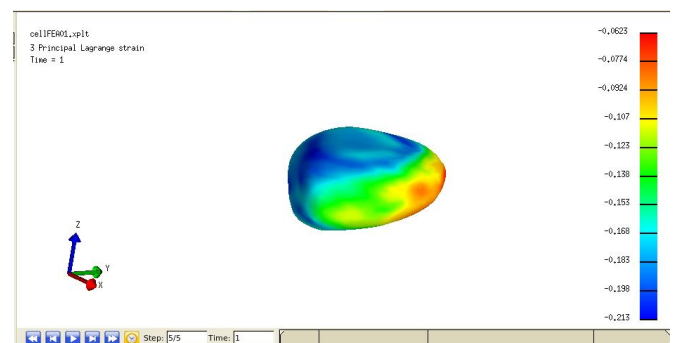


Figure 2: An example of a finite element analysis driven by the displacement field calculated by deformable image registration.

The software are open-source and freely available at github.com/siboles/pyCellAnalyst, distributed under the MIT license.

REFERENCES

1. Han et al. J Biomech. 2012.
2. Moo et al. J Biomech. 2013.
3. Dru et al. The Insight Journal. 2009.

ACKNOWLEDGEMENTS

The authors acknowledge Azim Jinha M.Sc. and Salvatore Federico Ph.D. for their contribution to discussions on this work. Also, funding from Canadian sources: NSERC, AIHS, and CIHR is appreciated.

UPPER EXTREMITY INJURIES IN LOW-SPEED MOTOR VEHICLE ACCIDENTS WITHOUT AIR BAG DEPLOYMENT

^{1,3} Kevin K. Toosi and ^{2,3} Pamela A. Chrissis

¹ The University of Pittsburgh, Pittsburgh, PA, USA

² Carnegie Mellon University, Pittsburgh, PA, USA

³ Pittsburgh Biomechanics, LLC, Pittsburgh, PA, USA

email: kktsoosi@pghbiomechanics.com, web: www.pghbiomechanics.com

INTRODUCTION

Research studies have demonstrated an increased risk of upper extremity injuries due the deployment of air bags, including fracture of the radius and ulna [1-3]. According to the National Automotive Sampling System (NASS), only 5.33% of injuries affecting the upper limbs result from low-speed vehicle impacts without air bag deployment [4]. While the upper extremity injuries are not commonly seen in low-speed collisions, forensic biomechanical engineers are frequently tasked to evaluate injuries involving upper limbs, such as rotator cuff pathologies, tear of the glenoid labrum, and carpal tunnel syndrome, that have been claimed as a result of low-speed motor vehicle accidents. The purpose of this study was to examine the real-world vehicle collisions, in order to have a better understanding of whether those claimed injuries could be attributed to the accident.

METHODS

Data were obtained from the NASS database [4] using the following criteria: vehicle body type (automobile), vehicle air bag deployment (not deployed), and occupant body region (upper limbs). This investigation resulted in 3192 automobile accidents, which all occurred over the time period from 2004 until 2011, with a higher concentration of reports found between 2004 and 2008. Only 170 applicable cases were matched the definition of low-speed impacts, i.e., vehicle barrier speed of less than 20 miles per hour (mph). From these specifications, various variables were selected for further analysis; these categories included number of vehicles, occupant injured, type of injury, and cause of injury.

RESULTS AND DISCUSSION

In the 170 cases observed, it was found that the impacts occurred by a single vehicle itself, the collision of two vehicles, or the collision of three vehicles. In the case of single vehicle accidents, 30 cases of the total were involved or approximately 17.8%. There were 117 cases, or 68.8%, of the total that occurred with a collision of two low speed vehicles. Finally, it was observed that 23 cases involved the collisions of three vehicles that amounted to 13.6% of the total number of cases observed. Following this classification of the cases, further analysis into the vehicle occupants' injuries took place. It was observed that out of all 170 cases, there were a total of 189 instances of injuries affecting the vehicle drivers, the vehicle passengers, or both. A total of 74 vehicle 1 drivers reported injury, which was 39.2% of the 189 instances occurring with primary vehicle drivers. Along with drivers, there were 29 instances, 15.3%, of primary vehicle passenger injuries reported in the database. There were reports of 62 secondary vehicle drivers injured, amounting to 32.8% of the total instances; additionally, 19 secondary vehicle passengers reported upper extremity injuries, which was 10.0%. Lastly, in the 23 cases involving three vehicles, 5 drivers of the tertiary vehicles reported injuries, 2.6%, and there were no reports of any passengers in the third vehicle being injured. From these observations, it appears that the majority of upper extremity injuries are incurred by those drivers of primary and secondary vehicles followed by those passengers in the primary vehicle.

Amongst the various injured occupants, several different areas throughout the upper extremities. The following categories were used to classify the

injuries reported in the cases: carpal-metacarpal joint sprain, finger fracture, wrist joint sprain, wrist joint fracture, radius fracture, elbow joint sprain, shoulder joint sprain, upper extremity muscle laceration, upper extremity muscle sprain, upper extremity skin abrasion, upper extremity skin contusion, upper extremity skin laceration, and upper extremity 2nd or 3rd degree burn. The most prominent injury resulting from a low speed vehicle collision was an upper extremity skin contusion with 104 instances from the 170 cases, or 61.18%. The next three highest injuries were upper extremity skin laceration with 23 instances (13.5%), upper extremity skin abrasion with 17 instances (10.0%), and shoulder joint sprain with 14 instances (8.2%). The remaining upper extremity injuries all occurred with a frequency of 3 instances or less: upper extremity muscle strain with 3 instances (1.76%), carpal-metacarpal joint sprain and wrist joint sprain each with 2 instances (1.18%), and finger fracture, wrist fracture, radius fracture, elbow joint sprain, upper extremity muscle laceration, and upper extremity 2nd or 3rd degree burn each with 1 instance (0.59%) throughout the applicable cases. Although many types of upper extremity injuries occur in low speed collisions, it appears that it is much more likely for certain injuries to occur, i.e. upper extremity skin contusions, lacerations, abrasions, and muscle joint sprains.

The above injuries resulted from several sources either inside of the vehicle itself or occasionally outside of it. The top cause of injury amongst the 170 cases observed was the seat belt webbing and/or buckle; 61 cases were reported equating to 35.9% of the total. The steering wheel rim was the second highest cause of injury in vehicle occupants with 20 instances or 11.8%. There were 13 instances, 7.65%, of a left side interior surface, excluding hardware or armrest, causing upper extremity injuries amongst occupants. These three injury types were the top categories observed throughout the data; the remaining injuries occurred with fewer than 10 instances. Either flying glass or the left B-pillar was the cause of injury in 9 instances each, contributing to 5.29% of the total. Closely following with 8 instances, the seat and/or back support caused injuries in 0.71% of the cases. The remaining sources contributed upper extremity

injuries in 5 or less observed instances: Steering wheel (combination of codes 004 and 005) with 5 instances (2.94%), right instrument panel and right-side interior surface excluding armrest and hardware each were found to cause 4 injuries (2.35%), the first row center console, left instrument panel and below, left rear upper quadrant, right instrument panel and below, and windshield each contributed to 3 instances (1.76%) of injuries, the left A(A1/A2)-pillar, left instrument panel, right rear upper quadrant, roof or convertible top, ground, other occupants, or other objects amounted to 2 instances each (1.18%), and lastly add on equipment, child safety seat, fire in vehicle, left armrest/hardware in forward upper quadrant, left armrest/hardware in rear upper quadrant, right B-pillar, right lower instrument panel, and steering wheel hub/spoke with 1 instance (0.59%) each. It can be noted that many of the left side injuries were mainly inflicted on the driver while most of the right side injuries occurred in passengers. Also, all steering wheel injuries resulted in injuries to the drivers of the vehicles.

CONCLUSIONS

The results of this study demonstrate that only 2.94% of the upper limb injuries occurring in low-speed motor vehicle collisions without air bag deployment were of moderate level while the rest were reported as minor upper extremity injuries; none of the observed injuries were categorized as major injuries. Therefore, it can be concluded that injuries such as acute traumatic tear of the rotator cuff, tear of the glenoid labrum, and acute carpal tunnel syndrome cannot be reasonably attributed to the low-speed vehicle accidents.

ACKNOWLEDGEMENTS

Support for this work was provided by Pittsburgh Biomechanics, LLC.

REFERENCES

1. Atkinson P, et al. *SAE Paper* 2002-01-0022, 2002.
2. Bass CR, et al. *SAE Paper* 973324, 1997.
3. Huelke DF, et al. *SAE Paper* 940716, 1994.
4. <http://www-nass.nhtsa.dot.gov/nass/cds/>

PRE-SHOT JITTER DURING SELF-PACED FIRING USING SMALL ARMS WEAPON SYSTEMS

Courtney A. Webster, Frank Morelli, Jennifer M. Neugebauer

U.S. Army Research Laboratory, Human Research and Engineering Directorate
Dismounted Warrior Branch
Aberdeen Proving Ground, MD, USA
Email: courtney.a.webster2.ctr@mail.mil

INTRODUCTION

Marksmanship is an essential skill for military personnel, and is a complex task that combines postural control, static load bearing, and fine motor control. Although training and practice can improve shooting performance, even expert marksmen exhibit subtle motion when acquiring or dwelling on a target. These small fluctuations in weapon aim can result in large shot errors and missed targets. Here, we use the term “jitter” to describe these fluctuations which may result from a number of factors including postural instability¹, physiological muscle tremor² and natural oscillations of the extended arms^{3,4}.

Another potential contributor to jitter may be the anticipation of recoil energy sustained from a particular weapon system. Recoil describes the backward momentum of a weapon following trigger pull. Factors influencing recoil include ammunition charge quantity, burn rate, weapon size and weight, and muzzle device design. Anticipatory perception of (and response to) recoil likely depends on shooting experience, individual differences in musculature, and tolerances for pressure and pain.

The U.S. Army Research Laboratory (ARL) has a vested interest in understanding all aspects of shooting performance in order to design technologies, interventions, or training regimens to optimize Soldier marksmanship. Human and weapon dynamics, recoil forces and accelerations, and shooting performance were quantified during militarily-relevant firing scenarios using three weapon conditions. Here, we report on pre-shot jitter during self-paced, single shots as recorded by tri-axial activity monitors. Jitter measures were analyzed to determine: 1) whether muzzle device affects jitter and its correlation to shooting accuracy

within each weapon condition, and 2) whether jitter differs for weapons of different calibers.

METHODS

Eight (8) male service members were recruited to participate in a marksmanship performance study conducted at the U.S. Army Marksmanship Unit (USAMU) Pool International Range Complex at Fort Benning in Columbus, GA. Subjects included volunteers from the U.S. Army 3rd Infantry Division and U.S. Army and Air Force Special Operations Forces. Four subjects (Q group) had completed a specialized training course qualifying them for the role of squad designated marksman (SDM) while the remaining four had not yet completed the course (NQ group). This distinction in shooting experience was used as a factor in the statistical analyses.

Subjects were instrumented with tri-axial wireless activity monitors (AM; Model GT3X+ ActiGraph Corp., Pensacola, FL) on segments of the shooting and support arms. Two additional AMs were secured to the buttstock and barrel of the weapon. Subjects fired each of three weapon conditions (listed from smallest to largest recoil): a standard M4 carbine firing 5.56 mm rounds (C556), an M4 carbine retrofitted to fire 6.8 mm rounds (C68), and a compact M110 rifle variant which fired 7.62 mm NATO rounds (C762). The C556 and C68 systems were fired with each of three muzzle device conditions including the standard-issue A2 “birdcage” flash hider (BC), a muzzle brake (MB; SureFire LLC, Fountain Valley, CA), and the muzzle brake with a suppressor adapter (SUP). Operationally, the C762 weapon is not typically fired without either a muzzle brake or a suppressor. Therefore, the C762 condition was fired with only the MB and SUP muzzle conditions. Targets were presented at a range of 50 m. Subjects fired 7

practice rounds with each system followed by 10 rounds at a self-selected pace, during which accelerations and shot accuracy were recorded.

Periods of pre-shot jitter were identified manually through visual inspection of the acceleration profiles. Jitter measures included mean resultant acceleration, the peak deviation from this mean (Peak), the difference between maximal and minimal acceleration magnitude (Range), the time-on-target, and the correlation of Range to shot accuracy. Pre-shot jitter measures from the barrel-mounted AM are presented here. Acceleration values are in units of gravity (g). To evaluate weapon or muzzle device effects, ANOVA analyses were conducted on linear mixed models which included experience (NQ, Q) and either condition (C556, C68, C762) or muzzle device (BC, MB, SUP) as fixed factors with a random effect of subject. Level of significance was set to 0.05.

RESULTS AND DISCUSSION

Between Muzzle Device Conditions - The data set was first blocked by weapon condition to analyze the effect of muzzle device when using a specific weapon system. Analyses revealed a significant interaction effect of muzzle device and experience for the C68 condition for Peak (X^2 (2, N = 236) = 12.73, $p < 0.002$) and Range (X^2 (2, N = 236) = 19.18, $p < 0.0001$) measures. Specifically, within the NQ group, the MB resulted in lower Peak and Range scores (0.041 ± 0.016 g and 0.074 ± 0.029 g, respectively) than either the BC or SUP options. Peak and Range scores were greater with the BC (0.058 ± 0.028 g and 0.100 ± 0.043 g) than with the SUP (0.051 ± 0.020 g and 0.089 ± 0.034 g).

Between Weapon Conditions - A second analysis was performed using the data set blocked by muzzle device condition which allowed us to examine differences between weapon conditions when the same muzzle device was used. Significant main and/or interaction effects were observed for the Range measure within each device option (Figure 1). Generally, Range measures varied between weapon conditions for the NQ group. Only for the SUP condition did the Q group exhibit differences in Range between weapons (C556 and C762).

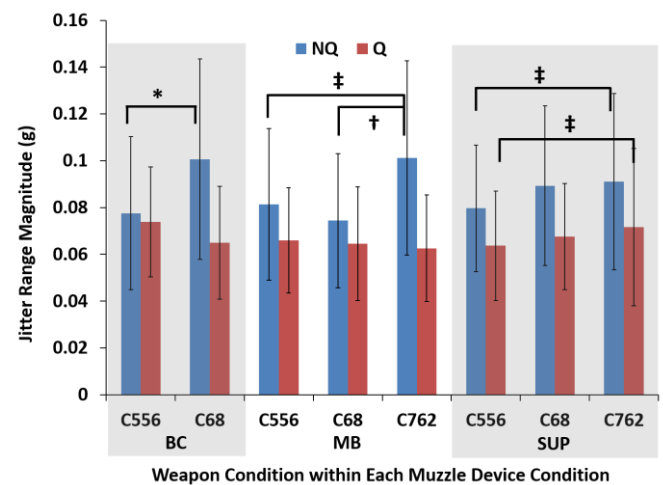


Figure 1. Jitter Range measures for each group, weapon, and muzzle device condition. Symbols denote statistically significant differences: * = $p < 0.0001$; † = $p < 0.001$; ‡ = $0.01 < p < 0.04$.

CONCLUSIONS

The Range jitter measure provides an estimate of the magnitude of postural correction during weapon aiming. Larger Range measures indicate poorer weapon stability. Results suggest that weapon type may affect jitter magnitude during aiming, and that the effect is more pronounced for those with less shooting experience. Additional analyses will investigate jitter from the body-mounted AMs and the relationship between these jitter magnitudes and shooting accuracy.

REFERENCES

1. Era P, et al. *J Biomechanics* **29**(3), 301-306, 1996.
2. Lakie M. *Plos Exp Physiol* **95**(3), 441-450, 2010.
3. Morrison S, Newell KM. *Clin Neurophysiol* **111**: 651-653, 2000.
4. Pellegrini B, et al. *J Neurosci Meth* **139**: 185-193, 2004.

ACKNOWLEDGEMENTS

Many thanks are owed to Mr. Troy Lawton and staff at the USAMU for their support of this work and for sharing their knowledge and expertise in marksmanship. Thanks also to Mr. Tom Fry, Mr. Doug Struve, and Mr. Sam Ortega for their invaluable assistance with this data collection, and to Mr. Jeff Nickel for his help with data processing.

AUTOMATIC SEGMENTATION AND RECONSTRUCTION OF EXTRAOCULAR MUSCLES FROM MRI USING SUPERPIXEL AND NORMALIZED CUT

¹ Qi Xing and ² Qi Wei

¹ Department of Computer Science, George Mason University, Fairfax, VA, USA

² Department of Bioengineering, George Mason University, Fairfax, VA, USA

email: qwei2@gmu.edu

INTRODUCTION

Extraocular muscles (EOMs) enlargement affects the biomechanics of eye movement and is a key factor of several orbital diseases [1]. Identification of EOM enlargement is important for clinical diagnosis and treatment, however, accurate and efficient quantification of EOM anatomy is challenge. We present a fully automatic method to segment and reconstruct 3D model of the EOMs. We design a novel algorithm which uses superpixels (i.e. clusters of pixels) as the basic units for segmentation. After obtaining the segmented EOM boundaries, we reconstruct 3D models of the EOMs. Our proposed method on automatically reconstructing patient-specific EOM models can be applied in clinical diagnosis and surgical planning.

METHODS

A few existing algorithms provided computer-assisted semi-automatic [2, 3, 4] methods to segment EOM boundaries, which are more efficient than manual segmentation. All of these approaches apply segmentation on discrete image pixels, which may not be the most natural representation of visual scenes. We suggest it would be more natural and efficient to process the EOM image with perceptually meaningful image patches that contains many pixels sharing similar image features. We represent local structures by using small patches obtained from superpixel over-segmentation [5] as the basic primitives for subsequent image processing. Each superpixel groups nearby pixels into one which have similar intensities and are more likely to belong to the same structure. Figure 1(b) illustrates the superpixels of the MR image in Figure 1(a). The orbital wall and the rectus muscles were manually outlined, each of which includes

several superpixels. The number of superpixels in one image obtained affects the accuracy and computational efficiency of the following segmentation procedure. The number of superpixels was optimized to be 1800 based on applying model selection theory on several training image sets, which is used as a fixed constant during later segmentation.

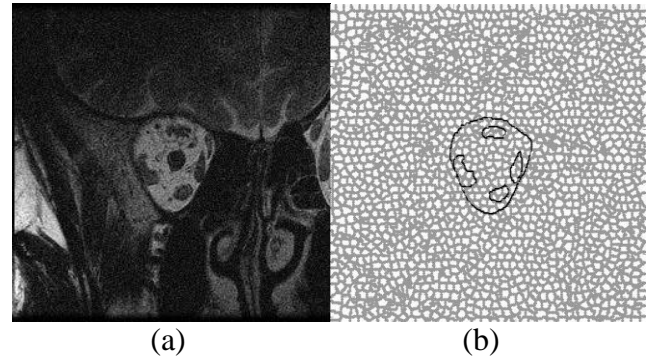


Figure 1: (a) MR Image of EOM; (b) Superpixel of MRI image in Fig. 1(a) with manually outlined structure boundaries.

We then constructed a region adjacency graph (RAG) for each image based on the neighborhood relationship among superpixels. Each superpixel was defined as a node in the RAG. Each node was connected to all its neighbor nodes through edges. The weight w_{ij} of the edge connecting two nodes n_i and n_j is defined as:

$$w_{ij} = \exp\left(\frac{-\|I_i - I_j\|^2}{\sigma^2}\right)$$

We applied the normalized cuts algorithm to the constructed RAG to partition the graph into two similar subgraphs. Then for each of the two parts, it recursively carries out the same procedure (Figure 2(a)) until all the labels were classified (Figure 2(b)). Applying the superpixel based normalized cut other than pixel level method is more accurate since the edge's weight between regions is larger than that between pixels. Moreover, the size of the

affinity matrix and the complexity of the RAG for image representation are significantly reduced, which makes the approach computationally more efficient.

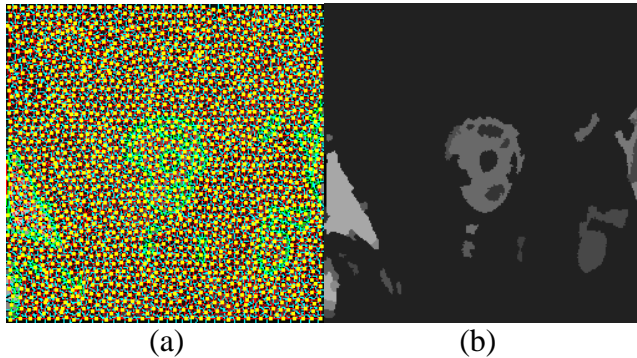


Figure 2: (a) RAG segmentation through normalized cut; (b) Labeled segmentation results after recursive segmentation using normalized cuts.

The Laplacian of Gaussian filter and the label connected component methods were then applied to determine the connected contours of the orbital wall (Figure 3(a)), EOMs and the optical nerve. The center of each contour was calculated. By using k-nearest algorithm ($k=2$), regions of the optical nerve and the orbital wall can be identified from the contours in image center. The orbital region was automatically extracted using convex hull with shape prior knowledge and defined as region of interest (ROI) (Figure 3(b)). By doing this, the EOMs with incomplete boundaries (lateral and medial rectus muscles in this example) can be segmented correctly from the background (Figure 3(c)). Finally, image region and hole filling algorithms were used to complete the EOM segmentation (Figure 3(c)). Once we have the segmented boundaries, we reconstructed the 3D extraocular muscle models using standard approaches, such as template based fitting [4].

RESULTS AND DISCUSSION

We applied our proposed method to two sets of orbital T2-weighted MR images of both eyes acquired from two normal subjects. All images used were digitized with 256×256 pixels and 16 bits gray-level of resolution at voxel size of $0.3 \text{ mm} \times 0.3 \text{ mm} \times 2.0 \text{ mm}$. We evaluated accuracy of our approach using the Boundary-based Directional Cut Discrepancy method by measuring the mean

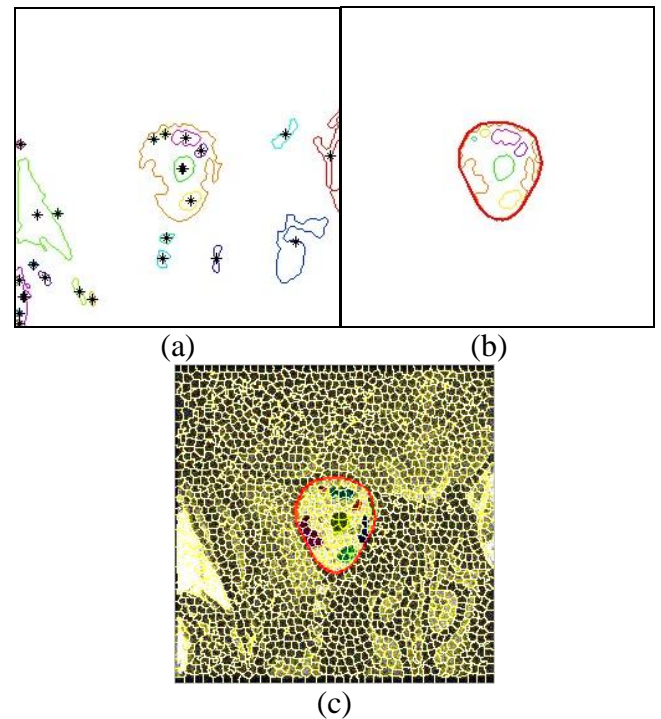


Figure 3: (a) Initial boundaries of the EOMs after normalized cut based on Fig. 2 (b); Orbit and EOM boundaries using convex hull; (c) Superpixels mapped with ROI and the detected EOM regions.

distance between our segmentation with manual segmentation. The average error was 2.75 ± 1.93 (mm). We plan to segment more data sets and perform more quantitative evaluation.

REFERENCES

1. Dal Canto AJ, et al. *Ophthalmology* **113**, 2324-2330, 2006.
2. Firbank MJ, et al. *Magn. Reson. Imaging* **19**, 257-265, 2001.
3. Souza ADA, et al. *Comput. Med. Imaging Graph* **31**, 39-45, 2007.
4. Wei Q, et al. *Proceeding of NACOB'08*, Ann Arbor, MI, USA, 2008.
5. Achanta R, et al. *IEEE Trans. Pattern Anal. Mach. Intell* **34**, 2274-2282, 2012

ACKNOWLEDGEMENTS

The anonymous MRI data was provided by Dr. Joseph Demer at UCLA. This study is supported by Jeffress Trust Awards.

INVESTIGATING THE MECHANISM OF NEONATAL BRACHIAL PLEXUS PALSY USING BIOMECHANICAL TESTING

¹ Thomas Zamorski, ¹ Lindsay Stoy, ² Malaeb Shadi, ² Maria Delivoria, ¹ Anita Singh

¹ Dept. of Biomedical Engineering, Widener University, Chester, PA

² Pediatrics, Physiology, Obstet. & Gynecol., Drexel College of Medicine, Philadelphia, PA
email: asingh2@widener.edu

INTRODUCTION

Despite considerable research and improvements in obstetrical care, permanent Neonatal Brachial Plexus Palsy (NBPP) continues to occur in 1.1-2.2 out of 10,000 births and remains a regular challenge for the affected families and treating physicians [1]. The brachial plexus (BP) is a network of nerves that originate in the neck and run through the shoulder to the arm [2]. Stretching of the BP or avulsion of the roots can occur during birth when the infant's shoulder impacts with the bony pelvis of the mother due to maternal (endogenous) forces as well as clinician-applied (exogenous) forces [2,3]. The effects of these forces on the BP are directly related to: magnitude, loading rate, surrounding tissue properties, and how the applied force is transmitted to the BP. Since *in vivo* measurements of the endogenous and exogenous forces, fetal shoulder deformation, and the response of the BP are difficult to assess during delivery, computational and physical models are used to simulate these events. However, a complete lack of biomechanical properties and data on the neonate BP limits the correct assessment of the risk of injury using these models. Thus, the goal of this study is to determine the biomechanical properties of the BP using a neonatal porcine model (piglets).

MATERIALS AND METHODS

Twenty fresh neonatal (3-5 days old) piglet BP cord segments were harvested and immediately preserved in 1% BSA (bovine serum albumin) until testing. A digital microscope was used to obtain images of harvested BP segments before stretch (5X; Digital Microscope, Elmwood Park, NJ). A 2mm scale (Leitz, Ernst-Leitz-Wetzlar GmbH, Germany) at the same magnification measured the segment diameter.

The BP segments were divided into two groups based on tensile loading rate. Group A (n=10) specimens were subjected to a stretch rate of 0.01 mm/s (quasistatic) and those in Group B (n=10) were subjected to a stretch rate of 10 mm/s (dynamic). Maximum stress, strain, and modulus of elasticity were calculated from the obtained load-displacement data during tensile testing. An ADMET material testing machine (eXpert 7600, ADMET Inc., Norwood, MA) was used to stretch the nerve (Fig. 1). Each BP segment was anchored by specially designed and fabricated clamps (Fig. 1). The design of the clamp allows for clamping of each segment firmly between the padded plexiglass and flat surface of the cylinder. The padded side facing the segment helped minimize the stress concentration at the clamping site [4,5,6]. The two clamps were initially set at a distance of 10-20 mm (depending on the initial length of the BP segment) and the segments were clamped with no initial tension prior to stretch. Stretch rates were controlled by built-in GaugeSafe software (ADMET Inc., Norwood, MA). The actuator was triggered, which stretched the BP segments at their assigned rates (0.01 mm/s or 10 mm/s) until complete failure. During this test, the load and displacement data was acquired at a sampling rate of 25 Hz for quasistatic and 1000 Hz for dynamic stretch rates. After completion of the experiment, the failure site was recorded and the clamps were checked for the presence of BP tissue. No tissue in the clamps implied that the tissue had completely slipped, and the results of those experiments were disregarded. Load data and the cross sectional area was used to calculate nominal stress. Displacement data was used to calculate the tensile strain that results from the applied tension. The load-displacement and stress-strain curves were plotted and the maximum and failure load, maximum and failure stress, strain at the point of maximum

failure and stress, and modulus of elasticity (the slope of the stress-strain curve after toe region and below the proportional limit, E) were determined.

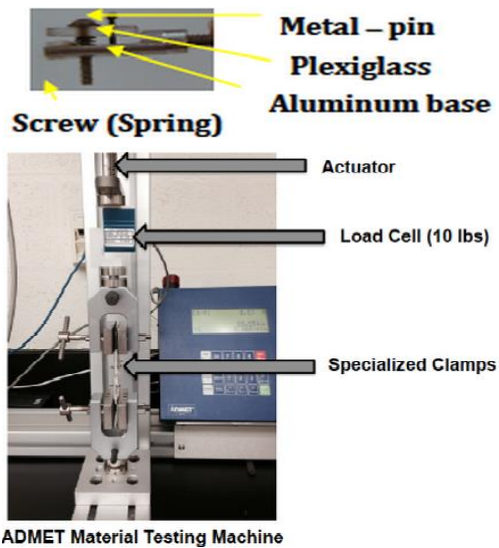


Figure 1: Biomechanical Testing Machine and Clamps

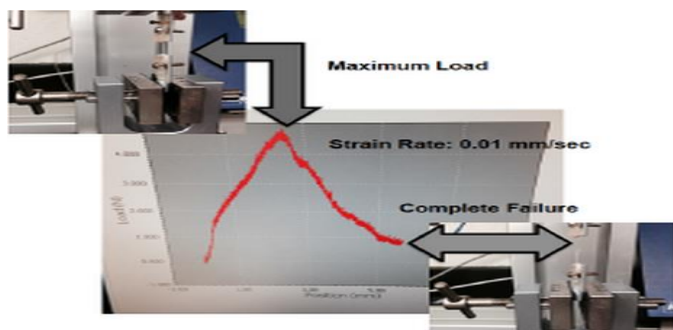


Figure 3: Preliminary Testing of BP Cord Segment at 0.01 mm/sec

Table 1: Mechanical Data of BP Segments

Rate	Failure Stress (MPa)	E (MPa)
Quasistatic (0.01 mm/sec)	11.7	48.5
Dynamic (10 mm/sec)	18.8	108.2

RESULTS

Stress at the proportional limit and apparent elastic modulus were used as indicators of strength, elasticity, and stiffness. Nerve rupture typically occurred immediately after reaching the proportional

limit as shown in Fig. 3. Table 1 contains experimental data for brachial plexus segments tested at both quasistatic and dynamic rates. The average values for the modulus of elasticity are greater for the dynamic rate data than the quasistatic rate data.

CONCLUSION

At a quasistatic strain rate, a lower modulus of elasticity and failure stress was observed and a higher stress and modulus of elasticity was observed at the dynamic rate. This is because the nerve tissue acts in a viscoelastic manner and becomes stiffer at a faster strain rate. Overall, the experimental data provides an accurate approximation to the biomechanical properties of the BP nerve tissue. The dynamics and quasistatic rates are good representations of the various forces acting on the infant during birth. The quasistatic rate could represent the maternal forces of the mother pushing during labor. The dynamic rate could represent sudden impact of the infant’s shoulder with the mother’s pelvis or a sudden clinician-applied force. The data obtained from studying the BP nerve at these two rates helps to better understand the biomechanical properties of the BP and assess the associated injury mechanisms associated with NBPP. This information can be used to develop a biofidelic computational model that accurately illustrates the predisposing risk factors for BP injury.

REFERENCES

1. Chauhan, SP, Blackwell SB, Ananth CV. Seminars in Perinatology, 2014, 8(4):210-218. PMID:24863027
2. N. Zhang, B. Gonik, and M. Grimm, Summer Bioengineering Conference, 2003.
3. M. Grimm, R. Costello, B. Gonik, Am J Obstet Gynecol 2010; 203:339.e1-5.
4. Singh, A, Lu Y, Chen, CY, Kallakuri, S, Cavanaugh, JM. 2006, 50: 601-623. SAE Paper # 2006-22-0023. PMID: 19271962
5. Singh, A, Lu, Y, Chen, C, Cavanaugh, JM. J of Biomechanics, 2006, 39: 1669- 1676. PMID: 15996674
6. Singh, A, Kallakuri, S, Chen, CY, Cavanaugh, JM. 2009, Journal of Neurotrauma, 26:1-14. PMID:17311179